

ORGANOMETALLICS

Volume 14, Number 7, July 1995

© Copyright 1995
American Chemical Society

Communications

The First Pb-Containing Cyclic Polysulfides, 1,2,3,4,5-Tetrathiaplumbolanes, Derived from Kinetically Stabilized Plumbylenes

Norihiro Tokitoh, Naokazu Kano, Kazusato Shibata, and Renji Okazaki*

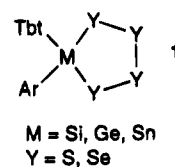
Department of Chemistry, Graduate School of Science, The University of Tokyo, 7-3-1 Hongo,
Bunkyo-ku, Tokyo 113, Japan

Received April 18, 1995[®]

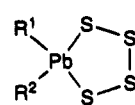
Summary: The first examples of Pb-containing cyclic polysulfides, 1,2,3,4,5-tetrathiaplumbolanes (R^1R^2 - PbS_4 : **2** ($R^1 = Tbt$, $R^2 = Tip$), **3** ($R^1 = Tbt$, $R^2 = Ttm$), and **4** ($R^1 = R^2 = Tip$); $Tbt = 2,4,6$ -tris[bis(trimethylsilyl)methyl]phenyl, $Tip = 2,4,6$ -triisopropylphenyl, and $Ttm = 2,4,6$ -tris[(trimethylsilyl)methyl]phenyl), were synthesized and isolated as stable crystalline compounds by sulfurization of the corresponding kinetically stabilized diarylplumbylenes $Tbt(Tip)Pb$: (**6**), $Tbt(Ttm)Pb$: (**7**), and Tip_2Pb : (**10**). The molecular structures of the novel lead-containing metallacycles **2** and **4** were determined by X-ray crystallographic analysis.

In contrast to the wide chemistry of the transition-metal polychalcogenido complexes,¹ cyclic polychalcogenides containing a main-group element had been unknown until we recently succeeded in the synthesis of novel tetrachalcogenolanes containing a group 14 element, $Tbt(Ar)MY_4$ (**1**: $M = Si, Ge, Sn$; $Y = S, Se$; $Ar = mesityl, 2,4,6$ -triisopropylphenyl (Tip)),² by taking advantage of a new steric protection group, 2,4,6-tris[bis(trimethylsilyl)methyl]phenyl (noted as Tbt hereafter).³

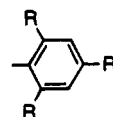
Furthermore, we have found that these overcrowded cyclic polychalcogenides are good precursors of stable group 14 element-chalcogen double-bond compounds,



$M = Si, Ge, Sn$
 $Y = S, Se$



2 ($R^1 = Tbt, R^2 = Tip$)
3 ($R^1 = Tbt, R^2 = Ttm$)
4 ($R^1 = R^2 = Tip$)



Tbt : $R = CH(SiMe_3)_2$
 Ttm : $R = CH_2SiMe_3$
 Tip : $R = CHMe_2$

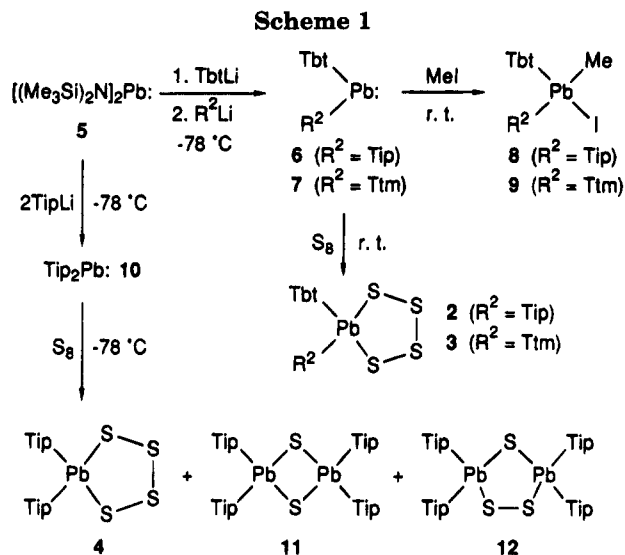
$Tbt(Ar)M=Y$.⁴ Here, we present the synthesis of novel Pb-containing cyclic tetrasulfides, 1,2,3,4,5-tetrathiaplumbolanes ($R^1R^2PbS_4$: **2** ($R^1 = Tbt$, $R^2 = Tip$), **3** ($R^1 = Tbt$, $R^2 = Ttm$), and **4** ($R^1 = R^2 = Tip$); $Ttm = 2,4,6$ -tris[(trimethylsilyl)methyl]phenyl), the heaviest congener of tetrathiolanes containing a group 14 element, together with their crystallographic structure analysis.

We employed kinetically stabilized diarylplumbylenes⁵ as starting materials for the preparation of the lead-containing cyclic polysulfides **2–4**. Ligand ex-

(2) (a) Tokitoh, N.; Suzuki, H.; Matsumoto, T.; Matsuhashi, Y.; Okazaki, R.; Goto, M. *J. Am. Chem. Soc.* **1991**, *113*, 7047. (b) Tokitoh, N.; Matsuhashi, Y.; Okazaki, R. *Tetrahedron Lett.* **1991**, *32*, 6151. (c) Tokitoh, N.; Matsumoto, T.; Okazaki, R. *Tetrahedron Lett.* **1992**, *33*, 2531. (d) Matsuhashi, Y.; Tokitoh, N.; Okazaki, R.; Goto, M.; Nagase, S. *Organometallics* **1993**, *12*, 1351. (e) Matsumoto, T.; Tokitoh, N.; Okazaki, R.; Goto, M. *Organometallics* **1995**, *14*, 1008. Although cyclic polysulfides containing silicon and germanium were prepared by Stuedel et al., they are reportedly stable only below -20 °C. See: Albertsen, J.; Stuedel, R. *Phosphorus, Sulfur, Silicon Relat. Elem.* **1992**, *65*, 165. Stuedel, R. In *The Chemistry of Inorganic Ring Systems*; Stuedel, R., Ed.; Elsevier: Amsterdam, 1992; p 233.

[®] Abstract published in *Advance ACS Abstracts*, June 15, 1995.

(1) Reviews of polychalcogenido complexes: (a) Draganjac, M.; Rauchfuss, T. B. *Angew. Chem., Int. Ed. Engl.* **1985**, *24*, 742. (b) Müller, A.; Diemann, E. *Adv. Inorg. Chem.* **1987**, *31*, 89. (c) Ansari, M. A.; Ibers, J. A. *Coord. Chem. Rev.* **1990**, *100*, 223. (d) Kolis, J. W. *Coord. Chem. Rev.* **1990**, *105*, 195.



change of bis[bis(trimethylsilyl)amino]plumbylene (**5**)^{7a} by sequential nucleophilic substitution with TbtLi and R²Li (R² = Tip, Ttm) in ether at -78 °C afforded the overcrowded diarylplumbylenes **6** and **7**, respectively. Plumbylenes **6** and **7** were found to be stable in solution even at room temperature, showing a characteristic purple color. They were readily trapped with methyl iodide at room temperature to afford the corresponding iodoplumbanes **8** and **9**⁹ in 43 and 33% yields, respectively.¹⁰ In ²⁰⁷Pb NMR, characteristic signals for **6** and **7** were observed as singlets in an extremely downfield region (δ_{Pb} (in toluene-*d*₆ relative to external Me₄Pb) +8888 for **6** and +8873 for **7**), which were unambiguously attributable to those for base-free monomeric plumbylenes.¹¹

The successful formation and the promising reactivity of the kinetically stabilized diarylplumbylenes **6** and **7** prompted us to examine their sulfurization with elemental sulfur, which was reported to be a useful

synthetic method for the lower homologues of tetrachalcogenolanes **1** containing a group 14 element.^{3a,4a} Thus, treatment of **6** and **7** with an excess amount of elemental sulfur gave the corresponding tetrathiaplumbolanes **2** and **3** as stable orange crystals in 68 and 52% yield, respectively.⁹ On the other hand, the reaction of the less hindered plumbylene Tip₂Pb: (**10**)¹² with sulfur in ether at -40 °C afforded the expected tetrathiaplumbolane **4** (20%)⁹ together with byproducts having two plumbylene units, *i.e.* 1,3,2,4-dithiadiplumbetane **11** (13%) and 1,3,4,2,5-trithiadiplumbolane **12** (14%),⁹ suggesting that the Tip group is less effective for steric protection than the Tbt group. All tetrathiaplumbolanes **2–4** here obtained were found to be stable toward air and moisture and could be purified by HPLC followed by silica gel chromatography. In ²⁰⁷Pb NMR the tetrathiaplumbolanes **2–4** showed singlet signals at 313.9, 311.6, and 288.6 ppm (relative to external Me₄Pb in CDCl₃), which are reasonably assigned to those for tetravalent lead compounds.

The tetrathiaplumbolanes **2–4** should be noted as the first examples of Pb-containing cyclic polysulfides, and the molecular structures of **2** and **4** were finally determined by X-ray crystallographic analysis.¹³ The con-

(3) We have recently found that the Tbt group is a useful steric protection group for the kinetic stabilization of a variety of highly reactive chemical species containing heavier typical elements: (a) Tokitoh, N.; Saito, M.; Okazaki, R. *J. Am. Chem. Soc.* **1993**, *115*, 2065. (b) Tokitoh, N.; Matsuhashi, Y.; Okazaki, R. *J. Chem. Soc., Chem. Commun.* **1993**, 407. (c) Tokitoh, N.; Suzuki, H.; Okazaki, R.; Ogawa, K. *J. Am. Chem. Soc.* **1993**, *115*, 10428. See also refs 2 and 4.

(4) (a) Tokitoh, N.; Matsumoto, T.; Manmaru, K.; Okazaki, R. *J. Am. Chem. Soc.* **1993**, *115*, 8855. (b) Matsuhashi, Y.; Tokitoh, N.; Okazaki, R. *Organometallics* **1993**, *12*, 2573. (c) Suzuki, H.; Tokitoh, N.; Nagase, S.; Okazaki, R. *J. Am. Chem. Soc.* **1994**, *116*, 11578. (d) Matsumoto, T.; Tokitoh, N.; Okazaki, R. *Angew. Chem., Int. Ed. Engl.* **1994**, *33*, 2316.

(5) Although Lappert et al. have already described the stable overcrowded dialkylplumbylene [(Me₃Si)₂CH]₂Pb,⁶ most of the other stable plumbylenes reported so far are restricted to the examples thermodynamically stabilized by the heteroatom-containing substituents.⁷ As for the aryl-substituted counterparts, there have been no stable plumbylenes except for the only isolable example, bis[2,4,6-tris(trifluoromethyl)phenyl]plumbylene, stabilized by the intramolecular coordination of the fluorine atoms of its four *o*-trifluoromethyl groups.⁸

(6) Cotton, J. D.; Davidson, P. J.; Lappert, M. F. *J. Chem. Soc., Dalton Trans.* **1976**, 2275.

(7) (a) Harris, D. H.; Lappert, M. F. *J. Chem. Soc., Chem. Commun.* **1974**, 895. (b) Gynane, M. J. S.; Harris, D. H.; Lappert, M. F.; Power, P. P.; Riviere, P.; Riviere-Baudet, M. *J. Chem. Soc., Dalton Trans.* **1977**, 2004. (c) Fjeldberg, T.; Hope, H.; Lappert, M. F.; Power, P. P.; Thorne, A. J. *J. Chem. Soc., Chem. Commun.* **1983**, 639. (d) Çetinkaya, B.; Gümrükçü, I.; Lappert, M. F.; Atwood, J. L.; Rogers, R. D.; Zaworotko, M. J. *J. Am. Chem. Soc.* **1980**, *102*, 2088. (e) Hitchcock, P. B.; Lappert, M. F.; Samways, B. J.; Weinberg, E. L. *J. Chem. Soc., Chem. Commun.* **1983**, 1492.

(8) Brooker, S.; Buijink, J. -K.; Edelman, F. T. *Organometallics* **1991**, *10*, 25.

(9) All the new organolead compounds here obtained showed satisfactory spectral and analytical data, which are described in the supporting information together with the experimental details for their preparation. In the following the preparation of diarylplumbylene **6** and its reaction with elemental sulfur are described as representative examples. *Preparation of 6*: To an ether solution (200 mL) of [(Me₃Si)₂N]₂Pb (**5**), synthesized from PbCl₂ (1.39 g, 5.0 mmol) and lithium hexamethyldisilazide (10.0 mmol) according to the reported method,^{7a} was added at -40 °C an ether suspension (50 mL) of TbtLi, prepared by the treatment of TbtBr (3.16 g, 5.0 mmol) with *t*-BuLi (1.60 M pentane solution, 6.6 mL, 10.5 mmol) at -40 °C, by means of a transfer tube. To the resulting red-brown suspension was added, after gradual warming to -25 °C, an ether suspension (50 mL) of TipLi (prepared from TipBr (1.28 mL, 5.0 mmol) as in the case of TbtLi) to give the dark purple solution of Tbt(Tip)Pb: (**6**). *Reaction of 6 with elemental sulfur*: To the ether solution of **6** thus prepared was added 3.85 g (15.0 mmol as S₈) of elemental sulfur in portions at room temperature. Immediately after the addition of sulfur the reaction mixture turned yellow, and it was stirred for 10 min. After the filtration of insoluble materials with Celite, the filtrate was concentrated under reduced pressure to afford a brown oil, which was purified by GPLC followed by column chromatography (SiO₂/hexane) to give 3.69 g (68%) of **2** as orange crystals. **2**: mp 189–192 °C dec; ¹H NMR (CDCl₃, 500 MHz) δ 0.01 (s, 18H), 0.02 (s, 18H), 0.03 (s, 18H), 1.19 (d, *J* = 6.9 Hz, 6H), 1.23 (d, *J* = 6.5 Hz, 12H), 1.32 (s, 1H), 1.66 (s, ⁴J_{PbH} = 13.1 Hz, 1H), 1.71 (s, ⁴J_{PbH} = 14.7 Hz, 1H), 2.83 (sept, *J* = 6.9 Hz, 1H), 3.28 (sept, *J* = 6.5 Hz, 2H), 6.48 (s, ⁴J_{PbH} = 65.6 Hz, 1H), 6.59 (s, ⁴J_{PbH} = 64.8 Hz, 1H), 7.16 (s, ⁴J_{PbH} = 55.6 Hz, 2H); ¹³C NMR (CDCl₃, 125 MHz) δ 0.8 (q), 1.3 (q), 1.6 (q), 24.0 (q), 25.9 (q), 30.5 (d), 32.1 (d), 32.7 (d), 34.3 (d), 39.5 (d, ³J_{PbC} = 70.6 Hz), 124.1 (d, ³J_{PbC} = 89.7 Hz), 128.8 (d, ³J_{PbC} = 87.8 Hz), 145.2 (s, ⁴J_{PbC} = 20.7 Hz), 149.6 (s), 149.8 (s), 150.7 (s, ⁴J_{PbC} = 19.5 Hz), 152.4 (s, ²J_{PbC} = 89.7 Hz), 165.2 (s, ¹J_{PbC} = 368.6 Hz), 167.6 (s, ¹J_{PbC} = 307.6 Hz); ²⁰⁷Pb NMR (CDCl₃, 56.4 MHz) δ 313.9; high-resolution FABMS *m/z* calcd for C₄₂H₈₃²⁰⁸PbS₄Si₆ 1091.3760, found 1091.3604 (MH⁺). Anal. Calcd for C₄₂H₈₂PbS₄Si₆: C, 46.23; H, 7.57; S, 11.76. Found: C, 46.25; H, 7.70; S, 12.14.

(10) Among the carbene analogues of heavier group 14 elements, a plumbylene is most difficult to trap, since it easily polymerizes accompanying disproportionation. Attempted reaction of the Lappert plumbylene [(Me₃Si)₂CH]₂Pb: with methyl iodide gave no expected insertion product but resulted in the formation of PbI₂.^{7a} The successful isolation of the insertion products **8** and **9** in the present reactions is in sharp contrast to the case of the Lappert plumbylene.

(11) δ_{Pb} of [(Me₃Si)₂CH]₂Pb: (in benzene-*d*₆) was reportedly +9110 relative to external Me₄Pb: Wrackmeyer, B.; Horchler, K.; Zhou, H. *Spektrochim. Acta* **1990**, *46A*, 809. ²⁰⁷Pb NMR resonances of the heteroatom-substituted plumbylenes appear in a rather upfield region (δ_{Pb} +4916 for [(Me₃Si)₂N]₂Pb: (in benzene-*d*₆) and +4260 for ¹BuNSiMe₂N(¹Bu)Pb: (in toluene-*d*₆)). (a) Wrackmeyer, B. *J. Magn. Reson.* **1985**, *61*, 536. (b) Stader, C.; Wrackmeyer, B. *J. Magn. Reson.* **1987**, *72*, 544. For the ²⁰⁷Pb NMR resonance of bis[2,4,6-tris(trifluoromethyl)phenyl]plumbylene, see ref 8.

(12) We have recently reported the formation and several reactions of bis(2,4,6-triisopropylphenyl)plumbylene (**10**), which was found to be stable only below -40 °C: Shibata, K.; Tokitoh, N.; Okazaki, R. *Tetrahedron Lett.* **1993**, *34*, 1495.

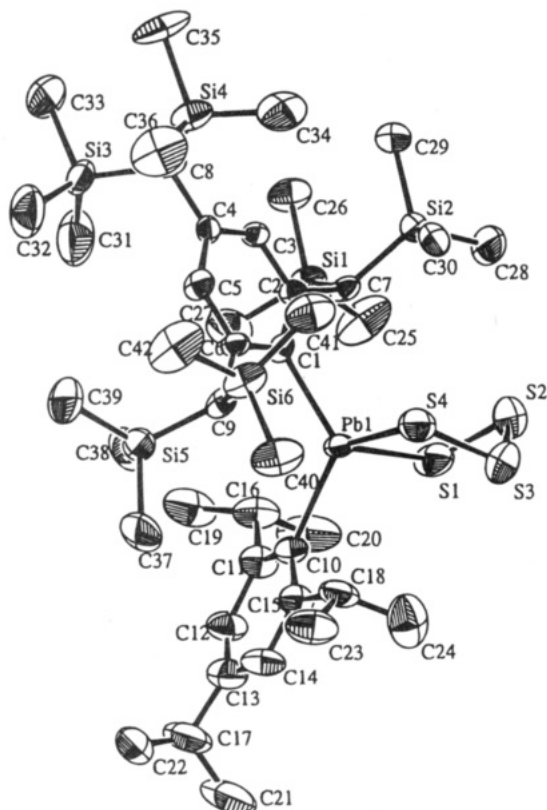


Figure 1. ORTEP drawing of Tbt(Tip)PbS₄ (**2**) with thermal ellipsoid plot (30% probability). Selected bond lengths (Å) and angles (deg): Pb(1)–S(1), 2.553(4); Pb(1)–S(4), 2.564(5); Pb(1)–C(1), 2.28(1); Pb(1)–C(10), 2.29(1); S(1)–S(2), 2.058(8); S(2)–S(3), 2.011(9); S(3)–S(4), 2.020(7); S(1)–Pb(1)–S(4), 92.7(2); S(1)–Pb(1)–C(1), 122.2(3); S(1)–Pb(1)–C(10), 97.5(3); S(4)–Pb(1)–C(1), 97.7(3); S(4)–Pb(1)–C(10), 120.5(4); C(1)–Pb(1)–C(10), 123.6(5); Pb(1)–S(1)–S(2), 99.6(2); S(1)–S(2)–S(3), 103.5(3); S(2)–S(3)–S(4), 102.4(3); Pb(1)–S(4)–S(3), 100.7(3).

formations of their tetrathiaplumbolane rings have almost half-chair geometry in contrast to the previously reported tetrachalcogenolanes **1** containing a group 14 element, the MS₄ rings of which were all found to have highly distorted half-chair (*i.e.*, nearly envelope) conformations.^{2,15}

In Figure 1 is shown an ORTEP drawing of **2** together with some selected bond lengths and angles. The central two sulfur atoms, S(2) and S(3), in the PbS₄ ring lie at almost equal distances (0.60 Å for S(2) and 0.63 Å for S(3)) on both sides of the plane that contains the central lead atom and the two coordinated sulfur atoms

S(1) and S(4).¹¹ Since the bond lengths between the central lead atom and the surrounding four atoms (two ipso carbons and two sulfur atoms in α -positions) are longer than those for the other group 14 element analogues of tetrathiaplumbolanes **1**, the conformation of the tetrathiaplumbolane ring is considered to be less affected by the bulky substituents than those of the other group 14 element analogues. It is quite interesting that the borderline for such noticeable conformational change lies between the tin and lead systems.

Since the plumbynes and tetrathiaplumbolanes here obtained are potentially good precursors for the synthesis of plumbanethiones, a novel class of lead–sulfur double-bond compounds, as in the cases of other group 14 element analogues,⁴ investigation on their further transformation is currently in progress.

Acknowledgment. This work was partially supported by Sumitomo Foundation (N.T.) and a Grant-in-Aid for Scientific Research (No. 05236102) from the Ministry of Education, Science and Culture of Japan. We are grateful to Shin-etsu Chemical Co., Ltd., and Tosoh Akzo Co., Ltd., for generous gifts of chlorosilanes and alkyllithiums, respectively.

Supporting Information Available: Text giving experimental details for the preparation of **2**–**12** together with their spectral and analytical data and tables of crystal data and structural refinement details, positional and thermal parameters, and bond lengths and angles for **2** and **4** (68 pages). Ordering information is given on any current masthead page.

OM950283H

(13) Crystal data for **2**: C₄₂H₈₂PbS₄Si₆, M_r = 1091.06, triclinic, space group P1̄, *a* = 11.653(6) Å, *b* = 24.207(4) Å, *c* = 10.690(2) Å, α = 98.26(1)°, β = 107.39(2)°, γ = 79.54(2)°, *V* = 2817(3) Å³, *Z* = 2, *D_c* = 1.286 g cm⁻³, μ = 33.10 cm⁻¹, *R* (*R_w*) = 0.056 (0.053). Crystal data for **4**: C₃₀H₄₆PbS₄, M_r = 742.13, orthorhombic, space group Pna2₁, *a* = 22.875(6) Å, *b* = 14.26(1) Å, *c* = 10.351(7) Å, α = β = γ = 90°, *V* = 3377(6) Å³, *Z* = 4, *D_c* = 1.460 g cm⁻³, μ = 52.89 cm⁻¹, *R* (*R_w*) = 0.048 (0.049). The intensity data were collected on a Rigaku AFC5R diffractometer with graphite-monochromated Mo K α radiation (λ = 0.710 69 Å). The structures were solved by direct methods with SHELXS-86.¹⁴ All non-hydrogen atoms were refined anisotropically. The final cycle of full-matrix least-squares refinement was based on 4211 (**2**) and 2139 (**4**) observed reflections (*I* > 3.00 σ (*I*)) and 478 (**2**) and 315 (**4**) variable parameters, respectively. Full details for the crystallographic analysis of **2** and **4** are described in the supporting information.

(14) Sheldrick, G. M. SHELXS-86; University of Göttingen: Göttingen, Germany, 1986.

(15) The central two sulfur atoms in the MS₄ ring of the analogous tetrathiaplumbolanes containing a group 14 element, Tbt(Ar)MS₄ (**1**; M = Si, Ge, Sn), are considerably apart from their M–S(1)–S(4) planes (0.21 and 1.02 Å for **1a** (M = Si, Ar = Mes), 0.26 and 0.99 Å for **1b** (M = Ge, Ar = Mes), and 0.31 and 0.93 Å for **1c** (M = Sn, Ar = Mes)).

(16) Also in the case of **4** the central two sulfur atoms S(2) and S(3) in the PbS₄ ring lie at about the same distances (0.59 Å for S(2) and 0.68 Å for S(3)) from the Pb(1)–S(1)–S(4) plane.

Derivative Chemistry of Cationic Triruthenium Carbonyl Cluster Compounds. Reactions Leading to a Neutral Hexanuclear Complex Consisting of Two Vertex-Linked Metal Triangles

Javier A. Cabeza,*[†] Ignacio del Río, and Víctor Riera

Instituto de Química Organometálica "Enrique Moles", Facultad de Química, Universidad de Oviedo-CSIC, E-33071 Oviedo, Spain

Fabrizia Grepioni*

Dipartimento di Chimica "G. Ciamician", Università degli Studi di Bologna, via Selmi 2, I-40126 Bologna, Italy

Received April 26, 1995[®]

Summary: $[Ru_6(\mu_3\text{-ampy})_2(CO)_{18}]$ (**1**; Humpy = 2-amino-6-methylpyridine), the first neutral hexanuclear carbonyl cluster complex consisting of two closed trimetal units connected by only one metal–metal bond (X-ray structure), has been prepared by (a) reaction of the cationic precursor $[Ru_3(\mu_3\text{-ampy})(CO)_{10}]^+$ (**2**) with aqueous NaOH, (b) reaction of complex **2** with the anion $[Ru_3(\mu_3\text{-ampy})(CO)_9]^-$, and (c) zinc reduction of complex **2**.

Recent reviews on structural and bonding aspects of metal cluster chemistry^{1,2} report examples for 22 different structural types corresponding to hexanuclear carbonyl cluster compounds, the most representative ones being those consisting of two closed metal triangles connected by six (octahedron **(A)**), bicapped tetrahedron **(B)**), five (capped square pyramid **(C)**), edge-sharing bi-tetrahedron **(D)**), four (basal edge-bridged square pyramid **(E)**), bi-semicapped square **(F)**), three (trigonal prism **(G)**), rhombic raft **(H)**), or two (bi-edge-bridged square **(I)**) metal–metal bonds (Chart 1).¹ However, only one carbonyl cluster compound corresponding to the simplest structure depicted in Chart 1 **(J)**, consisting of two metal triangles connected to each other by only one metal–metal bond, has been reported so far, namely, the mixed-metal anionic cluster $[Re_4Ir_2(\mu\text{-H})_2(CO)_{22}]^{2-}$.³ We now describe different synthetic approaches to the first neutral carbonyl compound of type **J**, the ruthenium complex $[Ru_6(\mu_3\text{-ampy})_2(CO)_{18}]$ (**1**, Chart 2; Humpy = 2-amino-6-methylpyridine), as well as its X-ray structure. Rational approaches to the preparation of high-nuclearity cluster compounds are now being actively investigated.⁴

The hexanuclear compound **1** was made during the course of a reactivity study of the cationic precursor

Chart 1

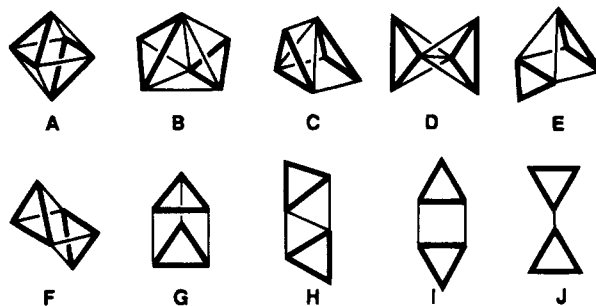
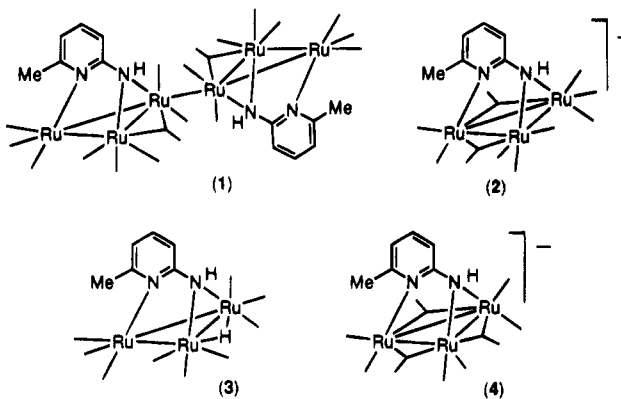


Chart 2



$[Ru_3(\mu_3\text{-ampy})(CO)_{10}][BF_4]$ (**2**; Chart 2).⁵ This compound is the only non-hydridic 48-electron cationic cluster compound reported to date and was expected to have an enhanced reactivity toward nucleophilic reagents due to its cationic nature.

Complex **2** reacts with an excess of aqueous NaOH in 1,2-dichloroethane (**2** is unstable in donor solvents such as alcohols, THF, or acetone) to give a mixture of the known $[Ru_3(\mu\text{-H})(\mu_3\text{-ampy})(CO)_9]$ (**3**; Chart 2) and complex **1**.⁷ A possible mechanism for this transformation is sketched in Scheme 1. It involves the nucleophilic attack of the hydroxide anion on a coordinated CO ligand of complex **2** to give an unstable hydroxycarbonyl derivative which rapidly releases CO_2 , rendering **3**.⁸ Before all complex **2** has been consumed,

(5) Cabeza, J. A.; del Río, I.; Llamazares, A.; Riera, V.; García-Granda, S.; Van der Maelen, J. F. *Inorg. Chem.* **1995**, *34*, 1620.

(6) Andreu, P. L.; Cabeza, J. A.; Riera, V.; Jeannin, Y.; Miguel, D. *J. Chem. Soc., Dalton Trans.* **1990**, 2201.

* E-mail: JAC@DWARF1.QUIMICA.UNIOVI.ES.

[®] Abstract published in *Advance ACS Abstracts*, June 15, 1995.

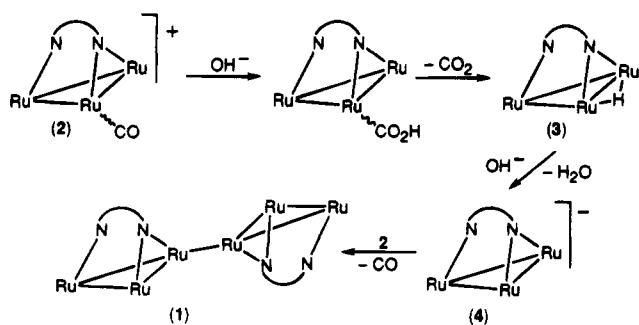
(1) Mingos, D. M. P.; May, A. S. In *The Chemistry of Metal Cluster Complexes*; Shriver, D. F., Kaesz, H. D., Adams, R. D., Eds.; VCH: New York, 1990; Chapter 2, p 11.

(2) (a) Mingos, D. M. P.; Wales, D. J. *Introduction to Cluster Chemistry*; Prentice-Hall International: Englewood Cliffs, NJ, 1990. (b) Farrar, D. H.; Goudsmit, R. J. In *Metal Clusters*; Moskovits, M., Ed.; Wiley: New York, 1986; Chapter 3, p 29.

(3) Beringhelli, T.; Ciani, G.; D'Alfonso, G.; Garlaschelli, L.; Moret, M.; Sironi, A. *J. Chem. Soc., Dalton Trans.* **1992**, 1865.

(4) For a review on the types of reactions that have been useful in preparing cluster complexes in a rational and systematic way, see: Adams, R. D. In *The Chemistry of Metal Cluster Complexes*; Shriver, D. F., Kaesz, H. D., Adams, R. D., Eds.; VCH: New York, 1990; Chapter 3, p 121.

Scheme 1



complex **3** deprotonates with more OH^- to give the anionic derivative $[\text{Ru}_3(\mu_3\text{-ampy})(\text{CO})_9]^-$ (**4**).⁹ Finally, complex **4** reacts with the remaining complex **2** to give **CO** and the hexanuclear cluster **1**.

This reaction sequence is supported by the fact that the reaction of complex **2** with complex **4** does yield the expected hexanuclear cluster **1**.¹⁰ It is interesting to point out that complexes **2** and **3** are insoluble in water and that no anionic complex **4** was formed (IR evidence) when a 1,2-dichloroethane solution of the neutral hydrido complex **3** was treated with an aqueous solution of NaOH unless $[\text{Et}_4\text{N}][\text{BF}_4]$ was added to the mixture. This confirms that the $[\text{BF}_4]^-$ anion is necessary to promote the phase transfer of the OH^- groups from the aqueous to the organic phase. It should also be noted that, in the reaction of complex **2** with aqueous NaOH , the organic phase contains initially only 1 equiv of the $[\text{BF}_4]^-$ anion; therefore, only 1 equiv of OH^- anion can be transferred to the organic phase. This and the observation of **1** and **3** (but not **2** and **4**) in the product mixture imply that at least $1/2$ equiv of OH^- reacts with complex **2** to give **3**; the remaining OH^- reacts with **3** to form the anion **4**, which finally couples with the unreacted **2** to give **1**.

The dimeric structure of the 94-electron cluster **1** (Figure 1) suggested that it could also be prepared by a

(7) Aqueous NaOH (0.2 mL, 10 M) was added to a solution of complex **2** (100 mg, 0.129 mmol) in 1,2-dichloroethane (20 mL). The color changed from dark red to brown. After it was stirred for 20 min, the solution was concentrated in vacuo to ca. 2 mL and chromatographed in a short column (10 \times 3 cm) of neutral alumina (activity IV). Elution with hexane-dichloromethane (3:1) afforded two bands. The second band (orange) contained complex **3** (IR, ^1H NMR).⁶ The first band (brown), which partially decomposed within the column to give **3**, afforded complex **1** as a very dark brown, nearly black, solid (16 mg, 24%). Anal. Found: C, 32.42; H, 1.23; N, 5.31. Calcd for $\text{C}_{30}\text{H}_{14}\text{N}_4\text{O}_{18}\text{Ru}_6$: C, 32.25; H, 1.37; N, 5.48. IR (CH_2Cl_2): $\nu(\text{CO})$: 2079 (w), 2061 (s), 2039 (vs), 1996 (s, br), 1975 (sh), 1853 (w, br) cm^{-1} . ^1H NMR (CDCl_3): 7.31 (t, $J = 7.8$ Hz, 1 H), 6.79 (d, $J = 7.8$ Hz, 1 H), 6.40 (d, $J = 7.8$ Hz, 1 H), 4.34 (s, br, 1 H, NH), 2.77 (s, 3 H, Me) ppm. $^{13}\text{C}\{^1\text{H}\}$ NMR (CD_2Cl_2): 240.7, 218.3, 203.1, 202.8, 202.4, 197.9, 196.8, 196.6, 188.1 (CO ligands), 174.9, 160.4, 138.9, 120.3, 111.2, 30.0 (ampy ligand) ppm.

(8) The nucleophilic attack of OH^- groups on coordinated CO ligands is well documented. See, for example: Schatz, W.; Neumann, H.-P.; Nuber, B.; Kanellakopolus, B.; Ziegler, M. L. *Chem. Ber.* **1991**, *124*, 453.

(9) (a) The deprotonation of neutral hydrido carbonyl cluster complexes with alcoholic solutions of KOH to give anionic derivatives has been reported. See, for example: Barner-Thorsen, C.; Hardcastle, K. I.; Rosenberg, E.; Siegel, J.; Manotti-Lanfredi, A. M.; Tiripicchio, A.; Tiripicchio-Camellini, M. *Inorg. Chem.* **1981**, *20*, 4306. (b) Complex **4** (PPN salt), as the analogous $[\text{PPN}][\text{Ru}_3(\mu_3\text{-ampy})(\text{CO})_9]$ (Hanpy = 2-anilinoypyridine), can also be made by reaction of its neutral precursor (**3**) with $[\text{PPN}][\text{BH}_4]$. See: Lugan, N.; Laurent, F.; Lavigne, G.; Newcomb, T. P.; Liimata, E. W.; Bonnet, J.-J. *J. Am. Chem. Soc.* **1990**, *112*, 8607.

(10) Equivalent amounts (0.076 mmol) of $[\text{Ru}_3(\mu_3\text{-ampy})(\text{CO})_{10}][\text{BF}_4]$ (**2**) and $[\text{PPN}][\text{Ru}_3(\mu_3\text{-ampy})(\text{CO})_9]$ (**4**)^{9b} were dissolved in 1,2-dichloroethane (10 mL) to give a dark brown solution which was worked up as in ref 7 to give complex **1** in 32% yield.

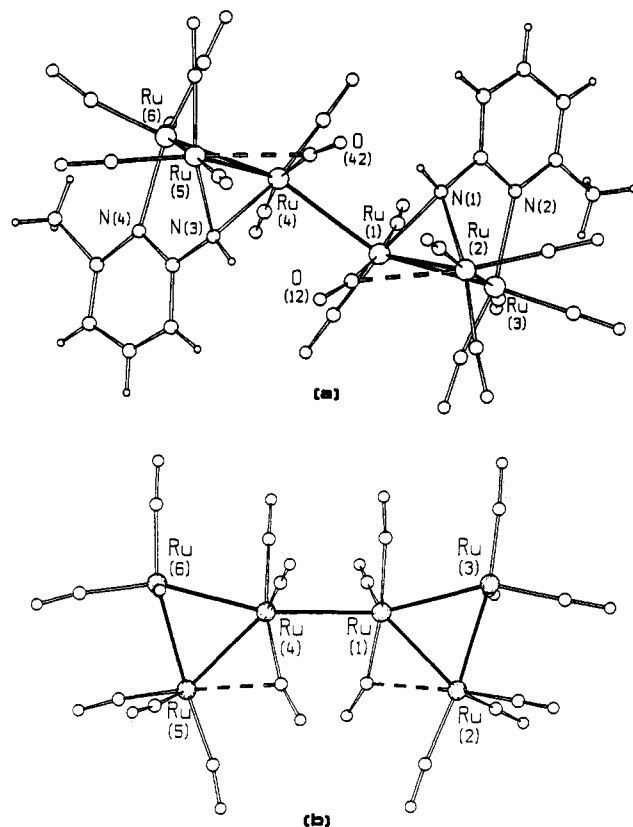


Figure 1. (a) Molecular structure of complex **1** viewed along the pseudo-2-fold axis. Relevant bond distances (\AA): Ru(1)–Ru(2), 2.734(4); Ru(1)–Ru(3), 2.778(4); Ru(2)–Ru(3), 2.732(4); Ru(4)–Ru(5), 2.726(4); Ru(4)–Ru(6), 2.777(4); Ru(5)–Ru(6), 2.726(4); Ru(1)–Ru(4), 2.855(4); N(1)–Ru(1), 2.18(2); N(1)–Ru(2), 2.10(2); N(2)–Ru(3), 2.21(2); N(3)–Ru(4), 2.18(2); N(3)–Ru(5), 2.09(2); N(4)–Ru(6), 2.22(2). (b) Projection in the metal frame main plane, showing the *cis* configuration of the two Ru_3 triangles. The two ampy ligands have been omitted for clarity.

1-electron reduction reaction of the cationic complex **2**, since this should lead to the 49-electron radical $[\text{Ru}_3(\mu_3\text{-ampy})(\text{CO})_{10}]$ which would lose CO and undergo dimerization to give **1**. In fact, complex **1** was also made by reacting complex **2** with zinc dust in 1,2-dichloroethane.¹¹ So far, we have been unable to prepare complex **1** by chemical oxidation of the anionic complex **4**.

The synthetic methods reported herein are significantly different from that used in the preparation of $[\text{Re}_4\text{Ir}_2(\mu\text{-H})_2(\text{CO})_{22}]^{2-}$, the only previously known hexanuclear carbonyl cluster of type **J**, which involves treatment of $[\text{Re}_2(\mu\text{-H})_2(\text{CO})_8]$ with $[\text{Ir}(\text{CO})_4]^-$ to give $[\text{Re}_2\text{IrH}(\mu\text{-H})(\text{CO})_{12}]^-$; subsequently, this trinuclear adduct releases CO and H_2 and undergoes dimerization, rendering the hexanuclear dianion.³

As the analytical and spectroscopic data of complex **1**⁷ were insufficient to unequivocally assign a structure, an X-ray diffraction study was carried out.¹² The solid-state molecular structure of compound **1** is shown in Figure 1. The metal frame consists of two Ru_3 triangular units linked by one Ru–Ru bond. The intertriangular Ru(1)–Ru(4) bond is appreciably longer than the average value of the remaining metal–metal bonds

(11) A mixture of complex **2** (50 mg, 0.065 mmol) and zinc dust (0.3 g) in 1,2-dichloroethane (15 mL) was stirred at reflux temperature for 45 min. The solids were filtered off, and the brown solution was worked up as in ref 7 to give complex **1** in 30% yield.

(2.855(4) vs 2.744(4) Å), as previously observed in the rhenium non-carbonyl cluster $[\text{Re}_6(\mu\text{-Cl})_6(\mu\text{-H})(\text{CH}_2\text{-SiMe}_3)_3]$ (intertriangle Re–Re distance 2.993(1) Å vs an average intriangle distance of 2.405(1) Å).¹³ In **1**, the two triangles are almost coplanar (maximum deviation from the mean plane of the six atoms 0.37 Å). The idealized molecular symmetry is C_2 , with the pseudo 2-fold axis bisecting the Ru(1)–Ru(4) bond and parallel to the plane defined by the two triangles. The two Ru₃ triangles adopt a *cis* configuration with respect to the Ru(1)–Ru(4) bond, as shown in Figure 1. In this aspect, the molecular geometry is different from that of the rhenium cluster previously mentioned,¹³ where the two coplanar Re₃ triangles conform to the geometry shown for structure **J** in Chart 1 and that of the anionic cluster $[\text{Re}_4\text{Ir}_2(\mu\text{-H})_2(\text{CO})_{22}]^{2-}$, where the two Re₂Ir triangles adopt a staggered *trans* configuration.³ Two CO ligands asymmetrically bridge two Ru–Ru bonds (Ru(1)–C(12) = 1.95(4), Ru(2)–C(12) = 2.56(3) Å; Ru(4)–C(42) = 1.99(3), Ru(5)–C(42) = 2.57(3) Å), while the remaining CO ligands are all terminally bound. The two ampy ligands bind to the two triangles on opposite sites and contribute five electrons each to the cluster. In both ligands, the two N–Ru bond distances associated with the bridging amido moiety are appreciably different (N(1)–Ru(1) = 2.18(2), N(1)–Ru(2) = 2.10(2) Å; N(3)–Ru(4) = 2.18(2), N(3)–Ru(5) = 2.09(2) Å). All N–Ru bond distances fall

(12) (a) Crystal and selected refinement data for **1**: $\text{C}_{30}\text{H}_{14}\text{N}_4\text{O}_{18}\text{-Ru}_6$, $M_r = 1324.87$, monoclinic, space group $P2_1/c$, $a = 13.192(7)$ Å, $b = 20.32(1)$ Å, $c = 17.876(4)$ Å, $\beta = 107.64(3)^\circ$, $V = 4567(4)$ Å³, $Z = 4$, $D_c = 1.927$ g cm⁻³, $F(000) = 2520$, $\mu(\text{Mo K}\alpha) = 20.02$ cm⁻¹, $2.5 < \theta < 25^\circ$, final $R1$ value (on F , $I > 2\sigma(I)$) = 0.077, $wR2$ (on F^2 , all data) = 0.281 for 7661 unique reflections. Data were collected at room temperature on an Enraf-Nonius CAD-4 diffractometer, equipped with a graphite monochromator (Mo K α radiation, $\lambda = 0.71069$ Å), by the ω - 2θ scan method. The structure was solved by direct methods^{12b} followed by difference Fourier syntheses and subsequent least-squares refinement on F^2 using SHELX93.^{12c} All non-H atoms were treated anisotropically. The H atoms were added in calculated positions and refined riding on their respective C atoms. Residual electron density (< 1.00 e Å⁻³) was found in the proximity of the molecules, indicating the presence of a disordered solvent. A detailed analysis of the crystal packing also revealed small cavities among the molecules in correspondence with the residual peaks. However, neither the nature nor the amount of this solvent could be unambiguously determined. The impossibility of locating and refining the solvent is partially responsible for the not quite satisfactory refinement result. (b) Walker, N.; Stuart, D. *Acta Crystallogr.* **1983**, *A39*, 158. (c) Sheldrick, G. M. SHELX93, Program for Crystal Structure Determination; University of Göttingen: Göttingen, Germany, 1993.

(13) Mertis, K.; Edwards, P. G.; Wilkinson, G.; Malik, K. M. A.; Hursthouse, M. B. *J. Chem. Soc., Dalton Trans.* **1981**, 705.

within the range observed for other Ru₃^{5,14} and Ru₆¹⁵ clusters containing the ampy ligand in the same coordination mode.

The observation of nine carbonyl resonances in the solution ¹³C NMR spectrum of complex **17** supports either a static C_2 structure, as in the solid state, or free rotation around the Ru(1)–Ru(4) bond. However, the X-ray diffraction study reveals that the proximity of the semibridging carbonyl ligands impedes such rotation. The proximity of these ligands may also account for their high ¹³C NMR chemical shift (240.7 ppm).

In conclusion, this communication reports the synthesis of a hexanuclear ruthenium cluster complex of a novel structural type using three different synthetic methods: (a) the reaction of a cluster cation with aqueous NaOH, (b) the reaction of a cluster anion with a cluster cation,¹⁶ and (c) the reduction of a cluster cation. These methods have never been used before for the synthesis of high-nuclearity clusters, and it is anticipated that they will be useful to many other cluster chemists. Further studies on the reactivity of the cationic complex **2** are in progress.

Acknowledgment. This research was supported by the DGICYT (Spain, Project PB92-1007) and the CNR (Italy).

Supporting Information Available: An ORTEP plot and tables of crystal data, atomic coordinates, bond distances and angles, anisotropic thermal parameters, and H-atom coordinates for complex **1** (11 pages). Ordering information is given on any current masthead page.

OM950303F

(14) See, for example: (a) Andreu, P. L.; Cabeza, J. A.; Riera, V.; Bois, C.; Jeannin, Y. *J. Chem. Soc., Dalton Trans.* **1990**, 3347. (b) Cabeza, J. A.; García-Granda, S.; Llamazares, A.; Riera, V.; Van der Maelen, J. F. *Organometallics* **1993**, *12*, 157. (c) Briard, P.; Cabeza, J. A.; Llamazares, A.; Ouahab, L.; Riera, V. *Organometallics* **1993**, *12*, 1006. (d) Cabeza, J. A.; Fernández-Colinas, J. M.; Llamazares, A.; Riera, V.; García-Granda, S.; Van der Maelen, J. F. *Organometallics* **1994**, *13*, 4352.

(15) Cabeza, J. A.; Fernández-Colinas, J. M.; García-Granda, S.; Llamazares, A.; López-Ortiz, F.; Riera, V.; Van der Maelen, J. F. *Organometallics* **1994**, *13*, 426.

(16) Treatment of anionic clusters with cationic mononuclear complexes has been used for the synthesis of "large" clusters. See, for example: (a) Reference 4. (b) Voss, E. J.; Stern, C. L.; Shriver, D. W. *Inorg. Chem.* **1994**, *33*, 1087 and references therein. (c) Lewis, J.; Li, C.-K.; Al-Mandhary, M. R. A.; Raithby, P. R. *J. Chem. Soc., Dalton Trans.* **1993**, 1915 and references therein. (d) Evans, J.; Stroud, P. M.; Webster, M. *J. Chem. Soc., Dalton Trans.* **1991**, 2027.

Hydroboration of Alkynes with Pinacolborane Catalyzed by HZrCp₂Cl

Schubert Pereira and Morris Srebnik*

Department of Chemistry, University of Toledo, Toledo, Ohio 43606

Received April 18, 1995[®]

Summary: Pinacolborane (1.05 equiv) hydroborates both terminal and internal alkynes, in the presence of 5 mol % zirconocene chloride hydride (HZrCp₂Cl) at 25 °C, in excellent yields and with excellent regio- and stereoselectivity. Without HZrCp₂Cl and under otherwise identical conditions, hydroboration proceeds to an extent of only 2–20%.

Catecholborane (CBH),¹ like other dioxaborolane or dioxaborinane² hydrides, is a sluggish hydroborating reagent, requiring elevated temperatures to assure an adequate rate of hydroboration of alkynes and alkenes. In 1985 Männig and Nöth reported that Rh(PPh₃)₃Cl catalyzes hydroboration of alkenes with CBH at ambient temperature and in the process different chemo- and regioselectivity was observed.³ Mechanistically, an oxidative-addition/reductive-elimination mechanism was postulated.⁴ In 1987 the rhodium-catalyzed hydroboration of acetylene by borazine was reported.⁵ In 1988 the enantioselective version of this reaction was reported,⁶ and in the same year diastereoselective studies with this reagent system were initiated.⁷ In 1992 organolanthanides were reported to catalyze hydroboration of alkenes with CBH.⁸ A different mechanism was presented. Metal-catalyzed hydroboration of alkynes or alkenes with other dioxaborolane or dioxaborinane hydrides apparently has not been investigated.⁹ However, in many instances the preferred boronic ester is pinacol since these esters are stable to aqueous workup and chromatography.¹⁰ Pinacol boronates can be prepared by hydroboration with HBBR₂SMe₂, followed by hydrolysis and esterification of the boronic ester with pinacol, or by transesterification.¹¹ However, HBBR₂ is quite Lewis acidic and may not be compatible with acid-sensitive groups. Recently, Knochel reported the preparation and reactivity of pinacolborane (PBH; **1**).¹² Hy-

Table 1. Hydroboration of Alkynes with PBH in the Presence of HZrCp₂Cl^a

entry no.	R ₁	R ₂	product ratio ^b 3:4:5:6	yield ^c (%)
1	2a CH ₃ (CH ₂) ₅ -	H	98:2:0:0	93.1
2	2b Cl(CH ₂) ₃ -	H	96.8:2.4:0:0.8	94.3
3	2c Me ₃ Si-	H	90.3:2.2:3.2:4.3	86.7
4	2d cyclopentyl	H	97.5:0.7:0:1.8	93.7
5	2e Me ₃ C-	H	100:0:0:0	95.2
6	2f Ph-	H	97.2:0.8:0.7:0.9	74.7
7	2g Ph(CH ₂) ₃ -	H	98.3:1.7:0:0	87.2
8	2h <i>i</i> -Pr-	CH ₃ -	96.9:2.2:0:0.9	93.8
9	2i Me ₃ C-	CH ₃ -	100:0:0:0	91.5
10	2j Et-	Et-	100:0:0:0	92.6
11	2k (EtO) ₂ CH-	H	81.9:10.8:7.3:0	82.2
12	2l MeOCH ₂ -	H	95.0:2.5:2.5:0	86.8
13	2m Me ₃ SiC≡CCH ₂ -	H	96.3:2.5:0.8:0.4	81.5

^a For general experimental conditions, see ref 14. ^b Determined by GC on a 30 m methylsilicone column and by integration of the corresponding methyl peaks in the 400 MHz ¹H NMR spectra. ^c Isolated yields.

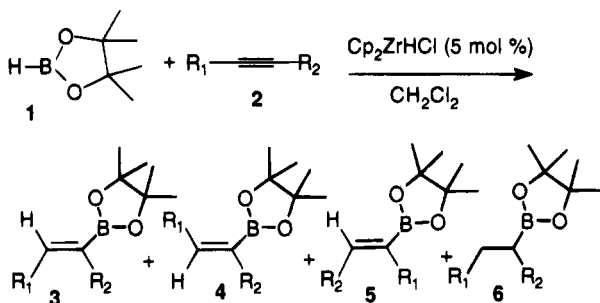
droboration of alkynes under Knochel's conditions requires 2 equiv of PBH. In the course of our studies on the reactions of borazirconocenes, we observed very facile boron migrations (apparently involving PBH) that suggested zirconium-mediated catalysis.¹³ In this communication we present our results on HZrCp₂Cl-catalyzed hydroboration of alkynes with PBH.¹⁴

When 1-octyne (1 equiv) was added to a solution of PBH (2 M, 1.05 equiv, CH₂Cl₂) containing 5 mol % HZrCp₂Cl, an orange color developed over time (2 h) that slowly disappeared. After the mixture was stirred for 24 h at 25 °C, aqueous workup afforded **3a** (Table 1, entry 1) in 93% yield as essentially pure material.¹⁵ (The same reaction without HZrCp₂Cl afforded **3a** in 2% yield when PBH prepared *in situ* was used or in 20% yield when PBH distilled and isolated was utilized in the hydroboration.) The sequence is outlined in Scheme 1.

In addition to the desired alkenylboronates **3**, other products were detected. The products of *anti* addition, **4**, were produced in small quantities. Indeed, *syn*

[®] Abstract published in *Advance ACS Abstracts*, June 1, 1995.
 (1) (a) Brown, H. C.; Gupta, S. K. *J. Am. Chem. Soc.* **1975**, *97*, 5249.
 (b) *Ibid.* **1972**, *94*, 4370.
 (2) (a) Woods, W. G.; Strong, P. L. *J. Am. Chem. Soc.* **1966**, *88*, 4667.
 (b) Fish, R. H. *J. Am. Chem. Soc.* **1968**, *90*, 4435.
 (3) Männig, D.; Nöth, H. *Angew. Chem., Int. Ed. Engl.* **1985**, *25*, 878.
 (4) The oxidative-addition product with Wilkinson's catalyst was isolated: Kono, H.; Ito, K. *Chem. Lett.* **1975**, 1095.
 (5) Lynch, A. T.; Sneddon, L. G. *J. Am. Chem. Soc.* **1987**, *109*, 5867.
 (6) Burgess, K.; Ohlmeyer, M. J. *J. Org. Chem.* **1988**, *53*, 5178.
 (7) Evans, D. A.; Fu, G. C.; Hoveyda, A. H. *J. Am. Chem. Soc.* **1988**, *110*, 6917.
 (8) Harrison, K. N.; Marks, T. J. *J. Am. Chem. Soc.* **1992**, *114*, 9220.
 (9) For a review, see: Burgess, K.; Ohlmeyer, M. J. *Chem. Rev.* **1991**, *91*, 1179.
 (10) For a review of the chemistry of organoboranes, see: (a) Matteson, D. S. In *The Chemistry of the Metal-Carbon Bond*; Hartley, F. R., Ed.; Wiley: Chichester, U.K., 1987; Vol 4, p 307. (b) Pelter, A.; Smith, K.; Brown, H. C. *Borane Reagents*. In *Best Synthetic Methods*; Katritzky, A. R., Meth-Cohn, O., Rees, C. W., Eds.; Academic Press: London, 1988.
 (11) Brown, H. C.; Bhat, N. G.; Somayaji, V. *Organometallics* **1983**, *2*, 1311.
 (12) Tucker, C. E.; Davidson, J.; Knochel, P. *J. Org. Chem.* **1992**, *57*, 3482.

(13) Pereira, S.; Srebnik, M. Unpublished results.
 (14) For other catalytic reactions involving zirconium, see: (a) Negishi, E.; Takahashi, T. *Acc. Chem. Res.* **1994**, *27*, 124. (b) Dzhe-milev, U. M.; Vostrikova, O. S.; Ibragimov, A. G. *Russ. Chem. Rev. (Engl. Transl.)* **1988**, *55*, 66.
 (15) **General experimental procedure for the hydroboration of alkynes by pinacolborane in the presence of HZrCp₂Cl:** A 2 mL round-bottom flask equipped with a side arm and stirring bar is charged with alkyne (0.5 mmol) and CH₂Cl₂ (0.25 mL), under an inert atmosphere, and cooled to 0 °C. Pinacolborane (0.525 mmol, 0.067 g) is then added dropwise via a syringe. After the mixture is stirred for 1 min, the reaction mixture is transferred by a double-ended needle to another 2 mL flask, immersed in an ice bath, containing Cp₂ZrHCl (0.025 mmol, 6.5 mg). After this mixture is warmed to ambient temperature, stirring is continued for 16 h, at which point the reaction is quenched with H₂O (0.5 mL). The mixture is extracted with ether (2 × 5 mL), washed with water (3 × 5 mL), dried with anhydrous MgSO₄ (0.5 g), filtered, and analyzed by GC. Isolation of products is achieved by removing volatile matter under reduced pressure followed by chromatography on a silica gel column if necessary.

Scheme 1. Hydroboration of Alkynes with PBH Catalyzed by HZrCp₂Cl


selectivity in the present case is among the best observed for hydroboration¹⁶ and is comparable to the results obtained with the uncatalyzed reaction.¹² Regioisomers **5** were occasionally observed, but in negligible quantities. The exception is **5k** (7.3%). This may be due to coordination of the hydroborating reagent with the oxygen atoms of the acetal.¹⁷ Nevertheless, the results indicate that the reaction is compatible with acid-sensitive functional groups. Hydrogenation products **6** were sometimes detected, but generally in very small amounts.¹⁸ Certainly, the lack of side products demonstrates the benefits associated with PBH over catechol, which often is accompanied by side products.¹⁹ The reaction works well for a variety of alkynes, both terminal and internal. Of importance is that only a slight excess of PBH is required. The results are summarized in Table 1.

Zirconocene dichloride was ineffective as a hydroboration catalyst and, indeed, appeared to retard the reaction.²⁰ Cole has demonstrated that vinyl groups from 1-alkenylzirconocene chlorides readily transfer to

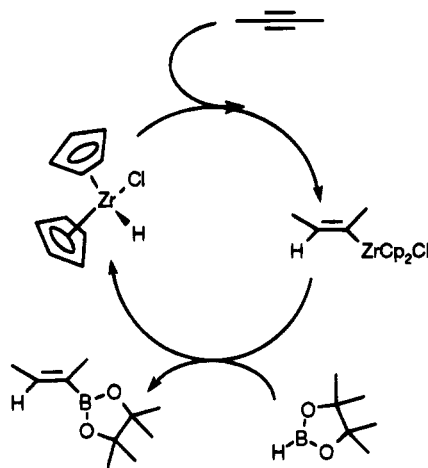
(16) For a review, see: Zaidlewicz, M. In *Comprehensive Organometallic Chemistry*; Wilkinson, G., Stone, F. G. A., Abel, E. W., Eds.; Pergamon Press: Oxford, U.K., 1982; Vol. 7, p 161.

(17) (a) Brown, H. C.; Unni, M. K. *J. Am. Chem. Soc.* **1968**, *90*, 2902. For additional examples of directive effects in hydroboration, see: (b) Still, W. C.; Barrish, J. C. *J. Am. Chem. Soc.* **1983**, *105*, 2489. (c) Harada, T.; Matsuda, Y.; Wada, I.; Uchimura, J.; Oku, A. *J. Chem. Soc. Chem. Commun.* **1990**, 21.

(18) Compounds **6** presumably arise from hydrolysis of the corresponding *gem*-borazirconocene alkanes: (a) Zheng, B.; Srebnik, M. *J. Organomet. Chem.* **1994**, *474*, 49. (b) Deloux, L.; Skrzypczak-Jankun, E.; Cheesman, B. V.; Sabat, M.; Srebnik, M. *J. Am. Chem. Soc.* **1994**, *116*, 10302.

(19) (a) For a discussion of the side reactions that occur in transition-metal-catalyzed hydroborations, see ref 9, p 1181. (b) Hydroboration of **2a** with 1.1 equiv of catecholborane in the presence of 5 mol % HZrCp_2Cl , using our general experimental procedure, gave products **3–6** in the ratio of 94.0:3.4:2.6:0, in 92% yield. Thus, *syn* selectivity is not as good as with PBH. Catecholboronates are water-sensitive and partially decompose on column chromatography. For the above reasons, PBH seems to be the reagent of choice in this reaction.

(20) Teuben has recently demonstrated that other zirconocene compounds, i.e., Cp_2ZrMe_2 , are not effective catalysts in the hydroboration of alkenes with CBH: Bijpost, E. A.; Duchateau, R.; Teuben, J. H. *J. Mol. Catal.* **1995**, *95*, 121.

Scheme 2. Proposed Cycle for HZrCp₂Cl-Catalyzed Hydroboration of Alkynes with Pinacolborane


B-chlorocatecholborane.²¹ ¹¹B NMR of an equimolar mixture of zirconocene dichloride and PBH in CH_2Cl_2 showed no change in the chemical shift or multiplicity of PBH over the course of 24 h.²² PBH, therefore, does not reduce zirconocene chloride under our conditions. Mechanistically, these observations are consistent with initial hydrozirconation of the alkyne to give a transient alkenylzirconocene chloride. Vinyl and hydride exchange then occur to give the product and regenerate HZrCp_2Cl in a manner not unlike the mechanism of lanthanide-catalyzed hydroboration of alkenes with catecholborane proposed by Marks.⁷ A proposed cycle is outlined in Scheme 2.²³

In conclusion, pinacolborane may be used in stoichiometric quantities to hydroborate alkynes at 25 °C by the novel use of HZrCp_2Cl as a catalyst. *syn* selectivity and regioselectivity are excellent. This intriguing catalysis is being further developed in our laboratories on related and other systems.

Acknowledgment. S.P. thanks the University of Toledo for a teaching fellowship. We thank Dr. Dean Giolando for useful discussions.

Supporting Information Available: Text giving general experimental details and figures giving ¹H NMR and ¹³C NMR spectra for pinacolboronates **3a–m** (34 pages). Ordering information is given on any current masthead page.

OM9502749

(21) Cole, T. E.; Quintanilla, R.; Rodewald, S. *Organometallics* **1991**, *10*, 3777.

(22) Catecholborane: ¹¹B NMR (CD_3Cl , 128.3 MHz) δ 27.9 (d, *J* = 175 Hz) (cf. ref 12).

(23) Indeed, hydrozirconation of the alkyne with 5 mol % HZrCp_2Cl followed by hydroboration with PBH yielded results identical with those obtained by using the protocol described in the general experimental procedure, in support of the contention that hydrozirconation is the first step.

Coordination Properties of Novel Tridentate Cyclopentadienyl Ligands in Titanium and Zirconium Complexes

Karen E. du Plooy, Ulrich Moll,[†] Sigrid Wocadlo, Werner Massa, and Jun Okuda*

Fachbereich Chemie der Philipps-Universität Marburg,
Hans-Meerwein-Strasse, D-35032 Marburg, Germany

Received April 6, 1995[®]

Summary: Tridentate-linked amido-cyclopentadienyl ligands $C_5Me_4SiMe_2NCH_2R$ with a neutral donor site R ($R = CH_2OMe, CH_2NMe_2, CH=CH_2$) have been synthesized and coordinated at tetravalent titanium and zirconium centers. The molecular structure of $Zr(\eta^5-\eta^1-C_5Me_4SiMe_2NCH_2CH_2NMe_2)Cl_2$ (**4b**) was determined by a single-crystal X-ray structural analysis, revealing an unusual trigonal-bipyramidal zirconium center with the $CH_2CH_2NMe_2$ moiety interacting with the zirconium center.

Bent metallocenes of early transition metals and lanthanides have led to the impressive recent development of homogeneous α -olefin polymerization catalysts. They contain an electronically and sterically constrained coordination sphere around the metal that restricts the substrate reactivity within the wedge created by the two cyclopentadienyl ligands.¹ Although mono(cyclopentadienyl)-transition-metal complexes can accommodate, in addition to one cyclopentadienyl ligand, as many as six ligands, a less crowded ligand sphere is commonly observed which should lead to potentially higher reactivity toward α -olefins.² For instance, the linked amido-cyclopentadienyl ligands introduced by Bercaw and Shapiro^{3,4} have provided scandium complexes ($(\eta^5-\eta^1-C_5Me_4SiMe_2NMe_2)ScR$) with significantly enhanced

Lewis acidity as compared to *ansa*-metallocenes. They represent the first examples of homogeneous single-component living α -olefin polymerization catalysts.^{3a-c} In order to better control the coordinative unsaturation in such strongly electrophilic metal complexes, we envisaged a ligand system in which a side chain with a weak neutral *additional donor site* is appended to the anchoring amido-cyclopentadienyl ligand framework.⁵ The use of such a semilabile ligand system may result in a reactivity pattern where the side chain can either interact with or expose the metal center.⁶ We report here that a linked amido-cyclopentadienyl ligand with an additional pendant neutral coordination site such as OMe, NMe₂, or C=C may act as a novel type of flexible tridentate ligand⁷ for tetravalent titanium and zirconium centers.

In analogy to the procedure for the synthesis of $C_5Me_4HSiMe_2NHCMe_3$,^{3c} the reaction of chlorodimethyl(tetramethylcyclopentadienyl)silane with the substituted lithium amides $Li(NHCH_2R)$ ($R = CH_2OMe, CH_2NMe_2, CH=CH_2$) straightforwardly gave the new ligand precursors **1** in excellent yields as distillable oils.⁸ Double deprotonation of analytically pure **1** with 2 equiv of *n*-butyllithium in hexane quantitatively yielded colorless solids of the dilithium "salts" $Li_2[C_5Me_4SiMe_2NCH_2R]$ (**2**). Reaction of **2a,b** with $TiCl_3(THF)_3$ in THF followed by oxidation with $PbCl_2^9$ afforded the titanium complexes **3a,b** in good yields as slightly air-sensitive, hexane-soluble, orange crystals.¹⁰ ¹H and ¹³C NMR spectra of **3a,b** recorded at ambient temperature revealed that the molecules possess a mirror plane. In

(5) For related bidentate amino- and imido-functionalized cyclopentadienyl ligands, see: (a) Clark, T. J.; Nile, T. A.; McPhail, D.; McPhail, A. T. *Polyhedron* **1989**, *8*, 1804. (b) Wang, T. F.; Lee, T. Y.; Wen, Y. S.; Liu, L. K. *J. Organomet. Chem.* **1991**, *403*, 353. (c) Wang, T. F.; Wen, Y. S. *J. Organomet. Chem.* **1992**, *439*, 155. (d) Wang, T. F.; Lee, T. Y.; Chou, J. W.; Ong, C. W. *J. Organomet. Chem.* **1992**, *423*, 31. (e) Jutzi, P.; Kristen, M. O.; Dahlhaus, J.; Neumann, B.; Stammier, H.-G. *Organometallics* **1993**, *12*, 2980. (f) van der Hende, J. R.; Hitchcock, P. B.; Lappert, M. F.; Nile, T. A. *J. Organomet. Chem.* **1994**, *472*, 79. (g) Antonelli, D. M.; Green, M. L. H.; Mountford, P. *J. Organomet. Chem.* **1992**, *438*, C4. (h) Flores, J. C.; Chien, J. C. W.; Rausch, M. D. *Organometallics* **1994**, *13*, 4140. (i) Jutzi, P.; Kleimeier, J. *J. Organomet. Chem.* **1995**, *486*, 287. (j) Herrmann, W. A.; Morawietz, M. J. A.; Priemer, T.; Mashima, K. *J. Organomet. Chem.* **1995**, *486*, 291.

(6) For a brief review on chelating cyclopentadienyl ligands, see: Okuda, J. *Comments Inorg. Chem.* **1994**, *16*, 185.

(7) During the course of this work, very similar tridentate cyclopentadienyl ligands appeared in the literature: (a) Fryzuk, M. D.; Mao, S. S. H.; Zaworotko, M. J.; MacGillivray, L. R. *J. Am. Chem. Soc.* **1993**, *115*, 5336. (b) Fryzuk, M. D.; Mao, S. S. H.; Duval, P. B.; Rettig, S. J. *Polyhedron* **1995**, *14*, 11. (c) Mu, Y.; Piers, W. E.; MacGillivray, L. R.; Zaworotko, M. J. *Polyhedron* **1995**, *14*, 1.

(8) $(C_5Me_4H)SiMe_2(NHCH_2CH_2NMe_2)$ (**1b**): yellow oil; 78% yield; bp 80 °C/10⁻² Torr. Anal. Calcd for $C_{15}H_{30}N_2Si$: C, 67.60; H, 11.35; N, 10.51. Found: C, 67.34; H, 11.55; N, 10.40.

(9) Luinstra, G. A.; Teuben, J. H. *J. Chem. Soc., Chem. Commun.* **1990**, 1470.

[†] Current address: BASF AG, ZKP, D-67056 Ludwigshafen, Germany.

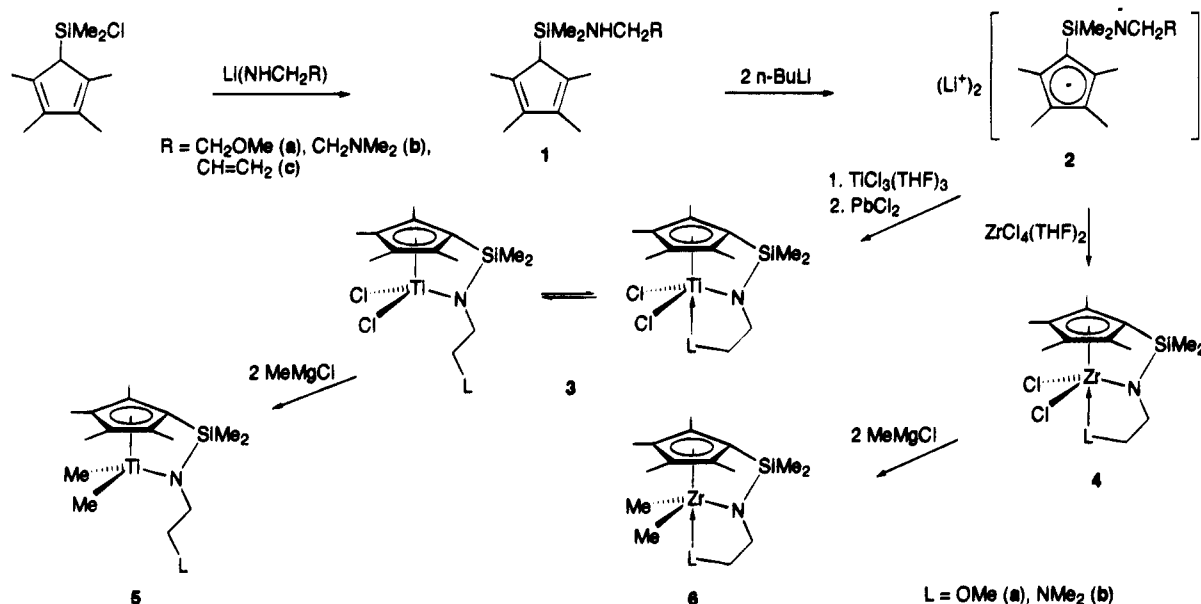
[®] Abstract published in *Advance ACS Abstracts*, June 1, 1995.

(1) Lauher, J. W.; Hoffmann, R. *J. Am. Chem. Soc.* **1976**, *98*, 1729.
(2) Syndiospecific styrene polymerization catalysts: (a) Ishihara, N.; Kuramoto, M.; Uoi, M. *Macromolecules* **1988**, *21*, 3356. (b) Chien, J. C. W.; Salajka, Z. *J. Polym. Sci., Part A* **1991**, *29*, 1243. (c) Pellecchia, C.; Longo, P.; Proto, A.; Zambelli, A. *Makromol. Chem., Rapid Commun.* **1992**, *13*, 265. (d) Kucht, A.; Kucht, H.; Barry, S.; Chien, J. C. W.; Rausch, M. D. *Organometallics* **1993**, *12*, 3075. (e) Ready, T. E.; Day, R. O.; Chien, J. C. W.; Rausch, M. D. *Macromolecules* **1993**, *26*, 5822. Olefin polymerization: (f) Quyoum, R.; Wang, Q.; Tudoret, M.-J.; Baird, M. C. *J. Am. Chem. Soc.* **1994**, *116*, 6435. (g) Pellecchia, C.; Immirzi, A.; Grassi, A.; Zambelli, A. *Organometallics* **1993**, *12*, 4473. (h) Chernega, A. N.; Gómez, R.; Green, M. L. H. *J. Chem. Soc., Chem. Commun.* **1993**, 1415. (i) Ricci, G.; Italia, S.; Giarusso, A.; Porri, L. *J. Organomet. Chem.* **1993**, *451*, 67. Alkyl cations: (j) Crowther, D. J.; Jordan, R. F.; Baenzigener, N. C.; Verma, A. *Organometallics* **1990**, *9*, 2574.

(3) (a) Shapiro, P. J.; Bunel, E.; Schaefer, W. P.; Bercaw, J. E. *Organometallics* **1990**, *9*, 867. (b) Piers, W. E.; Shapiro, P. J.; Bunel, E. E.; Bercaw, J. E. *Synlett* **1990**, *2*, 74. (c) Shapiro, P. J.; Cotter, W. D.; Schaefer, W. P.; Labinger, J. A.; Bercaw, J. E. *J. Am. Chem. Soc.* **1994**, *116*, 4632. (d) Schaefer, W. P.; Cotter, W. D.; Bercaw, J. E. *Acta Crystallogr., Sect. C* **1993**, *49*, 1489.

(4) (a) Okuda, J. *Chem. Ber.* **1990**, *123*, 1649. (b) Hughes, A. K.; Meetsma, A.; Teuben, J. H. *Organometallics* **1993**, *12*, 1936. (c) Okuda, J.; Schattenmann, F. J.; Wocadlo, S.; Massa, W. *Organometallics* **1995**, *14*, 789. (d) Canich, J. A. (Exxon Chemical Co.), U.S. Patent 5,026,798, 1991. (e) Stevens, J. C.; Timmers, F. J.; Rosen, G. W.; Knight, G. W.; Lai, S. Y. (Dow Chemical Co.), European Patent Application, EP 0 416 815 A2, 1991. (f) Stevens, J. C. *Metcon* **93**, Houston, May 26–28, 1993; p 157. (g) Woo, T. K.; Fan, L.; Ziegler, T. *Organometallics* **1994**, *13*, 2252. (h) Herrmann, W. A.; Morawietz, M. J. A. *J. Organomet. Chem.* **1994**, *482*, 169.

Scheme 1



particular, the CH₂CH₂ link gives rise to two tripletlike AA'X' signals in the ¹H NMR spectrum. These data do not allow one to distinguish whether the additional donor site in the side chain is rigidly coordinated in a symmetrical fashion, does not interact at all with the metal center, or is involved in a fluxional coordination (on the NMR time scale). On the basis of the temperature dependence of the NMR spectra, we presently favor the last possibility for **3a,b**.¹¹

The syntheses of the zirconium derivatives **4a,b** were performed by reacting **2** with ZrCl₄(THF)₂ in toluene, resulting in the isolation of toluene-soluble, colorless crystals in good yields.¹² ¹H and ¹³C NMR spectroscopic data again show the same basic feature as for the titanium complexes, **3a,b**, thus not unambiguously proving the coordination mode.¹³ A single-crystal X-ray structural analysis of the NMe₂-functionalized **4b** revealed, however, that the side chain is in fact coordinated.¹⁴ The coordination sphere of the linked amido-

cyclopentadienyl moiety in **4b** can be considered to be derived from the monomeric (η⁵:η¹-C₅Me₄SiMe₂NCMe₃)-ZrCl₂.^{4d-f} As in all scandium and group 4 complexes containing the C₅R'₄SiMe₂NCMe₃ ligand system,^{3,4} the amido nitrogen atom is planar as a result of the strong p_π-d_π bonding. The dimethylamino function of the side chain interacts with the 14-electron zirconium center to create a distorted trigonal bipyramid with the C₅Me₄ and the NMe₂ groups occupying the apical positions. It is noteworthy that mono(cyclopentadienyl)-metal complexes with this configuration are extremely scarce.^{15,16}

Treatment of the dichlorides **3a,b** with 2 equiv of methylmagnesium chloride gave quantitative yields of yellow, hexane-soluble dimethyl complexes **5a,b**, respectively. The resonance for both of the titanium methyl groups in **5b** is recorded in the ¹H NMR spectrum as a singlet at δ 0.33 and in the ¹³C NMR spectrum as a quartet at δ 48.8 with ¹J(C,H) = 118 Hz.¹⁷ The ¹H NOESY spectra (C₆D₆, 25 °C, t_{mix} = 2.0 s) of both **5a** and **5b** showed that NOE is absent between the TiMe signal and the OMe and NMe₂ groups, indicating that the side chain is not coordinated at the titanium center.¹⁸ The reaction of the zirconium dichlorides **4a,b** also smoothly afforded the dimethyl complexes **6a,b** as hexane-soluble, colorless crystals.¹⁷ In contrast to the titanium complexes **5a,b**, the zirconium complexes retain the intramolecular coordination in

(10) Ti(η⁵:η¹-C₅Me₄SiMe₂NCH₂CH₂NMe₂)Cl₂ (**3b**): 57% yield; mp 142 °C; ¹H NMR (C₆D₆, 25 °C) δ 0.34 (s, 6 H, SiCH₃), 2.06 (s, 6 H, ring CH₃), 2.14 (s, 6 H, ring CH₃), 2.31 (s, 6 H, N(CH₃)₂), 2.61 ("t", 2 H, CH₂NMe₂), 3.49 ("t", 2 H, SiNCH₂); ¹³C NMR (C₆D₆, 25 °C) δ 2.2 (SiCH₃), 13.2, 15.9 (ring CH₃), 47.1 (N(CH₃)₂), 53.4 (SiNCH₂), 60.7 (CH₂NMe₂), 105.3 (ring C attached to SiMe₂), 136.7, 137.6 (ring C). Anal. Calcd for C₁₅H₂₈Cl₂N₂SiTi: C, 47.00; H, 7.36; N, 7.31. Found: C, 47.00; H, 7.32; N, 6.83.

(11) In the unsubstituted analog Ti(η⁵:η¹-C₅H₄SiMe₂NCH₂CH₂NMe₂)Cl₂ the ligand is tridentate according to a preliminary X-ray crystal structural analysis.²²

(12) Zr(η⁵:η¹-C₅Me₄SiMe₂NCH₂CH₂NMe₂)Cl₂ (**4b**): colorless crystals from toluene; 65% yield; mp 125 °C; ¹H NMR (C₆D₆, 25 °C) δ 0.36 (s, 6 H, SiCH₃), 2.09 (s, 6 H, ring CH₃), 2.12 (s, 6 H, ring CH₃), 2.35 (s, 6 H, N(CH₃)₂), 2.52 ("t", 2 H, CH₂NMe₂), 2.92 ("t", 2 H, SiNCH₂); ¹³C NMR (C₆D₆, 25 °C) δ 2.3 (SiCH₃), 12.2, 14.4 (ring CH₃), 46.9 (SiNCH₂), 47.3 (N(CH₃)₂), 62.3 (CH₂NMe₂), 102.2 (ring C attached to SiMe₂), 129.1, 131.3 (ring C). Anal. Calcd for C₁₅H₂₈Cl₂N₂SiZr: C, 42.23; H, 6.62; N, 6.57. Found: C, 43.19; H, 6.08; N, 6.16.

(13) Tetravalent zirconium complexes containing the linked amido-cyclopentadienyl ligand may have a three-legged piano-stool structure or may coordinate another two-electron ligand.^{4e-f}

(14) Crystal data for **4b**: colorless cubes, C₁₅H₂₈Cl₂N₂SiZr, M_r = 426.60, monoclinic, space group P2₁/n, a = 8.456(1) Å, b = 13.699(1) Å, c = 16.686(1) Å, β = 96.59(1)°, V = 1920.1(3) Å³, Z = 4, D_{calcd} = 1.476 g cm⁻³, F(000) = 880. Data in the range 2 < 2θ < 24° were collected at 293(2) K using Mo Kα radiation on a Siemens P4 diffractometer. The structure was solved by direct methods and refined by full-matrix least-squares techniques against all F² data. GOF = 1.067, wR2 = 0.0751 for all 3021 reflections, and R = 0.0273 for 2623 observed reflections with I > 2σ(I).

(15) Kubacek, P.; Hoffmann, R.; Havlas, Z. *Organometallics* **1982**, *1*, 180. Despite the large number of half-sandwich complexes of the general type (C₅R₅)ML_{4-n}X_n (see: Poli, R. *Chem. Rev.* **1991**, *91*, 509), there is only a small amount of indirect evidence for trigonal-bipyramidal configuration; e.g.: Abugideiri, F.; Gordon, J. C.; Poli, R.; Owens-Waltermire, B. E.; Rheingold, A. L. *Organometallics* **1993**, *12*, 1575. We thank Professor R. Poli for kindly providing us with this information.

(16) Liu, A. H.; Murray, R. C.; Dewan, J. C.; Santarsiero, B. D.; Schrock, R. R. *J. Am. Chem. Soc.* **1987**, *109*, 4282.

(17) Ti(η⁵:η¹-C₅Me₄SiMe₂NCH₂CH₂NMe₂)Me₂ (**5b**): 43% yield; mp 45 °C. Anal. Calcd for C₁₇H₃₄N₂SiTi: 59.62; H, 10.01; N, 8.18. Found: C, 59.33; H, 9.75; N, 8.30. Zr(η⁵:η¹-C₅Me₄SiMe₂NCH₂CH₂NMe₂)Me₂ (**6b**): off-white microcrystals; 55% yield; mp 58 °C. Anal. Calcd for C₁₇H₃₄N₂SiZr: C, 52.93; H, 8.88; N, 7.26. Found: C, 52.55; H, 8.76; N, 7.13.

(18) As one possible consequence of the noncoordination of the side chain, the dimethyl complexes **5a,b** show modest activity for ring-opening polymerization of ε-caprolactone as well as for the syndiospecific polystyrene formation upon activation with methylaluminumoxane.

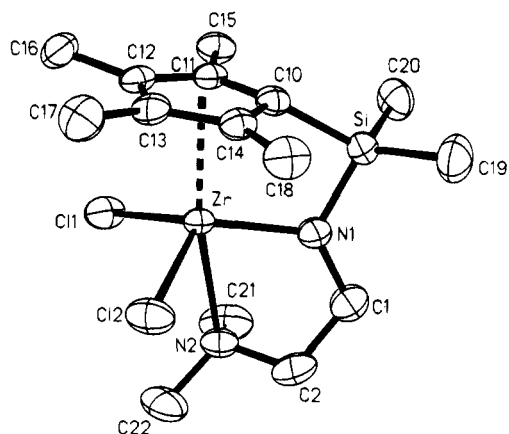
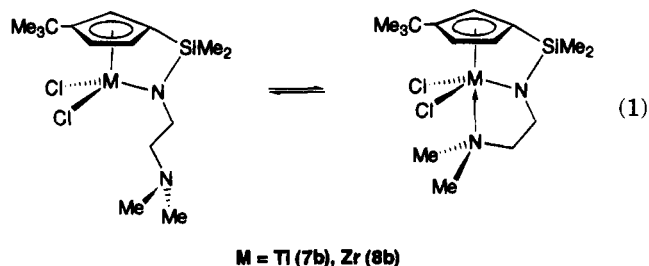


Figure 1. ORTEP view of the molecular structure of **4b**. Thermal ellipsoids are drawn at the 50% probability level. Hydrogen atoms are omitted for the sake of clarity. Selected bond distances (Å) and angles (deg): Zr–N1, 2.077(2); Zr–N2, 2.491(2); Zr–Cl(av), 2.450(1); Zr–C10, 2.443(3); Zr–C11, 2.501(3); Zr–C12, 2.629(3); Si–N1, 1.724(3); C11–Zr–C12, 109.60(3); N1–Zr–N2, 70.69(9); Si–N1–Zr, 108.9(1); C1–N1–Zr, 125.5(2); Si–N1–C1, 125.2(2).

solution, as deduced from the room-temperature NOE-SY spectra for **6a,b**. There is clearly an NOE between the proton signals for ZrMe₂ and both OMe and NMe₂.

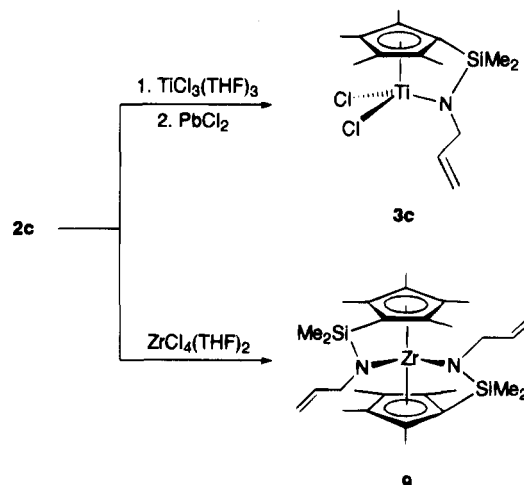
Since a rigid coordination of the NMe₂ group will prevent nitrogen inversion, the nonequivalence of the NMe₂ groups in the planar chiral derivative M{η⁵:η¹:η⁵-C₅(CMe₃)H₃SiMe₂NCH₂CH₂NMe₂}Cl₂ would directly reveal the presence of the intramolecular coordination of the NMe₂ function (eq 1). Thus, the titanium complex



7b shows one signal for both of the NMe₂ groups and for the zirconium analog **8b** two distinct resonances are recorded.¹⁹ In agreement with the data found for **3–6**, a fluxional coordination is found in **7b**, whereas a fairly rigid intramolecular coordination exists in **8b**.

In order to utilize the chelate effect to examine the possible intramolecular C=C bond coordination at a d⁰ metal center,²⁰ we also attempted to coordinate the allyl substituted ligands **1c** at titanium and zirconium, following the above described procedures. The titanium derivative **3c** could be isolated as a brown powder that lacks any direct evidence for a rigid coordination of the allyl group.²¹ Quite unexpectedly, the reaction of ZrCl₄(THF)₂ with **2c** resulted in the formation of the C₂-symmetric zirconocene derivative Zr(η⁵:η¹-C₅Me₄SiMe₂-NCH₂CH=CH₂)₂ (**9**) as highly hexane-soluble, beige crystals. At this time, we account for our failure to obtain the homolog of **3c** as due to the high solubility of the lithium salt **2c** in toluene.²² The high concentra-

Scheme 2



tion of **2c** relative to ZrCl₄(THF)₂ in the reaction mixture apparently resulted in the predominant formation of the metallocene derivative. We are continuing to utilize such flexible polydentate ligand systems in the context of designing coordination spheres that may support highly electrophilic early-metal centers.

Acknowledgment. Generous financial support by the Volkswagen-Foundation, the Fonds der Chemischen Industrie, the Deutsche Forschungsgemeinschaft (Grant No. SFB 260), and the donors of the Petroleum Research Fund, administered by the American Chemical Society, is gratefully acknowledged. K.E.D. thanks the Alexander-von-Humboldt Foundation and U.M. BASF for a scholarship.

Supporting Information Available: Listings of all crystal data and refinement parameters, atomic parameters (including hydrogen atoms), thermal parameters, and bond lengths and angles for **4b** (10 pages). Ordering information is given on any current masthead page.

OM9502493

(19) Ti(η⁵:η¹:η¹-C₅(CMe₃)H₃SiMe₂NCH₂CH₂NMe₂)Cl₂ (**7b**): orange-red oil; ¹H NMR (C₆D₆, 25 °C) δ 0.27 (br s, 6 H, SiCH₃), 1.34 (s, 9 H, C(CH₃)₃), 1.90 (s, 6 H, N(CH₃)₂), 2.34 (m, 2 H, CH₂NMe₂), 4.14 (m, 2 H, CH₂NSi), 6.23 (m, 1 H, ring H), 6.26 (m, 1 H, ring H), 6.85 (m, 1 H, ring H); ¹³C{¹H} NMR (C₆D₆, 25 °C) δ -2.4, -1.5 (SiCH₃), 30.9 (C(CH₃)₃), 33.6 (C(CH₃)₃), 45.6 (N(CH₃)₂), 55.4 (SiNCH₂), 60.0 (CH₂NMe₂), 111.0 (s, ring C attached to SiMe₂), 120.8, 125.1, 126.2, 153.3 (s, ring C); EI MS *m/z* 383 (25%, M⁺ + H), 382 (50%, M⁺ - CH₃). Zr(η⁵:η¹:η¹-C₅(CMe₃)H₃SiMe₂NCH₂CH₂NMe₂)Cl₂ (**8b**): white crystals; ¹H NMR (C₆D₆, 25 °C) δ 0.19, 0.25 (s, 3 H, SiCH₃), 1.47 (s, 9 H, C(CH₃)₃), 2.08, 2.55 (s, 3 H, N(CH₃)₂), 1.89, 3.20 (m, 1 H, CH₂NMe₂), 2.82, 2.90 (m, 1 H, CH₂NSi), 6.04 (m, 1 H, ring H), 6.30 (m, 1 H, ring H), 7.03 (m, 1 H, ring H); ¹³C{¹H} NMR (C₆D₆, 25 °C) δ -3.3, -2.0 (SiCH₃), 31.4 (C(CH₃)₃), 33.3 (C(CH₃)₃), 44.9, 48.7 (N(CH₃)₂), 47.3 (SiNCH₂), 62.6 (CH₂NMe₂), 107.0 (s, ring C attached to SiMe₂), 115.6, 118.1, 126.4, 146.9 (s, ring C); EI MS *m/z* 426 (24%, M⁺ + H), 424 (18%, M⁺ - CH₃), 368 (38%, M⁺ - C₄H₉), 366 (13%, M⁺ - C₃H₇N), 58 (100%, C₃H₈N⁺). Anal. Calcd for C₁₅H₂₈N₂Cl₂SiZr: C, 42.23; H, 6.62; N, 6.57. Found: C, 44.28; H, 7.17; N, 6.72.

(20) Okuda, J.; du Plooy, K. E.; Toscano, P. J. *J. Organomet. Chem.*, in press.

(21) Ti(η⁵:η¹-C₅Me₄SiMe₂NCH₂CH=CH₂)Cl₂ (**5c**): dark brown powder; 54% yield; mp 88 °C. Anal. Calcd for C₁₄H₂₃Cl₂NSiTi: C, 47.74; H, 6.58; N, 4.00. Found: C, 47.40; H, 6.44; N, 4.10.

(22) The same difficulty was encountered during the synthesis of the unsubstituted analogs of **3a,b**. However, reaction of Ti(η⁵-C₅H₄-SiMe₂Cl)Cl₃ (Ciruelos, S.; Cuenca, T.; Gomez-Sal, P.; Manzanero, A.; Royo, P. *Organometallics* **1995**, *14*, 177) with 1.33 equiv of Li(NCH₂R) led to the desired compounds. Okuda, J.; Rose, U.; du Plooy, K. E.; Kang, H.-C.; Massa, W., unpublished results.

Constrained-Geometry Titanium(II) Diene Complexes. Structural Diversity and Olefin Polymerization Activity

David D. Devore,* Francis J. Timmers, and Dennis L. Hasha

The Dow Chemical Company, Midland, Michigan 48674

Robert K. Rosen

The Dow Chemical Company, Freeport, Texas 77541

Tobin J. Marks,* Paul A. Deck, and Charlotte L. Stern

Department of Chemistry, Northwestern University, Evanston, Illinois 60208-3113

Received March 8, 1995[⊗]

Summary: Reduction of $(\eta^5\text{-}\eta^1\text{-C}_5\text{Me}_4\text{SiMe}_2\text{NR})\text{TiCl}_2$ with $n\text{BuLi}$ in the presence of various 1,3-dienes yields $(\eta^5\text{-}\eta^1\text{-C}_5\text{Me}_4\text{SiMe}_2\text{NR})\text{Ti}(\text{diene})$ complexes. The diene coordination mode (π , formally Ti(II), or metallacyclic, formally Ti(IV)) and the activity for olefin polymerization (which can be very high) are highly sensitive to the identity of R.

The recent development of "constrained geometry" catalysts has had a major impact on homogeneous olefin polymerization technologies¹ and necessitates a better understanding of basic organo-group 4 metal chemistry with $\eta^5\text{-}\eta^1\text{-C}_5\text{Me}_4\text{SiMe}_2\text{NR}$ ancillary ligation.^{2,3} Multi-hapto ligands such as 1,3-dienes, which engage in a variety of bonding modes, offer a direct probe of $(\text{C}_5\text{Me}_4\text{SiMe}_2\text{NR})\text{M}$ steric and electronic requirements which can then be compared to and contrasted with those of more conventional group 4 Cp_2M and CpM metal-diene ligand arrays.^{4,5} We communicate here the synthesis and unusual structural characteristics and diversities, as well as high olefin polymerization activities, of the first series of $(\text{C}_5\text{Me}_4\text{SiMe}_2\text{NR})\text{Ti}(\text{diene})$ complexes.

$(\text{C}_5\text{Me}_4\text{SiMe}_2\text{NR})\text{Ti}(\text{diene})$ complexes are readily synthesized by reduction of the $(\text{C}_5\text{Me}_4\text{SiMe}_2\text{NR})\text{TiCl}_2$ precursors (1) with 2 equiv of $n\text{BuLi}$ in the presence of dienes in refluxing hexane (eq 1).^{6,7} Isolated yields of the dark purple complexes range from 20 to 97% after optional recrystallization from hexane.⁷ As indicated

by NMR spectroscopy and X-ray diffraction (vide infra), minor changes in the ancillary ligation ($\text{R}_1 = t\text{Bu} \rightarrow \text{R}_1$

(7) (a) Generalized procedure (using **2b** as example): In an inert-atmosphere glovebox, 0.500 g (1.36 mmol) of $(\text{C}_5\text{Me}_4\text{SiMe}_2\text{N}^t\text{Bu})\text{TiCl}_2$ was dissolved into approximately 50 mL of dry, degassed hexane. To this yellow solution was added 2.70 mL of technical grade piperylene (27.1 mmol) followed by 1.09 mL of $n\text{BuLi}$ (2.72 mmol, 2.5 M in hexanes). Addition of the latter resulted in an immediate color change to dark red. The reaction mixture was heated to reflux for 45–60 min, after which time it was cooled to room temperature. The solution was filtered through Celite, using 10 mL of additional hexane to wash the insoluble byproducts. The combined hexane filtrate was taken to dryness under reduced pressure, yielding the product, $(\text{C}_5\text{Me}_4\text{SiMe}_2\text{N}^t\text{Bu})\text{Ti}(\text{prone-trans-1,3-pentadiene})$, as a red-purple solid in 97% yield (0.97 g). Analytical and spectroscopic data for complex **2b** are as follows. ¹H NMR (C_6D_6 , ppm): δ 4.01 (m, $\text{CHH}=\text{CHCH}=\text{CHCH}_3$, 1H); 3.84 (m, $\text{CHH}=\text{CHCH}=\text{CHCH}_3$, 1H); 2.97 (m, $\text{CHH}=\text{CHCH}=\text{CHCH}_3$, 1H); 2.13 (s, C_5Me_4 , 3H); 2.1 (multiplet, partly overlapped by two singlets, $\text{CHH}=\text{CHCH}=\text{CHCH}_3$, 1H); 2.05 (s, C_5Me_4 , 3H); 1.88 (d, $\text{CHH}=\text{CHCH}=\text{CHCH}_3$, 3H, $J_{\text{HH}} = 5.5$ Hz); 1.75 (dd, $\text{CHH}=\text{CHCH}=\text{CHCH}_3$, 1H, $J_{\text{HH}} = 13.3, 7.3$ Hz); 1.23, 1.21 (s each, C_5Me_4 , 3H each); 1.16 (s, $t\text{Bu}$, 9H); 0.76, 0.73 (s each, SiMe_2 , 3H each). ¹³C{¹H} NMR (C_6D_6 , ppm): δ 8.12, 8.88, 14.37, 16.08 (C_5Me_4); 11.60 (SiMe_2); 19.14 ($\text{CH}_2=\text{CHCH}=\text{CHCH}_3$); 35.27, 57.22 ($t\text{Bu}$); 61.75 ($\text{CH}_2=\text{CHCH}=\text{CHCH}_3$); 76.76 ($\text{CH}_2=\text{CHCH}=\text{CHCH}_3$); 103.73 (C_5 carbon attached to Si); 107.67, 114.99 ($\text{CH}_2=\text{CHCH}=\text{CHCH}_3$); 123.17, 123.44, 130.51 (C_5 ring, remaining resonance under C_6D_6). Anal. Calcd for $\text{C}_{20}\text{H}_{35}\text{NSiTi}$: C, 65.73; H, 9.65; N, 3.83. Found: C, 66.36; H, 9.73; N, 3.59. (b) Complex **2a** was prepared similarly to **2b** in 20% yield. ¹H NMR (C_6D_6 , ppm): δ 3.73 (m, $\text{CH}(\text{CH}_3)\text{CHCHCH}(\text{CH}_3)$, 2H); 2.1 (m, partially overlapped by a C_5Me_4 singlet, $\text{CH}(\text{CH}_3)\text{CHCHCH}(\text{CH}_3)$, 2H); 2.11 (s, C_5Me_4 , 6H); 1.89 (d, $\text{CH}(\text{CH}_3)\text{CHCHCH}(\text{CH}_3)$, 6H, $J_{\text{HH}} = 5.4$ Hz); 1.24 (s, C_5Me_4 , 6H); 1.13 (s, $t\text{Bu}$, 9H); 0.73 (s, SiMe_2 , 6H). ¹³C{¹H} NMR (C_6D_6 , ppm): δ 8.51, 11.74 (C_5Me_4); 14.50 (SiMe_2); 19.00 ($\text{CH}(\text{CH}_3)\text{CHCHCH}(\text{CH}_3)$); 35.32, 56.85 ($t\text{Bu}$); 76.60 ($\text{CH}(\text{CH}_3)\text{CHCHCH}(\text{CH}_3)$); 103.9 (C_5 carbon attached to Si); 110.39 ($\text{CH}(\text{CH}_3)\text{CHCHCH}(\text{CH}_3)$); 122.83 (C_5 , remaining resonance under C_6D_6). Anal. Calcd for $\text{C}_{21}\text{H}_{37}\text{NSiTi}$: C, 66.46; H, 9.83; N, 3.69. Found: C, 66.85; H, 9.48; N, 3.51. (c) The mixture **2c/3c** was prepared similarly to **2b** in 36% yield. Assignments for **2c** are as follows. ¹H NMR (C_6D_6 , ppm): δ 7.5–7.0 (m, Ph, 3H); 6.69 (d, Ph, 2H, $J_{\text{HH}} = 7.4$ Hz); 3.78 (m, $\text{CH}(\text{CH}_3)\text{CHCHCH}(\text{CH}_3)$, 2H); 2.19 (s, C_5Me_4 , 6H); 1.90 (m, partially overlapped by a CH_3 doublet, $\text{CH}(\text{CH}_3)\text{CHCHCH}(\text{CH}_3)$, 2H); 1.85 (d, $\text{CH}(\text{CH}_3)\text{CHCHCH}(\text{CH}_3)$, 6H, $J_{\text{HH}} = 4.6$ Hz); 1.24 (s, C_5Me_4 , 6H); 0.55 (s, SiMe_2 , 6H). Assignments for **3c** are as follows. ¹H NMR (C_6D_6 , ppm): δ 7.5–7.0 (m, Ph, 3H); 6.1 (d, Ph, 2H); 5.26 (m, $\text{CH}(\text{CH}_3)\text{CHCHCH}(\text{CH}_3)$, 2H); 2.36 (s, C_5Me_4 , 6H); 1.78 (d, $\text{CH}(\text{CH}_3)\text{CHCHCH}(\text{CH}_3)$, 6H, $J_{\text{HH}} = 6.0$ Hz); 1.46 (s, C_5Me_4 , 6H); 0.47 (s, SiMe_2 , 6H); 0.3 (m, $\text{CH}(\text{CH}_3)\text{CHCHCH}(\text{CH}_3)$, 2H). Anal. Calcd for $\text{C}_{22}\text{H}_{33}\text{NSiTi}$: C, 69.15; H, 8.33; N, 3.51. Found: C, 69.68; H, 8.08; N, 3.32. (d) The mixture **2d/3d** was prepared similarly to **2b** in 49% yield. Assignments for **2d** are as follows. ¹H NMR (C_6D_6 , ppm): δ 7.1 (m, Ph, 2H, partially overlapped by solvent); 6.85 (m, Ph, 1H); 6.70 (d, Ph, 2H, $J_{\text{HH}} = 8.4$ Hz); 4.05 (m, $\text{CHH}=\text{CHCH}=\text{CHCH}_3$, 1H); 3.92 (m, $\text{CHH}=\text{CHCH}=\text{CHCH}_3$, 1H); 3.17 (m, $\text{CHH}=\text{CHCH}=\text{CHCH}_3$, 1H); 2.22 (s, C_5Me_4 , 3H); 2.13 (s, C_5Me_4 , 3H); 1.82 (d, $\text{CHH}=\text{CHCH}=\text{CHCH}_3$, 3H, $J_{\text{HH}} = 2.0$ Hz); 1.8 (m, partly overlapped, $\text{CHH}=\text{CHCH}=\text{CHCH}_3$, 1H); 1.45 (m, partly overlapped, $\text{CHH}=\text{CHCH}=\text{CHCH}_3$, 1H); 1.23 (s, C_5Me_4 , 6H); 0.56, 0.55 (s each, SiMe_2 , 3H each). Assignments for **3d** are as follows. ¹H NMR (C_6D_6 , ppm): δ 7.01 (m, Ph, 2H); 6.8 (m, Ph, 1H); 6.10 (d, Ph, 2H, $J_{\text{HH}} = 8.3$ Hz); 5.4 (m, $\text{CHH}=\text{CHCH}=\text{CHCH}_3$, 2H); 3.05 (m, $\text{CHH}=\text{CHCH}=\text{CHCH}_3$, 1H); 2.34, 2.33 (s each, C_5Me_4 , 3H each); 1.70 (d, $\text{CHH}=\text{CHCH}=\text{CHCH}_3$, 3H, $J_{\text{HH}} = 5.9$ Hz); 1.50 (s, C_5Me_4 , 6H); 0.49, 0.48 (s each, SiMe_2 , 3H each); 0.4 (m, $\text{CH}_2=\text{CHCH}=\text{CHCH}_3$, 2H). Anal. Calcd for $\text{C}_{22}\text{H}_{31}\text{NSiTi}$: C, 68.55; H, 8.11; N, 3.63. Found: C, 69.01; H, 8.13; N, 3.44.

[⊗] Abstract published in *Advance ACS Abstracts*, June 1, 1995.

(1) (a) *Plast. Technol.* **1992**, 25 (Sept). (b) *Chem. Bus.* **1992**, 15 (Oct). (c) *Mod. Plast.* **1992**, 20 (Nov). (d) *Plast. Week* **1992**, 4 (Dec). (e) *Mod. Plast.* **1993**, 57 (Jan). (f) *Chemicalweek* **1995**, 8 (Feb).

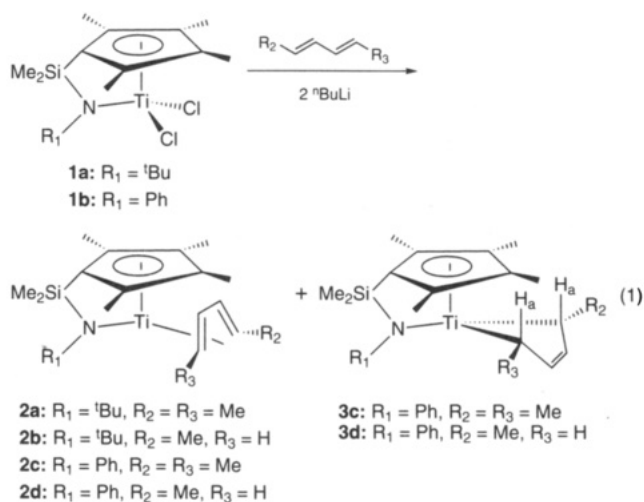
(2) (a) Woo, T. K.; Fan, L.; Ziegler, T. *Organometallics* **1994**, *13*, 432. (b) Woo, T. K.; Fan, L.; Ziegler, T. *Organometallics* **1994**, *13*, 2252.

(3) For studies in group 3, see: (a) Shapiro, P. J.; Cotter, W. D.; Schaefer, W. P.; Labinger, J. A.; Bercaw, J. E. *J. Am. Chem. Soc.* **1994**, *116*, 4623–4640 and references therein. (b) Coughlin, E. B.; Shapiro, P. J.; Bercaw, J. E. *Polym. Prepr.* **1992**, *33*, 1226–1227.

(4) (a) Erker, G.; Krüger, C.; Müller, G. *Adv. Organomet. Chem.* **1985**, *24*, 1 and references therein. (b) Yasuda, H.; Tatsumi, K.; Nakamura, A. *Acc. Chem. Res.* **1985**, *18*, 120 and references therein.

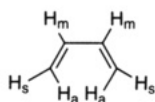
(5) For some recent examples, see: (a) Yamamoto, H.; Yasuda, H.; Tatsumi, K.; Lee, K.; Nakamura, A.; Chen, J.; Kai, Y.; Kasai, N. *Organometallics* **1989**, *8*, 105. (b) Blenkins, J.; Hessen, B.; van Boihuis, F.; Wagner, A. J.; Teuben, J. H. *Organometallics* **1987**, *6*, 459. (c) Krüger, C.; Müller, G.; Erker, G.; Dorf, U.; Engel, K. *Organometallics* **1985**, *4*, 215. (d) Erker, G.; Berg, K.; Krüger, C.; Müller, G.; Angermund, K.; Benn, R.; Schroth, G. *Angew. Chem., Int. Ed. Engl.* **1984**, *23*, 455. (e) Erker, G.; Wicher, J.; Engel, K.; Krüger, C. *Chem. Ber.* **1982**, *115*, 3300. (f) Dorf, U.; Engel, K.; Erker, G. *Organometallics* **1983**, *2*, 462.

(6) The dienes (Aldrich) were used as mixtures of isomers. 2,4-Hexadiene was a 62:35.7% mixture of the *cis,trans* and *trans,trans* isomers. 1,3-Pentadiene was a 57.3:31.6% mixture of the *trans* and *cis* isomers.



= Ph) effect significant perturbations in the diene bonding pattern as well as polymerization activity.

For R₁ = ^tBu, NMR indicates that eq 1 affords, at all stages, a single type of isomeric diene structure (**2a,b**). Thus, structurally diagnostic^{4,5} $\delta(H_a)$ and $\delta(H_m)$ occur at 2.10 and 3.73 ppm in **2a** and at 2.13, 1.75, 3.84, and 4.01 ppm in **2b**



in good agreement with data for the structurally characterized complexes Cp^{*}TiCl(1,3-butadiene)^{5a} and Cp₂Zr(*s-trans*-1,3-butadiene), which are predominantly π -diene in character.^{5e} $\delta(H_a) - \delta(H_m)$ exhibits a far greater dispersion in complexes such as Cp₂Zr(*s-cis*-1,3-butadiene)^{4a,5f} and Cp^{*}TiCl(supine-isoprene), which are predominantly σ -bound (metallacyclopentene) in character.^{5a,8} ¹J_{CH} data are less structurally definitive for group 4 diene complexes. Thus, ¹J_{CH_a} = 134 Hz in **2a** and ¹J_{CH_a} 137.8 (CH₃H_s), 134 (CH_aCH₃) Hz in **2b** would at first appear rather small in magnitude for "sp²" hybridization; however, the diffraction results for **2a** (vide infra) show the H_a's to be severely displaced from the diene plane. In contrast to these results, ¹J_{CH_a} = 159.4 Hz in **2b** is more consistent with sp² hybridization and is identical with the larger of the two geminal ¹J_{CH} values (159, 149 Hz) in π -bound Cp₂Zr(*s-trans*-1,3-butadiene).^{5e} However, note that ¹J_{CH_a} and ¹J_{CH_b} values of 129 and 152 Hz, respectively, are observed in the static (-75 °C) spectrum of the fluxional, formally metallacyclic Cp₂Zr(CH₂CMeCMeCH₂)^{5c} and that thorium metallacyclopentene parameters are similar.⁹ The ¹³C CPMAS spectrum of **2a** is consistent with the solution-phase spectrum, arguing that the solid-state structure persists in solution.

X-ray structural analysis of **2a**¹⁰ (Figure 1) shows the 2,4-hexadiene ligand to be coordinated in a "prone" π -fashion.^{4,11} The two Ti-C(terminal) diene distances (Ti-C17 = 2.187(6) and Ti-C20 = 2.176(7) Å) differ from

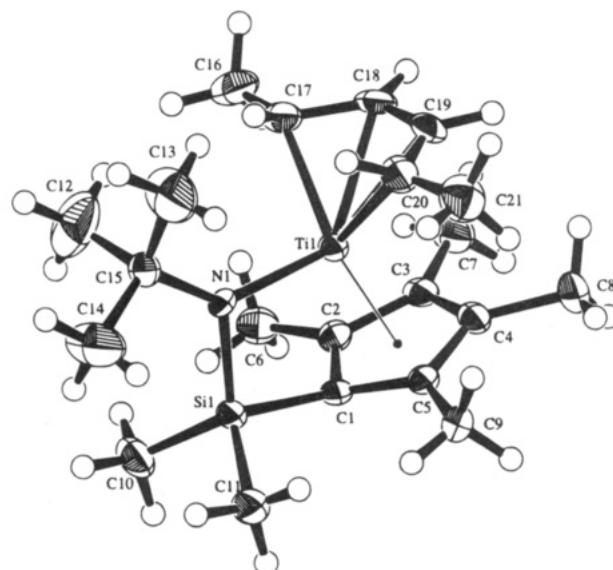


Figure 1. Crystal structure of (C₅Me₄SiMe₂N^tBu)Ti(prone-2,4-hexadiene) (**2a**). Selected bond distances (Å) and angles (deg) are as follows: Ti-C17 = 2.187(6), Ti-C18 = 2.298(6), Ti-C19 = 2.288(6), Ti-C20 = 2.176(7), C17-C18 = 1.402(9), C18-C19 = 1.404(9), C19-C20 = 1.391(9), Ti-N1 = 2.007(4), Si1-N1 = 1.733(5), Si1-C1 = 1.869(6), Ti-C1 = 2.228(5), Ti-C2 = 2.304(6), Ti-C3 = 2.481(6), Ti-C4 = 2.483(6), Ti-C5 = 2.331(6); Cp(Cg)-Ti-N = 109.8, Cp(Cg)-C1-Si1 = 153.2, C17-Ti-C20 = 90.0(3), N1-Si1-C1 = 94.5(2). Thermal ellipsoids are drawn at the 35% probability level.

the two Ti-C(internal) diene distances (Ti-C18 = 2.298(6) and Ti-C19 = 2.288(6) Å) by only 0.112 Å. This difference¹² ($\Delta d = -0.11$ Å) is similar to that reported for the Zr(II) π -butadiene complex CpZr(η^3 -allyl)(supine-butadiene) ($\Delta d = -0.103$ Å). The C-C distances in the 2,4-hexadiene ligand of **2a** (C17-C18 = 1.402(9), C18-C19 = 1.404(9), C19-C20 = 1.391(9) Å) also support the assignment of a predominantly π -bound diene ligand. This C-C bonding sequence is similar to that observed in typical M(CO)₃(η^4 -diene) (M = Fe, Ru) structures^{9,13} and is in sharp contrast to patterns observed in typical metallacyclopentenes, such as Cp₂Zr(CH₂CMeCMeCH₂).^{5c} Another important 2,4-hexadiene feature in **2a** concerns the coplanarity of atoms C17-C20. The two methyl substituents (C16 and C21) are displaced from the diene plane by only 0.032 (toward Ti) and -0.007 (away from Ti) Å, respectively. However, H34 and H37, which are the *anti* (H_a) protons of C17 and C20, respectively, are grossly displaced from the C17-C20 plane, away from Ti, by ~0.41 and ~0.44 Å, respectively. This distortion likely affects the magnitude of ¹J_{CH_a} (vide supra). The structural features of the constrained-geometry ligand also support a formal divalent Ti oxidation state assignment and reveal the

(10) Crystal data for C₂₁H₃₇NSiTi: triclinic system with cell dimensions at -120 °C of $a = 8.786(6)$ Å, $b = 9.760(6)$ Å, $c = 14.285(8)$ Å, $\alpha = 74.08(5)^\circ$, $\beta = 88.46(5)^\circ$, $\gamma = 66.18(5)^\circ$, and $V = 1072(1)$ Å³. The space group is $P\bar{1}$ (No. 2) with $Z = 2$ and $D_{\text{calcld}} = 1.175$ g/cm³. The structure was solved by direct methods and refined by full-matrix least-squares techniques using 3604 reflections having $I > 3.00\sigma(I)$ and resulting in $R = 0.073$ and $R_w = 0.085$.

(11) A "prone" diene is coordinated with the "cup" of the diene oriented away from the Cp ligand. A "supine" diene is coordinated with the "cup" of the diene oriented toward the Cp ligand.⁴

(12) $\Delta d = [(Ti-C17) + (Ti-C20)]/2 - [(Ti-C18) + (Ti-C19)]/2$.

(13) Cotton, F. A.; Day, V. W.; Frenz, B. A.; Hardcastle, K. I.; Troop, J. M. *J. Am. Chem. Soc.* **1973**, *95*, 4522 and references therein.

(8) The chemical shifts for H_a and H_m in Cp₂Zr(*s-cis*-1,3-butadiene)^{4a,d} and Cp^{*}TiCl(supine-isoprene)^{5a} occur at δ -0.70 and 4.85 ppm and δ 1.23, 1.10, and 5.68 ppm, respectively.

(9) Smith, G. M.; Suzuki, H.; Sonnenberger, D. C.; Day, V. W.; Marks, T. J. *Organometallics* **1986**, *5*, 549. ¹J_{CH} values for Cp^{*}Th(η^4 -C₄H₆), at low temperature: 131, 153 Hz.

effects of linking the amide substituent to the cyclopentadienyl ring via the silane bridge. The Ti–N distance in **2a** is 2.007(4) Å, which is significantly longer than in typical Ti(IV) amide complexes.^{14ab} In Ti(IV) constrained-geometry complexes, typical Ti–N distances of 1.895–1.957 Å are observed.^{14c–e} The present Ti–N distance is more consistent with those in lower valent (\leq II) Ti amide complexes (Ti–N = 2.023–2.066 Å).¹⁵ The N–Ti–Cp(Cg) bond angle contraction to 109.8° in **2a** is doubtless due to the silane bridge. The effect of constraining the amide substituent is also seen in the displacement of the Si from the plane of the cyclopentadienyl ring (Cp(Cg)–C1–Si = 153.2°) as well as a slight slipping of the ring toward the silane bridge, as evidenced by the dispersion in the Ti–C(ring) distances.

Simple replacement of $R_1 = ^t\text{Bu}$ by Ph drastically alters the products of eq 1. Thus, 2,4-hexadiene yields a 70/30 mixture of **2c** and **3c**, while 1,3-pentadiene yields 55/45 **2d** and **3d**. It was not possible to separate these mixtures by fractional crystallization. ¹H NMR data^{7c,d} supplemented by 2-D NOESY experiments indicate that **2c** and **2d** have prone, predominantly π -diene character similar to **2a** and **2b**, while the parameters for minor isomers **3c** and **3d**^{7c,d} are characteristic of structures with predominant metallacyclopentene character having the diene fragment in the supine orientation. Thus, in **2d**, NOESY data reveal a close proximity of H_m to the Cp methyl groups farthest from the Si bridge and H_a to the Ph *ortho* protons; exactly the opposite relationship is observed in **3d**. All attempts to observe **2c** \rightleftharpoons **3c** and **2d** \rightleftharpoons **3d** equilibration by variable-temperature DNMR/2-D EXSY or prolonged heating (displacement of the equilibrium) experiments have been unsuccessful, arguing that the **2c/3c**, **2d/3d** pairs are kinetic products of eq 1 related by a large

kinetic barrier.¹⁶ This relationship stands in marked contrast to more typical group 4 diene complexes, where structural interconversions are frequently facile.^{4,5}

When activated with cocatalysts such as $\text{B}(\text{C}_6\text{F}_5)_3$, $(\text{HNMe}_2\text{Ph})[\text{B}(\text{C}_6\text{F}_5)_4]$, or MAO, complexes **2a** and **2b** are highly active olefin polymerization catalysts. Under typical conditions¹⁷ with $\text{B}(\text{C}_6\text{F}_5)_3$ as a cocatalyst, **2a** and **2b** effect the random copolymerization of 1-octene-ethylene with activities of 7.7×10^6 ^{18a} and 6.8×10^6 g/(mol·h·atm),^{18b} respectively. In contrast, **2d/3d** exhibits an activity of only 0.3×10^6 g/(mol·h·atm)^{18c} under the same conditions.

These results demonstrate that constrained-geometry ancillary ligands can stabilize Ti–diene coordination in both predominantly π -diene (formally Ti(II)) and predominantly metallacyclopentene (formally Ti(IV)) bonding geometries and that such complexes exhibit a variety of interesting structural and catalytic characteristics. Further exploratory studies of constrained-geometry group 4 chemistry are in progress.

Acknowledgment. Research at Northwestern was supported by the U.S. Department of Energy (Grant DE-FG02-86ER13511). P.A.D. thanks the Dow Chemical Co. and the National Science Foundation for postdoctoral fellowships.

Supporting Information Available: Text giving details of the X-ray study, tables of crystal data and refinement details, positional and thermal parameters, and bond distances and angles, and a fully labeled structure diagram for compound **2a** (15 pages). Ordering information is given on any current masthead page.

OM9501788

(16) In contrast, $R_1 = ^t\text{Bu}$ complexes with internally substituted dienes (isoprene, 2,3-dimethylbutadiene) undergo rapid **2** \rightleftharpoons **3** interconversion, presumably via inversion^{5c} of the diene/metallacyclic structures. (Devore, D. D.; Timmers, F. J. Unpublished observations).

(17) In a typical polymerization, a 2 L Parr reactor was charged with 740 g of Isopar E solvent and 118 g of 1-octene. Hydrogen was added for molecular weight control by differential pressure expansion from a 75 L addition tank at 25 psi. The reactor was heated to 140 °C and saturated with ethylene at 500 psig. Then 2.0 μmol each of catalyst and cocatalyst (0.005 M in toluene) were premixed in the drybox; the solution was transferred to a catalyst addition tank and injected into the reactor. Polymerization conditions were maintained for 15 min with ethylene on demand. The resulting polymer solutions were removed from the reactor, and a phenol antioxidant (Irganox 1010) was added. Polymers were recovered by removal of solvent in vacuo at 120 °C for 20 h. Yields of polymer were 131 g (**2a**), 116 g (**2b**), and 5.3 g (**2d/3d**).

(18) (a) $M_w/M_n = 2.19$; $M_w = 77\,000$. (b) $M_w/M_n = 2.40$; $M_w = 89\,000$. (c) $M_w/M_n = 4.90$; $M_w = 116\,000$.

(14) (a) Lappert, M. F.; Power, P. P.; Sanger, A. R.; Srivastava, R. C. *Metal and Metalloid Amides*; Ellis Horwood: West Sussex, U.K., 1980; pp 472–475. (b) Brauer, D. J.; Bürger, H.; Essig, E.; Geschwandtner, W. *J. Organomet. Chem.* **1980**, *190*, 343. (c) Stevens, J. C.; Timmers, F. J.; Wilson, D. R.; Schmidt, G. F.; Nickias, P. N.; Rosen, R. K.; Knight, G. W.; Lai, S. European Patent Application EP-416-815-A2, March 13, 1991. (d) Wilson, D. R.; Rudolf, P. R. Unpublished results. (e) Ti–N distances: $(\text{C}_5\text{Me}_4\text{SiMe}_2\text{NPh})\text{TiCl}_2$, 1.906(3) Å; $[\text{C}_5\text{Me}_4\text{SiMe}_2\text{N}(\text{C}_6\text{H}_4\text{-4-CH}_3)]\text{TiCl}_2$, 1.905(4) Å; $(\text{C}_5\text{Me}_4\text{SiMe}_2\text{N}^t\text{Bu})\text{TiCl}_2$, 1.909(6) Å; $(\text{C}_5\text{Me}_4\text{SiMe}_2\text{N}^i\text{Bu})\text{TiMe}_2$, 1.957(7) Å; $(\text{C}_5\text{Me}_4\text{SiMe}_2\text{N}^i\text{Pr})\text{TiMe}_2$, 1.895(4) Å.

(15) (a) Duchateau, R.; Gambarotta, S.; Beydoun, N.; Bensimon, C. *J. Am. Chem. Soc.* **1991**, *113*, 8986. (b) Scoles, L.; Minhas, R.; Duchateau, R.; Jubb, J.; Gambarotta, S. *Organometallics* **1994**, *13*, 4978.

Protected (Fluoroaryl)borates as Effective Counteranions for Cationic Metallocene Polymerization Catalysts

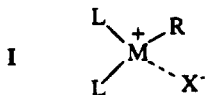
Li Jia, Xinmin Yang, Atsushi Ishihara, and Tobin J. Marks*

Department of Chemistry, Northwestern University, Evanston, Illinois 60208-3113

Received April 13, 1995*

Summary: The functionalized (fluoroaryl)borate salts $Ph_3C^+B(C_6F_4TBS)_4^-$ and $Ph_3C^+B(C_6F_4TIPS)_4^-$ (TBS = $t\text{-BuMe}_2\text{Si}$; TIPS = $i\text{-Pr}_3\text{Si}$) are prepared in three steps from 1,4- $\text{HC}_6\text{F}_4\text{Br}$. Reaction with zirconocene dimethyls yields crystalline, thermally stable, soluble $L_2\text{ZrCH}_3^+\text{B}(\text{C}_6\text{F}_4\text{SiR}_3)_4^-$ and $L_2\text{ZrH}^+\text{B}(\text{C}_6\text{F}_4\text{SiR}_3)_4^-$ salts ($L = \eta^5\text{-C}_5\text{H}_5$; $\eta^5\text{-1,2-Me}_2\text{C}_5\text{H}_3$; $L' = \eta^5\text{-Me}_5\text{C}_5$) which function as highly active ethylene polymerization catalysts.

Recent observations suggest that many of the properties of highly active cationic metallocene olefin polymerization catalysts^{1,2} are closely connected with the nature of the cation–anion tight ion pairing (I).^{3,4}



L = cyclopentadienyl ligand

Despite numerous efforts to “engineer” the cationic portion of such catalysts, far less attention has been devoted to the charge-compensating anion (X^-). Of the existing anions, $B(\text{C}_6\text{F}_5)_4^-$ -derived base-free catalysts exhibit some of the highest reported catalytic activities^{3a,4h,5} but have proven difficult to characterize in the pure state.⁶ In our hands, they exhibit poor thermal

stability (as judged by exceedingly complex, time-dependent 25 °C NMR spectra) and poor crystallizability (insoluble, hard to purify oils are frequently obtained).⁷ We report here on the interesting properties of “protected” fluoroarylborates designed to address some of these issues and to enforce greater cation–anion separations as a potential means to modulate cation reactivity.^{8,9}

Low-temperature halogen–metal interchange using 1-bromo-2,3,5,6-tetrafluorobenzene and $n\text{BuLi}$ ¹⁰ followed

(5) (a) Chien, J. C. W.; Tsai, W. M.; Rausch, M. D. *J. Am. Chem. Soc.* **1991**, *113*, 8570–8571. (b) Resconi, L.; Bossi, S.; Abis, L. *Macromolecules* **1990**, *23*, 4489–4491. (c) Turner, H. W.; Hlatky, G. G. PCT Int. Appl. WO 88/05793 (Eur. Pat. Appl. EP 211004, 1988). (d) Ewen, J. A.; Elder, M. J. Eur. Pat. Appl. 427697, 1991.

(6) Canich, J. Lecture, Contemporary Inorganic Chemistry Symposium, College Station, TX, March 12–15, 1995.

(7) Giardello, M. A.; Eisen, M.; Yang, X.; Marks, T. J. Unpublished observations.

(8) Communicated in part: Jia, L.; Marks, T. J. *Abstracts of Papers*, 207th National Meeting of the American Chemical Society, San Diego, CA, 1994; American Chemical Society: Washington, DC, 1994; INOR 41.

(9) For reviews of weakly coordinating anions, see: (a) Strauss, S. H. *Chem. Rev.* **1993**, 927–963 and references therein. (b) Seppelt, K. *Angew. Chem., Int. Ed., Engl.* **1993**, *32*, 1025–1027 and references therein. (c) Boehmann, M. *Angew. Chem., Int. Ed. Engl.* **1992**, *31*, 1181–1182 and references therein.

(10) Tamborski, C.; Soloski, E. J. *J. Org. Chem.* **1966**, *31*, 743–745.

(11) TBS triflate (Aldrich, 17.0 g, 64.6 mmol) was injected into a suspension of LiC_6HF_4 (prepared from C_6HBrF_4 (14.8 g, 64.6 mmol) and $n\text{BuLi}$ (40 mL, 1.6 M in hexanes) with stirring at -78°C . The mixture was slowly warmed to 25 °C over a period of 8 h and the resulting suspension filtered. After the solvent was removed at 25 °C under reduced pressure, the nonvolatile residue was distilled (45 °C/0.8 mm) and a colorless liquid was collected. Yield of **1a**: 80%. ^1H NMR (CD_2Cl_2): δ 0.40 (“t”, 6H), 0.93 (s, 9H), 7.10 (m, 1H). ^{19}F NMR (CD_2Cl_2): δ -128.2 (b), -132.4 (b). ^{13}C NMR (CD_2Cl_2): δ -3.7, 18.1, 26.5, 108.0, 144.8, 148.1, 151.4. Compound **1a** (5.4 g, 20.4 mmol) was dissolved in Et_2O , and $n\text{BuLi}$ (13 mL, 1.6 M in hexanes) was then added dropwise with stirring at -78°C . After 2 h, BCl_3 (4.2 mL, 1.0 M in hexanes) was injected. The mixture was warmed to room temperature over a period of 16 h, and the resulting suspension was filtered. The product was recrystallized from Et_2O /pentane and collected as large colorless crystals. Yield of **2a**: 74%. ^1H NMR (C_6D_6): δ 0.20 (s, 24H), 0.80 (m, 12H), 0.82 (s, 36H), 3.05 (q, $J = 7.1$ Hz, 8H). ^{19}F NMR (C_6D_6): δ -129.4 (b), -133.8 (b). Compound **2a** (3.8 g, 3.1 mmol) and $(\text{C}_6\text{H}_5)_3\text{CCl}$ (0.88 g, 3.1 mmol) were suspended in pentane and stirred for 6 h at 25 °C, and the orange product was collected by filtration. The crude product was then dissolved in CH_2Cl_2 and filtered to remove LiCl , followed by pentane addition to precipitate the orange solid. Yield of **3a**: 86%. ^1H NMR (CDCl_2D_2): δ 0.31 (s, 24H), 0.88 (s, 36H), 7.64 (d, $J = 6.9$ Hz, 6H), 7.85 (t, $J = 6.9$ Hz, 6H), 8.25 (“t”, $J = 6.9$ Hz, 3H). ^{19}F NMR (CD_2Cl_2): δ -133.0 (b), -144.5 (b). ^{13}C NMR (CD_2Cl_2): δ -3.8, 17.8, 26.4, 108.4, 131.0, 140.2, 143.0, 144.0, 147.4 ($J_{\text{C-F}} = 262$ Hz), 149.6 ($J_{\text{C-F}} = 262$ Hz), 211.3. Anal. Calcd for $\text{C}_{67}\text{H}_{75}\text{BF}_{16}\text{Si}_4$: C, 61.55; H, 5.78. Found: C, 61.83; H, 5.61. The same procedures were used in the syntheses of **1b**, **2b**, and **3b**. **1b**: ^1H NMR (CDCl_2D_2) δ 0.98 (d, $J = 7.5$ Hz, 24H), 1.50 (“p”, $J = 7.5$ Hz, 12H), 7.10 (m, 1H); ^{19}F NMR (CDCl_3) δ -128.2 (b), -132.4 (b). **2b**: ^1H NMR (CDCl_3) δ 0.80 (t, $J = 7.1$ Hz, 12H), 1.08 (d, $J = 7.5$ Hz, 24H), 1.52 (“p”, $J = 7.5$ Hz, 12H), 3.05 (q, $J = 7.1$ Hz, 8H); ^{19}F NMR (CDCl_3) δ -131.3 (b), -132.1 (b). **3b**: ^1H NMR (CDCl_3) δ 1.09 (d, $J = 7.5$ Hz, 24H), 1.51 (“p”, $J = 7.5$ Hz, 12H), 7.60 (d, $J = 6.9$ Hz, 6H), 7.85 (t, $J = 6.9$ Hz, 6H), 8.25 (“t”, $J = 6.9$ Hz, 3H); ^{19}F NMR (CDCl_3) δ -131.3 (b), -132.1 (b); ^{13}C NMR (CDCl_3) δ 12.8, 18.8, 108.6, 130.6, 139.2, 142.4, 144.0, 146.8 ($J_{\text{C-F}} = 261$ Hz), 148.9 ($J_{\text{C-F}} = 259$ Hz), 211.3. Anal. Calcd for $\text{C}_{79}\text{H}_{99}\text{BF}_{16}\text{Si}_4$: C, 64.30; H, 6.76. Found: C, 64.57; H, 6.89.

* Abstract published in *Advance ACS Abstracts*, June 15, 1995.

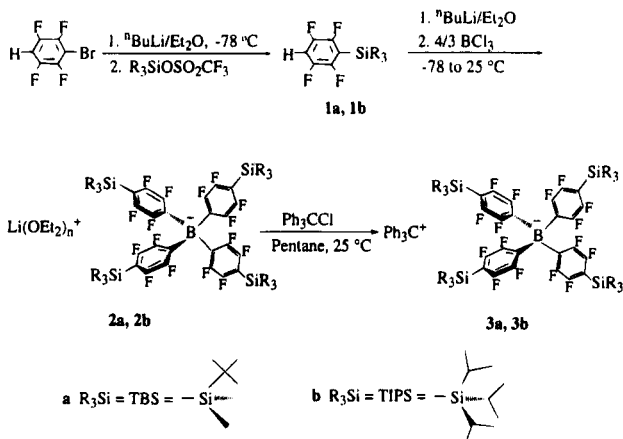
(1) (a) Möhring, P. C.; Coville, N. J. *J. Organomet. Chem.* **1994**, *479*, 1–29 and references therein. (b) Kaminsky, W. *Catal. Today* **1994**, *20*, 257–271 and references therein. (c) Quirk, R. P., Ed. *Transition Metal Catalyzed Polymerizations*; Cambridge University Press: Cambridge, U.K., 1988. (d) Kaminsky, W.; Sinn, H., Eds. *Transition Metals and Organometallics for Catalysts for Olefin Polymerization*; Springer: New York, 1988. (e) Keii, T.; Soga, K., Eds. *Catalytic Polymerization of Olefins*; Elsevier: Amsterdam, 1986.

(2) (a) Jordan, R. F. *Adv. Organomet. Chem.* **1991**, *32*, 325–387 and references therein. (b) Marks, T. J. *Acc. Chem. Res.* **1992**, *25*, 57–65 and references therein.

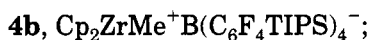
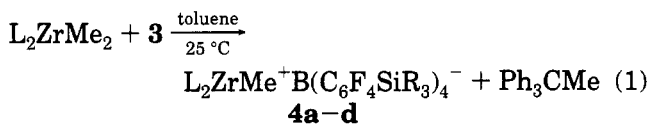
(3) (a) Vizzini, J. C.; Chien, J. C. W.; Gaddam, N. B.; Newmark, R. A. *J. Polym. Sci. A, Polym. Chem.* **1994**, *32*, 2049–2056 (anion effects on propylene polymerization activity and isospecificity). (b) Chien, J. C. W.; Song, W.; Rausch, M. D. *J. Polym. Sci. A, Polym. Chem.* **1994**, *32*, 2387–2393 (solvent effects on propylene polymerization activity and isospecificity). (c) Giardello, M. A.; Eisen, M. S.; Stern, S. L.; Marks, T. J. *J. Am. Chem. Soc.* **1993**, *115*, 3326–3327 (anion effects on propylene polymerization activity, chain transfer, and isospecificity). (d) Herfert, N.; Fink, G. *Makromol. Chem.* **1992**, *193*, 773–778 (solvent effects on propylene polymerization activity and syndiospecificity).

(4) For recent structural/spectroscopic studies of metallocene ion pairing see refs 1 and 2 and: (a) Yang, X.; Stern, C. L.; Marks, T. J. *J. Am. Chem. Soc.* **1994**, *116*, 10015–10031. (b) Boehmann, M.; Lancaster, S. J.; Hursthouse, M. B.; Malik, K. M. A. *Organometallics* **1994**, *13*, 2235–2243. (c) Yang, X.; King, W. A.; Sabat, M.; Marks, T. J. *Organometallics* **1993**, *12*, 4254–4258. (d) Eisch, J. J.; Pombrink, S. I.; Zheng, G.-X. *Organometallics* **1993**, *12*, 3856–3863. (e) Sishita, C.; Hathorn, R. M.; Marks, T. J. *Organometallics* **1993**, *12*, 4254–4258. (f) Hlatky, G. G.; Eckman, R. R.; Turner, H. W. *Organometallics* **1992**, *11*, 1413–1416. (g) Yang, X.; Stern, C. L.; Marks, T. J. *Angew. Chem., Int. Ed. Engl.* **1992**, *31*, 1375–1377. (h) Yang, X.; Stern, C. L.; Marks, T. J. *Organometallics* **1991**, *10*, 840–842. (i) Siedle, A. R.; Newmark, R. A.; Lamanna, W. M.; Shroepfer, J. N. *Polyhedron* **1990**, *9*, 301–308. (j) Hlatky, G. G.; Turner, H. W.; Eckman, R. R. *J. Am. Chem. Soc.* **1989**, *111*, 2728–2729.

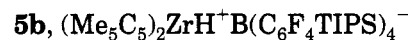
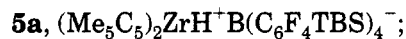
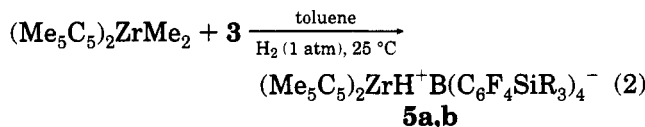
Scheme 1



by quenching with a trialkylsilyl triflate (Scheme 1) yields silyl-substituted tetrafluoroarenes.¹¹ Subsequent $n\text{-BuLi}$ metalation, reaction with BCl_3 , and cation metathesis affords the corresponding tetraarylborates¹¹ as crystalline trityl salts ($\text{B}(\text{C}_6\text{F}_4\text{TBS})_4^-$, **3a**; $\text{B}(\text{C}_6\text{F}_4\text{TIPS})_4^-$, **3b**). Zirconocenium salts **4** are then cleanly and rapidly obtained using these methide abstraction reagents^{5a} and the corresponding zirconocene dimethyls (eq 1).¹² The

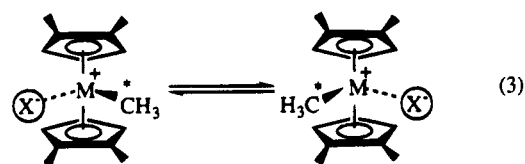


only exception is $(\text{Me}_5\text{C}_5)_2\text{ZrMe}_2$, for which the abstraction process is sluggish (presumably for steric reasons). However, the corresponding hydride^{4g} cations are readily obtained under H_2 (eq 2).¹¹ Complex classes **4** and **5** are crystalline solids and have been characterized by stan-



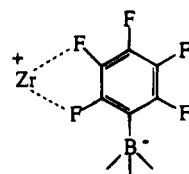
dard spectroscopic and analytical techniques.¹¹ The methyl derivatives exhibit low-field $\text{Zr}-^{13}\text{CH}_3$ NMR resonances characteristic of zirconocene methyl cations.^{4a} In contrast to the aforementioned $\text{B}(\text{C}_6\text{F}_5)_4^-$ analogues, **4** and **5** exhibit *high thermal stability*, as evidenced by negligible ^1H NMR spectroscopic changes over the course of several hours at $100\text{ }^\circ\text{C}$ in toluene- d_8 and half-lives on the order of 1 h at $130\text{ }^\circ\text{C}$ in toluene- d_8 .

In regard to tight ion pair structure in solution, variable-temperature ^1H NMR studies of **4c,d** in toluene- d_8 reveal diastereotopic $\text{Cp}-\text{Me}$ group permutation indicative of rapid reorganization/symmetrization of the evidently dissymmetric ground-state ion pairing (eq 3).



Derived ΔG^\ddagger values of 15.1(8) (**4c**) and 15.8(5) kcal/mol (**4d**) ($60\text{ }^\circ\text{C}$) are significantly lower than in $(1,2\text{-Me}_2\text{Cp})_2\text{ZrMe}^+\text{MeB}(\text{C}_6\text{F}_5)_3^-$ ($\Delta G^\ddagger = 18.3(2)$ kcal/mol at $80\text{ }^\circ\text{C}$),^{4a} indicating substantially "looser" ion pairing in the case of the functionalized borates. At $-90\text{ }^\circ\text{C}$ in toluene- d_8 , the ^{19}F NMR spectrum of **4a** reveals 12 signals (not all of equal intensity), indicating a low-symmetry instantaneous cation-anion structure. Significant displacements of the aryl ^{19}F resonances from the $\delta -130$ ppm region of **3**, with signals at $\delta -167.6$ and -162.0 , suggest weak $\text{Zr}^+\cdots\text{F}(\text{aryl})$ interactions as identified crystallographically in $(1,2\text{-Me}_2\text{Cp})_2\text{ZrH}^+\text{MeB}(\text{C}_6\text{F}_5)_3^-$ (**II**).^{4a,g} As the temperature is raised, spectral line

(12) $[(\text{C}_6\text{H}_5)_3\text{C}][\text{B}(\text{C}_6\text{F}_4\text{TBS})_4]^-$ (390 mg, 0.30 mmol) and Cp_2ZrMe_2 (82 mg, 0.32 mmol) were stirred in toluene for 8 h. Then, pentane was added to precipitate the product, which was collected after filtration and washed with pentane. Yield of **4a**: 310 mg, 75%. **4a**: ^1H NMR (C_6D_6) δ 0.23 (s, 24H), 0.56 (s, 3H), 0.85 (s, 36H), 5.75 (s, 10H); ^{19}F NMR (C_6D_6): δ -128.2 (b), -130.6 (b); ^{13}C NMR ($\text{C}_6\text{D}_4\text{Cl}_2$) δ -4.4, 17.2, 25.8, 49.6, 111.6, 114.8, 119.8, 147.0, 149.8. Anal. Calcd for $\text{C}_{59}\text{H}_{73}\text{BF}_4\text{Si}_4\text{Zr}$: C, 54.49; H, 5.66. Found: C, 54.30; H, 5.35. The same procedures were used to synthesize **4b-d**. Similar procedures were used to synthesize **5a,b**, except that the reactions were carried out under 1 atm of H_2 . **4b**: ^1H NMR (C_6D_6) δ 0.54 (s, 3H), 1.01 (d, $J = 7.5$ Hz, 72H), 1.43 ("p", $J = 7.5$ Hz, 12H), 5.75 (s, 10H); ^{19}F NMR (C_6D_6) δ -130.1 (b), -131.4 (b); ^{13}C NMR ($\text{C}_6\text{D}_4\text{Cl}_2$) δ 12.0, 19.2, 111.6, 114.8, 120, 146.6, 150. Anal. Calcd for $\text{C}_{71}\text{H}_{97}\text{BF}_4\text{Si}_4\text{Zr}$: C, 58.06; H, 6.66. Found: C, 58.32; H, 6.79. **4c**: ^1H NMR (C_6D_6) δ 0.21 (s, 24H), 0.34 (s, 3H), 0.83 (s, 36H), 1.37 (s, 6H), 1.61 (s, 6H), 5.00 (b, 2H), 5.69 (b, 2H), 5.97 (t, 2H); ^{13}C NMR (C_6D_6) δ -3.9, 12.5, 17.7, 26.4, 45.9, 108.1, 110.1, 111.8, 119.8, 133.5, 147.7, 150.9. Anal. Calcd for $\text{C}_{69}\text{H}_{81}\text{BF}_4\text{Si}_4\text{Zr}$: C, 55.78; H, 6.02. Found: C, 55.56; H, 6.01. **4d**: ^1H NMR (toluene- d_8) δ 0.37 (s, 3H), 1.08 (d, $J = 7.5$ Hz, 72H), 1.43 (s, 6H), 1.51 ("t", $J = 7.5$ Hz, 12H), 1.73 (s, 6H), 5.08 (b, 4H), 5.75 (b, 4H), 6.01 (t, $J = 1.0$ Hz, 2H); ^{13}C NMR (toluene- d_8) δ 12.0, 12.8, 19.2, 47.0, 109.1, 110.1, 113.8, 121.4, 149.8, 152.7. Anal. Calcd for $\text{C}_{75}\text{H}_{105}\text{BF}_4\text{Si}_4\text{Zr}$: C, 59.07; H, 6.95. Found: C, 59.34; H, 6.98. **5a**: ^1H NMR (C_6D_6) δ 0.25 (s, 24H), 0.87 (2, 36H), 1.63 (s, 30H), 7.90 (b, 1H); ^{13}C NMR (C_6D_6) δ -3.9, 11.2, 17.7, 26.5, 110.1, 122.5, 147.7, 151.0. Anal. Calcd for $\text{C}_{68}\text{H}_{91}\text{BF}_4\text{Si}_4\text{Zr}$: C, 57.24; H, 6.43. Found: C, 56.87; H, 6.46. **5b**: ^1H NMR (C_6D_6) δ 1.12 (d, $J = 7.5$ Hz, 72H), 1.50 ("p", $J = 7.5$ Hz, 12H), 1.72 (s, 30H), 7.96 (b, 1H); ^{13}C NMR (toluene- d_8) δ 12.0, 12.5, 18.8, 109.8, 111.9, 148.2, 150.6. Anal. Calcd for $\text{C}_{90}\text{H}_{115}\text{BF}_4\text{Si}_4\text{Zr}$: C, 60.46; H, 7.33. Found: C, 60.56; H, 6.98.



broadening and coalescence ultimately give rise to two aryl ^{19}F signals by $25\text{ }^\circ\text{C}$. Although all members of the **4**, **5** series are crystalline, severe disordering and twinning have to date frustrated attempts at high-quality diffraction analyses.

Ethylene polymerization experiments and polymer characterization were carried out using previously described procedures.^{4a,c} Polymerization activity assays are carried out under rigorously anhydrous/anaerobic high-vacuum-line conditions,^{4a,c} are designed to minimize mass transport effects (rapid mixing, short reaction times),¹³ and aim for constant polymer yields to allow catalyst activity comparisons. All polymeric products exhibit the characteristic $^1\text{H}/^{13}\text{C}$ NMR spectroscopic

Table 1. Ethylene Polymerization Characteristics of Metallocene Cations Having Various Anions^a

entry no.	metallocene cation	anion	[cat.] (mM)	reacn time (s)	polymer yield ^b (g)	activity ($\times 10^6$ g PE/mol of Zr atm \cdot h)	M_w^c ($\times 10^5$)	M_n^c ($\times 10^5$)
1	Cp ₂ ZrMe ⁺ ^d	MeB(C ₆ F ₅) ₃ ⁻	0.32	40	1.6	4.5(4)	1.24	0.61
2	(1,2-Me ₂ Cp) ₂ ZrMe ⁺ ^d	MeB(C ₆ F ₅) ₃ ⁻	0.14	66	1.7	6.8(6)	5.21	3.67
3	(Me ₅ C ₅) ₂ ZrMe ⁺ ^d	MeB(C ₆ F ₅) ₃ ⁻	0.14	62	0.9	3.8(5)	2.55	1.26
4	Cp ₂ ZrMe ⁺	B(C ₆ F ₄ TBS) ₄ ⁻	0.14	62	1.4	5.7(6)	8.78	5.12
5	Cp ₂ ZrMe ⁺	B(C ₆ F ₄ TIPS) ₄ ⁻	0.14	60	1.5	6.2(6)	5.65	4.29
6	(1,2-Me ₂ Cp) ₂ ZrMe ⁺	B(C ₆ F ₄ TBS) ₄ ⁻	0.14	10	1.9	50(20)	8.29	5.29
7	(1,2-Me ₂ Cp) ₂ ZrMe ⁺	B(C ₆ F ₄ TIPS) ₄ ⁻	0.14	10	1.6	42(20)	6.02	3.03
8	(Me ₅ C ₅) ₂ ZrH ⁺	B(C ₆ F ₄ TBS) ₄ ⁻	0.14	20	0.9	11(2)	21.6	10.8
9	(Me ₅ C ₅) ₂ ZrH ⁺	B(C ₆ F ₄ TIPS) ₄ ⁻	0.14	20	0.8	10(2)	12.8	4.5
10	Cp ₂ ZrMe ⁺ ^e	B(C ₆ F ₅) ₄ ⁻	0.20	60	2.1	6.4(6)	9.87	7.13
11	(1,2-Me ₂ Cp) ₂ ZrMe ⁺ ^e	B(C ₆ F ₅) ₄ ⁻	0.20	22	3.2	28(6)	7.03	4.38
12	(Me ₅ C ₅) ₂ ZrMe ⁺ ^e	B(C ₆ F ₅) ₄ ⁻	0.20	20	1.1	10(2)	5.32	3.20

^a Procedure of ref 4c; toluene solvent (100 mL). ^b Average yield of ≥ 3 runs. ^c By GPC relative to polystyrene. ^d Data of ref 4c. ^e Catalyst generated by in situ reaction of the corresponding zirconocene dimethyl with Ph₃C⁺B(C₆F₅)₄⁻ in toluene for 5 min. Longer reaction times gave lower catalytic activities. For example, the activity of the B(C₆F₅)₄⁻ catalyst in entry 11 declines by 90% on standing in toluene solution for 3 h at 25 °C.

signatures of highly linear polyethylene.¹⁴ Molecular weight characteristics (Table 1) are unexceptional for single-site metallocene catalysts operating under these conditions.¹⁻⁴ With regard to catalyst characteristics, the polymerization activity and polymer characterization data reveal several noteworthy trends (Table 1). In comparison to CH₃B(C₆F₅)₃⁻-derived zirconocene catalysts, the corresponding B(C₆F₄TBS)₄⁻ and B(C₆F₄TIPS)₄⁻-derived catalysts exhibit significantly higher polymerization activity and yield polyethylenes of significantly higher molecular weight. Particularly striking are the results for the (1,2-Me₂Cp)₂ZrCH₃⁺ systems, in which ethylene polymerization activities rival or exceed any values previously measured in this laboratory.^{3c,15} The cation and anion structure-reactivity

trends in Table 1 likely reflect subtle electronic effects and matching/mismatching of steric encumbrances about the cation olefin activation zone¹⁶ of the tight ion pair. The data in Table 1 also reveal that *freshly prepared* B(C₆F₅)₄⁻-based catalysts have polymerization activities roughly similar to those of the B(C₆F₄TBS)₄⁻ and B(C₆F₄TIPS)₄⁻ analogues; however, standing at room temperature significantly erodes the catalytic performance (Table 1, footnoted), in accord with the aforementioned thermal stability observations.

The present results indicate that the properties of metallocene cation-anion ion pairs can be substantially modified by functionalization of the weakly coordinating anion. Trialkylsilyl substitution of the (fluoroaryl)-borate framework can be effectively employed to enhance catalyst stability, polymerization activity, and solubility.

Acknowledgment. This research was supported by the U.S. Department of Energy (Grant DE-FG02-86ER13511). L.J. thanks Akzo-Nobel Chemicals for a predoctoral fellowship. We thank Dr. D. A. Kershner of Akzo-Nobel for GPC analyses.

OM9502695

(14) Bovey, F. A. *Chain Structure and Conformation of Macromolecules*; Academic: New York, 1982; pp 78-91.

(15) Jia, L.; Yang, X.; Stern, C. L.; Marks, T. J. *Organometallics* **1994**, *13*, 3755-3757.

(16) (a) Castonguay, L. A.; Rappé, A. K. *J. Am. Chem. Soc.* **1992**, *114*, 5832-5842. (b) Prosenic, M.-H.; Janiak, C.; Brintzinger, H. H. *Organometallics* **1992**, *11*, 4036-4041. (c) Kawamura-Kuribayash, H.; Koga, N.; Morokuma, K. *J. Am. Chem. Soc.* **1992**, *114*, 8687-8694. (d) Hart, J. R.; Rappé, A. K. *J. Am. Chem. Soc.* **1993**, *115*, 6159-6164. (e) Bierwagen, E. P.; Bercaw, J. E.; Goddard, W. A. *J. Am. Chem. Soc.* **1994**, *116*, 1481-1489. (f) Woo, T. K.; Fan, L.; Ziegler, T. *Organometallics* **1994**, *13*, 2252-2261.

Fragmentation of, and Oxygen Atom Abstraction by, $\{\text{Cp}^*\text{Re}(\text{O})\}_2(\mu\text{-O})_2$

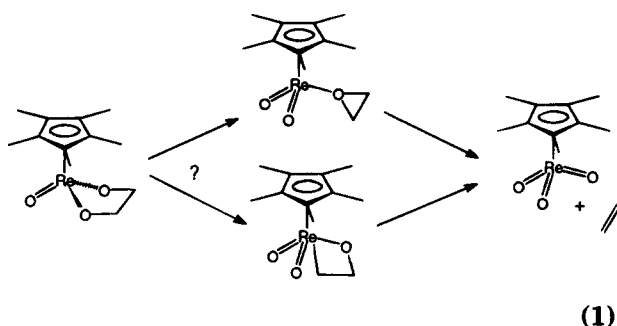
Kevin P. Gable,^{*,1} Jerrick J. J. Juliette, and Michael A. Gartman

Department of Chemistry, Oregon State University, Corvallis, Oregon 97331

Received March 17, 1995[®]

Summary: The dimeric oxo complex $(\text{Cp}^*\text{ReO})_2(\mu\text{-O})_2$ is found to be in equilibrium with a monomeric form, proposed to be Cp^*ReO_2 . The mixture of monomer and dimer stereospecifically abstracts oxygen from epoxides to make alkene plus Cp^*ReO_3 .

Transition-metal oxo complexes have been the subject of intense scrutiny as reagents and catalysts for a variety of oxidations of organic molecules,² particularly epoxidation³ and bishydroxylation^{4–6} of alkenes. We have undertaken mechanistic investigations and have focused on the microscopic reverse of bishydroxylation, alkene extrusion from rhenium(V) diolates.⁷ In the course of this study, it became necessary to consider whether a coordinated epoxide was a viable intermediate in the process (eq 1). This led us to investigate



closely the chemistry of $(\text{Cp}^*\text{ReO})_2(\mu\text{-O})_2$.⁸ We report here that fragmentation of this dimer is observable by both NMR and UV–visible spectroscopy and that the

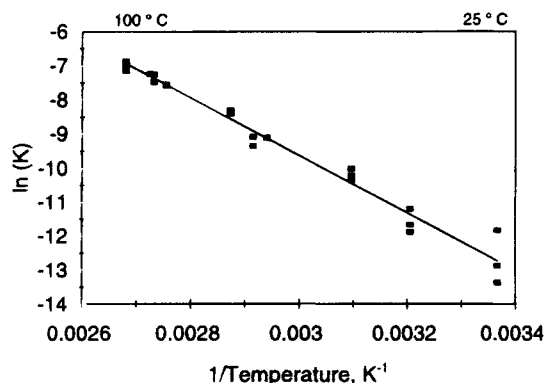


Figure 1. van't Hoff plot for dimer \rightleftharpoons monomer equilibrium: slope -8450 , intercept 15.717 , $r^2 = 0.9745$.

monomeric Cp^*ReO_2 is capable of several oxygen atom abstraction processes.

At room temperature, solutions of $(\text{Cp}^*\text{ReO})_2(\mu\text{-O})_2$ (C_6D_6 , sealed under vacuum) exhibit a single ^1H NMR signal at δ 1.96 ppm. However, when the temperature is raised, a new signal appears at δ 1.66 ppm. This is clearly distinct from the signal for Cp^*ReO_3 , which occurs at δ 1.60 ppm. When the solutions are cooled, this new peak slowly disappears, and that for the dimer regains its original intensity.⁹ If the initial concentration of dimer is varied, one observes that small concentrations and high temperatures favor the formation of this new compound. At 373 K, a solution initially 0.007 M in dimer showed a ratio of Cp^* methyl peaks of 100:17.6. The fragmentation shows a minor dependence on solvent; in $\text{THF-}d_3$ at 373 K (initially 0.0106 M in dimer), the ratio of peaks is 100:22.5.

The ^{13}C NMR also shows two new signals at 12.4 and 109.3 ppm. These are distinct from those of the dimer (11.4 and 108.5 ppm), as well as from Cp^*ReO_3 (9.9 and 119.3 ppm).

This concentration vs composition relationship fits an equilibrium constant expression for fragmentation of a dimer: $K = [\text{monomer}]^2/[\text{dimer}]$. At 366 K, the equilibrium constant is calculated to be $(6.05 \pm 1.29) \times 10^{-4}$ M. Furthermore, evaluation of K at various temperatures and concentrations yields the van't Hoff plot seen in Figure 1; from this, the thermodynamic parameters $\Delta H^\circ = 16.8 \pm 0.3$ kcal/mol and $\Delta S^\circ = +31.2 \pm 1.4$ cal/(mol K) may be calculated.

Electronic spectra of the mixture (toluene solution) were obtained over a similar temperature range. A decrease of the peak at 418 nm is observed at higher

(9) It is possible to find a small peak (intensity $<1\%$ of that of the dimer) at δ 1.66 ppm.

[®] Abstract published in *Advance ACS Abstracts*, June 1, 1995.

(1) E-mail: gablek@ccmail.orst.edu (internet).

(2) (a) Sheldon, R. A.; Kochi, J. K. *Metal Catalyzed Oxidations of Organic Chemistry*; Academic Press: New York, 1981. (b) *Organic Synthesis by Oxidation with Metal Compounds*; Mijs, W. J., deJonghe, C. R. H. I., Eds.; Plenum: New York, 1986.

(3) (a) Palucki, M.; Pospisil, P. J.; Zhang, W.; Jacobsen, E. N. *J. Am. Chem. Soc.* **1994**, *116*, 9333–9334. (b) Ostovic, D.; Bruice, T. C. *Acc. Chem. Res.* **1992**, *25*, 314–320. (c) Meunier, B. *Chem. Rev.* **1992**, *92*, 1411–1456. (d) Schurig, U.; Betschinger, F. *Chem. Rev.* **1992**, *92*, 873–888.

(4) (a) Schröder, M. *Chem. Rev.* **1990**, *80*, 187–213. (b) Jorgensen, K. A.; Schiott, B. *Chem. Rev.* **1990**, *90*, 1483–1506.

(5) (a) Göbel, T.; Sharpless, K. B. *Angew. Chem., Int. Ed. Engl.*, **1993**, *32*, 1329–1331. (b) Kolb, H. C.; Andersson, P. G.; Sharpless, K. B. *J. Am. Chem. Soc.* **1994**, *116*, 1278–1291. (c) Norrby, P.-O.; Kolb, H. C.; Sharpless, K. B. *Organometallics* **1994**, *13*, 344–347.

(6) Corey, E. J.; Jardine, P. D.; Virgil, S.; Yuen, P.-W.; Connell, R. D. *J. Am. Chem. Soc.* **1989**, *111*, 9243–9244. (b) Corey, E. J.; Noe, M. C.; Sarshar, S. *J. Am. Chem. Soc.* **1993**, *115*, 3828–3829.

(7) Gable, K. P.; Phan, T. N. *J. Am. Chem. Soc.* **1994**, *116*, 833–839.

(8) (a) Herrmann, W. A.; Flöel, M.; Kulpe, J.; Felixberger, J. K.; Herdtweck, E. *J. Organomet. Chem.* **1988**, *355*, 297–313. (b) Herrmann, W. A.; Serrano, R.; Küsthardt, U.; Ziegler, M. L.; Guggolz, E.; Zahn, T. *Angew. Chem., Int. Ed. Engl.* **1984**, *7*, 515–517. (c) Herrmann, W. A.; Serrano, R.; Küsthardt, U.; Guggolz, E.; Nuber, B.; Ziegler, M. L. *J. Organomet. Chem.* **1985**, *287*, 329–344.

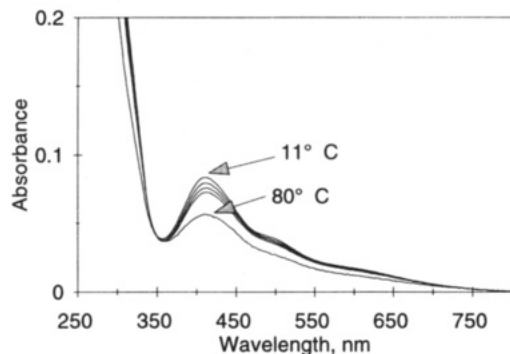
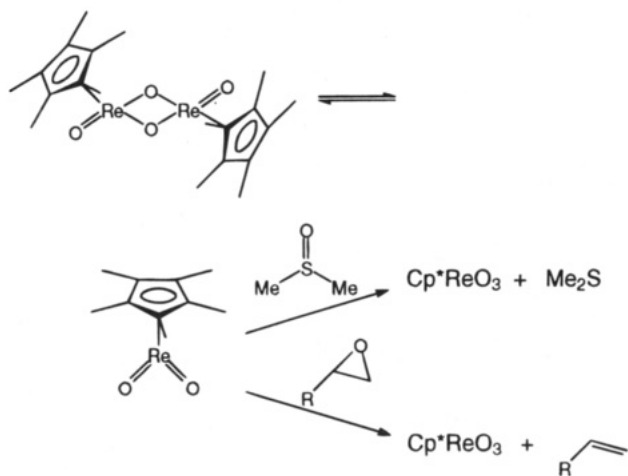


Figure 2. UV-vis spectra vs temperature (toluene, 0.057 mM).

Scheme 1



temperatures; an isosbestic point is observed at 349 nm (see Figure 2). This feature is likely due to the metal-metal bond that has been suggested for the dimer.¹⁰ On the basis of the NMR behavior, analysis of these spectra gave a calculated¹¹ molar absorptivity of $\epsilon = 1550 \text{ M}^{-1} \text{ cm}^{-1}$ for the dimer. The monomer has a calculated absorptivity of $\epsilon = 100 \text{ M}^{-1} \text{ cm}^{-1}$ at 418 nm, probably due to the tailoff of the ligand-to-metal charge transfer band seen below 300 nm for this system. Subtraction of spectra revealed no new features unequivocally attributable to the monomer.¹²

Reaction of dimer (in equilibrium with monomer) with an excess of dimethyl sulfoxide at 65 °C gave Cp^*ReO_3 and dimethyl sulfide (Scheme 1).¹³ The system also reacted with several epoxides at 50–105 °C, including styrene oxide, cyclohexene oxide, 1,1-dimethyloxirane, and (*E*)- and (*Z*)-1,2-dimethyloxirane. Formation of Cp^*ReO_3 was quantitative by ¹H NMR (no other Cp* methyl signals were observed). The alkene was also observed, though loss of volatile alkene to the head

space made quantitation impractical. (*E*)- and (*Z*)-dimethyloxirane each give the corresponding 2-butene with retention of configuration; ¹H signals for (*E*)-2-butene were seen at 5.35 (m) and 1.42 (d) ppm, while signals for (*Z*)-2-butene were seen at 5.48 and 1.48 ppm. The relative reactivity was styrene oxide > 1,1-dimethyloxirane > (*Z*)-1,2-dimethyloxirane > (*E*)-1,2-dimethyloxirane.

Evaluation of the rate law for deoxygenation of styrene oxide was performed. When run with a large excess of epoxide (pseudo-first-order conditions), there was a half-order dependence on $(\text{Cp}^*\text{ReO}_2)_2(\mu\text{-O})_2$. This is expected if monomeric Cp^*ReO_2 is responsible for oxygen atom abstraction. There was also a first-order dependence on epoxide concentration between 0.3 and 2.0 M. This leads to a rate law of the form

$$-d[(\text{Cp}^*\text{ReO}_2)_2(\mu\text{-O})_2]/dt = k_{\text{obs}}[\text{epoxide}][(\text{Cp}^*\text{ReO}_2)_2(\mu\text{-O})_2]^{1/2} \quad (2)$$

At 50.1 °C, k_{obs} was found to be $6.4 \times 10^{-8} \text{ M}^{-1/2} \text{ s}^{-1}$ for deoxygenation of styrene oxide in C_6D_6 . This corresponds to a second-order rate of $2.1 \times 10^{-5} \text{ M}^{-1} \text{ s}^{-1}$ for conversion of monomer plus epoxide to trioxo plus alkene. Such a rate corresponds to $\Delta G^\ddagger = 25.6 \text{ kcal/mol}$. In THF-*d*₈ at the same temperature, the rate is marginally faster, $k_{\text{obs}} = 8.7 \times 10^{-8} \text{ M}^{-1/2} \text{ s}^{-1}$.

These observations can be interpreted on the basis of an analysis performed by Holm and Donahue.¹⁴ The dimer $(\text{Cp}^*\text{ReO}_2)_2(\mu\text{-O})_2$ is formed from Cp^*ReO_3 and PPh_3 .¹⁵ Since both DMSO and epoxides are thermodynamically better O atom donors than Ph_3PO , and given that oxo transfer to DMSO from Cp^*ReO_3 to yield Me_2SO_2 is not observed, we can estimate the average $\text{Re}=\text{O}$ bond enthalpy in the trioxide at 120–141 kcal/mol, consistent with other third-row metal oxo compounds.¹⁶

There are several possible mechanisms for these deoxygenations (Scheme 2). The simplest is a concerted fragmentation of the coordinated epoxide. This parallels Bercaw's investigation of a tantalum-based epoxide deoxygenation¹⁷ and Mayer's studies on L_4WCl_2 ¹⁸ and is also suggested by the facile reduction of DMSO we observe; however, one expects that a coordinating solvent such as THF should have a larger effect either on the rate of deoxygenation (by inhibiting coordination of the epoxide) or on the monomer-dimer equilibrium. One alternative would be a radical process, such as that observed by Nugent and co-workers.¹⁹ However, this appears incompatible with the high stereospecificity of the reaction. Finally, oxidative addition of the three-membered ring to form a metallaoxetane²⁰ offers a third possibility. This last possibility could also include the

(10) Herrmann, W. A.; Küsthardt, U.; Flöel, M.; Kulpe, J.; Herdtweck, E.; Voss, E. *J. Organomet. Chem.* **1986**, *314*, 151–162.

(11) A two-component Beer's law plot was generated using variable-temperature UV-vis data for different initial concentrations of dimer. Concentrations of monomer and dimer were calculated using the van't Hoff plot shown in Figure 1.

(12) In addition to LMCT bands, the expected feature of this d² species is a weak, long-wavelength d-d transition. Given the low concentrations of monomer generated in this system, the inability to identify this feature is unremarkable.

(13) Brown, S. M.; DuMez, D. D.; Mayer, J. M. *Abstracts of Papers*, 207th National Meeting of the American Chemical Society, San Diego, CA, Spring 1994, American Chemical Society: Washington, DC, 1994; INOR 168.

(14) Holm, R. H.; Donahue, J. P. *Polyhedron* **1993**, *12*, 571–589.

(15) Reference 8c.

(16) Glidewell, C. *Inorg. Chim. Acta* **1977**, *24*, 149–157.

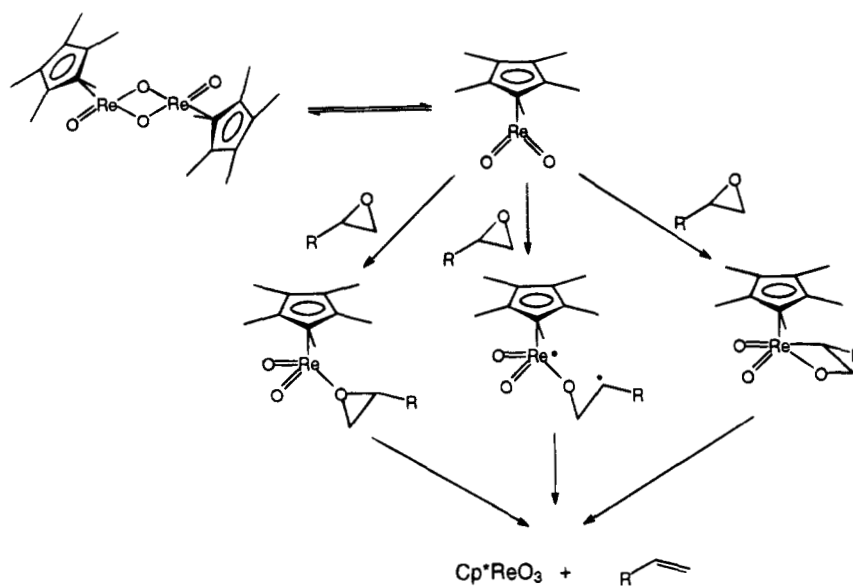
(17) Whinnery, L. L.; Henling, L. M.; Bercaw, J. E. *J. Am. Chem. Soc.* **1991**, *113*, 7575–7582.

(18) Atagi, L. M.; Over, D. E.; McAlister, D. R.; Mayer, J. M. *J. Am. Chem. Soc.* **1991**, *113*, 870–874.

(19) (a) RajanBabu, T. V.; Nugent, W. A.; Beattie, M. S. *J. Am. Chem. Soc.* **1990**, *112*, 6408–6409. (b) RajanBabu, T. V.; Nugent, W. A. *J. Am. Chem. Soc.* **1994**, *116*, 986–997.

(20) Calhorda, M. J.; Galvão, A. M.; Unalerglu, C.; Zlota, A. A.; Frolow, F.; Milstein, D. M. *Organometallics* **1993**, *12*, 3316–3325.

Scheme 2



coordinated epoxide as a precursor. Each of these has ramifications concerning the mechanism of fragmentation of diolates; we are currently evaluating the reaction energetics to discern the relationship between the two processes.

Acknowledgment. Support from the National Science Foundation (Grant CHE-9312650) is gratefully acknowledged.

OM950200X

4-Methyl-1,4-thiaborin, an Aromatic Boron–Sulfur Heterocycle

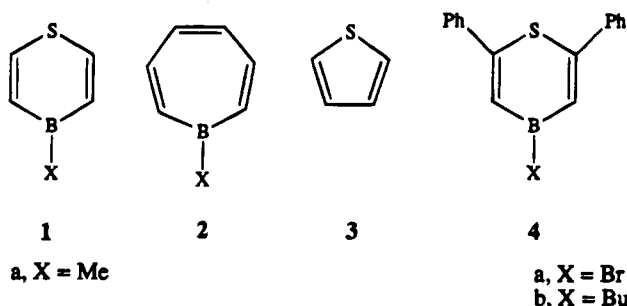
Arthur J. Ashe, III,* Jeff W. Kampf, and Jack R. Waas

Department of Chemistry, The University of Michigan, Ann Arbor, Michigan 48109-1055

Received March 6, 1995[®]

Summary: The base-catalyzed hydrostannation of diethynyl sulfide with dibutylstannane affords 4,4-dibutyl-1,4-thiastannin, which reacts with methylboron dibromide to give 4-methyl-1,4-thiaborin. The thiaborin has been converted to tricarbonyl(η^6 -4-methyl-1,4-thiaborin)-molybdenum, which has been characterized by single-crystal X-ray diffraction.

The boron–sulfur heterocycle 1,4-thiaborin (**1**) is a potentially six- π -electron aromatic compound. Comparison of **1** with the better known six- π -electron heterocycles borepin (**2**)¹ and thiophene (**3**)² should be intrinsically interesting. Although the synthesis of 4-butyl- and 4-bromo-2,6-diphenyl-1,4-thiaborins (**4a,b**) was reported by Meller in 1982,³ the chemistry of thiaborins has been virtually unexplored. We report here on the synthesis of a C-unsubstituted thiaborin and on structural data which show that thiaborin can serve as an η^6 -aromatic ligand toward transition metals.



The preparation of **1** relies on the general synthesis of boron heterocycles from diacetylenes via organotin intermediates.^{4,5} The precursor diacetylene, diethynyl sulfide (**6**),^{5a} is easily obtained by desilylation of bis((trimethylsilyl)ethynyl) sulfide⁶ (**5**) with Bu_4NF in methanol. Since **6** is extremely labile, it is not isolated

but is extracted with pentane/toluene and the dried extracts are subject to base-catalyzed hydrostannation using dibutylstannane, powdered KOH, and 18-crown-6 ether at 25 °C.^{4c} The resulting 4,4-dibutyl-1,4-thiastannin (**7**) is obtained as a stable distillable yellow oil in 20% yield from **5**. The reaction of **7** with methylboron dibromide in pentane affords 4-methyl-1,4-thiaborin (**1a**) as an air-sensitive volatile oil in 57% yield.⁷

The most widely used criterion of aromaticity involves ¹H NMR spectroscopy. The protons of planar aromatic rings show low-field chemical shift values which are attributed to the presence of a diamagnetic ring current.⁸ By this measure **1a** seems to be aromatic. The chemical shift values for **1a** (δ 7.99 (H₂) and 7.40 (H₃))

(6) Verboom, W.; Schoufs, M.; Meijer, J.; Verkruisje, H. D.; Brandsma, L. *Recl. Trav. Chim. Pays-Bas* **1979**, *97*, 245.

(7) Experimental procedures and characterization of new compounds are as follows. (a) 4,4-Dibutyl-1,4-thiastannin (**7**): A solution of $\text{Bu}_4\text{NF}\cdot\frac{1}{3}\text{H}_2\text{O}$ (12.6 g, 36.2 mmol) in 40 mL of methanol was added dropwise with stirring to a solution of bis((trimethylsilyl)ethynyl) sulfide (**5**) (3.9 g, 17.2 mmol) in 80 mL of methanol under a nitrogen atmosphere. No discernible color change occurred. The mixture was then poured onto 150 mL of pentane and extracted twice with 200 mL of water. Then, 20 mL of toluene was added to the organic layer, which was thereafter dried over K_2CO_3 and decanted. Careful concentration of the solution on a rotary evaporator (water bath temperature did not exceed 25 °C) gave 24.6 g of a light yellow solution. Analysis by ¹H NMR spectroscopy indicated that the solution contained approximately 3.4% (830 mg, 59% yield) of diethynyl sulfide (**6**). ¹H NMR (C_6D_6 , 300 MHz): δ 3.22(s). To this solution was added dibutylstannane (2.62 g, 11.2 mmol), powdered KOH (285 mg, 5.07 mmol), and 18-crown-6 ether (134 mg, 0.51 mmol). The mixture was then stirred vigorously for 3 h under N_2 . Removal of volatiles in vacuo and distillation (bp 68–70 °C/0.1 torr) gave 920 mg of **7**; 20% yield based on **5**. ¹H NMR (C_6D_6 , 200 MHz): δ 6.66 (dd, $J = 11.0, 2.0$ Hz, $J_{\text{19SnH}} = 96$ Hz, 2H), 6.14 (dd, $J = 11.0, 2.0$ Hz, $J_{\text{19SnH}} = 64$ Hz, 2H), 1.45–0.86 (m, 18H). ¹³C NMR (CDCl_3 , 50.3 MHz): δ 137.2 ($J_{\text{19SnC}} = 9$ Hz), 122.4 ($J_{\text{19SnC}} = 186$ Hz), 28.7, 26.8, 13.6, 11.4. HRMS (EI, 70 eV): calcd for $\text{C}_{12}\text{H}_{22}\text{S}^{120}\text{Sn}$ 318.0464, found 318.0477. Anal. Calcd for $\text{C}_{12}\text{H}_{22}\text{SSn}$: C, 45.46; H, 6.99. Found: C, 45.33, 45.29; H, 6.92, 6.81. (b) 4-Methyl-1,4-thiaborin (**1a**): Methylboron dibromide (132 mg, 710 μmol) was added dropwise with stirring to a solution of **7** (250 mg, 788 μL) in 1 mL of pentane at 25 °C. The solvent was removed under vacuum, and the product was pot-to-pot distilled at 25 °C under a high vacuum into a cold (–78 °C) receiver. The product (44 mg, 57% yield) was a colorless oil. ¹H NMR (CDCl_3 , 300 MHz): δ 7.99 (d, $J = 12.2$ Hz, 2H), 7.40 (dd, $J = 2.5, 12.4$ Hz, 2H), 0.82 (s, 3H). ¹³C NMR (CDCl_3 , 90.6 MHz): δ 141.8, 136 (br), 9 (br). ¹¹B NMR (CDCl_3 , 115.5 MHz): δ 50.1. HRMS (EI, 70 eV): calcd for $\text{C}_5\text{H}_7^{11}\text{BS}$ 110.0362, found 110.0363. (c) Tricarbonyl(η^6 -4-methyl-1,4-thiaborin)molybdenum (**8**): As above, the reaction of **7** (330 mg, 1.04 mmol) and methylboron dibromide (193 mg, 1.04 mmol) in 0.5 mL of pentane afforded volatile products, which were taken up in 4 mL of ether. Tricarbonyltris(pyridine)molybdenum (520 mg, 1.25 mmol) was added with stirring at 25 °C, followed by $\text{BF}_3\cdot\text{OEt}_2$ (0.64 mL, 5.2 mmol). The mixture was heated to reflux for 1 h, and after cooling to 25 °C volatile material was removed under high vacuum. The residue was extracted with pentane. After separation and removal of solvent, the product was recrystallized from hexane, yielding 124 mg (41%) of orange cubes, mp 116–119 °C. ¹H NMR (C_6D_6 , 300 MHz): δ 4.32 (d, $J = 10.6$ Hz, 2H), 4.01 (dd, $J = 10.6, 1.6$ Hz, 2H), 0.93 (s, 3H). ¹³C NMR (C_6D_6 , 50.3 MHz): 201.0 (CO), 100.0, 95 (br), signal for the Me not observed. ¹¹B NMR (C_6D_6 , 115.5 MHz): 22.3. IR (hexane): $\nu(\text{CO})$ 2002, 1936, 1931 cm^{-1} . HRMS (EI, 70 eV): calcd for $\text{C}_5\text{H}_7^{11}\text{BMoO}_3\text{S}$ 291.9263; found 291.9268. Anal. Calcd for $\text{C}_5\text{H}_7\text{BMoO}_3\text{S}$: C, 33.14; H, 2.43. Found: C, 32.82, 32.96; H, 2.36, 2.28.

(8) Garratt, P. J. Aromaticity. In *Comprehensive Organic Chemistry*; Barton, D., Ollis, W. D., Eds.; Pergamon Press: Oxford, U.K., 1979; Vol. 1, pp 215–240.

[®] Abstract published in *Advance ACS Abstracts*, June 15, 1995.

(1) Ashe, A. J., III; Klein, W.; Rousseau, R. *Organometallics* **1993**, *12*, 3225 and references cited therein.

(2) (a) Gronowitz, S., Ed. Thiophene and Its Derivatives. In *The Chemistry of Heterocyclic Compounds*; Taylor, E. C., Weissberger, A., Eds.; Wiley: New York, 1986, 1987; Vol. 44. (b) Bird, C. W.; Cheeseman, G. W. H. In *Comprehensive Heterocyclic Chemistry*; Katritzky, A. R., Rees, C. W., Eds.; Pergamon Press: Oxford, U.K., 1984; Vol. 4, pp 1–38.

(3) Habben, C.; Maringgele, W.; Meller, A. *Z. Naturforsch., B: Anorg. Chem. Org. Chem.* **1982**, *37B*, 43.

(4) (a) Noltes, J. G.; van der Kerk, G. J. M. *Recl. Trav. Chim. Pays-Bas* **1962**, *81*, 41. Leusink, A. J.; Noltes, J. G.; Budding, H. A.; van der Kerk, G. J. M. *Recl. Trav. Chim. Pays-Bas* **1964**, *83*, 1036. Leusink, A. J.; Drenth, W.; Noltes, J. G.; van der Kerk, G. J. M. *Tetrahedron Lett.* **1967**, 1263. (b) Ashe, A. J., III; Shu, P. *J. Am. Chem. Soc.* **1971**, *93*, 1804. (c) Ashe, A. J., III; Drone, F. *J. Am. Chem. Soc.* **1987**, *109*, 1879; **1988**, *110*, 6599. Ashe, A. J., III; Kampf, J. W.; Kausch, C. M.; Konishi, H.; Kristen, M. O.; Kroker, J. *Organometallics* **1990**, *9*, 2944. (d) Sugihara, Y.; Yagi, T.; Murata, I.; Imamura, A. *J. Am. Chem. Soc.* **1992**, *114*, 1479.

(5) Also see: (a) Meijer, J.; Vermeer, P.; Verkruisje, H. D.; Brandsma, L. *Recl. Trav. Chim. Pays-Bas* **1973**, *92*, 1326. (b) Schoufs, M.; Meijer, J.; Vermeer, P.; Brandsma, L. *Recl. Trav. Chim. Pays-Bas* **1974**, *93*, 244.

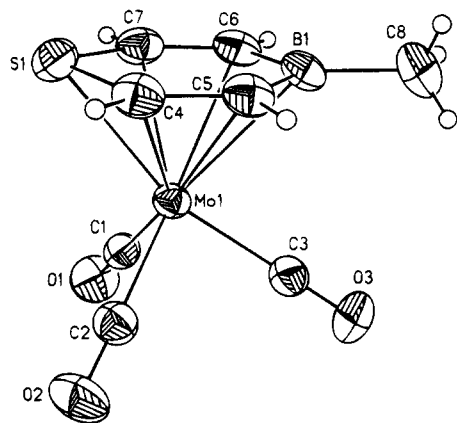
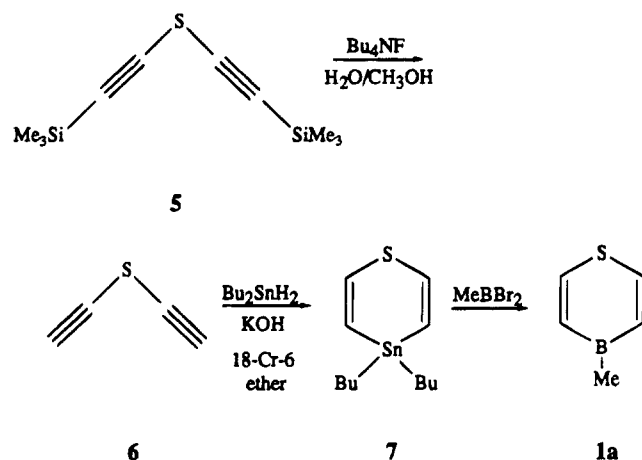
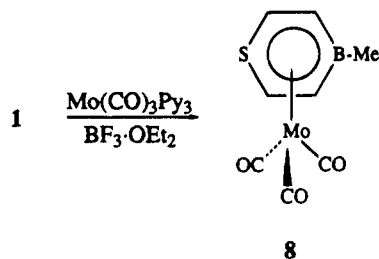


Figure 1. Solid-state structure of **8** (ORTEP). Selected distances (Å) and angles (deg): Mo–B, 2.523(4); Mo–C4, 2.339(4); Mo–C5, 2.414(3); Mo–C6, 2.426(4); Mo–C7, 2.334(4); Mo–S, 2.512(1); B–C5, 1.520(6); B–C6, 1.523(4); B–C8, 1.578(7); C4–C5, 1.375(5); C6–C7, 1.369(6); C4–S, 1.754(3); C7–S, 1.750(4); C5–B–C6, 115.0(3); C4–S–C7, 101.3(2).

Scheme 1



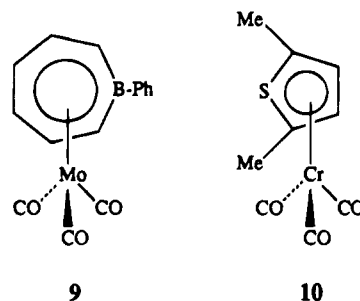
Scheme 2



are comparable to those of the aromatic 1-methylborepin (**2a**; δ 7.66 (H_2) and 7.73 (H_3)) and thiophene (**3**; δ 7.30 (H_2) and 7.10 (H_3)). In addition, electron donation to the boron atom of **1a** seems indicated by the observed ^{11}B chemical shift (δ 50.1) upfield from that of **2a** (δ 54.8).¹ Surprisingly, the ^{11}B chemical shift of **4b** (δ 66.8) is at much lower field.³

The reaction of **1a** with tricarbonyltris(pyridine)-molybdenum and $BF_3 \cdot OEt_2$ gives adduct **8** as dark red crystals in 40% yield. The X-ray structure of **8** illustrated in Figure 1 shows that the nearly planar thiaborin ring is η^6 -coordinated to the molybdenum atom.⁹ The boron and four carbon atoms lie in a common plane, but the sulfur atom is displaced out of this plane away from the metal by 0.11 Å. This is a likely consequence of the larger size of sulfur and is analogous to the out-of-plane displacement (0.096 Å

found in tricarbonyl(η^5 -2,5-dimethylthiophene)chromium (**10**).¹⁰ The juxtaposition of the metal tricarbonyl group relative to the ring in **8** resembles that of **10**, where one CO group is trans to sulfur,¹⁰ and **9**, where a CO group eclipses boron.¹¹ This conformational feature has been found for other boron^{4c,12,13} and sulfur^{13,14} heterocycles and has been treated by MO studies^{10,15,16} which probably apply to **8**.



It is striking that all corresponding ring bonds of **8–10** are essentially of the same length. Compare the C–C bond distances of **8** (1.37, 1.38 Å) with the C–C bonds adjacent to the heteroatoms in **9** (1.39 Å) and **10** (1.38 Å). Similarly, the endocyclic C–B bonds of **8** and **9** (1.52, 1.53 Å) and the C–S bonds of **8** and **10** (1.75, 1.76 Å) are identical within experimental error. Thus the structural parameters of **8–10** indicate that the compounds are very similar π -complexes of aromatic rings.

Finally we note that **8** is the only structurally characterized complex involving sulfur π -bonding to molybdenum. Mo π -bound thiophene complexes have figured prominently in mechanistic speculation about the mode of action of molybdenum-based hydrodesulfurization catalysis.¹⁷ The preparation of a related Mo π -bound sulfur complex may be relevant to these studies.

Acknowledgment. We thank Ms. Heather Crocker for performing the initial experiments on the desilylation of **5**. We thank the National Science Foundation (Grant No. CHE-9224967) for financial support of our work.

Supporting Information Available: Tables of crystallographic data, positional and thermal parameters, and interatomic distances and angles for **8** (5 pages). Ordering information is given on any current masthead page.

OM950171Q

(9) Crystal data for **8**: $C_8H_7BMoO_3S$, monoclinic, $P2_1/n$ (No. 14), $a = 8.634(2)$ Å, $b = 9.997(2)$ Å, $c = 12.471(3)$ Å, $\beta = 104.80(2)^\circ$, $V = 1040.7(4)$ Å³, $Z = 4$, $D_c = 1.85$ g cm⁻³, $T = 298$ K, $\mu(Mo K\alpha) = 13.98$ cm⁻¹. Data were collected on a Syntex P2₁m/v diffractometer using the 2θ scan range 5–52°; of the 2417 reflections measured, 2067 were unique ($R_{int} = 0.0146$) and 1695 with $F \geq 4\sigma(F)$ were used in the refinement. The structure was solved by Patterson techniques and refined by full-matrix least squares. $R = 0.0257$, $R_w = 0.0356$, and $GO F = 0.93$.

(10) Sanger, M. J.; Angelici, R. J. *Organometallics* **1994**, *13*, 1821.

(11) Ashe, A. J., III; Kampf, J. W.; Nakadaira, Y.; Pace, J. M. *Angew. Chem., Int. Ed. Engl.* **1992**, *31*, 1255. Ashe, A. J., III; Kampf, J. W.; Klein, W.; Rousseau, R. *Angew. Chem., Int. Ed. Engl.* **1993**, *32*, 1065.

(12) Huttner, G.; Krieg, B. *Chem. Ber.* **1972**, *105*, 3437.

(13) Siebert, W.; Augustin, G.; Full, R.; Krüger, C.; Tsay, Y.-H. *Angew. Chem., Int. Ed. Engl.* **1975**, *14*, 262. Siebert, W.; Full, R.; Edwin, J.; Kinberger, K.; Krüger, C. *J. Organomet. Chem.* **1977**, *131*, 1.

(14) Bailey, M. F.; Dahl, L. F. *Inorg. Chem.* **1965**, *4*, 1306.

(15) Albricht, T. A.; Hoffmann, R. *Chem. Ber.* **1978**, *111*, 1578.

(16) Böhm, M. C.; Gleiter, R.; Herberich, G. E.; Hessner, B. *J. Phys. Chem.* **1985**, *89*, 2129.

(17) (a) Rauchfuss, T. B. *Prog. Inorg. Chem.* **1991**, *39*, 259. (b) Angelici, R. J. *Acc. Chem. Res.* **1988**, *21*, 387; *J. Coord. Chem. Rev.* **1990**, *105*, 61. (c) References cited in ref 10. (d) Blackman, A. *Adv. Heterocycl. Chem.* **1993**, *58*, 147–153.

A Stable Palladium(I) Dimer with One 14e Palladium Center and Its Reversible Reaction with CS₂, Affording a New Complex with a Planar Four-Coordinate Carbon

Piero Leoni*

Scuola Normale Superiore, Piazza dei Cavalieri 7, I-56100 Pisa, Italy

Marco Pasquali* and Giuseppe Pieri

Dipartimento di Chimica e Chimica Industriale, Università di Pisa,
via Risorgimento 35, I-56126 Pisa, Italy

Alberto Albinati*

Istituto di Chimica Farmaceutica, Università di Milano, I-20131 Milano, Italy

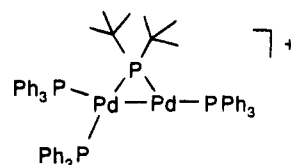
Paul S. Pregosin* and Heinz Rügger

Laboratorium für Anorganische Chemie, ETH Zentrum, CH-8092 Zürich, Switzerland

Received February 17, 1995[®]

Summary: Two new stable dinuclear Pd(I) complexes, $[Pd_2(\mu-PBu^t_2)(PPh_3)_3]X$ and $[Pd_2(\mu-PBu^t_2)(PPh_3)_2(\mu,\eta^2-\eta^2-CS_2)]X$ ($X = BF_4, CF_3SO_3$), have been synthesized and characterized. The former has one 14e Pd center, and the latter, which has been characterized by X-ray diffraction, contains a CS₂ molecule with a four-coordinate planar CS₂ carbon.

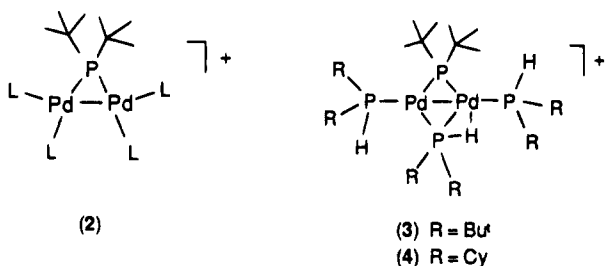
14e configuration, the first of its kind for a dinuclear Pd(I) complex.



(5)X

a, X = CF₃SO₃
b, X = BF₄

In our studies on Pd(I) dinuclear complexes^{1–4} we have utilized the fragment $[Pd_2(\mu-PBu^t_2)]^+$, (**1**), as a building block. This moiety can be stabilized by accepting electrons from four additional ligands to afford the 30e cationic complexes of type **2**. In some interesting complexes the fragment **1** can be stabilized by three secondary phosphine ligands, as shown by **3** and **4**; however, as one of the secondary phosphines is serving as a four-electron donor, these cations can still be considered as 30e species.



(2)

(3) R = Bu^t
(4) R = Cy

We report here the synthesis of **5**, a 28e dinuclear cationic species, in which one of the Pd centers has a

A violet suspension of **3** (as its BF₄ salt¹) in dimethoxyethane was reacted with a 10-fold excess of PPh₃ for 12h at 70 °C to afford (**5**)BF₄ as a red microcrystalline solid in 90% yield. The ³¹P, ¹⁹F, ¹³C, and ¹H NMR data⁵ for this complex are consistent with the proposed formulation. There is no evidence for an η² interaction from one of the phosphine phenyl groups. Figure 1 shows one of the first examples of a ³¹P, ¹³C correlation in a transition-metal complex.⁶ The ³¹P spin in a position pseudo-trans to the bridging ligand is correlated to its aryl ¹³C partners. The vertical axis with all of the ¹³C PPh₃ signals shows (a) all the PPh₃ ligands have three equivalent rings and, via the correlation, (b) the *ortho* carbons for the selected ³¹P spin are all equivalent. It is worth noting that all of the *ortho* ¹³C signals appear at relatively high frequency. In an η²-olefin complex one would expect some low-frequency shift (even if there were an equilibrium involving exchange of different

(5) The *ortho* and *meta* ¹³C signals for all three PPh₃ ligands have been assigned. NMR spectra (acetone-*d*₆, 293 K) of (**5**)BF₄: ¹H, δ (ppm) 7.2 (m, 45H, Ph), 0.95 (d, ³J_{PH} = 14 Hz, 18H, Bu^t); ¹⁹F, δ (ppm) -154.8 (s); ³¹P{¹H}, ABMX spin system, δ (ppm) 350.6 (P₃, ²J_{P₃P₁} = 210, ²J_{P₃P₂} = 54, ²J_{P₃P₁} = 66 Hz), 23.4 (P₄, ²J_{P₄P₁} = 210, ²J_{P₄P₂} = 25, ³J_{P₄P₃} = 20 Hz), 18.1 (P₂, ³J_{P₂P₁} = 135 Hz, ³J_{P₂P₃} = 20, ²J_{P₂P₃} = 54 Hz), 17.5 (P₁, ³J_{P₁P₂} = 135, ³J_{P₁P₃} = 25, ²J_{P₁P₃} = 66 Hz) (see eq 1 for the numbering scheme). IR (Nujol, KBr): 3040 m (ν_{C-H}), 1590 m, 1440m (ν_{C=C}), 1063 br vs (ν_{BF}) cm⁻¹. Anal. Calcd for C₆₂H₆₃BF₄P₄Pd₂: C, 60.5; H, 5.16; P, 10.1. Found: C, 60.3; H, 5.35; P, 10.4.

(6) Mention of a hitherto unpublished ¹³C, ³¹P correlation of a palladium–phosphine complex was made in: Bast, P.; Berger, S.; Günther, H. *Magn. Reson. Chem.* **1992**, *30*, 587.

[®] Abstract published in *Advance ACS Abstracts*, May 15, 1995.
(1) Albinati, A.; Lianza, F.; Pasquali, M.; Sommovigo, M.; Leoni, P.; Pregosin, P. S.; Rügger, H. *Inorg. Chem.* **1991**, *30*, 4690.
(2) Leoni, P.; Pasquali, M.; Sommovigo, M.; Laschi, F.; Zanello, P.; Albinati, A.; Lianza, F.; Pregosin, P. S.; Rügger, H. *Organometallics* **1993**, *12*, 1702.
(3) Leoni, P.; Pasquali, M.; Sommovigo, M.; Albinati, A.; Lianza, F.; Pregosin, P. S.; Rügger, H. *Organometallics* **1993**, *12*, 4503.
(4) Leoni, P.; Pasquali, M.; Sommovigo, M.; Albinati, A.; Lianza, F.; Pregosin, P. S.; Rügger, H. *Organometallics* **1994**, *13*, 4017.

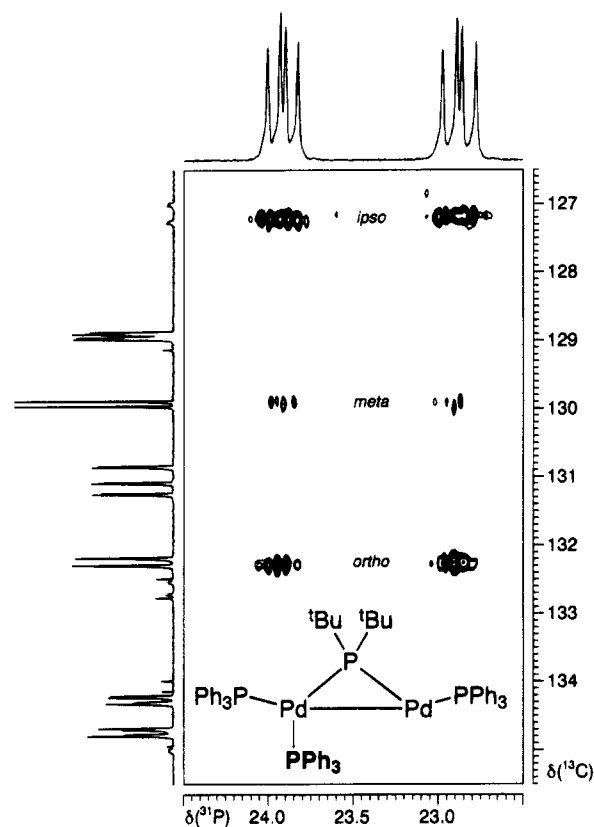
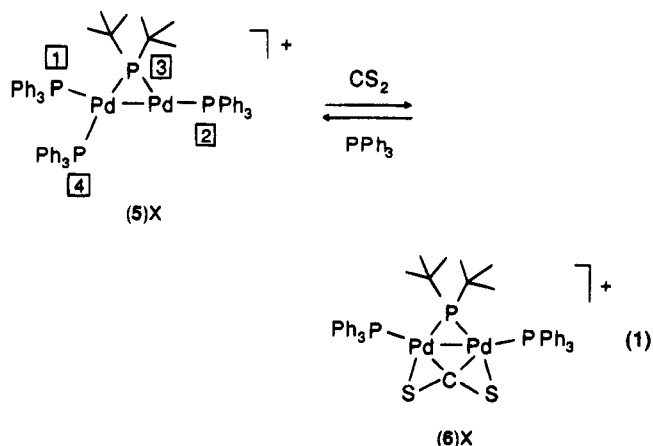


Figure 1. ^{31}P , ^{13}C correlation for the PPh_3 pseudo-trans to the $\mu\text{-PBu}_2$ group. From the ^{13}C NMR signals in the aromatic region, one can deduce that, within a given PPh_3 , all three phenyl groups are equivalent.

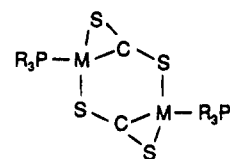
interacting carbons). The ^{19}F NMR spectrum, in both the solid and solution states, is a singlet,⁵ thus ruling out a complex with a bridging F atom from the BF_4^- anion;⁷ this is further confirmed by the strong IR absorption⁵ at 1063 cm^{-1} , characteristic for an ionic BF_4^- anion.⁸ Moreover, the ^1H and ^{31}P NMR spectra of (5) BF_4 and of (5) CF_3SO_3 were identical. The ^{31}P NMR data are almost solvent-independent,⁹ thereby eliminating a structure with a solvent molecule in the open position. We attribute the relative stability of this 14e Pd center to the presence of two relatively large flanking PPh_3 ligands, i.e., steric inhibition to coordination.

Both (5a)X and (5b)X react with an excess of CS_2 to afford a yellow solid, (6)X.



The reaction is reversible in that addition of PPh_3 to a solution of (6)X in acetone affords (5)X. (6) CF_3SO_3

gave crystals suitable for X-ray diffraction,¹⁰ and an ORTEP plot for this cation is shown in Figure 2, with a few bond lengths and bond angles being given in the caption. The cation contains a four-coordinate, almost planar CS_2 molecule in which the CS_2 carbon is bonded nearly symmetrically¹¹ to both metal centers as well as to the two sulfur atoms. The two Pd-S distances are not significantly different, with the average being $2.351(3)\text{ \AA}$. Interestingly, the carbon is closer to the metal than are the two sulfurs. The three atoms of the CS_2 all lie in the plane defined by the two Pd and the bridging P atoms, with maximum deviations less than $\pm 0.7\text{ \AA}$. Although this is an unusual environment for a carbon atom, Erker and co-workers have also found complexes containing planar four-coordinate carbon.¹² Further, Bianchini^{13a} and Farrar^{13b,c} and their co-workers have found the dinuclear $\text{M}(0)$ complexes **7**, in which, however, the CS_2 molecules are not symmetrically bonded and are part of larger six-membered rings, with longer, nonbonding, MM distances.



(7) $\text{M} = \text{Ni, Pd, Pt}$

The Pd-S bond lengths in **7** ($\text{M} = \text{Pd}$)^{13b} are somewhat shorter at $2.314(1)\text{ \AA}$.

Other examples of cumulenes symmetrically $\mu, \eta^2:\eta^2$ -bonded to and coplanar with an M_2 system are the

(7) For example, (3) BF_4 gives a singlet at -154.8 ppm as do the complexes of formula $[\text{Pd}_2(\mu\text{-PBu}_2)(\text{PR}_3)_4]\text{BF}_4$ cited in ref 4. (b) Sünkel, K.; Urban, G.; Beck, W. *J. Organomet. Chem.* **1987**, *319*, C1. (c) Appel, M.; Beck, W. *J. Organomet. Chem.* **1987**, *319*, C1.

(8) Beck, W.; Sünkel, K. *Angew. Chem., Int. Ed. Engl.* **1988**, *27*, 1405.

(9) Only minor changes in $\delta(^{31}\text{P}\{^1\text{H}\})$ (with P,P coupling constant remaining practically unchanged) were observed for spectra in CH_2Cl_2 , DME, THF, acetone and benzene. In CH_3CN , however, we observed a significant change ($^{31}\text{P}\{^1\text{H}\}$ NMR (CD_3CN , 298 K) δ (ppm) 324.0 (ddd, $J_{\text{PP}} = 179, 44, 37\text{ Hz}$, P_3), 25.3 (ddd, $J_{\text{PP}} = 179, 19, 22\text{ Hz}$, P_4), 11.7 (ddd, $J_{\text{PP}} = 44, 19, 198\text{ Hz}$, P_1), 8.02 (ddd, $J_{\text{PP}} = 37, 22, 198\text{ Hz}$, P_2) attributable to the formation of $[\text{Pd}_2(\mu\text{-PBu}_2)(\text{PPh}_3)_3(\text{NCCH}_3)]\text{BF}_4$ with a solvent molecule occupying the free position *trans* to the phosphido. The nitrile complex was isolated as a yellow solid; the coordination is weak, however, and acetonitrile is easily lost under vacuum.

(10) Crystal data: $\text{C}_{46}\text{H}_{48}\text{F}_3\text{O}_3\text{P}_3\text{Pd}_2\text{S}_3$, $M_w = 1107.80$, monoclinic, space group $\text{P}2_1/c$, $a = 18.627(2)\text{ \AA}$, $b = 13.783(8)\text{ \AA}$, $c = 19.729(3)\text{ \AA}$, $\beta = 108.35(2)^\circ$, $V = 4808(3)\text{ \AA}^3$, $D_{\text{calc}} = 1.530$, $\mu(\text{Mo K}\alpha) = 10.102$, $Z = 4$. A total of 7502 unique data were collected using a CAD4 diffractometer ($2.5 < \theta < 24.0^\circ$) and empirically corrected for absorption (Ψ -scan method, transmission coefficient 0.8185–0.9985). The structure was solved by Patterson and Fourier methods and refined by full matrix least-squares (based on 4352 observed reflections with $|F_o| > 4\sigma(F_o)$) using anisotropic displacement parameters for all the atoms of the cation. The contribution of the H atoms, in calculated positions ($\text{C-H} = 0.95\text{ \AA}$), was taken into account but not refined. After convergence (511 parameters, largest $\Delta\rho/\sigma < 0.1$) $R = 0.040$ and $R_w = 0.055$. All calculations were carried out using the Enraf-Nonius MOLEN crystallographic package.

(11) The same symmetrical bonding situation is retained in solution; the $^{31}\text{P}\{^1\text{H}\}$ NMR spectrum of (6) BF_4 (acetone- d_6 , 293 K) consists simply of a triplet at 396.4 ppm and a doublet at 25.7 ppm ($^2J_{\text{PP}} = 21\text{ Hz}$) and is consistent with the presence of two equivalent phosphines bonded *cis* to the phosphido ligand. Anal. Calcd for $\text{C}_{46}\text{H}_{48}\text{BF}_4\text{P}_3\text{Pd}_2\text{S}_2$: C, 51.7; H, 4.63; P, 8.89. Found: C, 51.2; H, 4.62; P, 8.80. IR (Nujol, KBr): 3040 m (ν_{CH}), 1590 m, 1440 m ($\nu_{\text{C-C}}$), 1213 s (ν_{CS}), 1063 br vs (ν_{BF}) cm^{-1} . ^1H NMR (CD_2Cl_2 , 298 K): δ (ppm) 0.84 (d, $^3J_{\text{PH}} = 15.5\text{ Hz}$, 18 H, $\text{P}\{\text{C}(\text{CH}_3)\}$), 7.6 (m, 30 H, C_6H_5). When the complex (6*) BF_4 is prepared with $^{13}\text{CS}_2$, the low field ^{31}P signal appears as a doublet of triplets ($^2J_{\text{PC}} = 10\text{ Hz}$) and the high-field one as a double doublet ($^2J_{\text{PC}} = 26\text{ Hz}$). The $^{13}\text{C}\{^1\text{H}\}$ NMR spectrum shows a doublet of triplets at 211.9 ppm ($^2J_{\text{PC}} = 10$ and 26 Hz) assigned to the coordinated carbon of $^{13}\text{CS}_2$. The absorption in the IR spectrum of (6*) BF_4 is shifted to 1173 cm^{-1} .

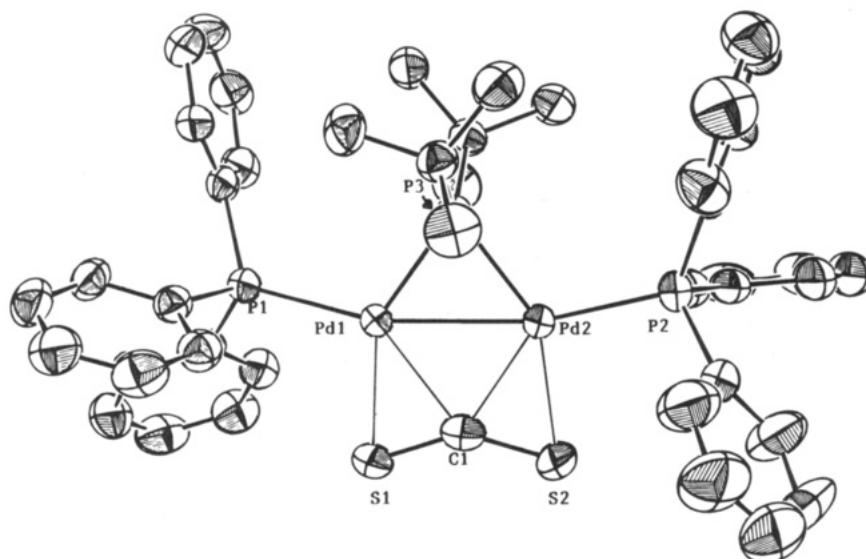


Figure 2. ORTEP diagram for $(6)CF_3SO_3$. Selected bond distances (Å) and angles (deg) are as follows: Pd1–Pd2 = 2.7077(7), Pd1–P1 = 2.309(2), Pd1–P3 = 2.272(1), Pd2–P2 = 2.307(2), Pd2–P3 = 2.306(2), Pd1–S1 = 2.354(2), Pd1–C1 = 2.331(9), Pd2–S2 = 2.349(3), Pd2–C1 = 2.280(7), C1–S1 = 1.606(7), C1–S2 = 1.618(9); Pd1–Pd2–P2 = 166.90(6), Pd2–Pd1–P1 = 165.42(5), P1–Pd1–S1 = 101.26(7), P2–Pd2–S2 = 97.27(8), P1–Pd1–C1 = 141.2(2), P2–Pd1–C1 = 138.1(2). Thermal ellipsoids are drawn at the 50% probability level.

allene¹⁴ in $W_2(\mu, \eta^2: \eta^2\text{-CH}_2\text{=C=CH}_2)(\text{OBU}^t)_6$ and a carbodiimide¹⁵ in $W_2(\mu, \eta^2: \eta^2\text{-ArN=C=NAr})(\text{OBU}^t)_6$.¹

The potential of the coordinatively unsaturated cation $(5)^+$ as a valuable synthetic precursor is now under investigation.

Acknowledgment. Financial support from the Ministero dell'Università e della Ricerca Scientifica e Tecnologica (MURST) and the CNR (Rome) is gratefully acknowledged; P.S.P. thanks the Swiss National Science Foundation and the ETHZ for support.

- (12) Erker, G.; Roettger, D. *Angew. Chem.* **1993**, *105*, 1691.
 (13) Bianchini, C.; Ghilardi, C. A.; Meli, A.; Midollini, S.; Orlandini, I. *J. Chem. Soc., Chem. Commun.* **1983**, 753. (b) Farrar, D. H.; Gukathasan, R. R.; Won, K. *J. Organomet. Chem.* **1984**, *275*, 263. (c) Farrar, D. H.; Gukathasan, R. R.; Morris, S. A. *Inorg. Chem.* **1984**, *23*, 3258.
 (14) Chacon, S. T.; Chisholm, M. H.; Folting, K.; Hoffmann, J. C.; Hampden-Smith, M. J. *Organometallics* **1991**, *10*, 3722.
 (15) Cotton, F. A.; Schwotzer, W.; Shamshoum, E. S. *Organometallics* **1985**, *4*, 461.

Supporting Information Available: Test giving details of the syntheses of $(5)X$, $(6)X$, and $(6^*)X$ and, for $(6)CF_3SO_3$, tables of X-ray experimental data, final atomic coordinates, anisotropic displacement parameters, bond distances and angles, and torsion angles and an ORTEP view of the molecule showing the numbering scheme (19 pages). Ordering information is given on any current masthead page.

OM950132E

Synthesis and Structure of 2,4,5-Trithia-1,3-disilabicyclo[1.1.1]pentane

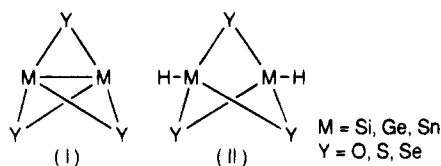
Nami Choi, Kumiko Asano, and Wataru Ando*

Department of Chemistry, University of Tsukuba, Tsukuba, Ibaraki 305, Japan

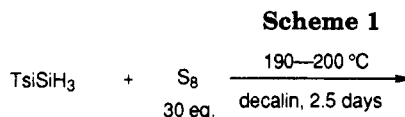
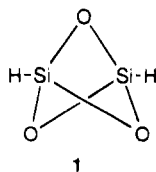
Received March 6, 1995[®]

Summary: The first 1,3-bis{tris(trimethylsilyl)methyl}-2,4,5-trithia-1,3-disilabicyclo[1.1.1]pentane (**2-S3**) was prepared by desulfurization of the corresponding 2,4,5,6-tetrathia-1,3-disilabicyclo[2.1.1]hexane (**2-S4**). The X-ray analysis clearly proved that the distance between the bridgehead silicon atoms of **2-S3** is 2.407 Å, which lies within the range of common Si–Si single bonds.

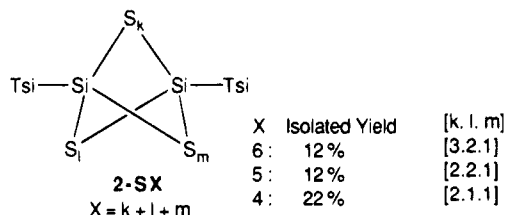
Although a large number of theoretical studies have been carried out on group IV propellanes and their derivatives in order to understand the nature of bridgehead bonds, few examples are known of experimental studies on these systems.^{1–3} Nagase and others suggested that the substitutions of electronegative groups (e.g., O, CH₂) at the peripheral positions could stabilize the central M–M interaction;² accordingly, the structures of [1.1.1]propellanes of the type M₂Y₃ (I; M = Si, Ge, Sn; Y = O, S, Se) and the corresponding bicyclo[1.1.1]pentanes H₂M₂Y₃ (II) should be similar.^{1–3} In-



terestingly, trioxadisilabicyclo[1.1.1]pentane (1) is predicted to have an extremely short distance between the bridgehead silicon atoms of only 2.06 Å, which is even smaller than that of Si=Si double bonds.² Nevertheless, the synthesis of neither 1 nor its sulfur analogue has been reported. We have already reported the first synthesis as well as the structure of the corresponding seleno analogue, namely, 1,3-bis-substituted 2,4,5-triseleno-1,3-disilabicyclo[1.1.1]pentane.⁴ Herein we report on the synthesis and structural features of 2,4,5-trithia-1,3-disilabicyclo[1.1.1]pentane.



Ts = C(SiMe₃)₃



A decalin solution of trisylsilane (tris(trimethylsilyl)methylsilane, TsSiH₃) and 30 equiv of elemental sulfur was heated to 190–200 °C for 2.5 days to give after chromatographic separation tetrathiadisilabicyclo[2.1.1]hexane (**2-S4**),⁵ pentathiadisilabicyclo[2.2.1]heptane (**2-S5**),⁶ and hexathiadisilabicyclo[3.2.1]octane (**2-S6**)⁷ as yellow solids in 22%, 12%, and 12% yields, respectively, which are stable toward air and moisture (Scheme 1). The structures of disilabicyclopolydisulfides **2-S4**, **2-S5**, and **2-S6** have been confirmed by X-ray structure analysis.⁸ When **2-S4** was irradiated in the presence of 1.9 equiv of triphenylphosphine for 4 h, 2,4,5-trithia-1,3-disilabicyclo[1.1.1]pentane (**2-S3**)⁹ was obtained in 64% yield. When **2-S4** was subjected to photolysis in the presence of a 10-fold excess of PPh₃, cyclodisilthiane **3**¹⁰ and **2-S3** could be isolated in 28% and 27% yields, respectively, while independently **2-S3** did not further react under identical conditions. Desulfurization of **2-S4** in *d*₈-toluene afforded *d*₁- or *d*₂-cyclodisilthiane and

(5) For **2-S4**: pale yellow crystals; mp >300 °C; sublimes at >250 °C; ¹H NMR (300 MHz, CDCl₃) δ 0.37 (s); ¹³C NMR (75 MHz, CDCl₃) δ 5.1 (q), 6.5 (s); ²⁹Si NMR (79.5 MHz, CDCl₃) δ 0.8 (SiMe₃), 25.7 (Si–S); UV (*n*-hexane) λ_{max}/nm 280 (ε 320), 366 (41); MS *m/z* 646 (M⁺). Anal. Calcd for C₂₀H₅₄Si₈S₄: C, 37.09; H, 8.40; S, 19.80. Found: C, 36.06; H, 8.40; S, 19.83.

(6) For **2-S5**: yellow crystals; mp >300 °C; sublimes at >250 °C; ¹H NMR (300 MHz, CDCl₃) δ 0.35 (s); ¹³C NMR (75 MHz, CDCl₃) δ 5.2 (q), 6.0 (s); ²⁹Si NMR (79.5 MHz, CDCl₃) δ 0.6 (SiMe₃), 37.3 (Si–S); UV (*n*-hexane) λ_{max}/nm 287 (ε 365), 375 (200); MS *m/z* 678 (M⁺), 646 (M⁺ – 32). Anal. Calcd for C₂₀H₅₄Si₈S₅: C, 35.35; H, 8.01; S, 23.59. Found: C, 35.65; H, 8.17; S, 23.30.

(7) For **2-S6**: yellow crystals; mp >300 °C; sublimes at >250 °C; ¹H NMR (500 MHz, CDCl₃) δ 0.35 (s); ¹³C NMR (75 MHz, CDCl₃) δ 5.5 (q), 6.0 (s); ²⁹Si NMR (79.5 MHz, CDCl₃) δ 0.1 (SiMe₃), 46.4 (Si–S); UV (*n*-hexane) λ_{max}/nm 265 (ε 2200), 350 (340); MS *m/z* 710 (M⁺), 678 (M⁺ – 32). Anal. Calcd for C₂₀H₅₄Si₈S₆: C, 33.75; H, 7.65; S, 27.02. Found: C, 34.02; H, 7.73; S, 26.70.

(8) Choi, N.; Asano, K.; Ando, W. To be submitted for publication.
(9) For **2-S3**: white crystals; mp 216–220 °C; ¹H NMR (400 MHz, C₆D₆) δ 0.45 (s); ¹³C NMR (100 MHz, C₆D₆) δ 4.2 (q), 6.9 (s); ²⁹Si NMR (79.5 MHz, C₆D₆) δ 1.0 (SiMe₃), 5.8 (Si–S); UV (*n*-hexane) λ_{max}/nm 224 (ε 1400), 257 (210), 290 (38); MS *m/z* 614 (M⁺). Anal. Calcd for C₂₀H₅₄Si₈S₃: C, 39.03; H, 8.84; S, 15.63. Found: C, 39.03; H, 8.89; S, 15.59.

(10) For **3**: white crystals; mp 262 °C; ¹H NMR (500 MHz, CDCl₃) δ 0.27 (s, 54H), 5.6 (s, 2H); ¹³C NMR (125 MHz, CDCl₃) δ 4.3 (q), 4.6 (s); ²⁹Si NMR (79.5 MHz, CDCl₃) δ 0.2 (SiMe₃), –7.6 (Si–H); MS *m/z* 584 (M⁺), 569 (M⁺ – 15); IR (KBr, cm^{–1}) ν 2130 (Si–H). Anal. Calcd for C₂₀H₅₆Si₈S₂: C, 41.03; H, 9.64; S, 10.95. Found: C, 40.62; H, 9.63; S, 11.29.

[®] Abstract published in *Advance ACS Abstracts*, June 15, 1995.

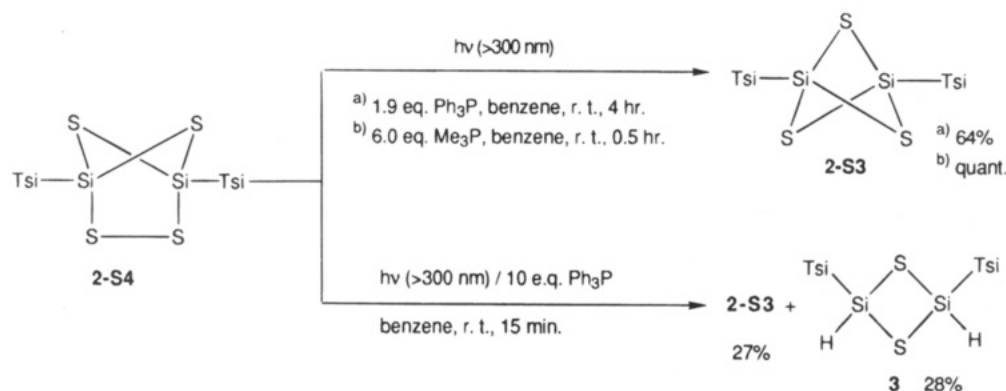
(1) Nguyen, K. A.; Carroll, M. T.; Gordon, M. S. *J. Am. Chem. Soc.* **1991**, *113*, 7924 and references cited therein.

(2) (a) Kudo, T.; Nagase, S. *J. Am. Chem. Soc.* **1985**, *107*, 2589. (b) Nagase, S.; Kudo, T.; Kurakake, T. *J. Chem. Soc., Chem. Commun.* **1988**, 1063. (c) Nagase, S.; Kudo, T. *Organometallics* **1987**, *6*, 2456. (d) Kitchen, D. B.; Jackson, J. E.; Allene, L. C. *J. Am. Chem. Soc.* **1990**, *112*, 3408. (e) Streitwieser, A. *J. Chem. Soc., Chem. Commun.* **1989**, 1261.

(3) Gordon, M. S.; Nguyen, K. A.; Carroll, M. T. *Polyhedron* **1991**, *10*, 1247.

(4) Yoshida, H.; Takahara, Y.; Erata, T.; Ando, W. *J. Am. Chem. Soc.* **1992**, *114*, 1098.

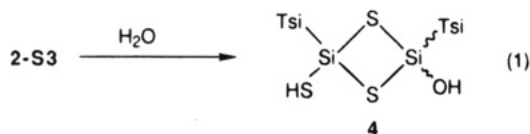
Scheme 2



cyclodisilthiane **3** (11% yield, D:H = 35:65) along with **2-S3** (29% yield). This suggested that proton sources for the formation of **3** are solvent or substituent.

The most likely initial step of the photochemical desulfurization of **2-S4** is cleavage of a S-S bond. Trapping of the resulting thiyl biradical by one or two molecules of PPh₃ would then lead to the formation of **2-S3** and **3**.

By irradiation in the presence of trimethylphosphine **2-S4** was quantitatively converted into **2-S3**. Separation by high-performance liquid chromatography (eluent toluene) followed by recrystallization from benzene, afforded **2-S3** as white crystals with mp 216–220 °C. **2-S3** is thermally quite stable (>300 °C) but is slowly hydrolyzed by moisture to provide 1,3-bis(tris(trimethylsilyl)methyl)-1-hydroxy-3-mercaptocyclodisilthiane¹¹ (**4**; eq 1). **2-S3** is the first example of 2,4,5-trithia-1,3-



disilabicyclo[1.1.1]pentane. The bicyclo[1.1.1]pentane structure of **2-S3** was deduced on the basis of the following spectroscopic properties: the EI mass spectrum indicated a M⁺ peak at *m/z* 614, in agreement with that calculated for C₂₀H₅₄Si₈S₃. Elemental analyses were also in agreement with the calculated values. The ¹H, ¹³C, and ²⁹Si NMR spectra of **2-S3** are fully consistent with the highly symmetrical structure.⁹ ²⁹Si NMR data of the bridgehead silicons in **2-S6**, **2-S5**, **2-S4**, and **2-S3** are 46.4, 37.3, 25.7, and 5.8 ppm, which are in order of the strain of silthiane rings. The structure of **2-S3** was unequivocally determined by single-crystal X-ray diffraction analysis.¹² The molecule has D_{3h} symmetry. The ORTEP drawing, selected bond lengths (Å), and angles (deg) are shown in Figure 1. The structure of **2-S3** is in good agreement with the results

(11) For **4**: white crystals; ¹H NMR (300 MHz, C₆D₆) δ 0.41 (s, 27H), 0.47 (s, 27H), 1.88 (1H, s), 5.08 (s, 1H); ¹³C NMR (75 MHz, C₆D₆) δ 5.6 (q), 5.7 (s), 10.4 (s), 12.1 (s); ²⁹Si NMR (59 MHz, C₆D₆) δ 11.4 (Si-OH), -0.1 (SiMe₃), -0.4 (SiMe₃), -3.4 (Si-SH); MS *m/z* 632 (M⁺); exact mass calcd for C₂₀H₅₆Si₈S₃O *m/z* 632.1648, found *m/z* 632.1666.

(12) Crystal data for **2-S3**: C₂₀H₅₄Si₈S₃, M_r = 615.53, monoclinic, *a* = 15.369(1) Å, *b* = 13.159(1) Å, *c* = 17.672(2) Å, β = 91.51(1)°, *V* = 3572.6 Å³, space group P2₁/c, *Z* = 4, μ(Mo Kα) = 4.7 cm⁻¹, ρ_{calcd} = 1.14 g/cm³. The 5200 independent reflections (*I*₀ > 3σ(*I*₀), θ < 50°) were measured on an Enraf-Nonius CAD4 diffractometer using Mo Kα radiation and a ω-2θ scan. The structure was solved by direct methods, and all non-hydrogen atoms were refined anisotropically by full-matrix least-squares to *R* = 0.036 and *R*_w = 0.037.

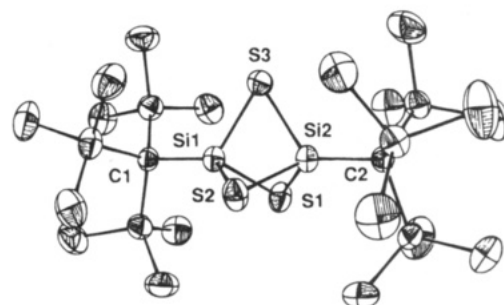
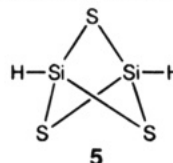


Figure 1. ORTEP drawing of **2-S3**. Selected bond lengths (Å) and angles (deg): Si1-S1, 2.174(1); Si1-S2, 2.181(1); Si1-S3, 2.182(1); Si1-C1, 1.838(3); Si2-S1, 2.171(1); Si2-S2, 2.186(1); Si2-S3, 2.180(1); Si2-C2, 1.833(3); Si1-Si2, 2.407(1); Si1-S1-Si2, 67.27(4); Si1-S2-Si2, 66.88(3); Si1-S3-Si2, 66.98(3); S1-Si1-S2, 92.68(4); S1-Si1-S3, 92.77(4); S2-Si1-S3, 91.87(4); S1-Si2-S2, 92.63(4); S1-Si2-S3, 92.89(4); S2-Si2-S3, 91.76(4); S1-Si1-C1, 122.21(9); S2-Si1-C1, 124.68(9); S3-Si1-C1, 123.67(9); S1-Si2-C2, 122.40(9); S2-Si2-C2, 124.15(9); S3-Si2-C2, 124.03(9); S1-Si1-Si2, 56.30(3); S1-Si2-Si1, 56.43(3); S2-Si1-Si2, 56.66(3); S2-Si2-Si1, 56.46(3); S3-Si1-Si2, 56.49(3); S3-Si2-Si1, 56.53(3).

Table 1. Experimental (**2-S3**) and Calculated (**5**) Bond Lengths (Å) and Angles (deg) of 2,4,5-Trithia-1,3-disilabicyclo[1.1.1]pentane (**2-S3**, **5**)

	2-S3 ^a	5 ^b
Si-Si	2.407(1)	2.363
Si-S	2.174(1)-2.182(1)	2.176
Si-S-Si	66.88(3)-67.27(4)	65.8
Si-Si-S	56.30(3)-56.66(3)	57.1

^a Single-crystal X-ray diffraction data. ^b Reference 1.



of quantum chemical calculations,¹ as reported by Gordon et al. and shown in Table 1. The bicyclo[1.1.1]pentane skeleton is constructed from three cyclobutanes (the dihedral angles of the cyclobutanes are 120.40, 119.75, and 118.85°; average 120.0°). The interesting feature is the acute Si-S-Si angle (66.88(3), 66.98(3), and 67.27(4)°), which can be regarded as angles of three-membered-ring compounds rather than those of normal four-membered-ring compounds; normal Si-S-Si angles of cyclodisilthianes¹³ are ca. 82°. One of the features of **2-S3** is a very short S-S distance, 3.15 Å, which is

within the sum of van der Waals radii of sulfur (3.70 Å). Interestingly, the bridgehead Si - -Si distance of 2.407(1) Å lies within the range of common Si-Si single-bond lengths (2.23–2.70 Å)¹⁴ and is ca. 0.1 Å shorter than that of its selenium analogue (2.515 Å).⁴ This value is very short relative to that of the cyclodisilathianes (2.78–2.83 Å).¹³ This unusual shortening of the Si - -Si distance is caused by the difference in electronegativity between the peripheral sulfur atom and the bridgehead silicon atom. Actually, no such shortening is observed in the corresponding silicon analogue, bicyclo[1.1.1]pentasilane (Si - -Si; 2.92 Å).¹⁵ The repul-

sion between sulfur atoms affects the shortening of the Si - -Si distance of **2-S3**. Then the unusual short Si - -Si distance is due to the geometrical factor; thus, there is a tug-of-war between the three Si-S-Si and six S-Si-S angles.

Acknowledgment. We are grateful to Shin-Etsu Co. Ltd. for their gifts of chlorosilanes. This work was supported in part by a Grant-in-Aid for Scientific Research from the Ministry of Education, Science and Culture of Japan.

Supporting Information Available: Detailed information on the X-ray crystal analysis of **2-S3** (26 pages). Ordering information is given on any current masthead page.

OM950175V

(13) (a) Wojnowski, W.; Peters, K.; Weber, D.; Von Schnering, H. *G. Z. Anorg. Allg. Chem.* **1984**, *519*, 134. (b) Schklower, W. E.; Strutschkow, Y. T.; Guselnikov, L. E.; Wolkowa, W. W.; Awakyan, W. *G. Z. Anorg. Allg. Chem.* **1983**, *501*, 153. (c) Peters, J.; Krebs, B. *Acta Crystallogr., Sect. B: Struct. Crystallogr. Cryst. Chem.* **1982**, *B38*, 1270. (d) Peters, J.; Mandt, J.; Meyring, M.; Krebs, B. *Z. Kristallogr.* **1981**, *156*, 90.

(14) Sheldrick, W. S. *The Chemistry of Organic Silicon Compounds*; Wiley: New York, 1989; Part 1, Chapter 3.

(15) (a) Kabe, Y.; Kawase, T.; Okada, J.; Yamashita, O.; Goto, M.; Masamune, S. *Angew. Chem., Int. Ed. Engl.* **1990**, *29*, 794. (b) Schleyer, P. v. R.; Janoschek, R. *Angew. Chem., Int. Ed. Engl.* **1987**, *26*, 1267. The distances between the bridgehead silicon atoms were investigated by ab initio level calculations (2.69–2.89 Å).

Formation of Mo–Pd and W–Pd Complexes. Insight into the Mechanism of Palladium-Catalyzed Metal–Carbon Bond Formation

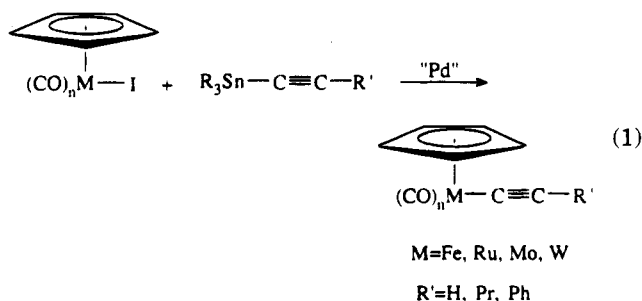
Luca Spadoni, Claudio Lo Sterzo,* Raffaella Crescenzi, and Giuseppe Frachey

Centro CNR di Studio sui Meccanismi di Reazione, c/o Dipartimento di Chimica, Università "La Sapienza", P.le A. Moro, 5-00185 Rome, Italy

Received February 8, 1995[®]

Summary: The oxidative addition of M–I moieties (M = Mo, W) at Pd⁰ was investigated in order to elucidate the mechanism of palladium-catalyzed metal–carbon bond formation. By the use of metal phosphine-substituted cyclopentadienyl iodo complexes of formula [η⁵-(Ph₂P)C₅H₄](CO)₃MI (M = Mo, W) it was possible to isolate and characterize a product of oxidative addition to zerovalent palladium, [η⁵-(Ph₂P)C₅H₄](CO)₃MPd-(PPh₃)I (M = Mo, W).

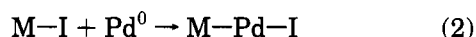
The use of zerovalent palladium catalysts in organic synthesis to form carbon–carbon bonds is a well-established procedure,¹ and the Stille coupling reaction itself represents one of the most important synthetic methodologies for transition-metal-mediated cross-coupling reactions.² We recently disclosed an unprecedented feature of palladium, showing that this metal can also promote metal–carbon bond formation. In the presence of a catalytic amount of Pd⁰ a σ-acetylide complex is formed by coupling of an iron–iodide complex and a trimethyltin acetylide.^{3a} Subsequently, we have shown that this coupling can be successfully carried out on a variety of tin acetylides and transition metals^{3b,4} (eq 1). These reactions occur under the same reaction conditions, leading to the formation of carbon–carbon bonds by palladium catalysis.



This new reaction gives easy access to an important class of compounds, the σ-metallaacetylides, and has revealed an unexpected and fascinating feature of palladium chemistry, a thus far unknown ability to catalyze

the formation of metal–carbon bonds. In addition to the synthetic utility of this new reaction, an intriguing aspect of the phenomenon is the understanding of the intimate role of palladium in these transformations.

The present work deals with the attempt of obtaining insight into the plausible working mechanism of these reactions. The first approach was to seek for a parallel to the well-known mechanism operating in the Stille coupling reaction⁵ initiated by the oxidative addition of an electrophile to a palladium(0) complex.⁶ If this parallel is true, in the present case the zerovalent palladium complex should insert, thus undergoing oxidative addition into the M–I bond, with formation of an M–Pd–I moiety (eq 2).



The electrophilicity of the M–I functionality in CpM(CO)_nI (Cp = η⁵-cyclopentadienyl; M = Fe, Mo, W) complexes has been previously demonstrated⁷ by its ability to oxidatively add zerovalent mercury with formation of the M–Hg–I array. On the other hand, several literature reports account for the insertion of palladium, and more generally zerovalent group 10 metals, into organomercurials and organometallic derivatives of group 14 elements.^{3b} Complexes such as M–Pd–X, containing Pd inserted between a transition metal and a halide (M = transition metal; X = Cl, Br, I), have been reported,⁸ and in some cases their formation has been rationalized as an oxidative addition of M–X moieties to Pd⁰.

In a series of preliminary experiments, we reacted CpFe(CO)₂I and a stoichiometric amount of the complex

(5) See ref 2a.

(6) Amatore, C.; Jutand, A.; Suarez, A. *J. Am. Chem. Soc.* **1993**, *115*, 9531.

(7) See refs 3–5 in: Coco, S.; Espinet, P.; Mayor, F.; Solans, X. *J. Chem. Soc., Dalton Trans.* **1991**, 2503.

(8) M–Pd–X complexes: (a) M = Mn: Hoskins, B. F.; Steen, R. J.; Turney, T. W. *J. Chem. Soc., Dalton Trans.* **1984**, 1831. Hoskins, B. F.; Steen, R. J.; Turney, T. W. *Inorg. Chim. Acta* **1983**, *77*, L69. (b) M = W: Engel, P. F.; Pfeffer, M.; Fischer, J.; Dedieu, A. *J. Chem. Soc., Chem. Commun.* **1991**, 1274. (c) M = Fe: Braunstein, P.; Knorr, M.; Tiripicchio, A.; Tiripicchio Carmellini, M. *Angew. Chem., Int. Ed. Engl.* **1989**, *28*, 1361. (d) M = Rh: Arena, C. G.; Rotondo, E.; Faraone, F.; Lanfranchi, M.; Tiripicchio, A. *Organometallics* **1991**, *10*, 3877 and references therein. Bailey, D. A.; Balch, A. L.; Fossett, L. A.; Olmstead, M. M.; Reedy, P. E., Jr. *Inorg. Chem.* **1987**, *26*, 2413 and references therein. (e) M = Mo: Zhang, Z. Z.; Wang, H. K.; Wang, H. G.; Wang, R. *J. Organomet. Chem.* **1986**, *314*, 357. Klaui, W.; Hamers, H.; Pfeffer, M.; de Cian, A.; Fischer, J. *J. Organomet. Chem.* **1990**, *394*, 213. Mashima, K.; Nakano, H.; Nakamura, A. *J. Am. Chem. Soc.* **1993**, *115*, 11632. (f) M = Pd: Rutherford, N. M.; Olmstead, M. M.; Balch, A. L. *Inorg. Chem.* **1984**, *23*, 2833 and references therein. Bender, R.; Braunstein, P.; Tiripicchio, A.; Tiripicchio-Carmellini, M. *J. Chem. Soc., Chem. Comm.* **1984**, 42. (g) M = Ru: Maisonnnet, A.; Farr, J. P.; Olmstead, M. M.; Hunt, C. T.; Balch, A. L. *Inorg. Chem.* **1982**, *21*, 3961 and references therein.

[®] Abstract published in *Advance ACS Abstracts*, May 1, 1995.

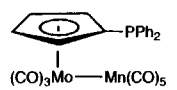
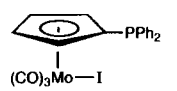
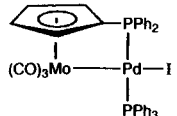
(1) (a) Heck, R. F. *Palladium in Organic Synthesis*; Academic Press: New York, 1985. (b) Schlosser, M., Ed. *Organometallics in Synthesis*; Wiley: Chichester, England, 1994.

(2) (a) Stille, J. K. *Angew. Chem., Int. Ed. Engl.* **1986**, *25*, 508. (b) Farina, V.; Krishnan, B.; Marshall, D. R.; Roth, G. P. *J. Org. Chem.* **1993**, *58*, 5434.

(3) (a) Lo Sterzo, C. *J. Chem. Soc., Dalton Trans.* **1992**, 1989. (b) Crescenzi, R.; Lo Sterzo, C. *Organometallics*, **1992**, *11*, 4301 and references therein. (c) Crescenzi, R. Tesi di Laurea, Università di Roma "La Sapienza", Rome, Italy, 1992.

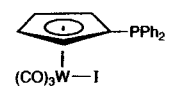
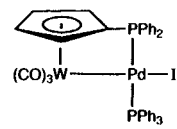
(4) (a) Viola, E.; Lo Sterzo, C.; Crescenzi, R.; Frachey, G. *J. Organomet. Chem.* **1995**, *493*, 55. (b) Viola, E.; Lo Sterzo, C.; Crescenzi, R.; Frachey, G. *J. Organomet. Chem.* **1995**, *493*, C9.

Table 1. ^1H , ^{13}C , and ^{31}P NMR and IR Data for Complexes 2, 3, and 6

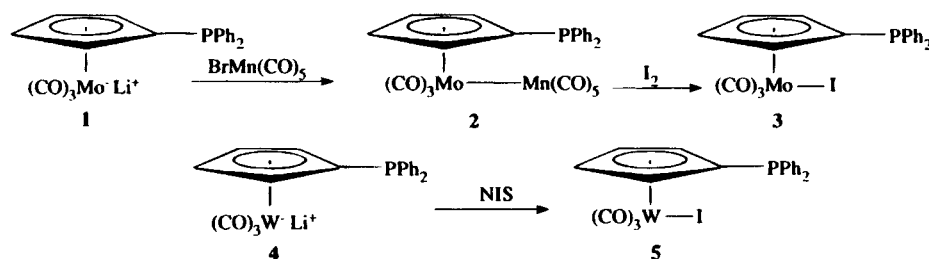
	^1H NMR ^a			^{13}C NMR ^b				^{31}P NMR ^c	IR ^d	
	Cp	PPh ₂	PPh ₃	Cp	PPh ₂	PPh ₃	CO			
	4.49, q, 2H, $J = 2.1$ Hz (β, β') 5.43, q, 2H, $J = 2.1$ Hz (α, α')	7.46–7.43, m, 6H (m, p) 7.97–7.90, m, 4H (o)		56.68, d, $J = 50.6$ Hz (<i>ipso</i>) 87.89, d, $J = 10.3$ Hz (α, α') 89.15, d, $J = 6.2$ Hz (β, β')	129.27, d, $J = 10.6$ Hz 131.42, d, $J = 12.4$ Hz 131.65, s 133.32, d, $J = 42.5$ Hz			231.03 225.73 215.34 (br)	58.74	2057.5 (s) 1988.0 (sh) 1971.8 (s) 1938.2 (m) 1908.7 (m) 1881.7 (m)
	5.56, q, 2H, $J = 2.1$ Hz (β, β') 5.75, m, 2H (α, α')	7.55–7.52, m, 6H (m, p) 7.97–7.90, m, 4H (o)		108.47, d, $J = 28.5$ Hz (<i>ipso</i>) 102.99, d, $J = 8.4$ Hz (α, α') 93.97, d, $J = 5.7$ Hz (β, β') 133.15, d, $J = 10.1$ Hz	129.05, d, $J = 9.8$ Hz 131.95, d, $J = 43.8$ Hz 132.23 s 133.15, d, $J = 10.1$ Hz		232.86 218.10	32.39	2085.9 (m) 2044.4 (s) 2017.8 (sh) 2004.7 (s) 1968.5 (s)	
	4.45, q, 2H, $J = 2.1$ Hz (β, β') 5.47, q, 2H, $J = 2.1$ Hz (α, α')	7.45–7.55, m, 6H (m, p) 8.09–8.16, m, 4H (o)	7.35–7.45, m, 9H (m, p) 7.58–7.90, m, 6H (o)	60.24, d, $J = 41.3$ Hz (<i>ipso</i>) 93.33, d, $J = 11.7$ Hz (α, α') 92.46, d, $J = 6.9$ Hz (β, β')	131.76, s 132.20, d, $J = 38.6$ Hz 135.58, d, $J = 11.7$ Hz		127.92, d, $J = 9.5$ Hz 128.53, d, $J = 11.5$ Hz 130.00, s	235.75 224.93	33.50, d, $J = 459$ Hz 17.00, d, $J = 459$ Hz	1966.1 (s) 1891.4 (m) 1867.7 (s)

^a CDCl₃, ppm, 298 K, 300 MHz, TMS reference. ^b CDCl₃, ppm, 298 K, 75.46 MHz, TMS reference. ^c CDCl₃, ppm, 298 K, 121.49 MHz, 85% H₃PO₄ reference. ^d CH₂Cl₂, cm⁻¹, s = strong, sh = shoulder, m = medium, w = weak.

Table 2. ^1H , ^{13}C , and ^{31}P NMR and IR Data for Complexes 5 and 7

	^1H NMR ^a			^{13}C NMR ^b				^{31}P NMR ^c	IR ^d
	Cp	PPh ₂	PPh ₃	Cp	PPh ₂	PPh ₃	CO		
	5.43, dt, 2H, $J_{\text{H-H}} = 2.2$ Hz, $J_{\text{P-H}} = 0.7$ Hz (α, α') 5.92, t, 2H, $J = 2.2$ Hz (β, β')	7.34–7.44, m, 10H		104.34, d, $J = 23.0$ Hz (<i>ipso</i>) 95.90, d, $J = 11.1$ Hz (α, α') 97.75, s (β, β')	128.87, d, $J = 6.8$ Hz 129.78, s 133.45, d, $J = 20.1$ Hz 135.87, d, $J = 11.0$ Hz		208.43 223.15, d, $J = 5.6$ Hz	-17.24	2036.9 (s) 1950.1 (s) 1892.8 (w)
	4.54, m, 2H (β, β') 5.38, m, 2H (α, α')	7.36–7.72, m, 20H 8.08–8.18, m, 5H		61.86, d, $J = 40.2$ Hz (<i>ipso</i>) 91.19, d, $J = 10.6$ Hz (α, α') 89.73, d, $J = 5.9$ Hz (β, β')	125.40–140.36, m		214.00 224.81, d, $J = 5.0$ Hz	24.68, d, $J = 461$ Hz 15.24, d, $J = 461$ Hz	1961.7 (s) 1940.1 (sh) 1882.0 (s) 1862.2 (s)

^a CDCl₃, ppm, 298 K, 300 MHz, TMS reference. ^b CDCl₃, ppm, 298 K, 75.46 MHz, TMS reference. ^c CDCl₃, ppm, 298 K, 121.49 MHz, 85% H₃PO₄ reference. ^d CH₂Cl₂, cm⁻¹, s = strong, sh = shoulder, w = weak.

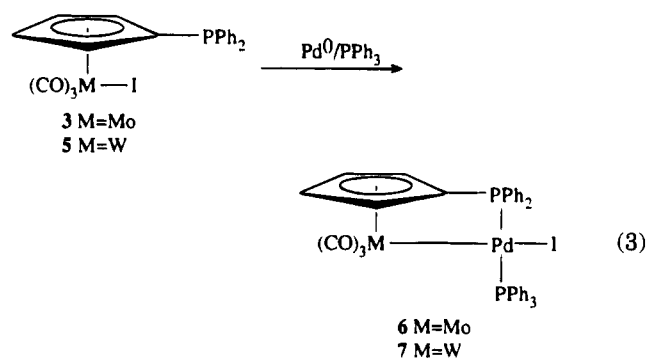
Scheme 1

$\text{Pd}[\text{P}(\text{Ph}_3)_4]$ under standard coupling conditions,^{3c} but we observed only formation of $\text{CpFe}(\text{CO})(\text{PPh}_3)\text{I}$ and $\text{CpFe}(\text{PPh}_3)_2\text{I}$, generated by phosphine replacement of the CO ligand on the starting iron complex. We have therefore used the bis(dibenzylideneacetone) complex $\text{Pd}(\text{dba})_2$ in order to avoid the inconvenience caused by PPh_3 , but it was only possible to monitor the consumption of starting materials without detection and/or isolation of intermediates or products.

A more suitable substrate to achieve our purpose was a cyclopentadienylmetal iodide complex having a diphenylphosphino group linked to the Cp ring. The (diphenylphosphino)cyclopentadienyl moiety has been widely used to hold two metal centers within the same molecular unit, one linked in an η^5 fashion to the Cp ring and the other coordinated in an η^1 mode to the phosphorus atom.⁹ Scheme 1 illustrates the reaction pathways for the preparation of the ((diphenylphosphino)cyclopentadienyl)tricarbonylmetal iodide complexes [η^5 -(Ph_2P) C_5H_5] $\text{M}(\text{CO})_3\text{I}$ (**3**, $\text{M} = \text{Mo}$; **6**, $\text{M} = \text{W}$).

The reaction of **1**¹⁰ with $\text{BrMn}(\text{CO})_5$ formed the Mo–Mn complex **2** in 46% yield; then the subsequent reaction with iodine quantitatively afforded complex **3**. In contrast, the tungsten complex **5** was formed by the direct reaction of anion **4**¹¹ with NIS (*N*-iodosuccinimide). However, the direct reaction of **1** with a source of I^+ such as NIS or 1,2-diiodoethane was unsuccessful.

Both complexes **3** and **5** reacted with a stoichiometric amount of zerovalent palladium complex, $\text{Pd}^0[(\text{PPh}_3)_4]$ or $\text{Pd}(\text{dba})_2$, in THF at room temperature within minutes¹² (eq 3). In the case of the reaction with $\text{Pd}(\text{dba})_2$,



1 equiv of PPh_3 was added to the reaction mixture in order to stabilize the product. Although ^1H NMR

spectra of the crude reaction mixtures showed complete conversion of starting material into product **6** or **7**, the following workup and chromatographic separation afforded a variable amount of pure material from run to run. The best results were 32% for the Mo–Pd complex **6** and 29% for the W–Pd complex **7**. Proof of identity of complexes **6** and **7** has been obtained by elemental analysis, IR, and ^1H , ^{13}C , and ^{31}P NMR. Very impressive are the NMR spectroscopic variations observed by comparing the spectra of compounds **3** and **5** with those of the corresponding products **6** and **7** obtained upon reaction with Pd^0 . The spectroscopic data for molybdenum complexes **2**, **3**, and **6** are reported in Table 1, while data for the tungsten complexes **5** and **7** are listed in Table 2. In the ^1H NMR spectrum of **3** the deshielding effect of the phosphorus atom imposes a marked downfield shift in the α, α' -protons of the Cp and in the ortho protons of the phenyl rings with respect to the Cp β, β' -protons and the meta and para phenyl protons.^{10,13} In **6**, due to the rigidity of the metallacycle formed and to the presence of the second phosphorus group, these differences became even larger. The ^{13}C NMR spectrum shows that the insertion of Pd^0 into the Mo–I bond of **3** produces heavy variations on the chemical shift of the Cp carbons. In **6** the C_{ipso} signal is shifted 48 ppm upfield with respect to that for **3**! The comparison of the ^{31}P NMR spectra of **3** and **6** clearly confirms the structural variations occurring around the Mo center of **3** upon reaction with Pd. The ^{31}P NMR spectrum of **3** appears as a broad singlet at 32.40 ppm, while in the spectrum of **6** the two nonequivalent phosphorus atoms bonded to palladium give rise to a simple first-order AB splitting pattern that produces two sets of doublets, centered respectively at 33.50 and 17.00 ppm, with a coupling constant of 459 Hz. This large value is characteristic of two different phosphorus atoms lying trans to each other, one of which is engaged in a four-membered metallo ring.¹⁴ Similar variations are observed for the tungsten pair **5**, **7**.

On the basis of these preliminary findings we have shown that Mo–I and W–I moieties can oxidatively add to zerovalent palladium to form the corresponding M–Pd–I species. These transformations can be viewed at as an oxidation of Pd^0 to Pd^{I} by Mo^{II} and W^{II} . In our opinion, complexes **6** and **7** afford a reasonable entry in the attempt to give a rational design to the mechanism of Pd-catalyzed metal–carbon coupling.¹⁵ Work is in progress to map other steps of the catalytic process.

Supporting Information Available: Text giving detailed synthetic procedures and analytical data and a figure giving ^1H , ^{13}C , and ^{31}P NMR spectra for complexes **3** and **6** (5 pages). Ordering information is given on any current masthead page.

OM950106G

(9) (a) Brumas, B.; de Caro, D.; Dahan, F.; de Montauzon, D.; Poilblanc, R. *Organometallics* **1983**, *12*, 1503. (b) Bullock, R. M.; Casey, C. P. *Acc. Chem. Res.* **1987**, *20*, 167 and references therein. (c) Tikkanen, W.; Fujita, Y.; Petersen, J. *Organometallics* **1986**, *5*, 888.

(10) Casey, C. P.; Bullock, R. M.; Fultz, W. C.; Rheingold, A. L. *Organometallics* **1982**, *1*, 1591.

(11) **4** was prepared analogously to **1** from $[(\text{Ph}_2\text{P})\text{C}_5\text{H}_4]^- \text{Li}^+$ and $(\text{CH}_3\text{CN})_3\text{W}(\text{CO})_3$.

(12) Complex **3** (0.72 g, 1.3 mmol) was dissolved in THF (40 mL), and to this solution were added $\text{Pd}(\text{dba})_2$ (0.74 g, 1.3 mmol) and $\text{P}(\text{C}_6\text{H}_5)_3$ (0.35 g, 1.3 mmol). After it was stirred for 2 h at room temperature, the reaction mixture was reduced to a minimum volume under vacuum and the residue chromatographed on silica gel by a gradient elution with a mixture of CH_2Cl_2 and hexane. Complex **6** (0.38 g, 32%) was obtained as a red solid. The same result was obtained by reacting an equivalent amount of **3** and $\text{Pd}[(\text{C}_6\text{H}_5)_3\text{P}]_4$ in THF under the same reaction conditions. Complex **7** (29%) was obtained in an identical procedure by reacting **5** with a stoichiometric amount of $\text{Pd}(\text{dba})_2/\text{P}(\text{C}_6\text{H}_5)_3$ or $\text{Pd}[(\text{C}_6\text{H}_5)_3\text{P}]_4$.

(13) Mathey, F.; Lampin, J. P. *Tetrahedron* **1975**, *31*, 2685.

(14) (a) Casey, C. P.; Bullock, R. M.; Nief, F. *J. Am. Chem. Soc.* **1983**, *105*, 7574. (b) Bianchini, C.; Masi, D.; Meli, A.; Peruzzini, M.; Zanobini, F. *J. Am. Chem. Soc.* **1988**, *110*, 6411.

(15) One reviewer raised the point that complexes **6** and **7** would be stabilized too much by the cyclopentadienylphosphine bridging ligand to act as true intermediates in the catalytic process. We recently found that these complexes smoothly undergo all the catalytic steps leading to metal–carbon bond formation. Narducci, V.; Cianfriglia, P.; Lo Sterzo, C.; Bocelli, G., manuscript in preparation.

Ruthenium(II)-Mediated Reaction of Phenylacetylene with Primary Amines To Give Ruthenium(II)–Isonitrile Complexes

Claudio Bianchini,* Maurizio Peruzzini, Antonio Romerosa, and Fabrizio Zanolini

Istituto per lo Studio della Stereochimica ed Energetica dei Composti di Coordinazione, CNR, Via J. Nardi 39, 50132 Firenze, Italy

Received April 18, 1995*

Summary: The Ru(II) fragment [(PNP)RuCl₂] assists the reaction of phenylacetylene with a variety of primary amines, including optically pure amines, to give Ru(II)–isonitrile complexes (PNP = CH₃CH₂CH₂N(CH₂CH₂PPh₂)₂). The reaction is initiated by 1-alkyne to vinylidene tautomerization at the ruthenium center, followed by attack of the primary amine on the vinylidene ligand to give Ru(II) aminocarbenes of the formula *fac,cis*-[(PNP)RuCl₂{=C(NHR)(CH₂Ph)}]. The latter compounds thermally convert to the corresponding isonitrile complexes *fac,cis*-[(PNP)RuCl₂(CNR)], while toluene is eliminated via C–C bond cleavage (R = CH₂CH₂CH₃, cyclo-C₆H₁₁, (R)-(+)-CH(Me)(Ph), (R)-(-)-CH(Me)(Et), (S)-(-)-CH(Me)(1-naphthyl)).

In a previous article,¹ we reported that the Ru(II) complex *mer,trans*-[(PNP)RuCl₂(PPh₃)₂]² (**1**) assists the coupling of phenylacetylene with H₂S to give the η¹-2-phenylethanthial ligand (PNP = CH₃CH₂CH₂N(CH₂CH₂PPh₂)₂). In this communication, we show that **1** mediates the addition of primary amines to phenylacetylene to yield isonitrile ligands. More importantly, the use of optically pure primary amines in the Ru(II)-assisted reaction herein described provides unprecedented access to optically pure Ru(II)–isonitrile complexes. Isonitriles are important substrates in organic and organometallic syntheses but are generally difficult to prepare by standard synthetic methods, owing to their propensity for spontaneous polymerization. Thus, alternative metal-assisted reactions have been developed which involve the attack of primary amines on thio- and dithiocarbene complexes.³

Heating **1** in tetrahydrofuran (THF) with phenylacetylene at reflux gives the vinylidene complex *fac,cis*-[(PNP)RuCl₂{C=C(H)Ph}] (**2**).¹ Complex **2** can be iso-

lated as pale orange crystals. However, without isolation, the following reaction step, which involves the addition of a slight excess of one of the primary amines listed in Scheme 1 at room temperature, can be also carried out. As a result, the corresponding aminocarbene derivatives *fac,cis*-[(PNP)RuCl₂{=C(NHR)(CH₂Ph)}] are quantitatively obtained (R = CH₂CH₂CH₃ (**3**), cyclo-C₆H₁₁ (**4**), (R)-(+)-CH(Me)(Ph) (**5**), (R)-(-)-CH(Me)(Et) (**6**), (S)-(-)-CH(Me)(1-naphthyl) (**7**)). The presence of the aminocarbene ligands in **3**–**7** is unambiguously demonstrated by both ¹H (δ_{NH} 10.62–11.46) and ¹³C-¹H NMR spectroscopy (δ_{Ru=C} 251.2–255.8; δ_{CH₂Ph} 56.5–59.5).^{4,5}

The aminocarbene complexes, which can be isolated as yellow crystals, are stable in THF at room temperature but quantitatively transform into the isonitrile complexes *fac,cis*-[(PNP)RuCl₂(CNR)] via elimination of toluene (¹H NMR, GC–MS) by stirring overnight at reflux temperature in THF (only for the 1-naphthyl complex **7** is a higher boiling solvent, such as monoglyme, required for a complete conversion to **12**) (R = CH₂CH₂CH₃ (**8**), cyclo-C₆H₁₁ (**9**), (R)-(+)-CH(Me)(Ph) (**10**), (R)-(-)-CH(Me)(Et) (**11**), (S)-(-)-CH(Me)(1-naphthyl) (**12**)). All isonitrile complexes can be isolated as cream-colored crystals which are air-stable in both the solid state and solution and were characterized by spectroscopic techniques (IR (Nujol mull) ν(C≡N) 2117–2085 cm⁻¹ (vs); ¹³C{¹H} NMR δ_{Ru–C≡N} 162.1–158.9).^{6,7}

(4) Dötz, K. H.; Fischer, H.; Hoffmann, P.; Kreissl, F. R.; Schubert, U.; Weiss, K. *Transition Metal Carbene Complexes*; Verlag Chemie: Weinheim, Germany, 1983.

(5) All spectroscopic and analytical data for the aminocarbene complexes **3**–**7** have been provided as supporting information. As an example, we report here analytical data and selected spectroscopic details for complex **5**. Anal. Calcd for C₄₇H₅₂N₂Cl₂P₂Ru: C, 64.23; H, 5.96; N, 3.19; Cl, 8.07. Found: C, 64.08; H, 5.89; N, 3.11; Cl, 7.90. IR: ν(NH) 3460 cm⁻¹ (br, w). ³¹P{¹H} NMR (22 °C, CD₂Cl₂, 81.01 MHz), AB system: δ_A 50.32, δ_B 48.04, J(P_AP_B) = 29.7 Hz. ¹H NMR (22 °C, CD₂Cl₂, 200.13 MHz): δ_{NH} 11.13 [br d, J(HH) = 9.6 Hz], δ_{CH₂Ph} 4.80, 4.48 [AB system, J(HH) = 16.8 Hz, 2H]. ¹³C{¹H} NMR (22 °C, CD₂Cl₂, 75.42 MHz): δ_{Ru=C} 255.3 [t, ²J(CP) = 11.3 Hz], δ_{CH₂Ph} 58.6 [t, ³J(CP) = 4.6 Hz].

(6) See for example: Singleton, E.; Oosthuizen, M. E. *Adv. Organomet. Chem.* **1983**, *22*, 209.

(7) All spectroscopic and analytical data for the isonitrile complexes **8**–**12** have been provided as supporting information. As an example, we report here analytical data and selected spectroscopic details for complex **10**. Anal. Calcd for C₄₀H₄₄N₂Cl₂P₂Ru: C, 61.07; H, 5.64; N, 3.56. Found: C, 60.94; H, 5.70; N, 3.38. IR ν(C≡N) 2100 cm⁻¹ (vs). ³¹P{¹H} NMR (22 °C, CDCl₃, 81.01 MHz), AB system: δ_A 58.02, δ_B 57.76, J(P_AP_B) = 26.1 Hz. ¹³C{¹H} NMR (20 °C, CD₂Cl₂, 75.42 MHz): δ_{C≡N} 160.9 [t, ²J(CP) = 15.2 Hz]. [α]_D²⁵ = -5.93 (c = 1.2, CHCl₃).

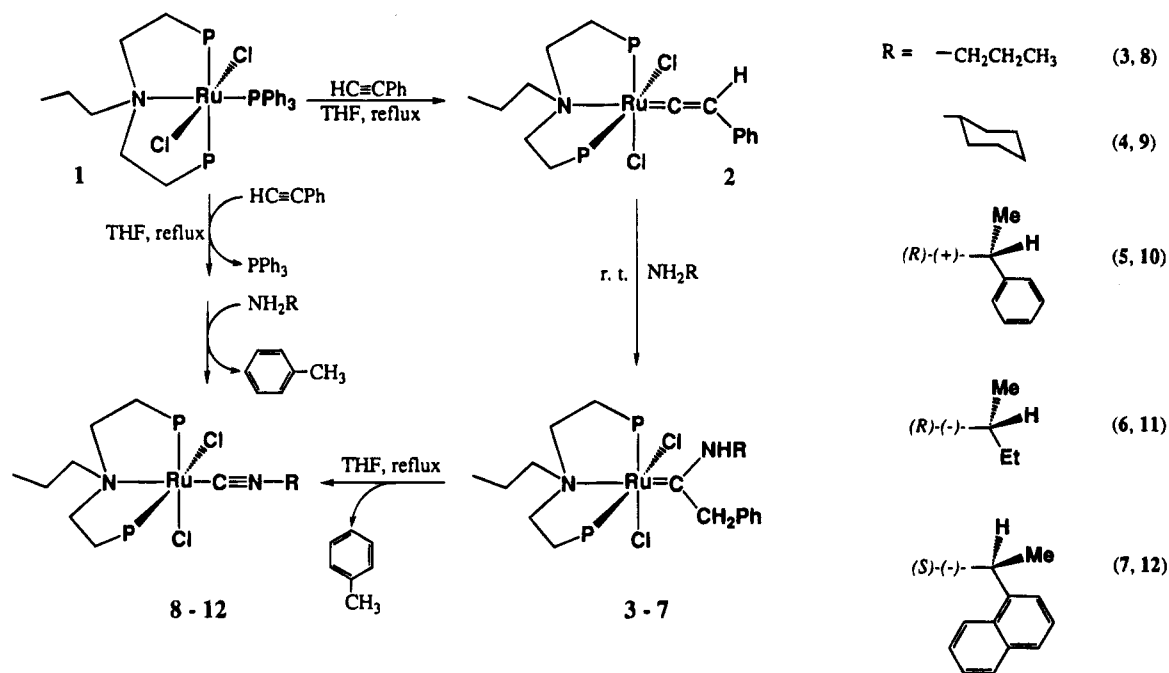
* Abstract published in *Advance ACS Abstracts*, July 1, 1995.

(1) Bianchini, C.; Glendenning, L.; Peruzzini, M.; Romerosa, A.; Zanolini, F. *J. Chem. Soc., Chem. Commun.* **1994**, 2219.

(2) Bianchini, C.; Innocenti, P.; Masi, D.; Peruzzini, M.; Zanolini, F. *Gazz. Chim. Ital.* **1992**, *122*, 461.

(3) McCormick, F. B.; Angelici, R. J. *Inorg. Chem.* **1979**, *18*, 1231. McCormick, F. B.; Angelici, R. J. *Inorg. Chem.* **1981**, *20*, 1118. Pickering, R. A.; Angelici, R. J. *Inorg. Chem.* **1981**, *20*, 2877. Steinmetz, A. L.; Hershberger, S. A.; Angelici, R. J. *Organometallic* **1984**, *3*, 461. Albano, V. G.; Bordoni, S.; Braga, D.; Busetto, C.; Palazzi, A.; Zanotti, V. *Angew. Chem., Int. Ed. Engl.* **1991**, *30*, 847. Faraone, F.; Piraino, P.; Marsala, V.; Sergi, S. *J. Chem. Soc., Dalton Trans.* **1977**, 859.

Scheme 1



The isonitrile ligands in complexes **8–12** are so strongly bound to ruthenium that their removal is not achieved either upon heating to 120 °C in monoglyme or upon pressurization under 15 atm of CO at 80 °C in THF solution.

Current investigations center upon finding a method for the removal of the isonitriles from the Ru(II) complexes. Preliminary results suggest that electrochemical oxidation may be successful.

Acknowledgment. This work was supported by Progetto Strategico "Tecnologie Chimiche Innovative", CNR, Rome, Italy, and the EC, Contract No. CHRX CT93-0147. A.R. thanks the Spanish Ministerio de Educación y Ciencia for a postdoctoral grant.

Supporting Information Available: Text giving experimental details of the synthesis and physicochemical characterization of the new complexes described in this paper (6 pages). Ordering information is given on any current masthead page.

OM950281X

Conformationally Rigid Diamide Complexes: Synthesis and Structure of Tantalum(III) Alkyne Derivatives[†]

Frédéric Guérin, David H. McConville,* and Jagadese J. Vittal

Department of Chemistry, University of Western Ontario, London, Ontario, Canada N6A 5B7

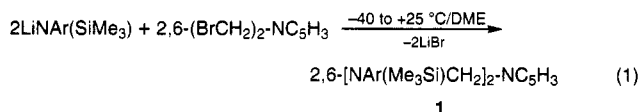
Received April 11, 1995[®]

Summary: The chelating diamide complexes *mer*-TaCl₃-(BDPP) (**2**), *mer*-TaCl₃(BDPP) (**3**), and (BDPP)Ta(η²-RC≡CR)Cl (**4a**, R = Pr; **4b**, R = Et; **4c**, R = Ph) (BDPP = 2,6-(ArNCH₂)₂-NC₅H₃; Ar = 2,6-*i*-Pr₂-C₆H₃), have been prepared. Proton and carbon NMR data suggest that the alkynes in **4a-c** rotate rapidly on the NMR time scale. An X-ray study of (BDPP)Ta(η²-PrC≡CPr)Cl (**4a**) revealed a distorted-square-pyramidal geometry with the chloride occupying the apical position.

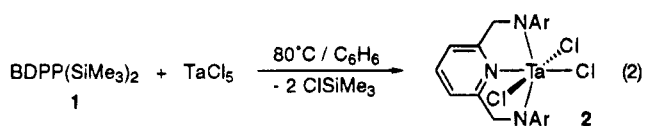
Certain group 5 metal complexes are active catalysts for the polymerization and cyclization of alkynes.¹⁻⁴ The polymerization of alkynes can occur by two different pathways: cycloaddition of an alkyne to a carbene to yield a vinylcarbene upon ring-opening⁵ and the insertion of an alkyne into a metal-carbon bond.⁶ Complexes of the type L_nTa(η²-RC≡CR)X (X = alkyl, hydride, chloride)⁷⁻¹⁰ are ideally suited for studying the latter mechanism. Cyclization reactions are highly dependent on the steric and electronic properties of the ancillary ligands. For example, the two-electron reduction of (DIPP)₂TaCl₃(OEt₂) (DIPP = 2,6-diisopropylphenoxide) in the presence of excess 3-hexyne yields the arene complex (DIPP)₂Ta(η⁶-C₆Et₆)Cl and hexaethylbenzene.⁴ Under similar conditions the complex (DIPP)₂-TaCl₂(OEt₂), which bears one additional bulky alkoxide ligand, yields only the metallacyclopentadiene complex (DIPP)₃Ta(C₄Et₄).¹¹ A flexible ligand array is common to the complexes mentioned above. Our interest in the steric and electronic effects of conformationally rigid ligands led us to explore the synthesis of bulky chelating diamide ancillaries,¹²⁻¹⁴ in particular, amides which bear the voluminous 2,6-diisopropylphenyl moiety. We

report here the synthesis of monoalkyne complexes of tantalum stabilized by a new conformationally rigid diamide ligand.

2,6-Bis(bromomethyl)pyridine¹⁵ was treated with 2 equiv of LiNAr(SiMe₃)¹⁶ to yield the silylated ligand precursor BDPP(SiMe₃)₂ (**1**)¹⁷ as a white crystalline solid (eq 1).

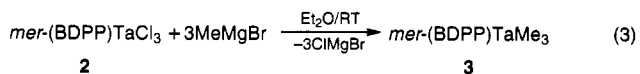


BDPP(SiMe₃)₂ reacts cleanly with TaCl₅ to give 2 equiv of ClSiMe₃ (confirmed by ¹H NMR spectroscopy) and the yellow trichloride complex *mer*-(BDPP)TaCl₃ (**2**) in high yield (eq 2).



Proton and carbon NMR spectra¹⁸ of complex **2** are consistent with a meridional coordination of the ligand, as evidenced by the singlet observed at 5.84 ppm for the methylene protons (CH₂N) of the BDPP unit. Interestingly, the isopropyl methyl groups of the arene are diastereotopic, which we interpret as a consequence of restricted rotation about the N-C_{ipso} bond. The proton NMR spectrum of complex **2** remains unchanged at 80 °C.

Compound **2** can be alkylated with 3 equiv of MeMgBr to give the trimethyl derivative *mer*-(DBPP)TaMe₃ (**3**), in good yield (eq 3; RT = room temperature).



[†] Dedicated to the memory of Professor Kenneth G. Rutherford.

[®] Abstract published in *Advance ACS Abstracts*, June 1, 1995.

(1) Cotton, F. A.; Hall, W. T.; Cann, K. J.; Karol, F. J. *Macromolecules* **1981**, *14*, 233.

(2) Masuda, T.; Isobe, E.; Higashimura, T.; Takada, K. *J. Am. Chem. Soc.* **1983**, *105*, 7473.

(3) Masuda, T.; Niki, A.; Isobe, E.; Higashimura, T. *Macromolecules* **1985**, *18*, 2109.

(4) Bruck, M. A.; Copenhaver, A. S.; Wigley, D. E. *J. Am. Chem. Soc.* **1987**, *109*, 6525.

(5) Katz, T. J.; Ho, T. H.; Shih, N.; Ying, Y.; Stuart, V. I. W. *J. Am. Chem. Soc.* **1984**, *106*, 2659.

(6) Taqui Kahn, M. M.; Martell, A. E. *Homogeneous Catalysis by Transition Metal Complexes*; Academic Press: New York, 1974; Vol. II.

(7) Labinger, J. A.; Schwartz, J.; Townsend, T. M. *J. Am. Chem. Soc.* **1974**, *96*, 4009.

(8) Green, M. L. H.; Jousseume, B. *J. Organomet. Chem.* **1980**, *193*, 339.

(9) Gibson, V. C.; Parkin, G.; Bercaw, J. *Organometallics* **1991**, *10*, 220.

(10) Chao, Y.-W.; Wexler, P. A.; Wigley, D. E. *Inorg. Chem.* **1989**, *28*, 3860.

(11) Strickler, J. R.; Wexler, P. A.; Wigley, D. E. *Organometallics* **1991**, *10*, 118.

(12) Cai, S.; Schrock, R. R. *Inorg. Chem.* **1991**, *30*, 4106.

(13) Kol, M.; Schrock, R. R.; Kempe, R.; Davis, W. M. *J. Am. Chem. Soc.* **1994**, *116*, 4382.

(14) Schubart, M.; O'Dwyer, L.; Gade, L. H.; Li, W.; McPartlin, M. *Inorg. Chem.* **1994**, *33*, 3893.

(15) A CH₂Cl₂ solution of 2,6-bis(bromomethyl)pyridine-HBr was extracted with saturated NaHCO₃ to yield 2,6-bis(bromomethyl)pyridine. Haeg, M. E.; Whitlock, B. J.; Whitlock, H. W., Jr. *J. Am. Chem. Soc.* **1989**, *111*, 692.

(16) Kennepohl, D. K.; Brooker, S.; Sheldrick, G. M.; Roesky, H. W. *Chem. Ber.* **1991**, *124*, 2223.

(17) BDPP(SiMe₃)₂ (**1**): ¹H NMR (C₆D₆, 300 MHz) δ 7.15 (t, 2H, Ar), 7.02 (d, 4H, Ar), 6.48 (t, 1H, py), 6.47 (d, 2H, py), 4.28 (s, 4H, NCH₂), 3.31 (sept, 4H, CHMe₂), 1.17 (d, 12H, CHMe₂), 0.90 (d, 12H, CHMe₂), 0.27 (s, 18H, SiMe₃); ¹³C{¹H} NMR δ 159.88, 148.69, 143.40, 135.88, 126.30, 124.24, 122.28, 58.78, 27.94, 25.18, 1.06; MS (EI) *m/z* 601.423 (M⁺), calcd for C₃₇H₅₈N₃Si₂ 601.424.

(18) *mer*-(BDPP)TaCl₃ (**2**): ¹H NMR (C₆D₆, 300 MHz) δ 7.14 (m, 6H, Ar), 6.84 (t, 1H, py), 6.38 (d, 2H, py), 5.84 (s, 4H, NCH₂), 3.80 (sept, 4H, CHMe₂), 1.52 (d, 12H, CHMe₂), 1.12 (d, 12H, CHMe₂); ¹³C{¹H} NMR δ 161.64, 148.84, 146.56, 139.66, 125.35, 122.28, 117.51, 71.78, 28.89, 27.57, 23.64. Anal. Calcd for C₃₁H₄₁N₃TaCl₃: C, 50.11; H, 5.56; N, 5.66. Found: C, 50.25; H, 5.68; N, 5.11.

The proton and carbon NMR spectra¹⁹ of compound **3** suggest that the meridional coordination of the BDPP ligand is retained. Furthermore, two different Ta–Me groups are observed: one trans to the pyridine of the BDPP unit and two cis. A similar restricted rotation about the N–C_{ipso} bond is proposed on the basis of the presence of diastereotopic isopropyl methyl groups. Other metathetical reactions involving larger alkylating reagents (e.g., PhCH₂MgCl and Me₃SiCH₂Li) yield intractable materials.

The reduction of *mer*-(BDPP)TaCl₃ with excess Na/Hg in the presence of alkynes yields the pseudo five-coordinate Ta(III) derivatives (BDPP)Ta(η²-RC≡CR)Cl (**4a**, R = Pr; **4b**, R = Et; **4c**, R = Ph) (eq 4).



A single low-field acetylenic carbon resonance is observed in the ¹³C{¹H} NMR spectra²⁰ of complexes **4a–c**, suggesting that the alkyne acts as a four-electron donor.²¹ The BDPP methylene protons (CH₂NAr) are diastereotopic in the ¹H NMR spectra of complexes **4a–c**, indicating some asymmetry above and below the N₃ plane of the ligand. However, the presence of two isopropyl methine and four isopropyl methyl resonances in the proton and carbon NMR spectra of complexes **4a–c** again supports the notion of a restricted rotation about the N–C_{ipso} bond. Given the above-mentioned asymmetry of the ligand and since both ends of the coordinated alkynes are equivalent by ¹H and ¹³C{¹H} NMR spectroscopy, a rapid rotation of the alkynes on the NMR time scale is advanced.

Yellow single crystals of (BDPP)Ta(η²-PrC≡CPr)Cl (**4a**) suitable for an X-ray analysis were grown from a saturated ether solution at –30 °C.²² The molecular structure of complex **4a** is shown in Figure 1, and selected bond distances and angles are given in Table 1. Overall, the molecular structure is best described as a distorted square pyramid with the chloride (Cl(1)) occupying the apical position. The 4-octyne unit is located trans to the pyridine of the BDPP ligand and is rotated by 50° with respect to the Cl(1)–Ta(1)–N(2) plane (Figure 1, bottom). The bond distances in the Ta–

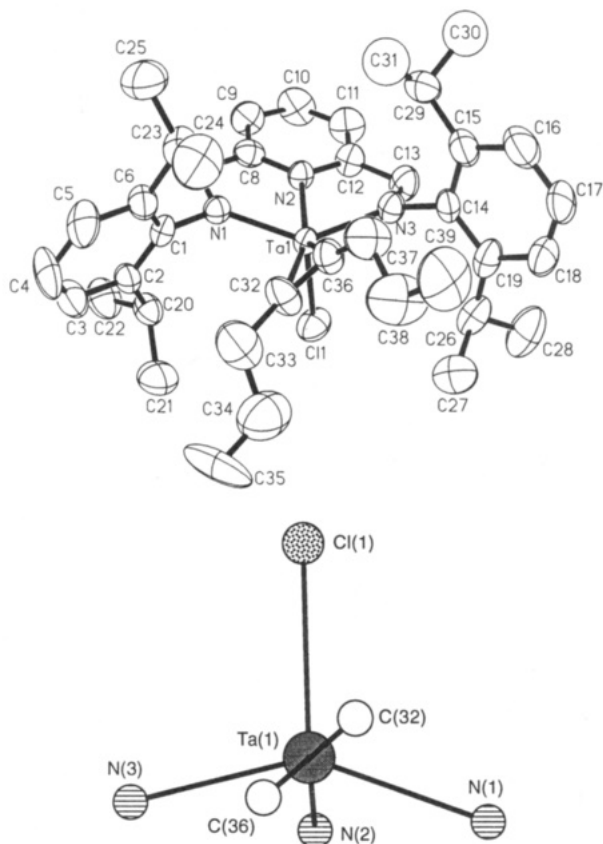


Figure 1. (top) ORTEP drawing of (BDPP)Ta(η²-PrC≡CPr)Cl (**4a**) with thermal ellipsoids at the 50% probability level. Three orientations of C(30) and C(31) were located in the final difference Fourier map. (bottom) Chem 3D Plus representation of the core of **4a**.

Table 1. Selected Bond Distances (Å) and Angles (deg) for (BDPP)Ta(η²-PrC≡CPr)Cl (**4a**)

Bond Distances			
Ta(1)–N(1)	2.053(6)	Ta(1)–N(2)	2.255(6)
Ta(1)–N(3)	2.033(6)	Ta(1)–Cl(1)	2.361(2)
Ta(1)–C(32)	2.062(7)	Ta(1)–C(36)	2.085(7)
C(32)–C(36)	1.287(11)	C(32)–C(33)	1.527(9)
C(36)–C(37)	1.522(8)	Acet*–Ta ^a	1.97
Bond Angles			
N(3)–Ta(1)–N(1)	137.2(2)	N(1)–Ta(1)–N(2)	71.4(2)
N(3)–Ta(1)–N(2)	71.9(2)	N(1)–Ta(1)–Cl(1)	106.6(2)
N(2)–Ta(1)–Cl(1)	93.7(2)	N(3)–Ta(1)–Cl(1)	96.9(2)
C(36)–C(32)–C(33)	132.6(8)	C(32)–C(36)–C(37)	137.2(8)
C(1)–N(1)–Ta(1)	126.3(5)	C(1)–N(1)–C(7)	108.7(5)
C(7)–N(1)–Ta(1)	124.5(5)	C(14)–N(3)–C(13)	109.3(6)
C(14)–N(3)–Ta(1)	130.2(5)	C(13)–N(3)–Ta(1)	120.4(5)

^a Acet* = midpoint of C(32)–C(36).

(19) *mer*-(BDPP)TaMe₃ (**3**): ¹H NMR (C₆D₆, 300 MHz) δ 7.14 (m, 6H, Ar), 6.84 (t, 1H, py), 6.63 (d, 2H, py), 5.04 (s, 4H, NCH₂), 3.56 (sept, 4H, CHMe₂), 1.42 (d, 12H, CHMe₂), 1.39 (s, 3H, TaMe), 1.16 (d, 12H, CHMe₂), 0.86 (s, 6H, TaMe), ¹³C{¹H} NMR (C₆D₆, 75.46 MHz) δ 161.27, 151.30, 145.28, 138.38, 126.36, 124.49, 116.78, 71.14, 69.09 (TaCH₃), 65.80 (TaCH₃), 28.44, 27.46, 23.95. Anal. Calcd for C₃₄H₅₀N₃Ta: C, 59.90; H, 7.39; N, 6.16. Found: C, 59.43; H, 7.35; N, 5.73.

(20) (BDPP)Ta(η²-PrC≡CPr)Cl (**4a**): ¹H NMR (C₆D₆, 300 MHz) δ 7.19 (t, 2H, Ar), 7.13 (d, 4H, Ar), 6.85 (t, 1H, py), 6.39 (d, 2H, py), 5.12 (AB quartet, ²J_{HH} = 20.1, 4H, NCH₂), 3.79 (sept, 2H, CHMe₂), 3.15 (sept, 2H, CHMe₂), 2.51 (m, 4H, =CCH₂), 1.46 (d, 6H, CHMe₂), 1.34 (m, 4H, CH₂CH₃), 1.32 (d, 6H, CHMe₂), 1.24 (d, 6H, CHMe₂), 1.01 (d, 6H, CHMe₂), 0.84 (t, 6H, CH₂CH₃); ¹³C{¹H} NMR δ 237.01 (C≡C), 160.77, 154.41, 145.19, 138.41, 125.49, 124.32, 123.57, 116.99, 70.95, 40.02, 28.60, 27.95, 26.66, 25.76, 24.61, 23.80, 21.94, 15.45. Anal. Calcd for C₃₉H₅₅N₃TaCl: C, 59.88; H, 7.09; N, 5.37. Found: C, 59.62; H, 7.19; N, 5.16. Spectroscopic details for compounds **4b** and **4c** are available in the supporting information.

(21) Templeton, J. L.; Ward, B. C. *J. Am. Chem. Soc.* **1980**, *102*, 3288.

alkyne moiety are comparable to those reported for other mononuclear Ta(III) alkyne complexes.^{11,23–25}

(22) X-ray data for (BDPP)Ta(η²-PrC≡CPr)Cl (**4a**): Data were collected at 23 °C on a Siemens P4 diffractometer using graphite-monochromated Mo Kα radiation. A total of 6078 reflections were collected in the θ range 1.9–23°, of which 5179 were unique (R_{int} = 0.0284). The structure was solved by a combination of Patterson and difference Fourier techniques. Non-hydrogen atoms were refined anisotropically, except C(30) and C(31), which were refined isotropically. In the final least-squares refinement cycle on F², the model converged at R1 = 0.0401, wR2 = 0.0946, and GOF = 1.037 for 4463 reflections with F_o ≥ 4σ(F_o) and 408 parameters. Crystal data: a = 9.936(2) Å, b = 11.558(1) Å, c = 17.689(2) Å, α = 74.997(6)°, β = 87.424(10)°, γ = 75.372(9)°, V = 1898.0(5) Å³, space group P1, Z = 2, mol wt 792.36, and ρ(calcd) = 1.386 g/cm³.

(23) Cotton, F. A.; Hall, W. T. *Inorg. Chem.* **1980**, *19*, 2352.

Each amide is sp^2 -hybridized, as evidenced by the sum of the angles about each nitrogen ($N(1) = 359.5^\circ$ and $N(3) = 359.9^\circ$). The rigid coordination of the ligand and enforced location of the aryl isopropyl groups creates a "pocket" opposite the pyridine and necessarily protects the metal above and below the N_3 plane.

Finally, we are also exploring the catalytic activity of derivatives of complex **4a**.²⁶ The alkyl complexes $(BDPP)Ta(\eta^2-PrC\equiv CPr)R$ ($R = \text{alkyl}$), where the apical chloride has been replaced with an alkyl group, are being pursued as alkyne polymerization catalysts.¹⁻³ In

addition, we are exploring the catalytic alkyne cyclization^{1,4} reactivity of *in situ* prepared cationic derivatives (e.g., $[(BDPP)Ta(\eta^2-PrC\equiv CPr)]^+$).

Acknowledgment. This work was supported by the NSERC (Canada) and a University of Western Ontario Internal Research Grant (to D.H.M.).

Supporting Information Available: Text giving experimental details for compounds **1-3** and **4a-c** and tables of crystal data, data collection details, final positional parameters, all bond distances and angles, torsion angles, and least-squares planes for **4a** (15 pages). Ordering information is given on any current masthead page.

OM950257J

(24) Smith, G.; Schrock, R. R.; Churchill, M. R.; Youngs, W. J. *Inorg. Chem.* **1981**, *20*, 387.

(25) Curtis, M. D.; Real, J.; Hirpo, W.; Butler, W. D. *Organometallics* **1990**, *9*, 66.

(26) Guérin, F.; McConville, D. H., to be submitted for publication.

Unprecedented Promoting Effect of a Ferrocenyl Group for the Oxidatively Induced Reductive Elimination in *cis*-Aryl(ferrocenyl acetylide)platinum(II) Complexes

Masaru Sato* and Emiko Mogi

Chemical Analysis Center, Saitama University, Urawa, Saitama 338, Japan

Shigekazu Kumakura

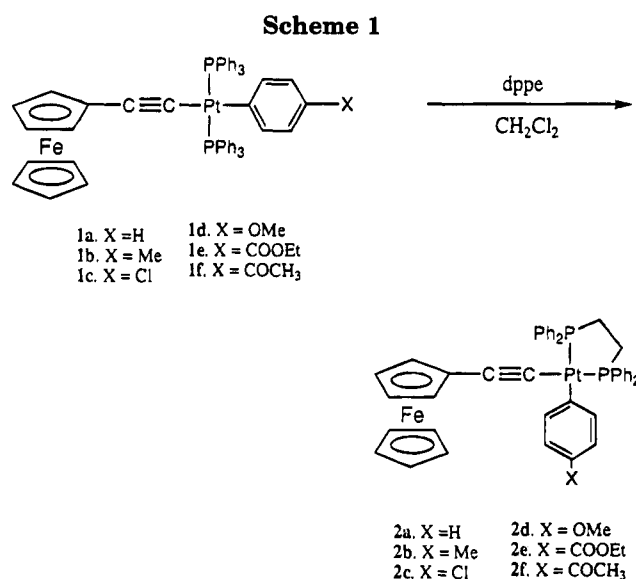
Department of Chemistry, Faculty of Science, Saitama University, Urawa, Saitama 338, Japan

Received December 19, 1994[⊗]

Summary: *cis*-Aryl(ferrocenyl acetylide)platinum(II) complexes very easily undergo oxidatively induced reductive elimination, which is induced by the oxidation of the ferrocenyl moiety and is promoted by the electron-donating substituent on the aryl ligand.

Reductive elimination is one of the key organometallic reactions for carbon-carbon bond formation.¹ It has been confirmed theoretically that a concerted reductive elimination from the *cis*-diorgano complexes MR₂L₂ of d⁸ metals is allowed, while that from the *trans* isomer is forbidden.² Oxidatively induced reductive eliminations are now commonly encountered because an increase in oxidation state of a metal center is apt to make reductive elimination susceptible. The oxidation activation is stimulated by the addition of a π -acid,³ oxidative addition of allyl halides,⁴ or electron transfer.⁵⁻⁸ Organoplatinum complexes are extremely stable toward reductive elimination.⁹ Recently *cis*-[PtMe(SiPh₃)(PMePh₂)₂] has been reported to undergo reductive elimination easily in the presence of π -acids,¹⁰ but the oxidation of a *cis*-dialkyl Pt(II) complex has been reported not to bring about reductive elimination.¹¹ We report here a fine example of oxidatively induced reductive elimination of Pt(II) complexes promoted by a ferrocenyl group.

cis-[Pt(C₆H₅)(C≡CfC)(dppe)] (**2a**) was prepared from the reaction of *trans*-[Pt(C₆H₅)(C≡CfC)(Ph₃P)₂] (**1a**)¹² with dppe in CH₂Cl₂ in 95% yield (dppe = 1,2-bis(diphenylphosphino)ethane; Fc = ferrocenyl).¹³ In a similar manner, *p*-MeC₆H₄- (**2b**), *p*-ClC₆H₄- (**2c**),



p-MeOC₆H₄- (**2d**), *p*-EtOCOC₆H₄- (**2e**), and *p*-MeCOC₆H₄ analogs (**2f**) were prepared in good yield.¹⁴ The ³¹P NMR spectrum of **2a**, for example, showed two singlets accompanied by the Pt satellite at δ 38.13 (¹J_{PtP} = 1531 Hz) and 44.19 (¹J_{PtP} = 2535 Hz), suggesting the square-planar *cis* configuration of the Pt atom in **2a**. This assignment was confirmed by the single-crystal analysis of **2e** (Figure 1).¹⁵ The ferrocenyl acetylide ligand is located *cis* to the phenyl ligand around the Pt(II) atom. The Pt-P distance (2.301(2) Å) *trans* to the acetylide ligand is somewhat longer than that (2.271(2) Å) *trans* to the phenyl group, which may reflect the different σ -donating abilities of both ligands. Other bond dis-

[⊗] Abstract published in *Advance ACS Abstracts*, June 1, 1995.

(1) Collmann, P.; Hegedus, L. S.; Norton, J. R.; Finke, R. G. *Principles and Applications of Organotransition Metal Chemistry*; University Science: Mill Valley, CA, 1987; p 322.

(2) Tatsumi, K.; Hoffmann, R.; Yamamoto, A.; Stille, J. K. *Bull. Chem. Soc. Jpn.* **1981**, *54*, 1857.

(3) (a) Yamamoto, T.; Yamamoto, A.; Ikeda, S. *J. Am. Chem. Soc.* **1971**, *93*, 3350. (b) Kurosawa, H.; Emoto, M.; Urabe, A.; Miki, K.; Kasai, N. *J. Am. Chem. Soc.* **1985**, *107*, 8253.

(4) Kurosawa, H.; Emoto, M.; Urabe, A. *J. Chem. Soc., Chem. Commun.* **1984**, 968.

(5) Tsou, T. T.; Kochi, J. K. *J. Am. Chem. Soc.* **1978**, *100*, 1634.

(6) Fukuzumi, S.; Ishikawa, K.; Tanaka, T. *J. Chem. Soc., Dalton Trans.* **1985**, 899.

(7) Almark, M.; Akermark, B. *J. Chem. Soc., Chem. Commun.* **1978**, 66.

(8) Pedersen, A.; Tilset, M. *Organometallics* **1993**, *12*, 56.

(9) Low, J. J.; Goddard, W. A., III. *J. Am. Chem. Soc.* **1986**, *108*, 6115 and references cited therein.

(10) Ozawa, F.; Hikida, T.; Hayashi, T. *J. Am. Chem. Soc.* **1994**, *116*, 2844.

(11) Chen, J. Y.; Kochi, J. K. *J. Am. Chem. Soc.* **1977**, *99*, 1450.

(12) Sato, M.; Mogi, E.; Katada, M. To be submitted for publication.

(13) *trans*-[Pt(C≡CfC)(C₆H₅)(PPh₃)₂] (**1a**; 50 mg, 0.05 mmol) was stirred with dppe (40 mg, 0.1 mmol) in CH₂Cl₂ (10 mL) at room temperature for 20 min. After the solvent was evaporated, the crude products were chromatographed on Al₂O₃ by elution of CH₂Cl₂/hexane to give *cis*-[Pt(C≡CfC)(C₆H₅)(dppe)] (**2a**) as orange crystals (38 mg, 95%).

(14) **2a**: orange crystals; mp 187-189 °C; IR (KBr) ν (C≡C) 2124, 2109 cm⁻¹; ¹H NMR (CDCl₃) δ 2.14-2.58 (m, 4H, CH₂), 3.89 (s, 5H, Cp-unsub), 3.92 (t, *J* = 1.7 Hz, 2H, Cp- β), 4.13 (t, *J* = 1.8 Hz, 2H, Cp- α), 6.73-6.88 (m, 2H, C₆H₅), 7.30-8.12 (m, 23H, C₆H₅, PPh₂); ¹³C NMR (CDCl₃) 26.76 (dd, *J*_{P-C} = 31.5, 12.4 Hz, CH₂), 30.25 (dd, *J*_{P-C} = 35.3, 16.6 Hz, CH₂), 66.70 (s, Cp- β), 69.37 (s, Cp-unsub), 70.57 (s, Cp- α), 72.40 (s, Cp-*ipso*), 107.20 (d, *J*_{P-C} = 34.6 Hz, C≡C), 108.70 (dd, *J*_{P-C} = 146.5, 15.2 Hz, C≡C), 122.06 (s, C₆H₅), 126.96 (d, *J*_{P-C} = 7.6 Hz, C₆H₅), 138.71 (s, C₆H₅), 153.31 (dd, *J*_{P-C} = 113.3, 8.0 Hz, C₆H₅); ³¹P NMR (CDCl₃) δ 38.13 (s, *J*_{Pt-P} = 1531 Hz, *trans* to Ar), 44.19 (s, *J*_{Pt-P} = 2535 Hz, *trans* to C≡C); ¹⁹⁵Pt NMR (CDCl₃) -3091.97 (dd, *J*_{Pt-P} = 2535, 1545 Hz). Anal. Found: C, 60.11; H, 4.36. Calcd for C₄₄H₃₈P₂FePt: C, 60.08; H, 4.36. Other products are similarly assigned by the spectroscopic data and satisfactory elemental analyses.

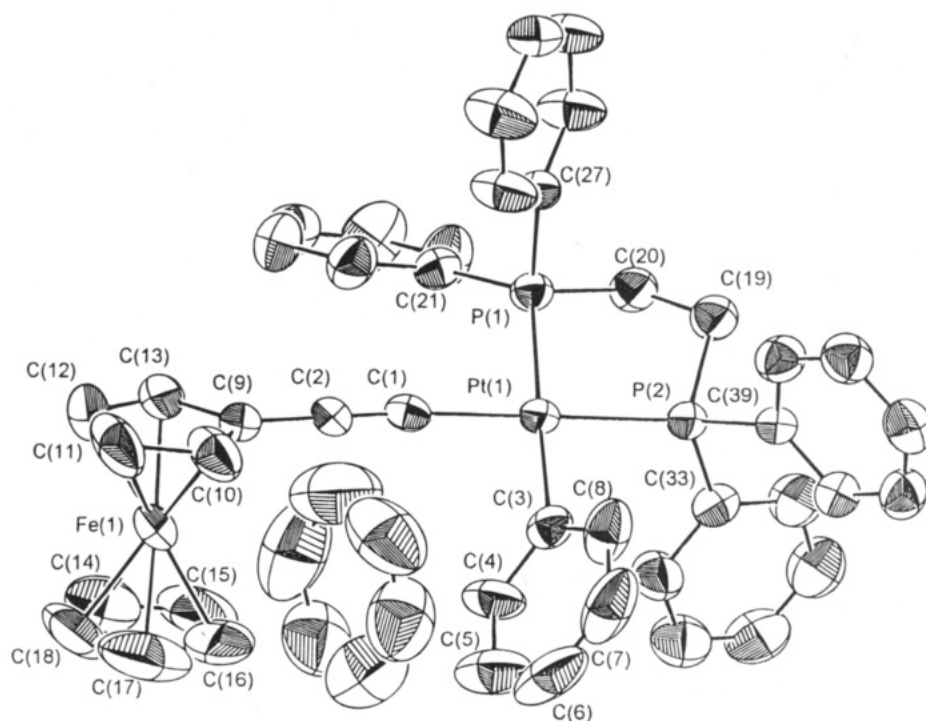


Figure 1. Crystal structure of **2a**. Selected bond distances (Å) and angles (deg): Pt–P(1) = 2.301(2), Pt–P(2) = 2.271(2), Pt–C(1) = 2.029(7), Pt–C(3) = 2.089(8), C(1)–C(2) = 1.185(10); P(1)–Pt–P(2) = 85.2(1), C(1)–Pt–C(3) = 86.1(3), Pt–C(1)–C(2) = 175.6(7).

tances and bond angles of **2e** are similar to those in *trans*-[PtH(C≡CfC)(PPh₃)₂]¹⁶ and *cis*-[Pt(CCFc)₂(PPh₃)₂].¹⁷ In the cyclic voltammogram, *trans* isomer **1a** showed a quasi-reversible wave at –0.16 V (Fe^{II}/Fe^{III}) and an irreversible wave at +0.90 V (Pt^{II}/Pt^{IV}).¹⁸ On the other hand, *cis* isomer **2a** showed one quasi-reversible wave at –0.07 V and one irreversible wave at +0.88 V. Also, an additional redox wave was observed at +0.10 V, whose redox potential is coincident with that of the coupling product **3a**. This wave appeared even when the scan turned back at +0.40 V and increased when the scan rate was decreased. Cyclic voltammograms of **2a–d** are shown in Figure 2. As seen clearly, the more electron-releasing the substituent, the larger the new wave appears, the potential of which is coincident with that of the corresponding coupling product. Such electrochemical behavior suggests that the one-electron-oxidized species of the *cis* complexes are unstable and are followed by a fast chemical reaction, producing the coupling product.

Complexes **2a–f** reacted smoothly with 1 equiv of DDQ or AgBF₄ in CH₂Cl₂ at room temperature to give

(15) Crystal structure data for **2a**: C₄₄H₃₈P₂FePtC₆H₆, fw = 957.75, triclinic, space group P1, *a* = 17.320(1) Å, *b* = 11.774(5) Å, *c* = 10.723(4) Å, α = 97.57(3)°, β = 74.37(4)°, γ = 89.57(5)°, *V* = 2086(2) Å³, *Z* = 2, ρ_{calcd} = 1.53 g cm⁻³, μ = 38.406 cm⁻¹, Mo Kα radiation, λ = 0.710 73 Å. Intensity data were collected on a Mac Science MXC18K diffractometer. Of 10 332 reflections collected, 9576 were unique, 7926 of which with *I* > 3.0σ(*I*) were used for refinement. The structure was solved by direct methods and refined by a full-matrix least-squares procedure. Absorption correction by the ψ-scan method and anisotropic refinement for non-hydrogen atoms were carried out. *R* = 0.046 and *R*_w = 0.053.

(16) Rosso, M. V.; Furlani, A.; Licocchia, S.; Paolesse, R.; Villa, A. C.; Guastini, C. *J. Organomet. Chem.* **1994**, 469, 245.

(17) Weigand, W.; Robl, C. *Chem. Ber.* **1993**, 126, 1807.

(18) Cyclic voltammograms of **2a–f** (1 mM) were measured in CH₂Cl₂ solution containing 0.1 M (*n*-Bu)₄NClO₄ at a Pt electrode and a sweep rate of 100 mV s⁻¹ at 25 °C. The potential is referred to FcH⁺/FcH. The waves were assigned in comparison with the reference compounds (+0.12 V for *p*-MeC₆H₄C≡CfC and +0.61 V for *trans*-[Pt(C₆H₄OMe-*p*)(C≡CPh)(Ph₃P)₂]).

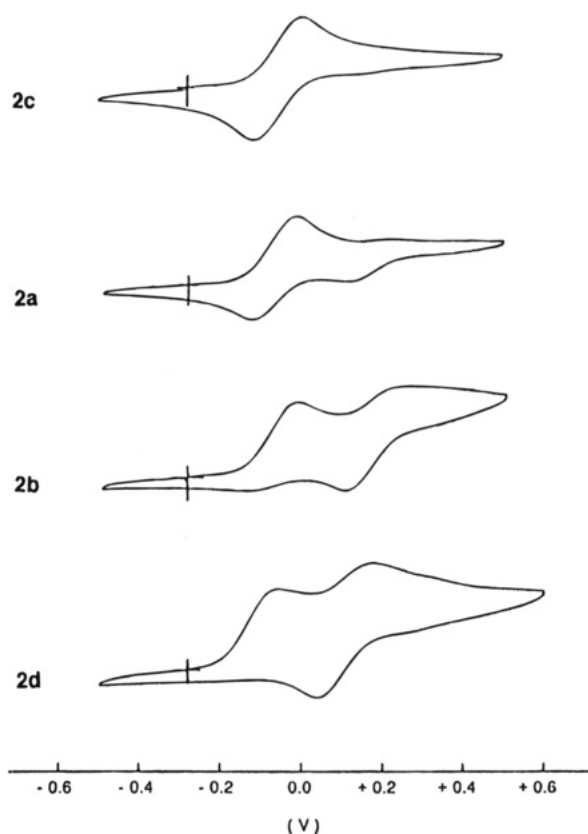
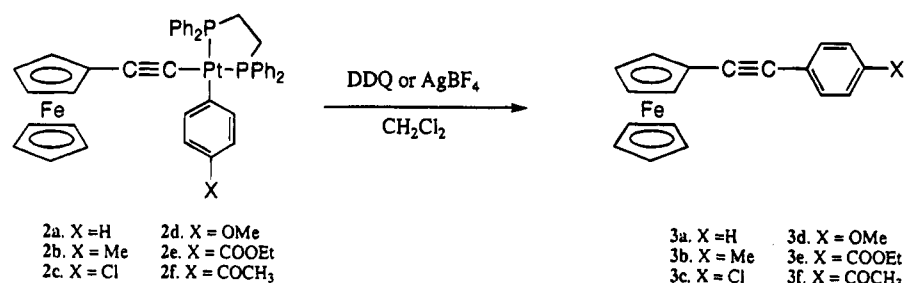


Figure 2. Cyclic voltammograms for **2a–d** (1 mM) in 0.1 M *n*-Bu₄NClO₄/CH₂Cl₂ at a Pt electrode and a sweep rate of 0.1 V s⁻¹.

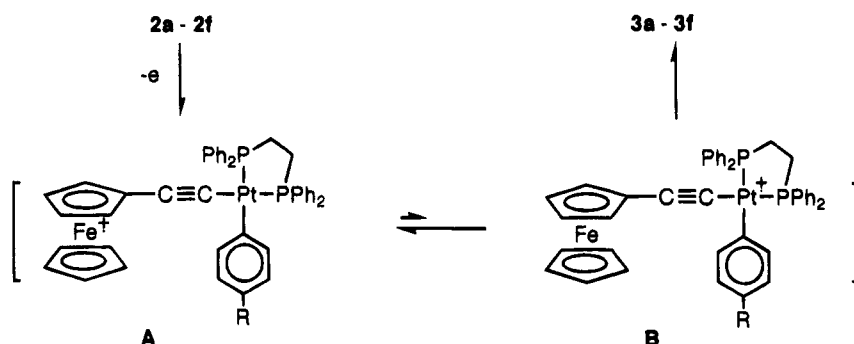
the corresponding coupling complexes *p*-XC₆H₄C≡CfC (**3a–f**), in excellent yield.¹⁹ The facile conversion of

(19) The electrochemical oxidation of **2a** also proceeded smoothly at 0.4 V to give the coupling product **3a**.

Scheme 2



Scheme 3



2a-f to the coupling product under the oxidative conditions is in striking contrast to the fact that the corresponding trans isomers **1a-f** give the stable one-electron-oxidized products under similar conditions in good yield.¹² That is, the oxidatively induced reductive elimination takes place only in the cis isomers. This fact is in good agreement with the theoretical prediction.³ When **2d** was refluxed in chloroform for 8 h without the oxidant, only a trace amount of **3d** was obtained. The reactions scarcely proceed in the presence of a catalytic amount of the oxidant. These indicate a remarkable oxidative activation by an equimolar amount of DDQ or AgBF₄ in the reductive elimination for the Pt(II) complexes **2a-f**. The electronic spectrum of **2e** immediately after the addition of 1 equiv of DDQ is, for example, different from that of **2e** and is quite similar to that of the one-electron-oxidized complex of the trans isomer **1e**. This suggests that the one-electron-oxidized species very rapidly formed on the addition of the oxidant, followed by its slow degradation to the coupling product. The decomposition of **2a-f** under oxidative conditions adopted first-order kinetics in CH₂Cl₂ solution.²⁰ The observed first-order rate constants (k_{obs} ; s⁻¹ at 0 °C) decreased in the following order: **2d** (8.9×10^{-2}) > **2b** (3.3×10^{-2}) > **2a** (1.9×10^{-2}) > **2c** (2.6×10^{-3}) > **2e,f** (1.3×10^{-3}). Curiously, the reaction is retarded by the electron-attracting substituent on the aryl ligand. The rate constants correlate with the substituent constant (σ_p) of the substituent on the aryl ligand in **2a-f** ($r = 0.96$). A similar but small substituent effect is observed in the AuMe₂Ar(PPh₃) complexes.²¹ The theo-

retical calculation suggests that the better the σ -donating capability of the leaving groups is, the more readily the elimination reaction proceeds.^{3a} A similar reaction of *cis*-[Pt(*p*-MeC₆H₄)(C≡CPh)(dppe)] with DDQ does not proceed successfully; instead, reaction occurs with AgBF₄ or FcHPF₆ in refluxing CH₂Cl₂ to give only a small yield of the coupling product. These results, along with the CV measurements, indicate a notable stimulating effect of the ferrocenyl group for the oxidatively induced reductive coupling in the Pt(II) complexes. The effect may be explained as follows (Scheme 3): the ferrocenyl part is first oxidized with a mild oxidant such as DDQ, which is not enough to oxidize the Pt(II) part, to give the one-electron-oxidized species **A**. Then, an electron transfer from the Pt(II) part through the C≡C bond produces the species **B**, in which the electron density on the Pt(II) atom is diminished. In this stage, the reductive elimination takes place rapidly, because the decrease of the electron density on the metal atom is known to accelerate the reductive elimination. A species such as **A** is confirmed to be predominant in the one-electron-oxidized species of the trans isomer,¹² and therefore the contribution of species **B** may be enhanced by the increase of electron density on the Pt(II) atom, so that the oxidatively induced reductive elimination in complexes **2a-f** is likely accelerated by the electron-releasing substituents on the aryl group. This seems to be a rare example which the chemical reaction is initiated by the metal-metal interaction.

Supporting Information Available: Text giving characterization data for **2a-f** and details of the X-ray crystal structure determination of **2e**, including tables of crystal data and data collection and refinement details, positional and thermal parameters, bond distances and angles, torsion angles, nonbonded distances, and least-squares planes and deviations therefrom and a figure giving the full atom-labeling scheme (50 pages). Ordering information is given on any current masthead page.

(20) The reaction was monitored spectroscopically. The spectrum of **2e**, for example, had three isosbestic points at 340, 360, and 400 nm. The reaction rate was followed up by the decrease of the peak near 460 nm, which was perhaps due to the charge-transfer band in the one-electron-oxidized species owing to the observation also in the corresponding trans isomer. The initial concentration of **2a-e** was 0.1 mmol with 2 equiv of DDQ. The rate was independent of the concentration of DDQ in the presence of more than 1 equiv of DDQ.

(21) Komiya, S.; Ozaki, S.; Shibue, A. *J. Chem. Soc., Chem. Commun.* **1986**, 1555.

Magnetic Behavior in Cluster-Based Organometallic Materials: Synthesis and Characterization of the Novel 1,1'-Bis(diphenylphosphino)ferrocene-Crippled Cluster Derivative $[\text{Ru}_6\text{C}(\text{CO})_{15}\{\mu\text{-Fe}(\text{C}_5\text{H}_4\text{PPh}_2)_2\}]$

Alexander J. Blake, Andrew Harrison, Brian F. G. Johnson,* Eric J. L. McInnes, Simon Parsons, Douglas S. Shephard, and Lesley J. Yellowlees

Department of Chemistry, The University of Edinburgh, West Mains Road, Edinburgh EH9 3JJ, U.K.

Received January 12, 1995[®]

Summary: The hexaruthenium carbido cluster derivative $[\text{Ru}_6\text{C}(\text{CO})_{15}\{\mu\text{-Fe}(\text{C}_5\text{H}_4\text{P}(\text{Ph})_2)_2\}]$, **3**, has been synthesized by direct reaction of the parent cluster $[\text{Ru}_6\text{C}(\text{CO})_{17}]$, **1**, with 1,1'-bis(diphenylphosphino)ferrocene (dppf). An X-ray crystallographic study revealed that the dppf ligand is coordinated in the vicinal form and the cluster core is greatly distorted from a regular octahedron. ³¹P NMR spectra of **3** at various temperatures show a high degree of stereochemically nonrigid behavior. Magnetic susceptibility measurements across a range of temperatures indicate that **3** is paramagnetic at all temperatures. An electrochemical study of **3** has demonstrated a significant degree of communication between the redox-active sites.

Metallocenes, in particular ferrocene, possess properties which have led to their use as ferromagnets,^{1,2b} molecular sensors,³⁻⁵ and electrochemical agents.⁶ Clusters have been shown to possess unusual magnetic^{7-9c} and redox properties¹⁰ which, as far as we are aware, have not been put to commercial use. The idea of combining the properties of these two sets of fascinating molecules has significant appeal, and in this communication we report the synthesis of the new cluster compound $[\text{Ru}_6\text{C}(\text{CO})_{15}\{\mu\text{-Fe}(\text{C}_5\text{H}_4\text{P}(\text{Ph})_2)_2\}]$, **3**, a 1,1'-bis(diphenylphosphino)ferrocene (dppf) derivative of the *closo* cluster $[\text{Ru}_6\text{C}(\text{CO})_{17}]$, **1**, which exhibits a major cluster deformation, interesting redox chemistry, and paramagnetic behavior.

There are many reports in the literature of dppf coordinated to single transition-metals.¹¹ Some of these heterobimetallic complexes show interesting cooperative effects between the two metal sites. Few corresponding

cluster derivatives of dppf have been reported to date, and those are mainly of low nuclearity.¹² Reports of paramagnetism in cluster complexes are also relatively few, and the phenomenon is poorly understood.^{7-9c}

The thermally initiated reaction of dppf with the parent cluster $[\text{Ru}_6\text{C}(\text{CO})_{17}]$, **1**, in tetrahydrofuran yields $[\text{Ru}_6\text{C}(\text{CO})_{15}\{\mu\text{-dppf}\}]$, **3**, as the major product along with a smaller amount of $[\text{Ru}_6\text{C}(\text{CO})_{16}\{\text{dppf}\}]$, **2**.^{10b} After separation by TLC using $\text{CH}_2\text{Cl}_2/\text{hexane}$ (1:4) as eluent, dark green **3** and red **2**^{10b} were tentatively identified on the basis of their IR spectra.^{10c} The ¹H

(10) (a) Schneider, J. J.; Goddard, R.; Krüger, C.; Werner, S.; Metz, B. *Chem. Ber.* **1991**, *124*, 301. (b) $[\text{Ru}_6\text{C}(\text{CO})_{16}\{\text{dppf}\}]$ will be described in full in a forthcoming paper. (c) Spectroscopic data for **3**: IR (CH_2Cl_2) $\nu(\text{CO})/\text{cm}^{-1}$: 2070 m, 2034 s, 2024 vs, 2012 s, 1997 m, 1969 w br; ³¹P NMR (CDCl_3 , 298 K): δ 43.78 (br s) ppm; ¹H NMR (CDCl_3 , 298 K): δ 7.58 (br m, 20H), δ 4.12 (br s, 8H) ppm. Anal. for $\text{C}_{50}\text{H}_{28}\text{FeO}_{15}\text{P}_2\text{Ru}_6\text{C}_2\text{CH}_2\text{Cl}_2$: found C, 37.43; H, 1.9 (calcd C, 37.32; H, 1.78). (d) Crystal data for **3**: $\text{C}_{50}\text{H}_{28}\text{FeO}_{15}\text{P}_2\text{Ru}_6\text{C}_2\text{CH}_2\text{Cl}_2$, $M = 1762.8$, monoclinic, space group $P2_1/n$ with $a = 17.280(3)$ Å, $b = 18.488(4)$ Å, $c = 17.359(3)$ Å, $\beta = 92.09(3)^\circ$, $U = 5542(2)$ Å³, $D_{\text{calcd}} = 2.101$ g cm⁻³, $Z = 4$, $\mu = 2.512$ mm⁻¹, $T = 150.0(2)$ K. Diffraction amplitudes were acquired using a Stoe-Stadi-4 four-circle diffractometer, graphite-monochromated Mo K α X-radiation, and an Oxford Cryosystems low-temperature device (Cosier, J.; Glazer, A. M. *J. Appl. Crystallogr.* **1986**, *19*, 105-108). Of 8872 reflections collected to $2\theta_{\text{max}} = 45^\circ$, 7213 were unique ($R_{\text{int}} = 0.064$). The structure was solved by automatic direct methods (Ru) (SHELXS-86; Sheldrick, G. M. *Acta Crystallogr.* **1990**, *A46*, 467) and developed through iterative cycles of least-squares refinement and difference Fourier synthesis. Dichloromethane solvate molecules occupy channels between molecules of **1**, and modeling of their substantial disorder was largely successful. Anisotropic refinement was allowed for Ru, Fe, P, and O atoms and nonsolvent H atoms were included in calculated positions and allowed to refine riding on their respective carbon atoms. (SHELXL-93: G. M. Sheldrick, University of Göttingen, Germany.) At final convergence with $R[F > 4\sigma(F)] = 0.074$, $wR_2[F^2, 7161 \text{ data}] = 0.1851$, and $S = 1.055$ for 465 refined parameters, and the final ΔF synthesis showed no feature lay outside the range $+1.44$ to -1.02 e Å⁻³. (e) Electrochemical experiments were carried out using a DSL 286-D PC with General Purpose Electrochemical System (GPES) Version 3 software coupled to an Autolab system containing a PSTAT 10 potentiostat. A conventional three-electrode cell was employed with Pt counter and microworking electrodes and a Ag/AgCl reference electrode against which the Fe/Fe⁺ couple was measured at $+0.55$ V. Coulometric studies employed a three-electrode H-type cell with a Pt basket working electrode. All electrochemical experiments were performed under an atmosphere of nitrogen. (f) Magnetic susceptibility measurements were performed on powder samples with a SQUID magnetometer (Quantum Design, model MPMS2) at temperatures between 1.8 and 310 K in an applied magnetic field of 0.1 T. The data were corrected for the response of the sample holder and the diamagnetic contributions of all atoms.¹⁸

(11) For examples, see: Millar, T. M.; Ahmed, K. J.; Wrighton, M. S. *Inorg. Chem.* **1989**, *28*, 2347. Housecroft, C. E.; Owen, S. O.; Raithby, P. R.; Shaykh, B. A. M. *Organometallics* **1990**, *9*, 1617. Butler, I. R.; Cullen, W. R.; Kim, T.-J.; Rettig, S. J.; Trotter, J. *Organometallics* **1985**, *4*, 972. Clemente, D. A.; Pillioni, G.; Corain, B.; Longato, B.; Tiripicchio-Camellini, M. *Inorg. Chim. Acta* **1986**, *115*, L9.

(12) (a) Draper, S. M.; Housecroft, C. E.; Rheingold, A. L. *J. Organomet. Chem.* **1992**, *435*, 9. (b) Chacon, S. T.; Cullen, W. R.; Bruce, M. I.; Shawkataly, O.; Einstein, F. W. B.; Jones, R. H.; Willis, A. C. *Can. J. Chem.* **1990**, *68*, 2001.

[®] Abstract published in *Advance ACS Abstracts*, June 1, 1995.

(1) Kollmar, C.; Couty, M.; Kahn, O. *J. Am. Chem. Soc.* **1991**, *113*, 7994.

(2) (a) Chi, K. M.; Calabrese, J. C.; Reiff, W. M.; Millar, J. S. *Organometallics* **1991**, *10*, 668. (b) Millar, J. S.; Epstein, A. *J. Angew. Chem., Int. Ed. Engl.* **1994**, *33*, 385.

(3) Wagner, R. W.; Brown, P. A.; Johnson, T. E.; Lindsey, J. S. *J. Chem. Soc., Chem. Commun.* **1991**, 1463.

(4) Constable, E. C. *Angew. Chem., Int. Ed. Engl.* **1991**, *30*, 407.

(5) Beer, P. D.; Chen, Z.; Drew, M. G. B.; Pilgrim, A. *J. Inorg. Chim. Acta* **1994**, *225*, 137.

(6) Butler, I. R. *Organometallic Chemistry*; Abel, E. W., Ed.; Special-ist Periodic Reports 21; Royal Society of Chemistry: Letchworth, U.K., 1992; p 338.

(7) (a) Rösch, N.; Ackermann, L.; Pacchioni, G.; Dunlap, B. I. *J. Chem. Phys.* **1991**, *95*, 7005. (b) Williams, I. H.; Spangler, D.; Femecc, D. A.; Maggiora, G. M.; Schowen, R. L. *J. Am. Chem. Soc.* **1980**, *102*, 6621.

(8) Johnson, D. C.; Edwards, P. P.; Benfield, R. E.; Nelson, W. J. H.; Vargas, M. D. *Nature* **1985**, *314*, 231.

(9) (a) Dahl, L. F.; Olsen, W. L.; Stacy, A. M. *J. Am. Chem. Soc.* **1986**, *108*, 7646. (b) Dahl, L. F.; Olsen, W. L. *J. Am. Chem. Soc.* **1986**, *108*, 7657. (c) Dahl, L. F.; Byers, L. R.; Uchtman, V. A. *J. Am. Chem. Soc.* **1981**, *103*, 1942.

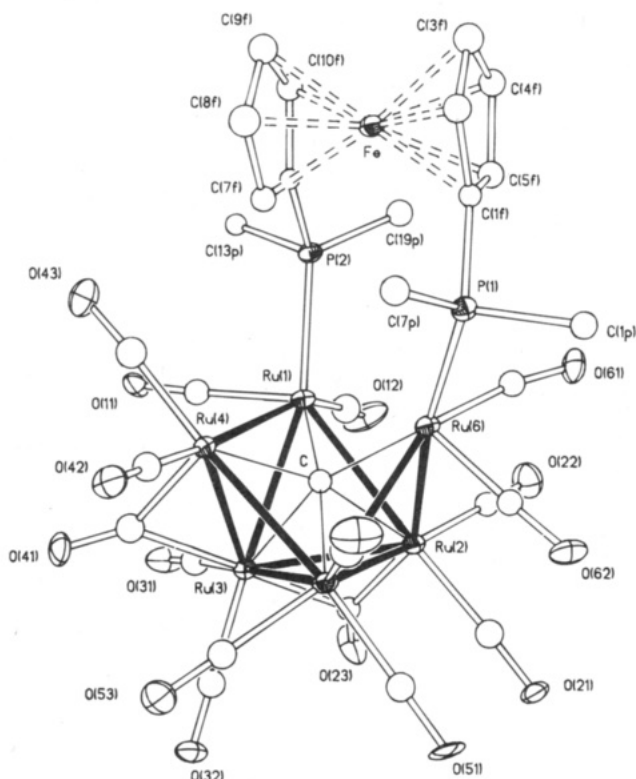


Figure 1. The solid state molecular structure of **3** as determined by X-ray crystallography. The hydrogens and phenyl groups have been omitted for clarity. Selected bond lengths (Å): Ru(1)–Ru(2), 2.968(1); Ru(1)–Ru(3), 2.912(1); Ru(1)–Ru(4), 2.870(1); Ru(2)–Ru(3), 2.767(1); Ru(2)–Ru(5), 2.971(1); Ru(2)–Ru(6), 2.816(1); Ru(3)–Ru(4), 2.854(1); Ru(3)–Ru(5), 2.914(1); Ru(4)–Ru(5), 2.827(1); Ru(5)–Ru(6), 2.861(1); Ru(1)–P(2), 2.391(2); Ru(6)–P(1), 2.389(2).

NMR spectrum of **3** in CDCl_3 showed exceptionally poor resolution of both the phenyl and cyclopentadienyl resonances at both room temperature and 223 K. This immediately suggested unusual behavior of the new cluster derivative. A ^{31}P NMR spectrum of **3** obtained at 298 K showed a single, slightly broadened signal at δ 44 ppm. This may be attributed to stereochemically nonrigid behavior producing equivalence of the two phosphorus nuclei on the NMR time scale (*vide infra*). At 198 K, however the ^{31}P NMR spectrum showed two signals at δ 41.07 and 52.96 ppm. The high-frequency signal was significantly broadened, possibly due to the presence of proximal unpaired electrons. The two signals observed at low temperature are consistent with the two phosphorus environments observed in the solid state structure of **3**. These observations perhaps indicate the itinerant nature of the unpaired electrons at ambient temperatures (*vide infra*).

A single-crystal X-ray analysis of **3** was undertaken to establish the molecular structure, and this is shown in Figure 1 along with some pertinent structural parameters.^{10d} Of striking significance is the distorted Ru_6C metal core. Two very long Ru–Ru distances [(Ru(1)–Ru(6), 3.171(1) Å, and Ru(4)–Ru(6), 3.450(1) Å)] are observed and show an “opening up” of the normally *closo* octahedron to give a hinged square-based pyramid. Ru(6) is hinged at the basal metal atoms Ru(2) and Ru(5) and supported by P(1) of the bridging dppf ligand. All remaining Ru–Ru contacts are within the normal range. The carbido carbon atom is displaced from the centroid of the four metals constituting the base of the

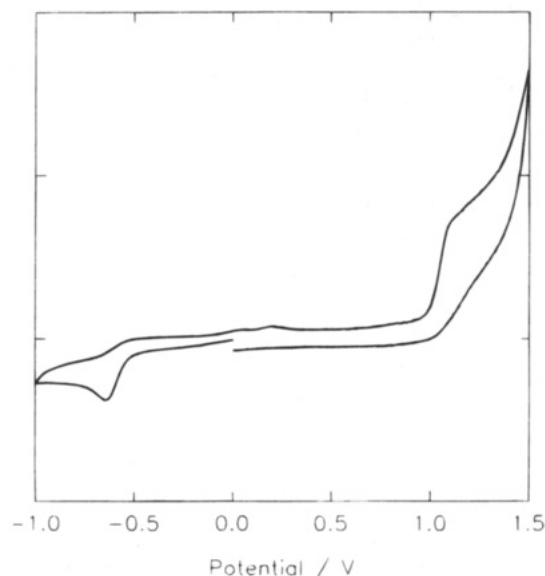


Figure 2. Cyclic voltammogram of **3** in 0.5 M $[\text{NBut}^n_4][\text{BF}_4]/\text{CH}_2\text{Cl}_2$ solution at room temperature.

square-based pyramid by 0.217(8) Å and toward Ru(6). The distorted cluster is surrounded by 13 terminal carbonyls and 2 μ -COs triangulating the Ru(2)–Ru(3) and Ru(3)–Ru(4) vectors. A single-crystal X-ray structural determination has shown that no comparable effect occurs in $[\text{Ru}_6\text{C}(\text{CO})_{15}\{\mu\text{-dppm}\}]^{13}$ or $[\text{H}_4\text{Ru}_4\text{C}(\text{CO})_{10}\{\mu\text{-diphos}\}]^{14}$.

The dppf is ligated in the vicinal form, bridging the hinged metal Ru(6) and the basal metal Ru(1). The P atoms each occupy slightly distorted tetrahedral environments which, due to the bonding mode and rearrangement of the metal core, are nonequivalent. The relative orientations of the P atoms with respect to the ferrocene moiety show a twist of 73.7°. The cyclopentadienyl rings are parallel to within estimated error, eclipsed to within 2.04°, and produce an average distance of 1.635(4) Å from their centroids to the iron. The crystal structure also contains highly disordered dichloromethane solvate molecules. Modeling of these was largely successful.

Shifts in the redox potential of the dppf ligand and Ru_6 cluster are of great interest and demonstrate in a complementary fashion electronic and/or electrostatic communication between redox-active sites.¹⁵ Cyclic voltammetry of **3** in 0.5 M $[\text{NBut}^n_4][\text{BF}_4]/\text{CH}_2\text{Cl}_2$ solution at room temperature reveals an irreversible two-electron reduction at -0.65 V vs Ag/AgCl with associated daughter peaks at +0.07 V and +0.25 V (Figure 2).^{10e} An irreversible oxidation is observed at *ca.* +1.15 V. Bulk electrolysis at -0.80 V confirms the reductive process as a two-electron step ($n = 1.95e$). Investigation is under way to characterize the daughter products of the reductive process. The parent cluster **1** exhibits no oxidative process but a two-electron reduction at -0.46 V to yield $[\text{Ru}_6\text{C}(\text{CO})_{16}^{2-}]$ which oxidizes at +0.45 V.¹⁶ Free dppf undergoes a quasi-reversible oxidation at

(13) Gracey, B. P.; Evans, J.; Jones, A. G.; Webster, M. *Acta Crystallogr.* **1987**, *C43*, 2286.

(14) Churchill, R. M.; Lashewycz, R. A.; Shapeley, J. R.; Richter, S. I. *Inorg. Chem.* **1980**, *19*, 1277.

(15) Colbert, M. C. B.; Ingham, S. L.; Lewis, J.; Long, N. J.; Raithby, P. R. *J. Chem. Soc., Dalton Trans.* **1994**, 2215.

(16) Drake, S. R.; Johnson, B. F. G.; Lewis, J. *J. Chem. Soc., Dalton Trans.* **1989**, 243.

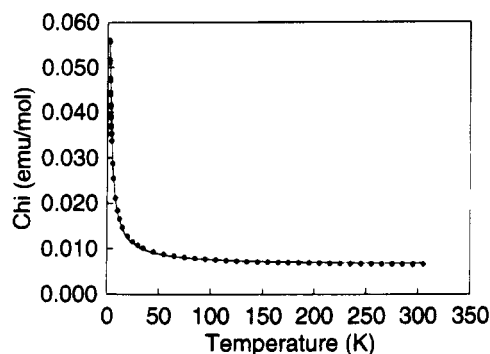


Figure 3. Variation of the molar magnetic susceptibility of **3** with temperature. Superimposed on the data points is a line of best fit utilizing the Curie–Weiss expression.

+0.75 V. We therefore assign the 2e reduction of **3** as primarily cluster-based and the oxidation as primarily dppf-based. These results show that the cluster and dppf moieties are more difficult to reduce and oxidize, respectively, than in the parent cluster and free dppf.

Variable temperature magnetic measurements^{10f} show **3** to be paramagnetic at all temperatures (Figure 3). The corrected data were fitted to both a Curie and a Curie–Weiss expression plus a temperature independent paramagnetic (TIP) term. The quality of the fit was appreciably better when a small Curie–Weiss constant Θ of -0.50 K was included, and the corresponding values of the Curie constant C and TIP contributions were 0.12 emu K mol⁻¹ and $0.052C$, respectively. The value of C corresponds to an effective magnetic moment of $0.99(5)$ Bohr magnetons at high temperatures. It appears therefore that the moment on the ferrocene/cluster unit is 35% of the moment that would arise from a spin triplet state and that there is a weak antiferromagnetic

coupling between the molecular units. The ESR spectrum of a solid sample of **3** appears silent at both 77 and 298 K. This is perhaps consistent with the high rate of relaxation that may be expected in both moieties.¹⁷

These results suggest that there is a strong interaction between the ferrocene and the cluster cage frontier orbitals. We propose the HOMO to be primarily ferrocene-based but with significant cage character which results in its more difficult oxidation. Concomitantly the LUMO is primarily cage-based but with a significant ferrocene admixture. Increased electron density at the cluster leads to the structural deformation of the formally 86e *closo* cluster framework observed in the solid state.

In the light of these results we have now begun a thorough investigation into a wide variety of systems designed to produce similar interactions between clusters and proximal redox-active centers.

Acknowledgment. We thank C. M. Grant and Dr. J. M. Rawson for magnetic data collection and processing, and also Dr. J. R. Galsworthy for helpful discussions. We gratefully acknowledge The University of Edinburgh and the EPSRC for financial support.

Supporting Information Available: Tables giving crystal data and structure refinement details, atomic coordinates, bond distances and angles, and anisotropic thermal parameters for **3** (11 pages). Ordering information is given on any current masthead page.

OM9500230

(17) Prins, R.; Reinders, F. J. *J. Am. Chem. Soc.* **1969**, *91*, 4929.

(18) König, E. In *Landholt-Börnstein New Series, Group 2 Atomic and Molecular Physics*; Hellwege, K. H. Ed.; Springer-Verlag, Berlin, 1966; Vol. 2.

Articles

New Synthesis of Functionalized Chromium Carbene Complexes using Zinc Organometallics

Heinz Stadtmüller and Paul Knochel*

Fachbereich Chemie der Philipps-Universität Marburg, D-35032 Marburg, Germany

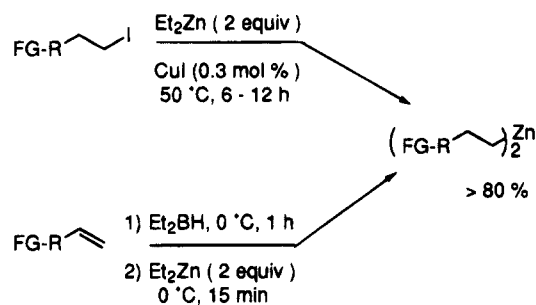
Received February 13, 1995[®]

The reaction of functionalized dialkylzincs with photochemically generated $\text{Cr}(\text{CO})_5\cdot\text{THF}$ affords, after carbonylation and methylation using Meerwein's reagent, polyfunctional chromium carbene complexes in 35%–45% overall yield. The hydroboration of the unsaturated chromium carbene complex **4e** followed by a boron–zinc exchange mediated by diethylzinc provides the dialkylzinc **6** bearing a chromium carbene functionality. This was reacted with deuterium oxide and iodine, affording the expected chromium carbene complexes in 67% and 43% yields, respectively.

Introduction

Heteroatom-stabilized chromium carbene complexes have proven to be versatile organometallics of interest for organic synthesis. They undergo unique synthetic transformations with unsaturated organic substrates allowing the performance of several new ring annulation reactions.¹ They can be prepared by two methods. The original procedure of Fischer² involves the addition of organolithium reagents to $\text{Cr}(\text{CO})_6$.^{1,2} Unfortunately, other less reactive organometallics (Grignard reagents, organoaluminums, organozincs) do not add to $\text{Cr}(\text{CO})_6$, limiting this approach to the preparation of relatively unfunctionalized chromium carbene complexes. This limitation does not exist for the second method, developed by Semmelhack³ and Hegedus,⁴ which allows the preparation of functionalized carbene complexes by using the reaction of $\text{M}_2\text{Cr}(\text{CO})_5$ ($\text{M} = \text{Na}, \text{K}$) with acid chlorides³ or amides.⁴ However, these two procedures require the laborious preparation of the sensitive dianion $\text{M}_2\text{Cr}(\text{CO})_5$. Cooper reported recently⁵ that $\text{Cr}(\text{CO})_5\cdot\text{NMe}_3$ reacts readily with phenyllithium and that the resulting chromium adduct can be converted to an anionic acyl chromium complex. This observation led us to reexamine the addition of organozinc derivatives to the readily available $\text{Cr}(\text{CO})_5\cdot\text{THF}$ complex. Herein, we wish to report the results of this study which led to the development of a new synthesis of polyfunctional chromium carbene complexes. An application of these carbene complexes to the preparation of new mixed

Scheme 1



dimetallic species of boron/chromium and zinc/chromium is also described.

Results and Discussion

The irradiation of $\text{Cr}(\text{CO})_6$ in THF at 25 °C with a high-pressure mercury lamp produces a deep orange solution of $\text{Cr}(\text{CO})_5\cdot\text{THF}$ in ca. 90% yield.⁶ This solution was treated with dialkylzinc **1** (2 equiv, 25 °C, 3–5 h), resulting in the formation of a deep red solution of the alkylchromium(0) complex of type **2**. The required polyfunctional diorganozincs can be prepared by iodine–zinc exchange⁷ or boron–zinc exchange⁸ in high yields^{7,8} (Scheme 1). The ate complexes **2** were treated under 1 atm of carbon monoxide for 2 h, producing the anionic acyl complexes of type **3** (Scheme 2).⁵ After removing the solvent in vacuum (0.1 mmHg, 25 °C), the residue was diluted in dry dichloromethane and treated with the Meerwein salt ($\text{Me}_3\text{O}^+ \text{BF}_4^-$) at –30 °C. The reaction mixture was stirred for 12 h at 0 °C, affording after workup (see experimental section) and chromatographic purification the chromium carbene complexes of type **4** (Scheme 2 and Table 1). This one-pot

[®] Abstract published in *Advance ACS Abstracts*, May 15, 1995.

(1) For excellent reviews, see: Dötz, K. H. *Angew. Chem., Int. Ed. Engl.* **1984**, *23*, 587. (b) Wulff, X. In *Comprehensive Organic Synthesis*; Trost, B. M., Fleming, I., Eds.; Pergamon: Oxford, 1991; Vol. 5, p 1065.

(2) Fischer, E. O.; Maasböl, A. *Angew. Chem., Int. Ed. Engl.* **1964**, *3*, 580. (b) Fischer, E. O.; Maasböl, A. *Chem. Ber.* **1967**, *100*, 2445. (c) Fischer, H. In *The Chemistry of the Metal–Carbon bond*; Hartley, F. R., Patai, S., Eds.; Wiley: New York, 1982; Vol. 1, p 181.

(3) Semmelhack, M. F.; Lee, G. R. *Organometallics* **1987**, *6*, 1839.

(4) (a) Imwinkelried, R.; Hegedus, L. S. *Organometallics* **1988**, *7*, 702. (b) Schwindt, M. A.; Lejon, T.; Hegedus, L. S. *Organometallics* **1990**, *9*, 2814.

(5) (a) Lee, I.; Cooper, N. J. *J. Am. Chem. Soc.* **1993**, *115*, 4389. (b) Maher, J. M.; Beatty, R. P.; Cooper, N. J. *Organometallics* **1985**, *4*, 1354.

(6) Strohmeier, W. *Angew. Chem., Int. Ed. Engl.* **1964**, *3*, 730.

(7) (a) Rozema, M. J.; AchyuthaRao, S.; Knochel, P. *J. Org. Chem.* **1992**, *57*, 1956. (b) Ostwald, R.; Chavant, P.-Y.; Stadtmüller, H.; Knochel, P. *J. Org. Chem.* **1994**, *59*, 4143.

(8) (a) Langer, F.; Waas, J. R.; Knochel, P. *Tetrahedron Lett.* **1993**, *34*, 5261. (b) Langer, F.; Devasagayaraj, A.; Chavant, P.-Y.; Knochel, P. *Synlett* **1994**, 410.

Scheme 2

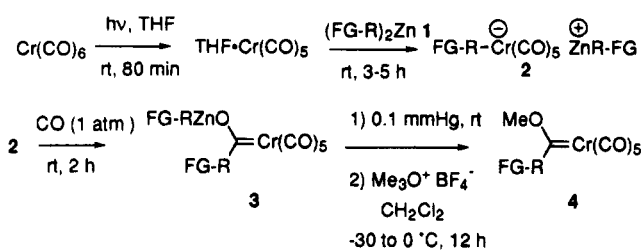


Table 1. One-Pot Preparation of Chromium Carbene Complexes 4a–i Obtained by the Reaction of Cr(CO)₅·THF with Diorganozincs 1

entry no.	(FG-R) ₂ Zn (FG-R)	product 4	yield (%) ^a
1	Et		41
2	Bu		43
3	i-Pr		45
4	Ph		35
5			37
6	Cl(CH ₂) ₄		41
7	Br(CH ₂) ₅		39
8	tBuCO ₂ (CH ₂) ₄		35
9	AcO(CH ₂) ₅		38

^a Isolated yields of analytically pure (>95%) chromium carbene complexes.

procedure allows the preparation of a range of functionalized carbene complexes **4** in satisfactory overall yields (35%–45%) based on chromium hexacarbonyl.

Primary, secondary, and aryl diorganozincs furnish the corresponding chromium carbene complexes **4a–d** in similar yields (entries 1–4 of Table 1). Interestingly, functionalities like a double bond, chloride, bromide, or ester are also readily tolerated (entries 5–9). Attempts to improve the yields by changing the quantities of diorganozincs, the reaction conditions (temperature, solvent, concentration), or the starting chromium carbonyl derivative (Cr(CO)₅NMe₃ instead of Cr(CO)₅·THF) were not successful. Similarly, the use of W(CO)₅·THF and (CpMe)Mn(CO)₂·THF instead of Cr(CO)₅·THF gave no reaction with diorganozincs.

The chromium carbene complex **4e** can be further converted into mixed bimetallic reagents. Thus, the hydroboration of **4e** with diethylborane^{8,9} (1 equiv, 0 °C, 2 h) produces the corresponding borane **5** which undergoes a smooth boron–zinc exchange reaction with diethylzinc (2 equiv, 0 °C, 20 min) leading to the mixed chromium/zinc bimetallic species **6** (Scheme 3). The treatment of **6** with D₂O at 0 °C affords the deuterated chromium complex **7** in 67% yield with 100% of deuterium incorporation. Iodolysis of **6** at –78 °C furnishes the iodinated chromium carbene complex **8** in 43% yield.

It is well-known that deprotonation at the carbon in the α-position of a carbene complex leads to an enolate equivalent,¹⁰ but this is, to our knowledge, the first time that a carbanionic center could be generated in a different position.

In summary, we have developed a new synthesis of chromium carbene complexes by using the addition of readily available diorganozincs to Cr(CO)₅·THF. Although the yields are moderate in comparison to the Fischer method (i.e., based on alkyl group transfer) our new approach shows a remarkable functional group tolerance. The preparation of mixed zinc/chromium bimetallics has been performed to demonstrate the potential utility of dialkylzincs in the chemistry of carbene complexes.

Experimental Section

General. All reactions were strictly carried out under an inert atmosphere. THF was freshly distilled over potassium/benzophenone. Ether was dried and distilled from sodium/benzophenone. Dichloromethane and hexane were dried and distilled over CaH₂. Fourier transform infrared spectra (FT-IR) were recorded on a Nicolet 511 spectrometer. Proton and carbon nuclear magnetic resonance spectra (¹H- and ¹³C-NMR) were recorded on Bruker AC-300, WH 400, and AMX 500 spectrometers. Radial chromatography was performed with a chromatotron (7924T, Harrison Research) on Merck silica gel (60 PF₂₅₀).

Starting Materials. The following starting materials were prepared according to literature procedures: 5-iodopentyl acetate,¹¹ 4-iodobutyl pivalate,¹¹ 5-bromopentene,¹² dibutylzinc,¹³ diisopropylzinc,¹³ bis(4-pentenyl)zinc,¹³ diphenylzinc,¹³ diethylborane,^{8,9} and trimethyloxonium tetrafluoroborate.¹⁴

General Procedure for the Preparation of Functionalized Dialkylzincs using an Iodine–Zinc Exchange. A Schlenk flask equipped with an argon inlet and a septum cap was charged with CuI (2 mg, ca. 0.01 mmol), the functionalized iodide (8.0 mmol), and Et₂Zn (1.2 mL, 12 mmol, 1.5 equiv). The reaction mixture was warmed to 50 °C and stirred for 8 h at this temperature. The Schlenk flask was connected to the vacuum (0.1 mmHg), and the excess Et₂Zn and formed EtI were collected in a trap cooled with liquid N₂. This operation required ca. 2 h at 50 °C. In the case of the bis(4-chlorobutyl)zinc, the removal of the by-products in vacuum was performed at 40 °C. The resulting dialkylzinc was diluted in THF (5 mL) and was ready to use. A yield of ca. 90% was found by running

(9) Köster, R.; Griasnow, G.; Larbig, W.; Binger, P. *Liebigs Ann. Chem.* **1964**, 627, 1.

(10) (a) Kreiter, C. G.; *Angew. Chem., Int. Ed. Engl.* **1968**, 7, 390. (b) Casey, C. P.; Boggs, R. A.; Anderson, R. L. *J. Am. Chem. Soc.* **1972**, 94, 8947.

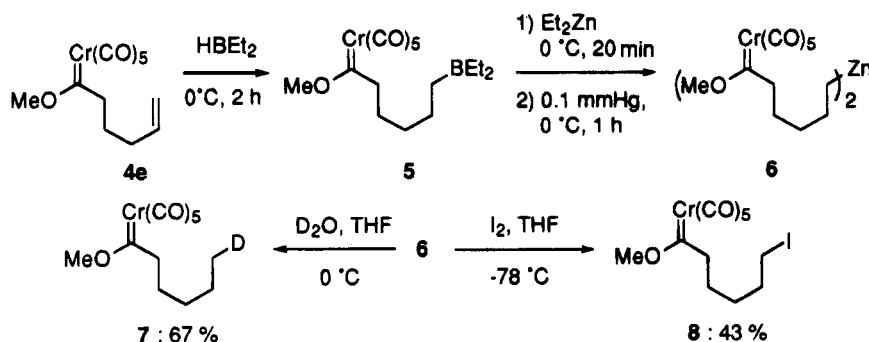
(11) Oku, A.; Harada, T.; Kita, K. *Tetrahedron Lett.* **1982**, 23, 681.

(12) (a) Brooks, L. A.; Snyder, H. R. *Organic Synthesis*; Pergamon: New York, 1945; Vol. 25, 84. (b) Smith, L. M.; Smith, R. G.; Loehr, T. M.; Daves, G. D. *J. Org. Chem.* **1978**, 43, 2464.

(13) Nützel, K. In *Methoden der Organischen Chemie*; Houben-Weyl Thieme Verlag: Stuttgart, Germany, 1973; Vol. 13/2, p 552.

(14) Curphy, T. J. *Organic Synthesis*; Pergamon: New York, 1988; Collective Vol. 6, 1019.

Scheme 3



the reaction in presence of an internal standard and by performing an iodolysis of a reaction aliquot.

General Procedure for the Preparation of Functionalized Dialkylzincs using a Hydroboration/Boron-Zinc Exchange Sequence. Bis(5-bromopentyl)zinc. A 25 mL two-neck flask equipped with an argon inlet and a rubber septum was charged with 5-bromopentene (1.20 g, 8.05 mmol) and cooled to 0 °C. Diethylborane (2.7 mL of a 3.0 molar solution in ether, 8.05 mmol) was added at once, and the solution was stirred for 0.5 h. The cooling bath was removed, and the solution was stirred for 0.3 h. The solvent was removed in vacuum for 1 h. The borane solution was cooled back to 0 °C, Et₂Zn (2.0 g, 1.6 mL, 16 mmol) was added, and the solution was stirred for 0.5 h. The excess Et₂Zn and the formed BEt₃ were carefully removed under vacuum at room temperature for 2 h. The resulting dialkylzinc was dissolved in THF (5 mL) and was ready to use. The yield of zinc reagent was determined by performing an iodolysis of a reaction aliquot.

General Procedure for the Preparation of the Chromium Carbene Complexes 4. Chromium hexacarbonyl (440 mg, 2.0 mmol) was dissolved in THF (180 mL). The solution was irradiated (Leybold Heraeus high-pressure mercury lamp, Pyrex) for 90 min at room temperature. The orange chromium pentacarbonyl tetrahydrofuran complex was obtained in ca. 90% yield as judged by IR spectroscopy. The dialkylzinc (ca. 4.0 mmol, 2 equiv) was then added. After stirring the reaction mixture for 2 h at room temperature, carbon monoxide was slowly bubbled through the deep red colored reaction mixture. The completion of the reaction was monitored by IR spectroscopy. After ca. 2 h of stirring, the yellow brown reaction mixture was connected to a vacuum and the solvent was evaporated. The residue was dissolved in dry CH₂Cl₂, cooled to -30 °C and trimethylxonium tetrafluoroborate (1.11 g, 8.40 mmol, 2.1 equiv) was added. The cooling bath was removed, and the heterogeneous reaction mixture was stirred for 10 h at 0 °C. The reaction mixture was filtered through a pad of silica gel, and the solvent was removed under vacuum. The crude residue was purified by radial chromatography affording the >95% pure chromium carbene complex as an orange oil.

Analytical Data for the Chromium Carbene Complexes 4a-i. **Pentacarbonyl(methoxyethylcarbene)chromium(0) (4a)**¹⁵ was prepared from diethylzinc (0.41 mL, 4.0 mmol). After radial chromatography (hexanes), **4a** (210 mg, 40% yield) was isolated as an orange oil. IR (hexanes): 2056 (m), 1963 (s), 1949 (s). ¹H-NMR (CDCl₃, 300 MHz): δ 4.72 (s, 3H), 3.28 (q, *J* = 7.4 Hz, 2H), 0.96 (t, *J* = 7.4 Hz, 3H). ¹³C-NMR (CDCl₃, 75 MHz): δ 363.7, 222.9, 216.3, 67.5, 55.8, 10.2. MS (EI): 264 (M⁺, 7), 152 (16), 124 (86), 109 (11). HRMS (EI) C₉H₈CrO₆: calcd, 263.9746; found, 263.9736.

Pentacarbonyl(butylmethoxycarbene)chromium(0) (4b) was prepared from dibutylzinc (720 mg, 4.0 mmol). After radial chromatography (hexanes), the carbene complex **4b** (250 mg, 43% yield) was isolated as an orange oil. IR (hexanes): 2064 (m), 1962 (s), 1948 (s). ¹H-NMR (CDCl₃, 300 MHz): δ

4.70 (s, 3H), 3.27–3.21 (m, 2H), 1.46–1.21 (m, 4H), 0.85 (t, *J* = 7.2 Hz, 3H). ¹³C-NMR (CDCl₃, 75 MHz): δ 363.9, 223.2, 216.4, 67.5, 62.8, 28.4, 22.4, 13.8. MS (EI): 292 (M⁺, 8), 236 (10), 180 (22), 152 (98), 107 (11). Anal. Calcd for C₁₁H₁₂CrO₆ (292.21): C, 45.21; H, 4.14. Found: C, 45.08; H, 4.22.

Pentacarbonyl(isopropylmethoxycarbene)chromium(0) (4c)¹⁶ was prepared from diisopropylzinc (610 mg, 4.0 mmol). After radial chromatography (hexanes), the carbene complex **4c** (250 mg, 0.90 mmol, 45% yield) was isolated as a yellow crystalline powder (mp 53 °C). IR (hexanes): 2065 (m), 1963 (s), 1948 (s). ¹H-NMR (CDCl₃, 300 MHz): δ 4.72 (s, 3H), 4.12 (septet, *J* = 6.6 Hz, 1H), 0.92 (d, *J* = 6.6 Hz, 6H). ¹³C-NMR (CDCl₃, 75 MHz): δ 367.6, 223.1, 216.2, 67.8, 18.0. MS (EI): 278 (M⁺, 5), 166 (14), 138 (55), 93 (20), 80 (21), 71 (11), 52 (100). Anal. Calcd for C₁₀H₁₀CrO₆ (278.18): C, 43.18; H, 3.62. Found: C, 43.41; H, 3.80.

Pentacarbonyl(methoxyphenylcarbene)chromium(0) (4d)¹⁷ was prepared from diphenylzinc (880 mg, 4.0 mmol). After radial chromatography (hexanes), the carbene complex **4d** (220 mg, 0.7 mmol, 35% yield) was isolated as an orange crystalline powder (mp 45 °C). IR (hexanes): 2064 (m), 1965 (s), 1955 (s), 1944 (s). ¹H-NMR (CDCl₃, 300 MHz): δ 7.40–7.19 (m, 5H), 4.65 (s, 3H). ¹³C-NMR (CDCl₃, 75 MHz): δ 351.1, 224.1, 216.2, 153.8, 130.3, 128.2, 123.0, 67.1. MS (EI): 312 (M⁺, 1), 256 (10), 200 (19), 172 (85), 157 (14), 129 (65). Anal. Calcd for C₁₃H₈CrO₆ (312.20): C, 50.01; H, 2.58. Found: C, 49.86; H, 2.70.

Pentacarbonyl[methoxy(4-pentenyl)carbene]chromium(0) (4e) was prepared from bis(4-pentenyl)zinc (820 mg, 4.0 mmol). After radial chromatography (hexanes), the carbene complex **4e** (230 mg, 0.76 mmol, 38% yield) was isolated as an orange oil. IR (hexanes): 2065 (m), 1963 (s), 1948 (s), 1638 (w). ¹H-NMR (CDCl₃, 300 MHz): δ 5.70 (ddt, *J* = 17.0, 10.2, 6.7 Hz, 1H), 5.00–4.92 (m, 2H), 4.71 (s, 3H), 3.28–3.23 (m, 2H), 2.04–1.97 (m, 2H), 1.60–1.47 (m, 2H). ¹³C-NMR (CDCl₃, 75 MHz): δ 363.4, 223.0, 216.3, 137.5, 115.5, 67.5, 62.3, 33.1, 25.4. MS (EI): 304 (M⁺, 11), 220 (13), 164 (43), 111 (20). Anal. Calcd for C₁₂H₁₂CrO₆ (304.22): C, 47.38; H, 3.97. Found: C, 47.30; H, 4.02.

Pentacarbonyl[(4-chlorobutyl)methoxycarbene]chromium(0) (4f) was prepared from bis(4-chlorobutyl)zinc (ca. 4 mmol). After radial chromatography (hexanes), the carbene complex **4f** (270 mg, 0.82 mmol, 35% yield) was isolated as an orange oil. IR (hexanes): 2065 (m), 1964 (s), 1950 (s), 663 (w). ¹H-NMR (CDCl₃, 300 MHz): δ 4.73 (s, 3H), 3.47 (t, *J* = 6.3 Hz, 2H), 3.31–3.26 (m, 2H), 1.79–1.53 (m, 4H). ¹³C-NMR (CDCl₃, 75 MHz): δ 363.3, 223.0, 216.3, 67.8, 61.9, 44.5, 31.9, 23.5. MS (EI): 328 (M⁺, 6), 326 (M⁺, 18), 186 (82), 118 (60), 99 (100). Anal. Calcd for C₁₁H₁₁ClCrO₆ (326.65): C, 40.45; H, 3.39. Found: C, 40.65; H, 3.32.

Pentacarbonyl[(5-bromopentyl)methoxycarbene]chromium(0) (4g) was prepared from bis(5-bromopentyl)zinc (ca. 4.0 mmol). After radial chromatography (hexanes), the

(16) Fischer, E. O.; Plabst, D. *Chem. Ber.* **1974**, *107*, 3326.

(17) Fischer, E. O.; Heckel, B.; Dütz, K. H.; Müller, J.; Werner, H. *J. Organomet. Chem.* **1969**, *16*, P 29.

(15) Fischer, E. O.; Fischer, H. *Chem. Ber.* **1974**, *107*, 657.

carbene complex (297 mg, 0.79 mmol, 39% yield) was isolated as an orange oil. IR (hexanes): 2065 (m), 1963 (s), 1949 (s), 649 (m). $^1\text{H-NMR}$ (CDCl_3 , 300 MHz): δ 4.72 (s, 3H), 3.33 (t, $J = 6.7$ Hz, 2H), 3.28–3.23 (m, 2H), 1.83–1.74 (m, 2H), 1.50–1.34 (m, 4H). $^{13}\text{C-NMR}$ (CDCl_3 , 75 MHz): δ 362.9, 222.9, 216.2, 67.5, 62.5, 33.1, 32.2, 27.5, 25.2. MS (EI): 386 ($M + 1$, 10), 385 (M^+ , 3), 384 ($M - 1$, 12), 244 (64), 162 (56), 113 (100). Anal. Calcd for $\text{C}_{12}\text{H}_{13}\text{BrCrO}_6$ (385.13): C, 37.42; H, 3.40. Found: C, 37.40; H, 3.41.

Pentacarbonyl[methoxy(4-pivaloxybutyl)carbene]chromium(0) (4h) was prepared from bis(4-pivaloxybutyl)zinc (ca. 4.0 mmol). After radial chromatography (hexanes/ether, 10:1) the carbene complex **4h** (273 mg, 0.7 mmol, 35% yield) was isolated as an orange oil. IR (hexanes): 2065 (m), 1962 (s), 1945 (s), 1737 (s). $^1\text{H-NMR}$ (CDCl_3 , 300 MHz): δ 4.72 (s, 3H), 4.00 (t, $J = 6.0$ Hz, 2H), 3.30–3.25 (m, 2H), 1.62–1.44 (m, 4H), 1.13 (s, 9H). $^{13}\text{C-NMR}$ (CDCl_3 , 75 MHz): δ 363.0, 222.9, 216.3, 178.4, 67.7, 63.7, 62.4, 38.7, 28.3, 27.1, 22.8. MS (EI): 392 (M^+ , 0.3), 308 (1), 252 (24), 237 (13), 209 (12), 153 (56), 103 (13). Anal. Calcd for $\text{C}_{16}\text{H}_{20}\text{CrO}_8$ (392.33): C, 48.98; H, 5.14. Found: C, 48.91; H, 5.24.

Pentacarbonyl[(5-acetoxypentyl)methoxycarbene]chromium(0) (4i) was prepared from bis(5-acetoxypentyl)zinc. After radial chromatography (hexanes/ether, 10:1 to 4:1) the carbene chromium complex **4i** (280 mg, 0.77 mmol, 38% yield) was isolated as an orange oil. IR (CDCl_3): 2062 (m), 1936 (s), 1729 (m). $^1\text{H-NMR}$ (CDCl_3 , 300 MHz): δ 4.72 (s, 3H), 4.00 (t, $J = 6.6$ Hz, 2H), 3.28–3.23 (m, 2H), 1.99 (s, 3H), 1.62–1.28 (m, 6H). $^{13}\text{C-NMR}$ (CDCl_3 , 75 MHz): δ 363.3, 223.1, 216.5, 171.2, 67.7, 64.1, 62.9, 28.4, 25.6, 21.0. MS (EI): 296 (13), 253 (23), 180 (12), 142 (22), 111 (39). Anal. Calcd for $\text{C}_{14}\text{H}_{16}\text{CrO}_8$ (364.27): C, 46.16; H, 4.43. Found: C, 45.98; H, 4.51.

Hydroboration and Boron–Zinc Exchange of the Unsaturated Chromium Carbene Complex 4e: Preparation of the Diorganozinc 6. A 10 mL two-neck flask equipped with an argon inlet and a rubber septum was charged with the chromium carbene complex **4e** (230 mg, 0.76 mmol) and was cooled to 0 °C. Diethylborane (0.26 mL of a 3 M solution in ether, 0.78 mmol) was added via syringe, and the resulting solution was stirred at 0 °C for 2 h. The solvent was pumped off under vacuum at room temperature for 1 h. The borane was cooled back to 0 °C, diethylzinc (0.20 g, 0.16 mL, 1.59 mmol, 2 equiv) was added, and the reaction mixture was stirred for 0.5 h. The triethylborane that formed was carefully removed under vacuum for 2 h, and the resulting zinc reagent **6** was dissolved in THF (3 mL) and was ready to use.

Deuteriation of 6: Preparation of Pentacarbonyl[(5-deuteriopentyl)methoxycarbene]chromium(0) (7). The zinc reagent **6** (0.38 mmol) prepared as described above was cooled to 0 °C, and deuterium oxide (200 mg, 0.2 mL, 10 mmol) was added dropwise. After 1 min, the reaction mixture was filtered through a pad of silica gel, and the residue obtained after evaporation (0.1 mmHg) of the solvent was purified by radial chromatography (hexane). The chromium carbene complex **7** (156 mg, 0.51 mmol, 67% yield) was isolated as an orange oil. IR (hexanes): 2064 (m), 1965 (s), 1922 (s). $^1\text{H-NMR}$ (CDCl_3 , 500 MHz): δ 4.74 (s, 3H), 3.30–3.25 (m, 2H), 1.48–1.42 (m, 2H), 1.28–1.22 (m, 4H), 0.87–0.81 (m, 2H). $^2\text{H-NMR}$ (CDCl_3 , 78 MHz): δ 0.90 (s, 1D). $^{13}\text{C-NMR}$ (CDCl_3 , 75 MHz): δ 363.8, 223.1, 216.4, 67.5, 63.0, 31.3, 26.0, 22.3, 13.5 (t, $J = 19.2$ Hz, $\text{CH}_2\text{-D}$). MS (EI): 308 ($M + 1$, 1), 307 (M^+ , 6), 279 (6), 195 (18), 167 (100). Anal. Calcd for $\text{C}_{12}\text{H}_{13}\text{DCrO}_6$ (307.24): C, 46.91; H, 4.92. Found: C, 46.67; H, 4.97.

Iodolysis of 6: Preparation of Pentacarbonyl[(5-iodopentyl)methoxycarbene]chromium(0) (8). The zinc reagent **6** (0.34 mmol) prepared as described above was cooled to –78 °C, and a solution of iodine (139 mg, 0.55 mmol) in THF (5 mL) was added at once. Diethylzinc (0.03 mL, 0.3 mmol) was added, and the reaction mixture was filtered after 1 min through a silica gel pad. The residue obtained after evaporation of the solvent was purified by radial chromatography, affording the chromium carbene complex **8** (127 mg, 0.29 mmol, 43% yield) as an orange oil. IR (hexanes): 2065 (m), 1963 (s), 1949 (s). $^1\text{H-NMR}$ (CDCl_3 , 400 MHz): δ 4.77 (s, 3H), 3.33–3.28 (m, 2H), 3.17 (t, $J = 6.9$ Hz, 2H), 1.84–1.76 (m, 2H), 1.53–1.35 (m, 4H). $^{13}\text{C-NMR}$ (CDCl_3 , 100 MHz): δ 363.0, 223.0, 216.3, 67.7, 62.6, 33.0, 30.0, 25.1, 6.4. MS (EI): 432 (M^+ , 3), 292 (60), 210 (37), 164 (33), 113 (100). Anal. Calcd for $\text{C}_{12}\text{H}_{13}\text{ICrO}_6$ (432.13): C, 33.35; H, 3.03. Found: C, 33.14; H, 3.19.

Acknowledgment. We thank the Fonds der Chemischen Industrie, the DFG (SFB 260) for generous support of this research, and WITCO (Bergkamen) and BASF AG (Ludwigshafen) for their generous gift of chemicals.

Supporting Information Available: ^1H - and ^{13}C -NMR spectral data for all products (23 pages). Ordering information is given on any current masthead page.

OM950120T

Organic Syntheses via Transition Metal Complexes. 79.¹ Aminomethylenation of [2-(NH-Amino)ethenyl]carbene Complexes of Chromium and Tungsten

Rudolf Aumann,* Beate Jasper, and Roland Fröhlich

Organisch-Chemisches Institut der Universität Münster,
Orléans-Ring 23, D-48149 Münster, Germany

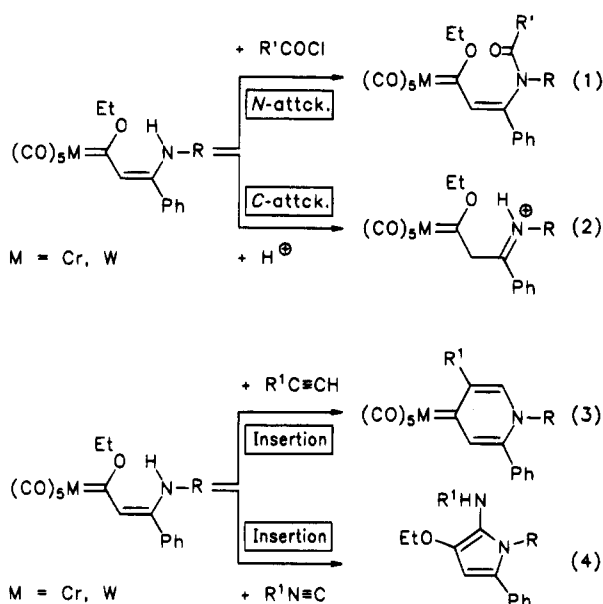
Received February 10, 1995[®]

[2-(NH-Amino)ethenyl]carbene complexes $(\text{CO})_5\text{M}=\text{C}(\text{OEt})-\text{CH}=\text{C}(\text{NHR})\text{Ph}$, **1a–d** ($\text{M} = \text{Cr}, \text{W}$; $\text{R} = \text{Ph}, p\text{-Tol}$), undergo a ring-closure to oxazin-6-ylidene complexes **3a–d** (60%–70%) on aminomethylenation with dimethylmethyleammonium iodide (**2**) in the presence of triethylamine. Compounds **1a,b** ($\text{R} = \text{Ph}$) afford [2-amino-1-(iminoacyl)ethenyl]carbene complexes $(\text{CO})_5\text{M}=\text{C}(\text{OEt})-\text{C}[\text{C}(\text{Ph})=\text{NPh}]=\text{CHNR}_2$ (*E*)-**5a–e** ($\text{NR}_2 = \text{NMe}_2$, pyrrolidine, morpholine) in 61%–83% yield by *C*-aminomethylenation with formamides $\text{HCO}-\text{NR}_2$, **4a–c**, in the presence of benzoyl chloride and triethylamine. Alkynylcarbene complexes **6** are obtained as by-products. The pyrrolidine tungsten derivative (*E*)-**5c** forms yellow and red crystals from pentane, which according to X-ray analyses are different modifications of the same molecule, $\text{C}_{27}\text{H}_{24}\text{N}_2\text{O}_6\text{W}$, red (yellow), monoclinic (triclinic), space group $\text{C}2/c$ (No. 15) ($\text{P}\bar{1}$ (No. 2)), $Z = 8$ (4), both of which contain a 1-metalla-1,3-diene unit in *s-cis* conformation. Thermolysis of the pentacarbonyl complex (*E*)-**5d** affords a tetracarbonyl chelate complex (*E*)-**7d**, in which the 1-metalla-1,3-diene unit is fixed in *s-trans* conformation. The latter compound is readily oxidized by air to give an aminoacrylate (*E*)-**8d** in >90% yield.

In connection with studies on the reactivity of aminocarbene complexes, we are currently probing the applicability of [2-(NH-amino)ethenyl]carbene complexes as building blocks for organic synthesis. Among the reactions studied so far are (a) the “activation” of the $\text{M}=\text{C}$ bond by *N*-acylation [which affords (2-acylaminoethenyl)carbene complexes (Scheme 1, eq 1)],² (b) the *C*-protonation at the β -carbon atom of the enamine unit [which yields stable iminium salts (Scheme 1, eq 2)],³ (c) the cyclization by addition of alkynes [with formation of 4(1*H*)-pyridinylidene complexes and pyridinium salts (Scheme 1, eq 3)],^{4,5} and (d) the cyclization by addition of isocyanides, which produces 2-aminopyrroles (Scheme 1, eq 4).⁶

[2-(NH-Amino)ethenyl]carbene complexes $(\text{CO})_5\text{M}=\text{C}(\text{OEt})-\text{CH}=\text{C}(\text{NHR})\text{R}^1$ ($\text{M} = \text{Cr}, \text{W}$) take an exceptional position within the class of enamino carbene complexes^{7–11} insofar as the *NH*-enamino carbene ligand may be modified by electrophilic attack at the β -carbon

Scheme 1. Selected Reactions of (2-(NH-Amino)ethenyl)carbene Complexes with Electrophiles



atom as well as at the nitrogen of the enamine unit. Not only are these compounds readily available as starting material [by Michael-addition of primary amines H_2NR to alkynylcarbene complexes $(\text{CO})_5\text{M}=\text{C}(\text{OEt})-\text{C}\equiv\text{CR}^{12}$ or by aminomethylenation of methylcarbene complexes $(\text{CO})_5\text{M}=\text{C}(\text{OEt})\text{CH}_3$ ($\text{M} = \text{Cr}, \text{W}$)

[®] Abstract published in *Advance ACS Abstracts*, June 1, 1995.

(1) Part 78: Aumann, R.; Jasper, B.; Fröhlich, R. *Organometallics* **1995**, in press.

(2) Aumann, R.; Jasper, B.; Goddard, R.; Krüger, C. *Chem. Ber.* **1994**, *127*, 717–724.

(3) Aumann, R.; Hinterding, P.; Krüger, C.; Betz, P. *Chem. Ber.* **1990**, *123*, 1847–1852.

(4) Aumann, R.; Hinterding, P. *Chem. Ber.* **1992**, *125*, 2765–2772.

(5) Duetsch, M.; Stein, F.; Funke, F.; Pohl, E.; Herbst-Irmer, R.; de Meijere, A. *Chem. Ber.* **1993**, *126*, 2535–2541.

(6) (a) Aumann, R. *Chem. Ber.* **1993**, *126*, 2325–2330. (b) Aumann, R. *Chem. Ber.* **1994**, *127*, 725–729.

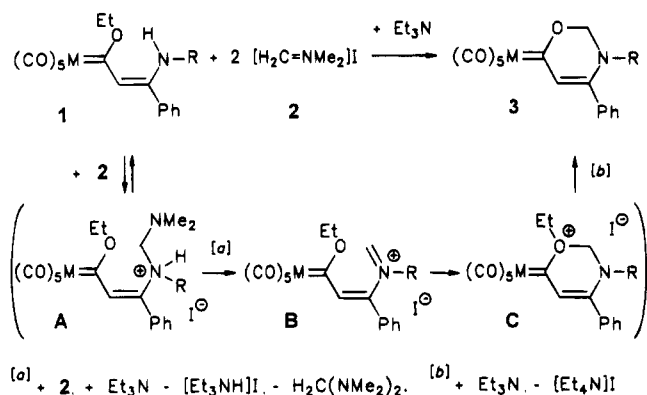
(7) (a) Fischer, E.-O.; Kreissl, F. R. *J. Organomet. Chem.* **1975**, *57*, C47–C52. (b) Fischer, E.-O.; Kalder, H. *J. Organomet. Chem.* **1977**, *131*, 57–64.

(8) Lattuada, L.; Licandro, E.; Papagni, A.; Maiorana, S.; Villa, A. C.; Guastini, C. *J. Chem. Soc., Chem. Commun.* **1988**, 1092–1093.

(9) (a) Stein, F.; Duetsch, M.; Pohl, E.; Herbst-Irmer, R.; de Meijere, A. *Organometallics* **1993**, *12*, 2556–2564. (b) Duetsch, M.; Stein, F.; Lackmann, R.; Pohl, E.; Herbst-Irmer, R.; de Meijere, A. *Chem. Ber.* **1992**, *125*, 2051–2065. (c) Duetsch, M.; Stein, F.; Lackmann, R.; de Meijere, A. *Synlett* **1992**, 324–326. (d) Stein, F.; Duetsch, M.; Noltemeyer, M.; de Meijere, A. *Synlett* **1993**, 486–488.

(10) (a) Camps, F.; Llebaria, A.; Moretó, J. M.; Ricart, S.; Viñas, J. M. *Tetrahedron Lett.* **1990**, *31*, 2479–2481. (b) Camps, F.; Jordi, L.; Moretó, J. M.; Ricart, S.; Castaño, A. M.; Echavarren, A. M. *J. Organomet. Chem.* **1992**, *436*, 189–192.

(11) Rahm, A.; Wulff, W. D.; Rheingold, A. L. *Organometallics* **1993**, *12*, 597–599.

Scheme 2. 1,3-Oxazin-6-ylidene Complexes 3 by Aminomethylation of 1 with Iminium Salt 2


with acid amides $\text{O}=\text{C}(\text{R}^1)\text{NHR}$,¹³ but they are also obtained stereochemically uniform in the (*Z*) configuration, which is stabilized by a hydrogen bridge between the NH group and the OEt moiety. By analogy to the *C*-aminomethylation of methylcarbene complexes,^{8,13} the *N*-aminomethylation of aminocarbene complexes $(\text{CO})_5\text{M}=\text{C}(\text{Ph})\text{NH}_2$ ($\text{M} = \text{Cr}, \text{W}$) with acid amides $\text{O}=\text{C}(\text{R})\text{NMe}_2$ leads to formation of iminocarbene complexes $(\text{CO})_5\text{M}=\text{C}(\text{Ph})\text{N}=\text{C}(\text{R})\text{NMe}_2$.¹⁴ Since aminomethylation has proven a powerful tool to organic synthesis,¹⁵ we have extended our studies of the aminomethylation of carbene complexes to include [2-(*NH*-amino)ethenyl]carbene derivatives 1. Considering conventional reactivity of an enamine function, one may anticipate *C*- and/or *N*-aminomethylation of these compounds, depending on the reagent used.

Aminomethylation of 1 with a Methyleneammonium Salt. [2-(*NH*-Amino)ethenyl]carbene complexes 1 react with dimethylmethyleneammonium iodide (2) in the presence of triethylamine to give 1,3-oxazin-6-ylidene complexes 3 (Scheme 2). It can be demonstrated by TLC that the red starting complex 1 is gradually transformed into the brown product 3 within 2–3 h at 0 °C. Taking into account that 2 equivs of 2 and also a base are required for the reaction to proceed, we tentatively suggest initial formation of an *N*-adduct A, from which an NMe_2 group is extracted by the second equivalent of 2 to give B [and an aminal $\text{H}_2\text{C}(\text{NMe}_2)_2$] (Scheme 2). Cyclization of B to 3 may involve the generation of an oxonium salt intermediate C, from which the ethyl group may be disengaged by nucleophilic attack, e.g., of Et_3N (or I^-). This route to compounds 3 gains interest in view of the high variability of the $\text{M}=\text{C}$ bond as a functional group and the attention that 1,3-oxazines have received as potential antitumor agents.¹⁶

(12) (a) For the stereochemistry of the addition of *secondary* amines, see refs. 7 and 9. (b) For the stereochemistry of the addition of *primary* amines, see: Aumann, R.; Hinterding, P. *Chem. Ber.* **1993**, *126*, 421–427.

(13) Aumann, R.; Hinterding, P. *Chem. Ber.* **1990**, *123*, 611–620.

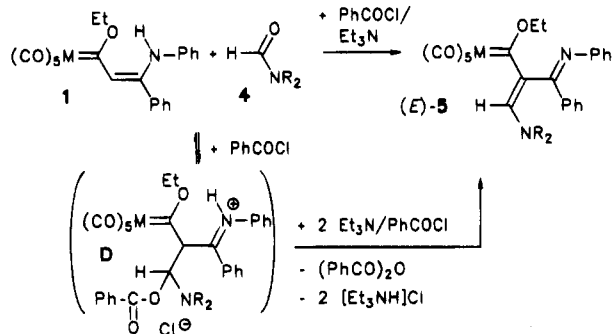
(14) Aumann, R.; Althaus, S.; Krüger, C.; Betz, P. *Chem. Ber.* **1989**, *122*, 357–364.

(15) (a) Böhme, H.; Viehe, H. In *Advances in Organic Chemistry: Methods and Results*; Taylor, E., Ed.; Wiley and Sons: New York, 1979; Vol. 9, pp 225–342. (b) Böhme, H.; Viehe, H. In *Advances in Organic Chemistry: Methods and Results*; Taylor, E., Ed.; Wiley and Sons: New York, 1979, 9, 393–526. (c) Danishefsky, S.; Kitahara, T.; McKee, R.; Schuda, P. *J. Am. Chem. Soc.* **1976**, *98*, 6715. (d) Kinast, G.; Tietze, L. *Angew. Chem., Int. Ed. Engl.* **1976**, *15*, 239.

(16) Motohashi, N.; Mitscher, L. A.; Meyer, R. *Med. Res. Rev.* **1991**, *11*, 239–294.

Scheme 3. Aminomethylation of 1 with Formamides 4

C-aminomethylation (*main rxn*):



N-aminomethylation (*side rxn*):

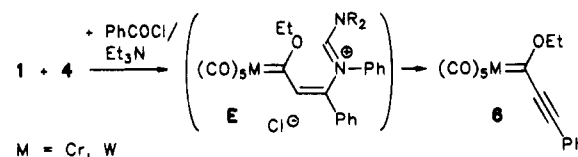


Table 1. Substitution Patterns and Chemical Yields of 3

1,3	M	R	3 [%]
a	W	Ph	65
b	Cr	Ph	70
c	W	p-Tol	60
d	Cr	p-Tol	64

Table 2. Substitution Patterns and Product Ratio (E)-5/6

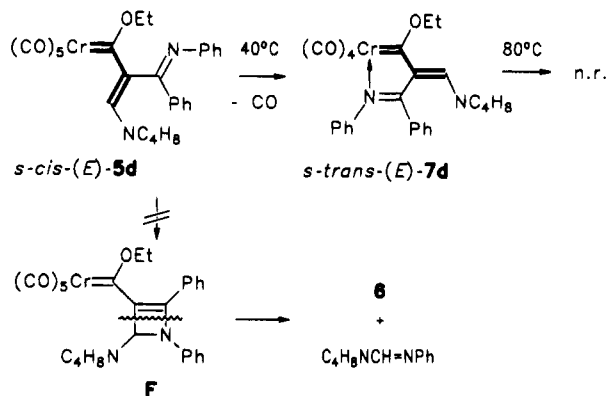
4	NR ₂	4	NR ₂
a	NMe ₂	c	morpholine
b	pyrrolidine		

(E)-5	M	NR ₂	(E)-5 [%]	6a,b [%]
a	W	NMe ₂	83	6
b	Cr	NMe ₂	78	9
c	W	pyrrolidine	65	25
d	Cr	pyrrolidine	61	30
e	W	morpholine	69	22

C- and N-Aminomethylation of 1 with Formamides. While *N*-aminomethylation of [2-(*NH*-amino)ethenyl]carbene complexes 1 can be achieved by reaction with an iminium salt 2 (Scheme 2), *C*-aminomethylation of compounds 1a,b to give [2-amino-1-(iminoacyl)ethenyl]carbene complexes (E)-5a–e becomes the major route if formamides 4a–c are added in presence of benzoyl chloride and triethylamine (Scheme 3). Compounds 5 seem to arise from Vilsmeier-like addition to the enamine unit of 1 via an intermediate of type D. Since benzoyl chloride/triethylamine is not commonly used in such connection, it should be noted that (stable) *N*-benzoyl derivatives² are obtained if the reaction is carried out in absence of a formamide 4.

Alkynylcarbene complexes 6a,b are produced as by-products (Scheme 3) in amounts that increase with the bulkiness of substituents on the nitrogen atom of the formamide 4 (Table 2). Since formation of alkynylcarbene complexes by β -elimination of, e.g., enolacetates, has been observed before,¹⁷ we assume that compounds 6 might arise from *N*-aminomethylation of 1 via an

Scheme 4. Configurational Change of Metalladiene Unit on Conversion of (*E*)-5d into Chelate Complex (*E*)-7d



iminium salt **E**, which is expected to be less prone to cyclization than a more electrophilic species **B** (Scheme 2), and therefore seems to undergo a (base-induced) β -elimination with formamidine $\text{CH}(\text{=NPh})\text{NR}_2$ as leaving group instead.

Chelate Complex (*E*)-7d. It can be excluded that pentacarbonyl complex (*E*)-5 serves as a precursor to **6**, e.g., via the fragmentation of a hypothetical azete intermediate **F**, since compound (*E*)-5d readily affords thermally quite stable tetracarbonyl chelate complex (*E*)-7d (Scheme 4) thermally (20–40 °C in C_6D_6) or if irradiated with 300 nm UV light. The *C*-aminomethylenation of **1a,b** with formamides **4a–c** is highly stereoselective and yields 1-metalla-1,3-dienes **5** of (*E*) configuration only.¹³ An (*E/Z*) interconversion to a significant extent could not be detected by ^1H NMR measurements even at 80 °C and after 20 h in C_6D_6 . By extrusion of carbon monoxide (*E*)-5d and subsequent chelation of the 1-metalladiene unit the conformation changes from *s-cis* in the (yellow) pentacarbonylchromium complex (*E*)-5d to *s-trans* in the (brown) chelate complex (*E*)-7d.

The structural assignment of (*E*)-7d is based on the ^{13}C NMR spectrum, above all on the 1:1:2 pattern of carbonyl signals typical for a *cis*- $\text{Cr}(\text{CO})_4$ group, and the low-field signal shift of the $\text{Cr}=\text{C}$ [(*E*)-7d, δ 323.6, (*E*)-5d, δ 293.8] and the $\text{C}=\text{N}$ group [(*E*)-7d, δ 176.7; (*E*)-5d, δ 167.8] compared to the nonchelate precursor (*E*)-5d. The strong upfield shifts of the ^1H NMR signals of the $=\text{CH}$ [(*E*)-7d, δ 6.28; (*E*)-5d, δ 8.16] and the β - CH_2 groups [(*E*)-7d, δ 1.06 and 0.94; (*E*)-5d, δ 2.50] are attributed to anisotropic shielding by the OCH_2 ¹³ and the 3-phenyl groups, respectively.

The tetracarbonyl complex (*E*)-7d is quite stable thermally, even at 80 °C for at least 50 h, but it is clearly more sensitive to oxidation than the pentacarbonyl complex (*E*)-5d. If exposed to air, compound (*E*)-7d appears to readily take up oxygen. It may form e.g. a π -complex **G**, which subsequently undergoes cleavage of the $\text{Cr}=\text{C}$ bond to give the aminoacrylate (*E*)-8d as the only detectable organic product (Scheme 5).

Crystal Structures of Alkenylcarbene Complexes *s-cis*-(*E*)-5c. The pyrrolidine tungsten derivative (*E*)-5c affords yellow and red crystals from pentane

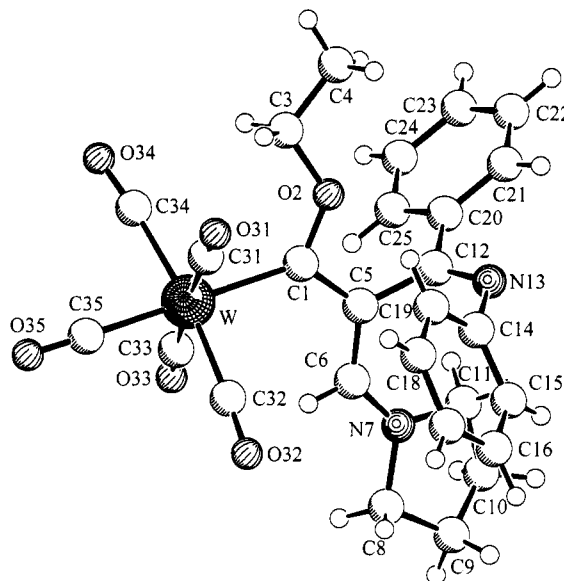


Figure 1. Molecular structure of the red modification of compounds *s-cis*-(*E*)-5c.

Scheme 5. Oxidation of (2-Aminoethenyl)carbene Complexes (*E*)-7d

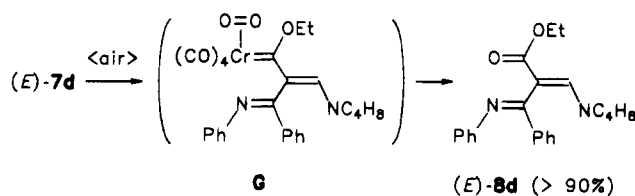


Table 3. Selected Bond Lengths [Å] and Angles [deg] of *s-cis*-(*E*)-5c and *s-trans*-(*E*)-5c

	red modification	yellow modification	
		molecule 1	molecule 2
W–C(1)	2.242(5)	2.275(8)	2.274(7)
C(1)–O(2)	1.347(6)	1.334(9)	1.345(9)
C(1)–C(5)	1.429(7)	1.440(10)	1.427(9)
O(2)–C(3)	1.437(6)	1.415(10)	1.440(9)
C(3)–C(4)	1.477(8)	1.419(13)	1.485(14)
C(5)–C(6)	1.384(7)	1.372(10)	1.385(10)
C(5)–C(12)	1.510(6)	1.509(10)	1.506(9)
C(6)–N(7)	1.326(6)	1.306(9)	1.314(9)
C(12)–N(13)	1.277(7)	1.290(10)	1.269(9)
N(13)–C(14)	1.426(7)	1.422(10)	1.433(9)
O(2)–C(1)–C(5)	105.2(4)	106.4(6)	106.5(6)
O(2)–C(1)–W	125.6(3)	125.7(5)	124.8(5)
C(5)–C(1)–W	129.1(4)	127.5(5)	127.7(5)
C(1)–O(2)–C(3)	124.6(4)	125.1(7)	123.5(6)
O(2)–C(3)–C(4)	107.2(5)	110.3(8)	107.9(8)
C(6)–C(5)–C(1)	121.5(4)	120.1(7)	118.5(6)
C(6)–C(5)–C(12)	120.6(4)	121.9(6)	124.1(6)
C(1)–C(5)–C(12)	117.6(4)	117.7(6)	117.4(6)
N(7)–C(6)–C(5)	128.5(5)	130.0(7)	132.2(7)
C(5)–C(12)–N(13)	122.1(5)	121.8(7)	126.8(6)
C(12)–N(13)–C(14)	117.6(4)	119.9(6)	122.1(6)

at –15 °C in approximately equal quantities. According to X-ray analysis (Tables 3–5), both crystal types contain the same molecular unit, in which the 1-metalla-1,3-diene adopts an *s-cis* conformation (Scheme 4). The $\text{W}=\text{C}=\text{C}=\text{N} \leftrightarrow \text{W}^--\text{C}=\text{C}=\text{C}=\text{N}^+$ unit is essentially planar [red modification, $\text{W}-\text{C}1-\text{C}5-\text{C}6$, $3.0(7)^\circ$, and $\text{C}1-\text{C}5-\text{C}6-\text{N}7$, $171.7(5)^\circ$; yellow modification, $\text{W}-\text{C}1-\text{C}5-\text{C}6$, $12.1(11)^\circ$, and $\text{C}1-\text{C}5-\text{C}6-\text{N}7$, $175.5(8)^\circ$]. The distances [e.g., red modification, $\text{W}-\text{C}1$, 2.242(5) Å; $\text{C}1-\text{C}5$, 1.429(7) Å; $\text{C}5-\text{C}6$, 1.384(7) Å; $\text{C}6-\text{N}7$, 1.326(6) Å]

(17) Aumann, R.; Jasper, B.; Läge, M.; Krebs, B. *Organometallics* 1994, 13, 3510–3516.

Table 4. Details of the X-ray Crystal Structure Analyses of (E)-5c: Data Collection and Structure Solution^a

	red modification	yellow modification
formula	C ₂₇ H ₂₄ N ₂ O ₆ W	C ₂₇ H ₂₄ N ₂ O ₆ W
a (Å)	13.399(1)	12.163(1)
b (Å)	32.970(4)	15.116(1)
c (Å)	11.999(1)	15.947(1)
α (deg)	90.00	110.82(1)
β (deg)	97.99(1)	92.68(1)
γ (deg)	90.00	101.09(1)
vol (Å ³)	5249.3(9)	2668.1(3)
diffractometer	Enraf-Nonius MACH III	
data coll temp (K)	223	223
λ (Å)	0.710 73	0.710 73
space group	C2/c (No.15)	P1̄ (No.2)
Z	8	4
μ (cm ⁻¹)	44.4	43.7
empirical abs corr	85.4%–99.9%	81.8%–99.9%
θ _{max} (deg)	26.3	26.3
no. of data collected	5554	11339
no. of unique data	5326	10807
R _{merge}	0.021	0.033
no. of data obsd (≥2σ(I))	4200	7624
no. of refined params	326	652
R1 (≥2σ(I))	0.025	0.044
wR2 (≥2σ(I))	0.075	0.142
goodness of fit	1.207	1.072

^a Programs used: SHELXS-86, SHELXL-93, and SCHAKAL-92.

are similar to those observed with cross-conjugated metallatrienes.¹⁸

Experimental Section

All operations were performed under argon. Solvents were dried by distillation from sodium/benzophenone. Melting points are uncorrected. Instrumentation: ¹H NMR and ¹³C NMR spectra were obtained with Bruker WM 300 and WP 360 spectrometers. Multiplicities were determined by DEPT. Chemical shifts refer to δ_{TMS} 0.00 ppm). Other analyses: IR Digilab FTS 45; MS Finnigan MAT 312; elemental analysis, Perkin-Elmer 240 elemental analyzer; column chromatography, Merck-Kieselgel 100; TLC, Merck DC-Alufolien Kieselgel 60 F 254. R_f values refer to TLC tests.

Pentacarbonyl(3,6-dihydro-3,4-diphenyl-1,3-oxazin-6-ylidene)tungsten (3a). To pentacarbonyl[1-ethoxy-3-phenyl-3-(phenylamino)propenylidene]tungsten¹⁹ (**1a**) (575 mg, 1.00 mmol) and dimethylmethyleammonium iodide (**2**) (463 mg, 2.50 mmol) in a 5-mL screw-top vessel is added triethylamine (404 mg, 4.00 mmol) in 3 mL of dry acetonitrile with magnetic stirring at 0 °C. A red solution is obtained, which becomes darker with reaction progress. According to a TLC test, approximately 90% of **1a** is consumed after 2 h at 20 °C. A total reaction time of 2.5–3 h is appropriate. Chromatography on silica gel with pentane/dichloromethane (10:1 to 2:1) affords a red-brown zone with **3a**: 363 mg, 65%, R_f = 0.5 in pentane/dichloromethane (3:1), brown crystals from pentane at –15 °C, mp 141 °C. ¹H NMR (C₆D₆): δ 7.43 (1 H, s, 5-H), 7.21, 6.85 and 6.76 (2:1:2 H, *o*:-*m*:-*p*-H, 4-Ph), 6.62 and 6.26 (3:2 H, *m* each, N-Ph), 4.43 (2 H, s, CH₂). ¹³C NMR (C₆D₆): δ 263.2 (W=C), 206.6 and 199.2 [1:4, *trans*- and *cis*-CO, W(CO)₅], 144.5 and 142.2 (C_q each, C4 and *i*-C N-Ph), 132.0 (C_q, *i*-C 4-Ph); 132.3, 130.3, 130.1, 129.7, 126.3, 125.1 (1:2:2:2:1:2, CH each, 2 Ph), 128.0 (CH, C-5), 82.1 (CH₂). IR (hexane), cm⁻¹ (%): ν̄ 2061.3 (30), 1975.3 (10), 1934.4 (100) [ν(C=O)]. MS (70 eV), *m/e* (%): ¹⁸⁴W: 559 (40) [M⁺], 503 (40), 475 (20), 447 (10), 419

Table 5. Atomic Coordinates (×10⁴) and Equivalent Isotropic Displacement Parameters (Å² × 10³) of (E)-5c

	x	y	z	U(eq) ^a
W	1924(1)	4587(1)	1480(1)	27(1)
C(1)	2466(4)	4105(2)	389(4)	29(1)
O(2)	3333(3)	4116(1)	-60(3)	37(1)
C(3)	3943(5)	4472(2)	-115(6)	47(2)
C(4)	4788(6)	4358(2)	-722(8)	74(2)
C(5)	2035(4)	3717(2)	85(4)	28(1)
C(6)	1136(4)	3596(2)	423(4)	30(1)
N(7)	587(3)	3270(1)	111(4)	33(1)
C(8)	-297(5)	3157(2)	648(6)	51(2)
C(9)	-646(7)	2770(3)	87(8)	89(3)
C(10)	-258(6)	2754(3)	-967(6)	75(3)
C(11)	709(5)	2991(2)	-819(5)	44(1)
C(12)	2652(4)	3425(2)	-505(4)	32(1)
N(13)	3117(3)	3126(1)	5(4)	36(1)
C(14)	3088(4)	3089(2)	1185(4)	37(1)
C(15)	2552(5)	2776(2)	1605(5)	42(1)
C(16)	2507(5)	2747(2)	2753(5)	49(2)
C(17)	3006(5)	3030(2)	3492(5)	51(2)
C(18)	3574(5)	3325(2)	3082(5)	49(2)
C(19)	3616(5)	3362(2)	1944(5)	45(1)
C(20)	2720(4)	3493(2)	-1715(5)	35(1)
C(21)	3465(5)	3302(2)	-2237(5)	47(1)
C(22)	3541(5)	3383(2)	-3351(5)	56(2)
C(23)	2885(6)	3649(2)	-3969(5)	56(2)
C(24)	2146(5)	3838(2)	-3461(5)	51(2)
C(25)	2061(5)	3761(2)	-2345(5)	42(1)
C(31)	3288(5)	4597(2)	2456(5)	53(2)
O(31)	4036(4)	4601(2)	3037(5)	107(3)
C(32)	1507(5)	4182(2)	2598(5)	42(1)
O(32)	1259(5)	3968(2)	3266(4)	70(2)
C(33)	551(4)	4542(2)	493(5)	33(1)
O(33)	-206(3)	4504(1)	-47(4)	56(1)
C(34)	2310(4)	5059(2)	507(5)	36(1)
O(34)	2499(4)	5338(1)	19(4)	52(1)
C(35)	1433(4)	5021(2)	2452(5)	37(1)
O(35)	1166(4)	5269(1)	3002(4)	57(1)

^a U(eq) is defined as one third of the trace of the orthogonalized U_{ij} tensor.

(100). Anal. Calcd for C₂₁H₁₃NO₆W (559.2): C, 45.11; H, 2.34; N, 2.50. Found: C, 45.23; H, 2.51; N, 2.62.

Pentacarbonyl(3,6-dihydro-3,4-diphenyl-1,3-oxazin-6-ylidene)chromium (3b). To pentacarbonyl[1-ethoxy-3-phenyl-3-(phenylamino)propenylidene]chromium (**1a**) (443 mg, 1.00 mmol) and dimethylmethyleammonium iodide (**2**) (463 mg, 2.50 mmol) in a 5-mL screw-top vessel is added triethylamine (404 mg, 4.00 mmol) in 3 mL of dry acetonitrile as described above. Data for **3b**: [289 mg, 70%, R_f = 0.5 in pentane/dichloromethane (3:1), brown crystals from pentane at –15 °C, mp 145 °C]. ¹H NMR (C₆D₆): δ 7.48 (1 H, s, 5-H); 7.26, 6.86 and 6.79 (2:1:2 H, *o*:-*m*:-*p*-H, 4-Ph), 6.66 and 6.33 (3:2 H, *m* each, N-Ph), 4.50 (2 H, s, CH₂). ¹³C NMR (C₆D₆): δ 288.4 (Cr=C), 224.8 and 218.8 [1:4, *trans*- and *cis*-CO, Cr(CO)₅], 142.1 and 140.2 (C_q each, C4 and *i*-C N-Ph), 132.0 (C_q, *i*-C 4-Ph); 131.7, 130.6, 129.8, 127.9, 127.2, 126.1 (1:2:2:2:1:2, CH each, 2 Ph), 129.2 (CH, C-5), 81.6 (CH₂). IR (hexane), cm⁻¹ (%): ν̄ 2054.5 (30), 1981.2 (10), 1940.5 (100) [ν(C=O)]. MS (70 eV), *m/e* (%): 427 (40) [M⁺], 371 (20), 343 (20), 315 (40), 287 (60) [M⁺ – 5 CO], 273 (20), 260 (20), 219 (40), 169 (60), 135 (60), 69 (100). Anal. Calcd for C₂₁H₁₃CrNO₆ (427.3): C, 59.02; H, 3.07; N, 3.28. Found: C, 59.05; H, 3.06; N, 3.35.

Pentacarbonyl(3,6-dihydro-4-phenyl-3-*p*-tolyl-1,3-oxazin-6-ylidene)tungsten (3c). Pentacarbonyl[1-ethoxy-3-phenyl-3-(*p*-tolylamino)propenylidene]tungsten (**1c**) (589 mg, 1.00 mmol) is reacted as described above with dimethylmethyleammonium iodide (**2**) (463 mg, 2.50 mmol) and triethylamine (404 mg, 4.00 mmol) in 3 mL of dry acetonitrile. Data for **3c**: 344 mg, 60%, R_f = 0.5 in pentane/dichloromethane (3:1), brown crystals from pentane at –15 °C, mp 146 °C. ¹H NMR (C₆D₆): δ 7.41 (1 H, s, 5-H); 7.24, 6.89 and 6.79 (2:1:2 H, *o*:-*m*:-*p*-H, 4-Ph), 6.48 and 6.26 (2:2 H, “d” each, *p*-tolyl),

(18) Aumann, R.; Roths, K.; Läge, M.; Krebs, B. *Synlett* **1993**, 667–669.

(19) Aumann, R. *Chem. Ber.* **1993**, *126*, 2325–2350.

4.48 (2 H, s, CH₂), 1.82 (3 H, s, CH₃). ¹³C NMR (C₆D₆): δ 261.3 (W=C), 205.1 and 199.7 [1:4, *trans*- and *cis*-CO, W(CO)₅], 144.6 (C_q, C-4), 139.7 and 137.7 (C_q each, *p*-tolyl), 132.2 (C_q, *i*-C 4-Ph); 131.9, 130.6, 129.3, 128.0, 125.8 (1:2:2:2:2, CH each, Ph and *p*-tolyl), 128.5 (CH, C-5), 82.1 (CH₂), 21.0 (CH₃). IR (hexane), cm⁻¹ (%): ν̄ 2061.7 (30), 1976.6 (10), 1936.7 (100) [ν(C=O)]. MS (70 eV), *m/e* (%) ¹⁸⁴W: 573 (40) [M⁺], 517 (40), 461 (10), 433 (60), 405 (50), 532 (60), 270 (70), 233 (60), 69 (100). Anal. Calcd for C₂₂H₁₅NO₆W (573.2): C, 46.10; H, 2.64; N, 2.44. Found: C, 46.32; H, 2.83; N, 2.57.

Pentacarbonyl(3,6-dihydro-4-phenyl-3-*p*-tolyl-1,3-oxazin-6-ylidene)chromium (3d). Pentacarbonyl[1-ethoxy-3-phenyl-3-(*p*-tolylamino)propenylidene]chromium (**1d**) (457 mg, 1.00 mmol) is reacted as described above with dimethylmethyleneammonium iodide (**2**) (463 mg, 2.50 mmol) and triethylamine (404 mg, 4.00 mmol) in 3 mL of dry acetonitrile. Data for **3d**: 282 mg, 64%, *R_f* = 0.4 in pentane/dichloromethane (5:1), brown crystals from pentane at -15 °C, mp 117 °C. ¹H NMR (C₆D₆): δ 7.49 (1 H, s, 5-H); 7.29, 6.83 and 6.80 (2:1:2 H, *o*-, *m*-, *p*-H, 4-Ph), 6.49 and 6.30 (2:2 H, *m* each, *p*-tolyl), 4.68 (2 H, s, CH₂), 2.02 (3 H, s, CH₃). ¹³C NMR (C₆D₆): δ 286.6 (Cr=C), 224.6 and 218.5 [1:4, *trans*- and *cis*-CO, Cr(CO)₅], 143.9 (C_q, C-4), 139.4 and 137.1 (C_q each, *p*-tolyl), 132.0 (C_q, *i*-C 4-Ph); 131.4, 130.5, 130.2, 128.7, 125.3 (1:2:2:2:2, CH each, Ph and *p*-tolyl), 128.6 (CH, C-5), 82.1 (CH₂), 21.0 (CH₃). IR (hexane), cm⁻¹ (%): ν̄ 2054.3 (25), 1979.8 (10), 1942.9 (100) [ν(C=O)]. MS (70 eV), *m/e* (%): 441 (40) [M⁺], 413 (3), 385 (20), 357 (20), 329 (40), 301 (60) [M⁺ - 5 CO], 52 (100). Anal. Calcd for C₂₂H₁₅CrNO₆ (441.4): C, 59.87; H, 3.43; N, 3.17. Found: C, 59.94; H, 3.64; N, 3.32.

Pentacarbonyl(2-[(*E*)-dimethylaminomethylene]-1-ethoxy-3-phenyl-3-(phenylimino)propan-1-ylidene)tungsten [(*E*)-5a] and Pentacarbonyl(1-ethoxy-3-phenylpropynylidene)tungsten (6a). To pentacarbonyl[1-ethoxy-3-phenyl-2-(phenylamino)propenylidene]tungsten¹⁹ (**1a**) (575 mg, 1.00 mmol) and dry dimethylformamide **4a** (146 mg, 2.00 mmol) in a 5-mL screw-top vessel is added with magnetic stirring at 20 °C a mixture of benzoyl chloride (422 mg, 3.00 mmol) and triethylamine (404 mg, 4.00 mmol) in 3 mL of dry dichloromethane. The solution gradually turns darker. According to a TLC test, compound **1a** is consumed within 20 min. The mixture is brought to dryness (20 °C, 15 Torr), and the residue is extracted with ether. Chromatography on silica with pentane/dichloromethane 2:1 yields a dark brown zone with **6a** (29 mg, 6%, brown crystals from pentane) and a yellow fraction of (*E*)-**5a**: 523 mg, 83%, *R_f* = 0.4 in pentane/dichloromethane (1:1), yellow crystals from pentane at -15 °C, mp 124 °C. ¹H NMR (C₆D₆): δ 7.90 (1 H, s, =CH); 7.73 and 7.31 (2:3 H, *m* each, 3-Ph); 7.15, 6.94 and 6.60 (2:1:2 H; "t", "t", "d", N-Ph), 4.60 (2 H, *m*, diastereotopic OCH₂), 3.15 and 3.05 (3 H each, *s* broad each, dynamically broadened NMe₂), 1.04 (3 H, *t*, CH₂CH₃). ¹³C NMR (C₆D₆): δ 278.1 (W=C), 203.4 and 200.3 [1:4, *trans*- and *cis*-CO, W(CO)₅], 169.3 (=CHNMe₂), 169.1 (C_q, C=N), 152.8 (C_q, *i*-C N-Ph), 141.0 (C_q, *i*-C 3-Ph); 131.2, 129.3, 129.1, 128.7, 124.8, 119.7 (1:2:2:2:1:2, CH each, 2 Ph), 125.5 (C_q, C-2), 72.1 (OCH₂), 49.2 and 41.2 (CH₃ each, dynamically broadened, NMe₂), 16.2 (CH₃). IR (hexane), cm⁻¹ (%): ν̄ 2058.9 (30), 1961.8 (10), 1921.1 (100) [ν(C=O)]. MS (70 eV), *m/e* (%) ¹⁸⁴W: 630 (10) [M⁺], 602 (40), 574 (40), 546 (60), 518 (20), 490 (60), 462 (50), 183 (80), 86 (100). Anal. Calcd for C₂₅H₂₂N₂O₆W (630.3): C, 47.64; H, 3.52; N, 4.44. Found: C, 47.85; H, 3.66; N, 4.62.

Pentacarbonyl(2-[(*E*)-dimethylaminomethylene]-1-ethoxy-3-phenyl-3-(phenylimino)propan-1-ylidene)chromium [(*E*)-5b] and Pentacarbonyl(1-ethoxy-3-phenylpropynylidene)chromium (6b). To pentacarbonyl[1-ethoxy-3-phenyl-3-(phenylamino)propenylidene]chromium (**1b**) (443 mg, 1.00 mmol) and dry dimethylformamide **4a** (146 mg, 2.00 mmol) in a 5-mL screw-top vessel is added with magnetic stirring at 20 °C a mixture of benzoylchloride (422 mg, 3.00 mmol) and triethylamine (404 mg, 4.00 mmol) in 3 mL of dry dichloromethane. According to a TLC test, compound **1b** is

consumed within 20 min. The mixture is brought to dryness (20 °C, 15 Torr), and the residue is extracted with ether. Chromatography on silica with pentane/dichloromethane 2:1 yields a violet zone with **6b** (32 mg, 9%, violet crystals from pentane) and a yellow zone with (*E*)-**5b**: 388 mg, 78%, *R_f* = 0.4 in pentane/dichloromethane (1:1), yellow crystals from pentane at -15 °C, mp 113 °C. ¹H NMR (C₆D₆): δ 7.87 (1 H, *s*, =CH); 7.70 and 7.29 (2:3 H, *m* each, 3-Ph); 7.14, 6.91 and 6.58 (2:1:2 H; "t", "t", "d", N-Ph), 4.55 and 4.42 (1 H each, *m* each, diastereotopic OCH₂), 2.83 and 2.79 (3 H each, *s* broad each, dynamically broadened NMe₂), 0.85 (3 H, *t*, CH₂CH₃). ¹³C NMR (C₆D₆): δ 294.1 (Cr=C), 221.3 and 216.9 [1:4, *trans*- and *cis*-CO, Cr(CO)₅], 166.3 (C_q, C=N), 164.0 (=CHNMe₂), 149.7 (C_q, *i*-C N-Ph), 138.1 (C_q, *i*-C 3-Ph); 131.3, 128.7, 128.6, 127.9, 124.9, 118.9 (1:2:2:2:1:2, CH each, 2 Ph), 125.6 (C_q, C-2), 71.8 (OCH₂), 46.1 and 38.1 (CH₃ each, dynamically broadened, NMe₂), 13.2 (CH₃). IR (hexane), cm⁻¹ (%): ν̄ 2050.0 (30), 1960.5 (10), 1925.3 (100) [ν(C=O)]. MS (70 eV), *m/e* (%): 498 (10) [M⁺], 470 (1), 442 (20), 414 (20), 386 (30), 359 (20), 197 (60), 105 (100), 77 (80). Anal. Calcd for C₂₅H₂₂CrN₂O₆ (498.5): C, 60.24; H, 4.45; N, 5.62. Found: C, 60.53; H, 4.40; N, 5.32.

Pentacarbonyl(1-ethoxy-3-phenyl-3-phenylimino-2-[(*E*)-pyrrolidinomethylene]propan-1-ylidene)tungsten [(*E*)-5c] and Pentacarbonyl(1-ethoxy-3-phenylpropynylidene)tungsten (6a). To pentacarbonyl[1-ethoxy-3-phenyl-3-phenylamino)propenylidene]tungsten¹⁹ (**1a**) (575 mg, 1.00 mmol) and dry *N*-formylpyrrolidine **4b** (198 mg, 2.00 mmol) in a 5-mL screw-top vessel is added with magnetic stirring at 20 °C a mixture of benzoyl chloride (422 mg, 3.00 mmol) and triethylamine (404 mg, 4.00 mmol) in 3 mL of dry dichloromethane. According to a TLC test, compound **1a** is consumed within 30 min. Chromatography on silica with pentane/dichloromethane 2:1 yields a dark brown zone with **6a** (120 mg, 25%, brown crystals from pentane, and a yellow fraction of (*E*)-**5c**: 427 mg, 65%, *R_f* = 0.5 in pentane/dichloromethane (1:1), yellow and dark-red crystals in equal amounts from pentane at -15 °C, mp 114 °C each. ¹H NMR (C₆D₆): δ 8.10 (1 H, *s*, =CH); 8.02 and 7.22 (2:3 H, *m* each, 3-Ph); 7.10, 6.92 and 6.75 (2:1:2 H; "t", "t", "d", N-Ph), 4.40 (2 H, *m*, diastereotopic OCH₂), 3.12 and 2.80 (2 H each, *m* each, dynamically broadened NCH₂), 2.30 (4 H, *m*, C-CH₂-CH₂, pyrrolidine), 0.79 (3 H, *t*, CH₂CH₃). ¹³C NMR (C₆D₆): δ 273.9 (W=C), 201.9 and 199.1 [1:4, *trans*- and *cis*-CO, W(CO)₅], 166.9 (C_q, C=N), 163.4 (=CHNMe₂), 151.5 (C_q, *i*-C N-Ph), 140.0 (C_q, *i*-C 3-Ph); 130.0, 128.4, 128.1, 127.8, 124.0, 119.0 (1:2:2:2:1:2, CH each, 2 Ph), 125.6 (C_q, C-2), 75.5 (OCH₂), 55.0 and 48.0 (NCH₂ each), 24.9 and 23.2 (C-CH₂-CH₂, pyrrolidine), 14.2 (CH₃). IR (hexane), cm⁻¹ (%): ν̄ 2058.5 (30), 1982.5 (5), 1924.8 (100) [ν(C=O)], 1582.4 [ν(C=N)]. MS (70 eV), *m/e* (%), ¹⁸⁴W: 656 (10) [M⁺], 628 (20), 600 (20), 572 (10), 544 (10), 516 (30) [M⁺ - 5 CO], 486 (20), 388 (30), 286 (40), 77 (100). Anal. Calcd for C₂₇H₂₄N₂O₆W (656.4): C, 49.41; H, 3.69; N, 4.27. Found: C, 49.33; H, 3.73; N, 4.36.

Pentacarbonyl(1-ethoxy-3-phenyl-3-(phenylimino)-2-[(*E*)-pyrrolidinomethylene]propan-1-ylidene)chromium [(*E*)-5d] and Pentacarbonyl(1-ethoxy-3-phenylpropynylidene)chromium (6b). To pentacarbonyl[1-ethoxy-3-phenyl-3-(phenylamino)propenylidene]chromium (**1b**) (443 mg, 1.00 mmol) and dry *N*-formylpyrrolidine **4b** (198 mg, 2.00 mmol) in a 5-mL screw-top vessel is added with magnetic stirring at 20 °C a mixture of benzoyl chloride (422 mg, 3.00 mmol) and triethylamine (404 mg, 4.00 mmol) in 3 mL of dry dichloromethane. According to a TLC test, compound **1b** is consumed within 30 min. Chromatography on silica with pentane/dichloromethane 2:1 yields a violet zone with **6b** (105 mg, 30%, violet crystals from pentane) and a yellow fraction of (*E*)-**5d**: 320 mg, 61%, *R_f* = 0.4 in pentane/dichloromethane (1:1), orange crystals from pentane at -15 °C, mp 111 °C, decomp. ¹H NMR (C₆D₆): δ 8.16 (1 H, *s*, =CH); 8.10 and 7.15 (2:3 H, *m* each, 3-Ph); 7.12, 6.85 and 6.59 (2:1:2 H; "t", "t", "d", N-Ph), 4.50 (2 H, *q*, OCH₂); 3.21, 2.75, 2.50 (2:2:4, *m* each,

pyrrolidine), 0.68 (3 H, t, CH₂CH₃). ¹³C NMR (C₆D₆): δ 293.8 (Cr=C), 223.7 and 219.7 [1:4, *trans*- and *cis*-CO, Cr(CO)₅], 167.8 (Cq, C=N), 161.9 (=CHNMe₂), 153.2 (Cq, *i*-C N-Ph), 140.8 (Cq, *i*-C 3-Ph); 131.0, 129.6, 129.2, 128.6, 124.6, 119.9 (1:2:2:2:1:2, CH each, 2 Ph), 124.5 (Cq, C-2), 73.9 (OCH₂), 55.7 and 48.7 (NCH₂ each, pyrrolidine), 25.8 and 24.0 (C-CH₂ each, pyrrolidine), 15.0 (CH₃). IR (hexane), cm⁻¹ (%): ν̄ 2049.3 (20), 1982.5 (5), 1928.1 (100) [ν(C=O)], 1588.3 [ν(C=N)]. MS (70 eV), *m/e* (%): 524 (10) [M⁺], 468 (20), 440 (20), 412 (30), 384 (40) [M⁺ - 5CO], 340 (40), 286 (40), 256 (40), 57 (100). Anal. Calcd for C₂₇H₂₄CrN₂O₆ (524.5): C, 61.83; H, 4.61; N, 5.34. Found: C, 61.95; H, 4.68; N, 5.43.

Pentacarbonyl{1-ethoxy-2-[(*E*)-morpholinomethylene]-3-phenyl-3-(phenylimino)propan-1-ylidene}tungsten [(*E*)-5e] and Pentacarbonyl(1-ethoxy-3-phenylpropynylidene)-tungsten (6a). To pentacarbonyl(1-ethoxy-3-phenyl-2-phenylamino-propynylidene)tungsten¹⁹ (**1a**) (575 mg, 1.00 mmol) and dry *N*-formylmorpholine **4c** (230 mg, 2.00 mmol) in a 5-mL screw-top vessel is added with magnetic stirring at 20 °C a mixture of benzoyl chloride (422 mg, 3.00 mmol) and triethylamine (404 mg, 4.00 mmol) in 3 mL of dry dichloromethane. According to a TLC test, compound **1a** is consumed within 30 min. Chromatography on silica with pentane/dichloromethane 2:1 yields a dark brown zone with **6a** (106 mg, 22%, brown crystals from pentane), and a yellow-orange fraction of (*E*)-**5e**: 464 mg, 69%, *R*_f = 0.4 in pentane/diethyl ether (3:1), yellow crystals from pentane at -15 °C, mp 121 °C, decomp. ¹H NMR (C₆D₆): δ 8.10 (1 H, s, =CH); 8.00, 7.21 and 7.14 (2:1:2 H, m each, 3-Ph); 7.11, 6.95 and 6.82 (2:1:2 H; "t", "t", "d", N-Ph), 4.40 (2 H, m, diastereotopic OCH₂), 2.90 and 2.80 (4 H each, s broad each, dynamically broadened NCH₂ and OCH₂ morpholine), 0.73 (3 H, t, CH₂CH₃). ¹³C NMR (C₆D₆): δ 276.5 (W=C), 200.8 and 197.9 [1:4, *trans*- and *cis*-CO, W(CO)₅], 165.7 (Cq, C=N), 164.9 (=CHNMe₂), 150.5 (Cq, *i*-C N-Ph), 138.0 (Cq, *i*-C 3-Ph); 131.8, 129.5, 129.2, 129.0, 125.0, 120.0 (1:2:2:2:1:2, CH each, 2 Ph), 122.8 (Cq, C-2), 75.0 (OCH₂), 64.8 (2 OCH₂), 51.0 and 49.5 (NCH₂ each, broad), 13.2 (CH₃). IR (hexane), cm⁻¹ (%): ν̄ 2059.4 (30), 1985.5 (5), 1925.5 (100) [ν(C=O)], 1590.0 [ν(C=N)]. MS (70 eV), *m/e* (%), ¹⁸⁴W: 672 (10) [M⁺], 644 (60), 616 (60), 588 (50), 560 (10), 532 (70) [M⁺ - 5CO], 504 (20), 445 (50), 292 (40) 77 (100). Anal. Calcd for C₂₇H₂₄N₂O₇W (672.4): C, 48.23; H, 3.60; N, 4.17. Found: C, 48.20; H, 3.55; N, 4.30.

Tetracarbonyl{1-ethoxy-3-phenyl-3-(phenylimino)-2-[(*E*)-pyrrolidinomethylene]propan-1-ylidene, *N*}chromium [(*E*)-7d]. Pentacarbonyl{1-ethoxy-3-phenyl-3-(phenylimino)-2-[(*E*)-pyrrolidinomethylene]propan-1-ylidene}chromium [(*E*)-5d] (262 mg, 0.50 mmol) in 1 mL of C₆D₆ in a 5-mL screw-top vessel is heated to 40 °C. The solution becomes dark red while a small pressure of carbon monoxide developing. A mixture of benzoyl chloride (422 mg, 3.00 mmol) and triethylamine (404 mg, 4.00 mmol) in 3 mL of dry dichloromethane is added. According to TLC tests, compound (*E*)-**5d** is consumed within 12 h, while red-brown compound (*E*)-**7d** is formed as the only detectable product. Isolation by crystallization from pentane yields 230 mg, 93%, *R*_f = 0.4 in pentane/

diethyl ether (1:1), brown crystals. ¹H NMR (C₆D₆): δ 6.94, 6.75 and 6.69 (4:4:2 H, m each, 2 Ph), 6.28 (1 H, s, =CH), 5.20 (2 H, q, OCH₂), 2.82 and 2.34 (2:2 H, m each, NCH₂, pyrrolidine), 1.40 (3 H, t, CH₂CH₃), 1.06 and 0.94 (2:2 H, m each, C-CH₂-CH₂-C, pyrrolidine). ¹³C NMR (C₆D₆): δ 323.6 (Cr=C); 232.9, 232.2 and 219.3 [1:1:2, Cr(CO)₄], 176.7 (Cq, C=N), 155.0 (Cq, *i*-C N-Ph), 147.3 (CHNMe₂), 136.6 (Cq, *i*-C 3-Ph); 129.0, 128.4, 128.1, 127.9, 124.0, 123.6 (1:2:2:2:1:2, CH each, 2 Ph), 125.9 (Cq, C-2), 76.4 (OCH₂), 55.5 and 54.7 (NCH₂ each, pyrrolidine), 25.8 and 24.0 (C-CH₂-CH₂-C, pyrrolidine), 16.2 (CH₃). IR (hexane), cm⁻¹ (%): ν̄ = 1999.2 (50), 1917.2 (60), 1897.3 (80), 1838.1 (60) [ν(C=O)], 1587.3 and 1549.0 [ν(C=N) of rotamers]. MS (70 eV), *m/e* (%): 496 (20) [M⁺], 468 (20), 440 (20), 412 (30), 384 (30) [M⁺ - 4 CO], 366 (20), 340 (30), 286 (30) 77 (100). Anal. Calcd for C₂₆H₂₄CrN₂O₆ (496.5): C, 62.90; H, 4.87; N, 5.64. Found: C, 62.95; H, 4.68; N, 5.43.

Ethyl{3-phenyl-3-(phenylimino)-2-[(*E*)-pyrrolidinomethylene]propanoate} [(*E*)-8d]. Tetracarbonyl{1-ethoxy-3-phenyl-3-phenylimino-2-[(*E*)-pyrrolidinomethylene]propan-1-ylidene, *N*}chromium [(*E*)-7d] (50 mg, 0.10 mmol) in 1 mL of C₆D₆ with a trace amount of hexamethylbenzene as an internal standard is heated in a sealed vial to 80 °C for 20 h. According to the ¹H NMR spectrum no detectable reaction has occurred. If the same solution is exposed to air (in a 15-mL screw-top vessel) and heated to 40 °C a smooth oxidation with formation of (*E*)-**8d** (>90% from integration of the NMR signals) as the only product takes place within minutes. ¹H NMR (C₆D₆): δ 8.35, 7.25, 7.20, 7.16, 6.92 (2:2:3:2:1 H, m each, 2 Ph); 7.56 (1 H, s, =CH), 4.09 (2 H, m, diastereotopic OCH₂), 2.82 and 2.39 (2:2 H, m each, dynamically broadened each, NCH₂, pyrrolidine), 1.35 and 0.92 (2:2 H, m each, dynamically broadened each, C-CH₂-CH₂-C, pyrrolidine), 0.95 (3 H, t, CH₂CH₃). ¹³C NMR (CDCl₃): δ 168.5 (Cq, OC=O), 165.6 (Cq, C=N), 154.2 (Cq, *i*-C N-Ph), 151.9 (CHNMe₂), 141.3 (Cq, *i*-C 3-Ph); 130.1, 128.5, 128.4, 128.1, 123.4, 120.0 (1:2:2:2:1:2, CH each, 2 Ph), 94.2 (Cq, C-2), 59.9 (OCH₂), 50.0 (2 NCH₂, pyrrolidine, dynamically broadened), 29.6 (C-CH₂-CH₂-C, pyrrolidine), 14.0 (CH₃). IR (diffuse reflexion), cm⁻¹ (%): ν̄ 1683.9 (30), 1591.9 (100) [ν(C=O), ν(C=C), and ν(C=N)]. MS (70 eV), *m/e* (%): 348 (20) [M⁺], 319 (10) [M⁺ - Et], 303 (10), 278 (60) [M⁺ - C₄H₉N], 256 (100), 210 (60), 206 (80), 183 (50), 180 (70) [PhCNPh⁺], 77 (100), 70 (40) [C₄H₉N⁺]. Exact mass: calcd for C₂₂H₂₄N₂O₂, 348.183778; found, 348.183793.

Acknowledgment. This work was supported by the Volkswagen-Stiftung and by the Fonds der Chemischen Industrie.

Supporting Information Available: Tables of crystal data and details of the structure solution, positional and displacement parameters, and bond distances and angles (26 pages). Ordering information is given on any current masthead page.

OM950111K

Organic Syntheses via Transition Metal Complexes. 80.¹ Allenylidene Complexes from [(2-Aminoethenyl)carbene]chromium Complexes

Rudolf Aumann,* Beate Jasper, and Roland Fröhlich

Organisch-Chemisches Institut der Universität Münster, Orléans-Ring 23,
D-48149 Münster, Germany

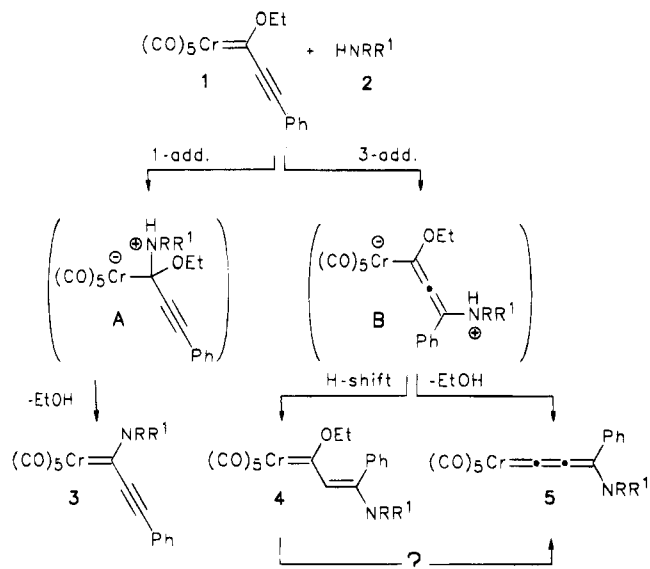
Received February 22, 1995[®]

Allenylidene complexes $(\text{CO})_5\text{Cr}=\text{C}=\text{C}=\text{C}(\text{NRR}^1)\text{Ph}$ (**5a–d**) ($\text{NRR}^1 = \text{NMe}_2, \text{NMePh}, \text{NEtPh}, \text{indolyl}$) are formed on reaction of (2-aminoalkenyl)carbene complexes $(\text{CO})_5\text{Cr}=\text{C}(\text{OEt})-\text{CH}=\text{C}(\text{NR}^1)\text{Ph}$ (**4a–d**) with aluminum chloride in carbon disulfide/dichloromethane in 53–73% isolated yield. The X-ray structure of complex **5d** [$\text{NRR}^1 = \text{NMePh}$; monoclinic space group $P2_1/c$ (No. 14), $a = 12.989(1) \text{ \AA}$, $b = 13.520(2) \text{ \AA}$, $c = 12.546(1) \text{ \AA}$, $Z = 4$, $R = 0.044$, $R_w = 0.143$] indicates that a polarized iminium–alkynyl structure $(\text{CO})_5\text{Cr}^--\text{C}\equiv\text{C}(\text{N}^+\text{MePh})\text{Ph}$ gives a more adequate description of the bond distances than the allenylidene structure.

Aminolysis of Alkynylcarbene Complexes

Alkynylcarbene complexes $(\text{CO})_5\text{M}=\text{C}(\text{X})\text{C}\equiv\text{CR}$ ($\text{M} = \text{Cr}, \text{W}$; $\text{X} = \text{OR}, \text{NR}_2$)² have gained much attention recently as building blocks for organic synthesis.^{3–9} Among various reactions studied so far are cycloadditions, ene-type reactions, and addition/eliminations.¹⁰ The aminolysis of alkynylcarbene complex **1** was investigated as early as 1972,² but it was shown only recently^{11–13} that altogether three competing reaction

Scheme 1. Three Routes for the Aminolysis of Alkynylcarbene Complexes



paths must be distinguished: (a) the 1-substitution to 1-aminocarbene complexes **3** via intermediates **A**, (b) the 3-addition to (2-aminoalkenyl)carbene complexes **4** via allenide intermediates **B**,¹⁴ and (c) the 3,1-substitution to (3-amino)allenylidene complexes **5** (Scheme 1).^{8g,h,11}

The isomerization of alkynylcarbene complexes $(\text{CO})_5\text{M}=\text{CX}-\text{C}\equiv\text{CR}$ to allenylidene complexes $(\text{CO})_5\text{M}=\text{C}=\text{C}=\text{CXR}$ deserves special attention. Compounds of the latter type were first prepared in 1976 ($\text{M} = \text{Cr}, \text{W}$; $\text{X} = \text{NR}_2$),¹⁵ and many allenylidene complexes became known since then ($\text{M} = \text{Cr}$,^{16,17} W ,^{18,19}

[®] Abstract published in *Advance ACS Abstracts*, June 1, 1995.

(1) Part 79: Aumann, R.; Jasper, B.; Fröhlich, R. *Organometallics* **1995**, *14*, 3167.

(2) (a) Fischer, E. O.; Kreissl, F. R. *J. Organomet. Chem.* **1972**, *35*, C47–C51. (b) Fischer, E. O.; Kalder, H. *J. Organomet. Chem.* **1977**, *131*, 57–64.

(3) Bao, J.; Wulff, W. D.; Dragisich, V.; Wenglowski, S.; Ball, R. G. *J. Am. Chem. Soc.* **1994**, *116*, 7616–7630.

(4) (a) Duetsch, M.; Stein, F.; Funke, F.; Pohl, E.; Herbst-Irmer, R.; de Meijere, A. *Chem. Ber.* **1993**, *126*, 2535–2541. (b) Duetsch, M.; Vidoni, S.; Stein, F.; Funke, F.; Pohl, E.; Noltemeyer, M.; de Meijere, A. *J. Chem. Soc., Chem. Commun.* **1994**, 1679–1680.

(5) (a) Christoffers, J.; Dötz, K.-H. *J. Chem. Soc., Chem. Commun.* **1993**, 1811–1812. (b) Christoffers, J.; Dötz, K.-H. *Chem. Ber.* **1995**, *128*, 157–161. (c) Christoffers, J.; Dötz, K.-H. *Organometallics* **1994**, *13*, 4189–4193.

(6) Fischer, H.; Meisner, T.; Hofmann, J. *Chem. Ber.* **1990**, *123*, 1799–1804.

(7) Camps, F.; Moretó, J. M.; Ricart, S.; Viñas, J. M. *Angew. Chem.* **1991**, *103*, 1540–1542; *Angew. Chem., Int. Ed. Engl.* **1991**, *30*, 1470–1472.

(8) (a) Aumann, R.; Jasper, B.; Fröhlich, R. *Organometallics* **1995**, *14*, 231–237. (b) Aumann, R.; Hinterding, P.; Krüger, C.; Goddard, R. *J. Organomet. Chem.* **1993**, *459*, 145–149. (c) Aumann, R. *Chem. Ber.* **1993**, *126*, 2325–2330. (d) Aumann, R.; Roths, K.; Läge, M.; Krebs, B. *Synlett* **1993**, 667–669. (e) Aumann, R.; Roths, K.; Läge, M.; Krebs, B. *Synlett* **1993**, 669–671. (f) Aumann, R.; Jasper, B.; Goddard, R.; Krüger, C. *Chem. Ber.* **1994**, *127*, 717–724. (g) Aumann, R. *Chem. Ber.* **1994**, *127*, 725–729. (h) Aumann, R.; Hinterding, P. *Chem. Ber.* **1993**, *126*, 421–427. (i) Aumann, R.; Jasper, B.; Läge, M.; Krebs, B. *Organometallics* **1994**, *13*, 3502–3509. (j) Aumann, R.; Kössmeier, M.; Roths, K.; Fröhlich, R. *Synlett* **1994**, 1041–1044.

(9) Weng, W.; Bartik, T.; Gladysz, J. A. *Angew. Chem.* **1994**, *106*, 2269–2271; *Angew. Chem., Int. Ed. Engl.* **1994**, *33*, 2199–2200.

(10) Review: Wulff, W. D. In *Comprehensive Organic Synthesis*; Trost, B. M.; Fleming, I., Eds.; Pergamon Press: Oxford, U.K., 1991; Vol. 5B, pp 1065–1113 (see also references cited therein).

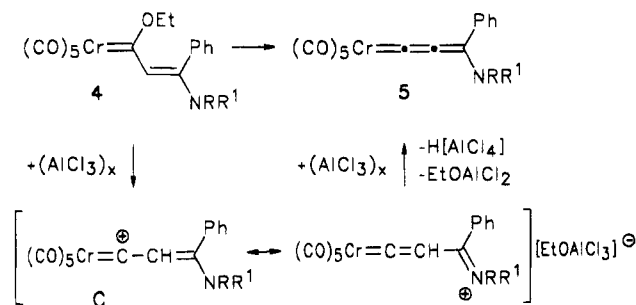
(11) (a) Stein, F.; Duetsch, M.; Pohl, E.; Herbst-Irmer, R.; de Meijere, A. *Organometallics* **1993**, *12*, 2556–2564. (b) Duetsch, M.; Stein, F.; Lackmann, R.; Pohl, E.; Herbst-Irmer, R.; de Meijere, A. *Chem. Ber.* **1992**, *125*, 2051–2065. (c) Duetsch, M.; Stein, F.; Lackmann, R.; de Meijere, A. *Synlett* **1992**, 324–326. (d) Stein, F.; Duetsch, M.; Noltemeyer, M.; de Meijere, A. *Synlett* **1993**, 486–488.

(12) (a) Camps, F.; Llebaria, A.; Moretó, J. M.; Ricart, S.; Viñas, J. M. *Tetrahedron Lett.* **1990**, *31*, 2479–2481. (b) Camps, F.; Jordi, L.; Moretó, J. M.; Ricart, S.; Castaño, A. M.; Echavarren, A. M. *J. Organomet. Chem.* **1992**, *436*, 189–192.

(13) Rahm, A.; Wulff, W. D.; Rheingold, A. L. *Organometallics* **1993**, *12*, 597–599.

(14) For stable phosphorus-analog compounds of this type see: Aumann, R.; Jasper, B.; Läge, M.; Krebs, B. *Chem. Ber.* **1994**, *127*, 2475–2482.

Scheme 2. Allenylidene Complexes 5 by 1,2-Elimination of EtOH from 4 with Aluminum Trichloride



Mn,^{20,21} Rh,²² Fe,²³ and Ru,^{24–26} and other metals^{27,28}). Except for the direct transformation of alkynyl into allenylidene complexes by 3,1-substitution (X = NR₂,¹¹ NHR,^{8g} OEt²⁹), little is known about the route to allenylidene from alkynylcarbene *via* (2-aminoalkenyl)carbene complexes (CO)₅M=C(OEt)-CH=CXR (4) by 1,2-elimination of EtOH (Scheme 1).¹⁵ We wish to describe experimental details for the efficient transformation of compounds 4 into 5 (Scheme 2).

The (orange) (2-aminoalkenyl)carbene complexes **4a–d** when reacted in a proper solvent mixture [=carbon-disulfide/dichloromethane (1:1)] with aluminum trichloride (3 equiv, 0 °C, 1.5 h) afford (violet) allenylidene complexes **5a–d** in 53–73% isolated yield after hydrolysis. Though this reaction is most straightforwardly performed, careful attention must be paid to the quality of aluminum trichloride and also to the hydrolytic workup of the reaction mixture. The elimination of EtOH may be initiated by coordination of aluminum chloride to the oxygen atom of the EtO group, thus favoring an *anti* elimination of EtOH *via* an intermediate **C** (Scheme 2).

Spectroscopy

Allenylidene complexes **5** are most conveniently distinguished from the corresponding alkynylcarbene complexes by the IR spectra. A strong absorption band at 1974–1988 cm⁻¹ [$\nu(\text{C}=\text{C})$] and a (usually very weak) A₁ $\nu(\text{C}=\text{O})$ band at 2071–2098 cm⁻¹ is typically ob-

served for allenylidene complexes **5**, while absorptions at 2165–2175 [$\nu(\text{C}\equiv\text{C})$] and 2058–2065 cm⁻¹ [A₁ $\nu(\text{C}=\text{O})$] are found in alkynylcarbene complexes. The structural assignment of compounds **5** is also based on the ¹³C NMR shift range of the Cr=C (δ 239–253) and C=C unit (δ 144–153, and 125–130, respectively) (Table 1).

¹H and ¹³C NMR spectra of the indolinyll derivative **5d** indicate the presence of a 3:2 mixture of stereoisomers **5A** and **5B** (Scheme 3). These isomers cannot be separated by chromatography, since they are configurationally unstable and slowly interconvert in solution. This process, though it does not lead to an appreciable line broadening in the ¹H NMR spectrum (C₆D₆, 360 MHz, 20 °C), is unambiguously indicated by spin saturation transfer experiments. The conformational assignment of the stereoisomers of **5d** is based on strong shift differences, e.g. of 7-H (**5A**, δ 9.40; **5B**, δ 6.05) and NCH₂ (**5A**, δ 3.00; **5B**, δ 4.00), due to the anisotropic influence of the 3-Ph group. The hindered rotation of the C=N⁺ bond in **5d** is attributed to the resonance contribution of a zwitterionic iminium structure but also to the sterical rigidity of the indolinyll ring. The ¹H and ¹³C NMR spectra of **5b,c** indicate the presence of one stereoisomer only. Crystallization of **5b** affords the isomer **5bB**, which structure has been determined by X-ray analysis.

Crystal Structure Analysis of 5b

Detailed information on the molecular structure of compounds **5** was obtained from its crystal structure analysis (Tables 2–4). The Cr–C(1)–C(2)–C(3) backbone of this compound is almost linear [Cr–C(1)–C(2) = 173.7(3)°, C(1)–C(2)–C(3) = 174.3(4)°]. The sums of valence angles at C(3) and N amount to 360.0 and 359.7°, respectively, which indicate an essentially planar coordination at these centers. Due to delocalization of the lone electron pair on the nitrogen atom into the adjacent C=C bond a short N–C(3) bond [1.323(4) Å] and a slightly elongation of the C(2)–C(3) bond [1.389(5) Å] is observed. The distance C(1)–C(2) = 1.224(5) Å is much shorter than in a C=C bond of 1,2-propadiene (1.312 Å) and corresponds to a C≡C bond.^{12a,15,24,26} Thus a polarized iminium–alkynyl structure **5A** (Scheme 3) gives a more adequate description of the bond distances than the allenylidene structure **5**.

Experimental Section

All operations were performed under argon. Solvents were dried by distillation from sodium/benzophenone. Melting points are uncorrected. Instrumentation: ¹H NMR and ¹³C NMR spectra were obtained with Bruker WM 300 and WP 360 spectrometers. Multiplicities were determined by DEPT. Chemical shifts refer to $\delta_{\text{TMS}} = 0.00$ ppm. Other analyses: IR Digilab FTS 45; MS Finnigan MAT 312; elemental analysis, Perkin-Elmer 240 elemental analyzer; column chromatography, Merck-Kieselgel 100; TLC, Merck DC-Alufolien Kieselgel 60 F 254. *R_f* values refer to TLC tests.

Pentacarbonyl[(2E)-1-ethoxy-3-(methylphenylamino)-3-phenylpropenylidene]chromium [(E)-4b]. Pentacarbonyl(3-phenylpropynylidene)chromium (**1**) (3.50 g, 10.00 mmol) in 5 mL of dry diethyl ether in a 25-mL centrifuge tube is reacted with *N*-methylaniline (**2b**) (1.06 g, 10.00 mmol) in 3 mL of diethyl ether at 20 °C. After addition of pentane (15 mL) yellow crystals of (*E*)-**4b** are obtained (4.33 g, 93%), which are removed by centrifugation after 2 h, washed 3 times with

(15) Fischer, E. O.; Kalder, H.-J.; Frank, A.; Köhler, F. H.; Huttner, G. *Angew. Chem.* **1976**, *88*, 683–684; *Angew. Chem., Int. Ed. Engl.* **1976**, *15*, 623–624.

(16) Berke, H.; Härter, P.; Huttner, G.; von Seyerl, J. *J. Organomet. Chem.* **1981**, *219*, 317–327.

(17) Berke, H.; Härter, P.; Huttner, G.; Zsolnai, L. *Z. Naturforsch., B* **1981**, *36B*, 929–938.

(18) Berke, H.; Härter, P.; Huttner, G.; Zsolnai, L. *Chem. Ber.* **1982**, *115*, 695–705.

(19) Fischer, H.; Roth, G.; Reindl, D.; Troll, C. *J. Organomet. Chem.* **1993**, *454*, 133–149.

(20) (a) Berke, H. *Z. Naturforsch., B* **1980**, *35B*, 86–90. (b) Berke, H. *Chem. Ber.* **1980**, *113*, 1370–1376.

(21) Berke, H. *Angew. Chem.* **1976**, *88*, 684–685; *Angew. Chem., Int. Ed. Engl.* **1976**, *15*, 624.

(22) Baum, M.; Mahr, N.; Werner, H. *Chem. Ber.* **1994**, *127*, 1877–1886.

(23) Kolobova, N. E.; Ivanov, L. L.; Zhvanko, O. S.; Aleksandrov, G. G.; Struchkov, Y. T. *J. Organomet. Chem.* **1982**, *228*, 265–270.

(24) Selegue, J. P. *Organometallics* **1982**, *1*, 217.

(25) Werner, H.; Stark, A.; Steinert, P.; Grünwald, C.; Wolf, J. *Chem. Ber.* **1995**, *128*, 49–62.

(26) Cadierno, V.; Gamasa, M., P.; Gimeno, J.; Borge, J.; García-Grande, S. *J. Chem. Soc., Chem. Commun.* **1994**, 2495–2496.

(27) Recent review: Bruce, M. I. *Chem. Rev.* **1991**, *91*, 197.

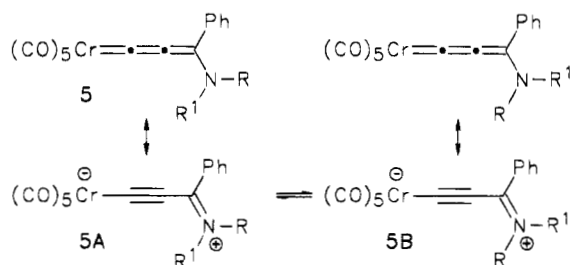
(28) Recent review: Werner, H. *J. Organomet. Chem.* **1994**, *475*, 45.

(29) Aumann, R. *Chem. Ber.* **1992**, *125*, 2773–2778.

Table 1. Selected ^{13}C NMR Chemical Shifts and IR Frequencies (cm^{-1}) of Allenylidenechromium Complexes $(\text{CO})_5\text{Cr}=\text{C}=\text{C}=\text{C}(\text{NRR}^1)\text{Ph}$

	R	R ¹	$\delta(\text{Cr}=\text{C})$	$\delta[\text{C}(3)]$	$\delta[\text{C}(2)]$	$\nu(\text{C}=\text{O})$	$\nu(\text{C}=\text{C}=\text{C})$	ref
	H	galacto ^a	252.7	147.0	127.8	2076, 1943	1977	8g
	<i>i</i> -Pr	<i>i</i> -Pr	238.3	152.0	65.8 ^b	2098, 1924	1976 ^c	11
5a	Me	Me	230.2	153.1	125.3	2078, 1939	1988	<i>d</i>
5b	Me	Ph	243.6	150.2	129.5	2071, 1943	1978	<i>d</i>
5c	Et	Ph	240.0	150.9	129.3	2075, 1943	1977	<i>d</i>
5d		indoliny	239.0 (243.0)	144.3 (143.9)	125.8 (125.1)	2072, 1940	1974	<i>d</i>

^a 2,3,4,6-tetra-*O*-pivaloyl- β -D-galactopyranosylamino. ^b We find $\delta = 126.7$ instead of $\delta = 65.8$ quoted in ref 11. ^c In ref 11 this band is assigned to $\nu(\text{C}=\text{O})$ instead of $\nu(\text{C}=\text{C}=\text{C})$. ^d This paper.

Scheme 3. Hindered Rotation of the $\text{C}=\text{NR}_2^-$ Bond of **5**

2 mL of pentane each, and dried (20 °C, 15 Torr). ^1H NMR [$\text{C}_6\text{H}_6/\text{CS}_2$ (1:1), 25 °C]: δ 7.10, 6.90 and 6.85 (5:3:2 H, m each, 2 Ph), 6.65 (1 H, s, 2-H), 4.20 (2 H, q broad, OCH_2), 3.03 (3 H, s broad, NCH_3), 0.50 (3H, t, CH_3 , Et). ^{13}C NMR [$\text{C}_6\text{H}_6/\text{CS}_2$ (1:1)]: δ 302.8 (Cr=C), 224.3 and 219.1 [1:4 C, *trans*- and *cis*-CO Cr(CO)₅], 153.4 (C_q, C3), 145.4 (C_q, *i*-C NPh), 137.7 (C_q, *i*-C 3-Ph); 137.6, 130.0, 129.2, 128.3, 127.9, 127.6, 127.0 (CH each, dynamically broadened, 2 Ph); 122.6 (CH, C2), 74.0 (OCH_2), 42.4 (NCH_3), 14.5 (CH_3 Et). IR (hexane) [cm^{-1} (%): 2049.1 (20), 1981.3 (5), 1932.1 (100) [$\nu(\text{C}=\text{O})$]. MS (70 eV) [m/e (%): 457 (20) [M^+], 429 (20), 401 (10), 373 (50), 345 (30), 317 (80) [$\text{M}^+ - 5\text{CO}$], 289 (30), 272 (30), 220 (80), 52 (100). Anal. Calcd for $\text{C}_{23}\text{H}_{19}\text{CrNO}_6$ (457.4): C, 60.40; H, 4.19; N, 3.06. Found: C, 60.60; H, 4.32; N, 3.33.

Pentacarbonyl[(2*E*)-1-ethoxy-3-(ethylphenylamino)-3-phenylpropynylidene]chromium [(*E*)-4c**].** Pentacarbonyl-(3-phenylpropynylidene)chromium (**1**) (3.50 g, 10.00 mmol) is reacted with *N*-ethylaniline (**2c**) (1.21 g, 10.00 mmol) as described above to give yellow crystals of (*E*)-**4c** [4.28 g, 91%, $R_f = 0.8$ in pentane/dichloromethane (4:1)]. ^1H NMR [$\text{C}_6\text{H}_6/$

Table 2. Crystal Data and Structure Refinement for **5b**

empirical formula	$\text{C}_{21}\text{H}_{13}\text{CrNO}_5$
fw	411.32
temp	223(2) K
wavelength	0.710 73 Å
cryst system	monoclinic
space group	$P2_1/c$ (No. 14)
unit cell dimens	$a = 12.989(1)$ Å
b	$b = 13.520(2)$ Å, $\beta = 116.41(1)^\circ$
c	$c = 12.546(1)$ Å
V	1973.3(4) Å ³
Z	4
$D(\text{calcd})$	1.385 Mg/m ³
abs coeff	0.610 mm ⁻¹
$F(000)$	840
cryst size	0.6 × 0.3 × 0.2 mm
θ range for data colln	2.31–26.31°
index ranges	$-16 \leq h \leq 14$, $-16 \leq k \leq 0$, $0 \leq l \leq 15$
reflens collcd	4198
independent reflens	4008 [$R(\text{int}) = 0.1061$]
refinement method	full-matrix least-squares on F^2
data/restraints/params	4000/0/254
goodness-of-fit on F^2	1.075
final R indices [$I > 2\sigma(I)$]	$R1 = 0.0441$, $R_w2 = 0.1429$
R indices (all data)	$R1 = 0.0889$, $R_w2 = 0.1726$
largest diff peak and hole	0.407 and $-0.492 \text{ e} \cdot \text{Å}^{-3}$

CS_2 (1:1), 25 °C]: δ 6.90 and 6.70 (7:3 H, m each, 2 Ph), 6.85 (1 H, s, 2-H), 4.23 (2 H, q, OCH_2), 3.03 (2 H, q broad, NCH_2), 0.80 (3 H, t, CH_3 NEt), 0.50 (3 H, t, CH_3 Oet). ^{13}C NMR (C_6D_6): δ 298.8 (Cr=C), 224.9 and 219.7 [1:4 C, *trans*- and *cis*-CO Cr(CO)₅], 154.2 (C_q, C3), 143.0 (C_q, *i*-C NPh), 137.6 (C_q, *i*-C 3-Ph); 129.9, 128.8, 128.5, 128.2, 128.0, 127.9 (CH each, dynamically broadened, 2 Ph); 121.8 (CH, C2), 73.9 (OCH_2),

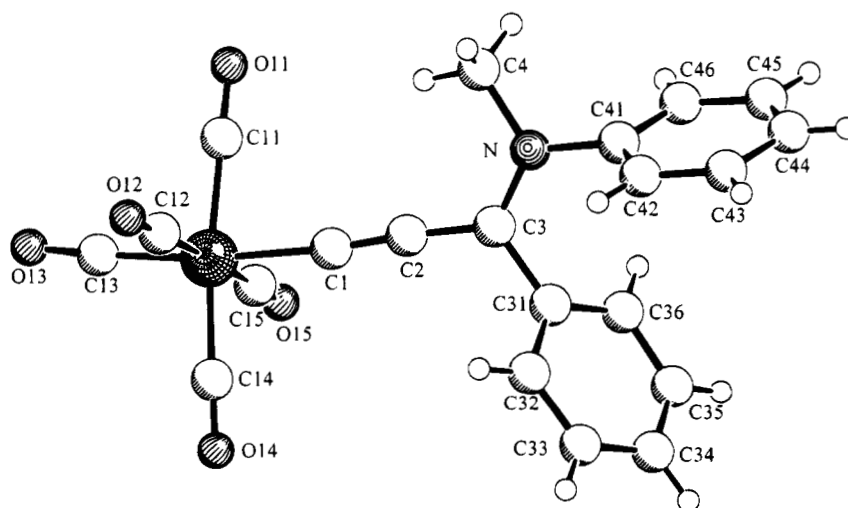


Figure 1. Molecular structure of allenylidene complex **5b** shown with 50% thermal ellipsoids. Selected bond distances (Å) and angles (deg): Cr–C(13) = 1.863(4), Cr–C(1) = 2.007(3), C(1)–C(2) = 1.224(5), C(2)–C(3) = 1.389(5), C(3)–N = 1.323(4), C(3)–C(31) = 1.487(5), N–C(4) = 1.464(5), N–C(41) = 1.450(4), C(2)–C(1)–Cr = 173.7(3), C(1)–C(2)–C(3) = 174.3(4), N–C(3)–C(2) = 122.3(3), N–C(3)–C(31) = 119.1(3), C(2)–C(3)–C(31) = 118.6(3), C(3)–N–C(41) = 121.6(3), C(3)–N–C(4) = 121.7(3), C(41)–N–C(4) = 116.4(3).

Table 3. Atomic Coordinates ($\times 10^4$) and Equivalent Isotropic Displacement Parameters ($\text{\AA}^2 \times 10^3$) for 5b

	x	y	z	U(eq)
Cr	1765(1)	1591(1)	-19(1)	33(1)
C(11)	1431(3)	500(3)	715(4)	48(1)
O(11)	1227(3)	-149(3)	1158(3)	83(1)
C(12)	2814(3)	2068(3)	1509(4)	44(1)
O(12)	3464(3)	2331(3)	2417(3)	71(1)
C(13)	2973(3)	882(3)	-69(3)	44(1)
O(13)	3716(2)	409(3)	-49(3)	68(1)
C(14)	1936(3)	2771(3)	-757(4)	44(1)
O(14)	2002(3)	3478(3)	-1217(3)	71(1)
C(15)	764(3)	1109(3)	-1558(3)	41(1)
O(15)	184(2)	820(3)	-2485(3)	60(1)
C(1)	417(3)	2217(3)	97(3)	37(1)
C(2)	-439(3)	2506(3)	178(3)	39(1)
C(3)	-1463(3)	2840(3)	147(3)	35(1)
C(31)	-2095(3)	3649(3)	-693(3)	36(1)
C(32)	-1556(3)	4542(3)	-615(4)	46(1)
C(33)	-2120(4)	5310(3)	-1369(4)	59(1)
C(34)	-3236(4)	5186(4)	-2229(4)	61(1)
C(35)	-3763(4)	4284(4)	-2327(4)	58(1)
C(36)	-3216(3)	3514(3)	-1569(3)	46(1)
N	-1898(2)	2458(2)	830(3)	37(1)
C(4)	-1336(4)	1639(3)	1647(4)	55(1)
C(41)	-2894(3)	2887(3)	890(3)	38(1)
C(42)	-2818(3)	3818(3)	1360(4)	51(1)
C(43)	-3778(4)	4236(4)	1388(5)	65(1)
C(44)	-4800(4)	3715(4)	944(4)	64(1)
C(45)	-4867(3)	2794(4)	478(4)	60(1)
C(46)	-3909(3)	2361(3)	450(4)	48(1)

^a U(eq) is defined as one-third of the trace of the orthogonalized U_{ij} tensor.

Table 4. Bond Lengths (\AA) and Angles (deg) for 5b

Cr-C(13)	1.863(4)	C(31)-C(32)	1.377(5)
Cr-C(11)	1.888(4)	C(31)-C(36)	1.392(5)
Cr-C(15)	1.900(4)	C(32)-C(33)	1.376(6)
Cr-C(12)	1.904(4)	C(33)-C(34)	1.379(7)
Cr-C(14)	1.908(4)	C(34)-C(35)	1.377(7)
Cr-C(1)	2.007(3)	C(35)-C(36)	1.375(6)
C(11)-O(11)	1.132(5)	N-C(41)	1.450(4)
C(12)-O(12)	1.132(5)	N-C(4)	1.464(5)
C(13)-O(13)	1.148(5)	C(41)-C(42)	1.375(6)
C(14)-O(14)	1.138(5)	C(41)-C(46)	1.379(5)
C(15)-O(15)	1.137(5)	C(42)-C(43)	1.383(5)
C(1)-C(2)	1.224(5)	C(43)-C(44)	1.383(7)
C(2)-C(3)	1.389(5)	C(44)-C(45)	1.361(7)
C(3)-N	1.323(4)	C(45)-C(46)	1.390(6)
C(3)-C(31)	1.487(5)		
C(13)-Cr-C(11)	89.6(2)	N-C(3)-C(2)	122.3(3)
C(13)-Cr-C(15)	89.7(2)	N-C(3)-C(31)	119.1(3)
C(11)-Cr-C(15)	91.5(2)	C(2)-C(3)-C(31)	118.6(3)
C(13)-Cr-C(12)	88.4(2)	C(32)-C(31)-C(36)	119.4(4)
C(11)-Cr-C(12)	89.4(2)	C(32)-C(31)-C(3)	119.4(3)
C(15)-Cr-C(12)	177.9(2)	C(36)-C(31)-C(3)	121.1(3)
C(13)-Cr-C(14)	97.6(2)	C(31)-C(32)-C(33)	120.9(4)
C(11)-Cr-C(14)	172.8(2)	C(32)-C(33)-C(34)	120.0(4)
C(15)-Cr-C(14)	88.2(2)	C(33)-C(34)-C(35)	119.0(4)
C(12)-Cr-C(14)	91.1(2)	C(36)-C(35)-C(34)	121.7(4)
C(13)-Cr-C(1)	173.7(2)	C(35)-C(36)-C(31)	119.0(4)
C(11)-Cr-C(1)	84.1(2)	C(3)-N-C(41)	121.6(3)
C(15)-Cr-C(1)	89.6(2)	C(3)-N-C(4)	121.7(3)
C(12)-Cr-C(1)	92.3(2)	C(41)-N-C(4)	116.4(3)
C(14)-Cr-C(1)	88.7(2)	C(42)-C(41)-C(46)	121.1(3)
O(11)-C(11)-Cr	179.4(4)	C(42)-C(41)-N	119.6(3)
O(12)-C(12)-Cr	177.8(4)	C(46)-C(41)-N	119.3(4)
O(13)-C(13)-Cr	176.0(4)	C(41)-C(42)-C(43)	119.4(4)
O(14)-C(14)-Cr	177.9(4)	C(44)-C(43)-C(42)	119.8(4)
O(15)-C(15)-Cr	178.6(3)	C(45)-C(44)-C(43)	120.4(4)
C(2)-C(1)-Cr	173.7(3)	C(44)-C(45)-C(46)	120.6(4)
C(1)-C(2)-C(3)	174.3(4)	C(41)-C(46)-C(45)	118.7(4)

48.8 (NCH₂), 14.3 (CH₃ OEt), 13.1 (CH₃ NEt). IR (hexane) [cm^{-1} (%): 2049.1 (20), 1981.3 (5), 1932.1 (100) [$\nu(\text{C}=\text{O})$]. MS (70 eV) [m/e (%): 471 (30) [M^+], 443 (20), 415 (10), 387 (50),

359 (30), 331 (30) [$\text{M}^+ - 5\text{CO}$], 234 (40), 219 (30), 170 (80), 57 (100). Anal. Calcd for C₂₄H₂₁CrNO₆ (471.5): C, 61.15; H, 4.49; N, 2.97. Found: C, 60.90; H, 4.68; N, 3.03.

Pentacarbonyl[(2E)-1-ethoxy-3-(1-indolinyl)-3-phenylpropenylidene]chromium [(E)-4d]. Pentacarbonyl(3-phenylpropenylidene)chromium (1) (3.50 g, 10.00 mmol) is reacted with indoline (2d) (1.19 g, 10.00 mmol) as described above to give yellow crystals of (E)-4d [4.27 g, 91%, $R_f = 0.2$ in pentane/dichloromethane (5:1), mp 119 °C]. ¹H NMR (C₆H₆, 25 °C): δ 7.20 and 6.90 (1:4 H, m each, Ph), 6.87 (1 H, s, 2-H), 6.65 (1 H, d, ³J = 7.3 Hz, 4'-H indoline), 6.60 (1 H, dd, ³J = 7.3 and 7.5 Hz, 5'-H indoline), 6.52 (1 H, dd dynamically broadened, 6'-H indoline), 5.70 (1 H, at 25 °C "s" broad; at 50 °C d, ³J = 7 Hz, 7'-H indoline), 4.30 (2 H, q, OCH₂), 3.33 (2 H, m, NCH₂), 2.50 (2 H, m, CH₂Ph), 0.55 (3 H, t, CH₃ Et). ¹³C NMR (C₆D₆): δ 300.6 (Cr=C), 223.0 and 217.7 [1:4 C, *trans*- and *cis*-CO Cr(CO)₅], 146.5 (Cq, C3); 141.2, 135.1 and 132.9 (Cq each; *i*-C 3-Ph and indoline); 129.6, 129.1, 128.5, 127.3, 125.7, 124.5, 123.4, 116.7 (CH each, 1:2:1:1:1:2:1:1 C; 3-Ph, indoline and C2), 74.3 (OCH₂), 53.7 (NCH₂), 27.7 (CH₂Ph), 14.3 (CH₃ Et). IR (hexane) [cm^{-1} (%): $\bar{\nu} = 2048.8$ (20), 1985.9 (5), 1933.6 (100) [$\nu(\text{C}=\text{O})$]. MS (70 eV) [m/e (%): 469 (20) [M^+], 441 (20), 413 (10), 385 (50), 357 (30), 329 (80) [$\text{M}^+ - 5\text{CO}$], 248 (60), 233 (40), 232 (50), 230 (60), 84 (100). Anal. Calcd for C₂₄H₁₉CrNO₆ (469.4): C, 61.41; H, 4.08; N, 2.98. Found: C, 61.44; H, 4.08; N, 2.98.

Pentacarbonyl[3-(dimethylamino)-3-phenyl-1,2-propadienylidene]chromium (5a). Pentacarbonyl[(2E)-1-ethoxy-3-(dimethylamino)-3-phenylpropenylidene]chromium [(E)-4a]³⁰ (350 mg, 1.00 mmol) in 2.0 mL of dichloromethane is added with stirring at 0 °C to a suspension of finely divided (yellow, crystalline!) aluminum chloride (400 mg, 3.00 mmol) in 2.0 mL of carbon disulfide. The reaction is followed by TLC. No evolution of gas (=CO) should occur, since this may an indication for a drastic drop of yield. After (E)-4a has been consumed completely (1.5 h at 0 °C) the reaction mixture is quenched by the dropwise addition to a rapidly stirred mixture of 10 g of ice and 3 g of sodium hydrogen carbonate. The organic layer is diluted with 20 mL of ether, separated, and brought to dryness (20 °C, 15 Torr). The residue is dissolved in 2 mL of dichloromethane, and 10 mL of pentane is added. Crystallization at -78 °C (1-3 d) yields 5a [223 mg, 64%, maroon crystals, $R_f = 0.5$ in dichloromethane/pentane (2:1), mp 122 °C, dec]. ¹H NMR (C₆D₆): δ 6.90 and 6.80 (2:3 H, Ph), 2.60 and 1.95 (3 H each, s each, NCH₃ each). ¹³C NMR (C₆D₆): δ 230.2 (Cr=C), 224.2 and 218.5 [1:4, *trans*- and *cis*-CO, Cr(CO)₅], 153.1 [C(q), C3], 134.4 [C(q), *i*-C Ph], 131.3 and 128.9 (1:4, CH each, Ph), 125.3 [C(q), C2], 43.8 and 41.4 (NCH₃ each). IR (hexane) [cm^{-1} (%): $\bar{\nu} = 2078.1$ (2), 1939.1 (100) [$\nu(\text{C}=\text{O})$], 1988.2 (80) [$\nu(\text{C}=\text{C}=\text{C})$]. MS (70 eV) [m/e (%): 349 (50) [M^+], 321 (10), 293 (20), 265 (40), 237 (50), 209 (80) [$\text{M}^+ - 5\text{CO}$], 166 (50), 127 (80), 93 (80), 86 (70), 77 (100). Anal. Calcd for C₁₆H₁₁CrNO₅ (349.3): C, 55.02; H, 3.17; N, 4.01. Found: C, 54.87; H, 3.29; N, 4.17.

Pentacarbonyl[3-(methylphenylamino)-3-phenyl-1,2-propadienylidene]chromium (5b). Pentacarbonyl[(2E)-1-ethoxy-3-(methylphenylamino)-3-phenylpropenylidene]chromium [(E)-4b] (457 mg, 1.00 mmol) is reacted as described above with aluminum chloride. Data for 5b [247 mg, 60%, violet crystals, $R_f = 0.4$ in dichloromethane/pentane (1:4), mp 112 °C, dec] are as follows. ¹H NMR (C₆D₆): δ 7.05 and 6.55 (2:3 H, m each, 3-Ph), 6.40 and 6.10 (3:2 H, m each, NPh), 3.25 (3 H, s, NCH₃). ¹³C NMR (C₆D₆): δ 243.6 (Cr=C), 224.9 and 218.1 [1:4, *trans*- and *cis*-CO, Cr(CO)₅], 150.2 [C(q), C3], 143.7 [C(q), *i*-C NPh], 135.0 [C(q), *i*-C 3-Ph]; 131.3, 130.3 and 129.5 (1:2:2, CH each, 3-Ph); 129.5 [C(q), C2]; 128.1, 127.7 and 125.3 (1:2:2, CH each, NPh), 46.5 (NCH₃). IR (hexane) [cm^{-1} (%): $\bar{\nu} = 2071.2$ (2), 1942.5 (100) [$\nu(\text{C}=\text{O})$], 1978.0 (60) [$\nu(\text{C}=\text{C}=\text{C})$]. MS (70 eV) [m/e (%): 411 (30) [M^+], 383 (10), 355 (20), 327 (40), 299 (50), 271 (80) [$\text{M}^+ - 5\text{CO}$], 219 (60),

179 (50), 127 (30), 77 (100). Anal. Calcd for $C_{21}H_{13}CrNO_5$ (411.3): C, 61.32; H, 3.19; N, 3.41. Found: C, 61.52; H, 3.25; N, 3.64.

Pentacarbonyl[3-(ethylphenylamino)-3-phenyl-1,2-propadienyldiene]chromium (5c). Pentacarbonyl[(2*E*)-1-ethoxy-3-(ethylphenylamino)-3-phenylpropenyldiene]chromium [(*E*)-**4c**] (471 mg, 1.00 mmol) is reacted as described above with aluminum chloride. Data for **5c** [225 mg, 53%, violet crystals, $R_f = 0.4$ in dichloromethane/pentane (1:4), mp 99 °C, dec] are as follows. 1H NMR (C_6D_6): δ 7.10 and 6.55 (2:3 H, m each, 3-Ph), 6.40 and 6.15 (3:2 H, m each, NPh), 3.80 (2 H, q, NCH_2), 1.00 (3 H, t, NCH_3). ^{13}C NMR (C_6D_6): δ 240.0 (Cr=C), 225.6 and 218.9 [1:4, *trans*- and *cis*-CO, $Cr(CO)_5$], 150.9 [C(q), C3], 142.8 [C(q), *i*-C NPh], 135.7 [C(q), *i*-C 3-Ph]; 131.9, 131.2 and 130.5 (1:2:2, CH each, 3-Ph); 129.3 [C(q), C2]; 129.0, 128.7 and 127.0 (1:2:2, CH each, NPh), 55.5 (NCH_2), 12.5 (NCH_3). IR (hexane) [cm^{-1} (%): $\bar{\nu} = 2075.2$ (2), 1943.2 (100) [$\nu(C=O)$], 1976.6 (60) [$\nu(C=C=C)$]. MS (70 eV) [m/e (%): 425 (30) [M^+], 397 (10), 369 (20), 341 (40), 313 (40), 285 (80) [$M^+ - 5CO$], 256 (30), 233 (20), 179 (30), 127 (30), 77 (100). Anal. Calcd for $C_{22}H_{15}CrNO_5$ (425.3): C, 62.12; H, 3.55; N, 3.29. Found: C, 62.00; H, 3.56; N, 3.38.

Pentacarbonyl[3-(1-indolinyl)-3-phenyl-1,2-propadienyldiene]chromium (5d). Pentacarbonyl[(2*E*)-1-ethoxy-3-indolinyl-3-phenylpropenyldiene]chromium [(*E*)-**4d**] (469 mg, 1.00 mmol) is reacted as described above with aluminum chloride. Data for **5c** [309 mg, 73%, violet crystals, $R_f = 0.4$ in dichloromethane/pentane (1:4), mp 132 °C, dec] are as follows. The NMR spectra at 20 °C indicate a 2:3 isomer mixture. The chemical shifts of the minor product are given

in parentheses. 1H NMR (C_6D_6): δ 9.40 (6.05) [1 H, d, $J = 8.0$ Hz, 7'-H], 7.30 and 7.10 (6.80 and 6.60) [1 H each, dd each, $J = 8.0$ and 7.5 Hz each, 5'-H and 6'-H], 6.80 (6.65) [1 H, d, $J = 8.0$ Hz, 4'-H], 7.10 and 6.95 (7.14 and 6.90) [2:3 H, m each, 3-Ph], 3.00 (4.00) [2 H, t, NCH_2], 2.00 (2.32) [2 H, t, NCH_2CH_2]. ^{13}C NMR (C_6D_6): δ 239.0 (243.0) [Cr=C], 224.9 and 217.9 (225.5 and 218.2) [1:4, *trans*- and *cis*-CO, $Cr(CO)_5$], 144.3 (143.9) [C(q), C3], 142.0 (140.4) [C(q), 7'a indoline], 137.1 (136.6) [C(q), 3'a indoline], 135.3 (134.9) [C(q), *i*-C 3-Ph]; 128.6, 126.1 and 125.4 (129.0, 126.4 and 125.9) [1:2:2, CH each, 3-Ph], 125.8 (125.1) [C(q), C2]; 126.4, 125.0, 122.6 and 116.0 (124.6, 124.3, 123.6 and 115.0) [CH each, C4-C7 indoline], 52.1 (54.3) [NCH_2], 24.8 (24.1) [Ar CH_2 indoline]. IR (hexane) [cm^{-1} (%): $\bar{\nu} = 2071.7$ (2), 1940.1 (100) [$\nu(C=O)$], 1973.8 (40) [$\nu(C=C=C)$]. MS (70 eV) [m/e (%): 423 (30) [M^+], 395 (10), 367 (20), 339 (40), 311 (40), 283 (80) [$M^+ - 5CO$], 230 (30), 117 (60), 89 (60), 63 (50), 52 (100). Anal. Calcd for $C_{22}H_{13}CrNO_5$ (423.3): C, 62.42; H, 3.10; N, 3.31. Found: C, 62.12; H, 3.00; N, 3.30.

Acknowledgment. This work was supported by the Volkswagen-Stiftung and by the Fonds der Chemischen Industrie.

Supporting Information Available: Tables of crystal data and details of the structure solution, hydrogen positional and *U* parameters, anisotropic displacement parameters, and bond distances and angles (5 pages). Ordering information is given on any current masthead page.

OM950142F

Reactions of Diazo Carbonyls with [PtX(CH₃)(chiral diphosphine)] (X = Cl, Br, I): Chemoselectivity and Diastereoselectivity of Pt–C and Pt–X Carbene Insertion

Paola Bergamini* and Emiliana Costa

Dipartimento di Chimica dell'Università di Ferrara e Centro di Studio su Fotoreattività e Catalisi del CNR, Via L. Borsari 46, 44100 Ferrara, Italy

A. Guy Orpen, Paul G. Pringle,* and Martin B. Smith

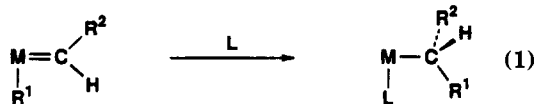
School of Chemistry, University of Bristol, Cantocks Close, Bristol BS8 1TS, U.K.

Received January 18, 1995*

In polar solvents (e.g. MeCN), ethyl diazoacetate reacts with [PtXMe(*S,S*-diop)], where X = Cl, Br, I, to give the corresponding [PtX(CHMeCO₂Et)(*S,S*-diop)] as a 2:1 mixture of diastereoisomers in high yields. The major diastereoisomer of [PtCl(CHMeCO₂Et)(*S,S*-diop)] is readily separated in crystalline form, and its crystal structure reveals that the configuration at the α -carbon is *R*; it is configurationally stable in CDCl₃ for at least 14 days. The factors that influence the diastereoselectivity have been examined by comparing (by ³¹P NMR spectroscopy) the ratio of diastereoisomers formed in the reactions between [PtXMe(diphos*)] and N₂CHCOR: X = Cl, Br, I; diphos* = *S,S*-diop, *R,R*-diop, *S,S*-skewphos, *S,S*-chiraphos; R = OEt, O(*l*-menthyl), Ph. In MeCN, the diastereoselectivity is independent of halogen but is a sensitive function of the chiral diphosphine and diazo carbonyl, though no systematic correlations have been divined. In solvents of lower polarity (e.g. CH₂Cl₂), diazo carbonyls react with [PtXMe(diphos*)] to give the products derived from Pt–X insertion as well as Pt–C insertion. When C₆H₆ is used as the solvent, the compounds [PtMe(CHICOR)(*S,S*-diop)], where R = OEt, O(*l*-menthyl), Ph, are formed in high yields and have been isolated. Redissolving these compounds in MeCN did not lead to isomerization to the Pt–C insertion species [PtI(CHMeCOR)(*S,S*-diop)]. Several trends have been found relating the extent of Pt–C insertion to the nature of the solvent and the structure of the reagents: the proportion of Pt–C insertion increases with (i) increasing polarity of the solvent (C₆H₆ < CHCl₃ < CH₂-Cl₂ < (CH₃)₂SO), (ii) increasing nucleofugacity of the halogen (I < Br < Cl), (iii) decreasing bite angle of the diphosphine (diop < chiraphos, skewphos), and (iv) diazo ketone < diazo ester. A mechanism which is consistent with these observations is discussed. Many of the compounds discussed here have been observed in solution only by ³¹P NMR, but representative species have been isolated and fully characterized by a combination of elemental analysis, IR spectroscopy, and ¹H, ¹³C, ³¹P, and ¹⁹⁵Pt NMR spectroscopy.

Introduction

One of the most important processes in organometallic chemistry, particularly in relation to organic synthesis and homogeneous catalysis, is the formation of a C–C bond within the coordination sphere of a transition metal.¹ The migration of an alkyl group to a coordinated carbene (eq 1) is an important C–C bond forming



step in the Fischer–Tropsch synthesis,² and recently this reaction (eq 1) has been exploited in organic and organometallic syntheses.³ We were interested in the insertion of substituted carbenes (RCH) into the Pt–C bonds of chiral methylplatinum(II) complexes because

of the possibility of controlling the configuration at the stereogenic center created α to the metal. In this paper we report that the reaction between diazo carbonyls and substrates of the type [PtX(CH₃)(chiral diphosphine)] (eq 2) can result in both Pt–C and Pt–X insertion occurring and in most cases these reactions are diastereoselective. A preliminary account of some of this work has been given.⁴

Results and Discussion

When [PtX(CH₃)(*S,S*-diop)] (X = Cl (**1a**), Br (**1b**), I (**1c**)) is treated with 1 equiv of N₂CHCO₂Et in CD₃CN or (CD₃)₂SO, nitrogen is evolved and, in each case, two products in the ratio 2:1 are observed by ³¹P NMR spectroscopy (see Table 1 for the data) whose structures have been assigned as **2a–c** and **3a–c** (Scheme 1) on

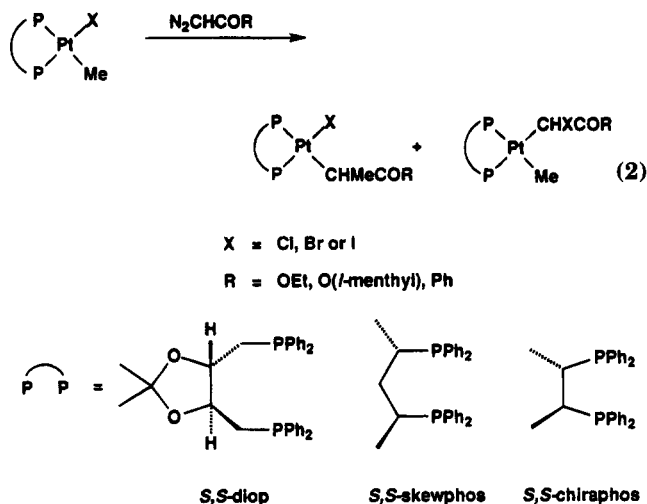
(3) For leading references see: (a) Hoover, J. F.; Stryker, J. M. *J. Am. Chem. Soc.* **1990**, *112*, 464. (b) Trace, R. L.; Sanchez, J.; Young, J.; Yim, S.; Jones, W. M. *Organometallics* **1992**, *11*, 1440. (c) Adams, H.; Bailey, N. A.; Bentley, G. W.; Tattershall, C. E.; Taylor, B. F.; Winter, M. J. *J. Chem. Soc., Chem. Commun.* **1992**, 533.

(4) Bergamini, P.; Costa, E.; Cramer, P.; Hogg, J.; Orpen, A. G.; Pringle, P. G. *Organometallics* **1994**, *14*, 1058.

* Abstract published in *Advance ACS Abstracts*, May 1, 1995.

(1) For leading references see: Collman, J. P.; Hegedus, L. S.; Norton, J. R.; Finke, R. G. *Principles of Organotransition Metal Chemistry*; University Science Books: Mill Valley, CA, 1987.

(2) Brady, R. C.; Pettit, R. *J. Am. Chem. Soc.* **1980**, *102*, 6181.



the following evidence. The major product from the reaction of **1a** was crystallized and its structure determined to be **2a** by X-ray crystallography (see below). The minor product is assigned the diastereoisomeric structure **3a** on the basis of the similarity of the spectroscopic data for **2a** and **3a** (Table 1 and Experimental Section). Reaction of the appropriate halide salt with pure **2a** gave the pure bromo and iodo analogues (**2b** and **2c**), and with 2:1 mixtures of **2a** and **3a**, 2:1 mixtures of **2b** and **3b** and of **2c** and **3c** were formed. Though it has previously been suggested⁵ that complexes containing a chiral CHMeCO₂Et ligand would be susceptible to racemization via a β-hydrogen elimination mechanism, no epimerization was observed when solutions of pure chloro complex **2a** or bromo complex **2b** in CDCl₃ were left to stand for 14 days. The iodo complexes **2c** and **3c** are more labile: after a few hours in CDCl₃, significant decomposition had taken place and one of the byproducts was identified as the diiodo complex [PtI₂(S,S-diop)].

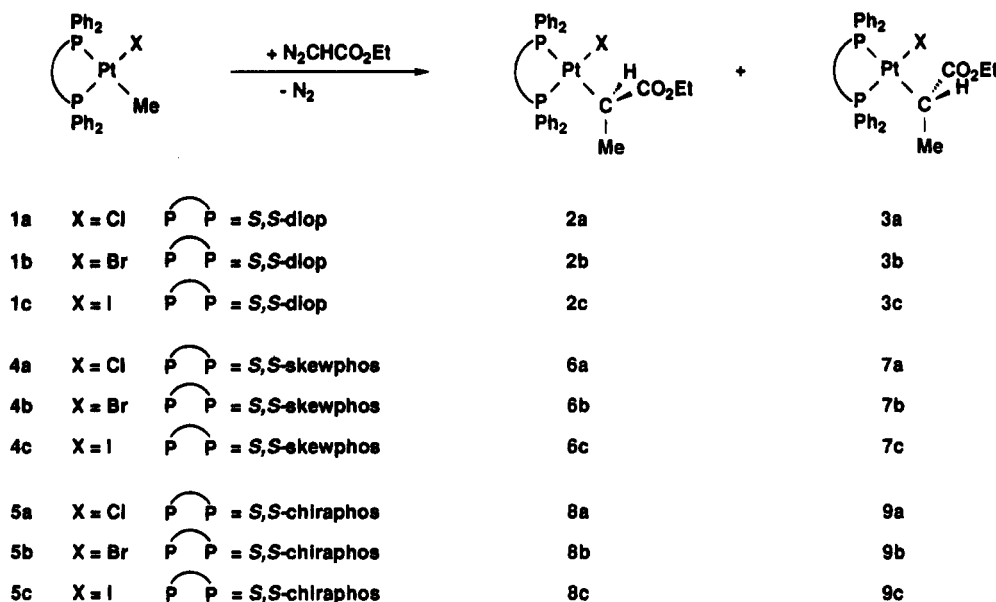
X-ray Crystal Structure of 2a. The molecular structure of **2a**, as present in the solid state, is shown in Figure 1, and the molecular dimensions are listed in Table 2. The crystal structure consists of isolated molecules of **2a** separated by normal contacts. The molecule **2a** consists of a platinum atom which is

chelated by a diop ligand and further ligated by a chloride ligand and σ-bonded to the chiral alkyl ligand through C(8) (Pt-C(8) = 2.171(14) Å). The variation in *trans* influence is indicated by the different Pt-P distances for the two diop phosphorus atoms (Pt-P(1) = 2.227(4) *trans* to Cl(1) and Pt-P(2) = 2.331(4) *trans* to C(8)). As is to be expected for a platinum(II) complex, the coordination at Pt is slightly distorted from planar (mean deviation of 0.112 Å) with a slight twist (10.8°) in the coordination plane between the PtP₂ and the PtCCl units. The *cis* and *trans* angles deviate slightly from 90 and 180°, the largest deviation for a *cis* angle being for the diop ligand (P(2)-Pt(1)-P(1) = 100.1(1°). The conformation adopted by the chiral alkyl has the α-hydrogen near the coordination plane of the platinum and pointing toward P(1) (torsion angle P(1)-Pt-C(8)-H(8a) = 16.5°). This orientation allows the bulkier Me and CO₂Et substituents at C(8) to avoid the crowded Pt coordination plane. Rather similar gross geometry was observed in [PtCl(*R*-CHClCO₂Et)(*R,R*-diop)], albeit with the opposite absolute structure.⁶ It should be noted that the favored diastereomeric configuration at the chiral α-carbon is the same in [PtCl(*R*-CHClCO₂Et)(*R,R*-diop)] and [PtCl(*R*-CHMeCO₂Et)(*S,S*-diop)] (**2a**).

Diastereoselectivity. In order to map the factors that influence the diastereoselectivity of the Pt-C insertions, we have systematically varied the ancillary diphosphine ligand, the halogen ligand, the solvent, and the diazo reagent as described below.

The complexes [PtX(CH₃)(*S,S*-skewphos)] (**4a-c**) and [PtX(CH₃)(*S,S*-chiraphos)] (**5a-c**) were treated with 1 equiv of N₂CHCO₂Et and the ratios of the diastereoisomeric products (Scheme 1) determined by the integration of the ³¹P NMR signals (Table 1). The chloro complexes **6a**, **7a** and **8a**, **9a** were isolated, but the bromo and iodo analogues were characterized only in solution by ³¹P NMR spectroscopy. The configuration of the α-carbon in the major isomer **6a** was determined to be *R* by observing that treatment of pure **2a** with *S,S*-skewphos in CH₂Cl₂ (eq 3) gave only **6a**. In DMSO, the skewphos substrates **4a-c** gave greater (5:1) diastereoselectivity than the diop substrates (2:1), while the chiraphos substrates **5a-c** gave negligible (1:1) diaste-

Scheme 1



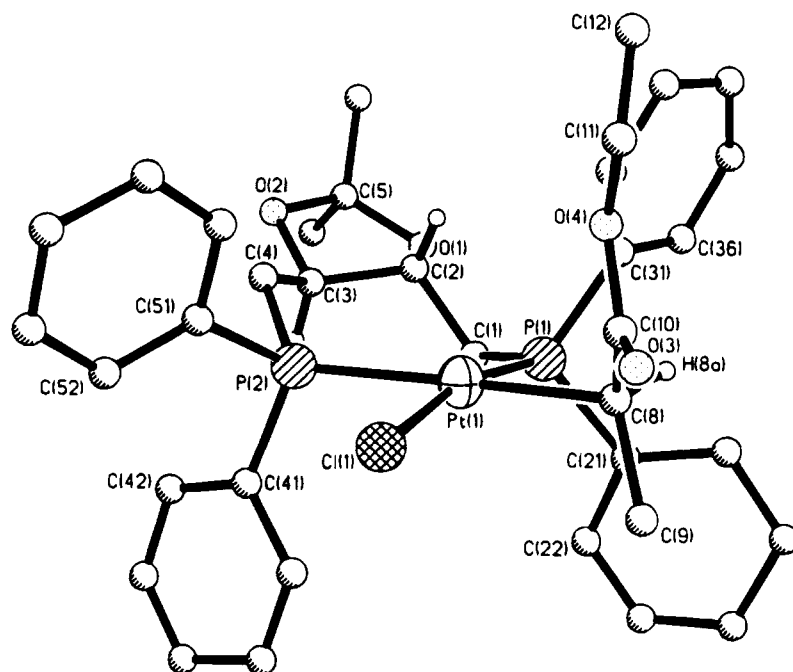
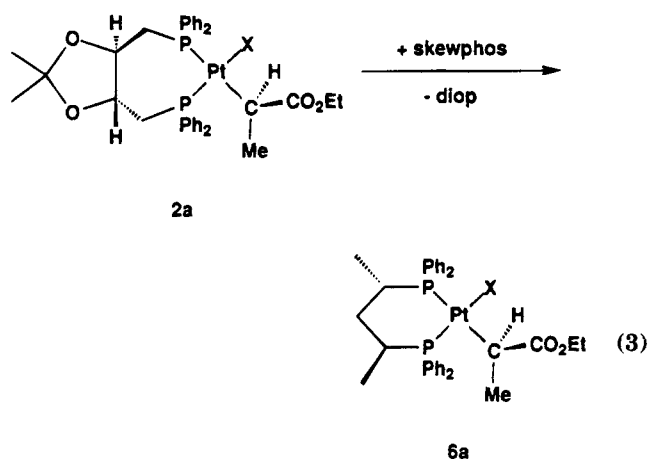


Figure 1. Molecular geometry of **2a**, showing the atom-labeling scheme. Non-hydrogen atoms are represented as ellipsoids enclosing 30% probability density. All hydrogens other than H(2a), H(3a), and H(8a) have been omitted for clarity.



reoselectivity. Hence, as expected, the diastereoselectivity of the Pt–C insertion is a function of the chiral ligand.

It was noted in the reactions shown in Scheme 1 that in polar solvents (MeCN, DMSO), the ratio of diastereoisomers was independent of the halogen. However, in less polar solvents (CHCl₃, CH₂Cl₂, C₆H₆) the ratios differ from those in polar solvents and depend on the halogen. For example, in DMSO and MeCN, the ratio of the skewphos products **6a–c**:**7a–c** is 5:1 for each of the halogens while in CDCl₃ the ratios are as follows: **6a**:**7a**, 2.5:1; **6b**:**7b**, 1.5:1; **6c**:**7c**, 1:1. This rather complex dependence of the diastereoselectivity on solvent and halogen will be discussed later.

To probe the effect of changing the diazo carbonyl reagent, [PtX(CH₃)(S,S-diop)] (**1a–c**) or the enantiomers [PtX(CH₃)(R,R-diop)] (**1a'–c'**) were treated with diazoacetophenone or *l*-menthyl diazoacetate to give **10–15** (Scheme 2). The complexes **12a**, **13a** and **14a**, **15a** have been isolated, but the other products of the

reactions shown in Scheme 2 were identified only by ³¹P NMR spectroscopy, and none of the absolute configurations have been determined. The ratio of diastereoisomers is sensitive to the structure of the diazo carbonyl: the ratio of the products derived from diazoacetophenones **10a–c** and **11a–c** was essentially 1:1 while for the menthyl ester complexes **12a–c** and **13a–c** the ratio was 4:1 (*cf.* 2:1 for the products from N₂CHCO₂Et). The subtlety of this sensitivity is illustrated by the reaction of [PtX(CH₃)(R,R-diop)] (**1a'–c'**) with *l*-menthyl diazoacetate, which in MeCN gives the products **14a–c**:**15a–c** in the ratio of 2:1. This discrimination between the enantiomers by *l*-menthyl diazoacetate indicates that some double diastereoselectivity is operating in this reaction; i.e. *l*-menthyl diazoacetate and **1a** are matched reagents.⁷ Interestingly, when a 1:1 mixture of the enantiomers **1a** and **1a'** is treated with 1 equiv of *l*-menthyl diazoacetate at 20 °C, reaction takes place preferentially with **1a**: the ratio of the products derived from **1a** and **1a'** is 2:1 (see Experimental Section).

The reaction of N₂CHCO₂Et with the bromo complex **1b** in CDCl₃ was carried out at +60, +20, and –15 °C and the diastereomeric ratio of the Pt–C insertion products found to be 2:1, 3:1, and 4:1 respectively; i.e., this reaction is more diastereoselective at lower temperatures.

Chemoselectivity. It was shown by ³¹P NMR spectroscopy that addition of N₂CHCO₂Et to [PtI(CH₃)(S,S-diop)] (**1c**) in CH₂Cl₂ gave not only the expected mixture of **2c** and **3c** but also the new species **16c** and **17c**, the products of carbene insertion into the Pt–I bond (Scheme 3). It was found that the relative proportions of the two sets of products (**2c**, **3c** and **16c**, **17c**) was a function of the solvent in which the reaction was carried out (see below). Thus, treatment of **1c** with N₂CHCO₂Et in DMSO or MeCN gave **2c** and **3c** exclusively, while in benzene **16c** and **17c** constitute *ca.* 85% of the product.

(5) Flood, T. C. In *Topics in Inorganic and Organometallic Stereochemistry*; Wiley: New York, 1981; p 37.

(6) Bergamini, P.; Costa, E.; Sostero, S.; Orpen, A. G.; Pringle, P. G. *Organometallics* **1992**, *11*, 3879.

(7) Masamune, S.; Choy, W.; Petersen, J. S.; Sita, L. R. *Angew. Chem., Int. Ed. Engl.* **1985**, *24*, 1.

Table 1. ^{31}P and ^{195}Pt NMR Data^a

	$\delta(\text{P}_A)$	$^1J(\text{PtP}_A)$	$\delta(\text{P}_B)$	$^1J(\text{PtP}_B)$	$^2J(\text{P}_A\text{P}_B)$	ratio ^b	$\delta(\text{Pt})$
1a	7.33	4318	10.10	1675	13		
1b	8.18	4295	7.70	1710	13		
1c	7.04	4104	3.49	1762	14		
2a	5.56	4305	5.07	1807	15	2.0 (2.0)	
3a	2.77	4296	3.30	1769	17		
2b	4.93	4294	2.74	1832	16	3.5 (2.0)	
3b	1.74	4282	0.23	1802	17		
2c	0.70	4113	-1.96	1868	16	3.0 (2.0)	
3c	-3.50	4107	-4.91	1827	17		
4a	18.43	4219	15.64	1611	22		
4b	18.94	4206	13.73	1633	22		
4c	17.34	4040	10.12	1670	22		
5a	44.14	4191	47.56	1678	11		
5b	44.71	4170	46.88	1680	11		
5c	43.85	4006	45.29	1684	12		
6a	13.77	4158	11.03	1749	25	2.5 (5.0)	
7a	13.63	4112	13.63	1824	24		
6b, 7b	12.86	4151	8.78	1756	26	1.5 (5.0)	
	13.62	4113	12.42	1842	24		
6c, 7c ^c	8.62	4000	5.06	1678	26	1.0 (5.0)	
	10.42	3976	9.89	1867	24		
8a, 9a	42.60	4169	43.38	1883	14	1.0 (1.0)	
	43.27	4109	43.47	1855	14		
8b, 9b	43.25	4098	42.54	1845	14	1.0 (1.0)	
	42.80	4143	42.55	1874	14		
8c, 9c ^c	41.04	3940	41.17	1833	13	1.0 (1.0)	
	40.60	3987	40.64	1857	13		
10a, 11a ^c	3.34	4280	1.29	1866	17	1.5	
	2.04	4448	2.58	1811	18		
10b, 11b ^d	4.18	4256	-1.82	1828	18	1.0	
	2.04	4237	0.68	1864	17		
10c, 11c ^d	0.11	4109	-7.77	1823	18	1.0	
	-2.51	4087	-4.24	1884	17		
12a, 13a	5.61	4316	4.34	1770	16	4.0 (4.0)	
	2.28	4248	3.63	1760	17		
12b, 13b ^c	4.57	4285	1.82	1839	17	4.0 (4.0)	
	1.51	4201	0.77	1817	17		
12c, 13c	0.52	4113	-2.90	1811	16	1.5 (4.0)	
	1.61	3915	-2.84	1930	16		
14a, 15a	5.43	4269	3.55	1766	16	2.5 (2.0)	
	3.69	4306	2.37	1762	17		
14b, 15b ^d	4.58	4247	0.10	1819	17	2.0 (2.0)	
	2.87	4278	-0.78	1811	18		
14c, 15c	0.81	4064	-3.90	1824	16	2.5 (2.0)	
	-2.59	4105	-5.96	1780	17		
16b, 17b	8.54	2440	8.54	1804	11	nr	
16c, 17c	9.49	2483	7.39	1801	11	12	-205
	8.48	2461	7.78	1783	11		-199
18c, 19c	9.72	2463	7.84	1783	11	n.r.	-235
20c, 21c	9.33	2454	7.45	1778	11	10	-208, -238
22a, 23a	8.92	2527	9.98	1811	10	nr	
22b, 23b	9.46	2560	9.31	1804	11	nr	
22c, 23c	11.10	2609	7.89	1812	11	25	-207, 218
24c, 25c ^f	19.11	2458	14.25	1707	19	nr	
26c, 27c ^f	47.85	2413	47.97	1768	10	1.0	
	46.58	2393	46.11	1737	10		
28	130.28	4531	52.47	1753	10		
29	151.14	1987	51.12	4224	10		
30	50.44	4214	143.92	2158	15		
31	131.07	4482	50.44	1948	10		

^a ^{31}P (81 MHz) and ^{195}Pt (85 MHz) NMR spectra were measured in CDCl_3 at 28 °C unless otherwise stated. Chemical shifts (δ) are in ppm (± 0.1) to high frequency of 85% H_3PO_4 or $\Xi(\text{Pt}) = 21.4$ MHz. Coupling constants (J) are in Hz (± 3). P_A is trans to the halogen, and P_B is trans to the carbon. ^b In cases where two diastereoisomers are formed, numbers in this column refer to ratios of the intensities of the ^{31}P NMR signals (data for the major isomer are given first unless stated otherwise); values in parentheses are ratios determined in MeCN instead of CDCl_3 . nr = not resolved, because either the signals for the minor isomer are too weak or they are coincident with those of the major isomer. ^c In CH_2Cl_2 (C_6D_6 in a capillary as lock). ^d In DMSO (C_6D_6 in a capillary as lock). ^e In a 1:1 $\text{CH}_2\text{Cl}_2/\text{MeCN}$ mixture (C_6D_6 in a capillary as lock). ^f In C_6D_6 .

A mixture of **16c** and **17c** was isolated from benzene, and their structures were assigned on the basis of elemental analysis, IR, ^1H , and especially ^{31}P and ^{195}Pt NMR (see Table 1 and Experimental Section), though the absolute stereochemistry is unknown. The related complexes derived from *l*-menthyl diazoacetate (**18c**, **19c**; **20c**, **21c**) and diazoacetophenone (**22c**, **23c**) have been isolated and characterized (see Table 1 and Experimental Section). In each of the Pt-I insertion

reactions studied, where the diastereoisomers have been observed, the diastereoselectivity is high (see Table 1); e.g., for the acetophenone derivatives **22c** and **23c** the ratio of diastereoisomers is ca. 25:1.

Complexes **2c** and **3c** are the products of insertion of CHCO_2Et into the Pt-C bonds of **1c**, and complexes **16c** and **17c** are the products of insertion of CHCO_2Et into the Pt-I bonds of **1c**. As in the diastereoselectivity study above, the effects of solvent, halogen ligand,

Scheme 2

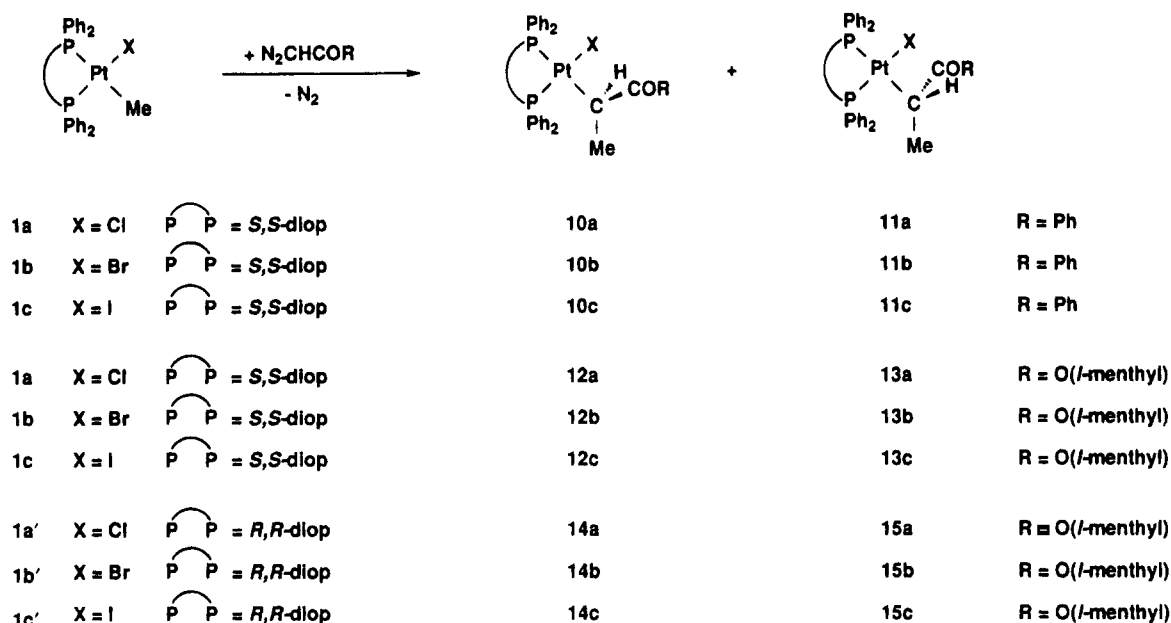


Table 2. Selected Bond Lengths (Å) and Bond Angles (deg)

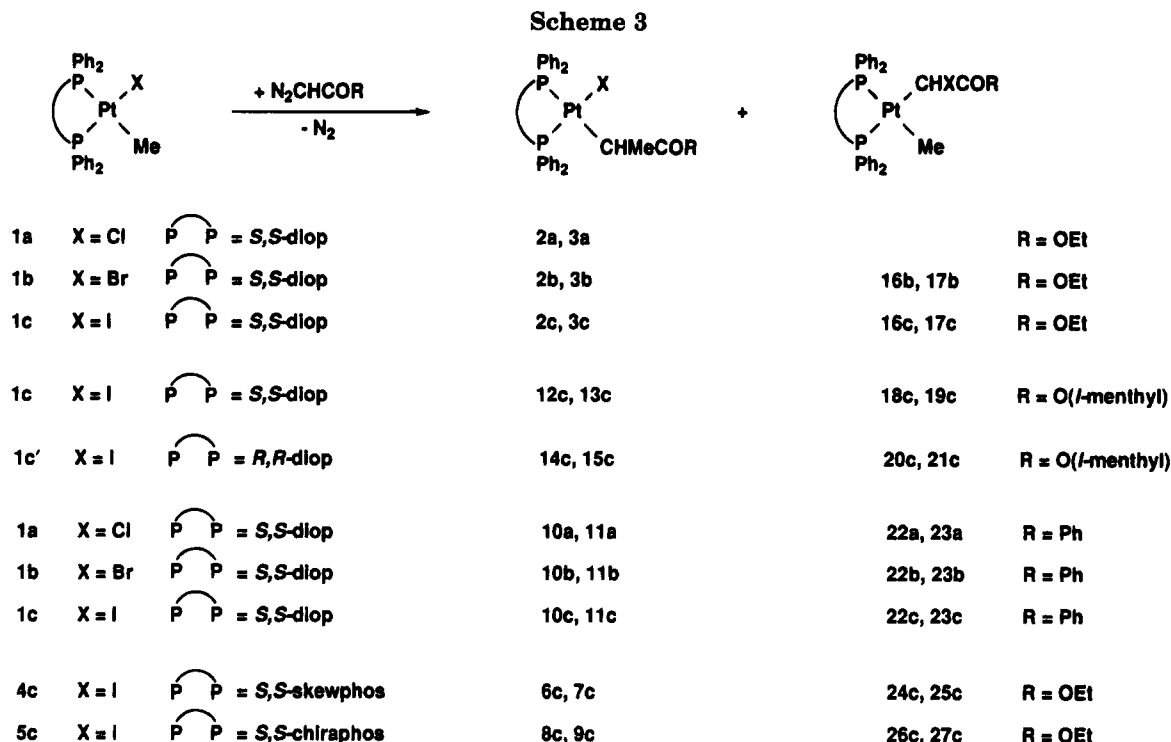
Pt(1)–Pt(1)	2.227(4)	Pt(1)–P(2)	2.331(4)	Pt(1)–Cl(1)	2.364(4)
Pt(1)–C(8)	2.171(14)	P(1)–C(1)	1.844(19)	P(1)–C(21)	1.808(17)
P(1)–C(31)	1.819(13)	P(2)–C(4)	1.855(15)	P(2)–C(41)	1.836(16)
P(2)–C(51)	1.843(15)	C(1)–C(2)	1.533(25)	C(2)–C(3)	1.494(19)
C(2)–O(1)	1.416(17)	C(3)–C(4)	1.471(20)	C(3)–O(2)	1.456(20)
O(1)–C(5)	1.431(24)	O(2)–C(5)	1.465(19)	C(5)–C(6)	1.487(29)
C(5)–C(7)	1.504(33)	C(8)–C(9)	1.552(21)	C(8)–C(10)	1.507(21)
C(10)–O(3)	1.195(20)	C(10)–O(4)	1.357(20)	O(4)–C(11)	1.454(22)
C(11)–C(12)	1.421(30)				
P(1)–Pt(1)–P(2)	100.1(1)	P(1)–Pt(1)–Cl(1)	167.4(2)		
P(2)–Pt(1)–Cl(1)	86.5(1)	P(1)–Pt(1)–C(8)	87.2(4)		
P(2)–Pt(1)–C(8)	172.6(4)	Cl(1)–Pt(1)–C(8)	86.4(4)		
Pt(1)–P(1)–C(1)	118.6(6)	Pt(1)–P(1)–C(21)	110.1(5)		
C(1)–P(1)–C(21)	102.0(8)	Pt(1)–P(1)–C(31)	116.9(4)		
C(1)–P(1)–C(31)	102.4(7)	C(21)–P(1)–C(31)	105.0(7)		
Pt(1)–P(2)–C(4)	123.2(5)	Pt(1)–P(2)–C(41)	112.5(6)		
C(4)–P(2)–C(41)	104.5(7)	Pt(1)–P(2)–C(51)	111.0(5)		
C(4)–P(2)–C(51)	96.5(7)	C(41)–P(2)–C(51)	107.2(7)		
P(1)–C(1)–C(2)	112.8(12)	C(1)–C(2)–C(3)	114.5(14)		
C(1)–C(2)–O(1)	106.4(14)	C(3)–C(2)–O(1)	103.6(11)		
C(2)–C(3)–C(4)	119.9(13)	C(2)–C(3)–O(2)	102.7(11)		
C(4)–C(3)–O(2)	109.5(14)	P(2)–C(4)–C(3)	121.4(12)		
C(2)–O(1)–C(5)	106.4(13)	C(3)–O(2)–C(5)	105.7(13)		
O(1)–C(5)–O(2)	107.2(13)	O(1)–C(5)–C(6)	107.6(19)		
O(2)–C(5)–C(6)	107.4(14)	O(1)–C(5)–C(7)	114.5(16)		
O(2)–C(5)–C(7)	106.5(18)	C(6)–C(5)–C(7)	113.3(18)		
Pt(1)–C(8)–C(9)	109.9(10)	Pt(1)–C(8)–C(10)	108.4(10)		
C(9)–C(8)–C(10)	113.7(12)	C(8)–C(10)–O(3)	125.1(14)		
C(8)–C(10)–O(4)	110.8(13)	O(3)–C(10)–O(4)	124.1(15)		
C(10)–O(4)–C(11)	117.1(13)	O(4)–C(11)–C(12)	111.8(17)		

diphosphine ligand, and diazo carbonyl reagent on the chemoselectivity for Pt–C or Pt–X insertion have been explored. The reactions shown in Scheme 3 were followed by ^{31}P NMR spectroscopy (see Table 1 for the data). In general, products derived from Pt–C and Pt–X insertion were observed and their relative proportions estimated by integration of the ^{31}P NMR signals. From the results collected in Table 3, it can be seen that the following trends in the proportion of Pt–C insertion products formed are discernible: (1) $\text{C}_6\text{D}_6 < \text{CDCl}_3 < \text{CD}_2\text{Cl}_2 < (\text{CD}_3)_2\text{SO}$; (2) $\text{I} < \text{Br} < \text{Cl}$; (3) diop < skewphos, chiraphos; (4) $\text{N}_2\text{CHCOPh} < \text{N}_2\text{CHCO}_2\text{Et}$.

The proportion of product derived from Pt–C insertion, in the reaction of $\text{N}_2\text{CHCO}_2\text{Et}$ with the bromo complex **1b** in CDCl_3 , increased at lower temperatures

(65% at +60 °C, 80% at +20 °C, 90% at –15 °C); i.e., this reaction is more chemoselective at lower temperatures.

Mechanistic Considerations. When $[\text{Pt}(\text{CH}_3)_2(S,S\text{-diop})]$ (**1c**) is treated with N_2CHCOPh in DMSO or MeCN, the Pt–C and Pt–I insertion products **10c**, **11c** and **22c**, **23c** are formed rapidly and simultaneously, in the ratio *ca.* 4:1. The isolated, pure mixture of **22c** and **23c** redissolved in DMSO or MeCN does not isomerize to **10c**, **11c** over a period of 14 days. Similarly, no isomerization is observed when any of the other Pt–I insertion products **16c**–**21c** are dissolved in MeCN or DMSO.⁸ This demonstrates that (i) the Pt–I insertion products are not intermediates in the formation of Pt–C insertion products and therefore they are formed



by parallel mechanisms and (ii) the chemoselectivity of the insertions is under kinetic control.

We propose the mechanism in Scheme 4 for the Pt-C insertion in polar solvents; it consists of nucleophilic substitution of halide by the diazo carbonyl to form the cationic intermediate **A** (step i) and then migration of the methyl group to form the new C-C bond, promoted either by recoordination of the halide (step ii) or by coordination of solvent (step iii) followed by halide substitution (step iv).⁹ Intermediate **A** has canonical forms **A**₁ and **A**₂, and the C-C bond-forming step from **A** can be viewed in two valid ways (Scheme 5): (a) as an alkyl to carbene migration which emphasizes form **A**₁ where the driving force is the formation of the strong C-C bond or (b) as a Wagner-Meerwein-like rearrangement of the carbonium ion, which emphasizes the alternative canonical form **A**₂ where the driving force is the formation of a more stable cation. McCrindle et al.^{10a} have proposed an alkyl to carbene migration in a cationic platinum(II) complex in the [PtCl(CH₃)(COD)]-catalyzed polymerization of CH₂N₂, and Stryker et al.^{3a}

(8) Addition of AgX ($X = PF_6, CF_3SO_3$) to the Pt-I insertion products **16c-23c** promoted the migration of the Me group from Pt to C quantitatively, as shown by ³¹P NMR spectroscopy (see Experimental Section). It is tempting to suggest that addition of Ag⁺ yields a cationic carbene complex (such as **A** in Scheme 4) and Me migration then occurs rapidly. However, this inference is obfuscated by the observation that the diastereomeric ratios obtained by this Ag⁺-promoted route are very different (see Experimental Section) from those obtained by direct insertions (Schemes 1 and 2). One plausible explanation of this behavior is that an intermediate iodocarbon-silver(I) complex is involved, but extensive further work would be required to elucidate this point.

(9) The possibility that methyl migration takes place within the diazoalkane complex intermediate [PtMe(N₂CHR)(diphosphine)]⁺ has also been explored using ³¹P NMR. It was reasoned that such an intermediate would be more readily formed by treatment of the labile complex [PtMe(NCMe)(S,S-dlophos)](O₃SCF₃) with N₂CHCO₂R ($R = Et, l\text{-menthyl}$). This procedure (see Experimental Section) yielded the complexes [Pt(CHMeCO₂R)(NCMe)(S,S-dlophos)](O₃SCF₃) rapidly and quantitatively, as shown by their independent synthesis upon treatment of the corresponding [PtCl(CHMeCO₂R)(S,S-dlophos)] mixture with AgO₃SCF₃. However, the ratios of diastereoisomers obtained from the MeCN complexes were different (see Experimental Section) from those obtained with the halide complexes (Scheme 1), from which it was deduced that Me migration within a diazoalkane complex does not make a major contribution to the reactions in Scheme 1.

Table 3. Ratio of Pt-C to Pt-X Insertion Products Formed in the Reaction of [PtX(CH₃)(diphos)] with N₂CHCOR in Various Solvents Expressed as a Percentage^a

X	R	diphos	(CH ₃) ₂ SO	CH ₂ Cl ₂	CHCl ₃	C ₆ H ₆
Cl	Ph	S,S-diop	100	80	65	0
Br	Ph	S,S-diop	100	65	10	0
I	Ph	S,S-diop	80	0	0	0
Cl	EtO	S,S-diop	100	100	100	100
Br	EtO	S,S-diop	100	80	80	45
I	EtO	S,S-diop	100	60	55	15
I	EtO	S,S-skew	100	100	nd	80
I	EtO	S,S-chiraphos	100	100	nd	85

^a The percentages are estimated from integration of the ³¹P signals with an error of ca. 5%. Values of 100 or 0 indicate that only one isomer was detected in the ³¹P NMR spectrum, implying that there was less than ca. 2% of the other isomer present. nd = not determined.

have described an ylide to carbene migration as a step in a platinum-mediated synthesis of (oxapentylidene)-triphenylphosphonium tetrafluoroborate. Moreover, it has been shown that alkyl to carbene migration occurs particularly readily when the complex is cationic.¹⁰

The intermediacy of **A** in the Pt-C insertion reaction (Scheme 4) can be used to rationalize the following observations:

(1) Solvents that would promote the formation of an ionic intermediate **A** (i.e. polar solvents of high dielectric constant) promote Pt-C insertion.

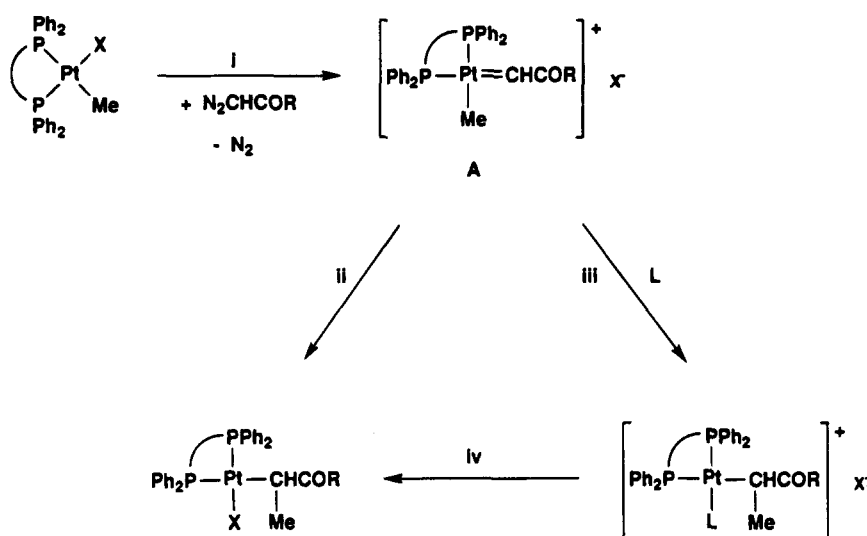
(2) The order of increasing nucleofugacity from platinum(II) ($I < Br < Cl$)¹¹ is the same as the order of increasing tendency to Pt-C insertion because the better the leaving group, the easier the formation of intermediate **A**.¹²

(3) In DMSO or MeCN, the diastereomeric ratio of Pt-C insertion products is independent of the halogen

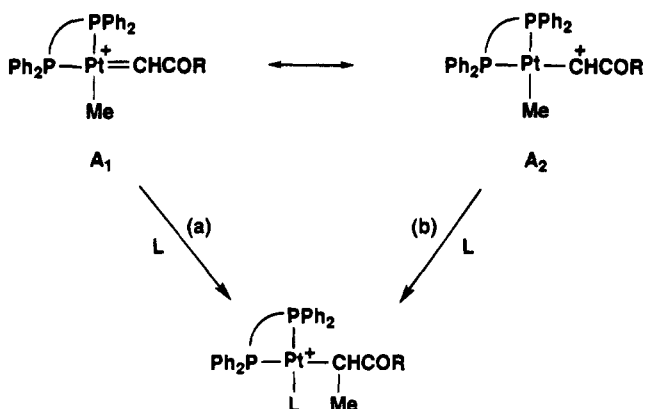
(10) (a) McCrindle, R.; Arsenault, G. J.; Farwaha, R.; Hampden-Smith, M. J.; McAlees, A. J. *J. Chem. Soc., Chem. Commun.* **1986**, 943. (b) Thorn, D. L.; Tulip, T. H. *J. Am. Chem. Soc.* **1981**, *103*, 5984. (c) Hubbard, J. L.; Morneau, A.; Burns, R. M.; Nadeau, O. W. *J. Am. Chem. Soc.* **1991**, *113*, 9180.

(11) Tobe, M. L. *Inorganic Reaction Mechanisms*; Nelson: London, 1972.

Scheme 4



Scheme 5



Scheme 7. It is proposed that Pt–X insertion occurs directly from a neutral, trigonal-bipyramidal carbene complex such as **B**.¹³ Therefore, Pt–X insertion should be favored by factors that stabilize **B** relative to the cationic carbene **A**. Clearly, nonpolar solvents would relatively stabilize neutral species **B**. Iodide is well-known to stabilize five-coordinate platinum(II),¹⁴ and the equatorial angle of 120° will be more easily spanned by diop than by skewphos or chiraphos.¹⁵ Explanations for the effect of the diazo carbonyl reagent on the chemoselectivity and the observed high diastereoselectivity for the Pt–X insertions (Table I) remain elusive.

It had been previously noted (see above) that the ratio of diastereoisomers from the reaction of [PtX(CH₃)-(chiral diphos)] was independent of halogen X when the reaction was carried out in MeCN or DMSO, but this was no longer true when the reactions were carried out in less polar solvents. This suggests that, in nonpolar solvents, the halogen is coordinated at the C–C bond-forming step, indicating that some Pt–C insertion may derive from methyl migration within a neutral intermediate such as **B** (Scheme 7).¹³

Conclusion. It has been demonstrated that a new C–C bond can be diastereoselectively created within the coordination sphere of platinum(II) by the insertion of a substituted carbene into a Pt–C bond. While the factors that control the chemoselectivity (Pt–C versus Pt–X) are well understood, the diastereoselectivity of these reactions is not a simple function of substrate or diazo reagent and is influenced strongly by solvent effects.

Experimental Section

All reactions were carried out under an atmosphere of nitrogen, though the products could be handled in air. CH₂-

for each of the reactions shown in Schemes 1 and 2, as expected if the halogen is lost to give intermediate **A**.

(4) The geometric isomers **28** and **29** (see Scheme 6) are available as 1:1 and a 1:3 mixtures (see Experimental Section). Treatment of these mixtures with N₂-CHCO₂Et in CDCl₃ gave a 1:1 and 1:3 mixture of the products **30** and **31**, respectively, as shown unambiguously by ³¹P NMR spectroscopy (see Table 1 and Experimental Section for the characterization data). These observations are consistent with **28** giving **30** and **29** giving **31** (Scheme 6), and therefore these reactions involve an inversion of configuration at the platinum. This is precisely what would be predicted from the mechanism in Scheme 4. Substitution of the chloride in **28** would give a cationic species similar to **A** from which the product **30** would be formed by methyl migration and chloride recoordination (as in Scheme 6). Using the same reasoning, **31** would be the predicted product from **29**.

Though investigation of the Pt–C insertions was the principal thrust of this work, we have also considered the Pt–X insertions that occur simultaneously. The factors that promote Pt–X insertion, which are (see above) (a) nonpolar solvents, (b) I > Br > Cl, (c) diop rather than skewphos or chiraphos complexes, and (d) N₂CHCOPh rather than N₂CHCO₂R, can be largely accounted for by the unified mechanism shown in

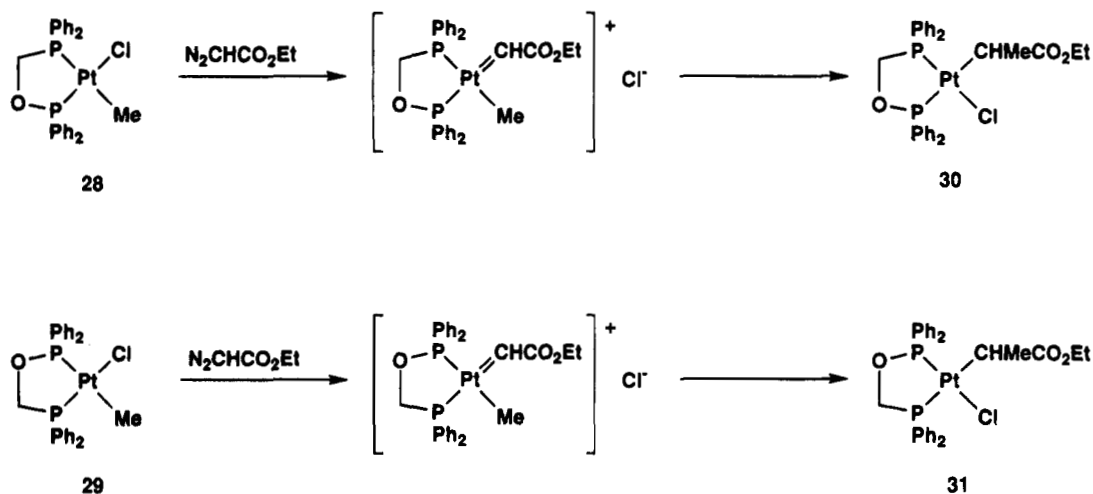
(12) No reaction took place between [Pt(CH₃)₂(*R,R*-diop)] and N₂-CHCO₂Et in CDCl₃ even after reflux for 2 h, consistent with the requirement for a labile group on the platinum.

(13) It is possible that a proportion of the Pt–X insertion products and the Pt–C insertion products in nonpolar solvents are derived from diazoalkane complexes such as **C** (Scheme 7), since the features discussed here that should stabilize **B** would also stabilize **C**. The distinction between routes via **B** and **C** is a question of whether migration of X or Me is synchronous with N₂ loss. It has previously been suggested that, in nonpolar solvents, complexes of the type [Pt(CH₃)(CHCl₂)(dppe)] rearrange by alkyl migration to [PtCl(CHClCH₃)(dppe)]; see: van Leeuwen, P. W. N. M.; Roobeek, C. F.; Huis, R. J. *Organomet. Chem.* **1977**, *142*, 243.

(14) Favez, R.; Roulet, R.; Pinkerton, A. A.; Schwarzenbach, D. *Inorg. Chem.* **1980**, *19*, 1356.

(15) Casey, C. P.; Whiteker, G. T.; Melville, M. G.; Petrovich, L. M.; Gavney, J. A.; Powell, D. R. *J. Am. Chem. Soc.* **1992**, *117*, 5535.

Scheme 6



Cl₂ was distilled from CaH₂ under nitrogen. All the diphosphines (Aldrich) and N₂CHCO₂Et (Fluka) were used as purchased, and N₂CHCO₂(*l*-menthyl),¹⁶ N₂CHCOPh,¹⁷ and [PtX(CH₃)(COD)] (COD = 1,5-cyclooctadiene; X = Cl, Br, I)¹⁸ were made by literature methods. FT-IR spectra were obtained using a Nicolet 510P spectrometer. ³¹P (81 MHz) and ¹H NMR spectra were measured in CDCl₃ at +22 °C using a Bruker AM200 spectrometer (200 MHz) or at +25 °C using a Varian Gemini 300 spectrometer (300 MHz). ¹⁹⁵Pt NMR spectra were measured at 85.6 MHz in CDCl₃ at 25 °C using a JEOL GX400 spectrometer; chemical shifts (δ) are to high frequency of 85% H₃PO₄, Si(CH₃)₄, or Ξ(Pt) = 21.4 MHz.

Preparation of [PtI(CH₃)(S,S-diop)] (1c). A solution of 179 mg (0.36 mmol) of *S,S*-diop in 20 mL of CH₂Cl₂ was added dropwise over 30 min to a solution of 160 mg (0.36 mmol) of [PtI(CH₃)(COD)] in 30 mL of CH₂Cl₂, and the mixture was stirred for 1 h. The solvent was then stripped under reduced pressure, and the yellow solid product (277 mg, 92%) was triturated with 5 mL of Et₂O and then filtered off. All the complexes **1a–c**, **4a–c**, and **5a–c** were made similarly in yields of 85–90%.

Preparation of [PtCl(CHMeCO₂Et)(S,S-diop)] (2a, 3a). A 1.4 mL amount of a 0.438 M solution of N₂CHCO₂Et (0.6 mmol) in CH₂Cl₂ was added to a solution of 200 mg (0.27 mmol) of [PtCl(CH₃)(S,S-diop)] in 8 mL of CH₂Cl₂ and the mixture stirred for 16 h. The solution was then evaporated to 0.5 mL and 15 mL of *n*-pentane added to precipitate the white solid product (182 mg, 82%). The isomer **2a** was crystallized by layering a CH₂Cl₂ solution of the mixture of **2a** and **3a** with Et₂O. Characterization data for **2a** and **3a** (see Table 1 for ³¹P NMR) are as follows. Anal. Found (calcd) for C₃₆H₄₁ClO₄P₂Pt·CH₂Cl₂: C, 48.65 (48.55); H, 4.80 (4.75). IR (CsI pellet): ν(CO) 1701 (s), ν(PtCl) 290 (m) cm⁻¹. ¹H NMR (CDCl₃) for **2a**: δ 0.66 (³J_{Pt-H} = 32.6 Hz, ³J_{H-H} = 7.7 Hz, ⁴J_{P-H} = 7.7 Hz, 3H, PtCHCH₃), 2.15 (assigned from COSY to PtCHCH₃). ¹³C NMR (CDCl₃) for **2a**: δ 15.3 (²J_{Pt-C} = 57.6 Hz, PtCHCH₃), 32.0 (assigned from DEPT to PtCHCH₃). ¹H NMR (CDCl₃) for **3a**: δ 0.9 (³J_{Pt-H} not resolved, ³J_{H-H} = 7.5 Hz, ⁴J_{P-H} = 7.5 Hz, 3H, PtCHCH₃).

The following were made similarly: **6a**, **7a** (67%), **8a**, **9a** (67%), **12a**, **13a** (62%), **14a**, **15a** (68%). Elemental analysis and IR (CsI disk) data are as follows. **6a**, **7a**: Anal. Found (calcd for C₃₃H₃₇ClO₂P₂Pt·0.25CH₂Cl₂): C, 51.25 (51.25); H, 5.15 (4.80). ν(CO): 1695 (s) cm⁻¹. **8a**, **9a**: Anal. Found (calcd for C₃₂H₃₅ClO₂P₂Pt·0.25CH₂Cl₂): C, 51.05 (50.65); H, 5.00 (4.65). ν(CO): 1688 (s) cm⁻¹. **12a**, **13a**: Anal. Found (calcd for C₄₅H₅₃ClO₄P₂Pt·0.75CH₂Cl₂): C, 53.95 (54.15); H, 5.75 (5.45). ν(CO): 1701 (s) cm⁻¹. **14a**, **15a**: Anal. Found (calcd

for C₄₄H₅₅ClO₄P₂Pt·0.25CH₂Cl₂): C, 54.90 (55.25); H, 5.90 (5.80). ν(CO): 1696 (s) cm⁻¹. The configuration of the α-carbon in **6a** was determined to be *R* by adding skewphos (1 equiv) to a CDCl₃ solution of pure **2a**, and after 5 h the formation of **6a** (and no **7a**) was detected by ³¹P NMR spectroscopy.

Preparation of [PtBr(CHMeCO₂Et)(S,S-diop)] (2b, 3b) and [PtI(CHMeCO₂Et)(S,S-diop)] (2c, 3c). **Procedure A.** A 1.0 mL portion of a 0.438 M solution of N₂CHCO₂Et (0.44 mmol) in CH₂Cl₂ was added to a solution of 165 mg (0.21 mmol) of [PtBrMe(S,S-diop)] in 4 mL of MeCN, and the mixture was stirred for 3 h. The solution was then evaporated to dryness to leave a colorless oil. Addition of 2 mL of Et₂O and 15 mL of *n*-pentane gave the white solid product (140 mg, 76%). Characterization data for **2b**, **3b** are as follows. Anal. Found (calcd for C₃₆H₄₁BrO₄P₂Pt·CH₂Cl₂): C, 49.65 (49.45); H, 4.85 (4.70). IR (CsI pellet): ν(CO) 1701 (s) cm⁻¹. ¹H NMR (CDCl₃) for **2b**: δ 0.64 (³J_{Pt-H} = 34.4 Hz, ³J_{H-H} = 7.7 Hz, ⁴J_{P-H} = 7.7 Hz, 3H); it was not possible to assign any other signals because of the complex overlapping multiplets associated with diop resonances in the δ 1–4 region.

Procedure B. A solution of 174 mg (2.0 mmol) of LiBr in 1 mL of MeCN was added to a solution of 166 mg (0.20 mmol) of [PtCl(CHMeCO₂Et)(S,S-diop)] in 1 mL of CH₂Cl₂ and 4 mL of MeCN, and the mixture was stirred at ambient temperature for 1 h. The solvent was then removed under reduced pressure, water and CH₂Cl₂ were added, and the organic layer was separated, dried over Na₂SO₄, and then reduced to dryness. Trituration of the residue with Et₂O gave the white solid product (150 mg, 81%).

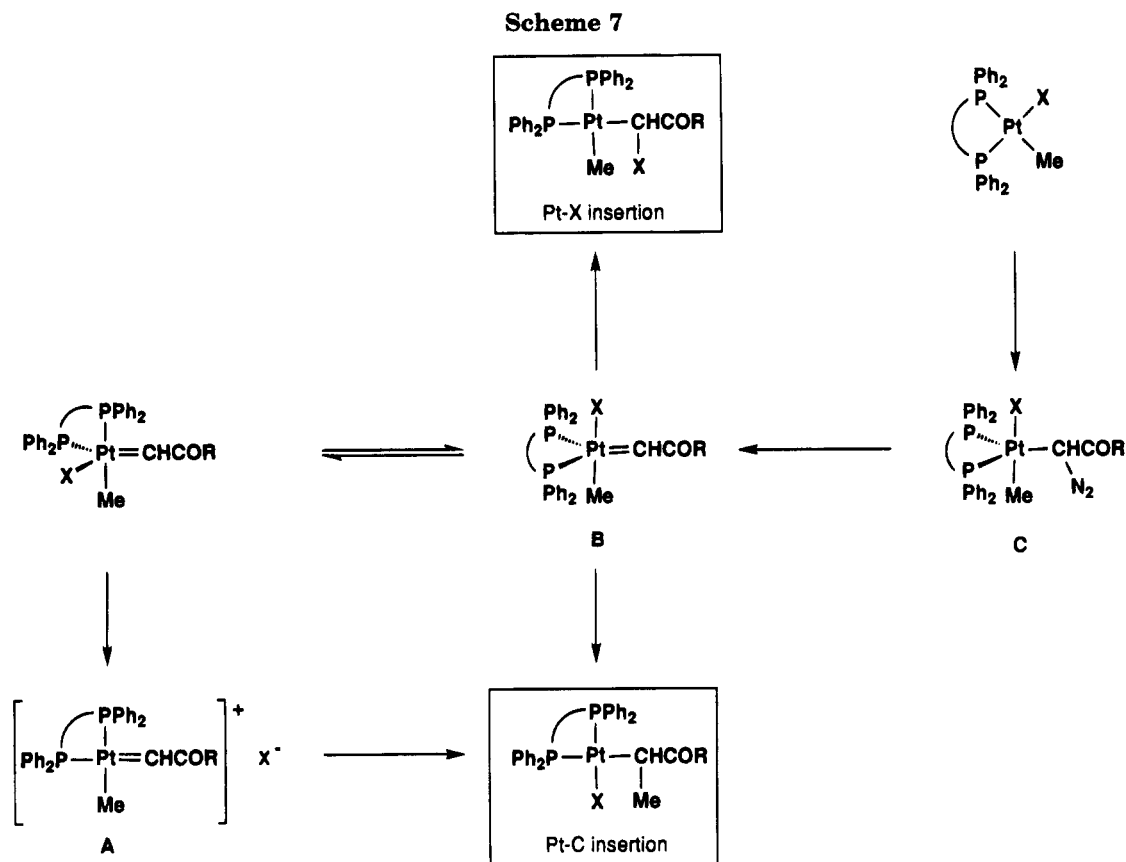
The iodo species **2c** and **3c** can be made similarly by either procedure A or B, but the product was always contaminated with small amounts (5–10%) of [PtI₂(S,S-diop)] and other decomposition products and was not obtained in pure form (see Table 1 for ³¹P NMR data). The bromo complexes **6b–9b** and **12b–15b** and the iodo complexes **6c–9c** and **12c–15c** were made by procedure A and characterized in solution only by ³¹P NMR (see Table 1).

Preparation of [PtMe(CHICO₂Et)(S,S-diop)] (16c, 17c). A solution of 80 mg (0.70 mmol) of N₂CHCO₂Et in 1 mL of C₆H₆ was added to a solution of 180 mg (0.21 mmol) of [PtIme(S,S-diop)] in 4 mL of C₆H₆ and the mixture stirred for 4 h. The solution was then evaporated to dryness to give a yellow oil, and 2 mL of Et₂O and 15 mL of *n*-pentane were added to give the off-white solid product (120 mg, 62%). Characterization data for **16c**, **17c** are as follows. Anal. Found (calcd for C₃₆H₄₁IO₄P₂Pt·0.75CH₂Cl₂): C, 44.85 (44.75); H, 4.35 (4.30). IR (CsI pellet): ν(CO) 1709 (s) cm⁻¹. ¹H NMR (CDCl₃): δ 0.50 (³J_{Pt-H} = 63.3 Hz, 3H, PtCH₃). The following were made similarly: **18c**, **19c** (71%), **20c**, **21c** (70%), **22c**, **23c** (62%) (made in CH₂Cl₂). ³¹P and ¹⁹⁵Pt NMR data are given in Table 1 but the ¹H NMR spectra of these complexes were uninforma-

(16) Fritschi, H.; Leutenegger, U.; Pfaltz, A. *Helv. Chim. Acta* **1988**, *71*, 1553.

(17) Scott, L. T.; Minton, M. A. *J. Org. Chem.* **1977**, *42*, 3757.

(18) Clark, H. C.; Manzer, L. E. *J. Organomet. Chem.* **1973**, *59*, 411.



tive because the PtCHMe signals were obscured by the diop and menthyl resonances. Elemental analysis and IR (CsI disk) data are as follows. **18c, 19c**: Anal. Found (calcd for $C_{44}H_{55}IO_4P_2Pt \cdot CH_2Cl_2$): C, 48.65 (48.35); H, 5.10 (5.25). $\nu(\text{CO})$: 1702 (s) cm^{-1} . **20c, 21c**: Anal. Found (calcd for $C_{44}H_{55}IO_4P_2Pt \cdot 0.5CH_2Cl_2$): C, 49.65 (49.70); H, 5.40 (5.35). $\nu(\text{CO})$: 1705 (s) cm^{-1} . **22c, 23c**: Anal. Found (calcd for $C_{40}H_{41}IO_3P_2Pt$): C, 50.60 (50.35); H, 4.30 (4.30). $\nu(\text{CO})$: 1651 (s) cm^{-1} .

Reaction of *rac*-[PtCl(CH₃)(diop)] with *l*-Menthyl Diazoacetate. To a mixture of 20 mg (0.027 mmol) of [PtCl(CH₃)-(*S,S*-diop)] and 20 mg (0.027 mmol) of [PtCl(CH₃)-(*R,R*-diop)] dissolved in 0.4 mL of $CDCl_3$ in an NMR tube was added 6 mg (0.027 mmol) of *l*-menthyl diazoacetate and the progress of the reaction followed by measuring the ^{31}P NMR spectrum at regular intervals. The reaction was complete after 10 h.

NMR Reactions To Determine Chemoselectivity/Diastereoselectivity. In a typical experiment a solution of 0.025 mmol of platinum substrate [PtX(CH₃)-(*S,S*-diop)] in 0.4 mL of solvent (DMSO, CH_2Cl_2 , $CHCl_3$, C_6H_6) in an NMR tube (containing a capillary tube of C_6D_6 for lock) was treated with 0.025 mmol of a 0.438 M solution of N_2CHCO_2Et in the same solvent and the mixture shaken. All other combinations of reagents shown in Table 3 were studied in the same way.

Preparation of [PtClMe(Ph₂PCH₂OPPh₂)] (28, 29**).** A solution of 89 mg (0.27 mmol) of [Pt(CH₃)(COD)] in 25 mL of dry, deoxygenated CH_2Cl_2 was cooled to -20°C , and then 59 mg (0.27 mmol) of Ph_2PCH_2OH and 50 μL (0.28 mmol) of Ph_2PCl were added in rapid succession. The resulting solution was stirred for 1 h, and then the solution was warmed slowly to room temperature. The solution was then concentrated to 1–2 mL, and 50 mL of Et_2O was added to precipitate the white solid product, which was filtered off in air and washed with 5 mL of Et_2O . The product (113 mg, 65%) was a 1:1 mixture of geometric isomers **28** and **29**. The filtrate contained a 1:3 mixture of **28** and **29**, respectively. Anal. Found (calcd for $C_{26}H_{25}ClO_2Pt$): C, 48.40 (48.35); H, 3.90 (3.90). IR (CsI pellet): $\nu(\text{PtCl})$ 295 (m) cm^{-1} .

Preparation of [PtCl(CHMeCO₂Et)(Ph₂PCH₂OPPh₂)] (30, 31**).** A 48 μL (0.46 mmol) portion of N_2CHCO_2Et was

added to a suspension of a 1:1 mixture of **28** and **29** in 0.7 mL of CD_2Cl_2 in an NMR tube. The progress of the reaction was monitored by ^{31}P NMR spectroscopy. After 4 h the reaction was complete and the yellow solution was added to 20 mL of *n*-pentane to precipitate the white solid mixture of isomers **30** and **31** (81 mg, 75%), which was filtered off and washed with 5 mL of *n*-pentane. Anal. Found (calcd for $C_{30}H_{31}ClO_3P_2Pt$): C, 49.00 (49.20); H, 4.35 (4.30). IR (CsI pellet): $\nu(\text{PtCl})$ 305 (m) cm^{-1} ; $\nu(\text{CO})$ 1695(s), 1670(s) cm^{-1} .

Reaction of [PtMe(CHICO₂Et)(*S,S*-diop)] with Silver Salts. A 6.8 mg (0.027 mmol) amount of AgO_3SCF_3 was added to a solution of 25 mg (0.027 mmol) of [PtMe(CHICO₂Et)-(*S,S*-diop)] in 0.5 mL of a 1:1 mixture of CH_2Cl_2 and MeCN. After 5 min the solution was filtered free of the pale yellow AgI precipitate and the product examined by ^{31}P NMR spectroscopy. Addition of 25 mg (0.057 mmol) of [AsPh₄]Cl·H₂O to the solution generated **2a** and **3a** exclusively. The results were exactly the same when $AgPF_6$ or $AgBF_4$ was used in place of silver triflate. Similar experiments were carried out between silver salts and [PtMe(CHICO₂R*)(*S,S*-diop)] or [PtMe(CHICO₂R*)(*R,R*-diop)] ($R^* = l$ -menthyl). In each of these experiments, the ratio of the diastereomeric products differed significantly from those obtained via the route shown in Scheme 1. The ratios of the products were as follows (ratios obtained via Scheme 1 shown in parentheses for comparison): **2a, 3a**, 1:2 (2:1); **12a, 13a**, 1:1 (4:1); **14a, 15a**, 1:4 (2:1).

Reaction of [PtMe(NCMe)(*S,S*-diop)][O₃SCF₃] with *N*-CHCO₂Et. A solution of 25 mg (0.034 mmol) of [PtCl(CH₃)-(*S,S*-diop)] in 0.4 mL of MeCN (C_6D_6 capillary for lock) was treated with 12 mg (0.034 mmol) of AgO_3SCF_3 (identical results were obtained when $AgBF_4$ was used). After 5 min, the resulting suspension was filtered free of AgCl and then 0.034 mmol of a 0.438 M solution of N_2CHCO_2Et in MeCN was added; the products were assigned by ^{31}P NMR spectroscopy to diastereoisomers of [Pt(CHMeCO₂Et)(NCMe)-(*S,S*-diop)][O₃SCF₃]. (Precisely the same products were obtained upon treatment of [PtCl(CHMeCO₂Et)-(*S,S*-diop)] (**2a** and **3a**) with AgO_3SCF_3 in MeCN). Addition of 15 mg (0.034 mmol) of [AsPh₄]Cl to the solutions of [Pt(CHMeCO₂Et)(NCMe)-(*S,S*-diop)][O₃SCF₃] gave the familiar resonances for **2a** and **3a**,

Table 4. Atomic Coordinates ($\times 10^4$) and Equivalent Isotropic Displacement Parameters ($\text{\AA}^2 \times 10^3$)

atom	x	y	z	U_{eq}^a
Pt(1)	2634(1)	2197(1)	1965(1)	39(1)
P(1)	3119(2)	1217(2)	2379(4)	38(1)
P(2)	2360(3)	2552(2)	4020(4)	43(1)
Cl(1)	2399(3)	3273(2)	1315(4)	65(2)
C(1)	3322(11)	995(9)	4043(18)	68(6)
C(2)	2546(11)	907(6)	4823(14)	54(5)
C(3)	2368(12)	1447(6)	5721(13)	56(5)
C(4)	1932(10)	2022(6)	5271(15)	52(5)
O(1)	2684(10)	373(5)	5635(10)	78(5)
O(2)	1897(10)	1131(5)	6709(13)	90(5)
C(5)	2152(15)	453(7)	6695	80(6)
C(6)	2632(16)	338(10)	7868(17)	106(7)
C(7)	1391(15)	56(11)	6629(27)	126(8)
C(8)	2818(9)	1981(7)	-31(13)	45(4)
C(9)	3601(9)	2315(7)	-513(16)	54(5)
C(10)	2068(10)	2176(8)	-749(15)	54(5)
O(3)	2042(7)	2582(5)	-1554(10)	59(4)
O(4)	1419(7)	1825(6)	-365(12)	66(4)
C(11)	666(11)	1919(9)	-1055(21)	74(6)
C(12)	103(12)	1415(12)	-810(28)	126(8)
C(21)	4105(10)	1119(7)	1658(17)	56(5)
C(22)	4762(11)	1401(8)	2238(26)	84(7)
C(23)	5497(14)	1388(11)	1694(37)	135(9)
C(24)	5624(17)	1166(13)	559(39)	151(9)
C(25)	4968(17)	827(10)	-103(24)	114(8)
C(26)	4180(11)	808(9)	484(19)	74(6)
C(31)	2528(8)	534(6)	1814(12)	41(4)
C(32)	1723(11)	621(8)	1432(18)	64(6)
C(33)	1248(15)	107(10)	1068(27)	119(8)
C(34)	1559(15)	-503(11)	992(23)	99(8)
C(35)	2308(14)	-594(8)	1431(20)	85(7)
C(36)	2803(10)	-93(7)	1790(16)	56(5)
C(41)	3239(9)	2935(7)	4773(16)	48(5)
C(42)	3321(11)	3047(9)	6079(17)	64(6)
C(43)	3995(13)	3345(10)	6511(21)	82(7)
C(44)	4598(12)	3544(10)	5789(23)	81(7)
C(45)	4546(12)	3431(10)	4470(19)	73(6)
C(46)	3874(11)	3143(8)	3989(21)	65(6)
C(51)	1532(9)	3149(7)	4024(16)	42(5)
C(52)	1627(10)	3746(7)	4567(19)	59(5)
C(53)	955(13)	4166(9)	4479(22)	85(7)
C(54)	231(12)	3978(10)	3973(20)	76(7)
C(55)	153(11)	3379(10)	3419(19)	75(6)
C(56)	813(10)	2958(8)	3478(21)	73(6)

^a Equivalent isotropic U , defined as one-third of the trace of the orthogonalized U_{ij} tensor.

but in the ratio 1:2.5 (cf. 2:1 in the direct reaction shown in Scheme 1). A similar experiment was carried out between $\text{N}_2\text{-CHCO}_2(l\text{-menthyl})$ and $[\text{PtMe}(\text{NCMe})(\text{S,S-diop})][\text{O}_3\text{SCF}_3]$, and the products **12a** and **13a** were obtained in the ratio 1:4 (cf. 2:1 via Scheme 1).

Structure Analysis of $[\text{PtCl}\{\text{R-CHClCO}_2\text{Et}\}(\text{S,S-diop})]$ (2a**).** Crystal data for **2a**: $\text{C}_{36}\text{H}_{41}\text{ClO}_4\text{P}_2\text{Pt}$, $M_r = 830.2$, orthorhombic, space group $P2_12_12$ (No. 18), $a = 16.520(5)$ \AA , $b = 20.722(6)$ \AA , $c = 10.535(4)$ \AA , $V = 1930.8(7)$ \AA^3 , $Z = 4$, $D_x = 1.53$ g cm^{-3} , $\lambda = 0.71073$ \AA , $\mu(\text{Mo K}\alpha) = 40.9$ cm^{-1} , $F(000) = 1656$, $T = 293$ K. A single crystal of **2a** (approximate dimensions $0.20 \times 0.50 \times 0.60$ mm) was mounted in a thin-walled glass capillary under N_2 and held in place with epoxy glue. All diffraction measurements were made at room temperature (293 K) on a Siemens R3m/V diffractometer, using graphite-monochromated Mo K α X-radiation. Unit cell dimensions were determined from 49 centered reflections in the range $14.0 < 2\theta < 31.0^\circ$. A total of 3808 diffracted intensities, including check reflections, were measured in a unique octant of reciprocal space for $4.0 < 2\theta < 50.0^\circ$ by Wyckoff ω scans.

Three check reflections (1,5,-3; 127; 3,2,-4) remeasured after every 50 ordinary data showed no decay and a variation of $\pm 4\%$ over the period of data collection. Of the 3577 intensity data (other than checks) collected, 3360 unique observations remained after averaging of duplicate and equivalent measurements and deletion of systematic absences; of these, 2802 with $I > 2\sigma(I)$ were retained for use in structure solution and refinement. An absorption correction was applied on the basis of 350 azimuthal scan data; maximum and minimum transmission coefficients were 0.727 and 0.292, respectively. Lorentz and polarization corrections were applied.

The structure was solved by Patterson and Fourier methods. All non-hydrogen atoms were assigned anisotropic displacement parameters and all hydrogen atoms fixed isotropic displacement parameters. All non-hydrogen atoms were refined without positional constraints. All hydrogen atoms were constrained to idealized geometries ($\text{C-H} = 0.96$ \AA , $\text{H-C-H} = 109.5^\circ$) with fixed isotropic displacement parameters. A parameter (η) defining the absolute structure, and hence the molecular chirality,¹⁹ was refined to 0.94(4), thereby confirming the handedness of the molecules of **2a** in the crystal studied. Full-matrix least-squares refinement of this model (398 parameters) converged to final residual indices $R = 0.047$, $R_w = 0.054$, and $S = 1.34$.²² Weights, w , were set equal to $[\sigma_c^2(F_o) + gF_o^2]^{-1}$, where $\sigma_c^2(F_o)$ is the variance in F_o due to counting statistics and $g = 0.0008$ was chosen to minimize the variation in S as a function of $|F_o|$. Final difference electron density maps showed no features outside the range $+1.2$ to -1.2 e \AA^{-3} , the largest of these being close to the platinum atom. Table 4 lists the final atomic positional parameters for the freely refined atoms and Table 2 the selected derived bond lengths and inter-bond angles. Tables in the supplementary material provide the final atomic positional parameters for the non-hydrogen atoms, full lists of the derived bond lengths and interbond angles, the anisotropic displacement parameters, and hydrogen atomic parameters. All calculations were carried out using programs of the SHELXTL-PLUS package.²⁰ Complex neutral-atom scattering factors were taken from ref 21.

Acknowledgment. We thank the following for experimental assistance: Ms. K. L. Mason (synthesis), Mr. J. K. Hogg and Mr. P. Cramer (X-ray crystallography), and Prof. S. Sostero (NMR). In addition, P.G.P. thanks Ciba-Geigy for the Senior Research Fellowship and the staff at the Dipartimento di Chimica at the Università di Ferrara for making the stay so enjoyable. Further financial support was given by Prof. O. Traverso, The Foundation Stiftelsen Blanceflor Boncompagni-Ludovisi f6dd Bildt (grant to E.C.), NATO (travel grant to P.G.P. and P.B.), and Johnson-Matthey (loan of platinum salts).

Supporting Information Available: Text giving additional details of the X-ray study and tables giving additional bond distances and angles, anisotropic thermal parameters, and H atom coordinates for **2a** (7 pages). Ordering information is given on any current masthead page.

OM950040P

(19) Rogers, D. *Acta Crystallogr., Sect. A* **1981**, *37*, 734.

(20) Sheldrick, G. M. SHELXTL-PLUS Rev. 2.4; University of G6ttingen, G6ttingen, FRG, 1988.

(21) *International Tables for X-ray Crystallography*; Kynoch Press: Birmingham, U.K., 1974; Vol. IV.

(22) $R = \sum |\Delta| / \sum |F_o|$; $R_w = [\sum w\Delta^2 / \sum wF_o^2]^{1/2}$; $S = [\sum w\Delta^2 / (\text{NO} - \text{NV})]^{1/2}$; $\Delta = F_o - F_c$.

An Unusual Example of CH Oxidative Addition following Phosphine Association: Mechanism of Formation and Reactivity of $\text{Cp}^*\text{Ru}(\mu\text{-H})(\mu\text{-}\eta^3, \eta^1\text{-}i\text{PrNC}(\text{Me})\text{CHH}_{\text{agostic}})\text{RuCp}^*$

Roger Kuhlman, Kirsten Folting, and Kenneth G. Caulton*

Department of Chemistry and Molecular Structure Center, Indiana University,
Bloomington, Indiana 47405-4001

Received April 10, 1995*

$(\text{Cp}^*\text{RuCl})_4$ reacts with lithium diisopropylamide (LDA) by dehydrogenation (i.e., -2H) of one isopropyl group to form the title complex (1). Full spectroscopic characterization and an X-ray structure determination are reported for this compound (triclinic $P\bar{1}$, $a = 10.939(1) \text{ \AA}$, $b = 15.242(2) \text{ \AA}$, $c = 8.422(1) \text{ \AA}$, $\alpha = 101.78(1)^\circ$, $\beta = 109.75(1)^\circ$, $\gamma = 83.58(1)^\circ$, $Z = 2$, $R(F) = 0.0370$, $R_w(F) = 0.0408$). Mechanistic studies with LDA deuterated at the methine positions suggest that the mechanism of this reaction is (1) metathesis of N^iPr_2 for Cl, (2) β -CH activation, (3) γ -CH activation, and (4) dehydrohalogenation by a second equivalent of LDA. The bridging hydride was found to exchange slowly with the two vinyl hydrogens. CO replaces the agostic interaction in 1 to form a CO adduct of a bimetallic azaallyl. However, the products of 1 with small phosphines are methyldiene-bridged dihydrides; i.e., the CH bond of the agostic interaction is broken in the phosphine-containing products.

Introduction

The ability of heteroatomic anions to stabilize metal centers with low coordination number has been demonstrated, and lies mainly in their ability to have metal–ligand multiple-bond character, in either a σ or a π fashion. Bergman et al. have observed the formation of “one-legged” piano stools via $t\text{BuNHLi}$ metathesis reactions, forming $\text{Cp}^*\text{IrN}^t\text{Bu}^1$ and $(\text{C}_6\text{Me}_6)\text{OsN}^t\text{Bu}^2$. One well-investigated class of two-legged piano stools is dimers of the form $[\text{Cp}^*\text{RuX}]_2$ ($\text{X} = \text{NHPH}$,³ SR ,⁴ $\text{OR}^{3,5}$), which have the ability to react with CH bonds.⁶ In nearly all cases, if the lone pairs of the heteroatom are assumed to donate to the metal center(s), these complexes can be considered to have 18-electron metal centers. For example, $\text{Cp}^*\text{IrN}^t\text{Bu}$ is 18e if Ir–N is considered to be a triple bond. Similarly, it has been shown by Fenske–Hall molecular orbital calculations that three orbitals on each oxygen overlap with metal orbitals in $(\text{Cp}^*\text{RuOMe})_2$, although overlap with one O π orbital is very small. If all three are considered, the Ru centers count to 18e, although the term “ π -stabilized unsaturated”⁷ is probably more appropriate. The amide $[\text{Cp}^*\text{Ru}(\text{NHPH})]_2^3$ is an exception, in that the bridging nitrogen has only one lone pair (two orbitals) available

for donation. Nevertheless, it has a structure quite similar to that of the alkoxide analogs; with no Ru–Ru bond (the Ru–Ru distance is $2.945(4) \text{ \AA}$), the metal centers are “truly” 16e.

The degree of oligomerization generally decreases with increasing steric bulk of ligands. It seemed plausible then that, using R groups with sufficient steric bulk and donor ability, Cp^*RuNR_2 could be isolated as a monomer. This would almost certainly require rehybridization at N for donation from a π -type lone pair (planar nitrogen) and require a very strong “dative” π -bond (ligand to metal). However, we report here that attempted synthesis of such a species (with $\text{R} = ^i\text{Pr}$) yields a product which is bimetallic and contains only one amide per Ru_2 unit, with the electron count at the metals satisfied by activating a pendant alkyl group, including the formation of an agostic interaction.⁸

Agostic CH bonds are generally considered very weak ligands, whose chemistry is dominated by displacement by incoming nucleophiles. Here we describe reactions of the title complex, some of which violate this general principle.

Experimental Section

General Procedures. Manipulations were performed under argon or in vacuo using standard Schlenk and glovebox techniques. All glassware was silylated using $(\text{Me}_3\text{Si})_2\text{NH}$ and flame-dried under vacuum prior to use. Solvents were dried, distilled, and stored in bulbs with Teflon valves. Microanalysis was performed by Oneida Research Services. IR spectra were recorded on a Nicolet 510P FT-IR spectrometer. NMR spectra were obtained on either a Bruker 500 MHz (^{13}C), a Nicolet 360 MHz (^{31}P , ^2H), or a Varian 300 MHz instrument (^1H), with chemical shifts referenced to residual solvent peaks (^1H , ^2H ,

(8) Kuhlman, R.; Folting, K.; Caulton, K. G. *J. Am. Chem. Soc.* **1993**, *115*, 5813.

* Abstract published in *Advance ACS Abstracts*, June 1, 1995.

(1) Glueck, D. S.; Hollander, F. J.; Bergman, R. G. *J. Am. Chem. Soc.* **1989**, *111*, 2719. Dobbs, D. A.; Bergman, R. G. *J. Am. Chem. Soc.* **1993**, *115*, 3836.

(2) Michelman, R. I.; Bergman, R. G.; Andersen, R. A. *Organometallics* **1993**, *12*, 2741.

(3) Blake, R. E.; Heyn, R. H.; Tilley, T. D. *Polyhedron* **1992**, *11*, 709.

(4) Koelle, U.; Rietmann, C.; Englert, U. *J. Organomet. Chem.* **1992**, *423*, C20.

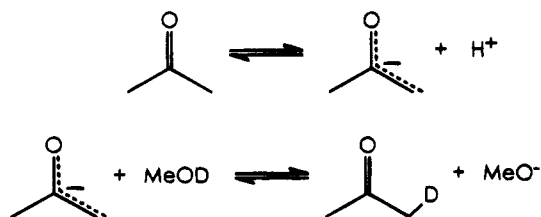
(5) (a) Koelle, U.; Kossakowski, J. *J. Chem. Soc., Chem. Commun.* **1988**, 549. (b) Loren, S. D.; Campion, B. K.; Heyn, R. H.; Tilley, T. D.; Bursten, B. E.; Luth, K. W. *J. Am. Chem. Soc.* **1989**, *111*, 4712.

(6) (a) Kang, B.-S.; Koelle, U.; Thewalt, U. *Organometallics* **1991**, *10*, 2569. (b) Loren, S. D.; Campion, B. K.; Heyn, R. H.; Tilley, T. D.; Bursten, B. E.; Luth, K. W. *J. Am. Chem. Soc.* **1989**, *111*, 4712.

(7) Caulton, K. G. *New J. Chem.* **1994**, *18*, 25.

^{13}C) or external H_3PO_4 (neat, ^{31}P). $(\text{Cp}^*\text{RuCl})_4$ was synthesized according to the literature.⁹ Lithium diisopropylamide was formed by slowly adding 1 equiv of $^n\text{BuLi}$ to a pentane solution of diisopropylamine, decanting the solvent, and drying in vacuo. Tertiary phosphines and CO were used as received. NMR tube reactions requiring equilibration between solution and head-space gas were subjected to tumbling end-over-end (ca. 0.2 revolution s^{-1}) with an electric stirrer motor.

$\text{Li}\{\text{N}(\text{CDMe}_2)_2\}$ (LDA- d_2) was synthesized the general method of Borch et al.,¹⁰ by sodium cyanoborodeuteride reduction of the imine formed from acetone and ammonia. However, it is important that the reaction be carried out in CH_3OH , rather than CH_3OD , as reported by Newcomb et al.¹¹ Using CH_3OD as solvent significantly scrambles deuterium into the methyl positions, presumably by reaction with acetone:



Isotopic purity of the LDA- d_2 was found to be ca. 95% by ^1H and ^2H NMR.

$(\text{Cp}^*\text{Ru})(\mu\text{-H})(\mu\text{-}\eta^3, \eta^1\text{-}^i\text{PrNC}(\text{Me})\text{CHH}_{\text{agostic}})(\text{RuCp}^*)$ (1). In a drybox, $(\text{Cp}^*\text{RuCl})_4$ (250 mg, 0.230 mmol) and LiN^iPr_2 (LDA) (98.5 mg, 0.919 mmol) were combined in a Schlenk flask. The flask was removed from the drybox, and THF (10 mL) was added. After 12 h of stirring, the THF was removed in vacuo. The resulting oily brown residue was extracted with pentane (3×15 mL), and the extract was filtered through a pipet containing glass wool and Celite. Removal of the pentane in vacuo provided the product as a brown solid (195 mg, 0.340 mmol, 74%).¹² Crystals suitable for X-ray diffraction were grown by sublimation in a sealed glass tube (2×10^{-4} Torr, 86–89 °C) over a period of 6 weeks. ^1H NMR (C_6D_6): δ 2.62 (apparent sept, $J = 6.6$, 1H, CHMeMe), 2.05 (s, 3H, NCMe), 1.89 (s, 15H, C_5Me_5), 1.81 (s, 15H, C_5Me_5), 1.63 (d, $J = 6.6$, 3H, CHMeMe), 0.64 (d, $J = 6.6$, 3H, CHMeMe), 0.24 (d, $J = 5.1$, 1H, $\text{CHH}_{\text{agostic}}$), -2.77 (d, $J = 5.1$, 3.3, 1H, $\text{H}_{\text{agostic}}$), -6.09 (d, $J = 3.3$, 1H, Ru-H-Ru). ^{13}C NMR (C_6D_6): δ 97.96 (s, $\text{NC}(\text{Me})\text{CH}_2$), 86.50 (m, C_5Me_5), 74.67 (m, C_5Me_5), 53.10 (dsept, $^1J_{\text{CH}} = 132.9$, $^2J_{\text{CH}} = 3.5$, CHMe_2), 26.73 (qdq, $^1J_{\text{CH}} = 125.2$, $^2J_{\text{CH}} = 4.8$, $^3J_{\text{CH}} = 3.1$, CHCH_3CH_3), 23.17 (qdq, $^1J_{\text{CH}} = 125.8$, $^2J_{\text{CH}} = 4.9$, $^3J_{\text{CH}} = 1.6$, CHCH_3CH_3), 19.75 (q apparent t, $^1J_{\text{CH}} = 125.8$, $^3J_{\text{CH}} = 2.0$, NCCH_3), 13.02 (q, $^1J_{\text{CH}} = 125.8$, $\text{C}_5(\text{CH}_3)_5$), 11.87 (q, $^1J_{\text{CH}} = 125.8$, $\text{C}_5(\text{CH}_3)_5$), 3.46 (ddm, $^1J_{\text{CH}} = 142.6$, $^1J_{\text{CH}} = 155.1$, CH_2). $m/e = 571$. Anal. Calcd: C, 54.62; H, 7.58; N, 2.45. Found: C, 54.27; H, 7.48; N, 2.17.

$(\text{Cp}^*\text{Ru})(\mu\text{-H}^i)\{\mu\text{-}\eta^3, \eta^1\text{-}(\text{CH}_3)_2\text{CDNC}(\text{CH}_3)\text{CH}^i\text{H}^i_{\text{agostic}}\}(\text{RuCp}^*)$ (1 i).¹⁴ The reaction was performed as for the perproton product, except that $\text{LiN}\{\text{CD}(\text{CH}_3)_2\}$ (LDA- d_2) was used instead of LDA. ^2H NMR (C_6H_6): δ 2.59 (s, 1H), 0.24 (s, 0.29 H), -2.63 (s, 0.27 H), -6.03 (s, 0.15 H). Relative intensities given are for the product after complete workup (ca. 16 h in THF and ca. 1 h in pentane).

$\text{Cp}^*\text{Ru}(\text{CO})(\mu\text{-H})(\mu\text{-}\eta^3, \eta^1\text{-}^i\text{PrNC}(\text{Me})\text{CH}_2)\text{RuCp}^*$ (2). In a Schlenk flask, **1** (85.0 mg, 149 mmol) was dissolved in benzene (6 mL), and CO was bubbled through the solution for

15 s and then blown over (about 1 mm from the surface) the solution, with vigorous stirring, for an additional 5 min. Evaporation of the solvent left **2** as a dark brown oily solid. Due to the stickiness of **2**, the yield was not measured. However, repeating the reaction in an NMR tube showed the conversion to be quantitative. Compound **2** sublimes very slowly at 75 °C and 5×10^{-5} Torr. However, the temperature required also leads to decomposition of **2**. When **2** was sublimed at 95 °C (to increase rate of sublimation) and 5×10^{-5} Torr for 4 h, only about 20% of the material had sublimed. While the sublimate was pure (^1H NMR), the residue was significantly contaminated. ^1H NMR (C_6D_6): δ 3.37 (sept, $J = 6.0$, 1H, CHMeMe), 1.94 (s, 3H, NCMe), 1.91 (s, 15H, C_5Me_5), 1.74 (s, 15H, C_5Me_5), 1.69 (d, $J = 1.5$, 1H, CHH), 1.39 (d, $J = 6.0$, 3H, CHMeMe), 1.24 (d, $J = 6.0$, 3H, CHMeMe), 0.60 (dd, $J = 1.5$, 1H, CHH), -15.65 (s, 1H, RuH). ^{13}C NMR (C_6D_6): δ 204.64 (d, $^2J_{\text{CH}} = 6.7$, CO), 110.05 (s, NCMeCH_2), 93.85 (s, $\text{C}_5\text{-Me}_5$), 86.10 (s, C_5Me_5), 57.95 (d, $J = 132$, CHMe_2), 37.81 (dd, $J = 160$, $J = 148$, NCMeCH_2), 28.33 (q, $J = 124$, CHCH_3Me), 25.07 (q, $J = 125$, CHMeCH_3), 21.93 (q, $J = 125$, NCMeCH_2), 11.74 (q, $J = 125$, C_5Me_5), 11.63 (q, $J = 126$, C_5Me_5). IR (KBr): $\nu_{\text{CO}} = 1893 \text{ cm}^{-1}$.

$\text{Cp}^*\text{Ru}(\text{CO})(\mu\text{-H})(\mu\text{-}\eta^3, \eta^1\text{-}^i\text{PrNC}(\text{Me})\text{CH}_2)\text{RuCp}^*$ (2*). In a drybox, **1** (7.5 mg, 0.013 mmol) was dissolved in C_6D_6 , and the solution was transferred to an NMR tube fitted with a Teflon valve. The solution was first subjected to three freeze-pump-thaw degas cycles, and then an excess of ^{13}CO (1 atm, ca. 8 equiv) was added. The product formation was complete after 15 min, as judged by ^1H NMR. No CO exchange was observed (^1H NMR) after vigorously bubbling ^{13}CO through a solution of **2*** in C_6H_6 for 10 min or after tumbling for 1 day in C_6D_6 under 1 atm of ^{13}CO in an NMR tube. Selected ^1H NMR (C_6D_6): δ -15.65 (d, $J_{\text{RuH}} = 6.7$). IR (KBr): $\nu_{\text{CO}} = 1848 \text{ cm}^{-1}$.

$\text{Cp}^*\text{Ru}(\text{PMe}_3)(\text{H})_2(^i\text{PrNC}(\text{Me})\text{CH})\text{RuCp}^*$ (3). Ten milligrams of **1** was dissolved in C_6D_6 in an NMR tube, and an excess (10 equiv) of PMe_3 was added. After 15 min, approximately 50% conversion to **3** was observed. After tumbling of the NMR tube for 1 day, all of the signals for **1** had disappeared and only **3** and free PMe_3 were observed in solution. Removal of the solvent (and excess PMe_3) in vacuo allowed isolation of **3**. However, if **3** is dissolved in C_6D_6 without excess PMe_3 present, slow (24 h, 25 °C) conversion can be seen back to **1**. In addition, if 1 atm of CO is added, complete conversion to **2** can be effected in about 1 day. Unlike **1**, **3** reacts very quickly with CD_2Cl_2 . $^{31}\text{P}\{^1\text{H}\}$ NMR (C_6D_6): δ 6.6 (s). ^1H NMR (C_6D_6): δ 6.92 (d, $J_{\text{PH}} = 21.3$, 1H, $\mu\text{-CH}$), 2.67 (sept, $J = 6.9$, 1H, CHMeMe), 2.46 (s, 3H, NCMe), 1.94 (d, $J_{\text{PH}} = 3.3$, 15H, C_5Me_5), 1.78 (s, 15H, C_5Me_5), 1.8¹⁶ (RuH), 1.08 (d, $J = 7.8$, 3H, CHMeMe), 1.05 (d, $J = 6.3$, 3H, CHMeMe), -15.98 (d, $J_{\text{PH}} = 12.6$, 1H, RuH). ^{13}C NMR (C_6D_6): δ 136.43 (d, $J_{\text{CH}} = 139$, $J_{\text{CP}} = 16.4$, $\mu\text{-CH}$), 97.64 (d, $^2J_{\text{CH}} = 3.5$, C_5Me_5), 87.41 (d, $^2J_{\text{CP}} = 80.8$, C_5Me_5), 81.58 (s, NCMe), 48.19 (d, $J_{\text{CH}} = 136$, CHMeMe), 24.74 (q, $J_{\text{CH}} = 127$, CHMeMe), 23.63 (q, $J_{\text{CH}} = 114$, NCMe), 22.51 (q, $J_{\text{CH}} = 124$, CHMeMe), 22.24 (dq, $J_{\text{PC}} = 21.3$, $J_{\text{CH}} = 120$, PMe_3), 13.28 (q, $J_{\text{CH}} = 125$, C_5Me_5), 12.28 (q, $J_{\text{CH}} = 125$, C_5Me_5).

$\text{Cp}^*\text{Ru}(\text{PMe}_2\text{Ph})(\text{H})_2(^i\text{PrNC}(\text{Me})\text{CH})\text{RuCp}^*$ (4). $\text{PMe}_2\text{-Ph}$ (5 equiv) reacts with **1** to form a product analogous to that formed with PMe_3 . By ^1H NMR, 70% conversion was observed after 2 h, and 100% conversion, after 1 day. $^{31}\text{P}\{^1\text{H}\}$ NMR (C_6D_6): δ 25.9 (s). ^1H NMR (C_6D_6): δ PMe_2Ph : 8.16 (t, $J = 8.6$, 1H), 7.36 (t, $J = 6.8$, 1H), 7.29 (t, $J = 7.4$, 1H), 7.12 (d, $J = 6.8$, 1H), 7.08 (d, $J = 7.0$, 1H), 7.06 (d, $J_{\text{HP}} = 19.8$, 1H, $\mu\text{-CH}$), 2.72 (sept, $J = 6.0$, 1H, CHMeMe), 2.50 (s, 3H, NCMe), 1.84 (d, $J_{\text{HP}} = 1.0$, 15H, C_5Me_5), 1.69 (s, 15H, C_5Me_5), 1.55 (d, $J_{\text{HP}} = 7.5$, 3H, PMe), 1.50 (d, $J_{\text{HP}} = 7.8$, 3H, PMe), 1.12 (d, $J = 6.0$,

(9) Fagan, P. J.; Mahoney, W. S.; Calabrese, J. C.; Williams, I. C. *Organometallics* **1990**, *9*, 1843.

(10) Borch, R. F.; Bernstein, M. D.; Durst, H. D. *J. Am. Chem. Soc.* **1971**, *93*, 2897.

(11) Newcomb, M.; Varick, T. R.; Goh, S.-H. *J. Am. Chem. Soc.* **1990**, *112*, 5186.

(12) The reaction has been repeated several times, with yields ranging from 65% to 75%.

(13) All couplings are given in Hz and refer to H-H coupling (^1H NMR) or C-H coupling (^{13}C NMR) unless otherwise specified.

(14) H^i indicates partial deuterium labeling.

(15) No other J_{CH} couplings were observed.

(16) This signal is not observed in ^1H NMR, presumably because of overlap with Cp^* resonances. When PMe_3 is added to **1**, ^2H signals are observed at 2.7, 1.8, and -16 ppm.

Table 1. Crystallographic Data for (Cp*Ru)₂(μ-H)(μ-¹PrNC₃H₅)

chem formula	C ₂₆ H ₄₃ NRu ₂	fw	571.77
a, Å	10.939(1)	space group	P1̄
b, Å	15.242(2)	T, °C	-90
c, Å	8.422(1)	λ, Å	0.710 69
α, deg	101.78(1)	ρ _{calcd} , g cm ⁻³	1.469
β, deg	109.75(1)	R ^a	0.0370
γ, deg	83.58(1)	R _w ^b	0.0408
V, Å ³	1292.44		
Z	2		

^a $R = \sum ||F_o| - |F_c|| / \sum |F_o|$. ^b $R_w = [\sum w(|F_o| - |F_c|)^2 / \sum w|F_o|^2]^{1/2}$ where $w = 1/\sigma^2(|F_o|)$.

3H, CHMeMe), 1.09 (d, $J = 6.0$, 3H, CHMeMe), -15.77 (d, $J_{HP} = 11.7$, 1H, RuH).

Cp*Ru(PMePh₂)(H)₂(¹PrNC(Me)CH)RuCp* (5). PMePh₂ (2 equiv) was added to **1**, and the reaction was followed by ¹H NMR. The reaction was very slow and apparently reached equilibrium after about 7 days, when consecutive measurements found [1]:[5] of about 1:1. ³¹P{¹H} NMR (C₆D₆): δ 45.9 (s). ¹H NMR (C₆D₆): δ 8.5–6.9 (several resonances, 11H, PMePh₂ and μ-CH), 2.77 (sept, $J = 4.6$, 1H, CHMeMe), 2.57 (s, 3H, NCMe), 1.68 ($J_{PH} = 1.0$ Hz, 15H C₅-Me₅), 1.58 (s, 15H, C₅Me₅), 1.13 (d, $J = 5.1$, 3H, CHMeMe), 1.08 (d, $J = 4.2$, 3H, CHMeMe), -15.69 (d, $J_{HP} = 11.4$, 1H, RuH).

Cp*Ru(P(OEt)₃)(H)₂(¹PrNC(Me)CH)RuCp* (6). This was synthesized as above for **3**, with quantitative conversion after 1 h. ³¹P{¹H} NMR (C₆D₆): δ 173.5 (s). ¹H NMR (C₆D₆): δ 7.04 (d, $J_{HP} = 2.1$, 1H, μ-CH), 3.90 (m, 6H, POCH₂CH₃), 2.61 (qq, $J = 6.0$, 5.2, 1H, CHMeMe), 2.30 (s, 3H, NCMe), 2.05 (d, $J_{HP} = 3.6$, 15H, C₅Me₅), 1.78 (s, 15H, C₅Me₅), 1.19 (t, $J = 7.1$, 9H, POCH₂CH₃), 1.15 (d, $J = 6.0$, 3H, CHMeMe), 1.08 (d, $J = 5.2$, 3H, CHMeMe), -16.27 (d, $J_{HP} = 24.3$, 1H, RuH).

Structure Determination of 1. A crystal of suitable size was attached to a glass fiber with silicone grease in a nitrogen atmosphere glovebag. It was then transferred to the goniostat and cooled to -150 °C. Due to some "abnormal" reflections at -150 °C, it was suspected that the crystal might be undergoing a phase transition.¹⁷ The crystal was therefore warmed to -90 °C, at which point the "abnormal" reflections had disappeared. A systematic search of a limited hemisphere of reciprocal space yielded a set of reflections which exhibited no systematic extinctions and no symmetry, other than $\bar{1}$. Plots of the four standard reflections (040, $\bar{5}00$, 33 $\bar{3}$, 00 $\bar{2}$) measured every 400 reflections showed no significant trends. Details of the data collection ($6^\circ < 2\theta < 45^\circ$) and refinement are given in Table 1. No correction for absorption was made.

The structure was solved using a combination of direct methods (SHELXS-86) and Fourier techniques. Initial attempts at solving the structure in $P\bar{1}$ failed. The Ru atoms were located by finding the four Ru atoms in the acentric space group $P\bar{1}$. When the atoms were located, the center of symmetry was readily located and the structure solution proceeded normally in $P\bar{1}$. Following initial refinement of all of the non-hydrogen atoms, almost all of the hydrogen atoms (on C atoms) were located in a difference Fourier map. In a subsequent difference map, the bridging hydrogen atom was located as well as all of the hydrogen atoms on the ¹PrNC₃H₅ group. The full-matrix least-squares refinement was completed using anisotropic thermal parameters on all non-hydrogen atoms and isotropic thermal parameters on the hydrogen atoms.¹⁸ The total number of variables was 375 (including the scale factor and an overall isotropic extinction parameter). All of the unique reflections were used. Reflec-

(17) The structure was actually solved later using data collected at -150 °C, in the space group $P\bar{1}$, but with a cell of twice the volume as that at -90 °C. Results of this structure determination were nearly identical in all ways to those at -90 °C and are available as supporting information (formerly known as supplementary material). In particular, the bridging hydride and the agostic hydrogen were evident in both independent molecules in the unit cell at -150 °C.

Table 2. Fractional Coordinates^a and Isotropic Thermal Parameters^b for Selected Atoms of (Cp*Ru)₂(μ-H)(μ-¹PrNC₃H₅)

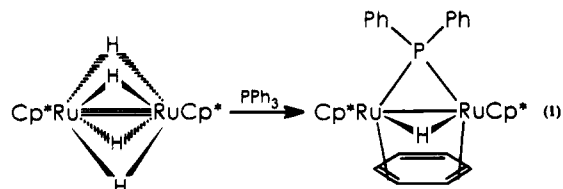
	x	y	z	10B _{iso} , Å ²
Ru1	9114.1(4)	7833.2(3)	7367(1)	18
Ru2	6797.3(4)	7246.4(3)	7243(1)	19
N3	7255(4)	8512(3)	6851(6)	18
C4	6868(5)	8626(4)	8288(7)	22
C5	7807(6)	8189(4)	9539(9)	29
C6	5733(7)	9202(5)	8582(11)	35
C7	6537(6)	9003(4)	5453(8)	26
C8	6583(8)	8463(6)	3758(9)	36
C9	7097(8)	9925(5)	5839(11)	38
C10	11147(5)	7792(4)	8732(8)	25
C11	10859(5)	8530(4)	7787(7)	22
C12	10334(5)	8152(4)	6019(8)	24
C13	10284(5)	7204(4)	5865(8)	26
C14	10829(5)	6978(4)	7567(9)	30
C15	11715(8)	7894(7)	10624(10)	42
C16	11180(8)	9482(5)	8511(11)	37
C17	10070(8)	8647(6)	4559(10)	36
C18	9831(9)	6555(6)	4192(11)	43
C19	11059(9)	6054(6)	7982(15)	49
C20	4774(6)	6870(4)	6083(9)	33
C21	5549(10)	6296(6)	5186(9)	56
C22	6457(8)	5829(4)	6508(17)	62
C23	6185(8)	6146(6)	8002(11)	48
C24	5212(6)	6744(5)	7742(9)	35
C25	3603(8)	7467(7)	5267(19)	106
C26	5311(20)	6166(12)	3281(13)	179
C27	7420(14)	5109(7)	6065(35)	219
C28	6884(13)	5793(11)	9667(20)	141
C29	4547(12)	7183(8)	9071(16)	92
H1	836(6)	688(4)	717(8)	47(12)

^a Fractional coordinates are $\times 10^4$ for non-hydrogen atoms and $\times 10^3$ for hydrogen atoms. ^b Isotropic values for those atoms refined anisotropically are calculated using the formula given by: Hamilton, W. C. *Acta Crystallogr.* **1959**, *12*, 609.

tions having $F < 3.0\sigma(F)$ were given zero weight. The final difference map was essentially featureless, with the largest peak at 0.95 e/Å³ and the deepest hole at -0.75 e/Å³. The majority of the peaks were in the area of the methyl groups of one Cp* (atoms C20–C29).

Results and Discussion

Bimetallic Cp*Ru complexes have displayed impressive ability to cleave strong bonds. For example, Suzuki et al. have shown that (Cp*Ru)₂(μ-H)₄ reacts with PPh₃ by breaking a C–P bond to form (Cp*Ru)₂(μ-H)(μ-PPh₂)-(μ-η²,η²-C₆H₆)¹⁹ (eq 1). Girolami et al. have observed the

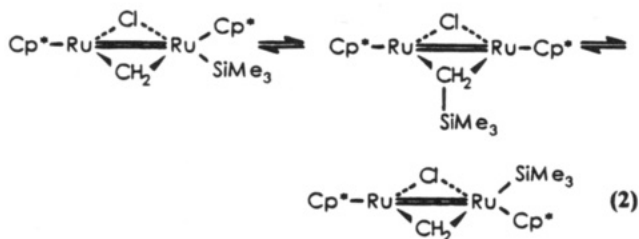


reversible cleavage of a C–Si bond in the product of a reaction between (Cp*RuCl)₄ and Mg(CH₂SiMe₃)₂.²⁰ The resulting product exhibits a fluxional process, which is explained by migration at Me₃Si from one face of Ru to the other via bridging methylene (eq 2). In this work, formation of the dimer [Cp*RuCH₂SiMe₃]₂ is ruled out

(18) Atoms H29–H43 were excluded. The carbon atoms C20–C29 had rather large thermal parameters, presumably due to rotation of the Cp* group.

(19) Omari, H.; Suzuki, H.; Takei, Y.; Moro-oka, Y. *Organometallics* **1989**, *8*, 2270.

(20) Lin, W.; Wilson, S. R.; Girolami, G. S. *Organometallics* **1994**, *13*, 2309.



since alkyl is a very unlikely bridging ligand. In this sense, our result is similar to Girolami's: inhibited dimerization leads to activation of a ligand.

Synthesis of $(\text{Cp}^*\text{Ru})_2(\mu\text{-H})(\mu\text{-}^i\text{PrNC}_3\text{H}_5)$ (1). The reaction of $(\text{Cp}^*\text{RuCl})_4$ with 4 equiv of LiN^iPr_2 (one LDA per Ru atom)²¹ in THF at room temperature gives **1** in 74% yield, after extraction with pentane. The other products of this reaction are LiCl and $^i\text{Pr}_2\text{NH}$ (see Scheme 1). The generation of $^i\text{Pr}_2\text{NH}$ was confirmed by repeating the experiment in THF- d_8 , where ^1H NMR signals corresponding to this amine were observed. The compound is inert to reaction with alkanes or CH_2Cl_2 for at least a week, and for a few days in arene solvents (C_6H_6 , $\text{C}_6\text{H}_5\text{CH}_3$). It reacts quickly with O_2 to form uncharacterized products and is unstable in the presence of protic solvents (H_2O , CH_3OH).

Crystal Structure of 1. Although **1** is often isolated as an oily solid, X-ray-quality crystals are best obtained by very slow sublimation in a sealed tube. The structure has been successfully determined (Figure 1) both at -150°C and at -90°C . It undergoes a phase transition on warming from -150 to -90°C , to a cell of half the volume and with one independent molecule instead of two. The bond distances and angles are virtually identical at the two temperatures. All hydrogen atoms were located except for those on the cyclopentadienyl ligand of Ru2, where disorder problems precluded their detection.

The molecule has no symmetry axis of rotation nor plane of symmetry and therefore belongs to point group C_1 . The two Cp^*Ru moieties are joined at an Ru–Ru separation of 2.743(1) Å and are additionally linked by a bridging hydride and a bridging nitrogen atom. The Ru1–N3 distance (2.124(4) Å) is slightly shorter than Ru2–N3 (2.161(4) Å). One intact isopropyl group remains on N, while the other has been doubly dehydrogenated. Multiple-bond character which results from this dehydrogenation is shared among N3, C4, and C5, so that both N3–C4 (1.385(7) Å) and C4–C5 (1.418(9) Å) have bond lengths intermediate between the normal ranges for single and double bonds; these three atoms comprise an azaallyl moiety.²² Correspondingly, the atoms N3, C4, C5, and C6 are coplanar. A remarkable feature of the structure is the agostic interaction of C5–H2 with Ru1. This interaction satisfies the 18-electron rule for Ru1, which would otherwise be formally 16e. Ru1–C5 (2.622(7) Å) and Ru1–H2 (2.24(7) Å) bonds are certainly longer than normal σ bonds, yet within the range for an agostic interaction.²³ To our knowledge, all other η^3 -azaallyl complexes have

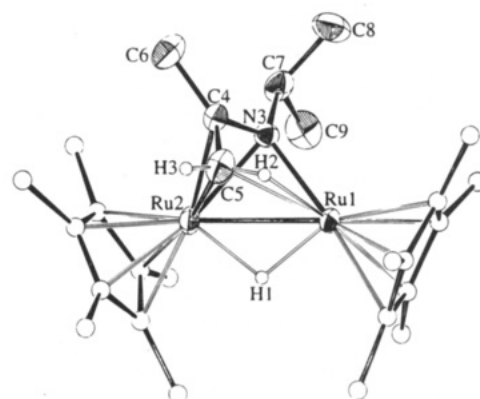


Figure 1. ORTEP drawing of $(\text{Cp}^*\text{Ru})_2(\mu\text{-H})(\mu\text{-}^i\text{PrNC}_3\text{H}_5)$, showing selected atom labeling.

Scheme 1

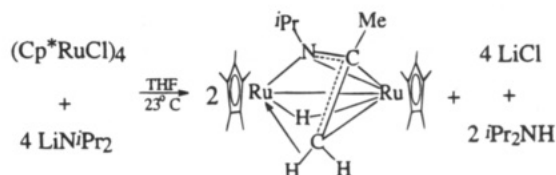


Table 3. Selected Bond Distances (Å) and Angles (deg) for $(\text{Cp}^*\text{Ru})_2(\mu\text{-H})(\mu\text{-}^i\text{PrNC}_3\text{H}_5)$

Ru1–Ru1	2.7431(7)	Ru2–C22	2.160(6)
Ru1–N3	2.124(4)	Ru2–C23	2.156(7)
Ru1–C5	2.622(7)	Ru2–C24	2.166(6)
Ru1–C10	2.131(6)	N3–C4	1.385(7)
Ru1–C11	2.178(5)	N3–C7	1.472(7)
Ru1–C12	2.168(6)	C4–C5	1.418(9)
Ru1–C13	2.117(6)	C4–C6	1.499(9)
Ru1–C14	2.139(6)	C7–C8	1.509(10)
Ru2–N3	2.161(4)	C7–C9	1.525(9)
Ru2–C4	2.107(6)	Ru1–H1	1.70(7)
Ru2–C5	2.192(7)	Ru2–H1	1.76(7)
Ru2–C20	2.186(6)	Ru1–H2	2.24(7)
Ru2–C21	2.187(7)		
Ru2–Ru1–N3	50.79(12)	C4–N3–C7	119.5(4)
Ru1–Ru2–N3	49.62(11)	N3–C4–C5	108.8(5)
Ru1–Ru2–C4	71.75(15)	N3–C4–C6	126.3(6)
Ru1–Ru2–C5	63.04(19)	C5–C4–C6	124.5(6)
Ru1–N3–Ru2	79.60(15)	N3–C7–C8	110.1(5)
Ru1–N3–C4	109.0(3)	N3–C7–C9	109.1(5)
Ru1–N3–C7	130.1(4)	C8–C7–C9	112.6(6)
Ru2–N3–C4	69.0(3)	Ru1–H1–Ru2	105(3)
Ru2–N3–C7	127.5(4)		

N–C–C angles ranging from 110 to 116° .²⁴ The observed N3–C4–C5 angle of $108.8(5)^\circ$ in **1** is slightly below this range, which supports the idea of C5 "reaching" toward Ru2 to form the agostic interaction. Crabtree has used the distance of the CH bond from one covalent radius of the metal (r_{bp}) as a semiquantitative measure of the extent of agostic interactions.²⁵ For **1**, $r_{\text{bp}} = 1.05$ Å,²⁶ indicating a relatively weak agostic

(23) Bond lengths of a Ru–CH_{agostic} moiety for comparison: Ru–C = 2.315(5), Ru–H (idealized) = 1.786(6) Å. See: Arliquie, T.; Chaudret, B.; Jalon, F. A.; Otero, A.; Lopez, J. A.; Lahoz, F. J. *Organometallics* **1991**, *10*, 1888.

(24) (a) Adams, R. D.; Chodosh, D. F. *J. Am. Chem. Soc.* **1977**, *99*, 6544. (b) Muller, F.; van Koten, G.; Kraakman, M. J. A.; Vrieze, K.; Heijdenrijk, D.; Zoutberg, M. C. *Organometallics* **1989**, *8*, 1331. (c) Muller, F.; van Koten, G.; Vrieze, K.; Duineveld, K. A. A.; Heijdenrijk, D.; Mak, A. N. S.; Stam, C. H. *Organometallics* **1989**, *8*, 1324. (d) Green, M.; Mercer, R. J.; Morton, C. E.; Orpen, A. G. *Angew. Chem., Int. Ed. Engl.* **1985**, *24*, 422. (e) Filippou, A. C.; Grünleitner, W.; Kiprof, P. *J. Organomet. Chem.* **1991**, *410*, 175. (f) Yang, G.-M.; Lee, G.-H.; Peng, S.-M.; Liu, R.-S. *Organometallics* **1991**, *10*, 1305. (25) Crabtree, R. H.; Holt, E. M.; Lavin, M.; Morehouse, S. M. *Inorg. Chem.* **1985**, *24*, 1986.

(21) It was later found that **1** is unreactive with LDA, and therefore excess LDA can be used to ensure complete conversion, in the event of accidental hydrolysis of part of the LDA.

(22) Bond lengths are quite comparable to those of a previously reported Ru–azaallyl complex: Polm, L. H.; van Koten, G.; Vrieze, K.; Stan, C.; van Tunnen, W. C. *J. Chem. Soc., Chem. Commun.* **1983**, 1177.

interaction. The r_{bp} of 1 is longer than those of 11 of the 17 complexes reviewed by Crabtree.

Spectroscopic Characterization of 1. ^1H and ^{13}C NMR experiments are consistent with retention of the solid-state molecular structure in C_6D_6 solution. In the ^1H NMR spectrum, two singlets at 1.89 and 1.81 ppm are easily assigned to the Cp^* hydrogens. A septet at 2.62 ppm and doublets at 1.63 and 0.64 ppm correspond to the methine and diastereotopic methyl hydrogens of the isopropyl group, respectively. Remaining are a singlet at 2.05 ppm, which represents the methyl of the dehydrogenated isopropyl group, and three unit intensity upfield resonances at 0.24 (d, $J = 5.1$), -2.76 (dd, $J = 5.1, 3.3$), and -6.09 ppm (d, $J = 3.3$). The assigned coupling was confirmed by selective spin decoupling studies. The doublet of doublets must correspond to the agostic hydrogen (H2), which shows coupling to the hydride (H1) and the other methylene hydrogen (H3). This upfield shift is characteristic of an agostic interaction.²⁷ It seems very unlikely (in fact, it would be unprecedented) that H1 would resonate upfield of H2, so the signal at 0.24 ppm is assigned to H3. Therefore, the hydride (H1) is the most upfield, at -6.09 ppm. Although this assignment requires an unusually large gem coupling constant²⁸ ($^2J_{\text{H}_2-\text{H}_3} = 5.5$ Hz), this phenomenon has been seen before in a similar system.²⁹

The gated-coupled ^{13}C NMR spectrum also shows some diagnostic features. A doublet of doublets (3.46 ppm, $^1J_{\text{CH}} = 143$ Hz, 155 Hz) is seen for C_5 . Quite often, $^1J_{\text{CH}}$ is significantly (ca. 30–60 Hz) lower for bonds involved in agostic interactions. However, the magnitude of this effect is quite variable.³⁰ The retention of a large coupling constant provides more evidence that this agostic interaction is a rather weak one. In sharp contrast to that for C_5 , the signal for C_4 appears at very low field (98 ppm, multiplet), which is more typical for "innocent" sp^2 carbon in this coordination mode. The remaining ^{13}C peak assignments are straightforward.

No signal is seen in the IR spectrum between 1800 and 2600 cm^{-1} , which is consistent with the assignment of the hydride to a bridging position.

Mechanism of Formation of 1. This product is quite different from the $(\text{Cp}^*\text{RuNHPPh})_2$, $(\text{Cp}^*\text{RuOR})_2$, and $(\text{Cp}^*\text{RuSR})_2$ products of analogous simple metathesis reactions.³¹ On the basis of these known structures, it does seem likely that metathesis of one N^iPr_2 for Cl occurs, segregating the tetramer to a dimer, $\text{Cp}^*\text{Ru}(\mu\text{-Cl})(\mu\text{-}^i\text{Pr}_2\text{N})\text{RuCp}^*$ but that further chloride metathesis

(26) r_{bp} was calculated according to the equation $r_{bp} = d_{bp} - 1.25$, where 1.25 is the covalent radius of Ru, and $d_{bp} = [d_{\text{RuH}}^2 + r^2 d_{\text{CH}}^2 - r(d_{\text{RuH}}^2 + d_{\text{CH}}^2 - d_{\text{RuC}}^2)]^{1/2}$. Here d_{XY} indicates the bond distance from X to Y and $r = 0.291$. Corrections were made for bond lengths determined by X-ray according to the equations

$$d_{\text{MH}} = l_{\text{MH}} + 0.1[(l_{\text{CH}}^2 + l_{\text{MH}}^2 - d_{\text{MC}}^2)/2l_{\text{CH}}l_{\text{MH}}]$$

$$d_{\text{CH}} = l_{\text{CH}} + 0.1$$

where l_{XY} is the bond length found by X-ray diffraction.

(27) Brookhart, M.; Green, M. L. H.; Wong, L.-L. *Prog. Inorg. Chem.* **1988**, *36*, 1.

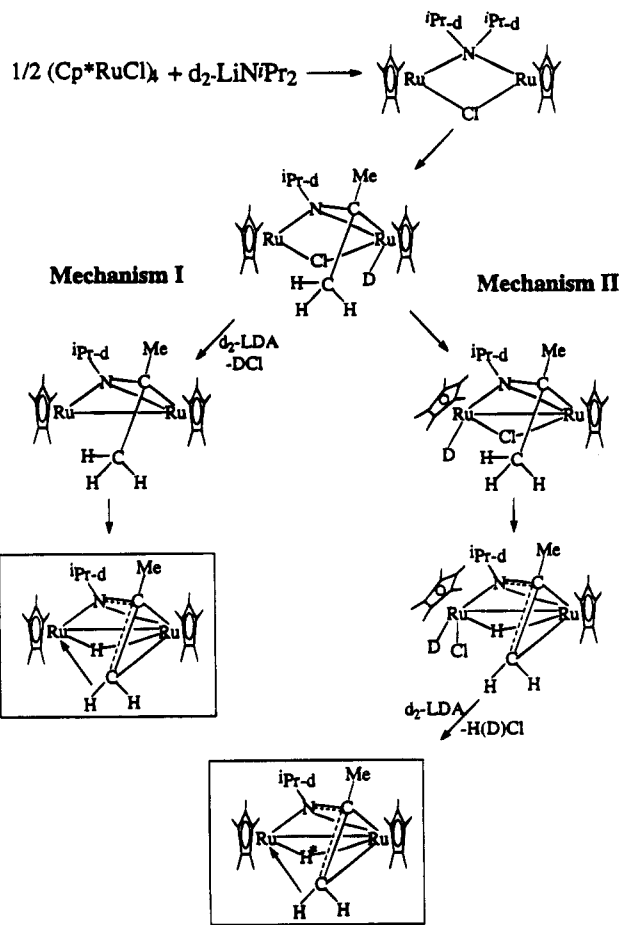
(28) These constants generally fall in the range 1–3.5 Hz: Loudon, G. M. *Organic Chemistry*; Addison-Wesley: Reading, MA, 1984; p 413.

(29) Horton, A. D.; Mays, M. J.; Raithby, P. R. *J. Chem. Soc., Chem. Commun.* **1985**, 247.

(30) In one instance, the difference in J-values was too small to be measured. Cracknell, R. B.; Orpen, A. G.; Spencer, J. L. *J. Chem. Soc., Chem. Commun.* **1984**, 326.

(31) Another interesting dimer for comparison is $[\text{Ru}(\eta\text{-C}_6\text{H}_6)(\text{N}-2,6\text{-}^i\text{Pr}_2\text{C}_6\text{H}_3)_2]$: Kee, T. P.; Park, L. Y.; Robbins, J.; Schrock, R. R. *J. Chem. Soc., Chem. Commun.* **1991**, 121.

Scheme 2

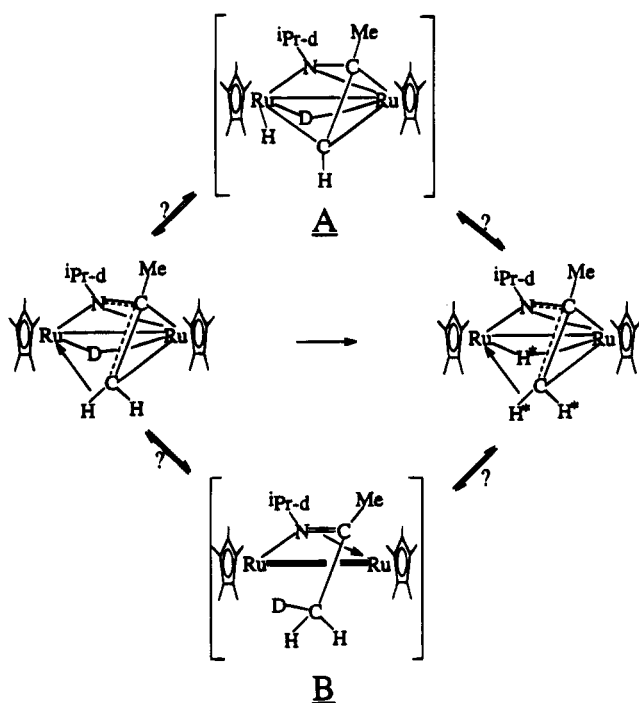


is frustrated sterically. From this proposed intermediate, the follow steps must occur to yield the final product: β -CH activation, γ -CH activation, and dehydrohalogenation.

Some reasonable assumptions about the order of occurrence of these three reaction steps can be made *a priori*. Certainly, at least one CH activation *must* precede dehydrohalogenation, in order to provide a hydrogen atom at Ru. For entropic reasons, β -CH activation is faster than γ -CH activation. Therefore, the reaction step immediately following metathesis can be reasonably assigned as β -CH activation. However, it remains quite uncertain which of the remaining two steps (dehydrohalogenation or γ -CH activation) precedes the other (see Scheme 2).

In order to distinguish between the two proposed mechanisms (mechanism I and mechanism II in Scheme 2), the reaction was repeated using selectively deuterium-labeled lithium diisopropylamide, $\text{Li}[\text{N}(\text{CDMe}_2)_2]$ ($\text{LDA-}d_2$). It was hoped that this reagent could be used to determine whether the hydride in the product is derived from hydrogen in the methine group (which would incorporate deuterium in the hydride position using $\text{LDA-}d_2$) or from hydrogen in a methyl group (which would remain deuterium-free at the hydride position using $\text{LDA-}d_2$). According to mechanism I, CD activation would be followed by dedeuteriohalogenation, and the product would have no deuterium in the hydride or vinylic positions. However, in mechanism II, CD activation is followed by CH activation. Therefore, both hydrogen and deuterium are available at the metal(s)

Scheme 3



in the dehydro- or dedeuteriohalogenation, and some deuterium should remain at the hydride position in the product.

In order to make this distinction, the reaction was monitored in THF in an NMR tube by ^2H NMR. After 2 h, a ^2H signal could be seen at -6 ppm for D-incorporation at the hydride position.³² This observation demonstrates conclusively that γ -CH activation precedes dehydrohalogenation (mechanism II), and mechanism I can be dismissed.

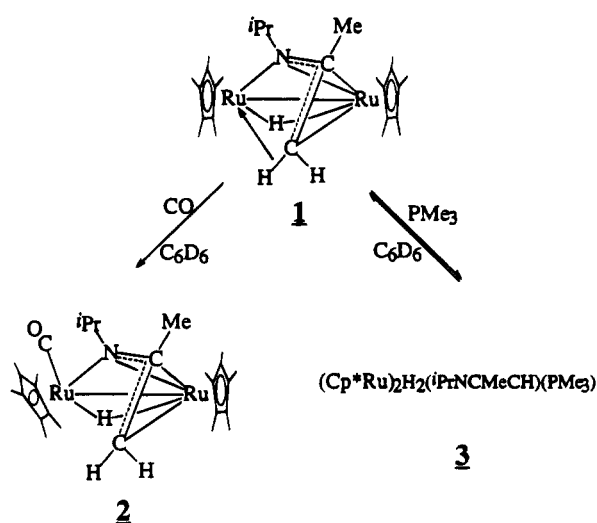
Exchange of Hydride with Methylene Hydrogens. After longer periods of time (> 4 h), additional information is obtained from this experiment. ^2H signals appear and increase in intensity at $\delta 0$ and -3 ppm, while the signal at -6 ppm decreases. This indicates a slow exchange (deuterium scrambling) of these three positions.³³ Integration of the ^2H resonances for this compound at equilibrium shows a preference for deuterium on carbon, rather than on ruthenium (29% D in the CH position, 27% D in the agostic position, and 15% D in the hydride position). The fact that the total deuterium incorporation (D atom/molecule of **1**) is only 0.71 is consistent with an intermediate containing chloride, hydride, and deuteride ligands before dehydrohalogenation. Because deuterium incorporation is observed first at the hydride position and only later in the methylene positions, the scrambling cannot occur in an intermediate step of the synthetic reaction (Scheme 1). That is, the exchange is intrinsic to the final product and not to the mechanism of formation of **1**.

The mechanism of this scrambling could be "completing" oxidative addition of the agostic CH bond and return to agostic CH or CD (Scheme 3, intermediate A). This scrambling mechanism is preferred to its converse: reductive elimination and re-formation of agostic

(32) There was also a signal at $\delta 2.6$ for the methine deuterium of the unperturbed isopropyl group.

(33) No significant broadening of these signals was observed in ^1H NMR even at $+90$ °C in toluene- d_6 .

Scheme 4



CH or CD (Scheme 3, intermediate B). The products of **1** with small tertiary phosphines (see below) are very similar in appearance to A. In fact, they can be considered trapped versions of intermediate A. Few studies have demonstrated such an exchange of hydride and agostic hydrogen.³⁴ Again, this exchange in **1** is slower than that in other known examples, which could be a result of the weak interaction (in early stages of CH activation) in **1**.

Reaction of **1 with CO.** Compound **1** reacts with CO quickly and irreversibly to form the adduct, **2**. On the basis of its stretching frequency (1893 cm^{-1}), the CO is assigned to a terminal position. Upon coordination of CO, the chemical shifts of the two vinylic hydrogens move to a region common for simple allyl-like coordination:³⁵ $\delta 1.69$ (d, $J = 1.5$) and 0.60 (apparent, t, $J = 1.5$).³⁶ Similarly, the ^{13}C signal for the vinylic carbon moves from $\delta 3.46$ in **1** to $\delta 37.82$ in **2**. This type of reactivity is quite common, since agostic CH is a very weak ligand and easily replaced. We assign the structure shown in Scheme 4 to the CO adduct. The hydride is shown bridging since no infrared band is observed between 1800 and 2700 cm^{-1} . In the ^{13}CO analog, ^{13}C -coupling is observed only to the hydride (^1H NMR). In $^{13}\text{C}\{^1\text{H}\}$ NMR, no coupling is observed from ^{13}C to any other resonance (natural abundance spectrum). This provides excellent evidence for CO bound to the Ru *without* the azaallyl ligand. In short, this reaction must simply be a displacement of the agostic interaction by the incoming CO ligand.

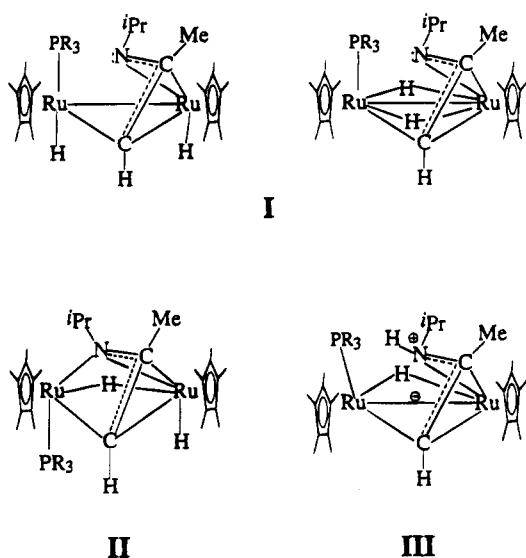
Even in the presence of excess CO, no further reaction is observed. Furthermore, no ^{12}CO incorporation is observed (^1H NMR) after treating a C_6D_6 solution of the ^{13}C -labeled adduct with 1 atm of CO for 1 day or after vigorously bubbling CO through a solution for 10 min.

(34) (a) Cree-Uchiyama, M.; Shapley, J. R.; St. George, G. M. *J. Am. Chem. Soc.* **1986**, *108*, 1316. (b) Crabtree, R. H.; Hamilton, D. G. *Adv. Organomet. Chem.* **1988**, *28*, 299.

(35) (a) Magashima, H.; Mukai, K.; Shiota, Y.; Yamaguchi, K.; Ara, K.; Fukahori, T.; Suzuki, H.; Akita, M.; Moro-oka, Y.; Itoh, K. *Organometallics* **1990**, *9*, 799. (b) Koelle, U.; Kang, B.-S.; Spaniol, T. P.; Englert, U. *Organometallics* **1992**, *11*, 249.

(36) One resonance for a methylene hydrogen appears as a doublet of doublets, even though the hydride signal appears as a singlet. Collapse of this methylene ^1H signal to a doublet upon irradiation of the hydride signal during acquisition confirmed the hydride as the source of the additional coupling. The line width of the hydride is 3.2 Hz, while $J = 1.5$ Hz.

Chart 1



Reaction of 1 with PR_3 . In contrast to its fast, irreversible reaction with CO, **1** reacts relatively slowly (several hours) and reversibly with PMe_3 to form an adduct, **3** (Scheme 4). Analogous products are formed from PMe_2Ph (**4**), PMePh_2 (**5**), and $\text{P}(\text{OEt})_3$ (**6**). Furthermore, PMe_3 is found not to displace the agostic interaction but to effect oxidative addition of this CH bond. The best evidence for this bond scission is the observation of a doublet (not a doublet of doublets) at 136.43 ppm in the gated-coupled ^{13}C spectrum, characteristic of an alkylidene carbon. Correspondingly, the signal for one hydride shifts upfield to -15.98 ppm (d, $J_{\text{PH}} = 12.6$) and a signal for one methine hydrogen appears at 6.92 ppm (d, $J_{\text{PH}} = 21.3$ Hz).³⁷ Unfortunately, one hydride resonance is obscured by a Cp^* signal. A signal at 1.8 ppm was observed in ^2H NMR for the product of reaction of deuterium-labeled **1**⁺ (see Experimental Section) and PMe_3 .

There are several reasonable structures for the phosphine adducts of **1** (Chart 1). In **I**, the phosphine has displaced nitrogen from its bridging position, while in **II**, the Ru–Ru bond is broken by the incoming ligand. According to electron-counting rules, the hydrides in **I** should be either both bridging or both terminal, while **II** would be expected to have one hydride bridging and one terminal. Because no terminal hydride stretch is seen in the IR, we favor **I** with both bridging hydrides. This structure is also relieved sterically by allowing the *i*Pr group on N the freedom to move away from the bulky phosphine ligand. One final possibility is a zwitterionic structure (**III**) with a bridging hydride and the other hydrogen attached to nitrogen. This would have a formal +1 charge on nitrogen, and a –1 charge distributed among the two metal centers.

Despite some remaining uncertainty about the eventual fate of the hydrogens, it is clear that phosphines effect a new type of reaction for agostically held CH

bonds. There are several explanations for the differences in structure of **1**, **2**, and **3–6**, based on the differences in size and electronic properties of the ligands. The bulkier PR_3 ligands may require some sort of internal “pre-equilibrium” to allow reaction. It was noted that H1, H2, and H3 will exchange positions over time (see Scheme 2). If this is the case, then products **3–6** can be seen as traps of the intermediate in this exchange. Furthermore, it may be true that significant van der Waals interactions exist between the R groups of the phosphine and the isopropyl group to essentially “hold” the amide moiety out of the bridging position. Of course, no such interactions exist when the incoming ligand is CO.

A contributing factor in the comparison of **1** and **3** is the donor ability of the ligand. The phosphine lone pair is more electron-donating than the nitrogen lone pair. Therefore, upon phosphine association, the metal center becomes more electron-rich and effects the oxidative addition. To test this, we investigated the possibility that less electron-rich phosphines may behave more like CO and simply displace agostic CH. However, reactions analogous to that with PMe_3 are observed for PMe_2Ph and PMePh_2 , and there is no observable reaction with PPh_3 . Even the very electron-poor $\text{P}(\text{OEt})_3$ effects CH bond scission, while $\text{P}(\text{O}^i\text{Pr})_3$ does not bind. Sterics seem to determine the rate and extent of binding, since reaction with $\text{P}(\text{OEt})_3$ is fast and quantitative, while the better donor PMePh_2 binds very slowly and incompletely. No reaction is observed with NH_3 or pyridine. We have been unable to grow crystals of **3–6** for X-ray structure determination.

Conclusions

In contrast to many other metathesis reactions with $(\text{Cp}^*\text{RuCl})_4$, reaction with LiN^iPr_2 does not lead to a simple heteroatom-bridged dimer. Instead, the ruthenium metal center dehydrogenates one isopropyl group of one diisopropylamide moiety. Such activations of CH bonds attendant to N are of interest to hydrodenitrogenation³⁸ (HDN) chemistry. This study represents one of few reactions to remove H both α and β to nitrogen³⁹ and is especially remarkable since it does not require elevated temperature. Both CH activations occur in consecutive mechanistic steps in this reaction. This propensity for “naked” Cp^*Ru to break strong bonds has been seen by others.⁴⁰ Dehydrogenation of the N^iPr_2 functionality has also been reported recently for a 3d element (vanadium).⁴¹

In the present case, a third C–H bond is broken upon addition of phosphine. This result is at first counter-

(38) For a description of the importance of HDN chemistry, see: Hirschon, A. S.; Wilson, R. B., Jr. *Appl. Organomet. Chem.* **1992**, *6*, 421.

(39) (a) Adams, R. D.; Tanner, J. T. *Appl. Organomet. Chem.* **1992**, *6*, 449. (b) Tanner, J. T.; Adams, R. D. *Organometallics* **1988**, *7*, 2241. (c) Day, M.; Hajela, S.; Hardcastle, K. I.; McPhillips, T.; Rosenberg, E.; Botta, M.; Gobetto, R.; Milone, L.; Osella, D.; Gellert, R. W. *Organometallics* **1990**, *9*, 913.

(40) (a) Omori, H.; Suzuki, H.; Take, Y.; Moro-oka, Y. *Organometallics* **1989**, *8*, 2270. (b) Kakigano, T.; Suzuki, H.; Igarashi, M.; Moro-oka, Y. *Organometallics* **1990**, *9*, 2192. (c) Lin, W.; Wilson, S. R.; Girolami, G. S. *J. Am. Chem. Soc.* **1993**, *115*, 3022. (d) Rondon, D.; Chaudret, B.; He, X.-D.; Labroue, D. *J. Am. Chem. Soc.* **1991**, *113*, 5671. (e) Masuda, K.; Ohkita, H.; Kurumatani, S.; Itoh, K. *Organometallics* **1993**, *12*, 2221.

(41) Song, J.; Berno, P.; Gambarotta, S. *J. Am. Chem. Soc.* **1994**, *116*, 6927.

(37) While three-bond HP coupling through a metal generally falls in the range 0–10 Hz, there are a few examples of values >20 Hz: (a) $^3J_{\text{HP}} = 35.7, 31.5, 29.6$; Cherkas, A. A.; Mott, G. N.; Granby, R.; Maclaughlin, S. A.; Yule, J. E.; Taylor, N. J.; Carty, A. J. *Organometallics* **1988**, *7*, 1115. (b) $^3J_{\text{HP}} = 29.8, 29.7, 28.5$; Cherkas, A. A.; Hoffman, D.; Taylor, N. J.; Carty, A. J. *Organometallics* **1987**, *6*, 1466. (c) $^3J_{\text{HP}} = 27$; Jeffery, J. C.; Moore, I.; Stone, F. G. A. *J. Chem. Soc., Dalton Trans.* **1984**, 1571. (d) $^3J_{\text{HP}} = 21.8$; Horton, A. D.; Mays, M. J.; McPartlin, M. *J. Chem. Soc., Chem. Commun.* **1987**, 424.

intuitive: generally, one thinks of phosphine *dissociation* (thereby creating unsaturation) leading to oxidative addition.⁴² However, it is not so surprising when one considers that the C–H bond already occupies a metal orbital in the preceding molecule, via an agostic interaction. For complete oxidative addition of the agostic CH, then, no ligand dissociation is needed (which is generally required to free a metal orbital). Only a more electron-donating ligand is needed to supply electron density to the metal center.

The complexes presented here are a nice representation of the approach and activation of a CH bond. In **2**, CH has no significant bonding interaction with the

metal. In **1**, the CH bond is closer and is held to the metal by an agostic interaction. In **3**, the bond has been broken and the oxidative addition is complete.

Acknowledgment. This work was supported by the NSF and by a material grant from Johnson Matthey/Aesar. R.K. is the recipient of an NSF graduate fellowship.

Supporting Information Available: Additional structural diagrams and listings of full crystallographic data, anisotropic thermal parameters, positional and isotropic thermal parameters, bond distances, and bond angles (19 pages). Ordering information is given on any current masthead page.

OM950252M

(42) Lehmkuhl, H.; Bellenbaum, M.; Grundke, J.; Mauermann, H.; Krüger, C. *Chem. Ber.* **1988**, *121*, 1719 and references therein.

C-S Bond Scission of Substituted Thiophenes at Rhodium. Factors Influencing the Regioselectivity of the Insertion and the Stability of the Resulting Metallathiacycles

Claudio Bianchini,* M. Victoria Jiménez, Andrea Meli, and Francesco Vizza

Istituto per lo Studio della Stereochimica ed Energetica dei Composti di Coordinazione, ISSECC-CNR, Via J. Nardi 39, 50132 Firenze, Italy

Received January 23, 1995[⊗]

The fragment [(triphos)RhH], generated *in situ* by thermolysis of the trihydride (triphos)-RhH₃ in refluxing tetrahydrofuran, reacts with a variety of substituted thiophenes to give C-S insertion products of the formula (triphos)Rh(η^3 -SCR=CR'CH=CH₂) (R' = H, R = Me, Et, COMe, CO₂Et; R = H, R' = Me, COMe, OMe; triphos = MeC(CH₂PPh₂)₃). Irrespective of the position and electronic character of the substituent in the thiophene, insertion is seen exclusively into the C-S bond away from the substituent, consistent with a determinant steric control. The electronic properties of the substituent in the thiophene play an important role in determining the stability of the C-S insertion products in chlorinated solvents. Among the thiophenes investigated, only 2,5-Me₂T, for steric reasons, and 2-OMeT, for electronic reasons, do not form butadienethiolate complexes by reaction with [(triphos)RhH]. The competitive reactivity of various substituted thiophenes toward the fragment [(triphos)-RhH] has been studied by NMR spectroscopy. The reactivity decreases in the order: 2-CO₂EtT > 2-COMeT > 3-COMeT \gg 3-OMeT > T \approx 2-MeT > 3-MeT, consistent with a predominant electronic effect.

Introduction

In recent years, an intense effort has been devoted to the fundamental understanding of the mechanisms which are operative in the hydrodesulfurization (HDS) reaction of fossil fuels.¹

A mechanistic approach which continues to attract considerable attention is the study of the coordination and reactivity of simple model substrates such as thiophene (T) with soluble metal complexes.²⁻⁸ However, since alkyl-substituted thiophenes in fossil fuels are much more prevalent than T itself, it is expected that information of effective practical relevance can best

be obtained from studies of the reactions between substituted thiophenes and metal fragments. Indeed, through an approach of this type, some research groups have recently answered important questions about the HDS mechanism.

Angelici has shown, *inter alia*, that methyl-substituted thiophenes are $\eta^1(S)$ - and/or η^5 -adsorbed to the catalyst surface through a comparison of their adsorption coefficients on a sulfided Co-Mo/Al₂O₃ HDS catalyst, with the equilibrium constants for thiophene binding in model complexes.⁹ Jones has proved that an S-bound species is an intermediate precursor to thiophene C-S bond cleavage just by looking at the different selectivities of the reactions between a unique metal fragment and various alkyl-substituted thiophenes.^{6,10}

Homogeneous reactions of substituted thiophenes with metal complexes have been investigated by a few other researchers.^{7,11-15} Scheme 1 summarizes all the known reactions leading to C-S bond scission.

An inspection of Scheme 1 clearly shows that both steric and electronic factors can interfere with the observed regioselectivities of the metal insertion into C-S bonds of different thiophenes. However many fundamental questions about C-S cleavage of substi-

[⊗] Abstract published in *Advance ACS Abstracts*, May 15, 1995.

(1) (a) Mitchell, P. C. H. *The Chemistry of Some Hydrodesulfurization Catalysts Containing Molybdenum*; Climax Molybdenum Co. Ltd.: London, 1967. (b) Schuman, S. C.; Shalit, H. *Catal. Rev.* **1970**, *4*, 245. (c) Weisser, O.; Landa, O. *Sulfide Catalysts: Their Properties and Applications*; Pergamon: Oxford, U.K., 1973. (d) Gates, B. C.; Katzer, J. R.; Schuit, G. C. A. *Chemistry of Catalytic Properties*; McGraw-Hill: New York, 1979. (e) Satterfield, C. N. *Heterogeneous Catalysis in Practice*; McGraw-Hill: New York, 1980. (f) *Geochemistry of Sulfur in Fossil Fuels*; Orr, W. L., White, C. M., Eds.; ACS Symposium Series 429; American Chemical Society: Washington, DC, 1990. (g) McCulloch, D. C. In *Applied Industrial Catalysis*; Leach, B. E., Ed.; Academic: New York, 1983; Vol. 1, p 69. (h) Lyapina, N. K. *Russ. Chem. Rev. (Engl. Transl.)* **1982**, *51*, 189. (i) Challenger, F. *Aspects of the Organic Chemistry of Sulfur*; Butterworths: London, 1959.

(2) (a) Sánchez-Delgado, R. A. *J. Mol. Catal.* **1994**, *86*, 287. (b) Rauchfuss, T. B. *Prog. Inorg. Chem.* **1991**, *39*, 259. (c) Angelici, R. J. *Coord. Chem. Rev.* **1990**, *105*, 61. (d) Angelici, R. J. *Acc. Chem. Res.* **1988**, *21*, 387.

(3) Bianchini, C.; Meli, A.; Peruzzini, M.; Vizza, F.; Frediani, P.; Herrera, V.; Sánchez-Delgado, R. A. *J. Am. Chem. Soc.* **1993**, *115*, 2731.

(4) Jones, W. D.; Chin, R. M. *J. Am. Chem. Soc.* **1994**, *116*, 198.

(5) Jones, W. D.; Chin, R. M.; Crane, T. W.; Baruch, D. M. *Organometallics* **1994**, *13*, 4448.

(6) Dong, L.; Duckett, S. B.; Ohman, K. F.; Jones, W. D. *J. Am. Chem. Soc.* **1992**, *114*, 151.

(7) Chen, J.; Daniels, L. M.; Angelici, R. J. *J. Am. Chem. Soc.* **1990**, *112*, 199.

(8) Selnau, H. E.; Merola, J. S. *Organometallics* **1993**, *12*, 1583.

(9) (a) Benson, J. W.; Angelici, R. J. *Organometallics* **1993**, *12*, 680.

(b) Benson, J. W.; Angelici, R. J. *Organometallics* **1992**, *11*, 922.

(10) Jones, W. D.; Dong, L. *J. Am. Chem. Soc.* **1991**, *113*, 559.

(11) Jones, W. D.; Chin, R. M. *J. Am. Chem. Soc.* **1992**, *114*, 9851.

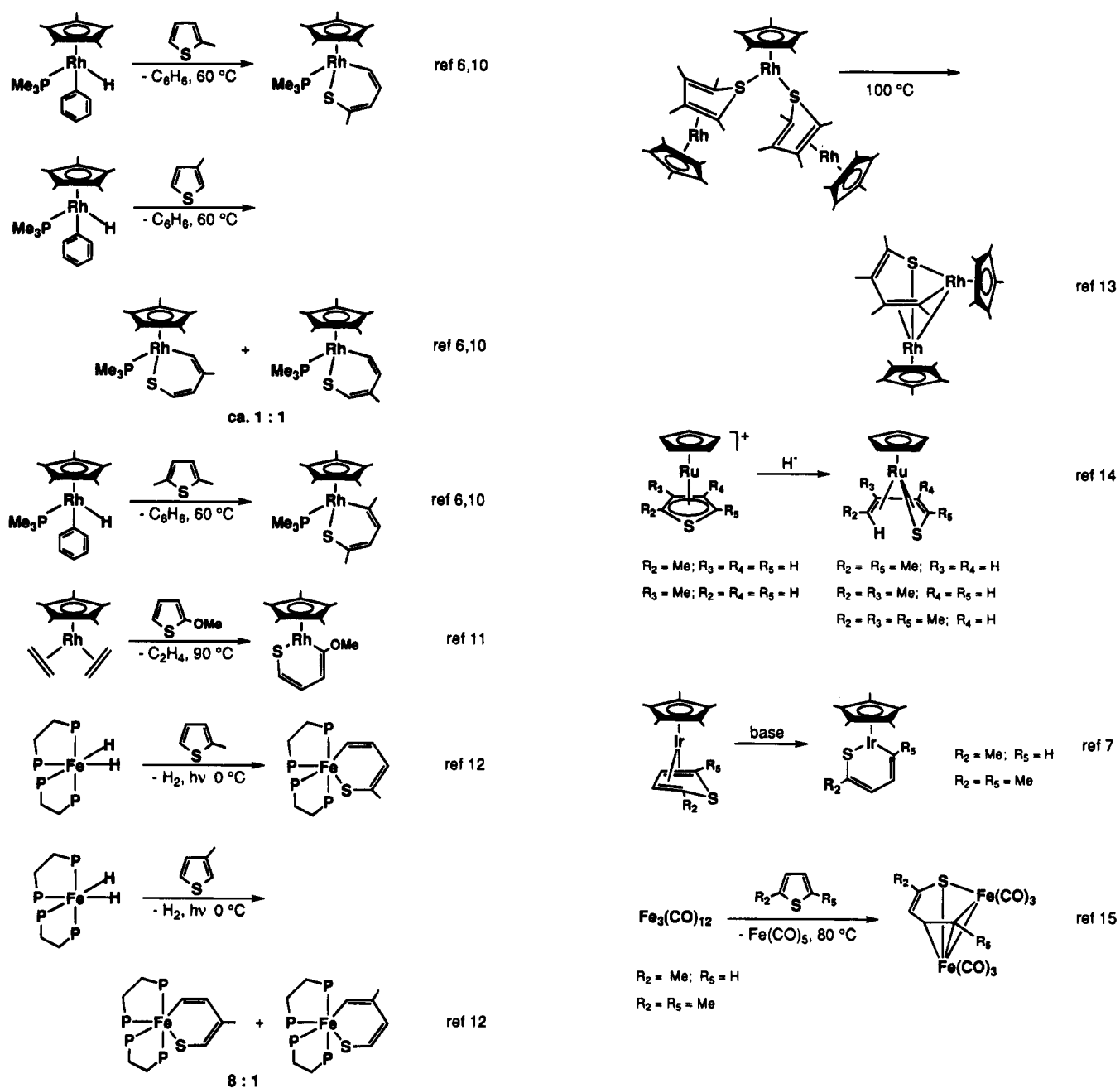
(12) Buys, I. E.; Field, L. D.; Hambley, T. W.; McQueen, A. E. D. *J. Chem. Soc., Chem. Commun.* **1994**, 557.

(13) Luo, S.; Skaugset, A. E.; Rauchfuss, T. B.; Wilson, S. R. *J. Am. Chem. Soc.* **1992**, *114*, 1732.

(14) Hachgenei, J. W.; Angelici, R. J. *J. Organomet. Chem.* **1988**, *355*, 359.

(15) Ogilvy, A. E.; Draganjac, M.; Rauchfuss, T. B.; Wilson, S. R. *Organometallics* **1988**, *7*, 1171.

Scheme 1



tuted thiophenes are still unanswered; for example, it is still not understood what the competitive selectivities of different thiophenes are and what the relative stabilities of the C-S insertion products as a function of the electronic and steric nature of the substituent(s) in the thiophene are.

This paper describes our effort to address some of these questions through a comparative study of the reactions of various substituted thiophenes with the 16-electron metal fragment [(triphos)RhH] (triphos = MeC(CH₂PPh₂)₃).¹⁶

Experimental Section

General Information. All reactions and manipulations were routinely performed under a nitrogen atmosphere by

using standard Schlenk techniques. Tetrahydrofuran (THF) was distilled from LiAlH₄ and *n*-heptane from sodium. The solvents were stored over molecular sieves and purged with nitrogen prior to use. 2-MeT, 2-EtT, 3-MeT, 2,5-Me₂T, 2-OMeT, 3-OMeT, 2-COMeT, 3-COMeT, and 2-CO₂EtT were purchased from Aldrich and used without further purification. All other chemicals were commercial products and were used as received without further purification. The literature method was used for the preparation of (triphos)RhH₃ (1).¹⁷ All metal complexes were collected on sintered-glass frits and washed with appropriate solvents before being dried under a stream of nitrogen. Infrared spectra were recorded on a Perkin-Elmer 1600 Series FT-IR spectrophotometer using samples mullied in Nujol between KBr plates. Deuterated solvents for NMR measurements were dried over molecular sieves. ¹H NMR spectra were obtained on a Bruker ACP 200 (200.13 MHz) spectrometer. ¹H NMR shifts are recorded relative to residual ¹H resonance in the deuterated solvent. ¹³C{¹H} NMR spectra were recorded on the Bruker ACP 200 instrument operating

Table 1. $^{31}\text{P}\{^1\text{H}\}$ NMR Spectral Data for the New Complexes^a

complex	pattern	chem shift, ppm ^b			coupling const, Hz					
		$\delta(\text{A})$	$\delta(\text{M})$	$\delta(\text{Q})$	$J(\text{AM})$	$J(\text{AQ})$	$J(\text{MQ})$	$J(\text{ARh})$	$J(\text{MRh})$	$J(\text{QRh})$
2 ^c	AMQX	31.4	0.2	-4.0						
	AMQX ^d	31.4	-0.3	-3.5	34.6	29.1	39.4	108.3	119.4	106.4
3	AMQX	30.8	-1.7	-4.3	33.3	30.0	44.3	108.4	118.3	107.8
4	AMQX	31.2	-1.4	-5.5						
	AMQX ^d	31.5	-1.6	-5.6	34.2	29.3	42.7	108.6	118.4	107.4
5	AMQX	30.3	3.4	-4.3						
	AMQX ^d	30.7	3.7	-4.2	33.9	30.9	27.9	106.2	123.6	104.0
6	AMQX	30.9	2.3	-4.3						
	AMQX ^d	31.4	0.5	-4.2	33.6	31.1	28.1	106.6	122.5	104.6
7	AMQX	30.8	0.2	-5.4	36.4	31.4	44.5	111.1	119.8	107.5
8	AMQX	31.2	2.1	-4.0						
	AMQX ^d	31.8	2.2	-3.9	35.4	32.0	34.9	108.7	120.3	104.6
9	AMQX	30.3	0.6	-5.7	35.4	28.5	41.5	107.4	120.0	105.6

^a All spectra were recorded at 20 °C in CD₂Cl₂ solutions unless otherwise stated. ^b The chemical shifts (δ 's) are relative to 85% H₃PO₄; downfield values are assumed as positive. ^c See ref 16a. ^d At -10 °C.

at 50.32 MHz. The $^{13}\text{C}\{^1\text{H}\}$ NMR shifts are given relative to the solvent resonance. $^{31}\text{P}\{^1\text{H}\}$ NMR spectra were recorded on a Bruker ACP 200 spectrometer operating at 81.01 MHz. Chemical shifts are relative to external 85% H₃PO₄ with downfield values reported as positive. Broad band and selective $^1\text{H}\{^{31}\text{P}\}$ NMR experiments were carried out on the Bruker ACP 200 instrument equipped with a 5-mm inverse probe and a BFX-5 amplifier device. ^{13}C DEPT, ^1H - ^{13}C 2D HETCOR, and ^1H - ^1H 2D COSY NMR experiments were conducted on the Bruker ACP 200 spectrometer. The computer simulation of NMR spectra was carried out with a locally developed package containing the programs LAOCN3¹⁸ and Davins¹⁹ running on a Compaq Deskpro 386/25 personal computer. The initial choices of shifts and coupling constants were refined by iterative least-squares calculations using experimental digitized spectra. The final parameters gave a satisfactory fit between experimental and calculated spectra, the agreement factor *R* being less than 1% in all cases.

General Procedure for the Preparation of (triphos)-Rh(η^3 -SCR-CH=CH₂) (R' = H, R = Me (3), Et (4), COMe (5), CO₂Et (6); R = H, R' = Me (7), COMe (8), OMe (9)). To a stirred suspension of (triphos)RhH₃ (1; 0.50 g, 0.68 mmol) in THF (40 mL) was added a 10-fold excess of the appropriate thiophene, and then the mixture was heated at reflux temperature. Within a few minutes the solid dissolved. After ca. 5 h, the resulting orange-brown solution was concentrated to ca. 10 mL. Whereas 4 and 9 precipitated during the concentration process, the precipitation of the other compounds was accomplished by portionwise addition of *n*-heptane (20 mL). All the compounds, obtained as orange microcrystals, were collected by filtration and washed with *n*-pentane; yield 70–85%. In independent isothermal reactions, carried out in THF-*d*₃ in the temperature range from 60 to 120 °C, only the isomer formed by 1–5 insertion was observed by $^{31}\text{P}\{^1\text{H}\}$ NMR spectroscopy.

Characterization of 3–9. Selected NMR spectral data for the metal complexes are collected in Table 1 ($^{31}\text{P}\{^1\text{H}\}$ NMR) and Table 2 (^1H , $^{13}\text{C}\{^1\text{H}\}$ NMR). ^{13}C DEPT, ^{13}C - ^1H 2D HETCOR, and ^1H - ^1H 2D COSY spectra allowed the total and unequivocal assignment of all hydrogen and carbon resonances for all metal complexes as labeled in Tables 1 and 2.

(triphos)Rh(η^3 -SC(Me)=CHCH=CH₂) (3). Anal. Calcd (found) for C₄₆H₄₆P₃RhS: C, 66.83 (66.65); H, 5.61 (5.58); Rh, 12.45 (12.22); S, 3.88 (3.59). IR: $\nu(\text{C}=\text{C})$ 1568 (m) cm⁻¹.

(triphos)Rh(η^3 -SC(Et)=CHCH=CH₂) (4). Anal. Calcd (found) for C₄₇H₄₈P₃RhS: C, 67.14 (67.00); H, 5.75 (5.78); Rh, 12.24 (12.00); S, 3.81 (3.61). IR: $\nu(\text{C}=\text{C})$ 1565 (m) cm⁻¹.

(triphos)Rh(η^3 -SC(OMe)=CHCH=CH₂) (5). Anal. Calcd (found) for C₄₇H₄₆OP₃RhS: C, 66.04 (65.83); H, 5.42 (5.31); Rh, 12.04 (12.00); S, 3.75 (3.57). IR: $\nu(\text{C}=\text{O})$ 1650 (s), $\nu(\text{C}=\text{C})$ 1536 (m) cm⁻¹.

(18) (a) Bothner-By, A. A.; Castellano, S. *QCPE* 1967, 11, 111. (b) Castenello, S.; Bothner-By, A. A. *J. Chem. Phys.* 1964, 41, 3863.

(19) Stephenson, D. S.; Binsch, G. *J. Magn. Reson.* 1980, 37, 409.

(triphos)Rh(η^3 -SC(CO₂Et)=CHCH=CH₂) (6). Anal. Calcd (found) for C₄₈H₄₈O₂P₃RhS: C, 65.16 (64.88); H, 5.47 (5.39); Rh, 11.63 (11.39); S, 3.62 (3.52). IR: $\nu(\text{C}=\text{O})$ 1690 (s), $\nu(\text{C}=\text{C})$ 1561 (m) cm⁻¹.

(triphos)Rh(η^3 -SCH=C(Me)CH=CH₂) (7). Anal. Calcd (found) for C₄₆H₄₆P₃RhS: C, 66.83 (66.55); H, 5.61 (5.54); Rh, 12.45 (12.26); S, 3.88 (3.64). IR: $\nu(\text{C}=\text{C})$ 1570 (m) cm⁻¹.

(triphos)Rh(η^3 -SCH=C(OMe)CH=CH₂) (8). Anal. Calcd (found) for C₄₇H₄₆OP₃RhS: C, 66.04 (65.74); H, 5.42 (5.32); Rh, 12.04 (11.90); S, 3.75 (3.61). IR: $\nu(\text{C}=\text{O})$ 1611 (s), $\nu(\text{C}=\text{C})$ 1510 (m) cm⁻¹.

(triphos)Rh(η^3 -SCH=C(OMe)CH=CH₂) (9). Anal. Calcd (found) for C₄₆H₄₆OP₃RhS: C, 65.56 (65.53); H, 5.50 (5.43); Rh, 12.21 (12.08); S, 3.80 (3.67). IR: $\nu(\text{C}=\text{C})$ 1550 (m), $\nu(\text{C}-\text{O})$ 1136 (s) cm⁻¹.

Reaction of 1 with 2,5-Me₂T. Following a procedure analogous to that reported above, the reaction between 1 and 2,5-Me₂T led to the formation of the known dimeric complex (triphos)RhH(μ -H)₂HRh(triphos).^{16b}

Reaction of 1 with 2-OMeT. Under the reaction conditions reported above, the reaction between 1 and 2-OMeT led to a mixture of several unidentified compounds.

General Procedure for the Intermolecular Competition Reaction of 1 with Two Different Thiophenes. A 5-mm NMR tube was charged under nitrogen with a solution of 1 (20 mg, 0.027 mmol) and a 10-fold excess of a 1:1 mixture of two different thiophenes in THF-*d*₃ (0.7 mL), flame-sealed, and kept at 70 °C (oil bath). After 5 h, the tube was cooled to room temperature and the product composition was determined by $^{31}\text{P}\{^1\text{H}\}$ NMR spectroscopy. The results obtained are reported in Table 3. The product ratios reported in the table are invariant with time up to 100 °C, which was the highest temperature investigated.

Results

Thermolysis of the Trihydride (triphos)RhH₃ in the Presence of Substituted Thiophenes. The complex (triphos)RhH₃ (1) has previously been shown to behave as a thermal precursor for the generation of the 16-electron fragment [(triphos)RhH],¹⁶ which is active toward the oxidative addition of C–S bonds from T or benzo[*b*]thiophene (BT).^{16a}

Thermolysis of 1 in THF occurs already at 60 °C and produces H₂. In the absence of substrates able to trap the unsaturated Rh(I) fragment, the latter dimerizes to the known complex (triphos)RhH(μ -H)₂HRh(triphos).^{16b} This reaction path is observed for the thermal reaction of 1 with 2,5-Me₂T (Scheme 2).

With the exception of 2-OMeT, all the other substituted thiophenes shown in Chart 1 react with [(triphos)-RhH] to give orange C–S insertion products of the

Table 2. ^1H and $^{13}\text{C}\{^1\text{H}\}$ NMR Spectral Data for the New Complexes^a

complex	^1H NMR		$^{13}\text{C}\{^1\text{H}\}$ NMR	
	assignt	δ (multiplicity, J) ^{b,c}	assignt	δ (multiplicity, J) ^b
	H ₄	5.98 (m, $^3J(\text{H}_4\text{Rh}) = 1.0$, $^3J(\text{H}_4\text{H}_3) = 4.5$)	C ₃	65.7 (dt, $^2J(\text{CP}) = 33.8$, 9.2 , $^1J(\text{CRh}) = 9.2$)
	H ₅	5.87 (m, $^3J(\text{H}_5\text{Rh}) = 2.0$, $^3J(\text{H}_5\text{H}_4) = 6.1$)	C ₂	40.8 (br d, $^2J(\text{CP}) = 32.0$)
	H ₃	3.26 (m, $^2J(\text{H}_3\text{Rh}) = 1.1$, $^3J(\text{H}_3\text{H}_2) = 7.5$)	C ₄	e
	H _{2d}	2.86 (m, $^2J(\text{H}_2\text{Rh}) = 2.0$, $^3J(\text{H}_2\text{H}_3) = 9.3$)	C ₅	e
	H ₂	1.63 (m, $^2J(\text{H}_2\text{Rh}) = 1.7$, $^2J(\text{H}_2\text{H}_2) = 0.5$)		
	H ₄	5.86 (m, $^3J(\text{H}_4\text{Rh}) = 1.2$, $^3J(\text{H}_4\text{H}_3) = 5.3$)	C ₃	63.1 (br d, $^2J(\text{CP}) = 32.8$)
	H _{2f}	3.11 (m, $^2J(\text{H}_2\text{Rh}) = 2.1$, $^3J(\text{H}_2\text{H}_3) = 9.1$)	C ₂	41.2 (br d, $^2J(\text{CP}) = 36.2$)
	H ₃	3.00 (m, $^2J(\text{H}_3\text{Rh}) = 1.2$, $^3J(\text{H}_3\text{H}_2) = 6.8$)	C ₆	24.0 (s)
	H ₆	2.00 (br s, $^4J(\text{H}_6\text{H}_4) = 1.1$)	C ₄	e
	H ₂	1.75 (m, $^2J(\text{H}_2\text{Rh}) = 1.3$, $^2J(\text{H}_2\text{H}_2) = 0.5$)	C ₅	e
	H ₄	5.87 (m, $^3J(\text{H}_4\text{Rh}) = 1.0$, $^3J(\text{H}_4\text{H}_3) = 4.2$)	C ₃	64.9 (m)
	H _{2g}	3.10 (m, $^2J(\text{H}_2\text{Rh}) = 2.1$, $^3J(\text{H}_2\text{H}_3) = 9.2$)	C ₂	42.4 (dd, $^2J(\text{CP}) = 24.4$, 10.1)
	H ₃	3.00 (m, $^2J(\text{H}_3\text{Rh}) = 1.5$, $^3J(\text{H}_3\text{H}_2) = 7.5$)	C ₆	31.5 (s)
	H ₆	2.3 ^h	C ₇	16.6 (s)
	H ₂	1.61 (m, $^2J(\text{H}_2\text{Rh}) = 1.0$)	C ₄	e
	H ₇	1.16 (t)	C ₅	e
	H ₄	7.4 ⁱ	C ₆	198.2 (s)
	H ₃	3.13 (m, $^2J(\text{H}_3\text{Rh}) = 1.4$, $^3J(\text{H}_3\text{H}_4) = 5.2$)	C ₃	59.5 (m)
	H ₂	3.05 (m, $^2J(\text{H}_2\text{Rh}) = 1.9$, $^3J(\text{H}_2\text{H}_3) = 9.2$)	C ₂	40.0 (m)
	H ₇	2.38 (s)	C ₇	27.8 (s)
	H ₂	1.74 (m, $^2J(\text{H}_2\text{Rh}) = 1.4$), $^3J(\text{H}_3\text{H}_2) = 7.6$)	C ₄	e
	H ₄	7.7 ⁱ ($^3J(\text{H}_4\text{H}_3) = 4.6$)	C ₆	168.5 (s)
	H ₇	4.18 (q, $^3J(\text{H}_7\text{H}_8) = 7.2$)	C ₇	60.7 (s)
	H ₃	3.12 (m, $^2J(\text{H}_3\text{Rh}) = 1.5$, $^3J(\text{H}_3\text{H}_2) = 7.1$)	C ₃	59.6 (dd, $^2J(\text{CP}) = 20.7$, 9.4)
	H _{2f}	3.02 (m, $^2J(\text{H}_2\text{Rh}) = 1.8$, $^3J(\text{H}_2\text{H}_3) = 9.4$)	C ₂	40.0 (dd, $^2J(\text{CP}) = 18.5$, 11.8)
	H ₂	1.70 (m, $^2J(\text{H}_2\text{Rh}) = 1.1$, $^2J(\text{H}_2\text{H}_2) = 0.5$)	C ₈	15.1 (s)
	H ₈	1.31 (t)	C ₄	e
			C ₅	e
	H ₅	5.51 (m, $^3J(\text{H}_5\text{Rh}) = 0.43$, $^4J(\text{H}_5\text{H}_3) = 1.13$)	C ₃	68.6 (dd, $^2J(\text{CP}) = 36.0$, 15.8)
	H _{2j}	3.01 (m, $^2J(\text{H}_2\text{Rh}) = 2.04$, $^3J(\text{H}_2\text{H}_3) = 9.11$)	C ₂	41.8 (br d, $^2J(\text{CP}) = 34.8$)
	H ₃	2.96 (m, $^2J(\text{H}_3\text{Rh}) = 0.90$, $^3J(\text{H}_3\text{H}_2) = 8.31$)	C ₆	24.1 (s)
	H ₆	1.94 (d, $^4J(\text{H}_6\text{H}_5) = 1.24$)	C ₄	e
	H ₂	1.68 (m, $^2J(\text{H}_2\text{Rh}) = -1.28$, $^2J(\text{H}_2\text{H}_2) = -1.81$)	C ₅	e
	H ₅	7.7 ⁱ ($^4J(\text{H}_5\text{H}_3) = 1.3$)	C ₆	190.1 (s)
	H ₃	4.11 (m, $^2J(\text{H}_3\text{Rh}) = 1.3$, $^3J(\text{H}_3\text{H}_2) = 7.7$)	C ₃	60.8 (dd, $^2J(\text{CP}) = 19.8$, 10.7)
	H _{2k}	2.62 (m, $^2J(\text{H}_2\text{Rh}) = 1.9$, $^3J(\text{H}_2\text{H}_3) = 9.6$)	C ₂	41.1 (br d, $^2J(\text{CP}) = 18.5$)
	H ₇	2.28 (s)	C ₇	26.8 (s)
	H ₂	1.58 (m, $^2J(\text{H}_2\text{Rh}) = 1.6$, $^2J(\text{H}_2\text{H}_2) = 0.5$)	C ₄	e
	H ₅	4.86 (br d, $^3J(\text{H}_5\text{Rh}) = 1.0$, $^4J(\text{H}_5\text{H}_3) = 1.2$)		
	H ₆	3.62 (s)		
	H _{2l}	3.04 (m, $^2J(\text{H}_2\text{Rh}) = 2.1$, $^3J(\text{H}_2\text{H}_3) = 8.9$)		
	H ₃	2.87 (m, $^2J(\text{H}_3\text{Rh}) = 1.4$, $^3J(\text{H}_3\text{H}_2) = 7.3$)		
	H ₂	1.63 (m, $^2J(\text{H}_2\text{Rh}) = 1.2$, $^2J(\text{H}_2\text{H}_2) = 0.5$)		

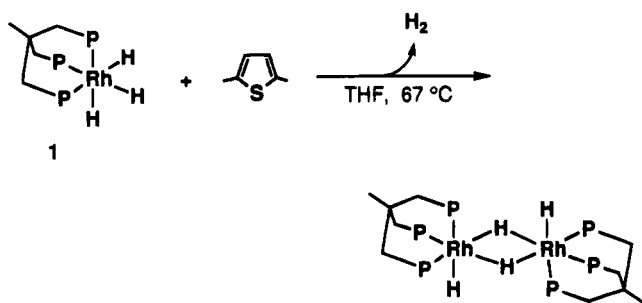
^a All spectra were recorded at room temperature in CD_2Cl_2 solutions at 200.13 (^1H NMR) and 50.32 MHz ($^{13}\text{C}\{^1\text{H}\}$ NMR) unless otherwise stated. ^b Chemical shifts are given in ppm and are relative to either residual ^1H resonance in the deuterated solvent (^1H NMR) or the deuterated solvent resonance ($^{13}\text{C}\{^1\text{H}\}$ NMR). Key: s, singlet; d, doublet; t, triplet; q, quartet; qt, quintet; m, multiplet; br, broad. Coupling constants (J) are in hertz. ^c The $J(\text{HH})$ values were determined on the basis of $^1\text{H}\{^{31}\text{P}\}$ NMR experiments. ^d See ref 16a. ^e Masked by the phenyl carbons of the triphos ligands. ^f The $^{13}\text{C}\{^1\text{H}\}$ NMR spectrum was recorded in $\text{DMF}-d_7$. ^g The $^{13}\text{C}\{^1\text{H}\}$ NMR spectrum was recorded in benzene- d_6 . ^h The two H_6 protons are masked by the aliphatic chain protons of the triphos ligand. In benzene- d_6 , however, they clearly appear as a second-order multiplet that was computed as the AB part of an ABX_3 spin system with the following magnetic parameters: $^2J(\text{H}_6\text{H}_6) = 14.4$ Hz, $^3J(\text{H}_6\text{H}_7) = ^3J(\text{H}_6\text{H}_7) = 7.4$ Hz. ⁱ Masked by the aromatic protons of the triphos ligand. The chemical shift was determined from a $^1\text{H}-^1\text{H}$ 2D COSY experiment. ^j The $^1\text{H}\{^{31}\text{P}\}$ NMR resonances of H_2 and H_3 were computed as the AB part of an ABCDE_3F spin system with $\text{F} = \text{Rh}$. ^k The $^{13}\text{C}\{^1\text{H}\}$ NMR spectrum was recorded in $\text{THF}-d_8$. ^l Due to the instability of **9** in CD_2Cl_2 and its low solubility in all the other organic solvents, no $^{13}\text{C}\{^1\text{H}\}$ NMR spectrum could be recorded.

general formula $(\text{triphos})\text{Rh}(\eta^3\text{-SCR}=\text{CR}'\text{CH}=\text{CH}_2)$ ($\text{R}' = \text{H}$, $\text{R} = \text{Me}$ (**3**), Et (**4**), COMe (**5**), CO_2Et (**6**); $\text{R} = \text{H}$, $\text{R}' = \text{Me}$ (**7**), COMe (**8**), OMe (**9**)) (Scheme 3).

Irrespective of the position and electronic character of the substituent in the thiophene, insertion is seen exclusively into the C-S bond away from the substituent. In fact, though the butadienethiolate substituents perturb the local magnetic field of the neighboring nuclei

differently (*vide infra*), the spectroscopic data of the η^3 -(S,C,C)-butadienethiolate complexes **3-9** are in excellent correlation with those of $(\text{triphos})\text{Rh}(\eta^3\text{-SCH}=\text{CH}-\text{CH}=\text{CH}_2)^{16a}$ (**2**) and $(\text{triphos})\text{Ir}(\eta^3\text{-SCH}=\text{CH}-\text{CH}=\text{CH}_2)^{16a}$ (**10**) obtained by reaction of $[(\text{triphos})\text{RhH}]$ and $[(\text{triphos})\text{IrH}]$ with **T**, respectively. Thus, like **2** and **10**, complexes **3-9** are assigned octahedral structures in which the rhodium center is coordinated by the three

Scheme 2

Table 3. Thermolysis of **1** in the Presence of a 1:1 Mixture of Different Thiophenes

mixture	products (ratio)
2-MeT/3-MeT	3/7 (60:40)
3-OMeT/2-MeT	9/3 (80:20)
2-COMeT/2-MeT	5
2-COMeT/3-COMeT	5/8 (80:20)
3-COMeT/3-MeT	8
T/2-MeT	2/3 (50:50)
3-COMeT/T	8
3-COMeT/3-OMeT	8
3-OMeT/3-MeT	9/7 (90:10)
2-CO ₂ EtT/2-COMeT	6/5 (60:40)

phosphorus atoms of a *fac* triphos and by a 2- or 3-substituted butadienethiolate ligand which uses the sulfur atom and the distal olefinic end to bind the metal. As previously found for **2** and **10**,^{3,16a} the olefinic moieties of the butadienethiolate ligands form quite robust bonds to the metal center due to a significant $d\pi$ (metal) $\rightarrow \pi^*$ (ligand) back-bonding. The metallacyclopropane character of the Rh-C₂-C₃ ring appears to be more pronounced for the complexes with thio ligands bearing electron-donating substituents ($^2J(C_{2,3}P) \approx 24$ – 36 Hz) than for the complexes obtained from thiophenes bearing electron-withdrawing substituents ($^2J(C_{2,3}P) \approx 18$ – 20 Hz). This effect may be explained

by considering that the substituent is closer to the sulfur atom than to the bound double bond. Accordingly, electron-withdrawing substituents decrease the electron density at the sulfur atom, thus ultimately decreasing the basicity of the rhodium center.

The nature of the substituent also affects the chemical shifts of the neighboring carbon and hydrogen nuclei, particularly of H₄ and H₅, which, as compared to the analogous resonances in the ¹H NMR spectrum of the unsubstituted complex **2**, move either upfield or downfield depending on the electron-donating/electron-withdrawing character of the substituent (see Table 2).

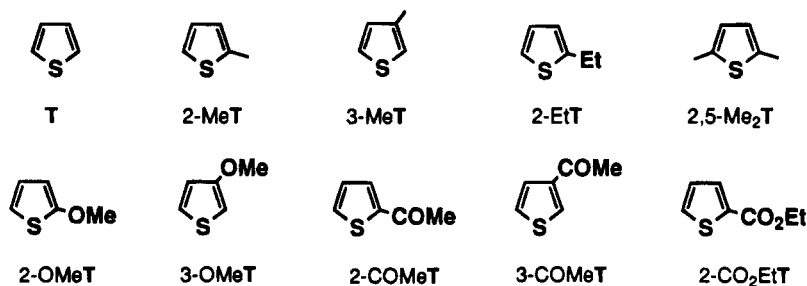
No intermediate Rh species was observed to traverse the conversion of **1** to **3**–**9** when the progress of the reactions was followed by ³¹P{¹H} NMR spectroscopy at a constant temperature of 60 °C.

Compounds **3**–**9** are stable both in the solid state, even for a short exposure to air, and in solution with non-halogenated solvents. In halogenated solvents (CH₂Cl₂, CHCl₃), the complexes containing electron-donating substituents (Me, Et, OMe) on the butadienethiolate ligand decompose at a rate that increases as the electron-donating character of the substituent in the thio ligand increases.

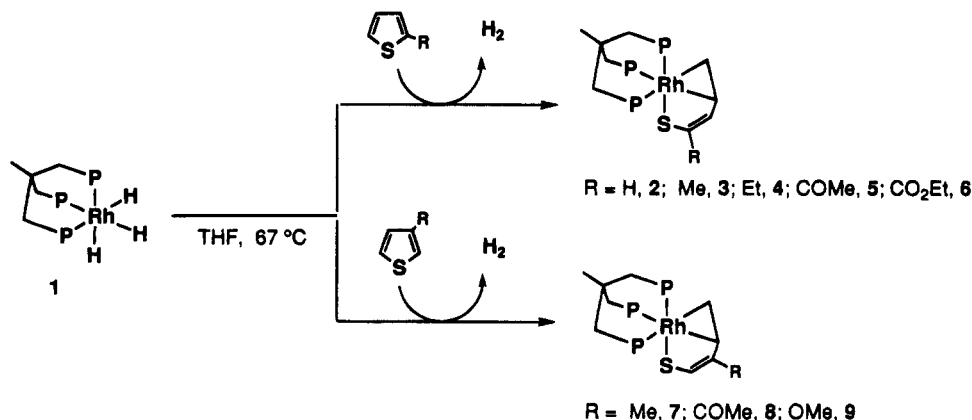
Among the various thiophenes investigated, 2-MeOT is the only one to react with [(triphos)RhH] without yielding a butadienethiolate complex; extensive decomposition occurs with formation of various, undefined rhodium compounds.

Thermolysis of the Trihydride **1 in the Presence of Mixtures of Substituted Thiophenes.** The competitive reactivity of substituted thiophenes toward the fragment [(triphos)RhH] has been followed in THF-*d*₈ in sealed NMR tubes charged with 1:1 mixtures of the following thiophene couples: T/2-MeT, T/3-COMeT, 2-MeT/3-MeT, 2-MeT/3-OMeT, 3-MeT/3-OMeT, 3-COM-

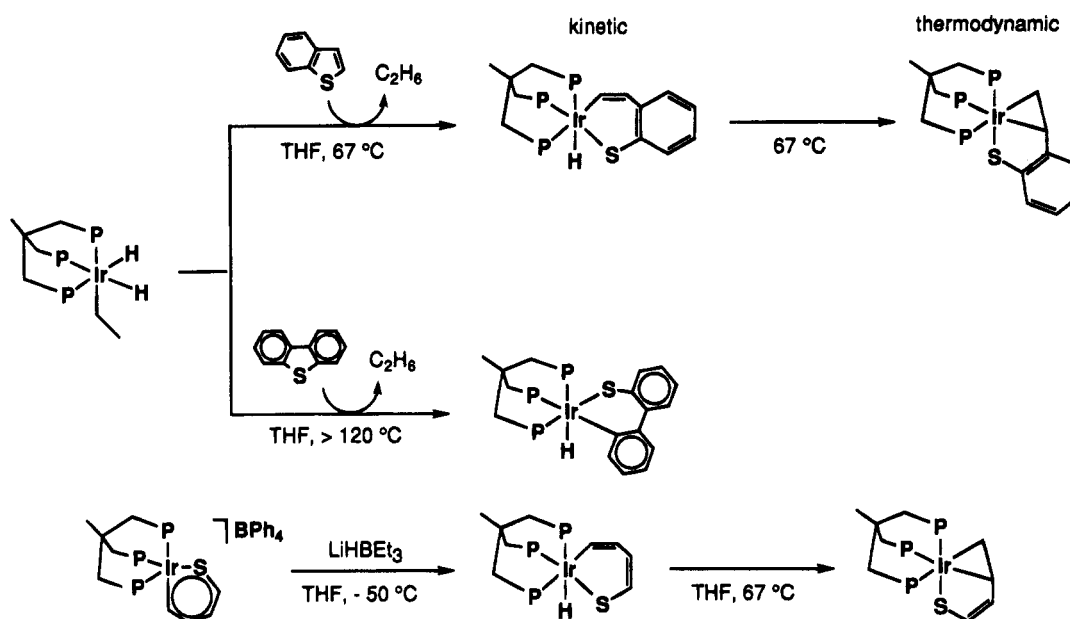
Chart 1



Scheme 3



Scheme 4



eT/3-OMeT, 2-MeT/2-COMeT, 3-MeT/3-COMeT, 2-COMeT/3-COMeT, and 2-CO₂EtT/2-COMeT.

At the complete disappearance of the starting trihydride, the product distribution of each run was determined by ³¹P{¹H} NMR integration. The results obtained, reported in Table 3, give the following trend of competitive reactivity: 2-CO₂EtT > 2-COMeT > 3-COMeT > 3-OMeT > T ≈ 2-MeT > 3-MeT.

The product ratios reported in Table 3 are invariant with time up to 100 °C, which is the highest temperature investigated. Consistently, the C-S insertion reactions are irreversible in the same temperature range. As an example, the butadienethiolate complex **2** is stable when refluxed in THF in the presence of 2-CO₂EtT. In conclusion, the observed product ratios represent kinetic distributions, which was confirmed by a preliminary study of the competitive reactions of the [(triphos)RhH] fragment, photochemically generated at 20 °C, with various substituted thiophenes.²⁰

Discussion

Opening of Substituted Thiophenes by [(triphos)RhH]. A possible mechanism for the formation of the C-S insertion products **3-9** can be proposed in light of previous studies on the opening of **T**, **BT**, or dibenzothiophene (**DBT**) by the [(triphos)RhH]^{16a} and [(triphos)IrH] fragments.^{3,21a,22}

Valuable mechanistic information was obtained with the use of the more kinetically inert iridium system. The fragment [(triphos)IrH] inserts into a C-S bond of **BT**

or **DBT** to give the complexes (triphos)Ir(H)(η²(S,C)-SC_xH_y) (x = 8, y = 6; x = 12, y = 8) as kinetic products.^{21,22} The **T** analog (triphos)Ir(H)(η²(S,C)-SC₄H₄) was prepared by hydride addition to the iridathiabenzene complex [(triphos)Ir(η²(S,C)-SC₄H₄)]BPh₄ (Scheme 4).³ From these **T** and **BT** hydrido iridathiacycles, the formation of the thermodynamically more stable butadienethiolate and 2-vinylthiophenolate products proceeds as a thermal step upon hydride migration to the α-carbon of the vinyl moiety of the metalated C₄H₄S and C₈H₆S systems (Scheme 4).

As previously discussed for the formation of **2** and **10**,^{3,16a} the lack of detectable intermediates in the course of the transformation of **1** into **3-9** can be ascribed to the higher energy of activation required to promote the reductive elimination of H₂ from **1**, as compared to the energies necessary to accomplish both the C-S bond scission and the migration of the terminal hydride to the α-carbon of the metallathiacycle.

In this paper, we have shown that variation of the substituents in the thiophene gives rise to insertion selectivities which are exclusively subject to steric control. Indeed, both electron-donating (*i.e.* methoxy) or electron-withdrawing (*i.e.* carboalkoxy) groups in the thiophene do not alter the direction of insertion, which invariably occurs away from the substituent.

Such a rigid control of the regioselectivity of the C-S bond scission has never been observed and is most likely due to the steric repulsions between the bulky PPh₂ groups in the triphos ligand and the substituent in either the 2- or 3-position. In fact, unsaturated metal fragments with minor steric demand do not exhibit the same selectivity of insertion: the 16-electron fragments [(C₅Me₅)Rh(PMe₃)]^{6,10} and [Fe(dmpe)₂]¹² react with 3-MeT to give isomeric mixtures of the 1,2- and 1,5-insertion products (Scheme 1).

Within this context, the lack of reactivity of 2,5-Me₂T with [(triphos)RhH] can reasonably be ascribed to steric repulsion between the six phenyl rings of triphos and the methyl groups in the thiophene.

Insertion into the more hindered side of the thiophene has been observed uniquely in the reaction of [(C₅Me₅)Rh(PMe₃)] with 2-OMeT and explained in terms of a

(20) A 5-mm NMR quartz tube, charged with a solution of **1** (20 mg, 0.027 mmol) and a 10-fold excess of a 1:1 mixture of two different thiophenes in THF-*d*₈ (0.7 mL), was irradiated with UV light at 20 °C. The photolysis source was a 135-W (principal emission wavelength 366 nm) high-pressure mercury vapor immersion lamp equipped with a water filter to remove excess heat. After 4 h, the product composition was determined by ³¹P{¹H} NMR spectroscopy. The selectivity trend of the competitive reactions was analogous to that observed in the thermal reactions at 70 °C, whereas a different product distribution, still invariant with time and temperature, was observed in some cases.

(21) (a) Bianchini, C.; Jiménez, M. V.; Meli, A.; Moneti, S.; Vizza, F. *J. Organomet. Chem.*, in press. (b) Bianchini, C.; Meli, A.; Peruzzini, M.; Vizza, F.; Moneti, S.; Herrera, V.; Sánchez-Delgado, R. A. *J. Am. Chem. Soc.* **1994**, *116*, 4370.

(22) Bianchini, C.; Jiménez, M. V.; Meli, A.; Moneti, S.; Vizza, F.; Herrera, V.; Sánchez-Delgado, R. A. *Organometallics*, in press.

stabilizing contribution of a delocalized resonance form (methoxycarbene moiety).¹¹ This remarkable electronic control on the insertion, driven by the methoxy substituent in the 2-position, is likely responsible for the unsuccessful reaction of **1** with 2-OMeT. The steric hindrance of the metal fragment in favor of 1,5-insertion is an antithesis to the electronic preference of the substrate for 1,2-insertion.

Although electronic effects are not the determining factors at work in the selectivity of the C–S insertions described in this paper, the electronic properties of the substituent in the thiophene remarkably affect the chemistry of the butadienethiolate products.

In CH₂Cl₂ or CHCl₃, the complexes containing electron-withdrawing substituents (COMe, CO₂Et) are fairly stable, whereas those containing electron-donating substituents rapidly decompose. Although the nature of the decomposition products has not been studied, we strongly suspect that compounds **3**, **4**, **7**, and **9** react by nucleophilic attack of the thiolate sulfur atom at the electrophilic carbon atom of the chlorinated solvent.

The remarkable nucleophilic character of the unsubstituted derivatives **2** and **10** has recently been demonstrated experimentally and theoretically.^{3,16a} Actually, each complex molecule contains two nucleophilic sites: the sulfur atom and the C₂ carbon atom of the distal olefinic moiety.^{16a} Alkyl halides such as MeI selectively react with the sulfur atom to give S-methylated adducts of the formula [(triphos)M(η^3 -(Me)-SCH=CHCH=CH₂)]BPh₄ (M = Rh,^{16a} Ir³). An increase of the nucleophilic character of the butadienethiolate ligand, produced by replacing a hydrogen with alkyl or methoxy groups, would make the sulfur atom sufficiently nucleophilic to attack the carbon atom of CH₂-Cl₂.²³ As a matter of fact, the methylated adducts [(triphos)Rh(η^3 -(Me)SCR=CR'CH=CH₂)]BPh₄ (R' = H, R = Me, Et; R = H, R' = Me, OMe), independently prepared by treatment of **3**, **4**, **7**, or **9** with MeI, are fully stable in chlorinated solvents.²⁴

Our observation that electron-donating substituents in the starting thiophene increase the basicity, and thus the reactivity of the butadienethiolate products, nicely fits with previous studies in which the relative HDS reactivity of alkyl-substituted thiophenes on Co–Mo/Al₂O₃ catalysts increases in the order T < 2-MeT < 3-MeT < 2,5-Me₂T. Indeed, as widely suggested,^{2d,25} if heterolytic splitting of H₂ is operative in hydrotreating catalysis, the major reactivity of alkyl-substituted thiophenes may be explained in terms of a more facile attack by H⁺ at either the sulfur or the C₂ carbon atom^{3,16a,21a} of the C–S insertion product once the latter has been reduced to butadienethiolate by H⁻.

Competitive Reactivity of Substituted Thiophenes with [(triphos)RhH]. Studies which compare C–S bond scission reactions between a unique metal system and thiophenes substituted at different positions by electronically different groups are limited indeed.

Jones has examined the thermal reaction of [(C₅Me₅)Rh(PMe₃)] with a 1:1 mixture of T and 2,5-Me₂T,

(23) Merola, J. S.; Grieb, A.; Ladipo, F. T.; Selnau, H. E. *Symposium on Mechanism of HDS/HDN Reactions*, 206th National Meeting of the American Chemical Society, Chicago, IL, August 22–27, 1993; Division of Petroleum Chemistry, Inc., American Chemical Society: Washington, DC, 1993; p 674.

(24) Bianchini, C.; Meli, A., to be submitted for publication.

(25) (a) Anderson, A. B.; Al-Saigh, Z. Y.; Hall, W. K. *J. Phys. Chem.* **1988**, *92*, 803. (b) Lacroix, M.; Yuan, S.; Breysse, M.; Dorémieux-Morin, C.; Fraissard, J. *J. Catal.* **1992**, *138*, 409. (c) Neurock, M.; van Santen, R. A. *J. Am. Chem. Soc.* **1994**, *116*, 4427.

showing that there is preferential C–S cleavage of the unsubstituted thiophene (2:1 product ratio).^{6,10}

The order of competitive reactivity of the present substituted thiophenes toward [(triphos)RhH] is as follows: 2-CO₂EtT > 2-COMeT > 3-COMeT ≫ 3-OMeT > T ≅ 2-MeT > 3-MeT. From this trend, one may readily conclude that (i) the insertion of rhodium into the C–S bond is facilitated by thiophene substituents exhibiting electron-withdrawing ability; (ii) for identical substituents, the C–S opening is easier for 2-substituted thiophenes than for 3-substituted thiophenes.

A qualitative explanation of the role exerted by the electronic nature of the substituents on the competitive reactions is provided by assuming that the mechanism reported by Jones for the insertion that the mechanism reported by Jones for the insertion [(C₅Me₅)Rh(PMe₃)] into a thiophene C–S bond is operative also for [(triphos)RhH] (this assumption is acceptable, as the two metal systems are isoelectronic and isolobal and generally exhibit the same chemistry). In Jones's mechanism, C–S insertion proceeds by S-coordination of the thiophene, followed by attack by the electron-rich Rh(I) metal on the adjacent carbon atom (*via* donation into the C–S antibonding orbital). In this mechanistic picture, electron-donating substituents in the thiophene are expected to destabilize the transition state,^{6,26} and as a consequence, insertion would be disfavored, consistent with what we observe experimentally. The anomalous position of 3-OMeT in the order of competitive reactivity is ascribed to the capability of the OMe substituent to stabilize the insertion product *via* a delocalized methoxycarbene resonance form.¹¹

In conclusion, the electronic control exerted by the thiophene substituent on the transition state for the C–S bond cleavage brought about by the [(triphos)RhH] fragment seems to be more determinant than the electronic influence on the nucleophilicity of the thiophene. In fact, it is well-known that electron-donating substituents in the thiophene strengthen the donor ability of the sulfur,⁹ thus favoring the formation of the η^1 (S) intermediate that precedes the C–S insertion reaction.

Apparently, our conclusions are in contrast with those of previous heterogeneous studies, according to which the greater the number of alkyl substituents in the thiophene, the easier the adsorption on the catalyst surface and the higher the HDS reactivity.^{27–29} This contrast may simply mean that our HDS model is poor indeed. On the other hand, it has also been suggested that the assumption of η^1 (S) binding of thiophene, made in the adsorption studies, may be incorrect and that η^5 coordination of thiophene may be a better form of adsorption on the HDS catalysts investigated.^{9,27–30}

Acknowledgment. We thank the Progetto Strategico "Tecnologie Chimiche Innovative", CNR, Rome, Italy, for financial support. A postdoctoral grant to M.V.J. from the Ministerio de Educación y Ciencia of Spain is gratefully acknowledged.

OM950054V

(26) Harris, S.; Chianelli, R. R. *J. Catal.* **1984**, *86*, 400.

(27) (a) Zdrzil, M. *Collect. Czech. Chem. Commun.* **1977**, *42*, 1484. (b) Zdrzil, M. *Catal. Today* **1988**, *3*, 269.

(28) Zdrzil, M. *Collect. Czech. Chem. Commun.* **1975**, *40*, 3491.

(29) Desikan, P.; Amberg, C. H. *Can. J. Chem.* **1963**, *41*, 1966.

(30) Angelici, R. J. In *Encyclopedia of Inorganic Chemistry*; King, R. B., Ed.; Wiley: New York, 1994; Vol. 3, p 1433.

Reactions of the Rhenium(I) Fragment $[\{\text{MeC}(\text{CH}_2\text{PPh}_2)_3\}\text{Re}(\text{CO})_2]^+$. Synthesis and Characterization of a Stable Cationic $\eta^2\text{-H}_2$ Complex of Rhenium[†]

Claudio Bianchini,^{*,‡} Andrea Marchi,[§] Lorenza Marvelli,[§] Maurizio Peruzzini,^{*,‡} Antonio Romerosa,[‡] Roberto Rossi,^{*,§} and Alberto Vacca^{||}

Istituto per lo Studio della Stereochimica ed Energetica dei Composti di Coordinazione, CNR, Via Jacopo Nardi 39, 50132 Firenze, Italy, Laboratorio di Chimica Nucleare ed Inorganica, Dipartimento di Chimica, Università di Ferrara, Via Borsari 46, 44100 Ferrara, Italy, and Dipartimento di Chimica, Università di Firenze, Via Monagliano 75, 50100 Firenze, Italy

Received January 27, 1995[⊗]

Reaction of $\text{Re}(\text{CO})_3(\text{PPh}_3)_2\text{Cl}$ with $\text{MeC}(\text{CH}_2\text{PPh}_2)_3$ (triphos) gives $(\text{triphos})\text{Re}(\text{CO})_2\text{Cl}$ (**1**) which is converted to the hydride $(\text{triphos})\text{Re}(\text{CO})_2\text{H}$ (**2**) by treatment with LiAlH_4 . An X-ray diffraction analysis of **2** shows that the rhenium atom is octahedrally coordinated by triphos, which occupies a triangular face of the coordination polyhedron, by two carbonyl groups and by a terminal hydride ligand. Treatment of **2** with Me_3OBF_4 results in the evolution of methane and formation of the unsaturated complex $[(\text{triphos})\text{Re}(\text{CO})_2]\text{BF}_4$ (**4**) which is stabilized by an agostic interaction between the rhenium center and a phenyl C–H bond of triphos. The $\eta^2\text{-H}_2$ complex $[(\text{triphos})\text{Re}(\text{CO})_2(\text{H}_2)]\text{BF}_4$ (**3**) is obtained either by protonation of **2** or by addition of H_2 to the agostic complex **4**. The presence of an intact dihydrogen ligand in **3** is unambiguously shown by ^1H NMR spectroscopy [$T_{\text{min}} = 8.6$ ms (CD_2Cl_2 , 300 MHz, -58 °C); J_{HD} of 30.8 Hz for the monodeuteriated isotopomer $[(\text{triphos})\text{Re}(\text{CO})_2(\text{HD})]\text{BF}_4$ (**3-d**₁)]. Vinylidene derivatives of the formula $[(\text{triphos})\text{Re}(\text{CO})_2\{\text{C}=\text{C}(\text{H})\text{R}\}]\text{BPh}_4$ ($\text{R} = \text{Ph}$, **8**; CO_2Et , **9**; C_6H_{13} , **10**) are obtained by reaction of either the $\eta^2\text{-H}_2$ complex **3** or the agostic complex **4** with terminal alkynes in the presence of NaBPh_4 . The preference for the coordination of neutral groups at rhenium in the $[(\text{triphos})\text{Re}(\text{CO})_2]^+$ fragment follows the order $\text{N}_2 < \text{C}-\text{H}_{(\text{agostic})} < \text{H}_2 < \text{HC}\equiv\text{CR} < \text{CH}_3\text{CN} < \text{CO}$. All the reactions described have been carried out in tetrahydrofuran or dichloromethane.

Introduction

The organometallic chemistry of rhenium has literally exploded over the past few years.¹ The principal reason for the attractive chemistry of rhenium is provided by its position in the periodic table. As a metal of the third row, the outer 5d orbitals of rhenium are relatively exposed and, thus, their electronic occupancy is strongly susceptible to the nature of the ligands. Also, due to its central position in the d block, rhenium can attain all oxidation states from $-III$ to VII .²

Rhenium has turned out to be an ideal metal for mechanistic studies due to the high strength of its bonds to other elements as well as its reluctance to form coordinatively unsaturated complexes. Some of the most recent and innovative applications of rhenium complexes in organometallic chemistry include (i) the formation of linear carbon chains C_n ($n = 1-5$) between

two metals;³ (ii) the synthesis of a large variety of homo- and heterometallic polyhydrido complexes with either classical or nonclassical structures;^{4,5} (iii) the reductive coupling of carbon monoxide with alkynes through C–O bond formation;⁶ (iv) the rearrangement of a hydroxide ligand to an oxo–hydride species;⁷ (v) the condensation of allyl, vinyl, and CO ligands at metal centers;⁸ and (vi) the synthesis of chiral-at-metal complexes for use in diastereo- and enantioselective syntheses.⁹

If, on the one hand, the electronic characteristics of rhenium, enhancing the stability of ordinarily reactive species, have permitted the observation of new types of reaction mechanisms, they, on the other hand, have not encouraged the use of rhenium compounds in homogeneous catalysis. Only recently have a number of exciting advances in organorhenium chemistry disclosed the world of rhenium-centered homogeneous catalysis.^{1a} Among the most significant rhenium-assisted catalytic reactions, one may cite olefin and alkyne metathesis reactions,^{10,11} the epoxidation of olefins,¹² the oxidation of sulphides,¹³ the olefination of aldehydes,¹⁴ and alkane dehydrogenations.¹⁵

Among the ligands which are used in rhenium organometallic chemistry, the cyclopentadienyl anion (Cp),

[†] Dedicated to the memory of Luciano Magon, Professor of Chemistry at the University of Ferrara, Italy.

[‡] CNR.

[§] Università di Ferrara.

^{||} Università di Firenze.

[⊗] Abstract published in *Advance ACS Abstracts*, June 15, 1995.

(1) (a) Casey, C. P. *Science* **1993**, *259*, 1552. (b) Stack, J. C.; Simpson, R. D.; Hollander, F. J.; Bergman, R. G.; Heathcock, C. Y. *J. Am. Chem. Soc.* **1990**, *112*, 2716. (c) Romão, C. C. In *Encyclopedia of Inorganic Chemistry*; King, R. B., Ed.; J. Wiley: Chichester, England, 1994; Vol. 6, p 3437.

(2) (a) Connerand, K. A.; Walton, R. A. In *Comprehensive Coordination Chemistry*; Wilkinson, G.; Gillard, R. D.; McCleverty, J. A., Eds.; Pergamon Press: Oxford, England, 1987; Vol. 4. (b) Greenwood, N. N.; Earnshaw, A. *Chemistry of the Elements*; Pergamon Press: Oxford, England, 1984.

(3) (a) Weng, W.; Bartik, T.; Gladysz, J. A. *Angew. Chem., Int. Ed. Engl.* **1994**, *33*, 2199. (b) Lang, H. *Angew. Chem., Int. Ed. Engl.* **1994**, *33*, 547. (c) Seyler, J. W.; Weng, W.; Zhou, Y.; Gladysz, J. A. *Organometallics* **1993**, *12*, 3802. (d) Zhou, Y.; Seyler, J. W.; Weng, W.; Ramsden, J. A.; Arif, A. M.; Gladysz, J. A. *J. Am. Chem. Soc.* **1993**, *115*, 3824.

either unsubstituted or permethylated, and tertiary phosphines play a predominant role.^{1,16} A phosphorus ligand that closely resembles the coordination and electronic properties of Cp is the triphosphine MeC(CH₂-PPh₂)₃ (triphos).¹⁷ Indeed, both ligands share a number of characteristics: excellent bonding ability as six-electron donors; formation of stable complexes in a variety of metal oxidation states, adaptability to many different coordination numbers, high nucleophilicity at the coordinated metal centers, and last, but not least, the stereoselective occupation of a triangular face of the coordination polyhedron. In spite of the similar bonding

properties of Cp and triphos, the chemistry of rhenium with the latter ligand is much less developed than that with the former.^{5,18} Thus, we decided to carry out a systematic study of the organometallic chemistry of rhenium in combination with triphos.

Actually, triphos may offer several advantages over the Cp ligand. These include (i) more rigid control of the stereochemistry and stoichiometry of the resulting complexes; (ii) the possibility of following organometallic reactions of the soluble complexes *via* ³¹P NMR spectroscopy; (iii) high stability toward electrophiles that, conversely, may attack the cyclopentadienyl ring; and (iv) increased thermal stability of the metal complexes. The latter feature alone has recently permitted the use of triphos complexes in catalytic processes which require very drastic reaction conditions such as the hydrogenation and hydrodesulfurization of thiophenic molecules.¹⁹

Following a recent report on the synthesis of hydrido rhenium complexes with hydride contents ranging from 3 to 7,⁵ we report here a study of the coordination and organometallic chemistry of the [(triphos)Re(CO)₂]⁺ fragment. The results obtained show that the marriage between triphos and rhenium will be long-lasting and satisfying.

Results and Discussion

The preparations and principal reactions described in this report are summarized in Schemes 1 and 2. Selected spectroscopic data are collected in Table 1 (³¹P-{¹H} NMR, IR) or are given in the Experimental Section (¹H and ¹³C{¹H} NMR).

Synthesis and Characterization of [(triphos)Re(CO)₂H] (2). Reaction of Re(CO)₃(PPh₃)₂Cl with a slight excess of triphos in refluxing toluene for 7 h gives pale yellow microcrystals of (triphos)Re(CO)₂Cl (1) in 80% yield. The IR spectrum of 1 as a KBr pellet shows two strong bands at 1948 and 1887 cm⁻¹ due to the symmetrical and antisymmetrical stretching vibrations of the two mutually *cis* CO ligands.²⁰ The ³¹P{¹H} NMR spectrum in dichloromethane-*d*₂ at room temperature shows a well-resolved AM₂ pattern (*J*_{AM} = 14.7 Hz), consistent with an octahedral environment about the metal center.²¹ The ¹³C{¹H} NMR spectrum of 1 is characterized by the presence, in the low-field region (δ 198.7), of a well-resolved 10-line multiplet with a relative intensity pattern of 1:1:2:2:2:2:2:1:1 due to the carbon atoms of carbonyl ligands. The observed multiplicity arises from an AXX'Y spin system in which a carbonyl carbon atom (A) couples to the three phospho-

(4) (a) Fontaine, X. L. R.; Layzell, T. P.; Shaw, B. L. *J. Chem. Soc., Dalton Trans.* **1994**, 379. (b) Leeaphon, M.; Rohl, K.; Thomas, R. J.; Fanwick, P. E.; Walton, R. A. *Inorg. Chem.* **1993**, *32*, 5562 and references therein. (c) Luo, X. L.; Crabtree, R. H. *J. Am. Chem. Soc.* **1990**, *112*, 6912. (d) Feracin, S.; Bürgi, T.; Bakhmutov, V. I.; Eremenko, I.; Vorontsov, E. V.; Yimenits, A. B.; Berke, H. *Organometallics* **1994**, *13*, 4194. (e) Cotton, F. A.; Luck, R. L. *J. Am. Chem. Soc.* **1989**, *111*, 5757. (f) Cotton, F. A.; Luck, R. L.; Root, D. R.; Walton, R. A. *Inorg. Chem.* **1990**, *29*, 43. (g) Allen, D. L.; Green, M. L. H.; Bandy, J. A. *J. Chem. Soc., Dalton Trans.* **1990**, 541. (h) Cotton, F. A.; Luck, R. L. *Inorg. Chem.* **1989**, *28*, 8. (i) Cotton, F. A.; Luck, R. L. *Inorg. Chem.* **1991**, *30*, 767. (j) Cotton, F. A.; Luck, R. L. *Inorg. Chem.* **1989**, *28*, 2181. (k) Bakhmutov, V.; Bürgi, T.; Burger, P.; Ruppli, U.; Berke, H. *Organometallics* **1994**, *13*, 4203. (l) Jia, G.; Lough, A. J.; Morris, R. H. *J. Organomet. Chem.* **1993**, *461*, 147. (m) Michos, D.; Luo, X. L.; Crabtree, R. H. *J. Chem. Soc., Dalton Trans.* **1992**, 1735. (n) Luo, X. L.; Crabtree, R. H. *Inorg. Chem.* **1989**, *28*, 3775. (o) Kim, Y.; Dang, H.; Meek, D. W.; Wojcicki, A. *J. Am. Chem. Soc.* **1990**, *112*, 2798. (p) Howard, J. A. K.; Mason, S. A.; Johnson, O.; Diamond, I. C.; Crennell, S.; Keller, A. P.; Spencer, J. L. *J. Chem. Soc., Chem. Commun.* **1988**, 1502. (q) Brammer, L.; Howard, J. A. K.; Johnson, O.; Koetzle, T. F.; Spencer, J. L.; Stringer, A. M. *J. Chem. Soc., Chem. Commun.* **1991**, 241. (r) Kim, Y.; Gallucci, J.; Wojcicki, A. *J. Am. Chem. Soc.* **1990**, *112*, 8600. (s) Kristjánsdóttir, S. S.; Loendorf, A. J.; Norton, J. R. *Inorg. Chem.* **1991**, *30*, 4470. (t) Luo, X. L.; Crabtree, R. H. *J. Chem. Soc., Dalton Trans.* **1991**, 587. (u) Luo, X. L.; Crabtree, R. H. *J. Am. Chem. Soc.* **1990**, *112*, 4813. (v) Michos, D.; Luo, X. L.; Howard, J. A. K.; Crabtree, R. H. *Inorg. Chem.* **1992**, *31*, 3914. (w) Haynes, G. R.; Martin, R. L.; Hay, P. J. *J. Am. Chem. Soc.* **1992**, *114*, 28. (x) Luo, X. L.; Michos, D.; Crabtree, R. H. *Inorg. Chem.* **1991**, *30*, 4286.

(5) Bianchini, C.; Peruzzini, M.; Zanobini, F.; Magon, L.; Marvelli, L.; Rossi, R. *J. Organomet. Chem.* **1993**, *451*, 97.

(6) Shih, K. Y.; Fanwick, P. E.; Walton, R. A. *J. Am. Chem. Soc.* **1993**, *115*, 9319.

(7) (a) Tahmassebi, S. K.; Conry, R. R.; Mayer, J. M. *J. Am. Chem. Soc.* **1993**, *115*, 7553. (b) Brown, S. N.; Mayer, J. M. *J. Am. Chem. Soc.* **1994**, *116*, 2219.

(8) Casey, C. P.; Vosejka, P. C.; Gavney, J. A. *J. Am. Chem. Soc.* **1990**, *112*, 4083.

(9) See for example: (a) Johnson, T. J.; Arif, A. M.; Gladysz, J. A. *Organometallics* **1994**, *13*, 3182. (b) Johnson, T. J.; Arif, A. M.; Gladysz, J. A. *Organometallics* **1993**, *12*, 4728.

(10) (a) Herrmann, W. A.; Kuchler, J. G.; Felixberger, J. F.; Herdtweck, E.; Wagner, W. *Angew. Chem., Int. Ed. Engl.* **1988**, *27*, 394. (b) Herrmann, W. A.; Wagner, W.; Flessner, U. N.; Volkhardt, U.; Komber, H. *Angew. Chem., Int. Ed. Engl.* **1991**, *30*, 1636.

(11) (a) Toreki, R.; Schrock, R. R.; Davis, W. M. *J. Am. Chem. Soc.* **1992**, *114*, 3367. (b) Toreki, R.; Schrock, R. R. *J. Am. Chem. Soc.* **1990**, *112*, 2448. (c) Weinstock, I. M.; Schrock, R. R. *J. Am. Chem. Soc.* **1991**, *113*, 135.

(12) See for example (a) Herrmann, W. A. *Abstracts of Papers*, 9th International Symposium on Homogeneous Catalysis, Jerusalem, Israel, August 21–26, 1994; Abstract K-3, p 5. (b) Herrmann, W. A.; Fischer, R. W.; Marz, D. W. *Angew. Chem., Int. Ed. Engl.* **1991**, *30*, 1638.

(13) Vassell, K. A.; Espenson, J. H. *Inorg. Chem.* **1994**, *33*, 5491.

(14) Herrmann, W. A.; Wang, M. *Angew. Chem., Int. Ed. Engl.* **1991**, *30*, 1641.

(15) Loza, M. L.; de Gala, S. R.; Crabtree, R. H. *Inorg. Chem.* **1994**, *33*, 5073 and references therein.

(16) (a) Peng, T.-S.; Winter, C. H.; Gladysz, J. A. *Inorg. Chem.* **1994**, *33*, 2534 and references therein. (b) Boag, N. M. and Kaesz, H. D. In *Comprehensive Organometallic Chemistry*; Wilkinson, G., Stone, F. G. A., Abel, E. W., Eds.; Pergamon Press: New York, 1982; Vol. 4, Chapter 30, p 205.

(17) Some leading references on triphos and other tripodal polyphosphines include: (a) Sacconi, L.; Mani, F. *Transition Met. Chem.* **1982**, *8*, 179. (b) Bianchini, C.; Meli, A.; Peruzzini, M.; Vizza, F.; Zanobini, F. *Coord. Chem. Rev.* **1992**, *120*, 193. (c) Cotton, F. A.; Hong, B. *Prog. Inorg. Chem.* **1992**, *40*, 179. (d) Bianchini, C. *Comments Inorg. Chem.* **1988**, *8*, 27. (e) Mayer, H.; Kaska, W. *Chem. Rev.* **1994**, *94*, 1239.

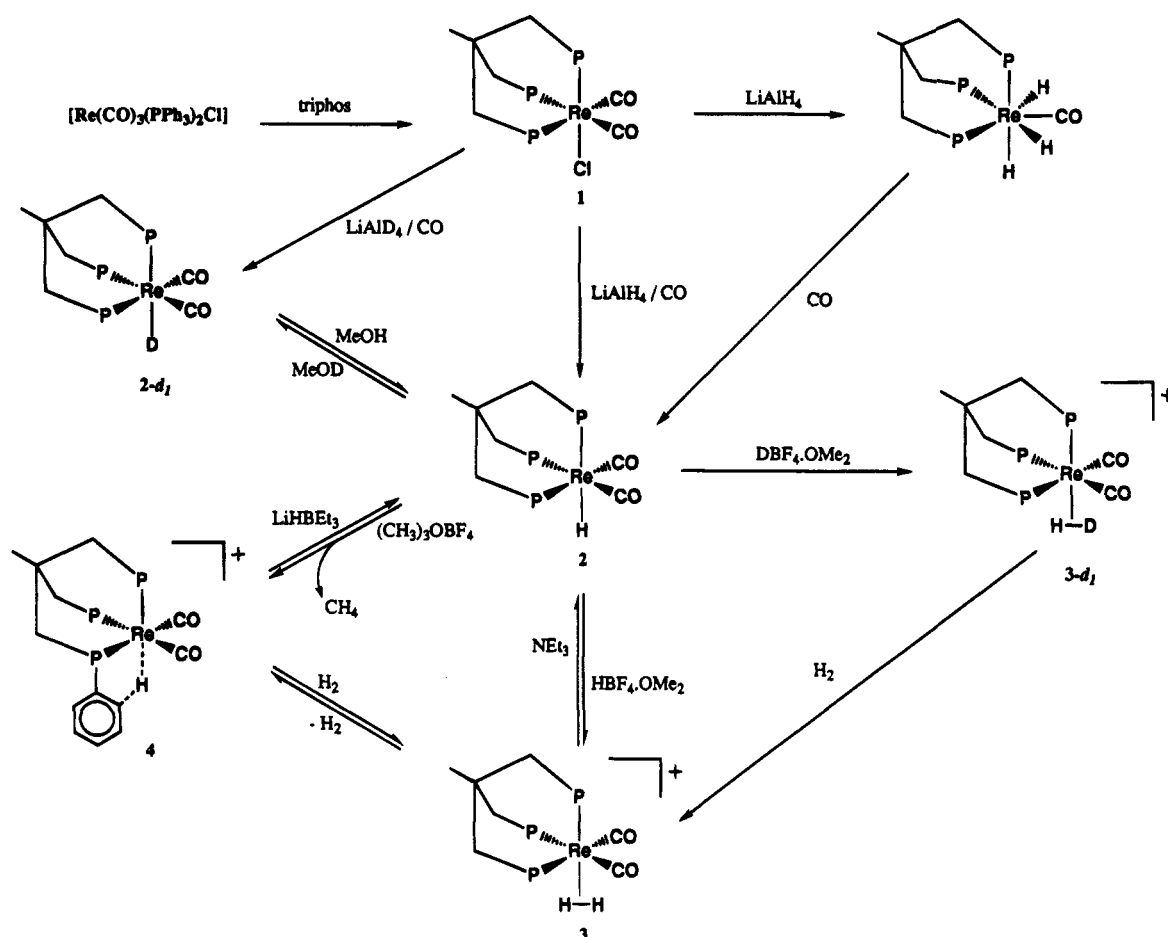
(18) (a) Ginsberg, A. P.; Abrahams, S. C.; Marsh, P.; Ataka, K.; Sprinkle, C. R. *J. Chem. Soc., Chem. Commun.* **1984**, 1321. (b) Abrahams, S. C.; Ginsberg, A. P.; Koetzle, T. F.; Marsh, P.; Sprinkle, C. R. *Inorg. Chem.* **1986**, *25*, 2500. (c) Lin, S. C.; Cheng, C. P.; Lee, T.-Y.; Lee, T.-J.; Peng, S.-M. *Acta Crystallogr.* **1986**, *C42*, 1733. (d) Costello, M. T.; Fanwick, P. E.; Green, M. A.; Walton, R. A. *Inorg. Chem.* **1992**, *31*, 2359.

(19) (a) Bianchini, C.; Meli, A.; Peruzzini, M.; Vizza, F.; Frediani, P.; Herrera, V.; Sánchez-Delgado, R. A. *J. Am. Chem. Soc.* **1993**, *115*, 7505. (b) Bianchini, C.; Meli, A.; Peruzzini, M.; Vizza, F.; Moneti, S.; Herrera, V.; Sánchez-Delgado, R. A. *J. Am. Chem. Soc.* **1994**, *116*, 4370. (c) Bianchini, C.; Jiménez, M. V.; Meli, A.; Vizza, F.; Moneti, S.; Herrera, V.; Sánchez-Delgado, R. A. *Organometallics* **1995**, *14*, 2342.

(20) Wehman-Coyevaar, I. C. M.; Kapteijn, G. M.; Grove, D. M.; Smeets, W. J. J.; Spek, A. L.; van Koten, G. *J. Chem. Soc., Dalton Trans.* **1994**, 703.

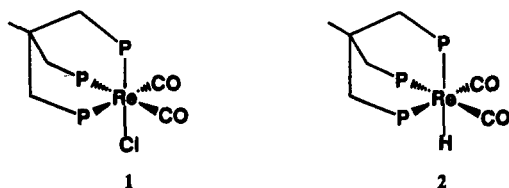
(21) A similar pattern has been reported for the isoelectronic [(triphos)Ru(CO)₂X]⁺ complexes (X = Cl, Br, I, H, Me, PhCH₂, CHO); Hommeltoft, S. I.; Cameron, A. D.; Shackleton, T. A.; Fraser, M. E.; Fortier, S.; Baird, M. C. *Organometallics* **1986**, *5*, 1380.

Scheme 1



rus donor atoms of the triphos ligand, two of which (X and X') lie in the "Re(CO)₂" plane and are chemically but not magnetically equivalent.²¹ Resonances of this type are present in the $^{13}\text{C}\{^1\text{H}\}$ NMR spectra of all of the Re(I) complexes described in this paper ($204.8 \leq \delta_{\text{CO}} \leq 189.6$) (*vide infra*).

Reaction of 1 with a large excess of LiAlH_4 in refluxing THF for 24 h yields the monohydride complex (triphos)Re(CO)₂H (2). The formation of 2 is invariably accompanied by that of a small amount ($\leq 10\%$) of the known trihydride complex (triphos)Re(CO)₂H₃.^{5,18c} Compound 2 can be obtained in pure form when the reaction is carried out under 1 atm of carbon monoxide. Under these experimental conditions 2 is isolated in fairly good yield as air-stable, off-white microcrystals.



The IR spectrum of 2 shows two carbon monoxide absorptions at lower frequencies than those of the parent complex 1 (ν_{CO} : 1921, 1856 cm^{-1}) as a consequence of the replacement of chloride by hydride. The $\nu_{\text{Re-H}}$ band is not visible, most likely because of overlapping with the more intense ν_{CO} bands. However, in the corresponding monodeuteriated isotopomer (triphos)Re(CO)₂D (2- d_1), a medium intensity $\nu_{\text{Re-D}}$ band is clearly

visible at 1345 cm^{-1} . From this value one can estimate that the Re-H stretching frequency in 2 should fall near 1900 cm^{-1} , just in the region of the more intense ν_{CO} absorptions.

The ^1H NMR spectrum of 2 (dichloromethane- d_2 , 20 °C) shows, in the hydride region, a broad triplet resonance at $\delta -5.83$ with a $^2J_{\text{HP}}$ value of 20.0 Hz, typical of a hydride ligand *cis* to two phosphorus atoms.²² This splitting pattern does not change with temperature from +30 to -90 °C, thus indicating the absence of a dynamic process involving a phosphine-arm dissociation.²³⁻²⁵ The three components of the triplet exhibit an unusually broad line width (*ca.* 5 Hz) which is invariant with temperature from +20 to -70 °C. A slight broadening of the triplet components is observed at lower temperature; however, this may simply be due to increased inhomogeneity of the mag-

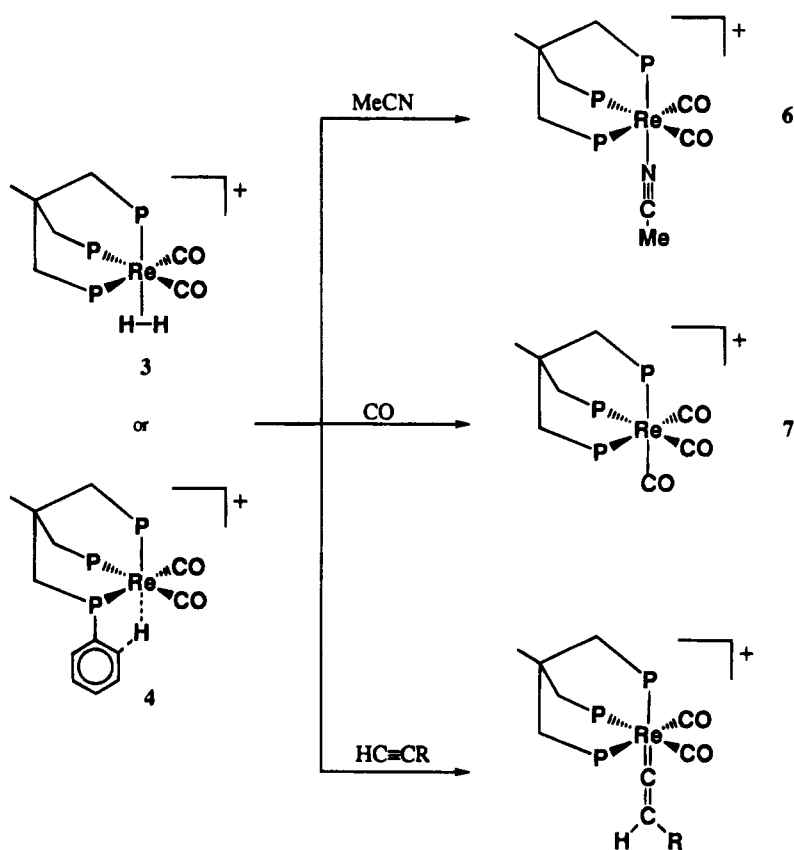
(22) (a) Bianchini, C.; Meli, A.; Peruzzini, M.; Vizza, F.; Frediani, P.; Ramirez, J. A. *Organometallics* **1990**, *9*, 226. (b) Bianchini, C.; Meli, A.; Peruzzini, M.; Vizza, F.; Albinati, A. *Organometallics* **1990**, *9*, 2283. (c) Bianchini, C.; Meli, A.; Peruzzini, M.; Vizza, F. *J. Am. Chem. Soc.* **1990**, *112*, 6726. (d) Bianchini, C.; Meli, A.; Peruzzini, M.; Vizza, F.; Frediani, P.; Herrera, V.; Sánchez-Delgado, R. A. *J. Am. Chem. Soc.* **1993**, *115*, 2731. (e) Barbaro, P.; Bianchini, C.; Meli, A.; Peruzzini, M.; Vacca, A.; Vizza, F. *Organometallics* **1991**, *10*, 2227. (f) Bianchini, C.; Barbaro, P.; Meli, A.; Peruzzini, M.; Vacca, A.; Vizza, F. *Organometallics* **1993**, *12*, 2505.

(23) (a) Thaler, E. G.; Folting, K.; Caulton, K. G. *J. Am. Chem. Soc.* **1990**, *112*, 2664. (b) Thaler, E. G.; Caulton, K. G. *Organometallics* **1990**, *9*, 1871.

(24) (a) Bianchini, C.; Meli, A.; Peruzzini, M.; Frediani, P.; Bohanna, C.; Esteruelas, M. A.; Oro, L. A. *Organometallics* **1992**, *11*, 138. (b) Bianchini, C.; Masi, D.; Meli, A.; Peruzzini, M.; Zanobini, F. *J. Am. Chem. Soc.* **1988**, *110*, 6411.

(25) Kiss, G.; Horvath, J. *Organometallics* **1991**, *10*, 3798.

Scheme 2

R = Ph, 8; CO₂Et, 9; C₆H₁₃, 10Table 1. ³¹P{¹H} NMR and Selected IR Spectral Data for the Complexes^a

compound	pattern	³¹ P{ ¹ H} NMR			IR, cm ⁻¹		
		chem. shift, ppm	δ_{PA}	δ_{PM}	J_{AM} , Hz	$\nu_{C=O}$	ν_{other}
(triphos)Re(CO) ₂ Cl	(1)	AM ₂	2.40	-18.23	14.7	1948, 1887	
(triphos)Re(CO) ₂ H	(2)	AM ₂ ^b	-4.05	-3.51	18.6	1921, 1856	
[(triphos)Re(CO) ₂ (H ₂)]BF ₄	(3)	AM ₂	-6.11	-11.22	24.8	1965, 1900	
[(triphos)Re(CO) ₂ (HD)]BF ₄	(3-d ₁)	AM ₂	-6.50	-11.32	24.5		
[(triphos)Re(CO) ₂]BF ₄	(4)	AM ₂	3.04	-4.55	16.6	1956, 1891	
(triphos)Re(CO) ₂ (OSO ₂ CF ₃)	(5)	AM ₂	-6.20	-10.11	14.7	1964, 1888	1320 (η^1 -OSO ₂ CF ₃)
[(triphos)Re(CO) ₂ (MeCN)]BPh ₄	(6)	AM ₂	-4.41	-9.28	19.7	1956, 1897	
[(triphos)Re(CO) ₃]BF ₄	(7)	A ₃	-16.38			2034, 1964, 1955	
[(triphos)Re(CO) ₂ {C=C(H)Ph}]BPh ₄	(8)	AM ₂	-20.46	-15.98	25.5	2013, 1961	1654 (C=C)
[(triphos)Re(CO) ₂ {C=C(H)CO ₂ Et}]BPh ₄	(9)	AM ₂	-21.80	-15.22	25.9	2036, 1970	1607 (C=C), 1701 (C=O), 1223 (COC)
[(triphos)Re(CO) ₂ {C=C(H)C ₆ H ₁₃ }]BPh ₄	(10)	AM ₂	-18.99	-15.24	24.2	2007, 1952	1663 (C=C)

^a All spectra have been recorded in dichloromethane-*d*₂ at room temperature (22 °C). ^b Second-order spin system.

netic field and solution viscosity. A proton NMR spectrum recorded in a diluted acetonitrile-*d*₃ solution (in which **2** is poorly soluble) also provides evidence for the invariance of the triplet resonance (δ -5.80, J_{HP} = 18.9 Hz) in a coordinating solvent.

The ¹H NMR T_1 values of the hydride resonance in **2** were measured in dichloromethane-*d*₂ at 300 MHz by the inversion-recovery method using a standard 180°- τ -90° pulse sequence. The results of the variable temperature longitudinal relaxation measurements on complex **2** are reported in Table 2. At room temperature, the triplet signal exhibits a T_1 value of 265 ms, consistent with the presence of a terminal hydride ligand.²⁶ As the temperature is decreased, the T_1 value steadily decreases but does not attain a minimum even

at the lowest temperature investigated (98 ms at -90 °C).

The ³¹P{¹H} NMR spectrum is temperature-invariant from +30 to -90 °C and consists of a second-order AB₂ spin system which has been computationally simulated with the following parameters: δ_A -4.05, δ_B -3.51, J_{AB} = 18.6 Hz. At lower temperatures, a small high-field shift of all resonances occurs (at -75 °C, a computer simulation of the multiplet gave the following spectral parameters: δ_A -4.14, δ_B -3.75, J_{AB} = 18.6 Hz). The second-order pattern did not allow a proton NMR

(26) Crabtree, R. H. *Acc. Chem. Res.* **1990**, *23*, 95. (b) Hamilton, D. G.; Crabtree, R. H. *J. Am. Chem. Soc.* **1988**, *110*, 41. (c) Bautista, H. T.; Earl, K. A.; Maltby, P. A.; Morris, R. H.; Schweitzer, C. T.; Sella, A. *J. Am. Chem. Soc.* **1988**, *110*, 7031.

Table 2. Measurements of T_1 (ms) for the Complexes (triphos)Re(CO) $_2$ H (2), [(triphos)Re(CO) $_2$ (H $_2$)]BF $_4$ (3), and [(triphos)Re(CO) $_2$ (HD)]BF $_4$ (3-d $_1$)

T (°C)	T_1 (ms)		
	2 ^a	3 ^a	3-d $_1$ ^a
20	265	16	220
0	215	13	160
-20	165	10	120
-40	135	9	92
-60	116	8	80
-80	102	10	73
-90	98	12	78

^a In CD $_2$ Cl $_2$ at 300 MHz, inversion-recovery sequence.

Table 3. Selected Bond Lengths (Å) and Angles (deg) for the Complex (triphos)Re(CO) $_2$ H (2)

Re-C(6)	1.886(11)	P(3)-C(3)	1.844(8)
Re-C(7)	1.895(10)	C(1)-C(4)	1.558(11)
Re-P(3)	2.403(2)	C(2)-C(4)	1.554(11)
Re-P(1)	2.431(2)	C(3)-C(4)	1.559(11)
Re-P(2)	2.438(2)	C(4)-C(5)	1.548(11)
P(1)-C(1)	1.831(8)	C(6)-O(1)	1.176(12)
P(2)-C(2)	1.839(8)	C(7)-O(2)	1.165(12)
C(6)-Re-C(7)	83.7(5)	C(6)-Re-P(2)	95.1(4)
C(6)-Re-P(3)	100.9(3)	C(7)-Re-P(2)	175.5(3)
C(7)-Re-P(3)	99.4(3)	P(3)-Re-P(2)	85.04(7)
C(6)-Re-P(1)	173.0(3)	P(1)-Re-P(2)	87.46(7)
C(7)-Re-P(1)	93.2(3)	O(1)-C(6)-Re	174.3(10)
P(3)-Re-P(1)	85.74(7)	O(2)-C(7)-Re	176.6(9)

spectrum with selective decoupling of the phosphorus resonances to be recorded. As expected, a broad-band phosphorus decoupling experiment gave a singlet at -5.80 ppm with almost the same line width ($\omega_{1/2} = 4.8$ Hz).

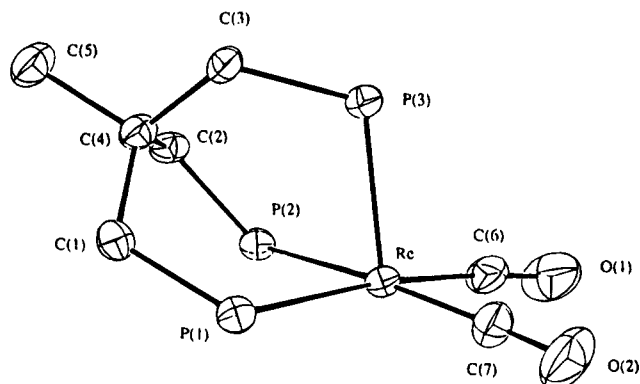
The absence of a large $^2J_{\text{HP}}$ coupling constant in **2** is intriguing indeed. Actually, all ^{31}P NMR spectra of known octahedral hydrido metal complexes with triphos exhibit a large $^2J_{\text{HP}}$ coupling constant due to the magnetic interaction between the mutually *trans* hydride and phosphorus ligands.^{22,27}

The most straightforward interpretation of the unusually small, if any, coupling constant of the hydride to the *trans*-P nucleus is to think of an anomalous orientation of the Re-H vector in solution which, moving out from the axis perpendicular to the plane containing the Re(CO) $_2$ moiety, could reduce or even null out the magnetic interaction to the *trans* phosphorus atom. In an attempt to elucidate this point, a single-crystal X-ray diffraction analysis has been carried out on **2**.

Crystals suitable for an X-ray analysis were obtained by recrystallization from a diluted THF/EtOH solution. The crystal structure of **2** consists of discrete (triphos)-Re(CO) $_2$ H molecules without trapped solvent molecule in the lattice. A selected list of bond angles and distances is given in Table 3, while an ORTEP view is presented in Figure 1. From an analysis of the Fourier difference map, it was not possible to locate the terminal hydride ligand in **2**, which is not surprising, due to the limitations of the X-ray technique in locating hydride ligands coordinated to a third-row transition metal.

The coordination polyhedron around the Re center can be described as a slightly distorted octahedron, in which the major deviations from the idealized geometry are

(27) Pregosin, P. S.; Kunz, R. W. ^{31}P and ^{13}C NMR of Transition Metal Phosphine Complexes; Diehl, P., Fluck, E., Kosfeld, R., Eds.; Springer-Verlag: Heidelberg, 1979.

**Figure 1.** ORTEP drawing of (triphos)Re(CO) $_2$ H (**2**). The phenyl rings of triphos are omitted for clarity.

due to the structural constraints of the tridentate ligand, as shown by the three P-Re-P angles which are significantly smaller than 90°. The Re-P bond distances *trans* to CO (Re-P(1), 2.431(2) Å; Re-P(2), 2.438(2) Å) reflect the strong π -acceptor character of the carbon monoxide ligands and are slightly longer than the Re-P distance *trans* to the hydride (Re-P(3), 2.403(2) Å). This finding matches well with previous crystallographic reports on hydride complexes containing tripodal polyphosphine ligands.^{22f,28} The three Re-P distances ($d_{\text{Re-P(ave)}} = 2.42$ Å) compare well with analogous separations in phosphine Re complexes, for example in *mer*-Re(CO) $_2$ (PMe $_3$) $_3$ H $_2$ ²⁹ (Re-P $_{\text{av}}$, 2.40 Å) and (triphos)ReCl $_3$ ^{18c} ($d_{\text{Re-P(ave)}} = 2.45$ Å). The Re-C bond lengths ($d_{\text{Re-C(ave)}} = 1.89$ Å) suggest the presence of multiple-bond character, which is confirmed by the relatively long C-O distances ($d_{\text{C-O(ave)}} = 1.17$ Å) as compared to the value of 1.13 Å in free CO. All other bond distances and angles are normal and do not require further discussion.

The inability to locate the terminal hydride ligand and the lack of dramatic geometrical distortions in the structure of **2** do not help in rationalizing the anomalous NMR resonance of the hydride ligand. As previously suggested, this phenomenon may simply be due to a solution effect. However, one cannot exclude *a priori* an intramolecular interaction which is steric in nature.

Synthesis and Characterization of [(triphos)Re(CO) $_2$ (H $_2$)]BF $_4$ (3**).** Protonation of **2** with HBF $_4$ ·OMe $_2$ in dichloromethane at 22 °C under a dihydrogen atmosphere gives the nonclassical dihydrogen complex [(triphos)Re(CO) $_2$ (H $_2$)]⁺, which is isolated as off-white microcrystals of the tetrafluoroborate salt [(triphos)Re(CO) $_2$ (H $_2$)]BF $_4$ (**3**).³⁰ The protonation reaction is reversible, and, like most η^2 -H $_2$ metal complexes, **3** is deprotonated by bases such as NEt $_3$ to regenerate the starting hydride complex **2**.

The IR spectrum of **3** contains two strong $\nu(\text{CO})$ absorptions at 1965 and 1900 cm $^{-1}$, whereas no band ascribable to either $\nu_{\text{Re-H}}$ or to $\nu_{\text{Re-H}_2}$ is detectable in

(28) (a) Bianchini, C.; Elsevier, C. J.; Ernstring, J. M.; Peruzzini, M.; Zanolini, F. *Inorg. Chem.* **1995**, *34*, 84. (b) Bianchini, C.; Frediani, P.; Masi, D.; Peruzzini, M.; Zanolini, F. *Organometallics* **1994**, *13*, 4616. (c) Di Vaira, M.; Rovai, D.; Stoppioni, P.; Peruzzini, M. *J. Organomet. Chem.* **1991**, *420*, 135.

(29) Gusev, D. G.; Nietlispach, D.; Eremenko, I. L.; Berke, H. *Inorg. Chem.* **1993**, *32*, 3628.

(30) For comprehensive reviews on molecular hydrogen complexes, see: (a) Kubas, G. J. *Acc. Chem. Res.* **1988**, *21*, 120. (b) Crabtree, R. H.; Hamilton, D. G. *Adv. Organomet. Chem.* **1988**, *28*, 299. (c) Ginsburg, A. G.; Bagaturyan, A. A. *Metalloorg. Khim.* **1989**, *2*, 249. (d) Jessop, P. G.; Morris, R. H. *Coord. Chem. Rev.* **1992**, *121*, 155. (e) Heinekey, D. M.; Oldham, W. J., Jr. *Chem. Rev.* **1993**, *93*, 913.

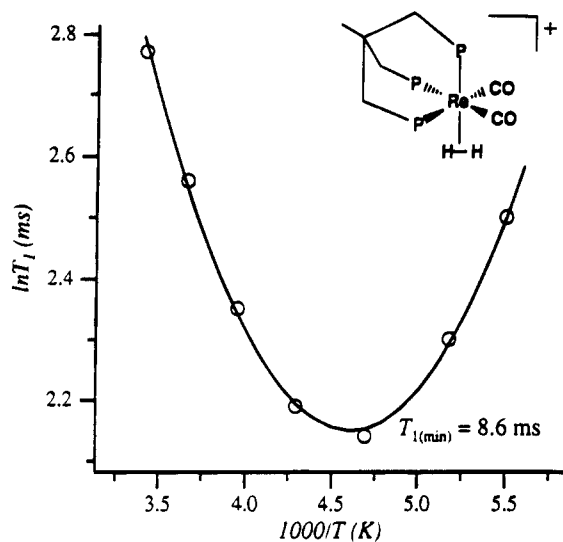


Figure 2. Plot of $\ln T_1$ vs $1000/T$ for $[(\text{triphos})\text{Re}(\text{CO})_2(\text{H}_2)]^+$.

the spectrum. The carbonyl-stretching frequencies are higher than those of **2**, consistent with the positive charge of **3** decreasing the Re to CO π -back-bonding.

The $^{31}\text{P}\{^1\text{H}\}$ NMR spectrum of **3** in dichloromethane- d_2 at 22 °C consists of a temperature-invariant AM_2 spin system ($J_{\text{PP}} = 24.8$ Hz) as expected for an octahedral metal complex with triphos.^{21,22} In the hydride region, the ^1H NMR spectrum in the same solvent contains a unique resonance ($\delta -4.85$, $w_{1/2} = 26$ Hz) apparently broadened by fast proton relaxation. This resonance, which does not show any resolvable coupling to the ^{31}P nuclei, is typical of $\eta^2\text{-H}_2$ complexes.³⁰

The presence of a η^2 -bonded H_2 ligand in **3** is confirmed by ^1H NMR T_1 measurements carried out in dichloromethane- d_2 at 300 MHz in the temperature range from -90 to $+20$ °C (Table 2). Figure 2 shows the temperature-dependence of T_1 for this complex. The plot of $\ln T_1(\text{s})$ vs $1000/T(\text{K})$ consists of a well-defined V-shaped curve in good agreement with a relaxation rate dominated by dipole-dipole interactions.^{26,31} Indirectly, the observed V-shaped curve rules out the existence of a tautomeric equilibrium between η^2 -dihydrogen and dihydride forms. Indeed, a fast equilibration between these two tautomers would cause a severe distortion of the T_1 plot due to the temperature-dependence of the equilibrium constant. Analysis of the plot gives an estimated $T_{1\text{min}}$ value of ca. 8.6 ms at -58 °C. This value is close to those of Berke's nonclassical dihydrides $[\text{Re}(\text{CO})_{x+1}(\text{PMe}_3)_{4-x}(\text{H}_2)]^+$ ($x = 0, 1$) ($T_{1\text{min}}$ from 8.2 to 9 ms at 300 MHz).²⁹ For complex **3**, assuming rapid spinning of the H_2 ligand around the Re- H_2 axis, an H-H distance of ca. 0.81 Å may be calculated.^{31a,32} This calculated H-H distance is comparable with the short $r_{\text{H-H}}$ value of 0.8–0.9 Å reported by Crabtree for $[\text{Re}(\text{CO})_2(\text{PMe}_2\text{Ph})_3(\text{H}_2)]^+$,³³ and more generally, with the H-H separations (0.80–0.85 Å) in some molecular hydrogen complexes which have been authenticated by neutron diffraction analyses.^{34,35}

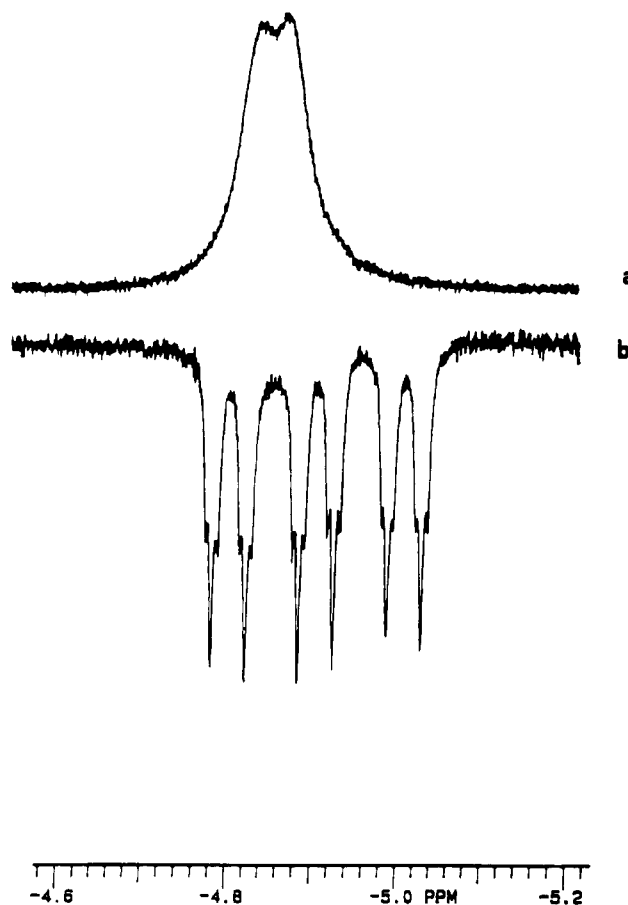


Figure 3. ^1H NMR spectra of $[(\text{triphos})\text{Re}(\text{CO})_2(\text{H}_2)]^+$ (trace a) and of $[(\text{triphos})\text{Re}(\text{CO})_2(\text{HD})]^+$ (trace b) (300 MHz, dichloromethane- d_2 , 24 °C) in the high-field region. The ^1H NMR spectrum of the monodeuteriated isotopomer was obtained by using an inversion-recovery experiment with a delay (τ) set to 16 ms to null out the residual signal of the $\eta^2\text{-H}_2$ isotopomer.

The ^1H NMR spectrum of the isotopomer $[(\text{triphos})\text{Re}(\text{CO})_2(\text{HD})]^+$ (**3-d**) prepared by protonation of **2** with a stoichiometric amount of $\text{DBF}_4\text{-OMe}_2$ in dichloromethane- d_2 , is unequivocally consistent with the nonclassical structure of **3**. As is evident from Figure 3, the signal of the dihydrogen ligand undergoes a dramatic change on changing from **3** (trace a) to **3-d** (trace b).

The broad resonance of the $\eta^2\text{-H}_2$ ligand at $\delta -4.846$ is split by deuterium ($I = 1$) into a 1:1:1 triplet at -4.904 ppm with $^1J_{\text{HD}} = 30.8$ Hz. The secondary isotope shift ($\Delta\delta = \delta_{\text{HD}} - \delta_{\text{H}_2}$) of 58 ppb corresponds well to the data reported for other $\eta^2\text{-HD}$ complexes.^{30,36} Remarkably,

(34) (a) Kubas, G. J.; Burns, C. J.; Eckert, J.; Johnson, S. W.; Larson, A. C.; Vergamini, P. J.; Unkefer, C. J.; Khalsa, G. R. K.; Jackson, S. A.; Eisenstein, O. *J. Am. Chem. Soc.* **1993**, *115*, 569. (b) Ricci, J. S.; Koetzle, T. F.; Bautista, M. T.; Hofstede, T. M.; Morris, R. H.; Sawyer, J. F. *J. Am. Chem. Soc.* **1989**, *111*, 8823. (c) Kubas, G. J.; Unkefer, C. J.; Swanson, B. I.; Fukushima, E. *J. Am. Chem. Soc.* **1986**, *108*, 7000. (d) Van der Sluys, L. S.; Eckert, J.; Eisenstein, O.; Hall, J. H.; Huffman, J. C.; Jackson, S. A.; Koetzle, T. F.; Kubas, G. J.; Vergamini, P. J.; Caulton, K. G. *J. Am. Chem. Soc.* **1990**, *112*, 4831. (e) Kubas, G. J.; Ryan, R. R. *Polyhedron* **1986**, *5*, 473.

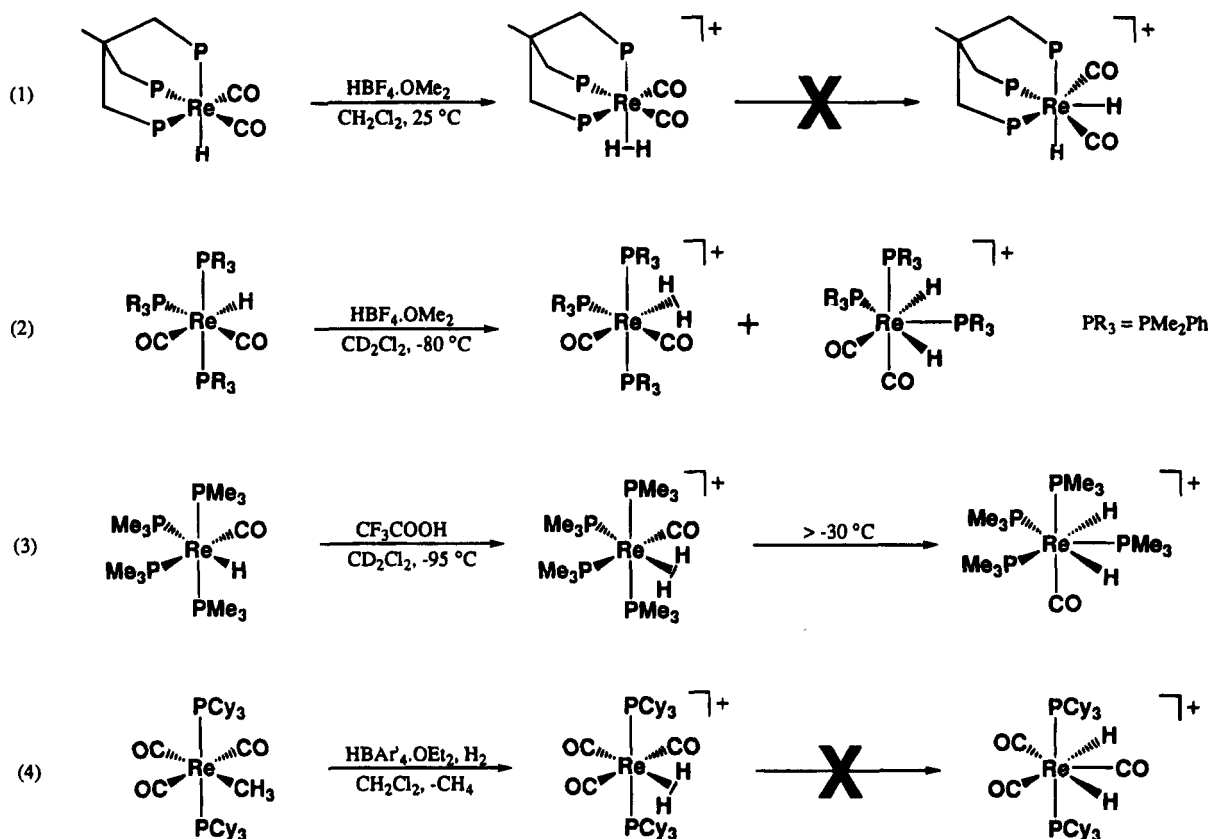
(35) Elongated H-H separations have recently been found in $[\text{Ir}(\text{H}_2)(\text{HCl})_2\text{P}(i\text{-Pr})_3]_2$ (Albinati, A.; Bakmutov, V. I.; Caulton, K. G.; Clot, E.; Eckert, J.; Eisenstein, O.; Gusev, D. G.; Grushin, V. V.; Hanger, B. E.; Klooster, W. T.; Koetzle, T. F.; McMullan, R. K.; O'Loughlin, T. J.; Pelissier, M.; Ricci, J. S.; Sigalas, M. P.; Vymenits, A. B. *J. Am. Chem. Soc.* **1993**, *115*, 7300), in $[\text{Os}(\eta^2\text{-H}_2)\text{en}_2(\text{CH}_3\text{CO}_2)_2]\text{-PF}_6$ (Hasegawa, T.; Li, Z.; Parkin, S.; Hope, H.; McMullan, R. K.; Koetzle, T. F.; Taube, H. *J. Am. Chem. Soc.* **1994**, *116*, 4352), and in $[\text{Ru}(\text{H}_2)(\text{Cp})(\text{dppe})]\text{BF}_4$ (Klooster, W. T.; Koetzle, T. F.; Jia, G.; Fong, T. P.; Morris, R. H.; Albinati, A. *J. Am. Chem. Soc.* **1994**, *116*, 7677).

(31) (a) Desrosiers, P. J.; Cai, L.; Lin, Z.; Richards, R.; Halpern, J. *J. Am. Chem. Soc.* **1991**, *113*, 4173. (b) Gusev, D. G.; Vymenits, A. B.; Bakmutov, V. I. *Inorg. Chem.* **1991**, *30*, 3116.

(32) (a) Luo, X. L.; Howard, J. A. K.; Crabtree, R. H. *Magn. Reson. Chem.* **1991**, *29*, 589. (b) Earl, K. A.; Jia, G.; Maltby, P. A.; Morris, R. H. *J. Am. Chem. Soc.* **1991**, *113*, 3027.

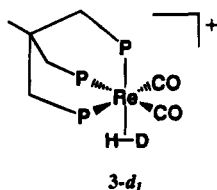
(33) Luo, X. L.; Michos, D.; Crabtree, R. H. *Organometallics* **1992**, *11*, 237.

Scheme 3



the HD resonance also exhibits well-resolved geminal couplings to the triphos phosphorus nuclei so that the overall multiplet appears as a triplet of doublets of triplets. In fact, each component of the H–D triplet is doubled by coupling to the phosphorus atom *trans* to the HD ligand ($^2J_{\text{HPtrans}} = 12.7$ Hz) and is additionally split into narrower triplets by coupling to the two chemically equivalent P atoms lying in the equatorial plane of the complex ($^2J_{\text{HPcis}} = 2.3$ Hz). This multiplicity is therefore consistent with an AMX_2Y spin system ($M = ^2\text{D}$) and with an octahedral structure for the complex, in which the H–D ligand lies *trans* to one phosphorus atom of the triphosphine.

The appearance of H–P coupling constants have previously been observed for only a few η^2 -HD complexes since the line width of the hydride/ η^2 -HD resonance is significantly reduced when compared to that of the corresponding protonated isotopomer.³⁰ Broadband and selective phosphorus decoupling NMR experiments were consistent with the interpretation of the proton spectrum of **3-d**₁.



Of great importance in the confirmation of the structure of **3** is the value of the $^1J_{\text{HD}}$ coupling constant (30.8

Hz) which lies at the upper end of the range commonly found for molecular hydrogen complexes.³⁰ This relatively high value points to an only slightly elongated H–H ligand in **3** and is more consistent with a $r_{\text{H-H}}$ distance of 0.81 Å, calculated from the T_1 data (*vide supra*) by assuming fast rotation of the H_2 ligand than with the longer H–H distance of 1.02 Å which can be calculated for a static nonspinning hydrogen ligand.³²

T_1 relaxation analysis of the ^1H nucleus in **3-d**₁ provides a V-shaped curve (Table 2) from which a minimum value of *ca.* 73 ms may be calculated at -75 °C. A T_1 value of this magnitude is in agreement with a ^2H – ^1H dipole–dipole interaction significantly less efficient than that commonly found for ^1H – ^1H interaction in η^2 - H_2 complexes.^{31,33}

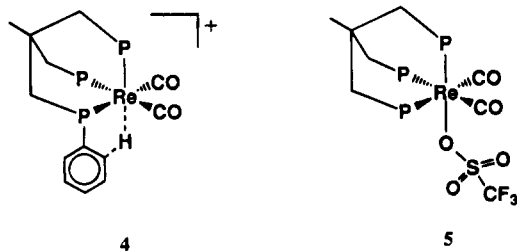
There is no NMR evidence for the conversion of **3** in solution to its classical dihydride form $[(\text{triphos})\text{Re}(\text{CO})_2\text{H}_2]^+$ over the temperature range from -90 to $+35$ °C (Scheme 3). Examples of equilibrium mixtures between classical and nonclassical dihydride tautomers have been reported recently by Crabtree for $[\text{Re}(\text{CO})_2(\text{PMe}_2\text{Ph})_3\text{H}_2]^+$ ³³ while Berke has shown that the nonclassical complex $[\text{Re}(\text{CO})(\text{PMe}_3)_4(\text{H}_2)]^+$ transforms irreversibly into the corresponding Re(III) classical dihydride $[\text{Re}(\text{CO})(\text{PMe}_3)_4\text{H}_2]^+$ at temperatures above -30 °C (see Scheme 3).²⁹

In complex **3**, the rigid and sterically demanding triphos ligand and the two π -acceptor CO groups (an overall donor atom set less basic than three PMe_2Ph or PMe_3 monophosphines) are expected to provide steric and electronic stabilization to the η^2 - H_2 ligand. Indeed, a similar conclusion has been made by Heinekey for the cationic hydrogen complexes $[\text{Re}(\text{PR}_3)_2(\text{CO})_3(\text{H}_2)]\text{BAR}_4$ ($\text{PR}_3 = \text{PCy}_3, \text{PPr}_3, \text{PPh}_3$; $\text{Ar} = [3,5-(\text{CF}_3)_2\text{C}_6\text{H}_3]$) (see equation 4 in Scheme 3).³⁷

(36) (a) Bianchini, C.; Linn, K.; Masi, D.; Peruzzini, M.; Polo, A.; Vacca, A.; Zanolini, F. *Inorg. Chem.* **1993**, *32*, 2366. (b) Panque, M.; Poveda, M. L.; Taboada, S. *J. Am. Chem. Soc.* **1994**, *116*, 4519 and references therein.

Synthesis and Characterization of [(triphos)Re(CO)₂]BF₄ (4). When the proton NMR spectrum of **3** is acquired at room temperature under a nitrogen or argon atmosphere, the appearance of a broad resonance at 4.60 ppm due to free H₂ can be observed. The intensity of this signal increases with time, showing that the H₂ ligand slowly dissociates in solution.

The H₂ ligand in complex **3** is also moderately labile in the solid state, requiring an H₂-enriched atmosphere for long storage. When the product is stored under nitrogen or argon, the loss of H₂ occurs quantitatively within 3–4 days to give the complex [(triphos)Re(CO)₂]BF₄ (**4**). Alternatively, compound **4** can be prepared by



reacting **2** in THF with a stoichiometric amount of Me₃OBF₄. When the alkylation of **2** is carried out using MeOSO₂CF₃, the η¹-O-trifluoromethanesulfonate complex (triphos)Re(CO)₂(η¹-OSO₂CF₃) (**5**) is obtained. *In situ* NMR experiments confirm that in both reactions 1 equiv of CH₄ is eliminated upon methylation of **2**. The neutral complex **5** can also be prepared in quantitative yield by treating a THF solution of **3** with various triflate salts or by reacting **2** with an excess of triflic acid in dichloromethane under nitrogen.

The η¹-O-coordination of the triflate ion in **5** is demonstrated by the IR spectrum, which contains a diagnostic band at 1320 cm⁻¹.³⁸ In contrast, there is no evidence for the coordination of the BF₄⁻ anion in **4**, which, in fact, behaves as a typical 1:1 electrolyte in dichloroethane solution.³⁹ Exposure of dichloromethane solutions of either **4** or **5** to an H₂ atmosphere quantitatively regenerates the molecular-hydrogen complex **3**.

While the formation of **5** from **3** is unremarkable in view of the lability of the H₂ ligand in solution (*vide infra*), the formation of the formally 16-electron complex **4** is intriguing because it apparently contrasts with the well-known reluctance of rhenium to form unsaturated complexes.¹ However, in this case too, there is no exception to the general rule. In fact, there is little doubt that an agostic interaction⁴⁰ between the rhenium center and a phenyl C–H bond of the triphosphine ligand provides electronic stabilization to the complex in both the solid state and solution.

Agostic interactions are widely encountered in molybdenum and tungsten compounds which are precursors to molecular hydrogen complexes.⁴¹ Some of these complexes, including Kubas' seminal complex W(CO)₃(

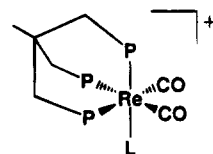
(PCy₃)₂, have been studied by either X-ray or neutron diffraction techniques.⁴²

The presence of an agostic interaction Re·H–C in **4** is strongly supported by the ³¹P{¹H} NMR spectrum. At room temperature, the spectrum shows the expected AM₂ splitting pattern. However, as the temperature is decreased, the low-field doublet at –4.55 ppm, which is temperature-invariant for all of the other Re(I) complexes described in this paper, broadens, loses its multiplicity, and finally coalesces into the baseline at –90 °C. Upon further cooling to –110 °C (CD₂Cl₂/CDCl₃, 7:3 v/v), two broad humps begin to appear at *ca.* 3.0 and –12.8 ppm, suggesting the onset of decoalescence and indicating that the slow-exchange spectrum is approaching an AMQ spin system. Freezing of the solution prevented us from recording spectra at lower temperatures and thus reaching the slow-exchange regime for the system. At the coalescence point a Δ*G*[‡] value of *ca.* 7.7 kcal mol⁻¹ can be calculated, which points to a very low energy barrier for the dynamic process averaging the two phosphorus atoms.³⁷ When the sample is heated to room temperature, the initial AM₂ splitting pattern is restored, demonstrating the complete reversibility of the dynamic process which in the fast motion regime averages the two phosphorus atoms *trans* to the carbonyl ligands. The observation of an AM₂ spin system at high temperature is thus attributed to a dynamic process in which the agostic hydrogen exchanges with the other *ortho*-phenyl protons of the two equatorial PPh₂ groups.

The structure of **4** as well as its ³¹P NMR behavior is essentially similar to those recently described by Heinekey in {Re(PCy₃)₂(CO)₃}BF₄ in which an agostic interaction between a C–H bond of a pendant cyclohexyl group and the metal center was authenticated in the solid-state by low-temperature X-ray crystallography.³⁷

The agostic interaction between a phenyl C–H bond and rhenium observed in **4** suggests that the phenyl substituents on the equatorial phosphorus atoms are quite close to the metal center and thus may eventually sterically interact with an axial ligand in [(triphos)Re(CO)₂(L)]⁺ complexes. In a sense, this may explain the anomalous NMR multiplicity of the terminal hydride ligand in **2**.

Reactivity of the Nonclassical Dihydride 3. The agostic interaction in **4** is weak in solution and can be eliminated by a variety of ligands.³⁰ For example, addition of PPNCl, LiHBet₃, or NaOSO₂CF₃ to THF solutions of **4** results in the formation of complexes **1**, **2**, or **5**, respectively. In a similar way, addition of neutral molecules to **4** provides an easy method for the synthesis of a variety of octahedral complexes of the formula [(triphos)Re(CO)₂(L)]Y (Y = BF₄, BPh₄). As an example, we describe here the reactions of **4** with acetonitrile and carbon monoxide which give the corresponding adducts [(triphos)Re(CO)₂(CH₃CN)]BPh₄ (**6**) and [(triphos)Re(CO)₃]BF₄ (**7**), respectively.



L = MeCN, **6**; CO, **7**

(37) Heinekey, D. M.; Schomber, B. M.; Radzewich, C. E. *J. Am. Chem. Soc.* **1994**, *116*, 4515.

(38) Lawrance, G. A. *Chem. Rev.* **1986**, *86*, 17.

(39) Strauss, H. S. *Chem. Rev.* **1993**, *93*, 927.

(40) (a) Brookhart, M.; Green, M. L. H. *J. Organomet. Chem.* **1983**, *250*, 395. (b) Brookhart, M.; Green, M. L. H.; Wong, L.-L. *Prog. Inorg. Chem.* **1988**, *36*, 1.

(41) (a) Luo, X.-L.; Kubas, G. J.; Burns, C. J.; Eckert, J. *Inorg. Chem.* **1994**, *33*, 5219. (b) Kubas, G. J.; Ryan, R. R.; Wroblewski, D. A. *J. Am. Chem. Soc.* **1986**, *108*, 1339. (c) Sato, M.; Tatsumi, T.; Kodama, T.; Hidai, M.; Uchida, T.; Uchida, Y. *J. Am. Chem. Soc.* **1978**, *100*, 4447.

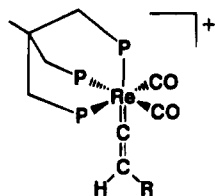
(42) Wasserman, H. J.; Kubas, G. J.; Ryan, R. R. *J. Am. Chem. Soc.* **1986**, *108*, 2294.

Interestingly, there is no evidence for coordination of dinitrogen; complex **4** can be manipulated under nitrogen in different solvents.

Monitoring the transformation of **3** into **4** by ^{31}P NMR spectroscopy under a nitrogen atmosphere shows that the process occurs without the intermediacy of a dinitrogen complex even when the NMR tube is pressurized with 3 atm of N_2 . This result is apparently anomalous in view of the high affinity for dinitrogen coordination of metal fragments which are capable of forming $\eta^2\text{-H}_2$ complexes. In fact, H_2 displacement by N_2 is a ubiquitous process for nonclassical hydrides to the extent that the value of the infrared absorption $\nu(\text{N}\equiv\text{N})$ in dinitrogen metal complexes has been taken as a diagnostic tool for predicting the thermodynamic stability of the corresponding molecular hydrogen complexes.⁴³

In the present case, a dinitrogen complex does not form because the metal center is saturated by a stronger agostic interaction. Similar behavior is exhibited by the agostic complex $[\text{Re}(\text{PCy}_3)_2(\text{CO})_3]\text{BAR}_4$, which is capable of strongly binding H_2 but is reluctant to coordinate N_2 .³⁷

Synthesis and Characterization of the Vinylidene Complexes $[(\text{triphos})\text{Re}(\text{CO})_2\{\text{C}=\text{C}(\text{H})\text{R}\}]\text{BPh}_4$ (R = Ph, **8; CO_2Et , **9**; C_6H_{13} , **10**).** Treatment of the molecular hydrogen complex **3** with a stoichiometric amount of a terminal alkyne $\text{HC}\equiv\text{CR}$ (R = Ph, CO_2Et , C_6H_{13}) in dichloromethane at room temperature results in an immediate color change from pale yellow to deep violet (R = Ph) or pink (R = CO_2Et , C_6H_{13}). Addition of NaBPh_4 in ethanol to the solutions leads to precipitation of crystals of the vinylidene complexes $[(\text{triphos})\text{Re}(\text{CO})_2\{\text{C}=\text{C}(\text{H})\text{R}\}]\text{BPh}_4$ (R = Ph, **8**; CO_2Et , **9**; C_6H_{13} , **10**) in excellent yields. Alternatively, compound **8–10**



R = Ph, **8**; CO_2Et , **9**; C_6H_{13} , **10**

can be prepared in comparable yields by reacting the agostic complex **4** with 1 equiv of the appropriate terminal alkyne, whereas no reaction occurs with the acetonitrile or carbonyl derivatives **6** and **7**. On the basis of the results presented in this paper, one may conclude that the binding preference of Re(I) in $[(\text{triphos})\text{Re}(\text{CO})_2]^+$ fragment is as follows: $\text{N}_2 < \text{C}-\text{H}_{(\text{agostic})} < \text{H}_2 < \text{HC}\equiv\text{CR} < \text{CH}_3\text{CN} < \text{CO}$.

The presence of a vinylidene ligand in **8–10** was unambiguously confirmed by spectroscopic techniques (IR and NMR).^{44,45} In fact, in addition to the typical

(43) Morris, R. H.; Earl, K. A.; Luck, R. L.; Lazarowych, N. J.; Sella, A. *Inorg. Chem.* **1987**, *26*, 2674.

(44) For a review on vinylidene complexes, see: Bruce, M. I. *Chem. Rev.* **1991**, *91*, 197.

(45) Rhenium vinylidene complexes include: (a) Kolobova, N. E.; Antonova, A. B.; Khitrova, O. M.; Antipin, M. Yu.; Struchkov, Yu. T. *J. Organomet. Chem.* **1977**, *137*, 69. (b) Senn, D. R.; Wong, A.; Patton, A. T.; Marsi, M.; Strouse, C. T.; Gladysz, J. A. *J. Am. Chem. Soc.* **1988**, *110*, 6096. (c) Pombeiro, A. J. L.; Almeida, S. S. P. R.; Silva, M. F. C. G.; Jeffrey, J. C.; Richards, R. L. *J. Chem. Soc., Dalton Trans.* **1989**, 2381. (d) Kowalczyk, J. J.; Arif, A. M.; Gladysz, J. A. *Organometallics* **1991**, *10*, 1079. (e) Ramsden, J. A.; Weng, W.; Gladysz, J. A. *Organometallics* **1992**, *11*, 3635. (f) Terry, M. R.; Mercado, L. A.;

absorptions of the carbonyl ligands, the IR spectra contain a couple of medium-intensity bands which fall in the proper range for the vinylidene $\text{C}=\text{C}$ moiety ($1663\text{--}1607\text{ cm}^{-1}$). The positions of the CO absorptions (from 2036 to 1952 cm^{-1}) confirm that the vinylidene ligand is a good π -acceptor ligand (Table 1).⁴⁶ The highest $\nu(\text{CO})$ values (2036 and 1970 cm^{-1}) are found for **9** as a consequence of the electron-withdrawing character of the CO_2Et substituent.

The $^{31}\text{P}\{^1\text{H}\}$ NMR spectra (dichloromethane- d_2) of **8–10** exhibit the expected AM_2 splitting pattern for an octahedral geometry about rhenium. Given the steric requirements of the (triphos)Re(CO)₂ moiety there is little doubt that the $\text{C}=\text{C}(\text{H})\text{R}$ ligand is located in the axial position from which the H_2 molecule in **3** is displaced by $\text{HC}\equiv\text{CR}$. The spectra are temperature-invariant down to $-90\text{ }^\circ\text{C}$, thus indicating that even at low temperature the vinylidene fragment is freely rotating in solution about the rhenium–vinylidene axis. This phenomenon is not unusual for metal–vinylidene complexes and has been ascribed to the existence of very low energy barriers for the different vinylidene rotamers.^{44,47}

The ^1H NMR spectra (dichloromethane- d_2) are clearly consistent with the presence of a vinylidene ligand. In particular, the spectra of **8** and **9** exhibit a one-proton quartet (**8**, δ 4.23, $^4J_{\text{HP}} = 2.9\text{ Hz}$; **9**, δ 3.92, $^4J_{\text{HP}} = 3.0\text{ Hz}$) in the expected region for vinylidene hydrogens. In keeping with this interpretation, these NMR signals do not correlate with any other proton resonance in the 2D-COSY H,H NMR spectrum and transform into a narrow singlet in the broad-band phosphorus-decoupled ^1H NMR spectrum. The vinylidene hydrogen of **10** appears as a well-resolved triplet of quartets at 3.41 ppm. This multiplicity arises from coupling of the vinylidene hydrogen to both the three phosphorus nuclei ($^4J_{\text{HP}} = 2.8\text{ Hz}$) and the proximal CH_2 protons of the n -hexyl substituent ($^3J_{\text{HH}} = 8.3\text{ Hz}$). Consistently, the vinylidene resonance transforms into a triplet in the $^1\text{H}\{^{31}\text{P}\}$ NMR spectrum and becomes a quartet when homodecoupling of the internal $\text{CH}_2(n\text{-hexyl})$ resonance is performed.

The $^{13}\text{C}\{^1\text{H}\}$ NMR spectra (dichloromethane- d_2) of complexes **8–10** display several interesting features. In particular, a downfield resonance ($351.0 \leq \delta \leq 339.5$), characteristic of the highly electron-deficient C_α carbon, appears as a doublet of triplets with $J_{\text{CPtrans}} > J_{\text{CPcis}}$.⁴⁷ In a similar way, the β -carbons of the vinylidene ligands also appear as a doublet of triplets in the expected range ($116.3 \leq \delta \leq 109.2$) with a relatively large coupling to the *trans* phosphorus atom ($^3J_{\text{CP}} \approx 13.5\text{ Hz}$). Finally, the carbonyl region of the spectrum shows the AXX'Y CO multiplet typical of the present rhenium(I) complexes. As an example, the carbonyl resonance of the phenylvinylidene derivative (**8**) is shown in Figure 4 with the computed spectrum.

Three possible product, namely, π -alkyne, σ -alkynyl hydride, and vinylidene complexes, may form upon the

Kelley, C.; Geoffrey, G. L.; Nombel, P.; Lugan, N.; Mathieu, R.; Olander, R. L.; Owens, B. E.; Rheingold, A. L. *Organometallics* **1994**, *13*, 843. (g) Casey, C. P.; Ha, Y.; Powell, D. R. *J. Organomet. Chem.* **1994**, *472*, 185.

(46) Kostic, N. M.; Fenske, R. F. *Organometallics* **1982**, *1*, 974.

(47) See for example: (a) Barbaro, P.; Bianchini, C.; Peruzzini, M.; Polo, A.; Zanobini, F.; Frediani, P. *Inorg. Chim. Acta* **1994**, *5*, 220. (b) Bianchini, C.; Meli, A.; Peruzzini, M.; Zanobini, F.; Zanello, P. *Organometallics* **1990**, *9*, 241. (c) Bianchini, C.; Peruzzini, M.; Vacca, A.; Zanobini, F. *Organometallics* **1991**, *10*, 3697.

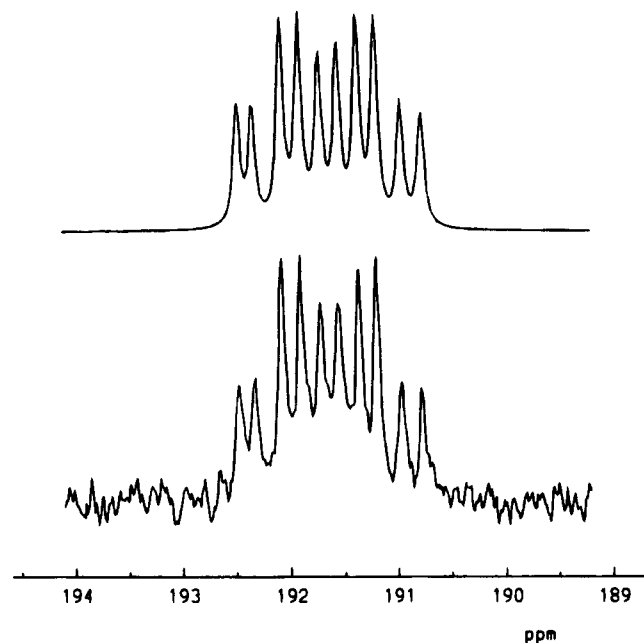


Figure 4. Experimental (lower) and computed (upper) $^{13}\text{C}\{-^1\text{H}\}$ NMR resonances of the carbonyl ligands of **8** (50.32 MHz, dichloromethane- d_2 , 22 °C).

stoichiometric reaction between unsaturated metal fragments and 1-alkynes, and evidence has been provided for both reversible and irreversible interconversion of the three isomers.^{44,47,48}

With a few exceptions,^{22f,49} it is believed that in the initial step the alkyne coordinates to the metal center. From the π -intermediate, the system can eventually convert to hydride alkynyl (C–H oxidative addition) and/or vinylidene (1,3-hydrogen shift/1,2-hydrogen shift) derivatives. Experimental and theoretical studies agree to favor the 1,3-hydrogen shift mechanism for $d^8 \text{ML}_4$ metal fragments, while the 1,2-hydrogen shift mechanism is favored for $d^6 \text{ML}_5$ metal fragments.⁵⁰ To date, no reaction intermediates have been observed when the reaction between **3** and $\text{HC}\equiv\text{CPh}$ is monitored by $^{31}\text{P}\{-^1\text{H}\}$ NMR spectroscopy at a temperature as low as –50 °C. While it is not possible at this time to provide experimental evidence for or against the two different mechanisms of acetylene to vinylidene tautomerization, we strongly favor the 1,2-hydrogen shift mechanism from a π -alkyne precursor based on the established reluctance of the $[(\text{triphos})\text{Re}(\text{CO})_2]^+$ fragment to undergo oxidative addition reactions.

Experimental Section

General Procedures. Diethyl ether, toluene, and tetrahydrofuran were purified by distillation under nitrogen over $\text{Na}/\text{Ph}_2\text{CO}$. Dichloromethane and ethanol were distilled from CaH_2 . Phenylacetylene, ethyl propiolate, and 1-octyne were purchased from Aldrich, their purity was checked by ^1H NMR spectroscopy, and, when necessary, the reagents were distilled

(48) Werner, H. *J. Organomet. Chem.* **1994**, 475, 45 and references therein.

(49) Hackett, M.; Whitesides, G. M. *J. Am. Chem. Soc.* **1988**, 110, 1449.

(50) See for example: (a) Werner, H.; Dirnberger, T.; Höhn, A. *Chem. Ber.* **1991**, 124, 1957. (b) Fryzuk, M. D.; Huang, L.; McManus, N. T.; Paglia, P.; Rettig, S. J.; White, G. S. *Organometallics* **1992**, 11, 2979. (c) Lomphey, J. R.; Selegue, J. P. *J. Am. Chem. Soc.* **1992**, 114, 5518. (d) For a theoretical study, see: Silvestre, J.; Hoffmann, R. *Helv. Chim. Acta* **1985**, 68, 1461.

under nitrogen prior to use. All the other reagents and chemicals were reagent grade and, unless otherwise stated, were used as received from commercial supplies. All reactions and manipulations were routinely performed under a dry nitrogen atmosphere by using standard Schlenk-tube techniques. The solid complexes were collected on sintered glass-frits and washed with ethanol and diethyl ether before being dried in a stream of nitrogen. The ligand 1,1,1-tris(diphenylphosphinomethyl)ethane (triphos)⁵¹ and the complexes $\text{Re}(\text{CO})_2(\text{PPh}_3)_2\text{Cl}$ ⁵² and $(\text{triphos})\text{Re}(\text{CO})\text{H}_3$ ⁵ were prepared as described in the literature. $\text{DBF}_4\cdot\text{OMe}_2$ was prepared *in situ* from $\text{HBF}_4\cdot\text{OMe}_2$ and D_2O as reported in the literature.^{32b} Deuteriated solvents for NMR measurements (Aldrich and Merck) were dried over molecular sieves. ^1H and $^{13}\text{C}\{-^1\text{H}\}$ NMR spectra were recorded on Varian VXR 300 or Bruker AC 200P spectrometers operating at 299.94 or 200.13 and 75.42 or 50.32 MHz, respectively. Peak positions are relative to tetramethylsilane and were calibrated against the residual solvent resonance (^1H) or the deuteriated solvent multiplet (^{13}C). $^{31}\text{P}\{-^1\text{H}\}$ NMR spectra were recorded on the same instruments operating at 121.42 and 81.01 MHz, respectively. Chemical shifts were measured relative to external 85% H_3PO_4 with downfield values taken as positive. Proton NMR spectra with broad-band phosphorus decoupling were recorded on the Bruker instrument equipped with a 5 mm inverse probe and a BFX-5 amplifier device using the wide-band phosphorus-decoupling sequence GARP. The spin–lattice relaxation time (T_1) measurements were carried out in CD_2Cl_2 at 300 MHz by the inversion–recovery method using standard $180^\circ\text{--}\tau\text{--}90^\circ$ pulse sequences. Computer simulations of NMR spectra were carried out with a locally developed package containing the programs LAOCN3⁵³ and DAVINS⁵⁴ run on a Compaq Deskpro 386/25 personal computer. The initial choices of shifts and coupling constants were refined by iterative least-squares calculations using the experimental digitized spectrum. The final parameters gave a satisfactory fit between experimental and calculated spectra, the agreement factor R being less than 1% in all cases. Infrared spectra were recorded in KBr pellets on a Nicolet 510 P spectrometer operating in the FT mode or as Nujol mulls on a Perkin-Elmer 1600 series FT-IR spectrometer between KBr plates. Conductivities were measured with an ORION model 990101 conductance cell connected to a model 101 conductivity meter. The conductivity data were obtained at sample concentrations of $ca. 1 \times 10^{-3}$ M in dichloroethane or nitroethane solutions at room temperature (21 °C). Elemental analyses were performed using a Carlo Erba model 1106 elemental analyzer.

Synthesis of the Complexes. **(triphos)Re(CO) $_2$ Cl (1).** To a suspension of $\text{Re}(\text{CO})_3(\text{PPh}_3)_2\text{Cl}$ (2.0 g, 2.40 mmol) in 150 mL of toluene was added with stirring solid triphos (2.0 g, 3.20 mmol). The resulting mixture was heated at reflux temperature for 7 h to give a pale yellow solution, which was concentrated under reduced pressure to $ca. 10$ mL. Addition of ethanol (30 mL) led to the precipitation of pale yellow microcrystals of $(\text{triphos})\text{Re}(\text{CO})_2\text{Cl}$ (**1**); yield 80%. Anal. Calcd for $\text{C}_{43}\text{H}_{39}\text{ClO}_2\text{P}_3\text{Re}$: C, 57.21; H, 4.36; Cl, 3.93. Found: C, 57.05; H, 4.20; Cl, 3.84. IR (KBr): ν_{COsym} 1948 cm^{-1} (s), $\nu_{\text{COantisym}}$ 1887 cm^{-1} (s). $^{31}\text{P}\{-^1\text{H}\}$ NMR (CD_2Cl_2 , 22 °C, 81.01 MHz): AM_2 system, δ_A 2.40, δ_M –18.23, $J_{\text{AM}} = 14.7$ Hz. ^1H NMR (CD_2Cl_2 , 22 °C, 200.13 MHz): δ 1.45 (q, $J_{\text{HP}} = 2.5$ Hz, CH_3 , 3H); δ 2.48 (m, CH_2 , 6H). $^{13}\text{C}\{-^1\text{H}\}$ NMR (CD_2Cl_2 , 22 °C, 75.42 MHz): δ 198.7 (AXX'Y spin system, $J_{\text{AX}} = 55.6$ Hz, $J_{\text{AX}'} = -8.8$ Hz, $J_{\text{AY}} = 7.1$ Hz, $J_{\text{X}'\text{Y}} = 28.5$ Hz, CO); δ 40.2 (q, $J_{\text{CP}} = 10.0$ Hz, CH_3); δ 39.8 (q, $J_{\text{CP}} = 3.5$ Hz, CH_3C); δ 37.3 (dt, $J_{\text{CPaxial}} = 26.3$ Hz; $J_{\text{CPequatorial}} = 3.1$ Hz, CH_2Paxial); δ 34.3 (td, $N =$

(51) Hewertson, W.; Watson, H. R. *J. Chem. Soc.* **1962**, 1490.

(52) Chatt, J.; Dilworth, J. R.; Gunz, H. P.; Leigh, G. J. *J. Organomet. Chem.* **1974**, 84, 245.

(53) Castellano, S.; Bothner-By, A. A. *J. Chem. Phys.* **1964**, 41, 3863.

(54) (a) Stephenson, D. S.; Binsch, G. A. *J. Magn. Reson.* **1980**, 37, 395. (b) Stephenson, D. S.; Binsch, G. A. *J. Magn. Reson.* **1980**, 37, 409.

$(J_{\text{C}^{\text{P}^{\text{equatorial}}}} + J_{\text{C}^{\text{P}^{\text{axial}}}}) = 15.3 \text{ Hz}$; $J_{\text{C}^{\text{P}^{\text{axial}}}} = 4.9 \text{ Hz}$, $\text{CH}_2\text{P}^{\text{equatorial}}$).

(triphos)Re(CO)₂H (2). **Method A.** Solid LiAlH₄ (0.29 g, 7.70 mmol) was added in small portions to a stirred suspension of **1** (1.0 g, 1.10 mmol) in tetrahydrofuran (50 mL), cooled to 0 °C, and saturated with carbon monoxide. The reaction mixture was slowly brought to room temperature and refluxed for 24 h. The mixture was filtered through Celite, and the pale yellow filtrate solution was evaporated to dryness in vacuo. The crude solid was dissolved in dichloromethane (3 × 10 mL), and the solution was filtered through Celite and concentrated to 10 mL. Addition of ethanol (20 mL) gave (triphos)Re(CO)₂H (**2**) as an off-white solid; yield 60%. Crystals suitable for an X-ray diffraction analysis were obtained by slow recrystallization from a tetrahydrofuran-ethanol solution.

Method B. To a suspension of **1** (1.0 g, 1.20 mmol) in 100 mL of tetrahydrofuran was added LiHBEt₃ (24.0 mL, 1.0 M THF solution, 24.0 mmol) at room temperature. The reaction mixture was heated at reflux for 24 h under CO atmosphere. The excess of LiHBEt₃ was hydrolyzed by careful addition of ethanol (3 × 10 mL), and the volume of the solution was reduced to 5 mL, during which time **2** began to separate. Addition of ethanol (20 mL) completed the precipitation of **2**; yield 67%.

Method C. A stream of CO (1 atm) was bubbled for 2 h into a solution of [(triphos)Re(CO)H₃] (0.20 g, 24 mmol) in refluxing tetrahydrofuran (20 mL). The solution was reduced to half of its original volume by vacuum concentration, and then ethanol (20 mL) was added to precipitate **2**; yield 85%.

Anal. Calcd for C₄₃H₄₀O₂P₃Re: C, 59.43; H, 4.64. Found: C, 59.06; H, 4.35. IR (KBr): $\nu_{\text{COsym}} = 1921 \text{ cm}^{-1}$ (s), $\nu_{\text{COantisym}} = 1856 \text{ cm}^{-1}$ (s). $\nu_{\text{Re-H}}$ not observed (masked by CO absorptions). ³¹P{¹H} NMR (CD₂Cl₂, 22 °C, 81.01 MHz): AM₂ system, $\delta_{\text{A}} -4.05$, $\delta_{\text{M}} -3.51$, $J_{\text{AM}} = 18.6 \text{ Hz}$. ¹H NMR (CD₂Cl₂, 22 °C, 200.13 MHz): δ 1.43 (q, $J_{\text{HP}} = 2.5 \text{ Hz}$, CH₃, 3H); δ 2.23, (m, CH₂, 4H); δ 2.42, (d, $J_{\text{HP}} = 7.2 \text{ Hz}$, CH₂, 2H); δ -5.83, (t, $J_{\text{HP}} = 20.0 \text{ Hz}$, ReH, 1H); ¹³C{¹H} NMR (CD₂Cl₂, 22 °C, 75.42 MHz): δ 204.8 (br m, CO); δ 36.3 (q, $J_{\text{CP}} = 9.2 \text{ Hz}$, CH₃); δ 36.6 (q, $J_{\text{CP}} = 5.3 \text{ Hz}$, CH₃C); δ 31.9 (dt, $J_{\text{CPaxial}} = 22.1 \text{ Hz}$; $J_{\text{C}^{\text{P}^{\text{equatorial}}}} = 4.9 \text{ Hz}$, CH₂P_{axial}); δ 30.3 (td, $N = (J_{\text{C}^{\text{P}^{\text{equatorial}}}} + J_{\text{C}^{\text{P}^{\text{axial}}}}) = 13.7 \text{ Hz}$; $J_{\text{C}^{\text{P}^{\text{axial}}}} = 5.0 \text{ Hz}$, CH₂P_{equatorial}).

(triphos)Re(CO)₂D (2-d₁). **Method A.** This compound was prepared starting from complex **1** (0.20g, 0.22 mmol) following the method reported above but using lithium aluminum deuteride and ethanol-d₁ instead of LiAlH₄ and ethanol, respectively.

Method B. The isotopomer **2-d₁** was obtained in quantitative yield from the corresponding protiated complex **2** by H/D exchange at room temperature with CH₃OD in CH₂Cl₂. The H/D exchange was monitored by ¹H NMR spectroscopy, and the solvent mixture was evaporated in vacuo after completion of the reaction. IR (KBr): $\nu_{\text{COsym}} 1921 \text{ cm}^{-1}$ (s), $\nu_{\text{COantisym}} 1856 \text{ cm}^{-1}$ (s), $\nu_{\text{Re-D}} 1345 \text{ cm}^{-1}$ (br, m).

[(triphos)Re(CO)₂(H₂)BF₄ (3). HBF₄·OMe₂ (33 μL , ca. 0.27 mmol) was added *via* microsyringe to a stirred suspension of **2** (0.25 g, 0.26 mmol) in dichloromethane (5.0 mL) cooled to -20 °C under a dihydrogen atmosphere. Stirring was continued for 5 min during which time all the monohydride dissolved to produce a pale yellow solution which was brought to room temperature. Addition of *n*-pentane (10 mL) yielded **3** as a pale yellow microcrystalline product, which was dried and stored under H₂; yield 70%. Anal. Calcd for C₄₃H₄₁BF₄O₂P₃Re: C, 54.04; H, 4.32. Found: C, 54.00; H, 4.35. IR (KBr): $\nu_{\text{COsym}} 1965 \text{ cm}^{-1}$ (s), $\nu_{\text{COantisym}} 1900 \text{ cm}^{-1}$ (s). ³¹P{¹H} NMR (CD₂Cl₂, 22 °C, 81.01 MHz): AM₂ system, $\delta_{\text{A}} -6.11$, $\delta_{\text{M}} -11.22$, $J_{\text{AM}} = 24.8 \text{ Hz}$. ¹H NMR (CD₂Cl₂, 22 °C, 200.13 MHz): δ 1.75 (br s, CH₃, 3H); δ 2.78, (m, CH₂, 6H); δ -4.85, (br s, Re-H₂, 2H).

Reaction of **3 with NEt₃.** Addition of a 2-fold excess of NEt₃ to a dichloromethane-d₂ (0.7 mL) solution of **3** in a 5-mm

NMR tube gave **2** immediately as shown by ¹H and ³¹P{¹H} NMR spectroscopy.

[(triphos)Re(CO)₂(HD)]BF₄ (3-d₁). Complex **2** (25.0 mg, 0.028 mmol) was dissolved in CD₂Cl₂ (0.4 mL) in a screw-cap 5-mm NMR tube. After the tube was cooled to 0 °C, DBF₄·OMe₂ (4 μL , ca. 0.03 mmol) was added by syringe to the solution. ³¹P{¹H} NMR (CD₂Cl₂, 22 °C, 81.01 MHz): AM₂ system, $\delta_{\text{A}} -6.50$, $\delta_{\text{M}} -11.32$, $J_{\text{AM}} = 24.5 \text{ Hz}$. ¹H NMR (CD₂Cl₂, 22 °C, 200.13 MHz): δ 1.75 (br s, CH₃, 3H); δ 2.76 (m, CH₂, 6H); δ -4.90 (tdt, Re-HD, 1H, $J_{\text{HD}} = 30.8 \text{ Hz}$, $J_{\text{HPA}} = 12.7 \text{ Hz}$, $J_{\text{HPM}} = 2.3 \text{ Hz}$).

[(triphos)Re(CO)₂]BF₄ (4). Me₃OBF₄ (80 mg, 0.54 mmol) was added to a stirred suspension of **2** (0.50 g, 0.52 mmol) in dichloromethane (15.0 mL) cooled to -10 °C under a nitrogen atmosphere. Stirring was continued for 5 min during which time all the monohydride dissolved to produce a pale yellow solution, which was brought to room temperature. Addition of *n*-pentane (10 mL) yielded **4** as a pale yellow microcrystalline product; yield 88%. Anal. Calcd for C₄₃H₃₉BF₄O₂P₃Re: C, 54.15; H, 4.12. Found: C, 53.95; H, 4.01. IR (KBr): $\nu_{\text{COsym}} 1956 \text{ cm}^{-1}$ (s), $\nu_{\text{COantisym}} 1891 \text{ cm}^{-1}$ (s). ³¹P{¹H} NMR (CD₂Cl₂, 22 °C, 81.01 MHz): AM₂ system, $\delta_{\text{A}} 3.04$, $\delta_{\text{M}} -4.55$, $J_{\text{AM}} = 16.6 \text{ Hz}$. ¹H NMR (CD₂Cl₂, 22 °C, 200.13 MHz): δ 1.59 (br s, CH₃, 3H); δ 2.60, (m, CH₂, 6H). $\Lambda_{\text{m}}(\text{dichloroethane}) = 27 \Omega^{-1} \text{ cm}^2 \text{ mol}^{-1}$.

[(triphos)Re(CO)₂(η^1 -OSO₂CF₃)] (5). To a solution of **3** (0.25 g, 0.26 mmol) in dichloromethane (5.0 mL) cooled to -20 °C was added MeSO₃CF₃ (30 μL , ca. 0.26 mmol) *via* microsyringe. The reaction mixture was stirred for 15 min, and the addition of ethanol (10 mL) resulted in the precipitation of a white solid; yield 85%. Anal. Calcd for C₄₄H₃₉F₃O₅P₃SRe: C, 52.02; H, 3.87. Found: C, 52.06; H, 3.79. IR (KBr): $\nu_{\text{COsym}} 1964 \text{ cm}^{-1}$ (s), $\nu_{\text{COantisym}} 1888 \text{ cm}^{-1}$ (s), $\nu_{\text{OSO}_2\text{CF}_3} 1320 \text{ cm}^{-1}$ (m). ³¹P{¹H} NMR (CD₂Cl₂, 22 °C, 81.01 MHz): AM₂ system, $\delta_{\text{A}} 6.20$, $\delta_{\text{M}} -10.11$, $J_{\text{AM}} = 14.7 \text{ Hz}$. ¹H NMR (CD₂Cl₂, 22 °C, 200.13 MHz): δ 1.54 (br s, CH₃, 3H); δ 2.47-2.63 (m, CH₂, 6H). ¹³C{¹H} NMR (CD₂Cl₂, 22 °C, 75.42 MHz): δ 197.5 (AXXY spin system, $J_{\text{AX}} = 52.8 \text{ Hz}$, $J_{\text{AX'}} -8.2 \text{ Hz}$, $J_{\text{AY}} = 6.6 \text{ Hz}$, $J_{\text{XX'}} = 26.5 \text{ Hz}$, CO); δ 39.9 (q, $J_{\text{CP}} = 9.9 \text{ Hz}$, CH₃); δ 39.4 (q, $J_{\text{CP}} = 3.3 \text{ Hz}$, CH₃C); δ 37.9 (dt, $J_{\text{CPaxial}} = 28.0 \text{ Hz}$; $J_{\text{C}^{\text{P}^{\text{equatorial}}}} = 4.0 \text{ Hz}$, CH₂P_{axial}); δ 33.7 (td, $N = (J_{\text{C}^{\text{P}^{\text{equatorial}}}} + J_{\text{C}^{\text{P}^{\text{axial}}}}) = 15.7 \text{ Hz}$; $J_{\text{C}^{\text{P}^{\text{axial}}}} = 5.1 \text{ Hz}$, CH₂P_{equatorial}).

Reaction of [(triphos)Re(CO)₂]BF₄ with H₂. A dichloromethane-d₂ solution of **4** in a 5-mm NMR tube was saturated with dihydrogen at 0 °C. ¹H and ³¹P NMR spectroscopy showed the quantitative formation of **3**.

Reaction of [(triphos)Re(CO)₂]BF₄ with N₂. A similar experiment carried out in a 5-mm NMR tube pressurized with 3 atm of dinitrogen showed no transformation of **4** over 48 h.

Reaction of [(triphos)Re(CO)₂]BF₄ with PPNCl. A slight excess of PPNCl was added to a solution of **4** in dichloromethane-d₂. ¹H and ³¹P NMR spectra showed the quantitative formation of **1**.

Reaction of [(triphos)Re(CO)₂]BF₄ with LiHBEt₃. A slight excess of LiHBEt₃ (1.0 M THF solution) was added to a solution of **4** in THF-d₈. ¹H and ³¹P NMR spectra showed the quantitative transformation into **2**.

Reaction of [(triphos)Re(CO)₂]BF₄ with NaOSO₂CF₃. A slight excess of sodium triflate was added to a solution of **4** in THF-d₈. ¹H and ³¹P NMR spectra showed the quantitative transformation into **5**.

[(triphos)Re(CO)₂(CH₃CN)]BPh₄ (6). HBF₄·OMe₂ (25 μL , ca. 0.26 mmol) was added to a stirred suspension of **2** (0.21 g, 0.25 mmol) in CH₃CN (4.0 mL) cooled to 0 °C with an ice-bath in a Schlenk tube. The resulting pale yellow solution was brought to room temperature and stirred for 15 min. Addition of NaBPh₄ (0.17 g, 0.5 mmol) in 5 mL of ethanol gave an off-white solid. Yield 97%. Anal. Calcd for C₆₉H₆₂BNO₂P₃Re: C, 67.53; H, 5.09; N, 1.14. Found: C, 67.51; H, 5.01; N, 1.10. IR (KBr): $\nu_{\text{COsym}} 1956 \text{ cm}^{-1}$ (s), $\nu_{\text{COantisym}} 1897 \text{ cm}^{-1}$ (s). ³¹P{¹H} NMR (CD₂Cl₂, 22 °C, 81.01 MHz): AM₂ system, $\delta_{\text{A}} -4.41$, $\delta_{\text{M}} -9.28$, $J_{\text{AM}} = 19.7 \text{ Hz}$. ¹H NMR (CD₂Cl₂, 22 °C, 200.13 MHz):

δ 1.08 (s, Re–NCMe, 3H); δ 1.45 (q, J_{HP} = 2.9 Hz, CH₃, 3H); δ 2.25–2.75 (m, CH₂, 6H). $\Lambda_{M(\text{nitroethane})} = 51 \Omega^{-1} \text{ cm}^2 \text{ mol}^{-1}$.

Reaction of [(triphos)Re(CO)₂(CH₃CN)]BPh₄ with H₂. A dichloromethane-*d*₂ solution of **6** in a 5-mm NMR tube was saturated with dihydrogen at 0 °C. ¹H and ³¹P NMR spectroscopy showed the complete stability of **6** over 24 h at room temperature.

[(triphos)Re(CO)₃]BF₄ (7). Method A. Carbon monoxide (1 atm) was bubbled for 5 min into a dichloromethane solution (5 mL) of **4** (0.2 g, 0.20 mmol). Addition of *n*-pentane (5.0 mL) gave off-white microcrystals of **8**; yield 98%.

Method B. The tricarbonyl complex **8** was obtained in comparable yield also by replacing **4** with **3** in the above preparation. Anal. Calcd for C₄₄H₃₉BF₄O₃P₃Re: C, 53.76; H, 4.00; Found: C, 53.79; H, 4.07; IR (KBr): ν_{CO} 2034 cm⁻¹ (m), 1964 and 1955 cm⁻¹ (s, br). ³¹P{¹H} NMR (CD₂Cl₂, 22 °C, 81.01 MHz): A₃ system, δ_A -16.38. ¹H NMR (CD₂Cl₂, 22 °C, 200.13 MHz): δ 1.66 (br s, CH₃, 3H), δ 2.60 (br s, CH₂, 6H).

[(triphos)Re(CO)₂{C=C(H)Ph}]BPh₄ (8). Method A. A dichloromethane (1.0 mL) solution of **4** (0.20 mmol) was prepared in a Schlenk-tube under nitrogen as previously above (*vide supra*). Addition of a slight excess of phenylacetylene (28 μ L, ca. 0.25 mmol) caused an immediate color change from pale yellow to deep violet. The resulting solution was stirred for about 1 h, during which time it was slowly brought to room temperature. Concentration under vacuum to ca. 0.2 mL and addition of *n*-pentane (1.0 mL) gave a lilac powder. The crude product was dissolved in THF (5 mL), and solid NaBPh₄ (0.10 g, 0.29 mmol) was added. Addition of ethanol (3 mL) and slow concentration under nitrogen gave violet crystals of **8**; yield 90%.

Method B. A slight excess of phenylacetylene (26 μ L, ca. 0.23 mmol) was added by syringe to a stirred dichloromethane solution (0.7 mL) of **3** (0.20 g, 0.21 mmol) at -20 °C. Within a few minutes the starting pale yellow color disappeared to produce a violet solution. After stirring for 30 min, addition of NaBPh₄ (0.10 g, 0.29 mmol) in ethanol (5 mL) gave **8**; yield 90%.

Method C. Substitution of the complex **3** for **5** in the above reaction did not change the nature of the final product; yield 95%. Anal. Calcd for C₇₅H₆₅BO₂P₃Re: C, 69.93; H, 5.08. Found: C, 69.82; H, 4.99. IR (KBr): $\nu_{CO_{\text{sym}}}$ 2013 cm⁻¹ (s), $\nu_{CO_{\text{antisym}}}$ 1961 cm⁻¹ (s), ν_{C-C} 1654 cm⁻¹ (m). ³¹P{¹H} NMR (CD₂Cl₂, 22 °C, 81.01 MHz): AM₂ system, δ_A -20.46, δ_M -15.98, J_{AM} = 25.5 Hz. ¹H NMR (CD₂Cl₂, 22 °C, 200.13 MHz): δ 1.75 (q, J_{HP} = 3.0 Hz, CH₃, 3H); δ 2.70 (m, CH₂, 6H), δ 4.23 (q, J_{HP} = 2.9 Hz, CH, 1H); ¹³C{¹H} NMR (CD₂Cl₂, 22 °C, 75.42 MHz): δ 351.0 (dt, $J_{CP_{\text{trans}}}$ = 30.7; $J_{CP_{\text{cis}}}$ = 11.6 Hz, C _{α}); δ 191.6 (AXX'Y spin system, J_{AX} = 47.4 Hz, $J_{AX'}$ = -12.0 Hz, J_{AY} = 8.4 Hz, J_{XY} = 24.9 Hz, CO); δ 116.3 (dt, $J_{CP_{\text{trans}}}$ = 13.3 Hz; $J_{CP_{\text{cis}}}$ = 2.7 Hz, C _{β}); δ 39.8 (q, J_{CP} = 10.9 Hz, CH₃); δ 39.9 (q, J_{CP} = 2.7 Hz, CH₃C); δ 32.7 (m, CH₂P_{axial}); δ 33.2 (br d, J_{CP} = 4.0 Hz, CH₂P_{equatorial}). $\Lambda_{M(\text{nitroethane})} = 55 \Omega^{-1} \text{ cm}^2 \text{ mol}^{-1}$.

[(triphos)Re(CO)₂{C=C(H)CO₂Et}]BPh₄ (9). Complex **9** was prepared as a pink crystalline compound following the methods described above (A–C) by using ethyl propiolate in place of phenylacetylene; yield 95%. Anal. Calcd for C₇₂H₆₅BO₄P₃Re: C, 67.35; H, 5.10. Found: C, 67.25; H, 5.15. IR (KBr): $\nu_{CO_{\text{sym}}}$ 2036 cm⁻¹ (s), $\nu_{CO_{\text{antisym}}}$ 1970 cm⁻¹ (s), ν_{COEt} 1701 cm⁻¹ (m), ν_{COC} 1223 cm⁻¹ (m), ν_{C-C} 1607 cm⁻¹ (m). ³¹P{¹H} NMR (CD₂Cl₂, 22 °C, 81.01 MHz): AM₂ system, δ_A -21.80, δ_M -15.22, J_{AM} = 25.9 Hz. ¹H NMR (CD₂Cl₂, 22 °C, 200.13 MHz): δ 1.32 (t, J_{HP} = 7.1 Hz, CO₂CH₂CH₃, 3H); δ 1.58 (q, J_{HP} = 3.0 Hz, CH₃, 3H); δ 2.62 (m, CH₂, 6H); δ 3.92 (q, J_{HP} = 3.0 Hz, CH, 1H), δ 4.30 (q, J_{HP} = 7.1 Hz, CO₂CH₂CH₃, 2H); ¹³C{¹H} NMR (CD₂Cl₂, 22 °C, 75.42 MHz): δ 339.5 (dt, $J_{CP_{\text{trans}}}$ = 33.8; $J_{CP_{\text{cis}}}$ = 10.6 Hz, C _{α}); δ 189.6 (AXX'Y spin system, J_{AX} = 45.7 Hz, $J_{AX'}$ = -10.0 Hz, J_{AY} = 8.8 Hz, J_{XY} = 25.6 Hz, CO); δ 163.4 (s, COEt); δ 109.2 (dt, $J_{CP_{\text{trans}}}$ = 13.9; $J_{CP_{\text{cis}}}$ = 2.0 Hz, C _{β}); δ 61.6 (br s, OCH₂CH₃); δ 40.0 (q, J_{CP} = 9.9 Hz, CH₃); δ 39.8 (q, J_{CP} = 3.3 Hz, CH₃C); δ 33.5 (br t, J_{CP} = 4.0 Hz, CH₂P_{axial}); δ 32.6 (td, $N = (J_{CP_{\text{equatorial}}} + J_{CP_{\text{equatorial}}'}) = 15.9$

Table 4. Summary of Crystal Data for (triphos)Re(CO)₂H (2)

formula	C ₄₃ H ₄₀ O ₂ P ₃ Re
fw	869.88
cryst size, mm	0.50 × 0.12 × 0.05
temp, K	273
cryst syst	monoclinic
space group	P2 ₁ /n (No. 14)
<i>a</i> , Å	10.447(1)
<i>b</i> , Å	18.199(1)
<i>c</i> , Å	19.729(1)
α , deg	90
β , deg	95.76(1)
γ , deg	90
<i>V</i> , Å ³	3732.0(5)
<i>Z</i>	4
ρ_{calcd} , g cm ⁻³	1.548
abs coeff, cm ⁻¹	0.7861
radiation; λ , Å	graphite-monochromated Cu K α , 1.5418
θ range, deg	4.50 $\leq \theta \leq$ 60.11
<i>F</i> (000)	1744
scan type	ω -2 θ
index ranges	-11 $\leq h \leq$ 11, 0 $\leq k \leq$ 20, 0 $\leq l \leq$ 22
no. of reflns colld	5085
no. of ind reflns	4928 [<i>R</i> _{int} = 0.0290]
refinement method	full-matrix least-squares on <i>F</i> ²
data/restraints/params	4971/0/265
goodness-of-fit on <i>F</i> ²	1.09
final <i>R</i> indices [<i>I</i> > σ (<i>I</i>)]	<i>R</i> ₁ = 0.052, <i>wR</i> ₂ = 0.108
<i>R</i> indices (all data)	<i>R</i> ₁ = 0.056, <i>wR</i> ₂ = 0.114
largest diff peak and hole, e Å ⁻³	0.76 and -1.02

H; $J_{CP_{\text{axial}}} = 5.3$ Hz, CH₂P_{equatorial}), δ 15.1 (s, OCH₂CH₃). $\Lambda_{M(\text{nitroethane})} = 52 \Omega^{-1} \text{ cm}^2 \text{ mol}^{-1}$.

[(triphos)Re(CO)₂{C=C(H)C₆H₁₃}]BPh₄ (10). Complex **10** was obtained as a pink crystalline product by using 1-octyne in the above preparation (Methods A–C); yield 95%. Anal. Calcd for C₇₅H₇₃BO₂P₃Re: C, 69.49; H, 5.68. Found: C, 69.21; H, 5.18. IR (KBr): $\nu_{CO_{\text{sym}}}$ 2007 cm⁻¹ (s), $\nu_{CO_{\text{antisym}}}$ 1952 cm⁻¹ (s), ν_{C-C} 1663 cm⁻¹ (m). ³¹P{¹H} NMR (CD₂Cl₂, 22 °C, 81.01 MHz): AM₂ system, δ_A -18.99, δ_M -15.24, J_{AM} = 24.2 Hz. ¹H NMR (CD₂Cl₂, 22 °C, 200.13 MHz): δ 0.89 (t, J_{HH} = 6.6 Hz, CH₃(hexyl), 3H); δ 1.1–1.3 (m, CH₂(hexyl), 10 H), δ 1.53 (br s, CH₃, 3H), δ 2.38 (m, CH₂, 6H), δ 3.41 (tq, J_{HH} = 8.3 Hz, J_{HP} = 2.8 Hz, CH, 1H); ¹³C{¹H} NMR (CD₂Cl₂, 22 °C, 75.42 MHz): δ 344.6 (dt, $J_{CP_{\text{trans}}} = 32.6$ Hz, $J_{CP_{\text{cis}}} = 9.9$ Hz, C _{α}); δ 191.9 (br m, CO); δ 111.5 (dt, $J_{CP_{\text{trans}}} = 13.3$; $J_{CP_{\text{cis}}} = 2.9$ Hz, C _{β}); δ 40.2 (q, J_{CP} = 10.0 Hz, CH₃); δ 39.9 (q, J_{CP} = 3.2 Hz, CH₃C); δ 32.6 (m, CH₂P_{axial}); δ 33.4 (td, $N = (J_{CP_{\text{equatorial}}} + J_{CP_{\text{equatorial}}'}) = 15.3$ Hz; $J_{CP_{\text{axial}}} = 4.5$ Hz, CH₂P_{equatorial}); δ 32.3, δ 32.2, δ 29.6, δ 23.4, δ 20.3 (all singlets, CH₂(hexyl)); δ 14.6 (s, CH₃(hexyl)). $\Lambda_{M(\text{nitroethane})} = 49 \Omega^{-1} \text{ cm}^2 \text{ mol}^{-1}$.

Reaction of [(triphos)Re(CO)₂(CH₃CN)]BPh₄ with 1-Alkynes. A 3-fold excess of HC≡CR (R = Ph, CO₂Et, C₆H₁₃) was added to a dichloromethane-*d*₂ solution of **6** in a 5-mm NMR tube under nitrogen. ³¹P{¹H} NMR spectroscopy showed that no reaction occurs between **6** and 1-alkynes within 48 h.

X-ray Diffraction Study. A summary of crystal and intensity data for compound **2** is presented in Table 4. Experimental data were collected at room temperature on a Philips PW1100 diffractometer with an upgraded computer control (FEBO system) using graphite-monochromated Cu K α radiation. A set of 25 carefully centered reflections was used for determining the lattice constants. As a general procedure, the intensities of three standard reflections were measured periodically ever 2 h for orientation and intensity control. This procedure did not reveal an appreciable decay of intensities of the specimen. The data were corrected for Lorentz and polarization effects. Atomic scattering factors were those tabulated by Cromer and Waber⁵⁵ with anomalous dispersion

corrections taken from reference 56. An empirical absorption correction was applied *via* a ψ scan procedure. The computational work was performed with a Digital Dec 5000/200 workstation using the programs SIR92⁵⁷ and SHELX-93.⁵⁸ The program ORTEP was also used.⁵⁹ Final atomic coordinates of all atoms and structure factors are provided as supporting information.

Crystals suitable for X-ray diffraction analysis were grown by slow evaporation from a diluted THF–EtOH solution (1:1 v/v). The structure was solved by direct methods using the program SIR92, and all of the non-hydrogen atoms were found through a series of F_o Fourier maps. Refinement was done by full-matrix least-squares calculations, initially with isotropic thermal parameters, and then with anisotropic thermal parameters for Re, P, O, and C with the exception of those pertaining to the phenyl rings. The phenyl rings were treated

as rigid bodies with D_{6h} symmetry and C–C distances fixed at 1.39 Å. Hydrogen atoms bonded to the carbon atoms were introduced in calculated positions using C–H bond values of 0.97 and 0.93 Å for the sp^3 -hybridized carbons and the phenyl rings, respectively. The final Fourier difference map did not show any peak in an acceptable position for a terminal hydride ligand which could be reasonably retained and refined.

Acknowledgment. Thanks are expressed to Mr. Dante Masi for collecting X-ray data and to Dr. Paola Bergamini, University of Ferrara, for NMR technical assistance. Authors thank Progetto Strategico "Tecnologie Chimiche Innovative" C.N.R., Rome Italy, the EU (Contract ERBCHRXCT930147), and MURST, Rome, Italy, for financial support.

(56) *International Tables for X-ray Crystallography*; Kynoch Press: Birmingham, U.K., 1974; Vol. 4, p 99.

(57) Altomare, A.; Burla, M. C.; Camalli, G.; Cascarano, G.; Giacovazzo, C.; Guagliandi, A.; Polidori, G. *J. Appl. Crystallogr.* **1994**, *27*, 435.

(58) Sheldrick, G. M. *SHELX93, Program for Structure Refinement*; University of Göttingen: Göttingen, Germany, 1993.

(59) Johnson, C. K. Technical Report ORNL-5138; Oak Ridge National Laboratory: Oak Ridge, TN, 1976.

Supporting Information Available: Tables of final positional parameters and isotropic and anisotropic displacement parameters for all atoms and bond lengths and angles for **2** (7 pages). Ordering information is given on any current masthead page.

OM950074X

Synthesis of σ,η^2 -Alkynyl-Bridged Bimetallic Complexes Containing *ansa*-Metallocene and Low-Valent Nickel–Monocarbonyl Entities

H. Lang,* S. Blau, B. Nuber, and L. Zsolnai

Ruprecht-Karls-Universität Heidelberg, Anorganisch-Chemisches Institut, Im Neuenheimer Feld 270, D-69120 Heidelberg, Germany

Received February 7, 1995[®]

The reaction of the *ansa*-titanocene dichlorides $[(\eta^5\text{-C}_5\text{H}_3\text{R}^1)(\eta^5\text{-C}_5\text{H}_3\text{R}^2)\text{SiMeR}^3]\text{TiCl}_2$ (**1a**, $\text{R}^1 = \text{R}^2 = \text{H}$, $\text{R}^3 = \text{Me}$; **1b**, $\text{R}^1 = \text{H}$, $\text{R}^2 = \text{SiMe}_3$, $\text{R}^3 = \text{Me}$; **1c**, $\text{R}^1 = \text{R}^2 = \text{SiMe}_3$, $\text{R}^3 = \text{Ph}$) with 2 equiv of $\text{LiC}\equiv\text{CSiMe}_3$ (**2**) yields the bis(alkynyl) *ansa*-titanocenes $[(\eta^5\text{-C}_5\text{H}_3\text{R}^1)(\eta^5\text{-C}_5\text{H}_3\text{R}^2)\text{SiMeR}^3]\text{Ti}(\text{C}\equiv\text{CSiMe}_3)_2$ (**3a**, $\text{R}^1 = \text{R}^2 = \text{H}$, $\text{R}^3 = \text{Me}$; **3b**, $\text{R}^1 = \text{H}$, $\text{R}^2 = \text{SiMe}_3$, $\text{R}^3 = \text{Me}$; **3c**, $\text{R}^1 = \text{R}^2 = \text{SiMe}_3$, $\text{R}^3 = \text{Ph}$). These compounds react with $\text{Ni}(\text{CO})_4$ (**4**) to afford $\{[(\eta^5\text{-C}_5\text{H}_3\text{R}^1)(\eta^5\text{-C}_5\text{H}_3\text{R}^2)\text{SiMeR}^3]\text{Ti}(\text{C}\equiv\text{CSiMe}_3)_2\}\text{Ni}(\text{CO})$ (**5a**, $\text{R}^1 = \text{R}^2 = \text{H}$, $\text{R}^3 = \text{Me}$; **5b**, $\text{R}^1 = \text{H}$, $\text{R}^2 = \text{SiMe}_3$, $\text{R}^3 = \text{Me}$; **5c**, $\text{R}^1 = \text{R}^2 = \text{SiMe}_3$, $\text{R}^3 = \text{Ph}$) in high yields. Compounds **5a–c** contain a low-valent nickel-monocarbonyl fragment, which is stabilized by the chelating effect of both alkynyl ligands of **3**. In contrast, the *ansa*-zirconocene dichloride $[(\eta^5\text{-C}_5\text{H}_4)(\eta^5\text{-C}_5\text{H}_3\text{SiMe}_3)\text{SiMe}_2]\text{ZrCl}_2$ (**6**) leads with 2 equiv of $\text{LiC}\equiv\text{CSiMe}_3$ (**2**) to a variety of reaction products, of which the σ,η^2 -doubly alkynyl-bridged dinuclear zirconocene $\{[(\eta^5\text{-C}_5\text{H}_4)(\eta^5\text{-C}_5\text{H}_3\text{SiMe}_3)\text{SiMe}_2]\text{Zr}(\text{C}\equiv\text{CSiMe}_3)_2\}_2$ (**7**) can be crystallized. Compound **7** can be synthesized in much better yields by reacting **6** first with $\text{LiC}\equiv\text{CSiMe}_3$ and secondly with *n*-butyllithium; a possible mechanism for the formation of **7** will be discussed. In **7** the alkynyl ligands act both as σ - and π -donors. Compound **7** contains two formal Zr^{III} centers. The X-ray structure analyses of **1b**, **3a**, and **7** are reported. Crystals of **1b** and **3a** are monoclinic, space group $P2_1/n$ (**1b**) and $P2_1/a$ (**3a**): **1b**, cell constants $a = 7.516(2)$ Å, $b = 19.862(6)$ Å, $c = 12.275(3)$ Å, $\beta = 91.47(2)^\circ$, $V = 1831.8$ Å³, and $Z = 4$; **3a**, cell constants $a = 10.786(6)$ Å, $b = 20.01(2)$ Å, $c = 11.88(2)$ Å, $\beta = 99.86(9)^\circ$, $V = 2526.2$ Å³, and $Z = 4$. Complex **7** crystallizes in the triclinic space group $P\bar{1}$ with the cell constants $a = 12.354(6)$ Å, $b = 19.15(1)$ Å, $c = 20.28(1)$ Å, $\alpha = 68.59(5)^\circ$, $\beta = 89.30(5)^\circ$, $\gamma = 86.77(5)^\circ$, $V = 4458.1$ Å³, and $Z = 4$. The properties of the MeRSi-bridged titanocenes **3** and **5** in comparison to the appropriate unbridged species are discussed.

Introduction

Recently, we described the application of 1-titanopenta-1,4-diyne $\text{Me}_3\text{SiC}\equiv\text{C}-[\text{Ti}]-\text{C}\equiv\text{CSiMe}_3$ $\{[\text{Ti}] = (\eta^5\text{-C}_5\text{H}_4\text{SiMe}_3)_2\text{Ti}\}$ as an organometallic chelating ligand (organometallic π -tweezers) for the stabilization of low-valent $\text{M}(\text{CO})$ moieties ($\text{M} = \text{Ni},^{1,2} \text{Co}^{2,3}$) as well as monomeric MX ($\text{M} = \text{Cu}, \text{Ag};^{4-7} \text{X} =$ singly bonded inorganic or organic ligand) and MCl_2 ($\text{M} = \text{Fe}, \text{Co}, \text{Ni}^{8,9}$) entities. In the so-assembled $[(\eta^5\text{-C}_5\text{H}_4\text{SiMe}_3)_2\text{Ti}(\text{C}\equiv\text{CSiMe}_3)_2]\text{ML}_n$ species both alkynyl ligands of the $(\eta^2\text{-C}\equiv\text{CSiMe}_3)_2\text{ML}_n$ entity are η^2 -coordinated to a monomeric ML_n building block. The most striking fea-

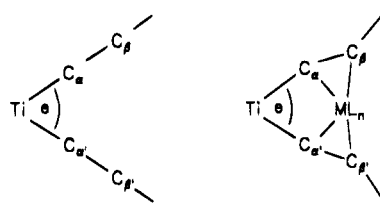


Figure 1. Schematic representation of $(\eta^5\text{-C}_5\text{H}_4\text{SiMe}_3)_2\text{Ti}(\text{C}\equiv\text{CSiMe}_3)_2$ (left) and $[(\eta^5\text{-C}_5\text{H}_4\text{SiMe}_3)_2\text{Ti}(\text{C}\equiv\text{CSiMe}_3)_2]\text{ML}_n$ (right).

ture about this coordination mode is the decrease of the bite angle θ ($\text{C}_\alpha\text{-Ti-C}_{\alpha'}$) of the bis(alkynyl) titanocene fragment,^{1–9} which results in a *trans*-deformation of the $\text{Ti-C}\equiv\text{C-Si}$ unit, due to the tweezers effect of the $[\text{Ti}]-(\text{C}\equiv\text{CSiMe}_3)_2$ moiety (Figure 1).

The bite angle θ , which provides a suitable geometry for the η^2 -coordination of the $\text{Me}_3\text{SiC}\equiv\text{C}$ ligands to monomeric ML_n species, should be decisively influenced by changing from unbridged to, e.g., silyl-bridged cyclopentadienyl ligands, a context already established for unbridged metallocene dichlorides and their appropriate bridged derivatives by Brintzinger et al.¹⁰

(10) Smith, J. A.; v. Seyerl, J.; Huttner, G.; Brintzinger, H. H. *J. Organomet. Chem.* **1979**, *173*, 175 and literature cited therein.

[®] Abstract published in *Advance ACS Abstracts*, June 1, 1995.
(1) (a) Yasufuku, K.; Yamazaki, H. *Bull. Chem. Soc. Jpn.* **1972**, *45*, 2664. (b) Lang, H.; Herres, M.; Imhof, W. *J. Organomet. Chem.* **1994**, *465*, 283.

(2) Lang, H.; Imhof, W. *Chem. Ber.* **1992**, *125*, 1307.

(3) Lang, H.; Herres, M.; Zsolnai, L. *Bull. Chem. Soc. Jpn.* **1993**, *66*, 429.

(4) Lang, H.; Köhler, K.; Blau, S. *Coord. Chem. Rev.* **1995**, in press, and literature cited therein.

(5) Janssen, M. D.; Herres, M.; Dedieu, A.; Spek, A. L.; Grove, D. M.; Lang, H.; van Koten, G. *J. Chem. Soc., Chem. Commun.*, in press.

(6) Janssen, M. D.; Herres, M.; Zsolnai, L.; Dedieu, A.; Spek, A. L.; Grove, D. M.; Lang, H.; van Koten, G. *Inorg. Chem.*, Submitted for publication.

(7) Lang, H.; Herres, M.; Zsolnai, L. *Organometallics* **1993**, *12*, 5008.

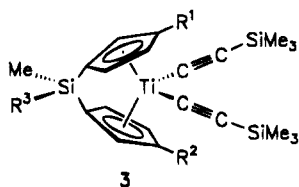
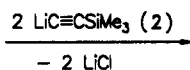
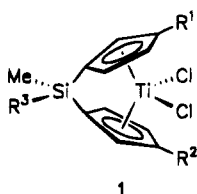
(8) Lang, H.; Herres, M.; Zsolnai, L.; Imhof, W. *J. Organomet. Chem.* **1991**, *409*, C7.

(9) Herres, M.; Lang, H. *J. Organomet. Chem.* **1994**, *480*, 235.

In this respect, we describe the synthesis of bis-(alkynyl) *ansa*-metallocenes and their suitability for the stabilization of low-valent nickel–monocarbonyl building blocks.

Results and Discussion

Bis(alkynyl) *ansa*-Titanocenes. $[(\eta^5\text{-C}_5\text{H}_3\text{R}^1)(\eta^5\text{-C}_5\text{H}_3\text{R}^2)\text{SiMeR}^3]\text{TiCl}_2$ (**1a**, $\text{R}^1 = \text{R}^2 = \text{H}$, $\text{R}^3 = \text{Me}$; **1b**, $\text{R}^1 = \text{H}$, $\text{R}^2 = \text{SiMe}_3$, $\text{R}^3 = \text{Me}$; **1c**, $\text{R}^1 = \text{R}^2 = \text{SiMe}_3$, $\text{R}^3 = \text{Ph}$)¹² reacts with 2 equiv of $\text{LiC}\equiv\text{CSiMe}_3$ (**2**) in Et_2O at 25 °C to yield the bis(alkynyl) *ansa*-titanocenes **3a–c**, the only isolated products obtained by extraction of the reaction residues with *n*-pentane, followed by filtration through a pad of Celite.



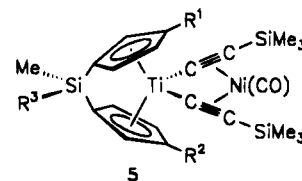
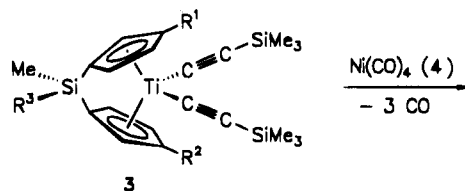
- 1a, 3a:** $\text{R}^1 = \text{R}^2 = \text{H}$, $\text{R}^3 = \text{Me}$
1b, 3b: $\text{R}^1 = \text{H}$, $\text{R}^2 = \text{SiMe}_3$, $\text{R}^3 = \text{Me}$
1c, 3c: $\text{R}^1 = \text{R}^2 = \text{SiMe}_3$, $\text{R}^3 = \text{Ph}$

Complexes **3a** and **3c** were isolated as orange air stable solids, while **3b** was obtained as an oil which decomposes on prolonged exposition to air. Compounds **3a–c** are soluble in most polar and nonpolar organic solvents.

Treatment of **3a–c** with equimolar amounts of $\text{Ni}(\text{CO})_4$ at 25 °C in toluene affords in 87%–95% yield the appropriate golden-brown complexes $\{[(\eta^5\text{-C}_5\text{H}_3\text{R}^1)(\eta^5\text{-C}_5\text{H}_3\text{R}^2)\text{SiMeR}^3]\text{Ti}(\text{C}\equiv\text{CSiMe}_3)_2\}\text{Ni}(\text{CO})$ (**5a**, $\text{R}^1 = \text{R}^2 = \text{H}$, $\text{R}^3 = \text{Me}$; **5b**, $\text{R}^1 = \text{H}$, $\text{R}^2 = \text{SiMe}_3$, $\text{R}^3 = \text{Me}$; **5c**, $\text{R}^1 = \text{R}^2 = \text{SiMe}_3$, $\text{R}^3 = \text{Ph}$), which are soluble in *n*-pentane.

In **5a–c** a low-valent nickel–monocarbonyl building block is stabilized by the η^2 -coordination of both $\text{Me}_3\text{SiC}\equiv\text{C}$ ligands of the bis(alkynyl) *ansa*-titanocene fragment $[(\eta^5\text{-C}_5\text{H}_3\text{R}^1)(\eta^5\text{-C}_5\text{H}_3\text{R}^2)\text{SiMeR}^3]\text{Ti}$. Low-valent NiL moieties ($\text{L} = \text{CO}$, PMe_3) could be independently stabilized by using tripodal ligands of type $\text{XM}'(\text{OCH}_2\text{PMe}_2)_n(\text{CH}_2\text{CH}_2\text{PMe}_2)_{3-n}$ ($\text{M}' = \text{Si}$, Ge , $n = 0\text{--}3$)^{11a} and 1,6-heptadiyne.^{11b}

The ^1H NMR and ^{13}C NMR spectra of **1**, **3**, and **5** consist of sharp and well-resolved signals for each of the organic groupings present. The most informative feature about the ^1H NMR spectra is the appearance of



- 3a, 5a:** $\text{R}^1 = \text{R}^2 = \text{H}$, $\text{R}^3 = \text{Me}$
3b, 5b: $\text{R}^1 = \text{H}$, $\text{R}^2 = \text{SiMe}_3$, $\text{R}^3 = \text{Me}$
3c, 5c: $\text{R}^1 = \text{R}^2 = \text{SiMe}_3$, $\text{R}^3 = \text{Ph}$

an AA'XX' resonance pattern for compounds **1a**, **3a**, and **5a**, while in **1b**, **3b**, and **5b** an ABX ($\eta^5\text{-C}_5\text{H}_3\text{SiMe}_3$) as well as an ABXY ($\eta^5\text{-C}_5\text{H}_4$) resonance pattern for the cyclopentadienyl protons in the δ 5.1–7.5 region is observed.¹² In compounds **1c**, **3c**, and **5c**, which contain exclusively ($\eta^5\text{-C}_5\text{H}_3\text{SiMe}_3$) cyclopentadienyl ligands, only ABX resonance patterns appear.¹²

For the MeRSi links ($\text{R} = \text{Me}$, Ph) the ^1H NMR spectra show the expected simplicity with the resonance signals of the methyl groups at around δ 0.4 and 0.9 as well as of the phenyl protons in the δ 7.3–7.9 region. As expected for the symmetrically substituted compounds **1a**, **3a**, and **5a** the methyl groups of the Me_2Si links are equivalent, whereas in the unsymmetrically substituted metallocenes **1b**, **3b**, and **5b** two resonance signals are observed.

Due to the η^2 -coordination of the $\text{Me}_3\text{SiC}\equiv\text{C}$ units to the nickel atom in **5a–c** the ^{13}C NMR signals of the C_α atoms in the $\text{Ti}(\text{C}\equiv\text{CSiMe}_3)_2$ entity (at about δ 170 in **3a,b**) shift downfield (at δ 190 in **5b,c**), a phenomenon typical for this type of compounds.^{2–10} The resonance signals for the C_β atoms could not be clearly assigned, since they appear in the cyclopentadienyl and phenyl region. The carbon atom of the nickel-bonded carbonyl ligand in **5a–c** shows a resonance signal at δ 200–204.

A much better hint for the η^2 -coordination of both $\text{Me}_3\text{SiC}\equiv\text{C}$ ligands to the $\text{Ni}(\text{CO})$ building block is given by the IR spectra. The $\text{C}\equiv\text{C}$ stretching vibration at about 2015 cm^{-1} in **3a–c** is shifted to lower wavenumbers in **5** (**5a,b**, 1834 cm^{-1} ; **5c**, 1831 cm^{-1}), thus indicating a weakening of the $\text{C}\equiv\text{C}$ triple bonds of the alkynyl ligands. This observation is generally made by changing from noncoordinating to η^2 -coordinating $\text{Me}_3\text{SiC}\equiv\text{C}$ ligands and is in agreement with the increasing participation of the back-bonding component in alkyne-to-nickel bondings.^{1–3} The CO stretching vibration in **5a–c** is observed at 1995 cm^{-1} (**5a,b**) and 2003 cm^{-1} (**5c**), respectively (for comparison, the CO -stretching frequency of $\text{Ni}(\text{CO})_4$ is 2052 cm^{-1}).

These spectroscopic data, given for the silyl-bridged titanocenes **5a–c**, are in agreement with those found for their unbridged equivalents.^{1,2} However, the latter compounds are stable in the solid state as well as in solution, while compounds **5a–c** tend to decompose in solution. This empirical observation has to be regarded in respect of the different bridging situations that may have an important influence on the specific geometrical properties of the molecules.

(11) (a) Grobe, J.; Krummen, N.; Wehmschulte, R.; Krebs, B.; Läge, M. Z. Anorg. Allg. Chem. 1994, 620, 1645. (b) Proft, B., Pörschke, K.-R.; Lutz, F.; Krüger, C. Chem. Ber. 1994, 127, 653.

(12) Compounds **1a–c** (Blau, S.; Zsolnai, L.; Neugebauer, U.; Weiss, K.; Lang, H. Manuscript in preparation) were prepared according to well-established procedures by H. H. Brintzinger and H. Köpf. For detailed information see, for example: (a) Wiesenfeldt, H.; Reinmuth, A.; Barsties, E.; Evertz, K.; Brintzinger, H. H. J. Organomet. Chem. 1989, 369, 359 and literature cited therein. (b) Smith, J. A.; v. Seyerl, J.; Huttner, G.; Brintzinger, H. H. J. Organomet. Chem. 1979, 173, 175. (c) Klouras, N.; Köpf, H. Monatsh. Chem. 1981, 112, 887 and literature cited therein. (d) Köpf, H.; Kahl, W. J. Organomet. Chem. 1974, 64, C37.

To reinforce this statement, X-ray structure analyses were carried out on single crystals of **1b**, **3a**, and **5c**. The structures of **1b** and **3a** are shown in Figure 2; crystallographic parameters and selected geometrical details are listed in Tables 1–5. The needle-like habitus of the crystals of **5c** resulted in *R*-values in the 20% region. For this reason the interatomic bond distances and angles of **5c** are only given for comparison.¹³

Compound **1b** crystallizes in the monoclinic space group $P2_1/n$, whereas **3a** crystallizes in the monoclinic space group $P2_1/a$. The geometrical environment of the Ti(1) center in **1b** is fixed by the arrangement of the two chloro groups [Cl(1), Cl(2)] and the η^5 -coordinated silyl-bridged cyclopentadienyl ligands. In comparison to their unbridged equivalents, in which the same grouping of ligands is present, different D1–Ti(1)–D2 (D1, D2 = centroids of the cyclopentadienyl ligands) and Cl(1)–Ti(1)–Cl(2) angles are found (Table 2). As is typical for these molecules,¹² the D1–Ti(1)–D2 angle decreases slightly by changing from $(\eta^5\text{-C}_5\text{H}_4\text{SiMe}_3)_2\text{-TiCl}_2$ ¹⁴ (131.0°) to **1b** (128.8°), simultaneously increasing the Cl(1)–Ti(1)–Cl(2) angle from 91.63°¹⁴ [in unbridged $(\eta^5\text{-C}_5\text{H}_4\text{SiMe}_3)_2\text{-TiCl}_2$] to 97.4(1)° in **1b** (Table 2).

Replacement of the chloro groups in $(\eta^5\text{-C}_5\text{H}_4\text{SiMe}_3)_2\text{-TiCl}_2$ and $[(\eta^5\text{-C}_5\text{H}_3\text{R}^1)(\eta^5\text{-C}_5\text{H}_3\text{R}^2)\text{SiMeR}^3]\text{TiCl}_2$ (**1**) by alkynyl building blocks leads to the formation of the appropriate bis(alkynyl) titanocenes $(\eta^5\text{-C}_5\text{H}_4\text{SiMe}_3)_2\text{-Ti}(\text{C}\equiv\text{CSiMe}_3)_2$ ⁷ and $[(\eta^5\text{-C}_5\text{H}_3\text{R}^1)(\eta^5\text{-C}_5\text{H}_3\text{R}^2)\text{SiMeR}^3]\text{-Ti}(\text{C}\equiv\text{CSiMe}_3)_2$ (**3**). As in compound $(\eta^5\text{-C}_5\text{H}_4\text{SiMe}_3)_2\text{-Ti}(\text{C}\equiv\text{CSiMe}_3)_2$,^{7,15} the bis(alkynyl) *ansa*-titanocene **3a** exhibits linear Ti–C≡C–Si units (Table 3). Compared

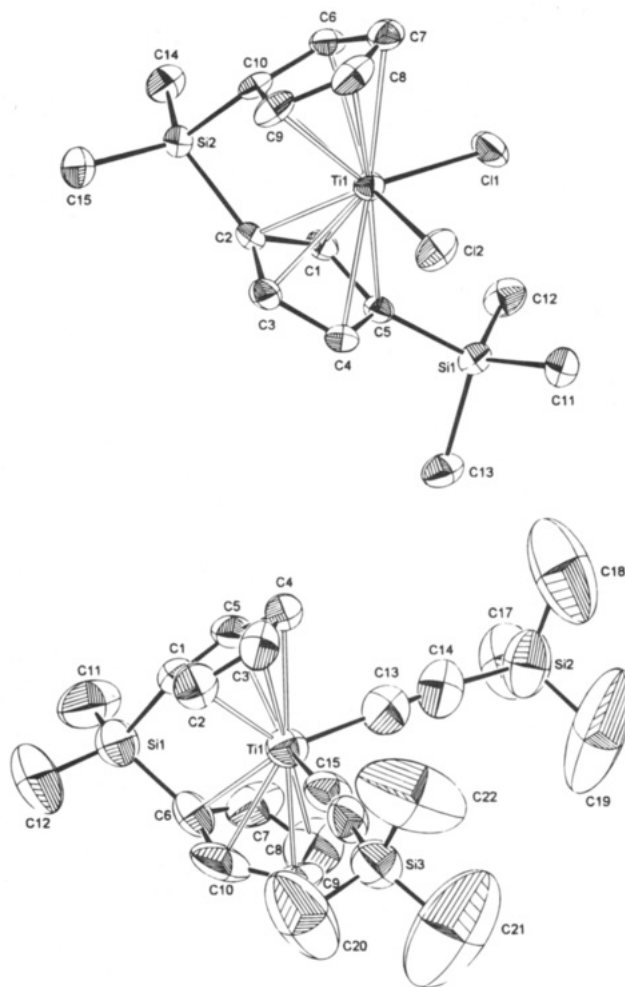


Figure 2. ORTEP drawings (drawn at 50% probability level) of **1b** (top) and **3a** (bottom) (with exclusion of the hydrogen atoms) with the atom numbering schemes.

to the titanocene dichlorides $(\eta^5\text{-C}_5\text{H}_4\text{SiMe}_3)_2\text{-TiCl}_2$ ¹⁴ and $[(\eta^5\text{-C}_5\text{H}_4)(\eta^5\text{-C}_5\text{H}_3\text{SiMe}_3)\text{SiMe}_2]\text{-TiCl}_2$ (**1b**) the angle D1–Ti–D2 (D1, D2 = centroids of the cyclopentadienyl ligands) in the bis(alkynyl) compounds is even more reduced in size (Tables 2 and 3). However, the angle $\text{C}_\alpha\text{-Ti-C}_\alpha'$ (Figure 1) does not depend on the bridging situation of the cyclopentadienyl ligands.

The interatomic distances of the C≡C moieties in **3a** [C(13)–C(14), 1.20(2) Å; C(15)–C(16), 1.21(2) Å] correspond to typical C≡C separations found in organic as well as organometallic alkynes (e.g., HC≡CH 1.21 Å;¹⁶ $\text{Me}_2\text{InC}\equiv\text{CMe}$, 1.207(2) Å;¹⁷ $[(\eta^5\text{-C}_5\text{Me}_5)_2\text{SmC}\equiv\text{C}^t\text{Bu}]_2$, 1.209(8) Å;¹⁸ $[(\text{Me}_3\text{N})(\text{MeC}\equiv\text{C})\text{Be}(\mu\text{-C}\equiv\text{CMe})_2]$, 1.198(5) Å;¹⁹ $(\eta^5\text{-C}_5\text{H}_5)_2\text{Zr}(\mu\text{-}\eta^1\text{-}\eta^2\text{-MeC}\equiv\text{CC}_6\text{H}_{11})(\mu\text{-C}\equiv\text{C-C}_6\text{H}_{11})\text{AlMe}_2$, 1.195(6) Å;²⁰ $(\eta^5\text{-C}_5\text{H}_4\text{SiMe}_3)_2\text{-Ti}(\text{C}\equiv\text{C-SiMe}_3)_2$, 1.203(9) Å, 1.214(6) Å⁷ (Table 3)). The Ti(1)–C(13) and Ti(1)–C(15) distances at 2.08(1) and 2.08(2) Å in **3a** are similar to those found in $(\eta^5\text{-C}_5\text{H}_4\text{SiMe}_3)_2\text{-Ti}(\text{C}\equiv\text{C-SiMe}_3)_2$.

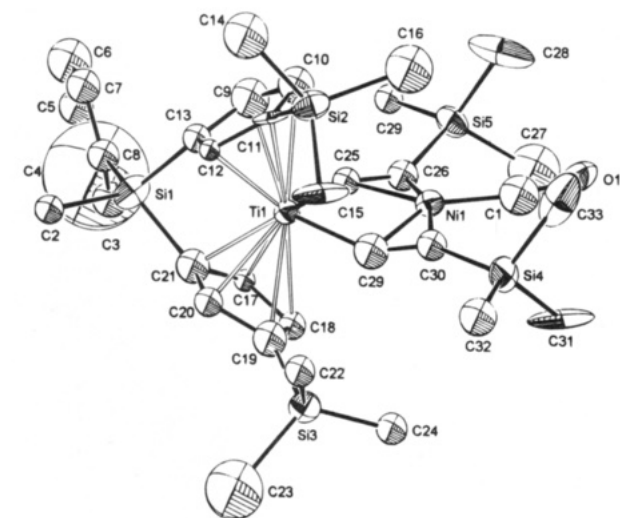
(16) Dale, J. Properties of Acetylenic Compounds. In *Chemistry of Acetylenes*; Viehe, H. G., Ed.; Marcel Dekker: New York, 1969; p 53.

(17) Fries, W.; Schwarz, W.; Hausen, H.-D.; Weidlein, J. *J. Organomet. Chem.* **1978**, *159*, 373. See also: Stucky, G. D.; McPherson, A. M.; Rhine, W. E.; Eisch, J. J.; Considine, J. L. *J. Am. Chem. Soc.* **1974**, *96*, 1941.

(18) Evans, W. J.; Keyer, R. A.; Ziller, J. W. *Organometallics* **1993**, *12*, 2618.

(19) Bell, N. A.; Nowell, J. W.; Coates, G. E.; Shearer, H. M. M. *J. Organomet. Chem.* **1984**, *273*, 179.

(20) Erker, G.; Albrecht, M.; Krüger, C.; Nolte, M.; Werner, S. *Organometallics* **1993**, *12*, 4979.



Selected bond lengths [Å] and angles [deg] (average values) are as follows: Ti–C_α, 2.1 Å; C_α–C_β, 1.28 Å; Ti–Ni, 2.85 Å; Ni–MP(C≡C), 1.89 Å (MP = mid-points of the alkynyl ligands C_α–C_β); C_α–Ti–C_α, 92°; Ti–C_α–C_β, 152°; C_α–C_β–Si, 145°; D1–Ti–D2, 130.6° (D1, D2 = centroids of the cyclopentadienyl ligands).

(14) Klouras, N.; Nastopoulos, V. *Monatsh. Chem.* **1991**, *122*, 551.

(15) Lang, H.; Seyferth, D. *Z. Naturforsch.* **1990**, *45b*, 212.

Table 1. Crystallographic Parameters for 1b, 3a, and 7

	1b	3a	7
formula	C ₁₅ H ₂₂ Cl ₂ Si ₂ Ti	C ₂₂ H ₃₂ Si ₃ Ti	C ₄₀ H ₆₂ Si ₆ Zr ₂
fw	377.30	428.63	893.89
cryst syst	monoclinic	monoclinic	triclinic
space group	P2 ₁ /n (No. 14)	P2 ₁ /a (No. 14)	P1 (No. 2)
a, Å	7.516(2)	10.786(6)	12.354(6)
b, Å	19.862(6)	20.01(2)	19.15(1)
c, Å	12.275(3)	11.88(2)	20.28(1)
α , deg			68.59(5)
β , deg	91.47(2)	99.86(9)	89.30(5)
γ , deg			86.77(5)
V, Å ³	1831.8	2526.2	4458.1
ρ_{calcd} , g cm ⁻³	1.1	1.13	1.33
Z	4	4	4
cryst size, mm ³	0.30 × 0.25 × 0.25	0.25 × 0.30 × 0.50	0.3 × 0.3 × 0.25
diff model	Siemens R3m/V	Siemens R3m/V	Siemens R3m/V
μ , mm ⁻¹	0.04	0.48	0.04
radiation (λ , Å)	Mo K α (0.710 73)	Mo K α (0.710 73)	Mo K α (0.710 73)
temp, K	198	276	190
scan mode	ω -scan	ω -scan	ω -scan
scan range $\Delta\omega$, deg	0.75	1.2	0.65
scan speed, deg min ⁻¹	2.4–29.3	3–29.3	7–29.3
2 θ range, deg	2.0–45.0	3.0–48	2.5–42.1
index ranges	0 ≤ h ≤ 8 0 ≤ k ≤ 21 –13 ≤ l ≤ 13	0 ≤ h ≤ 13 0 ≤ k ≤ 23 –14 ≤ l ≤ 14	–12 ≤ h ≤ 12 –19 ≤ k ≤ 19 –20 ≤ l ≤ 20
no. of unique data	2369	4109	9555
no. obsd	2128 [I ≥ 2.0 σ (I)]	1631 [I ≥ 2.5 σ (I)]	7270 [I ≥ 2.0 σ (I)]
no. refined params	185	236	975
R ₁ ^a	0.027	0.097	0.041
R _w , wR ₂ ^b	0.025	0.076	0.124

^a R₁ = $[\sum||F_o| - |F_c|| / \sum|F_o|]$ only for observed reflections. ^b 1b, 3a: R_w = $[\sum||F_o| - |F_c||w^{0.5}] / \sum|F_o|w^{0.5}$. 7: wR₂ = $[\sum|F_o|^2 - F_c^2| / \sum[w(F_o^2)^2]^{0.5}$ for all reflections.

Table 2. Selected Bond Lengths (Å) and Angles (deg) for [(η^5 -C₅H₄)(η^5 -C₅H₃SiMe₃)SiMe₂]₂TiCl₂ (1b) and Its Unbridged Equivalent, (η^5 -C₅H₄SiMe₃)₂TiCl₂¹⁴

	1b	(η^5 -C ₅ H ₄ SiMe ₃) ₂ TiCl ₂ ¹⁴
Bond Lengths		
Ti(1)–Cl(1)	2.345(1)	2.367(1)
Ti(1)–Cl(2)	2.344(1)	2.362(1)
C(2)–Si(2)	1.859(3)	
C(10)–Si(2)	1.863(3)	
D1–Ti(1) ^a	2.078	2.063
D2–Ti(1) ^a	2.068	2.061
Angles		
Cl(1)–Ti(1)–Cl(2)	97.4(1)	91.63
C(2)–Si(2)–C(10)	90.1(1)	
D1–Ti(1)–D2 ^a	128.8	131.0

^a D1, D2 = centroids of the cyclopentadienyl ligands

Ti(C≡CSiMe₃)₂⁷ (Table 3) but are remarkably shorter than those titanium-to-carbon bonds involving sp³-hybridized carbon atoms, as found in, e.g., (η^5 -C₅H₅)₂Ti(CH₂Ph)₂, 2.239(6) and 2.210(5) Å;²¹ (η^5 -C₅H₅)₂TiMe₂, 2.170(2) and 2.181(2) Å;²² (η^5 -C₅H₄SiMe₃)Ti(Cl)(CH₂-SiMe₃), 2.209(6) Å;²³ and (η^5 -C₉H₇)₂TiMe₂, 2.21(2) Å.²⁴ These data indicate some π -conjugation between the d⁰-configured 16-valence electron titanocene fragment and the π -system of the organic alkynyl ligands C≡CSiMe₃ in 3a due to a conjugative interaction of a vacant orbital available at the metallocene fragment²⁵ with the π -systems of the adjacently bonded alkynyl

Table 3. Selected Bond Lengths (Å) and Angles (deg) for [(η^5 -C₅H₄)₂SiMe₂]₂Ti(C≡CSiMe₃)₂ (3a) and Its Unbridged Equivalent, (η^5 -C₅H₄SiMe₃)₂Ti(C≡CSiMe₃)₂⁷

	3a	(η^5 -C ₅ H ₄ SiMe ₃) ₂ Ti(C≡CSiMe ₃) ₂ ⁷
Bond Lengths		
Ti(1)–C(13)	2.08(2)	2.124(5)
Ti(1)–C(15)	2.08(1)	2.103(5)
C(13)–C(14)	1.20(2)	1.214(6)
C(15)–C(16)	1.21(2)	1.203(9)
C(1)–Si(1)	1.87(1)	
C(6)–Si(1)	1.83(2)	
D1–Ti(1) ^a	2.03	2.06
D2–Ti(1) ^a	2.04	2.05
Angles		
C(13)–Ti(1)–C(15)	100.8(5)	102.8(2)
Ti(1)–C(13)–C(14)	176(1)	178.2(5)
Si(2)–C(14)–C(13)	176(1)	178.3(5)
Ti(1)–C(15)–C(16)	177(1)	175.8(4)
Si(3)–C(16)–C(15)	178(1)	174.8(4)
C(1)–Si(1)–C(6)	91.9(7)	
D1–Ti(1)–D2 ^a	128.8	134.7

^a D1, D2 = centroids of the cyclopentadienyl ligands.

ligands. As a consequence the bite angles C(13)–Ti(1)–C(15) in 3a (100.8(5)°) as well as in (η^5 -C₅H₄SiMe₃)₂Ti(C≡CSiMe₃)₂⁷ (102.8(2)°) are significantly larger than those found in complexes containing Ti–C(sp³) σ -bonds, e.g., (η^5 -C₅H₅)₂TiMe₂, 91.2(1)°;²² (η^5 -C₅H₄SiMe₃)₂Ti(Cl)(CH₂SiMe₃), 92.8(2)°;²³ (η^5 -C₉H₇)₂TiMe₂, 93.5(2)°;²⁴ (η^5 -C₅H₅)₂Ti(CH₂Ph)₂, 91.0(2)°.²¹

As is typical for [(η^5 -C₅H₄SiMe₃)₂Ti(C≡CSiMe₃)₂]ML_n compounds it is found that the Ni(CO) entity in 5a–c is stabilized by the η^2 -coordination of both alkynyl ligands in 3a–c.¹³ As result, the linear Ti–C≡C–SiMe₃ units in 3a are deformed. The tweezers effect of the bis(alkynyl) *ansa*-titanocene induces a *trans*-deformation of the Ti–C≡C–Si moieties (for comparison, see

(21) Scholz, J.; Rehbaum, F.; Thiele, K.-H.; Goddard, R.; Betz, P.; Krüger, K.-H. *J. Organomet. Chem.* **1993**, *443*, 93.

(22) Thewalt, U.; Wöhrlé, T. *J. Organomet. Chem.* **1994**, *464*, C17.

(23) Lang, H.; Blau, S.; Nuber, B. Manuscript in preparation.

(24) Atwood, J. L.; Hunter, W. E.; Hrnčir, D. C.; Samuel, E.; Alt, H.; Rausch, M. D. *Inorg. Chem.* **1975**, *14*, 1757.

(25) Erker, G.; Frömberg, W.; Benn, R.; Mynott, R.; Angermund, K.; Krüger, C. *Organometallics* **1989**, *8*, 911.

Table 4. Atomic Coordinates and Equivalent Isotropic Displacement Parameters (Å²) for 1b^a

atom	x/a	y/b	z/c	U(eq) ^a
Ti(1)	0.12119(6)	0.74463(3)	0.74416(4)	0.023
Cl(1)	0.2569(1)	0.67239(4)	0.87249(6)	0.039
Cl(2)	-0.17094(9)	0.70555(4)	0.76172(7)	0.041
Si(1)	0.2650(1)	0.56430(4)	0.65426(7)	0.028
Si(2)	0.3461(1)	0.85839(4)	0.60931(6)	0.026
C(1)	0.3521(4)	0.7108(1)	0.6296(2)	0.024
C(2)	0.2767(4)	0.7699(1)	0.5832(2)	0.026
C(3)	0.0984(4)	0.7518(1)	0.5530(2)	0.031
C(4)	0.0744(4)	0.6827(1)	0.5756(2)	0.029
C(5)	0.2301(4)	0.6559(1)	0.6238(2)	0.023
C(6)	0.2851(4)	0.8297(1)	0.8382(2)	0.029
C(7)	0.1416(4)	0.8162(2)	0.9061(2)	0.037
C(8)	-0.0125(4)	0.8344(2)	0.8496(3)	0.042
C(9)	0.0327(4)	0.8583(1)	0.7461(3)	0.034
C(10)	0.2221(3)	0.8583(1)	0.7388(2)	0.025
C(11)	0.0767(4)	0.5307(2)	0.7332(2)	0.038
C(12)	0.4860(4)	0.5508(2)	0.7232(2)	0.040
C(13)	0.2591(4)	0.5226(2)	0.5180(2)	0.040
C(14)	0.5878(4)	0.8667(2)	0.6375(2)	0.037
C(15)	0.2518(4)	0.9173(2)	0.5069(2)	0.049

^a U(eq) is defined as one-third of the trace of the orthogonalized U_{ij} tensor.

Table 5. Atomic Coordinates (×10⁴) and Equivalent Isotropic Displacement Parameters (Å² × 10³) for 3a^a

atom	x	y	z	U(eq)
Ti(1)	2041(2)	914(1)	9080(2)	56(1)
Si(1)	1790(4)	2293(2)	7678(4)	82(2)
Si(2)	2974(5)	543(2)	13373(4)	100(2)
Si(3)	1923(4)	-1427(2)	7404(4)	85(2)
C(1)	651(10)	1725(6)	8218(12)	55(6)
C(2)	240(11)	1113(6)	7754(11)	63(6)
C(3)	-183(10)	728(6)	8562(13)	63(6)
C(4)	9(10)	1082(7)	9581(11)	59(6)
C(5)	540(10)	1705(6)	9369(11)	53(6)
C(6)	3114(14)	1744(8)	8222(16)	73(7)
C(7)	3639(14)	1719(8)	9387(20)	93(10)
C(8)	4242(17)	1115(12)	9603(18)	116(11)
C(9)	4086(17)	745(8)	8666(23)	115(12)
C(10)	3404(15)	1126(10)	7800(15)	91(8)
C(11)	1906(11)	3113(6)	8328(12)	120(8)
C(12)	1507(14)	2336(8)	6130(12)	170(11)
C(13)	2352(12)	741(6)	10834(12)	74(6)
C(14)	2561(13)	677(7)	11851(13)	84(7)
C(15)	1962(11)	-62(6)	8461(10)	67(6)
C(16)	1923(12)	-617(6)	8043(11)	67(6)
C(17)	3710(13)	1289(7)	14041(12)	141(9)
C(18)	1630(15)	366(9)	14043(12)	223(14)
C(19)	3957(20)	-174(9)	13606(13)	339(19)
C(20)	1969(17)	-1358(8)	5938(12)	218(14)
C(21)	3238(18)	-1890(8)	8062(17)	321(19)
C(22)	611(16)	-1888(7)	7622(16)	251(16)

^a U(eq) is defined as one-third of the trace of the orthogonalized U_{ij} tensor.

Figure 1). Similar observations were made for all other [(η⁵-C₅H₄SiMe₃)₂Ti(C≡CSiMe₃)₂]ML_n compounds.¹⁻¹⁰

Alkynyl *ansa*-Zirconocenes. Using the reaction conditions already described for the preparation of the bis(alkynyl) *ansa*-titanocenes **3a-c**, the *ansa*-zirconocene dichloride [(η⁵-C₅H₄)(η⁵-C₅H₃SiMe₃)SiMe₂]ZrCl₂ (**6**) leads with 2 equiv of LiC≡CSiMe₃ (**2**) to a multitude of reaction products, of which the dimeric alkynyl-bridged complex {[(η⁵-C₅H₄)(η⁵-C₅H₃SiMe₃)SiMe₂]Zr(C≡CSiMe₃)₂}₂ (**7**) can be crystallized in 10% yield. Spectroscopic measurements of the reaction mixture show unreacted **6**, which gives rise to the formation of the expected bis(alkynyl) *ansa*-zirconocene [(η⁵-C₅H₄)(η⁵-C₅H₃SiMe₃)SiMe₂]Zr(C≡CSiMe₃)₂ (**8**) as well as the monoalkynyl-

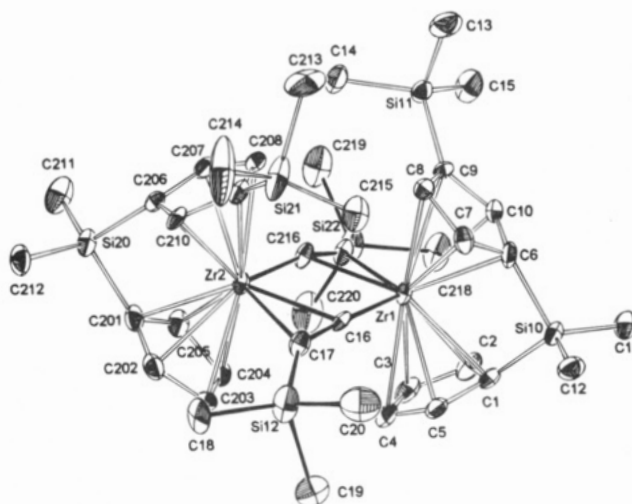
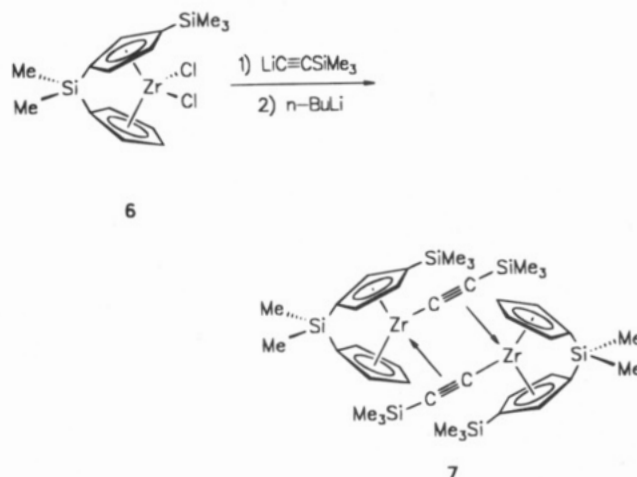


Figure 3. ORTEP drawing (drawn at 50% probability level) of **7** (with exclusion of the hydrogen atoms) with the atom-numbering scheme (Tables 1, 6, and 7).

substituted zirconocene [(η⁵-C₅H₄)(η⁵-C₅H₃SiMe₃)SiMe₂]Zr(C≡CSiMe₃)(Cl) (**9**).

In much better yields **7** is accessible by the reaction of [(η⁵-C₅H₄)(η⁵-C₅H₃SiMe₃)SiMe₂]ZrCl₂ (**6**) with first 1 equiv of LiC≡CSiMe₃ (**2**) and secondly with 1 additional equiv of *n*-butyllithium. Analytically pure **7** can be obtained by filtration of the crude reaction material through a pad of Celite with *n*-pentane. Crystallization at -30 °C affords **7** as orange crystals in 45% yield. The



diamagnetic complex **7** is soluble in polar solvents (THF, Et₂O) and slightly soluble in toluene or *n*-pentane. While solid **7** is stable in air for days, solutions of **7** decompose on exposition to air and in chlorinated solvents.

One hint on the diamagnetic structure of **7** is given by the proton NMR spectrum. It shows a 3:3:1:1 ratio of the protons of the methyl resonances of the η⁵-C₅H₃-SiMe₃, C≡CSiMe₃, and SiMe₂ units. The EI mass spectrum of **7** confirms its dimeric nature, with the M⁺ ion observed at *m/e* = 892 as its base peak. Another spectroscopic proof of dimeric **7** is the appearance of an IR-absorption band at 1741 cm⁻¹, a region typical for C≡C triple bonds η²-coordinated to group 4 metallocene fragments, suggesting a significantly reduced C≡C bond order.²⁵⁻²⁹

The result of the X-ray structure analysis of **7**, depicted in Figure 3 (crystallographic parameters are

Table 6. Selected Bond Lengths (Å) and Angles (deg) for 7 (Molecule 1)^a

Distances			
Bond Lengths		NonBonding Distances	
Zr(1)–C(16)	2.177(6)	Zr(1)–Zr(2)	3.489
Zr(1)–C(217)	2.394(6)	Zr(1)–MP2 ^b	2.3084
Zr(1)–C(216)	2.394(5)	Zr(2)–MP1 ^b	2.3124
Zr(2)–C(216)	2.187(6)	Zr(1)–D1 ^c	2.238
Zr(2)–C(16)	2.394(5)	Zr(1)–D1' ^c	2.256
Zr(2)–C(17)	2.397(6)	Zr(2)–D2 ^c	2.234
C(16)–C(17)	1.254(8)	Zr(2)–D2' ^c	2.250
C(216)–C(217)	1.270(8)		
Angles			
C(16)–Zr(1)–C(216)	80.9(2)	C(217)–C(216)–Zr(2)	167.5(5)
C(216)–Zr(2)–C(16)	80.7(2)	Zr(2)–C(216)–Zr(1)	99.1(2)
C(17)–C(16)–Zr(1)	168.7(5)	C(216)–C(217)–Si(22)	145.2(5)
Zr(1)–C(16)–Zr(2)	99.4(2)	C(216)–C(217)–Zr(1)	74.6(3)
C(16)–C(17)–Zr(2)	74.7(3)	D1–Zr(1)–D1' ^c	125.1
C(16)–(17)–Si(12)	143.7(5)	D2–Zr(2)–D2' ^c	124.7

^a Molecule 1 and molecule 2 are essentially identical; the set of data on molecule 2 is available as supporting information. ^b MP1, MP2 = midpoints of the C≡C triple bonds. ^c D1, D1', D2, D2' = centroids of the cyclopentadienyl ligands.

given in Table 1; bond lengths and angles are given in Table 6), explains these features. Compound **7** crystallizes in the triclinic space group $P\bar{1}$ with two crystallographically independent molecules, both being essentially identical. Only the numbering of molecule 1 is shown in Figure 3. Final atomic coordinates and equivalent isotropic thermal parameters for non-hydrogen atoms are presented in Table 7. The most representative bond distances and angles are given in Table 6. In **7** two identical $[(\eta^5\text{-C}_5\text{H}_4)(\eta^5\text{-C}_5\text{H}_3\text{SiMe}_3)\text{SiMe}_2]\text{-Zr}(\text{C}\equiv\text{CSiMe}_3)$ building blocks have dimerized to form a central organometallic framework consisting of two early transition metal centers (Zr(1), Zr(2)) and four acetylide carbon atoms (C(16), C(17), C(216), C(217)). These atoms form a plane (maximum deviation: 0.156 Å). The Zr(1)–C(216)–C(217) plane is folded by 21.51° relative to the Zr(2)–C(16)–C(17) plane. As compared to²⁷ $[(\eta^5\text{-C}_5\text{H}_5)_2\text{Zr}(\text{C}\equiv\text{CSiMe}_3)]_2$ ²⁸ (5.4°) the folding in **7** (molecule 1) is much larger, which can be best explained by the bulkiness of the *ansa*-zirconocene building blocks $[(\eta^5\text{-C}_5\text{H}_4)(\eta^5\text{-C}_5\text{H}_3\text{SiMe}_3)\text{SiMe}_2]\text{Zr}$. The Zr–D1 and Zr–D2 distances (D1, D2 = centroids of the cyclopentadienyl ligands) are in the range of 2.234–2.250 Å, the angles D1–Zr–D2 are 124.7° and 125.1° (Table 6) and are thereby similar to other compounds of this type.^{25,28}

The structure of **7** is similar to that of $[(\eta^5\text{-C}_5\text{H}_4\text{-Me})_2\text{Zr}(\text{C}\equiv\text{CPh})]_2$,²⁵ $[(\eta^5\text{-C}_5\text{H}_5)_2\text{Zr}(\text{C}\equiv\text{CSiMe}_3)]_2$,²⁸ and $[(\eta^5\text{-C}_5\text{H}_5)_2\text{Ti}(\text{C}\equiv\text{CSiMe}_3)]_2$,^{26,27,29} respectively. The Zr(1)–Zr(2) distance of 3.489 Å is in the nonbonding region. The carbon–carbon triple-bond length in **7** is with 1.270(8) Å [C(216)–C(217)] due to the η^2 -coordination to a zirconium atom somewhat longer than that found in $(\eta^5\text{-C}_5\text{H}_5)_2\text{Zr}(\text{C}\equiv\text{CMe})_2$ ²⁵ [1.206(4) Å]. The Zr–C_α bonds are with 2.177(6) Å and 2.187(6) Å [Zr(1)–C(16), Zr(2)–C(216)] significantly shorter than the zirconium–carbon distances found in $(\eta^5\text{-C}_5\text{H}_4\text{SiMe}_3)_2\text{-Zr}(\text{Cl})[\text{CH}(\text{SiMe}_3)_2]$ ³⁰ (2.327(3) Å) or $(\eta^5\text{-C}_5\text{H}_5)_2\text{Zr}(\text{CHPh})_2$ ³¹ (2.396(6) and, 2.379(6) Å), but almost as

Table 7. Atomic Coordinates ($\times 10^4$) and Equivalent Isotropic Displacement Parameters ($\text{Å}^2 \times 10^3$) for 7

atom	x	y	z	U(eq)
Zr(1+)	2709(1)	2791(1)	1171(1)	17(1)
Zr(2)	365(1)	3225(1)	1954(1)	16(1)
Si(10)	4022(1)	1974(1)	190(1)	25(1)
Si(11)	4443(1)	1838(1)	3092(1)	25(1)
Si(12)	–1159(1)	2431(1)	680(1)	47(1)
Si(20)	–1140(1)	3945(1)	2956(1)	24(1)
Si(21)	–217(2)	927(1)	2999(1)	51(1)
Si(22)	4042(1)	4340(1)	1713(1)	29(1)
C(1)	3349(4)	2921(3)	–36(3)	23(1)
C(2)	3786(5)	3524(3)	111(3)	29(2)
C(3)	2957(5)	4041(3)	114(3)	28(2)
C(4)	1988(5)	3780(3)	–10(3)	29(2)
C(5)	2223(5)	3091(3)	–98(3)	23(1)
C(6)	3857(4)	1686(3)	1161(3)	23(1)
C(7)	2906(5)	1398(3)	1527(3)	24(1)
C(8)	2901(4)	1480(3)	2183(3)	20(1)
C(9)	3854(4)	1819(3)	2247(3)	21(1)
C(10)	4430(4)	1969(3)	1608(3)	23(1)
C(11)	5473(5)	2025(4)	–55(3)	46(2)
C(12)	3256(5)	1378(3)	–161(3)	33(2)
C(13)	4603(6)	847(4)	3707(3)	43(2)
C(14)	3615(5)	2360(4)	3548(3)	34(2)
C(15)	5796(5)	2235(4)	2895(3)	41(2)
C(16)	996(4)	2568(3)	1208(3)	16(1)
C(17)	–18(5)	2577(3)	1178(3)	24(1)
C(18)	–2479(9)	2789(8)	922(7)	39(3)
C(19)	–936(13)	3166(8)	–336(7)	41(4)
C(20)	–751(26)	1575(22)	421(18)	58(8)
C(18X) ^c	–2284(13)	1960(12)	1406(8)	75(6)
C(19X) ^c	–1657(17)	3126(10)	28(10)	86(7)
C(20X) ^b	–1169(23)	1545(19)	645(17)	51(7)
C(201)	–765(5)	4339(3)	2000(3)	24(1)
C(202)	–1240(5)	4130(3)	1469(3)	28(2)
C(203)	–545(5)	4288(3)	888(3)	26(2)
C(204)	378(5)	4569(3)	1056(3)	24(1)
C(205)	249(5)	4600(3)	1730(3)	25(1)
C(206)	–440(4)	3007(3)	3133(3)	18(1)
C(207)	673(4)	2833(3)	3251(3)	25(1)
C(208)	930(5)	2161(3)	3137(3)	23(1)
C(209)	–8(5)	1909(3)	2946(3)	22(1)
C(210)	–864(4)	2451(3)	2925(3)	20(1)
C(211)	–528(6)	4429(4)	3487(3)	43(2)
C(212)	–2616(5)	3863(3)	3097(3)	34(2)
C(213)	850(18)	388(9)	3835(8)	71(6)
C(214)	–1452(15)	633(9)	3342(12)	97(8)
C(23X) ^c	–97(12)	288(8)	3834(8)	43(4)
C(24X) ^c	–1784(10)	960(8)	2702(7)	32(3)
C(215)	401(5)	600(3)	2335(3)	38(2)
C(216)	2083(4)	3457(3)	1911(3)	20(1)
C(217)	3043(5)	3655(3)	1742(3)	23(1)
C(218)	5331(5)	4197(4)	1276(3)	38(2)
C(219)	4316(5)	4296(4)	2620(4)	47(2)
C(220)	3460(6)	5288(4)	1189(4)	49(2)

^a Molecule 1 and molecule 2 are essentially identical; the set of data on molecule 2 is available as supporting information. ^b U_{eq} is defined as one-third of the trace of the orthogonalized U_{ij} tensor. ^c Two of the trimethylsilyl groups [C(18)–C(20); C(213), C(214)] are disordered.

short as the Zr–C_{sp} bond in $(\eta^5\text{-C}_5\text{H}_5)_2\text{Zr}(\text{CO})_2$.³² This suggests that compound **7** can be described by the resonance formulae **A**, **B**, and **C** as shown in Scheme 1, attributing a π -interaction between the zirconium centers and the adjacent alkynyl π -system via the connecting Zr–C σ -bond.

Due to the η^2 -coordination of the Zr–C≡C–Si units in **7** to an adjacent zirconium atom the C≡C–Si

(30) Lappert, M. F.; Riley, P. I.; Yarrow, P. I. W.; Atwood, J. L.; Hunter, W. E.; Zaworotko, M. J. *J. Chem. Soc., Dalton Trans.* **1981**, 814.

(31) Atwood, J. L.; Barker, G. K.; Holton, J.; Hunter, W. E.; Lappert, M. F.; Pearce, R. *J. Am. Chem. Soc.* **1977**, *99*, 6645.

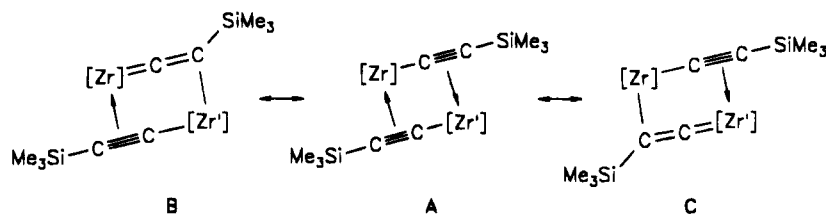
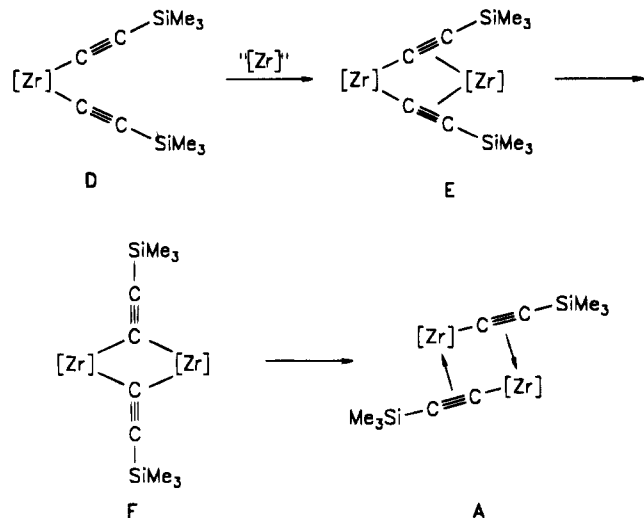
(32) Atwood, J. L.; Rogers, R. D.; Hunter, W. E.; Floriani, C.; Fachinetti, G.; Chiesi-Villa, A. *Inorg. Chem.* **1980**, *19*, 3812.

(26) Rosenthal, U.; Görls, H. *J. Organomet. Chem.* **1992**, *439*, C36.

(27) Wood, G. L.; Knobler, C. B.; Hawthorne, M. F. *Inorg. Chem.* **1989**, *28*, 382.

(28) Metzler, N.; Nöth, H. *J. Organomet. Chem.* **1993**, *454*, C5.

(29) Cuenca, T.; Gómez, R.; Gómez-Sal, P.; Rodríguez, G. M.; Royo, P. *Organometallics* **1992**, *11*, 1229.

Scheme 1. Possible Resonance Formulae of $\{[(\eta^5\text{-C}_5\text{H}_4)(\eta^5\text{-C}_5\text{H}_3\text{SiMe}_3)\text{SiMe}_2]\text{Zr}(\text{C}\equiv\text{CSiMe}_3)_2\}_2$ (7)Scheme 2. Possible Mechanism for the Formation of 7 by the Reaction of 6 with 2 and ${}^n\text{C}_4\text{H}_9\text{Li}$; $[\text{Zr}] = [(\eta^5\text{-C}_5\text{H}_4)(\eta^5\text{-C}_5\text{H}_3\text{SiMe}_3)\text{SiMe}_2]\text{Zr}$ 

moieties are deformed from linearity ($\text{C}\equiv\text{C}-\text{SiMe}_3$: $143.7(5)^\circ$ and $145.2(5)^\circ$). This deformation is consistent with the previously reported structure of $[(\eta^5\text{-C}_5\text{H}_4\text{-Me})_2\text{Zr}(\text{C}\equiv\text{CPh})_2]^{25}$ ($146.8(2)^\circ$) and $[(\eta^5\text{-C}_5\text{H}_5)_2\text{Zr}(\text{C}\equiv\text{CSiMe}_3)_2]^{28}$ ($142.5(4)^\circ$). The $\text{Zr}-\text{C}\equiv\text{C}$ angles are almost linear at $167.5(5)^\circ$ and $168.7(5)^\circ$. Usually both the $\text{Zr}-\text{C}\equiv\text{C}$ and $\text{C}\equiv\text{C}-\text{Si}$ angles are decreased on η^2 -coordination of the C_2 unit to a transition metal atom. In the case of 7, the $\text{Zr}-\text{C}\equiv\text{C}$ angle is not that much affected, which can be explained by using a geometrical argument: Additional deformation of the $\text{Zr}-\text{C}\equiv\text{C}$ entity would weaken the alkyne-to-metal (Zr') π -interaction.

A possible way for the formation of dimeric 7 by the reaction of $[(\eta^5\text{-C}_5\text{H}_4)(\eta^5\text{-C}_5\text{H}_3\text{SiMe}_3)\text{SiMe}_2]\text{ZrCl}_2$ (6) with $\text{LiC}\equiv\text{CSiMe}_3$ (2) and ${}^n\text{C}_4\text{H}_9\text{Li}$ is given in Scheme 2. Presumably in the first step, the bis(alkynyl) zirconocene D acts as an organometallic chelating ligand (organometallic π -tweezers compound) and affords with "[Zr]" ($[\text{Zr}] = [(\eta^5\text{-C}_5\text{H}_4)(\eta^5\text{-C}_5\text{H}_3\text{SiMe}_3)\text{SiMe}_2]\text{Zr}$, generated from $[(\eta^5\text{-C}_5\text{H}_4)(\eta^5\text{-C}_5\text{H}_3\text{SiMe}_3)\text{SiMe}_2]\text{ZrCl}_2$ (6) and ${}^n\text{C}_4\text{H}_9\text{Li}$) the dinuclear intermediate E (Scheme 2). E contains two bridging σ, π -alkynyl ligands between two zirconium atoms. Structural type E molecules are well defined for compounds of general type $[\text{L}_x\text{M}(\text{C}\equiv\text{CR})_2]\text{M}'\text{L}_n$ [$\text{L}_x\text{M} = (\eta^5\text{-C}_5\text{H}_4\text{SiMe}_3)_2\text{Ti}$, $(\eta^5\text{-C}_5\text{H}_4\text{SiMe}_3)_2\text{Hf}$, $\text{Re}(\text{CO})_3(\text{PPh}_3)$, $(\eta^5\text{-C}_5\text{H}_5)\text{Ru}$, $\text{Ir}(\text{PPh}_3)_2(\text{C}\equiv\text{CR})_2$, $\text{Rh}(\text{PPh}_3)_2(\text{C}\equiv\text{CR})_2$, $(\text{C}_5\text{F}_5)_2\text{Pt}$, $(\text{dppe})\text{Pt}$, $\text{Pt}(\text{PPh}_3)_2$; $\text{M}'\text{L}_n = \text{Ni}(\text{CO})$, $\text{Co}(\text{CO})$; CuX , AgX ; X = singly bonded inorganic or organic ligand; R = singly bonded organic ligand] $^{1-7,33-36}$ and could be isolated if the chelated organometallic building block provides a center with low Lewis-acidity, e.g., $\text{Ni}(\text{CO})$, 1,2 FeCl_2 , 4 or Cu , Ag . 6,7

Fragments with a higher electrophilicity, e.g., $(\eta^5\text{-C}_5\text{-Me}_5)_2\text{Ln}$ ($\text{Ln} = \text{Sm}$, Eu , Yb), tend to coordinate preferentially to the C_α atom of the $\{[\text{Ti}](\text{C}_\alpha\equiv\text{C}\beta\text{SiMe}_3)_2\}$ moiety, giving rise to a bonding situation better described as asymmetric bridging of $\text{Me}_3\text{SiC}\equiv\text{C}$ groups between two metal centers (in analogy to intermediate F). Compounds of this type could be crystallographically characterized, involving main group elements, 37 f-orbital centers, 38 or platinum atoms. 39 Symmetrical cleavage of F by breaking of two zirconium- C_α -acetylide bonds, which afterwards can recombine to form dimeric $\{[(\eta^5\text{-C}_5\text{H}_4)(\eta^5\text{-C}_5\text{H}_3\text{SiMe}_3)\text{SiMe}_2]\text{Zr}(\text{C}\equiv\text{CSiMe}_3)_2$ (type A molecule).

Experimental Section

General Comments. All reactions were carried out under an atmosphere of nitrogen using standard Schlenk techniques. Tetrahydrofuran (THF) and diethylether (Et_2O) were purified by distillation from sodium/benzophenone ketyl; toluene and *n*-pentane were purified by distillation from calcium hydride. Infrared spectra were obtained with a Perkin-Elmer 983G spectrometer. ^1H NMR spectra were recorded on a Bruker AC 200 spectrometer operating at 200.132 MHz in the Fourier transform mode, and ^{13}C NMR spectra were recorded at 50.323 MHz. Chemical shifts are reported in δ units (parts per million) downfield from tetramethylsilane with the solvent as the reference signal. EI mass spectra were recorded on a Finnigan 8230 mass spectrometer operating in the positive-ion mode. Melting points were determined with use of analytically pure samples, which were sealed in nitrogen-purged capillaries on a Gallenkamp MFB 595 010 M melting point apparatus. Microanalyses were performed by the Organisch-Chemisches Institut der Universität Heidelberg.

(A) Synthesis of 3a-c. The *ansa*-titanocene dichlorides 1a-c (1a, 1.6 g; 1b, 2.0 g; 1c, 2.7 g; 5.3 mmol) 14 were added at 25°C in one portion to a solution of $\text{LiC}\equiv\text{CSiMe}_3$ (2) 40 (1.1 g, 10.6 mmol) in 100 mL of Et_2O (to dissolve compound 1a an additional 100 mL portion of THF had to be added). After stirring for 2 h at 25°C all volatile materials were removed in vacuo, and the residues were each extracted with 100 mL

(33) (a) Abu Salah, O. M.; Bruce, M. I. *Aust. J. Chem.* **1976**, *29*, 531. (b) Abu Salah, O. M.; Bruce, M. I. *Aust. J. Chem.* **1977**, *30*, 2639. (c) Abu Salah, O. M.; Bruce, M. I. *J. Chem. Soc., Chem. Commun.* **1974**, 688. (d) Abu Salah, O. M.; Bruce, M. I.; Redhouse, A. D. *J. Chem. Soc., Chem. Commun.* **1974**, 855. Abu Salah, O. M.; Bruce, M. I. *J. Chem. Soc., Dalton Trans.* **1975**, 2311.

(34) (a) Fornies, J.; Lalinde, E.; Martinez, F.; Moreno, M. T.; Welch, A. J. *J. Organomet. Chem.* **1993**, *455*, 271. (b) Berenguer, J. R.; Fornies, J.; Lalinde, E.; Martin, A. *Angew. Chem.* **1994**, *106*, 2196.

(35) Ciriano, M.; Howard, J. A. K.; Spencer, J. L.; Stone, F. G. A.; Wade, H. J. *J. Chem. Soc., Dalton Trans.* **1979**, 1749.

(36) Troyanov, S. I.; Varga, V.; Mach, K. *Organometallics* **1993**, *12*, 2820.

(37) Erker, G.; Albrecht, M.; Krüger, C.; Nolte, M.; Werner, S. *Organometallics* **1993**, *12*, 4979.

(38) (a) Evans, W. J.; Drummond, D. K.; Hanusa, T. P.; Olofson, J. M. *J. Organomet. Chem.* **1989**, *376*, 311. (b) Evans, W. J.; Keyser, R. A.; Ziller, J. W. *Organometallics* **1993**, *12*, 2618 and literature cited therein.

(39) Berenguer, J. R.; Falvello, L. R.; Fornies, J.; Lalinde, E.; Tomas, M. *Organometallics* **1993**, *12*, 6.

(40) Lang, H.; Keller, H.; Imhof, W.; Martin, S. *Chem. Ber.* **1990**, *123*, 417.

of *n*-pentane and filtered through a pad of Celite. Crystallization at $-30\text{ }^\circ\text{C}$ yielded **3a** and **3c** (**3a**, 0.8 g, 1.75 mmol, 35%; **3c**, 2.9 g, 4.54 mmol, 86%) as orange-colored solids; **3b** (2.4 g, 4.77 mmol, 90%), an intense orange-colored oil, could not be crystallized. Data for **3a**: mp $176\text{ }^\circ\text{C}$; IR (KBr) $\nu(\text{C}\equiv\text{C})$ 2015 cm^{-1} ; $^1\text{H NMR}$ (CDCl_3) δ 0.10 (s, 18 H, SiMe_3), 0.58 (s, 6 H, SiMe_2), 5.65 (pt, $J_{\text{HH}} = 2.1\text{ Hz}$, 4 H, C_5H_4), 7.40 (pt, $J_{\text{HH}} = 2.1\text{ Hz}$, 4 H, C_5H_4); $^{13}\text{C}\{^1\text{H}\}$ NMR (CDCl_3) δ -5.5 (s, SiMe_2), 0.5 (s, SiMe_3), 97.3 (s, C_5H_4), 98.2 (s, $\text{C}\equiv\text{C}$), 115.7 (s, C_5H_4), 126.1 (s, C_5H_4), 170.0 (s, $\text{C}\equiv\text{C}$); EI mass spectrum, m/e (relative intensity) M^+ , 428 (23); $\text{M}^+ - \text{C}_2\text{SiMe}_3$, 330 (40); $\text{M}^+ - 2\text{C}_2\text{SiMe}_3$, 234 (100). Anal. Calcd for $\text{C}_{22}\text{H}_{32}\text{Si}_3\text{Ti}$ (428.63): C, 61.65; H, 7.52. Found: C, 61.08; H, 7.27. For **3b**: IR (neat, NaCl plates) $\nu(\text{C}\equiv\text{C})$ 2017 cm^{-1} ; $^1\text{H NMR}$ (CDCl_3) δ 0.09 (s, 18 H, $\text{C}\equiv\text{CSiMe}_3$), 0.37 (s, 9 H, $\text{C}_5\text{H}_3\text{SiMe}_3$), 0.49 (s, 3 H, SiMe_2), 0.60 (s, 3 H, SiMe_2), 5.65 (m, 1 H, C_5H_4), 5.84 (pt, $J_{\text{HH}} = 2.3\text{ Hz}$, 1 H, $\text{C}_5\text{H}_3\text{SiMe}_3$), 5.91 (m, 2 H, C_5H_4 , $\text{C}_5\text{H}_3\text{SiMe}_3$), 7.09 (m, 1 H, C_5H_4), 7.45 (m, 2 H, C_5H_4 , $\text{C}_5\text{H}_3\text{SiMe}_3$); $^{13}\text{C}\{^1\text{H}\}$ NMR (CDCl_3) δ -6.7 , -3.9 (s, SiMe_2); -0.3 (s, $\text{C}_5\text{H}_3\text{SiMe}_3$); 0.1, 0.3 (s, $\text{C}\equiv\text{CSiMe}_3$); 99.5, 101.0, 111.8, 116.2, 120.7, 123.1, 125.0, 127.6, 132.7, 134.9 (s, C_5H_4 , $\text{C}_5\text{H}_3\text{SiMe}_3$, $\text{C}\equiv\text{C}$), 169.0 (s, $\text{C}\equiv\text{C}$); EI mass spectrum, m/e (relative intensity) M^+ , 501 (22); $\text{M}^+ - \text{Me}$, 486 (8); $\text{M}^+ - \text{C}_2\text{SiMe}_3$, 402 (100); $\text{M}^+ - 2\text{C}_2\text{SiMe}_3$, 306 (60); SiMe_3^+ , 73 (18). Anal. Calcd for $\text{C}_{25}\text{H}_{40}\text{Si}_4\text{Ti}$ (500.82): C, 59.96; H, 8.05. Found: C, 59.15; H, 7.91. For **3c**: mp $140\text{ }^\circ\text{C}$; IR (KBr) $\nu(\text{C}\equiv\text{C})$ 2014 cm^{-1} ; $^1\text{H NMR}$ (CDCl_3) δ 0.06 (s, 9 H, $\text{C}\equiv\text{CSiMe}_3$), 0.11 (s, 9 H, $\text{C}\equiv\text{CSiMe}_3$), 0.39 (s, 9 H, $\text{C}_5\text{H}_3\text{SiMe}_3$), 0.40 (s, 9 H, $\text{C}_5\text{H}_3\text{SiMe}_3$), 0.68 (s, 3 H, SiMe), 5.62 (pt, $J_{\text{HH}} = 1.8\text{ Hz}$, 2 H, $\text{C}_5\text{H}_3\text{SiMe}_3$), 5.78 (pt, $J_{\text{HH}} = 2.3\text{ Hz}$, 2 H, $\text{C}_5\text{H}_3\text{SiMe}_3$), 5.84 (pt, $J_{\text{HH}} = 2.3\text{ Hz}$, 2 H, $\text{C}_5\text{H}_3\text{SiMe}_3$), 5.97 (pt, $J_{\text{HH}} = 1.8\text{ Hz}$, 2 H, $\text{C}_5\text{H}_3\text{SiMe}_3$), 6.17 (pt, $J_{\text{HH}} = 2.3\text{ Hz}$, 2 H, $\text{C}_5\text{H}_3\text{SiMe}_3$), 6.60 (pt, $J_{\text{HH}} = 1.8\text{ Hz}$, 2 H, $\text{C}_5\text{H}_3\text{SiMe}_3$), 7.3–7.9 (m, 5 H, Ph); EI mass spectrum, m/e (relative intensity) M^+ , 634 (28); $\text{M}^+ - \text{C}_2\text{SiMe}_3$, 537 (100); $\text{M}^+ - 2\text{C}_2\text{SiMe}_3$, 440 (20); SiMe_3^+ , 73 (19). Anal. Calcd for $\text{C}_{33}\text{H}_{50}\text{Si}_5\text{Ti}$ (635.07): C, 62.41; H, 7.94. Found: C, 61.90; H, 8.20.

(B) Synthesis of 5a–c. The bis(alkynyl) *ansa*-titanocenes **3a–c** (**3a**, 215 mg; **3b**, 250 mg; **3c**, 320 mg; 0.5 mmol) were dissolved in toluene (50 mL), and $\text{Ni}(\text{CO})_4$ (100 mg, 0.58 mmol) was added at $25\text{ }^\circ\text{C}$ in one portion. After stirring for 1 h at $25\text{ }^\circ\text{C}$ all volatile materials were removed in vacuo, and the residues were each extracted with 50 mL of *n*-pentane. Crystallization at $-30\text{ }^\circ\text{C}$ yielded compound **5c** (315 mg, 0.44 mmol, 87%) as brown-golden solid; compounds **5a** (230 mg, 0.45 mmol, 90%) and **5b** (280 mg, 0.48 mmol, 95%) could not be crystallized. Data for **5a**: IR (neat, NaCl plates) $\nu(\text{CO})$ 1995 cm^{-1} (s), $\nu(\text{C}\equiv\text{C})$ 1834 cm^{-1} (m); $^1\text{H NMR}$ (CDCl_3) δ 0.32 (s, 9 H, SiMe_3), 0.33 (s, 9 H, SiMe_3), 0.59 (s, 3 H, SiMe_2), 0.60 (s, 3 H, SiMe_2), 5.33 (pt, $J_{\text{HH}} = 2\text{ Hz}$, 4 H, C_5H_4), 5.68 (pt, $J_{\text{HH}} = 2\text{ Hz}$, 4 H, C_5H_4); EI mass spectrum, m/e (relative intensity) $\text{M}^+ - \text{CO}$, 486 (64); $\text{M}^+ - \text{NiCO} - 2\text{C}_2\text{SiMe}_3$, 234 (100); $\text{Me}_2\text{SiC}_5\text{H}_5^+$, 123 (84); SiMe_3^+ , 73 (76). Anal. Calcd for $\text{C}_{23}\text{H}_{32}\text{NiOSi}_3\text{Ti}$ (515.33): C, 53.61; H, 6.26. Found: C, 53.41; H, 6.42. Data for **5b**: IR (neat, NaCl plates) $\nu(\text{CO})$ 1995 cm^{-1} (vs), $\nu(\text{C}\equiv\text{C})$ 1834 cm^{-1} (s); $^1\text{H NMR}$ (CDCl_3) δ 0.01 (s, 9 H, $\text{C}_5\text{H}_3\text{SiMe}_3$), 0.31 (s, 18 H, $\text{C}\equiv\text{CSiMe}_3$), 0.57 (s, 3 H, SiMe_2), 0.60 (s, 3 H, SiMe_2), 5.11 (m, 1 H, C_5H_4), 5.33 (pt, $J_{\text{HH}} = 2.0\text{ Hz}$, 1 H, $\text{C}_5\text{H}_3\text{SiMe}_3$), 5.39 (m, 1 H, C_5H_4), 5.60 (m, 1 H, C_5H_4), 5.64 (pt, $J_{\text{HH}} = 2.0\text{ Hz}$, 1 H, $\text{C}_5\text{H}_3\text{SiMe}_3$), 5.67 (m, 1 H, C_5H_4), 5.88 (pt, $J_{\text{HH}} = 2.0\text{ Hz}$, 1 H, $\text{C}_5\text{H}_3\text{SiMe}_3$); $^{13}\text{C}\{^1\text{H}\}$ NMR (CDCl_3) δ -5.2 (s, SiMe_2); -0.3 , 0.6, 0.8 (s, SiMe_3); 81.3, 82.1, 105.2, 106.4, 109.3, 110.1, 110.4, 115.4, 117.1, 120.4, 125.3 (s, C_5H_4 , $\text{C}_5\text{H}_3\text{SiMe}_3$, $\text{C}\equiv\text{C}$); 189.8 (s, $\text{C}\equiv\text{C}$), 200.8 (s, CO); EI mass spectrum, m/e (relative intensity) M^+ , 586 (4); $\text{M}^+ - \text{CO}$, 557 (100); M^+

$- \text{C}_5\text{H}_5\text{SiMe}_3$, 447 (16); $\text{M}^+ - \text{C}_5\text{H}_5\text{SiMe}_3 - \text{SiMe}_3$, 373 (14); $\text{Si}(\text{C}_5\text{H}_4)_2\text{Ti}^+$, 202 (24); SiMe_3^+ , 73 (20). Anal. Calcd for $\text{C}_{26}\text{H}_{40}\text{NiOSi}_4\text{Ti}$ (587.52): C, 53.15; H, 6.86. Found: C, 53.17; H, 6.42. Data for **5c**: mp $62\text{ }^\circ\text{C}$; IR (KBr) $\nu(\text{CO})$ 2003 cm^{-1} (s), $\nu(\text{C}\equiv\text{C})$ 1831 cm^{-1} (m); $^1\text{H NMR}$ (CDCl_3) δ 0.07 (s, 18 H, $\text{C}_5\text{H}_3\text{SiMe}_3$), 0.28 (s, 9 H, $\text{C}\equiv\text{CSiMe}_3$), 0.33 (s, 9 H, $\text{C}\equiv\text{CSiMe}_3$), 0.84 (s, 3 H, SiMe), 5.05 (pt, $J_{\text{HH}} = 1.9\text{ Hz}$, 2 H, $\text{C}_5\text{H}_3\text{SiMe}_3$), 5.65 (pt, $J_{\text{HH}} = 1.9\text{ Hz}$, 2 H, $\text{C}_5\text{H}_3\text{SiMe}_3$), 5.95 (pt, $J_{\text{HH}} = 1.9\text{ Hz}$, 2 H, $\text{C}_5\text{H}_3\text{SiMe}_3$), 7.51 (m, 3 H, C_6H_5), 7.93 (m, 2 H, C_6H_5); $^{13}\text{C}\{^1\text{H}\}$ NMR (CDCl_3) δ -4.8 (s, SiMe); 0.0, 0.6, 0.8 (s, SiMe_3); 109.9, 111.9, 112.9, 119.5, 127.1, 128.3, 130.3, 134.7 (s, C_6H_5 , $\text{C}_5\text{H}_3\text{SiMe}_3$, $\text{C}\equiv\text{C}$); 190.1 (s, $\text{C}\equiv\text{C}$), 203.5 (s, CO); EI mass spectrum, m/e (relative intensity) M^+ , 721 (2); $\text{M}^+ - \text{CH}_3$, 707 (2); $\text{M}^+ - \text{CO}$, 693 (100); SiMe_3^+ , 73 (10). Anal. Calcd for $\text{C}_{34}\text{H}_{50}\text{NiOSi}_5\text{Ti}$ (721.77): C, 56.58; H, 6.98. Found: C, 56.38; H, 7.23.

(C) Synthesis of 7. To $[(\eta^5\text{-C}_5\text{H}_3\text{SiMe}_3)(\eta^5\text{-C}_5\text{H}_4\text{SiMe}_2)\text{-ZrCl}_2]$ (**6**)¹⁴ (2.0 g, 4.8 mmol) in THF (50 mL) were added at $25\text{ }^\circ\text{C}$ in one portion $\text{LiC}\equiv\text{CSiMe}_3$ (**2**)⁴⁰ (0.5 g, 4.8 mmol, 20 mL Et_2O), and after 5 min, $^n\text{C}_4\text{H}_7\text{Li}$ (1.9 mL, 4.8 mmol; 2.5 M in hexane) in 100 mL of Et_2O . After stirring for 2 h at $25\text{ }^\circ\text{C}$ the solvents were evaporated under high vacuum; the residue was extracted with 50 mL of *n*-pentane and filtered through a pad of Celite. Crystallization from Et_2O at $-30\text{ }^\circ\text{C}$ yielded **7** (0.96 g, 1.1 mmol; 45%) as an orange-colored solid: mp $131\text{ }^\circ\text{C}$; IR (KBr) $\nu(\text{C}\equiv\text{C})$ 1741 cm^{-1} ; $^1\text{H NMR}$ (CDCl_3) δ 0.14 (s, 9 H, SiMe_3), 0.45 (s, 9 H, SiMe_3), 0.52 (s, 3 H, SiMe_2), 0.70 (s, 3 H, SiMe_2), 4.16 (m, 2 H, C_5H_4), 4.99 (pt, $J_{\text{HH}} = 2\text{ Hz}$, 2 H, $\text{C}_5\text{H}_3\text{SiMe}_3$), 5.79 (m, 2 H, C_5H_4), 5.99 (pt, $J_{\text{HH}} = 2\text{ Hz}$, 2 H, $\text{C}_5\text{H}_3\text{SiMe}_3$), 6.03 (m, 6 H, C_5H_4 , $\text{C}_5\text{H}_3\text{SiMe}_3$); EI mass spectrum, m/e (relative intensity) M^+ , 892 (100); $\text{M}^{2+} - \text{C}_2\text{SiMe}_3$, 348 (28). Anal. Calcd for $\text{C}_{40}\text{H}_{62}\text{Si}_6\text{Zr}_2$ (893.89): C, 53.75; H, 6.99. Found: C, 53.73; H, 7.07.

X-ray Structure Determinations of 1b, 3a, and 7. The structures of compounds **1b**, **3a**, and **7** were determined from single-crystal X-ray diffraction data, which were collected using a Siemens R3m/V (Nicolet Syntex) diffractometer. Crystallographic data for **1b**, **3a**, and **7** are given in Table 1. All structures were solved by direct methods (SHELXTL PLUS; Sheldrick, G. M. University of Göttingen: Göttingen, Germany, 1988). An empirical absorption correction was applied. The structures of **1b** and **3a** were refined by the least-squares method based on F with all reflections (SHELXTL PLUS) the structure of **7** was refined by the least-squares method based on F^2 with all reflections (SHELXL 93; Sheldrick, G. M. University of Göttingen: Göttingen, Germany, 1993). All non-hydrogen atoms were refined anisotropically; the hydrogens were placed in calculated positions. Two of the trimethylsilyl groups (C(18)–C(20); C(213), C(214)) in **7** are disordered.

Acknowledgment. We are grateful to the Deutsche Forschungsgemeinschaft, the Volkswagenstiftung and the Fonds der Chemischen Industrie for financial support. We thank Th. Jannack for carrying out the MS measurements.

Supporting Information Available: Tables of crystal data and structure refinement, bond lengths and bond angles, and anisotropic displacement factors for **1b**, **3a**, and **7** (21 pages). Ordering information is given on any current masthead page.

OM9500984

Solid–Gas Reactions of the “Lightly Stabilized” $\text{Os}_3(\text{CO})_{11}\text{L}$ ($\text{L} = \text{NCCH}_3$, C_2H_4) Clusters with CO , NH_3 , and H_2

Silvio Aime,* Walter Dastrù, Roberto Gobetto, Jochen Krause, and Enrico Sappa

Dipartimento di Chimica Inorganica, Chimica Fisica e Chimica dei Materiali, Università di Torino, Via Pietro Giuria 7, 10125 Torino, Italy

Received December 27, 1994[®]

The solid–gas reactions of the “lightly stabilized” $\text{Os}_3(\text{CO})_{11}\text{L}$ ($\text{L} = \text{NCCH}_3$ (**1**), $\text{L} = \text{C}_2\text{H}_4$ (**2**)) clusters with gaseous reactants as CO , NH_3 , and H_2 have been investigated. At 80 °C polycrystalline samples (ca. 50 mg) of **1** and **2** undergo substitution of the axially bound acetonitrile ligand and the equatorially coordinated ethene ligand by the gaseous reactants. **1** and **2** react with ^{13}CO to form $\text{Os}_3(\text{CO})_{11}(^{13}\text{CO})$ (**3a**), but no site selectivity is observed for the labeled carbonyl ligand (as shown by ^{13}C MAS NMR). On reaction with NH_3 both **1** and **2** afford $\text{Os}_3(\text{CO})_{11}(\text{NH}_3)$ (**4**) with the ammonia ligand coordinated in an axial position. The observed stereochemistry of the reaction products of **1** and **2** with CO and NH_3 suggests the presence of an unsaturated intermediate $\text{Os}_3(\text{CO})_{11}$, which displays an intramolecular axial–equatorial exchange of the vacant coordination site. Reaction with dihydrogen of solid $\text{Os}_3(\text{CO})_{11}(\text{NCCH}_3)$ (**1**) or $\text{Os}_3(\text{CO})_{11}(\text{C}_2\text{H}_4)$ (**2**) gives $\text{H}_2\text{Os}_3(\text{CO})_{11}$ as first product, which under the experimental conditions affords $\text{Os}_3(\text{CO})_{12}$ and $\text{H}_2\text{Os}_3(\text{CO})_{10}$.

Introduction

The development of solid–gas reactions^{1–6} is of great interest not only for the positive ecological impact associated with the possibility of avoiding the use of organic solvents. As far as possible applications are concerned, a better knowledge of solid–gas reactions may provide useful insights into the design of novel sensor devices for gases. Furthermore, the investigation of stoichiometric transformations of organometallic solids may lead to the development of catalytic reactions in the solid state; this would be a viable alternative to heterogeneous catalysis using organometallic compounds supported on inorganic surfaces.

For a solid–gas reaction two general pathways can be envisaged: (a) The crystalline solid is loosely packed and contains channels through which small gaseous molecules can diffuse and flood the whole solid. (b) The gaseous molecules react at the surface of the solid disrupting the crystalline order and allowing more gaseous reactant to penetrate the interlayer spaces and interact with further substrate molecules. To get bulk reactivity, such a process may require the sliding of the product species over the surface of the solid; this step should be favored by an increase in temperature.

In principle, for organometallic compounds one would expect solid–gas reactions to take place readily if the

solid substrate is coordinatively unsaturated. This has recently been shown⁷ by the solid state reactions of $\text{H}_2\text{Os}_3(\text{CO})_{10}$ ($46 e^-$) with gaseous Lewis bases L ($\text{L} = \text{CO}$, NH_3 , H_2S) which give rise to the electron precise adducts $\text{H}_2\text{Os}_3(\text{CO})_{10}\text{L}$ ($48 e^-$). We are interested in extending this approach through the use of organometallic compounds which may easily afford coordinatively unsaturated species upon spontaneous release of coordinated groups. Metal carbonyl clusters containing nitrile or olefin ligands as leaving groups have been shown to be very reactive^{8–10} in solution, and for this reason, these derivatives are sometimes denoted as “lightly stabilized” systems.

In order to assess if these systems are also reactive in the solid state, we have studied the reactions between solid $\text{Os}_3(\text{CO})_{11}\text{L}$ ($\text{L} = \text{NCCH}_3$, C_2H_4) clusters and gaseous reactants such as CO , NH_3 , and H_2 .

Results and Discussion

Reactions of $\text{Os}_3(\text{CO})_{11}(\text{NCCH}_3)$ (1**) and $\text{Os}_3(\text{CO})_{11}(\text{C}_2\text{H}_4)$ (**2**) with Carbon Monoxide.** When crystalline yellow $\text{Os}_3(\text{CO})_{11}(\text{NCCH}_3)$ (**1**) is reacted with CO (1 atm) at 80 °C, a pale yellow powder of $\text{Os}_3(\text{CO})_{12}$ (**3**) is formed. The conversion is complete after several hours (12–24 h) as can be shown by IR. When **1** is reacted under the same conditions with ^{13}CO (Scheme 1), $\text{Os}_3(\text{CO})_{11}(^{13}\text{CO})$ (**3a**) is obtained. The ^{13}C MAS NMR spectrum of **3a** shows that the ^{13}CO ligand is equally distributed over axial (ax) and equatorial (eq) sites as shown by integra-

[®] Abstract published in *Advance ACS Abstracts*, May 1, 1995.

(1) Thomas, J. M.; Moro, S. E.; Desvergne, J. P. *Adv. Phys. Org. Chem.* **1977**, *15*, 63.

(2) Siedle, A. R.; Newmark, R. A. *J. Am. Chem. Soc.* **1989**, *111*, 2058.

(3) Bianchini, C.; Peruzzini, M.; Zanobini, F. *Organometallics* **1991**, *10*, 3415.

(4) Chin, C. S.; Lee, B.; Kim, S. *Organometallics* **1993**, *12*, 1462.

(5) Bianchini, C.; Zanobini, F.; Aime, S.; Gobetto, R.; Psaro, R.; Sordelli, L. *Organometallics* **1993**, *12*, 4757.

(6) Bianchini, C.; Farnetti, E.; Graziani, M.; Kaspar, J.; Vizza, F. *J. Am. Chem. Soc.* **1993**, *115*, 1753.

(7) Aime, S.; Dastrù, W.; Gobetto, R.; Arce, A. *J. Organometallics* **1994**, *13*, 4232.

(8) Adams, A. D.; Selegue, J. P. In *Comprehensive Organometallic Chemistry*; Pergamon Press: Oxford, U.K., 1982; p 1025.

(9) Johnson, B. F. G.; Lewis, J.; Pippard, D. A. *J. Chem. Soc., Dalton Trans.* **1989**, 407.

(10) Tachikawa, M.; Shapley, J. R. *J. Organomet. Chem.* **1977**, *124*, C19.

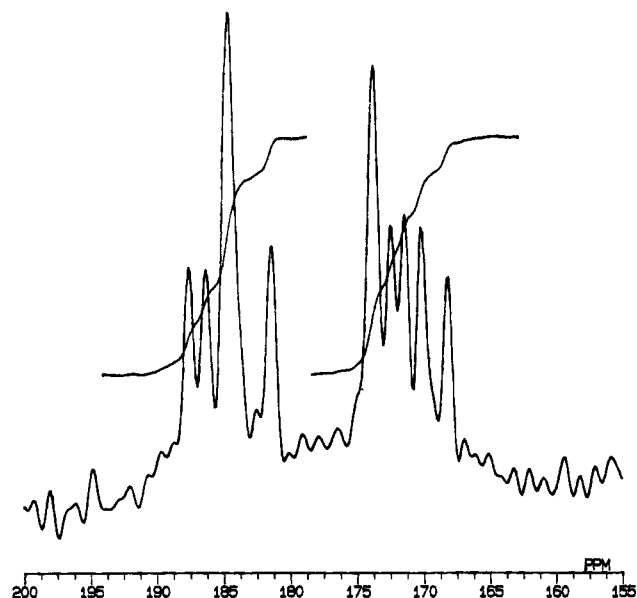
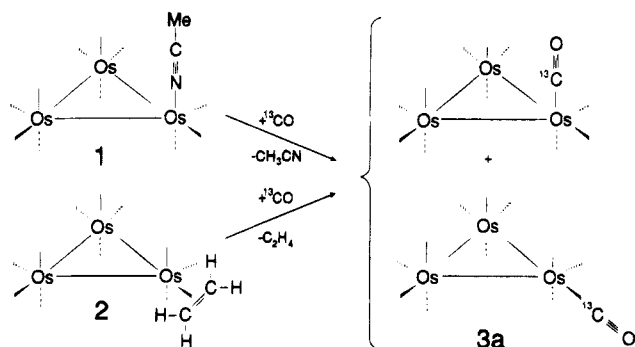


Figure 1. ¹³C MAS spectrum (isotropic region only) of Os₃(CO)₁₁(¹³CO) (**3a**) obtained by the solid-gas reaction of **1** with ¹³CO. Experimental conditions: spinning speed 6000 Hz, recycle time 120 s, pulse width 1 μs (20° pulse), ambient temperature.

Scheme 1



tion of the relative areas of the two regions previously assigned to axial (from 188 to 180 ppm) and equatorial (from 175 to 167 ppm) carbonyls, respectively (Figure 1). Like **1**, Os₃(CO)₁₁(C₂H₄) (**2**) reacts with CO at 80 °C to form Os₃(CO)₁₂ (**3**). The reaction of **2** with ¹³CO affords Os₃(CO)₁₁(¹³CO) (**3a**) (Scheme 1), the ¹³C MAS NMR spectrum of which is equal to the spectrum shown in Figure 1. The observed minor line broadening of the ¹³C resonances of **3a** with respect to the published spectrum of Os₃(CO)₁₂¹¹ appears to be associated with the powdery nature (microcrystals) of the product.

In principle, if a dissociative pathway for the reaction mechanism is assumed,¹² the axial coordination site of the acetonitrile ligand¹³ in **1** and the equatorial coordination site of the ethene ligand¹⁴ in **2** should confer an axial or equatorial site specificity, respectively, on the substitution product. Since solid Os₃(CO)₁₂ does not show any intermolecular exchange with ¹³CO (80 °C, 24 h), the observed equal distribution of ¹³CO over axial

and equatorial sites indicates that fluxional behavior occurs at some stage during the reaction. Three possible fluxional processes may be taken into consideration: (1) a fluxionality at the Os(CO)₃L (L = NCCH₃, C₂H₄) unit in the starting material (**1**, **2**) preceding the release of the acetonitrile/ethene ligand; (2) an axial-equatorial CO rearrangement in Os₃(CO)₁₂; (3) a fluxional behavior involving the vacant site of the Os(CO)₃ unit in the postulated reaction intermediate Os₃(CO)₁₁.

Although ax-eq CO exchange in **1** and **2** (process 1) is known to occur in solution, VT-¹³C CPMAS spectroscopy over the temperature range 25–80 °C has shown that the solid compounds are rigid on the NMR time scale. A fast (NMR detectable) ax-eq CO exchange in solid Os₃(CO)₁₂ (process 2) can be ruled out since no line broadening is observed in the ¹³C MAS spectra of Os₃(CO)₁₂ upon raising the temperature (spectra were recorded up to 120 °C).

However, complete scrambling of ¹³CO could also be achieved by a slow ax-eq CO exchange during the long reaction times necessary for complete conversion. Therefore, the reactions of **1** and **2** with ¹³CO were interrupted after shorter reaction times (e.g. 2 h, corresponding to ca. 40% conversion) and the products were analyzed by ¹³C MAS NMR. In both cases equal distribution of ¹³CO over axial and equatorial sites was observed already at such early stages of the reaction. On the basis of these results, also a slow ax-eq rearrangement in Os₃(CO)₁₂ does not seem to be responsible for the observed equilibration of ¹³CO at ax and eq sites. Although there is still the possibility of a rearrangement process having an intermediate rate, we think that it is more likely that the lack of site specificity in the solid state reactions of both **1** and **2** with ¹³CO is due to a fluxionality of the common unsaturated Os₃(CO)₁₁ intermediate (process 3): the vacant coordination site exchanges between axial and equatorial positions both of which are trapped by reaction with ¹³CO to yield the isoenergetical ax- and eq-(¹³CO)Os₃(CO)₁₁ in a 1:1 ratio.

The species Os₃(CO)₁₁ has already been observed by Wrighton et al.¹⁵ in a hydrocarbon glass at *T* ≤ 110 K as the product of photochemically induced loss of CO by Os₃(CO)₁₂. For Os₃(CO)₁₁ a rearrangement of the vacant coordination site from an equatorial to an axial position has been found, although no fluxional behavior was observed under the applied experimental conditions.

In order to further investigate the solid-gas reaction mechanism, we have studied the reaction of **1** and **2** with a gaseous reactant (NH₃) for which the two possible substitution products (ax or eq) would be energetically different.

Reactions of Os₃(CO)₁₁(NCCH₃) (1**) and Os₃(CO)₁₁(C₂H₄) (**2**) with Ammonia.** It is known that **1** reacts in solution with NH₃ to form Os₃(CO)₁₁(NH₃)¹⁶ (**4**). The same product is obtained when a CH₂Cl₂ solution of **2** is reacted with NH₃. (We have obtained slightly different IR and ¹H NMR data for **4** even when synthesizing **4** according to ref 16 (see Experimental Section).) Since its stereochemistry has not been assigned previously, we carried out a detailed NMR characterization

(11) Aime, S.; Botta, M.; Gobetto, R.; Osella, D.; Milone, L. *Inorg. Chim. Acta* **1988**, *146*, 151.

(12) Hudson, R. H. E.; Poë, A. J.; Sampson, C. L.; Siegel, A. *J. Chem. Soc., Dalton Trans.* **1989**, 2235.

(13) Dawson, P. A.; Johnson, B. F. G.; Lewis, J.; Puga, J.; Raithby, P. R.; Rosales, M. J. *J. Chem. Soc., Dalton Trans.* **1982**, 233.

(14) Evans, J.; McNulty, J. S. *J. Chem. Soc., Dalton Trans.* **1984**, 79.

(15) Bentson, J. G.; Wrighton, M. S. *J. Am. Chem. Soc.* **1987**, *109*, 4518.

(16) Suess-Fink, G. Z. *Naturforsch.* **1980**, *35b*, 454.

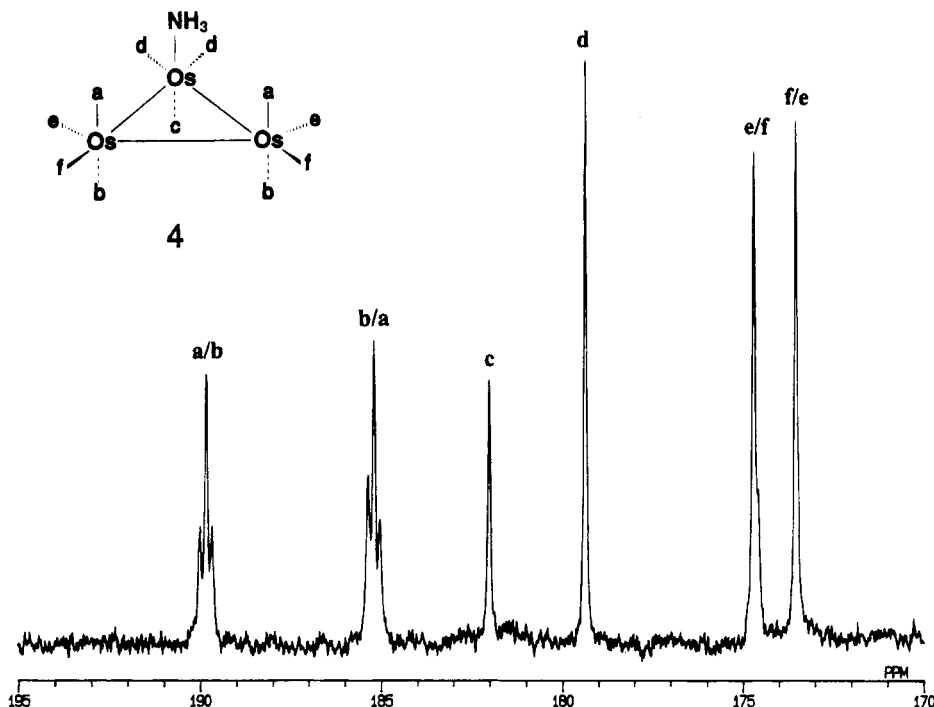


Figure 2. Structure and ^{13}C NMR spectrum (CD_2Cl_2 , -70°C) of a ^{13}CO -enriched sample ($\sim 40\%$) of $\text{Os}_3(\text{CO})_{11}(\text{NH}_3)$.

of **4**. In solution **4** is fluxional and the ^{13}C NMR spectrum (CD_2Cl_2) corresponding to its "frozen" structure is observed at -70°C (Figure 2). It shows six resonances in the region for terminally bound CO ligands at $\delta = 189.8$ (2C, **a/b**), 185.2 (2C, **b/a**), 182.0 (1C, **c**), 179.4 (2C, **d**), 174.7 (2C, **e/f**), and 173.5 (2C, **f/e**). The number and relative intensities of the CO resonances clearly indicate that the ammonia ligand is bound in an axial position; for $\text{M}_3(\text{CO})_{11}\text{L}$ complexes with L coordinated in an equatorial position eight CO resonances are expected. The signals at $\delta = 189.8$ and 185.2 show satellites due to ^{13}C - ^{13}C J -coupling (36.6 Hz) characteristic of two carbonyl ligands in a trans arrangement¹⁷ and are therefore attributed to the axial carbonyls **a** and **b**. The remaining resonance in the axial CO region which has an intensity of 1 is assigned to the carbonyl trans to the ammonia ligand. The signals at $\delta = 179.4$, 174.7 , and 173.5 correspond to the equatorial CO ligands labeled **d**, **e**, and **f**; their partial assignment follows from the dynamic behavior of **4**.¹⁸ The structure of **4** derived from the low-temperature ^{13}C limiting spectrum is analogous to that of the starting complex **1**, and it is in agreement with the expectation that nitrogen donor ligands always occupy axial coordination sites in trimetallic carbonyl clusters.^{7,19,20}

When solid **1** or **2** are reacted with NH_3 at 80°C for several hours (12–24 h), yellow powdery solids are obtained, the solution spectra (IR, ^1H , ^{13}C) of which are identical to those of **4** (Scheme 2). The substitutions of the acetonitrile/ethene ligands in **1** and **2**, respectively, by ammonia therefore occur in solution as well as in the solid state. The solid state reactions afford an analytical pure product (complete conversion into **4**).

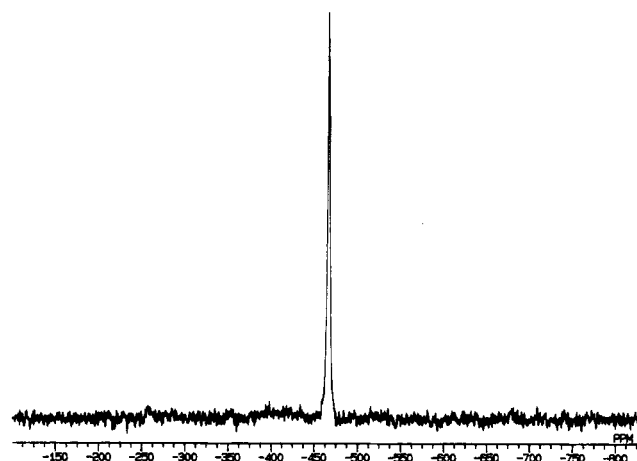
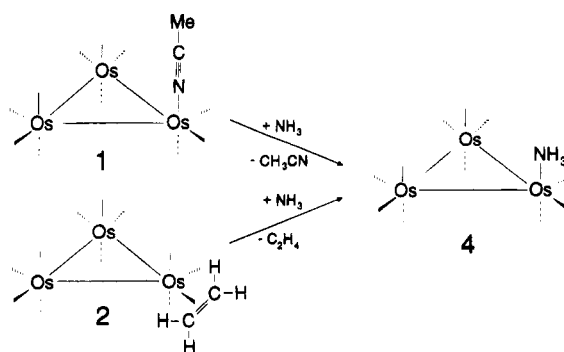


Figure 3. ^{15}N CPMAS spectrum (26°C) of $\text{Os}_3(\text{CO})_{11}({}^{15}\text{NH}_3)$ (**4a**). Experimental conditions: spinning speed 6000 Hz, recycle time 12 s, contact time 3 ms, ambient temperature.

Scheme 2



For the assignment of the stereochemistry of the solid state reactions the products had to be characterized in the solid state, since in solution **4** is fluxional and isomerization processes are likely to occur. Therefore, **1** and **2** were reacted at the solid state with $^{15}\text{NH}_3$ and

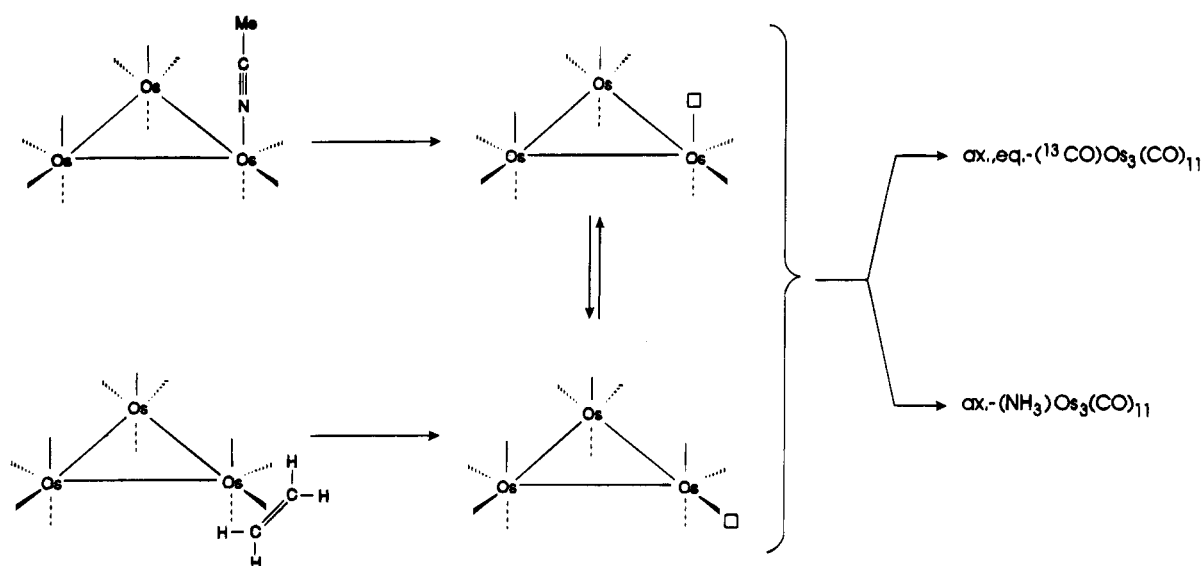
(17) Cotton, F. A.; Hanson, B. E.; Jamerson, J. D. *J. Am. Chem. Soc.* **1977**, *99*, 6588.

(18) Aime, S.; Dastrù, W.; Gobetto, R.; Krause, J.; Milone, L. Manuscript in preparation.

(19) Aime, S.; Dastrù, W.; Gobetto, R.; Krause, J.; Violano, L. *Inorg. Chim. Acta* **1995**, *235*, 357.

(20) Keister, J. B.; Shapley, J. R. *Inorg. Chem.* **1982**, *21*, 3304.

Scheme 3



the products were analyzed by ¹⁵N CPMAS spectroscopy. In both cases a sharp signal at $\delta = -467.0$ was observed (Figure 3) indicating that both **1** and **2** lead to the same stereoisomer of **4** (¹⁵NH₃ in an axial or equatorial coordination site should result in a different chemical shift). Furthermore the same ¹⁵N CPMAS spectrum is observed for Os₃(CO)₁₁(¹⁵NH₃) (**4a**) obtained by the solution reactions. Thus, also at the solid state only the ax-Os₃(CO)₁₁(NH₃) isomer is formed irrespective of the coordination site of the leaving group in the starting complexes.

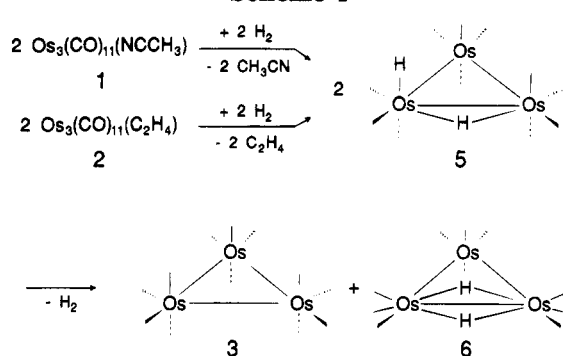
For the observed site selectivity of the NH₃ ligand a fluxional behavior at some stage of the reactions has to occur as already found for the analogous reactions with CO. Also for the reactions with NH₃ a fluxional intermediate Os₃(CO)₁₁ would account for the observed stereochemistry (Scheme 3). Whereas the reaction of the Os₃(CO)₁₁ intermediate with ¹³CO leads to the two isoenergetic isomers ¹³CO in an axial or equatorial coordination site, the NH₃ ligand clearly favors the axial position (thermodynamically more stable).

No signal for a (hypothetical) equatorial isomer of Os₃(CO)₁₁(¹⁵NH₃) is observed in the ¹⁵N CPMAS spectrum even when the reaction is interrupted after short reaction times (e.g. 2 h, corresponding to ca. 40% conversion). There are two possible interpretations for this observation: (i) the Os₃(CO)₁₁ reacts with ammonia only when the vacant coordination site is in an axial position (kinetically controlled reaction), or (ii) both the ax and eq isomers are formed, but the less stable equatorial one reacts back or rearranges quickly to give the axial isomer (thermodynamically controlled reaction).

Since no other isomer is observed during the reaction, we cannot decide whether the formation of ax-Os₃(CO)₁₁(NH₃) is due to a site specificity of the NH₃ addition to Os₃(CO)₁₁ or to a rearrangement of the equatorially substituted isomer.

Reaction of Os₃(CO)₁₁(NCCH₃) (1**) and Os₃(CO)₁₁(C₂H₄) (**2**) with Dihydrogen.** It has been shown by Poë et al.¹² that **1** reacts in solution with H₂ at 26 °C to form (μ-H)(H)Os₃(CO)₁₁ (**5**). When solid **1** and **2** are reacted with H₂ (1 atm) at 80 °C for 24 h a light yellow solid of Os₃(CO)₁₂ (**3**) and a violet sublimate of H₂Os₃(CO)₁₀ (**6**) in an equimolar ratio are formed. The two products are nicely separated in the reaction apparatus and are obtained as pure compounds.

Scheme 4



(CO)₁₀ (**6**) in an equimolar ratio are formed. The two products are nicely separated in the reaction apparatus and are obtained as pure compounds.

It can be assumed that the initial reaction with H₂ forms (μ-H)(H)Os₃(CO)₁₁ (**5**), which under the experimental conditions affords **3** and **6**. In fact, when an authentic sample of **5** is heated to 80 °C, it completely converts into **3** and **6** within 24 h. Thus we propose that the solid state reactions of **1** and **2** proceed according to Scheme 4.

Conclusions

The results obtained in this work show that the "lightly stabilized" organometallic complexes **1** and **2**, which are known to be very reactive in solution, also react readily in the solid state with gaseous reactants such as CO, NH₃, and H₂. The reactions apparently proceed via the coordinatively unsaturated species Os₃(CO)₁₁, which is formed upon release of the acetonitrile/ethene ligand (dissociative reaction pathway).

Since in the substitution reactions of the stereochemically different Os₃(CO)₁₁L clusters **1** and **2** with ¹³CO and NH₃ the stereochemistry is lost (¹³CO) or selectively only one product stereoisomer is formed (NH₃), the unsaturated intermediate is proposed to be fluxional; in principle, both axial and equatorial coordination sites are therefore accessible for the incoming ligand.

In summary, these findings show that it is possible to generate coordinatively unsaturated, highly reactive organometallic species "in situ". Acetonitrile and ethene

have been found to be good leaving groups; however, it may be interesting to explore systems containing bulkier groups as they are expected to be more labile. An alternative route to improve reaction rates may be provided by the control of the physical state of the solid substrate, such as its deposition in thin films on the walls of the reaction vessel or its physisorption on inert cellulosic supports.

In this account we dealt with simple addition reaction at the vacant site; however, one would expect that a number of chemical transformations could be carried out on the surface of metal clusters once suitable substrates have entered its coordination sphere.

Experimental Section

Materials. CO, NH₃, and H₂ were purchased from SIAD (Bergamo, Italy) and used without further purification. ¹³CO (99% enriched) and ¹⁵NH₃ (99% enriched) were purchased from Isotec (Miamisburg, OH). Os₃(CO)₁₁(NCCH₃),²¹ Os₃(CO)₁₁(C₂H₄),⁹ and H₂Os₃(CO)₁₁²² were prepared according to published methods. ¹³CO-enriched metal carbonyls were prepared by using as starting material ¹³C-enriched (ca. 40%) Os₃(CO)₁₂ obtained by direct exchange of ¹³CO with Os₃(CO)₁₂ (200 mg), in *n*-octane (100 mL) at 110 °C for 3 days in sealed vials (250 mL).

Spectra. Infrared spectra were recorded on a Perkin-Elmer 580B spectrometer. ¹H and ¹³C NMR spectra in solution were obtained on a JEOL EX400 spectrometer operating at 399.65 and 100.25 MHz, respectively. The high-resolution solid state ¹³C and ¹⁵N NMR experiments were performed on a JEOL GSE 270 (6.34 T) spectrometer operating at 67.8 and 27.4 MHz, respectively. Cylindrical 6 mm o.d. zirconia rotors with a sample volume of 120 μL were employed with a spinning speed in the range from 5.5 to 6.0 kHz. For all samples the magic angle was carefully adjusted from the ⁷⁹Br MAS (magic angle spinning) spectrum of KBr by minimizing the line width of the spinning side bands from the satellite transitions.

The MAS technique was used for ¹³C, whereas in the case of ¹⁵N the CPMAS technique was employed with a contact time

of 3 ms and a recycle time of 12 s. Conditions and scale reference for ¹⁵N measurement were refined by using a 98% isotopically enriched (¹⁵NH₄)₂SO₄ sample (δ = -360 with respect to CH₃NO₂ as a reference: δ = 0).

Reactions of Os₃(CO)₁₁(NCCH₃) (1) and Os₃(CO)₁₁(C₂H₄) (2) with CO. A 50 mg amount of 1 (2) was introduced in a Schlenk tube apparatus (25 mL). The system was evacuated and refilled with CO (1 atm). The Schlenk apparatus was placed in an oil bath at 80 °C. After 24 h Os₃(CO)₁₂ was formed quantitatively. The product was identified by IR (KBr pellets).²³

Reactions of Os₃(CO)₁₁(NCCH₃) (1) and Os₃(CO)₁₁(C₂H₄) (2) with NH₃. A 50 mg amount of 1 (2) was exposed to NH₃ gas (1 atm) at 80 °C in a Schlenk tube apparatus (25 mL). After 24 h yellow Os₃(CO)₁₁(NH₃) (4) was formed quantitatively. The product was identified by IR and NMR. IR: ν(CO) (cm⁻¹) (CH₂Cl₂) 2104 (w), 2050 (s), 2034 (vs), 1919 (m), 1996 (s), 1985 (sh), 1960 (sh); ν(NH₃) (cm⁻¹) (KBr) 3390, 3316; δ(NH₃) (cm⁻¹) 1626, 1290, 1277. ¹H NMR (acetone-*d*₆, 25 °C): δ = 4.09 (broad). ¹³C NMR (CD₂Cl₂, -70 °C): δ = 189.8 (2), 185.2 (2), 182.0 (1), 179.4 (2), 174.7 (2), 173.5 (2).

Reactions of Os₃(CO)₁₁(NCCH₃) (1) and Os₃(CO)₁₁(C₂H₄) (2) with H₂. A 50 mg amount of solid 1 was exposed to H₂ (1 atm) at 80 °C. After 24 h the starting material was completely converted into a violet sublimate (H₂Os₃(CO)₁₀) and a light yellow solid (Os₃(CO)₁₂) in an equimolar ratio. The products were identified by IR (KBr pellets).^{23,24}

Os₃(CO)₁₁(¹³CO) (3a) and Os₃(CO)₁₁(¹⁵NH₃) (4a) were obtained as described above using ¹³CO and ¹⁵NH₃, respectively. The reaction times for the solid state reactions indicate only the order of magnitude as they depend upon the particle size of the solid substrate.

Acknowledgment. We thank the Ministero dell'Università e della Ricerca Scientifica e Tecnologica (MURST, Rome) for financial support. The European Community (Commission-DG XII, HCM program) is gratefully acknowledged for providing a postdoctoral grant to J.K.

OM940987B

(21) Nicholls, J. N.; Vargas, M. D. *Inorganic Syntheses*; Angelici, R. J., Ed.; John Wiley & Sons: New York, 1990; Vol. 28, p 232.

(22) (a) Demming, A. J.; Hasso, S. *J. Organomet. Chem.* **1975**, *88*, C21. (b) Deeming, A. J.; Hasso, S. *J. Organomet. Chem.* **1976**, *114*, 313.

(23) Drake, S. R.; Loveday, P. A. *Inorganic Syntheses*; Angelici, R. J., Ed.; John Wiley & Sons: New York, 1990; Vol. 28, p 230.

(24) Kaesz, H. D. *Inorganic Syntheses*; Angelici, R. J., Ed.; John Wiley & Sons: New York, 1990; Vol. 28, p 238.

Synthesis, Structure, and Characterization of the $[\text{Fe}_5\text{S}_4(\text{CO})_{12}]^{2-}$ Ions and Studies on the Oxidative Conversion of the Dianion to $[\text{Fe}_6\text{S}_6(\text{CO})_{12}]^{2-}$

Daniel E. Barber,[†] Michal Sabat, Ekkehard Sinn,[‡] and Bruce A. Averill^{*,§}

Department of Chemistry, University of Virginia, Charlottesville, Virginia 22901

Received March 8, 1995[®]

The compounds $(\text{Pr}_4\text{N})_2[\text{Fe}_5\text{S}_4(\text{CO})_{12}]$ ($(\text{Pr}_4\text{N})_2\text{IV}$) and $(\text{Pr}_4\text{N})[\text{Fe}_5\text{S}_4(\text{CO})_{12}]\cdot 0.5\text{THF}$ ($(\text{Pr}_4\text{N})\text{V}\cdot 0.5\text{THF}$, THF = tetrahydrofuran) have been prepared and structurally characterized. Crystals of $(\text{Pr}_4\text{N})\text{IV}$ are monoclinic, space group $C2/c$ ($a = 34.16(1)$ Å, $b = 19.446(8)$ Å, $c = 17.902(8)$ Å, $\beta = 121.40(2)^\circ$, $R = 0.056$, $R_w = 0.064$, 2368 reflections with $I > 3\sigma(I)$); crystals of $(\text{Pr}_4\text{N})\text{V}\cdot 0.5\text{THF}$ are triclinic, space group $P1$ ($a = 11.745(1)$ Å, $b = 11.807(1)$ Å, $c = 15.198(2)$ Å, $\alpha = 68.58(1)^\circ$, $\beta = 85.99(1)^\circ$, $\gamma = 75.46(1)^\circ$, $R = 0.023$, $R_w = 0.038$, 5296 reflections with $I > 3\sigma(I)$). The two anions have similar structures, with a central Fe atom (Fe(II) and Fe(III) for **IV** and **V**, respectively) coordinated in a distorted tetrahedral geometry by two $[\text{Fe}_2\text{S}_2(\text{CO})_6]^{2-}$ ligands. Cluster **IV** undergoes an O_2 -specific oxidation to the known cluster $[\text{Fe}_6\text{S}_6(\text{CO})_{12}]^{2-}$ (**VI**) by an undetermined mechanism. Cluster **VI** can be prepared cleanly by reaction of $\text{Fe}_2\text{S}_2(\text{CO})_6$ (**I**) with $[\text{Fe}_4\text{S}_4(\text{CO})_{12}]^{2-}$ (**II**), and a mechanism involving oxidative addition of **I** to **II** is postulated. $(\text{Pr}_4\text{N})_2\text{VI}$ has been obtained in crystalline form (orthorhombic, space group $Cmc2_1$; $a = 18.870(8)$ Å, $b = 17.307(13)$ Å, $c = 16.430(3)$ Å, $R = 0.057$, $R_w = 0.076$, 2689 reflections with $I > 3\sigma(I)$) and structurally characterized. Oxidative addition of **II** is also suggested as an important step in the formation of the previously reported cluster $[\text{MoOF}_5\text{S}_6(\text{CO})_{12}]^{2-}$, which insight has resulted in an improved synthesis for the latter cluster. This newly-discovered reactivity of $[\text{Fe}_4\text{S}_4(\text{CO})_{12}]^{2-}$ makes the compound a potentially useful reagent in preparing a variety of mixed M–Fe–S clusters having new stoichiometries and structures.

Introduction

The reductive chemistry of the butterfly cluster $\text{Fe}_2\text{S}_2(\text{CO})_6$ (**I**)¹ has been well established for several years, primarily due to the efforts of Seyferth and co-workers.^{2,3} Their work and additional studies in our laboratory have shown that reduction of the neutral complex **I** with 1 equiv of a reducing agent yields the disulfide-bridged dimeric compound $[\text{Fe}_4\text{S}_4(\text{CO})_{12}]^{2-}$ (**II**),⁴ and further reaction of **II** with a second 1 equiv of reductant yields the dianion $[\text{Fe}_2\text{S}_2(\text{CO})_6]^{2-}$ (**III**).² The bridging sulfides of both **II** and **III** possess nucleophilic character, as demonstrated by their reactions with alkyl halides to form S-alkylated products^{3a,4} and, in the case of the fully reduced dianion **III**, by reaction with a variety of metal halides to yield metal clusters in which the $[\text{Fe}_2\text{S}_2(\text{CO})_6]^{2-}$ unit acts as a bidentate ligand coordinated via the bridging sulfides.³

In our research, we have used the dianion **III** as an iron and sulfur source in reactions with molybdenum halides to yield molybdenum–iron–sulfur clusters with high iron and sulfur content. Examples of the unusual clusters prepared by this method include the $[\text{MoOF}_5\text{S}_6(\text{CO})_{12}]^{2-}$,^{5a} $[\text{MoFe}_4\text{S}_3(\text{CO})_{14}]^{2-}$,^{5b} and $[\text{MoFe}_6\text{S}_6(\text{CO})_{16}]^{2-}$ ions.^{5b,c} Until recently,^{5b} the rearrangements involved in the formation of these clusters were poorly understood. In this paper, the preparation and characterization of the $[\text{Fe}_5\text{S}_4(\text{CO})_{12}]^{2-}$ (**IV**) and $[\text{Fe}_5\text{S}_4(\text{CO})_{12}]^-$ (**V**) ions and studies of the oxidative conversion of **IV** to the known cluster $[\text{Fe}_6\text{S}_6(\text{CO})_{12}]^{2-}$ (**VI**)⁶ are presented. During this work, novel reactivity of the $[\text{Fe}_4\text{S}_4(\text{CO})_{12}]^{2-}$ ion (**II**) was observed, and the chemistry of **II** has subsequently been shown to be important in many of the aforementioned cluster formation reactions.

Experimental Section

All reactions were carried out under a dry nitrogen atmosphere (except where otherwise indicated) using standard Schlenk techniques. Solvents were distilled under N_2 ; acetonitrile (MeCN) was distilled from CaH_2 , tetrahydrofuran (THF) was distilled from Na–benzophenone ketyl, methanol (MeOH) was distilled from magnesium methoxide, and 2-propanol (*i*-PrOH) was distilled from $\text{Al}(\text{O-}i\text{-Pr})_3$. Hexane and diethyl ether were reagent grade and were used without further purification. Tetraalkylammonium halide salts were generally

[†] Current address: Department of Chemistry, Oberlin College, 130 West Lorain Street, Oberlin, OH 44074.

[‡] Current address: School of Chemistry, University of Hull, Cottingham Road, Hull HU6 7RX, U.K.

[§] Current address: E. C. Slater Instituut, Universiteit van Amsterdam, Plantage Muidergracht 12, 1018 TV Amsterdam, NL.

[®] Abstract published in *Advance ACS Abstracts*, May 1, 1995.

(1) (a) Hieber, W.; Gruber, J. Z. *Anorg. Allg. Chem.* **1958**, 296, 91. (b) Wei, C.-H.; Dahl, L. F. *Inorg. Chem.* **1965**, 4, 1.

(2) (a) Seyferth, D.; Henderson, R. S.; Song, L.-C. *Organometallics* **1982**, 1, 125. (b) Seyferth, D.; Kiwan, A. M.; Sinn, E. *J. Organomet. Chem.* **1985**, 281, 111.

(3) (a) Cowie, M.; DeKock, R. L.; Wagenmaker, T. R.; Seyferth, D.; Henderson, R. S.; Gallagher, M. K. *Organometallics* **1989**, 8, 119. (b) Day, V. W.; Lesch, D. A.; Rauchfuss, T. B. *J. Am. Chem. Soc.* **1982**, 104, 1290. (c) Seyferth, D.; Henderson, R. S.; Gallagher, M. K. *J. Organomet. Chem.* **1980**, 193, C75. (d) Bogan, L. E., Jr.; Lesch, D. A.; Rauchfuss, T. B. *J. Organomet. Chem.* **1983**, 250, 429.

(4) Bose, K. S.; Sinn, E.; Averill, B. A. *Organometallics* **1984**, 3, 1126.

(5) (a) Bose, K. S.; Lamberty, P. C.; Kovacs, J. A.; Sinn, E.; Averill, B. A. *Polyhedron* **1986**, 5, 393. (b) Eldredge, P. A.; Bose, K. S.; Barber, D. E.; Bryan, R. F.; Sinn, E.; Rheingold, A.; Averill, B. A. *Inorg. Chem.* **1991**, 30, 2365. (c) Eldredge, P. A.; Bryan, R. F.; Sinn, E.; Averill, B. A. *J. Am. Chem. Soc.* **1988**, 110, 5573.

(6) Lilley, G. L.; Sinn, E.; Averill, B. A. *Inorg. Chem.* **1986**, 25, 1073.

dried for several hours under vacuum at 60–70 °C and were stored in a Vacuum Atmospheres drybox under argon. Iron pentacarbonyl, iron(II) bromide, Superhydride (1 M LiEt₃BH in THF), and sublimed sulfur were obtained from Aldrich and were used as received. The compounds Fe₂S₂(CO)₆ (I)^{3d} and [Fe₂S₂(CO)₆]²⁻ (III)² were prepared by published procedures; (Ph₄As)₂[Fe₄S₄(CO)₁₂] ((Ph₄As)₂II) was prepared by the method of Bose et al.⁴ The peroxide compound DABCO·2H₂O₂ (DABCO = 1,4-diazabicyclo[2.2.2]octane) was prepared as described,⁷ and [Fe(phen)₃][BF₄]₃ was a gift from Phyllis Hunt (University of Virginia).

Infrared spectra were recorded in an NaCl solution IR cell on a Mattson Cygnus 1000 FTIR spectrometer using EXPERT software. Electronic spectra were recorded on a Cary 219 UV–visible spectrophotometer. Electrochemical measurements were performed using a Princeton Applied Research Model 175 universal programmer and Model 173 potentiostat and a Yokogawa 3023 plotter; the working and auxiliary electrodes were Pt wire. All values are referenced to a saturated calomel electrode (SCE). Elemental analyses were obtained from Galbraith Laboratories, Inc. (Knoxville, TN).

Preparation of (Pr₄N)₂[Fe₅S₄(CO)₁₂], (Pr₄N)₂[IV]. To a solution of 2 mmol of [Fe₂S₂(CO)₆]²⁻, III, in ca. 40 mL of THF at –78 °C was added a room temperature (RT) suspension of 0.22 g (1 mmol) FeBr₂ in ca. 5 mL of MeCN. The solution was allowed to warm to RT, during which time the deep green solution changed to dark greenish-brown color. The solvent was removed under vacuum, the residue was dissolved in ca. 3 mL of MeCN, and a solution of 0.80 g (3 mmol) of (Pr₄N)Br in ca. 30 mL of *i*-PrOH was added. The solution was filtered immediately to remove the microcrystalline product; larger X-ray-quality crystals separated from the filtrate upon standing (total isolated yield ca. 70%). IR (MeCN), ν_{CO} (cm⁻¹): 2021 (s), 1997 (vs), 1945 (s, sl br). Electronic spectrum (MeCN), λ (nm) (ε (M⁻¹ cm⁻¹)): 700 (2126), 480 (sh), 425 (4930, sh), 330 (>20 000). Anal. Calcd (found) for C₃₆H₅₆N₂Fe₅S₄O₁₂: C, 38.73 (38.01); H, 5.06 (5.49); N, 2.51 (2.22); S, 11.49 (12.36); Fe, 25.01 (24.49).

Preparation of (Pr₄N)[Fe₅S₄(CO)₁₂], (Pr₄N)[V]. Method A. A solution of 1.12 g (1 mmol) of (Pr₄N)₂IV in ca. 20 mL of MeCN at RT was treated with 1 equiv of Cp₂Fe⁺ (prepared by reaction of ferrocene with NOBF₄ (1 equiv)); the color of the solution changed to deep bluish-green, and the conversion of IV to product was observed in the IR spectrum. The product was precipitated as X-ray-quality crystals (which contain 1/2 equiv of THF solvent) in nearly quantitative yield (92%) by slow diffusion of hexane into a concentrated THF solution of V. IR (MeCN), ν_{CO} (cm⁻¹): 2046 (s), 2020 (vs), 1982 (s, br). Electronic spectrum (MeCN), λ (nm) (ε (M⁻¹ cm⁻¹)): 663 (4600), 486 (4900), 330 (22 300).

Method B. A solution of 0.69 g (2 mmol) of Fe₂S₂(CO)₆, I, in ca. 20 mL of THF at –78 °C was treated with 3 mL (3 mmol) of Superhydride. To this solution was added a RT suspension of 0.44 g (2 mmol) of FeBr₂ in ca. 10 mL of MeCN, and the solution was warmed to RT. The solvent was removed under vacuum, and the residue was redissolved in a minimum volume of MeCN. The product was precipitated by addition of 0.8 g (3 mmol) of (Pr₄N)Br in *i*-PrOH and was shown to be identical to that obtained by method A (yield ca. 60%).

Method C. To a solution of 2 mmol of III in ca. 30 mL of THF at –78 °C was added a solution of 0.30 g (1 mmol) of FeBr₃ in ca. 7 mL of MeCN at RT. The deep bluish-green solution was warmed to RT, during which time the color changed to brownish-green. The solvent was removed under vacuum, and the residue was dissolved in MeCN. Solution IR spectra of the mother liquor showed ν_{CO} bands due to V with small amounts of IV and [Fe₆S₆(CO)₁₂]²⁻ (VI) as contaminants.

Preparation of (Pr₄N)₂[Fe₆S₆(CO)₁₂], (Pr₄N)₂[VI]. Method A. A solution of (Pr₄N)₂IV in MeCN was prepared, and

O₂(g) was bubbled through the solution via syringe until the solution color had changed to deep purple and the IR spectrum showed no ν_{CO} bands due to IV. The solution volume was reduced, and *i*-PrOH was added to precipitate (Pr₄N)₂VI in ca. 12% yield. X-ray-quality crystals were grown by slow cooling of saturated MeCN/*i*-PrOH solutions of the cluster. IR (MeCN), ν_{CO} (cm⁻¹): 2042 (m), 2012 (vs), 1969 (ms, sl br).

Method B. An equimolar solution of 0.17 g (0.5 mmol) of Fe₂S₂(CO)₆, I, and (Ph₄As)₂[Fe₄S₄(CO)₁₂], (Ph₄As)₂II, was prepared in ca. 30 mL of MeCN at RT. The reaction was monitored by IR spectroscopy over ca. 3–4 h, during which time the solution changed from orange-green to deep purple. The product was spectroscopically identical to that obtained by method A.

Preparation of (Ph₄As)₂[MoOF₆S₆(CO)₁₂]. To a solution of 1.03 g (3 mmol) of Fe₂S₂(CO)₆ (I) in ca. 30 mL of THF at –78 °C was added 4 mL (4 mmol) of Superhydride in 0.5 mL increments over 30 min. To the resulting deep green solution was added rapidly a solution of 0.38 g (1 mmol) of MoOCl₃·(THF)₂ in ca. 3 mL of MeCN. The initial deep orange reaction mixture turned brown upon warming to room temperature. The solvent was removed under vacuum, the residue was dissolved in ca. 2 mL of MeCN, and excess (Ph₄As)Cl in ca. 30 mL of *i*-PrOH was added, resulting in precipitation of a microcrystalline solid. The solid was filtered out, washed with *i*-PrOH, and dried under vacuum. The solution IR spectrum of this product (MeCN (cm⁻¹): ν_{CO}, 2042 (m), 2008 (s), 1966 (ms); ν_{Mo=O}, 930) was identical to that of the previously reported compound.^{5a} Yield: 0.93 g (55%).

X-ray Analyses. All X-ray measurements were carried out on an Enraf-Nonius CAD4 diffractometer using Mo radiation. Unit cell dimensions were determined using the setting angles of 25 high-angle reflections. The intensities of three standard reflections were measured every 3 h of X-ray exposure and showed no significant fluctuations. Intensities were corrected for absorption by applying the program DIFABS.⁸ Crystallographic calculations were performed by using the TEXSAN 5.0 software package.⁹ Crystal data and collection and refinement parameters are summarized in Table 1 for (Pr₄N)₂[Fe₅S₄(CO)₁₂] ((Pr₄N)₂IV), (Pr₄N)[Fe₅S₄(CO)₁₂]·0.5THF ((Pr₄N)V·0.5THF), and (Pr₄N)₂[Fe₆S₆(CO)₁₂] ((Pr₄N)₂VI). In the first two structures, the cations were crystallographically ordered with no unusual features. Tables of all positional and thermal parameters and selected distances and angles are available as supplementary material.

(Pr₄N)₂IV. MULTAN was used to locate 4 of the 5 iron atoms, and the other atoms were located via successive Fourier syntheses.¹⁰ All heavy atoms were refined isotropically using full-matrix least-squares refinement; no account was taken of H atoms.

(Pr₄N)V·0.5THF. Data collection and refinement were performed as for (Pr₄N)₂IV, except that structure solution was by direct methods (SIR-88)¹¹ and all heavy atoms were refined anisotropically. The THF molecule was found to be disordered between two positions on the center of symmetry, such that C atoms in the 2 and 4 positions of the rings in the two orientations were superimposed (C26 and C26*). The atoms of the THF were refined anisotropically in these two positions with occupancy factors of 0.5 for the nonoverlapped atoms and 1.0 for the overlapped atoms.

(Pr₄N)₂VI. Data collection and refinement were performed as for (Pr₄N)V·0.5THF, except that the heavy atoms of the cations were refined isotropically using the following model for disorder of one of the cations. While the mirror plane

(8) Walker, N.; Stuart, D. *Acta Crystallogr., Sect. A* **1983**, *39*, 158.

(9) TEXSAN: *Single Crystal Structure Analysis Software*; Version 5.0; Molecular Structure Corp.: The Woodlands, TX 77381, 1989.

(10) Freyberg, D. P.; Mockler, G. M.; Sinn, E. *J. Chem. Soc., Dalton Trans.* **1976**, 447.

(11) SIR88: Burla, M. C.; Camalli, M.; Cascarano, G.; Giacovazzo, C.; Polidori, G.; Spagna, R.; Viterbo, D. *J. Appl. Crystallogr.* **1989**, *22*, 389.

Table 1. Summary of Crystal Data, Intensity Measurements, and Structure Solution and Refinement

compd	(Pr ₄ N) ₂ IV	(Pr ₄ N)V·0.5THF	(Pr ₄ N) ₂ VI
A. Crystal Data			
formula	C ₃₆ H ₅₆ N ₂ O ₁₂ S ₄ Fe ₅	C ₂₆ H ₃₀ NO _{12.5} S ₄ Fe ₅	C ₃₆ H ₅₆ N ₂ O ₁₂ S ₆ Fe ₆
fw	1116	962	1236
cryst color, habit	black prism	black prism	black prism
cryst dimens (mm)	0.35 × 0.35 × 0.30	0.46 × 0.39 × 0.32	0.43 × 0.32 × 0.28
cryst system	monoclinic	triclinic	orthorhombic
<i>a</i> (Å)	34.26	11.745(1)	18.870(8)
<i>b</i> (Å)	19.446(8)	11.807(1)	17.307(3)
<i>c</i> (Å)	17.902(8)	15.198(2)	16.430(6)
α (deg)	90	68.58(1)	90
β (deg)	121.40(2)	85.99(1)	90
γ (deg)	90	75.46(1)	90
<i>V</i> (Å ³)	10150	1899	5366
space group	<i>C</i> 2/ <i>c</i> (No. 2)	<i>P</i> 1 (No. 1)	<i>C</i> mc2 ₁ (No. 36)
<i>Z</i>	8	2	4
<i>d</i> _{calc} (g/cm ³)	1.46	1.69	1.53
μ(Mo Kα) (cm ⁻¹)	1.64	21.32	18.56
B. Intensity Measurements			
diffractometer	Enraf-Nonius CAD4	Enraf-Nonius CAD4	Enraf-Nonius CAD4
radiation	Mo Kα	Mo Kα	Mo Kα
<i>T</i> (°C)	23	-120	23
scan type	ω-2θ	ω-2θ	ω-2θ
2θ _{max} (deg)	50	48	50
no. of reflns	total: 8153	total: 6287 unique: 5957 (<i>R</i> _{int} = 0.010)	total: 4145
corrs	Lorentz-polarization absorption	Lorentz-polarization absorption	Lorentz-polarization absorption
transm factors		0.80-1.25	0.69-1.31
C. Structure Solution and Refinement			
struct solution	Multan	direct methods (SIR88)	direct methods (SIR88)
refinement	full-matrix least squares	full-matrix least squares	full-matrix least squares
function minimized	Σw(<i>F</i> _o - <i>F</i> _c) ²	Σw(<i>F</i> _o - <i>F</i> _c) ²	Σw(<i>F</i> _o - <i>F</i> _c) ²
no. observns with <i>I</i> > 3σ(<i>I</i>)	2368	5296	2689
no. variables	241	432	235
reflncs/param	9.8	12.3	11.4
<i>R</i> ; <i>R</i> _w	0.056; 0.054	0.023; 0.038	0.057; 0.076
goodness of fit	1.62	1.28	2.22
max peak (e/Å ³) in final diff map	0.28	0.72	1.25

symmetry of the ion requires two propyl groups to be located on the plane, the presence of several peaks in difference Fourier maps suggested that carbon atoms C11, C12, C14, and C15 were disordered between two equally populated locations outside the symmetry plane. The final difference Fourier map showed a peak of 1.25 e/Å³ intensity in the vicinity of the disordered propyl groups.

Results and Discussion

Syntheses of Clusters. The cluster [Fe₅S₄(CO)₁₂]²⁻, **IV**, see Chart 1, was originally observed as one of four products in the reaction of MoCl₅ with the dianion **III**.^{5a} In addition, reaction of MoOCl₃(THF)₂ with 3 equiv of **III** to form [MoOF₅S₆(CO)₁₂]²⁻ also yields significant amounts of cluster **IV** and, to a lesser extent, the known cluster^{5c} [MoFe₆S₆(CO)₁₆]²⁻. A direct synthesis of **IV** was achieved by the straightforward reaction of FeBr₂ with 2 equiv of **III**. Cluster **IV** can be isolated in ca. 70% yield as its Pr₄N⁺ salt and can be identified readily by characteristic ν_{CO} bands at 2027, 1989, and 1945 cm⁻¹ in its infrared spectrum. Solutions of the cluster are dark greenish-brown due to absorptions at 700 and 425 nm and an intense absorption at ca. 330 nm. The crystal structure and physical properties of **IV** are consistent with the formulation of the cluster as a central Fe^{II} chelated by two [Fe₂S₂(CO)₆]²⁻ ligands (vide infra).

Electrochemical measurements of **IV** (in MeCN, 0.1 M (Bu₄N)ClO₄) reveal a nearly reversible oxidation at *E*_{1/2} = -0.465 V vs SCE (Δ*E*_p = 120 mV, *i*_{pa}/*i*_{pc} = 1.02).

The value of *E*_{1/2} for the oxidation process is at the upper limit of the range reported for the Fe^{II/III} redox couple of mononuclear four-coordinate iron complexes with thiolate ligands,¹² and therefore the existence of a stable Fe^{III} analog of **IV** was investigated. One-electron oxidation of **IV** by ferrocenium or [Fe(phen)₃]³⁺ (in MeCN at room temperature) resulted in quantitative conversion to the monoanionic analog [Fe₅S₄(CO)₁₂]⁻, **V**. The conversion was monitored easily by observing the disappearance of the IR spectrum of the starting material and the appearance of the product's spectrum at 2047, 2021, and 1987 cm⁻¹; in addition, the color of the solution changed to deep bluish-green, reflecting shifts in the cluster's visible absorptions to 660 and 488 nm. Cluster **V** can be isolated (also as its Pr₄N⁺ salt) in >90% yield by precipitation from THF/hexane. The cluster is somewhat less stable in solution than is the dianionic analog, and this property has hampered efforts to obtain analytically pure samples. The cluster is isostructural with cluster **IV**, and the physical properties of **V** indicate that the oxidation is localized on the central Fe atom (vide infra).

Cluster **V** can also be synthesized in good yield by reaction of 1 equiv of FeBr₂ with a solution containing 1 equiv of **III** and 0.5 equiv of [Fe₄S₄(CO)₁₂]²⁻ (**II**), prepared as described in the Experimental Section, or by reaction of FeBr₃ with 2 equiv of **III**; thus the Fe²⁺

(12) (a) Lane, R. W.; Ibers, J. A.; Frankel, R. B.; Holm, R. H. *Proc. Natl. Acad. Sci. U.S.A.* **1975**, *72*, 2868. (b) Millar, M.; Lee, J. F.; Koch, S. A.; Fikar, R. *Inorg. Chem.* **1982**, *21*, 4105. (c) Hagen, D. S.; Reynolds, J. G.; Holm, R. H. *J. Am. Chem. Soc.* **1981**, *103*, 4054.

Chart 1. Schematic Drawings of the Clusters Referred to in This Work with Terminal CO Ligands Indicated by Straight Lines Attached to Fe

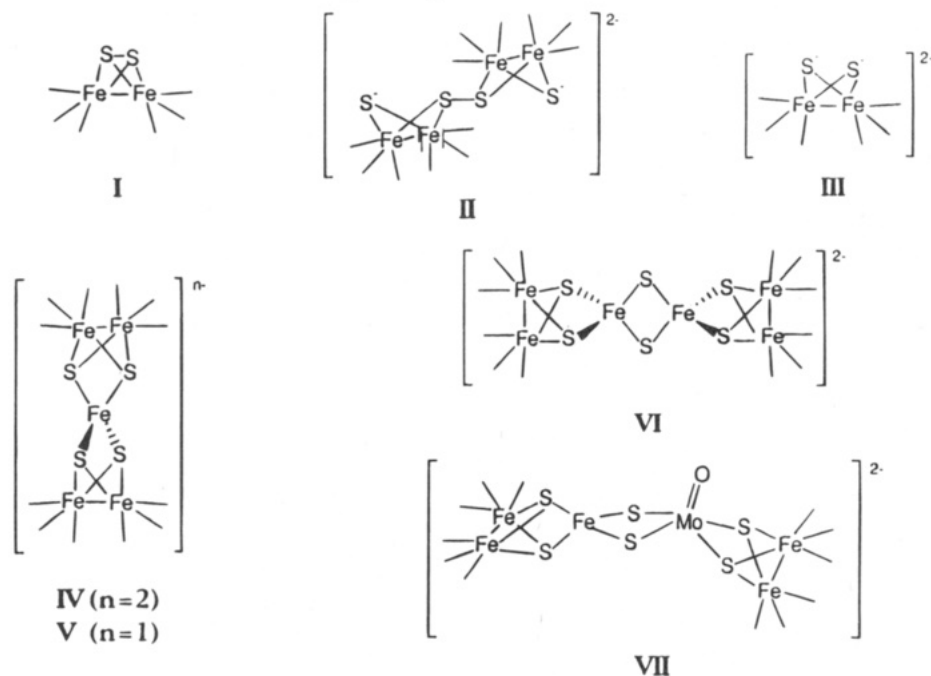


Table 2. Selected Bond Distances (Å) and Angles (deg) for $[\text{Fe}_5\text{S}_4(\text{CO})_{12}]^{2-}$ (IV) and $[\text{Fe}_5\text{S}_4(\text{CO})_{12}]^{-}$ (V)^a

	IV	V
Fe-S1	2.345(4)	2.2674(8)
Fe-S2	2.338(5)	2.2691(8)
Fe-S3	2.340(5)	2.2689(8)
Fe-S4	2.345(4)	2.2673(8)
S1-Fe-S2	82.0(2)	87.76(3)
S3-Fe-S4	81.9(2)	87.84(3)
S1-Fe-S3	107.6(2)	120.25(3)
S1-Fe-S4	149.0(2)	120.48(3)
S2-Fe-S3	144.7(2)	120.79(3)
S2-Fe-S4	107.6(2)	123.55(3)

^a Fe refers to the central Fe atom, Fe3 and Fe1 in IV and V, respectively.

ion acts as a one-electron reductant toward the $[\text{Fe}_4\text{S}_4(\text{CO})_{12}]^{2-}$ species present in solution. In both reactions the initial color of the solution was deep bluish-green, consistent with formation of exclusively V, but the color became more brownish-green upon warming to room temperature. Infrared spectroscopy indicated that small amounts of IV and $[\text{Fe}_6\text{S}_6(\text{CO})_{12}]^{2-}$, VI (vide infra), were produced. Over several days the spectrum of V disappeared and bands at 2063, 2018, 1991, and 1929 cm^{-1} appeared; these belong to as yet unidentified clusters, and their appearance reflects the relative instability of this cluster.

Structural Characterization of New Clusters. Crystals of $(\text{Pr}_4\text{N})_2\text{IV}$ suitable for X-ray diffraction were obtained from saturated MeCN/*i*-PrOH (ca. 1:8) solutions. The relevant crystal data are summarized in Table 1; the room-temperature intensity data were refined satisfactorily to final residuals of $R = 5.6\%$ and $R_w = 6.4\%$. The structure of the dianion IV, shown in Figure 1, consists of a central Fe atom coordinated by four S atoms from the two $\text{Fe}_2\text{S}_2(\text{CO})_6$ ligands; Table 2 summarizes important bond distances and angles within the cluster. The average $\text{Fe}^{\text{II}}-\text{S}$ distance is 2.343(5) Å, which is slightly shorter than the corresponding value

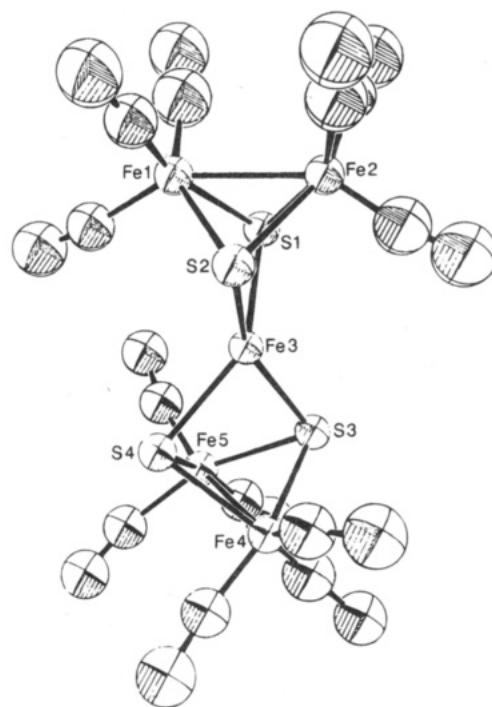


Figure 1. Structure of the $[\text{Fe}_5\text{S}_4(\text{CO})_{12}]^{2-}$ ion, IV (50% probability thermal ellipsoids).

found for other $\text{Fe}^{\text{II}}-\text{S}_4$ complexes which contain thiolate-type ligands ($[\text{Fe}(\text{S}_2\text{-o-xy})_2]^{2-}$, 2.37 Å;^{13a} $[\text{Fe}(\text{SPh})_4]^{2-}$, 2.36 Å; $[\text{Fe}(\text{S}_2\text{C}_4\text{O}_2)_2]^{2-}$, 2.39 Å^{13b,c}). The geometry about the central Fe (Fe3) is severely distorted from tetrahedral with S-Fe3-S "bite" angles (due to the $\text{Fe}_2\text{S}_2(\text{CO})_6$ ligands) of 82.0(2)° (average); the remaining S-Fe3-S angles are grouped as two smaller

(13) (a) Lane, R. W.; Ibers, J. A.; Frankel, R. B.; Papaefthymiou, G. C.; Holm, R. H. *J. Am. Chem. Soc.* **1977**, *99*, 84. (b) Coucouvanis, D.; Swenson, D.; Baenziger, N. C.; Holah, D. G.; Kostikas, A.; Simopoulos, A.; Petrouleas, V. *J. Am. Chem. Soc.* **1976**, *98*, 5721. (c) Coucouvanis, D.; Swenson, D.; Baenziger, N. C.; Murphy, C.; Holah, D. G.; Sfarnas, N.; Simopoulos, A.; Kostikas, A. *J. Am. Chem. Soc.* **1981**, *103*, 3350.

Table 3. Comparison of Structural Parameters of Chelated Fe₂S₂(CO)₆ Units in Selected Complexes

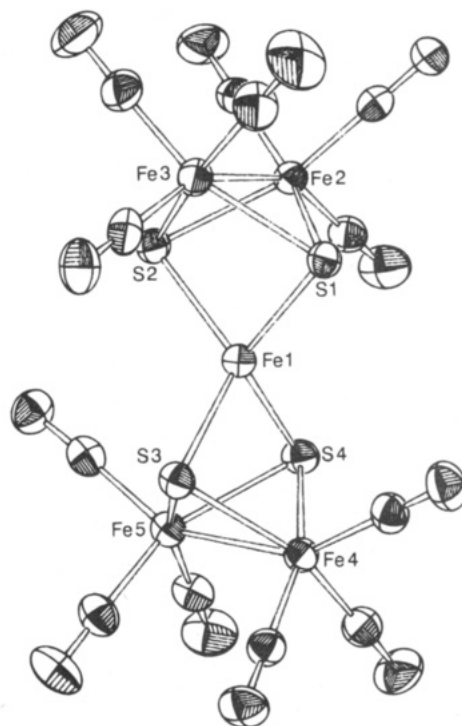
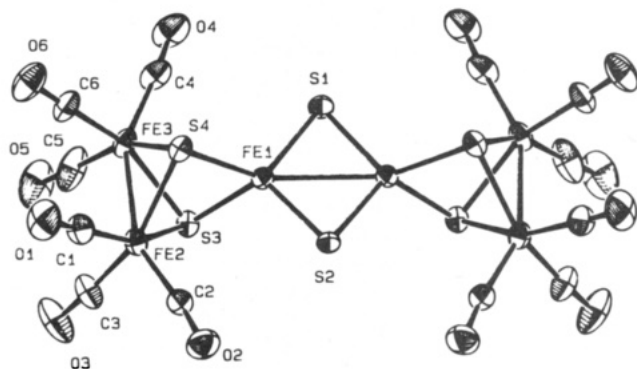
	bond length (av, Å)		bond angle (av, deg)		
	Fe-Fe	Fe-S	Fe-S-Fe	S-Fe-S	Fe ₂ S (dihedral)
[Fe ₅ S ₄ (CO) ₁₂] ²⁻ (IV)	2.483	2.301	65.2	83.7	104.9
[Fe ₅ S ₄ (CO) ₁₂] ⁻ (V)	2.500	2.307	65.62	85.98	108.61
[Fe ₆ S ₆ (CO) ₁₂] ²⁻ (VI)	2.504	2.307	65.80	83.6	104.99
Ge[Fe ₂ S ₂ (CO) ₆] ₂ ^a	2.49	2.30	65.6	95.3	

^a Reference 14.

(average 107.6(2)°) and two larger (average 147°) angles, with an overall average value of 127.3°. The latter observation is a result of the distortion of the central Fe from idealized *D*_{2d} symmetry, as can also be seen by the dihedral angle of 128.4° between the Fe3-S1-S2 and Fe3-S3-S4 planes (*D*_{2d} symmetry requires that this angle be 90°). Similar distortions have not been observed in other iron(II)-thiolate complexes.¹³ The two Fe₂S₂(CO)₆ units are identical within experimental error; the average Fe-Fe and Fe-S distances (2.48 and 2.30 Å, respectively) and the Fe-S-Fe angle (average 65.3°) are similar to the corresponding parameters in other structurally characterized complexes containing the Fe₂S₂(CO)₆ unit (see Table 3). The S-Fe-S angle shows the most variability among the compounds listed; the value for IV is 83.7° (average) and results in a dihedral angle of 104.9° (average) between the two Fe₂S planes.

The structure of the monoanionic analog V has also been determined. Crystals of (Pr₄N)V·0.5THF suitable for X-ray diffraction studies were obtained by slow diffusion of hexane into a THF solution of the cluster. Relevant crystal data are summarized in Table 1; the intensity data (-120 °C) were refined to residuals of *R* = 2.4% and *R*_w = 3.9%. The structure of V is shown in Figure 2; selected bond distances and angles are compared in Table 2. Again the geometry about the central Fe is distorted tetrahedral, with an S-Fe1-S bite angle of 87.80(3)° (average); in this case the remaining S-Fe1-S angles are all nearly equal, with an average value of 121.3°. This is because the symmetry about the central iron approaches idealized *D*_{2d}, with a dihedral angle between the S1-Fe1-S2 and S3-Fe1-S4 planes of 88.9°. In addition, the Fe1-S bond distance of 2.27(1) Å (average) is nearly 0.1 Å shorter than that in the dianion IV and is typical of other Fe^{III}-S₄ bond distances.^{13a,15} The Fe₂S₂(CO)₆ units again are identical to each other and have Fe-S and Fe-Fe distances (2.31 Å (average) and 2.50 Å (average), respectively) and Fe-S-Fe angles (65.6° (average)) similar to those of other complexes containing this unit; the S-Fe-S angle (86.0° (average)) is more than 2 deg larger than the corresponding angle in the reduced cluster IV (see Table 3).

Although the structure of (BzEt₂MeN)₂[Fe₆S₆(CO)₁₂], (BzEt₂MeN)₂VI, has been reported, the data only allowed for refinement to residuals of *R* = 9.9% and *R*_w = 10.8% due to disorder in the cations.⁶ The current work has provided crystals of (Pr₄N)₂VI that have allowed significantly better refinement (*R* = 5.7%, *R*_w = 7.6%). The resulting structure, shown in Figure 3, is essentially the same as that reported previously. The

**Figure 2.** Structure of the [Fe₅S₄(CO)₁₂]⁻ ion, V (50% probability thermal ellipsoids).**Figure 3.** Structure of the [Fe₆S₆(CO)₁₂]²⁻ ion, VI (50% probability thermal ellipsoids). Important distances and angles: Fe(1)-S(1)(av), 2.210(4) Å; Fe(1)-S(2,3)(av), 2.304(4) Å; S(1)-Fe(1)-S(1'), 104.9° (see also Table 3).

most noteworthy differences are that the S3-Fe1-S4 angle is significantly smaller in the refined structure of the Pr₄N⁺ salt (83.7(1)° vs 86.8° (in BzEt₂MeN)₂VI) and that the average Fe-S distance in the Fe₂S₂(CO)₆ ligands is more in keeping with the value observed in other compounds that contain this moiety. The structural parameters of the Fe₂S₂(CO)₆ unit in VI are compared with those of other clusters in Table 3. Both the S-Fe-S angles (average 83.6°) and the dihedral angle between the two Fe₂S planes (105°) are more similar to the corresponding values obtained in IV; this average C-O distance (1.14 Å) is identical to that found

(14) Nametkin, N. S.; Tyurin, V. D.; Aleksandrov, G. G.; Kuz'min, O. V.; Nekhaev, A. I.; Andrianov, V. G.; Mavlonov, M.; Struchkov, Y. T. *Izv. Akad. Nauk SSSR, Ser. Khim.* **1979**, 6, 1353.

(15) Koch, S. A.; Maelis, L. E.; Millar, M. *J. Am. Chem. Soc.* **1983**, 105, 5944.

in **V**. The Fe1–S3,S4 average distance (2.304 Å) is near the average of the corresponding distances in clusters **IV** and **V**. Complete structural data are provided in the supplementary material.

Reaction of $[\text{Fe}_5\text{S}_4(\text{CO})_{12}]^{2-}$ (IV**) with Oxidants.** During routine manipulation of solutions of **IV**, it was observed that these solutions changed from dark greenish-brown to the characteristic deep purple color of the known compound $[\text{Fe}_6\text{S}_6(\text{CO})_{12}]^{2-}$, **VI**,⁶ upon exposure to air. More careful investigation of this phenomenon showed that the conversion could be effected by bubbling pure $\text{O}_2(\text{g})$ via syringe through an MeCN solution of **IV**. Infrared spectroscopy indicated that **VI** was the only detectable CO-containing product of this reaction; no CO-containing intermediates were observed (see Figure 4). Similarly, reaction of the monoanion **V** with O_2 resulted in the formation of a small amount of **VI**, but a large amount of $\text{Fe}_2\text{S}_2(\text{CO})_6$, **I**, was also formed; this enhanced susceptibility to oxidative decomposition is consistent with the observed lower stability of **V** in solution. Because the oxidative conversion of **IV** to **VI** must involve a novel rearrangement, this reaction was investigated in more detail.

Oxidations of **IV** with ferrocenium and $[\text{Fe}(\text{phen})_3]^{3+}$ were performed in order to determine whether the role of oxygen was as an outer-sphere oxidant. Cluster **V** was first produced during initial experiments with ferrocenium as oxidant; later experiments utilized the more powerful oxidant $[\text{Fe}(\text{phen})_3]^{3+}$. The latter experiments showed that, upon oxidation of **V** with $[\text{Fe}(\text{phen})_3]^{3+}$, a significant amount of **I** was produced as well as a mixture of several other unidentified clusters. At no time was any formation of **VI** detected either by IR spectroscopy or by changes in the color of the solution. Thus, O_2 is not merely an outer-sphere oxidant but must play a more direct role in the conversion of **IV** to **VI**.

The reactions of both **IV** and **V** with superoxide and H_2O_2 were examined in order to determine whether oxidants related to O_2 could also induce the conversion of these clusters to **VI**. Slow addition of 1 equiv of KO_2 (solubilized in a 0.1 M DMSO solution of 18-crown-6¹⁶) to **V** in MeCN, a reaction which formally involves the same number of electrons as $\text{IV} + \text{O}_2$, resulted immediately in nearly quantitative conversion (by IR) of **V** to **IV**, with a small amount of **VI** also formed; further addition of KO_2 resulted only in precipitation of an insoluble black solid. These observations indicate that superoxide acts as a reductant toward **V**, with formation of **VI** due to reaction of the redox products **IV** and O_2 , and that reaction of superoxide with **IV** does not yield **VI** but produces only insoluble decomposition products.

Both **IV** and **V** reacted with H_2O_2 (as DABCO- $2\text{H}_2\text{O}_2$)⁷ to yield mixtures of compounds; in both cases a large excess of H_2O_2 was required before significant reaction was observed (>8 equiv and >7 equiv for the two reactions, respectively). Although the mixtures in both reactions displayed infrared bands at 2040, 2007, and 1964 cm^{-1} , the relative intensities of these bands were different in each case; also, the mixture obtained from the reaction with **IV** was more complex, with additional lower-energy bands at 1930 and 1904 cm^{-1} . No formation of **VI** was observed in either case by IR spectroscopy or by detection of the characteristic purple color of the

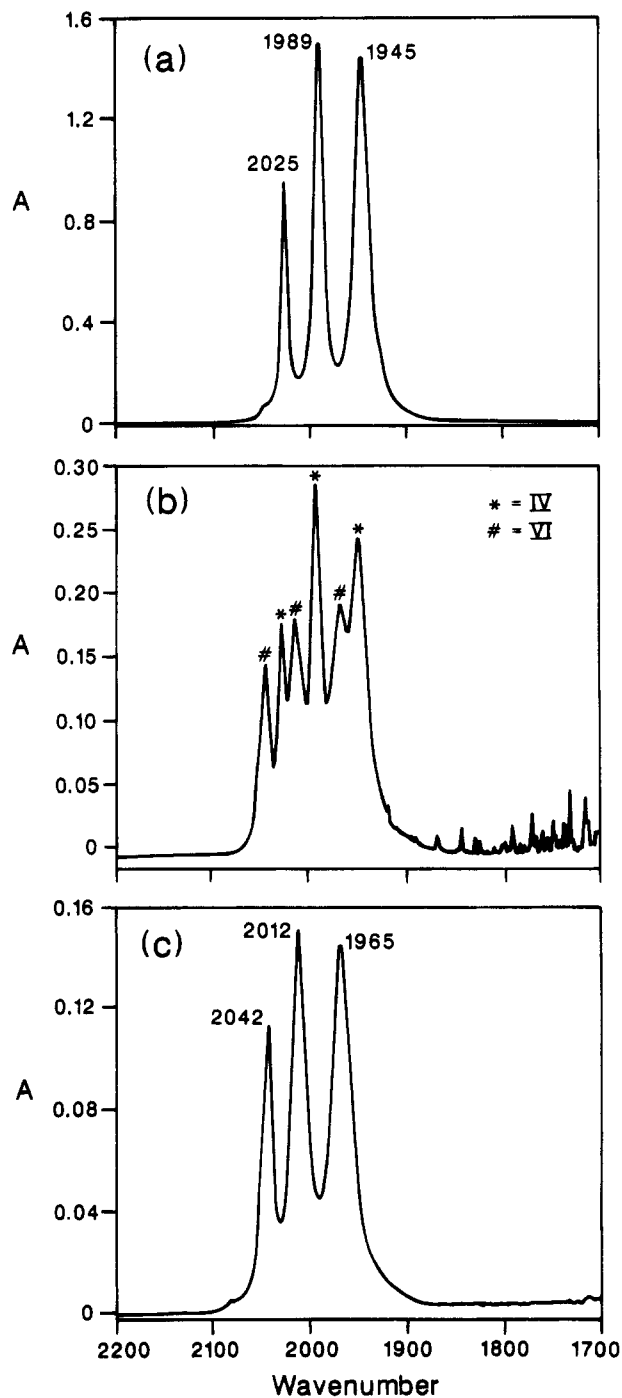


Figure 4. Infrared spectra (ν_{CO} region, MeCN solution) of (a) **IV**, (b) **IV** + O_2 (incomplete reaction), and (c) **IV** + O_2 (final product). Starred peaks in (b) correspond to **IV**; those indicated by # correspond to **VI**.

cluster. The products from these reactions have not been further characterized; no evidence for formation of **VI** was noted, even upon exposure of the solutions to the atmosphere.

The stoichiometry of the reaction of **IV** with O_2 was evaluated by two separate experiments. Since the ν_{CO} infrared absorbances of **VI** (in MeCN) obeyed Beer's law in the concentration range 0–1 mM, the concentration of **VI** present in solution could be determined using infrared spectroscopy. Therefore, a solution containing a known amount of **IV** was reacted slowly with O_2 until the IR absorbances of the starting material had disappeared, and the amount of **VI** produced was determined by the sample's infrared absorbance at 2043 cm^{-1} . This

(16) Valentine, J. S.; Curtis, A. B. *J. Am. Chem. Soc.* **1975**, *97*, 224.

Table 4. Reactions of IV and V with Possible Oxidation Products

reactants	products
[Fe ₅ S ₄ (CO) ₁₂] ²⁻ (IV) + 2Fe ₂ S ₂ (CO) ₆ (I)	I + V + [Fe ₆ S ₆ (CO) ₁₂] ²⁻ (VI)
[Fe ₅ S ₄ (CO) ₁₂] ²⁻ (IV) + [Fe ₄ S ₄ (CO) ₁₂] ²⁻ (II)	no reaction
[Fe ₅ S ₄ (CO) ₁₂] ⁻ (V) + Fe ₂ S ₂ (CO) ₆ (I)	no reaction
[Fe ₅ S ₄ (CO) ₁₂] ⁻ (V) + [Fe ₄ S ₄ (CO) ₁₂] ²⁻ (II)	I + V + [Fe ₆ S ₆ (CO) ₁₂] ²⁻ (VI)
Fe ₂ S ₂ (CO) ₆ (I) + [Fe ₄ S ₄ (CO) ₁₂] ²⁻ (II)	[Fe ₆ S ₆ (CO) ₁₂] ²⁻ (VI)

experiment indicated that 4 equiv of IV was required for the formation of 1 equiv of VI. The amount of O₂ needed for this transformation was also determined by titration of a known amount of IV (in MeCN) with an O₂-saturated acetone solution;¹⁷ IR spectroscopy indicated that the conversion was complete after addition of 5 equiv of O₂. These values should be considered as upper limits since slow oxidative decomposition of VI by O₂ would result in the values being too high. Presumably several Fe–O and/or Fe–S species are also present, but the nature of these products has not been determined.

Reactions of Possible Oxidation Products. The possibility was considered that the formation of VI is a result of the rapid reaction of two transiently formed oxidation products of IV. The known clusters Fe₂S₂(CO)₆ (I), [Fe₄S₄(CO)₁₂]²⁻ (II), and [Fe₅S₄(CO)₁₂]⁻ (V) were considered as possible oxidation products of IV, and the reactions among these four compounds were examined to determine if this postulate was feasible. All reactions were performed in MeCN at room temperature, since these are the conditions under which the reactivity of IV with O₂ is observed, and were monitored by IR spectroscopy. The results of these studies are summarized in Table 4 and are discussed in detail below.

Reaction of an equimolar mixture of IV and I resulted immediately in a mixture of V and II in addition to the starting materials. Addition of an extra 1 equiv of I to this orange-green solution resulted in no spectroscopic changes other than an increase in the intensity of the bands associated with this cluster. This solution changed to the purplish color of VI over ca. 4 h; IR spectroscopy confirmed the presence of a large amount of VI as well as V and a small amount of I. Presumably I is acting as an oxidant toward IV in the initial step of this reaction, and VI is formed by a relatively slow reaction of some of the clusters present in solution.

Similar results were obtained in the reaction of 1 equiv of [Fe₅S₄(CO)₁₂]⁻ (V) with 1 equiv of [Fe₄S₄(CO)₁₂]²⁻ (II). The initial reaction mixture again contained a mixture of all four clusters and gradually converted to a mixture of VI, V, and a small amount of IV. In this case, V acts as an oxidant toward II to produce IV and I. Further evidence for the observation that the two forms of [Fe₅S₄(CO)₁₂]ⁿ⁻ (n = 1, 2) act as electron-transfer reagents comes from the absence of reactivity either between IV and II (the two more reduced species) or between V and I (the two more oxidized species) after several hours at room temperature.

The final entry in Table 4 clearly indicates that the source of [Fe₆S₆(CO)₁₂]²⁻ (VI) in the preceding experiments is the reaction of Fe₂S₂(CO)₆ (I) with [Fe₄S₄(CO)₁₂]²⁻ (II) at room temperature. An equimolar mixture of I and II cleanly reacted over ca. 4 h to yield

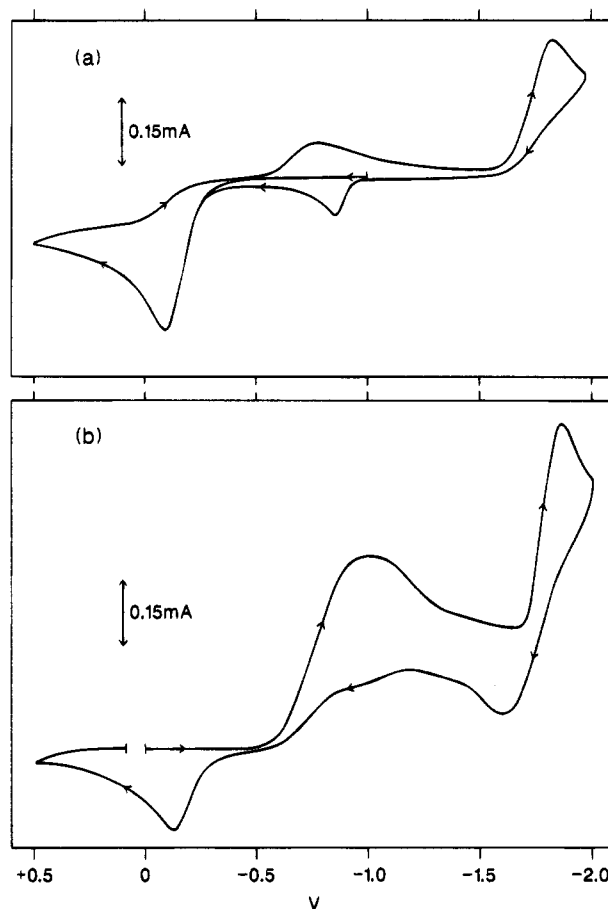


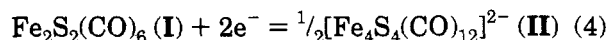
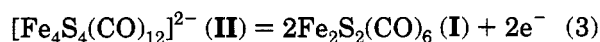
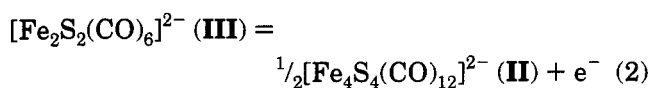
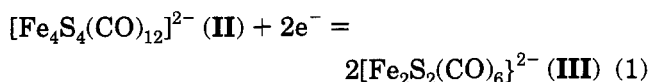
Figure 5. Cyclic voltammograms (0.1 M Bu₄NClO₄ in MeCN, scan rate = 100 mV/s) of (a) [Fe₄S₄(CO)₁₂]²⁻ (II) and (b) Fe₂S₂(CO)₆ (I).

VI, with only a small amount of either II or IV (produced by slow decomposition of II in solution) as a minor contaminant. This result indicates that the role of the [Fe₅S₄(CO)₁₂]ⁿ⁻ species is to act as a "redox buffer" to maintain a supply of both I and II for the production of VI. A similar role for the "o-xylyl dithiolate-disulfide" mixture was suggested in the previously reported synthesis of VI.⁶

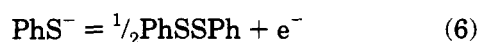
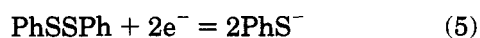
The electrochemical properties of I and II were studied by cyclic voltammetry. Figure 5a shows the cyclic voltammogram of II (MeCN, 0.1 M (Bu₄N)ClO₄); the initial potential sweep is anodic, with an initial potential of -1.0 V (vs SCE). The first cycle revealed an irreversible oxidation at $E_{pa} = -0.087$ V, a somewhat broadened irreversible reduction at $E_{pc} \approx -0.75$ V, and an irreversible reduction at $E_{pc} = -1.84$ V; subsequent cycles revealed an additional irreversible oxidation at $E_{pa} = -0.86$ V. More careful examination of this system revealed that the oxidation wave at -0.86 V was not observed if the reduction at -1.84 V was not performed; similarly, the broad reduction at ca. -0.75 V was not observed if the oxidation at -0.087 V did not occur. These observations indicate that two additional electroactive species are produced upon reduction at -1.87

(17) Ebsworth, E. A. V.; Connor, J. A.; Turner, J. J. *Comprehensive Inorganic Chemistry*; Pergamon Press Ltd.: Oxford, U.K., 1973; Vol. 2, p 709.

V and oxidation at -0.087 V. The voltammogram can be interpreted in terms of the known chemistry of the $\text{Fe}_2\text{S}_2(\text{CO})_6$ species. The reduction at -1.84 V is assumed to correspond to the formation of $[\text{Fe}_2\text{S}_2(\text{CO})_6]^{2-}$ (**III**) via eq 1, whereas the oxidation at -0.86 V cor-



responds to re-oxidation of **III** and subsequent dimerization as shown in eq 2. Likewise, the oxidation wave at -0.087 V and the broad reduction wave at -0.75 V correspond to similar cleavage and dimerization reactions as shown in eqs 3 and 4, respectively. These four reactions are also assumed to explain the cyclic voltammogram of $\text{Fe}_2\text{S}_2(\text{CO})_6$ (Figure 5b), which displayed a broad, irreversible reduction at $E_{pc} \approx -1.0$ V, a nearly irreversible reduction at $E_{pc} = -1.87$ V, and an irreversible oxidation at -0.12 V that was absent if the first reduction at -1.0 V did not occur. By analogy to the cyclic voltammogram of **II**, these electrode processes are assigned to eqs 4, 1, and 3, respectively. The breadth of the reduction wave at -1.0 V and the presence of a weak shoulder at ca. -1.0 V in the oxidative sweep in the voltammogram of **I** (see Figure 5b) indicate that the chemistry at the electrode surface is complex; more detailed electrochemical studies would be required to allow meaningful statements to be made about the mechanisms of these electrode processes. The interpretation of this electrochemistry is supported both by the known chemistry of $\text{Fe}_2\text{S}_2(\text{CO})_6$ species and by the qualitative similarity of these voltammograms to that of diphenyl disulfide, which displays an irreversible reduction at -1.54 V and an irreversible oxidation at -0.20 V assigned to the reactions shown in eqs 5 and 6,



respectively.¹⁸ Our electrochemical results demonstrate that **I–III** can be formed by purely electrochemical means and provide support for the idea that the role of the $[\text{Fe}_5\text{S}_4(\text{CO})_{12}]^{2-}$ couple in the reactions described in Table 4 is that of an electron-transfer reagent.

The reaction of **I** with **II** to form **VI** provides a clear explanation of the reactions listed in Table 4 and of the published synthesis of **VI** from **I** and the *o*-xylyl dithiolate–disulfide mixture.⁶ However, this reaction alone is far too slow to account for the production of **VI** by oxidation of **IV**. This reactivity could be responsible if the reaction between **I** and **II** were catalyzed by a third species in solution. Several postulated catalysts (H^+ (as

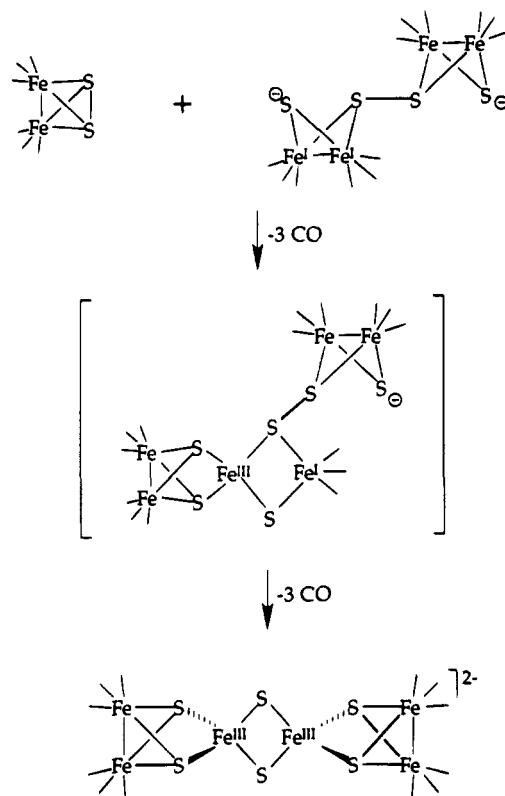


Figure 6. Possible mechanism for formation of $[\text{Fe}_6\text{S}_6(\text{CO})_{12}]^{2-}$, **VI**.

$\text{CH}_3\text{CO}_2\text{H}$), FeBr_2 , FeBr_3 , OH^- (as $(\text{Me}_4\text{N})\text{OH}$ in MeOH), $\text{FeBr}_2 + \text{OH}^-$, and $\text{FeBr}_3 + \text{OH}^-$) were added to equimolar solutions of **I** and **II**, and the colors of the solutions were observed to determine qualitatively whether **VI** was formed. Both H^+ and OH^- were considered since the air and oxygen used in the previous reactions were not dried and perhaps contained traces of moisture; the Fe^{II} and Fe^{III} salts were considered as possible side products in the degradation of **IV**, and $\text{Fe}-\text{OH}^-$ mixtures could conceivably result in the formation of catalytically active iron–oxo compounds. In no case was the immediate formation of **VI** noted upon addition of the potential catalyst. Upon addition of the Fe^{II} solutions to the mixture an immediate bluish-green color was noted, consistent with the formation of **V** from Fe^{II} and **II** (as described in the synthesis section). Thus, there is no evidence to suggest that the observed reaction of **IV** with O_2 involves a catalyzed reaction between **I** and **II**.

Proposed Mechanisms for Cluster Formation. A straightforward mechanism can be proposed to explain the formation of $[\text{Fe}_6\text{S}_6(\text{CO})_{12}]^{2-}$ (**VI**) from $\text{Fe}_2\text{S}_2(\text{CO})_6$ (**I**) and $[\text{Fe}_4\text{S}_4(\text{CO})_{12}]^{2-}$ (**II**). The mechanism, shown in Figure 6, features an initial oxidative decarbonylation of **II** by the disulfide bond of **I**; as mentioned in the Introduction, oxidative addition of **I** to metal carbonyls has been observed previously.³ The intermediate thus formed then undergoes an intramolecular oxidative addition via the remaining disulfide bond to yield the final product. The first oxidative addition is most likely rate limiting since no intermediates can be detected in the reaction mixture. Intramolecular oxidative addition is a novel mode of reactivity recognized in our laboratory, and this reaction has been found to be important in the syntheses of several other $\text{Mo}-\text{Fe}-\text{S}$ clusters.^{5b}

(18) (a) Krüger, H.-J.; Holm, R. H. *Inorg. Chem.* **1989**, *28*, 1148. (b) Bradbury, J. R.; Masters, A. F.; McDonnell, A. C.; Brunette, A. A.; Bond, A. M.; Wedd, A. G. *J. Am. Chem. Soc.* **1981**, *103*, 1959.

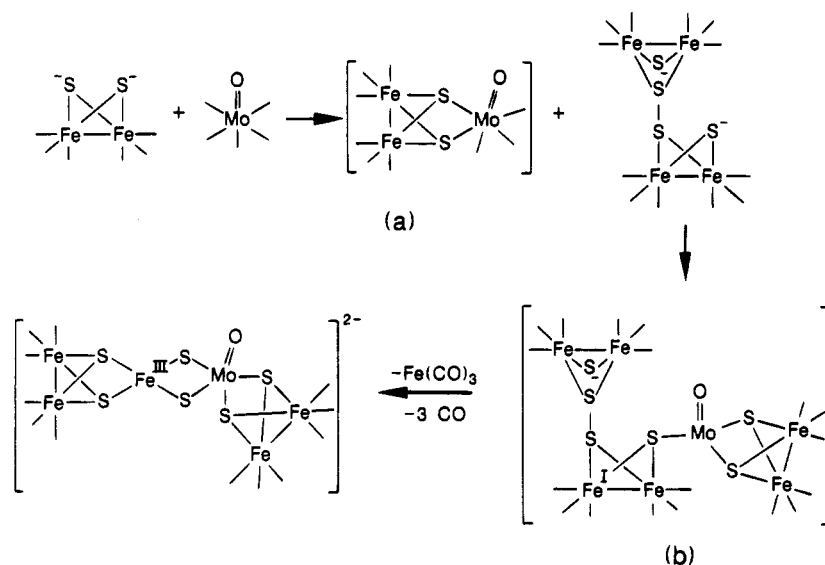


Figure 7. Possible mechanism for formation of [MoOFe₅S₆(CO)₁₂]²⁻.

The observed importance of the oxidative addition chemistry of **II** led to a reexamination of the synthesis of [MoOFe₅S₆(CO)₁₂]²⁻. The reported synthesis of this cluster^{5a} involves reaction of 3 equiv of [Fe₂S₂(CO)₆]²⁻ (**III**) with 1 equiv of the Mo^V species MoOCl₃(THF)₂ and results in the production of a significant amount of [Fe₅S₄(CO)₁₂]²⁻ (**IV**) as a byproduct. The desired product [MoOFe₅S₆(CO)₁₂]²⁻ contains a central Fe^{III}(μ-S)₂-Mo^VO core ligated by two Fe₂S₂(CO)₆ ligands (see Chart 1). The presence of an [Fe₂S₂(CO)₆]²⁻Fe^{III}(μ-S)₂ unit similar to that observed in [Fe₆S₆(CO)₁₂]²⁻ (**VI**) strongly suggests that an oxidative addition reaction is operative in the formation of [MoOFe₅S₆(CO)₁₂]²⁻. A plausible mechanism for formation of this cluster is outlined in Figure 7. The first two steps involve facile ligand displacement by [Fe₂S₂(CO)₆]²⁻ and [Fe₄S₄(CO)₁₂]²⁻ to yield intermediate **b**. Intramolecular oxidative addition to Fe^I then occurs, with the formal elimination of an [Fe(CO)₃]⁺ species and formation of the observed product. Intermediate **b** is structurally similar to intermediates proposed in the formation of [MoFe₄S₃(CO)₁₄]²⁻ and [MoFe₆S₆(CO)₁₆]²⁻,^{5b} however, in those cases oxidative addition was proposed to occur at the low-valent Mo centers. In this case, the intramolecular oxidative addition cannot occur at the high-valent Mo^V center and so must occur at Fe as shown in Figure 7.

The mechanism in Figure 7 requires 1 equiv of **II** and 1 equiv of **III** as opposed to the 3 equiv of **III** reported in the published synthesis. Therefore a solution of 3 equiv of **I** was reacted with 4 equiv of Superhydride in THF at -78 °C to produce formally the required mixture of **II** and **III**. Reaction of this mixture with 1 equiv of MoOCl₃(THF)₂ resulted in the immediate formation of a deep orange solution that gradually turned brown upon warming to room temperature. The IR spectrum of the mother liquid in MeCN shows strong ν_{CO} bands due to the expected product with additional very weak bands at 2080, 2062, 2016, and 2000 cm⁻¹; no formation of **IV** is observed, unlike the reported preparation utilizing only the fully-reduced cluster **III**. In addition, because of the higher purity of the reaction mixture, the desired product can be isolated in >50% yield as opposed to routine yields of ca. 30% by the published procedure. The success of the postulated mechanism in predicting conditions that result in a higher yield of the desired

product argues for the importance of oxidative addition in the cluster formation mechanism.

Summary

The novel clusters **IV** and **V** have been shown to be structurally analogous compounds related by a one-electron redox couple. Structural parameters suggest that the redox process is associated solely with the Fe^{II/III} couple of the central iron atom; the redox potential of this couple (*E*_{1/2} = -0.465 V vs NaCl SCE) is the highest yet reported for any Fe-S₄ compound. Clusters **IV** and **V** also represent one of the few examples in which both the oxidized and reduced analogs have been isolated and structurally characterized.

Cluster **IV** displays an unprecedented reactivity with O₂, which results in formation of **VI**. This transformation is not merely an outer-sphere oxidation but has been shown to be an O₂-specific process that must involve a complicated rearrangement; therefore the lack of any observable intermediates is somewhat surprising. The clean reaction of **I** with **II** to yield **VI** is too slow to be solely responsible for the observed reactivity of **IV** and is only a plausible mechanism if the reaction between **I** and **II** is catalyzed by some Fe-O/S species that is present in the reaction mixture upon O₂ oxidation.

Finally, it is proposed that the species **II** plays a more significant role in reactions utilizing the dianion **III** than has previously been recognized. The proposed mechanisms for formation of **VI** and [MoOFe₅S₆(CO)₁₂]²⁻ demonstrate that oxidative addition may occur at either Fe or Mo, dependent upon the oxidation states of the metal centers. This newly-discovered reactivity of [Fe₄S₄(CO)₁₂]²⁻ makes the compound a potentially useful reagent in preparing a variety of mixed M-Fe-S clusters having new stoichiometries and structures.

Acknowledgment. We thank Dr. K. S. Bose and Dr. Steve Chmielewski for helpful discussions and advice. This research was supported by NSF Grant No. CHE-89-01474 to B.A.A.

Supporting Information Available: Tables of positional and thermal parameters and bond distances and angles for (Pr₄N)₂**IV**, (Pr₄N)**V**·0.5THF, and (Pr₄N)₂**VI** (21 pages). Ordering information is given on any current masthead page.

Systematic Kinetic Studies of Nucleophile Addition to $(\mu_2\text{-H})_2\text{Os}_3(\text{CO})_{10}$

Robert H. E. Hudson and Anthony J. Poë*

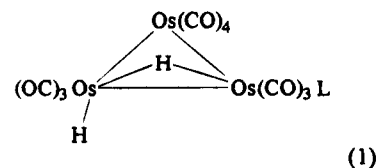
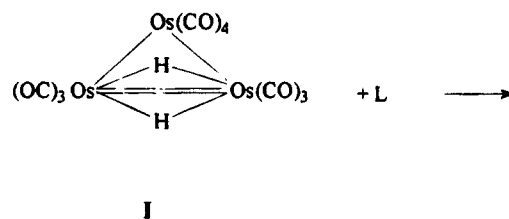
J. Tuzo Wilson Research Laboratories, Erindale Campus, University of Toronto, Mississauga, Ontario, Canada L5L 1C6

Received March 3, 1995[⊙]

The addition of P-donor ligands to the unsaturated cluster $(\mu_2\text{-H})_2\text{Os}_3(\text{CO})_{10}$ in heptane proceeds by simple bimolecular concerted attack to form $(\mu_2\text{-H})(\text{H})\text{Os}_3(\text{CO})_{10}\text{L}$. The second-order rate constants, at 30 °C, for 16 nucleophiles fit very well to the equation $\log k_2 = \alpha + \beta(\text{p}K'_a + 4) + \gamma(\theta - \theta_{\text{th}})\lambda$, where $\text{p}K'_a$ measures the σ -donicity and θ the Tolman cone angle of each nucleophile. The steric threshold is quite sharply defined by $\theta_{\text{th}} = 142 \pm 2^\circ$, so that no steric effects are observed when $\theta < 142^\circ$ (switching function (λ) = 0) but a large steric effect ($\gamma = -0.163 \pm 0.014 \text{ deg}^{-1}$) is found when $\theta > \theta_{\text{th}}$ ($\lambda = 1$). The sensitivity of the rates to $\text{p}K'_a$ is high ($\beta = 0.433 \pm 0.020$), and the standard reactivity, SR (defined by the value, α , of $\log k_2$ for a hypothetical weak and small nucleophile, i.e. with $\text{p}K'_a = -4$ and $\theta < \theta_{\text{th}}$) is also high (-0.50 ± 0.16). The sharpness of the steric threshold and the value of θ_{th} imply the existence in the transition state of an isomeric form (the transition isomer, TSI) of the $(\mu_2\text{-H})_2\text{Os}_3(\text{CO})_{10}$ cluster. This contains a well-defined and large open space into which nucleophiles with $\theta \leq \theta_{\text{th}}$ can fit without steric repulsions. The substantially negative value of γ shows that the TSI strongly resists further opening and this, combined with the high value of β , suggests a relatively late transition state. The values of ΔH^\ddagger ($7.4 \pm 0.3 \text{ kcal mol}^{-1}$) and ΔH° ($-23 \text{ kcal mol}^{-1}$, reported elsewhere) for reactions with $\text{P}(\text{O}^i\text{Pr})_3$ can be coupled with data for reaction with CO to estimate that up to ca. 50% of the available 58 kcal mol^{-1} of Os–P bond strength in $(\mu_2\text{-H})(\text{H})\text{Os}_3(\text{CO})_{10}\{\text{P}(\text{O}^i\text{Pr})_3\}$ is released on forming the transition state. The criteria for judging the success of the data analyses are explored and the use of an alternative steric parameter, $\theta' = 103.8 + 0.553E_R$, is shown to have a negligible effect on the values of θ_{th} and γ . (E_R is Brown's ligand repulsion parameter, and its values has been rescaled and normalized to $\theta' = \theta = 145^\circ$ for PPh_3 so that steric effects can be expressed in the same units, whichever steric parameter is used.) The value of θ_{th} implies that ligands which in $\text{Cr}(\text{CO})_5\text{L}$ experience a repulsion energy of up to 70 kcal mol^{-1} undergo no steric repulsion in the TSIs of these reactions. The value of γ indicates that ΔG^\ddagger increases by 0.12 kcal mol^{-1} for every increase of 1 kcal mol^{-1} in E_R . Kinetic isotope effects, $k_{\text{H}}/k_{\text{D}}$, range from 1.04 ± 0.01 (for $\text{P}(\text{OCH}_2)_3\text{C}^i\text{Et}$) to 1.28 ± 0.02 for PEt_3 . Reactions in chlorobenzene are generally slightly slower than in heptane, and kinetic data for reactions with AsPh_3 and SbPh_3 are also reported.

Introduction

The hydrido carbonyl cluster $(\mu_2\text{-H})_2\text{Os}_3(\text{CO})_{10}$ is the parent of a significant group of related clusters that are electronically unsaturated in terms of common electron-counting rules.¹ As such, it undergoes rapid and often complete addition reactions² with a wide variety of Lewis bases, as indicated in eq 1. Alkene isomerization is catalyzed by this cluster, and the rate-determining step is believed to involve the addition of the alkene as a Lewis base to form $(\mu_2\text{-H})(\text{H})\text{Os}_3(\text{CO})_{10}(\eta^2\text{-alkene})$.³



The thermodynamics of CH_3CN addition⁴ and the kinetics and thermodynamics of reversible addition of CO have recently been reported.⁵ The enthalpies of addition of a few P-donor ligands have been measured.⁶

* To whom correspondence should be addressed at Lash Miller Chemical Laboratories, University of Toronto, 80 St. George St., Toronto, Ontario, Canada M5S 1A1.

[⊙] Abstract published in *Advance ACS Abstracts*, May 15, 1995.

(1) Adams, R. D.; Selegue, J. P. In *Comprehensive Organometallic Chemistry*; Wilkinson, G., Stone, F. G. A., Abel, E., Eds.; Pergamon: Oxford, U.K., 1982; Vol. 4, and references therein. Deeming, A. J. *Adv. Organomet. Chem.* **1986**, *26*, 1–96. Vargas, M. D.; Nicholls, J. N. *Adv. Inorg. Chem. Radiochem.* **1986**, *30*, 123–222. Mingos, D. M. P.; May, A. S. In *The Chemistry of Metal Cluster Complexes*; Shriver, D. F., Kaesz, H. D., Adams, R. D., Eds.; VCH: New York, 1990; Chapter 2.

(2) Deeming, A. J.; Hasso, S. J. *Organomet. Chem.* **1975**, *88*, C21–C23. Keister, J. B.; Shapley, J. R. *Inorg. Chem.* **1982**, *21*, 3304–3310.

It has been established very clearly that systematic studies of associative reactions of metal carbonyls with a wide variety of P-donor nucleophiles are capable of providing clear quantitative electronic and steric profiles based on the electronic and steric properties of the nucleophiles.⁷ The dependence of the rates on these properties provides a number of parameters that are characteristic of the dynamic natures of the carbonyl complexes and so help complete our understanding of their chemical natures. This applies particularly to metal carbonyl clusters, which are exceptionally susceptible to nucleophilic attack even when they are not electronically unsaturated.^{7b-e} Since virtually no such studies⁸ have been reported for electronically unsaturated clusters, and since $(\mu_2\text{-H})_2\text{Os}_3(\text{CO})_{10}$ is the archetype of such clusters, we have carried out extensive kinetic studies on this cluster in order to verify that the methodology of the data analysis is successful in this case as well and to see whether the parameters so obtained show any special features compared to those for electronically saturated clusters. Alternative methods of representing the effective sizes of P-donor nucleophiles are considered. Results for reactions with AsPh_3 and SbPh_3 are also reported.

Experimental Section

Chemicals. $\text{Os}_3(\text{CO})_{12}$ (Strem) was used as received. AsPh_3 , SbPh_3 (Matheson, Coleman and Bell) and PPh_3 (British Drug Houses; BDH) were recrystallized from 95% ethanol and dried *in vacuo* before use. PET_3 (Strem) and $\text{P}(n\text{-Bu})_3$ (Aldrich) were distilled from sodium under dry argon and stored under argon in a septum-sealed Schlenk tube. $\text{P}(\text{OPh})_3$ (Caledon Laboratories), $\text{P}(\text{OEt})_3$ (BDH), PCl_2Ph and PClPh_2 (K&G), and $\text{P}(\text{O-}i\text{-Pr})_3$ (Strem) were distilled and stored similarly. Etpb ($\text{P}(\text{OCH}_2)_3\text{CEt}$; Strem) was sublimed under reduced pressure. PCy_3 (Strem) was purified by way of its CS_2 adduct. $\text{P}(t\text{-Bu})_3$, $\text{P}(m\text{-tolyl})_3$, $\text{P}(o\text{-tolyl})_3$, and $\text{P}(\text{NMe}_2)_3$ (Strem) and $\text{P}(\text{CH}_2\text{Ph})_3$, $\text{P}(p\text{-XC}_6\text{H}_4)_3$ ($\text{X} = \text{CF}_3, \text{F}, \text{Cl}, \text{Me}, \text{and MeO}$), and CS_2 (Digital Specialty Chemicals) were used as received. The purity of the nucleophiles was established by ^{31}P or ^1H NMR or IR spectroscopy as necessary. Trimethylamine *N*-oxide (Aldrich) was sublimed and stored under dry argon.

Heptane (Caledon) was distilled from sodium-benzophenone ketyl, and chlorobenzene (Aldrich) and 1,2-dichloroethane (BDH) were distilled from P_2O_5 . All were stored over activated molecular sieves. Gases (Matheson or Canox) were prepurified or research grade.

(3) Deeming, A. J.; Hasso, S. J. *Organomet. Chem.* **1976**, *114*, 313–324.

(4) Hudson, R. H. E.; Poë, A. J.; Sampson, C. N.; Siegal, A. *J. Chem. Soc., Dalton Trans.* **1989**, 2235–2240.

(5) Poë, A. J.; Sampson, C. N.; Smith, R. T.; Zheng, Y. *J. Am. Chem. Soc.* **1993**, *115*, 3174–3181.

(6) Stradella, L. *J. Therm. Anal.* **1986**, *31*, 671–673.

(7) (a) Woska, D. C.; Wilson, M.; Bartholomew, J.; Eriks, K.; Prock, A.; Giering, W. P. *Organometallics* **1992**, *11*, 3343–2050 and references therein. (b) Poë, A. J. In *Metal Clusters*; Moskovits, M., Ed.; Wiley: New York, 1986; Chapter 4. (c) Poë, A. J.; Farrar, D. H.; Zheng, Y. *J. Am. Chem. Soc.* **1992**, *114*, 5146–5142 and references therein. (d) Farrar, D. H.; Poë, A. J.; Zheng, Y. *J. Am. Chem. Soc.* **1994**, *116*, 6252–6261. (e) Chen, L. Ph.D. Thesis, University of Toronto, Toronto, Canada, 1991. (f) Chen, L.; Poë, A. J. *Coord. Chem. Rev.*, in press.

(8) Data from systematic kinetic studies⁹ of associative reactions of the 33-electron $\text{Fe}_2(\text{CO})_7(\mu\text{-PPh}_2)$ have been successfully analyzed^{7e,10} in terms of steric and electronic properties of the nucleophiles and show⁹ a rate enhancement of $\geq 10^5$ for this odd-electron molecule compared with closely analogous electronically saturated complexes.

(9) Baker, R. T.; Calabrese, J. C.; Krusic, P. J.; Therien, M. J.; Troger, W. C. *J. Am. Chem. Soc.* **1988**, *110*, 8392–8412.

(10) Liu, H.-Y.; Eriks, K.; Prock, A.; Giering, W. P. *Organometallics* **1990**, *9*, 1758–1766.

The cluster $(\mu_2\text{-H})_2\text{Os}_3(\text{CO})_{10}$ was most conveniently prepared by bubbling H_2 through a refluxing, saturated solution of $\text{Os}_3(\text{CO})_{12}$ in toluene or *n*-octane for several minutes. Cooling to room temperature led to precipitation of unreacted $\text{Os}_3(\text{CO})_{12}$. $(\mu_2\text{-H})_2\text{Os}_3(\text{CO})_{10}$ crystallized slowly at reduced temperatures in pure form with yields of 60–65%, the purity being confirmed by IR spectroscopy.⁵ The cluster $(\mu_2\text{-D})_2\text{Os}_3(\text{CO})_{10}$ was prepared from $\text{Os}_3(\text{CO})_{10}(\text{NCMe})_2$ ⁴ in rigorously dried solvents and equipment to avoid the possibility of ^2H – ^1H exchange. A solution in acetonitrile (100 mg, 15 mL) was diluted with isooctane or cyclohexane (100 mL) in a two-necked round-bottomed flask. The acetonitrile was removed by distillation into a Dean–Stark apparatus under a flow of D_2 . Once the acetonitrile was removed, the reaction proceeded rapidly at ca. 60 °C to form $(\mu_2\text{-D})_2\text{Os}_3(\text{CO})_{10}$. The crude product, isolated by evaporation of the solvent, was purified by recrystallization from solution and obtained in overall yields of 60–70%. This product was shown to be chemically pure by IR spectroscopy. An identical sample was used for all the measurements of the kinetic isotope effect so that the presence of any of the ^1H isotopomer would serve only to decrease the magnitude of the KIE by the same amount for all reactions. This method could also be used to prepare $(\mu_2\text{-H})_2\text{Os}_3(\text{CO})_{10}$, but the direct method is to be preferred because, although the yields are similar, unreacted $\text{Os}_3(\text{CO})_{12}$ can be recovered for future use in the latter case and it is more rapid.

Instruments. IR spectra were measured with Nicolet 5DX or 10DX FTIR or Perkin-Elmer 298 spectrophotometers using matched 1 mm path length cells with NaCl windows. Proton (^1H) NMR spectra were recorded with Varian XL60, XL200, or XL400 spectrometers, and ^{31}P NMR spectra were measured with the Varian XL200 instrument. UV–vis spectra were measured with a Hewlett-Packard 8452A or Unicam SP1800 spectrophotometer. A Beckman DU-40 UV–vis spectrophotometer was also used for kinetic monitoring of suitably slow reactions. Fast reactions were monitored by using a Durrum 110 stopped-flow instrument interfaced with a Tektronix 4051 computer and driven by custom software (Analytical Services Laboratory, University of Toronto). The temperature was externally controlled by a Tamson TX-9 circulating water bath and a Neslab Instruments BC-4 bath cooler.

Kinetics. Solutions of complex and nucleophiles were prepared by standard anaerobic procedures. Concentrations of the nucleophiles were established by weighing, and at least three independently prepared solutions of each nucleophile of different concentrations were employed. Other concentrations were obtained by dilution. The concentration of complex ($(1 - 10) \times 10^{-5}$ M, depending on the monitoring technique employed) was based on individual weighings or on the value $\epsilon = 8125 \text{ M}^{-1} \text{ cm}^{-1}$ at 328 nm in heptane.

Slower reactions ($t_{1/2} > \text{ca. } 30 \text{ min}$) were monitored in quartz cells in the thermostated multicell compartment of the Beckman spectrophotometer. Temperatures were measured with an iron–constantan thermocouple, and the temperature variation over the course of reactions was established to be $\leq \pm 0.1$ °C by continuous monitoring. Several reactions could be followed simultaneously. For faster reactions ($t_{1/2} > \text{ca. } 30 \text{ s}$) a Helma tandem-mix quartz cell was used. The cell with the separated solutions of complex and nucleophile was first thermostated in the cell holder of the HP 8452A spectrophotometer. The reactions were then initiated by agitating the cell vigorously before replacing it in the cell holder and immediately initiating absorbance monitoring. Absorbance versus time data were recorded digitally (Hewlett-Packard software; program version 1.0). Still faster reactions ($t_{1/2} < \text{ca. } 30 \text{ s}$) were monitored by stopped-flow methods. Wavelengths were chosen so that all absorbance changes were maximized ($\Delta A \approx 0.5$).

For reactions monitored with the Beckman or Hewlett-Packard spectrophotometers, rate constants for individual runs

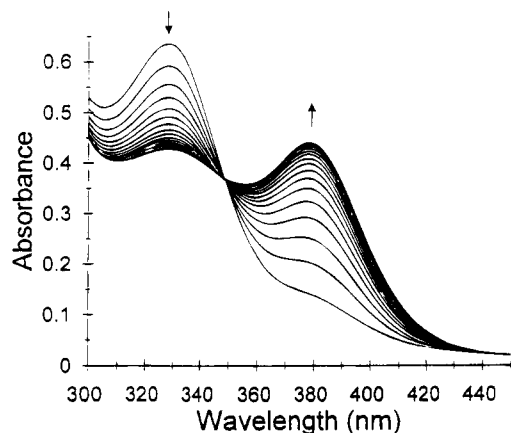


Figure 1. UV-vis spectral changes during the reaction of $(\mu_2\text{-H})_2\text{Os}_3(\text{CO})_{10}$ with P(OPh)_3 in heptane at 22 °C.

were obtained by analyzing the absorbance versus time changes by use of the nonlinear least-squares KORE program.¹¹ In cases where aromatic moieties were not present in the nucleophiles, it was possible to monitor the decrease of absorbance at low wavelengths (328 nm) as well as the increase of absorbance at higher wavelengths (ca. 385 nm), and excellent agreement was obtained (ca. $\pm 5\%$).

For reactions monitored by the stopped-flow method, the increase in absorbance with time was monitored and data were usually collected for 6–8 reactions of identical pairs of reactant solutions. Rate constants were obtained for each reaction individually by a nonweighted linear least-squares computer analysis of $\ln(A_\infty - A_t)$ vs t , the values of A_∞ being those measured experimentally at the end of each reaction. For rate constants within each set reproducibility was generally better than $\pm 1\%$.

Results

In all cases the reactions proceeded cleanly according to eq 1. Subsequent reactions are much slower, and no intermediates were detectable. The isolated products of reaction were identified by IR and UV-vis spectrophotometry after independent isolation and spectroscopic characterization of previously synthesized compounds ($\text{L} = \text{PPh}_3$, P(Cy)_3 , P(OMe)_3).^{2,12} Reaction with P(OPh)_3 was slow enough to be monitored by repetitive FTIR spectroscopy at ambient temperatures, and the changes accompanying formation of $(\mu_2\text{-H})(\text{H})\text{Os}_3(\text{CO})_{10}\{\text{P(OPh)}_3\}$ show the growth of characteristic bands at 2114 w, 2051 m, 2035 s, 1988 w, and 1973 w cm^{-1} . Sharp isosbestic points were observed at 2057 and 2030 cm^{-1} . When the same reaction was monitored by UV-vis spectrophotometry, the reactant band at 328 nm was replaced by the product band at 378 nm, and there was a sharp isosbestic point at 346 nm (Figure 1). Similarly clean changes in the UV-vis spectra were obtained for slower reactions with other nucleophiles. Faster reactions, for which monitoring over the whole spectral range was not possible, gave excellent pseudo-first-order rate plots. There seems to be no reason why these faster reactions were not equally well behaved. The values of the pseudo-first-order rate constants, k_{obs} , for reac-

tions with a given nucleophile, L, always increase linearly with $[\text{L}]$ according to eq 2. Linear least-squares analysis of the data led to the values of α ¹⁴ and k_2 shown in Tables 1 and 2 for reactions in heptane and chlorobenzene, respectively.

$$k_{\text{obs}} = \alpha + k_2[\text{L}] \quad (2)$$

The values of k_{obs} for a given nucleophile were all weighted according to the assumption of a constant standard error, expressed as a percentage. The resulting standard errors show that the kinetic data are generally of excellent precision. All reactions were monitored at 30.0 °C and, for $\text{L} = \text{P(OPh)}_3$, at 10.0 and 20.0 °C as well. The activation parameters are given in footnote *h* of Table 1.

Reactions with $\text{P(CH}_2\text{Ph)}_3$ were carried out in 1,2-dichloroethane, because this ligand is not sufficiently soluble in heptane. The results can be compared with others in heptane if it is assumed that the solvent effect for this ligand is negligible, as was found to be the case for P(OPh)_3 , for which $k_2(\text{heptane})/k_2(\text{DCE}) = 0.96 \pm 0.10$ at 20.0 °C. Reactions with AsPh_3 and SbPh_3 also gave good kinetic data (Table 1). Attempts were made to study the reactions with the weakly basic nucleophiles $\text{PCl}_n\text{Ph}_{3-n}$ ($n = 1-3$). Reactions with PCl_3 were not spectroscopically clean and led to unidentifiable products. Reactions with PCl_2Ph and PClPh_2 appeared to lead cleanly to monosubstituted products according to FTIR and UV-vis spectroscopic changes, and reaction with PClPh_2 showed a very clean isosbestic point at 348 nm. The kinetics of the last reaction showed a reasonable fit to eq 2, but with a large negative value of α . It seems likely that data for the more dilute solutions were less reliable, and the value of k_2 obtained from runs at higher concentrations is reported in Table 1. Reactions with $(\mu\text{-D})_2\text{Os}_3(\text{CO})_{10}$ were all carried out with the same cluster sample. For $\text{L} = \text{P(OPh)}_3$ and PEt_3 , two quite separate sets of runs were performed with different sets of nucleophile solutions, and the data were analyzed according to eq 2. These results are included in Table 1 and lead to values of $k_2(\text{H})/k_2(\text{D})$ of 1.21 ± 0.02 and 1.28 ± 0.02 , respectively. Reactions of $(\mu_2\text{-H})_2\text{Os}_3(\text{CO})_{10}$ and $(\mu_2\text{-D})_2\text{Os}_3(\text{CO})_{10}$ with etpb were carried out at the same time with identical concentrations of etpb , 4.96×10^{-3} or 16.3×10^{-3} M. The ratio of $\{k_{\text{obs}}(\text{H})/k_{\text{obs}}(\text{D})\}_{\text{av}}$ obtained at the former concentration from 14 runs with $(\mu_2\text{-H})_2\text{Os}_3(\text{CO})_{10}$ and 12 runs with $(\mu_2\text{-D})_2\text{Os}_3(\text{CO})_{10}$ was 1.025 ± 0.008 , while the value from 8 runs on each complex at the latter concentration was 1.049 ± 0.012 . The weighted average is 1.03 ± 0.01 . A similar analysis of data for $\text{L} = \text{P(OEt)}_3$ ($[\text{L}] = 3.60 \times 10^{-3}$ M) and $\text{L} =$

(14) The same values of α are not found for all nucleophiles; therefore, α cannot correspond to the rate constant for a ligand-independent process undergone by the cluster itself. In those cases in which a statistically significant positive value of α is obtained, it is conceivable that the reactions are approaching an equilibrium mixture of reactant and product. In this case k_{obs} will be equal to the sum of the pseudo-first-order rate constant, $k_2[\text{L}]$, for adduct formation and the first-order rate constant, k_{-L} , for loss of L from the adduct, i.e. $\alpha = k_{-L}$. However, no attempts were made to obtain spectroscopic evidence for the existence of equilibrium mixtures at low values of $[\text{L}]$, and this question remains to be investigated further. Similar but rather better evidence was found for approach to equilibrium mixtures in the reactions of P(OPh)_3 and SbPh_3 with $\text{Fe}_2(\text{CO})_6(\text{NO})(\mu\text{-AsMe}_2)$,¹⁵ when the Fe-Fe bond is broken heterolytically by the approaching nucleophile.

(15) Jackson, R. A.; Kanlun, R.; Poë, A. *J. Inorg. Chem.* **1984**, *23*, 523–527.

(11) Swain, C. G.; Swain, M. S.; Berg, L. F. *J. Chem. Inf. Comput. Sci.* **1980**, *20*, 47–51.

(12) These syntheses¹³ will be described elsewhere.

(13) Hudson, R. H. E. M.Sc. Thesis, University of Toronto, Toronto, Canada, 1990.

Table 1. Kinetic Data for Addition of Nucleophiles, L, to $(\mu_2\text{-H})_2\text{Os}_3(\text{CO})_{10}$ in Heptane (at 30 °C Unless Otherwise Indicated)

L	θ ($^\circ$), ^a deg	$\text{p}K_a'$ ^b	$10^4[\text{L}]$, M	N (n) ^c	α , s^{-1}	k_2 , $\text{M}^{-1} \text{s}^{-1}$	$\sigma(k_{\text{obs}})$, ^d %
ETPB (1)	101 (118)	-0.30	4.96-163	30 (3)	$-(1.2 \pm 0.2) \times 10^{-2}$	$(2.18 \pm 0.02) \times 10^1$	2.5
P(OEt) ₃ (2)	109 (136)	1.64	360-1200	39 (3)	$(2.2 \pm 1.3) \times 10^{-1}$	$(1.38 \pm 0.01) \times 10^2$	3.9
P(OPh) ₃ (3)	128 (140)	-2.79	45-225	10 (5)	$(4.8 \pm 0.9) \times 10^{-4}$	$(5.56 \pm 0.11) \times 10^{-1}$	3.1
			91.3-457	7 (3) ^e	$(6.1 \pm 0.8) \times 10^{-4}$	$(4.96 \pm 0.03) \times 10^{-1}$	1.1
			45-225	12 (6) ^f	$-(6.44 \pm 92) \times 10^{-5}$	$(3.69 \pm 0.09) \times 10^{-1}$	4.6
			45-225	10 (5) ^{g,h}	$(1.7 \pm 5.2) \times 10^{-5}$	$(1.65 \pm 0.06) \times 10^{-1}$	6.7
P(O- <i>i</i> -Pr) ₃ (4)	130 (145)	3.38	152-510	37 (3)	$(3.8 \pm 0.6) \times 10^{-1}$	$(1.50 \pm 0.03) \times 10^2$	5.1
PEt ₃ (5)	132 (138)	7.96	22.2-91.6	43 (5)	1.8 ± 0.7	$(2.32 \pm 0.03) \times 10^4$	1.4
			45.5-60.3	28 (2) ^e	0	$(1.82 \pm 0.03) \times 10^4$ ⁱ	4.3
P(<i>p</i> -F ₃ CC ₆ H ₄) ₃ (6)	145 (145)	-1.39	63.2-173	19 (5)	$-(1.6 \pm 0.4) \times 10^{-3}$	$(9.9 \pm 0.50) \times 10^{-1}$	8.0
P(<i>p</i> -ClC ₆ H ₄) ₃ (7)	145 (145)	0.87	3.10-6.19	9 (3)	$-(2.1 \pm 1.0) \times 10^{-4}$	6.4 ± 0.30	3.5
P(<i>p</i> -FC ₆ H ₄) ₃ (8)	145 (145)	1.63	42.2-135	25 (3)	$-(1.6 \pm 0.3) \times 10^{-3}$	$(1.66 \pm 0.01) \times 10^1$	0.6
PPh ₃ (9)	145 (145)	3.28	154-455	43 (4)	$-(2.8 \pm 1.3) \times 10^{-2}$	$(9.49 \pm 0.05) \times 10^1$	1.4
P(<i>p</i> -tol) ₃ (10)	145 (145)	4.46	5.06-9.66	33 (3)	$(4.9 \pm 0.3) \times 10^{-3}$	$(2.15 \pm 0.04) \times 10^2$	2.1
P(<i>p</i> -MeOC ₆ H ₄) ₃ (11)	145 (145)	5.13	18.3-30.1	32 (3)	$(6.0 \pm 14) \times 10^{-3}$	$(7.53 \pm 0.05) \times 10^2$	0.8
P(<i>m</i> -tol) ₃ (12)	148 ^f (147)	4.23	28.0-96.5	25 (3)	$-(2.0 \pm 0.9) \times 10^{-2}$	$(2.5 \pm 0.02) \times 10^2$	2.1
P(NMe ₂) ₃ (13)	157 (-)	8.20	174-355	30 (4)	$(7.3 \pm 0.9) \times 10^{-1}$	$(1.31 \pm 0.02) \times 10^2$	4.8
P(CH ₂ Ph) ₃ (14)	165 (149)	5.23	76.4	6 (1)	0	1.91 ± 0.09 ⁱ	11.0
P(C ₆ H ₁₁) ₃ (15)	170 (168)	11.26	2.42-47.8	26 (4)	$-(2.3 \pm 1.1) \times 10^{-1}$	$(8.84 \pm 0.23) \times 10^1$	8.9
P(<i>t</i> -Bu) ₃ (16)	182 (189)	12.20	146-708	13 (3)	$(1.5 \pm 0.7) \times 10^{-4}$	$(8.7 \pm 0.30) \times 10^{-2}$	13.4
P(<i>o</i> -tol) ₃ (17)	194 (166)	5.03	187-331	19 (7)	$-(1 \pm 10) \times 10^{-6}$	$(1.1 \pm 0.10) \times 10^{-2}$	15.3
PPh ₂ Cl (18)	137 (130)	-4.9	6.06-9.10	3 (2)	0	$(8.3 \pm 0.6) \times 10^1$ ⁱ	
AsPh ₃ (19)	142		133-608	25 (3)	$(1.2 \pm 3) \times 10^{-4}$	$(1.41 \pm 0.01) \times 10^1$	0.5
SbPh ₃ (20)	138		59.8-108	21 (3)	$-(8 \pm 2) \times 10^{-3}$	$(3.37 \pm 0.02) \times 10^1$	0.7
CO (21)	95					$(6.4 \pm 0.16) \times 10^{-2}$ ^h	3.1

^a Tolman cone angles ("cone angles" based on Brown's E_R values; see text). ^b These $\text{p}K_a'$ values^{7c,e,f} are measures of the σ -donicities of the nucleophiles appropriate to associative reactions in nonpolar solvents (see Discussion). ^c N is the total number of k_{obs} measurements ($k_{\text{obs}} = \alpha + k_2[\text{L}]$), and n is the number of different values of [L] used. ^d Standard error of an individual measurement of k_{obs} . ^e Reactions of $(\mu_2\text{-D})_2\text{Os}_3(\text{CO})_{10}$. ^f Reactions at 20 °C. ^g Reactions at 10 °C. ^h When our results were combined with data obtained elsewhere (see ref 39), it was found that the results at 10 °C were significantly low. A combination of our data at 20 and 30 °C with others at 20.4, 26.2, 30.2, 40.5, and 46.7 °C (a total of 44 values of $k_{\text{obs}}/[\text{L}]$ with [L] varying from 4.5 to 495 mM) led to $\Delta H^\ddagger = 7.37 \pm 0.27$ kcal mol⁻¹ and $\Delta S^\ddagger = -35.3 \pm 0.9$ cal K⁻¹ mol⁻¹, with a standard error of $\pm 8.6\%$ for the determination of an individual value of k_{obs} . ⁱ Obtained from $k_{\text{obs}}/[\text{L}]$. ^j Revised Tolman cone angle (see ref 32 and text). ^h Obtained from ref 5.

Table 2. Kinetic Data for Addition of Nucleophiles, L, to $(\mu_2\text{-H})_2\text{Os}_3(\text{CO})_{10}$ in Chlorobenzene at 30 °C

L ^a	$10^3[\text{L}]$, M	N (n) ^b	α , s^{-1}	k_2 , $\text{M}^{-1} \text{s}^{-1}$	$\sigma(k_{\text{obs}})$, ^c %	$k_{\text{H}}/k_{\text{CB}}$ ^d
P(OPh) ₃ (3)	6.8-60.8	12 (3)	$(2.12 \pm 0.71) \times 10^{-4}$	$(1.93 \pm 0.02) \times 10^{-1}$	12.0	2.99
P(O- <i>i</i> -Pr) ₃ (4)	20.2-58.0	35 (3)	$(4.80 \pm 0.90) \times 10^{-2}$	$(5.09 \pm 0.27) \times 10^1$	1.5	2.95
PEt ₃ (5)	1.97-6.99	38 (3)	$(4.1 \pm 8.0) \times 10^{-1}$	$(1.52 \pm 0.03) \times 10^4$	5.3	1.53
P(<i>p</i> -F ₃ CC ₆ H ₄) ₃ (6)	3.71-23.5	8 (4)	$-(4.8 \pm 2.5) \times 10^{-4}$	$(8.0 \pm 0.5) \times 10^{-1}$	8.0	1.24
P(<i>p</i> -ClC ₆ H ₄) ₃ (7)	1.29-6.06	14 (5)	$(8.7 \pm 1.8) \times 10^{-4}$	3.51 ± 0.30	7.9	1.82
P(<i>p</i> -FC ₆ H ₄) ₃ (8)	1.39-6.97	8 (3)	$-(3.8 \pm 1.8) \times 10^{-4}$	9.22 ± 0.05	1.5	1.81
PPh ₃ (9)	13.1-29.4	24 (3)	$-(9.3 \pm 2.5) \times 10^{-3}$	$(2.23 \pm 0.05) \times 10^1$	1.0	4.26
P(<i>p</i> -tol) ₃ (10)	3.94-11.0	24 (3)	$(4.4 \pm 1.6) \times 10^{-2}$	$(1.07 \pm 0.04) \times 10^2$	3.5	2.01
P(<i>p</i> -MeOC ₆ H ₄) ₃ (11)	4.02-16.3	24 (3)	$(4.8 \pm 1.3) \times 10^{-2}$	$(2.36 \pm 0.05) \times 10^2$	2.0	3.19

^a Numbering of nucleophiles corresponds to numbering in Table 1. ^b N is the total number of measurements of k_{obs} , and n is the number of different values of [L] used. ^c Standard error of an individual measurement of k_{obs} . ^d Ratio of values of k_2 in heptane (k_{H}) and chlorobenzene (k_{CB}).

PCy₃ ($10^3[\text{L}] = 2.92, 4.35, \text{ and } 4.48$ M) leads to $k_2(\text{H})/k_2(\text{D}) = 1.08 \pm 0.01$ in both cases.

Dependence of the Rates on the Electronic and Steric Properties of the P-Donor Nucleophiles. The values of k_2 show a pronounced dependence on both the electronic and the steric properties of the nucleophiles L. The value of k_2 for reaction of the cluster with PEt₃ (Tolman cone angle $\theta = 132^\circ$, $\text{p}K_a = 8.69$)¹⁶ is 4×10^4 times larger than that for the nearly isosteric but much less basic nucleophile P(OPh)₃ ($\theta = 128^\circ$, $\text{p}K_a = -2.0$). On the other hand, the value of k_2 for reaction with P(*t*-Bu)₃ ($\theta = 182^\circ$, $\text{p}K_a = 11.4$) is 3×10^5 times slower than that for the somewhat less basic but very much smaller nucleophile PEt₃. The importance of Os-L bond making in determining the energy of the transition state is therefore very clear.

The dependence of k_2 on the electronic and steric properties of the nucleophiles can be expressed more

generally by the plot of the values of $\log k_2$ against corresponding values of $\text{p}K_a'$ for the nucleophiles, as shown by the electronic profile in Figure 2. The values of $\text{p}K_a'$ are not simply the same as the $\text{p}K_a$ values for dissociation of the proton from the conjugate acids PH⁺ in aqueous solution but are related to the σ -donicity of the P-donors in a way that is more appropriate to associative reactions of P-donor nucleophiles in nonpolar organic solvents.^{7c} They are derived as follows. Giering et al. showed¹⁰ that, for ligands that they classified as pure σ -donors, the values of $\text{p}K_a$ are related^{10,16} to the values of $\chi^{10,17}$ by an equation that includes a term in θ . This appears to be required because $\text{p}K_a$ values are affected by the different sizes of the phosphonium ions and, presumably, the consequent differences in hydration energies. The values of χ are clearly not subject to such effects. We find that the data for a set of 17 ligands very slightly different from Giering's¹⁰ give a good fit

(16) Rahman, Md. M.; Liu, H.-Y.; Ericks, K.; Prock, A.; Giering, W. *P. Organometallics* **1989**, *8*, 1-7.

(17) Bartik, T.; Himmler, T.; Schulte, H.-G.; Seevogel, K. *J. Organomet. Chem.* **1984**, *272*, 29-41.

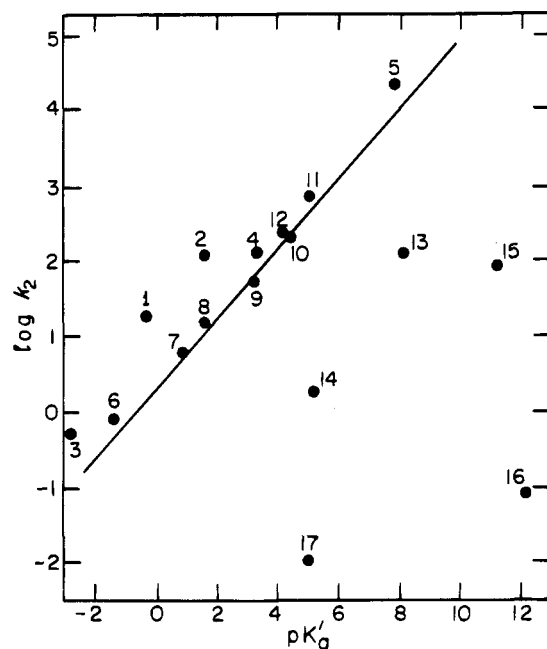


Figure 2. Electronic profile for the reactions of $(\mu_2\text{-H})_2\text{-Os}_3(\text{CO})_{10}$ with L in heptane at 30 °C. The numbers correspond to those listed in Table 1, and the line is drawn through the data for the nucleophiles $\text{P}(p\text{-XC}_6\text{H}_4)_3$.

to eq 3, which is essentially identical with the equation derived by Giering et al.¹⁰

$$pK_a = (18.93 \pm 1.65) - (0.673 \pm 0.035)\chi - (0.0464 \pm 0.0104)\theta \quad (3)$$

$$\text{RMSD} = 0.480; R^2 = 0.970$$

The values of pK_a' for these σ -donor ligands are defined by eq 4, where the last term is included so that the pK_a' values are scaled in a way that makes them close to those of pK_a .

$$pK_a' = 18.93 - 0.673\chi - (0.0464 \times 145) \quad (4)$$

For ligands that are classified¹⁰ as being π -acids as well as σ -donors, it is not possible to use χ as a measure of the pure σ -donicity and it is necessary to use eq 5, where the pK_a' values are derived from pK_a values by correcting for the size and hydration effects that are not operative in nonpolar solvents.

$$pK_a' = pK_a + 0.0464(\theta - 145) \quad (5)$$

The correction is made relative to ligands with $\theta = 145^\circ$, and a combination of eqs 4 and 5 leads to eq 3; thus, the two ways of deriving values for pK_a' are self-consistent. What is different is that the values of pK_a' for purely σ -donor ligands have all the precision associated with χ values¹⁷ while the pK_a' values for ligands that are π -acids as well as σ -donors are related to the experimental pK_a values by correcting for hydration effects. In this they resemble the χ_d values listed by Giering et al.¹⁰

Figure 2 shows that the data for the six isosteric nucleophiles $\text{P}(p\text{-XC}_6\text{H}_4)_3$ ($\theta = 145^\circ$) exhibit an excellent linear free energy relationship (LFER), and an unweighted linear least-squares analysis provides a value of 0.433 ± 0.020 for the gradient β ($\text{RMSD} = 0.089$, R^2

$= 0.992$). The values of $\log k_2$ for the smaller nucleophiles 1–5 ($\theta = 101\text{--}132^\circ$) lie an average of 0.57 ± 0.15 above the plot for nucleophiles 6–11 and fall on an LFER with a gradient of 0.40 ± 0.04 ($\text{RMSD} = 0.281$, $R^2 = 0.964$) which is indistinguishable from the value for the “ 145° nucleophiles”. Four of these five nucleophiles are phosphites, which might show transition-state stabilization that is enhanced by their π -acidity, but all of the 145° nucleophiles are arylphosphines, which might show diminished transition-state stabilization because of the “aryl effect”.¹⁸ However, neither of these effects has yet been established as being significant for reactions such as these,^{7c-f,19} and it therefore seems more straightforward to suppose that the smaller nucleophiles react more rapidly, at rates dependent only on their basicities and not on their sizes, because they all lie below a steric threshold. The 145° nucleophiles, and those with even higher cone angles, react more slowly because they lie above the steric threshold.

This type of behavior can be described by eq 6, which successfully accounts for the data obtained for over 50 different sets of second-order reactions^{7c-f} of metal carbonyls with P-donor nucleophiles. The parameter λ

$$\log k_2 = \alpha + \beta(pK_a' + 4) + \gamma(\theta - \theta_{th})\lambda \quad (6)$$

is a switching function¹⁰ that is set to zero when the nucleophile cone angles are less than a critical threshold value, θ_{th} , below which no steric effects are evident, and when $\log k_2^\circ = \log k_2 - \beta(pK_a' + 4) = \alpha$. When $\theta > \theta_{th}$, $\lambda = 1$ and $\log k_2^\circ$ is proportional to θ . Just as the parameter β is a measure of the sensitivity of the substrate carbonyl to the σ -donicity of the nucleophiles, so γ measures the substrate's sensitivity to the size of the nucleophiles when their cone angles exceed θ_{th} . The value, α , of $\log k_2^\circ$ when $\theta \leq \theta_{th}$ is a measure of the standard reactivity, SR, of the carbonyl with respect to a standard, hypothetical, and small nucleophile of low basicity ($pK_a' = -4$).^{7c-f} In order to get the best fit of data to eq 6, the goodness of fit is examined as a function of various chosen values of θ_{th} . The value that leads to a minimum for the root mean square deviation (RMSD)²⁰ is accepted as the best one, and the corresponding values of SR, β , and γ are also then the best ones available by this method.

(18) Wilson, M. R.; Woska, D. C.; Prock, A.; Giering, W. P. *Organometallics* **1993**, *12*, 1742–1752.

(19) Unpublished results available on request from Professor W. P. Giering.

(20) $\text{RMSD} = \{\sum[\log k_2(\text{expt}) - \log k_2(\text{calc})]^2\}^{1/2}$. In a few cases two minima are observed in plots of RMSD versus the various chosen values of θ_{th} , but the value of θ_{th} that leads to the lower minimum is deemed to be the better one.^{7e}

(21) Poë, A. J.; Twigg, M. V. *J. Chem. Soc., Dalton Trans.* **1974**, 1860–1866.

(22) Dahlinger, K.; Falcone, F.; Poë, A. J. *Inorg. Chem.* **1986**, *25*, 2654–2658.

(23) Original data taken from: Kennedy, J. R.; Seltz, P.; Rheingold, A. L.; Trogler, W. C.; Basolo, F. *J. Am. Chem. Soc.* **1989**, *111*, 3615–3627.

(24) Original data taken from: Ellgen, P. C.; Gerlach, J. N. *Inorg. Chem.* **1974**, *13*, 1944–1947.

(25) Jackson, R. A.; Kanluen, R.; Poë, A. J. *Inorg. Chem.* **1981**, *20*, 1130–1133.

(26) Original data taken from: Chang, C.-Y.; Johnson, C. E.; Richmond, T. G.; Chen, Y.-T.; Trogler, W. C.; Basolo, F. *Inorg. Chem.* **1981**, *20*, 3167–3172.

(27) Original data taken from: Shi, Q.-Z.; Richmond, T. G.; Trogler, W. C.; Basolo, F. *J. Am. Chem. Soc.* **1984**, *106*, 71–76.

(28) References to sources of the appropriate data are given in ref 29.

(29) Basolo, F. *Polyhedron* **1990**, *9*, 1503–1535.

Table 3. Characteristic Kinetic Parameters for Associative Reactions of Metal Carbonyls at 25 °C^a

complex (solvent)	no. of L's	θ_{th} , deg	SR	β	γ , deg ⁻¹	RMSD	R^2	ref
$(\mu_2\text{-H})_2\text{Os}_3(\text{CO})_{10}$ (heptane)	16 ^b	142 ± 2	-0.53 ± 0.15	0.42 ± 0.04	-0.163 ± 0.014	0.375	0.918	this work
	6 ^c		> -1.2	0.433 ± 0.020		0.089	0.992	
	16 ^d	139 ± 3	-0.43 ± 0.33	0.43 ± 0.06	-0.161 ± 0.018	0.582	0.858	
	15 ^e	142 ± 3	-0.51 ± 0.21	0.41 ± 0.04	-0.160 ± 0.013	0.370	0.960	
	15 ^f	139 ± 3	-0.26 ± 0.30	0.40 ± 0.05	-0.145 ± 0.018	0.508	0.856	
$(\mu_2\text{-H}_2)\text{Os}_3(\text{CO})_{10}$ (chlorobenzene)	6 ^c			0.37 ± 0.03		0.116	0.980	
Ru ₃ (CO) ₁₂ (decalin)	10	122	-3.4 ± 0.2	0.16 ± 0.03	-0.06 ± 0.01	0.21	0.837	21 ^g
Ru ₆ C(CO) ₁₇ (heptane)	14	119	1.51 ± 0.26	0.41 ± 0.04	-0.20 ± 0.01	0.41		7c
Ru ₆ C(CO) ₁₇ (chlorobenzene)	8	≤ 130	≥ -0.10 ± 0.19	0.29 ± 0.03	-0.19 ± 0.01	0.19		7c
Ru ₅ C(CO) ₁₅ (heptane)	8 ^h	117	2.86 ± 0.18	0.21 ± 0.04	-0.068 ± 0.013	0.13	0.939	7d
Ru ₅ C(CO) ₁₅ (heptane)	9 ⁱ	148	-2.30 ± 0.13	0.59 ± 0.03	-0.233 ± 0.012	0.12	0.912	7d
Ir ₄ (CO) ₁₂ (chlorobenzene)	7	≤ 101	≥ -3.4 ± 0.3	0.31 ± 0.05	-0.09 ± 0.01	0.30	0.953	22 ^g
Rh ₄ (CO) ₉ {μ ₃ -HC(PPh ₂) ₃ } (CH ₂ Cl ₂)	4	121	0.64 ± 0.01	0.40 ± 0.01	-0.155 ± 0.001	0.004	1.000	23 ^g
Fe ₂ (CO) ₆ {μ-RN(CO)NR} (toluene)	6	113	-3.5 ± 0.4	0.42 ± 0.06	-0.07 ± 0.02	0.36	0.937	24 ^g
Fe ₂ (CO) ₇ {μ-PPh ₂ } (CH ₂ Cl ₂)	7	131	-1.5 ± 0.1	0.15 ± 0.02	-0.064 ± 0.005	0.08	0.982	9 ^g
FeCo(CO) ₇ {μ-AsMe ₂ } ₂ (decalin)	8	140	-3.2 ± 0.1	0.16 ± 0.02	-0.03 ± 0.01	0.17	0.914	25 ^g
Fe(CO) ₃ (N ₄ Me ₂) ^j (toluene)	10	121	-5.2 ± 0.5	0.55 ± 0.08	-0.19 ± 0.02	0.57	0.931	26 ^g
V(CO) ₆ (hexane)	7	138	-1.7 ± 0.5	0.30 ± 0.07	-0.15 ± 0.03	0.37	0.884	27 ^g
V(CO) ₅ (NO) (hexane)	4	≥ 145	-2.3 ± 0.2	0.23 ± 0.04		0.12	0.910	28 ^g
Mn(CO) ₄ (NO) (<i>p</i> -xylene)	3	≥ 145	-5.3 ± 0.2	0.24 ± 0.04		0.14	0.984	28 ^g
Co(CO) ₃ (NO) (toluene)	11	136	-4.5 ± 0.2	0.31 ± 0.03	-0.06 ± 0.01	0.23	0.951	28 ^g
CpRh(CO) ₂ (toluene)	8	139	-4.9 ± 0.1	0.17 ± 0.02	-0.08 ± 0.01	0.16	0.953	28 ^g

^a Where data were obtained at temperatures other than 25 °C, the SR values were adjusted to 25 °C by use of available activation enthalpies, but the values of the other parameters are generally as given at the temperature of measurement. These values are not very sensitive to the temperature. Thus, the values of β and γ for Ir₄(CO)₁₂ were obtained over a range of temperature and are 0.25 ± 0.04 and -0.080 ± 0.008 deg⁻¹, respectively, at 80 °C; i.e., they are the same, within the quoted precision, as those at 25 °C. ^b Nucleophiles 1–16 from Table 1. ^c $\theta = 145^\circ$ nucleophiles only. ^d Analysis using θ' values (see text) and nucleophiles 1–12 and 14–17. ^e Analysis using θ and nucleophiles 1–12 and 14–16. ^f Analysis using θ' and the same nucleophiles as in footnote e. ^g These references are to the sources of the original data that have been analyzed ^{7e} according to eq 6. ^h Nucleophiles with $\theta \leq 133^\circ$. These react initially to form adducts Ru₅C(CO)₁₅L. ⁱ Nucleophiles with $\theta \geq 136^\circ$. These react *via* a different path from smaller nucleophiles and form the substitution products Ru₅C(CO)₁₄L in a single concerted step. ^j N₄Me₂ = 1,4-dimethyltetraazabutadiene.

Data for nucleophiles 12–16 can be analyzed independently by using eq 6 with $\lambda = 1$ and $\theta_{\text{th}} < 148^\circ$, and the value obtained for β is 0.34 ± 0.18 . Although this is less precise, it is entirely compatible with the two other values of β found above; therefore, a common β value seems to be operating over the whole range of cone angles as required by eq 6. Data for all the nucleophiles 1–16 can therefore be fitted to eq 6 by the method described above, and the RMSDs vary with the chosen θ_{th} as follows: θ_{th} (RMSD) = 135° (0.557), 140° (0.406), 141° (0.386), 142° (0.376), 143° (0.377), and 145° (0.416). The parameters corresponding to the best value of θ_{th} (142°) are given in Table 3, where the R^2 value shows that only 8.3% of the dependence of the values of $\log k_2$ on the basicity and size of the nucleophiles remains unexplained by the model represented by eq 6 and the parameters $\text{p}K_{\text{a}}'$ and θ . This is not at all unsatisfactory, but the situation is even better than this indicates. If the inadequacy of the model to account completely for the data when $\theta > \theta_{\text{th}}$ is ascribed solely to uncertainties in the cone angles, then an average adjustment of $\pm 2.0^\circ$ in the cone angles would lead to a *perfect description* of these data by the model. The only ligands that require an adjustment of more than 3° are PCy₃ (-3.9°), PBz₃ (-4.0°), and *P-t*-Bu₃ (+5.0°); thus, the adjustments are generally very close to the intrinsic uncertainty in the estimates of the cone angles in the first place.³⁰ The much larger adjustments suggested³¹ for ligands such as P(OEt)₃, PEt₃, and, by implication, other phosphites would have no effect on the data analysis for these reactions because even the higher cone angles would still leave those ligands below the steric threshold. The inability of the model to account completely for the rates

of reaction of these nucleophiles can be overcome by applying an average deviation of ± 0.64 to $\text{p}K_{\text{a}}'$, which is only 4% of the total range covered by this parameter. Similarly, the average deviation in $\text{p}K_{\text{a}}'$ for the P(*p*-XC₆H₄)₃ nucleophiles alone is 0.18, or 2.7% of the range covered by these ligands. These considerations suggest that values of RMSD and R^2 are not entirely satisfactory indicators of the goodness of fit of the model to the data when small and perfectly reasonable adjustments of the two variable parameters can reduce the deviations essentially to zero and increase R^2 to unity. This is particularly true when it is recognized that the effective relative cone angles could vary from system to system because of different extents of bond making in the transition states. It also has implications for the estimates of the uncertainties in the parameters SR, β , and γ , which can also be reduced to zero. However, since these parameters are of interest for comparative purposes, it seems best to accept a consistent set of values for $\text{p}K_{\text{a}}'$ and θ , as well as the uncertainties in the derived parameters that they lead to. In this regard the uncertainty in θ_{th} , which is not explicitly given by the analysis described above, can be estimated to be ca. $\pm 2^\circ$ by examination of the range of θ_{th} values that corresponds to the uncertainty in the value of SR. The steric profile that results from the analysis of the data described above is shown in Figure 3.

The existence of the steric threshold in the first place is confirmed by a separate analysis of the data for the 11 nucleophiles with $\theta \geq 145^\circ$ and the use of the parameters obtained to predict what the rate constants should be for the five nucleophiles with $\theta \leq 132^\circ$. All the calculated values of $\log k_2^\circ$ are much higher than those observed, viz. etpb (6.4), P(OEt)₃ (5.1), P(OPh)₃ (2.6), P(*O-i*-Pr)₃ (2.4), and PEt₃ (1.7 high). Even if the suggested adjustments³¹ to the cone angles of P(OEt)₃

(30) Tolman, C. A. *Chem. Rev.* 1977, 77, 313–348; *J. Am. Chem. Soc.* 1970, 92, 2956–2965.

(31) Stahl, L.; Ernst, R. D. *J. Am. Chem. Soc.* 1987, 109, 5673–5680.

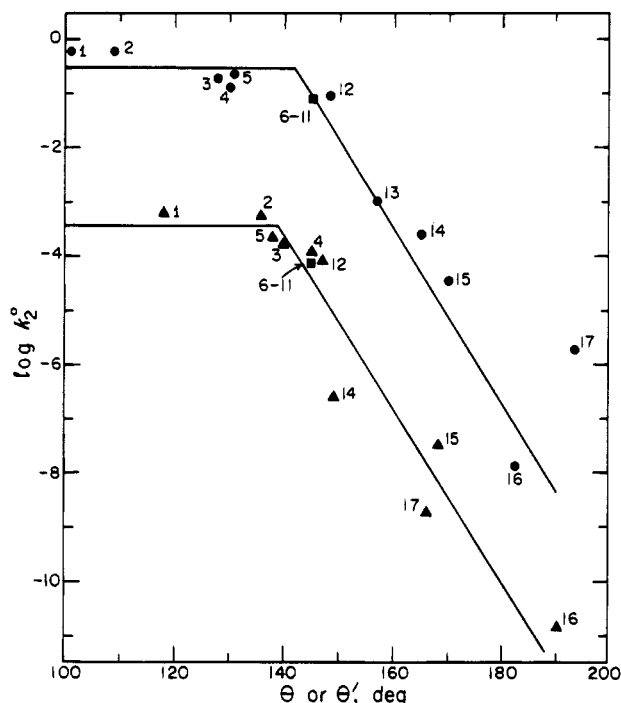


Figure 3. Steric profiles for the reactions of $(\mu_2\text{-H})_2\text{Os}_3\text{-(CO)}_{10}$ with L in heptane at 30 °C: (●) $\log k_2^\circ$ vs θ ; (▲) $\log k_2^\circ - 3$ vs θ' . The nucleophile numbering is taken from Table 1. (■ is the average value of $\log k_2^\circ$ or $\log k_2^\circ - 3$ for nucleophiles 6–11.)

and PET_3 are made, the calculated values of k_2° for those nucleophiles are still over an order of magnitude too high. The value of $\log k_2^\circ$ for etpb, for which there is no controversy over its Tolman cone angle,³¹ by itself shows the existence of the steric threshold quite dramatically.

The only data omitted from the above analyses were those for $\text{P}(o\text{-tol})_3$, which clearly do not fit on the steric profile in Figure 3, and PPh_2Cl , which will be considered later. It seems likely that the deviation of $\text{P}(o\text{-tol})_3$ is due to a considerable overestimate of its Tolman cone angle. The original cone angle for $\text{P}(m\text{-tol})_3$ (165°) would have caused the data for this nucleophile also to deviate strongly from the steric profile, but this value has recently been revised downward³² after reconsideration of the appropriate conformation to use. The revised value was obtained by a computer method that essentially mimicked Tolman's method and that led to exactly the same cone angle for PPh_3 as Tolman's. Deviations from similar correlations of data for $\text{P}(o\text{-tol})_3$, and for $\text{P}(m\text{-tol})_3$ when using Tolman's original cone angle, have been observed before.³³

Use of an Alternative Steric Parameter. The successful use of Tolman cone angles in analyzing the data for this system and many others^{7c-f,19} is remarkable in view of the simplicity, if not downright crudity, of the model on which they are based. Other more theoretically sophisticated and agreeable estimates of ligand size (a.k.a. steric requirements) have been suggested but are available only for relatively few ligands. The situation has recently been reviewed,³⁴ and a notable extension is the availability of E_R values cal-

culated by Brown³⁵ for a very wide range of ligands. These are estimates of the repulsion energies experienced by the ligands in the complexes $\text{Cr}(\text{CO})_5\text{L}$.³⁶ Being a repulsion energy, it is a more rational parameter to correlate with energetic parameters such as activation free energies, in contrast to cone angles, which would not be expected to relate linearly to energetic parameters. However, this aspect of the relative merits of cone angles and E_R values is of less importance than it might seem because of the excellent linear correlation found between their values for a wide range of ligands. Thus, a set of 37 alkyl, mixed-alkyl, aryl, and mixed-alkyl-aryl phosphines (including $\text{P}(m\text{-tol})_3$) fit closely to eq 7, with an RMSD value of $\pm 3.8^\circ$ and $R^2 = 0.934$.

$$\theta = (101.3 \pm 2.1) + (0.553 \pm 0.025)E_R \quad (7)$$

PET_3 and $\text{P-}n\text{-Bu}_3$ (which were included in the correlation) lie 3 and 5° low, while PCy_2H and PCyH_2 (which were not) also fall close to the correlation (θ being 5 and 4° high, respectively). Values of θ for the following important ligands are high by 6° (PPh_2H), 10° (PPh_2Bz and PPh_2Cl), 18° (PBz_3), 21° ($\text{P}(m\text{-ClC}_6\text{H}_4)_3$), and 30° ($\text{P}(o\text{-tol})_3$). In contrast, the values of θ for phosphite and mixed-phosphine-phosphite ligands are often lower than expected from the correlation, the deviations being -14° (etpb), -23° ($\text{P}(\text{OMe})_3$), -25° ($\text{P}(\text{OEt})_3$), -27° ($\text{P}(\text{O-}n\text{-Bu})_3$), -12° ($\text{P}(\text{O-}i\text{-Pr})_3$), -9° ($\text{P}(\text{OPh})_3$), +16° ($\text{P}(\text{O-}t\text{-Bu})_3$), +19° ($\text{PPh}(\text{OMe})_2$), and +3° ($\text{PPh}_2(\text{OMe})$ and $\text{PPh}_2(\text{OEt})$).

These results suggest that it would be convenient to calculate values of a new set of "cone angles", θ' , that fit exactly to eq 8, established by the 37 phosphine ligands but with the first term being 2.5° higher than that in eq 7 so as to make the average of θ' for the $\text{P}(p\text{-XC}_6\text{H}_4)_3$ ligands equal to 145°. This normalizes the θ'

$$\theta' = 103.8 + 0.553E_R \quad (8)$$

values around the Tolman cone angle for these very common, useful, and mid-sized ligands. The results are included in Table 1, where it can be seen that no value is available for $\text{P}(\text{NMe}_2)_3$. No value of E_R is known for $\text{P}(p\text{-F}_3\text{CC}_6\text{H}_4)_3$ either, but the value of θ' is based on comparison with the values for the other $\text{P}(p\text{-XC}_6\text{H}_4)_3$ ligands. The values of θ' are thus directly based on the corresponding E_R values, but the latter have been transformed by a scaling process into equivalent angles. These are comparable to Tolman cone angles and can be used in stereoelectronic analyses in exactly the same way. The parameters so obtained will be in the same units and can be directly compared. The relationship between θ' and θ is, therefore, not dissimilar to that between $\text{p}K_a'$ and χ (see above).

Analysis of the data for the 16 nucleophiles 1–12 and 14–17 according to eq 6 (but with θ and θ_{th} replaced by θ' and θ'_{th}) can be carried out exactly as before. The best fit (RMSD = 0.582, $R^2 = 0.858$) is obtained for $\theta'_{\text{th}} = 139^\circ$, and the values of SR, β , and γ are given in Table 3. The uncertainty in θ'_{th} is estimated as $\pm 3^\circ$ by the

(32) White, D.; Carlton, L.; Coville, N. J. *J. Organomet. Chem.* **1992**, *440*, 15–25.

(33) Romeo, R.; Arena, G.; Scolaro, L. M. *Inorg. Chem.* **1992**, *31*, 4879–4884.

(34) White, D.; Coville, N. J. *Adv. Organomet. Chem.* **1994**, *36*, 95–158. Brown, T. L.; Lee, K. J. *Coord. Chem. Rev.* **1993**, *128*, 89–116.

(35) Brown, T. L. *Inorg. Chem.* **1992**, *31*, 1286–1294.

(36) Values of repulsion energies, E_R , have also been reported by Brown et al.³⁷ for ligands in $\text{CpRh}(\text{CO})\text{L}$.

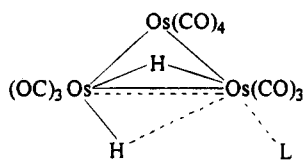
(37) Choi, M.-G.; Brown, T. L. *Inorg. Chem.* **1993**, *32*, 5603–5610.

method described above for θ_{th} . This fit is not nearly as good as when θ was used, although the parameters obtained are not significantly different. An average adjustment of $\pm 2.9^\circ$ in the value of θ' when $\theta' > \theta_{\text{th}}'$ will lead to a perfect description of the data by the model. Much of the adjustment needed is caused by $\text{P}(o\text{-tol})_3$ and PBz_3 , which require increases of 6.8 and 10.4° , respectively, in their θ' values. The data for these nucleophiles otherwise lie below the steric profile by 1.10 and 1.65 log units, respectively. The steric profile drawn in terms of θ' is included in Figure 3.

In making a comparison between the success of the model when using θ or θ' values, it would be fairer to use exactly the same set of nucleophiles. In the comparison made above, the data for $\text{P}(o\text{-tol})_3$ had to be omitted to get any reasonable fit when using θ values, while the analysis using θ' values also omitted data for one nucleophile ($\text{P}(\text{NMe}_2)_3$) for which a θ' value was not available. Omitting the data for these nucleophiles led to best fits characterized by RMSD (and R^2) values of 0.508 (0.925) and 0.370 (0.960), respectively, when θ' and θ values were used. Only when data for PBz_3 were also omitted from both analyses was the result better using θ' , viz. 0.187 (0.990) vs 0.348 (0.996), but the parameters, including θ_{th}' and θ_{th} , were quite indistinguishable.

Discussion

Stoichiometric Mechanisms. The reactions all proceed very cleanly according to eq 1 with straightforward pseudo-first-order kinetics and with excellent fits to eq 2. In this they resemble the reactions of $(\mu_2\text{-H})_2\text{Os}_3(\text{CO})_{10}$ with CO to form $(\mu_2\text{-H})\text{Os}_3(\text{CO})_{11}$.⁵ The activation parameters for reactions with $\text{P}(\text{OPh})_3$ (Table 1) are typical of associative reactions of P-donor nucleophiles.^{7c,29} It can therefore be concluded that the reactions involve concerted addition of the nucleophiles to form the electronically and coordinatively saturated adducts $(\mu_2\text{-H})(\text{H})\text{Os}_3(\text{CO})_{10}\text{L}$ just as is the case for addition of CO,⁵ and the transition states can be represented in a similar way by III, which is intermediate between I and II.



III

Although the ultimate products of the reactions have the added ligands in equatorial positions,³⁸ i.e. in the plane defined by the Os_3 cluster, it appears likely that the nucleophile enters the cluster from above (or below) the Os_3 plane to form an axial isomer that subsequently isomerizes to form the more stable equatorial product.³⁹

Success of the Model. The data analyses presented above show that eq 6 provides a good description of the data for 16 nucleophiles when using Tolman cone angles, but data for $\text{P}(o\text{-tol})_3$ and PPh_2Cl do not fit.

When the θ' parameters, based directly on Brown's E_R values,³⁵ are used instead, the data for 16 nucleophiles (now including $\text{P}(o\text{-tol})_3$ but not PPh_2Cl or $\text{P}(\text{NMe}_2)_3$, for which there is no E_R or θ' value) are not described as well by eq 6 (Table 3). Even when identical sets of nucleophiles are used, the analysis using θ' is not as good unless data for one further nucleophile, PBz_3 , are omitted. The E_R value for this ligand must be considered to be suspect. In all cases the values of θ_{th} , SR, β , and γ are indistinguishable, only their uncertainties varying with the details of the analysis. This is largely accounted for by the fact that the phosphite ligands, which are most likely to show which of θ or θ' is the better steric parameter, all lie below the steric thresholds θ_{th} or θ_{th}' , and this system is therefore not a good one for making this comparison. However, the relationship between θ , θ' , and E_R , and the value $\theta_{\text{th}} = 142^\circ$, enables the conclusion to be reached that ligands which in $\text{Cr}(\text{CO})_5\text{L}$ experience repulsion energies of up to 70 kcal mol⁻¹ undergo no repulsion in the transition states of these reactions.

Intimate Mechanisms of the Reactions. The good fit of the data to eq 6 provides quite precise values for the parameters θ_{th} , SR, β , and γ as shown in Table 3. These values are unique to this cluster and therefore provide the dynamic characterization mentioned in the Introduction. They do, however, a great deal more than this, since they can also provide considerable insight into the details of the intimate mechanisms of such reactions.

Values of β have, for a long time,²¹ been considered to provide relative estimates of the "extents" of bond making in associative reactions of metal carbonyls. Ideally, the dependence of $\log k_2$ (or ΔG^\ddagger) on $\log K$ (or ΔG°) for formation of the products would provide a more rigorously defined LFER and a better estimate of the extent of bond making, but systematic equilibrium data are not available for such comparisons. Instead, the values of $\log k_2$ are compared effectively with the values of $\log K$ estimated^{7c,e,f} for formation of the $\text{H}^+ - \text{P}$ bond in the phosphonium ion in nonpolar solvents. In this way the values of β provide a measure of the energetic stabilization of the transition state by partial $\text{M} - \text{P}$ bond formation compared to the stabilization of the phosphonium ion by complete $\text{H}^+ - \text{P}$ bonding. Their absolute significance is not, therefore, particularly precise, but the relative values do provide a good indication of the relative extents of transition-state stabilization by $\text{M} - \text{P}$ bond making.⁴⁰ It should be noted that a higher β value could be obtained for one system when the proportion of bond making is actually less than that in another system for which there is

(40) In effect, the values could be regarded as being compared to the value of β for some hypothetical reference compound for which $\log k_2$ values for all the nucleophiles used have been obtained. In this sense the values of β are similar to those of S found for associative reactions of Pt(II) complexes where the linear dependence of $\log k_2$ on n^2_{Pt} defines the relative selectivity toward the nucleophiles of the complex being studied compared with that of the standard *trans*- $\text{PtCl}_2(\text{py})_2$.⁴¹ The relative value of β defined by the dependencies of $\log k_2$ on $\text{p}K'_a$ are therefore linked by the $\text{p}K'_a$ values without necessarily being conceptually dependent on them, only the empirical linearity of the various dependencies being important. A similar point was made in the study of associative reactions of $\text{Co}_2(\text{CO})_8(\mu\text{-C}_2\text{Ph}_2)$.⁴²

(41) Shriver, D. F.; Atkins, P. W.; Langford, C. H. *Inorganic Chemistry*, 2nd ed.; Freeman: New York, 1994; Chapter 15. Cattalini, L. *Prog. Inorg. Chem.* **1970**, *13*, 263-327.

(42) Cobb, M. A.; Hungate, B.; Poë, A. J. *J. Chem. Soc., Dalton Trans.* **1976**, 2226-2229.

(38) Churchill, M. R.; DeBoer, B. G. *Inorg. Chem.* **1977**, *16*, 2397-2403.

(39) Neubrand, A.; Poë, A. J.; van Eldik, R. *Organometallics* **1995**, *14*, 3249.

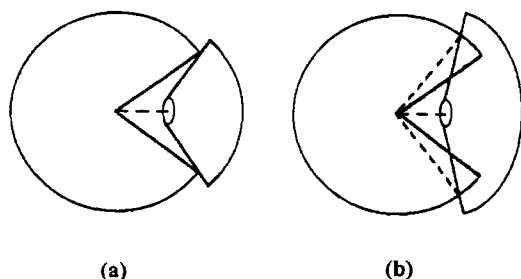


Figure 4. (a) Representation of a TSI with its opened space occupied by a partially coordinated P-donor nucleophile, drawn as a truncated cone, with $\theta = \theta_{th}$. (b) The same TSI with a partially bonded nucleophile with $\theta > \theta_{th}$. The broken line shows how the TSI has to open up to accommodate the nucleophile while maintaining the same M - P bond length as in (a).

proportionally more bond making. This could arise if the fully formed M-P bond in the former case were considerably stronger than the fully formed M-P bond in the second case; i.e., a smaller fraction of a stronger M-P bond could provide more energetic stabilization of the transition state than a larger fraction of a weaker M-P bond.

The significance of the values of θ_{th} has been discussed previously.^{7c,d,f} The packing of carbonyl and other ligands around metal clusters, in particular, is sufficiently compact that it is difficult to see how attack, even by relatively small nucleophiles, could occur without any steric difficulties at all. This led it to be suggested^{7c} that the approach of the nucleophile is accompanied by an opening up of the ligand polytope to form a higher energy isomer (the transition-state isomer, TSI) of the ground-state cluster that contains a rather well-defined open space into which all nucleophiles with $\theta < \theta_{th}$ can fit without the occurrence of any steric repulsion. Values of θ_{th} are related to the size of this opened space in the TSI. When $\theta > \theta_{th}$, the space available in the TSI is not great enough for M - P bonds of the same length to be formed unless there is a further opening up of the ligand polytope, and the value of γ found when $\theta > \theta_{th}$ is a measure of the energetic difficulty of this process; i.e., γ is a measure of the flexibility of the TSI. This situation is illustrated by the sketch in Figure 4. It is possible that the slower rates observed when $\theta > \theta_{th}$ may be due to the inability of these larger nucleophiles to approach as close to the electrophilic center in the TSI, the latter being quite rigid in this case. In principle this would lead to larger β values for nucleophiles with $\theta < \theta_{th}$ than for those with $\theta > \theta_{th}$, but that might be difficult to detect.⁴³

Values of γ in deg^{-1} at 25 °C can be transformed into dimensionless numbers by multiplying by $-1.36 \times 0.553 = -0.75$, i.e. by transforming $\log k_2^\circ$ values into equivalent free energies of activation and by taking account of the relationship shown in eq 8. This means that a γ value of -0.1 deg^{-1} corresponds to an increase of $0.075 \text{ kcal mol}^{-1}$ in the free energy of the TSI for every 1 kcal mol^{-1} increase in E_R .

The analysis also leads to a clear indication of the meaning of the standard (SR) and intrinsic (IR) reac-

tivities. The SR is a measure of the energy required for the isomerization process less the amount of energy released by formation of the M - P bond with the hypothetical small and weak nucleophile of $pK_a' = -4$. The IR is the energy required to produce the TSI without any stabilization of the isomer by M-P bond formation, but this can only be quantified at all accurately for those cases where β approaches zero; i.e., stabilization by M - P bond making is negligible for any nucleophile. As β becomes larger, so the SR will overestimate the IR to an increasing extent but, if the β values for two systems are similar, the relative values of SR will also be a good measure of their relative intrinsic reactivities.

One might expect there to be systematic relationships between the values of θ_{th} and β . If two complexes have similar β values, but one has a lower θ_{th} , then the latter complex must have a smaller opened space. But, if two complexes have TSIs with the same extent of opened-up space, then the one with the higher β value (greater bond making) would be expected to have the lower value of θ_{th} .

Turning to the parameters (Table 3) for the $(\mu_2\text{-H})_2\text{-Os}_3(\text{CO})_{10}$ cluster studied here (and for the selection of other metal carbonyls), we can see that the value of β is very high. It is exceeded so far only by the values for $\text{Fe}(\text{CO})_3(\text{N}_4\text{Me}_2)$ and for the concerted substitution reactions of $\text{Ru}_5\text{C}(\text{CO})_{15}$ with larger nucleophiles.^{7d} Values for the 17-electron $\text{V}(\text{CO})_6$ or various $\eta^5\text{-C}_5\text{H}_5$, $\eta^5\text{-indenyl}$, or NO-containing mononuclear carbonyls^{7e} do not even approach it. It is equaled or approached only by values for $\text{Fe}_2(\text{CO})_6(\mu_2\text{-RN}(\text{CO})\text{NR})$ ($\text{R} = p\text{-MeOC}_6\text{H}_4$) and $\text{Rh}_4(\text{CO})_9\{\mu_3\text{-HC}(\text{PPh}_2)_3\}$.

In spite of this high degree of bond making, the well-defined value of θ_{th} is also high, only those for $\text{Mn}(\text{CO})_4(\text{NO})$, $\text{V}(\text{CO})_5(\text{NO})$, and $\text{Cr}(\text{CO})_6$ ⁴⁴ exceeding 145° , but to an unknown extent.⁴⁵ The value of β for $\text{Cr}(\text{CO})_6$ is very low (0.04 ± 0.01)^{7e} so that its high value of θ_{th} could be associated with the very small contribution of bond making, but the values of β for $\text{Mn}(\text{CO})_4(\text{NO})$ and $\text{V}(\text{CO})_5(\text{NO})$ are significant (Table 3). Bond making is therefore quite pronounced in these cases, and the high value of θ_{th} must indicate quite a high degree of opening up of the transition state isomers. The only carbonyl cluster to show a comparable value of θ_{th} is $\text{Ru}_5\text{C}(\text{CO})_{15}$ in its concerted substitution reactions with larger nucleophiles (Table 3),^{7d} and because of its even higher value of β , this cluster must open up even more than $(\mu_2\text{-H})_2\text{Os}_3(\text{CO})_{10}$.

The negative value of γ for $(\mu_2\text{-H})_2\text{Os}_3(\text{CO})_{10}$ is surpassed only by those for $\text{Fe}(\text{CO})_3(\text{N}_4\text{Me}_2)$ and $\text{Ru}_6\text{C}(\text{CO})_{17}$ and for $\text{Ru}_5\text{C}(\text{CO})_{15}$ in its concerted substitution reactions. The flexibility of the very open TSI of $(\mu_2\text{-H})_2\text{Os}_3(\text{CO})_{10}$ is therefore very low in a comparative sense. However, in other terms, the value of γ corresponds to a destabilization of the transition state by only $0.12 \text{ kcal mol}^{-1}$ for every 1 kcal mol^{-1} destabilization of $\text{Cr}(\text{CO})_6\text{L}$.

The standard reactivity is larger than those of $\text{Ru}_3(\text{CO})_{12}$ and, quite certainly, $\text{Os}_3(\text{CO})_{12}$ (which undergoes

(44) Original data taken from: Graham, J. R.; Angelici, R. J. *Inorg. Chem.* **1967**, *6*, 2082-2085.

(45) Only nucleophiles with $\theta \leq 145^\circ$ were used in these studies, and all nucleophiles lie on the LFER; thus, there is no evidence available for any steric deviations.

(43) Thus, in this case, β from the 145° nucleophiles (which are only just above the steric threshold) is 0.433 ± 0.020 , and from the five larger nucleophiles it is 0.34 ± 0.18 , which is consistent with the former value, but it could also be significantly smaller.

Table 4. Enthalpy Data for Reactions of $(\mu_2\text{-H})_2\text{Os}_3(\text{CO})_{10}$ (I) with CO and P(OPh)₃

reacn	ΔH , kcal mol ⁻¹
I + CO → III (L = CO)	15.7 ± 0.04 ^a
I + CO → II (L = CO)	-9.5 ± 0.3 ^a
I + P(OPh) ₃ → III (L = P(OPh) ₃)	7.4 ± 0.3 ^b
I + P(OPh) ₃ → II (L = P(OPh) ₃)	-23 ^c

^a Data from ref 5. ^b See footnote *h* in Table 1. ^c Data from ref 6.

substitution reactions very much more slowly,⁴⁶ although data for a full analysis are not available). It is less than that for $\text{Ru}_6\text{C}(\text{CO})_{17}$ ^{7c} and is considerably less than that for reactions of $\text{Ru}_5\text{C}(\text{CO})_{15}$ with smaller nucleophiles to form the adducts $\text{Ru}_5\text{C}(\text{CO})_{15}\text{L}$, the latter value being the highest found so far.

Enthalpy Changes during Reactions with P(OPh)₃. A more penetrating insight into the energy changes involved in the $(\mu_2\text{-H})_2\text{Os}_3(\text{CO})_{10}\text{-L}$ system can be obtained by considering the values of ΔH^\ddagger and ΔH° ⁶ for reaction with P(OPh)₃, together with those for the reaction with CO⁵ as shown in Table 4.

The energy of the newly formed Os-CO bond in II (L = CO) can be taken to be 45 kcal mol⁻¹ or slightly more,⁵ so that the rearrangement required for conversion of $(\mu_2\text{-H})_2\text{Os}_3(\text{CO})_{10}$ to the $(\mu_2\text{-H})(\text{H})\text{Os}_3(\text{CO})_{10}$ moiety in the product II (L = CO) is ca. 45-9.5, i.e. ca. 35 kcal mol⁻¹.⁵ If we assume that the same energy is required to produce the $(\mu_2\text{-H})(\text{H})\text{Os}_3(\text{CO})_{10}$ moiety in II (L = P(OPh)₃),⁴⁷ then the strength of the newly formed Os-P bond is ca. 58 kcal mol⁻¹. We can now consider the relative extents of $\text{H}_2\text{Os}_3(\text{CO})_{10}$ rearrangement and Os-P bond formation in forming III (L = P(OPh)₃). At one extreme all of the activation enthalpy (7.4 kcal mol⁻¹) could be used to rearrange $\text{H}_2\text{Os}_3(\text{CO})_{10}$ to an (energetic) extent of ca. $7/35 = 20\%$ of the way toward the $\text{H}_2\text{Os}_3(\text{CO})_{10}$ moiety in II (L = P(OPh)₃) without there being any offsetting enthalpy released through Os-P bond formation. In view of the high value of β this extreme is quite unacceptable. At the other extreme we could envisage the value of ΔH^\ddagger to be made up of a complete rearrangement of the $(\mu_2\text{-H})_2\text{Os}_3(\text{CO})_{10}$ to the form it would have in the product, offset by the energy released by Os-P bond formation. This would require ca. $35 - 7 = \text{ca. } 28$ kcal mol⁻¹ of enthalpy to be released by Os-P bond formation. This implies that the Os-P bond enthalpy in the transition state is ca. $28/58 = \text{ca. } 50\%$ of the enthalpy released by complete formation of the Os-P bond. This represents the maximum contribution of Os-P bond formation in the transition state and is essentially the same as the maximum extent of Os-CO bonding in III (L = CO) estimated previously.⁵ In that case, however, there was no way of disallowing the possibility of a much smaller amount of rearrangement and virtually no enthalpy release from Os-CO bond formation. In this case (see above) we know that Os-P bond formation is well advanced because of the high β value, so that something approaching complete rearrangement of the $(\mu_2\text{-H})_2\text{Os}_3(\text{CO})_{10}$ and 50% of Os-P bond formation is much more

likely.⁴⁹ A large extent of $(\mu_2\text{-H})_2\text{Os}_3(\text{CO})_{10}$ rearrangement is in good accord with the high value of θ_{th} , which indicates a large amount of opened-up space in the TSI.

These data also provide some quantitative evidence for the large difference between the SR and IR values, which must apply generally in cases when β is large. The IR value, as given by the enthalpy of formation of the TSI, is equal to the rearrangement enthalpy of up to ca. 35 kcal mol⁻¹ estimated above by assuming virtually complete rearrangement of $(\mu_2\text{-H})_2\text{Os}_3(\text{CO})_{10}$. Even the weak nucleophile P(OPh)₃ ($\text{p}K_{\text{a}}' = -2.79$) stabilizes the transition state by up to ca. 28 kcal mol⁻¹ (see above), and the hypothetical standard nucleophile with $\text{p}K_{\text{a}}' = -4$ would not stabilize the transition state by very much less than this. The extrapolation of SR values to IR values (when the transition state is not stabilized at all by M-P bond formation) is therefore a particularly long one when β values are large, and the uncertainty in the IR values that results from the extrapolation is correspondingly large.

Kinetic Isotope Effects (KIEs). The KIEs for the five nucleophiles studied are all normal, showing that the combined H (D) bonding of the two sorts of hydride in the transition states is weaker than in the reactant cluster. The KIEs seem to vary rather randomly with the electronic and steric properties of the nucleophiles. The difference between the lower values for etpb (1.03 ± 0.01), P(OEt)₃ (1.08 ± 0.01), and PCy₃ (1.08 ± 0.01) and the higher values for P(OPh)₃ (1.21 ± 0.02) and PEt₃ (1.28 ± 0.02) seems likely to be statistically significant. The precision is high, because of extensive replication of k_{obs} values that have low individual standard errors of measurement, and systematic errors are likely to be small because identical samples of $\text{D}_2\text{Os}_3(\text{CO})_{10}$ were used and runs with the D₂ and H₂ clusters were carried out almost simultaneously under identical conditions. The difficulty of assessing the significance of these data may arise from the fact that there are two sorts of hydride ligands involved in the transition states (one bridging and one semibridging or even terminal) and the KIEs will be determined by the changes of the bonding involved in forming each of these.

Results for Other Nucleophiles. The values of k_2 for reactions with AsPh₃ and SbPh₃ are not very much less than that for PPh₃ and are much greater than that for P(OPh)₃. These relative rates are very similar to those observed for the nucleophile-induced heterolysis of the Fe-CO and Fe-Fe bonds in $\text{FeCo}(\text{CO})_7(\mu\text{-AsMe}_2)$ and $\text{Fe}_2(\text{CO})_6(\text{NO})(\mu\text{-AsMe}_2)$, respectively, but not to those observed for nucleophilic attack on most other carbonyls.⁵⁰ The behavior of these ligands as nucleophiles seems to be quite erratic. The value of k_2 for PPh₂Cl is approximately the same as that for PPh₃ in spite of its very low basicity, and the value of the log k_2 is ca. 3 log units larger than expected. This nucleophile is not commonly used in such studies, and the significance of this unexpectedly large rate is not obvious. More measurements involving this ligand should be

(46) Poë, A. J.; Sekar, V. *Inorg. Chem.* **1985**, *24*, 4376-4380.

(47) This seems reasonable in view of the facts that the average Os-CO bond lengths in $(\mu_2\text{-H})_2\text{Os}_3(\text{CO})_{11}$ and $(\mu_2\text{-H})\text{Os}(\text{CO})_{10}\text{PPh}_3$, for instance, are virtually identical and the average Os-Os bond lengths are nearly so.^{38,48}

(48) Churchill, M. R.; Deboer, B. G. *Inorg. Chem.* **1977**, *16*, 878-884.

(49) A similar amount of bond making can be estimated from the data for reactions with PPh₃,^{6,39} but the values of ΔH^\ddagger for reactions with P(*i*-Pr)₃ and PPhEt₂ (-108 and -90 kcal mol⁻¹)⁶ would lead to negative values of ΔH^\ddagger for 50% bond making. These values of ΔH^\ddagger imply Os-P bond strengths of 143 and 125 kcal mol⁻¹, respectively, which seem excessively high compared with those for P(OPh)₃ (58 kcal mol⁻¹) and PPh₃ (65 kcal mol⁻¹) in spite of their higher basicity ($\text{p}K_{\text{a}}' = 9.89$ and 5.94, respectively).

(50) See refs 9, 12, 14, 15, and 21 in ref 15.

made. The data for $P(o\text{-tol})_3$ have been discussed above.

Chlorobenzene as Solvent. Aromatic solvents are useful for studying associative reactions of carbonyls with P-donor nucleophiles when the associative reactions occur together with a CO-dissociative path. This situation necessitates the use of relatively high concentrations of the nucleophiles, so that $k_2[L]$ can be made comparable to k_{-CO} , and this is hard to attain in paraffin solvents in some cases, e.g. $L = P(p\text{-XC}_6\text{H}_4)_3$. Although this situation does not obtain with $(\mu_2\text{-H})_2\text{Os}_3(\text{CO})_{10}$, it is useful to compare the kinetic data obtained in a paraffin hydrocarbon such as heptane and an aromatic solvent such as chlorobenzene. Reactions of $(\mu_2\text{-H})_2\text{Os}_3(\text{CO})_{10}$ are generally slightly slower in chlorobenzene than those in heptane, with an average ratio $k_2(\text{heptane})/k_2(\text{chlorobenzene})$ of 2.4 ± 0.3 for those nucleophiles common to both solvents. The highest and the lowest ratios are 4.26 for PPh_3 and 1.24 for $P(p\text{-F}_3\text{-CC}_6\text{H}_4)_3$, respectively. The variations are quite random,

and essentially the same β value is obtained in both solvents (Table 3). More extensive data are available elsewhere.³⁹ The very small differential effects of these two solvents makes any discussion unprofitable, except for it to be noted that chlorobenzene is a perceptibly better donor than heptane.⁵¹ Reactions in better donor solvents might be even slower because of the need for prior removal of a solvent molecule, S, from what might be the partially formed adducts $\text{H}_2\text{Os}_3(\text{CO})_{10}\text{S}$.

Acknowledgment. The Natural Science and Engineering Research Council, Ottawa, Ontario, Canada, is gratefully acknowledged for financial support of this work and for the award of a postgraduate fellowship (to R.H.E.H.). Thanks are also due to Ms. L. Paine for assistance in the preparation of this paper.

OM9501687

(51) Dobson, G. R.; Zhang, S. *J. Coord. Chem.* **1990**, *21*, 155–165.

Activation Parameter Correlations for Nucleophile Addition to $(\mu_2\text{-H})_2\text{Os}_3(\text{CO})_{10}$

Anton Neubrand,^{1a} Anthony J. Poë,^{*,1b} and Rudi van Eldik^{*,1a}

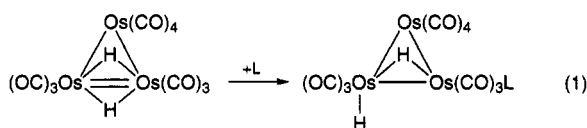
Institute for Inorganic Chemistry, University of Erlangen-Nürnberg, Egerlandstrasse 1, 91058 Erlangen, Germany, and Lash Miller Chemical Laboratories, University of Toronto, 80 St. George Street, Toronto, Ontario, Canada M5S 1A1

Received December 15, 1994[®]

Kinetic studies of the addition reactions of a large number of P-donor nucleophiles to the unsaturated cluster $(\mu_2\text{-H})_2\text{Os}_3(\text{CO})_{10}$ were performed as a function of pressure and temperature. The second-order rate constants, k_2 , for reactions in chlorobenzene at 30 °C follow the same empirical equation, $\log k_2 = \alpha + \beta(\text{p}K'_a + 4) + \gamma(\theta - \theta_{\text{th}})\lambda$, that has been reported elsewhere for reactions in heptane. $\text{p}K'_a$ represents the σ -donicity of the nucleophiles in nonpolar solvents and θ the Tolman cone angle for the individual P-donors. No steric effect was observed for ligands with cone angles below the steric threshold ($\theta \leq \theta_{\text{th}} = \text{ca. } 147^\circ$; $\lambda = 0$). For larger ligands ($\theta > \theta_{\text{th}}$; $\lambda = 1$) k_2 is strongly affected by the size of the nucleophile, as shown by the large, negative γ value of $-0.18 \pm 0.02 \text{ deg}^{-1}$. Reactions with PPh_3 in heptane and nitromethane show that the rate constant is independent of the polarity of the solvent at ambient temperatures. In chlorobenzene as solvent the rate constants are slightly smaller, possibly due to the solvent donor properties, but the β and γ values and, therefore, the transition states of the addition step remain essentially unchanged. The volumes of activation, ΔV^\ddagger , determined in chlorobenzene are all negative. They show no significant dependence on the $\text{p}K'_a$ values, which indicates that the volume collapse is controlled by steric rather than electronic factors. The ΔV^\ddagger values show a remarkable correlation with the cone angles. For $\theta < 160^\circ$, ΔV^\ddagger decreases linearly ($R = 0.91$) with $\tan^2(\theta/2)$, a measure of the relative volumes of the nucleophiles. This suggests that the $\text{Os}\cdots\text{P}$ bond lengths in the transition states are the same for all these nucleophiles, and the slope of the correlation enables a rough estimate to be made of the penetration (ca. 24 pm) of the P-donor ligands inside the periphery of the cluster in the transition state. Extrapolation to $\tan^2(\theta/2) = 0$ shows that formation of the cluster moiety in the transition state unexpectedly involves a compression of the ligand polytope. At $\theta = 160^\circ$ there appears to be a new type of steric threshold (defined in terms of ΔV^\ddagger rather than $\log k_2$ or ΔG^\ddagger) above which the ΔV^\ddagger values become less negative, the penetration of the nucleophiles becomes less, and the $\text{Os}\cdots\text{P}$ bond lengths become progressively longer. Other correlations of the activation parameters are considered.

Introduction

The hydrido carbonyl cluster $(\mu_2\text{-H})_2\text{Os}_3(\text{CO})_{10}$ has been known for some time to react with a wide variety of Lewis bases according to the overall reaction (1).²



Detailed studies have been undertaken on the thermodynamics of the addition of MeCN,³ the kinetics and thermodynamics of the reversible addition of CO,⁴ the

enthalpies of addition of some P-donor ligands,⁵ and the kinetics of the addition of a wide variety of P-donor nucleophiles.^{6a} In the last study^{6a} it was possible to provide clear quantitative electronic and steric profiles for such associative reactions based on the electronic and steric properties of the nucleophiles,⁷ something that had not been done for electronically unsaturated clusters such as $(\mu_2\text{-H})_2\text{Os}_3(\text{CO})_{10}$ before.⁸

The second-order rate constants k_2 of reaction 1 for a series of P-donor ligands were correlated with the $\text{p}K'_a$ values for the nucleophiles to account for electronic effects, where $\text{p}K'_a$ is related to the σ -donicity of the P-donors and can be derived^{7a} from χ_d values^{8b} for the ligands in the complexes $\text{Ni}(\text{CO})_3\text{L}$. These values are related to the $\text{p}K_a$ values in aqueous solution that have

[®] Abstract published in *Advance ACS Abstracts*, May 15, 1995.

(1) (a) University of Erlangen-Nürnberg. (b) University of Toronto.

(2) (a) Adams, R. D.; Selegue, J. P. In *Comprehensive Organometallic Chemistry*; Wilkinson, G., Stone, F. G. A., Abel, E., Eds.; Pergamon: Oxford, U.K., 1982; Vol. 4, and references therein. (b) Deeming, A. J. *Adv. Organomet. Chem.* **1986**, *26*, 1–96. (c) Lavigne, G. In *The Chemistry of Metal Cluster Complexes*; Shriver, D. F., Kaesz, H. D., Adams, R. D., Eds.; VCH: New York, 1990; Chapter 2.

(3) Hudson, R. H. E.; Poë, A. J.; Sampson, C. N.; Siegel, A. *J. Chem. Soc., Dalton Trans.* **1989**, 2235.

(4) Poë, A. J.; Sampson, C. N.; Smith, R. T.; Zheng, Y. *J. Am. Chem. Soc.* **1993**, *115*, 3174.

(5) Stradella, L. *J. Therm. Anal.* **1986**, *31*, 671.

(6) (a) Hudson, R. H. E.; Poë, A. J. *Organometallics* **1995**, *14*, 3238.

(b) References 2b and 6b in ref 6a.

(7) (a) Poë, A. J.; Farrar, D. H.; Zheng, Y. *J. Am. Chem. Soc.* **1992**, *114*, 5146 and references cited therein. (b) Farrar, D. H.; Poë, A. J.; Zheng, Y. *J. Am. Chem. Soc.* **1994**, *116*, 6252. (c) Waska, D. C.; Wilson, M.; Bartholomew, J.; Eriks, K.; Prock, A.; Giering, W. P. *Organometallics* **1992**, *11*, 3343 and references cited therein.

(8) (a) Baker, R. T.; Calabrese, J. C.; Krusic, P. J.; Therein, M. J.; Trogler, W. C. *J. Am. Chem. Soc.* **1988**, *110*, 8392. (b) Liu, H.-Y.; Eriks, K.; Prock, A.; Giering, W. P. *Organometallics* **1990**, *9*, 1758.

been corrected for varying hydration energies due to the varying sizes of the phosphonium ions, PH^+ .⁹ It was found that data for nucleophiles with Tolman cone angle¹⁰ $\theta \leq 145^\circ$ fit reasonably well to a linear free energy relationship (LFER), but larger nucleophiles reacted considerably more slowly than was expected from their σ -donicity.^{6a} Such a behavior has been observed for many different sets of bimolecular reactions of metal carbonyls with P-donor nucleophiles,⁷ and the data can always be fitted to eq 2. The parameter λ is a

$$\log k_2 = \alpha + \beta(\text{p}K_a' + 4) + \gamma(\theta - \theta_{\text{th}})\lambda \quad (2)$$

switching function that is set to zero when the nucleophile cone angles are less than a critical threshold value, θ_{th} , below which no steric effects are evident. λ is set to unity for $\theta > \theta_{\text{th}}$ and $\log k_2^0 (= \log k_2 - \beta(\text{p}K_a' + 4))$ is proportional to θ . The value of α is taken^{7a,b} as a measure of the standard reactivity, SR, of the cluster, defined by the value of $\log k_2$ for reaction with a hypothetical, small ($\theta \leq \theta_{\text{th}}$), and weakly basic ($\text{p}K_a' = -4$) P-donor nucleophile. The parameter β measures the sensitivity of the carbonyl complex to the σ -donicity of the nucleophiles, and γ measures the substrate's sensitivity to the size of the nucleophile when the cone angle exceeds θ_{th} .^{6a,7} Thus, the success in fitting the data to eq 2 allows individual complexes to be characterized electronically and sterically by their separate responses (as measured by β and by θ_{th} and γ , respectively) to the electronic and steric properties ($\text{p}K_a'$ and θ) of the nucleophiles. It follows from eq 2 that for $\theta \leq \theta_{\text{th}}$ no steric effects influence the value of k_2 , whereas at $\theta > \theta_{\text{th}}$, k_2 depends on the size of the nucleophile. This implies^{7a} that in the transition state the cluster provides a well-defined open space in the coordination sphere, into which relatively small donors ($\theta \leq \theta_{\text{th}}$) can enter with negligible repulsion. The opened form of the cluster is called the transition state isomer (TSI).

The ability to correlate such electronic and steric effects for a wide range of P-donor nucleophiles, based on k_2 data for reaction 1, raised the question whether the corresponding activation parameters ΔH^\ddagger , ΔS^\ddagger , and ΔV^\ddagger , determined from the temperature and pressure dependence of k_2 , exhibit similar correlations. This would enable a further classification of the nature of the transition state for the addition of nucleophiles to carbonyl clusters. In the present study we have determined these activation parameters for a total of 18 different P-donor nucleophiles and report electronic and steric correlations based on these values for reaction 1. The values of ΔV^\ddagger , in particular, are found to provide a novel and especially detailed picture of the nature of the transition states in these reactions.

Experimental Section

Materials. $\text{Os}_3(\text{CO})_{12}$ (Strem) was used as received. The cluster $\text{H}_2\text{Os}_3(\text{CO})_{10}$ was synthesized according to Kaesz's method¹¹ by bubbling hydrogen (Messer Griesheim, grade 2.0) through a solution of $\text{Os}_3(\text{CO})_{10}$ in boiling toluene for 2 h. Cooling to 0 °C led to the precipitation of unreacted $\text{Os}_3(\text{CO})_{12}$.

(9) Rahman, Md. M.; Liu, H.-Y.; Eriks, K.; Prock, A.; Giering, W. P. *Organometallics* **1989**, *8*, 1.

(10) (a) Tolman, C. A. *Chem. Rev.* **1977**, *77*, 313. (b) Tolman, C. A. *J. Am. Chem. Soc.* **1970**, *92*, 2956.

(11) Knox, S. A. R.; Koepke, J. W.; Andrews, M. A.; Kaesz, H. D. *J. Am. Chem. Soc.* **1975**, *97*, 3942.

The remaining solution was decanted, the solvent removed by distillation under reduced pressure, and the resulting product dried in vacuo. The yield was calculated to be 70%, and the purity was checked by IR spectroscopy.¹¹

Liquid phosphorus nucleophiles $\text{P}(\text{OMe})_3$, $\text{P}(\text{O}i\text{Bu})_3$, $\text{P}(\text{O}^i\text{Pr})_3$, and $\text{P}(\text{OPh})_3$ (Fluka), $\text{PPh}_2(\text{OEt})$ (Aldrich), and P^nBu_3 and $\text{P}(\text{NMe}_2)_3$ (Strem) were purified by distillation under argon at ambient or reduced pressure, as appropriate. PPh_3 , SbPh_3 , and AsPh_3 (Strem) were recrystallized from dry methanol and dried in vacuo for 12 h. 4-Ethyl-2,6,7-trioxo-1-phosphabicyclo-[2.2.2]octane (etpb) (Strem) was sublimed under reduced pressure prior to use. Tricyclohexylphosphine (PCy_3) was obtained from $\text{PCy}_3\text{-CS}_2$ (Strem) by dissolving the adduct in refluxing ethanol followed by distilling to remove the CS_2 . The pure phosphine was obtained quantitatively by cooling the solution to -18°C and drying the precipitate in vacuo for 48 h. All other solid phosphines, $\text{P}(p\text{-X-C}_6\text{H}_4)_3$ ($\text{X} = \text{CF}_3$, F, Cl, Me, MeO), tribenzylphosphine (PBz_3), dicyclohexylphenylphosphine (PCy_2Ph), PPh_2Cy , PBzPh_2 , $\text{P}(m\text{-tol})_3$, and $\text{P}(o\text{-tol})_3$ (Strem), were used without further purification. The purity of all phosphorus nucleophiles was checked by ^{31}P NMR spectroscopy.

n-Heptane (Baker, p.A. grade) was distilled over potassium-sodium alloy, chlorobenzene (Merck, p.A. grade) was distilled and stored over molecular sieves (4 Å), and nitromethane (Merck, p.A. grade) was distilled twice and dried with molecular sieves. All solvents were stored under argon.

Sample solutions were transferred to optical cuvettes and pillbox cells¹² for UV-vis spectroscopic and kinetic measurements under anaerobic conditions.

Instrumentation. IR spectra were recorded on Nicolet 5SX and Perkin-Elmer 397 spectrophotometers with 1 mm path length cells with KBr windows. For ^{31}P and ^1H NMR measurements a Bruker 400 AM-WB (400 MHz) NMR spectrometer was used with CDCl_3 or C_6D_6 as solvent. UV-vis spectra were obtained from HP8452A and CARY13 spectrophotometers. UV-vis repetitive scan spectra were recorded on a Durrum D110 stopped-flow device equipped with a J&M detector connected to a TIDAS 16-416 spectrophotometer.

Slow kinetic measurements were performed in the cell compartment of the HP8452A spectrophotometer at ambient pressure and in a high-pressure cell¹³ built into a Zeiss PMQ II spectrophotometer for pressures up to 150 MPa. Fast reactions were studied on Durrum D 110 and Hi-Tech SF-51 stopped-flow instruments at ambient pressure and on a homemade high-pressure stopped-flow unit,¹⁴ at pressures up to 175 MPa. The reactions were monitored by analyzing the increase of the product band at ca. 384 nm in thermostated ($\pm 0.1^\circ\text{C}$) cuvettes or high-pressure cells attached to on-line computer systems for data acquisition and handling.

The OLIS KINFIT (Bogart, GA) program was used to calculate k_{obs} values for absorbance vs time traces by fitting single- or double-exponential functions through the data points. Also, the TKINETIK^{15a} program for an analysis according to the Kezdy-Swinbourne method^{15b,c} was applied for slow reactions when a constant infinity absorbance was not reached.

All addition reactions were carried out under pseudo-first-order conditions, i.e. an at least 15-fold excess of nucleophile, and the resulting plots of $\log(A_\infty - A_t)$ versus t were linear for at least 3 half-lives when a one-exponential fit was appropriate.

(12) le Noble, W. J.; Schlott, R. *Rev. Sci. Instrum.* **1976**, *47*, 770.

(13) van Eldik, R.; Palmer, D. A.; Schmidt, R.; Kelm, H. *Inorg. Chim. Acta* **1981**, *50*, 131.

(14) Kraft, J.; Wieland, S.; Kraft, U.; van Eldik, R. *GIT Fachz. Lab.* **1987**, *31*, 560.

(15) (a) Programmed by A. Neubrand. (b) Kezdy, F. J.; Jaz, J.; Bruylants, A. *Bull. Soc. Chim. Belg.* **1958**, *67*, 687. (c) Swinbourne, E. G. *J. Chem. Soc.* **1960**, 2371.

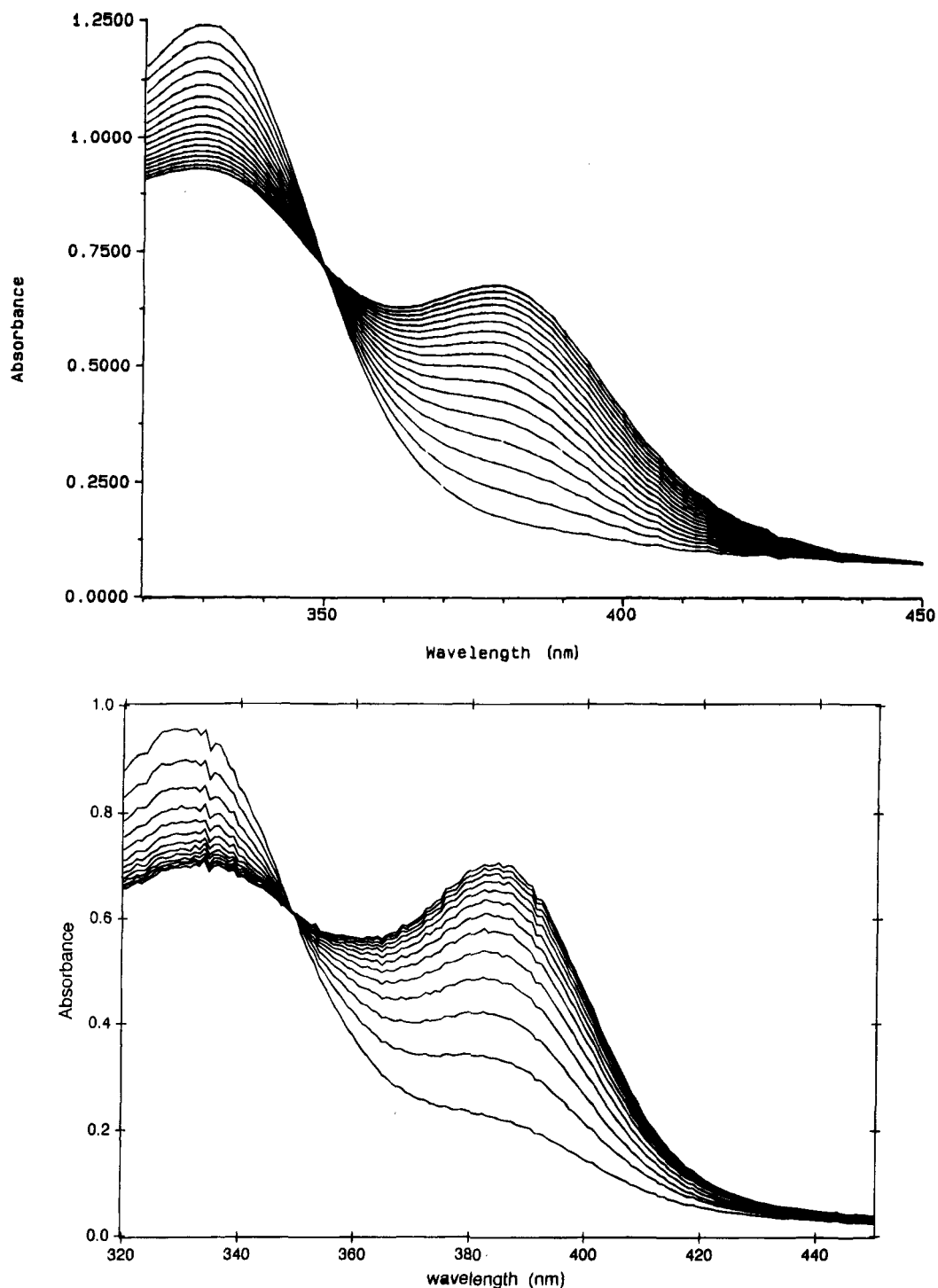


Figure 1. (a, top) UV-vis spectral changes observed after mixing a 5×10^{-6} M $\text{H}_2\text{Os}_3(\text{CO})_{10}$ and 3.6×10^{-6} M $\text{P}(\text{OPh})_3$ solution in chlorobenzene at 30°C in a tandem quartz cell at 3 min intervals. (b, bottom) UV-vis rapid-scan spectra observed after mixing of a solution of 5×10^{-6} M $\text{H}_2\text{Os}_3(\text{CO})_{10}$ and 1.2×10^{-4} M PBU_3 in chlorobenzene at 30°C (time interval between two traces: 24 ms).

Results and Discussion

General Observations. All the reactions proceed rapidly with quantitative formation of the very well-known adducts $(\mu_2\text{-H})(\text{H})\text{Os}_3(\text{CO})_{10}\text{L}$,^{6b} all of which have been isolated and spectroscopically characterized by comparison with known compounds.^{6b} Very sharp isosbestic points were observed in both IR and UV-vis spectra (see Figure 1a) during the relatively slow reactions with $\text{P}(\text{OPh})_3$. For the faster reaction with PBU_3 an isosbestic point was also found in the UV-vis spectrum (Figure 1b). The adducts undergo slow loss

of CO to form $(\mu_2\text{-H})_2\text{Os}_3(\text{CO})_9\text{L}$, but no evidence of the latter was observed on the time scale of the reactions studied here.

The UV-vis absorbance changes observed during the reactions were generally analyzable by means of a single-exponential function, as observed elsewhere,^{6a} from which values of k_{obs} were readily obtained. The values of k_{obs} increased with nucleophile concentration, $[\text{L}]$, but at higher $[\text{L}]$ values, the absorbance changes were sometimes found to be better analyzed according to a double-exponential function. This was most clearly

Table 1. Kinetic Data for the Concentration Dependence of the Addition of P(OMe)₃ to H₂Os₃(CO)₁₀ in Chlorobenzene at 30.2 °C

[P(OMe) ₃], mM	<i>k</i> _{obs} , ^a s ⁻¹	<i>k</i> _{fast} , ^b s ⁻¹	<i>k</i> _{slow} , ^b s ⁻¹	<i>k</i> _{fast} / <i>k</i> _{slow}
4.48	0.134 ± 0.001			
11.3	0.366 ± 0.003			
19.2	0.619 ± 0.002			
40.6	1.273 ± 0.006			
58.3	1.640 ± 0.002			
70.3	2.02 ± 0.01			
154.7	3.73 ± 0.02	7.06 ± 0.04	2.50 ± 0.03	2.8
304.1	7.61 ± 0.12	12.1 ± 0.5	3.59 ± 0.09	3.4
663	11.9 ± 0.4	25.4 ± 0.5	3.32 ± 0.53	7.7
1008	21.7 ± 0.6	38.0 ± 0.8	2.71 ± 0.34	14
2127		81.1 ± 1.5	2.69 ± 0.13	30
2806		108.7 ± 4.3	1.99 ± 0.12	54

^a Calculated from a single-exponential fit. ^b Calculated from a double-exponential fit.

evident for the reaction of P(OMe)₃, for which the results are shown in Table 1. The values of *k*_{obs} for the faster step continue to increase with [L], but those for the slower step remain essentially constant. This explains why single-exponential behavior is observed at lower [L], since the first step is then appreciably slower than the second so that the latter is not observed.

The double-exponential behavior was only observed clearly for a minority of the P-donor nucleophiles due to limitations imposed by their solubility and by instrumental limitations in measuring fast rates. It was also made difficult to detect by the relatively small absorbance change during reactions. Thus, with PPh₃, the second stage involved only 20% of the total absorbance change. For most of the nucleophiles where this behavior is observed, the ratios of the first to the second rate constant obtained from the double-exponential fit are between 1.0 and 2.3, even at the highest values of [L]; thus, the second one cannot generally be accurately resolved. It was also found for these nucleophiles that the deviation from single-exponential behavior becomes greater with increasing temperature.

These observations strongly suggest that the reactions proceed by initial [L]-dependent formation of a form of the adduct (μ₂-H)Os₃(CO)₁₀L that is less stable thermodynamically than the final product and that is, presumably, a stereochemically different isomer of that product. Since (μ₂-H)Os₃(CO)₁₀PPh₃ is known¹⁶ to have the PPh₃ ligand in the equatorial plane defined by the Os₃ cluster, it seems plausible to conclude that the kinetic product probably has the P-donor in an axial position. The temperature dependence data suggest that the activation enthalpies for the bimolecular formation of the less stable isomer must be greater than those for the isomerization step, as might be expected.

The values of *k*_{obs} for the initial step vary with [L] over a very wide concentration range according to eq 3, where the constant *a* is usually negligible (Table 2).

$$k_{\text{obs}} = a + k_2[\text{L}] \quad (3)$$

Since *a* is not the same for all nucleophiles, it cannot represent a simple [L]-independent rate process common to all reactions and its possible significance, discussed elsewhere,^{6a} will not be considered any further

here, where we shall focus only on the bimolecular reactions characterized by the *k*₂ values.

Solvent Dependence. For kinetic investigations of reaction 1 nonpolar and noncoordinating solvents are preferably used to prevent direct interaction with the electrophilic metal center. Both the cluster compound and the aromatic nucleophiles, however, are only sparingly soluble in nonpolar hydrocarbons, such as heptane. The high-pressure stopped-flow instrument requires relatively high absorption changes and therefore high cluster concentrations. Consequently, we performed most of our measurements in chlorobenzene, a substantially better solvent for both the complex and most of the ligands, but still a relatively weak donor solvent compared with acetonitrile, for example, which actually forms an adduct with the cluster.³

The reactions studied here at 30 °C in chlorobenzene are generally slower than corresponding reactions in heptane, except for P(*o*-tol)₃. In any case the differential effects of these two solvents on the rates are rather small. Differences in the activation parameters (Table 3) are also variable and are of borderline statistical significance.

The reactions of PPh₃ were also studied in nitromethane, and the rates at 30 °C (Table 3) are again closely comparable with those in heptane and chlorobenzene, showing that its much greater dipole moment has a negligible effect on the rates, as expected for nonpolar transition states. However, the values of Δ*H*[‡] and Δ*S*[‡] in nitromethane (Table 4) are respectively much higher and much less negative than those in heptane, and this compensation effect seems to be statistically quite significant.

Current theories of solvent effects¹⁷ suggest that isokinetic temperatures for reactions in different solvents should only exist if "all solvents in the series have the same vibrational frequency". The similarity of the rate constants in heptane, chlorobenzene, and nitromethane at the experimental temperatures used in our studies would not seem to fulfill this requirement. In view of the absence of activation parameters for reactions of the other nucleophiles in nitromethane, any further discussion would not be justified at this stage, but the absence of solvent effects at the temperature used for analysis of the nucleophile dependence of the values of *k*₂ and Δ*V*[‡] suggest that the discussion need not take such effects into account.

Nucleophile Dependence of the Rates. The dependence of the rates of reaction 1 on the electronic and steric nature of the P-donor nucleophiles (Table 4) is very close to that reported elsewhere^{6a} and is in good agreement with that expected on the basis of eq 2. The plot of log *k*₂ against p*K*_a' in Figure 2 shows an excellent linear free energy relationship (*R* = 0.996) for the isosteric nucleophiles P(*p*-XC₆H₄)₃ with cone angles of 145°. Larger nucleophiles react more slowly and a few smaller ones react slightly more rapidly. The gradient of the LFER provides a value of β = 0.40 ± 0.02, which is in excellent agreement with the value 0.43 ± 0.02 found for corresponding reactions in heptane.^{6a} The values of β allow calculation of values of log *k*₂⁰ = log *k*₂ - β(p*K*_a' + 4), which can then be plotted against the corresponding value of θ to give a steric profile. This immediately shows that the data for P(*o*-tol)₃ deviate

Table 2. Kinetic Parameters for the Addition of Nucleophiles to $\text{H}_2\text{Os}_3(\text{CO})_{10}$

no. ^a	ligand	solvent	[L] range, mM	temp, °C	$\alpha,^b 10^3 \text{ s}^{-1}$	$k_2,^b \text{ M}^{-1} \text{ s}^{-1}$	$k_2,^c \text{ M}^{-1} \text{ s}^{-1}$
2	P(OMe) ₃	chlorobenzene	4.48–2806	30.2	29 ± 16	35.2 ± 1.4	
3	P(OBu) ₃	heptane	70.9	20.5			207.6 ± 1.8
				25.2			228.2 ± 3.5
				30.2			270.8 ± 4.5
				38.1			368.4 ± 5.4
				42.2			456.1 ± 9.4
				49.6			484.1 ± 19.2
3	P(OBu) ₃	chlorobenzene	3.3–35.2	20.2	70 ± 30	35.7 ± 3.7	
				26.9	60 ± 30	47.6 ± 4.7	
				30.2	30 ± 20	55.4 ± 2.9	
				35.4	230 ± 1	63.4 ± 0.2	
4	P(OPh) ₃	heptane	4.37–495	20.4	0.41 ± 0.06	0.402 ± 0.005	
				26.2	1.4 ± 1.0	0.500 ± 0.07	
				30.2	1.5 ± 0.1	0.575 ± 0.08	
				35.2	1.8 ± 0.3	0.685 ± 0.02	
				40.5	2.1 ± 0.3	0.88 ± 0.02	
				46.7	3.3 ± 0.6	1.12 ± 0.04	
4	P(OPh) ₃	chlorobenzene	4.41–294	20.2	0.32 ± 0.03	0.098 ± 0.003	
				26.2	0.71 ± 0.05	0.131 ± 0.003	
				30.2	1.17 ± 0.05	0.154 ± 0.003	
				35.2	1.6 ± 0.2	0.183 ± 0.008	
				40.2	1.49 ± 0.08	0.219 ± 0.005	
7	PPh ₂ (OEt)	chlorobenzene	8.7–32.9	30.2	120 ± 50	292 ± 3.7	
8	PPh ₃	heptane	3.2–29.1	22.4	47 ± 10	69.7 ± 1.5	
				30.2	28 ± 4	91.5 ± 0.6	
				37.2	29 ± 3	112.5 ± 0.5	
8	PPh ₃	chlorobenzene	5.75–41.75	20.4	50 ± 30	26.0 ± 2.9	
				26.2	10 ± 40	33.5 ± 3.3	
				30.2	-0.2 ± 4	40.0 ± 3.4	
				35.2	20 ± 70	43.9 ± 6.8	
				40.2	-40 ± 60	62.0 ± 6.6	
8	PPh ₃	nitromethane	19.0	20.2			52.6 ± 0.5
				26.5			74.1 ± 0.5
				30.2			88.7 ± 1.6

^a Nucleophile number. This numbering will be used throughout the paper. ^b Data fitted according to $k_{\text{obs}} = \alpha + k_2[\text{L}]$. ^c Data fitted according to $k_2 = k_{\text{obs}}/[\text{L}]$.

Table 3. Thermal Activation Parameters for the Addition of Nucleophiles to $\text{H}_2\text{Os}_3(\text{CO})_{10}$

no.	ligand	solvent	$\Delta G^\ddagger(25^\circ\text{C}), \text{ kJ mol}^{-1}$	$\Delta H^\ddagger, \text{ kJ mol}^{-1}$	$\Delta S^\ddagger, \text{ J mol}^{-1} \text{ K}^{-1}$	temp range, °C	remarks
2	P(OMe) ₃	chlorobenzene	65.5	36.1 ± 2.3	-99 ± 8	7.4–62.7	a
3	P(OBu) ₃	chlorobenzene	63.6	26.4 ± 2.2	-125 ± 7	20.2–35.4	b
3	P(OBu) ₃	heptane	59.5	22.9 ± 2.2	-123 ± 7	20.5–49.6	c
4	P(OPh) ₃	chlorobenzene	78.2	27.9 ± 1.2	-169 ± 4	20.2–40.2	b
		heptane	74.8	28.6 ± 1.0	-155 ± 3	20.4–46.7	b
5	P(O ⁱ Pr) ₃	chlorobenzene	64.0	35.4 ± 0.7	-96 ± 2	7.8–54.4	a
7	PPh ₂ (OEt)	chlorobenzene	59.2	32.4 ± 0.9	-90 ± 3	5.9–54.1	a
8	PPh ₃	chlorobenzene	64.4	29.8 ± 1.4	-116 ± 4	9.5–47.9	a
		chlorobenzene	64.6	29.1 ± 3.4	-119 ± 10	20.4–40.2	b
		heptane	62.3	22.2 ± 0.8	-134 ± 3	22.4–37.2	b
		nitromethane	62.5	36.3 ± 0.8	-88 ± 3	20.2–30.2	a
11	P(<i>p</i> -ClC ₆ H ₄) ₃	chlorobenzene	69.5	34.3 ± 0.2	-118 ± 1	9.1–49.9	c
12	P(<i>p</i> -tol) ₃	chlorobenzene	61.4	31.2 ± 1.2	-101 ± 4	17.3–46.8	a
13	P(<i>p</i> -MeOC ₆ H ₄) ₃	chlorobenzene	60.3	23.3 ± 2.9	-124 ± 9	12.9–63.2	a
17	P(NMe ₂) ₃	chlorobenzene	57.8	59 ± 5	+6 ± 15	13.6–58.3	a
18	PCy ₂ Ph	chlorobenzene	65.1	26.9 ± 1.6	-128 ± 5	9.4–50.1	a
19	PBz ₃	chlorobenzene	69.7	35.4 ± 1.2	-115 ± 4	6.3–42.3	a
21	P(<i>o</i> -tol) ₃	chlorobenzene	94.2	62.2 ± 1.4	-107 ± 4	13.0–50.0	a

^a From $k_{\text{obs}}/[\text{L}]$, one concentration. ^b From the concentration dependence of k_{obs} . ^c From $k_{\text{fast}}/[\text{L}]$, one concentration.

significantly from the profile when its Tolman cone angle (194°) is used. The same is true of the data for P(*m*-tol)₃ ($\theta = 165^\circ$), but in this case, a revised cone angle of 148° has recently been estimated¹⁸ by what was essentially a geometrical method analogous to Tolman's but which used an improved conformation of the *m*-tol groups. The same method successfully reproduced the Tolman cone angle of 145° for PPh₃, and the data for P(*m*-tol)₃ fit well to the steric profile when the reestimated cone angle is used. (Deviations of the data for P(*o*-tol)₃ and P(*m*-tol)₃ from steric profiles have been

observed elsewhere when Tolman cone angles were used.¹⁹) This means that the data for 19 out of the 20 P-donor nucleophiles can be fitted to eq 2 in order to obtain values of α (=SR), β , and γ . The fitting requires^{7a} the minimization of the RMSDs (root mean square deviations), or the maximization of the correlation coefficient R , as a function of varying inputted values of θ_{th} . It turns out that the value of θ_{th} is not very well defined because of the scatter of the data at lower cone angles, and a value of $147 \pm 4^\circ$ is the best that can be obtained. Fortunately, this uncertainty has a very

(18) White, D.; Carlton, L.; Coville, N. J. *J. Organomet. Chem.* **1992**, *440*, 15.

(19) Romeo, R.; Arena, G.; Monsù Scolaro, L. *Inorg. Chem.* **1992**, *31*, 4879.

Table 4. Volumes of Activation and Second-Order Rate Constants (k_2) for the Addition of Nucleophiles to $(\mu_2\text{-H})_2\text{Os}_3(\text{CO})_{10}$ in Chlorobenzene at 30.2 °C

no.	ligand	cone angle, deg	$\text{p}K_a$	$\text{p}K_a'$	k_2 , $\text{M}^{-1} \text{s}^{-1}$	ΔV^\ddagger , $\text{cm}^3 \text{mol}^{-1}$
1	etbp	101	1.74	-0.30	12.3	-16.6 ± 2.4
2	P(OMe) ₃	107	2.60	0.83	35.2	-13.2 ± 1.6
3	P(OBu) ₃	109	3.31	1.64	55.4	
4	P(OPh) ₃	128	-2.0	-2.79	0.154	-12.8 ± 0.7
5	P(O ⁱ Pr) ₃	130	4.08	3.38	50.4	-12.7 ± 0.5
6	P(ⁿ Bu) ₃	132	8.43	8.67	6600	-16.1 ± 1.1
7	PPh ₂ (OEt)	133	2.91	1.99	292	-14.9 ± 1.7
8	PPh ₃	145	2.73	3.28	40.0	-20.2 ± 0.2
9	P(<i>p</i> -F ₃ CC ₆ H ₄) ₃	145	-1.55	-1.39	0.81	-20.4 ± 0.6
10	P(<i>p</i> -FC ₆ H ₄) ₃	145	1.97	1.63	10.3	-21.0 ± 1.0
12	P(<i>p</i> -MeC ₆ H ₄) ₃	145	3.84	4.46	153.8	-19.3 ± 0.4
13	P(<i>p</i> -MeOC ₆ H ₄) ₃	145		5.13	378	-19.0 ± 0.8
14	P(<i>m</i> -tol) ₃	148	3.30	4.23	68.4	-16.4 ± 0.7
15	PBzPh ₂	152		3.92	134.7	-20.9 ± 0.8
16	PCyPh ₂	153	5.05	5.87	255.4	-26.2 ± 1.0
17	P(NMe ₂) ₃	157	7.6	8.20	110	-31.8 ± 0.9
18	PCy ₂ Ph	162	5.55	8.46	39.9	-22.9 ± 1.0
19	PBz ₃	165	4.2	5.23	0.21	-20.4 ± 0.7
20	PCy ₃	170	9.70	11.26	5.9	
21	P(<i>o</i> -tol) ₃	194	3.08	5.03	0.015	-8.1 ± 1.4
12	SbPh ₃	138 ^c			13.46	-20.8 ± 2.1
23	AsPh ₃	142 ^c			5.6	-20.4 ± 1.7

^a These data are taken from: Imyanitov, N. S. *Sov. J. Coord. Chem. (Engl. Transl.)* **1985**, *11*, 663.

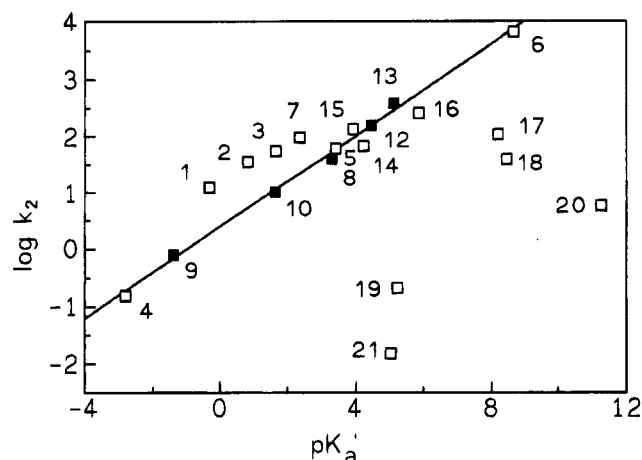


Figure 2. Electronic profile for the addition reaction of P-donor nucleophiles with $(\mu_2\text{-H})_2\text{Os}_3(\text{CO})_{10}$ in chlorobenzene at 30.2 °C. The numbers of the ligands correspond to those given in Tables 2–4. Filled squares represent isosteric nucleophiles with a cone angle of 145°.

small effect on the values of the other parameters, which are found to be $\text{SR} = -0.70 \pm 0.23$, $\beta = 0.38 \pm 0.04$, and $\gamma = -0.18 \pm 0.02 \text{ deg}^{-1}$ ($\text{RMSD} = 0.43$, $R = 0.922$) when $\theta_{\text{th}} = 147^\circ$. The value of β is in excellent agreement with that found by using only the isosteric nucleophiles with $\theta = 145^\circ$, and all the parameters are in excellent agreement with those found from reactions in heptane.^{6a} The steric profile in Figure 3 has been drawn in accordance with these parameters.

The validity of the steric threshold can be demonstrated as follows. Simply taking $\theta_{\text{th}} = 0$ leads to a very poor fit of the data ($R = 0.699$), and the value of β (0.25 ± 0.07) disagrees strongly with that found by using the data for the isosteric nucleophiles P(*p*-XC₆H₄)₃. It is true that some of the nucleophiles with $\theta < \theta_{\text{th}}$ have had their cone angles revised upward by as much as 25°, and this would bring their values of $\log k_2^0$ closer

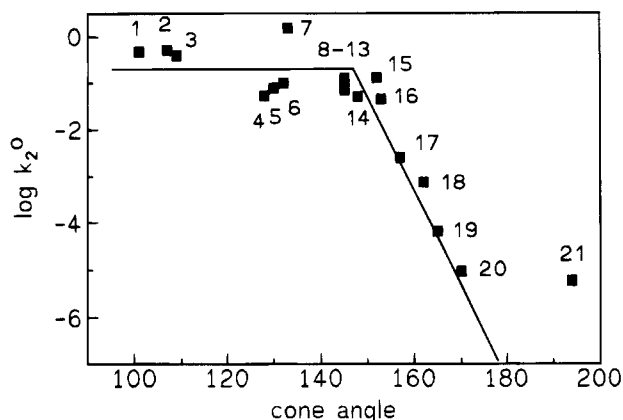


Figure 3. Steric profile for the addition reaction of P-donor nucleophiles with $(\mu_2\text{-H})_2\text{Os}_3(\text{CO})_{10}$ in chlorobenzene at 30.2 °C. $\log k_2^0 = \log k_2 - \beta(\text{p}K_a' + 4)$.

to the sloping line in Figure 3. This is not the case, however, for etpb, which has a very well-defined conformation and cone angle.^{10,20} When the value of k_2 for etpb is calculated by using the data for nucleophiles with $\theta \geq 145^\circ$, it is found to be over 6 orders of magnitude too high. When the higher proposed²⁰ cone angles for P(OMe)₃ and P(ⁿBu)₃ are used, together with comparably increased cone angles for the other phosphites (apart from etpb), the analysis still requires a steric threshold falling in the same range as that found previously, largely because the adjustments simply lead to movement of the data along the horizontal part of the steric profile. Omitting altogether the data for the phosphites that have dubious cone angles results in the best fit ($R = 0.974$) being found for $\theta_{\text{th}} = 152^\circ$, which is close to the upper limit of the ranges found from the other analyses. The existence of a steric threshold that is quite large^{6a,7a,b} is therefore unambiguously demonstrated.

Apart from cone angles (modified or not), other ways of characterizing the "sizes" of P-donor ligands have been reviewed.²¹ In particular, Brown has proposed²² the use of repulsion energies (E_R values), derived from molecular mechanics calculations on a standard reference compound ($\text{Cr}(\text{CO})_5\text{L}$), as a measure of ligand steric effects. E_R values are available²² for 18 of the 20 nucleophiles used here, including P(*o*-tol)₃ and P(*m*-tol)₃ but not P(NMe₂)₃ or P(*p*-F₃CC₆H₄)₃. The average E_R value of the five P(*p*-XC₆H₄)₃ ligands considered by Brown is $314 \pm 2 \text{ kJ mol}^{-1}$, and we can take that value for P(*p*-F₃CC₆H₄)₃, but no comparable estimate can be made for P(NMe₂)₃. The fit of the data for the remaining 19 nucleophiles to eq 2, with θ replaced by E_R , is not very good ($R = 0.872$), but a plot of $\log k_2^0$ vs E_R shows clearly that this is largely because the data for PBz₃ deviate strongly from the steric profile plotted using the data for the other 18 nucleophiles. These lead to $E_R = 289 \text{ kJ mol}^{-1}$, $\text{SR} = -0.64 \pm 0.20$, $\beta = 0.40 \pm 0.04$, and $\gamma = -0.41 \pm 0.03 \text{ kJ mol}^{-1}$ ($\text{RMSD} = 0.369$; $R = 0.957$). The value of E_R for PBz₃ has to be increased by 105 kJ mol^{-1} for it to fit on the steric profile. The values of SR and β are essentially the same as those found by using cone angles, but the values of E_R and γ

(20) Stahl, L.; Ernst, R. D. *J. Am. Chem. Soc.* **1987**, *109*, 5657.

(21) (a) Brown, T. L.; Lee, K. *J. Coord. Chem. Rev.* **1993**, *128*, 89.

(b) White, D.; Coville, N. *J. Adv. Organomet. Chem.* **1994**, *36*, 95.

(22) Brown, T. L. *Inorg. Chem.* **1992**, *92*, 1286.

have different units and cannot be compared directly with values obtained using cone angles. (However, a rather similar group of nucleophiles lies below the steric threshold in both cases.) The values of RMSD and R are somewhat better than those based on cone angles, although data for one nucleophile (PBz_3) still have to be omitted for this to be true.

The RMSD and R values cannot, however, be accepted at face value as criteria for judging which steric parameter leads to the better fit of the model to the data. Thus, the data for nucleophiles with $\theta > \theta_{\text{th}} = 144^\circ$ require an average change of only $\pm 2.3^\circ$ in the cone angles for them to fit the steric profile perfectly, in which case the RMSD would be determined solely by those nucleophiles with $\theta < 144^\circ$ and would be reduced from 0.452 to 0.298 ($R = 0.963$) which is a somewhat better fit than when E_R values are used. These adjustments to θ are of the same magnitude as their intrinsic uncertainties;¹⁰ therefore, they are certainly not unreasonable. Corresponding average adjustments of $\pm 8.8 \text{ kJ mol}^{-1}$ to the E_R values lead to a decrease in the RMSD to 0.282 ($R = 0.975$), and these are probably not unreasonable in view of the complexity of the calculations. For these data it appears that either steric parameter can lead to a good fit of the model to the data.

It is, in any case, quite clear that the dependence of the rates of reaction 1 in chlorobenzene on the electronic and steric natures of the nucleophiles is in excellent accord with eq 2 and is virtually identical with that observed for reactions in heptane.^{6a} The high^{7a,b} value of the steric threshold, θ_{th} , shows that the space opened up in the ligand polytope surrounding the Os_3 cluster is quite large. In view of the conclusion that the nucleophiles end up in an axial position in the initial product, it must be easier to create an axial opening in the TSI than an equatorial one and this facilitates the entry of an approaching nucleophile into an axial position. The high value^{7a,b} of β corresponds to a high degree of stabilization of the transition states by $\text{M}\cdots\text{P}$ σ -bond making, and the large,^{7a,b} negative value of γ suggests that the TSI is exceptionally resistant toward further stereochemical distortion. The parameters all serve to indicate that the transition states involved occur "late" along a concerted path to the initially formed axially substituted product.

Temperature and Pressure Dependence. The values of ΔH^\ddagger and ΔS^\ddagger for many of the reactions were determined in the usual way and are summarized in Table 3. The pressure dependence of these reactions was studied under similar conditions, and the activation volumes are summarized in Table 4. The activation parameters in Tables 3 and 4 show that the addition reactions are all characterized by significantly negative ΔS^\ddagger and ΔV^\ddagger values, in line with an associative bond formation process. Figure 4 shows a general compensation effect in the plot of ΔH^\ddagger vs ΔS^\ddagger , although the scatter around a regression line is large. Any possible isokinetic temperature that might be characteristic of these reactions is sufficiently uncertain that no insight is provided as to whether the reactions are entropy- or enthalpy-controlled. However, ligand 17 ($\text{P}(\text{NMe}_2)_3$) is exceptional in showing a low positive ΔS^\ddagger value, which contrasts with a large negative value of ΔV^\ddagger . If the values of ΔH^\ddagger and ΔS^\ddagger for this nucleophile are omitted from the plot, then the remaining data suggest that the

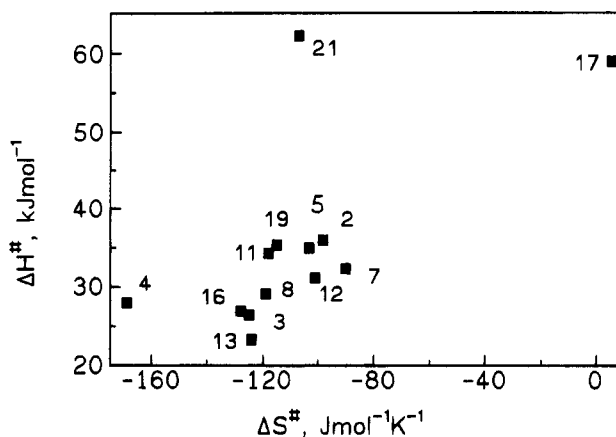


Figure 4. ΔH^\ddagger vs ΔS^\ddagger plot for reaction 1 under the same conditions as outlined in Figure 1.

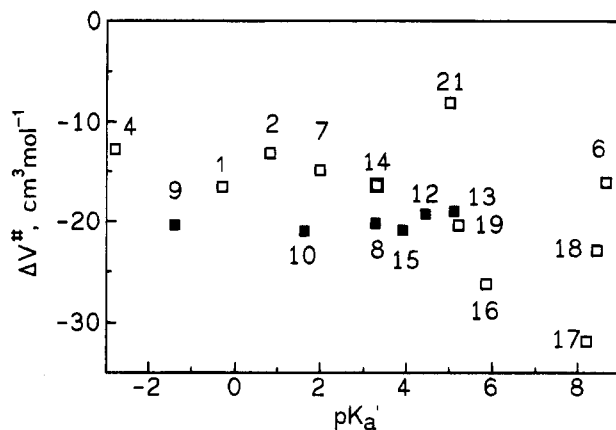


Figure 5. Plot of the volumes of activation against $\text{p}K_a'$ for the nucleophiles under the conditions outlined in Figure 1.

rates are largely entropy-controlled, the range of $T\Delta S^\ddagger$ at 330 K being ca. 26 kJ mol^{-1} and that of ΔH^\ddagger being 13 kJ mol^{-1} . In spite of the occasional deviations from this trend, it seems most likely that all these closely related reactions proceed via a common mechanism.

On the basis of an associative process, the values for the activation volume for reaction 1 should be large and negative. Our measured values range from -12 to $-31 \text{ cm}^3 \text{ mol}^{-1}$ and are in good agreement with other associative reactions^{23,24} (e.g.: Michael addition, $-33 \text{ cm}^3 \text{ mol}^{-1}$; insertion reactions, -17 to $-25 \text{ cm}^3 \text{ mol}^{-1}$; [2 + 2]-cycloadditions, -20 to $-55 \text{ cm}^3 \text{ mol}^{-1}$). Our ΔV^\ddagger data are correlated with the electronic and steric parameters in Figures 5 and 6, respectively. The data points for isosteric ligands (see Figure 5) do not exhibit any significant change in ΔV^\ddagger with increasing σ -donicity (basicity). Thus, for the $\theta = 145^\circ$ nucleophiles, ΔV^\ddagger has an average value of $-20.0 \pm 0.4 \text{ cm}^3 \text{ mol}^{-1}$ for the five different nucleophiles, covering a wide basicity range from $\text{p}K_a' = -1.4$ to $+4.6$. This value of ΔV^\ddagger is the same, within experimental error, as the values of AsPh_3 and SbPh_3 , which in general show rather varied nucleophilic character depending on the particular carbonyls involved.^{6a} This constancy of ΔV^\ddagger with widely varying

(23) van Eldik, R.; Neubrand, A. In *Mechanisms of Inorganic and Organometallic Reactions*; Twigg, M. V., Ed.; Plenum Press: New York, in press; Vol. 9.

(24) (a) le Noble, W. J.; Kelm, H. *Angew. Chem.* **1980**, *92*, 887. (b) Asano, T.; le Noble, W. J. *Chem. Rev.* **1978**, *78*, 407. (c) van Eldik, R.; Asano, T.; le Noble, W. J. *Chem. Rev.* **1989**, *89*, 549.

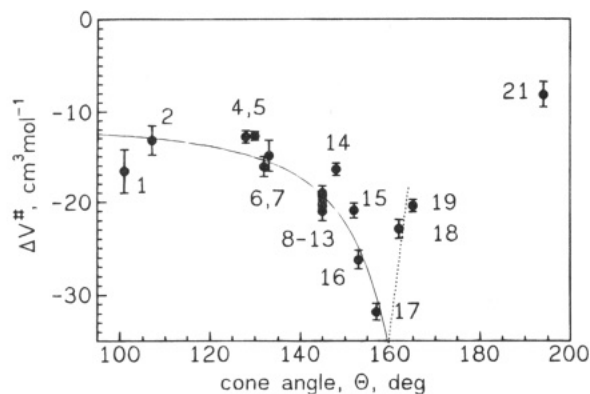


Figure 6. Plot of the volumes of activation versus the cone angle of a set of nucleophiles. The line connecting ligands 1–17 represents the theoretical fit to eq 5 as derived from the data in Figure 7 (see below). Error bars indicate the standard deviation of the volume of activation.

nucleophile basicity means that the volume collapse on forming the transition state is not dependent on electronic factors but only on steric factors, as shown in Figure 6.

Initial inspection of Figure 6 suggests a remarkable similarity to the steric profile in Figure 3. Thus, ΔV^\ddagger is essentially independent of θ for $\theta < \text{ca. } 140^\circ$ and becomes steadily more negative from 140 to 160° . The observation of essentially identical values of ΔV^\ddagger for the isosteric nucleophiles $\text{P}(p\text{-XC}_6\text{H}_4)_3$ ($\theta = 145^\circ$) is very important in demonstrating that the $\text{Os}\cdots\text{P}$ bond lengths in the transition states are effectively identical in spite of their wide range of basicities (see above) and, therefore, of $\text{Os}\cdots\text{P}$ bond strengths. As θ exceeds 160° , the values of ΔV^\ddagger become steadily less negative.

The overall behavior suggests rather little variation of ΔV^\ddagger in the cone angle region where the steric profile in Figure 3 shows there to be negligible steric repulsion. When steric repulsion appears to become more pronounced, ΔV^\ddagger becomes more negative, indicating progressively greater overlap between the TSI and the entering nucleophiles, this overlap reaching a maximum with the most negative ΔV^\ddagger at $\theta = 157^\circ$. Above $\theta = 160^\circ$ it must be inferred that steric repulsion becomes so great that the $\text{Os}\cdots\text{P}$ bond lengths in the transition state have to increase steadily so that the overlap of the nucleophiles with the TSI decreases and ΔV^\ddagger becomes less negative.

However, the data in Figure 6 for $\theta \leq 157^\circ$ can be treated in a more quantitative way. The volume of a cone with angle θ can be expressed as in eq 4, where x

$$V_{\text{cone}} = (\pi x^3/3) \tan^2(\theta/2) \quad (4)$$

represents the height of the cone. Our experimental values for ΔV^\ddagger do correlate quite well ($R = 0.91$, $\text{RMSD} = 2.1 \text{ cm}^3 \text{ mol}^{-1}$) with $\tan^2(\theta/2)$ according to eq 5 and as shown in Figure 7.

$$\Delta V^\ddagger = [-11.6(\pm 1.1)] - [0.76(\pm 0.10)] \tan^2(\theta/2) \quad (5)$$

The correlation is fully consistent with the conclusion^{7a} that clusters in such reactions open up to form a TSI with a space of essentially constant size into which nucleophiles with $\theta < \theta_{\text{th}}$ can fit with a constant $\text{M}\cdots\text{P}$ bond length, without any steric repulsion or further distortion. As the size of the nucleophile increases, the

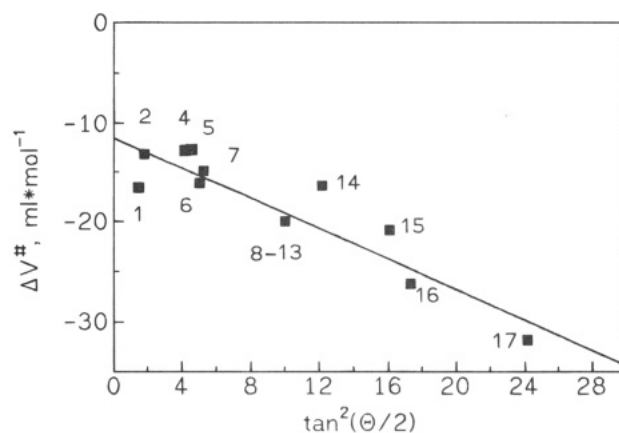


Figure 7. Plot of the volumes of activation versus the function that measures the dependence of the volume of a cone on its inner angle θ , according to eq 5.

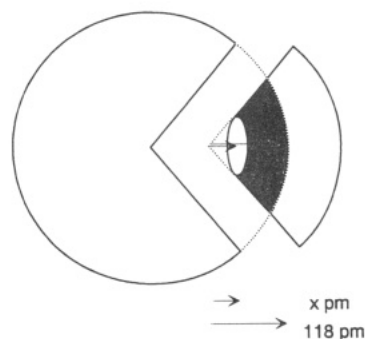


Figure 8. Schematic representation of the geometrical situation during the addition reaction and the origin of the ΔV^\ddagger values.

volume of it that is incorporated within the space in the TSI will increase so that a progressive decrease in the volume of the system will result on forming the transition states even when $\theta < \theta_{\text{th}}$. This is illustrated in Figure 8.

An unexpected feature of eq 5 is that, when θ and $\tan^2(\theta/2) = 0$, ΔV^\ddagger is still negative at $-11.6(\pm 1.1) \text{ cm}^3 \text{ mol}^{-1}$ in spite of the cluster's having opened up to form the TSI without a nucleophile of finite size entering the space created. This value of ΔV^\ddagger can be called the intrinsic volume of activation, $\Delta V^\ddagger_{\text{intr}}$. Its negative value implies that even though the ligand polytope has rearranged to create the open space in the TSI it has done so with an overall *compression* of the cluster as a whole. Any increased interligand repulsion that follows from this compression will be included in the contribution to the activation energy that results from formation of the TSI. However, since the overall volume of the cluster calculated from crystal structure data²⁵ is $245 \text{ cm}^3 \text{ mol}^{-1}$, the net compression in forming the TSI is only 5% of the total cluster volume. Nevertheless, this effect is quite unexpected and may result from the presence of the large and very polarizable hydridic ligands in the cluster. It would be interesting to see whether or not such negative values of $\Delta V^\ddagger_{\text{intr}}$ are found for clusters without hydride ligands.

The second term in eq 5 represents the additional volume collapse due to the entry of the conical nucleophile into the opened space in the TSI. The slope of

(25) Churchill, M. R.; Hollander, F. J.; Hutchinson, J. P. *Inorg. Chem.* **1977**, *16*, 2697.

0.78 can be used to estimate how deeply the P-donor nucleophile penetrates into the cluster sphere. The Tolman cone angle is defined for P-donor nucleophiles attached to a metal with a covalent radius of 118 pm. From this it follows that the actual nucleophile represents a truncated cone with a cut apex of 118 pm in height, so that

$$\Delta V_{\text{obs}}^{\ddagger} = \Delta V_{\text{intr}}^{\ddagger} - [N_A \pi (x^3 - 118^3) / 3] \tan^2(\theta/2) \quad (6)$$

With the Avogadro constant $N_A = 6.022 \times 10^{23} \text{ mol}^{-1}$, x can be estimated to be ca. 142 pm and indicates a penetration of $142 - 118 = \text{ca. } 24 \text{ pm}$ of the P atom into the opened cluster in the transition state. Although a number of simplifications were made in the above treatment, the convincing fit of the data to eq 5 does show that the cone angles of the nucleophiles do lead to an effective measure of the size of the cone that is included within the overall surface of the cluster in the transition state.

The relationship of the correlation in Figure 6 to that in Figure 3 can now be understood. The apparent constancy of ΔV^{\ddagger} for nucleophiles 1–7 results from the rather narrower range of $\tan^2(\theta/2)$ values as compared with the range of θ . Indeed, a plot of the values of ΔV^{\ddagger} (calculated from eq 5) against θ goes smoothly through the data in Figure 6 for $\theta < \text{ca. } 160^\circ$.

In principle, one would expect that ΔV^{\ddagger} would correlate better with a nucleophile volume parameter since a proportion of the total volume of the nucleophile will become enveloped within the substrate during an associative reaction. Correlation with θ , which (through its own correlation with the energy parameter²² E_R) is an energy parameter, is more to be expected of $\log k_2$ (or ΔG^{\ddagger}), which is an energy parameter.

It is also interesting that the values of ΔV^{\ddagger} , calculated according to eq 5 for AsPh_3 ($-18.4 \text{ cm}^3 \text{ mol}^{-1}$) and SbPh_3 ($-17.1 \text{ cm}^3 \text{ mol}^{-1}$), are very close to the measured values when their uncertainties are taken into account.

The size of the nucleophiles that fit with the correlation in Figure 6 extends to one which shows a substantial steric repulsion effect in Figure 3. This fit is what would be expected if this nucleophile persists in attaining the same $\text{Os} \cdots \text{P}$ bond length in spite of the fact that the TSI has to undergo some energetically significant distortion to accommodate this, the volume change accompanying this distortion being ignored to a first approximation. However it is clear that, as steric effects increase still further, the amount of $\text{Os} \cdots \text{P}$ bonding in the transition state must decrease substantially. Indeed, the data for $\text{P}(o\text{-tol})_3$ suggests that the $\text{Os} \cdots \text{P}$ bonding may have become virtually nonexistent. This shows that at least part of the steric effect, observed in Figure 3 for higher θ values, must be due to longer $\text{Os} \cdots \text{P}$ bonds in the transition state instead of it all being due to increased distortion of the TSI. This effect is probably related to the fact that $\tan^2(\theta/2)$ increases very substantially from $\theta = 160^\circ$ ($\tan^2(\theta/2) = 32$) to $\theta = 170^\circ$ ($\tan^2(\theta/2) = 131$) so that it is no longer possible for the space in the TSI to be expanded sufficiently to incorporate ligands of such large volumes unless their penetration into that space is greatly reduced. In fact, it is hard to imagine a nucleophile with $\theta = 180^\circ$, and $\tan^2(\theta/2) \rightarrow \infty$, being able to penetrate at all into the space. The relationship of steric profiles based on \log

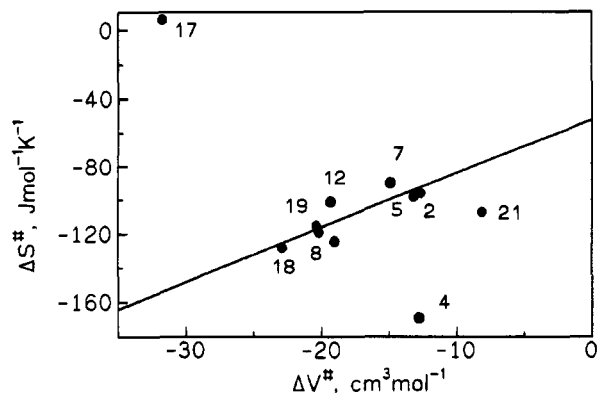


Figure 9. Plot of the Gibbs activation energies, ΔS^{\ddagger} , versus the volumes of activation for reaction 1.

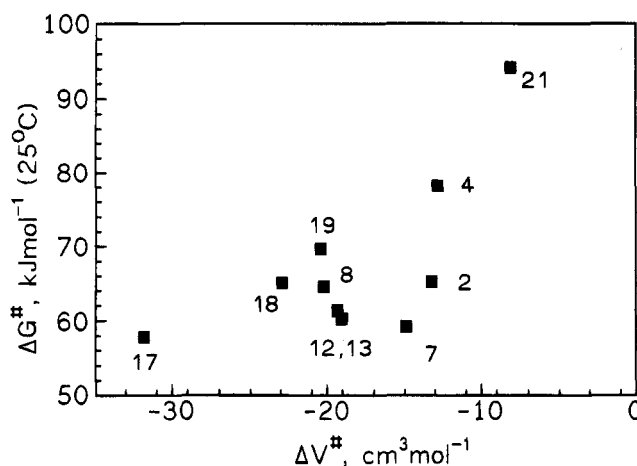


Figure 10. Plot of ΔS^{\ddagger} versus ΔV^{\ddagger} for reaction 1 under the same conditions as described in Figure 1.

k_2 and ΔV^{\ddagger} is obviously one that will repay further investigation.

In considering other possible correlations, one can see (Figure 9) that values of ΔS^{\ddagger} become more negative as values of ΔV^{\ddagger} decrease, with the exception of the data for $\text{P}(\text{NMe}_2)_3$, which has already been shown to be anomalous, and for $\text{P}(\text{OPh})_3$, which seems to have a substantially more negative ΔS^{\ddagger} value and, therefore, a correspondingly lower ΔH^{\ddagger} value than would be expected from the correlation. One would not necessarily expect any correlation between ΔG^{\ddagger} and ΔV^{\ddagger} (Figure 10) because the former is strongly dependent on the electronic properties of the nucleophiles (Figure 2) as well as on their size, whereas the latter is only dependent on their size. However, the rather rough correlation that is shown would suggest that mainly steric factors control the addition process and, therefore, both ΔG^{\ddagger} and ΔV^{\ddagger} .

Conclusions

(1) The reactions of $(\mu_2\text{-H})_2\text{Os}_3(\text{CO})_{10}$ with at least some of the P-donors (L) proceed in two stages. The initial step is first order in [L] and yields what is probably an axial isomer, which subsequently isomerizes to the more stable equatorial isomer.¹⁶

(2) The rates of initial adduct formation in chlorobenzene depend on the electronic and steric properties of the nucleophiles in exactly the same way as reactions in heptanes.^{6a} The transition state isomer (TSI)^{7a} has a rather large open space for approach by a nucleophile,

and further distortion of the TSI for nucleophiles that are larger than the steric threshold, θ_{th} , is very difficult.

(3) The volumes of activation depend only on the size of the nucleophiles and not on their basicities.

(4) For nucleophiles with $\theta < 160^\circ$ the Os \cdots P bond lengths in the transition state are constant and ΔV^\ddagger decreases linearly with $\tan^2(\theta/2)$.

(5) The extent of penetration of these smaller nucleophiles within the periphery of the opened cluster can be estimated roughly to be ca. 24 pm.

(6) There is a quite sharp threshold for ΔV^\ddagger at $\theta \approx 160^\circ$, above which penetration of the nucleophile within the open space in the TSI becomes progressively more difficult so that the Os \cdots P bond length increases and ΔV^\ddagger become less negative. The steric threshold observed for ΔV^\ddagger values is conceptually different from that based on $\log k_2$ (or ΔG^\ddagger) values. However, this conclusion implies that values of γ (eq 2) may in general be determined by the extent to which M \cdots P bond lengths increase as well as, or instead of, the energetic difficulty of further distortion of the TSI.

(7) Extrapolation of ΔV^\ddagger to $\theta = 0$ shows that formation of the TSI is actually accompanied by a compression of the ligand polytope which is sufficient to overcome the extra volume opened up in the TSI to allow approach of the nucleophile.

The richness and depth of the inferences that can be drawn on the basis of ΔV^\ddagger measurements for reactions

of a sufficiently wide variety of nucleophiles with a common substrate have been well illustrated by this study, which is the first of its kind. Measurements of ΔH^\ddagger and ΔS^\ddagger do not provide nearly as much insight into the intimate mechanisms of the reaction. Some questions, however, remain unanswered. It was not possible to establish a volume profile for reactions of individual ligands, since dilatometric reaction volume measurements require inordinately large quantities of the cluster. This would, in principle, be very valuable in order to reveal evidence for a possible change from an early to a late transition state along the series of nucleophiles of increasing size, since both electronic and steric effects can control the position of the transition state along the reaction coordinate.

Acknowledgment. We gratefully acknowledge financial support from the Deutsche Forschungsgemeinschaft, the Fonds der Chemischen Industries, the Volkswagen-Foundation, and the Natural Science and Engineering Research Council, Ottawa, Ontario, Canada.

Supporting Information Available: Table giving values of k_{obs} as a function of nucleophile concentration, temperature, pressure, and solvent for all reactions investigated in this study (9 pages). Ordering information is given on any current masthead page.

OM940959T

The First Isolable Organopalladium Formate Complexes: Synthesis, Characterization, and X-ray Structure. Facile and Convenient Thermal Generation of Coordinatively Unsaturated Palladium(0) Species

Vladimir V. Grushin, Corinne Bensimon, and Howard Alper*

Department of Chemistry, University of Ottawa, 10 Marie Curie, Ottawa, Ontario, Canada K1N 6N5

Received February 3, 1995[®]

$[\text{L}_2\text{Pd}_2(\text{R})_2(\mu\text{-OH})_2]$ complexes ($\text{L} = \text{PPh}_3$, $\text{R} = \text{Ph}$, Me) react with formic acid in benzene to give the first stable organopalladium formates, $[\text{L}_2\text{Pd}_2(\text{R})_2(\mu\text{-HCOO})_2]$ (**1**, $\text{R} = \text{Ph}$; **2**, $\text{R} = \text{Me}$). Addition of L to **1** and **2** results in the formation of the less stable, but still isolable, $[\text{L}_2\text{Pd}(\text{R})(\text{HCOO})]$ (**3**, $\text{R} = \text{Ph}$; **4**, $\text{R} = \text{Me}$). Complexes **1**–**4** have been characterized by elemental analysis and NMR and IR spectral data. The structure of **2** has been confirmed by X-ray analysis of its 1:1.5 benzene solvate: monoclinic, space group $P2_1/n$; $a = 9.785(4)$ Å, $b = 24.909(8)$ Å, $c = 18.854(7)$ Å, $\beta = 102.92(3)^\circ$; $V = 4479(3)$ Å³, $Z = 4$; $D_{\text{calc}} = 1.441$ g/cm³; $R = 0.044$, $R_w = 0.066$. The thermal decomposition of **1**–**4** in benzene or toluene at 30–55 °C gives CO_2 , RH , and highly reactive $[\text{L}_n\text{Pd}]$ ($n = 1, 2$). An exchange between the $\sigma\text{-Me}$ groups and phenyls of the PPh_3 ligand is observed in the course of the thermal decomposition of **2** in toluene at 55 °C. The thermolysis of **1** in the presence of PhI gives rise to $[\text{L}_2\text{Pd}_2(\text{Ph})_2(\mu\text{-I})_2]$ (**5**); likewise, the decomposition of **2** in the presence of MeI furnishes $[\text{L}_2\text{Pd}_2(\text{Me})_2(\mu\text{-I})_2]$ (**6**). However, when **1** is decomposed in the presence of MeI , both **5** and **6** are formed, with the ratio of **5** to **6** being higher at higher concentrations of MeI . A similar effect is observed when **2** is thermolyzed in the presence of PhI . This “reverse” selectivity leads to the recognition of two distinct mechanisms governing the Pd-catalyzed reductive dehalogenation of aryl halides with formate anion.

Organopalladium formate complexes have been proposed as key catalytic intermediates in a number of synthetically valuable processes, such as the preparation of terminal olefins from allylic esters and formic acid,^{1,2} the reductive dehalogenation of haloarenes with formate anion,³ and some carbonylation reactions.⁴ Both the unique catalytic properties of palladium⁵ and the importance of transition-metal formates in the

Table 1. Crystallographic Data for $[(\text{Ph}_3\text{P})_2\text{Pd}_2\text{Me}_2(\mu\text{-HCOO})_2] \cdot 1.5\text{C}_6\text{H}_6$ (**2**·1.5 C_6H_6)

formula	$\text{C}_{49}\text{H}_{47}\text{O}_4\text{P}_2\text{Pd}_2$
fw	974.62
cryst shape	cube
cryst dimens, mm	$0.2 \times 0.2 \times 0.2$
cryst syst	monoclinic
lattice params	$a = 9.785(4)$ Å $b = 24.909(8)$ Å $c = 18.854(7)$ Å $\beta = 102.92(3)^\circ$
space group	$P2_1/n$
Z	4
V , Å ³	4479(3)
d_{calc} , g/cm ³	1.441
T , K	143
radiation (λ , Å)	$\text{Mo K}\alpha$ (0.709 30)
μ , mm ⁻¹	0.89
R (R_w), %	4.4 (6.6)

activation of CO_2 ⁶ provide a special challenge for the synthesis and characterization of (formate)palladium complexes. In the present paper we wish to report the preparation, isolation, full characterization (including X-ray analysis), and some properties of the first (σ -organo)palladium formates. There has been only one report⁷ in the literature, describing the generation (at –30 °C) and in situ characterization of (π -allyl)palla-

(7) Oshima, M.; Shimizu, I.; Yamamoto, A.; Ozawa, F. *Organometallics* 1991, 10, 1221.

(8) (a) Darnesbourg and co-workers^{8b} reported the preparation of $[(\text{Cy}_3\text{P})_2\text{Pd}(\text{H})(\text{HCOO})]$ for kinetic studies. The complex was characterized by ¹H NMR spectroscopy; however, elemental analysis was not performed, probably due to the instability of the compound. (b) Darnesbourg, D. J.; Wiegrefe, P.; Riordan, C. G. *J. Am. Chem. Soc.* 1990, 112, 5759.

[®] Abstract published in *Advance ACS Abstracts*, May 15, 1995.
(1) For reviews see: (a) Tsuji, J. *Pure Appl. Chem.* 1982, 54, 197.
(b) Tsuji, J. *Pure Appl. Chem.* 1986, 58, 869. (c) Tsuji, J.; Takahashi, T. *Yakugaku Zasshi* 1987, 107, 87. (d) Shimizu, I.; Oshima, M.; Nagasawa, K.; Tsuji, J.; Mandai, T. *Yuki Gosi Kagaku Kyokaiishi* 1991, 49, 526; *Chem. Abstr.* 1991, 115, 70866d.
(2) For the most recent references see: (a) Hayashi, T.; Iwamura, H.; Uozumi, Y. *Tetrahedron Lett.* 1994, 35, 4813. (b) Hayashi, T.; Iwamura, H.; Naito, M.; Matsumoto, Y.; Uozumi, Y.; Miki, M.; Yanagi, K. *J. Am. Chem. Soc.* 1994, 116, 775. (c) Mandai, T.; Matsumoto, T.; Kawada, M.; Tsuji, J. *Tetrahedron* 1993, 49, 5483. (d) Mandai, T.; Matsumoto, T.; Kawada, M.; Tsuji, J. *Tetrahedron Lett.* 1993, 34, 2161.
(3) (a) Cortese, N. A.; Heck, R. F. *J. Org. Chem.* 1977, 42, 3491. (b) Helquist, P. *Tetrahedron Lett.* 1978, 1913. (c) Pri-Bar, I.; Buchman, O. *J. Org. Chem.* 1986, 51, 734. (d) Anwer, M. K.; Sherman, D. B.; Roney, J. G.; Spatola, A. F. *J. Org. Chem.* 1989, 54, 1284. (e) Ben-David, Y.; Gozin, M.; Portnoy, M.; Milstein, D. *J. Mol. Catal.* 1992, 73, 173.

(4) (a) Pri-Bar, I.; Buchman, O. *J. Org. Chem.* 1988, 53, 624. (b) Ben-David, Y.; Portnoy, M.; Milstein, D. *J. Chem. Soc., Chem. Commun.* 1989, 1816. (c) El Ali, B.; Alper, H. *J. Mol. Catal.* 1992, 77, 7. (d) El Ali, B.; Alper, H. *J. Org. Chem.* 1993, 58, 3595. (e) Zargarian, D.; Alper, H. *Organometallics* 1993, 12, 712.

(5) (a) Tsuji, J. *Organic Synthesis with Palladium Compounds*; Springer: Heidelberg, Germany, 1980. (b) Heck, R. F. *Palladium Reagents in Organic Synthesis*; Academic Press: New York, 1985.
(6) (a) Behr, A. *Carbon Dioxide Activation by Metal Complexes*; VCH: Weinheim, Germany, 1988. (b) For the most recent references see: Jessop, P. G.; Ikariya, T.; Noyori, R. *Nature* 1994, 368, 231. Leitner, W.; Dinjus, E.; Gassner, F. *J. Organomet. Chem.* 1994, 475, 257. Gassner, F.; Leitner, W. *J. Chem. Soc., Chem. Commun.* 1993, 1465. Graf, E.; Leitner, W. *J. Chem. Soc., Chem. Commun.* 1992, 623.

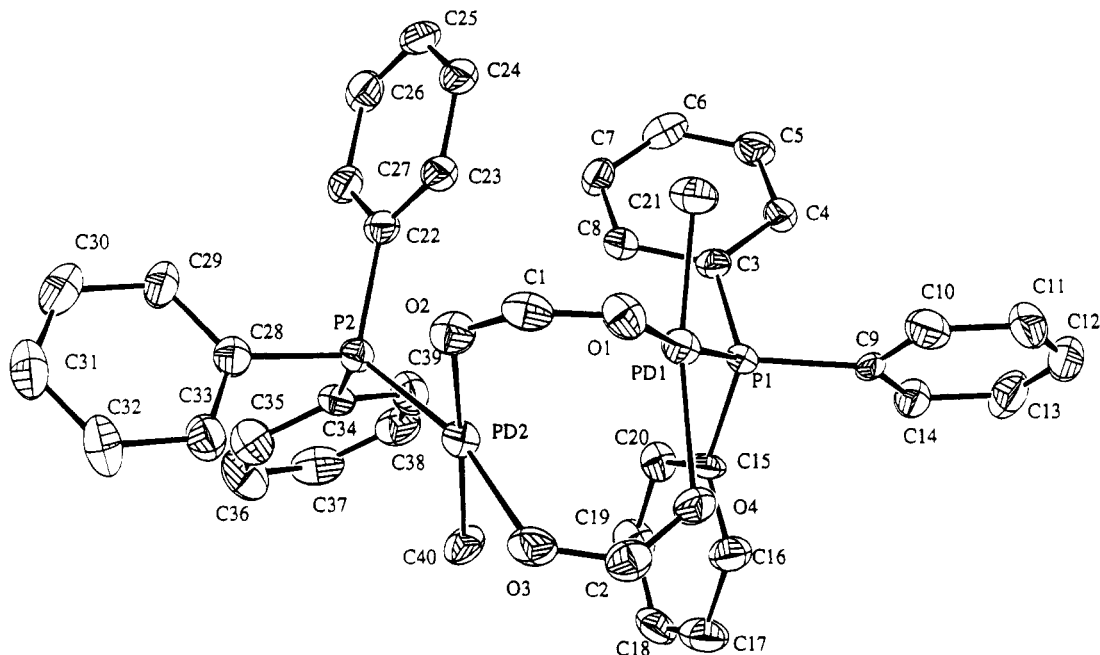
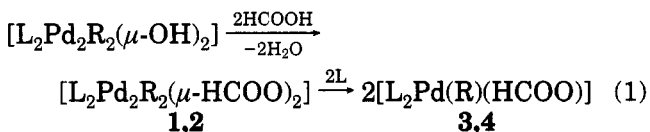


Figure 1. ORTEP drawing for the metal complex part of $2 \cdot 1.5\text{C}_6\text{H}_6$ (hydrogen atoms are omitted). Selected bond lengths (Å) and angles (deg): Pd(1)–P(1), 2.2144(21); Pd(1)–O(1), 2.124(5); Pd(1)–O(4), 2.151(5); Pd(1)–C(21), 2.036(8); Pd(2)–P(2), 2.2266(21); Pd(2)–O(2), 2.183(5); Pd(2)–O(3), 2.117(5); Pd(2)–C(40), 2.027(8); O(1)–C(1), 1.251(10); O(2)–C(1), 1.239(10); O(3)–C(2), 1.256(10); O(4)–C(2), 1.238(10); P(1)–Pd(1)–O(1), 173.58(15); P(1)–Pd(1)–O(4), 98.06(16); P(1)–Pd(1)–C(21), 87.61(24); O(1)–Pd(1)–C(21), 86.4(3); P(2)–Pd(2)–O(2), 96.07(15); P(2)–Pd(2)–O(3), 165.66(16); P(2)–Pd(2)–C(40), 89.12(24); O(2)–Pd(2)–O(3), 85.99(21); O(2)–Pd(2)–C(40), 171.9(3); O(3)–Pd(2)–C(40), 87.5(3); Pd(1)–O(1)–C(1), 125.0(5); Pd(2)–O(2)–C(1), 124.7(5); Pd(2)–O(3)–C(2), 123.8(5); Pd(1)–O(4)–C(2), 126.3(5); O(1)–C(1)–O(2), 129.1(7); O(3)–C(2)–O(4), 128.3(7).

dium formates in solution by low-temperature NMR spectroscopy.⁸ These complexes, however, cannot be isolated, as they decompose rapidly at ambient temperature.⁷

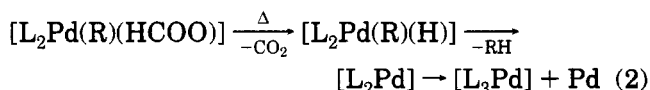
Treatment of $[(\text{Ph}_3\text{P})_2\text{Pd}_2(\text{R})_2(\mu\text{-OH})_2]$, where R = Ph⁹ or Me (see Experimental Section), with a 1.5–7-fold excess of formic acid in benzene results in direct and clean formation of the corresponding *binuclear* organopalladium complexes with two bridging η^2 -formate ligands, **1** and **2**. Both **1** and **2** readily add triphenylphosphine to give the corresponding *mononuclear* organopalladium η^1 -formates, **3** and **4** (eq 1).



Complexes **1–4** were isolated in high yields (85–98%) and characterized by elemental analysis and IR and NMR spectroscopy. The structure of **2** was confirmed by a single-crystal diffraction study of its benzene solvate (Table 1). As shown in Figure 1, the two Pd atoms in **2** are held in one molecule by two bridging η^2 -formate ligands *cis* to each other, as previously found for the closely related Pd benzoato dimer $[(\text{Ph}_3\text{P})_2\text{Pd}_2\text{Ph}_2(\mu\text{-PhCOO})_2]$.¹⁰

The binuclear complexes **1** and **2** are considerably more stable than the mononuclear **3** and **4**. In the solid state, both **1** and **2** do not decompose at room temperature for several days, whereas crystalline **3** decomposes slowly at 20 °C and solid **4** is even less stable. However,

all the formate complexes **1–4** can be stored at –15 °C for a few weeks without any sign of decomposition. In benzene or toluene solution, mononuclear **3** and **4** start decomposing above 15 °C, to give CO₂, Pd metal, tris(triphenylphosphine)palladium(0), and benzene or methane, respectively. This reaction likely occurs via CO₂ loss, followed by reductive elimination of the corresponding hydrocarbon, RH, and disproportionation of the thus generated $[(\text{Ph}_3\text{P})_2\text{Pd}]$ (eq 2). It is noteworthy that benzoato¹⁰ and acetato (see Experimental Section) analogues of **1–4** are stable at up to 70–90 °C in benzene and toluene solutions under N₂, showing no sign of decomposition for at least 10–15 min.



Unlike *trans*-alkyl- or *trans*-arylbis(phosphine)platinum hydrides,^{11a} their Pd analogues are too unstable for isolation or even spectral characterization *in situ*, decomposing immediately upon generation (eq 2).^{11b} The resulting bis(triphenylphosphine)palladium¹² was not observed by ³¹P NMR spectroscopy due to its facile disproportionation to $[(\text{Ph}_3\text{P})_3\text{Pd}]$ under the reaction conditions. Similarly, $[(\text{Ph}_3\text{P})_2\text{Pt}]$, generated by various means, readily transforms to $[(\text{Ph}_3\text{P})_3\text{Pt}]$.¹³ However, the *in situ* generation of $[(\text{Ph}_3\text{P})_2\text{Pd}]$ was confirmed by

(11) (a) Arnold, D. P.; Bennett, M. A. *J. Organomet. Chem.* **1980**, *199*, C17. (b) Two complexes, *trans*- $[\text{L}_2\text{Pd}(\text{H})\text{Me}]$, where L = Cy₃P or *i*-Pr₃P, are relatively stable due to the bulky electron-rich phosphine ligands. See: Abis, L.; Santi, R.; Halpern, J. *J. Organomet. Chem.* **1981**, *215*, 263.

(12) Urata, H.; Suzuki, H.; Moro-oka, Y.; Ikawa, T. *J. Organomet. Chem.* **1989**, *364*, 235.

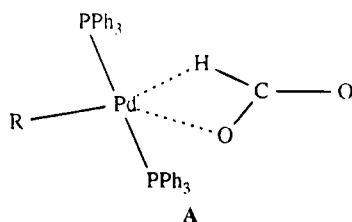
(13) (a) Abis, L.; Sen, A.; Halpern, J. *J. Am. Chem. Soc.* **1978**, *100*, 2915. (b) Grushin, V. V.; Akhrem, I. S.; Vol'pin, M. E. *J. Organomet. Chem.* **1989**, *371*, 403.

(9) Grushin, V. V.; Alper, H. *Organometallics* **1993**, *12*, 1890.

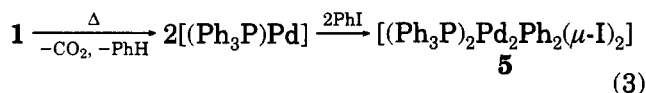
(10) Grushin, V. V.; Alper, H. *J. Am. Chem. Soc.* **1995**, *117*, 4305.

running the decomposition of **3** in the presence of iodobenzene, which furnished $[(\text{Ph}_3\text{P})_2\text{Pd}(\text{I})\text{Ph}]^{14}$ in quantitative yield.

The thermal decomposition of binuclear **1** in benzene or toluene starts at 50–55 °C to give CO_2 , PhH , Pd metal, and a mixture of $[(\text{Ph}_3\text{P})_3\text{Pd}]$ and $[(\text{Ph}_3\text{P})_4\text{Pd}]$ in a ca. 2:1 ratio.¹⁵ It is noteworthy that thermal decomposition reactions of **1** and **2** exhibit a well-pronounced autocatalytic effect which is due to the release of free phosphine in the course of the reaction.¹⁶ The free phosphine adds to as yet unreacted **1** (eq 1) to give the more labile mononuclear **3**. This significant difference in stability of the monomeric and dimeric formates is a consequence of the facile attainment of the transition state **A**^{8b} for **3** and **4** bearing η^1 -formate ligands, whereas cleavage of the η^2 -formate bridges in **1** and **2** is required before β -elimination can occur.



As anticipated, no autocatalytic effect was observed when the decomposition of **1** was conducted in the presence of iodobenzene (eq 3) since the presumably generated $[(\text{Ph}_3\text{P})\text{Pd}]$ was trapped with PhI prior to decomposition.

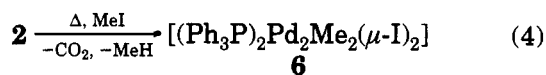


Only traces of Pd metal, if any, were formed in the course of reaction 3, which furnished $[(\text{Ph}_3\text{P})_2\text{Pd}_2\text{Ph}_2(\mu\text{-I})_2]^9$ (**5**) in quantitative yield. Therefore, oxidative addition of PhI to the highly coordinately unsaturated $[(\text{Ph}_3\text{P})\text{Pd}]$ is substantially faster than the disproportionation to Pd metal and $[(\text{Ph}_3\text{P})_n\text{Pd}]$ ($n = 3, 4$). No noticeable difference was observed when reaction 3 was carried out in the absence, or in the presence, of 1,1-diphenylethylene (5-fold excess) as a radical trap.¹⁷ This observation provides evidence against a free-radical mechanism for both the decomposition of **1** and the oxidative addition of PhI to the generated Pd(0) species.

A remarkable exchange between the σ -methyl groups and phenyls of the PPh_3 ligands was observed in the course of the thermal decomposition of **2** in toluene at 55 °C. A similar aryl/aryl exchange reaction¹⁸ likely took place when **1** decomposed under the same conditions, but because of its degenerate nature this exchange

was not detected. Two singlets at -0.5 and 22.0 ppm (3:1 integral intensity) were observed in the ^{31}P NMR spectrum when **2**, in toluene, was decomposed at 55 °C. Cooling this solution down to -92 °C resulted in transformation of the downfield signal into a singlet at 22.7 ppm and a doublet at 23.2 ppm with $J(\text{P-P}) = 94.5$ Hz, whereas a number of resonances in the range of 0–2 ppm replaced the singlet (-0.5 ppm) originally observed at 55 °C. The major low-temperature upfield resonance was a 1:2:1 triplet at 0.9 ppm, with the same coupling constant and half the intensity of the simultaneously observed doublet at 23.2 ppm. Clearly, the singlet at 22.7 ppm was due to $[(\text{Ph}_3\text{P})_3\text{Pd}]$,^{15b} whereas the doublet (23.2 ppm) and the triplet (0.9 ppm) appeared from an AB_2 spin system such as $[(\text{Ph}_3\text{P})_2(\text{Ph}_2\text{PMe})\text{Pd}]$. Unambiguous evidence for the methyl/phenyl exchange was observed by monitoring (^{13}C NMR) the decomposition of $[(\text{Ph}_3\text{P})_2\text{Pd}_2(^{13}\text{CH}_3)_2(\mu\text{-H}^{13}\text{COO})_2]$ (**2a**) in benzene- d_6 at 55 °C. In addition to the singlets at -4.3 ppm ($^{13}\text{CH}_4$) and 125.1 ppm ($^{13}\text{CO}_2$),¹⁹ a very broad, intense resonance at 14 ppm and two sharp doublets at 16.8 ppm (major, $J(\text{C-P}) = 73.5$ Hz) and 18.3 ppm (minor, $J(\text{C-P}) = 71.6$ Hz) were observed in the ^{13}C NMR spectrum after the decomposition of **2a**. While the broad resonance could be assigned to various Pd(0) methylphosphine complexes in rapid exchange (see above), the doublets were clearly due to $\text{Ph}_2\text{P}(^{13}\text{CH}_3)\text{O}$ and $\text{PhP}(^{13}\text{CH}_3)_2\text{O}$,²⁰ respectively, which likely formed due to the traces of molecular oxygen present in the sample. No evidence was obtained for the formation of any $[\text{L}_2\text{Pd}(\text{CO}_2)]$ ($\text{L} =$ tertiary phosphine) complexes, which are stable only under excess CO_2 at low temperature.²¹

The methyl/phenyl exchange process was totally suppressed when the thermolysis of **2** or **2a** was carried out in the presence of PhI or MeI at the same temperature. Thus, complex **6** formed quantitatively upon decomposition of **2** in benzene containing methyl iodide (eq 4).



When **2** was decomposed in the presence of PhI , surprisingly both **5** and **6** were formed (in 100% overall yield), with the ratio of **5** to **6** being dependent on the concentration of iodobenzene. Quite striking was also the fact that higher concentrations of PhI resulted in lower ratios of **5** to **6**! In other words, the more PhI that was present, the less the σ -Ph complex formed. For instance, when the molar ratio of PhI to **2** was varied from 2.4 to 21, and further to ∞ (decomposition in pure iodobenzene), the observed (^{31}P NMR) ratios of **5** to **6** were 2.4, 1.9, and 1.6, respectively. Even more pronounced was the influence of the iodomethane concentration on the result of its reaction with **1** in benzene at 60 °C: the ratios of **5** to **6** were found to be 1.7 and 13.1 for the MeI to **1** molar ratios of 19 and ∞ (thermolysis in a 1:1 by volume mixture of MeI and benzene), respectively. These results can be rationalized in terms

(14) Garrou, P. E.; Heck, R. F. *J. Am. Chem. Soc.* **1976**, *98*, 4115.

(15) (a) This ratio was determined by measuring the ^{31}P NMR spectrum of the decomposed **1** in toluene at -90 °C, the chemical shifts of the tri- and tetracoordinate Pd(0) complexes being 22.2 and 17.0 ppm.^{15b} (b) Mann, B. E.; Musco, A. *J. Chem. Soc., Dalton Trans.* **1975**, 1673.

(16) At ambient temperature, $[(\text{Ph}_3\text{P})_4\text{Pd}]$ is completely dissociated in solution to $[(\text{Ph}_3\text{P})_3\text{Pd}]$ and PPh_3 . See ref 15b and: Kurran, W.; Musco, A. *Inorg. Chim. Acta* **1975**, *12*, 187.

(17) See for example: Lubinkowski, J. J.; Gomez, M.; Calderon, J. L.; McEwen, W. E. *J. Org. Chem.* **1978**, *43*, 2432. Grushin, V. V.; Shcherbina, T. M.; Tolstaya, T. P. *J. Organomet. Chem.* **1985**, *292*, 105.

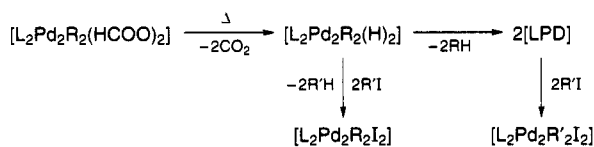
(18) Kong, K.-C.; Cheng, C.-H. *J. Am. Chem. Soc.* **1991**, *113*, 6131. See also: Gillie, A.; Stille, J. K. *J. Am. Chem. Soc.* **1980**, *102*, 4933.

(19) Günther, H. *NMR Spectroscopy: An Introduction*; Wiley: New York, 1980; p 398.

(20) Albright, T. A.; Freeman, W. J.; Schweizer, E. E. *J. Org. Chem.* **1975**, *40*, 3437.

(21) Sakamoto, M.; Shimizu, I.; Yamamoto, A. *Organometallics* **1994**, *13*, 407.

Scheme 1



of two competing processes shown in Scheme 1. Before the reductive elimination of RH occurs, the Pd hydrido intermediate may reduce the organic iodide, thus giving the "anomalous" metal product. As the reduction should be of positive order in the organic iodide, an increase of [R'I] would favor its reduction rate, thus decreasing the "normal" to "anomalous" product ratio.²² These results shed light on the intimate process of the palladium-catalyzed reductive dehalogenation of haloarenes with formate anion,³ indicating that *two* different mechanisms (Scheme 1; R = R') equally resulting in the arene production, can govern the catalytic process.

In conclusion, organopalladium formate complexes have been isolated and fully characterized for the first time. The facile thermal decomposition of these complexes results in smooth and clean generation of the highly reactive, coordinatively unsaturated species [(Ph₃P)_nPd] (n = 1, 2). An investigation of the thermal decomposition of organopalladium formates, in the presence of organic iodides, disclosed the existence of two distinct mechanisms for the Pd-catalyzed reductive dehalogenation of aryl halides with formate anion.

Experimental Section

Physical measurements were carried out using the following equipment: Varian XL 300 (¹H, ¹³C, and ³¹P NMR), Bomem MB-100 (FT-IR), and Rigaku AFC6S (X-ray diffraction). All chemicals were purchased from commercial sources (Aldrich, Strem, and Organometallics) and used as received.

Synthesis of [(Ph₃P)₂Pd₂(Me)₂(μ-OH)₂]. A mixture of [(Ph₃P)₂PdCl₂] (1.10 g; 1.57 mmol), 50% KOH (4 g), benzene (8 mL), and MeI (1 mL) was stirred under nitrogen at room temperature for 20 h. The reaction mixture first turned dark brown and then gradually decolorized, and colorless precipitate formed. The workup was performed in air. Water (15 mL) and dichloromethane (50 mL) were added, the mixture was stirred until all the solid dissolved, and the organic layer was separated and evaporated. The residual oil was dried under vacuum and then stirred under nitrogen with dichloromethane (10 mL) and 50% KOH (8 g) for 3 h (small amounts of Pd metal precipitated). The yellow organic phase was separated, filtered through cotton, and evaporated. The residue was dried under vacuum until solidified, and treated with acetone (4 mL), to give a grayish white microcrystalline solid which was thoroughly washed with acetone (3 × 3 mL) and dried under vacuum. The yield of [(Ph₃P)₂Pd₂(Me)₂(μ-OH)₂] (monohydrate) was 0.46–0.58 g (70–90%). In chloroform solution, the complex exists as a 1:1 mixture of *cis* and *trans* isomers. ¹H NMR (CDCl₃; δ): -3.3 (br s, 0.5H, *cis*-OH); -2.1 (br s, 1H, *trans*-OH); -0.7 (br s, 0.5H, *cis*-OH); 0.0 (d, 3H, J = 2.6 Hz, Pd-CH₃); 0.2 (d, 3H, J = 2.6 Hz, Pd-CH₃); 7.5 (m, 30H, C₆H₅).

(22) It is conceivable that the intermediate organopalladium hydrido species and the already formed organopalladium iodides undergo an intermolecular *σ*-Me/*σ*-Ph exchange similar to that described for the cross-coupling reactions of diorganopalladium complexes and organic halides.²³ We thank a reviewer for bringing this possibility to our attention.

(23) Ozawa, F.; Fujimori, M.; Yamamoto, T.; Yamamoto, A. *Organometallics* **1986**, *5*, 2144. Ozawa, F.; Hidaka, T.; Yamamoto, T.; Yamamoto, A. *J. Organomet. Chem.* **1987**, *330*, 253. Ozawa, F.; Kurihara, K.; Fujimori, M.; Hidaka, T.; Toyoshima, T.; Yamamoto, A. *Organometallics* **1989**, *8*, 180.

³¹P (CDCl₃; δ): 39.4 (s, 0.5P); 39.6 (s, 0.5P). IR (Nujol; cm⁻¹): 3610 (OH). Anal. Calcd for C₃₈H₄₀O₃P₂Pd₂: C, 55.7; H, 4.9. Found: C, 55.7; H, 4.9.

Synthesis of [(Ph₃P)₂Pd₂(Ph)₂(μ-HCOO)₂] (1). Formic acid (30 mg; 0.65 mmol) was added to a stirred mixture of [(Ph₃P)₂Pd₂(Ph)₂(μ-OH)₂] (0.20 g; 0.22 mmol) and benzene (8 mL), causing immediate dissolution of the solid. The resulting benzene solution was filtered, reduced in volume to ca. 2 mL (the temperature of the bath should not exceed 35 °C), and treated with hexane (dropwise) until the solution grew turbid. After some crystals formed, more hexane (25 mL) was added, and the mixture was kept at -17 °C for 1 h. The yellowish crystals were separated, washed with hexane (3 × 3 mL), and dried under vacuum. The yield of **1** was 0.193 g (91%). Anal. Calcd for C₅₀H₄₂O₄P₂Pd₂: C, 61.2; H, 4.3. Found: C, 61.5; H, 4.5. ¹H NMR (benzene-*d*₆, 18 °C; δ): 7.0 (m, 18H, 3,4,5-C₆H₅P); 7.1 (m, 6H, 3,4,5-C₆H₅Pd); 7.65 (m, 12H, 2,6-C₆H₅P); 7.85 (m, 4H, 2,6-C₆H₅Pd); 8.3 (s, 2H, HCOO). ³¹P NMR (C₆H₆; δ): 30.3 (s). IR (Nujol; cm⁻¹): 2825 (shoulder; H-COO); 1593, 1353 (CO).

Synthesis of [(Ph₃P)₂Pd₂(Me)₂(μ-HCOO)₂] (2). Formic acid (45 mg; 1 mmol) was added to a stirred suspension of [(Ph₃P)₂Pd₂(Me)₂(μ-OH)₂·H₂O] (0.23 g; 0.28 mmol) in benzene (10 mL). The solid dissolved immediately, and the mixture was stirred for another 5 min. The yellow benzene solution was filtered and reduced in volume to 2–3 mL (the temperature of the bath should not exceed 35 °C). Hexane was added dropwise until the solution turned cloudy, and the mixture was left until a considerable amount of yellowish crystals formed (10–20 min). More hexane (15 mL) was added portionwise; the crystals were separated, washed with hexane (3 × 4 mL), and dried under vacuum. The yield of **2**·1.5C₆H₆ was 0.252 g (92%). Anal. Calcd for C₄₉H₄₇O₄P₂Pd₂: C, 60.4; H, 4.9. Found: C, 60.3; H, 5.0. ¹H NMR (CDCl₃, 18 °C; δ): 0.65 (s, 6H, CH₃); 7.3 (m, 18H, 3,4,5-C₆H₅); 7.6 (m, 12H, 2,6-C₆H₅); 7.95 (br s, 2H, HCOO). ³¹P NMR (C₆H₆; δ): 37.8 (s). IR (Nujol; cm⁻¹): 2810 (H-COO); 1595, 1349 (CO).

Complex **2a** was prepared similarly from [(Ph₃P)₂PdCl₂], ¹³CH₃I, and H¹³COOH. ¹³C NMR (benzene-*d*₆, 18 °C; δ): 3.1 (s, ¹³CH₃), 170.6 (s, H¹³COO).

Synthesis of [(Ph₃P)₂Pd(Ph)(HCOO)] (3). Formic acid (45 mg; 1 mmol) was added to a stirred mixture of [(Ph₃P)₂Pd₂(Ph)₂(μ-OH)₂] (0.125 g; 0.135 mmol) and benzene (4 mL). After the solid dissolved, the resulting lemon yellow benzene solution was filtered, reduced in volume to ca. 2 mL (the temperature of the bath should not exceed 35 °C), and treated with PPh₃ (0.10 g; 0.38 mmol) at 5–10 °C (ice bath). The addition of triphenylphosphine caused immediate decolorization of the solution. While the mixture was kept in the ice bath, cold (0–5 °C) hexane was added dropwise until the solution turned cloudy. After colorless, well-shaped crystals started growing, more cold hexane (10 mL) was added portionwise, and the mixture was kept at ca. 0 °C for 1 h. The crystals were separated, washed with hexane, and dried under vacuum at room temperature. The yield of **3** was 0.20 g (98%). Anal. Calcd for C₄₃H₃₆O₂P₂Pd: C, 68.6; H, 4.8. Found: C, 69.1; H, 4.9. ¹H NMR (benzene-*d*₆, 7 °C; δ): 6.5 (m, 3H, 3,4,5-C₆H₅Pd); 6.7 (m, 2H, 2,6-C₆H₅Pd); 7.1 (m, 18H, 3,4,5-C₆H₅P); 7.85 (m, 12H, 2,6-C₆H₅P); 8.25 (s, 1H, HCOO). ³¹P NMR (C₆H₆, 7 °C; δ): 22.0 (s). IR (Nujol; cm⁻¹): 2803 (H-COO); 1609, 1313 (CO).

Synthesis of [(Ph₃P)₂Pd(Me)(HCOO)] (4). Formic acid (45 mg; 1 mmol) was added to a suspension of [(Ph₃P)₂Pd₂(Me)₂(μ-OH)₂·H₂O] (0.115 g; 0.14 mmol) in benzene (2 mL), with stirring. After the solid dissolved, the yellow benzene solution was separated, the flask was rinsed with benzene (1 mL), and the combined benzene solutions were filtered and placed on an ice bath. When benzene started crystallizing, PPh₃ (0.11 g; 0.42 mmol) was added, and the mixture was carefully warmed and stirred until the crystallized benzene melted and the PPh₃ dissolved. Cold (0 °C) hexane (3 mL) was added, and the mixture was kept at -17 °C until yellowish crystals started

depositing. More hexane (2 mL) was added, and the mixture was kept at $-17\text{ }^{\circ}\text{C}$ for another 1 h, after which the crystals were separated, washed with hexane, and dried under vacuum. The yield of the spectroscopically (^1H , ^{31}P NMR) pure **4** was 0.138 g (85%). Satisfactory elemental analysis was not obtained due to the instability of the complex at ambient temperature. ^1H NMR (benzene- d_6 , $7\text{ }^{\circ}\text{C}$; δ): 0.55 (t, 3H, $J(\text{H}-\text{P}) = 6.2\text{ Hz}$), CH_3); 7.2 (m, 18H, 3,4,5- C_6H_5); 8.0 (m, 12H, 2,6- C_6H_5); 8.2 (s, 1H, HCOO). ^{31}P NMR (benzene, $7\text{ }^{\circ}\text{C}$; δ): 29.7 (s). IR (Nujol; cm^{-1}): 2787 ($\text{H}-\text{COO}$); 1606, 1302 (CO).

Decomposition of 2 in the Presence of MeI (Synthesis of 6). An oxygen-free mixture of $2 \cdot 1.5\text{C}_6\text{H}_6$ (70 mg; 0.07 mmol), benzene (5 mL), and MeI (0.5 mL) was heated at $60\text{ }^{\circ}\text{C}$ in a closed flask under N_2 for 2 h. The brownish solution was filtered hot and evaporated, and the residue was treated with acetone to give 60 mg (82%) of brownish **6**, which was washed with acetone and dried under vacuum. Anal. Calcd for $\text{C}_{38}\text{H}_{36}\text{I}_2\text{P}_2\text{Pd}_2$: C, 44.7; H, 3.6. Found: C, 45.1; H, 3.6. ^1H NMR (CDCl_3 , $18\text{ }^{\circ}\text{C}$; δ): 0.8 (d, 6H, $J(\text{H}-\text{P}) = 3.2\text{ Hz}$, CH_3); 7.4 (m, 18H, 3,4,5- C_6H_5); 7.65 (m, 12H, 2,6- C_6H_5). ^{31}P NMR (C_6H_6 , $18\text{ }^{\circ}\text{C}$; δ): 38.0 (s).

Synthesis of $[(\text{Ph}_3\text{P})_2\text{Pd}_2(\text{Ph})_2(\mu\text{-CH}_3\text{COO})_2]$. Acetic acid (35 mg; 0.58 mmol) was added to a stirred mixture of $[(\text{Ph}_3\text{P})_2\text{Pd}_2(\text{Ph})_2(\mu\text{-OH})_2]$ (0.17 g; 0.18 mmol) and benzene (6 mL), causing fast dissolution of the solid. The resulting benzene solution was evaporated, and the residual crystals were washed with hexane and dried under vacuum. The yield of $[(\text{Ph}_3\text{P})_2\text{Pd}_2(\text{Ph})_2(\mu\text{-CH}_3\text{COO})_2] \cdot 1.5\text{C}_6\text{H}_6$ was 0.204 g (98.5%). Anal. Calcd for $\text{C}_{61}\text{H}_{55}\text{O}_4\text{P}_2\text{Pd}_2$: C, 65.0; H, 4.9. Found: C, 65.0; H, 4.9. ^1H NMR (benzene- d_6 , $18\text{ }^{\circ}\text{C}$; δ): 1.6 (s, 6H, CH_3); 7.0 (m, 24H, 3,4,5- C_6H_5); 7.5 (m, 12H, 2,6- $\text{C}_6\text{H}_5\text{P}$); 7.8 (m, 4H, 2,6- $\text{C}_6\text{H}_5\text{Pd}$). ^{31}P NMR (C_6H_6 ; δ): 30.4 (s). IR (Nujol; cm^{-1}): 1580, 1377 (CO).

Synthesis of $[(\text{Ph}_3\text{P})_2\text{Pd}(\text{Ph})(\text{CH}_3\text{COO})]$. A mixture of $[(\text{Ph}_3\text{P})_2\text{Pd}_2(\text{Ph})_2(\mu\text{-CH}_3\text{COO})_2] \cdot 1.5\text{C}_6\text{H}_6$ (0.08 g; 0.07 mmol), benzene (5 mL), and PPh_3 (0.055 g; 0.21 mmol) was stirred at room temperature for a few minutes until all the solid dissolved and a clear, colorless solution formed. The solution was reduced in volume to ca. 2 mL, and the residue was treated with hexane (10 mL, portionwise). After 1 h, the colorless crystals were separated, washed with hexane, and dried under vacuum. The yield of $[(\text{Ph}_3\text{P})_2\text{Pd}(\text{Ph})(\text{CH}_3\text{COO})]$ was 0.106 g (97%). Anal. Calcd for $\text{C}_{44}\text{H}_{38}\text{O}_2\text{P}_2\text{Pd}$: C, 68.9; H, 5.0. Found: C, 68.9; H, 4.9. ^1H NMR (benzene- d_6 ; δ): 1.4 (s, 3H, CH_3); 6.4 (m, 3H, 3,4,5- $\text{C}_6\text{H}_5\text{Pd}$); 6.6 (m, 2H, 2,6- $\text{C}_6\text{H}_5\text{P}$); 7.0 (m, 18H, 3,4,5- $\text{C}_6\text{H}_5\text{P}$); 7.7 (m, 12H, 2,6- $\text{C}_6\text{H}_5\text{P}$). ^{31}P NMR (C_6H_6 ; δ): 21.7 (s). IR (Nujol; cm^{-1}): 1605, 1324 (CO).

Single-Crystal Diffraction Study of $2 \cdot 1.5\text{C}_6\text{H}_6$. A well-shaped crystal of $2 \cdot 1.5\text{C}_6\text{H}_6$ having approximate dimensions

of $0.2 \times 0.2 \times 0.2\text{ mm}$ was mounted on a glass capillary. The measurements were made at $-130\text{ }^{\circ}\text{C}$ with Mo K α radiation and a graphite monochromator. During the data collection, standard reflections were measured after every 150 reflections to check the stability of the crystal. No crystal decay was noticed. A total of 5025 reflections were measured. The unique set contained 4633 reflections. Using the criterion $I > 2.5\sigma(I)$, where $\sigma(I)$ is the estimated standard deviation derived from the counting statistics, 4067 out of 5025 reflections were used. The data were corrected for Lorentz and polarization effects.²⁴ An absorption correction (ψ -scan) was made. The minimum and maximum transmission factors were 0.8168 and 0.8175.

The structure was solved by direct methods. All the atoms were refined anisotropically, except for the hydrogens. The hydrogen atoms were found by a difference Fourier map. To increase the ratio of reflections to parameters, the benzene rings were all refined as rigid groups. One of the solvent molecules (C(47)–C(52)) has an occupancy of 0.5, and the other one (C(41)–C(46)) has an occupancy of 1. The value of 0.5 (confirmed by elemental analysis, see above) was obtained by refining the occupancy and fixing the thermal parameter to a value close to that of the other solvent molecule. There were still some residues around the solvent molecule with an occupancy of 0.5, which could be due to a small disorder. The final cycle of full-matrix least-squares refinement was based on 4067 observed reflections and 416 parameters. Weights based on counting statistics were used. The maximum and minimum peaks on the final Fourier map corresponded to 0.960 and $-0.620\text{ e}/\text{\AA}^3$, respectively. All the calculations were performed using the NRCVAX crystallographic software package.²⁵

Acknowledgment. We thank the Natural Sciences and Engineering Research Council of Canada (NSERC) for support of this research.

Supporting Information Available: Tables and text giving X-ray crystallographic data for $2 \cdot 1.5\text{C}_6\text{H}_6$ (19 pages). This material is contained in many libraries on microfiche, immediately follows this article in the microfilm version of the journal, and can be ordered from the ACS; see any current masthead page for ordering information.

OM950090U

(24) Grant, D. F.; Gabe, E. J. *J. Appl. Crystallogr.* **1978**, *11*, 114.
(25) Gabe, E. J.; Lee, F. L.; Le Page, Y. *J. Appl. Crystallogr.* **1989**, *22*, 384.

Synthesis and Characterization of the σ -Bonded, Quasi-Linear, Metal(II) Diaryls MMes^*_2 ($\text{M} = \text{Mg, Mn, Fe}$; $\text{Mes}^* = 2,4,6\text{-}t\text{-Bu}_3\text{C}_6\text{H}_2\text{-}$)

Rudolf J. Wehmschulte and Philip P. Power*

Department of Chemistry, University of California, Davis, California 95616

Received March 10, 1995*

Disproportionation of a THF solution of Mes^*MgBr ($\text{Mes}^* = 2,4,6\text{-}t\text{-Bu}_3\text{C}_6\text{H}_2\text{-}$) with 1,4-dioxane affords MgMes^*_2 (**1**). The treatment of activated MnCl_2 or FeBr_2 with MgMes^*_2 in ether, and in the presence of 1,4-dioxane, affords the manganese(II) and iron(II) diaryls MnMes^*_2 (**2**) and FeMes^*_2 (**3**) as thermally stable pale yellow or yellow crystals in moderate yield. The X-ray crystal structures of **1–3** feature rare examples of two-coordinate metal(II) diaryls. The Mg–C, Mn–C, and Fe–C distances are 2.116(3), 2.108(2), and 2.058(4) Å, respectively, and the C–M–C angles are in the range 157.9(2)–159.66(10)°. There are also close (*ca.* 2.2–2.3 Å) contacts involving the metal and hydrogens from the ortho-*t*-Bu groups. No reactions were observed between MMes^*_2 and THF, pyridine, or acetonitrile. Crystal data at 130 K with Mo K α ($\lambda = 0.71073$ Å) (**2** and **3**) or Cu K α ($\lambda = 1.54178$ Å) (**1**) radiation: $\text{C}_{36}\text{H}_{58}\text{Mg}$ (**1**), $M_r = 515.13$, $a = 9.823(2)$ Å, $b = 15.571(8)$ Å, $c = 22.501(4)$ Å, $\alpha = 96.88(3)^\circ$, $\beta = 97.85(2)^\circ$, $\gamma = 98.77(3)^\circ$, triclinic, space group $P\bar{1}$, $Z = 4$, $R = 0.059$ for 6304 ($I > 2\sigma(I)$) data; $\text{C}_{36}\text{H}_{58}\text{Mn}$ (**2**), $M_r = 545.76$, $a = 17.705(10)$ Å, $b = 8.576(4)$ Å, $c = 23.252(11)$ Å, $\beta = 108.51(4)^\circ$, monoclinic, space group $C2/c$, $Z = 4$, $R = 0.047$ for 3133 ($I > 2\sigma(I)$) data; $\text{C}_{36}\text{H}_{58}\text{Fe}$ (**3**), $M_r = 546.67$, $a = 17.763(12)$ Å, $b = 8.593(4)$ Å, $c = 23.365(13)$ Å, $\beta = 109.49(4)^\circ$, monoclinic, space group $C2/c$, $Z = 4$, $R = 0.067$ for 2740 ($I > 2\sigma(I)$) data.

Introduction

Well-characterized, two-coordinate, open-shell (i.e. $d^0\text{--}d^9$), transition metal organometallic species are confined to the three manganese dialkyls $\text{Mn}\{\text{CH}_2(t\text{-Bu})\}_2$,¹ $\text{Mn}\{\text{CH}(\text{SiMe}_3)_2\}_2$,² and $\text{Mn}\{\text{C}(\text{SiMe}_3)_3\}_2$.³ The X-ray crystal structure of the latter shows that it is a linear monomer in the solid.³ Electron diffraction studies of $\text{Mn}\{\text{CH}_2(t\text{-Bu})\}_2$ ¹ and $\text{Mn}\{\text{CH}(\text{SiMe}_3)_2\}_2$ ² demonstrate that they are linear and monomeric in the vapor, but there is evidence that indicates that they are associated in the condensed phase.^{2,4} In this paper the synthesis and characterization of the new monomeric, two-coordinate, d^5 and d^6 manganese(II) and iron(II) diaryls, MnMes^*_2 (**2**) and FeMes^*_2 (**3**)⁵ ($\text{Mes}^* = 2,4,6\text{-}t\text{-Bu}_3\text{C}_6\text{H}_2\text{-}$), are reported. They were synthesized by the addition of the novel magnesium diaryl MgMes^*_2 (**1**) with the appropriate metal dihalides. The monomeric diorganomagnesium species **1**, which has a two-coordinate Mg(II) center in the crystal phase, is only predated in the literature by the crystal structure of $\text{Mg}\{\text{C}(\text{SiMe}_3)_3\}_2$.⁶

Experimental Section

General Procedures. All work was performed under anaerobic and anhydrous conditions by using Schlenk techniques or a Vacuum Atmospheres HE-43-2 drybox. Solvents were distilled from sodium/potassium alloy and degassed twice prior to use.

Physical Measurements. ¹H NMR and ¹³C NMR spectra were obtained on a General Electric QE-300 spectrometer using either C₆D₆ or C₇D₈ solvent. Magnetic measurements were performed with a Johnson-Mathey magnetic balance. UV–visible spectra were obtained on a Hitachi U-2000 spectrophotometer.

Starting Materials. Magnesium turnings and FeBr₂ were purchased from commercial suppliers and used as received. Activated MnCl₂⁷ and Mes^{*}Br⁸ were synthesized by literature procedures.

Synthesis of MgMes^*_2 (1**).** Magnesium turnings (0.04 g, 16.4 mmol) were activated by grinding with a mortar and pestle followed by a 1–2 h of stirring under reduced pressure at *ca.* 60 °C. They were then treated with 50–100 μL of BrCH₂CH₂Br in THF (20 mL) at reflux temperature. After 30 min Mes^{*}Br (5.35 g, 16.4 mmol) in THF (100 mL) was added dropwise. Continued refluxing for 3 h resulted in almost complete consumption of the magnesium. The Grignard solution was then treated with 1,4-dioxane (0.73 g, 8.2 mmol) and refluxed for 24 h. The volatile components were removed under reduced pressure, and the resultant colorless solid was then extracted with 2 \times 60 mL of *n*-hexane to give a cloudy solution. Filtration and reduction of the volume to *ca.* 30 mL, followed by storage for several days in a –20 °C freezer, afforded the product MgMes^*_2 as colorless crystals. Yield:

(6) Al-Juaid, S. S.; Eaborn, C.; Hitchcock, P. B.; McGeary, C. A.; Smith, J. D. *J. Chem. Soc., Chem. Commun.* **1989**, 273.

(7) Horvath, B.; Möseler, R.; Horvath, E. G. *Z. Anorg. Allg. Chem.* **1979**, *450*, 165.

(8) Pearson, D. E.; Frazer, M. G.; Frazer, V. S.; Washburn, C. L. *Synthesis* **1976**, 621.

* Abstract published in *Advance ACS Abstracts*, June 1, 1995.

(1) Andersen, R. A.; Haaland, A.; Rypdal, K.; Volden, H. V. *J. Chem. Soc., Chem. Commun.* **1985**, 1807.

(2) Andersen, R. A.; Berg, D. J.; Fernhold, L.; Faegri, K.; Green, J. C.; Haaland, A.; Lappert, M. F.; Leung, W.-P.; Rypdal, K. *Acta Chem. Scand.* **1988**, *42A*, 554.

(3) Buttrus, N. H.; Eaborn, C.; Hitchcock, P. B.; Smith, J. D.; Sullivan, A. C. *J. Chem. Soc., Chem. Commun.* **1985**, 1380.

(4) Andersen, R. A.; Carmona-Guzman, E.; Gibson, J. F.; Wilkinson, G. *J. Chem. Soc., Dalton Trans.* **1976**, 2204.

(5) After this work had been submitted, we became aware that a very recent report also disclosed the synthesis and structure of FeMes^*_2 , which was made by the treatment of $\text{FeBr}_2\cdot\text{THF}_2$ with the Grignard reagent. It is apparent from a comparison of the data for this compound and **3** that they are identical: Müller, H.; Seidel, W.; Görls, H. *Angew. Chem., Int. Ed. Engl.* **1995**, *36*, 325.

Table 1. Selected Crystallographic Data for 1-3^a

	1	2	3
formula	C ₃₆ H ₅₈ Mg	C ₃₆ H ₅₈ Mn	C ₃₆ H ₅₈ Fe
fw	515.13	545.76	546.67
cryst syst	triclinic	monoclinic	monoclinic
a, Å	9.823(2)	17.705(10)	17.763(12)
b, Å	15.571(8)	8.576(4)	8.593(4)
c, Å	22.501(4)	23.252(11)	23.365(13)
α, deg	96.88(3)		
β, deg	97.85(2)	108.51(4)	109.49(4)
γ, deg	98.77(3)		
V, Å ³	3335(2)	3348(3)	3362(3)
space group	P $\bar{1}$	C2/c	C2/c
Z	4	4	4
d _{calc} , g cm ⁻³	1.026	1.083	1.080
μ, mm ⁻¹	0.586	0.415	0.469
2θ range, deg	0-114	0-55	0-55
no. of obsd rflns	6304 (I > 2σ(I))	3133 (I > 2σ(I))	2740 (I > 2σ(I))
no. of variables	761	227	208
R, R _w ^b	0.059/0.145	0.047/0.111	0.067/0.164

^a Data were collected at 130 K with Mo Kα (λ = 0.710 73 Å) (2 and 3) or Cu Kα (λ = 1.541 78 Å) (1) radiation. ^b Based on F_o² and F₂² values.

1.85 g, 44%. Mp: softens at 200 °C, turns red at 250 °C. ¹H NMR (C₆D₆): 7.57 (s, m-H, 4H), 1.48 (s, o-CH₃, 36H), 1.43 (s, p-CH₃, 18H). ¹³C{¹H} NMR (C₆D₆): 159.3 (o-C), 148.2 (p-C), 146.3 (i-C), 119.6 (m-C), 38.2 (o-C(CH₃)₃), 34.9 (p-C(CH₃)₃), 34.0 (o-CH₃), 31.9 (p-CH₃).

MnMes*₂ (2). A slurry of 0.31 g (2.5 mmol) of activated MnCl₂⁷ in 30 mL of THF and 0.5 mL (5.9 mmol) of 1,4-dioxane was treated dropwise with a solution of 1.29 g (2.5 mmol) of MgMes*₂ in Et₂O (30 mL) at -20 °C. After 1 h at -20 °C, and slow warming to room temperature, the resultant clear pale yellow solution was stirred for another 22 h during which time the solution became cloudy. The volatile components were removed, and the resulting solid was extracted with 100 mL of n-hexane. Concentration of the hexane solution to 10-15 mL followed by cooling in a -20 °C freezer leads to the isolation of 0.25 g of MnMes*₂ in the form of large (2-5 mm) pale yellow air-sensitive crystals. Yield: 18%. Mp: 205-210 °C (melts and turns black). μ_{eff} = 5.90(0.1) μ_B. UV/vis (benzene): no absorption 400-1100 nm. ¹H NMR (ca. 15 mg in 0.3 mL of C₆D₆): 8.3 (s, broad, Δν_{1/2} = 270 Hz). An additional broad, weak signal at 48 ppm with ν_{1/2} ~ 2000 Hz could not be well resolved due to phasing problems.

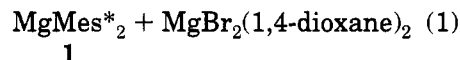
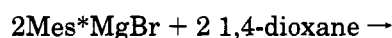
FeMes*₂ (3). A 0.65 g (3.0 mmol) amount of FeBr₂ was added via solid addition funnel to a solution of MgMes*₂ (1.58 g, 3.07 mmol) in Et₂O (80 mL) at 0 °C. The mixture was slowly warmed to room temperature and stirred for 16 h. To the pale yellow solution, which still contained unreacted FeBr₂ (brownish solid), was added 1,4-dioxane (0.34 mL, 4.0 mmol, 0.35 g), and the resulting yellow green mixture was heated to reflux for 3 h. Filtration of the bright yellow solution, concentration under reduced pressure to ca. 5 mL, and crystallization in a -20 °C freezer for 1 week leads to the formation of yellow, extremely air-sensitive, X-ray-quality crystals. Yield: 0.72 g (43.9%). Mp: darkens at 185 °C, melts with decomposition at 193-195 °C (turns black). μ_{eff} = 5.18(0.1) μ_B. UV/vis: intense absorption (log ε > 10⁴) between 400 and 200 nm with a shoulder at 460 nm. ¹H NMR (C₆D₆, 22 °C, 40 mg in ca. 0.4 mL, 300 MHz): 121.0 (s, br, Δν_{1/2} = 680 Hz, m-H, 4H), 61.0 (s, br, Δν_{1/2} = 2600 Hz, o-CH₃, 36H), 26.2 (s, Δν_{1/2} = 270 Hz, p-CH₃, 18H).

X-ray Crystallographic Studies. The X-ray data were collected on a Siemens R3m/V (2, 3) or a Syntex P2₁ (1) diffractometer equipped with a locally modified Enraf-Nonius LT device. The data were collected by using graphite-monochromated Mo Kα (λ = 0.710 73 Å) (2 and 3) or Cu Kα (λ = 1.541 78 Å) (1) radiation. Calculations were those of SHELXTL-94 installed on an IBM 386 PC. Scattering factors were

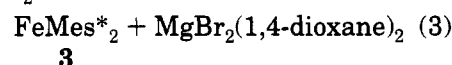
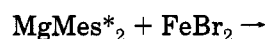
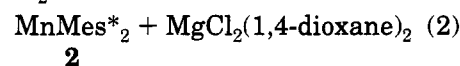
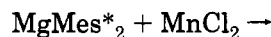
obtained from ref 9. An absorption correction was applied by using the method described in ref 10. All structures were solved by direct methods and Fourier difference maps. They were refined by full-matrix least-squares procedures. All non-hydrogen atoms were refined anisotropically at calculated positions using a riding model with the parameters given in SHELXTL-94. The structures showed disorder either in a para-*t*-Bu group (1 and 3) or in *ortho* and para-*t*-Bu groups (2). These were refined successfully with split occupancies. Some details of the crystallographic data are given in Table 1, coordinates for important atoms are given in Table 2, and selected bond distances and angles are provided in Table 3.

Results and Discussion

Syntheses. The compound MgMes*₂ was synthesized by the addition of 1,4-dioxane to the Grignard reagent Mes**Mg*Br (eq 1). The isolation of 1 as an



uncomplexed species from THF solution is remarkable since diorganomagnesium compounds normally complex strongly with two donor molecules to give a distorted tetrahedral coordination at the magnesium.¹¹ The compound 1 smoothly converts MnCl₂ or FeBr₂ to MnMes*₂ (2) or FeMes*₂ (3) by stirring in ether at room temperature in the presence of 2 equiv of 1,4-dioxane (eqs 2 or 3). The use of 1,4-dioxane helps to drive the



reaction to completion by precipitating the magnesium halide as a 1,4-dioxane complex. Similar experiments involving the treatment of MgMes*₂ with VBr₂, CrCl₂, or CoCl₂ have not yet afforded stable diaryl derivatives of V, Cr, or Co.

Structures. The structures of 1 (Figure 1), 2 (Figure 2), and 3 (Table of Contents illustration) are very similar, and in fact, the crystals of 2 and 3 are isomorphous. The close relationship between the three structures is evident from the data in Table 3. The basic structural motif consists of a two-coordinate metal bound to two Mes* groups (with a crystallographically required 2-fold axis, which bisects the C-M-C angle, in the case of 2 and 3). There are further secondary interactions between the metals and *ortho-t*-Bu hydrogens as listed in Table 3. The M-C bond lengths vary only slightly, and the Mg-C and Mn-C distances are within three standard deviations of each other. The Fe-C distance is slightly shorter, having a value of 2.058(4) Å, which is in keeping with the smaller size of the Fe²⁺ ion. Each compound has a bent geometry with C-M-C angles in the narrow range 157.9(2)-

(9) *International Tables for X-Ray Crystallography*; D. Reidel Publishing Co.: Dordrecht, The Netherlands, 1993; Vol. C.

(10) Parkin, S. R.; Moezzi, B.; Hope, H. *J. Appl. Crystallogr.* **1995**, *28*, 53.

(11) Markie, P. R.; Akkerman, O. S.; Bickelhaupt, F.; Smeets, W. J. J.; Spek, A. L. *Adv. Organomet. Chem.* **1991**, *37*, 47.

Table 2. Atomic Coordinates ($\times 10^4$) for 1,^a 2, and 3

	x	y	z		x	y	z
Compound 1							
Mg(1)	3846(1)	1299(1)	7522(1)	C(21)	1533(3)	983(2)	9047(1)
C(1)	4405(3)	577(2)	6759(1)	C(21)	1533(3)	983(2)	9047(1)
C(2)	3428(3)	-83(2)	6367(1)	C(22)	828(3)	1690(2)	9096(1)
C(3)	3857(3)	-722(2)	5983(1)	C(23)	1176(3)	2339(2)	8747(1)
C(4)	5252(3)	-751(2)	5952(1)	C(24)	2147(3)	2283(2)	8351(1)
C(5)	6212(3)	-87(2)	6316(1)	C(25)	3220(3)	84(2)	8673(1)
C(6)	5818(3)	566(2)	6709(1)	C(26)	4297(4)	43(2)	8255(2)
C(7)	1830(3)	-133(2)	6322(1)	C(27)	2112(3)	-747(2)	8484(2)
C(8)	1173(3)	-1013(2)	6492(1)	C(28)	3968(3)	82(2)	9318(1)
C(9)	1410(3)	599(2)	6733(2)	C(29)	-242(3)	1760(2)	9530(1)
C(10)	1205(3)	-60(2)	5671(1)	C(30)	-1334(5)	942(3)	9406(2)
C(11)	5672(3)	-1462(2)	5514(1)	C(31)	-1005(5)	2552(3)	9451(2)
C(12)	5042(4)	-2369(2)	5634(2)	C(32)	527(5)	1895(3)	10182(2)
C(13)	5139(4)	-1350(2)	4863(1)	C(30A)	-523(12)	900(7)	9847(5)
C(14)	7252(3)	-1411(2)	5585(2)	C(32A)	257(12)	2499(7)	10013(5)
C(16)	7755(3)	1743(2)	6588(1)	C(32A)	257(12)	2499(7)	10013(5)
C(16)	7755(3)	1743(2)	6588(1)	C(33)	2431(3)	3083(2)	8015(1)
C(17)	8075(3)	872(2)	7456(1)	C(34)	1092(3)	3187(2)	7609(1)
C(18)	6548(3)	1990(2)	7467(2)	C(35)	3545(3)	3017(2)	7610(2)
C(19)	2834(3)	1550(2)	8282(1)	C(36)	2690(3)	3912(2)	8483(1)
C(20)	2515(3)	907(2)	8660(1)				
Compound 2							
Mn(1)	5000	2512(1)	2500	C(13)	9014(2)	1170(6)	4422(2)
C(1)	6011(1)	2078(2)	3257(1)	C(14)	8354(3)	-1377(5)	4382(2)
C(2)	6751(1)	2804(2)	3314(1)	C(12A)	8674(3)	1456(6)	4956(2)
C(3)	7464(1)	2211(2)	3708(1)	C(13A)	8829(3)	-186(7)	4103(2)
C(4)	7491(1)	912(2)	4066(1)	C(14A)	8198(3)	-1284(6)	4816(2)
C(5)	6765(1)	240(2)	4038(1)	C(15)	5284(1)	-32(2)	3695(1)
C(6)	6039(1)	799(2)	3654(1)	C(16)	4512(2)	673(4)	3295(2)
C(7)	6840(1)	4307(2)	2977(1)	C(17)	5286(2)	90(5)	4349(1)
C(8)	7367(1)	4015(3)	2578(1)	C(18)	5314(2)	-1741(3)	3527(1)
C(9)	7209(1)	5582(3)	3449(1)	C(16A)	4680(2)	1124(3)	3797(3)
C(10)	6051(1)	4974(3)	2569(1)	C(17A)	5372(4)	-1256(3)	4217(1)
C(11)	8283(1)	282(2)	4492(1)	C(18A)	4902(3)	-1047(3)	3106(1)
C(12)	8286(3)	570(6)	5157(2)				
Compound 3							
Fe(1)	5000	2528(1)	2500	C(11)	8270(2)	265(5)	4505(2)
C(1)	5986(2)	2068(4)	3248(2)	C(12)	8288(6)	583(13)	5158(4)
C(2)	6731(2)	2781(4)	3310(2)	C(13)	9008(5)	1153(12)	4436(5)
C(3)	7449(2)	2187(4)	3710(2)	C(14)	8354(5)	-1384(11)	4390(4)
C(4)	7472(2)	898(4)	4074(2)	C(12A)	8661(6)	1443(12)	4966(56)
C(5)	6749(2)	235(4)	4039(2)	C(13A)	8798(6)	-207(14)	4132(4)
C(6)	6015(2)	792(4)	3645(2)	C(14A)	8173(6)	-1278(11)	4837(5)
C(7)	6818(2)	4269(4)	2967(2)	C(15)	5261(2)	-51(4)	3679(2)
C(8)	7323(2)	3933(5)	2560(2)	C(16)	4486(3)	667(7)	3728(2)
C(9)	7217(2)	5555(5)	3430(2)	C(17)	5249(3)	43(7)	4326(2)
C(10)	6021(2)	4945(5)	2567(2)	C(18)	5287(3)	-1758(6)	3504(2)

^a Data for only one molecule in the asymmetric unit are given.

Table 3. Selected Bond Distances (Å) and Angles (deg) for 1-3

	MgMes* ₂ (1)	MnMes* ₂ (2)	FeMes* ₂ (3)
M-C	2.120(3) (C(1)) 2.118(3) (C(19)) 2.118(3) (C(37)) 2.109(3) (C(55))	2.108(2)	2.058(4)
C-M-C	158.35(10) 158.03(10)	159.66(10)	157.9(2)
H...M	2.28 (H18A) 2.28 (H70B)	2.27 (H10B) 2.29 (H16C)	2.18 (H10B) 2.23 (H16C)
C...M	2.72 (C35) 2.71 (C53)	2.78 (C16)	2.73 (C10)
torsion angle C ₂ M-Ar	46.7 (C1-C6) 43.8 (C19-C24) 45.0 (C37-C42) 48.0 (C55-C60)	45.8	46.4
torsion angle Ar-Ar	73.3 75.0	74.5	75.5
angle between M-C and vector C(ipso)-C(para)	15.9 (C1-C4) 14.7 (C19-C22) 15.4 (C37-C40) 16.1 (C55-C58)	15.6	15.1

159.66(10)°. The angles between the perpendiculars to the aromatic ring planes when viewed along an M-C

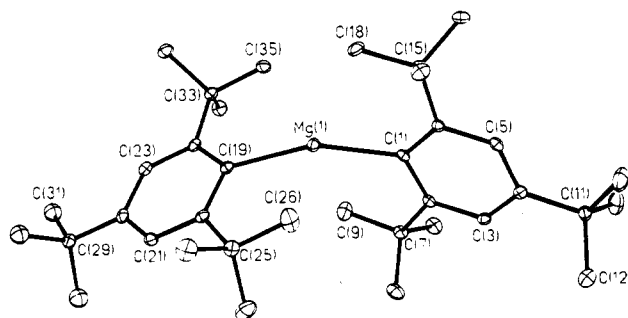


Figure 1. Thermal ellipsoidal plot of one of the molecules in the asymmetric unit of 1. Hydrogen atoms are not shown for clarity. Important bond distances and angles are given in Table 3.

bond vary from 73.3 to 75.5°. Some steric strain is also suggested by the fact that all the ring planes (exemplified by the C(ipso)-C(para) vector) are bent by ca. 15° from the line of the M-C(ipso) bond.

Discussion. The compounds 1-3 represent very rare examples of structurally authenticated two-coor-

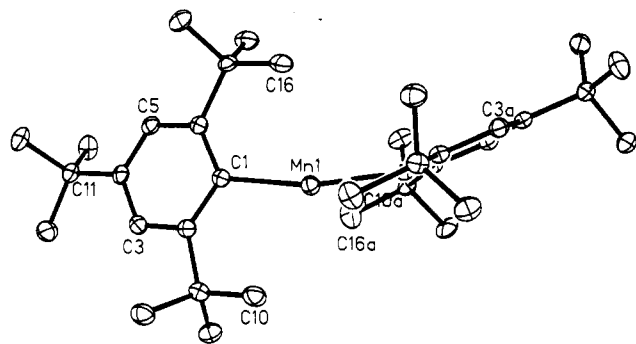


Figure 2. Thermal ellipsoidal plot of one of **2**. Hydrogen atoms are not shown for clarity. Important bond distances and angles are given in Table 3.

dinate Mg, Mn, or Fe centers in the solid state.¹² The low coordination is a consequence of the large steric requirements of the Mes* group. In the case of magnesium, the only¹³ crystal structures of two-coordinate species are Mg{C(SiMe₃)₃}₂⁶ (**4**) and Mg{N(SiMePh₂)₂}₂¹⁴ (**5**). The compound **4** has a linear geometry and an Mg–C distance of 2.166(2) Å which is slightly longer than that observed in **1**. Interestingly, the amido complex **5** has an interligand angle of 162.8(3)° which is close to that measured for **1**. MgMes*₂ does not form stable complexes with THF or Et₂O, and this behavior may be contrasted with the bis(tetrahydrofuran) complexes formed by Mg(2,4,6-R₃C₆H₂)₂ (R = Me or *i*-Pr).¹⁵

The structure of the manganese species **2** is preceded by those of the alkyl derivatives mentioned in the Introduction. Only the two-coordinate derivative Mn{C(SiMe₃)₃}₂ (linear geometry) has been structurally characterized in the solid state,³ however, and the Mn–C distance 2.101(4) Å is practically identical to the 2.109(2) Å found for **2**. The steric effect of the large size of the Mes* ligand in MnMes*₂ may be contrasted with that of the Mes ligand, which results in the isolation of the trimer MesMn(μ-Mes)₂Mn(μ-Mes)₂MnMes.¹⁶ Two-coordination at iron has precedent only in the solid state structures of the related amides and thiolates Fe{N(SiMePh₂)₂}₂,^{17,18} Fe{N(SiMe₂Ph)₂}₂,¹⁸ Fe(N-MesBMes₂)₂,¹⁹ Fe{N(SiMe₃)₂}SR,²⁰ and Fe(SR)₂²⁰ (R = 2,6-Mes₂C₆H₃–) and in the vapor-phase structure of Fe{N(SiMe₃)₂}₂.²¹ These molecules feature interligand angles at iron that vary from *ca.* 120° in the thiolate derivatives to 180° in Fe{N(SiMe₃)₂}₂. The Fe–C distance in **1**, 2.058(4) Å, is significantly longer than the Fe–N distances in Fe{N(SiMe₂Ph)₂}₂¹⁷ (1.903(7) Å)

or Fe{N(SiMePh₂)₂}₂^{17,18} (1.917(2) Å). The difference in metal–ligand bond lengths (*ca.* 0.14–0.15 Å), which is much greater than the difference between the radii of carbon (0.77 Å) and nitrogen (0.73 Å), can be attributed in part to the greater ionic character of the Fe–N bond.

The quasi-linear structures observed for **2** and **3** suggest high spin d⁵- or d⁶-electron configurations. This is confirmed by magnetic moments of 5.90(0.1) and 5.18(0.1) μ_B at 25 °C, which are consistent with the presence of five and four unpaired electrons, respectively. The ¹H NMR spectrum of **2** displays a broad singlet at 8.3 ppm and a further, much broader, signal at 48 ppm. The ¹H NMR spectrum of **3**, however, displays three assignable paramagnetically shifted peaks at δ = 121.0 (*m*-H), 61.0 (*o*-C(CH₃)₃), and 26.2 (*p*-C(CH₃)₃) in C₆D₆ at 25 °C. The UV–vis spectrum of **3** in hexane displayed a rise in absorption toward higher energy with a shoulder observed at 460 nm, whereas the corresponding spectrum of **2** was essentially featureless between 400 and 1100 nm.

Unlike M{N(SiMe₃)₂}₂ (M = Mn or Fe), which are dimers in the solid^{22,23} and form complexes with THF²² or pyridine,²⁴ neither MnMes*₂ nor FeMes*₂ forms complexes with THF, pyridine, or acetonitrile. It therefore appears that the MMes*₂ molecules are quite sterically encumbered and much more hindered than the less crowded dimeric, diaryl analogues such as (MnMes₂)₃,¹⁶ (FeMes₂)₂,²⁵ and (FeTrip)₂.²⁶ (Mes = 2,4,6-Me₃C₆H₂ and Trip = 2,4,6-*i*-Pr₃C₆H₂). The similar bending in **1**–**3** is probably due to weak interactions between ortho C–H groups and the metal orbitals. This may be contrasted with the almost linear structure observed (C–Hg–C 173.4(2)°, Hg–C = 2.080(6) Å) for HgMes*₂.²⁷ The compounds **1**–**3** are stable for several weeks when stored in a nitrogen atmosphere. The chromium(II) (d⁴) and a cobalt(II) (d⁷) analogues of **2** and **3** are significantly less stable and apparently decompose under ambient conditions.²⁸ The properties of these and reactivity studies of **1**–**3** will be described in a future publication.

Acknowledgment. We thank the National Science Foundation and the donors of the Petroleum Research Fund, administered by the American Chemical Society, for financial support.

Supporting Information Available: Tables of data collection parameters, complete atom coordinates and *U* values, bond distances and angles, and anisotropic thermal parameters, and ORTEP diagrams (34 pages). Ordering information is given on any current masthead page.

OM950268C

(12) Power, P. P. *Comments Inorg. Chem.* **1989**, *8*, 177; *Chemtracts: Inorg. Chem.*, in press.

(13) It could be argued that the species [Mg{CH(SiMe₃)₂}{CH(SiMe₃)–SiMe₂–μ-Me}]_n has a two-coordinate Mg center. It has, however, been described as associated with intermolecular agostic interactions. Moreover, the C–Mg–C angle is 140.0(2)°: Hitchcock, P. B.; Howard, J. A. K.; Lappert, M. F.; Leung, W. P.; Mason, S. A. *J. Chem. Soc., Chem. Commun.* **1990**, 847.

(14) Bartlett, R. A.; Olmstead, M. M.; Power, P. P. *Inorg. Chem.* **1994**, *33*, 4800.

(15) Waggoner, K.; Power, P. P. *Organometallics* **1992**, *11*, 3209.

(16) Gambarotta, S.; Floriani, C.; Chiesi-Villa, A.; Guastini, C. *J. Chem. Soc., Chem. Commun.* **1983**, 1128.

(17) Bartlett, R. A.; Power, P. P. *J. Am. Chem. Soc.* **1987**, *109*, 7563.

(18) Chen, H.; Bartlett, R. A.; Dias, H. V. R.; Olmstead, M. M.; Power, P. P. *J. Am. Chem. Soc.* **1989**, *111*, 4338.

(19) Chen, H.; Bartlett, R. A.; Olmstead, M. M.; Power, P. P. *J. Am. Chem. Soc.* **1990**, *112*, 1048.

(20) Ellison, J. J.; Ruhlandt-Senge, K.; Power, P. P. *Angew. Chem., Int. Ed. Engl.* **1994**, *33*, 1178.

(21) Andersen, R. A.; Faegri, K.; Green, J. C.; Haaland, A.; Lappert, M. F.; Leung, W.-P.; Rypdal, K. *Inorg. Chem.* **1988**, *27*, 1782.

(22) (a) Bradley, D. C.; Hursthouse, M. B.; Malik, K. M. A.; Mösele, R. *Transition Met. Chem. (Weinheim, Ger.)* **1978**, *3*, 253. (b) Murray, B. D.; Power, P. P. *Inorg. Chem.* **1984**, *23*, 4584.

(23) Olmstead, M. M.; Power, P. P.; Shoner, S. C. *Inorg. Chem.* **1991**, *30*, 2547.

(24) Olmstead, M. M.; Power, P. P.; Shoner, S. C. Unpublished results.

(25) (a) Machelett, B. *Z. Chem.* **1976**, *16*, 116. (b) Müller, H.; Seidel, W.; Görls, H. *J. Organomet. Chem.* **1993**, *445*, 133.

(26) Klose, A.; Solari, E.; Floriani, C.; Chiesi-Villa, A.; Rizzoli, C.; Re, N. *J. Am. Chem. Soc.* **1994**, *116*, 9123.

(27) Huffman, J. C.; Nugent, W. A.; Kochi, J. K. *Inorg. Chem.* **1980**, *19*, 2749.

(28) Wehmschulte, R. J.; Power, P. P. Unpublished results.

Matrix Photochemistry of $\text{Ru}(\text{CO})_2(\text{PMe}_3)_2\text{H}_2$ and $\text{Ru}(\text{CO})_3(\text{PMe}_3)_2$: Formation of $\text{Ru}(\text{CO})_2(\text{PMe}_3)_2 \cdot \cdot \text{S}$ ($\text{S} = \text{Ar}, \text{CH}_4, \text{Xe}$)

Roger J. Mawby, Robin N. Perutz,* and Michael K. Whittlesey

Department of Chemistry, University of York, Heslington, York YO1 5DD, U.K.

Received March 2, 1995[⊗]

The photochemical reactions of $\text{Ru}(\text{CO})_2(\text{PMe}_3)_2\text{H}_2$ (**I**) and $\text{Ru}(\text{CO})_3(\text{PMe}_3)_2$ (**II**) have been studied in low-temperature Ar, CH_4 , and Xe matrices by IR and UV–visible spectroscopy. UV photolysis ($\lambda > 200$ nm) of **I** and **II** results in the formation of $\text{Ru}(\text{CO})_2(\text{PMe}_3)_2 \cdot \cdot \text{S}$ ($\text{S} =$ matrix host), which shows a distinctive UV–visible absorption band with λ_{max} dependent on S (Ar, 423 nm; CH_4 , 385 nm; Xe, 352 nm). The reactions are partially reversed by irradiation with $\lambda > 360$ nm. ^{13}C isotopic labeling studies and trapping experiments in H_2 -doped and N_2 -doped Ar and CO matrices prove that the intermediate is a dicarbonyl species. In the structure proposed for $\text{Ru}(\text{CO})_2(\text{PMe}_3)_2 \cdot \cdot \text{S}$, the C–Ru–C bond angle must exceed 130° .

Introduction

The photodissociation of dihydrogen from transition metal dihydride complexes represents a facile and well-documented route to highly reactive, coordinatively unsaturated species. This methodology has been used with particular success in generating the $\text{M}(\eta^5\text{-C}_5\text{R}_5)\text{L}$ fragments from $\text{M}(\eta^5\text{-C}_5\text{R}_5)\text{LH}_2$ complexes ($\text{R} = \text{H}, \text{CH}_3$; $\text{M} = \text{Rh}, \text{Ir}$; $\text{L} = \text{PMe}_3$). These intermediates are well-known for their ability to react with hydrocarbon C–H bonds.¹

Our recent matrix isolation and laser flash photolysis work has demonstrated that 16-electron $\text{M}(\text{dmpe})_2$ ($\text{M} = \text{Fe}, \text{Ru}$; $\text{dmpe} = \text{Me}_2\text{PCH}_2\text{CH}_2\text{PMe}_2$) fragments can be produced similarly by photolysis of the dihydride precursors $\text{M}(\text{dmpe})_2\text{H}_2$.² The iron and ruthenium fragments exhibit a remarkable difference in reactivity: $\text{Fe}(\text{dmpe})_2$ reacts with C–H bonds in alkanes (including methane in a matrix at 12 K) while $\text{Ru}(\text{dmpe})_2$ does not. Kinetic experiments with laser flash photolysis have shown that $\text{Ru}(\text{dmpe})_2$ reacts over 10^4 times more rapidly with H_2 than does $\text{Fe}(\text{dmpe})_2$. The stereochemistry and electronic ground state of these intermediates appear to be decisive in determining the reactivity toward C–H and H–H bonds. The insensitivity of the vibrational modes of the dmpe ligands to structure and oxidation state has prevented us from determining the exact geometries of $\text{Fe}(\text{dmpe})_2$ and $\text{Ru}(\text{dmpe})_2$ by IR spectroscopy in matrices. Nevertheless, there is now considerable evidence that $\text{Ru}(\text{dmpe})_2$ is square planar.

Our continuing interest in metal dihydride complexes of Fe, Ru, and Os has led us to examine the matrix photochemistry of the related ruthenium complex

$\text{Ru}(\text{CO})_2(\text{PMe}_3)_2\text{H}_2$, which has two mutually *cis* hydride ligands. Photo-induced loss of H_2 in a matrix would generate the 16-electron species, $\text{Ru}(\text{CO})_2(\text{PMe}_3)_2$, and thus offer an intermediate directly comparable with $\text{Ru}(\text{dmpe})_2$. The presence of carbonyl “reporter” ligands would, more importantly, assist in the determination of the geometry of the molecule by IR spectroscopy.

In this paper, we report on the matrix photochemistry of $\text{Ru}(\text{CO})_2(\text{PMe}_3)_2\text{H}_2$ in inert and reactive low-temperature matrices. We also describe the matrix photochemistry of the tricarbonyl complex $\text{Ru}(\text{CO})_3(\text{PMe}_3)_2$, which proved to be a more selective precursor to $\text{Ru}(\text{CO})_2(\text{PMe}_3)_2$.

Results

1. Preparation, Characterization, and Reactivity of $\text{Ru}(\text{CO})_2(\text{PMe}_3)_2\text{H}_2$ (I**).** Treatment of an ethanol suspension of $\text{Ru}(\text{CO})_2(\text{PMe}_3)_2\text{Cl}_2$ with excess NaBH_4 resulted in the formation of a yellow-orange oil. Sublimation onto a liquid nitrogen cooled finger at room temperature yielded a white, volatile, mildly air-sensitive solid. The compound slowly turned yellow even when stored at low temperature under argon, although the process was reduced by cold storage under hydrogen. NMR, IR, and mass spectral data (Table 1 and Experimental Section) were consistent with formulation of the solid as $\text{Ru}(\text{CO})_2(\text{PMe}_3)_2\text{H}_2$ (**I**). The ^1H NMR spectrum of the compound in C_6D_6 shows a “virtual” triplet for the PMe_3 protons and a triplet resonance at $\delta -7.32$ for the hydride ligands coupled to two equivalent phosphorus nuclei. In the $^{13}\text{C}\{^1\text{H}\}$ NMR spectrum, the magnitude of $^2J(\text{P}-\text{C})$ for the carbonyl ligands shows that they are *cis* to the PMe_3 groups. The IR spectrum shows that the carbonyl groups are *cis* to one another, so that the structure of **I** must be as shown below.

$\text{Ru}(\text{CO})_2(\text{PMe}_3)_2\text{H}_2$ reacted with CO (1 atm) in benzene at room temperature over weeks to give $\text{Ru}(\text{CO})_3(\text{PMe}_3)_2$ (**II**) in quantitative yield. Photolysis of **I** in alkane or arene solution at room temperature under argon also resulted in the formation of **II**. The tricar-

[⊗] Abstract published in *Advance ACS Abstracts*, June 1, 1995.

(1) (a) Buchanan, J. M.; Stryker, J. M.; Bergman, R. G. *J. Am. Chem. Soc.* **1986**, *108*, 1537. (b) Periana, R. A.; Bergman, R. G. *J. Am. Chem. Soc.* **1986**, *108*, 7332. (c) Jones, W. D.; Feher, F. J. *J. Am. Chem. Soc.* **1984**, *106*, 1650. (d) Jones, W. D.; Feher, F. J. *J. Am. Chem. Soc.* **1986**, *108*, 4814. (e) Partridge, M. G.; McCamley, A.; Perutz, R. N. *J. Chem. Soc., Dalton Trans.* **1994**, 3519.

(2) (a) Whittlesey, M. K.; Mawby, R. J.; Osman, R.; Perutz, R. N.; Field, L. D.; Wilkinson, M. P.; George, M. W. *J. Am. Chem. Soc.* **1993**, *115*, 8627. (b) Hall, C.; Jones, W. D.; Mawby, R. J.; Osman, R.; Perutz, R. N.; Whittlesey, M. K. *J. Am. Chem. Soc.* **1992**, *114*, 7425.

Table 1. NMR Data for $Ru(CO)_2(PMe_3)_2H_2$ (I) and $Ru(CO)_3(PMe_3)_2$ (II)^a

	I	II
¹ H	δ -7.32 (t, [² J(P-H)] = 26.4 Hz, 2H), Ru-H δ 1.21 (t, [² J(P-H) + ⁴ J(P-H)] = 7.2 Hz, 18H), PMe ₃	δ 1.45 (t, [² J(P-H) + ⁴ J(P-H)] = 7.7 Hz), PMe ₃
³¹ P{ ¹ H}	δ -2.6 (s)	δ 0.9 (s)
¹³ C{ ¹ H}	δ 24.9 (t, [¹ J(P-C) + ³ J(P-C)] = 32.6 Hz), PMe ₃ δ 202.7 (t, [² J(P-C)] = 10.0 Hz), CO	δ 24.7 (t, [¹ J(P-C) + ³ J(P-C)] = 33.0 Hz), PMe ₃ δ 211.0 (t, [² J(P-C)] = 17.1 Hz), CO

^a All data are for benzene-*d*₆ solutions at 298 K.



bonyl complex, **II**, was first reported by Jones et al.³ as the product of reaction of the complex $Ru_2(\mu-CH_2)_3-(PMe_3)_6$ with CO. It was shown to have a trigonal bipyramidal structure with axial phosphines. We found that **II** reacted slowly with H_2 (1 atm) in solution over weeks to re-form **I**.

2. Photochemistry of $Ru(CO)_2(PMe_3)_2H_2$ (I) and $Ru(CO)_3(PMe_3)_2$ (II) in Low-Temperature Argon Matrices. The IR spectrum of **I** in an argon matrix at 12 K exhibited major bands at 2014 and 1968 cm^{-1} corresponding to the a_1 and b_1 carbonyl stretching modes. A bond angle of 110° between the carbonyl groups may be deduced from the relative intensities of these two bands.⁴ The Ru-H stretching mode appeared as a much weaker band at 1826 cm^{-1} (Figure 1a). The assignment of bands in the lower frequency region of the IR spectrum (Table 2) is based upon a comparison with the IR spectrum of free trimethylphosphine.⁵ The UV-visible absorption spectrum of the white compound **I** in the same matrix was broad and featureless.

Broad band UV photolysis of the matrix (30 min) resulted in a 50% loss of the carbonyl bands of **I** and a depletion of the Ru-H stretching band. A new band with several components was observed centered at 1849 cm^{-1} . In addition, other much weaker bands appeared at 2023, 1941, 1918, and 1900 cm^{-1} (Figure 1b). A band for free CO at 2138 cm^{-1} was also observed. No distinct new bands were observed in the low-frequency region of the IR spectrum. The UV-visible spectrum showed the appearance of a strong new band in the visible region at 423 nm and a much weaker feature at ca. 610 nm.

The IR data suggest that loss of both H_2 and CO takes place, making the unambiguous assignment of product bands difficult. Use of $Ru(CO)_3(PMe_3)_2$ (**II**) as an alternative precursor was explored since it should exhibit a single photochemical pathway, loss of CO.

The IR spectrum of **II** in an argon matrix at 12 K contained a split carbonyl band centered at ca. 1900 cm^{-1} (Table 2). This splitting must result from multiple conformations and trapping sites in the matrix. The UV-visible spectrum of **II** in the same matrix showed weak bands at 300, 280, and 250 nm. UV irradiation ($\lambda > 200$ nm, 90 min) caused depletion of the carbonyl

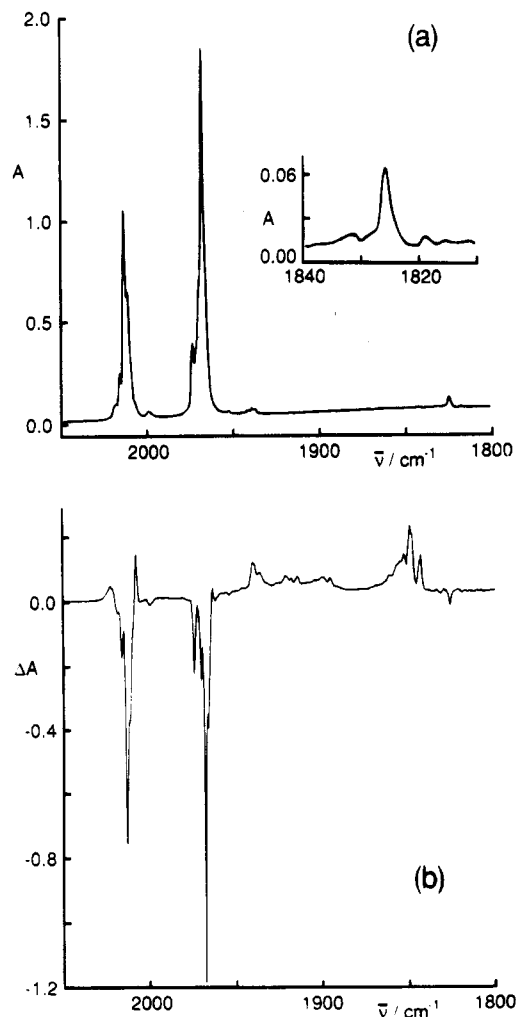


Figure 1. IR spectrum of $Ru(CO)_2(PMe_3)_2H_2$ (**I**) isolated in an argon matrix at 12 K (a) before photolysis showing the carbonyl region and (inset) the Ru-H stretching mode and (b) after 30 min of photolysis with $\lambda > 200$ nm presented as a difference spectrum relative to the deposition spectrum.

band and formation of a weaker split band at 1849 cm^{-1} , along with a band for free CO at 2138 cm^{-1} . As in the case of **I**, the UV-visible spectrum showed the formation of a new band in the visible at 423 nm along with a very much weaker and broader absorption at ca. 610 nm.

Subsequent longer wavelength irradiation ($\lambda = 360$ –378 nm, 205 min), designed to select the blue side of the 423 nm band, resulted in a slight bleach of this band but had no effect on the low energy absorption at 610 nm. The IR spectrum showed a small decrease in the band at 1849 cm^{-1} and an equally small growth in the band of **II** at ca. 1900 cm^{-1} . A similar experiment was performed in which the initial UV photolysis was followed by selective visible irradiation on the red side ($\lambda = 475$ –508 nm, 720 min). This method resulted in a

(3) Jones, R. A.; Wilkinson, G.; Galas, A. M. R.; Hursthouse, M. B.; Abdul Malik, K. M. *J. Chem. Soc., Dalton Trans.* **1980**, 1771.

(4) Braterman, P. S. *Metal Carbonyl Spectra*; Academic Press: London, 1975. The calculation of the bond angle assumes that there is no change in the relative intensity of the $\nu(CO)$ modes as a result of mixing with the $\nu(RuH)$ modes.

(5) Park, P. J. D.; Hendra, P. J. *Spectrochim. Acta* **1968**, 24A, 2081.

Table 2. IR Bands (ν/cm^{-1}) for I and II in Argon Matrices at 12 K

I	assgnt	II	assgnt
2982 m	$\nu(\text{CH})$	2976 m	$\nu(\text{CH})$
2913 m	$\nu(\text{CH})$	2911 m	$\nu(\text{CH})$
2014 vs	$\nu(^{12}\text{CO})_2 \text{ sym}$	1903, 1898 vs	$\nu(^{12}\text{CO})_3 \text{ asym}$
2000 w	$\nu(^{13}\text{CO})(^{12}\text{CO})$	1429 m	$\delta(\text{CH}_3)_{\text{asym}}$
1968 vs	$\nu(^{12}\text{CO})_2 \text{ asym}$	1288 s	$\delta(\text{CH}_3)_{\text{sym}}$
1940 w	$\nu(^{13}\text{CO})(^{12}\text{CO})$	947 vs	$\rho(\text{CH}_3)$
1826 w	$\nu(\text{RuH}_2)$	855 w	
1435 w	$\delta(\text{CH}_3)_{\text{asym}}$	741, 734 vw	$\nu(\text{PC})_{\text{asym}}$
1426, 1422 w	$\delta(\text{CH}_3)_{\text{asym}}$	677 m	$\nu(\text{PC})_{\text{sym}}$
1285 m	$\delta(\text{CH}_3)_{\text{sym}}$	584 m	
946 s	$\rho(\text{CH}_3)$		
857, 854 m			
783 w	$\delta(\text{RuH}_2)$		
754 vw	$\delta(\text{RuH}_2)$		
734, 730 vw	$\nu(\text{PC})_{\text{asym}}$		
678 m	$\nu(\text{PC})_{\text{sym}}$		
552 vw			

much larger depletion of the band at 1849 cm^{-1} and growth of the band at $1890\text{--}1910 \text{ cm}^{-1}$, along with a bleach of the 423 nm band in the UV-visible spectrum. No effect on the band at 610 nm was observed.

The species corresponding to the IR band at 1849 cm^{-1} may therefore be formed from both $\text{Ru}(\text{CO})_2(\text{PMe}_3)_2\text{H}_2$ and $\text{Ru}(\text{CO})_3(\text{PMe}_3)_2$. This excludes assignment of the band to a metal-hydride stretch and implies that it must be due to a carbonyl mode in a ruthenium carbonyl phosphine fragment. The band is shifted to low frequency of the antisymmetric CO-stretching mode of I by 119 cm^{-1} . This dramatic shift demonstrates that the oxidation state of the photoproduct is zero and is consistent with either $\text{Ru}(\text{CO})_2(\text{PMe}_3)_2$ or $\text{Ru}(\text{CO})(\text{PMe}_3)_2$. No changes are observed in the low-frequency region of the IR spectrum on photolysis that could be attributed to dissociation of PMe_3 which thus excludes a species containing one phosphine ligand. The selective photolysis experiments establish that the visible absorption band at 423 nm can be assigned to this species. The reversible photochemistry which takes place upon long wavelength irradiation is typical of a coordinatively unsaturated species.

In order to determine the number of carbonyl ligands present in the photoproduct, matrix experiments on isotopically labeled I were carried out. The IR spectrum of a mixture of isotopomers $\text{Ru}(^{13}\text{CO})_x(^{12}\text{CO})_{2-x}(\text{PMe}_3)_2\text{H}_2$ ($x = 0, 1, 2$) in an argon matrix (190 min deposition) contained 5 bands in the carbonyl region (Figure 2a). These bands are readily assigned to the isotopomers with $x = 0, 1, \text{ and } 2$. The calculated positions and intensities of the isotopomers were found by standard methods with a CO-factored force field^{4,6} (Table 3). From the relative intensities of the all ^{12}CO and all ^{13}CO isotopomers, the ratio of ^{12}CO to ^{13}CO was found to be 1.04, i.e. 51% ^{12}CO and 49% ^{13}CO .

Broad band photolysis (30 min) of the matrix resulted in depletion of all five bands. Bands for free ^{12}CO and ^{13}CO (2138 and 2091 cm^{-1}) were observed, together with new product bands centered at $1903, 1849, 1821, \text{ and } 1807 \text{ cm}^{-1}$ (Figure 2b).⁷ The presence of the band at 1821 cm^{-1} between the all ^{12}CO band at 1849 cm^{-1} and

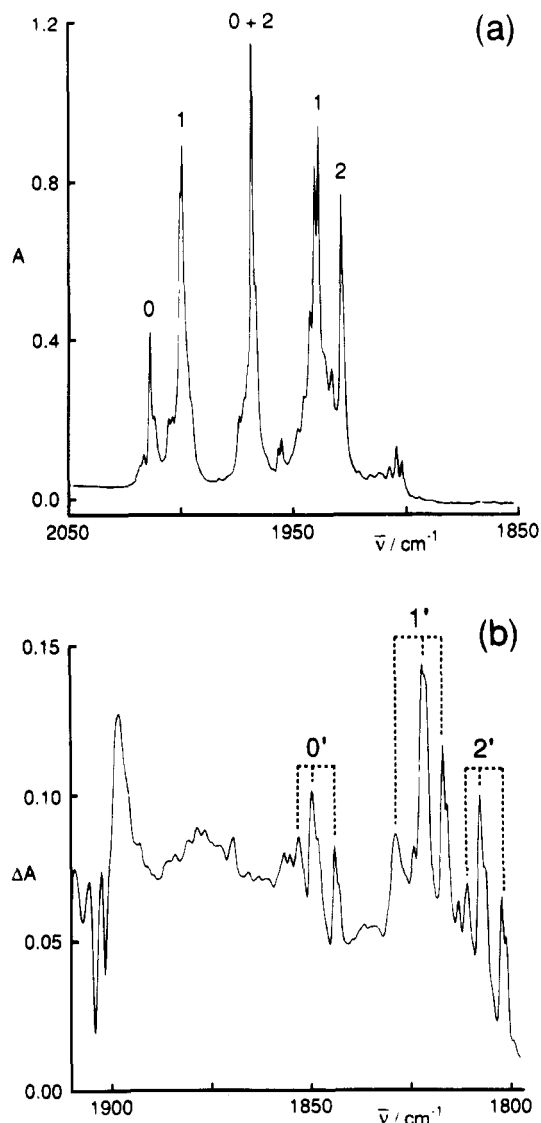


Figure 2. (a) IR spectrum of $\text{Ru}(^{13}\text{CO})_x(^{12}\text{CO})_{2-x}(\text{PMe}_3)_2\text{H}_2$ in an argon matrix at 12 K ($0 = \text{Ru}(^{12}\text{CO})_2(\text{PMe}_3)_2\text{H}_2$, $1 = \text{Ru}(^{12}\text{CO})(^{13}\text{CO})(\text{PMe}_3)_2\text{H}_2$, $2 = \text{Ru}(^{13}\text{CO})_2(\text{PMe}_3)_2\text{H}_2$). (b) IR spectrum after 30 min of photolysis ($\lambda > 200 \text{ nm}$) showing isotopomers of $\text{Ru}(^{13}\text{CO})_x(^{12}\text{CO})_{2-x}(\text{PMe}_3)_2 \cdot \text{Ar}$ presented as a difference spectrum relative to the deposition spectrum ($0' = \text{Ru}(^{12}\text{CO})_2(\text{PMe}_3)_2$, $1' = \text{Ru}(^{12}\text{CO})(^{13}\text{CO})(\text{PMe}_3)_2$, $2' = \text{Ru}(^{13}\text{CO})_2(\text{PMe}_3)_2$). Note that (a) and (b) have different abscissa scales.

Table 3. Calculated and Observed Carbonyl Stretching Modes (ν/cm^{-1}) for the Isotopomers of I in an Argon Matrix at 12 K^a

calcd	obsd	error	assgnt
2013.0	2013.9	0.9	$\nu(^{12}\text{CO})_2 \text{ sym}$
1970.8	1968.3	-2.5	$\nu(^{12}\text{CO})_2 \text{ asym}$
2000.2	1999.2	-1.0	$\nu(^{12}\text{CO})_2(^{13}\text{CO})$
1939.2	1939.2	0.0	$\nu(^{12}\text{CO})(^{13}\text{CO})$
1968.2	1968.0	-0.2	$\nu(^{13}\text{CO})_2 \text{ sym}$
1926.9	1928.3	1.4	$\nu(^{13}\text{CO})_2 \text{ asym}$

^a Stretching force constant 1603 N m^{-1} ; interaction force constant 34 N m^{-1} ; RMS error 1.3 cm^{-1} .

the all ^{13}CO analogue at 1807 cm^{-1} implies that the product cannot be a monocarbonyl fragment and suggests that it is a dicarbonyl species. The spectrum can indeed be fitted satisfactorily to a dicarbonyl species (Table 4).⁸ The position of the unobserved symmetric stretching mode of the all ^{12}CO molecule is estimated

(6) Perutz, R. N.; Turner, J. J. *Inorg. Chem.* **1975**, *14*, 262.

(7) The intensity behavior of the band at 1890 cm^{-1} in Figure 2b implies that it is not associated with the product at 1849 cm^{-1} nor any of its isotopomers. We assign this band to the ^{13}CO isotopomer of the species produced on photolysis of I which shows a band at 1941 cm^{-1} (see main text).

Table 4. Calculated and Observed Carbonyl Stretching Modes (ν/cm^{-1}) for the Isotopomers of $\text{Ru}(\text{CO})_2(\text{PMe}_3)_2$ in an Argon Matrix at 12 K^a

calcd	obsd	error	assgnt
1901.9	n.o.		$\nu(^{12}\text{CO})_2$ sym
1849.0	1849.6	0.6	$\nu(^{12}\text{CO})_2$ asym
1887.9	n.o.		$\nu(^{12}\text{CO}^{13}\text{CO})$
1821.0	1821.6	0.6	$\nu(^{12}\text{CO}^{13}\text{CO})$
1859.4	n.o.		$\nu(^{13}\text{CO})_2$ sym
1807.7	1807.4	-0.3	$\nu(^{13}\text{CO})_2$ asym

^a n.o. = not observed. Stretching force constant 1421 N m^{-1} ; interaction force constant 40 N m^{-1} ; RMS error 0.5 cm^{-1} .

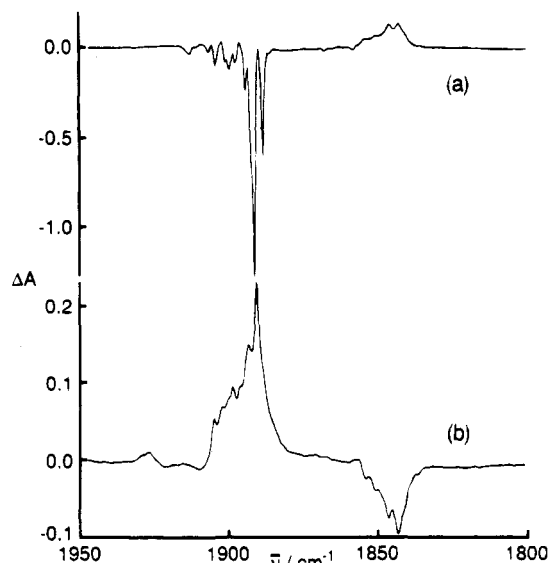


Figure 3. IR spectrum of $\text{Ru}(\text{CO})_2(\text{PMe}_3)_2$ (**II**) isolated in a methane matrix at 12 K (a) after 20 min of photolysis ($\lambda > 200 \text{ nm}$) presented as a difference spectrum relative to the deposition spectrum and (b) after 120 min of photolysis ($\lambda = 360\text{--}378 \text{ nm}$) shown as a difference spectrum relative to the spectrum recorded after UV photolysis.

to be 1902 cm^{-1} , but the fit of the observed bands is not very sensitive to its position.

3. Photochemistry of I and II in Low-Temperature Methane Matrices. Photolysis of **I** isolated in a methane matrix ($\lambda > 290 \text{ nm}$, 120 min) resulted in the appearance of a band at 2020 cm^{-1} and a weaker, split feature at 1846 cm^{-1} . The decrease in intensity of the two starting carbonyl bands of **I** (2007 and 1964 cm^{-1}) was found to be greater for the higher than for the lower frequency band (21% and 7%, respectively), suggesting overlap of a product carbonyl band with the lower frequency mode of **I**.

Additional broad band photolysis (60 min) resulted in further depletion of **I** and in loss of the band at 2020 cm^{-1} . The product band at 1846 cm^{-1} increased in intensity, and very weak, new bands appeared at 2135 , 1930 , 1912 , and 1899 cm^{-1} .

Complex **II** proved to be more photosensitive in methane than in argon. Broad band irradiation (20 min) effected 45% depletion of the split carbonyl stretching band (1891 and 1889 cm^{-1}) and resulted in the formation of a new band at 1846 cm^{-1} (Figure 3a). A UV-visible difference spectrum showed a strong prod-

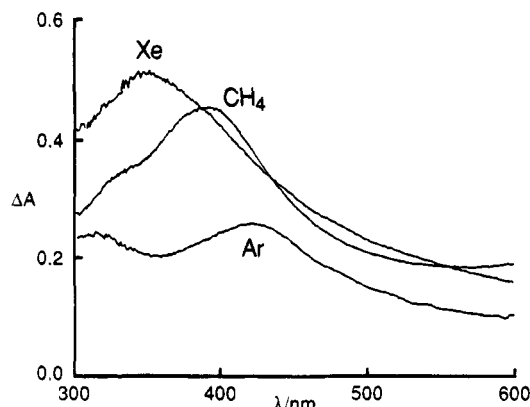


Figure 4. UV-visible spectra of $\text{Ru}(\text{CO})_2(\text{PMe}_3)_2 \cdot \text{S}$ for $\text{S} = \text{Ar}$, CH_4 , and Xe . The spectra were obtained by subtraction of the deposition spectrum from that recorded after UV photolysis.

uct band at 385 nm , along with a broader, weaker feature at 610 nm (Figure 4). The shift of the high energy band found on changing the matrix host from argon to methane (423 nm to 385 nm , $\Delta\nu = 2330 \text{ cm}^{-1}$) strongly suggests that $\text{Ru}(\text{CO})_2(\text{PMe}_3)_2$ is not a "naked" fragment like $\text{Ru}(\text{dmpe})_2$ but is solvated by the matrix (see Discussion).

Selective photolysis experiments ($\lambda = 360\text{--}378 \text{ nm}$ and $\lambda = 420\text{--}450 \text{ nm}$), similar to those carried out in argon matrices, resulted in both cases in depletion of the photoproduct band at 385 nm in the UV-visible spectrum, loss of the IR band at 1846 cm^{-1} , and growth of IR bands of the starting material **II** (Figure 3b). The visible band at 610 nm was unaffected.

Photolysis into the low-energy visible band ($\lambda > 580 \text{ nm}$, 210 min) was found to have no effect on the band at 1846 cm^{-1} in the IR spectrum, although there was an increase in the intensity of the carbonyl bands of the starting material **II**. Thus the behavior of the 610 nm UV-visible band on long wavelength photolysis does not match that of the band in the IR spectrum at 1846 cm^{-1} , implying that it belongs to another species, perhaps a dinuclear product.

The IR spectrum of the partially ^{13}CO labeled **II**, $\text{Ru}(^{13}\text{CO})_x(^{12}\text{CO})_{3-x}(\text{PMe}_3)_2$ ($x = 0, 1, 2, 3$), in a methane matrix revealed a $\nu(\text{CO})$ band for the $x = 3$ isotopomer at 1848 cm^{-1} which coincides with the $x = 0$ product band (1846 cm^{-1}) making **II** a poor precursor for isotopic analysis. However, upon broad band photolysis (50 min), a weak new band was observed at 1804 cm^{-1} , which was assigned to the $x = 2$ isotopomer of the photoproduct. It was not possible to observe the IR band for the corresponding $x = 1$ species (expected at 1821 cm^{-1}) as a $^{13}\text{C}^{18}\text{O}$ isotopomer of **II** shrouded this region.

4. Photochemistry of I and II in More Reactive Low-Temperature Matrices. The large shift in the position of the strong visible band on changing the matrix host from argon to methane prompted us to investigate the photochemistry of **II** in a xenon matrix. The IR spectrum of **II** in a xenon matrix showed a highly split carbonyl band with peaks between 1910 and 1880 cm^{-1} . Broad band irradiation (60 min) resulted in some alteration of the relative intensities of the component bands with a strong growth at 1891 cm^{-1} . At the same time, appearance of a new band at 1844 cm^{-1} (along

(8) The appearance of each band as more than a single component is due to matrix splittings. This is evident from Figure 2b where the bands for 0', 1', and 2' each show the same "triplet" appearance.

with a band for free CO at 2138 cm^{-1}) confirmed the formation of $\text{Ru}(\text{CO})_2(\text{PMe}_3)_2$.

The UV-visible difference spectrum now showed a strong band with $\lambda_{\text{max}} = 352 \text{ nm}$, blue-shifted compared to both argon (423 nm) and methane (385 nm) (Figure 4). There was no evidence for the formation of a longer wavelength band in the xenon matrix.

Upon photolysis of **I** in a CO matrix ($\lambda > 200 \text{ nm}$, 10 min), loss of starting material bands at 2007 and 1964 cm^{-1} was observed and a new intense split band appeared; this was centered at 1890 cm^{-1} , with components at 1897, 1884, and 1879 cm^{-1} . The band was readily assigned to **II**. No bands arising from free HCO were seen in the matrix,⁹ implying that loss of H_2 from $\text{Ru}(\text{CO})_2(\text{PMe}_3)_2\text{H}_2$ must occur in a concerted process.

Irradiation of **II** in a nitrogen-doped argon matrix (10% nitrogen:90% argon, $\lambda > 200 \text{ nm}$, 60 min) generated new bands at 1870 and 2138 cm^{-1} (free CO) and a broad feature at 2159 cm^{-1} . The bands at 2159 cm^{-1} and 1870 cm^{-1} are assigned to $\nu(\text{NN})$ and $\nu(\text{CO})$, respectively, of $\text{Ru}(\text{CO})_2(\text{PMe}_3)_2(\text{N}_2)$.

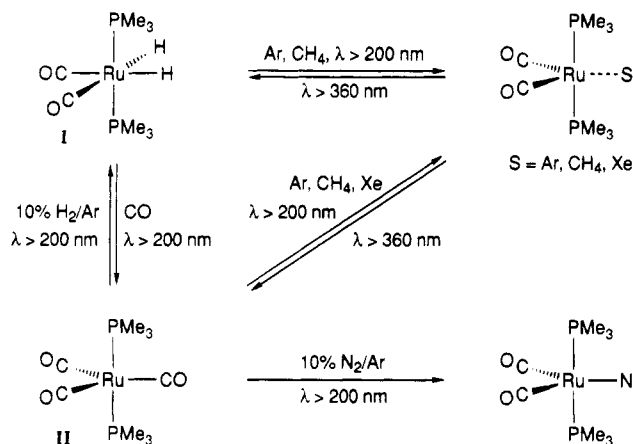
Broad band photolysis of **II** in a hydrogen-doped argon matrix (10% H_2 :90% Ar) for 10 min resulted in the appearance of new bands at 2138 (free CO), 2022, 2013, and 1968 cm^{-1} . The liberation of CO and the positions and relative intensity of the two low-frequency bands imply the formation of **I**. There is no evidence for formation of isomers of **I**.

Discussion

Photolysis of $\text{Ru}(\text{CO})_2(\text{PMe}_3)_2\text{H}_2$ (**I**) or $\text{Ru}(\text{CO})_3(\text{PMe}_3)_2$ (**II**) in inert low-temperature matrices results in the formation of a common product showing a single carbonyl band in the IR spectrum at 1849 cm^{-1} in argon or 1846 cm^{-1} in methane. This species is assigned to the 16-electron complex $\text{Ru}(\text{CO})_2(\text{PMe}_3)_2$ on the basis of ^{13}C isotopic labeling experiments and trapping experiments in more reactive matrices. The reversibility of the photochemistry upon long wavelength irradiation is behavior common among 16-electron coordinatively unsaturated species.¹⁰ The photochemistry of **I** and **II** in low-temperature matrices is summarized in Scheme 1.

Photolysis of the dihydride complex results in the loss of both H_2 and CO to give not only $\text{Ru}(\text{CO})_2(\text{PMe}_3)_2$ but also additional products. These are seen by the appearance of carbonyl bands at 2023, 1941, 1918, and 1900 cm^{-1} . The positions of these bands are consistent with a ruthenium(II) species, although there are too many bands for a single product. This suggests a number of isomers of the monocarbonyl complex $\text{Ru}(\text{CO})(\text{PMe}_3)_2\text{H}_2$. The photochemical loss of both H_2 and CO from **I** is mirrored by the chemical behavior of the analogous complex $\text{Ru}(\text{CO})_2(\text{PMe}_2\text{Ph})_2\text{H}_2$, which reacts with $\text{PhC}(\text{O})\text{CH}=\text{CHPh}$ under UV irradiation to give $\text{Ru}(\text{CO})\{\eta^4\text{-PhC}(\text{O})\text{CH}=\text{CHPh}\}(\text{PMe}_2\text{Ph})_2$ in high yield, with $\text{Ru}(\text{CO})_3(\text{PMe}_2\text{Ph})_2$ as a byproduct.¹¹ The matrix experiments reported here demonstrate that $\text{Ru}(\text{CO})_3(\text{PMe}_3)_2$ represents a far more selective precursor to $\text{Ru}(\text{CO})_2(\text{PMe}_3)_2$.

Scheme 1. Matrix Photochemistry of $\text{Ru}(\text{CO})_2(\text{PMe}_3)_2\text{H}_2$ (**I**) and $\text{Ru}(\text{CO})_3(\text{PMe}_3)_2$ (**II**) at 12 K



There are several matrix studies of carbonyl hydride complexes available for comparison.¹² In the case of monohydride complexes, such as $\text{Mn}(\text{CO})_5\text{H}$ and $\text{Mo}(\eta^5\text{-C}_5\text{H}_5)(\text{CO})_3\text{H}$, photolysis may result in the loss of hydrogen atoms.¹³ Among dihydride complexes, Sweany has shown¹⁴ that photolysis of $\text{Fe}(\text{CO})_4\text{H}_2$ in an argon matrix at 12 K results solely in loss of H_2 to generate $\text{Fe}(\text{CO})_4$. Photolysis with a Nernst glower brings about partial photoreversal of the reaction, a process that can be taken to completion in an H_2 -doped argon matrix. Rest et al.¹⁵ and McCamley et al.¹⁶ have shown more recently that photolysis of $\text{Ir}(\eta^5\text{-C}_5\text{H}_5)(\text{CO})\text{H}_2$ and $\text{Os}(\eta^6\text{-C}_6\text{H}_3\text{Me}_3)(\text{CO})\text{H}_2$, respectively, also yields products resulting from loss of H_2 . Geoffroy and Bradley¹⁷ have reported that UV photolysis of $\text{Ru}(\text{CO})(\text{PPh}_3)_3\text{H}_2$ in benzene solution at room temperature results in loss of H_2 only.

The UV-visible spectrum of $\text{Ru}(\text{CO})_2(\text{PMe}_3)_2$ in argon shows only a single band at 423 nm, a very different result from the three band visible spectrum obtained for $\text{Ru}(\text{dmpe})_2$ in an argon or methane matrix. The appearance of a low-energy band at 745 nm for $\text{Ru}(\text{dmpe})_2$ was cited as evidence for the square planar geometry.² On the basis of the UV-visible spectra recorded in the present study, $\text{Ru}(\text{CO})_2(\text{PMe}_3)_2$ would not appear to be square planar.

The visible band observed for $\text{Ru}(\text{CO})_2(\text{PMe}_3)_2$ in argon at 423 nm is significantly shifted to the blue on changing the matrix host to methane (385 nm) and then to xenon (352 nm). Such behavior was originally reported for $\text{M}(\text{CO})_5$ ($\text{M} = \text{Cr}, \text{Mo}, \text{W}$)¹⁸ and has since been observed for other 16-electron metal carbonyls such as $\text{Mn}(\text{CH}_3)(\text{CO})_4$.¹⁹ It is therefore more accurate to represent $\text{Ru}(\text{CO})_2(\text{PMe}_3)_2$ not as a four coordinate fragment but as the pseudo five coordinate species $\text{Ru}(\text{CO})_2(\text{PMe}_3)_2 \cdot \text{S}$, where S is Ar, CH₄, or Xe. Such

(12) Sweany, R. L. *Transition Metal Hydrides*; Dedieu, A., Ed.; VCH: Weinheim, Germany, 1992.

(13) (a) Church, S. P.; Poliakoff, M.; Timney, J. A.; Turner, J. J. *Inorg. Chem.* **1983**, *22*, 3259. (b) Mahmoud, K. A.; Rest, A. J.; Alt, H. G. *J. Organomet. Chem.* **1983**, *246*, C37.

(14) Sweany, R. L. *J. Am. Chem. Soc.* **1981**, *103*, 2410.

(15) Rest, A. J.; Whitwell, I.; Graham, W. A. G.; Hoyano, J. K.; McMaster, A. D. *J. Chem. Soc., Dalton Trans.* **1987**, 1181.

(16) McCamley, A.; Perutz, R. N.; Stahl, S.; Werner, H. *Angew. Chem., Int. Edit. Engl.* **1989**, *28*, 1690.

(17) Geoffroy, G. L.; Bradley, M. G. *Inorg. Chem.* **1977**, *16*, 744.

(18) Perutz, R. N.; Turner, J. J. *J. Am. Chem. Soc.* **1975**, *97*, 4971.

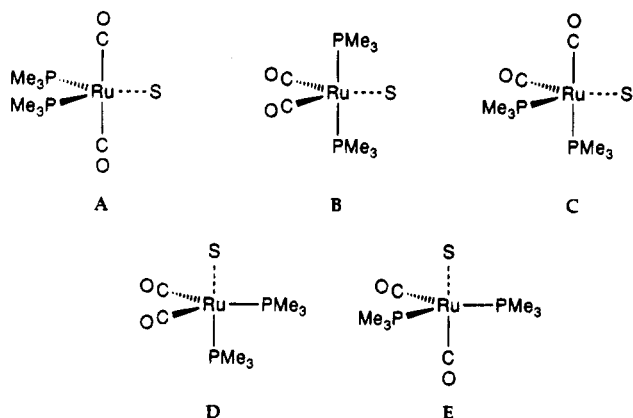
(19) Horton-Mastin, A.; Poliakoff, M. *Organometallics* **1986**, *5*, 405.

(9) Milligan, D. E.; Jacox, M. E. *J. Chem. Phys.* **1964**, *42*, 3032.

(10) Hitam, R. B.; Mahmoud, K. A.; Rest, A. J. *Coord. Chem. Rev.* **1984**, *55*, 1.

(11) Lynam, J.; Weston, W. S.; Mawby, R. J. Unpublished results.

shifts in UV-visible absorption bands with changes in the nature of a token ligand are typical of 16-electron d^6 molecules with five conventional ligands although the shifts in band energy (Ar to CH_4 , 2330 cm^{-1} ; Ar to Xe, 4770 cm^{-1}) are considerably larger than those observed for $\text{Cr}(\text{CO})_5$.¹⁸ Interaction with the matrix or solvent has also been detected for $\text{Fe}(\text{CO})_4$, which has a d^8 configuration,²⁰ but in that case it was manifested by changes in the IR spectrum. The enthalpy of interaction of $\text{Fe}(\text{CO})_2(\text{PMe}_3)_2$ with cyclohexane solvent is postulated to be stronger than that of $\text{Fe}(\text{CO})_4$.^{20c} The results presented here show that $\text{Ru}(\text{CO})_2(\text{PMe}_3)_2 \cdot \text{S}$ shows UV-visible behavior more like $\text{Cr}(\text{CO})_5 \cdot \text{S}$ although its structure must resemble that of $\text{Fe}(\text{CO})_4 \cdot \text{S}$. Five ligand arrangements are possible within a trigonal bipyramidal structure:



Structure A is the only one which at first sight is compatible with the appearance of a single carbonyl band. However, structure B would also be possible provided that the OC-Ru-CO bond angle is large enough for the intensity of the symmetric CO -stretching band to be lowered to a point where it could be obscured. Although a weak band was observed at 1900 cm^{-1} in the region anticipated for the symmetric stretching mode of $\text{Ru}(\text{CO})_2(\text{PMe}_3)_2 \cdot \text{S}$ (Table 4), the intensity behavior of this band suggested that it did not belong to the same species as the 1849 cm^{-1} band. We conclude that the symmetric stretching mode must be weaker than other minor peaks leading to an estimate that $I_{\text{antisym}}/I_{\text{sym}} > 5$ and that $\text{OC-Ru-CO} > 130^\circ$.

Recent results by Caulton, Eisenstein, and co-workers²¹ have added weight to the argument. The crystal structure of the stable species $\text{Ru}(\text{CO})_2(\text{P}^t\text{Bu}_2\text{Me})_2$ shows a C-Ru-C bond angle of 133° and a P-Ru-P angle of 166° . This would imply a ratio of ca. 5.3:1 in the relative intensities of the antisymmetric and symmetric carbonyl stretching modes, large enough to be consistent with our observations on $\text{Ru}(\text{CO})_2(\text{PMe}_3)_2$. *Ab initio* calculations on the model complex $\text{Ru}(\text{CO})_2(\text{PH}_3)_2$ by the same authors have reproduced the bond angles in the $\text{P}^t\text{Bu}_2\text{Me}$ complex, indicating that the steric bulk of the phosphine is not responsible for the disposition of the ligands at the metal center. Walsh diagrams demonstrate that it is the stabilization of the high-energy d

orbitals of the $\text{Ru}(0)$ fragment by the π^* orbitals of CO that is crucial to the distortion away from a square planar geometry. On the basis of our experimental evidence, the angles in $\text{Ru}(\text{CO})_2(\text{PMe}_3)_2 \cdot \text{S}$ may be very close to those in $\text{Ru}(\text{CO})_2(\text{P}^t\text{Bu}_2\text{Me})_2$, a version of B distorted toward a square pyramid.

The shift in the UV-visible spectra of $\text{Ru}(\text{CO})_2(\text{PMe}_3)_2 \cdot \text{S}$ upon changing S from Ar to CH_4 to Xe may reflect both a change in the strength of the $\text{Ru} \cdot \text{S}$ bonding interaction and a change in bond angles. The sensitivity of the HOMO-LUMO transition to bond angle is shown by Walsh diagrams for $d^8 \text{M}(\text{CO})_4$.²²

Our observations on $\text{Ru}(\text{CO})_2(\text{PMe}_3)_2$ can be put into context alongside several other d^8 4-coordinate complexes of ruthenium. $\text{Ru}(\text{CO})_4$ has been observed in the gas phase by time-resolved infrared spectroscopy. Although it was not possible to determine the structure from these experiments,²³ density functional calculations have suggested that $\text{Ru}(\text{CO})_4$ should have a C_{2v} ground state geometry.²⁴ $\text{Ru}(\text{CO})_3\text{PPh}_3$ may be formed in a methylcyclohexane glass at 100 K upon photolysis of $\text{Ru}(\text{CO})_4\text{PPh}_3$.²⁵ The 16-electron tricarbonyl complex shows two UV-visible bands at 425 and 342 nm (relative intensity 1:2) and is postulated to have a C_{3v} geometry on the basis of its IR spectrum. In this paper, we have reported on $\text{Ru}(\text{CO})_2(\text{PMe}_3)_2$. The last member of the series, $\text{Ru}(\text{dmpe})_2$, has been shown to have a square planar geometry.² Clearly the exchange of carbonyl and phosphine ligands has a dramatic effect on the geometry of the complexes.

Experimental Section

General Methods and Materials. The compounds were synthesized and handled using standard Schlenk and high-vacuum techniques. Solvents were dried by refluxing over sodium/benzophenone and then distilling under an argon atmosphere. Deuterated solvents (Goss Scientific Instruments Ltd.) were dried by stirring over potassium/benzophenone and then distilled. Gases used in syntheses (H_2 and CO) were BOC standard grade (99.9% purity). Gases used for the matrix experiments (Ar, CH_4 , Xe, CO , N_2) were BOC research grade (99.999% purity). ^{13}C (99 atom % ^{13}C) was obtained from Amersham International. Ruthenium trichloride hydrate and trimethylphosphine were obtained from Aldrich. $\text{Ru}(\text{CO})_2(\text{PMe}_3)_2\text{Cl}_2$ was prepared by a modification of the procedure used by Jenkins et al.²⁶ Spectroscopic data for this complex are already reported in the literature.²⁷

NMR spectra were recorded on either Bruker MSL 300 MHz or JEOL FX90-Q 90 MHz spectrometers. ^1H spectra were referenced to residual protonated benzene $\text{C}_6\text{D}_5\text{H}$ at δ 7.13. ^{13}C spectra were referenced to C_6D_6 at δ 128.0 ppm. ^{31}P NMR chemical shifts were referenced externally to 85% H_3PO_4 at δ = 0.

Matrix Isolation Experiments. The matrix isolation apparatus is described in detail elsewhere.²⁸ Samples for IR

(22) Albright, T. A.; Burdett, J. K.; Whangbo, M. H. *Orbital Interactions in Chemistry*; John Wiley and Sons: New York, 1985.

(23) Bogdan, P. L.; Weitz, E. J. *Am. Chem. Soc.* **1989**, *111*, 3163.

(24) (a) Ziegler, T.; Tshinke, V.; Fan, L.; Becke, A. D. *J. Am. Chem. Soc.* **1989**, *111*, 9177. (b) Li, J.; Schreckenbach, G.; Ziegler, T. *J. Am. Chem. Soc.* **1995**, *117*, 486.

(25) (a) Liu, D. K.; Wrighton, M. S.; McKay, D. R.; Maciel, G. R. *Inorg. Chem.* **1984**, *23*, 212. (b) Liu, D. K.; Brinkley, C. G.; Wrighton, M. S. *Organometallics* **1984**, *3*, 1449.

(26) Jenkins, J. M.; Lupin, M. S.; Shaw, B. L. *J. Chem. Soc. (A)* **1966**, 1787.

(27) Krassowski, D. W.; Nelson, J. H.; Brower, K. R.; Hauenstein, D.; Jacobson, R. A. *Inorg. Chem.* **1988**, *27*, 4294.

(28) Haddleton, D. M.; McCamley, A.; Perutz, R. N. *J. Am. Chem. Soc.* **1988**, *110*, 1810.

(20) (a) Poliakoff, M.; Turner, J. J. *J. Chem. Soc., Dalton Trans.* **1974**, 2276. (b) Poliakoff, M. *Chem. Soc. Rev.* **1978**, *7*, 527. (c) Nayak, S. K.; Burkey, T. J. *J. Am. Chem. Soc.* **1993**, *115*, 6391.

(21) Ogasawara, M.; Macgregor, S. A.; Streib, W. E.; Folting, K.; Eisenstein, O.; Caulton, K. G. *J. Am. Chem. Soc.*, submitted for publication.

spectroscopy alone were deposited onto a CsI window cooled by an Air Products CS202 closed-cycle refrigerator to 12–35 K. A BaF₂ window was used for combined IR and UV–vis spectroscopy. The outer windows of the vacuum shroud were chosen to match. Ru(CO)₂(PMe₃)₂H₂ and Ru(CO)₃(PMe₃)₂ were sublimed from right-angled glass tubes (at 267 and 303 K, respectively) at the same time as a gas stream entered the vacuum shroud through a separate inlet. Typical deposition temperatures and rates were 20 K for Ar (2 mmol h⁻¹), 25 K for CH₄ (2 mmol h⁻¹), and 35 K for Xe (1.7 mmol h⁻¹). The samples were then cooled to 12 K before recording IR spectra on a Mattson Sirius or a Mattson Research Series FTIR spectrometer fitted with a TGS detector and KBr beam splitter, which was continuously purged with dry CO₂-free air. Spectra were recorded at 1 cm⁻¹ resolution with 128 scans coaveraged (25K data points with two-times zero-filling). UV–vis spectra were recorded on the same sample at the same temperature on a Perkin-Elmer Lambda 7G spectrometer. Matrices were photolyzed through a quartz window with a Philips HPK 125 W medium-pressure mercury arc, using a quartz focusing lens and water filter or an ILC 302UV 300 W Xe arc equipped with either UV-reflecting (240–400 nm) or visible-reflecting (400–800 nm) mirrors and a water filter. Photolysis wavelengths were selected with cutoff or interference filters.

Synthesis. Ru(CO)₂(PMe₃)₂H₂. Ru(CO)₂(PMe₃)₂Cl₂ (0.2 g, 0.58 mmol) was dissolved in 50 cm³ of degassed ethanol. Excess NaBH₄ (0.16 g, 4.23 mmol) was added, and the mixture was stirred under a flow of hydrogen for 3 h. The solvent was removed *in vacuo* and the residue extracted exhaustively with benzene. The combined extracts were stripped of solvent under reduced pressure to leave an orange-brown oil. Subli-

mation at room temperature (10⁻⁴ mbar) onto a liquid nitrogen cooled finger afforded Ru(CO)₂(PMe₃)₂H₂ as a white solid. The product was stored under hydrogen at -20 °C. The sensitivity of the complex, as is evident from its discoloration, has prevented us from obtaining a satisfactory elemental analysis. The red-brown crude product could also be purified by chromatography on alumina with pentane, although the yield was extremely low. NMR data are given in Table 1. IR (pentane, cm⁻¹): ν(CO) 2010, 1960. MS: *m/e* 310, (M - H₂)⁺.

Ru(CO)₃(PMe₃)₂. Ru(CO)₂(PMe₃)₂H₂ (0.05 g, 0.16 mmol) was dissolved in C₆D₆ in an NMR tube fitted with a PTFE Young's tap. The solution was placed under 1 atm of CO, and the reaction was followed by ³¹P{¹H} NMR spectroscopy. After 3 weeks at room temperature, conversion of the dihydride to Ru(CO)₃(PMe₃)₂ was complete. The compound was purified by removal of the solvent and sublimation of the residue at 306 K to give a white product. NMR data are given in Table 1. IR (pentane, cm⁻¹): ν(CO) 1895.

Isotopically Labeled I and II. ¹³CO incorporated **II** was produced as described above from **I** and ¹³CO. ¹³CO-labeled **I** was produced by reaction of this sample of isotopically labeled **II** with H₂.

Acknowledgment. We wish to thank Professors K. G. Caulton and O. Eisenstein for disclosing results prior to publication. We are pleased to acknowledge the support of the SERC, the European Commission, NATO, British Gas and the Royal Society.

OM950167E

Electron Transfer Catalysis in the Activation of C–H Bonds by Iridium Complexes

Pietro Diversi,^{*,†} Stefania Iacononi,[†] Giovanni Ingrosso,[†] Franco Laschi,[‡]
Antonio Lucherini,[†] Calogero Pinzino,[§] Gloria Uccello-Barretta,^{||} and
Piero Zanello[‡]

Dipartimento di Chimica e Chimica Industriale, Università di Pisa, Via Risorgimento 35,
56126 Pisa, Italy, Dipartimento di Chimica, Università di Siena, Pian dei Mantellini 44,
53100 Siena, Italy, Istituto di Chimica Quantistica ed Energetica Molecolare del CNR,
Via Risorgimento 35, 56126 Pisa, Italy, and Centro del CNR per lo Studio delle Macromolecole
Stereordinate ed Otticamente Attive, Via Risorgimento 35, 56126 Pisa, Italy

Received January 26, 1995[⊗]

Iridium(III) dimethyl complexes, $\text{Cp}^*\text{Ir}(\text{PR}_3)_2\text{Me}_2$ ($\text{Cp}^* = \eta^5\text{-C}_5\text{Me}_5$; $\text{R} = \text{Ph}$ (**1a**), Me (**1b**)), react slowly (**1a**), or not at all (**1b**), with C–H bonds of aromatic hydrocarbons under severe conditions (110 °C, 2 weeks) to give methane and the new methyl aryl derivatives $\text{Cp}^*\text{Ir}(\text{PPh}_3)(\text{Me})(\text{Ar})$ ($\text{Ar} = \text{C}_6\text{H}_5$, $\text{C}_6\text{H}_4\text{Me}$, $\text{C}_6\text{H}_4\text{CF}_3$, $\text{C}_6\text{H}_3\text{Me}_2$). With benzene and trifluorotoluene, the diaryl complexes $\text{Cp}^*\text{Ir}(\text{PPh}_3)\text{Ar}_2$ are also formed. In contrast, the reaction of both **1a** and **1b** with arenes, in the presence of catalytic amounts of an oxidant ($\text{Cp}_2\text{Fe}^+\text{PF}_6^-$, AgBF_4 , or $\text{Ph}_3\text{C}^+\text{BF}_4^-$), proceeds rapidly at room temperature: the corresponding methyl aryl derivatives $\text{Cp}^*\text{Ir}(\text{PR}_3)(\text{Me})(\text{Ar})$ ($\text{R} = \text{Ph}$; $\text{Ar} = \text{C}_6\text{H}_5$, C_6D_5 , $\text{C}_6\text{H}_4\text{Me}$, $\text{C}_6\text{H}_4\text{CF}_3$, $\text{C}_6\text{H}_3\text{Me}_2$. $\text{R} = \text{Me}$; $\text{Ar} = \text{C}_6\text{H}_5$, C_6D_5 , $\text{C}_6\text{H}_4\text{Cl}$, $\text{C}_6\text{H}_4\text{Br}$, $\text{C}_6\text{H}_4\text{F}$, $\text{C}_6\text{H}_4\text{CF}_3$, $\text{C}_6\text{H}_4\text{NO}_2$, $\text{C}_6\text{H}_4\text{Me}$, $\text{C}_6\text{H}_3\text{Me}_2$) are produced. In the reaction with benzene-*d*₆, a mixture of CH_4 and CH_3D is obtained. When substituted arenes are used, only the meta and para C–H bonds react. In the case of **1a**, the methyl aryl derivative is in equilibrium with the orthometalated compound $\text{Cp}^*\text{Ir}(\text{C}_6\text{H}_4\text{PPh}_2)\text{Me}$ (**12**), which is the primary reaction product. Evidence is provided for a facile one-electron oxidation of **1a** and **1b**. The electrochemical oxidation of **1a**, **1b**, and related iridium(III) dialkyls in CH_2Cl_2 involves a 1-electron process, yielding the corresponding iridium(IV) paramagnetic cations, as shown by coupled electrochemical–ESR studies. AgBF_4 oxidation of **1a** and **1b** in CH_2Cl_2 gives instead radical species, which have been shown by ESR spectroscopy to have the “tucked-in” structure $\text{Ir}(\eta^5\text{-C}_5\text{Me}_4\text{CH}_2)$. Such species are proved to be involved as intermediates in the above arene C–H activation reactions.

Introduction

The role of odd-electron species in transition-metal organometallic chemistry has only been fully recognized recently despite the pioneering studies by Kochi.¹ Odd-electron complexes may have reactivity patterns, which are forbidden for species obeying the 16/18-electron rule but which proceed easily through radical (mainly 17- and 19-electron) intermediates.^{1,d,f,g} Taking advantage of these ideas, it has been shown that many reactions, such as ligand substitution,² CO insertion,³ and isomerizations of complexes,⁴ which occur slowly for 18-electron closed-shell species, may be dramatically accelerated in the presence of electron transfer reagents, which can give rise to 17- and 19-electron intermediates.

In the course of our investigations on the cyclometalation reactions of half-sandwich iridium(III) dialkyl derivatives,^{5a,b} we have found that the methyl complexes $\text{Cp}^*\text{Ir}(\text{PR}_3)_2\text{Me}_2$ ($\text{R} = \text{Ph}$ (**1a**), Me (**1b**)), which are able to activate C–H bonds of arenes only under rather drastic conditions or not at all, become strongly reactive in the presence of catalytic amounts of one-electron oxidants.^{5c} These C–H activation reactions have features which make them analogous to the “ σ -bond metathesis”⁶ of M–R bonds and hydrocarbon C–H

(3) (a) Magnuson, R. H.; Meirowitz, R.; Zulu, S.; Giering, P. *J. Am. Chem. Soc.* **1982**, *104*, 5790. (b) Magnuson, R. H.; Meirowitz, R.; Zulu, S. J.; Giering, W. P. *Organometallics* **1983**, *2*, 460. (c) Therien, M. J.; Trogler, W. C. *J. Am. Chem. Soc.* **1987**, *109*, 5127. (d) Prock, A.; Giering, W. P.; Greene, J. E.; Meirowitz, R. E.; Hofmann, S. L.; Woska, D. C.; Wilson, M.; Chang, R.; Chen, J.; Magnuson, R. H.; Eriks, K. *Organometallics* **1991**, *10*, 3479.

(4) (a) Bond, A. M.; Colton, R.; Mann, T. F. *Organometallics* **1988**, *7*, 749. (b) Bond, A. M.; Colton, R.; Feldberg, S. W.; Mahon, P. J.; Whyte, T. *Organometallics* **1991**, *10*, 3320.

(5) (a) Andreucci, L.; Diversi, P.; Ingrosso, G.; Lucherini, A.; Marchetti, F.; Adovasio, V.; Nardelli, M. *J. Chem. Soc., Dalton Trans.* **1986**, 803. (b) Diversi, P. *Abstracts of the Italian-Portuguese-Spanish Meeting in Inorganic Chemistry*, Gandia (Valencia), Spain, June 25–29, 1990; p 60. (c) Diversi, P.; Iacononi, S.; Ingrosso, G.; Laschi, F.; Lucherini, A.; Zanello, P. *J. Chem. Soc., Dalton Trans.* **1993**, 351.

(6) (a) Watson, P. L.; Parshall, G. W. *Acc. Chem. Res.* **1985**, *18*, 51. (b) Fendrick, C. M.; Marks, T. J. *J. Am. Chem. Soc.* **1986**, *108*, 425. (c) Thompson, M. E.; Baxter, S. E.; Ray Bulls, A.; Burger, B. J.; Nolan, M. C.; Santarsiero, B. D.; Schaefer, W. P.; Bercaw, J. E. *J. Am. Chem. Soc.* **1987**, *109*, 203. (d) Rothwell, I. P. In *Activation and Functionalization of Alkanes*; Hill, C. L., Ed.; Wiley: New York, 1989; p 151.

[†] Università di Pisa.

^{||} Università di Siena.

[§] Istituto di Chimica Quantistica ed Energetica Molecolare del CNR.

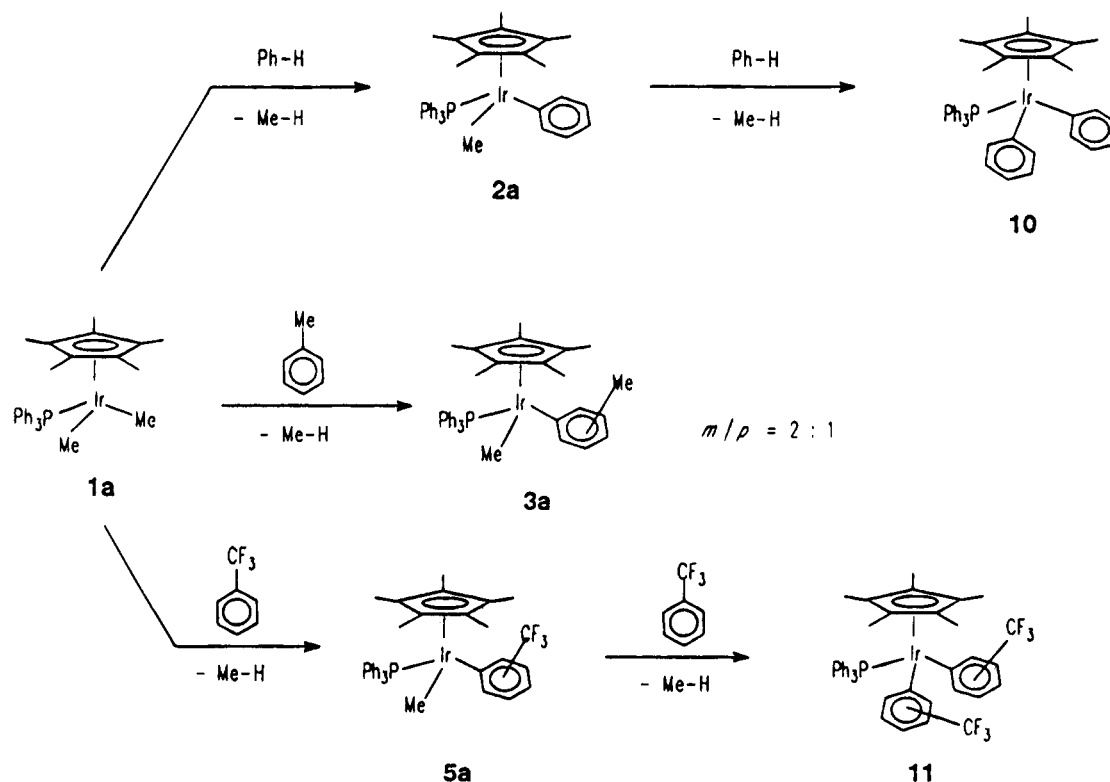
^{||} Centro del CNR per lo Studio delle Macromolecole Stereordinate ed Otticamente Attive.

[⊗] Abstract published in *Advance ACS Abstracts*, May 15, 1995.

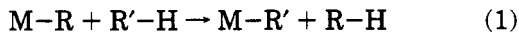
(1) (a) Kochi, J. K. *Organometallic Mechanism and Catalysis*; Academic Press: New York, 1978. (b) Chanon, M.; Tobe, M. L. *Angew. Chem., Int. Ed. Engl.* **1982**, *21*, 1. (c) Astruc, D. *Angew. Chem., Int. Ed. Engl.* **1988**, *27*, 643. (d) Astruc, D. *Chem. Rev.* **1988**, *88*, 1189. (e) Tyler, D. R. *Prog. Inorg. Chem.* **1988**, *36*, 125. (f) Tyler, D. R. *Acc. Chem. Res.* **1991**, *24*, 325. (g) Astruc, D. *Acc. Chem. Res.* **1991**, *24*, 36.

(2) Kochi, J. K. *J. Organomet. Chem.* **1986**, *300*, 139.

Scheme 1



bonds (eq 1). This reaction has been more commonly



observed for early transition or f-block⁶ and also for a few late⁷ transition metals under conditions of thermal activation.

Since the oxidation behavior of **1a** and **1b** is peculiar if compared with that of other one-electron oxidative cleavages of metal-carbon bonds reported in the literature for late d-block metals, e.g., organoruthenium,⁸ organocobalt,⁹ organorhodium,^{9c,10} organopalladium,¹¹ and organoplatinum¹² complexes, we decided to study more thoroughly the chemical and electrochemical oxidation of **1a** and **1b** both in the presence and in absence of arenes. The results of this study compared with the data of the thermolysis of **1a** and **1b** in arenes are reported in this paper.¹³

Results and Discussion

Thermolysis of 1a and 1b. The reactivity of **1a** and **1b** toward arenes has been studied under conditions of

(7) (a) Gomez, M.; Yarrow, P. I.; Robinson, D. J.; Maitlis, P. M. *J. Organomet. Chem.* **1985**, *279*, 115. (b) Lehmkuhl, H.; Bellenbaum, M.; Grundke, J.; Mauermann, H.; Krüger, C. *Chem. Ber.* **1988**, *121*, 1719. (c) Lehmkuhl, H.; Schwickardi, R.; Mehler, G.; Krüger, C.; Goddard, R. *Z. Anorg. Allg. Chem.* **1991**, *606*, 141.

(8) Aase, T.; Tilset, M.; Parker, V. D. *J. Am. Chem. Soc.* **1990**, *112*, 4974.

(9) (a) Witman, M. W.; Weber, J. H. *Inorg. Chim. Acta* **1977**, *23*, 263. (b) Tamblin, W. H.; Klingler, R. J.; Hwang, W. S.; Kochi, J. K. *J. Am. Chem. Soc.* **1981**, *103*, 3161. (c) Åkermark, B.; Almemark, M.; Jutand, A. *Acta Chem. Scand.* **1982**, *B36*, 451. (d) Vol'pin, M. E.; Levitin, I. Ya.; Sigán, A. L.; Nikitaev, A. T. *J. Organomet. Chem.* **1985**, *279*, 263. (e) Fukuzumi, S.; Ishikawa, K.; Tanaka, T. *J. Chem. Soc., Dalton Trans.* **1985**, 899.

(10) Pedersen, A.; Tilset, M. *Organometallics* **1993**, *12*, 56.

(11) Seligson, A. L.; Trogler, W. C. *J. Am. Chem. Soc.* **1992**, *114*, 7085.

(12) Chen, J. Y.; Kochi, J. K. *J. Am. Chem. Soc.* **1977**, *99*, 1450.

(13) (a) When this paper was at the point of being submitted for publication, a study of the oxidation chemistry of $\text{Cp}^*\text{Ir}(\text{PPh}_3)\text{Me}_2$ (**1a**) in acetonitrile was reported.^{13b} Owing to the coordination ability of acetonitrile, the reactivity is quite different from that described here.

(b) Pedersen, A.; Tilset, M. *Organometallics* **1994**, *13*, 4887.

(14) Tolman, C. A. *Chem. Rev.* **1977**, *77*, 313.

thermal activation. While **1b** is stable for months toward aliphatic and aromatic hydrocarbons at temperatures up to 140 °C (above this temperature decomposition starts to be significant), **1a** reacts slowly with arenes at temperatures higher than 70 °C; the thermolysis has been typically studied at 110 °C, this temperature providing a convenient reaction rate without appreciable decomposition (Scheme 1). Reaction with benzene gives methane and the methyl phenyl complex **2a**, which reacts further with benzene to give methane and the diphenyl derivative **10**.

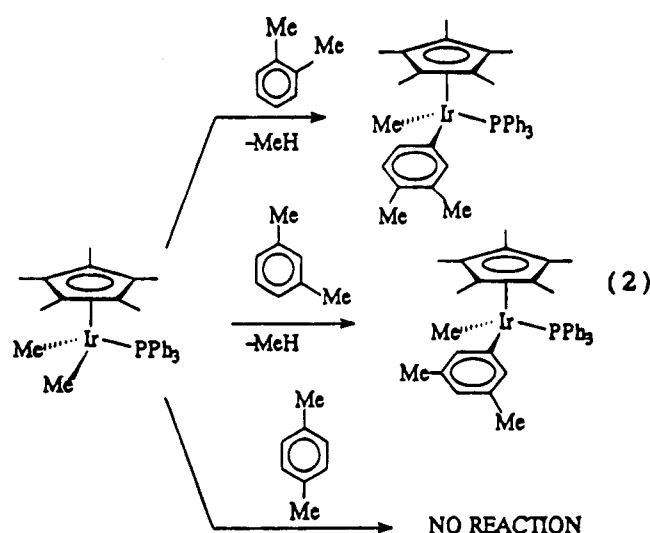
The reaction with benzene-*d*₆ is conveniently followed by ¹H NMR spectroscopy, and it is well described by a pseudo-first-order kinetic law for over 4 half-lives ($k = 2.55 \times 10^{-2} \text{ h}^{-1}$, $t_{1/2} = 27.2 \text{ h}$, $110 \pm 0.5 \text{ °C}$), **1a** being completely converted after 2 weeks. Since only MeD is formed and no intramolecular activation product has been detected, we suggest the hypothesis of a reaction intermediate deriving from the temporary loss of triphenylphosphine. This is consistent also with the complete inhibition of the reaction by an excess of free phosphine ($\text{PPh}_3/\mathbf{1a} = 4$) and with the thermal stability of **1b**, which is presumably only slightly dissociated in solution because of the smaller cone angle of trimethylphosphine with respect to the bulky triphenylphosphine.¹⁴ Analogously Maitlis et al.^{7a} have proposed that, in reactions of arene thermal activation by the related complex $\text{Cp}^*\text{Ir}(\text{DMSO})\text{Me}_2$ (DMSO = dimethyl sulfide), the loss of the DMSO ligand is a prerequisite for the oxidative addition of the arene C-H bond.

1a is able to activate other arenes (Scheme 1). The reaction of toluene is slightly slower than that of benzene ($k = 2.32 \times 10^{-2} \text{ h}^{-1}$, first-order rate law, $t_{1/2} = 29.9 \text{ h}$, in the case of toluene-*d*₈, by ¹H NMR spectroscopy), and the reaction product is a mixture of the *m*- and *p*-tolyl derivatives **3a** in a 2/1 ratio. The two isomers were identified by analysis of the ¹H NMR spectra of the reaction mixtures and by comparison with

the spectra of authentic samples prepared by stepwise alkylation of the dichloro complex $\text{Cp}^*\text{Ir}(\text{PPh}_3)\text{Cl}_2$. There is no evidence for the activation of the *ortho*, and benzyl C–H bonds, as well as for the formation of a diaryl complex.

Trifluorotoluene behaves like benzene since the methyl trifluorotolyl derivatives *m*- and *p*-**5a** (3/2 mixture) initially formed react further with the arene to be converted into the diaryl isomers **11** (95%, after 2 weeks at 110 °C). The regiochemistry of both reaction steps seems to be regulated by steric effects, only the *meta* and *para* C–H bonds being activated. The three major diaryl isomers **11** (four isomers have been actually detected, one of these being present in very low amounts) have not been isolated, and the mixture has been analyzed by ^1H NMR two-dimensional exchange (NOESY) spectroscopy, in benzene- d_6 solution at 25 °C. As shown in Table 1, the Cp^* protons gave distinct resonances for the three isomers at 1.19, 1.16, and 1.13 ppm; each of them gives rise to intramolecular interligand NOEs on the aromatic protons of the trifluorotolyl groups, thus allowing us to perform a complete structural assignment. The Cp^* protons at δ 1.19 gave NOEs only on the singlet at δ 7.95 and on the doublet at δ 7.42 and hence were attributed to the isomer containing two *m*-trifluorotolyl groups (**m,m'**-**11**). The Cp^* protons at δ 1.13, which gave NOEs only on the doublet at δ 7.01, were assigned to the isomer containing two *para*-substituted aromatic groups (**p,p'**-**11**). Finally, the Cp^* methyls at δ 1.16 originated the most complex NOE pattern: at δ 7.96 (singlet), 7.02 (doublet), and 7.41 (doublet); the signals at δ 7.02 and 7.41 showed *J*-coupling with the triplet at δ 6.60 and with the doublet at δ 7.05, respectively, thus indicating that this isomer contains one *m*- and one *p*-trifluorotolyl group (**m,p'**-**11**).

1a was also reacted with xylenes, giving selectively and almost quantitatively the methyl aryl derivative **m,m**-**4a** in the case of *m*-xylene and the **m,p**-**4a** isomer from *o*-xylene (*p*-xylene does not react at all) (eq 2).



These results clearly show the importance of steric factors on the course of the reaction and in particular the inertia of the C–H bonds *ortho* to the substituents.

Oxidatively Promoted Arene C–H Activation by **1a and **1b**.** Treatment of **1a** with benzene in the presence of small amount (10–15%) of $\text{Cp}_2\text{Fe}^+\text{PF}_6^-$ produces, after an induction period of a few seconds, a

rapid evolution of gas and a transient red-violet color at the solid–oxidant surface. Monitoring the reaction by ^1H NMR, we have observed the formation of ferrocene and CH_4 together with a new organometallic compound, which has been identified as the orthometal-

lated complex $\text{Cp}^*\text{Ir}(\text{C}_6\text{H}_4\text{PPh}_2)\text{Me}$ (**12**) (92% after 2 h) (Scheme 2). In fact the aromatic region of the ^1H NMR spectrum shows the typical pattern of the orthometalated triphenylphosphine, and the high-field resonance in the ^{31}P NMR spectrum ($\delta = -57.50$ in benzene- d_6) is consistent¹⁵ with the presence of a phosphorus atom in a four-membered ring (Table 1). Compound **12**, which is stable for months in benzene at 110 °C, when left in the presence of the oxidant, adds benzene, thus restoring the monohapto phosphine ligand and giving $\text{Cp}^*\text{Ir}(\text{PPh}_3)(\text{Me})(\text{Ph})$ (**2a**), which has been characterized by comparison with an authentic sample prepared by sequential alkylation of $\text{Cp}^*\text{Ir}(\text{PPh}_3)\text{Cl}_2$ first with MeMgI and then with PhMgBr . By monitoring the reaction with ^1H NMR, one finds that a maximum of 85% conversion of **12** in **2a** is reached after 16 h. The same product ratio (**2a**/**12** = 85/15) has been obtained by reaction of pure **2a** or **12** in benzene- d_6 in the presence of the oxidant. If the concentrations of **2a** and **12** are expressed as molar fractions, then $K_{\text{eq}} = \chi_{12}\chi_{\text{C}_6\text{H}_6}/\chi_{2a} = 0.18$ (molar $K_{\text{eq}} = 2.0$ M) and $\Delta G^\circ = 1.01$ kcal/mol (as a term of comparison, see the data by Jones and Feher for the reaction $\text{Cp}^*\text{Rh}(\text{PMe}_2\text{CH}_2\text{Ph})(\text{Ph})\text{H} \rightleftharpoons \text{Cp}^*\text{Rh}(\text{C}_6\text{H}_4\text{CH}_2\text{PMe}_2)\text{H} + \text{PhH}$, in which a relatively more stable five-membered ring is involved: $K_{\text{eq}} = 36.7$, $\Delta G^\circ = -2.32$ kcal/mol).¹⁶ This shows that the intermolecular reaction product **2a** is thermodynamically favored and that the intramolecular C–H activation product **12** is only kinetically preferred.

Pure **12** can be conveniently prepared and isolated by reaction of **1a** in dichloromethane in the presence of the ferrocenium cation: only the intramolecular activation product **12** is obtained, and no reaction with the solvent takes place.

The amount of $\text{Cp}_2\text{Fe}^+\text{PF}_6^-$ necessary to catalyze the reaction is only a fraction of the quantity employed, corresponding to 4–6% of the moles of **1a**, as evaluated by ^1H NMR on the basis of the ferrocene which is formed. A saturated benzene solution of the poorly soluble ferrocenium salt catalyzes the cyclometalation of **1** to **12** (although *ca.* 10^2 times less rapidly than in the presence of solid oxidant) but is not able to induce further reaction of **12** with benzene. In the presence of the ferrocenium salt, **1a** reacts also with several other arenes (toluene, xylenes, trifluorotoluene) to give the corresponding methyl aryl derivative *via* the formation of the intramolecular activation product **12**. The presence of the substituent on the ring introduces a complication due to the isomerism. The products have been identified by analysis of the $^1\text{H}\{^1\text{H}\}$ NOE difference or 2D NOESY spectra (benzene- d_6 , 25 °C), as previously described in detail for isomers **11**. The NMR spectral data are reported in Table 1. Part of the structural assignments were made by comparison with authentic samples prepared by a different route (see Experimental

(15) Garrou, P. E. *Chem. Rev.* **1981**, *81*, 229.

(16) (a) Jones, W. D.; Feher, F. J. *J. Am. Chem. Soc.* **1984**, *106*, 1650. (b) Jones, W. D.; Feher, F. J. *J. Am. Chem. Soc.* **1985**, *107*, 620. (c) Jones, W. D. In *Activation and Functionalization of Alkanes*; Hill, C. L., Ed.; Wiley: New York, 1989; p 111.

Table 1. NMR Spectral Data^a

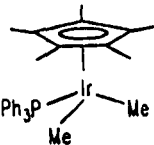
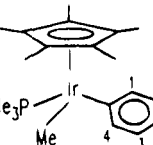
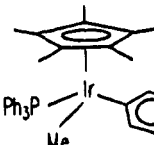
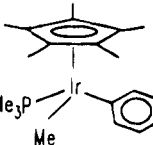
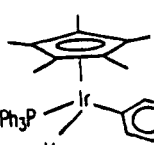
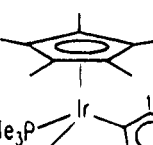
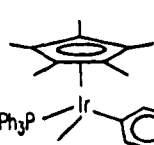
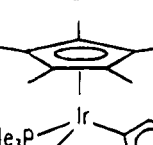
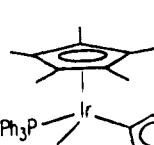
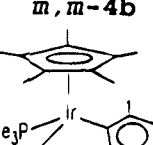
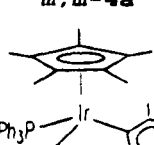
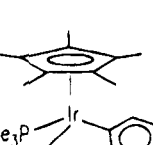
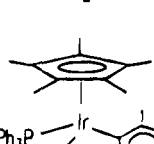
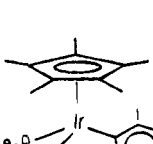
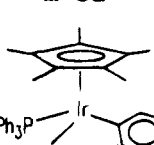
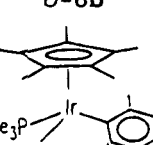
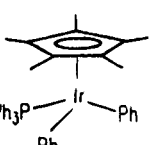
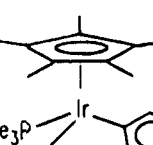
	¹ H	³¹ P		¹ H	³¹ P
	0.64 [d, 6 H, <i>J</i> (PH) 5.0, Ir-Me] 1.40 [d, 15 H, <i>J</i> (PH) 1.9, C ₅ Me ₅] 6.95-7.15 (m, 9 H, PPh ₃) 7.44-7.56 (m, 6 H, PPh ₃)	10.77		0.64 [d, 3 H, <i>J</i> (PH) 6.7, Ir-Me] 0.99 [d, 9 H, <i>J</i> (PH) 9.8, PMe ₃] 1.52 [d, 15 H, <i>J</i> (PH) 1.8, C ₅ Me ₅] 2.36 (s, 3 H, Me) 7.4-7.85 (m, 4 H, H ₁ - H ₂ - H ₃ + H ₄)	
1a			m-3b		
	0.86 [d, 3 H, <i>J</i> (PH) 6.0, Ir-Me] 1.34 [d, 15 H, <i>J</i> (PH) 1.8, C ₅ Me ₅] 6.8-7.5 (m, 20 H, PPh ₃ + Ph)	10.72		0.62 [d, 3 H, <i>J</i> (PH) 6.7, Ir-Me] 0.99 [d, 9 H, <i>J</i> (PH) 9.7, PMe ₃] 1.52 [d, 15 H, <i>J</i> (PH) 1.8, C ₅ Me ₅] 2.33 (s, 3 H, Me) 7.01 [d, <i>J</i> (HH) 7.7, H ₂], 7.38 [d, 2 H, <i>J</i> (PH) 7.9, H ₁]	
2a			p-3b		
	0.89 [d, 3 H, <i>J</i> (PH) 6.0, Ir-Me] 1.36 [d, 15 H, <i>J</i> (PH) 1.8, C ₅ Me ₅] 2.17 (s, 3 H, Me) 6.8-7.35 (m, 19 H, Ph)	10.89		0.66 [d, 3 H, <i>J</i> (PH) 6.6, Ir-Me] 1.01 [d, 9 H, <i>J</i> (PH) 9.6, PMe ₃] 1.54 [d, 15 H, <i>J</i> (PH) 1.8, C ₅ Me ₅] 2.24 (s, 3 H, Me) 2.29 (s, 3 H, Me) 6.97 [d, 1 H, <i>J</i> (HH) 7.5, H ₂] 7.01 [d, <i>J</i> (HH) 7.7, H ₃] 7.23 (s, 1 H, H ₁)	-38.07
m-3a			m, p-4b		
	0.89 [d, 3 H, <i>J</i> (PH) 6.0, Ir-Me] 1.36 [d, 15 H, <i>J</i> (PH) 1.8] 2.25 (s, 3 H, Me) 6.8-7.35 (m, 19 H, Ph)	10.67		0.66 [d, 3 H, <i>J</i> (PH) 6.6, Ir-Me] 1.01 [d, 9 H, <i>J</i> (PH) 9.7, PMe ₃] 1.54 [d, 15 H, <i>J</i> (PH) 1.8, C ₅ Me ₅] 2.36 (s, 6 H, Me) 6.73 (s, 2 H, H ₁) 7.16 (s, 1 H, H ₂)	
p-3a			m, m-4b		
	0.88 [d, 3 H, <i>J</i> (PH) 5.9, Ir-Me] 1.38 [d, 15 H, <i>J</i> (PH) 1.7, 15 H] 2.19 (s, 6 H, Me) 6.64 (s, 1 H, H ₂) 6.92 (s, 2 H, H ₁) 6.95-7.10 (m, 15 H, PPh ₃)			0.52 [d, 3 H, <i>J</i> (PH) 6.8, Ir-Me] 0.88 [d, 9 H, <i>J</i> (PH) 9.7, PMe ₃] 1.41 [d, 15 H, <i>J</i> (PH) 1.8, C ₅ Me ₅] 6.97 [t, 1 H, <i>J</i> (HH) 7.8, H ₃] 7.31 [d, 1 H, <i>J</i> (HH) 7.8, H ₂] 7.52 [d, 1 H, <i>J</i> (HH) 8.0, H ₄] 7.84 (s, 1 H, H ₃)	-38.36
m, m-4a			m-5b		
	0.89 [d, 3 H, <i>J</i> (PH) 6.0, Ir-Me] 1.37 [d, 15 H, <i>J</i> (PH) 1.8, C ₅ Me ₅] 2.08 (s, 3 H, Me) 2.19 (s, 3 H, Me) 6.87 [d, 1 H, <i>J</i> (HH) 8.1, H ₂] 7.02 (s, 1 H, H ₁) 7.14 [d, 1 H, <i>J</i> (HH) 7.9, H ₃] 6.95-7.10 (m, 15 H, PPh ₃)	10.77		0.50 [d, 3 H, <i>J</i> (PH) 7.1, Ir-Me] 0.86 [d, 9 H, <i>J</i> (PH) 9.5, PMe ₃] 1.40 [d, 15 H, <i>J</i> (PH) 1.8, C ₅ Me ₅] 7.32 [d, 2 H, <i>J</i> (PH) 8.2, H ₂] 7.43 [d, 2 H, <i>J</i> (HH) 8.2, H ₁]	-38.48
m, p-4a			p-5b		
	0.78 [d, 3 H, <i>J</i> (PH) 5.9, Ir-Me] 1.27 [d, 15 H, <i>J</i> (PH) 1.8, C ₅ Me ₅] 6.86 [t, 1 H, <i>J</i> (HH) 7.8, H ₃] 7.30 [d, 1 H, <i>J</i> (HH) 7.5, H ₂] 7.47 [d, 1 H, <i>J</i> (HH) 7.5, H ₄] 7.70 (s, 1 H, H ₁) 6.9-7.3 (b, 15 H, PPh ₃)			0.57 [d, 3 H, <i>J</i> (PH) 7.1, Ir-Me] 1.06 [d, 9 H, <i>J</i> (PH) 9.8, PMe ₃] 1.53 [d, 15 H, <i>J</i> (PH) 1.7, C ₅ Me ₅] 6.75-7.05 (m, 3 H, H ₂ + H ₃ - H ₄) 7.38 [dd, 1 H, <i>J</i> (HH) = <i>J</i> (HF) = 5.9, H ₁]	
m-5a			o-6b		
	0.78 [d, 3 H, <i>J</i> (PH) 6.0, Ir-Me] 1.25 [d, <i>J</i> (PH) 1.8, C ₅ Me ₅] 7.15 [d, 2 H, <i>J</i> (HH) 8.1, H ₂] 7.38 [d, 2 H, <i>J</i> (HH) 8.1, H ₁] 6.9-7.3 (m, 15 H, PPh ₃)			0.53 [d, 3 H, <i>J</i> (PH) 6.8, Ir-Me] 0.91 [d, 9 H, <i>J</i> (PH) 9.8, PMe ₃] 1.44 [d, 15 H, <i>J</i> (PH) 1.7, C ₅ Me ₅] 7.18 [d, 1 H, <i>J</i> (HH) 7.6, H ₄] 6.75-7.05 (m, 2 H, H ₂ + H ₃) 7.30 [d, 1 H, <i>J</i> (FH) 11.7, H ₁]	
p-5a			m-6b		
	1.32 [d, 15 H, <i>J</i> (PH) 1.9, C ₅ Me ₅] 6.9-7.6 (b m, 25 H, Ph - PPh ₃)	7.21		0.53 [d, 3 H, <i>J</i> (PH) 6.6, Ir-Me] 0.92 [d, 9 H, <i>J</i> (PH) 9.8, PMe ₃] 1.46 [d, 15 H, <i>J</i> (PH) 1.7, C ₅ Me ₅] 6.75-7.05 (m, 2 H, H ₂) 7.24 [dd, 2 H, <i>J</i> (HH) 6.8, <i>J</i> (FH) 6.6, H ₁]	
10			p-6b		

Table 1. (Continued)

	¹ H	³¹ P		¹ H	³¹ P
	1.19 [d, 15 H, <i>J</i> (PH) 1.4, C ₅ Me ₅] 6.67 [t, 2 H, <i>J</i> (HH) 5.0, H ₃] 7.19 [d, 2 H, <i>J</i> (HH) 5.6, H ₂] 7.42 [d, 2 H, <i>J</i> (HH) 5.6, H ₄] 7.95 (s, 2 H, H ₁) 6.9–7.3 (m, 15 H, PPh ₃)			0.52 [d, 3 H, <i>J</i> (PH) 6.6, Ir–Me] –39.23 0.90 [d, 9 H, <i>J</i> (PH) 9.9, PMe ₃] 1.43 [d, 15 H, <i>J</i> (PH) 1.8, C ₅ Me ₅] 6.88 [t, 1 H, <i>J</i> (HH) 8.5, H ₃] 7.14 [d, 1 H, <i>J</i> (HH) 8.8, H ₂] 7.25 [d, 1 H, <i>J</i> (HH) 8.5, H ₄] 7.58 (s, 1 H, H ₁)	
	1.16 [d, 15 H, <i>J</i> (PH) 1.2, C ₅ Me ₅] 6.60 [t, 1 H, <i>J</i> (HH) 5.0, H ₃] 7.02 [d, 1 H, <i>J</i> (HH) 4.8, H ₄] 7.05 [d, 2 H, <i>J</i> (HH) 5.4, H ₆] 7.18 [d, 1 H, <i>J</i> (HH) 5.4, H ₂] 7.41 [d, 2 H, <i>J</i> (HH) 5.4, H ₅] 7.96 (s, 1 H, H ₁) 6.9–7.3 (m, 15 H, PPh ₃)			0.50 [d, 3 H, <i>J</i> (PH) 6.9, Ir–Me] –39.40 0.90 [d, 9 H, <i>J</i> (PH) 9.6, PMe ₃] 1.44 [d, 15 H, <i>J</i> (PH) 1.6, C ₅ Me ₅] 7.13 [d, 2 H, <i>J</i> (HH) 8.5, H ₂] 7.25 [d, 2 H, <i>J</i> (HH) 8.5, H ₁]	
	1.13 [d, 15 H, <i>J</i> (PH) 1.4, C ₅ Me ₅] 7.01 [d, 4 H, <i>J</i> (HH) 5.0, H ₁] 7.30 [d, 4 H, <i>J</i> (HH) 5.0, H ₂] 6.9–7.3 (m, 15 H, PPh ₃)			0.50 [d, 3 H, <i>J</i> (PH) 6.9, Ir–Me] –39.25 0.91 [d, 9 H, <i>J</i> (PH) 9.7, PMe ₃] 1.42 [d, 15 H, <i>J</i> (PH) 1.8, C ₅ Me ₅] 6.82 [t, 1 H, <i>J</i> (HH) 7.5, H ₃] 7.25 [d, 1 H, <i>J</i> (HH) 7.5, H ₂] 7.27 [d, 1 H, <i>J</i> (HH) 7.5, H ₄] 7.73 (s, 1 H, H ₁)	
	0.76 [d, 3 H, <i>J</i> (PH) 6.3, Ir–Me] 1.62 [d, 15 H, <i>J</i> (PH) 2.3, C ₅ Me ₅] 6.85–7.25 (m, 10 H, PPh ₂) 7.27–7.35 (m, 2 H, H ₁ + H ₄) 7.72 [dt, 2 H, <i>J</i> (HH) 9.5, H ₂ + H ₃]	–57.50		0.48 [d, 3 H, <i>J</i> (PH) 6.7, Ir–Me] –39.44 0.88 [d, 9 H, <i>J</i> (PH) 9.6, PMe ₃] 1.43 [d, 15 H, <i>J</i> (PH) 1.7, C ₅ Me ₅] 7.19 [d, 2 H, <i>J</i> (HH) 8.5, H ₁] 7.30 [d, 2 H, <i>J</i> (HH) 8.5, H ₂]	
	0.43 [d, 6 H, <i>J</i> (PH) 5.7, Ir–Me] 1.04 [d, 9 H, <i>J</i> (PH) 9.5, PMe ₃] 1.63 [d, 15 H, <i>J</i> (PH) 1.8, C ₅ Me ₅]	–41.92		0.48 [d, 3 H, <i>J</i> (PH) 6.6, Ir–Me] 0.84 [d, 9 H, <i>J</i> (PH) 9.6, PMe ₃] 1.35 [d, 15 H, <i>J</i> (PH) 1.8, C ₅ Me ₅] 6.83 [t, 1 H, <i>J</i> (HH) 7.5, H ₂] 7.54 [d, 1 H, <i>J</i> (HH) 7.5, H ₄] 7.89 [d, 1 H, <i>J</i> (HH) 7.5, H ₂] 8.43 (s, 1 H, H ₁)	
	0.62 [d, 3 H, <i>J</i> (PH) 6.8, Ir–Me] 0.97 [d, 9 H, <i>J</i> (PH) 9.5, PMe ₃] 1.51 [d, 15 H, <i>J</i> (PH) 1.8, C ₅ Me ₅] 7.1–7.25 (m, 3 H, H ₂ + H ₃) 7.48 [dd, 2 H, <i>J</i> (HH) 7.9, <i>J</i> (HH) 1.6, H ₁]	–38.92		0.43 [d, 3 H, <i>J</i> (PH) 6.6, Ir–Me] 0.81 [d, 9 H, <i>J</i> (PH) 9.3, PMe ₃] 1.37 [d, 15 H, <i>J</i> (PH) 1.8, C ₅ Me ₅] 7.33 [d, 2 H, <i>J</i> (HH) 8.4, H ₁] 7.89 [d, 2 H, <i>J</i> (HH) 8.4, H ₂]	

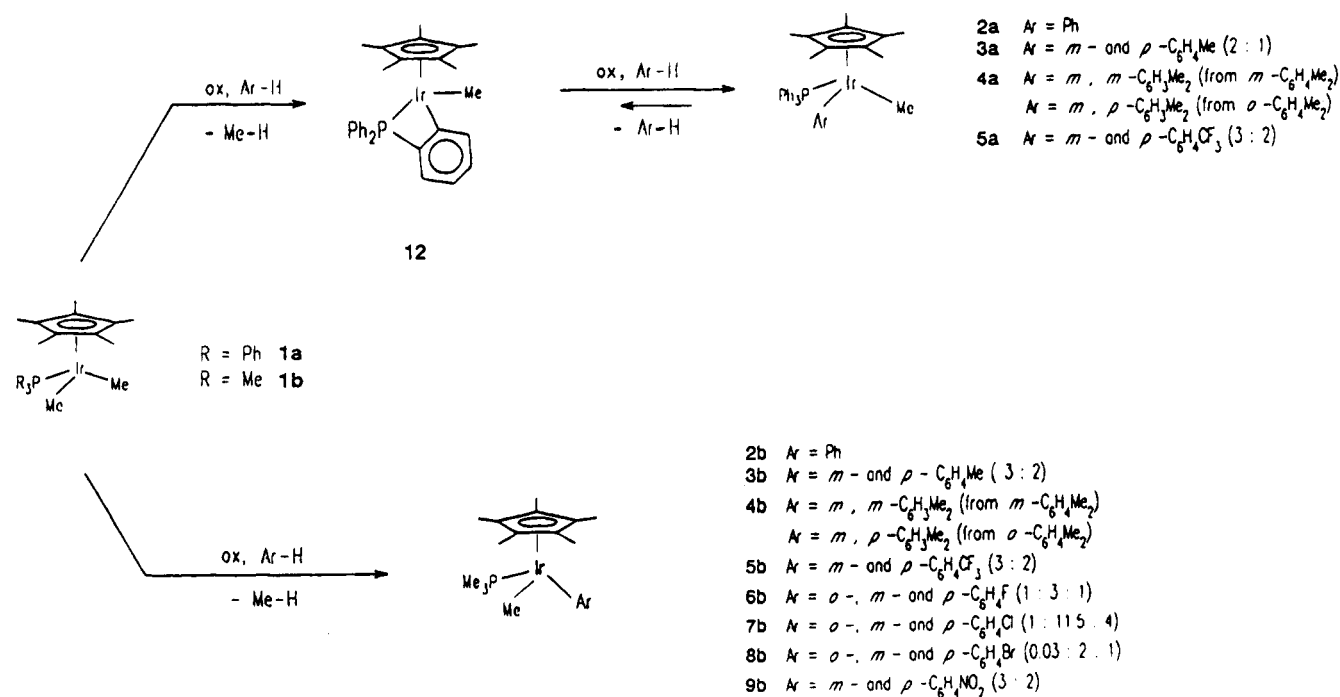
^a Spectra obtained in benzene-*d*₆; given as chemical shift (δ) [multiplicity, relative intensity, coupling (*J* in Hz), assignment]. ¹⁹F NMR, δ: *m*-5b, 7.70; *p*-5b, 8.52.

Section). As already noted for the thermolysis reactions of **1a**, in all cases the *ortho* positions do not react, presumably for steric reasons. So in toluene only the *meta* and *para* C–H bonds are activated with the *meta/para* ratio (2/1) corresponding to the statistical value, and in the case of xylenes only *o*- and *m*-xylene react to give respectively *m,p*- and *m,m*-**4a**. No evidence for benzylic C–H activation has been acquired. The equilibrium between the inter- and intramolecular activation product seems to depend on the number of reactive C–H bonds: the conversion of **12** into the intermolecular product is 75% in the reaction with toluene, 60% with *o*-xylene, 40% with *m*-xylene, and 0% with *p*-xylene. Unexpectedly, reaction of **1a** with trifluorotoluene (having almost identical steric requirements as toluene) only affords the intermolecular activation

product Cp*Ir(PPh₃)(Me)(C₆H₄CF₃) (**5a**) as a (3/2) mixture of the *meta* and *para* isomers.

In order to study the potentiality of the reaction and to avoid complications due to orthometalation of the phosphine, we have examined the reactions of the complex Cp*Ir(PMe₃)Me₂ (**1b**), which is expected to be more resistant to cyclometalation. In fact **1b** reacts with benzene in the presence of ferrocenium hexafluorophosphate under the same conditions given above to give (quantitatively, in 1 h) Cp*Ir(PMe₃)(Me)(Ph) (**2b**), which can be easily isolated by column chromatography followed by crystallization. When treated with benzene-*d*₆, a mixture of CH₄ and CH₃D is produced, the relative amounts being 2/3. This is a clear indication of two competitive patterns: a direct reaction between **1b** and benzene-*d*₆ and a ligand C–H activation to an unstable

Scheme 2



product, followed by fast reaction with benzene-*d*₆ to give **3b-d**₆. ²H NMR spectroscopy shows indeed the presence of deuterium on the pentamethylcyclopentadienyl ligand ($\delta = 3.98$) (in addition to the Ir-C₆D₅ resonances), thus giving evidence of this ligand as a source of hydrogen atoms. It has already been observed in the literature^{10c,d} that, in some C-H activation reactions by cyclopentadienylmetal derivatives, metalation of the Cp* ligand can occur to give a transient "tucked-in" derivative (see below). It is plausible that Cp* activation, in addition to direct orthometalation of the phosphine, is also operating in the case of **1a**. An estimate of the kinetic isotopic effect has also been made by reacting **1b** with benzene/benzene-*d*₆ mixtures in various proportions and evaluating the Ir-C₆H₅/Ir-C₆D₅ ratio by ¹H NMR spectroscopy: a rather moderate value of 2.2 was found for k_H/k_D .

The reaction works equally well with substituted arenes (Scheme 2), thus providing a facile route to the synthesis of methylaryliridium derivatives. In the case of toluene, a mixture of the *m*- and *p*-isomers Cp*Ir(PMe₃)(Me)(C₆H₄Me) (**3b**) is obtained in a 3/2 ratio, while in the case of xylenes, only Cp*Ir(PMe₃)(Me)(*m,p*-C₆H₃Me₂) (**4b**) is formed from *o*-xylene, Cp*Ir(PMe₃)(Me)(*m,m*-C₆H₃Me₂) (**4b**) from *m*-xylene, and nothing from *p*-xylene. Other monosubstituted arenes (fluorobenzene, chlorobenzene, bromobenzene, trifluorotoluene, nitrobenzene) react to give a mixture of the *m*- and *p*-isomers, their ratio being always close to the statistical value, independent of the electron-withdrawing or -releasing power of the group.

The kinetic selectivity of **1b** toward substituted arenes was also investigated. An ¹H NMR study of the reaction with benzene-*d*₆ or toluene-*d*₈ under pseudo-first-order conditions showed good first-order plots, although the rate constants are not very reproducible owing to the heterogeneity of the system. We therefore followed the reaction of equimolar mixtures of arenes, and assuming that the same first-order law is valid in all cases, we have derived the following relative scale of reactivity (the values of the relative kinetic constants are given

in parentheses): Ar-H (8.8) > Ar-F (4.4) > Ar-Me = Ar-Cl = Ar-Br (4) > Ar-CF₃ = ArNO₂ (1). All these data seem to exclude the influence of electronic factors in determining the selectivity of the reaction. The regiochemistry too does not seem to depend on electronic factors, since in the reactions with benzene, toluene, and xylenes the kinetic constants relative to the number of active positions of the arene are practically identical.

k_{rel}	6.6	3	2	1
$k_{rel}/act. pos$	1.1	1	1	1

In order to exclude a thermodynamic control of the observed selectivity operating through scrambling reactions between the σ -bonded aryl group and free arene, the methyl aryl derivatives have been treated with benzene in the presence of the oxidant. Since in no case has the σ -aryl ligand been substituted by the phenyl group, we must conclude that the selectivity is kinetic indeed.

Other 1-electron oxidants have been tested as promoters for the activation of benzene by **1a** and **1b**. While Fe(acac)₃ and methylviologen dichloride do not give any reaction, AgBF₄ and Ph₃C⁺BF₄⁻ behave like ferrocenium hexafluorophosphate, giving **2b** from **1b** and a 15/85 mixture of **12** and **2a** from **1a** (the same equilibrium composition obtained with the ferrocenium cation).

With the aim of establishing if the above reactivity could be exhibited by other metal dialkyls, we have also studied the reactivity of related iridium(III) and rhodium(III) dialkyl derivatives, Cp*Ir(PPh₃)R₂ (R = CH₂-SiMe₃ (**13**); R₂ = CH₂SiMe₂CH₂ (**14**), Cp*Rh(PR'₃)Me₂ (R' = Ph (**15a**), Me (**15b**)), and Cp*Rh(PPh₃)R₂ (R = CH₂SiMe₃ (**16**); R₂ = CH₂CMe₃CH₂ (**17**)), with Cp₂Fe⁺-

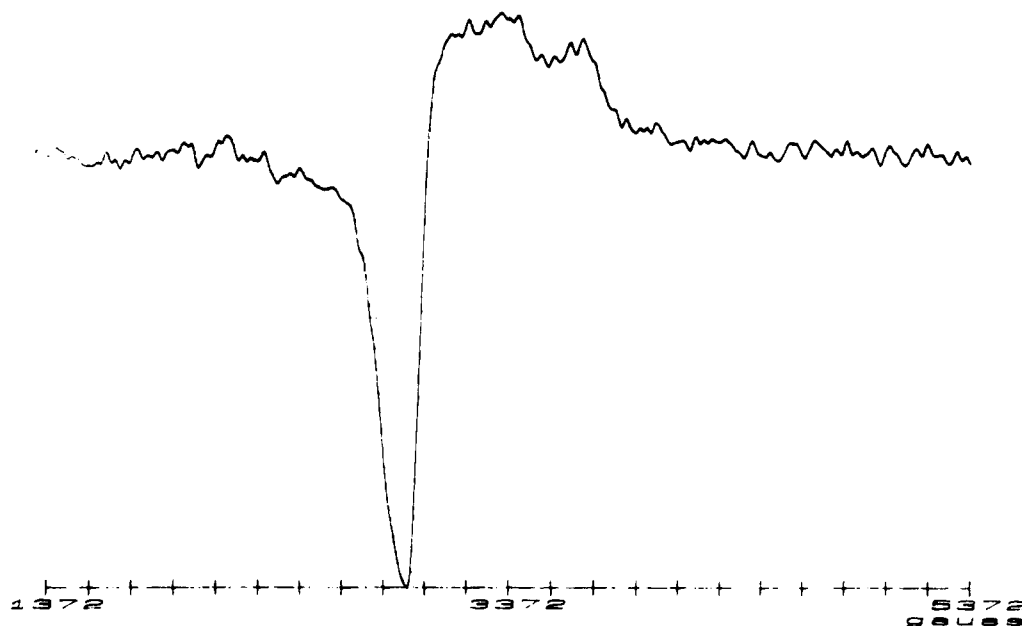


Figure 1. ESR spectrum at 120 K of the species obtained by reaction of **1a** with AgBF_4 in CH_2Cl_2 .

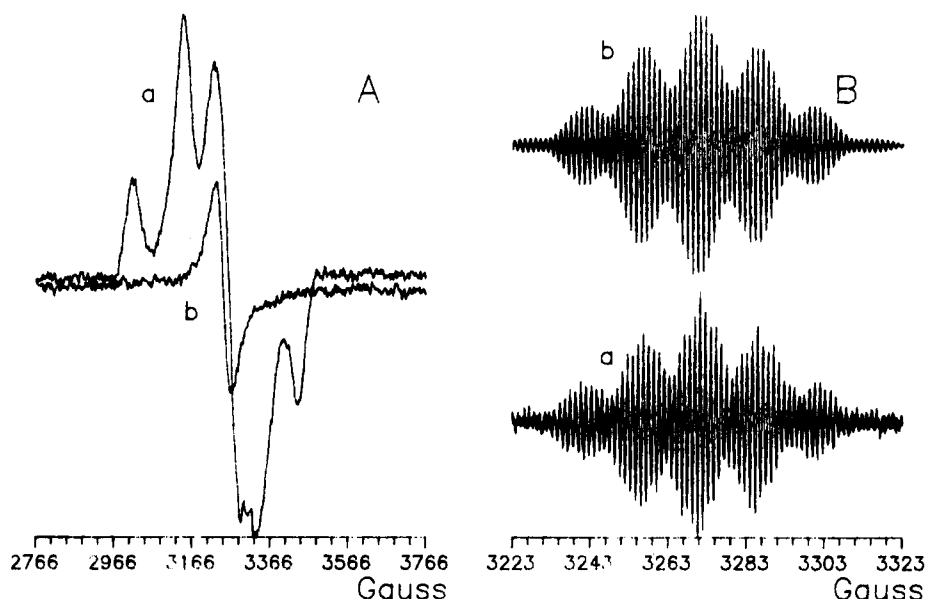


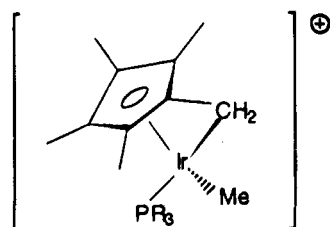
Figure 2. ESR spectra of the species obtained by reaction of **1b** with AgBF_4 in CH_2Cl_2 .

PF_6^- in benzene: we never observed activation of aromatic C-H bonds. The reaction leads to the almost stoichiometric oxidation (on the basis of the amounts of formed ferrocene) of the dialkyl complex, yielding a deep-red/deep-green gummy solid. Oxidation is accompanied by decomposition of the dialkyl groups, as shown by the formation of SiMe_4 and CH_4 in the case of complexes **13**, **14**, **16**, and **17** and of C_2H_6 and CH_4 in the case of rhodium compounds **15a** and **15b** (analogous results have been reported by Tilstet¹⁰ for the oxidation of **15a** in CH_2Cl_2). We were unable to isolate the resulting organometallic products.

ESR Studies of the Chemical Oxidation of **1a, **1b**, and Related Iridium Dialkyls.** In order to acquire some mechanistic information on the above reactions, we initiated an ESR study of the oxidation of **1a** and **1b**. Preliminary experiments, carried out using various ferrocenium salts, revealed that the presence of iron(III) centers could mask the observation of spectra associated with the *in situ* generated iridium paramagnetic species, perhaps as a consequence of intermolecu-

lar spin-spin interactions. Moreover, because of the poor solubility of the cationic iridium oxidation products in arenes, we chose to use CH_2Cl_2 as the solvent. AgBF_4 in CH_2Cl_2 was conveniently used. Under these conditions, the oxidation of **1a** proceeds easily even at low temperature (120 K, solid state), generating a species **1a**⁺, the ESR spectrum of which ($g_{\perp} = 2.1720$; $g_{\parallel} = 1.8120$) is reported in Figure 1. Analogously, by oxidation of **1b** at 173 K an ESR-active species **1b**⁺ which gives rise to a single-line signal centered at $g_{\text{iso}} = 2.0090$ (Figure 2a) is obtained. When the sample is cooled to 82 K, the spectrum appears as the superposition of two sets of signals, each having three different g values (this could be due to the presence of two isomeric forms resulting from the existence of two different positions of the Cp ring with respect to the other ligands). Due to the lack of hyperfine structure, a detailed determination of the structure of the primary 1-electron-oxidation products **1a**⁺ and **1b**⁺ is not possible. Raising the temperature above 173 K causes the intensity of the above ESR patterns to decrease slowly in both cases

until, at 253 K, vigorous evolution of methane starts to occur and new spectra appear. The spectra of the two species are practically identical, but owing to the longer lifetime, only in the case of the cation radical deriving from **1b** is the spectrum ($\Delta H_{pp} = 0.8$ G) sufficiently intense to be satisfactorily compared to a computer-simulated one (Figure 2B(b)), which is consistent with a radical having a spin delocalization confined to two sets of two methyl groups ($a_H = 14.6$ G and $a_H = 2.7$ G), to the iridium atom ($a_{Ir} = 2.7$ G), and finally to one methylene group ($a_H = 1.35$ G). Furthermore, oxidation of $Cp^*Ir(PMe_3)(CD_3)_2$ **1b-d₆** gives a radical displaying almost the same spectrum, apart from a small decrease of the signal width. On this basis, we attribute to these radicals the "tucked-in"^{6c,d} structure



This is nicely consistent with the observed partial substitution of a hydrogen by a deuterium atom in the Cp^* ligand after the reaction of **1b** with benzene- d_6 and strongly supports the role of the "tucked-in" intermediate in the intramolecular mechanistic pathway of the arene activation reactions (see above). It is worthwhile to stress that, according to ESR evidence, the Cp^* methyl groups are metalated even in the case of **1a**, where chemical oxidation in dichloromethane eventually causes metalation of the triphenylphosphine ligand.

Similar experiments performed on the dialkyl derivatives **13** and **14** have shown the formation at low temperature (113 K, solid state) of the corresponding paramagnetic species **13⁺** ($g_{\perp} = 2.191$, $g_{\parallel} = 1.963$) and **14⁺** ($g_{\perp} = 1.9642$, $g_{\parallel} = 2.2101$). At 233 K the spectrum of **13⁺** appears as a single-line signal ($g = 2.139$). The signals slowly disappear when the temperature is raised, and no new signals are detected.

Electrochemical Oxidation of 1a, 1b, and Related Rhodium and Iridium Dialkyls. The cyclic voltammetric responses shown in Figure 3 give evidence for the different redox aptitudes of **1a** and **1b**, in dichloromethane solution, at ambient temperature.

Both complexes undergo an anodic process, which, in controlled-potential coulometry, consumes 1 electron/molecule; in the case of **1a**, the oxidation process displays features of chemical reversibility, whereas for **1b**, fast chemical complications follow the electron transfer.

Analysis¹⁷ of the cyclic voltammetric responses relative to **1a**, with the scan rate v varying from 0.02 to 20.48 $V s^{-1}$, shows that (i) the peak current ratio i_{pc}/i_{pa} is constantly equal to 1, (ii) the peak-to-peak separation, ΔE_p , progressively increases from 68 to 374 mV, and (iii) the current function $i_{pa}/v^{1/2}$ remains substantially constant. Taking into account that, under the same experimental conditions, the 1-electron oxidation of ferrocene displays a similar increase of ΔE_p with scan rate, one can conclude that the **1a/1a⁺** oxidation involves a chemically and electrochemically reversible 1-electron removal, at least in the short time scale of cyclic voltammetry [$t_{1/2}(\mathbf{1a}^+) \approx 30$ s]. As a matter of

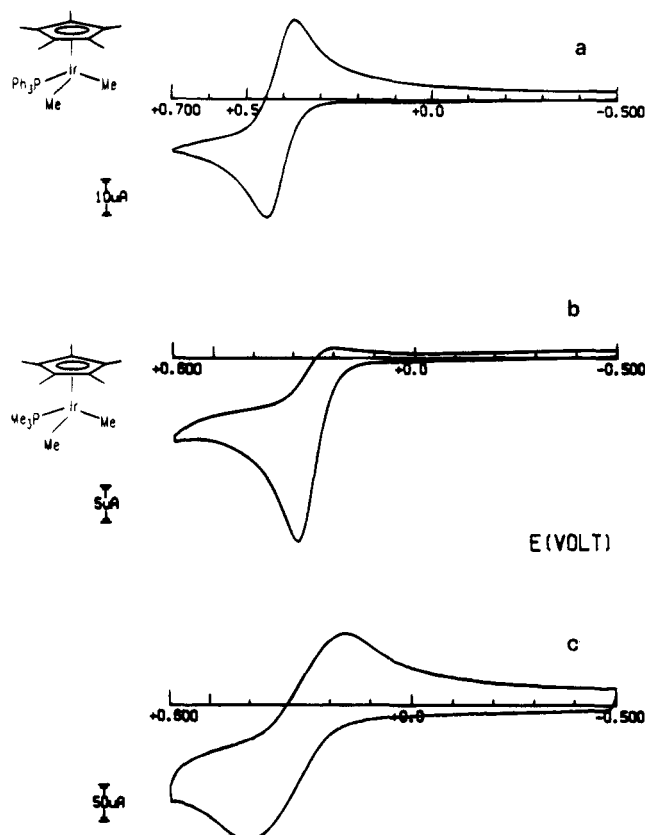


Figure 3. Cyclic voltammograms recorded at a platinum electrode on CH_2Cl_2 solutions containing $[NBu_4][ClO_4]$ (0.2 mol dm^{-3}) and (a) **1a** (2.1×10^{-3} mol dm^{-3}) or (b, c) **1b** (1.5×10^{-3} mol dm^{-3}). Scan rates: (a, b) 0.2 $V s^{-1}$; (c) 20.48 $V s^{-1}$.

fact, in the longer times of macroelectrolysis at ambient temperature, full decomposition of the exhaustively electrogenerated cation **1a⁺** occurs. During the test, the starting pale yellow solution first turns red-violet and then degrades slowly to yellow. Quite similar results have been obtained by Tilset.^{13b} At the end of the electrolysis, cyclic voltammetry shows no more evidence of the presence of the **1a/1a⁺** couple. Nevertheless, by performing the macroelectrolysis test at -20 °C, we see that the red-violet color of the 1-electron-oxidized species **1a⁺** persists in solution for a time sufficiently long to allow its ESR spectrum to be recorded (see below). It has to be noted that the initial red-violet color was also obtained at the first stages of the above described chemical oxidation.

As for the analysis of the cyclic voltammetric responses of **1b** at increasing scan rates, the most significant parameter, the i_{pc}/i_{pa} ratio, progressively increases from 0.26 at 0.2 $V s^{-1}$ to 1 at 20.48 $V s^{-1}$. This allows us¹⁷ to assign a lifetime ($t_{1/2}$) of about 0.05 s to the primarily electrogenerated monocation **1b⁺**.

Table 2 summarizes the redox potentials for the electron removals exhibited by the complexes here studied.

Interestingly, the presence of the more basic PMe_3 ligand in **1b** favors the thermodynamic access to the corresponding Ir(IV) cation, which however is kinetically more labile. A similar difference in kinetic stability of the 1-electron-oxidized species holds for the iridium

(17) Brown, E. R.; Sandifer, J. In *Physical Methods of Chemistry. Electrochemical Methods*; Rossiter, B. W., Hamilton, J. F., Eds.; Wiley: New York, 1986; Vol. 2, Chapter 4.

Table 2. Electrochemical Characteristics of the Oxidation Processes of the Iridium and Rhodium Complexes

complex	$E^{o'}$ (0/+) (V, vs SCE)	E_p (mV)	i_{pc}/i_{pa}^a	$t_{1/2}$ (mono- cation) ^b (s)	solvent
1a	+0.41	82 ^a	1	≥ 30	CH ₂ Cl ₂
	+0.42 ^c				CH ₂ Cl ₂
	+0.64	108 ^a	1	≥ 30	THF
	+0.41 ^c				MeCN
1b	+0.28	114 ^d	0.26	≈ 0.05	CH ₂ Cl ₂
12	+0.51	116 ^d	0.21	≈ 0.04	CH ₂ Cl ₂
13	+0.31	80 ^a	0.55	≈ 1	CH ₂ Cl ₂
	+0.54	170 ^b	0.50	≈ 1	THF
14	+0.09	70 ^a	1	≥ 30	CH ₂ Cl ₂
15a	+0.49 ^{a,e}		<i>f</i>	≤ 0.01	CH ₂ Cl ₂
	+0.5 ^c				MeCN/CH ₂ Cl ₂
15b	+0.36	126 ^d	0.34	≈ 0.2	CH ₂ Cl ₂
16	+0.34 ^{a,e}		<i>f</i>	≤ 0.01	CH ₂ Cl ₂
17	+0.14 ^{a,e}		<i>f</i>	≤ 0.01	CH ₂ Cl ₂

^a Measured at 0.2 V s⁻¹. ^b Cyclic voltammetric time scale. ^c Reference 13b. ^d Measured at 1.0 V s⁻¹. ^e Peak potential value. ^f No associated peak in the reverse scan.

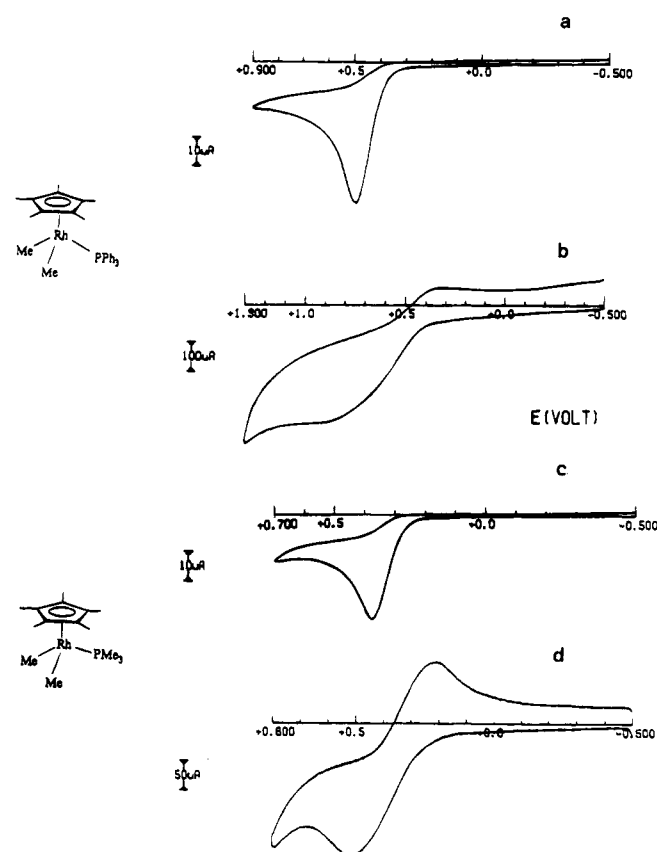


Figure 4. Cyclic voltammograms recorded at a platinum electrode on CH₂Cl₂ solutions containing [NBu₄][ClO₄] (0.2 mol dm⁻³) and (a, b) **15a** (2.1 × 10⁻³ mol dm⁻³) or (c, d) **15b** (1.7 × 10⁻³ mol dm⁻³). Scan rates: (a, c) 0.2 V s⁻¹; (b) 51.20 V s⁻¹; (d) 20.48 V s⁻¹.

dialkyls **13** and **14**. As a matter of fact, the cyclic voltammogram of **14** shows features of chemical reversibility, whereas that of **13** shows evidence of relatively fast complications following the electron removal.

Nevertheless, the most dramatic difference in redox properties is found between iridium and rhodium analogues. As an example, Figure 4 shows the cyclic voltammetric behavior of the rhodium dimethyl complexes **15a** and **15b**, analogues of the iridium complexes **1a** and **1b**. As illustrated, the 1-electron oxidation is again coupled to fast chemical complications, but in this case, the presence of the electron-donating PMe₃ ligand

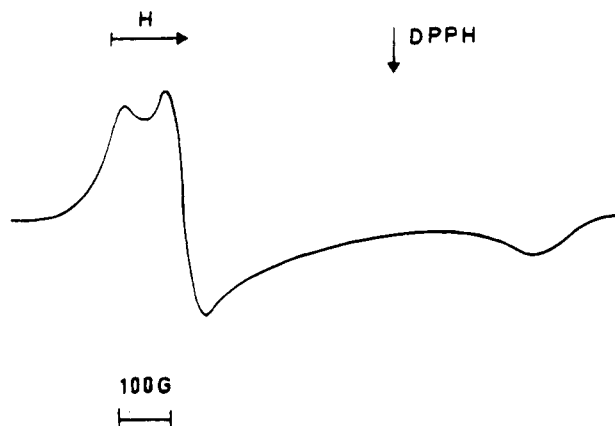


Figure 5. X-band ESR spectrum of the electrogenerated monocation [**1a**]⁺ in CH₂Cl₂ solution at $T = 100$ K.

favors both thermodynamically and kinetically the formation of the monocation.

Analogously, complex **16**, the rhodium congener of **13**, and complex **17** exhibit a response qualitatively similar to that of **15a**.

An interesting question arises from the fact that we were unable to electrochemically induce the chemically induced catalytic conversion of **1a** to **12** via loss of methane. In fact, in dichloromethane solution, **12** undergoes a 1-electron oxidation complicated by subsequent chemical reactions at potential values only slightly more anodic than that for **1a** ($\Delta E \approx 0.1$ V). This means that the driving force of the expected catalytic process should be rather low.^{1c} Nevertheless, even with the macroelectrolysis test performed at potential values corresponding to the rising part of the wave of **1a** (0.33 V $\leq E_w \leq 0.40$ V), in order to avoid the concomitant oxidation of the possibly electrogenerated species **12**, 1 electron/molecule is slowly consumed and the resulting solution does not exhibit any more significant redox properties. These electrochemical results prelude the fact that chemical and electrochemical oxidations follow different pathways. This was confirmed by the coupled electrochemical/ESR measurements.

ESR Characterization of the Electrogenerated Iridium(IV) Species 1a⁺, 13⁺, and 14⁺. Figure 5 shows the liquid nitrogen (100 K) X-band ESR spectrum of the monocation **1a**⁺, obtained by macroelectrolysis in CH₂Cl₂ solution at 253 K. The sample was withdrawn at the first stages of electrolysis (0.3 electron/molecule).

The anisotropic signal displays a well-resolved spectral pattern with orthorhombic symmetry, which can be suitably interpreted in terms of a $S = 1/2$ spin Hamiltonian. The relevant parameters have been evaluated by computer-simulated line shape analysis and are reported in Table 3.⁴

These glassy-solution parameters are characteristic of significant orbital contribution and are evidence for the metal-in nature of the $S = 1/2$ unpaired electron. There is no evidence for hyperfine (hpf) couplings of the unpaired electron with the magnetically active ¹⁹¹Ir and ¹⁹³Ir nuclei ($I = 3/2$), as well as for superhyperfine (shpf) coupling with the ³¹P nucleus ($I = 1/2$), probably because of the relatively large overall linewidth which overlaps any less separated hpf and shpf signals.¹⁸

When the temperature is raised, the signal rapidly drops out at the glassy/liquid phase transition, but upon

Table 3. X-Band ESR Parameters of the Electrogenerated Iridium(IV) Species in CH₂Cl₂ Solution

species	100 K				300 K	
	g_i	g_m	g_h	$\langle g \rangle$	g_{iso}	ΔH (G ^a)
[1a] ⁺	2.387	2.315	1.846	2.183		
[13] ⁺	2.326	2.239	1.943	2.169	2.015 ^d	160 ^a
[14] ⁺	2.160 ^b	2.011 ^c		2.110	2.111	80

^a ± 5 G. ^b ⊥ absorption. ^c || absorption. ^d $g_{averaged} \pm 0.008$. $g_i \pm 0.004$.

freezing again, the starting absorption signal is restored. This reversible temperature dependence is highly indicative of the stability of the electrogenerated 1a⁺ complex while the corresponding spectral features give ESR evidence that active molecular distortions around the paramagnetic metal center are present, particularly under fast-motion conditions.

The paramagnetic cation 13⁺ displays a liquid-nitrogen X-band ESR spectrum similar to that of 1a⁺, with a large metal-in character signal (although of slightly reduced rhombic symmetry) and a significant orbital contribution. The relevant parameters are reported in Table 3. When the temperature is raised, the overall anisotropic line shape rapidly loses its rhombic pattern before the glassy/liquid phase transition, displaying a large, unresolved signal at $T > 180$ K (at 300 K, $\Delta H = 160$ G and $g_{av} = 2.015$). Again line shape analysis does not give evidence of hpf or shpf splittings because of the broad absorption pattern.

Finally, the monocation 14⁺ shows some interesting differences in terms of line shape analysis, at both liquid-nitrogen and room temperatures. Figure 6a shows the relevant X-band ESR spectrum recorded at 100 K.

The well-shaped axial parameters ($g_{\perp} > g_{\parallel}$) can be interpreted in terms of a $S = 1/2$ spin Hamiltonian and are indicative of an arrangement around the metal-centered unpaired electron more symmetrical than the previous rhombic ones. The corresponding computed spectrum is shown in Figure 6b, and the relevant parameters are reported in Table 3.

As illustrated in Figure 6c, when the temperature is raised, the line shape evolves to a single, relatively narrow unresolved isotropic signal centered at $g_{iso} = 2.111$, which displays a significant reduction of the spectral intensity, probably as a consequence of the chemical instability of the monocation. Once again, the actual large isotropic absorption pattern ($\Delta H = 80$ G) likely does not permit the detection of the magnetic couplings with the ¹⁹¹Ir, ¹⁹³Ir, and ³¹P nuclei. On the other hand, the peak-to-peak separation (ΔH) at 300 K, narrower than that of 13⁺, is indicative of longer electron spin relaxation times, in agreement with a more symmetric arrangement of the overall molecular framework around the unpaired electron.¹⁸ Thus the bulk of evidence shows that all the above electrochemically generated cations are metal-centered paramagnetic species and do not evolve to the AgBF₄-generated radicals.

Conclusions

The large increase in the reactivity toward arenes that the dimethyl complexes 1a and 1b exhibit in the presence of catalytic amounts of oxidants places the C–H activation reaction here described among the

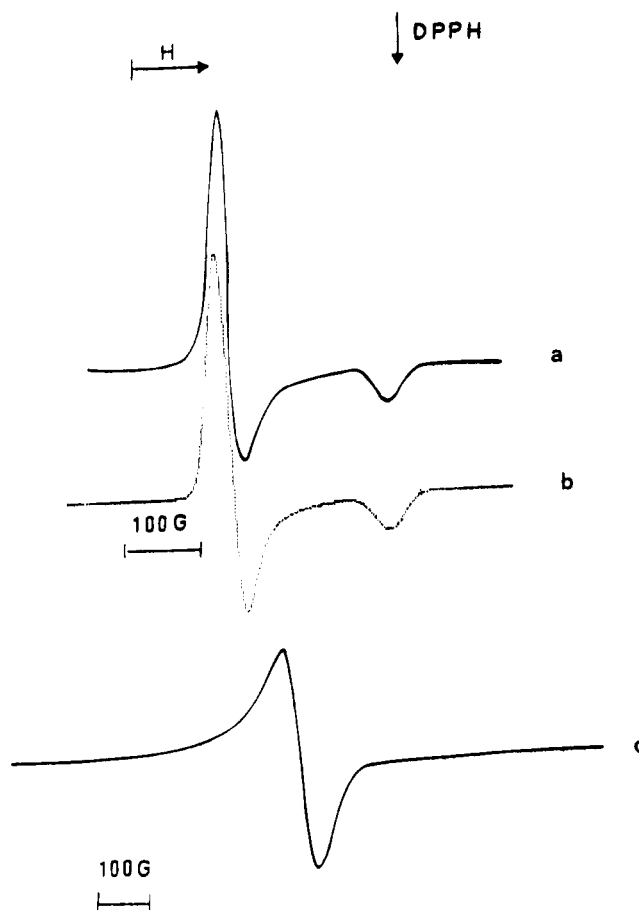
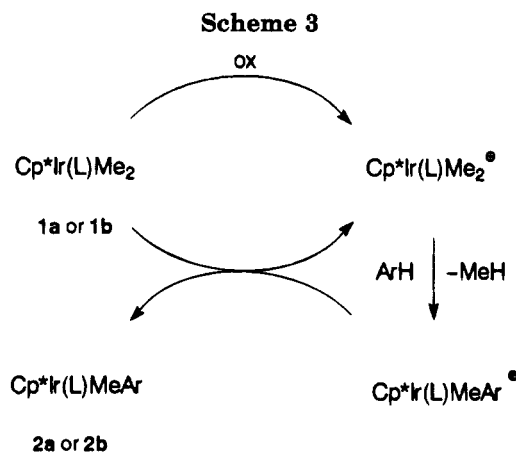


Figure 6. X-band ESR spectra of [14]⁺ in CH₂Cl₂ solution: (a) experimental and (b) simulated spectra at $T = 100$ K; (c) experimental spectrum at $T = 300$ K.



restricted number of electron transfer chain (ETC) catalyzed organometallic reactions.^{1b,c} According to this mechanistic scheme, the iridium species $\text{Cp}^*\text{Ir}(\text{L})\text{Me}_2^+$ ($\text{L} = \text{PPh}_3, \text{PMe}_3$), deriving from a 1-electron oxidation of 1a or 1b, reacts rapidly with arenes to yield a cationic iridium derivative; this in turn oxidizes 1a or 1b and gives rise to the final methyl aryl compound 2a or 2b (Scheme 3).

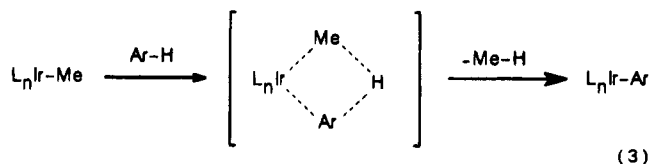
The cross-ET propagation step should probably be only slightly exergonic (and then rather slow) since the methyl ligand is just a bit more electron-releasing than an aryl one. As a consequence, the reactions are not very fast if compared with other more exergonic ETC reactions reported in the literature.¹ Fortunately, side reactions, a serious problem in ETC catalysis, do not seem to be too important in our cases.

Unfortunately electrochemical studies, which are generally quite informative about ETC reactions, are not very helpful in this case in supporting the reliability of such scheme; actually voltammetric techniques in CH_2Cl_2 show that $\mathbf{1a}^+$ does not convert to the ortho-metalated complex $\mathbf{12}$ as happens in the chemically induced reaction of $\mathbf{1a}$ in dichloromethane.

On the other hand, the radicals generated by Ag^+ oxidation of $\mathbf{1a}$ and $\mathbf{1b}$, which are best described in terms of a "tucked-in" structure (see above), should be mechanistically significant, also on the basis of the results obtained from the reaction of $\mathbf{1b}$ with deuterated benzene. In the ESR experiments carried out in the absence of aromatics, the intramolecular pattern obviously becomes the only one operative, and thus only the "tucked-in" radical is observed. The formation of this radical may reflect an electron-transfer mechanism, which substantially proceeds through the Cp^* ligand. Thus the bulk of evidence strongly supports the idea that chemical oxidation proceeds through a Cp^* -mediated inner-sphere mechanism, whereas the electrochemical oxidation involves the common outer-sphere mechanism.¹⁹ This would easily explain the different fate of the electrochemically and chemically generated species, which is known to depend in some cases on the nature of the oxidant.²⁰ Therefore it is possible that activation of arenes by these systems proceeds via two different intermediates, the "tucked-in" radical along the intramolecular pathway and another cationic derivative, perhaps the iridium(IV) cation, along the bimolecular route. The reason of the increased reactivity of the Cp^* -centered radical species obtained from chemical oxidation probably lies in the release of energy from the strained "tucked-in" intermediate which triggers the activation of the arene C–H bond. Instead the reactivity of the iridium(IV) system could most probably be related to the overcoming of the energy restrictions imposed by the saturated electron configuration in $\mathbf{1a}$ or $\mathbf{1b}$,^{1e,f} which prevent arene coordination. Alternatively, the access of arene to the iridium center can be thermally achieved by inducing the release of the phosphine ligand from $\mathbf{1a}$, and this easily explains the absence of the orthometalated product in the reaction mixture.

As for the mechanism of the aromatic C–H activation, we are inclined to disregard the oxidative addition pattern (quite common for late d transition metals and particularly for the iridium d^8 systems). The high oxidation state and some formal analogies are rather reminiscent of the " σ -bond metathesis" reactions, which have been described for early d transition metal systems. Moreover the following features are similar for the two systems: (i) the reaction is almost insensitive to the electron-donating or -attracting properties of the substituent on the arene but depends substantially on the number of arene reactive sites; (ii) the ratio (close to 2/1) of the *meta* vs *para* attack is almost purely statistic; (iii) the isotopic effect of the reaction with benzene ($k_{\text{H}}/k_{\text{D}} = 2.2$) implies a moderate but significant involvement of the cleavage of the C–H bond in the transition state of the slow step; (iv) the rate is well described by a first-order equation, which reflects two competitive pathways (intra- and intermolecular).

These features are consistent with the hypothesis of a concerted mechanism based on the formation of a four-center transition state as proposed for the " σ -bond metathesis" of C–H and M–C bonds by scandocene systems (eq 3).⁶



There is however a striking difference between the two systems, and this is the lack of reactivity toward nonaromatic C–H bonds. At the moment, we ignore whether this is just because of the poor solubility of the oxidant in aliphatic hydrocarbons or because of the intrinsic inactivity of the system. However it must be remembered that, in the reactions between arenes and the iridium dimethyl derivatives $\mathbf{1a}$ and $\mathbf{1b}$, the C–H bonds of the pentamethylcyclopentadienyl methyls are also activated to give a transient "tucked-in" intermediate. This suggests that even alkane activation may occur, but this could be masked by a rapid equilibration with other thermodynamically more favored reactions. Work is in progress in order to verify these ideas.

Experimental Section

General Procedures. The reactions and manipulation of organometallics were carried out under dinitrogen or argon, using standard techniques. The solvents were dried and distilled prior to use. The compounds $\text{Cp}^*\text{Ir}(\text{PPh}_3)\text{Cl}_2$,²¹ $\text{Cp}^*\text{Ir}(\text{PMe}_3)\text{Cl}_2$,²² $\text{Cp}^*\text{Ir}(\text{PMe}_3)\text{MeCl}$,²³ $\text{Cp}^*\text{Rh}(\text{PPh}_3)\text{Me}_2$,²¹ $\text{Cp}^*\text{Ir}(\text{PPh}_3)(\text{CH}_2\text{SiMe}_3)_2$,²⁴ $\text{Cp}^*\text{Ir}(\text{CH}_2\text{SiMe}_2\text{CH}_2)(\text{PPh}_3)$,²⁴ $\text{Cp}^*\text{Rh}(\text{PPh}_3)(\text{CH}_2\text{SiMe}_3)_2$,²⁴ $\text{Cp}^*\text{Rh}(\text{CH}_2\text{CMe}_2\text{CH}_2)(\text{PPh}_3)$,²⁴ and $\text{Cp}_2\text{Fe}^+\text{PF}_6^-$ ²⁵ were prepared according to literature procedures. AgBF_4 , $\text{Ph}_3\text{C}^+\text{BF}_4^-$, and methylviologen dichloride were Aldrich products. The ^1H NMR spectra were recorded using Varian Gemini 200 and VXR 300 spectrometers, operating respectively at 200 and 300 MHz. The ^1H NMR chemical shifts were referenced to residual protiated solvent as follows: benzene- d_6 , $\delta = 7.15$; dichloromethane- d_2 , $\delta = 5.32$. The ^{19}F , ^{31}P , and ^2H spectra were recorded on the VXR 300 instrument at 282, 121, and 46 MHz, respectively; the ^{19}F chemical shifts were referred to CFCl_3 as external standard, the ^{31}P chemical shifts to H_3PO_4 (external standard), and the ^2H data to benzene- d_6 (external standard). The 2D NOESY spectra were recorded in the phase-sensitive mode on the Varian VXR 300 spectrometer, and the temperature was controlled to ± 0.1 °C. A spectral width of about 3000 Hz was used in both ω_1 and ω_2 dimensions, and the mixing time was 800 ms. The pulse delay was maintained at 10 s; 512 hypercomplex increments of 8 scans and 2K data points each were collected. The data matrix was zero-filled at $2\text{K} \times 2\text{K}$ and multiplied by a shifted Gaussian function in both dimensions. The monodimensional $^1\text{H}\{^1\text{H}\}$ NOE experiments were performed in the difference mode. The decoupler was placed at the required frequency to saturate the proton of interest. The decoupling power was the minimum required to saturate the spin. A waiting time of 10

(21) Kang, J. W.; Moseley, K.; Maitlis, P. M. *J. Am. Chem. Soc.* **1969**, *91*, 5970.

(22) Isobe, K.; Bailey, P. M.; Maitlis, P. M. *J. Chem. Soc., Dalton Trans.* **1981**, 2003.

(23) Buchanan, J. M.; Stryker, J. M.; Bergman, R. G. *J. Am. Chem. Soc.* **1986**, *108*, 1537.

(24) Andreucci, L.; Diversi, P.; Ingrosso, G.; Lucherini, A.; Marchetti, F.; Adovasio, V.; Nardelli, M. *J. Chem. Soc., Dalton Trans.* **1986**, 477.

(25) Brauer, G. *Handbuch der Präparativen Anorganischen Chemie*; Ferdinand Enke Verlag: Stuttgart, Germany, 1981; p 1845.

(19) *Electron-Transfer and Electrochemical Reactions; Photochemical and Other Energized Reactions*; Zuckerman, J. J., Ed.; Inorganic Reactions and Methods, Vol. 15; VCH Publishers: New York, 1986.

(20) Kochi, J. K. *Angew. Chem., Int. Ed. Engl.* **1988**, *27*, 1227.

s was used. ESR spectra for the chemical oxidation reactions were obtained by using an EPR Varian E 112 instrument equipped with a Varian E 257 for temperature control. The spectrometer was interfaced to an AST Premium 486/25 by means of a data acquisition system consisting of an acquisition board capable of acquiring up to 500 000 12-bit samples/s, including 32-bit add-to memory, thus giving on-line signal averaging and a software package specially designed for ESR experiments.²⁶ Materials and methods for electrochemistry and EPR spectroscopy of the electrogenerated species have been described elsewhere.²⁷ All potential values are referred to the saturated calomel electrode (SCE). Under the present experimental conditions, the 1-electron oxidation of ferrocene occurs at $E^{\circ} = +0.45$ v in CH_2Cl_2 and at $E^{\circ} = +0.54$ V in THF solutions. X-band EPR spectra at $T = 100$ K and at room temperature were computed by the SIM14a computer simulation program.²⁸ Elemental analyses were performed by the Laboratorio di Microanalisi of the Istituto di Chimica Organica, Facoltà di Farmacia, University of Pisa.

Cp*Ir(PPh₃)Me₂ (1a). A suspension of Cp*Ir(PPh₃)Cl₂ (1 g, 1.55 mmol) in pentane (20 mL) was treated with MeMgI (120 mL of a 0.335 M solution in diethyl ether, 40 mmol) at room temperature for 20 h. 1,4-Dioxane (3.5 mL) was added and the suspension stirred for further 5 h. The reaction mixture was hydrolyzed with water, and the pentane extracts were collected and dried. The product was purified by column chromatography on alumina using pentane/ether (1/1) as the eluant to give 0.88 g (94% yield) of **1a**, which was crystallized from pentane to give pale-yellow crystals having the same ¹H NMR spectrum as that of the compound prepared by a different route.²⁹

Cp*Ir(PMe₃)Me₂ (1b). MeMgI (90 mL of a 0.30 M diethyl ether solution, 27 mmol) was added slowly to Cp*Ir(PMe₃)Cl₂ (1 g, 2.1 mmol). The mixture was stirred for 24 h at room temperature and then evaporated to dryness, extracted with pentane, and treated with 1,4-dioxane (1 mL). After removal of the magnesium salts, the resulting solution was evaporated to dryness. The residue was extracted with pentane and hydrolyzed with water at 0 °C. The organic extracts were dried over sodium sulfate and evaporated to dryness under vacuum, to give pale-yellow crystals (0.7 g, 77%) of **1a** having the same properties as those of a sample prepared by an alternative route.²³

Cp*Ir(PMe₃)Me-d₃)₂ (1b-d₆). According to the above procedure, Cp*Ir(PMe₃)Cl₂ (0.15 g, 0.32 mmol) in pentane (5 mL) was reacted with (Me-d₃)MgI (2.5 mL of a 1 M solution in diethyl ether, 2.5 mmol) for 9 h at room temperature to give 0.1 g of **1b-d₆** (72%) having the same ¹H NMR spectrum as that reported in the literature for an authentic sample.²³

Cp*Rh(PMe₃)Me₂ (15b). Cp*Rh(PMe₃)Cl₂ (0.39 g, 1 mmol) in pentane (15 mL) was treated with MeMgI (10 mL of a 0.33 M solution in diethyl ether, 3.3 mmol). After 16 h, the mixture was evaporated to dryness, extracted with pentane, and hydrolyzed with water. The pentane extracts were dried over sodium sulfate and concentrated. By crystallization at -30 °C yellow crystals of **15b** were obtained (0.24 g, 70%). Anal. Calcd for C₁₅H₃₀PRh: C, 52.31; H, 8.79; P, 9.00. Found: C, 52.15; H, 8.76; P, 8.70. ¹H NMR (benzene-d₆): δ 0.15 (6 H, dd, $J(\text{PH})$ 5.3 Hz, $J(\text{RhH})$ 2.5 Hz, Rh-Me) 0.89 (9 H, dd, $J(\text{PH})$ 9.2 Hz, $J(\text{RhH})$ 1.0 Hz, PMe₃), 1.63 (15 H, d, $J(\text{PH})$ 2.3 Hz, Cp*).

Cp*Ir(PPh₃)(Me)(Ph)(2a). A suspension of Cp*Ir(PPh₃)Cl₂ (0.21 g, 0.3 mmol) was reacted with MeMgI (20 mL of a 0.3 M solution in diethyl ether, 6 mmol). After 40 h, the suspension was hydrolyzed, and the collected pentane extracts were dried over sodium sulfate. The crude product was transferred to the top of a chromatography column (alumina).

Benzene eluted a band of the pure halomethyl derivative. ¹H NMR (benzene-d₆): δ 1.36 (15 H, d, $J(\text{PH})$ 1.94 Hz, Cp*), 1.57 (3 H, d, $J(\text{PH})$ 6.35, Ir-Me), 7.02 (9 H, m, Ph), 7.72 (6 H, m, Ph). This product was added to pentane (5 mL) and treated with PhMgBr (1 mL of a 1.7 M solution in diethyl ether, 1.7 mmol). After 2 h, 1,4-dioxane was added and the reaction mixture stirred for 36 h. After hydrolysis and extraction with pentane, a solid residue was obtained that was chromatographed on alumina with pentane/benzene (2/1) to give a pale-yellow band from which green-yellow crystals of **2a** (50% yield) were obtained. Anal. Calcd for C₃₃H₃₈IrP: C, 61.65; H, 5.62; P, 4.54. Found: C, 61.61; H, 5.60; P, 4.49.

Cp*Ir(PPh₃)Ph₂ (10). A suspension of Cp*Ir(PPh₃)Cl₂ (0.17 g, 0.26 mmol) in pentane (5 mL) was treated with PhMgBr (2.5 mL of a 1.7 M solution in diethyl ether, 4.25 mmol), and the mixture was stirred for 2 h. 1,4-Dioxane was added, and the suspension was stirred for 24 h. After the usual workup and column chromatography on alumina by eluting with pentane/ether, a central yellow band was collected, which was evaporated to dryness and then extracted with pentane. The residue was crystallized from pentane/ether to give yellow crystals of **10** (20% yield). Anal. Calcd for C₄₀H₄₀IrP: C, 64.58; H, 5.42; P, 4.16. Found: C, 64.47; H, 5.41; P, 4.05.

Cp*Ir(PPh₃)(Me)(m-C₆H₄Me) (m-3a). A suspension of Cp*Ir(PPh₃)Cl₂ (0.31 g, 0.45 mmol) in diethyl ether (15 mL) was treated with (*m*-C₆H₄Me)MgBr (1.0 M solution in diethyl ether, 1.15 mmol), and the mixture was stirred at room temperature for 40 h. The mixture was then evaporated to dryness under vacuum, and the solid residue was hydrolyzed at 0 °C with water, extracted with ether, and chromatographed on a column of alumina. Pentane/benzene (1/1) eluted a yellow band which by crystallization from pentane gave orange crystals of Cp*Ir(PPh₃)(Br)(*m*-C₆H₄Me) (0.19 g, 55% yield). Anal. Calcd for C₃₅H₃₇BrIrP: C, 55.26; H, 4.90; Br, 10.50. Found: C, 55.41; H, 4.82; Br, 10.01. ¹H NMR (benzene-d₆): δ 1.26 (15 H, d, $J(\text{HP})$ 1.9 Hz, Cp*), 2.17 (3 H, s, C₆H₄Me), 6.80–7.35 (18 H, b m, PPh₃, C₆H₄Me), 7.90 (1 H, b s, C₆H₄Me). These crystals were suspended in pentane (1 mL) and treated with MeMgI (4 mL of a 0.3 M solution in diethyl ether, 1.2 mmol). After 14 h at room temperature, the mixture was evaporated to dryness, extracted with pentane, and hydrolyzed with water. The organic phase was dried over Na₂SO₄ and chromatographed on an alumina column to give yellow crystals (0.1 g, 57%). Anal. Calcd for C₃₆H₄₀IrP: C, 62.13; H, 5.79. Found: C, 62.26; H, 5.86.

Cp*Ir(PPh₃)(Me)(p-C₆H₄Me) (p-3a). Cp*Ir(PPh₃)Cl₂ (0.33 g, 0.48 mmol) was reacted with MeMgI (30 mL of a 0.3 M solution in diethyl ether, 9 mmol) by the procedure described for **2a** to give the monomethyl derivative, which was suspended in pentane (7 mL) and treated with Mg(*p*-tolyl)Br (3 mL of a 1 M solution in diethyl ether, 3 mmol). After 16 h, 1 mL of 1,4-dioxane was added, and the mixture was stirred for further 24 h. The solvent was removed under vacuum, and the residue was taken up in pentane and hydrolyzed. The combined pentane/ether (5/1) extracts were dried over sodium sulfate and evaporated to dryness. The crude yellow solid was dissolved in a minimum amount of benzene. Column chromatography on alumina, eluting with pentane, gave yellow-brown crystals of **p-3a** (0.16 g, 47%). Anal. Calcd for C₃₆H₄₀IrP: C, 62.13; H, 5.79. Found: C, 61.96; H, 5.75.

Cp*Ir(PMe₃)(Me)(p-C₆H₄Me) (p-3b). Cp*Ir(PMe₃)(Me)(Cl) (0.065 g) in diethyl ether (2 mL) was treated with (*p*-C₆H₄Me)MgBr (1 mL of a 1 M solution in diethyl ether, 1 mmol) for 20 h. The suspension was evaporated to dryness and extracted with pentane. The pentane extracts were hydrolyzed, and the organic layer was dried over sodium sulfate and evaporated to dryness to give **p-3b** as a yellow solid (42 mg, 57%). Anal. Calcd for C₂₁H₃₄IrP: C, 49.49; H, 6.72. Found: C, 49.28; H, 6.70.

Cp*Ir(PMe₃)(Me)(m-C₆H₄Me) (m-3b). According to the above procedure, Cp*Ir(PMe₃)(Me)(Cl) (0.066 g, 0.15 mmol) was reacted with (*m*-C₆H₄Me)MgBr (1 mL of a 1 M solution

(26) Ambrosetti, R.; Ricci, D. *Rev. Sci. Instrum.* **1991**, *62*, 2281; ESR-ENDOR, ICQEM-CNR, 1992.

(27) Osella, D.; Ravera, M.; Nervi, C.; Housecroft, C. E.; Raithby, P. R.; Zanillo, P.; Laschi, F. *Organometallics* **1991**, *10*, 3253.

(28) Lozos, J. P.; Hoffman, B. M.; Franz, C. G. *QCPE* **1973**, *11*, 243.

(29) Glueck, D. S.; Bergman, R. G. *Organometallics* **1991**, *10*, 1479.

in diethyl ether, 1 mmol) to give after crystallization from pentane yellow crystals of **m-3b** (0.036 g, 47%). Anal. Calcd for $C_{21}H_{34}IrP$: C, 49.49; H, 6.72. Found: C, 49.37; H, 6.69.

Cp*Ir(PMe₃)(Me)(*o*-C₆H₄Me) (o-3b). According to the above procedure, Cp*Ir(PMe₃)(Me)(Cl) (0.061 g, 0.13 mmol) was reacted with (*o*-C₆H₄Me)MgBr (0.5 mL of a 2 M solution in diethyl ether, 1 mmol) to give yellow crystals of **o-3b** (0.027 g, 39%). Anal. Calcd for $C_{21}H_{34}IrP$: C, 49.49; H, 6.72. Found: C, 49.44; H, 6.74.

Thermolysis of 1a in Benzene. **1a** (0.02 g) and benzene (1 mL), or benzene-*d*₆ when the reaction was monitored by ¹H NMR spectroscopy, were loaded into an NMR tube, and the tube was sealed off under argon. It was then immersed in a thermostated oil bath. The progress of the reaction was evaluated by monitoring the signal of CH₃D [δ 0.13 (t, *J*(HD) 2 Hz)] and the integrated intensities of the Cp* resonances for **1a** (δ 1.40), **2a** (δ 1.34), and **10** (δ 1.32). After 2 weeks at temperatures below 70 °C, no reaction was found to occur. After **1a** was heated in benzene for 12 days at 110 ± 0.5 °C, the tube was cracked open, the solvent was removed, and benzene-*d*₆ was added. The ¹H NMR spectrum revealed a mixture of **1a** (10%), **2a** (24%), and **10** (66%).

Under the same conditions, **1a** was reacted with toluene or toluene-*d*₈ to give the *m*- and *p*-tolyl derivatives **3a** (2/1, 95%) and with trifluorotoluene to give the diaryl derivatives.

Reaction of Cp*Ir(PPh₃)Me₂ (1a) with Cp₂Fe⁺PF₆⁻ in

Dichloromethane-*d*₂: Formation of Cp*Ir(C₆H₄PPh₂)Me (12). **1a** (0.038 g, 0.062 mmol) in dichloromethane-*d*₂ (2 mL) was treated in an NMR tube with Cp₂Fe⁺PF₆⁻ (6 × 10⁻³ mmol). After a few seconds, a gas was evolved from the surface of the solid oxidant, which was shown to be CH₄ by GLC and ¹H NMR (δ 0.2), while signals due to **1a** decreased to give a new product. The reaction was complete in 30 min. The solution was filtered and dried under vacuum. Crystallization from pentane at -30 °C gave yellow crystals of **12** (0.028 g, 75%).

Reaction of Cp*Ir(PPh₃)Me₂ (1a) with Cp₂Fe⁺PF₆⁻ in Benzene: Formation of Cp*Ir(C₆H₄PPh₂)Me (12) and Cp*Ir(PPh₃)(Me)(Ph) (2a). **1a** (0.02 g, 0.032 mmol) and Cp₂Fe⁺PF₆⁻ (1.1 mg, 0.0032 mmol) were reacted similarly in

benzene or, when the reaction was monitored by ¹H NMR spectroscopy, in benzene-*d*₆ using hexamethylbenzene as internal standard. CH₄ (δ 0.14) was evolved, and **1a** was converted with 92% yield after 2 h to a mixture of the orthometalated compound **12** (15%) and the methyl phenyl derivative Cp*Ir(PPh₃)(Me)(Ph) (**2a**) (85%), both identified by comparison of the ¹H NMR spectral data with those of an authentic sample prepared as described above. The same equilibrium composition was obtained by reacting pure **12** or **2a** with Cp₂Fe⁺PF₆⁻ or AgBF₄ in benzene.

Reaction of Cp*Ir(PMe₃)Me₂ (1b) with Cp₂Fe⁺PF₆⁻ in Benzene: Formation of Cp*Ir(PMe₃)(Me)(Ph) (2b). The reaction was carried out as described for **1a**, except that the conversion of **1b** (0.042 g, 0.097 mmol) was complete in 1 h. The solution was separated from the oxidant by filtration and pumped to dryness. Crystallization from pentane at -30 °C gave yellow crystals of **2b** (0.041 g, 85%).

The isotope effect ($k_H/k_D = 2.2$) was evaluated by carrying out the reaction in benzene/benzene-*d*₆ mixtures of different compositions (1/1, 2.5/1, and 4/1) and comparing the ¹H NMR signals' integrated areas of the phosphine and pentamethylcyclopentadienyl ligand of **3b** and **3b-d to those of the phenyl group.**

ESR Spectral Studies of the Chemical Oxidation of 1a, 1b, 13, and 14. The reaction mixtures were prepared by placing a weighed amount of metal complex (typically, 5 mg) and AgBF₄ (1 mg) into a quartz tube (o.d. 3 mm; i.d. 2 mm) fitted with a quartz-Pyrex joint and a Corning Rotaflo Teflon tap (DISA, Milan). The tube was then attached to a vacuum line and degassed by standard vacuum/argon techniques; afterward, it was immersed in a dry ice-cooled acetone bath and then charged with dichloromethane under pure argon atmosphere. The hyperfine coupling constants and line widths were obtained by computer simulation of the ESR spectra.

Acknowledgment. We thank the CNR (Rome) for financial support.

OM950070S

Anion Recognition by Redox-Responsive Ditopic Bis-Cobaltocenium Receptor Molecules Including a Novel Calix[4]arene Derivative That Binds a Dicarboxylate Dianion

Paul D. Beer,* Dusan Heseck, Justine E. Kingston, David K. Smith, and Sally E. Stokes

Inorganic Chemistry Laboratory, University of Oxford, South Parks Road, Oxford OX1 3QR, U.K.

Michael G. B. Drew

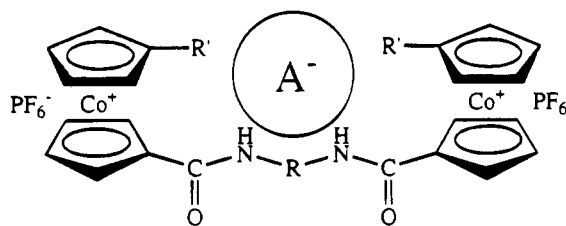
Department of Chemistry, The University, Whiteknights, P.O. Box 224, Reading RG6 2AD, U.K.

Received February 23, 1995[⊗]

A series of novel ditopic bis-cobaltocenium receptor molecules containing alkyl, aryl, and calix[4]arene spacers have been synthesized via the reaction of the new synthon 1-(ethylcarboxy)-1'-(chlorocarbonyl)cobaltocenium chloride (**3**) or 1-(chlorocarbonyl)cobaltocenium chloride (**9**) with the appropriate diamine. Proton NMR halide anion coordination studies reveal that the ethyl- (**4**), propyl- (**5**), and butyl-linked (**6**) derivatives form 1:1 stoichiometric complexes in acetonitrile solutions. Stability constant determinations suggest that the ethyl derivative **4** exhibits selectivity for the chloride anion in preference to bromide or iodide. Receptors containing larger aryl (**7,8,10**) and alkylamino (**11**) spacers form complexes of 2:1 halide anion:receptor stoichiometry. An X-ray crystal structure of the bis-cobaltocenium calix[4]arene derivative **15** is described. This receptor forms extremely stable 1:1 anion complexes with chloride, bromide, and H_2PO_4^- in dimethylsulfoxide solutions and with the dicarboxylate dianion adipate in acetone. All the bis-cobaltocenium systems were found to display electrochemical recognition of varied anion guests, as shown by cyclic voltammetric experiments. Receptor **15** was also found to redox-respond to the presence of adipate.

Introduction

The synthesis of positively charged^{1,2} or neutral^{1,3} electron deficient abiotic receptor molecules designed to coordinate anionic guest species is an area of intense current research activity. This is because anions are known to play numerous fundamental roles in chemical and biochemical processes. For example, the majority of enzymes bind anions as either substrates or cofactors,⁴ and many anions act as nucleophiles, bases, redox agents, and phase transfer catalysts. We have recently reported the synthesis of the first redox-responsive class of anion receptor based on the redox-active, pH-



R = Alkyl, Aryl, calix[4]arene spacer

R' = CO_2Et , H

Figure 1. Schematic representation of anion recognition by a ditopic bis-cobaltocenium receptor.

independent positively charged cobaltocenium moiety. Simple acyclic amide-linked cobaltocenium host molecules have been demonstrated to bind and electrochemically recognize halide, hydrogen sulfate, and dihydrogen phosphate guest anions⁵ via favorable mutual electrostatic interactions and ubiquitous amide $-\text{CONH}-$ hydrogen-bonding effects. In an effort to impart selectivity and enhance complex stability for this class of anion receptor we describe here the synthesis, anion coordination, and electrochemical properties of novel ditopic bis-cobaltocenium receptor molecules. The two positively charged metallocene centers, linked via various alkyl, aryl, and calix[4]arene spacers, may cooperate in the molecular recognition of mono- or dianionic guest substrates (Figure 1).

* Abstract published in *Advance ACS Abstracts*, June 1, 1995.

(1) (a) Dietrich, B. *Pure Appl. Chem.* **1993**, *65*, 1457. (b) Schmidtchen, F. P. *Nachr. Chem. Tech. Lab.* **1988**, *36*, 8.

(2) (a) Park, C. H.; Simmons, H. E. *J. Am. Chem. Soc.* **1968**, *90*, 2431. (b) Lehn, J.-M.; Sonveaux, E.; Willard, A. K. *J. Am. Chem. Soc.* **1978**, *100*, 4914. (c) Dietrich, B.; Hosseini, M. W.; Lehn, J.-M.; Sessions, R. B. *J. Am. Chem. Soc.* **1981**, *103*, 1282. (d) Gelb, R. I.; Lee, B. T.; Zompa, L. J. *J. Am. Chem. Soc.* **1985**, *107*, 909. (e) Heyer, D.; Lehn, J.-M. *Tetrahedron Lett.* **1986**, *27*, 5869. (f) Hosseini, M. W.; Lehn, J.-M. *Helv. Chim. Acta.* **1986**, *69*, 587. (g) Hosseini, M. W.; Blacker, A. J.; Lehn, J.-M. *J. Am. Chem. Soc.* **1990**, *112*, 3896. (h) Sessler, J. L.; Furuta, H.; Král, V. *Supramol. Chem.* **1993**, *1*, 209 and references therein.

(3) (a) Katz, H. E. *Organometallics* **1987**, *6*, 1134. (b) Wuest, J. D.; Zacharie, B. *J. Am. Chem. Soc.* **1987**, *109*, 4714. (c) Newcomb, M.; Horner, J. H.; Blanda, M. T. *J. Am. Chem. Soc.* **1987**, *109*, 7878. (d) Jung, M. E.; Xia, H. *Tetrahedron Lett.* **1988**, *29*, 297. (e) Yang, X.; Johnson, S. E.; Khan, S. I.; Hawthorne, M. F. *J. Am. Chem. Soc.* **1993**, *115*, 193. (f) Rudkevich, D. M.; Brzozka, Z.; Palys, M.; Visser, H.; Verboom, W.; Reinhoudt, D. N. *Angew. Chem., Int. Ed. Engl.* **1994**, *33*, 467–468. (i) Scheerder, J.; Fochi, M.; Engbersen, J. F. J.; Reinhoudt, D. N. *J. Org. Chem.* **1994**, *59*, 7815.

(4) Lang, L. G.; Riordon, J. F.; Vallee, B. L. *Biochemistry* **1974**, *13*, 4361.

Experimental Section

Instrumentation. Nuclear magnetic resonance spectra were obtained on a Bruker AM300 instrument using the solvent deuterium signal as internal reference. Fast atom bombardment mass spectrometry was performed by the SERC mass spectrometry service at University College, Swansea, U.K. Electrochemical measurements were carried out using an E.G. and G. Princeton Applied Research 362 scanning potentiostat. Elemental analyses were performed at the Inorganic Chemistry Laboratory, University of Oxford.

Solvent and Reagent Pretreatment. Where necessary, solvents were purified prior to use and stored under nitrogen. Acetonitrile was predried over class 4A molecular sieves (4–8 mesh) and then distilled from calcium hydride. Unless stated to the contrary commercial grade chemicals were used without further purification.

1,1'-Bis(ethylcarboxyl)cobaltocenium hexafluorophosphate (**1**),⁶ 1-(chlorocarboxyl)cobaltocenium chloride (**9**),⁶ and 25,27-dihydroxy-26,28-dimethoxy-11,23-dinitrocalix[4]arene (**13**)⁷ were prepared according to literature procedures.

Syntheses. *N,N'*-Bis(1-carboxyl-1'-(ethylcarboxy)cobaltoceniumyl)-1,2-diaminoethane bis(hexafluorophosphate) (**4**), *N,N'*-bis(1-carboxyl-1'-(ethylcarboxy)cobaltoceniumyl)-1,3-diaminopropane bis(hexafluorophosphate) (**5**), and *N,N'*-bis(1-carboxyl-1'-(ethylcarboxy)cobaltoceniumyl)-1,4-diaminobutane bis(hexafluorophosphate) (**6**) were prepared using the following procedure.

1,1'-Bis(ethylcarboxy)cobaltocenium hexafluorophosphate (0.5 g, 1 mmol) was dissolved in ethanol with 1 equiv of KOH (0.058 g, 1 mmol). The mixture was then refluxed for 6 h. The color was observed to change from yellow to red to green over this time. The mixture was evaporated to dryness, and the residue was dissolved in water (40 mL). The aqueous solution was filtered, and the filtrate acidified. The water was then removed in vacuo to yield cobaltocenium "monoacid-monoester" **2**, which was thoroughly dried in vacuo and then refluxed with thionyl chloride for 12 h. The mixture was observed to change color from yellow to green. The thionyl chloride was removed in vacuo, and the green product "mono acid chloride-monoester" **3** was dried in vacuo. A solution of this product in dry CH₃CN was then added dropwise to a stirred solution of half an equivalent of the appropriate diamine in CH₃CN. A color change was observed, and a precipitate formed. The solution was filtered and then evaporated to dryness. The resultant solid product was columned on Sephadex using MeOH/CH₃CN (50/50) as eluent. To each column fraction were added a few drops of aqueous ammonium hexafluorophosphate solution, and the products slowly crystallized as the solvent evaporated. Yields: **4**, 25%, **5**, 15%, and **6**, 20%. Analytical data for **4**. ¹H NMR (CD₃CN): δ 1.38 (t, *J* = 7.1 Hz, 6H, CH₂CH₃), 3.53 (d, *J* = 5.7 Hz, 4H, N-CH₂), 4.36 (q, *J* = 7.1 Hz, 4H, OCH₂CH₃), 5.84 (dd, *J* = 2.1 Hz, 4H, Cp H), 5.86 (dd, *J* = 2.1 Hz, 4H, Cp H), 6.09 (dd, *J* = 2.1 Hz, 4H, Cp H), 6.13 (dd, *J* = 2.1 Hz, 4H, Cp H), 7.47 (s, 2H, N-H). Anal. Found: C, 38.97; H, 3.33; N, 3.52. Calcd for C₆₂H₃₀N₂O₆P₂F₁₂: C, 38.98; H, 3.49; N, 3.03. IR ν_{max}/cm⁻¹: 3441 (N-H), 1728 (C=O_{ester}), 1667 (C=O_{amide}), 838 (PF₆⁻). FAB MS *m/z*: 779 (M - PF₆)⁺, 634 (M - 2PF₆)⁺. Data for **5**. ¹H NMR (CD₃CN): δ 1.37 (t, *J* = 7.2 Hz, 6H, CH₂CH₃), 3.42 (dt, *J* = 6.4 Hz, NCH₂), 4.36 (q, *J* = 7.2 Hz, 4H, OCH₂CH₃), 5.85 (dd, *J*

= 2.1 Hz, 8H, Cp H), 5.88 (dd, *J* = 2.1 Hz, 4H, Cp H), 6.13 (dd, *J* = 2.1 Hz, 4H, Cp H), 7.53 (s, 2H, N-H). ¹³C NMR (CD₃CN): δ 14.27 (CH₂CH₃), 29.23 (NCH₂CH₂), 37.96 (NCH₂), 63.72 (OCH₂CH₃), 86.00 (Cp C-H), 87.47 (Cp C-H), 88.04 (Cp C-H), 88.73 (Cp C-H), 91.4 (Cp C-C), 96.4 (Cp C-C), 161.4 (C=O), 163.4 (C=O). Anal. Found: C, 37.33; H, 3.43; N, 3.60. Calcd for C₆₂H₃₀N₂O₆P₂F₁₂: C, 38.30; H, 3.32; N, 3.07. IR ν_{max}/cm⁻¹: 3438 (N-H), 1733 (C=O_{ester}), 1678 (C=O_{amide}), 836 (PF₆⁻). FAB MS *m/z*: 793 (M - PF₆)⁺, 648 (M - 2PF₆)⁺. Data for **6**. ¹H NMR (CD₃CN): δ 1.37 (t, *J* = 7.2 Hz, 6H, CH₂CH₃), 1.66 (t, 4H, NCH₂CH₂), 3.37 (dt, 4H, NCH₂), 4.35 (q, *J* = 7.2 Hz, 4H, OCH₂CH₃), 5.83 (m, 8H, Cp H), 6.10 (m, 8H, Cp H), 7.40 (s, 2H, N-H). ¹³C NMR (CD₃CN): δ 14.25 (CH₂CH₃), 27.09 (NCH₂CH₂), 40.42 (NCH₂), 63.69 (OCH₂CH₃), 86.00 (Cp C-H), 87.40 (Cp C-H), 87.95 (Cp C-H), 88.60 (Cp C-H), 91.40 (Cp C-C), 96.57 (Cp C-C), 161.12 (C=O), 163.35 (C=O). Anal. Found: C, 39.72; H, 3.68; N, 3.14. Calcd for C₆₂H₃₀N₂O₆P₂F₁₂: C, 40.35; H, 3.81; N, 2.94. IR ν_{max}/cm⁻¹: 3436 (N-H), 1729 (C=O_{ester}), 1668 (C=O_{amide}), 834 (PF₆⁻). FAB MS *m/z*: 807 (M - PF₆)⁺, 662 (M - 2PF₆)⁺.

***N,N'*-Bis(1-carboxyl-1'-(ethylcarboxy)cobaltoceniumyl)-4,4'-diaminodiphenylmethane Bis(hexafluorophosphate) (**7**).** 4,4'-Diaminodiphenylmethane (0.085 g, 4.2 × 10⁻⁴ mol) was dissolved in dry CH₃CN (60 mL) under a nitrogen atmosphere. To this solution was added 1-(ethylcarboxy)-1'-(chlorocarboxy)cobaltocenium chloride (**3**) (0.39 g, 8.4 × 10⁻⁴ mol) in dry CH₃CN (50 mL) dropwise and under nitrogen. Once addition was complete, the mixture was stirred at room temperature for 18 h. After this time the mixture was filtered to yield a small amount of cream-colored powder and a golden yellow filtrate. The filtrate was evaporated to dryness to give the crude product, which was purified by column chromatography on Sephadex LH20 using an eluting solvent system of CH₃CN/MeOH (1:1). To each of the seven fractions collected from the column were added a few drops of a dilute aqueous solution of NH₄PF₆. On standing, the pure product crystallized out (as the more volatile solvent evaporated) as gold/yellow crystals (0.20 g, 1.9 × 10⁻⁴ mol, yield: 45%). ¹H NMR (CD₃CN): δ 1.26 (t, *J* = 7.7 Hz, 6H, OCH₂CH₃), 3.99 (s, 2H, ArCH₂-Ar), 4.23 (q, *J* = 7.8 Hz, 4H, OCH₂CH₃), 5.87 (m, 8H, Cp H), 6.14 (t, *J* = 2.3 Hz, 4H, Cp H), 6.25 (t, *J* = 2.3 Hz, 4H, Cp H), 7.28 (d, *J* = 9.4 Hz, 4H, Ar H), 7.66 (d, *J* = 9.4 Hz, 4H, Ar H), 8.78 (s, 2H, N-H). ¹³C NMR (75.42 MHz, CD₃CN): δ 14.1 (CH₂CH₃), 41.2 (ArCH₂Ar), 63.7 (CH₂CH₃), 86.2, 87.5, 88.1, 88.7 (Cp C-H), 91.5, 97.0 (Cp C-C=O), 121.7, 130.1 (Ar C-H), 137 (Ar C-CH₂), 139.5 (Ar C-N), 159.5, 163.0 (C=O). Anal. Found: C, 46.03; H, 3.7; N, 2.90. Calcd for C₄₁H₃₈N₂O₆-C₆₂H₃₀P₂F₁₂: C, 46.35; H, 3.6; N, 2.64. IR ν_{max}/cm⁻¹: 3410 (N-H), 1723 (C=O_{ester}), 1684 (C=O_{amide}), 852 (PF₆⁻). FAB MS *m/z*: 772 (M - 2PF₆)²⁺, 917 (M - PF₆)⁺.

***N,N'*-Bis(1-carboxyl-1'-(ethylcarboxy)cobaltoceniumyl)-4,4'-diaminodiphenyl Ether Bis(hexafluorophosphate) (**8**).** 4,4'-Diaminodiphenyl ether (0.042 g, 2.1 × 10⁻⁴ mol) was dissolved in dry CH₃CN (50 mL) under a nitrogen atmosphere. To this solution was added 1-(ethylcarboxy)-1'-(chlorocarboxy)-cobaltocenium hexafluorophosphate (**3**) (0.2 g, 4.3 × 10⁻⁴ mol) in dry CH₃CN (50 mL) dropwise and under nitrogen. Once addition was complete, the mixture was stirred at room temperature for 24 h. After this time the mixture was filtered to yield a small amount of brown-colored powder and a golden brown filtrate. The filtrate was evaporated to dryness to give the crude product, which was purified by column chromatography on Sephadex LH20 using an eluting solvent system of CH₃CN/MeOH (1:1). Four major bands were eluted (yellow, orange, mid-brown, and red/burgandy), and to each of the fractions collected from the column were added a few drops of a dilute aqueous solution of NH₄PF₆. On standing, the pure product crystallized out of the last two fractions (as the more volatile solvent evaporated) to give red/brown crystals (0.053 g, 5 × 10⁻⁵ mol, yield: 23%). ¹H NMR (CD₃CN): δ 1.25 (t, *J* = 7.8 Hz, 6H, OCH₂CH₃), 4.23 (q, *J* = 7.8 Hz, 4H, OCH₂CH₃), 5.88 (m, 8H, Cp H), 6.14 (t, *J* = 2.22 Hz, 4H, Cp H), 6.26 (t, *J*

(5) (a) Beer, P. D.; Heseck, D.; Hodacova, J.; Stokes, S. E. *J. Chem. Soc., Chem. Commun.* **1992**, 270. (b) Beer, P. D.; Hazlewood, C.; Heseck, D.; Hodacova, J.; Stokes, S. E. *J. Chem. Soc., Dalton Trans.* **1993**, 1327. (c) Beer, P. D.; Drew, M. G. B.; Hazlewood, C.; Heseck, D.; Hodacova, J.; Stokes, S. E. *J. Chem. Soc., Chem. Commun.* **1993**, 229. (d) Beer, P. D.; Dickson, C. A. P.; Fletcher, N.; Goulden, A. J.; Grieve, A.; Hodacova, J.; Wear, T. *J. Chem. Soc., Chem. Commun.* **1993**, 828. (e) Beer, P. D.; Drew, M. G. B.; Graydon, A. R.; Smith, D. K.; Stokes, S. E. *J. Chem. Soc., Dalton Trans.* **1995**, 403.

(6) Sheats, J. E.; Rausch, M. D. *J. Org. Chem.* **1970**, *35*, 3245.

(7) Loon, J.-D.; Arduini, A.; Coppi, A.; Verboom, W.; Pochini, A.; Ungaro, R.; Harkenna, S.; Reinhoudt, D. N. *J. Org. Chem.* **1990**, *55*, 5639.

= 2.4 Hz, 4H, Cp H), 7.27 (d, $J = 7.6$ Hz, 4H, Ar H), 7.66 (d, $J = 7.6$ Hz, 4H, Ar H), 8.88 (s, 2H, N-H). ^{13}C NMR (75.42 MHz, CD_3CN): δ 14.1 (CH_2CH_3), 63.7 (CH_2CH_3), 86.1, 87.5, 87.9, 88.6 (Cp C-H), 91.5, 97.0 (Cp C-C=O), 116.2, 123.4 (Ar C H), 130.9 (Ar C-O), 155.3 (Ar C-N), 159.4, 161.0 (C=O). Anal. Found: C, 44.48; H, 3.34; N, 2.85. Calcd for $\text{C}_{40}\text{H}_{36}\text{N}_2\text{O}_7\text{Co}_2\text{P}_2\text{F}_{12}$: C, 45.13; H, 3.41; N, 2.63. IR $\nu_{\text{max}}/\text{cm}^{-1}$: 3398 (N-H), 1728 (C=O_{ester}), 1674 (C=O_{amide}), 840 (PF_6^-). FAB MS m/z : 774 ($\text{M} - 2\text{PF}_6^+$), 919 ($\text{M} - \text{PF}_6^-$).

***N,N'*-Bis(1-carbonylcobaltoceniumyl)-4,4'-diaminodiphenylmethane Bis(hexafluorophosphate) (10).** 4,4'-Diaminodiphenylmethane (0.15 g, 6×10^{-4} mol) and four drops of triethylamine were dissolved in dry CH_3CN (60 mL) and stirred under a nitrogen atmosphere. To this solution was added 1-(chlorocarbonyl)cobaltocenium chloride (9) (0.5 g, 1.3 mmol) in CH_3CN (50 mL), dropwise and under nitrogen. On addition of the acid chloride, the solution changed from colorless to yellow/orange and an orange precipitate formed. The mixture was stirred for 12 h, and the crude product was isolated as an orange solid. The crude product was taken up in hot water, and a saturated solution of NH_4PF_6 was added to precipitate the pure product as a bright orange powder (0.26 g, 2.8×10^{-4} mol, yield: 47%). ^1H NMR (CD_3CN): δ 3.98 (s, 2H, ArCH_2Ar), 5.60 (s, 10H, Cp H), 5.74 (t, $J = 2.3$ Hz, 4H, Cp H), 6.13 (t, $J = 2.3$ Hz, 4H, Cp H), 7.28 (d, $J = 9.3$ Hz, 4H, Ar H), 7.65 (d, $J = 9.3$ Hz, 4H, Ar H), 8.76 (s, 2H, N-H). Anal. Found: C, 45.72; H, 3.49; N, 3.31. Calcd for $\text{C}_{35}\text{H}_{30}\text{N}_2\text{O}_2\text{Co}_2\text{P}_2\text{F}_{12}$: C, 45.77; H, 3.29; N, 3.05. FAB MS m/z : 773 ($\text{M} - \text{PF}_6^-$), 628 ($\text{M} - 2\text{PF}_6^+$).

***N,N'*-Bis(1-carbonylcobaltoceniumyl)-*N*-methyl-*N*-propylamine-1,3-propanediamine Bis(hexafluorophosphate) (11).** Bis(*N*-methyl-*N*-propylamine)-1,3-propanediamine (0.07 g, 3.24×10^{-4} mol) and triethylamine (0.06 g, 5.9×10^{-4} mol) were dissolved in dry CH_3CN (60 mL) and stirred under a nitrogen atmosphere. To this was added 1-(chlorocarbonyl)cobaltocenium chloride (9) (0.24 g, 6.0×10^{-4} mol) in CH_3CN (40 mL), dropwise and under nitrogen, and the yellow solution that resulted was stirred overnight. The solvent was removed to give the crude product as a yellow powder. The crude product was purified by column chromatography using Sephadex LH20 and $\text{CH}_3\text{CN}/\text{MeOH}$ (4:1) as eluting solvent. Two fractions were collected, brown and bright yellow. The yellow fraction from the column was evaporated to dryness, taken up in hot water, and a saturated solution of NH_4PF_6 was added to precipitate the pure product as a bright yellow powder (0.17 g, 1.8×10^{-4} mol, yield: 80%). ^1H NMR (CD_3CN): δ [1.97 (m), 2.87 (s), 3.15 (t, $J = 8$ Hz), 3.43 (t, $J = 6.8$ Hz), 2.4H, CH_2 and CH_3], 5.72 (s, 10H, Cp H), 5.78 (t, $J = 2$ Hz, 4H, Cp H), 6.06 (t, $J = 2$ Hz, 4H, Cp H), 7.48 (s, 2H, N-H). ^{13}C NMR (75.42 MHz, CD_3CN): δ 18.6 (CH_3), 23.6, 36.6, 52.1, 53.4 (CH_2), 83.8, 85.7, 85.9 (Cp C-H), 93.7 (Cp C-C=O), 161.6 (C=O). Anal. Found: C, 42.73; H, 4.01; N, 4.42. Calcd for $\text{C}_{33}\text{H}_{44}\text{N}_4\text{O}_2\text{Co}_2\text{P}_2\text{F}_{12}$: C, 42.32; H, 4.64; N, 4.74. IR $\nu_{\text{max}}/\text{cm}^{-1}$: 3412 (NH), 1647 (C=O), 834 (PF_6^-). FAB MS m/z : 646 ($\text{M} - 2\text{PF}_6^+$), 791 ($\text{M} - \text{PF}_6^-$).

11,23-Diamino-25,27-dihydroxy-26-28-dimethoxycalix[4]arene (14). Hydrazine hydrate was slowly added to a stirred mixture of 13 (1.08 g, 2 mmol) and wet Raney nickel in methanol at 60 °C. After the reaction had changed to a reddish color, the Raney nickel was separated and the filtrate was concentrated to dryness in vacuo. The residue was dissolved in DMF and filtered with charcoal, and the volatile components were evaporated under reduced pressure. The solid was treated with methanol to give a light red powder of 14 in 55–70% yield. ^1H NMR (CD_2Cl_2): 3.28 (d, $J = 13$ Hz, 4H, $\text{CH}_{2(e)}$), 3.95 (s, 6H, CH_3), 4.26 (d, 4H, $\text{CH}_{2(a)}$), 6.47 (s, 4H, CH-arom), 6.77 (t, 2H, CH-arom), 6.94 (d, 4H, $J = 7.6$ Hz, CH-arom), 7.03 (br, 6H, N-H, O-H). ^{13}C NMR (DMSO- d_6): 153.4, 143.8 (Ar C), 140.7 (Ar C), 128.6 (Ar C), 128.4 (Ar C), 124.8 (d, Ar C), 114.5 (Ar C), 63.2 (CH_3), 30.6 (CH_2).

11,23-Bis((cobaltoceniumyl)carbonyl)amino)-25,27-dihydroxy-26,28-dimethoxycalix[4]arene (15). Aminocalix-

[4]arene 14 (0.49 g, 1 mmol) was dissolved in dry DMF (5 mL), and acetonitrile (15 mL) was slowly added under nitrogen to 1-(chlorocarbonyl)cobaltocenium chloride. The temperature was raised to 40 °C for 0.5 h, and then triethylamine (0.45 mL) was added. The dark red solution was stirred for 5 h at room temperature. Methanol (10 mL) was added, and the volatile components were evaporated under reduced pressure. To the black oil was added water (80 mL), and the solid precipitate was filtered off. After dissolving the crude sample in a minimum amount of DMF, the liquid phase was treated with NaPF_6 (0.3 g) and the mixture was filtered through a short silica gel column with acetonitrile/dichloromethane (4:1) as eluent to give an orange powder of 15 as the main fraction in 61% (0.73 g) yield. ^1H NMR (DMSO- d_6): δ 3.47 (d, $J = J = 13$ Hz, 4H, $\text{CH}_{2(e)}$), 3.95 (s, 6H, CH_3), 4.24 (d, 4H, $\text{CH}_{2(a)}$), 5.90 (s, 10H, CH-cp), 5.97 (t, $J = 2.0$ Hz, 4H, CH-cp), 6.63 (dd, $J = 7.4$ Hz, $J = 7.6$ Hz, 2H, CH-arom), 7.02 (d, 4H, CH-arom), 7.47 (s, 4H, CH-arom), 8.07 (s, 2H, OH), 10.17 (s, 2H, -NHCO-). ^{13}C NMR (DMSO- d_6): δ 153.4, 149.6 (Ar C), 133.1, 129.3 (Ar C), 128.9 (Ar C), 127.0 (Ar C), 125.1 (Ar C), 121.3 (Ar C), 94 (Cp C), 85.9 (Cp C), 85.5 (d, Cp C), 84.0 (Cp C), 63.6 (CH_3), 30.5 (CH_2). Anal. Found: C, 51.98; H, 3.84; N, 3.06. Calcd for $\text{C}_{52}\text{H}_{46}\text{Co}_2\text{N}_2\text{O}_6\text{P}_2\text{F}_{12}$: C, 52.30; H, 3.86; N, 2.40. FAB MS $m/z = 1192$ (M^+).

Crystal Structure Determination of 15. Crystal data for 15·2MeCN, $\text{Co}_2\text{C}_{54}\text{N}_3\text{O}_6\text{H}_{49}\text{P}_2\text{F}_{12}$, $M_w = 1243.2$, $a = 20.117(16)$ Å, $b = 8.977(9)$ Å, $c = 34.288(23)$ Å, $\beta = 118.7(1)^\circ$, $U = 5431.4$ Å³, $F(000) = 2536$, $d_m = 1.50$ g cm⁻³, $d_c = 1.52$ g cm⁻³, $Z = 4$, Mo K radiation ($\lambda = 0.7107$ Å), $\mu(\text{Mo K}\alpha) = 7.94$ cm⁻¹, spacegroup $C2/c$.

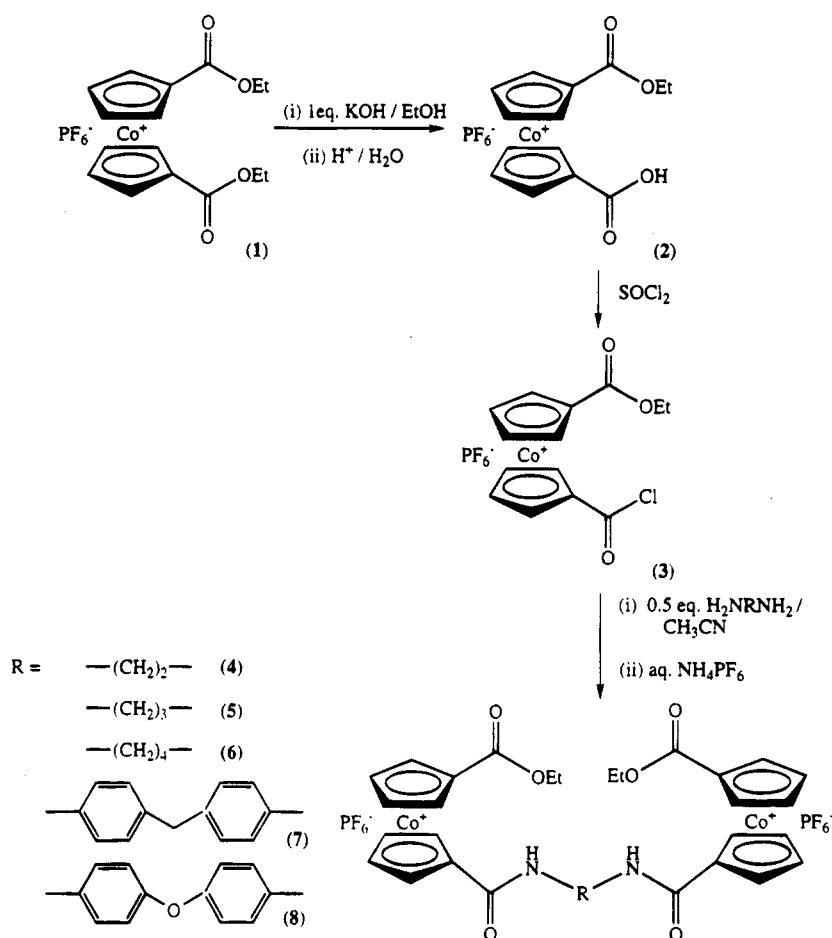
A crystal of approximate size $0.3 \times 0.3 \times 0.3$ mm³ was mounted on a STOE-2 diffractometer to be rotated around the a axis. Data were measured via ω scan with a 2θ maximum of 50°. Background counts were for 2θ s and a scan rate of 0.0333°/s was applied to a width of $(1.5 + \sin u/\tan \Theta)$. No decay in intensity was observed for the standard reflections. A total of 5200 independent reflections were measured of which 1926 with $I > 2\sigma(I)$ were used in subsequent calculations. The structure was solved by heavy atom methods. The cation contains crystallographically imposed C_2 symmetry. Hydrogen atoms on the cation were placed in calculated positions. All non-hydrogen atoms in the cation and anion were refined anisotropically. The acetonitrile solvent was given an occupancy of 50% and refined isotropically. The structure was refined by full matrix least squares with a weighting scheme $w = 1/[\sigma^2(F) + 0.003F_2]$. In the final cycle of refinement the maximum shift error ratio was 0.1. In the final difference Fourier map, maximum and minimum peaks were at 0.75 and -0.53 e Å⁻³, respectively. Calculations were performed using SHELX76⁸ and some of our own programs on the Amdahl 5870 Computer at the University of Reading. The final R value was 0.079 ($R_w = 0.077$). Positional coordinates, molecular dimensions, thermal parameters, and hydrogen atom positions are provided in the supporting information (formerly known as supplementary material).

Results and Discussion

Syntheses. 1,1'-Bis(ethylcarboxy)cobaltocenium hexafluorophosphate (1)⁶ was selectively monohydrolyzed by addition of 1 equiv of potassium hydroxide in refluxing ethanol. Upon reaction with thionyl chloride the ester-acid compound 2 was converted to the ester-acid chloride derivative 3. A 2 equiv amount of compound 3 in an acetonitrile solution was added dropwise to 1 equiv of an appropriate diamine in acetonitrile solution to produce the respective crude ditopic bis-cobaltocenium receptor. This was typically purified via Sephadex

(8) Sheldrick, G. M. *SHELX-76. Programs for Crystallographic Calculations*; University of Cambridge: Cambridge, England, 1976.

Scheme 1

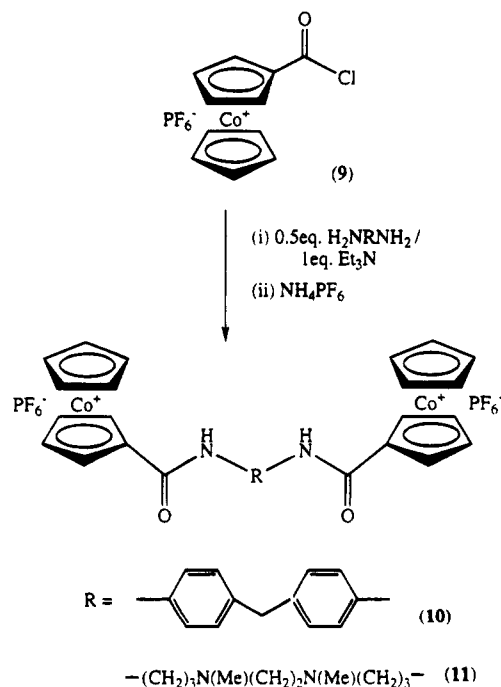


column chromatography and converted to the bis-(hexafluorophosphate) salt product using aqueous NH_4PF_6 (Scheme 1). The overall yields from **1** ranged between 10% and 25%, and all these new compounds **4–9** gave analytical and spectroscopic data in accordance with the proposed structures (See Experimental Section).

The related ditopic receptors **10** and **11** were prepared in an analogous fashion via condensation of 2 equiv of (chlorocarbonyl)cobaltocenium chloride (**9**)⁶ with 1 equiv of the respective diamine (Scheme 2). Sephadex column chromatography and conversion to the hexafluorophosphate salts gave **10** and **11** in 47% and 80% yields, respectively.

The calixarenes⁹ are attractive host molecules on which to construct additional recognition sites for target guests **2**. Although the calix[4]arene host structural unit has been modified at the lower rim for the recognition of metal cations,¹⁰ the design and synthesis of calix[4]arene anion receptors is still relatively rare.¹¹ The reaction of 1,3-dimethoxy-calix[4]arene **12**⁷ with nitric acid and acetic acid in dichloromethane produced the dinitro calix[4]arene derivative **13**⁷ in 50% yield. Reduction of **13** using Raney nickel and hydrazine hydrate gave the new diamino compound **14** in 70% yield. Condensation of **14** and 2 equiv of **9**⁶ in a dimethylformamide–acetonitrile solvent mixture ini-

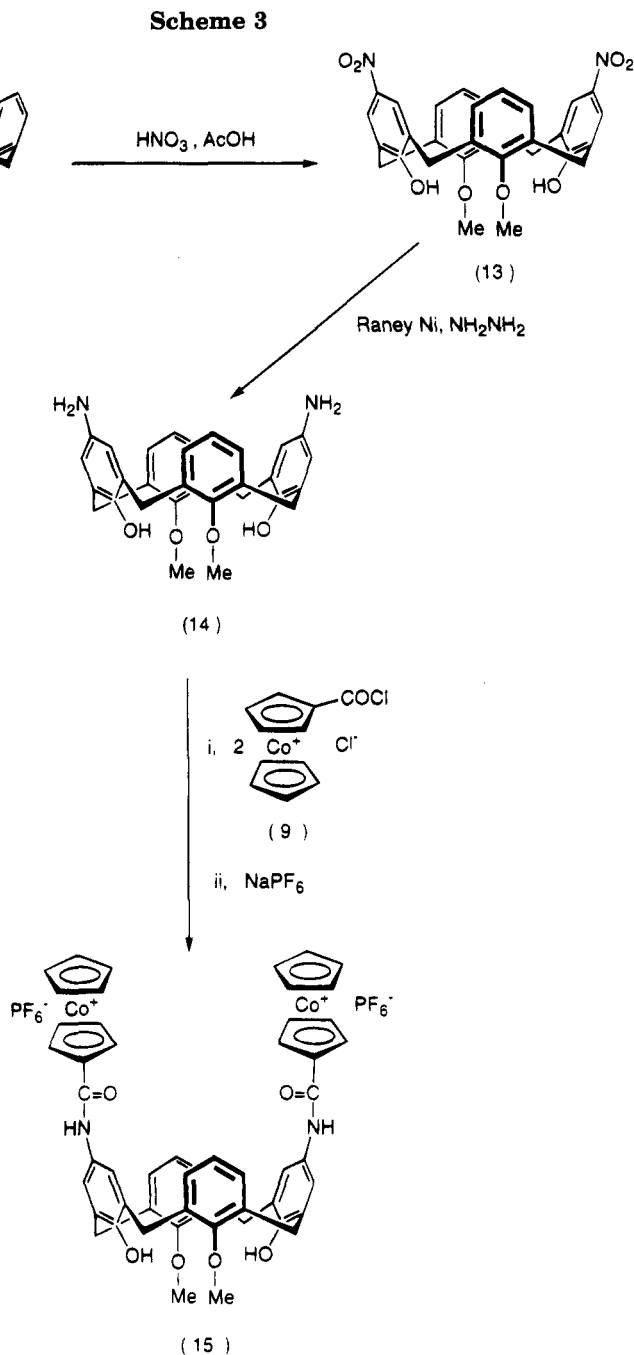
Scheme 2



tially produced a crude dark-red oil which, on treatment with an excess amount of sodium hexafluorophosphate

(9) Gutsche, C. D. *Calixarenes*; Stoddart, J. F., Ed.; Monographs in Supramolecular Chemistry; The Royal Society of Chemistry: Cambridge, England, 1989; Vol. 1.

(10) Ungaro, R.; Pochini, A. *Calixarenes, A Versatile Class of Macrocyclic Compounds*; Vicens, J., Böhrer, V., Eds.; Kluwer: Dordrecht, The Netherlands, 1990; p 133 and references therein.



followed by silica gel column chromatography (acetonitrile–dichloromethane, 4:1), afforded **15** as a red crystalline solid in 61% yield (Scheme 3).

X-ray Structural Investigation of 15. Crystals of **15** suitable for an X-ray structural determination were grown from an acetonitrile–methanol solvent mixture (Figure 2). The calix[4]arene has the cone conformation stabilized by two O–H···O hydrogen bonds (2.80 Å) around the bottom of the cone. The calix[4]arene is asymmetric in that the unique C_{ar}–C_{ar}–CH₂–CH₂ torsion angles are –81.4°, –110.2°, 98.5°, and –71.5°. At the top of the cone the Ph–NH–CO–C₅H₅ moieties are closely planar with torsion angles around the C_{ar}–

N, N–C(O), and C(O)–C_{ar} bonds of –18.3°, 178.9°, and 3.6°, respectively. The acetonitrile solvent molecules are positioned inside the cavity as shown in Figure 2 between the unattached cyclopentadienyl ring and the calixarene. The closest contacts are from N(81) to the cyclopentadienyl ring [C(61) at 3.44 and C(62) at 3.30 Å] and to a phenyl ring of the calixarene [C(32) 3.42 and C(33) at 3.54 Å]. In the Co(cyclopentadienyl)₂ moiety, the Co–C distances are as expected, ranging from 1.94 to 2.06 Å. The two rings are staggered across the metal atom.

Anion Coordination Studies and Stability Constant Determinations from ¹H NMR Titration Investigations. The addition of tetrabutylammonium halides to deuterated acetonitrile ¹H NMR solutions of **4–6** resulted in significant shifts of the respective protons of all three receptors. Remarkable downfield shifts of the amide and cyclopentadienyl protons are

(11) (a) Beer, P. D.; Chen, Z.; Goulden, A. J.; Graydon, A. R.; Stokes, S. E.; Wear, T. *J. Chem. Soc., Chem. Commun.* **1993**, 1834. (b) Morzherin, Y.; Rudkevich, D. M.; Verboom, W.; Reinhoudt, D. N. *J. Org. Chem.* **1993**, *88*, 7602. (c) Beer, P. D.; Chen, Z.; Goulden, A. J.; Grieve, A.; Heseck, D.; Szemes, F.; Wear, T. *J. Chem. Soc., Chem. Commun.* **1994**, 1269.

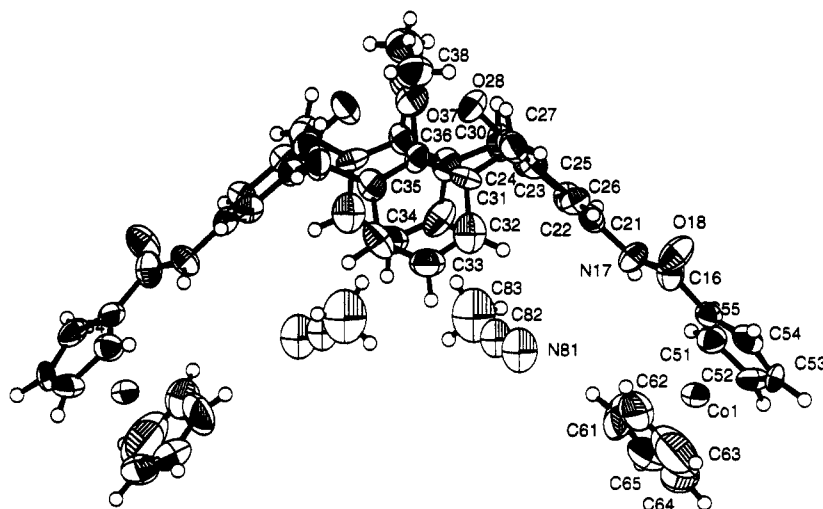


Figure 2. Structure of $15 \cdot 2\text{MeCN}$.

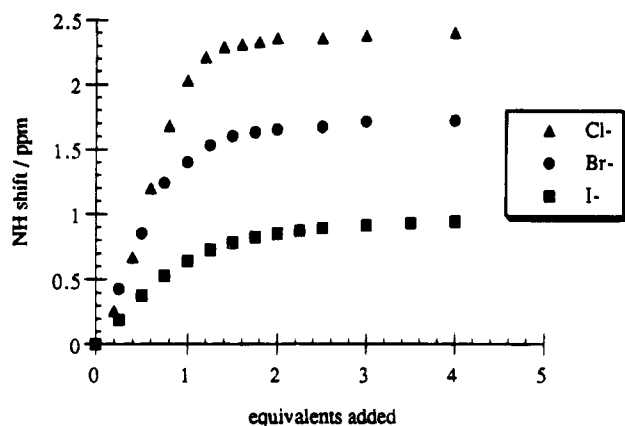


Figure 3. Proton NMR titration curves of **4** with halide anions in CD_3CN .

Table 1. Stability Constant Data for **4–6** and Halide Anions in CD_3CN

receptor	$K/\text{dm}^3 \text{mol}^{-1}$ ^a		
	Cl^-	Br^-	I^-
4	2500	330	450
5	1300	270	275
6	280	260	100

^a Errors estimated to be $\leq 10\%$.

especially noteworthy, and the resulting titration curves suggest a stoichiometry of 1:1 ditopic bis-cobaltocenium receptor:halide anion (Figure 3). The computer program EQNMR¹² was used to estimate stability constants from the ^1H NMR titration data, and the results are summarized in Table 1. Receptor **4** clearly exhibits a degree of selectivity for chloride \gg bromide \approx iodide. It is interesting that as the size of the methylene linker increases from ethyl (**4**) to propyl (**5**) or butyl (**6**) a dramatic reduction in the magnitude of the chloride anion stability constant value results. This is also observed for the bromide anion, although with the larger iodide anion all three receptors exhibit relatively low stability constant values of similar magnitudes. Consequently, whereas **4** is selective for chloride, receptors **5** and **6**, within experimental error, exhibit virtually no selectivity for any of the halide anion guests. These observations may indicate the cavity of **4** being suf-

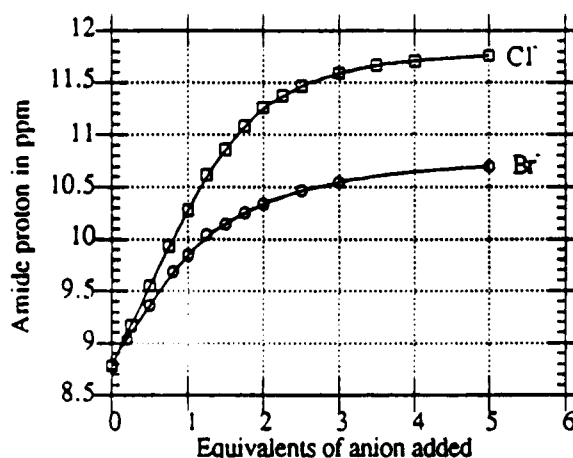


Figure 4. Proton NMR titration curves of **7** with Cl^- and Br^- in CD_3CN .

Table 2. Stability Constant Data for **7, 8, 10, and 11** and Halide Anions in CD_3CN ^a

receptor	anion	$K_1/\text{dm}^3 \text{mol}^{-1}$	$K_2/\text{dm}^3 \text{mol}^{-1}$	log K overall
7	Cl^-	1260	250	5.5
7	Br^-	1000	65	4.8
8	Cl^-	1260	400	5.7
8	Br^-	800	130	5.0
10	Cl^-	2500	130	5.5
10	Br^-	950	50	4.7
11^b	Cl^-	3160	90	5.4
11^b	Br^-	3160	50	5.2

^a *Errors estimated to be $\leq 15\%$. ^b Titration performed in DMSO.

ficiently preorganized and of complementary size and shape for chloride but being relatively too small for the larger halide anions. With the more flexible and larger ditopic receptors **5** and **6** this degree of preorganization and cavity size selection is lost, and as a result little selectivity is observed.

Analogous ^1H NMR titrations of receptors **7, 8, 10,** and **11** with chloride and bromide anions were undertaken in deuterated acetonitrile solutions. It is noteworthy that EQNMR¹² analysis of the titration data revealed 2:1 halide anion receptor stoichiometry (See Figure 4); the larger aryl and alkylamino spacers negating the possibility of cooperative 1:1 stoichiometric binding. The resulting stability constants are shown in Table 2. As predicted on statistical and electrostatic grounds K_1 values are larger than those of K_2 . Gener-

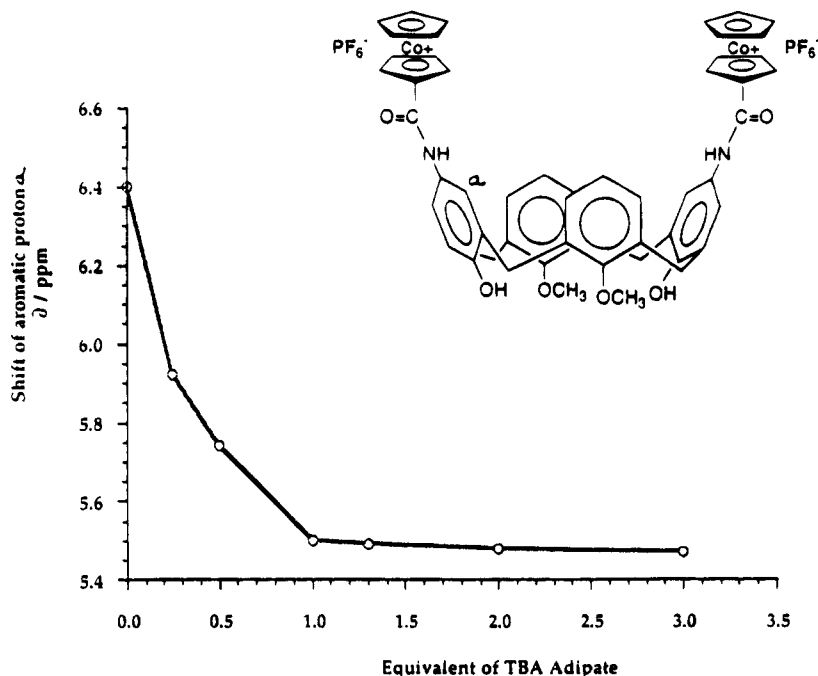


Figure 5. Proton NMR titration curve of **15** and adipate [$^{-}\text{O}_2\text{C}(\text{CH}_2)_4\text{CO}_2^{-}$] in acetone- d_6 .

Table 3. Stability Constant Data for **15 and Various Anions in DMSO- d_6**

anion	$K/\text{dm}^3 \text{mol}^{-1}$ ^a
Cl^-	5035
Br^-	1680
H_2PO_4^-	2800
HSO_4^-	$K_1 = 990; K_2 = 495$
$^{-}\text{O}_2\text{C}(\text{CH}_2)_4\text{CO}_2^{-}$ ^b	11510

^a Errors estimated to be $\leq 10\%$. ^b Titration performed in acetone- d_6 .

ally the overall log K values are larger for Cl^- than Br^- . Comparing the respective stability constant values for receptors **7** and **10** suggests the presence of the ester functionality has little effect on the halide anion recognition process.

Disappointingly ^1H NMR titrations of **7**, **8**, **10**, and **11** with other anions such as HSO_4^- and H_2PO_4^- in acetonitrile or DMSO solutions led to precipitation of the respective complexes. Consequently it was not possible to calculate stability constants from the resulting incomplete titration curves.

^1H NMR titrations of the novel calix[4]arene receptor **15** with various anions were performed in deuteriated dimethyl sulfoxide solutions due to solubility problems. Large downfield perturbations of the receptor's protons were observed on addition of halides, hydrogen sulfate, and dihydrogen phosphate anions. For example, with HSO_4^- downfield shifts of $\Delta\delta = 0.25 - 0.4$ ppm for the aryl protons of the calix[4]arene structural framework were observed, suggesting anion complexation takes place within the upper rim of the calix cavity of **15**. EQNMR¹² analysis of the resulting titration curves suggested 1:1 anion complexes are formed with Cl^- , Br^- , and H_2PO_4^- . Hydrogen sulfate anions, however, formed a 1:2 host molecule:anion complex. The calculated stability constant values, shown in Table 3, are large in magnitude, especially considering they were determined in the highly polar DMSO- d_6 solvent medium.

With the dicarboxylate dianion adipate, although significant interactions were observed with acetonitrile,

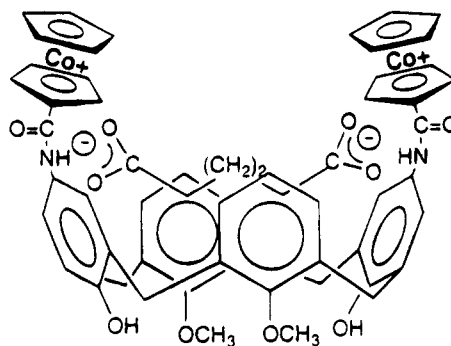


Figure 6. Proposed solution complex structure of **15** and adipate.

acetone, and DMSO solutions of **7**, **8**, **10**, and **11**, precipitation problems of the resulting receptor-dianion complexes again thwarted their respective stoichiometries being elucidated. A ^1H NMR titration curve of **15** and adipate was, however, obtained in acetone- d_6 solution (Figure 5). In addition to upfield perturbations of the substituted cyclopentadienyl protons, significant shifts of the calix aryl protons were observed, suggesting the adipate guest dianion coordinates within the confines of the upper rim cavity of **15** (Figure 6). The calculated stability constant of $K = 11\,510$ (Table 3) implies a thermodynamically stable 1:1 **15**-adipate complex exists in acetone solution. Disappointingly, repeated attempts at obtaining crystals of X-ray quality of the **15**-adipate complex from a variety of solvent mixtures failed.

Electrochemical Anion Recognition Studies. The electrochemical properties of all these new bis-cobaltocenium receptor molecules were investigated in acetonitrile or acetone using cyclic voltammetry with Bu_4NBF_4 as the supporting electrolyte. Each compound exhibited a reversible two-electron redox reduction wave in the -0.8 to -1.1 V region (Table 4). Cyclic voltammograms were also recorded after progressively adding stoichiometric equivalents of anion guests to the electrochemical solutions, and the results are summarized

Table 4. Electrochemical Data

receptor	E_f/V^a	$\Delta E_f(Cl^-)/mV^b$	$\Delta E_f(Br^-)/mV^b$	$\Delta E_f(HSO_4^-)^b$	$\Delta E_f(H_2PO_4^-)^b$
4	-0.88	60	40		
5	-0.89	45	30		
6	-0.89	40	30		
7	-0.85	70		65	165
8	-0.79	65		35	200
10	-0.90	70		<i>c</i>	<i>c</i>
11	-1.04	50		115	250
16^d	-0.85 ^d	55 ^d	30 ^d	50 ^d	<i>c</i>

^a Obtained in acetonitrile solution containing 0.2 mol of NBu_4BF_4 per dm^{-3} as supporting electrolyte. Solutions were ca. 1×10^{-3} mol dm^{-3} in receptor, and potentials were obtained with reference to a Ag/Ag^+ electrode. Coulometric investigations suggest E_f values represent a two-electron reduction process. ^b Cathodic shift in reduction potential produced by presence of anions (up to 4 equiv) added as their tetrabutylammonium salts. ^c Precipitation of complex observed; no c.v. could be obtained. ^d Obtained in acetone solution.

in Table 4. Substantial one-wave cathodic shifts of the respective cobaltocenium/cobaltocene redox couple are generally observed with most anionic guest species. The complexed anion effectively stabilizes the positive charge of the cobaltocenium unit. It is noteworthy that chloride, by virtue of its higher charge density, causes relatively larger cathodic perturbations than bromide (see examples of **4–6** in Table 4). Interestingly, as observed with monosubstituted cobaltocenium derivatives,⁵ the dihydrogenphosphate anion produces the largest magnitudes of cathodic shifts.

The addition of tetrabutylammonium adipate to electrochemical solutions of **15** led to a cathodic shift of 50 mV, suggesting this receptor can electrochemically recognize this dianionic guest in acetone solution. Similar electrochemical experiments with the other bis-cobaltocenium receptors gave, because of solubility problems, inconclusive results.

Conclusions

A series of novel ditopic bis-cobaltocenium receptor molecules containing alkyl, aryl, and calix[4]arene spacers have been synthesized, and a crystal structure of the calix[4]arene derivative **15** has been determined. Proton NMR halide anion coordination studies revealed that the alkyl-linked derivatives **4–6** form 1:1 stoichiometric complexes. Stability constant evaluations suggested that as the length of the alkyl chain increased the selectivity preference for chloride and the general stability of the halide complex decreased. Receptors **7**, **8**, **10**, and **11** containing larger linking moieties produced anion complexes of 2:1 halide anion:receptor stoichiometry. The bis-cobaltocenium calix[4]arene derivative **15** forms thermodynamically stable 1:1 anion complexes with Cl^- , Br^- , and $H_2PO_4^-$ in polar DMSO solutions and adipate in acetone. Electrochemical investigations showed all the bis-cobaltocenium systems can electrochemically recognize a variety of anions, including **15** sensing adipate.

Acknowledgment. We thank the SERC for a postdoctoral fellowship to D.H., for studentships to J.E.K. and S.E.S., and for use of the mass spectrometry service at University College, Swansea, U.K. The University of Reading and the SERC are gratefully acknowledged for funding toward the crystallographic Image Plate System.

Supporting Information Available: Tables of atom coordinates, bond distances and angles, and anisotropic thermal parameters for **15** (9 pages). Ordering information is given on any current masthead page.

OM950147C

Comparative Study of the Structures and Reactivity of the π -Cyclopentadienyl-Bonded and Metal-Bonded Succinimidyl Ester Complexes (Metal = Mo, Fe): X-ray Molecular Structures of $[(\eta^5\text{-C}_5\text{H}_4\text{COONS})\text{Mo}(\text{CO})_3\text{Me}]$ and $[(\eta^5\text{-C}_5\text{H}_5)\text{Mo}(\text{CO})_3(\eta^1\text{-CH}_2\text{COONS})]$ ($-\text{NS} = \text{N-Succinimidyl}$)

Bouchra El Mouatassim,[†] Hani Elamouri,^{*,†} Jacqueline Vaissermann,[‡] and Gérard Jaouen^{*,†}

Ecole Nationale Supérieure de Chimie de Paris, URA CNRS 403, 11, rue Pierre et Marie Curie, 75231 Paris Cedex 05, France, and Université Pierre et Marie Curie, Place Jussieu, 75231 Paris Cedex 05, France

Received March 3, 1995[⊗]

The activated ester compounds $[(\eta^5\text{-C}_5\text{H}_4\text{COONS})\text{Mo}(\text{CO})_3\text{Me}]$ (**5**) and $[(\eta^5\text{-C}_5\text{H}_4\text{COONS})\text{Fe}(\text{CO})_2\text{Me}]$ (**6**) were obtained by treatment of the novel organometallic carboxylic acid complexes $[(\eta^5\text{-C}_5\text{H}_4\text{COOH})\text{Mo}(\text{CO})_3\text{Me}]$ (**2**) and $[(\eta^5\text{-C}_5\text{H}_4\text{COOH})\text{Fe}(\text{CO})_2\text{Me}]$ (**4**) with *N*-hydroxysuccinimide in THF in the presence of DCC (dicyclohexylcarbodiimide) or with DSC (disuccinimidyl carbonate) in CH_3CN in the presence of pyridine. These activated ester complexes were identified spectroscopically, and in addition, the X-ray molecular structure of **5** was determined. Compound **5** crystallizes in the triclinic space group $P\bar{1}$: $a = 8.684(4)$ Å, $b = 12.764(8)$ Å, $c = 16.522(10)$ Å, $\alpha = 65.13(4)^\circ$, $\beta = 72.52(4)^\circ$, $\gamma = 71.34(4)^\circ$, $V = 1544.6$ Å³, $Z = 4$. Similarly, the metal-activated ester complex $[(\eta^5\text{-C}_5\text{H}_5)\text{Mo}(\text{CO})_3(\eta^1\text{-CH}_2\text{COONS})]$ (**7**) was obtained by treatment of the dimer $[\text{Cp}_2\text{Mo}_2(\text{CO})_6]$ with Na/Hg followed by addition of 2 equiv of $\text{ClCH}_2\text{COONS}$ in THF; in this compound the ester unit is bonded directly to the metal center rather than to the π -bonded cyclopentadienyl. Complex **7** was characterized by spectroscopic methods, and its molecular structure was ascertained by X-ray crystallography which showed that it belongs to the well-known carbon-bound molybdenum 2-oxaalkyl (η^1 -enolate) category. Complex $[(\eta^5\text{-C}_5\text{H}_5)\text{Mo}(\text{CO})_3(\eta^1\text{-CH}_2\text{COONS})]$ (**7**) crystallizes in the monoclinic space group $C2/c$: $a = 19.484(2)$ Å, $b = 11.393(2)$ Å, $c = 13.694(2)$ Å, $\beta = 98.91(2)^\circ$, $V = 3000$ Å³, $Z = 8$. The reactivity of π -bonded activated ester complexes **5** and **6** with ISiMe_3 gave respectively the iodo derivatives $[(\eta^5\text{-C}_5\text{H}_4\text{COONS})\text{Mo}(\text{CO})_3\text{I}]$ (**9**) and $[(\eta^5\text{-C}_5\text{H}_4\text{COONS})\text{Fe}(\text{CO})_2\text{I}]$ (**10**) as deep red microcrystalline solids. The reactivity of the π -bonded activated ester complexes **5** and **6** and that of the metal-bonded activated ester **7** with amino esters are presented and discussed.

Introduction

Recently, there has been considerable interest toward the synthesis of organometallic synthons which form stable conjugates with amino acids and proteins.¹ An important objective is their potential use as labeling agents: the introduction of such species helps to bring about the crystallization of the corresponding adduct and hence its identification by X-ray analysis.² Such perspective has been demonstrated with success, particularly with amino acids and nucleotides; for instance, the stable conjugates $[\text{Cp}^*\text{Ir}(\text{glycine})]$ and $[\text{Cp}^*(\text{phenyl-}$

glycine)] have been isolated and identified by X-ray determination.^{2b}

An interesting class of synthons are η^5 -cyclopentadienyl metallocarbonyl complexes, where the π -bonded cyclopentadienyl is attached to an activated *N*-succinimidyl ester function. Such species have been used for the selective labeling of amino acids in peptide chains and proved to be a valuable method to assay the number of such amino acids which are exposed and available for reaction.^{1b,3} The metal-carbonyl bands absorb in the range of 1900–2100 cm^{-1} , where biological molecules are transparent. Hence the labeling of proteins by these complexes can be achieved by monitoring the metallocarbonyl bands using FT infrared techniques. In this paper we report on the syntheses of the novel *N*-succinimidyl ester complexes $[(\eta^5\text{-C}_5\text{H}_4\text{COONS})\text{Mo}$

[†] Ecole Nationale Supérieure de Chimie de Paris.

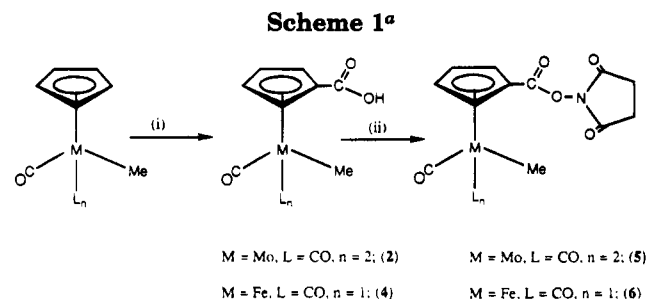
[‡] Université Pierre et Marie Curie.

[⊗] Abstract published in *Advance ACS Abstracts*, June 15, 1995.

(1) (a) Laurie, S. H. *Amino Acids, Peptides and Proteins*. In *Comprehensive Coordination Chemistry*; Wilkinson, G., Ed.; Pergamon: Oxford, England, 1987; Vol. 2, p 739. (b) Jaouen, G.; Vessières, A.; Butler, I. S. *Acc. Chem. Res.* **1993**, *26*, 361 and references therein. (c) Sloop, F. V.; Brown, G. M.; Sachleben, R. A.; Garrity, M. L.; Elbert, J. E.; Jacobson, K. B. *New J. Chem.* **1994**, *18*, 317. (d) Craver, J. A.; Fates, B.; Kane-Maguire, L. A. P. *J. Chem. Soc., Chem. Commun.* **1993**, 928. (e) Anson, C. E.; Creaser, C. S.; Egyed, O.; Fey, M. A.; Stephenson, G. R. *J. Chem. Soc., Chem. Commun.* **1994**, 39. (f) Lavastre, I.; Besancon, J.; Brossier, P.; Moise, C. *Appl. Organomet. Chem.* **1991**, *5*, 143.

(2) (a) Elamouri, H.; Gruselle, M.; Vaissermann, J.; McGlinchey, M. J.; Jaouen, G. *J. Organomet. Chem.* **1995**, *485*, 79. (b) Grotjahn, D. B.; Groy, T. L. *J. Am. Chem. Soc.* **1994**, *116*, 6969. (c) Beck, W.; Kramer, R. *Angew. Chem., Int. Ed. Engl.* **1991**, *30*, 1467.

(3) (a) Wang, Z.; Roe, B. A.; Nicholas, K. M.; White, R. L. *J. Am. Chem. Soc.* **1993**, *115*, 4399. (b) Salmain, M.; Gunn, M.; Gorfti, A.; Top, S.; Jaouen, G. *Bioconjugate Chem.* **1993**, *4*, 425.



^a Reagents and conditions: (i) (a) THF, *s*-BuLi (1.7 equiv), -78°C , 15 min, (b) THF, dry ice (excess), -30°C , 10 min, (c) HCl (10%), THF, room temperature; (ii) CH_3CN , DSC (1 equiv), pyridine (1 equiv), room temperature.

$(\text{CO})_3\text{Me}$ (**5**) and $[(\eta^5\text{-C}_5\text{H}_4\text{COONS})\text{Fe}(\text{CO})_2\text{Me}]$ (**6**) from their organometallic carboxylic acids $[(\eta^5\text{-C}_5\text{H}_4\text{COOH})\text{Mo}(\text{CO})_3\text{Me}]$ (**2**) and $[(\eta^5\text{-C}_5\text{H}_4\text{COOH})\text{Fe}(\text{CO})_2\text{Me}]$ (**4**). The molecular structure of **5** has been ascertained by X-ray analysis; furthermore the reactivity of these new succinimidyl ester complexes with ISiMe_3 and with various amino esters are reported. On the other hand we have also prepared the metal-activated ester complex $[(\eta^5\text{-C}_5\text{H}_5)\text{Mo}(\text{CO})_3(\eta^1\text{-CH}_2\text{COONS})]$ (**7**), where the ester unit is bonded directly to the metal center rather than to the π -bonded cyclopentadienyl. The molecular structure of **7** was identified by X-ray analysis. Finally, the structure and the reactivity of the latter complex are compared to those of $[(\eta^5\text{-C}_5\text{H}_4\text{COONS})\text{Mo}(\text{CO})_3\text{Me}]$ (**5**) and $[(\eta^5\text{-C}_5\text{H}_4\text{COONS})\text{Fe}(\text{CO})_2\text{Me}]$ (**6**).

Results and Discussion

Synthesis and NMR Characterization. The cornerstone for the preparation of these functionalized η^5 -cyclopentadienyl metalcarbonyl complexes **5** and **6** is the synthesis of the parent organometallic carboxylic acids $[(\eta^5\text{-C}_5\text{H}_4\text{COOH})\text{Mo}(\text{CO})_3\text{Me}]$ (**2**) and $[(\eta^5\text{-C}_5\text{H}_4\text{COOH})\text{Fe}(\text{CO})_2\text{Me}]$ (**4**). The latter reacts either with NHS (*N*-hydroxysuccinimide) in the presence of DCC (dicyclohexylcarbodiimide) or with DSC (disuccinimidyl carbonate) in the presence of pyridine to give the target compounds (Scheme 1).

Rausch et al. have prepared the organometallic carboxylic acid complexes $(\eta^5\text{-C}_5\text{H}_4\text{COOH})\text{ML}_n$ ($M = \text{Co}, \text{W}$) by saponification of the corresponding ester derivatives with aqueous potassium hydroxide in methanol, followed by acidification with hydrochloric acid;⁴ however, the previous experimental conditions have been shown to be unsuccessful for preparing the compound $[(\eta^5\text{-C}_5\text{H}_4\text{COOH})\text{Mo}(\text{CO})_3\text{Me}]$ (**2**); the authors attributed this behavior to the instability of **2** in basic medium.⁵ We also note that complexes of the type $[(\eta^5\text{-C}_5\text{H}_4\text{COOH})\text{Fe}(\text{CO})_2\text{R}]$ ($R = \text{-Ph}; \text{-CpMn}(\text{CO})_3$) have been reported but using a different synthetic procedure.⁶

In our case, the organometallic acid complexes $[(\eta^5\text{-C}_5\text{H}_4\text{COOH})\text{Mo}(\text{CO})_3\text{Me}]$ (**2**) and $[(\eta^5\text{-C}_5\text{H}_4\text{COOH})\text{Fe}(\text{CO})_2\text{Me}]$ (**4**) were prepared in good yields, 62% and 63%, respectively, by treatment of $[(\eta^5\text{-C}_5\text{H}_5)\text{Mo}(\text{CO})_3\text{Me}]$ (**1**) and $[(\eta^5\text{-C}_5\text{H}_5)\text{Fe}(\text{CO})_2\text{Me}]$ (**3**) with *s*-BuLi fol-

lowed by addition of dry ice (CO_2) and acidification with aqueous HCl solution (Scheme 1). Although the preparation of the iron derivative **4** was attained without difficulties, the molybdenum derivative $[(\eta^5\text{-C}_5\text{H}_4\text{COOH})\text{Mo}(\text{CO})_3\text{Me}]$ (**2**), reported for the first time, could only be obtained by avoiding its recrystallization in basic medium. A brief communication has already been reported concerning their synthesis and their pK_a values.⁷ The $^1\text{H-NMR}$ spectra of **2** and **4** show a pair of triplets in the area (5–6 ppm) characteristic of a functionalized π -bonded cyclopentadienyl ring; there is also a singlet peak at 0.44 and 0.25 ppm attributed to the metal-bonded methyl groups of **2** and **4**, respectively. The organic carbonyl stretching absorptions in these compounds are shifted to a lower frequency when compared to organic carboxylic acids, and they absorb at 1680 cm^{-1} for **2** and 1676 cm^{-1} for **4**.

When the carboxylic acid complex $[(\eta^5\text{-C}_5\text{H}_4\text{COOH})\text{Fe}(\text{CO})_2\text{Me}]$ (**4**) was treated with *N*-hydroxysuccinimide in the presence of DCC (dicyclohexylcarbodiimide) in THF solution (see Scheme 1), the succinimidyl ester derivative $[(\eta^5\text{-C}_5\text{H}_4\text{COONS})\text{Fe}(\text{CO})_2\text{Me}]$ (**6**) was isolated in 62% yield. Similarly, the analogous molybdenum derivative $[(\eta^5\text{-C}_5\text{H}_4\text{COONS})\text{Mo}(\text{CO})_3\text{Me}]$ (**5**) was obtained but in a low yield. We have found that **5** can be prepared in 57% yield by treatment of $[(\eta^5\text{-C}_5\text{H}_4\text{COOH})\text{Mo}(\text{CO})_3\text{Me}]$ (**2**) with DSC (disuccinimidyl carbonate) in CH_3CN in the presence of pyridine. In general the iron compounds **4** and **6** exhibit higher stabilities in solution than the molybdenum derivatives **2** and **5**. The structures of these activated ester complexes were proposed on the basis of spectroscopic data as well as X-ray analysis carried out on $[(\eta^5\text{-C}_5\text{H}_4\text{COONS})\text{Mo}(\text{CO})_3\text{Me}]$ (**5**) (vide infra).

The $^1\text{H-NMR}$ spectra of complexes **5** and **6** show a pair of triplets characteristic of these functionalized π -complexed Cp rings which appear in the area 5–6.2 ppm and a singlet attributed to the *N*-succinimidyl fragment around 2.8–2.9 ppm; finally, the methyl group attached to the metal center appears as a singlet upfield in the range 0.4–0.6 ppm. The organic carbonyls of **5** and **6** show three strong stretching vibrations in the area of $1730\text{--}1812\text{ cm}^{-1}$.

X-ray Molecular Structure of $(\eta^5\text{-C}_5\text{H}_4\text{COONS})\text{Mo}(\text{CO})_3\text{Me}$ (5**).** Suitable crystals for X-ray analysis were obtained from cooling a solution of **5** in an ether/hexane mixture. The unit cell contains two independent molecules (a) and (b) (see Figure 1). A view of molecule a is shown in Figure 2; the unit cell was found to be triclinic $P\bar{1}$, and crystallographic data collection parameters and selected bond lengths and angles are listed in Tables 1–3. The complex exhibits four-legged piano stool geometry (vide infra); the carbonyls and the methyl group serve as legs. The structure shows also that the plane containing the succinimidyl moiety is almost orthogonal to that of the Cp ring with $\theta = 82^\circ$ (a) and 85° (b). The $\text{Mo-Cp}_{\text{centroid}}$ bond distance is 2.02 (a) and 2.01 Å (b) and compares well to that of $(\eta^5\text{-C}_5\text{H}_4\text{COMe})\text{Mo}(\text{CO})_3\text{Me}$ with an $\text{Mo-Cp}_{\text{centroid}}$ bond distance of 2.01 Å reported by Rausch et al.⁸

The activated ester complexes **5** and **6** react with excess ISiMe_3 in THF for 16 h at $T = 60^\circ\text{C}$ to give

(4) (a) Hart, W. P.; Macomber, D. W.; Rausch, M. D. *J. Am. Chem. Soc.* **1980**, *102*, 1196. (b) Hart, W. P.; Rausch, M. D. *J. Organomet. Chem.* **1988**, *355*, 455.

(5) Macomber, D. W.; Rausch, M. D. *J. Organomet. Chem.* **1983**, *258*, 331.

(6) Orlova, T. Yu.; Setkina, V. N.; Kursanov, D. N. *J. Organomet. Chem.* **1984**, *267*, 309.

(7) El Mouatassim, B.; Elamouri, H.; Salmain, M.; Jaouen, G. *J. Organomet. Chem.* **1994**, *479*, C18.

(8) Rodgers, R. D.; Atwood, J. L.; Rausch, M. D.; Macomber, D. W. *J. Cryst. Spectrosc. Res.* **1990**, *20*, 555.

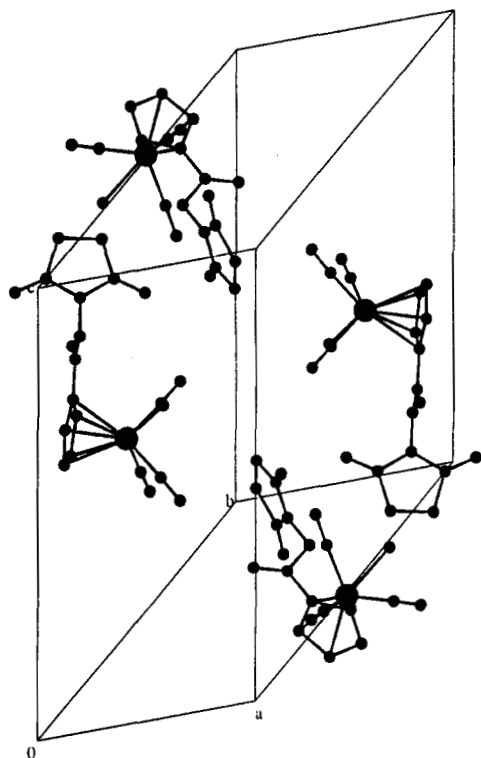


Figure 1. Unit cell of **5** showing two independent molecules (a) and (b).

Table 1. Crystallographic Data for $[(\eta^5\text{-C}_5\text{H}_4\text{COONS})\text{Mo}(\text{CO})_3\text{Me}]$ (**5**)

chemical formula	$\text{C}_{14}\text{H}_{11}\text{O}_7\text{NM}_6$
fw	401.18
cryst syst	triclinic
space group	$P\bar{1}$
Z	4
a, Å	8.684(4)
b, Å	12.764(8)
c, Å	16.522(10)
α , deg	65.13(4)
β , deg	72.52(4)
λ , deg	71.34(4)
V, Å ³	1544.6
F(000)	800
ρ (calcd), g cm ⁻³	1.72
μ (Mo K α) cm ⁻¹	8.61
diffractometer	Philips PW1100
monochromator	graphite
radiation (λ , Å)	Mo K α (0.710 70)
temp, °C	20
scan type	$\omega/2\theta$
scan range θ , deg	1.1 + 0.34 tan θ
2 θ range, deg	4–50
no. of refctn colld	5395
no. of refctn used (criteria)	4323 ($I > 3\sigma(I)$)
R	0.0253
R_w^a	0.0269
abs corr	min 0.85, max 1.15
secondary ext	51×10^{-6}
weighting scheme	unit weights
rms (shift/esd) (last ref)	0.34
Is params	484

^a $R_w = [\sum W_i(F_o - F_c)^2 / \sum W_i F_o^2]^{1/2}$. ^b Difabs. Walker, N.; Stuart, D. *Acta Crystallogr.* **1983**, *A39*, 159.

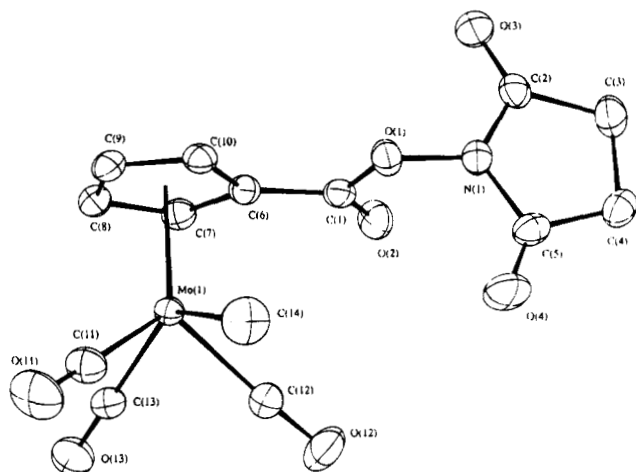


Figure 2. Molecular structure and atom labeling for $[(\eta^5\text{-C}_5\text{H}_4\text{COONS})\text{Mo}(\text{CO})_3\text{Me}]$ (**5**).

respectively the iodo derivatives $[(\eta^5\text{-C}_5\text{H}_4\text{COONS})\text{Mo}(\text{CO})_3\text{I}]$ (**9**) and $[(\eta^5\text{-C}_5\text{H}_4\text{COONS})\text{Fe}(\text{CO})_2\text{I}]$ (**10**) as deep red microcrystals. The infrared data were the most informative, which show a higher wavenumber shift for the metal–carbonyl bands of 30–40 cm^{-1} ; this is due to the presence of the electron-withdrawing iodo atom which is bonded to the metal center instead of the methyl group. The ¹H-NMR spectra of these complexes show the usual pair of triplets but appearing slightly downfield relative to the parent molecules **5** and **6** in the area 5.2–6.6 ppm as well as the singlet attributed to the succinimidyl moiety; we also note the disappearance of the singlet signals in the 0.4–0.6 ppm range characteristic of the metal-bonded methyl groups.

On the other hand we have prepared another type of metal-activated ester, in which the ester unit bonded directly to the metal center and not to the cyclopentadienyl fragment. The main objective of this work is to

compare the reactivity and the stability of both systems toward amino acids labeling. Thus $[(\eta^5\text{-C}_5\text{H}_5)\text{Mo}(\text{CO})_3(\eta^1\text{-CH}_2\text{COONS})]$ (**7**) was obtained as the major product in 45% yield by a one-pot reaction from the cleavage of the dimer $[\text{Cp}_2\text{Mo}_2(\text{CO})_6]$ with Na/Hg followed by addition of 2 equiv of $\text{ClCH}_2\text{COONS}$ in THF (Scheme 2).

We have also isolated a minor compound as an orange material; attempts to identify this unstable species have been so far unsuccessful, since it transforms to the starting material $[\text{Cp}_2\text{Mo}_2(\text{CO})_6]$. Similar results were obtained by Bailey, Winter and co-workers, when $[\text{CpMo}(\text{CO})_3][\text{Na}]$ prepared in situ, was treated with 2 equiv of $\text{BrCH}_2\text{CH}_2\text{CH}_2\text{Br}$ in THF. The authors obtained the expected alkyl derivative $\text{CpMo}(\text{CO})_3\text{CH}_2\text{CH}_2\text{CH}_2\text{Br}$, as well as an unstable orange compound, which transforms to give the starting material $[\text{Cp}_2\text{Mo}_2(\text{CO})_6]$.⁹

It is worth mentioning that preparation of tungsten and molybdenum 2-oxaallyl(η^1 -(C)-enolate) complexes by the above procedure has been well investigated by King, Green, and co-workers.¹⁰ Recently, a detailed and improved synthesis of such complexes as well as their reactivity have been reported by Bergman, Heathcock, and co-workers;¹¹ in general the authors observed the formation of only one product in 50–80% yield, but we are not aware of any previous example in the literature in which the enolate ester complex possesses an N-succinimidyl fragment.

(9) Adams, H.; Bailey, N. A.; Winter, M. J. *J. Chem. Soc., Dalton Trans.* **1984**, 273.

(10) (a) King, R. B.; Bisnette, M. B.; Fronzaylia, A. *J. Organomet. Chem.* **1966**, *5*, 341. (b) Ariyarante, J. K. P.; Bierrum, A. M.; Green, M. L. H.; Ishaq, M.; Prout, C. K.; Swainwick, M. G. *J. Chem. Soc. A* **1969**, 1309. (c) Hillis, J.; Ishaq, M.; Gorewit, B.; Tsutsui, M. *J. Organomet. Chem.* **1976**, *116*, 91.

(11) (a) Doney, J. J.; Bergman, R. G.; Heathcock, C. H. *J. Am. Chem. Soc.* **1985**, *107*, 3724. (b) Burkhardt, E. R.; Doney, J. J.; Bergman, R. G.; Heathcock, C. H. *J. Am. Chem. Soc.* **1987**, *109*, 2022.

Table 2. Collection Parameters for $[(\eta^5\text{-C}_5\text{H}_4\text{COONS})\text{Mo}(\text{CO})_3\text{Me}]$ (5**)**

atom	<i>x/a</i>	<i>y/b</i>	<i>z/c</i>	<i>U</i> (eq), Å ²
Molecule a				
Mo(1)	0.19459(3)	0.23280(2)	0.52333(2)	0.0315
O(1)	0.0020(3)	0.2072(2)	0.7825(2)	0.0446
O(2)	-0.1707(3)	0.3597(2)	0.6950(2)	0.0505
O(3)	-0.2908(4)	0.2029(3)	0.9092(2)	0.0579
O(4)	0.1502(4)	0.3745(3)	0.7799(2)	0.0676
O(11)	0.5257(4)	0.1399(3)	0.4087(3)	0.0774
O(12)	0.2248(5)	0.4683(3)	0.5264(2)	0.0763
O(13)	0.1505(4)	0.3998(3)	0.3248(2)	0.0638
N(1)	-0.0538(4)	0.2708(3)	0.8404(2)	0.0438
C(1)	-0.0737(4)	0.2665(3)	0.7063(2)	0.0375
C(2)	-0.2037(5)	0.2649(3)	0.8999(2)	0.0420
C(3)	-0.2275(5)	0.3503(4)	0.9454(3)	0.0535
C(4)	-0.0872(5)	0.4148(3)	0.8967(3)	0.0502
C(5)	0.0237(5)	0.3565(3)	0.8311(3)	0.0453
C(6)	-0.0199(4)	0.1959(3)	0.6482(2)	0.0356
C(7)	-0.0824(4)	0.2273(3)	0.5693(2)	0.0396
C(8)	-0.0034(4)	0.1382(3)	0.5321(2)	0.0407
C(9)	0.1063(5)	0.0504(3)	0.5884(3)	0.0413
C(10)	0.0970(4)	0.0849(3)	0.6599(2)	0.0380
C(11)	0.4048(5)	0.1753(4)	0.4506(3)	0.0512
C(12)	0.2142(5)	0.3837(4)	0.5227(3)	0.0506
C(13)	0.1634(5)	0.3397(3)	0.3974(3)	0.0441
C(14)	0.4001(6)	0.1892(4)	0.6016(3)	0.0660
Molecule b				
Mo(51)	-0.33644(3)	0.90997(3)	0.84385(2)	0.0309
O(51)	0.0639(3)	0.6570(2)	0.8316(2)	0.0484
O(52)	0.1808(3)	0.8115(2)	0.7896(2)	0.0462
O(53)	0.1507(5)	0.7042(4)	0.6439(3)	0.0902
O(54)	0.3266(5)	0.4999(3)	0.9114(2)	0.0703
O(61)	-0.4290(4)	1.1876(2)	0.7602(2)	0.0618
O(62)	-0.2285(4)	0.9476(3)	0.6373(2)	0.0624
O(63)	-0.7217(3)	0.9590(3)	0.8726(2)	0.0603
N(51)	0.2105(4)	0.6067(3)	0.7855(2)	0.0422
C(51)	0.0682(4)	0.7655(3)	0.8309(2)	0.0354
C(52)	0.2405(5)	0.6318(4)	0.6929(3)	0.0554
C(53)	0.4029(6)	0.5512(4)	0.6738(3)	0.0577
C(54)	0.4643(5)	0.4861(4)	0.7626(3)	0.0573
C(55)	0.3330(5)	0.5270(3)	0.8318(3)	0.0429
C(56)	-0.0821(4)	0.8062(3)	0.8897(2)	0.0337
C(57)	-0.2026(4)	0.7404(3)	0.9521(2)	0.0395
C(58)	-0.3167(5)	0.8114(4)	0.9991(2)	0.0445
C(59)	-0.2706(5)	0.9212(3)	0.9666(2)	0.0418
C(60)	-0.1245(4)	0.9170(3)	0.8999(2)	0.0377
C(61)	-0.3946(5)	1.0869(3)	0.7900(3)	0.0429
C(62)	-0.2691(4)	0.9363(3)	0.7127(2)	0.0411
C(63)	-0.5804(4)	0.9413(3)	0.8610(2)	0.0414
C(64)	-0.3961(5)	0.7603(4)	0.8218(3)	0.0540

The metal-activated ester complex $[(\eta^5\text{-C}_5\text{H}_5)\text{Mo}(\text{CO})_3(\eta^1\text{-CH}_2\text{COONS})]$ (**7**) was obtained as light yellow crystals and was identified spectroscopically; in addition, the X-ray molecular structure was determined.

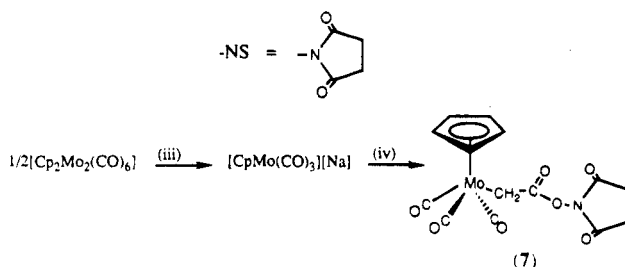
X-ray Molecular Structure of $(\eta^5\text{-C}_5\text{H}_5)\text{Mo}(\text{CO})_3(\eta^1\text{-CH}_2\text{COONS})$ (7**).** Recrystallization of **7** from ether/hexane gave a sample suitable for an X-ray crystallographic diffraction study. Figure 3 shows a view of $[(\eta^5\text{-C}_5\text{H}_5)\text{Mo}(\text{CO})_3(\eta^1\text{-CH}_2\text{COONS})]$ (**7**), and crystallographic data collection parameters and selected bond lengths and angles are listed in Tables 4–6.

Complex $[(\eta^5\text{-C}_5\text{H}_5)\text{Mo}(\text{CO})_3(\eta^1\text{-CH}_2\text{COONS})]$ (**7**) displays a piano stool structure well-known for half-sandwich complexes with Cp as the seat and the four legs occupied by the carbonyl ligands and the $\eta^1\text{-C}$ -enolate unit. The carbonyl oxygen is not coordinated to the metal center, similar to that observed for the methyl ester enolate derivative $(\eta^5\text{-C}_5\text{H}_5)\text{W}(\text{CO})_3(\eta^1\text{-CH}_2\text{COOMe})$ or the more recently reported structure of $(\eta^5\text{-C}_5\text{H}_5)\text{W}(\text{CO})_3(\eta^1\text{-CH}_2\text{COOEt})$. The term "enolate" as applied to compounds such as **7** and the interaction between carbon–metal bonding electrons and the car-

Table 3. Selected Intramolecular Distances (Å) and Angles (deg) for $[(\eta^5\text{-C}_5\text{H}_4\text{COONS})\text{Mo}(\text{CO})_3\text{Me}]$ (5a,b**)**

Distances			
Mo1–C6	2.320(3)	Mo51–C61	2.000(4)
Mo1–C8	2.338(3)	Mo51–C62	1.976(4)
Mo1–C7	2.310(3)	Mo51–C63	1.980(4)
Mo1–C9	2.389(3)	Mo51–C64	2.321(4)
Mo1–CP ^a	2.02		
Mo1–C12	1.983(4)	C1–O1	1.403(4)
Mo1–C14	2.305(4)	C1–O2	1.194(4)
		O1–N1	1.390(4)
Mo51–C56	2.345(3)		
Mo51–C57	2.370(3)	C56–C51	1.466(5)
Mo51–C58	2.367(4)	C51–O51	1.392(4)
Mo51–C59	2.335(3)	C51–O52	1.182(4)
Mo51–C60	2.335(3)	O51–N51	1.385(4)
Mo51–CP ^a	2.01		
C6–C7	1.413(5)		
C7–C8	1.406(5)		
C8–C9	1.416(5)		
C9–C10	1.398(5)		
C6–C10	1.430(5)		
C56–C57	1.431(5)		
C57–C58	1.401(5)		
C58–C59	1.417(5)		
C59–C60	1.412(5)		
C56–C60	1.412(5)		
Angles			
C7–Mo1–C6	35.5(1)	C6–C1–O2	127.2(3)
C8–Mo1–C7	35.2(1)	C1–O1–O2	122.6(3)
C9–Mo1–C7	58.2(1)	C1–O1–N1	110.7(3)
C10–Mo1–C6	35.4(1)	C56–Mo51–C64	98.3(1)
C10–Mo1–C8	57.8(1)	C59–Mo51–C60	35.2(1)
C11–Mo1–C10	114.9(1)	C12–Mo–C13	78.1(1)
C12–Mo1–C7	107.5(2)	C57–Mo51–C59	58.2(1)
C12–Mo1–C9	154.8(1)	C57–Mo51–C63	118.0(1)
C14–Mo1–C7		C60–Mo51–C62	111.3(1)
C12–Mo1–C11	105.5(2)	C58–Mo51–C62	155.3(1)
C13–Mo1–C7	91.6(1)	C60–Mo51–C64	133.2(1)
C13–Mo1–C9	118.8(1)		
C13–Mo1–C11	78.6(2)		
C14–Mo1–C11	73.2(2)		
C14–Mo1–C12	72.2(2)		
C14–Mo1–C13	132.4(2)		
C13–Mo1–C12	79.6(2)		

^a CP is the centroid of the cyclopentadienyl ring plane.

Scheme 2^a

^a Reagents and conditions: (iii) THF, Na/Hg, 2h, room temperature; (iv) THF, ClCH₂COONS (1 equiv), -78 °C, 5 min, then 1 h at room temperature.

bonyl π -orbital have been invoked previously by Bergman, Heathcock, and co-workers on the basis of spectroscopic and crystallographic data.^{11b} In this regard, we feel, in our case, that such an interaction is also valid; for instance, the carbonyl absorptions for complex **7** are shifted toward lower energy when compared to those of the isomer **5** where the ester unit is attached to the π -Cp ligand. Confirmation of this interaction is displayed by the structure of **7** in the solid state where the (C=O)–C bond (1.46 Å) is shorter than the normal ester value of 1.48–1.51 Å, although the –C=O bond

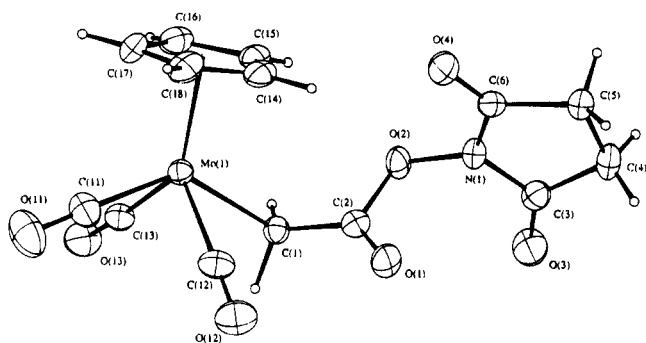


Figure 3. Molecular structure and atom labeling for $[(\eta^5\text{-C}_5\text{H}_5)\text{Mo}(\text{CO})_3(\eta^1\text{-CH}_2\text{COONS})]$ (**7**).

Table 4. Crystallographic Data for $[(\eta^5\text{-C}_5\text{H}_5)\text{Mo}(\text{CO})_3(\eta^1\text{-CH}_2\text{COONS})]$ (**7**)

chemical formula	$\text{C}_{14}\text{H}_{11}\text{O}_7\text{NMo}$
fw	401.18
cryst syst	monoclinic
space group	$C2/c$
Z	8
a , Å	19.484(2)
b , Å	11.393(2)
c , Å	13.694(2)
β , deg	98.91(2)
V , Å ³	3000
$F(000)$	1600
$\rho(\text{calcd})$, gcm ⁻³	1.79
$\mu(\text{Mo K}\alpha)$ cm ⁻¹	8.92
diffractometer	Philips PW1100
monochromator	graphite
radiation (λ , Å)	Mo K α (0.710 70)
temp, °C	20
scan type	$\omega/2\theta$
scan range θ , deg	$1.0 + 0.34 \tan \theta$
2θ range, deg	4–57
no. of reflctn collected	3801
no. of reflctn used (criteria)	2946 ($I > 3\sigma(I)$)
R	0.027
R_w^a	0.029
abs corr ^b	min 0.88, max 1.11
secondary ext	99.9×10^{-6}
weighting scheme	unit weights
rms (shift/esd) (last ref)	0.10
Is params	243

^a $R_w = [\sum_i W_i(F_o - F_c)^2 / \sum_i W_i F_o^2]^{1/2}$. ^b Difabs. Walker, N.; Stuart, D. *Acta Crystallogr.* **1983**, *A39*, 159.

distance is 1.194 Å, typical of a carbonyl function. We also note that the plane of the *N*-succinimidyl unit forms an angle $\theta = 54^\circ$ with that of the π -bonded cyclopentadienyl ligand; this value is smaller than that observed in **5** (vide supra). The Mo–Cp_{centroid} bond distance is 1.99 Å, slightly shorter than that of its isomer **5** and comparable to that reported for the tungsten enolate $(\eta^5\text{-C}_5\text{H}_5)\text{W}(\text{CO})_3(\eta^1\text{-CH}_2\text{COOEt})$ (1.998 Å); further, the (C=O)–O2 bond distance is 1.42 Å, longer than that in **5** (C=O)–O1 (a) 1.40 Å and –(b) 1.39 Å. Although there were no differences in the bond lengths of the *N*-succinimidyl unit between **5** and **7** in the solid state, their behaviors in solution, in particular their reactivity toward amino esters, showed stark contrast.

Reactivity of 5–7 with Benzylamine and Various Amino Esters. We have studied the reactivity of the above organometallic species with β -alanine ethyl ester, amphetamine, and benzylamine. The labeling of amino esters by our organometallic *N*-succinimidyl esters is described by Scheme 3.

Complex $[(\eta^5\text{-C}_5\text{H}_4\text{COONS})\text{Mo}(\text{CO})_3\text{Me}]$ (**5**) reacted with β -alanine ethyl ester in THF to give the conjugate

Table 5. Collection Parameters for $[(\eta^5\text{-C}_5\text{H}_5)\text{Mo}(\text{CO})_3(\eta^1\text{-CH}_2\text{COONS})]$ (**7**)

atom	x/a	y/b	z/c	$U(\text{eq})$, Å ²	$U(\text{iso})$, Å ²
Mo(1)	0.16001(1)	0.04854(2)	0.08387(2)	0.0302	
O(1)	0.3549(1)	0.0131(2)	0.0977(2)	0.0442	
O(2)	0.3131(1)	-0.1138(2)	-0.0239(2)	0.0381	
O(3)	0.3231(1)	0.0786(2)	-0.1494(2)	0.0544	
O(4)	0.4433(1)	-0.2209(2)	0.0157(2)	0.0563	
O(11)	0.2761(1)	0.1745(2)	0.2319(2)	0.0554	
O(12)	0.0783(2)	0.1908(3)	0.2248(2)	0.0716	
O(13)	0.0974(1)	-0.1516(2)	0.2004(2)	0.0548	
N(1)	0.3705(1)	-0.0841(2)	-0.0663(2)	0.0363	
C(1)	0.2483(1)	-0.0928(3)	0.1065(2)	0.0315	
C(2)	0.3101(1)	-0.0550(3)	0.0670(2)	0.0316	
C(3)	0.3700(2)	0.0105(3)	-0.1302(2)	0.0403	
C(4)	0.4393(2)	0.0072(4)	-0.1660(3)	0.0463	
C(5)	0.4785(2)	-0.0961(3)	-0.1135(3)	0.0429	
C(6)	0.4322(2)	-0.1452(3)	-0.0452(2)	0.0382	
C(11)	0.2353(2)	0.1269(3)	0.1783(2)	0.0395	
C(12)	0.1082(2)	0.1396(3)	0.1730(3)	0.0496	
C(13)	0.1218(2)	-0.0789(3)	0.1599(2)	0.0377	
C(14)	0.1858(2)	0.1230(3)	-0.0647(3)	0.0438	
C(15)	0.1652(2)	0.0067(3)	-0.0838(2)	0.0420	
C(16)	0.0954(2)	-0.0048(4)	-0.0698(2)	0.0455	
C(17)	0.0733(2)	0.1056(4)	-0.0418(3)	0.0451	
C(18)	0.1297(2)	0.1854(3)	-0.0394(3)	0.0473	
H(11)	0.261(2)	-0.102(3)	0.173(3)		0.057(3)
H(12)	0.231(2)	-0.169(3)	0.078(3)		0.057(3)
H(14)	0.224(2)	0.148(3)	-0.069(3)		0.057(3)
H(15)	0.192(2)	-0.060(3)	-0.104(3)		0.057(3)
H(16)	0.075(2)	-0.073(3)	-0.076(3)		0.057(3)
H(17)	0.027(2)	0.122(3)	-0.028(3)		0.057(3)
H(18)	0.134(2)	0.267(4)	-0.025(3)		0.057(3)
H(41)	0.569(2)	0.004(3)	0.228(3)		0.057(3)
H(42)	0.040(2)	0.411(3)	0.150(3)		0.057(3)
H(51)	0.486(2)	-0.159(3)	-0.157(3)		0.057(3)
H(52)	0.526(2)	-0.073(3)	-0.076(3)		0.057(3)

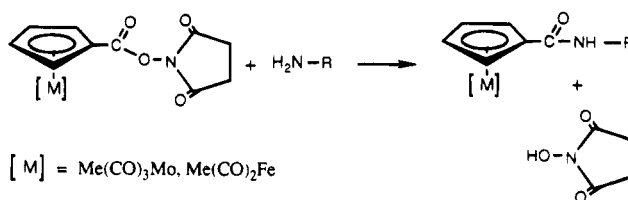
Table 6. Selected Intramolecular Distances (Å) and Angles (deg) for $[(\eta^5\text{-C}_5\text{H}_5)\text{Mo}(\text{CO})_3(\eta^1\text{-CH}_2\text{COONS})]$ (**7**)

Distances			
Mo–C14	2.330(3)	C6–O4	1.197(4)
Mo–C15	2.363(3)	N1–C3	1.387(4)
Mo–C16	2.358(3)	C3–O3	1.198(4)
Mo–C17	2.310(3)	C3–C4	1.507(4)
Mo–C18	2.307(3)	C4–C5	1.521(5)
		C5–C6	1.505(4)
Mo–C1	2.341(3)	C1–C2	1.461(4)
Mo–C11	2.008(3)	C2–O1	1.194(3)
Mo–C12	1.992(4)	C2–O2	1.422(3)
Mo–C13	1.997(3)	O2–N1	1.380(3)
Mo–Cp ^a	1.99	N1–C6	1.381(4)

Angles			
C1–Mo–C11	76.8(1)	Mo–C1–C2	112.3(2)
C1–Mo–C12	135.1(1)	C1–C2–O1	131.3(3)
C1–Mo–C13	75.9(1)	C2–O2–N1	113.4(2)
C11–Mo–C12	76.3(1)	N1–C6–O4	124.6(3)
C11–Mo–C13	106.4(1)	N1–C3–O3	124.9(3)
C12–Mo–C13	78.1(1)		

^a CP is the centroid of the cyclopentadienyl ring plane.

Scheme 3



adduct $[(\eta^5\text{-C}_5\text{H}_4\text{CONH}(\text{CH}_2)_2\text{COOEt})\text{Mo}(\text{CO})_3\text{Me}]$ (**11**) as yellow microcrystalline solids in 36% yield. We have found that the Fe derivative **6** is more stable than its

Mo analog **5** and particularly in basic medium (vide supra); thus **6** reacted with benzylamine and amphetamine to give the amide counterpart complexes $[(\eta^5\text{-C}_5\text{H}_4\text{CONHCH}_2\text{Ph})\text{Fe}(\text{CO})_2\text{Me}]$ (**12**) and $[(\eta^5\text{-C}_5\text{H}_4\text{CONHC}(\text{H})(\text{Me})\text{CH}_2\text{Ph})\text{Fe}(\text{CO})_2\text{Me}]$ (**13**) in 25% and 32% yields respectively, while $[(\eta^5\text{-C}_5\text{H}_4\text{COONS})\text{Mo}(\text{CO})_3\text{Me}]$ (**5**) failed to give any stable product, instead decomposing during the reaction course.

On the other hand the *N*-succinimidyl enolate derivative $[(\eta^5\text{-C}_5\text{H}_5)\text{Mo}(\text{CO})_3(\eta^1\text{-CH}_2\text{COONS})]$ (**7**) was inactive toward amino acid labeling. Thus treatment of **7** with β -alanine ethyl ester in THF for 2 days failed to give any defined product; only decomposition of the starting material was noticed. It should be mentioned that the analogous Fe-activated succinimidyl ester $[(\eta^5\text{-C}_5\text{H}_5)\text{Fe}(\text{CO})_2(\eta^1\text{-COONS})]$ (**8**) requires 1 week to react with amino acids. This difference in reactivity between the two families, for instance $\eta^5\text{-Cp}$ -bonded activated ester complexes and metal-bonded ester complexes, could be related to the enolate character of the latter complexes. As pointed out in this work and previously in the literature for the enolate species, there is an association of the metal (M-C) with the oxoallyl unit whereby the carbon-metal bonding electrons interact with the carbonyl π -orbital; we feel that this interaction influences their reactivity. In this respect we also note that the pK_a values of the parent acid molecules of the type $(\eta^5\text{-C}_5\text{H}_5)\text{M}(\text{CO})_n(\text{CH}_2\text{COOH})$ (M = Mo, $n = 3$; M = Fe, $n = 2$) are in the range 8.2–8.7^{10b} and are weaker acids than those of $(\eta^5\text{-C}_5\text{H}_4\text{COOH})\text{M}(\text{CO})_n\text{Me}$ (M = Mo, $n = 3$ (**2**); M = Fe, $n = 2$ (**5**)) with pK_a values of 4–4.5,⁷ and hence are less reactive. In general the previous trend remains valid also for the corresponding *N*-succinimidyl esters; therefore the activated ester complexes, for instance $(\eta^5\text{-C}_5\text{H}_4\text{COONS})\text{M}(\text{CO})_n\text{Me}$ (M = Mo, $n = 3$ (**3**); M = Fe, $n = 2$ (**6**)) should be more reactive toward the addition-elimination reaction that took place during the labeling process of amino acids.

We are currently pursuing our research toward the labeling of proteins by the above complexes and also to enhance the stability of **5** by changing the ancillary ligands around the metal center.

Experimental Section

General Procedures. All manipulations were carried out under argon atmosphere using Shlenck techniques. Solvents were purified and dried prior to use by conventional distillation techniques. All reagents obtained from commercial sources were used without further purification, and $[\text{Na}][\text{CpMo}(\text{CO})_3]^{12}$ and $[\text{Na}][\text{CpFe}(\text{CO})_2]^{13}$ were prepared according to published procedures. ¹H- and ¹³C-NMR were recorded on a Bruker AM 250 MHz instrument. ¹H-NMR chemical shifts are reported in parts per million referenced to the residual solvent proton resonance. Infrared spectra were obtained on a FT Bomem Michelson 100 spectrometer from samples prepared either on KBr disks or in CH₂Cl₂ solutions. All absorptions are expressed in wavenumbers (cm⁻¹). Elemental analyses were performed by the Microanalytical Laboratory of the CNRS of the University of Paris VI.

Synthesis on $[(\eta^5\text{-C}_5\text{H}_4\text{COOH})\text{Mo}(\text{CO})_3\text{Me}]$ (2**).** A solution of *s*-BuLi (3.45 mmol, 1.8 mL) in hexane was added

dropwise to a solution of CpMo(CO)₃Me (**1**) (2 mmol, 500 mg) in 50 mL of THF at -80 °C. The mixture was left under stirring for 30 min, then an excess of dry ice (CO₂) was added, and the resulting mixture was stirred for further 15 min, while the temperature was kept at -80 °C. The reaction mixture was allowed to reach room temperature, followed by acidification with 8 mL of 10% HCl solution. The organometallic carboxylic acid **2** was extracted with 15 mL of CH₂Cl₂ and then dried over MgSO₄, filtered, and evaporated to dryness under vacuum; the yellow powder was washed with pentane to remove starting material **1**. Further purification was attained when the product was dissolved in acetone and the solution filtered through Celite. The solvent was removed under vacuum, and recrystallization from CHCl₃/pentane gave a yellow microcrystalline solid. Yield: 550 mg, 61%. IR, ν/cm^{-1} (KBr): M-CO 2025, 1950, 1917; C=O 1680. ¹H-NMR ((CD₃)₂CO): δ 5.90 (t, $J_{\text{H-H}} = 2.5$ Hz, 2H, -C₅H₄), 5.68 (t, $J_{\text{H-H}} = 2.5$ Hz, 2H, -C₅H₄), 0.44 (s, 3H, -CH₃). ¹³C-NMR ((CD₃)₂CO): δ 239, 227 (M-CO), 165.40 (C=O), 99.33, 96.15, 95.99 (-C₅H₄), -19.60 (-CH₃). Anal. Calcd for C₁₀H₈O₅Mo: C, 39.47; H, 2.63. Found: C, 38.81; H, 2.61.

Synthesis of $[(\eta^5\text{-C}_5\text{H}_4\text{COOH})\text{Fe}(\text{CO})_2\text{Me}]$ (4**).** A THF solution of *s*-BuLi (1.69 mmol, 1 mL) was added dropwise to a solution of CpFe(CO)₂Me (**3**) (600 mg, 1.69 mmol) in 50 mL of THF at $T = -80$ °C. The reaction mixture was stirred for 20 min, then an excess of solid CO₂ was added, and the resulting mixture was stirred for a further 15 minutes. The system was allowed to reach room temperature, and the mixture was acidified by 10 mL of 10% HCl and then extracted with 10 mL of CH₂Cl₂. The organic phase was hydrolyzed with 20% Na₂CO₃ and acidified with 15 mL of 5% HCl; then the organic phase was again extracted with 10 mL of CH₂Cl₂. The solvent was removed under vacuum, and the product was recrystallized from acetone/pentane. Yield: 62%, 380 mg. IR, ν/cm^{-1} (KBr): M-CO 2012, 1951; C=O, 1676. ¹H-NMR ((CD₃)₂CO): δ 5.43 (t, $J_{\text{H-H}} = 2.5$ Hz, 2H, -C₅H₄), 5.13 (br, 2H, -C₅H₄), 0.25 (s, 3H, CH₃). ¹³C-NMR ((CD₃)₂CO): δ 216.75 (M-CO), 166.22 (C=O), 91.50, 87.96, 85.96 (-C₅H₄), -21.41 (-CH₃). Anal. Calcd for C₉H₈O₄Fe: C, 45.69; H, 3.39. Found: C, 45.69; H, 3.47.

Synthesis of $[(\eta^5\text{-C}_5\text{H}_4\text{COONS})\text{Mo}(\text{CO})_3\text{Me}]$ (5**).** A solution of DSC (0.33 mmol, 84 mg) and pyridine (0.33 mmol, 26 μL) in 2 mL of CH₃CN was added dropwise to a solution of **2** (100 mg, 0.33 mmol) in 10 mL of CH₃CN, and the reaction was stirred for 18 h; then the solvent was removed under vacuum, and the product was eluted on silica gel using CHCl₃ as eluent. The solvent was removed under vacuum to give a yellow microcrystalline solid. Yield: 74 mg, 57%. IR, ν/cm^{-1} (KBr): M-CO 2028, 1936, C=O 1802, 1769, 1736. ¹H-NMR ((CD₃)₂CO): δ 6.10 (t, $J_{\text{H-H}} = 2.5$ Hz, 2H, -C₅H₄), 5.83 (t, $J_{\text{H-H}} = 2.5$ Hz, 2H, -C₅H₄), 2.92 (s, 4H, -CH₂-CH₂-, -NS), 0.55 (s, 3H, CH₃). ¹³C-NMR ((CD₃)₂CO): δ 235.71, 223.15 (M-CO), 166.76, 160.38 (C=O), 95.94, 94.60, 90.47 (-C₅H₄), 25.50 (-CH₂-CH₂-, -NS), -19.36 (-CH₃). Anal. Calcd for C₁₄H₁₁O₇NMo: C, 41.89; H, 2.74; N, 3.49. Found: C, 41.98; H, 2.58; N, 3.59.

Synthesis of $[(\eta^5\text{-C}_5\text{H}_4\text{COONS})\text{Fe}(\text{CO})_2\text{Me}]$ (6**).** *N*-Hydroxysuccinimide (NHS) (49 mg, 0.42 mmol) was added to a yellow solution of **4** (100 mg, 0.42 mmol) in 10 mL of THF, in the presence of dicyclohexylcarbodiimide (DCC) (88 mg, 0.42 mmol), and the mixture was stirred for 10 h. The solution was filtered through Celite, and the residue was chromatographed on silica gel and eluted with acetone, hexane (10:3) to give a yellow band which afforded yellow-orange crystals of **6**. Yield: 86 mg, 61%. IR, ν/cm^{-1} (KBr): M-CO 2024, 1970, C=O 1811, 1780, 1738. ¹H-NMR (CDCl₃): δ 5.50 (t, $J_{\text{H-H}} = 2.0$ Hz, 2H, -C₅H₄), 5.03 (t, $J_{\text{H-H}} = 2.0$ Hz, 2H, -C₅H₄), 2.89 (s, 4H, -CH₂-CH₂-, -NS), 0.46 (s, 3H, CH₃). ¹³C-NMR ((CD₃)₂CO): δ 213.76 (M-CO), 168.58, 160.70, 91.44, 85.10, 78.15 (-C₅H₄), 25.29 (-CH₂-CH₂-, -NS), -20.70 (-CH₃). Anal. Calcd for C₁₃H₁₁O₆NFe: C, 46.87; H, 3.30; N, 4.21. Found: C, 47.22; H, 3.42; N, 4.12.

(12) (a) Ellis, J. E. *J. Organomet. Chem.* **1975**, *86*, 1. (b) Patil, H. R. H.; Graham, W. A. G. *Inorg. Chem.* **1966**, *5*, 1401. (c) Hayter, R. G. *Inorg. Chem.* **1963**, *2*, 1031.

(13) Zhen, Y. Q.; Feighery, W. G.; Lai, C. K.; Atwood, J. D. *J. Am. Chem. Soc.* **1989**, *111*, 7832.

Synthesis of $[(\eta^5\text{-C}_5\text{H}_5)\text{Mo}(\text{CO})_3(\eta^1\text{-CH}_2\text{COONS})]$ (7). A solution of $[\text{CpMo}(\text{CO})_3]_2$ (500 mg, 1.02 mmol) in 30 mL of THF was cleaved by 10% NaHg amalgam, and after 1 h the yellow solution of $[\text{Na}][\text{CpMo}(\text{CO})_3]$ was filtered into a Schlenk tube kept under argon. To this mixture was added dropwise a solution of $\text{ClCH}_2\text{COONS}$ (2 mmol, 383 mg) in 12 mL of THF while the temperature was kept at -78°C . The mixture was stirred for 1 h at -78°C , and then the mixture was filtered to remove the precipitate salt, followed by evaporation to dryness using the vacuum line. The residue was then eluted on silica gel using ether/hexane (5/1), the yellow band was collected, and the solvent mixture was concentrated under vacuum. Upon cooling overnight at -20°C , yellow crystals were obtained. Yield: 200 mg, 45%. IR, ν/cm^{-1} (KBr): M–CO 2031, 1965, 1954, 1927, C=O 1791, 1731. $^1\text{H-NMR}$ ((CDCl_3)): δ 5.54 (s, 5H, $-\text{C}_5\text{H}_5$), 2.82 (s, 4H, $-\text{CH}_2-\text{CH}_2-$, $-\text{NS}$), 1.92 (s, 2H, $-\text{CH}_2-$). $^{13}\text{C-NMR}$ ($(\text{CD}_3)_2\text{CO}$): δ 228.24 (M–CO), 177.16, 171.39 (C=O), 95.36 ($-\text{C}_5\text{H}_4$), 26.23 ($-\text{CH}_2-\text{CH}_2-$, $-\text{NS}$), -9.51 ($-\text{CH}_2-$). Anal. Calcd for $\text{C}_{14}\text{H}_{11}\text{O}_7\text{NMo}$: C, 41.89; H, 2.74; N, 3.49. Found: C, 41.71; H, 2.82; N, 3.47.

Synthesis of $[(\eta^5\text{-C}_5\text{H}_4\text{COONS})\text{Mo}(\text{CO})_3\text{I}]$ (9). The preparation of **9** was performed, following the synthetic procedure described by Rausch et al. for the compound $[(\eta^5\text{-C}_5\text{H}_4\text{COOMe})\text{W}(\text{CO})_3\text{I}]$.⁵ A solution of ISiMe_3 (70 μL , 0.5 mmol) was added to a solution of $[(\eta^5\text{-C}_5\text{H}_4\text{COONS})\text{Mo}(\text{CO})_3\text{Me}]$ (**5**) (100 mg, 0.25 mmol) in 15 mL of CH_3CN , and the reaction mixture was stirred at $T = 60^\circ\text{C}$ for 16 h. At this stage the solvent was removed and the residue was eluted on silica gel using toluene/acetone (10:3) as eluent. Compound **9** was obtained as a deep red microcrystalline solid. Yield: 58 mg, 45%. IR, ν/cm^{-1} (KBr): M–CO 2050, 1973, C=O 1803, 1769, 1737. $^1\text{H-NMR}$ ($(\text{CD}_3)_2\text{CO}$): δ 6.42 (t, $J_{\text{H-H}} = 2.5$ Hz, 2H, $-\text{C}_5\text{H}_4$), 6.19 (t, $J_{\text{H-H}} = 2.5$ Hz, 2H, $-\text{C}_5\text{H}_4$), 2.92 (s, 4H, $-\text{CH}_2-\text{CH}_2-$, $-\text{NS}$). $^{13}\text{C-NMR}$ ($(\text{CD}_3)_2\text{CO}$): δ 237, 230, 223 (M–CO), 174.31, 165.32 (C=O), 105.68, 101.28, 96.04 ($-\text{C}_5\text{H}_4$), 30.79 ($-\text{CH}_2-\text{CH}_2-$, $-\text{NS}$).

Synthesis of $[(\eta^5\text{-C}_5\text{H}_4\text{COONS})\text{Fe}(\text{CO})_2\text{I}]$ (10). This compound was prepared in a fashion similar to that of **9**; thus an excess of ISiMe_3 was added dropwise at room temperature to a solution of **6** (100 mg, 0.3 mmol) in 10 mL of CH_3CN . Then the mixture was stirred for 24 h while the temperature was kept at 60°C . At this stage the reaction was stopped and the excess of ISiMe_3 was hydrolyzed followed by extraction with CH_2Cl_2 . The organic phase was concentrated under vacuum, and the residue was chromatographed on silica gel and eluted with toluene/acetone (10:8) to give a brown-red microcrystalline solid. Yield: 77 mg, 58%. IR, ν/cm^{-1} (KBr): M–CO 2055, 2012, C=O 1798, 1769, 1736. $^1\text{H-NMR}$ (CDCl_3): δ 5.83 (t, $J_{\text{H-H}} = 2.5$ Hz, 2H, $-\text{C}_5\text{H}_4$), 5.29 (t, $J_{\text{H-H}} = 2.5$ Hz, 2H, $-\text{C}_5\text{H}_4$), 2.90 (s, 4H, $-\text{CH}_2-\text{CH}_2-$, $-\text{NS}$). $^{13}\text{C-NMR}$ ($(\text{CD}_3)_2\text{CO}$): δ 210, 53 (M–CO), 168.46, 160.38 (C=O), 90.17, 85.78, 75.22 ($-\text{C}_5\text{H}_4$), 25.70 ($-\text{CH}_2-\text{CH}_2-$, $-\text{NS}$).

Synthesis of $[(\eta^5\text{-C}_5\text{H}_4\text{CONH}(\text{CH}_2)_2\text{COOEt})\text{Mo}(\text{CO})_3\text{Me}]$ (11). A solution of β -alanine ethyl ester (46 mg, 0.3 mmol) in 8 mL of THF was added dropwise to a solution of **5** (120 mg, 0.3 mmol) in 12 mL of THF, and the reaction mixture was stirred for 12 h. The solution was concentrated under vacuum, and the residue was chromatographed on silica gel plates with toluene/acetone (10:1) as eluent. A yellow band was separated, which afforded a yellow microcrystalline solid. Yield: 36 mg, 30%. IR, ν/cm^{-1} (KBr): M–CO 2023, 1936, C=O 1726, CON 1664, 1522. $^1\text{H-NMR}$ (CDCl_3): δ 6.64 (m, 1H, $-\text{NH}$), 5.67 (t, $J_{\text{H-H}} = 2.5$ Hz, 2H, $-\text{C}_5\text{H}_4$), 5.29 (t, $J_{\text{H-H}} = 2.5$ Hz, 2H, $-\text{C}_5\text{H}_4$), 4.19 (q, 2H, $-\text{N}-\text{CH}_2$), 2.59 (t, 2H, $-\text{O}-\text{CH}_2$), 1.26 (q, 3H, $-\text{OCH}_2-\text{CH}_3$), 0.44 (s, 3H, $\text{Mo}-\text{CH}_3$).

Synthesis of $[(\eta^5\text{-C}_5\text{H}_4\text{CONHCH}_2\text{Ph})\text{Fe}(\text{CO})_2\text{Me}]$ (12). A solution of benzylamine (16 μL , 0.15 mmol) in 2 mL of THF was added dropwise to a solution of **6** (50 mg, 0.15 mmol) in 4 mL of THF, and the mixture was stirred for 10 h. Then solvent was removed, and the residue was chromatographed on a silica gel column and eluted with toluene/acetone (10:1) to give a yellow band which afforded yellow crystals of **12**. Yield: 12 mg, 25%. IR, ν/cm^{-1} (KBr): NH 3289, M–CO 2001, 19461, CON 1636, 1555. $^1\text{H-NMR}$ ($(\text{CD}_3)_2\text{CO}$): δ 7.32–7.45 (m, 5H, phenyl Hs), 5.53 (t, $J_{\text{H-H}} = 2.0$ Hz, 2H, $-\text{C}_5\text{H}_4$), 5.06 (t, $J_{\text{H-H}} = 2.0$ Hz, 2H, $-\text{C}_5\text{H}_4$), 4.52 (d, $J_{\text{H-H}} = 6.0$ Hz, 2H, $-\text{N}-\text{CH}_2$), 0.24 (s, 3H, $\text{Fe}-\text{CH}_3$).

Synthesis of $[(\eta^5\text{-C}_5\text{H}_4\text{CONH}(\text{H})(\text{Me})\text{CH}_2\text{Ph})\text{Fe}(\text{CO})_2\text{Me}]$ (13). This compound was prepared in a fashion similar to that of **12** using an equimolar concentration of **6** and amphetamine. The product was separated on silica gel plates using ether/hexane (10:5) as eluent, which afforded a yellow microcrystalline solid of **13**. Yield: 32%. IR, ν/cm^{-1} (CHCl_3): M–CO 2016, 1960, CON 1658, 1519. $^1\text{H-NMR}$ ($(\text{CD}_3)_2\text{CO}$): δ 7.26–7.20 (m, 5H, phenyl Hs), 5.60 (t, 2H, $-\text{C}_5\text{H}_4$), 5.10 (t, 2H, $-\text{C}_5\text{H}_4$), 4.29 (m, 1H, $-\text{CH}_{\text{asy}}$), 2.94 (m, 1H, $-\text{CH}_{\text{A}(\text{H}_\text{B})}$), 2.53 (m, 1H, $-\text{CH}_{\text{A}(\text{H}_\text{B})}$), 1.20 (d, 3H, $-\text{Me}$), 0.18 (s, 3H, $\text{Fe}-\text{CH}_3$).

Structure Determination of $[(\eta^5\text{-C}_5\text{H}_4\text{COONS})\text{Mo}(\text{CO})_3\text{Me}]$ (5) and of $[(\eta^5\text{-C}_5\text{H}_5)\text{Mo}(\text{CO})_3(\eta^1\text{-CH}_2\text{COONS})]$ (7). Single crystals were grown from cooling a hexane solution of $[(\eta^5\text{-C}_5\text{H}_4\text{COONS})\text{Mo}(\text{CO})_3\text{Me}]$ (**5**) and from ether/hexane for $[(\eta^5\text{-C}_5\text{H}_5)\text{Mo}(\text{CO})_3(\eta^1\text{-CH}_2\text{COONS})]$ (**7**). Crystallographic data for **5** and **7** are collected in Tables 1 and 4, respectively. Accurate cell dimensions and orientation matrices were obtained by least-squares refinement of 25 accurately centered reflections on a Nonius CAD4 diffractometer equipped with graphite-monochromated Mo $\text{K}\alpha$ radiation. No significant variations were observed in the two check reflections during data collection. The data were corrected for Lorentz and polarization effects; an empirical absorption correction (DI-FABS)¹⁴ was applied. Computations were performed by using CRYSTALS¹⁵ modified locally for a Microvax II Computer.¹⁶ The structures were resolved by direct methods (SHELXS)¹⁷ and refined by full-matrix least squares with anisotropic thermal parameters for all non-hydrogen atoms. All hydrogen atoms were then located on a difference Fourier map and their coordinates refined with an isotropic thermal parameter. The structures of $[(\eta^5\text{-C}_5\text{H}_4\text{COONS})\text{Mo}(\text{CO})_3\text{Me}]$ (**5**) and $[(\eta^5\text{-C}_5\text{H}_5)\text{Mo}(\text{CO})_3(\eta^1\text{-CH}_2\text{COONS})]$ (**7**) were refined to $R = 0.0253$, $R_w = 0.0269$ and $R = 0.027$, $R_w = 0.029$, respectively, with use of 4323 and 2946 reflections of 484 and 243 least-squares parameters.

Acknowledgment. We would like to thank CNRS (France) for supporting this work.

Supporting Information Available: Anisotropic displacement parameters (Tables S1 and S4) and bond distances and angles (Tables S2 and S5) for **5** and **7**, respectively (5 pages). Ordering information is given on any current masthead page.

OM950170Y

(14) Walker, N.; Stuart, D. *Acta Crystallogr.* **1983**, *A39*, 159.

(15) Watkin, D. J.; Carruthers, J. R.; Betteridge, P. W. *Crystals User Guide*; Chemical Crystallography Laboratory: University of Oxford: Oxford, England, 1986.

(16) *International Tables for X-ray Crystallography*; Kynoch Press: Birmingham, England, 1974; Vol. IV.

(17) Sheldrick, G. M. SHELXS86, Program for Crystal Structure Solution. University of Göttingen, 1986.

Variable Temperature IR Spectroelectrochemical Investigation of the Stability of the Metal–Metal-Bonded Radical Anions $[(\text{CO})_5\text{MnRe}(\text{CO})_3(\text{L})]^{•-}$ (L = 2,2'-Bipyridine (BPY), 2,2'-Bipyrimidine (BPYM), 2,3-Bis(2-pyridyl)pyrazine (DPP)) and $[(\text{CO})_5\text{MnRe}(\text{CO})_3(\text{L})\text{Re}(\text{Br})(\text{CO})_3]^{•-}$ (L = BPYM, DPP) Controlled by the Lowest π^* (α -Diimine) Orbital Energy

J. W. M. van Outersterp, F. Hartl,* and D. J. Stufkens

Anorganisch Chemisch Laboratorium, Universiteit van Amsterdam, J. H. van 't Hoff Research Institute, Nieuwe Achtergracht 166, 1018 WV Amsterdam, The Netherlands

Received November 14, 1994[®]

Cyclic voltammetry in combination with IR thin-layer spectroelectrochemistry was employed for detection and characterization of the radical anionic complexes $[(\text{CO})_5\text{MnRe}(\text{CO})_3(\text{L})]^{•-}$ (L = 2,2'-bipyridine (BPY), 2,2'-bipyrimidine (BPYM), and 2,3-bis(2-pyridyl)pyrazine (DPP)) and $[(\text{CO})_5\text{MnRe}(\text{CO})_3(\mu\text{-L})\text{Re}(\text{Br})(\text{CO})_3]^{•-}$ ($\mu\text{-L} = \mu\text{-BPYM}, \mu\text{-DPP}$) as the primary products formed upon one-electron reduction of the neutral parent compounds. The stability of the radical anions is determined by the degree of polarization of the Mn–Re bond which increases in the order Mn–Re($\mu\text{-BPYM}$)Re < Mn–Re($\mu\text{-DPP}$)Re < Mn–Re(BPYM) ~ Mn–Re(DPP) < Mn–Re(BPY), i.e., with increasing energy of the π^* LUMO of the α -diimine ligand in the parent complexes and with increasing σ - and π -donor character of the α -diimine anion in the reduced species. In the same order, the unpaired electron in the metal–metal-bonded radical anions becomes more delocalized over the (Mn)Re–L chelate bond. This delocalization in turn also considerably destabilizes the d_{z^2} orbital of Re(L) involved in the Mn–Re bonding, making its occupation no more energetically convenient. Consequently, the Mn–Re bond will split heterolytically to give $[\text{Mn}(\text{CO})_5]^-$ and $[\text{Re}(\text{CO})_3(\text{L})]^+$. The trinuclear radical anion with $\mu\text{-L} = \mu\text{-BPYM}$ was found to be stable already at room temperature and could be characterized also by UV–vis and ESR spectroscopy. The related radical anion with $\mu\text{-DPP}$ could only be stabilized at properly low temperatures, just as for the compounds with nonbridging BPYM and DPP. In the case of the BPY compound, the metal–metal-bonded radical anion could not be detected at all. Descriptions of the secondary reaction pathways of the radicals $[\text{Re}(\text{CO})_3(\text{L})]^{•+}$, formed in the course of the irreversible reduction of the above Mn–Re-bonded complexes, are given as well.

Introduction

It is a well-established fact that metal–metal-bonded complexes with the lowest unoccupied molecular orbital (LUMO) of a $\sigma^*(\text{M}–\text{M})$ character are prone to cleavage of the metal–metal bond upon reduction. In the absence of a bridging ligand, both metal centers are usually reduced in a direct two-electron step, and the only observable products are negatively charged fragments. Thus no evidence has so far been obtained for the existence of the radical anionic complexes $[\text{M}_2(\text{CO})_{10}]^{•-}$ (M = Mn, Re). The only product detected by cyclic voltammetry and spectroelectrochemistry in the course of the 2e reduction of parent $\text{Mn}_2(\text{CO})_{10}$ is $[\text{Mn}(\text{CO})_5]^-$ which may be reoxidized at a considerably more positive potential to give back $\text{Mn}_2(\text{CO})_{10}$.^{1–4}

The W–W-bonded dimer $[\text{W}_2(\text{SBz})_2(\text{CO})_8]$ (SBz = μ -phenylmethanethiolate) also undergoes 2e reduction localized on the $\sigma^*(\text{W}–\text{W})$ orbital.⁵ However, due to the presence of the two bridging SBz ligands, it was still possible to distinguish between the individual 1e reduction steps. As a result, the primary reduction product, $[\text{W}_2(\text{SBz})_2(\text{CO})_8]^{•-}$, could even be detected by IR spectroelectrochemistry.^{5b} However, it was generated only in a very low concentration corresponding to a large value of the disproportionation constant described by eq 1. Consequently, it could not be established whether the radical anion still possesses an intact W–W bond or whether it contains the $\text{W}(\text{CO})_4$ units linked only by the bridging SBz ligands, as was found in the final reduction product $[\text{W}_2(\text{SBz})_2(\text{CO})_8]^{2-}$.⁵

$$K_{\text{disp}} = \{[\text{W}_2(\text{SBz})_2(\text{CO})_8]^{2-}\} \cdot \{[\text{W}_2(\text{SBz})_2(\text{CO})_8]\} / \{[\text{W}_2(\text{SBz})_2(\text{CO})_8]^{•-}\}^2 = 7500 \quad (1)$$

Opening of a metal–metal bond as a consequence of the population of the $\sigma^*(\text{M}–\text{M})$ LUMO also accompanies

(4) Lee, K. Y.; Kuchynka, D. J.; Kochi, J. K. *Organometallics* 1987, 6, 1886.

* To whom correspondence should be addressed.

[®] Abstract published in *Advance ACS Abstracts*, June 1, 1995.

(1) Dessy, R. E.; Weissman, P. M.; Pohl, R. C. *J. Am. Chem. Soc.* 1966, 88, 5117.

(2) Krejčík, M.; Daněk, M.; Hartl, F. *J. Electroanal. Chem. Interfacial Electrochem.* 1991, 317, 179.

(3) Lacombe, D. A.; Anderson, J. E.; Kadish, K. M. *Inorg. Chem.* 1986, 25, 2074.

one-electron reduction of the cluster $\text{Ru}_3(\text{CO})_{12}$. In this case the overall mechanism is more complex. The primary reduction product, $[\text{Ru}_3(\text{CO})_{12}]^{\cdot-}$, is a very short-lived species which transforms to an open-structure isomer prone to dissociation of a CO ligand. Finally, the stable cluster, $[\text{Ru}_3(\text{CO})_{11}]^{2-}$, with a CO-bridged triangular metal core is formed.⁶

From the above-mentioned examples it is apparent that stabilization of such radical anionic metal-metal-bonded complexes will require the presence of another redox active center (ligand) which is able to accommodate the unpaired electron in its low-lying LUMO, thus bypassing the labilizing effect of population of the $\sigma^*(\text{M}-\text{M})$ orbital at a higher energy.

Van der Graaf et al.⁷ studied reduction of several $[(\text{CO})_5\text{MnMn}(\text{CO})_3(\alpha\text{-diimine})]$ complexes ($\alpha\text{-diimine}$ = a series of substituted 2,2'-bipyridine, 1,4-diaza-1,3-butadiene, and pyridine-2-carbaldehyde imine ligands). Coordination of an $\alpha\text{-diimine}$ ligand will have a stabilizing influence on the metal-metal bond in the singly reduced species since the SOMO is then the lowest π^* orbital of the $\alpha\text{-diimine}$ and not $\sigma^*(\text{M}-\text{M})$. Furthermore, the presence of an $\alpha\text{-diimine}$ ligand also results in sufficient separation between the first and second one-electron reduction steps. However, the primary radical anionic products, formed during the one-electron reduction of the above-mentioned complexes, have never been observed spectroscopically, not even in the case of the related compound $[(\text{CO})_5\text{MnRe}(\text{CO})_3(\text{BPY}')]^{\cdot-}$ (BPY' = 4,4'-dimethyl-2,2'-bipyridine) with the more stable Mn-Re bond.⁸ Instead, the metal-metal bond was instantaneously split with formation of $\text{Mn}(\text{CO})_5^{\cdot-}$ and $[\text{Mn}(\text{CO})_3(\alpha\text{-diimine})]^{\cdot-}$ radicals. The latter species quickly dimerized to give $[\text{Mn}_2(\text{CO})_6(\alpha\text{-diimine})_2]$. Likewise, one-electron reduction of $[(\text{CO})_5\text{MnRu}(\text{Me})(\text{CO})_2(\text{i-Pr-DAB})]$ (i-Pr-DAB = N,N' -diisopropyl-1,4-diaza-1,3-butadiene) at 193 K yielded directly $\text{Mn}(\text{CO})_5^{\cdot-}$ and the radical species $[\text{Ru}(\text{Me})(\text{n-PrCN})(\text{CO})_2(\text{i-Pr-DAB})]^{\cdot-}$. The radical anion $[(\text{CO})_5\text{MnRu}(\text{Me})(\text{CO})_2(\text{i-Pr-DAB})]^{\cdot-}$ was not even observed in traces.⁹ The instantaneous fragmentation of the above reduced $\alpha\text{-diimine}$ complexes is very similar to the release of Br^- from the radical anions $[\text{Re}(\text{Br})(\text{CO})_3(\alpha\text{-diimine})]^{\cdot-}$.^{10,11}

In order to find out if variation of the $\pi^*(\alpha\text{-diimine})$ LUMO energy is responsible for differences in the stability of the metal-metal bond upon reduction, complexes of the type $[(\text{CO})_5\text{MnRe}(\text{CO})_3(\text{L})]$ (L = 2,2'-bipyridine [BPY], 2,2'-bipyrimidine [BPYM], and 2,3-bis(2-pyridyl)pyrazine [DPP]) and $[(\text{CO})_5\text{MnRe}(\text{CO})_3(\mu\text{-L})\text{Re}(\text{Br})(\text{CO})_3]$ ($\mu\text{-L}$ = $\mu\text{-BPYM}$, $\mu\text{-DPP}$) were selected for this spectroelectrochemical study. The general structures of the complexes and the $\alpha\text{-diimine}$ ligands are depicted in Figure 1. In particular, the complexes

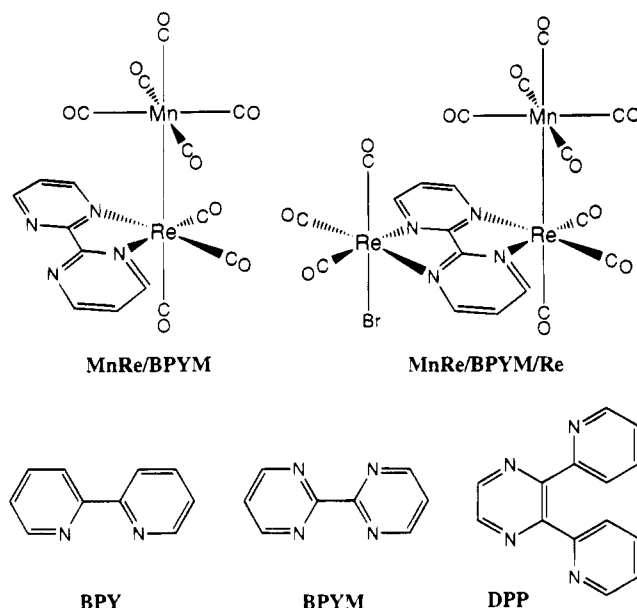


Figure 1. Molecular structures of the complexes MnRe/BPYM and MnRe/BPYM/Re and the $\alpha\text{-diimine}$ ligands L used.

with the bridging BPYM and DPP ligands were supposed to be good candidates for the reversible 1e reduction as the π^* LUMO of these ligands is known to be very low-lying.¹²⁻¹⁴ In the text below the abbreviated formulas MnRe/L and MnRe/L/Re denote the dinuclear complexes $[(\text{CO})_5\text{MnRe}(\text{CO})_3(\text{L})]$ and the trinuclear complexes $[(\text{CO})_5\text{MnRe}(\text{CO})_3(\mu\text{-L})\text{Re}(\text{Br})(\text{CO})_3]$, respectively.

Experimental Section

Materials and Preparations. Tetrahydrofuran (THF, Janssen Chimica) and butyronitrile (n-PrCN, Fluka) were distilled prior to use from a Na/benzophenone mixture and from CaH_2 , respectively. The supporting electrolyte, Bu_4NPF_6 (Fluka), was dried overnight under vacuum at 80 °C. $\text{Co}(\text{Cp})_2$ (Aldrich), Ferrocene (Fc, BDH), BPY (Merck), DPP (Aldrich), BPYM (Johnson & Matthey), Ag^+Otf^- (Otf^- = CF_3SO_3^- , Aldrich) were used as received.

The complexes MnRe/L (L = BPY, BPYM, DPP)^{15,16} and MnRe/L/Re (L = BPYM, DPP)¹⁷ were synthesized according to literature procedures and purified by column chromatography on Silica 60 (Merck), activated by heating overnight under vacuum at 180 °C, with gradient elution by n-hexane/THF. The complexes $[\text{Re}(\text{X})(\text{CO})_3(\text{L})]$ (X = Cl^- , L = BPY,¹⁸ X = Br^- , L = BPYM¹⁹) were prepared as reported in the literature. The complexes $[\text{Re}(\text{Otf})(\text{CO})_3(\text{L})]$ (L = BPY, BPYM) were synthesized as previously described,²⁰ except for Ag^+Otf^- which was used as a reactant instead of H^+Otf^- .

All electrochemical and spectroelectrochemical samples were degassed by several freeze-pump-thaw cycles and handled

(5) (a) Smith, D. A.; Zhuang, B.; Newton, W. E.; McDonald, J. W.; Schultz, F. A. *Inorg. Chem.* **1987**, *26*, 2524. (b) Hill, M. G.; Rosenheim, L. D.; Mann, K. R.; Mu, X. H.; Schultz, F. A. *Inorg. Chem.* **1992**, *31*, 4108.

(6) Cyr, J. C.; DeGray, J. A.; Gosser, D. K.; Lee, E. S.; Rieger, P. H. *Organometallics* **1985**, *4*, 950.

(7) van der Graaf, T.; Hofstra, R.; Schilder, P. G. M.; Rijkhoff, M.; Stufkens, D. J.; van der Linden, J. G. M. *Organometallics* **1991**, *10*, 3668.

(8) Meckstroth, W. K.; Ridge, D. P. *J. Am. Chem. Soc.* **1985**, *107*, 2281.

(9) Nieuwenhuis, H. A.; Hartl, F.; Stufkens, D. J. To be published.

(10) Stor, G. J.; Hartl, F.; van Outersterp, J. W. M.; Stufkens, D. J. *Organometallics* **1995**, *14*, 1115.

(11) Vogler, C. Ph.D. Thesis, Universität Stuttgart, Stuttgart, Germany, 1990.

(12) Creutz, C.; Taube, H. *J. Am. Chem. Soc.* **1969**, *91*, 3988.

(13) Ruminiski, R. R.; Petersen, J. D. *Inorg. Chem.* **1982**, *21*, 3706.

(14) Braunstein, C. H.; Baker, A. D.; Streckas, T. C.; Gafney, H. D. *Inorg. Chem.* **1984**, *23*, 857.

(15) Morse, D. L.; Wrighton, M. S. *J. Am. Chem. Soc.* **1976**, *98*, 3931.

(16) Staal, L. H.; van Koten, G.; Vrieze, K. *J. Organomet. Chem.* **1979**, *175*, 73.

(17) van Outersterp, J. W. M.; Stufkens, D. J.; Fraanje, J.; Goubitz, K.; Vlček, A. *Inorg. Chem.*, submitted for publication.

(18) Staal, L. H.; Oskam, A.; Vrieze, K. *J. Organomet. Chem.* **1979**, *170*, 135.

(19) Baiano, J. A.; Carlson, D. L.; Wolosh, G. M.; DeJesus, D. E.; Knowles, C. F.; Zabo, E. G.; Murphy, W. R. *Inorg. Chem.* **1990**, *29*, 2327.

(20) Sullivan, B. P.; Meyer, T. J. *J. Chem. Soc., Chem. Commun.* **1984**, 1244.

carefully under a nitrogen atmosphere. The solutions of the light-sensitive di- and trinuclear complexes were prepared in the dark.

Spectroscopic Measurements and Instrumentation. IR spectra were measured on a BioRad FTS-7 FTIR spectrometer (16 scans, resolution of 2 cm⁻¹). Electronic absorption spectra were recorded on a Perkin Elmer Lambda 5 UV-vis spectrophotometer attached to a 3600 data station. An OTTLE cell,² equipped with a Pt minigrad working electrode (32 wires/cm) was used for IR and UV-vis spectroelectrochemical experiments at room temperature. Spectroelectrochemistry at low temperatures (LT) was performed in a home-made cryostat OTTLE cell, which has been described in detail elsewhere.²¹ Quartz/CaF₂ and NaCl/CaF₂ windows were employed for UV-vis and IR OTTLE measurements, respectively. The working electrode surroundings were masked carefully to avoid passing the spectral beam through the nonelectrolyzed solution. Cyclic voltammetry and controlled potential electrolysis within the OTTLE cells were carried out by using PAR model 174 and PA4 (Ekono, Czech Republic) potentiostats. For all spectroelectrochemical samples the concentrations of the complexes and Bu₄NPF₆ were 5 × 10⁻³ and 4 × 10⁻¹ M, respectively. Cyclic voltammograms were recorded at 293 and 213 K under the following conditions: 5 × 10⁻⁴ M redox active compound in n-PrCN or THF in the presence of 10⁻¹ M Bu₄NPF₆, Pt disk electrode of 0.38 mm² area, Pt gauze auxiliary electrode, Ag wire pseudoreference electrode, a ligh-protected CV cell. All potentials are reported with respect to the ferrocene/ferrocenium (Fc/Fc⁺) standard redox couple.²²

Results

The MnRe/L and MnRe/L/Re complexes are reduced with one electron to give the corresponding radical anions which are stable or undergo secondary chemical reactions. In the latter case, a complete description of the reduction pathways of the metal-metal-bonded species also required spectroelectrochemical investigation of selected mononuclear complexes [Re(X)(CO)₃(α-diimine)] (X = Cl⁻, Br⁻, Otf⁻) (vide infra).

The ν(CO) frequencies of all complexes studied are collected in Table 1. The reduction potentials of the compounds are presented in Table 2.²³

Cyclic Voltammetry. The reduction of MnRe/BPYM/Re at E_{p,c} = -0.87 V is apparently electrochemically (ΔE_p = 80 mV vs 80 mV for Fc/Fc⁺ at ν = 100 mV/s; E_{p,c} is independent of scan rate) as well as chemically (I_{p,a}/I_{p,c} = 1) reversible at room temperature on the cyclic voltammetry (CV) time scale. This reduction step is diffusion-controlled, as I_{p,c} varies linearly with the square root of the scan rate in the range 10 < ν < 500 mV/s. Comparison with the reversible oxidation of ferrocene, present in the solution in equimolar concentration, revealed that the reduction of MnRe/BPYM/Re is a one-electron process. This result also agrees with the spectroelectrochemical reduction of MnRe/BPYM/Re (vide infra).

A peak showed up at E_{p,a} = -0.64 V during the anodic sweep after passing through the chemically irreversible reduction of [MnRe/BPYM/Re]^{•-} at E_{p,c} = -1.50 V. This peak can reasonably be assigned to reoxidation of

Table 1. CO-Stretching Frequencies of MnRe/L and MnRe/L/Re and Their Reduction Products in n-PrCN (Unless Stated Otherwise)

compd	ν(CO) (cm ⁻¹)
MnRe/BPY ^a	2055 m, 1997 s, 1948 vs, 1899 sh, 1890 m
[Re(n-PrCN)(CO) ₃ (BPY)] ^{•+} ^b	2039 s, 1936 s, br
[Re(n-PrCN)(CO) ₃ (BPY)] ^{•-} ^b	2010 s, 1905 s, 1885 s
[Re(CO) ₃ (BPY)] ⁻ ^a	1944 s, 1843 s, br
[Re(n-PrCN)(CO) ₃ (BPY)] ⁻ ^a	1980 s, 1861 s, 1851 s
[Re(Cl)(CO) ₃ (BPY)] ^c	2021 s, 1916 m, 1897 m
[Re(Cl)(CO) ₃ (BPY)] ^{•-} ^c	1996 s, 1881 m, 1865 m
MnRe/BPYM/Re ^b	2059 m, 2029 s, 2005 s, 1959 s, br, 1930 m, sh, 1917 s
[MnRe/BPYM/Re] ^{•-} ^b	2050 m, 2016 s, 1996 s, br, 1939 s, br, 1910 m, 1896 s
MnRe/BPYM ^c	2056 m, 2001 s, 1949 vs, 1901 m
[MnRe/BPYM] ^{•-} ^c	2044 m, 1985 s, 1939 s, br, 1864 m
[Re(Otf)(CO) ₃ (BPYM)] ^{b,d}	2040 s, 1934 s, br
[Re(THF)(CO) ₃ (BPYM)] ^{•+} ^{b,d}	2026 s, 1941 s, 1915 s
[Re(THF)(CO) ₃ (BPYM)] ^{•-} ^{b,d}	2012 s, 1914 s, 1893 s
[Re(Br)(CO) ₃ (BPYM)] ^{•-} ^b	2004 s, 1897 m, 1877 m
[Re(THF)(CO) ₃ (BPYM)] ^{•-} ^{b,d}	1992 s, 1874 s, 1862 s
[Re(n-PrCN)(CO) ₃ (BPYM)] ⁻ ^c	1987 s, 1873 s, 1864 s
MnRe/DPP/Re ^c	2057 m, 2024 s, 2001 s, 1957 m, 1924 m, 1909 m
[MnRe/DPP/Re] ^{•-} ^c	2049 m, 2007 s, 1991 s, 1943 s, br, 1897 sh, 1885 m
MnRe/DPP ^c	2055 m, 2000 s, 1952 vs, 1901 m
[MnRe/DPP] ^{•-} ^a	2043 m, 1984 s, 1935 s, br, 1864 m
[(Re(Br)(CO) ₃) ₂ (μ-DPP)] ^b	2022 s, 1920 s, br
[Re(n-PrCN)(CO) ₃ (μ-DPP)-Re(Br)(CO) ₃] ^{•+} ^b	2012 sh, 2004 s, 1903 s, 1890 s
[Mn(CO) ₅] ⁻	1902 s, 1862 s

^a Measured at 183 K. ^b Measured at 293 K. ^c Measured at 213 K. ^d Measured in THF.

Table 2. Reduction Potentials (V vs Fc/Fc⁺) of the Complexes MnRe/L, MnRe/L/Re, and Selected [Re(X)(CO)₃(L)]^{0/-} (X = Halide, Solvent; L = BPY, BPYM) (5 × 10⁻⁴ M) in 10⁻¹ M Bu₄NPF₆/n-PrCN Solution (ν = 100 mV/s, Pt Disk Electrode)

compd	E _{p,c} ^g	(ΔE _p)	(ΔE _p) of Fc/Fc ⁺
MnRe/BPY	-1.73 (irr) ^a		
	-1.79 (irr) ^b	(111)	(85)
MnRe/BPYM	-1.53 (irr) ^a		
	-1.49 (rev) ^b	(115)	(115)
MnRe/DPP	-1.48 (irr) ^a		
	-1.46 (rev) ^b	(85)	(85)
MnRe/BPYM/Re	-0.87 (rev) ^a	(80)	(80)
	-0.87 (rev) ^b	(110)	(95)
MnRe/DPP/Re	-1.04 (rev) ^a	(115)	(115)
	-1.07 (rev) ^b	(190)	(160)
[(Re(Br)(CO) ₃) ₂ (μ-DPP)]	-0.98 (rev) ^a	(65)	(65)
[Re(Br)(CO) ₃ (BPYM)] ^c	-1.42 (rev) ^{a,d}	(80)	
[Re(THF)(CO) ₃ (BPYM)] ^{•+}	-1.28 (rev) ^a	(85)	(85)
[Re(Br)(CO) ₃ (BPYM)] ^{•-} ^e	-2.04 (irr) ^{a,d}		
[Re(THF)(CO) ₃ (BPYM)] ^{•-}	-1.73 (rev) ^a		
[Re(Cl)(CO) ₃ (BPY)] ^f	-1.91 (rev) ^{a,c}	(110)	
[Re(Cl)(CO) ₃ (BPY)] ^{•-} ^f	-2.38 (irr) ^{a,c}		
[Re(n-PrCN)(CO) ₃ (BPY)] ^{•+}	-1.62 (rev) ^a	(100)	(100)
[Re(n-PrCN)(CO) ₃ (BPY)] ^{•-}	-1.97 (irr) ^a		

^a Measured at 293 K. ^b Measured at 213 K. ^c Measured in THF. ^d Measured in DMF. ^e See ref 11. ^f See ref 10. ^g Chemical reversibility (rev)/irreversibility (irr) indicated in brackets.

[Mn(CO)₅]⁻.^{3,4} This observation points to inherent instability of the dianion [MnRe/BPYM/Re]²⁻.

All the other Mn-Re-bonded complexes under study also showed diffusion-controlled, electrochemically reversible one-electron reduction. The reduction of MnRe/DPP/Re was chemically reversible on the time scale of cyclic voltammetry (ν = 20–500 mV/s) already at room temperature, whereas the dinuclear complexes MnRe/

(21) Hartl, F.; Luyten, H.; Nieuwenhuis, H. A.; Schoemaker, G. C. *Appl. Spectrosc.* **1995**, *48*, 1522.

(22) Cagné, R. R.; Koval, C. A.; Lisensky, C. G. *Inorg. Chem.* **1980**, *19*, 2854.

(23) Electrochemical reversibility of all investigated electrode processes was compared with that of the Fc/Fc⁺ couple²² used as an internal standard to account for effects such as uncompensated iR drop, electrode passivation, etc.

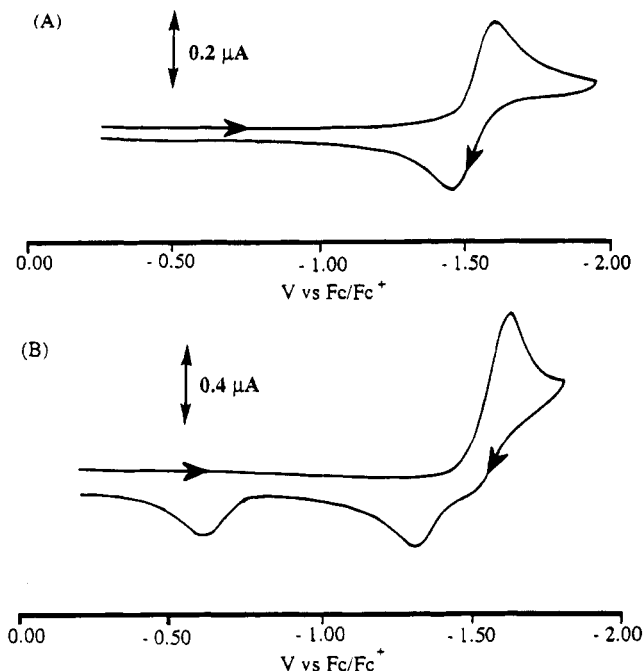


Figure 2. Cyclic voltammograms of MnRe/BPYM measured in n-PrCN at 213 K (A) and 293 K (B). Conditions: 5×10^{-4} M solution in n-PrCN in the presence of 10^{-1} M Bu_4NPF_6 , Pt disk electrode (real surface area of 0.38 mm^2), $\nu = 100 \text{ mV/sec}$.

BPYM (Figure 2A) and MnRe/DPP were reversibly reduced only at 213 K. At room temperature the reduction of the latter complexes was chemically irreversible ($I_{p,a}/I_{p,c} < 1$) (Figure 2B). The reduction of MnRe/BPY was chemically irreversible even at 213 K. This irreversibility indicates that the primary reduction product $[\text{MnRe/BPY}]^{\cdot-}$ undergoes a very fast scission of the Mn–Re bond with a rather low activation energy which increases in the order $\text{MnRe/BPY} < \text{MnRe/L} \ll \text{MnRe/L/Re}$ ($\text{L} = \text{DPP, BPYM}$). For, the irreversible cathodic processes were associated in all MnRe/L cases with the appearance of two new anodic peaks on the reverse scan (see Figure 2B) due to reoxidation of the secondary products $\text{Mn}(\text{CO})_5^-$ at $E_{p,a} = -0.6 \text{ V}$ ^{3,4} and $[\text{Re}(\text{n-PrCN})(\text{CO})_3(\text{L})]^{\cdot-}$ at more negative potentials (see Table 2).

Spectroelectrochemistry. MnRe/BPYM/Re. Electrochemical reduction of MnRe/BPYM/Re in n-PrCN within the IR OTTL cell at room temperature gave a product with bands in the $\nu(\text{CO})$ region at 2050 m, 2016 s, 1996 s,br, 1939 s,br, 1910 m,sh, and 1896 s cm^{-1} . The band pattern is identical to that of the parent compound MnRe/BPYM/Re (Table 1, Figure 3), and the product is therefore assigned as the radical anionic complex $[\text{MnRe/BPYM/Re}]^{\cdot-}$. The shift of the $\nu(\text{CO})$ bands to lower frequencies upon reduction of MnRe/BPYM/Re can obviously be ascribed to an increased π -back-donation from the metal centers toward the CO ligands. The magnitude of the $\nu(\text{CO})$ shifts of $\sim 15\text{--}20 \text{ cm}^{-1}$ agrees with the expected value for α -diimine-localized one-electron reduction steps¹⁰ and points to a weak π -donation from the bis-chelated $[\text{BPYM}]^{\cdot-}$ radical anionic ligand to both Re centers.

The radical anion $[\text{MnRe/BPYM/Re}]^{\cdot-}$ is stable at room temperature. It could also be obtained chemically by smooth reduction of MnRe/BPYM/Re with 1 equiv of $\text{Co}(\text{Cp})_2$ in THF ($\text{Co}(\text{Cp})_2/\text{Co}(\text{Cp})_2^+$ possesses $E_{1/2} =$

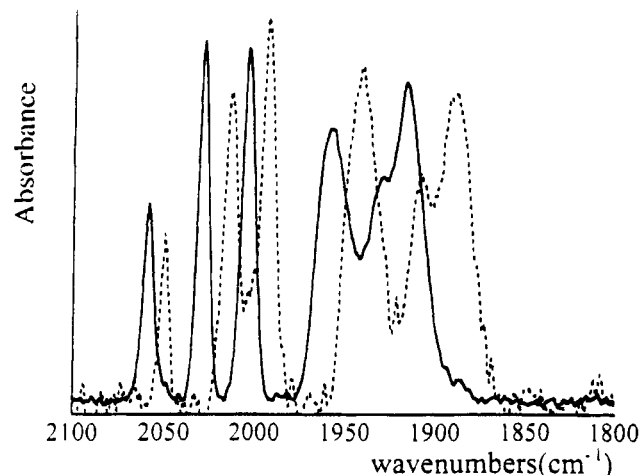


Figure 3. IR spectra of MnRe/BPYM/Re (—) and $[\text{MnRe/BPYM/Re}]^{\cdot-}$ (···) in the $\nu(\text{CO})$ region; in n-PrCN at 293 K.

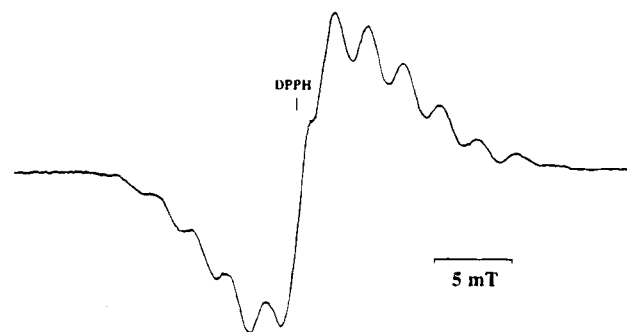


Figure 4. ESR spectrum of $[\text{MnRe/BPYM/Re}]^{\cdot-}$ in THF at 293 K.

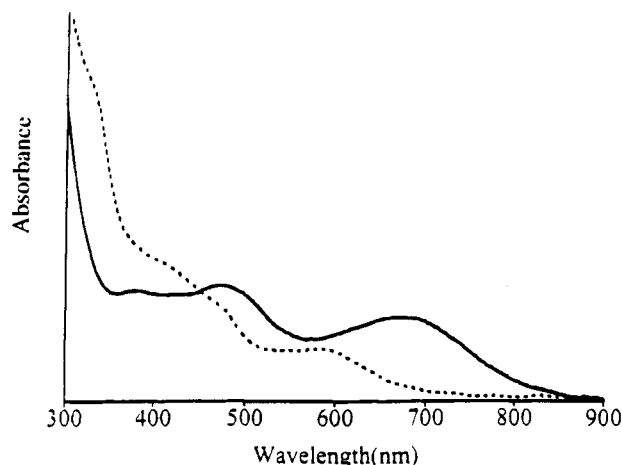


Figure 5. UV-vis spectra of MnRe/BPYM/Re (—) and $[\text{MnRe/BPYM/Re}]^{\cdot-}$ (···) in n-PrCN at 293 K.

$-1.33 \text{ V vs Fc/Fc}^+$). In this way it was possible to characterize $[\text{MnRe/BPYM/Re}]^{\cdot-}$ by ESR (Figure 4) and UV-vis spectroscopy (Figure 5).

The radical anion $[\text{MnRe/BPYM/Re}]^{\cdot-}$ exhibits a partially resolved ESR spectrum at $g = 1.9990$ (Figure 4). The spectrum has apparently an asymmetric shape which may be ascribed to second-order effects (deviations in spacing between lines and in line width) due to insufficient averaging of anisotropic contributions (g factors, splitting constants), not uncommon for the coupling from the $^{185,187}\text{Re}$ nuclei.²⁴ This feature in combination with possible hyperfine splitting due to the large number of nuclei (two inequivalent ^{185}Re ($I = 5/2$, 37.07%) or ^{187}Re ($I = 5/2$, 62.93%) nuclei, one ^{55}Mn

nucleus ($I = 5/2$), one ^{79}Br ($I = 3/2$, 50.54%) or ^{81}Br ($I = 3/2$, 49.46%) nucleus, four ^{14}N ($I = 1$, 99.63%) and two (of six) 25 ^1H ($I = 1/2$, 100%) nuclei of the BPYM heterocycle) make the computer simulation of the ESR spectrum rather difficult. The best result has been obtained with the following parameters: the coupling constants $a_{\text{Re}(\text{Mn})} = a_{\text{Re}(\text{Br})} = 2.4$ mT (sextets of the line-intensity pattern 1:2:3:3:2:1), $a_{\text{Mn}} = a_{\text{Br}} = 0.9$ mT, line width of 1.4 mT. For comparison, the ESR spectrum of the related BPYM-centered radical anion $[(\text{Re}(\text{Br})(\text{CO})_3)_2(\mu\text{-BPYM})]^{*-}$ has been recorded²⁶ at $g = 2.0005$, and the computer simulation inferred $a_{\text{Re}} = 1.2$ mT and $a_{\text{Br}} = 0.8$ mT. The rhenium coupling constant (a_{Re}) of approximately 2.4 mT for $[\text{MnRe}/\text{BPYM}/\text{Re}]^{*-}$ clearly indicates that this radical anion is also BPYM-centered since a rhenium-centered radical would possess much larger a_{Re} (≥ 20 mT).^{24,27} The relatively small isotropic g factor of $[\text{MnRe}/\text{BPYM}/\text{Re}]^{*-}$ (see above) with respect to the value $g_e = 2.0023$ of the free electron reflects mixing of the singly occupied MO (SOMO) of the $[\text{BPYM}]^{*-}$ ligand, b_{2u}^* ,²⁵ with a low-lying unoccupied MO (which might be²⁵ the a_u^* LUMO of $[\text{BPYM}]^{*-}$) through the spin-orbit coupling²⁸ due to the presence of the heavy Re atoms.

The UV-vis spectrum of $\text{MnRe}/\text{BPYM}/\text{Re}$ (Figure 5) shows two MLCT transitions at 473 and 671 nm in THF. A resonance Raman study on this complex¹⁷ revealed that the lower-energy MLCT band originates from the (Mn)Re metal center whereas the higher-energy MLCT transitions originate mainly from the Re(Br) metal center. Upon the one-electron reduction the lowest energy band shifts approximately 2600 cm^{-1} to higher energy. Provided that the SOMO of $[\text{MnRe}/\text{BPYM}/\text{Re}]^{*-}$ still has $\pi^*(\text{BPYM})$ character, which is indicated by ESR spectroscopy (vide supra) and the stability of the radical, this shift of the MLCT band may be ascribed to a larger destabilization of the $\pi^*(\text{BPM})$ frontier orbital upon single occupation with respect to the filled $d_{\gamma}(\text{Re}(\text{Mn}))$ orbitals.

Further reduction of $[\text{MnRe}/\text{BPYM}/\text{Re}]^{*-}$ ($E_{\text{p,c}} = -1.50$ V vs Fc/Fc^+) led to instantaneous splitting of the Mn-Re bond, as was indicated by the appearance of the characteristic $\nu(\text{CO})$ bands of $\text{Mn}(\text{CO})_5^-$ accompanied by the generation of yet unidentified product(s) ($\nu(\text{CO})$ at 2018 s, 1932 s, and 1915 s cm^{-1}).

MnRe/DPP/Re. At room temperature, $[\text{MnRe}/\text{DPP}/\text{Re}]^{*-}$ was not as stable on the OTTLE time scale of minutes as $[\text{MnRe}/\text{BPYM}/\text{Re}]^{*-}$ since it slowly decomposed into $\text{Mn}(\text{CO})_5^-$ and a product with $\nu(\text{CO})$ bands at 2012 sh, 2004 s, 1903 s, and 1890 s cm^{-1} . The latter frequencies are tentatively assigned to $[\text{Re}(\text{n-PrCN})(\text{CO})_3(\mu\text{-DPP})\text{Re}(\text{Br})(\text{CO})_3]^{*-}$. A product with the same $\nu(\text{CO})$ frequencies is formed upon one-electron reduction of $[(\text{Re}(\text{Br})(\text{CO})_3)_2(\mu\text{-DPP})]^{29,30}$. At 213 K, however, the

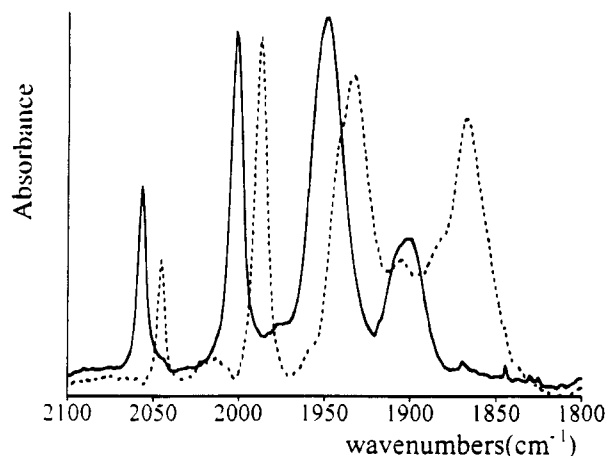


Figure 6. IR spectra of MnRe/BPYM (—) and $[\text{MnRe}/\text{BPYM}]^{*-}$ (···) in the $\nu(\text{CO})$ region; in n-PrCN at 193 K.

one-electron reduction of $\text{MnRe}/\text{DPP}/\text{Re}$ was also completely reversible on the OTTLE time scale. This was indicated by the isosbestic appearance of the $\nu(\text{CO})$ bands of $[\text{MnRe}/\text{DPP}/\text{Re}]^{*-}$ (Table 1) which persisted in the solution at the reduced temperature for more than 10 min without any apparent decomposition. Only further reduction of the radical anion at $E_{\text{p,c}} = -1.50$ V vs Fc/Fc^+ led again to the formation of $\text{Mn}(\text{CO})_5^-$ and some unidentified products with $\nu(\text{CO})$ at 2031 (sh), 2026, 2011, and 1906 (broad) cm^{-1} .

MnRe/BPYM. Figure 6 shows the IR spectral changes in the $\nu(\text{CO})$ region accompanying the reduction of MnRe/BPYM in n-PrCN at 213 K. Using the same reasoning as for $[\text{MnRe}/\text{BPYM}/\text{Re}]^{*-}$ (vide supra) the product formed is assigned to the radical anion $[\text{MnRe}/\text{BPYM}]^{*-}$ (Table 1). Although stable on the CV time scale ($v = 20\text{--}500$ mV/s) at 213 K, $[\text{MnRe}/\text{BPYM}]^{*-}$ slowly decomposed during electrolysis within the LT OTTLE cell into $\text{Mn}(\text{CO})_5^-$ and $[\text{Re}(\text{n-PrCN})(\text{CO})_3(\text{BPYM})]^{*-}$. The latter product could not, however, be observed spectroscopically since it was immediately reduced further to give $[\text{Re}(\text{n-PrCN})(\text{CO})_3(\text{BPYM})]^{*-}$. The identity of the latter product was confirmed by independent reduction of $[\text{Re}(\text{Otf})(\text{CO})_3(\text{BPYM})]$ in THF and of $[\text{Re}(\text{Br})(\text{CO})_3(\text{BPYM})]$ in n-PrCN (see Scheme 1).

$[\text{Re}(\text{Otf})(\text{CO})_3(\text{BPYM})]$ was completely converted prior to its one-electron reduction in THF to $[\text{Re}(\text{THF})(\text{CO})_3(\text{BPYM})]^{*-}$. For the description of the mechanism of this electrocatalyzed substitution we refer to previous works of Kochi et al.³¹ and Stor et al.¹⁰ Subsequent one-electron reduction of the latter cationic compound gave smoothly the radical complex $[\text{Re}(\text{THF})(\text{CO})_3(\text{BPYM})]^{*-}$. In a subsequent one-electron reduction step this radical was converted into $[\text{Re}(\text{THF})(\text{CO})_3(\text{BPYM})]^{*-}$ upon retention of isosbestic points in the IR $\nu(\text{CO})$ region. Importantly, the $\nu(\text{CO})$ frequencies of $[\text{Re}(\text{THF})(\text{CO})_3(\text{BPYM})]^{*-}$ strongly resemble those of the final Re product formed upon reduction of MnRe/BPYM in n-PrCN (see Scheme 1), thus proving its assignment to $[\text{Re}(\text{n-PrCN})(\text{CO})_3(\text{BPYM})]^{*-}$ (Table 1).

The anion $[\text{Re}(\text{n-PrCN})(\text{CO})_3(\text{BPYM})]^{*-}$ was also spectroelectrochemically generated by stepwise reduction of $[\text{Re}(\text{Br})(\text{CO})_3(\text{BPYM})]$ in n-PrCN at room temperature. The first one-electron reduction step led to the formation of stable $[\text{Re}(\text{Br})(\text{CO})_3(\text{BPYM})]^{*-}$. Its subsequent one-

(24) deLearie, L. A.; Haltiwanger, R. C.; Pierpont, C. G. *Inorg. Chem.* **1987**, *26*, 817.

(25) Kaim, W.; Kohlmann, S.; Lees, A.; Snoeck, T. L.; Stufkens, D. J.; Zulu, M. M. *Inorg. Chim. Acta* **1993**, *210*, 159.

(26) Kaim, W.; Kohlmann, S. *Inorg. Chem.* **1990**, *29*, 2909.

(27) Al-Mowali, A.; Porte, A. L. *J. Chem. Soc., Dalton Trans.* **1975**, 250.

(28) Kaim, W. *J. Coord. Chem. Rev.* **1987**, *76*, 187.

(29) The uptake of one electron probably leads to a heterolytic splitting of only one of the Re-Br bonds and a concomitant replacement of Br⁻ by a donor solvent molecule, as was indicated by a different $\nu(\text{CO})$ pattern of the asymmetric radical product with respect to that found for parent $[(\text{Re}(\text{Br})(\text{CO})_3)_2(\mu\text{-DPP})]$ (see Table 1).

(30) van Outersterp, J. W. M. Unpublished results.

(31) Hershberger, J. W.; Klingler, R. J.; Kochi, J. K. *J. Am. Chem. Soc.* **1983**, *105*, 61.

by IR and UV-vis spectra ($\nu(\text{CO})$ at 1988 s, 1951 s, 1887 s, and 1859 cm^{-1} ; λ_{max} 805, 600, and 470 nm).¹⁰ In n-PrCN at room temperature, however, formation of the dimer [Re₂(CO)₆(BPY)₂] was not observed. Instead, one-electron reduction of MnRe/BPY led to the formation of Mn(CO)₅⁻ and [Re(n-PrCN)(CO)₃(BPY)]⁺ (see Scheme 2).

The assignment of the above Re/BPY products was supported by the results of independent spectroelectrochemical reduction of [Re(OTf)(CO)₃(BPY)] in n-PrCN at room temperature and [Re(Cl)(CO)₃(BPY)] in n-PrCN at 213 K. [Re(OTf)(CO)₃(BPY)] immediately converted in n-PrCN at room temperature into [Re(n-PrCN)(CO)₃(BPY)]⁺. The one-electron reduction of the latter species gave the stable radical [Re(n-PrCN)(CO)₃(BPY)][•] as the only product. The one-electron reduction of [Re(Cl)(CO)₃(BPY)] at 213 K in n-PrCN resulted in the formation of the stable radical anion [Re(Cl)(CO)₃(BPY)]^{•-}. [Re(Cl)(CO)₃(BPY)]^{•-} was further reduced to give a product with $\nu(\text{CO})$ bands at 1980 s, 1861 s, and 1851 cm^{-1} and a minor amount of a product with $\nu(\text{CO})$ bands at 1944 s and 1843 s, br cm^{-1} . The $\nu(\text{CO})$ frequencies of the former product strongly resemble those of [Re(n-PrCN)(CO)₃(DAPA)]^{•-} (DAPA = 2,6-diacetylpyridine bis-(anil) ($\nu(\text{CO})$ at 1980 s, 1856 s, and 1842 cm^{-1})¹⁰ and those of [Re(n-PrCN)(CO)₃(BPYM)]^{•-} (Table 1). The complex is therefore assigned to [Re(n-PrCN)(CO)₃(BPY)]^{•-}. The latter product corresponds to pentacoordinated [Re(CO)₃(BPY)]^{•-}, in accordance with the results of Stor et al.¹⁰ Scheme 2 summarizes the various events taking place upon reduction of MnRe/BPY, [Re(Cl)(CO)₃(BPY)], and [Re(OTf)(CO)₃(BPY)].

Discussion

The (spectro)electrochemical data presented in the previous section clearly show that the cleavage of a metal-metal bond in transition metal complexes upon reduction may successfully be avoided by coordination of π -acceptor ligands which are able to accommodate the added electrons in their low-lying empty π^* orbitals. The α -diimine ligands proved to be suitable candidates for this strategy. It is noted that they possess a similar stabilizing effect for the Re-X bond in the complexes [Re(X)(CO)₃(α -diimine)]^{•-} (X = halide)¹⁰ depending on their basicity in the singly reduced form.

A comparison of the reduction potentials of the complexes MnRe/ α -diimine revealed that BPY ($E_{\text{p,c}}$ (MnRe/BPY) = -1.73 V vs Fc/Fc⁺ at 293 K) possesses the highest-energy π^* LUMO and has, therefore, the weakest π -acceptor character. BPYM and DPP in MnRe/L are comparable in their π -acceptor capacity ($E_{\text{p,c}}$ (MnRe/BPYM) = -1.53 V vs Fc/Fc⁺ at 293 K; $E_{\text{p,c}}$ (MnRe/DPP) = -1.48 V vs Fc/Fc⁺ at 293 K). Their π -acceptor character becomes much stronger in MnRe/L/Re where they act as bridges between the two Re central atoms ($E_{\text{p,c}}$ (MnRe/BPYM/Re) = -0.87 V vs Fc/Fc⁺ at 293 K; $E_{\text{p,c}}$ (MnRe/DPP/Re) = -1.04 V vs Fc/Fc⁺ at 293 K). The decrease of the π^* orbital energy of the bridging versus nonbridging BPYM or DPP is a well-known phenomenon¹²⁻¹⁴ caused by coordination of a second electron-withdrawing metal center. The effect is also apparent from the UV-vis spectra of the di- and trinuclear BPYM and DPP compounds.¹⁷ The d((Mn)-Re) $\rightarrow \pi^*(\text{BPYM})$ CT band of MnRe/BPYM at 523 nm (in THF, room temperature) shifts to 671 nm in MnRe/

BPYM/Re and an extra MLCT band, originating mainly from the Re center of the Re(Br)(CO)₃ fragment, is observed at 473 nm for the trinuclear compound. The d₇((Mn)Re) $\rightarrow \pi^*(\text{DPP})$ CT band at 557 nm shifts to 636 nm going from MnRe/DPP to MnRe/DPP/Re, and an extra MLCT band shows up at 474 nm for the latter compound due to the coordination of the Re(Br)(CO)₃ metal fragment.

The radical anion [MnRe/BPYM/Re]^{•-} is stable at room temperature, whereas the radical anion [MnRe/DPP/Re]^{•-} could only be stabilized at 213 K. This difference in reactivity implies that the bridging BPYM ligand offers a lower-lying π^* LUMO than bridging DPP and is, therefore, more suitable for accommodation of the extra electron. This is in accordance with the reduction potentials of the neutral compounds which are $E_{\text{p,c}} = -0.87$ V and $E_{\text{p,c}} = -1.04$ V for MnRe/BPYM/Re and MnRe/DPP/Re, respectively.

Considering the dinuclear species, the most stable radical anion is formed by the one-electron reduction of MnRe/BPYM. [MnRe/BPYM]^{•-} could already be stabilized at 213 K whereas for [MnRe/DPP]^{•-} the temperature had to be decreased to 183 K. This is rather surprising since the reduction potentials of MnRe/BPYM ($E_{\text{p,c}} = -1.53$ V) and MnRe/DPP ($E_{\text{p,c}} = -1.48$ V) are very similar. Apparently, other effects play a role. For the [BPYM]^{•-} ligand it is known from MO calculations³² that the electron density on its π^* SOMO (b_{2u}^*) should be localized on the inter-ring C-C bond. Complexes with α -diimine ligands of the type [R-DAB]^{•-} (R = alkyl, aryl; DAB = 1,4-diaza-1,3-butadiene) are expected to have the electron density in their π^* SOMO delocalized over the C=N bonds.^{33,34} Supposing this is also true for the [DPP]^{•-} ligand, the π^* electron will then be more delocalized over the (Mn)-Re-DPP chelate bond than in the complex with the [BPYM]^{•-} ligand. Consequently, the increased electron density on the Re atom will result in stronger polarization and hence in more facile cleavage of the Mn-Re bond (see below).

[MnRe/BPY]^{•-} was not even observed at low temperatures since [BPY]^{•-} ($E_{\text{p,c}}$ (MnRe/BPY) = -1.73 V vs Fc/Fc⁺) is apparently a much stronger σ, π -donor in this case. This particular property of the BPY ligand was also demonstrated by several other authors.^{9-11,35} For example, Stor et al.¹⁰ reported a facile loss of Br⁻ from [Re(Br)(CO)₃(BPY)]^{•-} at room temperature whereas the related complexes with the [DPP]^{•-} and [APY]^{•-} ligands are inherently stable. In this respect we have shown in this study that the related [Re(Cl)(CO)₃(BPY)]^{•-} radical anions could in fact be stabilized by simply lowering the temperature to 213 K. This temperature was sufficiently low to inhibit completely the follow-up dissociation of the chloride ligand, even in the absence of excess Cl⁻ anions in the solution, which is otherwise required at room temperature.³⁶

The above results illustrate that the heterolytic splitting of the Mn-Re bond in [MnRe/L]^{•-} and [MnRe/

(32) (a) Kaim, W.; Kohlmann, S. *Inorg. Chem.* **1987**, *26*, 187. (b) Matheis, W.; Kaim, W. *Inorg. Chim. Acta* **1991**, *181*, 15.

(33) Andréa, R. R.; de Lange, W. G. J.; van der Graaf, T.; Rijkhoff, M.; Stufkens, D. J.; Oskam, A. *Organometallics* **1988**, *7*, 1100.

(34) van der Graaf, T.; Stufkens, D. J.; Oskam, A.; Goubitz, K. *Inorg. Chem.* **1991**, *30*, 599.

(35) tom Dieck, H.; Franz, K.-D.; Hohmann, F. *Chem. Ber.* **1975**, *108*, 163.

(36) Shu, C.-F.; Wrighton, M. S. Unpublished manuscript.

$L/Re]^{\bullet-}$ has its origin in a strong polarization of this bond by a charge "leakage" from the reduced α -diimine ligand. The basicity,²⁴ i.e., the σ - and π -donor character of the α -diimine radical anion, increases in the order $[BPYM]^{\bullet-} < [DPP]^{\bullet-} < [BPY]^{\bullet-}$. In the same order the unpaired electron becomes more delocalized over the Re–L chelate bond which will in turn considerably destabilize also the d_{z^2} orbital of Re involved in the Mn–Re σ -bonding. The doubly-occupied $\sigma(Mn-Re)$ orbital will then also rise in energy and will obtain an increasing $d_{z^2}(Mn)$ contribution. The Mn–Re bond will therefore be polarized to such an extent that it will split heterolytically into $Mn^{\bullet-} \cdots Re^+(L^{\bullet-})$, which has indeed been confirmed by the observed formation of $[Mn(CO)_5]^-$ and the reactive radicals $[Re(CO)_3(L)]^{\bullet}$ (see Schemes 1 and 2). The same mechanism of the σ -bond polarization probably applies also for the dissociation of Br^- from $[Re(Br)(CO)_3(L)]^{\bullet-}$.¹⁰

The strong influence of the increased basicity of the α -diimine ligand on the lability of a metal–metal bond can also be demonstrated by the formation of $[(CO)_5ReRe(CO)_3(L_2)]$ upon reaction of $[Re(CO)_5]^-$ with $[Re(Cl)(CO)_3-$

$(L_2)]^{\bullet}$.³⁷ The Re–Re bond was formed for $L_2 = BPY$ whereas no reaction was observed for the significantly more basic pyridine (PY) ligands ($E_{1/2}(PY/PY^{\bullet-}) - E_{1/2}(BPY/BPY^{\bullet-}) = -690 \text{ mV}^{37}$).

Conclusions

The radical anionic complexes $[MnRe/L]^{\bullet-}$ and $[MnRe/L/Re]^{\bullet-}$ can be stabilized by coordination of strong π -acceptor α -diimine ligands ($L = BPYM, DPP$) and by sufficiently decreasing the temperature. These compounds are the first radical–anionic metal–metal-bonded complexes of this type characterized spectroscopically.

Acknowledgment. The Netherlands Foundation for Chemical Research (SON) and the Netherlands Organisation for Pure Research (NWO) are thanked for financial support.

OM940856A

(37) Morse, D. L.; Wrighton, M. S. *J. Organomet. Chem.* **1977**, *125*, 71.

Palladium π -Allyl Chemistry of New P,S Bidentate Ligands. Selective but Variable Dynamics in the Isomerization of the η^3 -C₃H₅ and η^3 -PhCHCHCHPh π -Allyl Ligands

Jörg Herrmann, Paul S. Pregosin,* and Renzo Salzmann

Laboratorium für Anorganische Chemie, ETH Zentrum, Zürich 8092, Switzerland

Alberto Albinati

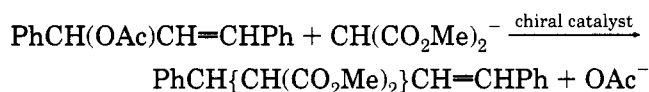
Chemical Pharmacy, University of Milan, I-20131 Milan, Italy

Received January 25, 1995[®]

A series of palladium(II) complexes based on new P,S bidentate ligands have been prepared. One of these, *exo*-8-((*o*-(diphenylphosphino)benzyl)thio)borneol (**3**), is chiral. PdCl₂(**3**), [Pd(η^3 -C₃H₅)(**3**)](CF₃SO₃) (**9**), [Pd(η^3 -PhCHCHCHPh)(**3**)](BF₄) (**10**), and other complexes of P,S ligands with cyclohexyl and ethyl substituents (in place of the *exo*-borneol fragment) have been prepared. The cationic complex [Pd(η^3 -C₃H₅)(**3**)]⁺ exists as two isomers in solution and reveals selective allyl dynamics which are controlled by *electronic* effects. [Pd(η^3 -PhCHCHCHPh)(**3**)]⁺ exists in four forms and also shows selective dynamics which are controlled by *steric* effects. The solid-state structure of [Pd(η^3 -C₃H₅)(**3**)](CF₃SO₃) (**9**), has been determined by X-ray diffraction methods. Complex **10** was used as a catalyst for both the allylic alkylation and the allylic amination. Although the chemical yields are high, the reactions are very slow and the ee's poor.

Introduction

New chiral auxiliaries are of increasing interest in that they may find application in synthetic organic chemistry.¹ It is well-known² that chiral chelating diphosphines are excellent auxiliaries for a variety of transformations, although in the chemistry of the allylic alkylation reaction



several different chelate types have been incorporated into the catalyst precursor, including diphosphine,³ diamine,⁴ and diimine⁵ ligands. Recently, "mixed" ligand chelates, e.g., P–N⁶ and S–N⁷ combinations, have been successfully employed with >90% enantiomeric excesses often reported.

We report here the synthesis and characterization of some new P,S chelating ligands, one of which contains an optically active center, together with preparative results for several of their Pd(II) complexes. Our emphasis, as in previous studies,⁸ is on the structure and dynamics of their π -allyl complexes and specifically the potential application to the catalytic allylic alkylation shown above.

Results and Discussion

The new ligands **1–3** were prepared by reaction of the (2-(chloromethyl)phenyl)diphenylphosphine compound together with the sulfur-anion of the thiol as shown in Scheme 1.

The dichloro complexes were readily prepared from PdCl₂(CH₃CN)₂, and the allyl complexes were prepared by treating the chloride-bridged dinuclear allyl compound with Ag⁺ and then with the appropriate ligand. Ligands **1** and **2** were included so as to have a measure of the electronic effects (via ¹³C NMR) of P,S ligands of smaller size. The new chelates **1–3**, together with their dichloro- and allylpalladium complexes, were characterized via elemental analyses, FAB mass spectra, and ³¹P, ¹³C, and ¹H NMR spectra. The FAB mass spectra show relatively intense signals for the molecular ions of the cationic π -allyl complexes and, for the neutral PdCl₂-(P,S) type complexes, quite strong signals for the cations corresponding to the molecular ion minus Cl, i.e., PdCl-

[®] Abstract published in *Advance ACS Abstracts*, June 1, 1995.

(1) Noyori, R. *Asymmetric Catalysis in Organic Synthesis*; Wiley: New York, 1994.

(2) Hayashi, T. In *Catalytic Asymmetry Synthesis*; Ojima, I., Ed.; VCH: Weinheim, Germany, 1993; p 325.

(3) Mackenzie, P. B.; Whelan, J.; Bosnich, B. *J. Am. Chem. Soc.* **1985**, *107*, 2046. Auburn, P. R.; Mackenzie, P. B.; Bosnich, B. *J. Am. Chem. Soc.* **1985**, *107*, 2033. Hayashi, T.; Yamamoto, A. *Tetrahedron Lett.* **1988**, *29*, 669. Hayashi, T.; Yamamoto, A.; Ito, Y.; Nishioka, E.; Miura, H.; Yanagi, K. *J. Am. Chem. Soc.* **1989**, *111*, 6301. Sawamura, M.; Nagata, H.; Sakamoto, H.; Ito, Y. *J. Am. Chem. Soc.* **1992**, *114*, 2586.

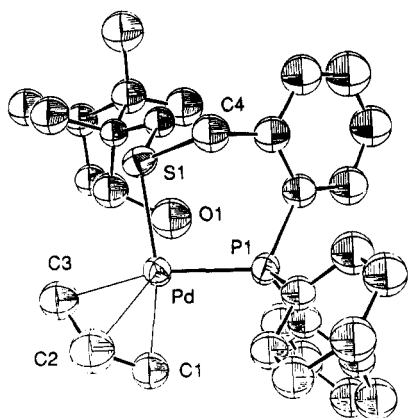
(4) Togni, A. *Tetrahedron: Asymmetry* **1991**, *2*, 683. Tanner, D. *Angew. Chem., Int. Ed. Engl.* **1994**, *106*, 625.

(5) Pfaltz, A. *Acc. Chem. Res.* **1993**, *26*, 339. von Matt, P.; Pfaltz, A. *Angew. Chem., Int. Ed. Engl.* **1993**, *32*, 566. Ohkita, K.; Kurosawa, H.; Hasegawa, T.; Hirao, T.; Ikeda, I. *Organometallics* **1993**, *12*, 3211.

(6) Sprinz, J.; Kiefer, M.; Helmchen, G.; Reggelein, M.; Huttner, G.; Zsolnai, L. *Tetrahedron Lett.* **1994**, *35*, 1523. Dawson, G.; Frost, C. G.; Williams, J. M. J. *Tetrahedron Lett.* **1993**, *34*, 3149.

(7) Frost, C. G.; Williams, J. M. J. *Tetrahedron Lett.* **1993**, *34*, 1785. Frost, C. G.; Williams, J. M. J. *Tetrahedron Lett.* **1993**, *34*, 2015.

(8) (a) Breutel, C.; Pregosin, P. S.; Salzmann, R.; Togni, A. *J. Am. Chem. Soc.* **1994**, *116*, 4067. (b) Pregosin, P. S.; Rügger, H.; Salzmann, R.; Albinati, A.; Lianza, F.; Kunz, R. W. *Organometallics* **1994**, *13*, 83; **1994**, *13*, 5040. (c) Rügger, H.; Pregosin, P. S. *Magn. Reson. Chem.* **1994**, *32*, 297. (d) Pregosin, P. S.; Salzmann, R. *Magn. Reson. Chem.* **1994**, *32*, 128. (e) Ammann, C. J.; Pregosin, P. S.; Rügger, H.; Albinati, A.; Lianza, F.; Kunz, R. W. *J. Organomet. Chem.* **1992**, *423*, 415. (f) Rügger, H.; Kunz, R. W.; Ammann, C. J.; Pregosin, P. S. *Magn. Reson. Chem.* **1992**, *29*, 197.

Figure 1. ORTEP view of **9**.

Scheme 1. Ph₂(2-(RSCH₂)C₆H₄)P Ligands and Their Pd Complexes

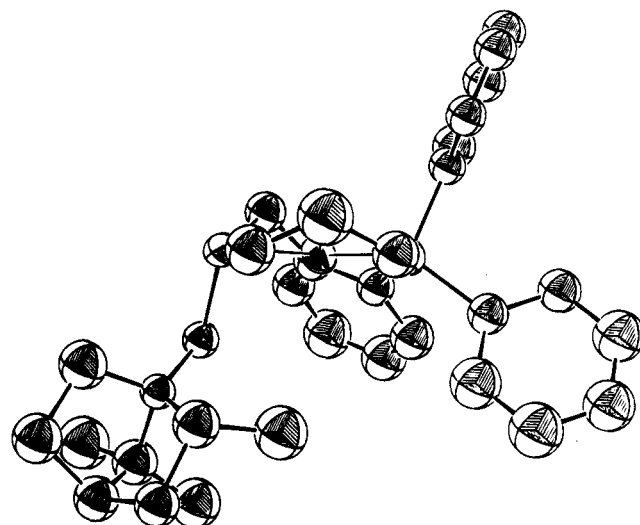
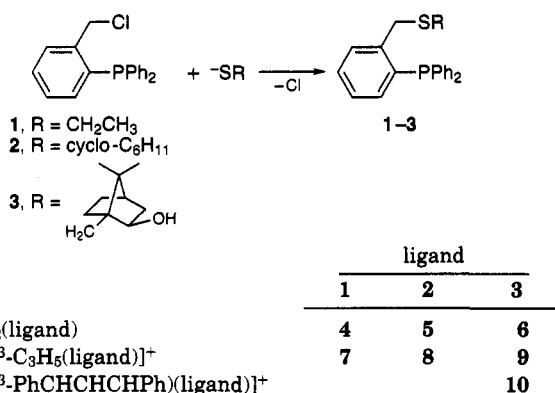
Figure 2. ORTEP view of **9** showing the axial orientation of the sulfur substituent.

Table 1. Selected Bond Lengths (Å) and Bond Angles (deg) for **9**

Pd-S1	2.350(2)	S1-C4	1.859(9)
Pd-P1	2.287(2)	S1-C5	1.826(6)
Pd-C1	2.145(9)	P1-C111	1.819(7)
Pd-C2	2.13(1)	P1-C121	1.829(7)
Pd-C3	2.198(7)	P1-C131	1.841(8)
S1-Pd-P1	95.41(7)	P1-Pd-C3	165.1(3)
S1-Pd-C1	167.2(2)	C1-Pd-C3	67.9(3)
S1-Pd-C2	131.2(3)	Pd-S1-C4	103.3(3)
S1-Pd-C3	99.4(3)	Pd-S1-C5	112.0(2)
P1-Pd-C1	97.2(2)	C1-C2-C3	124.6(9)

(P,S)⁺. In the dichloro derivatives we find three strong bands in the Pd-Cl stretching region of the IR, two of which overlap.

As indicated, our primary interest lies in the π -allyl chemistry of these ligands so that we have prepared the simple η^3 -C₃H₅ cationic compounds **7-9**, plus the 1,3-diphenylallyl cationic compound [Pd(η^3 -PhCHCHCHPh)(**3**)]⁺ (**10**). This latter complex is an intermediate in the allylic alkylation using **3** as chiral auxiliary. The molecular structure for the [Pd(η^3 -C₃H₅)(**3**)](CF₃SO₃) compound, **9**, has been determined by X-ray diffraction methods.

X-ray Structure of 9. Suitable crystals of **9** were obtained from dichloromethane/ether, and two ORTEP views of the molecule are shown in Figures 1 and 2. Tables 1-3 contain selected bond lengths and bond angles, experimental details of the structure determination, and positional parameters, respectively.

For **9**, the local geometry at the palladium atom is distorted square planar with the Pd, P, S, and two terminal carbon atoms comprising the coordination sphere. The two terminal allyl carbons are ca. 0.092(9) and 0.074(9) Å (C(1) and C(3), respectively) below the plane defined by the Pd, P, and S atoms. Interestingly, the central allyl carbon is also below this plane, by 0.68(1) Å, thus placing the entire allyl ligand on one side of the coordination plane. Since the *exo*-borneol methylene carbon, S-CH₂, is ca. 1.69(1) Å above this plane, we can conclude (a) that the *exo*-borneol substituent on sulfur is in a pseudo-axial position (see Figure 2) and (b) the solid-state structure corresponds to the major allyl rotational isom. in solution (*vide infra*) and represents that isomer in which the central

allyl carbon and the *exo*-borneol S-CH₂ are on opposite sides of the molecule. The *P*-phenyl ipso carbons, C(111) and C(121), of the C₆H₅ groups, are in pseudo-equatorial and pseudo-axial positions, respectively, with the latter on the same side as the allyl central carbon. The allyl plane makes an angle of ca. 110° with the coordination plane.

The three Pd-C(allyl) bond distances in **9** (2.145(8), 2.130(10), and 2.198(7) Å, for C(1)-C(3), respectively) are in keeping with the literature⁹⁻¹⁴ for Pd- η^3 -C₃H₅ allyl derivatives, allowing that a tertiary phosphine has a larger trans influence than a thioether. Thus, the Pd-C(3) bond trans to P (2.198(7) Å) is longer than the Pd-C(1) bond trans to S (2.145(9) Å). The Pd-P bond length (2.287(2) Å) and the Pd-S distance (2.350(2) Å) are both normal. In the dicationic bis(thioether) complexes [Pd(crown thioether)₂]²⁺, one finds Pd-S separations of ca. 2.27-2.33 Å.¹⁵ For the dication [Pd{P(2-MeSC₆H₄)₃}₂]²⁺, which has two coordinated P,S chelates and which has the trans geometry for the two P and S atoms, the two Pd-S separations are 2.324(5) and 2.383(4) Å.¹⁶ In the cyclometalated complexes with the

(9) Facchin, G.; Bertani, R.; Calligaris, M.; Nardin, G.; Mari, M. *J. Chem. Soc., Dalton Trans.* **1987**, 1381.

(10) Gozum, J. E.; Pollina, D. M.; Jensen, J.; Girolami, G. S. *J. Am. Chem. Soc.* **1988**, *110*, 2688.

(11) Musco, A.; Pontellini, R.; Grassi, M.; Sironi, A.; Meille, S. V.; Ruegger, H.; Ammann, C.; Pregosin, P. S. *Organometallics* **1988**, *7*, 2130.

(12) Albinati, A.; Kunz, R. W.; Ammann, C.; Pregosin, P. S. *Organometallics* **1991**, *10*, 1800.

(13) Ozawa, F.; Son, T.; Ebina, S.; Osakada, K.; Yamamoto, A. *Organometallics* **1992**, *11*, 171.

(14) Knierzinger, A.; Scholzer, P. *Helv. Chim. Acta* **1992**, *75*, 1211.

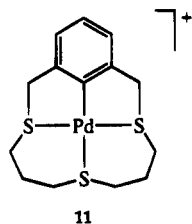
(15) Grant, G. J.; Sanders, K. A.; Setzer, W. N.; VanDerveer, D. G. *Inorg. Chem.* **1991**, *30*, 4053.

Table 2. Experimental Data for the X-ray Diffraction Study of **9**

formula	C ₃₂ H ₃₈ F ₃ O ₄ PPdS ₂
mol wt	745.15
cryst dimens, mm	0.30 × 0.40 × 0.45
data collect T, °C	25
cryst syst	orthorhombic
space group	P2 ₁ 2 ₁ 2 ₁
a, Å	11.0351(9)
b, Å	16.5551(9)
c, Å	18.840(2)
V, Å ³	3442(2)
Z	4
ρ (calcd), g cm ⁻³	1.438
radiation	Mo K α (graphite monochromated, $\lambda = 0.710 69$ Å)
μ , cm ⁻¹	7.416
transmissn coeff	0.9982–0.9695
measd rflns	+h,+k,+l
θ range, deg	2.5 < θ < 25.0
scan type	$\omega/2\theta$
scan width, deg	1.1 + 0.35 tan θ
max counting time, s	110
bkgd time, s	0.5 × scan time
max scan speed, deg min ⁻¹	21.5
prescan rejection limit	0.55 (1.82 σ)
prescan acceptance limit	0.025 (40.0 σ)
horiz receiving slit, mm	1.80 + tan θ
vert receiving slit, mm	4.0
no. of indep data collected	3375
no. of obsd rflns (n_o)	2525 ($ F_o ^2 > 3.0\sigma(F ^2)$)
no. of params refined (n_v)	307
fudge factor, f	0.050
max param shift $\Delta p/\sigma$ (at convergence)	<0.1
R^a	0.036
R_w^b	0.051
GOF ^c	1.817

^a $R = \sum(|F_o| - (1/k)|F_c|)/\sum|F_o|$. ^b $R_w = [\sum w(|F_o| - (1/k)|F_c|)^2/\sum w|F_o|^2]^{1/2}$, where $w = [\sigma^2(F_o)]^{-1}$ and $\sigma(F_o) = [\sigma^2(F_o^2) + \mu^2(F_o^2)]^{1/2}/2F_o$. ^c GOF = $[\sum w(|F_o| - (1/k)|F_c|)^2/(n_o - n_v)]^{1/2}$.

coordination sphere [Pd(P,S)(N,C)]⁺ (P,S = Ph₂PCH₂-CH₂SMe),¹⁷ with S trans to "C", the observed Pd–S values fall in the range 2.396(3)–2.421(3) Å. In **11**, the



11

values for the three different Pd–S distances are 2.267(2), 2.369(2), and 2.275(2) Å, with the longest having the thioether S atom trans to the carbon ligand.¹⁸ Consequently, **9** seems to have a Pd–S bond whose length lies toward the middle of its expected range, and the presence of the *exo*-borneol fragment in no way interferes with coordination (see Figure 2), especially as the pseudo-axial arrangement of the sulfur substituent minimizes its contact with the remaining ligand moieties. The two S–C bonds (S(1)–C(4) and S(1)–C(5)) have lengths of 1.859(9) and 1.826(6) Å, which are

(16) Abel, E. A.; Dormer, J. C.; Ellis, D.; Orrell, K. G.; Sik, V.; Hursthouse, M. B.; Mazid, M. A. *J. Chem. Soc., Dalton Trans.* **1992**, 1073.

(17) Chooi, S. Y.; Andy Hor, T. T.; Leung, P.; Mok, K. F. *Inorg. Chem.* **1992**, *31*, 1494.

(18) Giesbrecht, G. R.; Hanan, G. S.; Kieckham, J. E.; Loeb, S. L. *Inorg. Chem.* **1992**, *31*, 3286.

Table 3. Final Positional and Isotropic Equivalent Parameters for **9**^a

Pd	0.26630(4)	0.00666(3)	0.19032(2)	3.232(8)
S1	0.4498(2)	0.07777(9)	0.2007(1)	3.64(3)
P1	0.2718(2)	-0.0027(1)	0.06923(8)	3.54(3)
O1	0.1778(5)	0.1936(5)	0.1893(4)	7.6(2)
C1	0.1025(8)	-0.0608(5)	0.2062(5)	5.1(2)
C2	0.173(2)	-0.0696(6)	0.2632(6)	7.6(2)
C3	0.220(1)	-0.0053(5)	0.3034(4)	6.4(2)
C4	0.5303(7)	0.0527(5)	0.1168(5)	4.9(2)
C5	0.4301(6)	0.1857(4)	0.1846(4)	3.6(1)
C6	0.3703(6)	0.2315(4)	0.2442(4)	3.5(1)
C7	0.2354(8)	0.2136(5)	0.2556(4)	5.0(2)
C8	0.1858(8)	0.2921(6)	0.2916(5)	5.4(2)
C9	0.3012(8)	0.3413(4)	0.3014(5)	5.1(2)
C10	0.377(1)	0.3002(6)	0.3579(5)	6.9(2)
C11	0.4265(9)	0.2246(6)	0.3161(5)	6.3(2)
C12	0.3698(7)	0.3248(4)	0.2325(6)	5.4(2)
C13	0.308(1)	0.3522(6)	0.1667(5)	8.0(3)
C14	0.499(1)	0.3597(6)	0.2339(9)	10.7(4)
C111	0.1219(6)	0.0056(5)	0.0297(4)	4.1(1)*
C112	0.0857(8)	-0.0427(5)	-0.0257(5)	4.8(2)*
C113	-0.031(1)	-0.0377(6)	-0.0514(5)	6.3(2)*
C114	-0.1105(9)	0.0168(7)	-0.0224(6)	6.9(2)*
C115	-0.075(1)	0.0663(7)	0.0323(6)	7.8(3)*
C116	0.042(1)	0.0596(7)	0.0578(6)	7.0(2)*
C121	0.3321(7)	-0.0981(4)	0.0354(4)	3.8(1)*
C122	0.4139(8)	-0.1003(5)	-0.0190(5)	5.5(2)*
C123	0.4572(8)	-0.1752(6)	-0.0473(5)	5.7(2)*
C124	0.4193(9)	-0.2447(6)	-0.0128(5)	5.4(2)*
C125	0.3403(8)	-0.2429(5)	0.0432(5)	4.9(2)*
C126	0.2977(7)	-0.1686(5)	0.0665(4)	4.5(1)*
C131	0.3662(7)	0.0757(5)	0.0275(4)	4.2(1)*
C132	0.4809(7)	0.0904(5)	0.0537(4)	4.4(2)*
C133	0.5500(9)	0.1512(6)	0.0187(5)	6.0(2)*
C134	0.504(1)	0.1918(7)	-0.0352(6)	7.1(2)*
C135	0.394(1)	0.1779(7)	-0.0604(6)	7.1(2)*
C136	0.3205(9)	0.1187(6)	-0.0295(5)	5.7(2)*
S2	-0.1648(2)	0.1835(1)	0.2418(1)	4.93(5)
O2	-0.0591(6)	0.1716(6)	0.2001(5)	9.4(2)
O3	-0.149(1)	0.2352(4)	0.2991(5)	9.9(3)
O4	-0.2657(7)	0.1967(5)	0.1961(5)	11.5(2)
C15	-0.1941(9)	0.0879(5)	0.2810(6)	6.2(2)
F1	-0.2932(8)	0.0856(5)	0.3166(4)	12.6(2)
F2	-0.2061(9)	0.0307(4)	0.2361(5)	12.0(2)
F3	-0.1056(8)	0.0634(4)	0.3218(5)	13.4(2)

^a Estimated standard deviations are given in parentheses. Starred values denote atoms refined isotropically. Anisotropically refined atoms are given in the form of the isotropic equivalent displacement parameter, defined as $\frac{1}{3}[a^2\beta_{11} + b^2\beta_{22} + c^2\beta_{33} + ab(\cos \gamma)\beta_{12} + ac(\cos \beta)\beta_{13} + bc(\cos \alpha)\beta_{23}]$.

not significantly different but are slightly on the long side, perhaps reflecting some relief of steric strain.

Allyl Dynamics. As the solution NMR spectra for the dichloro complexes are of a routine nature, we begin with a discussion for the [Pd(η^3 -C₃H₅)(**3**)]⁺ cation (**9**). The ³¹P spectrum for **9** is a broad singlet at ambient temperature. At 260 K there are two well-resolved signals in the ratio ca. 1:1, although one of these is considerably broader than the other. The ¹H spectrum at ambient temperature reveals resolved signals for two isomers, although several of the π -allyl proton resonances are very broad. At 260 K, the proton signals for one isomer are relatively sharp, but several allyl proton absorptions are still somewhat broad. Lowering the temperature successively to 233 K does not help in that almost all of the ¹H resonances increasingly broaden, leaving little or no definition. We note that the allyl protons trans to phosphorus are the broadest. At ambient temperature the terminal allyl ¹³C signals are fairly sharp, and a ¹³C,¹H correlation showed that, for both isomers, the terminal carbons trans to phosphorus, coincidentally, have identical chemical shifts

Table 4. Selected ^1H NMR Data (δ) for the $\eta^3\text{-C}_3\text{H}_5$ Allyl Complexes

position	7	8	9a	9b
1s	4.94	4.93	4.90	5.06
1a	3.81	3.73	3.85	3.62
2	5.91	5.90	5.86	5.89
3s	4.00	4.01	3.95	4.01
3a	3.47	3.46	3.39	3.29

Table 5. Selected ^1H NMR Data (δ) for **9** and **10**^a

position	9a	9b	10a	10b
1s	4.90	5.06		
1a	3.85	3.62	5.73	5.73
2	5.86	5.89	6.60	6.65
3s	3.95	4.01		
3a	3.39	3.29	4.97	5.06
a	4.03	4.00	3.65	3.57
OH	4.06	4.01	2.27	2.31
b(exo)	1.79	1.78	1.66	1.66
b(endo)	1.79	1.78	1.66	1.66
c	1.72	1.70	1.58	1.58
d(exo)	1.75	1.78	1.34	1.45
d(endo)	1.10	1.08	0.74	0.83
e(exo)	1.60	1.64	0.30	0.77
e(endo)	1.40	1.44	0.47	0.68
i	0.97	0.98	0.84	0.84
h	0.76	0.76	0.63	0.53
j	3.07/2.46	3.17/2.45	2.81/2.45	2.78/2.18
k	3.75–3.90	3.75–3.90	4.33/3.46	4.10/3.72

allylic ortho protons

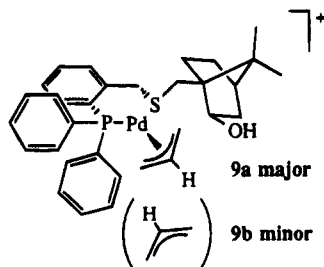
trans to P 7.69 7.70

trans to S 6.86 6.88

^a The numbering of the borneol starts with the CHOH proton (=a) and proceeds toward the CH_2 (=b) etc.

(there are four well-resolved protons in the ^{13}C , ^1H correlation). At 260 K these two terminal carbons trans to phosphorus are both quite broad, but the two terminal carbons trans to sulfur are relatively sharp. We summarize some of the most important ^1H NMR details for **9** as well as for **7** and **8** in Table 4. We have also assigned the ^1H ligand signals for ligand **3**, in both **9** and **10** (see Table 5).

The temperature dependence of the line widths within the two isomers suggests that, for **9**, there are several dynamic processes occurring simultaneously. On the basis of previous experience, and the discussion for **10**, we assign the structures of the two species to the usual rotational isomers:¹⁹



The major isomer was assigned using 2-D NOE spectroscopy. Its central allyl proton shows an NOE to

(19) Two allyl rotational isomers is a common occurrence when the chiral auxiliary does not have C_2 symmetry; see: (a) Cesarotti, E.; Grassi, M.; Prati, L.; Demartin, F. *J. Chem. Soc., Dalton Trans.* **1991**, 2073. However, isomers are also well-known in organometallic chemistry; see: (b) Vrieze, K. In *Dynamic Nuclear Magnetic Resonance Spectroscopy*; Jackman, L. M., Cotton, F. A., Eds.; Academic Press: New York, 1975. (c) Faller, J. W. In *Determination of Organic Structures by Physical Methods*; Nachod, F. C., Zuckerman, J. J., Eds.; Academic Press: New York, 1973; Vol. 5, p 75.

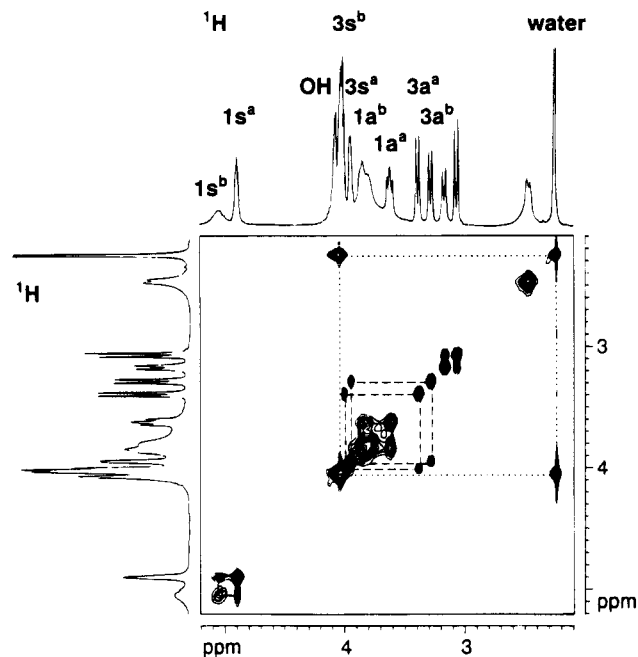


Figure 3. 2-D NOESY (CDCl_3 , 260 K) of **9** showing the various exchange peaks. In the lower left hand corner, one can clearly see the exchange between the two isomers. The analysis of these data is shown in Scheme 2.

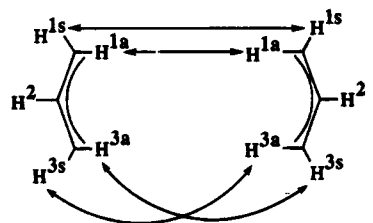
the axial ortho PPh_2 protons, whereas the minor isomer showed no such contact. This develops since one of the two P-phenyl groups in the major isomer is on the same side as the central allyl proton but on the opposite side relative to the S substituent.

It is not immediately obvious that the two isomers must stem from the orientation of the allyl ligand. The S-atom in the ligand is prochiral and complexation can afford diastereomers. Consequently, one could be confronting structures arising from the position of the CH_2 -*exo*-borneol substituent, relative to a "static" allyl ligand. There are many examples of isomers arising from S inversion in thioethers in the literature.^{16,20} However, (a) we know from the NOE cross-peaks (*vide infra*) that the allyl does change its position relative to the PPh_2 moiety and (b) the selective allyl NOE's provide a clear picture, as noted above.

Phase-sensitive 2-D NOESY also provides exchange information, and we indicate several of the exchange cross-peaks for the allyl protons in Figure 3 and summarize these exchange results in Scheme 2. The exchange is selective in that for the protons trans to phosphorus (labeled H^1) there is syn \rightarrow syn, anti \rightarrow anti exchange; however, for those trans to sulfur (labeled H^3) there is syn \rightarrow anti isomerization. Consequently, the $\eta^3\text{-}\eta^1$ opening is selective, with the double bond retained trans to phosphorus:



(20) Abel, E. W.; Ellis, D.; Orrell, K. G.; Sik, V. *J. Chem. Soc., Dalton Trans.* **1992**, 3497. Abel, E. W.; Coston, T. P. J.; Higgins, K. M.; Ellis, D.; Orrell, K. G.; Sik, V.; Cameron, T. S. *J. Chem. Soc., Dalton Trans.* **1989**, 701. Abel, E. W.; Moss, I.; Orrell, K. G.; Sik, V.; Stephanson, D.; Bates, P. A.; Hursthouse, M. B. *J. Chem. Soc., Dalton Trans.* **1988**, 521 and references therein.

Scheme 2. Selective Exchange within the Two Isomers of 9


H¹ is trans to phosphorus, H³ trans to sulfur

The formation of the η^1 complex, by itself, is not sufficient to achieve isomerization. For an η^3 -C₃H₅ allyl, η^1 formation followed by rotation around the sp³-sp² C-C bond, and then re-formation of the η^3 -C₃H₅ allyl, is sufficient to afford the other isomer. For the prochiral PhCHCHCHPh allyl ligand, a modification of this mechanism is necessary for a complete understanding of the dynamics (*vide infra*).

The selectivity in the η^3 - η^1 opening resembles that which we observed previously in several allyl complexes of the chiral phosphorus bidentate JOSIPHOS^{8a,21a} (structure shown in Table 6). In this set of molecules steric effects were shown to be important.^{21a} We note that, for **9**, the η^3 - η^1 opening is in accord with the expected differences in donor strength between tertiary phosphine and thioether donors; i.e., the η^1 -carbon bond forms opposite to the weaker of the two donors, leaving the open position trans to the stronger donor. This isomerization brings the allyl ligand closer to the relatively large PPh₂ moiety in **9**. We know that the PPh₂ moiety is larger (and comes closer to the allyl) than the S substituent since, apart from the X-ray data, there are stronger NOE contacts between the two P-phenyls and the allyl than between the *exo*-borneol and the η^3 -C₃H₅ allyl. Consequently, the η^1 -allyl develops toward the sterically more crowded side of the molecule. Therefore, although the isomerization selectivity is similar to that found in the ferrocene-based JOSIPHOS bidentate complexes,²¹ the source of this selectivity differs; i.e., *electronic and not steric factors are more important in 9*.

The dynamics for the 1,3-diphenylallyl complex [Pd-(PhCHCHCHPh)(**3**)](BF₄) (**10**) are quite different. There are two ³¹P signals in the ratio ca. 4:3, with the minor component having a somewhat broadened signal at ambient temperature. We assign these to the rotational isomers **10a** and **10b**. They possess syn/syn local allyl structures; however, they differ with respect to the positions of the allyl phenyl groups relative to coordinated **3**.

The ¹H spectrum also shows two sets of signals, with all of the proton lines seeming reasonably sharp; nevertheless, the 2-D exchange spectrum (with a mixing time of 0.8 s) reveals that (a) the two major isomers are selectively exchanging with two minor species, **10c** and **10d**, which otherwise would have gone unnoticed (see Figure 4) and (b) the two major isomers are **not** exchanging with each other.

(21) (a) Pregosin, P. S.; Salzmann, R.; Togni, A. *Organometallics* **1995**, *14*, 842. (b) We thank the reviewer for his/her suggestion with respect to **10**. Further, he/she has pointed out that the allyl isomerization data may reflect steric control of allyl isomerization thermodynamics.

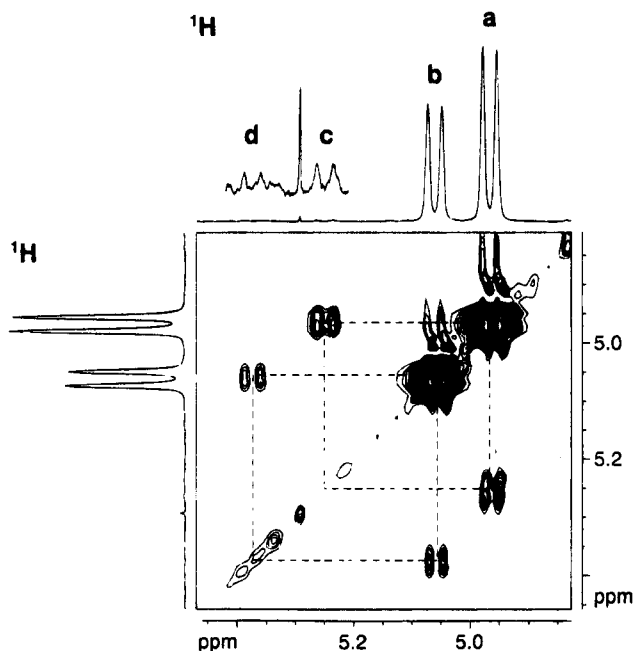


Figure 4. Section of the 2-D NOESY (CDCl₃, 296 K) of **10** showing the various exchange peaks. The protons a and b are trans to sulfur. Note the almost invisible signals (d and c) with which the two major isomers exchange.

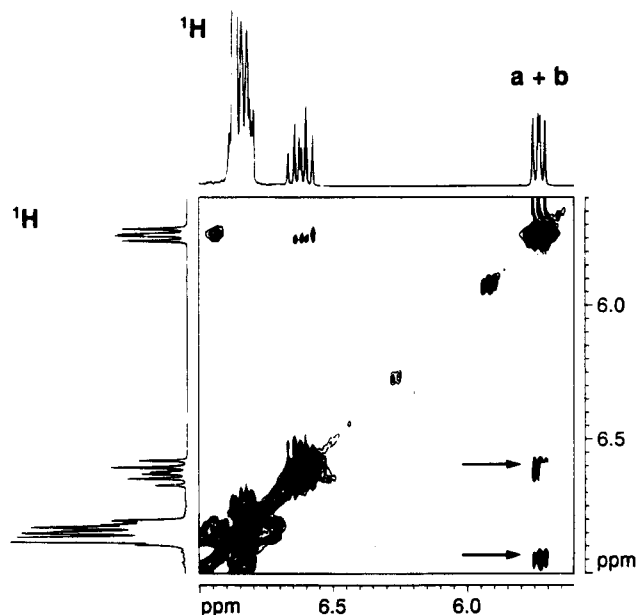
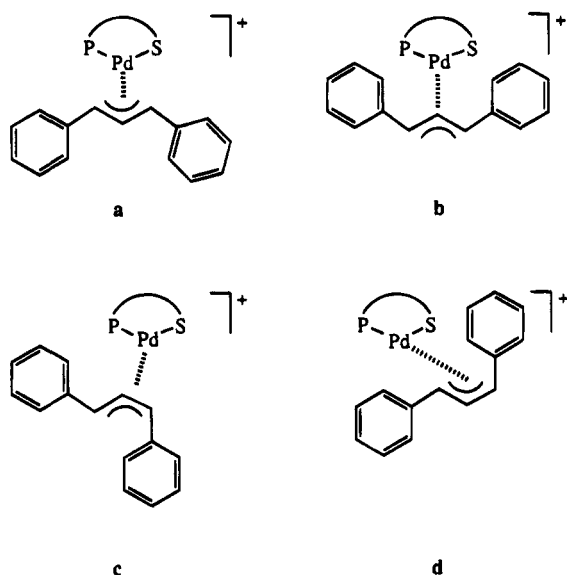


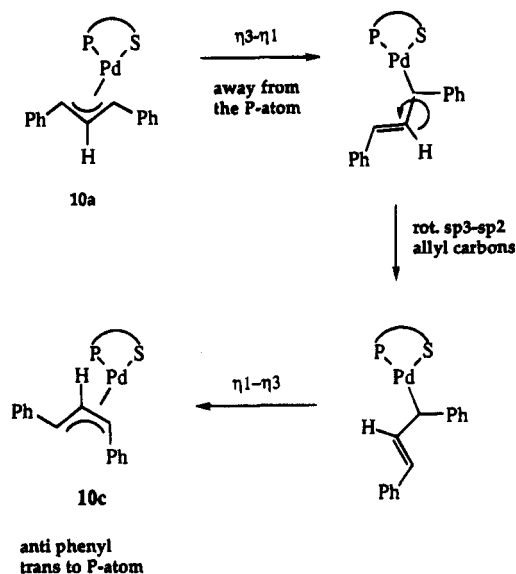
Figure 5. Section of the 2-D NOESY (CDCl₃, 296 K) of **10** showing several exchange peaks. The peaks marked a and b (trans to phosphorus) stem from the *two* major isomers (in a different solvent they are resolved). Signals a and b are in exchange with signals which are buried (indicated by the arrows).

An analysis of the ³J(H,H) values for the allyl protons trans to the sulfur donor in **10c** and **10d** shows that these must be in anti positions with respect to the allyl central proton (phenyl in syn position). The same exchange spectrum (see Figure 5) shows that the anti protons trans to the phosphorus donor for the major isomers, **10a** and **10b**, exchange with two new resonances which are buried in the aromatic region. These high-frequency chemical shifts are typical for syn protons^{8,19} (phenyl in anti position), so that we assign the

Chart 1. Isomers of 10^a

^a The ligand **3** is abbreviated.

Scheme 3. Isomerization Pathway for 10a to 10c

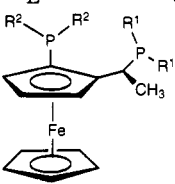


structures of **10c** and **10d** to syn/anti isomers of the type shown in Chart 1.

The appearance of an anti allyl phenyl group, trans only to phosphorus (cis to sulfur), implies selectivity in the isomerization. Scheme 3 shows the pathway to this isomer. Since this isomerization arises due to the formation of an η^1 -carbon trans to the stronger donor, phosphorus (cis to the sulfur), the allyl is opening away from the larger P substituent and we have just the opposite of what we observed in the C_3H_5 allyl isomerization, described above; i.e., this process is *sterically and not electronically controlled*. It is possible that the η^3 - η^1 opening trans to the S atom is as fast as the η^3 - η^1 isomerization trans to the P donor; however, the back-reaction may be rapid enough so that we do not observe it.^{21b}

We believe this to be the first characterized example of such a reversal in the Pd-allyl chemistry of a given bidentate ligand (and certainly the first for a chiral complex). One can argue that this change in mechanism is reasonable in that the 1,3-diphenylallyl ligand

Table 6. ¹³C NMR Chemical Shifts^a for [Pd(η^3 -C₃H₅)L¹L²]⁺ Complexes

compd	δ (terminal)	δ (central)	ref
L ¹ = L ² = μ -OAc	54.8	110.5	22
L ¹ = L ² = acac	60.7	113.2	23
L ¹ = L ² = μ -Cl	62.8	111.3	23
L ¹ = L ² = bis(oxazoline) (chiral complex, N donors)	60.1, 62.0	117.0	25
L ¹ = L ² = PMe ₃ ^b	69.7	137.1	13
L ¹ = L ² = PPh ₃	78.9	127.3	26
L ¹ = L ² = PEt ₂ Ph	71.6	122.6	26
L ¹ = L ² = 	66.9, 76.3 (major); 65.6, 78.2 (minor)	121.9	21a
7	69.5, ^d 76.8 ^e	122.6	this work
8	69.9, ^d 76.9 ^e		this work
9	68.7, ^d 79.3 ^e	122.8	this work

^a Chemical shifts relative to TMS; CDCl₃ solutions. ^b For CH₂C(Me)CH₂ allyl ligand. ^c R¹ = Cy, R² = Ph; the 66.9 ppm resonance is trans to the PPh₂ moiety, and the 76.3 ppm resonance is trans to the PCy₂ moiety. ^d Trans to S ligand. ^e Trans to P ligand.

is larger than η^3 -C₃H₅, with the result that the PPh₂ moiety interacts more strongly with this allyl than with a smaller C₃H₅ allyl ligand. Put slightly differently, it would appear that both electronic and steric effects can operate in an allyl isomerization, with the nature of the allyl ligand providing one determining factor. Given our different results with JOSIPHOS, it seems that both the chiral auxiliary and the allyl ligand will play important roles. This implies that the catalytic allylic alkylation using the, now classical, 1,3-diphenylallyl ligand may have no generality; i.e., the auxiliary is tuned to the substrate. With respect to catalytic allylic alkylation using different chiral auxiliaries, together with a 1,3-diphenylallyl substrate, it will also be necessary to consider the consequences of attack of the nucleophile at one of the terminal carbons of a syn/anti isomer. This may or may not give the same enantiomer.

Allyl ¹³C Parameters. Table 6 shows ¹³C data for the η^3 -C₃H₅ cationic compounds together with comparison data from the literature.^{21a,22-26} Concentrating on the terminal carbons, one notices that these cover the range δ 54.8–79.3, with the lowest frequencies associated with poor donors (weak trans influence). A comparison of **7** and **8** with **9** shows that the presence of the *exo*-borneol fragment does not significantly change the δ value of the allyl carbon trans to the sulfur donor (δ 69.5, 69.9, and 68.7 for **7**–**9**, respectively). As expected, in all three compounds, the S donor shows a trans allyl carbon shift at lower frequency than for the P-donor, with the former suggesting a trans influence between that for a phosphorus donor and that for a Cl⁻

(22) Brown, R. G.; Chaudhari, R. V.; Davidson, J. M. *J. Chem. Soc., Dalton Trans.* **1977**, 176.

(23) Hoberg, H.; Gotor, V.; Mynott, R. *J. Organomet. Chem.* **1978**, 149, 1.

(24) Farnell, L.; Randall, E. W.; Rosenberg, E. *J. Chem. Soc. D* **1971**, 1078.

(25) von Matt, P.; Lloyd-Jones, G. C.; Minidis, A. B. E.; Pfaltz, A.; Macko, L.; Neuburger, M.; Zehnder, M.; Rügger, H.; Pregosin, P. S. *Helv. Chim. Acta* **1995**, 78, 265.

(26) Axelson, D. E.; Holloway, C. E. *J. Chem. Soc., Chem. Commun.* **1973**, 455.

or oxazoline nitrogen. The chemical shifts of the terminal allyl carbon trans to the P donors (δ 76.8, 76.9, and 79.3 for **7**–**9**, respectively) are not very different from that found for the bis-PPh₃ complex (78.9 ppm). It is interesting, and somewhat unexpected, that the allyl ¹³C chemical shifts for the PMe₃ and PEt₂Ph complexes (δ 69.7 and 71.6 ppm) are at relatively low frequency. Also noteworthy is that the terminal allyl carbon trans to the PPh₂ donor in the chiral ferrocene chelate JOSIPHOS, at 66.9 ppm, is not much different from that for the carbon trans to the S donor in either **7** or **9**, and we have discussed this separately.²¹

Catalysis. For completeness, we have used **10** as a catalyst in the allylic alkylation and allylic amination reactions with CH(CO₂Me)₂⁻ and NH₂CH₂Ph as nucleophiles to afford PhCH{CH(CO₂Me)₂}CH=CHPh and PhCH{NH₂CH₂Ph}CH=CHPh, respectively. Neither of these reactions gave substantial ee's. In CH₂Cl₂ solution, for the allylic alkylation at room temperature, we find a 93% conversion after 4 days and a ca. 22% ee. For the amination in THF solution at 70 °C after 1 day, we note ca. 86% conversion to product and an ee of ca. 5%. In a second run after 8 days, at room temperature, the chemical yield is 98% and the ee ca. 23%. As might be expected on the basis of the presence of substantial amounts of the rotational isomers **10a** and **10b** as well as the syn/anti isomers **10c** and **10d**, ligand **3** is not especially useful in either the allylic alkylation or allylic amination reactions.

Experimental Section

IR spectra were measured on a Perkin-Elmer 883 instrument. FAB mass spectra and microanalyses were performed in the analytical laboratories of the ETH Zürich. The chloride-bridged complexes were prepared as described in the literature.

The NMR experiments were carried out using a Bruker AMX 500 spectrometer on 0.02 mmol samples in CDCl₃. Resonances are given in δ units (ppm), and coupling constants are given in hertz. The frequencies: 500.13, 202.47, and 125.75 MHz were employed for ¹H, ¹³C, and ³¹P, respectively. Standard pulse sequences were employed for the ¹H 2D-NOESY,²⁷ ¹³C–¹H,²⁸ and ³¹P–¹H²⁹ correlation studies. The phase-sensitive NOESY experiments used mixing times of 0.8 s.

***o*-(Diphenylphosphino)benzyl Chloride.** *o*-(Diphenylphosphino)benzyl dimethylamine³⁰ (14.789 g, 0.046 mol) was dissolved in 25 mL of degassed benzene and then treated with 1.3 equiv of ethyl chloroformate (6.49 g, 0.060 mol). The solution was refluxed for 2 h and then the solvent distilled. Addition of a small amount of methanol with stirring afforded 7.57 g (53%) of a white precipitate which could be dried in vacuo; mp 84 °C. ¹H NMR (CDCl₃): 7.6–7.2 (m, 14H, arom H), 4.94 (d, *J* = 2.0, 2H, –CH₂Cl). ³¹P NMR (CDCl₃): –17.2. ¹³C NMR (CDCl₃): 142–128 (arom C), 44.3 (d, *J* = 29.4). EI-MS: *m/z* 309.0 (molecular ion – 1, 100%), 275.0 (2.5%). Anal. Calcd for C₁₉H₁₆PCl (310.76): C, 73.44; H, 5.19. Found: C, 73.35; H, 5.23.

***o*-(Diphenylphosphino)benzyl Ethyl Thioether (1).** A 3 mL portion of ethanethiol (2.52 g, 40.0 mmol) at ca. 0 °C was reacted with lithium (10 mg, 1.4 mmol). After the lithium

dissolved, *o*-(diphenylphosphino)benzyl chloride (164 mg, 0.53 mmol) was added with stirring. After 3 h the excess thiol was distilled into a cold trap, the residue was dissolved in ether, and the ethereal solution was washed three times with 10 mL of water saturated with NaCl. The ether extract was dried over MgSO₄ and then chromatographed through silica gel using dichloromethane as eluent (*R_f* 0.73). A total of 177.6 mg (89.7%) of the product as a pungent smelling oil was obtained. ¹H NMR (CDCl₃): 7.6–6.9 (14H, arom H), 4.05 (d, *J* = 1.7, 2H, PhCH₂), 2.48 (q, *J* = 7.4, 2H, CH₂CH₃), 1.22 (t, *J* = 7.4, 3H, CH₃). ³¹P NMR (CDCl₃): –16.9. ¹³C NMR (CDCl₃): 144–126 (arom C), 34.2 (d, *J* = 25.1, PCH₂), 25.6 (SCH₂), 14.4 (CH₃). EI-MS: *m/z* 307.1 (100%, M⁺ – C₂H₅). Anal. Calcd for C₂₁H₂₁PS (336.44): C, 74.97; H, 6.29. Found: C, 75.03; H, 6.48.

***o*-(Diphenylphosphino)benzyl Cyclohexyl Thioether (2).** A procedure similar to that described above for the ethyl ether was followed. From cyclohexanethiol (0.5 mL, 474 mg, 4.1 mmol), sodium (50 mg, 2.2 mmol), and (diphenylphosphino)benzyl chloride (200 mg, 0.64 mmol) a white suspension is obtained. Addition of 30 mL of water was followed by extraction with 3 × 50 mL of ether. Washing with 30 mL of a saturated NaCl solution was followed by drying of the ether layer over MgSO₄. The ether was distilled and the residue chromatographed over silica gel using hexane/ethyl acetate (97:3) (*R_f* 0.32). The product (250.4 mg, 99.6%) was obtained as a viscous oil. ¹H NMR (CDCl₃): 7.6–6.8 (14H, arom H), 4.02 (d, *J* = 2.0, 2H, PhCH₂), 1.70 (m, 1H), 2.0–1.0 (m, 10H). ³¹P NMR (CDCl₃): –15.8. ¹³C NMR (CDCl₃): 146–126 (m, arom C), 43.6, 33.6, 26.1, 25.9. EI-MS: *m/z* 389.2 (M⁺ – 1), 307.1 (M⁺ – cyclohexyl), 275.1 (M⁺ – cyclohexanethiolate). Anal. Calcd for C₂₆H₂₇PS (390.52): C, 76.89; H, 6.97. Found: C, 76.77; H, 6.82.

***exo*-8-((*o*-(Diphenylphosphino)benzyl)thio)borneol (3).** *exo*-8-Thioborneol (785.5 mg, 4.3 mmol) in 25 mL of THF was cooled to –60 °C. Sodium hydride (171.9, 1 equiv, 4.3 mmol) in oil was added, and the suspension was warmed slowly to 0 °C over 0.5 h. Addition of *o*-(diphenylphosphino)benzyl chloride (1550 mg, 5.0 mmol) was followed by stirring for 8 h. Concentration to ca. 20% of the volume, addition of ether, and washing with a saturated NaCl solution gave a crude product after separating and drying the ether phase over MgSO₄. Chromatography over silica gel using hexane/ethyl acetate (9:1) (*R_f* 0.37) afforded 863.4 mg (41.9%) of **3**, as a viscous oil which slowly solidified. [α]_D²⁰ = –43.4° (*c* = 8.8, in CHCl₃). ¹H NMR (CDCl₃): 7.6–6.9 (14H, arom H), 4.07 (d, 2H, *J* = 1.2) 3.78 (m, 1H), 2.77 (d, 1H, *J* = 11.0), 2.60 (d, 1H, *J* = 11.0), 2.48 (br, 1H), 1.8–0.9 (m, 7H), 1.04 (s, 3H), 0.81 (s, 3H). ³¹P NMR (CDCl₃): –16.0. ¹³C NMR (CDCl₃): 144–126 (arom C), 76.7, 52.2, 47.6, 45.1, 39.1, 36.8 (d, *J* = 24.2), 32.2, 30.9, 27.2, 20.7, 20.0. EI-MS: *m/z* 459.2 (M⁺ – 1), 307.1 (M⁺ – (borneol – 1)). Anal. Calcd for C₂₉H₃₃OPS·H₂O (478.62): C, 72.77; H, 7.37. Found: C, 72.72; H, 7.30.

[PdCl₂(*o*-(diphenylphosphino)benzyl) cyclohexyl thioether] (5). Compound **2** (28.0 mg, 0.072 mmol) and 18.6 mg (0.072 mmol) of PdCl₂(NCCCH₃)₂ were refluxed for 2 h in 2 mL of benzene. The yellow suspension was filtered and the solid washed with pentane and then dried to afford 38.2 mg (93.8%) of product. ¹H NMR (CD₂Cl₂): 7.6–6.7 (14H, arom H), 3.9–3.0 (m, 3H), 2.4–0.7 (m, 13H). ³¹P NMR (CD₂Cl₂): 25.4. IR (CsI pellet): 332 s, 293 (sh), 292 s cm⁻¹. FAB-MS: *m/z* 533.0 (M⁺ – Cl). Anal. Calcd for C₂₅H₂₇PSCl₂Pd (567.85): C, 52.88; H, 4.79. Found: C, 52.91; H, 4.75.

[PdCl₂(*o*-(Diphenylphosphino)benzyl ethyl thioether] (4). This synthesis followed that given for **5**. From *o*-(diphenylphosphino)benzyl ethyl thioether (19.5 mg, 0.058 mmol) and PdCl₂(NCCCH₃)₂ (15.0 mg, 0.058 mmol) a white suspension is obtained after refluxing in benzene for 1 h. After filtration and drying in vacuo there remains 27.8 mg (93.5%) of product. ¹H NMR (CD₂Cl₂): 7.8–6.7 (m, 14H, arom H), 3.75 (m, 1H), 3.42 (m, 1H), 3.07 (m, 1H), 2.78 (m, 1H), 1.28 (t, 3H, *J* = 7.3). ³¹P NMR (CD₂Cl₂): 26.2. ¹³C NMR (CD₂Cl₂): 136–

(27) Sklener, V.; Miyashiro, H.; Zon, G.; Miles, H. T.; Bax, A. *FEBS Lett.* **1986**, *208*, 94.

(28) Summers, M. F.; Marzilli, L. G.; Bax, A. *J. Am. Chem. Soc.* **1986**, *108*, 4285.

(29) Jeener, J.; Meier, G. H.; Bachmann, P.; Ernst, R. *J. Chem. Phys.* **1979**, *71*, 4545.

(30) Rauchfuss, T. B.; Patino, F. T.; Roundhill, M. *Inorg. Chem.* **1975**, *14*, 652.

127 (arom C), 33.9 ($J = 11.7$), 32.7, 13.6. IR (CsI pellet): 341, 287 (Pd-Cl) cm^{-1} . FAB-MS: m/z 476.9 ($M^+ - \text{Cl}$). Anal. Calcd for $\text{C}_{21}\text{H}_{21}\text{PSCl}_2\text{Pd}$ (513.76): C, 49.09; H, 4.12. Found: C, 46.06; H, 4.42.

[PdCl₂{*exo*-8-(*o*-(diphenylphosphino)benzyl)thio)borneol} (6). Ligand **3** (47.0 mg, 0.098 mmol) in 5 mL of benzene and PdCl₂(NCCH₃)₂ (25.4 mg, 0.098 mmol) were stirred for 3 h. The solid which resulted was filtered and washed with ether and pentane. Recrystallization from dichloromethane/ether afforded 30.9 mg (49.4%) of product **8**. ¹H NMR (CDCl₃): 7.9–7.4 (13H, arom H), 6.93 (m, 1H, arom H), 4.05 (m, 1H), 3.99 (m, 1H), 3.75 (m, 1H), 3.53 (m, 1H), 3.35 (m, 1H), 2.22 (m, 1H), 1.28 (m, 1H), 1.7–1.1 (m, 3H), 0.99 (s, 3H, CH₃), 0.69 (s, 3H, CH₃). ³¹P NMR (CDCl₃): 26.7. IR (CsI pellet): 322 (m, Pd-Cl), 277 (m, Pd-Cl) cm^{-1} . FAB-MS: 602.3 ($M^+ - \text{Cl}$). Anal. Calcd for $\text{C}_{29}\text{H}_{33}\text{OPSCl}_2\text{Pd}$ (637.95): C, 54.60; H, 5.21. Found: C, 54.64; H, 5.25.

[Pd(η^3 -C₃H₅)₂{*o*-(diphenylphosphino)benzyl cyclohexyl thioether}](CF₃SO₃) (8). [Pd(η^3 -C₃H₅)(μ -Cl)]₂ (12.4 mg, 0.034 mmol) in 2 mL of methanol was treated with silver triflate (17.8 mg, 0.069 mmol) in 2 mL of methanol. After 10 min the AgCl was filtered and the resulting solution treated with *o*-(diphenylphosphino)benzyl cyclohexyl thioether (26.9 mg, 0.069 mmol) in 0.5 mL of dichloromethane. After 1 h, the solvents were removed and the residue recrystallized from dichloromethane/ether to afford 32.8 mg (67.7%) of a white powder. ¹H NMR (CDCl₃): 7.6–6.8 (14H, arom H), 5.90 (h, 1H), 4.93 (m, 1H), 4.05 (m, 1H), 3.83 (s, broad, 3H), 3.73 (m, 1H), 3.46 (m, 1H), 2.81 (m, 1H), 2.00–1.20 (m, 11H). ³¹P NMR (CDCl₃): 17.7. ¹³C NMR (CDCl₃): 140–126 (arom C), 76.9 (d, $J = 26.8$ Hz), 69.9, 49.9, 34.3 (d, $J = 15.0$), 33.4, 33.2, 26.1, 25.0. FAB-MS: m/z 537.1 ($M^+ - \text{triflate}$). Anal. Calcd for $\text{C}_{29}\text{H}_{32}\text{O}_4\text{F}_3\text{PS}_2\text{Pd}$ (703.09): C, 49.50; H, 4.59. Found: C, 48.96; H, 4.76.

[Pd(η^3 -C₃H₅)₂{*o*-(diphenylphosphino)benzyl ethyl thioether}](CF₃SO₃) (7). This synthesis follows closely that shown above for **8**. From [Pd(η^3 -C₃H₅)(μ -Cl)]₂ (13.2 mg, 0.036 mmol) and silver triflate (18.6 mg, 0.072 mmol) in methanol followed by addition of **1** (23.9 mg, 0.072 mmol) in dichloromethane, one obtains after recrystallization from CH₂Cl₂/ether 34.4 mg (75.1%) of a white powder. ¹H NMR (CDCl₃): 7.9–6.7 (14H, arom H), 6.85 (1H), 4.91 (m, 1H), 3.99 (m, 1H), 3.9–3.6 (m, 3H), 3.35 (m, 1H), 3.0–2.7 (m, 2H), 1.31 (t, 1H, $J = 7.3$). ³¹P NMR (CDCl₃): 17.0. ¹³C NMR (CDCl₃): 138–124 (arom C), 122.6 ($J = 5.5$), 76.8 ($J = 26.5$), 69.5, 35.3 ($J = 14.6$), 32.2, 14.1. FAB-MS: m/z 483.1 ($M^+ - \text{triflate}$). Anal. Calcd for $\text{C}_{25}\text{H}_{25}\text{O}_3\text{F}_3\text{PS}_2\text{Pd}$ (631.99): C, 47.51; H, 3.99. Found: C, 47.28; H, 4.09.

[Pd(η^3 -C₃H₅)₂{*exo*-8-(*o*-(diphenylphosphino)benzyl)thio)borneol}](CF₃SO₃) (9). Complex **9** was prepared from [Pd(η^3 -C₃H₅)(μ -Cl)]₂ (31.9 mg, 0.087 mmol) in 3 mL of dichloromethane with silver triflate (45.0 mg, 0.175 mmol) in 3 mL of methanol. After 10 min the silver chloride was filtered and the filtrate treated with **3** (80.5 mg, 0.175 mmol). Stirring for 2 h, removal of the solvents, and recrystallization from dichloromethane/ether gave 132.3 mg (quantitative conversion) of the product **9**. The details of the NMR spectroscopy are given in the tables and in the text. FAB-MS: m/z 607 ($M^+ - \text{triflate}$). Anal. Calcd for $\text{C}_{33}\text{H}_{38}\text{O}_4\text{F}_3\text{PS}_2\text{Pd}$ (757.18): C, 52.34; H, 5.06. Found: C, 52.15; H, 5.22.

[Pd(1,3-diphenylallyl)(3)]BF₄ (10). Solid [(1,3-diphenylallyl)PdCl]₂ (60 mg, 0.09 mmol) was added to a solution of **3** (80 mg, 0.18 mmol) in CH₂Cl₂ (10 mL). A solution of AgBF₄ (35 mg, 0.18 mmol) in MeOH (5 mL) was then added. The mixture was stirred in the dark for 15 min and filtered over Celite. After the solvent was evaporated to ca. one-third of the total volume under a stream of nitrogen, diethyl ether/*n*-pentane (1/1, 30 mL) was added, causing precipitation of a yellow solid. A total of 120 mg (80% yield) of pure compound was obtained after recrystallization from CH₂Cl₂/diethyl ether/

n-pentane under a stream of nitrogen. FAB-MS: m/z 759.1 ($M^+ - \text{BF}_4$). Anal. Calcd for $\text{C}_{44}\text{H}_{46}\text{BOF}_4\text{PSPd}$ (847.08): C, 62.39; H, 5.47. Found: C, 62.06; H, 5.63.

Crystallography. Crystals of compound **9** were obtained by crystallization from dichloromethane/ether and are air-stable.

An Enraf-Nonius diffractometer was used for the unit cell and space group determination and for the data collection. Unit cell dimensions were obtained by a least-squares fit of the 2 θ values of 25 high-order reflections ($9.4 < \theta < 16.3^\circ$). Selected crystallographic and other relevant data are listed in Table 2.

Data were measured with variable scan speed to ensure constant statistical precision on the collected intensities. Three standard reflections were used to check the stability of the crystal and of the experimental conditions and measured every 1 h; no significant variation was detected. The orientation of the crystal was checked by measuring 3 reflections every 360 measurements.

Data were corrected for Lorentz and polarization factors and, empirically, for absorption³¹ (azimuthal (ψ) scans of four reflections having $\chi > 86^\circ$, $10.9 < \theta < 17.7^\circ$). The standard deviations on intensities were calculated in term of statistics alone, while those on F_o were calculated as reported in Table 2.

The structure was solved by Patterson and Fourier methods and refined by full-matrix least squares, using anisotropic displacement parameters for all atoms except the carbon atoms of the phenyl rings.

The contribution of the hydrogen atoms in their idealized positions ($C-H = 0.95 \text{ \AA}$, $B = 1.5[B(\text{carbon})] \text{ \AA}^2$) was taken into account but not refined.

The function minimized was $[\sum w(|F_o| - 1/k|F_c|)^2]$ with $w = [\sigma^2(F_o)]^{-1}$. No extinction correction was found to be necessary. The scattering factors used, corrected for the real and imaginary parts of the anomalous dispersion, were taken from the literature.³²

Upon convergence the final Fourier difference map showed no significant peaks. All calculations were carried out by using the Enraf-Nonius MOLEN crystallographic programs.³³ The handedness of the crystal was tested by refining the two enantiomorphs. The two sets of coordinates gave significantly different values for the agreement factors, based on the Hamilton test³⁴ ($R_w = 0.053$ and $R_w = 0.057$, respectively), thus establishing the absolute configuration of the molecule. Final atomic coordinates and equivalent thermal factors are given in Table 3.

Acknowledgment. P.S.P. thanks the Swiss National Science Foundation as well as the ETH for support and the Johnson-Matthey Research Foundation, Reading, England, for the loan of precious metals. A.A. thanks CNR for support. We also thank Dr. Pierluigi Barbaro, CNR, Florence, Italy, for preparing complex **10**.

Supporting Information Available: Figure giving the complete numbering scheme for the ORTEP drawing and calculated hydrogen positions (Table S1), anisotropic displacement parameters (Table S2), extended list of bond lengths and bond angles (Table S3), for **9** (11 pages). Ordering information is given on any current masthead page.

OM950064W

(31) North, A. C. T.; Philips, D. C.; Mathews, F. S. *Acta Crystallogr., Sect. A* **1968**, *A24*, 351.

(32) *International Tables for X-ray Crystallography*; Kynoch: Birmingham, England, 1974; Vol. IV.

(33) MOLEN, Enraf-Nonius Structure Determination Package; Enraf-Nonius: Delft, The Netherlands, 1990.

(34) Hamilton, W. C. *Acta Crystallogr.* **1965**, *13*, 502.

Functional Ruthenium(II) Allenylidene and Diynyl (Arene) Derivatives Formed by Activation of a Diyne via a Ru=C=C=C=CR₂ Intermediate

Daniel Péron,[†] Antonio Romero,[‡] and Pierre H. Dixneuf^{*,†}

Laboratoire de Chimie de Coordination Organique, URA CNRS 415, Campus de Beaulieu, Université de Rennes, 35042 Rennes, France, and Instituto de Quimica Fisica, Rocasolano, CSIC, Calle Serrano, 119, 28006 Madrid, Spain

Received February 8, 1994[®]

The activation of the diyne HC≡CC≡CC(OSiMe₃)Ph₂ (**II**) by a variety of RuCl₂(PR₃)(C₆Me₆) complexes **1** [PR₃ = PMe₃(**a**), PMe₂Ph (**b**), PMePh₂(**c**)], in the presence of the salt NaPF₆, selectively leads either to [L_nRu=C(OMe)CH=C=C=CR₂]PF₆ (**3**), [L_nRu=C=C=C(OR)CH=CR₂]PF₆ (**4–6**), [L_nRu=C=C=C(NR'₂)CH=CR₂]PF₆ (**7**), or [L_nRu=C≡CC≡CC(OSiMe₃)Ph₂]PF₆ (**8**), (L_nRu = RuCl(PR₃)(C₆Me₆)). In methanol **1a** leads to the buta-1,2,3-trienylcarbene complex **3** and the 3-alkenylallenylidene derivative **4a**. In ethanol and 2-propanol the complexes containing the 3-alkenylallenylidene moiety **5a–c** and **6a–c** are generated from **1a–c**. In the presence of HNPh₂ the derivatives [L_nRu=C=C=C(NPh₂)CH=CPh₂]PF₆ (**7a–c**) are obtained, whereas in the presence of HN^tPr₂, NEt₃ or, Bu^tNH₂ and NaPF₆ the diynyl derivatives **8a–c** are selectively produced. The protonation with HBF₄ of the diynyl complexes **8** in the presence of alcohol or diphenylamine is shown to displace the OSiMe₃ group and generate (3-alkenylallenylidene)ruthenium derivatives **6–7***. The activation of the diyne **II** by complexes **1** and NaPF₆ can be rationalized in terms of the formation of the electrophilic penta-1,2,3,4-tetraenylidene intermediate [(C₆Me₆)(PR₃)Cl Ru=C=C=C=C=CPh₂]⁺ (**2**), which is reactive toward weak nucleophiles.

Introduction

Organometallic compounds containing a π-conjugated unsaturated chain have recently attracted interest for their unusual intrinsic properties, such as cumulenyln-metal derivatives,¹ but also for liquid crystal² and nonlinear optic³ properties, such as [MC≡CC=C]_n polymers,⁴ or bis(alkynyl)platinum(II) derivatives,⁵ respectively. They also have potential for the synthesis of highly unsaturated molecules.^{6,7} Metal–vinylidene M=C=CR₂ and their metal–allenylidene M=C=C=CR₂ homologs constitute the simplest examples of unsaturated organometallics with a M=C bond. By contrast to the development of the chemistry of vinylidene complexes during the last decade,⁸ the allenylidene complexes have not been the source of many chemical discoveries, even if the first examples are known since

1976.⁹ However, metal allenylidenes have potential for the access to unusual molecules by ligand transfer to unsaturated molecules by analogy to the chemistry of M=C bond containing complexes,¹⁰ by polymerization of the unsaturated chain by analogy to that of alkenylcarbenes,¹¹ and by homogeneous catalysis. The first example of the involvement of a M=C=C=CR₂ species in catalysis has just been reported for coupling of allylic alcohols with propargylic alcohol derivatives in the presence of the RuCl(PPh₃)₂(C₅H₅) catalyst.¹²

Actually the use of metal allenylidenes is limited by the lack of general methods of preparation. They have been obtained *via* (i) transformation of alkenyl^{9a} and alkynylcarbene¹³ complexes, and (ii) coordination of a (C)₃ skeleton dianion, either [C≡CCR₂O]²⁻^{9b,14} or Li₂C₃Ph₂.¹⁵ The most straightforward method of access to

[†] Université de Rennes.

[‡] CSIC.

[®] Abstract published in *Advance ACS Abstracts*, June 1, 1995.

(1) (a) Stang, P. J.; Datta, A. K.; Dixit, V.; Wistiand, L. G. *Organometallics* **1989**, *8*, 1020. (b) Stang, P. J.; Datta, A. K. *Organometallics* **1989**, *8*, 1024. (c) Heeres, H. J.; Nijhoff, J.; Teuben, J. H.; Rogers, R. D. *Organometallics* **1993**, *12*, 2609.

(2) Giroud-Godquin, A. M.; Maitlis, P. M. *Angew. Chem., Int. Ed. Engl.* **1991**, *30*, 375.

(3) Chemla, D. S. *Non-Linear Optical. Properties of Organic Molecules and Crystals*; Zyss, J., Ed.; Academic: Orlando, FL, 1987; Vol. 1.

(4) Takahashi, S.; Takai, Y.; Morimoto, H.; Sonogashira, K. *J. Chem. Soc., Chem. Commun.* **1984**, 3.

(5) Sonogashira, K.; Fujikura, Y.; Yatake, T.; Toyoshima, N.; Takahashi, S.; Hagihara, N. *J. Organomet. Chem.* **1978**, *145*, 101.

(6) Wakatsuki, Y.; Yamazaki, H.; Kumegawa, N.; Satoh, T.; Satoh, J. Y. *J. Am. Chem. Soc.* **1991**, *113*, 9604.

(7) Iyoda, M.; Kuwatami, Y.; Oda, M. *J. Am. Chem. Soc.* **1989**, *111*, 3761.

(8) (a) Bruce, M. I.; Swincer, A. G. *Adv. Organomet. Chem.* **1983**, *22*, 59. (b) Bruce, M. I. *Chem. Rev.* **1991**, *91*, 197. (c) Antonova, A. B.; Ioganson, A. A. *Russ. Chem. Rev.* **1989**, *58* (7), 693.

(9) (a) Fischer, E. O.; Kalder, H.-J.; Franck, A.; Köhler, F. H.; Huttner, G. *Angew. Chem., Int. Ed. Engl.* **1976**, *15*, 623. (b) Berke, H. *Angew. Chem., Int. Ed. Engl.* **1976**, *15*, 624.

(10) (a) Murray, C. K.; Yang, D. C.; Wulff, W. D. *J. Am. Chem. Soc.* **1990**, *112*, 5660. (b) Harvey, D. F.; Brown, M. F. *J. Am. Chem. Soc.* **1990**, *112*, 7806. (c) Wiens, A.; Reissig, H.-U. *Chem. Ber.* **1991**, *124*, 957.

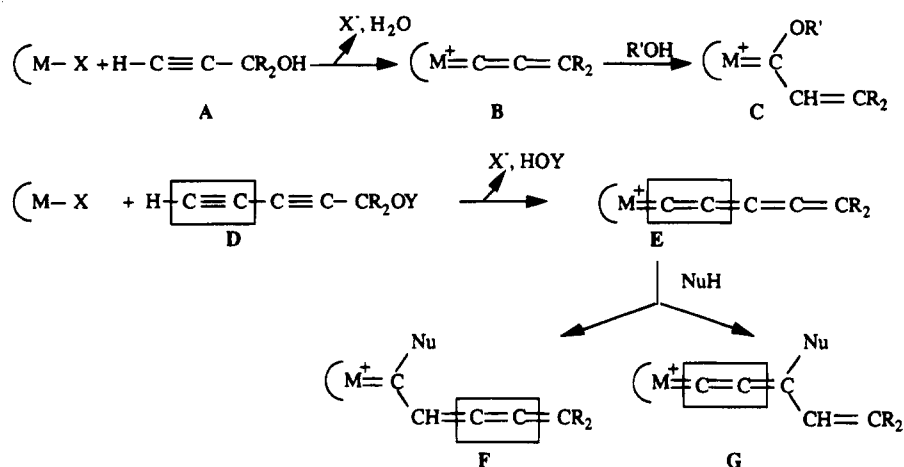
(11) Macomber, D. W.; Hung, M.-H.; Liang, M.; Verma, A. G.; Madhukar, P. *Macromolecules* **1988**, *21*, 1189.

(12) Trost, B. M.; Flygare, J. A. *J. Am. Chem. Soc.* **1992**, *114*, 5476.

(13) (a) Duetsch, M.; Stein, F.; Lackmann, R.; Pohl, E.; Herbst-Irmer, R.; de Meijere, A. *Chem. Ber.* **1992**, *125*, 2051. (b) Stein, F.; Duetsch, M.; Noltemeyer, M.; de Meijere, A. *Synlett* **1993**, 486. (c) Stein, F.; Duetsch, M.; Pohl, E.; Herbst-Irmer, R.; de Meijere, A. *Organometallics* **1993**, *12*, 2556. (d) Aumann, R. *Chem. Ber.* **1992**, *125*, 2773.

(14) (a) Berke, H. *Chem. Ber.* **1980**, *113*, 1370. (b) Berke, H.; Härter, P.; Huttner, G.; Seyerl, J. V. *J. Organomet. Chem.* **1981**, *219*, 317. (c) Berke, H.; Härter, P.; Huttner, G.; Zsolnai, L. *Z. Naturforsch.* **1981**, *36 b*, 929. (d) Berke, H.; Härter, P.; Huttner, G.; Zsolnai, L. *Chem. Ber.* **1982**, *115*, 695. (e) Berke, H.; Grössmann, U.; Huttner, G.; Zsolnai, L. *Chem. Ber.* **1984**, *117*, 3432. (f) Berke, H.; Härter, P.; Huttner, G.; Zsolnai, L. *Chem. Ber.* **1984**, *117*, 3423. (g) Berke, H.; Härter, P. *Angew. Chem., Int. Ed. Engl.* **1980**, *19*, 225. (h) Fischer, H.; Reindl, D.; Roth, G. *Z. Naturforsch.* **1984**, *49b*, 1207.

Scheme 1



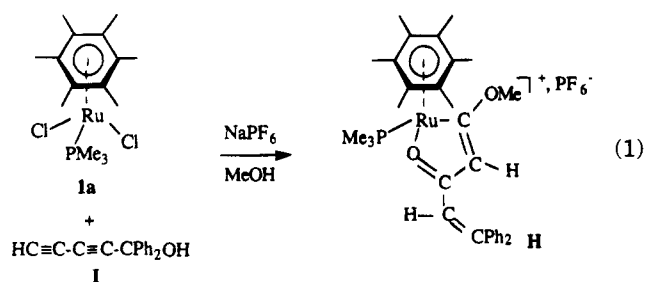
the allenylidene–metal intermediate appears to be the direct dehydration of propargyl alcohol derivatives **A** using ruthenium(II) complexes $\text{RuCl}_2(\text{PMe}_3)_2(\text{C}_5\text{H}_5)$,¹⁶ $\text{RuCl}_2(\text{PR}_3)(\text{arene})$,¹⁷ $\text{RuCl}_2(\text{Ph}_2\text{PCH}_2\text{PPh}_2)_2$,^{18a} $\text{RuCl}_2(\text{Ph}_2\text{PCH}_2\text{CH}_2\text{PPh}_2)_2$,^{18b} $\text{N}(\text{CH}_2\text{CH}_2\text{PPh}_2)_3\text{RuCl}_2$,^{18c} $\text{RuCl}(\text{PR}_3)_2(\eta^5\text{-C}_9\text{H}_7)$,¹⁹ and $\text{Ru}_2(\mu_2\text{-S}^i\text{Pr})_2(\text{C}_5\text{Me}_5)_2$.²⁰ They are expected to arise from the dehydration of 3-hydroxyvinylidene–metal intermediates^{16,21} as it has been shown with rhodium²² and group 6^{14h} derivatives.

The metallacumulenes **B** are thus obtained from propargyl alcohols and easily available ruthenium(II) precursors, and their stability depends on the electron richness of the ruthenium complexes (Scheme 1). They can be isolated with electron-rich ruthenium(II) complexes^{16a,18} whereas with the electrophilic precursors $\text{RuCl}_2(\text{PR}_3)(\text{arene})$ the intermediates **B** are very reactive toward weak nucleophiles and unsaturated carbenes **C** are produced¹⁷ (Scheme 1). This reaction sequence suggested a very simple strategy for the access to higher alkapolenylenide–metal intermediates. Similar ruthenium(II) precursors should be able to activate diyne derivatives of type **D** containing a leaving group OY to generate the novel penta-1,2,3,4-tetraenylidene–metal reactive species **E** able to produce new cumulenes **F** and functional allenylidenes **G** on addition of weak nucleophiles.

Following our preliminary results^{23,24} we report here our first general study based on this strategy of the activation of diyne compounds $\text{HC}\equiv\text{CC}\equiv\text{CCR}_2\text{OY}$ with $\text{RuCl}_2(\text{PR}_3)(\text{arene})$ complexes and we show a general route to new functional ruthenium allenylidene and diynyl complexes.

Results and Discussion

1. Synthesis of Ruthenium Buta-1,2,3-trienylcarbene Complex 3. The first attempt to activate a diyne with a ruthenium(II) complex was performed with (arene)ruthenium(II) derivative **1a** and the diyne $\text{HC}\equiv\text{CC}\equiv\text{CCPh}_2\text{OH}$ (**I**) in methanol and led to the unexpected formation of a (3-oxopentadienyl)ruthenium complex (**H**)²³ (eq 1). This transformation suggested the formation of a penta-1,2,3,4-tetraenylidene intermediate of type (**E**) *via* dehydration and successive addition of methanol at carbon C₁ and of the released water at carbon C₃.



In order to decrease the formation of water during the reaction, and thus generate a cumulene, the activation of the diyne $\text{HC}\equiv\text{CC}\equiv\text{CCPh}_2(\text{OSiMe}_3)$ (**II**) containing the OSiMe_3 leaving group was studied. The reaction of **II** with **1a**, in methanol and in the presence of a slight excess of NaPF_6 , led, at room temperature, to the formation of two compounds which were separated by fractional precipitation and identified as the first butatrienylcarbene **3** (40%) and 3-alkenylallenylidene–ruthenium **4** (11%) complexes, respectively (Scheme 2). The reaction required the presence of a noncoordinating anion-containing salt (NaPF_6) otherwise complex **1a** was

(23) Romero, A.; Vegas, A.; Dixneuf, P. H. *Angew. Chem., Int. Ed. Engl.* **1990**, *29*, 215.

(24) Romero, A.; Péron, D.; Dixneuf, P. H. *J. Chem. Soc., Chem. Commun.* **1990**, 1410.

(15) Binger, P.; Müller, P.; Wenz, R.; Mynott, R. *Angew. Chem., Int. Ed. Engl.* **1990**, *9*, 1037.

(16) (a) Selegue, J. P. *Organometallics* **1982**, *1*, 217. (b) Selegue, J. P.; Young, B. A.; Logan, S. L. *Organometallics* **1991**, *10*, 1972. (c) Selegue, J. P. *J. Am. Chem. Soc.* **1983**, *105*, 5921.

(17) (a) Le Bozec, H.; Ouzzine, K.; Dixneuf, P. H. *J. Chem. Soc., Chem. Commun.* **1989**, 219. (b) Devanne, D.; Dixneuf, P. H. *J. Chem. Soc., Chem. Commun.* **1990**, 641. (c) Pilette, D.; Ouzzine, K.; Le Bozec, H.; Dixneuf, P. H.; Rickard, C. E. F.; Roper, W. R. *Organometallics* **1992**, *11*, 809. (d) Le Bozec, H.; Pilette, D.; Dixneuf, P. H. *New J. Chem.* **1990**, *14*, 793.

(18) (a) Pirio, N.; Touchard, D.; Toupet, L.; Dixneuf, P. H. *J. Chem. Soc., Chem. Commun.* **1991**, 980. (b) Touchard, D.; Morice, C.; Cadierno, V.; Haquette, P.; Toupet, L.; Dixneuf, P. H. *J. Chem. Soc., Chem. Commun.* **1994**, 859. (c) Wolinska, A.; Touchard, D.; Dixneuf, P. H.; Romero, A. *J. Organomet. Chem.* **1991**, *420*, 217.

(19) (a) Cadierno, V.; Gamasa, M. P.; Gimeno, J.; Lastra, E. *J. Organomet. Chem.* **1994**, *474*, C27. (b) Cadierno, V.; Gamasa, M. P.; Gimeno, J.; Lastra, E.; Borge, J.; Garcia-Granda, S. *Organometallics* **1994**, *13*, 745.

(20) (a) Matsuzaka, H.; Koizumi, H.; Takagi, Y.; Nishio, M.; Hidai, M. *J. Am. Chem. Soc.* **1993**, *115*, 10396. (b) Matsuzaka, H.; Takagi, Y.; Hidai, M. *Organometallics* **1994**, *13*, 13.

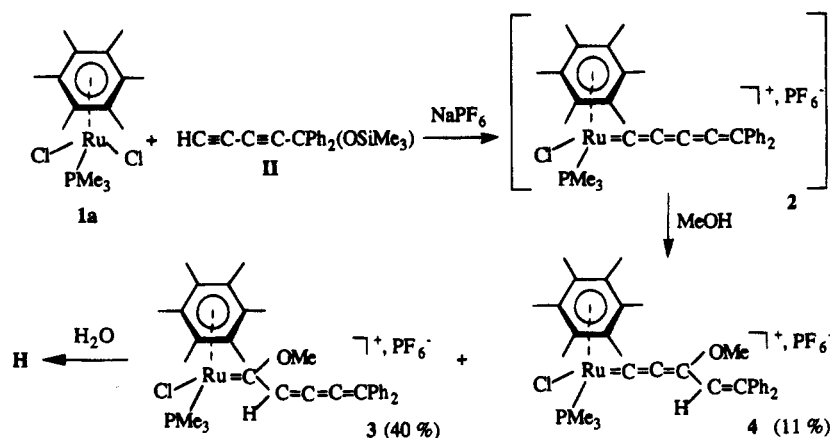
(21) Le Lagadec, R.; Roman, E.; Toupet, L.; Müller, U.; Dixneuf, P. H. *Organometallics* **1994**, *13*, 5030.

(22) (a) Werner, H.; Rappert, T. *Chem. Ber.* **1993**, *126*, 669. (b) Werner, H.; Rappert, T.; Wiedemann, R.; Wolf, J.; Mahr, N. *Organometallics* **1994**, *13*, 2721.

Table 1. ^{13}C NMR Data (δ , ppm) of the $[\text{Ru}=\text{C}_1=\text{C}_2=\text{C}_3(\text{YR}')\text{C}_4\text{H}=\text{C}_5\text{Ph}_2]$ Complexes 4–6

PR_3	compd	YR'	C_1 ($^2J_{\text{PC}}$, Hz)	C_2	C_4 ($^1J_{\text{CH}}$, Hz)	C_3, C_5
PMe_3	4	OMe	233.74 (28.4)	134.05	123.00 (162)	162.55, 161.43
PMe_3	5a	OEt	231.20 (28.6)	133.55	123.12 (162)	162.12, 161.13
PMe_2Ph	5b	OEt	229.93 (28.8)	133.80	123.02 (163)	162.28, 161.40
PMePh_2	5c	OEt	229.18 (30.3)	132.91	123.04 (163)	162.25, 161.55
PMe_3	6a	O ⁱ Pr	229.00 (30.5)	131.88	123.67 (163)	161.60, 161.12
PMe_2Ph	6b	O ⁱ Pr	227.99 (28.8)	132.13	123.63 (163)	161.72, 161.40
PMePh_2	6c	O ⁱ Pr	227.11 (30.0)	132.66	123.51 (163)	161.80, 161.71
PMe_3	7a	NPh_2	213.04 (33.0)	121.02	123.67 (165)	153.95, 152.10
PMe_2Ph	7b	NPh_2	210.37 (32.2)	120.68	123.22 (167)	154.92, 150.16
PMePh_2	7c	NPh_2	210.62 (32.0)	122.75	123.16 (166)	154.98, 150.85

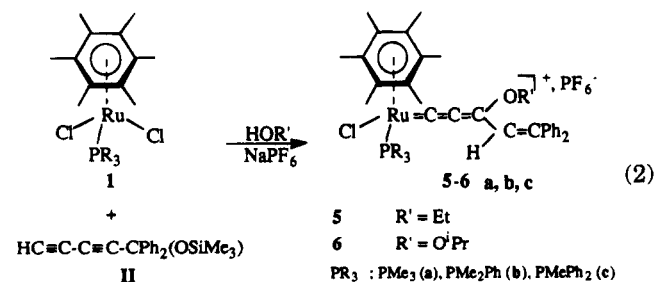
Scheme 2



recovered. The nature of **3** [IR (KBr): $\nu_{\text{C}=\text{C}=\text{C}}$: 2080 cm^{-1}] and **4** [$\nu_{\text{C}=\text{C}=\text{C}}$: 1980 cm^{-1}], established by NMR spectroscopy, suggested that the activation of **II** by **1a** proceeded *via* dissociation of the RuCl bond in a polar solvent, coordination of the diene *via* the terminal $\text{C}\equiv\text{CH}$ bond, and "HOSiMe₃" elimination to give the cumulene intermediate **2**, analogous to **E**. This cationic heterocumulene **2** is likely to be electrophilic and add methanol either at carbon C_1 and C_3 , to give complexes **3** and **4** after protonation at carbon C_2 or C_4 , respectively.

Whereas complex **4** is inert toward the addition of water, complex **3** reacts rapidly with water affording the corresponding complex of type **H**.²³ (eq 1, Scheme 2)

2. Preparation of Alkoxyalkenylallenylidene Derivatives 5 and 6. Complex **1a** and NaPF_6 also reacted with the diene **II** in the presence of the bulkier alcohols, ethanol and 2-propanol. Complexes **5a** (45%) and **6a** (57%) were isolated respectively (eq 2). The crude



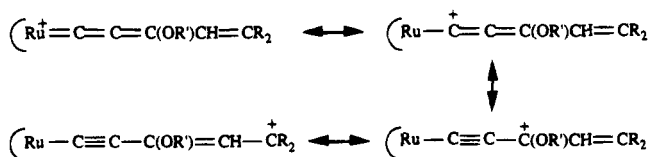
product of the reaction performed in ethanol showed an infrared absorption at 1995 cm^{-1} ($\nu_{\text{C}=\text{C}=\text{C}}$, **5a**) and at 2070 cm^{-1} . The latter absorption disappeared after one crystallization and was likely due to the presence of a small amount of the product analogous to **3** ($\nu_{\text{C}=\text{C}=\text{C}}$: 2080 cm^{-1}).

For solubility reasons the reaction of complexes **1b,c** with the diene **II** and NaPF_6 was performed in dichloromethane. After 3 h at room temperature, the red solution had turned into a dark blue one; then an excess of ethanol or 2-propanol was added and the mixture turned immediately violet. The violet allenylidene complexes **5b** (58%), **6b** (49%), **5c** (43%), and **6c** (36%) were isolated (eq 2). The formation of allenylidene complexes **5-6** is consistent with the addition of the alcohol (EtOH or ⁱPrOH) at carbon ($\text{C}(3)$) of the cumulene intermediate **2**. It shows that the steric hindrance of both the PR_3 ligand and alcohol disfavors the addition at carbon $\text{C}(1)$ of **2** and the formation of a complex analogous to **3**.

The $^{13}\text{C}\{^1\text{H}\}$ NMR spectrum of **3** shows a low-field doublet δ 295.13 ppm typical of a carbene ($\text{Ru}=\text{C}$) carbon nucleus.¹⁷ Four lines for the $\text{C}=\text{C}=\text{C}=\text{C}$ arrangement are observed, and the $^1J_{\text{CH}} = 172$ Hz ($\delta = 109.79$ ppm) and $^2J_{\text{CH}} = 6.8$ Hz ($\delta = 148.42$ ppm) are measured on the undecoupled ^{13}C NMR spectrum. By contrast the ^{13}C NMR spectra of the allenylidene complexes **4-6** show a higher field doublet for the $\text{Ru}=\text{C}$ carbon nucleus at $\delta \sim 230$ ppm ($^2J_{\text{PC}} \approx 30$ Hz) (Table 1). Whereas the $\text{C}(3)$ and $\text{C}(5)$ singlets are close to each other, the $\text{C}(4)$ signal is easily identified from the undecoupled ^{13}C spectrum at $\delta \sim 123$ ppm ($^1J_{\text{CH}} \sim 162$ Hz). Thus the chemical shift sequence is $\delta(\text{C}_1) > \delta(\text{C}_3, \text{C}_5) > \delta(\text{C}_2) > \delta(\text{C}_4)$. The most deshielded signals correspond to the electron-deficient carbon according to the canonical forms (Scheme 3). For the first reported allenylidene-metal complex $(\text{OC})_5\text{W}=\text{C}_1=\text{C}_2=\text{C}_3(\text{NMe}_2)-(\text{Ph})^{9a}$ the closely related sequence $\delta(\text{C}_1) > \delta(\text{C}_3) > \delta(\text{C}_2)$ was established on the basis of the $^nJ_{\text{WC}}$ coupling constants.²⁵

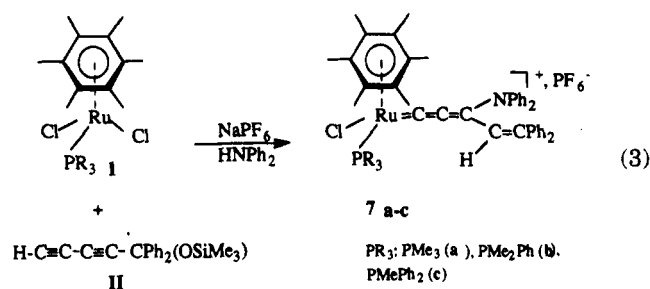
(25) $^nJ_{\text{WC}}$ (Hz): $^1J = 102.5$; $^2J = 26.9$; $^3J = 5$ Hz.^{9a}

Scheme 3



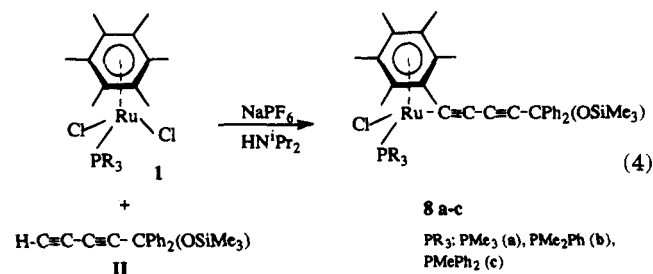
It is thus likely that the alkenylallenylidene complexes 4–6 are stabilized by the presence of an heteroatom electron-releasing group at the electrophilic carbon C(3) as are the Fischer type carbene complexes.

3. Preparation of Ruthenium 3-Amino 3-alkenylallenylidene Complexes 7a–c. As an amino group at C(3) is expected to better stabilize the alkenylallenylidene complexes than an alkoxy group, the addition of amines to the cumulene intermediate 2 was attempted. The diyne II was activated by complex 1a in the presence of NaPF₆ and the weak base HNPh₂ in dichloromethane. The brown complex 7a was formed (52%). Analogously from 1b,c the complexes 7b,c were isolated in 67% and 81% yield, respectively (eq 3). The complexes 7 show in ¹³C NMR a chemical shift sequence analogous to that of 5 and 6, but for C(1) a doublet is observed at slightly higher field than for the complexes 5–6 [δ = 213.04 (7a), 210.37 (7b), 210.62 (7c) ppm] (Table 1). This shift is consistent with the electron donating capability of the NPh₂ group.



It is noteworthy that complexes of type 7 could not be obtained with a more basic secondary amine as another process took place.

4. Preparation of Ruthenium Diynyl Complexes 8. The reaction of 1a with II and NaPF₆ but in the presence of HNⁱPr₂ (pK_a = 10.96), instead of HNPh₂ (pK_a = 0.79), led to the formation of the orange neutral ruthenium diynyl derivative 8a isolated in 57% yield (eq 4). Similarly, complexes 1b,c afforded the diynyl



complexes 8b (56%) and 8c (42%). Complexes 8 could also be obtained when another basic amine was used. Thus in the presence of the tertiary amine NEt₃ (pK_a =

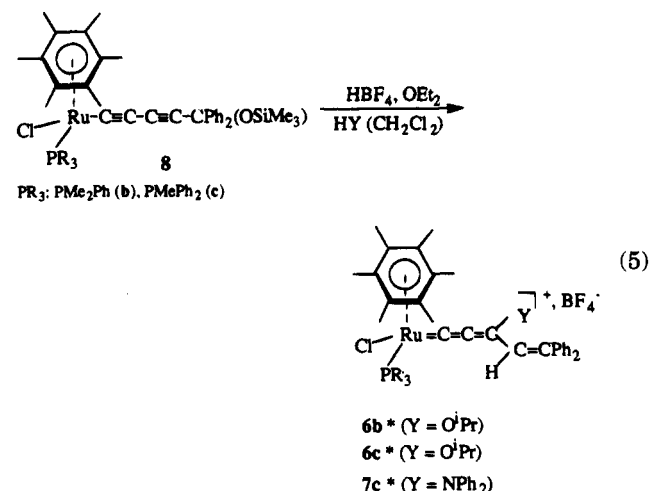
(26) Complex 7b was also obtained from 1b by activation of Me₃Si(C₄C(OSiMe₃)Ph₂): Péron, D.; Romero, A.; Dixneuf, P. H. *Gazz. Chim. Ital.* **1994**, *124*, 497.

11.01) complexes 8a (26%), 8b (49%), and 8c (59%) were obtained. The use of the primary amine ^tBuNH₂ (pK_a = 10.83) led to complexes 8a (20%), 8b (23%), and 8c (25%). HNⁱPr₂ appears to be the best compromise.

Thus, the reaction corresponds to the formal substitution of one chloride by the "acetylide" expected to be generated by deprotonation of the terminal alkyne II with a base. However, the same reaction performed in the absence of NaPF₆ does not lead to complexes 8 and the starting complex 1 is recovered (92% of 1a). Complexes 8a–c show in their infrared spectrum two absorptions at ν ~2185 and ~2025 cm⁻¹ typical of C≡C bonds. The ¹H NMR spectrum shows the retention of the OSiMe₃ group, and in ¹³C NMR the RuC₁C₂ chemical shifts [8a (δ , ppm): C₁, 121.12 (²J_{PC} = 39.5 Hz); C₂, 78.28 (³J_{PC} = 3.9 Hz)] are quite consistent with a RuC₁≡C₂ arrangement.

An X-ray diffraction study of a single crystal of 8a was undertaken. It established that the molecular structure of 8a contains an almost linear RuC≡CC≡CC-(OSiMe₃)Ph₂ arrangement.²⁴ However, the quality of the crystal structure (R = 0.076) does not allow significant discussion of the influence of the replacement of the (HC≡C) H atom of II by the Ru(Cl)(PMe₃)(C₆Me₆) moiety.^{24,27}

5. Synthesis of Alkenylallenylidenes from Ruthenium Diynyl Complexes 8. The facile displacement of a leaving group attached at the C₃ carbon of an alkynyl–metal complex is a well-known process, and for instance, the cationic allenylidenes [Mn=C=C=CPh₂-(CO)₂(C₅H₄Me)]⁺²⁹ or [Ru=C=C=CAr₂(Cl)(Ph₂PCH₂-PPh₂)₂]⁺¹⁸ were prepared by elimination of the OMe group from the corresponding MC≡CCR₂OMe moiety with an acid and Ph₃C⁺PF₆⁻, respectively. Complexes 8b,c, in dichloromethane and an excess of 2-propanol, were treated with HBF₄·OEt₂. Dark blue complexes 6b*,c* formed immediately and were isolated in 46% and 42% yield, respectively (eq 5). Complex 8c, in the



presence of HNPh₂, on protonation with HBF₄·OEt₂

(27) From the X-ray structure of 8a,²⁴ the distances (Å) Ru–C₁ [1.93(3)], C₁–C₂ [1.26(4)], C₂–C₃ [1.40(5)], C₃–C₄ [1.13(6)], C₄–C₅ [1.53(6)] of the RuC₁C₂C₃C₄C₅(OSiMe₃)Ph₂ moiety can be compared with those of *trans*-Ru(C₁≡C₂C₃≡C₄H)₂(CO)₂(PEt₃)₂:²⁸ Ru–C₁, 2.078(2); C₁–C₂, 1.194(2); C₂–C₃, 1.386(3); C₃–C₄, 1.196(3).

(28) Sun, Y.; Taylor, N. J.; Carty, A. J. *J. Organomet. Chem.* **1992**, *423*, C43; *Organometallics* **1992**, *11*, 4293.

(29) Berke, H.; Huttner, G.; Seyerl, J. v. *Z. Naturforsch.* **1981**, *36b*, 1277.

Half of the solvent was evaporated, and 0.38 g of a red-violet solid was obtained by filtration on a frit. Its infrared spectrum showed two intense absorptions at 2080 and 1980 cm^{-1} . The product was dissolved in 20 mL of dichloromethane, 10 mL of diethyl ether was first added, and 0.22 g of orange crystals of **3** (40%) (2080 cm^{-1}) was obtained. Further addition of ether led to the crystallization of the deep red crystals of **4** (0.06 g, 11%) (1980 cm^{-1}).

[Ru(C(OMe)CH=C=C=CPh₂)(PMe₃)(Cl)(η^6 -C₆Me₆)]PF₆ (3**). IR (KBr): 2080 (s, $\nu_{\text{C}=\text{C}}$), 855 (vs, $\nu_{\text{P}-\text{F}}$) cm^{-1} . ¹H NMR (CD₂Cl₂, 297 K, 300.133 MHz) (δ , ppm): 7.69–7.47 (m, 10 H, Ph), 7.29 (s, 1 H, =CH), 4.51 (s, 3 H, OMe), 2.06 (d, ²J_{(P,H)}} = 0.7 Hz, 18 H, C₆Me₆), 1.40 (d, ²J_{(P,H)}} = 10.6 Hz, 9 H, PMe₃). ³¹P{¹H} NMR (CD₂Cl₂, 297 K, 121.496 MHz) (δ , ppm): 10.54 (s, PMe₃), -143.45 (sept, PF₆⁻). ¹³C{¹H} NMR (CD₂Cl₂, 297 K, 75.469 MHz) (δ , ppm): 295.13 (d, ²J_{(P,C)}} = 21.2 Hz, Ru=C), 166.88, 148.83, (s, C=C=C), 148.42 (s, CH=C), ²J_{CH} = 6.8 Hz), 109.79 (s, HC=), (¹J_{(C,H)}} = 172 Hz), 106.47 (s, C₆Me₆), 67.43 (s, OMe), 16.41 (s, C₆Me₆), 16.05 (d, ¹J_{(P,C)}} = 34.6, PMe₃). Anal. Calcd (found) for C₃₃H₄₁ClOP₂F₆Ru·1/2CH₂Cl₂: C, 49.76 (49.64); H, 5.24 (5.21); Cl, 8.76 (7.89).**

[Ru(C=C=C(OMe)HC=CPh₂)(Cl)(PMe₃)(η^6 -C₆Me₆)]PF₆ (4**). IR (KBr): 1982 (s, $\nu_{\text{C}=\text{C}}$), 855 (vs, $\nu_{\text{P}-\text{F}}$) cm^{-1} . ¹H NMR (CD₂Cl₂, 297 K, 300.133 MHz) (δ , ppm): 7.45–7.23 (m, 10 H, Ph), 6.73 (s, 1 H, =CH), 3.94 (s, 3 H, OMe), 2.13 (s, 18 H, C₆Me₆), 1.54 (d, 9 H, ²J_{(P,H)}} = 11 Hz, PMe₃). ³¹P{¹H} NMR (CD₂Cl₂, 297 K, 121.496 MHz) (δ , ppm): 12.14 (s, PMe₃), -143.45 (sept, PF₆⁻). ¹³C{¹H} NMR (CD₂Cl₂, 297 K, 75.469 MHz) (δ , ppm): 233.74 (d, ²J_{(P,C)}} = 28.4 Hz, Ru=C), 162.55, 161.43 (s, C=C=C), -CPh₂), 141.02, 139.26 (s, C₆Me₆), 134.05 (s, C=C=C), 123.00 (s, =CH), ¹J_{(C,H)}} = 162 Hz), 109.78 (s, C₆Me₆), 61.85 (s, OMe), 16.80 (s, C₆Me₆), 16.77 (d, ¹J_{(P,C)}} = 36.9 Hz, PMe₃).**

Preparation of Complexes 5a and 6a. A 1 mmol (0.41 g) amount of complex **1a** and of NaPF₆ in 20 mL of dry alcohol (ethanol or 2-propanol) were stirred at room temperature, and then compound **II** (3 mmol) was introduced with a syringe. The solution turned rapidly from red to violet, and a violet product progressively precipitated. After 3 h of stirring, half of the solvent was evaporated and the violet complex was obtained by filtration on a frit. The product was dissolved in 20 mL of dichloromethane, 20 mL of ether was added, and the mixture was kept at room temperature for 2 days. Violet crystals of compounds **5a** and **6a** were formed and isolated by removal of the supernatant through a filter paper tipped cannula.

[Ru(C=C=C(OEt)HC=CPh₂)(Cl)(PMe₃)(η^6 -C₆Me₆)]PF₆ (5a**). From 0.41 g (1 mmol) of **1a**, 0.18 g (1 mmol) of NaPF₆, 20 mL of ethanol, and 3 mmol of compound **II**, complex **5a** was obtained in 45% yield (0.35 g). IR (KBr): 1995 (s, $\nu_{\text{C}=\text{C}}$), 855 (vs, $\nu_{\text{P}-\text{F}}$) cm^{-1} . ¹H NMR (CD₂Cl₂, 297 K, 300.134 MHz) (δ , ppm): 7.48–7.32 (m, 8 H, Ph), 7.23–7.20 (m, 2 H, Ph), 6.74 (s, 1 H, =CH), 4.33 (m, ³J_{(H,H)}} = 7.1 Hz, 2 H, CH₂), 2.14 (s, 18 H, C₆Me₆), 1.58 (d, ²J_{(P,H)}} = 10.1 Hz, 9 H, PMe₃), 0.94 (t, ³J_{(H,H)}} = 7.1 Hz, 3 H, CH₂Me). ³¹P{¹H} NMR (CD₂Cl₂, 297 K, 121.496 MHz) (δ , ppm): 12.39 (s, PMe₃), -143.49 (sept, PF₆⁻). ¹³C{¹H} NMR (CD₂Cl₂, 297 K, 75.469 MHz) (δ , ppm): 231.20 (d, ²J_{(P,C)}} = 28.6 Hz, Ru=C), 162.12, 161.13, (s, C=C=C, -CPh₂), 140.67, 139.49 (s, C₆Me₆), 123.12 (s, CH=), ¹J_{(C,H)}} = 162 Hz), 109.60 (d, ²J_{(P,C)}} = 2 Hz, C₆Me₆), 71.88 (s, CH₂), 16.81 (s, C₆Me₆), 16.79 (d, ¹J_{(P,C)}} = 36.9 Hz, PMe₃), 13.71 (s, CH₂Me). Anal. Calcd (found) for C₃₄H₄₃ClF₆OP₂Ru: C, 52.34 (52.24); H, 5.55 (5.56).**

[Ru(C=C=C(OⁱPr)CH=CPh₂)(Cl)(PMe₃)(η^6 -C₆Me₆)]PF₆ (6a**). From 0.41 g (1 mmol) of **1a**, 0.18 g (1 mmol) of NaPF₆, 20 mL of 2-propanol, and 3 mmol of compound **2**, the violet complex **6a** was obtained in 57% yield (0.45 g). IR (KBr): 1996 (vs, $\nu_{\text{C}=\text{C}}$), 840 (vs, $\nu_{\text{P}-\text{F}}$) cm^{-1} . ¹H NMR (CD₂Cl₂, 297 K, 300.134 MHz) (δ , ppm): 7.49–7.32 (m, 8 H, Ph), 7.21–7.18 (m, 2 H, Ph), 6.77 (s, 1 H, =CH), 5.21 (sept, 1 H, ³J_{(H,H)}} = 6.2 Hz, OCHMe₂), 2.15 (s, 18 H, C₆Me₆), 1.55 (d, ²J_{(P,H)}} = 11 Hz, 9 H, PMe₃), 1.04 (d, ³J_{(H,H)}} = 6.2 Hz, 6 H, OCHMe₂).**

³¹P{¹H} NMR (CD₂Cl₂, 297 K, 121.496 MHz) (δ , ppm): 12.47 (s, PMe₃), -143.46 (sept, PF₆⁻). ¹³C{¹H} NMR (CD₂Cl₂, 297 K, 75.469 MHz) (δ , ppm): 229.00 (d, ²J_{(P,C)}} = 30.5 Hz, Ru=C), 161.60, 161.12 (s, C=C=C, -CPh₂), 140.50, 139.55 (s, C₆Me₆), 131.88 (s, C=C=C), 123.67 (s, CH=), ¹J_{(C,H)}} = 163 Hz), 109.38 (d, ²J_{(P,C)}} = 2.3 Hz, C₆Me₆), 80.69 (s, OCHMe₂), 21.60 (s, OCHMe₂), 21.45 (s, OCHMe₂), 16.85 (d, ¹J_{(P,C)}} = 36.6 Hz, PMe₃), 16.81 (s, C₆Me₆). Anal. Calcd (found) for C₃₅H₄₅ClF₆OP₂Ru·1/2CH₂Cl₂: C, 50.96 (50.86); H, 5.54 (5.48).

Preparation of Complexes 5b,c, and 6b,c. In a Schlenk tube were successively introduced **1b** or **1c**, NaPF₆, 15 mL of dry dichloromethane, and an excess of diyne **II** (4–5 equiv). The reaction mixture was stirred at room temperature for 3 h and turned from orange-red to deep blue. On addition of the alcohol (ethanol or 2-propanol) the solution became violet. After 2 h of stirring the solution was filtered and transferred with a cannula. The solvents were removed under vacuum, and 15 mL of CH₂Cl₂, 30 mL of diethyl ether, and 30 mL of *n*-pentane were successively added. After 24 h at room temperature the complexes **5** or **6** precipitated. The complexes were obtained by removing the supernatant solution with a cannula, washing with diethyl ether, and drying under vacuum.

[Ru(C=C=C(OEt)CH=CPh₂)(Cl)(PMe₂Ph)(η^6 -C₆Me₆)]PF₆ (5b**). From 0.24 g (0.51 mmol) of **1b**, 0.11 g (0.65 mmol) of NaPF₆, 2 mmol of **II**, and 0.3 mL of ethanol, complex **5b** was obtained in 58% yield (0.25 g). IR (KBr): 1977 (s, $\nu_{\text{C}=\text{C}}$), 840 (vs, $\nu_{\text{P}-\text{F}}$) cm^{-1} . ¹H NMR (CDCl₃, 297 K, 300.134 MHz) (δ , ppm): 7.60–6.95 (m, 15 H, Ph), 6.80 (s, 1 H, CH=), 4.38 (ABX₃, ²J_{(H,H)}} = 22.5 Hz, ³J_{(H,H)}} = 7.1 Hz, 2 H, OCH₂), 1.86 (s, 18 H, C₆Me₆), 1.76 (d, ²J_{(P,H)}} = 10.6 Hz, 6H, PMe₂), 0.94 (t, ³J_{(H,H)}} = 7.1 Hz, 3 H, CH₂Me). ³¹P{¹H} NMR (CDCl₃, 297 K, 121.496 MHz) (δ , ppm): 19.80 (s, PMe₂Ph), -143.94 (sept, PF₆⁻). ¹³C{¹H} NMR (CD₂Cl₂, 297 K, 75.469 MHz) (δ , ppm): 229.93 (d, ²J_{(P,C)}} = 28.8 Hz, Ru=C), 162.28, 161.40 (s, C=C=C, -CPh₂), 140.57, 139.47 (s, C₆Me₆), 133.88 (s, C=C=C), 123.02 (s, CH=), (¹J_{(C,H)}} = 162.7 Hz), 109.84 (s, C₆Me₆), 72.01 (s, OCH₂), 16.09 (s, C₆Me₆), 13.71 (s, OCH₂CH₃). Anal. Calcd (found) for C₃₉H₄₅ClF₆OP₂Ru: C, 55.62 (55.80); H, 5.38 (5.39).**

[Ru(C=C=C(OEt)CH=CPh₂)(Cl)(PMePh₂)(η^6 -C₆Me₆)]PF₆ (5c**). From 0.25 g (0.45 mmol) of **1c**, 0.11 g (0.65 mmol) of NaPF₆, 2 mmol of **II** and 0.8 mL of ethanol, complex **5c** was obtained in 43% yield (0.185 g). IR (KBr): 1978 (s, $\nu_{\text{C}=\text{C}}$), 839 (vs, $\nu_{\text{P}-\text{F}}$) cm^{-1} . ¹H NMR (CD₂Cl₂, 297 K, 300.134 MHz) (δ , ppm): 7.56–7.34 (m, 14 H, Ph), 7.19–7.15 (m, 6 H, Ph), 6.40 (s, 1 H, CH=), 4.15 (ABX₃, ²J_{(H,H)}} = 22.5 Hz, ³J_{(H,H)}} = 7.1 Hz, 2 H, OCH₂), 2.14 (d, ²J_{(P,H)}} = 10.7 Hz, 3 H, PMe), 1.86 (s, 18 H, C₆Me₆), 0.80 (t, ³J_{(H,H)}} = 7.1 Hz, 3 H, CH₂Me). ³¹P{¹H} NMR (CD₂Cl₂, 297 K, 121.496 MHz) (δ , ppm): 33.22 (s, PMePh₂), -143.80 (sept, PF₆⁻). ¹³C{¹H} NMR (CD₂Cl₂, 297 K, 75.469 MHz) (δ , ppm): 229.18 (d, ²J_{(P,C)}} = 30.3 Hz, Ru=C), 162.25, 161.55 (s, C=C=C, -CPh₂), 140.37, 139.31 (s, C₆Me₆), 132.91 (s, C=C=C), 123.04 (s, CH=), ¹J_{(C,H)}} = 163 Hz), 110.28 (s, C₆Me₆), 71.87 (s, OCH₂), 17.81 (d, ¹J_{(P,C)}} = 39.1 Hz, PMePh₂), 16.11 (s, C₆Me₆), 13.57 (s, CH₂Me). Anal. Calcd (found) for C₄₄H₄₅ClF₆OP₂Ru·0.25 CH₂Cl₂: C, 57.42 (57.06); H, 5.17 (5.28).**

[Ru(C=C=C(OⁱPr)CH=CPh₂)(Cl)(PMe₂Ph)(η^6 -C₆Me₆)]PF₆ (6b**). From 0.24 g (0.45 mmol) of **1b**, 0.11 g (0.65 mmol) of NaPF₆, 2 mmol of **II**, and 0.3 mL of 2-propanol, complex **6b** was obtained in 49% yield (0.21 g). IR (KBr): 1975 (s, $\nu_{\text{C}=\text{C}}$), 838 (vs, $\nu_{\text{P}-\text{F}}$) cm^{-1} . ¹H NMR (CD₂Cl₂, 297 K, 300.134 MHz) (δ , ppm): 7.67–7.56 (m, 3 H, Ph), 7.51–7.21 (m, 12 H, Ph), 6.85 (s, 1 H, CH=), 5.30–5.23 (m, 1 H, OCHMe₂), 1.88 (s, 18 H, C₆Me₆), 1.82 (d, ²J_{(P,H)}} = 9.2 Hz, 3 H, PMe), 1.75 (d, ²J_{(P,H)}} = 10 Hz, 3 H, PMe), 1.08 (d, ³J_{(H,H)}} = 5.7 Hz, 3 H, OCHMe₂), 1.06 (d, ³J_{(H,H)}} = 5.8 Hz, 3 H, OCHMe₂). ³¹P{¹H} NMR (CD₂Cl₂, 297 K, 121.496 MHz) (δ , ppm): 20.10 (s, PMe₂Ph), -143.93 (sept, PF₆⁻). ¹³C{¹H} NMR (CD₂Cl₂, 297 K, 75.469 MHz) (δ , ppm): 227.99 (d, ²J_{(P,C)}} = 28.8 Hz, Ru=C), 161.72, 161.40 (s, C=C=C, -CPh₂), 132.13 (s, C=C=C), 123.63 (s, CH=), ¹J_{(C,H)}} = 163 Hz), 109.64 (d, ²J_{(P,C)}} = 2.3 Hz, C₆Me₆), 80.90 (s, OCHMe₂), 21.69, 21.49 (s, OCHMe₂), 17.20 (d, ¹J_{(P,C)}} = 41.4 Hz, PMe), 16.13 (s, C₆Me₆), 13.35 (d, ¹J_{(P,C)}} = 38.1 Hz, PMe). Anal.**

Calcd (found) for $C_{40}H_{47}ClF_6OP_2Ru$: C, 56.11 (56.21); H, 5.53 (5.37); Cl, 4.14 (4.51).

[Ru(C=C=C(OPr)CH=CPh₂)(Cl)(PMePh₂)(η^6 -C₆Me₆)]PF₆ (6c). From 0.24 g (0.45 mmol) of **1c**, 0.11 g (0.65 mmol) of NaPF₆, 2 mmol of **II**, and 0.2 mL of 2-propanol, complex **6c** was obtained in 36% yield (0.15 g). IR (KBr): 1978 (s, ν_{C-C}), 839 (vs, ν_{P-F}) cm^{-1} . ¹H NMR (CD₂Cl₂, 297 K, 300.134 MHz) (δ , ppm): 7.54–7.10 (m, 20 H, Ph), 6.50 (s, 1 H, CH=), 4.96 (sept, ³J_{(H,H)} = 6.2 Hz, 1 H, OCHMe₂), 2.05 (d, ²J_{(P,H)} = 10.6 Hz, 3 H, PMe), 1.86 (d, ⁴J_{(P,H)} = 0.7 Hz, 18 H, C₆Me₆), 0.94 (d, ³J_{(H,H)} = 6.2 Hz, 3 H, OCHMe), 0.78 (d, ³J_{(H,H)} = 6.2 Hz, 3 H, OCHMe). ³¹P{¹H} NMR (CD₂Cl₂, 297 K, 121.496 MHz) (δ , ppm): 34.06 (s, PMe₃), -143.51 (sept, PF₆⁻). ¹³C{¹H} NMR (CD₂Cl₂, 297 K, 75.469 MHz) (δ , ppm): 227.11 (d, ²J_{(P,C)} = 30 Hz, Ru=C), 161.80, 161.71 (s, C=C=C, =CPh₂), 140.23, 139.40 (s, C₁ Ph), 133.50 (s, C=C=C), 123.51 (s, HC=, ¹J_{(C,H)} = 163.1 Hz), 110.09 (d, ²J_{(P,C)} = 2.5 Hz, C₆Me₆), 80.97 (s, OCHMe₂), 21.51 (s, OCHMe), 21.33 (s, OCHMe), 18.06 (d, ¹J_{(P,C)} = 39.4 Hz, PMe), 16.11 (s, C₆Me₆). Anal. Calcd (found) for C₄₅H₄₉ClF₆OP₂Ru: C, 58.86 (58.77); H, 5.38 (5.31); Cl, 3.86 (3.94).}}}}}}}}}

Preparation of Complexes 7a-c. [Ru(C=C=C(NPh₂)-HC=CPh₂)(Cl)(PMe₃)(η^6 -C₆Me₆)]PF₆ (7a). A 0.6 mmol (0.25 g) amount of complex **1a** and 0.65 mmol (0.11 g) of NaPF₆, 15 mL of dry CH₂Cl₂, and 0.61 mmol of **II** were successively introduced in a Schlenk tube. The mixture was stirred at room temperature and turned rapidly from red to blue. After 1 h of stirring, 0.65 mmol of diphenylamine in 2 mL of dichloromethane was added and the mixture became dark red. After 1 h the solvent was evaporated and the complex was dissolved in 15 mL of dichloromethane and filtered through a filter paper tipped cannula. A 30 mL volume of ether and 30 mL of *n*-pentane were added. The red complex precipitated at room temperature and was isolated by removal of the supernatant solution with a cannula. Dark red complex **7a** was obtained in 53% yield (0.29 g). IR (KBr): 1996 (s, ν_{C-C}), 837 (vs, ν_{P-F}) cm^{-1} . ¹H NMR (CD₂Cl₂, 297 K, 300.133 MHz) (δ , ppm): 7.48–6.76 (m, 20 H, Ph), 6.46 (s, 1 H, =CH), 1.92 (s, 18 H, C₆Me₆), 1.29 (d, ²J_{(P,H)} = 10.8 Hz, PMe₃), ³¹P{¹H} NMR (CD₂Cl₂, 297 K, 121.496 MHz) (δ , ppm): 11.10 (s, PMe₃), -143.41 (sept, PF₆⁻). ¹³C{¹H} NMR (CD₂Cl₂, 297 K, 75.469 MHz) (δ , ppm): 213.04 (d, ²J_{(P,C)} = 33 Hz, Ru=C), 153.95, 152.10 (s, C=C=C, =CPh₂), 123.67 (s, HC=, ¹J_{(C,H)} = 165.5 Hz), 121.02 (s, C=C=C), 106.59 (d, ²J_{(P,C)} = 2.2 Hz, C₆Me₆), 16.51 (s, C₆Me₆), 16.41 (d, ¹J_{(P,C)} = 35.8 Hz, PMe₃). Anal. Calcd (found) for C₄₄H₄₈ClF₆NP₂Ru: C, 58.50 (58.48); H, 5.35 (5.47); N, 1.55 (1.42).}}}}}

[Ru(C=C=C(NPh₂)HC=CPh₂)(PMe₂Ph)(Cl)(η^6 -C₆Me₆)]PF₆ (7b). From 0.24 g (0.51 mmol) of **1b**, 0.11 g (0.65 mmol) of NaPF₆, and 4.3 mmol of **II**, stirring for 4 h, and addition of 0.09 g (0.59 mmol) of HNPh₂, stirring for 2 h, 0.33 g (67%) of **7b** was obtained. IR (KBr): 1996 cm^{-1} (s, ν_{C-C}), 840 (s, ν_{P-F}) cm^{-1} . ³¹P{¹H} NMR (CD₂Cl₂, 121.496 MHz, 297 K) (δ , ppm): 19.08 (s, PMe₂Ph), -143.60 (sept, ¹J_{(P,F)} = 710 Hz, PF₆⁻). ¹H NMR (CD₂Cl₂, 300.134 MHz, 297 K) (δ , ppm): 7.48–6.97 (m, 25 H, Ph), 6.55 (s, 1 H, CH=), 1.66 (s, C₆Me₆), 1.47 (d, ²J_{(P,H)} = 10.3 Hz, 6 H, PMe₂). ¹³C{¹H} NMR (CDCl₃, 75.472 MHz, 297 K) (δ , ppm): 210.37 (d, ²J_{(P,C)} = 32.2 Hz, Ru=C), 154.92, 150.16 (s, C=C=C, =CPh₂), 123.22 (¹J_{(C,H)} = 167 Hz, CH=), 120.68 (s, C=C=C), 106.49 (d, ²J_{(P,C)} = 2.8 Hz, C₆Me₆), 15.55 (s, C₆Me₆), 14.38 (d, ¹J_{(P,C)} = 38.6 Hz, PMe), 14.13 (d, ¹J_{(P,C)} = 39.6 Hz, PMe).}}}}}}}

[Ru(C=C=C(NPh₂)HC=CPh₂)(PMePh₂)(Cl)(η^6 -C₆Me₆)]PF₆ (7c). From 0.25 g (0.47 mmol) of **1c**, 0.11 g (0.65 mmol) of NaPF₆, and 2.6 mmol of **II**, stirring for 4 h, and addition of 0.10 g (0.59 mmol) of HNPh₂, stirring for 2 h, the complex **7c** was obtained in 81% yield (0.39 g). IR (KBr): 1995 (s, ν_{C-C}), 841 (vs, ν_{P-F}) cm^{-1} . ¹H NMR (CD₂Cl₂, 297 K, 300.133 MHz) (δ , ppm): 7.58–6.54 (m, 30 H, Ph), 6.33 (s, 1 H, CH=), 1.71 (d, ²J_{(P,H)} = 10.5 Hz, 3 H, PMe), 1.63 (s, 18 H, C₆Me₆). ³¹P{¹H} NMR (CD₂Cl₂, 297 K, 121.496 MHz) (δ , ppm): 35.46 (s, PMePh₂), -143.46 (sept, PF₆⁻). ¹³C{¹H} NMR (CD₂Cl₂, 297 K, 75.469 MHz) (δ , ppm): 210.62 (d, ²J_{(P,C)} = 32.2 Hz, Ru=C),}}

154.98, 150.86 (s, C=C=C, =CPh₂), 123.16 (s, HC=, ¹J_{(C,H)} = 166.4 Hz), 122.75 (s, C=C=C), 107.67 (s, C₆Me₆), 17.76 (d, ¹J_{(P,C)} = 39.7 Hz, PMe), 15.78 (s, C₆Me₆). Anal. Calcd (found) for C₅₄H₅₂ClF₆NP₂Ru: C, 62.07 (61.71); H, 5.10 (5.04); Cl, 3.45 (3.44).}}

Preparation of Complexes 8a-c. Method A. RuC=C-C=CC(OSiMe₃)Ph₂(Cl)(PMe₃)(η^6 -C₆Me₆) (8a). To a mixture of 0.70 mmol (0.29 g) of **1a** and 0.71 mmol (0.12 g) of NaPF₆ were successively added 15 mL of dichloromethane, an excess (3 equiv) of **II**, and 1.07 mmol of diisopropylamine. The solution was stirred at room temperature for 2 h and turned from brown to a red color. After evaporation of the solvent and amine, chromatography of the products on an 8 cm alumina column (eluent: dichloromethane, ether, *n*-pentane, 3:1:1) afforded complex **8a**. The pure orange complex was obtained by crystallization after evaporation of the eluent and dissolution in 10 mL of dichloromethane followed by addition of 20 mL of diethyl ether and 20 mL of *n*-pentane. The complex **8a** was obtained in 57% yield (0.27 g). IR (KBr): 2186 (s, $\nu_{C=C}$), 2035 (m, $\nu_{C=C}$) cm^{-1} . ¹H NMR (CD₂Cl₂, 297 K, 300.134 MHz) (δ , ppm): 7.56–7.16 (m, 10 H, Ph), 2.05 (s, 18 H, C₆Me₆), 1.45 (d, ²J_{(P,H)} = 10 Hz, 9 H, PMe₃), 0.12 (s, 9 H, OSiMe₃). ³¹P{¹H} NMR (CD₂Cl₂, 297 K, 121.496 MHz) (δ , ppm): 8.19 (s, PMe₃). ¹³C{¹H} NMR (CD₂Cl₂, 297 K, 75.469 MHz) (δ , ppm): 121.11 (d, ²J_{(P,C)} = 39.5 Hz, Ru-C), 101.02 (d, ²J_{(P,C)} = 2.8 Hz, C₆Me₆), 86.38, 78.26, 76.75 (s, C=CC=C), 68.31 (s, CPh₂), 16.54 (d, ¹J_{(P,C)} = 34 Hz, PMe₃), 16.37 (s, C₆Me₆), 1.65 (s, OSiMe₃). Anal. Calcd (found) for C₃₅H₄₆ClOPRuSi: C, 61.97 (61.70), H, 6.83 (6.70), Cl, 5.23 (5.38).}}}}

Ru-C=CC=CC(OSiMe₃)Ph₂(Cl)(PMe₂Ph)(η^6 -C₆Me₆) (8b). From 1.05 mmol (0.50 g) of **1b**, 1.31 mmol (0.22 g) of NaPF₆, 6 mmol of **II**, and 1.14 mmol of HNⁱPr₂, the complex **8b** was obtained in 56% yield (0.78 g). IR (KBr): 2185 (s, $\nu_{C=C}$), 2033 (m, $\nu_{C=C}$) cm^{-1} . ¹H NMR (CD₂Cl₂, 297 K, 300.134 MHz) (δ , ppm): 7.72–7.15 (m, 15 H, Ph), 1.77 (d, ⁴J_{(P,H)} = 0.7 Hz, 18 H, C₆Me₆), 1.71 (d, ²J_{(P,H)} = 10.8 Hz, 3 H, PMe), 1.70 (d, ²J_{(P,H)} = 10.4 Hz, 3 H, PMe), 0.14 (s, 9 H, OSiMe₃). ³¹P{¹H} NMR (CDCl₃, 297 K, 121.496 MHz) (δ , ppm): 16.73 (s, PMe₂Ph). ¹³C{¹H} NMR (CDCl₃, 297 K, 75.469 MHz) (δ , ppm): 121.11 (d, ²J_{(P,C)} = 39.5 Hz, Ru-C), 101.25 (d, ²J_{(P,C)} = 3.2 Hz, C₆Me₆), 78.40 (d, ³J_{(P,C)} = 3.6 Hz, C=CC=C), 86.73, 76.80 (s, C=CC=C), 68.25 (s, CPh₂), 15.68 (s, C₆Me₆), 15.21 (d, ¹J_{(P,C)} = 36.7 Hz, PMe), 14.38 (d, ¹J_{(P,C)} = 38.9 Hz, PMe), 1.73 (s, OSiMe₃). Anal. Calcd (found) for C₄₀H₄₈ClOPRuSi: C, 64.89 (64.64); H, 6.53 (6.58); Cl, 4.79 (5.07).}}}}}}}}

RuC=CC=CC(OSiMe₃)Ph₂(Cl)(PMePh₂)(η^6 -C₆Me₆) (8c). From 0.47 mmol (0.25 g) of **1c**, 0.65 mmol (0.11 g) of NaPF₆, 2.6 mmol of **II**, and 1.43 mmol of HNⁱPr₂, the complex **8c** was obtained in 42% yield (0.16 g). IR (KBr): 2189 (s, $\nu_{C=C}$), 2038 (m, $\nu_{C=C}$) cm^{-1} . ¹H NMR (CD₂Cl₂, 297 K, 300.134 MHz) (δ , ppm): 7.72–7.14 (m, 20 H, Ph), 1.99 (d, ²J_{(P,H)} = 10.4 Hz, 3 H, PMe), 1.76 (s, 18 H, C₆Me₆), 0.13 (s, 9 H, OSiMe₃). ³¹P{¹H} NMR (CD₂Cl₂, 297 K, 121.496 MHz) (δ , ppm): 31.70 (s, PMePh₂). ¹³C{¹H} NMR (CD₂Cl₂, 297 K, 75.469 MHz) (δ , ppm): 120.22 (d, ²J_{(P,C)} = 37.2 Hz, Ru-C), 102.14 (d, ²J_{(P,C)} = 3.2 Hz, C₆Me₆), 78.30 (d, ³J_{(P,C)} = 3 Hz, C=CC=C), 87.83, 76.68 (s, C=CC=C), 68.37 (s, CPh₂), 18.18 (d, ¹J_{(P,C)} = 39.5 Hz, PMe), 15.64 (s, C₆Me₆), 1.67 (s, OSiMe₃). Anal. Calcd (found) for C₄₅H₅₀ClOPRuSi: C, 67.35 (66.88); H, 6.28 (6.41); Cl, 4.42 (4.26).}}}}}

Method B. Preparation of Complexes 8a-c Using Triethylamine or *tert*-Butylamine. When diisopropylamine in method A was replaced by triethylamine or *tert*-butylamine, an other color instantaneously appeared and, after 2.5 h at room temperature, workup as in method A afforded **8a-c**. From 0.61 mmol (0.25 g) of **1a**, 0.65 mmol (0.11 g) of NaPF₆, 3 mmol of **II**, and 0.61 mmol (0.08 mL) of NEt₃, complex **8a** was obtained in 26% yield (0.11 g). From 0.53 mmol (0.25 g) of **1b**, 0.65 mmol (0.11 g) of NaPF₆, 3 mmol of **II**, and 0.53 mmol (0.07 mL) of NEt₃, the complex **8b** was obtained in 49% yield (0.19 g). From 0.47 mmol (0.25 g) of **1c**, 0.65 mmol (0.11 g) of NaPF₆, 3 mmol of **II**, and 0.47 mmol

(0.06 mL) of NEt_3 , the complex **8c** was obtained in 59% yield (0.22 g). From 0.61 mmol (0.25 g) of **1a**, 0.65 mmol (0.11 g) of NaPF_6 , 3 mmol of **II**, and 0.57 mmol (0.06 mL) of $^i\text{BuNH}_2$, the complex **8a** was obtained in 20% yield (0.08 g). From 0.53 mmol (0.25 g) of **1b**, 0.65 mmol (0.11 g) of NaPF_6 , 3 mmol of **II**, and 0.57 mmol (0.06 mL) of $^i\text{BuNH}_2$, the complex **8b** was obtained in 23% yield (0.09 g). From 0.47 mmol (0.25 g) of **1c**, 0.65 mmol (0.11 g) of NaPF_6 , 3 mmol of **II**, and 0.47 mmol (0.05 mL) of $^i\text{BuNH}_2$, the complex **8c** was obtained in 25% yield (0.09 g). The complexes **8a-c** were identical to those prepared according to method A on the basis of their IR, ^1H NMR, and ^{31}P NMR spectra.

Preparation of Complexes 6* ($\text{X} = \text{BF}_4^-$) from Ruthenium Diynyl Complexes 8. Complex $[\text{Ru}(\text{C}=\text{C}=\text{C}(\text{O}^i\text{Pr})\text{HC}=\text{CPh}_2)(\text{PMe}_2\text{Ph})(\text{Cl})(\eta^6\text{-C}_6\text{Me}_6)]\text{BF}_4$ (**6b***). To a solution of 0.16 mmol (0.12 g) of **8b** in 15 mL of dichloromethane were added successively 1 mL of $^i\text{PrOH}$ and 30 μl of $\text{HBF}_4\cdot\text{OEt}_2$. The solution turned immediately from orange to dark blue and was stirred for 2.5 h at room temperature. The solvents were removed, and the solid residue was washed twice with 15 mL of diethyl ether and dissolved in 15 mL of dichloromethane. After addition of 15 mL of diethyl ether and 15 mL of *n*-hexane and after 24 h at room temperature, a violet compound precipitated. The supernatant solution was removed with a cannula, and the solid was washed with ether and dried under vacuum. Complex **7b*** was obtained in 46% yield (60 mg). IR (KBr): 1963 (s, $\nu_{\text{C}=\text{C}}$), 1060 (m, $\nu_{\text{B-F}}$) cm^{-1} . ^1H NMR (CD_2Cl_2 , 297 K, 300.134 MHz) (δ , ppm): 7.63–7.36 (m, 13 H, Ph), 7.22–7.19 (m, 2 H, Ph), 6.83 (s, 1 H, $\text{CH}=\text{}$), 5.25 (sept, $^3J_{\text{H,H}} = 6.2$ Hz, 1 H, OCHMe_2), 1.87 (d, $^4J_{\text{P,H}} = 0.5$ Hz, 18 H, $\text{C}_6\text{-}$

Me_6), 1.83 (d, $^2J_{\text{P,H}} = 11.1$ Hz, 3 H, PMe), 1.76 (d, $^2J_{\text{P,H}} = 10.7$ Hz, 3 H, PMe), 1.06 (d, $^3J_{\text{H,H}} = 6.2$ Hz, 3 H, OCHMe), 1.04 (d, $^3J_{\text{H,H}} = 6.3$ Hz, 3 H, OCHMe). Anal. Calcd (found) for $\text{C}_{40}\text{H}_{47}\text{BClF}_4\text{OPRu}$: C, 60.20 (60.42), H, 5.94 (6.04).

Complex $[\text{Ru}(\text{C}=\text{C}=\text{C}(\text{O}^i\text{Pr})\text{HC}=\text{CPh}_2)(\text{PMePh}_2)(\text{Cl})(\eta^6\text{-C}_6\text{Me}_6)]\text{BF}_4$ (6c***).** From 0.25 g (0.31 mmol) of **8c**, 1 mL of HO^iPr , and 42.10 μl of $\text{HBF}_4\cdot\text{OEt}_2$, 120 mg (42%) of **6c*** was obtained. IR (KBr): 1976 (s, $\nu_{\text{C}=\text{C}}$), 1055 (m, $\nu_{\text{B-F}}$) cm^{-1} . ^1H NMR (CD_2Cl_2 , 297 K, 300.134 MHz) (δ , ppm): 7.55–7.09 (m, 20 H, Ph), 6.50 (s, 1 H, $\text{CH}=\text{}$), 4.96 (sept, $^3J_{\text{H,H}} = 6.2$ Hz, 1 H, OCHMe_2), 2.06 (d, $^2J_{\text{P,H}} = 10.6$ Hz, 3 H, PMe), 1.86 (d, $^4J_{\text{P,H}} = 0.6$ Hz, 18 H, C_6Me_6), 0.94 (d, $^3J_{\text{H,H}} = 6.2$ Hz, 3 H, OCHMe). Anal. Calcd (found) for $\text{C}_{45}\text{H}_{49}\text{BClF}_4\text{OPRu}$: C, 62.83 (62.82), H, 5.74 (5.61), Cl, 4.12 (4.35).

Complex $[\text{Ru}(\text{C}=\text{C}=\text{C}(\text{NPh}_2)\text{HC}=\text{CPh}_2)(\text{PMePh}_2)(\text{Cl})(\eta^6\text{-C}_6\text{Me}_6)]\text{BF}_4$ (7c***).** From 0.25 g (0.31 mmol) of **8c**, 45 μl of $\text{HBF}_4\cdot\text{OEt}_2$, and diphenylamine (0.06 g, 0.35 mmol), 180 mg (64%) of **7c*** was obtained. IR (KBr): 1996 (s, $\nu_{\text{C}=\text{C}}$), 1053 (m, $\nu_{\text{B-F}}$) cm^{-1} . ^1H NMR (CD_2Cl_2 , 297 K, 300.134 MHz) (δ , ppm): 7.56–6.55 (m, 30 H, Ph), 6.33 (s, 1 H, $\text{CH}=\text{}$), 1.71 (d, $^2J_{\text{P,H}} = 10.5$ Hz, 3 H, PMe), 1.64 (s, 18 H, C_6Me_6). Anal. Calcd (found) for $\text{C}_{54}\text{H}_{52}\text{BClF}_4\text{OPRu}$: C, 66.77 (65.90), H, 5.40 (5.38); Cl, 3.65 (4.14).

Acknowledgment. The authors are grateful to the CNRS for support and the MRT for a thesis grant to D.P.

OM9501034

Does the Tetrahydroborate Species AuBH₄ Exist? Ab Initio MO Study of the Structure and Stability of CuBH₄, AgBH₄, and AuBH₄

Djamaladdin G. Musaev and Keiji Morokuma*

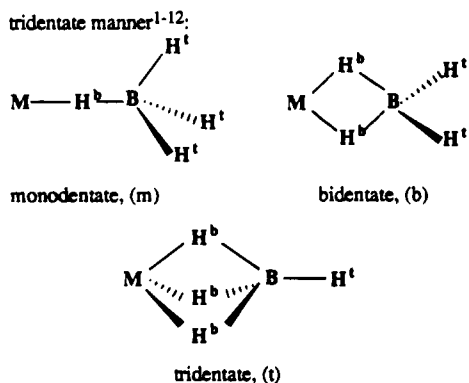
Cherry L. Emerson Center for Scientific Computation and Department of Chemistry,
Emory University, Atlanta, Georgia 30322

Received February 27, 1995[⊗]

The MP2, MP4(SDTQ), QCISD(T), and CCSD(T) methods in conjunction with the 19-valence electron Hay–Wadt relativistic effective core potential have been used to study geometries, energies, and possible rearrangements of tetrahydroborate compounds of Cu, Ag, and Au. For the CuBH₄ and AgBH₄ molecules only the tetrahydroborate structure MBH₄ can exist; the hydrido borane structure, HMBH₃, is thermodynamically (about 25–26 kcal/mol) and kinetically unstable and rearranges into the MBH₄ structure. The bidentate (b) and tridentate (t) MBH₄ structures are energetically very close and structurally nonrigid, and at ambient temperature their bridge and terminal hydrogen atoms will easily interchange by the pathway (b) ⇌ (t) ⇌ (b') ⇌ (t') ⇌ ... However, the Au analog cannot exist as a tetrahydroborate species, AuBH₄, which rearranges with a small (~1 kcal/mol) barrier to the hydrido(borane)gold, HAuBH₃, structure lying 11.7 kcal/mol lower. The thermal stability of MBH₄ (M = Cu, Ag, and Au) molecules for the lowest decomposition path, MH + BH₃, decreases in the order Cu > Ag > Au.

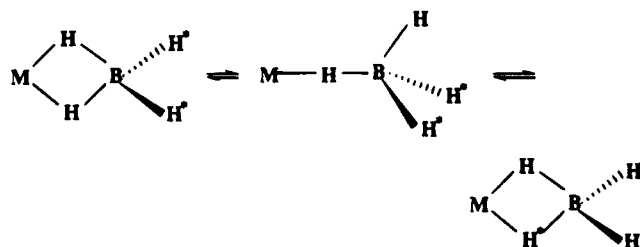
Introduction

The tetrahydroborate ion, BH₄⁻, is the simplest known anionic boron hydride, which is known to coordinate to a metal ion via a monodentate (only in one known case), bidentate, or tridentate manner:^{1–12}



Tetrahydroborate complexes of various metals have been synthesized, and their chemical and physical

properties have been studied.^{1–12} In general, the bridge H^b and terminal H^t hydrogen atoms of these complexes interchange at ambient temperatures. The actual rate of the process and the mechanism of rearrangement, however, has remained to be solved. Various possible pathways have been proposed. The first pathway suggested to explain stereochemical nonrigidity in a tetrahydroborate complexes involves permutation of bridge and terminal hydrogens via a monodentate intermediate or transition state:

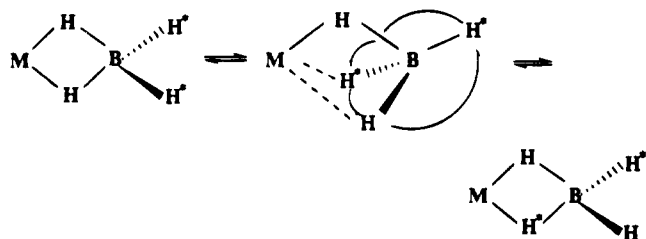


Certain empirical observations, as well as ab initio calculations^{13–30} have suggested that, at least for early

[⊗] Abstract published in *Advance ACS Abstracts*, June 1, 1995.
 (1) Muetterties, E. L. *Boron Hydride Chemistry*; Academic Press: New York, 1975.
 (2) Marks, T. J.; Kolb, J. R. *Chem. Rev.* **1977**, *77*, 263.
 (3) Housecroft, C. E.; Fehler, T. P. *Adv. Organomet. Chem.* **1981**, *21*, 57.
 (4) Edelstein, N. *Inorg. Chem.* **1981**, *20*, 299.
 (5) Corazza, F.; Floriani, A. G.; Cheisi-Villa A.; Guastini, C. *Inorg. Chem.* **1991**, *30*, 145.
 (6) Csaszar, A. G.; Hedberg, L.; Hedberg, K.; Burns, R.; Wen, A. T.; McGlinchey, M. J. *Inorg. Chem.* **1991**, *30*, 1371.
 (7) White, J. P.; Deng, H.; Shore, S. G. *Inorg. Chem.* **1991**, *30*, 2337.
 (8) Gozum, J. E.; Girolami, G. S. *J. Am. Chem. Soc.* **1991**, *113*, 3829.
 (9) Gozum, J. E.; Wilson, S. R.; Girolami, G. S. *J. Am. Chem. Soc.* **1992**, *114*, 9483.
 (10) *Electron Deficient Boron and Carbon Chemistry*; Olah, G. A., Wade, K., Williams, R. E., Eds.; Wiley Interscience: New York, 1990.
 (11) Kawashima, Y.; Yamada, C.; Hirota, E. *J. Chem. Phys.* **1991**, *94*, 7707.
 (12) Kawashima, Y.; Hirota, E. *J. Chem. Phys.* **1992**, *96*, 2460.

(13) Boldyrev, A. I.; Charkin, O. P.; Rambidi, N. G.; Avdeev, V. I. *Chem. Phys. Lett.* **1976**, *44*, 20.
 (14) Baranov, L. Ya.; Boldyrev, A. I. *Chem. Phys. Lett.* **1983**, *96*, 218.
 (15) Kello, V.; Urban, M.; Boldyrev, A. I. *Chem. Phys. Lett.* **1984**, *106*, 455.
 (16) Bonaccorsi, R.; Scrocco, E.; Tomasi, J. *Theor. Chim. Acta* **1979**, *52*, 113.
 (17) Dill, J. B.; Schleyer, P. v. R.; Binkley, J. S.; Pople, J. A. *J. Am. Chem. Soc.* **1977**, *79*, 6159.
 (18) Barone, V.; Dolcetti, G.; Lelj, F.; Russo, N. *Inorg. Chem.* **1981**, *20*, 1687.
 (19) Charkin, O. P.; Musaev, D. G.; Klimenko, N. M. *Russ. J. Coord. Chem.* **1985**, *11*, 728.
 (20) DeFrees, D. J.; Raghavachari, K.; Schlegel, H. B.; Pople, J. A.; Schleyer, P. v. R. *J. Phys. Chem.* **1987**, *91*, 1857.
 (21) Musaev, D. G.; Zyubin, A. S.; Charkin, O. P. *Russ. J. Coord. Chem.* **1988**, *14*, 638.

transition metals, bidentate and tridentate structures do not differ much in energy. The second suggested pathway is a concerted process for tetrahydroborates having bidentate reactant geometries to twist the BH_4 ligand about one of the $\text{B}-\text{H}^b$ bonds:



A similar twisting process can be written for a complex with a tridentate reactant structure; here the midpoint of the reaction coordinate resembles, with the exception of possible asymmetry in the bridge, a bidentate configuration. For the interchange process of bridge and terminal hydrogens, a Berry pseudorotation mechanism has also been suggested.²

The scope of dynamic molecular processes involving the coordinated tetrahydroborate moiety is not limited to intramolecular bridge-terminal hydrogen interchange. Hydrogen exchange between tetrahydroborate moiety and other ligands coordinated to transition metal atoms also may occur. This process has been widely studied in the literature. For example, variable-temperature ^1H NMR spectra of $(\eta^5\text{-C}_5\text{H}_5)_2\text{Zr}(\text{BH}_4)_2$, $(\eta^5\text{-C}_5\text{H}_5)_2\text{Hf}(\text{BH}_4)_2$, and $(\eta^5\text{-C}_5\text{H}_5)_2\text{Zr}(\text{H})\text{BH}_4$ exhibit a rapid interchange of C_5H_5 and BH_4 hydrogens at high temperature.³¹ In the present paper we will concentrate on the hydrogen exchange between the tetrahydroborate moiety and transition metal center, $\text{MBH}_4 \rightleftharpoons \text{HMBH}_3$ and study some possible mechanisms of the intermolecular exchange process for CuBH_4 , AgBH_4 , and AuBH_4 species.

The observed differences between the stability of the CuBH_4 , AgBH_4 , and AuBH_4 species also need to be elucidated. The CuBH_4 species³²⁻³⁵ and the AgBH_4 analog³⁶ have been synthesized at low temperature in diethyl ether and have been shown to be air sensitive and decompose to metal atoms, diborane, and hydrogen at -12 and -30 °C, respectively. These compounds can be stabilized by the addition of soft Lewis bases to form complexes of the type $(\text{R}_3\text{E})_2\text{MBH}_4$, where R_3E may be

the phosphine, arsine, or stibine ligand.^{37,38} However, their gold analog has not been prepared even at low temperature. The $\text{Au}(\text{BH}_4)_3$ species prepared at -120 °C in diethyl ether by reaction of gold(III) chloride with LiBH_4 is thermally very unstable and decomposes to gold metal, diborane, and hydrogen upon increasing the temperature.³⁹ Thus, it is apparent that the stability of the MBH_4 complexes decreases in the order of $\text{Cu} > \text{Ag} > \text{Au}$, and we believe that the quantum chemical calculations carried out in this paper for study of structure, stability, and possible mechanisms of intermolecular process of the CuBH_4 , AgBH_4 , and AuBH_4 species will be helpful for elucidation of this stability difference.

Calculation Procedure

All calculations have been performed by using the GAUSSIAN-92 program.⁴⁰ Geometries have been optimized by using the MP2 method in conjunction with the lan12dz (for transition metal atoms) and the 6-31G(d,p)⁴¹ (for other atoms) basis sets, which will be called basis set I. The lan12dz basis set taken from the GAUSSIAN-92 library includes Hay-Wadt effective core potential⁴² in which the 19 $nsnpnd(n+1)s$ electrons of the group 11 metals are explicitly considered, with the following basis sets of (8s5p5d/3s3p2d), (8s6p4d/3s3p2d), and (8s6p3d/3s3p2d) for Cu, Ag, and Au, respectively. Note that the present ECP takes into account the relativistic effects only for second- and third-row transition metal atoms. Due to the absence of the relativistic effects our results probably will underestimate the bonding energies by a few kcal/mol for the Cu complexes. However, it will not affect the calculated relative energies. Once the geometries were determined, energies have been recalculated by using QCISD(T), MP4-(SDTQ), and CCSD(T) methods with the lan12dz plus polarization f-functions for transition metal atoms and 6-311G(d,p) for other atoms, called basis set II. The exponents of the polarization f-functions have been taken from the recent paper of Ehlers et al.⁴³ Vibrational frequencies have been numerically calculated at the MP2/T level for characterization of the nature of the stationary points, zero-point correction (ZPC), and prediction of vibrational spectra. All the stationary points have been positively identified for minima (number of imaginary frequencies, NIMAG = 0), transition state (NIMAG = 1) and higher order stationary points. In some important cases, we have followed the "pseudo-intrinsic reaction coordinate (IRC)" from a given transition state to both directions to confirm the reactant and the product to which this transition state lead; we took a few steps of the IRC⁴⁴ from the transition state and then performed geometry optimization toward a local minimum. The final energy parameters given in the paper

(22) Charkin, O. P.; Bonaccorsi, R.; Tomasi, J.; Zyubin, A. S.; Musaev, D. G. *Russ. J. Inorg. Chem.* **1987**, *32*, 2644.

(23) Charkin, O. P.; Bonaccorsi, R.; Tomasi, J.; Zyubin, A. S.; Musaev, D. G. *Russ. J. Inorg. Chem.* **1987**, *32*, 2907.

(24) Musaev, D. G.; Charkin, O. P. *Russ. J. Inorg. Chem.* **1991**, *36*, 430.

(25) Ramondo, F.; Bencivenni, L.; Di Martino, V. *Chem. Phys.* **1991**, *158*, 41.

(26) Lledos, A.; Duran, M.; Jean, Y.; Volatron, F. *Inorg. Chem.* **1991**, *23*, 4440.

(27) Lledos, A.; Duran, M.; Jean, Y.; Volatron, F. *Bull. Soc. Chim. Fr.* **1992**, *129*, 216.

(28) Volatron, F.; Duran, M.; Lledos, A.; Jean, Y. *Inorg. Chem.* **1993**, *32*, 951.

(29) Jarid, A.; Lledos, A.; Jean, Y.; Volatron, F. *Inorg. Chem.* **1993**, *32*, 4695.

(30) Francisco, J. S.; Williams, I. H. *J. Phys. Chem.* **1992**, *96*, 7567.

(31) Marks, T. J.; Kolb, J. R. *J. Am. Chem. Soc.* **1975**, *97*, 3397.

(32) Wiberg, E. *Angew. Chem.* **1953**, *65*, 16.

(33) Klingen, T. *J. Inorg. Chem.* **1964**, *3*, 1058.

(34) Klingen, T. *J. J. Inorg. Nucl. Chem.* **1966**, *28*, 2243.

(35) Wiberg, E.; Henle, W. *Z. Naturforsch., B* **1952**, *7*, 582.

(36) Wiberg, E.; Henle, W. *Z. Naturforsch., B* **1952**, *7*, 575.

(37) Lippard, S. J.; Ucko, D. A. *Inorg. Chem.* **1968**, *7*, 1051.

(38) Carlati, F.; Naldini, L. *Gazz. Chim. Ital.* **1965**, *95*, 201.

(39) Puddephatt, R. J. *The Chemistry of Gold*; Elsevier: Amsterdam, 1978.

(40) GAUSSIAN-92: Frisch, M. J.; Trucks, G. W.; Head-Gordon, M.; Gill, P. M. W.; Wong, M. W.; Foresman, J. B.; Johnson, B. G.; Schlegel, H. B.; Robb, M. A.; Replogle, E. S.; Gomperts, R.; Andres, J. L.; Raghavachari, K.; Binkley, J. S.; Gonzales, C.; Martin, R. L.; Fox, D. J.; DeFrees, D. J.; Baker, J.; Stewart, J. J. A.; Pople, J. A. Gaussian Inc., Pittsburgh, PA, 1992.

(41) (a) Hariharan, P. C.; Pople, J. A. *Theor. Chim. Acta* **1973**, *28*, 213. (b) Francl, M. M.; Pietro, W. J.; Henre, W. J.; Binkley, J. S.; Gordon, M. S.; DeFrees, D. J.; Pople, J. A. *J. Chem. Phys.* **1982**, *77*, 3654.

(42) Hay, P. J.; Wadt, W. R. *J. Chem. Phys.* **1985**, *82*, 299.

(43) Ehlers, A. W.; Bohme, M.; Dapprich, S.; Gobbi, A.; Hollwarth, A.; Jonas, V.; Kohler, K. F.; Stegmann, R.; Veldkamp, A.; Frenking, G. *Chem. Phys. Lett.* **1993**, *208*, 111.

(44) (a) Ishida, K.; Morokuma, K.; Komornicki, A. *J. Chem. Phys.* **1977**, *66*, 2153. (b) Gonzales, C.; Schlegel, H. B. *J. Phys. Chem.* **1989**, *90*, 2154.

contain the ZPC calculated with the MP2/1 normal frequencies scaled by 0.95.⁴⁵

Results and Discussions

The MP2/1 optimized geometries are shown in Figures 1 and 2. The relative energies of various structures of MBH₄ calculated at several levels of theory are shown in Table 1. The calculated binding energies of M–H, M–BH₃, H–MBH₃, and HM–BH₃ bonds are given in Table 2. Results of Mulliken population analysis for these molecules are given in Table 3. The relative energies of all the structures involved are summarized in Figure 3.

Geometries of Intermediates and Transition States. Here we will consider geometries of all the critical points we find; their energies and nature (i.e., NIMAG) will be discussed in the next subsection. MP2/1 optimized geometrical parameters given in Figure 1 show that geometries of the BH₄ group in the C_{2v}-assumed bidentate (b) and C_{3v}-assumed tridentate (t) structures are weakly dependent on the nature of metal atoms; the distances $r(\text{B}-\text{H}^b)$ and $r(\text{B}-\text{H}^t)$ change only up to 0.007 and 0.02 Å, respectively, among M = Cu, Ag, and Au, and are 0.01–0.05 Å longer than in the isolated BH₄[−] anion, shown in Figure 2. On the other hand, the distance $r(\text{B}-\text{H}^b)$ in the C_{3v}-assumed monodentate (m) structures for M = Cu and Ag is about 0.1 Å longer than in isolated BH₄[−]. It is dramatically stretched for M = Au; the distance $r(\text{B}-\text{H}^b)$ in AuBH₄ (m) is about 0.40 and 0.50 Å longer than that in the (m) structure of and in isolated BH₄[−], respectively, with the bridged hydrogen H^b actually closer to Au (1.529 Å) than to B (1.757 Å). Upon optimization without any symmetry constraint the geometry of AuBH₄ converged to a structure having C_s symmetry between the monodentate and tridentate structures, (mt) in Figure 1, where $r(\text{B}-\text{H}^b)$ is 1.797 Å, about 0.57 Å longer than that in isolated BH₄[−]. One may say that in the AuBH₄ (m) and (mt) structures the B–H bond is already strongly activated.

The geometries of the HMBH₃ complex, (h), are different among M = Cu, Ag, and Au, as seen in Figure 1. For Cu it has a planar C_s structure, where two H atoms of BH₃ group are asymmetrically oriented to the metal atom. The structure for Ag is similar to that for Cu; two H atoms of BH₃ group are also asymmetrically oriented to the metal atom, but the entire molecule is slightly nonplanar with the H^tAgB angle of 169° and the H^tAgBH^b dihedral angle of 43°. Both for Cu and Ag the geometry of the BH₃ fragment is not much different from that in isolated BH₃ and the M–B distance is quite long, indicating that the interaction between MH and BH₃ is not strong. For Au, however, the structure is very different. It has a nonplanar C_s structure, with only one H atom of BH₃ directed to the metal atom. The interaction of Au with the bridging hydrogen atom H^b seems to be very strong, as indicated by the B–H^b bond elongated by 0.10 Å. The H^tMB angle decreases in the order of M: Cu (172°) ≈ Ag (169°) > Au (136°). These structural features will be discussed later in connection with the Mulliken population analysis.

The transition states (ts) for insertion of the Cu and Ag metal center into a B–H bond of BH₄ are located late, as seen in Figure 1, with their structures resembling more the structures (h) of the HMBH₃ product than the lowest structures (t) of the MBH₄ reactant. The Cu compound has C₁ symmetry and is quasiplanar, where two H atoms of the BH₃ fragment are oriented to the Cu atom. The Ag compound has C_s symmetry, with one H atom of the BH₃ fragment is oriented to the Ag atom. For Au the C_s transition state (ts) is tight with a short Au–H distance and resembles more the MBH₄ reactant.

Qualitative Characteristics of the Potential Energy Surface. Here we discuss the qualitative characteristics of the potential energy surface (PES) at the MP2/1 + ZPC level of theory. More quantitative energetics for critical structures at higher levels of theory will be discussed in the next subsection. For CuBH₄ and AgBH₄ the (t) structure is the global minimum. As shown in Figure 1, the (b) structure for CuBH₄ and AgBH₄ is only 0.58 and 0.24 kcal/mol, respectively, higher in energy than the (t) structure. The normal mode analysis shows that the (b) structure has one B₁ normal mode with a small imaginary frequency shown in Figure 1 and is the transition state between one (t) and another (t) structure. Thus, like their alkali and alkaline earth analogs,^{11–19,30} CuBH₄ and AgBH₄ are structurally nonrigid and at ambient temperatures should exchange bridge and terminal hydrogen atoms easily by the pathway (t) ⇌ (b) ⇌ (t') ⇌ (b') ⇌ ... With a smaller barrier, AgBH₄ is a little more fluxional than CuBH₄. The monodentate (m) structure lies about 21 and 13 kcal/mol higher than the (t) structure for M = Cu and Ag, respectively. The (m) structure has a doubly degenerate imaginary frequency connecting (t) and (b) structures. The hydridoborane metal, HMBH₃ (h), structure is a local minimum on the potential energy surface for CuBH₄ and AgBH₄. It lies 26.0 and 27.4 kcal/mol higher than the (t) structure, has a barrier of only 0.16 and 1.88 kcal/mol, respectively, at the transition state (ts) for rearrangement to the (t) structure, and most likely does not exist at moderate temperature.

The transition state (ts) separating the HMBH₃ (h) structure from the MBH₄ (t) or (b) structure has one small imaginary frequency of 146i and 151i cm^{−1} for CuBH₄ and AgBH₄, respectively, corresponding to migration of one of the hydrogen atoms (H^t) from B to the metal atom, as shown in Figure 1. For Cu, following this normal mode, the transition state can structurally easily reach the product (h) having a very similar structure. Pseudo-IRC following indicates that the path from the transition state back to the reactant leads to the reactant (t). For Ag, pseudo-IRC following shows that it can reach the product (h) by a 125° rotation of the BH₃ group accompanied by a concurrent 63° conrotatory motion of H^t. A large reversal rotational and translational motion of H^t from (ts) accompanied with the rotation of terminal the H^t atoms maintaining the overall C_s symmetry connects (ts) to the reactant (b), which can be converted to the global minimum (t) via rotation of BH₄.

For AuBH₄ the calculated potential energy picture is completely different from that for CuBH₄ or AgBH₄. Here the local minimum is the (mt) structure, and the structure (b), 1.7 kcal/mol higher with one B₂ imaginary

(45) Hehre, W. J.; Radom, L.; Schleyer, P. v. R.; Pople, J. A. *Ab initio Molecular Orbital Theory*; Wiley: New York, 1986.

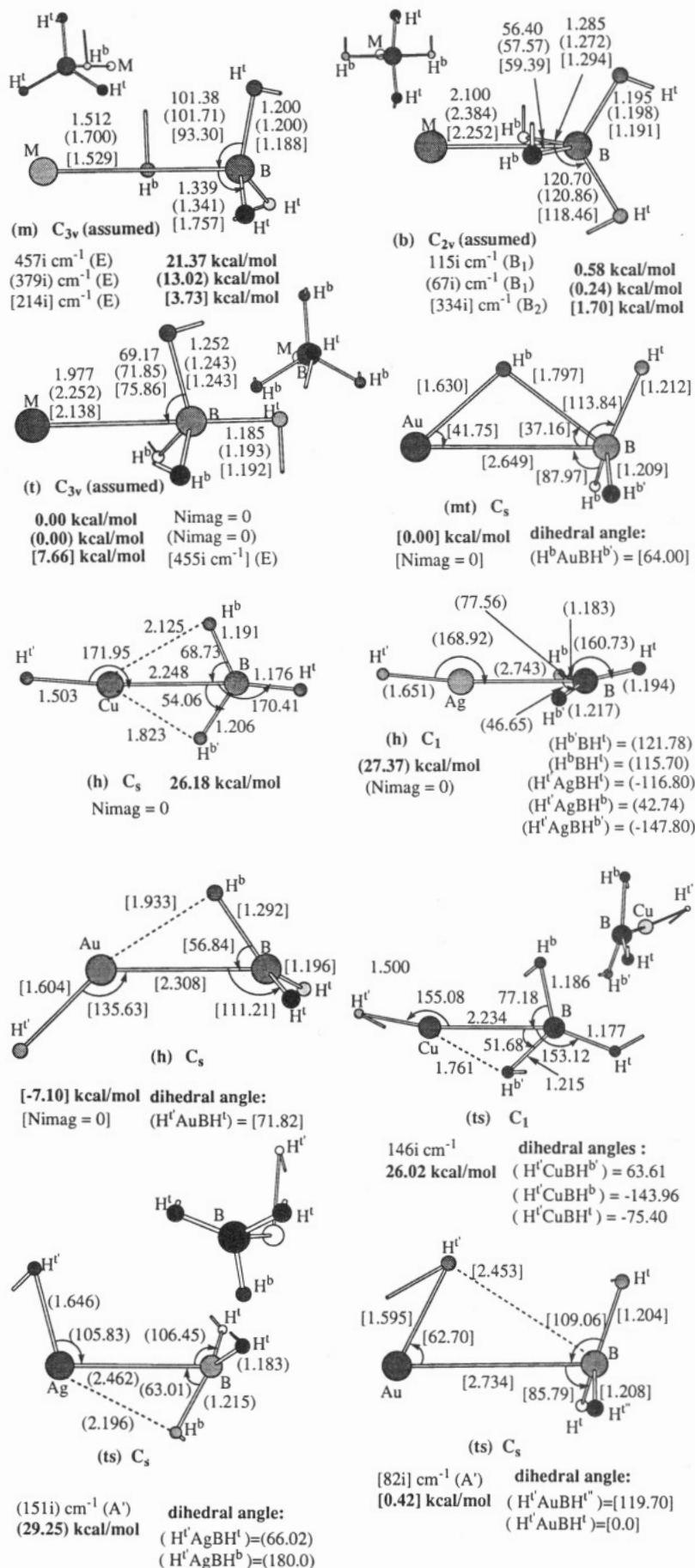


Figure 1. MP2/I optimized geometries (distances in Å and angles in deg) and the MP2/I + ZPC relative energies (in kcal/mol) of various structures of CuBH_4 , AgBH_4 (in parentheses), and AuBH_4 (in brackets).

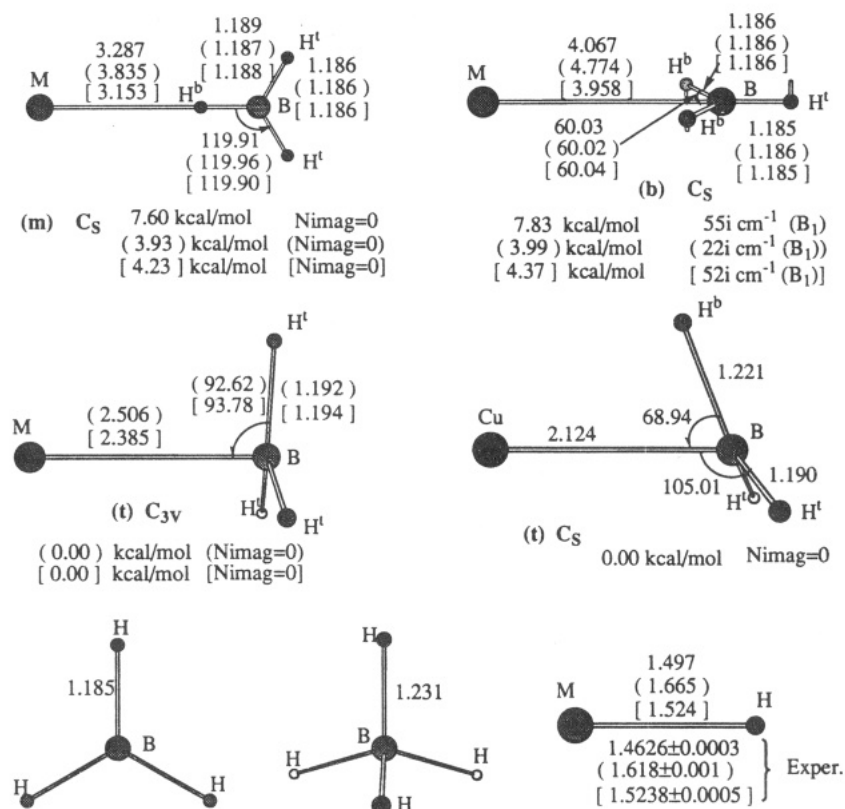


Figure 2. MP2/I optimized geometries (distances in Å and angles in deg) and the MP2/I + ZPC relative energies (in kcal/mol) of various structures of the MBH_3 , MH , BH_3 , and BH_4^- molecules, where $M = Cu, Ag$ (in parentheses), and Au (in brackets).

Table 1. Relative Energies (in kcal/mol) of Various Structures of Metal-Borane Complexes, $CuBH_4$, $AgBH_4$, and $AuBH_4$, at the MP2/I Optimized Geometries^a

molecule (struct)	basis set I			basis set II					
	MP2	NIMAG ^b	MP2 + ZPC	MP2	MP4 (SDTQ)	QCISD(T)	CCSD(T)	CCSD(T) + ZPC	
$CuBH_4$ (m)	20.41	2 457i E	21.37	21.46		26.32			
(b)	0.55	1 115i B_1	0.58	-0.66	-1.13	-0.37	-0.54	-0.51	
(t)	<i>-222.28951</i>	0	0.00	<i>-222.47381</i>	<i>-222.52725</i>	<i>-222.48480</i>	<i>-222.48714</i>	0.00	
(h)	25.81	0	26.18	24.93	15.58	41.01	24.37	24.74	
(ts)	25.99	1 146i A	26.02	24.93	14.53	35.75	23.97	24.00	
$AgBH_4$ (m)	12.93	2 379i E	13.02	13.21		12.93			
(b)	0.20	1 67i B_1	0.24	-0.20	-0.29	-0.27	-0.26	-0.22	
(t)	<i>-172.05552</i>	0	0.00	<i>-172.31039</i>	<i>-172.33549</i>	<i>-172.33484</i>	<i>-172.33435</i>	0.00	
(h)	25.37	0	27.37	24.94	24.04	24.12	24.13	26.13	
(ts)	26.79	1 151i A'	29.25	25.29	23.49	23.02	23.02	25.48	
$AuBH_4$ (m)	2.82	2 214i E	3.73	4.01		4.38			
(b)	1.24	1 334i B_2	1.70	-0.19	0.06	-0.06	-0.06	0.00	
(t)	7.39	2 455i E	7.66	8.63		8.30			
(mt)	<i>-161.69518</i>	0	0.00	<i>-161.92499</i>	<i>-161.94630</i>	<i>-161.94584</i>	<i>-161.94510</i>	0.00	
(h)	-6.90	0	-7.10	-11.92	-12.48	-11.73	-11.48	-11.68	
(ts)	0.19	1 82i A'	0.42	0.94	0.75	0.71	0.69	0.92	

^a ZPC was calculated at the MP2/I level and scaled by 0.95. Total energies (italic, in hartree) are given only for reference structures, and relative energies (in kcal/mol) for other structures are relative to the reference structures. ^b The first entry is the number of imaginary frequencies, the second their values, and the third their symmetry.

frequency, is the transition state between one (mt) and another (mt). The (mt) structure will be able to scramble its hydrides relatively easily through the (b) transition state. The (m) structure at 3.7 kcal/mol above (mt), as well as (t) structure at 7.7 kcal/mol above (mt), has a doubly degenerate imaginary frequency and connects (mt) and (b) structures. The most remarkable feature of the PES for Au is that the global minimum is the hydrido(borane)gold, $HAuBH_3$, structure (h), which is more stable than the (mt) $AuBH_4$ structure by 7.1 kcal/mol at this level of theory. The transition state (ts) separating the $AuBH_4$ (mt) structure from the $HAuBH_3$ (h) structure is only 0.42 kcal/mol above the (mt)

structure; the (mt) structure is not likely to exist at this level of theory. The (ts) can structurally easily reach the reactant (mt) by moving H^t onto the B atom. Pseudo-IRC following from the transition state (ts) to the product (h) indicates that the H atom to be transferred (H^t) has to move all the way from above the $Au-B$ axis in (ts) in Figure 1 to below the axis in (h) by making a 162° rotation around the Au atom, while the BH_3 fragment makes a 52° conrotatory motion.

Energetics at Higher Levels of Theory. Here we would like to discuss the energetics of critical structures of the present molecules calculated at higher levels of theory, MP4(SDTQ), QCISD(T), and CCSD(T), in con-

Table 2. Calculated M–H, M–BH₃, and M⁺–BH₄[–] Bond Dissociation Energies (in kcal/mol) for MH, MBH₃, and HMBH₃ Species with Various Basis Sets and Methods^a

molecule	basis set I			basis set II				exptl ^c
	MP2	MP2	MP4 (SDTQ)	QCISD(T)	CCSD(T)	CCSD(T) + ZPC ^b		
	<i>D_e(M–H)</i>							
CuH	49.0	54.2	62.1	46.4	57.8	60.1	66.4	
AgH	36.7	44.2	48.0	48.5	48.4	50.5	51.4 ± 2	
AuH	57.0	67.0	69.6	69.6	69.5	72.4	69.8 ± 2	
HCuBH ₃	52.8	57.3	68.3	207.1	59.0	62.9		
HAgBH ₃	40.6	45.7	48.7	48.5	48.5	51.9		
HAuBH ₃	66.6	82.0	84.3	82.8	87.8	87.6		
	<i>D_e(M–BH₃)</i>							
CuBH ₃	7.6	12.4	18.2	–163.0	13.6	14.2		
AgBH ₃	1.5	6.9	7.6	7.6	7.5	7.9		
AuBH ₃	4.1	10.1	10.4	10.1	10.5	10.2		
HCuBH ₃	11.4	15.5	24.4	6.8	14.9	16.6		
HAgBH ₃	5.5	8.4	8.3	7.6	7.5	9.2		
HAuBH ₃	13.7	25.2	25.1	23.3	25.7	25.4		
	<i>D_e(M⁺–BH₄[–])</i>							
CuBH ₄ (b)		171.3	178.0	167.4	170.1	171.4		
AgBH ₄ (b)		150.4	150.2	149.9	149.8	150.7		
AuBH ₄ (b)		188.2	186.9	186.3	186.1	185.8		

^a At the MP2/I optimized geometries of the molecules (shown in Figure 1) and fragments (in Figure 2). ^b ZPC at the scaled MP2/I level. ^c Experimental data were taken from ref 47.

Table 3. Transition Metal Valence s, p, and d Orbital Mulliken Gross Populations (M), Mulliken Overlap Populations (Q), Atomic Charges (Z^{*}), and Dipole Moments (μ) of MH, MBH₃, HMBH₃, and MBH₄ (M = Cu, Ag, Au) Calculated at the HF/II Level

molecule	M			Q			Z [*]				μ (D)	
	s	p	d	M–B	M–H ^c	M–H ^b (M–H ^b)	M	B	H ^c	H ^b (H ^b)		
CuH	0.75	0.15	9.95		0.75		+0.15					4.08
AgH	0.72	0.11	9.94		0.69		+0.23					4.34
AuH	1.08	0.06	9.77		0.75		+0.09					2.60
CuBH ₃	0.68	0.12	9.97	0.40		–0.01	+0.23	–0.11	–0.03	–0.05		2.95
AgBH ₃	0.83	0.01	9.99	0.25			+0.17	–0.06	–0.04	–0.04		1.94
AuBH ₃	0.88	0.04	9.94	0.29			+0.14					1.73
HCuBH ₃	0.78	0.34	9.91	0.13	0.77	0.05 (0.17)	+0.01	+0.19	–0.20	0.0 (+0.02)		5.45
HAgBH ₃	0.78	0.07	9.95	0.00	0.69	0.01	+0.20	+0.13	–0.30	–0.04		5.41
HAuBH ₃	1.01	0.26	9.56	0.48	0.73	0.10	+0.17	–0.14	–0.11	+0.07		1.92
CuBH ₄ (b)	0.32	0.27	9.96	0.25		0.28	+0.45	–0.16		–0.09		6.25
AgBH ₄ (b)	0.27	0.15	9.99	0.16		0.19	+0.59	–0.18		–0.14		7.65
AuBH ₄ (b)	0.56	0.25	9.89	0.30		0.29	+0.30	–0.32		+0.03		5.51
AuBH ₄ (mt)	0.91	0.15	9.81	0.12		0.70	+0.13	–0.02	–0.04 ^a	(0.0) (–0.04)		4.26

^a For the H^c atom.

junction with the larger basis set II with ZPC calculated from the scaled MP2/I frequencies. In these calculations we used the geometries optimized at the MP2/I level.

As seen in Table 1, at the highest level of theory, CCSD(T)/II + ZPC, for CuBH₄ and AgBH₄ the (b) and (h) structures are stabilized a few kcal/mol more than the (t) structure than at the MP2/I + ZPC level. As a result, the (b) structure becomes 0.51 and 0.22 kcal/mol, respectively, more stable than the (t) structure. The (ts) structure is stabilized a few kcal/mol more than the (h) structure; the HMBH₃ structure (h) lies 0.74 and 0.65 kcal/mol, respectively, higher than the (ts) separating of the (h) structure from (t) or (b) for CuBH₄ and AgBH₄. However, the main conclusion made above at the MP2 level does not change; CuBH₄ and AgBH₄ molecules exist only as tetrahydroborate species, MBH₄, with nearly degenerated (b) and (t) structures. They are nonrigid and at ambient temperature should exchange bridge and terminal hydrogen atoms very easily by the pathway (b) ⇌ (t) ⇌ (b') ⇌ (t') ⇌ AgBH₄ is still a little more fluxial than CuBH₄. The hydrido(borane)-metal HMBH₃ (h) structure is thermodynamically unfavorable by 25 and 26 kcal/mol for CuBH₄ and AgBH₄,

respectively, and kinetically unstable or only marginally stable; it is not likely to exist.

For the interest of theoreticians, here we would like to discuss briefly the total failure of the QCISD(T) method for copper complexes. As seen in Table 1, the calculated energy difference between (t) and (h) structures of CuBH₄ jumps to 41 kcal/mol at the QCISD(T) level from 15–20 kcal/mol at the other levels. As shown in Table 2, the HCu–BH₃ and Cu–BH₃ bonding energies calculated at the QCISD(T) level are 150–200 kcal/mol different from those obtained at the other levels. Note this erratic behavior of QCISD(T) arising from the (T) correction term has been recognized recently elsewhere,⁴⁶ and the user of the method should be warned of this problem.

For AuBH₄ at the highest CCSD(T) + ZPC level of theory the (b) and (mt) AuBH₄ structures are degenerate, and it is difficult to conclude which of them is energetically more stable. They are 11.7 kcal/mol higher than the hydrido(borane)gold complex HAuBH₃ (h), and they rearrange into (h) with a small barrier of 0.92 kcal/mol, at the best level. The barrier height is

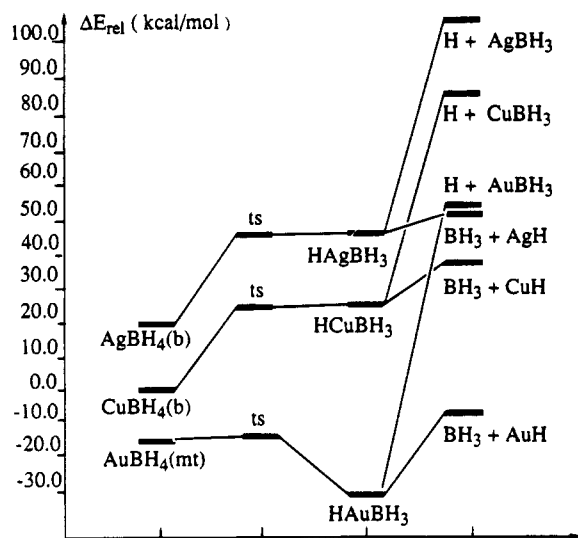


Figure 3. Relative energies ΔE_{rel} of the most stable MBH_4 structure, the transition state (ts), HMBH_3 , $\text{H} + \text{MBH}_3$, and $\text{MH} + \text{BH}_3$ (where $\text{M} = \text{Cu}, \text{Ag},$ and Au) calculated at the CCSD(T)/II + ZPC (scaled MP2/I) level at the MP2/I optimized geometries. The energy origin is arbitrarily shifted for each M.

quite small, and it is unlikely that any AuBH_4 structure, (mt) or (b), exists. Thus, one may conclude that the reactivity of Cu^+ , Ag^+ , and Au^+ cations with the BH_4^- anion would be very different; the reaction of Cu^+ and Ag^+ with BH_4^- leads to the tetrahydroborate complexes CuBH_4 and AgBH_4 , respectively, while the same reaction of Au^+ yields hydrido borane complex HAuBH_3 . Our conclusion is in good agreement with available experiments.^{32–39}

As seen in Table 2, the calculated M–H bonding energies at our best CCSD(T) + ZPC level are 60.1, 50.5, and 72.4 kcal/mol for the bare metal hydrides CuH , AgH , and AuH , respectively. The calculated numbers for $\text{M} = \text{Ag}$ and Au are in reasonable agreement with experimental values⁴⁷ of 51.4 ± 2 and 69.8 ± 2 kcal/mol, respectively. The value for $\text{M} = \text{Cu}$ is about 6 kcal/mol smaller than the experimental value,⁴⁷ 66.4 kcal/mol, which may be a result of the absence of the relativistic effects in our calculation for $\text{M} = \text{Cu}$. Addition of the BH_3 ligand to the metal atom M strengthens the H–M bond by 2.8, 1.4, and 15.2 kcal/mol for $\text{M} = \text{Cu}, \text{Ag},$ and Au , respectively, and as a result, the M–H bond in HMBH_3 structure becomes 24.7 and 35.9 kcal/mol stronger for Au than for Cu and Ag, respectively. While the calculated strengths of the M– BH_3 (14.2, 7.9, and 10.2 kcal/mol for Cu, Ag, and Au, respectively) and HM–BH_3 (16.6, 9.2, and 25.4 kcal/mol for Cu, Ag, and Au, respectively) bonds in MBH_3 and HMBH_3 , respectively, are significantly less than the metal–hydride bond, the HM–BH_3 bond for Au is about 8.8 and 16.2 kcal/mol stronger than for Cu and Ag, respectively. Thus, these results show that the M–X bonds (especially the M–H bond) are stronger for the first-row transition metal Cu than for the second-row Ag and that those for the third-row transition metal Au are the strongest of all, which is in good agreement with

the trend predicted earlier.^{48,49} As also seen in Table 2, the dissociation energy of the tetrahydroborate MBH_4 (b) structure to $\text{M}^+ + \text{BH}_4^-$ increases in the same order as the M–H bond energy in the MH molecules, i.e. AgBH_4 (151 kcal/mol) < CuBH_4 (171 kcal/mol) < AuBH_4 (186 kcal/mol).

According to the energy diagram given in Figure 3, the thermodynamically favorable channel of MBH_4 decomposition is $\text{MH} + \text{BH}_3$ for all metals considered. However, the mechanism of this process is different for $\text{M} = \text{Cu}$ and Ag and for $\text{M} = \text{Au}$. Since CuBH_4 and AgBH_4 exist only as tetrahydroborate species, the reaction $\text{MBH}_4 \rightarrow \text{MH} + \text{BH}_3$ should take place in two steps; at first, they need 24.7 and 26.1 kcal/mol of energy for $\text{M} = \text{Cu}$ and Ag , respectively, to rearrange into (metastable) the hydrido borane structure, HCuBH_3 and HAgBH_3 , from where the dissociation into MH and BH_3 fragments requires an additional 16.6 and 9.2 kcal/mol. The overall energy needed for decomposition of CuBH_4 and AgBH_4 into the MH and BH_3 fragments is large, 41.3 and 35.3 kcal/mol for Cu and Ag, respectively. On the other hand, the AuBH_4 complex exists only as a hydrido borane species, HAuBH_3 , and the decomposition reaction takes place by one step and leads to AuH and BH_3 products with an endothermicity of 25.4 kcal/mol. Thus, our calculations show that the thermal stability of the CuBH_4 , AgBH_4 , and AuBH_4 species increases in the order AuBH_4 (25.4 kcal/mol) < AgBH_4 (35.3 kcal/mol) < CuBH_4 (41.3 kcal/mol), which is consistent with available experiments.³⁹

The difference in fundamental features of the potential energy surface, i.e. the difference in reactivity of Cu^+ and Ag^+ , on one side, and Au^+ , on the other side, with BH_4^- is directly related to the differences among first-, second-, and third-row transition metals in binding energies $D_e(\text{M–H})$, $D_e(\text{M–BH}_3)$, $D_e(\text{HM–BH}_3)$, and $D_e(\text{H–MBH}_3)$ discussed above. The metal–ligand bonding energy in general changes in the following order: first row > second row < third row.⁴⁸ The fact that the metal–ligand bond of the first-row transition metal is stronger than that of the second row is often explained in terms of larger overlap of the first-row metal 4s orbital with the H 1s or ligand sp hybrid orbital than the second-row 5s orbital. The expectation value of radius (r) of the Cu 4s orbital is 1.92 Å, compared with 1.64 Å of Ag 5s and 1.56 Å of Au 6s, and the larger size of Cu 4s provides a better overlap with ligands.^{50–52} On the other hand, the fact that the metal–ligand bond of the third-row transition metal is stronger than that of the second row is explained in terms of the magnitude of d orbital contribution in bonding. At first, for heavier atoms s^1d^{n+1} and the s^0d^{n+1} states are energetically not very much higher, and sometimes even lower, than the s^2d^n states. In addition, the size of the d orbital, relative to the s orbital, increases as the metal becomes heavier. These factors result in better s–d hybridization and larger d involvement in the bonding of heavier transi-

(48) Walch S. P.; Bauschlicher, C. W., Jr. In *Comparison of Ab Initio Quantum Chemistry with Experiment*; Bartlett, R., Ed.; Reidel: Boston, MA, 1985; p 17.

(49) Langhoff, S. R.; Pettersson, L. G. M.; Bauschlicher, C. W., Jr.; Partridge, H. *J. Chem. Phys.* **1987**, *86*, 268.

(50) Schilling, J. B.; Goddard, W. A., III; Beauchamp, J. L. *J. Am. Chem. Soc.* **1986**, *108*, 582.

(51) Schilling, J. B.; Goddard, W. A., III; Beauchamp, J. L. *J. Am. Chem. Soc.* **1987**, *109*, 5565.

(52) Ohanessian, G.; Brusich, M. J.; Goddard, W. A., III. *J. Am. Chem. Soc.* **1990**, *112*, 7179.

(47) Huber, K. P.; Herzberg, G. *Molecular Spectra and Molecular Structure. IV. Constants of diatomic molecules*; Van Nostrand Reinhold Co.: New York, 1979.

tion metals. The relativistic effects, which cause the above differences and increases for heavier metals, have been explicitly evaluated in theoretical studies. For example, Schwerdtfeger et al.⁵³ have shown that the inclusion of relativistic effects decreases the Au–H bond length by 0.25 Å and, consequently, increases the Au–H binding energy as much as 15 kcal/mol.

Mulliken Population Analysis. The above discussed trends of bond energies can be related to the results of the Mulliken population analysis. As shown in Table 3, the metal atom in CuH, CuBH₃, AgH, and AgBH₃ molecules has a Mulliken population of $d^{9.95}s^{0.75}p^{0.15}$, $d^{9.97}s^{0.68}p^{0.12}$, $d^{9.94}s^{0.72}p^{0.11}$, and $d^{9.99}s^{0.83}p^{0.01}$, respectively. The d electrons are not significantly involved in the bonding. Thus $R(M-X)$ and D_e in these molecules are mainly determined by the overlap of the valence s orbital with the ligand. The radial overlap of the Cu 4s orbital with the H 1s orbital or B sp hybrid orbital is slightly better than the overlap of the Ag 5s orbital, as reflected in the difference in overlap population Q in Table 3, and consequently D_e is slightly larger in CuH and CuBH₃ than in AgH and AgBH₃, respectively. In contrast, the Mulliken population of Au in AuH and AuBH₃ is $d^{9.77}s^{1.08}p^{0.06}$ and $d^{9.94}s^{0.88}p^{0.04}$, respectively, and the d-electrons of Au are more strongly involved in bonding than those of Cu and Ag, which makes the Au–H and Au–BH₃ bonds different in nature and stronger compared with their Cu and Ag analogs.

As was discussed above, extra H and BH₃ ligands on the transition metal atom strengthens the metal–BH₃ and metal–H bonds, respectively. Though these changes are small, 2–3 kcal/mol, for Cu and Ag, they are quite large, about 15 kcal/mol, for Au. Similar results have been found for MCH₃⁺ and M(CH₃)₂⁺ of first- and second-row transition metal atoms by Rosi et al.⁵⁴ and for MH⁺, MCH₃⁺, and HMCH₃⁺ of Fe, Co, Rh, and Ir by us.^{55–57}

The origin of this effect is that the first ligand facilitates the involvement of low-lying $d^{n+1}s^1$ and $d^n s^1 p^1$ electronic configurations of the metal atom into the M–X bond, thus increasing the p and d character of the bond, and consequently makes the second bond stronger than the first. As seen in Table 3, the Mulliken population of metal atoms in HMBH₃ complexes of $d^{9.91}s^{0.78}p^{0.34}$, $d^{9.95}s^{0.78}p^{0.07}$, and $d^{9.56}s^{1.01}p^{0.26}$, respectively,

(53) Schwerdtfeger, P.; Dolg, M.; Schwarz, W. H. E.; Bowmaker, G. A.; Boyd, P. D. W. *J. Chem. Phys.* **1989**, *91*, 1762.

(54) Rosi, M.; Bauschlicher, C. W., Jr.; Langhoff, S. R.; Partridge, H. *J. Phys. Chem.* **1990**, *94*, 8656.

(55) Musaev, D. G.; Koga, N.; Morokuma, K. *J. Phys. Chem.* **1993**, *97*, 4064.

(56) Musaev, D. G.; Morokuma, K.; Koga, N.; Nguyen, K. A.; Gordon, M. S.; Cundari, T. R. *J. Phys. Chem.* **1993**, *97*, 11435.

(57) Musaev, D. G.; Morokuma, K. *Isr. J. Chem.* **1993**, *33*, 307.

for M = Cu, Ag, and Au substantiates the above arguments.

Conclusions

The following key points may be drawn from the calculations presented here.

1. The CuBH₄ and AgBH₄ molecules exist only as tetrahydroborate species, MBH₄. The lowest geometrical structures are (b) and (t) structures, of which the (b) structure is at the best level (CCSD(T) + ZPC) of theory, slightly (0.5 and 0.2 kcal/mol for CuBH₄ and AgBH₄, respectively) more stable than the (t) structure. The monodentate structure (m) lies about 20–25 and 13 kcal/mol higher than (b) or (t) structures for CuBH₄ and AgBH₄, respectively. For these molecules the HMBH₃ structure lies about 25–26 kcal/mol higher than the most stable MBH₄ structure and does not exist as an intermediate but rearranges into the tetrahydroborate structure, MBH₄, with a very small (or no) barrier.

2. The corresponding complex of Au, AuBH₄, exists only as hydrido(borane)gold, HAuBH₃. Its tetrahydroborate structure, about 12 kcal/mol higher, does not exist and rearranges to the hydrido(borane)gold, HAuBH₃, structure with a small barrier.

3. At the best level (CCSD(T) + ZPC) of theory the bond energies are calculated to be 60.1, 50.5, and 72.4 kcal/mol for the M–H bond, 14.2, 7.9, and 10.2 kcal/mol for the M–BH₃ bond, 62.9, 51.9, and 87.6 kcal/mol for the H–MBH₃ bond, 16.6, 9.2, and 25.4 kcal/mol for the HM–BH₃ bond, and 171.4, 150.7, and 185.8 kcal/mol for the M⁺–BH₄[−] bond, respectively, for M = Cu, Ag, and Au.

4. The thermal stabilities of CuBH₄, AgBH₄, and AuBH₄ complexes are calculated to be 41.3, 35.3, and 25.4 kcal/mol, i.e., decreases in the order CuBH₄ > AgBH₄ > AuBH₄, which is in good agreement with available experiment.^{36–39} The thermodynamically most favorable decomposition channel of the MBH₄ molecule is MH + BH₃ for all metals considered. It takes place by a two-step mechanism for the CuBH₄ and AgBH₄ species; at first the stable tetrahydroborate structure, MBH₄, rearranges into hydrido borane, HMBH₃, which dissociates into HM and BH₃ fragments. However, for AuBH₄ species the decomposition process takes place by a one-step mechanism, simple dissociation of the stable structure HAuBH₃ to AuH and BH₃ fragments.

Acknowledgment. The present research is in part supported by the Grant CHE-9409020 from the National Science Foundation.

OM9501539

Metal Carbene, Metal Vinylidene, and Metal Alkyne Complexes: Reaction of Acetylides with $(\eta^5\text{-C}_5\text{H}_5)\text{M}(\text{CO})_2(\text{NO})$ (M = Cr, Mo, W)

Junes Ipaktschi,^{*,†} Gabriele J. Demuth-Eberle,[†] Farzad Mirzaei,[†]
Burkhard G. Müller,[†] Johannes Beck,[‡] and Michael Serafin[‡]

*Institute of Organic Chemistry and Institute of Inorganic and Analytical Chemistry,
Justus-Liebig-University, Heinrich-Buff-Ring 58, D-35392 Giessen, Germany*

Received November 9, 1994[®]

Reaction of $(\eta^5\text{-C}_5\text{H}_5)\text{M}(\text{CO})_2(\text{NO})$ (M = Mo or W) (**1**) with $\text{LiC}\equiv\text{CR}$ (**2**) and subsequent addition of an electrophile leads either to a vinylidene or an η^2 -alkyne metal complex. $[(\eta^5\text{-C}_5\text{H}_5)(\text{CO})(\text{NO})]\text{M}=\text{C}=\text{C}(\text{R})(\text{R}')$ derivatives are formed when alkyl or aryl acetylides (R = alkyl or C_6H_5) and either C-electrophile or dilute acid (R' = CH_3 or H) are used. $[(\eta^5\text{-C}_5\text{H}_5)(\text{CO})(\text{NO})]\text{M}(\text{R}-\text{C}\equiv\text{C}-\text{R}')$ (R = $(\text{CH}_3)_3\text{Si}$, CH_3 , allyl, or C_6H_5 ; R' = $(\text{CH}_3)_3\text{Si}$) is formed either when $\text{LiC}\equiv\text{C}-\text{Si}(\text{CH}_3)_3$ is used and the addition product is trapped by allylbromide, trifluoromethanesulfonate, or (trimethylsilyl)chloride, or when the addition product of $\text{LiC}\equiv\text{C}-\text{C}_6\text{H}_5$ with **1** is trapped by (trimethylsilyl)chloride. The structure of $[(\eta^5\text{-C}_5\text{H}_5)(\text{CO})(\text{NO})]\text{W}[\text{H}_3\text{C}-\text{C}\equiv\text{C}-\text{Si}(\text{CH}_3)_3]$ was determined by X-ray diffraction. Under the conditions used here, independent of the identity of the acetylide or electrophile, $(\eta^5\text{-C}_5\text{H}_5)\text{Cr}(\text{CO})_2(\text{NO})$ leads only to the carbene complexes $[(\eta^5\text{-C}_5\text{H}_5)(\text{CO})(\text{NO})]\text{Cr}=\text{C}(\text{OCH}_3)(\text{C}\equiv\text{C}-\text{R})$ (R = C_6H_5 or $(\text{CH}_3)_3\text{Si}$). Addition of secondary amines to carbene complex $[(\eta^5\text{-C}_5\text{H}_5)(\text{CO})(\text{NO})]\text{Cr}=\text{C}(\text{OCH}_3)(\text{C}\equiv\text{C}-\text{C}_6\text{H}_5)$ is discussed. Synthesis of $[(\eta^5\text{-C}_5\text{H}_5)(\text{CO})(\text{NO})]\text{W}=\text{C}=\text{CH}_2$ is described.

Introduction

The classic preparation method of Fischer-type metal carbene complexes is based on the addition of the organolithium reagents to metal carbonyls and subsequent alkylation of the acyl anions with a strong electrophile.¹ A great number of carbene complexes with a variety of substituents can be prepared in this way.¹ In contrast to this behavior, however, we recently obtained, upon reaction of **2a** with the molybdenum carbonyl **1b** and subsequent alkylation with $\text{CF}_3\text{SO}_3\text{-CH}_3$, the vinylidene complex **5a** instead of the anticipated Fischer-type carbene complex.² With the intention of exploring the reactivity of the homologous chromium and tungsten carbonyl complexes **1a** and **1c**, we investigated the reaction of **1a–c** with a variety of lithium acetylides. Depending on the identity of the central metal atom in complex **1**, the substituent on the acetylides **2**, and the applied electrophiles, we found that carbene complexes, η^2 -alkyne metal complexes, or vinylidene derivatives are formed.³

Results and Discussion

The reaction of acetylide **2a** or **2e** with the chromium complex **1a** in THF at 0 °C produces, after treatment

with methyl trifluoromethanesulfonate, the Fischer-type carbene complexes **7a** and **7e** in 63% and 67% yields. These complexes are obtained as red (**7a**) and orange (**7e**) crystalline products.⁴ These results can be compared to the reaction of acetylide **2a** with $\text{Cr}(\text{CO})_6$ or $\text{W}(\text{CO})_6$, which also gives rise to the corresponding Fischer-type complexes.⁵ In contrast to this, the reaction of acetylides **2a–d** with the tungsten complex **1c** in THF at –30 °C led to a deep green solution.⁶ Treatment of this solution with an electrophile (methyl triflate or diluted HCl) resulted, after purification through chromatography and crystallization from pentane, the vinylidene complexes **6a–d** and **9a–c** in 48%–91% yield as orange to red crystalline products. NMR investigations of these products show the presence of rotamers. For complex **6a** a rotational barrier of $\Delta G^\ddagger > 20.4(\pm 0.3)$ kcal/mol was obtained by NMR experiments (see Scheme 1).

Obviously in the case of the chromium complex **1a**, acetylide attack at the carbonyl group forms an acyl metalate anion as an intermediate. This is subse-

(3) For general reviews see: (a) Werner, H. *Nachr. Chem., Tech. Lab.* **1992**, *40*, 435–442; (b) Bruce, M. I. *Chem. Rev.* **1991**, *91*, 197–257; (c) Werner, H. *Angew. Chem.* **1990**, *102*, 1109–1212; *Angew. Chem., Int. Ed. Engl.* **1990**, *29*, 1077. (d) Davies, S. G.; McNally, J. P.; Smallridge, A. J. *Adv. Organomet. Chem.* **1990**, *30*, 1–76. (e) Antonova, A. B.; Johansson, A. A. *Russ. Chem. Rev.* **1989**, *58*, 693. (f) Bruce, M. I.; Swinger, A. G. *Adv. Organomet. Chem.* **1983**, *22*, 59–128.

(4) Complex **7a** shows a temperature dependent ¹H NMR spectrum, and a rotational barrier of $\Delta G^\ddagger = 14.0(\pm 0.3)$ kcal/mol was obtained through dynamic NMR experiments.

(5) Aumann, R. *Chem. Ber.* **1994**, *127*, 725–729. Stein, F.; Duetsch, M.; Pohl, E.; Herbst-Irmer, R.; de Meijere, A. *Organometallics* **1993**, *12*, 2556–2564. Chan, K. S.; Wulff, W. D. *J. Am. Chem. Soc.* **1986**, *108*, 5229–5236. Dötz, K. H.; Kühn, W. *J. Organomet. Chem.* **1985**, *286*, C23–C26.

(6) The preparations of **5a** and **6b** were carried out at –78 and 0 °C; no other products were found. Chromium complex **1a** did not react at –78 °C. At room temperature only carbenes **7a** and **7e** were found in low yields (see also Experimental Section).

^{*} Institute of Organic Chemistry.

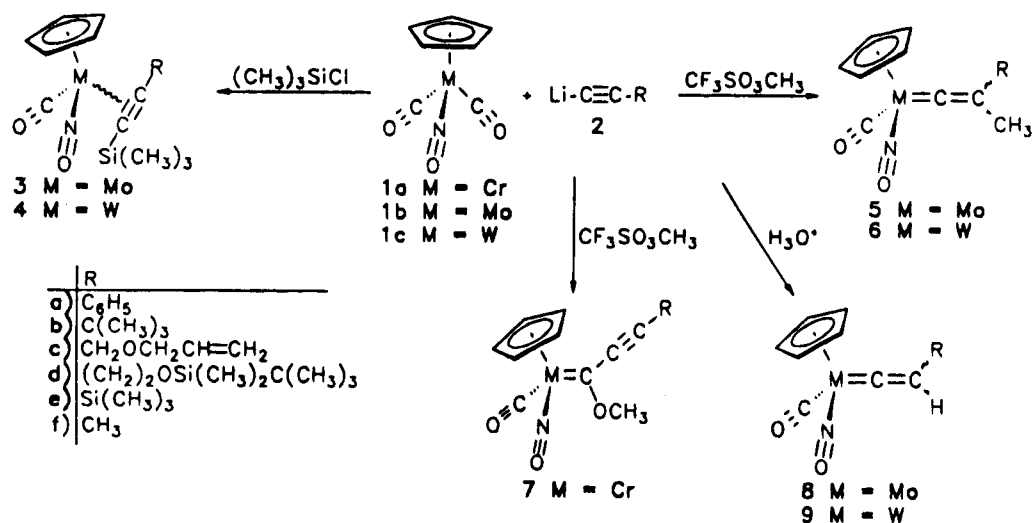
[†] Institute of Inorganic and Analytical Chemistry.

[®] Abstract published in *Advance ACS Abstracts*, June 1, 1995.

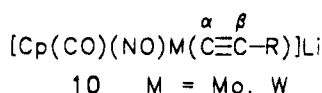
(1) For general reviews see: (a) Hegedus, L. S. *Transition Metals in the Synthesis of Complex Organic Molecules*; University Science Books: Mill Valley, CA, 1994. (b) Wulff, W. D. In *Comprehensive Organic Synthesis*; Trost, B. M., Fleming, I., Eds.; Pergamon Press: Oxford, England, 1991; Vol. 5, pp 1065–1113. (c) Rubetsov, A. Z. *Russ. Chem. Rev.* **1991**, *60*, 89–105. (d) Wulff, W. D. In *Advances in Metal-Organic Chemistry*; Liebeskind, L. S., Ed.; JAI Press: Greenwich, CT, 1989; Vol. 1, pp 209–393. (e) Dötz, K. H. In *Transition Metal Carbene Complexes*; Verlag Chemie: Deerfield Beach, FL, 1983; pp 191–226.

(2) Ipaktschi, J.; Müller, B. G.; Glaum, R. *Organometallics* **1994**, *13*, 1044–1046.

Scheme 1



quently alkylated by the electrophiles to yield the carbene complexes. It is known that compounds like **1a–c** are capable of losing one or both carbonyl ligands in reactions involving strong donor ligands when irradiated or heated.⁷ We believe, however, in case of the molybdenum and tungsten complexes **1b** and **1c**, that the reaction with the acetylides occurs directly at the metal center. The resulting complex then undergoes decarbonylation, generating the alkynyl metalate anion **10** as an intermediate for the vinylidene products. Such



attacks of electrophiles at the β -carbon atom of transition metal alkynyl complexes $\text{L}_n\text{M}-\text{C}\equiv\text{CR}$ are well documented in the literature and represent one of the main preparative routes to vinylidene metal complexes.^{3,8}

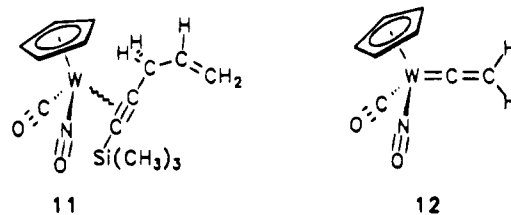
A possible reason for the different reactivity of the chromium complex **1a** with the acetylides on one hand and the molybdenum and tungsten complexes **1b** and **1c** on the other hand might be due to the relative strength of the metal to carbon monoxide bonds and the ease of the CO substitution reaction. Although the bond dissociation energies increase from $\text{Cr}(\text{CO})_6 < \text{Mo}(\text{CO})_6 < \text{W}(\text{CO})_6$, the rate of ligand substitution is often $\text{Cr} < \text{Mo} > \text{W}$, implying that a nondissociative mechanism is involved.^{9,10} This nondissociative substitution of carbon monoxide in the complexes **1b** and **1c** could be the result of an easier nucleophilic attack at the metal centers in **1b** and **1c** compared to **1a**. In agreement with this hypothesis, electrochemical measurements show a higher

reduction potential for **1a** ($E_{1/2} = -1.83 \text{ V}$) than for **1b** (-1.73 V) and **1c** (-1.77 V).¹¹

Ligand substitution from the 18-electron complexes **1b** and **1c** presumably occurs by (single) electron transfer into the $\text{M}-\text{NO} \pi^*$ -orbital and changing the geometry of $\text{M}-\text{NO}$ from a linear to a bent structure¹² so that a hypercoordinated (7-coordinate) $[\text{CpM}(\text{CO})_2\text{NO}-\text{nuc}]^-$ species is formed. Rehybridization of NO and dissociation of CO then generates the anionic intermediate **10**.

In this context it is interesting to mention that the reaction of the carbonyl compounds **1a–c** with LiC_6H_5 , independent of the identity of the central metal atom, leads in high yields to the corresponding carbene complexes as the only isolated product.¹³

Interestingly a new type of product is formed when the acetylide **2e**, bearing a trimethylsilyl group, is used instead of aryl- or alkyl-substituted lithium acetylides **2a–d**. Upon treating the green solution with $\text{CF}_3\text{SO}_3\text{CH}_3$ at -30°C in THF, the η^2 -alkyne complex **4f** was obtained in 68% yield (5:1 mixture of two rotamers; $\Delta G^\ddagger = 19.8(\pm 0.3) \text{ kcal/mol}$, measured by temperature dependent ^1H NMR experiments). Treatment of the green solution with allylbromide as electrophile produces the η^2 -alkyne complex **11** in 28% yield (4:1 mixture of



rotamers). Only η^2 -alkyne complexes are formed when the metalate anion (**10**, $\text{R} = \text{C}_6\text{H}_5$), generated by the addition of aryllithium acetylides to **1c**, is trapped by (trimethylsilyl)chloride as the electrophilic reagent. Treatment of **1c** with the acetylide **2a** or **2c** and

(11) Geiger, W. E.; Rieger, P. H.; Tulyathan B.; Rausch, M. D. *J. Am. Chem. Soc.* **1984**, *106*, 7000–7006. Legzdins, P.; Reina, R.; Shaw, M. J.; Batchelor, R. J.; Einstein, F. W. B. *Organometallics* **1993**, *12*, 1029–1037.

(12) Song, J.; Hall, M. B. *J. Am. Chem. Soc.* **1993**, *115*, 327–336. Legzdins, P.; Veltheer, J. E. *Acc. Chem. Res.* **1993**, *26*, 41–48.

(13) Fischer, E. O.; Beck, H. *J. Chem. Ber.* **1971**, *104*, 3101–3107.

(7) Richter-Addo, G. B.; Legzdins, P. *Chem. Rev.* **1988**, *88*, 991–1010.

(8) Silvestre, J.; Hoffmann, R. *Helv. Chim. Acta* **1985**, *68*, 1461–1506. Kostic, N. M.; Fenske, R. F. *Organometallics* **1982**, *1*, 974–982. Schilling, B. E. R.; Hoffmann, R.; Lichtenberger, D. L. *J. Am. Chem. Soc.* **1979**, *101*, 585–591. Delbecq, F. *J. Organomet. Chem.* **1991**, *406*, 171–182.

(9) Collman, J. P.; Hegedus, L. S.; Norton, J. R.; Finke, R. G. *Principles and Applications of Organotransition Metal Chemistry*; University Science Books: Mill Valley, CA, 1987.

(10) Harvey, D. F.; Grenzer, E. M.; Gantzel, P. K. *J. Am. Chem. Soc.* **1994**, *116*, 6719–6731. Ehlers, W. A.; Frenking, G. *Organometallics* **1995**, *14*, 423–426.

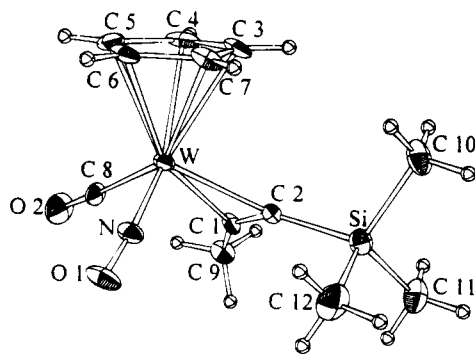
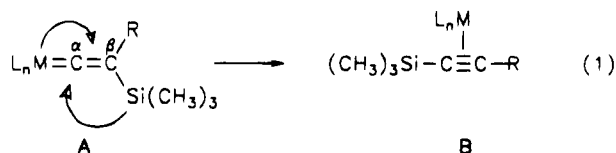


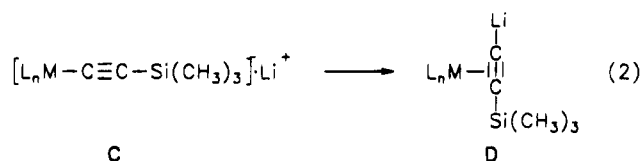
Figure 1. ORTEP diagram for $\{(\eta^5\text{-C}_5\text{H}_5)(\text{CO})(\text{NO})\text{W}[\text{H}_3\text{C}-\text{C}\equiv\text{C}-\text{Si}(\text{CH}_3)_3]\}$ (**4f**).

subsequent addition of (trimethylsilyl)chloride produced **4a** in 54% yield (3:2 rotamers) and **4c** in 25% yield (2:1 rotamers), respectively. Structural assignment of the η^2 -alkyne complexes **4a,c,f** and **11** is based on the characteristic IR-absorption¹⁴ at 1781, 1810, 1820, and 1823 cm^{-1} , respectively. In addition, the X-ray crystal structure of **4f** was determined (Figure 1).

The observation that η^2 -alkyne complexes are formed from the reaction of **1c** with the acetylides **2a** and **2e**, followed by alkylation with (trimethylsilyl)chloride, means that this reactivity needs further study. One explanation would be that the silylation of **10** (R = phenyl) or the alkylation of **10** (R = trimethylsilyl) occurs in both cases at the β -carbon atom, yielding the vinylidene derivative **A** (eq 1). This is followed by a



β -to- α carbon shift of the trimethylsilyl group to form the η^2 -alkyne complex **B**. The rearrangement of vinylidene metal complexes to η^2 -alkyne derivatives, however, is contradictory to experience and thermodynamic expectations.^{8,15} Extended Hückel and nonparameterized MO calculations support the thermodynamic stability of vinylidene complexes compared to the η^2 -alkyne complexes.⁸ An exception to this behavior is the recently observed isomerization of the cationic dicarbonyl(η^5 -cyclopentadienyl)iron (Fp) vinylidene complexes to the η^2 -alkyne derivatives.¹⁶ The tendency of Fp vinylidene complexes to rearrange is presumably due to the extreme electrophilicity of vinylidene α -carbon, the high π -acidity of carbonyl ligands, and the low electron density on the metal in Fp complexes. It is also conceivable, that the trimethylsilyl-substituted metalate anion **C** undergoes a σ/π rearrangement to form the π -coordinated alkynyl anion **D** prior to alkylation (eq 2). A similar rearrangement has been recently postu-



lated for polymetallic compounds to explain the conversion of an μ -acetylide complex into its η^2 -alkyne lithium derivative.¹⁷

The molybdenum complex **1b** shows a similar dichotomous reactivity with acetylides as the analogous tungsten complex **1c**. We have demonstrated previously that the addition of acetylide **2a** to **1b** and subsequent reaction with methyl trifluoromethanesulfonate, diluted HCl, or acetylchloride leads to the corresponding vinylidene complexes.² Treatment of **1b** at -30°C in THF with **2e** and addition of methyl trifluoromethanesulfonate or (trimethylsilyl)chloride to the metalate anion solution gave, analogous to the tungsten complex, the η^2 -alkyne derivatives **3f** (49%) and **3e** (50%). Attempts to prepare the tungsten complex **4e** were hitherto unsuccessful. Interestingly the reaction of **2e** with the tungsten complex **1c** resulted, after the anion was trapped with (trimethylsilyl)chloride and subsequently hydrolyzed with a solution of NaHCO_3 , in the unsubstituted vinylidene complex **12** as air stable orange crystals in 53% yield, instead of the expected **4e**. The corresponding η^2 -alkyne complex $[(\eta^5\text{-C}_5\text{H}_5)(\text{CO})(\text{NO})\text{W}(\text{HC}\equiv\text{CH})]^{18}$ could not be obtained from this reaction sequence.

Reactions of the Alkynylcarbene Complex 7a with Secondary Amines. Secondary amines react with pentacarbonyl(1-alkoxy-1-alkynylcarbene)chromium complexes to yield either the corresponding 1-aminocarbene- or β -aminovinylcarbene as well as allenylidene complexes.^{5,19,20} The product ratio is influenced by the size of the substituent on the acetylene terminus, the basicity of the amine, and the reaction temperature.^{5,20} In order to investigate the influence of the ligands on chromium we studied the addition reactions of secondary amines to **7a**.

The addition of dimethylamine to **7a** at -78 or -20°C yielded, independent of the reaction temperature, the 1-(dimethylamino) complex **13** as the only product in 50% yield. This complex shows a $\text{C}\equiv\text{C}$ stretching vibration at $\bar{\nu}$ 2171 cm^{-1} and a carbene carbon absorption at 262.7 ppm in the ^{13}C NMR spectra. Both these observations are in accordance with the structure **13**. Complex **7a** reacts with morpholine and piperidine at 20°C in a Michael-type addition to produce the vinylcarbene complexes **14** and **15**. The configuration of the $\text{C}=\text{C}$ double bond in complex **14** was established by NOE measurements (see Scheme 2).

To summarize, the reaction of molybdenum and tungsten complexes **1b** and **1c** with **2** give rise—in a CO substitution reaction, after addition of an electrophile—either to a vinylidene or an η^2 -alkyne metal complex. Vinylidene derivatives are formed when alkyl or aryl acetylides are used and the metalate anion is either trapped with a C-electrophile or with diluted acid. In

(14) Werner, H.; Rappert, T. *Chem. Ber.* **1993**, *126*, 669–678. Löwe, C.; Hund, H.-U.; Berke, H. *J. Organomet. Chem.* **1989**, *378*, 211–225.

(15) Werner, H.; Baum, M.; Schneider, D.; Windmüller, B. *Organometallics* **1994**, *13*, 1089–1097.

(16) Bly, R. S.; Zhong, Z.; Kane, C.; Bly, R. K. *Organometallics* **1994**, *13*, 899–908.

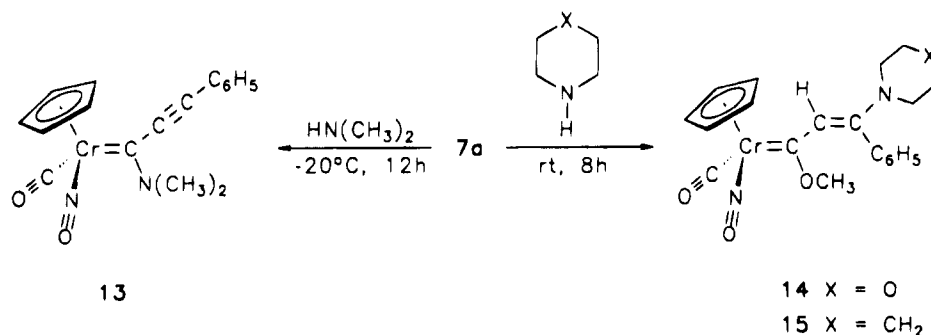
(17) Ferrer, M.; Rossel, O.; Seco, M.; Pellinghelli, M. A.; Tiripiccio, A. *Organometallics* **1995**, *14*, 57–62.

(18) Alt, H. G.; Hayen, H. I. *Angew. Chemie* **1983**, *95*, 1030–1031; *Angew. Chem., Int. Ed. Engl.* **1983**, *22*, 1008.

(19) Fischer, E. O.; Kreissl, F. R. *J. Organomet. Chem.* **1972**, *35*, C47–C51. Fischer, E. O.; Kalder, H. J. *J. Organomet. Chem.* **1977**, *131*, 57–64. Pipoh, R.; van Eldik, R.; Henkel, G. *Organometallics* **1993**, *12*, 2236–2242. Pipoh, R.; van Eldik, R. *Organometallics* **1993**, *12*, 2668–2671.

(20) Duetsch, M.; Stein, F.; Lackmann, R.; Pohl, E.; Herbst-Irmer, R.; de Meijere, A. *Chem. Ber.* **1992**, *125*, 2051–2065. Rahm, A.; Wulff, W. D.; Rheingold, A. L. *Organometallics* **1993**, *12*, 597–599.

Scheme 2

Table 1. Crystallographic Data for $\{(\eta^5\text{-C}_5\text{H}_5)(\text{CO})(\text{NO})\text{W}[\text{H}_3\text{C}-\text{C}\equiv\text{C}-\text{Si}(\text{CH}_3)_3]\}$ (**4f**)

cryst dimens	0.19 × 0.08 × 0.04 mm ³
color and habit	red, transparent, pinacoidal
cryst syst	triclinic
space group	P1 (No. 2)
lattice constants	$a = 10.80(1) \text{ \AA}$, $\alpha = 94.88(1)^\circ$ $b = 9.72(1) \text{ \AA}$, $\beta = 94.16(1)^\circ$ $c = 8.07(1) \text{ \AA}$, $\gamma = 114.09(1)^\circ$
vol	765.6(14) Å ³
formula units per unit cell	Z = 2
density (calcd)	1.818 g/cm ³
linear abs coeff	76.16 cm ⁻¹
diffractometer	four-circle (PW 1100, Philips)
radiation	Mo Kα ($\lambda = 0.71069 \text{ \AA}$)
monochromator	graphite
data collection	ω -scan, background-peak-background method, room temp
scan range	6° ≤ 2θ ≤ 50° -12 ≤ h ≤ 12, -11 ≤ k ≤ 11, -9 ≤ l ≤ 9
reflins collected	5403
goodness of fit (R_m)	0.0812
indpt reflins	2708
indpt reflins, $F_o > 4\sigma(F_o)$	1667
applied corrections	Lorentz and polarization coefficients
structure determination and refinement	W positional parameters from Patterson synthesis (program SHELXS-86 ^a), additional atoms from ΔF synthesis (program SHELXL-93 ^b), structure refinement by the anisotropic full-matrix least-squares procedure for all non-hydrogen atoms. Hydrogen position refinement by "riding" model, atomic scattering factors from footnote c.
no. of params	154
$R(F^2)$	0.1569
$R(F)$	0.1102 for all 2708 reflins
$R(F)$	0.0592 for all 1667 reflins with $F_o > 4\sigma(F_o)$

^a Sheldrick, G. M. *SHELXS-86, Program for the Solution of Crystal Structures*; Universität Göttingen: Göttingen, Germany, 1986.

^b Sheldrick, G. M. *SHELXL-93, Program for Crystal Structure Refinement*; Universität Göttingen: Göttingen, Germany, 1993. ^c *International Tables for Crystallography*; Wilson, A. J. C., Ed.; Kluwer Academic Publishers: Dordrecht, The Netherlands, 1992; Vol. C.

contrast to this behavior, η^2 -alkyne complexes are formed either when **1b** or **1c** react with an acetylide bearing a trimethylsilyl group, or the metalate anion is trapped with (trimethylsilyl)chloride as electrophile. Under the conditions used here, independent of the applied acetylide or electrophile, chromium complex **1a** leads only to the carbene complex.

Molecular Structure of Complex 4f. Crystallization of complex **4f** in pentane resulted in single-crystals. The X-ray diffraction study confirmed the structure of **4f** as an η^2 -alkyne complex. The ORTEP plot (Figure 1) reveals that the coordination geometry about the tungsten center in **4f** is a slightly distorted piano-stool structure. The most notable features of the structure parameters are bond distances W-C1 (2.23(2) Å) and W-C2 (2.20(2) Å) which are shorter than a W-C(sp³) bond.²¹ The bond length of C1-C2 is 1.27(2) Å, just between a C=C double- and a C≡C triple-bond length.

Table 2. Selected Bond Distances (Å) for $\{(\eta^5\text{-C}_5\text{H}_5)(\text{CO})(\text{NO})\text{W}[\text{H}_3\text{C}-\text{C}\equiv\text{C}-\text{Si}(\text{CH}_3)_3]\}$ (**4f**)

W-C(1)	2.23(2)	W-C(7)	2.36(2)
W-C(2)	2.20(2)	W-C(8)	1.99(2)
W-C(3)	2.40(2)	W-N	1.80(2)
W-C(4)	2.37(2)	N-O(1)	1.19(2)
W-C(5)	2.34(2)	C(8)-O(2)	1.11(2)
W-C(6)	2.32(2)	C(1)-C(2)	1.27(2)
C(2)-Si	1.82(2)	C(1)-C(9)	1.50(2)

The dihedral angle C8-W-C1-C2 = 11.3(1.3)° shows that the C1-C2 bond axis is nearly parallel to the W-CO axis. The C1-C2-Si angle of 145.2(14)° and C2-C1-C9 angle of 148.8(17)° shows that the C-C≡C-Si moiety is not linear. For crystallographic data and selected bond distances and angles, see Tables 1-4.

Experimental Section

General Considerations. All reactions were carried out under an argon atmosphere (99.99%, by Messer-Griesheim) with the use of standard Schlenk techniques. Solvents were

(21) Alt, H. G.; Han, J. S.; Rogers, R. D.; Thewalt, U. *J. Organomet. Chem.* **1993**, *459*, 209-217.

Table 3. Selected Bond Angles (deg) for $\{(\eta^5\text{-C}_5\text{H}_5)(\text{CO})(\text{NO})\text{W}[\text{H}_3\text{C}-\text{C}\equiv\text{C}-\text{Si}(\text{CH}_3)_3]\}$ (4f**)**

C(1)-W-C(2)	33.3(6)	C(2)-W-C(6)	134.3(8)
C(1)-W-C(3)	100.3(6)	C(2)-W-C(7)	99.2(8)
C(1)-W-C(4)	101.1(6)	C(2)-W-C(8)	107.6(7)
C(1)-W-C(5)	132.7(8)	C(2)-W-N	96.7(7)
C(1)-W-C(6)	156.7(6)	C(8)-W-N	92.6(8)
C(1)-W-C(7)	126.9(7)	W-N-O(1)	174.6(14)
C(1)-W-C(8)	74.9(7)	C-C(8)-O(2)	177(2)
C(1)-W-N	104.4(6)	W-C(1)-C(9)	139.3(13)
C(2)-W-C(3)	83.8(7)	W-C(2)-Si	138.3(9)
C(2)-W-C(4)	102.3(8)	C(1)-C(2)-Si	145.2(14)
C(2)-W-C(5)	138.2(7)	C(2)-C(1)-C(9)	148.8(17)

Table 4. Atomic Coordinates ($\times 10^4$) for $\{(\eta^5\text{-C}_5\text{H}_5)(\text{CO})(\text{NO})\text{W}[\text{H}_3\text{C}-\text{C}\equiv\text{C}-\text{Si}(\text{CH}_3)_3]\}$ (4f**)**

atom	x	y	z
W	1972(1)	4121(1)	1685(1)
Si	3182(6)	1147(6)	2714(8)
O1	1156(13)	2599(19)	-1846(16)
O2	3800(19)	7253(19)	667(26)
N	1542(14)	3201(19)	-440(19)
C1	4105(15)	4404(20)	2383(19)
C2	3305(17)	3046(19)	2519(19)
C3	1037(20)	3494(30)	4270(22)
C4	1475(20)	5031(33)	4254(24)
C5	623(25)	5225(27)	2864(30)
C6	-228(19)	3804(34)	2117(23)
C7	28(21)	2723(27)	2978(24)
C8	3151(21)	6110(22)	999(27)
C9	5533(17)	5606(21)	2525(24)
C10	2097(24)	278(26)	4381(32)
C11	4937(25)	1250(29)	3236(35)
C12	2395(30)	75(27)	667(34)

purified by standard methods and distilled under argon prior to use. Literature methods were used to prepare $(\eta^5\text{-C}_5\text{H}_5)\text{M}(\text{CO})_2(\text{NO})$ (**1**) ($\text{M} = \text{Cr}, \text{Mo}, \text{W}$)²² and allyl propargyl ether.²³ All other compounds were commercially available. NMR spectra were obtained on Bruker AM 400 and AC 200 spectrometers. Proton and carbon chemical shifts are referred to tetramethylsilane. MS measurements (70 eV) were performed on a Varian MAT 311-A. IR spectra were recorded on a Bruker FT-IR IFS 85. Microanalyses were done on a Carlo Erba 1104 elemental analyzer.

$\{(\eta^5\text{-C}_5\text{H}_5)(\text{CO})(\text{NO})\text{M}[(\text{CH}_3)_3\text{Si}-\text{C}\equiv\text{C}-\text{Si}(\text{CH}_3)_3]\}$ (**3e**). At -30°C , a solution of 7.5 mmol of ((trimethylsilyl)ethynyl)lithium (**2e**) in 15 mL of THF was added dropwise to the orange solution of **1b** (1.24 g, 5 mmol) in THF (50 mL). The progress of the reaction was monitored by IR. After complete disappearance of **1b** (4 h), 0.95 mL (7.5 mmol) of trimethylchlorosilane was added to the deep green reaction mixture at -30°C . After 6 h, the orange solution was washed with saturated aqueous sodium bicarbonate and saturated aqueous sodium chloride. After usual workup the residue was chromatographed (silica gel; pentane:ether 10:1) to yield 970 mg (50%) of **3e** as orange crystals, mp 102–103 $^\circ\text{C}$ (decomp). Anal. Calcd for $\text{C}_{14}\text{H}_{23}\text{MoNO}_2\text{Si}_2$: C, 43.18; H, 5.95; N, 3.60. Found: C, 43.25; H, 5.90; N, 3.53. ^1H NMR (CDCl_3) δ 5.46 (s, 5H, Cp), 0.36 (s, 9H, $\text{Si}(\text{CH}_3)_3$), 0.30 (s, 9H, $\text{Si}(\text{CH}_3)_3$); ^{13}C NMR (CDCl_3) δ 235.1 (C=O), 95.7 (Cp), 93.4 (alkyne), 1.1 ($\text{Si}(\text{CH}_3)_3$), 0.6 ($\text{Si}(\text{CH}_3)_3$); IR (KBr) $\bar{\nu}$ (cm^{-1}) 1954 (C=O), 1825 (C \equiv C), 1599 (N=O); MS (70 eV) m/e 389 (M^+ , ^{96}Mo), 361 ($\text{M}^+ - \text{CO}$), 331 ($\text{M}^+ - \text{CO} - \text{NO}$); high-resolution mass spectrum calcd for $\text{C}_{14}\text{H}_{23}^{92}\text{MoNO}_2\text{Si}_2$ (M^+) m/e 385.0335, found m/e 385.0321.

$\{(\eta^5\text{-C}_5\text{H}_5)(\text{CO})(\text{NO})\text{M}[\text{H}_3\text{C}-\text{C}\equiv\text{C}-\text{Si}(\text{CH}_3)_3]\}$ (**3f**). The preparation of **3f** is analogous to that for **3e**, but, instead of trimethylchlorosilane, 0.85 mL (7.5 mmol) of $\text{CF}_3\text{SO}_3\text{CH}_3$ was used. After 30 min, the orange solution was treated analogous to **3e**. Yield: 820 mg (49.5%) of **3f**, as orange crystals, mp

44–45 $^\circ\text{C}$. Anal. Calcd for $\text{C}_{12}\text{H}_{17}\text{MoNO}_2\text{Si}$: C, 43.51; H, 5.17; N, 4.23. Found: C, 43.61; H, 5.11; N, 4.40. ^1H NMR (CDCl_3) δ 5.52 (s, 5H, Cp), 2.69 (s, 3H, CH_3), 0.31 (s, 9H, $\text{Si}(\text{CH}_3)_3$); ^{13}C NMR (CDCl_3) δ 231.2 (C=O), 115.1 (alkyne), 96.2 (Cp), 90.2 (alkyne), 14.2 (CH_3), 0.5 ($\text{Si}(\text{CH}_3)_3$); IR (CCl_4) $\bar{\nu}$ (cm^{-1}) 1976 (C=O), 1853 (C \equiv C), 1624 (N=O); MS (70 eV) m/e 331 (M^+ , ^{96}Mo), 303 ($\text{M}^+ - \text{CO}$), 273 ($\text{M}^+ - \text{CO} - \text{NO}$).

$\{(\eta^5\text{-C}_5\text{H}_5)(\text{CO})(\text{NO})\text{W}[(\text{CH}_3)_3\text{Si}-\text{C}\equiv\text{C}-\text{C}_6\text{H}_5]\}$ (**4a**). At -30°C , a solution of 4.5 mmol of (phenylethynyl)lithium (**2a**) in 15 mL of THF was added dropwise to an orange solution of **1c** (1.0 g, 3 mmol) in THF (30 mL). The progress of the reaction was monitored by IR. After complete disappearance (3 h) of **1c**, 0.6 mL (4.5 mmol) of trimethylchlorosilane was added to the deep green reaction mixture at -30°C . After 6 h, the orange solution was washed with saturated aqueous sodium bicarbonate and saturated aqueous sodium chloride. After usual workup the residue was chromatographed (silica gel; pentane:ether 10:1) to yield 780 mg (54%) of **4a**, as orange crystals, mp 83 $^\circ\text{C}$. Anal. Calcd for $\text{C}_{17}\text{H}_{19}\text{NO}_2\text{SiW}$: C, 42.43; H, 3.98; N, 2.91. Found: C, 42.63; H, 3.66; N, 2.91. Two rotamers: ^1H NMR (CDCl_3) δ 7.66–7.23 (m, 5H, Ph), 5.74 and 5.59 (two s, 2:3, Cp), 0.37 and 0.35 (two s, 2:3, $\text{Si}(\text{CH}_3)_3$); ^{13}C NMR (CDCl_3) δ 218.4 and 217.9 (two C=O), 136.3, 135.6, 131.2, 128.5, 128.4, 128.2 (arom C), 129.4 and 127.5 (alkyne), 104.0 and 97.3 (alkyne), 96.3 and 95.9 (two Cp), 0.7 and 0.5 (two $\text{Si}(\text{CH}_3)_3$); IR (CCl_4) $\bar{\nu}$ (cm^{-1}) 1986 (C=O), 1792 (C \equiv C), 1610 (N=O); MS (70 eV) m/e 481 (M^+ , ^{184}W), 453 ($\text{M}^+ - \text{CO}$), 423 ($\text{M}^+ - \text{CO} - \text{NO}$); high-resolution mass spectrum calcd for $\text{C}_{17}\text{H}_{19}\text{NO}_2\text{Si}^{182}\text{W}$ (M^+) m/e 479.0667, found m/e 479.0632.

$\{(\eta^5\text{-C}_5\text{H}_5)(\text{CO})(\text{NO})\text{W}[(\text{CH}_3)_3\text{Si}-\text{C}\equiv\text{C}-\text{CH}_2\text{OCH}_2\text{-CH}=\text{CH}_2]\}$ (**4c**). The preparation of **4c** is analogous to that of **4a**, but, instead of (phenylethynyl)lithium, 4.5 mmol of lithium compound **2c** was used. Yield: 356 mg (25%) of **4c**, as a red oil. Two rotamers: ^1H NMR (CDCl_3) δ 6.07–5.84 (m, 1H, CH), 5.69 and 5.68 (two s, 1:2, Cp), 5.40–5.16 (m, 2H, CH_2), 5.10–4.80 (m, 2H, CH_2), 4.18–3.95 (m, 2H, CH_2), 0.33 and 0.26 (two s, 2:1, $\text{Si}(\text{CH}_3)_3$); ^{13}C NMR (CDCl_3) δ 218.2 and 217.3 (two C=O), 135.4 and 134.6 (two CH), 125.1 (alkyne), 117.1 and 117.0 (two CH_2), 98.9 (alkyne), 95.7 and 95.5 (two Cp), 71.3 and 71.2 (two CH_2), 70.9 and 70.3 (two CH_2), 0.6 and 0.0 (two $\text{Si}(\text{CH}_3)_3$); IR (cm^{-1}) 1977 (C=O), 1810 (C \equiv C), 1594 (N=O); MS (70 eV) m/e 475 (M^+ , ^{184}W), 447 ($\text{M}^+ - \text{CO}$), 417 ($\text{M}^+ - \text{CO} - \text{NO}$); high-resolution mass spectrum calcd for $\text{C}_{15}\text{H}_{21}\text{NO}_3\text{Si}^{182}\text{W}$ (M^+) m/e 473.0773, found m/e 473.0762.

$\{(\eta^5\text{-C}_5\text{H}_5)(\text{CO})(\text{NO})\text{W}[\text{H}_3\text{C}-\text{C}\equiv\text{C}-\text{Si}(\text{CH}_3)_3]\}$ (**4f**). The preparation of **4f** is analogous to that of molybdenum complex **3f**. A 1.0 g (3 mmol) amount of **1c** yielded 855 mg (68%), as red crystals, mp 68 $^\circ\text{C}$. Anal. Calcd for $\text{C}_{12}\text{H}_{17}\text{NO}_2\text{SiW}$: C, 34.38; H, 4.09; N, 3.34. Found: C, 34.30; H, 4.04; N, 3.15. Two rotamers: ^1H NMR (CDCl_3) δ 5.65 and 5.60 (two s, 5:1, Cp), 2.88 and 2.81 (two s, 1:5, CH_3), 0.31 and 0.22 (two s, 5:1, $\text{Si}(\text{CH}_3)_3$); ^{13}C NMR (CDCl_3) δ 219.7 (C=O), 132.4 and 122.5 (alkyne), 95.7 and 95.5 (two Cp), 92.5 and 87.0 (alkyne), 19.8 and 14.7 (two CH_3), 0.41 and 0.39 (two $\text{Si}(\text{CH}_3)_3$); IR (CCl_4) $\bar{\nu}$ (cm^{-1}) 1975 (C=O), 1812 (C \equiv C), 1605 (N=O); MS (70 eV) m/e 419 (M^+ , ^{184}W), 391 ($\text{M}^+ - \text{CO}$), 361 ($\text{M}^+ - \text{CO} - \text{NO}$); high-resolution mass spectrum calcd for $\text{C}_{12}\text{H}_{17}\text{NO}_2\text{Si}^{182}\text{W}$ (M^+) m/e 417.0511, found 417.0498.

$\{(\eta^5\text{-C}_5\text{H}_5)(\text{CO})(\text{NO})\text{Mo}=\text{C}-\text{C}(\text{CH}_3)[\text{C}(\text{CH}_3)_3]\}$ (**5b**). At -30°C , a solution of 7.5 mmol of (2,2-dimethylpropynyl)lithium (**2b**) in 15 mL of THF was added dropwise to the orange solution of **1b** (1.24 g, 5 mmol) in THF (50 mL). The progress of the reaction was monitored by IR. After complete disappearance of **1b** (4 h), 0.85 mL (7.5 mmol) of $\text{CF}_3\text{SO}_3\text{CH}_3$ was added to the deep green reaction mixture at -30°C . After 30 min, the orange solution was washed with saturated aqueous sodium bicarbonate and saturated aqueous sodium chloride. After usual workup the residue was chromatographed (silica gel; pentane:ether 10:1) to yield 1040 mg (66%) of **5b**, as orange crystals, mp 67–68 $^\circ\text{C}$ (decomp). Anal. Calcd for $\text{C}_{13}\text{H}_{17}\text{MoNO}_2$: C, 49.53; H, 5.44; N, 4.44. Found: C, 49.53; H, 5.16; N, 4.33. Two rotamers ($\Delta G^\ddagger = 19.7(\pm 0.3)$ kcal/mol

(22) Chin, T. T.; Hoyano, J. K.; Legzdins, P.; Malito, J. T. *Inorg. Synth.* **1990**, *28*, 196–198.

(23) Billington, D. C.; Willison, D. *Tetrahedron Lett.* **1984**, *36*, 4041–4044.

by temperature dependent ^1H NMR spectra): ^1H NMR (CDCl_3) δ 5.74 and 5.72 (two s, 2:1, Cp), 1.68 and 1.63 (two s, 1:2, CH_3), 1.13 and 1.08 (two s, 2:1, $\text{C}(\text{CH}_3)_3$); ^{13}C NMR (CDCl_3) δ 361.3 and 360.1 (two C_α), 219.6 and 219.3 (two $\text{C}=\text{O}$), 142.6 (C_β), 97.2 and 96.5 (two Cp), 35.5 and 34.1 (two $\text{C}(\text{CH}_3)_3$), 29.7 and 29.5 (two $\text{C}(\text{CH}_3)_3$), 12.6 and 10.9 (two CH_3); IR (CCl_4) $\bar{\nu}$ (cm^{-1}) 2010 ($\text{C}=\text{O}$), 1654 ($\text{N}=\text{O}$); MS (70 eV) m/e 315 (M^+ , ^{96}Mo), 287 ($\text{M}^+ - \text{CO}$), 257 ($\text{M}^+ - \text{CO} - \text{NO}$); high-resolution mass spectrum calcd for $\text{C}_{13}\text{H}_{17}^{92}\text{MoNO}_2$ (M^+) m/e 311.0327, found m/e 311.0306.

Preparation of 5b at Different Temperatures. The preparation was carried out as described above; the lithium compound **2b** was added at -78°C . The temperature was held at -78°C for 6–7 h to complete the reaction. All other steps were identical. Only vinylidene **5b** could be isolated. Preparation at 0°C led to vinylidene **5b** in 3 h but resulted in lower yields.

$(\eta^5\text{-C}_5\text{H}_5)(\text{CO})(\text{NO})\text{W}=\text{C}=\text{C}(\text{CH}_3)(\text{C}_6\text{H}_5)$ (6a**).** The preparation of **6a** is analogous to that of molybdenum complex **3f**. A 4.5 mmol amount of (phenylethynyl)lithium (**2a**) and 1.0 g (3 mmol) of **1c** yielded 647 mg (51%) of **6a**, as red crystals, mp 119°C . Anal. Calcd for $\text{C}_{15}\text{H}_{13}\text{NO}_2\text{W}$: C, 42.58; H, 3.10; N, 3.31. Found: C, 42.64; H, 2.75; N, 3.31. Two rotamers: ^1H NMR (CDCl_3) δ 7.40–7.08 (m, 5H, Ph), 5.84 (s, 5H, Cp), 2.05 and 1.96 (two s, 1:2, CH_3); ^{13}C NMR (CDCl_3) δ 344.9 and 344.8 (two C_α), 211.1 and 210.2 (two $\text{C}=\text{O}$), 136.9 (arom C), 136.6 and 135.4 (two C_β), 129.4, 126.6, 125.3, 125.0 (arom C), 96.4 and 96.1 (two Cp), 15.0 and 13.3 (two CH_3); IR (CCl_4) $\bar{\nu}$ (cm^{-1}) 2005 ($\text{C}=\text{O}$), 1647 ($\text{N}=\text{O}$); MS (70 eV) m/e 423 (M^+ , ^{184}W), 395 ($\text{M}^+ - \text{CO}$), 365 ($\text{M}^+ - \text{CO} - \text{NO}$); high-resolution mass spectrum calcd for $\text{C}_{15}\text{H}_{13}\text{NO}_2^{184}\text{W}$ (M^+) m/e 423.0456, found m/e 423.0457.

Preparation of 6a at Different Temperatures. The preparation was carried out as described for **3f**; the lithium compound **2a** was added at -78°C . The temperature was held at -78°C for 6 h to complete the reaction. All other steps were identical. Only vinylidene **6a** could be isolated. Preparation at 0°C led in 3 h to vinylidene **6a**.

$(\eta^5\text{-C}_5\text{H}_5)(\text{CO})(\text{NO})\text{W}=\text{C}=\text{C}(\text{CH}_3)[\text{C}(\text{CH}_3)_3]$ (6b**).** The preparation of **6b** is analogous to that of molybdenum complex **3f**. A 4.5 mmol amount of **2b** and 1.0 g (3 mmol) of **1c** yielded 810 mg (67%) of **6b**, as orange crystals, mp 102°C . Anal. Calcd for $\text{C}_{13}\text{H}_{17}\text{NO}_2\text{W}$: C, 38.73; H, 4.25; N, 3.47. Found: C, 38.84; H, 4.02; N, 3.72. Two rotamers: ^1H NMR (CDCl_3) δ 5.85 and 5.80 (two s, 2:1, Cp), 1.72 and 1.64 (two s, 1:2, CH_3), 1.14 and 1.08 (two s, 2:1, $\text{C}(\text{CH}_3)_3$); ^{13}C NMR (CDCl_3) δ 339.6 and 338.5 (two C_α), 212.6 and 211.9 (two $\text{C}=\text{O}$), 145.1 (C_β), 96.3 and 95.6 (two Cp), 35.1 and 33.6 (two $\text{C}(\text{CH}_3)_3$), 29.8 and 29.5 (two $\text{C}(\text{CH}_3)_3$), 13.0 and 11.5 (two CH_3); IR (CCl_4) $\bar{\nu}$ (cm^{-1}) 1997 ($\text{C}=\text{O}$), 1629 ($\text{N}=\text{O}$); MS (70 eV) m/e 403 (M^+ , ^{184}W), 375 ($\text{M}^+ - \text{CO}$); high-resolution mass spectrum calcd for $\text{C}_{13}\text{H}_{17}\text{NO}_2^{182}\text{W}$ (M^+) m/e 401.0742, found m/e 401.0753.

$(\eta^5\text{-C}_5\text{H}_5)(\text{CO})(\text{NO})\text{W}=\text{C}=\text{C}(\text{CH}_3)(\text{CH}_2\text{OCH}_2\text{CH}=\text{CH}_2)$ (6c**).** At -30°C , a solution of 1.5 mmol of lithium compound **2c** in 10 mL of THF was added dropwise to the orange solution of **1c** (335 mg, 1 mmol) in THF (20 mL). The progress of the reaction was monitored by IR. After complete disappearance of **1c** (3 h), 0.17 mL (246 mg, 1.5 mmol) of $\text{CF}_3\text{SO}_3\text{CH}_3$ was added to the deep green reaction mixture at -30°C . After 30 min, the orange solution was washed with saturated aqueous sodium bicarbonate and saturated aqueous sodium chloride. After usual workup, chromatography on silica gel (pentane: ether 3:1) yielded 200 mg (48%) of **6c** as orange crystals from pentane, mp $54\text{--}55^\circ\text{C}$. Anal. Calcd for $\text{C}_{13}\text{H}_{13}\text{NO}_3\text{W}$: C, 37.43; H, 3.62; N, 3.36. Found: C, 37.84; H, 3.39; N, 3.20. Two rotamers: ^1H NMR (CDCl_3) δ 5.98–5.90 (m, 1H, $\text{CH}_2=\text{CH}$), 5.87 and 5.86 (two s, 1:1, Cp), 5.34–5.18 (m, 2H, $\text{CH}_2=\text{CH}$), 4.03–3.93 (m, 4H, $\text{CH}_2\text{O}-\text{CH}_2$), 1.76 and 1.72 (two s, 1:1, CH_3); ^{13}C NMR (CDCl_3) δ 337.6 and 337.3 (C_α), 210.6 and 210.4 (CO), 135.0 and 134.7 ($\text{CH}=\text{CH}_2$), 133.5 (C_β), 117.0 and 116.9 ($\text{CH}=\text{CH}_2$), 96.0 (Cp), 70.2, 69.3 and 68.4 ($\text{CH}_2\text{O}-\text{CH}_2$), 13.6 and 12.9 (CH_3); IR (CCl_4) $\bar{\nu}$ (cm^{-1}) 2003 ($\text{C}=\text{O}$), 1664 ($\text{C}=\text{C}=\text{W}$),

1636 ($\text{N}=\text{O}$); MS (70 eV) m/e 417 (M^+ , ^{184}W), 318 ($\text{M}^+ - \text{C}_3\text{H}_5 - \text{CO} - \text{NO}$).

$(\eta^5\text{-C}_5\text{H}_5)(\text{CO})(\text{NO})\text{W}=\text{C}=\text{C}(\text{CH}_3)[(\text{CH}_2)_2\text{OSi}(\text{CH}_3)_2\text{C}(\text{CH}_3)_3]$ (6d**).** The preparation was carried out as described for **6c**, but, instead of **2c**, 1.5 mmol of lithium compound **2d** was used. Chromatography on silica gel (pentane: ether 3:1) yielded 293 mg (58%) of **6d** as orange crystals from pentane. Anal. Calcd for $\text{C}_{17}\text{H}_{27}\text{NO}_3\text{SiW}$: C, 40.40; H, 5.38; N, 2.77. Found: C, 40.66; H, 5.24; N, 2.68. Two rotamers: ^1H NMR (CDCl_3) δ 5.78 and 5.77 (two s, 5:6, Cp), 3.58–3.70 (m, 2H, $\text{CH}_2\text{CH}_2\text{O}$), 2.08–2.29 (m, 2H, $\text{CH}_2\text{CH}_2\text{O}$), 1.67 and 1.61 (two s, 6:5, CH_3), 0.85 and 0.82 (two s, 5:6, $\text{C}(\text{CH}_3)_3$), 0.02, 0.00 (two s, 5:6, $\text{Si}(\text{CH}_3)_2$); ^{13}C NMR (CDCl_3) δ 338.8 and 338.1 (C_α), 211.4 and 211.1 (CO), 134.0 and 133.9 (C_β), 96.0 and 95.8 (Cp), 61.9 and 61.8 ($\text{CH}_2\text{CH}_2\text{O}$), 35.4 and 35.1 ($\text{CH}_2\text{CH}_2\text{O}$), 25.9 and 25.8 [$\text{C}(\text{CH}_3)_3$], 18.3 and 18.2 [$\text{C}(\text{CH}_3)_3$], 16.1 and 15.0 ($\text{CH}_3-\text{C}_\beta$), -5.31 and -5.39 [$\text{Si}(\text{CH}_3)_2$]; IR (CCl_4) $\bar{\nu}$ (cm^{-1}) 1999 ($\text{C}=\text{O}$), 1633 ($\text{N}=\text{O}$); MS (70 eV) m/e 505 (M^+ , ^{184}W), 477 ($\text{M}^+ - \text{CO}$), 447 ($\text{M}^+ - \text{CO} - \text{NO}$).

$(\eta^5\text{-C}_5\text{H}_5)(\text{CO})(\text{NO})\text{Cr}=\text{C}(\text{OCH}_3)(\text{C}=\text{C}-\text{C}_6\text{H}_5)$ (7a**).** To a solution of 2 mmol of (phenylethynyl)lithium (**2a**) in 20 mL of THF at -78°C chromium carbonyl was added **1a** (203 mg, 1 mmol) in 5 mL of THF. After the mixture was stirred under exclusion of light for 15 h at 0°C , 0.23 mL (328 mg, 2 mmol) of methyl triflate was added at -30°C . The mixture was stirred for 30 min at 0°C . After removal of the solvent under reduced pressure the residue was dissolved in ether and then filtered. After removal of the ether under reduced pressure, chromatography of the residue on silica gel (at first with pentane and then with pentane: ether 10:1) yielded 201 mg (63%) of **7a** as dark red crystals from pentane, mp 49°C . Anal. Calcd for $\text{C}_{16}\text{H}_{13}\text{CrNO}_3$: C, 60.19; H, 4.10; N, 4.39. Found: C, 60.22; H, 3.91; N, 4.13. ^1H NMR (CDCl_3) δ 7.48–7.35 (m, 5H, C_6H_5), 5.32 (s, 5H, Cp), 4.26 (s, broad, CH_3); ^{13}C NMR (CDCl_3) (-30°C , two rotamers) δ 307.2 and 306.5 (C_α), 232.0 and 230.2 (CO), 132.5, 131.4, 129.7, 129.0, 128.6 and 128.4 (arom C), 122.0 and 121.6 ($\text{C}=\text{C}$), 96.8 and 95.1 (Cp), 92.2 (C_β), 88.4 (C_β), 64.2 and 62.4 (CH_3); IR (CCl_4) $\bar{\nu}$ (cm^{-1}) 2152 ($\text{C}=\text{C}$), 1992 ($\text{C}=\text{O}$), 1676 ($\text{N}=\text{O}$); MS (70 eV) m/e 319 (M^+ , ^{52}Cr), 291 ($\text{M}^+ - \text{CO}$), 261 ($\text{M}^+ - \text{CO} - \text{NO}$).

$(\eta^5\text{-C}_5\text{H}_5)(\text{CO})(\text{NO})\text{Cr}=\text{C}(\text{OCH}_3)(\text{C}=\text{C}-\text{Si}(\text{CH}_3)_3)$ (7e**).** The preparation of **7e** was carried out as described for **7a**, but, instead of (phenylethynyl)lithium, 2 mmol of ((trimethylsilyl)ethynyl)lithium (**2e**) was used. Chromatography on silica gel (benzene: pentane 2:1) yielded 211 mg (67%) of **7e** as orange crystals from pentane, mp $57\text{--}58^\circ\text{C}$. Anal. Calcd for $\text{C}_{13}\text{H}_{17}\text{CrNO}_3\text{Si}$: C, 49.51; H, 5.43; N, 4.44. Found: C, 49.52; H, 5.19; N, 4.02. ^1H NMR (CDCl_3) δ 5.25 (s, 5H, Cp), 4.34 (s, broad, 3H, CH_3), 0.29 (s, 9H, $\text{Si}(\text{CH}_3)_3$); ^{13}C NMR (CDCl_3) (-35°C) δ 308.4 (C_α), 229.4 (CO), 106.0 (C_β), 97.3 (Cp), 95.1 (C_β), 64.5 (OCH_3), 0.26 ($\text{Si}(\text{CH}_3)_3$); IR (CCl_4) $\bar{\nu}$ (cm^{-1}) 2082 ($\text{C}=\text{C}$), 1995 ($\text{C}=\text{O}$), 1683 ($\text{N}=\text{O}$); MS (70 eV) m/e 315 (M^+ , ^{52}Cr), 287 ($\text{M}^+ - \text{CO}$), 257 ($\text{M}^+ - \text{CO} - \text{NO}$).

Attempt to Prepare 7a and 7e at Different Temperatures. At -78°C no reaction could be observed; at room temperature the only observed products were the carbenes **7a** and **7e** described above in poor yields.

$(\eta^5\text{-C}_5\text{H}_5)(\text{CO})(\text{NO})\text{Mo}=\text{C}=\text{C}(\text{H})(\text{C}(\text{CH}_3)_3)$ (8b**).** At -30°C , a solution of 7.5 mmol of (2,2-dimethylpropynyl)lithium (**2b**) in 15 mL of THF was added dropwise to the orange solution of **1b** (1.24 g, 5 mmol) in THF (50 mL). The progress of the reaction was monitored by IR. After complete disappearance of **1b** (4 h), at room temperature 1 mL of concentrated HCl diluted with 20 mL of water was added to the deep green reaction mixture. The color changed immediately to orange. This solution was washed with saturated aqueous sodium bicarbonate and saturated aqueous sodium chloride. After usual workup the residue was chromatographed (silica gel; pentane: ether 10:1) to yield 843 mg (56%) of **8b**, as orange crystals, mp 51°C (decomp). Anal. Calcd for $\text{C}_{12}\text{H}_{15}\text{MoNO}_2$: C, 47.85; H, 5.02; N, 4.65. Found: C, 48.13; H, 4.79; N, 4.72. Two rotamers: ^1H NMR (CDCl_3) δ 6.02 and 6.01 (two s, 1:1,

$C_{\beta}H$), 5.84 and 5.83 (two s, 1:1, Cp), 1.20 and 1.16 (two s, 1:1, $C(CH_3)_3$); ^{13}C NMR ($CDCl_3$) δ 360.9 and 360.4 (two C_{α}), 219.0 and 217.9 (two $C=O$), 137.7 and 137.2 (two C_{β}), 97.2 and 97.0 (two Cp), 35.3 and 33.7 (two $C(CH_3)_3$), 31.4 and 31.2 (two $C(CH_3)_3$); IR (KBr) $\bar{\nu}$ (cm^{-1}) 2008 ($C=O$), 1617 ($N=O$); MS (70 eV) m/e 301 (M^+ , ^{96}Mo), 273 ($M^+ - CO$), 243 ($M^+ - CO - NO$); high-resolution mass spectrum calcd for $C_{12}H_{15}^{92}MoNO_2$ (M^+) m/e 297.0171, found m/e 297.0169.

[($\eta^5-C_5H_5$)(CO)(NO)]W=C=C(H)(C₆H₅) (9a). The preparation of **9a** was analogous to that of molybdenum complex **8b**. A 4.5 mmol amount of (phenylethynyl)lithium (**2a**) and 1.0 g (3 mmol) of **1c** yielded 933 mg (76%) of **9a**, as orange crystals, mp 129 °C. Anal. Calcd for $C_{14}H_{11}NO_2W$: C, 41.10; H, 2.71; N, 3.42. Found: C, 41.12; H, 2.40; N, 3.32. Two rotamers: 1H NMR ($CDCl_3$) δ 7.22–7.03 (m, 5H, Ph), 6.59 and 6.54 (two s, 5:4, H), 5.84 and 5.81 (two s, 4:5, Cp); ^{13}C NMR ($CDCl_3$) δ 344.6 (C_{α}), 210.6 and 209.2 (two $C=O$), 133.3 (arom C), 131.3 and 130.9 (two C_{β}), 128.7, 126.7, 126.1, 125.9 (arom C), 96.5 and 96.4 (two Cp); IR (CCl_4) $\bar{\nu}$ (cm^{-1}) 2010 ($C=O$), 1654 ($N=O$); MS (70 eV) m/e 409 (M^+ , ^{184}W), 381 ($M^+ - CO$), 351 ($M^+ - CO - NO$); high-resolution mass spectrum calcd for $C_{14}H_{11}NO_2^{182}W$ (M^+) m/e 407.0272, found m/e 407.0287.

[($\eta^5-C_5H_5$)(CO)(NO)]W=C=C(H)[C(CH₃)₃] (9b). Complex **9b** was prepared analogous to molybdenum complex **8b**, and a 1.0 g amount of **1c** yielded 1062 mg (91%) of **9b**, as orange crystals, mp 84 °C. Anal. Calcd for $C_{12}H_{15}NO_2W$: C, 37.04; H, 3.89; N, 3.60. Found: C, 37.19; H, 3.85; N, 3.58. Two rotamers: 1H NMR ($CDCl_3$) δ 5.83 and 5.81 (two s, 5:4, Cp), 5.73 and 5.69 (two s, 5:4, H), 1.10 and 1.08 (two s, 4:5, $C(CH_3)_3$); ^{13}C NMR ($CDCl_3$) δ 338.7 and 338.4 (two C_{α}), 211.8 and 210.8 (two $C=O$), 140.0 and 139.5 (two C_{β}), 96.2 and 96.0 (two Cp), 34.6 and 33.0 (two $C(CH_3)_3$), 31.2 and 31.0 (two $C(CH_3)_3$); IR (CCl_4) $\bar{\nu}$ (cm^{-1}) 2002 ($C=O$), 1624 ($N=O$); MS (70 eV) m/e 389 (M^+ , ^{184}W), 361 ($M^+ - CO$); high-resolution mass spectrum calcd for $C_{12}H_{15}NO_2^{182}W$ (M^+) m/e 387.0585, found m/e 387.0568.

[($\eta^5-C_5H_5$)(CO)(NO)]W=C=C(H)(CH₂OCH₂CH=CH₂) (9c). The preparation was analogous to that of molybdenum complex **8b**. A 4.5 mmol amount of **2c** and 1.0 g (3 mmol) of **1c** yielded 640 mg (53%) of **9c**, as orange oil. Anal. Calcd for $C_{12}H_{13}NO_3W$: C, 35.76; H, 3.25; N, 3.47. Found: C, 35.84; H, 2.92; N, 3.55. Two rotamers: 1H NMR ($CDCl_3$) δ 5.99–5.85 (m, 1H, CH), 5.89 and 5.88 (two s, Cp), 5.78 (m, 1H, CH), 5.37–5.16 (m, 2H, CH₂), 4.11–3.99 (m, 4H, two OCH₂); ^{13}C NMR ($CDCl_3$) δ 338.95 and 338.70 (two C_{α}), 209.95 and 209.49 (two $C=O$), 134.87 and 134.77 (two CH), 125.38 and 125.16 (two C_{β}), 117.08 and 117.00 (two CH₂), 96.32 and 96.07 (two Cp), 70.38 (OCH₂), 65.90 and 64.95 (two OCH₂); IR ($\bar{\nu}$ (cm^{-1}) 2003 ($C=O$), 1615 ($N=O$); MS (70 eV) m/e 403 (M^+ , ^{184}W), 375 ($M^+ - CO$), 345 ($M^+ - CO - NO$); high-resolution mass spectrum calcd for $C_{12}H_{13}NO_3^{182}W$ (M^+) m/e 401.0378, found m/e 401.0350.

[($\eta^5-C_5H_5$)(CO)(NO)]W[CH₂=CHCH₂-C=C-Si(CH₃)₃] (11). The preparation of **11** is proceeded analogous to that of molybdenum complex **3f**. Instead of trimethylchlorosilane 0.52 mL (6.0 mmol) of allylic bromide was used, and a 1.0 g (3 mmol) amount of **1c** yielded 374 mg (28%) of **11**, as orange crystals, mp 62 °C. Anal. Calcd for $C_{14}H_{19}NO_2SiW$: C, 37.77; H, 4.30; N, 3.15. Found: C, 37.47; H, 4.05; N, 2.94. Two rotamers: 1H NMR ($CDCl_3$) δ 6.0–5.88 (m, 1H, CH), 5.66 and 5.63 (two s, 4:1, Cp), 5.10–4.92 (m, 2H, CH₂), 4.01–3.91 (m, 1H, CH₂), 3.8–3.71 (m, 1H, CH₂), 0.31 and 0.25 (two s, 4:1, Si(CH₃)₃); ^{13}C NMR ($CDCl_3$) δ 219.24 ($C=O$), 136.0 and 135.4 (two CH), 125.2 (alkyne), 116.1 (=CH₂), 95.6 (Cp), 94.4 (alkyne), 38.6 and 34.3 (two CH₂), 0.7 and 0.2 (two Si(CH₃)₃); IR (CCl_4) $\bar{\nu}$ (cm^{-1}) 1976 ($C=O$), 1808 ($C=C$), 1605 ($N=O$); MS (70 eV) m/e 445 (M^+ , ^{184}W), 417 ($M^+ - CO$); high-resolution mass spectrum calcd for $C_{14}H_{19}NO_2Si^{182}W$ (M^+) m/e 443.0667, found m/e 443.0690.

[($\eta^5-C_5H_5$)(CO)(NO)]W=C=CH₂ (12). Complex **12** is prepared analogous to molybdenum complex **3e**, but, instead of trimethylchlorosilane, saturated aqueous sodium bicarbonate

was added; the color changed from green to orange. After usual workup 1.0 g (3 mmol) of **1c** yielded 530 mg (53%) of **12**, as orange crystals, mp 90 °C (decomp). Anal. Calcd for $C_8H_7NO_2W$: C, 28.86; H, 2.12; N, 4.21. Found: C, 29.26; H, 1.77; N, 4.10. 1H NMR ($CDCl_3$) δ 5.85 (d, 2 H, CH₂), 5.24 (s, 5H, Cp); ^{13}C NMR ($CDCl_3$) δ 341.2 (C_{α}), 209.9 ($C=O$), 112.9 (C_{β}), 96.3 (Cp); IR (CCl_4) $\bar{\nu}$ (cm^{-1}) 2008 ($C=O$), 1654 ($N=O$); MS (70 eV) m/e 333 (M^+ , ^{184}W), 305 ($M^+ - CO$), 275 ($M^+ - CO - NO$); high-resolution mass spectrum calcd for $C_8H_7NO_2^{186}W$ (M^+) m/e 335.0021, found m/e 335.0027.

[($\eta^5-C_5H_5$)(CO)(NO)]Cr=C[N(CH₃)₂](C=C-C₆H₅) (13). A 2 mL (1.36 g, 30 mmol) amount of condensed dimethyl amine was added to 319 mg (1 mmol) of **7a** in 15 mL ether at -20 °C. After 30 min the formation of dark red **13** could be detected by TLC (R_f = 0.48, pentane:ether 3:1). Complex **7a** is completely consumed after 4.5 h. After removal of the solvent under reduced pressure 166 mg (50%) of **13** was obtained as black crystals from ether:pentane 1:10, mp 116 °C (decomp). 1H NMR ($CDCl_3$) δ 7.39–7.36 (m, 5H, arom), 5.10 (s, 5H, Cp), 3.80 and 3.59 (two s, 6H, N(CH₃)₂); ^{13}C NMR ($CDCl_3$) δ 262.7 (C_{α}), 246.0 (CO), 130.7, 129.0, 128.6 and 124.2 (arom C), 123.1 (C.), 94.3 (Cp), 89.8 (C_{β}), 48.3 and 47.2 (N(CH₃)₂); IR (CCl_4) $\bar{\nu}$ (cm^{-1}) 2171 ($C=C$), 1948 ($C=O$), 1644 ($N=O$); MS (70 eV) m/e 332 (M^+ , ^{52}Cr), 304 ($M^+ - CO$), 274 ($M^+ - CO - NO$); high-resolution mass spectrum calcd for $C_{17}H_{16}^{52}CrN_2O_2$ (M^+) m/e 332.0619, found m/e 332.0605.

[($\eta^5-C_5H_5$)(CO)(NO)]Cr=C(OCH₃)[CH=C(C₆H₅)(N-morpholine)] (14). 0.35 mL (356 mg, 4 mmol) of morpholine was added to 319 mg (1 mmol) of **7a** in 15 mL ether at room temperature. After a few minutes the formation of red **14** could be detected by TLC (R_f = 0.02, pentane:ether 3:1). Complex **7a** was completely consumed after 8 h at room temperature. After removal of the solvent under reduced pressure 274 mg (67%) of **14** was obtained as black crystals from ether:pentane 1:5, mp 104 °C (decomp). Anal. Calcd for $C_{20}H_{22}CrN_2O_4$: C, 59.10; H, 5.45; N, 6.89. Found: C, 58.64; H, 5.33; N, 6.89. 1H NMR ($CDCl_3$) δ 7.18–7.34 (m, 5H, arom), 6.28 (s, 1H), 5.12 (s, 5H, Cp), 3.76 (s, 3H, CH₃), 3.70 (s, 4H, OCH₂CH₂), 3.04 (s, 4H, NCH₂CH₂); ^{13}C NMR ($CDCl_3$) δ 327.3 (C_{α}), 242.1 (CO), 146.8 (C.), 137.9 (C_{β}), 129.2, 128.2, 128.0 and 118.3 (arom C), 93.6 (Cp), 66.7 (CH₃), 63.4 (OCH₂CH₂), 49.9 (NCH₂CH₂); IR (CCl_4) $\bar{\nu}$ (cm^{-1}) 1951 ($C=O$), 1653 ($N=O$); MS (70 eV) m/e 406 (M^+ , ^{52}Cr) 378 ($M^+ - CO$), 348 ($M^+ - CO - NO$); high-resolution mass spectrum calcd for $C_{20}H_{22}^{52}CrN_2O_4$ ($M^+ - CO$) m/e 378.1036, found m/e 378.1036.

[($\eta^5-C_5H_5$)(CO)(NO)]Cr=C(OCH₃)[CH=C(C₆H₅)(N-piperidine)] (15). The preparation was carried out as described for **14**, but, instead of morpholine, 0.4 mL (341 mg, 4 mmol) of piperidine was used. After removal of the solvent under reduced pressure 260 mg (64%) of **15** was obtained as black crystals from ether:pentane 1:5, mp 122 °C (decomp). Anal. Calcd for $C_{21}H_{24}CrN_2O_3$: C, 62.36; H, 5.98; N, 6.92. Found: C, 62.19; H, 6.07; N, 6.91. 1H NMR ($CDCl_3$) δ 7.16–7.34 (m, 5H), 6.30 (s, 1H), 5.08 (s, 5H, Cp), 3.71 (s, 3H, CH₃), 3.10 (s, 4H, NCH₂), 1.60–1.58 (s, 6H, CH₂CH₂CH₂); ^{13}C NMR ($CDCl_3$) δ 323.0 (C_{α}), 245.0 (CO), 148.3 (C.), 138.6 (C_{β}), 128.9, 128.0, 127.9 and 117.2 (arom C), 93.3 (Cp), 63.2 (CH₃), 49.7 (NCH₂CH₂CH₂), 25.9 (NCH₂CH₂CH₂), 24.3 (NCH₂CH₂CH₂); IR (CCl_4) $\bar{\nu}$ (cm^{-1}) 1946 ($C=O$), 1647 ($N=O$); MS (70 eV) m/e 376 ($M^+ - CO$, ^{52}Cr); high-resolution mass spectrum calcd for $C_{19}H_{24}^{52}CrN_2O$ ($M^+ - CO$) m/e 376.1243, found m/e 376.1240.

Acknowledgment. This work was supported by the Fonds der Chemischen Industrie, Frankfurt/Main, Germany. F.M. thanks the Ministry of Culture and Higher Education, Tehran, Iran, for a Ph.D. grant.

Supporting Information Available: Data for crystal structure determination and refinement and tables of atomic coordinates, bond lengths, and angles for **4f** (3 pages). Ordering information is given on any current masthead page.

OM940851D

Alkyne, Triorganosilyl, and Triorganostannyl Derivatives of Anionic Triruthenium Carbonyl Cluster Complexes Containing Bridging Pyrazolyl Ligands

Javier A. Cabeza,* R. Jesús Franco, and Víctor Riera

Instituto de Química Organometálica "Enrique Moles", Facultad de Química, Universidad de Oviedo—CSIC, E-33071 Oviedo, Spain

Santiago García-Granda and Juan F. Van der Maelen

Departamento de Química Física y Analítica, Facultad de Química, Universidad de Oviedo, E-33071 Oviedo, Spain

Received April 12, 1995[®]

The anionic cluster complex $[\text{Ru}_3(\mu\text{-H})(\mu\text{-CO})(\text{CO})_{10}]^-$ reacts with 3,5-dimethylpyrazole (Hdmpz) to give $[\text{Ru}_3(\mu\text{-dmpz})(\mu\text{-CO})_3(\text{CO})_7]^-$ (**1**) in high yield. The reactivity of complex **1** with protic acids, alkynes, tertiary silanes, and tertiary stannanes is described. Complex **1** reacts with trifluoroacetic acid to give the known neutral hydrido derivative $[\text{Ru}_3(\mu\text{-H})(\mu\text{-dmpz})(\text{CO})_{10}]$ (**2**). With diphenylacetylene, complex **1** gives $[\text{Ru}_3(\mu\text{-dmpz})(\mu_3\text{-Ph}_2\text{C}_2)(\mu\text{-CO})_2(\text{CO})_6]^-$ (**3**), in which the alkyne ligand interacts with the three ruthenium atoms. An X-ray structure analysis of [PPN]**3** is reported. Complex **2** reacts with 2 equiv of tertiary silanes or stannanes to give $[\text{Ru}_3(\mu\text{-dmpz})(\mu\text{-H})_2(\text{ER}_3)_2(\text{CO})_8]^-$ ($\text{ER}_3 = \text{SiEt}_3$ (**4**), $\text{Si}(\text{OMe})_3$ (**5**), SiPh_3 (**6**), SnBu_3 (**7**), SnPh_3 (**8**)). Their spectroscopic data (IR, ^1H and ^{13}C NMR) indicate that the structure of the dihydrido disilyl complexes **4–6** (C_1 symmetry) is different from that of the dihydrido distannyl derivatives **7** and **8** (C_s symmetry). Compound **1** does not promote the hydrosilylation of alkynes; in fact, the reaction of complex **3** with tertiary silanes affords *cis*- and *trans*-stilbene as the only alkyne-derived products, and complexes **4–8** do not react with phenyl- or diphenylacetylene. All anionic cluster complexes have been prepared as $[\text{Et}_4\text{N}]^+$ and $[\text{PPN}]^+$ salts.

Introduction

Most of the reactions of organosilanes with unsaturated organic substrates are catalyzed by transition-metal compounds. These reactions have become important in organic synthesis,¹ and some of them are of interest in connection with industrial processes.^{1,2}

In the case of ruthenium carbonyl cluster complexes, $[\text{Ru}_3(\text{CO})_{12}]$ has been demonstrated to be an efficient catalyst precursor for alkene hydrosilylation³ and for the synthesis of vinylsilanes from alkenes.⁴ The anionic cluster $[\text{Ru}_3(\mu\text{-H})(\mu\text{-CO})(\text{CO})_{10}]^-$ has been found to promote the reaction of ethylene with CO and HSiEt_3 to give unsaturated silyl ethers,⁵ the coupling of silanes with CO_2 to give silyl formates,⁶ and the spirocyclization of isocyanates in the presence of HSiEt_3 .⁷ It has also been reported that a mixture of $[\text{Ru}_3(\mu\text{-H})(\mu_3\text{-NPhy})-$

$(\text{CO})_9]$ ($\text{HNPhy} = 2\text{-anilinopyridine}$) and HSiEt_3 promotes the polymerization of phenylacetylene.⁸ However, in contrast with this interesting catalytic activity, very little is known about the mechanisms governing these reactions and very few papers dealing with the reactivity of ruthenium carbonyl cluster complexes with organosilanes have been published.^{9–13}

It is known that tertiary silanes react with $[\text{Ru}_3(\text{CO})_{12}]$ to give mono-, bi-, and trinuclear derivatives.⁹ Analogous reactions with $[\text{Ru}_3(\mu\text{-H})(\mu\text{-CO})(\text{CO})_{10}]^-$ only give trinuclear products.¹⁰ Recently, we have described the reactivity of tertiary silanes with $[\text{Ru}_3(\mu\text{-H})(\mu_3\text{-ampy})(\text{CO})_9]$ ($\text{Hampy} = 2\text{-amino-6-methylpyridine}$),¹¹ $[\text{Ru}_3(\mu\text{-pydz})(\mu\text{-CO})_3(\text{CO})_7]$ ($\text{pydz} = \text{pyridazine}$),¹² and $[\text{Ru}_3(\mu\text{-NO})(\text{CO})_{10}]^-$,¹³ in these three cases, the products are also trinuclear derivatives. From these examples,

* E-mail: jac@dwarf1.quimica.uniovi.es.

[®] Abstract published in *Advance ACS Abstracts*, June 15, 1995.

(1) See, for example: (a) *Comprehensive Handbook on Hydrosilylation*; Marciniec, B., Ed.; Pergamon: Oxford, U.K., 1992. (b) Ojima, I. In *The Chemistry of Organic Silicon Compounds*; Patay, S., Rappoport, Z., Eds.; Wiley: New York, 1989; Chapter 25.

(2) Noels, A. F.; Hubert, A. J. In *Industrial Applications of Homogeneous Catalysis*; Mortheux, A., Petit, F., Eds.; Reidel: Boston, MA, 1988; Chapter 3.

(3) (a) Tanaka, M.; Hayashi, T.; Mi, Z.-Y. *J. Mol. Catal.* **1993**, *81*, 207. (b) Hilal, H. S.; Khalaf, S.; Jondi, W. *J. Organomet. Chem.* **1993**, *452*, 167.

(4) (a) Kakiuchi, F.; Tanaka, Y.; Chatani, N.; Murai, S. *J. Organomet. Chem.* **1993**, *456*, 45. (b) Seki, Y.; Takeshida, K.; Kawamoto, K.; Murai, S.; Sonoda, N. *J. Org. Chem.* **1986**, *51*, 3890. (c) Ojima, I.; Fuchikami, T.; Yatabe, M. *J. Organomet. Chem.* **1984**, *260*, 335.

(5) Süß-Fink, G. *Angew. Chem., Int. Ed. Engl.* **1982**, *21*, 73.

(6) Süß-Fink, G.; Reiner, J. *J. Organomet. Chem.* **1981**, *221*, C36.

(7) Herrmann, G.; Süß-Fink, G. *Chem. Ber.* **1985**, *118*, 3959.

(8) Nombel, P.; Lukan, N.; Mulla, F.; Lavigne, G. *Organometallics* **1994**, *13*, 4673.

(9) (a) Cotton, J. D.; Knox, S. A. R.; Stone, F. G. A. *Chem. Commun.* **1967**, 965. (b) Knox, S. A. R.; Stone, F. G. A. *J. Chem. Soc. A* **1969**, 2559. (c) Vancea, L.; Graham, W. A. G. *Inorg. Chem.* **1974**, *13*, 511. (d) Van Buuren, G. N.; Willis, A. C.; Einstein, F. W. B.; Peterson, L. K.; Pomeroy, R. K.; Sutton, D. *Inorg. Chem.* **1981**, *20*, 4361.

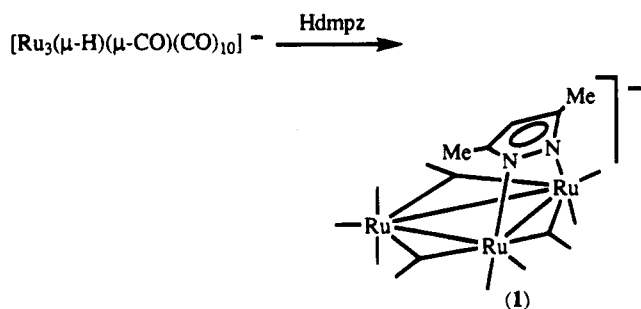
(10) (a) Süß-Fink, G.; Ott, J.; Schmidkonz, B.; Guldner, K. *Chem. Ber.* **1982**, *115*, 2487. (b) Klein, H.-P.; Thewalt, U.; Herrmann, G.; Süß-Fink, G.; Moinet, C. *J. Organomet. Chem.* **1985**, *286*, 225.

(11) (a) Cabeza, J. A.; Llamazares, A.; Riera, V.; Triki, S.; Ouahab, L. *Organometallics* **1992**, *11*, 3334. (b) Cabeza, J. A.; García-Granda, S.; Llamazares, A.; Riera, V.; Van der Maelen, J. F. *Organometallics* **1993**, *12*, 2973.

(12) Cabeza, J. A.; Franco, R. J.; Llamazares, A.; Riera, V.; Bois, C.; Jeannin, Y. *Inorg. Chem.* **1993**, *32*, 4640.

(13) Cabeza, J. A.; Franco, R. J.; Riera, V. *Inorg. Chem.* **1994**, *33*, 5952.

Scheme 1



it seems clear that the presence of bridging ligands is important in order to maintain the cluster nuclearity.

Although the reactions of tertiary stannanes with unsaturated organic molecules usually are not metal-catalyzed,¹⁴ the reactivity of mononuclear transition-metal complexes with tertiary silanes and stannanes can be compared in many respects.^{15,16} However, we still know very little about the reactivity of metal cluster complexes with these two reagents,^{15,16} therefore, more reactivity studies of metal clusters with silanes and stannanes are needed in order to rationalize their behavior.

This article reports the synthesis of a new anionic ruthenium carbonyl cluster, $[\text{Ru}_3(\mu\text{-dmpz})(\mu\text{-CO})_3(\text{CO})_7]^-$ (**1**; Hdmpz = 3,5-dimethylpyrazole), its reactions with protic acids, alkynes, silanes, and stannanes, and some attempts to hydrosilylate alkynes using complex **1** as catalyst precursor. We initially used HSiEt_3 , $\text{HSi}(\text{OMe})_3$, and HSnBu_3 as reagents, but since their products were oils which proved to be very difficult to crystallize, we also carried out the reactions using HSiPh_3 and HSnPh_3 . We chose complex **1** as starting material because anionic compounds are more prone to undergo oxidative addition reactions than their neutral precursors and because *N*-donor ligands are good cis-labilizers, facilitating the substitution of CO ligands.^{11–13} Furthermore, the methyl groups on the pyrazolyl ligand help to monitor the reactions by NMR spectroscopy.

Only a few trinuclear pyrazolyl derivatives of ruthenium carbonyl have been reported to date. They are the neutral compounds $[\text{Ru}_3(\mu\text{-H})(\mu\text{-}3,5\text{-R}_2\text{C}_3\text{HN}_2)(\text{CO})_{10}]$ ($\text{R} = \text{H}, \text{Me}, \text{CF}_3$).¹⁷

Results and Discussion

The cluster anion $[\text{Ru}_3(\mu\text{-dmpz})(\mu\text{-CO})_3(\text{CO})_7]^-$ (**1**) has been prepared in good yield (65–85%), as the $[\text{Et}_4\text{N}]^+$ or $[\text{PPN}]^+$ salt, by treating $[\text{Ru}_3(\mu\text{-H})(\mu\text{-CO})(\text{CO})_{10}]^-$ with 3,5-dimethylpyrazole in THF at reflux temperature (Scheme 1). The cluster contains terminal and bridging CO ligands (IR) and has a symmetric structure (C_s), as indicated by its ¹H and ¹³C NMR spectra, which confirm the presence of a symmetry plane perpendicular to the pyrazolyl ring. The structure proposed in Scheme 1 is also based on that reported for the related anionic triruthenium carbonyl cluster $[\text{Ru}_3(\mu\text{-Opy})(\mu\text{-CO})_3(\text{CO})_7]^-$ (HOpy = 2-pyridone), which has been characterized by

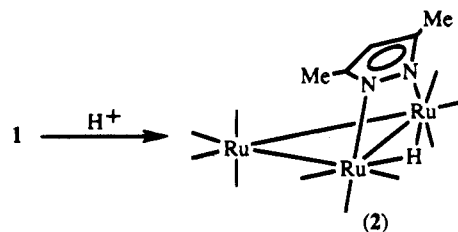
(14) Pereire, M.; Quintard, J. P.; Rahm, A. *Tin in Organic Synthesis*; Butterworths: London, U.K., 1986.

(15) Holt, M. S.; Wilson, W. L.; Nelson, J. H. *Chem. Rev.* **1989**, *89*, 11.

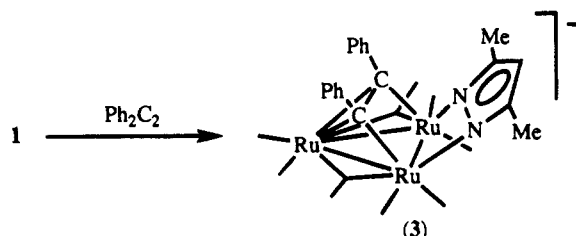
(16) Stille, J. K. *Angew. Chem., Int. Ed. Engl.* **1986**, *25*, 508.

(17) Bruce, M. I.; Humphrey, M. G.; Snow, M. R.; Tiekink, E. R. T.; Wallis, R. C. *J. Organomet. Chem.* **1986**, *314*, 311.

Scheme 2



Scheme 3



X-ray diffraction methods.¹⁸ Very few anionic ruthenium cluster complexes containing *N*-donor heterocycles have been reported to date.^{18,19}

The efficient preparation of anion **1**, described above, allowed a study of its reactivity. In order to confirm that **1** is a decacarbonyl derivative, its reaction with protic acids was studied. This was expected to lead to the known,¹⁷ neutral hydrido derivative $[\text{Ru}_3(\mu\text{-H})(\mu\text{-dmpz})(\text{CO})_{10}]$ (**2**; Scheme 2). Effectively, the reaction of complex **1** with trifluoroacetic acid gives complex **2** in excellent yield (80%, based on initial $[\text{Ru}_3(\text{CO})_{12}]$). Analogous results are obtained when $\text{HBF}_4\cdot\text{OEt}_2$ is substituted for trifluoroacetic acid. It is interesting to note that, under thermal conditions, the reaction of $[\text{Ru}_3(\text{CO})_{12}]$ with 3,5-dimethylpyrazole, in a 1:1 mole ratio, only affords small amounts (<20%) of complex **2**,^{17,20} whereas the use of an excess of pyrazole ligand leads to the binuclear derivative $[\text{Ru}_2(\mu\text{-dmpz})_2(\text{CO})_6]$.^{20–22} The synthetic strategy consisting of (a) transformation of $[\text{Ru}_3(\text{CO})_{12}]$ into $[\text{Ru}_3(\mu\text{-H})(\mu\text{-CO})(\text{CO})_{10}]^-$, (b) reaction of $[\text{Ru}_3(\mu\text{-H})(\mu\text{-CO})(\text{CO})_{10}]^-$ with a protic *N*-donor ligand, and (c) protonation of the resulting anionic complex has been used before to prepare neutral hydridocarbonyl-triruthenium clusters containing bridging *N*-donor ligands which are not conveniently made by direct reaction of $[\text{Ru}_3(\text{CO})_{12}]$ with the appropriate ligand.¹⁸

The thermal reaction of complex **1** with phenylacetylene (1:1 mole ratio, THF, reflux temperature, 30 min) gives a mixture of at least three compounds (NMR evidence) which we could not separate and identify. However, a similar reaction with diphenylacetylene renders the anionic alkyne derivative $[\text{Ru}_3(\mu\text{-dmpz})(\mu_3\text{-Ph}_2\text{C}_2)(\mu\text{-CO})_2(\text{CO})_6]^-$ (**3**) in quantitative spectroscopic yield (Scheme 3). Its IR spectrum shows terminal and bridging CO ligands, and its ¹H and ¹³C NMR spectra are consistent with a structure in which a symmetry

(18) Lugan, N.; Laurent, F.; Lavigne, G.; Newcomb, T. P.; Liimata, E. W.; Bonnet, J. *J. Organometallics* **1992**, *11*, 1351.

(19) For a review on ruthenium clusters containing *N*-donor ligands, see: Bruce, M. I.; Cifuentes, M. P.; Humphrey, M. G. *Polyhedron* **1991**, *10*, 277.

(20) Cabeza, J. A.; Landázuri, C.; Oro, L. A.; Tiripicchio, A.; Tiripicchio-Camellini, M. *J. Organomet. Chem.* **1987**, *322*, C16.

(21) Neumann, F.; Süß-Fink, G. *J. Organomet. Chem.* **1989**, *367*, 175.

(22) Cabeza, J. A.; Landázuri, C.; Oro, L. A.; Belletti, D.; Tiripicchio, A.; Tiripicchio-Camellini, M. *J. Chem. Soc., Dalton Trans.* **1989**, 1093.

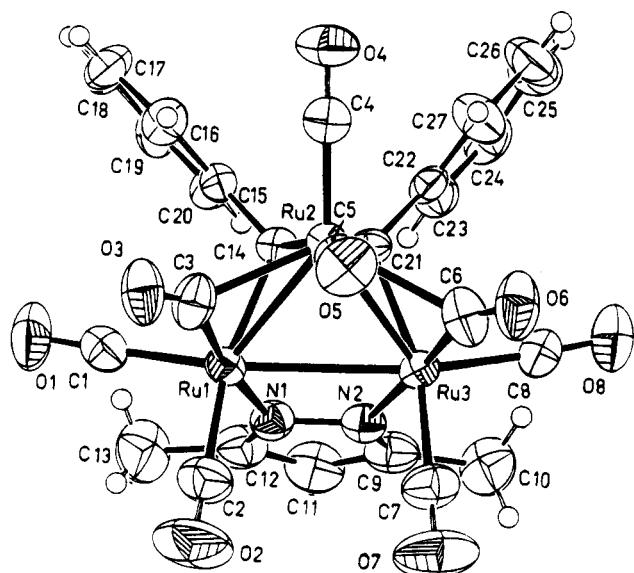


Figure 1. EUCLID structural plot of the anion $[\text{Ru}_3(\mu\text{-dmpz})(\mu_3\text{-Ph}_2\text{C}_2)(\mu\text{-CO})_2(\text{CO})_6]^-$ (**3**) in $[\text{PPN}]\text{3}$. Thermal ellipsoids are drawn at the 50% probability level.

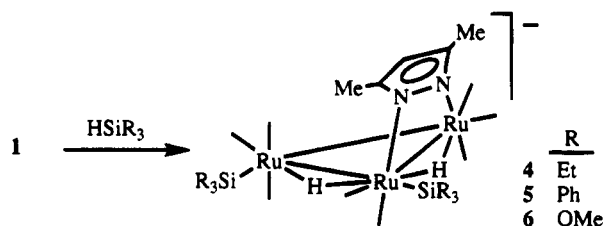
Table 1. Selected Bond Lengths and Bond Angles in $[\text{PPN}]\text{3}$

Bond Lengths (Å)			
Ru(1)–Ru(2)	2.753(1)	Ru(1)–Ru(3)	2.865(1)
Ru(2)–Ru(3)	2.769(1)	Ru(1)–N(1)	2.131(4)
Ru(3)–N(2)	2.135(4)	Ru(1)–C(1)	1.917(5)
Ru(1)–C(2)	1.939(6)	Ru(1)–C(3)	2.030(6)
Ru(1)–C(14)	2.126(4)	Ru(2)–C(3)	2.181(6)
Ru(2)–C(4)	1.864(5)	Ru(2)–C(5)	1.868(5)
Ru(2)–C(6)	2.352(6)	Ru(2)–C(14)	2.288(4)
Ru(2)–C(21)	2.286(4)	Ru(3)–C(6)	1.942(6)
Ru(3)–C(7)	1.947(5)	Ru(3)–C(8)	1.931(6)
Ru(3)–C(21)	2.133(4)	C(1)–O(1)	1.132(6)
C(2)–O(2)	1.118(7)	C(3)–O(3)	1.149(7)
C(4)–O(4)	1.141(6)	C(5)–O(5)	1.145(6)
C(6)–O(6)	1.150(6)	C(7)–O(7)	1.130(6)
C(8)–O(8)	1.26(7)	C(14)–C(21)	1.371(6)
Bond Angles (deg)			
Ru(1)–Ru(2)–Ru(3)	62.50(3)	Ru(1)–Ru(3)–Ru(2)	58.48(3)
Ru(2)–Ru(1)–Ru(3)	59.02(3)	Ru(1)–C(3)–Ru(2)	81.6(2)
Ru(1)–C(3)–O(3)	146.6(5)	Ru(2)–C(3)–O(3)	131.8(5)
Ru(2)–C(6)–Ru(3)	79.7(2)	Ru(2)–C(6)–O(6)	125.6(5)
Ru(3)–C(6)–O(6)	154.6(5)	Ru(1)–C(14)–Ru(2)	77.1(1)
Ru(2)–C(21)–Ru(3)	77.5(1)	C(14)–Ru(2)–C(21)	24.9(2)
C(15)–C(14)–C(21)	126.0(4)	C(14)–C(21)–C(22)	125.5(4)

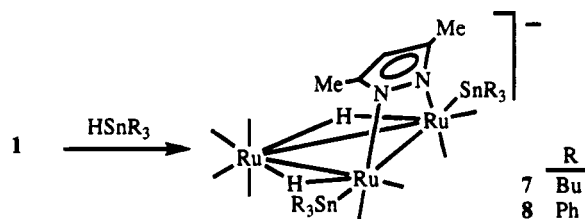
plane cuts the pyrazolyl and alkyne ligands into identical halves. As these spectroscopic data are not sufficient to unequivocally assign a structure to this cluster, an X-ray diffraction study of the $[\text{PPN}]^+$ salt was carried out.

Figure 1 shows the structure of anion **3** in $[\text{PPN}]\text{3}$. A selection of bond distances and angles is given in Table 1. The anion consists of an isosceles triangle of ruthenium atoms in which one Ru–Ru distance, Ru(1)–Ru(3), is ca. 0.1 Å longer than the other two. The dmpz ligand spans the longest Ru–Ru edge, forming a dihedral angle of $150.5(1)^\circ$ with the Ru_3 plane. The structural features of this ligand are comparable to those previously observed in binuclear ruthenium carbonyl complexes.^{20–22} The alkyne ligand is placed on the same Ru_3 face as the pyrazolyl ligand, interacting with the three ruthenium atoms in such a way that the C(14)–C(21) vector is parallel to the Ru(1)–Ru(3) edge. The Ru(1)–C(14) and Ru(3)–C(21) distances are ca. 0.16 Å shorter than the Ru(2)–C(14) and Ru(2)–C(21)

Scheme 4



Scheme 5



distances. The alkyne C(14)–C(21) bond distance (1.371(6) Å) indicates a reduction of the C–C bond order upon coordination and correlates well with the C(14)–C(21)–C(22) and C(15)–C(14)–C(21) bond angles ($125.5(4)$ and $126.0(4)^\circ$, respectively).²³ The cluster shell is completed by six terminal CO ligands and two semibridging CO ligands. The latter span the shorter Ru–Ru edges, being closer to Ru(1) and Ru(3) than to Ru(2). Although many carbonyl metal clusters containing alkynes as ligands have been reported,^{23–25} to our knowledge, only two anionic derivatives of ruthenium have been structurally characterized, namely, $[\text{PPN}][\text{Ru}_3(\mu\text{-H})(\mu_3\text{-Ph}_2\text{C}_2)(\text{CO})_9]$ and $[\text{PPN}][\text{Ru}_3(\mu\text{-Cl})(\mu_3\text{-Ph}_2\text{C}_2)(\text{CO})_9]$.²⁵ In these two compounds, the alkyne ligands are coordinated to the three metal atoms and are parallel to a Ru–Ru edge, as occurs in complex **3**; however, although the chloride and pyrazolyl ligands behave as 3-electron donors in their respective complexes, the chloro complex $[\text{Ru}_3(\mu\text{-Cl})(\mu_3\text{-Ph}_2\text{C}_2)(\text{CO})_9]^-$ is an open 50-electron cluster, whereas complex **3** is a closed 48-electron species.

The reactions of complex **1** with tertiary silanes and stannanes (THF, reflux temperature) lead to the disilyl (Scheme 4) or distannyl (Scheme 5) dihydrido derivatives $[\text{Ru}_3(\mu\text{-dmpz})(\mu\text{-H})_2(\text{ER}_3)_2(\text{CO})_8]^-$ ($\text{ER}_3 = \text{SiEt}_3$ (**4**), $\text{Si}(\text{OMe})_3$ (**5**), SiPh_3 (**6**), SnBu_3 (**7**), SnPh_3 (**8**)). IR monitoring of the reactions indicated that at least 2 equiv of silane or stannane is needed to consume all complex **1**. No reaction intermediates can be detected by spectroscopic means (IR). A similar situation has been observed before for the clusters $[\text{Ru}_3(\mu\text{-H})(\mu\text{-CO})(\text{CO})_{10}]^-$ ¹⁰ and $[\text{Ru}_3(\mu\text{-pydz})(\mu\text{-CO})_3(\text{CO})_7]$,¹² which also take 2 equiv of silanes or stannanes. However, only 1 equiv of these reagents can be incorporated into the

(23) A correlation between the RC–CR distances and the C–C–R angles for a large number of complexes containing alkynes as ligands has been reported: Gervasio, G.; Rossetti, R.; Stanghellini, P. L. *Organometallics* **1985**, *4*, 1612.

(24) For reviews on alkyne-containing carbonyl metal clusters, see: (a) Sappa, E.; Tiripicchio, A.; Braunstein, P. *Chem. Rev.* **1983**, *83*, 203. (b) Raithby, P. R.; Rosales, M. J. *Adv. Inorg. Chem. Radiochem.* **1985**, *29*, 169. (c) Sappa, E.; Tiripicchio, A.; Braunstein, P. *Coord. Chem. Rev.* **1985**, *64*, 219. (d) Sappa, E.; Tiripicchio, A.; Carty, A. J.; Toogood, G. E. *Prog. Inorg. Chem.* **1987**, *35*, 437. (e) Osella, D.; Raithby, P. R. In *Stereochemistry of Organometallic and Inorganic Compounds*; Bernal, I., Ed.; Elsevier: Amsterdam, The Netherlands, 1989; Vol. 3. (f) Cauzzi, D.; Giorgano, R.; Sappa, E.; Tiripicchio, A.; Tiripicchio-Camellini, T. *J. Cluster Sci.* **1993**, *4*, 279. (g) Sappa, E. *J. Cluster Sci.* **1994**, *5*, 211.

(25) Rivomanana, S.; Lavigne, G.; Lugan, N.; Bonnet, J. J. *Organometallics* **1991**, *10*, 2285.

clusters [Ru₃(CO)₁₁(MeCN)]²⁶ and [Ru₃(μ-H)(μ₃-ampy)-(CO)₉]^{11,27} whereas in similar reactions with [Ru₃(μ-NO)(CO)₁₀]⁻, mono- and disilyl or distannyl derivatives can be obtained depending on the reaction conditions.¹³

The IR spectra of the silyl complexes 4–6 are different from those of the stannyl complexes 7 and 8. This suggests different structures. The ¹H NMR spectra of the silyl derivatives show two hydride and two methyl resonances, whereas those of the stannyl complexes only show one hydride²⁸ and one methyl resonance, indicating that the silyl derivatives are asymmetric (C₁) and that the stannyl derivatives are symmetric (C_s). This structural difference was confirmed by the ¹³C NMR spectra of these compounds, which, apart from the resonances of the organic fragments (that also reflect the symmetry of the complexes), show eight CO signals for the silyl derivatives and five CO signals for the stannyl compounds (unlike 1–3, the silyl and stannyl complexes are not fluxional at room temperature). The structures depicted in Schemes 4 and 5 for these compounds are consistent with their spectroscopic data, but unfortunately, they could not be confirmed by X-ray diffraction studies since the compounds could not be obtained as single crystals.²⁹

To date, apart from the examples described in this article, only one ruthenium cluster, [Ru₃(μ-pydz)(μ-CO)₃(CO)₇], is known to behave in a way similar to that for complex 1, giving asymmetric disilyl and symmetric distannyl complexes.¹² The disilyl and distannyl derivatives of [Ru₃(μ-H)(μ-CO)(CO)₁₀]⁻ are isostructural,^{10,30} whereas [Ru₃(μ-NO)(CO)₁₀]⁻ gives symmetric disilyl and asymmetric distannyl products.¹³ Interestingly, the cluster complexes which only add 1 equiv of HSiR₃ or HSnR₃ give isostructural products.^{11,13,27} This particular behavior of tertiary silanes and stannanes in their reactions with carbonyl cluster compounds is intriguing, and its explanation needs much more work in this area.

As the preparation of vinylsilanes is currently of great interest,^{1,31} we investigated the reactivity of the alkyne complex 3 with tertiary silanes, the reactivity of the silyl derivatives 4 and 5 with alkynes, and the activity of complex 1 as a catalyst precursor for the synthesis of vinylsilanes *via* hydrosilylation of alkynes.

The reaction of complex 3 with tertiary silanes (1,2-dichloroethane, reflux temperature) gives *cis*- and *trans*-stilbene, as the only alkyne-derived products, and an inseparable mixture of cluster compounds. A similar reaction with HSnPh₃ (1,2-dichloroethane, room temperature) gives diphenylacetylene and the distannyl complex 8. On the other hand, no reaction was observed between complexes 4–8 and phenyl- or diphenylacetylene. These results are in accordance with the fact that no vinylsilanes are produced when complex 1, HSiEt₃, and phenyl- or diphenylacetylene are allowed to react

in 1,2-dichloroethane under catalytic conditions (1:80:50 mole ratio, 80 °C, 1 h).

In conclusion, this paper reports an efficient synthesis of complex 1, a novel anionic ruthenium carbonyl cluster containing a bridging N-donor heterocyclic ligand (a thus far uncommon class of compound), and its reactivity with alkynes, tertiary silanes, and tertiary stannanes. The X-ray-characterized alkyne complex 3 adds a new example to the very few in which the coordination of alkynes to anionic clusters has been reported. Finally, the results of the reactivity studies of complex 1 with tertiary silanes and stannanes, although are far from being explainable, may contribute to shed light on the behavior of these reagents in their reactions with carbonyl cluster complexes.

Experimental Section

General Data. Solvents were dried over sodium diphenyl ketyl (THF, diethyl ether, hydrocarbons), magnesium (methanol), or CaH₂ (dichloromethane, 1,2-dichloroethane) and distilled under nitrogen prior to use. Unless otherwise stated, the reactions were carried out under nitrogen at room temperature, using Schlenk–vacuum-line techniques, and were routinely monitored by solution IR spectroscopy (carbonyl stretching region). All reagents were used as received from Aldrich. IR spectra were recorded in solution on a Perkin-Elmer FT 1720-X spectrophotometer, using 0.1-mm CaF₂ cells. ¹H and ¹³C NMR spectra were run at 20 °C with Bruker AC-200 and AC-300 instruments, using SiMe₄ as internal standard (δ 0 ppm). Microanalyses were obtained from the University of Oviedo Analytical Service. GC analyses were carried out at 175 °C on a Perkin-Elmer 8600 gas chromatograph, equipped with a 12-m AQ2 capillary column and a flame ionization detector.

The IR and NMR spectroscopic properties of the [Et₄N]⁺ and [PPN]⁻ salts of the same anionic complex are very similar; therefore, only data corresponding to one of these salts are given.

[Et₄N][Ru₃(μ-dmpz)(μ-CO)₃(CO)₇] ([Et₄N]1). A solution of Na[BH₄] (35 mg, 0.938 mmol) in methanol (5 mL) was added to a solution of [Ru₃(CO)₁₂] (400 mg, 0.625 mmol) in warm THF (40 mL, 40 °C). The color changed from orange to deep red. The solvent was evaporated under reduced pressure and the residue redissolved in THF (30 mL). At this point, an IR spectrum of the solution indicated only the presence of Na[Ru₃(μ-H)(μ-CO)(CO)₁₀]. After addition of Hdmpz (90 mg, 0.938 mmol), the solution was stirred at reflux temperature for 1.5 h. A solution of [Et₄N]Br (144 mg, 0.688 mmol) in methanol (5 mL) was added. The solvent was evaporated under reduced pressure and the residue extracted into dichloromethane (40 mL) to remove insoluble NaBr. The filtered solution was evaporated to dryness and the residue washed with hexane (3 × 3 mL) to give [Et₄N]1 as a yellow solid (417 mg, 83%). Anal. Calcd for C₂₃H₂₇N₃O₁₀Ru₃: C, 34.16; H, 3.36; N, 5.20. Found: C, 34.61; H, 3.40; N, 5.00. IR ν(CO) (THF): 2071 (w), 2015 (vs), 1987 (vs), 1950 (m), 1935 (s), 1852 (w), 1807 (sh), 1800 (s) cm⁻¹. ¹H NMR (CD₂Cl₂): 5.23 (s, 1H), 1.79 (s, 6H) (dmpz) ppm; 3.17 (q, 8 H), 1.31 (t, 12 H) (Et₄N) ppm. ¹³C{¹H} NMR (CD₂Cl₂): 227.1, 205.6, 202.0 (CO) ppm; 149.7, 106.8, 13.8 (dmpz) ppm; 54.2, 8.9 (Et₄N) ppm.

[PPN][Ru₃(μ-dmpz)(μ-CO)₃(CO)₇] ([PPN]1). A solution of [PPN][BH₄] (380 mg, 0.687 mmol) in dichloromethane (40 mL) was added to a solution of [Ru₃(CO)₁₂] (400 mg, 0.625 mmol) in THF (40 mL). The color changed from orange to deep red. After the mixture was stirred for 15 min, the solvent was evaporated under reduced pressure and the residue redissolved in THF (20 mL). At this point, an IR spectrum of the solution indicated only the presence of [PPN][Ru₃(μ-H)(μ-CO)(CO)₁₀]. After addition of Hdmpz (66 mg, 0.687 mmol), the solution was stirred at reflux temperature for 2 h. The solvent was removed

(26) Burgess, K.; Guerin, C.; Johnson, B. F. G.; Lewis, J. J. *Organomet. Chem.* **1985**, *295*, C3.

(27) Cabeza, J. A.; García-Granda, S.; Llamazares, A.; Riera, V.; Van der Maelen, J. F. *Organometallics* **1993**, *12*, 157.

(28) The *J*(^{119/117}Sn–¹H) coupling constants measured in the satellites of these hydride resonances (ca. 29 Hz) are indicative of a *cis* arrangement of the hydride and stannyl ligands.^{11–13}

(29) The structure proposed for the silyl derivatives is comparable to that of [Ru₃(μ-pydz)(μ-H)₂(SiEt₃)₂(CO)₈], which has been characterized by X-ray diffraction methods.¹²

(30) Watkins, S. F. *J. Chem. Soc. A* **1969**, 1552.

(31) Esteruelas, M. A.; Herrero, J.; Oro, L. A. *Organometallics* **1993**, *12*, 2377 and references therein.

under reduced pressure and the residue washed with hexane (3 × 4 mL) to give [PPN]1 as a yellow solid (490 mg, 64%). Anal. Calcd for C₅₁H₃₇N₃O₁₀P₂Ru₃: C, 50.33; H, 3.06; N, 3.45. Found: C, 49.94; H, 3.23; N, 3.31.

[Ru₃(μ-H)(μ-dmpz)(CO)₁₀] (2). Trifluoroacetic acid (1 mL) was added to a solution of Na[Ru₃(μ-dmpz)(μ-CO)₃(CO)₇] (prepared *in situ*, as described above, from [Ru₃(CO)₁₂] (1 g, 1.564 mmol), Na[BH₄] (89 mg, 2.35 mmol), and Hdmpz (225 mg, 2.35 mmol)) in dichloromethane (15 mL). The mixture was stirred for 25 min and evaporated to dryness. The residue was then extracted into dichloromethane (3 mL) and filtered through a short (5 × 2 cm) column of neutral alumina (activity I). The column was washed with dichloromethane and the resulting solution evaporated to dryness to give an oil which was redissolved in pentane. The solvent was again evaporated to give complex 2 as an orange solid (850 mg, 80%). Anal. Calcd for C₁₅H₈N₂O₁₀Ru₃: C, 26.52; H, 1.19; N, 4.12. Found: C, 26.60; H, 1.18; N, 4.08. IR ν(CO) (hexane): 2105 (w), 2067 (s), 2059 (s), 2026 (vs), 2016 (w), 2008 (m), 1993 (w), 1990 (s) cm⁻¹. ¹H NMR (CD₂Cl₂): 5.74 (s, 1 H), 2.06 (s, 6 H) (dmpz) ppm; -13.18 (s, 1 H, μ-H) ppm.

[Et₄N][Ru₃(μ-dmpz)(μ-Ph₂C₂)(μ-CO)₂(CO)₆] ([Et₄N]3). A solution of [Et₄N]1 (70 mg, 0.087 mmol) and diphenylacetylene (23 mg, 0.129 mmol) in THF (20 mL) was stirred at reflux temperature for 2.5 h. The color changed from yellow to orange. The solvent was removed and the residue washed with hexane (3 × 3 mL) to give [Et₄N]3 as an orange solid (70 mg, 86%). Anal. Calcd for C₃₅H₃₇N₃O₈Ru₃: C, 45.16; H, 4.00; N, 4.51. Found: C, 45.29; H, 4.33; N, 4.34. IR ν(CO) (THF): 2039 (m), 1996 (vs), 1977 (s), 1969 (sh), 1935 (m), 1898 (w), 1785 (w) cm⁻¹. ¹H NMR (CDCl₃): 7.6–6.6 (m, 10 H, Ph) ppm; 5.91 (s, 1 H), 2.12 (s, 6 H) (dmpz) ppm; 3.01 (q, br, 8 H), 1.18 (t, br, 12 H) (Et₄N) ppm.

The compound [PPN]3 was prepared in a similar way (78% yield), with [PPN]1 as starting material. Anal. Calcd for C₆₃H₄₇N₃O₈P₂Ru₃: C, 56.50; H, 3.54; N, 3.14. Found: C, 56.99; H, 3.71; N, 3.21. Selected ¹³C{¹H} NMR (CD₂Cl₂): 201.9, 193.1 (CO) ppm; 180.6 (Ph₂C₂), 156.2 (*ipso*-C of Ph₂C₂) ppm; 147.8, 106.3, 12.6 (dmpz) ppm.

[Et₄N][Ru₃(μ-dmpz)(μ-H)₂(SiEt₃)₂(CO)₈] ([Et₄N]4). A solution of [Et₄N]1 (80 mg, 0.099 mmol) and HSiEt₃ (40 μL, 0.256 mmol) in THF (15 mL) was stirred at reflux temperature for 45 min. The color changed from yellow to red. The solvent was removed and the residue washed with hexane (2 × 4 mL) to give the complex [Et₄N]4 as a red oil which could not be crystallized. IR ν(CO) (THF): 2054 (m), 2015 (m), 1999 (vs), 1969 (s), 1957 (m), 1932 (m) cm⁻¹; ¹H NMR (CDCl₃): 5.44 (s, 1 H), 2.00 (s, 3 H), 1.95 (s, 3 H) (dmpz) ppm; 3.12 (q, 8 H), 1.18 (t, 12 H) (Et₄N) ppm; 0.95 (m, 30 H, SiEt₃) ppm; -11.12 (d, *J* = 2 Hz, 1 H), -11.77 (d, *J* = 2 Hz, 1 H) (μ-H) ppm. ¹³C-¹H NMR (CDCl₃): 211.7, 209.7, 208.5, 207.2, 206.6, 205.4, 199.0, 192.9 (CO) ppm; 147.8, 147.2, 104.9, 12.9, 12.8 (dmpz) ppm; 52.3, 7.2 (Et₄N) ppm; 12.4, 11.1, 9.0, 8.8 (SiEt₃) ppm.

The compound [PPN]4 (red oil) was prepared in a similar way, with [PPN]1 as starting material.

[Et₄N][Ru₃(μ-dmpz)(μ-H)₂(SiPh₃)₂(CO)₈] ([Et₄N]5). A solution of [Et₄N]1 (80 mg, 0.099 mmol) and HSiPh₃ (44 mg, 0.247 mmol) in THF (20 mL) was stirred at reflux temperature for 2 h. The color changed from yellow to red. The solvent was removed and the residue extracted into diethyl ether (2 × 10 mL). The filtered solution was evaporated to dryness and the residue washed with hexane (2 × 5 mL) to give [Et₄N]5 as a red-orange solid (74 mg, 59%). Anal. Calcd for C₅₇H₅₉N₃O₈Ru₃Si₂: C, 53.76; H, 4.67; N, 3.30. Found: C, 53.98; H, 4.80; N, 3.31. IR ν(CO) (THF): 2062 (m), 2036 (sh), 2016 (s), 1983 (vs), 1971 (m), 1951 (sh), 1933 (sh) cm⁻¹. ¹H NMR (CDCl₃): 7.8–7.0 (m, 30 H, SiPh₃) ppm; 5.38 (s, 1 H), 1.95 (s, 3 H), 1.59 (s, 3 H) (dmpz) ppm; 2.97 (q, br, 8 H), 1.14 (t, br, 12 H) (Et₄N) ppm; -10.97 (s, 1 H), -11.76 (s, 1 H) (μ-H) ppm. Selected ¹³C{¹H} NMR (CD₂Cl₂): 202.9, 199.3, 199.2, 197.9, 197.1, 196.2, 190.6, 182.1 (CO) ppm; 146.8, 145.0, 107.3, 13.1, 12.7 (dmpz) ppm; 54.6, 7.7 (Et₄N) ppm.

Table 2. Crystallographic and Refinement Data for [PPN]3

formula	C ₆₃ H ₄₇ N ₃ O ₈ P ₂ Ru ₃
fw	1339.19
cryst syst	monoclinic
space group	P2 ₁
<i>a</i> , <i>b</i> , <i>c</i> , Å	15.718(9), 9.580(3), 19.957(12)
<i>β</i> , deg	108.39(4)
<i>V</i> , Å ³	2852(3)
<i>Z</i>	2
<i>F</i> (000)	1344
<i>D</i> _{calcd} , g/cm ³	1.560
<i>μ</i> , mm ⁻¹	0.899
cryst size, mm	0.36 × 0.33 × 0.13
radiation (λ, Å)	Mo Kα (0.710 73)
diffractometer	Enraf-Nonius CAD4
monochromator	graphite
temp, K	293(2)
scan method	ω-2θ
θ limits, deg	1.08–24.97
<i>h</i> , <i>k</i> , <i>l</i> ranges	0 to +18, 0 to +11, -23 to +22
no. of rflns collected	5503
no. of indep rflns	5338
<i>R</i> _{int} = Σ(<i>I</i> - ⟨ <i>I</i> ⟩)/Σ <i>I</i>	0.022
no. of rflns with <i>I</i> > 2σ(<i>I</i>)	4976
no. of restraints, params	1, 759
<i>R</i> (<i>F</i>) _{<i>I</i>>2σ(<i>I</i>)^a}	0.0218
<i>R</i> _w (<i>F</i>) ² _{all data^b}	0.0589
GOF ^c	1.065
Δ/ <i>σ</i>	0.002
max, min Δ <i>ρ</i> , e/Å ³	+0.602, -0.248

^a *R*(*F*) = Σ||*F*_o| - |*F*_c||/Σ|*F*_o|. ^b *R*_w(*F*)² = [Σ*w*(*F*_o² - *F*_c²)²]/Σ*w*(*F*_o²)^{1/2}. ^c Goodness of fit (GOF) = [Σ*w*(*F*_o² - *F*_c²)²/(*N* - *P*)]^{1/2}.

The compound [PPN]5 was prepared in a similar way (71% yield), with [PPN]1 as starting material. Anal. Calcd for C₈₅H₆₉N₃O₈P₂Ru₃Si₂: C, 60.70; H, 4.13; N, 2.50. Found: C, 61.07; H, 4.13; N, 2.70.

[PPN][Ru₃(μ-dmpz)(μ-H)₂(Si(OMe)₃)₂(CO)₈] ([PPN]6). A solution of [PPN]1 (90 mg, 0.074 mmol) and HSi(OMe)₃ (20 μL, 0.155 mmol) in THF (10 mL) was stirred at reflux temperature for 2 h. The color changed from yellow to orange. The solution was evaporated to dryness and the residue washed with hexane (2 × 5 mL) to give [PPN]6 as an orange air-sensitive oil which could not be crystallized. IR ν(CO) (THF): 2066 (m), 2018 (sh), 2012 (vs), 1984 (s), 1972 (sh), 1952 (m), 1930 (sh) cm⁻¹. ¹H NMR (CDCl₃): 7.7–7.3 (m, 30 H, PPN) ppm; 5.28 (s, 1 H), 1.99 (s, 3 H), 1.96 (s, 3 H) (dmpz) ppm; 3.56 (s, 9 H), 3.30 (s, 9 H) (OMe₃) ppm; -11.63 (s, 1 H), -12.34 (s, 1 H) (μ-H) ppm.

[Et₄N][Ru₃(μ-dmpz)(μ-H)₂(SnBu₃)₂(CO)₈] ([Et₄N]7). A solution of [Et₄N]1 (80 mg, 0.099 mmol) and HSnBu₃ (67 μL, 0.247 mmol) in THF (20 mL) was stirred at reflux temperature for 1.5 h. The color changed from yellow to violet. The solvent was removed and the residue washed with hexane (3 × 5 mL) to give the complex [Et₄N]7 as a violet oil which could not be crystallized. IR ν(CO) (THF): 2080 (w), 2006 (s), 1991 (s), 1972 (s), 1926 (s), 1906 (sh) cm⁻¹. ¹H NMR (CDCl₃): 5.46 (s, 1 H), 1.99 (s, 6 H) (dmpz) ppm; 3.13 (q, br, 8 H), 1.5–0.8 (m, 66 H) (Et₄N and SnBu₃) ppm; -11.09 (s with satellites, *J* = 28 Hz, 2 H, μ-H) ppm.

The compound [PPN]7 (violet oil) was prepared in a similar way, with [PPN]1 as starting material.

[Et₄N][Ru₃(μ-dmpz)(μ-H)₂(SnPh₃)₂(CO)₈] ([Et₄N]8). A solution of [Et₄N]1 (80 mg, 0.099 mmol) and HSnPh₃ (74 mg, 0.211 mmol) in THF (20 mL) was stirred at reflux temperature for 2 h. The color changed from yellow to red-violet. The solvent was removed and the residue washed with diethyl ether (2 × 5 mL) to give [Et₄N]8 as a violet solid (97 mg, 67%). Anal. Calcd for C₅₇H₅₉N₃O₈Ru₃Sn₂: C, 47.06; H, 4.09; N, 2.89. Found: C, 46.91; H, 4.23; N, 2.85. IR ν(CO) (THF): 2089 (w), 2031 (vs), 2015 (s), 2000 (sh), 1954 (s, br), 1942 (sh, br) cm⁻¹. ¹H NMR (CDCl₃): 7.6–7.0 (m, 30 H, SnPh₃) ppm; 5.50 (s, 1 H), 1.54 (s, 6 H) (dmpz) ppm; 2.38 (q, br, 8 H), 0.75 (t, br, 12

Table 3. Atomic Coordinates ($\times 10^4$) and Equivalent Isotropic Displacement Parameters ($\text{\AA}^2 \times 10^3$) for the Non-H Atoms of [PPN]3

atom	<i>x/a</i>	<i>y/b</i>	<i>z/c</i>	<i>U</i> _{eq} ^a	atom	<i>x/a</i>	<i>y/b</i>	<i>z/c</i>	<i>U</i> _{eq} ^b
Ru(1)	7068(1)	1310(1)	7825(1)	38(1)	P(1)	7257(1)	1447(1)	1559(1)	38(1)
Ru(2)	8021(1)	1937(1)	6919(1)	36(1)	P(2)	7648(1)	1157(1)	3141(1)	36(1)
Ru(3)	8703(1)	-121(1)	7919(1)	37(1)	N(3)	7568(3)	732(5)	2359(2)	47(1)
C(1)	5810(3)	1645(6)	7624(3)	54(1)	C(28)	6095(3)	671(6)	1119(2)	44(1)
O(1)	5076(2)	1926(6)	7489(3)	85(1)	C(29)	5756(4)	-503(6)	1336(3)	63(2)
C(2)	7448(4)	2181(7)	8749(3)	64(2)	C(30)	4875(4)	-908(8)	989(3)	78(2)
O(2)	7671(4)	2734(7)	9269(2)	117(2)	C(31)	4347(4)	-154(9)	431(3)	77(2)
C(3)	7149(3)	3161(6)	7354(3)	56(1)	C(32)	4691(4)	1005(8)	227(3)	77(2)
O(3)	6935(3)	4312(4)	7286(2)	68(1)	C(33)	5564(3)	1436(7)	561(3)	58(1)
C(4)	7801(3)	2289(5)	5961(3)	47(1)	C(34)	7353(3)	2982(5)	1398(2)	43(1)
O(4)	7679(3)	2516(5)	5377(2)	67(1)	C(35)	7978(4)	3488(7)	1104(3)	62(2)
C(5)	8709(3)	3566(5)	7100(2)	45(1)	C(36)	8064(4)	4910(9)	1030(4)	86(2)
O(5)	9148(3)	4546(4)	7221(2)	68(1)	C(37)	7552(5)	5841(8)	1269(4)	86(2)
C(6)	9451(4)	1105(6)	7570(3)	59(1)	C(38)	6929(5)	5334(7)	1555(3)	74(2)
O(6)	10121(2)	1511(5)	7527(3)	75(1)	C(39)	6821(4)	3940(6)	1616(3)	52(1)
C(7)	9341(4)	475(7)	8879(3)	60(1)	C(40)	7909(3)	183(5)	1119(2)	43(1)
O(7)	9713(3)	866(7)	9428(2)	105(2)	C(41)	7558(4)	-162(8)	419(3)	69(2)
C(8)	9486(3)	-1597(6)	7813(3)	52(1)	C(42)	8069(5)	-878(9)	83(3)	81(2)
O(8)	9981(3)	-2351(5)	7710(3)	78(1)	C(43)	8938(4)	-1235(7)	453(3)	68(2)
N(1)	7049(2)	-759(4)	8212(2)	42(1)	C(44)	9287(4)	-890(7)	1145(3)	61(1)
N(2)	7824(2)	-1426(4)	8267(2)	41(1)	C(45)	8786(3)	-180(7)	1483(2)	52(1)
C(9)	7776(4)	-2747(5)	8467(2)	51(1)	C(46)	8653(3)	402(5)	3732(2)	42(1)
C(10)	8532(4)	-3749(7)	8602(3)	72(2)	C(47)	9000(3)	926(6)	4413(2)	56(1)
C(11)	6928(4)	-2926(7)	8535(3)	61(1)	C(48)	9772(4)	330(7)	4867(3)	71(2)
C(12)	6493(3)	-1660(7)	8374(3)	54(1)	C(49)	10184(4)	-735(7)	4653(3)	67(2)
C(13)	5572(4)	-1253(8)	8361(4)	81(2)	C(50)	9850(4)	-1252(7)	3986(3)	64(2)
C(14)	6957(3)	270(4)	6860(2)	35(1)	C(51)	9069(3)	-692(6)	3515(3)	50(1)
C(15)	6073(3)	50(5)	6308(2)	36(1)	C(52)	7727(3)	3017(5)	3301(2)	40(1)
C(16)	5655(3)	1078(6)	5830(2)	49(1)	C(53)	8449(3)	3751(6)	3212(3)	51(1)
C(17)	4810(3)	850(6)	5353(3)	55(1)	C(54)	8505(4)	5150(7)	3301(3)	68(2)
C(18)	4377(3)	-401(6)	5339(3)	53(1)	C(55)	7857(5)	5868(7)	3485(3)	71(2)
C(19)	4782(3)	-1416(6)	5815(3)	49(1)	C(56)	7160(5)	5175(7)	3582(3)	68(2)
C(20)	5614(3)	-1186(5)	6297(2)	44(1)	C(57)	7086(4)	3744(6)	3491(3)	54(1)
C(21)	7740(3)	-407(4)	6901(2)	36(1)	C(58)	6706(3)	531(5)	3386(2)	42(1)
C(22)	7848(3)	-1480(5)	6400(2)	38(1)	C(59)	6818(4)	-162(7)	4018(3)	62(1)
C(23)	7523(3)	-2822(5)	6442(3)	47(1)	C(60)	6062(5)	-577(8)	4184(4)	79(2)
C(24)	7591(3)	-3861(6)	5990(3)	55(1)	C(61)	5213(4)	-326(8)	3727(3)	72(2)
C(25)	8001(4)	-3610(7)	5490(3)	68(2)	C(62)	5114(4)	349(7)	3107(3)	62(2)
C(26)	8354(5)	-2321(7)	5459(3)	73(2)	C(63)	5843(3)	787(6)	2934(3)	51(1)
C(27)	8283(4)	-1257(6)	5913(3)	60(1)					

^a *U*_{eq} is defined as one-third of the trace of the orthogonalized *U*_{ij} tensor.

H) (Et₄N) ppm; -10.33 (s with satellites, *J* = 30 Hz, 2 H, *μ*-H) ppm. Selected ¹³C{¹H} NMR (CD₂Cl₂): 205.8, 199.9, 199.5, 199.3, 198.8 (CO) ppm; 146.9, 106.9, 13.6 (dmp) ppm; 54.6, 7.7 (Et₄N) ppm.

The compound [PPN]8 was prepared in a similar way (66% yield), with [PPN]1 as starting material. Anal. Calcd for C₈₅H₆₉N₃O₈P₂Ru₃Sn₂: C, 54.80; H, 3.73; N, 2.25. Found: C, 55.08; H, 3.80; N, 2.38.

Reaction of [NEt₄]3 with HSiPh₃. A solution of [NEt₄]3 (50 mg, 0.0053 mmol) and HSiPh₃ (38 mg, 0.107 mmol) in 1,2-dichloroethane (10 mL) was stirred for 20 min at room temperature. As no reaction was observed, the solution was then heated at reflux temperature for 20 min. The color changed from red to orange. The solution was evaporated to dryness and the residue washed with diethyl ether. A ¹H NMR spectrum of the solid revealed a mixture of complexes in which [Et₄N]5 was the major component. A GC analysis of the ethereal solution indicated the presence of *cis*- and *trans*-stilbene. Analogous results were obtained when HSiEt₃ was substituted for HSiPh₃.

Reaction of [NEt₄]3 with HSnPh₃. A solution of [NEt₄]3 (100 mg, 0.107 mmol) and HSnPh₃ (86 mg, 0.247 mmol) in 1,2-dichloroethane (10 mL) was stirred for 20 min. The color changed from red to violet. The solution was evaporated to dryness and the residue washed with diethyl ether. A ¹H NMR spectrum of the solid revealed the presence of [Et₄N]8. A GC analysis of the ethereal solution indicated the presence of diphenylacetylene.

Crystal Structure of [PPN]3. A dark red crystal, obtained by layering pentane on a solution of the complex in

diethyl ether at -20 °C, was used for the X-ray diffraction study. A selection of crystal and refinement data is given in Table 2.

The cell dimensions were determined by least-squares refinement of 25 reflections with 15 < *θ* < 20°. The space group *P*2₁ was found from systematic absences. Intensities were collected with a variable scan rate and a maximum scan time of 60 s per reflection. Three standard reflections were monitored every 60 min, revealing no intensity fluctuations. Final drift correction factors were between 0.98 and 1.03. Profile analysis was performed on all reflections.³² An empirical absorption correction based on *ψ*-scans was applied;³³ *μ*(Mo K α) = 8.99 cm⁻¹ (minimum, maximum correction factors 0.945, 1.000). Lorentz and polarization corrections were applied, and data were reduced to |*F*_o| values.

The structure was solved by Patterson interpretation using DIRDIF92.³⁴ Isotropic least-squares refinement, using a local version³⁵ of SHELX,³⁶ was followed by a semiempirical absorp-

(32) (a) Lehman, M. S.; Larsen, F. K. *Acta Crystallogr.* **1974**, *A30*, 580. (b) Grant, D. F.; Gabe, E. J. *J. Appl. Crystallogr.* **1978**, *11*, 114.

(33) North, A. C. T.; Phillips, D. C.; Mathews, F. S. *Acta Crystallogr.* **1968**, *A24*, 351.

(34) Beurskens, P. T.; Admiraal, G.; Beurskens, G.; Bosman, W. P.; Garcia-Granda, S.; Gould, R. O.; Smits, J. M. M.; Smykalla, C. *The DIRDIF91 Program System*; University of Nijmegen: Nijmegen, The Netherlands, 1992.

(35) Van der Maalen, J. F. Ph.D. Thesis; University of Oviedo: Oviedo, Spain, 1991.

(36) Sheldrick, G. M. *SHELX, a Program for Crystal Structure Determination*; University Chemical Laboratory; Cambridge, U.K., 1976.

tion correction³⁷ (minimum, maximum correction factors 0.28, 0.34). Full-matrix anisotropic least-squares refinement over F^2 , using the program SHELXL93,³⁸ followed by a difference Fourier synthesis allowed the location of all the hydrogen atoms. After refinement of the positional and anisotropic thermal parameters of the non-hydrogen atoms, the hydrogen atoms were refined isotropically, using a riding model, with free distances to the parent atoms and free rotation for the methyl groups. The thermal parameter used for the hydrogens of the methyl groups was different from that used for the remaining hydrogen atoms. The function minimized was $\sum w(F_o^2 - F_c^2)^2$, $w = 1/[\sigma^2(F_o^2) + (0.0368P)^2 + 0.5332P]$, with $\sigma(F_o)$ from counting statistics and $P = (F_o^2 + 2F_c^2)/3$. Atomic scattering factors were taken from ref 39. Geometrical calculations were made with PARST.⁴⁰ The structure plot was

drawn with the EUCLID package.⁴¹ Final atomic coordinates are given in Table 3. All calculations were carried out on a MicroVax3400 computer at the Scientific Computer Center of the University of Oviedo.

Acknowledgment. This research was supported by the DGICYT (Spain, Grant PB92-1007). R.J.F. is grateful to MUTIS and the Instituto de Cooperación Iberoamericana for postgraduate scholarships.

Supporting Information Available: Tables of bond distances and angles, anisotropic thermal parameters, and H-atom coordinates for [PPN]3 (11 pages). This material is contained in many libraries on microfiche, immediately follows this article in the microfilm version of the journal, and can be ordered from the ACS; see any current masthead page for ordering information.

OM950263F

(37) Walker, N.; Stuart, D. *Acta Crystallogr.* **1983**, A39, 158.

(38) Sheldrick, G. M. In *Crystallographic Computing 6*; Flack, H. D., Párkányi, L., Simon, K., Eds.; International Union of Crystallography & Oxford University Press: Oxford, U.K., 1993; p 100.

(39) *International Tables for X-Ray Crystallography*; Kynoch Press: Birmingham, U.K., 1992 (present distributor: Kluwer Academic: Dordrecht, The Netherlands); Vol. C, Tables 4.2.6.8 and 6.1.1.4.

(40) Nardelli, M. *Comput. Chem.* **1983**, 7, 95.

(41) Spek, A. L. In *Computational Crystallography*; Sayre, D., Ed.; Clarendon Press: Oxford, U.K., 1982; p 528.

Tetraphenylborate Anion as a Phenylating Agent: Chemical and Electrochemical Reactivity of BPh_4^- -Rh Complexes toward Mono- and Dienes and Carbon Dioxide

Michele Aresta,* Eugenio Quaranta, and Immacolata Tommasi

Dipartimento di Chimica and Centro CNR MISO, Campus Universitario, 70126 Bari, Italy

Sylvie Dérien

Laboratoire de Chimie de Coordination Organique, CNRS, UR 415, Université Rennes-1, Campus de Beaulieu, 35042 Rennes, France

Elizabeth Duñach

Laboratoire de Chimie Moléculaire, CNRS, URA 426, Université de Nice "Sophia Antipolis", 06108 Nice, France

Received October 17, 1994[®]

A few aspects of the chemical and electrochemical reactivity of mono-, di-, and trinuclear η^6 -tetraphenylborate-Rh complexes $[(\text{C}_2\text{H}_4)_2\text{Rh}(\eta^6\text{-PhBPh}_3)]$ (**1**), $\{[(\text{C}_2\text{H}_4)_2\text{Rh}(\eta^6\text{-Ph})]_2\text{BPh}_2\}\text{O}_3\text{-SCF}_3$ (**2**), and $\{[(\text{C}_2\text{H}_4)_2\text{Rh}(\eta^6\text{-Ph})]_3\text{BPh}\}(\text{O}_3\text{SCF}_3)_2$ (**3**) are described. The factors governing the phenyl transfer reaction from coordinated BPh_4^- anion to monoenes and dienes are highlighted. Phenyl transfer to ethylene affords, among other products, styrene and ethylbenzene; styrene is converted into *trans*-stilbene. Complexes **1** and **2** react with isoprene affording 1,1-dimethylindene and 1,2-dihydro-2-methyl- and 1,2-dihydro-3-methyl-naphthalene, species formally involving phenyl transfer from boron to coordinated isoprene and intramolecular cyclization of the resulting intermediate. The reactivity of **1–3** toward carbon dioxide has been investigated and compared with that of (diphos)Rh(η^6 -PhBPh₃). Using complexes **1–3**, coordinated ethylene competes with CO₂ toward coupling with phenyl. The electrochemical behavior of the dinuclear complex, **2**, has been investigated. It undergoes two consecutive irreversible one-electron reductions at -1.53 and -1.74 V *vs* SCE, respectively. Analogous experiments carried out in the presence of CO₂ have clearly shown that the reduced species are both able to react catalytically with the heterocumulene under controlled-potential conditions (-1.5 and -1.8 V). CO₂ was coupled with both ethylene and phenyl affording propionic and benzoic acid. The former species was the only product under an ethylene/carbon dioxide atmosphere.

Introduction

The coordination chemistry of the tetraphenylborate anion binding to metal centers¹ represents an area of

growing interest due to the structural aspects related to the variety of binding modes shown by this anion when coordinated to a transition metal ion, the fluxional character shown by several BPh_4^- -metal complexes,^{1,i,l,m,r,s,2} and the prospects that such a chemistry opens in the fields of molecular engineering,^{1k} catalysis,^{1m,3} and both organometallic^{1g,4–8} and organic^{2,9–11} synthesis.

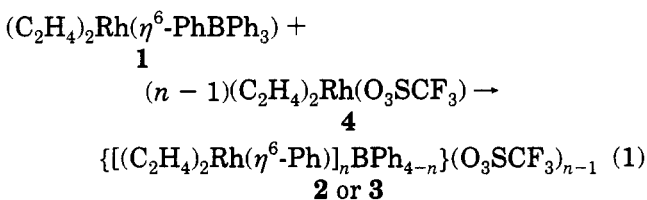
[®] Abstract published in *Advance ACS Abstracts*, April 15, 1995.
 (1) (a) Nolte, M. J.; Gafner, G.; Haines, L. M. *J. Chem. Soc., Chem. Commun.* **1969**, 1406. (b) Schrock, R. R.; Osborn, J. A. *Inorg. Chem.* **1970**, *9*, 2339. (c) Gosser, L. W.; Parshall, G. W. *Inorg. Chem.* **1974**, *13*, 1947. (d) Kruger, G. J.; du Preez, A. L.; Haines, R. J. *J. Chem. Soc., Dalton Trans.* **1974**, 1302. (e) Ashworth, T. V.; Nolte, M. J.; Reimann, R. H.; Singleton, E. *J. Chem. Soc., Chem. Commun.* **1977**, 937. (f) Hossain Bilayet, M.; van der Helm, D. *Inorg. Chem.* **1978**, *17*, 2893. (g) Albano, P.; Aresta, M.; Manassero, M. *Inorg. Chem.* **1980**, *19*, 1069. (h) Pasquali, M.; Floriani, C.; Gaetani-Manfredotti, A. *Inorg. Chem.* **1980**, *19*, 1191. (i) Dartinguenave, M.; Dartinguenave, I.; Beauchamp, A. L. *J. Am. Chem. Soc.* **1984**, *106*, 6849. (j) Fachinetti, G.; Funaioli, T.; Zanazzi, P. F. *J. Chem. Soc., Chem. Commun.* **1988**, 1100. (k) Fagan, P. J.; Ward, M. D.; Calabrese, J. C. *J. Am. Chem. Soc.* **1989**, *111*, 1698. (l) Bochmann, M.; Karger, G.; Jaggar, A. G. *J. Chem. Soc., Chem. Commun.* **1990**, 1038. (m) Horton, A. D.; Frijns, J. H. G. *Angew. Chem., Int. Ed. Engl.* **1991**, *30*, 1152. (n) Thomas, B. J.; Noh, S. K.; Schulte, G. K.; Sendlinger, S. C.; Theopold, K. H. *J. Am. Chem. Soc.* **1991**, *113*, 893. (o) Longato, B.; Pilloni, G.; Graziani, R.; Casellato, U. *J. Organomet. Chem.* **1991**, *407*, 369. (p) Calderazzo, F.; Englert, U.; Pampaloni, G.; Rocchi, L. *Angew. Chem., Int. Ed. Engl.* **1992**, *31*, 1235. (q) Bochmann, M. *Angew. Chem., Int. Ed. Engl.* **1992**, *31*, 1181. (r) Albinati, A.; Aresta, M.; Quaranta, E. *Organometallics* **1993**, *12*, 2032. (s) Aresta, M.; Quaranta, E. *J. Organomet. Chem.* **1993**, *463*, 215.

(2) Aresta, M.; Quaranta, E.; Tommasi, I. *Gazz. Chim. Ital.* **1993**, *123*, 271.
 (3) (a) Albano, P.; Aresta, M. *J. Organomet. Chem.* **1980**, *190*, 243. (b) Aresta, M.; Quaranta, E.; Ciccarese, A. C. *Mol. Chem.* **1985**, *1*, 283.
 (4) (a) Clark, H. C.; Manzer, L. E. *Inorg. Chem.* **1971**, *10*, 2669. (b) Siegmund, K.; Pregosin, P. S.; Venanzi, L. M. *Organometallics* **1989**, *8*, 2659.
 (5) Coates, G. E. *Organometallic Compounds*, J. Wiley: New York, 1960.
 (6) Haines, R. J.; Du Preez, A. L. *J. Chem. Soc., Dalton Trans.* **1972**, 944.
 (7) Sacconi, L.; Dapporto, P.; Stoppioni, P. *Inorg. Chem.* **1976**, *15*, 325.
 (8) Feng Chin, P. K.; Hartley, F. R. *Inorg. Chem.* **1976**, *15*, 982.
 (9) Crociani, B.; Nicolini, M.; Richards, R. L. *J. Organomet. Chem.* **1976**, *104*, 259.
 (10) Taylor, S. H.; Maitlis, P. M. *J. Am. Chem. Soc.* **1978**, *100*, 4700.
 (11) Crociani, B.; Di Bianca, F.; Uguagliati, P.; Canovese, L.; Berton, A. *J. Chem. Soc., Dalton Trans.* **1991**, 71.

Recently, we have reported the isolation from $(C_2H_4)_2-Rh(\eta^6-PhBPh_3)^{12}$ (**1**) of $\{[(C_2H_4)_2Rh(\eta^6-Ph)]_2BPh_2\}O_3SCF_3$ (**2**) and $\{[(C_2H_4)_2Rh(\eta^6-Ph)]_3BPh\}(O_3SCF_3)_2$ (**3**), examples of a tetraphenylborate anion bridging two and three metal centers, respectively. Compounds **2** and **3** have been characterized in the solid state and solution.^{1r} As an extension of our studies on the use of coordinated BPh_4^- as a phenylating agent,² we wish to describe in this paper a few aspects of the chemical reactivity of complexes **1–3** toward monoenes (ethylene, styrene), dienes (isoprene) and the use of **2** as an electrochemical catalyst for ethylene–CO₂ coupling.

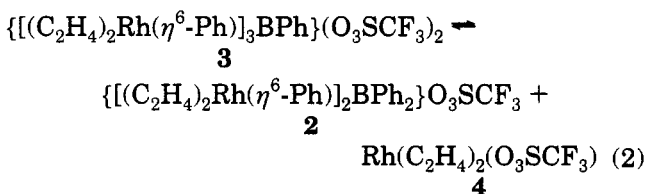
Results and Discussion

Stability of Coordinated Tetraphenylborate Anion. $(C_2H_4)_2Rh(\eta^6-PhBPh_3)$ (**1**), synthesized from $[(C_2H_4)_2RhCl]_2$ and $NaBPh_4$, can be conveniently used as the starting material for the synthesis of di-, tri-, and tetranuclear η^6-BPh_4-Rh complexes according to eq 1.



$$n = 1-4; n = 2, \mathbf{2}; n = 3, \mathbf{3}$$

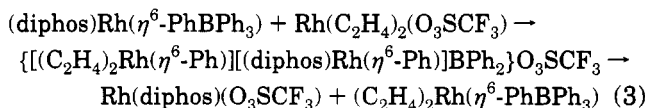
In the solid state, compounds **1–3** are stable for a long time, even in the presence of oxygen or moisture. In solution, their behavior strongly depends on the nature of the solvent and the experimental conditions. Coordinating solvents (CH₃CN, DMF) easily displace the tetraphenylborate anion from the metal center to afford the ionic species $[(C_2H_4)_2Rh(S)_n]O_3SCF_3$ and $[(C_2H_4)_2Rh(S)_n]BPh_4$ (*S* is solvent), the formation of which has been monitored by means of NMR and conductometric techniques.^{1,2} However, loss of the BPh_4^- anion can be observed also in less coordinating solvents (THF, dichloromethane) when more than two $Rh(C_2H_4)_2$ moieties are coordinated to the BPh_4^- anion and according to the temperature. As a matter of fact, we have ascertained by ¹H NMR (see the Experimental Section) that complex **3** is partially dissociated (38% at 293 K) in CD₂Cl₂ according to equilibrium 2, which is shifted to right upon



increasing temperature (43% at 301 K). No evidence for a dissociative equilibrium analogous to (2) has been found for complexes **1** and **2** at temperatures lower than 310 K, both in CH₂Cl₂ and THF.¹³ In our opinion such a different behavior can be related to the steric encum-

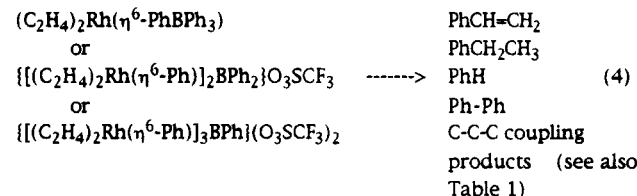
berment around the boron atom that increases in the order **1** < **2** < **3** < $\{[(C_2H_4)_2Rh(\eta^6-Ph)]_4B\}(O_3SCF_3)_3$.

Such a view is supported by the fact that substitution of ethylene with dipy or diphos as ancillary ligands allows the coordination of only one Rh atom to BPh_4^- . Indeed, when $(diphos)Rh(\eta^6-PhBPh_3)$ is reacted with $Rh(C_2H_4)_2(O_3SCF_3)$ (**4**), the dinuclear complex $\{[(C_2H_4)_2Rh(\eta^6-Ph)][(diphos)Rh(\eta^6-Ph)]BPh_2\}O_3SCF_3$ is formed¹⁴ but not isolated, as it converts quickly into **1** and $Rh(diphos)(O_3SCF_3)$ (eq 3).



This reaction represents the first example of coordinated tetraphenylborate transfer between two metal centers.

Reactivity of Complexes 1–3. (A) Phenyl Transfer from Boron to Monoolefins. When THF or CH₂Cl₂ solutions of one of the complexes **1–3** are left at room temperature (293 K) *in vacuo* or under an inert gas atmosphere (N₂, Ar), a black precipitate (probably containing metal Rh) slowly separates within a few hours. The GC–MS analysis of these solutions reveals the formation of diphenyl, benzene, ethylbenzene, and styrene (eq 4). The formation of styrene and ethylben-



zene is particularly interesting as it requires a two-step mechanism based on (a) phenyl transfer from boron to coordinated ethylene with formation of a new C–C bond and (b) hydrogen transfer. Owing to the potentiality of using the tetraphenylborate anion as a stable, nontoxic, commercially available phenylating agent, we have further investigated this reaction at temperatures higher than 293 K focusing our attention on compounds **1** and **2**, as **3** shows a high tendency to give **2** upon dissociation. In Table 1 we summarize the findings on the reactivity of **1** and **2** under C₂H₄ (0.1 MPa) at 338 K.

After heating of THF solutions of **1** or **2** under the conditions given in Table 1 (entries 1 and 2) for about 12 h or less, benzene, diphenyl, styrene, and ethylbenzene were formed, together with minor amounts of other products. The phenyl group and ethylene itself can compete as hydrogen acceptors to afford benzene and ethane, respectively.¹⁵ The total balance of phenylated products shows that at least three phenyl groups *per*

(14) The formation of $\{[(C_2H_4)_2Rh(\eta^6-Ph)][(diphos)Rh(\eta^6-Ph)]BPh_2\}O_3SCF_3$ is justified considering that $(diphos)Rh(\eta^6-PhBPh_3)$ in solution does not generate free BPh_4^- , as demonstrated by conductivity and NMR (¹¹B, ¹H) measurements.^{14,2} The addition of $Rh(C_2H_4)_2(O_3SCF_3)$ to the solution of $(diphos)Rh(\eta^6-PhBPh_3)$ causes the change of the ¹H spectrum in the region of the co-ordinated and free phenyl groups accounting for an intermediate with two Rh atoms co-ordinated to tetraphenylborate. This species finally evolves to afford the limit isolated complexes $(diphos)Rh(O_3SCF_3)$ and **1**, with the elimination from the tetraphenylborate co-ordination sphere of the most encumbered moiety “(diphos)Rh”.

(15) The ¹H NMR (200 MHz) spectrum of a THF-*d*₃ solution of **1** heated at 338 K *in vacuo* or under ethylene shows a signal(s) at 0.85 ppm indicative of the presence of ethane.

(12) This complex was first prepared by Osborn and Schrock (see ref 1b). In ref 1r we have described a new synthetic procedure and reported the complete IR and NMR characterization.

(13) Studies at temperatures markedly higher than 310 K were prevented from the reactivity shown by **1** and **2** (see later, in the text).

Table 1. Reactivity of 1, 2, or NaBPh₄ under Ethylene (0.1 MPa) at 338 K^{a,b}

entry	compd	solvent	products ^c				
			PhH	Ph-Ph	PhCH=CH ₂	PhEt	others ^d
1	1 (0.098 mmol)	THF (3 mL)	0.90	0.47	0.71	0.20	e
2	2 (0.072 mmol)	THF (3 mL)	1.15	0.23	0.63	0.14	e
3	2 (0.061 mmol)	CH ₃ CN (3 mL)	0.68	0.35	0.32	0.04	f
4	NaBPh ₄ (1.42 mmol)	THF (3 mL)	traces	0.03			g
5	1 (0.042 mmol) + BPh ₃ (0.080 mmol) ^h	THF (3 mL)	2.81	0.60	0.47	0.36	

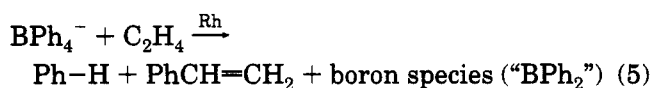
^a The reaction time was equal to 12 h in all runs. ^b The reacting system was very sensitive to oxygen: some phenol has been detected among the products when air was left to enter the reaction vessel. In the latter case, 2-OH-THF and/or γ -butyrolactone were also formed as side products when the reaction solvent was THF. ^c Yields are expressed in moles of product per mole of BPh₄⁻ anion. ^d These products have been identified by GC-MS analysis on the basis of their fragmentation pattern and by comparison with the mass spectra of pure compounds. ^e Butylbenzenes (*m/z* 134), phenylbutenes (*m/z* 132), 1-methyl-2,3-dihydroindene (*m/z* 132), and *trans*-stilbene were also formed in yields lower than 1–2%. ^f Traces of PhCH₂CH₂CN were found. The formation of this compound was not observed when a CH₃CN solution of NaBPh₄ was heated at 338 K under an ethylene atmosphere for 12 h. ^g Traces of terphenyls were detected in the reaction mixture. ^h The GC-MS analysis of the reaction mixture, once the reaction was stopped, did not show the presence of residual amounts of BPh₃.

Table 2. Reactivity of 1, 2, (diphos)Rh(η^6 -PhBPh₄), or NaBPh₄ toward Styrene at 343 K^{a,b,c,d}

entry	Rh complex	PhH	Ph-Ph	PhEt	<i>trans</i> -PhCH=CHPh	others ^e	styrene conv (%)
1	1 (0.034 mmol)	0.86	0.49	0.66	0.50	f	20
2	2 (0.035 mmol)	1.19	0.17	0.38	0.21	g	89
3	(diphos)Rh(η^6 -PhBPh ₃) (0.036 mmol)	1.27	0.19	0.77	1.53	h	19
4	NaBPh ₄ (0.139 mmol)	traces	traces				

^a The free styrene/BPh₄⁻ molar ratio was approximately equal to 20 in all runs, except run 4 where it was equal to 60. ^b The reaction time was equal to 6.5 h in all runs. ^c All runs were performed in THF (3 mL) under a dinitrogen atmosphere (0.1 MPa). ^d Yields are expressed in moles of product per mole of BPh₄⁻ anion. ^e These products have been identified by GC-MS analysis on the basis of their fragmentation pattern and by comparison with the mass spectra of pure compounds. ^f The GC-MS analysis of the reaction mixture showed the formation of small amounts of isomeric products with a mass/charge ratio of *m/z* 132 (formally involving styrene-ethylene coupling), Ph₂CHCH₃, Ph₂C=CH₂, and PhCH₂CH₂Ph. Dimers of styrene (*m/z* 208), a few of which partially hydrogenated (*m/z* 210), were also formed in variable yields: among them we have identified 1,3-diphenyl-1-butene, 1,4-diphenyl-1-butene, and 1,4-diphenylbutane. ^g The GC-MS analysis of the reaction mixture showed the formation of small amounts of isomeric products with a mass/charge ratio of *m/z* 132 (see footnote f, this Table), Ph₂CHCH₃, Ph₂C=CH₂, and PhCH₂CH₂Ph. Dimers, trimers, and higher oligomers of styrene were also found in the reaction mixture. ^h The GC-MS analysis of the reaction mixture showed the formation of Ph₂CHCH₃, Ph₂C=CH₂, and PhCH₂CH₂Ph, styrene oligomers [*m/z* 208 and 210 (1,3-diphenyl-1-butene and 1,4-diphenylbutane), *m/z* 312], and other products formally involving phenylation of styrene dimers (*m/z* 286).

BPh₄⁻ are converted into organic products. This result matches our previous findings of four phenyls per BPh₄⁻ used in the phenylation of aldehydes.² Interestingly, under an ethylene atmosphere styrene is preferentially produced with respect to ethylbenzene with an overall reaction given in eq 5. However, the analysis of the data in Table 1 shows that benzene can be formed by other independent routes.



The formation of all above mentioned organic compounds is, without a doubt, promoted by the Rh center. In fact, no formation of styrene, ethylbenzene, stilbene, and other substituted benzenes was observed when a THF solution of NaBPh₄ was heated under ethylene at 338 K (entry 4, Table 1): only trace amounts of benzene and diphenyl were formed in this case. In runs 1–3 (Table 1) BPh₃ was never found at the end of the reaction. More interestingly, when free BPh₃ was added to the reaction mixture (entry 5, Table 1), it was involved into the phenylation reaction and influenced the styrene/ethylbenzene molar ratio (the overall phenyl-ethylene coupling yield was practically unchanged). This result is quite intriguing. It was reported that BPh₃ can coordinate to an electron-rich metal center through boron.¹⁶ The Rh species that are generated in solution do not appear to fully meet this requirement. In fact, we have demonstrated that Rh(C₂H₄)₂(O₃SCF₃),

a possible daughter species, reacts with BPh₃, which can coordinate to Rh through the phenyl π -electron system.¹⁷ This might explain the BPh₃ reactivity, although at the present state we cannot exclude a boron coordination.

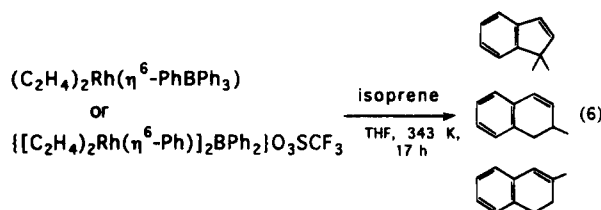
In CH₃CN (entry 3, Table 1), which is able to promote the decoordination of BPh₄⁻ anion from the rhodium center and afford ionic species, 2 slowly converts into [Rh(C₂H₄)₂(CH₃CN)₂]BPh₄ and [Rh(C₂H₄)₂(CH₃CN)₂]O₃SCF₃. Under these conditions, the formation of styrene results to be repressed and only traces of ethylbenzene were detected in the reaction mixture. Moreover, stilbene and other benzene derivatives were not formed. The lower yield of phenylated products in CH₃CN with respect to THF supports the idea that coordination of BPh₄⁻ to the metal center promotes the phenyl transfer. A coordinating solvent can, thus, affect markedly both the distribution of products and the yield of the olefin-phenyl coupling reaction.

The formation of minor amounts of *trans*-stilbene and phenylbutenes can be explained as a further conversion of the styrene generated by Ph/C₂H₄ coupling.

Table 2 (entries 1 and 2) shows the results obtained when complexes 1 and 2 were reacted with pure styrene. *trans*-Stilbene was formed in this case, and the yield was significantly affected by suitably changing the ancillary ligands at rhodium (entry 3, Table 2). The phenyl transfer reaction from boron to styrene is both regio- and stereoselective as no formation of *cis*-stilbene has been observed, whereas 1,1-diphenyl-ethylene was

formed only in traces. The phenylation of styrene is accompanied by an oligomerization reaction. The formation of styrene oligomers was particularly important when **2** was used as catalyst (see below).

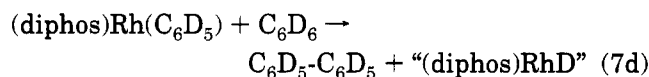
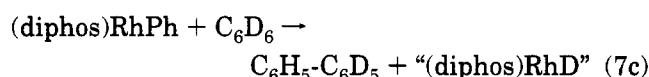
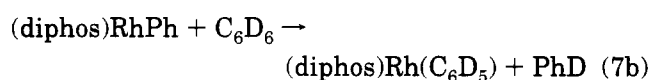
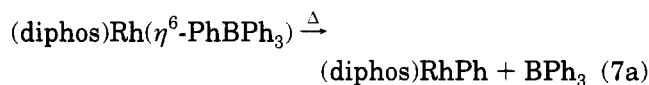
(B) Phenyl Transfer from Boron to Isoprene. The reaction of **1** or **2** with isoprene (diene/BPh₄⁻ molar ratio = 30–50) in THF at 343 K (17 h) affords 1,1-dimethylindene, the major product, and a mixture of 1,2-dihydro-3-methyl- and 1,2-dihydro-2-methylnaphthalene (product distribution: 1:0.7:0.4, respectively). All these species formally involve phenyl transfer from boron to isoprene followed by the intramolecular cyclization of the resulting intermediate (eq 6). Other



isoprene phenylation products (*m/z* 146) were formed in very low yield. One mole of isoprene was phenylated *per* mole of phenyl transferred. The formation of both styrene and ethylbenzene is completely repressed under these conditions (see below paragraph D). It may be of interest to note that complexes **1** and **2** show a different behavior toward isoprene. The mononuclear complex **1** shows a negligible ability to oligomerize isoprene, while the dinuclear complex afforded dimers (*m/z* 136), trimers (*m/z* 202 and 204), and tetramers (*m/z* 272) as well species involving the coupling of some of these oligomers with ethylene. The most abundant of all these species is 1,5,9-trimethyl-1,5,9-cyclododecatriene. Moreover, benzene was formed only in traces in both cases, and the dinuclear complex **2** produced diphenyl in smaller amounts (practically traces) than the mononuclear homologue **1**. In order to get further information about the role of the metal center in these phenyl transfer processes, we have carried out the same reaction using NaBPh₄. When NaBPh₄ was reacted with isoprene (5.0 mmol) in THF, coupling products were not formed nor were isoprene oligomers.¹⁸

(C) Role of Solvents as the Source of Hydrogen Atoms. In the reactions discussed above, part of the BPh₄⁻ phenyls gave rise to benzene and diphenyl. In order to throw light on the reaction mechanism and the source of hydrogen demanded by benzene, we have investigated the thermal behavior of **1** in deuterated solvents. The GC–MS of a THF-*d*₈ solution of **1** heated at 348 K shows the presence of benzene-*d*_{*n*} [*n* = 0 and 1 (less abundant)] and diphenyl-*d*₀.¹⁹ The relative amounts of these products demonstrates that the hydrogen atom source is essentially ethylene itself or a phenyl group bound to boron but less probably the solvent. The generation of benzene and diphenyl seems to be a general feature of the reactivity of the tetraphenylborate anion η⁶-coordinated to Rh centers.² In fact, we have observed the formation of benzene-*d*_{*n*}, diphenyl-*d*_{*n*}, and terphenyls-*d*_{*n*} (*n* = 0, 1) when a THF-*d*₈ solution of (diphos)Rh(η⁶-PhBPh₃) was heated at 348 K under

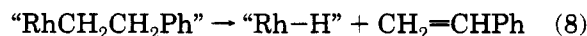
N₂. The partial involvement of the solvent is clearly demonstrated by the fact that when (diphos)Rh(η⁶-PhBPh₃) was heated in C₆D₆ at 348 K (under N₂), diphenyl-*d*₀, diphenyl-*d*₅, and diphenyl-*d*₁₀, besides small amounts of terphenyl-*d*_{*n*} (*n* = 0, 4, 5), were found in the reaction mixture. Diphenyl can be formed by the coupling of two phenyl groups coming from the tetraphenylborate anion or generated from the benzene-*d*₆ present in the reaction mixture. The formation of diphenyl-*d*₁₀ from C₆D₆ suggests that, upon heating, (diphos)Rh(η⁶-PhBPh₃) is able to promote the activation of aromatic C–D bonds. Most probably, the reaction involves Rh–Ph^{1g} species according to eq 7a–d. The formation of (diphos)RhPh has been clearly documented and reported in a previous paper.^{1g}



(D) Mechanistic Considerations. The phenyl transfer to Rh from BPh₄⁻ (eq 7a) is expected to take place much more easily with complexes **1**–**3** with respect to Rh(diphos)(η⁶-PhBPh₃), because of the higher electrophilicity of the Rh centers resulting from both the different donor–acceptor properties of ethylene with respect to diphos and, in the case of complexes **1** and **2**, the net positive charge on the Rh atoms.²⁰ Noteworthy, a species of type (C₂H₄)₂RhPh (**5**) could not be isolated or detected spectroscopically, probably because of a higher kinetic lability with respect to the isolated^{1g} (diphos)RhPh.

Starting from complexes **2** and **3**, besides (C₂H₄)₂RhPh, (C₂H₄)₂Rh(O₃SCF₃) (**4**) and BPh₃ may be generated. In an *ad hoc* study we have found evidence that triphenylboron can react with **4** affording a new adduct in which BPh₃ is η-coordinated to rhodium.¹⁷ This finding can, in part, explain the reactivity of BPh₃ as a source of phenyl groups reported above.

The intermediate (C₂H₄)₂RhPh can be generated from any of the complexes **1**–**3**. Insertion of ethylene in the Rh–Ph bond of **5** can produce a “RhCH₂CH₂Ph” species that can evolve to give styrene (eq 8).²¹ The formation



of PhEt or also ethane can be explained on the basis of

(20) In THF-*d*₈ solution, indeed, (diphos)Rh(η⁶-PhBPh₃) shows a much higher thermal stability than compounds **1**–**3**.

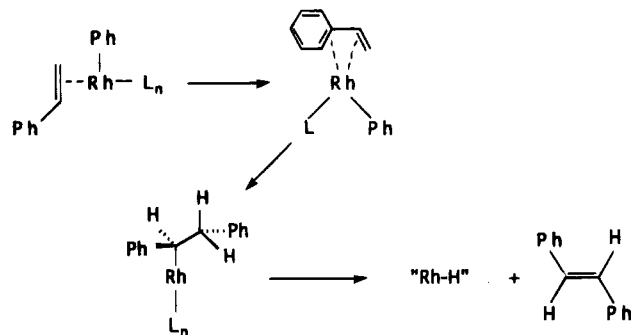
(21) The above described reactions are all Rh-mediated and do not appear to be initiated by radical species. As a matter of fact, when benzoyl peroxide was heated in THF in the presence of an excess of styrene or isoprene, in conditions suitable for the production of phenyl radicals (373 K),²² we have not observed the formation of any coupling product such as ethylbenzene, stilbene, 1,1-dimethylindene, and 1,2-dihydro-2-methyl- and 1,2-dihydro-3-methylnaphthalene.

(22) Detar, D. F.; Long, R. A. J.; Rendceman, J.; Bradley, J.; Duncan, P. *J. Am. Chem. Soc.* **1967**, *89*, 4051.

(18) The GC–MS analysis of the reaction mixture showed the presence of diphenyl and traces of benzene.

(19) Diphenyl-*d*₁ could not be unequivocally confirmed despite a number of attempts changing the reaction conditions.

Scheme 1



a hydrogen transfer to styrene or ethylene. As far as PhEt formation is concerned, it may be worth to emphasize the following: significant amounts of PhEt were formed when **1** or **2** were reacted with styrene (Table 2); ethylbenzene was preferentially formed with respect to styrene when complexes **1** or **2** were heated in THF *in vacuo* or in an inert gas atmosphere, whereas the opposite took place in the presence of an excess of ethylene.

Very little hydrogen comes from the solvent as confirmed by the fact that minor amounts of PhCHDCH₃ and PhCHDCH₂D were formed when **1** was heated in THF-*d*₈ (both under ethylene and *in vacuo*).²³ These results agree with the above described role of solvent as source of hydrogen.

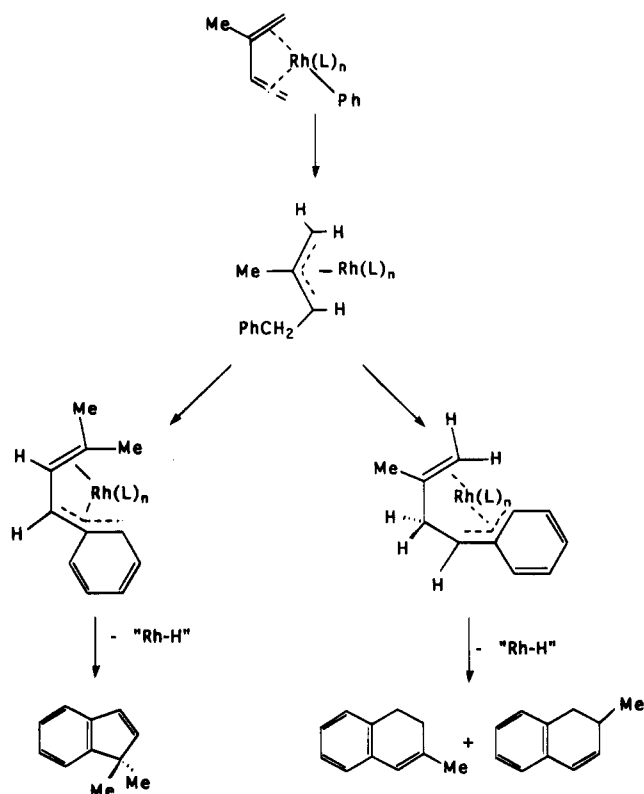
BPh₃ produced seems to be not involved in further production of styrene: more likely, it generates diphenyl and benzene. In fact, no increase of phenyl-ethylene coupling product has been observed when **1** was heated under ethylene in the presence of an excess of BPh₃, whereas both diphenyl and, more markedly, benzene formation resulted in being favored. The decomposition of triarylboron compounds to symmetric biaryls in the presence of Pd(0) has been reported by Chiusoli and co-workers,²⁴ who, however, have not described the formation of benzene. The mechanism through which these transformations can take place is still unclear; further investigation is needed also for clarifying the final fate of boron.

When isoprene or styrene are added to **1** or **2**, the ethylene substitution is a fast process that precedes the phenyl migration from boron to rhodium. This is supported by the fact that, in the reaction of **1** or **2** with isoprene, both styrene and ethylbenzene formation are almost totally repressed. If styrene is the substrate, the ligand substitution step results to be thermodynamically or kinetically less favored for **2** than for **1**, most probably because of the cationic character of the catalyst, as demonstrated by the significantly different yield of stilbene and PhEt in the two cases (entries 1 and 2, Table 2).

Schemes 1 and 2 summarily show the pathways for the formation of stilbene from styrene and 1,1-dimethylindene and 1,2-dihydro-2-methyl- and 1,2-dihydro-2-methylnaphthalene from isoprene.

The fact that **2** behaves as a good catalyst for the formation of styrene or isoprene oligomers is explained

Scheme 2



on the basis of the fact that **2** easily generates the complex L₂RhO₃SCF₃ (L = styrene, isoprene) that has been isolated. (C₂H₄)₂RhO₃SCF₃^{1r} was also prepared by an independent route and reacted with styrene or isoprene in conditions analogous to those used for their reaction with **1**²⁵ and shown to afford the same products discussed here.

(E) Complexes 1–3 vs (diphos)Rh(η⁶-PhBPh₃) Reactivity toward Carbon Dioxide. Our interest in carbon dioxide activation by metal centers and in carboxylation reactions of organic substrates using CO₂²⁶ pushed us to investigate the reactivity of complexes **1–3** toward CO₂. Differently from (diphos)Rh(η⁶-PhBPh₃), which has been shown to be able to coordinate CO₂ (CH₂Cl₂, 293 K, 1 MPa CO₂ pressure),^{1g} complexes **1–3** are not able to afford stable adducts with the heterocumulene. Complexes (diphos)Rh(η⁶-PhBPh₃) and **1–3** are all 18 e⁻ systems and, as judged by their NMR spectra,^{1r} the η⁶ → η⁴ → η² bound phenyl fluxional process, which would make available coordination sites on rhodium, is absent at room temperature. The interaction of L₂Rh(η⁶-Ph) moieties [L₂ = (C₂H₄)₂ or diphos] with carbon dioxide should involve, as in the case of Rh(diars)₂Cl,²⁷ a full orbital of the metal and an empty antibonding π-orbital of CO₂. The different behavior of compounds **1–3** toward CO₂ with respect to (diphos)Rh(η⁶-PhBPh₃) emphasizes the role and importance of the ancillary ligands in stabilizing the coordination of carbon dioxide to a metal center: the weaker σ-donor and better π-acceptor C₂H₄, with respect to diphos, does not favor the formation of a stable CO₂-

(23) The experiments in deuterated solvents also reveal the formation of low amounts of styrene-*d*₁ in addition to the more abundant styrene-*d*₀.

(24) Catellani, M.; Chiusoli, G. P.; Fornasari, V. *Gazz. Chim. Ital.* **1990**, *120*, 779.

(25) Aresta, M.; Quaranta, E. Manuscript in preparation.

(26) Aresta, M.; Quaranta, E.; Tommasi, I. *New J. Chem.* **1994**, *18*, 133 and references therein.

(27) Calabrese, J. C.; Herskovitz, T.; Kinney, J. B. *J. Am. Chem. Soc.* **1983**, *105*, 5914.

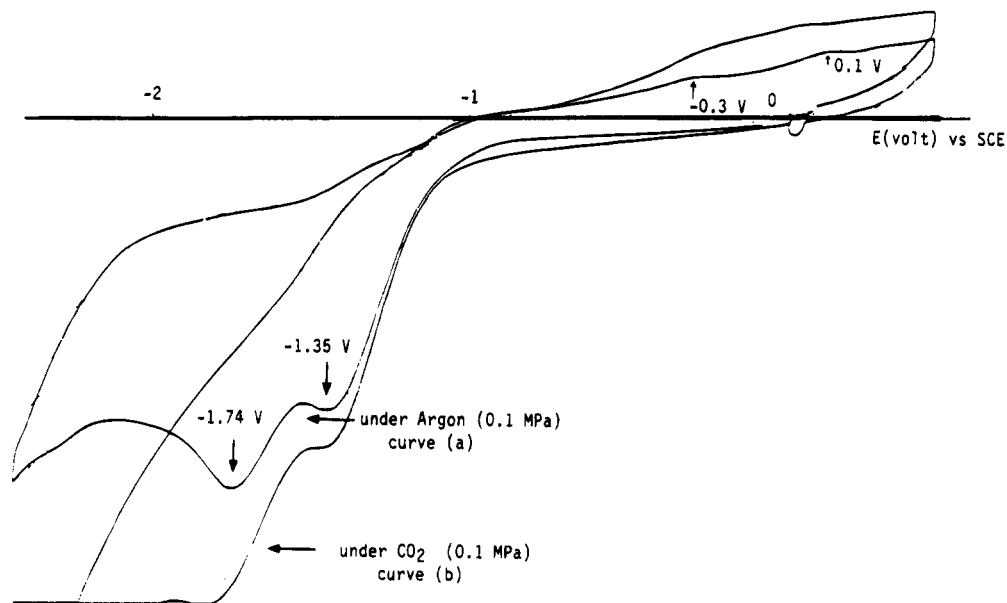


Figure 1. Cyclic voltammograms obtained with a freshly polished gold microelectrode (3 mm², Tacussel), at 293 K at a scan rate of 200 mV/s, for a solution of **2** (1.25 mM) in THF (20 mL) containing 0.15 M tetrabutylammonium tetrafluoroborate as supporting electrolyte: (a) solution under argon; (b) solution saturated with CO₂.

Rh adduct. Moreover, the stability of a $M-\eta^1(C)-CO_2$ adduct is strongly affected by the coulombic interaction between the net charge on the metal and the CO₂ carbon atom:²⁸ the more positive the charge on the metal, the more destabilizing the contribution of this energetic term. Consequently, the existence of a net positive charge on the Rh atoms of **1** (+ $1/2 e$) and **2** (+ $2/3 e$) represents a further action which contributes to determine the scarce reactivity of **1** and **2** toward carbon dioxide.

Heating (diphos)Rh(η^6 -PhBPh₃) under a carbon dioxide atmosphere produces in good yield the benzoato complex (diphos)Rh(O)CPh.¹⁸ The formation of this species has been rationalized as a result of the insertion of the heterocumulene in the Rh-Ph bond of (diphos)-RhPh, the product obtained upon transfer of a phenyl from boron to rhodium. No significant formation of carboxylation products has been observed when complexes **1-3** were reacted with CO₂ or C₂H₄/CO₂ mixtures at 353 K, but benzene, diphenyl, and the phenyl-ethylene coupling products were observed. This suggests that the ethylene-CO₂ competition for the phenyl moiety is resolved in favor of the olefin, most likely because ethylene is already in the coordination sphere of the metal. This result is a further demonstration of the fact that all the chemistry described above is not radical chemistry but takes place around the metal center. The higher π -acceptor character of C₂H₄ with respect to diphos is another point in favor of the ethylene-phenyl preferential coupling.²⁹

Electrochemical Behavior of [(C₂H₄)₂Rh(η^6 -Ph)₂BPh₂]₂O₃SCF₃. The poor tendency of complexes **1-3** to undergo a chemical interaction with CO₂ suggested us to investigate if the olefin-CO₂ coupling could be better achieved using other strategies. We have explored the electrochemical way, focusing our attention on complex **2**.

The cyclic voltammetry curves of complex **2** in THF containing tetrabutylammonium tetrafluoroborate as

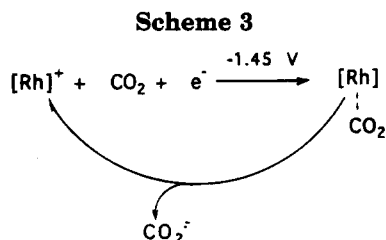
supporting electrolyte are presented in Figure 1, curve a. An irreversible one-electron reduction peak at -1.35 V vs SCE is followed by a second irreversible one-electron reduction peak at -1.74 V. Only low-intensity reoxidation peaks appear around -0.3 and +0.1 V. The addition of an internal alkyne such as 4-octyne to a solution of complex **2** in THF (alkyne/**2** molar ratio equal to 1) did not modify the electrochemical behavior of **2**. Thus, it appears that the alkyne does not coordinate to the rhodium complex, and ethylene ligands in **2** are not exchanged with the alkyne. Conversely, the addition of DMF (2 mL, 5% v/v) to the initial THF solution of **2** results in the shift of the reduction peaks to -1.30 and -1.60 V, respectively: the rhodium complex is now modified. Most probably, cationic complexes are formed with the highly coordinating DMF cosolvent (see above), which are more easily reducible. This behavior is in very good agreement with the chemical results. The further addition of DMF does not modify the reduction potentials.

Where the electron is located, if it is at the Rh atom or it is delocalized on the extended π -electron system involving the ethylene molecules and the coordinated phenyl, is difficult to say. We have in progress ESR studies to elucidate this point.

Bubbling CO₂ into a solution of **2** results in the modified cyclic voltammogram as illustrated in Figure 1, curve b. The first nonreversible reduction peak is shifted to -1.45 V, and its intensity is increased. The second peak appears at -1.80 V, also with a higher intensity. The increase of the peak intensities corresponds to a slight irreversible catalytic current both at -1.45 and -1.80 V.³⁰ The effect of CO₂ addition is reversible and does not decompose the rhodium complex. As a matter of fact, when the CO₂-containing solution

(29) A study by Darensbourg [Darensbourg, D. J.; Grottsch, C. G.; Wiegrefe, P.; Rheingold, A. L. *Inorg. Chem.* **1987**, *26*, 3827] has shown that CO₂ insertion in Rh(I)-Ph bond is favored by strong σ -donor ligands in the coordination sphere of Rh.

(30) As a comparison, the electrochemical reduction of [Rh(C₂H₄)₂-Cl]₂ in THF shows a single irreversible reduction peak at -1.65 V vs SCE, which is not modified in the presence of CO₂ (0.1 MPa).

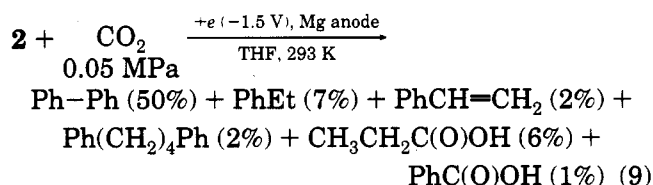


of curve b is degassed with argon, the initial electrochemical behavior of complex **2** is found (e.g. curve a). It is worth noting that the direct reduction of CO₂ occurs at potentials more negative than -2.2 V vs SCE, in agreement with literature data.³¹ Earlier work has shown that the catalytic process observed is characteristic of the reduction of coordinated CO₂ to its radical anion (Scheme 3).³²

The potential shift of **2** in the presence of CO₂ indicates an interaction between the rhodium and CO₂, by CO₂ coordination to the reduced species formed at -1.35 and -1.74 V. The reversibility of the CO₂ coordination supposes that the radical anion of CO₂ evolves to form species without modification of the Rh complex. The reduced CO₂ can then yield oxalate, by dimerization, or CO and carbonate, by disproportionation.^{31,32,33} The reduced complex **2** (both at 1 and 2e⁻) is, thus, a catalyst for the CO₂ reduction. However, the relatively small increase of the peak intensities under CO₂ indicates a slow CO₂ reduction process at the time scale of the cyclic voltammetry.

The reactivity of the electrogenerated species at the potentials shown in Figure 1 was examined in electrolyses carried out at room temperature in a single-compartment cell fitted with a consumable magnesium anode. Recent advances in catalyzed electrochemical reactions involving CO₂ activation have been associated with the use of sacrificial anodes.³⁴

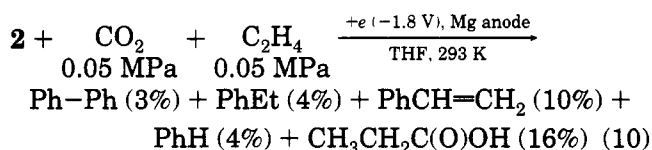
The electrolysis of **2** in THF, at -1.5 V, under a CO₂/Ar atmosphere (0.05 MPa CO₂ pressure, total pressure = 0.1 MPa) proceeded up to the consumption of 4 F/mol of **2**. The solution, initially sharp yellow, turned quickly to orange and, then, to dark-brown. The electrolysis was stopped, the solution was stirred for 2 h, and the organic products were analyzed by GC and GC-MS. The reactivity of **2** and CO₂ at -1.50 V is shown in eq 9. Diphenyl is formed in high yield together with several



phenyl-ethylene coupling products, which is reminiscent of their chemical behavior. Interestingly, ethylene could be carboxylated under the very mild reaction conditions, leading to propionic acid in 6% yield. CO₂

was also partially incorporated into phenyl groups yielding benzoic acid. The electricity consumption of 4 F/mol of **2** indicates a rhodium-catalyzed CO₂ reduction in agreement with the cyclic voltammetry experiments. The higher electron density at the metal center or the localized electron density on ethylene promote the interaction of the metal-ethylene moiety with the heterocumulene that results in its fixation.

In order to investigate if ethylene could be carboxylated to a higher extent, we have investigated the electrochemical behavior of a solution of **2** in THF under a 1:1 mixture of ethylene and carbon dioxide (0.1 MPa overall pressure) at -1.80 V up to the passage of 4 F/mol of **2**, when the intensity slowly started to decrease to zero. The CO₂ incorporation into ethylene afforded propionic acid (eq 10) in 16% yield. Benzoic acid was not formed, and the formation of benzene (4%) and diphenyl (3%) was repressed. Styrene is formed in higher yield than in absence of ethylene.



These results are in good agreement with the chemical findings and show that carbon dioxide interaction with the metal system takes place when an excess negative charge is present. Noteworthy, the ethylene carboxylation takes place easily and in the presence of free ethylene the yield is increased. The essential role of the metal is confirmed. Studies are in progress aimed at identifying the species obtained upon 1 or 2e⁻ transfer to **2**.

Experimental Section

General Comments. Unless otherwise stated, all reactions and manipulations were carried out under dinitrogen, argon, or carbon dioxide atmosphere (as specified in the text) with rigorous exclusion of both air and atmospheric moisture, by using vacuum line techniques. All solvents were dried as described in the literature³⁵ and stored under dinitrogen.

Complexes **1-3** and (diphos)Rh(η^6 -PhBPh₃) were prepared as previously described.^{18,r} Styrene and isoprene (from Fluka) were distilled before using. Tetrabutylammonium tetrafluoroborate (Fluka) was dried by heating overnight at 343 °C *in vacuo*. Magnesium used as the anode was of high purity (magnesium rod, 99.8%, 1 cm diameter, Prolabo). Ethylene (99.7% minimum) and CO₂ (99.99% pure) were from Matheson and SIO SpA, respectively.

Infrared spectra were obtained with a Perkin-Elmer 883 spectrophotometer. NMR spectra were recorded with a Varian XL 200 or a Bruker AM 500. GC-MS analyses were carried out with a HP 5890 gas chromatograph linked to a HP 5970 selective mass detector (capillary column: SE-30, 30 m × 0.000 32 m, 0.25 μ m film thickness). GC analyses were obtained with a DANI HR 3800 gas chromatograph equipped with a Carbowax C 0.1% packed column or a Durawax-DX1 capillary column (30 m × 0.000 329 m, 0.25 μ m). HPLC analyses were performed with a Perkin-Elmer Series 4 LC (column: Erbasil C18/M, 10 μ m, 250 × 4.6 mm) connected with a LC 290 UV/vis spectrophotometer detector. HPLC separation of the products was performed using a Perkin-Elmer LC Series 2 (column: Partisil M9 10/25 ODS).

(35) Perrin, D. D.; Armarego, W. L. F.; Perrin, D. R. *Purification of Laboratory Chemicals*; Pergamon Press: Oxford, England, 1986.

(31) Amatore, C.; Savéant, J. M. *J. Am. Chem. Soc.* **1981**, *103*, 5021 and references therein.

(32) (a) Daniele, S.; Ugo, P.; Bontempelli, G.; Fiorani, M. *J. Electroanal. Chem. Interfacial Electrochem.* **1987**, *219*, 259. (b) Gasnier, L.; Rollin, Y.; Perichon, J. *New J. Chem.* **1989**, *13*, 53.

(33) Dubois, D. L.; Miedanes, A. *J. Am. Chem. Soc.* **1987**, *109*, 113.

(34) (a) Dérien, S.; Duñach, E.; Périchon, J. *J. Am. Chem. Soc.* **1991**, *113*, 8447. (b) Dérien, S.; Clinet, J. C.; Duñach, E.; Périchon, J. *J. Org. Chem.* **1993**, *58*, 2578.

The electrochemical one-compartment cell is a cylindrical glass vessel of 40 mL volume such as that described in ref 36, equipped with a gold grid cathode (20 cm²), a magnesium-rod (immersed 3 cm) anode, and a SCE electrode. Cyclic voltammetric experiments and controlled-potential electrolyses were performed with the aid of Solea-Tacussel conventional equipment and were carried out at 293 K by utilizing a gold microelectrode (Tacussel). All potentials were quoted with respect to a saturated calomel electrode (SCE).

Behavior of 3 in Solution. The behavior of **3** in solution was studied by NMR. An analytically pure sample of **3** was dissolved in CD₂Cl₂, and the ¹H NMR spectrum of the resulting solution was recorded at both 293 and 301 K. The aromatic region showed, besides the signals of the trinuclear complex **3** [6.56 (t, H_{m,ip}^δ-Ph₁₃, ³J_{H_m-H_p} ≈ ³J_{H_m-H_p} = 5.9 Hz), 6.69 (d, H_{o,ip}^δ-Ph₁₃), 7.34 (m, H_{m,BPh}), 7.39 (m, H_{p,ip}^δ-Ph₁₃), 7.40 (m, H_{m,BPh}), 7.69 (d, H_{o,BPh}, ³J_{H_o-H_m} = 7.16 Hz)], also the resonances due to the dinuclear species **2** [6.36 (t, H_{m,ip}^δ-Ph₁₂, ³J_{H_m-H_p} ≈ ³J_{H_m-H_p} = 6.38 Hz), 6.52 (d, H_{o,ip}^δ-Ph₁₂), 7.13 (m, H_{p,BPh₂}), 7.24 (m, H_{m,BPh₂}), 7.26 (t, H_{p,ip}^δ-Ph₁₂), 7.40 (d, H_{o,BPh₂}, ³J_{H_o-H_m} = 6.84 Hz)]. The relative amounts of **2** and **3**, under equilibrium conditions at the given temperature, could be calculated from the integrals of the protons. H_{m,ip}^δ-Ph₁₂ (6.36 ppm, t) and H_{o,ip}^δ-Ph₁₃ (6.69 ppm, d), which do not overlap with the signals of other protons, are the most reliable.

Reaction of 1–3 with Ethylene: General Procedure. A THF (3 mL) solution of the complex (see Table 1) was prepared under ethylene (0.1 MPa) in a 10 mL glass tube. After the tube was sealed, the solution was stirred at 338 K for 12 h and then cooled to room temperature and analyzed by means of chromatographic techniques. The isolation of the products was performed by HPLC.

Reaction of 1–3 with Styrene or Isoprene: General Procedure. A THF (3 mL) solution of the complex and the substrate [reaction with styrene, see Table 2; reaction with isoprene, NaBPh₄ (0.051 05 g, 0.15 mmol), isoprene (0.5 mL, 5 mmol); **1** (0.049 05 g, 0.10 mmol), isoprene (0.3 mL, 3 mmol); **2** (0.023 g, 0.029 mmol), isoprene (0.15 mL, 1.5 mmol)] was prepared under dinitrogen in a 10 mL glass tube. After the tube was sealed, the solution was stirred at 343 K for 6.5 h (styrene) or 17 h (isoprene) and then cooled to room temperature and analyzed by means of chromatographic techniques. The isolation of pure products was performed by HPLC.

Electrocarboxylation: General Procedure. A THF (30 mL) solution containing **2** (0.097 g, 0.12 mmol) and tetrabutylammonium tetrafluoroborate (1 g, 3 mmol) was placed in the cell under CO₂ (or CO₂/C₂H₄) and stirred at 393 K. The desired potential was applied between the electrodes and the electrolysis continued until the intensity was negligible. Without the anode, the reaction mixture was stirred for 1–2 h under CO₂ (or CO₂/C₂H₄). The carboxylic acids of the mixture were directly esterified by adding anhydrous K₂CO₃ (0.5 mmol) and benzyl bromide (1 mmol) in THF/acetone (1:1 v/v, 60 mL) and stirring at 323 K for 10 h. The solution was hydrolyzed with 70 mL of 0.01 M HCl solution and extracted with diethyl ether. The organic layer was washed with water, dried over MgSO₄, and evaporated. The products were analyzed by GC and GC-MS, the carboxylic acids being analyzed as benzyl esters.

Acknowledgment. This work was supported by the Ministero dell'Università e della Ricerca Scientifica e Tecnologica (MURST, 40% and 60% funds) and the CNR (Progetto Finalizzato Chimica Fine II).

OM940795G

(36) Chaussard, J.; Folest, J. C.; Nédélec, J. Y.; Périchon, J.; Sibille, S.; Troupel, M. *Synthesis* **1990**, 5, 369.

Cyclopolymerization of 1,2-Diethynylperalkyldisilanes using Molybdenum Alkylidene Initiators

Jennifer L. Maciejewski, Guillermo C. Bazan,* and George Rodriguez

Department of Chemistry, University of Rochester, Rochester, New York 14627

Received February 10, 1995[®]

1,2-Diethynyl-1,1,2,2-tetraalkyldisilanes were polymerized using only the most active Schrock molybdenum alkylidene initiators ($\text{Mo}(\text{NAr})(\text{CHCMe}_2\text{Ph})(\text{OR})_2$ ($\text{OR} = \text{OC}(\text{CF}_3)_2\text{Me}$, $\text{Ar} = 2,6\text{-C}_6\text{H}_3\text{-}i\text{-Pr}_2$ or $2,6\text{-C}_6\text{H}_3\text{-Me}_2$)). Other less active initiators ($\text{Mo}(\text{NAr})(\text{CHCMe}_2\text{Ph})(\text{OCMe}_3)_2$) and monomers (1,2-dipropynyl-1,1,2,2-tetramethyldisilane) yielded monoinserted products that give insight into factors controlling the mechanism of these reactions.

Introduction

Well-defined organometallic initiators that polymerize substrates in a living fashion provide polymer science with a versatile new synthetic methodology¹ encompassing a range of reactivities, tolerance to functionalities, and stereoselectivity.² Particularly notable are the applications of various olefin metathesis catalysts in the preparation of conjugated polymers. The catalytic activity of these complexes can be implemented to effect the ring-opening metathesis polymerization (ROMP) of cyclic olefins to ultimately provide polyacetylene, polyenes, and poly(*p*-phenylenevinylene).³ A recent development has demonstrated that molybdenum-based olefin metathesis catalysts of the general type $\text{Mo}(\text{NAr})(\text{CHCMe}_2\text{Ph})(\text{OR})_2$ ($\text{R} = t\text{-Bu}$ with varying degrees of fluorine substitution, $\text{Ar} = 2,6\text{-C}_6\text{H}_3\text{-}i\text{-Pr}_2$ or $2,6\text{-C}_6\text{H}_3\text{-Me}_2$) can effect the living cyclopolymerization of 1,6-heptadiyne derivatives to produce polyacetylenes with long average conjugation lengths.⁴ These soluble materials serve as excellent models to study how the average degree of polymerization affects conjugation and cubic optical nonlinearity.⁵

The use of alkylidene reagents for the preparation of conjugated polymers incorporating main-group metals has received less attention than their all-organic counterparts.⁶ Classical catalysts have also been used to prepare related materials.⁷ Silicon substitution is particularly attractive because of the technological applications of polymers partly composed of these atoms.⁸ That this new generation of catalysts has not

been more extensively applied in the construction of hybrid main-group metal/conjugated polymer molecules is somewhat surprising in view of the tolerance toward functionalities displayed by these catalysts and the significant perturbation expected on the electronic structure of conjugated segments either by $\sigma\text{-}\pi$ delocalization or silicon d orbital participation.⁹ Potential benefits exist in applying modern catalyst technology to polymeric silicon materials; a view that has already been recognized by the groups of Sita who reported the stereospecific ROMP of 1,1,2,2-tetramethyl-1,2-disilacyclopent-3-ene and Wagener who applied ADMET technology to prepare poly(carbo(dimethyl)silanes).¹⁰

The cyclopolymerization of 1,2-diethynyl-1,1,2,2-tetramethyldisilane (**2a**) using classical metathesis catalysts such as MoCl_5 or $\text{WCl}_6/\text{SnMe}_4$ has been reported by Kusumoto and Hiyama.¹¹ The resulting polymers were described as soluble, air stable, and conductive upon doping. However, these catalysts did not control the reaction well as evidenced by erratic molecular weights and broad polydispersity values. Since one of the goals of synthetic polymer chemistry is to tailor polymer properties via regulation of the polymerization reaction at the molecular level, diethynyltetraalkyldisilanes lend themselves well to cyclopolymerization studies using modern well-defined, functionality tolerant catalysts. We report herein a series of studies concerning the synthesis of conjugated polymers with appended main-group metal containing cyclic side groups using molybdenum-based Schrock alkylidene initiators.

[®] Abstract published in *Advance ACS Abstracts*, June 1, 1995.

(1) (a) Keii, T.; Doi, Y.; Soga, K. *Encycl. Polym. Sci. Eng.* **1990** (Suppl.), 437. (b) Grubbs, R. H.; Novak, B. M. *Encycl. Polym. Sci. Eng.* **1990** (Suppl.), 420.

(2) (a) Schrock, R. R.; Murdzek, J. S.; Bazan, G. C.; Robbins, J.; DiMare, M.; O'Regan, M. *J. Am. Chem. Soc.* **1990**, *112*, 3875. (b) Toreki, R.; Schrock, R. R. *J. Am. Chem. Soc.* **1990**, *112*, 2448. (c) Johnson, L. K.; Virgil, S. C.; Grubbs, R. H. *J. Am. Chem. Soc.* **1990**, *112*, 5384. (d) Nguyen, S. T.; Johnson, L. K.; Grubbs, R. H. *J. Am. Chem. Soc.* **1992**, *114*, 3974. (e) Wallace, K. C.; Liu, A. H.; Davis, W. M.; Schrock, R. R. *Organometallics* **1989**, *8*, 644.

(3) (a) Miao, Y.; Bazan, G. C. *Macromolecules* **1994**, *27*, 1063. (b) Gorman, C. B.; Ginsburg, E. J.; Grubbs, R. H. *J. Am. Chem. Soc.* **1993**, *115*, 1397 and references therein. (c) Conticello, V. P.; Gin, D. L.; Grubbs, R. H. *J. Am. Chem. Soc.* **1992**, *114*, 9708. (d) Feast, W. J. *Makromol. Chem., Macromol. Symp.* **1991**, *53*, 317. (e) Feast, W. J.; Friend, R. H. *J. Mater. Sci.* **1990**, *25*, 3796. (f) Schrock, R. R. *Acc. Chem. Res.* **1990**, *23*, 158.

(4) Fox, H. H.; Wolf, M. O.; O'Dell, R.; Lin, B. L.; Schrock, R. R.; Wrighton, M. S. *J. Am. Chem. Soc.* **1994**, *116*, 2827.

(5) Samuel, I. D. F.; Ledoux, I.; Dhenaut, C.; Zyss, J.; Fox, H. H.; Schrock, R. R.; Silbey, R. J. *Science* **1994**, *265*, 1070.

(6) (a) Wagener, K. B.; Smith, D. W., Jr. *Macromolecules* **1991**, *24*, 6073. (b) Ginsburg, E. J.; Gorman, C. B.; Marder, S. R.; Grubbs, R. H. *J. Am. Chem. Soc.* **1989**, *111*, 7621.

(7) (a) Ohshita, J.; Matsuguchi, A.; Furumori, K.; Hong, R.; Ishikawa, M. *Macromolecules* **1992**, *25*, 2134. (b) Ni, Q.; Shinar, J.; Vardeny, Z. V.; Grigoras, S. *Phys. Rev. B: Condens. Matter* **1991**, *44*, 5939. (c) Wei, X.; Han, S. G.; Wong, K. S.; Hess, B. C.; Zheng, L. X.; Vardeny, Z. V.; Ni, Q.; Shinar, J.; Pang, Y.; Ijadi-Maghsoodi, S.; Barton, T. J. *Synth. Met.* **1991**, *42*, 1583. (f) Kim, Y. H.; Gal, Y.; Kim, U.; Choi, S. *Macromolecules* **1988**, *21*, 1991.

(8) Zeigler, J. M.; Fearon, F. W. G., Eds. *Silicon-Based Polymer Science: A Comprehensive Resource*; Advances in Chemistry Series 224; American Chemical Society: Washington, DC, 1990.

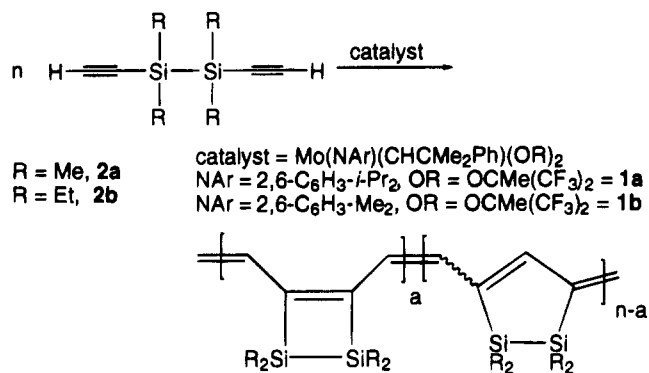
(9) (a) Ishikawa, M.; Hatano, T.; Hasegawa, Y.; Horio, T.; Kunai, A.; Miyai, A.; Ishida, T.; Tsukihara, T.; Yamanaka, T.; Koike, T.; Shiyo, J. *Organometallics* **1992**, *11*, 1604. (b) Tanaka, K.; Nakajima, K.; Okada, M.; Yamabe, T.; Ishikawa, M. *Organometallics* **1991**, *10*, 2679.

(10) (a) Sita, L. R.; Lyon, S. R. *J. Am. Chem. Soc.* **1993**, *115*, 10374. (b) Wagener, K. B.; Smith, D. W., Jr. *Macromolecules* **1991**, *24*, 6073.

(11) Kusumoto, T.; Hiyama, T. *Chem. Lett.* **1988**, *7*, 1149.

Results

Polymerizations. Addition of **2a** to a solution of Mo-(CHCMe₂Ph)(N-2,6-C₆H₃-i-Pr₂)(OCMe(CF₃)₂)₂ (**1a**) in



C₆D₆, toluene, or 1,2-dimethoxyethane (DME) causes an immediate color change from pale yellow to red that darkens over several minutes. No precipitation or discoloration of polymers has been observed in any of the reactions or subsequent products as long as the materials are maintained under an inert atmosphere. Monomer incorporation proceeds to approximately 30 equiv and then ceases as witnessed by ¹H NMR spectroscopy. The alkylidene resonance of the initiator appears at δ 12.13 ppm with new alkylidene signals observed at δ 12.48 and 12.68 ppm after reaction with 2-fold monomer excess. No alkylidene signals were detected in the case where 25 monomer equiv had been added. These combined observations indicate that at the beginning of the reaction some monomer is cyclo-polymerized to yield a new monosubstituted alkylidene, but apparently monomer incorporation into the growing polymer chain stops after a certain point. Similar results were obtained at the 10–20 equiv of monomer level in DME using the initiator Mo(CHCMe₂Ph)(N-2,6-C₆H₃-Me₂)(OCMe(CF₃)₂)₂ (**1b**).

After preparative scale reactions, polymers are readily purified by precipitation of the concentrated reaction solution into methanol, isolated by centrifugation in 50% yield, and placed *in vacuo* overnight to remove as much of the residual solvent as possible. The materials thus obtained are deep red powders that dissolve readily in solvents such as toluene or methylene chloride and are stable for a period of several months if stored cold (–30 °C) under nitrogen. Analysis by ¹³C NMR spectroscopy reveals two broad resonances between 143 and 146 ppm attributable to the polyene backbone. The ²⁹Si NMR spectrum displays multiple broad and complex resonances in the δ –6 to –30 ppm range, suggesting that the polymerization is not regioselective.

Gel permeation chromatography (GPC)¹² of isolated samples of poly-**2a** revealed that, unlike Schrock's polyheptadiyne analogs, M_n does not depend linearly on the number of equivalents of monomer added to the initiator (Table 1). Despite repeated attempts to optimize variables such as solvent, reaction time, amount of monomer, and choice of catalyst [**1a**, **1b**, Mo(CHCMe₂Ph)(N-2,6-C₆H₃-i-Pr₂)(OCMe₂(CF₃)₂)₂ (**1c**), and Mo(CHCMe₂Ph)(N-2,6-C₆H₃-i-Pr₂)(OCMe₃)₂ (**1d**)], we were not able to obtain poly-**2a** with $M_n > 9000$. Best results were obtained when dimethoxyethane (DME)

Table 1. GPC Data for Polymerizations using **1a**

no. of equiv of monomer	M_n	PDI
10 (2a) ^a	2033	1.98
20 (2a) ^a	2146	2.07
30 (2a) ^a	1691	2.45
50 (2a) ^a	4604	1.29
100 (2a) ^a	4260	1.29
1 (2a) ^b	1083	1.32
5 (2a) ^b	3286	1.33
10 (2a) ^b	3710	1.45
25 (2a) ^b	2297	2.16
50 (2a) ^b	1662	2.39
100 (2a) ^b	1981	2.45
10 (2b) ^a	3218	1.55
20 (2b) ^a	3911	1.32
30 (2b) ^a	7636	1.53
50 (2b) ^a	12046	1.64
100 (2b) ^a	13710	1.83
100 (2a) ^c	8550	1.70
100 (2b) ^c	14762	1.80

^a In DME. ^b In toluene. ^c Neat.

was used as a solvent. Addition of bases such as PMe₃ or pyridine effectively shuts down polymerization.

Increasing the size of the alkyl substituents on the monomer does not significantly improve the reaction. A series of GPC experiments was performed using 1,2-diethynyl-1,1,2,2-tetraethyl-disilane (**2b**). At first glance, there appears to be better correlation for **2b** (relative to **2a**) between M_n and added monomer, but the polymerization still does not qualify as living (Table 1). The largest M_n observed for these polymerizations was achieved by dissolving **1a** into neat monomer, but at this stage we are hesitant to claim a larger degree of polymerization, again relative to poly-**2a**, because the monomer is intrinsically larger. The ¹³C and ²⁹Si NMR data of poly-**2b** in C₆D₆ indicate the presence of a polyene backbone and a nonregioselective polymerization.

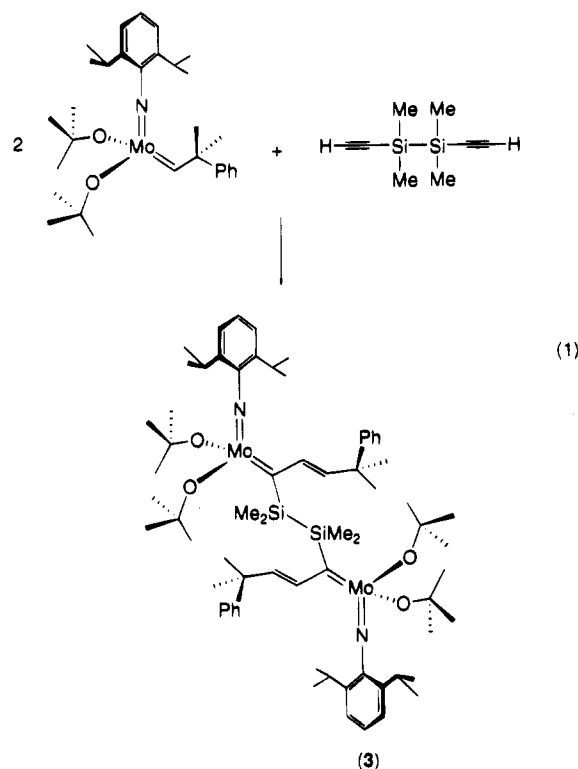
A significant difference between poly-**2a** and poly-**2b** is the degree of solubility in common organic solvents. Poly-**2a** is soluble in CHCl₃, aromatic solvents, and DME but is insoluble in methanol. When **2b** is polymerized, a portion of the product precipitates from DME as the concentration increases. However, this solid fraction is soluble in CHCl₃ and was characterized by GPC.

The polymers decompose on exposure to air and water, complicating the study of this system. The UV–vis absorption spectrum of a sample of **2b** in CHCl₃ obtained under inert conditions displays $\lambda_{\text{max}} = 512$ nm. After exposure to air, the absorption maximum shows a steady decline over time (Figure 1). For all polymers, λ_{max} values obtained using the GPC eluent detector were consistently lower than values procured as described above. We believe that this discrepancy is a result of backbone degradation with moisture, a problem that is augmented by the dilute requirements for GPC analysis. Qualitatively, poly-**2b** dissolved in CaH₂-dried chloroform maintained the initial color for longer periods than samples in HPLC grade solvent.

Characterization of Monoinserted Products. No polymer was formed upon addition of various amounts of **2a** to Mo(CHCMe₂Ph)(N-2,6-C₆H₃-i-Pr₂)(OCMe₃)₂ (**1d**). By ¹H NMR spectroscopy, a single product is generated that lacks the typical low-field H_α resonance of mono-substituted alkylidenes and displays a pair of characteristic doublets at 5.82 ppm (olefinic H) and 7.42 ppm (H_β). X-ray quality crystals of the product were ob-

(12) All GPC results are calibrated versus polystyrene standards.

tained by slowly cooling a pentane solution initially containing a substoichiometric amount of **2a** with **1d**. Structural characterization revealed a bimetallic dimer that contains two pseudotetrahedral molybdenum alkylidene fragments linked together by a disilane bridge (see **3** in eq 1 and Figure 2).¹³ There is a crystallo-



graphically imposed inversion center which relates the two halves of the dimer. Within the tetrahedral core the distances between the molybdenum atom and the two alkoxide and imido ligands are in the normal range for this type of alkylidene complex.¹⁴ Perhaps the most significant feature is the N–Mo–C_α–C_β torsion angle of 22(7)°. This last observation implies that optimum π overlap between molybdenum and C_α has not been achieved, and the final arrangement therefore is a compromise between competing steric and electronic effects.¹⁵ The overall structure of the dimer is significant in that it can arise only through α -insertion. In the presence of a 2:1 monomer excess a new species appears with similar spectral characteristics to **3** but with two doublets at 5.62 and 7.61 ppm and a new acetylenic resonance at 2.19 ppm.¹⁶ We take these data to indicate that, while a metal core structure similar to **3** is formed, it is most likely a monoinserted product with a dangling unreacted acetylene.

(13) Crystal data for **3**: space group $P2_1/c$ (No. 14) with $a = 11.472(3)$ Å, $b = 14.430(9)$ Å, $c = 21.911(1)$ Å, $\beta = 95.50(4)^\circ$, $Z = 2$, $f_w = 1265.66$, and $\rho = 1.164$ g/cm³. A total of 6977 reflections were collected (6626 unique) ($h, k, \pm l$) in the range of $4^\circ < 2\theta < 50^\circ$ with the 3428 reflections having $I > 3.00\sigma(I)$ being used in the structural refinement by full-matrix least-squares techniques (352 variables) using the TEXSAN crystallographic package from Molecular Structures Corporation. Final $R_1 = 0.064$, $R_2 = 0.077$.

(14) Bazan, G.; Khosravi, E.; Schrock, R. R.; Feast, W. J.; Gibson, V. C.; O'Regan, M. *J. Am. Chem. Soc.* **1990**, *112*, 8387.

(15) Schrock, R. R.; DePue, R.; Feldman, J.; Schaverien, C. J.; Dewan, J. C.; Liu, A. H. *J. Am. Chem. Soc.* **1988**, *110*, 1423.

(16) ¹H NMR (C₆D₆): δ 0.40 (s), 0.80 (s) (SiMe₂); 1.28 (s, CMe₂Ph), 1.29 (s, CHMe₂), 1.31 (s, OCM₂), 2.19 (s, ethynyl H), 4.05 (septet, CHMe₂), 5.62 (d, C_αCH), 7.04 (m) and 7.25 (d) (phenyl and aryl imido protons), 7.61 (d, olefin).

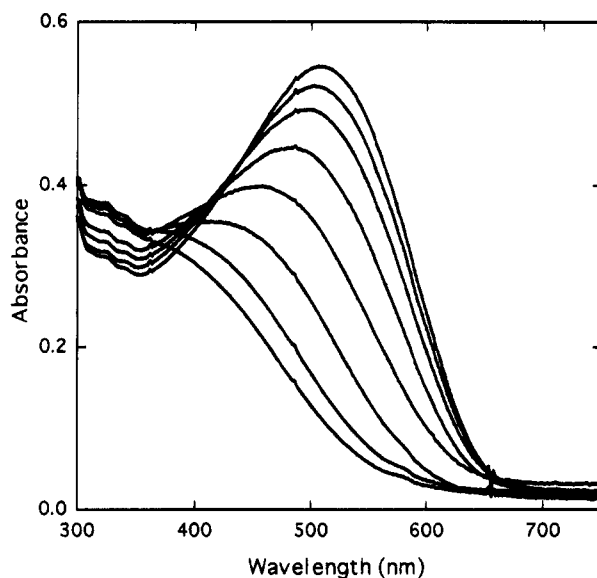


Figure 1. UV-vis decomposition of poly-**1b** upon exposure to air (60 min time delay between spectra).

The reaction of **2a** with **1c**, an initiator of intermediate activity, also leads to a monoinserted alkylidene. However, in this case two sets of doublets are observed in the ¹H NMR spectrum centered at 5.63 and 7.55 ppm and at 5.75 and 7.35 ppm in a 2:1 ratio (by integration). Our current thinking is that these signals are attributable to the presence of two rotamers, a type of isomerism that is well-known for this general class of alkylidenes.¹⁷

Dipropynyl analogues do not polymerize. We observed reactivity only between 1,2-dipropynyl-1,1,2,2-tetramethyldisilane (**4**) and **1a**. In this case, excess **4** slowly reacts with **1a** over a period of several days to provide a new complex that maintains the molybdenum core and has incorporated a single monomer unit. After this point no further reactivity is observed with excess **4**, even under forcing conditions. Slow recrystallization of the product from a concentrated pentane solution afforded crystals suitable for structural determination. Unfortunately, although the X-ray data set obtained for this compound is good, there is one-half of a molecule of pentane of crystallization in the asymmetric unit which is disordered, causing a high residual electron density, particularly in the region of the disordered pentane.¹⁸ However, the atoms connected to molybdenum were reliably located, delineating the important molecular features shown in Figure 3. The overall geometry about the metal is the standard pseudotetrahedral arrangement containing an sp²-hybridized imido nitrogen and a disubstituted alkylidene carbon. One of these substituents is a methyl group while the second, pointing toward the imido ligand, contains a five-membered ring with a disilane link. The carbon–carbon bond distances in the syn fragment of C_α are in agreement with an alternation of double and single bonds [in Å: C_α–C_β = 1.43(2), C_β–C_γ = 1.36(2), C_γ–C_δ = 1.53(2), C_δ–C_ε = 1.34(2)]. Therefore we propose the connectivity shown in eq 2, one which arises from β -insertion of monomer followed by intramolecular insertion of the pendant propynyl into the *disubstituted* alkylidene and finally breakup of the resulting metallacyclobutene (refer to right side of Scheme 1).

(17) Oskam, J. H.; Schrock, R. R. *J. Am. Chem. Soc.* **1993**, *115*, 11831.

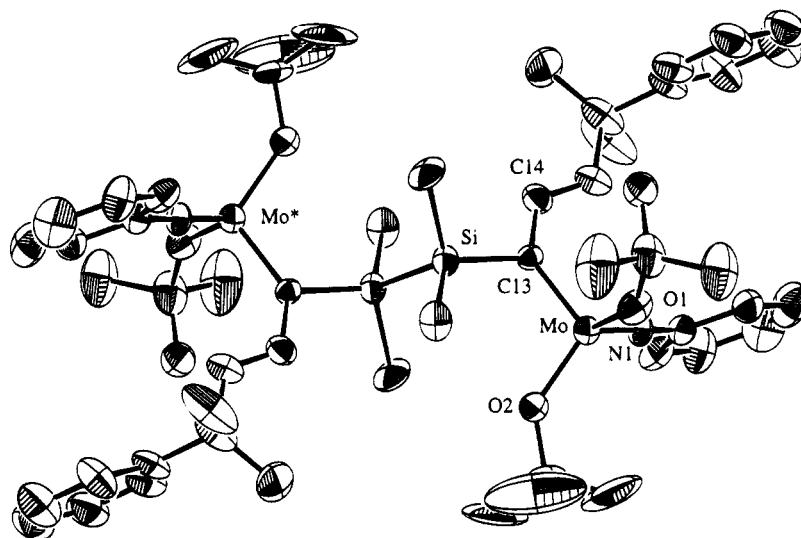


Figure 2. ORTEP diagram of **3** with CF_3 and *i*-Pr groups omitted for clarity. Important bond distances (Å) and bond angles (deg): Mo–O(1) = 1.899(6), Mo–O(2) = 1.882(6), Mo–C(13) = 1.906(9), Si–Si = 2.351(5), C(13)–C(14) = 1.48(1); Mo–C(13)–Si = 114.7(4), Mo–C(13)–C(14) = 133.3(7).

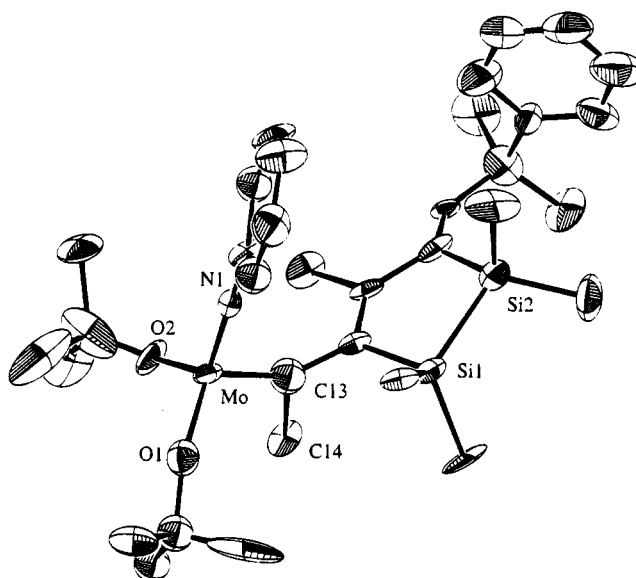
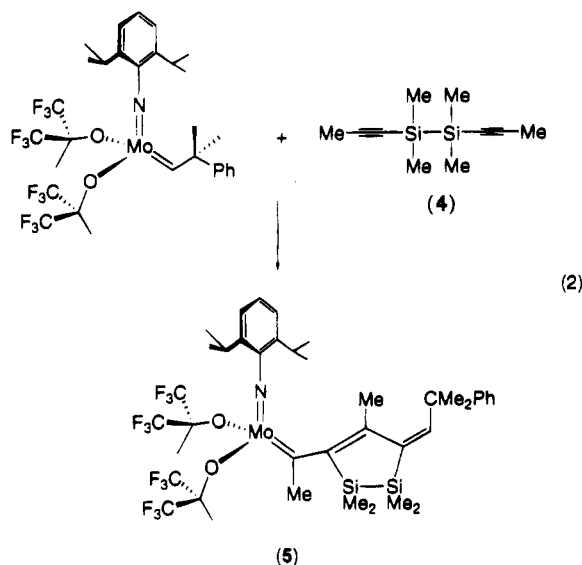


Figure 3. ORTEP diagram of **5** with *i*-Pr groups omitted for clarity.

Discussion

The results obtained from these studies serve to evaluate the polymerization of 1,2-diethynylperalkyl-disilanes with molybdenum alkylidene initiators. Ultimately, the goal of a living cyclopolymerization process was not obtained, the reasons for which remain inconclusive. One complication that may affect the kinetic competence of the propagating alkylidene arises from the mechanism of polymerization. It is important to realize that two types of metallacyclobutenes may form as a consequence of the nonsymmetric substitution of the reactive acetylene. Because of these two possible insertion regiochemistries, the mechanism of polymerization is branched and may result in different stereochemical outcomes (Scheme 1). Observation of multiple resonances by ^{29}Si NMR spectroscopy in the

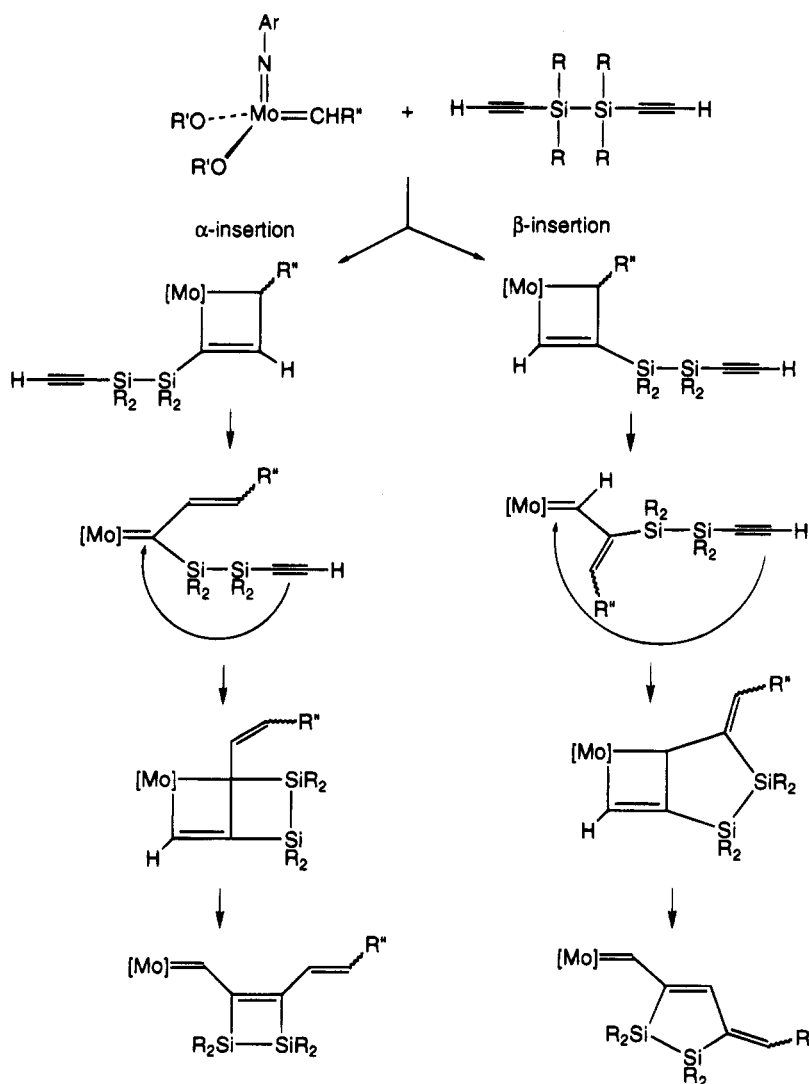
isolated polymers is consistent with the participation of four metallacyclobutenes; the complexity of the spectra points to the complexity of the polymerization. The presence of four- and five-membered rings would lead to multiple resonances, as observed, due to interactions with different neighboring rings. Unfortunately, lack of model compounds and the known difficulties of predicting ^{29}Si shifts from structural considerations alone¹⁹ make further analysis difficult and unreliable.

The decomposition of the polymers in air is interesting and attests to the inherent strain and instability of 1,2-disilacyclopent-3-enes and 1,2-disilacyclobut-3-enes. Many examples of variously substituted disilacyclobutenes are present in the literature, and it is well-known that they are easily oxidized to cyclic disiloxanes.²⁰ Additionally, certain mesityl-substituted disilacyclobutenes undergo ring contraction to disilacyc-

(18) Crystal data for **5**: space group $P\bar{1}$ (No. 2) with $a = 11.229(7)$ Å, $b = 12.391(6)$ Å, $c = 18.68(1)$ Å, $\beta = 104.44(5)^\circ$, $Z = 2$, $fW = 959.96$, and $\rho = 1.321$ g/cm³. A total of 8229 reflections were collected (7782 unique) ($h, \pm k, \pm l$) in the range $4^\circ < 2\theta < 50^\circ$ with the 3644 reflections having $I > 3.00\sigma(I)$ being used in the structural refinement by full-matrix least-squares techniques (539 variables) using the TEXSAN crystallographic package from Molecular Structures Corporation. Final $R_1 = 0.087$, $R_2 = 0.098$.

(19) (a) Marsmann, H. *NMR* **1981**, *17*, 65. (b) Schraml, J.; Bellama, J. M. *Determ. Org. Struct. Phys. Methods* **1976**, *6*, 203.

Scheme 1



lopropane species.²¹ 1,1,2,2-Tetramethyl-1,2-disilacyclopent-3-ene is the only example of a 1,2-disilacyclopent-3-ene reported in the literature.^{10a} This monomer is effectively used in ROMP, implying an inherent ring strain in this system. These patterns of reactivity described in the literature provide a potential basis for the observed decomposition of poly-**2a** and poly-**2b** on exposure to air and water.

Trends in reactivity thus far indicate that, as expected from steric considerations, disubstituted alkyldienes are less reactive than their monosubstituted counterparts in these catalytic cycles and once formed are reluctant to incorporate further monomer into the growing chain. The two structurally characterized insertion products illustrate these problems. In the formation of **3** one acetylenic functionality from **2a** reacts initially with **1d** via a substituted metallacyclobutene. Upon breakup, the resulting disubstituted β -disilylalkylidene does not react either bimolecularly or intramolecularly with additional substrate. In the case of **5**, β -insertion occurs

first leading to a disubstituted alkyldiene. The resulting intermediate can further react intramolecularly with the pendant propynyl functionality leading to the final unreactive product. It is safe to assume that the difference in regiochemistry of the initial insertion for these monoinserted examples is a consequence of increasing the fluorination of the alkoxides and not a function of monomer. There is negligible perturbation in the basicity of the alkyne in the two monomers, and the large disilyl bridge is still expected to dominate steric interferences in any intermediate metallacyclobutenes. The fact that β -substitution is favored as the extent of the steric shielding from coordinated ligands increases should not be surprising since this site locates the large disilane functionality away from the metal.

One major difference between the cyclopolymerization of diethynylperalkyldisilanes and 1,6-heptadiynes is the smaller size of the disubstituted alkyldienes in the catalytic cycle of the latter. It is plausible that these smaller intermediates are more reactive and function well to intramolecularly cyclize the monomer. Disilyl-substituted alkyldienes may fail in this step not only

(20) (a) Nakadaira, Y.; Sato, R.; Kida, N.; Sakurai, H. *Chem. Lett.* **1984**, 393. (b) Seyferth, D.; Annarelli, D. C.; Vick, S. C. *J. Organomet. Chem.* **1984**, 272, 123. (c) Sakurai, H.; Kobayashi, T.; Nadadaira, Y. *J. Organomet. Chem.* **1978**, 162, C43. (d) Seyferth, D.; Vick, S. C. *J. Organomet. Chem.* **1977**, 125, C11. (e) Barton, T. J.; Kilgour, J. A. *J. Am. Chem. Soc.* **1976**, 98, 7746. (f) Atwell, W. H.; Uhlmann, J. G. *J. Organomet. Chem.* **1973**, 52, C21.

(21) (a) Ishikawa, M.; Matsuzawa, S.; Sugisawa, H.; Yano, F.; Kamitori, S.; Higuchi, T. *J. Am. Chem. Soc.* **1985**, 107, 7706.

because of increased steric constraints but also because of inductive deactivation by the α -silicon atom.

It may be possible to further optimize initiator structure or reaction conditions to finally obtain a regioselective living polymerization system. However, in contrast to previous reports,¹¹ the materials are intrinsically unstable in air and decompose quickly (Figure 1). For this reason we have abandoned further investigations into their potential applications although it may still be useful to study the conductivities of pristine samples to properly evaluate the effect of silicon on delocalized organic fragments.

Experimental Section

General Procedures. All manipulations were carried out using either high-vacuum or glovebox techniques as described previously.²² ¹H, ¹³C, and ²⁹Si NMR spectra were recorded on a Bruker AMX-400 NMR spectrometer at 400.1, 100.6 and 79.5 MHz, respectively. Elemental analyses were performed by Desert Analytics Laboratory (Tucson, AZ). AlCl₃ and ethynylmagnesium chloride were purchased from Aldrich. Propynyllithium was obtained from Alfa Aesar and HCl from Air Products. All commercially available chemicals were used as received. Toluene, pentane, diethyl ether, and tetrahydrofuran were distilled from benzophenone ketyl. The preparations of **2a**²³ and **2b**²⁴ are available in the literature.

Preparation of 1,2-Dipropynyl-1,1,2,2-tetramethyldisilane (4). The preparation of **4** was adapted from the literature.²⁵ To a cooled suspension of propynyllithium (1 g, 22 mmol) in 40 mL of THF was added 1,2-dichloro-1,1,2,2-tetramethyldisilane²⁶ (1.87 g, 10 mmol) in 2 mL of THF. The solution became clear during the addition. The mixture was then warmed to room temperature and stirred overnight after which time the reaction was cooled and then quenched with 1 N HCl and washed with 100 mL of 1 N HCl and 100 mL of water. The product was dried over MgSO₄, concentrated, and distilled at 73 °C/3 mmHg to give 1.2 g (62%) of **4**. ¹H NMR (C₆D₆): δ 0.39 (s, 6H, Me₂Si), 1.51 (s, 3H, MeC). ¹³C NMR (C₆D₆): δ -2.5 (Me₂Si), 4.7 (terminal Me), 81.7, 105.6 (acetylenic carbons). Anal. Calcd for C₁₀H₁₈Si₂: C, 61.9; H, 9.3. Found: C, 59.88, 59.14; H, 9.22, 9.07.

Preparation of Monoinserted Products. Compound 3: **2a** (0.045 g, 0.27 mmol) and **1d** (0.2 g, 0.36 mmol) were individually dissolved in 0.5 g of pentane. The monomer was added dropwise to the initiator to give a deep red solution. After 2 h of stirring at room temperature, the reaction was cooled to -30 °C. Large, dark red crystals had formed after several hours. The reaction is quantitative by ¹H NMR, and a 50% isolated yield was realized due to the solubility of the product in pentane. ¹H NMR (C₆D₆): δ 0.88 (s, 6H, SiMe₂), 1.32 (s, 6H, CMe₂Ph), 1.34 (s, 12H, CHMe₂), 1.38 (s, 18H, OCM₂Ph), 4.09 (septet, 2H, CHMe₂), 5.82 (d, 1H, C _{α} CH), 7.06 (m) and 7.29 (d) (phenyl and aryl imido protons), 7.42 (d, 1H, olefin) ppm; ¹³C NMR (C₆D₆): δ 1.2 (SiMe₂); 23.8 (CHMe₂); 29.2

and 29.3 (CMe₂Ph, CHMe₂); 32.4 (OCMe₃); 41.1 (CMe₂Ph); 78.7 (OCMe₃); 122.9 and 125.6 (olefin); 126.3, 144.4 (aromatic), 138.1, 143.2, 149.7, 152.5 (aryl imido carbons); 258.8 ppm (C _{α}). Anal. Calcd for C₆₈H₁₀₈Mo₂N₂O₄Si₂: C, 64.53; H, 8.53. Found: C, 64.76; H, 8.07.

Compound 5: **4** (0.1 g, 0.52 mmol) and **1a** (0.4 g, 0.52 mmol) were each dissolved in 0.5 g of pentane. The reagents were combined and stirred at room temperature for 5 days. The reaction solution was concentrated, and the product redissolved in minimal pentane. The solution was cooled to -30 °C to yield red crystals. The reaction was quantitative by ¹H NMR; however, only a few crystals were ultimately obtained, which were difficult to isolate cleanly because of pentane solubility. Additionally, the product that recrystallizes contains pentane, further hindering analysis. The oily nature of the bulk product does not allow elemental analyses to be accurately obtained. ¹H NMR (C₆D₆): δ 0.03 (s) and 0.04 (s) (12H, SiMe₂); 1.19 (d, 6H, CHMe₂); 1.42 (s, 6H, CMe₂Ph); 1.46 (s, 6H, OCM₂(CF₃)₂); 1.88 (s, 3H, C=CMeR); 3.18 (s, 3H, C _{α} Me); 3.77 (septet, 2H, CHMe₂); 6.84 (s), 6.96 (s) (aryl imido); 7.09 (t), 7.18 (t), 7.28 (d) (phenyl). ¹³C NMR (C₆D₆): δ -4.2, -1.9 (SiMe₂); 19.2 (ArCHMe₂, Ar = C₆H₃); 19.8 (ArCHMe₂); 22.6 (CMe₂Ph); 24.2 (C=CMe); 28.5 (CMe(CF₃)₂); 31.5 (C _{α} Me); 42.6 (CMe₂Ph); 122.9, 123.3, 125.7, 126.3 (aryl imido); 126.9, 128.5 (phenyl); 141.3 (C=CMe); 147.2 (CMe(CF₃)₂); 148.7 (C=CH); 150.4 (C=CMe); 153.6; 154.7 (C=CH); 162.3 (CF₃); 292.94 ppm (C _{α}). Some signals may be obscured by the solvent peak.

Typical Polymerization Reaction. In DME: Stock solutions of monomer and initiator were prepared by dissolving 250 mg of 1,2-diethynyl-1,1,2,2-tetramethyldisilane and 25 mg of **1a** each in 1 mL of DME. An aliquot of initiator was put in a vial equipped with a stir bar and diluted so that the total amount of solvent would equal 2 mL. The monomer aliquot was added, and the red solution was stirred for 24 h. The reaction was quenched with 20 mL of benzaldehyde.

In Toluene: Toluene reactions were run analogously except that stock solutions were not employed; reagents were weighed out discretely.

GPC Sample Preparation. The solvent was removed and the crude product was dissolved in CHCl₃. An aliquot of concentrated sample was then diluted with CHCl₃ and filtered before analysis. The samples were treated as air-sensitive and were kept in the drybox until immediately before injection.

Characterization Data of Polymers. Poly-2a. ²⁹Si NMR (C₆D₆): δ -5.3, -17.4, -20.3, -21.2, -22.6, -26.2 ppm. ¹³C NMR (C₆D₆): δ broad resonances from -4.5 to -1 ppm attributable to the SiMe₂ functionalities and two broad resonances between 142 and 147 ppm due to the polyene backbone. ¹H NMR (C₆D₆): δ 0.34, 0.45 (overlapping broad resonances, SiMe₂); 0.96, 0.97 (overlapping broad resonances, SiMe₂); 6.6-8.3 (broad resonance, conjugated backbone) ppm. Anal. Calcd for poly(C₈H₁₄Si₂):²⁷ C, 57.88; H, 8.43; Si, 33.84. Found: C, 49.86; H, 7.14; Si, 12.35. Related silicon-containing polymeric precursors are pyrolyzed under argon to give silicon carbide.²⁸ The high temperatures required for elemental analysis are perhaps leading to just such an occurrence even under oxygen, thus showing lower percentages of carbon and silicon than expected.

Poly-2b: ²⁹Si NMR (C₆D₆): δ -11.4, -10.6, -10.2, -9.7, -7.5, -6.2, -5.7, 4.9, 5.8, 6.5, 7.1, 9.5, 9.8, 10.7, 11.1 ppm. ¹³C NMR (C₆D₆): δ 4.4 (broad), 5.2-5.6 (broad, multiple peaks), 5.8, 6.2, 6.4, 8.9, 9.0, 9.1, 9.2, 9.5, 9.6, 9.9; 141-148 (two broad polyene resonances) ppm. ¹H NMR (C₆D₆): δ 1.59 (s, broad, SiEt₂), 6.6-7.9 (broad resonance, conjugated backbone).

(27) Values do not take into account end-group effects.

(28) (a) Boury, B.; Corriu, R. J. P.; Douglas, W. E. *Chem. Mater.* **1991**, *3*, 487. (b) Corriu, R. J. P.; Guerin, C.; Henner, B.; Jean, A.; Mutin, H. *J. Organomet. Chem.* **1990**, *396*, C35. (c) Wu, H.; Interrante, L. V. *Chem. Mater.* **1989**, *1*, 564. (d) Hasegawa, Y.; Okamura, K. *J. Mater. Sci.* **1983**, *18*, 3633.

(29) Further analysis was not attempted because of polymer instability.

(22) Burger, B. J.; Bercaw, J. E. In *Experimental Organometallic Chemistry*; Wayda, A. L., Darensbourg, M. Y., Eds.; ACS Symposium Series 357; American Chemical Society: Washington, DC, 1987.

(23) Sebald, A.; Seiberlich, P.; Wrackmeyer, B. *J. Organomet. Chem.* **1986**, *303*, 73.

(24) Ishikawa, M.; Hatano, T.; Hasegawa, Y.; Horio, T.; Kunai, A.; Miyai, A.; Ishida, T.; Tsukihara, T.; Yamanaka, T.; Koike, T.; Shioya, J. *Organometallics* **1992**, *11*, 1604.

(25) Preparation of **4** is analogous to that of several well-characterized compounds. (a) Ishikawa, M.; Hatano, T.; Hasegawa, Y.; Horio, T.; Kunai, A.; Miyai, A.; Ishida, T.; Tsukihara, T.; Yamanaka, T.; Koike, T.; Shioya, J. *Organometallics* **1992**, *11*, 1604. (b) Oshita, J.; Matsuguchi, A.; Furumori, K.; Hong, R.; Ishikawa, M. *Macromolecules* **1992**, *25*, 2134. (c) Iwahara, T.; Hayase, S.; West, R. *Macromolecules* **1990**, *23*, 1298. (d) Kim, Y.; Gal, G.; Kim, U.; Choi, S. *Macromolecules* **1988**, *21*, 1991.

(26) Ishikawa, M.; Kumada, M.; Sakurai, H. *J. Organomet. Chem.* **1970**, *23*, 63.

Acknowledgment. J.L.M. thanks Bausch & Lomb/Xerox for an Advantage Internship and the Center for Photoinduced Charge Transfer at the University of Rochester for funding this work. G.C.B. thanks the Dreyfus Foundation for a Distinguished New Faculty Award. We thank Dr. Xian-Ping Zhang and Dr. Jiemin Sun for help in preparing starting materials and aid with supporting experiments.

Supporting Information Available: X-ray crystallographic determination of **3** and **5** (38 pages). This material is contained in many libraries on microfiche, immediately follows this article in the microfilm version of the journal, and can be ordered from the ACS; see any current masthead page for ordering information.

OM950115P

Synthesis and Structure of Hypervalent Antimony Compounds Bearing Antimony–Iron Bonds

Yohsuke Yamamoto, Michiko Okazaki, Yukiya Wakisaka, and Kin-ya Akiba*

Department of Chemistry, Faculty of Science, Hiroshima University,
1-3-1 Kagamiyama, Higashi-Hiroshima 739, Japan

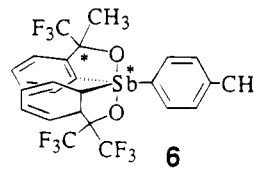
Received December 20, 1994[®]

A hypervalent stiborane with an Sb–Fe bond (**3**: $\text{Rf}_2\text{SbFeCp}(\text{CO})_2$ ($\text{Rf} = o\text{-C}_6\text{H}_4\text{C}(\text{CF}_3)_2\text{O}-$)) was synthesized by the reaction of stiboranide anion (**1-Et**, $\text{Rf}_2\text{Sb}^-\text{Et}_4\text{N}^+$) with $\text{CpFe}(\text{CO})_2\text{I}$ (**2b**) in the presence of AgBF_4 . The carbonyl group was replaced with phosphines such as triphenylphosphine or 1,2-(diphenylphosphino)ethane by irradiation with a tungsten lamp to give a mixture of diastereomers (**4a,b**) $\{\text{Rf}_2\text{SbFeCp}(\text{CO})(\text{PPh}_3)\}$ or **5** $\{\text{Rf}_2\text{SbFeCp}(\text{Ph}_2\text{PCH}_2\text{CH}_2\text{PPh}_2)\}$. X-ray crystallographic analysis of **3**, **4a,b**, and **5** showed that the apical Sb–O bond lengths of these compounds are much longer than those of Rf_2SbCl (**8**) or $\text{Rf}_2\text{Sb}(p\text{-CH}_3\text{C}_6\text{H}_4)$ (**9**). The order of elongation of the Sb–O bond is **5** > **4b**, **4a** > **3**, suggesting the order of the electron-donating property of the iron groups toward the hypervalent 3c–4e bond. The rate of isomerization of the diastereomers of **4** was very slow even at 145 °C, showing the strong equatophilicity of the iron group.

Introduction

Recently, examples of compounds containing transition metal atoms bound to pentacoordinate group 15 atoms have been reported,^{1–9} however, the number of structurally determined compounds with hypervalent group 15 element–transition metal ligands has been relatively few.^{1a,3b,c,8c,8g,8j,k,9} Here we report the prepara-

tion and X-ray structural analysis of stable 10-Sb-5¹⁰ compounds bearing two five-membered ligands ($\text{Rf} = o\text{-C}_6\text{H}_4\text{C}(\text{CF}_3)_2\text{O}-$), the so-called Martin ligand,¹¹ and a monodentate Fe ligand, focusing on the effects of the iron ligands on the structure and on the energy barrier in the pseudorotation of the hypervalent Sb moiety. The apical Sb–O bonds are elongated in the following order of Fe ligands, i.e., $\text{CpFe}(\text{CO})_2 < \text{CpFe}(\text{CO})(\text{PPh}_3) < \text{CpFe}(\text{Ph}_2\text{PCH}_2\text{CH}_2\text{PPh}_2)$, showing the increasing order of the electron-donating property of the iron group. The energy barrier of the pseudorotation of diastereomeric **4a,b** $\{\text{Rf}_2\text{SbFe}(\text{CO})(\text{PPh}_3)\}$ is larger than that of diastereomeric **6** $\{\text{Rf}(o\text{-C}_6\text{H}_4\text{C}^*\text{Me}(\text{CF}_3)\text{O}-)\text{Sb}^*(p\text{-CH}_3\text{C}_6\text{H}_4)\}$,¹² thus showing the stronger equatophilicity of the iron group than that of the tolyl group.



Results and Discussion

Preparation of 3 $\{\text{Rf}_2\text{SbFeCp}(\text{CO})_2$ ($\text{Rf} = o\text{-C}_6\text{H}_4\text{C}(\text{CF}_3)_2\text{O}-$)}. $\{\text{Bis}[\alpha,\alpha\text{-bis}(\text{trifluoromethyl})\text{benzenemethanolato}(2-)\text{-C}^2,\text{O}]\text{stiboranide-dicarbonylcyclopentadienyliron(II)}\}$ (**3**) was prepared by the method outlined in Scheme 1. The reaction of cyclopentadienyldicarbonyliron(**2b**)¹³ in the presence of silver tetrafluoroborate, which forms cyclopentadienyldicarbonyliron tetrafluoroborate (**2a**),¹⁴ with the tetraethylammonium

[®] Abstract published in *Advance ACS Abstracts*, June 1, 1995.

(1) (a) Chopra, S. K.; Martin, J. C. *Heteroatom Chem.* **1991**, *2*, 71. (b) Martin, J. C.; Chopra, S. K.; Moon, C. D.; Forbus, T. R., Jr. *Phosphorus, Sulfur, Silicon Relat. Chem.* **1993**, *76*, 347. (c) Montgomery, C. D. *Phosphorus, Sulfur, Silicon* **1993**, *84*, 23.

(2) Nakazawa, H.; Kubo, K.; Miyoshi, K. *J. Am. Chem. Soc.* **1993**, *115*, 5863.

(3) (a) Malisch, W.; Panster, P. *Angew. Chem., Int. Ed. Engl.* **1974**, *13*, 670. (b) Malisch, W.; Panster, P. *Chem. Ber.* **1975**, *108*, 700. (c) Malisch, W.; Kaul, H.-A.; Gross, E.; Thewalt, U. *Angew. Chem., Int. Ed. Engl.* **1982**, *21*, 549; *Angew. Chem. Suppl.* **1982**, 1281.

(4) Matsumura, Y.; Harakawa, M.; Okawara, R. *J. Organomet. Chem.* **1974**, *71*, 403.

(5) (a) Wachter, J.; Mentzen, B. F.; Riess, J. G. *Angew. Chem., Int. Ed. Engl.* **1981**, *20*, 284. (b) Jeanneaux, F.; Grand, A.; Riess, J. G. *J. Am. Chem. Soc.* **1981**, *103*, 4272. (c) Dupart, J.-M.; Grand, A.; Pace, S.; Riess, J. G. *J. Am. Chem. Soc.* **1982**, *104*, 2316. (d) Dupart, J.-M.; Grand, A.; Riess, J. G. *J. Am. Chem. Soc.* **1986**, *108*, 1167.

(6) (a) Ebsworth, E. A. V.; McManus, N. T.; Pilkington, N. J.; Rankin, D. W. H. *J. Chem. Soc., Chem. Commun.* **1983**, 484. (b) Ebsworth, E. A. V.; Holloway, J. H.; Pilkington, N. J.; Rankin, D. W. H. *Angew. Chem., Int. Ed. Engl.* **1984**, *23*, 630.

(7) Anand, B. N.; Bains, R.; Usha, K. *J. Chem. Soc., Dalton Trans.* **1990**, 2315.

(8) (a) Lattman, M.; Anand, B. N.; Garrett, D. R.; Whitener, M. A. *Inorg. Chim. Acta* **1983**, *76*, L139. (b) Lattman, M.; Morse, S. A.; Cowley, A. H.; Lasch, J. G.; Norman, N. C. *Inorg. Chem.* **1985**, *24*, 1364. (c) Lattman, M.; Chopra, S. K.; Cowley, A. H.; Arif, A. M. *Organometallics* **1986**, *5*, 677. (d) Burns, E. G.; Chu, S. S. C.; de Meester, P.; Lattman, M. *Organometallics* **1986**, *5*, 2383. (e) Lattman, M.; Burns, E. G.; Chopra, S. K.; Cowley, A. H.; Arif, A. M. *Inorg. Chem.* **1987**, *26*, 1926. (f) Khasnis, D. V.; Lattman, M.; Siriwardane, U. *J. Chem. Soc., Chem. Commun.* **1989**, 1538. (g) Khasnis, D. V.; Lattman, M.; Siriwardane, U. *Inorg. Chem.* **1989**, *28*, 681. (h) Khasnis, D. V.; Lattman, M.; Siriwardane, U. *Inorg. Chem.* **1989**, *28*, 2594. (i) Khasnis, D. V.; Lattman, M.; Siriwardane, U.; Chopra, S. K. *J. Am. Chem. Soc.* **1989**, *111*, 3103. (j) Khasnis, D. V.; Lattman, M.; Siriwardane, U. *Organometallics* **1991**, *10*, 1326. (k) Khasnis, D. V.; Lattman, M.; Siriwardane, U.; Zhang, H. *Organometallics* **1992**, *11*, 2074. (l) Khasnis, D. V.; Burton, J. M.; Zhang, H.; Lattman, M. *Organometallics* **1992**, *11*, 3745.

(9) (a) Dixon, D. A.; Arduengo, A. J., III. *J. Am. Chem. Soc.* **1987**, *109*, 338. (b) Arduengo, A. J., III.; Lattman, M.; Dias, H. V. R.; Calabrese, J. C.; Kline, M. *J. Am. Chem. Soc.* **1991**, *113*, 1799.

(10) For designation see: Perkins, C. W.; Martin, J. C.; Arduengo, A. J., III; Lau, W.; Alegria, A.; Kochi, J. K. *J. Am. Chem. Soc.* **1980**, *102*, 7753.

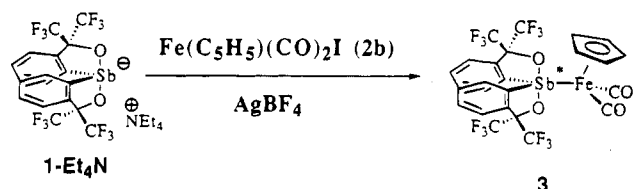
(11) Perrozzi, E. F.; Michalak, R. S.; Figuly, G. D.; Stevenson, W. H., III; Dess, D. B.; Ross, M. R.; Martin, J. C. *J. Org. Chem.* **1981**, *46*, 7049.

(12) (a) Kojima, S.; Nakata, H.; Takagi, R.; Yamamoto, Y.; Akiba, K.-y. Manuscript in preparation. (b) Kojima, S.; Doi, Y.; Okuda, M.; Akiba, K.-y. *Organometallics* **1995**, *14*, 1928.

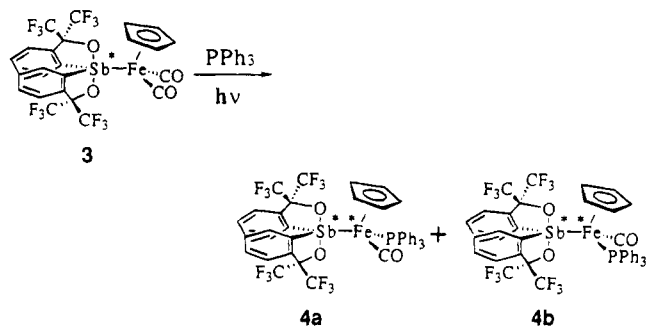
(13) King, R. B.; Stone, F. G. *Inorg. Synth.* **1963**, *7*, 110.

(14) Reger, D. L.; Coleman, C. J. *Organomet. Chem.* **1977**, *131*, 153.

Scheme 1



Scheme 2



stiboranide 10-Sb-4 anion (1-Et₄N⁺)¹⁵ gave **3** in good yield (76%). It should be noted that the activation of the Fe electrophile with silver(I) was necessary to obtain **3**. The reaction of **2b** with 1-Et₄N⁺ did not take place at all even after heating the mixture for 3 days under chloroform reflux, thus indicating that the stiboranide anion (1-Et₄N⁺) was much less reactive than the corresponding phosphoranide, which reacted with **2b** at room temperature to give **7**.^{1a}

Compound **3** was stable to atmospheric moisture and could be purified by column chromatography (SiO₂/ether). Assignment of the compound was carried out by NMR (¹³C, ¹H, and ¹⁹F), IR, elemental analysis, and X-ray structural analysis.

Preparation of Diastereomeric 4a,b {Rf₂SbFe(CO)PPh₃}. Photoirradiation of **3** in the presence of an equimolar amount of PPh₃ gave a mixture of diastereomers, **4a,b**, in 18% and 27% yields, respectively (Scheme 2). Separation of **4a** and **4b** was easily accomplished by flash column chromatography (SiO₂/1:3 AcOEt:*n*-hexane). No bis(triphenylphosphine) adduct was obtained in this case. Compounds **4a,b** were stable to atmospheric moisture, and assignment of each compound was carried out by NMR (¹H and ¹⁹F), IR, elemental analysis, and X-ray structural analysis.

Preparation of 5 {Rf₂SbFeCp(Ph₂PCH₂CH₂PPh₂)}. Photoirradiation of **3** in the presence of (diphenylphosphino)ethane gave a mixture of products, from which a 36% yield of **5** {Rf₂SbFeCp(Ph₂PCH₂CH₂PPh₂)} could be separated and purified by flash column chromatography (SiO₂/1:5 AcOEt:*n*-hexane) (Scheme 3). Compound **5** decomposed somewhat upon prolonged standing in the air at room temperature, but the assignment could be carried out by NMR (¹H and ¹⁹F), elemental analysis, and X-ray structural analysis.

Comparison of the Spectral Data of 3, 4a,b, and 5. Table 1 shows the NMR data (¹H, ¹⁹F, and ³¹P) and

(15) Akiba, K.-y.; Nakata, H.; Yamamoto, Y.; Kojima, S. *Chem. Lett.* **1992**, 1559. See also for 10-Sn-5 compounds: Akiba, K.-y.; Ito, Y.; Kondo, F.; Ohashi, N.; Sakaguchi, A.; Kojima, S.; Yamamoto, Y. *Chem. Lett.* **1992**, 1563.

(16) Coalescence of the two pairs of quartets to a pair of quartets was observed at ca. 80 °C. The differential four CF₃ groups observed at low temperatures may be due to the restricted Sb-Fe bond rotation.

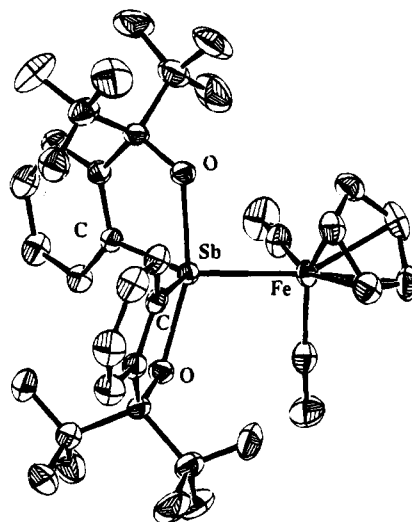
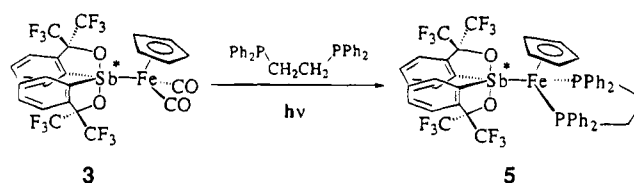


Figure 1. ORTEP diagram (30% probability ellipsoids) for **3** (one of the independent molecules).

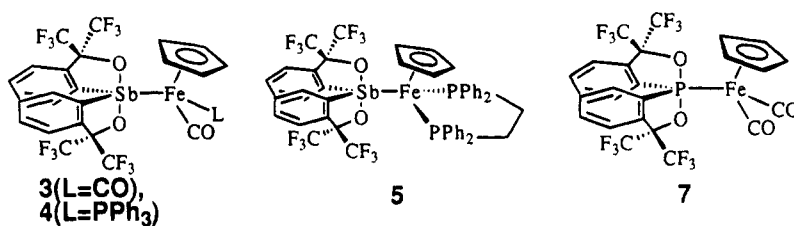
Scheme 3



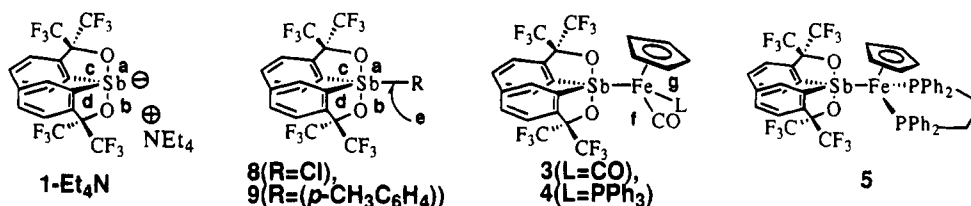
IR data (ν_{CO}) of **3**, **4a,b**, and **5** in addition to the reported data for the corresponding phosphorane **7**.^{1a} The protons of the Cp ligand appeared at δ 5.12 for **3**, 4.81 for **4a**, 4.42 for **4b**, and 4.50 for **5**, roughly reflecting the number of phosphines which should be more electron-donating than the CO group. The higher field chemical shift for Cp (δ 4.86) in the phosphorane **7** compared to that of **3** may reflect the stronger electron-donating property of the phosphoranide ligand in comparison with the stiboranide ligand. It may also be due to the fact that the averaged Fe-Cp bond length in **7** is larger than that in **3**. Probably one of the reasons for this stems from the steric repulsion due to the shorter P-Fe bond compared with Sb-Fe bond (vide infra). The ν_{CO} also shows the effect of triphenylphosphine in **4a,b** where the ν_{CO} value is lower than that in **3**.

X-ray Crystal Structures of 3, 4a,b, and 5. Crystals of **3**, **4a,b**, and **5** suitable for X-ray analysis were obtained by recrystallization from benzene-*n*-hexane for **3** and **4a**, ethyl acetate-*n*-hexane for **4b**, and dichloromethane-ether for **5**. Figures 1-4 show the crystal structures of **3**, **4a,b**, and **5**. Selected bond lengths and bond angles for the structures of **3** (two independent molecules), **4a,b**, and **5** in addition to compounds **1**, **8**, and **9** for comparison are listed in Table 2. The geometry about antimony in **3**, **4a,b**, and **5** was roughly similar to that in **1**, **8**, and **9** and could be considered as a distorted trigonal bipyramid (TBP) with the iron atom at the equatorial site of the TBP. However, distortion toward the square pyramid (SP) is generally higher in the phosphine-substituted compounds (**4a,b** and **5**) as is shown by the difference of the angles between the apical and the equatorial bonds ($\angle ab - \angle cd$, in Table 2; Δ angle¹⁷). Seppelt suggested

(17) Seppelt, K. In *Heteroatom Chemistry*; Block, E., Ed.; VCH Verlagsgesellschaft: Weinheim, Germany, 1990; p 335.

Table 1. Selected ^1H NMR and IR Data for 3, 4a,b, 5 and 7

3	4a	4b	5	7
2015	1978	IR (ν_{CO} , cm^{-1})		1992
2050		1981		2045
5.12 (s)	4.81 (d, $J = 1.8$ Hz)	^1H NMR (δ , ppm)		4.86 (s)
		4.42 (d, $J = 1.8$ Hz)	4.50 (t, $J = 1.5$ Hz)	
		^{19}F NMR (δ , ppm)		
-75.3 (q, 6F)	-73.7 (q, 6F)	-73.9 (q, 6F)	-72.28 (q, 3F) ^a	-74.07 (q, 6F)
-75.7 (q, 6F)	-75.7 (q, 6F)	-74.8 (q, 6F)	-72.95 (q, 3F)	-74.46 (q, 6F)
			-74.45 (q, 3F)	
			-75.06 (q, 3F)	
	65.2 (s)	^{31}P NMR (δ , ppm)		
		66.7 (s)	94.0 (d, $J = 21$ HZ)	
			94.9 (d, $J = 21$ HZ)	

^a Reference 16.Table 2. Selected Bond Lengths and Bond Angles for 1-Et₄N, 3, 4a,b, 5, 8, and 9

	1-Et ₄ N	8	9	3	4a	4b	5
Bond Lengths (Å)							
a	2.136(9)	2.016(2)	2.035(2)	2.091(3)	2.093(3)	2.129(2)	2.142(2)
b	2.147(9)	2.015(2)	2.042(3)	2.075(3)	2.087(3)	2.095(2)	2.148(2)
c	2.15(1)	2.073(2)	2.089(4)	2.116(3)	2.110(3)	2.140(3)	2.118(3)
d	2.16(1)	2.080(3)	2.094(4)	2.104(3)	2.110(3)	2.127(4)	2.114(4)
e		2.290(1)	2.094(4)	2.4801(5)	2.4790(5)	2.5204(5)	2.5106(6)
f				1.776(6)	1.768(6)	1.754(4)	1.749(4)
g				1.772(4)	1.751(4)	2.238(1)	2.230(1)
Bond Angles (deg)							
ab	158.6(4)	177.03(9)	170.6(1)	161.3(1)	163.69(9)	154.2(1)	152.36(9)
cd	103.4(5)	127.0(1)	121.5(1)	115.9(1)	111.1(1)	117.4(1)	114.1(1)
ac	77.3(4)	82.50(9)	81.5(1)	79.3(1)	78.9(1)	77.7(1)	77.3(1)
bd	77.1(4)	82.4(1)	81.2(1)	79.7(1)	79.4(1)	78.5(1)	76.9(1)
ad	90.0(4)	96.3(1)	94.0(1)	90.3(1)	90.4(1)	87.0(1)	86.6(1)
bc	89.0(4)	96.17(9)	94.0(1)	90.8(1)	92.8(1)	90.0(1)	89.2(1)
ce		115.16(8)	119.8(2)	118.95(9)	124.16(8)	125.5(1)	116.5(1)
de		117.78(8)	118.7(2)	125.10(9)	124.56(9)	116.96(7)	129.23(9)
ae		91.70(7)	95.7(1)	97.44(7)	96.42(7)	102.07(7)	100.97(7)
be		91.27(6)	93.7(1)	101.24(7)	99.85(7)	103.54(7)	106.64(6)

that compounds having **D** angles of more than 45° should be regarded as TBP and compounds having **D** of less than 15° as SP. On the basis of this discussion, the compounds **4a** (**D** angle: 36.8°), **4b** (44.9°), and **5** (38.26°) may be regarded as intermediate compounds although the structures of these compounds are much closer to TBP than to SP. The relatively small apical bond angle ($\angle\text{ab}$) of **3**, **4a,b**, and **5** should be the main reason for this deviation from the ideal TBP.

Compound **9** can be considered to be the standard molecule for the present series of compounds concerning the electronic effect and adopts an almost ideal TBP

structure, although the apical O–Sb–O bond angle (170.6°) deviates significantly from 180°. When the *p*-methylphenyl group is replaced with a chlorine atom (**8**), the Sb–O bond length is shortened (ca. 0.02 Å) and the O–Sb–O angle (177.0°) approaches the ideal one. On the other hand, when the *p*-methylphenyl group is replaced by a lone pair of electrons (1-Et₄N⁺), the Sb–O bond is elongated (ca. 0.10 Å) and both the O–Sb–O (158.6°) and C–Sb–C (103.4°) bond angles are reduced significantly. These facts clearly show such effects of an equatorial substituent that an electron-donating one elongates the apical O–Sb–O bond and an electron-

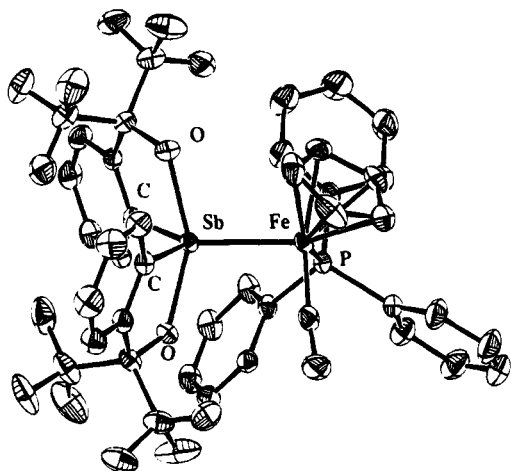


Figure 2. ORTEP diagram (30% probability ellipsoids) for 4a.

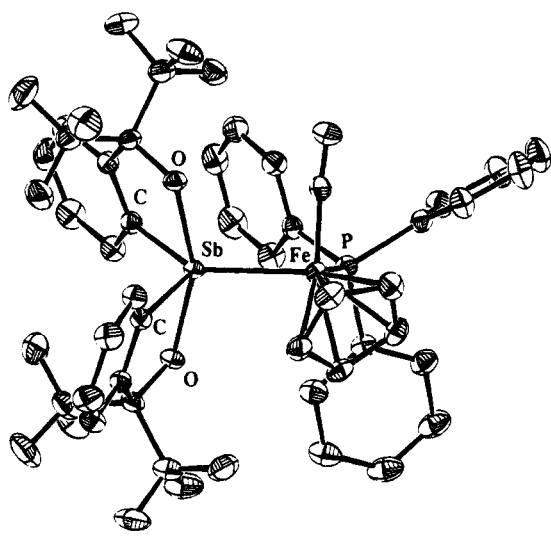


Figure 3. ORTEP diagram (30% probability ellipsoids) for 4b.

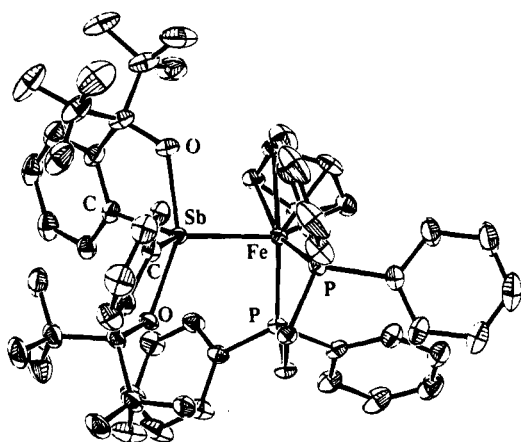


Figure 4. ORTEP diagram (30% probability ellipsoids) for 5.

withdrawing one shortens the bond. Strong electronic repulsion caused by the lone pair electrons decreases the corresponding bond angles (O–Sb–O and C–Sb–C) significantly, and the steric bulk of the ortho protons of the *p*-methylphenyl group affects the O–Sb–O bond angle considerably but does not affect the C–Sb–C angle so much.

Therefore, the fact that the apical Sb–O bond lengths

of **3** (2.075–2.093 Å) are much longer and the apical bond angles (161.3 and 163.69°) are much smaller than those of **9** (2.035 Å, 2.042 Å, 170.6°) would be due to the electron-donating property of the iron group {CpFe(CO)₂} even though the iron has two electron-withdrawing CO groups.^{1a} Among the series of **3**, **4a,b**, and **5** the order of the elongation of the Sb–O bond and the order of the reduction of the apical O–Sb–O bond angle is identical and follows the pattern **5** > **4a**, **4b** > **3**, reflecting an increase in electron donation from the equatorial ligand to the apical 3c–4e bond by increase in the number of the phosphine ligands in the place of the CO groups. The angle of Cl–Sb–Cl is also reduced in the two independent molecules of acyclic Me₂(Cl)₂-SbFe(Cp)(CO)(PMe₃) (163.2 and 163.8°).^{3c}

The Sb–Fe bond lengths in **3**, **4a,b**, and **5** are consistent with the reported Sb–Fe bond lengths (2.494–2.567 Å) in [Fe₂(CO)₈(μ-Sb)₂][Fe₂(CO)₆].¹⁸ These compounds also show the effect of the phosphine substitution with bond lengths in the order of **5** > **4a**, **4b** > **3**.

The Fe–CO bond lengths were shortened in **4a,b** in comparison with those of **3**, which can be due to the stronger back-donation from the iron to the CO in **4a,b**. The effect is also reflected in the relatively long C–O bond distances and the smaller ν_{CO} frequencies in **4a,b**.

The averaged Fe–Cp bond lengths (2.081 Å in **3**, 2.091 Å in **5**, 2.104 Å in **7**) may reflect the steric repulsion, while the chemical shift of the cyclopentadienyl group may depend on the averaged bond lengths besides the electron-donating property of the ligand. Thus, the higher field chemical shift of the Cp protons of **7** relative to **3** could be due to the longer averaged Fe–Cp distance on the basis of the steric repulsion and also to the stronger electron-donating ability of the phosphoranide anion than the stiboranide anion.

Pseudorotational Barrier of 4. With diastereomers **4a,b** in hand, the pseudorotational barrier of hypervalent stiboranes bearing two Martin ligands could be estimated. The pseudorotational barrier of **8** and **6** has been measured to be 14.1 kcal/mol for **8** at 313 K in toluene^{12a} and 27.3 kcal/mol for **6** (minor to major) at 298 K in *o*-dichlorobenzene.^{12b} Since the energy barrier has been considered to be dependent on the apicophilicity of the monodentate equatorial substituent in these kinds of bicyclic compounds,¹⁹ the apicophilicity of the carbon substituent could be considered to be less than that of the electronegative chlorine. An *o*-dichlorobenzene solution of **4a** or **4b** was heated separately in an NMR tube at 145 °C, but even after 3 h only slight (<5%) equilibration could be observed. At 160 °C equilibration was almost complete in 8 h to give about a 1.3:1 mixture of **4b** and **4a** with considerable (ca. 30%) decomposition. The equilibration of **6** was complete within a few hours at 100 °C; thus, the apicophilicity of the iron group can be considered to be much less than that of the carbon substituent although the exact barrier could not be determined.²⁰ The strong "equatophilicity" of the iron ligand could be due to its strong electron-donating property²¹ and steric

(18) Rheingold, A. L.; Geib, S. J.; Shieh, M.; Whitmire, K. H. *Inorg. Chem.* **1987**, *26*, 463.

(19) (a) Stevenson, W. H., III; Wilson, S.; Martin, J. C.; Farnham, W. B. *J. Am. Chem. Soc.* **1985**, *107*, 6340. (b) Holmes, R. R. *Pentacoordinated Phosphorus*; American Chemical Society: Washington, DC, 1980; Vols. I and II.

bulkiness. Further studies of the effect of the iron group by use of the same chiral ligand as **6** are now in progress.

Experimental Section

Melting points were taken on a Yanagimoto micro melting point apparatus and are uncorrected. ^1H NMR (400-MHz), ^{19}F NMR (376-MHz), and ^{13}C NMR (100-MHz) spectra were recorded on a JEOL EX-400 spectrometer. ^1H NMR (90-MHz) and ^{19}F NMR (85-MHz) spectra were recorded on a Hitachi R-90H spectrometer. Chemical shifts are reported (δ scale) from internal tetramethylsilane for ^1H and ^{13}C or from fluorotrichloromethane for ^{19}F . IR spectra were recorded on a Shimadzu 460 spectrometer. Elemental analysis was performed on a Perkin-Elmer 2400CHN elemental analyzer. Flash column chromatography was carried out on Merck silica gel 9385. Thin-layer chromatography was performed with Merck silica gel GF-254 plates. All reactions were carried out under N_2 or Ar.

Solvents and Reagents. The preparation of cyclopentadienyldicarbonyliron (**2b**)¹³ followed published procedures. The preparation of the tetraethylammonium stiboranide 10-Sb-4 anion ($1\text{-Et}_4\text{N}^+$) has been reported.¹⁵ Tetrahydrofuran (THF) and diethyl ether were distilled from sodium-benzophenone.

Bis[α,α -bis(trifluoromethyl)benzenemethanolato(2-)- C^2,O]stiboranide-Dicarbonylcyclopentadienyliiron(II) (3**).** A mixture of dicarbonylcyclopentadienyliodoiron **2b** (1.8 g, 6.0 mmol) and silver tetrafluoroborate (1.4 g, 7.2 mmol) in 10 mL of dry THF was stirred for 3 h at room temperature. To the suspension was added tetraethylammonium stiboranide ($1\text{-Et}_4\text{N}^+$) (3.8 g, 5.3 mmol) in 10 mL of dry THF. The mixture was heated under reflux for 14 h and was filtered through Celite. After the solvent was evaporated in vacuo the crude products were subjected to flash column chromatography (ether) to give **3**: 3.1 g, 76%; orange needles (recrystallized from benzene-*n*-hexane); mp 210–214 °C (dec); IR (KBr) 2015, 2050 cm^{-1} ; ^1H NMR (CDCl_3) 5.12 (s, 5 H), 7.53 (t, 2 H, $J = 7$ Hz), 7.61 (t, 2 H, $J = 7$ Hz), 7.73 (d, 2 H, $J = 7$ Hz), 8.14 (d, 2 H, $J = 7$ Hz); ^{19}F NMR (CDCl_3) -75.3 (q, 6 F, $J = 8$ Hz), -75.7 (q, 6 F, $J = 8$ Hz); ^{13}C NMR (CD_2Cl_2) 83.5 (sept, $J = 29$ Hz, $(\text{CF}_3)_2\text{C}$), 84.8 (s, Cp), 124.0 (q, $J = 289$ Hz, CF_3), 124.6 (q, $J = 287$ Hz, CF_3), 127.0 (d, $\text{SbCC}(\text{R})\text{C}$), 130.9 (d, SbCCC), 131.3 (d, $\text{SbCC}(\text{R})\text{C}$), 134.6 (d, SbCC), 136.8 (s, $\text{SbCC}(\text{R})$), 137.6 (s, SbC), 208.1 (s, CO), 209.5 (s, CO). Anal. Calcd for $\text{C}_{25}\text{H}_{13}\text{F}_{12}\text{O}_4\text{FeSb}$: C, 38.35; H, 1.67. Found: C, 38.37; H, 1.60.

Bis[α,α -bis(trifluoromethyl)benzenemethanolato(2-)- C^2,O]stiboranide-Carbonyl(triphenylphosphine)cyclopentadienyliiron(II) (4a,b**).** A solution of **3** (990 mg, 1.3 mmol) and triphenylphosphine (350 mg, 1.3 mmol) in 70 mL of 1,2-dichloroethane was irradiated with a tungsten lamp

for 6 h at room temperature. After the solvent was evaporated the crude products were subjected to flash column chromatography (1:3 ethyl acetate-*n*-hexane) to give less polar diastereomer **4a** ($R_f = 0.47$) and more polar diastereomer **4b** ($R_f = 0.33$). **4a**: 173 mg, 18%; orange needles (recrystallized from benzene-*n*-hexane); mp ca. 220 °C (dec); IR (KBr) 1978 cm^{-1} ; ^1H NMR (CDCl_3) 4.81 (d, 5 H, $J = 1.8$ Hz), 7.2–7.7 (m, 23 H); ^{19}F NMR (CDCl_3) -73.7 (q, 6 F, $J = 9$ Hz), -75.7 (q, 6 F, $J = 9$ Hz); ^{31}P NMR (CDCl_3) 65.2 (s, 1 P). Anal. Calcd for $\text{C}_{42}\text{H}_{28}\text{F}_{12}\text{O}_3\text{PFeSb}$: C, 49.59; H, 2.77. Found: C, 49.89; H, 2.63. **4b**: 260 mg, 27%; orange needles (recrystallized from ethyl acetate-*n*-hexane); mp ca. 220 °C (dec); IR (KBr) 1981 cm^{-1} ; ^1H NMR (CDCl_3) 4.42 (d, 5 H, $J = 1.8$ Hz), 7.2–7.7 (m, 23 H); ^{19}F NMR (CDCl_3) -73.9 (q, 6 F, $J = 9$ Hz), -74.8 (q, 6 F, $J = 9$ Hz); ^{31}P NMR (CDCl_3) 66.7 (s, 1 P). Anal. Calcd for $\text{C}_{42}\text{H}_{28}\text{F}_{12}\text{O}_3\text{PFeSb}$: C, 49.59; H, 2.77. Found: C, 49.38; H, 2.61.

Isomerization from **4a to **4b**.** A solution of **4a** (5 mg) in 1.7 mL of *o*-dichlorobenzene in an NMR tube was covered with aluminum foil and was heated at 60 °C for 1 h, at 70 °C for 1 h, at 85 °C for 1 h, at 120 °C for 1 h, and at 145 °C for 3 h in an oil bath. A slight amount of **4b** (<5%) was observed. A similar procedure was applied for a solution of **4b**, and only <5% isomerization was observed. Extensive decomposition took place after prolonged heating (12 h) at 145 °C.

Another solution of **4a** (3.8 mg) in 1 mL of *o*-dichlorobenzene was heated at 160 °C in an NMR probe to monitor the reaction by use of ^{19}F NMR. From the beginning a singlet which could be assigned to a decomposed product was observed, and after 8 h the equilibration was almost complete to give a 1:1.3 mixture of **4a** and **4b** with ca. 30% of the decomposition product.

Bis[α,α -bis(trifluoromethyl)benzenemethanolato(2-)- C^2,O]stiboranide-(Diphenylphosphino)ethane)cyclopentadienyliiron(II) (5**).** A solution of **2** (990 mg, 1.3 mmol) and 1,2-(diphenylphosphino)ethane (650 mg, 1.6 mmol) in 50 mL of 1,2-dichloroethane was irradiated with a tungsten lamp for 16 h at room temperature. After the solvent was evaporated the crude products were subjected to flash column chromatography (1:5 ethyl acetate-*n*-hexane) to give **5**: 530 mg, 36%; red-orange plates (recrystallized from dichloromethane-ether); mp 208–211 °C (dec); ^1H NMR (CDCl_3) 2.1–2.2 (m, 1 H), 2.7–2.8 (m, 2 H), 3.1–3.2 (m, 1 H), 4.50 (t, 5 H, $J = 1.5$ Hz), 6.9–7.7 (m, 28 H); ^{19}F NMR (CDCl_3) -72.28 (q, 3 F, $J = 10$ Hz), -72.95 (q, 3 F, $J = 10$ Hz), -74.45 (q, 3 F, $J = 10$ Hz), -75.06 (q, 3 F, $J = 10$ Hz); ^{31}P NMR (CDCl_3) 94.0 (d, 1 P, $J = 21$ Hz), 94.9 (d, 1 P, $J = 21$ Hz). Anal. Calcd for $\text{C}_{49}\text{H}_{37}\text{F}_{12}\text{O}_2\text{P}_2\text{FeSb}$: C, 52.30; H, 3.31. Found: C, 52.38; H, 3.31.

Crystallographic Studies. Crystal Structure of **3, **4a,b**, and **5**.** Crystal data and numerical details of the structure determinations are given in Table 3. Crystals suitable for X-ray structure determination were mounted on a Mac Science MXC3 diffractometer and irradiated with graphite-monochromated Mo K α radiation ($\lambda = 0.71073$ Å) for data collection. Lattice parameters were determined by least-squares fitting of 32 for **3**, of 31 for **4a**, of 24 for **4b**, and of 27 reflections for **5** with $31^\circ < 2\theta < 35^\circ$. Data were collected with the $2\theta/\omega$ scan mode. All data were corrected for absorption²² and extinction.²³ The structures were solved by direct methods with the program, Monte Carlo-Multan.²⁴ Refinement on F was carried out by full-matrix least-squares. All non-hydrogen atoms were refined with anisotropic thermal parameters. All hydrogen atoms in **3**, **4a,b**, and **5** could be found on a difference Fourier map; these coordinates were included in the refinement with isotropic thermal parameters. All the computations were carried out on a Titan-750 computer using the crystal-G program.²⁴

(20) The mechanism of equilibration of **4a/4b** by dissociation of one of the ligands on the iron group may also be possible. However, we recently synthesized [α,α -bis(trifluoromethyl)benzenemethanolato(2-)- C^2,O][α -(trifluoromethyl)- α -methylbenzenemethanolato(2-)- C^2,O]stiboranide-dicarbonyl(cyclopentadienyl)iron(II) (**10**) and measured the barrier for the equilibration. In **10**, the barrier (30.5 kcal mol $^{-1}$ at 110 °C) should be the inversion barrier at the central Sb atom because the ligands on the iron group are identical. Thus, we think the equilibration of **4a/4b** takes place also via inversion at the central Sb atom. The slightly lower temperature (110–130 °C) required for the equilibration of **10** in comparison with that (>145 °C) required for the equilibration of **4a/4b** is consistent with the higher apicophilicity of the iron group of **10** than that of **4a/4b** since the carbonyl group on the iron group of **10** should be more electron-withdrawing than the triphenylphosphine on the iron group of **4a/4b**.

(21) The origin of the donating property of the iron group may be explained in two ways: (i) donation from a filled d-orbital on Fe into the antibonding component of the axial MO on Sb in a π -fashion; (ii) strong σ -donation of the electropositive iron group into the central antimony atom. While we need more information to reach a conclusion, the second explanation is the preferred one at present because the donation by the first one might have decreased the longer Sb-Fe bond.

(22) Furusaki, A. *Acta Crystallogr.* **1979**, A35, 220.

(23) Katayama, C. *Acta Crystallogr.* **1986**, A42, 19.

(24) Coppens, P.; Hamilton, W. C. *Acta Crystallogr.* **1970**, A26, 71.

Table 3. Crystal Data for 3, 4a,b, and 5

	3	4a	4b	5
formula	C ₂₅ H ₁₃ O ₂ F ₁₂ FeSb	C ₄₂ H ₂₈ O ₃ F ₁₂ PFeSb	C ₄₂ H ₂₈ O ₃ F ₁₂ PFeSb +CH ₃ CO ₂ Et	C ₄₉ H ₃₇ O ₂ F ₁₂ P ₂ FeSb
mol wt	751.0	1017.2	1105.4	1125.4
cryst syst	monoclinic	triclinic	triclinic	monoclinic
space group	P2 ₁ /n	P $\bar{1}$	P $\bar{1}$	P2 ₁ /n
cryst dimens, mm	0.80 × 0.40 × 0.20	0.85 × 0.80 × 0.45	0.50 × 0.30 × 0.20	0.85 × 0.32 × 0.17
a, Å	19.502(6)	11.291(2)	13.467(3)	19.135(4)
b, Å	16.357(6)	12.028(2)	13.748(5)	13.064(4)
c, Å	18.596(6)	15.418(4)	14.141(4)	18.974(4)
α, deg	90	104.44(2)	84.42(3)	90
β, deg	115.75(2)	93.35(2)	64.28(2)	105.69(2)
γ, deg	90	92.37(1)	69.50(2)	90
V, Å ³	5343(3)	2020.8(8)	2205(1)	4566(2)
Z	8	2	2	4
D _{calc} , g cm ⁻³	1.87	1.67	1.66	1.64
abs coeff, cm ⁻¹	15.36	10.65	9.76	9.77
F(000)	2912	1008	1080	2248
radiation; λ, Å	Mo Kα; 0.710 73	Mo Kα; 0.710 73	Mo Kα; 0.710 73	Mo Kα; 0.710 73
temp, °C	23 ± 1	23 ± 1	23 ± 1	23 ± 1
2θ max, deg	50	50	50	50
scan rate, deg/min	4.0	14.0	8.0	4.0
linear decay, %	3			4
data collcd	±h, -k, +l	±h, ±k, +l	±h, ±k, +l	±h, +k, +l
tot. data collcd, unique,	10257, 9408,	7485, 7120,	8196, 7764,	8816, 8063,
obsd	8019 (I > 3σ(I))	6635 (I > 3σ(I))	6846 (I > 3σ(I))	6329 (I > 3σ(I))
R int	0.02	0.01	0.01	0.03
no. of params refined	859	631	685	721
R, R _w , S	0.033, 0.030, 1.39	0.042, 0.052, 2.10	0.033, 0.030, 2.39	0.035, 0.029, 1.40
max shift in final cycle	0.19	0.10	3.33	0.17
final diff map, max, e/Å ³	0.65	1.58	0.81	0.62

Acknowledgment. We are indebted, for partial support of this research, to Grants-in-Aid for Scientific Research on Priority Area of Organic Unusual Valency (Nos. 02247103, 03233104, and 04217105) administered by the Ministry of Education, Science, and Culture of the Japanese Government.

Supporting Information Available: Tables of crystallographic parameters, positional and thermal parameters, and complete interatomic distances and angles and ORTEP diagrams for 3, 4a,b and 5 (78 pages). Ordering information is given on any current masthead page.

OM940976I

A Novel Synthetic Route to Molybdenum Hydrido-Thiocarbamoyl and Hydrosulfido-Carbyne Complexes by Reactions of *trans*-Mo(N₂)₂(R₂PC₂H₄PR₂)₂ with *N,N*-Dimethylthioformamide

Xiao-Liang Luo,* Gregory J. Kubas,* Carol J. Burns, and Ray J. Butcher

Materials and Chemical Design Group (CST-10), Mail Stop C346, Los Alamos National Laboratory, Los Alamos, New Mexico 87545

Received February 27, 1995*

The reactions of bis(dinitrogen)molybdenum complexes *trans*-Mo(N₂)₂(R₂PC₂H₄PR₂)₂ (R = Ph, Et) with *N,N*-dimethylthioformamide (HC(S)NMe₂) in refluxing benzene under argon give the molybdenum hydrido-thiocarbamoyl complexes MoH(η²-C(S)NMe₂)(R₂PC₂H₄PR₂)₂ (R = Ph (**1a**), Et (**1b**)). On heating at 125 °C in toluene solutions, compounds **1a** and **1b** rearrange to form the molybdenum hydrosulfido-aminocarbyne complexes *trans*-Mo(SH)(≡CNMe₂)(R₂PC₂H₄PR₂)₂ (R = Ph (**2a**), Et (**2b**)). A mechanism is proposed for this thermal rearrangement which involves migration of the hydride ligand from molybdenum to the sulfur atom of the thiocarbamoyl ligand to give the 16-electron Fischer carbene intermediate Mo(=C(SH)NMe₂)(R₂PC₂H₄PR₂)₂, followed by migration of the hydrosulfido group from the carbene carbon to molybdenum. The molecular structures of compounds **1a** and **2a** have been determined by single-crystal X-ray diffraction studies. Crystallographic data for **1a**: monoclinic, space group C2/c, *a* = 19.536(4) Å, *b* = 15.950(3) Å, *c* = 15.793(3) Å, β = 105.54(3)°, *V* = 4741(2) Å³, *Z* = 4, and *R* = 0.037. Crystallographic data for **2a**: monoclinic, space group P2₁/c, *a* = 19.516(4) Å, *b* = 12.301(2) Å, *c* = 19.899(4) Å, β = 102.46(3)°, *V* = 4665 (2) Å³, *Z* = 4, and *R* = 0.062.

Introduction

The reactivity of bis(dinitrogen)molybdenum complexes of the type *trans*-Mo(N₂)₂(R₂PC₂H₄PR₂)₂ has been extensively studied.¹ Hidai and co-workers reported that the decarbonylation of *N,N*-dimethylformamide (DMF) by *trans*-Mo(N₂)₂(Ph₂PC₂H₄PPh₂)₂ gives *trans*-Mo(DMF)(CO)(Ph₂PC₂H₄PPh₂)₂, which is converted into *trans*-Mo(N₂)(CO)(Ph₂PC₂H₄PPh₂)₂ under dinitrogen and then into Mo(CO)(Ph₂PC₂H₄PPh₂)₂ under argon.²

Recently, we reported the one-step synthesis of a series of formally 16-electron complexes of the type Mo(CO)(R₂PC₂H₄PR₂)₂ by the reactions of bis(dinitrogen)molybdenum complexes *trans*-Mo(N₂)₂(R₂PC₂H₄PR₂)₂ with an ester such as ethyl acetate in refluxing benzene or toluene under argon.³ Some of the Mo(CO)(R₂PC₂H₄PR₂)₂ complexes, *i.e.*, for R = Ph,^{2b} Bu,⁴ CH₂Ph,^{3a} and CH₂C₆H₄-*m*-Me,^{3a} have been shown by X-ray crystallography or variable-temperature ¹H NMR spectroscopy to adopt an octahedral structure, in which an agostic Mo···H-C interaction occupies an otherwise vacant coordination site trans to the CO ligand.

The weak agostic Mo···H-C interaction in Mo(CO)(R₂PC₂H₄PR₂)₂ can be readily displaced by a wide

variety of small molecules.³⁻⁵ In particular, the reaction of Mo(CO)(R₂PC₂H₄PR₂)₂ with H₂ gives a dihydrogen complex Mo(η²-H₂)(CO)(R₂PC₂H₄PR₂)₂ when R is an electron-withdrawing phenyl or benzyl group or a dihydride complex MoH₂(CO)(R₂PC₂H₄PR₂)₂ when R is an electron-donating alkyl group.³ Thus, electronic control of η²-dihydrogen versus dihydride coordination has been achieved in this molybdenum system.

We were interested in synthesizing the formally 16-electron thiocarbonyl complexes of type Mo(CS)(R₂PC₂H₄PR₂)₂ with a wide range of steric and electronic properties and using these complexes for the binding and activation of small molecules. In an attempt to prepare Mo(CS)(R₂PC₂H₄PR₂)₂ by the reactions of *trans*-Mo(N₂)₂(R₂PC₂H₄PR₂)₂ with *N,N*-dimethylthioformamide (HC(S)NMe₂) using a procedure similar to that used for the synthesis of Mo(CO)(Ph₂PC₂H₄PPh₂)₂,² we have unexpectedly found a novel synthetic route to molybdenum hydrido-thiocarbamoyl and hydrosulfido-aminocarbyne complexes. Herein we report the synthesis and spectroscopic and crystallographic characterization of these complexes.

Results and Discussion

Synthesis and Spectroscopic Characterization of Molybdenum Hydrido-Thiocarbamoyl Complexes MoH(η²-C(S)NMe₂)(R₂PC₂H₄PR₂)₂ (R = Ph (1a**), Et (**1b**)).** Most complexes containing the thiocarbamoyl ligand C(S)NMe₂ have been prepared either by displacement of Cl⁻ from ClC(S)NMe₂ by metal carbonyl

* Abstract published in *Advance ACS Abstracts*, June 1, 1995.

(1) (a) Hidai, M.; Mizobe, Y. In *Reactions of Coordinated Ligands*; Braterman, P. S., Ed.; Plenum Press: New York, 1989; Vol. 2, p 53. (b) Georger, T. A. In *Homogeneous Catalysis with Metal Phosphine Complexes*; Pignolet, L. H., Ed.; Plenum Press: New York, 1983; p 405.

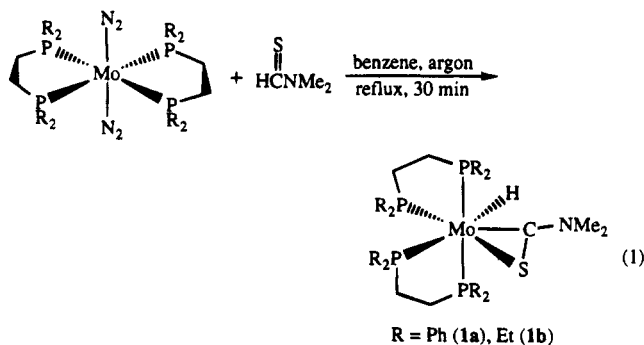
(2) (a) Tatsumi, T.; Tominaga, H.; Hidai, M.; Uchida, Y. *J. Organomet. Chem.* **1976**, *114*, C27. (b) Sato, M.; Tatsumi, T.; Kodama, T.; Hidai, M.; Uchida, T.; Uchida, Y. *J. Am. Chem. Soc.* **1978**, *100*, 4447.

(3) (a) Luo, X.-L.; Kubas, G. J.; Burns, C. J.; Eckert, J. *Inorg. Chem.* **1994**, *33*, 5219. (b) Kubas, G. J.; Burns, C. J.; Eckert, J.; Johnson, S. W.; Larson, A. C.; Vergamini, P. J.; Unkefer, C. J.; Khalsa, G. R. K.; Jackson, S. A.; Eisenstein, O. *J. Am. Chem. Soc.* **1993**, *115*, 569.

(4) Luo, X.-L.; Kubas, G. J.; Burns, C. J.; Bryan, J. C.; Butcher, R. J. *Inorg. Chem.*, submitted for publication.

(5) (a) Luo, X.-L.; Kubas, G. J.; Bryan, J. C.; Burns, C. J.; Unkefer, C. J. *J. Am. Chem. Soc.* **1994**, *116*, 10312. (b) Luo, X.-L.; Kubas, G. J.; Burns, C. J.; Bryan, J. C.; Unkefer, C. J. *J. Am. Chem. Soc.* **1995**, *117*, 1159.

anions⁶ or by oxidative addition of the C–X bonds of XC(S)NMe₂ (X = Cl,⁷ SMe,⁸ S₂CNMe₂,⁸ N(Ph)(C(S)NMe₂)⁸) to metal complexes. We have now found a convenient synthetic route to molybdenum thiocarbamoyl complexes, which involves the oxidative cleavage of the aldehydic C–H bond in HC(S)NMe₂ by bis(dinitrogen)molybdenum complexes of the type *trans*-Mo(N₂)₂(R₂PC₂H₄PR₂)₂. Thus, the reactions of *trans*-Mo(N₂)₂(R₂PC₂H₄PR₂)₂ (R = Ph, Et) with HC(S)NMe₂ in refluxing benzene under argon gave deep red solutions, from which the hydrido–thiocarbamoyl complexes MoH(η²-C(S)NMe₂)(R₂PC₂H₄PR₂)₂ (R = Ph (**1a**), Et (**1b**)) were isolated as red-brown solids in high yields and high purity (eq 1).



To our knowledge, only one hydrido–thiocarbamoyl complex, *i.e.*, [IrH(η²-C(S)NMe₂)(CO)(PPh₃)₂]⁺, has been reported,^{7c} but the compound was not characterized crystallographically. The tungsten hydrido–carbamoyl complex WH(η²-C(O)NMe₂)(Ph₂PC₂H₄PPh₂)₂, which is analogous to compounds **1a** and **1b**, has recently been prepared from the reaction of *trans*-W(N₂)₂(Ph₂PC₂H₄PPh₂)₂ with *N,N*-dimethylformamide.⁹

The ¹H NMR spectrum of **1a** in C₆D₅CD₃ at 298 K displays a binomial quintet resonance at δ –3.63 (²J_{HP} = 39.5 Hz) assignable to the hydride ligand, two singlet resonances at δ 2.69 and 2.34 due to the two inequivalent *N*-methyl groups, and resonances due to the diphosphine ligands. The observation of a quintet hydride resonance indicates that the four phosphorus atoms are equivalent at this temperature due to rapid fluxionality that is commonly observed for seven-coordinate complexes.¹⁰ When the sample is cooled, the hydride resonance broadens and then collapses at 188 K into a broad doublet (²J_{HP} = 85 Hz). The variable-temperature ³¹P{¹H} NMR spectra of **1a** in C₆D₅CD₃ are shown in Figure 1. At 298 K, a single resonance at δ 74.5 is observed. When the sample is cooled to 188 K, this resonance collapses into four resonances with equal intensity at δ 81.3, 77.2, 63.5, and 61.4. The two doublet

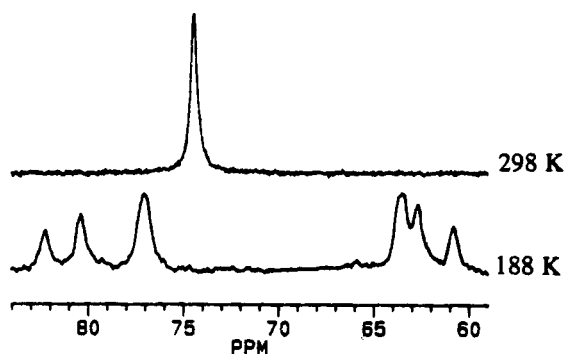


Figure 1. Variable-temperature ³¹P{¹H} NMR spectra (80.96 MHz) of MoH(η²-C(S)NMe₂)(Ph₂PC₂H₄PPh₂)₂ (**1a**) in C₆D₅CD₃.

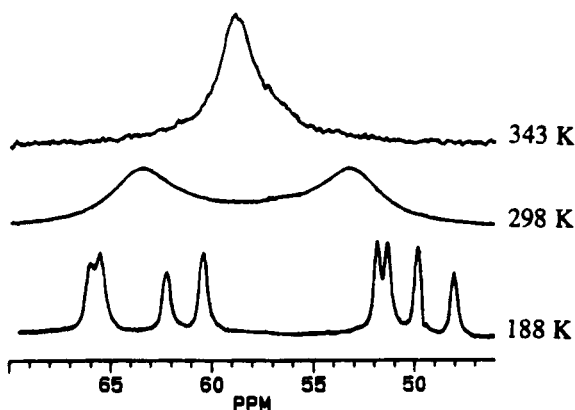


Figure 2. Variable-temperature ³¹P{¹H} NMR spectra (80.96 MHz) of MoH(η²-C(S)NMe₂)(Et₂PC₂H₄PEt₂)₂ (**1b**) in C₆D₅CD₃.

resonances at δ 81.3 and 61.4 show a very large ²J_{PP} coupling constant of 148 Hz, which suggests a *trans* disposition of two inequivalent phosphorus atoms. The ¹H and ³¹P{¹H} NMR spectroscopic data are consistent with a seven-coordinate pentagonal bipyramidal structure with two phosphorus atoms occupying the two *trans* axial sites as shown in eq 1.

The variable-temperature ¹H and ³¹P{¹H} NMR spectra of **1b** in C₆D₅CD₃ are quite similar to those of **1a**. The hydride region of the ¹H NMR spectrum at 298 K displays a quintet resonance at δ –6.44 (²J_{HP} = 36.7 Hz), which collapses at 188 K into a doublet (²J_{HP} = 93 Hz) of multiplets. The variable-temperature ³¹P{¹H} NMR spectra of **1b** are shown in Figure 2. At 298 K, two broad resonances at δ 63.5 and 53.0 are observed which coalesce into a broad peak at 343 K. When the sample is cooled to 188 K, four resonances with equal intensity are observed at δ 65.9, 61.4, 51.6, and 49.0. The two resonances at δ 61.4 and 49.0 show a very large *trans* ²J_{PP} coupling constant of 145 Hz. On the basis of the ¹H and ³¹P{¹H} NMR spectroscopic data, compound **1b** is isostructural with **1a** and adopts the pentagonal bipyramidal structure shown in eq 1.

The IR spectra of **1a** and **1b** in Nujol mulls show broad bands at 1886 and 1889 cm^{–1}, respectively, which are assigned to ν(Mo–H). The ν(C–N) bands for the thiocarbamoyl ligand appear at 1521 and 1524 cm^{–1}, respectively, for **1a** and **1b**. Both stretching frequencies are outside the range of 1575–1650 cm^{–1} typically found for an η²-bound C(S)NMe₂ group.^{6–8} Nevertheless, a similarly low C–N stretching frequency of 1526 cm^{–1}

(6) (a) Dean, W. K.; Treichel, P. M. *J. Organomet. Chem.* **1974**, *66*, 87. (b) Dean, W. K. *J. Organomet. Chem.* **1977**, *135*, 195.

(7) (a) Green, C. R.; Angelici, R. J. *Inorg. Chem.* **1972**, *11*, 2095. (b) Dean, W. K.; Charles, R. S.; VanDerveer, D. G. *Inorg. Chem.* **1977**, *16*, 3328. (c) Gal, A. W.; Ambrosius, H. P. M. M.; Ver Der Ploeg, A. F. M. J.; Bosman, W. P. *J. Organomet. Chem.* **1978**, *149*, 81. (d) Gal, W. K. *J. Organomet. Chem.* **1980**, *190*, 353. (e) Corain, B.; Martelli, M. *Inorg. Nucl. Chem. Lett.* **1972**, *8*, 39. (f) Gibson, J. A. E.; Cowie, M. *Organometallics* **1984**, *3*, 722.

(8) Gal, A. W.; Ver Der Ploeg, A. F. M. J.; Vollenbroek, F. A.; Bosman, W. P. *J. Organomet. Chem.* **1975**, *96*, 123.

(9) (a) Ishida, T.; Mizobe, Y.; Tanase, T.; Hidai, M. *J. Organomet. Chem.* **1991**, *409*, 355. (b) Ishida, T.; Mizobe, Y.; Tanase, T.; Hidai, M. *Chem. Lett.* **1988**, 441.

(10) Luo, X.-L.; Schulte, G. K.; Demou, P.; Crabtree, R. H. *Inorg. Chem.* **1990**, *29*, 4268 and references therein.

Table 1. Crystallographic Data for MoH(η^2 -C(S)NMe₂)(Ph₂PC₂H₄PPh₂)₂ (1a)

empirical formula	C ₅₅ H ₅₅ MoNP ₄ S
fw	981.88
cryst syst	monoclinic
space group	C2/c
a, Å	19.536(4)
b, Å	15.950(3)
c, Å	15.793(3)
β , deg	105.54(3)
V, Å ³	4741(2)
Z	4
ρ (calcd), g cm ⁻³	1.376
μ (Mo K α), cm ⁻¹	4.94
min/max transmissn coeff	0.72–0.79
T, K	203
R ^a	0.037
R _w ^b	0.055

$$^a R = \sum ||F_o| - |F_c|| / \sum |F_o|, \quad ^b R_w = [\sum w(|F_o| - |F_c|)^2 / \sum w F_o^2]^{1/2}.$$

Table 2. Selected Bond Lengths (Å) and Angles (deg) for MoH(η^2 -C(S)NMe₂)(Ph₂PC₂H₄PPh₂)₂ (1a)

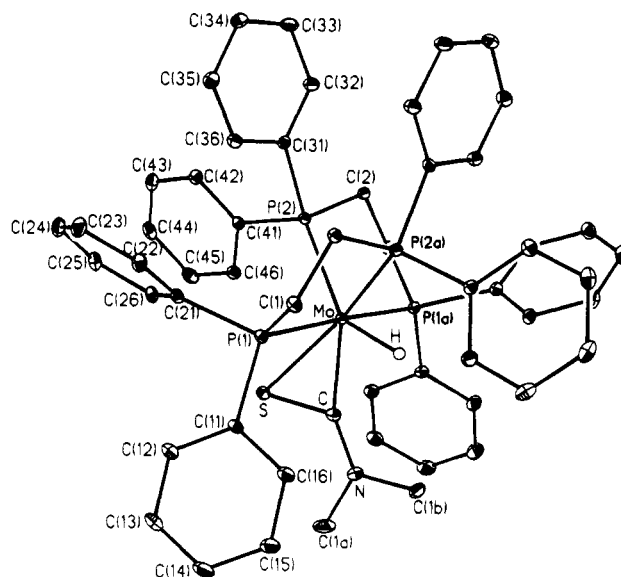
Bond Lengths			
Mo–P(1)	2.435(1)	Mo–P(2)	2.477(1)
Mo–P(2)	2.477(1)	Mo–P(2a)	2.477(1)
Mo–C	2.049(3)	Mo–S	2.626(1)
Mo–H	1.56(5)	C–S	1.755(1)
C–N	1.310(5)	N–C(1a)	1.438(5)
N–C(1b)	1.439(7)		
Bond Angles			
P(1)–Mo–P(1a)	177.4(1)	P(2)–Mo–P(1a)	79.6(1)
P(1)–Mo–P(2)	102.3(1)	P(1a)–Mo–P(2a)	102.3(1)
P(1)–Mo–P(2a)	79.6(1)	P(2)–Mo–P(2a)	87.0(1)
P(1)–Mo–C	88.7(1)	C–Mo–P(1a)	88.7(1)
P(2)–Mo–C	136.5(1)	C–Mo–P(2a)	136.5(1)
P(1)–Mo–S	82.5(1)	P(2)–Mo–S	97.4(1)
S–Mo–P(1a)	95.6(1)	S–Mo–P(2a)	162.1(1)
S–Mo–C	41.9(1)	Mo–S–C	51.2(1)
Mo–C–S	86.9(1)	Mo–C–N	151.4(2)
S–C–N	121.7(2)	C–N–C(1a)	125.5(3)
C–N–C(1b)	119.8(3)	C(1a)–N–C(1b)	114.7(3)
P(1)–Mo–H	100.4(20)	P(2)–Mo–H	145.0(20)
P(1a)–Mo–H	78.7(20)	P(2a)–Mo–H	71.3(20)
C–Mo–H	69.9(20)	S–Mo–H	111.8(20)

has been reported for W(η^2 -C(S)NEt₂)(S₂CNEt₂)(CO)-(PhCHS).¹¹

In the majority of mononuclear thiocarbamoyl complexes reported to date, the thiocarbamoyl ligand adopts the η^2 coordination mode.^{6–8} The η^1 coordination mode has been reported only for square-planar d⁸ species,^{7a,c,e} but no examples have been characterized by X-ray crystallography. The η^1 coordination of the C(S)NMe₂ group in **1a** and **1b** is unlikely since it would give less stable 16-electron octahedral complexes.

X-ray Crystal Structure of MoH(η^2 -C(S)NMe₂)(Ph₂PC₂H₄PPh₂)₂ (1a). In order to obtain more detailed information on the mode of coordination of the C(S)NMe₂ group in compounds **1a** and **1b**, an X-ray crystallographic study has been performed on a single crystal of **1a**. A summary of the crystallographic data is given in Table 1, and the selected bond lengths and angles are given in Table 2. An ORTEP drawing is shown in Figure 3. Compound **1a** is the first crystallographically characterized hydrido–thiocarbamoyl complex.

Consistent with the solution ¹H and ³¹P{¹H} NMR spectroscopic data (*vide supra*), the coordination geometry around the molybdenum atom in **1a** is best described as a distorted pentagonal bipyramid. The two

**Figure 3.** ORTEP drawing of MoH(η^2 -C(S)NMe₂)(Ph₂PC₂H₄PPh₂)₂ (**1a**).

trans axial sites are occupied by the two phosphorus atoms P(1) and P(1a), whereas the five equatorial sites are occupied by the hydride ligand, the η^2 -thiocarbamoyl ligand, and the two phosphorus atoms P(2) and P(2a). The molybdenum atom essentially lies on the least-squares plane defined by the atoms at the five equatorial sites, with an insignificant deviation of 0.002 Å from the plane. The position of the hydride ligand was determined in the difference Fourier map, and it behaved well on refinement. The hydride ligand occupies the equatorial site between the P(2a) and the C atom of the thiocarbamoyl ligand. The Mo–H distance of 1.56(5) Å is somewhat shorter than the value of 1.685–(3) Å found for (η^5 -C₅H₅)₂MoH₂ by a neutron diffraction study.¹² This is not surprising in view of the tendency of X-ray crystallography to give foreshortened metal–hydrogen distances.¹³

The MoCSNMe₂ unit in **1a** is virtually planar. Thus, the largest deviation from the least-squares plane defined by the atoms Mo, C, S, N, C(1a), and C(1b) is only 0.015 Å for S and C(1b). The five torsional angles, Mo–S–C–N, Mo–C–N–C(1a), Mo–C–N–C(1b), S–C–N–C(1a), and S–C–N–C(1b), are –179.6°, 180.0°, –1.0°, –0.9°, and 178.1°, respectively, confirming the near planarity of the MoCSNMe₂ moiety.

The C–N distance in **1a** is 1.310(5) Å, which is significantly shorter than the N–C(1a) and N–C(1b) distances of 1.438(5) and 1.439(7) Å, respectively, and is very similar to the C–N distances found in aminocarbene complexes¹⁴ and typical organic amides.¹⁵ This suggests the presence of substantial overlap between the nitrogen lone pair and the p_z orbital of the carbon atom and is consistent with the hindered rotation around the C–N bond as indicated by the inequivalence of the two N-methyl groups in ¹H NMR (*vide supra*).

(12) Schultz, A. J.; Stearley, K. L.; Williams, J. M.; Mink, R.; Stucky, G. D. *Inorg. Chem.* **1977**, *16*, 3303.

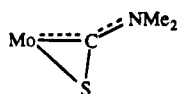
(13) Teller, R. G.; Bau, R. *Struct. Bonding (Berlin)* **1981**, *44*, 1.

(14) (a) Fischer, E. O. *Adv. Organomet. Chem.* **1976**, *14*, 1. (b) Gallop, M. A.; Roper, W. R. *Adv. Organomet. Chem.* **1986**, *25*, 121. (c) Brothers, P. J.; Roper, W. R. *Chem. Rev.* **1988**, *88*, 1293. (d) Nugent, W. A.; Mayer, J. M. *Metal-Ligand Multiple Bonds*; John Wiley & Sons: New York, 1988.

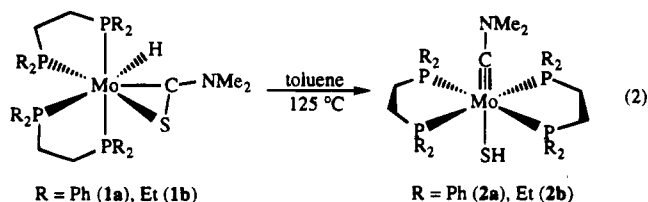
(15) Hamilton, W. C. *Acta Crystallogr.* **1965**, *18*, 866.

(11) Mayr, A.; McDermott, G. A.; Dorries, A. M.; Holder, A. K. J. *Am. Chem. Soc.* **1986**, *108*, 310.

The C–S distance of 1.755(1) Å in **1a** is significantly longer than those (1.61–1.69 Å) previously found for η^2 -thiocarbamoyl complexes.^{6–8} In fact, this distance is substantially longer than the C=S double-bond distances of 1.55–1.56 Å observed in CS₂,¹⁶ COS,¹⁷ CSTE,¹⁸ and HNCS¹⁹ and 1.61 Å in CH₂=S²⁰ and approaches the typical C–S single-bond distances of 1.78–1.82 Å that have been observed in several thioethers.²¹ The Mo–C distance of 2.049(3) Å is considerably shorter than the Mo–C single-bond distances of 2.2–2.4 Å found in molybdenum alkyl complexes²² and close to the range of Mo=C double-bond distances of 1.8–2.0 Å reported for molybdenum alkylidene complexes.¹⁴ Both the long C–S distance and the short Mo–C distance in **1a** indicate that the η^2 -thiocarbamoyl ligand has substantial carbenoid character as represented by



Synthesis and Spectroscopic Characterization of Molybdenum Hydrosulfido-Carbyne Complexes *trans*-Mo(SH)(=CNMe₂)(R₂PC₂H₄PR₂)₂ (R = Ph (2a**), Et (**2b**)).** When the red solutions of molybdenum hydrido–thiocarbamoyl complexes **1a** and **1b** in toluene were heated at 125 °C, greenish-yellow solutions were formed, from which the molybdenum hydrosulfido–aminocarbyne complexes *trans*-Mo(SH)(=CNMe₂)(R₂PC₂H₄PR₂)₂ (R = Ph (**2a**), Et (**2b**)) were isolated as greenish-yellow solids in high yields (eq 2).



Compounds **2a** and **2b** are obviously formed by thermally induced rearrangement of **1a** and **1b**, respectively. To our knowledge, this represents a new synthetic approach to carbyne complexes. Mononuclear transition metal complexes containing terminally bound hydrosulfido ligands (SH) are relatively rare. Many of the terminal hydrosulfido complexes tend to undergo decomposition to form dimeric or cluster species containing bridging SH or S²⁻ ligands. In contrast, com-

pounds **2a** and **2b** are remarkably stable toward thermal decomposition, as manifested by the high temperature at which they are synthesized. Only a few monomeric molybdenum terminal hydrosulfido complexes have been structurally characterized.²³

The high-field region of the ¹H NMR spectrum of **2a** in CD₂Cl₂ displays a quintet resonance at δ –3.98 (²J_{HP} = 6.7 Hz) which is assigned to the SH proton. The ³¹P{¹H} NMR spectrum shows only a single resonance at δ 62.3. The ¹³C{¹H} spectrum displays a very low-field binomial quintet resonance at δ 266.5 (²J_{CP} = 18.4 Hz) which is assigned to the carbyne carbon since this chemical shift is in the range typically observed for carbyne complexes.^{14d}

The NMR spectroscopic data of **2b** are similar to those of **2a**. The high-field region of the ¹H NMR spectrum of **2b** in C₆D₆ shows a quintet resonance at δ –3.66 (²J_{HP} = 7.1 Hz) which is assignable to the SH proton. The ³¹P{¹H} NMR spectrum displays a single resonance at δ 56.6. The ¹³C{¹H} spectrum shows a binomial quintet resonance at δ 226.5 (²J_{CP} = 17.6 Hz) assignable to the carbyne carbon.

All the NMR spectroscopic data of **2a** and **2b** are consistent with an octahedral structure with a *trans* disposition of the hydrosulfido and aminocarbyne ligands, as shown in eq 2. This *trans* geometry is adopted probably because the strong π -accepting capacity of the carbyne ligand²⁴ favors it being *trans* to the π -donating hydrosulfido ligand. In contrast, the carbyne complex [Mo(=CC₆H₄-*p*-Me)(CO)(Ph₂PC₂H₄PPh₂)₂]⁺ has been shown to adopt a *cis* octahedral structure in which the carbyne and carbonyl ligands are *cis* to each other due to the strong π -accepting properties of both ligands.²⁵

The IR spectra of **2a** and **2b** in Nujol mulls show weak bands at 2568 and 2571 cm⁻¹, respectively, which are attributable to ν (S–H). These ν (S–H) stretching frequencies are in the range observed for conventional organic thiols.²⁶ The ν (C–N) bands for the aminocarbyne ligands appear at 1509 and 1497 cm⁻¹, respectively, for **2a** and **2b**.

Mechanism for the Thermal Rearrangement of 1a and 1b to 2a and 2b. A proposed mechanism for the thermal rearrangement of the hydrido–thiocarbamoyl complexes **1a** and **1b** to the hydrosulfido–aminocarbyne complexes **2a** and **2b** is outlined in Scheme 1. The mechanism involves the initial migration of the hydride ligand from molybdenum to the sulfur atom of the thiocarbamoyl ligand to generate the 16-electron Fischer carbene intermediate Mo(=C(SH)NMe₂)(R₂PC₂H₄PR₂)₂, followed by migration of the hydrosulfido group from the carbene carbon to molybdenum to give the *cis* hydrosulfido–aminocarbyne complex which subsequently rearranges to the thermodynamically more stable *trans* isomer. Such a mechanism is plausible given the precedents for transformation of aminocarbene into

(16) Guenther, A. H. *J. Chem. Phys.* **1959**, *31*, 1095.
 (17) Callomon, H. J.; Thompson, H. W. *Proc. R. Soc. London, Ser. A.* **1959**, *222*, 431.
 (18) Hardy, W. A.; Silvey, G. *Phys. Rev.* **1954**, *95*, 385.
 (19) Dousmanis, G. C.; Sanders, T. M., Jr.; Townes, C. H.; Zeiger, H. J. *J. Chem. Phys.* **1953**, *21*, 1416.
 (20) Johnson, D. R.; Powell, F. X.; Kirchoff, W. H. *J. Mol. Spectrosc.* **1971**, *39*, 136.
 (21) (a) Maier, W. *Angew. Chem.* **1961**, *73*, 120. (b) Frank, G. W.; Degen, P. J. *Acta Crystallogr.* **1973**, *B29*, 1815. (c) Valle, G.; Busetti, V.; Mammi, M.; Carazzolo, G. *Acta Crystallogr.* **1969**, *B25*, 1432. (d) Valle, G.; Busetti, V.; Mammi, M.; Carazzolo, G. *Acta Crystallogr.* **1969**, *B25*, 1631. (e) Fleming, J. E.; Lynton, H. *Can. J. Chem.* **1967**, *45*, 353. (f) Cunningham, G. L., Jr.; Boyd, A. W.; Myers, R. J.; Gwinn, W. D.; Le Van, W. I. *J. Chem. Phys.* **1951**, *19*, 676.
 (22) (a) Churchill, M. R. *Perspect. Struct. Chem.* **1971**, *3*, 91. (b) Kirtley, S. W. In *Comprehensive Organometallic Chemistry*; Wilkinson, G.; Stone, F. G. A.; Abel, E. W., Eds.; Pergamon Press: Oxford, England, 1982; Vol. 3, Chapter 27.1. (c) Atwood, J. L.; Hunter, W. E.; Rogers, R. D.; Carmona, E.; Wilkinson, G. *J. Chem. Soc., Dalton Trans.* **1979**, 1519. (d) Ko, J. J.; Bockman, T. M.; Kochi, J. K. *Organometallics* **1990**, *9*, 1833. (e) Prout, K.; Cameron, T. S.; Forder, R. A.; Critchley, S. R.; Denton, B.; Rees, G. V. *Acta Crystallogr.* **1974**, *B30*, 2290.

(23) (a) DeSimone, R. E.; Glick, M. D. *Inorg. Chem.* **1978**, *17*, 3574. (b) Dupre, N.; Hendriks, H. M. J.; Jordanov, J. J. *Chem. Soc., Dalton Trans.* **1984**, 1463. (c) Kamenar, B.; Korpar-Colig, B.; Cindric, M.; Penavic, M.; Strukan, N. *J. Chem. Soc., Dalton Trans.* **1992**, 2093. (d) Kamenar, B.; Korpar-Colig, B.; Cindric, M.; Penavic, M.; Strukan, N. *J. Chem. Soc., Dalton Trans.* **1992**, 2093.
 (24) (a) Fischer, H.; Hofmann, P.; Kreissl, F. R.; Schrock, R. R.; Schubert, U.; Weiss, K. *Carbyne Complexes*; VCH Publishers: New York, 1988. (b) Mayr, A.; Hoffmeister, H. *Adv. Organomet. Chem.* **1991**, *32*, 227. (c) Kim, H. P.; Angelici, R. J. *Adv. Organomet. Chem.* **1987**, *27*, 51.
 (25) Dahlke, P.; Jeffery, J. C.; Mortimer, M. D. *Polyhedron* **1992**, *11*, 1587.
 (26) Patai, S., Ed. *The Chemistry of the Thiol Group*; Wiley: New York, 1974.

Scheme 1

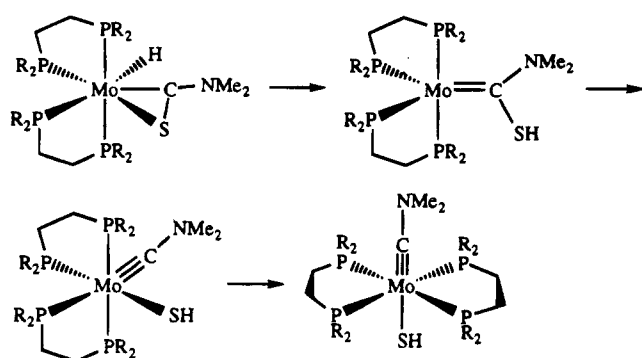
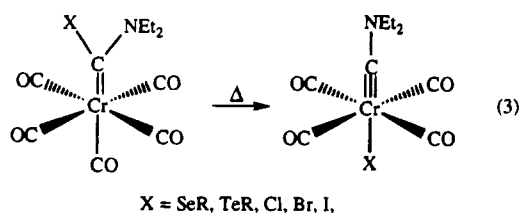


Table 3. Crystallographic Data for *trans*-Mo(SH)(=CNMe₂)(Ph₂PC₂H₄PPh₂)₂ (2a**)**

empirical formula	C ₅₅ H ₅₅ MoNP ₄ S
fw	981.89
cryst syst	monoclinic
space group	P2 ₁ /c
<i>a</i> , Å	19.516(4)
<i>b</i> , Å	12.301(2)
<i>c</i> , Å	19.899(4)
β , deg	102.46(3)
<i>V</i> , Å ³	4665(2)
<i>Z</i>	4
ρ (calcd), g cm ⁻³	1.397
μ (Mo K α), cm ⁻¹	5.02
min/max transmissn coeff	0.76–0.84
<i>T</i> , K	203
<i>R</i> ^a	0.062
<i>R</i> _w ^b	0.069

$$^a R = \sum ||F_o| - |F_c|| / \sum |F_o|. \quad ^b R_w = [\sum w(|F_o| - |F_c|)^2 / \sum w F_o^2]^{1/2}.$$

aminocarbene complexes, e.g., thermolysis of Cr(=C(X)-NEt₂)(CO)₅ results in extrusion of one CO ligand and concomitant migration of the X group from the carbene carbon to chromium to give *trans*-CrX(=CNEt₂)(CO)₄ (eq 3).²⁷



X-ray Crystal Structure of Mo(SH)(=CNMe₂)(Ph₂PC₂H₄PPh₂)₂ (2a**).** The formulation of **2a** as a hydrosulfido-aminocarbene complex has been confirmed by a single-crystal X-ray diffraction study. A summary of the crystallographic data is given in Table 3, and the selected bond lengths and angles are given in Table 4. An ORTEP drawing is shown in Figure 4.

Consistent with the solution NMR spectroscopic data (*vide supra*), the coordination geometry around the molybdenum atom in **2a** is best described as a slightly distorted octahedron, with the two diphosphine ligands lying on the equatorial plane and the hydrosulfido and the carbene ligands occupying the two trans apical positions. The least-squares plane of the aminocarbene ligand defined by C, N, C(1c), and C(2c) is only slightly tilted with respect to the plane defined by Mo, C, P(2a), S, and P(2b), the dihedral angle formed by intersection

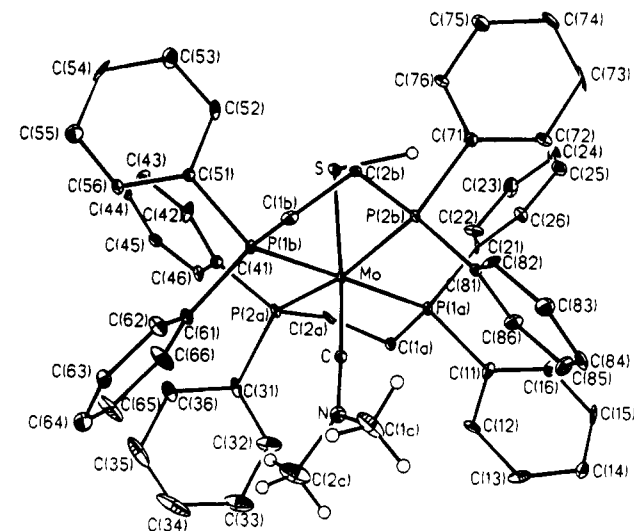


Figure 4. ORTEP drawing of *trans*-Mo(SH)(=CNMe₂)(Ph₂PC₂H₄PPh₂)₂ (**2a**).

Table 4. Selected Bond Lengths (Å) and Angles (deg) for *trans*-Mo(SH)(=CNMe₂)(Ph₂PC₂H₄PPh₂)₂ (2a**)**

Bond Lengths			
Mo–P(1a)	2.485(3)	Mo–P(1b)	2.438(3)
Mo–P(2a)	2.514(3)	Mo–P(2b)	2.504(3)
Mo–S	2.596(3)	Mo–C	1.830(11)
C–N	1.344(15)	N–C(1c)	1.422(20)
N–C(2c)	1.460(18)	S–H	1.63
Bond Angles			
P(1a)–Mo–P(1b)	178.2(1)	P(1a)–Mo–P(2a)	79.81(1)
P(1a)–Mo–P(2b)	98.7(1)	P(1b)–Mo–P(2a)	101.1(1)
P(1b)–Mo–P(2b)	80.8(1)	P(2a)–Mo–P(2b)	167.7(1)
P(1a)–Mo–S	86.7(1)	P(1b)–Mo–S	95.1(1)
P(2a)–Mo–S	79.2(1)	P(2b)–Mo–S	88.5(1)
P(1a)–Mo–C	96.9(4)	P(1b)–Mo–C	81.3(4)
P(2a)–Mo–C	100.3(4)	P(2b)–Mo–C	92.1(4)
S–Mo–C	176.2(4)	Mo–C–N	175.1(8)
C–N–C(1c)	125.1(10)	C–N–C(2c)	120.7(11)
C(1c)–N–C(2c)	113.8(11)	Mo–S–H	95.5

of the two planes being 9.2°. Since an orientation with a zero dihedral angle would be expected to maximize the π -bonding between the molybdenum and the aminocarbene ligand, the slight tilting is probably caused by steric repulsion between the NMe₂ group and the phenyl rings.

The aminocarbene ligand in **2a** is nearly planar, all of its atoms (C, N, C(1c), C(2c)) lying within 0.043 Å of the calculated least-squares plane. This suggests the presence of substantial overlap between the nitrogen lone pair and a p_{π} orbital of the carbene carbon, which is substantiated by the short C–N distance of 1.34(2) Å as compared to the N–C(1c) and N–C(2c) distances of 1.42(2) and 1.46(2) Å, respectively. The Mo–C–N angle (175.1(8)°) deviates slightly from linearity, which is not unusual for carbene ligands.²⁴ The Mo–C (carbene) distance of 1.83(1) Å is within the range previously reported for other molybdenum carbene complexes.²⁴

The Mo–S distance of 2.596(3) Å in **2a** unambiguously indicates a single bond between the molybdenum and sulfur atoms since the typical Mo=S double bond distances lie in the range of 2.08–2.13 Å.²⁸ It is noteworthy that the Mo–S distance in **2a** is significantly

(27) (a) Fischer, H.; Motsch, A.; Markl, R.; Ackermann, K. *Organometallics* **1985**, *4*, 726. (b) Fischer, H.; Fischer, E. O.; Himmelreich, D.; Cai, R.; Schubert, U.; Ackermann, K. *Chem. Ber.* **1981**, *114*, 3220.

(28) (a) Bunzey, G.; Enemark, J. H. *Inorg. Chem.* **1978**, *17*, 682. (b) Huneke, J. T.; Enemark, J. H. *Inorg. Chem.* **1978**, *17*, 3698.

longer than the distances of 2.37–2.48 Å previously reported for other molybdenum terminal hydrosulfido complexes.^{23,29} This lengthening reflects the high trans influence of the carbyne ligand²⁴ on the hydrosulfido ligand. The hydrogen of the hydrosulfido ligand was located in the difference Fourier map but was not refined. The S–H distance is 1.63 Å, and the Mo–S–H angle is 95.5°.

Conclusion

We have found a novel synthetic route to molybdenum hydrido–thiocarbamoyl and hydrosulfido–aminocarbyne complexes. The oxidative cleavage of the aldehydic C–H bond in *N,N*-dimethylthioformamide by *trans*-Mo(N₂)₂(R₂PC₂H₄PR₂)₂ (R = Ph, Et) affords the hydrido–thiocarbamoyl complexes MoH(η²-C(S)NMe₂)(R₂PC₂H₄PR₂)₂ (R = Ph (**1a**), Et (**1b**)). Compounds **1a** and **1b** undergo thermal rearrangement to give the hydrosulfido–aminocarbyne complexes *trans*-Mo(SH)(=CNMe₂)(R₂PC₂H₄PR₂)₂ (R = Ph (**2a**), Et (**2b**)). This rearrangement probably proceeds via migration of the hydride ligand from molybdenum to the sulfur atom of the thiocarbamoyl ligand to give the 16-electron Fischer carbene intermediate Mo(=C(SH)NMe₂)(R₂PC₂H₄PR₂)₂, followed by migration of the hydrosulfido group from the carbene carbon to molybdenum. Compounds **2a** and **2b** represent rare examples of terminal hydrosulfido complexes which are remarkably stable toward thermal decomposition. We are currently exploring the synthetic scope of the reactions described in this paper and the reactivity of the resulting molybdenum hydrido–thiocarbamoyl and hydrosulfido–aminocarbyne complexes.

Experimental Section

General Procedures. All manipulations were performed either under a helium atmosphere in a Vacuum Atmospheres glovebox or under an argon atmosphere using standard Schlenk techniques unless otherwise specified. Solvents were distilled from sodium benzophenone ketyl and stored in a glovebox under helium. All deuterated NMR solvents were distilled from CaH₂. *N,N*-Dimethylthioformamide was purchased from Fluka and dried over 4-Å activated molecular sieves before use. The bis(dinitrogen)molybdenum complexes *trans*-Mo(N₂)₂(R₂PC₂H₄PR₂)₂ (R = Ph, Et) were prepared as described previously.^{3b}

¹H, ³¹P{¹H}, and ¹³C{¹H} NMR spectra were recorded on a Bruker AM-200 spectrometer at 200.16, 81.03, and 50.25 MHz, respectively; ¹H and ¹³C chemical shifts were referenced to the solvent resonance relative to TMS; ³¹P chemical shifts were referenced to external 85% H₃PO₄. Infrared spectra were recorded on a Biorad FTS-40 FT-IR spectrometer as Nujol mulls between KBr plates unless otherwise specified. Elemental analyses were performed using a Perkin-Elmer PE2400 CHN elemental analyzer.

Synthesis of MoH(η²-C(S)NMe₂)(Ph₂PC₂H₄PPh₂)₂ (1a**).** *trans*-Mo(N₂)₂(Ph₂PC₂H₄PPh₂)₂ (1.37 g, 1.44 mmol) and HC(S)NMe₂ (0.23 mL, 2.88 mmol) in benzene (20 mL) were refluxed for 25 min with a slow stream of argon sweeping through the reaction flask (50 mL, with side arm) and exiting through the reflux condenser. The resulting deep-red solution was cooled to room temperature and concentrated in vacuo to ca. 5 mL. Addition of hexane (30 mL) resulted in the precipitation of **1a** as a red-brown solid, which was filtered off, washed with hexane (2 × 10 mL), and dried in vacuo.

Yield: 1.20 g (85%). Anal. Calcd for C₅₅H₅₅MoNP₄S: C, 67.28; H, 5.64; N, 1.43. Found: C, 66.55; H, 5.60; N, 1.53. IR (Nujol): ν(Mo–H) 1886 cm⁻¹, ν(C–N) 1521 cm⁻¹. ¹H NMR (C₆D₅CD₃, 298 K): δ 6.85–7.50 (m, Ph), 2.69 (s, NCH₃), 2.34 (s, NCH₃), 2.21 (m, PCH₂CH₂P), 2.01 (m, PCH₂CH₂P), –3.66 (qnt, ²J_{HP} = 37 Hz, Mo–H). ¹H NMR (C₆D₅CD₃, 188 K): δ 6.80–7.70 (m, Ph), 2.33 (s, NCH₃), 2.20 (m, PCH₂CH₂P), 1.90 (m, PCH₂CH₂P), –4.10 (br d, ²J_{HP} = 85 Hz, Mo–H). ³¹P{¹H} NMR (C₆D₅CD₃, 298 K): δ 74.5 (s). ³¹P{¹H} NMR (C₆D₅CD₃, 188 K): δ 81.3 (d, ²J_{PP} = 148 Hz), 77.2 (br s), 63.5 (br s), 61.4 (d, ²J_{PP} = 148 Hz).

Synthesis of MoH(η²-C(S)NMe₂)(Et₂PC₂H₄PEt₂)₂ (1b**).** *trans*-Mo(N₂)₂(Et₂PC₂H₄PEt₂)₂ (0.50 g, 0.89 mmol) and HC(S)NMe₂ (0.086 mL, 1.06 mmol) in benzene (10 mL) were refluxed for 25 min with a slow stream of argon sweeping through the reaction flask (25 mL, with side arm) and exiting through the reflux condenser. The resulting wine-red solution was cooled to room temperature and evaporated in vacuo to dryness, giving **1b** as a slightly tacky red solid which was contaminated with a small amount of unreacted HC(S)NMe₂. The solid was dried at 55 °C in vacuo overnight and then scraped off the bottom and wall of the reaction flask. Yield: 0.48 g (91%). The product is extremely soluble in all common organic solvents. Anal. Calcd for C₂₃H₅₅MoNP₄S: C, 46.23; H, 9.28; N, 2.34. Found: C, 46.81; H, 9.49; N, 2.20. IR (Nujol): ν(Mo–H) 1889 cm⁻¹, ν(C–N) 1524 cm⁻¹. ¹H NMR (C₆D₅CD₃, 298 K): 3.42 (s, 6 H, NCH₃), 0.9–1.8 (m, 48 H, PC₂H₄P, C₂H₅), –6.44 (qnt, ²J_{HP} = 36.7 Hz, 1 H, Mo–H). ¹H NMR (C₆D₅CD₃, 188 K): 3.20 (s, 6 H, NCH₃), 0.8–1.9 (m, 48 H, PC₂H₄P, C₂H₅), –6.77 (dm, ²J_{HP} = 93 Hz, 1 H, Mo–H). ³¹P{¹H} NMR (C₆D₅CD₃, 298 K): δ 63.5 (br s), 53.0 (br s). ³¹P{¹H} NMR (C₆D₅CD₃, 188 K): δ 65.9 (d, ²J_{PP} = 41 Hz), 61.4 (d, ²J_{PP} = 145 Hz), 51.6 (d, ²J_{PP} = 41 Hz), 49.0 (d, ²J_{PP} = 145 Hz).

Synthesis of *trans*-Mo(SH)(=CNMe₂)(Ph₂PC₂H₄PPh₂)₂ (2a**).** A solution of MoH(η²-C(S)NMe₂)(Ph₂PC₂H₄PPh₂)₂ (**1a**) (122 mg, 0.124 mmol) in toluene (10 mL) was heated at 125 °C in a 25-mL resealable glass vessel. The resulting green-yellow solution was cooled to room temperature. Addition of hexane (30 mL) resulted in the precipitation of **2a** as a greenish-yellow solid, which was filtered off, washed with hexane (2 × 10 mL), and dried in vacuo. Yield: 85 mg (70%). Anal. Calcd for C₅₅H₅₅MoNP₄S: C, 67.28; H, 5.64; N, 1.43. Found: C, 66.76; H, 5.48; N, 1.32. IR (Nujol): ν(S–H) 2568 cm⁻¹, ν(C–N) 1509 cm⁻¹. ¹H NMR (CD₂Cl₂, 298 K): δ 7.00–7.54 (m, 40 H, Ph), 2.67 (m, 4 H, PCH₂CH₂P), 2.35 (m, 4 H, PCH₂CH₂P), 1.52 (s, 6 H, NCH₃), –3.98 (qnt, ²J_{HP} = 6.7 Hz, SH). ³¹P{¹H} NMR (CD₂Cl₂, 298 K): δ 62.3 (s). ¹³C{¹H} NMR (CD₂Cl₂, 298 K): δ 266.8 (qnt, ²J_{CP} = 18.4 Hz, Mo≡C), 142.8 (m, C1 of Ph), 140.5 (m, C1 of Ph), 133.9 (br s, C2 of Ph), 133.6 (br s, C2 of Ph), 128.6 (s, C4 of Ph), 128.2 (s, C4 of Ph), 127.9 (br s, C3 of Ph), 127.4 (br s, C3 of Ph), 39.4 (br s, NCH₃), 30.2 (qnt, J_{CP} = 9.6 Hz, PC₂H₄P).

Synthesis of *trans*-Mo(SH)(=CNMe₂)(Et₂PC₂H₄PEt₂)₂ (2b**).** A solution of MoH(η²-C(S)NMe₂)(Et₂PC₂H₄PEt₂)₂ (**1b**) (0.48 g, 0.80 mmol) in toluene (10 mL) was heated at 125 °C in a 25-mL resealable glass vessel. The resulting green-yellow solution was cooled to room temperature and evaporated in vacuo to dryness. The residue was dissolved in Et₂O (2 mL). Addition of hexamethyldisiloxane (20 mL) and chilling of the mixture at –37 °C in a freezer for 1 h resulted in the precipitation of **2b** as a greenish-yellow solid, which was filtered off, washed with cold hexamethyldisiloxane (2 × 5 mL), and dried in vacuo. Yield: 0.43 g (89%). Anal. Calcd for C₂₃H₅₅MoNP₄S: C, 46.23; H, 9.28; N, 2.34. Found: C, 45.77; H, 9.22; N, 2.15. IR (Nujol): ν(S–H) 2571 cm⁻¹, ν(C–N) 1497 cm⁻¹. ¹H NMR (C₆D₆, 298 K): 2.32 (s, 6 H, NCH₃), 1.0–2.2 (m, 48 H, PC₂H₄P, C₂H₅), –3.66 (qnt, ²J_{HP} = 7.1 Hz, 1 H, Mo–H). ³¹P{¹H} NMR (C₆D₆, 298 K): δ 56.6 (s). ¹³C{¹H} NMR (C₆D₆, 298 K): δ 226.5 (qnt, ²J_{CP} = 17.6 Hz, Mo≡C), 41.3 (br s, NCH₃), 26.2 (br s, CH₂CH₃), 24.4 (qnt, J_{CP} = 9.2 Hz, PC₂H₄P), 19.8 (br s, CH₂CH₃), 9.6 (s, CH₂CH₃), 8.8 (s, CH₂CH₃).

(29) (a) Cragel, J.; Pett, V. B.; Glick, M. D.; DeSimone, R. E. *Inorg. Chem.* **1978**, *17*, 2885. (b) Tsuge, K.; Imoto, H.; Saito, T. *Inorg. Chem.* **1992**, *31*, 4715.

X-ray Crystallographic Analysis of $\text{MoH}(\eta^3\text{-C}(\text{S})\text{NMe}_2)\text{-}(\text{Ph}_2\text{PC}_2\text{H}_4\text{PPh}_2)_2$ (1a**).** Red crystals of **1a** suitable for X-ray diffraction measurements were grown from THF/hexamethyldisiloxane. A crystal having the approximate dimensions of $0.65 \times 0.35 \times 0.25 \text{ mm}^3$ was selected, mounted on a glass fiber with Apiezon "H" grease, and transferred to the goniostat cooled to -70°C . Data were collected on a Enraf-Nonius CAD4 diffractometer with graphite-monochromated Mo K α radiation ($\lambda = 0.71073 \text{ \AA}$). Cell constants and an orientation matrix were obtained by least-squares refinement, using the setting angles of 25 randomly selected reflections. A total of 7384 reflections were collected ($-4 \leq h \leq 27$, $0 \leq k \leq 22$, $-22 \leq l \leq 21$) in the range $3.34^\circ < 2\theta < 60.00^\circ$ with 6918 being unique ($R_{\text{int}} = 4.45\%$). A series of high χ (above 80°) reflections were scanned to provide the basis for an empirical absorption correction with the transmission coefficient ranging from 0.73 to 0.79. No crystal decay was evident during the data collection.

The structure was solved by direct methods and refined to convergence by full-matrix least-squares methods. It should be mentioned that the molybdenum atom lies on a crystallographically imposed 2-fold axis, which necessarily means that both the thiocarbonyl and hydride ligands must be disordered over two positions, with the 2-fold axis passing through the Mo, C, and one of the amido carbons (C(1a)). The positions of the hydride ligand and the hydrogen atoms on the ethylene linkage of the diphosphine ligand were determined in the difference Fourier maps and were refined anisotropically. The remaining hydrogen atoms were placed in the calculated positions (C-H fixed at 0.96 \AA) with their isotropic thermal parameters refined and were added to the structure factor calculations. The final residuals for the full-matrix least-squares refinement were $R = 3.69\%$, $R_w = 5.53\%$, and GOF = 0.86 for 336 variable parameters and 5396 reflections ($F > 4.0\sigma(F)$). All calculations were conducted using the SHELXTL-Plus software package.³⁰

X-ray Crystallographic Analysis of $\text{trans-Mo}(\text{SH})(\equiv\text{CNMe}_2)(\text{Ph}_2\text{PC}_2\text{H}_4\text{PPh}_2)_2$ (2a**).** Yellow crystals of **2a** suitable for X-ray diffraction measurements were grown by slowly cooling a saturated solution of **2a** in hot toluene. A

crystal having the approximate dimensions of $0.35 \times 0.42 \times 0.27 \text{ mm}^3$ was selected, mounted on a glass fiber with Apiezon "H" grease, and transferred to the goniostat cooled to -70°C . Data were collected on a Enraf-Nonius CAD4 diffractometer with graphite-monochromated Mo K α radiation ($\lambda = 0.71073 \text{ \AA}$). Cell constants and an orientation matrix were obtained by least-squares refinement, using the setting angles of 25 randomly selected reflections. A total of 8588 reflections were collected ($0 \leq h \leq 23$, $0 \leq k \leq 14$, $-25 \leq l \leq 25$) in the range $2.14^\circ < 2\theta < 54.88^\circ$ with 7882 being unique ($R_{\text{int}} = 7.49\%$). A series of high χ (above 80°) reflections were scanned to provide the basis for an empirical absorption correction with the transmission coefficient ranging from 0.76 to 0.84. No crystal decay was evident during the data collection.

The structure was solved by direct methods and refined to convergence by full-matrix least-squares methods. The calculated positions of the hydrogen atoms (except for the hydrogen of the hydrosulfido ligand) were added to the structure factor calculations (C-H fixed at 0.96 \AA) but were not refined. The difference Fourier maps revealed the position of the hydrosulfido hydrogen. The final residuals for the full-matrix least-squares refinement were $R = 6.15\%$, $R_w = 6.89\%$, and GOF = 1.09 for 525 variable parameters and 3314 reflections ($F > 4.0\sigma(F)$). All calculations were conducted using the SHELXTL-Plus software package.³⁰

Acknowledgment. This work was performed under the auspices of the Division of Chemical Sciences, Office of Basic Energy Sciences, Office of Energy Research, U.S. Department of Energy. We wish to thank Dr. Jeffrey C. Bryan (Oak Ridge National Laboratory) for helpful discussions.

Supporting Information Available: Tables of crystallographic data, positional and thermal parameters, bond lengths and angles, and atomic parameters of hydrogen atoms for **1a** and **2a** (18 pages). This material is contained in many libraries on microfiche, immediately follows this article in the microfilm version of the journal, and can be ordered from the ACS; see any current masthead page for ordering information.

(30) SHELXTL-Plus; Siemens Analytical X-Ray Instruments, Inc.: Madison, WI, 1988.

Norbornadiene on Pt(111) Is Not Bound as an $\eta^2:\eta^2$ Diene: Characterization of an Unexpected $\eta^2:\eta^1$ Bonding Mode Involving an Agostic Pt–H–C Interaction

Michael J. Hostetler,[†] Ralph G. Nuzzo,^{*,†,‡} Gregory S. Girolami,^{*,†} and Lawrence H. Dubois^{*,§}

School of Chemical Sciences, Frederick Seitz Materials Research Laboratory, and Department of Materials Science and Engineering, University of Illinois at Urbana-Champaign, Urbana, Illinois 61801, and AT & T Bell Laboratories, Murray Hill, New Jersey 07974

Received September 29, 1994[®]

The structure and reactivity of norbornadiene (NBD) adsorbed on Pt(111) has been studied by several physical techniques, including reflection–absorption infrared spectroscopy (RAIRS), high-resolution electron energy loss spectroscopy (HREELS), temperature-programmed reaction spectroscopy (TPRS), integrated desorption mass spectrometry (IDMS), and Auger electron spectroscopy (AES). At 130 K, NBD is bound to the surface in an unusual way: through only one C=C double bond and through an agostic interaction involving one of the C–H bonds of the bridging CH₂ group. The latter interaction is characterized by an intense, broad band centered at 2670 cm⁻¹ (fwhm \approx 50 cm⁻¹) in the RAIR spectra. The data strongly suggest that the other C=C double bond of NBD does not interact with the surface. This unusual binding mode, which may be adopted because steric factors favor it over the alternative $\eta^2:\eta^2$ geometry, persists to 220–260 K, whereupon the agostic C–H bond is cleaved to give a norbornadienyl intermediate that is stable to 400–450 K. In this latter temperature range the norbornadienyl intermediate decomposes, probably via a retro cyclization reaction, to give benzene and dihydrogen (which desorb) and a fractional monolayer of carbon (which remains on the surface). Comparisons of the low-frequency C–H stretching mode seen for NBD with those seen for other adsorbed hydrocarbons suggest that the line width of these modes is largely due to inhomogeneous broadening, not to dispersion or lifetime effects.

Introduction

The close relationship between organometallic chemistry and surface chemistry is illustrated by the large number of analogous adsorbate (ligand) binding configurations that have been documented in the two fields.¹ This relationship often proves useful: well-characterized molecular complexes can greatly assist in interpreting the vibrational spectra and identifying the structures of new surface-bound intermediates. Occasionally, however, the binding configuration of an adsorbate is different from that found in discrete organometallic complexes.²

The conversion of the bicyclic alkene norbornadiene (NBD) to benzene on Pt(111) was first described in 1982.³ On the basis of the available organometallic literature, it was proposed that NBD initially binds to Pt(111) in an $\eta^2:\eta^2$ fashion, i.e., via both C=C double bonds. From isotopic labeling studies (which showed that the bridging CH₂ group of NBD was not incorpo-

rated into the desorbing benzene), Muettterties and co-workers suggested that NBD must “roll over” to expose the CH₂ group to the surface; the surface then removes the CH₂ group from NBD to generate benzene. We report here that norbornadiene does not adopt an $\eta^2:\eta^2$ binding mode on Pt(111) surfaces; instead, the binding mode is distinct from the manner in which norbornadiene binds in any known organometallic complex. We show that one C–H bond of norbornadiene is involved in an “agostic” interaction with the surface and suggest that the manner in which norbornadiene is bound is related to the mechanism by which this molecule thermolytically decomposes on Pt(111).

The reactions of NBD on metal surfaces have a more general significance.⁴ The catalytic re-forming of large cyclic hydrocarbons (naphtha) into high-octane fuels is conducted on a large scale in the petroleum industry.⁵ The reactions are complex and involve the interplay of H–H, C–H, and C=C bond activation steps, adsorption/desorption equilibria, surface diffusion, and the organizational dynamics of multicomponent adsorbate systems. The present study provides insight into the energies and fundamental mechanisms of such processes.

Experimental Section

The ultra-high-vacuum (UHV) chambers used in this work have been described previously; a summary is given here. The

[†] School of Chemical Sciences and Materials Research Laboratory, University of Illinois.

[‡] Department of Materials Science and Engineering, University of Illinois.

[§] AT & T Bell Laboratories. Present address: Advanced Research Project Agency, ARPA/DSO, 3701 North Fairfax Drive, Arlington, VA 22203.

[®] Abstract published in *Advance ACS Abstracts*, January 15, 1995.

(1) Muettterties, E. L. *Chem. Soc. Rev.* **1982**, *11*, 283–320.

(2) Jenks, C. J.; Bent, B. E.; Bernstein, N.; Zaera, F. *Surf. Sci.* **1992**, *277*, L89–L94.

(3) (a) Muettterties, E. L. *Pure Appl. Chem.* **1982**, *54*, 83–96. (b) Tsai, M.-C.; Stein, J.; Friend, C. M.; Muettterties, E. L. *J. Am. Chem. Soc.* **1982**, *104*, 3533–3534.

(4) Lee, T. R.; Whitesides, G. M. *Acc. Chem. Res.* **1992**, *25*, 266–272.

(5) Satterfield, C. N. *Heterogeneous Catalysis in Industrial Practice*, 2nd ed.; McGraw-Hill: New York, 1991; Chapter 9.

mass spectrometric studies were performed in a stainless steel chamber equipped with diffusion, turbomolecular, titanium sublimation, and ion pumps. The base pressure in the chamber was $\sim 2.0 \times 10^{-10}$ Torr.⁶ The reflection-absorption infrared spectroscopic (RAIRS) studies were performed in a stainless steel chamber equipped with turbomolecular and titanium sublimation pumps; the base pressure was $\sim 3.0 \times 10^{-10}$ Torr.⁷ The high-resolution electron energy loss spectroscopic (HREELS) studies were performed in a stainless steel chamber equipped with diffusion, ion, and titanium sublimation pumps; the base pressure was $\sim 2.0 \times 10^{-10}$ Torr.⁸ All chambers were equipped for ion sputtering, Auger electron spectroscopy (AES), and, for the last chamber, low-energy diffraction (LEED). The Pt(111) crystal was purchased from Cornell Laboratories and was oriented to within 0.5° and polished to a fine mirror finish by standard metallographic techniques. The crystal was cleaned in the first and third chambers by sputtering with Ar^+ ions at 1050 K (current to the crystal $\sim 5 \mu\text{A}$), followed by annealing at 1050 K for 5 min. In the second chamber, the crystal was cleaned by heating it to 900 K in the presence of 1×10^{-6} Torr of O_2 for 2 min followed by annealing at 1000 K for 1 min. AES indicated, in all cases, that there was no detectable carbon on the crystal surface (<0.5 atom %).

Norbornadiene was purchased from Aldrich ($>98\%$ pure) and was thoroughly degassed before being introduced into the chamber. Dosing was accomplished by either back-filling the chamber through a variable-leak valve (HREELS and TPRS studies) or using an effusive doser positioned ~ 5 cm from the crystal face. Exposures, which are uncorrected for the relative sensitivity of the ion gauge, are reported in langmuirs (1 langmuir $\equiv 10^{-6}$ Torr s).

Results

Reflection-absorption infrared spectroscopy (RAIRS) and high-resolution electron energy loss spectroscopy (HREELS) were used to establish the structure and orientation of the surface-bound norbornadiene molecules. For RAIRS, the orientations of adsorbed molecules can be easily determined, since only those modes whose transition dipoles have a nonzero projection along the surface normal are observable.⁹ For HREELS, this dipole selection rule is not rigorously observed, owing to the occurrence of both impact and dipole scattering.¹⁰ As a consequence, modes which are inactive in the RAIR spectra of a hydrocarbon species can often be observed in HREEL spectra. Thus, these techniques are often complementary.

Characterization of Norbornadiene Multilayers. The exposures necessary to form multilayers of NBD on Pt(111) have been determined by temperature-programmed reaction spectroscopy (Figure 1). The TPRS profiles in the m/e 91 channel contain an NBD desorption peak at ~ 205 K that first appears following an exposure of 5 langmuir and a second NBD desorption peak at ~ 175 K that first appears following an exposure of 6 langmuir (Figure 1a,b). We assign these TPRS features to desorption of NBD from a partial monolayer and from a multilayer, respectively. Therefore, multilayers of NBD are generated at exposures of ~ 6 langmuir or greater.

(6) Hostetler, M. J.; Nuzzo, R. G.; Girolami, G. S.; Dubois, L. H. *J. Phys. Chem.* **1994**, *98*, 2952-2962.

(7) Wiegand, B. C.; Lohokare, S. P.; Nuzzo, R. G. *J. Phys. Chem.* **1993**, *97*, 11553-11562.

(8) Dubois, L. H.; Nuzzo, R. G. *Langmuir* **1985**, *1*, 663-669.

(9) Chabal, Y. J. *Surf. Sci. Rep.* **1988**, *8*, 211-357.

(10) Ibach, H.; Mills, D. L. *Electron Energy Loss Spectroscopy and Surface Vibrations*; Academic Press: New York, 1982.

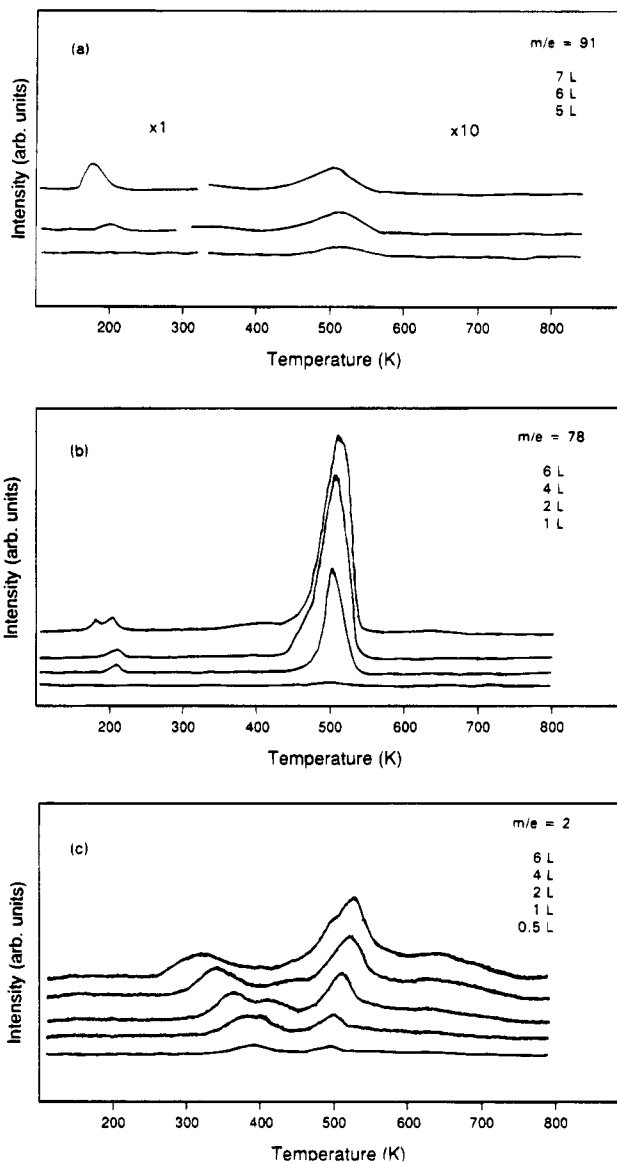


Figure 1. Temperature-programmed reaction spectra for norbornadiene on Pt(111) as a function of coverage for differing mass channels: (a) m/e 91, tracking norbornadiene desorption; (b) m/e 78, tracking benzene and norbornadiene desorption; (c) m/e 2, tracking the desorption of hydrogen.

The RAIR spectrum of a multilayer of NBD (~ 50 langmuir dose) adsorbed on Pt(111) at 132 K is shown in Figure 2. The mode assignments (Table 1) directly follow those detailed in the literature.¹¹⁻¹³ When the surface is heated to 182 K, the RAIR spectrum changes owing to desorption of the multilayer. The new spectrum, which corresponds to that of an NBD monolayer, will be discussed in the next section.

The HREEL spectrum of a multilayer of NBD (7 langmuir dose) adsorbed on Pt(111) at 100 K is shown in Figure 3a; mode assignments are given in Table 2. Except for the different resolution, the HREEL spectrum resembles the RAIR spectrum of an NBD multi-

(11) Aleksanyan, V. T.; Garbuzova, I. A.; Pryanishnikova, M. A.; Paturyan, I. N. *Bull. Acad. Sci. USSR, Div. Chem. Sci.* **1973**, 756-760.

(12) Levin, I. W.; Harris, W. C. *Spectrochim. Acta* **1973**, *29A*, 1815-1834.

(13) Maslowsky, E., Jr. *Vibrational Spectra of Organometallic Compounds*; Wiley: New York, 1977; pp 468-477.

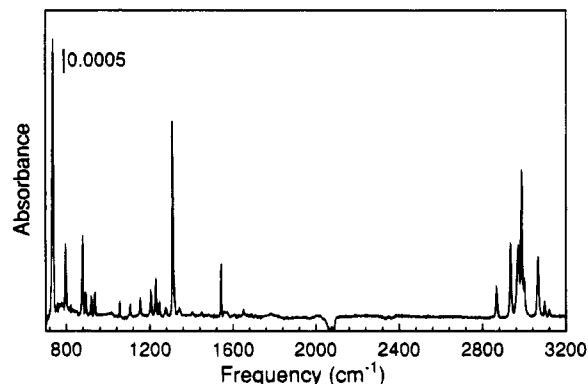


Figure 2. Reflection-absorption infrared spectrum of a multilayer coverage of norbornadiene on Pt(111).

Table 1. Vibrational Assignments for a Multilayer Coverage of NBD on Pt(111)

assignt	IR	
	solid ^a	multilayer 105 K
not assigned		3121
=C-H str Fermi ^b	3097	3098
=C-H str Fermi ^b	3067	3067
CH ₂ str	3002	3001
tertiary CH str	2987	2986
tertiary CH str	2969	2972
CH ₂ str Fermi ^c	2935	2934
CH ₂ str Fermi ^c	2867	2866
comb 879 + 773	1651	1651
skeletal stretch	1543	1543
CH ₂ bend	1451	1451
CH ₂ bend and =C-H bend	1345	1342
CH bridgehead deform and skeletal str	1309	1310
comb 735 + 549	1279	1277
CH bridgehead bend	1246	1248
	1240	1240
=CH bend	1228	1231
CH bridgehead bend	1205	1206
=CH bend	1154	1155
skeletal str and =CH bend	1103	1107
bridgehead deform and skeletal str	1055	1057
skeletal str and CH bridgehead bend	937	936
comb 503 + 428	919	918
CH ₂ bend	892	893
overtone 2 × 446	880	880
CH wag	800	797
skeletal str	735	737

^a See refs 11 and 12. ^b In Fermi resonance with $2 \times 1543 \text{ cm}^{-1}$.

^c In Fermi resonance with $2 \times 1451 \text{ cm}^{-1}$.

layer (Figure 2); in particular, the same skeletal stretching vibration near 730 cm^{-1} gives rise to the most intense band in each spectrum. Heating the sample to 221 K (Figure 3b) causes both the absolute and relative intensities of the HREELS bands to change substantially, owing to desorption of the NBD multilayer.

Characterization of Norbornadiene Monolayers. Identification of the Soft C-H Mode That Corresponds to an Agostic M-H-C Interaction. The coverage-dependent RAIR spectra of NBD adsorbed on Pt(111) at 110 K are presented in Figure 4; the relevant mode assignments are listed in Table 3. At the lowest coverage examined ($\theta \approx 0.1$), the most intense band in the C-H stretching region (Figure 4a) appears at 2605 cm^{-1} (fwhm $\approx 50 \text{ cm}^{-1}$). Broad bands that appear between 2400 and 2800 cm^{-1} have been assigned to stretching vibrations of C-H bonds participating in "agostic" M-H-C interactions with a metal surface.¹⁴⁻¹⁶ This shift to lower frequency is thought to result

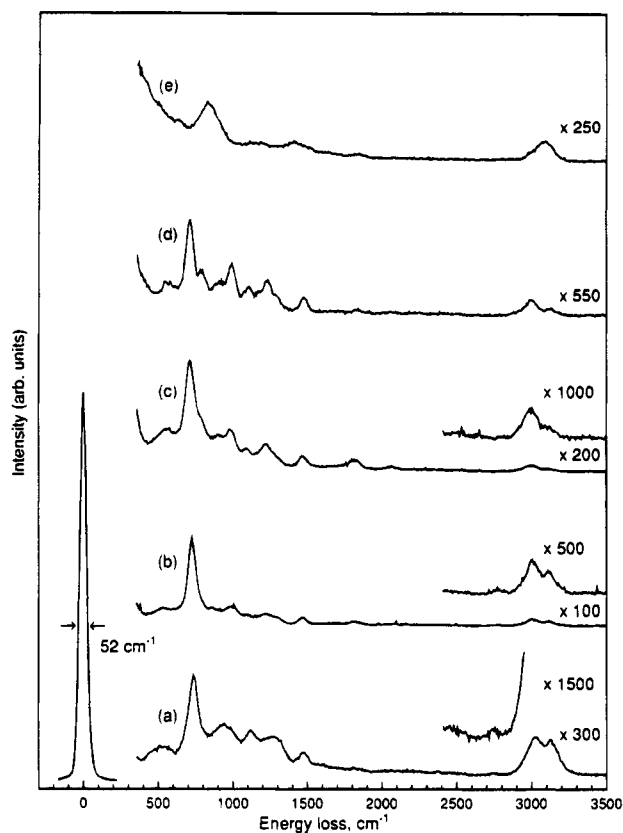
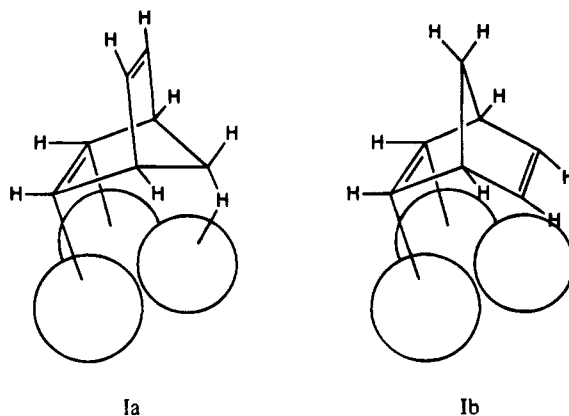


Figure 3. High-resolution electron energy loss spectra of a 7 langmuir dose of norbornadiene annealed to various temperatures on Pt(111): (a) 100 K; (b) 221 K; (c) 270 K; (d) 422 K; (e) 534 K.

from donation of conduction electrons at the Fermi level into the C-H σ^* orbitals. The interaction responsible for this mode softening¹⁷ most likely occurs at a specific surface site (an atop site; see Discussion).

The other bands in the RAIR spectra are most consistent with a configuration in which the CH₂ unit of NBD is involved in the agostic interaction (structure Ia). From the dipole selection rules and the local C_s



symmetry of the adsorbed molecule, one expects to see only two IR-active modes for this configuration: a symmetric C-H stretch for the vinylic group that is not

(14) Raval, R.; Parker, S. F.; Chesters, M. A. *Surf. Sci.* **1993**, *289*, 227-236.

(15) Chesters, M. A.; Gardner, P. *Spectrochim. Acta* **1990**, *46A*, 1011-1015.

(16) Hoffmann, F. M.; Upton, T. H. *J. Phys. Chem.* **1984**, *88*, 6209-6212.

Table 2. High-Resolution Electron Energy Loss Spectroscopy Vibrational Assignments for NBD on Pt(111)

assignt	100 K	221 K	270 K	422 K	534 K
—C—H str Fermi	3105	3090	3065	3100	
ν (C—H) benzene					3060
CH ₂ str	3010	2980	2975	2980	
CH ₂ softened mode	2740	2770			
CO		1800, 2050	1810, 2040		1820
ν (CC) benzene					1400
CH ₂ or CH bend	1455	1455	1455	1460	
—C—H bend	1250	1210, 1270	1210	1220, 1260	
ring vib benzene skeletal str	1110	1080	1080	1100	1140
C—H bridgehead bend	930	975	975	984	
ν (C—C)		855	900	904	
β (C—H) benzene skeletal str	730	720	700	780, 712	824
M—C str	520	530	560	560	640

interacting with the surface and a stretch for the "nonagostic" C—H bond of the CH₂ group.¹⁸ (Other modes, even though they are not rigorously forbidden by the dipole selection rules, should be very weak because their transition directions would be $\sim 70^\circ$ away from the surface normal: $\cos^2 \theta < 0.12$.) These predictions are confirmed by the data at higher coverages (Figure 4b): a vinylic C—H stretching mode at 3055 cm⁻¹ and a band associated with the nonagostic methylene C—H bond at ~ 2965 cm⁻¹ are evident. The large line width of the latter band may arise from coupling of this mode with modes associated with the Pt—H—C interaction.

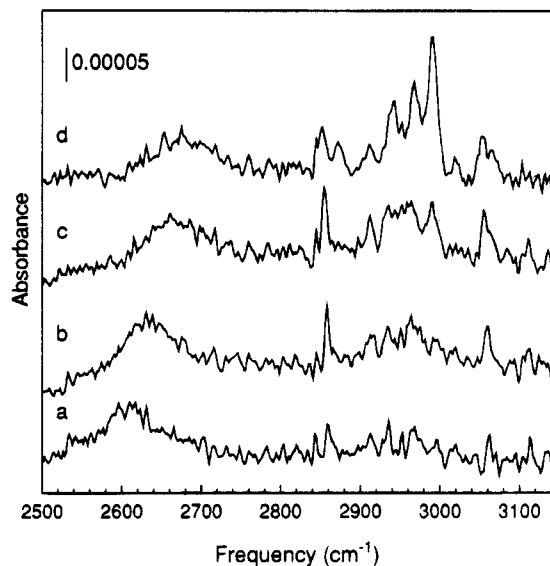
It is difficult to envision another arrangement of NBD that can explain the present data. Specifically, if both C=C double bonds of NBD were interacting with the surface (structure Ib), then the vinylic C—H stretching vibrations should be absent because their transition directions would be essentially perpendicular to the surface normal. These vinylic C—H stretching bands are, however, present both in the spectrum of a sub-monolayer coverage of NBD at 110 K and in the spectrum of a full monolayer coverage of NBD annealed to 182 K, which is above the multilayer desorption temperature (see Figure 5b). Thus, the presence of a vinylic C—H stretching band at 3051 cm⁻¹ in these spectra rules out structure Ib and provides strong evidence for structure Ia.

The lower frequency bands in the RAIR spectrum are readily assignable in a manner consistent with structure Ia. The band at 1447 cm⁻¹ is assigned to the C—H bending vibration for the methylene C—H bond not interacting with the surface. The totally symmetric

(17) Different meanings are attached to the terms "agostic" and "soft": the former refers to a structural feature whereas the latter refers to an electronic effect. Agostic bonds often exhibit soft modes; even so, the latter can not be used to unambiguously establish the former. In the present context, we are not aware of a definitive demonstration of the structural perturbations that occur when a hydrocarbon interacts with a metal surface.

(18) The feature at 2855 cm⁻¹ in Figure 4b may be an overtone (or a Fermi resonance involving the overtone) of the bending vibration for the CH₂ group. Such a Fermi resonance is observed in the IR spectrum of polycrystalline NBD.^{11,12}

(19) This binding mode for a norbornadienyl group has been previously observed in a nickel complex; see: Dahl, L. F.; Wei, C. H. *Inorg. Chem.* **1963**, *2*, 713–721.

**Figure 4.** Reflection-absorption infrared spectra of norbornadiene on Pt(111) at 110 K: (a) $\theta \approx 0.1$; (b) $\theta \approx 0.2$; (c) $\theta \approx 0.5$; (d) $\theta \approx 1$.**Table 3. Vibrational Assignments for Varying Coverages of NBD on Pt(111) at 110 K**

assignt	$\theta \approx 0.1$	$\theta \approx 0.2$	$\theta \approx 0.5$	$\theta \approx 1$
—C—H str Fermi ^a		3059	3055	3053, 3065 ^b
CH ₂ str			2990 ^b	2992 ^b
CH ₂ str		2965	2965	2953, 2968 ^b
CH ₂ str Fermi			2935	2943
bound —CH str			2912	2911
overtone 2×1447 cm ⁻¹		2855	2855	2853, 2872 ^b
CH ₂ softened mode	2610	2630	2660	2675

^a In Fermi resonance with 2×1545 cm⁻¹. ^b From NBD in the multilayer.

Table 4. Mode Assignments for RAIR Spectra of Norbornadiene on Pt(111) Annealed to the Listed Temperatures

mode assignts	110 K	182 K	261 K	338 K	401 K
—C—H str Fermi ^a	3107	3109	3109	3109	3107
—C—H str Fermi ^a	3055	3055	3053	3053	3051
CH ₂ str ^b	2992				
CH ₂ str ^{c,e}	2968	2953	2957		
CH str ^{d,f}			2934	2930	2932
CH ₂ str Fermi ^{b,e}	2940				
bound —CH str	2909	2911	2912	2912	2912
CH ₂ str Fermi ^{b,e}	2874				
CH ₂ str Fermi ^e	2854 ^c	2853 ^c	2853 ^{c,d}	2855 ^d	2853 ^d
CH ₂ softened mode ^c	2670	2690			
C=C skeletal str ^b	1545				
CH ₂ or CH bend skeletal str ^b	1443 ^c	1447 ^c	1447 ^{c,d}	1447 ^d	1447 ^d
skeletal str ^b	1314				
—CH bend	1206	1206	1207	1207	1207
not assigned	1011				
CH wag ^c		779			
skeletal str ^c	719	719	718		
skeletal str ^d			696	696	698
CH wag ^b	664				

^a In Fermi resonance with 2×1545 cm⁻¹. ^b From NBD in the multilayer. ^c From $\eta^2:\eta^1$ bound NBD. ^d From the norbornadienyl intermediate. ^e In Fermi resonance with 2×1443 (or 1447) cm⁻¹. ^f Metal-bound C—H unit.

C—H bending vibration for the noninteracting alkene appears at 1206 cm⁻¹. Finally, a skeletal vibration, which is the strongest band in the spectrum, appears at 719 cm⁻¹.

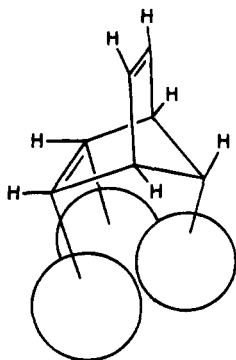
As the coverage of NBD is increased, the soft mode moves to higher frequency (Figure 4), presumably

because the energy of the Fermi level is coverage-dependent. Simultaneously, the peaks in the aliphatic C—H stretching region become sharper and relatively more intense. The formation of a multilayer at higher exposures is demonstrated by the appearance of the symmetric and antisymmetric C—H stretching vibrations of an unperturbed CH₂ group (Figure 4c,d).

The HREEL spectrum of an NBD monolayer resembles the corresponding RAIR spectrum, except that several extra bands are present, in part due to the relaxation of the selection rules. Most of these bands can be assigned straightforwardly. The band at 520 cm⁻¹, assigned to the Pt—C stretching vibration, shifts to higher frequency as the temperature is increased (Figure 3a–d). The bands at 730, 930, and 1110 cm⁻¹ arise from skeletal stretching vibrations.¹² The loss signal at ~1250 cm⁻¹ comprises both the vinylic CH bending and the bridgehead CH bending modes, which are observed at 1206 and 1230 cm⁻¹, respectively, in the RAIR spectrum of a NBD multilayer.

The soft C—H stretching mode is also seen in the HREEL spectra (Figure 3a,b), but it is much less prominent than in the RAIRS data. Such disparities in the relative intensities of soft C—H stretching modes in HREEL and RAIR spectra have been noted previously.¹⁴

Decomposition of Norbornadiene at Higher Temperatures. When the NBD-dosed surface is heated to 261 K, significant changes occur in the RAIR spectrum: the soft mode disappears, the broad band at 2953 cm⁻¹ diminishes significantly in intensity, the skeletal vibration at 719 cm⁻¹ virtually disappears, and a new skeletal vibration band at 696 cm⁻¹ is now evident. When taken together, these data suggest that the agostic C—H bond has been cleaved; a norbornadienyl group should be the result (structure II).¹⁹ Consistent



II

with this interpretation, TPRS profiles (Figure 1c) show a low-temperature dihydrogen desorption feature (~310 K) when a saturation coverage of NBD on Pt(111) is heated. The spectrum of the norbornadienyl group remains unchanged up to 401 K (Figure 5d,e). At 490 K, however, the RAIR spectrum is featureless, which suggests that the norbornadienyl intermediate has decomposed (data not shown).

Similar changes due to the formation of a norbornadienyl group are seen in the HREEL spectra when an NBD-dosed surface is heated from 100 to 270 K. For example, the soft mode (present at 221 K, Figure 3b) disappears as expected for a reaction in which the agostic C—H bond of NBD is cleaved (Figure 3c). The HREEL spectrum at 422 K (Figure 3d) is essentially

identical with that seen at 270 K, but at higher temperatures, the HREEL spectrum is substantially different (Figure 3e). As judged from previous work, the spectrum obtained after heating to 534 K arises from a combination of adsorbed benzene and C_xH_y fragments.⁶ These intermediates were not detectable by RAIRS, probably as a result of the dipole selection rule.

The dehydrogenation of NBD at temperatures above 220 K, which was suggested by the RAIR and HREEL spectra, has been confirmed by temperature-programmed reaction studies in which the *m/e* 2 channel was monitored (Figure 1c). At the lowest coverage of NBD examined (1/2 langmuir), hydrogen desorbs from the surface in two features, one centered at 380 K and the other at 482 K. At higher coverages of NBD, more complex TPRS profiles are seen. The low-temperature feature closely parallels the recombination-limited desorption of hydrogen from Pt(111). This result is consistent with our RAIRS and HREELS studies, which suggested that the agostic C—H bond of NBD is cleaved at temperatures ≥ 225 K. The feature centered at ~482 K (which moves to higher temperatures as the coverage of NBD is increased) coincides with the desorption of benzene (see below), which suggests that both C—C and C—H bonds are broken competitively in this latter product-forming process. A final hydrogen desorption peak is seen at ~620 K for exposures of NBD that are ≥ 1 langmuir. This latter feature is associated with the conversion of C_xH_y fragments to a carbonaceous overlayer.

We have also used TPRS to establish the identities of the hydrocarbons that desorb upon heating the NBD-dosed surface. We find that a small amount of NBD desorbs molecularly at ~205 K. No norbornene or norbornane desorbs from the surface: the integrated desorption mass spectrum (IDMS)²⁰ taken between 130 and 300 K is clearly due to NBD (Figure 6a). Thus, we conclude that self-hydrogenation reactions, which are commonly seen in this temperature range for alkenes adsorbed on Pt(111),^{21,22} do not occur for NBD. Small amounts of NBD can be hydrogenated to norbornane, however, if the Pt(111) surface is pretreated with H₂ (Figure 6b).

In addition, the TPRS traces in the *m/e* 78 channel indicate that a significant amount of the norbornadiene is converted to benzene (Figure 1b); this transformation has been reported previously by Muettterties and co-workers.³ The identity of the species desorbing between 400 and 550 K was rigorously confirmed to be >95% benzene (a small amount of NBD desorbs at the same temperature) by inspection of the IDM spectrum (Figure 6c). The yield of benzene is strongly coverage-dependent (Figure 1b). Little benzene desorbs from a surface exposed to 1 langmuir of NBD; much more desorbs if the exposure of NBD is increased to 2 langmuir. The formation of benzene is saturated at a NBD exposure of ~4 langmuir. The strong dependence of the benzene yield on coverage indicates that lateral repulsions play a significant role in the decomposition and desorption kinetics.

(20) Dubois, L. H. *Rev. Sci. Instrum.* **1989**, *60*, 410–413.

(21) Godbey, D.; Zaera, F.; Yeates, R.; Somorjai, G. A. *Surf. Sci.* **1986**, *167*, 150–166.

(22) Hostetler, M. J.; Nuzzo, R. G.; Girolami, G. S. *J. Am. Chem. Soc.*, in press.

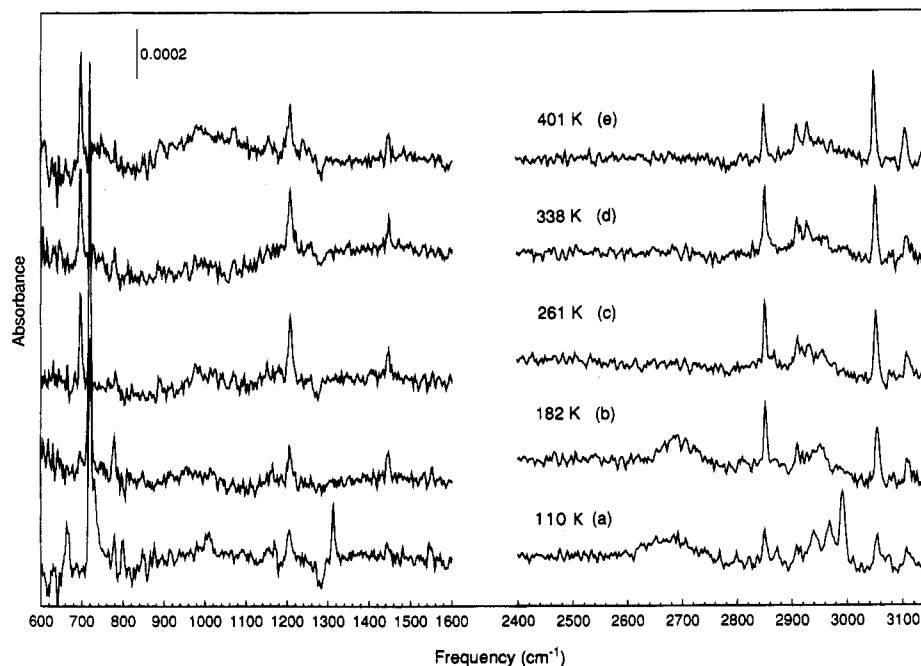


Figure 5. Reflection-absorption infrared spectra of norbornadiene ($\theta \approx 1$ monolayer) on Pt(111) annealed to the indicated temperature.

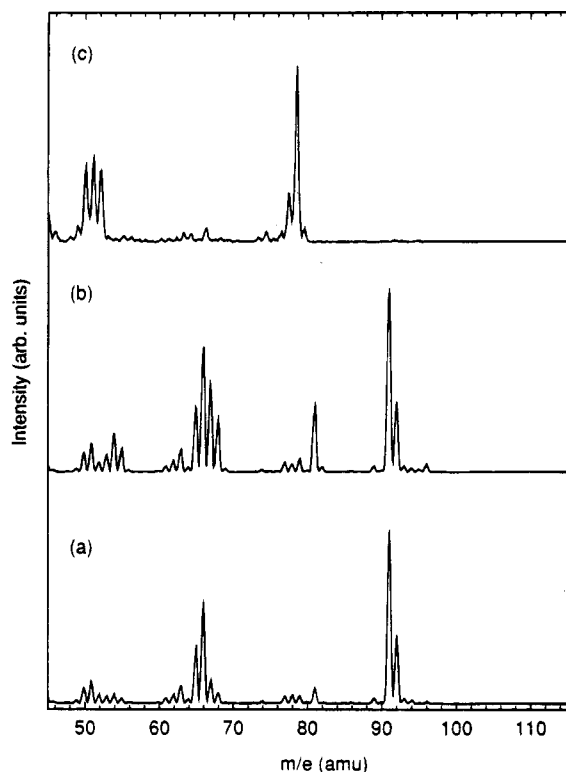


Figure 6. Integrated desorption mass spectra of the species desorbing from a Pt(111) surface over the indicated temperature range: (a) 130–330 K, following a 5 langmuir dose of NBD; (b) 130–300 K, following a dose of 20 langmuir of H_2 and then 5 langmuir of NBD; (c) 400–550 K, following a dose of 5 langmuir of NBD. Spectra a and c are identical with IDM spectra taken of NBD and benzene standards, respectively.

Auger electron spectroscopy establishes that heating a saturation coverage of NBD (8 L) to 850 K leaves a submonolayer of carbon on the surface.²³ By comparing this carbon yield to the amount of carbon atoms present in a closest packed monolayer of NBD, we can estimate

that approximately half of the adsorbate molecules initially present decompose to give desorbed benzene.

Discussion

Several conclusions can be drawn from the data presented above: (1) NBD bonds to Pt(111) in an unexpected $\eta^2:\eta^1$ manner involving a C=C double bond and an agostic Pt-H-C interaction, (2) this latter interaction is characterized by a red-shifted (soft) C-H stretching mode, and (3) the conversion of norbornadiene to benzene proceeds through a norbornadienyl intermediate. The factors responsible for these phenomena will be discussed in turn.

Molecular Orientation of NBD Adsorbed on Pt(111). The two most reasonable binding modes for NBD on Pt(111) are binding to the exo face (structure Ia) and binding to the endo face (structure Ib). The presence of vinylic C-H stretching vibrations in the RAIR spectrum for submonolayer coverages of NBD on Pt(111) is only consistent with structure Ia. We ask, why is this nonintuitive structure adopted in preference to structure Ib?

In both mono- and polynuclear organometallic complexes, norbornadiene is almost invariably bound to a single metal center by means of both C=C double bonds (i.e., $\eta^2:\eta^2$); NBD thus serves as a bidentate ligand and the metal is bound to the endo face of NBD.^{24,25} This bonding mode is most closely related to structure Ib. There are a few examples of NBD molecules that bind to metals by means of only one C=C double bond (η^2); in such cases, the metal is bound to the exo face of NBD.²⁶

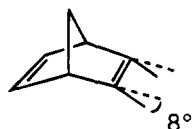
(23) The carbon yield is somewhat uncertain. Because the filaments of the AES system deposit some carbon on the surface, the value we measure, $\theta_c < 0.7$ monolayer, should be considered an upper limit. The carbon coverage was calculated by using the calibration parameters described in: Rodriguez, J. A.; Campbell, C. T. *J. Phys. Chem.* **1989**, *93*, 826–835.

(24) Abel, E. W.; Bennett, M. A.; Wilkinson, G. *J. Chem. Soc.* **1959**, 3178–3182.

(25) Alexander, R. A.; Baenziger, N. C.; Carpenter, C.; Doyle, J. R. *J. Am. Chem. Soc.* **1960**, *82*, 535–538.

Inspection of molecular models of NBD reveals that the $\eta^2:\eta^2$ bonding mode (structure Ib) must involve a single platinum atom: the short distance between the two C=C double bonds and the canting of the π -systems inward toward the endo face make it impossible for NBD to adopt a bridging geometry in which each C=C double bond interacts with a different metal atom.

More importantly, however, even if NBD were able to bind to a single surface Pt atom, the (111) surface would have to undergo a significant reconstruction to avoid the formation of unacceptably short Pt-H contacts with the vinylic hydrogen atoms. In free NBD, the vinylic C-H bonds are bent $\sim 8^\circ$ away from the exo face due to steric repulsions with the bridging CH₂ group.²⁷



This distortion makes the endo face more sterically hindered than the exo face, a fact which is reflected by the higher reactivity of the exo face of NBD toward many organic reagents.²⁸⁻³¹ For an NBD molecule bonded in a $\eta^2:\eta^2$ fashion via its endo face to a single platinum atom in an unreconstructed Pt(111) surface (with Pt-C distances to the olefinic carbon atoms of ~ 2.2 Å), the distances between the vinylic hydrogen atoms and the nearest neighbor platinum atoms would be ~ 1.0 Å; such distances are far too short to be acceptable. Thus, the principal factor that disfavors the $\eta^2:\eta^2$ bonding mode is the prohibitively large steric repulsions between the surface and the vinylic hydrogen atoms; this factor is a direct consequence of the rigid bicyclic structure of NBD.

In contrast, a similar analysis of the $\eta^2:\eta^1$ geometry (structure Ia) shows that no unfavorable secondary interactions are generated. For an NBD molecule bound via an interaction with the sterically more accessible exo face (in which only one C=C double bond is involved in a π or di- σ interaction with the surface), the other portion of the NBD molecule that comes in contact with the surface is a hydrogen atom of the bridging CH₂ group. The geometry of NBD dictates that the distance between this hydrogen atom and the surface is approximately 1.7-1.8 Å, which is within the range expected for an "agostic" M-H-C interaction.³²

The rigid bicyclic structure of NBD guarantees that the agostic C-H bond must point directly toward a specific site on the surface. The nature of this site depends upon how the C=C double bond interacts with the surface. If the C=C double bond bridges two Pt atoms in a di- σ fashion, then the agostic C-H bond points toward an atop site of an adjacent platinum atom. If, on the other hand, the C=C double bond interacts with only one Pt atom in a π fashion, the agostic C-H

bond points toward a 2-fold bridging site. Experimental and theoretical studies of a structurally diverse range of alkenes suggest that the di- σ bonding mode is predominant on Pt(111) surfaces.³³⁻³⁶ If one assumes that NBD behaves similarly, then the agostic interaction involves an atop site on the surface.

Soft C-H Stretching Modes and the Nature of the Agostic Bond. Other workers have discussed in detail the nature of the "agostic" interaction responsible for the soft C-H stretching modes seen for certain hydrocarbons on metal surfaces.^{14-16,37-43} RAIRS is a valuable tool for studying the structural basis of softened modes, because differences in the line widths of the modes seen from molecule to molecule can be accurately determined. For example, the full width at half-maximum (fwhm) of the soft mode for cyclohexane on a Pt(111) surface is ~ 300 cm⁻¹.¹⁵ In contrast, the soft mode for NBD is relatively narrow (fwhm ≈ 50 cm⁻¹). Several hypotheses have been advanced to explain why soft C-H stretching modes of adsorbed hydrocarbons often have large line widths: (1) inhomogeneous line broadening due to the presence of a large number of energetically similar binding sites, (2) dispersion arising from the coupling of the C-H stretching vibration with the low-frequency M-H stretching and bending vibrations, and (3) lifetime broadening.^{37,42,44}

The major difference in the way that saturated hydrocarbons and NBD adsorb is that the latter is firmly bound to the surface at a second point: the C=C double bond. The "pinning" of NBD to specific sites should reduce the amount of inhomogeneous line broadening but should not greatly affect the coupling to other low-frequency modes or the lifetime of the vibrational excited states. The data thus suggest that inhomogeneous line broadening is responsible for a substantial portion of the line width of the soft modes seen for weakly adsorbed hydrocarbons. Other factors must also contribute to the band structure, however, since the 50 cm⁻¹ line width seen for the soft mode of NBD is still larger than the line widths of the "normal" C-H stretching modes.

Conversion of NBD to Benzene. In the original report of the discovery that NBD is converted to benzene on Pt(111) at high temperatures,^{3b} Muetterties and his co-workers logically presumed that at low temperatures NBD is bound to Pt(111) in an $\eta^2:\eta^2$ fashion and that consequently the CH₂ group is remote from the surface. In order to afford the platinum surface an opportunity to cleave the CH₂ group from NBD and generate the

(26) Klein, H. F.; Fabry, L.; Witty, H.; Schubert, U.; Lueken, H.; Stamm, U. *Inorg. Chem.* **1985**, *24*, 683-688.

(27) Holthausen, M. C.; Koch, W. *J. Phys. Chem.* **1993**, *97*, 10021-10027.

(28) Schleyer, P. v. R. *J. Am. Chem. Soc.* **1967**, *89*, 701-703.

(29) Fahey, R. C. *Top. Stereochem.* **1968**, *3*, 237-342.

(30) Huisgen, R.; Ooms, P. H.; Mingin, M. N.; Allinger, N. L. *J. Am. Chem. Soc.* **1980**, *102*, 3951-3953.

(31) Huisgen, R. *Pure Appl. Chem.* **1981**, *53*, 171-187.

(32) Brown, R. K.; Williams, J. M.; Schultz, A. J.; Stucky, G. D.; Ittel, S. D.; Harlow, R. L. *J. Am. Chem. Soc.* **1980**, *102*, 981-987.

(33) Stuve, E. M.; Madix, R. J. *J. Phys. Chem.* **1985**, *89*, 3183-3185.

(34) (a) Sheppard, N. *J. Electron Spectrosc. Relat. Phenom.* **1986**, *38*, 175-186. (b) Sheppard, N. *Annu. Rev. Phys. Chem.* **1988**, *39*, 589-644.

(35) Bent, B. E.; Mate, C. M.; Kao, C.-T.; Slavin, A. J.; Somorjai, G. A. *J. Phys. Chem.* **1988**, *92*, 4720-4726.

(36) Paul, J.-F.; Sautet, P. *J. Phys. Chem.* **1994**, *98*, 10906-10912.

(37) Demuth, J. E.; Ibach, H.; Lehwald, S. *Phys. Rev. Lett.* **1978**, *40*, 1044-1047.

(38) Hoffmann, F. M.; Felner, T. E.; Thiel, P. A.; Weinberg, W. H. *Surf. Sci.* **1983**, *130*, 173-190.

(39) Kang, D. B.; Anderson, A. B. *J. Am. Chem. Soc.* **1985**, *107*, 7858-7861.

(40) Baetzold, R. C. *J. Am. Chem. Soc.* **1983**, *105*, 4271-4276.

(41) Raval, R.; Pemble, M. E.; Chesters, M. A. *Surf. Sci.* **1989**, *210*, 187-200.

(42) Raval, R.; Chesters, M. A. *Surf. Sci.* **1989**, *219*, L506-L514.

(43) Saillard, J.-Y.; Hoffmann, R. *J. Am. Chem. Soc.* **1984**, *106*, 2006-2026.

(44) Persson, B. N. J.; Ryberg, R. *Phys. Rev. Lett.* **1982**, *48*, 549-552.

observed thermolysis product benzene, Muettert and co-workers proposed that NBD must "roll over" at higher temperatures to place the CH₂ group next to the surface.

One of the problems with this hypothesis is that it is difficult to envision a mechanism that would allow the NBD molecule to roll over but not desorb. To reach the transition state of the roll-over process (i.e., from endo to exo binding), the strong metal-alkene π (or di- σ) interaction must be broken completely; at the transition state, the molecule would be weakly physisorbed at best. It is unclear whether such a process could efficiently interconnect the two bound states in a manner which would not result in desorption. We note that alkene roll-over processes are known to have high activation energies under catalytic conditions (high pressures and temperatures).⁴⁵ Perhaps the best evidence of this is derived from studies of the heterogeneously catalyzed isotopic H/D exchange of cyclic hydrocarbons. For example, at short contact times, H/D exchange in norbornane occurs only on one face of the alkane, which clearly suggests that there are significant energetic barriers that prohibit the roll over of adsorbed, unsaturated intermediates.⁴⁶ Whitesides and Lee also found that the dominant *d*₄ product obtained in the hydrogenation of NBD with D₂ is the all-exo *d*₄ isomer.⁴ This result strongly supports the importance of exo-binding of NBD (and the necessity for multiple adsorption/desorption steps for its complete reduction). In those cases where H/D exchange is not face-selective, adsorption/desorption equilibrium are clearly implicated. The importance of analogous dissociation/association equilibria is also well-established in the facial exchange processes of discrete metal-alkene complexes.⁴⁷

The mechanistic difficulties associated with a roll-over step are obviated by our conclusion that NBD is not bound to Pt(111) surfaces in an $\eta^2:\eta^2$ fashion. Instead, the thermodynamically preferred $\eta^2:\eta^1$ binding mode adopted by NBD places the CH₂ group that must be cleaved from the NBD skeleton in contact with the surface at low temperatures. The platinum surface then cleaves one of the C-H bonds of the methylene group between 220 and 260 K to generate a norbornadienyl intermediate bound to the surface; this intermediate is subsequently converted to benzene. It is of course relevant that the first C-H bond activated by the surface is the one that participates in the agostic interaction.

The spectroscopic data indicate that, as soon as benzene is generated on the surface, a significant fraction of it desorbs; the peak desorption temperature of ~495 K is likely reflective of a reaction-limited process. This temperature corresponds to an activation

energy of 30 kcal/mol, if one assumes that the desorption kinetics follow a first-order rate law and that the preexponential factor is 10¹³ s⁻¹.⁴⁸ The assumption of first-order kinetics appears reasonable in light of the weak dependence of the benzene desorption temperature on initial NBD coverage.

The RAIRS data and the TPRS profiles in the *m/e* 2 channel suggest that at least one C-H bond-breaking step precedes the formation of benzene and that others occur coincident with its desorption. The lower temperature C-H cleavage process is associated with the conversion of an $\eta^2:\eta^1$ -bound NBD to a norbornadienyl intermediate; this species is stable up to ~420 K. The higher temperature C-H bond-breaking step must by necessity be accompanied by the cleavage of two C-C bonds in order to convert the norbornadienyl group into benzene. The simplest mechanism for this latter process involves the retro-cyclization of a norbornadienyl group into a methine group (which remains on the surface) and benzene (which partially desorbs). This proposed mechanism finds precedent in the thermal extrusion reactions that occur when 7-substituted norbornadiene molecules decompose in the gas phase (yielding benzene and a carbene diradical; 420-620 K).⁴⁹

The remaining methine group is evidently dehydrogenated to hydrogen (which desorbs) and surface carbon. By 620 K, the remaining adsorbed hydrocarbon fragments have completely decomposed to yield a carbonaceous overlayer ($\leq 2/3$ of a monolayer).

Conclusions

Norbornadiene adopts an unexpected bonding configuration on Pt(111): rather than binding through both C=C double bonds, NBD is chemisorbed by means of a single C=C double bond and an agostic interaction between one of the methylene C-H bonds and an atop site on the platinum surface. Steric factors probably favor this unusual binding mode over the $\eta^2:\eta^2$ geometry that had been previously proposed for this adsorbate. The relatively small line width seen for the IR stretch associated with the agostic Pt-H-C interaction suggests that the large line widths seen for the soft modes of other adsorbed hydrocarbons are due to inhomogeneous broadening. The agostic C-H bond is cleaved by 260 K to give a norbornadienyl intermediate that is stable up to 450-500 K. In this temperature range, this norbornadienyl species evidently undergoes a retro-cyclization to give benzene, which partially desorbs, and a methine group. The hydrocarbon fragments that remain on the surface are finally thermolyzed to a carbonaceous overlayer by ~620 K.

Acknowledgment. We thank the Department of Energy (Grant DEFG02-91ER45439) for support of this work.

OM940758P

(45) Kamball, C. *Adv. Catal.* **1959**, *11*, 223-262.

(46) Burwell, R. L., Jr.; Shim, B. K. C.; Rowlinson, H. C. *J. Am. Chem. Soc.* **1957**, *79*, 5142-5148.

(47) James, B. R. In *Comprehensive Organometallic Chemistry*; Wilkinson, G., Stone, F. G. A., Abel, E. W., Eds.; Pergamon: New York, 1982; Vol. 8; pp 285-369.

(48) Redhead, P. A. *Vacuum* **1962**, *12*, 203-211.

(49) Hoffmann, R. W. *Acc. Chem. Res.* **1985**, *18*, 248-253.

Transition Metal Complexes of Diazenes. 35. Synthesis of 1-(Arylamino)indoles by Rhodium-Catalyzed Addition of Alkynes to 1,2-Diaryldiazenes^{†,1}

Uwe R. Aulwurm, Jörg U. Melchinger, and Horst Kisch*

Institut für Anorganische Chemie der Universität Erlangen–Nürnberg, Egerlandstrasse 1, D-91058 Erlangen, Germany

Received December 12, 1994[©]

Addition of 1,2-diaryldiazenes to aliphatic or aromatic internal alkynes in the presence of catalytic amounts of $\text{RhCl}(\text{PPh}_3)_3$ (Wilkinson's catalyst) in refluxing propanol affords *N*-(arylamino)indole derivatives. Electron-withdrawing substituents in the alkyne induce a decrease of the turnover rate, while electronic properties of the diazene have only a minor influence. When unsymmetrically substituted alkynes are employed, a mixture of regioisomers is obtained except in the case of very large substituents like *tert*-butyl and adamantyl which bring about a regioselective reaction. Steric alterations in the diazene induce significant effects. While the unsubstituted phenyl ring is attacked in the case of 3,5-dichloroazobenzene, no reaction occurs with 2,4,6-trimethylazobenzene. Kinetic measurements reveal a first-order dependence on $\text{RhCl}(\text{PPh}_3)_3$ and azobenzene, while a broken order of -0.3 is found for tolan. The activation parameters are $E_a = 75 \pm 6 \text{ kJ/mol}$ and $\Delta S^\ddagger = -96 \pm 14 \text{ J mol}^{-1} \text{ K}^{-1}$. A mechanism is proposed wherein the key steps are orthometalation of the diazene followed by insertion of the alkyne into a Rh–H bond and reductive $\text{C}(\text{sp}^2)\text{--C}(\text{sp}^2)$ elimination to afford a 2-vinylazobenzene intermediate. This is converted to the *N*-(arylamino)indole derivative in an acid-catalyzed reaction step.

Introduction

Due to the general importance of indole derivatives in biological systems, many synthetic pathways have been described in the literature. A few of them are transition metal catalyzed, and in no case has a 1-aryl-substituted derivative been obtained.^{2 a} Recently we found that 1-anilino-2,3-diphenylindole (**1**) is formed in 26% yield when azobenzene and tolan are refluxed in toluene solution in the presence of catalytic amounts of $\text{RhCl}(\text{PPh}_3)_3$.^{2 b} As a by-product 2,3-diphenylindole (**2**) is formed in 2–7% yield. It was found that silica gel or acetic acid acts as a cocatalyst inducing maximum turnover numbers (TON) in the range of 60. In order to clarify the role of the acid and the synthetic scope of the reaction in homogeneous solution, we report here on the catalytic preparation of a variety of substituted 1-(arylamino)indoles, on the solvent influence, and on kinetic measurements. A paper on the SiO_2 -supported system is in preparation.³

Results and Discussion

1. Influence of Solvents and Catalytic Amounts of Various Additives.

Addition of catalytic amounts of acetic acid (0.06 vol %) to the system azobenzene/tolan/ $\text{RhCl}(\text{PPh}_3)_3$ in refluxing toluene (110 °C) induces

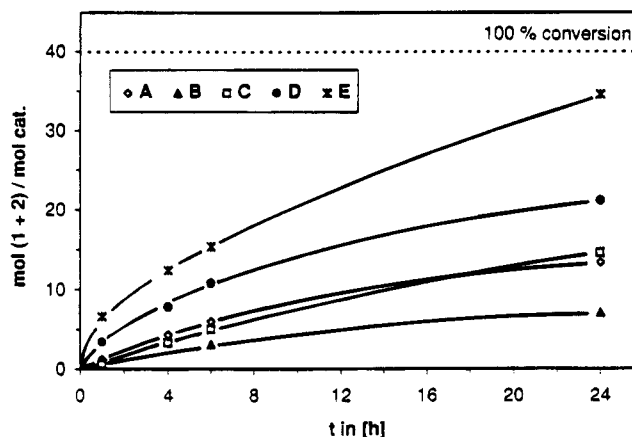


Figure 1. Product formation in the presence of 0.25 mmol of different additives, with 2 mmol of azobenzene and tolan and 0.05 mmol of $\text{RhCl}(\text{PPh}_3)_3$ in 25 mL of refluxing toluene: A, without additive; B, pyridine; C, 1-BuOH; D, NaOAc/HOAc; E, HOAc.

a turnover rate (TOR, turnover number after 1 h) of 6 and a TON of 34 (Figure 1). When equimolar catalytic amounts of sodium acetate and acetic acid are added, TOR and TON decrease to 3 and 17, respectively, while addition of pyridine leads to values of 0.6 (TOR) and 7 (TON). The use of a very weak acid like 1-BuOH does not increase the catalytic activity (TOR 1, TON 29) as compared to toluene, but a smaller amount of **2** is formed at the end of the reaction (1%). In all cases TOR and TON are given as the sum of **1** + **2**, the fraction of **2** amounting to about 5% unless otherwise mentioned.

To compare the pK_a values of the acidic cocatalysts with the catalytic activity, different benzoic acids were added to the azobenzene/tolan/ $\text{RhCl}(\text{PPh}_3)_3$ /toluene. Benzoic acid itself (pK_a 4.2) and the weaker anthranilic acid

[†] Dedicated to Professor H.-J. Bestmann on the occasion of his 70th birthday.

[©] Abstract published in *Advance ACS Abstracts*, June 1, 1995.

(1) For number 34, see: Halbritter, G.; Knoch, F.; Kisch, H. *J. Organomet. Chem.* **1995**, *492*, 87.

(2) (a) Robinson, B. *The Fischer Indole Synthesis*; J. Wiley & Sons: Chichester, 1982. Hegedus, L. S. *Angew. Chem.* **1988**, *100*, 1147. *Angew. Chem., Int. Ed. Engl.* **1988**, *27*, 1113. (b) Reisser, P.; Wakatsuki, Y.; Kisch, H. *Monatsh. Chem.* **1995**, *126*, 1.

(3) Westernacher, S.; Kisch, H. In preparation.

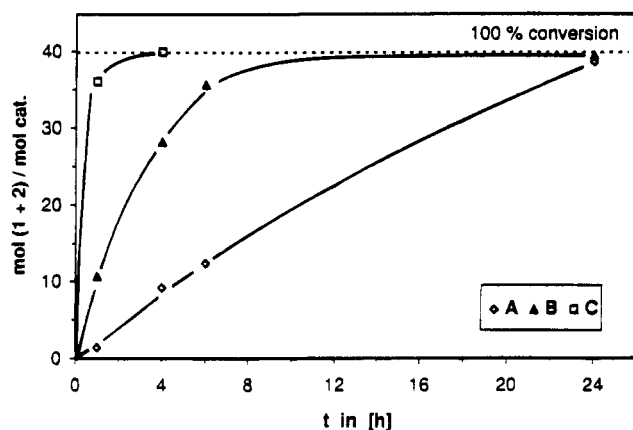


Figure 2. Product formation in alcohol solvents (25 mL); 2×10^{-3} M $\text{RhCl}(\text{PPh}_3)_3$, 8×10^{-3} M each of PhN_2Ph and PhC_2Ph . A, 1-PrOH (97 °C); B, 1-BuOH (118 °C); C, 1-pentanol (138 °C).

($\text{p}K_a$ 4.95) induce a TOR of 2. For the stronger 4-chlorobenzoic ($\text{p}K_a$ 3.98) and 4-nitrobenzoic acids ($\text{p}K_a$ 3.42) TOR values of 1 and 0 are obtained, respectively. The inhibiting effect of the strongest acid resembles the influence of mineral acids,^{2b} while the $\text{p}K_a$ value of the weakest acid is close to that of HOAc, which is the best cocatalyst.

When, instead of toluene, acetic acid is used as solvent, the catalyst is decomposed and no reaction occurs. In the basic solvent pyridine only a trace of **1** is found after 24 h. Since acetic acid decomposes the catalyst, alcohols were employed as weak acidic solvents. Refluxing 1-BuOH (118 °C) induces a 2-fold increase of catalytic activity (TOR 13, Figure 2 curve B) as compared to the toluene/HOAc (TOR 6) system. According to the lower boiling point of 1-PrOH (97 °C) the reaction therein is slower (TOR 1), but diminished catalyst deactivation and formation of fewer by-products give rise to a higher yield after 24 h (TON 38) (Figure 2, curve A) than in the toluene/HOAc (TON 34) system. In 1-pentanol (138 °C) as solvent (Figure 2, curve C) the reaction becomes very fast (TOR 36), whereas it is very slow (TOR 0 and, after 24 h, TON 2) in refluxing ethanol (79 °C). These results indicate that a reaction temperature above 90 °C is necessary to obtain a high catalytic activity.

In alcohol solvents the addition of catalytic amounts of acetic acid also induces an increase of the catalytic activity. In 1-PrOH/HOAc (0.06 vol %) a 3-fold (TOR 4) increase and in 1-BuOH/HOAc a 1.5-fold (TOR 20) increase of the initial rate are induced. When azobenzene and tolan are employed in a 120-fold excess as compared to $\text{RhCl}(\text{PPh}_3)_3$, the TON is increased through addition of HOAc by about 15%–20%. Maximum turnover numbers are in the range of 100 mol of product/mol of catalyst (1-PrOH/HOAc 0.03 vol %, TON 105).

The fraction of **2** produced depends on the solvent and increases with the reaction temperature. At the end of the reaction in toluene, usually after 24 h, 15% of the TON are due to **2**, while in 1-PrOH and 1-BuOH the corresponding percentages are only 2% and 4%, respectively. In 1-pentanol, the reaction is finished already after 4 h and 5% of the TON are due to **2**. In summary, the 1-PrOH/HOAc system affords the best results in terms of reaction rate and product yield.

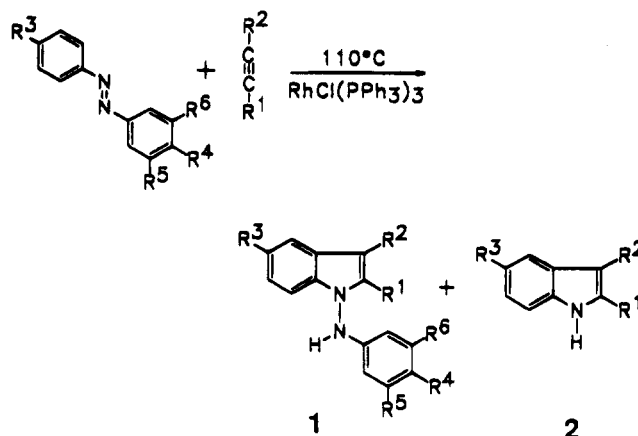


Figure 3.

Table 1. Substitution Pattern and Isolated Yields of 1a–w

indole ^a	R ¹	R ²	R ³	R ⁴	yield (%)
1a	C ₆ H ₅	C ₆ H ₅	H	H	90
1b	4-CH ₃ -C ₆ H ₄	4-CH ₃ -C ₆ H ₄	H	H	86
1c	4-CH ₃ O-C ₆ H ₄	4-CH ₃ O-C ₆ H ₄	H	H	78
1d	n-C ₃ H ₇	n-C ₃ H ₇	H	H	52
1e	C ₆ F ₅	C ₆ F ₅	H	H	16
1f	(CH ₃) ₃ C	C ₆ H ₅	H	H	18
1g	adamantyl-	C ₆ H ₅	H	H	29
1h	CH ₃	C ₆ H ₅	H	H	14
1i	C ₆ H ₅	CH ₃	H	H	8
1k	4-CH ₃ -C ₆ H ₄	C ₆ H ₅	H	H	42
1l	C ₆ H ₅	4-CH ₃ -C ₆ H ₄	H	H	31
1m	4-CH ₃ O-C ₆ H ₄	C ₆ H ₅	H	H	24
1n	C ₆ H ₅	4-CH ₃ O-C ₆ H ₄	H	H	35
1o	4-NO ₂ -C ₆ H ₄	C ₆ H ₅	H	H	6
1p	C ₆ H ₅	4-NO ₂ -C ₆ H ₄	H	H	14
1q	C ₆ H ₅	C ₆ H ₅	Cl	H	39
1r	C ₆ H ₅	C ₆ H ₅	H	Cl	8
1s	C ₆ H ₅	C ₆ H ₅	CH ₃	H	52
1t	C ₆ H ₅	C ₆ H ₅	H	CH ₃	26
1u	C ₆ H ₅	C ₆ H ₅	CH ₃	CH ₃	24
1v	C ₆ H ₅	C ₆ H ₅	Cl	Cl	26
1w	C ₆ H ₅	C ₆ H ₅	H	H	21

^a R⁵ = R⁶ = H except in the case of **1w** where R⁵ = R⁶ = Cl.

2. Syntheses. Refluxing a 1-PrOH/HOAc solution of various 1,2-diazenes and alkynes in the presence of $\text{RhCl}(\text{PPh}_3)_3$ affords the new indoles **1** as summarized in Figure 3 and Table 1. After 24 h, the reaction is stopped and the raw material obtained is purified by preparative HPLC. The products are worked up in the dark to avoid light-induced decomposition and cyclization reactions.⁴ Isolated yields are in the range of 55%–85% for symmetrically substituted alkynes with electron-releasing substituents and also for the 4-CH₃- and 4-CH₃O-monomethylated tolan. Unsymmetrically substituted alkynes with alkyl substituents and all alkynes with electron-withdrawing substituents afford yields in the range of 6%–30%.

When unsymmetrically substituted alkynes are employed, the reaction is regioselective. With *tert*-butylphenylacetylene and adamantylphenylacetylene only one isomer, with the bulky group in the 2-position, is obtained, whereas with 1-phenylpropyne two isomers in a ratio of 7:4 (**1h**/**1i**) arise. Thus, regioselectivity originates in steric effects and is also slightly sensitive to electronic factors. Accordingly, the regioisomers formed from 4-methyltolan, 4-methoxytolan, and 4-ni-

(4) Mudry, C. A.; Frasca, A. R. *Tetrahedron* **1974**, *30*, 2983.

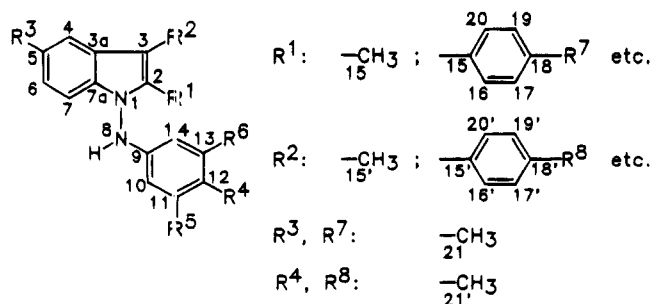


Figure 4.

Table 2. Characteristic ^1H - and ^{13}C -NMR Data of **1a-w** (Acetone- d_6)

	^1H -NMR				^{13}C -NMR			
	4-H	8-H	10-H/14-H	12-H	C-2	C-3	C-4	C-9
1a	7.73	8.51	6.49	6.74	138.4	114.6	120.1	149.1
1b	7.55	8.30	6.30	6.55	137.1	114.2	120.0	149.5
1c	7.68	8.45	6.48	6.74	137.9	113.8	119.9	149.2
1d	7.63	8.95	6.55	6.85	<i>a</i>	<i>a</i>	120.9	148.3
1e	7.55	8.30	6.43	6.77	138.4	110.7	119.1	149.4
1f	7.02	8.55	6.60	6.80	144.1	113.3	119.7	148.9
1g	6.98	8.54	6.60	6.80	143.9	113.5	119.8	149.1
1h	7.66	8.50	6.53	6.82	135.1	113.1	119.2	149.1
1i	7.62	8.39	6.40	6.70	138.1	108.1	119.6	149.3
1k	7.72	8.43	6.49	6.70	138.4	114.2	119.9	148.9
1l	7.72	8.43	6.49	6.70	138.0	114.5	120.1	148.9
1m	7.72	8.44	6.49	6.72	138.4	114.0	119.9	149.0
1n	7.72	8.44	6.49	6.72	137.9	114.3	120.1	149.0
1o	7.71	8.66	6.50	6.74	146.4	112.6	119.8	148.7
1p	7.82	8.58	6.50	6.74	137.7	116.7	120.5	148.7
1q	7.73	8.63	6.49	6.78	140.1	113.1	119.4	148.7
1r	7.76	8.72	<i>a</i>	<i>a</i>	138.2	114.4	120.2	147.9
1s	7.53	8.48	6.48	6.74	138.4	114.1	119.6	149.0
1t	7.72	8.38	6.42	<i>a</i>	<i>a</i>	115.0	120.0	146.8
1u	7.51	8.30	6.40	<i>a</i>	138.7	114.1	119.7	146.8
1v	7.55	8.64	6.35	<i>a</i>	139.9	114.6	119.5	147.9
1w	7.77	9.04	6.48	6.82	137.9	115.3	120.0	151.3

^a Signals not assigned. For atom numbering see Figure 4.

trotolan are in the ratios of 4:3 (**1k/1l**), 2:3 (**1m/1n**), and 2:5 (**1o/1p**), respectively. Complete separation of the regioisomers by preparative HPLC was not possible, but fractions with different isomeric ratios could be obtained. The determination of the isomeric ratio was performed by ^1H -NMR.

Symmetrically substituted azobenzenes induce yields of 24%–26%, unsymmetrically substituted azobenzenes afford 21%–78%. For 4-chloro- and 4-methylazobenzene both regioisomers can be isolated. A slight electronic influence is suggested by the ratios of **1q/1r** = 5:1 and **1s/1t** = 2:1. In both cases the substituted phenyl ring is attacked preferentially by the catalyst. Steric reasons may be responsible for the fact that, in the case of 3,5-dichloroazobenzene, only the isomer originating in attack at the unsubstituted phenyl ring is obtained.

The structures of the new compounds follow from single-crystal X-ray analyses of **1q** and **1u**⁵ and from comparison of extensive NMR data with those of 1-unsubstituted indoles (see Figure 4 and Table 2).⁶ In addition to this evidence, the presence of an *N*-arylamino group is demonstrated by the reductive cleavage of **1** to **2** by Zn/HCl .

In the ^1H -NMR spectra the signals of the hydrogen atoms 4-H, 8-H, 10-H/14-H, and 12-H are observed for all indoles **1** in the range 7–8 (m), 8.3–9 (s), 6.5 (d), and 6.7 ppm (t), respectively. The ^{13}C -NMR spectra contain the peaks of the carbon atoms C-2, C-3, C-5, and C-9 in the range 138, 113, 123, and 149 ppm, respectively. Replacing the phenyl group at the 2-position of **1a** by a *tert*-butyl (**1f**), an adamantyl (**1g**), or a 4-nitrophenyl group (**1o**) results in a shift of the C-2 signal to 144 ppm in the first two cases and to 146 ppm in the latter. Substituting the phenyl group at the 3-position of **1a** by a methyl (**1i**) or a 4-nitrophenyl (**1p**) group shifts the signal of C-3 to 108 and 117 ppm, respectively. For **1e** chemical shifts could not be assigned to C-2 and C-3 since the strong coupling with the fluorine atoms induces overlapping with other signals. When hydrogen at C-5 is substituted by a chloro (**1q**, **1v**) or methyl group (**1s**, **1u**), the signal is shifted slightly to lower field, 127 and 130 ppm, respectively. The peak of C-9 appears at higher field, 148 and 147 ppm, respectively, when C-12 is a chloro (**1r**, **1v**) or methyl group (**1t**, **1u**) but distinctly at lower field (151 ppm) in the case of **1w** ($\text{R}^5 = \text{R}^6 = \text{Cl}$).

In the NMR spectra of the isomeric mixtures obtained from unsymmetrically substituted alkynes, the signals could be unambiguously assigned in the case of **1h/1i** by comparison with the NMR data of the corresponding 1-unsubstituted indoles⁶ and in the case of **1k/1l** and **1m/1n** by comparison with the NMR data of **1a** and **1b**, and of **1a** and **1c**, respectively. For the isomeric mixture of **1o/1p** unambiguous assignment is based on ^1H -NOE difference spectra.

3. Kinetic Measurements. To obtain experimental evidence for the catalytic cycle postulated,^{2b} kinetic investigations were carried out in the azobenzene (0.08 M)/tolan (0.08 M)/ $\text{RhCl}(\text{PPh}_3)_3$ (0.002 M)/1-BuOH (50 mL)/HOAc (0.01 M) system at 110 ± 0.1 °C. Formation of **1** was followed by HPLC. Since a short induction period is observed, the amount of product formed between 10 and 20 min of reaction time, the time interval affording the highest turnover rates, was taken as the initial rate. The individual reaction orders of all components were obtained by measuring these rates as functions of increasing component concentration.⁷ From the slope of the plot of the logarithm of initial rate vs the logarithm of concentration the reaction order is obtained (Figure 5). However, it has been mentioned that in complex systems this initial-rate method may afford unreliable fractional orders.^{7,8}

In the case of azobenzene (0.2–0.12 mol/L) and $\text{RhCl}(\text{PPh}_3)_3$ ($(1-4) \times 10^{-3}$ mol/L) reaction orders of unity arise as indicated by the slopes of 0.9 ± 0.04 and 1.01 ± 0.08 , respectively. At higher catalyst concentrations the intermediate $\text{RhCl}(\text{PhC}_2\text{Ph})(\text{PPh}_3)_2$ complex precipitates from the solution, as indicated by IR and mass spectra. For tolan (0.02–0.08 mol/L) and HOAc ($2-100 \times 10^{-3}$ mol/L) orders of -0.3 and 0 are obtained from the corresponding slopes of -0.3 ± 0.02 and -0.008 ± 0.024 . From these results the rate law is formulated

(5) Aulwurm, U. R.; Knoch, F.; Kisch, H. In preparation.

(6) (a) Erra-Balsells, R. *J. Heterocycl. Chem.* **1988**, *25*, 1059. (b) Erra-Balsells, R.; Frasca, A. R. *Magn. Reson. Chem.* **1989**, *27*, 134. (c) Morales-Rios, M. S.; Espineira, J.; Joseph-Nathan, P. *Magn. Res. Chem.* **1987**, *25*, 377. (d) Mudry, C. A.; Frasca, A. R. *Tetrahedron* **1973**, *29*, 603.

(7) Jordan, R. B. *Mechanismen anorganischer und metallorganischer Reaktionen*; Teubner Studienbücher: Stuttgart, Germany, 1994.

(8) Wilkins, R. G. *Kinetics and Mechanism of Reactions of Transition Metal Complexes*, 2nd ed.; VCH-Verlagsgesellschaft: Weinheim, Germany, 1991.

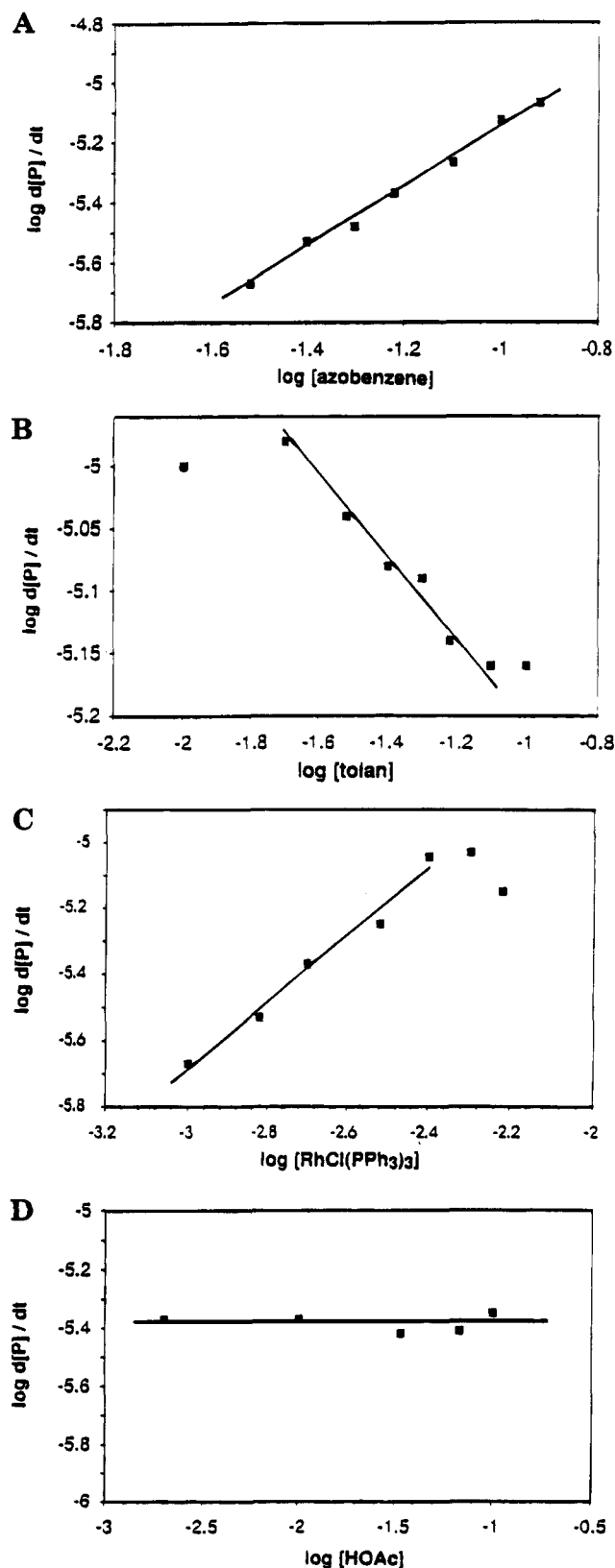


Figure 5. Plot of $\log(dP/dt)$ vs logarithm of the concentrations of azobenzene (A), tolan (B), $\text{RhCl}(\text{PPh}_3)_3$ (C), and HOAc (D).

according to eq 1. Measurement of the rate constant k

$$d[P]/dt = k[\text{Rh}][\text{PhN}_2\text{Ph}][\text{PhC}_2\text{Ph}]^{-0.3} \quad (1)$$

at four temperatures in the range 100–115 °C allows construction of an Arrhenius diagram from which the

activation parameters $E_a = 75 \pm 6$ kJ/mol and $\Delta S^\ddagger = -96 \pm 14$ J/mol K were calculated.⁹

4. Mechanism. Scheme 1 contains an extended version of the catalytic cycle postulated previously.^{2b}

In the boiling solvent $\text{RhCl}(\text{PPh}_3)_3$ is in equilibrium with $[\text{RhCl}(\text{PPh}_3)_2]$ and its dimer, $[\text{RhCl}(\text{PPh}_3)_2]_2$.¹⁰ $[\text{RhCl}(\text{PPh}_3)_2]$ can also be generated *in situ* from rhodium(III) chloride trihydrate and differing amounts of PPh_3 . A maximum is observed in a plot of rate vs concentration of PPh_3 when the latter is present in a 3-fold excess. Since 1 equiv is consumed for the reduction to rhodium(I), 2 equiv remain as ligands for one rhodium atom. Addition of more PPh_3 inhibits the reaction.¹¹ The dimer is only slightly soluble and precipitates as a crystalline orange solid. Upon addition of the substrates the solution becomes clear as tolan reacts with $[\text{RhCl}(\text{PPh}_3)_2]$ to afford **A**. An alternative reaction with azobenzene is unlikely, as indicated by the fact that azobenzene does not react with $\text{RhCl}(\text{PPh}_3)_3$, even in boiling mesitylene (163 °C). *Ab initio* calculations on $\text{RhCl}(\text{PH}_3)_2\text{L}$ indicate that the acetylene complex ($\text{L} = \text{C}_2\text{H}_2$) is more stable by 96 and 73 kJ/mol than the complex ($\text{L} = \text{N}_2\text{H}_2$), respectively.^{2b} Displacement of PPh_3 by azobenzene affords **B**, which then undergoes orthometalation to **C**. From the observed rate law (eq 1) one can conclude that the transition state of the rate-determining step⁸ contains azobenzene, tolan, and a rhodium complex fragment. It is therefore assumed that this step is the formation of **C**. The negative activation entropy of $\Delta S^\ddagger = -96 \pm 14$ J/mol K is in accord with this interpretation. The negative reaction order of tolan and the zero-order of HOAc suggest that the former undergoes a fast side reaction before the rate-determining step while the latter becomes involved thereafter. In a side reaction, **A** may react with a second molecule of tolan to produce a bis-(alkyne) complex. This rationalizes the negative reaction order found for tolan.

Substituents in the 4,4'-positions of azobenzene have only a minor influence, as indicated by the relative rates of 1, 1.4, and 1.4 obtained for the substituents H, CH_3 , and Cl, respectively. No reaction occurs with 2,2',4,4',6,6'-hexamethylazobenzene, which is lacking *ortho* H atoms, 2,4,6-trimethylazobenzene, 3,3',5,5'-tetrachloro-, or 3,3',5,5'-tetramethylazobenzene. Since the three latter compounds are orthometalated by $[\text{CoH}(\text{PPh}_3)_3]$,^{1,12} it is likely that steric hindrance by the alkyne ligand of **A** prevents the formation of **B** and **C** when a methyl or chloro group is present at the position *ortho* to the metalated carbon atom. In agreement with this rationalization the unsubstituted phenyl ring is attacked in the case of 3,5-dichloroazobenzene. When the two *ortho* positions are substituted as in 2,4,6-trimethylazobenzene, no indole formation is observed. In this case orthometalation requires attack of rhodium at the nitrogen atom bound to the substituted ring. However, due to steric hindrance by the methyl groups, attack at

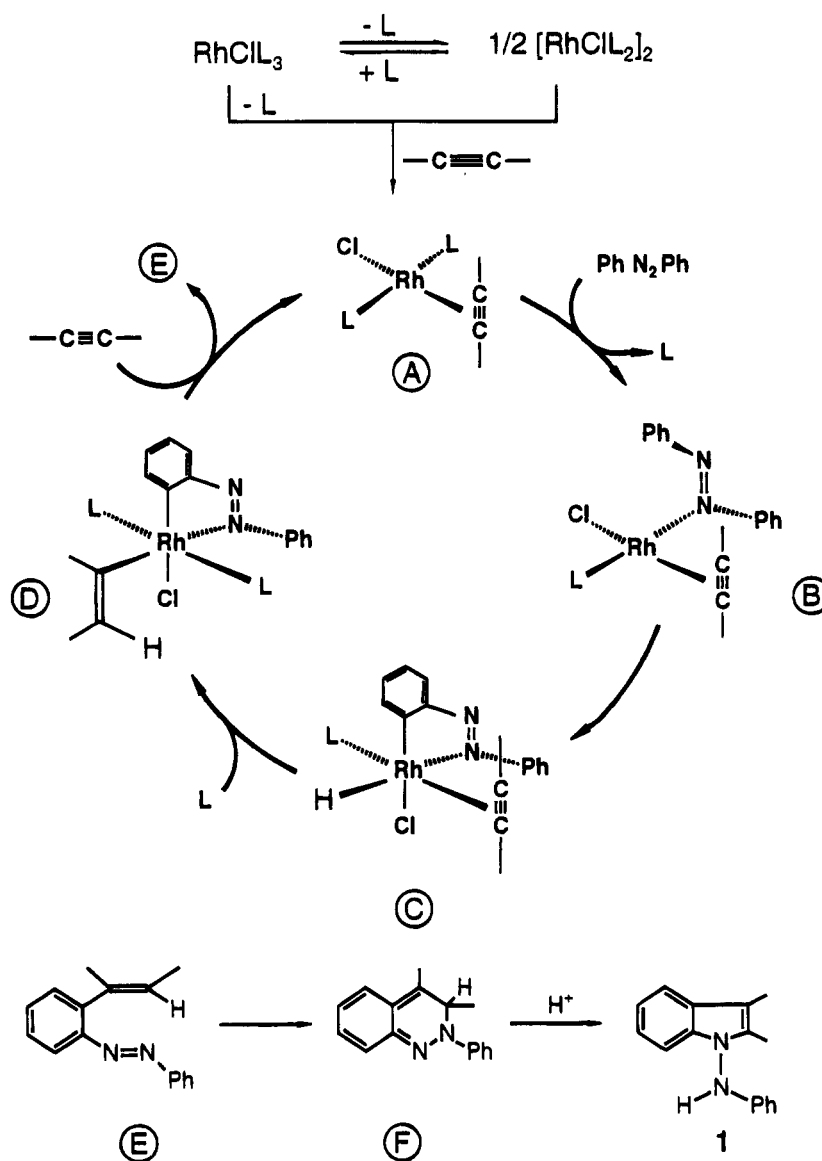
(9) Hoffmann, R. W. *Aufklärung von Reaktionsmechanismen*; Thieme Verlag: Stuttgart, 1976.

(10) Osborne, A.; Jardine, F. H.; Young, J. F.; Wilkinson, G. *J. Chem. Soc. A* **1966**, 1711.

(11) Reisser, P. Ph.D. Thesis, Universität Erlangen-Nürnberg, Nürnberg, Germany, 1992.

(12) Halbritter, G.; Knoch, F.; Wolski, A.; Kisch, H. *Angew. Chem.* **1994**, *106*, 1676; *Angew. Chem., Int. Ed. Engl.* **1994**, *33*, 1603.

Scheme 1. Catalytic Cycle of Indole Formation



the other nitrogen atom should be favored.¹³ Highly substituted azo dyes do not react. When azobenzene is monosubstituted in the 4-position, that regioisomer which originates from orthometalation of the substituted ring is favored. Thus ratios of **1q**/**1r** = 5:1 and **1s**/**1t** = 2:1 are found when the substituent is Cl or CH_3 , respectively.

¹H-NMR experiments with **A** and 4,4'-dimethylazobenzene in 1,4-dioxane-*d*₈ support these reaction steps. At room temperature all signals remain unchanged including the methyl group at 2.38 ppm. Upon heating to 60 °C a second singlet is observed at 2.26 ppm which most likely arises from the σ -coordinated ligand of **B**. A fast intramolecular 1,2-shift of the metal fragment^{13,14} explains the appearance of a singlet instead of the expected doublet. When heating is continued to 95 °C, additional methyl signals are formed in the range of 2.38–1.92 ppm. The shift to higher field is in agreement with the data of other cyclorhodated

azobenzene complexes¹⁵ and supports the orthometalation step from **B** to **C**. However, no hydride signal of the latter could be detected but rather the vinylic protons of the subsequent intermediates **D** and **E**, as suggested by two singlets at 6.27 and 5.94 ppm.

Insertion of the alkyne into the Rh–H bond and recoordination of a PPh_3 ligand affords the *cis*-stilbenyl complex **D**. It cannot be decided whether this complex or its *trans*-stilbenyl isomer undergoes the subsequent reaction. A related isomerization was reported for the alkyne insertion in $[\text{Rh}(\text{Cp})\text{H}(\text{PhC}_2\text{Ph})\text{P}(\text{i-Pr})_3]^+$.¹⁶

Electron-donating substituents R in the alkyne RC_2R increase the relative reaction rate after 4 h in the sequence F_3C_6 (0.17) < 4- $\text{CH}_3\text{O}-\text{C}_6\text{H}_4$ (0.66) < Ph (1) < 4- $\text{CH}_3-\text{C}_6\text{H}_4$ (2) < n-Pr (2.2). No indole formation occurs when R is CO_2H or 4- $\text{NO}_2-\text{C}_6\text{H}_4$. This parallels observations made on alkyne insertion into Rh–H bonds.^{17,18}

(15) Van Baar, J. F.; Vrieze, K.; Stufkens, D. J. *J. Organomet. Chem.* **1975**, *97*, 461.

(16) Werner, H.; Wolf, J.; Schubert, U.; Ackermann, K. *J. Organomet. Chem.* **1986**, *317*, 327.

(17) Van Gaal, H. L. M.; Graef, M. W. M.; van der Ent, A. *J. Organomet. Chem.* **1977**, *131*, 453.

(13) Abel, E. W.; Blackwell, E. S.; Orrell, K. G.; Šik, V. *J. Organomet. Chem.* **1994**, *464*, 163.

(14) Einstein, F. W. B.; Sutton, D.; Tyers, K. G. *Inorg. Chem.* **1987**, *26*, 111.

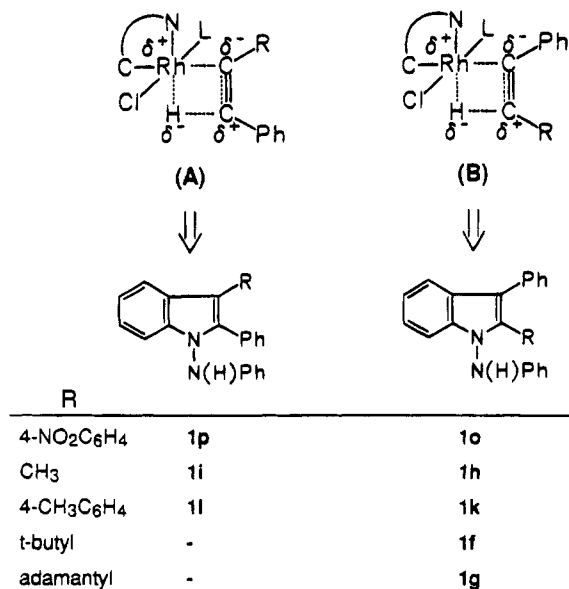


Figure 6. Transition states of alkyne insertion.

Decreasing π -back-bonding and the resulting diminished strength of the Rh to alkyne bond are responsible for the effect which may operate in the insertion (C to D) and orthometalation steps (B to C). In the case of unsymmetrically substituted alkynes RC_2Ph two *cis*-insertion products and therefore two regioisomeric indoles may be obtained. Assuming a negatively polarized hydride ligand, the four-membered transition state 6A (Figure 6) should be favored when R is more electron-withdrawing than the phenyl group.¹⁶ Accordingly, a 4-nitrophenyl substituent induces preferred formation of the regioisomer **1p** as indicated by the isomeric ratio of **1p/1o** = 5:2. Contrary to that, transition state 6B and the corresponding regioisomer should be favored when R is more electron-donating than the phenyl group. This is in the case when R is a methyl group and the ratio of **1i/1h** is 4:7. A methyl group at the 4-position of one phenyl ring has only a weak influence as demonstrated by the ratio **1l/1k** = 3:4. Sterically demanding substituents R should favor the transition state 6B wherein they are located further away from the metal than in 6A. The reaction therefore proceeds regioselectively to **1f** and **1g** when R is a *tert*-butyl or adamantyl group, respectively.

Reductive elimination of the 2-stilbenylazobenzene **E** leads to $[RhCl(PPh_3)_2]$, which takes up toluene to reform the catalyst **A**.¹⁹ **E** cyclizes to the 2,3-dihydrocinnoline **F**, a reaction known from 2,6-distilbenylazobenzene derivatives.^{12,20}

When the reaction of toluene with azobenzene in 1-BuOH or 1-PrOH is carried out in the absence of HOAc, formation and disappearance of the intermediate **F** can be observed by HPLC (8.5 min) (Figure 7). This is not possible when HOAc is present. In the higher boiling solvent the characteristic maximum of the concentration vs time curve is found at a much shorter reaction time.

Experiments to isolate this intermediate by preparative HPLC afforded a mixture containing **F** as the major component and smaller amounts of the indole **1a** and

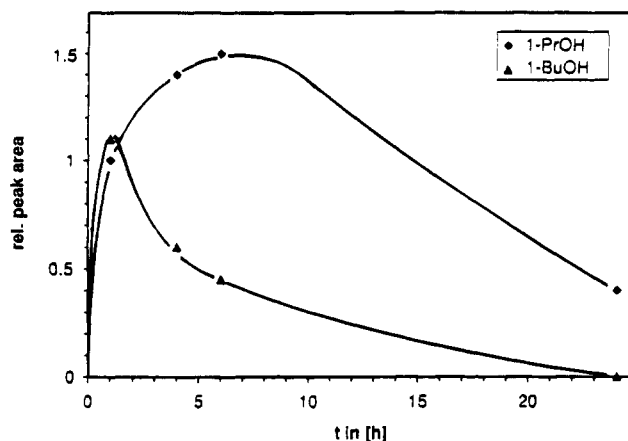


Figure 7. Concentration vs time curves for the intermediate **F** in 1-PrOH (97 °C) and 1-BuOH (117 °C).

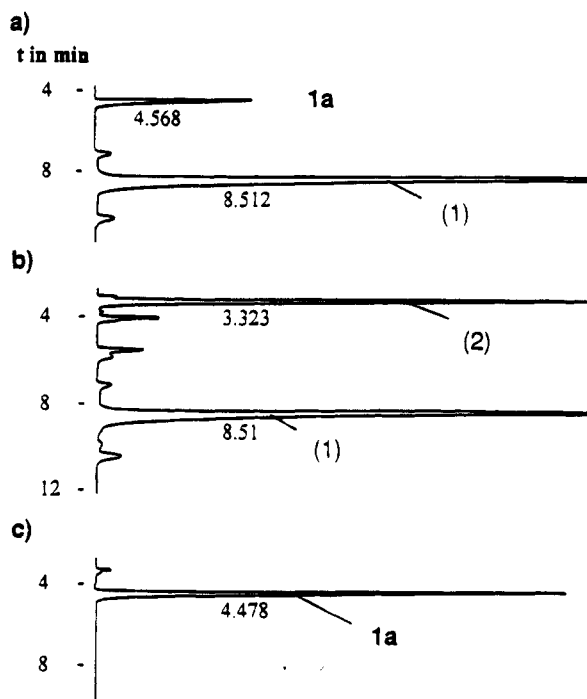


Figure 8. HPLC spectra ($CH_3CN/H_2O = 5/1$, 5 mL/min) of (a) the intermediate isolated from reaction of azobenzene with toluene, (1) = 2,3,4-triphenyl-2,3-dihydrocinnoline, (b) raw material from the Wittig–Horner reaction,²⁰ (2) = 2-benzoylazobenzene, and (c) products obtained after heating the isolated intermediate in BuOH/HOAc (110 °C) for 5 min.

two unidentified byproducts (Figure 8a). **F** is identified as 2,3,4-triphenyl-2,3-dihydrocinnoline by comparison with authentic material prepared by a Wittig–Horner reaction of 2-benzoylazobenzene and diethyl benzylphosphonate (Figure 8b).²¹ When the mixture that is isolated from the catalytic reaction is heated in 1-BuOH/HOAc (110 °C), complete conversion to **1** is observed after 5 min (Figure 8c). In the presence of HOAc the intermediate **F** cannot be observed in the reaction solution by HPLC.

The conversion of 1,2- and 1,4-dihydrocinnolines to 1-aminoindoles is described in the literature.²²

When the chloro ligand (X = Cl) in $RhX(PPh_3)_3$ is replaced by a bromo or iodo ligand, TOR values in the

(18) Halpern, J.; Okamoto, T. *Inorg. Chim. Acta* **1984**, *89*, 1984.
 (19) Wang, Z. Q.; Turner, M. L.; Kunicki, A. R.; Maitlis, P. M. *J. Organomet. Chem.* **1995**, *488*, C11.
 (20) Halbritter, G. Ph.D. Thesis, Universität Erlangen–Nürnberg, Nürnberg, Germany, 1994.

(21) This affords **E** in the first step, which cyclizes to **F**; see ref 20.
 (22) (a) Besford, L. S.; Bruce, M. I. *J. Chem. Soc.* **1964**, 4037. (b) Haddlesey, D. J.; Major, P. A.; Szinai, S. S. *J. Chem. Soc.* **1964**, 5269.

toluene/HOAc system increase in the order Cl (6) < Br (8) < I (10), while the TON vary in the sequence I (31) < Cl (34) < Br (35) due to the higher oxygen sensitivity of the iodo complex. The increase of TOR parallels the increasing trans-effect as observed for the same halide ligands in the rhodium catalyzed hydrogenation of olefins.¹⁰ In alcohols all three halogeno complexes are more sensitive toward oxidative decomposition, which increases in the order Cl < Br < I.²³ Due to this effect the TOR values change to Cl (1) < I (2) < Br (3) in the lower boiling solvent, ProH, and to I (3) < Br (8) < Cl (13) in the higher boiling solvent, BuOH. Addition of HOAc to BuOH increases the rate, and the dependence on the halide ligand becomes I (10) < Br (20) = Cl (20). It seems therefore more likely that the intrinsic influence of the halogeno ligand is reflected best by the results obtained in toluene solution. Although the trans effect can operate in the steps B to C and D to E, the latter one should be more important since it should labilize the Rh-C bond which has to be broken during reductive elimination.

Experimental Section

All reactions were conducted under a nitrogen atmosphere, and solvents were dried and purified by standard procedures and nitrogen-saturated after distillation. Acetonitrile (Ferak) used for the HPLC measurements was sonicated and stored under nitrogen. Column chromatography: SiO₂-60 (230–400 mesh ASTM, Merck); $l = 20$ cm, $\phi = 2.5$ cm, petroleum ether/diethylether = 5/1 (v/v) as eluting agent. HPLC: Knauer HPLC pump 64 with analytical and preparative pump head, Knauer UV/vis filter photometer at $\lambda = 220$ nm as detector. *Analytical measurements*: precolumn (30 × 8 mm²) attached to main column (250 × 8 mm²) and both filled with Spherisorb ODS 2.5 μ m (RP C18), eluting with CH₃CN/H₂O = 5/1 (v/v) at a flow rate of 5.0 mL/min. Sample preparation: 250 μ L of the reacting solution was withdrawn by a syringe, evaporated to dryness, and redissolved in 5.0 mL of CH₃CN; 20 μ L of this solution was then injected, and the concentration was determined via a calibration curve. *Preparative isolations*: 1 mL of a THF solution was injected; identical elution agent and filling material were used, while the sizes of precolumn and main column were 30 × 32 and 250 × 32 mm², respectively; the flow rate was 30 mL/min.

¹H and ¹³C NMR spectra were measured in acetone-*d*₆ solutions at 270 and 67 MHz, respectively, and IR spectra in KBr unless otherwise noted. The following instruments were used: NMR, Jeol FT-JNM-EX 270 and Jeol JNM-PXM 60; IR, Perkin-Elmer 983 and FT IR 1600; UV/vis, Shimadzu UV-3101 PC; MS, Varian MAT 212.

The compounds RhCl(PPh₃)₃,²⁴ RhBr(PPh₃)₃,²⁴ RhI(PPh₃)₃,¹⁰ 4,4'-dimethyltolan,²⁵ 4,4'-dimethoxytolan,²⁵ 4,4'-dinitrotolan,²⁶ decafluorotolan,²⁷ 4-methyltolan,²⁸ 4-methoxytolan,²⁸ 4-nitrotolan,²⁸ *tert*-butylphenylacetylene,²⁹ and adamantyl-phenylacetylene²⁹ were prepared according to literature. Symmetric diazenes were synthesized from the corresponding anilines, and asymmetric diazenes were synthesized from aniline and

nitrosobenzene derivatives.³⁰ All turnover numbers and turnover rates refer to total concentrations of 1 + 2 as obtained from HPLC analysis.

General Procedure of Reaction Monitoring in the System PhN₂Ph/PhC₂Ph with TON = 40. To a refluxing solution of 0.05 mmol of RhX(PPh₃)₃ (X = Cl, Br, I) in 10 mL of solvent are added 364 mg (2 mmol) of azobenzene and 357 mg (2 mmol) of tolan dissolved in 15 mL of solvent within 10 min. Refluxing is continued for 24 h, and samples for HPLC analysis are withdrawn after 1, 4, 6, and 24 or 48 h.

Product Yields in Different Solvents. With 46.1 mg of RhCl(PPh₃)₃ as catalyst the concentrations [10⁻³ mol/L] of 1 and 2, respectively, at the indicated reaction times are as follows: toluene, 2 and 0.4 (1 h), 7.6 and 1 (4 h), 9.8 and 2.1 (6 h), 22.8 and 4.0 (24 h); 1-ProH, 2.4 and 0.4 (1 h), 17.8 and 0.6 (4 h), 24.0 and 0.8 (6 h), 76.0 and 1.2 (24 h); 1-BuOH, 26.0 and 0.7 (1 h), 54.6 and 1.8 (4 h), 68.6 and 2.6 (6 h), 75.4 and 3.4 (24 h); 1-pentanol, 70.8 and 1.2 (1 h), 75.8 and 4.0 (4 h); ethanol, 3.0 and 0 (24 h); acetic acid, 0 and 0 (24 h); pyridine, 0.8 and 0 (24 h).

With 48.4 mg of RhBr(PPh₃)₃ as catalyst the concentrations [10⁻³ mol/L] of 1 and 2, respectively, at the indicated reaction times are as follows: 1-ProH, 6.0 and 0.2 (1 h), 27.6 and 0.7 (4 h), 36.6 and 0.9 (6 h), 75.0 and 1.1 (24 h); 1-BuOH, 14.8 and 0.3 (1 h), 39.2 and 0.6 (4 h), 54.0 and 1.0 (6 h), 60.8 and 5.0 (24 h).

With 50.8 mg of RhI(PPh₃)₃ as catalyst the concentrations [10⁻³ mol/L] of 1 and 2, respectively, at the indicated reaction times are as follows: 1-ProH, 3.6 and 0 (1 h), 23.2 and 1.6 (4 h) 32.4 and 3.2 (6 h) 49.2 and 7.6 (24 h); 1-BuOH, 6.8 and 0 (1 h), 24.4 and 2.0 (4 h), 32.4 and 3.2 (6 h), 49.2 and 7.6 (24 h).

Product Yields in Different Solvents in Presence of Catalytic Amounts of Additives. The additive was dissolved together with the catalyst in 10 mL of the refluxing solvent. With 46.1 mg of RhCl(PPh₃)₃ as catalyst the concentrations [10⁻³ mol/L] of 1 and 2, respectively, at the indicated reaction times are as follows: toluene/HOAc (0.25 mmol), 12.4 and 0.2 (1 h), 23.6 and 0.8 (4 h), 29.6 and 1.2 (6 h), 65.6 and 3.4 (24 h); toluene/pyridine (0.25 mmol), 1.2 and 0 (1 h) 4.4 and 1.8 (6 h), 12.4 and 1.8 (24 h); toluene/1-BuOH (0.25 mmol), 0.8 and 0.4 (1 h), 5.7 and 0.9 (4 h), 8.8 and 1.2 (6 h), 28 and 1.2 (24 h); toluene/benzoic acid (0.25 mmol), 4.4 and 0 (1 h), 7.4 and 0.1 (4 h), 9.0 and 0.3 (6 h), 10.5 and 1.2 (24 h); toluene/antranilic acid (0.25 mmol), 4.3 and 0 (1 h), 6.4 and 0.3 (4 h), 9.4 and 0.7 (48 h); toluene/4-nitrobenzoic acid (0.25 mmol), 0 and 0 (1 h), 1.0 and 0 (4 h), 2.1 and 0.2 (48 h); toluene/4-chlorobenzoic acid (0.25 mmol), 2.3 and 0 (1 h), 3.9 and 0.2 (4 h), 10.8 and 1.2 (48 h); 1-ProH/HOAc (0.25 mmol), 7.2 and 0.1 (1 h), 28.0 and 0.4 (4 h), 43.6 and 0.8 (6 h), 76.0 and 1.4 (24 h); 1-BuOH/HOAc (0.25 mmol), 37.2 and 2.0 (1 h), 73.4 and 3.2 (4 h), 75.2 and 4.6 (6 h).

With 48.4 mg of RhBr(PPh₃)₃ as catalyst the concentrations [10⁻³ mol/L] of 1 and 2, respectively, at the indicated reaction times are as follows: toluene/HOAc (0.25 mmol), 16.8 and 0.4 (1 h), 18.0 and 0.4 (4 h), 67.2 and 3.6 (24 h); 1-BuOH/HOAc (0.25 mmol), 39.6 and 0.4 (1 h), 75 and 2 (4 h), 77 and 3 (6 h).

With 50.8 mg of RhI(PPh₃)₃ as catalyst the concentrations [10⁻³ mol/L] of 1 and 2, respectively, at the indicated reaction times are as follows: toluene/HOAc (0.25 mmol), 20.4 and 0.4 (1 h), 36.0 and 0.6 (4 h), 60.0 and 2 (24 h); 1-BuOH/HOAc (0.25 mmol), 18.8 and 1.2 (1 h), 36.8 and 2.8 (4 h), 48.4 and 4.0 (6 h), 55.2 and 9.0 (24 h).

General Procedure of Reaction Monitoring in the System PhN₂Ph/PhC₂Ph with TON_{max} = 120. To 20 mL of a refluxing solution of 46.1 mg (0.05 mmol) of RhCl(PPh₃)₃ and 15 μ L (0.25 mmol) of HOAc are added 1092 mg (6 mmol) of azobenzene and 1068 mg (6 mmol) of tolan dissolved in 30 mL of solvent slowly within 15 min. Refluxing is continued

(23) Augustine, R. L.; van Peppen, J. F. *J. Chem. Soc. Chem. Commun.* **1970**, 497.

(24) Osborn, A.; Wilkinson, G. *Inorg. Synth.* **1967**, *10*, 67.

(25) (a) Mukaiyama, T.; Nambu, H.; Kumamoto, T. *J. Org. Chem.* **1964**, *29*, 2243. (b) Mukaiyama, T.; Nambu, H.; Okamoto, M. *J. Org. Chem.* **1962**, *27*, 3651.

(26) (a) Walden, P.; Kernbaum, A. *Chem. Ber.* **1890**, *23*, 1958. (b) Ruggli, P.; Lang, F. *Helv. Chim. Acta* **1938**, *21*, 38.

(27) Gastinger, R. G.; Tokas, E. F.; Rausch, M. D. *J. Org. Chem.* **1978**, *43*, 159.

(28) Stephens, R. D.; Castro, C. E. *J. Org. Chem.* **1963**, *28*, 3313.

(29) Capozzi, G.; Romeo, G.; Marcuzzi, F. *J. Chem. Soc., Chem. Commun.* **1982**, 959.

(30) Schundehütte, K. H. In *Houben-Weyl: Methoden der organischen Chemie*; Thieme Verlag: Stuttgart, Germany, 1965; Vol. 10/3, p 321.

for 48 h, and samples for HPLC analysis are withdrawn after 1, 4, 6, 24, and 48 h.

Different Solvents. The concentrations [10^{-3} mol/L] of **1** and **2**, respectively, at the indicated reaction times are as follows: toluene, 4.3 and 0 (1 h), 9.0 and 0 (4 h), 10.6 and 0 (6 h), 16.4 and 0.6 (48 h); 1-PrOH, 5.5 and 0 (1 h), 22.2 and 0.2 (4 h), 32.4 and 1.1 (6 h), 103.0 and 1.7 (48 h); 1-BuOH, 47.8 and 0.75 (4 h), 61.2 and 1.25 (6 h), 95.3 and 3.0 (48 h); 1-pentanol, 23.2 and 2.3 (1 h), 42.7 and 6.1 (4 h), 44.5 and 7.5 (6 h), 23.7 and 20.3 (24 h).

In Situ Preparation of Wilkinson's Catalyst in Dependence on the PPh_3 Concentration. A 13.1 mg (0.05 mmol) amount of $\text{RhCl}_3 \cdot 3\text{H}_2\text{O}$ and different concentrations of PPh_3 in 20 mL of 1-PrOH are refluxed for 20 min. Then a solution of 1.092 g (6 mmol) of azobenzene and 1.068 g (6 mmol) of tolan in 30 mL of 1-PrOH is added within 30 min. Refluxing is continued for 48 h, and samples for HPLC analysis are withdrawn after 6, 24, and 48 h. The concentrations [10^{-3} mol/L] of **1** and **2**, respectively, at the indicated reaction times are as follows: 13.1 mg (0.05 mmol) of PPh_3 , 1.0 and 0.7 (6 h), 3.2 and 6.0 (24 h), 4.4 and 10.1 (48 h); 26.2 mg (0.1 mmol) of PPh_3 , 1.1 and 1.2 (6 h), 4.2 and 6.0 (24 h), 7.2 and 9.0 (48 h); 39.3 mg (0.15 mmol) of PPh_3 , 12.5 and 2.0 (6 h), 38.2 and 10.0 (24 h), 85.1 and 22.7 (48 h); 52.4 mg (0.2 mmol) of PPh_3 , 5.5 and 3.6 (6 h), 18.0 and 15.0 (24 h), 29.3 and 24.0 (48 h).

Kinetic Measurements. For the measurement of the initial rate as a function of substrate concentration the following standard procedure was applied. A 92.2 mg (0.1 mmol) amount of $\text{RhCl}(\text{PPh}_3)_3$ and 30 μL (0.5 mmol) of HOAc in 20 mL of 1-BuOH are heated in a thermostated oil bath to 110 °C. Thereafter 30 mL of a 110 °C hot solution containing 728 mg (4 mmol) of azobenzene and 712 mg (4 mmol) of tolan in 1-BuOH are added as quickly as possible. Samples of 500 μL were withdrawn, evaporated to dryness, and redissolved in 4 mL of CH_3CN , and the concentration of **1** was determined by HPLC as described above. Reproducibility was within $\pm 10\%$. The concentrations of **1** within the first 40 min are 14.4×10^{-4} (10 min), 60.8×10^{-4} (20 min), 83.2×10^{-4} (30 min) and 108.2×10^{-4} mol/L (40 min). Since the rate is fastest between 10 and 20 min, the initial rate was calculated from the amount of **1** produced within this period.

Initial Rate as a Function of Azobenzene Concentration. 0.02 mol/L: 9.6×10^{-4} mol/L (10 min), 22.4×10^{-4} mol/L (20 min), $d[\text{P}]/dt = 2.13 \times 10^{-6}$ mol/L s. 0.03 mol/L: 4.0×10^{-4} mol/L (10 min), 21.6×10^{-4} mol/L (20 min), $d[\text{P}]/dt = 2.93 \times 10^{-6}$ mol/L s. 0.04 mol/L: 14.4×10^{-4} mol/L (10 min), 34.4×10^{-4} mol/L (20 min), $d[\text{P}]/dt = 3.33 \times 10^{-6}$ mol/L s. 0.05 mol/L: 9.6×10^{-4} mol/L (10 min), 35.2×10^{-4} mol/L (20 min), $d[\text{P}]/dt = 4.26 \times 10^{-6}$ mol/L s. 0.06 mol/L: 21.6×10^{-4} mol/L (10 min), 53.6×10^{-4} mol/L (20 min), $d[\text{P}]/dt = 5.33 \times 10^{-6}$ mol/L s. 0.08 mol/L: 23.2×10^{-4} mol/L (10 min), 67.2×10^{-4} mol/L (20 min), $d[\text{P}]/dt = 7.33 \times 10^{-6}$ mol/L s. 0.1 mol/L: 16.0×10^{-4} mol/L (10 min), 67.2×10^{-4} mol/L (20 min), $d[\text{P}]/dt = 8.53 \times 10^{-6}$ mol/L s.

Initial Rate as a Function of Tolane Concentration. 0.01 mol/L: 16.0×10^{-4} mol/L (10 min), 75.6×10^{-4} mol/L (20 min), $d[\text{P}]/dt = 9.96 \times 10^{-6}$ mol/L s. 0.02 mol/L: 33.6×10^{-4} mol/L (10 min), 96.8×10^{-4} mol/L (20 min), $d[\text{P}]/dt = 10.4 \times 10^{-6}$ mol/L s. 0.03 mol/L: 40.0×10^{-4} mol/L (10 min), 94.4×10^{-4} mol/L (20 min), $d[\text{P}]/dt = 9.06 \times 10^{-6}$ mol/L s. 0.04 mol/L: 32.0×10^{-4} mol/L (10 min), 81.6×10^{-4} mol/L (20 min), $d[\text{P}]/dt = 8.26 \times 10^{-6}$ mol/L s. 0.06 mol/L: 28.8×10^{-4} mol/L (10 min), 72.0×10^{-4} mol/L (20 min), $d[\text{P}]/dt = 7.2 \times 10^{-6}$ mol/L s. 0.08 mol/L: 26.2×10^{-4} mol/L (10 min), 68.0×10^{-4} mol/L (20 min), $d[\text{P}]/dt = 6.93 \times 10^{-6}$ mol/L s. 0.1 mol/L: 24.8×10^{-4} mol/L (10 min), 66.4×10^{-4} mol/L (20 min), $d[\text{P}]/dt = 6.93 \times 10^{-6}$ mol/L s.

Initial Rate as a Function of $\text{RhCl}(\text{PPh}_3)_3$ Concentration. 1.0 mmol/L: 2.4×10^{-4} mol/L (10 min), 15.2×10^{-4} mol/L (20 min), $d[\text{P}]/dt = 2.13 \times 10^{-6}$ mol/L s. 1.5 mmol/L: 18.4×10^{-4} mol/L (10 min), 36.0×10^{-4} mol/L (20 min), $d[\text{P}]/dt = 2.93 \times 10^{-6}$ mol/L s. 2.0 mmol/L: 12.0×10^{-4} mol/L (10

min), 37.6×10^{-4} mol/L (20 min), $d[\text{P}]/dt = 4.26 \times 10^{-6}$ mol/L s. 3.0 mmol/L: 34.4×10^{-4} mol/L (10 min), 68.0×10^{-4} mol/L (20 min), $d[\text{P}]/dt = 5.6 \times 10^{-6}$ mol/L s. 4.0 mmol/L: 33.6×10^{-4} mol/L (10 min), 88.8×10^{-4} mol/L (20 min), $d[\text{P}]/dt = 9.1 \times 10^{-6}$ mol/L s. 5.0 mmol/L: 32.0×10^{-4} mol/L (10 min), 88.0×10^{-4} mol/L (20 min), $d[\text{P}]/dt = 9.33 \times 10^{-6}$ mol/L s. 6.0 mmol/L: 28.8×10^{-4} mol/L (10 min), 71.2×10^{-4} mol/L (20 min), $d[\text{P}]/dt = 7.06 \times 10^{-6}$ mol/L s.

Initial Rate as a Function of HOAc Concentration. 0.002 mol/L: 6.4×10^{-4} mol/L (10 min), 32.0×10^{-4} mol/L (20 min), $d[\text{P}]/dt = 4.26 \times 10^{-6}$ mol/L s. 0.01 mol/L: 12.0×10^{-4} mol/L (10 min), 37.6×10^{-4} mol/L (20 min), $d[\text{P}]/dt = 4.26 \times 10^{-6}$ mol/L s. 0.033 mol/L: 28.8×10^{-4} mol/L (10 min), 51.2×10^{-4} mol/L (20 min), $d[\text{P}]/dt = 3.73 \times 10^{-6}$ mol/L s. 0.066 mol/L: 47.2×10^{-4} mol/L (10 min), 70.4×10^{-4} mol/L (20 min), $d[\text{P}]/dt = 3.86 \times 10^{-6}$ mol/L s. 0.1 mol/L: 32.0×10^{-4} mol/L (10 min), 58.4×10^{-4} mol/L (20 min), $d[\text{P}]/dt = 4.4 \times 10^{-6}$ mol/L s.

Initial Rate and Rate Constant as Functions of the Temperature. 373 K: 2.4×10^{-4} mol/L (10 min), 15.2×10^{-4} mol/L (20 min), $d[\text{P}]/dt = 2.1 \times 10^{-6}$ mol/L s; from eq 1 and the concentrations given above, the rate constants is calculated as $k = 5.4 \times 10^{-3}$ (mol/L) $^{-0.7}$ s $^{-1}$. 378 K: 23.2×10^{-4} mol/L (10 min), 42.4×10^{-4} mol/L (20 min), $d[\text{P}]/dt = 3.2 \times 10^{-6}$ mol/L s, $k = 8.26 \times 10^{-3}$ (mol/L) $^{-0.7}$ s $^{-1}$. 383 K: 12.0×10^{-4} mol/L (10 min), 37.6×10^{-4} mol/L (20 min), $d[\text{P}]/dt = 4.26 \times 10^{-6}$ mol/L s, $k = 11.11 \times 10^{-3}$ (mol/L) $^{-0.7}$ s $^{-1}$. 388 K: 28.82×10^{-4} mol/L (10 min), 62.42×10^{-4} mol/L (20 min), $d[\text{P}]/dt = 5.6 \times 10^{-6}$ mol/L s, $k = 14.4 \times 10^{-3}$ (mol/L) $^{-0.7}$ s $^{-1}$. A plot of $\log k$ vs $1/T$ affords a straight line (corr coeff = 0.98) with a slope of -8960 ± 670 K and an intercept of 18.8 ± 1.8 . The activation energy and activation entropy are calculated to $E_a = 75 \pm 6$ kJ/mol and $\Delta S^\ddagger = -96 \pm 14$ J/mol K, respectively.

General Procedure for Indole Syntheses. To a solution of 46.1 mg (0.05 mmol) of $\text{RhCl}(\text{PPh}_3)_3$ and 15 μL (0.25 mmol) of HOAc in 10 mL of refluxing 1-PrOH are added dropwise within 10 min 2 mmol each of the alkyne and diaryldiazene dissolved in 15 mL of 1-PrOH. After 24 h the solution is evaporated to dryness, and the residue is chromatographed with petroleum ether/ether = 5/1 (v/v) on a short SiO_2 column ($l \approx 15$ cm, $\phi = 3$ cm, Merck SiO_2 -60). The obtained raw material is purified by preparative HPLC as described above.

1-Anilino-2,3-diphenylindole, 1a: 357 mg of tolan and 364 mg of azobenzene were used. After 4 h 30% of the tolan had reacted, yielding 719 mg of raw material from which 263 mg was purified, affording 238 mg of a white crystalline solid. This corresponded to an overall yield of 90%. $^1\text{H-NMR}$: δ (ppm) 8.51 (s, 1H, NH); 7.73 (m, 1H, 4-H); 7.41–7.07 (m, 15H, 2 C_6H_5 at C-2 and C-3 plus 5-H, 6-H, 7-H, 11-H, and 13-H); 6.74 (t, 1H, 12-H); 6.49 (d, 2H, 10-H and 14-H). $^{13}\text{C-NMR}$: 111.0 (C-7); 113.0 (C-10 and C-14); 114.6 (C-3); 120.1 (C-4); 120.7 (C-12); 120.8 (C-6); 121.8 (C-5); 123.5 (C-18'); 126.3 (C-3a); 126.8 (C-18); 128.7 (C-16' and C-20'); 129.1 (C-16 and C-20); 129.9 (C-11 and C-13); 130.8 (C-17' and C-19'); 131.6 (C-15); 131.7 (C-17 and C-19); 135.7 (C-15'); 138.4 (C-2 and C-7a); 149.1 (C-9). IR $\nu(\text{NH}) = 3296$ cm^{-1} . MS (FD) m/z 360 (M^+). Calcd for $\text{C}_{26}\text{H}_{20}\text{N}_2$ (360.4): C, 86.64; H, 5.59; N, 7.77. Found: C, 86.76; H, 5.60; N, 7.80.

1-Anilino-2,3-bis-(4-methylphenyl)indole, 1b: 404 mg of 4,4'-dimethyltolan and 364 mg of azobenzene were used. After 4 h 70% of the azobenzene had reacted, yielding 830.6 mg of raw material from which 640 mg was purified, affording 496 mg of a white-brown crystalline solid (86% yield). $^1\text{H-NMR}$: 8.3 (s, 1H, NH); 7.55 (m, 1H, 4-H); 6.8–7.1 (m, 13H, 2 C_6H_4 at C-2 and C-3, 5-H, 6-H, 7-H, 11-H, and 13-H); 6.55 (t, 1H, 12-H); 6.3 (d, 2H, 10-H and 14-H); 2.15 (s, 3H, $-\text{CH}_3$ and C-18'); 2.08 (s, 3H, $-\text{CH}_3$ at C-18). $^{13}\text{C-NMR}$: 21.16 (C-21 and C-21'); 110.8 (C-7); 112.9 (C-10 and C-14); 114.2 (C-3); 120.0 (C-4); 120.6 (C-12); 121.5 (C-6); 123.2 (C-5); 126.4 (C-3a); 128.7 (C-15); 129.3 (C-11 and C-13); 129.8 (C-16, C-20, C-17', and C-19'); 130.3 (C-16' and C-20'); 131.5 (C-17 and C-19); 137.1 (C-2); 138.3 (C-18 and C-18'); 149.5 (C-9). IR $\nu(\text{NH}) = 3350$ cm^{-1} .

MS (FD) m/z 388 (M^+). Calcd for $C_{28}H_{24}N_2$ (388.4): C, 86.56; H, 6.22; N, 7.20. Found: C, 86.25; H, 6.48; N, 7.07.

1-Anilino-2,3-bis-(4-methoxyphenyl)indole, 1c: 476 mg of 4,4'-dimethoxytolan and 364 mg of azobenzene were used. After 4 h 23% of the tolan had reacted, yielding 931 mg of raw material from which 361 mg was purified, affording 254 mg of a white-brown crystalline solid (78% yield). 1H -NMR: 8.45 (s, 1H, NH); 7.68 (m, 1H, 4-H); 7.33–7.25 (m, 5H, 7-H, 16-H, 16'-H, 20-H, and 20'-H); 7.18–7.07 (m, 4H, 5-H, 6-H, 11-H, and 13-H); 6.92–6.71 (2d, t, 5H, 12-H forms the triplet, 17-H/19-H and 17'-H/19'-H form the two doublets); 6.48 (d, 2H, 10-H and 14-H); 3.78 (s, 3H, $-OCH_3$ at C-18'); 3.73 (s, 3H, $-OCH_3$ at C-18). ^{13}C -NMR: 55.4 (2 $-OCH_3$); 110.8 (C-7); 112.9 (C-10 and C-14); 113.8 (C-3); 114.2 (C-17 and C-19); 114.6 (C-17' and C-19'); 119.9 (C-4); 120.6 (C-12); 121.5 (C-6); 123.1 (C-5); 123.8 (C-15); 126.6 (C-3a); 128.1 (C-15'); 129.9 (C-11 and C-13); 131.8 (C-16' and C-20'); 132.9 (C-16 and C-20); 137.1 (C-7a); 137.9 (C-2); 149.2 (C-9); 158.9 (C-18'); 160.2 (C-18). IR $\nu(NH) = 3340\text{ cm}^{-1}$. MS (FD) m/z 420 (M^+). Calcd for $C_{28}H_{24}N_2O_2$ (420.5): C, 79.98; H, 5.75; N, 6.65. Found: C, 79.97; H, 5.83; N, 6.56.

1-Anilino-2,3-di-*n*-propylindole, 1d: 300 μL of 4-octyne and 364 mg of azobenzene were used. After 4 h 78% of the azobenzene had reacted, 556 mg of raw material from which 377 mg was purified, affording 202 mg of a white crystalline solid (52% yield). 1H -NMR: 8.3 (s, 1H, NH); 7.55 (m, 1H, 4-H); 7.15–6.95 (m, 5H, 5-H, 6-H, 7-H, 11-H, and 13-H); 6.77 (t, 1H, 12-H); 6.43 (d, 2H, 10-H and 14-H); 2.8–2.65 (m, 4H, 2 $-CH_2$ at C-2 and C-3); 1.75–1.6 (m, 4H, 2 $-CH_2$ at C-15 and C-15'); 1.0–0.9 (m, 6H, 2 $-CH_3$). ^{13}C -NMR: 14.3 (C-17'); 14.4 (C-17); 24.0 (C-16'); 24.9 (C-16); 26.7 (C-15'); 27.2 (C-15); 109.8 (C-7); 110.7 (C-3); 112.8 (C-10 and C-14); 119.1 (C-4); 120.1 (C-6); 120.5 (C-12); 121.6 (C-5); 127.3 (C-3a); 129.8 (C-11 and C-13); 136.4 (C-7a); 138.4 (C-2); 149.4 (C-9). IR $\nu(NH) = 3303\text{ cm}^{-1}$. MS (FD) m/z 292 (M^+). Calcd for $C_{20}H_{24}N_2$ (292.4): C, 82.14; H, 8.27; N, 9.57. Found: C, 82.20; H, 8.55; N, 9.72.

1-Anilino-2,3-bis(pentafluorophenyl)indole, 1e: 716 mg of decafluorotolan and 364 mg of azobenzene were used with a 45 h reaction time. After 20 h 50% of the azobenzene had reacted. A 177 mg amount of a white-brown crystalline solid was isolated (16% yield). 1H -NMR: 8.95 (s, 1H, NH); 7.63 (d, 1H, 4-H); 7.4–7.25 (m, 3H, 5-H, 6-H, and 7-H); 7.15 (t, 2H, 11-H and 13-H); 6.85 (t, 1H, 12-H); 6.55 (d, 2H, 10-H and 14-H). ^{13}C -NMR: 111.8 (C-7); 113.5 (C-10 and C-14); 120.9 (C-4); 121.9 (C-12); 122.9 (C-6); 125.2 (C-5); 126.1 (C-3a); 130.2 (C-11 and C-13); 137.4 (C-7a); 148.3 (C-9); no detailed assignment was possible for C-2, C-3, or the carbon atoms of the pentafluorophenyl rings which appeared as broad multiplets in the ranges 136.0–137.2, 139.4–141.2, 142.8–145.0, and 147.0–148.0. IR $\nu(NH) = 3338\text{ cm}^{-1}$. MS (FD) m/z 540 (M^+). Calcd for $C_{26}H_{10}N_2F_{10}$ (540.3): C, 57.79; H, 1.86; N, 5.18. Found: C, 57.54; H, 1.87; N, 5.06.

Reaction of Azobenzene with 4,4'-Dinitrotolan: 364 mg of azobenzene and 536 mg of 4,4'-dinitrotolan were used. Upon dropwise addition of the substrates the color of the solution changed immediately from cloudy orange to clear red and after 5 min to green yellow and cloudy again. After 24 h, about 5% of azobenzene had reacted but no indoles were present.

Reaction of Azobenzene with Acetylenedicarboxylic Acid: 364 mg of azobenzene and 228 mg of acetylenedicarboxylic acid were used. A few minutes after dropwise addition of the substrates the color of the solution changed from orange to yellow. After 6 h and 24 h no indole formation had occurred.

1-Anilino-2-*tert*-butyl-3-phenylindole, 1f: 350 μL of *tert*-butylphenylacetylene and 364 mg of azobenzene were used, yielding 538 mg of raw material from which 431 mg was purified, affording 97 mg of a white-brown crystalline solid (18% yield). 1H -NMR: 8.55 (s, 1H, NH); 7.45–7.33 (m, 5H, $-C_6H_5$ at C-3); 7.2 (t, 2H, 11-H and 13-H); 7.04–6.9 (m, 4H, 4-H, 5-H, 6-H, and 7-H); 6.8 (t, 1H, 12-H); 6.6 (br, 10-H and 14-H); 1.37 (s, 9H, 3 $-CH_3$). ^{13}C -NMR: 31.7 (3 $-CH_3$); 35.0 (C-15); 110.1 (C-7); 113.3 (C-3); 113.6 (C-10 and C-14); 119.7 (C-

4); 120.7 (C-12); 120.8 (C-6); 122.4 (C-5); 127.5 (C-18'); 128.5 (C-16' and C-20'); 129.2 (C-3a); 129.8 (C-11 and C-13); 132.3 (C-17'); 132.7 (C-19'); 136.1 (C-7a); 144.1 (C-2); 148.9 (C-9). IR $\nu(NH) = 3302\text{ cm}^{-1}$. MS (FD) m/z 340 (M^+). Calcd for $C_{24}H_{24}N_2$ (340.45): C, 84.66; H, 7.10; N, 8.22. Found: C, 84.62; H, 7.19; N, 8.26.

1-Anilino-2-adamantyl-3-phenylindole, 1g. Amounts of 472.7 mg of adamantylphenylacetylene and 364 mg of azobenzene were used, yielding 836 mg of raw material from which 418 mg was purified, affording 120 mg of a white-brown crystalline solid (29% yield). 1H -NMR: 8.54 (s, 1H, NH); 7.4–7.25 (m, 5H, $-C_6H_5$ at C-3); 7.2 (t, 2H, 11-H and 13-H); 7.0–6.85 (m, 4H, 4-H, 5-H, 6-H, and 7-H); 6.8 (t, 1H, 12-H); 6.6 (b, 10-H and 14-H); 2.3–1.5 (m, 10H, $-C_{10}H_{15}$). ^{13}C -NMR: 29.5 (C-19, C-20, and C-21); 37.3 (C-22, C-23, and C-24); 38.0 (C-15); 42.5 (C-16, C-17, and C-18); 110.0 (C-7); 113.5 (C-3); 113.8 (C-10 and C-14); 119.8 (C-4); 120.5 (C-6); 120.8 (C-12); 122.4 (C-5); 127.2 (C-18'); 128.3 (C-16' and C-20'); 129.4 (C-3a); 129.9 (C-11 and C-13); 132.3 (C-17'); 132.8 (C-19'); 136.0 (C-15'); 138.3 (C-7a); 143.9 (C-2); 149.1 (C-9). IR $\nu(NH) = 3307\text{ cm}^{-1}$. MS (FD) m/z 419 (M^+). Calcd for $C_{30}H_{30}N_2$ (418.6): C, 86.08; H, 7.22; N, 6.69. Found: C, 85.89; H, 7.38; N, 7.12.

Isomeric Mixture 1h/1i: 250 μL of phenylpropyne and 364 mg of azobenzene were used, and 131 mg of a white-brown crystalline solid was isolated (22% yield). 1H -NMR for 1h: 8.5 (s, 1H, NH); 6.8 (t, 1H, 12-H); 6.53 (d, 2H, 10-H and 14-H); 2.42 (s, 3H, $-CH_3$). For 1i: 8.37 (s, 1H, NH); 6.7 (t, 1H, 12-H); 6.4 (d, 2H, 10-H and 14-H); 2.36 (s, 3H, $-CH_3$); ambiguously assigned signals, 7.68–7.0 (m, 11H, $-C_6H_5$, 4-H, 5-H, 6-H, 7-H, 11-H, and 13-H). The isomeric ratio 1h/1i = 7:4 is obtained from the intensities of the two methyl singlets. ^{13}C -NMR assignment is based on the higher intensities of the 1h signals. For 1h: 10.4 (C-15); 110.0 (C-7); 113.0 (C-10 and C-14); 113.1 (C-3); 119.2 (C-4); 121.0 (C-12); 121.2 (C-6); 122.4 (C-5); 126.7 (C-18'); 129.3 (C-16' and C-20'); 129.6 (C-3a); 130.1 (C-11 and C-13); 130.2 (C-17' and C-19'); 135.1 (C-2); 136.7 (C-15'); 137.1 (C-7a); 149.1 (C-9). For 1i: 9.8 (C-15'); 108.1 (C-3); 110.5 (C-7); 112.8 (C-10 and C-14); 119.6 (C-4); 120.4 (C-12); 120.7 (C-6); 123.1 (C-5); 127.7 (C-3a); 128.2 (C-15); 128.7 (C-16 and C-20); 129.8 (C-11 and C-13); 131.0 (C-17 and C-19); 136.2 (C-2); 138.1 (C-7a); 149.3 (C-9). MS (FD) m/z 298 (M^+). Calcd for $C_{21}H_{18}N_2$ (298.4): C, 84.53; H, 6.08; N, 9.38. Found: C, 84.39; H, 6.12; N, 9.56.

Isomeric Mixture 1k/1l: 384 mg of 4-methyltolan and 364 mg of azobenzene were used, yielding 756 mg of raw material from which 620 mg was purified, affording 457 mg of a white-brown crystalline mixture (73% yield). The isomeric ratio of 1k/1l is 4:3. The NMR spectra are assigned corresponding to the signals of 1a and 1b. The isomeric ratio is calculated from the 1H -NMR signals of the CH_3 groups. In the 1H -NMR of the isomeric mixture, the only distinguishable and unambiguously assigned signals belong to the CH_3 groups: 2.2 (s, 3H, $-CH_3$ at C-18'); 2.3 (s, 3H, $-CH_3$ at C-18). Signals valid for both compounds: 8.43 (s, 1H, NH); 7.7 (m, 1H, 4-H); 6.7 (t, 1H, 12-H); 6.5 (d, 2H, 10-H and 14-H). Ambiguously assigned signals of both compounds: 7.4–7.0 (m, 14H, $-C_6H_4$, $-C_6H_5$, 5-H, 6-H, 7-H, 11-H, and 13-H). ^{13}C -NMR of the isomeric mixture. For 1k: 21.2 ($-CH_3$); 110.8 (C-7); 112.8 (C-10 and C-14); 114.2 (C-3); 119.9 (C-4); 120.6 (C-12); 121.6 (C-6); 123.3 (C-5); 126.2 (C-3a); 126.8 (C-18'); 128.5 (C-15); 129.0 (C-16' and C-20'); 129.3 (C-16 and C-20); 129.8 (C-11 and C-13); 130.6 (C-17' and C-19'); 131.5 (C-17 and C-19); 135.7 (C-15'); 137.1 (C-18); 138.2 (C-7a); 138.4 (C-2); 148.9 (C-9). For 1l: 21.1 ($-CH_3$); 110.8 (C-7); 112.8 (C-10 and C-14); 114.5 (C-3); 120.1 (C-4); 120.6 (C-12); 121.6 (C-6); 123.3 (C-5); 126.3 (C-3a); 128.5 (C-18); 128.6 (C-16' and C-20'); 129.2 (C-16 and C-20); 129.9 (C-11 and C-13); 130.5 (C-17' and C-19'); 131.6 (C-17 and C-19); 131.7 (C-15); 132.6 (C-15'); 136.0 (C-18'); 137.1 (C-7a); 138.0 (C-2); 148.9 (C-9). MS (FD) m/z 374 (M^+). Calcd for $C_{27}H_{22}N_2$ (374.5): C, 86.60; H, 5.92; N, 7.48. Found: C, 86.30; H, 6.08; N, 7.09.

Isomeric Mixture 1m/1n: 416 mg of 4-methoxytolan and 364 mg of azobenzene were used, and 461 mg of a white-brown

crystalline mixture was isolated (59% yield). The isomeric ratio of **1m/1n** is 2:3, calculated from the ¹H-NMR signals of the -OCH₃ groups. ¹H-NMR for **1m**: 6.78 (d, 2H, C-17 and C-19); 3.68 (s, 3H, -OCH₃). For **1n**: 6.88 (d, C-17' and C-19'); 3.73 (s, 3H, -OCH₃); 8.4 (s, 1H, NH); 7.7 (m, 1H, 4-H); 6.72 (m, 12-H); 6.5 (d, 2H, 10-H and 14-H); 7.4–7.0 (m, 12H, -C₆H₅ at C-2 or C-3, hydrogen atoms *meta* to OCH₃, and 5-H, 6-H, 7-H, 11-H, and 13-H). ¹³C-NMR for **1m**: 55.3 (-OCH₃); 110.8 (C-7); 112.9 (C-10 and C-14); 114 (C-3); 114.2 (C-17 and C-19); 119.9 (C-4); 120.6 (C-12); 121.7 (C-6); 123.2 (C-5); 123.6 (C-15); 126.3 (C-3a); 126.6 (C-18'); 129.1 (C-16' and C-20'); 129.9 (C-11 and C-13); 130.7 (C-17' and C-19'); 132.9 (C-16 and C-20); 135.9 (C-15'); 137.1 (C-7a); 138.4 (C-2); 149.0 (C-9); 160.2 (C-18). For **1n**: 55.3 (-OCH₃); 110.8 (C-7); 112.9 (C-10 and C-14); 114.3 (C-3); 114.6 (C-17' and C-19'); 120.1 (C-4); 120.6 (C-12); 121.6 (C-6); 123.4 (C-5); 126.5 (C-3a); 127.8 (C-15'); 128.6 (C-16 and C-20); 129.9 (C-11 and C-13); 131.6 (C-17 and C-19); 131.6 (C-15); 131.8 (C-16' and C-20'); 137.2 (C-7a); 137.9 (C-2); 149.0 (C-9); 158.9 (C-18'). MS (FD) *m/z* 390 (M⁺). Calcd for C₂₇H₂₂N₂O (390.5): C, 83.05; H, 5.68; N, 7.17. Found: C, 82.67; H, 5.85; N, 7.17.

Isomeric Mixture 1o/1p: 446 mg of 4-nitrotolan and 364 mg of azobenzene were used, and 160 mg of an orange crystalline mixture was isolated (20% yield). The isomeric ratio **1o/1p** is 2:5. ¹H-NMR of the isomeric mixture. For **1o**: 8.66 (s, 1H, NH); 8.08 (d, 2H, 17-H and 19-H); 7.71 (d, 1H, 4-H); 7.66 (d, 2H, 16-H and 20-H). For **1p**: 8.58 (s, 1H, NH); 8.16 (d, 2H, 17'-H and 19'-H); 7.82 (m, 1H, 4-H); 7.58 (d, 2H, 16'-H and 20'-H); the resonances of both isomers are isochrone: 7.08 (t, 2H, 11-H and 13-H); 6.74 (t, 1H, 12-H); 6.5 (d, 2H, 10-H and 14-H). Signals not assigned: 7.42–7.15 (m, 8H, -C₆H₅ at C-2 or C-3 and 5-H, 6-H, and 7-H). ¹H-NOE difference spectra (400 MHz): (1) Irradiation at 8.66 ppm (9-H, **1o**) causes intensity increases at 7.66 (16-H, 20-H, **1o**), 7.33 (7-H, **1o**), and 6.5 ppm (10-H, 14-H, **1o**). (2) Irradiation at 8.58 ppm (9-H, **1p**) causes intensity increases at 7.4 (16-H, 20-H, **1p**), 7.34 (7-H, **1p**), and 6.5 ppm (10-H, 14-H, **1p**). (3) Irradiation at 7.66 ppm (16-H, 20-H, **1o**) causes intensity increases at 8.66 (9-H, **1o**), 8.08 (17-H, 19-H, **1o**), and 6.5 ppm (10-H, 14-H, **1o**). (4) Irradiation at 7.58 ppm (16'-H, 20'-H, **1p**) causes intensity increases at 8.16 (17'-H, 19'-H, **1p**), 7.81 (4-H, **1p**), and 7.4 ppm (16-H, 20-H, **1p**). ¹³C-NMR for **1o**: 111.3 (C-7); 112.6 (C-3); 113.0 (C-10 and C-14); 119.8 (C-4); 121.1 (C-12); 122.5 (C-6); 124.1 (C-5); 124.4 (C-17 and C-19); 125.6 (C-3a); 129.1 (C-16' and C-20'); 129.4 (C-18'); 129.9 (C-11 and C-13); 131.1 (C-16 and C-20); 131.7 (C-17' and C-19'); 137.3 (C-15'); 140.3 (C-15); 143.3 (C-7a); 146.4 (C-2); 148.7 (C-18); 148.7 (C-9). For **1p**: 111.2 (C-7); 113.1 (C-10 and C-14); 116.7 (C-3); 120.5 (C-4); 121.2 (C-12); 122.3 (C-6); 123.5 (C-17' and C-19'); 124.5 (C-5); 126.3 (C-3a); 127.5 (C-18); 129.5 (C-16 and C-20); 130.0 (C-11 and C-13); 130.9 (C-17 and C-19); 132.6 (C-16' and C-20'); 134.9 (C-15); 136.0 (C-7a); 137.7 (C-2); 138.4 (C-15'); 147.9 (C-18'); 148.7 (C-9). MS (FD) *m/z* 405 (M⁺). Calcd for C₂₈H₁₉N₃O₂ (405.4): C, 77.05; H, 4.72; N, 10.36. Found: C, 76.66; H, 4.63; N, 10.18.

Isomeric Mixture 1q/1r: 357 mg of tolan and 433 mg of 4-chloroazobenzene were used, and 368 mg of a white solid was isolated (47% yield). ¹H-NMR for **1q**: 8.63 (s, 1H, NH); 7.73 (d, 1H, 4-H); 7.13 (t, 2H, 11-H and 13-H); 6.78 (t, 1H, 12-H); 6.49 (d, 2H, 10-H and 14-H). For **1r**: 8.72 (s, 1H, NH); 7.80–7.73 (m, 1H, 4-H). Signals not assigned: 7.50–7.18 (m, 12H, -C₆H₅, 6-H, 7-H of **1q**, and m, 17 H, -C₆H₅, 5-H, 6-H, 7-H, 10-H to 14-H of **1r**). An isomeric ratio **1q/1r** = 5:1 was obtained from the intensities of the NH signals in the ¹H-NMR spectrum. ¹³C-NMR assignment is based on higher intensities of **1q** resonances. For **1q**: 112.5 (C-7); 113.0 (C-10 and C-14); 113.1 (C-3); 119.4 (C-4); 121.0 (C-12); 123.7 (C-6); 127.1 (C-5); 127.2 (C-19'); 127.4 (C-3a); 128.9 (C-16' and C-20'); 129.0 (C-18); 129.4 (C-16 and C-20); 130.0 (C-11 and C-13); 130.8 (C-17' and C-19'); 131.1 (C-15); 131.7 (C-17 and C-19); 135.0 (C-15'); 135.8 (C-7a); 140.1 (C-2); 148.7 (C-9). For **1r**: 110.7 (C-7); 114.4 (C-3, C-10, and C-14); 120.2 (C-4); 121.9 (C-6); 123.7

(C-5); 124.3 (C-3a); 126.3 (C-12); 131.4 (C-15); 135.5 (C-15'); 137.0 (C-7a); 138.2 (C-2); 147.9 (C-9). Signals not assigned: C-11, C-13, C-16–20, and C-15'–20'. MS (FD) *m/z* 395 (M⁺). Calcd for C₂₆H₁₉N₂Cl (394.9): C, 79.08; H, 4.85; N, 7.09. Found: C, 78.60; H, 4.84; N, 7.00.

Isomeric Mixture 1s/1t: 357 mg of tolan and 392 mg of 4-methylazobenzene were used, and 590 mg of a white solid was isolated (78% yield). ¹H-NMR for **1s**: 8.48 (s, 1H, NH); 7.53 (s, 1H, 4-H); 6.74 (t, 1H, 12-H); 6.48 (d, 2H, 10-H and 14-H); 2.40 (s, 3H, -CH₃ at C-5). For **1t**: 8.38 (s, 1H, NH); 7.75–7.70 (m, 1H, 4-H); 6.92 (d, 2H, 11-H and 13-H); 6.42 (d, 2H, 10-H and 14-H); 2.15 (s, 3H, -CH₃ at C-12). Signals not assigned: 7.43–6.97 (m, -C₆H₅, 5-H, 6-H, 7-H, 11-H, 13-H, of **1s**, and m, 13H, -C₆H₅, 6-H, 7-H of **1t**). An isomeric ratio of **1s/1t** = 2:1 was obtained from the intensities of the NH signals. ¹³C-NMR assignment is based on higher intensities of **1s** signals. For **1s**: 21.5 (C-21); 110.6 (C-7); 112.8 (C-10 and C-14); 114.1 (C-3); 119.6 (C-4); 120.5 (C-12); 125.0 (C-6); 126.6 (C-18'); 128.4 (C-18); 128.5 (C-16' and C-20'); 129.0 (C-16 and C-20); 129.8 (C-11 and C-13); 130.3 (C-5); 130.7 (C-17' and C-19'); 131.6 (C-17 and C-19); 131.7 (C-15); 135.5 (C-15'); 135.9 (C-7a); 138.4 (C-2); 149.0 (C-9); signal not assigned for C-3a. For **1t**: 20.4 (C-21'); 110.9 (C-7); 113.0 (C-10 and C-14); 115.0 (C-3); 120.0 (C-4); 120.6 (C-6); 121.6 (C-5); 123.5 (C-18'); 126.4 (C-3a); 126.6 (C-18); 136.3 (C-15'); 137.1 (C-7a); 146.8 (C-9). Signals not assigned: C-2, C-11–13, C-15–17, C-19–20, C-15'–17', C-19', and 20'. MS (FD) *m/z* 374 (M⁺). Calcd for C₂₇H₂₂N₂ (374.5): C, 86.60; H, 5.92; N, 7.48. Found: C, 86.66; H, 5.90; N, 7.52.

Reaction of 4,4'-dimethoxyazobenzene with tolan: 357 mg of tolan and 484 mg of 4,4'-dimethoxyazobenzene were used. After 72 h, the reaction was stopped and analyzed for indole formation by DC and HPLC. Since retention times were too similar, no product isolation was attempted.

Reactions of 2,4,6-trimethyl-, 3,3',5,5'-tetrachloro-, 3,3',5,5'-tetramethyl-, and 2,2',4,4',6,6'-hexamethylazobenzene with tolan: 357 mg of tolan and 2.0 mmol of the corresponding diazene were employed. No indoles were detected after 24 h.

1-Toluidino-2,3-diphenyl-5-methylindole, 1u: 357 mg of tolan and 421 mg of 4,4'-dimethylazobenzene were used, and 187 mg of a white-brown solid was isolated (24% yield). ¹H-NMR: 8.30 (s, 1H, NH); 7.51 (s, 1H, 4-H); 7.43–7.19 (m, 10H, -C₆H₅); 7.15 (d, 1H, 7-H); 7.01 (d, 1H, 6-H); 6.91 (d, 2H, 11-H and 13-H); 6.40 (d, 2H, 10-H and 14-H); 2.36 (s, 3H, CH₃-21); 2.14 (s, 3H, CH₃-21'). ¹³C-NMR: 20.5 (C-21'), 21.6 (C-21); 110.9 (C-7); 113.1 (C-10 and C-14); 114.1 (C-3); 119.7 (C-4); 125.0 (C-6); 126.6 (C-18'); 128.5 (C-18); 128.6 (C-16' and C-20'); 129.0 (C-16 and C-20); 129.6 (C-3a and C-12); 130.3 (C-11 and C-13); 130.7 (C-5); 130.8 (C-17' and C-19'); 131.7 (C-17 and C-19); 131.9 (C-15); 135.7 (C-15'); 136.0 (C-7a); 138.7 (C-2); 146.8 (C-9). IR ν (NH) = 3350 cm⁻¹. MS (FD) *m/z* 389 (M⁺). Calcd for C₂₈H₂₄N₂ (388.5): C, 86.56; H, 6.23; N, 7.21. Found: C, 86.48; H, 6.25; N, 7.28.

1-(4-Chloroanilino)-2,3-diphenyl-5-chloroindole, 1v: 357 mg of tolan and 502 mg of 4,4-dichloroazobenzene were used, and 223 mg of a white solid was isolated (26% yield). ¹H-NMR: 8.64 (s, 1H, NH); 7.55 (d, 1H, 4-H); 7.35–7.05 (m, 12H, -C₆H₅, 6-H and 7-H); 7.00 (d, 2H, 11-H and 13-H); 6.35 (d, 2H, 10-H and 14-H). ¹³C-NMR: 112.4 (C-7); 114.5 (C-10 and C-14); 114.6 (C-3); 119.5 (C-4); 123.8 (C-6); 125.1 (C-12); 127.4 (C-5 and C-18'); 128.9 (C-16' and C-20'); 129.1 (C-18); 129.3 (C-16 and C-20); 129.9 (C-11 and C-13); 130.7 (C-17' and C-19'); 130.9 (C-15); 131.6 (C-17 and C-19); 134.8 (C-15'); 135.6 (C-7a); 139.9 (C-2); 147.6 (C-9). IR ν (NH) = 3347 cm⁻¹. MS (FD) *m/z* 429 (M⁺). Calcd for C₂₆H₁₈Cl₂N₂ (429.4): C, 72.74; H, 4.23; N, 6.53. Found: C, 72.69; H, 4.52; N, 6.52.

1-(3,5-Dichloroanilino)-2,3-diphenylindole, 1w: 357 mg of tolan and 502 mg of 3,5-dichloroazobenzene were used, and 180 mg of a white solid was isolated (21% yield). ¹H-NMR: 9.04 (s, 1H, NH); 7.77 (d, 1H, 4-H); 7.45–7.18 (m, 13H, -C₆H₅, 5-H, 6-H, and 7-H); 6.82 (t, 1H, 12-H); 6.48 (d, 2H, 10-H and

14-H). $^{13}\text{C-NMR}$: 110.6 (C-7), 111.2 (C-10 and C-14); 115.3 (C-3); 119.1 (C-5); 120.0 (C-4); 120.4 (C-12); 122.3 (C-6); 124.1 (C-18'); 126.3 (C-3a); 127.0 (C-18); 128.6 (C-16 and C-20); 129.2 (C-16' and C-20'); 130.7 (C-17' and C-19'); 131.1 (C-15), 131.6 (C-17 and C-19); 135.3 (C-15'); 136.2 (C-11 and C-13); 136.9 (C-7a); 137.9 (C-2); 151.3 (C-9). IR $\nu(\text{NH}) = 3337\text{ cm}^{-1}$. MS (FD) m/z 429 (M^+). Calcd for $\text{C}_{26}\text{H}_{18}\text{C}_{12}\text{N}_2$ (429.4): C, 72.74; H, 4.23; N, 6.53. Found: C, 73.27; H, 4.21; N, 6.06.

Reaction of azobenzene with $\text{RhCl}(\text{PPh}_3)_3$ in mesitylene: 46 mg (0.05 mmol) of $\text{RhCl}(\text{PPh}_3)_3$ and 9 mg (0.05 mmol) of azobenzene were refluxed for 2 h in mesitylene (bp 163 °C). After cooling to room temperature, the orange brown precipitate (13 mg) was filtered off and washed three times with light petroleum. The IR spectrum showed only the presence of $[\text{RhCl}(\text{PPh}_3)_2]_2$.

NMR experiment with $\text{RhCl}(\text{PPh}_3)_2(\text{PhC}_2\text{Ph})$: 8 mg (0.01 mmol) of the alkyne complex and 2 mg (0.01 mmol) of 4,4'-dimethylazobenzene were transferred into an NMR tube. After addition of 1,4-dioxane- d_8 the measurement was started at 21.4 °C (0 min), and then the solution was heated to 60.3 °C (11 min), 95.1 °C (17 and 51 min), and 95.0 °C (1 day).

Attempt to isolate 2,3,4-triphenyl-2,3-dihydrocinnoline: To a refluxing solution of 92.2 mg (0.1 mmol) of $\text{RhCl}(\text{PPh}_3)_3$ in 20 mL of 1-BuOH were added dropwise within 5 min 1092 mg (6 mmol) of azobenzene and 356 mg (2 mmol) of tolan dissolved in 30 mL of 1-BuOH. After 30 min a new peak appeared in the HPLC spectrum at a retention time of 8.5 min. The peaks of azobenzene, **1a**, and tolan appear at 4.05, 4.55, and 3.95 min, respectively. The reaction was interrupted, and after evaporation to dryness the residue was dissolved in 1 mL of THF. The red solution obtained after purification by

preparative HPLC partially decomposed during subsequent evaporation of the solvent. The HPLC spectrum of the resulting red mixture [4.527 min (relative intensity: 331 492) for 1-anilino-2,3-diphenylindole; 7.093 min (120 175) for an unknown; 8.463 min (3 911 643) for an isolated peak; 10.395 min (143 818) for an unknown] was very similar to that of the mixture obtained from the direct synthesis of the acyclic isomer 2-stilbenylazobenzene.¹⁶ Heating the red mixture in 3 mL of 1-BuOH containing 5 μL of HOAc to 110 °C induced complete conversion of the unknown peak to **1**.

The red mixture is photochromic in CH_2Cl_2 solution: The absorbance of 0.425 at the maximum of 494 nm decreases to 0.162 upon irradiating for 1 min with a 20 W/12 V tungsten-halogen lamp (Osram). After turning off the light, absorbance gradually recovers (0.230 after 5 min) and almost reaches the initial value (0.420) after 180 min. MS (FD): In the range of m/z 250–500 only one peak is found at m/z 360 (M^+).

Acknowledgment. We are grateful to Dr. M. Moll and Priv.-Doz. Dr. W. Bauer for measuring the NMR spectra. This work was supported by Degussa AG and Fonds der Chemischen Industrie.

Supporting Information Available: Text giving general procedure for syntheses of compounds **1a–w** with reaction scheme and tables of yields, elemental analyses, and $^{13}\text{C-NMR}$, MS, IR, and $^1\text{H-NMR}$ data (4 pages). Ordering information is given on any current masthead page.

OM940944V

Diastereoselective Synthesis of Nitrogen-Containing Heterobicyclic and -tricyclic Skeletons via Intramolecular Cyclization of (η^4 -diene)Fe(CO)₃ Complexes Bearing Amino Acid Derivatives

Ming-Chang P. Yeh,* L.-W. Chuang, C.-C. Hwu, J.-M. Sheu, and L.-C. Row

Department of Chemistry, National Taiwan Normal University, 88 Section 4, Ding-Jou Road, Taipei, Taiwan 117, ROC

Received March 6, 1995[⊗]

Addition of secondary amino acid derivatives to (η^5 -pentadienyl)tricarbonyliron cations gives (η^4 -diene)tricarbonyliron complexes in high yields with amino ester groups at the terminal position of the diene ligands. Treatments of the adducts containing a sarcosine, phenylalanine, or alanine moiety with lithium diisopropylamide (LDA), under an atmosphere of carbon monoxide, furnish fused 3-azabicyclo[3.3.0]octanecarboxylic acid derivatives. Under the same reaction conditions, intramolecular cyclizations of complexes containing a proline or pipercolinic acid derivative at the terminal position of the diene ligands give 6-azatricyclo[6.3.0.0^{2,6}]undecane and 7-azatricyclo[7.3.0.0^{2,7}]dodecane ring systems, respectively, whereas treatment of the complex containing a nipecotic acid derivative provides a bridged 8-azatricyclo[6.3.1.0^{2,6}]dodecanecarboxylic acid derivative.

Nitrogen-containing heterocyclic compounds have figured prominently in chemistry due to their useful pharmacological properties, their structural novelty, and their attendant rich chemistry.¹ In spite of the numerous literature on the synthesis of nitrogen-containing heterobicyclic compounds,² there have been few reports on the preparation of nitrogen-containing heterobicyclic and -tricyclic compounds promoted by transition metals. Of these reactions, however, formation of fused nitrogen-containing heterobicyclic compounds has so far been restricted to only cobalt,³ chromium,⁴ titanium,⁵ nickel,⁶ iron,⁷ or palladium-promoted⁸ cyclization of

unsaturated molecules. Only limited examples of cobalt-mediated (the Pauson–Khand reaction) coupling reactions of alkyne to alkene followed by radical cyclization to give angularly fused triquinanes containing a nitrogen atom^{9a} and a palladium-catalyzed cyclization of a polyenyne to give a linearly fused triquinane containing a nitrogen atom have been explored.^{9b} In this paper, we report that nitrogen-containing fused bicyclic, linearly fused tricyclic, and bridged tricyclic skeletons can be constructed by the intramolecular cyclization of the diene–iron complexes bearing amino acid derivatives at the terminal position of the diene ligands.

[⊗] Abstract published in *Advance ACS Abstracts*, June 1, 1995.

- (1) (a) Jutz, J. C. *Top. Curr. Chem.* **1978**, *73*, 125. (b) Katritzky, A. R. *Tetrahedron* **1980**, *36*, 679. (c) Boger, D. L. *Chem. Rev.* **1986**, *86*, 781. (d) Jones, G. In *Quinolines*; Jones, G., Ed.; Wiley-Interscience: London, 1977; p 1. (e) Dyke, S. F.; Kinsman, R. G. In *Isoquinolines*; Grethe, G., Ed.; Wiley-Interscience: New York, 1981; p 1. (f) Sundberg, R. J. *The Chemistry of Indoles*, Academic Press, New York, **1970**. (g) Cordell, G. A. *Introduction to Alkaloids*; Wiley-Interscience: New York, 1981. (h) Williams, D. R.; Brown, D. L.; Benbow, J. W. *J. Am. Chem. Soc.* **1989**, *111*, 1923. (i) Boger, D. L.; Mullican, M. D. *J. Org. Chem.* **1984**, *49*, 4033. (j) Williams, J. P.; St. Laurent, D. R.; Friedrich, D.; Pinard, E.; Roden, B. A.; Paquette, L. A. *J. Am. Chem. Soc.* **1994**, *116*, 4689. (k) Wang, Z.; Jimenez, L. S. *J. Am. Chem. Soc.* **1994**, *116*, 4977.
- (2) (a) Black, D. St. C.; Doyle, J. E. *Adv. Heterocycl. Chem.* **1980**, *27*, 1. (b) Mulzer, J.; Becker, R.; Brunner, E. *J. Am. Chem. Soc.* **1989**, *111*, 7500. (c) Pearson, W. H.; Walavalkar, R.; Schkeryantz, J. M.; Fang, W. K.; Blickensdorf, J. D. *J. Am. Chem. Soc.* **1993**, *115*, 10183. (d) Tückmantel, W.; Andree, G.; Seidel, A.; Schmickler, H.; Lex, J.; Kraka, E.; Haug, M.; Cremer, D.; Vogel, E. *Angew. Chem., Int. Ed. Engl.* **1985**, *24*, 592. (e) Kato, H.; Arikawa, Y.; Hashimoto, M.; Masuzawa, M. *J. Chem. Soc., Chem. Commun.* **1983**, 938. (f) Tokitoh, N.; Okazaki, R. *J. Am. Chem. Soc.* **1987**, *109*, 1856. (g) Shea, K. J.; Lease, T. G.; Ziller, J. W. *J. Am. Chem. Soc.* **1990**, *112*, 8627. (h) Overman, L. E.; Mendelson, L. T.; Jacobsen, E. J. *J. Am. Chem. Soc.* **1983**, *105*, 6629. (i) Overman, L. E.; Jacobsen, E. J.; Doedens, R. J. *J. Org. Chem.* **1983**, *48*, 3393. (j) Jacobsen, E. J.; Levin, J.; Overman, L. E. *J. Am. Chem. Soc.* **1988**, *110*, 4329.
- (3) (a) Jeong, N.; Hwang, S. H.; Lee, Y. *J. Am. Chem. Soc.* **1994**, *116*, 3159. (b) Chung, Y. K.; Lee, B. Y.; Jeong, N.; Hudecek, M.; Pauson, P. L. *Organometallics* **1993**, *12*, 220. (c) Brown, S. W.; Pauson, P. L. *J. Chem. Soc., Perkin Trans. 1* **1990**, 1205.
- (4) (a) Dötz, K. H.; Schäfer, T.; Harms, K. *Angew. Chem., Int. Ed. Engl.* **1990**, *29*, 176. (b) Audouin, M.; Blandinières, S.; Parlier, A.; Rudler, H. *J. Chem. Soc., Chem. Commun.* **1990**, 23.
- (5) Berk, S. C.; Grossman, R. B.; Buchwald, S. L. *J. Am. Chem. Soc.* **1993**, *115*, 4912.

Preparation of Starting Complexes

The addition of primary amines to the (η^5 -pentadienyl)Fe(CO)₃ cation (**1a**) is known to proceed by exo attack to produce (η^4 -*cis*-dienylamine)Fe(CO)₃ complexes and the binuclear species obtained by further reaction with the cation.¹⁰ This has been confirmed in our preliminary investigations; the reaction of the primary amino ester derivative H₂NCH₂CO₂Et with **1a** provided the binuclear species as the major product in 51% yield.

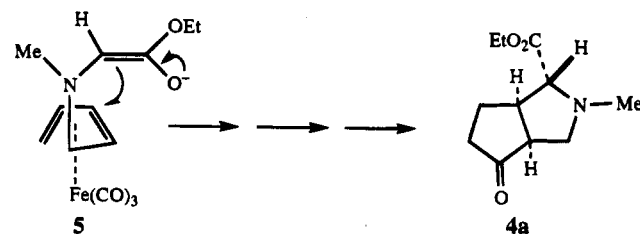
- (6) Tamao, K.; Kobayashi, K.; Ito, Y. *J. Am. Chem. Soc.* **1988**, *110*, 1286.
- (7) (a) Knölker, H.-J. *Synlett* **1992**, 371. (b) Knölker, H.-J.; Heber, J. *Synlett* **1993**, 924. (c) Knölker, H.-J.; El-Ahl, A.-A.; Weingärter, G. *Synlett* **1994**, 194.
- (8) (a) Hegedus, L. S. *Angew. Chem., Int. Ed. Engl.* **1988**, *27*, 1113. (b) van der Schaaf, P. A.; Sutter, J.-P.; Grellier, M.; van Mier, G. P. M.; Spek, A. L.; van Koten, G.; Pfeffer, M. *J. Am. Chem. Soc.* **1994**, *116*, 5134. (c) Bäckvall, J.-E.; Andersson, P. G. *J. Am. Chem. Soc.* **1990**, *112*, 3683. (d) Andersson, P. G.; Bäckvall, J. E. *J. Am. Chem. Soc.* **1992**, *114*, 8696. (e) Grigg, R.; Dorrity, M. J.; Malone, J. F.; Sridharan, V.; Sukirthalingam, S. *Tetrahedron Lett.* **1990**, *31*, 1343. (f) Trost, B. M.; Chen, S.-F. *J. Am. Chem. Soc.* **1986**, *108*, 6053. (g) Trost, B. M.; Scanlan, T. S. *J. Am. Chem. Soc.* **1989**, *111*, 4988. (h) Trost, B. M.; van Vranken, D. L. *J. Am. Chem. Soc.* **1993**, *115*, 444. (i) Trost, B. M.; Marrs, C. M. *J. Am. Chem. Soc.* **1993**, *115*, 6636.
- (9) (a) Clive, D. L. J.; Cole, D. C.; Tao, Y. *J. Org. Chem.* **1994**, *59*, 1396. (b) Trost, B. M.; Shi, Y. *J. Am. Chem. Soc.* **1993**, *115*, 9421.
- (10) (a) Maglio, G.; Palumbo, R. *J. Organomet. Chem.* **1974**, *76*, 367. (b) Maglio, G.; Musco, A.; Palumbo, R. *J. Organomet. Chem.* **1971**, *32*, 127.

With secondary amino ester derivatives, however, we were able to introduce an amino ester moiety at the C-5 position of the diene ligand under mild reaction conditions.¹¹ Thus, additions of protected amino acids **2a–h** (1.2 molar equiv) to a stirred suspension of cations **1a–c** at $-40\text{ }^{\circ}\text{C}$ for 20 min and $25\text{ }^{\circ}\text{C}$ for 30 min, followed by workup, gave (η^4 -*cis*-dienylamine)Fe(CO)₃ complexes **3a–j** as the major products after purification by flash column chromatography on silica gel. The yields of the additions were generally high (69–98%; Table 1). It must be mentioned that complexes **3b,d,i,j** were obtained as mixtures of diastereomers and were used for the intramolecular cyclization without further separation. The stereochemistry of **3** was assigned as *cis* on the basis of comparison of their ¹H NMR spectral data, which were close to those of *cis*-C-5-substituted (η^4 -diene)Fe(CO)₃ complexes made by addition of functionalized zinc–copper reagents to cation **1**¹² and were consistent with the ¹H NMR spectral data of (η^4 -*cis*-dienylamine)Fe(CO)₃ complexes reported in the literature.^{10b}

Intramolecular Cyclization Reactions

Our cyclization study began with complex **3a**. Treatment of **3a** with 1.2 molar equiv of LDA at $-78\text{ }^{\circ}\text{C}$ under an atmosphere of CO provided a major product in 50% yield, identified as the 3-azabicyclo[3.3.0]octanecarboxylic acid derivative **4a** with an incorporated CO at the C-6 position. It is important to note that three new stereogenic centers of compound **4a** are created; however, only the single diastereomer shown was isolated. NMR (nuclear magnetic resonance) spectroscopy studies provided the initial evidence for support of the structural assignments. The ¹H NMR spectrum of compound **4a** exhibited the following: two narrow quartets, centered at δ 4.16, assigned to the two diastereotopic methylene protons of C-10; a doublet of doublets, centered at δ 3.29, assigned to one of the diastereotopic methylene protons at C-4; a singlet at δ 2.97, assigned to the proton at C-2; a multiplet, centered at δ 2.95, assigned to the proton at C-1; a multiplet, centered at δ 2.80, assigned to the proton at C-5; a doublet of doublets, centered at δ 2.55, assigned to one of the diastereotopic methylene protons at C-4; a multiplet, centered at δ 2.36, assigned to the protons at C-7 and C-8; a singlet at δ 2.30, assigned to the methyl protons at the nitrogen atom; a multiplet, centered at δ 2.11, assigned to the protons at C-7; a multiplet, centered at δ 1.94, assigned to the protons at C-8; a triplet, centered at δ 1.24, assigned to the methyl group at C-11. The ¹³C NMR spectrum of complex **4a** exhibited the following: a signal at δ 219.9, assigned to C-6 (carbonyl of the keto functionality); a signal at δ 172.3, assigned to C-9 (carbonyl of the ester functionality); a signal at δ 73.0, assigned to C-2; a signal at δ 60.7, assigned to C-10; a signal at δ 57.5, assigned to C-4; a signal at δ 50.4, assigned to C-5; a signal at δ 45.7, assigned to C-1; a signal at δ 38.9,

assigned to C-7; a signal at δ 37.3, assigned to the methyl carbon at the nitrogen atom; a signal at δ 25.2, assigned to C-8; a signal at δ 14.4, assigned to C-11. Compound **4a** results from anti addition of the α -face of the kinetic enolate **5** at the internal position (C-3) of the diene ligand. None of the product arising from




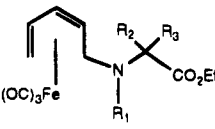
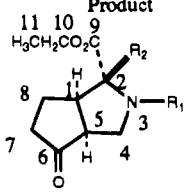

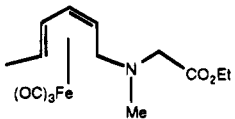
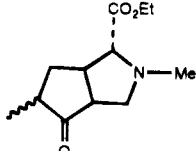
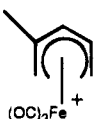
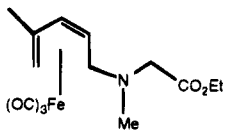
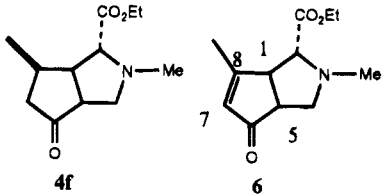
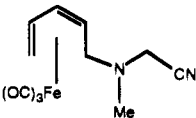
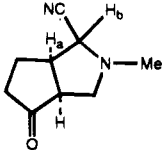
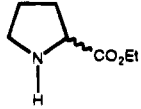
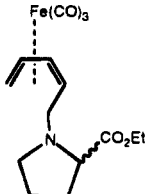
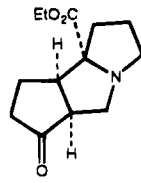
addition at the β -face of **5** has been found. This result agrees closely with the formation of a single diastereomer of fused bicyclo[3.3.0]octanecarboxylic acid derivatives obtained by the intramolecular cyclization of (η^4 -diene)Fe(CO)₃ complexes bearing functionalized side chains at the terminal position of the diene ligands.^{12a} Several examples of cyclization of diene–iron complexes bearing amino acid derivatives are summarized in Table 1.

Several entries in Table 1 deserve special mention. Substrates with tertiary α -carbons **3b–d** (obtained from additions of the phenylalanine and alanine derivatives to cation **1a**, respectively, entries 2–4, Table 1), also underwent intramolecular cyclization to produce 3-azabicyclo[3.3.0]octanecarboxylic acid derivatives **4b–d**, respectively, as the only diastereomeric product in each case. All exo carbethoxy groups of **4b–d** were assigned on the basis of the NOE difference spectrum of **4b** and **4c**. Irradiation of the benzylic protons of **4b** did not result in enhancement of the proton at C-1, while irradiation of the methyl protons at C-2 of **4c** provided enhancement of the exo proton at C-4. No enhancement of protons at C-1 and C-5 was observed. Attempts to assign the relative stereochemistry of **4d** using NOE analysis were unsuccessful. The generation of a single product from intramolecular cyclization of a mixture of diastereomeric dienylamine precursors further substantiates the formation of a common intermediate, *i.e.*, the planar enolate anion as mentioned above. However, intramolecular cyclization of the substrate with an additional methyl group at the terminal position of the diene ligand **3e** gave a mixture of diastereomers in a ratio of 1:1 (entry 5, Table 1), presumably derived from epimerization at the α -carbon (C-7) of the keto group during acid quenching and aqueous workup. The epimerization of the α -carbon (C-7) of the keto group during acid quenching had also been observed in the carbocyclic analog.^{12a} It must be mentioned that the ratio of the two diastereomeric products of the carbocyclic analog depended on the isolation processes. Isolation of the reaction mixture immediately after acid quenching afforded a single diastereomer. However, both diastereomers were obtained when the reaction mixture was stirred in trifluoroacetic acid for a long period of time (12 h). Thus, the difference may be due to the epimerization of the α -carbon (C-7) of the keto group during acid quenching. However, isolation of the reaction mixture from the intramolecular cyclization of **3e** with an amino acid derivative at the terminal position of the diene ligand immediately after acid

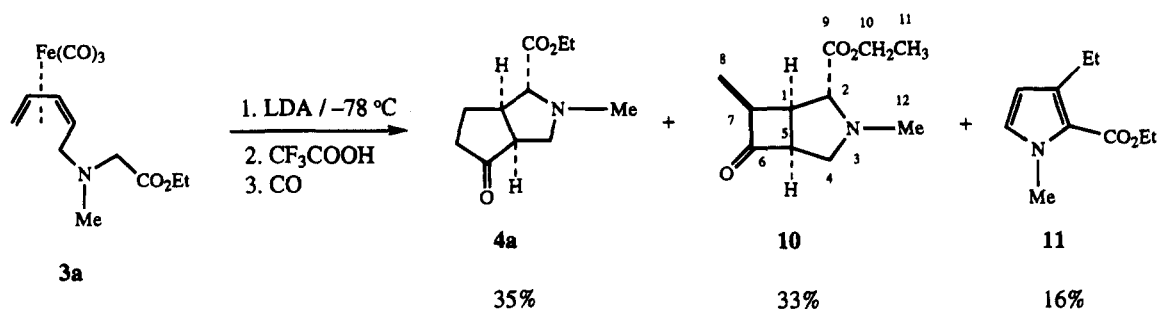
(11) C-Alkylation of protected amino acids to tricarbonyl(η^5 -dienyl)-iron cations were reported; see: (a) Dunn, M. J.; Jackson, R. F. W.; Stephenson, G. R. *Synlett* **1992**, 905. (b) Dunn, M. J.; Jackson, R. F. W. *J. Chem. Soc., Chem. Commun.* **1992**, 319. (c) Genet, J.-P.; Hudson, R. D. A.; Meng, W.-D.; Roberts, E.; Stephenson, G. R.; Thorimbert, S. *Synlett* **1994**, 631.

(12) (a) Yeh, M. C. P.; Sheu, B. A.; Fu, H. W.; Tau, S. I.; Chuang, L. W. *J. Am. Chem. Soc.* **1993**, *115*, 5941. (b) Yeh, M. C. P.; Sun, M.-L.; Lin, S.-K. *Tetrahedron Lett.* **1991**, *32*, 113.

Table 1. Synthesis and Intramolecular Cyclization of Complexes 3a-g

Entry	Cation	amino acid derivatives	Complex	Product	Yield (%)
1		HN(Me)CH ₂ CO ₂ Et·HCl 2a			50%
	1a		3a R ₁ = Me, R ₂ = R ₃ = H	4a R ₁ = Me, R ₂ = H	
2	1a	NH(Et)CH(CH ₂ Ph)CO ₂ Et 2b	3b R ₁ = Et, R ₂ = H, R ₃ = CH ₂ Ph	4b R ₁ = Et, R ₂ = CH ₂ Ph	33%
3	1a	NH(Et)CH(Me)CO ₂ Et 2c	3c R ₁ = Et, R ₂ = H, R ₃ = Me	4c R ₁ = Et, R ₂ = Me	44%
4	1a	NH(CH ₂ CH=CHCH ₃)CH(Me)CO ₂ Et 2d	3d R ₁ = CH ₂ CH=CHCH ₃ , R ₂ = H, R ₃ = Me	4d R ₁ = CH ₂ CH=CHCH ₃ , R ₂ = Me	69%
5		2a			36%
	1b		3e	4e	
6		2a			80%
	1c		3f	4f 4f : 6 = 1.2 : 1	
7	1a	HN(Me)CH ₂ CN·HCl 2e			65%
	1a		3g	4g exo : endo = 1.4 : 1	
8	1a				13%
	1a	2f	3h	7	

Scheme 1



quenching gave a mixture of diastereomers of **4e** in a ratio of 1:1. This difference is not understood. It was suggested that the basicity of the nitrogen atom in **4e** may facilitate the epimerization process at the α -carbon (C-7) of the keto group during the isolation process. Surprisingly, intramolecular cycloaddition of the substrate with a methyl group at the internal position (C-2) of the diene ligand, for example complex **3f**, produced the usual type of 3-azabicyclo[3.3.0]octanecarboxylic acid derivative **4f** (46%) along with the 3-azabicyclo[3.3.0]octenecarboxylic acid derivative **6** (34%) (entry 6, Table 1). The stereochemistry for the carboxy group in **4f** assigned as exo was based on the same hypothesis as for the formation of **4a**. Attempts to confirm the relative stereochemistry of **4f** using NOESY measurements were unsuccessful. The tentative assignment of the endo methyl group of **4f** was based on the previous report of the intermolecular nucleophilic addition/carbonylation of diene-iron complexes with either methoxy or methyl substituents at C-2 of the diene ligand.¹³ In both cases, cis-3,4-disubstituted cyclopentanones were obtained. Moreover, the stereochemistry for the methyl group at C-8 assigned as endo was consistent with anti addition of the enolate to the diene ligand as shown in Scheme 5. NMR and infrared spectra of **6** exhibited signal patterns corresponding to an α,β -unsaturated ketone. The proton at δ 5.95, a singlet, was assigned to the vinyl proton at C-7; a three-proton singlet at δ 2.19 was assigned to the methyl group at C-9. The carbon at δ 209.2 was assigned to the carbonyl of the keto functionality; two carbons at δ 171.7 and 131.3 were assigned to the vinyl carbons at C-8 and C-7, respectively. The typical absorption at 1703 cm⁻¹ for the keto functionality of an α,β -unsaturated ketone in the infrared spectrum of **6** also proved the structural assignments.

3g, a substrate with a (cyanomethyl)methylamino group, also underwent intramolecular cyclization to produce a mixture of exo and endo isomers in a ratio of 1.4:1 (entry 7, Table 1). Unlike an ester group, a cyano group is rather small. Thus, either one of the two α -protons is possibly removed by LDA under the kinetically controlled reaction conditions.^{12a} The major isomer assigned as exo is based on ¹H NMR studies. The proton at δ 3.71, a singlet, was assigned to H_b. The coupling constant for H_a-H_b (J_{ab}) of 0 Hz agrees with the 0 Hz coupling constant for similarly disposed trans hydrogens of **4a**. Furthermore, the dihedral angle of 95.26° for H_a-C₁-C₂-H_b analyzed by the molecular

modeling (Chem 3D program) of **4g** (exo) is consistent with the angle (95.30°) obtained by X-ray diffraction analysis, which proves the 0 Hz coupling constant for H_a-H_b. The coupling constant for H_a-H_b of the endo isomer of **4g** is 7.8 Hz, which agrees with a dihedral angle (H_a-C₁-C₂-H_b) of 37.5° analyzed by molecular modeling (Chem 3D).¹⁴

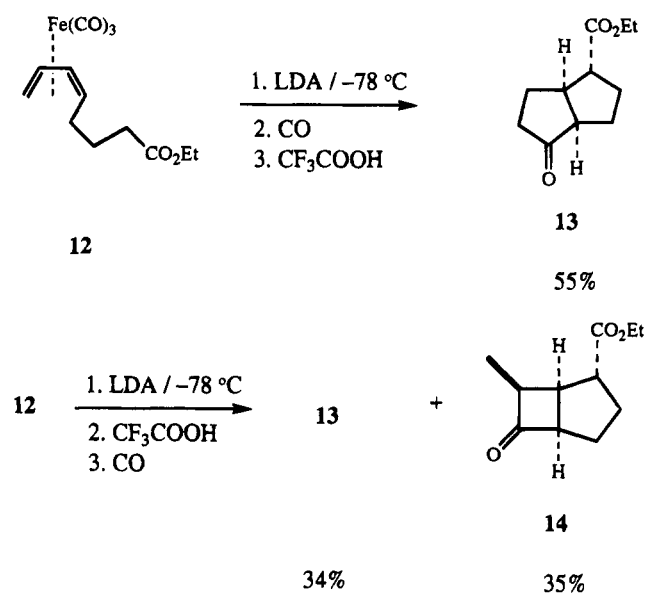
Under the same reaction conditions, we were able to construct the nitrogen-containing linearly fused tricyclo[6.3.0.0^{2,6}]undecanecarboxylic acid derivative **7**, linearly fused tricyclo[7.3.0.0^{2,7}]dodecanecarboxylic acid derivative **8**, and the bridged tricyclo[6.3.1.0^{2,6}]dodecanecarboxylic acid derivative **9** via intramolecular cyclization of (η^4 -1,3-diene)Fe(CO)₃ complexes bearing a proline, pipercolinic, and nipecotic acid derivatives, respectively, at the terminal positions of the diene ligands. Attempts to confirm stereochemistries of carboxy groups of tricyclic compounds **7-9** using various methods (NOE and NOESY spectra) were unsuccessful. All carboxy groups of **7-9** were tentatively assigned as exo on the basis of addition of the α -face of the kinetic enolate at the C-3 position of diene ligands. It is important to note that three new stereogenic centers of the fairly complicated tricyclic compounds **7-9** are created; however, only the single diastereomers shown were isolated.

Interestingly, the reaction undergoes different pathways by direct quenching of the reaction mixture with acid followed by addition of CO. Thus, treatment of complex **3a** with 1.2 molar equiv of LDA at -78 °C under nitrogen for 2 h followed by acid quenching and then addition of CO (14-18 psi) affords **4a** (35%), the 3-azabicyclo[3.2.0]heptanecarboxylic acid derivative **10** (33%), and the pyrrole derivative **11** (16%) after purification by flash column chromatography and distillation under reduced pressure (Scheme 1). NMR (nuclear magnetic resonance) spectroscopy studies provided the initial evidence for support of the structural assignments. The ¹H NMR spectrum of compound **10** exhibited the following: two narrow quartets, centered at δ 4.16, assigned to the two diastereotopic methylene protons of C-10; a multiplet, centered at δ 3.67, assigned to the proton at C-5; a singlet at δ 3.63, assigned to the proton at C-2; a multiplet, centered at δ 3.42, assigned to the proton at C-1; a doublet of doublets, centered at δ 3.12, assigned to one of the diastereotopic methylene protons at C-4; a multiplet, centered at δ 3.07, assigned to the proton at C-7; a doublet of doublets, centered at δ 3.02, assigned to one of the diastereotopic methylene protons at C-4; a singlet at δ 2.43, assigned to the

(13) (a) Semmelhack, M. F.; Bodurov, C. M.; Fewkes, E.; Herndon, J. W.; Knaus, G.; Le, H. T. M.; Sanner, M. *Chem. Scr.* **1985**, *25*, 131. (b) Semmelhack, M. F.; Herndon, J. W.; Liu, J. K. *Organometallics* **1983**, *2*, 1885.

(14) (a) Karplus, M. *J. Am. Chem. Soc.* **1963**, *85*, 2870. (b) Bothner-By, A. A. *Adv. Magn. Reson.* **1965**, *1*, 195.

Scheme 2



methyl protons at the nitrogen atom; a triplet, centered at δ 1.30, assigned to the methyl protons at C-11; a doublet, centered at δ 1.09, assigned to the methyl protons at C-8. The ^{13}C NMR spectrum of complex **10** exhibited the following: a signal at δ 215.3, assigned to C-6 (carbonyl of the keto functionality); a signal at δ 172.5, assigned to C-9 (carbonyl of the ester functionality); a signal at δ 64.8, assigned to C-2; a signal at δ 62.4, assigned to C-10; a signal at δ 60.2, assigned to C-4; a signal at δ 55.3, assigned to C-5; a signal at δ 55.0, assigned to C-1; a signal at δ 38.7, assigned to C-7; a signal at δ 36.8, assigned to the methyl carbon at the nitrogen atom; a signal at δ 14.4, assigned to C-11; a signal at δ 8.0, assigned to C-8. This result is consistent with the intramolecular cyclization of complex **12** to give the fused bicyclo[3.3.0]octanecarboxylic acid derivative **13** only or both **13** and the fused bicyclo[3.2.0]heptanecarboxylic acid derivative **14**, depending on the

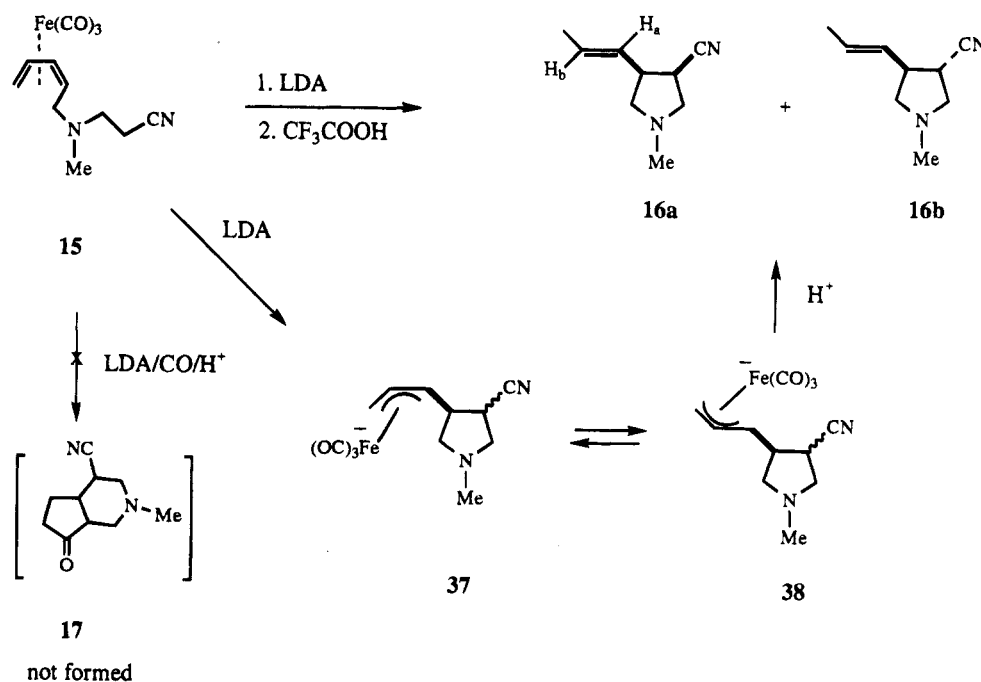
quenching process (Scheme 2). Thus, treatment of **12** with LDA under an atmosphere of CO at $-78\text{ }^{\circ}\text{C}$ for 2 h and $25\text{ }^{\circ}\text{C}$ for 2 h followed by acid quenching produced **13** as the major product in 55% yield,^{12a} whereas reaction of **12** with LDA at $-78\text{ }^{\circ}\text{C}$ for 2 h followed by acid quenching and then addition of an atmosphere of CO for 1 h at $-78\text{ }^{\circ}\text{C}$ provided **13** (34%) and **14** (35%) (Scheme 2) after purification by flash column chromatography and distillation under reduced pressure. Both methyl groups at C-7 of **10** and **14** were assigned as endo on the basis of their NOESY experiments. It is important to note that the formation of bicyclo[3.2.0]heptane skeletons is limited to the iron-diene complexes bearing no substituents at the C-1 or C-2 position of the diene ligands. For example, treatment of complexes with a methyl group at C-1 (**3e**) or C-2 (**3f**) with LDA at $-78\text{ }^{\circ}\text{C}$ followed by acid quenching did not generate bicyclo[3.2.0]heptane or bicyclo[3.3.0]octane skeletons. The major products isolated were cyclopentanecarboxylic acid derivatives; no carbonyl insertion products were obtained.

Increasing the tether length by 1 with complex **15** (Scheme 3) led to a 23% yield of an inseparable mixture of *cis* and *trans* isomers of pyrrolidine derivatives **16a,b** in a ratio of 4:3 (obtained by the integration of the ^1H NMR spectrum of the crude mixture). None of the desired internal addition product, for example **17**, was isolated under an atmosphere of N_2 or CO. The stereochemistry of the double bonds of **16a** and **16b** was assigned as *trans* on the basis of comparison of their ^1H NMR decoupling experiments. A coupling constant of 14.6 Hz for the two vicinal vinyl protons (H_a – H_b) suggested a *trans* relationship between H_a and H_b .

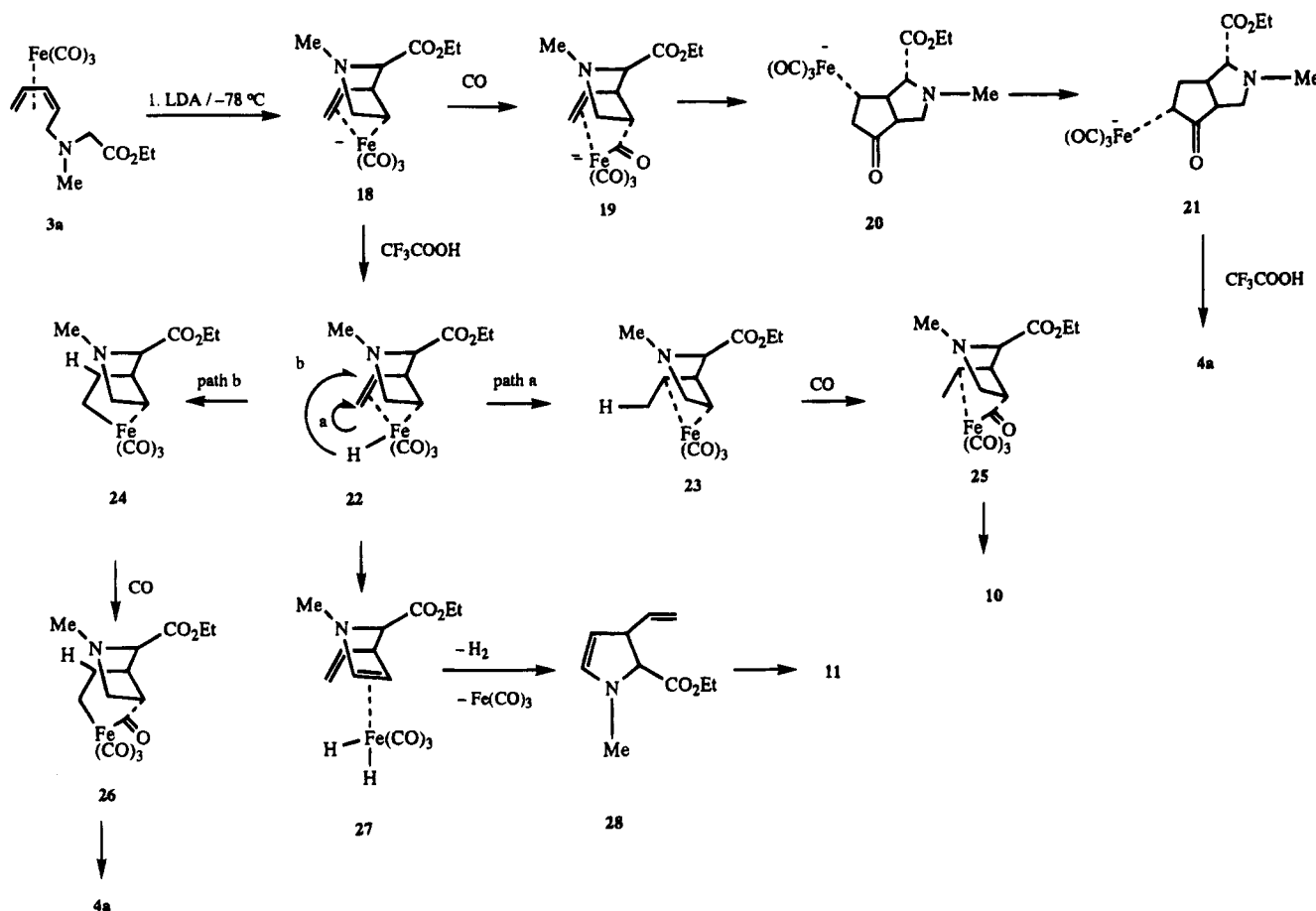
Discussion

The formation of aza-bicyclic and -tricyclic skeletons agrees closely with the mechanism proposed for the intramolecular addition of nucleophiles to acyclic (η^4 -diene) $\text{Fe}(\text{CO})_3$ complexes bearing functionalized side

Scheme 3



Scheme 4



chains at the terminal position of the diene ligands.^{12a} Anti addition of the stabilized α -amino enolate anion, obtained from treatment of **3a** with 1.2 molar equiv of LDA, at C-3 of the diene ligand gave the putative homoallyl anion intermediate **18** (Scheme 4). It is important to mention that an α -amino ester enolate anion such as α -lithio-*N,N*-dimethylglycine ethyl ester fails to add to $(\eta^4\text{-diene})\text{Fe}(\text{CO})_3$ complexes intermolecularly, under the same reaction conditions. Moreover, the intramolecular addition occurred exclusively at the C-3 position of the diene ligand, and no addition at C-2 was found. Carbonyl insertion was then enhanced by external CO (14–18 psi) to generate the acyliron anion intermediate **19** and intramolecular alkene insertion to give **20**. The postulated initial bicyclic intermediate **20** could rearrange rapidly to the enolate–iron derivative **21**, presumably via a β -hydride elimination/readdition process. Protonation of **21** produced the azabicyclic compound **4a**. Furthermore, intermolecular cyclization of both diastereomers of complexes **3b–d,h–j** under the same reaction conditions (LDA/CO, -78°C , THF/HMPA) gave only a single diastereomer of cycloadducts **4b–d**, **7**, **8**, and **9**, respectively. The reason for the isolation of a single isomer in each case may derive from the formation of the same kinetic enolates by treatment of both diastereomers with LDA under the kinetically controlled reaction conditions.¹⁵ However, the formation of compound **4a** in Table 1 and Scheme 1 may result from different reaction pathways. Iron–hydride species **22** could be obtained upon direct quenching of **18** with CF_3COOH (Scheme 4). Intramolecular alkene insertion into the iron–hydride bond of **22** would lead to the

formation of ferracyclobutane derivative **23** (path a) and ferracyclopentane derivative **24** (path b). Carbonyl insertion was then enhanced by external CO (14–18 psi) to produce ferracyclopentane intermediate **25** and ferracyclohexane intermediate **26**, which after reductive elimination produce the 3-azabicyclo[3.2.0]heptanecarboxylic acid derivative **10**^{16,17} and 3-azabicyclo[3.3.0]octanecarboxylic acid derivative **4a**, respectively. However, detachment of the iron tricarbonyl moiety from the olefin of **22** followed by β -hydride elimination would give **27**. Reductive elimination of **27** followed by decomplexation of the iron tricarbonyl moiety produced **28**. The initially formed product **28** presumably aromatized by migration of the double bond to provide pyrrole derivative **11**. However, insertion of the pendant olefin into the iron–hydride bond of **22** is limited to the complexes bearing no methyl group at the C-1 or C-2 positions of diene–iron complexes. For example, reaction of complexes with a methyl group at C-1 (**3e**) or C-2 (**3f**) with LDA at -78°C followed by acid quenching did not generate bicyclo[3.2.0]heptane or bicyclo[3.3.0]octane skeletons. The reason for the limitation may be due to the difficulty of insertion of a substituted olefin into the iron–hydride bond of intermediate **22**. Moreover, the

(15) Ireland, R. E.; Mueller, R. H.; Willard, A. K. *J. Am. Chem. Soc.* **1976**, *98*, 2868.

(16) 3-Azabicyclo[3.2.0]heptanone derivatives can also be obtained by intramolecular [2 + 2] cycloadditions of keteniminium salts derived from β -amino acids: Gobeaux, B.; Ghosez, L. *Heterocycles* **1989**, *28*, 29.

(17) Cyclobutanone derivatives can be isolated by intermolecular nucleophilic addition followed by acid quenching. Semmelhack, M. F.; Le, H. T. M. *J. Am. Chem. Soc.* **1984**, *106*, 2715.

ligand at $-78\text{ }^{\circ}\text{C}$ (kinetically controlled reaction conditions) to generate homoallyl anion species. When the temperature is raised to $25\text{ }^{\circ}\text{C}$ (thermodynamically controlled reaction conditions), anions reverse and add at the terminal position of the diene ligand to produce allyl anion intermediates. The anion intermediate **37** might undergo allyl syn-anti isomerization to give **38**.¹⁹ Protonation of **38** with acid gave pyrrolidine derivatives **16a,b**.

The reactions described herein demonstrate that intramolecular iron-mediated cycloaddition can be a convenient method for the formation of N-containing heterobicyclic and -tricyclic compounds. Although the yields of the N-containing heterotricyclic compounds **7–9** are only moderate, this facile and straightforward approach to the synthesis of fairly complicated systems, with promising relative stereocontrol, may have further applications.

Experimental Section

All reactions were run under a nitrogen atmosphere in oven-dried glassware unless otherwise indicated. Anhydrous solvents or reaction mixtures were transferred via an oven-dried syringe or cannula. Diethyl ether (ether) and tetrahydrofuran (THF) were distilled under nitrogen from a deep blue sodium benzophenone ketyl solution. Methylene chloride was distilled from calcium chloride. Copper cyanide (CuCN), sarcosine ethyl ester hydrochloride, (methylamino)acetonitrile hydrochloride, 3-(methylamino)propionitrile, DL-phenylalanine, DL-alanine, ethyl pipercolinate, ethyl nipecotate, fluoroboric acid (48% in water), and hexafluorophosphoric acid (60% in water) were purchased from Aldrich Chemical Co. and used as received. Cations **1a–c** were synthesized according to the literature procedure.²⁰ Amino acid derivatives **2b,c** were synthesized by protection of DL-alanine and DL-phenylalanine, respectively, following the literature procedure.²¹ Compound **2d** was obtained by treatment of DL-alanine with thionyl chloride in ethanol followed by protection of the amino group with *trans*-crotonaldehyde.²¹ Compound **2f** was obtained by protection of the acid group of DL-proline with thionyl chloride in ethanol. Flash column chromatography, following the method of Still,²² was carried out with E. Merck silica gel (Kieselgel 60, 230–400 mesh) using the indicated solvents. Analytical thin-layer chromatography was performed with silica gel 60 F₂₅₄ plastic plates of 0.2-mm thickness from E. Merck. The term "concentration" refers to the removal of solvent with an aspirator pump (Yamato Instrument Company Model WP-15) with a Buchi Rotovapor-R. The term "under nitrogen" implies that the apparatus was evacuated (oil pump) and then filled with nitrogen three times. The term "flash distillation" refers to a vacuum distillation at $25\text{ }^{\circ}\text{C}$ with a receiver at $-78\text{ }^{\circ}\text{C}$. The term "short-path distillation" refers to the process in which the entire distillation apparatus (a tube closed at one end, held horizontally) with the exception of the collection bulb was slowly heated in an air bath from 25 to $150\text{ }^{\circ}\text{C}$ under vacuum; the distillate was collected at $-78\text{ }^{\circ}\text{C}$, and boiling points for fractions refer to the bath temperature range. Melting points were determined in open capillaries with a Thomas-Hoover apparatus and are uncorrected. ¹H nuclear magnetic resonance (NMR) spectra were obtained with a JEOL EX 400

instrument (400 MHz). Chemical shifts are reported in parts per million with either tetramethylsilane (0.00 ppm) or CHCl₃ (7.26 ppm) as internal standard. ¹³C NMR spectra were recorded with JEOL EX 400 (100.4 MHz) spectrometers with CDCl₃ (77.0 ppm) as the internal standard. Infrared (IR) spectra were recorded with a JASCO IR-700 spectrometer. Mass spectra were acquired on a JEOL JMS-D 100 spectrometer at an ionization potential of 70 eV and are reported as mass/charge (*m/e*) with percent relative abundance. High-resolution mass spectra were obtained with an AEI MS-9 double-focusing mass spectrometer and a JEOL JMS-HX 110 spectrometer at the Department of Chemistry, Central Instrument Center, Taichung, ROC.

General Procedure for Addition of Amino Acid Derivatives 2a–h to (η^5 -pentadienyl)Fe(CO)₃ Cation Salts 1a–c. Amino acid derivatives **2** (1.2 molar equiv) and triethylamine (1.2 molar equiv; 2.2 molar equiv was added in the cases of **2a,e,g**) in 5.0 mL of THF at $-40\text{ }^{\circ}\text{C}$ was added to a stirred suspension of a cation salt (**1a–c**) in 20 mL of THF under nitrogen. A homogeneous solution was obtained after the reaction mixture was stirred at $-40\text{ }^{\circ}\text{C}$ for 20 min. The reaction mixture was further stirred at $25\text{ }^{\circ}\text{C}$ for 30 min and was then diluted with 100 mL of 50% ethyl acetate/hexanes. The resultant solution was washed with water (100 mL \times 3) and brine (100 mL \times 3), dried over anhydrous magnesium sulfate (10 g), and concentrated to give the crude mixture.

General Procedure for Intramolecular Cyclization of (η^4 -diene)Fe(CO)₃ Complexes 3a–j. In a typical procedure, to a solution of diisopropylamine (0.64 mL, 4.5 mmol) in 4.0 mL of THF under nitrogen at $-78\text{ }^{\circ}\text{C}$ was added rapidly, neat, via syringe, a solution of *n*-butyllithium (2.8 mL, 4.5 mmol, 1.6 M) in hexane followed by addition of 0.80 mL of hexamethylphosphoramide. The reaction mixture was stirred at $-78\text{ }^{\circ}\text{C}$ for 20 min. With the solution at $-78\text{ }^{\circ}\text{C}$, carbon monoxide was added to the system via a syringe needle and was pressurized to ca. 2 psig (always with a positive pressure kept on the system) as measured by a regulator at the CO cylinder. The CO pressure was then released via an additional needle, and the CO was allowed to flow through the system for 20 s. A solution of a diene-iron complex (**3a–j**, 4.0 mmol) in 3.0 mL of THF was added dropwise via syringe, the gas exit needle was removed, and the closed system was pressurized to ca. 14 psig with CO. The mixture was stirred at $-78\text{ }^{\circ}\text{C}$ for 2 h and $25\text{ }^{\circ}\text{C}$ for 2 h. After this time, the mixture was again cooled to $-78\text{ }^{\circ}\text{C}$, the CO needle was removed, and the system was depressurized via insertion of a syringe needle into the septum, which was quickly removed when gas flow could no longer be heard. The reaction mixture was quenched with trifluoroacetic acid (5.0 molar equiv) via a syringe needle and was stirred at $25\text{ }^{\circ}\text{C}$ for 2 h. After this time, the reaction mixture was diluted with a mixture of ethyl acetate/hexanes (1/2, 100 mL). The resultant solution was washed with water (100 mL \times 3) and brine (100 mL \times 3), dried over anhydrous magnesium sulfate (10 g), and concentrated to give the crude mixture.

[(2-5- η)-1-((Carbomethoxymethyl)methylamino)-2,4-pentadiene]tricarbonyliron (3a). The crude mixture obtained from the addition of **2a** (0.74 g, 4.8 mmol) to cation **1a** (1.2 g, 4.0 mmol) was purified via flash column chromatography (silica gel, 5% ethyl acetate/hexanes) to give **3a** (1.2 g, 3.7 mmol, 93%) as a yellow oil: IR (CH₂Cl₂) 3073, 2996, 2976, 2872, 2047, 1977, 1738, 1287, 1192, 1044 cm⁻¹; ¹H NMR (400 MHz, CDCl₃) δ 5.49–5.44 (m, 2 H), 4.17 (q, *J* = 7.3 Hz, 2 H), 3.24 (d, *J* = 16.6 Hz, 1 H), 3.14 (d, *J* = 16.6 Hz, 1 H), 2.87 (dd, *J* = 13.2, 9.3 Hz, 1 H), 2.56 (m, 1 H), 2.31 (s, 3 H, NCH₃), 2.07 (dd, *J* = 13.2, 10.3 Hz, 1 H), 1.81 (d, *J* = 7.8 Hz, 1 H), 1.49 (d, *J* = 9.7 Hz, 1 H), 1.27 (t, *J* = 7.3 Hz, 3 H); ¹³C NMR (100.4 MHz, CDCl₃) δ 210.7, 170.7, 91.1, 87.6, 60.5, 57.3, 56.0, 54.7, 41.6, 40.2, 14.2; MS (70 eV) *m/e* (relative intensity) 323 (M⁺, 5), 295 (15), 267 (27), 250 (32), 239 (83), 207 (100), 171 (52), 151 (62), 129 (98), 100 (32), 99 (73), 67 (92); HRMS (EI) *m/e* calcd for C₁₀H₁₇NO₂Fe (M⁺ - 3CO) 239.0608, found 239.0608.

(19) (a) Chang, S.; White, P. S.; Brookhart, M. *Organometallics* **1993**, *12*, 3636. (b) Brookhart, M.; Yoon, J.; Noh, S. K. *J. Am. Chem. Soc.* **1999**, *111*, 4117.

(20) Donaldson, W. A. *J. Organomet. Chem.* **1990**, *395*, 187.

(21) (a). Womack, E. B.; McWhirter, J. *Organic Syntheses*; Wiley: New York, 1955; Collect. Vol. III, p 714. (b) Groneberg, R. D.; Miyazaki, T.; Stylianides, N. A.; Schulze, T. J.; Stahl, W.; Schreiner, E. P.; Suzuki, T.; Iwabuchi, Y.; Smith, A. L.; Nicolaou, K. C. *J. Am. Chem. Soc.* **1993**, *115*, 7593.

(22) Still, W. C.; Kahn, M.; Mitra, A. *J. Org. Chem.* **1978**, *43*, 2923.

[(2-5- η)-1-((1-Carbethoxy-2-phenylethyl)ethylamino)-2,4-pentadiene]tricarbonyliron (3b). The crude mixture obtained from the addition of **2b** (1.4 g, 6.1 mmol) to cation **1a** (1.5 g, 5.1 mmol) was purified via flash column chromatography (silica gel, 7% ethyl acetate/hexanes) to give **3b** (2.0 g, 4.7 mmol, 92%) as a 1:1 mixture of diastereomers: IR (CH₂Cl₂) (mixture of diastereomers) 3066, 3030, 2978, 2935, 2872, 2042, 1973, 1724, 1604, 1494, 1454, 1377, 1344, 1286, 1172, 1095, 1068, 1034 cm⁻¹; ¹H NMR (400 MHz, CDCl₃) (mixture of diastereomers) δ 7.30–7.17 (m, 10 H, Ph), 5.45 (m, 2 H), 5.31 (dd, J = 7.8, 5.8 Hz, 1 H, 1 H), 5.22 (dd, J = 7.8, 5.4 Hz, 1 H), 4.06 (m, 4 H), 3.56 (t, J = 7.8 Hz, 2 H), 3.06–2.60 (m, 8 H), 2.50 (m, 1 H), 2.40–2.20 (m, 4 H), 2.09 (dd, J = 13.7, 9.8 Hz, 1 H), 1.78 (m, 2 H), 1.52 (m, 2 H), 1.16 (t, J = 7.3 Hz, 6 H), 0.99 (t, J = 7.3 Hz, 6 H); ¹³C NMR (100.4 MHz, CDCl₃) (mixture of diastereomers) δ 210.9, 172.6, 172.5, 136.6, 138.5, 129.3, 129.3, 128.2, 128.1, 126.2, 90.8, 90.8, 87.6, 87.6, 65.5, 64.1, 60.2, 60.0, 57.8, 57.2, 50.0, 49.9, 44.6, 43.8, 39.9, 39.8, 36.7, 35.8, 14.3, 14.2, 13.8, 13.7; MS (30 eV) (mixture of diastereomers) m/e (relative intensity) 427 (M⁺, 1), 399 (3), 371 (16), 343 (100), 275 (15), 252 (36), 214 (18), 196 (22); HRMS (EI) m/e calcd for C₁₈H₂₅FeNO₂ (M⁺ - 3CO) 343.1235, found 343.1234.

[(2-5- η)-1-(1-Carbethoxyethyl)ethylamino)-2,4-pentadiene]tricarbonyliron Complex (3c). The crude mixture obtained from the addition of **2c** (0.54 g, 3.7 mmol) to cation **1a** (0.90 g, 3.1 mmol) was purified via flash column chromatography (silica gel, 9% ethyl acetate/hexanes) to give **3c** (0.95 g, 2.7 mmol, 90%) as a yellow oil. Complex **3c** could be further separated into two diastereomers. Diastereomer 1: IR (CH₂Cl₂) 3047, 2991, 2980, 2937, 2046, 1983, 1726, 1452, 1375, 1296, 1280, 1178, 1113, 881, 860 cm⁻¹; ¹H NMR (400 MHz, CDCl₃) δ 5.46 (m, 1 H), 5.41 (dd, J = 7.3, 5.4 Hz, 1 H), 4.15 (q, J = 6.8 Hz, 2 H), 3.51 (q, J = 7.8 Hz, 1 H), 2.88 (dd, J = 14.2, 2.8 Hz, 1 H), 2.57 (m, 3 H), 2.17 (dd, J = 14.2, 9.8 Hz, 1 H), 1.80 (dd, J = 4.9, 2.0 Hz, 1 H), 1.54 (dd, J = 6.8, 2.0 Hz, 1 H), 1.27 (t, J = 7.3 Hz, 3 H), 1.18 (d, J = 7.8 Hz, 3 H), 1.03 (t, J = 7.3 Hz, 3 H); ¹³C NMR (100.4 MHz, CDCl₃) δ 210.0, 174.1, 90.9, 87.6, 60.4, 58.7, 57.2, 49.9, 44.6, 39.8, 14.6, 14.3, 13.8; MS (30 eV) m/e (relative intensity) 295 (M⁺ - 2CO, 14), 267 (100), 199 (98), 171 (71), 128 (73); HRMS (EI) m/e calcd for C₁₂H₂₁FeNO₂ (M⁺ - 3CO) 267.0922, found 267.0918. Diastereomer 2: IR (CH₂Cl₂) 3051, 2991, 2980, 2977, 2046, 1959, 1724, 1452, 1377, 1296, 1267, 1178, 1111, 1070, 1022, 829, 815 cm⁻¹; ¹H NMR (400 MHz, CDCl₃) δ 5.46 (m, 1 H), 5.42 (dd, J = 7.3, 4.9 Hz, 1 H), 4.11 (q, J = 6.8 Hz, 2 H), 3.50 (q, J = 6.8 Hz, 1 H), 2.92 (dd, J = 12.2, 3.9 Hz, 1 H), 2.68 (m, 1 H), 2.52 (m, 1 H), 2.43 (m, 1 H), 2.10 (dd, J = 13.7, 9.8 Hz, 1 H), 1.79 (dd, J = 4.9, 1.9 Hz, 1 H), 1.55 (dd, J = 9.3, 1.9 Hz, 1 H), 1.28 (d, J = 6.8 Hz, 3 H), 1.27 (t, J = 7.3 Hz, 3 H), 0.99 (t, J = 6.8 Hz, 3 H); ¹³C NMR (100.4 MHz, CDCl₃) δ 210.0, 173.8, 90.8, 87.6, 60.1, 57.5, 57.2, 49.3, 43.9, 39.8, 16.2, 14.3, 13.5; MS (30 eV) m/e (relative intensity) 295 (M⁺ - 2CO, 14), 267 (100), 238 (7), 207 (9), 171 (25); HRMS (EI) m/e calcd for C₁₂H₂₁FeNO₂ (M⁺ - 3CO) 267.0922, found 267.0920.

[(2-5- η)-1-((1-Carbethoxyethyl)(*E*)-2-butenyl)amino)-2,4-pentadiene]tricarbonyliron (3d). The crude mixture obtained from the addition of **2d** (0.20 g, 1.2 mmol) to cation **1a** (0.30 g, 1.0 mmol) was purified via flash column chromatography (silica gel, 9% ethyl acetate/hexanes) to give **3d** (0.26 g, 0.69 mmol, 69%) as a 1:1 mixture of diastereomers. The mixture of diastereomers was further purified by MPLC, and only one of the diastereomers was obtained as a pure compound: IR (CH₂Cl₂) 3055, 2993, 2980, 2939, 2046, 1981, 1724, 1448, 1423, 1377, 1246, 1195, 1151, 1059, 970, 866 cm⁻¹; ¹H NMR (400 MHz, CDCl₃) δ 5.55–5.39 (m, 4 H), 4.10 (q, J = 7.3 Hz, 2 H), 3.53 (q, J = 7.3 Hz, 1 H), 3.21 (br d, J = 14.1 Hz, 1 H), 2.91 (m, 2 H), 2.53 (m, 1 H), 2.08 (dd, J = 14.2, 4.4 Hz, 1 H), 1.78 (dd, J = 4.4, 2.0 Hz, 1 H), 1.68 (d, J = 6.3 Hz, 3 H), 1.52 (dd, J = 9.3, 2.0 Hz, 1 H), 1.26 (m, 6 H); ¹³C NMR (100.4 MHz, CDCl₃) δ 211.0, 173.8, 128.7, 128.6, 90.9, 87.7, 60.1, 57.2, 52.3, 49.1, 40.0, 39.9, 17.8, 16.0, 14.3; MS (30 eV) m/e (relative

intensity) 321 (M⁺ - 2CO, 1), 293 (100), 237 (90), 225 (80); HRMS (EI) m/e calcd for C₁₄H₂₃FeNO₂ (M⁺ - 3CO) 293.1078, found 293.1077.

[(2-5- η)-1-((Carbethoxymethyl)methylamino)-2,4-hexadiene]tricarbonyliron (3e). The crude mixture obtained from the addition of **2a** (1.2 g, 7.2 mmol) to cation **1b** (1.9 g, 6.0 mmol) was purified via flash column chromatography (silica gel, 20% ethyl acetate/hexanes) to give **3e** (1.9 g, 5.7 mmol, 95%) as a yellow oil: IR (CH₂Cl₂) 2963, 2932, 2861, 2020, 1979, 1736, 1454, 1379, 1194, 1125, 1032, 945, 781 cm⁻¹; ¹H NMR (400 MHz, CDCl₃) δ 5.19 (m, 2 H), 4.10 (q, J = 7.3 Hz, 2 H), 3.15 (d, J = 16.6 Hz, 1 H), 3.10 (d, J = 16.6 Hz, 1 H), 2.81 (dd, J = 13.2, 3.9 Hz, 1 H), 2.40 (m, 1 H), 2.34 (m, 1 H), 2.29 (s, 3 H, NCH₃), 2.05 (dd, J = 13.2, 10.3 Hz, 1 H), 1.35 (d, J = 5.9 Hz, 3 H), 1.20 (t, J = 7.3 Hz, 3 H); ¹³C NMR (100.4 MHz, CDCl₃) δ 211.4, 170.7, 94.9, 83.0, 60.5, 57.3, 56.4, 54.4, 41.7, 22.6, 20.3, 14.2; MS (70 eV) m/e (relative intensity) 337 (M⁺, 6), 281 (22), 252 (100), 220 (32), 170 (97), 142 (54), 128 (56), 98 (56), 81 (72), 54 (78), 44 (65); HRMS (EI) m/e calcd for C₁₂H₁₉FeNO₃ (M⁺ - 2CO) 281.0731, found 281.0709.

[(2-5- η)-1-((Carbethoxymethyl)methylamino)-4-methyl-2,4-pentadiene]tricarbonyliron (3f). The crude mixture obtained from the addition of **2a** (0.69 g, 4.5 mmol) to cation **1c** (1.2 g, 4.1 mmol) was purified via flash column chromatography (silica gel, 20% ethyl acetate/hexanes) to give **3f** (1.3 g, 3.9 mmol, 96%) as a yellow oil: IR (CH₂Cl₂) 3065, 3052, 2990, 2984, 2047, 1975, 1744, 1622, 1381, 1283, 1267, 1246, 1188, 1036, 905 cm⁻¹; ¹H NMR (400 MHz, CDCl₃) δ 5.36 (d, J = 7.3 Hz, 1 H), 4.17 (q, J = 7.3 Hz, 2 H), 3.24 (d, J = 16.6 Hz, 1 H), 3.14 (d, J = 16.6 Hz, 1 H), 2.82 (dd, J = 13.2, 3.9 Hz, 1 H), 2.41 (m, 1 H), 2.31 (s, 3 H, NCH₃), 2.18 (s, 3 H), 2.10 (dd, J = 13.2, 9.8 Hz, 1 H), 1.84 (s, 1 H), 1.51 (s, 1 H), 1.27 (t, J = 7.3 Hz, 3 H); ¹³C NMR (100.4 MHz, CDCl₃) δ 210.6, 170.7, 108.3, 87.3, 60.5, 57.4, 55.8, 51.1, 42.7, 41.7, 24.3, 14.2; MS (70 eV) m/e (relative intensity) 337 (M⁺, 92), 309 (52), 253 (71), 222 (82), 198 (89), 193 (100), 165 (92), 129 (75), 116 (97), 112 (91), 100 (89), 82 (96); HRMS (EI) m/e calcd for C₁₄H₁₉FeNO₃ (M⁺) 337.0611, found 337.0611.

[(2-5- η)-1-((Cyanomethyl)methylamino)-2,4-pentadiene]tricarbonyliron Complex (3g). The crude mixture obtained from the addition of **2e** (0.84 g, 7.2 mmol) to cation **1a** (1.8 g, 6.0 mmol) was purified via flash column chromatography (silica gel, 15% ethyl acetate/hexanes) to give **3g** (1.6 g, 5.9 mmol, 98%) as a yellow oil: IR (CH₂Cl₂) 3056, 3046, 2992, 2982, 2951, 2234, 2051, 1985, 1616, 1453, 1258, 1125, 1030, 895, 878 cm⁻¹; ¹H NMR (400 MHz, CDCl₃) δ 5.54 (m, 1 H), 5.44 (dd, J = 6.8, 5.9 Hz, 1 H), 3.57 (d, J = 17.1 Hz, 1 H), 3.44 (d, J = 17.1 Hz, 1 H), 2.68 (dd, J = 13.2, 4.9 Hz, 1 H), 2.47 (m, 1 H), 2.30 (s, 3 H, NCH₃), 2.00 (dd, J = 13.2, 9.8 Hz, 1 H), 1.88 (dd, J = 7.8, 3.4 Hz, 1 H), 1.53 (dd, J = 9.8, 3.4 Hz, 1 H); ¹³C NMR (100.4 MHz, CDCl₃) δ 210.3, 114.5, 91.6, 87.0, 54.6, 53.8, 43.9, 41.3, 40.5; MS (70 eV) m/e (relative intensity) 276 (M⁺, 12), 248 (100), 220 (92), 192 (97), 149 (80), 121 (60), 110 (70), 84 (89), 67 (74), 56 (80), 42 (78); HRMS (EI) m/e calcd for C₁₁H₁₂FeN₂O₃ (M⁺) 276.0196, found 276.0201.

[Ethyl *N*-((2-5- η)-2,4-pentadienyl)prolinate]tricarbonyliron (3h). The crude mixture obtained from the addition of **2f** (0.84 g, 6.0 mmol) to cation **1a** (1.5 g, 5.0 mmol) was purified via flash column chromatography (silica gel, 30% ethyl acetate/hexanes) to give **3h** (1.2 g, 3.3 mmol, 72%) as a yellow oil. Complex **3h** could be further separated into two diastereomers. Diastereomer 1: IR (CH₂Cl₂) 2992, 2984, 2048, 1979, 1736, 1267, 1254, 1097, 889, 869, 848 cm⁻¹; ¹H NMR (400 MHz, CDCl₃) δ 5.48 (m, 1 H), 5.40 (m, 1 H), 4.17 (q, J = 6.8 Hz, 2 H), 3.18 (m, 1 H), 3.08 (dd, J = 8.8, 6.4 Hz, 1 H), 2.99 (dd, J = 13.2, 4.9 Hz, 1 H), 2.64 (m, 1 H), 2.24 (m, 1 H), 2.08–1.74 (m, 6 H), 1.56 (dd, J = 9.3, 2.5 Hz, 1 H), 1.27 (t, J = 6.8 Hz, 3 H); ¹³C NMR (100.4 MHz, CDCl₃) δ 210.8, 173.7, 91.2, 87.4, 64.5, 60.6, 55.6, 52.5, 52.3, 40.2, 29.2, 22.8, 14.2; MS (20 eV) m/e (relative intensity) 294 (M⁺ - 2CO + 1, 55), 266 (78), 250 (22), 221 (33), 198 (100), 169 (23), 157 (34), 136 (35); HRMS (EI) m/e calcd for C₁₂H₁₉FeNO₂ (M⁺ - 3CO) 265.0770, found

265.0767. Diastereomer 2: IR (CH₂Cl₂) 2992, 2982, 2048, 1973, 1736, 1283, 1265, 1248, 1183, 910, 882, 833 cm⁻¹; ¹H NMR (400 MHz, CDCl₃) δ 5.49 (m, 1 H), 5.40 (m, 1 H), 4.18 (q, *J* = 6.8 Hz, 2 H), 3.09 (m, 2 H), 2.87 (dd, *J* = 12.7, 5.0 Hz, 1 H), 2.63 (m, 1 H), 2.41 (m, 1 H), 2.18 (t, *J* = 10.7 Hz, 1 H), 2.07 (m, 1 H), 1.88–1.84 (m, 4 H), 1.48 (dd, *J* = 8.3, 2.0 Hz, 1 H), 1.28 (t, *J* = 7.3 Hz, 3 H); ¹³C NMR (100.4 MHz, CDCl₃) δ 210.7, 174.0, 91.2, 87.6, 64.7, 60.6, 55.4, 53.3, 53.0, 40.4, 29.4, 23.1, 14.2; MS (20 eV) *m/e* (relative intensity) 294 (M⁺ - 2CO + 1, 25), 276 (31), 266 (75), 206 (36), 197 (86), 169 (81), 136 (67), 126 (100), 64 (25); HRMS (EI) *m/e* calcd for C₁₃H₁₉FeNO₃ (M⁺ - 2CO) 293.0719, found 293.0718.

[Ethyl N-((2-5-η)-2,4-pentadienyl)pipecolat]tricarboxyliron (3i). The crude mixture obtained from the addition of **2g** (1.2 g, 6.0 mmol) to cation **1a** (1.5 g, 5.0 mmol) was purified via flash column chromatography (silica gel, 30% ethyl acetate/hexanes) to give **3i** (1.3 g, 3.5 mmol, 70%) as a 1:1 mixture of diastereomers: IR (CH₂Cl₂) (mixture of diastereomers) 3065, 2989, 2049, 1975, 1713, 1275, 1182, 891, 828 cm⁻¹; ¹H NMR (400 MHz, CDCl₃) (mixture of diastereomers) δ 5.45 (m, 4 H), 4.19 (m, 4 H), 3.14–3.00 (m, 4 H), 2.83–2.59 (m, 5 H), 2.35 (m, 1 H), 2.17–1.93 (m, 3 H), 1.81–1.70 (m, 12 H), 1.54 (m, 1 H), 1.27 (m, 6 H), 0.88 (m, 1 H); ¹³C NMR (100.4 MHz, CDCl₃) (mixture of diastereomers) δ 210.8, 173.5, 173.3, 91.0, 87.9, 87.8, 64.3, 64.0, 60.5, 60.4, 55.3, 55.1, 54.5, 54.4, 50.8, 49.5, 40.3, 30.0, 29.6, 25.3, 25.1, 23.0, 22.4, 14.3; MS (20 eV) (mixture of diastereomers) *m/e* (relative intensity) 308 (M⁺ - 2CO + 1, 100), 291 (35), 280 (88), 265 (35), 223 (41), 211 (47), 184 (35), 170 (41), 139 (32); HRMS (EI) *m/e* calcd for C₁₄H₂₁FeNO₃ (M⁺ - 2CO) 307.0876, found 307.0863.

[Ethyl N-((2-5-η)-2,4-pentadienyl)nipecotate]tricarboxyliron (3j). The crude mixture obtained from the addition of **2h** (0.96 g, 6.0 mmol) to cation **1a** (1.5 g, 5.0 mmol) was purified via flash column chromatography (silica gel, 30% ethyl acetate/hexanes), to give **3j** (1.2 g, 3.2 mmol, 64%) as a 1:1 mixture of diastereomers: IR (CH₂Cl₂) (mixture of diastereomers) 3046, 2992, 2982, 2048, 1977, 1725, 1674, 1618, 1283, 1152, 1094, 912, 883 cm⁻¹; ¹H NMR (400 MHz, CDCl₃) (mixture of diastereomers) δ 5.46 (m, 4 H), 4.13 (m, 4 H), 3.02 (m, 1 H), 2.75 (m, 3 H), 2.55 (m, 4 H), 2.23 (m, 1 H), 2.02 (m, 2 H), 1.89–1.68 (m, 10 H), 1.55–1.43 (m, 6 H), 1.25 (m, 6 H), 0.86 (m, 1 H); ¹³C NMR (100.4 MHz, CDCl₃) (mixture of diastereomers) δ 210.8, 174.9, 90.9, 87.7, 60.2, 57.6, 57.6, 55.3, 55.0, 54.9, 54.0, 53.5, 52.2, 41.8, 41.7, 40.1, 40.0, 26.8, 26.7, 24.5, 24.3, 14.1; MS (20 eV) (mixture of diastereomers) *m/e* (relative intensity) 335 (M⁺ - CO, 1), 307 (15), 279 (100), 211 (31), 207 (16), 183 (12), 139 (36), 67 (15); HRMS (EI) *m/e* calcd for C₁₅H₂₁FeNO₄ (M⁺ - CO) 335.0827, found 335.0818.

[(2-5-η)-2,4-pentadienyl)methylamino]propionitrile]tricarboxyliron (15). The crude mixture obtained from the addition of 3-(methylamino)propionitrile (0.39 g, 4.2 mmol) to cation **1a** (1.2 g, 3.8 mmol) was purified via flash column chromatography (silica gel, 15% ethyl acetate/hexanes) to give **15** (1.0 g, 3.5 mmol, 91%) as a yellow oil: IR (CH₂Cl₂) 3065, 3029, 2994, 2934, 1998, 1732, 1605, 1464, 1375, 1337, 1238, 1136, 1046, 891, 774, 752 cm⁻¹; ¹H NMR (400 MHz, CDCl₃) δ 5.50 (m, 2 H), 2.79 (dd, *J* = 9.6, 4.2 Hz, 1 H), 2.70 (m, 1 H), 2.59–2.52 (m, 2 H), 2.40 (t, *J* = 6.8 Hz, 2 H), 2.21 (s, 3 H, NCH₃), 1.95 (dd, *J* = 13.3, 10.0 Hz, 1 H), 1.83 (d, *J* = 7.5 Hz, 1 H), 1.46 (d, *J* = 6.7 Hz, 1 H); ¹³C NMR (100.4 MHz, CDCl₃) δ 210.5, 118.6, 91.0, 87.5, 55.8, 54.1, 51.3, 40.6, 40.0, 16.2; MS (70 eV) *m/e* (relative intensity) 290 (M⁺, 5), 248 (15), 220 (80), 192 (100), 149 (98), 123 (43), 110 (97), 84 (53), 67 (95), 56 (75), 42 (52), 38 (54); HRMS (EI) *m/e* calcd for C₁₂H₁₄FeN₂O₃ (M⁺) 290.0353, found 290.0347.

(1R*,2R*,5S*)-2-Carboxy-3-methyl-6-oxo-3-azabicyclo[3.3.0]octane (4a). The crude mixture from intramolecular cyclization of complex **3a** (1.2 g, 3.7 mmol) was purified via flash column chromatography (silica gel, 7% ethyl acetate/hexanes) and short-path distillation (0.02 mmHg, 65–75 °C) to give **4a** (0.39 g, 1.9 mmol, 50%) as a colorless liquid: IR (CH₂Cl₂) 2967, 1738, 1449, 1262, 1184, 1100, 1032, 893,

843 cm⁻¹; ¹H NMR (400 MHz, CDCl₃) δ 4.19–4.13 (m, 2 H), 3.29 (dd, *J* = 9.8, 9.3 Hz, 1 H), 2.97 (s, 1 H), 2.95 (m, 1 H), 2.80 (m, 1 H), 2.55 (dd, *J* = 9.3, 4.9 Hz, 1 H), 2.36 (m, 2 H), 2.30 (s, 3 H, NCH₃), 2.11 (m, 1 H), 1.94 (m, 1 H), 1.24 (t, *J* = 6.8 Hz, 3 H); ¹³C NMR (100.4 MHz, CDCl₃) δ 219.9, 172.3, 73.0, 60.7, 57.5, 50.4, 45.7, 38.9, 37.3, 25.2, 14.4; MS (70 eV) *m/e* (relative intensity) 211 (M⁺, 10), 166 (30), 138 (100), 111 (30), 97 (40), 82 (50), 71 (60), 57 (100), 53 (80), 28 (20); HRMS (EI) *m/e* calcd for C₁₁H₁₇NO₃ (M⁺) 211.1207, found 211.1205.

(1R*,2R*,5S*)-2-Carboxy-3-ethyl-2-(phenylmethyl)-6-oxo-3-azabicyclo[3.3.0]octane (4b). The crude mixture from intramolecular cyclization of complex **3b** (0.85 g, 2.0 mmol) was purified via flash column chromatography (silica gel, 16% ethyl acetate/hexanes) to give **4b** (0.21 g, 0.66 mmol, 33%) as a colorless liquid: IR (CH₂Cl₂) 3067, 3045, 2991, 2980, 2937, 2874, 1738, 1714, 1637, 1604, 1496, 1452, 1381, 1296, 1209, 1184, 1159, 1093 cm⁻¹; ¹H NMR (400 MHz, CDCl₃) δ 7.23 (m, 3 H), 7.14 (d, *J* = 7.3 Hz, 2 H), 4.16 (q, *J* = 7.3 Hz, 2 H), 3.57 (d, *J* = 14.7 Hz, 1 H), 3.30 (dd, *J* = 7.3, 2.3 Hz, 1 H), 3.05 (q, *J* = 9.3 Hz, 1 H), 2.96 (m, 1 H), 2.84 (t, *J* = 9.3 Hz, 1 H), 2.70 (d, *J* = 14.7 Hz, 1 H), 2.43 (t, *J* = 9.8 Hz, 1 H), 2.21 (m, 2 H), 2.15 (m, 1 H), 1.88 (m, 2 H), 1.25 (t, *J* = 6.8 Hz, 3 H), 1.07 (t, *J* = 6.8 Hz, 3 H); ¹³C NMR (100.4 MHz, CDCl₃) δ 220.9, 171.6, 137.5, 129.2, 128.3, 126.3, 74.9, 60.4, 53.1, 48.5, 45.5, 43.0, 39.4, 37.2, 23.9, 14.9, 14.5; MS (70 eV) *m/e* (relative intensity) 315 (M⁺, 1), 261 (6), 242 (100), 224 (55), 214 (30), 128 (25); HRMS (EI) *m/e* calcd for C₁₉H₂₅NO₃ (M⁺) 315.1834, found 315.1827.

(1R*,2R*,5S*)-2-Carboxy-3-ethyl-2-methyl-6-oxo-3-azabicyclo[3.3.0]octane (4c). The crude mixture from intramolecular cyclization of complex **3c** (0.70 g, 2.0 mmol) was purified via flash column chromatography (silica gel, 9% ethyl acetate/hexanes) and short-path distillation (0.02 mmHg, 83–95 °C) to give **4c** (0.21 g, 0.88 mmol, 44%) as a colorless liquid: IR (CH₂Cl₂) 2993, 2974, 2939, 2845, 1724, 1641, 1467, 1448, 1412, 1379, 1290, 1238, 1159, 1136, 1076, 1022, 912, 881 cm⁻¹; ¹H NMR (400 MHz, CDCl₃) δ 4.14 (q, *J* = 7.0 Hz, 2 H), 3.22 (d, *J* = 6.9 Hz, 1 H), 2.98 (dt, *J* = 8.3, 7.8 Hz, 1 H), 2.83 (m, 2 H), 2.71 (m, 1 H), 2.29 (t, *J* = 8.8 Hz, 2 H), 2.22 (m, 1 H), 2.00 (m, 1 H), 1.87 (m, 1 H), 1.30 (s, 3 H), 1.28 (t, *J* = 7.3 Hz, 3 H), 1.02 (t, *J* = 7.3 Hz, 3 H); ¹³C NMR (100.4 MHz, CDCl₃) δ 221.0, 173.9, 70.5, 60.2, 53.3, 48.9, 48.0, 42.6, 39.2, 23.4, 17.2, 14.7, 14.4; MS (70 eV) *m/e* (relative intensity) 239 (M⁺, 4), 166 (100), 138 (18), 110 (98), 94 (24), 82 (61); HRMS (EI) *m/e* calcd for C₁₃H₂₁NO₃ (M⁺) 239.1521, found 239.1519.

(1R*,2R*,5S*)-2-Carboxy-3-(*E*)-2-butenyl-2-methyl-6-oxo-3-azabicyclo[3.3.0]octane (4d). The crude mixture from intramolecular cyclization of complex **3d** (0.26 g, 0.69 mmol) was purified via flash column chromatography (silica gel, 9% ethyl acetate/hexanes) to give **4d** (0.11 g, 0.42 mmol, 61%) as a colorless liquid: IR (CH₂Cl₂) 3043, 2997, 2972, 2939, 2876, 2854, 1726, 1635, 1446, 1413, 1377, 1288, 1230, 1136, 1074, 1020, 970 cm⁻¹; ¹H NMR (400 MHz, CDCl₃) δ 5.53 (dq, *J* = 15.2, 6.4 Hz, 1 H), 5.35 (m, 1 H), 4.14 (q, *J* = 6.8 Hz, 2 H), 3.30 (dd, *J* = 13.7, 4.9 Hz, 1 H), 3.14 (dd, *J* = 15.1, 8.8 Hz, 1 H), 3.00 (q, *J* = 7.8 Hz, 1 H), 2.79 (m, 2 H), 2.72 (dd, *J* = 13.7, 7.8 Hz, 1 H), 2.28 (dd, *J* = 9.3, 6.8 Hz, 2 H), 2.02 (m, 1 H), 1.88 (m, 1 H), 1.64 (d, *J* = 6.4 Hz, 3 H), 1.31 (s, 3 H), 1.28 (t, *J* = 7.3 Hz, 3 H); ¹³C NMR (100.4 MHz, CDCl₃) δ 221.0, 174.0, 129.1, 127.1, 70.1, 60.3, 53.8, 50.8, 48.8, 48.1, 39.2, 23.4, 17.7, 17.3, 14.5; MS (70 eV) *m/e* (relative intensity) 265 (M⁺, 3), 210 (3), 192 (98), 166 (100), 138 (97), 110 (42), 82 (51), 67 (29), 55 (96); HRMS (EI) *m/e* calcd for C₁₅H₂₃NO₃ (M⁺) 265.1679, found 265.1674.

2-Carboxy-3,7-dimethyl-6-oxo-3-azabicyclo[3.3.0]octane (4e). The crude mixture from intramolecular cyclization of complex **3e** (1.9 g, 5.7 mmol) was purified via flash column chromatography (silica gel, 20% ethyl acetate/hexanes) to give **4e** (0.46 g, 2.1 mmol, 36%) as a mixture of diastereomers in a 1:1 ratio: IR (CH₂Cl₂) (mixture of diastereomers) 2968, 1740, 1449, 1361, 1260, 1180, 1109, 1044, 894, 802 cm⁻¹; ¹H NMR (400 MHz, CDCl₃) (mixture of diastereomers) δ 4.30

(q, $J = 7.3$ Hz, 2 H), 4.18 (q, $J = 7.3$ Hz, 2 H), 3.41 (m, 1 H), 3.21 (s, 1 H), 3.00 (m, 1 H), 3.00–2.84 (m, 6 H), 2.54–2.40 (m, 5 H), 2.39 (s, 6 H), 2.39–2.21 (m, 2 H), 1.72 (m, 4 H), 1.35 (m, 2 H), 1.30 (t, $J = 7.3$ Hz, 3 H), 1.02 (d, $J = 6.8$ Hz, 3 H); ^{13}C NMR (100.4 MHz, CDCl_3) (mixture of diastereomers) δ 219.8, 219.4, 172.5, 172.1, 73.5, 73.0, 61.8, 60.2, 57.8, 57.2, 51.8, 50.2, 44.4, 43.8, 38.5, 38.2, 37.2, 37.0, 25.4, 25.1, 14.1, 13.3; MS (70 eV) m/e (relative intensity) (mixture of diastereomers) 225 (M^+ , 5), 195 (10), 162 (12), 150 (100), 122 (13), 108 (68), 94 (45), 85 (52), 82 (95), 67 (48), 55 (52), 51 (18); HRMS (EI) m/e calcd for $\text{C}_{12}\text{H}_{19}\text{NO}_3$ (M^+) 225.1364, found 225.1358.

(1R*,2R*,5S*,8R*)-2-Carbethoxy-3,8-dimethyl-6-oxo-3-azabicyclo[3.3.0]octane (4f). The crude mixture from intramolecular cyclization of complex **3f** (1.3 g, 4.0 mmol) was purified via flash column chromatography (silica gel, 20% ethyl acetate/hexanes) and short-path distillation (0.02 mmHg, 110–130 °C) to give **4f** (0.41 g, 1.8 mmol, 46%) and **6** (0.31 g, 1.4 mmol, 34%) as colorless liquids. **4f**: IR (CH_2Cl_2) 3054, 2994, 2980, 2944, 1740, 1624, 1478, 1445, 1433, 1304, 1182, 1123, 1096, 1059, 907, 893, 856, 845 cm^{-1} ; ^1H NMR (400 MHz, CDCl_3) δ 4.23 (q, $J = 7.3$ Hz, 2 H), 3.37 (dd, $J = 9.3, 8.3$ Hz, 1 H), 3.27 (d, $J = 6.4$ Hz, 1 H), 3.10 (q, $J = 7.3$ Hz, 1 H), 2.83 (dt, $J = 8.3, 3.4$ Hz, 1 H), 2.65 (dd, $J = 9.3, 3.9$ Hz, 1 H), 2.45 (m, 1 H), 2.35 (m, 1 H), 2.34 (s, 3 H, NCH_3), 2.09 (dd, $J = 17.5, 13.2$ Hz, 1 H), 1.31 (t, $J = 7.3$ Hz, 3 H), 1.18 (d, $J = 6.8$ Hz, 3 H); ^{13}C NMR (100.4 MHz, CDCl_3) δ 219.4, 172.7, 66.5, 60.3, 57.7, 52.7, 50.5, 44.2, 38.2, 31.1, 16.3, 14.0; MS (70 eV) m/e (relative intensity) 225 (M^+ , 100), 196 (15), 163 (18), 153 (100), 150 (100), 122 (10), 108 (58), 94 (32), 83 (50), 82 (100), 67 (95), 55 (50), 51 (12); HRMS (EI) m/e calcd for $\text{C}_{12}\text{H}_{19}\text{NO}_3$ (M^+) 225.1364, found 225.1359.

(1R*,2R*,5S*)-2-Carbethoxy-3,8-dimethyl-6-oxo-3-azabicyclo[3.3.0]oct-7-ene (6): IR (CH_2Cl_2) 3065, 3052, 2980, 2944, 2885, 1740, 1624, 1433, 1381, 1182, 1030, 895, 679 cm^{-1} ; ^1H NMR (400 MHz, CDCl_3) δ 5.95 (s, 1 H), 4.25 (q, $J = 6.8$ Hz, 2 H), 3.39 (d, $J = 4.9$ Hz, 1 H), 3.25 (m, 2 H), 3.03 (m, 1 H), 2.75 (dd, $J = 9.3, 4.9$ Hz, 1 H), 2.38 (s, 3 H, NCH_3), 2.19 (s, 3 H), 1.13 (t, $J = 6.8$ Hz, 3 H); ^{13}C NMR (100.4 MHz, CDCl_3) δ 209.2, 176.5, 171.7, 131.3, 67.6, 60.7, 55.4, 54.3, 50.4, 38.1, 18.0, 14.2; MS (70 eV) m/e (relative intensity) 223 (M^+ , 100), 208 (5), 194 (7), 152 (60), 150 (98), 122 (95), 107 (65), 82 (95), 68 (90), 55 (40); HRMS (EI) m/e calcd for $\text{C}_{12}\text{H}_{17}\text{NO}_3$ (M^+) 223.1207, found 223.1210.

(1R*,2R*,5S*)-2-Cyano-3-methyl-6-oxo-3-azabicyclo[3.3.0]octane (4g). The crude mixture from intramolecular cyclization of complex **3g** (1.5 g, 4.3 mmol) was purified via flash column chromatography (silica gel, 20% ethyl acetate/hexanes) and short-path distillation (0.02 mmHg, 65–75 °C) to give **4g** (exo) as a colorless solid (0.26 g, 1.6 mmol, 37%) and **4g** (endo) (0.19 g, 1.2 mmol, 28%) as a colorless liquid.

4g (exo): IR (CH_2Cl_2) 3065, 2966, 2957, 2226, 1744, 1607, 1451, 1304, 1258, 1163 cm^{-1} ; ^1H NMR (400 MHz, CDCl_3) δ 3.71 (s, 1 H), 3.21 (m, 1 H), 3.15 (d, $J = 9.5$ Hz, 1 H), 2.76 (dd, $J = 8.8, 8.5$ Hz, 1 H), 2.65 (dd, $J = 9.2, 8.8$ Hz, 1 H), 2.42 (s, 3 H, NCH_3), 2.42–2.32 (m, 3 H), 1.81 (m, 1 H); ^{13}C NMR (100.4 MHz, CDCl_3) δ 218.4, 116.3, 62.7, 56.8, 49.3, 45.1, 38.6, 37.9, 26.9; MS (70 eV) m/e (relative intensity) 164 (M^+ , 52), 138 (72), 119 (23), 95 (42), 85 (49), 82 (100), 67 (23), 55 (12); HRMS (EI) m/e calcd for $\text{C}_9\text{H}_{12}\text{N}_2\text{O}$ (M^+) 164.0949, found 164.0948.

4g (endo): IR (CH_2Cl_2) 3066, 2977, 2967, 2229, 1744, 1605, 1354, 1268, 1156 cm^{-1} ; ^1H NMR (400 MHz, CDCl_3) δ 3.39 (d, $J = 7.8$ Hz, 1 H), 3.17 (m, 2 H), 2.75 (dd, $J = 5.2, 4.5$ Hz, 1 H), 2.48 (dd, $J = 9.7, 5.2$ Hz, 1 H), 2.42 (s, 3 H, NCH_3), 2.39 (m, 1 H), 2.23 (m, 3 H); ^{13}C NMR (100.4 MHz, CDCl_3) δ 218.0, 116.7, 61.5, 58.7, 50.2, 42.3, 40.8, 38.7, 24.9; MS (70 eV) m/e (relative intensity) 164 (M^+ , 52), 138 (72), 119 (15), 95 (32), 85 (49), 82 (100), 67 (23), 55 (12); HRMS (EI) m/e calcd for $\text{C}_9\text{H}_{12}\text{N}_2\text{O}$ (M^+) 164.0949, found 164.0948.

(1R*,2R*,8S*)-2-Carbethoxy-9-oxo-6-azatricyclo[6.3.0.0^{2,6}]-undecane (7). The crude mixture from intramolecular cyclization of complex **3h** (1.2 g, 3.3 mmol) was purified via flash column chromatography (silica gel, 30% ethyl acetate/hexanes)

to give **7** (0.10 g, 0.42 mmol, 13%) as a pale yellow liquid: IR (CH_2Cl_2) 3067, 2991, 2982, 1738, 1423, 1186, 1114 cm^{-1} ; ^1H NMR (400 MHz, CDCl_3) δ 4.21 (q, $J = 7.3$ Hz, 2 H), 3.30 (dd, $J = 15.6, 9.8$ Hz, 1 H), 3.18 (m, 1 H), 3.08 (dd, $J = 15.1, 7.8$ Hz, 1 H), 2.86 (dd, $J = 13.7, 9.3$ Hz, 2 H), 2.75 (m, 1 H), 2.43 (m, 1 H), 2.36 (m, 1 H), 2.26 (m, 1 H), 2.12 (m, 1 H), 1.91 (m, 1 H), 1.79 (m, 1 H), 1.75 (m, 1 H), 1.66 (m, 1 H), 1.30 (t, $J = 7.3$ Hz, 3 H); ^{13}C NMR (100.4 MHz, CDCl_3) δ 218.5, 174.2, 82.2, 61.0, 56.5, 54.6, 51.0, 49.9, 38.5, 36.5, 24.3, 23.9, 14.3; MS (70 eV) m/e (relative intensity) 238 ($\text{M}^+ + 1$, 87), 164 (99), 135 (45), 125 (55), 100 (100), 79 (99), 67 (31), 55 (23); HRMS (EI) m/e calcd for $\text{C}_{13}\text{H}_{19}\text{NO}_3$ (M^+) 237.1365, found 237.1356.

(1R*,2R*,9S*)-2-Carbethoxy-10-oxo-7-azatricyclo[7.3.0.0^{2,7}]-dodecane (8). The crude mixture from intramolecular cyclization of complex **3i** (1.1 g, 2.9 mmol) was purified via flash column chromatography (silica gel, 30% ethyl acetate/hexanes) to give **8** (0.48 g, 0.93 mmol, 32%) as a pale yellow liquid: IR (CH_2Cl_2) 2943, 2860, 1736, 1444, 1334, 1265, 1224, 1141, 1024 cm^{-1} ; ^1H NMR (400 MHz, CDCl_3) δ 4.14 (m, 2 H), 3.34 (dd, $J = 9.8, 8.8$ Hz, 1 H), 2.98 (dd, $J = 9.8, 2.4$ Hz, 1 H), 2.93–2.85 (m, 2 H), 2.74 (dd, $J = 15.4, 6.3$ Hz, 1 H), 2.61 (dd, $J = 8.8, 2.4$ Hz, 1 H), 2.27 (d, $J = 8.8$ Hz, 1 H), 2.24 (d, $J = 2.9$ Hz, 1 H), 2.12 (d, $J = 12.7$ Hz, 1 H), 1.99 (m, 1 H), 1.91 (m, 1 H), 1.69 (d, $J = 13.7$ Hz, 1 H), 1.54 (d, $J = 12.2$ Hz, 1 H), 1.43–1.33 (m, 2 H), 1.25 (t, $J = 7.3$ Hz, 3 H), 1.17 (m, 1 H); ^{13}C NMR (100.4 MHz, CDCl_3) δ 220.9, 175.1, 70.7, 60.1, 54.1, 48.3, 48.1, 45.3, 39.4, 29.1, 24.6, 23.0, 21.5, 14.3; MS (70 eV) m/e (relative intensity) 252 ($\text{M}^+ + 1$, 22), 178 (100), 176 (23), 150 (6), 122 (18), 79 (8); HRMS (EI) m/e calcd for $\text{C}_{14}\text{H}_{21}\text{NO}_3$ (M^+) 251.1521, found 251.1514.

(1S*,2R*,6S*)-1-Carbethoxy-5-oxo-8-azatricyclo[6.3.1.0^{2,6}]-dodecane (9). The crude mixture from intramolecular cyclization of complex **3j** (1.1 g, 2.9 mmol) was purified via flash column chromatography (silica gel, 30% ethyl acetate/hexanes) to give **9** (0.36 g, 1.4 mmol, 50%) as a pale yellow liquid: IR (CH_2Cl_2) 3399, 3067, 2986, 1721, 1290, 1265, 1246, 1096, 895, 880, 858 cm^{-1} ; ^1H NMR (400 MHz, CDCl_3) δ 4.16 (m, 2 H), 3.26 (dd, $J = 18.5, 4.2$ Hz, 1 H), 3.10 (m, 1 H), 3.03 (m, 2 H), 2.94 (m, 2 H), 2.81 (d, $J = 13.2$ Hz, 1 H), 2.73 (m, 1 H), 2.40 (dd, $J = 18.5, 8.0$ Hz, 1 H), 2.20 (m, 1 H), 2.16 (m, 1 H), 1.95 (m, 2 H), 1.86 (m, 1 H), 1.55 (m, 1 H), 1.41 (t, $J = 7.3$ Hz, 1 H), 1.28 (t, $J = 7.3$ Hz, 3 H); ^{13}C NMR (100.4 MHz, CDCl_3) δ 214.3, 172.2, 61.7, 50.1, 48.1, 46.2, 43.3, 40.7, 40.5, 37.0, 32.5, 23.4, 19.5, 14.1; MS (70 eV) m/e (relative intensity) 251 (M^+ , 62), 194 (8), 178 (43), 169 (98), 140 (48), 97 (30), 96 (100), 56 (12); HRMS (EI) m/e calcd for $\text{C}_{14}\text{H}_{21}\text{NO}_3$ (M^+) 251.1521, found 251.1525.

(1R*,2R*,5S*,7S*)-2-Carbethoxy-7-methyl-6-oxo-3-azabicyclo[3.2.0]heptane (10). To a solution of diisopropylamine (0.85 mL, 6.0 mmol) in 4.0 mL of THF under nitrogen at -78 °C was added rapidly, neat, via syringe, a solution of *n*-butyllithium (3.8 mL, 6.0 mmol, 1.6 M) in hexane followed by addition of HMPA (1.8 mL). The reaction mixture was stirred at -78 °C for 20 min. A solution of complex **3a** (1.4 g, 4.3 mmol) in THF (3.0 mL) was added dropwise via syringe. The mixture was stirred at -78 °C for 2 h. The reaction mixture was quenched with trifluoroacetic acid (1.0 mL) via a syringe needle and was stirred at 25 °C under an atmosphere of CO for 2 h. After this time, the reaction mixture was diluted with an ethyl acetate/hexanes mixture (1/1, 100 mL). The resultant solution was washed with water (100 mL \times 3) and brine (100 mL \times 3), dried over anhydrous magnesium sulfate (10 g), and concentrated to give the crude mixture. The crude mixture was purified via flash column chromatography (silica gel, 25% ethyl acetate/hexanes) to give **11** (0.25 g, 1.8 mmol, 16%), **10** (0.30 g, 1.4 mmol, 33%), and **4a** (0.32 g, 1.5 mmol, 35%) as colorless oils. **10**: IR (CH_2Cl_2) 2984, 2936, 1775, 1728, 1275, 1254, 1192, 1098, 1030 cm^{-1} ; ^1H NMR (400 MHz, CDCl_3) δ 4.18 (q, $J = 7.3$ Hz, 2 H), 3.67 (m, 1 H), 3.63 (s, 1 H), 3.42 (m, 1 H), 3.12 (dd, $J = 9.3, 8.3$ Hz, 1 H), 3.07 (m, 1 H), 3.02 (dd, $J = 9.3, 6.8$ Hz, 1 H), 2.43 (s, 3 H, NCH_3), 1.30 (t, $J = 6.8$ Hz, 3 H), 1.09 (d, $J = 7.3$ Hz, 3 H); ^{13}C NMR (100.4 MHz,

CDCl_3) δ 215.3, 172.5, 64.8, 62.4, 60.2, 55.3, 55.0, 38.7, 36.8, 14.4, 8.0; MS (70 eV) *m/e* (relative intensity) 211 (M^+ , 10), 154 (30), 138 (95), 128 (10), 82 (10), 67 (15); HRMS (EI) *m/e* calcd for $\text{C}_{11}\text{H}_{17}\text{NO}_3$ (M^+) 211.1207, found 211.1213.

2-Carboethoxy-3-ethyl-1-methylpyrrole (11): IR (CH_2Cl_2) 3063, 3050, 2985, 1727, 1609, 1273, 1105, 895, 828, 818 cm^{-1} ; ^1H NMR (400 MHz, CDCl_3) δ 6.67 (d, $J = 2.4$ Hz, 1 H), 6.00 (d, $J = 2.4$ Hz, 1 H), 4.30 (q, $J = 7.3$ Hz, 2 H), 3.87 (s, 3 H, NCH_3), 2.78 (q, $J = 7.3$ Hz, 2 H), 1.36 (t, $J = 6.8$ Hz, 3 H), 1.19 (t, $J = 7.3$ Hz, 3 H); ^{13}C NMR (100.4 MHz, CDCl_3) δ 164.5, 128.2, 108.2, 76.7, 76.4, 59.9, 37.6, 21.4, 15.0, 14.4; MS (70 eV) *m/e* (relative intensity) 181 (M^+ , 37), 166 (12), 149 (100), 136 (34), 125 (32), 112 (26), 67 (28); HRMS (EI) *m/e* calcd for $\text{C}_{10}\text{H}_{15}\text{NO}_2$ (M^+) 181.1102, found 181.1108.

(1R*,2R*,5S*,7S*)-2-Carboethoxy-7-methyl-6-oxobicyclo[3.2.0]heptane (14). To a solution of diisopropylamine (0.85 mL, 6.0 mmol) in 4 mL of THF under nitrogen at -78 °C was added rapidly, neat, via syringe, a solution of *n*-butyllithium (3.8 mL, 6.0 mmol, 1.6 M) in hexane followed by addition of HMPA (1.8 mL). The reaction mixture was stirred at -78 °C for 20 min. A solution of complex **12** (1.5 g, 4.8 mmol) in THF (3.0 mL) was added dropwise via syringe. The mixture was stirred at -78 °C for 2 h. The reaction mixture was quenched with trifluoroacetic acid (1.0 mL) via a syringe needle and was stirred at 25 °C under an atmosphere of CO for 2 h. After this time, the reaction mixture was diluted with an ethyl acetate/hexanes mixture (1/1, 100 mL). The resultant solution was washed with water (100 mL \times 3) and brine (100 mL \times 3), dried over anhydrous magnesium sulfate (10 g), and concentrated to give the crude mixture. The crude mixture was purified via flash column chromatography (silica gel, 25% ethyl acetate/hexanes) to give **13**^{12a} (0.32 g, 1.6 mmol, 34%), and **14** (0.33 g, 1.7 mmol, 35%) as colorless oils. **14:** IR (CH_2Cl_2) 2971, 2876, 1769, 1449, 1375, 1352, 1192, 1157, 1136, 1032 cm^{-1} ; ^1H NMR (400 MHz, CDCl_3) δ 4.12 (q, $J = 7.2$ Hz, 2 H), 3.69 (ddd, $J = 6.8, 5.9, 3.4$ Hz, 1 H), 3.53 (dq, $J = 10.3, 7.8$ Hz, 1 H), 3.27 (dd, $J = 10.3, 5.9$ Hz, 1 H), 2.87 (d, $J = 7.8$ Hz, 1 H), 2.17 (dd, $J = 12.2, 5.8$ Hz, 1 H), 1.98 (dd, $J = 12.5, 6.1$ Hz, 1 H), 1.80–1.62 (m, 2 H), 1.27 (t, $J = 7.2$ Hz, 3 H), 1.02 (d, $J =$

7.8 Hz, 3 H); ^{13}C NMR (100.4 MHz, CDCl_3) δ 216.7, 175.1, 63.5, 60.6, 54.9, 43.9, 37.9, 30.5, 27.4, 14.1, 7.9; MS (70 eV) *m/e* (relative intensity) 196 (M^+ , 16), 167 (13), 150 (18), 141 (27), 95 (67), 67 (100), 54 (29); HRMS (EI) *m/e* calcd for $\text{C}_{11}\text{H}_{16}\text{O}_3$ (M^+) 196.1099, found 196.1100.

3-Cyano-4-(*E*)-1-propenyl-1-methylpyrrolidine (16).

The crude mixture from intramolecular cyclization of complex **15** (0.92 g, 2.7 mmol) was purified via flash column chromatography (silica gel, 7% ethyl acetate/hexanes) and short-path distillation (0.02 mmHg, 85–90 °C) to give **16** (0.15 g, 0.67 mmol, 25%) as an inseparable 4:3 mixture of syn and anti isomers: IR (CH_2Cl_2) (mixture of diastereomers) 3019, 2988, 2948, 2849, 2242, 1607, 1424, 1250, 1100, 895, 833, 828 cm^{-1} ; ^1H NMR (400 MHz, CDCl_3) (mixture of diastereomers) δ 5.62 (m, 2 H), 5.37 (m, 2 H), 3.42 (quin, $J = 6.8$ Hz, 1 H), 3.04 (quin, $J = 7.1$ Hz, 1 H), 2.88–2.79 (m, 6 H), 2.71 (m, 2 H), 2.36 (s, 3 H, NCH_3), 2.35 (s, 3 H, NCH_3), 2.34 (m, 2 H), 1.69 (d, $J = 6.4$ Hz, 3 H), 1.67 (d, $J = 6.8$ Hz, 3 H); ^{13}C NMR (100.4 MHz, CDCl_3) (mixture of diastereomers) δ 129.4, 127.1, 126.3, 120.7, 120.5, 60.8, 60.5, 58.3, 58.2, 46.6, 40.9, 40.6, 40.5, 33.9, 33.6, 16.8, 12.3; MS (70 eV) (mixture of diastereomers) *m/e* (relative intensity) 150 (M^+ , 86), 149 (39), 135 (16), 124 (15), 108 (27), 107 (31), 82 (18), 67 (10), 57 (100); HRMS (EI) *m/e* calcd for $\text{C}_9\text{H}_{14}\text{N}_2$ (M^+) 150.1156, found 150.1153.

Acknowledgment. Support for this research from the National Science Council (Grant No. NSC 83-0208-M-003-023) of the Republic of China is gratefully acknowledged.

Supporting Information Available: ORTEP diagrams showing the atom-numbering scheme and tables of crystallographic data, positional parameters, and bond lengths and angles for **4g** (8 pages). This material is contained in many libraries on microfiche, immediately follows this article in the microfilm version of the journal, and can be ordered from the ACS; see any current masthead page for ordering information.

OM9501743

ΔE – ΔC Analysis of Phosphine Basicity

Russell S. Drago

Department of Chemistry, University of Florida, Gainesville, Florida 32611

Received January 31, 1995*

The recently reported ΔE – ΔC substituent constant analysis is used to interpret 45 families of reactions involving substituted phosphines. Reported inductive substituent parameters that have been shown to be applicable to organic and inorganic systems can be summed for the three substituents on phosphine to predict their reactivity. In addition to good data fits, a very different interpretation of the chemistry is offered from that resulting with single-parameter scales of basicity. The traditional role of cone angles, *i.e.* an enthalpic type steric effect, is greatly diminished from that inferred by QALE analyses when a covalent contribution is added. Two new entropic steric effects are proposed to rationalize deviations in linear free energy relations. These same effects are seen to be operative in free energies of several different systems. The variations found in the covalent (soft or frontier controlled) component of the reactions studied make reported one-parameter scales of phosphine basicity poorly suited for analyses of many of these reactions. Increasing the diversity of systems shown to obey the electrostatic–covalent model serves to provide further support that the electrostatic–covalent model is the energy counterpart of the symmetry-based Woodward–Hoffmann rules for chemical reactivity.

Introduction

The extensive utilization of phosphines as ligands in organometallic chemistry has led to many attempts to evaluate the electronic and steric factors influencing the reactivity of these ligands. The reader is referred to refs 1–7 for a discussion of and references to the extensive literature in this area. Quantitative interpretations^{1–3} of the reactivity of substituted phosphines are based upon equations of the form

$$\Delta\chi_i^J = a_J E_i + b_J S_i + c_J \quad (1)$$

where $\Delta\chi_i^J$ is an energy related property (e.g. the log of the rate constant, for the *i*th ligand in the set *J*), E_i and S_i are the electronic and steric parameters, respectively, of the *i*th ligand, and a_J and b_J weight the relative importance of steric and electronic effects to the *J* set of measured properties. The c_J parameter is the value of the measured property for the hypothetical reference reactant in which E_i and S_i are zero. The E_i parameters are based on various collections and estimates of $\text{p}K_a$'s for phosphines, the ¹³C chemical shifts in $\text{X}_3\text{PNi}(\text{CO})_3$ complexes,⁴ or the A_1 IR stretching frequency of the nickel carbonyl complexes.^{5,6} The S_i parameters are based upon Tolman's⁵ cone angle, θ , or Brown's³ ligand repulsive parameter, E_R .

Considerable effort has gone into demonstrating that the factors contributing to σ bond strength can be grouped into two independent terms. These have been referred to as hard–soft (or charged–soft), frontier–charge controlled or electrostatic–covalent.^{8b} The only reported⁸ reactivity scale that incorporates these dual concepts uses the electrostatic–covalent terminology. Equation 1 uses E_i as a one-parameter scale of ligand σ donor properties. Work from this laboratory⁹ has shown that one-parameter scales of donor strength are valid only when the ratio of the covalent and electrostatic contributions to the reactions being analyzed are similar to those in the reactions used to establish the scale. When the ratios differ, poor correlations result or seemingly good correlations result in incorrect data interpretations.⁹ If E_i (eq 1) does not properly represent the covalent contribution in the property being correlated, deviations from incorrect parameters for donor strength could be compensated for and incorrectly attributed to steric effects in the data fit with b_J , producing a meaningless, good correlation of the data.

The recently reported⁸ successful correlations of over 58 reaction types and physicochemical properties with eq 2 has prompted a reanalysis of phosphine basicity.

$$\Delta\chi^X = d^E \Delta E^X + d^C \Delta C^X + \Delta\chi^H \quad (2)$$

In eq 2, $\Delta\chi^X$ is an energy related property in a *J* set of measurements of a family of compounds with an X substituent, and $\Delta\chi^H$ is the measurement for the parent hydrogen compound. The property can be any spectral or reactivity measure expressed in energy units. ΔE^X is the electrostatic substituent constant for the X group and ΔC^X the analogous quantity for the covalent contribution, d^E gauges the contribution made to the *J* data

* Abstract published in *Advance ACS Abstracts*, June 1, 1995.
 (1) Schenkluhn, H.; Berger, R.; Pittel, B.; Zahres, M. *Transition Met. Chem. (London)* **1981**, *6*, 277 and references therein.
 (2) (a) Tracey, A. A.; Eriks, K.; Prock, A.; Giering, W. P. *Organometallics* **1990**, *9*, 1399 and references therein. (b) Liu, H. Y.; Eriks, K.; Prock, A.; Giering, W. P. *Organometallics* **1990**, *9*, 1758. (c) Fernandez, A. L.; Prock, A.; Giering, W. P. *Organometallics* **1994**, *13*, 2767.
 (3) Brown, T. L. *Inorg. Chem.* **1992**, *31*, 1286 and references therein.
 (4) Bodner, G. M.; May, M. P.; McKinney, L. E. *Inorg. Chem.* **1980**, *19*, 1951 and references therein.
 (5) Tolman, C. A. *Chem. Rev.* **1977**, *77*, 313.
 (6) Chen, L.; Poe, A. J. *Inorg. Chem.* **1989**, *28*, 3641 and references therein.
 (7) (a) Bush, R. C.; Angelici, R. J. *Inorg. Chem.* **1988**, *27*, 681. (b) Sowa, J. R., Jr.; Angelici, R. J. *Inorg. Chem.* **1991**, *30*, 3534.

(8) (a) Drago, R. S.; Dadmun, A. P. *J. Am. Chem. Soc.* **1993**, *115*, 8592. (b) Drago, R. S. *Applications of Electrostatic-Covalent Models in Chemistry*; Surfside Scientific: P.O. Box 13413, Gainesville, FL, 1994. (c) Drago, R. S.; Zoltewicz, J. A. *J. Org. Chem.* **1994**, *59*, 2824.
 (9) Drago, R. S. *Inorg. Chem.* **1990**, *29*, 1379.

Table 1. Revised and New Inductive Substituent Parameters

substituent (n) ^a	3- ΔE	3- ΔC	substituent (n) ^a	3- ΔE	3- ΔC
3-OCH ₃ (0.2)	-0.015	0.158	3-CF ₃ CH ₂ (0.4)	-0.028	-0.118
3-N(CH ₃) ₂ (0.4)	0.041	0.431	3-CH ₃ CO ₂ CH ₂ (0.7)	-0.036	-0.166
3-C ₆ H ₅ (0.2)	0.011	0.058	3-(CH ₃) ₃ SiCH ₂ (0.5)	0.060	0.285
3- <i>n</i> -C ₃ H ₇ (0.4)	0.043	0.172	3-CH ₃ CH ₂ CH(CH ₃) (0.5)	0.057	0.233
3- <i>i</i> -C ₃ H ₇ (0.2)	0.059	0.254	3-C ₆ H ₅ CO (0.8)	-0.060	-0.252
3-OC ₂ H ₅ (0.5)	-0.006	0.269	3-(CH ₃) ₃ CCH ₂ (0.4)	0.048	0.204
3-SCH ₃ (0.5)	-0.035	-0.216	3-NO ₂ CH ₂ (0.6)	-0.118	-0.553
3- <i>n</i> -C ₄ H ₉ (0.4)	0.046	0.181	3-CHCl ₂ (0.8)	-0.127	-0.622
3-(CH ₃) ₂ CHCH ₂ (0.4)	0.039	0.141	3-N ₃ (0.8)	-0.171	-0.759
3- <i>t</i> -C ₄ H ₉ (0.4)	0.059	0.306	3-SCN- (0.6)	-0.110	-0.335
3-ClCH ₂ (0.4)	-0.045	-0.246	3-NCS- (0.6)	-0.125	-0.442
3-C ₆ H ₅ CH ₂ (0.5)	0.009	0.010	3-OCN- (0.5)	-0.099	-0.345
3-C ₆ H ₁₁ (0.4)	0.058	0.278	3-CCl ₃ (0.8)	-0.089	-0.372
3-OC ₆ H ₅ (0.5)	-0.049	0.094	3-OCH(CH ₃) ₂ (0.5)	0.001	0.195
3-Si(CH ₃) ₃ (0.5)	0.043	0.196	3- <i>p</i> -CH ₃ C ₆ H ₄ (0.3)	0.015	0.071
3-C ₂ H ₃ (0.4)	0.012	0.020	3- <i>p</i> -CH ₃ OC ₆ H ₄ (0.4)	0.017	0.078
3-CH ₃ OCH ₂ (0.6)	-0.003	-0.132	3- <i>p</i> -ClC ₆ H ₄ (0.5)	0.001	0.029
3-BrCH ₂ (0.4)	-0.041	-0.208	3- <i>p</i> -CF ₃ C ₆ H ₄ (0.7)	0.001	0.077
3-CH ₂ I (0.4)	-0.048	-0.243	3- <i>p</i> -N(CH ₃) ₂ C ₆ H ₄ (0.8)	0.038	0.064
3-NCCH ₂ (0.5)	-0.078	-0.357	3- <i>p</i> -FC ₆ H ₄ (0.4)	0.006	0.043

^a An n value of 0.2 indicates the parameters are well-known for this substituent. The larger the value, the less well-known. The weight given to a substituent in a data fit is given by $1/n$.

set by the electrostatic substituent constant and d^C that from the covalent substituent constant. The same ΔE^X and ΔC^X parameters are used on families of donor or acceptor molecules. When the nature of the interaction is known, a subscript is added to the d term to indicate if a donor (B) or acceptor (A) is the constant reactant in the J set of $\Delta\chi^X$ measurements.

The ΔE^X and ΔC^X parameters are derived from the data fit of over 58 different physicochemical properties, including data in poorly solvating solvents. A given substituent has parameters for its inductive influence, 3- ΔE^X and 3- ΔC^X , and different parameters when the mechanism for the substituent influence is mainly a conjugative interaction, 4- ΔE^X and 4- ΔC^X . The 3- and 4-labels refer to positions on a benzene ring, but the substituents are used on other families of compounds where inductive or conjugative mechanisms dominate.

Equation 2 is a two-parameter analogue of the Hammett equation.¹⁰ The dual-parameter analogues to σ are ΔE and ΔC , while the dual-parameter analogues to ρ are d^E and d^C . Interpretations of the parameters follow those of the Hammett equation, except information is now available on the covalent and electrostatic components of σ and ρ . The d parameter, like ρ , depends on the demand made by the constant reactant (its E^* and C^*) on the family of reactants and on the sensitivity of the family to the substituent change (s^E and s^C):

$$d^E = s^E E^* \quad (3)$$

$$d^C = s^C C^* \quad (4)$$

The components of d , like the components of ρ , often are not determined.

The E and C equation, which is the basis for eq 2, is given in eq 5. This equation is written to analyze

$$\Delta\chi^X = E_A^* E_B + C_A^* C_B + W \quad (5)$$

measurements in which the acceptor is held constant and donors are varied. Reported E_B and C_B parameters

for donors (the dual-parameter donor scale) are substituted into eq 5, and the series of simultaneous equations (one for each donor) are solved for E_A^* and C_A^* . The electrostatic-covalent model was imposed on the parameters in this data fit and carries over to ΔE^X and ΔC^X . Values of E_A^* and C_A^* from analyses with eq 5 for families of pyridine donors where s^C and s^E equal 1 are entered for d into eq 2 in the data fit used to determine ΔE and ΔC .

In the application of eq 5, the reactants are not limited to a family of compounds. Equation 2 is used instead of eq 5 to analyze data when the E_B and C_B or E_A and C_A values of a family of donors or acceptors are not known. This is the case for the family of substituted-phosphine donors. It is important to emphasize that E^* and C^* of eqs 3 and 4 are identical with E_A^* and C_A^* of eq 5.

In this article, dual-parameter substituent constant analyses (eq 2) will be made on data that have been previously analyzed with eq 1. A different interpretation of phosphine basicity will be offered that makes the interpretation of this chemistry consistent with the analysis of the many other physicochemical properties correlated with ΔE and ΔC .

Results and Discussion

Refinement of Parameters. The large amount of additional data on the reactivity and spectroscopy of phosphines has enabled us to combine these results with the data set used earlier to expand, and further refine, several of the inductive 3- ΔE and 3- ΔC parameters (see Calculation Section) that were not accurately known. The new parameters are reported in Table 1. The d^E and d^C parameters for the probes that have also been refined in the determination of these new parameters are reported in Table 2. Other reported probe parameters⁸ remain the same. The pK 's of 3-OCH₃- and 3-C₆H₅-substituted pyridines, quinuclidines, and anilines, which were fit in earlier studies, now deviate when the refined parameters are used. The misses are in a direction that suggests water hydrogen bonds to these substituents in the neutral base but not in the protonated species. This result illustrates the point that

(10) Exner, O. In *Correlation Analysis in Chemistry*; Chapman, N. B., Shorter, J. H., Eds.; Plenum Press: New York, 1978, and references therein.

Table 2. Revised d^E , d^C , and $\Delta\chi^H$ Parameters

family	d^E	d^C	$\Delta\chi^H$
XCoP dist	3.339	-0.723	2.397
XCoPy dist	1.877	-0.306	2.057
$\log[K(4\text{-CNC}_5\text{H}_4\text{NCo})]$	3.25	-0.84	1.72
$E^{1/2}(\text{XCo}(\text{DH})_2\text{H}_2\text{O})$	-2.56	-0.007	0.862
^{13}C XCoP	-76.43	14.98	52.88
^{13}C XCoPy	-24.76	3.85	137.74
^{13}C XCo- <i>t</i> -BuPy	-39.58	6.77	162.14
$\log[k(\text{C}_6\text{H}_5\text{C}(\text{CH}_3)_2\text{Cl})]$	9.33	0.788	-0.27
^{13}C Ni(CO)PX ₃ ^a	13.81	0.095	3.77

^a Parameters for the three X groups are summed and entered as the single ΔE^X and ΔC^X substituent parameter.

accommodating parameters can mask subtle effects when a limited set of data is available. None of the other interpretations in the earlier studies are changed by refinements of the parameters.

Table 3. Spectral Shifts of Metal Carbonyl-Phosphine Complexes

phosphine	^{13}C $\delta(\text{Ni}(\text{CO})_3\text{PX}_3)$		$\nu(\text{Ni}(\text{CO})_3\text{PX}_3)$, cm^{-1}		^{13}C $\delta(\text{cis-Cr}(\text{CO})_5\text{PX}_3)$		^{13}C $\delta(\text{trans-Cr}(\text{CO})_5\text{PX}_3)$	
	exptl	calcd ^a	exptl	calcd ^b	exptl	calcd ^c	exptl	calcd ^d
P(OCH ₃) ₃	3.18	3.21	2079	2078	3.89	3.98	7.90	8.00
P(OC ₂ H ₅) ₃	3.61	3.61	2076	2078	4.28	4.32	8.24	8.04
P(O- <i>i</i> -C ₃ H ₇) ₃	3.90	3.88	2076	2074	4.67	4.55	9.22	8.56
P(OPh) ₃	1.69	1.76	2085	2088	2.59	2.75	6.93	6.74
P(NMe ₂) ₃	5.68	5.59			6.17	6.00	9.67	9.51
PCl ₃	-1.41	-1.32	2097	2099	0.18	0.15	5.66	5.47
P(CH ₃) ₃	5.05	5.22	2064	2063	5.50	5.69		
P(C ₂ H ₅) ₃	5.54	5.43	2062	2062	5.96	5.87	9.89	10.28
P(CH=CH ₂) ₃	4.22	4.27	2069	2068	4.92	4.89	10.07	9.54
P(C ₃ H ₇) ₃	5.62	5.59			6.03	6.01	9.83	10.38
P(<i>i</i> -C ₃ H ₇) ₃	6.20	6.28	2059	2058				
PBu ₃	5.69	5.71	2060	2061	6.08	6.11	9.83	10.47
P- <i>i</i> -Bu ₃	5.40	5.43			6.05	5.87	9.77	10.32
P- <i>t</i> -Bu ₃	6.37	6.31	2056	2059	6.66	6.61	10.36	10.66
P(<i>c</i> -C ₆ H ₁₁) ₃	6.32	6.27	2056	2059	7.19	(6.43)	10.28	(10.62)
P(C ₆ H ₅) ₃	4.30	4.23	2069	2069	5.25	4.85	10.06	9.37
P(benzyl) ₃	3.98	4.14	2066	2069				
P(C ₆ H ₄ - <i>p</i> -CH ₃) ₃	4.50	4.41	2067	2068				
P(C ₆ H ₄ - <i>p</i> -OCH ₃) ₃	4.43	4.50	2066	2068				
P(C ₆ H ₄ - <i>p</i> -F) ₃	3.77	4.03	2071	2070				
P(C ₆ H ₄ - <i>p</i> -Cl) ₃	3.54	3.84	2073	2072				
PhP(OCH ₃) ₂	3.48	3.55	2079	2075				
PHP(OC ₂ H ₅) ₂	4.04	3.82	2074	2075				
PhP(O- <i>i</i> -C ₃ H ₇) ₂	4.23	4.00	2072	2074				
PhP(OPh) ₂	2.54	2.58	2080	2081				
PhP(NMe ₂) ₂	4.69	(5.14)			5.29	5.22		
PhPCl ₂	0.69	0.52	2092	2089	1.71	1.71	6.39	6.76
PhPH ₂	3.54	(3.93)	2077	(2071)	4.29	(4.60)		
PhP(CH ₃) ₂	4.76	4.88	2065	2065	5.26	5.40	10.01	9.87
PhP(C ₂ H ₅) ₂	5.36	(5.04)	2064	2065	5.59	5.54	10.01	9.98
PhP(CH=CH ₂) ₂	4.25	4.26			4.92	4.88	9.87	9.48
PhP(<i>c</i> -C ₆ H ₁₁) ₂	5.80	(5.47)			7.05	(5.91)	9.91	(10.28)
Ph ₂ P(OCH ₃)	3.96	3.89	2072	2072				
Ph ₂ P(OC ₂ H ₅)	4.27	4.03	2072	2072				
Ph ₂ P(OPh)	3.46	3.40	2080	2075				
Ph ₂ P(NMe ₂)	4.34	(4.68)						
Ph ₂ PCl	2.49	2.36	2081	2079	5.29	5.23		
Ph ₂ PH	3.93	4.08	2073	2070	3.59	3.27	7.40	(8.05)
Ph ₂ PCH ₃	4.53	4.55	2067	2067	4.81	4.72	9.71	9.28
Ph ₂ PC ₂ H ₅	4.78	4.62	2067	2067	5.20	5.13	9.95	9.62
Ph ₂ PCH=CH ₂	4.26	4.24	2069	2069	5.33	5.18	9.97	9.66
Ph ₂ P(<i>c</i> -C ₆ H ₁₁)	5.07	4.85			5.55	5.38	10.25	9.78
(<i>c</i> -C ₆ H ₁₁) ₂ PH ₂	4.07	(4.55)			4.80	(5.12)	10.01	(9.93)
(<i>c</i> -C ₆ H ₁₁) ₂ PH	5.35	5.32			6.03	5.78	9.74	10.11

^a Chemical shifts were measured⁴ in CDCl₃ solution and are reported in ppm downfield from Ni(CO)₄. All data reported have a precision of ± 0.03 ppm. Values were calculated with $\delta(^{13}\text{C}) = [13.81(\pm 0.13)]\Delta E + [0.095(\pm 0.03)]\Delta C + 3.77(\pm 0.02)$ and $\bar{x} = 0.08$; % fit = 1.1. Systems in parentheses were omitted from the fit. Also fit (phosphine/exptl/calcd): P-*s*-Bu₃/6.23/6.18; P(SiMe₃)₃/5.67/5.61; (MeO)PCl₂/0.17/0.18; (EtO)PCl₂/0.30/0.32; (*i*-PrO)PCl₂/0.38/0.41; (C₆H₅O)PCl₂/-0.33/-0.42; (MeO)₂PCl/1.69/1.70; (EtO)₂PCl/2.00/1.96; (*i*-PrO)₂PCl/2.15/2.14; (C₆H₅O)PCl₂/0.74/0.73; (C₆H₅O)P(OCH₃)₂/2.08/(2.73); (C₂H₅)P(OCH₃)₂/(4.36)/(3.96); C₆H₅P(C₃H₇)₂/5.29/5.14; C₆H₅P(*n*-C₄H₉)₂/5.29/5.22; (C₆H₅)₂P(O-*i*-C₃H₇)₂/4.26/4.11; (C₆H₅)₂PC₃H₇/4.76/4.69; (C₆H₅)₂PC₄H₉/4.74/4.73; (C₆H₅)₂P(*t*-C₄H₉)₂/4.80/4.92; P(*p*-N(CH₃)₂C₆H₄)₂/5.35/5.37. ^b A₁, CO stretching frequency^{5,6} of Ni(CO)₃PX₃. Values were calculated with $\Delta\nu = [-98.7(\pm 2.9)]\Delta E^X + [5.53(\pm 0.7)]\Delta C^X + 2071(\pm 1)$ and $\bar{x} = 1.4$; % fit = 3.3. ^c ^{13}C of the *cis* carbonyl of Cr(CO)₅PX₃ adducts reported⁴ in ppm downfield from Cr(CO)₆. Values were calculated with $\delta(^{13}\text{C}) = [11.76(\pm 0.32)]\Delta E^X + [0.06(\pm 0.07)]\Delta C^X + 4.47$ and $\bar{x} = 0.14$; % fit = 1.8. The Cr(CO)₅PH₃ adduct gives a calculated value of 4.47 compared to a measured value of 3.96. ^d ^{13}C of the *trans* carbonyl of Cr(CO)₅PX₃ adducts reported⁴ in ppm downfield from Cr(CO)₆. Values were calculated with $\delta(^{13}\text{C}) = [14.04(\pm 0.7)]\Delta E^X - [1.03(\pm 0.17)]\Delta C^X + 9.19(\pm 0.4)$ and $\bar{x} = 0.37$; % fit = 8.

Fit of ^{13}C and Infrared Shifts of Phosphine Adducts. The differences in the ^{13}C shifts of Ni(CO)₃PX₃ complexes⁴ and Ni(CO)₄, where PX₃ is a substituted phosphine, have been used for the basicity parameter, E_i , of eq 1. The fit of the ^{13}C NMR shifts ($\delta(\text{Ni}(\text{CO})_3\text{PX}_3) - \delta(\text{Ni}(\text{CO})_4)$) for an extensive series of nickel substituted-phosphine tricarbonyl complexes, XXX'PNi(CO)₃, to eq 2 was carried out by summing the 3- ΔE^X and the 3- ΔC^X substituent constants of X, X', and X'' (where X may or may not be the same as X' or X''). An excellent fit results (Table 3) with an average deviation of calculated and experimental values, \bar{x} , of 0.08 and a percent fit (100 \bar{x} /range of calculated values) of 1.1. The data fit is shown in Table 3. The resulting parameters $d^E = 13.80$, $d^C = 0.091$, and $\Delta\chi^H = 3.77$ of eq 2 indicate that the ^{13}C chemical shift

differences, induced by the substituents, are dominated by the changes in the electrostatic donor properties of the phosphine (the d^C/d^E ratio is 0.007). Thus, the use of $\text{Ni}(\text{CO})_3\text{PX}_3$, ^{13}C shifts as a one-parameter phosphine basicity scale is valid only for reactions or physicochemical properties in which the change from that of the parent compound is dominated by electrostatic interactions.

Two points should be made about the interpretation of d^E and d^C . Dominance by d^E does not imply that the nickel-phosphine interaction is mainly electrostatic but that the difference in the response of the measured property, $\Delta\chi^X$, for PX_3 from that of $\Delta\chi^H$ is most sensitive to the electrostatic component of the nickel-phosphine interaction. Furthermore, the good fit of ^{13}C shifts to d^E and d^C does not prove the absence of π -back-bonding in the nickel-phosphorus bond. However, if it does exist, π -back-bonding must change in a manner that is proportional to σ basicity or to the E_B or C_B values of the phosphine. An inverse correlation is a reasonable expectation because increased σ basicity is expected to correspond to a higher energy acceptor d orbital on phosphorus and less π -back-bonding. Since σ -donation and π -back-bonding (which is mainly covalent) have opposite influences on the ^{13}C shift, a small, net, d^C value could accommodate proportional effects in σ - and π -back-bonding.

There is no evidence of problems from steric effects in the fit of the $\text{Ni}(\text{CO})_3\text{PX}_3$ ^{13}C NMR data (Table 3). This is consistent with literature suggestions¹⁻⁵ for the use of this quantity as a measure of the electronic component of basicity. The question remaining is to what extent have interactions that involve more substantial covalent contributions been improperly attributed to steric effects when ^{13}C resonances of $\text{Ni}(\text{CO})_3\text{PX}_3$ are used as a measure of the electronic effect in eq 1? This question will be addressed by analyzing other reactions of phosphines.

Also contained in Table 3 is a fit of the ^{13}C chemical shifts for the *cis* carbonyl of $\text{Cr}(\text{CO})_5\text{PX}_3$ adducts. The data are fit almost as well as those for $\text{Ni}(\text{CO})_3\text{PX}_3$. Except for phosphines containing two or more hydrogen substituents, no pattern is obvious in the systems that deviate. Several of the deviant systems in $\text{Cr}(\text{CO})_5\text{PX}_3$ are bulky phosphines,⁵ but assignment of their misses to a steric effect is inconsistent with a good fit of the $(t\text{-C}_4\text{H}_9)_3\text{P}$ adduct which has the largest cone angle.⁵ Even when $(t\text{-C}_4\text{H}_9)_3\text{P}$ is omitted from the data fit, the d parameters are unchanged as is the calculated ^{13}C value for the *tert*-butyl adduct. The d^E and d^C values show that the changes in the $\text{Cr}(\text{CO})_5\text{PX}_3$ shifts are also dominated by changes in the electrostatic donor properties of the phosphine.

The *trans*- $\text{Cr}(\text{CO})_5\text{PX}_3$ shifts are poorly correlated. Consistent with results from other studies,¹¹⁻¹³ no pattern could be found which enables one to rationalize the cause of the poor data fit. Table 4 summarizes the results of the d^E and d^C analyses on molybdenum

carbonyls. The *cis* carbonyls in adducts⁴ of $\text{Mo}(\text{CO})_5\text{-PX}_3$ are well behaved, and *trans* carbonyls in these adducts are again poorly behaved.

The A_1 CO stretching frequency of $\text{Ni}(\text{CO})_3\text{PX}_3$ (Table 3) is fit very well by eq 2. The shift is dominated by the electrostatic term. An electron-releasing substituent (whose ΔE^X and ΔC^X values are positive) produces a frequency decrease from the electrostatic term and a frequency increase from the covalent term.

Phosphines containing two or three hydrogen substituents deviate in the data fits discussed above. The bond angles in PH_3 and RPH_2 compounds are close to 90° , while those in the PR_3 , PR_2H , and PX_3 compounds are close to 108° . Thus, in addition to the normal substituent effect of hydrogen, the poor P-H overlap leads to a weak P-H bond that results in more s character in the lone-pair orbital than would result if the inductive influence of hydrogen were the only effect influencing hybridization. The donor strength predicted with ΔE and ΔC values of 0 for hydrogen are those for a PH_3 molecule with bond angles close to 108° . Thus, these ΔE and ΔC values are inappropriate for PH_3 and RPH_2 molecules whose hybridization (and basicity) have changed from effects other than the inductive influence. It is interesting to note that if a 90° phosphine is assigned hydrogen parameters of $\Delta E = -0.015$ and $\Delta C = 0.2$, satisfactory fits result for the ^{13}C δ values for the $\text{Ni}(\text{CO})_3\text{PX}_3$ adducts of $\text{C}_6\text{H}_5\text{PH}_2$ and *c*-hex PH_2 , for the $\nu_{A_1}(\text{CO})$ value of $\text{C}_6\text{H}_5\text{PH}_2$, and for the ^{13}CO δ values for the *cis*- $\text{Cr}(\text{CO})_5\text{PX}_3$ adducts of $\text{C}_6\text{H}_5\text{PH}_2$, *c*-hex PH_2 , and PH_3 . Thus, in all of the correlations of phosphines with eq 2, the $\Delta\chi^H$ value calculated will correspond to that of a hypothetical PH_3 donor with bond angles close to 108° and with the corresponding phosphorus hybridization.

Common Phosphine Basicity Probes. The pK_A values of phosphines measured in nitromethane^{15,16} have been used as measures of σ -donicity in QALE analyses.² When all of the reported values for phosphines and phosphites are analyzed with eq 2, a poor data fit results.

The pK_B values of tertiary amines have been correlated with the E and C equation¹⁸ and those of primary amines with the ΔE - ΔC model.⁹ It was not possible to include tertiary, secondary, and primary amines or any combinations thereof in the same data fit. Hydrogen bonding of the water solvent molecule functioning as a Lewis base to the N-H proton of the ammonium ion gave rise to enthalpic and entropic contributions that make the combined data sets incompatible. These conclusions have also been reported¹⁴ in other analyses of amine pK_B data. Accordingly, the RPH_2 donors were omitted to try and improve the phosphine data fit. A poor data fit still results.

When phosphines containing phenyl groups and the phosphites are excluded, a good fit of the remaining pK_A 's for alkylphosphines is obtained as shown in Table 5. The deviations of the phenyl derivatives could be rationalized if one assumes that water (introduced by using 70% HClO_4) hydrogen-bonds to the phenyl group

(11) Bodner, G. M. *Inorg. Chem.* **1975**, *14*, 2694.

(12) Webb, M. J.; Graham, W. A. G. *J. Organomet. Chem.* **1975**, *93*, 119.

(13) Woodard, R. J.; Angelici, R. J.; Dombeck, B. D. *Inorg. Chem.* **1978**, *17*, 1634.

(14) (a) Taft, R. W.; Wolf, J. F.; Beauchamp, J. L.; Scorrano, G.; Arnett, E. M. *J. Am. Chem. Soc.* **1978**, *100*, 1240. (b) Kamlet, M. J.; Gal, J. F.; Marea, P. C.; Taft, R. W. *J. Chem. Soc., Perkin Trans. 2* **1985**, 1583.

(15) Henderson, W. A., Jr.; Streuli, C. A. *J. Am. Chem. Soc.* **1960**, *82*, 5791.

(16) Allman, T.; Goel, R. G. *Can. J. Chem.* **1982**, *60*, 716.

(17) Drago, R. S. *Inorg. Chem.*, in press.

(18) Drago, R. S.; Dadmun, A. P.; Vogel, G. C. *Inorg. Chem.* **1993**, *32*, 2473.

Table 4

system	d^E	d^C	$\Delta\chi^H$	\bar{x}	% fit	no. of phos ^a (classes)
¹³ C δ (<i>cis</i> -Mo(CO) ₅ PX ₃) ^b	10.76 ± 0.35	-0.01 ± 0.08	4.13	0.14	3.6	19 (4)
¹³ C δ (<i>trans</i> -Mo(CO) ₅ PX ₃) ^c	10.90 ± 0.99	-0.85 ± 0.22	8.49	0.45	9.7	19 (4)
- ΔH (HgCl ₂ -PX ₃) ^d	171 ± 6	-21.7 ± 1.5	17.3	0.6	5	9 (2)
- ΔH (HgBr ₂ -PX ₃) ^d	193 ± 6	-29.8 ± 1.5	18.3	0.6	5	9 (2)
- ΔH (HgI ₂ -PX ₃) ^d	87.0 ± 6.9	-6.2 ± 1.7	15.0	0.5	7	8 (2)
- ΔH_M (CpIr(CO)PX ₃) ^e	38.4 ± 2.7	1.1 ± 0.8	29.0	0.14	3.4	5 (2)
ΔH_M (Fe(CO) ₃ (PX ₃) ₂) ^f	117.6 ± 13	4.4 ± 4.4	10.0	0.5	5.2	5 (2)
log[k _r (V(CO) ₆)] ^g	19.4	5.7	-2.0	0.1	4	4 (3)
ΔH^\ddagger (V(CO) ₆) ^g	-20.1 ± 3.0	-0.95 ± 1	10.5	0.3	8	5 (3)
log[K(Cp ₂ Ti(CO) ₂)] ^h	19.9	3.6	-6.2	0.05	3	4 (3)
Δv [Cp ₂ Ti(CO)PX ₃] ^h	-18.6 ± 11	25.5 ± 2.6	1854	1	6	7 (3)
log[k _r (η^5 -C ₅ H ₅) ₃ CpRh(CO) ₂] ^h	11.0	7.1	-6.4	0.01	1	4 (2)
log[k _r (η^5 -C ₅ H ₅) ₃ CpCo(CO) ₂] ^h	13.5	6.9	-6.7	0.03	2	4 (2)
ΔH^\ddagger (CoNO(CO) ₃) ⁱ	-19.9(±1.2)	1.7(0.4)	15.6	0.1	2.5	4 (2)
log[k _r (THF)CoNO(CO) ₃] ⁱ	13.2(±0.6)	3.3(±0.5)	-3.6	0.1	2.4	6 (3)
log[k _r (CH ₃ NO ₂)CoNO(CO) ₃] ⁱ	14.0(±1)	2.9(±0.8)	-3.4	0.1	3	7 (3)
log[k _r (Ru(CO) ₃ (SiCl ₃) ₂)] ^j	4.3	-1.5	-4.2	0.15	11	7 (2)
log[k _r (Mo(CO) ₂ (PX ₃) ₂ Br ₂)] ^k	-19	-0.9	4.6	0.1	13	5 (1)
log[k _r (Ru(bpy) ₂ PX ₃)] ^l	-49	17	-5.4	0.1	3	5 (1)
log[k _r (Ru(bpy) ₂ PX ₃)] ^l	19.3	-0.9	-2.7	0.14	7	6 (1)
$E_{1/2}$ (Ru(bpy) ₂ (H ₂ O)PX ₃ ²⁺) ^l	-3.89(±0.10)	0.67(±0.03)	1.33	0.016	3.4	13 (2)
log[k _r (Cp ₂ Fe ₂ (CO) ₄)] ^m	-1.8(±0.8)	-3.6(±0.4)	7.4	0.09	4.5	6 (3)
log[k(Re(CO) ₄ L)] ⁿ	-2.32(±0.77)	-1.74(±0.5)	8.89	0.80	7.5	5 (2)

^a These are the phosphines retained in the fit. The footnotes and text give the total number fit and the extent of the miss by deviant systems. ^b ¹³C chemical shift of the *cis* carbonyl of Mo(CO)₅PX₃ adducts. ^c Deviant systems are as follows: (C₆H₅)₃P*/4.9/4.5; C₆H₅PCl₂/2.0/1.7; (C₆H₅)₂PCl*/3.4/3.1; *c*-hexPH₂*/4.1/4.7; (*c*-hex)₃P*/6.4/5.9. The asterisks indicate systems that deviated in the *cis*-Cr(CO)₅PX₃ fit. The data for deviant systems are listed in the order phosphine/exptl/calcd. ^d ¹³C chemical shift of the *trans* carbonyl of Mo(CO)₅PX₃ adducts. This fit was carried out by omitting those systems that deviated in the *cis*-Mo(CO)₅PX₃ fit. ^e Enthalpy of 1:1 adduct formation of HgX₂ with tertiary phosphines in benzene. ^f The average error in the data set is reported to be 0.6 kcal mol⁻¹. C₆H₅P(CH₃) was omitted from the HgCl₂ and HgI₂ data set, and (C₆H₅)₂PC₂H₅ was omitted from the HgBr₂ and HgI₂ data sets. ^g Enthalpy of protonation of the indicated complex with CF₃SO₃H in 1,2-dichloroethane. ^h Logarithms of the rate constant and enthalpies of activation of the second-order substitution of CO in V(CO)₆ to form V(CO)₅PX₃ in hexane solvent. ⁱ log K_r systems omitted and deviations: (*i*-C₃H₇)₃P/-1.0/5.76; (*n*-C₄H₉)₃P/1.7/3.7; (*i*-C₃H₇)₂O₃P/-0.03/1.4. ^j Logarithms of the equilibrium constant for the substitution of CO in Cp₂Ti(CO)₂ and Δv_{CO} for the Cp₂Ti(CO)PX₃ adducts. ^k The following were omitted from log *k*: (C₆H₅)₃P/-6.1/-4.9; (*n*-C₄H₉)₃P/-5.81/-1.5; (*i*-C₃H₇)₃P/-5.5/4.0. ^l Logarithms of the rate constant for the second-order substitution reaction of CO in η^5 -C₅(CH₃)₅M(CO)₂ in toluene where M = Rh, Co. ^m (*i*-C₄H₉)₃P, (C₂H₅O)₃P, (*n*-C₄H₉)₃P, and (*i*-C₃H₇)₃P were omitted from both fits. ⁿ Activation enthalpies²⁶ in toluene and logarithms rate constants in THF and CH₃NO₂ for the second-order substitution of CO by PX₃ in CoNO(CO)₃. ^o Logarithms of the rate constant²⁷ for substitution of the equatorial carbonyl by P(OMe)₃ by a dissociative mechanism in *mer*-Ru(CO)₃(PX₃)(SiCl₃)₂. All tris-phenyl-substituted compounds and C₆H₅P(*i*-C₃H₇)₂ were excluded. ^p Logarithms of the bimolecular rate constant for the photochemically generated Mo(CO)₂(PR)₂(Br)₂ species reacting with CO to form the tricarbonyl. ^q Only tris-phenyl-substituted phosphines were included. ^r Logarithms of the second-order rate constants for the exchange of water by CH₃CN in Ru^{II}(H₂O)(bpy)₂PX₃ in *o*-dichlorobenzene. ^s $E_{1/2}$ values were measured in CH₂Cl₂ vs SSCE reference electrode. The "al" superscript refers to aliphatic phosphines: (*i*-C₄H₉)₃P/-0.5/3.8; (C₆H₅CH₂)₃P/-0.8/-6.2. "ar" refers to aromatic phosphines. ^t Logarithms of the rate constants for reaction of Cp₂Fe₂(μ -CO)₃ with PX₃ in hexane:³⁰ (C₆H₅)₃P/5.5/6.7; (C₆H₅O)₃P/5.6/5.3. ^u Logarithms of the electron transfer rate constants³¹ for Re(CO)₄PX₃ with 1-methyl-4-cyanopyridinium ion: (*i*-C₄H₉)₃P/6.9/7.8.

π -system in the free phosphine and dissociates when the phosphine is protonated. The alkyl phosphites are not correlated by these parameters and deviate in the same direction as the phenyl derivatives.

Though nine data points were included in the pK_A fit, only phosphines with alkyl substituents were used. As discussed previously,¹⁷ substituents from at least three of the four different classes of substituents should be used in a data fit. Using only one or two classes not only leads to a poor definition of the minimum¹⁷ with misleading d^E and d^C values but could give an apparent data fit for a property that is not related to bond strength.

The difficulty in assessing the problem with the pK_A data is further illustrated by an alternative interpretation of this chemistry. If one eliminates long-chain substituents C₂H₅, C₃H₇, C₄H₉, and C₆H₁₁, the fit labeled "II calcd" results. In this interpretation the phenyl derivatives are well-behaved. The deviations for the long-chain alkyls are attributed to loss of conformational degrees of freedom from rotation of the alkyl chain in the phosphonium salt. The phosphonium cation is more effectively solvated than the phosphine by the polar solvent nitromethane. Furthermore, the phosphonium ion is more effectively solvated when the

alkyl chain is coiled up to afford the smallest radius. The negative entropy for coiling long-chain phosphines decreases the basicity in comparison to phosphines with methyl substituents. As was the case for analysis I, the phosphites are not accommodated by the data fit, suggesting that enthalpic and entropic solvation contributions differ for this family of donors.

When there are a large number of deviant systems in a data set, alternate interpretations will exist. This problem will be seen to arise when free energies of activation and free energies of donor-acceptor reactions are fit. In general, the entropic interpretations of free energies in an individual deviant system are arbitrary. It is only when the explanations appear as common patterns in phosphine reactivity in several systems and disappear when enthalpies and $E_{1/2}$ values on analogous systems are fit that the entropic interpretations become convincing. When the experimental results of more systems are discussed, the phosphine reactivity patterns will be seen to favor this latter interpretation, i.e. II calcd. Competitive hydrogen bonding of water to CH₃-NO₂ instead of the phenylphosphine also favors the II calcd interpretation.

The essential conclusion to be drawn from the pK_A fit is not ambiguous. The good fit of ¹³CO δ values for

Table 5. pK_A Values of X_3P Compounds Measured in CH_3NO_2

phosphine	pK_A (CH_3NO_2)			$\log k$ (EtI)		$-\Delta H$ (CF_3SO_3H)	
	exptl	I calcd ^{a,e}	II calcd ^{d,e}	exptl	calcd ^{c,e}	exptl	calcd ^{d,e}
(<i>c</i> - C_6H_{11}) ₃ P	9.70	9.81	(11.5)	-2.86	-3.11	33.2	(37.0)
(CH_3) ₃ P	8.65	8.67	8.56	-2.65	-2.70	31.6	31.9
(C_2H_5)P(CH_3) ₂	8.62	8.67	8.84	-2.09	(-2.7)		
(C_2H_5) ₂ PCH ₃	8.62	8.60	(9.23)	-2.37	-2.63		
(C_2H_5) ₃ P	8.69	8.65	(9.47)	-2.81	-2.64	33.7	33.5
(<i>n</i> - C_3H_7) ₃ P	8.64	8.63	(10.16)	-2.86	-2.59		
(<i>n</i> - C_4H_9) ₃ P	8.43	8.41	(10.80)	-2.79	-2.43		
(<i>i</i> - C_4H_9) ₃ P	7.97	8.00	(9.89)	-3.86	(-2.3)		
C_6H_5 P(CH_3) ₂	6.49	(9.6)	6.56	-3.12	-3.29	28.4	28.2
(C_6H_5) ₂ P(C_2H_5) ₂	6.25	(9.4)	(7.30)	-3.32	-3.16		
(C_6H_5) ₂ PC ₂ H ₅	4.90	(10.4)	4.95	-3.95	-3.81		
(C_6H_5) ₃ P	2.73	(11.2)	2.77	-4.42	-4.36		
(<i>t</i> - C_4H_9) ₃ P	11.4	11.4	11.4			21.2	21.3
(<i>p</i> - $CH_3OC_6H_4$) ₃ P	4.57	(10.5)	4.39	-3.57	-3.90	36.6	36.7
(<i>p</i> - $CH_3C_6H_4$) ₃ P	3.84	(10.7)	3.85			24.1	24.3
(<i>p</i> - FC_6H_4) ₃ P	1.97	(11.3)	1.49			23.2	23.3
(<i>p</i> - ClC_6H_4) ₃ P	1.03	(11.8)	0.79			19.6	19.3
						17.9	17.7

^a pK_A in CH_3NO_2 from 70% aqueous $HClO_4$ titration.^{15,16} Calculated with $pK_A = [-88.62(\pm 0.7)]\Delta E_B^X + [17.71(\pm 0.1)]\Delta C_B^X + 10.89; \bar{x} = 0.04$, % fit = 1.3. ^b Calculated with $pK_A = [115.24(\pm 1.4)]\Delta E_B^X - [11.09(\pm 0.29)]\Delta C_B^X + 1.07(\pm 0.5); \bar{x} = 0.14$, % fit = 1.3. ^c Logarithms of the rate constants for nucleophilic attack of the phosphine on C_2H_5I in acetone.¹⁹ Calculated with $\log k = [52.64(\pm 2.0)]\Delta E_B^X - [9.79(\pm 0.5)]\Delta C_B^X - 4.31; \bar{x} = 0.20$, % fit = 3.8. (*n*- C_4H_9)₂PH and (*i*- C_4H_9)₂PH were omitted and gave calculated/measured values of -3.05/-4.06 and -2.97/-4.42, respectively. ^d $-\Delta H$ for reaction with CF_3SO_3H in 1,2-dichloroethane.²² Calculated with $-\Delta H = [213.5(\pm 1.3)]\Delta E_B^X - [21.3(\pm 0.3)]\Delta C_B^X + 18.28; \bar{x} = 0.16$, % fit = 1.9. Errors calculated with (*c*- C_6H_{11})₃P omitted. (C_6H_5)₂PCH₃/24.7/calcd 24.8. ^e Systems in parentheses omitted from the fit and calculated with the d^E , d^C , and $\Delta\chi^H$ values in the above equations. The substituent ΔE and ΔC values are summed.

$Ni(CO)_3PX_3$ and the poor fit of pK_A to $\Delta E - \Delta C$ indicate that the pK_A values are not related to bond strengths and do not provide a reliable one-parameter estimate of the electronic component of basicity when used in eq 6.

The log of the rate constants¹⁹ for nucleophilic attack on ethyl iodide measured in acetone solvent is reported¹⁹ to be poorly correlated by the sum of the σ^* substituent constants. The fit to eq 2 is moderately good, except the rate for (*i*- C_4H_9)₃P is too slow and that for (C_2H_5)₂P(CH_3)₂ is surprisingly fast when compared to those for (CH_3)₃P and (C_2H_5)₃P. These two phosphines were omitted from the data fit. In the resulting fit, there is indication of a slowing of the rate with increasing chain length. Deviations between the calculated and experimental rates (Table 4) increase in the order (C_2H_5)₃P ($\theta = 132^\circ$) < (*n*- C_3H_7)₃P ($\theta = 132^\circ$) < (*n*- C_4H_9)₃P ($\theta = 132^\circ$) < (*i*- C_4H_9)₃P ($\theta = 143^\circ$). Since (C_6H_5)₃P has a larger cone angle ($\theta = 145^\circ$) than any of the above phosphines, and is fit well, a front strain, cone angle steric effect is excluded. Instead, this analysis suggests that the steric effect involves an entropy effect associated with rearranging the alkyl substituent chain for maximum interaction of the phosphine with ethyl iodide in the transition state. In the formation of the transition state, conformational degrees of freedom in the alkyl chains are lost. This steric effect will be referred to as a *conformational entropic steric effect* to distinguish it from an *enthalpic, front strain type of steric effect*. The existence of the conformational effect has profound implications for the interpretation of phosphine reactivity with eq 1. The conformational entropic steric contribution to free energy data cannot be treated with $b_j S_i$, for it is not proportional to the cone angle. The conformational entropic steric effect is not a new idea for structure-reactivity analyses. Brown²⁰ invoked a similar argument to explain the fact that, toward

$B(CH_3)_3$, $-\Delta G(CH_3NH_2) > -\Delta G(C_2H_5NH_2)$ but $-\Delta H(C_2H_5NH_2) > -\Delta H(CH_3NH_2)$.

Of the three probes presented in Table 5, the enthalpy of interaction of the phosphines with CF_3SO_3H in 1,2-dichloroethane⁷ is fit the best. The deviation of (*c*- C_6H_{11})₃P cannot be attributed to steric problems because (*t*- C_4H_9)₃P is fit very well and the deviation is larger than the possible error in the cyclohexyl parameters. The cause of the deviation is unknown but could result from enthalpic ring conformation changes upon protonation, conformation changes causing the substituent constants to be nonadditive, or variation in the extent of ion pairing in the protonated species. The excellent fit of these enthalpies compared to the pK_A fit is somewhat deceptive. Except for (*c*- C_6H_{11})₃P and (C_2H_5)₃P, the donors studied are those in the pK_A II fit. The fit of (C_2H_5)₃P is encouraging, suggesting that CF_3SO_3H has potential as a general measure of phosphine basicity. The measurements should be extended to long-chain phosphines, pyridines, and tertiary amines.

Other enthalpy probes involve the 1:1 adduct formation reaction²¹ of phosphines with $HgCl_2$, $HgBr_2$, and HgI_2 and the data fits for the enthalpies for protonation of $CpIr(CO)PX_3$ by CF_3SO_3H in 1,2-dichloroethane²² (Table 4). The reported enthalpies are fit as accurately as they have been measured. The enthalpies for protonation of $Fe(CO)_3PR_3$ are poorly fit relative to the experimental error. Significant enthalpy contributions may result from the reported²² decomposition reactions that occur.

It is significant to point out that, contrary to literature conclusions, the dual-parameter estimate of basicity suggests there is no evidence for the existence of a cone angle, front strain type of steric effect in the C_2H_5I and $Cr(CO)_5PX_3$ data sets. This conclusion is verified above, and in analyses to be presented, by omitting all the

(19) Henderson, W. A.; Buckler, S. A. *J. Am. Chem. Soc.* **1960**, *82*, 5794.

(20) Brown, H. C.; et al. *J. Am. Chem. Soc.* **1953**, *75*, 1.

(21) Gallagher, M. J.; Graddon, D. P.; Sheikh, A. R. *Aust. J. Chem.* **1976**, *29*, 759.

(22) Sowa, J. R., Jr.; Zanotti, V.; Facchin, G.; Angelici, R. J. *J. Am. Chem. Soc.* **1991**, *113*, 9185.

Table 6. ΔE and ΔC Analyses of Reactivity

phosphine	E° - (Cp*Mn)		log- [k_r (Cp*Mn)]		log- [k_r (Cp*Mn')		log- [k_r (Co(NO)(CO) ₃)]		ΔH^\ddagger - (RuSiCl ₃)		log- [k_r (RuSiCl ₃)]		log- k_r (Ru(CO) ₄ PX ₃)		
	exptl	calcd ^a	exptl	calcd ^b	exptl	calcd ^c	exptl	calcd ^d	exptl	calcd ^e	exptl	I calcd ^b	ii calcd ^g	exptl	calcd ^h
(CH ₃ O) ₃ P	0.68	0.68					-2.7	-2.7	27.4	27.3	-5.1		-5.2		
(C ₆ H ₅ O) ₃ P	0.85	0.85			1.1	1.3	-4.5	-4.9						-3.6	(-1.9)
(C ₂ H ₅) ₃ P	0.39	0.38	4.3	4.3			-0.5	-0.7						-3.7	-3.6
(<i>n</i> -C ₄ H ₉) ₃ P							-1.0	(-0.1)	28.7	(27.8)	-3.8	(-2.8)	(-5.4)	-3.6	-3.7
(C ₆ H ₅) ₃ P	0.49	0.50	1.2	1.3	4.1	4.1	-3.0	-3.1	27.1	27.2	-3.1	-3.1		-3.1	-3.1
(<i>p</i> -CH ₃ C ₆ H ₄) ₃ P	0.50	0.48	1.7	1.7	4.5	4.6			26.9	27.2	-3.1	-3.1		-3.1	-3.2
(<i>p</i> -CH ₃ OC ₆ H ₄) ₃ P	0.41	0.47	2.2	1.9					26.8	27.3	-3.1	-3.1		-3.2	-3.2
(<i>p</i> -FC ₆ H ₄) ₃ P									27.0	27.0	-3.1	-3.2			
(<i>p</i> -ClC ₆ H ₄) ₃ P	0.60	0.54			3.0	2.9			27.0	27.0	-3.1	-3.2			
(C ₆ H ₅) ₂ P(OCH ₃)	0.58	0.56	2.6	2.6	4.4	4.3			27.5	27.2	-4.6		-4.5		
(C ₆ H ₅) ₂ P(CH ₃)	0.46	0.47	3.0	(2.0)	>5	5.0			27.4	27.3	-4.1		-4.4	-3.5	-3.3
(C ₆ H ₅) ₂ P(C ₂ H ₅)	0.46	0.46	2.2	2.3			-2.2	2.3						-3.2	-3.2
(C ₆ H ₅) ₂ P(<i>n</i> -C ₄ H ₉)	0.45	0.45	2.1	(2.6)			-2.3	-2.1							
(C ₆ H ₅) ₂ P(<i>i</i> -C ₃ H ₇)			1.3	(3.4)					28.7	(27.5)	-3.2	(2.9)	(-4.8)		
(C ₆ H ₅) ₂ PCl							-4.0	(-7.1)	26.5	26.4	-3.8	-3.6			
C ₆ H ₅ P(C ₂ H ₅) ₂	0.42	0.42	3.3	3.3			-1.5	-1.5						-3.3	-3.4
C ₆ H ₅ P(CH ₃) ₂									27.5	27.4	-4.7		-4.4		
C ₆ H ₅ P(OCH ₃) ₂									26.9	27.2	-4.9		-4.9		
C ₆ H ₅ PCl ₂							-4.0	-3.8	25.5	25.6	-4.0	-4.0			

^a $E_{1/2}$ for CH₃CpMn(CO)₂PX₃ in CH₂Cl₂ vs SCE.^{23b} Calculated with $E_{1/2} = [-1.85(\pm 0.12)]\Delta E^X + [0.13(\pm 0.08)]\Delta C^X + 0.54$; $\bar{x} = 0.02$, % fit = 3.7. ^b Logarithms of the rate constants for the bimolecular displacement of 4-NO₂C₅H₄N from (η^5 -MeCp)Mn(CO)₂(4-NO₂C₅H₄N)⁺.^{23b} Calculated with $\log k_r^X = [1.11(\pm 0.54)]\Delta E^X + [10.3(\pm 0.5)]\Delta C^X - 0.55$; $\bar{x} = 0.06$, % fit = 1.9. ^c Logarithms of the rate constants for the bimolecular displacement of CH₃CN from (η^5 -MeCp)Mn(CO)₂(CH₃CN)⁺.^{23a} Calculated with $\log k_r^X = [19.9(\pm 0.9)]\Delta E^X + [6.9(\pm 0.8)]\Delta C^X + 2.55$; $\bar{x} = 0.1$, % fit = 2.8. ^d Logarithms of the rate constants for the bimolecular displacement of CO by PX₃ in Co(NO)(CO)₃.²⁶ Calculated with $\log k_r^X = [12.9(\pm 1.1)]\Delta E^X + [4.5(\pm 0.9)]\Delta C^X - 4.3$; $\bar{x} = 0.15$, % fit = 6. (C₆H₁₁)₃P/-2.0/1.2 and P([N(CH₃)₂]₃)/-4.5/3.1 are omitted. ^e Activation enthalpy for dissociation of CO from *mer*-Ru(CO)₃(SiCl₃)₂PX₃.²⁷ Calculated with $\Delta H^\ddagger = [2.4(\pm 0.9)]\Delta E^X + [0.94(\pm 0.2)]\Delta C^X + 26.9$; $\bar{x} = 0.17$; % fit = 8. ^f Logarithms of the rate constants for the reaction in footnote e,²⁷ bulky phenyl I. Calculated with $\log k_r^X = [4.0(\pm 0.4)]\Delta E^X - [0.14(\pm 0.1)]\Delta C^X - 3.2$; $\bar{x} = 0.07$, % fit = 7. ^g Logarithms of the constants for the reaction in footnote e small phenyl II. Calculated with $\log k_r^X = [0.54(\pm 1.9)]\Delta E^X - [3.6(\pm 1.1)]\Delta C^X - 3.5$; $\bar{x} = 0.14$, % fit = 17. ^h First-order dissociative substitution of CO in Ru(CO)₄PX₃.⁶ Calculated with $\log k_r^X = [-7.3(\pm 1.0)]\Delta E^X + [0.42(\pm 0.1)]\Delta C^X - 2.93$; $\bar{x} = 0.1$, % fit 10. [N(CH₃)₂]₃P/-3.3/-3.3; (C₆H₁₁)₃P/-2.4/(-3.8); (C₂H₅O)₃P/-3.9/(-2.5); (C₆H₅CH₂)₃P/-3.3/-3.1.

systems with large cone angles from a data fit and noting that the values calculated for the omitted systems from the resulting d^E , d^C , and $\Delta\chi^H$ values do not give rise to deviations that parallel cone angles.

It is informative to have a one-parameter quantity such as ρ to compare the demand made on the phosphines by the reactant. Since alkyl substituents generally have a $\Delta C/\Delta E$ ratio of 4, such a scale is given for hydrocarbon substituents with the quantity ρ_{CH} :

$$\rho_{CH} = 0.05d^E + 0.2d^C \quad (6)$$

It is the essence of the electrostatic-covalent model that the substituent response order for reactants could differ for substituents with different $\Delta C/\Delta E$ ratios as d^E and d^C change. Thus, ρ_{CH} is restricted to alkyl substituents with $\Delta E/\Delta C$ values of 4. The ¹³C shift of Ni(CO)₃PX₃ has a ρ_{CH} value of 0.7; Cr(CO)₅PX₃ has 0.6, and Mo(CO)₅PX₃ has 0.5.

The sign reversals for d^E and d^C in Table 5 will be considered next. As seen in eqs 3 and 4, a sign reversal for d^E and d^C can result from a sign reversal for s^E and s^C or from a sign reversal of E_A^* and C_A^* . If solvent-minimized enthalpies were available, E_A^* and C_A^* would be positive in a data fit and a sign reversal in d could be attributed to s^E and s^C . For the systems in Table 5, the charge transfer complexes of the phosphines with the solvent and variations in the extent of ion pairing as phosphine basicity changes could be reflected in a reversal in the signs of E_A^* and C_A^* . Thus, we are not able to attribute the sign reversal of d^E and d^C to either s , E^* , or C^* of eqs 3 and 4.

Correlations of Bimolecular Substitution Reactions. Bimolecular substitution reactions proceed faster

and have lower activation energies with increased basicity of the nucleophile. This corresponds to a dominance by positive d values for the log rates and negative d values for ΔH^\ddagger . Table 6 contains the results of the ΔE - ΔC analyses of several reactions²³ involving substituted phosphines. The rates of substitution of 4-nitropyridine in (η^5 -CH₃Cp)Mn(CO)₂(4-NO₂py)⁺ by a series of trisubstituted phosphines have been determined by electrochemical generation of the cation.²³ The substitution reaction of the cation follows a conventional S_N2 pathway. The data are fit poorly by eq 2 unless the three systems indicated in parentheses in Table 6 under the log k_r (Cp*Mn) calcd column are omitted. An excellent data fit of the remaining phosphines leads to d^E and d^C parameters which indicate that the covalent contributions of the substituents dominate the rate change. Thus, none of the scales of phosphine basicity in Table 3 are covalent enough to predict the electronic contribution to the free energy of this series of reactions ($d^C/d^E = 9$).

Two of the omitted phosphines give rates that are smaller than are predicted, while (C₆H₅)₂PCH₃ has a faster rate than is predicted. The deviations for (C₆H₅)₂P(*i*-C₃H₇) ($\theta = 150^\circ$) are entropic and enthalpic cone angle related. The cone angles of the systems that fit well vary from 132 to 145°, while the deviant systems (C₆H₅)₂PCH₃ and (C₆H₅)₂P(*n*-C₄H₉) have θ values of 136 and 140°, respectively.

It is proposed that the triphenyl- and (substituted-triphenyl)phosphines ($\theta = 145^\circ$) undergo an entropic

(23) (a) Herschberger, J. W.; Klingler, R. J.; Kochi, J. K. *J. Am. Chem. Soc.* **1983**, *105*, 61. (b) Zizelman, P. M.; Amatore, C.; Kochi, J. K. *J. Am. Chem. Soc.* **1984**, *106*, 3771.

steric effect associated with restricted rotation about the phosphorus–manganese bond formed in the transition state, slowing the rate. The entropic contributions from restricted rotation around the phosphorus–manganese bond in the $(C_2H_5)_3P$, $(C_6H_5)_2P(C_2H_5)_2$, $(C_6H_5)_2P(C_2H_5)$, and $(C_6H_5)_2P(OCH_3)$ transition states ($\theta = 132, 136, 140$, and 132° , respectively) also slows the rate to a comparable or proportional extent. As a result, the ethyl- and methoxyphosphines listed above correlate in the linear free energy data fit with the substituted triphenylphosphines. More rotational freedom around the phosphorus–manganese bond in the transition state leads to a smaller entropic steric contribution in $(C_6H_5)_2PCH_3$ that causes this system to react faster than predicted. Rearrangement of the $n-C_4H_9$ chain of $(C_6H_5)_2P(n-C_4H_9)$ in the transition state in addition to phosphorus–manganese restricted bond rotation causes this system to react slower. Contributions from an enthalpic steric effect in the transition state in triarylphosphines and from conformational steric effects in ethyl derivatives are possible contributions in the linear free energy fit.

The above interpretation is very different from that offered in the literature,^{23b} where the donor contribution is correlated with the pK_A of the phosphine and a cone angle steric contribution of 0.11θ is proposed in all systems. Recall pK_A II had a d^C/d^E ratio of -0.1 , a fairly electrostatic scale, that contained contributions from entropic steric effects for long-chain alkyls. Thus, an improper electronic scale based on pK_A with a built-in entropic steric effect is compensated with a 0.11θ steric term to fit the data. The possibility that ΔE and ΔC contain a disguised steric component is readily dismissed by the successful use of these parameters for CF_3SO_3H (Table 5), for ^{13}C δ values of $NiCO_3L$ (Table 3), and for the meta position of substituted phenyl compounds.⁸

The more limited data set^{23a} for the displacement of CH_3CN from $(\eta^5-CH_3Cp)Mn(CO)_2CH_3CN$ by phosphines is also shown in Table 6 as $\log[k(CpMn')]$. The data fit very well with the smaller CH_3CN , but on the basis of the above explanation the only system studied that could detect an entropic steric component is $(C_6H_5)_2PCH_3$, for which a $\log k$ value of >5 is reported, compared to the predicted value of 5.0.

The standard oxidation potentials in CH_2Cl_2 , of the product phosphine adducts of the above displacement reactions, give an excellent fit (Table 6). The stronger donor stabilizes the higher oxidation state, making it more difficult (smaller $E_{1/2}$) to reduce the complex. The signs of d^E and d^C show that the differences in the family for stabilization of the higher oxidation state relative to the lower one is dominated by the electrostatic term. The successful fit to $E_{1/2}$ of adducts in which an entropic steric effect was proposed for the rate data provides support for the entropic steric interpretation offered for these rate data. An entropic steric effect is not expected in $E_{1/2}$ because rotational and chain conformational degrees of freedom are not expected to change significantly with change in oxidation state. Accordingly, all the $E_{1/2}$ values are correlated with $\Delta E - \Delta C$. The good fit of the $(C_6H_5)_2PCH_3$ derivative with the other systems indicates that enthalpic strain does not influence the potentials and is absent in the ground state of $(\eta^5-CH_3Cp)Mn(CO)_2PX_3$ and the oxidized cation.

The rate constants^{24a} for displacement of CO from $V(CO)_6$ show a similar pattern to those discussed above for $(\eta^5-CH_3Cp)Mn(CO)_2PX_3^+$, but with less steric constraints from M–P bond rotation. The $\log k$ values for reactions of $(CH_3)_3P$, $(CH_3O)_3P$, $(C_6H_5)_3P$, and $(C_6H_5)_2PCH_3$ are predicted very well with the parameters given in Table 4. Conformational entropic steric effects are indicated with the $(n-C_4H_9)_3P$ and $(O-i-C_3H_7)_3P$ complexes, and both entropic and enthalpic steric strain occurs with the $(i-C_3H_7)_3P$ complex ($\theta = 160^\circ$). The calculated $\log k$ values for the above three phosphines deviate by 2, 1.4, and 6 kcal mol⁻¹, respectively, in the direction corresponding to slower rates.

Support for the entropic steric effect as the cause of the deviation in the $\log k$ fits is obtained from the fit of the enthalpies of activation for $V(CO)_6$ substitution. The entropic steric effect should not be reflected in the enthalpies. The enthalpy fit for $V(CO)_6$ (Table 4) includes four phosphines whose $\log k$ values were also accurately fit plus the deviating system in the $\log k$ fit, $(n-C_4H_9)_3P$. The enthalpies of activation for all five phosphines are fit as well by eq 2 as the reported experimental error.

The above reactivity patterns are seen in the equilibrium constants^{24b} for displacement of CO by phosphines in $CpTi(CO)_2$, where $(CH_3)_3P$, $(C_6H_5)_2PCH_3$, $C_6H_5P(CH_3)_2$, and $(C_2H_5O)_3P$ are fit very well (Table 4). Deviations of 1.2, 1.6, and 4.3 kcal mol⁻¹ are found for $(C_6H_5)_3P$, $(i-C_3H_7O)_3P$, and $(n-C_4H_9)_3P$, respectively. On the other hand, the infrared CO stretching frequency shifts for all of the adducts studied (Table 4) are accurately correlated by eq 2, suggesting the absence of enthalpic strain. The deviations in the equilibrium constants are attributed to a rotational entropic steric effect from loss of rotation about the metal–phosphorus bond in the former two adducts and this rotational effect as well ordering of the butyl chain in $(n-C_4H_9)_3P$.

The logarithms of the second-order rate constants for substitution of CO by phosphines in $(\eta^5-(CH_3)_5Cp)M(CO)_2$ complexes, where M is Rh and Co²⁵ (Table 4), show patterns of reactivity similar to those discussed above. The $(CH_3)_3P$, $(CH_3O)_3P$, $(C_6H_5)_2PCH_3$, and $C_6H_5P(CH_3)_2$ values correlate well, while those for $(i-C_4H_9)_3P$, $(n-C_4H_9)_3P$, $(C_2H_5O)_3P$, and $(i-C_3H_7O)_3P$ deviate by about 3 kcal mol⁻¹ in a direction corresponding to a slower rate.

Rate constants for the substitution of CO in $Co(NO)(CO)_3$ by a series of phosphines have been measured²⁶ in toluene, tetrahydrofuran, and nitromethane solvents. A bimolecular displacement mechanism is proposed for this reaction. An excellent data fit of eight phosphines in toluene solvent (Table 6) shows no steric problems even with $(C_6H_5)_3P$ but does show a conformational entropic steric problem from chain ordering in the transition state with $(n-C_4H_9)_3P$. The $(C_6H_5)_2PCl$ derivative misses in the direction of being too fast, for reasons unknown. Both $P[N(CH_3)_2]_3$ and $(C_6H_{11})_3P$ react slower than calculated. The enthalpies of activation of four phosphines, including $(C_6H_5)_2PCl$, are fit well by eq 2 (Table 4). The rate constants for $Co(NO)-$

(24) (a) Shi, Q.-Z.; Richmond, T. G.; Trogler, W. C.; Basolo, F. *J. Am. Chem. Soc.* **1984**, *106*, 71. (b) Palmer, G. T.; Basolo, F.; Kool, L. B.; Rausch, M. D. *J. Am. Chem. Soc.* **1986**, *108*, 4417.

(25) Rerek, M. E.; Basolo, F. *Organometallics* **1983**, *2*, 372.

(26) Thorsteinson, E. M.; Basolo, F. *J. Am. Chem. Soc.* **1966**, *88*, 3929.

(CO)₃ measured in THF and CH₃NO₂ involve only those phosphines that fit eq 2 in toluene. The data fit is essentially unchanged in these solvents (Table 4).

The ρ_{CH} values for logarithms of the rate give response orders of 2.4, 2.1, 2.1, 2.0, 2.1, and 1.6 for (η^5 -MeCp)Mn(CO)₂(CH₃CN)⁺, (η^5 -MeCp)Mn(CO)₂(4-NO₂-Py)⁺, V(CO)₆, (η^5 -(CH₃)₅Cp)Rh(CO)₂, (η^5 -(CH₃)₅Cp)Co(CO)₂, and Co(NO)(CO)₃, respectively. The $\Delta\chi^{\text{H}}$ values for the above order of reactants are 2.55, -0.55, -2.0, -6.4, -6.7, and 4.3. In the manganese system the substitution of 4-NO₂C₅H₄N by CH₃CN increases the acceptor strength, as reflected in both $\Delta\chi^{\text{H}}$ and ρ_{CH} . The similarities in substituent response reported^{23b} for (η^5 -CH₃Cp)Mn(CO)₂(4-NO₂py)⁺ and V(CO)₆ are evident with Co(NO)(CO)₃ showing a smaller sensitivity to substituent change on the phosphine than V(CO)₆.

Correlations of First-Order Dissociation and Flash Photolysis Studies. Rates and activation enthalpies have been reported²⁷ for the substitution of CO by P(OCH₃)₃ in *mer*-Ru(CO)₃PX₃(SiCl₃)₂, where the substituted phosphine located *trans* to SiCl₃ is varied. The CO group *trans* to SiCl₃ is replaced by a dissociative mechanism. Estimated errors in the activation enthalpies are ± 0.4 kcal/mol⁻¹. The average deviation of the data fit (Table 6, ΔH^{\ddagger} for Ru) is better than the estimated experimental error. With a positive d^{E} and d^{C} , electron-releasing substituents on phosphorus are seen to increase the CO bond dissociation energy and increase the activation enthalpy. This trend parallels the dominance of the Ru-CO bond strength by π -back-bonding. A larger than predicted enthalpy of activation is observed in (C₆H₅)₂P(*i*-C₃H₇)₂ and (*n*-C₄H₉)₃P. The former deviation is attributed to an enthalpic, cone angle type of steric effect. A mechanism change may occur²⁷ for (*n*-C₄H₉)₃P because (C₆H₅)₃P, with a larger cone angle than (*n*-C₄H₉)₃P, is fit in the correlation. The literature reports²⁷ that there is no correlation with the ¹³C Ni(CO)₃L electronic basicity scales for phosphines. We find a good correlation with $\Delta E - \Delta C$. The $d^{\text{C}}/d^{\text{E}}$ ratio of 0.4 shows the Ni(CO)₃L scale is not covalent enough to correlate the enthalpies.

The logarithm of the rate constant for this substitution reaction is very poorly fit relative to experimental error. With the full data set, an average deviation of 0.5 results, compared to an estimated experimental error of 0.1. The large SiCl₃ groups are expected to cause steric problems. For a dissociative mechanism, the entropic steric effects will have the opposite effect on the rate compared to that in the associative mechanism. More rotational degrees of freedom around the metal-phosphorus bond and less substituent ordering will occur in the transition state. All of the substituted triphenylphosphine derivatives have experimental rates that are faster than predicted. The data are divided into two data sets labeled I calcd and II calcd in Table 6. In data set I bulky phosphines give a good fit. In these reactions, the transition state is stabilized by gaining rotational freedom around the metal-P bond. The interaction is not detected in the enthalpy of activation; thus, it must be entropic in nature. Systems in group II do not gain as many degrees of rotational freedom in the transition state, for they have less restricted rotation in the ground state. As a result, they react slower than predicted from the d^{E} and d^{C} param-

eters of the group I phosphines. In each group, the trends are influenced by the electronic properties of the phosphines.

The species Mo(CO)₂(PR₃)₂Br₂ generated by flash photolysis²⁸ undergoes a rapid bimolecular reaction with CO to form the tricarbonyl. The logarithms of the reported²⁸ bimolecular rate constants are poorly fit to ΔE and ΔC (Table 4). When triphenyl- and substituted triphenylphosphines are correlated, an excellent fit results. The omitted phosphines (C₂H₅)₃P, C₆H₅P(C₂H₅)₂, and (C₆H₅)₂PCH₃ have experimental log k values 3.4, 3.3, and 2.6 kcal mol⁻¹ larger than predicted, corresponding to faster reactions. This result suggests that there is a constant contribution from loss of Mo-P rotational degrees of freedom in the transition state of the triphenyl- and substituted triphenylphosphines. A smaller loss of rotational freedom around the metal-phosphorus bond enables the reaction to proceed at a faster rate when phenyl groups are replaced by ethyl groups. The similarity in the deviations of (C₂H₅)₃P and (C₆H₅)₂P(C₂H₅)₂ suggests that entropic steric effects do not arise until the diphenyl derivative is employed. The limited number of systems with more rotational freedom precludes a meaningful data fit of these phosphines.

Dissociative substitution kinetics are reported⁶ for Ru(CO)₄PX₃. The logarithms of the rates were fit with an \bar{x} value of 0.09 when (C₆H₁₁)₃P, (C₆H₅O)₃P, and (C₂H₅O)₃P were omitted from the fit. The range of rates is very small, leading to a large percent fit. The experimental value for (C₆H₁₁)₃P is 1.4 kcal mol⁻¹ faster, and the last two systems are 1.7 and 1.4 kcal mol⁻¹ slower than predicted. As expected, steric influences on the rate are less important in this data set than in Ru(CO)₃PX₃(SiCl₃)₂.

Rate constants for the exchange of CH₃CN with coordinated water in Ru^{II}(H₂O)(bpy)₂(PR₃)₂²⁺ have been reported.²⁹ When the full data set is analyzed, a poor fit results. When tertiary phosphines with aliphatic substituents are fit, an excellent correlation results, (Table 4, (Ru(bpy)₂PR₃^{al})). The aromatic and isobutyl phosphines all have experimental rates that are faster than predicted. When the aromatic phosphines are treated separately, an excellent fit also results (Table 4, Ru(bpy)PR₃^{ar}). These results are consistent with an increase in rotational freedom for the aromatic phosphines that would occur in the transition state for the dissociative I_D mechanism reported. The aliphatic phosphines as a group are not as constrained in the ground state; they gain fewer degrees of rotational freedom in the transition state and have rates that are slower than those predicted.

The ruthenium(III/II) reduction potentials of Ru^{III}-(H₂O)(bpy)₂PR₃ complexes were reported.²⁹ An excellent data fit (Table 4) results for the combined aromatic and aliphatic substituted phosphines. Changes in rotational degrees of freedom accompanying the Ru(II) to Ru(III) oxidation state change do not differ for the aromatic and aliphatic classes.

Photochemical substitution reactions of phosphines with Cp₂Fe₂(CO)₄ have been reported.³⁰ A good data

(28) Herrick, R. S.; Peters, C. H.; Duff, R. R., Jr. *Inorg. Chem.* **1988**, *27*, 2214.

(29) Leising, R. A.; Ohman, J. S.; Takeuchi, K. *J. Inorg. Chem.* **1988**, *27*, 3804.

(30) Zhang, S.; Brown, T. L. *Organometallics* **1992**, *11*, 4166.

(31) Rushman, P.; Brown, T. L. *J. Am. Chem. Soc.* **1987**, *109*, 3632.

(27) Chalk, K. L.; Pomeroy, R. K. *Inorg. Chem.* **1984**, *23*, 444.

fit results for six of the eight substituted phosphines studied (Table 4). The $(C_6H_5)_3P$ system is 1.3 kcal mol⁻¹, smaller than predicted, and $(C_6H_5O)_3P$ is 1.5 kcal mol⁻¹ smaller than predicted. Since $(t-C_4H_9)_3P$ and $(n-C_4H_9)_3P$ are correlated, the deviations are not attributed to rotational or conformational steric effects.

Conclusions

Equation 2 is proposed as a dual-parameter estimate of the basicity of phosphines in preference to E_i in eq 1. Thirty-five different reactions or spectral shifts are analyzed to illustrate the relevance of these parameters to organometallic systems. In contrast to the prevalence in the literature interpretations of a cone angle type of enthalpic steric effect in these systems, very few instances are found in the 35 systems treated. The few systems where enthalpic steric effects clearly dominate reactivity, e.g. $-\Delta H$ for $CH_3Pt[P(C_6H_5)_3]_2B$ adducts, are not treated in this study. The analyses support a chain conformation, entropic steric effect in many of the reactions that is not cone angle related. Long-chain substituents on phosphines with small cone angles deviate in complexes where phosphines with larger cone angles are well-behaved in the data fit. The entropic steric effect is supported, in those instances where data are available, by being well-behaved when the corresponding enthalpies of activation or reduction potentials are fit. There clearly are reactions in which enthalpic steric effects are operative. When this is the case, the values calculated for bulky substituents using reactant d^E , d^C , and $\Delta\chi^H$ parameters from the fit of substituents with minimal steric contributions will deviate in proportion to the cone angle or E_R . The entropic steric effect is readily spotted by deviations in the data fit that increase as the chain length increases.

In several systems, entropic contributions are detected from changes in rotational degrees of freedom around the metal-phosphorus bond in going from the ground to the transition state. This speeds up reactions that are dissociative in nature, for the transition state is less ordered and the entropy is more positive. On the other hand, associative reactions produce a more ordered transition state and this effect slows the reactions. M-L rotational entropic contributions will occur in phosphines with three large substituents that have large cone angles. Enthalpies of activation and redox potentials are not influenced by this entropic steric effect. Clearly, if one is attempting to study the basicity of phosphines and the influence of enthalpic steric effects, rate studies are not recommended because of the diversity of entropic factors that can contribute.

In addition to the reinterpretation of a substantial body of rate and activation enthalpy data, the pK_A values for substituted phosphines are shown to have dominant contributions from factors that are not related to bond strength. This has a profound effect on the validity of analyses that use pK_A as an estimate of E_i in eq 1.

The d^C/d^E ratio of the ¹³C shift of $Ni(CO)_3PX_3$ adducts is 0.01. This measurement would provide a reasonable one-parameter scale of the phosphine electronic properties for physicochemical properties whose d^C/d^E ratios are in the range of -0.05 to 0.05. As can be seen in

Tables 4 and 6, several of the organometallic physicochemical properties fall in this range and give good correlations with ¹³C. However, the majority of the systems have more substantial covalent contributions and ¹³C is not a good gauge of the electronic component. As described in the literature,¹⁷ seemingly good fits could result when properties outside this range are correlated with a limited number of phosphines, but these fits are misleading. The reader is referred to ref 9 for an in-depth discussion of one-parameter basicity scales.

Clearly, the electrostatic-covalent model has led to a very different explanation of phosphine reactivity than eq 1. The analyses based on eq 2 would suggest that cone angle corrections with eq 1, in some instances, compensate for improper estimates of the covalency in the interaction that result from a one-parameter basicity scale. The data interpretations offered should aid in experiment design and stimulate further research. The role of symmetry in influencing chemical reactivity is well understood via the Woodward-Hoffman rules. The influences of the energetics of the reactants (HOMO-LUMO energies, overlap, etc.) on reactivity are less well understood. The widespread applications of the electrostatic-covalent model to aliphatic and aromatic hydrocarbons, inorganic systems and organometallic systems constitutes an empirical step toward gaining this understanding. The broader the applicability of the parameters, the greater the probability that they represent fundamental properties.

Calculation Section

A least-squares minimization program is used to find the best-fit d^E , d^C , and $\Delta\chi^H$ parameters of eq 2 for a J set of experimental $\Delta\chi^X$ values. The ΔE and ΔC values reported earlier were employed in the correlations of over 60 reaction types. The ΔE^X and ΔC^X values are not all known with equal degrees of certainty. The fit is weighted using the reported n values, which indicate the confidence to be placed in the parameters. The larger the n value, the less well known the parameter; thus, the weight given in the data fit is $1/n$.

As in any empirical correlation, the reactivity parameters should be refined as more data become available. When a single set of ΔE^X and ΔC^X substituent constants is refined, all of the known $\Delta\chi^X$ values for reactions of this X substituent are substituted into eq 2 along with the d^E , d^C , and $\Delta\chi^H$ values for the reaction. The set of simultaneous equations is solved for the refined ΔE^X and ΔC^X parameters.

In this article, so many new $\Delta\chi^X$ values became available that a master fit analysis^{8b} was employed for the changed substituents in Table 1. Simultaneous equations were written for each $\Delta\chi^X$ of the form of eq 1. The ΔE^X and ΔC^X substituents whose n values are reported to be 0.2 were entered and not allowed to vary. For those substituents with $n > 0.2$, all of the $\Delta\chi^X$ values for sets of reactions used in the original parameter determination were entered and the d^E , d^C , and $\Delta\chi^H$ values for these reactions were fixed at their reported values. Data points that showed large deviations in the data fit were eliminated and the fit rerun. The refined ΔE^X and ΔC^X parameters resulting from this analysis are reported in Table 1. Those not listed in Table 1 but reported earlier were used unchanged. These parameters, appropriately weighted, were then used in the data fit described in the first paragraph of this section for each of the reactions discussed in this article.

Synthesis and Characterization of Cationic Square-Planar Iridium(I) Complexes Containing Chiral Diphosphines

Franco Morandini* and Giuseppe Pilloni

Dipartimento di Chimica Inorganica, Metallorganica ed Analitica and Centro CNR, Via F. Marzolo 1, I-35131 Padova, Italy

Giambattista Consiglio

Technisch-Chemisches Laboratorium, E. T. H. Zentrum, Universitätsstrasse 6, CH-8092 Zurich, Switzerland

Antonio Mezzetti

Dipartimento di Scienze e Tecnologie Chimiche, Via del Cottonificio 108, I-33100 Udine, Italy

Received February 1, 1995*

Cationic square-planar complexes of the type $[\text{Ir}(\text{diphosphine})_2]\text{Cl}$ (diphosphine = (*R,R*)- and *rac*-cypenphos, (*S,S*)-chiraphos, (*R*)- and *rac*-prophos, (*R*)-phenphos) have been synthesized starting from $[\text{Ir}(\text{COE})_2\text{Cl}]_2$ or $[\text{Ir}(\text{C}_2\text{H}_4)_2\text{Cl}]_2$. The complexes were fully characterized through ^1H - and $^{31}\text{P}\{^1\text{H}\}$ -NMR spectroscopy. With the C_1 diphosphines both *cis* and *trans* isomers are formed with low selectivity. Using racemic cypenphos no diastereoselectivity in the formation of the complexes was observed. For the racemic prophos the diastereoselectivity is different for the two geometrical isomers formed. A study of the electrochemical behavior of these complexes in acetonitrile with some attention to the characteristics of the electron transfer process has been carried out. The results are compared with those previously obtained in the reduction of the corresponding dppe derivative and provide a tool for the determination of the relative basicity of the ligands. The reduction was found to proceed by a single two-electron step to a d^{10} anion, which is quenched by the protic solvent to give the final metal hydride derivative which in the case of complexes **2** and **3** were observed by NMR spectroscopy.

Introduction

Electron-rich transition metal complexes are believed to be efficient agents for stereospecific reactions of organic substrates both from a stoichiometric and a catalytic point of view.¹⁻⁵ In particular complexes of the type $[\text{Ir}(\text{diphosphine})_2]\text{Cl}$ (in which the diphosphine is chiral) can be of interest as catalyst precursors for enantioselective hydrogenation.⁶ During attempts to prepare compounds of the type $(\eta^5\text{-C}_9\text{H}_7)\text{Ir}(\text{diphosphine})$ to be compared with the previously reported analogous rhodium complexes⁷ via displacement of the diolefin from $(\eta^5\text{-C}_9\text{H}_7)\text{Ir}(\text{COD})$ (COD = 1,5-cyclooctadiene) or $(\eta^5\text{-C}_9\text{H}_7)\text{Ir}(\text{COE})_2$ (COE = cyclooctene) with chiral diphosphines (Chart 1), we observed formation of cationic complexes of the type $[\text{Ir}(\text{diphosphine})_2]^+$ as the

* Abstract published in *Advance ACS Abstracts*, June 1, 1995.

(1) Werner, H. *Angew. Chem., Int. Ed. Engl.* **1983**, *22*, 927.
(2) For example, compare: (a) Davies, S. G.; McNally, J. P.; Smallridge, A. J. *Adv. Organomet. Chem.* **1990**, *30*, 1. (b) Davies, S. G. *Pure Appl. Chem.* **1988**, *60*, 13. (c) Dalton, D. M.; Fernandez, J. M.; Emerson, K.; Larsen, R. D.; Arif, A. M.; Gladysz, J. A. *J. Am. Chem. Soc.* **1990**, *112*, 9198.

(3) Consiglio, G.; Morandini, F. *Chem. Rev.* **1987**, *87*, 761.

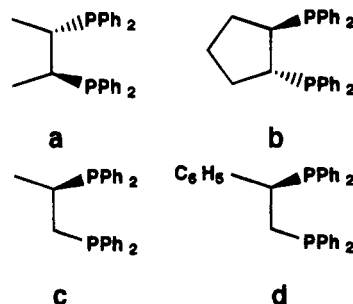
(4) Morandini, F.; Consiglio, G.; Sironi, A.; Moret, M. *J. Organomet. Chem.* **1989**, *370*, 305.

(5) Morandini, F.; Consiglio, G. *J. Organomet. Chem.* **1990**, *390*, C64.

(6) (a) Chang, Y. N. C.; Meyer, D.; Osborn, J. A. *J. Chem. Soc., Chem. Commun.* **1990**, 869. (b) Mashima, K.; Akutagawa, T.; Zhang, X.; Takaya, H.; Taketomi, T.; Kumobayashi, H.; Akutagawa, S. *J. Organomet. Chem.* **1992**, *428*, 213. (c) Zhang, X.; Taketomi, T.; Yoshizumi, T.; Kumobayashi, H.; Akutagawa, T.; Mashima, K.; Takaya, H. *J. Am. Chem. Soc.* **1993**, *115*, 3318.

(7) Morandini, F.; Pilloni, G.; Consiglio, G.; Sironi, A.; Moret, M. *Organometallics* **1993**, *12*, 3495.

Chart 1



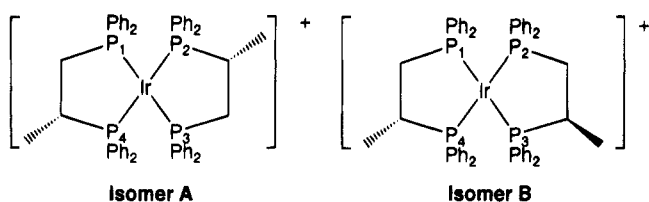
major component. These complexes are also of interest because of diastereoselectivity phenomena during complexation and of their relationship to possible nonlinear effects in catalysis.⁸ In the present work we report on the synthesis, the multinuclear NMR characterization, and the electrochemical behavior of iridium(I) complexes of formula $[\text{Ir}(\text{diphosphine})_2]\text{Cl}$ obtained by reacting the dimers $[\text{Ir}(\text{COE})_2\text{Cl}]_2$ or $[\text{Ir}(\text{C}_2\text{H}_4)_2\text{Cl}]_2$ with various chiral diphosphines.

Results and Discussion

Preparation and Spectroscopic Properties. In contrast to the similar reaction with triphenylphosphine, by reacting the complex $(\eta^5\text{-C}_9\text{H}_7)\text{Ir}(\text{COD})$ with the diphosphines of Chart 1, mixtures of compounds are

(8) Guillauneux, D.; Zhao, S.-H.; Samuel, O.; Rainford, D.; Kagan, H. B. *J. Am. Chem. Soc.* **1994**, *116*, 9430.

Chart 2



obtained in which it is possible to recognize by NMR analysis complexes of the type $[\text{Ir}(\text{diphosphine})_2]^+$ as the major component. The reaction seems to occur with displacement of the C_9H_7^- leading to formation of stable planar cationic complexes of the type $[\text{Ir}(\text{diphosphine})_2]^+$. In fact, we were unable to ascertain the previously observed formation of compounds corresponding to the migration of the cyclopentadienyl ligand to the cyclooctadiene ligand.¹⁰

The complexes $[\text{Ir}(\text{diphosphine})_2]\text{Cl}$ can be prepared in a pure form by reacting dimeric $[\text{Ir}(\text{COE})_2\text{Cl}]_2$ in toluene at room temperature with an excess of the appropriate diphosphine. Better results are obtained when the cyclooctene ligand is first substituted with ethylene at 0 °C in diethyl ether solution, followed by the addition of the appropriate diphosphine. In the latter case the yields of the reactions are quite high, normally close to 90%. The orange microcrystalline compounds behave as 1:1 electrolytes of the type $[\text{Ir}(\text{diphosphine})_2]\text{Cl}$ in methanol solution.¹¹

The $^{31}\text{P}\{^1\text{H}\}$ -NMR spectra of the complexes containing the optically pure C_2 chiral diphosphines (*S,S*)-chiraphos, **a**, (Chart 1) and (*R,R*)-cypenphos, **b**, contain a single signal for the four equivalent P atoms, as expected for a square-planar iridium(I) complex. The chemical shift value (δ 50.03) found for the singlet of $[\text{Ir}(\text{S,S-chiraphos})_2]\text{Cl}$, **1**, is close to that of $[\text{Ir}(\text{dppe})_2]\text{Cl}$, **2**,¹² (δ 50.28). Analogously, $[\text{Ir}(\text{R,R-cypenphos})_2]\text{Cl}$, **3**, exhibits only a singlet centered at δ 22.79.

The $^{31}\text{P}\{^1\text{H}\}$ -NMR spectrum of the compound prepared starting with racemic cypenphos shows two singlets with the same intensity at δ 22.79 and 24.71. The two species formed correspond to the two possible diastereomers $[\text{Ir}\{(R^*,R^*)\text{-cypenphos}\}_2]\text{Cl}$ and $[\text{Ir}\{(R,S)\text{-cypenphos}\}_2]\text{Cl}$, respectively, in which two homo- or heterochiral diphosphine molecules are coordinated to the metal. The equal intensity of the two lines shows that there is no diastereoselectivity in the formation of the bis(diphosphine) complex.

The complexes containing C_1 chiral phosphines give rise to more complicated $^{31}\text{P}\{^1\text{H}\}$ -NMR spectra since the two P atoms of the diphosphine are inequivalent, and the two geometrical isomers **A** and **B** are formed (Chart 2). Thus, the $^{31}\text{P}\{^1\text{H}\}$ -NMR spectrum of the prophan derivative, $[\text{Ir}\{(R)\text{-prophan}\}_2]\text{Cl}$, **4**, shows two sets of AA'XX' patterns that are characterized by the different magnitude of the $J(\text{P},\text{P}')$ coupling constants. The experimental spectrum together with the simulated spectra for both isomers **A** and **B** are reported in Figure 1.

The $^{31}\text{P}\{^1\text{H}\}$ -NMR spectrum of the *trans* isomer **A** shows only *cis*- $J(\text{P},\text{P}')$ coupling constants in the range

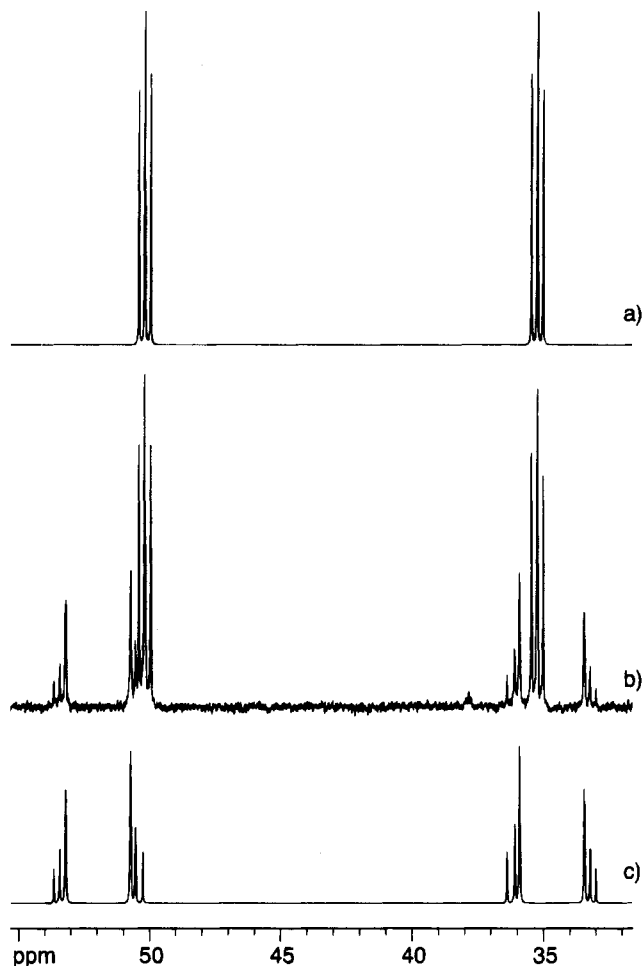


Figure 1. $^{31}\text{P}\{^1\text{H}\}$ -NMR spectrum of $[\text{Ir}\{(R)\text{-prophan}\}_2]\text{Cl}$, **4**: (a) simulated spectrum of isomer **A**; (b) experimental spectrum of the mixture of isomers **A** and **B** (CD_2Cl_2 , room temperature); (c) simulated spectrum of isomer **B**.

20–25 Hz, in agreement with the presence of two pairs of chemically equivalent *trans* P atoms. The resonances at lower field are due to the phosphorus atoms closer to the methyl group of the backbone.^{13,14} In isomer **B** the two chemically inequivalent P atoms occupy *trans* positions, as indicated by the large $J(\text{P},\text{P}')$ coupling constant of 271.6 Hz. The two geometrical isomers are present in a **A**:**B** molar ratio of 59:41. This ratio was also confirmed by integration of the signals due to the methyl protons of the prophan ligands centered at δ 0.86 and 0.79 in the ^1H -NMR spectrum.

When racemic prophan is used, four different isomers form, which correspond to the diastereomers (containing homo- or heterochiral ligands) of each geometrical isomer. The diastereomers containing the homochiral ligands are obviously formed as pairs of enantiomers ((*R,R*) and (*S,S*), respectively). The *cis*:*trans* molar ratio is 54:46 for the homochiral diastereomer (i.e., for the sum of the (*R,R*) and (*S,S*) compounds) and is 45:55 for the heterochiral diastereomer. On the other hand, the diastereomeric ratio $\{(R,S):(S,S) + (R,R)\}$ is different for the *cis* isomers, being larger for the *cis* isomer (62:38) than for the *trans* one (54:46). In both cases the diastereomer containing two heterochiral ligand molecules prevails.

(9) Marder, T. B.; Williams, I. D. *J. Chem. Soc., Chem. Commun.* **1987**, 1478.

(10) Merola, J. S.; Kacmarcik, R. T. *Organometallics* **1989**, *8*, 778.

(11) Geary, W. J. *Coord. Chem. Rev.* **1971**, *7*, 81.

(12) Vaska, L.; Catone, D. L. *J. Am. Chem. Soc.* **1966**, *88*, 5324.

(13) Morandini, F.; Consiglio, G.; Piccolo, O. *Inorg. Chim. Acta* **1982**, *57*, 15.

(14) Brunner, H.; Stumpf, A. *J. Organomet. Chem.* **1993**, *459*, 139.

The complex containing the phenphos **d** analogue, [Ir{(R)-phenphos}₂]Cl, **5**, displays a similar ³¹P{¹H}-NMR pattern and isomeric composition as observed for the (R)-prophos derivative **4**. The spectrum consists also in this case of two superimposed AA'XX' systems for the two isomers **A** and **B** with an **A**:**B** ratio of 56:44 as determined by integration of the ³¹P{¹H}-NMR spectrum. The subspectrum of the *trans* isomer appears as two *pseudotriplets* since the four *cis*-²J_{PP} coupling constants have fortuitously the same value.

We attempted to change the isomeric distribution obtained for the complexes [Ir{(R)-prophos}₂]Cl and [Ir{(R)-phenphos}₂]Cl by means of electrocatalytic cyclovoltammetry and/or controlled-potential coulometry experiments in acetonitrile–tetraethylammonium perchlorate (0.2 M) solution. These tests stemmed from the observation that the electrogenerated tetrahedral anion [Ir(prophos)₂]⁻ turned out long-lived enough to be potentially capable of triggering isomerization of the depolarizer (*t*_{0.5} = 3 s, *vide infra*). However, if the catholyte is dried under vacuum and the residue dissolved in deuterated dichloromethane, the ³¹P{¹H}-NMR spectrum shows no change in the isomeric composition both for the prophos and the phenphos derivatives.

Electrochemistry. The electrochemical reduction of square-planar bis(diphosphine) complexes of rhodium and iridium has been thoroughly studied by a number of research groups during the past 20 years.^{15–18} One of us first proposed and subsequently confirmed¹⁸ that the electrochemical reduction of these complexes in acetonitrile proceeds via a single two-electron step to the anionic intermediate [M(dppe)₂]⁻ quenched by proton abstraction from the medium to give the final hydride derivative HM(dppe)₂. Other groups^{16,17} envisaged the reduction to proceed *via* a one-electron transfer, generating the zero-valent compound followed by H atom abstraction from the solvent to give the metal hydride and subsequent reduction of the solvent radical. More recent work of Eisenberg et al.,¹⁹ employing a purely chemical approach to the reduction of [Rh(dppe)₂]⁺, concluded that the two-electron-reduction product does undergo reaction with protic solvents by acid–base chemistry, while H atom sources are not at all involved in the metal hydride formation.

As expected, the electrochemical behavior of the complexes [Ir{(S,S)-chiraphos}₂]⁺, **1**, [Ir{(R)-prophos}₂]⁺, **4**, and [Ir{(R)-phenphos}₂]⁺, **5**, is quite similar to that observed for the dppe analogue **2** under identical experimental conditions.^{15,18} Thus, the cyclic voltammograms always exhibit a single reduction peak with the directly associated oxidation response in the reverse scan, which is coupled to an irreversible chemical reaction (Figures 2–4). The occurrence of two-electron transfers has been verified chronoamperometrically by comparison of the diffusion currents with **2** and confirmed by controlled potential coulometries. That a concerted two-electron reaction, i.e., an EE mechanism

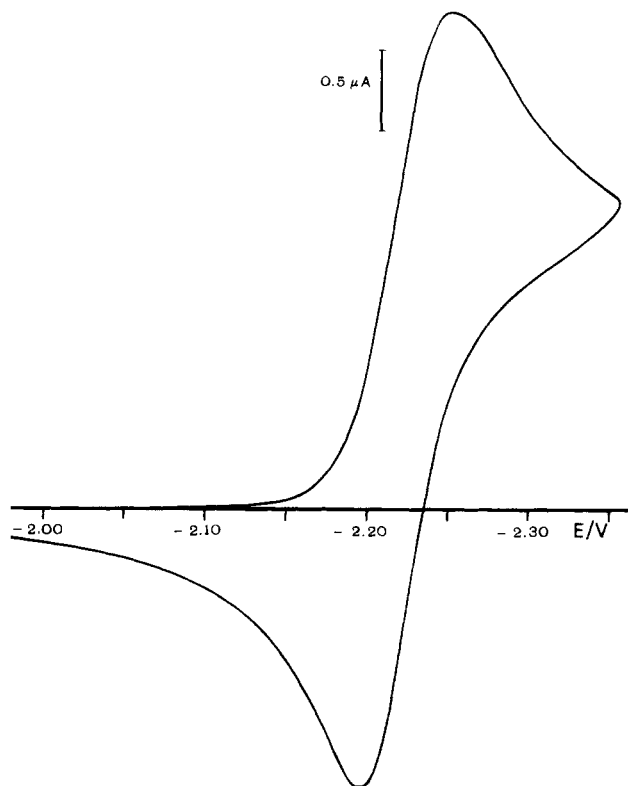


Figure 2. Cyclic voltammogram of 1.92 mM [Ir{(S,S)-chiraphos}₂]Cl, **1**, in CH₃CN, 0.2 M TEAP, at 25 °C and at a scan rate of 100 mV s⁻¹.

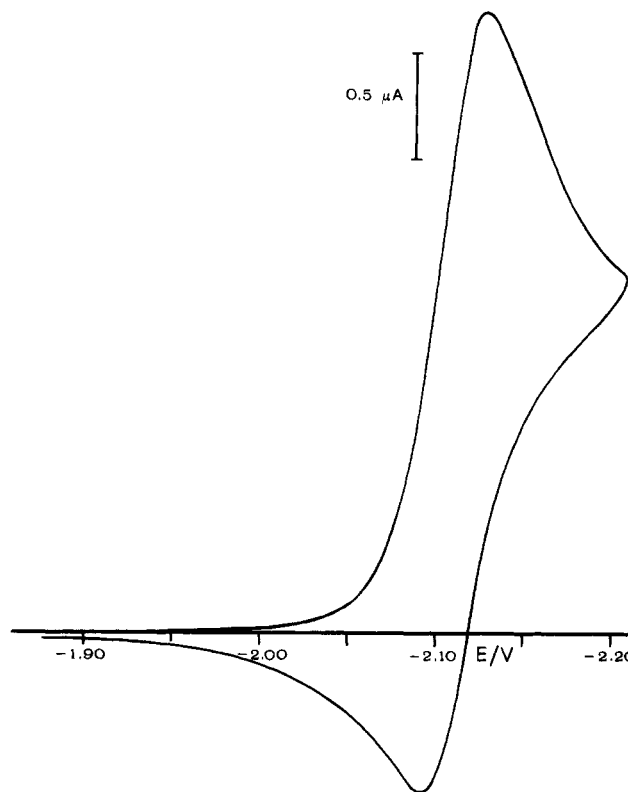


Figure 3. Cyclic voltammogram of 1.92 mM [Ir(dppe)₂]Cl, **2**, in CH₃CN, 0.2 M TEAP, at 25 °C and at a scan rate of 100 mV s⁻¹.

with *E*₂^o very anodic of *E*₁^o,²⁰ does occur in complex **2** as well as in its rhodium analogue has been already proved unambiguously.¹⁸

(15) Pilloni, G.; Vecchi, E.; Martelli, M. *J. Electroanal. Chem.* **1973**, *45*, 483.

(16) Teo, B. K.; Ginsberg, A. P.; Calabrese, J. C. *J. Am. Chem. Soc.* **1976**, *98*, 3027.

(17) Sofranko, J. A.; Eisenberg, R.; Kampmaier, J. A. *J. Am. Chem. Soc.* **1979**, *101*, 1042.

(18) Pilloni, G.; Zotti, G.; Martelli, M. *Inorg. Chem.* **1982**, *21*, 1283.

(19) Kunin, A. J.; Nanni, E. J.; Eisenberg, R. *Inorg. Chem.* **1985**, *24*, 1852.

(20) Myers, R. L.; Shain, I. *Anal. Chem.* **1969**, *41*, 980.

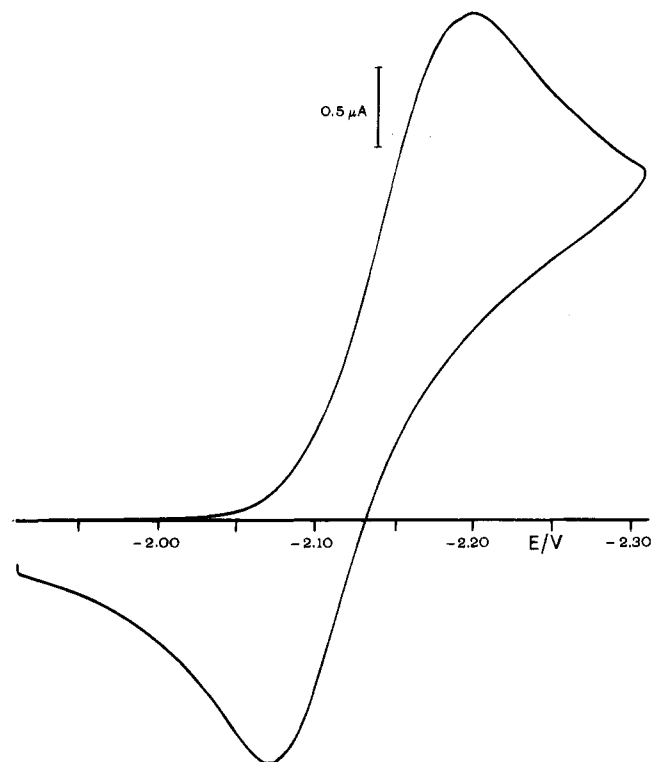


Figure 4. Cyclic voltammogram of 2.70 mM $[\text{Ir}\{(\text{R})\text{-phenphos}\}_2]\text{Cl}$, **5**, in CH_3CN , 0.2 M TEAP, at 25 °C and at a scan rate of 100 mV s^{-1} .

However, it is of interest to see how the modification in the backbone of the diphosphine affects the Ir(I)/Ir(-I) redox behavior. The redox couples are centered at $E_{1/2} = -2.11_0, -2.13_5, -2.15_5, -2.17_0,$ and -2.22_5 V (as mean values of the potentials for cathodic and anodic peak currents) for **2**, **5**, **4**, **3**, and **1**, respectively. The shifting of $E_{1/2}$ values to more negative potentials on going from R = H (dppe) to Ph (phenphos), Me (prophos), cypenphos, and finally to chiraphos (which has two methyl groups on the backbone) is in accordance with the relative electron-donating capacities of these substituents. Thus, the chiraphos ligand is expected to be the most electron-donating of the three ligands and $[\text{Ir}\{(\text{S,S})\text{-chiraphos}\}_2]^+$, **1**, is the most difficult of the five complexes to reduce.

Moreover, an inspection of the shape of the voltammetric responses (see Figures 2–4) clearly indicates that the electron transfer is essentially reversible for **2** (peak width, $E_{p/2} - E_p = 30$ mV, and peak to peak separation, $\Delta E_p = 38$ mV, at the scan rate used), while the wave is quasireversible for **1**, **4**, and **3** ($E_{p/2} - E_p = 40$ mV; $\Delta E_p = 60$ mV) and approaches the irreversible behavior in the case of **5** ($E_{p/2} - E_p = 65$ mV; $\Delta E_p = 130$ mV).²¹ In line with these observations, the shape and the position of the waves displayed by complexes **1**, **3**, **4**, and **5** are markedly dependent upon the cyclic scan rate over the experimental range used (20–1000 mV s^{-1}), while they are virtually independent for **2**. The slowed down rate of heterogeneous electron transfer in depolarizers **1**, **3**, **4**, and **5**, compared with that of **2**, apparently reflects the relative greater conformational rigidity arising from the steric demand of the substituents in the backbone.

Competing with and/or alternative to the multielectron transfer mechanism could be the disproportionation

mechanism.²¹ A detailed report by Eisenberg et al.¹⁹ describing the chemical reduction of $[\text{Rh}(\text{dppe})_2]^+$ through variation of solvent and temperature conditions established that the intermediate one-electron reduction product, $\text{Rh}(\text{dppe})_2^0$, is in equilibrium with the disproportionated $[\text{Rh}(\text{dppe})_2]^-/\text{Rh}(\text{dppe})_2^+$ ion pair. The ionic species appear to predominate by far in polar solutions and/or at low temperatures, while the radical species is favored in nonpolar solvents at room temperature. Since the shape and position of the voltammograms were found to be independent of the depolarizer concentration, the irreversible disproportionation reaction is not an important pathway under the conditions used.

Consistently, this result could reveal that the first electron transfer is the slow step in the electrochemical reduction of complex **5**, so that the zero-valent complex is rapidly reduced to the corresponding anion at the electrode surface. Unfortunately, the peak current ratios i_p^a/i_p^c were found to be always equal to unity at scan rates large enough (≥ 0.5 V s^{-1}) to make the wave irreversible and assure that the coupled chemical reaction is not occurring at any appreciable extent. Thus, the identity of the slow step remains still undetermined.²¹

So far as the chemical reaction following charge transfer, it can once again be ascribed to quenching of the primary two-electron reduction product by proton sources to give the hydride derivative. The final hydride products were recognized for the complexes **2** and **3** by $^1\text{H-NMR}$ spectroscopy. For both complexes the resonance of the hydride proton appears as a quintet centered at $\delta -12.47$ ppm ($J_{\text{PH}} = 8.5$ Hz) and $\delta -13.18$ ($J_{\text{PH}} = 7.3$ Hz) in toluene- d_8 solution, respectively.²² Indeed, in close analogy with our previous results for the $[\text{M}(\text{dppe})_2]^+$ systems,^{15,18} deliberate addition of increasing amounts of water leads to the stepwise disappearance of the coupled anodic peak, the cathodic one being unchanged, in the cyclic voltammograms of **1**, **3**, **4**, and **5**.

Owing to incomplete reversibility of the electron transfer processes, the rate constant value for the chemical step in the reduction of **1**, **3**, **4** and **5** has been determined by double-potential step chronoamperometry.²³ The pseudo-first-order rate constants at 25 °C in nominally anhydrous acetonitrile were found to be 0.17, 0.35, 0.24, and 0.13 s^{-1} for complexes **1**, **3**, **4**, and **5**, respectively. These values are compatible with the value of 0.40 s^{-1} that we previously obtained by cyclic voltammetry¹⁸ and here confirmed by chronoamperometric method for complex **2** under identical conditions.

Conclusion

We have reported here the preparation of new chiral bis(diphosphine) iridium complexes. The formation of these complexes is accompanied in the cases examined by a very low extent of diastereoselectivity. Of interest is the response of the electrochemical measurements which give information about the different basicity of the ligands investigated. These methods can be useful in finding a possible rationale for the difference in

(21) Rayan, M. D. *J. Electrochem. Soc.* **1978**, *125*, 547.

(22) Schnabel, R. C.; Roddick, D. M. *Organometallics* **1993**, *12*, 704 and references therein.

(23) Schwarz, W. M.; Shain, I. *J. Phys. Chem.* **1965**, *69*, 30.

reactivity shown by these ligands in stoichiometric and catalytic reactions.^{3,24}

Experimental Section

Materials. All reactions and manipulations were carried out under nitrogen. The solvents were dried and degassed before use. ¹H- and ³¹P{¹H}-NMR spectra were recorded on a JEOL FX 90 Q or on a AM 400 Bruker spectrometer. Positive δ values in ppm are downfield from internal Me₄Si (¹H) or external 85% H₃PO₄ (³¹P). Anhydrous CH₃CN was purchased from Aldrich and used as received. The electrolyte tetraethylammonium perchlorate (TEAP; C. Erba) was dried in vacuo at 75 °C prior to use. High-purity argon, further purified from oxygen by passage over reduced copper at 450 °C, was used in electrochemical experiments. Cyclooctene and 1,5-cyclooctadiene were obtained from Jansen, 1,2-bis(diphenylphosphino)ethane (dppe) and triphenylphosphine from Fluka and were used without purification. 1,2-Bis(diphenylphosphino)cyclopentane (cypenphos),²⁵ (2*S*,3*S*)-2,3-bis(diphenylphosphino)butane (chiraphos),^{26a} (*R*)-1,2-bis(diphenylphosphino)propane (propfos),^{26b} (*R*)-1-phenyl-1,2-bis(diphenylphosphino)ethane (phenphos),²⁷ [Ir(COE)₂Cl]₂,²⁸ [Ir(COD)Cl]₂,²⁹ (η^5 -C₉H₇)Ir(COD),¹⁰ and (η^5 -C₉H₇)Ir(COE)₂³⁰ were prepared according to published procedures. Spectral simulations were performed with PANIC (Bruker Spectrospin AG) using positive *trans*-²J_{PP} and negative *cis*-²J_{PP}. The *trans*-²J_{PP} values obtained for the *cis* isomers were used as starting values in the data set of the corresponding *trans* species.

The conductivity experiments were carried out at 25 °C with a Radiometer CDM3 instrument on a ca. 10⁻² methanol solution of the complexes.

General Procedure for the Preparation of the [Ir(diphos)₂Cl] Complexes. [Ir(C₂H₄)₂Cl]₂ was generated in situ by bubbling ethylene into a suspension of [Ir(COE)₂Cl]₂ (0.3 g, 0.33 mmol) in ethyl ether at 0 °C for 30 min as previously reported.³¹ The solution was then reacted with a 5-fold excess of the appropriate diphosphine in 20 mL of toluene or dichloromethane at room temperature. After 8 h, the solvent was removed under reduced pressure and 20 mL of *n*-hexane was added to the residue. The orange microcrystalline compounds were filtered off, washed with *n*-hexane, and dried in vacuo. Recrystallization was from dichloromethane/*n*-hexane. Yields are up to 90%. Elemental analyses and NMR parameters (δ , CD₂Cl₂) for the complexes are as follows.

[Ir{(S,S)-chiraphos}₂]Cl, 1. ¹H-NMR: 7.49–7.17 (m, 40H, C₆H₅); 1.83 (m, 4H, CH); 0.67 (m, 12H, CH₃). ³¹P-NMR: 50.03 (s). Anal. Found: C, 61.73; H, 5.07. Calcd for C₅₈H₅₆P₄ClIr: C, 62.24; H, 5.22.

(24) Visentin, G.; Piccolo, O.; Consiglio, G. *J. Mol. Catal.* **1990**, *61*, L1.

(25) Allen, D. L.; Gibson, V. C.; Green, M. L. H.; Skinner, J. F.; Bashkin, J.; Grebenik, P. D. *J. Chem. Soc., Chem. Commun.* **1983**, 895.

(26) (a) Fryzuk, M. D.; Bosnich, B. *J. Am. Chem. Soc.* **1977**, *99*, 6262. (b) Fryzuk, M. D.; Bosnich, B. *J. Am. Chem. Soc.* **1978**, *100*, 5491.

(27) (a) King, R. B.; Bakos, J.; Hoff, C. D.; Marko, L. *J. Org. Chem.* **1979**, *44*, 1729. (b) Brown, J. M.; Murrer, B. A. *Tetrahedron Lett.* **1979**, 4859.

(28) Van der Ent, A.; Onderdelinden, A. L. *Inorg. Synth.* **1990**, *28*, 90.

(29) Herde, J. L.; Lambert, J. C.; Senoff, C. V. *Inorg. Synth.* **1974**, *15*, 18.

(30) Merola, J. S.; Kacmarcik, R. T.; Van Engen, D. *J. Am. Chem. Soc.* **1986**, *108*, 329.

(31) Abad, J. A. *Inorg. Chim. Acta* **1986**, *121*, 213.

[Ir{(R,R)-cypenphos}₂]Cl, 3. ¹H-NMR: 7.76–7.14 (m, 40H, C₆H₅); 2.30–0.89 (m, 16H, CH + CH₂). ³¹P-NMR: 22.77 (s). Anal. Found: C, 62.78; H, 5.08. Calcd for C₅₈H₅₆P₄ClIr: C, 63.06; H, 5.10.

[Ir{(R*,R*)-cypenphos}₂]Cl + [Ir{(R,S)-cypenphos}₂]Cl, 3'. ¹H-NMR: 7.77–6.79 (m, 40H, C₆H₅); 2.27–0.93 (m, 16H, CH + CH₂). ³¹P-NMR: 24.71 (s); 22.77 (s). Anal. Found: C, 62.90; H, 5.16. Calcd for C₅₈H₅₆P₄ClIr: C, 63.06; H, 5.10.

[Ir{(R)-propfos}₂]Cl, 4. ¹H-NMR: 7.80–6.86 (m, 40H, C₆H₅); 2.45–2.09 (m, 6H, CH + CH₂); 0.86, 0.79 (m, 6H, CH₃). ³¹P-NMR: isomer A, *trans*-(*R,R*), AA'XX' pattern, 35.2 (P₁, P₃), 50.2 (P₂, P₄), (*J*_{1,2} = *J*_{3,4} = 24.2, *J*_{1,3} = 271.1, *J*_{1,4} = *J*_{2,3} = 20.7, *J*_{2,4} = 271.3 Hz); isomer B, *cis*-(*R,R*), AA'XX' pattern, 34.8 (P₁, P₂), 51.9 (P₃, P₄) (*J*_{1,2} = 25.1, *J*_{1,3} = *J*_{2,4} = 271.6, *J*_{1,4} = *J*_{2,3} = 20.7, *J*_{3,4} = 23.2 Hz). Anal. Found: C, 61.71; H, 5.08. Calcd for C₅₄H₅₂P₄ClIr: C, 61.62; H, 4.98.

[Ir{(R*,R*)-propfos}₂]Cl + [Ir{(R,S)-propfos}₂]Cl, 4'. ¹H-NMR: 7.70–6.80 (m, 40H, C₆H₅); 2.36–1.60 (m, 6H, CH + CH₂); 0.82 (m, 6H, CH₃). ³¹P-NMR: isomer A, *trans*-(*R,S*), AA'XX' pattern, 40.2 (P₁, P₃), 54.6 (P₂, P₄), (*J*_{1,2} = *J*_{3,4} = 17.4, *J*_{1,3} = 265.3, *J*_{1,4} = *J*_{2,3} = 21.8, *J*_{2,4} = 265.2 Hz); isomer B, *cis*-(*R,S*), AA'XX' pattern, 30.8 (P₁, P₂), 55.7 (P₃, P₄) (*J*_{1,2} = 25.4, *J*_{1,3} = *J*_{2,4} = 270.9, *J*_{1,4} = *J*_{2,3} = 23.4, *J*_{3,4} = 22.0 Hz). Anal. Found: C, 61.52; H, 4.92. Calcd for C₅₄H₅₂P₄ClIr: C, 61.62; H, 4.98.

[Ir{(R)-phenphos}₂]Cl, 5. ¹H-NMR: 7.51–6.35 (m, 40H, C₆H₅); 3.35–2.48 (m, 6H, CH + CH₂). ³¹P-NMR: isomer A, *trans*-(*R,R*), *pseudo* A₂X₂ pattern, 31.4 (t), 54.6 (t), (*J*_{PP} = 23.2 Hz); isomer B, *cis*-(*R,R*), AA'XX' pattern, 30.8 (P₁, P₂), 55.7 (P₃, P₄) (*J*_{1,2} = 25.4, *J*_{1,3} = *J*_{2,4} = 270.9, *J*_{1,4} = *J*_{2,3} = 23.4, *J*_{3,4} = 22.0 Hz). Anal. Found: C, 65.58; H, 4.86. Calcd for C₆₄H₅₆P₄ClIr: C, 65.33; H, 4.80.

Apparatus and Procedure for the Electrochemical Measurements. All experiments were performed on anhydrous deoxygenated acetonitrile solutions with 0.2 M TEAP as the supporting electrolyte, using a conventional three-electrode liquid-jacketed cell. Cyclic voltammetry measurements were performed with an Amel 551 potentiostat modulated by an Amel 566 function generator, and the recording device was either an Amel model 863 X-Y recorder or a Hewlett-Packard 7090 A measurement plotting system, depending on the scan rate employed. The working electrode was a planar platinum microelectrode (ca. 0.3 mm²) surrounded by a platinum spiral counter electrode.

Controlled potential electrolyses were performed with an Amel 552 potentiostat linked to an Amel 731 digital integrator. The working electrode was a mercury pool, and the counter was external, the connection being made through an appropriate salt bridge. In all cases silver/0.1 M silver perchlorate in CH₃CN, separated from the test solution by 0.2 M TEAP in CH₃CN solution sandwiched between two fritted disks, was used as the reference electrode. Compensation for *iR* drop was achieved by positive feedback. Ferrocene was added at the end of each experiment as the internal reference. All potentials are referred to the ferrocenium/ferrocene redox couple (*E*^o = +0.01_v relative to the actual Ag/AgClO₄ reference electrode and +0.42_v relative to SCE).

Acknowledgment. We thank Mr. A. Ravazzolo (CNR, Padua, Italy) for skillful technical assistance.

OM9500836

Synthesis and Theoretical Analysis of Palladium(II) Complexes Containing a η^1 Metallacarbyne Ligand

Philippus F. Engel and Michel Pfeffer*

Laboratoire de Synthèses Métallo-induites (URA 416 du CNRS), Université Louis Pasteur,
4, rue Blaise Pascal, F-67070 Strasbourg Cedex, France

Alain Dedieu*

Laboratoire de Chimie Quantique (UPR 139 du CNRS), Université Louis Pasteur,
4, rue Blaise Pascal, F-67070 Strasbourg Cedex, France

Received March 8, 1995[®]

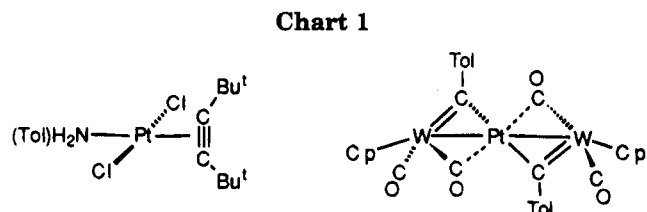
Metallacarbyne complexes such as $(\eta^5\text{-C}_5\text{H}_5)\text{M}(\text{CO})_2\equiv\text{CR}$ ($\text{M} = \text{Mo}, \text{W}$; $\text{R} = \text{p-Tol}$) afford simple adduct complexes when reacted with cyclopalladated compounds derived from benzo(*h*)quinoline, 8-alkylquinoline, or *N,N*-dimethylnaphthylamine. The interaction between the metallacarbyne and the palladium atom occurs primarily via the carbyne carbon atom, suggesting a η^1 interaction between the $\text{M}\equiv\text{C}$ unit and $\text{Pd}(\text{II})$. The bound metallacarbyne is easily displaced by two-electron donor ligands such as pyridine or trialkylphosphines. Comparison of the results of SCF calculations carried out on the $[\text{Cp}(\text{CO})_2\text{MoCH}]$ – $[\text{PdCl}_2(\text{NH}_3)]$, $[\text{Cp}(\text{CO})_2\text{MoCH}][\text{AlH}_3]$, and $[\text{Cp}(\text{CO})_2\text{MoCHCH}_3]^+$ model systems indicates that the bonding between the metallacarbyne and the palladium complex is best described as involving a Lewis acid–Lewis base interaction together with a strong electrostatic component. It is suggested that these adducts are intermediates in the coupling reaction that occurs between the carbyne atom and the palladated carbon atom of the cyclopalladated complexes.

Introduction

It is generally accepted¹ that the first step in the insertion of an alkyne into a $\text{Pd}-\text{C}$ bond is the formation of a complex in which the alkyne is η^2 -coordinated to the metal center. In this step, the alkyne simply substitutes a labile halogen substituent X on palladium (see Scheme 1; for example, the $\text{C}-\text{Y}$ represents a cyclopalladated ligand, $\text{X} = \text{Cl}, \text{I}$).² Recently, kinetic data have been obtained for these reactions,³ and the results support the formation of a halide-bridged bimetallic coordination complex (Scheme 1).

None of these proposed alkyne coordination complexes has been well-characterized. Only one complex, $[\text{Pd}_2\text{Cl}_4(\text{tBuC}\equiv\text{C}^t\text{Bu})_2]$, has been isolated, but no X-ray structure is available.⁴ In contrast, a number of planar $\text{M}^{\text{II}}\text{L}_3$ (olefin) complexes have been characterized, and their structures show that the olefin is coordinated perpendicularly to the metal plane.⁵ Since olefins and alkynes both possess π and π^* orbitals, it can be expected that alkynes are able to adopt similar coordination modes.

The intermediate η^2 complexes such as those depicted in Scheme 1 can also be advanced on the basis of known



alkyne complexes of $\text{Pt}(\text{II})$. For instance, in the complex $[(4\text{-Tol})\text{NH}_2]\text{Cl}_2\text{Pt}(\eta^2\text{-}^t\text{BuC}\equiv\text{C}^t\text{Bu})$, the carbon–carbon triple bond is coordinated symmetrically to the platinum center, the triple bond being perpendicular to the plane of the “ PtL_3 ” fragment (Chart 1).⁶

Another interesting model system is found in the coordination chemistry of certain metallacarbynes, $\text{L}_n\text{M}\equiv\text{CR}$. It is well-known that alkynes and metallacarbynes display analogous ligand properties toward zero-valent metal centers.^{7a} These properties can therefore be expected to apply to higher valent metals like $\text{Pd}(\text{II})$ as well. Unfortunately, complexes with a metallacarbyne coordinated to a $\text{Pd}(\text{II})$ center have never been reported. μ -Alkylidyne complexes of $\text{Pd}(0)$ are also very rare: only the labile complex $[\text{PdW}_2(\mu\text{-C}(4\text{-Tol}))_2(\text{CO})_4(\text{Cp})_2]$ has been isolated, but no X-ray structure could be obtained.^{7b}

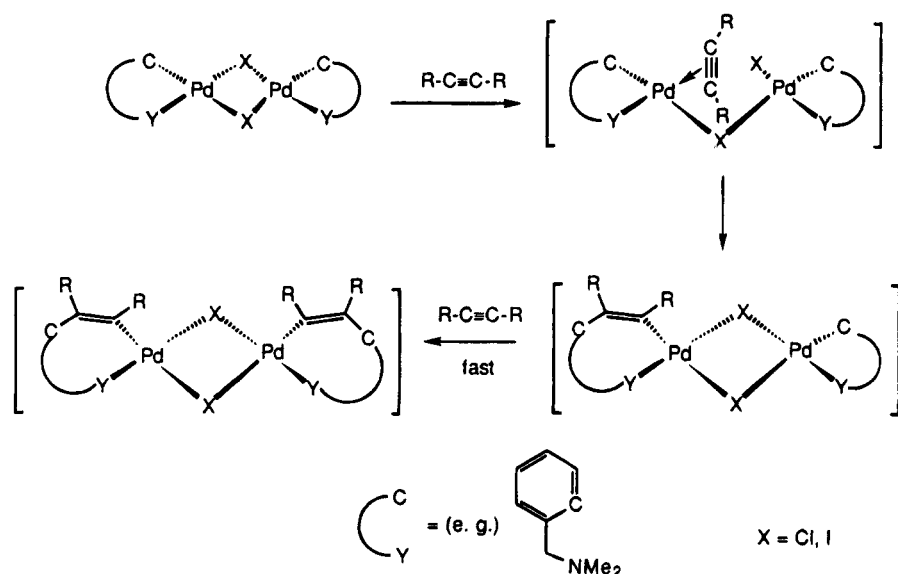
We have shown recently⁸ that some so-called “Fischer metallacarbynes” formally insert into the metal–carbon bond of cyclopalladated complexes. For example, the

* To whom correspondence should be addressed.

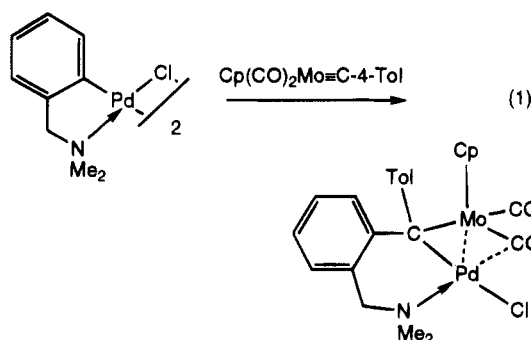
[®] Abstract published in *Advance ACS Abstracts*, May 15, 1995.
 (1) Maitlis, P. M. *Acc. Chem. Res.* **1976**, *9*, 93. Maitlis, P. M. *J. Organomet. Chem.* **1980**, *200*, 161. Huggins, J. M.; Bergman, R. G. *J. Amer. Chem. Soc.* **1981**, *103*, 3002. Samsel, E. G.; Norton, J. R. *J. Am. Chem. Soc.* **1984**, *106*, 5505.
 (2) Pfeffer, M. *Recl. Trav. Chim. Pays-Bas* **1990**, *109*, 567.
 (3) Ryabov, A. D.; Van Eldik, R.; Le Borgne, G.; Pfeffer, M. *Organometallics* **1993**, *12*, 1686.
 (4) Hosokawa, T.; Moritani, I.; Nishioka, S. *Tetrahedron Lett.* **1969**, 3833.
 (5) Allbright, T. A.; Hoffmann, R.; Thibeault, J. C.; Thorn, D. L. *J. Am. Chem. Soc.* **1979**, *101*, 3801.

(6) Davies, G. R.; Hewertson, W.; Mais, R. H. B.; Owston, P. G.; Patel, C. G. *J. Chem. Soc. A.* **1970**, 1873.
 (7) (a) Stone, F. G. A. *Angew. Chem., Int. Ed. Engl.* **1984**, *23*, 89.
 (b) Ashworth, T. V.; Chetcuti, M. J.; Howard, J. A. K.; Wisbey, S. J.; Stone, F. G. A. *J. Chem. Soc., Dalton Trans.* **1981**, 763.
 (8) Engel, P. F.; Pfeffer, M.; Fischer, J. *Organometallics* **1994**, *13*, 4751.

Scheme 1



chloride-bridged complex of *N,N*-dimethylbenzylamine (dmba) reacts smoothly with $\text{Cp}(\text{CO})_2\text{Mo}\equiv\text{C-4-Tol}$ to give a μ -alkylidene complex (eq 1). It corresponds to the



formal insertion of the metal-carbon triple bond into the palladium-carbon bond. The overall analogy between the insertions of alkynes and metallacarbynes is evidenced by a number of similar reactions. This puts the study of the insertion reaction of metallacarbynes in an interesting perspective, since it may shed some light upon the insertion reaction of alkynes as well.

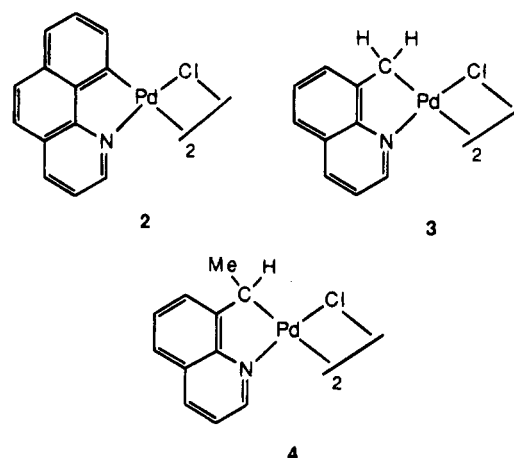
In the reactions between these metallacarbynes and some cyclopalladated ligands, transient, deeply colored complexes were observed prior to the actual C-C coupling between the carbyne carbon and the ligand.⁸ In this paper, we present the synthesis and characterization of some of these species, and their importance to the understanding of the mechanism of the insertion reaction will be discussed. Ab initio calculations have been carried out on a model of one of these complexes in order to obtain a detailed bonding description. Part of this study has been published in a preliminary form.⁹

Results and Discussion

Reactions of Cyclopalladated Quinoline Ligands.

While the cyclopalladated complexes undergo an insertion reaction with the metallacarbynes $\text{Cp}(\text{CO})_2$

Chart 2



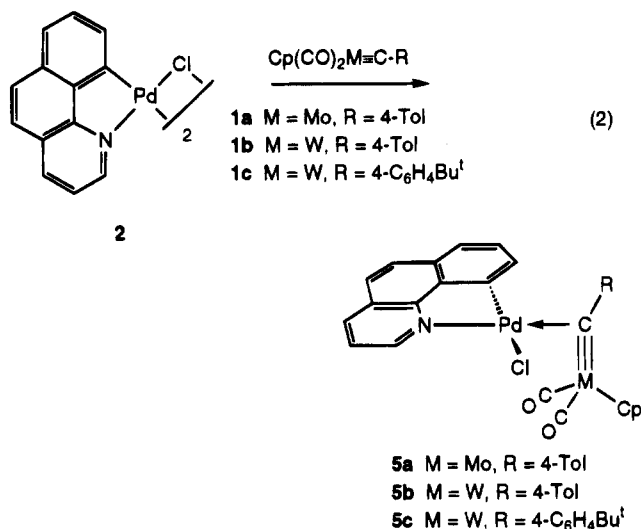
$\text{M}\equiv\text{C-4-Tol}$ (**1a**, $\text{M} = \text{Mo}$; **1b**, $\text{M} = \text{W}$) a rapid color change from orange to deep red brown is observed;⁸ at the same time, the insoluble dimeric palladium complex dissolves. This color then disappears during the formation of the final product, a μ -alkylidene compound similar to the dmba complex shown in eq 1.⁸ As a rule, these transient red brown complexes are difficult to characterize fully, due to this irreversible transformation.

However, it turns out that chloride-bridged complexes of benzo(*h*)quinoline (**2**), 8-methylquinoline (**3**), and 8-ethylquinoline (**4**) (Chart 2) are generally less reactive in the C-C coupling reaction than the other cyclopalladated complexes. It is also apparent that the tungsten metallacarbyne, **1b**, reacts more slowly with cyclopalladated ligands than its molybdenum analogue, **1a**. Therefore, the right combination of a metallacarbyne and a cyclopalladated ligand may result in slowing down the reaction, which allows for the isolation and full characterization of the transient complexes.

Benzo(*h*)quinoline Complexes. Adding 2 equiv of the metallacarbynes **1a** or **1b** to a suspension of the bhq complex **2** in dichloromethane results in a rapid dissolution of the poorly soluble palladium complex. Deep

(9) Engel, P. F.; Pfeffer, M.; Fischer, J.; Dedieu, A. *J. Chem. Soc., Chem. Commun.* **1991**, 1274.

red brown species are formed, which are stable enough to be isolated in about 77% yield. They have been characterized as the first Pd(II) μ -alkylidyne complexes [Cp(CO)₂M][μ -C(4-Tol)][Pd(bhq)Cl] (**5a**, M = Mo; **5b**, M = W; eq 2). Complex **5b** has been characterized by an



X-ray diffraction study, which has been discussed before.⁹ Clearly, the labile chloride bridge *trans* to the nitrogen donor atom in **2** has been substituted by the metal-carbon triple bond of the metallacarbyne. Complexes **5a,b** are therefore directly related to the proposed coordination complexes shown in Scheme 1. Complexes **5a,b** are stable for a few days in the solid state when kept at -20 °C, but they decompose in solution within 2 days at this latter temperature. When 2 equiv of **1a** are reacted with the iodide-bridged analogue of **2** in dichloromethane, a coordination complex similar to **5a** can be observed by infrared and proton NMR spectroscopy. It cannot be characterized further at room temperature, since the reaction proceeds rapidly to the μ -alkylidene complex [Cp(CO)(μ -CO)Mo][μ -C(4-Tol)(bhq)]Pd(I).⁸

To investigate the influence of the nature of the carbyne carbon in this coordination reaction, the metallacarbyne Cp(CO)₂W=C-4-C₆H₄^tBu, **1c**, has been prepared. The carbyne carbon in **1c** should be somehow more electron rich than in **1b**. As for **1b**, 2 equiv of **1c** reacts with the bhq complex **2** and rapidly forms a deep red brown complex, which can be isolated and characterized. Its spectral data suggest it to be the impure μ -alkylidyne complex [Cp(CO)₂W][μ -C(4-C₆H₄^tBu)][Pd(bhq)Cl], **5c** (eq 2). Clearly, the electronic differences between the *para* methyl group in **1b** and the *para tert*-butyl group in **1c** are not important in the formation of complexes **5**.

From the X-ray structure of **5b** it can be expected that bulky substituents on the *ortho* position of the carbyne phenyl ring will hinder the formation of the coordination complex. To verify this, the metallacarbyne Cp(CO)₂W=C-2,6-C₆H₃Me₂, **1d**, has been prepared, which possesses two methyl groups in the *ortho* position relative to the carbyne carbon. Addition of **1d** to a solution of the bhq complex **2** in dichloromethane does not result in a color change, the orange color of the metallacarbyne being maintained. The proton NMR spectrum of the reaction mixture in *d*-chloroform confirms that only the reactants **1d** and **2** are present in solution. If a

Chart 3

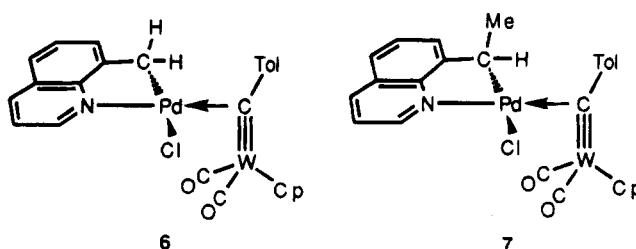
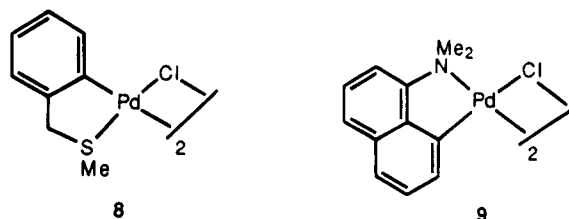


Chart 4



coordination complex similar to **5** is to be formed, it has a lifetime too short to allow observation by proton NMR.

It seems that the formation of coordination complexes like **5** is seriously hindered by the presence of bulky groups close to the carbyne carbon. This remarkable behavior of the metallacarbyne **1d** has been noted already in the C-C-coupling reaction between **1d** and a cyclopalladated complex of the ligand benzylmethylsulfide.⁸

Methyl- and Ethylquinoline Complexes. The 8-methylquinoline complex **3** is significantly more reactive toward the metallacarbynes **1** than is the bhq complex **2**, and only in the reaction between **3** and the less reactive tungsten metallacarbyne **1b** can a coordination complex be isolated. Complex **3** reacts instantaneously with 2 equiv of **1b** in dichloromethane to give the deep red brown μ -alkylidyne complex [Cp(CO)₂W][μ -C(4-Tol)][Pd(8mqin)Cl], **6** (Chart 3). Complex **3** is so reactive that during the isolation of **6** the μ -alkylidene complex is formed. Attempts to purify **6** *via* crystallization at -20 °C also afford some of the μ -alkylidene complex [Cp(CO)(μ -CO)W][μ -C(4-Tol)(8mqin)][PdCl].

Complexes containing the 8-ethylquinoline ligand **4** are the least reactive of the cyclopalladated complexes that undergo an insertion reaction with the metallacarbynes **1**.⁸ A 2 equiv amount of **1b** reacts instantaneously with **4** in dichloromethane to form a deep red brown solution. In the isolated solid, a μ -alkylidyne complex can be recognized as the major product, which is probably [Cp(CO)₂W][μ -C(4-Tol)][Pd(8sequin)Cl], **7**. Molecular models suggest that the bulky Cp(CO)₂W fragment will be in an *anti* position relative to the methyl group on the palladated carbon. Three minor products are also present, but the attempts to purify **7** *via* repeated precipitation from a dichloromethane-hexane mixture have only led to the formation of other undefined products.

Reactions of Other Cyclopalladated Ligands. Benzylmethylsulfide Complexes. The cyclopalladated complex with a benzylmethylsulfide ligand (bms, **8**, Chart 4) reacts almost instantaneously with the metallacarbynes **1a,b** to give the μ -alkylidene complexes [Cp(CO)(μ -CO)M][μ -C(4-Tol)(bms)][Pd(Cl)] (M = Mo, W). During this reaction, two rapid color changes from orange to deep red brown and back again to red orange

Chart 5

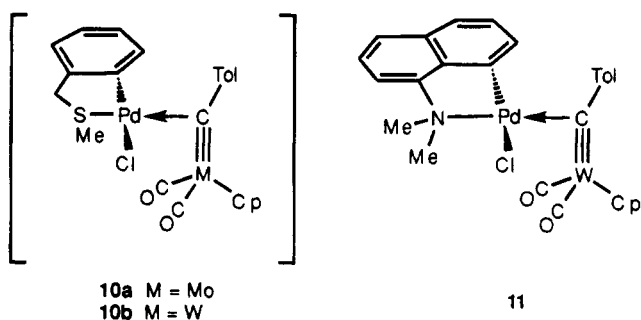


Table 1. Selected Spectral Data for Complexes 5-7 and 11

compd no.	IR ν_{CO} (cm^{-1}) ^a	¹ H NMR (ppm) ^b		
		Cp (s)	4-Me (s)	C ₆ H ₄ ^c
5a	1998, 1932	5.76	2.33	8.06
5b	1984, 1913	5.91	2.29	8.03, 7.10
5c	1984, 1910	5.90		8.05
6 ^d	1966, 1896	5.85	2.29	7.94-7.13
7	1961, 1891	5.78	2.29	8.06, 7.15
11	1982, 1913	5.85	2.31	7.99, 7.13

compd no.	¹³ C NMR (ppm) ^d			
	CO	μ -C	Cp	4-Me
5a	229.5, 227.7	312.8	95.9	22.0
5b	221.1, 219.1	303.3	95.1	22.3
5c	220.6, 218.3	302.9	94.5	
6	222.1, 221.4	302.1	94.0	21.9
7 ^e				
11	220.8, 218.6	306.5	94.3	22.0

^a In CH₂Cl₂. ^b In CDCl₃. ^c Doublets with ³J_{HH} = 8-9 Hz, not always visible. ^d In CD₂Cl₂. ^e Not available.

are observed. We assume that in this reaction the coordination complexes [Cp(CO)₂M][μ -C(4-Tol)]Pd-(bms)Cl (10a, M = Mo; 10b, M = W) are formed (Chart 5) although these complexes could obviously not be isolated because of the rapid insertion reaction that takes place with the cyclopalladated ligand.

N,N-Dimethylnaphthylamine Complexes. The ligand *N,N*-dimethylnaphthylamine (dmna) forms cyclopalladated complexes in which a rigid five-membered metallacycle is present, as in the quinoline complexes 2-4. Neither the chloride complex 9 nor its iodide-bridged analogue reacts cleanly with the metallacarbynes 1 to give μ -alkylidene complexes. However, in these reactions, the formation of deeply colored species was also observed upon mixing the palladium complex with 1, accompanied by the dissolution of the Pd dimer. For example, the reaction between 2 equiv of 1b and 9 in dichloromethane is instantaneous, and the deep red brown μ -alkylidene complex [Cp(CO)₂W][μ -C(4-Tol)]Pd-(dmna)Cl, 11, can be isolated in about 60% yield (Chart 5). As usual, the complex decomposes in solution at room temperature within a few hours, but it may be kept at -20 °C in the solid state for several weeks.

Characterization of the Complexes. Spectral Data. The metallacarbyne fragment in the complexes 5-7 and 11 displays very characteristic signals in the infrared and NMR spectra, which indicates that all these complexes belong to the same class of μ -alkylidene compounds. Table 1 lists selected spectral data of these complexes which concern the metallacarbyne fragment. The ¹³C NMR spectrum for 7 is not available because the complex could not be obtained sufficiently pure.

Cp(CO)₂M Fragment. In the infrared spectra, two stretching frequencies are found close to the values of the free metallacarbynes (1a, 1993, 1917 cm⁻¹; 1b, 1984, 1906 cm⁻¹; 1c, 1984, 1907 cm⁻¹), and they indicate the presence of two terminal carbonyl ligands. For compounds 5a-c and 11 they are found at somehow higher frequencies which indicate some electron release from the metallacarbyne unit when coordinated to Pd (see below, theoretical calculations).

The ν_{CO} values of complexes 6 and 7 are rather lower in energy, this being due to the least electron withdrawing groups, 8-alkylquinoline vs benzo(*h*)quinoline or naphthylamine. In the carbon NMR spectra, the carbonyl carbons are found as two signals around 220 ppm.

The cyclopentadienyl protons appear as a singlet between 5.91 and 5.76 ppm in the proton NMR spectra, slightly downfield of the values encountered for the free metallacarbynes (1a, 5.62 ppm; 1b, 5.67 ppm; 1c, 5.67 ppm). This small downfield shift of 0.14-0.24 ppm is typical for this coordination of the metallacarbyne to Pd(II), and it is a sign of the increased electron donation from the Cp ligand to its metal center. The chemical shift of the Cp ligand in the carbon NMR spectra, however, is not much affected, and it is found around 95 ppm.

The chirality of the μ -alkylidene complexes is reflected in compounds 6 and 11 by the diastereotopicity of the NMe₂ and CH₂ fragments of the cyclopalladated ligands. When a solution of 6 in *d*₆-benzene is quickly heated to 75 °C, the CH₂ protons of the metallated carbon remain diastereotopic, which confirms that the metallacarbyne is still coordinated to the palladium center.

The carbon bridging the two metals is found in the carbon NMR spectra around 300 ppm, which is a normal value for a free metallacarbyne (285-330 ppm).¹⁰ It indicates that the sp character of the carbyne carbon has been preserved and that the Cp(CO)₂MC-4-Tol fragment can still be considered as a metallacarbyne. It must be noted, however, that the sp² carbons of terminal metallacarbenes can also resonate above 300 ppm (240-370 ppm),¹¹ and that this chemical shift must thus be interpreted with care.

Solid State Structure of [Cp(CO)₂W][μ -C(4-Tol)]-[Pd(bhq)Cl], 5b. Complex 5b has been fully characterized by an X-ray diffraction study. Details of the crystal structure determination have been published.⁹ Some important features of the structure will be described here, however (see Table 2 and Figure 1).

It is at first sight apparent that 5b is built up from two fragments that are connected via a short contact between palladium and the carbyne carbon C₁₄. Neither the metallacarbyne nor the palladium fragment has undergone any major changes with respect to the starting complexes 1b and 2.

The geometry around the palladium atom is that of a square plane, the tungstacarbyne unit occupying the fourth coordination site. The W-C₁₄ bond is coordinated almost perpendicularly to the coordination plane of Pd(W-C₁₄-Pd = 89.27(2)°) as would be expected from the geometry of Pd(II) (alkyne) complexes. However, since the carbon C₁₄ is almost exactly in the fourth

(10) Fischer, E. O.; Schubert, U. *J. Organomet. Chem.* **1975**, *100*, 59. Heesook, P. K.; Angelici, R. *J. Adv. Organomet. Chem.* **1987**, *27*, 51.

(11) Herrmann, W. A. *Pure Appl. Chem.* **1982**, *1*, 65.

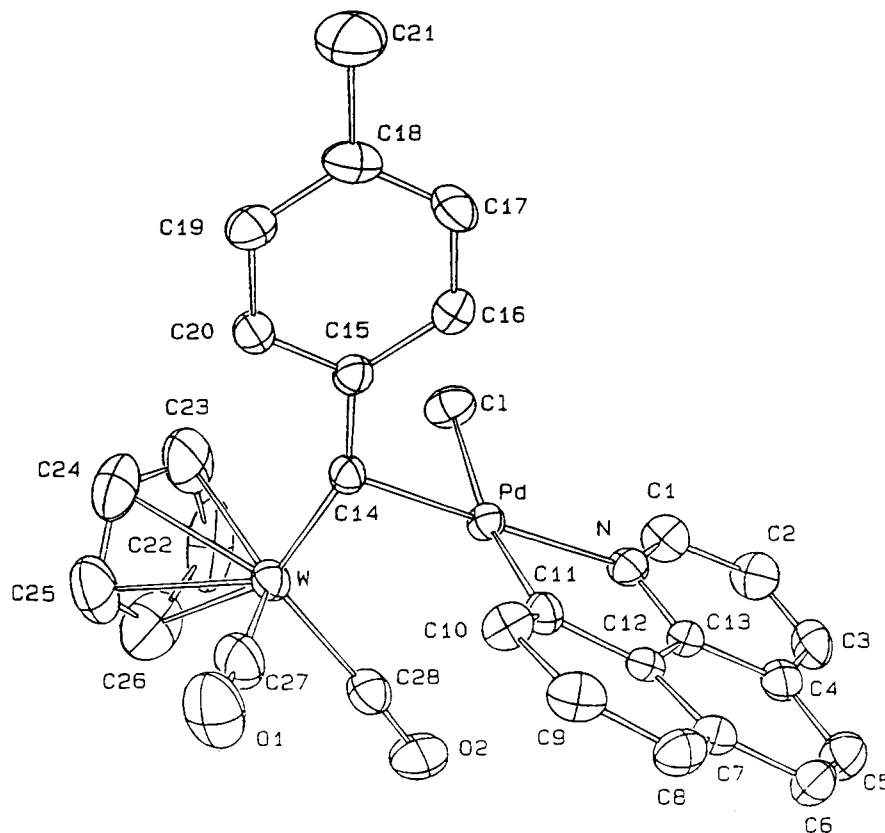


Figure 1. ORTEP diagram of $[\text{Cp}(\text{CO})_2\text{W}][\mu\text{-C}(4\text{-Tol})][\text{Pd}(\text{bhq})\text{Cl}]$, **5b**, with the corresponding atom-labeling scheme.

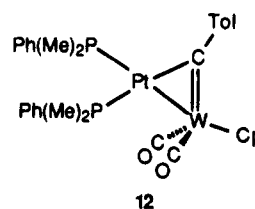
Table 2. Selected Bond Distances (Å), Angles (deg) and Dihedral Angles (deg) of **5b**^a

Bond Distances			
Pd-C ₁₄	2.084(7)	W-C ₁₄	1.897(7)
Pd-N	2.107(6)	W...Pd	2.8001(6)
Pd-Cl	2.400(2)	W-C ₂₇	1.95(1)
Pd-C ₁₁	1.998(7)	W-C ₂₈	1.995(9)
Pd...C ₂₇	3.839(7)	W-Cp' ^c	2.024(1)
Pd...C ₂₈	2.666(7)	C ₁₄ -C ₁₅	1.438(9)
Pd...H(C ₁₆) ^b	2.773(7)	C ₂₇ -O ₁	1.15(1)
Angles			
C ₁₁ -Pd-Cl	169.8(2)	C ₂₇ -W-C ₁₄	87.8(3)
C ₁₄ -Pd-N	172.7(2)	C ₂₈ -W-C ₁₄	109.1(3)
C ₁₁ -Pd-C ₁₄	92.4(3)	W-C ₁₄ -C ₁₅	151.9(4)
C ₁₁ -Pd-N	81.7(2)	W-C ₁₄ -Pd	89.27(2)
N-Pd-Cl	92.4(2)	Pd-C ₁₄ -C ₁₅	117.91(3)
C ₁₄ -Pd-Cl	92.8(2)	W-C ₂₇ -O ₁	176.84(5)
C ₂₇ -W-C ₂₈	91.0(4)	W-C ₂₈ -O ₂	173.53(5)
Cp'-W-C ₁₄ ^c	122.45(4)		
Dihedral Angles			
plane 1	plane 2		
Cp'-W-C ₁₄ ^c	W-C ₁₄ -Pd		122.9(3)
W-C ₁₄ -Pd	C ₁₅ -C ₁₆ -C ₁₇ -C ₁₈ -C ₁₉		7.3(1.5)
W-C ₁₄ -Pd	C ₁₄ -Pd(Cl)(C ₁₁)-N		83.9(2)

^a From ref 9. ^b H(C₁₆) is the hydrogen substituent of the tolyl carbon C₁₆. ^c Cp' is the centroid of the η⁵-C₅H₅ ligand.

coordination position of Pd *trans* to the nitrogen atom (C₁₄-Pd-N = 172.7(2)°), the interaction of the W≡C unit to the palladium atom may be considered as nonsymmetrical; a more symmetrical tungstacarbene to Pd interaction would correspond to a situation whereby W and C are roughly equidistant from the coordination plane of Pd. The W-Pd distance (2.8001(6) Å) is significantly smaller than the sum of the covalent radii of these atoms (2.986 Å),¹³ thus suggesting that there is some interaction between the two metals. The W-C₁₄

Chart 6



distance (1.897(7) Å) is intermediate between the W-C distances in the free metallacarbene $\text{Cp}(\text{CO})_2\text{W}=\text{C}-4\text{-Tol}$ (1.82(2) Å)¹⁴ and in the related dimetallacyclopropene complex $[\text{Cp}(\text{CO})_2\text{W}][\mu\text{-C}(4\text{-Tol})][\text{Pt}(\text{PMe}_2\text{Ph})_2]$, **12** (1.97 Å).^{15a,b} The fragment $\text{Cp}(\text{CO})_2\text{W}=\text{C}-4\text{-Tol}$ in **5b** seems thus to have preserved its metallacarbene character. The Pd-C₁₄ separation (2.084(7) Å) is within the range generally observed for Pd-C σ bonds (1.99–2.15 Å); however, it is somewhat longer than that normally found for such a bond *trans* to a pyridine nitrogen atom, *i.e.*, an atom that is known to have a rather small *trans* influence.¹²

The plane bisecting the Cp and both carbonyl ligands makes an unusual dihedral angle of 122.9(3)° with the

(12) For a selection of relevant references, see: Bruce, M. I. In *Comprehensive Organometallic Chemistry*; Pergamon Press: Oxford, U.K., 1982; Vol. 9, pp 1399–1405.

(13) Bender, R.; Braunstein, P.; Jud, J. M.; Dusausoy, Y. *Inorg. Chem.* **1983**, *22*, 3394.

(14) Huttner, G.; Frank, A.; Fischer, E. O. *Isr. J. Chem.* **1976**, *15*, 133.

(15) (a) Ashworth, T. V.; Howard, J. A. K.; Stone, F. G. A. *J. Chem. Soc., Dalton Trans.* **1980**, 1609. (b) We are not aware of any report of the molecular structure determination of a dimetallacyclopropene compound built up by the reaction of a metallacarbene compound with a palladium(0) complex. However, we have recently succeeded in obtaining the crystal structure of $\text{Pd}\{\mu\text{-CC}_6\text{H}_4\text{Me}_2\text{-2,6}(\text{CO})_2(\eta\text{-C}_5\text{H}_5)\}_2$, which contains two such units and which is isostructural to the closely related compounds of Pt and Ni^{7b} (Engel, P. F.; Pfeffer, M.; Fischer, J. Unpublished results, 1993).

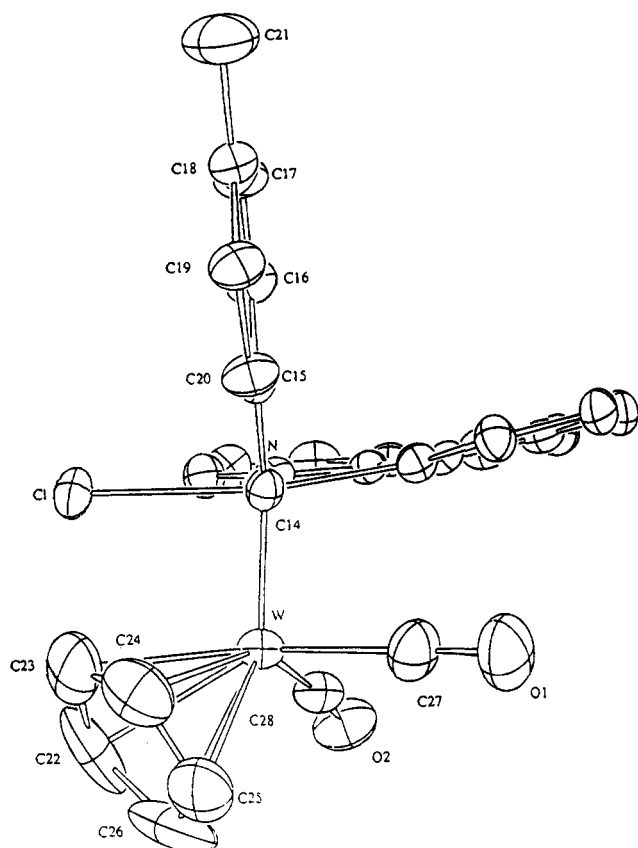
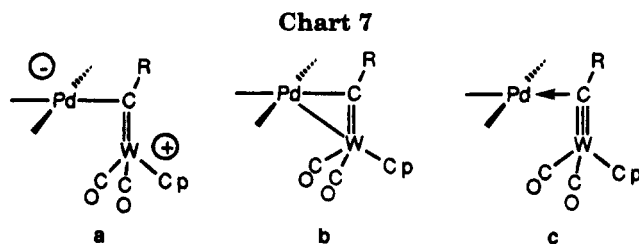


Figure 2. ORTEP diagram of **5b**, viewed along the C_{14} -Pd axis, from C_{14} to Pd (Pd is hidden behind C_{14}).

plane of the tolyl group, whereas this angle is 90° in the structure of the free metallacarbyne **1b**¹⁴ (Figure 2). It is not clear if this torsion around the W- C_{14} axis is due to steric interactions between the protons of the Cp ligand and other substituents in its vicinity. It is most likely, though, that an interaction between Cp and the chloride group forces the Cp(CO)₂M fragment in his position.

It is clear from Figure 2 that the plane of the tolyl ligand is almost parallel to the plane W- C_{14} -Pd ($7.31(1.48)^\circ$ between the planes), which is expected from the orbital interaction between the p orbitals on C_{14} and the d orbitals on Pd. The p orbital lying in the tolyl plane is not delocalized onto the aromatic ring, and it is therefore more available for the interaction with Pd than the p orbital perpendicular to the plane. To maximize the overlap between the p and d orbitals, the tolyl plane has to be oriented parallel to the C_{14} -Pd bond. In this orientation of the tolyl plane, the hydrogen substituent of the carbon C_{16} is positioned above the palladium plane (Pd-H(C_{16}) = $2.773(7)$ Å). This Pd-H distance compares well with those found in several other Pd complexes having an agostic interaction between the C-H bond and the Pd atom.¹⁶

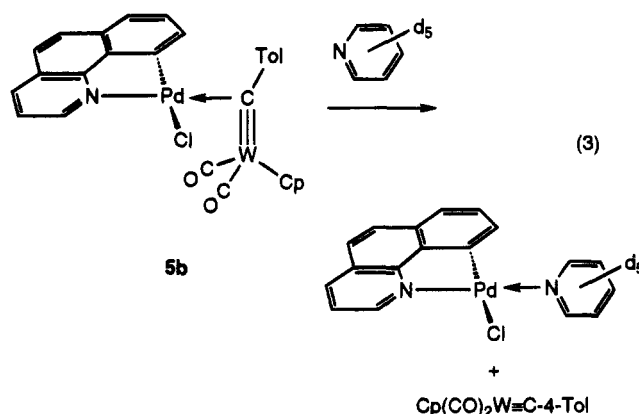
Lability of the Metallacarbyne Ligand. The complexes **5-7** and **11** have in common a weakly coordinated metallacarbyne ligand, which may be exchanged in solution for other donor ligands. The addition of the molybdenum metallacarbyne **1a** to a solution



of **5b** in *d*-chloroform results in a mixture of **1a,b** and **5a,b**, as is clear from the proton NMR spectrum. This confirms that **1a** can partially displace **1b** when the latter is coordinated to the palladium center. The fact that both **5a** and **5b** are present in solution indicates that the metallacarbynes **1a** and **1b** have the same ligating properties toward a Pd(II) center.

Another typical reaction of the μ -alkylidyne complexes is the displacement of the metallacarbyne by a two-electron donor ligand. Upon adding pyridine or triphenylphosphine to a solution of a μ -alkylidyne complex in dichloromethane, a rapid color change from deep red brown to orange is observed.

This reaction can be easily monitored by proton MMR spectroscopy. *d*₅-Pyridine reacts instantaneously with a solution of **5b** in CDCl₃, and the spectrum of the mixture obtained confirms that *d*₅-pyridine has displaced the metallacarbyne ligand entirely (eq 3). The



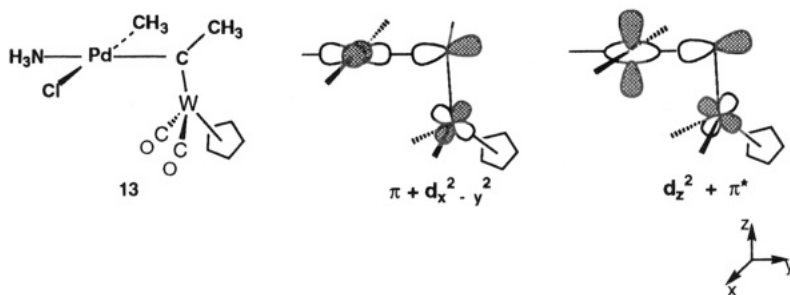
monomeric pyridine complex formed in this reaction is a well-known compound, which is easily obtained by reacting the dimeric complex **2** directly with pyridine. A similar monomeric complex has been obtained from the reaction between **2** and triethylphosphine. This pyridine complex does not react further with the metallacarbyne **1b** to form **5b**, which confirms that the substitution of the metallacarbyne by pyridine in **5b** is irreversible. It seems that the metallacarbynes **1** behave toward a Pd(II) center as simple, but unusual, two-electron donor ligands.

Discussion

The Nature of the Bonding: Structural and Theoretical Considerations. Three different limiting forms can be used to describe the structure of the coordination complex **5b**: a zwitterionic metallacarbene (a), a dimetallacyclopropene (b), and a complex in which the metallacarbyne binds mostly to the metal center via the carbyne carbon (c) (Chart 7, R = 4-Tol).

(16) (a) Dehand, J.; Fischer, J.; Pfeffer, M.; Mitschler, A.; Zinsius, M. *Inorg. Chem.* **1976**, *15*, 2675. (b) Brammer, L.; Chamoch, J. M.; Goggin, P. L.; Goodfellow, R. J.; Orpen, A. G.; Koetzle, T. F. *J. Chem. Soc., Dalton Trans.* **1991**, 1789 and references cited therein.

Chart 8

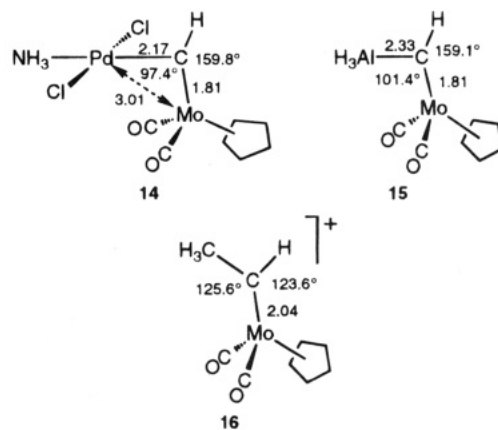


The W-C₁₄ distance in **5b** is significantly shorter than the W-C bond in a normal metallocarbene such as (CO)₅W=C(OMe)Ph (2.04 Å).¹⁷ Together with the fact that the Pd-C₁₄-W angle is 89.27(2)° this seems to exclude the metallocarbene structure **a** as an adequate description of **5b**. The nonsymmetric bonding mode of the W≡C unit with respect to the Pd coordination plane (*vide supra*) associated with the rather short W-C₁₄ distance and a relatively long Pd-C₁₄ interaction led us also to conclude that the dimetallacyclopropane limiting form is an inadequate structure for **5b**.

Related examples of bimetallic compounds in which carborane tungstacarbene derivatives are coordinated to Au(I),^{18a} Pt(II)^{18b} and Ru(II)^{18c} complexes and which display short W-C distances and long C-M interactions have been described earlier. These compounds were analyzed as containing a semibridging carbene carbon atom supporting a strong metal-metal interaction. But they all exhibit a disposition of the W≡C unit that is more symmetrical than the one found in **5b**. For instance, the P-Au-C angle in [AuW(μ-CC₆H₄Me-4)-(CO)₂(PPh₃)(η⁵-C₂B₉H₉Me₂)] amounts to 163°^{18a} whereas the corresponding N-Pd-C angle in **5b** amounts to 173°. It is in fact the whole palladium-metallacarbene unit which is rotated by about 10° in **5b**, thus leading to the observed asymmetry.

The third limiting form is **c** for **5b**, *i.e.*, a metallocarbene η¹-coordinated to a metal center via its carbene carbon. In this description, the metal-metal interaction would be the weakest, and the Pd-C bond would be the result of an electron transfer from the triple bond to palladium via the carbon C₁₄. Preliminary EHT calculations carried out on the [Cp(CO)₂WCCH₃][PdCl(NH₃)-(CH₃)] system, **13**,⁹ indeed indicated that a major component of the binding is a two-electron stabilizing interaction between the doubly occupied π type orbital of the metallocarbene and the empty d_{x²-y²} orbital of the T-shaped palladium fragment, see Chart 8. Compound **5b** can thus be considered as a Lewis acid (the palladium fragment) coordinating a Lewis base (the metallocarbene). A second interaction, although less important, was also found to be operative. This interaction is of σ back-donation type, between the d_{z²} orbital of palladium (doubly occupied) and the empty π* orbital of the metallocarbene, see Chart 8. Note at this stage

Chart 9



of the discussion that, given the geometry of the system and in particular because of the N-Pd-C linear arrangement, the positive overlap between the lower lobe of the Pd d_{z²} orbital and one upper lobe of the Mo d_{yz} orbital might give rise to some metal-metal bonding. In order to put these preliminary findings on more firm grounds, the geometry and the electronic structure of three related systems, *viz.* [Cp(CO)₂MoCH][PdCl₂(NH₃)], **14**, [Cp(CO)₂MoCH][AlH₃], **15**, and [Cp(CO)₂MoCH-CH₃]⁺, **16**, see Chart 9, were determined through SCF *ab initio* calculations. These three systems were chosen to scan various types of bonding. Compound **14** was taken as a model of the metallocarbene palladium complex **5b**. The substitution of the PdCl₂(NH₃) palladium fragment by the prototypical Lewis acid AlH₃ was aimed at assessing, through the comparison between **15** and **14**, the extent of Lewis acid/Lewis base type of binding. The substitution by CH₃⁺ to yield **16** should provide instead a reference for a true metallocarbene. The nature of the bonding in **14** was further investigated by analyzing the distribution of the fragment electron deformation density obtained by subtracting the electron density of the two fragments, PdCl₂(NH₃) and Cp(CO)₂MoCH, from the total electron density of the composite system, [Cp(CO)₂MoCH][PdCl₂(NH₃)]. A similar analysis was also performed for **15**.

Chart 9 displays the three computed geometries as obtained from the geometry optimization procedure (with the most important bond distances and bond angles). We first note the good agreement between the optimized structure of **14** and the related structure of **5b**. But the most salient feature of the chart is the strong similarity between **14** and **15**. In both structures the Mo-C bond is short, 1.81 Å, consistent with a triple-bond character.¹⁹ The angular disposition around the carbene atom is also similar in **14** and **15** with a Mo-

(17) Mills, O. S.; Redhouse, A. D. *J. Chem. Soc. A* **1968**, 642.

(18) (a) Green, M.; Howard, A. P. J.; Nunn, C. M.; Stone, F. G. A. *J. Chem. Soc., Dalton Trans.* **1987**, 61. Goldberg, J. E.; Mullica, D. F.; Sappenfield, E. L.; Stone, F. G. A. *J. Chem. Soc., Dalton Trans.* **1992**, 2495. (b) Devore, D. D.; Howard, J. A. K.; Jeffrey, J. C.; Pilotti, M. V.; Stone, F. G. A. *J. Chem. Soc., Dalton Trans.* **1989**, 303. Carr, N.; Gimeno, C.; Stone, F. G. A.; *J. Chem. Soc., Dalton Trans.* **1990**, 2617. (c) Green, M.; Howard, J. A. K.; Jelfs, A. N. de M.; Johnson, O.; Stone, F. G. A. *J. Chem. Soc., Dalton Trans.* **1987**, 73.

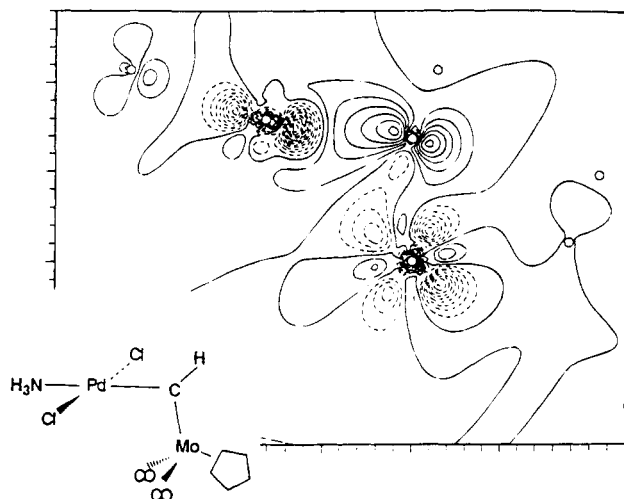


Figure 3. Map of the fragment electron deformation density of the $[\text{Cp}(\text{CO})_2\text{MoCH}][\text{PdCl}_2(\text{NH}_3)]$ system in the Mo-C-H-Pd plane. The fragments are $[\text{Cp}(\text{CO})_2\text{MoCH}]$ and $[\text{PdCl}_2(\text{NH}_3)]$. Solid lines for zero- and positive-density contours, dashed lines for negative-density contours; contour interval, $0.050 \text{ e } \text{\AA}^{-3}$.

C-H angle of about 160° and a Mo-C-Pd or Mo-C-Al angle of about 100° . We note, however, that the Pd-C bond in **14** is comparatively much shorter than the Al-C bond in **15** ($2.17 \text{ vs } 2.33 \text{ \AA}$). This points to a stronger interaction in the palladium case: the SCF heterolytic bond dissociation energies are 30.9 and 17.2 kcal/mol , respectively.²⁰ But the aforementioned geometrical features are clearly indicative of the retention of the sp character of the carbyne atom. This is in agreement with the chemical shift observed in the experimental system (*vide supra*). In contrast, the carbon atom in **16** is clearly of sp^2 character with the Mo-C-C and Mo-C-H angles amounting to 125.6° and 123.6° , respectively. The Mo-C bond length is also much greater, 2.04 \AA , *i.e.*, typical of a Mo-C double bond.

The two maps of the fragment deformation density are shown in the Figures 3 and 4 for **14** and **15**, respectively. They both display a buildup of electron density on the carbyne atom and between this carbyne atom and either Pd or Al. The buildup of electron density on the carbyne atom might seem contradictory with the Lewis base character of the metallacarbyne. But a closer look at the maps (and also at the population analysis) shows that, upon metallacarbyne coordination, a complete reorganization of the electron density takes place. This reorganization is shown schematically in Chart 10. It involves an electron flow from the Mo atom (and from the ligands attached to it) toward the palladium and its ligands (see, for instance, the increase of electron density on NH_3 *via* the carbyne atom. This accounts for the shifts observed experimentally in the carbonyl IR frequencies and the ^1NMR signal of the Cp protons (*vide supra*).

For **14** electron depletion is also found in the immediate vicinity of Pd. This is traced to the σ back-donation ($d_{z^2} \rightarrow \pi^*$) sketched in Chart 8. In **15** no such back-

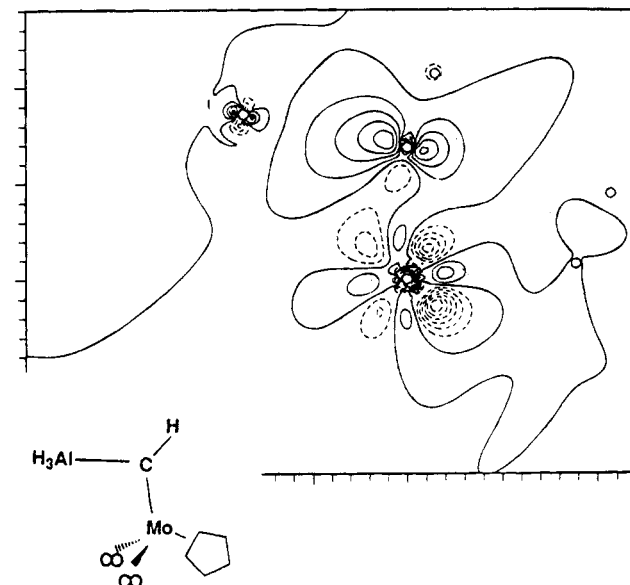
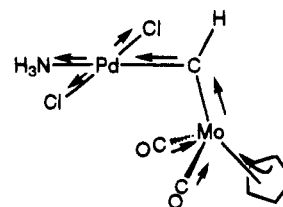


Figure 4. Map of the fragment electron deformation density of the $[\text{Cp}(\text{CO})_2\text{MoCH}][\text{AlH}_3]$ system in the Mo-C-H-Al plane. The fragments are $[\text{Cp}(\text{CO})_2\text{MoCH}]$ and $[\text{AlH}_3]$. Solid lines for zero- and positive-density contours, dashed lines for negative-density contours; contour interval, $0.050 \text{ e } \text{\AA}^{-3}$.

Chart 10



donation interaction can occur due to the lack of occupied d_σ orbitals in the AlH_3 fragment. The consequence is a smaller electron buildup between Mo and Al and the weaker Mo-Al bond. That the flow of electron density originating from the metallacarbyne will spread on the whole palladium fragment is a feature of interest. It explains in particular that the quinoline ligand with its framework of π^* accepting orbitals is well suited to stabilize the η^1 -coordination mode of the metallacarbyne ligand. Similarly the greater electronegativity of chlorine compared to iodine accounts for the greater stability of chlorine derivatives which is found experimentally (*vide supra*).

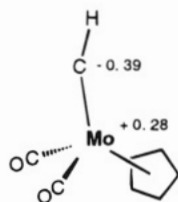
The differential density map of the $[\text{Cp}(\text{CO})_2\text{MoCH}][\text{PdCl}_2(\text{NH}_3)]$ system is also indicative of a slight electron buildup between the Mo and the Pd atom, see Figure 3. This buildup is traced, as mentioned above, to the positive overlap between the lower lobe of the Pd d_{z^2} orbital and one upper lobe of the Mo d_{yz} orbital in the $d_{z^2} + \pi^*$ combination, Chart 8. The palladium metallacarbyne complex may therefore be seen as having a weak $\text{Pd} \cdots \text{Mo}$ interaction. The optimized Pd-C-Mo angle is indeed somewhat smaller than the Al-C-Mo angle, see Chart 9. But this component of the bonding remains weak, and it cannot account for the overall stability of the system.

Finally, one should not overlook some additional contribution of the electrostatic interactions to the bonding. The metallacarbyne system is polarized, see Chart 11, the carbon atom being highly negative and

(19) The Mo=Co bond length was optimized to 1.80 \AA in the free $\text{Cp}(\text{CO})_2\text{Mo}=\text{CH}$ metallacarbyne system.

(20) These values computed with the full split valence basis set refer to unrelaxed fragments. The basis set superposition error is not taken into account.

Chart 11



the molybdenum atom being positively charged. We have seen that the η^1 -binding of the metallacarbonyne will reinforce this polarization. Since the palladium atom is positively charged, the electrostatics favor the η^1 rather than the η^2 mode of binding.

The above overall picture of the bonding for this class of systems is consistent with previous theoretical and experimental findings on other metallacarbonyne or alkyne complexes. Iron metallacarbonyne complex $[\text{Cp}(\text{CO})_2\text{M}(\text{C}=\text{R})][\text{Fe}(\text{CO})_3]$ and $[\text{Cp}(\text{CO})_2\text{M}(\text{C}=\text{R})][\text{Fe}(\text{CO})_4]$ ($\text{M} = \text{Mo}, \text{W}$) have been structurally characterized and theoretically analyzed by Stone and co-workers.²¹ They show a η^2 mode of binding, accounted for by the two stabilizing interactions sketched in Chart 12.

The main difference with our systems lies in the $d_{z^2} + \pi^*$ back-donative interaction of Chart 12. In the iron complexes the π^* metallacarbonyne orbital will interact preferentially with the d_{yz} orbital: this orbital is the HOMO of the $\text{Fe}(\text{CO})_3$ or $\text{Fe}(\text{CO})_4$ fragment, thus quite high in energy. It is also polarized toward the metallacarbonyne. In **13** and **14** the HOMO of the palladium fragment is not the d_{yz} but the d_{z^2} orbital (Chart 8). The d_{yz} orbital is not hybridized and lies at much lower energy, therefore precluding any strong interaction with the π^* metallacarbonyne orbital. Moreover, since the iron atom is in the 0 oxidation state, it is probably less positively charged (despite the back-donation to the carbonyls) than the palladium atom in the +2 oxidation state. It will therefore exert a much weaker electrostatic attraction on the carbon atom of the metallacarbonyne. The electrostatic contribution to the bonding is also best exemplified by our recent study of the $\text{PdCl}(\text{CH}_3)(\text{NH}_3)(\text{C}_2\text{H}_2)$ system:²² In C_2H_2 the two carbon atoms are equivalent and bear the same charge. A SCF geometry optimization starting from a η^1 geometry did not end with an intermediate having this coordination mode but led directly to the η^2 geometry.

The electronic structure of the $[\text{Cp}(\text{CO})_2\text{WCH}][\text{Au}(\text{PH}_3)]^+$ system taken as a model of various $[\text{Cp}(\text{CO})_2\text{W}(\text{C}\equiv\text{R})][\text{Au}(\text{PPh}_3)]^+$ and related complexes has been recently investigated through extended Hückel calculations.²³ No significant orbital interactions between the $[\text{Cp}(\text{CO})_2\text{WCH}]$ and the $[\text{Au}(\text{PH}_3)]^+$ fragment were found (due to the large energy gap between the d orbitals of

Au and the valence orbital of the metallacarbonyne), with the exception of a weak interaction between the empty sp hybrid of $[\text{Au}(\text{PH}_3)]^+$ and the doubly occupied π orbital of the metallacarbonyne. $\text{PdCl}_2(\text{NH}_3)$ is isolobal to $[\text{Au}(\text{PH}_3)]^+$ and the $\pi + d_{x^2-y^2}$ interaction (Chart 8) is the analog of the $\pi + sp$ interaction in the gold system. There is one difference, however: the d_{z^2} orbital is much higher in energy in $[\text{PdCl}_2(\text{NH}_3)]$ than in $[\text{Au}(\text{PH}_3)]^+$ and it can therefore interact with the π^* orbital of the metallacarbonyne, provided that a good overlap exists between the two orbitals. We have seen that this requirement is fulfilled if the carbon atom lies in the palladium coordination plane.

Stability of the μ -Alkyldiynes Complexes. The metallacarbonyne ligand in the μ -alkyldiynes complexes can be easily displaced by other donor ligands like pyridine. This seems to indicate that the $\text{Pd}-\mu\text{-C}$ bond is relatively fragile. However, when the 8mquin complex **6** is heated in d_6 -benzene to 75 °C, the chirality of the molecule is maintained, as is clear from the diastereotopic CH_2 protons in the proton NMR spectrum. This can mean either that the rotation of the metallacarbonyne ligand along the $\text{Pd}-\text{C}$ bond is slow on the NMR time scale or that the decoordination/recoordination of the metallacarbonyne to Pd is too slow a process to be observed.

Geometry of the μ -Alkyldiynes Complexes. In the structure of **5b**, the plane of the tolyl ring is virtually coplanar with the plane $\text{W}-\text{C}_{14}-\text{Pd}$. Orbital considerations show that this orientation of the tolyl ring is the most favorable for the overlap between the p orbitals on C_{14} and the d orbitals on palladium. An additional reason for the orientation may be the interaction between palladium and one of the ortho protons of the tolyl ring. This can be possibly described as a three-center four-electron interaction. The position of the $\text{Cp}(\text{CO})_2\text{W}$ unit must be influenced by the steric repulsions between the cyclopentadienyl ring on the one hand and the chloride and tolyl substituents on the other hand.

Implications for the C-C Coupling Reaction between Metallacarbonynes and Cyclopalladated Complexes. A number of cyclopalladated complexes react with the metallacarbonynes **1a** or **1b** to give μ -alkyldiene complexes, resulting from a carbon-carbon-coupling reaction between the carbonyne carbon and the cyclopalladated ligand.⁸ In the reactions of the quinoline complexes $[\text{Pd}(\text{bhq})\text{I}]_2$ and $[\text{Pd}(\text{8mquin})\text{X}]_2$ ($\text{X} = \text{Cl}, \text{I}$) transient species are formed, which are the analogues of the characterized coordination complexes **5** and **6**. In the coupling reaction between the bms complex **8** and the metallacarbonynes **1**, similar coordination complexes may be formed.

It is therefore tempting to assume that μ -alkyldiynes

Chart 12

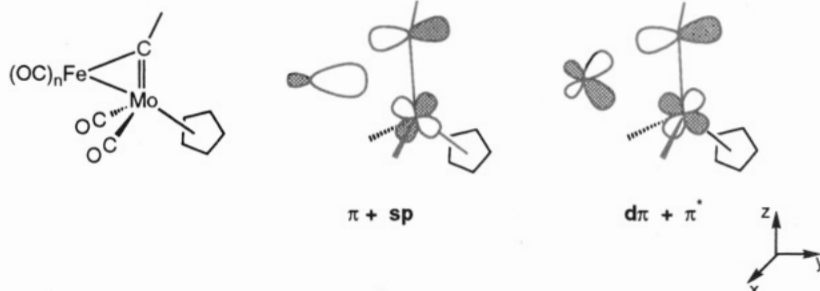
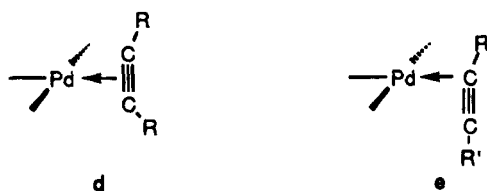


Chart 13



complexes like **5** are actual intermediates in these insertion reactions, and that the formation of these complexes is a necessary step in all coupling reactions of cyclopalladated ligands with the metallacarbene **1**.

However, no coordination complexes seem to be formed during the reaction of the cyclopalladated complexes of *N,N*-dimethylbenzylamine (dmba) or 2-benzylpyridine (bzpy) and **1a** or **1b**. When these reactions are monitored by proton NMR spectroscopy in CDCl_3 , only the starting materials and the final μ -alkylidene products are observed. Attempts to follow the reaction between $[\text{Pd}(\text{bhq})\text{I}]_2$ and **1a** by UV/vis spectroscopy have so far failed to prove whether a coordination complex can be transformed into a μ -alkylidene or not.

Still, the best working hypothesis remains that complexes like **5** are real intermediates, which undergo subsequent rotation around the Pd- μ -C bond, and then an insertion to form the μ -alkylidene products. It may be that the coordination complexes are formed in all of the coupling reactions but that their lifetimes are often too short to observe them by proton NMR spectroscopy. The fact that coordination complexes are formed with quinoline ligands and dmna may indicate that a rigid five-membered metallacycle stabilizes these structures. Other cyclopalladated ligands may not be able to stabilize the complexes sufficiently to be observed.

Another reason could be that the formation of the coordination complex is slow compared to the formation of the carbon-carbon bond. The proposed intermediate would then be consumed too rapidly to be observed. On the basis of the available data it is not possible to make a clear choice. Kinetic experiments will be required to gain further insight into the mechanism of these reactions.

Implications for Alkyne Complexes. As noted in the introduction, no alkyne complexes of Pd(II) have been structurally characterized. The metallacarbynes $\text{Cp}(\text{CO})_2\text{M}\equiv\text{C}-\text{R}$ ($\text{M} = \text{Mo}, \text{W}$) are isolobal with alkynes, and they can be considered as models for highly asymmetrical alkynes. The structure of complex **5b** thus provides a strong indication that alkyne complexes like **d** or **e** may actually exist, although they would be too labile to be isolated (Chart 13).

When the alkyne is symmetrical, the η^2 geometry **d** will probably be adopted, but the greater the difference between the alkyne substituents R and R', the more geometry **e** will be favored. As Silvestre and Hoffmann suggested,²⁴ the η^1 geometry **e** may also play a role in the course of the insertion reaction, even when it is less stable than the η^2 geometry **d**. Our recent theoretical study of the acetylene insertion into the palladium methyl bond of $\text{PdCl}(\text{CH}_3)(\text{NH}_3)(\text{C}_2\text{H}_2)$ indicated that at

least in the C_2H_2 case the η^1 geometry corresponds to the transition state.²²

Conclusions

In the reactions between the metallacarbynes $\text{Cp}(\text{CO})_2\text{M}\equiv\text{C}-4\text{-Tol}$ ($\text{M} = \text{Mo}, \text{W}$) and the cyclopalladated ligands benzo(h)quinoline, 8-methylquinoline, 8-ethylquinoline, and *N,N*-dimethylnaphthylamine, coordination complexes are formed, which are characterized as μ -alkylidyne complexes with a higher valent group 10 metal.

The X-ray data show that the metallacarbene is bound to Pd essentially through the carbon atom. A theoretical analysis based on ab initio SCF calculations reveals that this η^1 coordination mode results from the maximization of two bonding interactions: the first is due to the strong Lewis acid character of the $\text{Pd}(\text{II})\text{L}_3$ fragment, and the second is a weaker interaction involving donation from the Pd d_{z^2} orbital into the π^* orbital of the metallacarbene. This last interaction is peculiar to T-shaped $d^8 \text{ML}_3$ fragments. In addition to these orbital interactions, an electrostatic interaction between the positively charged palladium atom and the negatively charged carbene atom should also favor the η^1 coordination mode.

It can be advanced that these simple coordination complexes are actually intermediates in the C-C coupling reactions between metallacarbynes and cyclopalladated complexes. However, additional studies have to be carried out to test the validity of this hypothesis.

The structural features of the coordination complex **5b** imply that alkynes may also be able to form complexes in which the C-C triple bond is coordination perpendicularly to the palladium plane. This provides a support for the proposed intermediates in the reaction between alkynes and metal-carbon bonds.

Experimental Section

General Considerations. All reactions were performed in a nitrogen atmosphere, using standard Schlenck techniques. Solvents were dried on sodium (ether, hexane) or calcium dihydride (dichloromethane) prior to use. The NMR spectra were recorded on a Bruker WP 200 SY spectrometer or a Bruker AC 300 spectrometer. Infrared spectra were recorded on a Bruker IFS 66 spectrometer (in CH_2Cl_2 , ν in cm^{-1}). Microanalyses were carried out by the Service de Microanalyse du CNRS in Strasbourg. FAB (+) mass spectra were provided by the Service de spectrométrie de masse (URA 31 du CNRS) in Strasbourg (in 3-nitrobenzyl alcohol). The coordination complexes were often too labile to be characterized by elemental analysis. FAB mass spectrometry was preferable, and the complexes are prepared and characterized *in situ*. The metallacarbynes $\text{Cp}(\text{CO})_2\text{M}\equiv\text{C}-\text{R}$ (**1**, $\text{M} = \text{Mo}, \text{W}$; $\text{R} = 4\text{-Tol}, 4\text{-C}_6\text{H}_4\text{tBu}$) were prepared via a general method reported by Stone et al.¹⁹ The cyclopalladated complexes were prepared according to literature procedures: $[\text{Pd}(\text{bhq})\text{Cl}]_2$, **2**,²⁵ $[\text{Pd}(\text{8mquin})\text{Cl}]_2$, **3**,²⁶ $[\text{Pd}(\text{Sequin})\text{Cl}]_2$, **4**,²⁷ $[\text{Pd}(\text{bms})\text{Cl}]_2$, **8**,²⁸ and $[\text{Pd}(\text{dmna})\text{Cl}]_2$, **9**.²⁹

(25) Hartwell, G. E.; Laurence, R. V.; Smas, M. J. *Chem. Commun.* **1970**, 912.

(26) Pfeffer, M. *Inorganic Synthesis*; Kaesz, H. D., Ed.; Wiley-Interscience: New York, 1989; Vol. 26, pp 213.

(27) Sokolov, V. I.; Sorokina, T. A.; Troitskaya, L. L.; Solovieva, L. I.; Reutov, O. A. *J. Organomet. Chem.* **1972**, *36*, 389.

(28) Dupont, J.; Beydoun, N.; Pfeffer, M. *J. Chem. Soc., Dalton Trans.* **1989**, 1715.

(21) Dossett, S. J.; Hill, A. F.; Jeffrey, J. C.; Marken, F.; Sherwood, P.; Stone, F. G. A. *J. Chem. Soc., Dalton Trans.* **1988**, 2453.

(22) De Vaal, P.; Dedieu, A. *J. Organomet. Chem.* **1994**, *478*, 121.

(23) Jemmis, E. D.; Prasad, B. V. *Organometallics* **1992**, *11*, 2528.

(24) Silvestre, J.; Hoffmann, R. *Helv. Chim. Acta* **1985**, *68*, 1461.

Syntheses. [**Cp**(CO)₂Mo][μ -C(4-Tol)][Pd(bhq)Cl], **5a**. To a solution of Cp(CO)₂Mo \equiv C-4-Tol (102 mg 0.32 mmol) in dichloromethane (10 mL) was added [Pd(bhq)Cl]₂ (121 mg, 0.19 mmol), whereupon most of the dimer dissolved over 1 min, and a deep red brown color was formed. After being stirred 10 min, the mixture was filtered over a Celite pad, and the solvent was removed from the filtrate *in vacuo*. The oily residue was washed with diethyl ether (2 \times 10 mL) and hexane (2 \times 10 mL). The solid was filtered off, and drying *in vacuo* gave **5a** (156 mg, 77%) as a black powder. Anal. Calcd for C₂₈H₂₀ClMoNO₂Pd (MW 640.29): C, 52.52; H, 3.15; N, 2.19. Found: C, 51.8; H, 2.95; N, 2.3. FAB *m/z*: M⁺ invisible, 1245 (5, recombination), 656 (6), 606 (28, M-Cl), 585 (26), 548 (42), 440 (14), 322 ([Pd(bhq)Cl + H]⁺, 16), 281 (37), 180 (100). ¹H NMR (CDCl₃) δ 9.72 (d, 1 H arom, ³J_{HH} = 5.1), 8.39 (d, 1 H arom, ³J_{HH} = 8.2), 8.06 (d, 2 H, 4-Tol, ³J_{HH} = 8.1), 7.79–7.65 (m, 3 H arom), 7.55 (d, 1 H arom, ³J_{HH} = 7.7), 7.30–7.07 (m, 4 H arom), 5.76 (s, 5 H, Cp), 2.33 (s, 3 H, 4-Me); ¹³C NMR (CD₂Cl₂) δ 312.8 (μ -C), 229.5, 227.7 (CO), 154.1, 152.5, 148.6, 142.4, 138.4, 136.7, 135.0, 132.2, 129.2, 128.7, 127.2, 124.1, 122.6 (C arom), 95.9 (Cp), 22.0 (4-Me); IR ν_{CO} 1998, 1932.

[**Cp**(CO)₂W][μ -C(4-Tol)][Pd(bhq)Cl], **5b**. Following the same procedure as for **5a**, a black powder (77%) was obtained. Anal. Calcd for C₂₈H₂₀ClNO₂PdW (MW 728.20) (+0.5CH₂-Cl₂): C, 44.41; H, 2.75; N, 1.82. Found: C, 44.05; H, 2.71; N, 1.91. FAB *m/z*: M⁺ not visible, 1421 (4, recombination), 1013 (5, recombination), 692 (40, [M-Cl]⁺), 673 (21), 636 (46), 528 (10), 408 (100, [Cp(CO)₂WC-4-Tol]⁺), 380 (34), 351 (56), 284 (26, [Pd(bhq)]⁺), 180 (51). ¹H NMR (CDCl₃) δ 9.72 (d, 1 H arom, ³J_{HH} = 4.8), 8.39 (d, 1 H arom, ³J_{HH} = 7.9), 8.03 (d, 2 H, 4-Tol, ³J_{HH} = 8.0), 7.78–7.65 (m, 3 H arom), 7.55 (d, 1 H arom, ³J_{HH} = 6.8), 7.27–7.23 (m, 2 H arom), 7.10 (d, 2 H, 4-Tol, ³J_{HH} = 8.0), 5.91 (s, 5 H, Cp), 2.29 (s, 3 H, 4-Me); ¹³C NMR (CDCl₃) δ 303.3 (μ -C), 221.1, 219.1 (CO), 153.4, 152.6, 149.1, 142.9, 142.1, 139.1, 137.0, 135.5, 132.2, 129.9, 129.6, 128.0, 124.8, 123.2 (C arom), 95.2 (Cp), 22.3 (4-Me); IR ν_{CO} 1984, 1913.

[**Cp**(CO)₂W][μ -C(4-C₆H₄Bu)][Pd(bhq)Cl], **5c**. Following the same procedure as for **5a**, a brown powder was obtained. Complex **5c** is contaminated with some free metallacarbyne. Attempts to remove the latter with hexane remained unsuccessful, so the yield could not be determined. However, the product is pure enough to attribute the spectral data. ¹H NMR (CDCl₃) δ 9.71 (d, 1 H arom, ³J_{HH} = 5.1), 8.38 (d, 1 H arom, ³J_{HH} = 8.0), 8.05 (d, 2 H arom, ³J_{HH} = 8.3), 7.75 (d, 1 H arom, ³J_{HH} = 8.7), 7.70–7.64 (m, 2 H arom), 7.55 (d, 1 H arom, ³J_{HH} = 6.4), 7.36–7.24 (m, 4 H arom), 5.90 (s, 5 H, Cp), 1.26 (s, 9 H, t-Bu); ¹³C NMR (CD₂Cl₂) δ 302.9 (μ -C), 220.6, 218.3 (CO), 154.3, 151.7, 148.5, 138.4, 136.2, 134.9, 131.5, 129.3, 128.9, 127.2, 125.4, 124.1, 122.5 (C arom), 94.5 (Cp), 35.4 (CMe₃), 31.1 (CMe₃); IR ν_{CO} 1984, 1910.

[**Cp**(CO)₂W][μ -C(4-Tol)][Pd(8mquin)Cl], **6**. To a suspension of [Pd(8mquin)Cl]₂ (119 mg, 0.21 mmol) in dichloromethane (15 mL) was added Cp(CO)₂W \equiv C-4-Tol (154 mg, 0.38 mmol), whereupon most of the dimer dissolved instantaneously and a deep red brown color was formed. After being stirred 5 min, the mixture was filtered over a Celite pad and the solvent was concentrated to 3 mL. Addition of hexane (30 mL) gave a suspension, from which the supernatant was decanted. Washing the residue hexane (2 \times 15 mL) and drying *in vacuo* gave impure **6** as a light brown powder. The ¹H NMR spectrum confirmed that the solid was a mixture of **6** with about 6% of a μ -alkylidene complex, formed via the C–C-coupling reaction. It was thus deemed useless to try to purify **6** any further. ¹H NMR (CDCl₃) δ 9.72 (d, 1 H arom, ³J_{HH} = 4.9), 8.36 (d, 1 H arom, ³J_{HH} = 8.3), 7.98 (d, 2 H, 4-Tol, ³J_{HH} = 8.0), 7.70–7.46 (m, 4 H arom), 7.11 (d, 2 H, 4-Tol, ³J_{HH} = 8.0), 5.86 (s, 5 H, Cp), 3.15 (m, 2 H, CH₂), 2.28 (s, 3 H, 4-Me); ¹³C NMR (CD₂Cl₂) δ 303.4 (μ -C), 222.1, 220.6 (CO), 150.2, 147.2, 141.0, 139.0, 130.2, 129.8, 129.1, 128.3, 124.8, 122.2 (C arom), 94.0 (Cp), 36.2 (CH₂), 22.0 (4-Me); IR ν_{CO} 1966, 1896.

[**Cp**(CO)₂W][μ -C(4-Tol)][Pd(8equin)Cl], **7**. To a suspension of [Pd(8equin)Cl]₂ (88 mg, 0.15 mmol) in dichloromethane (10 mL) was added Cp(CO)₂W \equiv C-4-Tol (126 mg, 0.31 mmol), whereupon the dimer dissolved instantaneously, and a deep red brown color was formed. After being stirred 5 min, the mixture was filtered over a Celite pad and the solvent was concentrated near dryness. Addition of hexane (15 mL) gave a suspension, from which the supernatant was decanted. Washing the residue with hexane (4 \times 15 mL) and drying *in vacuo* gave impure **7** as a light brown powder. The proton NMR spectrum showed that the solid was a mixture of **7** with probably three other minor products. Attempts to purify **7** further *via* repeated precipitation from dichloromethane with hexane or *via* crystallization from dichloromethane–hexane only resulted in the decomposition of **7**. Complex **7** is therefore only partially characterized, by analogy with the spectral data of the bhq and 8mquin complexes. ¹H NMR (CDCl₃) δ 9.72 (d, H arom, ³J_{HH} = 4.0), 8.36 (d, H arom, ³J_{HH} = 8.2), 8.06, 7.15 (AB pattern, H arom, ³J_{HH} = 7.9), 7.8–7.3 (m, H arom), 5.77 (s, 5 H, Cp), 3.71 (q, 1 H, MeCH, ³J_{HH} = 7.2), 2.29 (s, 3 H, 4-Me), 0.75 (d, 3 H, HCMe, ³J_{HH} = 7.3); IR ν_{CO} 1961, 1891. The ¹³C NMR spectrum is difficult to interpret, due to the presence of several minor compounds.

[**Cp**(CO)₂W][μ -C(4-Tol)][Pd(dmna)Cl], **11**. To a solution of Cp(CO)₂WfC-4-Tol (126 mg, 0.31 mmol) in dichloromethane (10 mL) was added [Pd(dmna)Cl]₂ (118 mg, 0.19 mmol), whereupon the dimer dissolved instantaneously, and a deep red brown color was formed. After being stirred 5 min, the mixture was filtered over a Celite pad and the solvent was removed from the filtrate *in vacuo*. After drying the residue *in vacuo*, it was washed with hexane (2 \times 15 mL). Drying *in vacuo* gave **11** (128 mg, 58%) as a brown powder. Anal. Calcd for C₂₇H₂₄ClNO₂PdW (MW 720.22): C, 45.03; H, 3.36; N, 1.95. Found: C, 44.6; H, 3.1; N, 2.15. ¹H NMR (CDCl₃) δ 7.99 (d, 2 H arom, ³J_{HH} = 8.0), 7.67 (d, 1 H arom, ³J_{HH} = 7.4), 7.54–7.42 (m, 3 H arom), 7.13 (d, 2 H arom, ³J_{HH} = 8.0), 7.09–7.01 (d, 1 H arom, ³J_{HH} = 8.0), 6.89 (d, 1 H arom, ³J_{HH} = 7.3), 5.85 (s, 5 H, Cp), 3.62, 3.42 (s, 6 H, NMe₂), 2.31 (s, 3 H, 4-Me); ¹³C NMR (CD₂Cl₂) δ 306.5 (μ -C), 220.8, 218.5 (CO), 155.9, 151.8, 148.0, 141.7, 135.7, 135.5, 132.0, 129.0, 127.9, 126.4, 126.1, 124.1, 123.6, 117.2, 116.2 (C arom), 94.2 (Cp), 53.0, 51.7 (NMe₂), 22.0 (4-Me); IR ν_{CO} 1982, 1913.

Computational Details

The SCF calculations were carried out with the ASTERIX system of programs.³⁰ For the geometry optimization we used a split valence type basis set for the Mo \equiv C(H)Pd bonding unit and a minimal basis set for the ligands, *i.e.*, (15,10,8) contracted to (6,4,4) for the molybdenum and palladium atoms;³¹ (9,5) contracted to (3,2) for the carbyne atom,³³ (4) contracted to (2) for the hydrogen atom of the carbyne atom,³⁴ and STO-3G³⁵ for the cyclopentadienyl, the carbonyl, the amine, and the chlorine ligands. Single-point calculations were then carried out on these optimized geometries with the split valence basis set on all atoms (this corresponds to a (11,7) contracted to (4,3) basis set for the chlorine atom³³). We checked by a geometry optimization carried out on [Cp(CO)₂-MoCH] with both basis set sets that the smallest basis set gave reliable results for the geometry optimization. The electron density deformation maps were obtained with the split valence basis set.

(30) (a) Ernenwein, R.; Rohmer, M.-M.; Bénard, M. *Comp. Phys. Commun.* **1990**, *58*, 305. (b) Rohmer, M.-M.; Demuyck, J.; Bénard, M.; Wiest, R. *Ibid.* **1990**, *60*, 127. (c) Wiest, R.; Demuyck, J.; Bénard, M.; Rohmer, M.-M.; Ernenwein, R. *Ibid.* **1991**, *62*, 107.

(31) The original (15,9,8) basis set³² was modified by adding p function of exponent 0.15 and 0.08386 to describe the 5p shell of the molybdenum and palladium atoms, respectively.

(32) Veillard, A.; Dedieu, A. *Theoret. Chim. Acta* **1984**, *65*, 215.

(33) Huzinaga, S. Technical Report. University of Alberta: Edmonton, Canada, 1971.

(34) Huzinaga, S. *J. Chem. Phys.* **1965**, *42*, 1293.

(35) Hehre, W. J.; Stewart, R. F.; Pople, J. A. *J. Chem. Phys.* **1969**, *51*, 2657.

The geometry optimization was carried out from analytical energy first derivatives by using an implemented BFGS algorithm.³⁶ The convergence thresholds for the geometry optimization were set to 0.002 for the gradient norm and for each individual component of the energy gradient. This led in every optimized geometry to a value equal to or less than 0.001 for the gradient norm. Some internal coordinates were kept constant to insure an overall C_s symmetry and local C_{3v} symmetry for the NH_3 , CH_3 , and AlH_3 groups.

Acknowledgment. The calculations were carried out on the IBM 3090 computer of the Centre de Calcul de Strasbourg Cronenbourg and on the CRAY2 computer of the CCVR in Palaiseau. The calculations and the stay of P.E. in both laboratories were made possible through a grant of the European Community (Science Program, Contract No. SC1-0319-C(GDF)).

(36) de Vaal, P.; Bénard, M.; Pouchan, C. Unpublished results, 1992.

OM950182J

Synthesis, Structure, and Reactions of $(\eta^5\text{-C}_5\text{H}_5)_3\text{Zr}$

Wayne W. Lukens, Jr., and Richard A. Andersen*

Chemistry Department and Chemical Sciences Division of Lawrence Berkeley Laboratory,
University of California, Berkeley, California 94720

Received January 24, 1995[⊗]

Cp_3Zr was synthesized by the reduction of Cp_4Zr (where $\text{Cp} = \text{C}_5\text{H}_5$). Cp_3Zr is determined to be monomeric in the solid state by X-ray diffraction with three Cp rings bonded to zirconium in an η^5 fashion. The 19-electron metallocene has a single unpaired electron and an axial EPR spectrum in frozen solution. It does not appear to form base adducts but does react by atom abstraction. The observed spectra and reactions are explained using the MO model for Cp_3M developed by Bursten and Strittmatter and previously by Lauher and Hoffmann.

Introduction

Only a few tris(cyclopentadienyl) compounds of the d-transition metals have been described, and with the exception of the "pseudolanthanides" Cp_3Y^1 and Cp_3La ,² none of them have all three cyclopentadienyl ligands bound in an η^5 manner. The crystal structure of Cp_3Sc shows that it is a dimer with the two $(\eta^5\text{-Cp})_2\text{Sc}$ fragments bridged by a pair of C_5H_5 groups that are η^1 -bound to each Cp_2Sc fragment.³ The crystal structure of the d^1 Cp_3Ti shows that two rings are bound in an η^5 manner and that the third is η^2 -bound.⁴ While the crystal structure of the d^2 Cp_3V is not known, the ^1H NMR spectrum of this paramagnetic compound shows two resonances in a 2:1 ratio.⁵ The spectrum was interpreted as being due to two η^5 -Cp ligands and an η^1 -Cp ligand which is fluxional, making all of the protons of the η^1 ligand equivalent. The solid-state and solution structures of Cp_3Tc and Cp_3Re also show that two rings are η^5 and one is η^1 .^{6–8} Curiously, the two η^5 rings are not rotating on the NMR time scale, since all five protons are inequivalent, and the η^1 ring is not fluxional, since it has three inequivalent protons which are distinct at all temperatures studied.

In contrast to the d-metal complexes, the tris(cyclopentadienyl) compounds of the f metals (except for lutetium) all have three η^5 -Cp ligands,⁹ and unlike the d-block complexes, the f-block complexes form base adducts.¹⁰ As noted by Bursten, two factors are responsible for the difference in reactivity between the f- and

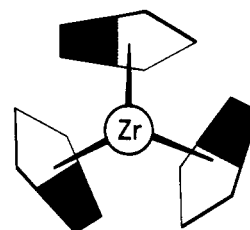


Figure 1. The nonbonding a' orbital of Cp_3Zr , in C_{3h} symmetry, which is the a_2' orbital in D_{3h} symmetry, the point group used in the text. The shadings represent opposite signs of the π -bonding p orbitals of the Cp ligands.

d-metal complexes.^{11,12} First, the f metals have larger radii, reducing steric congestion enough to allow all three Cp ligands to coordinate in an η^5 manner. Second, the presence of the low-lying f orbitals prevents these complexes from becoming electronically saturated by allowing the metal electrons to fill their f orbitals. The MO description of tris(η^5 -cyclopentadienyl) compounds has been described by Bursten and previously by Lauher and Hoffmann.^{13–15} For d transition metals, the three ligands contribute 13 electrons since one ligand-based orbital of a_2' symmetry, shown in Figure 1, has no overlap with s, p, or d orbitals. This orbital is entirely ligand-based and therefore relatively high in energy. Only one Cp to metal nonbonding metal-based orbital is available, and it is largely d_{z^2} . Any d-metal complex with more than two electrons is forced to place electrons in high-lying antibonding orbitals, therefore forcing the third cyclopentadienyl ligand to be something other than η^5 . As previously noted, the f-block metallocenes fill the f orbitals rather than the d orbitals, leaving the d_{z^2} orbital empty and available to interact with a Lewis base, which allows these metallocenes to form base adducts.

An interesting anomaly among the f-block metallocenes is $[(\text{Me}_3\text{Si})_2\text{C}_5\text{H}_3\text{Th}]$.¹⁶ This complex has a d^1

* To whom correspondence should be addressed at the Chemistry Department.

[⊗] Abstract published in *Advance ACS Abstracts*, June 1, 1995.

(1) Adam, M.; Behrens, U.; Fischer, R. D. *Acta Crystallogr.* **1991**, *C47*, 968–971.

(2) Eggars, S. H.; Kopf, J.; Fischer, R. D. *Organometallics* **1986**, *5*, 383–385.

(3) Atwood, J. L.; Smith, K. D. *J. Am. Chem. Soc.* **1973**, *95*, 1488.

(4) Lucas, C. R.; Green, M. L. H.; Forder, R. A.; Prout, K. W. *J. Chem. Soc., Chem. Commun.* **1973**, 97.

(5) Siegert, F. W.; de Meijer, H. J. *J. Organomet. Chem.* **1968**, *15*, 131–137.

(6) Apostolidis, C.; Kanellakopoulos, B.; Maier, R.; Rebizant, J.; Ziegler, M. L. *J. Organomet. Chem.* **1990**, *396*, 315–326.

(7) Apostolidis, C.; Kanellakopoulos, B.; Rebizant, J.; Ziegler, M. L. *J. Organomet. Chem.* **1991**, *411*, 171.

(8) Apostolidis, C.; Kanellakopoulos, B.; Maier, R.; Rebizant, J.; Ziegler, M. L. *J. Organomet. Chem.* **1991**, *409*, 243–254.

(9) Eggars, S. H.; Kopf, J.; Fischer, R. D. *Acta Crystallogr.* **1987**, *C43*, 2288–2290.

(10) Fischer, R. D. In *Organometallics of the f-Elements*; Marks, T. J., Fischer, R. D., Eds.; D. Reidel: Dordrecht, Holland, 1979.

(11) Bursten, B. E.; Rhodes, L. F.; Strittmatter, R. J. *J. Am. Chem. Soc.* **1989**, *111*, 2758–2766.

(12) Bursten, B. E.; Strittmatter, R. J. *Angew. Chem., Int. Ed. Engl.* **1991**, *30*, 1069–1085.

(13) Bursten, B. E.; Rhodes, L. F.; Strittmatter, R. J. *J. Am. Chem. Soc.* **1989**, *111*, 2756–2758.

(14) Strittmatter, R. J.; Bursten, B. E. *J. Am. Chem. Soc.* **1991**, *113*, 552–559.

(15) Lauher, J. W.; Hoffmann, R. *J. Am. Chem. Soc.* **1976**, *98*, 1729–1742.

(16) Blake, P. C.; Lappert, M. F.; Atwood, J. L.; Zhang, N. *J. Chem. Soc., Chem. Commun.* **1986**, 1148–1149.

rather than an f^1 electronic ground state and unlike the other f-block metallocenes does not appear to form base adducts.^{17,18} The analogous lanthanide metallocene tris(cyclopentadienyl)cerium has an f^1 electronic ground state and forms base adducts.¹⁹ We were interested in comparing the reactions of this $6d^1$ actinide metallocene to that of a transition-metal metallocene with a d^1 electronic ground state to assess the influence of the electronic ground state upon the reactivity. In order to do this, we had to prepare a compound with three η^5 -Cp ligands. Since zirconium(IV) complexes which have three η^5 -Cp ligands were known,^{14,20,21} and since Cp_3Ti was also known,²² it seemed likely that Cp_3Zr could be synthesized.

Results and Discussion

Cp_3Zr was synthesized by reducing Cp_4Zr ²⁰ with potassium graphite²³ in toluene, from which it was crystallized as shiny, brown, hexagonal plates. In this reaction, only the zirconium reactant and product are soluble, allowing for easy separation. Cp_3Zr was also made by reducing Cp_4Zr with sodium naphthalenide in tetrahydrofuran. However, while it was possible to prepare Cp_3Zr pure by the former method, the latter always gave Cp_3Zr contaminated with 5–10% Cp_3ZrH .²⁴ The purity was estimated by treating a C_6D_6 solution with CCl_4 and comparing the integration of the cyclopentadienyl resonance before addition of CCl_4 , i.e. due to Cp_3ZrH , to the integration of the cyclopentadienyl resonance after addition due to Cp_3ZrCl from the reaction of Cp_3Zr with CCl_4 . The purity could not be determined directly because Cp_3Zr is NMR silent. Attempts to reduce Cp_4Zr with t -BuLi analogously to the reduction of Cp_3UCl ^{25–28} or Cp_2ZrX_2 ²⁹ gave only Cp_3ZrH .

The EPR spectrum of Cp_3Zr at room temperature in 2-methyltetrahydrofuran was observed at $g_{iso} = 1.977$ with six satellites having $A_{iso} = 115$ MHz (41 G) presumably due to coupling to ^{91}Zr . As a frozen glass, the spectral parameters were $g_{||} = 1.999$ and $g_{\perp} = 1.970$; the spectrum is shown in Figure 2. These g values are consistent with the MO model, since an electron in a d_{z^2} orbital cannot change the value of $g_{||}$ from that of a free electron by spin-orbit coupling but spin-orbit

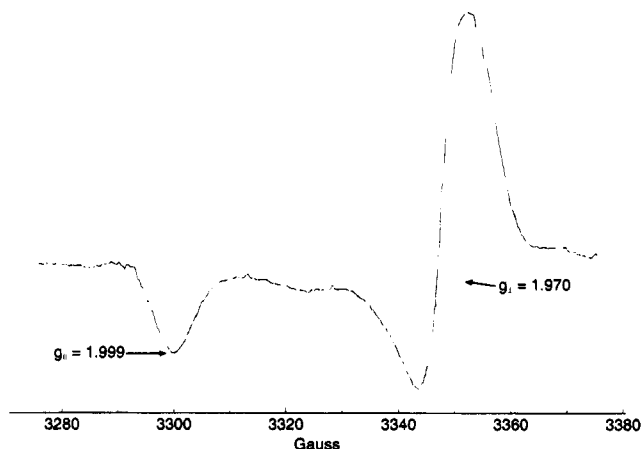


Figure 2. EPR spectrum of Cp_3Zr in 2-methyltetrahydrofuran at 100 K.

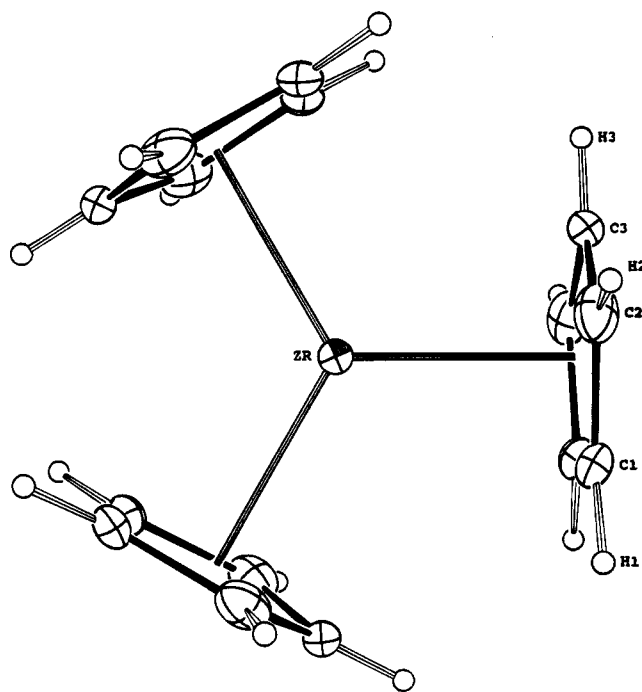


Figure 3. ORTEP drawing of Cp_3Zr with 50% thermal ellipsoids, except hydrogen atoms, which are shown as spheres of arbitrary size.

coupling to the d_{xz} and d_{yz} orbitals can lower g_{\perp} .³⁰ The magnetic moment of Cp_3Zr was determined by variable-temperature magnetic susceptibility and was found to be $1.64 \mu_B$ from 5 to 300 K with $\theta = -3.5$ K.

The solid-state structure of Cp_3Zr is shown in Figure 3. The data collection parameters are given in Table 1, the atomic positions in Table 2, and the distances and angles in Table 3. The molecule possesses crystallographic $\bar{6}(C_{3h})$ symmetry and is monomeric. The shortest intermolecular Zr–H and Zr–C distances are 4.29 and 5.00 Å, respectively. Surprisingly, the average Zr–C distance is 2.58 Å, the same as the average Zr–C distance for the three η^5 -Cp ligands in Cp_4Zr .²⁰ As noted above, the Cp rings of Cp_3Zr are postulated to have a high-lying nonbonding orbital of a_2' symmetry which is not stabilized by the metal center.¹⁴ The Cp rings of Cp_3Zr are distorted in a manner consistent with this

(17) Kot, W.; Shalimoff, G.; Edelstein, N.; Edelman, M.; Lappert, M. F. *J. Am. Chem. Soc.* **1988**, *110*, 986–987.

(18) Kot, W. Ph.D. Thesis, University of California, Berkeley, CA, 1991.

(19) Stults, S. D.; Andersen, R. A.; Zalkin, A. *Organometallics* **1990**, *9*, 115–122.

(20) Rogers, R. D.; Bynum, R. V.; Atwood, J. L. *J. Am. Chem. Soc.* **1978**, *100*, 5238–5239.

(21) Kopf, J.; Vollmer, H.-J.; Kaminsky, W. *Cryst. Struct. Commun.* **1980**, *9*, 985–990.

(22) Fischer, E. O.; Löchner, A. *Z. Naturforsch.* **1960**, *15B*, 266–267.

(23) Schwindt, M. A.; Lejon, T.; Hegedus, L. B. *Organometallics* **1990**, *9*, 2814–2819.

(24) Lokshin, B. V.; Klemenkova, Z. S.; Ezernitskaya, M. G.; Strunkina, L. I.; Brainina, E. M. *J. Organomet. Chem.* **1982**, *235*, 69–75.

(25) Brennan, J. G.; Andersen, R. A.; Zalkin, A. *Inorg. Chem.* **1986**, *25*, 1756–1760.

(26) Brennan, J. G. Ph.D. Thesis, University of California, Berkeley, CA, 1985.

(27) Marks, T. J.; Seyam, A. M.; Kolb, J. R. *J. Am. Chem. Soc.* **1973**, *95*, 5529–5539.

(28) Weydert, M. Ph.D. Thesis, University of California, Berkeley, CA, 1993.

(29) Wielstra, Y.; Gambarotta, S.; Meetsma, A. *Organometallics* **1989**, *9*, 2948–2952.

(30) McGarvey, B. R. In *Transition Metal Chemistry: A Series of Advances*; Carlin, R. L., Ed.; Marcel Dekker: New York, 1966; Vol. 3, pp 90–201.

Table 1. Crystal Data for Cp_3Zr

space group	$P6_3/m$
a (Å)	8.003(1)
b (Å)	8.003(1)
c (Å)	10.276(2)
α (deg)	90
β (deg)	90
γ (deg)	120
cell vol (cm ³)	570.0
Z	2
d (calcd) (g/cm ³)	1.668
μ (calcd) (cm ⁻¹)	9.148
radiation	Mo K α
monochromator	highly oriented graphite
scan range (deg), type	$3 \leq 2\theta \leq 45$, $\theta-2\theta$
scan speed (deg/min)	2.8
scan width (deg)	$\Delta\theta = 0.90 + 0.35 \tan \theta$
no. of rflns collected	851 ($\pm h, \pm k, \pm l$), 532 used
no. of unique rflns	266
no. of rflns, $F_o^2 > 3\sigma(F_o^2)$	245
R , %	2.97
R_w , %	3.25
R_{all} , %	3.20
GOF	1.179
largest Δ/σ in final least-squares cycle	0

Table 2. Atomic Coordinates and Isotropic Thermal Parameters for Cp_3Zr

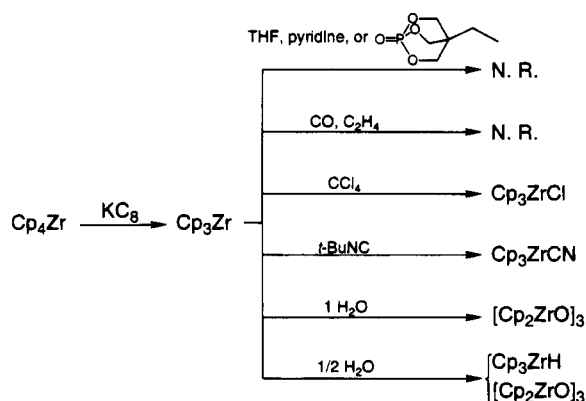
atom	x	y	z	B (Å ²)
Zr	-0.333	0.333	0.25	1.33(1)
C1	0.0168(3)	0.5827(3)	0.3170(3)	1.44(5)
C2	-0.1032(4)	0.6551(3)	0.3607(3)	1.66(6)
C3	-0.1683(5)	0.7062(5)	0.25	1.47(8)
H1	0.088(4)	0.538(3)	0.366(3)	2.1(6)
H2	-0.125(4)	0.670(3)	0.452(2)	2.4(6)
H3	-0.245(4)	0.749(5)	0.25	1.0(8)

Table 3. Selected Distances (Å) and Angles (deg) in Cp_3Zr

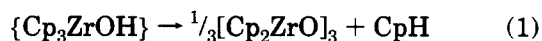
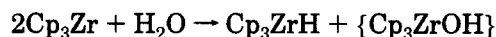
Zr-C1	2.592(3)	C3-H3	0.84(5)
Zr-C2	2.564(3)	C1-C2	1.420(5)
Zr-C3	2.590(4)	C2-C3	1.395(5)
C1-H1	0.95(4)	C1-C1'	1.376(7)
C2-H2	0.97(3)		
C1'-C1-C2	108.4(2)	C2-C3-C2	109.2(4)
C1-C2-C3	106.8(3)		

lack of stabilization. This orbital (Figure 1) possesses a node between C1 and C2, the presence of which is reflected in the longer C1-C2 distance of 1.420(5) Å relative to the shorter C2-C3 and C1-C1' distances of 1.395(5) and 1.376(7) Å, respectively. In the analogous $\text{Cp}^*\text{Sm}^{3+}$ (Cp^* is Me_5C_5), which crystallizes in the same space group also at a site of $\bar{6}$ symmetry, the Cp^* ligands are not distorted in this manner, consistent with stabilization of this orbital by the $f_{y(3x^2-y^2)}$ orbital as predicted by Bursten and Strittmatter.^{13,14} While other tris(cyclopentadienyl) compounds have been characterized by crystallography, these compounds do not have pentasubstituted Cp rings,³² substitution of the Cp removes the degeneracy in the e_2 orbital of the ligand, causing a distortion of the ligand.^{33,34}

Some reactions of Cp_3Zr are shown in Scheme 1. We were unable to isolate or obtain evidence for the exist-

Scheme 1. Reactions of Cp_3Zr 

ence of base adducts of Cp_3Zr with THF, pyridine, or $\text{OP}(\text{OCH}_2)_3\text{CET}$. In addition, Cp_3Zr did not appear to react with carbon monoxide or ethylene. In all cases, only Cp_3Zr was recovered as determined by EPR spectroscopy, and NMR spectroscopy showed no evidence of diamagnetic zirconium species. While Cp_3Zr did not form base adducts, it did react with CCl_4 and $t\text{-BuNC}$ to form the oxidation products Cp_3ZrCl and Cp_3ZrCN , respectively. When treated with 1 equiv of water in benzene, Cp_3Zr gave $[\text{Cp}_2\text{ZrO}]_3$ ³⁵ and CpH. When treated with 0.5 equiv of water, Cp_3Zr gave a mixture of $[\text{Cp}_2\text{ZrO}]_3$ ³⁵ and Cp_3ZrH ²⁴ presumably by the series of steps shown in eq 1.



Steric effects cannot account for the inability of Cp_3Zr to form base adducts, since compounds of Zr(IV) exist which have three $\eta^5\text{-Cp}$ ligands plus an additional ligand coordinated to the Zr center. In addition, Zr(III) should be larger than Zr(IV) for a given coordination number. Rather, the lack of reactivity is most likely due to its electronic structure. When a Lewis base interacts with Cp_3Zr , the d_{z^2} orbital is destabilized, becoming the σ^* orbital with respect to the incoming ligand. Since the unpaired electron occupies this orbital, the interaction with the incoming ligand becomes less favorable. However, the unpaired electron does not prevent single-electron reactions. When the ligand is a one-electron donor, as is the case for OH, CN, and Cl, the unpaired electron in the a_1 (d_{z^2} parentage) orbital in C_{3v} symmetry can share this bonding orbital with the electron from the one-electron ligand, while the antibonding orbital remains unoccupied.

In order to compare the reactivity of Cp_3Zr to that of a transition-metal complex in which all three Cp rings are not η^5 -coordinated Cp rings, the behavior of Cp_3Ti was briefly examined. The reactivity of Cp_3Ti ^{22,36,37} as shown in Scheme 2 is quite different from that of Cp_3Zr . While Cp_3Zr does not react with CO, Cp_3Ti forms $\text{Cp}_2\text{Ti}(\text{CO})_2$ when treated with CO.³⁸ Additionally, although Cp_3Ti reacts with CCl_4 and $t\text{-BuNC}$, the

(31) Evans, W. J.; Gonzales, S. L.; Ziller, J. W. *J. Am. Chem. Soc.* **1991**, *113*, 7423-7424.

(32) Schumann, H.; Glanz, M.; Hemling, H. *J. Organomet. Chem.* **1993**, *445*, C1-C3.

(33) Davies, A. G.; Lusztyk, E.; Lusztyk, J. *J. Chem. Soc., Perkin Trans. 2* **1982**, 729-736.

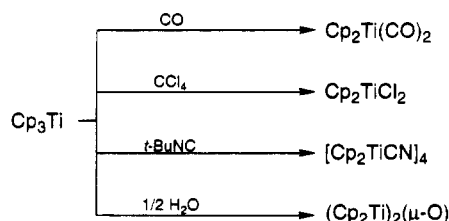
(34) Davies, A. G.; Jeffery, P. G.; Lusztyk, E.; Lusztyk, J. *J. Chem. Soc., Perkin Trans. 2* **1982**, 737-743.

(35) Fachinetti, G.; Floriani, C.; Chiesi-Villa, A.; Guastini, G. *J. Am. Chem. Soc.* **1979**, *101*, 1767-1775.

(36) Canty, A. J.; Coutts, R. S. P.; Wailes, P. C. *Aust. J. Chem.* **1968**, *21*, 807-810.

(37) Siebert, F. W.; de Meijer, H. J. *J. Organomet. Chem.* **1969**, *20*, 141-145.

(38) Fischer, E. O.; Löchner, A. *Z. Naturforsch.* **1960**, *15B*, 266.

Scheme 2. Reactions of Cp₃Ti

products are Cp₂TiCl₂ and [Cp₂TiCN]₄,³⁹ respectively. Treatment of Cp₃Ti with 0.5 equiv of water produced (Cp₂Ti)₂(μ-O) cleanly.⁴⁰ The reactivity of Cp₃Ti is consistent with a bent metallocene in which the η²-Cp ligand behaves somewhat analogously to a weakly bound alkyl group.

Conclusion

The synthesis, structure, and chemical behavior of Cp₃Zr have been described. Its reactivity is controlled by the presence of a electron in the d_{z²} orbital. Since [(Me₃Si)₂C₅H₃]₃Th behaves similarly,¹⁸ and since its electronic ground state is 6d¹, it seems likely that the electronic structure controls the reactivity in this case as well. Cp₃Ti, which also has a single d electron but does not have the same molecular structure, reacts differently. In light of the similarity of the reactivity of Cp₃Zr to that of the thorium metallocene, perhaps in this case it is useful to think of zirconium as "a little thorium".

Experimental Section

All reactions and manipulations were carried out in an inert atmosphere using standard Schlenk and drybox techniques as described previously.⁴⁰

Cp₃Zr. (a) From Cp₄Zr²⁰ and KC₈. Cp₄Zr (1.00 g, 2.84 mmol), dissolved in 200 mL of toluene, was added slowly to a slurry of KC₈ (0.42 g, 3.1 mmol) in 10 mL of toluene using a cannula. The reaction mixture was stirred overnight. The solution was filtered, giving a deep brown solution. The volume of the filtrate was reduced to ca. 175 mL, and the solution was heated to 80 °C to redissolve the solid. The solution was placed in a -20 °C freezer. After 3 days, the mother liquor was removed, yielding Cp₃Zr (0.46 g, 56%) as thin hexagonal plates. The compound did not melt up to 300 °C. IR: 3130 (m), 1023 (s), 1012 (s), 912 (s), 845 (s), 819 (s), 790 (s) 730 (m, sh), 285 (s), 250 (s) cm⁻¹. MS (found, calc): *m/e* 285 (100, 100), 286 (85, 39), 287 (80, 38), 288 (28, 6), 289 (75, 34). Anal. Calcd for C₁₅H₁₅Zr: C, 62.9; H, 5.28. Found: C, 63.1; H, 5.32.

(b) From Cp₄Zr²⁰ and NaC₁₀H₈. Naphthalene (0.37 g, 2.8 mmol) was added to a flask with a large excess of sodium slices followed by the addition of 50 mL of tetrahydrofuran. The solution quickly became green, and the contents of the flask were stirred for 12 h. The NaC₁₀H₈ solution was added, using a cannula, to Cp₄Zr (1.00 g, 2.84 mmol) dissolved in 100 mL of tetrahydrofuran. The reaction mixture became red-brown, and it was stirred for 12 h. The tetrahydrofuran was removed under reduced pressure, and the naphthalene was removed by heating the Schlenk tube to 80 °C under dynamic vacuum for 4 h. The solid residue was suspended in 200 mL of toluene and then filtered and cooled to -20 °C. After 10 days, brown plates were isolated (0.40 g), but they were contaminated with 12% Cp₃ZrH²⁴ as judged by the following method.

Reaction of Cp₃Zr with CCl₄. In an NMR tube, a benzene solution of Cp₃Zr was treated with an excess of CCl₄ using a syringe. The color immediately changed from green-brown to yellow-orange. The ¹H NMR spectrum of the reaction mixture showed it to be Cp₃ZrCl.⁴¹ In this way, the purity of the Cp₃Zr was estimated by comparing the integrations of the Cp peaks relative to benzene before and after the addition of CCl₄. It must be noted that the chemical shift of the protons of Cp₃ZrCl was reported as δ 6.05 ppm in CDCl₃.⁴¹ We find the resonance of Cp₃ZrCl, prepared as described in ref 41, at 5.67 ppm in C₆D₆.

Reaction of Cp₃Ti with CCl₄. In an NMR tube, a benzene solution of Cp₃Ti^{22,36,37} was treated with an excess of CCl₄ added using a syringe. The color immediately changed from dark green to dark red. The ¹H NMR spectrum of the reaction mixture showed it to be Cp₂TiCl₂.

Reaction of Cp₄Zr with *t*-BuLi. Cp₄Zr (0.50 g, 1.4 mmol) was dissolved in 125 mL of hot toluene, and the solution was cooled to room temperature. *t*-BuLi (0.64 mL, 2.24 M in hexane) was added by syringe. The solution became viscous, and a colorless precipitate appeared. After 1 h, the mixture was filtered, giving a pale yellow solution out of which white needles formed on standing. The solution was cooled to -80 °C to complete the crystallization. After 3 days, the mother liquor was removed from the small white needles using a cannula (0.29 g, 71%). ¹H NMR (not previously reported): δ 5.28 (15H), 2.83 (1H). The IR spectrum was identical with that previously reported.²⁴

Cp₃ZrCN^{1/3}C₇H₈. Cp₃Zr (0.30 g, 1.0 mmol) was dissolved in 100 mL of warm toluene. *t*-BuNC (0.10 g, 1.2 mmol) was added using a syringe. The solution instantly became dark and then lightened to red and finally to orange-red. The solution was filtered, although no precipitate was evident, and the volume was reduced to ca. 25 mL. The solution was cooled to -20 °C. After 2 weeks, the slightly cloudy solution was refiltered and cooled to -80 °C. After 3 weeks, the mother liquor was removed, yielding orange-red microcrystals (0.04 g, 12%). Mp: 220 °C dec. ¹H NMR: δ 5.39 (15H, C₅H₅), 2.10 (1H, H₃CC₅H₅). IR: 3100 (m), 3080 (w), 2130 (w), 1260 (w), 1020 (m), 1010 (m), 840 (m), 825 (s), 810 (s), 800 (s), 730 (w), 605 (w), 375 (w), 290 (m), 235 (m) cm⁻¹. MS (found, calc): *m/e* 311 (100, 100), 312 (43, 38), 313 (38, 37), 315 (34, 32). Anal. Calcd for C₅₅H₅₃N₃Zr₃: C, 64.2; H, 5.19; N, 4.08. Found: C, 63.7; H, 5.37; N, 3.81.

Reaction of Cp₃Ti with *t*-BuNC. Cp₃Ti^{22,36,37} (0.50 g, 2.1 mmol) was dissolved in 80 mL of toluene; *t*-BuNC (0.25 mL, 2.3 mmol) was added using a syringe. The green solution immediately became deep purple. The solution was allowed to stand for 4 h and then filtered and cooled to -20 °C. After 2 weeks, the mother liquor was removed using a cannula, leaving a purple powder. The IR spectrum, color, and solubility matched those reported for [Cp₂TiCN]₄.^{39,42} MS (found, calc): *m/e* 814 (36, 40), 815 (55, 53), 816 (100, 100), 817 (68, 71), 818 (42, 47), 819 (16, 21).

Reactions of Cp₃Zr with Water. (a) With 1 Equiv of Water. Cp₃Zr (1.8 mg, 6.4 μmol) was dissolved in 0.25 mL of C₆D₆. Water (0.1 μmol, 6 μmol) was added using a syringe. The initially green-brown solution became cloudy and a white precipitate formed. The only species present in solution were [Cp₂ZrO]₃ (δ 6.21 (s) ppm)³⁵ and C₅H₅ (δ 6.40 (m), 2.68 (m) ppm).

(b) With 0.5 Equiv of Water. Cp₃Zr (0.26 g, 0.91 mmol) was dissolved in 40 mL of tetrahydrofuran and cooled to -78 °C. Water (8.2 μL, 0.45 mmol) was dissolved in 30 mL of tetrahydrofuran and slowly added to the solution of Cp₃Zr. The solution was warmed to room temperature and became pale and cloudy as the temperature increased. After the mixture was stirred for 12 h, the tetrahydrofuran was removed under

(39) Schinnerling, P.; Thewalt, U. *J. Organomet. Chem.* **1992**, *431*, 41-45.

(40) Lukens, W. W.; Andersen, R. A. *Inorg. Chem.*, in press.

(41) Etievant, P.; Gautheron, B.; Tainturier, G. *Bull. Soc. Chim. Fr.* **1978**, 292-298.

(42) Coutts, R.; Wailes, P. C. *Inorg. Nucl. Chem. Lett.* **1967**, *3*, 1-5.

reduced pressure and 100 mL of toluene was added. The mixture was heated to 90 °C and then cooled to room temperature and allowed to settle, which gave a clear solution and a white precipitate which was removed by filtration. The white solid was almost insoluble in benzene, and its IR and ^1H NMR spectra matched those reported for $[\text{Cp}_2\text{ZrO}]_3$.³⁵ Cooling to -80 °C caused the precipitation of a white solid, which was found to be a mixture of $\text{Cp}_3\text{ZrH}^{24}$ and $[\text{Cp}_2\text{ZrO}]_3$ ³⁵ by IR and ^1H NMR spectroscopy.

Attempted Reactions of Cp_3Zr with Ligands. Cp_3Zr was dissolved in toluene. Ligands were added as toluene solutions ($\text{OP}(\text{OCH}_2)_3\text{CET}$), neat (pyridine), or as gases in a thick-walled pressure bottle (CO and C_2H_4). After the mixture was stirred for 12 h, no color change was noted. The solutions were filtered, and the volume of the mother liquor was reduced. Cooling to -20 °C produced the characteristic thin, brown, hexagonal crystals of Cp_3Zr . The spectra were identical with that of Cp_3Zr .

Solid-State Structure of Cp_3Zr . Small, brown, hexagonal prisms were grown by slowly cooling a diethyl ether solution of the compound. The crystals were placed in a Petri dish and covered with Paratone N. A crystal measuring $0.20 \times 0.20 \times 0.40$ mm was placed on the end of a 0.2 mm quartz capillary tube with a drop of Paratone N. The crystal was transferred to an Enraf-Nonius CAD-4 automated diffractometer and cooled to -108 °C under a cold stream of nitrogen previously calibrated by a thermocouple placed in the sample position. The crystal was centered in the beam. Automatic peak search and indexing procedures indicated that the crystal had a trigonal cell and yielded the unit cell parameters. The cell parameters and data collection parameters are given in Table 1.

The data collected were $(\pm h, +k, +l)$. The 851 raw intensity data were converted to structure factor amplitudes and their esds by correction for scan speed, background, and Lorentz-polarization effects. Inspection of the intensity standards showed a very severe decay at the middle of the data collection; therefore, the last half of the data was discarded (it was redundant). No decay correction was applied to the remaining 532 data. The reflection condition $(00l), l = 2n$, was observed and the five $(00l), l = 2n + 1$, reflections were discarded. Azimuthal scan data showed a difference of $I_{\text{min}}/I_{\text{max}} = 0.78$. An empirical absorption was applied. Finally, redundant data were averaged, yielding 266 unique data, of which 245 data had $F_o > 3\sigma(F_o)$.

The cell volume of 570 cm^3 indicated that $Z = 2$ by comparison with the known structure of Cp_3Ti . Systematic absences suggested that the space group was either $P6_3$ or $P6_3/m$ with the molecule sitting on a site with 3 or $\bar{6}$ symmetry. The zirconium position was obtained by solving the Patterson map. Initially, the solution was attempted in $P6_3$. The carbon positions were obtained by difference Fourier searches after refining on the zirconium position. With the carbon atoms refined isotropically and the zirconium atom refined anisotro-

pically, the R value was 0.051. However, when the carbon atoms were refined anisotropically, the thermal parameters seemed to be highly correlated, and the carbon atoms went nonpositive definite. Since the molecule appeared to have 6 symmetry, the space group was changed to $P6_3/m$. With the carbon atoms refined isotropically and the zirconium atom refined anisotropically, the R value was 0.052. In addition, the carbon atoms could be refined anisotropically. After the anisotropic refinement of the carbon and zirconium atoms had converged, a difference Fourier search located the three hydrogen atom positions. The hydrogen atoms were refined isotropically. Toward the end of the refinement, an examination of the extinction test listing showed that secondary extinction was occurring; therefore, a secondary extinction coefficient was included and refined upon.

The final residuals for 39 variables refined against the 245 data with $F_o > 3\sigma(F_o)$ were $R = 2.9\%$, $R_w = 3.25\%$, and $\text{GOF} = 1.179$. The R value for all data (including unobserved reflections) was 3.2%. The quantity minimized by the least-squares refinements was $w(|F_o| - |F_c|)^2$, where w is the weight given to a particular reflection. The p factor, used to reduce the weight of intense reflections, was set to 0.03 initially but later changed to 0.04. The analytical forms of the scattering factors for neutral atoms were used. All non-hydrogen scattering factors were corrected for both real and imaginary components of anomalous dispersion.

Inspection of the residuals in the range of $(\sin \theta/\lambda), |F_o|$, and parity and values of the individual indexes showed no trend other than the one previously mentioned in correction with secondary extinction. Three reflections had anomalously high values of $w\Delta^2$ and were weighted to zero toward the end of the refinement. The largest positive and negative peaks in the final difference Fourier map had electron densities of 0.58 and -0.65, respectively, and were associated with the zirconium atom.

Acknowledgment. We thank Dr. Fred Hollander for assistance with the crystallography and Drs. Norman Edelstein and Wing Kot for helpful discussions and for making the data on the reactivity of $[(\text{Me}_3\text{Si})_2\text{C}_5\text{H}_3]_3\text{-Th}$ available. W.W.L. thanks the National Science Foundation for a graduate fellowship. This work was partially supported by the Director, Office of Energy Research, Office of Basic Energy Sciences, Chemical Sciences Division, of the U.S. Department of Energy under Contract No. DE-AC03-76SF00098.

Supporting Information Available: Text giving all data reduction formulas and tables of bond lengths and angles and anisotropic thermal parameters for Cp_3Zr (4 pages). Ordering information is given on any current masthead page.

OM950061J

Kinetic Studies of Olefin Binding to Sulfido Sites in Dinuclear Molybdenum Complexes

C. R. Koval, L. L. Lopez, B. B. Kaul, S. Renshaw, K. Green, and
M. Rakowski DuBois*

Department of Chemistry and Biochemistry, University of Colorado,
Boulder, Colorado 80309-0215

Received March 2, 1995[®]

The reactions of olefins with a series of molybdenum complexes of the formula $(R-CpMo(\mu-S))_2S_2CHX$, where $R = H, CH_3, CO_2Na$, and $X = H, CN, CMe_3$, have been studied. Olefin reagents have included propene, 1-butene, *cis*- and *trans*-2-butene, and isomers of hexene. Olefin additions to the sulfido ligands in the dimers result in alkanedithiolate complexes. The rates of these reactions have been monitored by visible spectroscopy, and rate constants, k_{on} , have been compared as dimer substituent and olefin structure have been varied. The rate constants for olefin dissociation from the alkanedithiolate complexes, k_{off} , have also been determined by NMR spectroscopy. The studies have permitted us to probe the relative contributions of k_{on} and k_{off} to the equilibrium constants for reversible olefin binding as inductive and steric effects are varied. The potential for using these systems in olefin separation schemes is discussed.

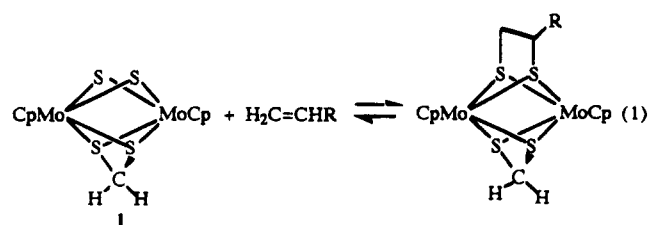
Introduction

Many metal ions have been reported to undergo reversible complexation reactions with olefins, and useful applications of this reaction have been developed. For example, silver-olefin complexes have been extensively studied¹ and have found use in chromatographic² and membrane-based olefin separation schemes.³ The nature of the interaction of the olefin π bond with the metal d orbitals in such systems has been the subject of detailed study and is well understood.⁴

In early studies of the dinuclear molybdenum complex $(CpMo(\mu-S))_2S_2CH_2$, **1**, we found that the sulfido ligands reacted with olefins to form a product with an alkanedithiolate ligand, eq 1.⁵ The reversible nature of

bonds makes this system fundamentally different from previously studied olefin-binding agents based on metal-olefin interactions, and significant differences in reaction rates, selectivities, or thermodynamic stabilities might be expected. For example, a preliminary study of olefin-binding constants for the molybdenum sulfide system revealed a very broad range of equilibrium constants ($0 \rightarrow 10^4 M^{-1}$) which varied as a function of olefin substituent and structure,⁵ while the binding constants for the silver ion, for example, were similar for most olefins.¹

A better understanding of the factors which influence olefin equilibria with **1** may permit us to tune equilibrium constants and maximize potential for selective olefin complexation and separation. For example, we wished to probe the relative contribution of k_{on} and k_{off} to the variation in equilibrium constants, and to determine whether electronic effects exerted by ligand substituents would significantly change either or both of these rate constants. We report here kinetic studies of olefin complexation and olefin dissociation reactions with **1** as substituents on the olefin and on the Cp and methanedithiolate ligands of **1** are varied. The variation of substituents on the molybdenum derivatives has altered solubilities and has also allowed us to investigate the influence of solvent on the rates of the reactions. In this study we have focused on a series of closely related olefins, including propene and the isomers of butene and hexene. Selective binding among these molecules, although potentially useful in commercial applications, is very difficult to achieve.



this reaction was established, and equilibrium constants for reactions with olefins in chloroform solution were determined. The reversible formation of covalent C-S

[®] Abstract published in *Advance ACS Abstracts*, June 1, 1995.

(1) (a) Beverwijk, C. D. M.; Van Der Kirk, G. J. M.; Leusink, A. J.; Noltes, J. G. *Organomet. Chem. Rev. A* **1970**, *5*, 215. (b) Hartley, F. R. *Chem. Rev.* **1973**, *73*, 163.

(2) (a) Bednas, M. E.; Russell, D. S. *Can. J. Chem.* **1958**, *36*, 1272. (b) Shabtai, J.; Herling, J.; Gil-Av, E. *J. Chromatogr.* **1962**, *8*, 349; **1963**, *11*, 32. (c) Cvetanovic, R. J.; Duncan, F. J.; Falconer, W. E. *Can. J. Chem.* **1963**, *41*, 2095. (d) Lawrence, B. M. *J. Chromatogr.* **1968**, *38*, 535.

(3) (a) LeBlanc, O. H., Jr.; Ward, W. J.; Matson, S. L.; Kimura, S. *G. J. Membrane Sci.* **1980**, *6*, 339. (b) Teramoto, M.; Matsuzama, H.; Yamashiro, T.; Katayama, Y. *J. Chem. Eng. Jpn.* **1986**, *19*, 419. (c) Koval, C. A.; Spontarelli, T. *J. Am. Chem. Soc.* **1988**, *110*, 293. (d) Koval, C. A.; Spontarelli, T.; Noble, R. D. *Ind. Eng. Chem. Res.* **1989**, *28*, 1020. (e) Valus, R. J.; Eshraghi, R.; Velikoff, A. E.; Davis, J. C. U.S. Patent 5,057,641, 1991. (f) Ho, W. S. W. U.S. Patent 5,015,268, 1991.

(4) (a) Mingos, D. M. P. In *Comprehensive Organometallic Chemistry*; Wilkinson, G., Stone, F. G. A., Abel, E. W., Eds.; Pergamon: New York, 1982; Vol. 3, p 1. (b) Dewar, M. J. S. *Bull. Soc. Chim. Fr.* **1951**, C71. (c) Chatt, J.; Duncanson, L. A. *J. Chem. Soc.* **1953**, 2939.

(5) McKenna, M.; Wright, L. L.; Miller, D. J.; Tanner, L.; Haltiwanger, R. C.; Rakowski DuBois, M. *J. Am. Chem. Soc.* **1983**, *105*, 5329.

(6) (a) Schroder, M. *Chem. Rev.* **1980**, *80*, 187. (b) Stewart, R. In *Oxidation in Organic Chemistry*; Weberg, K. B., Ed.; Academic: New York, 1965; Part A, p 1. (c) Sharpless, K. B.; Akashi, K. *J. Am. Chem. Soc.* **1976**, *98*, 1986.

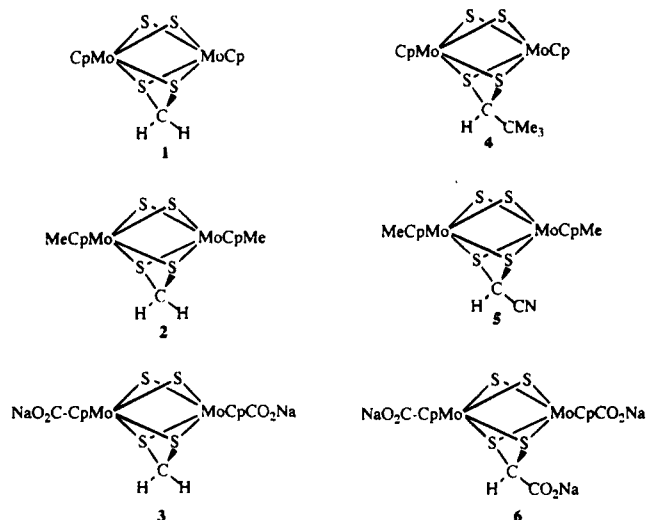


Figure 1. Structures of methanedithiolate derivatives used in this study.

The ligand-based reactions of the molybdenum sulfide systems with olefins can be compared to those of metal oxide complexes, such as OsO_4 , RuO_4 , and MnO_4^- . Reactions of olefins with the oxo ligands, which lead to metal diolate formation, have seen extensive development for the synthesis of free cis diols with modifications to achieve enantioselective diol formation.⁷ The formation of the diolate complexes is generally an irreversible process, but examples of cycloreversion reactions of metal diolate complexes have been reported.⁸ Kinetic studies have recently been reported for both olefin addition and olefin extrusion reactions with the Cp^*ReO_3 system.⁹

Results

Syntheses of Compounds. The methanedithiolate derivatives which have been included in this study are shown in Figure 1. Complexes with methyl and carboxylate groups on the Cp ligands have been reported previously.^{5,10} Several derivatives with substituents on the methanedithiolate ligand have also been reported previously.^{5,11} The new complexes $(\text{CpMo}(\mu\text{-S}))_2\text{S}_2\text{CHR}$, where R = t-Bu (4) and CN (5) were synthesized in low yields by a procedure similar to that reported for the parent complex 1, which involves the deprotonation of $[\text{CpMo}(\mu\text{-S})(\mu\text{-SH})_2]$ in the presence of Br_2CHR . Spec-

(7) (a) Norrby, P. O.; Kolb, H. C.; Sharpless, K. B. *J. Am. Chem. Soc.* **1994**, *116*, 8470. (b) Sharpless, K. B.; Teranishi, A. Y.; Backvall, J. E. *J. Am. Chem. Soc.* **1977**, *99*, 3120. (c) Hintges, S. G.; Sharpless, K. B. *J. Am. Chem. Soc.* **1980**, *102*, 4263. (d) Tokles, M.; Snyder, J. K. *Tetrahedron Lett.* **1986**, 3951. (e) Yamada, T.; Narasaka, K. *Chem. Lett.* **1986**, 131. (f) Carlsen, P. H. J.; Katsuki, T.; Martin, V. S.; Sharpless, K. B. *J. Org. Chem.* **1981**, *46*, 3936. (g) Tomioka, K.; Nakajima, M.; Koga, K. *J. Am. Chem. Soc.* **1987**, *109*, 6213.

(8) (a) Brown, S. N.; Mayer, J. M. *Inorg. Chem.* **1992**, *31*, 4091. (b) Herrmann, W. A.; Marz, D.; Herdtweck, E.; Schaefer, A.; Wagner, W.; Kneuper, H. *J. Angew. Chem.* **1987**, *99*, 462. (c) Herrmann, W. A.; Floel, M.; Kulpe, J.; Felixberger, J. K.; Herdtweck, E. *J. Organomet. Chem.* **1988**, *355*, 297. (d) Herrmann, W. A.; Marz, D. W.; Herdtweck, E. *J. Organomet. Chem.* **1990**, *394*, 285. (e) Okuda, J.; Murray, R. C.; Dewan, J. C.; Schrock, R. R. *Organometallics* **1986**, *5*, 1681 and references therein. (f) Pearlstein, R. M.; Davison, A. *Polyhedron* **1988**, *7*, 1981. (g) Bohm, G.; Wieghardt, K.; Naber, B.; Weiss, J. *Angew. Chem., Int. Ed. Engl.* **1990**, *29*, 787.

(9) (a) Gable, K. P.; Phan, T. N. *J. Am. Chem. Soc.* **1994**, *116*, 833. (b) Gable, K. P.; Juliette, J. J. *J. Am. Chem. Soc.* **1995**, *117*, 955.

(10) Allshouse, J.; Kaul, B. B.; Rakowski DuBois, M. *Organometallics* **1994**, *13*, 28.

(11) Lopez, L. L.; Gabay, J.; Haltiwanger, R. C.; Green, K.; Allshouse, J.; Casewit, C. J.; Rakowski DuBois, M. *Organometallics* **1993**, *12*, 4764.

Table 1. Cyclic Voltammetric Data for Methanedithiolate Derivatives^a

complex	V vs Fc (ΔE , mV)	
	oxidation	reduction
$(\text{CpMo}(\mu\text{-S}))_2\text{S}_2\text{CH}_2$	-0.13 (132)	-1.70 (96)
$(\text{CpMo}(\mu\text{-S}))_2\text{S}_2\text{CH}(\text{CMe}_3)$	-0.13 (140)	-1.71 (72)
$(\text{MeCpMo}(\mu\text{-S}))_2\text{S}_2\text{CH}_2$	-0.14 (90)	-1.73 (70)
$(\text{MeCpMo}(\mu\text{-S}))_2\text{S}_2\text{CH}(\text{CO}_2\text{Me})^b$	+0.04 (214)	-2.78 irrev
		-1.64 (68)
$(\text{MeCpMo}(\mu\text{-S}))_2\text{S}_2\text{CH}(\text{CN})^c$	+0.16 (84)	-2.24 irrev
		-1.56 (74)
		-2.37 irrev

^a Cyclic voltammograms were recorded in $\text{CH}_3\text{CN}/0.1$ M Bu_4NBF_4 with a platinum working electrode at a scan rate of 100 mV/s. Ferrocene was used as an internal standard. ^b Data taken from ref 11. ^c Decamethylferrocene was used as an internal standard. Potentials were converted to the ferrocene reference using $E_{\text{DMFC}} = -500$ mV vs Fc.²⁰

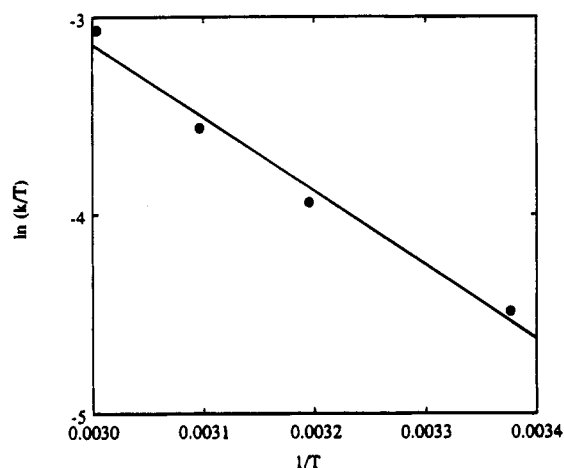


Figure 2. Eyring plot for the reaction of $(\text{NaO}_2\text{C-CpMo}(\mu\text{-S}))_2\text{S}_2\text{CH}_2$, 3, with 1-hexene in methanol; $r^2 = 0.982$. Similar plots were observed for *trans*-2-hexene ($r^2 = 0.998$) and *cis*-2-hexene ($r^2 = 0.982$).

troscopic data for 4 and 5 are given in the Experimental Section, and electrochemical data are included in Table 1.

The reactions of each of the complexes in Figure 1 with olefins proceeded as indicated in eq 1. In several cases, the alkanedithiolate complexes have been isolated and characterized by spectroscopic data.⁵ In other cases the dithiolate products were simply identified in situ by ^1H NMR spectroscopy. Representative characterization data are included in the Experimental Section.

Determination of Rate Constants for Olefin Addition Reactions. The reactions of $(\text{Cp}^*\text{Mo}(\mu\text{-S}))_2\text{S}_2\text{-CHR}$ derivatives with propene and the butene isomers in organic solvents were carried out with large excesses (50–150 equiv) of olefin. All derivatives of 1 are a deep blue color with strong absorbances in the visible spectrum near 720 and 580 nm, while the olefin adducts are pale brown complexes with no absorption in this region. The rates of the reactions were therefore readily monitored by visible spectroscopy, and plots of $\ln(A_t - A_\infty)$ vs time were linear with correlation coefficients of 0.98–0.99. The pseudo-first-order rate constants obtained in these studies were plotted vs 4–6 different initial olefin concentrations in order to determine the second order rate constant, k_{on} , for olefin binding at 20 °C. Values for these rate constants are given in Table 2. The kinetics of the reactions of $(\text{NaO}_2\text{CCpMo}(\mu\text{-S}))_2\text{S}_2\text{CH}_2$ with hexene isomers in MeOH were also monitored by visible spectroscopy under pseudo-first-order conditions

Table 2. Values of k_{on} ($M^{-1} s^{-1}$) at 20 °C for Reactions of Molybdenum Dimers with Olefins

entry	compd	solvent	ethene	propene	1-butene	cis-2-butene	trans-2-butene	1-hexene
1	(CpMo(μ -S)) ₂ S ₂ CH ₂	benzene	19 ± 1	1.0 ± 0.1	3.9 ± 0.4	0.97 ± 0.12	0.12	2.6 ± 0.2
2	(CpMo(μ -S)) ₂ S ₂ CH-t-Bu	benzene	15 ± 1.2	0.36 ± 0.04	1.6 ± 0.2	0.16 ± 0.02	0.024 ± 0.03	1.6 ± 0.4
3	(Me-CpMo(μ -S)) ₂ S ₂ CH ₂	benzene		1.3 ± 0.3	2.9 ± 0.3	0.49 ± 0.07	0.094 ± 0.012	
4	(Me-CpMo(μ -S)) ₂ S ₂ CH(CN)	benzene		2.9 ± 0.2	4.8 ± 0.3	0.82 ± 0.12	0.12 ± 0.02	
5	(CpMo(μ -S)) ₂ S ₂ CH ₂	CHCl ₃		0.55	0.75 ± 0.08	0.26 ± 0.03	0.11 ± 0.01	0.67 ± 0.07
6	(Me-CpMo(μ -S)) ₂ S ₂ CH ₂	CHCl ₃	6.0 ± 1.0	0.63 ± 0.1	0.42 ± 0.02	0.12 ± 0.01	0.034 ± 0.004	
7	(CpMo(μ -S)) ₂ S ₂ CH ₂	acetone		3.1 ± 0.1	2.3 ± 0.2		0.16 ± 0.01	

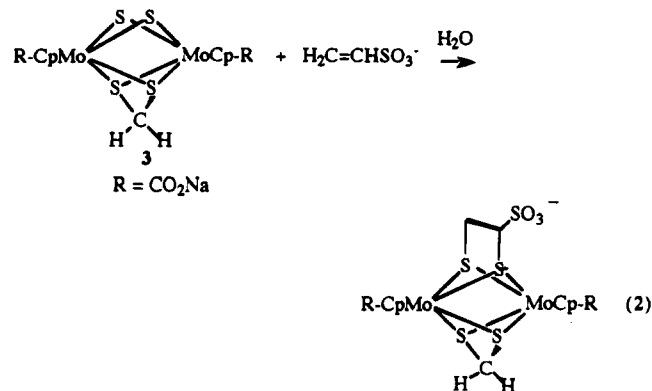
Table 3. Kinetic Data for the Reactions of (NaO₂C-CpMo(μ -S))₂S₂CH₂, **3, with Hexene Isomers in Methanol**

olefin	temp, °C	k_{on} , M ⁻¹ s ⁻¹	k_{off} , s ⁻¹ ^a	K_{eq} ^b	ΔH^\ddagger , kJ/mol	ΔS^\ddagger , J/mol K
1-hexene	22	3.3				
	40	6.1				
	50	9.2	3.1 × 10 ⁻³	3000		
	60	12.5	2.8 × 10 ⁻²	450	26 ^c	-150
trans-2-hexene	22.5	0.11	1.8 × 10 ⁻⁴	610		
	40	0.26	5.7 × 10 ⁻⁴	460		
	50	0.38	9.0 × 10 ⁻⁴	420		
	60	0.57	3.0 × 10 ⁻³	190	33	-150
cis-2-hexene	8.5	0.17				
	13	0.21	3.2 × 10 ⁻⁴	660		
	19.5	0.26	1.8 × 10 ⁻³	140		
	25	0.42	3.9 × 10 ⁻³	110		
	31	0.52	9.2 × 10 ⁻³	57	34	-140

^a Determined for reversible reactions from the intercept in plots of k_{obs} vs [hexene]. ^b Determined from the reported values of k_{on} and k_{off} . ^c See Figure 2.

over an olefin concentration range of 10⁻¹–10⁻³ M. Values for k_{on} are given in Table 3. In the latter systems the dependence of the rates on temperature was also investigated. Values of ln(k_{on}/T) vs 1/ T for each hexene isomer were plotted, see Figure 2, and the activation parameters for the hexene-binding reactions calculated from these data are also given in Table 3.

Several attempts to obtain kinetic data for the reactions of hexenes with (NaO₂C-CpMo(μ -S))₂S₂CH₂ in aqueous solution were made, but consistent kinetic data were not obtained, presumably because of the very low solubility of hexenes in water. In order to determine a rate of olefin addition in water, the reaction of **3** with excess vinyl sulfonate, eq 2, was monitored by visible

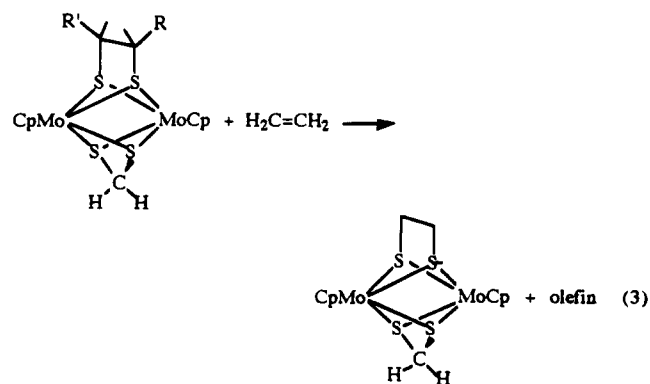


spectroscopy. Pseudo-first-order rate constants for reaction 2 were determined over an olefin concentration ranging from 10⁻³ M to 10⁻² M. From a plot of k_{app} values vs olefin concentrations, the second-order rate constant for the vinyl sulfonate addition to **1** was found to be 110 M⁻¹ s⁻¹ at 20 °C. This rate constant is about 2–3 orders of magnitude larger than those reported in Tables 2 and 3 for the butene and hexene isomers. This increase was tentatively attributed to the effect of the electron-withdrawing olefin substituent rather than to the difference in solvents. In order to compare the effect of an electron-withdrawing substituent in a nonaque-

ous solvent, we attempted to monitor the reaction of **1** with excess acrylonitrile in benzene solution. The reaction appeared complete in 2–3 s and could not be adequately monitored by the spectroscopic methods used in this study.

Determination of Rate Constants for Olefin Dissociation Reactions. The interactions of the 2-hexene isomers with (NaO₂C-CpMo(μ -S))₂(S₂CH₂), described above, were reversible reactions. In addition to the values for k_{on} determined from the slope of k_{obs} vs [olefin], a value for k_{off} could also be determined from the intercept of these plots. The values for k_{off} at the different reaction temperatures, as well as the resulting equilibrium constants, are included in Table 3.

For several of the more stable alkanedithiolate systems it was possible to study the rates of olefin dissociation directly and to independently determine values of k_{off} for these reactions. These studies provided a more accurate measure of the rate constants for olefin dissociation than those derived from the intercepts of the reversible reactions. For example, in our studies of the organic soluble derivatives, the olefin adducts were isolated and then reacted with a large excess of ethene to form the ethanedithiolate complex, eq 3. The reac-



tions were carried out in deuterated solvents in NMR tubes, and the rates were monitored by integrations of

Table 4. Values of $k_{\text{off}} \times 10^4 \text{ (s}^{-1}\text{)}$ at 18 °C for Dissociation of Olefin Adducts^a

entry no.	product	solvent	propene	1-butene	<i>trans</i> -2-butene	<i>cis</i> -2-butene
1	(CpMo(μ -S)) ₂ S ₂ CH ₂	C ₆ D ₆	1.6	1.5	0.98	28 ± 3 ^b
2	(CpMo(μ -S)) ₂ S ₂ CH(CN)	C ₆ D ₆	7.0 ± 0.9 ^b		1.7	
3	(CpMo(μ -S)) ₂ S ₂ CH(<i>t</i> -Bu)	C ₆ D ₆	1.6	5.2	1.7	54 ± 21
4	(CpMo(μ -S)) ₂ S ₂ CH ₂	CDCl ₃	3.6 ± 0.04	1.6 ± 0.2 ^c	0.92 ± 0.04 ^d	61 ± 11
5	(Me-CpMo(μ -S)) ₂ S ₂ CH ₂	CDCl ₃	3.5	5.6	5.3	
6	(CpMo(μ -S)) ₂ S ₂ CH ₂	<i>d</i> ₈ -acetone	1.8	6.8	0.75	
7	(Me-CpMo(μ -S)) ₂ S ₂ CHCN	C ₆ D ₆				72 ± 8
8	(Me-CpMo(μ -S)) ₂ S ₂ CH ₂	C ₆ D ₆				20 ± 4

^a Values for propene, 1-butene, and *trans*-2-butene were obtained by monitoring the rate of eq 3. Values for *cis*-2-butene were obtained from the values of k_{apparent} in the olefin addition studies and independently determined equilibrium constants, as described in the Results section. ^b Because of the extended times required for these experiments, only a few of the runs were repeated (three times) in order to obtain representative standard deviations. ^c Value obtained in the presence of excess acetylene was $1.4 \times 10^{-4} \text{ s}^{-1}$. ^d Value obtained in the presence of excess acetylene was $0.85 \times 10^{-4} \text{ s}^{-1}$.

Table 5

A. Rate Dependence of Reaction 4 on Vinyl Sulfonate Concentration at 21 °C

[complex 3] × 10 ²	[vinyl sulfonate] × 10 ²	$k_{\text{obs}} \times 10^5 \text{ (s}^{-1}\text{)}$
2.41	2.4	6.46
2.41	7.4	6.99
2.41	14.8	6.38

B. Values of k_{off} for the Dissociation of the Propene Adduct of (NaO₂C-CpMo(μ -S))₂S₂CHX, Eq 4, in Aqueous Solution

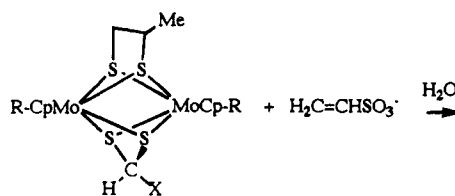
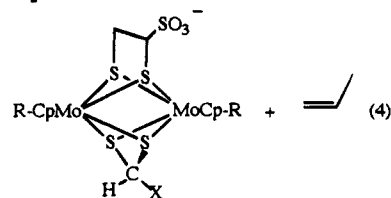
complex	temp, °C	$k \times 10^4 \text{ (s}^{-1}\text{)}$	ΔH^\ddagger (kJ/mol)	ΔS^\ddagger J/mol K
3 (X = H)	25	0.70		
	30	1.35	89.3 ± 0.2	-24.2 ± 0.5
	35	2.38		
	40	4.04		
	50	12.8		
6 (X = CO ₂ Na)	25	0.53	110 ± 1	42.6 ± 2.6
	30	1.02		
	35	2.33		
	40	3.53		
	50	18.90		

appropriate resonances of the starting reagent or of product. Plots of ln(Integration) vs time gave linear plots with a slope of k_{off} . Previous mechanistic studies of related alkanedithiolate molybdenum complexes have established that olefin dissociation is the rate-determining step in the olefin exchange reactions.¹³ The large excess of ethene (which has the largest value of k_{on} of the series of olefins studied) therefore allowed us to measure k_{off} under conditions in which the reverse reaction with the displaced olefin is not significant. In two of the systems studied here, the rates of the reactions with acetylene were also monitored. In these cases, olefins were displaced and alkenedithiolate complexes were formed irreversibly. First-order rate constants, k_{off} , were found to be identical within experimental error to those observed for the olefin dissociation in the presence of ethene, (see Table 4) supporting our assumption that olefin dissociation is rate determining.

Using this approach, the rates of dissociation of propene, 1-butene, and *trans*-2-butene were measured for a series of molybdenum adducts in which substituents on the cyclopentadienyl and methanedithiolate ligands were varied. First-order rate constants determined at 18 °C are reported in Table 4. The adducts of *cis*-2-butene were not stable enough to be isolated for the type of substitution reaction shown in eq 3. The values of k_{off} for this olefin included in Table 4 were determined from the values of k_{app} in the olefin addition studies and independently determined equilibrium con-

stants (see below) according to the equation $k_{\text{off}} = k_{\text{app}} / \{K_{\text{eq}}[\text{olefin}] + 1\}$.¹²

Similar kinetic studies to determine k_{off} in aqueous solution were carried out with the carboxylate-Cp derivatives. Vinyl sulfonate was reacted with the isolated propene adduct of **3** or **6** in aqueous solution to form the vinyl sulfonate adduct and free propene, reaction 4 (eq 4). The rate of disappearance of the

Adduct of **3**: R = CO₂Na, X = HAdduct of **6**: R = CO₂Na, X = CO₂Na

starting propene adduct of **3** was found to be independent of the vinyl sulfonate concentration over a range of 10^{-1} to 10^{-2} M (Table 5, part A). These data are consistent with a dissociative mechanism for reaction 4 in which loss of propene is the rate-determining step, similar to that proposed above for the organic soluble systems. Because of the large excess of vinyl sulfonate present and its rapid rate of addition to the intermediate complex **3**, the reverse reaction of propene addition to **3** is not significant under these conditions. Rate constants for reaction 4, determined from plots of ln(integration) vs time over 2–3 half lives and over a temperature range of 25–50 °C are given in Table 5. A plot of ln k/T vs $1/T$ (Figure 3) permitted us to calculate activation parameters for the propene dissociation, which are also included in the table.

An alternate method for determining the rate of olefin dissociation was also explored with the 1-hexene adduct of (NaO₂C-CpMo(μ -S))₂S₂CH₂. A methanol solution of the adduct in a cuvette cell was maintained at a constant elevated temperature, and the solution was purged with MeOH-saturated nitrogen. The rate of formation of the absorbance band at 742 nm corresponding to (NaO₂C-CpMo(μ -S))₂S₂CH₂ was monitored, and values of k_{off} were determined from linear plots of ln A vs time. The rate constants determined by this

(12) Espenson, J. H. *Chemical Kinetics and Reaction Mechanisms*; McGraw Hill: New York, 1981; p 45.

(13) DuBois, D. L.; Miller, W. K.; Rakowski DuBois, M. *J. Am. Chem. Soc.* **1981**, *103*, 3429.

Table 6. Values of K_{eq} Estimated from ^1H NMR Spectroscopy and from Rate Constants^a

complex	solvent	propene	1-butene	<i>trans</i> -2-butene	<i>cis</i> -2-butene	1-hexene
(CpMo(μ -S)) ₂ S ₂ CH ₂	benzene	1.8×10^4 6.2×10^3	1.9×10^4 2.6×10^4	3.5×10^3 1.2×10^3	3.3×10^2	
(CpMo(μ -S)) ₂ S ₂ CHt-Bu	benzene	1.1×10^3 2.2×10^3	1.0×10^3 3.1×10^3	2.7×10^1 1.4×10^2	2.0×10^1	
(CpMo(μ -S)) ₂ S ₂ CHCN	benzene	4.3×10^3	2.6×10^3	2.3×10^3	4.4×10^2	
(Me-CpMo(μ -S)) ₂ S ₂ CHCN	benzene	3.9×10^3	1.2×10^3	1.2×10^3	1.3×10^2	5.2×10^3
(Me-CpMo(μ -S)) ₂ S ₂ CH ₂	benzene	1.6×10^3	5.5×10^2	5.2×10^2	5.2×10^1	
(CpMo(μ -S)) ₂ S ₂ CH ₂	CDCl ₃		6.1×10^3	1.4×10^3	5.0×10^1	1.9×10^3
(CpMo(μ -S)) ₂ S ₂ CH ₂	(CD ₃) ₂ CO	1.5×10^3 6.4×10^3	4.7×10^3 5.6×10^3	1.2×10^3 2.3×10^3	1.6×10^2	
(Me-CpMo(μ -S)) ₂ S ₂ CH ₂	CDCl ₃	1.7×10^4 1.2×10^3	3.4×10^3 6.2×10^2	2.1×10^3 2.3×10^2	2.2×10^1	1.3×10^3
(NaO ₂ C-CpMo(μ -S)) ₂ S ₂ CH ₂	D ₂ O	1.8×10^3 3.2×10^3	7.5×10^2 3.6×10^4	5.6×10^1 4.0×10^3		
(NaO ₂ C-CpMo(μ -S)) ₂ S ₂ CH ₂	CD ₃ OD	5.3×10^3	4.0×10^4	1.9×10^3	2.8×10^2	

^a First values listed are from NMR integrations of equilibrium solutions at ambient temperature. The second values listed in some cases are calculated from independently determined k_{on} and k_{off} data.

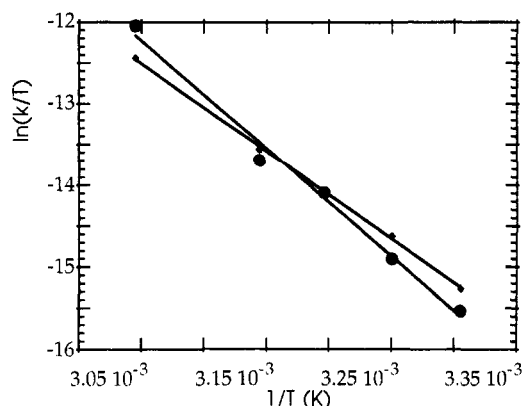


Figure 3. Eyring plots for the dissociation of propene from the adducts of (NaO₂C-CpMo(μ -S))₂S₂CH₂, **3** (■), and (NaO₂C-CpMo(μ -S))₂S₂CHCO₂Na, **6** (●). Correlation coefficients were 0.999 and 0.994, respectively.

method were $(5.0 \pm 1) \times 10^{-3} \text{ s}^{-1}$ at 50 °C and $(1.4 \pm 0.2) \times 10^{-2} \text{ s}^{-1}$ at 60 °C. These values agreed within a factor of 2 with the rate constants determined from the intercepts of the plots for the equilibrium reactions, Table 3.

Determination of Equilibrium Constants. The reactions of propene, 1-butene, and *cis*- and *trans*-2-butene with the molybdenum dimers were carried out in sealed tubes, and adduct formation was monitored by NMR spectroscopy. Unlike most olefin interactions with metal complexes, the reactions were slow on the NMR time scale. Integration values of all species in solution were compared to that of an internal standard, and equilibrium constants at room temperature were estimated from these values when concentrations reached a constant level (Table 6). In a few cases the dissociation of olefin from the isolated adduct was also monitored in the same solvent, and equilibrium constants determined from these reactions were similar to those from the forward reactions.

A second estimate of equilibrium constants is possible for those systems for which k_{on} and k_{off} have been determined independently. These values are included in Table 6 as second entries. These K_{eq} values are approximate because slightly different temperatures were maintained in the kinetic studies of olefin binding and olefin dissociation. However, in most cases, the orders of magnitude agreed well with the NMR determinations.

Discussion

Mechanistic aspects of olefin binding to and dissociation from the molybdenum sulfide dimers have been studied previously.¹³ Neither *cis*-*trans* nor terminal-internal olefin isomerizations were observed, and reactions were proposed to involve concerted additions and eliminations. Extended Huckel molecular orbital calculations have shown that the interaction between the sulfido ligands in the molybdenum dimer and the olefin involves a vacant orbital with both metal and sulfur character which accepts electron density from the olefin π orbital. In addition, a filled orbital on the dimer with primarily sulfur p character has appropriate symmetry for back-donation to the π^* orbital of the olefin.

In order to obtain a measure of the inductive effects involved in the substituted derivatives studied here, the derivatives of **1** with substituted methanedithiolate ligands have been characterized by cyclic voltammetry. The data are listed in Table 1. Each of the complexes showed a quasi-reversible oxidation and a reversible reduction process. The potentials of these waves reflect the energy of the metal-based HOMO and of the LUMO, which has both metal and sulfur character. In the complexes with electron-withdrawing substituents (CO₂-Me, CN), the potentials for both these processes were shifted to more anodic values. This effect was most pronounced for the cyano substituent where anodic shifts of 200–300 mV were observed relative to the methanedithiolate complex **1**. In contrast, for a *tert*-butyl substituent on the methanedithiolate ligand or a methyl group on the Cp ligand, only a slight cathodic shift was observed in the reduction potentials.

As the substituents on the molybdenum dimer were varied, the rate constants determined for the olefin binding reactions in organic solvents, Table 2, showed a small but consistent trend. Electron-donating substituents on the methanedithiolate ligand, entry 2, or to a lesser extent, on the cyclopentadienyl ligand, entry 3, resulted in slower rates of most olefin additions relative to the unsubstituted molybdenum complex, entry 1. Entries 5 and 6 also followed this trend. In contrast small increases in rate constants were observed for the complex with the electron-withdrawing cyano substituent on the methanedithiolate ligand (entry 4 vs 3). On the basis of these substituent effects, the acceptance of electron density from the olefin appears to be an important interaction that influences the rate of addition for a given olefin.

In a reported study of the rates of olefin addition to the metal center in $\text{HCo}[\text{PPh}(\text{OEt})_2]_3$, the values of k ($\text{M}^{-1} \text{s}^{-1}$) at 23 °C varied from 1.2×10^8 for 1-hexene to 2.5×10^7 for *cis*-2-hexene and 2.4×10^6 for *trans*-2-hexene.^{14a} For the molybdenum sulfide systems studied here, rates were much slower, but the rate constants for olefin addition also varied by approximately 2 orders of magnitude for the series including ethene, propene, and butene and hexene isomers. Rates of reactions with ethene ($k = 5\text{--}20 \text{ M}^{-1} \text{s}^{-1}$) and the 1-normal olefins ($k = 0.3\text{--}5 \text{ M}^{-1} \text{s}^{-1}$) were found to be faster than those for the internal olefins. In addition, rate constants for the addition of the *cis*-2-isomers of butene and hexene were consistently faster than the rates of addition of the *trans* isomers (by factors of 2–8). The differences in rates between terminal and internal olefins can be rationalized on the basis of steric effects. Similarly, *trans* substituents on an olefin are expected to have greater steric interactions with the Cp ligands on approaching the sulfur sites, while a small rotation of the *cis* isomer may permit a decrease in steric repulsions. In the related addition of olefins to MnO_4^- , OsO_4 , and RuO_4 to form diolate complexes, steric effects do not appear to play a dominant role, and the relative rates of the *trans* internal olefins were found to be larger than those of the *cis* isomers.^{14b}

A comparison of the rate constants for the addition of butene isomers to **1** in benzene (Table 2) and the constants for the addition of hexene isomers to **3** in MeOH (at 22 °C) (Table 3) shows that the values are remarkably similar for the respective isomers. Although the variations in solvent, Cp substituents and olefin chain length may have fortuitously similar effects on rates in these systems, it appears that the magnitude of these effects is relatively small.

Much larger variations in rate constants appear to result when inductive effects on the olefin are varied. For example, the reaction of $(\text{NaO}_2\text{C}-\text{CpMo}(\mu\text{-S})_2\text{S}_2\text{CH}_2)$, **3**, with vinyl sulfonate proceeded with a k_{on} of $110 \text{ M}^{-1} \text{s}^{-1}$ at 20 °C while k_{on} for propene in the same system is estimated (from K_{eq} and k_{off} data) to be ca. $0.2 \text{ M}^{-1} \text{s}^{-1}$. Similarly in our study of the nonaqueous system involving the reaction of **1** with acrylonitrile in benzene solution, a value of k_{on} of $>300 \text{ M}^{-1} \text{s}^{-1}$ was estimated. The electron-withdrawing groups on the olefin decrease the energy of both the π and π^* orbitals,¹⁵ and extended Huckel calculations have shown that this favors both the donor and acceptor olefin interactions with the molybdenum sulfide dimers.¹⁶

Activation parameters for the additions of the three hexene isomers to **3** in methanol are summarized in Table 3. The values are similar to those determined previously for the addition of benzyl isocyanide to the sulfido ligand sites in $[\text{CpMo}(\mu\text{-S})(\mu\text{-SH})_2]$ in chloroform solution¹³ and are consistent with the proposed associative mechanism. The internal olefins were found to have a larger ΔH^\ddagger than normal 1-hexene, and this is attributed to the greater steric interactions of the 2-olefins with the Cp ligands of the dimer. We have not found for comparison the report of activation

parameters for the addition of a similar series of isomeric olefins to a transition metal center. In general, we would predict that the ΔS^\ddagger for the olefin additions to the molybdenum sulfide dimers would be much more negative than the ΔS^\ddagger values for olefin additions to a metal center, because the bound olefin in the alkanedithiolate ligand is much more constrained than $\text{M}-\eta^2$ -olefin systems. In the latter, rotation about the metal–olefin bond is often observed. A comparison can be made with the reported activation parameters for the addition of a chelating olefin $\text{Ph}(\text{H})\text{C}=\text{C}(\text{CO}_2\text{Me})(\text{NHCOMe})$ to a cationic square planar $\text{Rh}(\text{I})$ complex.¹⁷ While the ΔH^\ddagger for the latter system of 29 kJ/mol was similar to values reported here, the ΔS^\ddagger (-75 J/mol of C) was much less negative. As expected, the ΔS^\ddagger for the addition of norbornene to two oxy ligands of Cp^*ReO_3 , which was proposed to involve stepwise formation of C–O bonds via a metallooxetane intermediate, was large and negative, -126 J/mol K . The ΔH^\ddagger for this last reaction, 76.1 kJ/mol, was significantly larger than the values for the olefin additions to the metal sulfide complexes, discussed above.⁹

Rates of Olefin Dissociation. The first-order rate constants for the dissociation of propene, 1-butene, or *trans*-2-butene from the molybdenum dimers, determined by NMR data, did not change very much or in a systematic way as the molybdenum complex, olefin, or solvent was varied, and values close to $1 \times 10^{-4} \text{ s}^{-1}$ were observed at room temperature for all of these systems (Table 4). Similar rates were observed for the dissociation of propene from the adducts of **3** and **6** in aqueous solution (Table 5).

The molybdenum sulfide adducts of the *cis*-2-olefins were significantly more labile than the adducts of the other olefins and were not readily isolated. Direct determinations of the k_{off} values for these adducts by monitoring the reaction in eq 3 was therefore not possible. Values of k_{off} determined as described above from kinetic studies of *cis* olefin binding and independently determined equilibrium constants indicate that the rate constants for *cis* olefin elimination are approximately an order of magnitude larger than those for the other olefins. Unfavorable steric interactions between adjacent substituents on the sp^3 -hybridized carbon atoms of the *cis*-alkanedithiolate ligand may contribute to the observed lability.

The dissociations of propene from adducts of **3** and **6** in aqueous solutions were studied over a temperature range of 25–50 °C, and the activation parameters for these reactions were determined (Table 5, part B). It is interesting that both the activation enthalpy and entropy for propene loss from **6** are significantly more positive than those of **3**. In addition to the electronic effect exerted by the additional carboxylate substituent in **6**, variations in net ionic charge and in acidities¹⁰ also distinguish **3** and **6** and may influence the activation parameters.¹⁸ Data for a broader range of complexes should be obtained before attempts are made to interpret these effects. It may be noted that the values for ΔH^\ddagger and ΔS^\ddagger reported for the loss of ethylene from a five-coordinate Pt(II) complex, $\text{Pt}(\text{C}_2\text{H}_4)(\text{Cl}_2)(\text{bipy})$, in dichloromethane solution, 77.8 kJ/mol and -33 J/mol

(14) (a) Oishi, S.; Kihara, N.; Hosaka, A. *J. Organomet. Chem.* **1984**, 276, C33. (b) Sharpless, K. B.; Williams, D. R. *Tetrahedron Lett.* **1975**, 3045.

(15) Dragutan, V.; Balaban, A. T.; Dimonie, M. *Olefin Metathesis and Ring-Opening Polymerization of Cyclo-Olefins*; Wiley: New York, 1985; pp 288–289.

(16) Kvietok, F. A. Ph.D. Thesis, University of Colorado, Boulder, Colorado, 1993.

(17) Landis, C. R.; Halpern, J. *J. Am. Chem. Soc.* **1987**, 109, 1746.

(18) For example, propene addition to and dissociation from **6** in water could be accompanied by protonation and deprotonation, respectively, of the $\text{S}_2\text{CH}(\text{CO}_2^-)$ ligand.

K, respectively,¹⁹ were similar to the values reported here for propene dissociation from **3**. In contrast the ΔH^\ddagger and ΔS^\ddagger values for the extrusion of olefins from Cp*ReO(diolate) derivatives have been found to be near 125 kJ/mol and -4 to -8 J/mol K, respectively.⁹

Equilibrium Constants. The equilibrium constants for the olefin interactions with the molybdenum sulfide complexes show a notable trend as the olefin isomers are varied. Largest values of K_{eq} are observed for ethene and for the terminal olefins, and the differences in K observed for the series of molybdenum dimers in Table 6 largely reflect the variations in k_{on} in the kinetic data for these olefins. However in the case of the internal olefins, the thermodynamic stabilities of the adducts ($K_{(trans)} > K_{(cis)}$) show the inverse order to that of the rate constants for olefin binding ($k_{on(cis)} > k_{on(trans)}$). This reversal reflects our proposals that the trans isomer is more sterically hindered in entering the binding site while the cis isomer is more sterically unfavorable in the sp^3 -hybridized product. The significantly larger binding constants for the trans olefin isomers in the olefin-sulfur adducts show the opposite trend to that observed for metal-olefin adducts, in which the cis isomer is generally more stable.^{1b}

Summary and Conclusions. Kinetic and thermodynamic parameters have been determined for the reversible interactions of olefins with μ -sulfido ligands in cyclopentadienylmolybdenum dimers, and the effects of electron-withdrawing and electron-donating substituents on the Cp and thiolate ligands have been probed. The inductive properties of ligand substituents were found to have a relatively small effect on rates of olefin binding. Electron-withdrawing substituents resulted in somewhat larger values of k_{on} relative to the unsubstituted parent complex, while slightly slower rates were observed for derivatives with electron-donating substituents. For a series of closely related C_3 - C_6 olefins, values of k_{on} varied over ca. 2 orders of magnitude as follows: ethene > 1-olefin > *cis*-2-olefin > *trans*-2-olefin. Equilibrium constants for the same systems were determined and showed the following order: $K_{ethene} > K_{1-olefin} > K_{trans-2-olefin} > K_{cis-2-olefin}$.

The reversible olefin binding by these molybdenum sulfide systems has potential application in the separation of low-molecular weight olefins from alkanes, and perhaps in some cases for selective separation of olefin isomers. The slow rates of olefin dissociation from the adducts ($k_{off} = 10^{-2}$ – 10^{-4} s⁻¹) make these systems unsuitable for separations in flow systems, but possible applications for fixed-bed reactors, which may be reactivated by temperature or pressure swings, are being pursued. The results of the studies reported here suggest that greater selectivity as well as faster olefin dissociation rates may be achieved by increasing the steric demands around the sulfur ligand binding site. Synthetic work to prepare appropriately substituted derivatives is in progress.

Experimental Section

Materials and Procedures. Most of the molybdenum complexes in Figure 1 were synthesized according to published methods.^{5,10} The syntheses of **4** and **5** are described below.

(19) Natile, G.; Maresca, L.; Cattalini, L.; Belluco, U.; Uguagliati, P.; Croatto, U. *Inorg. Chim. Acta* **1976**, *20*, 49.

(20) Koval, C. A.; Austermann, R. L. *J. Electrochem. Soc.* **1985**, *132*, 2656.

Olefins were purchased from commercial suppliers and used without purification. NMR spectra were recorded on a Varian VXR-300 NMR instrument. Visible spectra were recorded on a Hewlett-Packard 8451-A diode array spectrophotometer. Both FAB and EI mass spectra were obtained on a VG Analytical 7070 EQ-HF spectrometer.

Synthesis of (CpMo(μ -S))₂(μ -S₂CHCMe₃), **4.** (CpMo)₂(μ -S)₂(μ -SH)₂ (0.25 g, 0.55 mmol) was dissolved in 100 mL of distilled THF. I₂CHCMe₃ (84 μ L, 5.5×10^{-4} mol) was added to the solution with stirring. A fresh solution of NaOCH₃ (30 mg Na in 5 mL of CH₃OH) was added dropwise to the solution under positive N₂ flow and with continued stirring. The burgundy color of the solution turned green/brown upon addition of the base, and the reaction mixture was stirred at room temperature for 10 min. After the reaction mixture was filtered through Celite, the solvent was removed and the brown residue was dried under dynamic vacuum for 48 h. This solid was then redissolved in a minimum amount of CH₂Cl₂ and chromatographed on neutral alumina. A gradient elution was carried out from 100% hexanes to 100% ether. The first brown fraction was discarded, and the blue second fraction eluted with ether was collected and evaporated to dryness to give a blue solid. Yield: ca. 4%. ¹H NMR (300 MHz, CDCl₃): δ 6.50 (s, 5, Cp), 6.43 (s, 5, Cp), 2.93 (s, 1, S₂CHR), 0.79 (s, 9, (CH₃)₃). UV-vis (CDCl₃): 586 nm ($\epsilon = 2.1 \times 10^3$ M⁻¹ cm⁻¹), 728 nm ($\epsilon = 3.6 \times 10^3$ M⁻¹ cm⁻¹). MS (EI+): *m/e* 520 (P), 418 (P - SCHC(CH₃)₃), 353 (P - Cp, SCHC(CH₃)₃). Anal. Calcd for 4 \cdot 1/2H₂O (water (0.5 equiv) is detected in NMR spectrum of sample), C₁₅H₂₁Mo₂O_{0.5}S₄: C, 34.03; H, 4.00; S, 24.22. Found: C, 33.05; H, 3.88; S, 23.61.

Synthesis of (Me-CpMo(μ -S))₂S₂CHCN, **5.** [(MeCpMo(μ -S)(μ -SH))₂] (0.49 g, 1.0 mmol) was dissolved in dried THF, and Br₂CH₂CN (100 μ L, 1.1 mmol) was added. Upon addition of NEt₃ (300 μ L, 2.1 mmol), the solution turned blue green. The solution was stirred at room temperature for 3 h, and solvent was removed in vacuo. The resulting solid was purified on a neutral alumina column under N₂, using dichloromethane to elute the blue band. Yield: 6%. ¹H NMR (CDCl₃): δ 6.36, 6.55 (2 m, 8 H, C₅H₄); 3.10 (s, 1 H, S₂CHCN); 2.45, 2.40 (2s, 6 H, Cp-Me). ¹³C NMR (CDCl₃): δ 119.9, 119.8, 118.8, (CN and C_{cp}-Me); 101.4, 100.9, 98.7, 98.0 (C₅H₄); 26.7 (S₂CHCN); 17.0, 16.9 (Me-Cp). IR (KBr): 2203 cm⁻¹ (ν_{CN}). MS (EI) *m/e*: 517 (P); 478 (P - CH(CN)); 446 (P - SCH(CN)). Anal. Calcd for C₁₄H₁₅NS₄Mo₂: C, 32.49; H, 2.93; S, 24.78; N, 2.71. Found: C, 32.56; H, 2.92; S, 24.73; N, 2.68.

Synthesis and Characterization Data for Representative Olefin Adducts. (a) **Propene Adduct of (NaO₂C-CpMo(μ -S))₂S₂CH₂.** (NaO₂C-CpMo(μ -S))₂S₂CH₂, **3**, (50 mg, 0.063 mmol) was dissolved in 1 mL of H₂O. Propylene was bubbled through the solution for 5 min. During this time the color of the solution changed to dark orange. Water was removed in vacuo at room temperature, and the brown orange residue was dried in vacuo. ¹H NMR (D₂O): δ 5.74 (m, 1 H, C₅H₄); 5.70 (AB, $J = 8.8$ Hz, S₂CH₂); 5.57 (m, 1 H, C₅H₄); 5.55 (m, 1 H, C₅H₄); 5.49 (m, 1 H, C₅H₄); 5.44 (m, 1 H, C₅H₄); 5.38 (m, 1 H, C₅H₄); 5.33 (m, 1 H, C₅H₄); 5.25 (m, 1 H, C₅H₄); 2.18, 1.02 (2 dd, AM spin system, $J_{AM} = 13$ Hz, SCH₂-); 2.0 (apparent sextet, 1 H, X of AMX spin system, $J_{AX} = 6$ Hz, $J_{MX} = 8$ Hz, SCHCH₃); 0.92 (d, $J = 6$ Hz, 3 H, CH₃). Anal. Calcd for C₁₆H₁₆O₄S₂Na₂Mo₂: C, 30.10; H, 2.52; S, 20.08. Found: C, 29.78; H, 2.63; S, 18.38.

(b) **1-Hexene Adduct of (NaO₂C-CpMo(μ -S))₂S₂CH₂.** Excess hexene was added to an aqueous solution of **3** with stirring. The color of the solution changed from blue to tan and the resulting hexene adduct was isolated as a tan crystalline solid by partial removal of solvent. ¹H NMR (D₂O): δ 5.2–5.75 (8 m, inequivalent Cp H's); 8.8 (s, S₂CH₂); 2.19, 1.92, 1.13, 0.61 (m, SCH₂CHSC₄H₉). MS (FAB⁺): 680 (P); 657 (P - Na); 596 (P - C₆H₁₂ (base)); 573 (P - C₆H₁₂-Na); 550 (P - C₆H₁₂ - 2Na). Attempts to dry the product under vacuum led to loss of hexene and correct elemental analyses were not obtained.

¹H NMR Data for Olefin Adducts of (CpMo(μ -S))₂S₂CH₂(CN) in C₆D₆. Propene adduct: δ 5.33, 5.24 (2s, Cp); 5.784 (AB spin system, $J_{AB} = 7.2$ Hz, S₂CH₂); 1.95, 0.84 (2 dd, AM spin system, $J_{AM} = 11.8$ Hz, SCH₂-); 1.65 (X of AMX spin system, apparent sextet, $J_{AX} = 6.6$ Hz, $J_{MX} = 7.9$ Hz, SCHCH₃); 0.96 (d, $J = 6.6$ Hz, CH₃). 1-Butene adduct: δ 5.38, 5.32 (2s, Cp); 5.85 (AB, $J = 7.0$ Hz, S₂CH₂); 2.05, 0.98 (2 dd, AM spin system, $J_{AM} = 11.4$, SCH₂-); 1.58 (apparent quint, X of AMX spin system, $J_{AX} = 8.2$, $J_{MX} = 6.9$, SCHCH₃); 1.33, 1.09 (2m, YZ spin system, $J_{YZ} = 13.2$ Hz, J_{XZ} , $J_{XY} = 7.5$ Hz, CH₂CH₃); 0.91 (t, $J = 7.3$ Hz, CH₃). *trans*-2-Butene adduct: δ 5.28 (s, Cp); 5.74 (s, S₂CH₂); 1.17 (m, SCHCH₃); 0.98 (m, SCHCH₃). *cis*-2-Butene adduct: δ 5.40, 5.23 (2s, Cp); 5.81 (br, S₂CH₂); 1.80 (m, A₂ portion of A₂B₆ pattern, SCHCH₃); 0.80 (m, B₆ portion of pattern, $J_{AB} = 6.9$ Hz, SCHCH₃).

¹H NMR Data for Olefin Adducts of (CpMo(μ -S))₂S₂CH(CN) in C₆D₆. Ethene adduct: δ 5.47, 5.08 (2s, Cp); 5.90 (s, S₂CHCN); 1.3 (AA'BB', SC₂H₄S). Propene adduct, two isomers in a 1.1:1 ratio. Isomer 1: δ 5.49, 5.18 (2s, Cp); 5.94 (s, S₂CHCN); 0.87 (d, $J = 6.6$ Hz, CH₃). Isomer 2: 5.59, 5.10 (2s, Cp); 5.90 (s, S₂CHCN); 0.84 (d, $J = 6.6$ Hz, CH₃). Other resonances were not well resolved. 1-Butene adduct, two isomers in a 1.1:1 ratio. Isomer 1: 5.49, 5.17 (2s, Cp); 5.94 (s, S₂CHCN); 1.80, 1.15 (AX, SCH₂); 0.79 (t, $J = 6.6$ Hz, CH₃). Isomer 2: 5.58, 5.10 (2s, Cp); 5.91 (s, S₂CHCN); 0.76 (t, $J = 6.6$ Hz, CH₃). (Other aliphatic resonances not assigned to individual isomers include multiplets at 1.9, 1.8, 1.35, 1.15, and 0.9). *trans*-2-Butene adduct: 5.60, 5.18 (2s, Cp); 5.92 (s, S₂CHCN); 0.84 (m, SCHCH₃). *cis*-2-Butene adduct, two isomers in a 3:2 ratio. Isomer 1: 5.48, 5.24 (2s, Cp); 5.96 (s, S₂CHCN); 0.85 (d, $J = 7.3$ Hz, SCHCH₃). Isomer 2: 5.70, 5.08 (2s, Cp); 5.94 (s, S₂CHCN), 0.85 (d, $J = 5.4$ Hz, SCHCH₃). (Other resonances were not resolved).

General Procedure for the Determination of the Rates of Reactions of Dinuclear Complexes with Olefins. (a) **Gaseous Olefins.** Olefin was bubbled into 5 mL of deuteriated solvent containing a known quantity (5–10 mM) of the internal standard CH₃NO₂. The absolute concentration of the resultant olefin solution was determined by ¹H NMR spectroscopy by comparing intensities of olefin resonances to those of the standard. This olefin solution was further diluted with non-deuteriated solvent to make several solutions which varied in concentration from 10⁻¹ to 10⁻² M. A 2.5–3 mL aliquot of each solution was placed in a quartz cuvette equipped with a stir bar. A constant temperature of 21–22 °C was maintained by means of water circulation used to stir the solution during UV–visible measurements. A millimolar stock solution of Mo–S dimer was made by dissolving the dimer in solvent. A 50–70 μ L aliquot of this stock solution was introduced to the olefin solution in the cuvette by means of a calibrated pipette. Pseudo first order conditions were maintained by keeping the olefin in a large (50–150-fold) excess with respect to the dimer. After allowing a few seconds for mixing, the decreases in absorbance maxima of 1 at 588 and 724 nm were monitored as a function of time. (Solutions of the molybdenum complexes were found to obey Beer's law over the concentration range studied.) The absorbance measurements were recorded every 1–2 s over at least 2–3 half lives. A plot of ln[absorbance – absorbance at t_∞] vs time (s) was used to obtain k_{observed} for a specific olefin concentration. Four to seven different olefin concentrations were used in a plot of k_{observed} vs [olefin] to determine k_1 .

(b) **Liquid Olefins:** A 10⁻⁴ M stock solution of dimer was prepared, and a 2.5–3 mL aliquot of the dimer solution was placed in a standard quartz cuvette or in one equipped with an attached 25 mL reservoir and Teflon stopcock. The cuvette holder was equipped with a magnetic stirring plate and was thermally equilibrated using a constant temperature bath. Different amounts of olefin were introduced to the dimer solution via a microsyringe, ensuring a large excess. Absorbance measurements were recorded over the course of the

reaction, and values for k_{on} were determined in the same manner as above. Raw data were subjected to linear analysis, and linear correlation coefficients were 0.99 or better. The standard deviation was calculated from three to seven measurements of the rate constant.

General Procedure for the Determination of the Rates of Olefin Dissociation from Olefin Adducts. (a) **Reactions in Organic Solvents.** Deuteriated solvent containing a standard, such as CH₃NO₂ in 5–10 mM concentration, was added to the olefin adduct in an NMR tube. After three freeze–pump–thaw cycles, a large excess of ethylene or acetylene (700–760 mmHg) was vacuum transferred to the tube and the tube was sealed at –196 °C. Upon thawing, the tube was kept at 18 °C in the NMR probe, and ¹H NMR spectra were obtained at intervals during the course of the reaction. Using the internal standard, molar concentrations of reactants and products were calculated and k_{-1} was determined from a plot of ln[concentration of a product or a reactant] vs time (s). Data were subjected to linear analysis, and linear correlation coefficients were 0.99 or better. Because of the lengthy nature of the k_{off} measurements, only a small number were repeated (three times) to determine standard deviations. These are included in Table 4.

(b) **Reactions in Aqueous Solution.** In a typical experiment, a D₂O solution of complex 3 or 6, 10⁻²–10⁻³ M, and excess vinylsulfonic acid, sodium salt (25 wt % solution in water (3–6 equiv)) were placed in a flame sealable NMR tube, and an internal standard of CH₃CN (1 μ L) was added by syringe. The solution was freeze–pump–thaw degassed three times and flame sealed under vacuum. The reaction mixture was shaken on a Thermolyne shaker at ambient temperature or maintained at constant temperature in the NMR probe. Plots of natural logarithm of the concentration of the starting complex vs time were linear, checked through 90% reaction, with correlation coefficients of 0.98–0.99+.

General Procedure for the Determination of K_{eq} for the Reactions of Dinuclear Complexes with Olefins. A known amount of methanedithiolate complex was placed in an NMR tube and dissolved in deuteriated solvent (resulting in a mM solution). An internal standard, such as (CH₃O)₂CO or CH₃NO₂, was used in the solution, usually as a standard stock solution of a 5–10 mM concentration of the standard dissolved in the deuteriated solvent. After three freeze–pump–thaw cycles, olefin (<1 atm) was vacuum transferred to the tube and the tube sealed under vacuum at –196 °C. Alternatively, the olefin adduct was dissolved in deuteriated solvent containing an internal standard, such as (CH₃O)₂CO or CH₃NO₂. After three freeze–pump–thaw cycles, the tube was sealed under vacuum at –196 °C. Reaction tubes were thawed and allowed to come to equilibrium at room temperature. ¹H NMR spectra were recorded at ambient temperature over a period of days until no further changes in the spectra were measured and the reaction had reached equilibrium. K_{eq} values were calculated by relating integration or peak height values of the reactants and products to that of the standard and calculating molar concentrations. Some of the constants have large errors because of the relatively low precision of the integration values of low concentration species. On the basis of several repetitive measurements for each system, the equilibrium constants are estimated to have a standard deviation of ca. $\pm 20\%$.

Acknowledgment. This work was supported by the Office of Industrial Technology, Office of Energy Research, U.S. Department of Energy, by the NSF I/U CRC Center for Separations Using Thin Films, and by a grant from Chevron Research and Technology Company.

OM950166M

Synthesis and Characterization of a Series of Organoindium Phosphides, Including Molecular Structures of $[(\text{Me}_3\text{CCH}_2)_2\text{InPET}_2]_2$ and $[(\text{Me}_3\text{CCH}_2)_2\text{InP(H)(C}_6\text{H}_{11})]_3$

O. T. Beachley, Jr.,* John D. Maloney, and Michael A. Banks

Department of Chemistry, State University of New York at Buffalo, Buffalo, New York 14260

Robin D. Rogers*

Department of Chemistry, Northern Illinois University, DeKalb, Illinois 60115

Received February 15, 1995[®]

A series of organoindium phosphides including $(\text{Me}_3\text{CCH}_2)_2\text{InPRR}'$ ($\text{R} = \text{R}' = \text{Et}$, C_6H_{11} ; $\text{R} = \text{C}_6\text{H}_{11}$, $\text{R}' = \text{H}$; $\text{R} = \text{Me}$, $\text{R}' = \text{Ph}$) and $(\text{Me}_3\text{SiCH}_2)_2\text{InP(Me)Ph}$ have been prepared and characterized. The characterization data include partial elemental analyses (C, H), ^1H and ^{31}P NMR and IR spectral studies, physical properties, cryoscopic molecular weight studies (with the exception of $(\text{Me}_3\text{CCH}_2)_2\text{InP(C}_6\text{H}_{11})_2$), and X-ray structural studies of $[(\text{Me}_3\text{CCH}_2)_2\text{InPET}_2]_2$ and $[(\text{Me}_3\text{CCH}_2)_2\text{InP(H)(C}_6\text{H}_{11})]_3$. The compound $(\text{Me}_3\text{CCH}_2)_2\text{InPET}_2$ is observed to be a dimer in benzene solution; $(\text{Me}_3\text{CCH}_2)_2\text{InP(H)(C}_6\text{H}_{11})$ exists as a dimer–trimer equilibrium mixture, whereas $(\text{Me}_3\text{CCH}_2)_2\text{InP(Me)(Ph)}$ and $(\text{Me}_3\text{SiCH}_2)_2\text{InP(Me)(Ph)}$ are trimers. NMR studies are consistent with $(\text{Me}_3\text{CCH}_2)_2\text{InP(C}_6\text{H}_{11})_2$ being a dimer in benzene solution, but the concentration was too low to confirm the conclusion by cryoscopic molecular weight studies. The compound $[(\text{Me}_3\text{CCH}_2)_2\text{InPET}_2]_2$ contains a planar In_2P_2 core with In–P distances of 2.623(2) and 2.641(2) Å. The compound $[(\text{Me}_3\text{CCH}_2)_2\text{InP(H)(C}_6\text{H}_{11})]_3$ has an In_3P_3 six-membered ring which is in the twist-boat conformation with In–P distances ranging from 2.613(3) to 2.659(2) Å.

Group 13–15 compounds of the type $\text{R}_2\text{MER}'_2$ have been used as single-source precursors^{1–7} for ceramic and/or electronic materials and as amphoteric ligands for main-group element compounds^{8–16} and for transition metal compounds.^{17,18} In order for these types of compounds to be used most effectively for either of these

purposes, it is necessary to first understand the advantages, disadvantages, and limitations of the available preparative routes. Secondly, as these compounds are typically associated as dimers but occasionally trimers, the nature of their association and the thermodynamic factors that influence the different degrees of association and their stabilities in the different states of matter must be defined and fully understood. The monomer should be the more useful species for the preparation of materials by chemical vapor deposition because it should be more volatile. Furthermore, it is only the monomer that can be nominally classified as an amphoteric ligand. Since very few monomeric compounds^{19,20} of the type $\text{R}_2\text{MER}'_2$ have been observed, experimental observations of compounds which identify the existence of different degrees of association under different conditions or which identify equilibria between species of different degrees of association under a given set of conditions might be important for using these compounds for the above purposes.

A series of organoindium phosphides, some of which are substituted with bulky ligands, $(\text{Me}_3\text{CCH}_2)_2\text{InPET}_2$, $(\text{Me}_3\text{CCH}_2)_2\text{InP(C}_6\text{H}_{11})_2$, $(\text{Me}_3\text{CCH}_2)_2\text{InP(H)(C}_6\text{H}_{11})$, $(\text{Me}_3\text{CCH}_2)_2\text{InP(Me)(Ph)}$, and $(\text{Me}_3\text{SiCH}_2)_2\text{InP(Me)(Ph)}$, have been prepared in nearly quantitative yields by elimination reactions between the appropriate indium derivative (InR_3) and the phosphine. All reactions were carried out in heated benzene solutions such that the

[®] Abstract published in *Advance ACS Abstracts*, June 15, 1995.

(1) Cowley, A. H.; Benac, B. L.; Ekerdt, J. G.; Jones, R. A.; Kidd, K. B.; Lee, J. Y.; Miller, J. E. *J. Am. Chem. Soc.* **1988**, *110*, 6248.

(2) Andrews, D. A.; Davies, G. J.; Bradley, D. C.; Faktor, M. M.; Frigo, D. M.; White, E. A. D. *Semicond. Sci. Technol.* **1988**, *3*, 1053.

(3) Hwang, J.-W.; Hanson, S. A.; Britton, D.; Evans, J. F.; Jensen, K. F.; Gladfelter, W. L. *Chem. Mater.* **1990**, *2*, 342.

(4) Miller, J. E.; Kidd, K. B.; Cowley, A. H.; Jones, R. A.; Ekerdt, J. G.; Gysling, H. J.; Weinberg, A. A.; Blanton, T. N. *Chem. Mater.* **1990**, *2*, 589.

(5) Cowley, A. H.; Harris, P. R.; Jones, R. A.; Nunn, C. M. *Organometallics* **1991**, *10*, 652.

(6) Miller, J. E.; Ekerdt, J. G. *Chem. Mater.* **1992**, *4*, 7.

(7) Miller, J. E.; Mardones, M. A.; Nail, J. W.; Cowley, A. H.; Jones, R. A.; Ekerdt, J. G. *Chem. Mater.* **1992**, *4*, 447.

(8) Wells, R. L.; Holley, W. K.; Shafieezad, S.; McPhail, A. T.; Pitt, C. G. *Phosphorus, Sulfur Silicon Relat. Elem.* **1989**, *41*, 15.

(9) Holley, W. K.; Wells, R. L.; Shafieezad, S.; McPhail, A. T.; Pitt, C. G. *J. Organomet. Chem.* **1990**, *381*, 15.

(10) Wells, R. L.; Pasterczyk, J. W.; McPhail, A. T.; Johansen, J. D.; Alvanipour, A. J. *J. Organomet. Chem.* **1991**, *407*, 17.

(11) Holley, W. K.; Pasterczyk, J. W.; Pitt, C. G.; Wells, R. L. *Heteroat. Chem.* **1990**, *1*, 475.

(12) Wells, R. L.; Jones, L. J.; McPhail, A. T.; Alvanipour, A. *Organometallics* **1991**, *10*, 2345.

(13) Wells, R. L.; McPhail, A. T.; Self, M. F. *Organometallics* **1991**, *11*, 221.

(14) Wells, R. L.; McPhail, A. T.; Pasterczyk, J. W.; Alvanipour, A. *Organometallics* **1992**, *11*, 226.

(15) Wells, R. L.; Aubuchon, S. R.; Self, M. F.; Jasinski, J. P.; Woudenberg, R. C.; Butcher, R. J. *Organometallics* **1992**, *11*, 3370.

(16) Wells, R. L.; McPhail, A. T.; Self, M. F. *Organometallics* **1993**, *12*, 3363.

(17) Tessier-Youngs, C.; Bueno, C.; Beachley, O. T., Jr.; Churchill, M. R. *Inorg. Chem.* **1983**, *22*, 1054.

(18) Tessier-Youngs, C.; Youngs, W. J.; Beachley, O. T., Jr.; Churchill, M. R. *Organometallics* **1983**, *2*, 1128.

(19) Byrne, E. K.; Parkanyi, L.; Theopold, K. H. *Science* **1988**, *241*, 332.

(20) Higa, K. T.; George, C. *Organometallics* **1990**, *9*, 275.

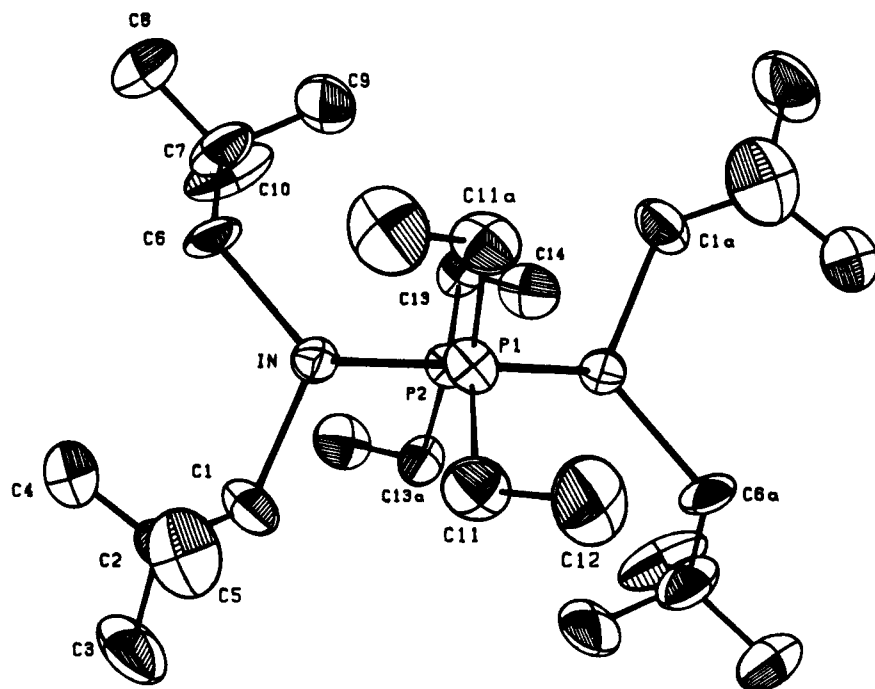


Figure 1. Labeling of atoms in $[(Me_3CCH_2)_2InPEt_2]_2$ (ORTEP diagram; 50% ellipsoids).

eliminated hydrocarbon (CMe_4 or $SiMe_4$) could be isolated, identified, and weighed. The less bulky phosphines, $HPeEt_2$ and $H_2P(C_6H_{11})_2$, were heated with $In(CH_2CMe_3)_3$ at 50 °C for 40 h each to achieve 96% yields of the corresponding products, whereas $HP(Me)(Ph)$ had to be heated with either $In(CH_2CMe_3)_3$ or $In(CH_2SiMe_3)_3$ at 80 °C for 4 days to achieve better than 95% product yields. In contrast, when the most bulky phosphine, $HP(C_6H_{11})_2$, was reacted with $In(CH_2CMe_3)_3$, heating for 21 days at 60 °C was required to achieve a yield of higher than 90%. Heating for only 7 days provided a 43% yield, whereas an additional 7 days increased the yield to only 78%. Thus, the elimination reaction between the organoindium compound and the phosphine appears to be the best reaction for preparing the indium phosphide products of highest purity for potential utilization as precursors for the chemical vapor deposition of electronic materials. This preparative method should not introduce any impurity which was not previously present in the indium or phosphorus precursors, the simplest reagents for the OMCVD process.

All compounds prepared in this investigation were characterized as fully as possible. X-ray structural studies, cryoscopic molecular weight studies in benzene solution, and ^{31}P and 1H NMR spectral studies of $[(Me_3CCH_2)_2InPEt_2]_2$ and $[(Me_3CCH_2)_2InP(H)(C_6H_{11})]_3$, including some variable temperature studies, were used to define the degrees of association of the compounds in the solid state and in solution, as appropriate. Physical properties, partial elemental analyses (C and H), and infrared spectra were used to define the identity and purity of the products.

Crystals of dineopentylindium diethylphosphide are composed of discrete dimeric units of the formula $[(Me_3CCH_2)_2InPEt_2]_2$. The labeling of the atoms in the molecule are shown in Figure 1 and the interatomic bond distances and angles are listed in Tables 1 and 2. There are no abnormally close contacts in the unit cell. The $In-P$ bond distances, 2.623(2) and 2.641(2) Å, are compared with the $In-P$ distances in a variety of other

Table 1. Interatomic Distances (Å) for $[(Me_3CCH_2)_2InPEt_2]_2$

(A) Indium-Phosphorus Distances			
$In-P(1)$	2.623(2)	$In-P(2)$	2.641(2)
(B) Indium-Carbon Distances			
$In-C(1)$	2.211(8)	$In-C(6)$	2.17(2)
$In-C(6)'$ ^a	2.29(3)		
(C) Phosphorus-Carbon Distances			
$P(1)-C(11)$	1.869(9)	$P(2)-C(13)$	1.835(8)

^a The neopentyl group $C(6)-C(10)$ is disordered.

Table 2. Angles (deg) for $[(Me_3CCH_2)_2InPEt_2]_2$ ^a

(A) Angles around the Indium Atom			
$P(1)-In-P(2)$	82.91(6)	$P(1)-In-C(1)$	111.1(2)
$P(1)-In-C(6)$	115.7(4)	$P(1)-In-C(6)'$	101.2(7)
$P(2)-In-C(1)$	100.5(2)	$P(2)-In-C(6)$	124.6(4)
$P(2)-In-C(6)'$	118.1(6)	$C(1)-In-C(6)$	116.9(5)
$C(1)-In-C(6)'$	132.2(7)		
(B) Angles around the Phosphorus Atoms			
$In-P(1)-In(a)$	97.51(9)	$In-P(2)-In(a)$	96.66(8)
$In-P(1)-C(11)$	113.5(3)	$In-P(2)-C(13)$	120.4(3)
$In-P(1)-C(11a)$	113.5(3)	$In-P(2)-C(13a)$	107.9(3)
$C(11)-P(1)-C(11a)$	105.5(5)	$C(13)-P(2)-C(13a)$	104.5(5)
(C) Indium-Carbon-Carbon Angles			
$In-C(1)-C(2)$	118.7(6)	$In-C(6)-C(7)$	123(1)
		$In-C(6)'-C(7)$	119(1)
(D) Phosphorus-Carbon-Carbon Angles			
$P(1)-C(11)-C(12)$	112.1(7)	$P(2)-C(13)-C(14)$	113.3(6)

^a Symmetry code denoted by the prime: $-x, y, 1/2 - z$.

dimers and trimers in Table 3. The four-membered ring is planar as are all other $(R_2InPR_2)_2$ compounds which have been structurally characterized (Table 3). The angles within the ring are smaller than the regular tetrahedral angle with observed values of $In-P(1)-In(a) = 97.51(9)^\circ$, $In-P(2)-In(a) = 96.66(8)^\circ$, and $P(1)-In-P(2) = 82.91(6)^\circ$.

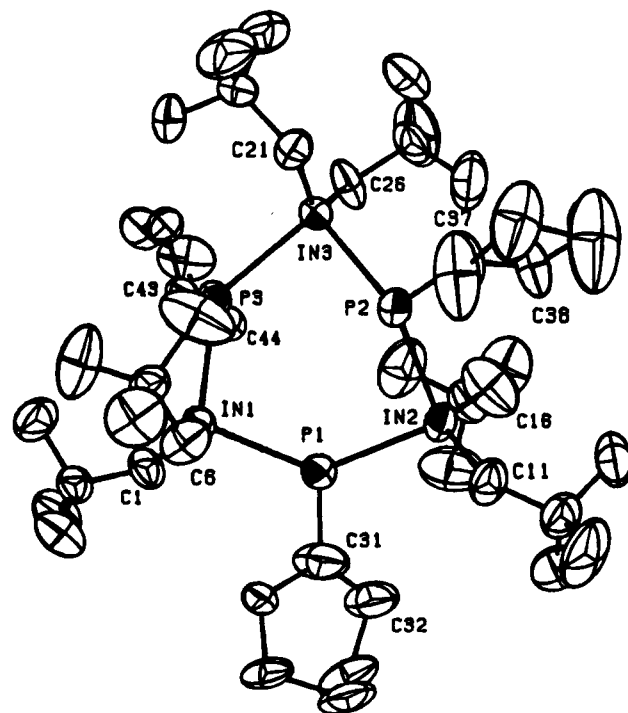
Cryoscopic molecular weight studies and NMR spectral data indicate that $(Me_3CCH_2)_2InPEt_2$ exists as dimeric species in benzene solution, as was observed in the solid state. The molecular weight and NMR (1H and ^{31}P) spectral data were independent of concentration,

Table 3. Indium–Phosphorus Bond Distances for Compounds of the Type $[\text{R}_2\text{InPR}'_2]_n$

compd	$d(\text{InP})$ (Å)		ref
$[(\text{Me}_3\text{CCH}_2)_2\text{InPET}_2]_2$	2.623(2)		this work
	2.641(2)		
$[(\text{Me}_3\text{CCH}_2)_2\text{InP}(\text{H})(\text{C}_6\text{H}_{11})]_3$	2.613(3)	2.637(3)	this work
	2.625(3)	2.645(3)	
	2.644(3)	2.659(2)	
$[(\text{Me}_3\text{CCH}_2)_2\text{InPPh}_2]_3$	2.677(1)		21
	2.699(2)		
$[(\text{Me}_3\text{SiCH}_2)_2\text{InPPh}_2]_2$	2.664(2)	2.659(2)	22
	2.643(2)	2.632(2)	
$[\text{Me}_2\text{InP}(\text{t-Bu})_2]_2$	2.656(4)		23
	2.637(4)		
$[\text{Et}_2\text{InP}(\text{t-Bu})_2]_2$	2.635(2)		24
$[(\text{Me}_3\text{SiCH}_2)_2\text{InP}(\text{SiMe}_3)_2]_2$	2.654(2)		13
	2.656(2)		
$[(\text{Me}_3\text{SiCH}_2)_2\text{InP}(\text{H})(\text{t-Bu})]_2$	2.633(1)		25
	2.638(1)		
$[(\text{C}_5\text{Me}_5)(\text{Cl})\text{InP}(\text{SiMe}_3)_2]_2$	2.648(2)		26
	2.594(1)		

an observation which suggests the absence of species other than dimer. The ^1H spectrum had lines for the methyl and methylene protons on phosphorus which were a triplet of doublets of doublets and a quartet of doublets of doublets, respectively. Thus, the lines for methyl group appeared as a pentet centered at 1.02 ppm with a coupling constant of 7.4 Hz and the methylene lines as an apparent quartet of triplets at 1.79 ppm ($^2J_{\text{HCH}} = 7.5$ Hz, $^2J_{\text{PCH}} = 2.0$ Hz). The methyl protons of the neopentyl groups were a singlet at 1.22 ppm, whereas the methylene protons of the neopentyl groups were a triplet at 1.20 ppm ($^3J_{\text{PGa-CH}} = 2.1$ Hz). The triplet for the methylene protons of the neopentyl group has been observed previously for other related derivatives^{21,27} and arises from coupling between the protons and the two phosphorus atoms. Similar coupling may explain the multiplicities of the lines for the CH_2 and CH_3 protons of the ethyl groups bound to phosphorus. The $^{31}\text{P}\{^1\text{H}\}$ NMR spectrum in d_6 -benzene was a single line at -52.2 ppm.

The monocyclohexylphosphide derivative $(\text{Me}_3\text{CCH}_2)_2\text{-InP}(\text{H})(\text{C}_6\text{H}_{11})$ was isolated as a colorless crystalline solid which sublimed at 80°C under high vacuum. Upon further heating, the compound underwent a glass transition at $120\text{--}125^\circ\text{C}$ and then melted over the relatively broad range $131\text{--}140^\circ\text{C}$. Similar phase changes or glass transitions have been observed for other group 13–15 compounds,^{28–31} including some neopentyl derivatives.^{22,27} A glass transition, however, was not observed for $[(\text{Me}_3\text{CCH}_2)_2\text{InPET}_2]_2$. These glass

**Figure 2.** Labeling of atoms in $[(\text{Me}_3\text{CCH}_2)_2\text{InP}(\text{H})(\text{C}_6\text{H}_{11})]_3$ (ORTEP diagram; 50% ellipsoids).**Table 4. Interatomic Distances (Å) for $[(\text{Me}_3\text{CCH}_2)_2\text{InP}(\text{H})(\text{C}_6\text{H}_{11})]_3$**

(A) Indium–Phosphorus Distances			
In(1)–P(1)	2.644(3)	In(1)–P(3)	2.613(3)
In(2)–P(2)	2.645(3)	In(2)–P(1)	2.637(3)
In(3)–P(3)	2.659(2)	In(3)–P(2)	2.625(3)
(B) Indium–Carbon Distances			
In(1)–C(1)	2.195(8)	In(1)–C(6)	2.22(1)
In(2)–C(11)	2.20(1)	In(2)–C(16)	2.19(2)
In(3)–C(21)	2.188(9)	In(3)–C(26)	2.16(1)
(C) Phosphorus–Carbon Distances			
P(1)–C(31)	1.83(2)	P(2)–C(37)	1.88(1)
P(3)–C(43)	1.871(7)		

transitions have been suggested to be due to changes in the degree of association of the compound with heating.^{29,30} After $(\text{Me}_3\text{CCH}_2)_2\text{InP}(\text{H})(\text{C}_6\text{H}_{11})$ melted, further heating caused the sample to turn yellow with bubbling at $150\text{--}170^\circ\text{C}$. Then the sample resolidified. These observations suggest the elimination of additional neopentane, but further investigations of this reaction were not pursued.

Crystals of dineopentylindium monocyclohexylphosphide consisted of discrete trimeric units of the formula $[(\text{Me}_3\text{CCH}_2)_2\text{InP}(\text{H})(\text{C}_6\text{H}_{11})]_3$, which are mutually separated by normal van der Waals distances. The labeling of the atoms in the molecule is shown in Figure 2, whereas interatomic bond distances and angles are listed in Tables 4 and 5. The In_3P_3 ring for $[(\text{Me}_3\text{CCH}_2)_2\text{-InP}(\text{H})(\text{C}_6\text{H}_{11})]_3$ has a twist-boat conformation. The internal ring angles are distorted from the regular tetrahedral angle and range from $128.90(9)^\circ$ to $132.18(8)^\circ$ for In–P–In and from $92.85(8)^\circ$ to $101.18(9)^\circ$ for P–In–P, respectively. The ring conformation shown in Figure 2 reveals that the cyclohexyl substituents occupy the E,E,A (equatorial, equatorial, axial) positions on the In_3P_3 ring (twist-boat). Similar observations of E,E,A

(21) Banks, M. A.; Beachley, O. T., Jr.; Buttrey, L. A.; Churchill, M. R.; Fetting, J. C. *Organometallics* **1991**, *10*, 1901.

(22) Beachley, O. T., Jr.; Kopasz, J. P.; Zhang, H.; Hunter, W. E.; Atwood, J. L. *J. Organomet. Chem.* **1987**, *325*, 69.

(23) Aitchison, K. A.; Baker-Dirks, J. D. J.; Bradley, D. C.; Faktor, M. M.; Frigo, D. M.; Hursthouse, M. B.; Hussain, B.; Short, R. L. *J. Organomet. Chem.* **1989**, *336*, 11.

(24) Alcock, N. W.; Degan, I. E.; Wallbridge, M. G. H.; Powell, H. R.; McPartlin, M.; Sheldrick, G. M. *J. Organomet. Chem.* **1989**, *361*, C33.

(25) Dembowski, U.; Noltemeyer, M.; Rockensüss, W.; Stuke, M.; Roesky, H. W. *Chem. Ber.* **1990**, *123*, 2335.

(26) Theopold, K. H.; Douglas, T. *Inorg. Chem.* **1991**, *30*, 594.

(27) Beachley, O. T., Jr.; Banks, M. A.; Churchill, M. R.; Feighery, W. G.; Fetting, J. C. *Organometallics* **1991**, *10*, 3036.

(28) Coates, G. E.; Graham, J. *J. Chem. Soc.* **1963**, 233.

(29) Beachley, O. T., Jr.; Coates, G. E. *J. Chem. Soc.* **1965**, 3241.

(30) Beachley, O. T., Jr.; Coates, G. E.; Kohnstam, G. *J. Chem. Soc.* **1965**, 3248.

(31) Beachley, O. T., Jr.; Tessier-Youngs, C. *Organometallics* **1983**, *2*, 796.

(32) Janik, J. F.; Duesler, E. N.; McNamara, W. F.; Westerhausen, M.; Paine, R. T. *Organometallics* **1989**, *8*, 506.

Table 5. Angles (deg) for $[(Me_3CCH_2)_2InP(H)(C_6H_{11})]_3$

(A) Angles around the Indium Atoms			
P(1)-In(1)-P(3)	101.18(9)	P(1)-In(1)-C(1)	98.1(3)
P(3)-In(1)-C(1)	106.5(3)	P(1)-In(1)-C(6)	104.4(3)
P(3)-In(1)-C(6)	113.3(3)	C(1)-In(1)-C(6)	128.6(5)
P(1)-In(2)-P(2)	92.85(8)	P(1)-In(2)-C(11)	105.5(3)
P(2)-In(2)-C(11)	104.5(3)	P(1)-In(2)-C(16)	118.3(4)
P(2)-In(2)-C(16)	103.5(5)	C(11)-In(2)-C(16)	125.9(5)
P(2)-In(3)-P(3)	93.69(8)	P(2)-In(3)-C(21)	98.4(3)
P(3)-In(3)-C(21)	108.0(3)	P(2)-In(3)-C(26)	113.9(3)
P(3)-In(3)-C(26)	107.0(3)	C(21)-In(3)-C(26)	129.9(5)
(B) Angles around the Phosphorus Atoms			
In(1)-P(1)-In(2)	130.1(1)	In(2)-P(1)-C(31)	107.2(5)
In(2)-P(2)-In(3)	132.18(8)	In(1)-P(1)-C(31)	107.6(6)
In(2)-P(2)-C(37)	112.1(4)	In(3)-P(2)-C(37)	107.0(4)
In(1)-P(3)-In(3)	128.90(9)	In(1)-P(3)-C(43)	105.8(3)
In(3)-P(3)-C(43)	115.1(3)		
(C) Indium-Carbon-Carbon Angles			
In(1)-C(1)-C(2)	120.4(6)	In(1)-C(6)-C(7)	120.5(8)
In(2)-C(11)-C(12)	119.7(7)	In(2)-C(16)-C(17)	125(1)
In(3)-C(21)-C(22)	121.3(6)	In(3)-C(26)-C(27)	119.4(6)
(D) Phosphorus-Carbon-Carbon Angles			
P(1)-C(31)-C(32)	114(1)	P(1)-C(31)-C(36)	122(1)
P(1)-C(31)-C(36)'	117(1)	P(2)-C(37)-C(38)	112.4(8)
P(2)-C(37)-C(42)	113(1)	P(3)-C(43)-C(44)	110.6(6)
P(3)-C(43)-C(48)	111.6(6)		

positions for the cyclohexyl group in $[(Me_3Si)_2AlP(H)(C_6H_{11})]_3$ ³² have been reported also. It has been suggested that the cyclohexyl groups in the E,E,A positions on the twist-boat conformation minimize the steric interactions between the cyclohexyl groups and the substituents on the metal.³² Other angles including C-In-C (range from 125.9(5)° to 129.9(5)°) and In-C-C (range from 119.4(6)° to 125(1)°) are also distorted from the ideal tetrahedral value of 109.47°.

Comparisons between the In-P bond lengths in $[(Me_3CCH_2)_2InP(H)(C_6H_{11})]_3$ and indium phosphide dimers (Table 3) suggest that no correlation exists between In-P bond distances and the degree of association. The In-P bond distances for $[(Me_3CCH_2)_2InP(H)(C_6H_{11})]_3$ range from 2.613(3) to 2.659(2) Å. These In-P distances are comparable to the In-P bond distances in $[(Me_3CCH_2)_2InPEt_2]_2$ of 2.623(2) Å and 2.641(2) Å and all the other indium phosphide dimers. However, the In-P bond distances for $[(Me_3CCH_2)_2InPPh_2]_3$ ²¹ of 2.677(1) and 2.699(2) Å are longer.

Concentration dependent ³¹P NMR spectra and molecular weight studies suggest that $(Me_3CCH_2)_2InP(H)(C_6H_{11})_2$ exists as a dimer-trimer equilibrium in benzene solution. Two sets of lines were observed in the ³¹P-{¹H} NMR spectrum at molal concentrations of 0.043-0.151 m. The ³¹P-{¹H} NMR spectrum of the 0.043 m solution exhibited two lines at -82.6 and -90.7 ppm, assigned to phosphorus atoms of the *cis* and *trans* isomers of the dimer, and eight lines from -112.3 to -114.4 ppm, assigned to the phosphorus atoms in the multiple conformations of the ring and/or orientations of substituents on the trimer. The ratio of the peak heights for the dimer to trimer lines was 1.0:5.3. When the concentration was increased to 0.151 m, the spectrum revealed similar lines, but the ratio of the peak heights for the dimer to trimer decreased (1.0:14.8) while the chemical shifts of the lines did not change. The ³¹P-{¹H} NMR spectrum of the 0.043 m solution was also investigated as a function of temperature, 20-60 °C. As the temperature increased, the ratio of peak heights of the dimer to trimer increased. This observa-

tion suggests the dimer to be more stable relative to the trimer at the higher temperature. Thus, enthalpies of solvation and entropies should be important factors. Since the ¹H NMR spectrum revealed multiple lines for both the neopentyl and the cyclohexyl groups that overlapped, assignments of the resonances to specific protons was not attempted.

The compounds $(Me_3CCH_2)_2InP(Me)Ph$ and $(Me_3SiCH_2)_2InP(Me)Ph$ were prepared readily by elimination reactions between $HP(Me)Ph$ and $In(CH_2CMe_3)_3$ or $In(CH_2SiMe_3)_3$, respectively. Dineopentylindium methylphenylphosphide was a colorless glassy solid which melted to a viscous oil at 30-52 °C whereas $(Me_3SiCH_2)_2InP(Me)Ph$ was a colorless viscous oil at room temperature. Cryoscopic molecular weight studies suggested that both $(Me_3CCH_2)_2InP(Me)Ph$ and $(Me_3SiCH_2)_2InP(Me)Ph$ were trimeric in benzene solution. The complexity of the ¹H and ³¹P NMR spectra of $(Me_3CCH_2)_2InP(Me)Ph$ and $(Me_3SiCH_2)_2InP(Me)Ph$ indicate a mixture of isomers of trimeric species in benzene. These isomers arise from the different orientations of the methyl and phenyl groups and/or different conformations of the ring.

The elimination reaction has also been utilized for the preparation of $(Me_3CCH_2)_2InP(C_6H_{11})_2$ from $In(CH_2CMe_3)_3$ and $HP(C_6H_{11})_2$, but heating in benzene at 60 °C for 21 days was required. The product was isolated in high yield (ca. 89%) as a colorless crystalline solid that was insoluble at room temperature in typical solvents, including hydrocarbons, THF, Et₂O, and aromatic solvents. These solubility characteristics precluded cryoscopic molecular weight studies and extensive NMR studies. The crystalline solid had elemental analyses consistent with the empirical formula.

The limited experimental observations suggest that $(Me_3CCH_2)_2InP(C_6H_{11})_2$ exists as a dimer. The ³¹P-{¹H} NMR spectrum of $(Me_3CCH_2)_2InP(C_6H_{11})_2$ in *d*₈-toluene at 70 °C revealed a singlet at -13.00 ppm. Since the chemical shift for $(Me_3CCH_2)_2InP(C_6H_{11})_2$ was only 2.43 ppm downfield from the corresponding gallium analog,³³ $[(Me_3CCH_2)_2GaP(C_6H_{11})_2]_2$, which was dimeric in benzene solution, $(Me_3CCH_2)_2InP(C_6H_{11})_2$ might be expected to be dimeric also. The weak Lewis basicity and large size of dicyclohexylphosphide would be expected to favor a low degree of association. It should be noted that $(Me_3CCH_2)_2InP(C_6H_{11})_2$ does not melt below 200 °C but decomposes at 225-229 °C. These observations suggest that $(Me_3CCH_2)_2InP(C_6H_{11})_2$ is not a simple monomer. It is noteworthy that $[Me_2InP(t-Bu)_2]_2$ exists as a dimer in the solid state and that it is also insoluble in Et₂O, hydrocarbons, and aromatic solvents.²³

Experimental Section

All compounds described in this investigation were extremely sensitive to oxygen and moisture and were manipulated in a standard vacuum line or under a purified argon atmosphere. The compounds $In(CH_2SiMe_3)_3$ ³⁴ and $In(CH_2CMe_3)_3$ ³⁵ were prepared and purified by literature methods. Dicyclohexylphosphine was purchased from Alfa Products, $HP(Me)Ph$ was purchased from Strem Chemicals, Inc., and $HPEt_2$ and $H_2P(C_6H_{11})$ were generous gifts from the Eastman Kodak

(33) Maloney, J. D., Ph.D. Thesis, State University of New York at Buffalo, Buffalo, NY, 1991.

(34) Beachley, O. T., Jr.; Rusinko, R. N. *Inorg. Chem.* **1979**, *18*, 1966.

(35) Beachley, O. T., Jr.; Spiegel, E. F.; Kopasz, J. P.; Rogers, R. D. *Organometallics* **1989**, *8*, 1915.

Table 6. Crystal Data and Summary of Intensity Data Collection and Structure Refinement of $[(\text{Me}_3\text{CCH}_2)_2\text{InPET}_2]_2$

molecular formula	$\text{C}_{28}\text{H}_{64}\text{In}_2\text{P}_2$
color/shape	colorless/parallelepiped
mol wt	684.34
space group	$C2/c$
temp, °C (K)	22 (295)
cell constants ^a	
<i>a</i> , Å	12.972(2)
<i>b</i> , Å	15.539(5)
<i>c</i> , Å	18.255(3)
β , deg	99.84(1)
<i>V</i> , Å ³	3625.6
<i>Z</i>	4
<i>D</i> _{calcd} , g cm ⁻³	1.25
μ _{calcd} , cm ⁻¹	13.6
diffractometer/scan	Enraf-Nonius CAD-4/ $\omega-2\theta$
range of rel transmissn factors, %	89/100
radiation, graphite monochromator (λ , Å)	Mo K α ($\lambda = 0.71073$)
max cryst dimens, mm ³	0.20 × 0.30 × 0.35
scan width	0.80 + 0.35 tan θ
no. of std reflns	600; 080; 0, 0, 14
no. of std reflns measd	±2%
no. of reflns measd	3454
2 θ range, deg	2 ≤ 2 θ ≤ 50
range of <i>h</i> , <i>k</i> , <i>l</i>	+15, +18, ±21 (<i>h</i> + <i>k</i> = 2 <i>n</i> only)
no. of reflns obsd	2261
[<i>F</i> _o ≥ 5 σ (<i>F</i> _o)] ^b	
computer programs ^c	SHELX ³⁷
structure solution	SHELXS ³⁸
no. of params varied	175
weights	[$\sigma(F_o)^2 + 0.002F_o^2$] ⁻¹
GOF	1.10
$R = \sum F_o - F_c / \sum F_o $	0.045
<i>R</i> _w	0.076
largest feature in final diff map, e Å ⁻³	0.6

^a Least-squares refinement of $(\sin \theta / \lambda)^2$ values for 25 reflections $\theta > 19^\circ$. ^b Corrections: Lorentz-polarization and absorption (empirical, ψ scan). ^c Neutral scattering factors and anomalous dispersion corrections from ref 39.

Company. All phosphines were purified by distillation prior to use. Solvents were dried by conventional procedures. Elemental analyses were performed by E+R Microanalytical Laboratory, Inc., Corona, NY, or Schwarzkopf Microanalytical Laboratory, Woodside, NY. Infrared spectra of Nujol mulls between CsI plates were recorded by means of a Perkin-Elmer 683 spectrometer. The ¹H spectra were recorded at 300 MHz by using a Varian Gemini-300 spectrometer. Proton chemical shifts are reported in δ units (ppm) and are referenced to SiMe₄ at δ 0.00 and C₆D₆ at δ 7.15. The ³¹P NMR spectrum was recorded at 161.9 MHz on a Varian VXR-400 spectrometer. Proton-decoupled ³¹P NMR spectra were referenced to 85% H₃PO₄ at δ 0.00. All samples for NMR spectra were contained in sealed NMR tubes. Melting points were observed in sealed capillaries. Molecular weights were measured cryoscopically in benzene by using an instrument similar to that described by Shriver and Drezdson.³⁶

Synthesis of $(\text{Me}_3\text{CCH}_2)_2\text{InPET}_2$. A tube with a Teflon valve was charged with 0.641 g (7.11 mmol) of HPET₂. A 100-mL Schlenk flask equipped with a 20-mm Solv-Seal joint was charged with 2.335 g (7.111 mmol) of In(CH₂CMe₃)₃ in the

Table 7. Final Fractional Coordinates for $[(\text{Me}_3\text{CCH}_2)_2\text{InPET}_2]_2$

Atom	<i>x/a</i>	<i>y/b</i>	<i>z/c</i>	<i>B</i> (eq ²)
In	0.15096(4)	0.87403(3)	0.24587(3)	2.47
P(1)	0.0000	0.7627(2)	0.2500	2.65
P(2)	0.0000	0.9870(2)	0.2500	2.25
C(1)	0.2453(7)	0.8929(6)	0.3576(5)	3.66
C(2)	0.3422(6)	0.8353(5)	0.3815(4)	2.68
C(3)	0.393(1)	0.8615(9)	0.4616(7)	6.01
C(4)	0.4219(8)	0.8468(8)	0.3304(6)	4.78
C(5)	0.3114(9)	0.7398(6)	0.3801(7)	5.26
C(6)	0.236(1)	0.860(1)	0.1540(8)	3.33
C(6) [']	0.196(2)	0.843(2)	0.133(1)	5.24
C(7)	0.2110(8)	0.9139(7)	0.0823(5)	4.35
C(8)	0.2780(9)	0.8895(7)	0.0234(6)	5.09
C(9)	0.093(1)	0.889(2)	0.050(1)	5.21
C(10)	0.208(2)	1.004(1)	0.091(1)	6.26
C(9) [']	0.125(2)	0.956(2)	0.048(1)	7.72
C(10) [']	0.293(2)	0.988(2)	0.136(1)	7.15
C(11)	0.0242(7)	0.6899(5)	0.3327(5)	3.59
C(12)	-0.070(1)	0.6320(6)	0.3376(8)	5.40
C(13)	-0.0419(6)	1.0592(5)	0.1710(4)	3.10
C(14)	-0.1284(9)	1.1242(6)	0.1846(6)	4.56

^a $B(\text{eq}) = 4/3[a^2\beta_{11} + b^2\beta_{22} + c^2\beta_{33} + ab(\cos \gamma)\beta_{12} + ac(\cos \beta)\beta_{13} + bc(\cos \alpha)\beta_{23}]$. ^b Primed and unprimed atoms of like numbers are disordered. C(6), C(9), and C(10) are present at 55% occupancy, while their primed counterparts have 45% occupancy.

glovebox. The Schlenk flask was capped, cooled to -196 °C, and evacuated. The HPET₂ was vacuum distilled into the Schlenk flask along with 30 mL of benzene. The reaction mixture was warmed to ambient temperature, and then the Schlenk flask was immersed into a 50 °C oil bath for 6 days. The volatile components were removed and fractionated through two -78 °C traps into a -196 °C trap. Neopentane (0.466 g, 6.46 mmol, 90.9% yield based on In(CH₂CMe₃)₃) was isolated in the -196 °C trap and identified by ¹H NMR spectroscopy. The Schlenk flask was fitted with a medium frit equipped with a Schlenk receiving vessel. One extraction with 30 mL of benzene provided a soluble, colorless solid (Me₃CCH₂)₂InPET₂ (2.080 g, 6.907 mmol, 97.13% yield based on In(CH₂CMe₃)₃). Crystallographic quality crystals were obtained from a saturated pentane solution maintained at -10 °C. Mp: 105–106 °C, sublimes at 70 °C/0.01 mmHg. ¹H NMR (C₆D₆, δ): 1.02 (tdd, see Discussion, ²*J*_{HCH} = 7.4 Hz, 2.7 H, -CH₃), 1.20 (t, ³*J*_{PGACH} = 2.1 Hz, 2.0 H, In-CH₂-), 1.22 (s, 7.0 H, -CMe₃), 1.79 (qdd, see Discussion, ²*J*_{HCH} = 7.5 Hz, ²*J*_{PCH} = 2.0 Hz, 1.7 H, P-CH₂-). ³¹P{¹H} NMR (C₆D₆, δ): -52.19 (s). Anal. Calcd: C, 48.45; H, 9.24. Found: C, 48.44; H, 9.37. Cryoscopic molecular weight, fw 346.52 (obsd molality, obsd mol wt, association): 0.0805, 746, 2.15; 0.0658, 744, 2.15; 0.0529, 745, 2.15. IR (Nujol mull, cm⁻¹): 2725 (vw), 2698 (vw), 1412 (m), 1352 (vs), 1210 (sh), 1105 (m), 1092 (m), 1036 (s), 1020 (m), 1008 (m), 968 (m), 926 (w), 907 (w), 757 (m), 739 (m), 717 (m), 689 (vs), 680 (vs), 660 (m), 568 (m), 555 (sh), 448 (w), 258 (vw), 237 (w).

Synthesis of $(\text{Me}_3\text{CCH}_2)_2\text{InP(H)(C}_6\text{H}_{11})$. The compound (Me₃CCH₂)₂InP(H)(C₆H₁₁) was prepared from In(CH₂CMe₃)₃ (1.941 g, 5.912 mmol) and H₂PC₆H₁₁ (0.687 g, 5.91 mmol) in benzene by using the method previously described for (Me₃CCH₂)₂InPET₂. After the reaction mixture was maintained at 50 °C for 40 h, neopentane CMe₄ (0.409 g, 5.67 mmol, 95.9% yield based on In(CH₂CMe₃)₃) was collected. Two extractions with 30 mL of benzene yielded a colorless solid (Me₃CCH₂)₂InP(H)(C₆H₁₁) (1.919 g, 5.156 mmol, 90.9% yield based on In(CH₂CMe₃)₃). Crystallographic quality crystals were obtained from a saturated benzene solution that was prepared by heating the same sample to 50 °C and then cooling the solution to ambient temperature. Mp: glass transition at 120–125 °C, melts at 131–140 °C, bubbles at 150–170 °C. ¹H NMR (C₆D₆, δ): 1.18 (m, -CH₂-), 1.23 (s, -CMe₃), 1.28 (s, -CMe₃), 1.41 (s, C₆H₁₁), 1.47 (s, C₆H₁₁), 1.51 (d, ²*J*_{HCH} = 10.5 Hz, C₆H₁₁), 1.67 (s, C₆H₁₁), 2.07 (d, ²*J*_{HCH} = 10.5 Hz, C₆H₁₁), 2.21 (m, C₆H₁₁), 2.48 (m, P-H), 3.32 (m, P-H). ³¹P{¹H} NMR

(36) Shriver, D. F.; Drezdson, M. A. *The Manipulation of Air Sensitive Compounds*; Wiley: New York, 1986; p 38.

(37) Sheldrick, G. M. *SHELX 76*, Programs for X-ray Structure Determination as Locally Modified, University of Cambridge: Cambridge, England, 1976.

(38) Sheldrick, G. M. *SHELXS. Acta Crystallogr.* **1990**, *A46*, 467.

(39) *International Tables for X-ray Crystallography*; Kynoch Press: Birmingham, England, 1974; Vol. 4, 1974, pp 72, 99, 149. (Present distributor: Kluwer Academic Publishers: Boston, MA.)

Table 8. Crystal Data and Summary of Intensity Data Collection and Structure Refinement of [(Me₃CCH₂)₂InP(H)(C₆H₁₁)]₃

molecular formula	C ₄₈ H ₆₉ In ₃ P ₃
color/shape	colorless/parallelepiped
mol wt	1116.7
space group	P $\bar{1}$
temp, °C (K)	20 (293)
cell constants ^a	
<i>a</i> , Å	11.272(3)
<i>b</i> , Å	13.992(5)
<i>c</i> , Å	20.539(9)
α, deg	95.37(5)
β, deg	104.83(4)
γ, deg	109.14(4)
V, Å ³	2901.9
Z	2
D _{calcd} , g cm ⁻³	1.28
μ _{calcd} , cm ⁻¹	12.87
diffractometer/scan	Enraf-Nonius CAD-4/ω-2θ
range of rel transmissn factors, %	85/100
radiation, graphite monochromator (λ, Å)	Mo Kα (λ = 0.710 73)
max cryst dimens, mm ³	0.15 × 0.30 × 0.35
scan width	0.80 + 0.35 tan θ
no. of std reflns	400; 030; 006
decay of std reflns	±3%
no. of reflns measd	10 246
2θ range, deg	2 ≤ 2θ ≤ 50
range of <i>h, k, l</i>	+9, +12, ±17
no. of reflns obsd [<i>F</i> _o ≥ 5σ(<i>F</i> _o)] ^b	6051
computer programs ^c	SHELX ³⁷
structure solution	SHELXS ³⁸
no. of params varied	523
weights	[σ(<i>F</i> _o) ² + 0.008 <i>F</i> _o ²] ⁻¹
GOF	0.40
<i>R</i> = Σ <i>F</i> _o - <i>F</i> _c /Σ <i>F</i> _o	0.054
<i>R</i> _w	0.078
largest feature in final diff map, e Å ⁻³	1.2 near In(2)

^a Least-squares refinement of ((sin θ)/λ)² values for 25 reflections θ > 20°. ^b Corrections: Lorentz-polarization and absorption (empirical, ψ scan). ^c Neutral scattering factors and anomalous dispersion corrections from ref 39.

(0.043 M, C₆D₆, δ): -82.62 (s, 2.9), -90.68 (s, 1.7), -106.2 (s, 0.5), -106.7 (s, 0.4), -112.3 (s, 1.0), -112.7 (s, 1.0), -112.9 (s, 1.6), -113.2 (s, 2.3), -113.3 (s, 5.5), -113.8 (s, 8.0), -114.2 (s, 2.8), -114.4 (s, 2.3). ³¹P{¹H} NMR (0.043 M at 40 °C, C₆D₆, δ): -82.95 (s, 5.4), -90.90 (s, 3.5), -112.3 (s, 1.0), -112.7 (s, 1.0), -112.9 (s, 1.8), -113.3 (s, 7.1), -113.8 (s, 7.0), -114.2 (s, 2.9), -114.4 (s, 2.4). ³¹P{¹H} NMR (0.043 m at 60 °C, C₆D₆, δ): -83.30 (s, 9.1), -91.17 (s, 6.8), -112.2 (s, 1.0), -112.6 (s, 1.2), -112.9 (s, 1.8), -113.3 (s, 10.9), -113.7 (s, 6.8), -114.0 (s, 2.6), -114.3 (s, 1.8). ³¹P{¹H} NMR (0.151 m, C₆D₆, δ): -82.3 (s, 1.7), -90.4 (s, 1.0), -106.2 (s, 0.4), -106.7 (s, 0.3), -112.3 (s, 1.1), -112.8 (s, 1.4), -112.9 (s, 2.2), -113.2 (s, 7.9), -113.3 (s, 5.7), -114.0 (s, 13.4), -114.4 (s, 4.4), -114.5 (s, 3.8). Anal. Calcd: C, 51.62; H, 9.21. Found: C, 51.77; H, 9.22. Cryoscopic molecular weight, fw 371.78 (obsd molality, obsd mol wt, association): 0.0754, 1041, 2.80; 0.0584, 1052, 2.83; 0.0441, 1029, 2.76. IR (Nujol mull, cm⁻¹): 2325 (m), 2303 (m), 2290 (m), 1354 (vs), 1292 (m), 1258 (m), 1230 (vs), 1190 (m), 1173 (m), 1105 (s), 1090 (s), 1068 (w), 1045 (w), 1008 (m), 995 (s), 928 (vw), 914 (w), 907 (w), 892 (m), 885 (m), 848 (m), 820 (m), 805 (m), 740 (m), 719 (m), 686 (s), 670 (s), 620 (w), 600 (w), 568 (s), 506 (vw), 445 (m), 375 (w), 343 (m), 290 (m).

Synthesis of (Me₃CCH₂)₂InP(Me)Ph. The compound (Me₃CCH₂)₂InP(Me)Ph was prepared from In(CH₂CMe₃)₃ (3.321 g, 10.118 mmol) and HP(Me)Ph (1.256 g, 10.118 mmol) in benzene by using the method previously described for (Me₃CCH₂)₂InPEt₂. Heating at 80 °C for 4 days gave 0.714 g CMe₄, 9.90 mmol, 97.8% yield based on In(CH₂CMe₃)₃. The crude product was extracted with 45 mL of anhydrous pentane to yield (Me₃CCH₂)₂InP(Me)Ph as a colorless material (3.202 g,

Table 9. Final Fractional Coordinates for [(CH₃CH₂)₂InP(H)(C₆H₁₁)]₃

atom	<i>x/a</i>	<i>y/b</i>	<i>z/c</i>	B(eq ²)
In(1)	0.11661(6)	0.51323(4)	0.24386(3)	2.77
In(2)	0.15441(6)	0.83677(5)	0.17487(3)	3.27
In(3)	-0.01876(6)	0.74770(4)	0.36161(3)	3.21
P(1)	0.1225(2)	0.6398(2)	0.1559(1)	3.40
P(2)	0.1579(2)	0.8441(2)	0.3045(1)	3.39
P(3)	-0.0307(2)	0.5618(2)	0.3106(1)	3.02
C(1)	-0.010(1)	0.3687(7)	0.1708(5)	3.93
C(2)	0.0029(9)	0.2664(7)	0.1849(5)	3.54
C(3)	0.138(1)	0.269(1)	0.1906(7)	6.03
C(4)	-0.037(1)	0.2435(9)	0.2503(6)	5.98
C(5)	-0.103(1)	0.1781(9)	0.1218(7)	5.75
C(6)	0.326(1)	0.5599(9)	0.3072(5)	4.55
C(7)	0.3606(9)	0.5631(7)	0.3839(5)	3.56
C(8)	0.329(1)	0.648(1)	0.4187(7)	7.11
C(9)	0.511(1)	0.583(1)	0.4120(7)	5.82
C(10)	0.282(2)	0.463(1)	0.4006(8)	7.60
C(11)	0.3602(9)	0.9202(8)	0.1804(6)	4.32
C(12)	0.392(1)	1.0013(8)	0.1354(6)	4.56
C(13)	0.332(2)	0.951(1)	0.0582(7)	6.58
C(14)	0.341(1)	1.0861(9)	0.1515(8)	6.19
C(15)	0.545(1)	1.049(1)	0.156(1)	8.61
C(16)	-0.014(1)	0.880(1)	0.1282(8)	7.44
C(17)	-0.137(1)	0.8091(9)	0.0746(6)	4.80
C(18)	-0.240(1)	0.858(1)	0.0584(9)	8.11
C(19)	-0.117(2)	0.750(2)	0.0157(8)	8.78
C(20)	-0.200(1)	0.720(1)	0.112(1)	8.67
C(21)	0.108(1)	0.7916(7)	0.4684(5)	4.08
C(22)	0.059(1)	0.7421(7)	0.5257(5)	4.35
C(23)	-0.051(1)	0.775(1)	0.5379(7)	6.94
C(24)	0.019(2)	0.6281(9)	0.5103(7)	7.10
C(25)	0.180(2)	0.784(1)	0.5945(6)	6.61
C(26)	-0.211(1)	0.7545(7)	0.3177(6)	4.57
C(27)	-0.232(1)	0.8600(8)	0.3306(6)	4.87
C(28)	-0.204(2)	0.897(1)	0.4052(8)	8.20
C(29)	-0.147(2)	0.937(1)	0.299(1)	9.11
C(30)	-0.381(2)	0.837(1)	0.292(1)	9.50
C(31)	0.234(2)	0.624(1)	0.1080(6)	8.11
C(32)	0.210(1)	0.657(1)	0.0396(6)	7.38
C(33)	0.264(2)	0.596(2)	-0.010(1)	6.18
C(34)	0.395(3)	0.626(3)	0.027(2)	8.22
C(35)	0.375(2)	0.534(2)	0.0716(9)	4.46
C(36)	0.272(3)	0.535(2)	0.107(1)	5.81
C(33) ^Y	0.332(3)	0.668(2)	0.007(2)	9.60
C(34) ^Y	0.360(3)	0.560(2)	0.016(2)	7.76
C(35) ^Y	0.420(2)	0.580(2)	0.096(1)	6.48
C(36) ^Y	0.344(2)	0.621(2)	0.1433(9)	5.77
C(37)	0.248(1)	0.9778(8)	0.3571(6)	5.01
C(38)	0.224(1)	1.0568(8)	0.3191(7)	5.32
C(39)	0.300(2)	1.167(1)	0.3615(8)	6.58
C(40)	0.435(2)	1.188(1)	0.3982(9)	9.92
C(41)	0.450(1)	1.108(1)	0.4444(7)	6.79
C(42)	0.389(1)	0.997(1)	0.3940(8)	7.59
C(43)	-0.2012(8)	0.4643(6)	0.2694(5)	3.29
C(44)	-0.263(1)	0.4868(7)	0.2018(5)	3.94
C(45)	-0.400(1)	0.4012(9)	0.1661(6)	4.86
C(46)	-0.489(1)	0.397(1)	0.2118(8)	6.44
C(47)	-0.427(1)	0.3745(9)	0.2797(8)	5.81
C(48)	-0.287(1)	0.4570(7)	0.3175(5)	4.23

^a B(eq) = ⁴/3[*a*²β₁₁ + *b*²β₂₂ + *c*²β₃₃ + *ab*(cos γ)β₁₂ + *ac*(cos β)β₁₃ + *bc*(cos α)β₂₃]. ^b Primed atoms are disordered with 50% occupancy each.

8.421 mmol, 83.23% yield based on In(CH₂CMe₃)₃. Mp: 30–52 °C (169–172 °C, decomp); material was glass-like in appearance and melted to a thick oil over a broad range. ¹H NMR (C₆D₆, δ): 0.95, 1.00, 1.01, 1.05, 1.08 (s, 18 H, -CMe₃); 1.20, 1.21, 1.23, 1.26 (4.1 H, -CH₂-); 1.72, 1.76 (m, 2.6 H, PMe). ³¹P{¹H} NMR (C₆D₆, δ): -97.6 (s, 11.4), -98.1 (s, 1.00), 98.5 (s, 2.19), -98.7 (s, 8.98), -98.9 (s, 5.07), -99.1 (s, 2.05). Anal. Calcd: C, 53.69; H, 7.97. Found: C, 53.72; H, 8.26. Cryoscopic molecular weight, fw 380.26 (obsd molality, obsd mol wt, association): 0.0787, 1099, 2.89; 0.0657, 1065, 2.80. IR (Nujol mull, cm⁻¹): 3078 (w), 3058 (w), 1955 (vw), 1938 (vw), 1795 (vw), 1582 (w), 1480 (s), 1431 (s), 1357 (s), 1308 (vw), 1295 (vw), 1270 (vw), 1265 (w), 1233 (m), 1210 (w), 1199

(vw), 1188 (vw), 1152 (vw), 1108 (w), 1095 (w), 1070 (vw), 1025 (w), 1010 (m), 998 (m), 960 (vw), 928 (vw), 908 (vw), 878 (s), 732 (vs), 689 (vs), 675 (m, sh), 665 (m, sh), 612 (vw), 568 (m), 478 (m), 448 (w), 404 (w), 378 (vw), 330 (vw), 310 (vw), 282 (vw).

Synthesis of $(\text{Me}_3\text{SiCH}_2)_2\text{InP}(\text{Me})\text{Ph}$. The compound $(\text{Me}_3\text{SiCH}_2)_2\text{InP}(\text{Me})\text{Ph}$ was prepared from $\text{In}(\text{CH}_2\text{SiMe}_3)_3$ (0.820 g, 2.18 mmol) and $\text{HP}(\text{Me})\text{Ph}$ (0.271 g, 2.18 mmol) in benzene by using the method previously described for $(\text{Me}_3\text{CCH}_2)_2\text{InPEt}_2$. Heating at 80 °C for 4 days gave 0.181 g CMe_4 , 1.84 mmol, 84.4% yield based on $\text{In}(\text{CH}_2\text{CMe}_3)_3$. The product was extracted with 45 mL of anhydrous pentane to yield $(\text{Me}_3\text{SiCH}_2)_2\text{InP}(\text{Me})\text{Ph}$ as a viscous oil (0.892 g, 2.16 mmol, 99.3% yield based on $\text{In}(\text{CH}_2\text{SiMe}_3)_3$). $^1\text{H NMR}$ (C_6D_6 , δ): -0.01, 0.03, 0.06, 0.08, 0.10, 0.16, 0.17, 0.18, 0.20, 0.24, 0.26, 0.28, 0.29, 0.37, 0.38 (s, combined lines 22 H, $-\text{CH}_2\text{SiMe}_3$); 1.81, 1.82, 1.84, 1.87 (s, 3 H, $-\text{PMe}$). $^{31}\text{P}\{^1\text{H}\}$ NMR (C_6D_6 , δ): -69.6 (s, 1.6), -69.9 (s, 3.1), -70.5 (s, 3.0), -70.8 (s, 1.3), -92.2 (s, 7.9), -98.7 (s, 50.7), -99.2 (s, 96.3). Anal. Calcd: C, 43.68; H, 7.35. Found: C, 43.49; H, 7.43. Cryoscopic molecular weight, fw 412.42 (obsd molality, obsd mol wt, association): 0.0702, 1196, 2.90; 0.0562, 1192, 2.89; 0.0438, 1233, 2.99. IR (Nujol mull, cm^{-1}): 3072 (w), 3056 (vw), 1562 (w), 1480 (m), 1431 (m), 1424 (m, sh), 1349 (w), 1330 (vw), 1308 (vw), 1275 (w, br), 1252 (m), 1240 (vs), 1152 (vw), 1068 (vw), 1022 (vw), 996 (vw), 955 (m, br), 878 (m), 848 (vs), 820 (vs), 745 (m), 731 (s), 718 (m), 688 (m), 678 (m), 605 (vw), 560 (w), 550 (w), 475 (w), 352 (vw), 345 (vw), 338 (vw), 325 (vw).

Synthesis of $(\text{Me}_3\text{CCH}_2)_2\text{InP}(\text{C}_6\text{H}_{11})_2$. In the glovebox, tared screw-cap vials were charged with 0.721 g (3.64 mmol) of $\text{HP}(\text{C}_6\text{H}_{11})_2$ and 1.194 g (3.636 mmol) of $\text{In}(\text{CH}_2\text{CMe}_3)_3$. The contents of each vial was transferred quantitatively into a 100-mL Schlenk flask equipped with a 20-mm Solv-Seal joint by using five separate 3 mL washings of benzene. The Schlenk flask was capped, cooled to -196 °C, and evacuated. The reaction mixture was heated with a 60 °C oil bath for 7 days. The volatile component were removed and fractionated through two -78 °C traps into a -196 °C trap. Neopentane (0.112 g, 1.56 mmol, 42.9% yield based on $\text{In}(\text{CH}_2\text{CMe}_3)_3$) was isolated in the -196 °C trap. The neopentane and benzene were vacuum distilled back into the original Schlenk reaction flask and heated at 60 °C for another 7 days. Fractionation yielded 0.206 g of CMe_4 , 3.42 mmol, 78.4% yield based on $\text{In}(\text{CH}_2\text{CMe}_3)_3$. Again, the neopentane and benzene were vacuum distilled into the original flask and heated at 60 °C. After another week (21 days total) fractionation yielded 0.247 g of CMe_4 , 3.42 mmol, 94.1% yield based on $\text{In}(\text{CH}_2\text{CMe}_3)_3$. The product was washed with 20 mL of anhydrous pentane to leave $(\text{Me}_3\text{CCH}_2)_2\text{InP}(\text{C}_6\text{H}_{11})_2$ as a colorless crystalline solid (1.466 g, 3.227 mmol, 88.76% yield based on $\text{In}(\text{CH}_2\text{CMe}_3)_3$). Mp 225–229 °C (decomp). $^{31}\text{P}\{^1\text{H}\}$ NMR (70 °C, $\text{C}_6\text{D}_5\text{CD}_3$, δ): -13.00 (s). Anal. Calcd: C, 58.15; H, 9.76. Found: C, 58.41; H, 9.41. IR (Nujol mull, cm^{-1}): 2700 (vw), 1340 (m), 1334 (m), 1327 (m), 1296 (w), 1290 (m), 1257 (m), 1227 (s), 1208 (m), 1186 (m), 1172 (s), 1163 (m), 1094 (m), 1089 (sh), 1065 (w), 1042 (w), 1036 (vw), 1020 (w), 1009 (m), 995 (s), 922 (vw), 910 (w), 901 (w), 880 (m), 844 (s), 813 (vw), 780 (vw), 737 (s), 725

(m), 671 (vs), 640 (s), 507 (w), 448 (m), 430 (sh), 380 (w), 350 (w), 318 (vw), 288 (m). Solubility: trace solubility in aromatic solvents and insoluble in Et_2O , THF, and hydrocarbons.

X-ray Data Collection, Structure Determination, and Refinement for $[(\text{Me}_3\text{CCH}_2)_2\text{InPEt}_2]_2$. A transparent single crystal of $[(\text{Me}_3\text{CCH}_2)_2\text{InPEt}_2]_2$ was mounted in a thin-walled glass capillary under Ar and transferred to the goniometer. The space group was determined to be either the centric $C2/c$ or acentric Cc from the systematic absences. The subsequent solution and successful refinement of the structure was carried out in the centric space group $C2/c$. A summary of data collection parameters is given in Table 6.

Least-squares refinement with isotropic thermal parameters led to $R = 0.066$. Disorder was obvious in the neopentyl group C(6)–C(10). The disorder resolved itself into two orientations of C(6), C(9), and C(10). C(7) and C(8) were common to both. Refinement of the occupancy factors gave C(6), C(9), and C(10) at 55% and their primed counterparts at 45%. The two orientations were refined in alternate least-squares cycles. The hydrogen atoms were not included in the final refinement. Refinement of non-hydrogen atoms with anisotropic temperature factors led to the final values of $R = 0.045$ and $R_w = 0.076$. The final values of the positional parameters are given in Table 7.

X-ray Data Collection, Structure Determination, and Refinement for $[(\text{Me}_3\text{CCH}_2)_2\text{InP}(\text{H})(\text{C}_6\text{H}_{11})]_2$. A transparent single crystal of $[(\text{Me}_3\text{CCH}_2)_2\text{InP}(\text{H})(\text{C}_6\text{H}_{11})]_2$ was mounted in a thin-walled glass capillary under Ar and transferred to the goniometer. The space group was determined to be either the centric $P\bar{1}$ or acentric $P1$. The subsequent solution and successful refinement of the structure was carried out in the centric space group $P\bar{1}$. A summary of data collection parameters is given in Table 8.

High thermal motion was noted for almost all C atoms. The only resolvable disorder was two orientations for the C(31)–C(36) cyclohexyl group. C(34)–C(36) and C(34)'–C(36)' were refined with 50% occupancy in alternate least-squares cycles. Due to the thermal motion and disorder, the hydrogen atoms were not included in the final refinement. Refinement of non-hydrogen atoms with anisotropic temperature factors led to the final values of $R = 0.054$ and $R_w = 0.078$. The final values of the positional parameters are given in Table 9.

Acknowledgment. This work was supported in part by the Office of Naval Research (O.T.B.) and by a generous grant from Eastman Kodak Company. We thank Dr. Henry J. Gysling for his work on the synthesis and characterization of $(\text{Me}_3\text{CCH}_2)_2\text{InP}(\text{Me})\text{Ph}$.

Supporting Information Available: Listings of anisotropic thermal parameters and bond distances and angles for $[(\text{Me}_3\text{CCH}_2)_2\text{InPEt}_2]_2$ and $[(\text{Me}_3\text{CCH}_2)_2\text{InP}(\text{H})(\text{C}_6\text{H}_{11})]_2$ (10 pages). Ordering information is given on any current masthead page.

OM950124Y

Quantitative Study of the Interconversion of S and U Isomers of Cp(η^5 -pentadienyl)Cr(CO) in 18- and 17-Electron Complexes: Cyclic Voltammetric Study of an Organometallic Square Scheme

Timothy T. Wooster and William E. Geiger*

Department of Chemistry, University of Vermont, Burlington, Vermont 05405

Richard D. Ernst*

Department of Chemistry, University of Utah, Salt Lake City, Utah 84112

Received February 13, 1995[®]

Electrochemical investigations have been performed on 17- and 18-electron complexes of structural type $[\text{Cp}(\eta^5\text{-Pd})\text{Cr}(\text{CO})]^n$ ($\text{Cp} = \text{C}_5\text{H}_5$, Pd = pentadienyl, $n = 0, 1+$) as well as related complexes. Two such complexes are shown to interconvert via a square scheme by cyclic voltammetry (CV) and bulk electrolysis data. CV in THF shows that the 17e/18e couple is ca. 550 mV more positive when the Pd ligand is bound in the S conformation compared to the U conformation, implying that the latter comparatively stabilizes the 17e complex by about 12 kcal/mol. Rate constants for isomerizations to the more stable isomer have been measured for both 17e and 18e complexes using digital simulation techniques. Whereas the 17e complexes are stable with the U-bonded Pd ligand, they are prone to rapid decomposition when the pentadienyl group is S-bonded.

Introduction

Metal pentadienyl (Pd) compounds have proven to possess remarkably different properties compared to their cyclopentadienyl analogues.¹ They generally display greater back-bonding abilities, preference for low-oxidation-state metals, steric crowding, and reactivity toward ligand coupling reactions. Pentadienyl ligands are also more prone to adopt a variety of bonding modes, including not only the expected η^1 , η^3 , and η^5 forms (the last designated as $\eta^5\text{-U}$, **A**), but also localized η^3 (through the 1-, 4-, and 5-positions)^{1a,c} and $\eta^5\text{-S}$ (**B**) forms. The letters U and S denote U- and S-shaped forms, respectively.



To date, the $\eta^5\text{-S}$ bonding mode seems favorable for 18e metal complexes having d^4 configurations, such as $(2,4\text{-C}_7\text{H}_{11})_2\text{M}(\text{L})$ ($\text{M} = \text{Mo}, \text{W}$; $2,4\text{-C}_7\text{H}_{11}$ = dimethylpentadienyl), $(\text{C}_5\text{R}_5)(\text{Pd})\text{Cr}(\text{L})$ ($\text{R} = \text{H}, \text{Me}$; Pd = C_5H_7 , $3\text{-C}_6\text{H}_9$ (C_6H_9 = methylpentadienyl), $2,3\text{-C}_7\text{H}_{11}$, $2,4\text{-C}_7\text{H}_{11}$, $1,5\text{-}[(\text{Me}_3\text{Si})_2\text{C}_5\text{H}_5]$),³ $(\text{Pd})\text{W}(\text{CO})_3\text{Br}$,⁴ $(\text{C}_5\text{Me}_5)(\text{Pd})\text{ReCl}$,⁵ and $(\text{C}_5\text{H}_5)(\text{Pd})\text{Mo}(\text{CO})$.⁶ Interestingly, whereas the $\eta^5\text{-S}$ bonding mode has been established

exclusively for wide varieties of Pd and L ligands ($\text{L} = \text{CO}, \text{PF}_3, \text{PR}_3, \text{RNC}$) in the $(\text{C}_5\text{R}_5)(\text{Pd})\text{Cr}(\text{L})$ species,³ oxidation of these compounds to cationic 17e complexes reestablishes the "normal" $\eta^5\text{-U}$ bonding mode for the crystallographically determined $(\text{C}_5\text{H}_5)(2,4\text{-C}_7\text{H}_{11})\text{Cr}(\text{CO})^+{}^3$ and $[(\text{C}_5\text{Me}_5)(3\text{-C}_6\text{H}_9)\text{Cr}(\text{CO})]^+{}^3$ and presumably for all others as well. The isomerization of the pentadienyl ligand from $\eta^5\text{-S}$ to $\eta^5\text{-U}$ in the one-electron oxidation reveals a rather narrow window of stability for the $\eta^5\text{-S}$ bonding mode.

The cationic Cr complexes are of interest in other respects as well. They are rare examples of metal pentadienyl complexes involving "higher" oxidation states. Furthermore, like their isoelectronic vanadium analogues,⁷ but unlike most other 17e complexes,⁸ these species undergo very slow ligand substitution reactions. In view of the considerable interest in the structures and properties of these 17e and 18e complexes, we were

(3) (a) Freeman, J. W.; Hallinan, N. C.; Arif, A. M.; Gedridge, R. W.; Ernst, R. D.; Basolo, F. *J. Am. Chem. Soc.* **1991**, *113*, 6509. (b) Bovino, S. C.; Coates, G. W.; Banovetz, J. P.; Waymouth, R. M.; Straus, D. A.; Ziller, J. W. *Inorg. Chim. Acta* **1993**, *203*, 179. (c) Shen, J. K.; Freeman, J. W.; Hallinan, N. C.; Rheingold, A. L.; Arif, A. M.; Ernst, R. D.; Basolo, F. *Organometallics* **1992**, *11*, 3215.

(4) Sivavec, T. M.; Katz, T. J.; Chiang, M. Y.; Yang, G. X.-Q. *Organometallics* **1989**, *8*, 1620.

(5) Herrmann, W. A.; Fischer, R. A.; Herdtweck, E. *Organometallics* **1989**, *8*, 2821.

(6) (a) Lee, G. H.; Peng, S.-M.; Lee, T.-W.; Liu, R.-S. *Organometallics* **1986**, *5*, 2378. (b) Green, M.; Nagle, K. R.; Woolhouse, C. M.; Williams, D. J. *J. Chem. Soc., Chem. Commun.* **1987**, 1793.

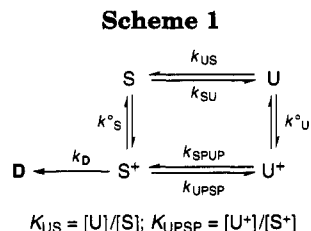
(7) Kowaleski, R. M.; Basolo, F.; Trogler, W. C.; Gedridge, R. W.; Newbound, T. D.; Ernst, R. D. *J. Am. Chem. Soc.* **1987**, *109*, 4860.

(8) (a) Kochi, J. K. *Organometallic Mechanisms and Catalysis*; Academic Press: New York, 1978. (b) Brown, T. L. *Ann. N.Y. Acad. Sci.* **1980**, *333*, 80. (c) Trogler, W. C. In *Organometallic Radical Processes*; Trogler, W. C., Ed.; Elsevier: Amsterdam, 1990; Chapter 9. (d) Lappert, M. F.; Lednor, P. W. *Adv. Organomet. Chem.* **1976**, *14*, 345.

[®] Abstract published in *Advance ACS Abstracts*, June 15, 1995.

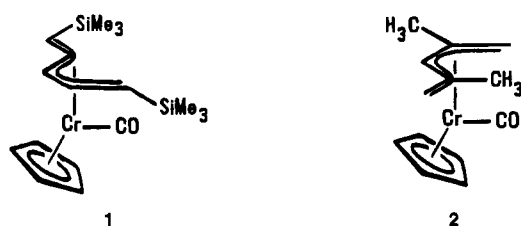
(1) (a) Ernst, R. D. *Chem. Rev.* **1988**, *88*, 1255. (b) Melendez, E.; Arif, A. M.; Rheingold, A. L.; Ernst, R. D. *J. Am. Chem. Soc.* **1988**, *110*, 8703. (c) Bleeke, J. R.; Boorsma, D.; Chiang, M. Y.; Clayton, T. W., Jr.; Haile, T.; Beatty, A. M.; Xie, Y.-F. *Organometallics* **1991**, *10*, 2391.

(2) Waldman, T. E.; Stahl, L.; Wilson, D. R.; Arif, A. M.; Hutchinson, J. P.; Ernst, R. D. *Organometallics* **1993**, *12*, 1543.



interested in obtaining more detailed information about their behavior during redox interconversions. This paper contains results of electrochemical experiments which yielded thermodynamic and kinetic data on the redox-coupled isomerizations of chromium pentadienyl complexes.

Cyclic voltammetry measurements indeed establish a square scheme (see Scheme 1) interrelating four chemical forms (two isomers in two oxidation states). Experimental results also require an irreversible side reaction of the S^+ isomer. Through changes in scan rates, all four members of the square scheme were detected, and digital simulations of experimental data yielded isomerization rates of the less stable to the more stable thermodynamic isomer in both oxidation states. The presence of a side reaction involving the decomposition of S^+ was also detected and quantified. The systems considered were $\text{Cp}[1,5-(\text{SiMe}_3)_2\text{C}_5\text{H}_5]\text{Cr}(\text{CO})$ (**1**) and $\text{Cp}(2,4\text{-Me}_2\text{C}_5\text{H}_5)\text{Cr}(\text{CO})$ (**2**).



Experimental Section

Chemicals. The preparations of the Cr complexes investigated in this work have been described previously.³ The 17e cation 2^+ was handled as the BF_4^- salt. All procedures were conducted under an atmosphere of nitrogen in a glovebox. Electrochemical solvents were dried and twice distilled: CH_2Cl_2 from CaH_2 and THF from potassium. The final distillation was conducted under static vacuum, the vessel with the resulting distillate being opened after transfer to the glovebox. The supporting electrolyte was 0.1 M $[\text{NBu}_4][\text{PF}_6]$ or 0.1 M $[\text{NBu}_4][\text{CF}_3\text{SO}_3]$. For solubility reasons, the latter was employed for THF solutions below about 270 K.

Electrochemistry. Commercial potentiostats (PARC 173 and PARC 273) interfaced with personal computers were used for data acquisition. Charging current subtraction was performed on all voltammograms used for quantitative purposes, by subtraction of the blank response (solvent plus electrolyte) from that of the test solution. Aqueous SCE or Ag/AgCl reference electrodes were employed, but potentials in this paper are referenced to the ferrocene(Fc)/ferrocenium couple. Ferrocene was added as an internal reference at an appropriate point in each experiment. Conversion to SCE values requires addition of +0.56 V for THF solutions. Pt working electrodes were employed: a gauze basket for bulk electrolyses and a bead of ca. 1 mm diameter for cyclic voltammetry experiments. Solutions were generally 0.5–1.5 mM in the test compound, and no effects of concentration variations on voltammetry response were noted. Voltammograms treated theoretically (e.g., Figures 3 and 6) were background-subtracted for electrolyte response using a digital acquisition system. No attempt was made to correct for residual iR

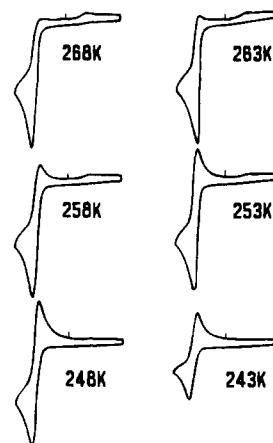


Figure 1. CV scans of 1.23 mM **1** in THF/0.1 M $[\text{NBu}_4][\text{CF}_3\text{SO}_2]$ at subambient temperatures ($\nu = 0.2$ V/s, Pt electrode). Originally recorded vs Ag/AgCl , these scans are from ca. -1.4 V to 0 V vs Fc.

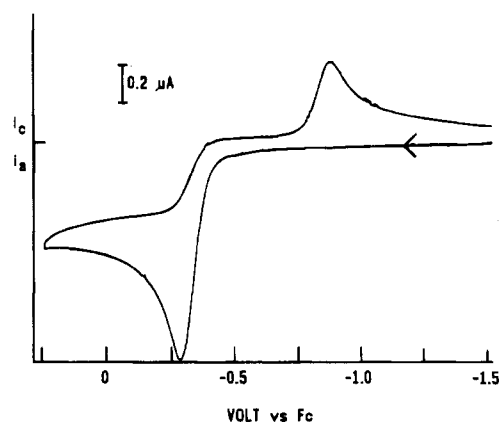


Figure 2. CV scan ($\nu = 0.2$ V/s) of 1.0 mM **1** in THF/0.1 M $[\text{NBu}_4][\text{PF}_6]$ (Pt electrode, ambient temperature).

distortions in voltammograms. Theoretical simulations were obtained with the recently developed method of Rudolph et al.,⁹ marketed by Bioanalytical Systems as DigiSim.

Results

Voltammetry of $\text{Cp}[1,5-(\text{SiMe}_3)_2\text{C}_5\text{H}_5]\text{Cr}(\text{CO})$ (1**).** Since complex **1** is stable (in the S conformation) in THF at room temperature for extended periods, this solvent was chosen for voltammetry studies. As shown in Figure 1, oxidation of **1** is chemically irreversible at 268 K but reversible at 243 K ($\nu = 0.2$ V/s). The formal potential of the $1S/1S^+$ couple is -0.33 V vs Fc. When the return scan was carried to a more negative potential (Figure 2), a second cathodic wave was seen ($E_{pc} = \text{ca. } -0.9$ V), which is ascribed to reduction of the corresponding cationic U isomer ($E^\circ = -0.87$ V). The basis of the assignment is that virtually the same value is found for the unequivocally identified U isomer of complex 2^+ (vide infra). This pattern of two quasi-Nernstian couples, one for each isomer, each less than fully chemically reversible, separated by 0.5–0.6 V, holds for both **1** and **2**. Variations in wave shapes and current intensities with scan rate were used to obtain quantitative values for the interconversion rates of the various isomers.

(9) (a) Rudolph, M. J. *Electroanal. Chem. Interfacial Electrochem.* **1991**, *314*, 13. (b) Rudolph, M.; Reddy, D. P.; Feldberg, S. W. *Anal. Chem.* **1994**, *66*, 589A.

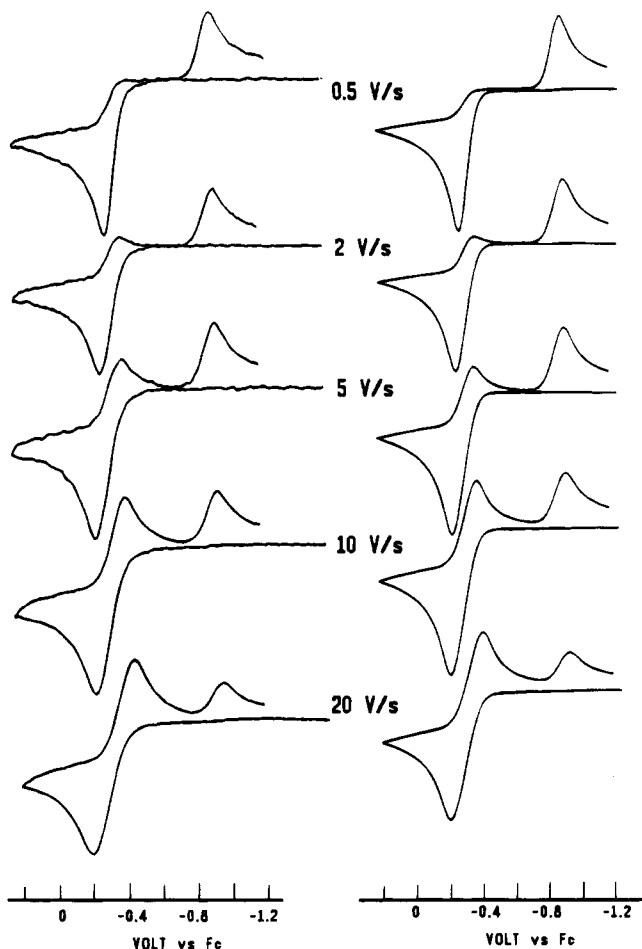


Figure 3. Comparison of CV experiment (left column) and theory (right column) at different scan rates for **1**. Experimental conditions: 1.0 mM **1** in THF/0.1 M [NBu₄][PF₆], Pt-bead electrode, 298 K. Theoretical details: digital simulations employing the parameters in Table 1 and k_s values of 0.1 cm/s, α values of 0.5, and $R_u = 40 \Omega$, $K_{US} = 0.01$, $K_{USP} = 100$.

Increases in scan rate resulted in a more nearly chemically reversible response for the **1S**/**1S**⁺ couple, with the decomposition rate of **1S**⁺ being estimated at ca. 10 s⁻¹ from the manner in which the reverse current for the wave at -0.33 V responded to v .¹⁰ Digital simulation of the voltammetric responses, including both (S and U) couples, gave a fuller accounting of the rates and mechanism of the isomeric interconversions, however, and we now consider those results.

The CV responses encompassing both waves are given as a function of v in Figure 3 (left), and digital simulations are shown in the adjacent column. The simulations are based on a model involving a square scheme (see Scheme 1) for interconversion of the two isomers in the two oxidation states, with addition of a side reaction for decomposition of **S**⁺. The model is general for both **1** and **2**, and the rate and equilibrium constants are as defined in Scheme 1. If the side reactions were not included in the simulations, reverse currents for the **S**⁺/**S** couple would be consistently larger than are experimentally observed. As we shall see, this effect is much more pronounced in CV simulations of complex **2**, owing to its slower **S**⁺ to **U**⁺ conversion and concomitant greater sensitivity to side reactions of **S**⁺.

Table 1. Relevant Square Scheme Parameters (Scheme 1) for **1 and **2**^a**

compd	E°_S, V	E°_U, V	k_{US}, s^{-1}	k_{SPUP}, s^{-1}	k_D, s^{-1}
Cp[(SiMe ₃) ₂ C ₅ H ₅]Cr(CO) (1)	-0.33	-0.87	5	13	2.0
Cp(Me ₂ C ₅ H ₅)Cr(CO) (2)	-0.32	-0.88	0.15	1.2	1.8

^a Potentials vs ferrocene, in THF/0.1 M [NBu₄][PF₆] at room temperature.

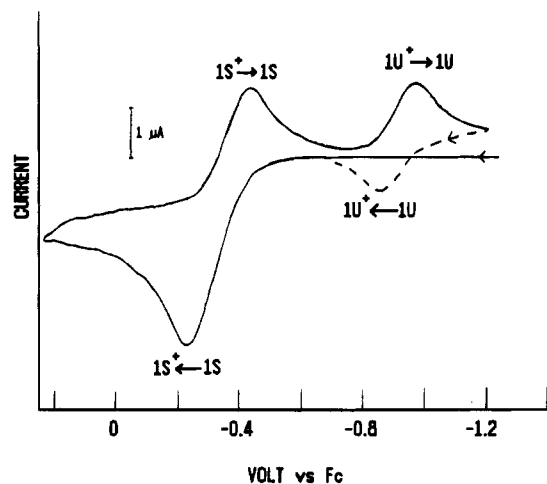


Figure 4. CV scan of 1.0 mM **1** (same experiment as Figure 3) with the beginning of the second positive-direction scan initiated immediately after completion of the first cycle, ($v = 10$ V/s).

As demonstrated in Figure 3, adequate agreement between theory and experiment was found by employing the parameters in Table 1. The salient features of this parameter set are the rates of isomerizations of 18e **1U** to **1S** ($k_{US} = 5$ s⁻¹) and 17e **1S**⁺ to **1U**⁺ ($k_{SPUP} = 13$ s⁻¹), and that of the side reaction **1S**⁺ to **D** ($k_D = 2.0$ s⁻¹). The last two rate constants are obtained from single-cycle experiments; the former constant is obtained from double-cycle scans (Figure 4, *vide infra*). Iterative simulation fits at different scan rates suggested that the k values are good to better than 50% (relative). The simulations employed heterogeneous electron transfer parameters (k_s , α values) typical of quasi-Nernstian couples with symmetric transition states, because the wave shapes and ΔE_p values ($\Delta E_p = E_{pa} - E_{pc}$) were approximately the same as those observed for ferrocene under the same conditions.¹¹ As long as the equilibrium constants employed for [S]/[U], [U⁺]/[S⁺], and [D]/[S⁺] were large (≥ 100 , reflecting the known thermodynamic preferences), their exact values did not affect the simulations.

Figure 4 is a trace in which a second CV scan was recorded immediately after completion of the first, in order to probe the chemical reversibility of the reduction of **1U**⁺. Some reverse (now anodic) current is observed at higher scan rates (dashed line in Figure 4) for the **1U**⁺/**1U** couple which is absent at lower scan rates. This enables estimation of the rate of isomerization of **1U** to **1S** ($k_{US} =$ ca. 5 s⁻¹) under the assumption that side reactions of **1U** are unimportant.

We do not know the identity of the side product which has been labeled **D** in Scheme 1. Bulk oxidations of

(11) The values of $E_{pc} - E_{pa}$ for equivalent concentrations of ferrocene ranged from about 70 mV with $v = 0.1$ V/s to 150 mV with $v = 20$ V/s in THF at ambient temperatures.

(10) Nicholson, R. S.; Shain, I. *Anal. Chem.* **1964**, *36*, 706.

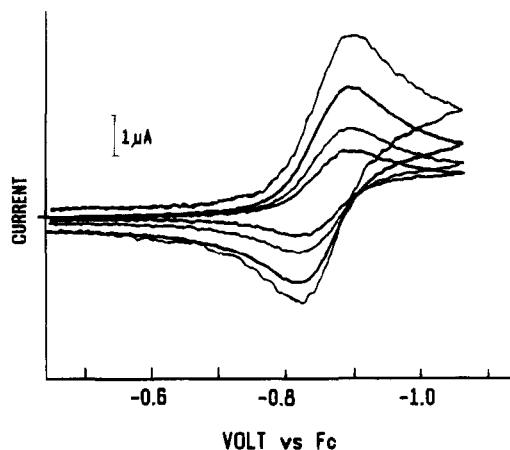


Figure 5. CV scans at variable v values for 1.0 mM 2^+ in $\text{CH}_2\text{Cl}_2/0.1 \text{ M } [\text{NBu}_4][\text{PF}_6]$ at ambient temperature (Pt-bead electrode). Currents increase at scan rates of 0.1, 0.2, 0.5, and 1 V/s.

either **1S** or **2S** produce blue solutions devoid of detectable quantities of CO-containing complexes (IR data). The color is reminiscent of reactions of half-open chromocenes with I_2 , Br_2 , or HgCl_2 , which lead to $(\text{C}_5\text{R}_5)\text{-CrX}_2$ complexes.¹² For $\text{X} = \text{I}$, the complexes are green, whereas for $\text{X} = \text{Br}$ or Cl , they are deep blue. Thus, a possible identity of the final side product is $(\text{C}_5\text{R}_5)\text{CrF}_2$ when PF_6^- is used as the supporting electrolyte anion. Of course, species **D** might be an intermediate on the route to the final side product, since we have no information about what occurs between the demise of the S^+ complex and the appearance of the final side product. Another structural possibility to consider is that involving intermolecular pentadienyl–pentadienyl coupling to form a dinuclear decatetraene moiety with both metals still coordinated in an η^4 fashion. Whatever the decomposition pathway(s) of the 17e complexes may be, they appear to be limited to the **S** isomer. Once the pentadienyl ligand has successfully isomerized to the η^5 -**U** form, the complex is not subject to such decomposition pathways.

Electrochemistry of $[\text{Cp}(2,4\text{-Me}_2\text{C}_5\text{H}_5)\text{Cr}(\text{CO})]^{+0}$ (2⁺** and **2**).** This complex is isolated in the 17e cationic form as the pure **U** isomer 2U^+ , which is stable in THF or CH_2Cl_2 .³ Voltammetry of 2U^+ gave a quasi-Nernstian, apparently one-electron CV which was fully chemically reversible only when the scan rate was above several volts per second in either THF ($E^\circ_{\text{U}} = -0.88 \text{ V}$ vs Fc) or CH_2Cl_2 (-0.86 V). From the i_a/i_c ratios as a function of v (typical CV scans in Figure 5), a rate constant for disappearance of the 18e isomer **2U** (equal to k_{US} in the absence of side reactions) was calculated as ca. 0.15 s^{-1} , a value much smaller than the 5 s^{-1} estimated for $\text{U} \rightarrow \text{S}$ conversion in **1**. This value gave an independent starting point for digital simulations of the fuller CV window of **2**.

We produced solutions of **2S**, the thermodynamically stable 18e isomer, by coulometric reduction of the 17e precursor 2U^+ . This was accomplished in ca. 70% yield by bulk cathodic reduction of 2U^+ at -1.2 V at a Pt-gauze electrode at 270 K. CV and rotating-Pt-electrode scans after electrolysis showed less than 2% of the starting material, with a new reversible oxidation wave

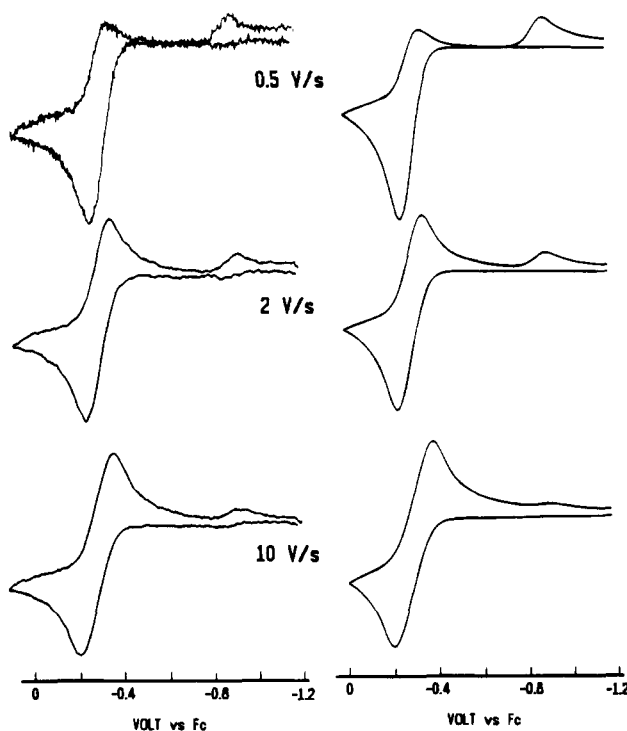


Figure 6. Comparison of CV experiment (left column) and theory (right column) at different scan rates for **2**. Experimental conditions: 1.0 mM **2** in THF/0.1 M $[\text{NBu}_4][\text{PF}_6]$, Pt-bead electrode, 298 K. Theoretical details: digital simulations employing the parameters in Table 1 and k_s values of 0.1 cm/s, α values of 0.5, and $R_u = 45 \Omega$, $K_{\text{US}} = 0.01$, $K_{\text{UPSP}} = 100$.

at $E^\circ = -0.32 \text{ V}$ attributed to 2S^{0+} . These reduced solutions were used for variable-scan-rate CV experiments (Figure 6) and gave quantitative information about the square scheme for compound **2**.

The electrolysis of 2U^+ to **2S** gave the color change orange to yellow, consistent with the known colors of these two isomers.^{3a,7} When, after ca. 2 h, **2S** was reoxidized to 2U^+ , only about 50% of the original amount of the latter was regenerated, the solution being the light blue color of **D**. Since **2S** is stable under these conditions, the loss of half of the starting material arises from the instability of 2S^+ .

CV scans of solutions of **2S** were qualitatively similar to those of complex **1S**, showing two redox couples separated by ca. 560 mV. The morphologies of these waves changed with sweep rate (Figure 6), and the experimental traces were once again simulated using the mechanism of Scheme 1.

Quite adequate agreement between theory and experiment was obtained, and the extracted parameters for **2** are given in Table 1. It is noteworthy that the isomerization rate (k_{SPUP}) for the 17e complex (2S^+ to 2U^+) is only 1.2 s^{-1} , 1 order of magnitude slower than that of the SiMe_3 derivative 1^+ (13 s^{-1}). This is the reason chemical reversibility is observed for the S^+/S couple at lower scan rates for **2** (Figure 6) compared to **1** (Figure 3).

Interestingly, the CV scans of **2** must take into account a side reaction of 2S^+ with a rate constant, k_{D} , of 2.0 s^{-1} , virtually the same as seen for 1S^+ . The effect of the side reaction on the CV scans of **2** is much more dramatic because the isomerization and side reactions of 2S^+ occur at competitive rates ($k_{\text{SPUP}} = 1.2 \text{ s}^{-1}$, $k_{\text{D}} =$

Table 2. Other Potentials Relevant to This Study, Converted to volts vs Ferrocene

compound	E° of oxidn	ref
Cp(2,4-Me ₂ C ₅ H ₅)Cr (3)	-0.6 (irrev)	this work
Cp(C ₅ H ₇)Cr(PF ₃) (4)		
S	-0.51	this work
U	-1.11	this work
Cp ₂ Cr	-1.16 (CH ₃ CN)	15
Cp ₂ Cr	-1.28 (THF)	16
Cp ₂ Cr(CO)	-1.1 (irrev)	15

2.0 s⁻¹). The similar S⁺ → D rates for **1** and **2** suggest that the S⁺ isomers share the fate of the same side reaction. This fact, and the observation that the voltammetric reversibilities were not concentration dependent, favor the loss of a ligand, rather than pentadienyl coupling, as the decomposition route of the 17e S isomers.

Voltammetry of Other Half-Open Complexes.

Two other complexes were briefly investigated (Table 2). The 16e compound Cp(2,4-Me₂C₅H₅)Cr (**3**) in THF showed an irreversible (to $v = 10$ V/s) oxidation at $E_{pa} = ca. -0.6$ V. The 18e compound Cp(C₅H₇)Cr(PF₃) (**4**) gave voltammetry results very similar to those for **1**, with the apparent values $E^\circ_U = -1.11$ V and $E^\circ_S = -0.51$ V.

Discussion

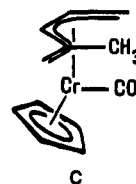
These studies verify the isomeric tendencies surmised from synthetic studies of the pentadienylchromium complexes.³ The voltammetric measurements confirm that the S isomer is thermodynamically favored in the neutral 18e complexes, and the U isomer is favored in the cationic 17e complexes. Quite surprising to us was the large separation of formal potentials for the U and S isomers, 540 mV for **1** and 560 mV for **2**. This is similar to the potential differences between cis and trans isomers for oxidation of some 18e octahedral complexes such as Cr(dppm)₂(CO)₂ (dppm = diphenylphosphinomethane)¹³ or *fac* and *mer* isomers of Mn(CO)₃(dppm)Cl.¹⁴ A stabilization of 550 mV is 12.3 kcal/mol when expressed in heat units, an impressive value for the stabilization energy of the 17e form in the U configuration compared to the S configuration relative to the 18e forms of the same isomers.

Two sources for this stabilization are considered, involving the overall abilities of the two pentadienyl configurations to remove electron density from the metal. IR data on other compounds suggest that a U-bonded pentadienyl group is more effective at back-bonding than is an S-bonded pentadienyl group.^{3a,15} If that is so, our observation that the U^{0/+} couple is negative of the S^{0/+} couple is hard to rationalize unless (a) the relative ability of U-Pdl to back-bond greatly decreases in the 17e structure or (b) the favoring of U-Pdl in the 17e form arises from a better spatial overlap of its orbitals with the metal. The latter seems more likely, since the splayed-out S-pentadienyl moiety

should have less favorable overlap with the smaller orbital of the Cr in the higher oxidation state.

In both configurations, the pentadienyl ligands are more electron-withdrawing than a cyclopentadienyl ligand. The E° values compared to chromocene analogues provide the basis for this statement. The 17e/18e couple Cp₂Cr(CO)⁺⁰ has an estimated¹⁶ E° value of -1.12 V vs Fc, considerably negative of the values of ca. -0.9 V observed for the pentadienyl U⁺⁰ couples and ca. -0.3 V for the pentadienyl S⁺⁰ couples. Confirmation of this trend is found in comparison of the E° value for the chromocene oxidation, Cp₂Cr^{0/+} (ca. -1.2 V),¹⁷ relative to that of Cp(2,4-Me₂C₅H₅)Cr (-0.6 V, irreversible).

Given the similar thermodynamic properties of complexes **1** and **2** (virtually identical potentials for both U and S isomers), the differences in kinetics of isomerizations are especially noteworthy. The rates at which the less stable isomers convert to the more stable ones (U to S and S⁺ to U⁺) are 1 order of magnitude faster in the bis-SiMe₃ derivative **1** than in the dimethyl derivative **2**. The approximate half-lives at ambient temperatures for the isomeric interconversions are 0.14 s for **1U** compared to 4.6 s for **2U** and 0.05 s for **1S⁺** compared to 0.6 s for **2S⁺**. This is consistent with the clear steric problems that are encountered by having an endo-oriented methyl group in an η^5 -S-2,4-C₇H₁₁ ligand. As the twist to an η^5 -U form will replace the endo-oriented methyl group (see **C**) by an endo-oriented metal-bound CH₂ group, a twist in either direction could lead to steric interference with either the CO or C₅H₅ ligand.



The most serious complication to efficient, reversible cycling around the square scheme is found in the fate of the S⁺ isomer, which undergoes, in addition to isomerization to U⁺, a parallel reaction to an unassigned side product (**D** in Scheme 1), which is not electroactive in the potential window scanned. Clear-cut evidence for this process is found in the CV scans of **2**, which require two rate-competitive reactions of **2S⁺** to account for the observed peak heights over a range of scan rates. The evidence for the reaction **1S⁺** → **D** is less clear, owing to the fact that the rate constant for the reaction is much less than that for the **1S⁺** → **1U⁺** isomerization. The fact that a side reaction occurs for the S⁺ isomers also rationalizes (a) the moderate yields (40–60%) for cyclic bulk oxidations and re-reductions of S isomers, (b) the 25–40% yields of U⁺ isomers upon chemical oxidation of S isomers,^{3c} and (c) the blue side products formed under these reaction conditions.

It is possible that the side reactions of S⁺ isomers involve initial CO loss, for this process is known to occur

(13) (a) Bond, A. M.; Colton, R.; Jackowski, J. J. *Inorg. Chem.* **1975**, *14*, 274. (b) Bond, A. M.; Grabaric, B. S.; Jackowski, J. J. *Inorg. Chem.* **1978**, *17*, 2153.

(14) Bond, A. M.; Colton, R.; McCormick, M. J. *Inorg. Chem.* **1977**, *16*, 155.

(15) Compare ν_{CO} for Cp₂Cr(CO) (1900 cm⁻¹) vs Cp(S-C₅H₇)Cr(CO) (1919 cm⁻¹) and Cp₂V(CO) (1881 cm⁻¹) vs Cp(U-C₅H₇)V(CO) (1938 cm⁻¹): (a) Wong, K. L. T.; Brintzinger, H. H. *J. Am. Chem. Soc.* **1975**, *97*, 5143. (b) Calderazzo, F.; Fachinetti, G.; Floriani, C. *J. Am. Chem. Soc.* **1974**, *96*, 3695. (c) Gedridge, R. W.; Hutchinson, J. P.; Rheingold, A. L.; Ernst, R. D. *Organometallics* **1993**, *12*, 1553.

(16) van Raaij, E. U.; Mönkeberg, S.; Kiesele, H.; Brintzinger, H. H. *J. Organomet. Chem.* **1988**, *356*, 307.

(17) (a) Holloway, J. D. L.; Bowden, W. L.; Geiger, W. E. *J. Am. Chem. Soc.* **1977**, *99*, 7089. (b) Holloway, J. D. L.; Sentfleber, F. C.; Geiger, W. E. *Anal. Chem.* **1978**, *50*, 1010. (c) Kölle, U. *J. Organomet. Chem.* **1978**, *157*, 327.

slowly in the 18e complexes, and oxidation would be expected to lower the strength of the metal-carbon bond. Although Basolo and co-workers have shown that CO loss is slow in 17e U^+ complexes of the type under discussion,^{3c} the behavior of the 17e S isomers may be quite different. If "D" is $[Cp(\eta^5-R_2C_5H_5)Cr]^+$ (note the positive charge: the formation of S^+ from S requires a potential positive of the oxidation of $Cp(\eta^5-R_2C_5H_5)Cr$), it would be subject to immediate decomposition, as was learned from the irreversible oxidation of the 16e neutral compound **3**, reported in Table 2. Indeed, if the final side product is a Cr(III) complex (vide supra), a decomposition mechanism involving more than one step from S^+ to D to the final side product is likely.

Conclusions

The S and U isomers of the complexes $[Cp(Pd)Cr(CO)]^n$ ($n = 0, 1+$) interconvert through a square scheme mechanism involving redox-induced isomerizations. The thermodynamically favored structures involve S-Pd coordination in the 18e complexes and U-Pd coordination in the 17e complexes. The interconversions of the less stable to more stable isomers (U to S and S^+ to U^+) occur with half-lives of 50 ms to 5 s at ambient temperatures for the two complexes studied. The much slower isomerization rates (in both oxidation states) for **2** compared to those for **1** are in line with other observations, both kinetic and thermodynamic,³ that demonstrate a significant steric effect brought about by endo-oriented methyl groups.

In terms of electronic factors, the U-bonded pentadienyl ligand significantly stabilizes the 17e structure, compared to the S-bonded pentadienyl ligand, at least for these Cr complexes.

Of the four chemical forms (U, U^+ , S, S^+), only one, namely S^+ , is prone toward decomposition on the time scale of the voltammetry. In fact, decomposition of S^+ is competitive with isomerization to U^+ for complex **1**⁺, thereby rationalizing the observation that chemical oxidation of **1** or **2** gives the corresponding cations **1**⁺ and **2**⁺ in poor yields.^{3c}

Given that metal-polyolefin complexes and intermediates are important in a diverse and important set of reactions,¹⁸ it is of interest to see how changes in metal electronic configurations affect bonding preferences in these complexes. The present work adds to a sparse knowledge base¹⁹ concerning this question. The demonstration of dramatically reversed conformational preferences exhibited by the neutral and cationic monoligand adducts of the half-open chromocenes substantiates the conclusions reached during earlier spectroscopic and structural investigations.³ We note, however, that the factors leading to stabilization of the η^5 -S coordination in various 18e d^4 pentadienyl complexes are still not clear. Molecular orbital calculations are in progress in hopes of developing a better understanding of these factors.

Acknowledgment. We are grateful to the National Science Foundation for the support of this research (Grant No. CHE 91-16332 at the University of Vermont and Grant No. CHE 92-21040 at the University of Utah).

OM950117+

(18) Collman, J. P.; Hegedus, L. S.; Norton, J. R.; Finke, R. G. *Principles and Applications of Organotransition Metal Chemistry*; University Science Books: Mill Valley, CA, 1987; Chapter 11.

(19) Geiger, W. E. In Lippard, S. J. (ed) *Progress in Inorganic Chemistry*; Lippard, S. J., Ed.; Wiley: New York, 1985; Vol. 33, pp 275ff.

Synthesis and Characterization of Trimetalloenes and Trimetalloenium Salts

Stephen Barlow, Vincent J. Murphy, John S. O. Evans, and Dermot O'Hare*

Inorganic Chemistry Laboratory, University of Oxford, South Parks Road, Oxford OX1 3QR, U.K.

Received March 8, 1995[⊗]

A range of trinuclear metallocene and metallocenium complexes have been prepared using the ferrocene-functionalized lithium salts $\text{Li}^+(\text{FcCMe}_2\text{C}_5\text{H}_4)^-$ (**2**; $\text{Fc} = \text{Fe}(\eta\text{-C}_5\text{H}_5)(\eta\text{-C}_5\text{H}_4)$), $\text{Li}^+\{\text{FcC}(\text{=CH}_2)\text{C}_5\text{H}_4\}^-$ (**4**), and $\text{Li}^+(\text{Fc}''\text{CH}_2\text{C}_5\text{H}_4)^-$ (**8**; $\text{Fc}'' = \text{Fe}(\eta\text{-C}_5\text{Me}_4\text{H})(\eta\text{-C}_5\text{Me}_4)$). The triferrocenes $(\text{FcCMe}_2\text{C}_5\text{H}_4)_2\text{Fe}$ (**3**) and $\{\text{FcC}(\text{=CH}_2)\text{C}_5\text{H}_4\}_2\text{Fe}$ (**5**) consist of a central ferrocene linked by single-carbon bridges to two terminal ferrocene units, whereas $(\text{Fc}''\text{CH}_2\text{C}_5\text{H}_4)_2\text{M}$ ($\text{M} = \text{Fe}$ (**9**), Co (**10**), Cr (**11**)) have terminal octamethylferrocene units. Cyclic voltammetry experiments reveal that **3** and **5** exhibit three reversible redox processes, indicating significant electrostatic interactions between the metal centers in these complexes. For **9** and **10** two redox events are observed. A range of metallocenium salts with diamagnetic and paramagnetic anions has also been synthesized from these trimetalloenes. Variable-temperature magnetic susceptibility data on paramagnetic trimetalloenes and trimetalloenium salts all obey the Curie–Weiss law, with no evidence for significant spin-spin exchange interactions between metal centers. The charge-transfer salts $\{(\text{Fc}''\text{CH}_2\text{C}_5\text{H}_4)_2\text{Fe}\}^{2+}(\text{TCNE}^-)_2$ (**17**; $\text{TCNE} = \text{tetracyanoethylene}$) and $\{(\text{Fc}''\text{CH}_2\text{C}_5\text{H}_4)_2\text{Co}\}^{3+}(\text{TCNE}^-)_3$ (**18**) have been prepared and their magnetic properties investigated.

Introduction

Soluble molecular systems containing more than one metallocene unit have attracted much interest for a number of reasons: as partially oxidized species, which may exhibit either mixed-valence behavior or electronic delocalization,^{1–4} as species exhibiting intramolecular magnetic exchange interactions,⁵ and, more recently, as models for poly(ferrocenyl)silane materials.^{6,7}

Here we report the rational synthesis and characterization of a range of fulvene-derived trimetallic species comprising three metallocene units linked by single-carbon bridges. Although a few such molecules, as shown in Figure 1, have been previously reported,^{8–11} they have been relatively little studied and no crystal structures have been reported. The trimetalloene systems reported here offer general routes to a range of heterometallic complexes exhibiting a wide range of oxidation states. The more highly methylated trimet-

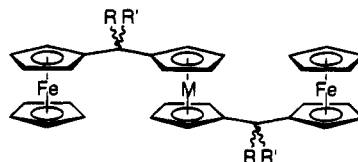


Figure 1. Generalized trimetalloene with single-carbon bridges. Those previously synthesized are as follows: $\text{R} = \text{R}' = \text{H}$, $\text{M} = \text{Fe}$;^{9,11} $\text{R} = \text{Ph}$, $\text{R}' = \text{H}$, $\text{M} = \text{Fe}$;⁸ $\text{R} = \text{Ph}$, $\text{R}' = \text{H}$, $\text{M} = \text{Co-PF}_6^-$;⁸ $\text{R} = \text{Me}$, $\text{R}' = \text{H}$, $\text{M} = \text{Fe}$.¹⁰

alocenes have been investigated as components of molecular radical cation–radical anion salts.

Experimental Section

General Procedures. Operations involving oxygen- or water-sensitive species were carried out under nitrogen or *in vacuo*, using standard Schlenk procedures or a Vacuum Atmospheres glovebox. Where necessary, solvents were dried and purified by refluxing over sodium–potassium alloy (pentane, petroleum ether (bp 40–60 °C), diethyl ether), potassium (THF), P_2O_5 (dichloromethane), or P_2O_5 followed by K_2CO_3 (acetonitrile), distilled under nitrogen, stored under nitrogen over activated type 4 Å molecular sieves, and degassed before use. Acetylferrocene¹² and octamethylformylferrocene¹³ were prepared by literature procedures. $\text{FeCl}_2 \cdot 1.5\text{THF}$ was prepared by dehydration of $\text{FeCl}_2 \cdot 4\text{H}_2\text{O}$, followed by Soxhlet extraction of the anhydrous material into THF. Ferrocenium hexafluorophosphate was prepared by oxidation of ferrocene by aqueous FeCl_3 , followed by filtration and precipitation by addition of ammonium hexafluorophosphate. LiAlH_4 (Aldrich) was purified by recrystallization from diethyl ether. $\text{Co}(\text{acac})_2$ (Janssen Chimica) was dehydrated and purified by sublimation from a furnace at 400 °C in a 10^{-5} Torr vacuum. TCNE (Aldrich) was sublimed *in vacuo* prior to use. Methyl lithium,

(12) Harwood, L. M.; Moody, C. J. *Experimental Organic Chemistry*; Blackwell Scientific Publications: Oxford, U.K., 1989.

(13) Zou, C.; Wrighton, M. S. *J. Am. Chem. Soc.* **1990**, *112*, 7578–7584.

[⊗] Abstract published in *Advance ACS Abstracts*, June 15, 1995.

(1) Morrison, W. H.; Hendrickson, D. N. *Inorg. Chem.* **1975**, *14*, 2331–2346.

(2) Iijima, S.; Motoyama, I.; Sano, H. *Bull. Chem. Soc. Jpn.* **1980**, *53*, 3180–3183.

(3) Reiff, W. M.; Manriquez, J. M.; Ward, M. D.; Miller, J. S. *Mol. Cryst. Liq. Cryst.* **1989**, *176*, 423–428.

(4) Reiff, W. M.; Manriquez, J. M.; Miller, J. S. *Hyperfine Interact.* **1990**, *53*, 397–402.

(5) Bergerat, P.; Blümel, J.; Fritz, M.; Hiermeier, J.; Hudeczek, P.; Kahn, O.; Köhler, F. H. *Angew. Chem., Int. Ed. Engl.* **1992**, *31*, 1258–1260.

(6) Rulkens, R.; Lough, A. J.; Manners, I. *J. Am. Chem. Soc.* **1994**, *116*, 797–798.

(7) Pannell, K. H.; Dementiev, V. V.; Li, H.; Cervantes-Lee, F.; Nguyen, M. T.; Diaz, A. F. *Organometallics* **1994**, *13*, 3644–3650.

(8) Knox, G. R.; Munro, J. D.; Pauson, P. L.; Smith, G. H.; Watts, W. E. *J. Chem. Soc.* **1961**, 4619–4624.

(9) Pauson, P. L.; Watts, W. E. *J. Chem. Soc.* **1962**, 3880–3886.

(10) Neuse, E. W.; Quo, E.; Howells, W. G. *J. Org. Chem.* **1965**, *30*, 4071.

(11) Barr, T. H.; Lentzner, H. L.; Watts, W. E. *Tetrahedron* **1969**, *25*, 6001–6013.

tert-butyllithium, ferrocene, silver trifluoromethanesulfonate, ammonium hexafluorophosphate, and anhydrous CrCl₂ were supplied by Aldrich.

Instrumental Techniques. Elemental microanalyses were performed by the analytical department of the Inorganic Chemistry Laboratory, Oxford, U.K. NMR spectra were recorded using a Bruker AM 300 spectrometer. Mass spectra were recorded using an electron impact AEI MS 9802 mass spectrometer, calibrated using perfluorokerosene. IR spectra were obtained using a Mattson Instruments Polaris FT spectrometer, as Nujol mulls or strong solutions between KBr plates. CV data were obtained using a glassy-carbon working electrode, a platinum-gauze auxiliary electrode, and a silver-wire pseudo reference electrode. Measurements were made on degassed dry dichloromethane solutions *ca.* 5×10^{-4} M in sample and 0.1 M in Buⁿ₄N⁺PF₆⁻ at scan rates of 20–200 mV s⁻¹. The reversibility of redox processes was judged by comparison with the behavior of ferrocene under identical conditions. Potentials were referenced to the ferrocenium/ferrocene couple by adding ferrocene to the cell. ESR measurements were performed on microcrystalline solids, solutions, or glasses in high-purity Spectrosil quartz tubes using an X-band Varian spectrometer; peaks were referenced by using a microcrystalline sample of 1,1-diphenyl-2-picrylhydrazyl. Solid-state magnetic moment data were measured over the temperature range 2.5–290 K, at fields of 0.1–1.5 T using a Cryogenic Consultants SCU500 SQUID magnetometer. Samples were loaded in high-purity Spectrosil quartz buckets, with polythene seals; after correction for the diamagnetism of these sample holders, data were corrected for the diamagnetism of the sample, either by graphical extrapolation of the measured susceptibility to infinite temperature or by use of Pascal's constants. The field independence of susceptibility data was verified by measurement at two different fields. Unless otherwise stated, the room-temperature values of μ_{eff} are quoted.

Synthesis. FcMeC=C(CH)₄ (Fc = Ferrocenyl, Fe(η -C₅H₅)(η -C₅H₄)) (1). A degassed solution of excess cyclopentadiene (*ca.* 30 mL, *ca.* 0.3 mol) and KOH (*ca.* 11 g) in 90 mL of ethanol was added to a degassed solution of acetylferrocene (12.8 g, 56 mmol) in 80 mL of ethanol; the reaction mixture was then stirred under nitrogen for 20 h. The mixture was transferred to a separating funnel, together with 300 mL each of water and diethyl ether. The layers were separated, and the aqueous layer was back-extracted with 2 \times 200 mL of diethyl ether. The combined ethereal extracts were then washed with 200 mL of water and 2 \times 200 mL of 2 M NaCl solution. The organic layer was dried over MgSO₄, filtered, and evaporated to dryness *in vacuo* to yield a blood-red oil. Repeated addition of petroleum ether (bp 40–60 °C), followed by evaporation to dryness, caused the oil to crystallize to give an essentially quantitative yield of the air-stable blood-red fulvene (pure by ¹H NMR). NMR and IR data were in agreement with literature values.¹⁴

Li⁺(FcCMe₂C₅H₄)⁻ (2). An 8 mL (11.2 mmol) amount of a 1.4 M solution of MeLi in diethyl ether was added dropwise to a solution of **1** (2.725 g, 9.87 mmol) in 100 mL of diethyl ether at 0 °C. The reaction mixture was warmed to room temperature and stirred for 20 h. The orange-yellow precipitate was collected on a sintered-glass frit, washed with 100 mL of diethyl ether, and dried *in vacuo* to give **2** (2.375 g, 7.97 mmol, 80% assuming no solvent is incorporated into the solid). The salt may also be prepared in THF, in which case the solvent must be removed and the solids washed with diethyl ether. Satisfactory analytical data were not obtained due to the air and moisture sensitivity of the material.

(FcCMe₂C₅H₄)₂Fe (3). A solution of **2** (691 mg, 2.32 mmol) in 25 mL of THF was added slowly to a slurry of FeCl₂·1.5THF (300 mg, 1.28 mmol) in 10 mL of THF. After 20 h the solvent was removed *in vacuo* and the residue extracted with 300 mL

of diethyl ether. The ether extracts were filtered through Celite and cooled to -80 °C to yield **3** (382 mg, 0.60 mmol, 52%) as a golden orange microcrystalline powder. An analytically pure sample was obtained by recrystallization from toluene at -25 °C. X-ray-quality single crystals of **3** were obtained by slow evaporation of a dichloromethane solution. Anal. Found (calcd): C, 67.49 (67.75); H, 5.92 (6.00). ¹H NMR (C₆D₆): δ 1.59 (s, 12H, CH₃), 3.95 (m, 16H, C₅H₄), 4.06 (s, 10H, C₅H₅). ¹³C{¹H} NMR (C₆D₆): δ 30.7 (CH₃), 33.6 (CMe₂), 66.4 (C₅H₄ CH), 66.8 (C₅H₄ CH), 67.0 (C₅H₄ CH), 67.9 (C₅H₄ CH), 68.7 (C₅H₅), 101.4 (C₅H₄ quat), 101.6 (C₅H₄ quat). MS (EI): *m/z* 638 (M⁺).

Li⁺{FcC(=CH₂)C₅H₄}⁻ (4). Method A. A solution of **1** (2.232 g, 8.1 mmol) in 30 mL of THF was added dropwise to a solution of lithioferrocene, prepared from ferrocene (1.5 g, 8.06 mmol) and BuⁿLi (4 mL of a 1.7 M pentane solution, 6.8 mmol),¹⁵ in 15 mL of THF at 0 °C. The resulting solids were collected on a sintered-glass frit and washed with 200 mL of diethyl ether before drying *in vacuo* to yield **4** (514 mg, 1.1 mmol, 13%) as an orange-red powder.

Method B. A 13 mL (22.1 mmol) amount of a 1.7 M solution of BuⁿLi in pentane was added dropwise to a solution of **1** (5.775 g, 20.9 mmol) in 25 mL of THF at 0 °C. After it was warmed to room temperature, the mixture was stirred for 2 days before solvent removal *in vacuo*. The resulting solids were collected on a sintered-glass frit and washed with 200 mL of petroleum ether (bp 40–60 °C) before drying *in vacuo* to yield **4** (1.926 g, 6.83 mmol, 31%) as an orange-yellow powder. Satisfactory analytical data were not obtained due to the air and moisture sensitivity of the material.

{FcC(=CH₂)C₅H₄}₂Fe (5). A slurry of FeCl₂·1.5THF (260 mg, 1.12 mmol) in 15 mL of THF was added slowly to a solution of **4** (514 mg, 1.82 mmol) in 15 mL of THF. After 20 h the solvent was removed and the residue was extracted with toluene. After filtration through Celite the toluene was removed *in vacuo* to yield a brown-red oily material which was then extracted with diethyl ether. The ether extracts were filtered through Celite, reduced in volume, and cooled to -80 °C to yield **5** (267 mg, 0.440 mmol, 48%). Anal. Found (calcd): C, 67.16 (67.37); H, 5.18 (4.98). ¹H NMR (C₆D₆): δ 4.06 (s, 10H, C₅H₅), 4.11 (m, 4H, C₅H₄), 4.18 (m, 4H, C₅H₄), 4.62 (m, 8H, C₅H₄), 5.52 (d, 2H, CH₂), 5.54 (d, 2H, CH₂). ¹³C-{¹H} NMR (C₆D₆) (assigned by DEPT): δ 68.4 (C₅H₄ CH), 68.5 (C₅H₄ CH), 69.7 (C₅H₄ CH), 69.9 (C₅H₄), 70.8 (C₅H₄ CH), 86.3 (C₅H₄ quat), 87.0 (C₅H₄ quat), 110.2 (CH₂), 143.4 (quat). Selected IR (CH₂Cl₂, cm⁻¹): 3106 (m), 3084 (m), 1596 (s).

{(FcCMe₂C₅H₄)₂Fe}³⁺(CF₃SO₃⁻)₃ (6). A solution of CF₃SO₃⁻Ag⁺ (124 mg, 0.48 mmol) in 15 mL of THF was added dropwise to a stirred solution of **3** (104 mg, 0.16 mmol) in 15 mL of THF. The solution immediately darkened. After 24 h a blue-black precipitate and a silver mirror were present, the THF was removed *in vacuo*, and the resulting solids were extracted with degassed acetone. The acetone extracts were filtered through a bed of Celite; the resulting green-red dichroic solution was reduced in volume to *ca.* 20 mL. The product was precipitated by addition of 100 mL of diethyl ether to the stirred acetone solution. The precipitate was allowed to settle, and the supernatant was decanted off. After it was washed with 2 \times 40 mL of diethyl ether, the dark green microcrystalline solid was dried *in vacuo* to yield analytically pure, slightly air-sensitive **6** (86 mg, 0.079 mmol, 50%). Single crystals of **6** were grown by diffusion of pentane into a concentrated acetone solution. Anal. Found (calcd): C, 43.32 (43.15); H, 3.57 (3.52). Magnetic moment: $\mu_{\text{eff}} = 4.4 \mu_{\text{B}}$, $\Theta = -2.7$ K.

Fc''CH=C(CH)₄ (Fc'' = Octamethylferrocenyl, Fe(η -C₅Me₄H)(η -C₅Me₄)) (7). A degassed solution of cyclopentadiene (*ca.* 10 mL, *ca.* 0.1 mol) and KOH (*ca.* 4 g) in 40 mL of ethanol was added to a stirred solution of octamethylferrocene (4.97 g, 15.2 mmol) in 40 mL of degassed ethanol.

(14) Rausch, M. D.; Wang, Y.-P. *Organometallics* **1991**, *10*, 1438–1443.

(15) Rebiere, F.; Samuel, O.; Kagan, H. B. *Tetrahedron Lett.* **1990**, *31*, 3121–3124.

Table 1. Summary of the Crystallographic Data for 3, 6, and 18

	3	6	18
formula	C ₃₆ H ₃₈ Fe ₃	C ₃₉ H ₃₈ Fe ₃ O ₉ S ₃	C ₆₆ H ₆₂ CoFe ₂ N ₁₂
fw	638.24	1085.43	1193.92
cryst appearance	orange block	blue-black plate	black plate
cryst size/mm	0.3 × 0.3 × 0.5	0.21 × 0.54 × 0.99	0.12 × 0.36 × 1.02
space group	P2 ₁ /a	C2	Cc
a/Å	14.409(1)	12.3274(8)	36.193(4)
b/Å	11.5831(6)	10.0383(8)	10.612(2)
c/Å	16.979(1)	16.935(1)	15.695(4)
β/deg	92.212(6)	95.097(6)	92.77(2)
cell vol/Å ³	2831.6(3)	2087.4(3)	6021(2)
Z	4	2	4
D _c /g mL ⁻¹	1.50	1.45	1.32
μ/cm ⁻¹	15.4	12.2	7.96
F(000)	1328	940	2484
θ limits/deg	0–33	0–32	0–24
scan mode	ω–2θ	ω–2θ	ω
total no. of data measd	13 711	6241	7559
total no. of unique data	10 652	3775	4708
no. of observns (I > 3σ(I))	6587	2023	2376
weighting scheme	Chebychev (11.7, –1.51, 9.60)	Chebychev (16.6, –3.95, 12.2)	unit weights
largest residual/e Å ⁻¹	0.5 near Fe(2)	0.6 near S(3)	0.4 near Fe(1)
R ^a	0.037	0.063	0.039
R _w ^b	0.044	0.074	0.038

$$^a R = \sum |F_o| - |F_c| / \sum |F_o|. \quad ^b R_w = \{ \sum (|F_o| - |F_c|)^2 / \sum |F_o|^2 \}^{1/2}.$$

The reaction mixture soon became purple. After 20 h the mixture was transferred to a separating funnel together with 200 mL each of water and diethyl ether. The layers were separated, and the lower aqueous layer was extracted with 2 × 100 mL of diethyl ether. The combined diethyl ether layers were washed with 200 mL of water and 2 × 200 mL of 2 M NaCl solution before drying over MgSO₄. After the MgSO₄ was filtered off, the solvent was removed *in vacuo* to give pure (by ¹H NMR) 6-(octamethylferrocenyl)fulvene, which is a deep purple oil, in essentially quantitative yield. ¹H NMR (CDCl₃): δ 1.67 (s, 6H, CH₃), 1.72 (s, 6H, CH₃), 1.65 (s, 6H, CH₃), 1.95 (s, 6H, CH₃), 3.36 (s, 1H, C₅Me₄H), 6.31 (m, 2H, fulvene ring CH), 6.48 (m, 1H, fulvene ring CH), 6.54 (m, 1H, fulvene ring CH), 7.10 (s, 1H, bridge CH). MS (EI): *m/z* 374 (M⁺). Selected IR (CH₂Cl₂, cm⁻¹): 3057 (m), 2962 (s), 2915 (s), 1612 (s).

Li⁺(Fc''CH₂C₅H₄)⁻ (8). LiAlH₄ (594 mg, 15.7 mmol) was stirred in 80 mL of diethyl ether; the resulting solution was added slowly to a stirred solution of 6-(octamethylferrocenyl)fulvene (5.70 g, 15.2 mmol) in 20 mL of diethyl ether; after 15 min a fine precipitate began to form. When the purple color of the fulvene had disappeared (ca. 40 h), the precipitate was collected on a sintered-glass frit, washed with 3 × 50 mL of diethyl ether, and dried *in vacuo*. A 5.295 g amount of a highly moisture- and oxygen-sensitive creamy yellow powder was obtained; assuming no solvent is incorporated in the product, this is 13.9 mmol (91% yield) of **8**. Satisfactory analytical data were not obtained due to the air and moisture sensitivity of the material.

(Fc''CH₂C₅H₄)₂Fe (9). A golden brown solution of **8** (0.713 g, 1.87 mmol, assuming no solvent is included in the compound) in 30 mL of THF was added in small portions to a slurry of FeCl₂·1.5THF (0.71 g, 3.51 mmol) in 20 mL of THF; the mixture immediately darkened. After this mixture was stirred for 15 h, the solvent was removed *in vacuo*; the resulting solids were extracted with portions of petroleum ether (bp 40–60 °C) until the extracts were almost colorless. The petroleum ether extracts were filtered through a bed of Celite and reduced in volume until the solution became slightly turbid. Slow cooling to –80 °C produced a yellow microcrystalline solid, from which the solution was decanted before washing with 2 × 10 mL of cold petroleum ether to give analytically pure, air-stable **9**. Two further batches were obtained to give a total yield of 565 mg (0.701 mmol, 75%). Anal. Found (calcd): C, 71.79 (71.48); H, 7.61 (7.75). ¹H NMR (C₆D₆): δ 1.68 (s, 12H, CH₃), 1.73 (s, 12H, CH₃), 1.62 (s, 12H, CH₃), 1.70 (s, 12H, CH₃), 3.29 (s, 2H, C₅Me₄H), 3.51 (s, 4H, CH₂), 3.97 (m, 4H, C₅H₄), 4.09 (m, 4H, C₅H₄). ¹³C{¹H} NMR

(C₆D₆) (assigned by DEPT): δ 9.7 (CH₃), 10.1 (CH₃), 10.8 (CH₃), 11.7 (CH₃), 26.5 (CH₂), 68.2 (C₅H₄ CH), 69.6 (C₅H₄ CH), 71.2 (C₅Me₄H CH), 78.3 (quat), 79.4 (quat), 79.7 (quat), 80.0 (quat), 83.6 (quat), 89.6 (quat).

(Fc''CH₂C₅H₄)₂Co (10). Co(acac)₂ (185 mg, 0.720 mmol) was slurried in 20 mL of THF; a solution of **8** (502 mg, 1.31 mmol, assuming no solvent is included in the compound) in 40 mL of THF was added in small portions. The reaction mixture soon became dark, and a fine white precipitate of Li(acac) appeared. After 12 h the solvent was removed *in vacuo*; the resulting solids were extracted with portions of petroleum ether (bp 40–60 °C) until the extracts were almost colorless. The petroleum ether extracts were filtered through a bed of Celite and reduced in volume until the solution became slightly turbid. Cooling to –25 °C produced **10** as an air-sensitive golden brown powder. The supernatant from the powder was further reduced in volume to yield more **10** on cooling to –80 °C, this time as analytically pure dark brown-red microcrystals. The total yield of **10** was 303 mg (0.37 mmol, 57%). Anal. Found (calcd): C, 71.41 (71.21); H, 7.73 (7.72). Magnetic moment: μ_{eff} = 1.65 μ_B at 200 K.

(Fc''CH₂C₅H₄)₂Cr (11). A solution of **8** (512 mg, 1.34 mmol) in 25 mL of THF was added slowly to a suspension of anhydrous CrCl₂ (86 mg, 0.70 mmol) in 15 mL of THF; the reaction mixture slowly took on a reddish appearance. After 3 days the solvent was removed *in vacuo* and the solids were extracted with petroleum ether (bp 40–60 °C); the orange-brown solution was filtered through Celite, reduced in volume, and crystallized at –80 °C. A total of 325 mg (62%) of **11** was obtained, as very air-sensitive orange-gold-brown microcrystals. The extreme oxygen and moisture sensitivity of this compound meant analysis could not be obtained within acceptable limits. Anal. Found (calcd): C, 69.93 (71.82); H, 7.67 (7.78). Magnetic moment: μ_{eff} = 2.6 μ_B, Θ = –6.2 K.

{(Fc''CH₂C₅H₄)₂Fe}³⁺(CF₃SO₃⁻)₃ (12). A solution of CF₃SO₃⁻Ag⁺ (90 mg, 0.35 mmol) in 8 mL of THF was added dropwise to a stirred solution of **9** (87 mg, 0.11 mmol) in 10 mL of THF; the reaction mixture soon became green and a silver mirror and gray precipitate slowly formed. After 4 h of stirring the solution was very pale green and the solids were gray-green. The THF was removed *in vacuo*, and the resulting solids were extracted with dichloromethane. The dichloromethane extracts were filtered through a bed of Celite and reduced in volume to ca. 15 mL. The product was precipitated by addition of 80 mL of diethyl ether to the stirred dichloromethane solution. The precipitate was allowed to settle and the almost colorless supernatant was decanted off using a cannula. An 85 mg (0.067 mmol, 62%) amount of a blue-green

Table 2. Fractional Atomic Coordinates and Equivalent Isotropic Temperature Factors (\AA^2) for 3^a

atom	<i>x/a</i>	<i>y/b</i>	<i>z/c</i>	<i>U</i> (equiv) ^b
Fe(1)	0.10068(2)	0.28633(3)	0.55234(2)	0.0315
Fe(2)	0.00165(2)	0.18049(2)	0.23131(2)	0.0284
Fe(3)	0.13342(2)	-0.31233(2)	0.09799(2)	0.0315
C(1)	0.1125(2)	0.3716(3)	0.6576(1)	0.0477
C(2)	0.1374(2)	0.2559(3)	0.6676(2)	0.0559
C(3)	0.2139(2)	0.2336(3)	0.6183(2)	0.0548
C(4)	0.2344(2)	0.3373(2)	0.5791(1)	0.0448
C(5)	0.1714(2)	0.4217(2)	0.6037(1)	0.0435
C(6)	0.0722(2)	0.1645(2)	0.4679(1)	0.0388
C(7)	0.0009(2)	0.1683(3)	0.5233(1)	0.0480
C(8)	-0.0370(2)	0.2803(3)	0.5224(1)	0.0474
C(9)	0.0101(1)	0.3466(2)	0.4664(1)	0.0374
C(10)	0.0784(1)	0.2754(2)	0.4316(1)	0.0288
C(11)	0.1385(1)	0.3091(2)	0.3642(1)	0.0302
C(12)	0.2233(1)	0.2291(2)	0.3603(1)	0.0411
C(13)	0.1731(2)	0.4348(2)	0.3746(1)	0.0408
C(14)	0.0802(1)	0.3065(1)	0.2870(1)	0.0315
C(15)	-0.0145(2)	0.3414(2)	0.2777(1)	0.0363
C(16)	-0.0405(2)	0.3416(2)	0.1959(1)	0.0445
C(17)	0.0379(2)	0.3061(2)	0.1542(1)	0.0453
C(18)	0.1124(2)	0.2849(2)	0.2097(1)	0.0388
C(19)	-0.0569(1)	0.0466(2)	0.1684(1)	0.0326
C(20)	-0.1155(1)	0.0813(2)	0.2293(1)	0.0406
C(21)	-0.0653(2)	0.0686(2)	0.3023(1)	0.0377
C(22)	0.0239(1)	0.0246(2)	0.2861(1)	0.0315
C(23)	0.0302(1)	0.0112(1)	0.2030(1)	0.0263
C(24)	0.1081(1)	-0.0471(2)	0.1599(1)	0.0277
C(25)	0.1151(2)	0.0041(2)	0.0774(1)	0.0403
C(26)	0.2018(1)	-0.0321(2)	0.2041(2)	0.0414
C(27)	0.0805(1)	-0.1738(2)	0.1565(1)	0.0296
C(28)	0.1089(2)	-0.2621(2)	0.2106(1)	0.0427
C(29)	0.0595(2)	-0.3643(2)	0.1917(2)	0.0541
C(30)	0.0002(2)	-0.3405(2)	0.1272(3)	0.0529
C(31)	0.0122(1)	-0.2229(2)	0.1045(2)	0.0416
C(32)	0.1833(2)	-0.2978(3)	-0.0128(2)	0.0526
C(33)	0.2519(2)	-0.2647(3)	0.0438(2)	0.0479
C(34)	0.2699(2)	-0.3588(3)	0.0951(2)	0.0501
C(35)	0.2117(2)	-0.4507(2)	0.0698(2)	0.0521
C(36)	0.1581(2)	-0.4123(3)	0.0028(2)	0.0560

^a Esd's are given in parentheses. ^b *U*(equiv) = one-third of the trace of the orthogonalized U_{ij} tensor.

powder was obtained after washing the precipitate with 2 × 50 mL of diethyl ether and drying *in vacuo*. Analytically pure dark green needles of **12** were grown by layering a solution of ca. 30 mg of the crude product in 20 mL of acetone with 80 mL of diethyl ether. Anal. Found (calcd): C, 49.05 (48.86); H, 4.79 (4.98). Magnetic moment: $\mu_{\text{eff}} = 4.1 \mu_{\text{B}}$, $\Theta = -1.7$ K.

Dark green needles of $12x\text{CH}_2\text{Cl}_2$ were grown by layering a solution of ca. 45 mg of the crude product in 15 mL of dichloromethane with 150 mL of diethyl ether. The presence of dichloromethane was shown by ¹H NMR spectroscopy in CD₃CN: C/H/N analysis suggested a stoichiometry of $x \approx 0.5$. Anal. Found (calcd): C, 47.49 (47.72); H, 4.80 (4.90). ¹H NMR (CD₃CN): δ 5.46 (s, CH₂Cl₂). Magnetic moment: $\mu_{\text{eff}} = 3.9 \mu_{\text{B}}$, $\Theta = -1.8$ K.

{(Fc''CH₂C₅H₄)₂Co}⁺PF₆⁻ (**13**). A solution of NH₄⁺PF₆⁻ (ca. 450 mg, 2.8 mmol) in 15 mL of THF was added dropwise to a stirred solution of **10** (400 mg, 0.494 mmol) in 20 mL of THF. After 24 h the solution had become purple and some precipitation had occurred. The solvent was removed *in vacuo*, and the resulting solids were extracted with dichloromethane. The filtered extracts were concentrated to ca. 35 mL and layered with 200 mL of diethyl ether. When the solvents had completely mixed, the supernatant was decanted from the resulting fine needles by cannula; the needles were then washed with 2 × 100 mL of diethyl ether and dried *in vacuo* to yield **13** (350 mg, 0.367 mmol, 74%) as air-stable purple microcrystals. Analytically pure crystals were grown by a second dichloromethane/diethyl ether layering. Anal. Found (calcd): C, 60.36 (60.39); H, 6.38 (6.55). ¹H NMR (CD₃CN): δ 1.71 (s, 12H, CH₃), 1.72 (s, 12H, CH₃), 1.77 (s, 12H, CH₃), 1.83 (s, 12H, CH₃), 3.33 (s, 2H, C₅Me₂H), 3.37 (s, 4H, CH₂), 5.40

Table 3. Selected Bond Lengths (\AA) for 3^a

Fe(1)-C(1)	2.044(2)	C(4)-C(5)	1.408(4)
Fe(1)-C(2)	2.040(2)	C(6)-C(7)	1.422(4)
Fe(1)-C(3)	2.037(2)	C(6)-C(10)	1.429(3)
Fe(1)-C(4)	2.050(2)	C(7)-C(8)	1.408(5)
Fe(1)-C(5)	2.047(2)	C(8)-C(9)	1.418(4)
Fe(1)-C(6)	2.043(2)	C(9)-C(10)	1.429(3)
Fe(1)-C(7)	2.032(2)	C(10)-C(11)	1.514(3)
Fe(1)-C(8)	2.030(2)	C(11)-C(12)	1.537(3)
Fe(1)-C(9)	2.044(2)	C(11)-C(13)	1.547(3)
Fe(1)-C(10)	2.067(2)	C(11)-C(14)	1.531(3)
Fe(2)-C(14)	2.056(2)	C(14)-C(15)	1.427(3)
Fe(2)-C(15)	2.041(2)	C(14)-C(18)	1.432(3)
Fe(2)-C(16)	2.047(2)	C(15)-C(16)	1.425(3)
Fe(2)-C(17)	2.040(2)	C(16)-C(17)	1.418(4)
Fe(2)-C(18)	2.048(2)	C(17)-C(18)	1.422(4)
Fe(2)-C(19)	2.047(2)	C(19)-C(20)	1.418(3)
Fe(2)-C(20)	2.042(2)	C(19)-C(23)	1.426(3)
Fe(2)-C(21)	2.039(2)	C(20)-C(21)	1.419(3)
Fe(2)-C(22)	2.052(2)	C(21)-C(22)	1.421(3)
Fe(2)-C(23)	2.065(2)	C(22)-C(23)	1.426(2)
Fe(3)-C(27)	2.050(2)	C(23)-C(24)	1.522(2)
Fe(3)-C(28)	2.044(2)	C(24)-C(25)	1.528(3)
Fe(3)-C(29)	2.040(3)	C(24)-C(26)	1.530(3)
Fe(3)-C(30)	2.029(3)	C(24)-C(27)	1.522(3)
Fe(3)-C(31)	2.038(2)	C(27)-C(28)	1.426(3)
Fe(3)-C(32)	2.047(3)	C(27)-C(31)	1.416(3)
Fe(3)-C(33)	2.048(2)	C(28)-C(29)	1.412(4)
Fe(3)-C(34)	2.042(2)	C(29)-C(30)	1.390(5)
Fe(3)-C(35)	2.028(2)	C(30)-C(31)	1.429(4)
Fe(3)-C(36)	2.032(2)	C(32)-C(33)	1.405(4)
C(1)-C(2)	1.396(5)	C(32)-C(36)	1.404(4)
C(1)-C(5)	1.399(4)	C(33)-C(34)	1.414(4)
C(2)-C(3)	1.435(5)	C(34)-C(35)	1.411(5)
C(3)-C(4)	1.410(4)	C(35)-C(36)	1.421(5)

^a Esd's are given in parentheses.

Table 4. Selected Bond Angles (deg) for 3^a

C(2)-C(1)-C(5)	108.6(2)	C(20)-C(19)-C(23)	108.7(2)
C(1)-C(2)-C(3)	107.5(3)	C(19)-C(20)-C(21)	108.0(2)
C(2)-C(3)-C(4)	107.6(2)	C(20)-C(21)-C(22)	107.6(2)
C(3)-C(4)-C(5)	107.6(2)	C(21)-C(22)-C(23)	108.9(2)
C(1)-C(5)-C(4)	108.7(2)	C(19)-C(23)-C(22)	106.7(2)
C(7)-C(6)-C(10)	108.5(2)	C(19)-C(23)-C(24)	125.7(2)
C(6)-C(7)-C(8)	108.1(2)	C(22)-C(23)-C(24)	126.9(2)
C(7)-C(8)-C(9)	108.2(2)	C(23)-C(24)-C(25)	110.2(2)
C(8)-C(9)-C(10)	108.6(2)	C(23)-C(24)-C(26)	111.5(2)
C(6)-C(10)-C(9)	106.6(2)	C(25)-C(24)-C(26)	108.5(2)
C(6)-C(10)-C(11)	127.3(2)	C(23)-C(24)-C(27)	104.5(1)
C(9)-C(10)-C(11)	125.9(2)	C(25)-C(24)-C(27)	111.4(2)
C(10)-C(11)-C(12)	110.9(2)	C(26)-C(24)-C(27)	110.7(2)
C(10)-C(11)-C(13)	110.4(2)	C(24)-C(27)-C(28)	126.9(2)
C(12)-C(11)-C(13)	108.6(2)	C(24)-C(27)-C(31)	125.9(2)
C(10)-C(11)-C(14)	109.4(1)	C(28)-C(27)-C(31)	106.8(2)
C(12)-C(11)-C(14)	111.2(2)	C(27)-C(28)-C(29)	109.0(3)
C(13)-C(11)-C(14)	106.3(2)	C(28)-C(29)-C(30)	107.6(2)
C(11)-C(14)-C(15)	125.5(2)	C(29)-C(30)-C(31)	108.9(2)
C(11)-C(14)-C(18)	127.1(2)	C(27)-C(31)-C(30)	107.7(3)
C(15)-C(14)-C(18)	106.9(2)	C(33)-C(32)-C(36)	108.0(3)
C(14)-C(15)-C(16)	108.8(2)	C(32)-C(33)-C(34)	108.6(3)
C(15)-C(16)-C(17)	107.6(2)	C(33)-C(34)-C(35)	107.6(3)
C(16)-C(17)-C(18)	108.4(2)	C(34)-C(35)-C(36)	107.8(3)
C(14)-C(18)-C(17)	108.3(2)	C(32)-C(36)-C(35)	108.0(3)

^a Esd's are given in parentheses.

(m, 4H, C₅H₄), 5.43 (m, 4H, C₅H₄). ¹³C{¹H} NMR (CD₃CN): δ 9.5 (CH₃), 9.8 (CH₃), 10.6 (CH₃), 11.5 (CH₃), 24.7 (CH₂), 71.6 (C₅Me₂H CH), 78.8 (quat), 80.8 (quat), 81.0 (quat), 82.0 (quat), 84.6 (C₅H₄ CH), 84.8 (C₅H₄ CH), 108.1 (C₅H₄ quat). Selected IR (Nujol, cm⁻¹): 821.

{(Fc''CH₂C₅H₄)₂Co}³⁺(PF₆⁻)₃ (**14**). A solution of **13** (217 mg, 0.227 mmol) in 40 mL of dichloromethane was added dropwise to a stirred slurry of FcH⁺PF₆⁻ (153 mg, 0.462 mmol) in 40 mL of dichloromethane, resulting instantly in a green precipitate. After 18 h the solvent was removed *in vacuo*; this also removed some of the ferrocene byproduct. The remaining ferrocene was removed by washing with 3 × 75 mL of diethyl ether; the resulting solids were then dried *in vacuo* before

Table 5. Fractional Atomic Coordinates, Equivalent Isotropic Thermal Parameters (\AA^2), and Occupancies for 6^a

atom	<i>x/a</i>	<i>y/b</i>	<i>z/c</i>	<i>U</i> (equiv) ^b	occ
Fe(1)	1.0000	0.2055(4)	0.0000	0.0304	1.0000
Fe(2)	0.71994(8)	0.2099(4)	-0.34633(6)	0.0458	1.0000
S(1)	0.7794(2)	0.2146(2)	0.3864(2)	0.0705	0.7264
S(2)	0.7973(3)	0.1993(3)	0.2783(3)	0.0680	0.2736
S(3)	0.5577(1)	0.2024(1)	0.0437(1)	0.0514	0.5000
F(1)	0.5069(5)	0.191(2)	0.1101(4)	0.0945	1.0000
F(2)	0.6170(6)	0.3205(9)	0.0289(6)	0.0632	1.0000
F(3)	0.6112(9)	0.095(1)	0.031(1)	0.0908	1.0000
F(4)	0.845(2)	0.303(2)	0.261(1)	0.1144	1.0000
F(5)	0.865(1)	0.089(1)	0.2638(9)	0.0931	1.0000
F(6)	0.7068(9)	0.175(2)	0.2423(6)	0.1428	1.0000
O(1)	0.708(1)	0.315(1)	0.394(1)	0.0880	1.0000
O(2)	0.743(2)	0.091(2)	0.404(1)	0.1126	1.0000
O(3)	0.8790(9)	0.199(4)	0.4223(5)	0.1309	1.0000
C(1)	1.004(1)	0.092(2)	-0.0986(9)	0.0493	1.0000
C(2)	1.108(1)	0.129(1)	-0.0772(9)	0.0417	1.0000
C(3)	1.1178(8)	0.269(1)	-0.0698(8)	0.0364	1.0000
C(4)	1.0117(7)	0.318(1)	-0.1062(6)	0.0264	1.0000
C(5)	0.9430(5)	0.195(1)	-0.1229(4)	0.0292	1.0000
C(6)	0.8268(5)	0.210(2)	-0.1618(3)	0.0383	1.0000
C(7)	0.764(1)	0.329(2)	-0.138(1)	0.0655	1.0000
C(8)	0.765(1)	0.081(1)	-0.1387(8)	0.0354	1.0000
C(9)	0.8409(5)	0.208(2)	-0.2500(4)	0.0395	1.0000
C(10)	0.8525(8)	0.321(1)	-0.2990(6)	0.0361	1.0000
C(11)	0.8703(9)	0.280(2)	-0.3783(9)	0.0485	1.0000
C(12)	0.866(1)	0.144(2)	-0.375(1)	0.0643	1.0000
C(13)	0.849(1)	0.092(2)	-0.299(1)	0.0675	1.0000
C(14)	0.5885(9)	0.318(1)	-0.367(1)	0.0490	1.0000
C(15)	0.604(1)	0.265(2)	-0.4346(8)	0.0646	1.0000
C(16)	0.606(2)	0.128(3)	-0.428(2)	0.0998	1.0000
C(17)	0.564(1)	0.098(2)	-0.352(2)	0.0704	1.0000
C(18)	0.5617(9)	0.215(4)	-0.3135(7)	0.0803	1.0000
C(19)	0.7973(3)	0.1993(3)	0.2783(3)	0.0680	0.7264
C(20)	0.7794(2)	0.2146(2)	0.3864(2)	0.0705	0.2736
C(21)	0.5579(1)	0.2029(1)	0.0439(1)	0.0514	0.5000

^a Esd's are given in parentheses. ^b *U*(equiv) = one-third of the trace of the orthogonalized U_{ij} tensor.

extracting into 100 mL of acetone. The acetone extracts were filtered into a Young's ampule, reduced *in vacuo* to 80 mL, and layered with 220 mL of pentane. After the layers had completely mixed, the colorless supernatant was decanted by cannula from the resulting solids, which were then washed with 2 × 80 mL of pentane before drying *in vacuo* to yield green platelike microcrystals (217 mg, 0.174 mmol, 78%), analyzed as **14**. Anal. Found (calcd): C, 46.16 (46.32); H, 4.89 (5.02). ESR (MeCN glass, 4.5 K): $g_{\perp} = 1.40$, $g_{\parallel} = 3.93$, $\langle g \rangle = 2.54$. Magnetic moment: $\mu_{\text{eff}} = 3.2 \mu_B$, $\Theta = -3.6$ K.

{(Fc⁺CH₂C₅H₄)₂Cr⁺}PF₆⁻ (**15**). A solution of FcH⁺PF₆⁻ (78 mg, 0.24 mmol) in 15 mL of acetonitrile was added dropwise to a solution of **11** (210 mg, 0.26 mmol) in 20 mL of THF. After 20 h the solvents were removed *in vacuo*, together with most of the ferrocene. The solids were washed with 3 × 150 mL of diethyl ether to remove excess **11** and residual ferrocene, dried *in vacuo*, and extracted with dichloromethane. The rich brown extracts were filtered, concentrated to 25 mL, and layered with 125 mL of diethyl ether. When the solvents had completely mixed, they were decanted from the resulting solids, which were then washed with 2 × 100 mL of diethyl ether and dried *in vacuo* to yield dark brown-black crystals (115 mg, 0.12 mmol, 47%). Both solid and solution rapidly decompose to a blue material on exposure to air. Anal. Found (calcd): C, 59.95 (60.84); H, 6.54 (6.59). ESR (CH₂Cl₂ glass, 22 K): $g_{\parallel} = 1.99$, $g_{\perp} = 4.08/2$, $\langle g \rangle = 2.02$.

{(Fc⁺CH₂C₅H₄)₂Cr⁺}³⁺(PF₆⁻)₃ (**16**). A slurry of FcH⁺PF₆⁻ (121 mg, 0.36 mmol) in 100 mL of THF was added to a solution of **11** (97 mg, 0.12 mmol) in 15 mL of THF; the solution slowly became green and a green precipitate formed. After 20 h the solvent was removed and the solids were dried overnight *in vacuo*. This also removed most of the ferrocene. The solids were washed with 2 × 15 mL of diethyl ether to remove the remaining ferrocene, dried *in vacuo*, and then extracted with

Table 6. Selected Bond Lengths (\AA) and Angles (deg) for 6^a

Fe(1)-C(1)	2.03(2)	C(2)-C(3)	1.42(1)
Fe(1)-C(2)	2.09(1)	C(3)-C(4)	1.48(1)
Fe(1)-C(3)	2.05(1)	C(4)-C(5)	1.52(2)
Fe(1)-C(4)	2.14(1)	C(5)-C(6)	1.530(9)
Fe(1)-C(5)	2.140(6)	C(6)-C(7)	1.50(2)
Fe(2)-C(9)	2.110(6)	C(6)-C(8)	1.56(2)
Fe(2)-C(10)	2.08(1)	C(6)-C(9)	1.520(8)
Fe(2)-C(11)	2.10(1)	C(9)-C(10)	1.43(2)
Fe(2)-C(12)	2.01(2)	C(9)-C(13)	1.43(2)
Fe(2)-C(13)	2.09(2)	C(10)-C(11)	1.44(2)
Fe(2)-C(14)	1.96(1)	C(11)-C(12)	1.37(2)
Fe(2)-C(15)	2.05(1)	C(12)-C(13)	1.42(3)
Fe(2)-C(16)	2.05(2)	C(14)-C(15)	1.29(2)
Fe(2)-C(17)	2.22(1)	C(14)-C(18)	1.44(3)
Fe(2)-C(18)	2.08(1)	C(15)-C(16)	1.38(3)
C(1)-C(2)	1.35(2)	C(16)-C(17)	1.47(3)
C(1)-C(5)	1.32(2)	C(17)-C(18)	1.34(4)
C(2)-C(1)-C(5)	111.4(14)	C(6)-C(9)-C(10)	126.0(15)
C(1)-C(2)-C(3)	111.9(13)	C(6)-C(9)-C(13)	126.6(16)
C(2)-C(3)-C(4)	103.0(13)	C(10)-C(9)-C(13)	107.3(7)
C(3)-C(4)-C(5)	105.4(10)	C(9)-C(10)-C(11)	110.0(13)
C(1)-C(5)-C(4)	106.8(7)	C(10)-C(11)-C(12)	103.8(17)
C(1)-C(5)-C(6)	134.2(14)	C(11)-C(12)-C(13)	114.4(19)
C(4)-C(5)-C(6)	119.1(12)	C(9)-C(13)-C(12)	104.4(16)
C(5)-C(6)-C(7)	116.7(11)	C(15)-C(14)-C(18)	108.8(17)
C(5)-C(6)-C(8)	105.6(12)	C(14)-C(15)-C(16)	110.1(21)
C(7)-C(6)-C(8)	108.5(6)	C(15)-C(16)-C(17)	105.9(23)
C(5)-C(6)-C(9)	103.7(6)	C(16)-C(17)-C(18)	105.4(19)
C(7)-C(6)-C(9)	112.4(13)	C(14)-C(18)-C(17)	108.1(14)
C(8)-C(6)-C(9)	109.6(12)		

^a Esd's are given in parentheses.

dichloromethane. The dichloromethane extracts were filtered, reduced *in vacuo* (to ca. 25 mL), and layered with 150 mL of diethyl ether. The resulting precipitate was washed with 2 × 30 mL of diethyl ether and dried *in vacuo* to yield a pale green air-sensitive powder (64 mg, 0.052 mmol, 43%) analyzed as **16**. Anal. Found (calcd): C, 46.44 (46.58); H, 5.02 (5.05). Selected IR (Nujol, cm⁻¹): 840. ESR (CH₂Cl₂ glass, 4.7 K): Fe, $g_{\perp} = 1.42$, $g_{\parallel} = 4.12$, $\langle g \rangle = 2.64$; Cr, $g_{\parallel} = 2.02$. Magnetic moment: $\mu_{\text{eff}} = 5.1 \mu_B$, $\Theta = -2.0$ K.

{(Fc⁺CH₂C₅H₄)₂Fe⁺}²⁺(TCNE⁻)₂ (**17**; TCNE = Tetracyanoethylene). **Method A (17a)**. A solution of TCNE (49 mg, 0.38 mmol) in 10 mL of THF was added dropwise to a stirred solution of **9** (148 mg, 0.18 mmol) in 20 mL of THF. After 20 h the green solution was filtered into a Young's ampule and layered with 200 mL of diethyl ether. After several weeks the supernatant was decanted from the resulting crystals, which were then washed with 2 × 50 mL of diethyl ether and dried *in vacuo*. Green to purple iridescent plates (ca. 60 mg, ca. 0.06 mmol, ca. 30%), analyzed as **17**, were obtained. Anal. Found (calcd): C, 68.02 (67.81); H, 5.80 (5.88); N, 10.27 (10.54). Selected IR (Nujol, cm⁻¹): 2145, 2182. ESR (THF solution, room temperature): TCNE⁻, $g = 2.00$. Magnetic moment: $\mu_{\text{eff}} = 4.0 \mu_B$, $\Theta = -0.8$ K.

Method B (17b). A solution of TCNE (49 mg, 0.38 mmol) in 20 mL of dichloromethane was added dropwise to a stirred solution of **9** (153 mg, 0.19 mmol) in 5 mL of dichloromethane; the solution became dark green. After 15 h the solution was filtered into a Young's ampule and layered with 80 mL of diethyl ether. When the solvents had completely mixed, the supernatant was filtered from the resulting fine purple needles. After these needles were washed with 2 × 50 mL of diethyl ether and dried *in vacuo*, a dark green microcrystalline powder (87 mg, 0.082 mmol, 43%), analyzed as **17**, was obtained. Anal. Found (calcd): C, 67.55 (67.81); H, 5.92 (5.88); N, 10.27 (10.54). Selected IR (Nujol, cm⁻¹): 2146, 2183. ESR (CH₂Cl₂ glass, 9.9 K): cation, $g_{\parallel} = 4.12$, $g_{\perp} = 1.33$, $\langle g \rangle = 2.61$; TCNE⁻, $g = 2.00$. Magnetic moment: $\mu_{\text{eff}} = 4.1 \mu_B$, $\Theta = +0.1$ K.

{(Fc⁺CH₂C₅H₄)₂Co⁺}³⁺(TCNE⁻)₃ (**18**). A solution of TCNE (39 mg, 0.30 mmol) in 10 mL of THF was added dropwise to a

Table 7. Fractional Atomic Coordinates and Equivalent Isotropic Temperature Factors (\AA^2) for 18^a

atom	<i>x/a</i>	<i>y/b</i>	<i>z/c</i>	<i>U</i> (equiv) ^b	atom	<i>x/a</i>	<i>y/b</i>	<i>z/c</i>	<i>U</i> (equiv) ^b
Co(1)	0.5643(2)	0.0001(6)	0.1318(4)	0.0547	C(27)	0.5972(7)	0.159(2)	0.137(2)	0.0810
Fe(1)	0.4184(2)	0.2931(4)	-0.0002(4)	0.0534	C(28)	0.6114(6)	0.066(2)	0.199(1)	0.0528
Fe(2)	0.7096(2)	-0.2904(5)	0.2628(4)	0.0559	C(29)	0.6190(5)	-0.048(2)	0.155(1)	0.0384
N(1)	0.317(1)	0.223(3)	0.535(2)	0.1419	C(30)	0.6322(5)	-0.164(2)	0.204(1)	0.0362
N(2)	0.4272(9)	0.172(3)	0.644(2)	0.1339	C(31)	0.6719(5)	-0.159(2)	0.223(1)	0.0309
N(3)	0.3554(9)	0.289(2)	0.309(2)	0.1186	C(32)	0.6862(6)	-0.133(2)	0.313(1)	0.0525
N(4)	0.466(1)	0.222(2)	0.405(2)	0.1045	C(33)	0.6664(8)	-0.109(3)	0.389(2)	0.0861
N(5)	0.5300(8)	0.392(3)	0.211(2)	0.1572	C(34)	0.7240(7)	-0.112(2)	0.311(1)	0.0485
N(6)	0.567(1)	0.695(1)	0.386(2)	0.1086	C(35)	0.7512(9)	-0.086(3)	0.387(2)	0.0907
N(7)	0.5636(9)	0.130(1)	0.372(2)	0.0858	C(36)	0.7336(5)	-0.118(2)	0.228(2)	0.0596
N(8)	0.6030(8)	0.417(4)	0.552(2)	0.1252	C(37)	0.7735(5)	-0.109(2)	0.181(2)	0.0592
N(9)	0.819(1)	0.229(3)	0.236(3)	0.1804	C(38)	0.6991(6)	-0.149(2)	0.173(1)	0.0487
N(10)	0.705(1)	0.175(3)	0.107(2)	0.1250	C(39)	0.7006(8)	-0.161(3)	0.074(2)	0.0530
N(11)	0.7714(7)	0.288(2)	0.455(2)	0.0866	C(40)	0.7464(6)	-0.438(3)	0.263(3)	0.0764
N(12)	0.664(1)	0.215(3)	0.340(2)	0.1155	C(41)	0.785(1)	-0.424(3)	0.278(5)	0.1701
C(1)	0.4291(9)	0.467(3)	0.066(2)	0.0920	C(42)	0.716(1)	-0.462(3)	0.211(1)	0.0912
C(2)	0.4466(5)	0.471(2)	-0.013(3)	0.0509	C(43)	0.731(2)	-0.489(2)	0.126(1)	0.1366
C(3)	0.4857(6)	0.487(3)	-0.001(2)	0.1092	C(44)	0.6860(7)	-0.459(3)	0.260(2)	0.0778
C(4)	0.420(1)	0.446(3)	-0.078(1)	0.0565	C(45)	0.657(1)	-0.503(3)	0.206(3)	0.1585
C(5)	0.429(2)	0.424(4)	-0.154(3)	0.2126	C(46)	0.6979(9)	-0.437(3)	0.341(2)	0.0935
C(6)	0.3860(7)	0.438(3)	-0.042(2)	0.0727	C(47)	0.684(1)	-0.449(3)	0.431(1)	0.0747
C(7)	0.3503(9)	0.435(3)	-0.093(3)	0.1542	C(48)	0.7355(9)	-0.421(3)	0.342(2)	0.0977
C(8)	0.3923(7)	0.458(3)	0.049(1)	0.0776	C(49)	0.349(1)	0.217(2)	0.524(1)	0.1058
C(9)	0.3575(9)	0.448(3)	0.097(3)	0.1135	C(50)	0.3848(6)	0.215(2)	0.515(1)	0.0623
C(10)	0.4399(5)	0.124(2)	-0.050(1)	0.0326	C(51)	0.4088(9)	0.190(3)	0.587(3)	0.1572
C(11)	0.4649(8)	0.120(2)	-0.127(1)	0.0496	C(52)	0.3735(6)	0.263(2)	0.365(2)	0.0696
C(12)	0.4008(6)	0.121(2)	-0.046(1)	0.0632	C(53)	0.3985(5)	0.239(2)	0.439(1)	0.0702
C(13)	0.3734(9)	0.091(3)	-0.116(2)	0.0847	C(54)	0.4355(5)	0.223(1)	0.425(1)	0.0550
C(14)	0.3919(5)	0.135(2)	0.044(1)	0.0456	C(55)	0.5426(7)	0.428(2)	0.277(2)	0.1079
C(15)	0.3566(8)	0.122(3)	0.069(2)	0.0913	C(56)	0.5582(6)	0.459(2)	0.352(1)	0.0787
C(16)	0.4225(6)	0.147(2)	0.089(1)	0.0467	C(57)	0.562(1)	0.594(2)	0.376(2)	0.1078
C(17)	0.4310(6)	0.167(3)	0.182(2)	0.0654	C(58)	0.5647(6)	0.239(2)	0.387(2)	0.0735
C(18)	0.4545(4)	0.139(2)	0.028(1)	0.0361	C(59)	0.5710(6)	0.368(2)	0.406(1)	0.0935
C(19)	0.4949(7)	0.164(2)	0.065(1)	0.0481	C(60)	0.5884(9)	0.402(2)	0.490(2)	0.1084
C(20)	0.5113(7)	0.046(2)	0.106(2)	0.0677	C(61)	0.788(1)	0.224(2)	0.241(2)	0.0995
C(21)	0.5183(7)	0.042(3)	0.194(1)	0.0504	C(62)	0.7466(6)	0.214(3)	0.249(2)	0.1299
C(22)	0.5291(7)	-0.080(3)	0.214(2)	0.0604	C(63)	0.7217(7)	0.194(2)	0.169(1)	0.0482
C(23)	0.5308(6)	-0.145(3)	0.139(2)	0.0387	C(64)	0.7561(8)	0.266(3)	0.392(2)	0.0873
C(24)	0.5206(7)	-0.077(3)	0.075(2)	0.0628	C(65)	0.7328(7)	0.233(3)	0.319(2)	0.1188
C(25)	0.6108(5)	-0.027(2)	0.068(1)	0.0506	C(66)	0.691(1)	0.227(3)	0.327(2)	0.1417
C(26)	0.5955(7)	0.102(3)	0.057(2)	0.0690					

^a Esd's are given in parentheses. ^b *U*(equiv) = one-third of the trace of the orthogonalized U_{ij} tensor.

stirred solution of **10** (81 mg, 0.10 mmol) in 15 mL of THF. After 18 h the solution was green and a fine brown precipitate had formed. The solvent was removed *in vacuo*, and the resulting solids were washed with 3 × 25 mL of diethyl ether. The solids were then extracted back into THF. The resulting green-red dichroic solution was filtered into a Young's ampule, reduced *in vacuo* to 60 mL, and layered with 150 mL of diethyl ether. When the solvents had completely mixed, the supernatant was decanted from the resulting shiny black platelets, which were then washed with 3 × 30 mL of diethyl ether and dried *in vacuo*. Ca. 45 mg (ca. 0.04 mmol, ca. 40%) of analytically pure crystals was obtained. A crystal suitable for X-ray structure analysis was selected and sealed in a glass capillary under a nitrogen atmosphere. Anal. Found (calcd): C, 66.25 (66.40); H, 5.39 (5.23); N, 13.33 (14.08). Selected IR data (Nujol, cm^{-1}): 2143, 2183. ESR (CH_2Cl_2 glass, 5.3 K): cation, $g_{\perp} = 1.38$, $g_{\parallel} = 4.06$, $\langle g \rangle = 2.60$; TCNE^- , $g = 2.00$. Magnetic moment: $\mu_{\text{eff}} = 4.5 \mu_{\text{B}}$, $\Theta = -5.8$ K.

Crystal Structure Determinations. General Considerations. X-ray structure determinations for **3**, **6**, **18** have been performed. A summary of the crystal data, data collection, and processing parameters is given in Table 1. The general procedure was as follows. A crystal was mounted in a Lindemann tube (0.7 mm), in the cases of **6** and **18** under dinitrogen, which was sealed with a small flame. This tube was transferred to the goniometer head of an Enraf-Nonius CAD4 diffractometer, employing graphite-monochromated $\text{Mo K}\alpha$ ($\lambda = 0.71069 \text{ \AA}$) radiation. Unit cell parameters were calculated from the setting angles of 25 carefully centered reflections. Three reflections were chosen as intensity standards and were measured every 3600 s of X-ray exposure time, and 3 orientation controls were measured every 250 reflections.

The data were corrected for Lorentz and polarization effects.¹⁶ For all structures the heavy-atom positions were determined by direct methods. Subsequent Fourier difference syntheses revealed the positions of the other non-hydrogen atoms. Non-hydrogen atoms were refined with anisotropic thermal parameters by full-matrix least-squares procedures. The hydrogen atoms were fixed in geometrically idealized positions and allowed to ride on their attached carbon atoms. The hydrogen atoms were given isotropic thermal parameters according to the atom to which they were attached (these were not refined). An absorption correction using DIFABS¹⁷ was applied. A Chebyshev weighting scheme¹⁸ was applied in the cases of **3** and **6**, and in all cases the data were corrected for the effects of anomalous dispersion and isotropic extinction (*via* an overall extinction parameter)¹⁹ in the final stages of refinement. All crystallographic calculations were performed using the Oxford CRYSTALS system²⁰ running on a Vax 11/750 or a Silicon Graphics Indigo R3000 computer. Neutral atom scattering factors were taken from the usual sources.²¹

Structure of 3. For crystals of **3** the systematic absences uniquely indicated the space group $P2_1/a$. Fractional atomic coordinates, selected bond lengths, and selected bond angles are shown in Tables 2–4, respectively.

(16) North, A. C. T.; Phillips, D. C.; Matthews, F. S. *Acta Crystallogr.* **1968**, *A24*, 351–359.

(17) Walker, N.; Stuart, D. *Acta Crystallogr.* **1983**, *A39*, 159–166.

(18) Carruthers, J.; Watkin, D. W. *Acta Crystallogr.* **1979**, *A35*, 698–699.

(19) Larson, A. C. *Acta Crystallogr.* **1967**, *23*, 664–665.

(20) Carruthers, J.; Watkin, D. W. *CRYSTALS Users Manual*; Oxford University Computer Centre: Oxford, U.K., 1975.

(21) *International Tables for X-ray Crystallography*; Kynoch Press: Birmingham, U.K., 1974.

Table 8. Selected Bond Lengths (Å) for 18^a

Co(1)–C(20)	2.00(3)	C(6)–C(8)	1.44(3)
Co(1)–C(21)	2.02(2)	C(10)–C(12)	1.42(2)
Co(1)–C(22)	2.04(2)	C(10)–C(18)	1.32(2)
Co(1)–C(23)	1.97(2)	C(12)–C(14)	1.47(3)
Co(1)–C(24)	1.95(2)	C(14)–C(16)	1.29(3)
Co(1)–C(25)	2.02(2)	C(16)–C(18)	1.54(2)
Co(1)–C(26)	1.98(2)	C(18)–C(19)	1.57(3)
Co(1)–C(27)	2.06(2)	C(19)–C(20)	1.51(3)
Co(1)–C(28)	2.09(2)	C(20)–C(21)	1.40(3)
Co(1)–C(29)	2.06(2)	C(20)–C(24)	1.44(3)
Fe(1)–C(1)	2.15(2)	C(21)–C(22)	1.38(4)
Fe(1)–C(2)	2.16(2)	C(22)–C(23)	1.36(4)
Fe(1)–C(4)	2.04(2)	C(23)–C(24)	1.28(3)
Fe(1)–C(6)	2.02(3)	C(25)–C(26)	1.48(3)
Fe(1)–C(8)	2.15(2)	C(25)–C(29)	1.41(3)
Fe(1)–C(10)	2.12(2)	C(26)–C(27)	1.38(3)
Fe(1)–C(12)	2.05(2)	C(27)–C(28)	1.47(3)
Fe(1)–C(14)	2.07(2)	C(28)–C(29)	1.43(3)
Fe(1)–C(16)	2.09(2)	C(29)–C(30)	1.51(3)
Fe(1)–C(18)	2.12(2)	C(30)–C(31)	1.45(2)
Fe(2)–C(31)	2.03(2)	C(31)–C(32)	1.50(2)
Fe(2)–C(32)	2.05(2)	C(31)–C(38)	1.29(3)
Fe(2)–C(34)	2.09(2)	C(32)–C(34)	1.38(3)
Fe(2)–C(36)	2.11(2)	C(34)–C(36)	1.37(3)
Fe(2)–C(38)	2.07(2)	C(36)–C(38)	1.52(3)
Fe(2)–C(40)	2.05(3)	C(40)–C(42)	1.36(3)
Fe(2)–C(42)	2.01(3)	C(40)–C(48)	1.33(3)
Fe(2)–C(44)	1.99(3)	C(42)–C(44)	1.35(3)
Fe(2)–C(46)	2.04(3)	C(44)–C(46)	1.35(3)
Fe(2)–C(48)	2.06(3)	C(46)–C(48)	1.37(3)
N(1)–C(49)	1.18(5)	C(49)–C(50)	1.33(4)
N(2)–C(51)	1.10(5)	C(50)–C(51)	1.42(4)
N(3)–C(52)	1.11(4)	C(50)–C(53)	1.34(3)
N(4)–C(54)	1.16(3)	C(52)–C(53)	1.45(3)
N(5)–C(55)	1.17(4)	C(53)–C(54)	1.38(3)
N(6)–C(57)	1.10(2)	C(55)–C(56)	1.32(4)
N(7)–C(58)	1.18(2)	C(56)–C(57)	1.48(2)
N(8)–C(60)	1.10(3)	C(56)–C(59)	1.35(2)
N(9)–C(61)	1.12(5)	C(58)–C(59)	1.42(2)
N(10)–C(63)	1.13(3)	C(59)–C(60)	1.47(3)
N(11)–C(64)	1.14(3)	C(61)–C(62)	1.50(4)
N(12)–C(66)	1.04(5)	C(62)–C(63)	1.53(3)
C(1)–C(2)	1.41(3)	C(62)–C(65)	1.25(4)
C(1)–C(8)	1.35(3)	C(64)–C(65)	1.43(4)
C(2)–C(4)	1.41(3)	C(65)–C(66)	1.51(5)
C(4)–C(6)	1.37(3)		

^a Esd's are given in parentheses.

Structure of 6. The structure of **6** was refined in the three possible space groups indicated by systematic absences: *C*2, *C*m, and *C*2/*m*. The most satisfactory refinement was obtained in *C*2. In this space group the asymmetric unit consists of half a trication and one complete and one half triflate anion; the "half" triflate anion is required to be disordered, since there is a 2-fold axis perpendicular to the principal axis of the anion. The "half" triflate was modeled as a carbon atom and a sulfur atom, each at a fixed occupancy of 0.5; both the temperature factors of these two atoms and their coordinates were treated as equivalent. The other atoms of the triflate were all treated as fluorine atoms. In addition, the complete triflate molecule was found to be disordered between the sulfur and carbon ends of the anion. This disorder, which is not crystallographically imposed, was modeled by placing S1 and C20 on one of the two C/S positions and S(2) and C(19) at the other site, all with equal temperature factors and at occupancy 0.5; refinement of occupancies, constrained so that $\text{occ}(\text{S}(1)) = \text{occ}(\text{C}(19)) = 1 - \text{occ}(\text{S}(2)) = 1 - \text{occ}(\text{C}(20))$, showed that 73% of the anions were oriented in one direction, whereas 27% were oriented in the opposite sense. In subsequent cycles of refinement, temperature factors were kept equivalent between S(1) and C(20) and between S(2) and C(19); occupancy was not refined. Given the similarity in scattering factors, no attempt was made to differentiate between the fluorines and oxygens of this anion. Fractional atomic coordinates are given in Table 5; bond lengths and angles are listed in Table 6.

Structure of 18. The space group could not be determined unambiguously from systematic absences, and therefore, solu-

Table 9. Selected Bond Angles (deg) for 18^a

C(2)–C(1)–C(8)	108.2(5)	C(42)–C(40)–C(48)	108.2(10)
C(1)–C(2)–C(4)	108.0(5)	C(40)–C(42)–C(44)	108.0(5)
C(2)–C(4)–C(6)	107.5(5)	C(42)–C(44)–C(46)	107.8(5)
C(4)–C(6)–C(8)	107.6(5)	C(44)–C(46)–C(48)	107.9(5)
C(1)–C(8)–C(6)	108.0(5)	C(40)–C(48)–C(46)	108.0(5)
C(12)–C(10)–C(18)	108.1(5)	N(1)–C(49)–C(50)	176.6(11)
C(10)–C(12)–C(14)	108.1(5)	C(49)–C(50)–C(51)	119.2(13)
C(12)–C(14)–C(16)	108.1(5)	C(49)–C(50)–C(53)	120.1(9)
C(14)–C(16)–C(18)	108.0(5)	C(51)–C(50)–C(53)	120.8(10)
C(17)–C(16)–C(18)	119.4(16)	N(2)–C(51)–C(50)	179.4(11)
C(10)–C(18)–C(16)	107.7(5)	N(3)–C(52)–C(53)	175.3(10)
C(10)–C(18)–C(19)	133.6(15)	C(50)–C(53)–C(52)	119.9(9)
C(16)–C(18)–C(19)	118.3(15)	C(50)–C(53)–C(54)	121.3(9)
C(18)–C(19)–C(20)	111.1(21)	C(52)–C(53)–C(54)	118.2(12)
C(19)–C(20)–C(21)	119.7(22)	N(4)–C(54)–C(53)	171.2(10)
C(19)–C(20)–C(24)	134.6(25)	N(5)–C(55)–C(56)	175.4(10)
C(21)–C(20)–C(24)	105.6(18)	C(55)–C(56)–C(57)	120.6(12)
C(20)–C(21)–C(22)	106.4(18)	C(55)–C(56)–C(59)	119.7(9)
C(21)–C(22)–C(23)	108.5(17)	C(57)–C(56)–C(59)	119.7(9)
C(22)–C(23)–C(24)	111.0(24)	N(6)–C(57)–C(56)	172.9(11)
C(20)–C(24)–C(23)	108.4(21)	N(7)–C(58)–C(59)	172.7(11)
C(26)–C(25)–C(29)	107.9(5)	C(56)–C(59)–C(58)	120.9(9)
C(25)–C(26)–C(27)	108.0(5)	C(56)–C(59)–C(60)	120.3(9)
C(26)–C(27)–C(28)	108.0(5)	C(58)–C(59)–C(60)	118.4(14)
C(27)–C(28)–C(29)	108.1(5)	N(8)–C(60)–C(59)	173.3(11)
C(25)–C(29)–C(28)	107.9(5)	N(9)–C(61)–C(62)	178.8(11)
C(25)–C(29)–C(30)	131.9(17)	C(61)–C(62)–C(63)	119.7(14)
C(28)–C(29)–C(30)	120.2(17)	C(61)–C(62)–C(65)	119.8(10)
C(29)–C(30)–C(31)	111.3(17)	C(63)–C(62)–C(65)	120.2(9)
C(30)–C(31)–C(32)	119.5(18)	N(10)–C(63)–C(62)	175.5(10)
C(30)–C(31)–C(38)	130.8(18)	N(11)–C(64)–C(65)	172.4(10)
C(32)–C(31)–C(38)	108.2(5)	C(62)–C(65)–C(64)	120.1(10)
C(31)–C(32)–C(34)	108.1(5)	C(62)–C(65)–C(66)	120.6(10)
C(32)–C(34)–C(36)	107.8(5)	C(64)–C(65)–C(66)	119.3(14)
C(34)–C(36)–C(38)	107.9(5)	N(12)–C(66)–C(65)	171.5(11)
C(31)–C(38)–C(36)	107.9(5)		

^a Esd's are given in parentheses.

tion was attempted in both *C*2/*c* and *C*c (in the former space group the cation lies on the crystallographic inversion center). Refinement in the noncentrosymmetric space group *C*c led to the more satisfactory solution, especially with regard to the TCNE anions. Unfortunately, the low ratio of data to variables meant noncrystallographic restraints had to be employed to regularize the cyclopentadienyl rings and the TCNE anions; therefore, a detailed discussion of bond lengths and angles is not possible. Fractional atomic coordinates, selected bond lengths, and selected bond angles for **18** are shown in Tables 7–9, respectively.

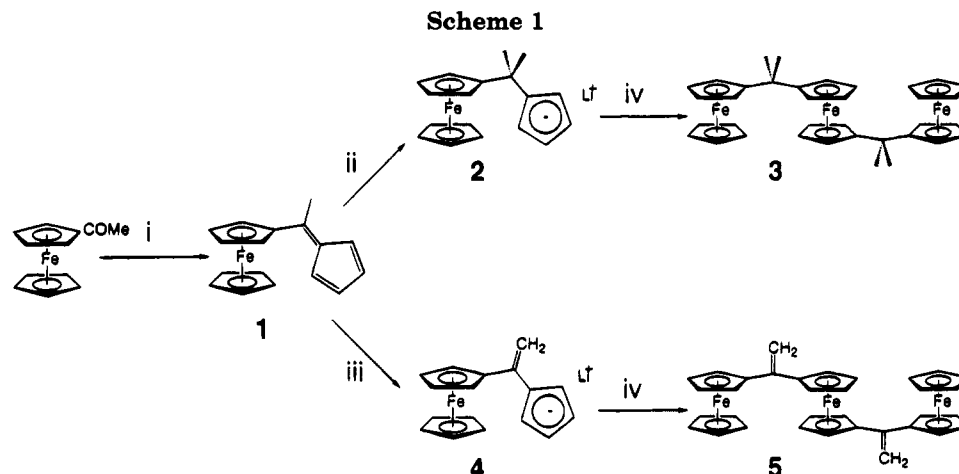
Results and Discussion

Synthesis of Trimetalloenes 3 and 5 from 6-Ferrocenyl-6-methylfulvene. The reactions of fulvenes with a variety of nucleophiles, bases, and reducing agents allow the preparation of many substituted cyclopentadienyl anions.²² Here we exploit some of these reactions to synthesize trimetalloene molecules.

6-ferrocenyl-6-methylfulvene (**1**) was prepared, as shown in Scheme 1, from acetylferrocene in a modification of a literature procedure,¹⁴ but using potassium hydroxide in place of sodium metal. Reaction with methyllithium in diethyl ether gives an orange precipitate of the ferrocene-functionalized lithium cyclopentadienide **2**, which was characterized by its reaction with $\text{FeCl}_2 \cdot 1.5\text{THF}$ in THF to yield the triferrocene **3**.

In contrast, treatment of **1** with either lithioferrocene or *tert*-butyllithium gives low yields of an alternative lithium salt, **4**, which on reaction with $\text{FeCl}_2 \cdot 1.5\text{THF}$ in THF gives the triferrocene **5**. The infrared spectrum of **5** indicates the presence of a C=C double bond in the

(22) Knox, G. R.; Pauson, P. L. *J. Chem. Soc.* **1961**, 4610–4615 and references therein.



^a Legend: (i) excess C₅H₆, KOH, EtOH; (ii) MeLi, Et₂O; (iii) Bu^tLi or FeLi, THF; (iv) FeCl₂·1.5THF.

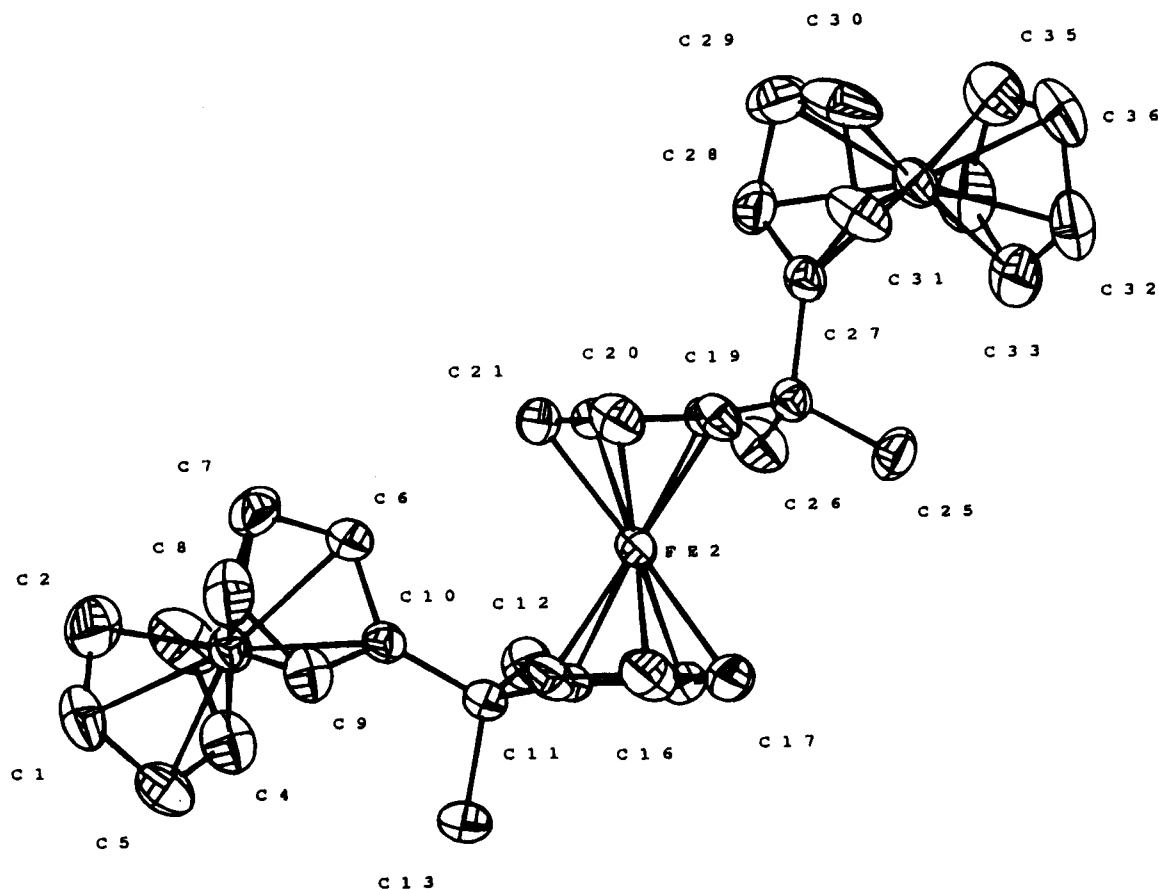


Figure 2. Crystal structure of **3** (50% thermal probability ellipsoids).

molecule. Use of methyllithium in THF gives a mixture of products, which is presumably due to the competition between the more basic and less nucleophilic character of methyllithium in the more polar solvent. **3** is air stable and is soluble in aromatic solvents, dichloromethane and THF, rather less soluble in diethyl ether, and insoluble in hexanes and very polar solvents such as acetone. **5** is slightly more soluble than **3**, and although it is air stable in the solid state, solutions exposed to air slowly decompose to deposit a brown precipitate.

X-ray Crystal Structure of the Triferrocene **3**.

Crystals of **3** were grown by slow evaporation of a dichloromethane solution. Compound **3** crystallizes in the monoclinic space group *P2₁/a*. Figure 2 gives a view of the molecular structure; fractional atomic coordinates are shown in Table 2, and selected distances and angles

are given in Tables 3 and 4, respectively. The Fe–ring centroid distances fall in the range 1.647(2)–1.704(2) Å, with a mean of 1.661(2) Å. The Fe–ring C distances fall in the range 2.028(2)–2.067(2) Å, with a mean of 2.044(2) Å. These distances are typical for ferrocenes; for example, ferrocene,²³ octamethylferrocene,²⁴ and dexamethylferrocene^{24,25} have average Fe–ring C distances of 2.04(2), 2.054(3), and 2.050(2) Å, respectively.

It is interesting to compare the structure of **3** with the related structurally characterized silicon-bridged analogues **19**⁷ and **20**⁶ (Figure 3). Pannell *et al.*⁷ have also performed molecular mechanics calculations on the

(23) Dunitz, J. D.; Orgel, L. E.; Rich, A. *Acta Crystallogr.* **1956**, *9*, 373–375.

(24) Struchkov, Y. T.; Adrianov, V. G.; Sal'nikova, T. N.; Lyatifov, I. R.; Materikova, R. B. *J. Organomet. Chem.* **1978**, *145*, 213–223.

(25) Freyberg, D. P.; Robbins, J. L.; Raymond, K. N.; Smart, J. C. *J. Am. Chem. Soc.* **1979**, *101*, 892–897.

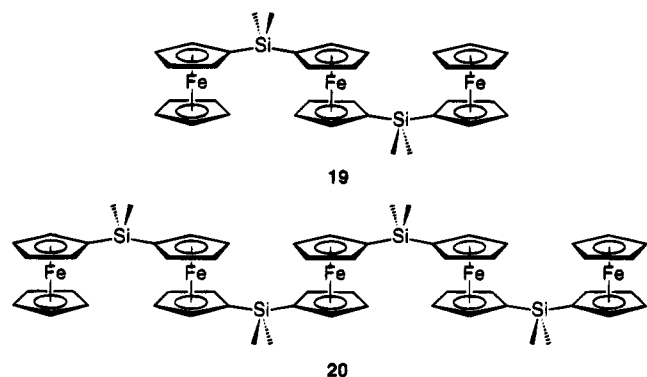


Figure 3. Si-bridged analogues of 3: 19 and 20.

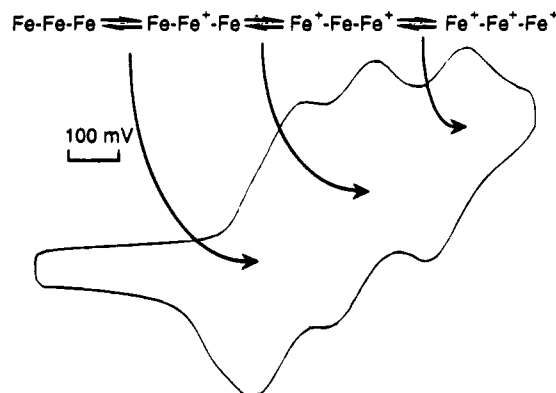


Figure 4. Cyclic voltammogram of 3 in CH_2Cl_2 . The scan rate is 200 mV s^{-1} .

structures of such oligomers in order to gain insight into the conformations of poly(ferrocenylsilane) materials. Pannell *et al.* found that 19 adopts a conformation in which the two terminal ferrocenes lie perpendicular to the central ferrocene; this conformation was also calculated to be one of several possible energy minima. However, 3 adopts an unsymmetrical conformation very different to any of Pannell's minima, in which the substituents of the central ferrocene are not perfectly staggered and in which the two intramolecular Fe-Fe separations are inequivalent at 5.716(1) and 6.456(1) Å.

Redox Chemistry of 3 and 5. The cyclic voltammogram of 3 in dichloromethane solution is shown in Figure 4. Three reversible redox events are resolvable at -0.14 , 0.00 , and $+0.20 \text{ V}$ (relative to the ferrocenium/ferrocene couple under the same conditions). The three reversible waves are in the ratio 1:1:1, with separations between successive waves ($\Delta E_{1/2}$) of 14 and 20 mV, respectively; these waves can be assigned to successive redox events at each iron center. The data indicate significant electrostatic interactions between the iron centers; in the absence of any interaction one would expect two waves in a 1:2 ratio, corresponding to the two ferrocene environments present. We believe that the central ferrocene unit will be the first center to be oxidized, as it bears two alkyl substituents; oxidation potentials of methylated ferrocenes have been found to decrease in steps of approximately 0.05 V on addition of each methyl substituent.²⁶ The second potential presumably corresponds to generation of a dication in which the charge is borne by the terminal ferrocenes and the third to the formation of the trication.

The cyclic voltammogram of 5 also shows three waves; these are at -0.11 , $+0.15$, and $+0.27 \text{ V}$ relative to ferrocene/ferrocenium. Interestingly, in this case the first and second oxidations are more widely separated than the second and third, whereas in 3 the reverse is true.

Interestingly, the SiMe_2 -bridged analogue of 3, 19 (Figure 3), which has been synthesized recently by two different groups, using three different strategies,^{6,7} shows radically different electrochemistry. Rulkens *et al.*⁶ have observed two waves in 1:1 dichloromethane/acetonitrile, in a 2:1 ratio, at -0.03 and 0.23 V (relative to ferrocenium/ferrocene); however, Pannell *et al.*⁷ have been able to resolve the -0.03 V wave into two using dichloromethane as a solvent. Silicon substituents on ferrocenes are neither strongly electron donating nor withdrawing.²⁶ Hence, the first oxidation potential is close to that of ferrocene itself, and there will be only a small difference between the potentials at which a monocation (central or terminal) or a dication (on both terminal ferrocenes) will form. Indeed, whether or not a terminal-terminal dication or a monocation (central or terminal) is the first species to be generated may depend on subtle factors, such as solvent choice. Rulkens *et al.* also studied a range of analogous species containing between two and eight ferrocene units. They found the CV data were always consistent with oxidation of alternate ferrocenes, with subsequent oxidation of intervening sites. Thus, 20 (Figure 3) shows two waves in a 3:2 ratio, attributable to oxidation of the central and two terminal ferrocenes to give a trication, followed by oxidation of the intervening ferrocenes at higher potential.

We have been able to chemically oxidize 3 to the paramagnetic triferrocenium salt 6 (Scheme 3) by the addition of 3 equiv of silver trifluoromethanesulfonate in THF. 6 is soluble in acetone and acetonitrile and slightly soluble in water but is insoluble in dichloromethane, THF, and other less polar solvents. ESR spectra of crystals of 6 are silent at 300 K; this is typical of ferrocenium salts and is generally attributed to rapid spin-lattice relaxation.²⁷ At 8.5 K the ESR spectrum of an acetonitrile glass of 6 consists of a series of overlapping broad anisotropic signals from the different ferrocenium environments, precluding accurate determination of the g tensors. Variable-temperature (6–290 K) solid-state magnetic susceptibility data show that there are no significant magnetic interactions between the metal centers; 6 obeys the Curie-Weiss law with a Curie constant (C) and Weiss constant (Θ) of $2.46 \text{ emu K mol}^{-1}$ and -2.7 K , respectively. The derived magnetic moment is $4.4 \mu_B$. Assuming the averaged g value ($\langle g \rangle$) for each iron center to be the same, the theoretical moment is given by

$$\mu_{\text{eff}}(\text{total})^2 = 3[\langle g \rangle^2(S(S+1))]$$

If we substitute $S = 1/2$ and $\langle g \rangle = 2.7$, typical for a methylferrocenium or 1,1'-dimethylferrocenium ion,^{28,29} this gives an expected μ_{eff} of $4.05 \mu_B$. The small discrepancy between this value and the observed value

(27) Fritz, H. P.; Keller, H. J.; Schwarzhan, K. E. *J. Organomet. Chem.* **1967**, *7*, 105–111.

(28) Prins, R. *Mol. Phys.* **1970**, *19*, 603–620.

(29) Duggan, D. M.; Hendrickson, D. N. *Inorg. Chem.* **1975**, *14*, 955–969.

(26) Hoh, G. L. K.; McEwen, W. E.; Kleinberg, J. *J. Am. Chem. Soc.* **1961**, *83*, 3949–3953.

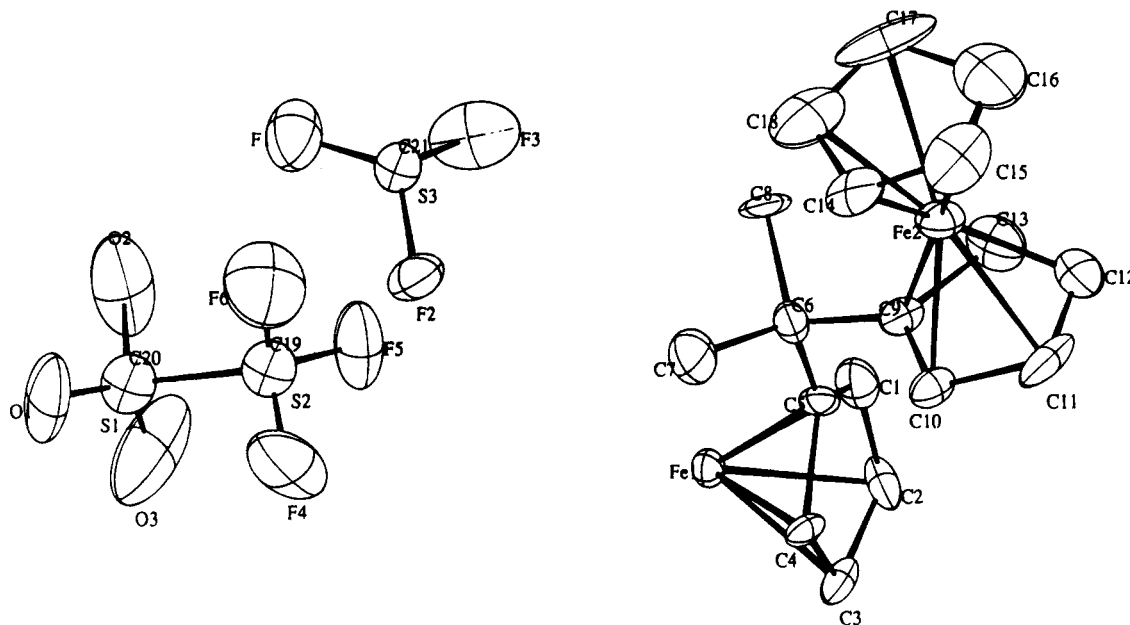


Figure 5. Asymmetric unit of the crystal structure of **6**, showing the atom-labeling scheme (50% thermal probability ellipsoids).

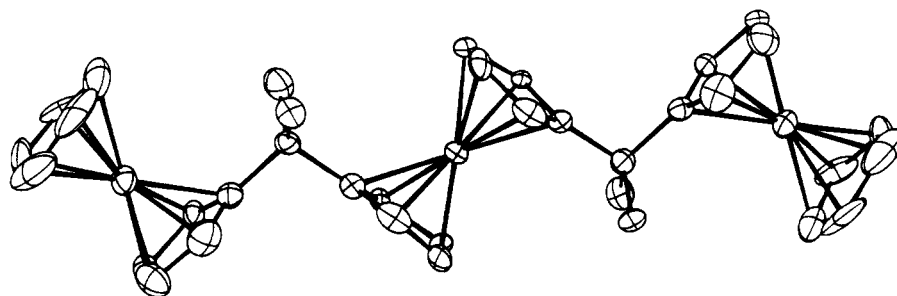


Figure 6. View of the 3^{3+} trication in the crystal structure of **6** (50% thermal probability ellipsoids).

may be due to preferential alignment of the platelike crystallites in the sample tube or to values of $\langle g \rangle$ greater than 2.7; unfortunately, as discussed above, the g values cannot be established independently by ESR.

X-ray Crystal Structure of the Tri-ferrocenium Salt 6. Single crystals of **6** were grown by slow diffusion of pentane vapor into an acetone solution of **6**. Compound **6** crystallizes in the monoclinic space group $C2$. Figure 5 shows the asymmetric unit and atomic numbering scheme, while Figure 6 clearly shows the conformation adopted by the trication. Fractional atomic coordinates and selected distances and angles are given in Tables 5 and 6, respectively. The two intramolecular Fe–Fe separations are constrained to be identical by crystallographic symmetry; the separation is 6.536(1) Å. The closest intermolecular Fe–Fe distance is 8.326(1) Å. The Fe–ring centroid distances range from 1.69(1) to 1.71(1) Å, with a mean of 1.70(1) Å; the average Fe–ring C distance is 2.08(1) Å. These distances are slightly longer than the corresponding average centroid distances found for the neutral parent molecule **3** (*vide supra*), whereas the intra-ring C–C distances are similar to those of the parent compound. Similar changes in bond lengths on oxidation have previously been observed for other ferrocenes, including ferrocene itself,³⁰ octamethylferrocene,³¹ and decamethylferrocene.³²

6 adopts one of Pannell's low-energy conformations (*vide supra*), but one with Fe–Fe separations larger than those adopted by **19**; it is possible that electrostatic repulsion between the cation centers of **6** is a contributory factor, although crystal packing considerations will also be important. **3**, however, adopts an unsymmetrical conformation with two different Fe–Fe separations (*vide supra*). We are currently carrying out our own molecular modeling calculations on these systems to calculate the relative energy of the various possible conformers.

Synthesis of Methylated Trimetalloenes 9–11 from 6-(Octamethylferrocenyl)fulvene. 6-(octamethylferrocenyl)fulvene (**7**) is a purple oil and may be obtained in essentially quantitative yield by the potassium hydroxide catalyzed reaction of octamethylferrocene with excess cyclopentadiene in ethanol. NMR and IR data are consistent with those for other fulvenes. Reaction with lithium aluminum hydride in diethyl ether gives a yellow lithium salt, **8**, which reacts in THF with $\text{FeCl}_2 \cdot 1.5\text{THF}$, $\text{Co}(\text{acac})_2$, or CrCl_2 to give good yields of **9**, **10**, or **11**, respectively (Scheme 2).

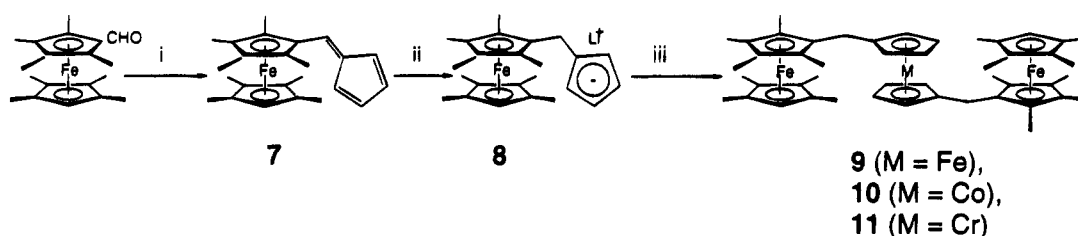
Unlike **3** and **5**, these trimetalloenes are soluble in petroleum ether, presumably owing to the methyl substituents of the terminal ferrocene units. Compound **9** is air stable and yellow, **10** is oxygen sensitive and red-brown, and **11** is extremely air sensitive and orange-

(30) Sullivan, B. W.; Foxman, B. M. *Organometallics* **1983**, *2*, 187–189.

(31) Miller, J. S.; Glatzhofer, D. T.; O'Hare, D. M.; Reiff, W. M.; Chakraborty, A.; Epstein, A. J. *Inorg. Chem.* **1989**, *28*, 2930–2939.

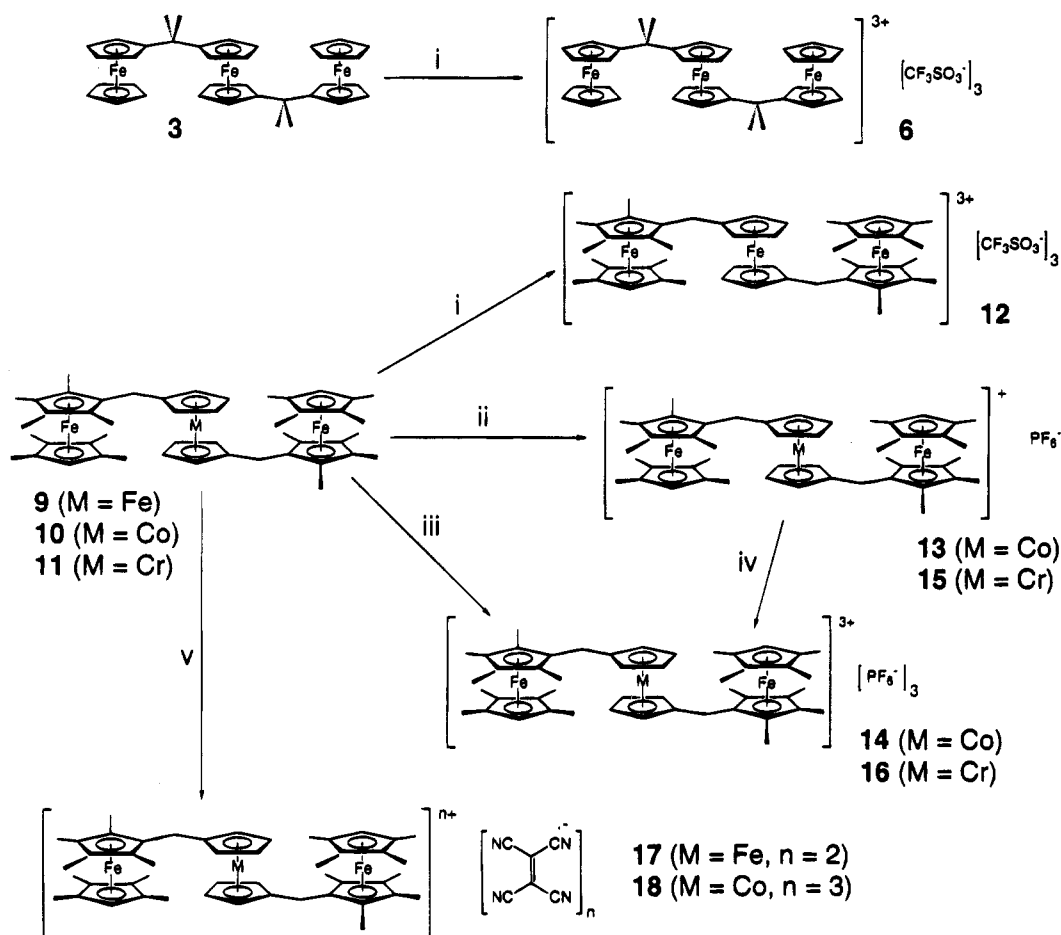
(32) Miller, J. S.; Calabrese, J. C.; Rommelmann, H.; Chittipeddi, S. R.; Zhang, J. H.; Reiff, W. M.; Epstein, A. J. *J. Am. Chem. Soc.* **1987**, *109*, 769–781.

Scheme 2



^a Legend: (i) excess C₅H₆, KOH, EtOH; (ii) LiAlH₄, Et₂O; (iii) for M = Fe, FeCl₂·1.5THF, THF; for M = Co, Co(acac)₂, THF; for M = Cr, CrCl₂, THF.

Scheme 3



^a Legend: (i) 3 equiv of CF₃SO₃⁻Ag⁺, THF; (ii) for M = Co, excess NH₄⁺PF₆⁻, THF; for M = Cr, 1 equiv of [Fe(Cp)₂]⁺PF₆⁻, THF/MeCN; (iii) for M = Cr, 3 equiv of [Fe(Cp)₂]⁺PF₆⁻, THF; (iv) for M = Co, 2 equiv of [Fe(Cp)₂]⁺PF₆⁻, CH₂Cl₂; (v) for M = Fe, 2 equiv of TCNE, THF or CH₂Cl₂; for M = Co, 3 equiv of TCNE, THF.

brown. Variable-temperature solid-state magnetic susceptibility measurements have been performed on the paramagnetic compounds **10** and **11**. The temperature dependence of the molar susceptibility of **10** can be fitted to the Curie-Weiss law in the temperature range 50–200 K with $C = 0.357 \text{ emu K mol}^{-1}$, corresponding to an effective magnetic moment of $1.69 \mu_B$, and $\Theta = -13 \text{ K}$, similar to the Weiss temperature of -15 K observed by König *et al.* for cobaltocene.³³ The overall temperature dependence of the effective magnetic moment is also similar to that observed for cobaltocene.^{33,34}

The extreme air sensitivity of **11** is a complication in the measurement of reliable magnetic data; however, the molar susceptibility data from 6 to 290 K can be fitted to the Curie-Weiss law, with $C = 0.856 \text{ emu K}$

mol^{-1} and $\Theta = -6.2 \text{ K}$. The observed high-temperature effective moment of $2.6 \mu_B$ is consistent with an $S = 1$ ground state, as has been found for other chromocenes.^{33–37}

Redox Chemistry of 9, 10, and 11. The cyclic voltammogram of **9** in dichloromethane exhibits two reversible waves, in a 2:1 ratio, at -0.47 and -0.07 V relative to the ferrocenium/ferrocene couple. The two-electron process corresponds to the simultaneous oxidation of the two terminal methylated ferrocenes, which are too far apart to significantly interact; the $E_{1/2}$ value lies between those for octamethylferrocene (-0.34 V)³¹ and dexamethylferrocene (-0.53 V).³⁶ The one-electron

(35) Ammeter, J. H. *J. Magn. Reson.* **1978**, *30*, 299–325.

(36) Robbins, J. L.; Edelstein, N.; Spencer, B.; Smart, J. C. *J. Am. Chem. Soc.* **1982**, *104*, 1882–1893.

(37) Castellani, M. P.; Geib, S. J.; Rheingold, A. L.; Troglor, W. C. *Organometallics* **1987**, *6*, 1703–1712.

(33) König, E.; Schnakig, R.; Kremer, S. *Chem. Phys.* **1978**, *27*, 331–344.

(34) Warren, K. D. *Struct. Bonding* **1976**, *27*, 45–160.

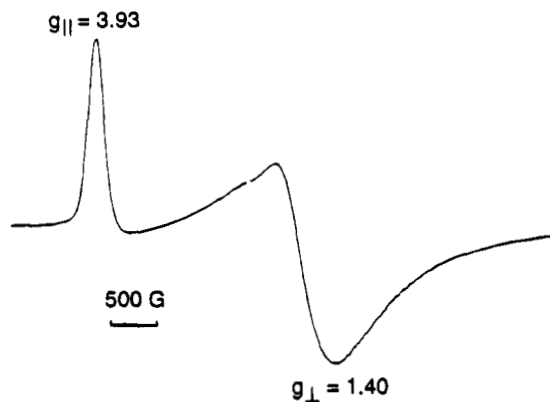


Figure 7. X-Band ESR spectrum of an acetonitrile glass of **14** at 4.5 K.

process corresponds to the oxidation of the central iron; this is at slightly lower potential than ferrocene itself, owing to a balancing of the electron-donating effect of the alkyl bridges with electrostatic interactions with the terminal cations.

The electrochemistry of **10** was investigated by measuring the cyclic voltammogram of its air-stable oxidized derivative **13** (*vide infra*) in dichloromethane. This shows two reversible redox processes at -1.50 and -0.45 V (relative to the ferrocenium/ferrocene couple), the waves being in a 1:2 ratio, corresponding to the couples for the cobalt and iron units, respectively. The $E_{1/2}$ value for the cobalt couple lies between those for cobaltocene (-1.32 V)³⁸ and decamethylcobaltocene (-1.89 V).³⁶

Compound **9** can be chemically oxidized to the trication **12** with 3 equiv of silver trifluoromethanesulfonate (Scheme 3). The salt is insoluble in THF and less polar solvents, sparingly soluble in water, soluble in dichloromethane and methanol, and very soluble in acetone and acetonitrile. Variable-temperature (6–290 K) magnetic susceptibility data are consistent with the presence of three noninteracting ferrocenium centers; the data can be fitted to the Curie–Weiss law, with $C = 3.74$ emu K mol⁻¹ and $\Theta = -1.7$ K, giving a magnetic moment of $4.1 \mu_B$. ESR spectra pose the same difficulties in interpretation as those of **6** (*vide supra*).

Oxidation of **10** with excess ammonium hexafluorophosphate in THF results in the precipitation of purple **13** (Scheme 3). The diamagnetic air-stable salt is almost completely insoluble in THF but soluble in acetone, acetonitrile, and dichloromethane.

14 may be prepared in good yield by the reaction of **13** with ferrocenium hexafluorophosphate in dichloromethane. The air-stable green salt is insoluble in THF, alcohols and water, almost insoluble in dichloromethane, sparingly soluble in chloroform and pyridine, moderately soluble in acetone, and very soluble in acetonitrile. ESR measurements on an acetonitrile glass at 4.5 K yield an axially symmetric powder pattern (shown in Figure 7) characterized by $g_{\perp} = 1.40$ and $g_{\parallel} = 3.93$, giving $\Delta g = 2.53$ and $\langle g \rangle = 2.54$; these are values similar to those reported for other ferrocenium ions slightly distorted from axial symmetry.³¹ Variable-temperature (6–290 K) magnetic susceptibility measurements show Curie–Weiss behavior ($C = 1.36$ emu K mol⁻¹, $\Theta = -3.6$ K) with no significant interactions

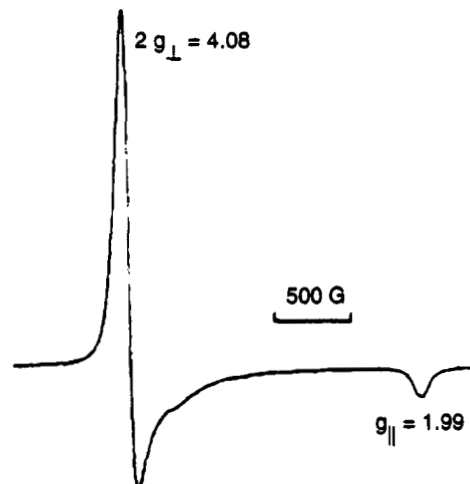


Figure 8. X-band ESR spectrum of a dichloromethane glass of **15** at 22 K.

between the metal centers; the effective magnetic moment of $3.2 \mu_B$ is in excellent agreement with the $3.1 \mu_B$ expected for a molecule containing two noninteracting ferrocenium ions with $\langle g \rangle = 2.54$.

11 may be oxidized by 1 or 3 equiv of ferrocenium hexafluorophosphate to yield the very air-sensitive salts **15** and **16**, respectively. This oxidation behavior of **11** is in contrast to the reaction of chromocene with ferrocenium hexafluorophosphate, where extensive decomposition is found.³⁹ In fact, salts of the unsubstituted chromocenium cation have only been formed by oxidation with allyl iodide⁴⁰ and carbon tetrachloride (to give $[\text{Cr}(\text{Cp})_2]^+[\text{Cr}(\text{Cp})\text{Cl}_3]^-$).⁴¹ In contrast, decamethylchromocene³⁶ and octaphenylchromocene³⁷ have been smoothly oxidized to their hexafluorophosphate salts by ferrocenium and silver(I) hexafluorophosphates, respectively. The difference in behavior between **11** and chromocene is probably due to the great steric bulk of the substituents in the former compound.

The ESR spectrum of **15** in a dichloromethane glass at 22 K is shown in Figure 8. An axially symmetric powder pattern is observed with g tensors of 1.99 and 4.08/2. This is in general agreement with findings for other chromocenium species,^{35–37} where a ${}^4A_{2g}(e_{2g}^2 a_{1g}^1)$ nondegenerate ground state results in resonances near $g = 2$ and $g = 4$, corresponding to the $m_s = -3/2 \rightarrow m_s = -1/2$ and $m_s = -3/2 \rightarrow m_s = +1/2$ transitions, respectively.

The ESR spectrum of **16** in a dichloromethane glass at 4.7 K shows signals at $g = 1.29$, 2.01, and 4.12. The signals at 1.29 and 4.12 are broad and correspond to g_{\perp} and g_{\parallel} , respectively, for the iron units, giving $\Delta g = 2.83$ and $\langle g \rangle = 2.60$. These values are similar to those found for the octamethylferrocenium units of other salts in this paper (some variation is generally found between ESR parameters of the same ferrocenium ion with different counterions or host lattices^{28,29}). The sharper signal at $g = 2.01$ is assigned to the g_{\parallel} chromocenium signal. Presumably we do not observe the $g = 4$ chromocenium signal due to overlap with the broad g_{\parallel} signal of the terminal iron units.

Variable-temperature (6–290 K) magnetic susceptibility measurements show that the compound displays Curie–Weiss behavior, with no significant interactions

(39) Pinsky, B. L., personal communication, cited in ref 36.

(40) Fischer, E. O.; Ulm, K. *Chem. Ber.* **1962**, *95*, 692–694.

(41) Fischer, E. O.; Ulm, K.; Kuzel, P. *Z. Anorg. Allg. Chem.* **1963**, *319*, 253–265.

(38) Koelle, U.; Khouzami, F. *Angew. Chem., Int. Ed. Engl.* **1980**, *19*, 640–641.

between the metal centers; the room-temperature magnetic moment is $5.1 \mu_B$. The total magnetic moment expected for a powdered sample is given by

$$\mu_{\text{eff}}(\text{total})^2 = 2\mu_{\text{eff}}(\text{Fe unit})^2 + \mu_{\text{eff}}(\text{Cr unit})^2$$

or

$$\mu_{\text{eff}}(\text{total})^2 = 2[\langle g_{\text{Fe}} \rangle^2 (1/2 \times 3/2)] + [\langle g_{\text{Cr}} \rangle^2 (3/2 \times 5/2)]$$

Substituting the values of g determined from ESR measurements for Fe, and assuming the Cr center to have a typical $\langle g \rangle$ close to 2, this gives a value of $5.01 \mu_B$, in excellent agreement with the experimental data.

Synthesis of TCNE Salts of Trimetalloenes.

Molecular solids exhibiting cooperative magnetism have attracted much interest; examples include the radical anion-radical cation salts formed by various redox-active metallocene donors with organic electron acceptors, notably with TCNE (tetracyanoethylene).⁴² Those ferromagnetically ordered metallocenium salts to have been structurally characterized share a common motif of stacks consisting of alternating cations and anions. The trimetallics **9**, **10**, and **11** all appear to be suitable candidates for the synthesis of related materials.

Addition of 2 equiv of tetracyanoethylene to **9** gives green solutions of $\{(\text{Fc}''\text{CH}_2\text{C}_5\text{H}_4)_2\text{Fe}\}^{2+}(\text{TCNE}^-)_2$ (**17**); the reaction may be performed in either THF or dichloromethane. Crystallization of the THF-prepared material, **17a**, from THF/diethyl ether yields purple-green iridescent plates; crystallization of the dichloromethane-prepared material, **17b**, from dichloromethane/diethyl ether yields fine green needles. Due to their apparently different crystal morphologies, these two materials were treated as separate compounds for following investigations. It has been found that the properties of salts of polycyano acceptor molecules are often critically dependent on the methods employed in their preparation and crystallization.^{32,43-45} Infrared spectroscopy has proved to be an invaluable tool in identification of the degree of reduction and oligomerization of polycyano anions; for both **17a** and **17b** the $\text{C}\equiv\text{N}$ stretching frequencies indicate TCNE is present as isolated radical anions. Room-temperature ESR spectra of microcrystalline samples and solutions of **17a** and **17b** all show a resonance centered at $g = 2$, indicating that, both in the solid state and in solution, **17a** and **17b** contain isolated TCNE^- radical anions (in THF solutions characteristic hyperfine coupling can be resolved). The ESR spectrum of a dichloromethane glass of **17b** at 9.9 K shows the TCNE^- radical anion $g = 2$ signal superimposed upon an axially symmetric ferrocenium spectrum characterized by $g_{\parallel} = 4.12$, $g_{\perp} = 1.33$, and hence $\langle g \rangle = 2.61$. These values are similar to those found for other salts in this paper containing octamethylferrocenium units and to those found for octamethylferrocenium tetrafluoroborate.³¹ Variable-temperature magnetic susceptibility data indicate both **17a** and **17b** obey the Curie-Weiss law from 5 to 290 K, with no evidence of

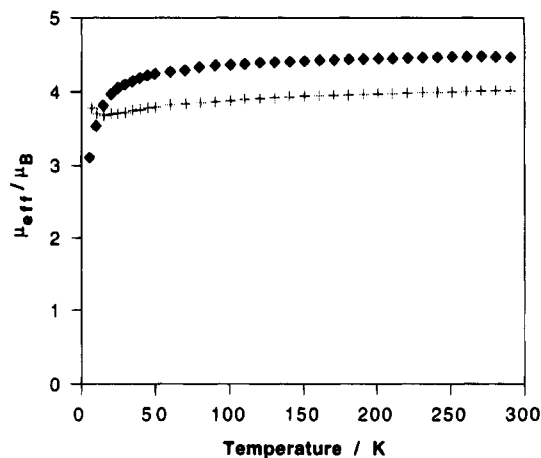


Figure 9. Plot of magnetic moment (μ_{eff}) vs temperature for **17a** (+) and **18** (◆).

any magnetic ordering phenomena. For **17a**, $C = 1.81 \text{ emu K mol}^{-1}$ and $\Theta = -0.8 \text{ K}$; the room-temperature magnetic moment is $4.0 \mu_B$. For **17b** (Figure 9) $C = 1.85 \text{ emu K mol}^{-1}$ and $\Theta = +0.1 \text{ K}$, with a room-temperature magnetic moment of $4.1 \mu_B$. These values of effective moment are consistent with the moment of $4.03 \mu_B$ calculated for a salt comprising two $S = 1/2$ cations with $\langle g \rangle = 2.61$ and two $S = 1/2$, $g = 2.00$ TCNE^- radical anions. Unfortunately, crystals suitable for structure determination have not been obtained; therefore, it is not clear if the absence of ordering is due to the absence of donor-acceptor stacks.

The reaction of **10** and 3 equiv of tetracyanoethylene in THF yields $\{(\text{Fc}''\text{CH}_2\text{C}_5\text{H}_4)_2\text{Co}\}^{3+}(\text{TCNE}^-)_3$ (**18**). Crystals may be obtained as shiny black plates from THF/diethyl ether. As in the cases of **17a** and **17b**, IR, ESR, and magnetic susceptibility measurements all indicate the presence of TCNE^- radical anions. The room-temperature ESR spectrum of a THF or dichloromethane solution of **18** shows a resonance split into nine lines, centered at $g = 2.00$, characteristic of the TCNE^- radical anion. The ESR spectrum of a dichloromethane glass of **18** at 5.5 K shows broad signals at $g = 1.38$ and $g = 4.06$, corresponding to g_{\perp} and g_{\parallel} , respectively, for the iron units, giving $\langle g \rangle = 2.60$. These are values similar to those obtained for **14** in acetonitrile, which contains the same trication, especially when it is realized that the ESR spectra of ferrocenium systems have often been found to be host and counterion dependent.^{28,29} Variable-temperature magnetic susceptibility data obey the Curie-Weiss law, with a significantly negative Weiss constant of -5.8 K , indicating the presence of antiferromagnetic interactions. A plot of magnetic moment against temperature (Figure 9) reveals a significant drop in μ_{eff} at low temperatures, again consistent with the presence of substantial antiferromagnetic interactions; the large number of paramagnetic centers in the compound means there are a number of possible origins for this antiferromagnetism. The high-temperature magnetic moment of $4.5 \mu_B$ is in good agreement with the $4.37 \mu_B$ calculated for three $S = 1/2$ TCNE^- anions, a diamagnetic cobaltocenium ion, and two ferrocenium ions with $\langle g \rangle = 2.60$.

Unfortunately the reaction of **11** and TCNE results in decomposition, a result often found in the oxidation of chromocenes.³⁹

X-ray Crystal Structure of the Trimetalloenium TCNE Salt 18. Black platelike crystals of $\{(\text{Fc}''\text{CH}_2-$

(42) Miller, J. S.; Epstein, A. J. *Angew. Chem., Int. Ed. Engl.* **1994**, *33*, 385-415 and references therein.

(43) Miller, J. S.; Zhang, J. H.; Reiff, W. M.; Dixon, D. A.; Preston, L. D.; Reis, A. H., Jr.; Gebert, E.; Extine, M.; Troup, J.; Epstein, A. J.; Ward, M. D. *J. Phys. Chem.* **1987**, *91*, 4344-4360.

(44) Miller, J. S.; O'Hare, D. M.; Chakraborty, A.; Epstein, A. J. *J. Am. Chem. Soc.* **1989**, *111*, 7853-7859.

(45) Ward, M. D.; Fagan, P. J.; Calabrese, J. C.; Johnson, D. C. *J. Am. Chem. Soc.* **1989**, *111*, 1719-1732.

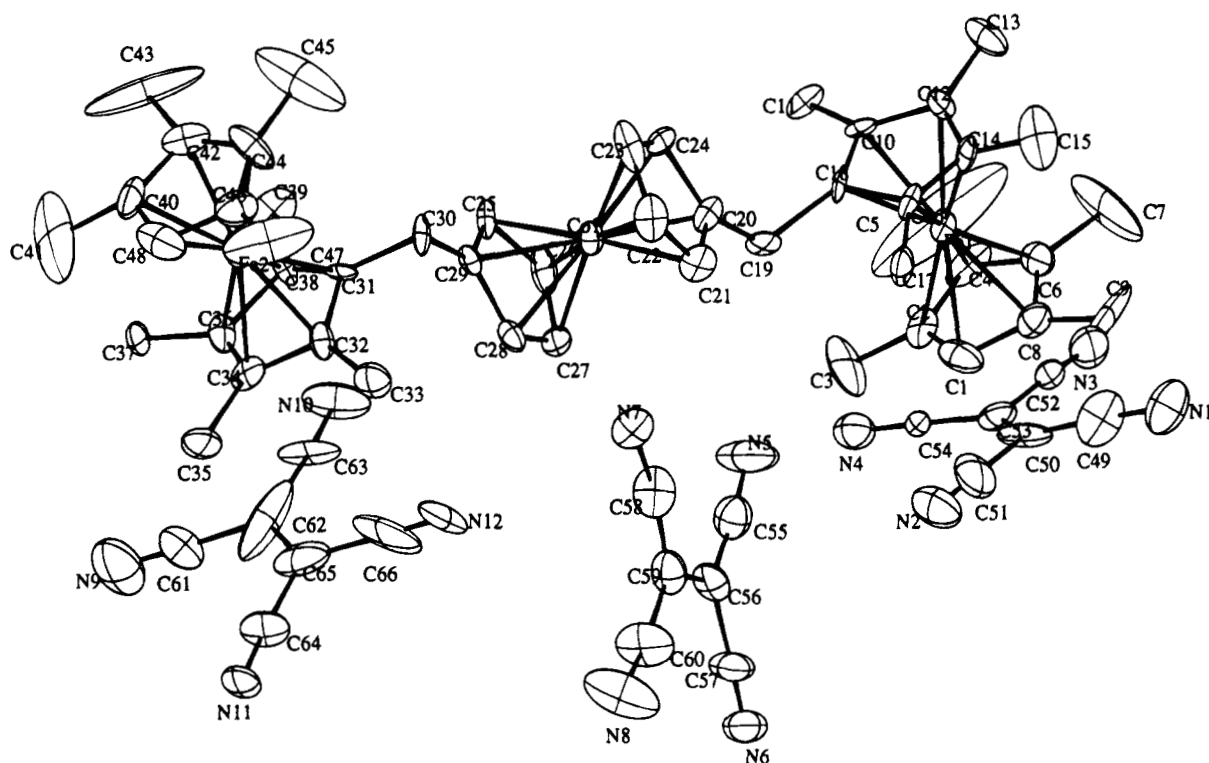


Figure 10. Crystal structure of **18** showing the atom-labeling scheme. Thermal ellipsoids are shown at the 25% probability level for clarity.

$C_5H_4)_2Co\}^{3+}(TCNE^-)_3$ (**18**) were obtained by layering a THF solution of **18** with diethyl ether. Fractional atomic coordinates are given in Table 7; selected bond lengths and angles are listed in Tables 8 and 9, respectively. The compound is confirmed as containing isolated $TCNE^-$ anions; however, the structure lacks the one-dimensional alternate stacking of anions and cations determined in all of the metallocenium salts found to exhibit ferromagnetic behavior, so that the absence of ferromagnetic coupling in **18** is not surprising. The conformation of the cation is similar to that of the triferrocenium ion in **6**; the two intramolecular Fe–Co distances are very similar at 6.386(8) and 6.352(8) Å and similar to the Fe–Fe separations in **6**. The Fe–ring C distances average 2.07(2) Å, similar to those for other ferrocenium systems.^{30–32} The average Co–ring centroid distance of 2.02(2) Å is similar to the 2.051(7) Å reported for the decamethylcobaltocenium cation.⁴⁶ As discussed in the Experimental Section, noncrystallographic restraints had to be employed, owing to the low ratio of data to variables. Thus, further discussion of intra-ring C–C bond lengths and of the geometry of the $TCNE^-$ radical anions is not justified.

(46) Dixon, D. A.; Miller, J. S. *J. Am. Chem. Soc.* **1987**, *109*, 3656–3664.

Conclusions

A general synthetic route for preparing trimetalocene complexes has been outlined. These molecules exhibit a rich redox chemistry, and a range of fully and partially oxidized species have been prepared and characterized. The solution electrochemistry of the triferrocene complexes show multi-redox events and evidence for electrostatic interactions between metal centers. However, in general the magnetic properties of the materials show no significant magnetic exchange interactions between the metal centers. The $TCNE$ salts of **9** and **10** do not exhibit any evidence of any long-range spin–spin ferromagnetic ordering at low temperatures, unlike those of $M(Cp^*)_2$ ($M = Cr, Mn, Fe$; $Cp^* = \eta-C_5Me_5$).

Acknowledgment. We thank the EPSRC for financial support, Dr. David White for help in recording the CV data, Dr. Simon Clarke for help with ESR measurements, and Dr. John Pudelski for helpful discussions.

Supporting Information Available: Listings of anisotropic thermal parameters and all bond angles and distances for **3**, **6**, and **18** (8 pages). Ordering information is given on any current masthead page.

OM950181R

Synthesis and Study of the $(\text{Ph}_3\text{P})_2\text{Pt}$ Complexes of Three Members of a Series of Highly Pyramidalized Alkenes

Athanassios Nicolaidis, Joseph M. Smith, Alok Kumar, David M. Barnhart, and Weston Thatcher Borden*

Department of Chemistry, University of Washington, Seattle, Washington 98195

Received April 18, 1995[⊗]

The $(\text{Ph}_3\text{P})_2\text{Pt}$ complexes (**3**) of three members of a homologous series of tricyclo[3.3.*n*.0^{3,7}]-alk-3(7)-enes (**2a–c**) have been prepared by allowing these highly pyramidalized alkenes to displace ethylene from $(\text{Ph}_3\text{P})_2\text{PtC}_2\text{H}_4$. The X-ray crystal structures of **3a–c** show that pyramidalization angles at the carbons bonded to platinum increase from an average of $\phi = 48.3^\circ$ in **3c** to $\phi = 55.1^\circ$ in **3b** to 62.3° in **3a**. In addition, as predicted computationally, the lengths of the bonds between the carbons attached to platinum increase and the C–Pt bond lengths decrease from **3c** to **3a**. The ^1H , ^{13}C , ^{31}P , and ^{195}Pt NMR spectra of **3a–c** provide information about how pyramidalization at these carbons affects the electronic structures of the complexes. The changes in the ^{13}C , ^{31}P , and ^{195}Pt chemical shifts and also the changes in the ^{13}C – ^{31}P and ^{31}P – ^{195}Pt coupling constants are consistent with the expected increase in back-bonding from the HOMO of $(\text{Ph}_3\text{P})_2\text{Pt}$ into the empty, π^* LUMO of the alkene as pyramidalization increases from **3c** to **3a**. The increase in the one-bond ^{13}C – ^{195}Pt coupling constant from **3c** to **3a** is found to be linearly related to the decrease in the ^{31}P – ^{195}Pt coupling constant. This finding indicates that, with increasing pyramidalization, donation from the π HOMO of the alkene into the 6s orbital of platinum also increases but at the expense of donation into platinum 6s from the in-phase combination of phosphine lone pair orbitals.

A number of organic molecules, containing highly reactive π bonds, have been isolated as $(\text{Ph}_3\text{P})_2\text{Pt}$ complexes. $(\text{Ph}_3\text{P})_2\text{Pt}$ complexes of cycloalkynes that have bent triple bonds—cyclopentyne, cyclohexyne, and cycloheptyne,¹ two isomers of cycloheptadienyne,² and the tropylium analog of benzyne²—have been prepared. $(\text{Ph}_3\text{P})_2\text{Pt}$ complexes of strained cyclic allenes, 1,2-cycloheptadiene³ and 1,2,4,6-cycloheptatetraene,⁴ have also been isolated. Among the deformed alkenes that have been isolated as $(\text{Ph}_3\text{P})_2\text{Pt}$ complexes are torsionally strained bridgehead olefins that violate Bredt's rule,^{5,6} bicyclo[2.2.0]hex-1(4)-ene,⁷ and, most recently, fullerene (C_{60}).^{8,9}

The spherical shape of C_{60} causes each of the carbons in it to have a pyramidal, rather than planar, geometry. The effect of pyramidalization on the bonding in non-conjugated alkenes has been investigated, both compu-

tationally and experimentally.¹⁰ *Ab initio* calculations predict that pyramidalization should result in raising the energy of the π HOMO and lowering the energy of the π^* LUMO.¹¹ However, the increase in the energy of the HOMO is computed to be only a fraction of the size of the decrease in the energy of the LUMO. These computational predictions have recently been confirmed by PES and ETS experiments.¹²

The existence of a low-lying, unfilled, π^* orbital in an alkene would be expected to result in particularly strong back-bonding from a d^{10} metal, such as Pt(0).¹³ The results of *ab initio* calculations on the effect of olefin pyramidalization in the $(\text{H}_3\text{P})_2\text{Pt}$ complex of ethylene give computational credibility to this qualitative prediction.¹⁴ Experimental confirmation might come from a study of the effects of increasing olefin pyramidalization on $(\text{Ph}_3\text{P})_2\text{Pt}$ complexes of a homologous series of pyramidalized alkenes.

We have prepared such a series of tricyclo[3.3.*n*.0^{3,7}]-alk-3(7)-enes (**2a–c**) with $n = 1,^{15} 2,^{16}$ and $3,^{12,17}$ and we have reported in a preliminary fashion the synthesis and X-ray structure of the $(\text{Ph}_3\text{P})_2\text{Pt}$ complex (**3a**) of **2a**.¹⁸ In this paper we describe the preparation of the

[⊗] Abstract published in *Advance ACS Abstracts*, June 15, 1995.

(1) (a) Bennett, M. A.; Yoshida, T. *J. Am. Chem. Soc.* **1978**, *100*, 1750. (b) Bennett, M. A.; Schwemlein, H. P. *Angew. Chem., Int. Ed. Engl.* **1989**, *28*, 1296. (c) Bennet, M. A. *Pure Appl. Chem.* **1989**, *61*, 1695.

(2) Lu, Z.; Abboud, K. A.; Jones, W. M. *J. Am. Chem. Soc.* **1992**, *114*, 10991.

(3) Visser, J. P.; Ramakers, J. E. *J. Chem. Soc., Chem. Commun.* **1972**, 178.

(4) Winchester, W. R.; Jones, W. M. *Organometallics* **1985**, *4*, 2228.

(5) Stamm, E.; Becker, K. B.; Engel, P.; Ermer, O.; Keese, R. *Angew. Chem., Int. Ed. Engl.* **1979**, *18*, 685.

(6) Godleski, S. A.; Gundlach, K. B.; Valpey, R. S. *Organometallics* **1985**, *4*, 296.

(7) Jason, M. E.; McGinnety, J. A.; Wiberg, K. B. *J. Am. Chem. Soc.* **1974**, *96*, 6531.

(8) (a) Fagan, P. J.; Calabrese, J. C.; Malone, B. *Science*, **1991**, *252*, 1160. (b) *J. Am. Chem. Soc.* **1991**, *113*, 9408. (c) *Acc. Chem. Res.* **1992**, *25*, 134.

(9) The $(\text{Ph}_3\text{P})_2\text{Pt}$ complex of a disilene has also been isolated: Pham, E. K.; West, R. *J. Am. Chem. Soc.* **1989**, *111*, 7667.

(10) Review: Borden, W. T. *Chem. Rev.* **1989**, *89*, 1095.

(11) Hrovat, D. A.; Borden, W. T. *J. Am. Chem. Soc.* **1988**, *110*, 4710.

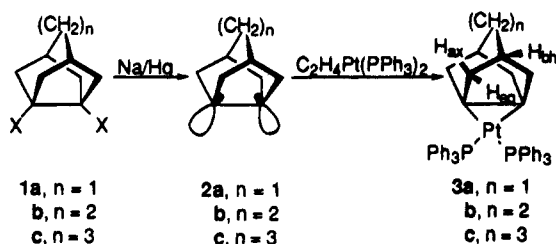
(12) Smith, J. M.; Hrovat, D. A.; Borden, W. T.; Allan, M.; Asmis, K. R.; Bulliard, C.; Haselbach, E.; Meier, U. C. *J. Am. Chem. Soc.* **1993**, *115*, 3816.

(13) Albright, T. A.; Hoffmann, R.; Thibault, J. C.; Thorn, D. L. *J. Am. Chem. Soc.* **1979**, *101*, 3801 and references therein.

(14) Morokuma, K.; Borden, W. T. *J. Am. Chem. Soc.* **1991**, *113*, 1912.

(15) (a) Renzoni, G. E.; Yin, T.-K.; Borden, W. T. *J. Am. Chem. Soc.* **1986**, *108*, 7121. (b) Radziszewski, J. G.; Yin, T.-K.; Renzoni, G. E.; Hrovat, D. A.; Borden, W. T.; Michl, J. *J. Am. Chem. Soc.* **1993**, *115*, 1454.

(Ph₃P)₂Pt complexes of **2b,c**, and we report the chemical shifts and coupling constants obtained from the ¹H, ¹³C, ³¹P, and ¹⁹⁵Pt NMR spectra of all three complexes (**3a-c**).

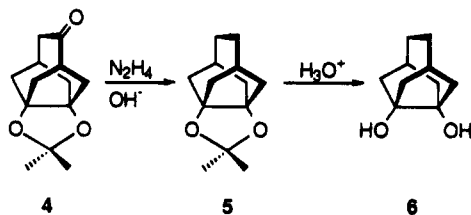


Because **3a-c** differ only in the degree to which the carbons bonded to platinum are forced to be pyramidalized, the NMR spectra of these three complexes provide detailed information about how pyramidalization of these carbons affects the electronic structures of the complexes. The differences in the chemical shifts and coupling constants, found in the ¹H, ¹³C, ³¹P, and ¹⁹⁵Pt NMR spectra of **3a-c**, are discussed in this light. The X-ray structures of **3a-c**, which are also reported, confirm that the changes in the chemical shifts and coupling constants can, in fact, be attributed to increased pyramidalization of the carbons bonded to platinum from **3c** to **3a**.

Results and Discussion

Preparation of the (Ph₃P)₂Pt Complexes. The synthesis of each complex was accomplished by reducing a diiodide (**1a**, X = I)¹⁵ or dimesylate (**1b,c**, X = OMs) precursor with sodium amalgam and allowing the olefin (**2**) thus formed to displace ethylene from (Ph₃P)₂PtC₂H₄.¹⁹ The generation and *in situ* trapping of **3a** by this method have already been described in a preliminary fashion.¹⁸

Alkene **2b** has been prepared previously by β -lactone pyrolysis;¹⁶ but for the purpose of trapping the olefin with (Ph₃P)₂Pt to form **3b**, the elevated temperatures required for decarboxylation of the β -lactone made development of a different method for generating **2b** highly desirable. Therefore, ketoacetone **4**, an inter-



mediate in the synthesis of **2c**,¹² was subjected to Wolff-Kishner reduction; and the acetonide group in the product (**5**) was then hydrolyzed to form diol **6**. Reaction with methyllithium converted **6** to the dilithio salt,

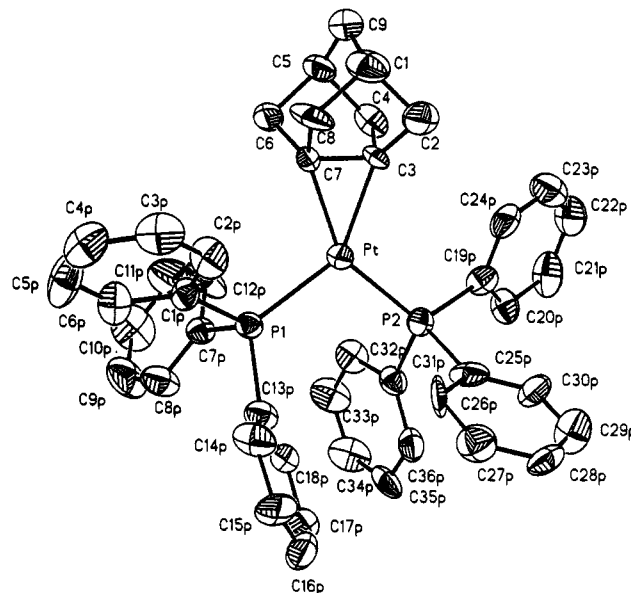


Figure 1. ORTEP drawing of the X-ray structure of **3a**. Hydrogens have been omitted for conciseness and clarity.

which, upon treatment with excess mesyl chloride afforded **1b**, X = OMs. Reduction of this dimesylate with sodium amalgam in the presence of (Ph₃P)₂PtC₂H₄ gave **3b**.

Unlike **2a,b**, **2c** is stable toward dimerization at room temperature. Therefore, it was not necessary to perform the sodium amalgam reduction of dimesylate **1c**, X = OMs, in the presence of (Ph₃P)₂PtC₂H₄. Instead, the dimesylate was first reduced and the olefin formed then added to a solution of (Ph₃P)₂PtC₂H₄ to yield **3c**.

Tetrasubstituted alkenes would not ordinarily be expected to form stable complexes with (Ph₃P)₂Pt.²⁰ In order to verify that it is the pyramidalization of the olefinic carbon atoms in **2a-c** which allows these alkenes to form very stable complexes with (Ph₃P)₂Pt,²¹ the unbridged olefin, bicyclo[3.3.0]oct-1(5)-ene,^{22,23} was stirred overnight with (Ph₃P)₂PtC₂H₄. As expected, no trace of the (Ph₃P)₂Pt complex of bicyclo[3.3.0]oct-1(5)-ene was detected.

X-ray Structures of the Complexes. The chemistry observed for alkenes **2a-c** leaves little doubt that, as expected,¹¹ alkene pyramidalization increases as n decreases.^{12,15-17} Nevertheless, in order to confirm experimentally that pyramidalization in the (Ph₃P)₂Pt complexes of these alkenes also increases in the same order, we obtained X-ray structures of **3a-c**.

The X-ray structure of **3a** has been reported previously.¹⁸ However, despite the convergence of the final structure refinement to $R_f = 0.059$, the accuracy of the structure of the olefinic portion of the molecule was not completely satisfactory. For example, one allylic C-C bond length to an olefinic carbon was found to be 1.63(4) Å, and the other was found to be 1.46(3) Å. One

(16) (a) Renzoni, G. E.; Yin, T.-K.; Miyake, F.; Borden, W. T. *Tetrahedron*, **1986**, *42*, 1581. (b) Radziszewski, J. G.; Yin, T.-K.; Miyake, F.; Renzoni, G. E.; Borden, W. T.; Michl, J. *J. Am. Chem. Soc.* **1986**, *108*, 3544. (c) Yin, T.-K.; Radziszewski, J. G.; Renzoni, G. E.; Downing, J. W.; Michl, J.; Borden, W. T. *J. Am. Chem. Soc.* **1987**, *109*, 820.

(17) A bis(ethano) derivative of $n = 0$ has also been prepared: Branam, B. M.; Paquette, L. A.; Hrovat, D. A.; Borden, W. T. *J. Am. Chem. Soc.* **1992**, *114*, 774.

(18) Kumar, A.; Lichtenhan, J. D.; Critchlow, S. C.; Eichinger, B. E.; Borden, W. T. *J. Am. Chem. Soc.* **1990**, *112*, 5633.

(19) Prepared by the following method: Nagel, U. *Chem. Ber.* **1982**, *115*, 1998.

(20) Complexes of olefins with transition metals have been reviewed: Ittel, S. D.; Ibers, J. A. *Adv. Organomet. Chem.* **1976**, *14*, 33.

(21) We have found **3a-c** to be much more stable than the (Ph₃P)₂Pt complex of ethylene toward decomposition via alkene loss. This is not surprising, since the pyramidalized alkenes in these complexes are predicted to be much more strongly bonded to (Ph₃P)₂Pt than is ethylene.¹⁴

(22) (a) Corey, E. J.; Bloch, E. *J. Org. Chem.* **1969**, *34*, 1233. (b) Paquette, L. A.; Houser, R. W. *J. Am. Chem. Soc.* **1969**, *91*, 3870. (c) Borden, W. T.; Ravindranathan, T. *J. Org. Chem.* **1971**, *36*, 4125.

(23) Prepared by sodium amalgam reduction of the dimesylate formed from bicyclo[3.3.0]octan-1,5-diol.^{22c}

Table 1. Atomic Coordinates ($\times 10^4$) and Equivalent Isotropic Displacement Coefficients ($\text{\AA}^2 \times 10^3$) for **3a**

atom	x	y	z	$U(\text{eq})^a$
Pt	2491(1)	9590(1)	1291(1)	29(1)
C(1)	1609(10)	8406(5)	-286(5)	57(4)
C(2)	2532(16)	9068(4)	-232(3)	51(3)
C(3)	3009(8)	8979(4)	472(4)	33(3)
C(4)	4197(11)	8430(6)	496(6)	49(4)
C(5)	3306(10)	7726(5)	465(4)	52(4)
C(6)	2375(15)	7891(3)	1041(4)	52(3)
C(7)	1865(9)	8649(4)	844(4)	34(3)
C(8)	729(11)	8531(7)	328(6)	54(5)
C(9)	2519(16)	7717(4)	-180(4)	53(3)
P(1)	1207(2)	9646(1)	2245(1)	31(1)
C(1P)	-461(8)	9177(4)	2192(4)	34(3)
C(2P)	-1142(8)	9183(5)	1590(5)	46(3)
C(3P)	-2415(14)	8871(4)	1524(5)	58(3)
C(4P)	-3011(9)	8532(5)	2047(6)	59(4)
C(5P)	-2342(13)	8506(5)	2644(6)	65(4)
C(6P)	-1079(9)	8829(5)	2713(5)	54(4)
C(7P)	2006(9)	9208(4)	2953(4)	35(3)
C(8P)	1738(9)	9355(4)	3607(4)	54(3)
C(9P)	2343(15)	8974(5)	4105(4)	73(4)
C(10P)	3228(12)	8426(7)	3964(6)	84(5)
C(11P)	3544(13)	8265(7)	3312(5)	90(5)
C(12P)	2958(9)	8668(5)	2832(5)	58(4)
C(13P)	703(8)	10534(4)	2568(4)	36(3)
C(14P)	-587(9)	10830(5)	2410(5)	49(4)
C(15P)	-852(10)	11547(5)	2560(6)	55(4)
C(16P)	122(11)	11961(5)	2871(6)	61(5)
C(17P)	1329(10)	11669(5)	3030(5)	50(4)
C(18P)	1644(9)	10955(4)	2888(4)	39(3)
P(2)	3923(2)	10564(1)	1298(1)	34(1)
C(19P)	5500(8)	10510(4)	779(4)	34(3)
C(20P)	6744(9)	10794(5)	971(5)	48(4)
C(21P)	7879(9)	10735(6)	567(5)	59(4)
C(22P)	7812(9)	10400(6)	-43(5)	61(5)
C(23P)	6563(12)	10121(5)	-228(6)	67(5)
C(24P)	5418(11)	10177(5)	171(5)	50(4)
C(25P)	3164(11)	11412(7)	1017(7)	41(4)
C(26P)	1747(12)	11520(7)	1129(6)	47(4)
C(27P)	1127(13)	12170(6)	944(6)	61(5)
C(28P)	1876(15)	12697(7)	637(7)	53(4)
C(29P)	3266(14)	12590(8)	521(7)	59(5)
C(30P)	3884(12)	11953(5)	719(6)	49(4)
C(31P)	4702(9)	10779(5)	2101(4)	35(3)
C(32P)	5226(11)	10227(5)	2469(5)	47(4)
C(33P)	5821(10)	10337(6)	3072(4)	62(4)
C(34P)	5862(9)	11011(6)	3334(5)	59(4)
C(35P)	5318(11)	11580(7)	2996(5)	56(4)
C(36P)	4752(9)	11479(5)	2364(5)	45(4)

^a Equivalent isotropic U defined as one-third of the trace of the orthogonalized U_{ij} tensor.

would have expected both bonds to have lengths that were nearly the same and approximately the average of these two different bond lengths.

In order to see if another independent structure determination would produce better results, we prepared **3a** again. Crystals were grown, the X-ray data recollected, and the structure solved again. After refinement $R_f = 0.0275$ was obtained; and although some pairs of allylic C-C bond lengths still differed by as much as 0.04 Å, the results of this determination of the structure of **3a** were definitely an improvement over the previous one.¹⁸

An ORTEP drawing of the structure of **3a** is shown in Figure 1. Table 1 gives the refined atomic coordinates and isotropic displacement coefficients, and Table 4 gives the values of important bond lengths and bond angles that were obtained from the redetermination of the structure of **3a**. The values in Table 4 agree well

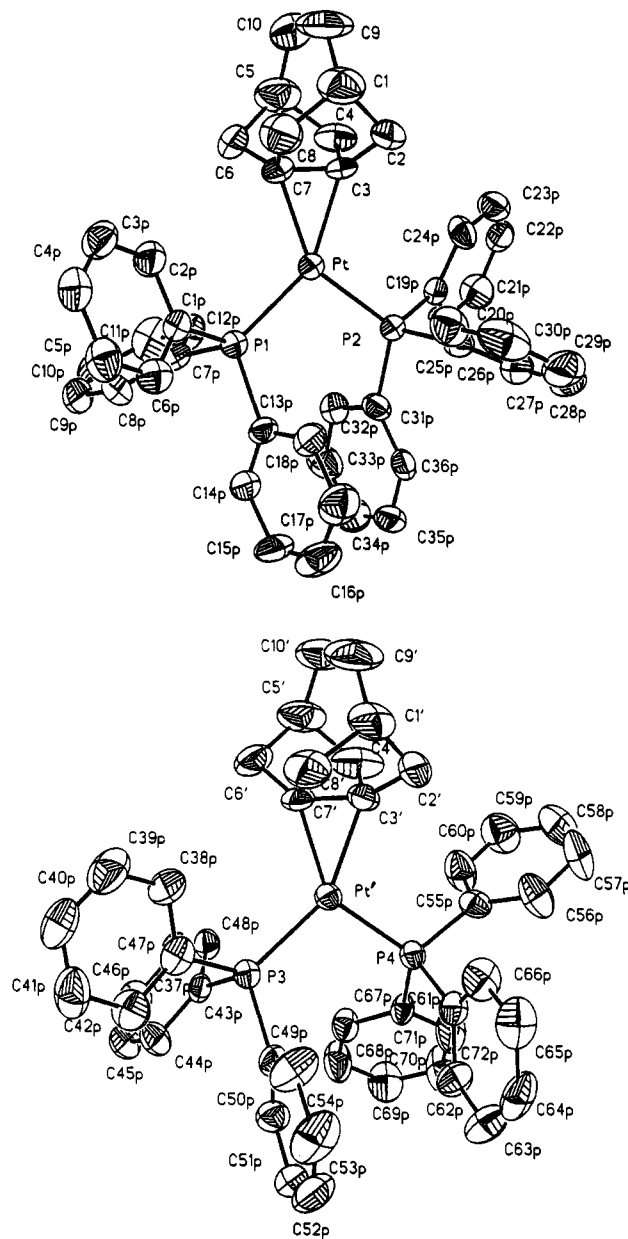


Figure 2. ORTEP drawings of the X-ray structures of the two independent molecules of **3b** in the unit cell. Hydrogens have been omitted for conciseness and clarity.

with those found previously.¹⁸ A complete listing of all the bond lengths and bond angles, obtained from the redetermination of the structure of **3a**, is available as supporting information.²⁴

Crystals of **3b** were found to contain two independent molecules in the unit cell. As shown in Figure 2, the two molecules differ in the way the two triphenylphosphine groups in each are oriented. Table 2 lists the refined atomic coordinates and isotropic displacement coefficients for both molecules, and the values of important bond lengths and bond angles in both are given in Table 4. The remaining bond lengths and bond angles in **3b** can be found in the supporting information.²⁴

The X-ray structure obtained for **3c** was better than those obtained for either **3a** or **3b**. Refinement converged to $R_f = 0.0195$, and bond lengths and bond angles that should have been nearly the same were generally found to be identical to within the precision of the structure determination. Table 3 provides the refined

Table 2. Atomic Coordinates ($\times 10^4$) and Equivalent Isotropic Displacement Coefficients ($\text{\AA}^2 \times 10^3$) for Both Molecules of **3b in the Unit Cell**

atom	x	y	z	$U(\text{eq})^a$	atom	x	y	z	$U(\text{eq})^a$
Pt	-1923(1)	2863(1)	2160(1)	33(1)	Pt'	3125(1)	-2655(1)	2675(1)	32(1)
C(1)	-1464(10)	4633(6)	2896(5)	75(5)	C(1')	3929(9)	-3989(7)	1487(5)	72(5)
C(2)	-1902(8)	3707(5)	3266(4)	58(4)	C(2')	3326(8)	-3120(7)	1348(5)	65(5)
C(3)	-1163(7)	3255(5)	2823(4)	41(3)	C(3')	3962(7)	-2716(6)	1729(4)	45(4)
C(4)	-9(7)	2860(6)	3034(5)	59(4)	C(4')	4979(9)	-2129(8)	1328(6)	89(6)
C(5)	869(9)	3595(8)	2584(6)	83(6)	C(5')	6003(8)	-2773(8)	1467(6)	85(6)
C(6)	415(8)	3866(7)	1902(5)	76(5)	C(6')	5651(7)	-3302(8)	2237(5)	79(6)
C(7)	-902(7)	3882(5)	2144(4)	45(3)	C(7')	4340(7)	-3437(5)	2312(4)	45(4)
C(8)	-1442(10)	4734(6)	2162(5)	73(5)	C(8')	3957(9)	-4270(6)	2259(5)	73(5)
C(9)	-248(13)	4744(8)	3054(7)	112(8)	C(9')	5150(10)	-3918(10)	1057(7)	113(8)
C(10)	848(11)	4305(9)	2859(6)	95(7)	C(10')	6131(9)	-3347(9)	1044(6)	96(7)
P(1)	-2261(2)	3095(1)	1087(1)	36(1)	P(3)	2877(2)	-3134(1)	3841(1)	31(1)
C(1P)	-2397(6)	4231(5)	526(4)	39(3)	C(37P)	3269(6)	-4250(5)	4323(4)	41(3)
C(2P)	-1567(7)	4815(5)	501(4)	50(4)	C(38P)	3948(8)	-4739(6)	3992(5)	62(4)
C(3P)	-1602(8)	5675(5)	63(4)	55(4)	C(39P)	4255(9)	-5580(6)	4374(6)	75(5)
C(4P)	-2431(7)	5960(5)	-358(4)	49(4)	C(40P)	3939(9)	-5928(6)	5058(6)	66(5)
C(5P)	-3237(8)	5363(5)	-330(4)	54(4)	C(41P)	3279(8)	-5453(7)	5376(5)	70(5)
C(6P)	-3227(7)	4519(5)	102(4)	49(4)	C(42P)	2917(8)	-4613(5)	5034(4)	56(4)
C(7P)	-1082(6)	2735(5)	552(4)	39(3)	C(43P)	3785(6)	-2525(4)	4131(3)	33(3)
C(8P)	-1001(8)	2996(6)	-149(4)	54(4)	C(44P)	3677(7)	-2579(5)	4808(4)	45(3)
C(9P)	-72(9)	2707(7)	-530(5)	71(5)	C(45P)	4432(7)	-2094(5)	4979(4)	51(4)
C(10P)	749(9)	2162(7)	-202(6)	73(5)	C(46P)	5292(7)	-1593(5)	4503(4)	51(4)
C(11P)	691(9)	1898(6)	501(6)	70(5)	C(47P)	5428(7)	-1548(5)	3831(4)	47(3)
C(12P)	-235(7)	2192(5)	864(4)	52(4)	C(48P)	4684(6)	-2009(5)	3659(4)	37(3)
C(13P)	-3582(6)	2596(5)	1029(4)	38(3)	C(49P)	1389(6)	-3107(5)	4302(4)	38(3)
C(14P)	-3586(8)	2015(6)	701(4)	52(4)	C(50P)	989(7)	-2538(5)	4617(4)	48(4)
C(15P)	-4638(9)	1634(6)	723(5)	68(5)	C(51P)	-127(8)	-2573(7)	4969(4)	62(4)
C(16P)	-5651(9)	1833(6)	1038(6)	75(5)	C(52P)	-890(9)	-3190(8)	4996(5)	78(5)
C(17P)	-5686(8)	2434(7)	1365(5)	69(5)	C(53P)	-527(8)	-3769(7)	4682(6)	85(6)
C(18P)	-4631(7)	2788(5)	1357(4)	48(4)	C(54P)	615(7)	-3726(6)	4334(5)	67(5)
P(2)	-2907(2)	1607(1)	2816(1)	34(1)	P(4)	1844(2)	-1551(1)	2356(1)	33(1)
C(19P)	-2263(6)	911(5)	3550(3)	33(3)	C(55P)	2018(7)	-961(5)	1428(4)	41(3)
C(20P)	-2033(7)	38(5)	3693(4)	47(4)	C(56P)	1256(9)	-995(6)	1016(4)	64(4)
C(21P)	-1568(8)	-463(6)	4271(4)	59(4)	C(57P)	1484(10)	-548(7)	316(5)	79(5)
C(22P)	-1340(7)	-103(5)	4711(4)	48(4)	C(58P)	2492(10)	-51(7)	29(5)	74(5)
C(23P)	-1591(8)	761(6)	4583(4)	59(4)	C(59P)	3251(9)	-11(7)	423(5)	76(5)
C(24P)	-2046(8)	1252(5)	4020(4)	48(3)	C(60P)	3010(8)	-456(6)	1111(4)	66(4)
C(25P)	-4375(7)	1777(5)	3253(4)	41(3)	C(61P)	326(6)	-1957(5)	2609(4)	39(3)
C(26P)	-4792(8)	2612(6)	3059(5)	60(4)	C(62P)	-485(7)	-1711(5)	3071(4)	51(4)
C(27P)	-5009(7)	1116(6)	3769(4)	55(4)	C(63P)	-1623(8)	-2052(6)	3281(5)	68(5)
C(28P)	-6115(8)	1270(8)	4063(5)	72(6)	C(64P)	-1931(8)	-2633(6)	3016(5)	67(5)
C(29P)	-6554(9)	2076(10)	3875(7)	87(7)	C(65P)	-1141(8)	-2907(6)	2580(5)	66(4)
C(30P)	-5922(9)	2756(8)	3381(6)	80(6)	C(66P)	4(8)	-2574(6)	2382(5)	59(4)
C(31P)	-3175(7)	831(5)	2429(4)	42(3)	C(67P)	1777(6)	-623(4)	2632(4)	35(3)
C(32P)	-2196(7)	518(5)	2099(4)	51(4)	C(68P)	2375(7)	-631(5)	3131(4)	44(3)
C(33P)	-2314(10)	-115(6)	1837(5)	66(5)	C(69P)	2363(9)	54(6)	3347(5)	68(5)
C(34P)	-3384(10)	-426(6)	1882(5)	72(5)	C(70P)	1752(9)	776(6)	3056(5)	68(5)
C(35P)	-4364(9)	-81(6)	2155(4)	58(4)	C(71P)	1140(10)	818(6)	2558(5)	81(5)
C(36P)	-4261(8)	542(5)	2434(4)	46(3)	C(72P)	1188(9)	129(6)	2329(5)	69(5)

^a Equivalent isotropic U defined as one-third of the trace of the orthogonalized U_{ij} tensor.

atomic coordinates and isotropic displacement coefficients. Important bond lengths and bond angles are given in Table 4, and the remainder are available as supporting information.²⁴

The ORTEP drawings of the structures of **3a-c**, shown in Figures 1-3, clearly reveal that pyramidalization of the carbons bonded to Pt in these complexes does, indeed, increase as n decreases. A convenient measure of the degree to which an olefin is pyramidalized is the pyramidalization angle, ϕ , which is defined as the angle between the extension of the bond between the olefinic carbons and the plane containing one of these carbons and the two substituents attached to it.¹⁰ The pyramidalization angles at C(3) and C(7) in each complex are given in Table 4. The average values of ϕ for **3a-c** are respectively 62.3, 55.1, and 48.3°. These values provide quantitative confirmation that, as indicated qualitatively by the drawings in Figures 1-3, olefin pyramidalization decreases from **3a** to **3c**.

Calculations on a $(\text{Ph}_3\text{P})_2\text{PtC}_2\text{H}_4$ model predict that increased olefin pyramidalization in **3** should be ac-

companied by a decrease in the Pt-C bond lengths, an increase in the length of the C-C bond between the olefinic carbons, and little change in the P-Pt bond length or the P-Pt-P bond angle.¹⁴ Table 4 shows that these predictions compare well with experiment.

With the exception of one long P-Pt bond in **3a**, the P-Pt bond lengths do seem to remain quite constant in **3a-c**. Although the P-Pt-P bond angles appear to vary slightly, there is no obvious trend, since the two different molecules of **3b** each have a smaller P-Pt-P bond angle than either **3a** or **3c**. The 3.1° difference between the P-Pt-P bond angles in the two molecules of **3b** in the same crystal suggests that the differences found between the P-Pt-P bond angles in **3a-c** are not structurally significant.

As predicted,¹⁴ the C-Pt bond lengths in **3** do decrease with increased pyramidalization. The decrease could be due to stronger bonding between the olefin and platinum and/or to a decrease in steric repulsion between the allylic CH_2 groups and the $(\text{Ph}_3\text{P})_2\text{Pt}$ moiety as pyramidalization increases. The fact that the C-Pt

Table 3. Atomic Coordinates ($\times 10^4$) and Equivalent Isotropic Displacement Coefficients ($\text{\AA}^2 \times 10^3$) for 3c

atom	x	y	z	$U(\text{eq})^a$
Pt	1849(1)	2582(1)	2202(1)	31(1)
C(1)	-1381(4)	1227(4)	407(4)	53(2)
C(2)	-935(4)	1503(4)	1534(4)	49(2)
C(3)	-60(4)	2645(4)	1781(3)	35(2)
C(4)	-392(5)	3790(4)	2122(4)	50(2)
C(5)	-685(5)	4328(5)	1205(4)	57(2)
C(6)	242(5)	3953(4)	772(4)	50(2)
C(7)	352(4)	2771(4)	989(3)	36(2)
C(8)	-232(5)	1717(5)	203(4)	49(2)
C(9)	-2517(5)	1755(5)	-84(4)	70(3)
C(10)	-2738(5)	2854(6)	419(5)	77(3)
C(11)	-2023(5)	3992(5)	522(5)	66(3)
P(1)	3490(1)	2725(1)	1705(1)	36(1)
C(1P)	3177(4)	2199(4)	409(3)	41(2)
C(2P)	2340(4)	2698(5)	-258(4)	52(2)
C(3P)	2045(5)	2345(5)	-1233(4)	61(2)
C(4P)	2584(6)	1499(6)	-1569(4)	74(3)
C(5P)	3432(6)	1034(5)	-938(4)	65(3)
C(6P)	3744(5)	1392(5)	66(4)	57(2)
C(7P)	4183(4)	4202(4)	1813(3)	41(2)
C(8P)	4937(4)	4518(5)	1307(4)	52(2)
C(9P)	5382(5)	5653(5)	1353(4)	63(3)
C(10P)	5039(6)	6490(5)	1891(4)	67(3)
C(11P)	4293(6)	6189(5)	2390(4)	67(3)
C(12P)	3864(5)	5060(4)	2347(4)	51(2)
C(13P)	4760(4)	2004(5)	2282(3)	48(2)
C(14P)	5983(5)	2498(6)	2659(4)	73(3)
C(15P)	6870(7)	1905(8)	3095(5)	92(4)
C(16P)	6556(9)	806(10)	3151(5)	110(5)
C(17P)	5331(9)	259(7)	2781(6)	101(5)
C(18P)	4430(6)	861(5)	2329(5)	70(3)
P(2)	2464(1)	2204(1)	3732(1)	36(1)
C(19P)	1908(4)	2980(4)	4614(3)	40(2)
C(20P)	2653(5)	3513(5)	5547(4)	57(2)
C(21P)	2135(6)	4056(5)	6160(4)	73(3)
C(22P)	917(6)	4061(5)	5879(4)	60(3)
C(23P)	149(5)	3524(5)	4955(4)	57(2)
C(24P)	636(5)	2989(4)	4326(4)	48(2)
C(25P)	1834(4)	720(4)	3709(3)	40(2)
C(26P)	1557(5)	371(5)	4474(4)	51(2)
C(27P)	990(5)	-751(5)	4380(5)	62(3)
C(28P)	734(5)	-1518(5)	3546(4)	58(2)
C(29P)	1045(5)	-1201(4)	2792(4)	57(2)
C(30P)	1579(4)	-68(4)	2870(4)	47(2)
C(31P)	4114(4)	2399(4)	4467(3)	44(2)
C(32P)	4853(4)	3402(5)	4492(4)	52(2)
C(33P)	6083(5)	3642(5)	5045(4)	64(3)
C(34P)	6604(5)	2829(5)	5529(4)	67(3)
C(35P)	5914(5)	1821(5)	5492(4)	65(3)
C(36P)	4657(5)	1594(4)	4956(4)	50(2)

^a Equivalent isotropic U defined as one-third of the trace of the orthogonalized U_{ij} tensor.

bond length in the (Ph₃P)₂Pt complex of ethylene (2.11 Å)²⁵ is actually slightly shorter than the average of those in the more highly pyramidalized²⁶ complex of 2c (2.12 Å) indicates that steric effects probably do have some influence on C–Pt bond lengths.

The amount of bonding between platinum and a complexed alkene does not appear to have a profound effect on the C–Pt bond length. These bond lengths are nearly the same in the (Ph₃P)₂Pt complexes of ethylene (2.11 Å)²⁵ and TCNE (2.10 Å),²⁷ despite the 32 kcal/mol stronger platinum–olefin bond in the latter.²⁸ The

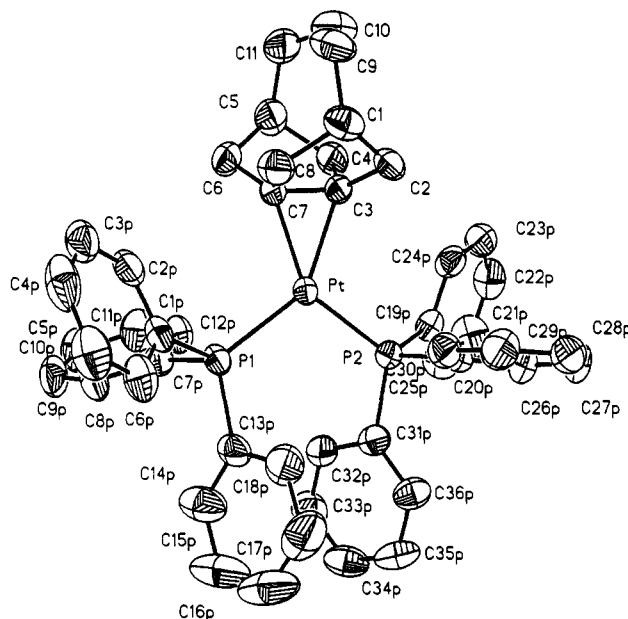
(25) Cheng, P. T.; Nyburg, S. C. *Can. J. Chem.* **1972**, *50*, 912.

(26) It is known that planar alkenes pyramidalize upon coordination to transition metals.²⁰ Although the X-ray structure of the (Ph₃P)₂Pt complex of ethylene has been published,²⁵ the hydrogen atoms were not located, so that the degree of pyramidalization at carbon in this complex is not known. However, in the optimized geometry of (H₃P)₂PtC₂H₄, obtained from *ab initio* calculations,¹⁴ the pyramidalization angle, ϕ (the angle between the H–C–H plane and the extension of the C–C bond), is 27.1°.

Table 4. Selected Bond Lengths (Å) and Bond Angles (deg) Obtained from the X-ray Structures of 3a–c

	3a	3b	3b' ^a	3c
Pt–P(1)	2.298(2)	2.284(2)	2.283(2)	2.274(1)
Pt–P(2)	2.279(2)	2.266(2)	2.272(2)	2.276(1)
Pt–C(3)	2.068(8)	2.105(9)	2.086(8)	2.129(4)
Pt–C(7)	2.056(8)	2.115(8)	2.095(8)	2.113(4)
C(3)–C(7)	1.475(11)	1.441(9)	1.467(9)	1.421(7)
C(2)–C(3)	1.503(11)	1.527(12)	1.539(14)	1.536(6)
C(3)–C(4)	1.539(13)	1.521(10)	1.504(10)	1.539(7)
C(6)–C(7)	1.541(11)	1.520(11)	1.517(11)	1.520(6)
C(7)–C(8)	1.535(13)	1.522(11)	1.527(13)	1.521(5)
P(1)–Pt–P(2)	106.8(1)	103.1(1)	106.2(1)	108.7(1)
$\phi(3)^b$	60.4(14)	55.4(12)	53.0(12)	47.8(8)
C(2)–C(3)–C(4)	109.5(8)	116.7(7)	115.4(7)	122.6(4)
C(2)–C(3)–C(7)	107.2(8)	107.2(6)	108.1(7)	109.6(3)
C(4)–C(3)–C(7)	105.9(7)	107.5(6)	109.4(6)	108.0(4)
$\phi(7)^b$	64.2(14)	53.5(12)	58.3(12)	48.8(8)
C(6)–C(7)–C(8)	106.1(8)	118.2(7)	115.8(7)	120.8(4)
C(3)–C(7)–C(6)	105.6(8)	107.7(6)	106.2(6)	109.5(4)
C(3)–C(7)–C(8)	104.7(7)	107.9(6)	106.2(7)	108.4(4)

^a Second independent molecule in the unit cell. ^b The pyramidalization angle, $\phi(n)$, at C(n), ($n = 3$ and 7) is defined¹⁰ as the angle between the C($n - 1$)–C(n)–C($n + 1$) plane and the extension of the C(3)–C(7) bond.

**Figure 3.** ORTEP drawing of the X-ray structure of 3c. Hydrogens have been omitted for conciseness and clarity.

greater steric requirements of a cyano group, compared to a hydrogen atom, may tend to equalize the C–Pt bond lengths in these two complexes.

The C–C bond length in the (Ph₃P)₂Pt complex of ethylene (1.43 Å) is about 0.06 Å shorter than that between the olefinic carbons in the (Ph₃P)₂Pt complex of TCNE. The longer olefinic C–C bond in the latter complex has been attributed to the greater back-bonding in it between a filled metal d orbital and the empty π^* orbital with which it interacts.²⁸

An increase of 0.08 Å in the C–C bond length in the (H₃P)₂Pt complex of ethylene has also been computed for a (H₃P)₂PtC₂H₄ model for 3a,¹⁴ and a difference of 0.05 Å has been calculated between this bond length in

(27) Panattoni, C.; Bombieri, G.; Belluco, U.; Baddley, W. H. *J. Am. Chem. Soc.* **1968**, *90*, 798. Bombieri, G.; Forsellini, E.; Panattoni, C.; Graziani, R.; Bardoli, G. *J. Chem. Soc. A* **1970**, 1313.

(28) Evans, A.; Mortimer, C. T.; Puddephat, R. *J. Organomet. Chem.* **1974**, *72*, 295.

the $(\text{H}_3\text{P})_2\text{PtC}_2\text{H}_4$ models for **3a,c**.²⁹ As predicted from these calculations on models, the data in Table 4 do show an increase in the C–C bond lengths between the olefinic carbons in **3** with increasing pyramidalization. The difference between the length of the C(3)–C(7) bond in **3c** and **3a**, is, within experimental error, the same as the 0.05 Å difference computed between the bond lengths in the models.

The pyramidalization angles at C(3) and C(7) in **3c** are not required to be exactly the same, even in the gas phase, but they differ by only 1.0° in the crystal. This is smaller than the 3.8° difference between the pyramidalization angles at C(3) and C(7) in the crystal of **3a**. The latter pyramidalization angles would, of course, be expected to be identical in gas-phase molecules of **3a**.

In contrast to the $(\text{Ph}_3\text{P})_2\text{Pt}$ complex of **2c** (**3c**), the 10-methyl-10-selenonia analog of olefin **2c** shows an 8° difference between the values of ϕ (20.3 and 12.3°) at C(3) and C(7).³⁰ In both compounds the less pyramidalized carbon is found *syn* to the three-atom bridge.

Since olefin **2c** is computed to have nearly identical values of ϕ (25.2 and 25.0°),¹¹ it has been suggested that the 8° difference in the values of ϕ at the olefinic carbons in the selenonium salt is due to an attraction between the positively charged selenium atom and the π electrons at the doubly-bonded carbon *syn* to it.^{11,31} The very small difference between the values of ϕ at the much more highly pyramidalized olefinic carbons in $(\text{Ph}_3\text{P})_2\text{Pt}$ complex **3c** tends to support this suggestion.

The most important result of the determinations by X-ray crystallography of the structures of **3a–c** is the confirmation of the expected increase in pyramidalization angle, ϕ , with decreasing *n* in these $(\text{Ph}_3\text{P})_2\text{Pt}$ complexes. This enabled us to interpret the changes in the NMR spectra of the complexes in terms of the changes in the geometry and the electronic structure of the alkene moiety that an increase in ϕ produces.^{11,12}

¹H NMR Spectra of the Complexes. The assignments of the resonances in the ¹H spectrum of **3a** were straightforward, except for determining which of the four-proton resonances belonged to the pseudoaxial protons (H_{ax}) of the six-membered rings and which belonged to the pseudoequatorial protons (H_{eq}). This assignment was made on the basis of an NOE experiment in which the methylene protons of the one-carbon bridge at δ 2.06 were irradiated. The much greater enhancement observed for the four protons at δ 2.20 than for those at δ 2.37 identified the former as being pseudoaxial and the latter as being pseudoequatorial.

This assignment is consistent with the observation that axial protons generally appear at higher field than equatorial protons.³² It is also consistent with the finding that, as shown in Table 5, the protons at δ 2.20 show very weak coupling to ¹⁹⁵Pt, whereas those at δ 2.37 exhibit a coupling constant of 52.2 Hz. Inspection of a model of **3a** shows that the dihedral angle between a pseudoaxial C–H bond and the adjacent C–Pt bond

Table 5. ¹H Chemical Shifts (ppm) and $J_{\text{H-Pt}}$ Coupling Constants (Hz) for **3a–c**

complex	δ_{Hax}	$^3J_{\text{Hax-Pt}}$	δ_{Heq}	$^3J_{\text{Heq-Pt}}$	δ_{Hbh}	$^4J_{\text{Hbh-Pt}}$
3a ^a	2.20	<10	2.37	52.2	3.46	60.3
3b ^a	1.84	13.8	2.47	69.3	2.97	39.1
3c ^b	2.36/2.10	20.1	2.88/2.54	80.6	2.80	<20

^a Benzene-*d*₆, 298 K. ^b Toluene-*d*₈, 245 K.

is close to 90°, but the pseudoequatorial C–H and C–Pt bonds are more nearly eclipsed. Therefore, the Karplus relationship for three-bond coupling constants³³ predicts small ¹⁹⁵Pt–¹H coupling for H_{ax} and large ¹⁹⁵Pt–¹H coupling for H_{eq} in **3a**.

The largest ¹⁹⁵Pt–¹H coupling constant in this complex is for the two bridgehead protons (H_{bh}). A model shows the existence of a “W” relationship between each of the bridgehead C–H bonds and both of the C–Pt bonds. This type of spatial relationship generally leads to large coupling constants.³⁴ The chemical shift of H_{bh} is also rather low, further suggesting the possibility of some interaction between the bridgehead C–H and the C–Pt bonds.

In the ¹H NMR spectrum of the $(\text{Ph}_3\text{P})_2\text{Pt}$ complex of **2b** the resonance for H_{ax} is found about 0.4 ppm upfield from those in the complexes of **2a** or **2c**. This upfield position of the H_{ax} resonance is not unique to **3b** but seems to be a general feature of the tricyclo[3.3.2.0^{3,7}]-decane skeleton. For example, the H_{ax} resonance in acetonide **5** is found at δ 1.88, 0.37 ppm upfield from that in the homologous acetonide precursor of **2c**.¹²

The H_{eq} resonance in **5**, which appears at δ 2.16, is also upfield from that in the acetonide precursor of **2c**.¹² The difference in chemical shift is 0.18 ppm, and a similar difference in chemical shift is found between H_{eq} in **3b,c**. Therefore, the data in Table 5 indicate that the $(\text{Ph}_3\text{P})_2\text{Pt}$ group in **3a–c** does not have a dramatic effect on the chemical shifts of H_{ax} and H_{eq} in the complexed alkenes.

The upfield position of the resonance for H_{ax} in **3b** causes H_{ax} to have essentially the same chemical shift as the four protons of the ethano bridge. Consequently, it was difficult to extract the ¹ H_{ax} –¹⁹⁵Pt coupling constant from the ¹H NMR spectrum. Therefore, the ¹H–¹⁹⁵Pt NMR spin echo difference (SED) spectrum³⁵ of **3b** was obtained.

In a ¹H–¹⁹⁵Pt SED spectrum only those protons that are coupled to ¹⁹⁵Pt appear. In the SED spectrum of **3b**, the resonance for H_{ax} appeared as a triplet with J = 13.8 Hz, indicating that the three-bond ¹ H_{ax} –¹⁹⁵Pt and the geminal ¹ H_{ax} –¹ H_{eq} coupling constants are both about this size.

The $(\text{Ph}_3\text{P})_2\text{Pt}$ complex of **3c**, like the olefin from which it is formed and other derivatives of tricyclo[3.3.3.0^{3,7}]undecane, undergoes a conformational change, involving flipping of the trimethylene bridge.³⁶ In the 500 MHz ¹H NMR spectrum of **3c**, this process is frozen out at 245 K, so that two different sets of pseudoaxial and pseudoequatorial protons can be observed at this temperature. On warming, coalescence occurs around 300 K, giving $\Delta G^\ddagger \approx 14$ kcal/mol.³⁶ The chemical shifts

(29) RHF optimization of the geometry of $(\text{H}_3\text{P})_2\text{PtC}_2\text{H}_4$ with the pyramidalization angle frozen at $\phi = 49.0^\circ$: Hrovat, D. A.; Borden, W. T. Unpublished results.

(30) Hrovat, D. A.; Miyake, F.; Trammell, G.; Gilbert, K. E.; Mitchell, J.; Clardy, J.; Borden, W. T. *J. Am. Chem. Soc.* **1987**, *109*, 5524.

(31) For a discussion of and leading references to interactions between cations and π bonds, see: Kearney, P. C.; Mizoue, L. S.; Kumpf, R. A.; Forman, J. E.; McCurdy, A.; Dougherty, D. A. *J. Am. Chem. Soc.* **1993**, *115*, 9907.

(32) See, for example: Günther, H. *NMR Spectroscopy, An Introduction*; Wiley: New York, 1980; p 72.

(33) See, for example, p 106 of ref 32.

(34) See, for example, pp 115–116 of ref 32.

(35) Emshwiller, M.; Hahn, E. L.; Kaplan, D. *Phys. Rev.* **1959**, *118*, 414.

(36) Smith, J. M.; Hrovat, D. A.; Borden, W. T. *Tetrahedron Lett.* **1993**, *34*, 5991.

Table 6. ³¹P and ¹⁹⁵Pt Chemical Shifts (ppm) and ¹J_{P-Pt} Coupling Constants (Hz) for **3a-c** and for (Ph₃P)₂PtC₂H₄ in Benzene-*d*₆ at 25 °C

complex	δ _P ^a	δ _{Pt} ^b	¹ J _{P-Pt}
3a	30.5	-467	2960
3b	31.1	-514	3115
3c	32.2	-501	3332
(Ph ₃ P) ₂ PtC ₂ H ₄	34.1	-555	3740

^a Relative to 85% H₃PO₄. ^b δ_{Pt} in **3a-c** was measured relative to δ_{Pt} in (Ph₃P)₂PtC₂H₄, for which δ_{Pt} was taken from ref 38.

and coupling constants from the low-temperature spectrum, taken at 245 K, are given in Table 5.

Proton decoupling and use of the SED pulse sequence allowed all the resonances in the 500 MHz ¹H NMR spectrum of **3c** at both 245 and 338 K to be assigned and the ¹H-¹⁹⁵Pt coupling constants to be measured. The SED experiment confirmed that the bridgehead protons are coupled to ¹⁹⁵Pt. However, a single broad resonance for these protons was observed in the SED spectrum, so that the precise ¹H_{bh}-¹⁹⁵Pt coupling constant could not be obtained. The entry for this coupling constant in Table 5 is an upper limit, based on the width of H_{bh} peak in the SED spectrum and the absence of detectable splitting in it. The same is true of the entry for the ¹H_{ax}-¹⁹⁵Pt coupling constant in **3a**.

Table 5 shows that from **3a** to **3c** the ¹H_{ax}-¹⁹⁵Pt and ¹H_{eq}-¹⁹⁵Pt coupling constants both increase but the ¹H_{bh}-¹⁹⁵Pt coupling constant decreases. Molecular models indicate that these changes in the ¹H-¹⁹⁵Pt coupling constants can be attributed to the changes in the geometry of the carbon skeleton of **3**, rather than to changes in the C-Pt bonding.

From **3a** to **3c** the five-membered rings flatten, so that the dihedral angle between the pseudoequatorial C-H bonds and the C-Pt bonds moves closer to zero. This change is presumably responsible for the monotonic increase in the ¹H_{eq}-¹⁹⁵Pt coupling constant. Flattening of the five-membered rings also increases the dihedral angle between the pseudoaxial C-H bonds and the C-Pt bonds past 90°, which is probably why, although the ¹H_{ax}-¹⁹⁵Pt coupling constant remains small, it too increases monotonically. Finally, the "W" relationship between the bridgehead C-H and the C-Pt bonds is lost as the rings flatten. For this reason the ¹⁹⁵Pt-¹H_{bh} coupling constant would be expected to decrease with increasing *n*, as is observed.

³¹P and ¹⁹⁵Pt NMR Spectra of the Complexes.

The data obtained from the ³¹P and ¹⁹⁵Pt NMR spectra of **3a-c** are contained in Table 6. Also given are the ³¹P and ¹⁹⁵Pt chemical shifts and the ³¹P-¹⁹⁵Pt coupling constant for the (Ph₃P)₂Pt complex of ethylene, which serves as a model for the (Ph₃P)₂Pt complex of a planar alkene.²⁶ Although the (Ph₃P)₂Pt complex of bicyclo-[3.3.0]oct-1(5)-ene would have been a better reference for **3a-c**, as noted above, we were unable to prepare a stable complex of (Ph₃P)₂Pt with this olefin.

Table 6 shows that, as olefin pyramidalization increases from (Ph₃P)₂PtC₂H₄ to **3a**, the ³¹P chemical shift in the (Ph₃P)₂Pt complex moves to higher field. As discussed in the introduction, since olefin pyramidalization lowers the energy of the π* MO,^{11,12} increased pyramidalization should result in increased back-bonding between the HOMO of (Ph₃P)₂Pt (the antibonding combination of a 5d AO on Pt with the out-of-phase combination of phosphine lone pairs)¹³ and the LUMO

(π*) of a coordinated alkene. *Ab initio* calculations on (H₃P)₂PtC₂H₄ confirm that increased pyramidalization does, in fact, result in transfer of electron density from the (H₃P)₂Pt moiety to the olefin.¹⁴ Therefore, one might have expected increased olefin pyramidalization in **3** to result in deshielding of phosphorus and a consequent shift of the ³¹P resonance to lower field. However, just the opposite—an upfield shift of ³¹P with decreasing *n*—is what is actually observed.

The factors responsible for ³¹P chemical shifts appear not to be entirely understood,³⁷ but there is experimental evidence that transfer of electron density from (Ph₃P)₂Pt to a complexed olefin does, indeed, shift the ³¹P resonances to higher field. It has been found in the (Ph₃P)₂Pt complexes of a series of cyanoethylenes that, as the number of electron-withdrawing cyano groups increases, the ³¹P resonances move upfield.³⁸ Therefore, the upfield ³¹P shifts that are observed in **3**, as pyramidalization of the complexed olefin increases, are, in fact, quite consistent with increased electron donation from (Ph₃P)₂Pt to the olefin. Upfield ³¹P shifts have also been reported in (Ph₃P)₂Pt complexes of cyclic acetylenes as bending of the triple bond increases with decreasing ring size.^{1c}

Unlike the ³¹P chemical shifts, the ¹⁹⁵Pt resonances in **3** move to lower field as olefin pyramidalization increases, although the change in ¹⁹⁵Pt chemical shifts is not monotonic.³⁹ Nevertheless, the general trend is consistent not only with the naive expectation that increasing transfer of charge from (Ph₃P)₂Pt to the olefin should deshield Pt but also with the observation that the ¹⁹⁵Pt chemical shifts of (Ph₃P)₂Pt complexes of cyanoethylenes move to lower field as the number of cyano groups increases.³⁸

Table 6 shows that the ³¹P-¹⁹⁵Pt coupling constants in **3** decrease monotonically with the increase in olefin pyramidalization that occurs from **3c** to **3a**. Interestingly, unlike the trends in ³¹P and ¹⁹⁵Pt chemical shifts, this trend in ³¹P-¹⁹⁵Pt coupling constants is not found in (Ph₃P)₂Pt complexes of cyanoethylenes as the number of cyano groups increases.³⁸ The cyanoethylene complexes show only small variations in the ³¹P-¹⁹⁵Pt coupling constants as the number of cyano groups increases, and the ³¹P-¹⁹⁵Pt coupling constant of the tetracyanoethylene (TCNE) complex is actually 27 Hz larger than that found in the complex of ethylene.

An important factor in the size of ³¹P-¹⁹⁵Pt coupling constants in these complexes is the amount of bonding between the symmetric combination of the lone-pair orbitals on each phosphorus and the empty 6s orbital on platinum.³⁷ The simplest interpretation of the experimental data for **3** and for the (Ph₃P)₂Pt complexes of cyanoethylenes³⁸ is that the bonding between the phosphine lone pairs and the 6s AO on Pt decreases with increasing olefin pyramidalization in **3** but remains

(37) Pregosin, P. S.; Kunz, R. W. *³¹P and ¹³C NMR of Transition Metal Complexes*; Springer-Verlag: New York, 1979.

(38) Pellizer, G.; Graziani, M.; Lenarda, M.; Heaton, B. T. *Polyhedron* **1983**, *2*, 657.

(39) One possible explanation is that the Pt-C bonding in **3b** is anomalous, because, unlike olefins **2a,c**, **2b** is predicted to have a double bond that is not only pyramidalized but also slightly twisted. Both molecular models and *ab initio* calculations¹¹ indicate that the two carbon bridge in **2b** prefers a geometry in which this molecule has only C₂ rather than C_{2v} symmetry. The IR spectrum of the matrix-isolated alkene confirms this prediction.^{16b} The twisting of the two-carbon bridge in **2b** is predicted to result in some torsion about the double bond, which is calculated to amount to 3.8°. However, the X-ray data (*vide supra*) do not indicate any more torsion about this C-C bond in **3b** than in **3a** or **3c**.

relatively constant as the number of cyano groups increases in the cyanoethylene complexes.

This interpretation allows one to draw some inferences about bonding between the metal and the olefins in these complexes, since bonding between the phosphine lone pair orbitals and the 6s AO on platinum should decrease as bonding between the filled olefin π MO and the 6s AO increases.^{37,40} Direct experimental evidence for this competition between the phosphine lone pairs and the π MO of the olefin for the 6s AO of platinum comes from the finding that in **3**, as the ^{31}P – ^{195}Pt coupling constants decrease, there is a linear increase in the ^{13}C – ^{195}Pt coupling constants (*vide infra*).

The decrease in the ^{31}P – ^{195}Pt coupling constants with the increase in olefin pyramidalization in **3** thus implies that the interaction between π and 6s increases with increasing pyramidalization. Similarly, the nearly constant value of the ^{31}P – ^{195}Pt coupling constant in the cyanoethylenes implies that the interaction between π and 6s remains nearly constant as the number of cyano groups attached to the double bond increases.

Upon superficial consideration, neither of these conclusions seems very reasonable. As noted in the introduction, although pyramidalization of the doubly bonded carbons does raise the energy of the π MO, both calculations¹¹ and experiments¹² find the changes in the π orbital energies to be small. In addition, increasing the number of cyano groups attached to a double bond is, as expected, found not to raise but to lower the energy of the π MO. Applying Koopman's theorem to the photoelectron spectra of ethylene and TCNE shows that four cyano groups lower the energy of the π MO by 1.3 eV.⁴¹

There is a logical resolution of this apparent conflict between what can be inferred about the energies of the π orbitals in **3** and in the $(\text{Ph}_3\text{P})_2\text{Pt}$ complexes of the cyanoethylenes from the changes in the ^{31}P – ^{195}Pt coupling constants and what is known about the energies of the π orbitals in the isolated alkenes. The resolution is simply that the effective energies of the π MOs of the olefins in the complexes are significantly different from the π MO energies of the uncomplexed alkenes.

For this explanation to be correct, the effective energies of the olefin π MOs in **3** would have to increase much faster with increased olefin pyramidalization than is indicated by the rather small changes in the energies of the π orbitals in the isolated alkenes (**2**). In addition, a similar type of increase in the effective π orbital energies of the cyanoethylenes in their $(\text{Ph}_3\text{P})_2\text{Pt}$ complexes would be required to approximately cancel the decrease of the energies of the π MOs with increasing numbers of cyano groups in the isolated olefins.

We suggest that the cause of the greater effective π MO energies in the complexed, than in the free alkenes is back-donation from the $(\text{Ph}_3\text{P})_2\text{Pt}$ HOMO¹³ into π^* . Lowering the energy of π^* , by increasing either the pyramidalization of the olefin or the number of cyano groups attached to the doubly bonded carbons, makes the alkene a better electron acceptor, so that more electron density is transferred from the $(\text{Ph}_3\text{P})_2\text{Pt}$ HOMO into the olefin LUMO. The transfer of electron

Table 7. ^{13}C Chemical Shifts (ppm) of the Olefinic Carbons and $^1J_{\text{C-Pt}}$, $^2J_{\text{C-P}}$, and $^2J_{\text{P-P}}$ Coupling Constants (Hz) for **3a–c** and for $(\text{Ph}_3\text{P})_2\text{PtC}_2\text{H}_4$

complex	δ_{C}	$^1J_{\text{C-Pt}}$	$^2J_{\text{C-P}}^{\text{trans}}$	$^2J_{\text{C-P}}^{\text{cis}}$	$^2J_{\text{P-P}}$
3a ^a	66.9	407	67	-10	-27
3b ^a	74.9	343	56	-9	-41
3c	78.8, 79.2 ^b	296 ^c	48 ^c	-9 ^c	-55 ^c
$(\text{Ph}_3\text{P})_2\text{PtC}_2\text{H}_4$ ^a	39.2	194	27	-3	-58

^a Benzene-*d*₆, 298 K. ^b Toluene-*d*₈, 229 K. ^c Toluene-*d*₈, 338 K.

density into π^* should result in a greater Coulombic energy for the electrons in the π MO and thus raise the effective energy of this orbital.

Increased transfer of charge from the $(\text{Ph}_3\text{P})_2\text{Pt}$ HOMO into the π^* MO of an olefin thus serves to enhance synergistically electron donation from the π MO of the olefin into empty AOs of the same symmetry on the metal. The consequences of enhanced donation from the olefin π MO into the 6s AO on platinum with increasing olefin pyramidalization in **3** are seen indirectly in the decrease of the ^{31}P – ^{195}Pt coupling constants. However, as discussed in the next section, direct evidence for increased donation from π to 6s is provided by the linear increase in the ^{13}C – ^{195}Pt coupling constants that accompanies the decrease in the ^{31}P – ^{195}Pt coupling constants.

^{13}C NMR Spectra of the Complexes. Table 7 gives the ^{13}C chemical shifts and the ^{13}C – ^{195}Pt and ^{13}C – ^{31}P coupling constants for the olefinic carbons of **3a–c**. The ^{31}P – ^{31}P coupling constants, which can be obtained from the ^{13}C NMR spectra (*vide infra*), are also given. The ^{13}C chemical shifts and all the coupling constants change monotonically with the increase in olefin pyramidalization that accompanies the decrease in *n*.

Pyramidalization appears to move the ^{13}C resonances for olefinic carbons to lower field in uncomplexed alkenes,¹² but the trend for the olefinic carbons of the complexed alkenes in **3** is just the opposite—the ^{13}C chemical shifts move toward higher field as pyramidalization increases. We attribute the upfield shifts of these carbons in **3** to increased back-donation of electron density from the $(\text{Ph}_3\text{P})_2\text{Pt}$ HOMO into the π^* LUMO of the olefin, which increases the diamagnetic shielding of these carbons.

The ^{13}C – ^{195}Pt coupling constants for the olefinic carbons increase by 38% on going from *n* = 3 to *n* = 1 in **3**, and the ^{13}C – ^{195}Pt coupling constant for the olefinic carbons in **3a** is more than a factor of 2 larger than that measured in the $(\text{Ph}_3\text{P})_2\text{Pt}$ complex of ethylene. These ^{13}C – ^{195}Pt coupling constants should be roughly proportional to the amount of bonding between the 2s orbital on each carbon and the 6s orbital on platinum.³⁷ The coupling constants will therefore be affected not only by the amount of electron donation from the filled π orbital of each olefin to the 6s orbital of platinum but also by the extent to which the carbon 2s orbitals contribute to bonding to platinum in the complex. Both of these factors are expected to increase with increased pyramidalization of the complexed olefin.

As discussed in the previous section, the observation that the ^{31}P – ^{195}Pt coupling constant decreases by 21% on going from the $(\text{Ph}_3\text{P})_2\text{Pt}$ complex of ethylene to **3a** indicates that bonding between the phosphine lone pairs and the 6s orbital of platinum decreases with increasing olefin pyramidalization. The decrease in the ^{31}P – ^{195}Pt coupling constants thus provides good evidence⁴⁰ that

(40) (a) Pidcock, A.; Richards, R. E.; Venanzi, L. M. *J. Chem. Soc. A* **1966**, 1707. (b) Allen, F. H.; Pidcock, A. *J. Chem. Soc. A* **1968**, 2700. (c) Church, M. J.; Mays, M. J. *J. Chem. Soc. A* **1968**, 3074; **1970**, 1938.

(41) Houk, K. N.; Munchausen, L. L. *J. Am. Chem. Soc.* **1976**, *98*, 937.

the 110% increase in the ¹³C–¹⁹⁵Pt coupling constant for the olefinic carbons cannot be due solely to an increased contribution of the carbon 2s AOs to carbon–platinum bonding. At least some of the increase in the ¹³C–¹⁹⁵Pt coupling constant must be due to increased bonding between the π MO and the 6s AO on platinum.

In fact, a plot of the ³¹P–¹⁹⁵Pt coupling constants in **3a–c**, and in the (Ph₃P)₂Pt complex of ethylene, against the ¹³C–¹⁹⁵Pt coupling constants in these complexes gives a good straight line. The equation $J_{P-Pt} = 4460 \text{ Hz} - 3.8J_{C-Pt}$ gives the best least squares fit for the four points with $R^2 = 0.991$. This equation provides evidence that, with increased pyramidalization in **3**, the increase in the π–6s bond order results in a linear decrease in the bond order between 6s and the phosphine lone pairs.

For (Ph₃P)₂Pt not coordinated to an alkene, $J_{C-Pt} = 0$; so the equation predicts $J_{P-Pt} = 4460 \text{ Hz}$ for this species. In fact, this is about the average of the ³¹P–¹⁹⁵Pt coupling constants in bis(phosphine) complexes of Pt(0), which range from 4202 to 4592 Hz.⁴² Perhaps not surprisingly, the equation is less successful when applied to *cis*-dimethylbis(phosphine)platinum compounds, in which $J_{C-Pt} \approx 600 \text{ Hz}$.⁴³ The equation predicts $J_{P-Pt} = 2180 \text{ Hz}$, but the observed ³¹P–¹⁹⁵Pt coupling constants are somewhat lower, falling in the range 1800–1900 Hz.^{40b,43}

The ³¹P splittings of the resonances for the olefinic carbons in the ¹³C spectra of the (Ph₃P)₂Pt complexes also provide information about the changes in the electronic structure that occur with increasing olefin pyramidalization. The ³¹P nuclei that are *cis* and *trans* to the olefinic carbons in **3** are magnetically nonequivalent. As expected for such an AXX' system, five-line patterns are observed for the olefinic carbons in all the ¹³C spectra, but the appearance of these resonances changes dramatically with increasing pyramidalization of the olefin.

The central portion of the ¹³C spectrum for the olefinic carbons in the (Ph₃P)₂Pt complex of ethylene is a 1:2:1 triplet, flanked by a very weak pair of resonances. The spectrum was simulated using PANIC,⁴⁴ and the values of $J_{C-P^{cis}}$, $J_{C-P^{trans}}$, and J_{P-P} that give the best fit are shown in Table 7. The simulation provides only the relative signs of the coupling constants and does not identify which ¹³C–³¹P coupling is $J_{C-P^{cis}}$ and which is $J_{C-P^{trans}}$. However, *trans* coupling constants to phosphines are usually positive and larger in magnitude than *cis*,³⁷ and use of this additional piece of information allowed the assignments in Table 7 to be made.

As shown in Table 7, in the (Ph₃P)₂Pt complex of ethylene $|J_{P-P}| > |J_{C-P^{cis}} - J_{C-P^{trans}}|$. The much larger magnitude of the coupling of the phosphines to each other than to carbon results in the ¹³C resonances appearing as a 1:2:1 triplet. Only the presence of the very weak pair of resonances that flank this triplet indicate that the phosphines are magnetically nonequivalent and that the peak separations in the triplet are really the average of $J_{C-P^{cis}}$ and $J_{C-P^{trans}}$.⁴⁵

With increasing pyramidalization, the central resonance decreases in intensity, and the outer pair increase. In **3a**, these three peaks have nearly equal

intensity, which is roughly 2/3 that of the inner pair of two peaks. The ¹³C spectra for the olefinic carbons in **3a–c** were also simulated with PANIC, and the coupling constants in Table 7 were obtained.

As shown in Table 7, as pyramidalization increases, the magnitudes of $J_{C-P^{cis}}$ and $J_{C-P^{trans}}$ increase, while the magnitude of J_{P-P} decreases. As $|J_{C-P^{cis}} - J_{C-P^{trans}}|$ becomes increasingly larger than $|J_{P-P}|$, the ¹³C resonances for the olefinic carbons should eventually become doublets of doublets,⁴⁵ with the two different splittings corresponding to $J_{C-P^{cis}}$ and $J_{C-P^{trans}}$. Although, even in **3a**, this limit is not reached, the transition from the triplet expected for $|J_{P-P}| \gg |J_{C-P^{cis}} - J_{C-P^{trans}}|$ to the doublet of doublets expected for $|J_{P-P}| \ll |J_{C-P^{cis}} - J_{C-P^{trans}}|$ is what is being observed in the ¹³C resonances for the olefinic carbons on going from the (Ph₃P)₂Pt complex of ethylene to **3a**.

The observed changes in J_{C-P} and J_{P-P} are consistent with the predicted increase in the interaction of the HOMO of a (R₃P)₂Pt fragment with the π* LUMO of an olefin with increasing pyramidalization.¹⁴ The HOMO of (R₃P)₂Pt consists of the antisymmetric (b₂) combination of phosphorus lone pair orbitals, mixed in an antibonding fashion with 5d_{xz} on Pt and in a bonding fashion with 6p_x.¹³ Therefore, as transfer of electron density from the (R₃P)₂Pt HOMO into π* of an olefin increases, all the ³¹P coupling constants should be affected.³⁷ The transfer of electron density from phosphorus to carbon should cause the magnitude of J_{P-P} to decrease and the magnitude of both $J_{C-P^{cis}}$ and $J_{C-P^{trans}}$ to increase. Greater donation from the filled olefin π orbital into the empty 6s and 6p_z AOs on the metal with increased olefin pyramidalization may also contribute to the changes in these coupling constants, and the greater contribution of the carbon 2s AOs to both π and π* is probably responsible for part of the observed increases in the magnitudes of the ¹³C–³¹P coupling constants.

Conclusions

The X-ray structures of the (Ph₃P)₂Pt complexes (**3**) of pyramidalized olefins **2a–c** show what the ¹⁹⁵Pt–¹H coupling constants for these complexes in solution suggest—the amount of pyramidalization of the carbons that are bonded to platinum increases substantially from **3c** to **3b** to **3a**. The degree to which these carbons are pyramidalized has a profound effect on the chemical shifts and coupling constants observed in the ³¹P, ¹⁹⁵Pt, and ¹³C NMR spectra of **3a–c**. The changes found in these chemical shifts and coupling constants provide confirmatory evidence that a major effect of alkene pyramidalization is to lower the energy of the π* MO.^{11,12}

Experimental Section

General Methods. Dry deoxygenated diethyl ether and tetrahydrofuran (THF) were distilled from sodium/benzophenone. Hexane and pentane, used in flash chromatographic separations, were distilled. Other reagents and solvents were used as obtained, unless otherwise stated.

Flash chromatography was carried out using Silica Gel 60, 40–63 μm (230–400 mesh). Thin-layer chromatography (TLC) was performed on glass supported Silica Gel 60 plates (0.25 mm thick). Gas chromatographic analyses were carried out on a Hewlett-Packard 5790A series gas chromatograph,

(42) Mann, B. E.; Musco, A. *J. Chem. Soc., Dalton Trans.* **1980**, 776.

(43) Cheney, A. J.; Mann, B. E.; Shaw, B. L. *J. Chem. Soc., Chem. Commun.* **1971**, 431; Harris, R. K.; McNaught, I. J.; Reams, P.; Packer, K. *J. Magn. Reson. Chem.* **1991**, *29*, S60.

(44) Bruker Instruments, Billerica, MS.

(45) See, for example, ref 32, pp 160–70.

equipped with a 30 m x 0.32 mm i.d., FSOT SE-54, 0.25 μm , capillary column and coupled to a Hewlett-Packard 3390A integrator.

NMR spectra were obtained on Bruker 200, 300, and 500 MHz instruments. ^1H chemical shifts are reported in ppm downfield from internal TMS, and ^{13}C chemical shifts were obtained using CDCl_3 as an internal standard. ^{31}P NMR chemical shifts are reported in ppm, relative to 85% H_3PO_4 , and $(\text{Ph}_3\text{P})_2\text{PtC}_2\text{H}_4$ (δ -555)³⁸ served as the standard for ^{195}Pt chemical shifts.

FAB high-resolution mass spectra were obtained on a VG Analytical 70-SEQ instrument with a 11-250J data system, using a xenon gun. EI spectra were measured either on the same spectrometer or on a medium-resolution Kratos Analytical GCMS with a Mach 3 data system, on a Kratos Analytical GC/MS, on a Hewlett-Packard 5985 GC/MS, or on a Hewlett-Packard 5971A GC/MS.

Infrared absorption spectra were obtained using a Perkin-Elmer 1600 series FTIR and were recorded in solution, versus a solvent reference cell. UV-Vis absorption spectra were measured on a Hewlett-Packard 8452A diode array UV-Vis spectrophotometer.

(Tricyclo[3.3.1.0^{3,7}]non-3(7)-ene)bis(triphenylphosphine)platinum (3a). Diiodide **1a**, $\text{X} = \text{I}$,¹⁵ 100 mg (0.27 mmol), and $(\text{Ph}_3\text{P})_2\text{PtC}_2\text{H}_4$,¹⁹ 200 mg (0.27 mmol), were placed in a flame-dried, nitrogen-purged, two-necked, round-bottom flask. To one neck was attached a dropping funnel containing 8 g of Na/Hg (0.4% Na by weight). The other neck was attached to a vacuum line, the flask was evacuated, and 15 mL of dry THF was distilled in. The flask was then filled with argon and removed from the vacuum line. The sodium amalgam was added in one portion, and the contents of the flask were stirred for 36 h. The reaction mixture was filtered through Celite, and the solids were washed with 20 mL of THF. The THF solutions were combined and evaporated under reduced pressure to give a brown oil. On trituration with ethanol, a beige colored powder was obtained (120 mg, 54%), which was recrystallized from THF-ethanol to give needlelike crystals, mp 192–94 °C, which were pure by NMR. ^1H NMR (500 MHz, C_6D_6): δ 2.06 (s, 2H), 2.20 (d, $J = 10.3$ Hz, 4H), 2.37 (td, $J_{\text{H-Pt}} = 52.2$ Hz, $J_{\text{H-H}} = 10.3$ Hz), 3.46 (t, $J_{\text{H-Pt}} = 60.3$ Hz, 2H), 7.12 (m, 18H), 7.22 (m, 12H). ^{13}C NMR (75.4 MHz, C_6D_6): δ 138.2, 134.8, 66.9 (t of m, $J_{\text{Pt-C}} = 407.4$ Hz), 61.2 (t, $J_{\text{Pt-C}} = 106.7$ Hz), 52.5 (s), 39.3 (s). ^{31}P NMR (121 MHz, C_6D_6): δ 30.5 (t of m, $J_{\text{Pt-P}} = 2960$ Hz). ^{195}Pt NMR (42.8 MHz, C_6D_6): δ -467 (t, $J_{\text{Pt-Pt}} = 2960$ Hz). The FAB mass spectrum showed the parent ion at $(\text{M} + \text{H})^+ = 840$ (exact mass: calcd for $\text{C}_{45}\text{H}_{43}\text{P}_2\text{Pt}$, m/e 840.2486; found, m/e 840.2497), with peaks at m/e 839 and 841 for the two other abundant isotopes of Pt. Anal. Calcd for $\text{C}_{45}\text{H}_{42}\text{P}_2\text{Pt}$: C, 64.35; H, 5.04; P, 7.37. Found: C, 64.39; H, 5.01; P, 7.64.

Acetonide of Tricyclo[3.3.2.0^{3,7}]decane-3,7-diol (5). Into a 250 mL round bottom flask, fitted with a condenser, was added 647 mg (2.91 mmol) of ketone **4**, 1.42 mL (29.2 mmol) of hydrazine monohydrate, 1.04 g (26.0 mmol) of sodium hydroxide, and 140 mL of diethylene glycol. The mixture was heated at 185 °C under nitrogen for 30 h. The reaction was worked up by cooling to room temperature, adding water, extracting three times with diethyl ether, washing the combined ether extracts twice with water, and drying the ether phase over magnesium sulfate. Diethyl ether was also used to rinse a significant amount of acetonide that had sublimed on the inside wall of the condenser. Solvent removal at reduced pressure on a rotary evaporator gave 629 mg of a solid, which GC and GCMS analysis showed to be 97% acetonide **5** (retention time = 3.28 min at 165 °C). Attempts to recrystallize **5** were unsuccessful. Purification was effected by flash chromatography on 45 g of silica, using diethyl ether-hexane (1:10) as the eluent. This yielded 538 mg (88.7%) of solid white acetonide **5**, mp 45.5–46.5 °C, in fractions collected when 160–260 mL of solvent had passed through the column. This material was pure by GC, TLC ($R_f = 0.30$ in 1:10 ether-hexane), and NMR. ^1H NMR (CDCl_3 , 500 MHz): δ 1.47 (s, 6

H), 1.70 (m, 4 H), 1.88 (d, $J = 11.7$ Hz, 4 H), 2.16 (dd, $J = 11.7$ Hz, $J = 6.1$ Hz, 4 H), 2.39 (m, 2 H). ^{13}C NMR (CDCl_3 , 50 MHz): δ 29.67 (CH_2), 30.10 (CH_3), 35.50 (CH), 47.66 (CH_2), 98.46 (C), 118.01 (C). IR (CHCl_3 , cm^{-1}): 3018, 2943, 2861, 1454, 1372, 1199, 1052. MS (EI): m/e 193 ($\text{M}^+ - \text{CH}_3$, 100), 151 (13.5), 133 (14.6), 109 (15.5), 93 (31.8), 79 (30.3), 67 (28.9), 55 (22.9), 43 (63.2). Exact mass (EI): calcd. for $\text{C}_{12}\text{H}_{17}\text{O}_2$ ($\text{M}^+ - \text{CH}_3$), m/e 193.1227; found, m/e 193.1220.

Tricyclo[3.3.2.0^{3,7}]decane-3,7-diol (6). A mixture of 49.0 mg (0.236 mmol) of acetonide **5** and 40 mL of 20% aqueous acetic acid was heated at 85 °C for 48 h in a 100 mL round bottom flask, fitted with a condenser. The solution was cooled, and the solvent was removed at reduced pressure on a rotary evaporator. The resulting solid residue was dissolved in 20 mL of chloroform and washed with 20 mL of saturated aqueous sodium bicarbonate. The aqueous phase was extracted with two 20 mL portions of chloroform, and the combined organic phases were dried over magnesium sulfate. Solvent removal at reduced pressure on a rotary evaporator gave 32.9 mg of solid white diol **6** (83.1%), which was pure by GC (retention time = 3.16 min at 165 °C), TLC ($R_f = 0.06$, diethyl ether-pentane, 1:1), and NMR. The diol was recrystallized from diethyl ether to give crystals, mp > 260 °C (sublimation begins around 220 °C at 1 atm). ^1H NMR (CDCl_3 , 500 MHz): δ 1.68 (m, 4 H), 1.85–1.95 (8 H), 2.10 (m, 2 H), 2.26 (s, 2 H, exchangeable with D_2O). ^{13}C NMR (CDCl_3 , 50 MHz): δ 29.15 (CH_2), 29.41 (CH), 48.04 (CH_2), 83.21 (C). IR (CHCl_3 , cm^{-1}): 3578, 3402 (broad), 3015, 2936, 2861, 1451, 1322, 1114. MS (EI): m/e 168 (M^+ , 100), 166 (40.8), 150 (9.8), 138 (30.1), 123 (14.5), 111 (60.6), 109 (63.4), 108 (58.8), 95 (62.0), 81 (61.8), 67 (20.5), 55 (17.8). Exact mass (EI): calcd for $\text{C}_{10}\text{H}_{16}\text{O}_2$, m/e 168.1149; found, m/e 168.1144.

Tricyclo[3.3.2.0^{3,7}]decane-3,7-diol Dimesylate (1b, X = OMs). To a stirred solution of 37.2 mg (0.221 mmol) of diol **6** in 14 mL of dry THF under argon at 0 °C was added 0.5 mL (0.70 mmol) of a 1.4 M solution of methylithium in diethyl ether. After 20 min, 0.056 mL (0.724 mmol) of methanesulfonyl chloride was added dropwise. After 3 h, most of the solvent was removed at reduced pressure on a rotary evaporator. To the remaining mixture was added 25 mL water, and the aqueous phase was extracted with 3–25 mL portions of chloroform. The combined organic phases were dried over magnesium sulfate. Solvent removal at reduced pressure on a rotary evaporator gave 59.1 mg of a white solid. Purification by flash chromatography on 7 g of silica, using ethyl acetate-hexane, 4:3, as the eluent, gave 37 mg (51.7%) of the dimesylate ($R_f = 0.43$ in ethyl acetate-hexane, 4:3) in fractions collected when 35–45 mL of solvent had passed through the column. Also isolated was 17 mg of monomesylate ($R_f = 0.18$) from fractions collected when 50–100 mL of solvent had passed through the column. Recrystallization of the dimesylate from chloroform-pentane (1:4) gave clear crystals, mp 134–135 °C, which were pure by NMR. ^1H NMR (CDCl_3 , 500 MHz): δ 1.71 (m, 4 H), 2.22 (d, $J = 11.8$ Hz, 4 H), 2.37 (m, 2 H), 2.60 (dd, $J = 11.8$ Hz, $J = 6.7$ Hz, 4 H), 3.09 (s, 6 H). ^{13}C NMR (CDCl_3 , 50 MHz): δ 28.23 (CH_2), 30.39 (CH), 40.70 (CH_3), 45.70 (CH_2), 96.90 (C). IR (CHCl_3 , cm^{-1}): 3025, 2937, 2865, 1343, 1168, 1036, 931, 846. MS (EI): m/e 245 (17.6), 149 (100), 121 (24.0), 109 (33.4), 107 (54.1), 91 (23.3), 79 (32.0). Exact mass (FAB): calcd for $\text{C}_{12}\text{H}_{21}\text{O}_6\text{S}_2$, m/e 325.0778; found, m/e 325.0775. Anal. Calcd for $\text{C}_{12}\text{H}_{20}\text{S}_2\text{O}_6$: C, 44.43; H, 6.22; S, 19.73. Found: C, 44.42; H, 6.25; S, 19.41.

(Tricyclo[3.3.2.0^{3,7}]dec-3(7)-ene)bis(triphenylphosphine)platinum (3b). A round bottom flask containing dimesylate **1b**, $\text{X} = \text{OMs}$ (201 mg, 0.62 mmol), Na/Hg (prepared by adding 100 mg of Na to 22 g of Hg under inert atmosphere), and $(\text{Ph}_3\text{P})_2\text{PtC}_2\text{H}_4$ (520 mg, 0.70 mmol) was attached to a vacuum line and evacuated. Dry ether (50 mL) was distilled in, the flask was filled with Ar, and the reaction mixture was stirred overnight. Filtration through Celite (under an Ar atmosphere) gave a clear yellow solution. The Celite bed was washed with dry ether (2 x 10 mL). The combined ether solutions were evaporated under vacuum to

Table 8. Crystal, Data Collection, and Refinement Information for X-ray Crystallography of 3a-c

	3a	3b	3c
empirical formula	C ₄₅ H ₄₂ P ₂ Pt	C ₄₆ H ₄₄ P ₂ Pt	C ₄₇ H ₄₆ P ₂ Pt
cryst color and habit	clear rhomb	clear rhomb	clear rhomb
cryst size (mm)	0.1 × 0.15 × 0.2	0.25 × 0.35 × 0.35	0.2 × 0.25 × 0.3
cryst system	orthorhombic	triclinic	triclinic
space group	P2 ₁ 2 ₁ 2 ₁	P $\bar{1}$	P $\bar{1}$
unit cell dimens	<i>a</i> = 9.714(2) Å <i>b</i> = 18.533(4) Å <i>c</i> = 20.208(4) Å	<i>a</i> = 11.656(2) Å <i>b</i> = 16.548(3) Å <i>c</i> = 20.208(4) Å α = 68.37(3)° β = 79.33(3)° γ = 86.70(3)°	<i>a</i> = 11.715(2) Å <i>b</i> = 12.015(2) Å <i>c</i> = 18.878(3) Å α = 97.76(3)° β = 109.36(3)° γ = 96.90(3)°
Z	4	4	2
abs coeff (mm ⁻¹)	3.976	3.846	3.756
2 θ range (deg)	2.0–50.0	3.0–45.0	3.0–45.0
index range	0 ≤ <i>h</i> ≤ 12 0 ≤ <i>k</i> ≤ 22 -4 ≤ <i>l</i> ≤ 24	0 ≤ <i>h</i> ≤ 11 -17 ≤ <i>k</i> ≤ 17 -22 ≤ <i>l</i> ≤ 22	0 ≤ <i>h</i> ≤ 11 -12 ≤ <i>k</i> ≤ 12 -16 ≤ <i>l</i> ≤ 15
reflens colld	4439	10 339	5307
independent reflens	4309 (<i>R</i> _{int} = 1.85%)	9814 (<i>R</i> _{int} = 1.85%)	5011 (<i>R</i> _{int} = 1.42%)
obsd reflens [<i>F</i> > 4.0 σ (<i>F</i>)]	2954	6851	4355
abs corr	semiempirical	semiempirical	semiempirical
<i>R</i> (<i>R</i> _w)	0.0275 (0.0242)	0.0280 (0.0288)	0.0195 (0.0235)

afford a yellowish powder, which was washed with pentane (2 × 5 mL), ethanol (4 mL), and then recrystallized from THF/ethanol (1:3) to afford yellowish crystals (220 mg, 42% yield), mp (sealed tube) 185–190 °C (dec), which were pure by NMR. ¹H-NMR (300 MHz, C₆D₆): δ 7.59 (m, 12 H), 6.95 (m, 18 H), 2.97 (bt, 2 H, *J*_{H-Pt} = 39.1 Hz), 2.47 (t of m, 4 H, *J*_{H-Pt} = 69.3 Hz), 1.83 (m, 8 H). ¹³C NMR (50.3 MHz, C₆D₆): δ 138.0 (m, C), 134.3 (m, CH), 129.1 (s, CH), 128.0 (s, CH), 74.9 (t of m, *J*_{Pt-C} = 343 Hz, C), 53.1 (t, *J*_{Pt-C} = 105 Hz, CH), 48.4 (t, *J*_{Pt-C} = 24 Hz, CH₂), 31.6 (s, CH₂). ³¹P NMR (81 MHz, C₆D₆): δ 31.1 (t of m, *J*_{P-Pt} = 3115 Hz). ¹⁹⁵Pt NMR (42.8 MHz, C₆D₆): δ -514 (t, *J*_{P-Pt} = 3115 Hz). The FAB mass spectrum showed the parent ion at (*M* + *H*)/*e* = 854 (exact mass: calcd for C₄₆H₄₄P₂Pt, *m/e* 854.2644; found, *m/e* 854.2598), with peaks at *m/e* 853 and 855 for the two other abundant isotopes of Pt. Anal. Calcd for C₄₆H₄₄P₂Pt: C, 64.71; H, 5.19; P, 7.25. Found: C, 64.71; H, 5.11; P, 7.56.

(Tricyclo[3.3.3.0^{3,7}]undec-3(7)-ene)bis(triphenylphosphine)platinum (3c). A round bottom flask containing dimesylate **1c**, X = OMs¹¹ (212 mg, 0.63 mmol) and Na/Hg (prepared by adding 100 mg of Na to 22 g of Hg under inert atmosphere) was attached to a vacuum line and evacuated. Dry ether (40 mL) was distilled in, the flask was filled with Ar, and the reaction mixture was stirred overnight. The reaction mixture was concentrated to about half its volume by bubbling Ar through it, and then it was filtered through Celite (under Ar atmosphere) into a solution of (Ph₃P)₂PtC₂H₄ (420 mg, 0.56 mmol) in dry THF (30 mL). Removal of the solvent under vacuum afforded a yellowish powder which was recrystallized from THF/ethanol (1:3) to give yellowish crystals (235 mg, 43% yield based on the (Ph₃P)₂Pt complex of ethylene), mp (sealed tube) 145–148 °C (dec), which were pure by NMR. ¹H-NMR (500 MHz, toluene-*d*₈, 245 K): δ 7.54 (m, 12 H), 6.96 (m, 18 H), 2.88 (t of m, 2 H, *J*_{H-Pt} = 80.6 Hz), 2.80 (m, 2 H), 2.54 (t of m, 2 H, *J*_{H-Pt} = 80.6 Hz), 2.36 (t of d, 2H, *J*_{H-Pt} = 20.1 Hz, *J*_{H-H} = 13.7 Hz), 2.10 (t of d, 2H, *J*_{H-Pt} = 20.1 Hz, *J*_{H-H} = 14.0 Hz), 1.98 (bm, 3 H), 1.67 (m, 1 H), 1.52 (t, 2H, *J* = 13.5 Hz). ¹H-NMR (500 MHz, C₆D₆, 338 K): δ 7.58 (m, 12 H), 6.98 (m, 18 H), 2.71 (bm, 2 H), 2.64 (bt, 4 H, *J*_{H-Pt} = 80 Hz), 2.14 (bd, 4 H, *J*_{H-Pt} = 20.1 Hz), 1.75–1.69 (b, 6 H). ¹³C NMR (50.3 MHz, toluene-*d*₈, 229 K): δ 138.3 (m, C), 134.2 (m, CH), 129.0 (s, CH), 128.0 (s, CH), 79.2 (m, C), 78.8 (m, C), 52.2 (t, *J*_{Pt-C} = 32 Hz, CH₂), 50.7 (t, *J*_{Pt-C} = 76 Hz, CH), 41.5 (t, *J*_{Pt-C} = 32 Hz, CH₂), 36.9 (s, CH₂), 23.1 (s, CH₂). ¹³C NMR

(50.3 MHz, toluene-*d*₈, 338 K): δ 138.6 (m, C), 134.4 (b, CH), 129.0 (s, CH), 128.0 (s, CH), 79.2 (t of m, *J*_{Pt-C} = 296 Hz, C), 50.8 (t, *J*_{Pt-C} = 76 Hz, CH), 47.4 (b, CH₂), 36.9 (s, CH₂), 23.1 (s, CH₂). ³¹P NMR (81 MHz, C₆D₆): δ 32.2 (t of m, *J*_{P-Pt} = 3332 Hz); ¹⁹⁵Pt NMR (toluene-*d*₈, 42.8 MHz): δ -501 (t, *J*_{P-Pt} = 3332 Hz). The FAB mass spectrum showed the parent ion at *M*⁺/*e* = 867 (exact mass: calculated for C₄₇H₄₆P₂Pt, *m/e* 867.2646, found *m/e* 867.2630), with peaks at *m/e* 866 and 868 for the two other abundant isotopes of Pt. Anal. Calcd for C₄₇H₄₆P₂Pt: C, 65.04; H, 5.34; P, 7.14. Found: C, 64.85; H, 5.21; P, 7.15.

X-ray Structures of (Tricyclo[3.3.1.0^{3,7}]non-3(7)-ene)-bis(triphenylphosphine)platinum (3a),¹⁸ (Tricyclo[3.3.2.0^{3,7}]dec-3(7)-ene)bis(triphenylphosphine)platinum (3b), and (Tricyclo[3.3.3.0^{3,7}]undec-3(7)-ene)bis(triphenylphosphine)platinum (3c). Suitable crystals of all three complexes were chosen and mounted with grease in capillaries, which were sealed with a torch. Descriptions of the crystals and the X-ray data collection are contained in Table 8. Reflections were collected for the three crystals, using an Enraf-Nonius CAD4 diffractometer with Mo K α radiation (λ = 0.710 73 Å) and a highly oriented graphite crystal monochromator. Data reduction was performed using the program XCAD4, followed by Siemen's SHELX XEMP for making absorption corrections, based on ψ -scan data. Structures were solved using direct and Fourier transform methods. Solutions and subsequent refinements were carried out using the PC version of SHELX. The Laue merging *R* factors for equivalent reflections were good, and densities agreed with the space groups found. The crystal of **3b** gave two independent molecules per unit cell in P $\bar{1}$. This result was examined carefully, but no higher space group was possible for the observed intensities. Additional information about the X-ray structure determinations is available as supporting information.²⁴

Acknowledgment. We thank the National Science Foundation for support of this research.

Supporting Information Available: Tables of bond lengths, bond angles, anisotropic displacement coefficients, and hydrogen atom coordinates and *U* values for **3a–c** (15 pages). Ordering information is given on any current masthead page.

OM9502751

Oxidative Addition of HSnR_3 ($\text{R} = \text{Ph}, ^n\text{Bu}$) to the Square-Planar Iridium(I) Compounds $\text{Ir}(\text{XR})(\text{TFB})(\text{PCy}_3)$ ($\text{XR} = \text{OMe}, \text{OEt}, \text{O}^i\text{Pr}, \text{OPh}, \text{S}^n\text{Pr}$) and $\text{Ir}(\text{C}_2\text{Ph})\text{L}_2(\text{PCy}_3)$ ($\text{L}_2 = \text{TFB}, 2\text{CO}$)

Miguel A. Esteruelas,* Fernando J. Lahoz, Montserrat Oliván, Enrique Oñate, and Luis A. Oro

Departamento de Química Inorgánica, Instituto de Ciencia de Materiales de Aragón, Universidad de Zaragoza, CSIC, 50009 Zaragoza, Spain

Received February 17, 1995[®]

The synthesis of the compounds $\text{Ir}(\text{OR})(\text{TFB})(\text{PCy}_3)$ ($\text{R} = \text{Et}$ (2), ^iPr (3), Ph (4); $\text{TFB} =$ tetrafluorobenzobarrelene), $\text{Ir}_2(\text{CO})_6(\text{PCy}_3)_2$ (5), $\text{Ir}(\text{S}^n\text{Pr})(\text{TFB})(\text{PCy}_3)$ (6), $[\text{Ir}(\mu\text{-S}^n\text{Pr})(\text{CO})(\text{PCy}_3)]_2$ (7), $\text{Ir}(\text{C}_2\text{R})(\text{TFB})(\text{PCy}_3)$ ($\text{R} = \text{Ph}$ (9), Cy (10), CO_2Me (11), SiMe_3 (12)), and $\text{Ir}(\text{C}_2\text{Ph})(\text{CO})_2(\text{PCy}_3)$ (13) is described. The complexes 2–4 and 6 react with HSnR'_3 in a 1:2 molar ratio to give $\text{IrH}_2(\text{SnR}'_3)(\text{TFB})(\text{PCy}_3)$ ($\text{R}' = \text{Ph}$ (14), ^nBu (15)) and RXSnR'_3 ($\text{X} = \text{O}, \text{S}$). The structure of 14 was determined by an X-ray investigation. Compound 14 crystallizes in the space group $P\bar{1}$ (No. 2) with $a = 10.923(1) \text{ \AA}$, $b = 10.943(1) \text{ \AA}$, $c = 19.679(1) \text{ \AA}$, $\alpha = 75.076(5)^\circ$, $\beta = 77.504(5)^\circ$, $\gamma = 72.606(5)^\circ$, and $Z = 2$. The coordination geometry around the iridium atom could be rationalized as being derived from a highly distorted octahedron with the triphenylstannyl group and the tricyclohexylphosphine ligand occupying pseudo-trans positions ($\text{Sn}-\text{Ir}-\text{P} = 129.46(3)^\circ$). In solution 14 and 15 are fluxional. The fluxional process, with values for ΔH^\ddagger of 13.4 ± 0.9 (14) and 12.7 ± 0.7 (15) kcal/mol and for ΔS^\ddagger of 3.0 ± 3.0 (14) and -1.6 ± 2.0 (15) eu, involves the relative positions of the diolefin atoms. The alkynyl derivative 9 reacts with HSnR'_3 to afford $\text{IrH}(\text{C}_2\text{Ph})(\text{SnR}'_3)(\text{TFB})(\text{PCy}_3)$ ($\text{R}' = \text{Ph}$ (19), ^nBu (20)). Under carbon monoxide atmosphere, 19 leads to $\text{IrH}(\text{C}_2\text{Ph})(\text{SnPh}_3)(\text{CO})_2(\text{PCy}_3)$ (21) and tetrafluorobenzobarrelene. Compound 21, and the related derivative $\text{IrH}(\text{C}_2\text{Ph})(\text{Sn}^n\text{Bu}_3)(\text{CO})_2(\text{PCy}_3)$ (22) can be also obtained by oxidative addition of the corresponding stannanes to 13. The complexes 14, 19, and 21 catalyze the addition of HSnPh_3 to phenylacetylene, and from all experiments *cis*- $\text{PhCH}=\text{CH}(\text{SnPh}_3)$ and *trans*- $\text{PhCH}=\text{CH}(\text{SnPh}_3)$ were obtained.

Introduction

Vinylsilanes and vinylstannanes have been shown to be versatile intermediates in organic synthesis.¹ Vinylsilanes are usually prepared by catalytic addition of silanes to alkynes. From a mechanistic point of view, the hydrosilylation reactions involve conventional oxidative addition, insertion, and reductive elimination steps.² In this respect, the investigation of the oxidative addition of silanes to unsaturated transition metal complexes is of great interest and has received increasing attention in recent years.³

The stereoselective formation of vinylstannanes by addition of alkyl- or arylstannanes to alkynes requires the presence of a transition metal catalyst.⁴ Although, at first glance, there should not be a great difference between the catalytic hydrosilylation and hydrostannation of alkynes, the applicability of catalyst precursors related to those used in hydrosilylation has been scarcely investigated in hydrostannation reactions. If these catalyst precursors were active as hydrostannation catalysts, one would expect mechanistic similarities. However, the oxidative addition of alkyl- or arylstannanes to unsaturated transition metal complexes has received less attention than the oxidative addition of silanes.⁵ In addition, it should be noted that the comparison of physical and chemical properties for

[®] Abstract published in *Advance ACS Abstracts*, June 15, 1995.

(1) (a) Chan, T. H. *Acc. Chem. Res.* **1977**, *10*, 442. (b) Hurdlike, P. F. in *New Applications of Organometallic Reagents in Organic Synthesis*; Seyferth, D., Ed.; Elsevier: Amsterdam, The Netherlands, 1976. (c) Cook, F.; Moerk, R.; Schwindeman, J.; Magnus, P. *J. Org. Chem.* **1980**, *45*, 1406. (d) Negishi, E. *Organometallics in Organic Synthesis*, John Wiley and Sons: New York, 1980. (e) Neumann, W. P. *Synthesis* **1987**, 665. (f) Fleming, I.; Dunogues, J.; Smithers, R. H. *Org. React.* **1989**, *37*, 57. (g) Kumar Das, V. G.; Chu C.-K. In *The Chemistry of the Metal-Carbon Bond*; Hartley, F. R., Patai, S., Eds.; Wiley: New York, 1985; Vol. 3.

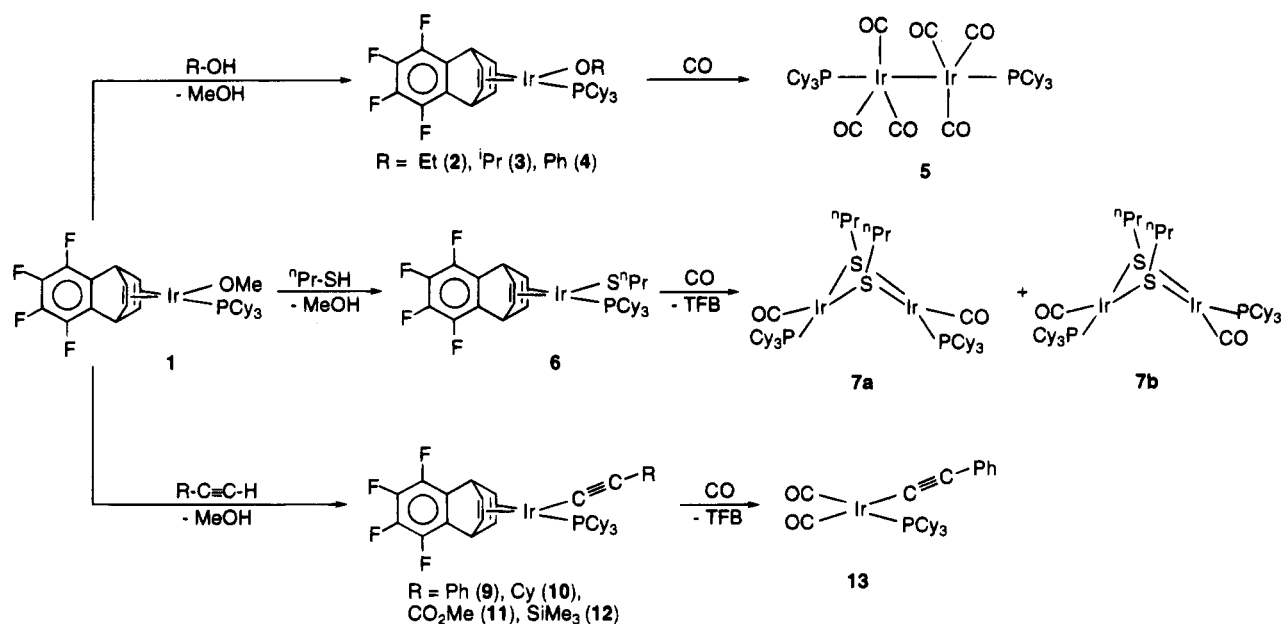
(2) Chalk, A. J.; Harrod, J. F. *J. Am. Chem. Soc.* **1965**, *87*, 16. (b) Schroeder, M.; Wrighton, M. S. *J. Organomet. Chem.* **1977**, *128*, 345. (c) Dickers, H. M.; Haszeldine, R. N.; Mather, A. P.; Parish, R. V. *J. Organomet. Chem.* **1978**, *161*, 91. (d) Randolph, C. L.; Wrighton, M. S. *J. Am. Chem. Soc.* **1986**, *108*, 3366. (e) Seitz, F.; Wrighton, M. S. *Angew. Chem., Int. Ed. Engl.* **1988**, *27*, 289. (f) Ojima, I.; Cios, N.; Donovan, R. J.; Ingallina, P. *Organometallics* **1990**, *9*, 3127. (g) Esteruelas, M. A.; Oro, L. A.; Valero, C. *Organometallics* **1991**, *10*, 462. (h) Duckett, S. B.; Perutz, R. N. *Organometallics* **1992**, *11*, 90. (i) Esteruelas, M. A.; Herrero, J.; Oro, L. A. *Organometallics* **1993**, *12*, 2377.

(3) (a) Tilley, T. D. In *The Chemistry of Organic Silicon Compounds*; Patai, S., Rappoport, Z., Eds.; Wiley: New York, 1989. (b) Schubert, U. *Transition Met. Chem.* **1991**, *16*, 136.

(4) (a) Stille, J. K. *Angew. Chem., Int. Ed. Engl.* **1986**, *25*, 508. (b) Mitchell, T. N.; Amamria, A.; Killing, H.; Rutschow, D. *J. Organomet. Chem.* **1986**, *304*, 257. (c) Kikukawa, K.; Umekawa, H.; Wada, F.; Matsuda, T. *Chem. Lett.* **1988**, 881. (d) Zhang, H. X.; Guibé, F.; Balavoine, G. *J. Org. Chem.* **1990**, *55*, 1857. (e) Mitchell, T. N.; Schneider, U. *J. Organomet. Chem.* **1991**, *405*, 195.

(5) (a) Lappert, M. F.; Travers, N. F. *J. Chem. Soc., Chem. Commun.* **1968**, 1569. (b) Luo, X.-L.; Schulte, G. K.; Demou, P.; Crabtree, R. H. *Inorg. Chem.* **1990**, *29*, 4268. (c) Cabeza, J. A.; Llamazares, A.; Riera, V.; Triki, S.; Ouahab, L. *Organometallics* **1992**, *11*, 3334. (d) Schubert, U.; Gilbert, S.; Mock, S. *Chem. Ber.* **1992**, *125*, 835. (e) Seebald, S.; Mayer, B.; Schubert, U. *J. Organomet. Chem.* **1993**, *462*, 225. (f) Clark, G. R.; Flower, K. R.; Rickard, C. E. F.; Roper, W. R.; Salter, D. M.; Wright, L. J. *J. Organomet. Chem.* **1993**, *462*, 331.

Scheme 1



analogous series of hydridosilyl and hydridostannyl complexes may be used in developing a better understanding of bonding interactions in these systems.

We have previously reported that the treatment of $\text{IrCl}_3 \cdot x\text{H}_2\text{O}$ with tetrafluorobenzobarrelene (TFB) in refluxing methanol/water leads to $\text{IrCl}(\text{TFB})_2$ in nearly quantitative yield.⁶ The accessibility of this compound has promoted the development of an extensive chemistry of neutral and cationic complexes, including $\text{Ir}(\eta^1\text{-OC}(\text{O})\text{CH}_3)(\text{TFB})(\text{PR}_3)$ ($\text{PR}_3 = \text{PPh}_3, \text{PCy}_3, \text{P}^i\text{Pr}_3$) and $\text{Ir}(\eta^1\text{-OC}(\text{O})\text{CH}_3)(\text{CO})_2(\text{PCy}_3)$, which show significant differences with respect to the chemistry of the typical iridium-1,5-cyclooctadiene moiety.^{6,7} Recently, we have also observed that the oxidative addition of HSiR_3 to $\text{Ir}(\eta^1\text{-OC}(\text{O})\text{CH}_3)\text{L}_2(\text{PCy}_3)$ ($\text{L}_2 = \text{TFB}, 2\text{CO}$) affords the dihydrosilyl derivatives $\text{IrH}_2(\text{SiR}_3)\text{L}_2(\text{PCy}_3)$ ($\text{L}_2 = \text{TFB}, 2\text{CO}$), which have been found to promote silicon-carbon bond formation in hydrosilylation and dehydrogenative silylation of phenylacetylene.⁸ As a continuation of our work in this field, we have now investigated the oxidative addition of HSnPh_3 and HSn^nBu_3 to the new square-planar complexes $\text{Ir}(\text{XR})(\text{TFB})(\text{PCy}_3)$ ($\text{XR} = \text{OMe}, \text{OEt}, \text{O}^i\text{Pr}, \text{OPh}, \text{S}^n\text{Pr}$) and $\text{Ir}(\text{C}_2\text{Ph})\text{L}_2(\text{PCy}_3)$ ($\text{L}_2 = \text{TFB}, 2\text{CO}$). In this paper, we describe the results obtained from this study, as well

as the catalytic activity of some of the prepared compounds in the hydrostannation of phenylacetylene with HSnPh_3 .

Results and Discussion

Synthesis and Characterization of $\text{Ir}(\text{XR})(\text{TFB})(\text{PCy}_3)$ ($\text{XR} = \text{OEt}, \text{O}^i\text{Pr}, \text{OPh}, \text{S}^n\text{Pr}$), $\text{Ir}(\text{C}_2\text{R})(\text{TFB})(\text{PCy}_3)$ ($\text{R} = \text{Ph}, \text{Cy}, \text{CO}_2\text{Me}, \text{SiMe}_3$), and $\text{Ir}(\text{C}_2\text{Ph})(\text{CO})_2(\text{PCy}_3)$. These compounds were prepared according to the reactions shown in Scheme 1. Treatment of $\text{Ir}(\text{OMe})(\text{TFB})(\text{PCy}_3)$ (1) with ethanol, 2-propanol, and phenol leads to the terminal alkoxide compounds 2–4, which were isolated as orange solids in 58%–71% yield. The most noticeable absorption in the IR spectra in Nujol are very strong bands between 1255 and 1055 cm^{-1} , assigned to the $\nu(\text{C}-\text{O})$ vibration of the alkoxide groups. The ^1H NMR spectra in benzene- d_6 are compatible with the square-planar structures shown in Scheme 1. The characteristic resonances of the tetrafluorobenzobarrelene diene are two broad signals at about 5.2 and 3.5 ppm. The first signal is attributable to the tertiary CH protons and the second signal to the olefinic protons trans to the tricyclohexylphosphine ligand. The resonances due to the olefinic protons trans to the alkoxide group are masked by the aliphatic resonances (2.00–1.10 ppm) of the tricyclohexylphosphine ligand. The $^{31}\text{P}\{^1\text{H}\}$ NMR spectra show singlets at 19.0 (2), 18.8 (3), and 19.6 (4) ppm.

The preparation of several iridium(I) alkoxide compounds of the type *trans*- $\text{Ir}(\text{OR})(\text{CO})(\text{PPh}_3)_2$ has been previously reported. They were obtained by metathesis of chlorides.¹⁰

Under carbon monoxide atmosphere, the complexes 2 and 3 evolve to the hexacarbonyl derivative 5, which was isolated as a yellow solid in 40% yield. In agreement with the IR spectra previously reported for related

(6) Usón, R.; Oro, L. A.; Carmona, D.; Esteruelas, M. A.; Foces-Foces, C.; Cano, F. H.; García-Blanco, S. *J. Organomet. Chem.* **1983**, *254*, 249.

(7) (a) Usón, R.; Oro, L. A.; Carmona, D.; Esteruelas, M. A. *J. Organomet. Chem.* **1984**, *263*, 109. (b) Usón, R.; Oro, L. A.; Carmona, D.; Esteruelas, M. A.; Foces-Foces, C.; Cano, F. H.; García-Blanco, S.; Vázquez de Miguel, A. *J. Organomet. Chem.* **1984**, *273*, 111. (c) Oro, L. A.; Carmona, D.; Esteruelas, M. A.; Foces-Foces, C.; Cano, F. H. *J. Organomet. Chem.* **1986**, *307*, 83. (d) Fernández, M. J.; Esteruelas, M. A.; Covarrubias, M.; Oro, L. A. *J. Organomet. Chem.* **1986**, *316*, 343. (e) Esteruelas, M. A.; Oro, L. A.; Apreada, M. C.; Foces-Foces, C.; Cano, F. H.; Claramunt, R. M.; López, C.; Elguero, J.; Begtrup, M. *J. Organomet. Chem.* **1988**, *344*, 93. (f) García, M. P.; López, A. M.; Esteruelas, M. A.; Lahoz, F. J.; Oro, L. A. *J. Chem. Soc., Dalton Trans.* **1990**, 3465. (g) García, M. P.; López, A. M.; Esteruelas, M. A.; Lahoz, F. J.; Oro, L. A. *J. Organomet. Chem.* **1990**, *388*, 365. (h) Esteruelas, M. A.; García, M. P.; López, A. M.; Oro, L. A. *Organometallics* **1991**, *10*, 127.

(8) Esteruelas, M. A.; Nürnberg, O.; Oliván, M.; Oro, L. A.; Werner, H. *Organometallics* **1993**, *12*, 3264.

(9) Esteruelas, M. A.; Lahoz, F. J.; Oliván, M.; Oñate, E.; Oro, L. A. *Organometallics* **1994**, *13*, 4246.

(10) (a) Rees, W. M.; Churchill, M. R.; Fettinger, J. C.; Atwood, J. S. *Organometallics* **1985**, *4*, 2179. (b) Rees, W. M.; Atwood, J. D. *Organometallics* **1985**, *4*, 402. (c) Churchill, M. R.; Fettinger, J. C.; Rees, W. M.; Atwood, J. D. *J. Organomet. Chem.* **1986**, *308*, 361. (d) Bryndza, H. E.; Tam, W. *Chem. Rev.* **1988**, *88*, 1163.

$M_2(CO)_6(PR_3)_2$ ($M = Co, Rh, Ir$) complexes,¹¹ the IR spectrum of **5** in dichloromethane shows a very strong $\nu(CO)$ absorption at 1945 cm^{-1} . The $^{31}P\{^1H\}$ NMR spectrum in benzene- d_6 contains a singlet at 21.1 ppm. While this work was in progress, Atwood *et al.* reported that the carbonylation of *trans*- $Ir(CO)(OR)\{P(p\text{-tolyl})_3\}_2$ ($R = H, Me, C_6H_4Me$) yields $Ir_2(CO)_6\{P(p\text{-tolyl})_3\}_2$.¹²

The reaction of **1** with propanethiol in acetone affords the thiopropoxide compound **6** as an orange solid. The presence of the thiolato ligand in this complex is supported by the 1H NMR spectrum, which shows a triplet at 2.59 ppm ($J_{H-H} = 7.1\text{ Hz}$), assigned to the protons of the $-CH_2S$ group. The $^{31}P\{^1H\}$ NMR spectrum shows a singlet at 16.7 ppm.

When a slow stream of carbon monoxide is passed through a dichloromethane solution of **6**, the dicarbonyl compound **7** is formed. Complex **7** was isolated as an orange solid in 78% yield. According to the 1H and $^{31}P\{^1H\}$ NMR spectra, it is a mixture of the isomers **7a** and **7b** in a 7:3 molar ratio. In the 1H NMR spectrum the isomer **7a**, with inequivalent thiolato groups, gives rise to two $-CH_2S$ signals at 3.80 and 2.99 ppm. The first signal, assigned to the thiolato group *trans* to the phosphine ligands, appears as a multiplet due to coupling with the phosphine ligands and the protons of the $-CH_2-CH_2S$ group. The second signal, assigned to the thiolato group *trans* to the carbonyl ligands, appears as a triplet with a H-H coupling constant of 7.5 Hz. The $-CH_2S$ protons of the isomer **7b**, with magnetically inequivalent thiolato groups, appear at 3.25 ppm as the $A_2A'_2$ part of a second order $A_2A'_2B_2B'_2-XX'$ splitting pattern. The $^{31}P\{^1H\}$ NMR spectrum of **7** contains two singlets at 29.1 (**7a**) and 30.9 (**7b**) ppm.

The bent configurations shown in Scheme 1 are proposed on the basis of the above mentioned spectroscopic data and are in agreement with X-ray diffraction studies previously carried out on related compounds.¹³

The reaction of formation of **7**, which can be easily monitored by IR spectroscopy in dichloromethane solutions, proceeds via the *cis*-dicarbonyl intermediate $Ir(S^iPr)(CO)_2(PCy_3)$ (**8**), which by loss of a carbon monoxide molecule affords **7**. In the IR spectrum, the intermediate **8** gives rise to two $\nu(CO)$ absorptions at 2035 and 1960 cm^{-1} .

Treatment of **1** with the stoichiometric amount of phenylacetylene, cyclohexylacetylene, methylpropiolate, and trimethylsilylacetylene, in acetone, yields the alkynyl compounds **9–12**, which were isolated as red or brown-red solids in 40%–70% yield. The presence of an alkynyl ligand in these compounds is mainly supported by the IR and $^{13}C\{^1H\}$ NMR spectra. The IR spectra in Nujol contain a $\nu(C\equiv C)$ absorption between 2020 and 2080 cm^{-1} . While the $^{13}C\{^1H\}$ NMR spectra show doublets between 110 and 144 ppm with P-C

coupling constants of about 12 Hz, which were assigned to the α -carbon atom of the alkynyl groups. The β -carbon atoms appear as singlets between 118 and 134 ppm. In agreement with the structure shown in Scheme 1, the $^{13}C\{^1H\}$ NMR spectra also contain two resonances due to the olefinic carbon atoms of the tetrafluorobenzobarrelene ligand at about 62 and 45 ppm. The resonances at lower field were assigned to the carbon atoms disposed *trans* to the phosphine ligand, and appear as doublets with P-C coupling constants of about 12 Hz. While the resonances at higher field were assigned to the carbon atoms disposed *trans* to the alkynyl ligands, and appear as singlets. In the 1H NMR spectra, the diolefin ligand gives rise to three broad resonances at about 5.25 (CH), 4.00 (CH= *trans* to PCy_3), and 2.50 (CH= *trans* to $C\equiv CR$) ppm. The $^{31}P\{^1H\}$ NMR spectra show singlets between 22 and 24 ppm.

The tetrafluorobenzobarrelene diolefin of **9** can be displaced by carbon monoxide. Thus, the passage of a slow stream of this gas through a dichloromethane solution of **9**, affords the *cis*-dicarbonyl complex **13**. This compound was isolated as a yellow solid in 66% yield. In accordance with the mutually *cis* disposition of both carbonyl ligands, the IR spectrum in Nujol shows two $\nu(CO)$ bands at 2045 and 1970 cm^{-1} . In addition, it should also be mentioned the absorption at 2100 cm^{-1} , assigned to the $\nu(C\equiv C)$ vibration of the terminal alkynyl ligand. The $^{31}P\{^1H\}$ NMR spectrum in benzene- d_6 contains a singlet at 27.6 ppm.

Reactions of $Ir(OR)(TFB)(PCy_3)$ ($R = Me, Et, ^iPr, Ph$) and $Ir(S^iPr)(TFB)(PCy_3)$ with $HSnPh_3$ and HSn^iBu_3 . The complexes **1–4** react with $HSnPh_3$ and HSn^iBu_3 in a 1:2 molar ratio in toluene to give the dihydrido(stannyl)iridium(III) derivatives **14** and **15** (Scheme 2), which were isolated as white air-stable powders in high yields (60%–90%). These reactions also lead to the formation of the corresponding $ROSnR'_3$, characterized for $R = Me, ^iPr, Ph$ and for $R' = Ph$ by mass spectroscopy. Similarly, the treatment of **6** with $HSnPh_3$ in a 1:2 molar ratio in toluene yields **14** and iPrSSnPh_3 .

The formation of **14** and **15** from the reactions of **1–4** or **6** with $HSnPh_3$ and HSn^iBu_3 , respectively, most probably involves the oxidative addition of the stannane to the starting material to give $Ir(XR)H(SnR'_3)(TFB)(PCy_3)$ (**16**). Thus, the subsequent elimination of $RXSnR'_3$ followed by the oxidative addition of a second stannane molecule to the intermediate $IrH(TFB)(PCy_3)$ (**17**) should afford **14** and **15** (Scheme 2). We have tried to detect the intermediates **16** and **17** by addition of 1 equiv of $HSnPh_3$ to an NMR tube containing a solution of **1** in benzene- d_6 . However, under these conditions, only a mixture of the starting material, **14**, and $MeOSnPh_3$ was observed.

Compounds **14** and **15** were identified by elemental analysis and IR and 1H and $^{31}P\{^1H\}$ NMR spectroscopies. Complex **14** was, furthermore, characterized by an X-ray crystallographic study. An ORTEP drawing of the molecular structure of **14** is presented in Figure 1. Selected bond distances and angles are listed in Table 1.

The coordination geometry around the iridium atom could be rationalized as derived from a highly distorted octahedron with the triphenylstannyl and the tricyclo-

(11) (a) Ibers, J. A. *J. Organomet. Chem.* **1968**, *14*, 423. (b) Whyman, R. *J. Chem. Soc., Dalton Trans.* **1972**, 1375. (c) Malatesta, L.; Angoletta, M.; Caglio, G. *J. Organomet. Chem.* **1974**, *73*, 265.

(12) Randall, S. L.; Miller, C. A.; See, R. F.; Churchill, M. R.; Janik, T. S.; Lake, C. H.; Atwood, J. D. *Organometallics* **1994**, *13*, 5088.

(13) (a) Bonnet, J. J.; Kalck, P.; Poilblanc, R. *Inorg. Chem.* **1977**, *16*, 1514. (b) Cruz-Garriz, D.; Rodríguez, B.; Torrens, H.; Leal, J. *Transition Met. Chem.* **1984**, *9*, 284. (c) Claver, C.; Masdeu, A. M.; Ruiz, N.; Foces-Foces, C.; Cano, F. H.; Apreada, M. C.; Oro, L. A.; García-Alejandre, J.; Torrens, H. *J. Organomet. Chem.* **1990**, *398*, 177. (d) Polo, A.; Claver, C.; Castillón, S.; Ruiz, A.; Bayón, J. C.; Real, J.; Mealli, C.; Masi, D. *Organometallics* **1992**, *11*, 3525. (e) Masdeu, A. M.; Ruiz, A.; Castillón, S.; Claver, C.; Hitchcock, P. B.; Chaloner, P. A.; Bó, C.; Poblet, J. M.; Sarasa, P. *J. Chem. Soc., Dalton Trans.* **1993**, 2689.

Scheme 2

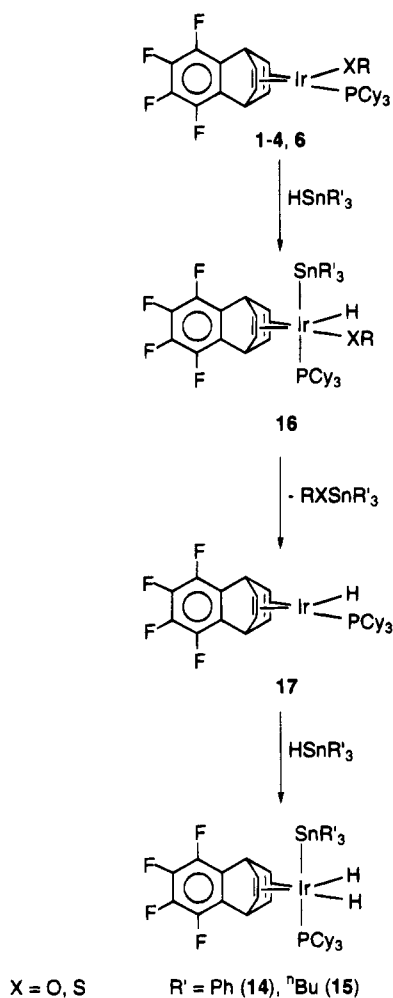


Table 1. Selected Bond Lengths (Å) and Angles (deg) for the Complex IrH₂(SnPh₃)(TFB)(PCy₃) (14)^a

Ir-Sn	2.6122(5)	Ir-C(12)	2.231(4)
Ir-P	2.363(1)	Ir-H(1)	1.48(5)
Ir-C(8)	2.235(6)	Ir-H(2)	1.55(5)
Ir-C(9)	2.241(6)	C(8)-C(9)	1.397(6)
Ir-C(11)	2.210(4)	C(11)-C(12)	1.409(6)
Sn-Ir-P	129.46(3)	M(1)-Ir-H(2)	99(2)
Sn-Ir-M(1)	107.5(1)	M(2)-Ir-H(1)	95(2)
Sn-Ir-M(2)	105.9(1)	M(2)-Ir-H(2)	161(2)
Sn-Ir-H(1)	68(2)	H(1)-Ir-H(2)	96(3)
Sn-Ir-H(2)	64(2)	C(8)-C(7)-C(12)	99.5(4)
P-Ir-M(1)	110.1(1)	C(7)-C(8)-C(9)	112.4(4)
P-Ir-M(2)	119.3(1)	C(8)-C(9)-C(10)	113.3(4)
P-Ir-H(1)	86(2)	C(9)-C(10)-C(11)	98.3(4)
P-Ir-H(2)	77(2)	C(10)-C(11)-C(12)	113.3(4)
M(1)-Ir-M(2)	66.9(2)	C(11)-C(12)-C(7)	112.0(4)
M(1)-Ir-H(1)	160(2)		

^a M(1) and M(2) represent the midpoints of the C(8)-C(9) and C(11)-C(12) olefinic double bonds, respectively.

hexylphosphine ligands occupying pseudo-trans positions (Sn-Ir-P = 129.46(3)°), at opposite sides of an ideal coordination plane defined by the two *cis*-hydrido ligands (H(1)-Ir-H(2) = 96(3)°) and the chelate di-olefinic molecule.

The small Sn-Ir-P angle is notable, and may be due to the different steric requirements, relatively small for the hydridos and comparatively large for the diene molecule and PCy₃ and SnPh₃ ligands. Angular distortions in hydrido complexes are not unusual. We note

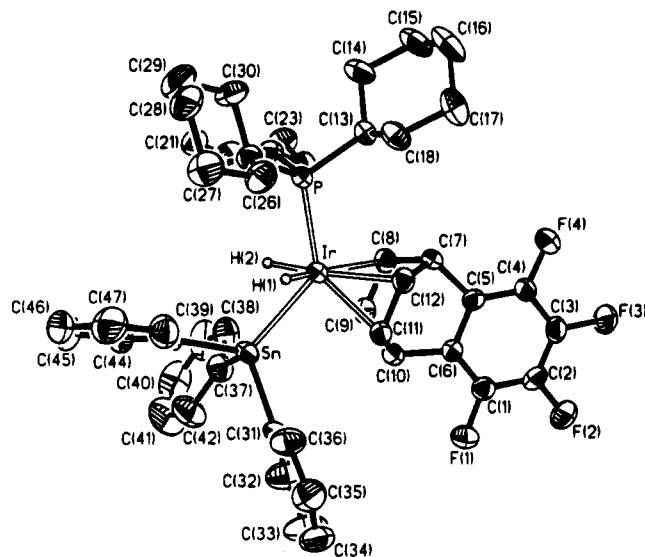


Figure 1. Molecular diagram of complex 14. Thermal ellipsoids are shown at the 50% level.

that in the complex IrH₂(SiEt₃)(COD)(AsPh₃) (COD = 1,5-cyclooctadiene) the angle between the triethylsilyl and the triphenylarsine ligands is 133.40(4)°.¹⁴ A similar observation has been reported for the complex IrH₂(SnCl₃)(PPh₃)₃, in which the major deviation from the ideal octahedral geometry arises from the P-Ir-P angle (145.95(9)°) involving two chemically equivalent phosphine groups, which are pseudo-trans to one other.¹⁵ Values about 150° have been also reported for the related angle in the complexes *mer*-IrH₃(PPh₃)₃,¹⁶ [(PPh₃)₃-Au(μ -H)IrH₂(PPh₃)₃]⁺,¹⁷ *mer*-[IrH₂(CO)(PPh₃)₃]⁺,¹⁸ and [IrH₂(PPh₃)₂(C₄H₈S)₂]⁺.¹⁹

The Ir-Sn distance (2.6122(5) Å) is significantly shorter than the value of 2.75 Å suggested for an iridium-tin single bond and, thus, indicates the presence of some partial multiple bond character.²⁰

The Ir-P, Ir-C, and Ir-H distances are clearly in the expected range and deserve no further comment.

In agreement with the structure shown in Figure 1, the IR spectra of 14 and 15 in Nujol contain one (15) or two (14) absorptions at about 2100 cm⁻¹, attributable to ν (Ir-H). In the ¹H NMR spectra in toluene-*d*₈ the hydrido resonances appear as a doublet at -15.37 (14) and -15.98 (15) with P-H coupling constants of 20.1 and 21.3 Hz, respectively. The ³¹P{¹H} NMR spectra show singlets at 14.8 (14) and 13.1 (15), along with the satellites due to ¹¹⁷Sn and ¹¹⁹Sn isotopes. In accordance with the pseudo-trans positions of the stannyl and phosphine ligands, the values of the P-¹¹⁹Sn coupling constants are 737.0 (14) and 528.4 (15) Hz, while the values of P-¹¹⁷Sn coupling constants are 641.8 (14) and 504.1 (15) Hz. Under off-resonance conditions, both singlets are split into triplets due to the P-H coupling.

(14) Fernández, M. J.; Esteruelas, M. A.; Oro, L. A.; Apreda, M. C.; Foces-Foces, C.; Cano, F. H. *Organometallics* **1987**, *6*, 1751.

(15) Kretschmer, M.; Pregosin, P. S.; Albinati, A.; Togni, A. *J. Organomet. Chem.* **1985**, *281*, 365.

(16) Clark, G. R.; Skelton, B. W.; Waters, T. N. *Inorg. Chim. Acta* **1975**, *12*, 235.

(17) Lehner, H.; Matt, D.; Pregosin, P. S.; Venanzi, L. M.; Albinati, A. *J. Am. Chem. Soc.* **1982**, *104*, 6825.

(18) Bird, P.; Harrod, J. F.; Than, K. A. *J. Am. Chem. Soc.* **1974**, *96*, 1222.

(19) Sánchez-Delgado, R. A.; Herrera, V.; Bianchini, C.; Masi, D.; Mealli, C. *Inorg. Chem.* **1993**, *32*, 3766.

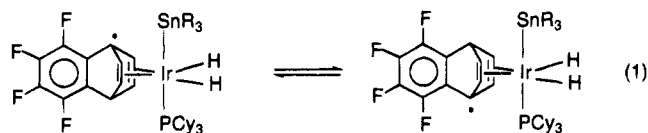
(20) Churchill, M. R.; Lin, K.-K. *J. Am. Chem. Soc.* **1974**, *96*, 76.

Table 2. Activation Parameters for Complexes 14, 15, and 18

complex	T_c , K	ΔG_c^\ddagger , kcal/mol ^a	ΔH^\ddagger , kcal/mol ^b	ΔS^\ddagger , eu ^b
14	273 ± 1	12.8 ± 0.1	13.4 ± 0.9	3.0 ± 3.0
15	293 ± 1	13.6 ± 0.1	12.7 ± 0.7	-1.6 ± 2.0
18	263 ± 1	13.0 ± 0.1	16.5 ± 0.7	13.6 ± 2.6

^a Calculated from T_c and $\Delta\nu_0$ with the equations $k_c = (\pi/\sqrt{2})\Delta\nu_0$ and $\Delta G_c^\ddagger/RT_c = \ln(\sqrt{2R/\pi N h}) + \ln(T_c/\Delta\nu_0)$. Errors shown are propagated from the estimated errors in T_c . ^b Calculated from the slopes and intercepts of the Eyring plots. Error ranges listed correspond to one standard deviation.

The disposition of ligands as shown in Figure 1 leads to a situation in which the aliphatic CH protons of the tetrafluorobenzobarrelene diolefin are chemically inequivalent; furthermore, the protons of each carbon-carbon double bond are also mutually inequivalent, although both olefin bonds are chemically equivalent. As would be expected for this arrangement, the ¹H NMR spectra of 14 and 15 display two aliphatic and two olefinic signals at -60 °C. However, at room temperature, the spectra only contain an aliphatic and an olefinic resonance. This behavior suggests that the complexes 14 and 15 have a rigid structure only at low temperature. At room temperature an intramolecular exchange process takes place which involves the relative positions of the diolefin atoms (eq 1).²¹



A similar fluxional process has been previously observed for the dihydrosilyl complex $\text{IrH}_2(\text{SiPh}_3)(\text{TfB})(\text{PCy}_3)$ (18).⁸ We suggest that the intramolecular exchange process involving the relative positions of diene atoms could proceed *via* the five-coordinate intermediate $\text{IrH}_2(\text{SiPh}_3)(\text{TfB})$, which should be formed by dissociation of the phosphine ligand. In accordance with this, we observed that the addition of P^iPr_3 to a benzene-*d*₆ solution of 18 in a 1:1 molar ratio leads to a mixture of the starting material, $\text{IrH}_2(\text{SiPh}_3)(\text{TfB})(\text{P}^i\text{Pr}_3)$, PCy_3 , and P^iPr_3 in a 1:1:1:1 molar ratio after 22 h. Under the same conditions, the addition of P^iPr_3 to benzene-*d*₆ solutions of 14 and 15 does not affect the spectra of these compounds. This indicates that, during the fluxional process of 14 and 15, the dissociation of the phosphine does not take place.

The free energies of activation for the intramolecular exchange of the diolefin at coalescence (ΔG_c^\ddagger) for 14, 15, and 18 were calculated using the temperature of coalescence (T_c) of the olefinic resonances and the chemical shift difference of these resonances projected from the slow-exchange limit ($\Delta\nu_0$). The resulting values, listed in Table 2, show that the free energy barriers for the three compounds are similar. In order to obtain additional information, we have utilized line-shape analysis as an alternative procedure. As an example, the observed resonances for 15 as a function of the temperature are shown in Figure 2. Linear least-squares analysis of the Eyring plots for the kinetic data provides values of ΔH^\ddagger and ΔS^\ddagger (Table 2) for the three compounds.

(21) The ³¹P{¹H} NMR spectra and the signal of the hydrido ligands are temperature invariant.

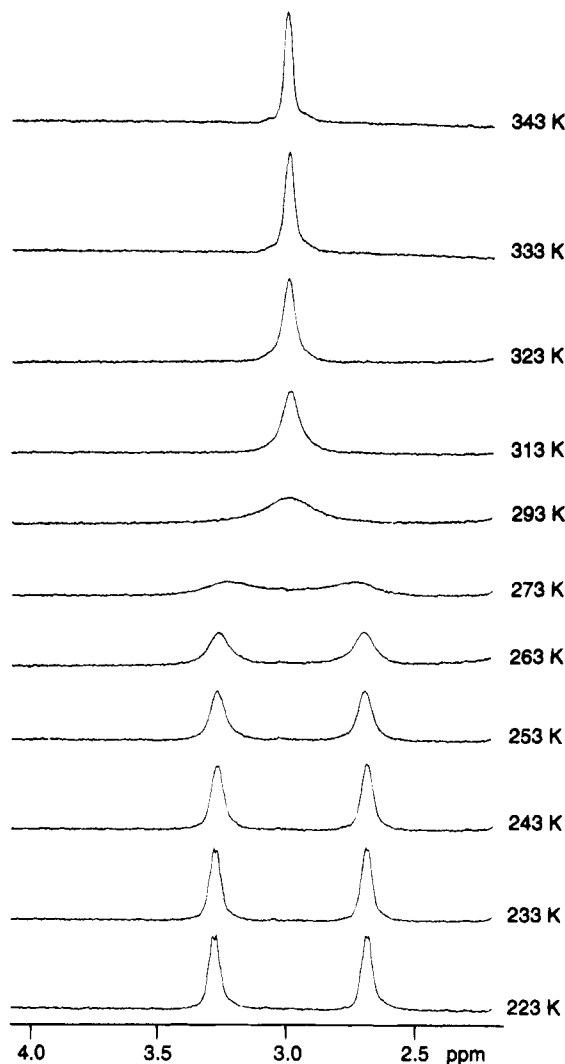


Figure 2. Variable-temperature ¹H NMR study (in toluene-*d*₈) at 299.949 MHz of the olefinic protons of the tetrafluorobenzobarrelene ligand of 15.

For the silyl complex 18 the significant positive value for the entropy of activation (13.6 ± 2.6 eu) is in agreement with the dissociation of the phosphine ligand during the fluxional process while, for 14 and 15, the values for the entropy of activation, close to zero, are in agreement with the fact that the dissociation of phosphine does not take place.

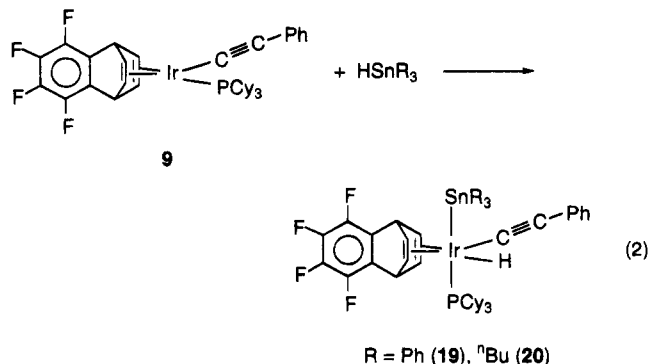
If the dissociation of phosphine from 14 and 15 does not occur during the intramolecular exchange of the diolefin atoms, it could be proposed that for the stannyl compounds the fluxional process involves the dissociation of one arm of the chelating tetrafluorobenzobarrelene diolefin, followed by rotation of the diene around the other iridium-olefin bond. This implies that the iridium-tetrafluorobenzobarrelene bond is more labile for 14 and 15 than for 18. In favor of this, we have found that the reaction of 14 with carbon monoxide produces the displacement of the diene and the formation of $\text{Ir}(\text{SnPh}_3)(\text{CO})_3(\text{PCy}_3)$, while under the same conditions 18 affords $\text{Ir}(\eta^1:\eta^2\text{-C}_{12}\text{F}_4\text{H}_7)(\text{CO})_2(\text{PCy}_3)$ and HSiPh_3 .⁸ The complex $\text{Ir}(\text{SiPh}_3)(\text{CO})_3(\text{PCy}_3)$ is also known and can be easily prepared by reaction of $\text{Ir}(\eta^1\text{-OC(O)CH}_3)(\text{CO})_2(\text{PCy}_3)$ with HSiPh_3 .⁹

For late transition metal-silicon and metal-tin bonds, some multiple bond character has been

suggested.^{3a,20,22} This multiple-bond character has been generally attributed to $d_{\pi}-d_{\pi}$ bonding involving donation of d-electron density from the transition metal to empty silicon or tin orbitals of appropriate symmetry. Because the energy difference between the iridium and tin d-orbitals (5d–5d) is smaller than that between the iridium and silicon d-orbitals (5d–3d), one should expect a better iridium–tin overlap and, therefore, a stronger iridium–tin bond. The behavior of **14** and **18** toward carbon monoxide is in agreement with this.

The higher contribution of the $d_{\pi}-d_{\pi}$ interaction to the iridium–tin bond compared to the iridium–silicon bond could also explain the different behavior of these compounds in solution. Thus, the transfer of electron density from the iridium to the stannyl groups should increase the electron-donor capacity of the phosphine hindering its dissociation, while the capacity of the iridium to back bond to the diolefin should decrease, favoring the dissociation of one arm of the tetrafluorobenzobarrelene ligand. The lability of one arm of the diene in **14** and **15** may also be a result of the steric demands of the tin atom compared to the silicon one.

Reactions of Ir(C₂Ph)(TFB)(PCy₃) and Ir(C₂Ph)(CO)₂(PCy₃) with HSnPh₃ and HSnⁿBu₃. The alkynyl–diolefin complex **9** also reacts with HSnPh₃ and HSnⁿBu₃. Thus, the treatment of a toluene solution of this complex with HSnPh₃ or HSnⁿBu₃ leads immediately to the formation of a light yellow solution from which the complexes **19** or **20** can be isolated as white solids (eq 2).

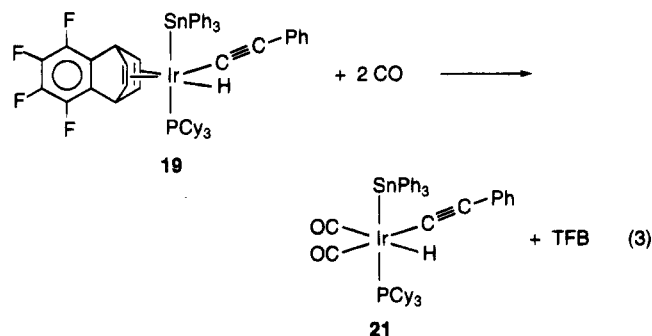


Complex **19** was isolated in 83% yield, and characterized by elemental analysis, IR, and ¹H, ³¹P{¹H}, and ¹³C{¹H} NMR spectroscopy. The most noticeable absorptions in the IR spectrum in Nujol are two bands at 2113 and 2058 cm⁻¹, which were assigned to the vibrations $\nu(\text{Ir}-\text{H})$ and $\nu(\text{C}\equiv\text{C})$, respectively. In the ¹H NMR spectrum, in benzene-*d*₆ at room temperature, the hydrido ligand gives rise to a broad resonance at -13.32 ppm. In toluene-*d*₈ at -60 °C, this signal is a broad doublet with a P–H coupling constant of 21.6 Hz. In agreement with the structure proposed for **19** in eq 2, ¹H NMR spectra at room temperature and at -60 °C show six resonances for the protons of the diene at 5.21 and 4.98 (CH) and at 3.72, 3.47, 3.42, and 2.07 (CH=) ppm. In the ¹³C{¹H} NMR spectrum, the olefinic carbon atoms of the tetrafluorobenzobarrelene ligand display four signals at 43.90, 39.80, 36.25, and 36.10 ppm, while the C_β and C_α carbon atoms of the alkynyl group appear at 109.01 and 72.30 ppm, respectively. The second signal as a doublet with a P–C coupling constant of 17.5

Hz. The ³¹P{¹H} NMR spectrum contains a singlet at -1.9 ppm, together with the satellites due to the ¹¹⁷Sn and ¹¹⁹Sn isotopes. In accordance with the trans position of the stannyl and phosphine ligands, the values of P–¹¹⁷Sn and P–¹¹⁹Sn coupling constants are 715.9 and 735.6 Hz, respectively. Under off-resonance conditions the singlet is split into a doublet due to P–H coupling.

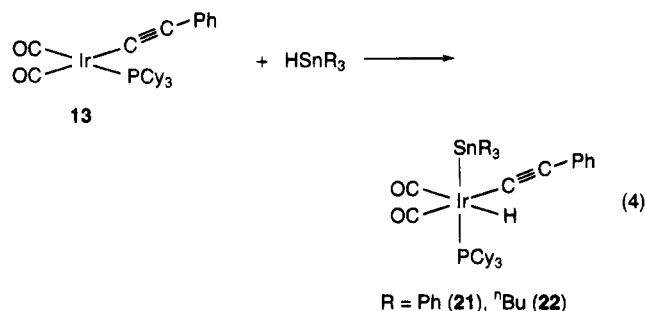
Complex **20** was isolated in 74% yield. In the IR spectrum in Nujol, the $\nu(\text{Ir}-\text{H})$ and $\nu(\text{C}\equiv\text{C})$ absorptions appear at 2085 and 2020 cm⁻¹. The ¹H NMR spectrum shows the expected resonances of the phosphine and stannyl ligands along with six resonances due to the diene at 5.31 and 5.08 (CH) and at 3.54, 3.31, 3.21, and 2.30 (CH=) ppm, and a doublet at -13.68 ppm with a P–H coupling constant of 26.1, which was assigned to the hydrido ligand. In the ¹³C{¹H} NMR spectrum, the diolefinic carbon atoms of the diene give rise to four signals at 37.80, 37.40, 36.57, and 35.85 ppm, while the C_β and C_α carbon atoms of the alkynyl group appear at 107.29 and 76.95 ppm as doublets with P–C coupling constants of 3.7 and 18.4 Hz, respectively. The ³¹P{¹H} NMR spectrum contains a singlet at -2.0 ppm along with the corresponding tin satellites ($J_{\text{P}-^{119}\text{Sn}} = 550.5$ Hz, $J_{\text{P}-^{117}\text{Sn}} = 525.9$ Hz). Under off-resonance conditions, this singlet is split into a doublet due to the P–H coupling.

The tetrafluorobenzobarrelene diolefin of **19** is also labile. Thus, under carbon monoxide atmosphere, this compound yields the dicarbonyl derivative **21** and tetrafluorobenzobarrelene (eq 3), according with the above mentioned dissociation of one arm of the chelating diolefin.



Complex **21** was isolated as a white solid in 75% yield. In agreement with the mutually cis disposition of the two carbonyl ligands, the IR spectrum of **21** in Nujol has two $\nu(\text{CO})$ absorptions at 2040 and 2000 cm⁻¹. The ¹H NMR spectrum in benzene-*d*₆ shows at -9.42 ppm a doublet with a P–H coupling constant of 14.8 Hz. The satellites due to the tin isotopes are also observed near of this resonance. The value of the Sn–H coupling constant, 30 Hz, strongly supports the cis disposition of the triphenylstannyl group and the hydrido ligand. In the ¹³C{¹H} NMR spectrum the C_β and C_α carbon atoms of the alkynyl group display doublets at 110.62 and 66.60 ppm with P–C coupling constants of 4.1 and 14.7 Hz, respectively. The ³¹P{¹H} NMR spectrum contains a singlet at 13.9 ppm along with the corresponding tin satellites. In agreement with the trans disposition of the tricyclohexylphosphine and stannyl ligands the values of the P–¹¹⁷Sn and P–¹¹⁹Sn coupling constants are 908.8 and 968.6 Hz, respectively.

Complex **21** can be also prepared in quantitative yield by addition of 1 equiv of HSnPh_3 to a NMR tube containing a benzene- d_6 solution of **13**. Similarly, the addition of 1 equiv of HSn^nBu_3 to an NMR tube containing **13** quantitatively yields **22** (eq 4).



Complex **22** was characterized by ^1H , $^{31}\text{P}\{^1\text{H}\}$, and $^{13}\text{C}\{^1\text{H}\}$ NMR spectroscopy. The ^1H NMR spectrum of the solution formed by addition of one equiv of HSn^nBu_3 to a benzene- d_6 solution of **13** shows in the higher field region, at -9.80 ppm, a doublet with a P-H coupling constant of 15.7 Hz, along with the satellites due to the tin isotopes. The value of the Sn-H coupling constant, 32.7 Hz, is in agreement with the structure shown in eq 4. The most noticeable signals in the $^{13}\text{C}\{^1\text{H}\}$ NMR of this solution are those corresponding to the C_α and C_β carbon atoms of the alkynyl ligand, which appear at 108.89 and 69.65 ppm. The first signal as a singlet and the second one as a doublet with a P-C coupling constant of 15.7 Hz. The $^{31}\text{P}\{^1\text{H}\}$ NMR spectrum contains a singlet at 11.1 ppm along with the satellites due to the ^{117}Sn and ^{119}Sn isotopes. In accordance with a mutually trans disposition for the phosphine and stannyl ligands, the values of the P- ^{117}Sn and P- ^{119}Sn coupling constants are 641.9 and 671.7 Hz, respectively. Under off-resonance conditions, the singlet is split into a doublet as a result of the P-H coupling. The IR spectrum of the solution formed by addition of 1 equiv of HSn^nBu_3 to a dichloromethane solution of **13** shows between 2200 and 1900 cm^{-1} four bands. Two strong absorptions at 2035 and 1995 cm^{-1} , assigned to the vibration $\nu(\text{CO})$ of two carbonyls ligands mutually cis disposed and two weak absorptions at 2135 and 2110 cm^{-1} , assigned to the vibrations $\nu(\text{Ir}-\text{H})$ and $\nu(\text{C}=\text{C})$, respectively.

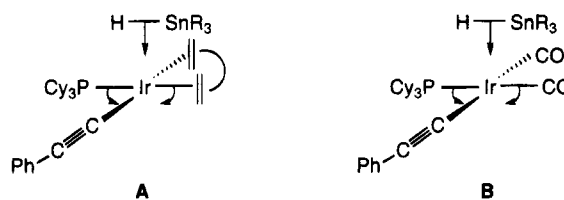
The oxidative addition of silanes to iridium(I) complexes is generally viewed as a concerted cis addition.²³ Furthermore, Johnson and Eisenberg have proved that the addition of HSiR_3 to the iridium(I) *cis*-phosphine complexes $\text{IrX}(\text{CO})(\text{dppe})$ ($\text{X} = \text{Br}, \text{CN}$; $\text{dppe} = 1,2$ -bis(diphenylphosphino)ethane) is a diastereoselective process with specific substrate orientation.²⁴ The exclusive and quantitative formation of **19**–**22**, with the hydrido and stannyl ligands mutually *cis* disposed, is also in agreement with a concerted *cis* addition of HSnPh_3 and HSn^nBu_3 to **9** and **13**, with specific substrate orientation. The addition of HSnPh_3 and HSn^nBu_3 to **9** seems to take place along the olefin-Ir-P axis with the tin

Table 3. Hydrostannylation of Phenylacetylene^a

catalyst	[prod], M	yield, % ^b	
		<i>cis</i> - PhCH=CH(SnPh ₃)	<i>trans</i> - PhCH=CH(SnPh ₃)
15	0.084	15	85
19	0.052	60	40
21	0.054	60	40

^a [Catalyst] = 1×10^{-3} M; [hydroquinone] = 4×10^{-3} M; [$\text{PhC}\equiv\text{CH}$] = [HSnPh_3] = 0.1 M; *n*-octane (0.125 M) is used as internal standard. Solvent: 1,2-dichloroethane. Argon atmosphere, temperature 60 °C. Time of reaction 20 min. In presence of hydroquinone (4×10^{-3} M) and in absence of catalyst no reaction occurs. In absence of catalyst and hydroquinone the reaction gives the *trans* product. ^b The relative amount of each product was measured in the ^{119}Sn spectra.

atom on the olefinic bond (A), and the oxidative addition to **13** seems to occur along the OC-Ir-P axis with the tin atom on the carbonyl group (B). The basis of this preference is probably steric and involves minimizing nonbonded interactions between the stannyl ligand and the cyclohexyl groups of the phosphine.



Addition of HSnPh_3 to Phenylacetylene Catalyzed by $\text{IrH}_2(\text{SnPh}_3)(\text{TfB})(\text{PCy}_3)$, $\text{IrH}(\text{C}_2\text{Ph})(\text{SnPh}_3)(\text{TfB})(\text{PCy}_3)$, and $\text{IrH}(\text{C}_2\text{Ph})(\text{SnPh}_3)(\text{CO})_2(\text{PCy}_3)$. The complexes $\text{IrH}_2(\text{SiEt}_3)(\text{TfB})(\text{PR}_3)$ ($\text{PR}_3 = \text{PCy}_3, \text{P}^i\text{Pr}_3, \text{PPh}_3$) catalyze the addition of HSiEt_3 to phenylacetylene in 1,2-dichloroethane at 60 °C, to give $\text{PhCH}=\text{CH}_2$, *cis*- $\text{PhCH}=\text{CH}(\text{SiEt}_3)$, *trans*- $\text{PhCH}=\text{CH}(\text{SiEt}_3)$, $\text{Ph}(\text{SiEt}_3)\text{C}=\text{CH}_2$, and $\text{PhC}\equiv\text{C}(\text{SiEt}_3)$. The major product, about 65%, in almost all cases is *cis*- $\text{PhCH}=\text{CH}(\text{SiEt}_3)$, resulting from *anti* addition of the silane to the alkyne. Under the same experimental conditions the related dihydrido-stannyl compound **14** catalyzes the addition of HSnPh_3 to phenylacetylene. In this case, the major product is *trans*- $\text{PhCH}=\text{CH}(\text{SnPh}_3)$ (Table 3), resulting from *syn* addition of the stannane to the alkyne. The formation of the dehydrogenative stannylation product, $\text{PhC}\equiv\text{CSnPh}_3$, is not observed.

We note from our previous reports that the formation of the dehydrogenative silylation product takes place when the *cis*-vinylsilane is an important product of the catalytic reaction.^{8,25–27} A recent study on the addition of HSiEt_3 to phenylacetylene catalyzed by $[\text{Ir}(\text{COD})(\eta^2\text{-}^i\text{Pr}_2\text{PCH}_2\text{CH}_2\text{OME})\text{BF}_4]$ reveals that the hydrido-alkynyl $[\text{IrH}(\text{C}_2\text{Ph})(\text{COD})(\eta^2\text{-}^i\text{Pr}_2\text{PCH}_2\text{CH}_2\text{OME})\text{BF}_4]$ is the key intermediate for the formation of $\text{PhC}\equiv\text{CSiEt}_3$ while $[\text{IrH}(\text{SiEt}_3)(\text{COD})(\eta^2\text{-}^i\text{Pr}_2\text{PCH}_2\text{CH}_2\text{OME})\text{BF}_4]$ is the key intermediate in the formation of *cis*- $\text{PhCH}=\text{CH}(\text{SiEt}_3)$.²⁶ So, one could think that, for some systems, the formation of the *anti*-addition product is favored by the presence of transition metal-alkynyl compounds.

(23) (a) Sommer, L. H.; Lyons, J. E.; Fujimoto, H. *J. Am. Chem. Soc.* **1969**, *91*, 7051. (b) Harrod, J. F.; Smith, C. A.; Than, K. A. *J. Am. Chem. Soc.* **1972**, *94*, 8321. (c) Fawcett, J. P.; Harrod, J. F. *J. Organomet. Chem.* **1976**, *113*, 245. (d) Bennet, M. A.; Charles, R.; Fraser, P. J. *Aust. J. Chem.* **1977**, *30*, 1201.

(24) Johnson, C. E.; Eisenberg, R. *J. Am. Chem. Soc.* **1985**, *107*, 6531.

(25) Esteruelas, M. A.; López, A. M.; Oro, L. A.; Tolosa, J. I. *J. Mol. Catal.*, **A. Chem.** **1995**, *96*, 21.

(26) Esteruelas, M. A.; Oliván, M.; Oro, L. A.; Tolosa, J. I. *J. Organomet. Chem.* **1995**, *487*, 143.

(27) (a) Fernández, M. J.; Oro, L. A.; Manzano, B. R. *J. Mol. Catal.* **1988**, *45*, 7. (b) Jun, C. H.; Crabtree, R. H. *J. Organomet. Chem.* **1993**, *447*, 177.

In order to find some relationship between the presence of metal-alkynyl compounds and the formation of the dehydrogenative stannation and *anti*-addition products, in the hydrostannation of terminal alkynes, we have explored the catalytic activity of the alkynyl derivatives **19** and **21** in the hydrostannation of phenylacetylene with HSnPh_3 . Although under these conditions the formation of the dehydrogenative stannation product is not observed, the results presented in Table 3 clearly show that in the presence of the alkynyl derivatives **19** and **21**, the amount of the *anti*-addition product (*cis*- $\text{PhCH}=\text{CH}(\text{SnPh}_3)$) formed is important (60%).

At this moment additional work is carried out in our laboratory, in order to determine whether the presence of a transition metal-alkynyl compound can affect the formation of the *anti*-addition product in the hydrosilylation and hydrostannation of terminal alkynes.

Concluding Remarks

This study has shown that the reaction of the compounds $\text{Ir}(\text{XR})(\text{TFB})(\text{PCy}_3)$ ($\text{XR} = \text{OMe}, \text{OEt}, \text{O}^i\text{Pr}, \text{OPh}, \text{S}^n\text{Pr}$) with HSnR'_3 leads to the dihydridostannyl derivatives $\text{IrH}_2(\text{SnR}'_3)(\text{TFB})(\text{PCy}_3)$ ($\text{R}' = \text{Ph}, ^n\text{Bu}$). In the solid state, these compounds have an octahedral structure with the stannyl group and the phosphine ligand occupying pseudo-*trans* positions (for $\text{SnR}'_3 = \text{SnPh}_3$, $\text{Sn}-\text{Ir}-\text{P} = 129.45(3)^\circ$). In solution, they have a rigid structure only at low temperature; at room temperature an intramolecular exchange process takes place which involves the relative positions of the diolefin atoms. The values for ΔH^\ddagger and ΔS^\ddagger of the fluxional processes are in agreement with a mechanism involving the dissociation of one arm of the diene, followed by rotation of the diolefin around of the other iridium-olefin bond.

The square-planar alkynyl compounds $\text{Ir}(\text{C}_2\text{Ph})\text{L}_2(\text{PCy}_3)$ also react with HSnR'_3 to afford $\text{IrH}(\text{C}_2\text{Ph})(\text{SnR}'_3)\text{L}_2(\text{PCy}_3)$ ($\text{L}_2 = \text{TFB}, 2\text{CO}$; $\text{R}' = \text{Ph}, ^n\text{Bu}$). These reactions are diastereoselective *cis* addition processes with specific substrate orientation.

The complexes $\text{IrH}_2(\text{SnPh}_3)(\text{TFB})(\text{PCy}_3)$, $\text{IrH}(\text{C}_2\text{Ph})(\text{SnPh}_3)(\text{TFB})(\text{PCy}_3)$ and $\text{IrH}(\text{C}_2\text{Ph})(\text{SnPh}_3)(\text{CO})_2(\text{PCy}_3)$ catalyze the addition of HSnPh_3 to phenylacetylene to give *cis*- and *trans*- $\text{PhCH}=\text{CH}(\text{SnPh}_3)$. Interestingly, the formation of the dehydrogenative stannation product is not observed. This is in contrast with that previously reported for related hydrosilylation reactions, in which the formation of $\text{PhC}\equiv\text{CSiEt}_3$ accompany to the formation of the *syn*- and *anti*-addition products.

Experimental Section

General Data. All reactions were carried out with the use of standard Schlenk procedures. Solvents were dried and purified by known procedures and distilled under argon prior to use. Elemental analyses were performed with a Perkin-Elmer 240 microanalyzer. ^1H , $^{13}\text{C}\{^1\text{H}\}$, $^{31}\text{P}\{^1\text{H}\}$, and ^{119}Sn NMR spectra were recorded on Varian UNITY 300 or Varian XL 200 spectrometers. Chemical shifts are expressed in parts per million upfield from SiMe_4 (^1H and $^{13}\text{C}\{^1\text{H}\}$ NMR spectra), 85% H_3PO_4 ($^{31}\text{P}\{^1\text{H}\}$ NMR spectra), or SnMe_4 (^{119}Sn NMR spectra). Infrared spectra were obtained from a Perkin-Elmer 783 spectrophotometer, as either solids (Nujol mulls on polyethylene sheets) or solutions (NaCl cell windows). The catalytic reactions were followed by measuring the phenylacetylene consumption as a function of time using *n*-octane

as the internal standard with a FFAP on Chromosorb GHP 80/100 mesh column at 170 °C. Mass spectra analyses were performed with a VG Auto Spec instrument. In FAB^+ mode (used for complexes **5** and **7**) ions were produced with the standard Cs^+ gun at *ca.* 30 kV, and 3-nitrobenzyl alcohol (NBA) was used as the matrix. Electron impact MS (operating at 70 eV) was used for MeOSnPh_3 , $^i\text{PrOSnPh}_3$, PhOSnPh_3 , and $^n\text{PrSSnPh}_3$. The starting material $\text{Ir}(\text{OMe})(\text{TFB})(\text{PCy}_3)$ (**1**) was prepared by published method.²⁸

Preparation of $\text{Ir}(\text{OEt})(\text{TFB})(\text{PCy}_3)$ (2**).** A suspension of **1** (100 mg, 0.137 mmol) in 5 mL of ethanol was stirred for 1 h at room temperature. The solution was decanted, and the orange solid was washed with ethanol and dried in vacuo; yield 67 mg (66%). Anal. Calcd for $\text{C}_{32}\text{H}_{44}\text{F}_4\text{IrOP}$: C, 51.68; H, 5.96. Found: C, 52.17; H, 6.66. IR (Nujol, cm^{-1}): $\nu(\text{C}-\text{O})$ 1055 (m). ^1H NMR (C_6D_6 , 20 °C): δ 5.31 (br, 2H, $-\text{CH}$), 4.12 (q, 2H, $J_{\text{H}-\text{H}} = 6.7$ Hz, OCH_2CH_3), 3.58 (br, 2H, $-\text{CH}$), 2.00–1.10 (m, 35 H, $-\text{CH}$, Cy), 1.40 (t, 3H, $J_{\text{H}-\text{H}} = 6.7$ Hz, OCH_2CH_3); this signal is partially masked by Cy resonances. $^{31}\text{P}\{^1\text{H}\}$ NMR (C_6D_6 , 20 °C): δ 19.0 (s).

Preparation of $\text{Ir}(\text{O}^i\text{Pr})(\text{TFB})(\text{PCy}_3)$ (3**).** A suspension of **1** (100 mg, 0.137 mmol) in a mixture of acetone/2-propanol 1:10 (11 mL) was stirred for 1 h at room temperature, and the suspension was concentrated to dryness. Acetone was added to afford an orange solid, the solution was decanted, and the solid was washed with acetone and dried in vacuo; yield 74 mg (71%). Anal. Calcd for $\text{C}_{33}\text{H}_{46}\text{F}_4\text{IrOP}$: C, 52.30; H, 6.12. Found: C, 52.53; H, 6.65. IR (Nujol, cm^{-1}): $\nu(\text{C}-\text{O})$ 1125 (m). ^1H NMR (C_6D_6 , 20 °C): δ 5.26 (br, 2H, $-\text{CH}$), 3.73 (sept, 1H, $J_{\text{H}-\text{H}} = 5.9$ Hz, $\text{OCH}(\text{CH}_3)_2$), 3.55 (br, 2H, $-\text{CH}$), 2.00–1.10 (m, 35 H, $-\text{CH}$, Cy), 1.36 (d, 6H, $J_{\text{H}-\text{H}} = 5.9$ Hz, $\text{OCH}(\text{CH}_3)_2$); this signal is partially masked by Cy resonances. $^{31}\text{P}\{^1\text{H}\}$ NMR (C_6D_6 , 20 °C): δ 18.8 (s).

Preparation of $\text{Ir}(\text{OPh})(\text{TFB})(\text{PCy}_3)$ (4**).** A suspension of **1** (100 mg, 0.137 mmol) in 10 mL of acetone was treated with an excess of PhOH (52 mg, 0.55 mmol). The resulting suspension was stirred for 2 h at room temperature. After concentrating to dryness, acetone was added to afford an orange solid. The solution was decanted, and the solid was washed with acetone and dried in vacuo; yield 63 mg (58%). Anal. Calcd for $\text{C}_{36}\text{H}_{44}\text{F}_4\text{IrOP}$: C, 54.60; H, 5.60. Found: C, 54.21; H, 5.48. IR (Nujol, cm^{-1}): $\nu(\text{C}=\text{C}, \text{Ph})$ 1590 (s), $\nu(\text{C}-\text{O})$ 1255 (s). ^1H NMR (C_6D_6 , 20 °C): δ 7.26–6.78 (m, 5H, Ph), 5.09 (br, 2H, $-\text{CH}$), 3.44 (br, 2H, $-\text{CH}$), 1.96–1.07 (m, 35H, $-\text{CH}$, Cy). $^{31}\text{P}\{^1\text{H}\}$ NMR (C_6D_6 , 20 °C): δ 19.6 (s).

Preparation of $\text{Ir}_2(\text{CO})_6(\text{PCy}_3)_2$ (5**).** A solution of **2** (200 mg, 0.27 mmol) or **3** (204 mg, 0.27 mmol) in 8 mL of CH_2Cl_2 was stirred under CO atmosphere for 30 min. The resulting pale yellow solution was concentrated to *ca.* 0.5 mL, and addition of hexane precipitated a pale yellow solid. The solution was decanted, and the solid was washed with hexane and dried in vacuo; yield 75 mg (40%). Anal. Calcd for $\text{C}_{42}\text{H}_{66}\text{Ir}_2\text{O}_6\text{P}_2$: C, 45.31; H, 5.97. Found: C, 45.68; H, 6.24. IR (Nujol, cm^{-1}): $\nu(\text{CO})$ 1940 (vs). IR (CH_2Cl_2 , cm^{-1}): $\nu(\text{CO})$ 1945 (vs). $^{31}\text{P}\{^1\text{H}\}$ NMR (C_6D_6 , 20 °C): δ 21.1 (s). MS (FAB^+): *m/e* 1056 ($\text{M}^+ - 2\text{CO}$), 557 ($\text{M}^+/2$).

Preparation of $\text{Ir}(\text{S}^n\text{Pr})(\text{TFB})(\text{PCy}_3)$ (6**).** This compound was prepared analogously as described for **4**, starting from **1** (100 mg, 0.137 mmol) with an excess of $^n\text{PrSH}$ (0.5 mL). Compound **6** was isolated as an orange microcrystalline solid; yield 93 mg (82%). The crystals contained 1 mol of acetone/mol of **6**. Anal. Calcd for $\text{C}_{36}\text{H}_{52}\text{F}_4\text{IrOPS}$: C, 51.96; H, 6.30. Found: C, 52.48; H, 7.19. ^1H NMR (C_6D_6 , 20 °C): δ 5.28 (br, 2H, $-\text{CH}$), 3.46 (br, 2H, $-\text{CH}$), 2.59 (t, 2H, $J_{\text{H}-\text{H}} = 7.1$ Hz, $\text{SCH}_2\text{CH}_2\text{CH}_3$), 2.00–1.09 (m, 40 H, $-\text{CH}$, Cy, $\text{SCH}_2\text{CH}_2\text{CH}_3$). $^{31}\text{P}\{^1\text{H}\}$ NMR (C_6D_6 , 20 °C): δ 16.7 (s).

Preparation of an Isomeric Mixture of $[\text{Ir}(\mu\text{-S}^n\text{Pr})(\text{CO})(\text{PCy}_3)]_2$ (7**).** This compound was prepared analogously as described for **5**, starting from **6** (100 mg, 0.12 mmol).

Compound **7** was isolated as an orange solid: yield 54 mg (78%). Anal. Calcd for $C_{44}H_{80}Ir_2O_2P_2S_2$: C, 45.88; H, 7.00. Found: C, 45.96; H, 7.16. IR (Nujol, cm^{-1}): $\nu(CO)$ 1955–1935 (vs). IR (CH_2Cl_2 , cm^{-1}): $\nu(CO)$ 1945 (vs), 1930 (vs). MS (FAB⁺): m/e 1151 (M^+). Data for **7a** are as follows. 1H NMR (C_6D_6 , 20 °C): δ 3.80 (m, 2H, $SCH_2CH_2CH_3$), 2.99 (t, $J_{H-H} = 7.5$ Hz, $SCH_2CH_2CH_3$), 2.40–0.86 (m, 76H, PCy_3 and $SCH_2CH_2CH_3$). $^{31}P\{^1H\}$ NMR (C_6D_6 , 20 °C): δ 29.1 (s). Data for **7b** are as follows. 1H NMR (C_6D_6 , 20 °C): δ 3.25 (m, 4H, $SCH_2CH_2CH_3$), 2.40–0.86 (m, 76H, PCy_3 and $SCH_2CH_2CH_3$). $^{31}P\{^1H\}$ NMR (C_6D_6 , 20 °C): δ 30.9 (s).

Preparation of Ir(C_2Ph)(TFB)(PCy_3) (9). $PhC\equiv CH$ (14 μL , 0.137 mmol) was added to a suspension of **1** (100 mg, 0.137 mmol) in 10 mL of acetone. The resulting red solution was stirred for 1 h at room temperature and cooled at –20 °C for 24 h. The solution was decanted, and the brown-red solid was washed with acetone and dried in vacuo; yield 72 mg (66%). Anal. Calcd for $C_{38}H_{44}F_4IrP$: C, 57.05; H, 5.54. Found: C, 56.90; H, 5.78. IR (Nujol, cm^{-1}): $\nu(C\equiv C)$ 2080 (s), $\nu(C=C, Ph)$ 1595 (s). 1H NMR (C_6D_6 , 20 °C): δ 7.63–6.94 (m, 5H, Ph), 5.32 (br, 2H, –CH), 4.12 (br, 2H, =CH), 2.52 (br, 2H, =CH), 2.15–1.09 (m, 33H, Cy). $^{13}C\{^1H\}$ NMR (C_6D_6 , 20 °C): δ 130.91 (s, Ph), 128.89 (s, C_β , C=C), 128.39 (s, Ph), 125.56 (s, Ph), 125.05 (d, $J_{P-C} = 12.9$ Hz, C_α , C=C), 62.84 (d, $J_{P-C} = 11.9$ Hz, CH=), 45.32 (s, CH=), 40.93 (s, –CH), 35.50 (d, $J_{P-C} = 26.7$ Hz, PCH, PCy_3), 30.62 (s, PCy_3), 27.99 (d, $J_{P-C} = 10.6$ Hz, PCHCH₂, PCy_3), 26.79 (s, PCy_3). $^{31}P\{^1H\}$ NMR (C_6D_6 , 20 °C): δ 23.2 (s).

Preparation of Ir(C_2Cy)(TFB)(PCy_3) (10). $CyC\equiv CH$ (18 μL , 0.137 mmol) was added to a suspension of **1** (100 mg, 0.137 mmol) in 10 mL of acetone. The resulting red solution was stirred for 4 h at room temperature and concentrated to 5 mL, yielding a brown-red solid. The solution was decanted, and the solid was washed with acetone and dried in vacuo; yield 77 mg (70%). Anal. Calcd for $C_{38}H_{50}F_4IrP$: C, 56.63; H, 6.25. Found: C, 57.05; H, 6.69. 1H NMR (C_6D_6 , 20 °C): δ 5.30 (br, 2H, –CH), 4.10 (br, 2H, =CH), 3.00 (br, 1H, C=CCH), 2.39 (br, 2H, =CH), 2.20–1.19 (m, 43H, Cy). $^{13}C\{^1H\}$ NMR (C_6D_6 , 20 °C): δ 133.50 (s, C_β , C=C), 111.10 (d, $J_{P-C} = 12.6$ Hz, C_α , C=C), 62.41 (d, $J_{P-C} = 12.4$ Hz, CH=), 42.02 (s, CH=), 40.71 (s, –CH), 35.47 (s, Cy), 35.39 (d, $J_{P-C} = 25.7$ Hz, PCH, PCy_3), 30.57 (s, PCy_3), 27.99 (d, $J_{P-C} = 10.6$ Hz, PCHCH₂, PCy_3), 26.91 (s, Cy), 26.83 (s, Cy), 26.76 (s, PCy_3), 25.55 (s, Cy). $^{31}P\{^1H\}$ NMR (C_6D_6 , 20 °C): δ 22.5 (s).

Preparation of Ir(C_2CO_2Me)(TFB)(PCy_3) (11). This compound was prepared analogously as described for **9**, starting from **1** (100 mg, 0.137 mmol) and $MeO_2CC\equiv CH$ (12 μL , 0.137 mmol). Compound **11** was isolated as a red solid: yield 44 mg (41%). Anal. Calcd for $C_{34}H_{42}F_4IrO_2P$: C, 52.23; H, 5.41. Found: C, 52.45; H, 5.69. IR (Nujol, cm^{-1}): $\nu(C\equiv C)$ 2065 (s), $\nu(C=O)$ 1680 (s). 1H NMR (C_6D_6 , 20 °C): δ 5.20 (br, 2H, –CH), 3.87 (br, 2H, =CH), 3.46 (s, 3H, $-CO_2CH_3$), 2.62 (br, 2H, =CH), 2.03–1.15 (m, 33H, Cy). $^{13}C\{^1H\}$ NMR (C_6D_6 , 20 °C): δ 154.24 (s, $-CO_2CH_3$), 129.71 (d, $J_{P-C} = 12.0$ Hz, C_α , C=C), 119.72 (s, C_β , C=C), 63.65 (d, $J_{P-C} = 11.5$ Hz, CH=), 51.04 (s, $-CO_2CH_3$), 50.13 (s, CH=), 40.97 (s, –CH), 35.48 (d, $J_{P-C} = 26.5$ Hz, PCH, PCy_3), 30.56 (s, PCy_3), 27.79 (d, $J_{P-C} = 10.7$ Hz, PCHCH₂, PCy_3), 26.69 (s, PCy_3). $^{31}P\{^1H\}$ NMR (C_6D_6 , 20 °C): δ 23.9 (s).

Preparation of Ir(C_2SiMe_3)(TFB)(PCy_3) (12). This compound was prepared analogously as described for **10**, by starting from **1** (100 mg, 0.137 mmol) and $Me_3SiC\equiv CH$ (19.4 μL , 0.137 mmol). Compound **12** was isolated as a brown-red solid; yield 50 mg (46%). Anal. Calcd for $C_{35}H_{48}F_4IrPSi$: C, 52.81; H, 6.08. Found: C, 52.47; H, 6.23. IR (Nujol, cm^{-1}): $\nu(C\equiv C)$ 2020 (s). 1H NMR (C_6D_6 , 20 °C): δ 5.25 (br, 2H, –CH), 4.02 (br, 2H, =CH), 2.54 (br, 2H, =CH), 2.10–1.19 (m, 33H, Cy), 0.38 (s, 9H, $-SiMe_3$). $^{13}C\{^1H\}$ NMR ($CDCl_3$, 20 °C): δ 143.76 (d, $J_{P-C} = 11.5$ Hz, C_α , C=C), 131.14 (s, C_β , C=C), 62.06 (d, $J_{P-C} = 12.0$ Hz, CH=), 47.69 (s, CH=), 40.70 (s, –CH), 34.86 (d, $J_{P-C} = 26.2$ Hz, PCH, PCy_3), 30.14 (s, PCy_3), 27.67 (d, J_{P-C}

= 10.6 Hz, PCHCH₂, PCy_3), 26.40 (s, PCy_3), 1.50 (s, $-SiMe_3$). $^{31}P\{^1H\}$ NMR (C_6D_6 , 20 °C): δ 22.6 (s).

Preparation of Ir(C_2Ph)(CO)₂(PCy_3) (13). A solution of **9** (100 mg, 0.125 mmol) in 8 mL of CH_2Cl_2 was stirred under CO until the color of the solution change from deep red to yellow (2 min). The solution was concentrated to ca. 0.5 mL, and addition of hexane caused the precipitation of a yellow solid. The solution was decanted, and the solid washed with hexane and dried in vacuo; yield 52 mg (66%). Anal. Calcd for $C_{28}H_{38}IrO_2P$: C, 53.40; H, 6.08. Found: C, 53.75; H, 6.55. IR (Nujol, cm^{-1}): $\nu(C\equiv C)$ 2100 (m), $\nu(CO)$ 2045 (s), 1970 (vs), $\nu(C=C, Ph)$ 1590 (m). IR (CH_2Cl_2 , cm^{-1}): $\nu(CO)$ 2050 (s), 1980 (vs). 1H NMR ($CDCl_3$, 20 °C): δ 7.39–7.15 (m, 5H, Ph), 2.60–1.20 (m, 33H, Cy). $^{31}P\{^1H\}$ NMR ($CDCl_3$, 20 °C): δ 27.6 (s).

Preparation of IrH₂(SnPh₃)(TFB)(PCy_3) (14). A solution of **1** (100 mg, 0.137 mmol) in 6 mL of toluene was treated with H_2SnPh_3 (96 mg, 0.274 mmol), and an immediate color change from orange to pale yellow was observed. This solution was stirred for 30 min at room temperature. The solution was concentrated to ca. 0.5 mL, and addition of hexane caused the precipitation of a white solid. The solution was decanted, and the solid was washed with hexane and dried in vacuo; yield 134 mg (93%). Anal. Calcd for $C_{48}H_{55}F_4IrPSn$: C, 54.92; H, 5.28. Found: C, 55.09; H, 5.51. IR (Nujol, cm^{-1}): $\nu(Ir-H)$ 2118 (m), 2093 (m); $\nu(Sn-Ph)$ 253 (s). 1H NMR (C_6D_6 , 20 °C): δ 8.01–7.22 (m, 15H, Ph), 4.88 (br, 2H, –CH), 3.11 (br, 4H, =CH), 1.85–1.04 (m, 33H, Cy), –15.37 (d, 2H, $J_{P-H} = 20.1$ Hz, Ir–H). 1H NMR (C_7D_8 , –60 °C): δ 4.88 (br, 1H, –CH), 4.82 (br, 1H, –CH), 3.22 (br, 2H, =CH), 2.77 (br, 2H, =CH), the other resonances are the same as that at 20 °C. $^{31}P\{^1H\}$ NMR (C_6D_6 , 20 °C): δ 14.8 (s with tin satellites, $J_{P-^{119}Sn} = 737.0$ Hz, $J_{P-^{117}Sn} = 641.8$ Hz; triplet in off-resonance). MS (EI) analysis of the mother liquors shows the presence of $MeOSnPh_3$. Mass fragmentation pattern of $MeOSnPh_3$: 382 (M^+), 351 ($M^+ - 31$, Ph_3Sn), 274 ($M^+ - 108$, Ph_2Sn), 197 ($M^+ - 185$, $SnPh$).

This complex may also be prepared from **3** (100 mg, 0.132 mmol; yield 102 mg (74%)), **4** (100 mg, 0.126 mmol; yield 102 mg (77%)), and **6** (100 mg, 0.12 mmol; yield 101 mg (80%)) as starting materials. MS (EI) analysis of the mother liquors show the presence of iPrOSnPh_3 , $PhOSnPh_3$, and nPrSSnPh_3 , respectively. Mass fragmentation pattern of iPrOSnPh_3 : 380 ($M^+ - 30$, Ph_3SnOCH), 351 ($M^+ - 59$, Ph_3Sn), 274 ($M^+ - 136$, Ph_2Sn), 197 ($M^+ - 213$, $SnPh$). Mass fragmentation pattern of $PhOSnPh_3$: 444 (M^+), 351 ($M^+ - 93$, Ph_3Sn), 197 ($M^+ - 247$, Ph_2Sn). Mass fragmentation pattern of nPrSSnPh_3 : 426 (M^+), 383 ($M^+ - 43$, Ph_3SnS), 351 ($M^+ - 75$, Ph_3Sn), 274 ($M^+ - 152$, Ph_2Sn), 229 ($M^+ - 197$, $PhSnS$), 197 ($M^+ - 229$, $PhSn$).

Preparation of IrH₂(SnⁿBu₃)(TFB)(PCy_3) (15). This compound was prepared analogously as described for **14**, starting from **1** (100 mg, 0.137 mmol) and $H_2Sn^iBu_3$ (74 μL , 0.274 mmol). Compound **15** was isolated as a white solid: yield 79 mg (57%). Anal. Calcd for $C_{42}H_{68}F_4IrPSn$: C, 50.91; H, 6.92. Found: C, 50.79; H, 6.98. IR (Nujol, cm^{-1}): $\nu(Ir-H)$ 2102 (m). 1H NMR (C_6D_6 , 20 °C): δ 5.10 (br, 2H, –CH), 3.00 (br, 4H, =CH), 2.00–1.10 (m, 60H, Cy, ⁿBu), –15.98 (d, 2H, $J_{P-H} = 21.3$ Hz). 1H NMR (C_7D_8 , –60 °C): δ 5.19 (br, 1H, –CH), 4.87 (br, 1H, –CH), 3.21 (br, 2H, =CH), 2.61 (br, 2H, =CH), the other resonances are the same as that at 20 °C. $^{31}P\{^1H\}$ NMR (C_6D_6 , 20 °C): δ 13.1 (s with tin satellites, $J_{P-^{119}Sn} = 528.4$ Hz, $J_{P-^{117}Sn} = 504.1$ Hz; triplet in off-resonance).

Reaction of 14 with CO: Formation of Ir(SnPh₃)(CO)₃(PCy_3). A solution of **14** (100 mg, 0.095 mmol) in dichloromethane (10 mL) was stirred under CO atmosphere during 16 h. The solution was concentrated to ca. 0.5 mL, and addition of hexane precipitated a white solid. The solution was decanted, and the solid was washed with hexane and dried in vacuo; yield 60 mg (70%). IR (Nujol, cm^{-1}): $\nu(CO)$ 1950 (vs), $\nu(Sn-Ph)$ 260 (s). IR (CH_2Cl_2 , cm^{-1}): $\nu(CO)$ 1945 (s). 1H NMR (C_6D_6 , 20 °C): δ 8.10–7.10 (m, 15H, Ph), 1.90–0.90 (m, 33H, PCy_3). $^{31}P\{^1H\}$ NMR (C_6D_6 , 20 °C): δ 21.9 (s with tin satellites, $J_{P-^{119}Sn} = 584.0$ Hz, $J_{P-^{117}Sn} = 560.0$ Hz).

Preparation of IrH(C₂Ph)(SnPh₃)(TFB)(PCy₃) (19). A solution of **9** (100 mg, 0.125 mmol) in 6 mL of toluene was treated with HSnPh₃ (44 mg, 0.125 mmol), and an immediate color change from red to light yellow was observed. The solution was stirred for 15 min and concentrated to ca. 0.5 mL. Addition of methanol precipitated a white solid. The solution was decanted, and the solid was washed with methanol and dried in vacuo; yield 119 mg (83%). Anal. Calcd for C₅₆H₆₀F₄IrPSn: C, 58.44; H, 5.25. Found: C, 58.16; H, 5.15. IR (Nujol, cm⁻¹): ν(Ir-H) 2113 (s), ν(C≡C) 2058 (m), ν(C=C, Ph) 1599 (m), ν(Sn-Ph) 246 (s). ¹H NMR (C₆D₆, 20 °C): δ 8.22–6.85 (m, 20H, Ph), 5.21 (br, 1H, -CH), 4.98 (br, 1H, -CH), 3.72 (br, 1H, =CH), 3.47 (br, 1H, =CH), 3.42 (br, 1H, =CH), 2.43–1.01 (m, 34H, =CH and PCy₃), -13.32 (br, 1H; this resonance is a doublet with J_{P-H} = 21.6 Hz in the ¹H NMR spectrum at -60 °C in toluene-d₆). ¹³C{¹H} NMR (C₆D₆, 20 °C): δ 145.18 (d, J_{P-C} = 5.5 Hz, C_{ipso} SnPh₃), 137.95 (s, SnPh₃), 131.53 (s, Ph), 131.49 (s, Ph), 128.41 (s, SnPh₃), 128.24 (s, SnPh₃), 128.13 (overlapping, Ph), 125.58 (s, Ph), 109.01 (br, C_β, C=C), this signal was only observed in the spectrum at -60 °C), 72.30 (d, J_{P-C} = 17.5 Hz, C_α, C=C), 43.90 (br s, CH=), 39.80 (br s, CH=), 37.59 (d, J_{P-C} = 21.6 Hz, PCy₃), 36.25 (br s, CH=), 36.10 (br s, CH=), 30.68 (s, PCy₃), 29.95 (s, PCy₃), 28.15 (d, J_{P-C} = 11.5 Hz, PCy₃), 28.00 (d, J_{P-C} = 11.5 Hz, PCy₃), 26.97 (s, PCy₃). ³¹P{¹H} NMR (C₆D₆, 20 °C): δ -1.9 (s with Sn satellites, J_{P-¹¹⁹Sn} = 735.6 Hz, J_{P-¹¹⁷Sn} = 715.9 Hz, doublet in off-resonance).

Preparation of IrH(C₂Ph)(SnⁿBu₃)(TFB)(PCy₃) (20). This compound was prepared analogously as described for **19**, starting from **9** (100 mg, 0.125 mmol) and HSnⁿBu₃ (34 μL, 0.125 mmol). Compound **20** was isolated as a white solid: yield 101 mg (74%). Anal. Calcd for C₅₀H₇₂F₄IrPSn: C, 55.04; H, 6.93. Found: C, 55.37; H, 6.43. IR (Nujol, cm⁻¹): ν(Ir-H) 2085 (s), ν(C≡C) 2020 (m), ν(C=C, Ph) 1590 (m). ¹H NMR (C₆D₆, 20 °C): δ 7.39–6.87 (m, 5H, Ph), 5.31 (br, 1H, -CH), 5.08 (br, 1H, -CH), 3.54 (br, 1H, =CH), 3.31 (br, 1H, =CH), 3.21 (br, 1H, =CH), 2.30 (br, 1H, =CH), 2.20–1.04 (m, 60H, ⁿBu, Cy), -13.68 (d, 1H, J_{P-H} = 26.1 Hz, J_{Sn-H} = 28.6 Hz, Ir-H). ¹³C{¹H} NMR (C₆D₆, 20 °C): δ 131.23 (s, Ph), 131.20 (s, Ph), 129.28 (s, Ph), 129.24 (s, Ph), 125.21 (s, Ph), 107.29 (d, J_{P-C} = 3.7 Hz, C_β, C=C), 76.95 (d, J_{P-C} = 18.4 Hz, C_α, C=C), 37.80 (br s, CH=), 37.40 (br s, CH=), 37.36 (d, J_{P-C} = 19.8 Hz, PCy₃), 36.57 (br s, CH=), 35.85 (br s, CH=), 31.03 (s, ⁿBu), 30.55 (s, PCy₃), 29.77 (s, PCy₃), 28.25 (s, ⁿBu), 28.18 (d, J_{P-C} = 10.6 Hz, PCy₃), 27.09 (s, PCy₃), 14.13 (s, ⁿBu), 13.49 (s, ⁿBu). ³¹P{¹H} NMR (C₆D₆, 20 °C): δ -2.0 (s with Sn satellites, J_{P-¹¹⁹Sn} = 550.5 Hz, J_{P-¹¹⁷Sn} = 525.9 Hz, doublet in off-resonance).

Preparation of IrH(C₂Ph)(SnPh₃)(CO)₂(PCy₃) (21). This complex can be prepared by using two different procedures. (a) To a 5 mm NMR tube containing a solution of **13** (50 mg, 0.079 mg) in 0.5 mL of benzene-d₆ was added HSnPh₃ (28 mg, 0.079 mg). After 2 h, ¹H and ³¹P{¹H} NMR spectra were recorded. (b) A solution of **19** (100 mg, 0.087 mmol) in CH₂Cl₂ (10 mL) was stirred under CO for 30 min, and the pale yellow solution was concentrated to ca. 0.5 mL. Addition of hexane caused the precipitation of a white solid. The solution was decanted, and the solid was washed with hexane and dried in vacuo; yield 64 mg (75%). Anal. Calcd for C₄₆H₅₄IrO₂PSn: C, 56.33; H, 5.50. Found: C, 55.93; H, 5.68. IR (Nujol, cm⁻¹): ν(Ir-H) 2140 (w), ν(C≡C) 2110 (s), ν(CO) 2040 (s), 2000 (s). IR (CH₂Cl₂, cm⁻¹): ν(Ir-H) 2130 (w), ν(C≡C) 2115 (w), ν(CO) 2050 (s), 2000 (s). ¹H NMR (C₆D₆, 20 °C): δ 8.06–6.82 (m, 20H, Ph), 2.20–1.10 (m, 33H, Cy), -9.42 (d, 1H, J_{P-H} = 14.8 Hz, J_{Sn-H} = 29.0 Hz, Ir-H). ¹³C{¹H} NMR (C₆D₆, 20 °C): δ 173.09 (br, CO), 171.22 (d, J_{P-C} = 4.6 Hz, CO), 143.96 (d, J_{P-C} = 6.9 Hz, C_{ipso} SnPh₃), 137.70 (s, SnPh₃), 131.45 (s, Ph), 131.42 (s, Ph), 128.58 (s, Ph), 128.18 (s, SnPh₃), 127.85 (s, SnPh₃), 125.88 (s, Ph), 110.62 (d, J_{P-C} = 4.1 Hz, C_β, C=C), 66.60 (d, J_{P-C} = 14.7 Hz, C_α, C=C), 34.78 (d, J_{P-C} = 22.5 Hz, PCy₃), 29.68 (s, PCy₃), 29.60 (s, PCy₃), 27.59 (d, J_{P-C} = 10.1 Hz, PCy₃), 27.49 (d, J_{P-C} = 10.6 Hz, PCy₃), 26.56 (s, PCy₃). ³¹P{¹H} NMR (C₆D₆,

Table 4. Atomic Coordinates (Å × 10⁴; × 10⁵ for Ir, P, and Sn Atoms) and Equivalent Isotropic Displacement Coefficients (Å² × 10³; × 10⁴ for Ir, P, and Sn Atoms) for the Compound IrH₂(SnPh₃)(TFB)(PCy₃) (14)

atom	x/a	y/b	z/c	U _{eq} ^a
Ir	11352(2)	6968(2)	29050(1)	286(7)
Sn	22318(3)	-12779(3)	22762(2)	334(1)
P	-2945(11)	27301(11)	24942(6)	282(4)
F(1)	4756(3)	-2318(3)	4921(2)	51(1)
F(2)	4883(3)	-1430(3)	6054(2)	56(1)
F(3)	3251(4)	850(3)	6332(2)	62(2)
F(4)	1442(3)	2256(3)	5484(2)	54(1)
C(1)	3919(5)	-1181(5)	5043(3)	37(2)
C(2)	3995(5)	-747(5)	5631(3)	39(2)
C(3)	3170(5)	410(5)	5770(3)	41(2)
C(4)	2244(5)	1131(4)	5327(3)	36(2)
C(5)	2176(5)	702(4)	4745(2)	34(2)
C(6)	3027(5)	-480(4)	4601(2)	32(2)
C(7)	1300(5)	1402(4)	4184(2)	33(2)
C(8)	2148(5)	1576(4)	3452(2)	34(2)
C(9)	2988(5)	394(5)	3314(3)	36(2)
C(10)	2853(5)	-784(4)	3922(3)	34(2)
C(11)	1417(5)	-695(5)	3929(2)	34(2)
C(12)	570(5)	489(5)	4080(2)	34(2)
C(13)	-1021(5)	3831(4)	3149(2)	35(2)
C(14)	-1542(6)	5301(5)	2853(3)	55(2)
C(15)	-1952(6)	6061(6)	3456(3)	63(3)
C(16)	-2900(6)	5545(6)	4052(4)	68(3)
C(17)	-2373(7)	4094(6)	4340(3)	62(3)
C(18)	-2013(5)	3335(5)	3740(3)	45(2)
C(19)	517(4)	3804(4)	1748(2)	32(2)
C(20)	892(5)	3336(5)	1030(2)	43(2)
C(21)	1496(6)	4310(6)	462(3)	50(2)
C(22)	2687(6)	4519(6)	666(3)	61(3)
C(23)	2330(6)	4956(6)	1366(3)	52(2)
C(24)	1713(5)	4006(5)	1951(3)	39(2)
C(25)	-1621(5)	2572(5)	2091(3)	36(2)
C(26)	-2454(5)	1685(6)	2556(3)	49(2)
C(27)	-3322(6)	1398(6)	2133(4)	61(3)
C(28)	-4181(6)	2657(6)	1783(4)	63(3)
C(29)	-3411(7)	3604(6)	1329(4)	65(3)
C(30)	-2513(5)	3853(5)	1743(3)	50(2)
C(31)	2551(5)	-3190(4)	2986(3)	38(2)
C(32)	3778(6)	-3975(6)	3082(4)	67(3)
C(33)	3945(7)	-5205(6)	3559(4)	77(3)
C(34)	2898(7)	-5622(6)	3937(3)	63(3)
C(35)	1673(6)	-4832(6)	3863(3)	58(3)
C(36)	1510(5)	-3638(5)	3391(3)	51(2)
C(37)	4069(5)	-1247(5)	1607(3)	46(2)
C(38)	4498(6)	-124(7)	1365(3)	59(3)
C(39)	5586(7)	-51(9)	850(4)	77(4)
C(40)	6256(7)	-1148(10)	568(4)	87(4)
C(41)	5869(8)	-2257(9)	789(4)	95(4)
C(42)	4769(7)	-2330(7)	1312(4)	73(3)
C(43)	1123(6)	-1438(5)	1535(3)	46(2)
C(44)	1645(7)	-1399(6)	817(3)	56(3)
C(45)	955(8)	-1586(7)	349(4)	74(3)
C(46)	-245(9)	-1803(7)	581(4)	83(4)
C(47)	-805(7)	-1822(7)	1291(4)	74(3)
C(48)	-116(6)	-1639(6)	1753(3)	58(3)

^a Equivalent isotropic U defined as one-third of the trace of the orthogonalized U_{ij} tensor.

20 °C): δ 13.9 (s with Sn satellites, J_{P-¹¹⁹Sn} = 968.6 Hz, J_{P-¹¹⁷Sn} = 908.8 Hz).

Preparation of IrH(C₂Ph)(SnⁿBu₃)(CO)₂(PCy₃) (22). This compound was prepared analogously as described for **21** (method a), starting from **13** (50 mg, 0.079 mmol) and HSnⁿBu₃ (21 μL, 0.079 mmol). IR (CH₂Cl₂, cm⁻¹): ν(Ir-H) 2135 (w), ν(C≡C) 2110 (w), ν(CO) 2035 (s), 1995 (s). ¹H NMR (C₆D₆, 20 °C): δ 7.53–6.92 (m, 5H, Ph), 2.24–0.97 (m, 60H, ⁿBu, Cy), -9.80 (d, 1H, J_{P-H} = 15.7 Hz, J_{Sn-H} = 32.7 Hz, Ir-H). ¹³C{¹H} NMR (C₆D₆, 20 °C): δ 175.00 (s, CO), 173.28 (s, CO), 131.41 (s, Ph), 128.97 (s, Ph), 125.65 (s, Ph), 108.89 (s, C_β, C=C), 69.65 (d, J_{P-C} = 15.7 Hz, C_α, C=C), 34.80 (d, J_{P-C} = 21.1 Hz, PCy₃), 30.99 (s, SnⁿBu₃), 29.86 (s, PCy₃), 29.60 (s, PCy₃), 27.87 (s,

Table 5. Crystal Data and Data Collection and Refinement for IrH₂(SnPh₃)(TFB)(PCy₃) (14)

Crystal Data	
formula	C ₄₈ H ₅₆ F ₄ PSnIr
mol wt	1050.85
color and habit	pale yellow, transparent prism
crystal size, mm ³	0.38 × 0.18 × 0.18
cryst syst	triclinic
space group	P $\bar{1}$ (No. 2)
a, Å	10.923(1)
b, Å	10.943(1)
c, Å	19.679(1)
α , °	75.076(5)
β , °	77.504(5)
γ , °	72.606(5)
V, Å ³	2144.0(3)
Z	2
D(calcd), g cm ⁻³	1.628
Data Collection and Refinement	
diffractometer	four-circle Siemens-P4
λ (Mo K α), Å; technique	0.710 73, bisecting geometry
monochromator	graphite-oriented
μ , mm ⁻¹	3.76
scan type	$\theta/2\theta$
2 θ range, deg	2 ≤ 2 θ ≤ 50
temp, K	293
no. of data collected	8796
no. of unique data	7492 (R_{int} 0.0237)
unique obsd data	6398 ($F_o \geq 4.0\sigma(F_o)$)
no. of params refined	505
R, R_w^a	0.0292, 0.0310

$$^a R = (\sum[|F_o| - |F_c|]) / \sum F_o; R_w = (\sum(|F_o| - |F_c|)w^{1/2}) / \sum(F_o w^{1/2}), w^{-1} = \sigma^2(F_o) + 0.000602(F_o)^2.$$

SnⁿBu₃), 27.69 (d, $J_{P-C} = 8.7$ Hz, PCy₃), 27.57 (d, $J_{P-C} = 8.7$ Hz, PCy₃), 26.50 (s, PCy₃), 13.91 (s, SnⁿBu₃), 12.72 (s, SnⁿBu₃). ³¹P{¹H} NMR (C₆D₆, 20 °C): δ 11.1 (s with Sn satellites, $J_{P-^{119}\text{Sn}} = 671.7$ Hz, $J_{P-^{117}\text{Sn}} = 641.9$ Hz; doublet in off-resonance).

Catalytic Studies. The hydrostannation reactions were performed under argon at 60 °C. The reaction were carried out in a two-necked flask fitted with a condenser and a magnetic stirring bar. The second neck was capped with a septum to allow periodical samples to be taken without opening the system.

In a typical procedure, a solution (4 mL) of HSnPh₃ and hydroquinone in 1,2-dichloroethane was added to a second solution of 1,2-dichloroethane (4 mL) containing PhC≡CH, *n*-octane, and the catalyst. The flask was then immersed in a bath at 60 °C, and the reaction mixture was magnetically stirred for 20 min. Tin-containing products were characterized by ¹¹⁹Sn NMR. ¹¹⁹Sn NMR (*trans*-PhCH=CH(SnPh₃), CDCl₃): δ -132.4. ¹¹⁹Sn NMR (*cis*-PhCH=CH(SnPh₃), CDCl₃): δ -151.2.

X-ray Structure Analysis of IrH₂(SnPh₃)(TFB)(PCy₃) (14). Crystals suitable for an X-ray diffraction experiment were obtained by slow diffusion of methanol into a concentrated solution of 14 in toluene. Atomic coordinates and U_{eq} values are listed in Table 4. A summary of crystal data, intensity collection procedures, and refinement data are reported in Table 5. The prismatic crystal studied was glued on a glass fiber and mounted on a Siemens-P4 diffractometer. Cell constants were obtained from the least-squares fit on the setting angles of 74 reflections in the range 10 ≤ 2 θ ≤ 30°. The 8796 recorded reflections were corrected for Lorentz and polarization effects. Three orientation and intensity standards were monitored every 100 measured reflections; no variation was observed. Reflections were also corrected for absorption by a semiempirical method (Ψ scan).²⁹

The structure was solved by Patterson (Ir atom) and conventional Fourier techniques. Refinement was carried out by full-matrix least-squares with initial isotropic thermal parameters. Anisotropic thermal parameters were used in the last cycles of refinement for all non-hydrogen atoms. Hydrogen atoms bonded to the C atoms were observed or calculated and included in the refinement riding on carbon atoms with a common isotropic thermal parameter. The two hydrido ligands were clearly found in the difference Fourier map and refined as free isotropic atoms. Atomic scattering factors, corrected for anomalous dispersion for Ir, Sn, and P, were taken from ref 30. The function minimized was $\sum w([F_o] - [F_c])^2$, with the weight defined as $w^{-1} = \sigma^2(F_o) - 0.000602[F_o]^2$. Final *R* and R_w values were 0.0292 and 0.0310. All calculations were performed using SHELXTL-PLUS.³¹

Acknowledgment. We thank the DGICYT (Project PB92-0092, Programa de Promoción General del Conocimiento) and the E.U. (Project: *Selective Processes and Catalysis involving Small Molecules*). M.O. and E.O. thank the Diputación General de Aragón (DGA) for grants.

Supporting Information Available: Tables of anisotropic thermal parameters, atomic coordinates for hydrogen atoms, experimental details of the X-ray study, bond distances, and angles (13 pages). Ordering information is given on any current masthead page.

OM9501337

(29) North, A. C. T.; Phillips, D. C.; Mathews, F. S. *Acta Crystallogr.* **1968**, *A24*, 351.

(30) *International Tables for X-Ray Crystallography*; Kynoch Press: Birmingham, England, 1974; Vol. 4.

(31) Sheldrick, G. M. *SHELXTL-PLUS*; Siemens Analytical X-ray Instruments, Inc.: Madison, WI, 1990.

**Reactions of Monocyclopentadienyl
Pentafluorobenzenethiolato Complexes of Molybdenum
and Tungsten with Group 11 Metal Derivatives:
Crystal and Molecular Structures of
[Au(PPh₃)₃][Mo(SC₆F₅)₄(η⁵-C₅H₅)] and
[Cu(PPh₃)₃][Mo(SC₆F₅)₄(η⁵-C₅H₅)]**

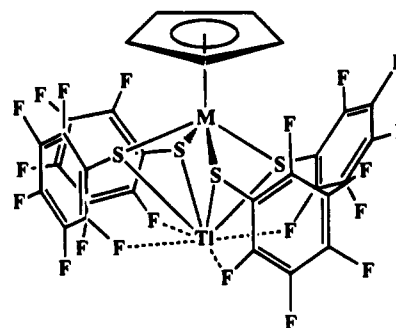
Jack L. Davidson,* W. Edward Lindsell,* Kevin J. McCullough,* and
Calum H. McIntosh

Department of Chemistry, Heriot-Watt University, Riccarton, Edinburgh EH14 4AS, U.K.

Received January 18, 1995[®]

Displacement of coordinated Tl(I) as TlCl from [TlM(SC₆F₅)₄Cp] (M = Mo, W; Cp = η⁵-C₅H₅) by gold complexes [AuCl(PR₃)] (R = Ph, Et) in dichloromethane or acetone solution affords ionic products [Au(PR₃)₃][M(SC₆F₅)₄Cp], isolable in higher yields from reactions carried out in the presence of three molar equiv of free phosphine, PR₃. Ligand exchange between [Au(PPh₃)₃][M(SC₆F₅)₄Cp] and diphosphines produces derivatives [Au(Ph₂P(CH₂)_n-PPh₂)₂][M(SC₆F₅)₄Cp] {n = 2 dppe (4); n = 3 dppp (5); M = Mo, W}. A related reaction of [CuCl(PPh₃)₃] and [TlMo(SC₆F₅)₄Cp] forms the copper derivative [Cu(PPh₃)₃][Mo(SC₆F₅)₄Cp] as the major product. Attempts to isolate derivatives with group 11 metal cations coordinated by anions [M(SC₆F₅)₄Cp]⁻ have been unsuccessful. Molecular structures of crystalline bimetallic species [M'(PR₃)₃][Mo(SC₆F₅)₄Cp]·0.5CH₂Cl₂ {M' = Au (2a), Cu (6)} have been determined by X-ray diffraction and are essentially isomorphous. Both contain approximately trigonal-planar [M'(PPh₃)₃]⁺ cations with P–Au–P angles of 123.83(5)°, 122.28(5)°, and 113.62(5)° and an average Au–P distance 2.386(2) Å or P–Cu–P angles 121.24(7)°, 123.44(8)° and 115.11(7)° and an average Cu–P bond length 2.295(2) Å, respectively. The discrete anions [Mo(SC₆F₅)₄Cp]⁻ in 2a and 6 are similar, with “four-legged piano-stool” geometry and average Mo–S distances of 2.421(2) or 2.420(3) Å, respectively. Spectroscopic studies of complexes 4 and 5 support ionic constitutions with four-coordinated [Au(Ph₂P(CH₂)_nPPh₂)₂]⁺ cations. Variable temperature ¹⁹F NMR studies of anions [M(SC₆F₅)₄Cp]⁻ of gold derivatives give barriers to fluxional rotation/inversion of SC₆F₅ groups, ΔG[‡] ca. 40–41 kJ mol⁻¹ (208–228 K), M = Mo, or ΔG[‡] ca. 43–44 kJ mol⁻¹ (223–245 K), M = W, comparable with ΔG[‡] values for salts [N(PPh₃)₂][M(SC₆F₅)₄Cp], which are essentially independent of solvent (CD₂Cl₂, (CD₃)₂CO, or C₆D₅CD₃), in contrast to barriers for coordinated species [TlM(SC₆F₅)₄Cp].

Previously we have described the synthesis of molybdenum and tungsten tetrathiolate anions [M(SC₆F₅)₄Cp]⁻ (Cp = η⁵-C₅H₅) which reversibly coordinate thallium(I) in solution,^{1,2} and more recently we have observed reversible coordination of alkali metal ions.³ These results are interesting in view of the differing soft and hard acid characteristics, respectively, of the two types of metal cations. A feature of the complex anions which promotes coordination to metal ions is the presence of a cavity defined by the transition metal, the four sulfurs, and four of the eight *ortho* fluorines of the thiolate C₆F₅ substituents. An X-ray diffraction study of [TlM(SC₆F₅)₄Cp] (1a, M = Mo) suggests that the primary bonding between the anion and Tl⁺ involves the four sulfurs, i.e., a soft acid/base system, whilst the four fluorine-



(1a) M = Mo;
(1b) M = W

thallium interactions are probably minimal.¹ The nature of the alkali metal–anion bonding has not yet been definitively established by a crystal structure but it is likely that fluorine–cation interactions are more important here.^{3,4} It is of interest to extend the chemistry of the anions [M(SC₆F₅)₄Cp]⁻ (M = Mo, W) by studying

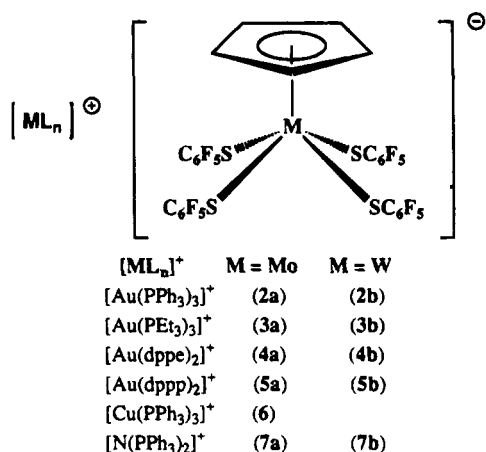
(4) Cf.: Plenio, H.; Burth, D. *J. Chem. Soc., Chem. Commun.* **1994**, 2297.

[®] Abstract published in *Advance ACS Abstracts*, June 1, 1995.
(1) Bakar, W. A. W. A.; Davidson, J. L.; Lindsell, W. E.; McCullough, K. J.; Muir, K. W. *J. Chem. Soc., Dalton Trans.* **1989**, 991.
(2) Bakar, W. A. W. A.; Davidson, J. L.; Lindsell, W. E.; McCullough, K. J. *J. Chem. Soc., Dalton Trans.* **1990**, 61.
(3) Davidson, J. L.; McIntosh, C. H.; Leverd, P. C.; Lindsell, W. E.; Simpson, N. J. *J. Chem. Soc., Dalton Trans.* **1994**, 2423. Boyd, A. S. F.; Davidson, J. L.; McIntosh, C. H.; Leverd, P. C.; Lindsell, W. E.; Simpson, N. J. *J. Chem. Soc., Dalton Trans.* **1992**, 2531.

their interactions with a wider range of metal derivatives and to investigate the limits of their coordination capabilities. We now report the results of some of these studies with systems containing the soft acid metal ions of group 11.

Results and Discussion

Synthetic studies. Reactions of $[\text{TlM}(\text{SC}_6\text{F}_5)_4\text{Cp}]$ ($\text{M} = \text{Mo}, \text{W}$) with $[\text{AuCl}(\text{PR}_3)]$ ($\text{R} = \text{Ph}, \text{Et}$). The complex $[\text{AuCl}(\text{PPh}_3)]$, as a soluble source of Au(I), was reacted with an equimolar quantity of $[\text{TlMo}(\text{SC}_6\text{F}_5)_4\text{Cp}]$ (**1a**) in tetrahydrofuran. From this reaction the only new, isolable product was obtained as orange-red crystals, incorporating PPh_3 and Cp in the stoichiometric ratio 3:1, as shown by the ^1H NMR spectrum. Reaction with an additional 3 equiv (i.e., an excess) of free triphenylphosphine gave the same orange-red crystals but in a considerably increased yield (>40%). It had been anticipated that the cationic gold center might coordinate to the soft sulfur sites of the tetrathiolate anion after elimination and precipitation of TiCl_4 , possibly accompanied by the loss of PPh_3 . However, elemental and NMR spectroscopic analyses were consistent with the ionic formulation $[\text{Au}(\text{PPh}_3)_3][\text{Mo}(\text{SC}_6\text{F}_5)_4\text{Cp}]$ (**2a**) solvated in the crystals with 0.5 mol of CH_2Cl_2 ,



as confirmed by X-ray analysis (see below). The analogous tungsten reaction with $[\text{TiW}(\text{SC}_6\text{F}_5)_4\text{Cp}]$ (**1b**) gave yellow crystals which showed similar NMR spectra to those of **2a**; elemental analyses of these crystals also corresponded to a related, but unsolvated, compound, $[\text{Au}(\text{PPh}_3)_3][\text{W}(\text{SC}_6\text{F}_5)_4\text{Cp}]$ (**2b**), obtained in 62% yield.

Reaction of $[\text{TlMo}(\text{SC}_6\text{F}_5)_4\text{Cp}]$ with $[\text{AuCl}(\text{PEt}_3)]$ and three equivalents of PEt_3 in CH_2Cl_2 yielded orange-red crystals for which the ^1H NMR spectrum showed that PEt_3 and Cp were present in a molar ratio of 3:1. The complex is formulated as an ionic species $[\text{Au}(\text{PEt}_3)_3][\text{Mo}(\text{SC}_6\text{F}_5)_4\text{Cp}]$ (**3a**), similar to **2a**, and this is supported by elemental analysis and dynamic ^{19}F NMR studies (see below). The related reaction of $[\text{TiW}(\text{SC}_6\text{F}_5)_4\text{Cp}]$ with $[\text{AuCl}(\text{PEt}_3)]$ and 3 equiv of PEt_3 in acetone yielded two new crystalline species. The major product was obtained in the form of yellow crystals, with the minor product as light green crystals, and these were separated by hand. Both types of crystal gave identical IR, UV/VIS, and NMR spectra in solution and the spectroscopic and analytical data of both forms indicated the same stoichiometric formula $[\text{Au}(\text{PEt}_3)_3][\text{W}(\text{SC}_6\text{F}_5)_4\text{Cp}]$ (**3b**), analogous to the molybdenum derivative **3a**.

(PEt_3) $_3$][$\text{W}(\text{SC}_6\text{F}_5)_4\text{Cp}]$ (**3b**), analogous to the molybdenum derivative **3a**.

Reactions of $[\text{Au}(\text{PPh}_3)_3][\text{M}(\text{SC}_6\text{F}_5)_4(\text{Cp})]$ ($\text{M} = \text{Mo}, \text{W}$) with diphosphines. Initially $[\text{Au}(\text{PPh}_3)_3][\text{Mo}(\text{SC}_6\text{F}_5)_4\text{Cp}]$ (**2a**) was reacted with 1 molar equiv of the potentially bidentate ligand 1,2-bis(diphenylphosphino)ethane (dppe) in CH_2Cl_2 . The product that separated first from solution formed orange needlelike crystals (**4a**) which contained dppe and Cp ligands in a 2:1 molar ratio, as shown by the ^1H NMR spectrum, and only one type of C_6F_5 group was evident from the ^{19}F NMR spectrum; further crystallization from the mother liquor only produced unreacted starting complex **2a**. The reaction was therefore repeated with 2 molar equiv of dppe to form **4a** in almost double the yield (95%). Reaction between tungsten complex **2b** and 2 equiv of dppe gave green, needlelike crystals which showed similar spectroscopic data to those of the molybdenum analogue. On the basis of analytical and spectroscopic analyses the complexes were formulated as $[\text{Au}(\text{dppe})_2][\text{M}(\text{SC}_6\text{F}_5)_4\text{Cp}]$ ($\text{M} = \text{Mo}$ (**4a**), W (**4b**)). Similarly, reactions of $[\text{Au}(\text{PPh}_3)_3][\text{M}(\text{SC}_6\text{F}_5)_4\text{Cp}]$ (**2a** or **2b**) with 2 molar equiv of 1,3-bis(diphenylphosphino)propane (dppp) in acetone gave new products as orange ($\text{M} = \text{Mo}$) or yellow ($\text{M} = \text{W}$) microcrystals for which NMR spectra and analytical data indicated a formula $[\text{Au}(\text{dppp})_2][\text{M}(\text{SC}_6\text{F}_5)_4(\text{Cp})]$ ($\text{M} = \text{Mo}$ (**5a**), W (**5b**)).

Reaction of $[\text{TlMo}(\text{SC}_6\text{F}_5)_4\text{Cp}]$ with $[\text{CuCl}(\text{PPh}_3)_3]$. Reaction of $[\text{TlMo}(\text{SC}_6\text{F}_5)_4\text{Cp}]$ with 1 molar equiv of $[\text{CuCl}(\text{PPh}_3)_3]$ in CH_2Cl_2 produced a mixture of two isolable crystalline species. The major product was obtained as red crystals (25%), which were contaminated with a small amount of dark crystals. The products were separated by hand, with the red crystals being suitable for structural analysis by X-ray diffraction (see below). The ^1H and ^{19}F NMR spectra of these red crystals in CD_2Cl_2 at ambient temperature included several resonances assignable to Cp and C_6F_5 groups, suggesting that more than one species exists in solution at this temperature; however, elemental analyses of the isolated crystalline product were consistent with the formula $[\text{Cu}(\text{PPh}_3)_3][\text{Mo}(\text{SC}_6\text{F}_5)_4\text{Cp}] \cdot 0.5\text{CH}_2\text{Cl}_2$ (**6**), and this was supported by low-temperature NMR spectra. The yield of dark crystals was too low for satisfactory characterization.

Other Reactions Involving Group 11 Metal Derivatives. Attempts were made to form simple complexes containing the group 11 ions, such as $[\text{M}'\text{M}(\text{SC}_6\text{F}_5)_4\text{Cp}]$ ($\text{M}' = \text{Au}, \text{Ag}, \text{Cu}$), in the absence of phosphorus ligands. Thallium derivatives $[\text{TlM}(\text{SC}_6\text{F}_5)_4\text{Cp}]$ ($\text{M} = \text{Mo}$ (**1a**), W (**1b**)) can be prepared by ligand exchange reactions in polar organic solvents between TlSC_6F_5 and $\text{M}(\text{IV})$ cyclopentadienyl halides, such as $[\text{MCl}_3(\text{CO})_2\text{Cp}]$, or between TlSC_6F_5 and $\text{Mo}(\text{II})$ species, e.g., $[\text{MoCl}(\text{CO})_3\text{Cp}]$, followed by oxidation.¹⁻³ However, related reactions of AuSC_6F_5 with $\text{M}(\text{IV})$ or $\text{Mo}(\text{II})$ derivatives in tetrahydrofuran, under various conditions, did not produce stable, isolable products; in several reactions impure, blue-green paramagnetic species were formed, and much AuSC_6F_5 was recovered, mixed with metallic gold. Related reactions with various $\text{Ag}(\text{I})$ and $\text{Cu}(\text{I})$ salts also gave uncharacterizable products. Since AuSC_6F_5 is extremely insoluble, reac-

(5) Peach, M. E. *Can. J. Chem.* **1968**, *46*, 2699. Beck, W.; Stetter, K. H.; Tadros, S.; Schwarzthans, K. E. *Chem. Ber.* **1967**, *100*, 3944.

Table 1. Fractional Coordinates of Atoms and U_{eq} Values (Å²) with Estimated Standard Deviations for Complex 2a

atom	x	y	z	U _{eq}	atom	x	y	z	U _{eq}
Mo(1)	0.078 27(4)	0.563 71(3)	0.211 37(3)	0.0387(3)	C(2)	-0.202 7(3)	-0.061 70(22)	0.173 42(19)	0.066(5)
S(1)	0.132 35(13)	0.547 64(10)	0.328 21(8)	0.0479(9)	C(3)	-0.308 6(3)	-0.052 89(22)	0.138 24(19)	0.077(6)
C(55)	-0.017 9(3)	0.436 80(19)	0.380 28(18)	0.048(4)	C(4)	-0.333 5(3)	0.019 90(22)	0.112 45(19)	0.078(6)
F(55)	0.030 6(3)	0.380 38(19)	0.342 04(18)	0.070(3)	C(5)	-0.252 4(3)	0.083 88(22)	0.121 86(19)	0.065(5)
C(56)	-0.102 6(3)	0.414 68(23)	0.419 65(19)	0.056(4)	C(6)	-0.146 4(3)	0.075 05(22)	0.157 06(19)	0.041(3)
F(56)	-0.136 3(3)	0.337 47(23)	0.419 11(19)	0.090(3)	C(7)	0.082 2(3)	0.244 27(19)	0.087 58(17)	0.051(4)
C(57)	-0.159 1(3)	0.471 0(3)	0.455 78(19)	0.066(5)	C(8)	0.133 7(3)	0.257 01(19)	0.028 03(17)	0.062(5)
F(57)	-0.238 3(3)	0.448 6(3)	0.497 27(19)	0.094(4)	C(9)	0.121 5(3)	0.198 82(19)	-0.025 52(17)	0.063(5)
C(58)	-0.116 4(3)	0.548 66(25)	0.460 34(19)	0.053(4)	C(10)	0.057 8(3)	0.127 85(19)	-0.019 52(17)	0.061(5)
F(58)	-0.170 4(3)	0.604 52(25)	0.496 14(19)	0.087(3)	C(11)	0.006 3(3)	0.115 12(19)	0.040 02(17)	0.049(4)
C(59)	-0.038 6(3)	0.571 40(20)	0.416 96(17)	0.050(4)	C(12)	0.018 5(3)	0.173 31(19)	0.093 58(17)	0.038(3)
F(59)	-0.003 9(3)	0.648 61(20)	0.419 62(17)	0.073(3)	C(13)	-0.177 6(3)	0.282 24(19)	0.129 23(15)	0.050(4)
C(60)	0.018 0(5)	0.516 4(4)	0.375 9(3)	0.045(4)	C(14)	-0.254 0(3)	0.343 50(23)	0.138 44(15)	0.062(5)
S(2)	0.250 59(14)	0.652 23(10)	0.224 54(8)	0.0495(10)	C(15)	-0.285 7(3)	0.366 78(23)	0.202 69(15)	0.071(5)
C(61)	0.363 0(3)	0.667 63(20)	0.352 05(18)	0.050(4)	C(16)	-0.241 0(3)	0.328 77(23)	0.257 74(15)	0.067(5)
F(61)	0.286 0(3)	0.722 42(20)	0.367 04(18)	0.075(3)	C(17)	-0.164 5(3)	0.267 51(23)	0.248 53(15)	0.054(4)
C(62)	0.444 5(3)	0.651 72(24)	0.400 10(19)	0.057(4)	C(18)	-0.132 8(3)	0.244 25(23)	0.184 27(15)	0.039(3)
F(62)	0.446 1(3)	0.690 50(24)	0.461 01(19)	0.093(3)	P(2)	0.301 03(12)	0.162 80(9)	0.255 43(7)	0.0362(8)
C(63)	0.521 3(3)	0.594 23(25)	0.387 85(21)	0.063(5)	C(19)	0.286 4(3)	0.311 12(23)	0.321 75(20)	0.051(4)
F(63)	0.605 0(3)	0.581 11(25)	0.434 56(21)	0.096(4)	C(20)	0.326 8(3)	0.377 01(23)	0.364 35(20)	0.067(5)
C(64)	0.523 5(3)	0.558 87(24)	0.324 34(21)	0.057(4)	C(21)	0.440 9(3)	0.381 51(23)	0.391 53(20)	0.066(5)
F(64)	0.598 5(3)	0.501 90(24)	0.311 66(21)	0.091(4)	C(22)	0.514 6(3)	0.320 13(23)	0.376 13(20)	0.060(4)
C(65)	0.435 9(3)	0.570 53(23)	0.277 52(18)	0.054(4)	C(23)	0.474 1(3)	0.254 25(23)	0.333 52(20)	0.051(4)
F(65)	0.437 4(3)	0.532 47(23)	0.216 48(18)	0.082(3)	C(24)	0.360 0(3)	0.249 74(23)	0.306 34(20)	0.039(3)
C(66)	0.352 5(5)	0.627 8(3)	0.287 6(3)	0.044(4)	C(25)	0.417 0(4)	0.018 82(25)	0.242 14(15)	0.064(5)
S(3)	0.003 97(14)	0.669 43(10)	0.148 28(9)	0.0526(10)	C(26)	0.462 2(4)	-0.049 81(25)	0.266 83(15)	0.087(6)
C(67)	0.192 8(3)	0.720 19(25)	0.076 79(19)	0.061(5)	C(27)	0.470 9(4)	-0.058 11(25)	0.335 74(15)	0.075(5)
F(67)	0.201 4(3)	0.644 25(25)	0.052 98(19)	0.084(3)	C(28)	0.434 4(4)	0.002 23(25)	0.379 96(15)	0.059(4)
C(68)	0.272 0(4)	0.775 0(3)	0.061 50(21)	0.070(5)	C(29)	0.389 2(4)	0.070 86(25)	0.355 27(15)	0.046(4)
F(68)	0.352 4(4)	0.754 0(3)	0.019 31(21)	0.109(4)	C(30)	0.380 5(4)	0.079 15(25)	0.286 36(15)	0.041(3)
C(69)	0.268 3(4)	0.852 7(3)	0.086 50(25)	0.082(6)	C(31)	0.302 4(3)	0.117 00(21)	0.121 05(19)	0.048(4)
F(69)	0.344 3(4)	0.908 2(3)	0.068 84(25)	0.127(5)	C(32)	0.341 0(3)	0.118 02(21)	0.056 61(19)	0.057(4)
C(70)	0.183 4(4)	0.873 5(3)	0.127 36(25)	0.076(6)	C(33)	0.427 0(3)	0.173 84(21)	0.043 20(19)	0.075(5)
F(70)	0.175 6(4)	0.949 7(3)	0.150 60(25)	0.124(5)	C(34)	0.474 4(3)	0.228 63(21)	0.094 23(19)	0.097(7)
C(71)	0.104 0(4)	0.818 35(21)	0.141 97(20)	0.062(5)	C(35)	0.435 7(3)	0.227 60(21)	0.158 66(19)	0.069(5)
F(71)	0.023 7(4)	0.840 22(21)	0.184 00(20)	0.082(3)	C(36)	0.349 7(3)	0.171 79(21)	0.172 06(19)	0.042(4)
C(72)	0.110 2(5)	0.737 6(4)	0.122 6(3)	0.054(4)	P(3)	0.0457 7(12)	0.087 94(8)	0.364 43(7)	0.0332(8)
S(4)	-0.112 26(14)	0.562 52(10)	0.253 90(8)	0.0508(10)	C(37)	-0.045 3(3)	-0.068 44(22)	0.376 08(20)	0.051(4)
C(73)	-0.265 6(3)	0.614 21(25)	0.151 44(20)	0.059(5)	C(38)	-0.041 0(3)	-0.151 41(22)	0.368 51(20)	0.064(5)
F(73)	-0.218 6(3)	0.563 44(25)	0.107 35(20)	0.082(3)	C(39)	0.052 1(3)	-0.186 56(22)	0.339 05(20)	0.060(4)
C(74)	-0.340 3(4)	0.668 7(3)	0.127 31(23)	0.070(5)	C(40)	0.140 9(3)	-0.138 75(22)	0.317 14(20)	0.060(4)
F(74)	-0.382 6(4)	0.658 2(3)	0.063 29(23)	0.119(5)	C(41)	0.136 6(3)	-0.055 77(22)	0.324 70(20)	0.050(4)
C(75)	-0.392 3(3)	0.719 70(25)	0.171 26(25)	0.072(5)	C(42)	0.043 6(3)	-0.020 62(22)	0.354 16(20)	0.038(3)
F(75)	-0.472 1(3)	0.768 38(25)	0.148 36(25)	0.115(4)	C(43)	0.198 9(3)	0.059 37(15)	0.474 49(18)	0.041(3)
C(76)	-0.353 0(4)	0.726 7(3)	0.236 7(3)	0.074(6)	C(44)	0.284 6(3)	0.083 32(15)	0.524 77(18)	0.051(4)
F(76)	-0.397 2(4)	0.780 4(3)	0.279 5(3)	0.117(4)	C(45)	0.320 3(3)	0.163 69(15)	0.535 79(18)	0.057(4)
C(77)	-0.268 0(3)	0.680 17(21)	0.258 83(21)	0.059(5)	C(46)	0.270 2(3)	0.220 09(15)	0.496 55(18)	0.057(4)
F(77)	-0.233 7(3)	0.687 37(21)	0.324 25(21)	0.084(3)	C(47)	0.184 4(3)	0.196 13(15)	0.446 27(18)	0.046(4)
C(78)	-0.217 3(5)	0.622 2(4)	0.216 9(3)	0.051(4)	C(48)	0.148 7(3)	0.115 77(15)	0.435 24(18)	0.033(3)
C(79)	0.174 4(4)	0.449 4(3)	0.191 78(23)	0.066(5)	C(49)	-0.190 9(3)	0.094 91(23)	0.350 62(15)	0.049(4)
C(80)	0.054 2(4)	0.430 2(3)	0.192 09(23)	0.063(5)	C(50)	-0.300 4(3)	0.111 94(23)	0.371 31(15)	0.061(5)
C(81)	-0.002 2(4)	0.462 1(3)	0.135 51(23)	0.063(5)	C(51)	-0.312 3(3)	0.145 96(23)	0.435 95(15)	0.067(5)
C(82)	0.083 3(4)	0.501 0(3)	0.100 24(23)	0.064(5)	C(52)	-0.214 7(3)	0.162 97(23)	0.479 91(15)	0.063(5)
C(83)	0.192 4(4)	0.493 1(3)	0.135 02(23)	0.067(5)	C(53)	-0.105 3(3)	0.145 94(23)	0.459 22(15)	0.046(4)
Au(1)	0.096 60(2)	0.141 59(1)	0.262 41(1)	0.0329(1)	C(54)	-0.093 4(3)	0.111 93(23)	0.394 57(15)	0.038(3)
P(1)	-0.042 35(12)	0.159 07(9)	0.173 34(7)	0.0356(8)	Cl(1)	0.501 2(3)	0.469 73(24)	0.065 31(21)	0.1663(14)
C(1)	-0.121 6(3)	0.002 26(22)	0.182 83(19)	0.048(4)	C(84)	0.414 4(18)	0.530 4(12)	0.007 8(10)	0.108(6)

tions were also investigated between **1b** or [N(PPh₃)₂]-[Mo(SC₆F₅)₄Cp] (**7a**)² and the soluble complex [AuCl(SMe₂)], from which the thioether can be displaced: despite visual and spectroscopic evidence for reactions taking place, no pure products could be isolated from these synthetic experiments.

Solid State Structural Investigations. Structural analyses by X-ray diffraction were carried out on orange-red crystals of [Au(PPh₃)₃][Mo(SC₆F₅)₄Cp]·0.5CH₂Cl₂, **2a**·0.5CH₂Cl₂, and red crystals of [Cu(PPh₃)₃][Mo(SC₆F₅)₄Cp]·0.5CH₂Cl₂, **6**·0.5CH₂Cl₂, both obtained from dichloromethane-hexane solutions at -15 to -20 °C. Fractional atomic coordinates for **2a** and **6** are given in Tables 1 and 3, respectively, and selected geometrical parameters with standard deviations in Tables 2 and

4. The two crystal structures are isomorphous, and the lattices contain discrete ions [M'(PPh₃)₃]⁺ and [Mo(SC₆F₅)₄Cp]⁻ along with noninteracting, disordered molecules of CH₂Cl₂ as solvent of crystallization (one molecule per unit cell). The packing arrangement of ions in **2a**·0.5CH₂Cl₂ is depicted in Figure 1, and there are no significant non-bonding interionic contacts less than 3.5 Å. The anion [Mo(SC₆F₅)₄Cp]⁻, as illustrated in Figure 2 for **2a** and in Figure 3 for **6**, has a "piano-stool" geometry closely related to that observed in [N(PPh₃)₂][Mo(SC₆F₅)₄Cp] (**7a**)² and [TlMo(SC₆F₅)₄Cp] (**1a**).¹ The Mo-S bond lengths in complexes **2a** and **6**, average 2.421 and 2.420 Å, respectively, are essentially the same as in **7a** and **1a** although there is a small displacement of the S atoms toward the central axis in

Table 2. Derived Geometrical Parameters for Complex 2a

Bond Lengths (Å) with Standard Deviations			
Au(1)–P(1)	2.3673(15)	Mo(1)–S(1)	2.4203(17)
Au(1)–P(2)	2.3990(15)	Mo(1)–S(2)	2.4336(17)
Au(1)–P(3)	2.3918(14)	Mo(1)–S(3)	2.4080(18)
P(1)–C(6)	1.819(4)	Mo(1)–S(4)	2.4201(17)
P(1)–C(12)	1.816(4)	Mo(1)–C(79)	2.281(5)
P(1)–C(18)	1.817(4)	Mo(1)–C(80)	2.252(5)
P(2)–C(24)	1.805(4)	Mo(1)–C(81)	2.326(5)
P(2)–C(30)	1.834(4)	Mo(1)–C(82)	2.399(5)
P(2)–C(36)	1.813(4)	Mo(1)–C(83)	2.372(5)
P(3)–C(42)	1.821(4)	S(1)–C(60)	1.770(6)
P(3)–C(48)	1.816(4)	S(2)–C(66)	1.755(6)
P(3)–C(54)	1.810(4)	S(3)–C(72)	1.776(7)
Cl(1)–C(84)	1.866(21)	S(4)–C(78)	1.768(7)

Angles (deg) with Standard Deviations			
P(1)–Au(1)–P(2)	123.83(5)	Au(1)–P(3)–C(54)	117.43(13)
P(1)–Au(1)–P(3)	122.28(5)	C(42)–P(3)–C(48)	105.42(17)
P(2)–Au(1)–P(3)	113.62(5)	C(42)–P(3)–C(54)	105.28(17)
Au(1)–P(1)–C(6)	113.08(13)	C(48)–P(3)–C(54)	104.64(17)
Au(1)–P(1)–C(12)	114.30(13)	P(3)–C(42)–C(37)	122.4(3)
Au(1)–P(1)–C(18)	116.26(13)	P(3)–C(42)–C(41)	117.6(3)
C(6)–P(1)–C(12)	105.58(18)	P(3)–C(48)–C(43)	122.3(3)
C(6)–P(1)–C(18)	103.42(18)	P(3)–C(48)–C(47)	117.46(25)
C(12)–P(1)–C(18)	102.89(18)	P(3)–C(54)–C(49)	117.6(3)
P(1)–C(6)–C(1)	119.3(3)	P(3)–C(54)–C(53)	122.4(3)
P(1)–C(6)–C(5)	120.6(3)	S(1)–Mo(1)–S(2)	81.30(6)
P(1)–C(12)–C(7)	117.8(3)	S(1)–Mo(1)–S(3)	135.72(6)
P(1)–C(12)–C(11)	122.2(3)	S(1)–Mo(1)–S(4)	81.02(6)
P(1)–C(18)–C(13)	121.1(3)	S(2)–Mo(1)–S(3)	82.33(6)
P(1)–C(18)–C(17)	118.7(3)	S(2)–Mo(1)–S(4)	136.30(6)
Au(1)–P(2)–C(24)	113.00(13)	S(3)–Mo(1)–S(4)	83.12(6)
Au(1)–P(2)–C(30)	111.28(14)	Mo(1)–S(1)–C(60)	115.08(21)
Au(1)–P(2)–C(36)	116.13(13)	S(1)–C(60)–C(55)	124.2(4)
C(24)–P(2)–C(30)	105.04(19)	S(1)–C(60)–C(59)	121.2(4)
C(24)–P(2)–C(36)	106.52(18)	Mo(1)–S(2)–C(66)	113.98(21)
C(30)–P(2)–C(36)	103.92(18)	S(2)–C(66)–C(61)	122.9(4)
P(2)–C(24)–C(19)	118.3(3)	S(2)–C(66)–C(65)	123.4(4)
P(2)–C(24)–C(23)	121.6(3)	Mo(1)–S(3)–C(72)	115.21(23)
P(2)–C(30)–C(25)	121.0(3)	S(3)–C(72)–C(67)	126.1(5)
P(2)–C(30)–C(29)	118.3(3)	S(3)–C(72)–C(71)	118.8(4)
P(2)–C(36)–C(31)	117.3(3)	Mo(1)–S(4)–C(78)	118.24(22)
P(2)–C(36)–C(35)	122.6(3)	S(4)–C(78)–C(73)	127.4(5)
Au(1)–P(3)–C(42)	109.43(13)	S(4)–C(78)–C(77)	118.0(4)
Au(1)–P(3)–C(48)	113.68(12)		

the latter species (mean *trans* angles S–Mo–S: 136.0° in **2a**, 136.1° in **6**, 132.0° in **1a**) which is consistent with Tl⁺ coordination to the sulfur atoms in **1a**. A structurally related anion has previously been characterized in the bis(1,2-dithiolene) complex, [PPh₄][Mo{S₂C₂(CN)₂}₂Cp], with a mean Mo–S bond length of 2.407 Å and a mean *trans* S–Mo–S angle of 135.5°, indicative of a species in which the unsaturated chelating sulfur ligands act as dinegative dithiolate ligands.⁶

The three triphenylphosphine ligands of **2a** are trigonally disposed about the Au atom in the cation [Au(PPh₃)₃]⁺, and the Au atom is displaced from the P₃ plane by 0.072 Å, see Figure 2. There is a degree of asymmetry, as indicated by P–Au–P angles of 123.83(5)°, 122.28(5)°, and 113.62(5)°, giving an average P–Au–P angle of 119.9°. These angles and the average Au–P bond length of 2.386 Å are comparable with those reported for the trigonal cation in the structurally characterized ionic thiaborane species [Au(PPh₃)₃][B₃H₁₂S]: P–Au–P angles 124.1(2), 121.5(2), and 112.3(2)° {average 119.3°}; mean Au–P bond length 2.382(5) Å.⁷ The cation [Cu(PPh₃)₃]⁺ of **6** contains Cu(I) in

an essentially trigonal planar coordination geometry with Cu located 0.061 Å out of the P₃ plane, see Figure 3. As in the cation [Au(PPh₃)₃]⁺ of **2a**, there is some asymmetry in the disposition of triphenylphosphine ligands around Cu with P–Cu–P angles of 121.24(7)°, 123.44(8)°, and 115.11(7)° (mean 119.9°) and an average Cu–P bond length of 2.295 Å.

Examples of simple tri-coordinated Cu(I) complexes are relatively rare. Phosphine halide complexes [CuX(PPh₃)₃] have distorted tetrahedral coordination geometries,⁸ and even in compounds [Cu(PPh₃)₃][BF₄]⁹ and [Cu(PPh₃)₃][ClO₄]¹⁰ the formal cations [Cu(PPh₃)₃]⁺ interact, albeit weakly, with the poorly η¹-bonded anions, OClO₃[−] and FBF₃[−], respectively, to generate four-coordinate Cu(I) centers. These distorted four-coordinate complexes show average Cu–P distances in the range 2.30–2.35 Å and P–Cu–P angles in the range 110–116°.¹⁰ However, distorted trigonal-planar geometry is observed in anionic trihalogenocuprates [CuX₃]^{2−},¹¹ and, more significantly in the context of this work, [Cu(PPh₃)₃][V(CO)₆] contains discrete trigonal cations [Cu(PPh₃)₃]⁺ and octahedral anions [V(CO)₆][−].¹² The geometrical parameters of the cation in [Cu(PPh₃)₃][V(CO)₆] are closely related to those in **6**, which has a mean Cu–P distance of 2.295 Å and mean P–Cu–P angle of 120.0°.¹²

Both yellow and light green crystals of [Au(PEt₃)₃][W(SC₆F₅)₄Cp] (**3b**) show indistinguishable properties in solution so that any structural difference is a solid state phenomenon. It is possible that an interaction between the Au(I) cation and the tetrathiolate anion in one of these forms, e.g., *via* the sulfur atoms, could account for the observed difference. The less bulky PEt₃ groups of the Au(I) cation in complex **3b** could conceivably permit such a cation–anion interaction which is precluded by the more sterically demanding PPh₃ ligands of complex **2a**. However, the IR spectra of both crystalline forms of **3b** are virtually identical, e.g., strong C₆F₅ vibrations at 1506 and 1463 cm^{−1} or at 1505 and 1461 cm^{−1} for the yellow or green forms, respectively. Moreover, the UV/vis spectra for both solids in Nujol mulls are very similar, with one broad absorption band in the visible region, λ_{max} *ca.* 435 nm (yellow form) or *ca.* 440 nm (green form). These data suggest that any differences in structure between the two solid state forms are relatively minor. Preliminary results from an X-ray structural investigation of a crystal of the green form indicates that it contains discrete [Au(PEt₃)₃]⁺ cations and [W(SC₆F₅)₄Cp][−] anions with a structure analogous to that of complex **2a**. The PEt₃ groups were, however, too disordered to permit satisfactory refinement of this structure.

NMR Spectroscopic Studies in Solution. NMR data for all new compounds are reported in the Experimental Section and are consistent with the ionic con-

(7) Guggenberger, L. J. *J. Organomet. Chem.* **1974**, *81*, 271.(8) Barron, P. F.; Dyason, J. C.; Healy, P. C.; Engelhardt, L. M.; Pakawatchai, C.; Patrick, V. A.; White, A. H. *J. Chem. Soc., Dalton Trans.* **1987**, 1099.(9) Gaughan, A. P.; Dori, Z.; Ibers, J. A. *Inorg. Chem.* **1974**, *13*, 1657.(10) Dyason, J. C.; Engelhardt, L. M.; Healy, P. C.; Klich, H. L.; White, A. H. *Aust. J. Chem.* **1986**, *39*, 2003.(11) Bowmaker, G. A.; Clark, G. R.; Rogers, D. A.; Camus, A.; Marsich, N. *J. Chem. Soc., Dalton Trans.* **1984**, 37.(12) Doyle, G.; Eriksen, K. A.; Engen, D. V. *Organometallics* **1985**, *4*, 2201.(6) (a) Locke, J.; McCleverty, J. A. *Inorg. Chem.* **1966**, *5*, 1157. (b) Churchill, M. R.; Cooke, J. *J. Chem. Soc. A* **1970**, 2046. (We thank a reviewer for drawing our attention to this work.)

Table 3. Fractional Coordinates of Atoms and U_{eq} Values (Å²) with Estimated Standard Deviations for Complex 6

atom	x	y	z	U _{eq}	atom	x	y	z	U _{eq}
Mo(1)	0.076 86(6)	0.561 61(4)	0.209 26(3)	0.0380(4)	C(2)	0.057 9(4)	0.128 78(25)	-0.016 97(24)	0.060(6)
S(1)	0.002 53(18)	0.665 03(13)	0.144 34(11)	0.0526(13)	C(3)	0.122 0(4)	0.199 43(25)	-0.022 34(24)	0.066(6)
C(55)	0.195 7(4)	0.713 2(3)	0.075 48(23)	0.057(6)	C(4)	0.136 5(4)	0.256 00(25)	0.032 46(24)	0.062(6)
F(55)	0.198 8(4)	0.639 1(3)	0.047 08(23)	0.086(4)	C(5)	0.087 0(4)	0.241 96(25)	0.092 64(24)	0.050(5)
C(56)	0.271 4(5)	0.769 0(3)	0.057 0(3)	0.073(7)	C(6)	0.022 9(4)	0.171 33(25)	0.098 01(24)	0.039(4)
F(56)	0.354 2(5)	0.747 9(3)	0.016 2(3)	0.112(5)	C(7)	-0.252 4(5)	0.083 5(3)	0.128 0(3)	0.066(6)
C(57)	0.267 6(5)	0.847 2(3)	0.080 9(3)	0.081(8)	C(8)	-0.334 0(5)	0.020 0(3)	0.118 8(3)	0.085(8)
F(57)	0.347 5(5)	0.901 5(3)	0.065 8(3)	0.130(6)	C(9)	-0.307 0(5)	-0.053 4(3)	0.141 8(3)	0.076(7)
C(58)	0.183 8(5)	0.867 1(3)	0.123 6(3)	0.076(7)	C(10)	-0.198 3(5)	-0.063 3(3)	0.174 1(3)	0.062(6)
F(58)	0.175 3(5)	0.943 2(3)	0.146 1(3)	0.119(6)	C(11)	-0.116 7(5)	0.000 2(3)	0.183 3(3)	0.049(5)
C(59)	0.107 3(4)	0.811 72(25)	0.140 39(23)	0.054(6)	C(12)	-0.143 7(5)	0.073 6(3)	0.160 3(3)	0.041(5)
F(59)	0.023 6(4)	0.834 81(25)	0.179 82(23)	0.076(4)	C(13)	-0.161 3(5)	0.264 3(3)	0.252 95(20)	0.056(6)
C(60)	0.109 3(7)	0.731 9(5)	0.118 2(4)	0.046(5)	C(14)	-0.238 8(5)	0.324 6(3)	0.262 05(20)	0.070(7)
S(2)	0.250 03(18)	0.649 77(12)	0.222 02(10)	0.0499(13)	C(15)	-0.284 3(5)	0.361 8(3)	0.206 60(20)	0.070(7)
C(61)	0.436 8(4)	0.571 5(3)	0.276 49(24)	0.055(6)	C(16)	-0.252 4(5)	0.338 7(3)	0.142 04(20)	0.064(6)
F(61)	0.436 2(4)	0.529 6(3)	0.216 74(24)	0.086(4)	C(17)	-0.174 9(5)	0.278 4(3)	0.132 94(20)	0.043(5)
C(62)	0.517 7(4)	0.555 4(3)	0.325 3(3)	0.056(6)	C(18)	-0.129 4(5)	0.241 2(3)	0.188 39(20)	0.039(4)
F(62)	0.597 9(4)	0.502 4(3)	0.312 5(3)	0.093(4)	P(2)	0.045 81(15)	0.086 77(11)	0.361 53(9)	0.0330(10)
C(63)	0.522 6(4)	0.597 4(3)	0.386 41(25)	0.064(6)	C(19)	-0.192 5(4)	0.091 8(3)	0.349 13(19)	0.046(5)
F(63)	0.601 1(4)	0.580 7(3)	0.435 30(25)	0.100(5)	C(20)	-0.302 1(4)	0.108 4(3)	0.370 19(19)	0.059(6)
C(64)	0.443 2(4)	0.652 4(3)	0.399 54(25)	0.059(6)	C(21)	-0.313 2(4)	0.144 1(3)	0.434 63(19)	0.063(6)
F(64)	0.447 3(4)	0.692 8(3)	0.460 12(25)	0.100(5)	C(22)	-0.214 7(4)	0.163 2(3)	0.478 02(19)	0.060(6)
C(65)	0.361 5(4)	0.666 6(3)	0.350 46(22)	0.053(6)	C(23)	-0.105 2(4)	0.146 6(3)	0.456 95(19)	0.047(5)
F(65)	0.286 7(4)	0.723 1(3)	0.364 07(22)	0.079(4)	C(24)	-0.094 0(4)	0.110 9(3)	0.392 50(19)	0.037(4)
C(66)	0.353 5(6)	0.626 3(5)	0.286 0(4)	0.046(5)	C(25)	0.183 3(4)	0.194 41(23)	0.444 87(23)	0.044(5)
S(3)	0.131 20(17)	0.547 37(13)	0.327 07(10)	0.0470(12)	C(26)	0.268 7(4)	0.218 34(23)	0.495 93(23)	0.058(6)
C(67)	-0.020 0(4)	0.439 35(25)	0.379 86(21)	0.049(5)	C(27)	0.318 5(4)	0.162 33(23)	0.535 54(23)	0.058(6)
F(67)	0.031 1(4)	0.382 20(25)	0.344 04(21)	0.068(3)	C(28)	0.283 0(4)	0.082 39(23)	0.524 11(23)	0.054(5)
C(68)	-0.104 2(4)	0.416 9(3)	0.420 57(24)	0.057(6)	C(29)	0.197 7(4)	0.058 46(23)	0.473 05(23)	0.041(5)
F(68)	-0.136 1(4)	0.340 1(3)	0.422 59(24)	0.093(4)	C(30)	0.147 8(4)	0.114 48(23)	0.433 43(23)	0.031(4)
C(69)	-0.154 1(4)	0.472 8(3)	0.460 33(24)	0.064(6)	C(31)	-0.045 3(4)	-0.068 7(3)	0.375 10(25)	0.049(5)
F(69)	-0.240 9(4)	0.452 0(3)	0.497 66(24)	0.098(5)	C(32)	-0.041 0(4)	-0.151 2(3)	0.368 07(25)	0.065(6)
C(70)	-0.122 0(4)	0.551 5(3)	0.456 89(22)	0.058(6)	C(33)	0.051 7(4)	-0.186 3(3)	0.338 08(25)	0.065(6)
F(70)	-0.169 2(4)	0.606 2(3)	0.497 31(22)	0.087(4)	C(34)	0.140 1(4)	-0.139 0(3)	0.315 13(25)	0.060(6)
C(71)	-0.036 9(4)	0.572 8(3)	0.417 43(21)	0.053(6)	C(35)	0.135 8(4)	-0.056 5(3)	0.322 17(25)	0.048(5)
F(71)	-0.006 0(4)	0.650 1(3)	0.417 55(21)	0.076(4)	C(36)	0.043 1(4)	-0.021 3(3)	0.352 16(25)	0.035(4)
C(72)	0.017 2(6)	0.517 8(5)	0.375 9(4)	0.042(5)	P(3)	0.294 22(16)	0.157 17(12)	0.255 57(9)	0.0365(11)
S(4)	-0.114 06(17)	0.561 39(13)	0.251 74(11)	0.0513(13)	C(37)	0.279 3(3)	0.306 1(3)	0.319 7(3)	0.053(5)
C(73)	-0.266 4(8)	0.677 4(6)	0.256 2(5)	0.061(6)	C(38)	0.319 4(3)	0.373 1(3)	0.361 0(3)	0.067(7)
F(73)	-0.232 5(5)	0.687 5(3)	0.322 3(3)	0.088(4)	C(39)	0.433 4(3)	0.378 6(3)	0.389 2(3)	0.067(7)
C(74)	-0.352 3(5)	0.727 0(3)	0.233 7(3)	0.082(8)	C(40)	0.507 4(3)	0.317 1(3)	0.375 9(3)	0.062(6)
F(74)	-0.397 0(5)	0.779 9(3)	0.276 9(3)	0.125(6)	C(41)	0.467 4(3)	0.250 1(3)	0.334 6(3)	0.049(5)
C(75)	-0.390 0(5)	0.719 8(3)	0.168 2(3)	0.086(8)	C(42)	0.353 4(3)	0.244 6(3)	0.306 5(3)	0.037(4)
F(75)	-0.473 8(5)	0.765 5(3)	0.145 4(3)	0.115(5)	C(43)	0.300 2(4)	0.111 9(3)	0.120 53(25)	0.043(5)
C(76)	-0.349 1(5)	0.661 8(3)	0.126 3(3)	0.077(7)	C(44)	0.340 7(4)	0.113 1(3)	0.056 23(25)	0.058(6)
F(76)	-0.381 3(5)	0.658 7(3)	0.060 3(3)	0.121(6)	C(45)	0.425 7(4)	0.169 8(3)	0.043 42(25)	0.083(8)
C(77)	-0.259 6(4)	0.616 9(3)	0.149 1(3)	0.065(7)	C(46)	0.470 2(4)	0.225 3(3)	0.094 89(25)	0.092(8)
F(77)	-0.227 2(4)	0.558 7(3)	0.106 0(3)	0.091(5)	C(47)	0.429 7(4)	0.224 1(3)	0.159 20(25)	0.073(7)
C(78)	-0.218 3(7)	0.620 2(5)	0.214 7(4)	0.048(5)	C(48)	0.344 7(4)	0.167 3(3)	0.172 00(25)	0.043(5)
C(79)	0.083 0(7)	0.496 4(3)	0.098 00(24)	0.064(6)	C(49)	0.410 9(5)	0.014 4(3)	0.241 96(19)	0.064(6)
C(80)	0.191 8(7)	0.489 3(3)	0.134 10(24)	0.066(7)	C(50)	0.456 2(5)	-0.053 8(3)	0.266 71(19)	0.079(7)
C(81)	0.172 1(7)	0.447 6(3)	0.191 92(24)	0.062(6)	C(51)	0.467 3(5)	-0.061 3(3)	0.336 06(19)	0.073(7)
C(82)	0.051 3(7)	0.429 0(3)	0.191 55(24)	0.063(6)	C(52)	0.433 0(5)	-0.000 7(3)	0.380 67(19)	0.057(6)
C(83)	-0.003 8(7)	0.459 1(3)	0.133 51(24)	0.062(6)	C(53)	0.387 7(5)	0.067 5(3)	0.355 92(19)	0.045(5)
Cu(1)	0.097 74(7)	0.137 83(5)	0.263 77(4)	0.0338(5)	C(54)	0.376 6(5)	0.075 0(3)	0.286 57(19)	0.036(4)
P(1)	-0.037 95(16)	0.156 97(11)	0.178 18(9)	0.0357(11)	Cl(1)	0.503 3(5)	0.468 3(3)	0.065 0(3)	0.1895(20)
C(1)	0.008 4(4)	0.114 74(25)	0.043 20(24)	0.050(5)	C(84)	0.577 8(23)	0.467 5(16)	-0.010 1(13)	0.1200(0)

stitutions proposed above. ¹H NMR spectra show a singlet resonance for cyclopentadienyl H atoms and contain resonances assignable to H atoms of phosphine ligands and of solvated CH₂Cl₂, when present. ³¹P{¹H} NMR spectra of species 2–5 comprise one singlet resonance shifted to high frequency from the resonance of the free ligand and assignable to equivalent phosphine ligands coordinated to Au(I); observed coordination shifts are PPh₃ 43, PEt₃ 56–58, dppe 39, and dppp 14.5 ppm.

At ambient temperature the ¹⁹F NMR spectra of all compounds in a range of solvents show simple spectra of four equivalent pentafluorophenyl groups in which *ortho* F atoms and, separately, *meta* F atoms are magnetically equivalent, as illustrated in Figure 4a for

compound 3b. At low temperatures both the *ortho* and *meta* signals split into two equal-intensity resonances (e.g., see Figure 4) and the spectra correspond to stereochemically rigid C₆F₅ systems in which all five F atoms are inequivalent, as expected from the solid state structures. This fluxionality, previously observed in related derivatives,^{1–3} involves concerted rotation of the C₆F₅ rings (or rotation/inversion of C₆F₅S ligands) with pairwise interchange of *ortho* and *meta* F atoms. From the coalescence temperatures of *ortho* and/or *meta* ¹⁹F-resonances values of ΔG[‡] for this process can be calculated,¹³ (Table 5). Values of ΔG[‡] are temperature

Table 4. Derived Geometrical Parameters for Complex 6

Bond Lengths (Å) with Standard Deviations			
Cu(1)–P(1)	2.2890(20)	Mo(1)–S(1)	2.4036(23)
Cu(1)–P(2)	2.2945(20)	Mo(1)–S(2)	2.4363(21)
Cu(1)–P(3)	2.3019(21)	Mo(1)–S(3)	2.4210(22)
P(1)–C(6)	1.817(5)	Mo(1)–S(4)	2.4182(22)
P(1)–C(12)	1.827(6)	Mo(1)–C(79)	2.410(6)
P(1)–C(18)	1.816(5)	Mo(1)–C(80)	2.375(6)
P(2)–C(24)	1.821(5)	Mo(1)–C(81)	2.275(6)
P(2)–C(30)	1.815(5)	Mo(1)–C(82)	2.249(6)
P(2)–C(36)	1.823(5)	Mo(1)–C(83)	2.335(6)
P(3)–C(42)	1.814(5)	S(1)–C(60)	1.771(8)
P(3)–C(48)	1.819(5)	S(2)–C(66)	1.768(8)
P(3)–C(54)	1.837(5)	S(3)–C(72)	1.769(8)
Cl(1)–C(84)	1.78(3)	S(4)–C(78)	1.753(8)
Angles(deg) with Standard Deviations			
P(1)–Cu(1)–P(2)	121.24(7)	Cu(1)–P(3)–C(54)	112.40(18)
P(1)–Cu(1)–P(3)	123.44(8)	C(42)–P(3)–C(48)	105.29(23)
P(2)–Cu(1)–P(3)	115.11(7)	C(42)–P(3)–C(54)	104.83(24)
Cu(1)–P(1)–C(6)	113.89(17)	C(48)–P(3)–C(54)	103.49(23)
Cu(1)–P(1)–C(12)	113.24(19)	P(3)–C(42)–C(37)	117.9(4)
Cu(1)–P(1)–C(18)	118.01(18)	P(3)–C(42)–C(41)	122.1(4)
C(6)–P(1)–C(12)	104.97(24)	P(3)–C(48)–C(43)	117.0(4)
C(6)–P(1)–C(18)	102.51(23)	P(3)–C(48)–C(47)	122.8(4)
C(12)–P(1)–C(18)	102.64(24)	P(3)–C(54)–C(49)	120.8(4)
P(1)–C(6)–C(1)	122.5(4)	P(3)–C(54)–C(53)	118.4(4)
P(1)–C(6)–C(5)	117.5(4)	S(1)–Mo(1)–S(2)	82.49(7)
P(1)–C(12)–C(7)	121.2(4)	S(1)–Mo(1)–S(3)	135.99(8)
P(1)–C(12)–C(11)	118.6(4)	S(1)–Mo(1)–S(4)	83.06(8)
P(1)–C(18)–C(13)	118.3(4)	S(2)–Mo(1)–S(3)	81.24(7)
P(1)–C(18)–C(17)	121.4(4)	S(2)–Mo(1)–S(4)	136.18(8)
Cu(1)–P(2)–C(24)	118.50(17)	S(3)–Mo(1)–S(4)	81.08(7)
Cu(1)–P(2)–C(30)	113.44(16)	Mo(1)–S(1)–C(60)	114.9(3)
Cu(1)–P(2)–C(36)	110.06(17)	S(1)–C(60)–C(55)	126.2(5)
C(24)–P(2)–C(30)	103.65(22)	S(1)–C(60)–C(59)	118.6(5)
C(24)–P(2)–C(36)	105.02(22)	Mo(1)–S(2)–C(66)	114.2(3)
C(30)–P(2)–C(36)	105.01(22)	S(2)–C(66)–C(61)	123.8(5)
P(2)–C(24)–C(19)	117.4(3)	S(2)–C(66)–C(65)	121.8(5)
P(2)–C(24)–C(23)	122.6(3)	Mo(1)–S(3)–C(72)	115.6(3)
P(2)–C(30)–C(25)	117.4(3)	S(3)–C(72)–C(67)	123.7(5)
P(2)–C(30)–C(29)	122.4(3)	S(3)–C(72)–C(71)	121.2(5)
P(2)–C(36)–C(31)	122.7(4)	Mo(1)–S(4)–C(78)	118.4(3)
P(2)–C(36)–C(35)	117.3(4)	S(4)–C(78)–C(73)	117.5(6)
Cu(1)–P(3)–C(42)	112.14(18)	S(4)–C(78)–C(77)	128.0(6)
Cu(1)–P(3)–C(48)	117.54(18)		

dependent but only show small variations, virtually within experimental error, over the limited temperature ranges of coalescence points for comparable solvent/substrate systems studied here.

In CD₂Cl₂ solution, ionic molybdenum or tungsten species **3** and **5**, and the related salts [N(PPh₃)₂]-[M(SC₆F₅)₄Cp] (**7**), have ΔG[‡] values for C₆F₅ motion, which vary only with the metal M (M = Mo, ca. 41 kJ mol⁻¹; M = W ca. 43–44 kJ mol⁻¹), and show no dependence on counteranion. Derivatives (**1**) which coordinate Tl⁺ under these conditions^{1,2} show significantly higher ΔG[‡] values (M = Mo, 45.8 kJ mol⁻¹; M = W, 46.7 kJ mol⁻¹). Barriers to C₆F₅ rotation of all the ionic derivatives are essentially independent of solvent, being ca. 40–41 or 43–44 kJ mol⁻¹ for Mo or W species, respectively, in CD₂Cl₂, (CD₃)₂CO or C₆D₅CD₃ (see Table 5). In contrast, the thallium species (**1**) have significantly reduced barriers in acetone solution, with ΔG[‡] values marginally below those of the simple ionic systems, and this is consistent with the previously noted dissociation of Tl⁺ in this solvent; it is possible that the dissociating Tl⁺ ion may also assist in the rotation of C₆F₅ groups.

The singlet ³¹P{¹H} NMR resonance, δ 21.6 ppm, for complexes **4** in CD₂Cl₂ is virtually identical to that reported for the four-coordinate complex [Au(dppe)₂]-

SbF₆ in solution (20.8 ppm in CDCl₃).¹⁴ Also, complexes **5** give a singlet ³¹P{¹H} NMR resonance (–2.0 ppm) which is unchanged for **5b** on cooling to –80 °C, showing no evidence for uncoordinated phosphine functions at this temperature when any exchange process between free and complexed phosphorus groups should be slow on the NMR time scale. Therefore, it may be concluded that compounds **4** and **5** contain four-coordinate cations [Au(diphosphine)₂]⁺ of bidentate dppe or dppp, respectively, with five- or six-membered chelate rings, and this is supported by the complex ¹H resonances of the methylene H atoms of the phosphine ligands. Reports of chelated Au(I) complexes have mainly been confined to bidentate ligands with rigid backbones as in cations [Au{o-phenylenebis(dimethylarsine)}₂]⁺,¹⁵ and flexible, bidentate ligands such as dppe tend to preserve linear coordination of Au(I) by formation of annular binuclear complexes.¹⁴ However, bis-chelation of Au(I) by dppe has been established in crystalline [Au(dppe)₂]-SbF₆·Me₂CO¹⁴ and [Au(dppe)₂]Cl·2H₂O¹⁶ which contain approximately tetrahedral or flattened tetrahedral cations.

The ¹⁹F NMR spectrum of red compound (**6**) in CD₂-Cl₂ at –80 °C is dominated (>88%) by five broadened resonances of equivalent, rigid C₆F₅ groups which are most probably assignable to the dissolved ionic derivative, [Cu(PPh₃)₃][Mo(SC₆F₅)₄Cp], present in the solid state. At higher temperatures the resonances of *meta* and *ortho* F atoms pass through coalescence points, ca. –60 and –45 °C, respectively, to produce a spectrum of three broadened resonances from fluxional C₆F₅ groups at room temperature. However, even at low temperatures, small resonances due to other pentafluorophenyl species are present in these spectra and these bands increase in intensity at higher temperatures. It appears that ionic [Cu(PPh₃)₃]-[Mo(SC₆F₅)₄Cp] is somewhat unstable in solution and may be in equilibrium with decomposition products. It is likely that the three-coordinate cation [Cu-(PPh₃)₃]⁺ could undergo ligand redistribution reactions causing consequent interactions with the anion [Mo(SC₆F₅)₄Cp]⁻.

Conclusions

Complexes [TlM(SC₆F₅)₄Cp] (M = Mo, W) react with Au(I) species in the presence of phosphine ligands, PR₃ (R = Ph, Et), to form ionic derivatives [Au(PR₃)₂]-[M(SC₆F₅)₄Cp] as the only identifiable new products from reaction systems with molar ratios of reactants Au(I):PR₃ varying from 1:1 to 1:4. It therefore appears that the anions [M(SC₆F₅)₄Cp]⁻ do not compete effectively in the coordination to Au(I) in comparison with monodentate phosphine ligands or with bidentate phosphines (dppe, dppp) which readily form compounds [Au(Ph₂P(CH₂)_nPPh₂)₂][M(SC₆F₅)₄Cp]. It should be noted that phosphine ligands do interact with thallium derivatives (**1**) and decoordination of Tl(I) from the organometallic anions is observed under some conditions: dissociation of phosphine complexed Tl⁺ ions

(14) Berners-Price, S. J.; Mazid, M. A.; Sadler, P. J. *J. Chem. Soc., Dalton Trans.* **1984**, 969

(15) Uson, R.; Laguna, A.; Vicente, J.; Garcia, J.; Jones, P. G.; Sheldrick, G. M. *J. Chem. Soc., Dalton Trans.* **1981**, 655.

(16) Bates, P. A.; Waters, J. M. *Inorg. Chim. Acta* **1984**, *81*, 151

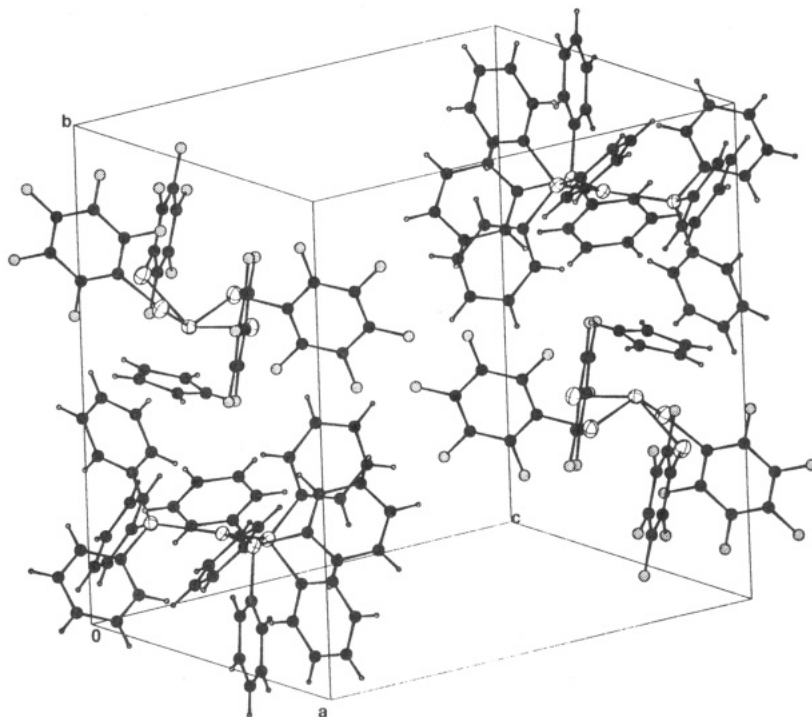


Figure 1. Packing diagram for complex **2a** depicting the unit cell contents. The disordered CH₂Cl₂ molecule has been omitted for clarity.

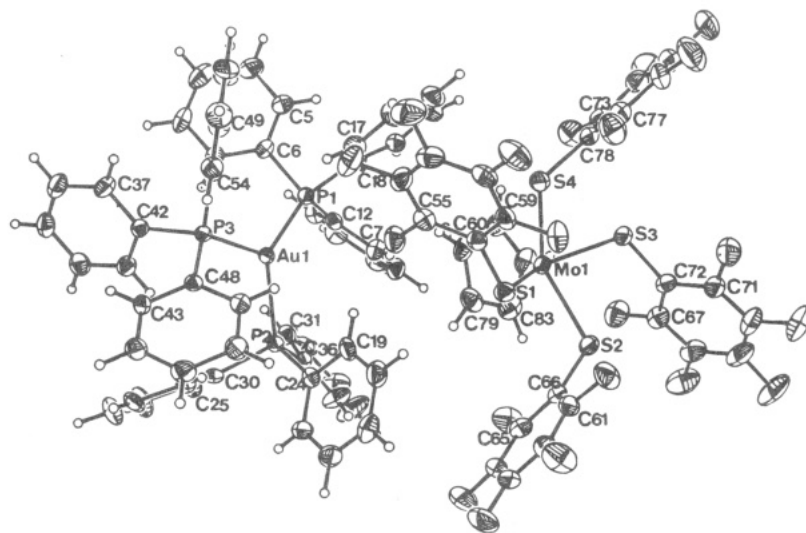


Figure 2. Molecular structure of complex **2a** (ORTEP 30% probability ellipsoids). Labels for the F and H atoms are taken from the carbon atom to which they are bonded.

is favored in polar solvents, such as acetone, and by more basic phosphine ligands, such as PEt₃ and PMe₂-Ph.^{1,2}

Attempts to characterize complexes of [M(SC₆F₅)₄Cp]⁻ with Au(I) or other coinage metals in the absence of phosphine ligands were unsuccessful, and it is possible that, in contrast to their facile coordination to Tl⁺, the complex anions are unexpectedly poor ligands towards these metals. Our failure to isolate complexes of the type [AuM(SC₆F₅)₄Cp] may be a result of unfavorable geometry of the cavity and the four planar S-donor sites since Au(I) does form complexes with other sulfur ligands under similar reaction conditions to those employed here. The fact that anions [M(SC₆F₅)₄Cp]⁻ (M = Mo, W) more readily form isolable, ionic solids with lattices containing relatively uncommon trigonal tri-coordinate complexes [Au(PR₃)₃]⁺ or [Cu(PPh₃)₃]⁺ as

countercations could be the result of favorable crystal packing of these ions.

Experimental Section

All reactions and operations were conducted under an atmosphere of dry, oxygen-free nitrogen gas, using Schlenk techniques, with solvents purified as described previously.^{1,2} The starting materials [AuCl(PR₃)] (R = PPh₃, PEt₃) and [AuCl(SMe₂)],¹⁷ [CuCl(PPh₃)₃],¹⁸ [TlM(SC₆F₅)₄Cp],^{1,2} [MCl₃(CO)₂-Cp], (M = Mo, W),¹⁹ and M'(SC₆F₅) (M' = Au, Ag, Cu)⁵ were prepared by literature methods. Compounds HAuCl₄, C₆F₅-SH, PPh₃, PEt₃, Ph₂P(CH₂)₂PPh₂ (dppe), Ph₂P(CH₂)₃PPh₂ (dppp), [N(PPh₃)₂]Cl, and Tl(O₂CMe) were obtained commercially (Strem or Aldrich) and used as supplied. IR spectra were recorded on a Perkin Elmer 580 or FT-1600 spectrometer, and UV/vis spectra were recorded on a Shimadzu UV-240 spectrometer. ¹H, ¹⁹F, and ³¹P{¹H} NMR spectra were recorded

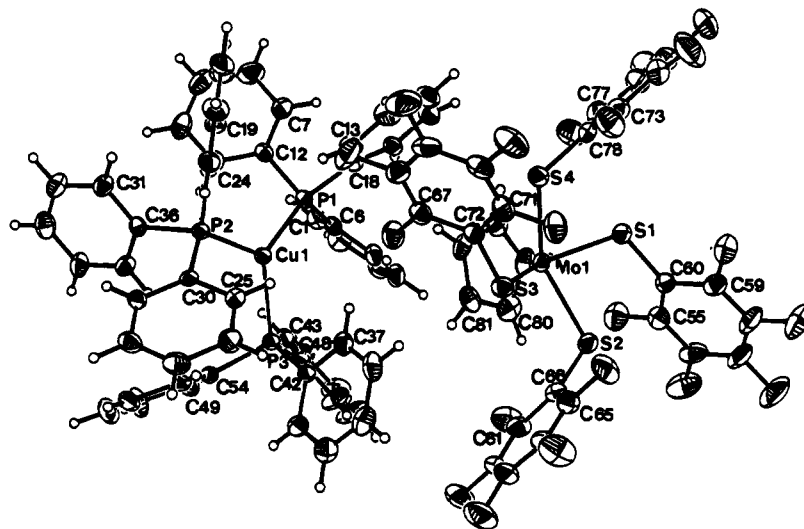


Figure 3. Molecular structure of complex **6** (ORTEP 30% probability ellipsoids). Labels for the F and H atoms are taken from the carbon atom to which they are bonded.

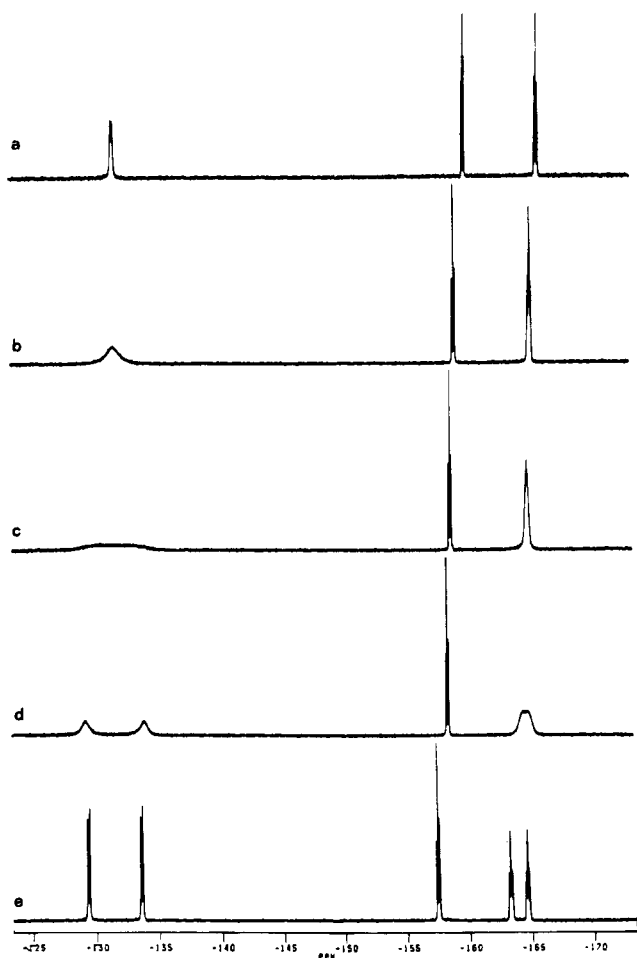


Figure 4. ^{19}F NMR spectra of $[\text{Au}(\text{PPh}_3)_3][\text{W}(\text{SC}_6\text{F}_5)_4\text{Cp}]$ in CD_2Cl_2 : (a) 20 °C; (b) -20 °C; (c) -30 °C; (d) -47 °C; (e) -80 °C.

at variable temperatures on a Bruker WP 200 SY instrument operating at 200.13, 188.31, and 80.32 MHz, respectively, using SiMe_4 , CCl_3F , and 85% aqueous H_3PO_4 as references (δ 0.0 ppm). Elemental analyses were carried out at UMIST, Manchester, U.K.

(17) See: Puddephatt, R. J. *The Chemistry of Gold*; Elsevier: Amsterdam, 1978. Puddephatt, R. J.; Treurnicht, I. J. *Organomet. Chem.* **1987**, 319, 129.

(18) Riechle, W. T. *Inorg. Chim. Acta* **1971**, 5, 325.

(19) Green, M. L. H.; Lindsell, W. E. *J. Chem. Soc., A* **1967**, 686.

Reaction of $[\text{TlMo}(\text{SC}_6\text{F}_5)_4\text{Cp}]$ with $[\text{AuCl}(\text{PPh}_3)]$. Complex **1a** (100 mg, 0.09 mmol), $[\text{AuCl}(\text{PPh}_3)]$ (44 mg, 0.09 mmol) and PPh_3 (68 mg, 0.26 mmol) were stirred in dichloromethane (40 cm^3) at room temperature for 15 min giving a dark cloudy solution. The mixture was filtered, hexane (10 cm^3) was added to the filtrate, and the resulting solution was concentrated *in vacuo* to give red crystals of $[\text{Au}(\text{PPh}_3)_3][\text{Mo}(\text{SC}_6\text{F}_5)_4\text{Cp}] \cdot 0.5\text{CH}_2\text{Cl}_2$ (**2a**) (72 mg, 41%). Anal. Found: C, 50.5; H, 2.8; S, 6.2. Calcd for $\text{C}_{83.5}\text{H}_{51}\text{ClF}_{20}\text{P}_3\text{S}_4\text{AuMo}$: C, 50.5; H, 2.6; S, 6.5. IR (CH_2Cl_2), C_6F_5 vibrations: 1507 (s) and 1478 (s) cm^{-1} . NMR: ^1H ($(\text{CD}_3)_2\text{CO}$, 19 °C), δ 7.2–7.6 (m, 45H, C_6H_5), 5.25 (s, 5H, C_5H_5) and 5.23 (s, 1H, CH_2Cl_2) ppm; ^{19}F ($(\text{CD}_3)_2\text{CO}$, 19 °C), δ -130.6 (br, d, $J = 20.3\text{ Hz}$, 8 *o*-F), -160.6 (t, $J = 20.6\text{ Hz}$, 4 *p*-F) and -166.2 (m, 8 *m*-F); ($(\text{CD}_3)_2\text{CO}$, -90 °C), -127.8 (dd, $J = 28.9, 6.8\text{ Hz}$, 4 *o*-F), -132.7 (dd, $J = 27.9, 6.2\text{ Hz}$, 4 *o*-F), -158.6 (t, $J = 21.9\text{ Hz}$, 4 *p*-F), -164.1 (~t, $J = 23.0\text{ Hz}$, 4 *m*-F), and -165.0 (~t, $J = 23.6\text{ Hz}$, 4 *m*-F); ^{31}P ($(\text{CD}_3)_2\text{CO}$, 20 °C) δ 37.7 (br s) ppm.

Reaction of $[\text{TlMo}(\text{SC}_6\text{F}_5)_4\text{Cp}]$ with $[\text{AuCl}(\text{PEt}_3)]$. Complex **1a** (100 mg, 0.09 mmol), $[\text{AuCl}(\text{PEt}_3)]$ (30 mg, 0.09 mmol) and PEt_3 (34 mg, 0.29 mmol) were stirred in dichloromethane (40 cm^3) under nitrogen at room temperature for 30 min giving an orange cloudy solution. The mixture was filtered, hexane (10 cm^3) was added, and the resulting solution was concentrated *in vacuo* to give red crystals of $[\text{Au}(\text{PEt}_3)_3][\text{Mo}(\text{SC}_6\text{F}_5)_4\text{Cp}]$ (**3a**) (70 mg, 54%). Anal. Found: C, 37.0; H, 3.0. Calcd for $\text{C}_{47}\text{H}_{50}\text{S}_4\text{P}_3\text{F}_{20}\text{MoAu}$: C, 37.4; H, 3.3. IR (CH_2Cl_2): C_6F_5 vibrations at 1508 (s) and 1477 cm^{-1} . NMR: ^1H (CDCl_3 , 20 °C) δ 5.29 (s, 5H, C_5H_5), 2.1–1.8 (br m, 18H, CH_2), and 1.4–1.0 (br m, 27H, CH_3); ^{19}F (CD_2Cl_2 , 18 °C) δ -131.3 (br d, $J = 20.8\text{ Hz}$, 8 *o*-F), -160.1 (m, 4 *p*-F), and -165.9 (m, 8 *m*-F); (CD_2Cl_2 , -80 °C), -129.3 (dd, $J = 29.2, 6.4\text{ Hz}$, 4 *o*-F), -133.1 (dd, $J = 27.7, 6.0\text{ Hz}$, 4 *o*-F), -157.5 (t, $J = 22.4\text{ Hz}$, 4 *p*-F), -163.2 (~t, $J = 24.5\text{ Hz}$, 4 *m*-F), and -164.6 (~t, $J = 23.7\text{ Hz}$, 4 *m*-F); ^{31}P (CD_2Cl_2 , 18 °C) δ 35.9 (s); (CD_2Cl_2 , -80 °C), 39.6 (s); ^{19}F ($(\text{CD}_3)_2\text{CO}$, 20 °C) δ -130.6 (dd, $J = 26.0\text{ Hz}$, 8 *o*-F), -160.9 (m, 4 *p*-F), and -166.4 (m, 8 *m*-F); ^{31}P ($(\text{CD}_3)_2\text{CO}$, 20 °C) δ 35.6 (br s) ppm.

Reaction of $[\text{TiW}(\text{SC}_6\text{F}_5)_4\text{Cp}]$ with $[\text{AuCl}(\text{PPh}_3)]$. Complex **1b** (100 mg, 0.08 mmol), $[\text{AuCl}(\text{PPh}_3)]$ (45 mg, 0.09 mmol) and PPh_3 (78 mg, 0.30 mmol) were stirred in dichloromethane (40 cm^3) under nitrogen at room temperature for 15 min giving a cloudy solution. The mixture was filtered, hexane (10 cm^3) was added, and the resulting solution was concentrated *in vacuo* to give yellow crystals of $[\text{Au}(\text{PPh}_3)_3][\text{W}(\text{SC}_6\text{F}_5)_4\text{Cp}]$ (**2b**) (100 mg, 62%). Anal. Found: C, 49.2; H, 2.0; S, 6.3. Calcd for $\text{C}_{83}\text{H}_{50}\text{F}_{20}\text{P}_3\text{S}_4\text{AuW}$: C, 49.1; H, 2.5; S, 6.3. IR (CH_2Cl_2): C_6F_5 vibrations at 1508 (s) and 1479 (s) cm^{-1} . NMR: ^1H ($(\text{CD}_3)_2\text{CO}$, 20 °C) δ 7.2–7.6 (m, 45H, C_6H_5) and 5.17 (s, 5H,

Table 5. Coalescence Temperatures (T_c) and Derived ΔG^\ddagger values from *ortho* and *meta* ¹⁹F NMR Resonances of C₆F₅ Groups of Pentafluorobenzenethiolato Complexes in Acetone or Dichloromethane Solutions

complex	resonance	acetone- <i>d</i> ₆		dichloromethane- <i>d</i> ₂	
		T_c (K)	ΔG^\ddagger (kJ mol ⁻¹) ^a	T_c (K)	ΔG^\ddagger (kJ mol ⁻¹) ^a
[TiMo(SC ₆ F ₅) ₄ Cp] (1a) ^b	<i>meta</i> - ¹⁹ F	203	38.8	243	45.8
[Au(PPh ₃) ₃][Mo(SC ₆ F ₅) ₄ Cp] (2a)	<i>meta</i> - ¹⁹ F	208	40.0		
	<i>ortho</i> - ¹⁹ F	224	40.1		
[Au(PET ₃) ₃][Mo(SC ₆ F ₅) ₄ Cp] (3a)	<i>meta</i> - ¹⁹ F			213	40.3
	<i>ortho</i> - ¹⁹ F			228	41.4
[N(PPh ₃) ₂][Mo(SC ₆ F ₅) ₄ Cp] (7a)	<i>meta</i> - ¹⁹ F			216	40.9
	<i>ortho</i> - ¹⁹ F			226	41.0
[TiW(SC ₆ F ₅) ₄ Cp] (1b)	<i>meta</i> - ¹⁹ F	220	42.1	248	46.7
	<i>ortho</i> - ¹⁹ F	~238	42.6		
[Au(PPh ₃) ₃][W(SC ₆ F ₅) ₄ Cp] (2b)	<i>meta</i> - ¹⁹ F	223	43.2		
	<i>ortho</i> - ¹⁹ F	241	43.1		
[Au(PET ₃) ₃][W(SC ₆ F ₅) ₄ Cp] (3b) ^c	<i>meta</i> - ¹⁹ F	223	43.0	226	42.9
	<i>ortho</i> - ¹⁹ F	243	43.5	243	44.0
[Au(dppp) ₂][W(SC ₆ F ₅) ₄ Cp] (5b)	<i>meta</i> - ¹⁹ F			~225	42.7
	<i>ortho</i> - ¹⁹ F			~245	44.4
[N(PPh ₃) ₂][W(SC ₆ F ₅) ₄ Cp] (7b)	<i>meta</i> - ¹⁹ F			229	43.4
	<i>ortho</i> - ¹⁹ F			245	44.4

^a Estimated error < 1.0 kJ mol⁻¹. ^b From ref 1. ^c In toluene-*d*₈: $\Delta G^\ddagger = 43.6$ kJ mol⁻¹ at 238 K.

C₅H₅); ¹⁹F ((CD₃)₂CO, 20 °C) δ -130.9 (br d, $J = 24.0$ Hz, 8 o-F), -160.5 (t, $J = 20.8$ Hz, 4 p-F), and -166.2 (m, 8 m-F); ((CD₃)₂CO, -80 °C), -127.9 (dd, $J = 29.0, 7.2$ Hz, 4 o-F), -133.4 (dd, $J = 28.5, 6.8$ Hz, 4 o-F), -158.7 (t, $J = 21.7$ Hz, 4 p-F), -164.2 (~t, $J = 24.3$ Hz, 4 m-F), and -165.1 (~t, $J = 23.2$ Hz, 4 m-F); ³¹P ((CD₃)₂CO, 20 °C) δ 37.9 (br s) ppm.

Reaction of [TiW(SC₆F₅)₄(Cp)] with [AuCl(PET₃)]. Complex **1b** (100 mg, 0.08 mmol), [AuCl(PET₃)₃] (29 mg, 0.08 mmol) and PET₃ (34 mg, 0.29 mmol) were stirred in acetone (30 cm³) under nitrogen at room temperature for 30 min giving a cloudy solution. The mixture was filtered and concentrated *in vacuo*. Hexane (10 cm³) was added, and the solution was cooled to -15 °C affording yellow and light green crystals of **3b**, which were separated by hand to give 75 mg of yellow product and 8 mg of green product. Anal. Found for yellow **3b**: C, 35.3; H, 3.2; S, 7.8. Calcd for C₄₇H₅₀F₂₀S₄P₃AuW: C, 35.4; H, 3.2; S, 8.0. IR (Nujol): C₆F₅ vibrations at 1506 (s) and 1463 (s) cm⁻¹. UV/vis (Nujol): λ_{\max} 435 ± 5 nm. NMR: ¹H (CDCl₃, 20 °C) δ 5.22 (s, 5H, C₅H₅), 2.1–1.8 (br m, 18H, CH₂), and 1.4–1.0 (br m, 27H, CH₃); ¹⁹F (C₇D₈, 20 °C) δ -130.8 (br d, $J = 22.3$ Hz, 8 o-F), -160.3 (t, $J = 21.4$ Hz, 4 p-F), and -165.9 (~t, $J = 21.3$ Hz, 8 m-F); (C₇D₈, -80 °C), -129.1 (br m, 4 o-F), -133.1 (br m, 4 o-F), -159.1 (br m, 4 p-F), -163.7 (br m, 4 m-F), and -166.3 (br m, 4 m-F); ³¹P(C₇D₈, 20 °C) δ 34.8 (br s); ¹⁹F (CD₂Cl₂, 20 °C) δ -131.6 (br d, $J = 25.5$ Hz, 8 o-F), -160.0 (t, $J = 21.2$ Hz, 4 p-F), and -165.9 (m, 8 m-F); (CD₂Cl₂, -80 °C), -129.4 (dd, $J = 29.4, 7.0$ Hz, 4 o-F), -133.6 (dd, $J = 28.6, 6.6$ Hz, 4 o-F), -157.5 (t, $J = 22.3$ Hz, 4 p-F), -163.3 (~t, $J = 25.0$ Hz, 4 m-F), and -164.7 (~t, $J = 25.5$ Hz, 4 m-F); ¹⁹F ((CD₃)₂CO, 19 °C) δ -130.91 (br d, $J = 23.8$ Hz, 8 o-F), -160.6 (t, $J = 20.7, 4 p-F$), and -166.2 (m, 8 m-F); ((CD₃)₂CO, -90 °C) -127.9 (dd, $J = 29.2, 7.4$ Hz, 4 o-F), -133.3 (dd, $J = 28.5, 6.9$ Hz, 4 o-F), -158.5 (t, $J = 21.8$ Hz, 4 p-F), -164.1 (~t, $J = 27.8$ Hz, 4 m-F), and -165.0 (~t, $J = 25.3$ Hz, 4 m-F); ³¹P ((CD₃)₂CO, 20 °C) δ 37.6 (br s) ppm. Anal. Found for light green **3b**: C, 35.8; H, 3.5. Calcd for C₄₇H₅₀F₂₀S₄P₃AuW: C, 35.4; H, 3.2. IR (Nujol): C₆F₅ vibrations at 1505 (s) and 1461 (s) cm⁻¹. UV/vis (Nujol): λ_{\max} 440 ± 5 nm. NMR: as for yellow form above.

Reaction of [Au(PPh₃)₃][Mo(SC₆F₅)₄Cp] with dppe. Complex **2a** (80 mg, 0.04 mmol) and dppe (34 mg, 0.085 mmol) were stirred in dichloromethane (30 cm³) at room temperature for 2 h. The solution was concentrated *in vacuo* and filtered, and hexane (10 cm³) was added to give orange crystals of [Au(dppe)₂][Mo(SC₆F₅)₄Cp] (**4a**) (74 mg, 95%). Anal. Found: C, 50.2; H, 2.9; S, 6.8. Calcd for C₈₁H₅₃F₂₀P₄S₄AuMo: C, 49.9; H, 2.7; S, 6.6. IR (CH₂Cl₂): C₆F₅ vibrations at 1507 (s) and 1477 (s) cm⁻¹. NMR: ¹H (CD₂Cl₂, 20 °C) δ 7.05–7.5 (br m, 40 H, C₆H₅), 5.25 (s, 5H, C₅H₅), and 2.4 (br, 8H, CH₂); ¹⁹F (CD₂Cl₂, 20 °C) δ -130.9 (br d, $J = 24.4$ Hz, 8 o-F), -159.3

(t, $J = 20.7$ Hz, 4 p-F) and -165.2 (~t, $J = 21.3$ Hz, 8 m-F); ³¹P (CD₂Cl₂, 20 °C) δ 21.6 (s) ppm.

Reaction of [Au(PPh₃)₃][W(SC₆F₅)₄Cp] with dppe. Complex **2b** (50 mg, 0.02 mmol) and dppe (20 mg, 0.05 mmol) were stirred in dichloromethane (30 cm³) at room temperature for 3 days. The solution was concentrated *in vacuo* and filtered, and hexane (10 cm³) was added to give green crystals of [Au(dppe)₂][W(SC₆F₅)₄Cp] (**4b**) (42 mg, 86%). Anal. Found: C, 48.1; H, 2.7; S, 7.1. Calcd for C₈₁H₅₃F₂₀P₄S₄AuW: C, 47.7; H, 2.9; S, 6.3. IR (CH₂Cl₂): C₆F₅ vibrations at 1507 (s) and 1477 (s) cm⁻¹. NMR: ¹H (CD₂Cl₂, 20 °C) δ : 7.1–7.45 (br m, 40 H, C₆H₅), 5.17 (s, 5H, C₅H₅), and 2.45 (br, 8 H, CH₂); ¹⁹F (CD₂Cl₂, 20 °C) δ -131.6 (br d, $J = 28.5$ Hz, 8 o-F), -160.0 (t, $J = 20.6$ Hz, 4 p-F), and -165.9 (m, 8 m-F); ³¹P(CD₂Cl₂, 20 °C) δ 21.6 (s) ppm.

Reaction of [Au(PPh₃)₃][Mo(SC₆F₅)₄Cp] with dppp. Complex **2a** (50 mg, 0.026 mmol) and dppp (22 mg, 0.053 mmol) were stirred in acetone (30 cm³) at room temperature for 3 d. The solution was concentrated *in vacuo* and filtered, and hexane (10 cm³) was added to give orange crystals of [Au(dppp)₂][Mo(SC₆F₅)₄Cp] (**5a**) (34 mg, 67%). Anal. Found: C, 50.6; H, 3.1; S, 6.8%. Calcd for C₈₃H₅₇F₂₀P₄S₄AuMo: C, 50.4; H, 2.9; S, 6.5. IR (CH₂Cl₂): C₆F₅ vibrations at 1507 (s) and 1477 (s) cm⁻¹. NMR: ¹H (CD₂Cl₂, 20 °C) δ 7.1–7.45 (br m, 40 H, C₆H₅), 5.24 (s, 5H, C₅H₅), 2.4–2.5 (br, 8H, CH₂-P), and 1.6–1.9 (br, 4H, CH₂); ¹⁹F (CD₂Cl₂, 20 °C) δ -131.3 (br d, $J = 21.2$ Hz, 8 o-F), -160.1 (t, $J = 21.2$ Hz, 4 p-F), and -165.9 (m, 8 m-F); ³¹P (CD₂Cl₂, 20 °C) δ -2.0 (s) ppm.

Reaction of [Au(PPh₃)₃][W(SC₆F₅)₄Cp] with dppp. Complex **2b** (50 mg, 0.025 mmol) and dppp (24 mg, 0.058 mmol) were stirred in acetone (30 cm³) at room temperature for 3 days. The solution was concentrated *in vacuo* and filtered, and hexane (10 cm³) was added to give yellow crystals of [Au(dppp)₂][W(SC₆F₅)₄Cp] (**5b**) (42 mg, 81%). Anal. Found: C, 48.9; H, 3.1; S, 6.2. Calcd for C₈₃H₅₇F₂₀P₄S₄WAu: C, 48.2; H, 2.8; S, 6.2. IR (CH₂Cl₂): C₆F₅ vibrations at 1507 (s) and 1477 (s) cm⁻¹. NMR: ¹H (CD₂Cl₂, 20 °C) δ 7.1–7.45 (br m, 40H, C₆H₅), 5.17 (s, 5H, C₅H₅), 2.35–2.55 (br, 8H, CH₂-P) and 1.6–1.9 (br, 4H, CH₂); ¹⁹F (CD₂Cl₂, 20 °C) δ -131.6 (br d, $J = 22.6$ Hz, 8 o-F), -160.0 (t, $J = 21.0$ Hz, 4 p-F), and -165.9 (m, 8 m-F); (CD₂Cl₂, -80 °C), -129.3 (dd, $J = 29.6, 6.1$ Hz, 4 o-F), -133.6 (br d, $J = 28.4$ Hz, 4 o-F), -157.5 (t, $J = 21.9$ Hz, 4 p-F), -163.3 (~t, $J = 24.8$ Hz, 4 m-F), and -164.6 (~t, $J = 25.0$ Hz, 4 m-F); ³¹P (CD₂Cl₂, 24 °C) δ : -1.95 (s) ppm.

Reaction of [TiMo(SC₆F₅)₄Cp] with [CuCl(PPh₃)₃]. Complex **1a** (500 mg, 0.43 mmol) and [CuCl(PPh₃)₃] (385 mg, 0.43 mmol) were stirred in dichloromethane (50 cm³) under nitrogen at room temperature for 1 h giving a dark cloudy solution. The mixture was filtered and concentrated *in vacuo*, and hexane (10 cm³) was added to give red crystals, which were

contaminated with a small amount of dark crystals. These were separated by hand to give ca. 200 mg of red crystals of $[\text{Cu}(\text{PPh}_3)_3][\text{Mo}(\text{SC}_6\text{F}_5)_4\text{Cp}] \cdot 0.5\text{CH}_2\text{Cl}_2$ (**6**) suitable for X-ray analysis. Anal. Found: C, 54.0; H, 2.8; S, 7.1. Calcd for $\text{C}_{83}\text{H}_{51}\text{ClF}_{20}\text{P}_3\text{S}_4\text{CuMo}$: C, 54.2; H, 2.8; S, 6.9. IR (CH_2Cl_2): C_6F_5 vibrations at 1511 (s) and 1480 (s) cm^{-1} . NMR analysis of these red crystals indicates several C_6F_5 -containing species existing in solution. The major species gives ^{19}F (CD_2Cl_2 , -20°C) δ -131.25 (br s, 8 o-F), -158.8 (br t, $J = 19.9$ Hz, 4 p-F), and -165.0 (m, 8 m-F); (CD_2Cl_2 , -80°C) δ -129.3 (br d, $J = 26.7$ Hz, 4 o-F), -133.0 (br d, $J = 26.0$ Hz, 4 o-F), -157.4 (br s, 4 p-F), -163.2 (br s, 4 m-F), and -164.6 (br s, 4 m-F) ppm.

Reaction of $[\text{TiW}(\text{SC}_6\text{F}_5)_4\text{Cp}]$ with $[\text{N}(\text{PPh}_3)_2]\text{Cl}$. Complex **1b** (100 mg, 0.08 mmol) and $[\text{N}(\text{PPh}_3)_2]\text{Cl}$ (52 mg, 0.09 mmol) were stirred in dichloromethane (40 cm^3) under nitrogen at room temperature for 1 h when the solution turned cloudy. The mixture was filtered, hexane (10 cm^3) was added, and the resulting solution was concentrated *in vacuo* to give yellow-green crystals of $[\text{N}(\text{PPh}_3)_2][\text{W}(\text{SC}_6\text{F}_5)_4\text{Cp}]$ (**7b**) (117 mg, 92%). Anal. Found: C, 50.0; H, 2.3; N, 1.0%. Calcd for $\text{C}_{85}\text{H}_{35}\text{F}_{20}\text{NWP}_2\text{S}_4$: C, 49.3; H, 2.2; N, 0.9. IR (CH_2Cl_2): C_6F_5 vibrations at 1507 (s) and 1478 (s) cm^{-1} . NMR: ^1H , (CD_2Cl_2 , 20°C) δ 7.4–7.7 (m, 30H, C_6H_5) and 5.17 (s, 5H, C_5H_5); ^{19}F (CD_2Cl_2 , 20°C) δ -131.6 (br d, $J = 22.1$ Hz, 8 o-F), -156.0 (t, $J = 21.3$ Hz, 4 p-F), and -165.9 (m, 8 m-F); (CD_2Cl_2 , -80°C) δ -129.3 (dd, $J = 29.6$, 6.6 Hz, 4 o-F), -133.5 (dd, $J = 28.6$, 5.5 Hz, 4 o-F), -157.3 (t, $J = 22.0$ Hz, 4 p-F), -163.1 (~t, $J = 24.8$ Hz, 4 m-F), and 164.5 (~t, $J = 25.1$ Hz, 4 m-F); ^{31}P (CD_2Cl_2 , 20°C) δ 23.7 (s) ppm.

Crystal Structure Determinations. A single crystal of **2a** (from petroleum ether/dichloromethane, approximate size $0.225 \times 0.25 \times 0.375$ mm^3), mounted in a Lindemann tube, was used for X-ray data collection.

Crystal Data. $\text{C}_{83}\text{H}_{50}\text{AuF}_{20}\text{P}_3\text{S}_4 \cdot 0.5\text{CH}_2\text{Cl}_2$, $M = 1983.6$, orange/red prisms, triclinic, space group $P\bar{1}$ (No. 2), $a = 11.6003(14)$ Å, $b = 16.805(3)$ Å, $c = 20.030(5)$ Å, $\alpha = 94.146(17)^\circ$, $\beta = 93.774(15)^\circ$, $\gamma = 92.213(12)^\circ$, $U = 3882.4(5)$ Å³, $Z = 2$, $D_{\text{calcd}} = 1.697$ g cm^{-3} , $F(000) = 1958$, $\mu(\text{Mo K}\alpha) = 23.32$ cm^{-1} .

Data Collection. The intensity data were collected on an Enraf-Nonius CAD4 diffractometer over the hemisphere (θ range: 1.50 – 23.0° ; h , -12 to $+12$; k , -18 to $+18$, l , 0 – 22) using graphite-monochromated Mo $\text{K}\alpha$ X-radiation ($\lambda = 0.710$ 693 Å) and ω – 2θ scanning. Of the 10 538 unique data measured, 8335 had $I > 2\sigma(I)$ and were used in subsequent structural solution and refinement. The data were corrected for Lorentz and polarization effects and for absorption (DIFABS²⁰).

Structure Solution. The approximate locations of the Au, Mo, and P atoms were determined by direct methods (SHELXS-86²¹). After two cycles of refinement, the remaining non-hydrogen atoms were subsequently located from a difference Fourier map phased on the refined heavy atom positions. The structure was refined by block-matrix least squares methods (SHELX76²²) using anisotropic temperature factors for all the non-hydrogen atoms except for the Cl and C atoms of the disordered dichloromethane solvent molecule. All the hydrogen atoms were located on difference Fourier maps and included in the refinement process at idealized positions. The

unsubstituted phenyl and cyclopentadienyl rings were treated as idealized hexagons ($\text{C}–\text{C} = 1.395$, $\text{C}–\text{H} = 0.95$ Å) and pentagons ($\text{C}–\text{C} = 1.42$, $\text{C}–\text{H} = 0.95$ Å), respectively. All C–F bonds were fixed at 1.34 Å. Fixed isotropic temperature factors were used for the hydrogen atoms ($U_{\text{iso}} = 0.10$ Å²). The solvent of crystallisation (one molecule of dichloromethane per unit cell) was disordered about the center of inversion at $[0.5, 0.5, 0.0]$. At convergence, the discrepancy factors R and R_w were 0.034 and 0.045, respectively. The weighting scheme, $w^{-1} = [\sigma^2(F) + 0.000 836(F)^2]$ was found to give satisfactory analyses of variance. The final difference Fourier map was essentially featureless (general noise level less than ± 0.3 e Å⁻³), apart from one peak ca. 0.89 e Å⁻³.

A single crystal of **6** (from petroleum ether/dichloromethane, approximate size $0.4 \times 0.2 \times 0.15$ mm^3), mounted in a Lindemann tube, was used for X-ray data collection.

Crystal Data. $\text{C}_{83}\text{H}_{50}\text{CuF}_{20}\text{P}_3\text{S}_4 \cdot 0.5\text{CH}_2\text{Cl}_2$, $M = 1850.2$, red prisms, triclinic, space group $P\bar{1}$ (No. 2), $a = 11.5695(22)$ Å, $b = 16.915(4)$ Å, $c = 19.928(3)$ Å, $\alpha = 94.204(16)^\circ$, $\beta = 93.774(16)^\circ$, $\gamma = 92.326(15)^\circ$, $U = 3876.4(16)$ Å³, $Z = 2$, $D_{\text{calcd}} = 1.585$ g cm^{-3} , $F(000) = 1858$, $\mu(\text{Mo K}\alpha) = 7.23$ cm^{-1} .

Data Collection, Structure Solution, and Refinement. The procedures for data collection, structure solution, and refinement were similar to that described above. The intensity data were collected on an Enraf-Nonius CAD4 diffractometer (θ range 1.0 – 25.0° ; h , 0 – $+13$; k , -20 to $+20$; l , -23 to $+23$; graphite-monochromated Mo $\text{K}\alpha$ X-radiation; ω – 2θ scanning). Of the 13 598 unique data measured, 6900 had $I > 3\sigma(I)$. The positions of the “heavy” and the non-hydrogen atoms were located and refined as described above. As for **2a**, one disordered molecule of dichloromethane per unit cell, present as solvent of crystallization, was found at the center of inversion at $[0.5, 0.5, 0.0]$. At convergence, the discrepancy factors R and R_w were 0.052 and 0.066, respectively, where $w^{-1} = [\sigma^2(F) + 0.000 112 9(F)^2]$. The final difference Fourier map was essentially featureless (general noise level less than ± 0.3 e Å⁻³), apart from four residual peaks ca. 0.5 e Å⁻³ in the vicinity of the heavy atoms.

Incidental crystallographic calculations and compilation of tables were carried out using the computer program CALC,²³ and Figures 1–3 were prepared using the crystallographic plotting programs CAMERON²⁴ and ORTEP.²⁵

Acknowledgment. We thank the SERC for financial support (to C.H.M.) and Professor M. B. Hursthouse (through the SERC service at University College Cardiff) and Dr. A. J. Welch (University of Edinburgh) for the collection of X-ray data for compounds **2a** and **6**, respectively.

Supporting Information Available: Tables of complete bond lengths and angles, anisotropic vibration parameters, and fractional coordinates of hydrogen atoms for complexes **2a** and **6** (19 pages). Ordering information is given on any current masthead page.

OM950039Q

(20) Walker, N. G.; Stuart, D. DIFABS. *Acta Crystallogr.* **1983**, *A39*, 158.

(21) Sheldrick, G. M. SHELXS-86. *Acta Crystallogr.* **1990**, *A46*, 467.

(22) SHELX76: University of Cambridge: Cambridge, England, 1976.

(23) Gould, R. O.; Taylor, P. CALC; University of Edinburgh: Edinburgh, Scotland, 1983.

(24) Pearce, L. J.; Watkins, D. J. CAMERON; University of Oxford: Oxford, England, 1993.

(25) Johnson, C. K. ORTEP. Report ORNL-5183; Oak Ridge National Laboratory: Oak Ridge, TN, 1976.

FT-IR Study of the Gas-Phase Thermolysis of Triethylgermane

Philip G. Harrison* and Ashley C. Torr

Department of Chemistry, University of Nottingham,
University Park, Nottingham NG7 2RD, U.K.

Received December 20, 1994[⊗]

Thermolysis of neat triethylgermane in the temperature range 628–653 K gives as products ethene, ethane, and diethylgermane in the ratio 48:14:1 and a silvery metallic film which contains some incorporated ethyl groups. Loss of triethylgermane over the whole temperature range follows second-order kinetics with an activation energy of 305(7) kJ mol⁻¹. Second-order rate constants vary from 1.35 mol⁻¹ L s⁻¹ at 628 K to 12.9 mol⁻¹ L s⁻¹ at 653 K. When the decomposition is performed in the presence of methyl iodide, the reaction occurs nearly 3 times faster. Ethene and nitrous oxide are the products when decomposition is carried out in the presence of nitric oxide, and the reaction proceeds at a 20th of the rate of the neat reaction. Decomposition in the presence of excess oxygen affords ethene, carbon monoxide, carbon dioxide, methane, water, formaldehyde, and hexaethyldigermoxane. Mechanisms involving intermediate radicals are proposed.

Introduction

Triethylgermane (TEG; (C₂H₅)₃GeH) is a possible alternative precursor for the formation of germanium films by MOCVD. Previous decomposition studies have been initiated by both thermal and photolytic techniques.¹ The susceptibility of ethylgermanes toward decomposition under photolysis increases with the number of ethyl groups attached to germanium (germane decomposes to only ca. 2% and triethylgermane decomposes up to 75% under the same conditions). However, little is known about the gas-phase chemistry of alkylgermanes at elevated temperatures. Compared to diethylgermane, the additional ethyl group in triethylgermane produces increased thermal stability. The byproducts of the gas-phase decomposition of triethylgermane as well as the characteristics of the resulting films have been noted. However, essentially no attention has been paid to the predeposition chemistry of the precursor, even though it has been established that the structure of the precursor molecule and the conditions under which its decomposition is carried out can have a profound effect on the nature and characteristics of the resulting film. In this paper, we describe a detailed account of the chemistry of triethylgermane at elevated temperatures in the gas phase. The reactions are rationalized on the basis of initial Ge–C bond homolysis followed by subsequent radical reactions.

Experimental Section

Triethylgermane was prepared² by the reduction of Et₃GeCl using LiAlH₄ (95+%, Aldrich Chemical Co. Ltd) in diethyl ether or tetrahydrofuran solvent under argon. The hydride was transferred to a conventional Schlenk line on which all

subsequent manipulations were carried out. For experiments involving neat hydride, a known pressure of hydride was admitted to the infrared cell at ambient temperature. Mixtures of the hydride with methyl iodide, nitric oxide, or oxygen were prepared using a gas bulb fitted with a small reservoir. A known pressure of the hydride was allowed into the bulb, which was then sealed. The hydride was then isolated in the reservoir by freezing at 77 K. The desired pressure of the second component was admitted into the remainder of the bulb prior to the opening of the reservoir, and the two components were allowed to mix. The general methodology of the infrared experiments has been described previously.³

All infrared measurements were carried out using a Nicolet 20SXC spectrometer. Mass spectra were recorded using a Micromass VG 7070E mass spectrometer.

Results

Infrared Spectrum and Beer–Lambert Characteristics of Triethylgermane. The gas-phase infrared spectral data of triethylgermane recorded at a pressure of 10.6 Torr at ambient temperature are listed in Table 1. For the purpose of studying quantitatively the thermal decomposition, the band centered at 2016 cm⁻¹ ($\nu(\text{Ge–H})^{4a}$) was used to quantify the gas-phase abundance of triethylgermane. This band is actually a composite of two conformers^{4b} with individual maxima at 2018 and 2012 cm⁻¹, although this does not affect the data. As the temperature is increased (prior to a temperature sufficient to initiate decomposition), the infrared bands characteristic of triethylgermane begin to broaden but suffer no diminution of integrated area. The limits of the envelope for the $\nu(\text{Ge–H})$ band increase from 2038–1987 cm⁻¹ to 2056–1971 cm⁻¹ as the temperature approaches that necessary to cause decomposition.

The Beer–Lambert plot (Figure 1) was constructed by allowing a known pressure of triethylgermane in the

[⊗] Abstract published in *Advance ACS Abstracts*, June 15, 1995.

(1) (a) Pola, J.; Parsons, J. P.; Taylor, R. *J. Chem. Soc., Faraday Trans. 1992*, 88, 1637. (b) Stanley, A. E.; Johnson, R. A.; Turner, J. B.; Roberts, A. H. *Appl. Spectrosc.* 1986, 40, 374. (c) Morancho, R.; Reynes, A.; El Boucham, J.; Sefiani, N.; Mazerolles, P. *Proc. Eur. Conf. Chem. Vap. Deposition* 1987, 6, 381.

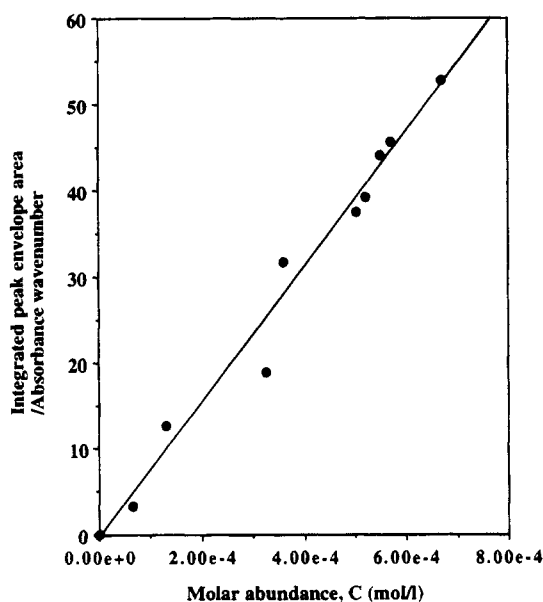
(2) Mochida, K.; Yoshida, Y. *Bull. Chem. Soc. Jpn.* 1988, 61, 1789.

(3) Harrison, P. G.; Ashworth, A.; Clarke, E. N.; McManus, J. *J. Chem. Soc., Faraday Trans.* 1990, 86, 4059–4063.

(4) (a) Mackay, K. M.; Watt, R. *J. Organomet. Chem.* 1966, 6, 336. (b) Mckean, D. C.; Torto, I.; Mackenzie, M. W.; Morrison, A. R. *Spectrochim. Acta* 1983, 39A, 387.

Table 1. Gas-Phase Infrared Data for Triethylgermane at Ambient Temperature

band position/cm ⁻¹	assign ^a
2961 vvvs	$\nu(\text{C-H})$
2921 vs	$\nu(\text{C-H})$
2883 vs	$\nu(\text{C-H})$
2836 w	$\nu(\text{C-H})$
2751 vvw	?
2018 vvvs	$\nu(\text{Ge-H})$
2012 vvvs	$\nu(\text{Ge-H})$
1470 mw	$\delta_{\text{as}}(\text{CH}_3)$
1435 w	$\delta_{\text{as}}(\text{CH}_3)$
1432 w	$\delta_{\text{as}}(\text{CH}_2)$
1384 vw	$\delta_{\text{s}}(\text{CH}_3)$
1235 vvw	$\delta_{\text{s}}(\text{CH}_2)$
1019 ms	$\nu(\text{C-C})$
969 m	$\nu(\text{C-C})$
751 vs	$\delta(\text{Ge-H}) + \rho(\text{Ge-Et})$
700 m	$\delta(\text{Ge-H}) + \rho(\text{Ge-Et})$
665 w	$\delta(\text{Ge-H}) + \rho(\text{Ge-Et})$
568 s	$\nu(\text{Ge-C}) + \rho(\text{Ge-H})$

^a Reference 4.**Figure 1.** Beer-Lambert plot for triethylgermane in the gas phase.

range 0.0–12.5 Torr at ambient temperature into the reaction cell and measuring the integrated area of the $\nu(\text{Ge-H})$ peak envelope. Least-squares analysis of the linear plot gave the relationship

$$A = -0.514 + (7.8735 \times 10^4)C$$

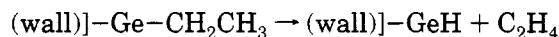
(correlation coefficient 0.977) where A is the integrated peak envelope area for $\nu(\text{Ge-H})$ (absorbance units cm^{-1}) and C the molar abundance (mol L^{-1}). From the gradient ϵl (7.87×10^4 (absorbance units cm^{-1}) mol^{-1} L) of the linear Beer-Lambert relationship, a value of 5.83×10^5 (absorbance units cm^{-1}) mol^{-1} L m^{-1} was determined for the extinction coefficient, ϵ .

Analysis of the Gas-Phase Reaction Products after Thermolysis of Triethylgermane in the Temperature Range 628–653 K. After the reaction cell had been conditioned by allowing triethylgermane to decompose at 648 K several times, kinetic runs were performed using neat triethylgermane in the temperature range 628–653 K. Although triethylgermane decomposes below 628 K, the reaction is extremely slow

and precludes a sufficient extent of reaction to be studied. The changes in the infrared spectrum during thermolysis at 633 K are illustrated in Figure 2. Expansions of the regions 3400–2700, 2200–1300, and 1300–400 cm^{-1} show the formation of ethene ($\nu_{\text{as}}(\text{CH}_2)$ at 3106 cm^{-1} , $\nu_{\text{s}}(\text{CH}_2)$ at 2989 cm^{-1} , CH_2 scis at 1444 cm^{-1} , and CH_2 wag at 949 cm^{-1}),⁵ ethane ($\nu(\text{C-H})$ at 2985 and 2895 cm^{-1}),⁶ and diethylgermane ($\nu(\text{Ge-H})$ at 2043 cm^{-1} , etc.) as products. Corroborative evidence of reaction products was obtained from mass spectrometry. No methane is detected. A typical time-resolved infrared spectrum in the region 2150–1950 cm^{-1} showing the decrease in intensity of the characteristic $\nu(\text{Ge-H})$ band of triethylgermane is illustrated in Figure 3. The shoulder at higher wavenumber (2043 cm^{-1}) due to diethylgermane also decreases with time.

In addition to the gaseous products, thermolysis of triethylgermane in this temperature range leads to the deposition of a silvery metallic film on the walls of the infrared cell. A typical mass balance using 4.84×10^{-4} mol L^{-1} of triethylgermane at 653 K (2000 s, >75% reaction) employing spectral subtraction of known pressures of authentic gaseous samples after the cell had been cooled to ambient temperature is presented in Table 2. The relatively flat spectrum base line after this procedure indicates that the major products of decomposition have been accounted for, although it is not possible to detect the presence of molecular hydrogen. Ethene is observed to be the major gaseous product of thermolysis, although a substantial quantity of ethane is also formed. Diethylgermane is formed only in trace molar quantities. The molar product ratio of ethene, ethane, and diethylgermane is approximately 48:14:1.

The mass balance analysis indicates approximately 35 mol % of carbon and approximately 46 mol % of hydrogen unaccounted for in the gas-phase products. Hence, one ethyl group (or its equivalent) on average is incorporated into the deposited solid film per triethylgermane molecule and, in addition, some gaseous hydrogen must also be formed. The presence of surface ethyl groups in the deposited film was demonstrated by cooling the reaction cell to room temperature after a kinetic run and then evacuating it for 30 s at $<10^{-3}$ Torr to remove all gaseous products and any products not chemisorbed to the solid film. After this treatment, the cell was reheated to 773 K, the temperature above which triethylgermane decomposes, and ethene was again produced. Under these conditions the production of ethene can only be from decomposition of the surface ethyl groups incorporated in the solid film:⁷



Rate Data and Determination of the Activation Energy. Plots of the decrease in gas-phase triethylgermane molar abundance⁸ with time over the temperature range 628–653 K are illustrated in Figure 4. These

(5) Smith, W. L.; Mills, I. M. *J. Chem. Phys.* **1963**, *40*, 2095.(6) Nakagawa, I.; Shimanouchi, T. *J. Mol. Spectrosc.* **1971**, *39*, 255.(7) Coon, P. A.; Wise, M. L.; Walker, Z. H.; George, S. M.; Roberts, D. A. *Appl. Phys. Lett.* **1992**, *60*, 2002.(8) The extinction coefficient, ϵ , and the time dependence of the integrated half-peak envelope area for the $\nu(\text{Ge-H})$ band between the limits 2011–1971 cm^{-1} were used to calculate the molar abundance for triethylgermane. Since the $\nu(\text{Ge-H})$ stretch for diethylgermane overlapped the hydride stretch for triethylgermane on the higher wavenumber side, this area was doubled to achieve a symmetric envelope, thereby eliminating possible errors due to band overlap.

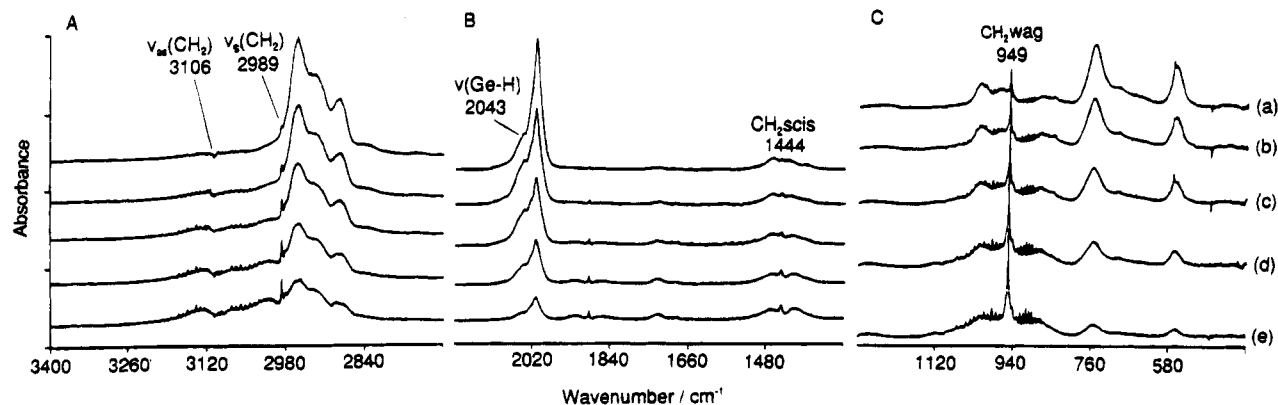


Figure 2. FT-IR spectra of triethylgermane in the gas phase (5 Torr) at 633 K in the regions 3400–2700 (A), 2200–1300 (B), and 1300–400 cm^{-1} (C) after the following times (s): (a) 0; (b) 500; (c) 1500; (d) 3500; (e) 5000.

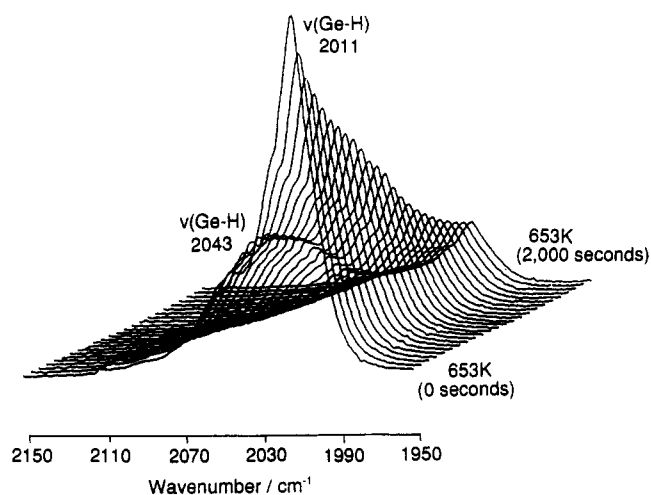


Figure 3. Time-resolved FT-IR spectra of triethylgermane in the $\nu(\text{Ge-H})$ region showing the diminution of the $\nu(\text{Ge-H})$ band of triethylgermane at 2011 cm^{-1} on heating at 653 K for 2000 s.

Table 2. Composition of the Gas-Phase Products after Thermolysis of Triethylgermane^a at 653 K for 2000 s

component	molar abundance/ $10^{-4} \text{ mol L}^{-1}$	mol of product/mol of triethylgermane reacted
triethylgermane	0.34	
diethylgermane	0.13	0.03
ethene	6.21	1.38
ethane	1.87	0.42

^a Initial molar abundance of triethylgermane $4.84 \times 10^{-4} \text{ mol L}^{-1}$.

data give excellent second-order kinetic fits with correlation coefficients ≥ 0.998 (Figure 5) and derived second-order rate constants varying from $1.35 \text{ mol}^{-1} \text{ L s}^{-1}$ at 628 K to $12.9 \text{ mol}^{-1} \text{ L s}^{-1}$ at 653 K. At lower temperatures the reactions exhibit an initial period of faster rate of loss of triethylgermane (Figure 5, inset). Rate data are summarized in Table 3.

Figure 6 shows the corresponding Arrhenius plot, which yields the relationship

$$\ln k = 58.56 - 3.66 \times 10^4/RT$$

($R^2 = 0.978$) leading to values for the activation energy, E_a , and the pre-exponential factor, A , of $305(7) \text{ kJ mol}^{-1}$ and $2.70 \times 10^{25} \text{ mol}^{-1} \text{ L s}^{-1}$, respectively.

Decomposition of Triethylgermane in the Presence of Methyl Iodide. The reaction of triethylger-

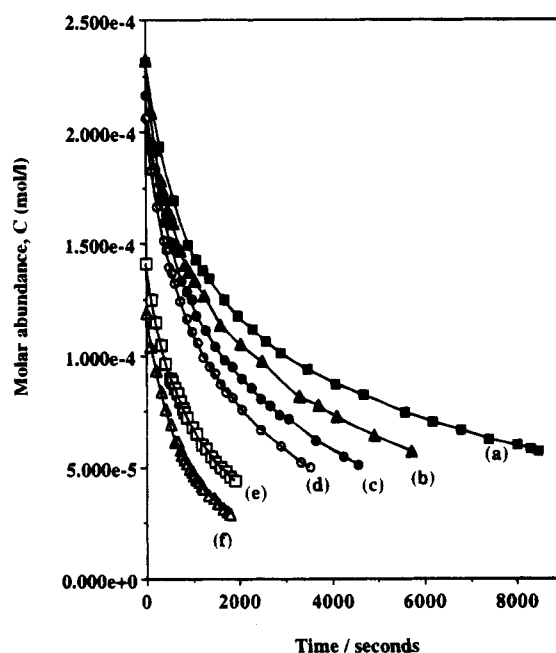


Figure 4. Plot of molar abundance of triethylgermane versus time for thermal decomposition: (a) 628 K; (b) 633 K; (c) 638 K; (d) 643 K; (e) 648 K; (f) 653 K.

mane and methyl iodide (molar ratio 4:1, combined pressure 10 Torr) was followed at 638 K to *ca.* >75% loss of triethylgermane. Infrared spectra show the growth of ethene (CH_2 wag 949 cm^{-1}), methane ($\nu(\text{C-H})$ 3019 cm^{-1} , $\delta(\text{H}_3\text{C-H})$ 1306 cm^{-1}), diethylgermane ($\nu(\text{Ge-H})$ 2043 cm^{-1}), and water (rotational fine structure $\nu_{\text{as}}(\text{O-H})$ centered at 3756 cm^{-1} and $\delta(\text{H}_2\text{O})$ centered at 1595 cm^{-1}). An unidentified product exhibiting a band at *ca.* 1730 cm^{-1} (which is neither formaldehyde ($\nu(\text{C=O})$ 1746 cm^{-1}) nor acetaldehyde ($\nu(\text{C=O})$ 1746 cm^{-1})) is also present throughout the reaction.

The decrease in the gas-phase abundance of triethylgermane at 638 K was followed by monitoring the integrated peak area of the $\nu(\text{Ge-H})$ band (Figure 7a). Under these conditions the loss of triethylgermane is also second order (Figure 8). However, a comparison of the corresponding rate constant ($8.23 \text{ mol}^{-1} \text{ L s}^{-1}$) with that of the thermolysis of neat triethylgermane at 638 K ($2.94 \text{ mol}^{-1} \text{ L s}^{-1}$) shows that the reaction is nearly 3 times faster when a small amount of methyl iodide is present.

In a second experiment, the reaction of triethylger-

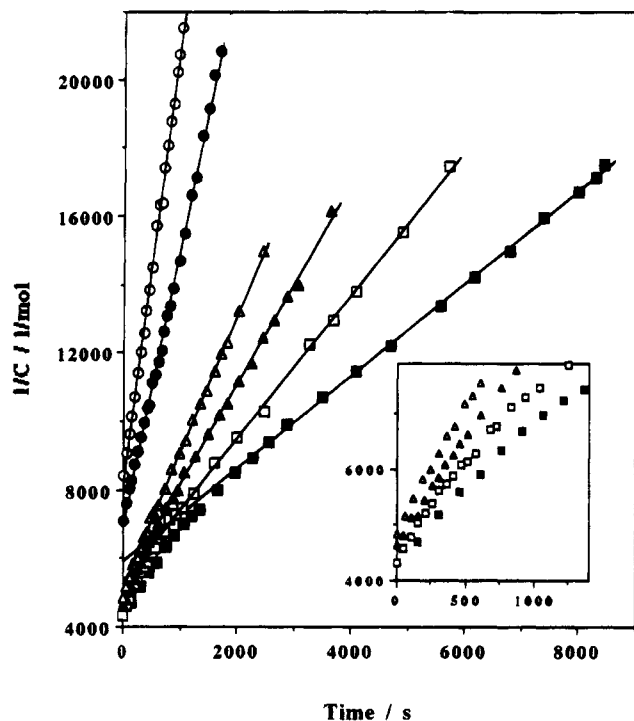


Figure 5. Second-order rate plots for the thermal decomposition of triethylgermane: (■) 628 K; (□) 633 K; (▲) 638 K; (△) 643 K; (●) 648 K; (○) 653 K.

Table 3. Second-Order Rate Constant and Arrhenius Data for the Thermolysis of Triethylgermane in the Temperature Range 628–653 K

temp/K	second-order rate constant, $k_2/\text{mol}^{-1} \text{L s}^{-1}$	correlation coeff
628	1.48	0.993
633	2.22	0.995
638	3.15	0.998
643	4.21	0.998
648	8.26	0.998
653	14.5	0.994

mane with excess methyl iodide (molar ratio 1:4, combined pressure 35 Torr) was followed. In this case, extensive decomposition of triethylgermane had already occurred by the time a temperature of 638 K was attained, and total decomposition was achieved after only 400 s at this temperature (Figure 7b). Products are methane ($\nu(\text{C-H})$ 3019 cm^{-1} , $\delta(\text{H}_3\text{C-H})$ 1306 cm^{-1}), ethene (CH_2 wag 949 cm^{-1}), water (rotational fine structure $\nu_{\text{as}}(\text{O-H})$ centered at 3756 cm^{-1} and $\delta(\text{H}_2\text{O})$ centered at 1595 cm^{-1}), and trace amounts of methanol ($\nu(\text{C-O})$ 1032 cm^{-1}) together with residual methyl iodide. No diethylgermane is formed. Unlike when neat triethylgermane decomposes thermally or when only small amounts of methyl iodide are present, the decomposition of triethylgermane with excess methyl iodide proceeds by *first-order kinetics* with a rate constant of $3.76 \times 10^{-3} \text{ s}^{-1}$ (Figure 9). In a similar experiment carried out at 553 K (molar ratio 1:4, combined pressure 25 Torr), the product distribution was essentially the same as at 638 K and the loss of triethylgermane was again first order with a rate constant of $8.71 \times 10^{-5} \text{ s}^{-1}$.

Decomposition of Triethylgermane in the Presence of Nitric Oxide. The reaction of triethylgermane and nitric oxide (1:1 molar ratio, combined pressure 12

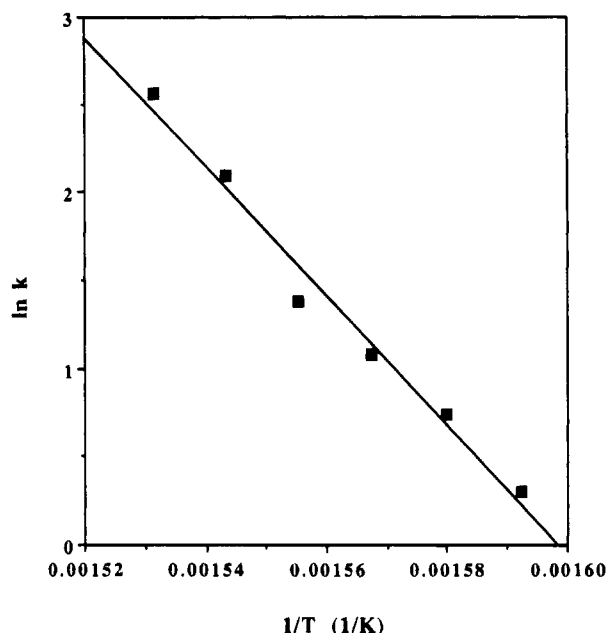


Figure 6. Arrhenius plot for the thermal decomposition of triethylgermane in the temperature range 628–653 K.

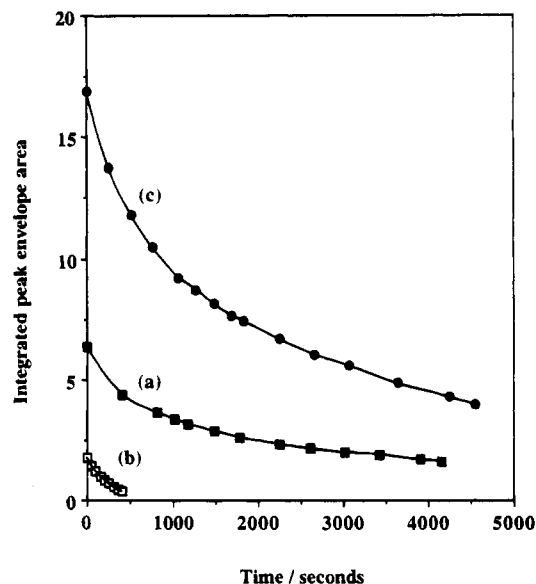


Figure 7. Comparison of the reaction rate profiles at 638 K: (a) for a 4:1 molar ratio mixture of triethylgermane and methyl iodide; (b) for a 1:4 molar ratio mixture of triethylgermane and methyl iodide; (c) for neat triethylgermane.

Torr) gave ethene (CH_2 wag 949 cm^{-1}) and nitrous oxide as products, but no diethylgermane. The fate of the germanium is uncertain due to the poor quality of the spectra. At large absorption in the $\nu(\text{GeOGe})$ region is observed, although unequivocal assignment is not possible. Decomposition of triethylgermane under these conditions is much slower than for neat triethylgermane. Whereas neat triethylgermane is almost totally decomposed after 1700 s, in the presence of nitric oxide only ca. 10% of triethylgermane has reacted after 3300 s (Figure 10) and the consumption of the germane follows second-order kinetics with a rate constant of $0.71 \text{ mol}^{-1} \text{L s}^{-1}$ (Figure 11).

Decomposition of Triethylgermane in the Presence of Oxygen. Infrared spectra (Figure 12) show that triethylgermane is totally absent from a mixture of triethylgermane and oxygen (1:10 molar ratio, com-

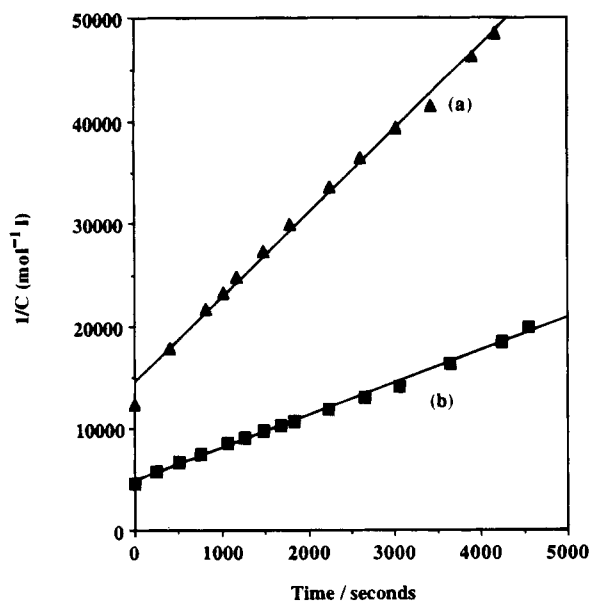


Figure 8. Second-order rate plots for the thermal decomposition at 638 K of (a) a 4:1 molar ratio mixture of triethylgermane and methyl iodide and (b) neat triethylgermane.

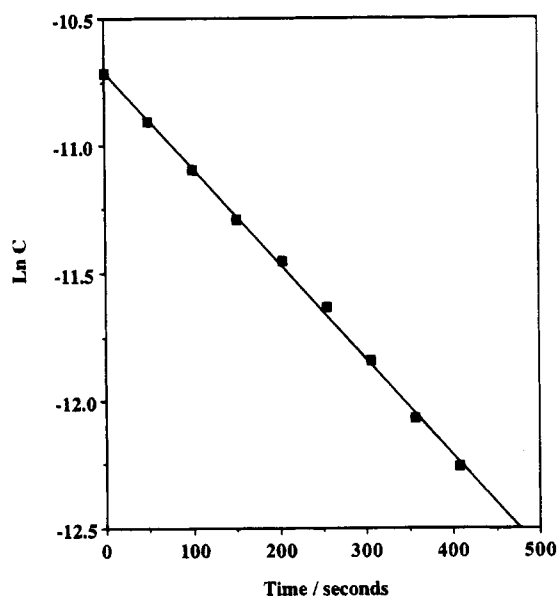


Figure 9. First-order rate plot for the thermal decomposition at 638 K of a 1:4 molar ratio mixture of triethylgermane and methyl iodide.

bined pressure 44 Torr) by the time a temperature of 643 K is reached. Identified products are ethene (CH_2 wag 949 cm^{-1}), carbon monoxide ($\nu(\text{CO})$ 2144 cm^{-1}), carbon dioxide ($\nu_{\text{as}}(\text{CO}_2)$ 2349 cm^{-1} , $\delta(\text{CO}_2)$ 667 cm^{-1}), methane ($\nu(\text{C-H})$ 3019 cm^{-1} , $\delta(\text{H}_3\text{C-H})$ 1306 cm^{-1}), water (rotational fine structure $\nu_{\text{as}}(\text{O-H})$ centered at 3756 cm^{-1} and $\delta(\text{H}_2\text{O})$ centered at 1595 cm^{-1}), and formaldehyde ($\nu_{\text{as}}(\text{CH}_2)$ 2843 cm^{-1} , $\nu_{\text{s}}(\text{CH}_2)$ 2783 cm^{-1} , $\nu(\text{C=O})$ 1746 cm^{-1} , CH_2 scis 1500 cm^{-1} , $\rho(\text{CH}_2)$ 1249 cm^{-1}).⁹ Even though decomposition of triethylgermane is complete, subsequent reactions occur as time elapses at 643 K. A second carbonyl compound (not identified) with a band at 1730 cm^{-1} is formed, and substantial band growth below 1400 cm^{-1} is also observed, as is the formation of hexaethyldigermoxane (Table 4). Carbon

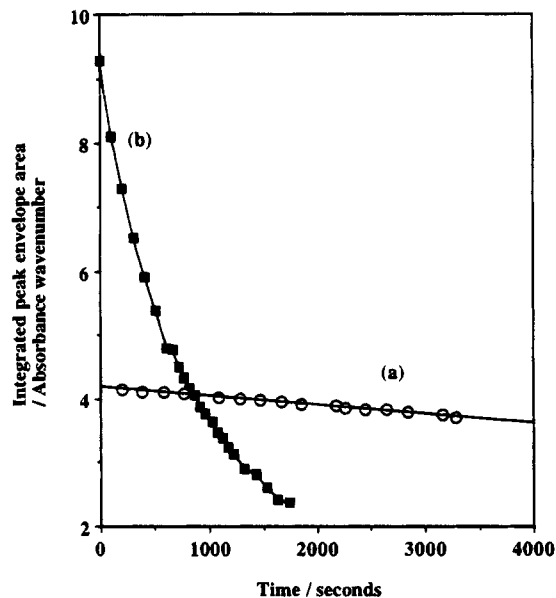


Figure 10. Comparison of the reaction rate profiles at 653 K (a) for a 1:1 molar ratio mixture of triethylgermane and nitric oxide and (b) for neat triethylgermane.

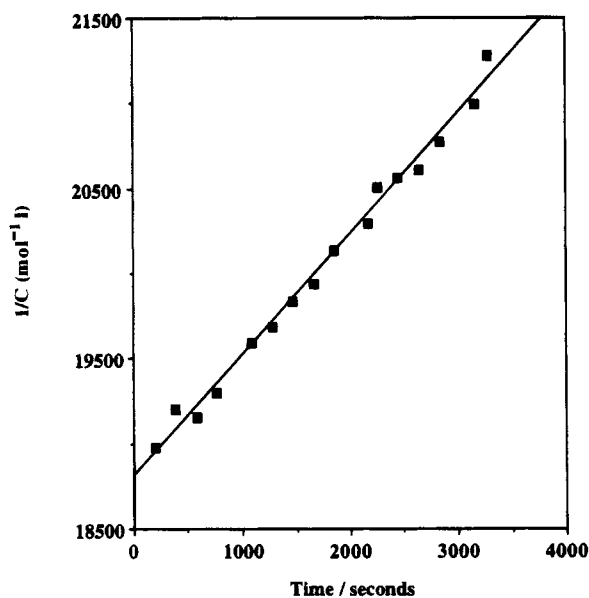


Figure 11. Second-order rate plot for the thermal decomposition at 638 K of a 1:1 molar ratio mixture of triethylgermane and nitric oxide.

monoxide and carbon dioxide continue to grow continuously up to 2000 s, after which time the abundance of both remains approximately constant.

Discussion

Product and kinetic data for the thermal decomposition of triethylgermane under a variety of conditions are summarized in Table 5.

Thermolysis of neat triethylgermane in the temperature range 628–653 K gives as gaseous products ethene, ethane, and diethylgermane in a typical molar ratio of 48:14:1. Simultaneously, a silvery metallic coating is deposited on the walls of the reaction cell, which from the mass balance contains *ca.* 33% carbon. The overall stoichiometry may be represented by the equation

(9) Harvey, K. B.; Ogilvie, J. F. *Can. J. Chem.* **1962**, *40*, 85.

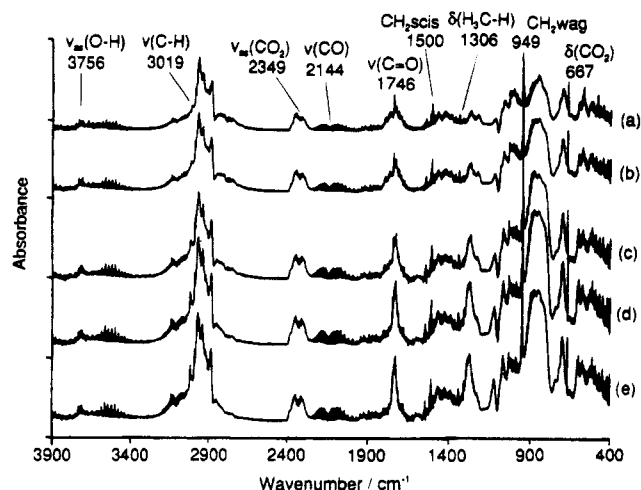
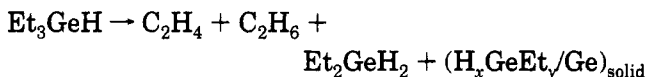


Figure 12. FT-IR spectra of a 1:10 molar ratio mixture of triethylgermane and oxygen in the gas phase at 643 K after (a) 0 s, (b) 300 s, (c) 1000 s, (d) 2200 s, and (e) 2900 s.

Table 4. Comparison of Infrared Data (1500–400 cm^{-1}) for Hexaethyldigermoxane^a and the Product from the Thermolysis of Triethylgermane in the Presence of Excess Oxygen

(Et ₃ Ge) ₂ O	product	assign
1451 (m)	1464 (m)	$\delta_a(\text{CH}_3)$
1414 (m)	1420 (m)	$\delta_a(\text{CH}_2)$
1374 (w)	1385 (m)	$\delta_s(\text{CH}_3)$
1218 (w)	1202 (w)	$\delta_s(\text{CH}_2)$
	1066 (s)	unassigned
1016 (m)	1031 (s)	$\nu(\text{C}-\text{C})/\rho(\text{C}-\text{Me})$
962 (w)	988 (m)	$\nu(\text{C}-\text{C})/\rho(\text{C}-\text{Me})$
855 (vs)	891 (vs)	$\nu(\text{GeOGe})$
699 (s)	699 (s)	$\rho(\text{CH}_2)$
582 (s)	600 (s)	$\nu_a(\text{Ge}-\text{C})$
536 (w)	572 (m)	$\nu_s(\text{Ge}-\text{C})$

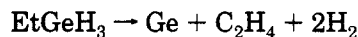
^a Cross, R. J.; Glockling, F. *J. Organomet. Chem.* **1965**, *3*, 146.



Loss of triethylgermane follows second-order kinetics over the whole of the temperature range studied, and rate constants vary from $1.35 \text{ mol}^{-1} \text{ L s}^{-1}$ at 628 K to $12.9 \text{ mol}^{-1} \text{ L s}^{-1}$ at 653 K. From the corresponding Arrhenius plot, the activation energy for the decomposition of triethylgermane under these conditions is $305(7) \text{ kJ mol}^{-1}$.

Similar product distributions have been observed for the decomposition of triethylgermane under photolytic conditions. Irradiation (excimer laser photolysis at 193 nm) of the ethylgermanes $\text{Et}_n\text{GeH}_{4-n}$ ($n = 1-3$) results in the formation of large quantities of ethane and ethene together with small quantities of ethylgermanes with a lower number of ethyl groups in the molecule.^{1a} The dominant gaseous product from photolysis of triethylgermane was ethane, and the ethane to ethene product ratio was (2.8–3.8):1. Trace amounts of *n*-butane and diethylgermane are also formed, and in addition to these products, a dark film was obtained on the inner surface of the photolysis reactor. Only very slight decomposition occurred with a barely visible deposition of the germanium during the CO_2 -laser-induced photolysis of triethylgermane (irradiation of the maximum vapor pressure for 15 s at 1075 cm^{-1} , 100 W/cm^2 output power), although germane, ethene, and hydrogen were observed as gas-phase products.^{1b}

Thermal decomposition of triethylgermane under dynamic conditions in a cold-wall CVD reactor has been shown to start at a minimum temperature of 623 K and also affords ethene and hydrogen as the gas-phase products.^{1c} The mechanism proposed involved successive elimination of ethene molecules and finally hydrogen:



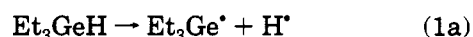
Products resulting from radicals (e.g. methane, propane, butane) were not observed.

In the present study, when a small amount of methyl iodide (TEG:MeI 4:1 molar ratio) is present as a radical initiator, decomposition of triethylgermane is again second order but occurs at a faster rate at the same temperature ($\times 2.8$ at 638 K). Under these conditions the gas-phase products are ethene, methane, diethylgermane, and water. When the decomposition is performed at 638 K in the presence of excess methyl iodide (1:4 molar ratio), the reaction is faster and becomes first order with respect to loss of triethylgermane and the constitution of the gas phase changes somewhat. Observed gas-phase products comprise methane, ethene, water, and trace methanol (together with residual unreacted methyl iodide), but no diethylgermane is formed. The presence of water and methanol in the gas phase indicates that adsorption/desorption reactions of methyl radicals must be occurring at the surface of the cell wall, since this is the only source of oxygen available in the system. The reaction is still first order when the decomposition is performed at 553 K using the same 1:4 molar ratio of reactants but is much slower ($0.023 \times$ rate at 638 K), and now the gaseous products comprise only methane, water, and methanol.

Nitric oxide usually inhibits radical reactions, functioning as a radical scavenger. The reaction of triethylgermane and nitric oxide (1:1 molar ratio) at 653 K is second order with respect to loss of triethylgermane and slower ($0.05 \times$ rate of neat decomposition at 653 K). Gaseous products are ethene and nitrous oxide together with residual nitric oxide.

Thus, since the decomposition of triethylgermane is promoted by methyl iodide, a radical reaction promoter, and inhibited by nitric oxide, a radical reaction inhibitor, it would appear that the mechanism involves a gas-phase radical process. A concerted molecular elimination of ethene from triethylgermane cannot be unequivocally excluded as a parallel reaction pathway, although the observation that no diethylgermane is formed serves to exclude this possibility. Some ethene is, however, formed by an elimination process from ethyl groups incorporated in the film at 773 K, which may or may not involve radicals.

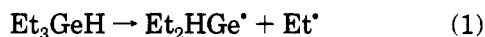
In the gas phase, the observed data indicate that the thermolysis of triethylgermane proceeds by a radical chain mechanism, the component steps of which are shown in Scheme 1. For the initiation step we prefer that involving Ge–C bond homolysis (step 1) rather than Ge–H homolysis



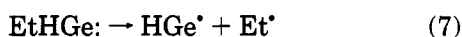
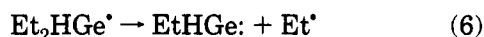
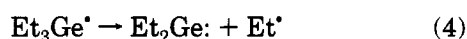
since Ge–C bond energies are *ca.* 20 kJ mol⁻¹ lower ($D(\text{Me}_3\text{Ge}-\text{Me}) = 320 \text{ kJ mol}^{-1}$, $D(\text{Me}_3\text{Ge}-\text{H}) = 344 \text{ kJ mol}^{-1}$, $D(\text{H}_3\text{Ge}-\text{H}) = 346 \text{ kJ mol}^{-1}$)^{10,11} and also the *A* factor for reaction 2 would be expected to be *ca.* 100 times lower than that for (1). Subsequent steps involve hydrogen abstraction from triethylgermane at germanium by ethyl radicals and hydrogen atoms to generate the Et₃Ge• radical¹⁰ (steps 2 and 3). Although β-hydrogen abstraction from tetraethylgermane by benzoyl radicals giving the •CH₂CH₂GeEt₃ radical has been observed,¹² the relative C–H (441 kJ mol⁻¹)¹⁰ and Ge–H (344 kJ mol⁻¹)¹⁰ bond energies suggest that hydrogen abstraction at germanium will be highly favored. Since we have no information concerning the evolution of molecular hydrogen, it is not possible to estimate the relative extents of hydrogen abstraction by hydrogen atoms (step 2) compared to abstraction by ethyl radicals (step 3), although it might be expected that the former is more important. Further propagation reactions involve the stepwise homolytic loss of ethyl ligands from ethylgermyl radicals (steps 4–7).

Scheme 1. Proposed Radical Mechanism for the Thermolysis of Triethylgermane

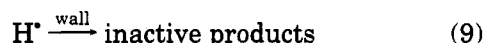
Initiation:



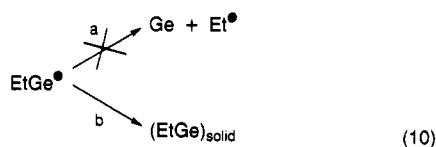
Propagation:



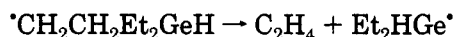
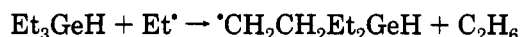
Termination:



Mass balance data indicate significant carbon and hydrogen incorporation in the deposited film, and evolution of ethene can be detected by the thermal decomposition of the film at 773 K. Approximately one ethyl group per germanium atom appears to be incorporated in the deposited film. It is, therefore, relatively unlikely that loss of the last ethyl ligand from germanium (path a in eq 10) takes place in the gas phase. Rather, it would appear that condensation from the gas phase takes place at this stage, giving a highly ethylated germanium film (path b in eq 10).



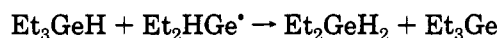
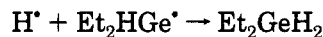
That ethene is formed in significantly greater amounts than ethane indicates that step 8 occurs extensively. Step 8 will be fast under these conditions (reported values of log *A*/s⁻¹ in the range 12.9–13.58 and *E* in the range 159–175 kJ mol⁻¹).^{13,14} With a half-life of <1 s at 628 K, this step is probably be the principal process responsible for removing ethyl radicals from the system. If this is indeed the case, hydrogen atoms would be generated in significant quantities, and therefore hydrogen abstraction (which would be more facile than by ethyl radicals) would be expected to be extensive (step 3). Ethene could be formed by the elimination of ethene from the •CH₂CH₂Et₂GeH radical resulting from abstraction at the β-carbon of the ethyl group, analogous to that reported¹² to occur for the •CH₂CH₂GeEt₃ radical:



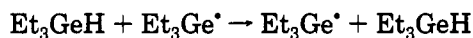
However, as stated above, we consider C–H abstraction to be unimportant in the case of triethylgermane.

Chain termination is by hydrogen atom deactivation at the cell wall (step 9). Since hydrogen atom elimination from ethyl radicals (step 8) is extensive, the flux of hydrogen atoms reaching the cell walls is likely to be much greater than the flux of ethyl groups, although impingement of the latter at the cell walls will also result in their removal from the system. Hydrogen atoms are known to interact strongly with surfaces and surface-bound organic species.^{15,16} Particularly relevant to the present discussion is the formation of surface l–Ge–H monohydride species upon adsorption of atomic hydrogen on germanium(111) surfaces at 500 K.¹⁷

The diethylgermane observed may be formed by either a combination reaction between H• atoms and Et₂HGe• radicals or by hydrogen abstraction from triethylgermane by a Et₂HGe• radical:



The identity reaction



(10) Jackson, R. A. *J. Organomet. Chem.* **1979**, *166*, 17.

(11) Clarke, K. B.; Griller, D. *Organometallics* **1991**, *10*, 746.

(12) Razuvaev, G. A.; Vyazankin, N. S.; Gladyshev, E. N. *Dokl. Akad. Nauk SSSR* **1963**, *153*, 104.

(13) Louchs, L. F.; Laidler, K. J. *Can. J. Chem.* **1967**, *45*, 2795.

(14) Trenwith, A. B. *J. Chem. Soc., Faraday Trans. 2*, **1986**, *82*, 457 and references therein.

(15) Cheng, C. C.; Lucas, S. R.; Gutleben, H.; Choyke, W. J.; Yates, J. T., Jr. *Surf. Sci. Lett.* **1992**, *273*, L441.

(16) Lutterloh, C.; Schenk, A.; Biener, J.; Winter, B.; Kuppers, J. *Surf. Sci.* **1994**, *316*, L1039.

(17) Crowell, J. E.; Lu, G. *J. Electron Spectrosc. Relat. Phenom.* **1990**, *54–55*, 1045.

Table 5. Summary of Reaction Data for the Pyrolysis of Triethylgermane under a Variety of Conditions

reactants	molar ratio	temp (K)/ pressure (Torr)	products	order wt loss of Et ₃ GeH	rate constant ^a
Et ₃ GeH		628–653/5	C ₂ H ₄ , C ₂ H ₆ , Et ₂ GeH ₂	2	1.48–14.5
Et ₃ GeH + MeI	4:1	638/10	C ₂ H ₄ , CH ₄ , Et ₂ GeH ₂ , H ₂ O	2	8.23
	1:4	638/35	C ₂ H ₄ , CH ₄ , H ₂ O, MeOH	1	3.76 × 10 ⁻³
	1:4	553/25	C ₂ H ₄ , CH ₄ , H ₂ O, MeOH	1	8.71 × 10 ⁻⁵
Et ₃ GeH + NO	1:1	653/12	C ₂ H ₄ , N ₂ O	2	0.71
Et ₃ GeH + O ₂	1:10	643/44	C ₂ H ₄ , CO, CO ₂ , CH ₄ , H ₂ O, HCHO, (Et ₃ Ge) ₂ O		

^a Second-order units mol⁻¹ L s⁻¹, first-order units s⁻¹.

almost certainly occurs, although it is not detectable in the present experimental arrangement.

According to Scheme 1, the rate of loss of triethylgermane from the system is given by the expression

$$-d[\text{Et}_3\text{GeH}]/dt = k_1[\text{Et}_3\text{GeH}] + k_2[\text{Et}^*][\text{Et}_3\text{GeH}] + k_3[\text{H}^*][\text{Et}_3\text{GeH}] \quad (11)$$

If (9) is the sole termination step, at steady state [Et*] and [H*] are given by the expressions

$$[\text{H}^*] = (k_1/k_9)[\text{Et}_3\text{GeH}] \quad (12)$$

$$[\text{Et}^*] = (k_1/k_9)[\text{Et}_3\text{GeH}]\{(k_3/k_8)[\text{Et}_3\text{GeH}] + k_9/k_8\} \quad (13)$$

which, after substitution in eq 11 affords the rate equation

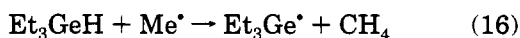
$$-d[\text{Et}_3\text{GeH}]/dt = (k_1 k_2/k_8)[\text{Et}_3\text{GeH}]^2\{(k_3/k_9)[\text{Et}_3\text{GeH}] + 1\} + (k_1 k_3/k_9)[\text{Et}_3\text{GeH}]^2 \quad (14)$$

Since $k_3[\text{Et}_3\text{GeH}]/k_9 \ll 1$, this expression reduces to

$$-d[\text{Et}_3\text{GeH}]/dt = k_1[k_2/k_8 + k_3/k_9][\text{Et}_3\text{GeH}]^2 \quad (15)$$

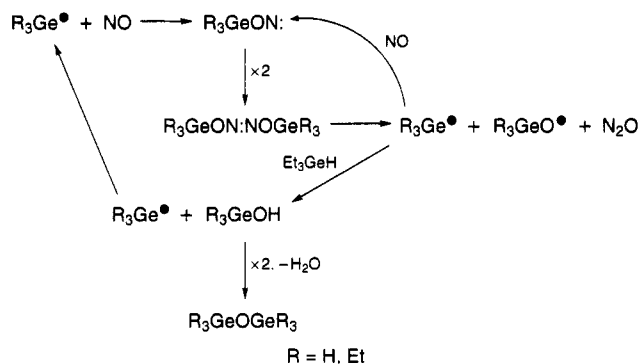
which shows second-order dependence of the rate on triethylgermane, as observed experimentally. The complex rate constant term involves, besides the rate constant for the initiation process, the rate constants for processes involving hydrogen atoms (steps 3 and 9) and ethyl radicals (steps 2 and 8). In the initial stages of reaction at lower temperatures, the first term in eq 14 is significant, and an apparent enhancement in rate is observed. The overall activation energy, E_{act} , for the process is determined experimentally to be 305(7) kJ mol⁻¹; however, the complexity of the rate constant term in eq 15 precludes discussion of the component contributions to the Arrhenius parameters.

In the presence of methyl iodide the rate of decomposition of triethylgermane increases, but the kinetic dependence changes from second order at low methyl iodide abundance to first order at high methyl iodide abundance. Significant quantities of methane are formed, and hence hydrogen abstraction by methyl radicals



is now important in addition to the other reactions in Scheme 1. At low abundances of methyl iodide this results in an enhancement of the rate of initiation; *i.e.*, the rate of initiation is now given by $k_1[\text{Et}_3\text{GeH}] +$

Scheme 2. Mechanism for the Formation of Nitrous Oxide in the Reaction of Triethylgermane with Nitric Oxide



$k_{16}[\text{Et}_3\text{GeH}][\text{MeI}]$. However, at high abundances of methyl iodide a very large concentration of methyl radicals is produced; these radicals are able to effectively scavenge Et₃Ge* radicals before any further ethyl group elimination can take place (step 17).



Hence, the rate of loss of triethylgermane is now given by the expression

$$-d[\text{Et}_3\text{GeH}]/dt = k_{17}[\text{Et}_3\text{GeH}][\text{Me}^*]$$

which, since [Me*] is very large and therefore constant, can be rewritten as

$$-d[\text{Et}_3\text{GeH}]/dt = k_{17}[\text{Et}_3\text{GeH}]$$

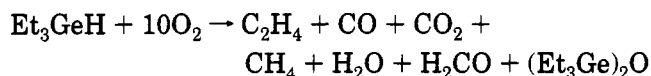
thereby rationalizing the change to first-order kinetics with loss of triethylgermane.

Reaction of triethylgermane with nitric oxide produces nitrous oxide and ethene. The formation of nitrous oxide most probably takes place via scavenging of germyl radicals by NO to form R₃GeON: intermediates, which then dimerize. Nitrous oxide is formed by elimination from the intermediate dimer (Scheme 2). Similar behavior has been observed in the reaction of trimethylsilyl radicals with nitric oxide to give nitrous oxide.¹⁸ Although it was not possible to unequivocally distinguish any germanium-containing products, it is most likely that an organodigermoxane is formed.

In the presence of excess oxygen the decomposition of triethylgermane is very fast. Reaction is complete by the time a temperature of 643 K is attained, affording as products ethene, carbon monoxide, carbon dioxide,

(18) Nay, M. A.; Woodall, G. N. C.; Strausz, O. P.; Gunning, H. E. *J. Am. Chem. Soc.* **1965**, *87*, 179.

methane, water, formaldehyde, and hexaethyldigermoxane:



Although kinetic data were not obtained in this present case, the mechanism most probably parallels that determined for the autoxidation of trimethylgermane in the temperature range 493–533 K.¹⁹ Over a wide molar ratio of reactants ($\text{Me}_3\text{GeH}:\text{O}_2$ ratio in the range 1:1 to 1:31) loss of Me_3GeH follows second-order kinetics, but the reaction was found to be independent of oxygen abundance. The products of the reaction are hexamethyldigermoxane ($\text{Me}_3\text{GeOGeMe}_3$) and water, and no other products are apparent. The principal features of the mechanism are (i) an initial abstraction of the hydridic hydrogen atom from germanium, (ii) reaction of the trimethylgermyl radical thus formed with oxygen, giving the (trimethylgermyl)peroxy radical, $\text{Me}_3\text{GeOO}^\bullet$, (iii) conversion into trimethylgermyl hydroperoxide, Me_3GeOOH , by further H abstraction from Me_3GeH , (iv) O–O bond fission to form (trimethylgermyl)oxyl ($\text{Me}_3\text{GeO}^\bullet$) and hydroxyl radicals, (v) propagation of the reaction by H abstraction from Me_3GeH , forming the intermediate Me_3GeOH and water, and (vi) self-condensation of two Me_3GeOH molecules to form hexamethyldigermoxane. Analogous processes are expected to take place in the present case with triethylgermane. The formation of products of more exhaustive oxidation is a consequence of the harsher reaction conditions.

It is pertinent to note that the reaction of triethylgermane with ozone at 195 K generates triethylgermanium hydrotrioxide, Et_3GeOOOH , which at higher temperatures eliminates oxygen to give Et_3GeOH and subsequently $(\text{Et}_3\text{Ge})_2\text{O}$.²⁰

Conclusions

1. Triethylgermane decomposes by a free-radical mechanism in the temperature range 628–653 K by second-order kinetics with an activation energy of 305(7) kJ mol^{-1} , giving as gaseous products ethene, ethane, and diethylgermane in a molar ratio of 48:14:1. Second-order rate constants vary from $1.35 \text{ mol}^{-1} \text{ L s}^{-1}$ at 628 K to $12.9 \text{ mol}^{-1} \text{ L s}^{-1}$ at 653 K.
2. In the presence of small amounts of methyl iodide the rate is enhanced and the kinetics are still second order, but with excess methyl iodide the kinetics change to first order.
3. Nitric oxide inhibits the decomposition, but the presence of oxygen accelerates the reaction substantially.

Acknowledgment. We thank the SERC for support in the form of a studentship (to A.C.T.). We thank the reviewers for some helpful suggestions.

OM940971L

(19) Harrison, P. G.; Podesta, D. M. *Organometallics* **1994**, *13*, 1569.

(20) Koenig, M.; Barrau, J.; Hamaida, N. B. *J. Organomet. Chem.* **1988**, *356*, 133.

Carborane Complexes of Ruthenium: A Convenient Synthesis of $[\text{Ru}(\text{CO})_3(\eta^5\text{-}7,8\text{-C}_2\text{B}_9\text{H}_{11})]$ and a Study of Reactions of This Complex[†]

Stephen Anderson, Donald F. Mullica, Eric L. Sappenfield, and
F. Gordon A. Stone*

Department of Chemistry, Baylor University, Waco, Texas 76798-7348

Received April 10, 1995[⊗]

Treatment of $[\text{Ru}_3(\text{CO})_{12}]$ with *nido*-7,8- $\text{C}_2\text{B}_9\text{H}_{11}$ in heptane at reflux temperatures affords $[\text{Ru}(\text{CO})_3(\eta^5\text{-}7,8\text{-C}_2\text{B}_9\text{H}_{11})]$ (**1**) in high yield. Heating thf (tetrahydrofuran) solutions of the latter with $[\text{NEt}_4][\text{RuI}(\text{CO})_2(\eta^5\text{-}7,8\text{-C}_2\text{B}_9\text{H}_{11})]$ (**2a**) which with AgBF_4 in thf yields the neutral complex $[\text{Ru}(\text{CO})_2(\text{thf})(\eta^5\text{-}7,8\text{-C}_2\text{B}_9\text{H}_{11})]$ (**3**). The latter reacts with molecular hydrogen to give, after addition of $[\text{NEt}_4][\text{BF}_4]$, the diruthenium species $[\text{NEt}_4][\text{Ru}_2(\mu\text{-H})(\text{CO})_4(\eta^5\text{-}7,8\text{-C}_2\text{B}_9\text{H}_{11})_2]$ (**4a**). The $[\text{K}(18\text{-crown-}6)]$ salt (**4b**) of the anionic diruthenium complex is formed on protonation ($\text{HBF}_4\cdot\text{Et}_2\text{O}$) of $[\text{K}(18\text{-crown-}6)][\text{RuH}(\text{CO})_2(\eta^5\text{-}7,8\text{-C}_2\text{B}_9\text{H}_{11})]$ in CH_2Cl_2 . The structure of **4a** was established by X-ray crystallography. Crystals are monoclinic, space group $P2_1/c$ (No. 14), with $a = 11.205(2)$ Å, $b = 20.736(2)$ Å, $c = 13.769(2)$ Å, $\beta = 96.69(2)^\circ$, and $Z = 4$. The Ru–Ru bond [3.189(6) Å] is bridged by the hydrido ligand. The *nido*-7,8- $\text{C}_2\text{B}_9\text{H}_{11}$ cages are transoid with respect to each other as are the two pairs of terminal CO groups on each ruthenium. The reaction between $[\text{K}(18\text{-crown-}6)][\text{RuH}(\text{CO})_2(\eta^5\text{-}7,8\text{-C}_2\text{B}_9\text{H}_{11})]$ and $[\text{AuCl}(\text{PPh}_3)]$ in thf in the presence of either AgBF_4 or TIPF_6 unexpectedly gives $[\text{Au}(\text{PPh}_3)_2][\text{RuCl}(\text{CO})_2(\eta^5\text{-}7,8\text{-C}_2\text{B}_9\text{H}_{11})]$ (**2b**) the structure of which was determined by X-ray crystallography. Crystals are triclinic, space group $P\bar{1}$ (No. 2), with $a = 11.167(2)$ Å, $b = 11.861(2)$ Å, $c = 17.103(3)$ Å, $\alpha = 99.50(2)^\circ$, $\beta = 105.01(2)^\circ$, $\gamma = 95.58(2)^\circ$, and $Z = 2$. The anion in **2b** has a piano stool configuration with ruthenium being coordinated on one side by the *nido*- $\text{C}_2\text{B}_9\text{H}_{11}$ cage in the usual pentahapto manner and on the other by the two CO groups and the Cl atom [Ru–Cl = 2.452(1) Å]. The salt **4b** is deprotonated with NaH in thf yielding $[\text{K}(18\text{-crown-}6)]_2[\text{Ru}_2(\mu\text{-CO})_2(\text{CO})_2(\eta^5\text{-}7,8\text{-C}_2\text{B}_9\text{H}_{11})_2]$ (**5**). An X-ray crystallographic study revealed that crystals are monoclinic, space group $P2_1/c$ (No. 14), with $a = 12.746(1)$ Å, $b = 18.116(4)$ Å, $c = 12.440(2)$ Å, $\beta = 109.58(1)^\circ$, and $Z = 2$. The Ru–Ru separation in the dianion is 2.793(1) Å. The metal atoms and the two terminal CO ligands lie in a mirror plane and the two $\eta^5\text{-}7,8\text{-C}_2\text{B}_9\text{H}_{11}$ groups are transoid on opposite sides of the plane, while the two mirror-related bridging CO groups lie on the crystallographic 2-fold axis. The reaction between $[\text{K}(18\text{-crown-}6)][\text{RuH}(\text{CO})_2(\eta^5\text{-}7,8\text{-C}_2\text{B}_9\text{H}_{11})]$ and $[\text{PtH}(\text{Cl})(\text{PEt}_3)_2]$ in thf in the presence of TIPF_6 yields $[\text{RuPt}(\mu\text{-H})(\mu\text{-}\sigma\text{-}\eta^5\text{-}7,8\text{-C}_2\text{B}_9\text{H}_{10})(\text{CO})_2(\text{PEt}_3)_2]$ (**6**), the structure of which was determined by X-ray crystallography. Crystals are monoclinic, space group $P2_1/c$ (No. 14), with $a = 18.774(4)$ Å, $b = 12.094(2)$ Å, $c = 13.429(3)$ Å, $\beta = 110.78(2)^\circ$, and $Z = 4$. The Ru–Pt bond [2.802(1) Å] is spanned on one side by the hydrido ligand and on the other by an exopolyhedral B–Pt linkage [2.069(7) Å] involving a cage boron atom which is in the α site with respect to the two carbon atoms in the CCBBB ring ligating the ruthenium. The latter carries two terminal CO ligands, and the platinum atom is in an essential planar environment defined by the Ru, B_α , and the two P atoms. The new complexes have been characterized by NMR spectroscopy in addition to the X-ray diffraction studies.

Introduction

The formal relationship between the pentahapto bonding modes of the ligands $\eta^5\text{-C}_5\text{R}_5$ and $\eta^5\text{-}7,n\text{-R}_2\text{-}7,n$

$\text{C}_2\text{B}_9\text{H}_9$ ($\text{R} = \text{H}$ or Me , $n = 8$ or 9) has long been known and has been exploited to prepare a host of complexes in which transition metal ions occupy vertices in *closo*-icosahedral cage structures.¹ We are exploring the reactivity of metal centers in certain icosahedral metallocarborane structures which are isolobally mapped with cyclopentadienylmetal species. Thus we have recently reported studies on the complexes $[\text{M}(\text{CO})_2(\eta^5\text{-}7,8\text{-C}_2\text{B}_9\text{H}_{11})]$ ($\text{M} = \text{Ni}$, Pd , or Pt)² which are related to

* To whom correspondence should be addressed.

[†] In the compounds described in this paper ruthenium atoms and *nido*- C_2B_9 cages form *closo*-1,2-dicarba-3-ruthenadodecaborane structures. However, use of this numbering scheme leads to an impossibly complex nomenclature for some of the metal complexes reported. Following precedent (Mullica, D. F.; Sappenfield, E. L.; Stone, F. G. A.; Woollam, S. F. *Organometallics* 1994, 13, 157), therefore, we treat the cage as a *nido* 11-vertex ligand with numbering as for an icosahedron from which the twelfth vertex has been removed. This has the added convenience of relating the metal carborane complexes to similar species with $\eta^5\text{-C}_5\text{H}_5$ ligands.

[⊗] Abstract published in *Advance ACS Abstracts*, June 15, 1995.

(1) (a) Hawthorne, M. F.; Young, D. C.; Andrews, T. D.; Howe, D. V.; Pilling, R. L.; Pitts, A. D.; Reintjes, M.; Warren, L. F.; Wegner, P. A. *J. Am. Chem. Soc.* 1968, 90, 879. (b) Hawthorne, M. F. *Pure Appl. Chem.* 1972, 29, 547; 1973, 33, 475. (c) Callahan, K. P.; Hawthorne, M. F. *Adv. Organomet. Chem.* 1976, 14, 145.

Table 1. Analytical and Physical Data

compd	color	yield/%	$\nu_{\max}(\text{CO})^c/\text{cm}^{-1}$	anal. ^b /%	
				C	H
[Ru(CO) ₃ (η^5 -7,8-C ₂ B ₉ H ₁₁)] ⁻ (1)	red	80	2114 s, 2058 s		
[NEt ₄][Ru(CO) ₂ (η^5 -7,8-C ₂ B ₉ H ₁₁)] (2a)	red	77	2037 s, 1981 s	26.1 (26.4) ^d	5.7 (5.7)
[Au(PPh ₃) ₂][RuCl(CO) ₂ (η^5 -7,8-C ₂ B ₉ H ₁₁)] (2b)	red	23	2037 s, 1981 s	45.5 (45.9)	3.6 (3.9)
[Ru(CO) ₂ (thf)(η^5 -7,8-C ₂ B ₉ H ₁₁)] (3)	yellow	60	2055 s, 2004 s	25.8 (26.6)	5.1 (5.3)
[NEt ₄][Ru ₂ (μ -H)(CO) ₄ (η^5 -7,8-C ₂ B ₉ H ₁₁) ₂] (4a)	yellow	77	2027 s, 1992 s	27.6 (27.0) ^e	6.6 (6.1)
[RuPt(μ -H)(μ - σ : η^5 -7,8-C ₂ B ₉ H ₁₀)(CO) ₂ (PET ₃) ₂] (6)	yellow	55	2025 s, 1970 s	27.4 (26.7)	5.6 (5.7)

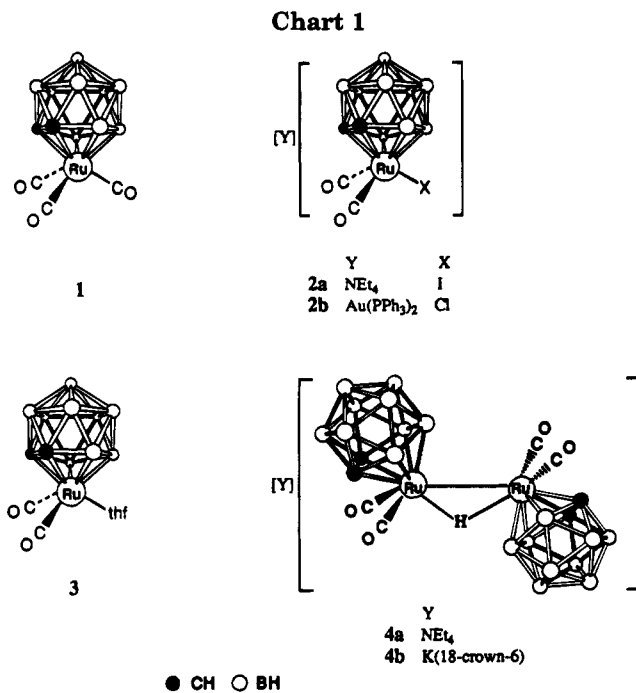
^a Measured in CH₂Cl₂. All complexes show a broad medium-intensity band at ca. 2550 cm⁻¹ due to cage B-H absorptions. ^b Calculated values are given in parentheses. ^c See ref 6. ^d N, 2.3 (2.6). ^e N, 2.0 (2.0).

the compounds [M(CO)₂(η^5 -C₅H₅)] (M = Co, Rh, or Ir). Although both neutral and anionic cyclopentadienyl-metal carbonyls are very important reagents in organometallic syntheses, studies on the chemistry of their metallocarborane analogs with icosahedral cage frameworks have been somewhat limited. However, salts of the anionic complexes [M(CO)₃(η^5 -7,8-C₂B₉H₁₁)]²⁻ (M = Mo or W), [M(CO)₃(η^5 -7,8-C₂B₉H₁₁)]⁻ (M = Mn or Re), [Fe(CO)₂(η^5 -7,8-C₂B₉H₁₁)]²⁻, and [Rh(CO)₂(η^5 -7,8-C₂B₉H₁₁)]⁻ are known and various reactions of these species have been reported.^{1a,3,4} These anionic complexes are formally analogs of [M(CO)₃(η^5 -C₅H₅)]⁻ (M = Mo or W), [M(CO)₃(η^5 -C₅H₅)] (M = Mn or Re), [Fe(CO)₂(η^5 -C₅H₅)]⁻, and [Rh(CO)₂(η^5 -C₅H₅)]⁻, respectively.

The neutral complexes [M(CO)₃(η^5 -7,8-C₂B₉H₁₁)] (M = Fe^{3a,b} or Ru^{5,6}) are of particular interest because of the ubiquitous and extensively explored chemistry of the fragments M(CO)_n(η^5 -C₅H₅) (n = 2 or 3). The synthesis of [Ru(CO)₃(η^5 -7,8-C₂B₉H₁₁)] (1) (Chart 1) was first reported by Siedle,⁵ who obtained it in very low yield (ca. 7%) from [Ru₂Cl₂(μ -Cl)₂(CO)₆] and Na₂[7,8-C₂B₉H₁₁]. Later Behnken and Hawthorne⁶ prepared 1 in good yield (ca. 65%) by treating [RuCl₂(CO)₃(thf)] (thf = tetrahydrofuran) with Na₂[7,8-C₂B₉H₁₁]. They were thereby able to study several reactions of this species, observing in particular the high reactivity of 1 toward nucleophiles. Neither of the reagents [Ru₂Cl₂(μ -Cl)₂(CO)₆] or [RuCl₂(CO)₃(thf)],⁷ however, are satisfactory precursors to 1 as they are not easy to prepare. Herein we describe a convenient high-yield synthesis of 1 allowing this compound to become a useful synthon for a variety of icosahedral ruthenacarborane complexes.

Results and Discussion

The reaction between [Ru₃(CO)₁₂] and cyclopentadiene under reflux in heptane initially gives [RuH(CO)₂(η -C₅H₅)] which subsequently releases hydrogen and forms [Ru₂(μ -CO)₂(CO)₂(η -C₅H₅)₂] in good yield.⁸ On the basis



of this synthesis, a related reaction between [Ru₃(CO)₁₂] and *nido*-7,8-C₂B₉H₁₃ in heptane at reflux was investigated and found to give [Ru(CO)₃(η^5 -7,8-C₂B₉H₁₁)] (1) in ca. 80% yield. The ¹¹B{¹H} NMR spectrum of 1 was identical with that reported previously.⁶ The IR spectrum measured in CH₂Cl₂ showed two terminal CO bands at 2114 and 2058 cm⁻¹, the latter peak being broad. In heptane, however, three CO absorptions are observed at 2108, 2058, and 2044 cm⁻¹. Compound 1 was further characterized by its ¹³C{¹H} and ¹H NMR spectra. The former spectrum displays a diagnostic resonance for the cage CH groups at δ 46.4 and a signal for the CO ligands at δ 188.9, while the ¹H NMR spectrum shows a peak at δ 3.54, corresponding to the chemical shift reported earlier for the CH vertices.⁵ Several reactions of 1 have been investigated.

Treatment of 1 with [NEt₄I] in thf gives [NEt₄][Ru(CO)₂(η^5 -7,8-C₂B₉H₁₁)] (2a), characterized by the data listed in Tables 1 and 2. As expected, the CO stretching frequencies in the IR spectrum of 2a are at noticeably lower frequency than those of 1 due to the former complex being anionic. Reaction between 2a and AgBF₄ in thf at room temperature leads to the rapid and apparently quantitative formation of [Ru(CO)₂(thf)(η^5 -7,8-C₂B₉H₁₁)] (3), AgI, and [NEt₄][BF₄]. Complex 3 is a useful reagent for preparing other ruthenacarborane compounds, and for this purpose it is best prepared and used *in situ*, with its formation being monitored by IR spectroscopy. Freshly generated neutral 3 shows $\nu_{\max}(\text{CO})$ at 2055 and 2004 cm⁻¹, higher frequencies than

(2) Carr, C.; Mullica, D. F.; Sappenfield, E. L.; Stone, F. G. A. *Inorg. Chem.* **1994**, *33*, 1666. Fallis, K. A.; Mullica, D. F.; Sappenfield, E. L.; Stone, F. G. A. *Inorg. Chem.* **1994**, *33*, 4927.

(3) (a) Lee, S.; Knobler, C. B.; Hawthorne, M. F. *Organometallics* **1991**, *10*, 670. (b) Lee, S.; Knobler, C. B.; Hawthorne, M. F. *Organometallics* **1991**, *10*, 1054. (c) Do, Y.; Knobler, C. B.; Hawthorne, M. F. *J. Am. Chem. Soc.* **1987**, *109*, 1853. (d) Kim, J.; Do, Y.; Sohn, Y. S.; Knobler, C. B.; Hawthorne, M. F. *J. Organomet. Chem.* **1991**, *418*, C1.

(4) (a) Pilotti, M. U.; Stone, F. G. A. *J. Chem. Soc., Dalton Trans.* **1990**, 2625. (b) Dossett, S. J.; Mullica, D. F.; Sappenfield, E. L.; Stone, F. G. A.; Went, M. J. *J. Chem. Soc., Dalton Trans.* **1993**, 281. (c) Dossett, S. J.; Li, S.; Stone, F. G. A. *J. Chem. Soc., Dalton Trans.* **1993**, 1585. (d) Mullica, D. F.; Sappenfield, E. L.; Stone, F. G. A.; Woollam, S. F. *J. Chem. Soc., Dalton Trans.* **1993**, 3559.

(5) Siedle, A. R. *J. Organomet. Chem.* **1975**, *90*, 249.

(6) Behnken, P. E.; Hawthorne, M. F. *Inorg. Chem.* **1984**, *23*, 3420.

(7) Bruce, M. I.; Stone, F. G. A. *J. Chem. Soc. A* **1967**, 1238.

(8) Humphries, A. P.; Knox, S. A. R. *J. Chem. Soc., Dalton Trans.* **1975**, 1710. Doherty, N. M.; Knox, S. A. R.; Morris, M. J. *Inorg. Synth.* **1990**, *28*, 189.

Table 2. Hydrogen-1, Carbon-13, and Boron-11 NMR Data^a

compd	¹ H/δ ^b	¹³ C/δ ^c	¹¹ B/δ ^d
1	3.54 (s, 2 H, cage CH)	188.9 (CO), 46.4 (cage CH)	8.9 (1 B), -3.6 (1 B), -4.8 (2 B), -8.7 (2 B), -17.6 (3 B)
2a	1.33 (m br, 12 H, NCH ₂ Me), 2.98 (s, 2 H, cage CH), 3.22 (m br, 8 H, NCH ₂)	197.7 (CO), 53.8 (NCH ₂), 46.4 (cage CH), 7.8 (NCH ₂ Me)	1.2 (1 B), -7.9 (1 B), -9.0 (4 B), -18.0 (1 B), -22.0 (2 B)
3	1.99 (m br, 4 H, OCH ₂ CH ₂), 3.29 (s, 2 H, cage CH), 3.90 (m br, 4 H, OCH ₂)	196.2 (CO), 71.3 (OCH ₂), 52.6 (cage CH), 27.6 (OCH ₂ CH ₂) ^d	3.6 (1 B), -7.0 (2 B), -8.5 (2 B), -12.1 (1 B), -18.2 (1 B), -20.7 (2 B)
4b	-14.67 (s, 1 H, μ-H), 3.11 (s, 2 H, cage CH), 3.62 (s, 24 H, 18-crown-6)	197.4 (CO), 70.4 (18-crown-6), 44.0 (cage CH)	2.9 (1 B), -4.0 (1 B), -7.8 (2 B), -9.0 (2 B), -18.9 (1 B), -20.7 (2 B)
6	-8.87 (d of d, 1 H, μ-H, J(PH)) 20, 49 Hz, J(PtH) = 190 Hz), 1.03 (m, 18 H, CH ₂ Me), 2.06 (m, 12 H, CH ₂), 3.20, 3.60 (s × 2, 2 H, cage CH)	198.4, 195.1 (CO), 40.0, 39.0 (cage CH), 20.8, 19.1 (m × 2, CH ₂ Me), 8.84 (CH ₂ Me)	49.1 (1 B, BPt, J(PtB) = 76 Hz), 0.4 (1 B), -2.7 (1 B), -3.6 (1 B), -9.2 (1 B), -14.5 (2 B), -17.9 (1 B), -28.0 (1 B)

^a Chemical shifts (δ) in ppm, coupling constants (J) in Hz, measurements in CD₂Cl₂ at room temperature. ^b Resonances for terminal BH protons occur as broad unresolved signals in the range δ ca. -2 to 3. ^c Hydrogen-1 decoupled, chemical shifts are positive to high frequency of SiMe₄. ^d Measured in thf-d₈.

those of **2a**. The ¹H NMR spectrum of **3** shows peaks at δ 3.29 for the cage CH groups and at δ 1.99 and 3.90 for ligated thf. The reagent **3** can be isolated if required by column chromatography, but if this is done, the yield is not quantitative. Interestingly, spectroscopic examination of solutions of **3** in nondonor solvents like CH₂-Cl₂ reveals the presence of another complex present in very minor amount. The latter shows CO peaks at 2064 and 2015 cm⁻¹ and resonances of weak intensity in the ¹H NMR spectrum at δ 3.11 for cage CH and at δ 1.83 and 3.69 for free thf. We suggest this labile species is the 16-electron complex [Ru(CO)₂(η⁵-7,8-C₂B₉H₁₁)], discussed further below.

It was shown earlier that reaction of **1** with KOH or K[BH(sec-Bu)₃] in the presence of 18-crown-6 gave the salt [K(18-crown-6)][RuH(CO)₂(η⁵-7,8-C₂B₉H₁₁)].⁶ We treated the latter in CH₂Cl₂ with 1 equiv of HBF₄·Et₂O in an attempt to obtain either a neutral dihydrido compound or an η²-H₂ complex of ruthenium, but we obtained instead the anionic diruthenium complex [Ru₂(μ-H)(CO)₄(η⁵-7,8-C₂B₉H₁₁)₂]⁻, which we isolated as the [NEt₄]⁺ (**4a**) or [K(18-crown-6)]⁺ (**4b**) salts. Data for **4** are given in Tables 1 and 2. The ¹H NMR spectrum displays a singlet for the μ-H group at δ -14.67, while the ¹³C{¹H} NMR spectrum shows resonances for the CO ligands at δ 197.4 and for the cage CH vertices at δ 44.1. Crystals of **4a** were the subject of an X-ray diffraction study to establish the structure of the anion. The results are given below after discussion of the routes by which **4** may be obtained.

Formation of **4** by protonating [K(18-crown-6)][RuH(CO)₂(η⁵-7,8-C₂B₉H₁₁)] can be readily understood by assuming that hydrogen is released, possibly by reductive elimination from a dihydride [Ru(H)₂(CO)₂(η⁵-7,8-C₂B₉H₁₁)]. This would produce the unsaturated species [Ru(CO)₂(η⁵-7,8-C₂B₉H₁₁)], mentioned above, which might then be captured by the unreacted [RuH(CO)₂(η⁵-7,8-C₂B₉H₁₁)]⁻ present in the solutions thus yielding **4b**. It is noteworthy that the compound [Ru(H)₂(PPh₃)₂(η⁵-7,8-C₂B₉H₁₁)] releases hydrogen to form the 16-electron coordinatively unsaturated complex [Ru(PPh₃)₂(η⁵-7,8-C₂B₉H₁₁)],⁹ closely related to the postulated species [Ru(CO)₂(η⁵-7,8-C₂B₉H₁₁)]. However, with phosphines ligating ruthenium, instead of carbonyls, the dihydride

would be more stable, it being well-known that replacement of CO groups by PPh₃ stabilizes metal-hydride bonds. Thus the dihydride [Ru(H)₂(PPh₃)₂(η⁵-7,8-C₂B₉H₁₁)] is readily re-formed from [Ru(PPh₃)₂(η⁵-7,8-C₂B₉H₁₁)] and hydrogen.⁹

Interestingly, if the ruthenium-tetrahydrofuran complex **3** is generated *in situ*, conditions under which the salt [NEt₄][BF₄] remains present, treatment of these solutions with hydrogen affords **4a** in over 70% yield. It seems likely that an η²-H₂ ruthenium complex is involved in the process, with the coordinated hydrogen being activated toward heterolytic cleavage by the thf present. Studies on isolobal cyclopentadienylruthenium complexes¹⁰ provide a good model for this proposal. The dihydrogen complex [Ru(CO)₂(η²-H₂)(η⁵-C₅Me₅)[BF₄] is readily deprotonated even by the very weak base Et₂O, forming [Ru₂(μ-H)(CO)₄(η⁵-C₅Me₅)₂][BF₄].^{11a} The cation of the latter is structurally and electronically related to the anion [Ru₂(μ-H)(CO)₄(η⁵-7,8-C₂B₉H₁₁)₂]⁻ present in **4a**. Hence an attractive pathway for the formation of **4a** by treating thf solutions of **3** with hydrogen, in the presence of the salt [NEt₄][BF₄], would involve a labile intermediate [Ru(CO)₂(η²-H₂)(η⁵-7,8-C₂B₉H₁₁)], akin to [Ru(CO)₂(η²-H₂)(η⁵-C₅Me₅)[BF₄]. The transient species [Ru(CO)₂(η²-H₂)(η⁵-7,8-C₂B₉H₁₁)] might be deprotonated by thf, the latter a stronger base than OEt₂. The [RuH(CO)₂(η⁵-7,8-C₂B₉H₁₁)]⁻ so formed would then combine with molecules of **3** or [Ru(CO)₂(η⁵-7,8-C₂B₉H₁₁)] to yield the [NEt₄]⁺ salt **4a** and HBF₄·thf.^{11a} Indeed, in a separate experiment we found that Behnken's and Hawthorne's⁶ salt [K(18-crown-6)][RuH(CO)₂(η⁵-7,8-C₂B₉H₁₁)] readily reacts with **3** to give **4b**.

In an attempt to clarify the nature of the intermediates involved in the formation of **4a** from **3** and H₂, solutions of **3** in CD₂Cl₂, with no [NEt₄][BF₄] present, were treated with H₂ and the ¹H NMR spectrum of the mixture was examined. In the ¹H NMR spectrum of [Ru(H)₂(PPh₃)₂(η⁵-7,8-C₂B₉H₁₁)] the resonance for the hydrido ligands occurs at δ -6.9,⁹ and in the tautomers [Ru(H)₂(PPh₃)₂(η⁵-C₅Me₅)]⁺ and [Ru(η²-H₂)(PPh₃)₂(η⁵-C₅Me₅)]⁺ the RuH and Ru(η²-H₂) signals are seen at δ -6.72 and -7.60, respectively.^{11b} In the hydrogen-

(10) Heinekey, D. M.; Oldham, W. J. *Chem. Rev.* **1993**, *93*, 913.(11) (a) Chinn, M. S.; Heinekey, D. M.; Payne, N. G. *Organometallics* **1989**, *8*, 1824. (b) Chinn, M. S.; Heinekey, D. M. *J. Am. Chem. Soc.* **1990**, *112*, 5166.

Table 3. Selected Internuclear Distances (Å) and Angles (deg) for [NEt₄][Ru₂(μ-H)(CO)₄(η⁵-7,8-C₂B₉H₁₁)₂] (4a), with Estimated Standard Deviations in Parentheses

Ru(1)–Ru(2)	3.189(6)	Ru(1)–H	1.809	Ru(1)–C(1)	2.256(4)	Ru(1)–C(2)	2.243(4)
Ru(1)–B(3)	2.245(5)	Ru(1)–B(4)	2.285(5)	Ru(1)–B(5)	2.305(5)	Ru(1)–C(3)	1.866(5)
Ru(1)–C(4)	1.862(4)	C(1)–C(2)	1.625(6)	C(1)–B(5)	1.723(6)	C(1)–B(6)	1.721(6)
C(1)–B(10)	1.695(7)	C(2)–B(3)	1.710(6)	C(2)–B(6)	1.717(7)	C(2)–B(7)	1.696(6)
B(3)–B(4)	1.810(7)	B(3)–B(7)	1.786(7)	B(3)–B(8)	1.746(7)	B(4)–B(5)	1.843(7)
B(4)–B(8)	1.763(7)	B(4)–B(9)	1.786(7)	B(5)–B(9)	1.751(7)	B(5)–B(10)	1.790(7)
B(6)–B(7)	1.753(8)	B(6)–B(10)	1.758(7)	B(6)–B(11)	1.760(8)	B(7)–B(8)	1.766(7)
B(7)–B(11)	1.779(8)	B(8)–B(9)	1.789(7)	B(8)–B(11)	1.782(8)	B(9)–B(10)	1.766(8)
B(9)–B(11)	1.779(7)	B(10)–B(11)	1.769(7)	H–Ru(2)	1.726	Ru(2)–C(23)	1.870(5)
Ru(2)–C(24)	1.870(5)	Ru(2)–C(21)	2.252(4)	Ru(2)–C(22)	2.233(4)	Ru(2)–B(23)	2.274(5)
Ru(2)–B(24)	2.296(5)	Ru(2)–B(25)	2.264(5)	C(21)–C(22)	1.634(6)	C(21)–B(25)	1.696(6)
C(21)–B(26)	1.708(7)	C(21)–B(30)	1.700(7)	C(22)–B(23)	1.690(7)	C(22)–B(26)	1.729(7)
C(22)–B(27)	1.707(7)	B(23)–B(24)	1.808(7)	B(23)–B(27)	1.783(8)	B(23)–B(28)	1.765(7)
B(24)–B(25)	1.809(7)	B(24)–B(28)	1.767(7)	B(24)–B(29)	1.773(7)	B(25)–B(29)	1.747(8)
B(25)–B(30)	1.788(8)	B(26)–B(27)	1.766(8)	B(26)–B(30)	1.750(7)	B(26)–B(31)	1.763(8)
B(27)–B(28)	1.765(7)	B(27)–B(31)	1.753(7)	B(28)–B(29)	1.785(7)	B(28)–B(31)	1.776(8)
B(29)–B(30)	1.779(8)	B(29)–B(31)	1.782(7)	B(30)–B(31)	1.786(8)	C(3)–O(3)	1.146(6)
C(4)–O(4)	1.151(5)	C(23)–O(23)	1.152(6)	C(24)–O(24)	1.138(6)		
H–Ru(1)–C(3)	89.7(1)	H–Ru(1)–C(4)	105.0(1)	C(3)–Ru(1)–C(4)	91.4(2)	Ru(1)–H–Ru(2)	128.8(1)
Ru(1)–C(3)–O(3)	177.1(4)	Ru(1)–C(4)–O(4)	172.4(4)	H–Ru(2)–C(23)	97.7(1)	H–Ru(2)–C(24)	80.6(1)
C(23)–Ru(2)–C(24)	88.8(2)	Ru(2)–C(23)–O(23)	175.3(4)	Ru(2)–C(24)–O(24)	174.9(4)		

saturated solutions of **3** no resonance was observed in the region δ –6 to –9 where peaks due to either Ru–H or Ru(η^2 -H₂) groups of the mononuclear ruthenium species [Ru(H)₂(CO)₂(η^5 -7,8-C₂B₉H₁₁)] or [Ru(CO)₂(η^2 -H₂)(η^5 -7,8-C₂B₉H₁₁)] would be expected. However, the solutions of **3** after treatment with H₂ did display in their ¹H NMR spectra two very broad peaks at δ –14.77 and –15.01. This is the chemical shift region diagnostic for a proton in a site bridging a Ru–Ru bond,¹² as typified by the very sharp resonance observed at δ –14.67 in the ¹H NMR spectra of the salts **4**. Cooling hydrogen-saturated solutions of **3** to –90 K resulted in the ¹H NMR resonance at δ –15.01 becoming sharp and that at δ –14.77 resolving into three sharper signals centered at δ –14.12. Measurement of relaxation times (*T*₁) on these signals provided no evidence for any being due to an Ru(μ - η^2 -H₂)Ru group,¹³ thus eliminating rapid equilibration between isomers with classical [Ru₂(μ -H)₂(CO)₄(η^5 -7,8-C₂B₉H₁₁)₂] and nonclassical [Ru₂(μ - η^2 -H₂)(CO)₄(η^5 -7,8-C₂B₉H₁₁)₂] structures. It is also noteworthy that in the ¹H NMR spectra of the hydrogen-saturated solutions measured both at room temperature and at –90 K there was a broad signal at δ 8.5, possibly ascribable to protons associated with thf molecules displaced from **3** by hydrogen. From this inconclusive data we infer that heterolytic cleavage of H₂ occurs via [Ru(CO)₂(η^2 -H₂)(η^5 -7,8-C₂B₉H₁₁)] immediately upon treatment of CH₂Cl₂ solutions of **3** with hydrogen and before addition of [NEt₄][BF₄] results in formation of **4a**. The solutions would contain protons and a dynamic equilibrating mixture of diruthenium species, probably including cis- and trans-isomers of the anion [Ru₂(μ -H)(CO)₄(η^5 -7,8-C₂B₉H₁₁)₂][–], thus accounting for the ¹H NMR signals seen in the region δ –14.77 to –15.01. Subsequent addition of [NEt₄][BF₄] displaces the equilibrium, producing **4a** as the most thermodynamically stable entity.

The structure of **4a** was determined by X-ray crystallography, and the anion is shown in Figure 1, with

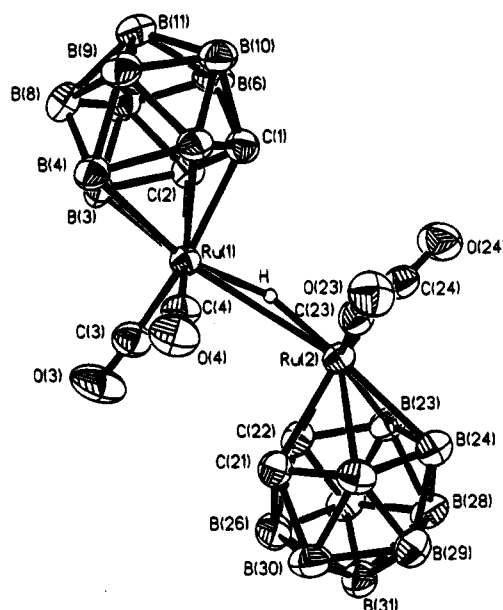


Figure 1. Structure of the anion [Ru₂(μ -H)(CO)₄(η^5 -7,8-C₂B₉H₁₁)₂][–] of **4a**, showing the crystallographic labeling scheme. Hydrogen atoms have been omitted for clarity, and thermal ellipsoids are shown at the 50% probability level.

selected structural parameters listed in Table 3. The hydrido ligand, located by difference Fourier mapping after all other H-atoms had been found, spans the Ru–Ru bond [3.189(6) Å] with μ -H–Ru(av) = 1.77 Å, a distance very similar to that (*ca.* 1.79 Å) in other species with Ru(μ -H)Ru groups.¹⁴ Each ruthenium atom is coordinated by a *nido*-7,8-C₂B₉H₁₁ group in the usual pentahapto manner with these cages being transoid to one another. The carbonyl ligands deviate perceptibly from linearity in their bonding to the ruthenium atoms [Ru–C–O angles, 172.4–177.1(4)^o].

The results of the protonation studies on [K(18-crown-6)][RuH(CO)₂(η^5 -7,8-C₂B₉H₁₁)] which afforded compound **4b**, and the isolobal mapping of H⁺ with Au(PPh₃)⁺, prompted us to study the reaction between the potassium salt of [RuH(CO)₂(η^5 -7,8-C₂B₉H₁₁)][–] and [AuCl(PPh₃)] in an attempt to obtain a ruthenium–gold

(12) Kaesz, H. D.; Saillant, R. B. *Chem. Rev.* **1972**, *72*, 231.

(13) Collman, J. P.; Wagenknecht, P. S.; Hutchison, J. E.; Lewis, N. S.; Lopez, M. A.; Guillard, R.; L'Her, M.; Bothner-By, A. A.; Mishra, P. K. *J. Am. Chem. Soc.* **1992**, *114*, 5654. Collman, J. P.; Hutchison, J. E.; Wagenknecht, P. S.; Lewis, N. S.; Lopez, M. A.; Guillard, R. *J. Am. Chem. Soc.* **1990**, *112*, 8206.

(14) Teller, R. G.; Bau, S. *Struct. Bonding* **1981**, *44*, 1.

Table 4. Selected Internuclear Distances (Å) and Angles (deg) for [Au(PPh₃)₂][RuCl(CO)₂(η⁵-7,8-C₂B₉H₁₁)] (2b), with Estimated Standard Deviations in Parentheses

Ru-C(1)	2.239(5)	Ru-C(2)	2.267(5)	Ru-B(3)	2.254(6)	Ru-B(4)	2.273(5)
Ru-B(5)	2.284(5)	Ru-C(3)	1.902(5)	Ru-C(4)	1.890(6)	Ru-Cl	2.452(1)
C(1)-C(2)	1.657(6)	C(1)-B(5)	1.708(6)	C(1)-B(6)	1.763(7)	C(1)-B(10)	1.724(7)
C(2)-B(3)	1.719(8)	C(2)-B(6)	1.733(8)	C(2)-B(7)	1.695(8)	B(3)-B(4)	1.860(7)
B(3)-B(7)	1.833(9)	B(3)-B(8)	1.796(8)	B(4)-B(5)	1.815(9)	B(4)-B(8)	1.837(8)
B(4)-B(9)	1.806(8)	B(5)-B(9)	1.773(8)	B(5)-B(10)	1.789(8)	B(6)-B(7)	1.784(10)
B(6)-B(10)	1.777(7)	B(6)-B(11)	1.799(8)	B(7)-B(8)	1.782(7)	B(7)-B(11)	1.781(8)
B(8)-B(9)	1.800(8)	B(8)-B(11)	1.771(9)	B(9)-B(10)	1.765(9)	B(9)-B(11)	1.797(7)
B(10)-B(11)	1.784(9)	C(3)-O(3)	1.155(6)	C(4)-O(4)	1.157(8)	Au-P(1)	2.319(1)
Au-P(2)	2.324(1)	P(1)-C(11)	1.835(4)	P(1)-C(21)	1.818(5)	P(1)-C(31)	1.825(5)
P(2)-C(41)	1.810(5)	P(2)-C(51)	1.840(5)	P(2)-C(61)	1.820(4)		
C(3)-Ru-C(4)	88.9(2)	C(3)-Ru-Cl	95.9(2)	C(4)-Ru-Cl	92.5(2)	Ru-C(3)-O(3)	173.3(4)
Ru-C(4)-O(4)	175.9(4)	P(1)-Au-P(2)	172.8(1)	Au-P(1)-C(11)	112.7(2)	Au-P(1)-C(21)	113.6(2)
C(11)-P(1)-C(21)	106.1(2)	Au-P(1)-C(31)	112.4(1)	C(11)-P(1)-C(31)	106.1(2)	C(21)-P(1)-C(31)	105.3(2)
Au-P(2)-C(41)	110.3(1)	Au-P(2)-C(51)	110.4(1)	C(41)-P(2)-C(51)	106.6(2)	Au-P(2)-C(61)	115.8(2)
C(41)-P(2)-C(61)	106.8(2)	C(51)-P(2)-C(61)	106.6(2)				

ring	distances (Ph)		angles (Ph)	
	mean	range	mean	range
C(11)-C(16)	1.39(1)	1.36-1.41	120.0(10)	119.0-122.0
C(21)-C(26)	1.39(2)	1.36-1.42	120.0(8)	118.7-121.1
C(31)-C(36)	1.39(2)	1.36-1.42	120.0(9)	119.2-121.4
C(41)-C(46)	1.39(1)	1.38-1.41	120.0(10)	118.7-121.2
C(51)-C(56)	1.39(1)	1.38-1.42	120.0(9)	118.4-120.8
C(61)-C(66)	1.40(1)	1.38-1.42	120.0(6)	119.3-120.9

complex of formulation [(η⁵-7,8-C₂B₉H₁₁)(OC)₂Ru(μ-H)-Au(PPh₃)]. Such a product would be formally related to [(OC)₅Cr(μ-H)Au(PPh₃)], obtained from the reaction between [N(PPh₃)₂][CrH(CO)₅] and [AuCl(PPh₃)],¹⁵ and would mimic the intermediate [Ru(CO)₂(η²-H₂)(η⁵-7,8-C₂B₉H₁₁)] mentioned above. The reaction between [K(18-crown-6)][RuH(CO)₂(η⁵-7,8-C₂B₉H₁₁)] and [AuCl(PPh₃)] in thf, in the presence of AgBF₄ to facilitate removal of Cl⁻ as AgCl, did not give the anticipated ruthenium-gold complex but instead yielded the salt [Au(PPh₃)₂][RuCl(CO)₂(η⁵-7,8-C₂B₉H₁₁)] (2b) together with what appeared to be a metallic residue of gold and silver. Compound 2b was also formed when TlPF₆ was used to remove Cl⁻ instead of AgBF₄, and the brown intractable residue produced in this reaction may have contained gold metal. In the absence of AgBF₄ or TlPF₆ the reaction did not proceed. Formation of the cation [Au(PPh₃)₂]⁺ in reactions of [AuCl(PPh₃)], carried out in the presence of TlPF₆ to remove chloride, has been observed previously¹⁶ and appears to involve displacement of solvent from [Au(sol)(PPh₃)]⁺ by PPh₃ molecules released when some of the gold reagent is reduced to the metal. Interestingly, compound 2b is also formed when 4a is treated with [AuCl(PPh₃)]. The IR and NMR data for 2b were essentially the same as those for 2a, apart from resonances in the NMR spectra due to the different cations.

Evidently a complex sequence of reactions occurs in the formation of 2b, and the nature of this product was not recognized until after a crystal structure determination had been made, the results of which are discussed below. Hawthorne and co-workers¹⁷ have observed that treatment of Na₂[Fe(CO)₂(η⁵-7,8-C₂B₉H₁₁)] with [AuCl(PPh₃)] affords [Fe(CO)₂(PPh₃)(η⁵-7,8-C₂B₉H₁₁)] in an electron-transfer process instead of the anticipated product with an Fe-Au bond from nucleophilic substi-

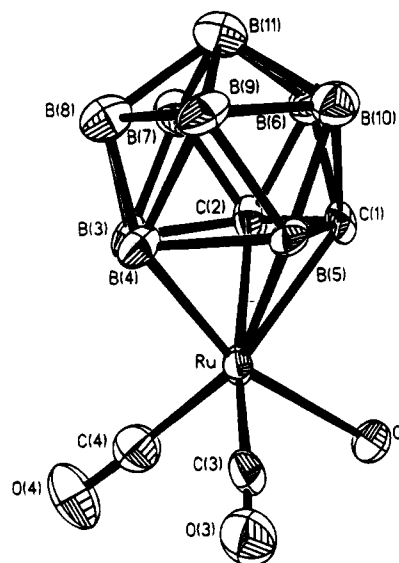


Figure 2. Structure of the anion [RuCl(CO)₂(η⁵-7,8-C₂B₉H₁₁)]⁻ of 2b, showing the crystallographic labeling scheme. Hydrogen atoms have been omitted for clarity, and thermal ellipsoids are shown at the 50% probability level.

tution. In our study failure of Ag⁺ or Tl⁺ to remove Cl⁻ as insoluble AgCl or TlCl in the reaction between [K(18-crown-6)][RuH(CO)₂(η⁵-7,8-C₂B₉H₁₁)] and [AuCl(PPh₃)], before chloride coordinates to the ruthenium to form 2b, is not fully explicable at present. However, if Ag⁺ or [Au(thf)(PPh₃)]⁺ were to oxidize [RuH(CO)₂(η⁵-7,8-C₂B₉H₁₁)]⁻ so generating [Ru(CO)₂(η⁵-7,8-C₂B₉H₁₁)] as an intermediate, the latter would then react rapidly with Cl⁻ to yield the anion of 2b, as in the similar formation of 2a from 1.

The structure of the anion of 2b is shown in Figure 2, and selected internuclear distances and angles are listed in Table 4. On one side the ruthenium atom is coordinated by the nido-7,8-C₂B₉H₁₁ cage and on the other by two essentially terminally bound CO ligands (Ru-C-O = 174°) and the chloride ligand [Ru-Cl = 2.437(19) Å]. The anion thus has the familiar piano

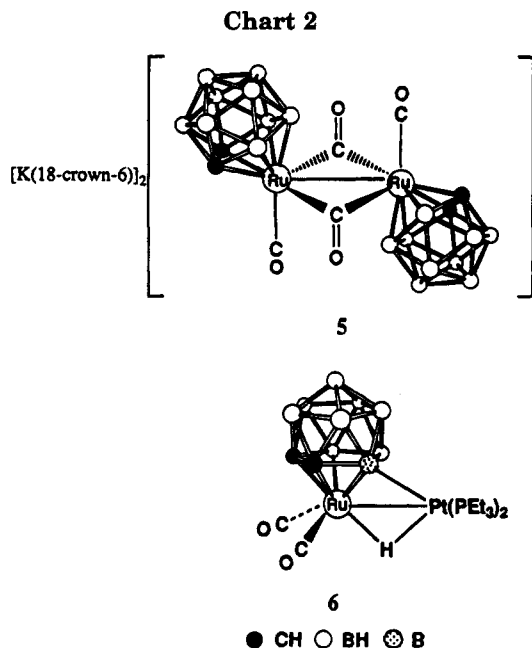
(15) Green, M.; Orpen, A. G.; Salter, I. D.; Stone, F. G. A. *J. Chem. Soc., Dalton Trans.* **1984**, 2497.

(16) Carriedo, G. A.; Howard, J. A. K.; Stone, F. G. A.; Went, M. J. *J. Chem. Soc., Dalton Trans.* **1984**, 2545.

(17) Lee, S. S.; Knobler, C. B.; Hawthorne, M. F. *Organometallics* **1991**, *10*, 1054.

Table 5. Selected Internuclear Distances (Å) and Angles (deg) for [K(18-crown-6)]₂[Ru₂(μ-CO)₂(CO)₂(η⁵-7,8-C₂B₉H₁₁)₂] (5), with Estimated Standard Deviations in Parentheses

Ru-C(1)	2.313(8)	Ru-C(2)	2.314(7)	Ru-B(3)	2.276(11)	Ru-B(4)	2.280(11)
Ru-B(5)	2.376(11)	Ru-C(3)	1.853(10)	Ru-C(4)	2.031(11)	Ru-Ru(a)	2.793(1)
Ru-C(4a)	2.088(10)	C(1)-C(2)	1.583(11)	C(1)-B(5)	1.758(13)	C(1)-B(6)	1.691(14)
C(1)-B(10)	1.739(15)	C(2)-B(3)	1.716(14)	C(2)-B(6)	1.707(14)	C(2)-B(7)	1.705(14)
B(3)-B(4)	1.844(12)	B(3)-B(7)	1.818(14)	B(3)-B(8)	1.810(15)	B(4)-B(5)	1.808(16)
B(4)-B(8)	1.793(13)	B(4)-B(9)	1.878(14)	B(5)-B(9)	1.723(17)	B(5)-B(10)	1.716(14)
B(6)-B(7)	1.761(17)	B(6)-B(10)	1.747(14)	B(6)-B(11)	1.760(17)	B(7)-B(8)	1.744(13)
B(7)-B(11)	1.761(14)	B(8)-B(9)	1.782(14)	B(8)-B(11)	1.737(15)	B(9)-B(10)	1.656(18)
B(9)-B(11)	1.714(12)	B(10)-B(11)	1.733(17)	C(3)-O(3)	1.143(12)	C(4)-O(4)	1.153(10)
C(4)-Ru(a)	2.088(10)						
C(3)-Ru-C(4)	93.5(4)	C(3)-Ru-Ru(a)	91.9(3)	C(4)-Ru-Ru(a)	48.2(3)	C(3)-Ru-C(4a)	89.1(4)
C(4)-Ru-C(4a)	94.6(3)	Ru(a)-Ru-C(4a)	46.5(3)	Ru-C(3)-O(3)	176.1(10)	Ru-C(4)-O(4)	141.0(9)
Ru-C(4)-Ru(a)	85.4(3)	O(4)-C(4)-Ru(a)	133.6(9)				



stool arrangement. In the isolobally mapped molecules [RuCl(PPh₃)₂(η⁵-C₅H₅)] and [RuCl(PPh₃)₂(η⁵-C₅Me₄CH₂-Cl)] the Ru-Cl distances are 2.453(2) Å^{18a} and 2.422(3) Å,^{18b} respectively. The atoms Ru, Cl, and B(3) and the midpoint of the cage C-C connectivity lie on a plane of symmetry. Consequently, in the ¹H and ¹³C{¹H} NMR spectra of the species **2** (Table 2) the CH groups of the cage are equivalent and therefore display a single resonance.

Treatment of compound **4b** in thf with NaH results in deprotonation and formation of the dianion [Ru₂(μ-CO)₂(CO)₂(η⁵-7,8-C₂B₉H₁₁)₂]²⁻ isolated as its [K(18-crown-6)]⁺ salt **5** (Chart 2). It has been previously shown⁶ that reduction of **1** with sodium amalgam also produces [Ru₂(μ-CO)₂(CO)₂(η⁵-7,8-C₂B₉H₁₁)₂]²⁻, and it was proposed, on the basis of the observation of only one terminal CO stretch in its IR spectrum (1910 cm⁻¹ in Nujol), that it has a centrosymmetric structure with a trans configuration of the carborane ligands. We can confirm this structure for the solid state as a result of an X-ray diffraction study.

The structure of the anion is depicted in Figure 3 and selected internuclear distances and bond angles are given in Table 5. In **5** the Ru-Ru distance is 2.793(1) Å and may be compared with the very similar metal-

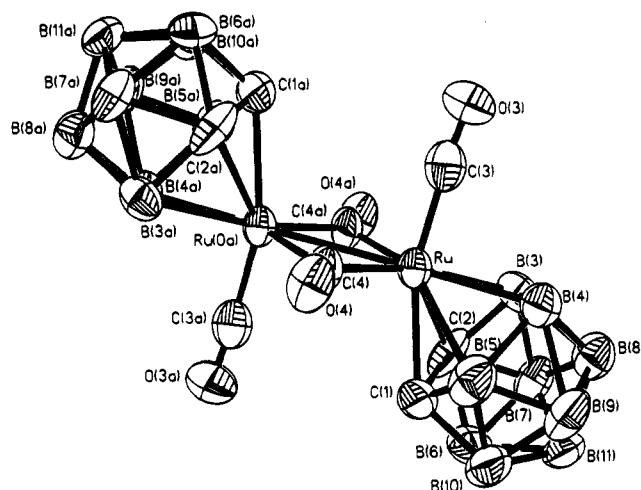


Figure 3. Structure of the anion [Ru(μ-CO)₂(CO)₂(η⁵-7,8-C₂B₉H₁₁)₂]²⁻ of **5**, showing the crystallographic labeling scheme. Hydrogen atoms have been omitted for clarity, and thermal ellipsoids are shown at the 50% probability level.

metal separations found in the isolobal cyclopentadienyl species [Ru₂(μ-CO)₂(CO)₂(η⁵-C₅H₅)₂] [2.735(2) Å]^{19a} and [Ru₂(μ-CO)₂(CO)₂(η⁵-C₅Me₄Et)₂] [2.7584(5) Å],^{19b} which have similar C_{2h} symmetry. The ruthenium atoms of the dianion of **5** and the two terminal CO groups lie in a mirror plane with the two pentahapto-bonded carborane groups lying across the mirror plane. The two mirror-related bridging CO ligands lie on the crystallographic 2-fold axis. Not surprisingly, the Ru-Ru distance in **5** is appreciably shorter than that in **4a** due to the presence of the μ-H group in the latter.¹⁴ The symmetrical molecular geometry of **5** found in the crystal evidently predominates in solutions of the complex since the IR spectrum displays a very strong terminal CO stretch (1974 cm⁻¹) when measured in thf. There is, however, a very weak absorption at 1930 cm⁻¹ indicating the presence of another isomer in low concentrations. A broad absorption for the bridging carbonyl groups is seen at 1760 cm⁻¹.

The reaction between [K(18-crown-6)][RuH(CO)₂(η⁵-7,8-C₂B₉H₁₁)] and [PtH(Cl)(PEt₃)₂] in thf in the presence of TlPF₆ was next investigated. In donor solvents, in the presence of the salts TlBF₄ or TlPF₆, the platinum complex affords the reactive species [PtH(solv)(PEt₃)₂]⁺ (solv = acetone or thf). Earlier results revealed that a combination of the reagents [PtH(Cl)(PEt₃)₂] and TlBF₄

(18) (a) Bruce, M. I.; Wong, F. S.; Skelton, B. W.; White, A. H. *J. Chem. Soc., Dalton Trans.* **1981**, 1398. (b) Fan, L.; Turner, M. L.; Adams, H.; Bailey, N. A.; Maitlis, P. M. *Organometallics* **1995**, *14*, 676.

(19) (a) Mills, O. S.; Nice, J. P. *J. Organomet. Chem.* **1967**, *9*, 339. (b) Bailey, N. A.; Radford, S. L.; Sanderson, J. A.; Tabatabaian, K.; White, C.; Worthington, J. M. *J. Organomet. Chem.* **1978**, *154*, 343.

Table 6. Selected Internuclear Distances (Å) and Angles (deg) for [RuPt(μ -H)(μ - σ - η^5 -7,8-C₂B₉H₁₀)(CO)₂(PEt₃)₂] (6), with Estimated Standard Deviations in Parentheses

Ru-H	1.817	Ru-C(1)	2.236(7)	Ru-C(2)	2.238(7)	Ru-B(3)	2.257(7)
Ru-B(4)	2.323(7)	Ru-B(5)	2.219(6)	Ru-C(3)	1.881(7)	Ru-C(4)	1.837(9)
Ru-Pt	2.802(1)	H-Pt	1.557	C(1)-C(2)	1.617(10)	C(1)-B(5)	1.791(11)
C(1)-B(6)	1.716(10)	C(1)-B(10)	1.698(9)	C(2)-B(3)	1.736(13)	C(2)-B(6)	1.704(11)
C(2)-B(7)	1.673(10)	B(3)-B(4)	1.830(10)	B(3)-B(7)	1.792(13)	B(3)-B(8)	1.782(10)
B(4)-B(5)	1.850(13)	B(4)-B(8)	1.774(10)	B(4)-B(9)	1.762(12)	B(5)-B(9)	1.807(10)
B(5)-B(10)	1.838(12)	B(5)-Pt	2.069(7)	B(6)-B(7)	1.738(14)	B(6)-B(10)	1.797(11)
B(6)-B(11)	1.758(12)	B(7)-B(8)	1.763(12)	B(7)-B(11)	1.761(11)	B(8)-B(9)	1.752(11)
B(8)-B(11)	1.747(14)	B(9)-B(10)	1.780(14)	B(9)-B(11)	1.763(11)	B(10)-B(11)	1.785(12)
C(3)-O(3)	1.157(9)	C(4)-O(4)	1.166(11)	Pt-P(1)	2.369(2)	Pt-P(2)	2.248(2)
P(1)-C(11)	1.792(8)	P(1)-C(13)	1.833(7)	P(1)-C(15)	1.859(10)	P(2)-C(21)	1.813(10)
P(2)-C(23)	1.826(7)	P(2)-C(25)	1.810(8)				
H-Ru-C(3)	82.4(2)	H-Ru-C(4)	89.3(2)	C(3)-Ru-C(4)	88.6(3)	H-Ru-Pt	31.0(1)
C(3)-Ru-Pt	106.5(2)	C(4)-Ru-Pt	108.8(2)	Ru-H-Pt	112.1(1)	Ru-B(5)-Pt	81.5(2)
Ru-C(3)-O(3)	176.2(8)	Ru-C(4)-O(4)	178.6(6)	Ru-Pt-H	36.9(1)	Ru-Pt-B(5)	51.6(2)
H-Pt-B(5)	88.4(2)	Ru-Pt-P(1)	107.0(1)	H-Pt-P(1)	70.7(1)	B(5)-Pt-P(1)	157.9(2)
Ru-Pt-P(2)	144.9(1)	H-Pt-P(2)	172.7(1)	B(5)-Pt-P(2)	93.6(2)	P(1)-Pt-P(2)	108.0(1)
Pt-P(1)-C(11)	110.8(3)	Pt-P(1)-C(13)	125.1(2)	C(11)-P(1)-C(13)	105.2(4)	Pt-P(1)-C(15)	108.2(3)
C(11)-P(1)-C(15)	101.1(4)	C(13)-P(1)-C(15)	103.8(4)	Pt-P(2)-C(21)	114.8(2)	Pt-P(2)-C(23)	115.1(2)
C(21)-P(2)-C(23)	103.8(4)	Pt-P(2)-C(25)	114.2(3)	C(21)-P(2)-C(25)	103.9(4)	C(23)-P(2)-C(25)	103.6(4)

reacts readily with [NEt₃][Rh(CO)(PPh₃)(η^5 -7,8-C₂B₉H₁₁)] to yield [RhPt(μ -H)(μ -CO)(PEt₃)₂(PPh₃)(η^5 -7,8-C₂B₉H₁₁)].^{20a} In view of this work it seemed likely that a metathetical reaction would occur between [RuH(CO)₂(η^5 -7,8-C₂B₉H₁₁)]⁻ and [PtH(solv)(PEt₃)₂]⁺ to yield a ruthenium-platinum complex. Moreover it would be interesting to establish if in any product of this reaction the cage adopts a spectator role as in [RhPt(μ -H)(μ -CO)(PEt₃)₂(PPh₃)(η^5 -7,8-C₂B₉H₁₁)] or whether it plays a nonspectator role as is often observed,²¹ as in for example [RhPt(μ - σ , η^5 -7,8-C₂B₉H₁₀)(CO)(PEt₃)₂(PPh₃)].^{20b}

It was found that if [K(18-crown-6)][RuH(CO)₂(η^5 -7,8-C₂B₉H₁₁)] and [PtH(Cl)(PEt₃)₂] are mixed in thf and TlPF₆ is added, hydrogen is released and the complex [RuPt(μ -H)(μ - σ , η^5 -7,8-C₂B₉H₁₀)(CO)₂(PEt₃)₂] (6) is obtained. The NMR data for this complex (Table 2) are in accord with the presence of a hydrido ligand bridging the Ru-Pt bond and with the cage forming an exopolyhedral B-Pt bond to the Pt(PEt₃)₂ group. The ¹H NMR spectrum has a diagnostic resonance for a μ -H group at δ -8.87 [*J*(PP) = 49 and 20 Hz, *J*(PtH) = 190 Hz] and the ¹¹B{¹H} NMR spectrum has a peak at δ 49.1 with ¹⁹⁵Pt satellite signals [*J*(PtB) = 590 Hz], a resonance pattern characteristic for a B-Pt σ -bond.²² In the complex [RhPt(CO)(μ - σ , η^5 -7,8-C₂B₉H₁₀)(PEt₃)₂(PPh₃)], which also has an exopolyhedral B-Pt bond, the signal for the boron nucleus is at δ 48.3 with *J*(PtB) = 598 Hz.^{20b}

It is very likely that the formation of 6 proceeds by a pathway which involves an intermediate species with an exo-polyhedral B-H-Pt linkage which then undergoes oxidative addition across the Ru-Pt bond yielding the Ru(μ -H)Pt and B-Pt groups present in the product. Exopolyhedral B-H-Pt linkages are common in species where a PtL₂ (L = PR₃ or CO) fragment is linked to a metal atom which forms a vertex in a *closo*-icosahedral

3,1,2-MC₂B₉ framework. Moreover, there is ample precedent for the facile transformation of such three-center two-electron bonds into structures having M(μ -H)Pt and B-Pt bonds.²⁰ However, it always remains to be established whether it is the boron atom in the α or β sites with respect to the two carbons in the

pentagonal CCB₃ face of the *nido*-C₂B₉ unit η^5 -coordinated to M which forms the B-H-Pt or B-Pt linkages. In the majority of instances it is the B $_{\beta}$ atom

in the CCB₃ ring which is involved in exopolyhedral bonding, especially if the *nido*-cage fragment is 7,8-Me₂-7,8-C₂B₉H₉ rather than 7,8-C₂B₉H₁₁. In compound 6, however, the ¹H and ¹³C{¹H} NMR data indicate asymmetry in the molecule providing strong evidence that it is the B $_{\alpha}$ atom which forms the B-Pt bond. The CH groups are nonequivalent with ¹H NMR resonances at δ 3.20 and 3.60 and ¹³C{¹H} NMR signals at δ 39.0 and 40.0. If a B $_{\beta}$ -Pt bond were present, the cage CH groups would lie on either side of a symmetry plane through the Pt, Ru, P, μ -H, and B $_{\beta}$ atoms and the midpoint of the C-C connectivity. This assumes the usual planar geometry around platinum with the two P atoms and the μ -H and B $_{\beta}$ atoms being coplanar with the Pt atom. The appearance of one resonance for CH in both the ¹H and ¹³C{¹H} NMR spectra would result from this geometry.

In order to unequivocally establish the structure of compound 6 a single-crystal X-ray diffraction study was carried out. Selected structural parameters are listed in Table 6, and the molecule is shown in Figure 4. It is immediately evident that it is the B $_{\alpha}$ atom which forms the exopolyhedral bond with a B(5)-Pt distance of 2.069(7) Å. Exopolyhedral B-Pt bonds are also found in [WPt(μ -H){ μ - σ , η^5 -7,8-Me₂-10-(CH₂C₆H₄Me-4)-7,8-C₂B₉H₇}(CO)₂(PMe₃)(PEt₃)₂] [2.123(5) Å],^{22a} [WPt(μ -CC₆H₃-Me₂-2,6)(μ - σ , η^5 -7,8-Me₂-7,8-C₂B₉H₈)(CO)₃(PEt₃)] [2.16(1) Å],^{22b} and [WPt(μ -CC₆H₄Me-4)(μ - σ , η^5 -7,8-Me₂-7,8-C₂B₉-H₈)(CO)₂(PMe₂Ph)₂] [2.17(1) Å].^{22c} The Ru-Pt bond [2.802(1) Å] in 6 is spanned by the hydrido ligand [Ru-H = 1.82, Pt-H = 1.56 Å] as expected. It was located by difference Fourier mapping after all other H-atoms were found. Most Ru-Pt separations occur in the range 2.609-2.875 Å, variations resulting from the presence or absence of bridging groups.²³ In [Ru₂Pt₂(μ -H)(μ_4 -CH)-

(20) (a) Goldberg, J. E.; Howard, J. A. K.; Müller, H.; Pilotti, M. U.; Stone, F. G. A. *J. Chem. Soc., Dalton Trans.* **1990**, 3055. (b) Goldberg, J. E.; Mullica, D. F.; Sappenfield, E. L.; Stone, F. G. A. *J. Chem. Soc., Dalton Trans.* **1992**, 2693.

(21) Stone, F. G. A. *Adv. Organomet. Chem.* **1990**, *31*, 53. Brew, S. A.; Stone, F. G. A. *Adv. Organomet. Chem.* **1993**, *35*, 135. Jelliss, P. A.; Stone, F. G. A. *J. Organomet. Chem.* **1995**, in press.

(22) (a) Atfield, M. J.; Howard, J. A. K.; Jelfs, A. N. de M.; Nunn, C. M.; Stone, F. G. A. *J. Chem. Soc., Dalton Trans.* **1987**, 2219. (b) Devore, D. D.; Howard, J. A. K.; Jeffery, J. C.; Pilotti, M. U.; Stone, F. G. A. *J. Chem. Soc., Dalton Trans.* **1989**, 303. (c) Carr, N.; Gimeno, M. C.; Stone, F. G. A. *J. Chem. Soc., Dalton Trans.* **1990**, 2617.

Table 7. Data for X-ray Crystal Structure Analyses^a

	2b	4a	5	6
cryst dimens/mm	0.20 × 0.28 × 0.44	0.21 × 0.25 × 0.61	0.12 × 0.48 × 0.59	0.13 × 0.49 × 0.53
formula	C ₄₀ H ₄₁ AuB ₉ ClO ₂ P ₂ Ru	C ₁₆ H ₄₃ B ₁₈ NO ₄ Ru ₂	C ₃₂ H ₇₀ B ₁₈ K ₂ O ₁₆ Ru ₂	C ₁₆ H ₄₁ B ₉ O ₂ P ₂ PtRu
<i>M_r</i>	1046.4	710.2	1185.8	720.9
cryst color, shape	orange irregular crystal	orange prism	orange irregular crystal	yellow triangular plate
cryst system	triclinic	monoclinic	monoclinic	monoclinic
space group (No.)	<i>P</i> 1 (No. 2)	<i>P</i> 2 ₁ / <i>c</i> (No. 14)	<i>P</i> 2 ₁ / <i>c</i> (No. 14)	<i>P</i> 2 ₁ / <i>c</i> (No. 14)
<i>a</i> /Å	11.167(2)	11.205(2)	12.746(1)	18.774(4)
<i>b</i> /Å	11.861(2)	20.736(2)	18.116(4)	12.094(2)
<i>c</i> /Å	17.103(3)	13.769(2)	12.440(2)	13.429(3)
α /deg	99.50(2)			
β /deg	105.01(2)	96.69(2)	109.58(1)	110.78(2)
γ /deg	95.58(2)			
<i>V</i> /Å ³	2134.6(6)	3177.5(8)	2706.4(8)	2850.8(10)
<i>Z</i>	2	4	2	4
<i>d</i> _{calcd} /g cm ⁻³	1.628	1.485	1.455	1.680
μ (Mo K α)/cm ⁻¹	39.40	9.58	7.57	55.96
<i>F</i> (000)/e	1024	1424	1212	1400
2 θ range/deg	3–40	3–40	3–40	3–40
<i>T</i> /K	292	292	292	292
no. of reflns measd	4229	3269	2771	2983
no. of unique reflns	3890	2951	2500	2652
no. of obsd reflns	3790	2571	2231	2396
criterion for obsd <i>n</i> [<i>F</i> _o ≥ <i>n</i> σ (<i>F</i> _o)]	<i>n</i> = 4	<i>n</i> = 4	<i>n</i> = 4	<i>n</i> = 4
weighting factor/ <i>g</i> (<i>w</i> ⁻¹ = [σ^2 (<i>F</i> _o) + <i>g</i> <i>F</i> _o ²])	0.0010	0.0007	0.0073	0.0012
refln limits				
<i>h</i>	0 to 10	0 to 10	0 to 11	-18 to 16
<i>k</i>	-11 to 11	0 to 19	0 to 17	0 to 11
<i>l</i>	-16 to 15	-13 to 13	-12 to 11	0 to 12
<i>R</i> (<i>R'</i>) ^b	0.0264 (0.0301)	0.0229 (0.0293)	0.0461 (0.0634)	0.0267 (0.0353)
final electron density diff features (max/min)/e Å ⁻³	1.47/-1.14	0.24/-0.22	1.07/-0.36	0.62/-0.79
<i>S</i> (goodness-of-fit)	1.06	1.14	1.14	1.13

^a Data collected on an Enraf-Nonius CAD4-F automated diffractometer operating in the ω -2 θ scan mode; graphite-monochromated Mo K α X-radiation, $\lambda = 0.71073$ Å. Refinement was block full-matrix least-squares on *F* with a weighting scheme of the form $w^{-1} = [\sigma^2(F_o) + g|F_o|^2]$ where $\sigma^2(F_o)$ is the variance in *F*_o due to counting statistics. ^b $R = \sum||F_o| - |F_c||/\sum|F_o|$, $R' = \sum w^{1/2}||F_o| - |F_c||/\sum w^{1/2}|F_o|$.

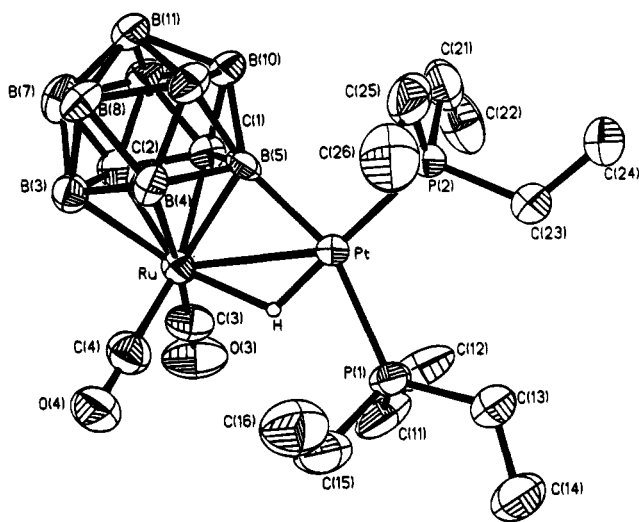


Figure 4. Structure of [RuPt(μ -H)(μ - σ : η^5 -7,8-C₂B₉H₁₀)(CO)₂(PEt₃)₂] (**6**), showing the crystallographic labeling scheme. Hydrogen atoms have been omitted for clarity, and thermal ellipsoids are shown at the 50% probability level.

(μ -CO)(CO)₂(PPRⁱ)₂(η^5 -C₅H₅)₂] the Ru–Pt bonds are bridged in a variety of ways, but the Ru–Pt linkage with a μ -H group is 2.820(1) Å,^{23b} very similar to that found in **6**. The ruthenium atom in **6** is ligated by the nido-7,8-C₂B₉ fragment in the usual η^5 -bonding mode but

with slight slippage toward B(5) [Ru–C(1) = 2.236(7), Ru–C(2) = 2.238(7), Ru–B(3) = 2.257(7), Ru–B(4) = 2.323(7), Ru–B(5) = 2.219(6) Å] as is usual in such systems. The Ru atom also carries two terminally bound CO groups (Ru–C–O(av) = 177.4°). The P–Pt distances are normal with P(1)–Pt [2.369(2) Å] transoid to the boron atom B(5) being longer than P(2)–Pt [2.248(2)] as expected.^{22a,c} Ignoring μ -H, the platinum atom lies in a plane defined by P(1), P(2), B(5), and Ru, and the maximum deviation of any atom from this plane is 0.11 Å.

As mentioned above, on the basis of earlier work²¹ formation of **6** likely proceeds through an intermediate having a B–H–Pt linkage, and because **6** has a B α –Pt bond the precursor would have a B α –H–Pt rather than a B β –H–Pt group. However, along the pathway to **6** the existence of a species with a B β –H–Pt bridge cannot be ruled out. Interconversion between B α –H–M and B β –H–M (M = Ir or Pt) groups has been observed, as has the overall transformation of a B β –H–Pt linkage into a product with B α –Pt and M(μ -H)Pt (M = Mo or W) units.^{4b,22b,24} The interconversion between a structure having an exopolyhedral B β –H–M linkage and one with a B α –H–M unit could be facile. It could occur *via* a momentarily breaking of these bridge bonds with concomitant rotation of the cage about an axis through the centroid of the C₂B₃ ring and the metal atom to which it is η^5 -coordinated, followed by re-formation of a B–H–M group in which the boron is in either the α or β site with respect to the carbons.

(23) (a) Davies, S. J.; Howard, J. A. K.; Pilotti, M. U.; Stone, F. G. A. *J. Chem. Soc., Dalton Trans.* **1989**, 303. (b) Davies, D. L.; Jeffery, J. C.; Miguel, D.; Sherwood, P.; Stone, F. G. A. *J. Organomet. Chem.* **1990**, 383, 463.

(24) Jeffery, J. C.; Ruiz, M. A.; Sherwood, P.; Stone, F. G. A. *J. Chem. Soc., Dalton Trans.* **1989**, 1845.

Table 8. Atomic Coordinates ($\times 10^4$) and Equivalent Isotropic Displacement Parameters ($\text{\AA}^2 \times 10^3$) for 4a

atom	x	y	z	$U(\text{eq})^a$
Ru(1)	7718(1)	6434(1)	4147(1)	28(1)
C(3)	6580(4)	6976(2)	4610(3)	44(2)
O(3)	5866(3)	7316(2)	4854(3)	73(2)
C(4)	8919(4)	6744(2)	5077(3)	36(2)
O(4)	9732(3)	6952(2)	5566(2)	52(1)
C(1)	8130(4)	5683(2)	3048(3)	37(2)
C(2)	6848(4)	6033(2)	2725(3)	35(2)
B(3)	7003(4)	6853(2)	2691(3)	34(2)
B(4)	8589(4)	7013(3)	3005(3)	36(2)
B(5)	9302(4)	6221(2)	3268(4)	37(2)
B(6)	7518(5)	5628(3)	1846(4)	45(2)
B(7)	6818(5)	6376(2)	1604(3)	41(2)
B(8)	7936(5)	6979(3)	1778(4)	42(2)
B(9)	9345(5)	6589(3)	2128(4)	41(2)
B(10)	9065(4)	5752(3)	2171(4)	42(2)
B(11)	8267(5)	6226(3)	1244(4)	42(2)
Ru(2)	7470(1)	5440(1)	5878(1)	31(1)
C(23)	9136(4)	5441(2)	5855(3)	37(2)
O(23)	0169(3)	5429(2)	5907(2)	52(1)
C(24)	7390(4)	4676(2)	5150(3)	42(2)
O(24)	7336(3)	4188(2)	4771(2)	62(1)
C(21)	6878(4)	6218(2)	6857(3)	40(2)
C(22)	5745(3)	5796(2)	6345(3)	38(2)
B(23)	5910(5)	4997(3)	6563(4)	43(2)
B(24)	7325(4)	4918(3)	7331(3)	38(2)
B(25)	7923(5)	5728(3)	7464(3)	39(2)
B(26)	5558(5)	6258(3)	7361(4)	48(2)
B(27)	4941(5)	5476(3)	7208(4)	43(2)
B(28)	5951(5)	4927(3)	7844(4)	44(2)
B(29)	7201(5)	5383(3)	8396(4)	43(2)
B(30)	6938(5)	6209(3)	8096(4)	48(2)
B(31)	5718(5)	5702(3)	8335(4)	45(2)
N	7843(3)	1815(2)	5730(2)	43(1)
C(51)	9023(4)	1545(2)	5435(3)	57(2)
C(52)	9013(5)	841(3)	5186(5)	90(3)
C(53)	7507(4)	1468(2)	6616(3)	53(2)
C(54)	8397(5)	1501(3)	7506(4)	81(3)
C(55)	8070(4)	2528(2)	5932(3)	56(2)
C(56)	7021(5)	2897(3)	6247(4)	71(2)
C(57)	6804(5)	1718(3)	4945(3)	66(2)
C(58)	6952(6)	2021(4)	3962(4)	111(3)

^a Equivalent isotropic U defined as one-third of the trace of the orthogonalized U_{ij} tensor.

Conclusions

The work described shows that compound **1** is capable of being the starting point for the synthesis of organoruthenium complexes having η^5 -7,8- $\text{C}_2\text{B}_9\text{H}_{11}$ ligands. The thf complex **3** in particular is likely to be a useful synthon, and preliminary studies indicate that it reacts readily with alkenes, alkynes, and alkylidyne-metal complexes. Moreover, the synthesis and exploration of the chemistry of $[\text{Ru}(\text{CO})_3(\eta^5$ -7,8- Me_2 -7,8- $\text{C}_2\text{B}_9\text{H}_9)]$ will also be important since previous results have demonstrated that the groups η^5 -7,8- $\text{C}_2\text{B}_9\text{H}_{11}$ and η^5 -7,8- Me_2 -7,8- $\text{C}_2\text{B}_9\text{H}_9$ often differ in their influence on the reactivity at metal centers just as η^5 - C_5H_5 and η^5 - C_5Me_5 ligands can promote different reactivity patterns.

Experimental Section

General Considerations. Solvents were distilled from appropriate drying agents under nitrogen prior to use. Petroleum ether refers to that fraction of boiling point 40–60 °C. All reactions were carried out under an atmosphere of dry nitrogen using Schlenk line techniques. Chromatography columns (ca. 15 cm in length and ca. 12 cm. in diameter) were packed with silica gel (Aldrich, 70–230 mesh). Celite pads for filtration were ca. 3 cm. thick. The reagents *nido*-7,8- $\text{C}_2\text{B}_9\text{H}_{13}$,²⁵ $[\text{AuCl}(\text{PPh}_3)]$,²⁶ and $[\text{PtH}(\text{Cl})(\text{PEt}_3)_2]$ ²⁷ were pre-

Table 9. Atomic Coordinates ($\times 10^4$) and Equivalent Isotropic Displacement Parameters ($\text{\AA}^2 \times 10^3$) for 2b

atom	x	y	z	$U(\text{eq})^a$
Ru	5488(1)	1700(1)	2025(1)	23(1)
C(1)	5445(4)	289(4)	2744(3)	25(2)
C(2)	5371(4)	-251(4)	1772(3)	30(2)
B(3)	6564(5)	426(5)	1475(3)	28(2)
B(4)	7534(5)	1448(5)	2423(3)	27(2)
B(5)	6733(5)	1310(4)	3207(3)	24(2)
B(6)	5786(5)	-1123(5)	2488(3)	33(2)
B(7)	6540(6)	-1036(5)	1695(4)	40(2)
B(8)	7922(5)	1(5)	2116(3)	35(2)
B(9)	8028(5)	565(5)	3179(3)	33(2)
B(10)	6710(5)	-134(5)	3388(4)	35(2)
B(11)	7468(5)	-934(5)	2729(3)	35(2)
C(3)	5907(5)	3260(5)	2608(3)	34(2)
O(3)	6278(3)	4183(3)	2992(2)	46(2)
C(4)	5330(5)	2238(4)	1028(3)	43(2)
O(4)	5306(4)	2599(3)	436(3)	66(2)
Cl	3232(1)	1569(1)	1874(1)	35(1)
Au	1718(1)	3041(1)	2859(1)	20(1)
P(1)	887(1)	3811(1)	1709(1)	21(1)
C(11)	280(4)	2703(4)	761(3)	24(2)
C(12)	788(4)	2686(4)	93(3)	26(2)
C(13)	296(5)	1804(4)	-608(3)	34(2)
C(14)	-673(5)	973(4)	-662(3)	34(2)
C(15)	-1201(4)	1000(4)	0(3)	35(2)
C(16)	-719(4)	1866(4)	711(3)	29(2)
C(21)	-400(4)	4604(3)	1798(3)	25(2)
C(22)	-411(4)	5230(4)	2575(3)	31(2)
C(23)	-1333(5)	5881(4)	2636(3)	40(2)
C(24)	-2291(5)	5945(4)	1936(3)	40(2)
C(25)	-2301(4)	5333(4)	1171(3)	34(2)
C(26)	-1357(4)	4670(4)	1095(3)	31(2)
C(31)	2043(4)	4834(4)	1505(3)	24(2)
C(32)	1771(5)	5914(4)	1296(3)	36(2)
C(33)	2688(5)	6626(4)	1099(3)	40(2)
C(34)	3815(5)	6289(4)	1098(3)	37(2)
C(35)	4081(5)	5237(5)	1304(3)	41(2)
C(36)	3219(4)	4517(4)	1521(3)	33(2)
P(2)	2311(1)	2286(1)	4049(1)	20(1)
C(41)	1138(4)	2394(4)	4605(3)	19(2)
C(42)	939(4)	1610(4)	5108(3)	25(2)
C(43)	-12(4)	1694(4)	5487(3)	29(2)
C(44)	-761(4)	2555(4)	5377(3)	32(2)
C(45)	-586(4)	3334(4)	4884(3)	33(2)
C(46)	369(4)	3260(4)	4509(3)	26(2)

^a Equivalent isotropic U defined as one-third of the trace of the orthogonalized U_{ij} tensor.

pared as previously described. Tetrafluoroboric acid was an 85% solution of $\text{HBF}_4 \cdot \text{Et}_2\text{O}$ in OEt_2 , as supplied by Aldrich. The NMR spectra were recorded in CD_2Cl_2 at ambient temperatures, unless otherwise stated, at the following frequencies: ^1H at 360.13 MHz, ^{13}C at 90.56 MHz, ^{31}P at 145.78 MHz, and ^{11}B at 115.5 MHz.

Synthesis of $[\text{Ru}(\text{CO})_3(\eta^5$ -7,8- $\text{C}_2\text{B}_9\text{H}_{11})]$ (1**).** The compounds $[\text{Ru}_3(\text{CO})_{12}]$ (3.0 g, 4.69 mmol) and *nido*-7,8- $\text{C}_2\text{B}_9\text{H}_{13}$ (1.92 g, 15 mmol) were heated in heptane (50 mL) for 4–5 h at reflux temperatures, during which time the mixture became dark red. After being cooled to room temperature, about half the heptane was removed *in vacuo* and the remaining solvent decanted from the residue. The latter was extracted with CH_2Cl_2 -petroleum ether (2:1, 30 mL) and the extracts filtered through a Celite pad. Solvent was removed *in vacuo* and the residue washed with petroleum ether (2 \times 10 mL) giving a dark red precipitate of **1** which is of satisfactory quality for most reactions without further purification. However, analytically pure $[\text{Ru}(\text{CO})_3(\eta^5$ -7,8- $\text{C}_2\text{B}_9\text{H}_{11})]$ (**1**) (3.59 g) can be obtained by column chromatography eluting with CH_2Cl_2 -

(25) Hlatky, G. G.; Crowther, D. J. *Inorg. Synth.*, in press. Young, D. A. T.; Wiersma, R. J.; Hawthorne, M. F. *J. Am. Chem. Soc.* **1971**, *93*, 5687.

(26) Usón, R.; Laguna, A. *Organomet. Synth.* **1986**, *3*, 325.

(27) Parshall, G. W. *Inorg. Synth.* **1970**, *12*, 28.

Table 10. Atomic Coordinates ($\times 10^4$) and Equivalent Isotropic Displacement Parameters ($\text{\AA}^2 \times 10^3$) for **5**

atom	x	y	z	$U(\text{eq})^a$
Ru	5548(1)	5295(1)	4296(1)	44(1)
C(1)	6238(6)	6425(4)	5085(7)	59(3)
C(2)	7226(6)	5854(5)	5286(7)	65(3)
B(3)	7233(8)	5425(5)	4059(9)	53(4)
B(4)	6079(8)	5869(5)	2929(8)	60(4)
B(5)	5463(8)	6530(6)	3630(9)	70(5)
B(6)	7536(9)	6773(6)	5393(10)	76(5)
B(7)	8200(8)	6161(6)	4729(9)	64(4)
B(8)	7474(7)	6207(6)	3267(9)	64(4)
B(9)	6406(8)	6883(6)	3045(10)	71(5)
B(10)	6436(9)	7181(6)	4314(11)	81(6)
B(11)	7679(8)	7009(5)	4077(9)	62(4)
C(3)	5136(7)	4502(6)	3302(8)	61(4)
O(3)	4924(6)	4027(4)	2659(6)	83(3)
C(4)	3983(8)	5446(5)	4339(8)	56(4)
O(4)	3170(4)	5757(3)	3870(5)	62(2)
K	2287(2)	6023(1)	1543(1)	64(1)
C(21)	1004(8)	4135(5)	905(9)	84(5)
C(22)	2058(8)	4072(6)	670(9)	83(5)
O(23)	2280(5)	4752(3)	228(5)	67(3)
C(24)	3241(9)	4701(5)	-94(9)	79(5)
C(25)	3316(9)	5393(6)	-749(9)	81(5)
O(26)	3392(4)	6019(4)	-37(5)	74(3)
C(27)	3535(9)	6680(7)	-589(9)	101(6)
C(28)	3602(9)	7301(7)	216(10)	103(6)
O(29)	2613(5)	7363(3)	454(5)	73(3)
C(30)	2553(9)	7972(5)	1083(8)	80(5)
C(31)	1503(10)	7983(6)	1297(9)	92(5)
O(32)	1459(4)	7376(3)	1998(4)	71(3)
C(33)	471(9)	7345(6)	2309(11)	97(5)
C(34)	489(8)	6691(6)	3005(8)	81(5)
O(35)	395(4)	6057(3)	2314(5)	66(2)
C(36)	358(8)	5407(6)	2920(8)	75(5)
C(37)	211(8)	4778(5)	2139(9)	79(5)
O(38)	1147(5)	4697(3)	1780(6)	69(3)

^a Equivalent isotropic U defined as one-third of the trace of the orthogonalized U_{ij} tensor.

petroleum ether (1:1), removing solvent *in vacuo*, and washing the residue with petroleum ether (20 mL).

Synthesis of $[\text{NET}_4][\text{Ru}(\text{CO})_2(\eta^5\text{-7,8-C}_2\text{B}_9\text{H}_{11})]$ (2a**).** A mixture of **1** (1.5 g, 4.7 mmol) and $[\text{NET}_4]\text{I}$ (1.21 g, 4.7 mmol) was heated in thf (30 mL) at reflux temperatures for 2–3 h. Solvent was removed *in vacuo* and the oily residue extracted with CH_2Cl_2 –light petroleum (2:1, 30 mL), and the extracts were filtered through a Celite pad. Solvent was then partially removed and light petroleum added (ca. 20 mL). The solution was cooled to give a red precipitate of $[\text{NET}_4][\text{Ru}(\text{CO})_2(\eta^5\text{-7,8-C}_2\text{B}_9\text{H}_{11})]$ (**2a**) (1.93 g), dried *in vacuo*.

Synthesis of $[\text{Ru}(\text{CO})_2(\text{thf})(\eta^5\text{-7,8-C}_2\text{B}_9\text{H}_{11})]$ (3**).** Compound **2a** (0.20 g, 0.36 mmol) in thf (20 mL) was treated with AgBF_4 (0.07 g, 0.36 mmol). After 10 min the solvent was removed *in vacuo* and the residue extracted with CH_2Cl_2 (20 mL), and the extract was filtered through a Celite pad to yield a solution of **3** in essentially quantitative yield and suitable for most purposes. Pure $[\text{Ru}(\text{CO})_2(\text{thf})(\eta^5\text{-7,8-C}_2\text{B}_9\text{H}_{11})]$ (**3**) (0.08 g, ca. 60%) if desired may be isolated by column chromatography at -20°C , eluting the broad yellow band which develops with CH_2Cl_2 –thf (5:1).

Synthesis of $[\text{NET}_4][\text{Ru}_2(\mu\text{-H})(\text{CO})_4(\eta^5\text{-7,8-C}_2\text{B}_9\text{H}_{11})_2]$ (4a**).** A CH_2Cl_2 (20 mL) solution of **3** was prepared as described above; under these conditions 1 molar equiv of $[\text{NET}_4][\text{BF}_4]$ is present. The mixture was treated with a stream of hydrogen, the color changing from yellow to red. Solvent was reduced in volume (ca. 5 mL) and the mixture chromatographed. Elution with CH_2Cl_2 removed a yellow fraction which on evaporation of solvent *in vacuo* and washing the residue with petroleum ether (20 mL) gave yellow microcrystals of $[\text{NET}_4][\text{Ru}_2(\mu\text{-H})(\text{CO})_4(\eta^5\text{-7,8-C}_2\text{B}_9\text{H}_{11})_2]$ (**4a**) (0.10 g).

Reactions of $[\text{K}(18\text{-crown-6})][\text{RuH}(\text{CO})_2(\eta^5\text{-7,8-C}_2\text{B}_9\text{H}_{11})]$. (i) The salt (0.20 g, 0.34 mmol) was dissolved in CH_2Cl_2 (20

Table 11. Atomic Coordinates ($\times 10^4$) and Equivalent Isotropic Displacement Parameters ($\text{\AA}^2 \times 10^3$) for **6**

atom	x	y	z	$U(\text{eq})^a$
Ru	3150(1)	2073(1)	3070(1)	37(1)
C(1)	1980(4)	2526(5)	3005(5)	44(1)
C(2)	2463(4)	3614(5)	2939(5)	46(1)
B(3)	2843(5)	3522(6)	1938(6)	43(1)
B(4)	2500(5)	2216(6)	1246(6)	41(1)
B(5)	1998(4)	1522(6)	2034(6)	36(1)
B(6)	1496(5)	3727(6)	2513(7)	52(1)
B(7)	2024(5)	4342(7)	1831(7)	56(1)
B(8)	2009(5)	3473(6)	769(6)	49(1)
B(9)	1499(5)	2276(6)	825(6)	46(1)
B(10)	1174(5)	2404(6)	1915(7)	46(1)
B(11)	1202(5)	3577(6)	1124(6)	47(1)
C(3)	3672(4)	2109(6)	4551(6)	58(1)
O(3)	4030(3)	2127(5)	5452(4)	94(1)
C(4)	4076(4)	2013(6)	2894(6)	58(1)
O(4)	4656(3)	1970(4)	2759(5)	82(1)
Pt	2456(1)	-9(1)	2602(1)	33(1)
P(1)	3409(1)	-1343(2)	3416(2)	48(1)
C(11)	3822(5)	-1113(7)	4824(6)	88(1)
C(12)	3260(5)	-1179(7)	5356(7)	106(1)
C(13)	3281(4)	-2843(6)	3262(7)	71(1)
C(14)	3979(5)	-3569(6)	3781(7)	84(1)
C(15)	4238(5)	-1060(7)	3004(7)	87(1)
C(16)	4060(5)	-910(8)	1873(7)	97(1)
P(2)	1353(1)	-907(1)	1791(2)	43(1)
C(21)	572(5)	-476(6)	2195(7)	69(1)
C(22)	768(5)	-604(7)	3358(7)	90(1)
C(23)	1394(4)	-2403(6)	1989(7)	59(1)
C(24)	647(4)	-3039(5)	1506(7)	72(1)
C(25)	979(5)	-756(6)	357(6)	75(1)
C(26)	1568(5)	-1054(7)	-150(6)	90(1)

^a Equivalent isotropic U defined as one-third of the trace of the orthogonalized U_{ij} tensor.

mL) at 0°C and treated dropwise with $\text{HBF}_4\cdot\text{Et}_2\text{O}$ (0.06 mL, 0.34 mmol). After the mixture was slowly warmed to room temperature, solvent was reduced in volume to ca. 5 mL, and the mixture was chromatographed as above for **4a**, yielding $[\text{K}(18\text{-crown-6})][\text{Ru}_2(\mu\text{-H})(\text{CO})_4(\eta^5\text{-7,8-C}_2\text{B}_9\text{H}_{11})_2]$ (**4b**) (0.12 g).

(ii) A 0.36 mmol sample of **3** was prepared *in situ* in CH_2Cl_2 (20 mL) at room temperature, and $[\text{K}(18\text{-crown-6})][\text{RuH}(\text{CO})_2(\eta^5\text{-7,8-C}_2\text{B}_9\text{H}_{11})]$ (0.20 g, 0.34 mmol) was added. After 1 h, solvent was reduced in volume to ca. 5 mL and the mixture chromatographed, as described above for **4a**, giving the salt **4b** (0.24 g, 74%).

(iii) A mixture of $[\text{K}(18\text{-crown-6})][\text{RuH}(\text{CO})_2(\eta^5\text{-7,8-C}_2\text{B}_9\text{H}_{11})]$ (0.20 g, 0.34 mmol), $[\text{AuCl}(\text{PPh}_3)]$ (0.17 g, 0.34 mmol), and AgBF_4 (0.06 g, 0.34 mmol) was stirred in thf (20 mL) at room temperature for 30 min. Solvent was removed *in vacuo* and the residue extracted with CH_2Cl_2 –petroleum ether (2:1, 2×15 mL). The extracts were filtered through a Celite pad, and the solvent was reduced in volume to ca. 5 mL and chromatographed. Elution with CH_2Cl_2 –thf (5:1) removed a yellow fraction from which red microcrystals of $[\text{Au}(\text{PPh}_3)_2][\text{RuCl}(\text{CO})_2(\eta^5\text{-7,8-C}_2\text{B}_9\text{H}_{11})]$ (**2b**) (0.08 g) were recovered after evaporation of solvent and washing the product with petroleum ether (20 mL).

(iv) A mixture of $[\text{K}(18\text{-crown-6})][\text{RuH}(\text{CO})_2(\eta^5\text{-7,8-C}_2\text{B}_9\text{H}_{11})]$ (0.15 g, 0.25 mmol) and $[\text{PtH}(\text{Cl})(\text{PEt}_3)_2]$ (0.12 g, 0.25 mmol) in thf (20 mL) was treated with TiPF_6 (0.09 g, 0.25 mmol). A precipitate formed instantly, but the reactants were stirred together for 1 h before removal of solvent *in vacuo*. The residue was extracted with CH_2Cl_2 –petroleum ether (2:1, 2×15 mL), and the extracts were filtered through a Celite pad. The volume was reduced to ca. 5 mL before chromatography. Elution with CH_2Cl_2 –petroleum ether (2:1) gave, after removal of solvent, yellow crystals of $[\text{RuPt}(\mu\text{-H})(\mu\text{-}\sigma\text{-}\eta^5\text{-7,8-C}_2\text{B}_9\text{H}_{10})\text{(CO)}_2(\text{PEt}_3)_2]$ (**6**) (0.11 g).

Crystal Structure Determinations and Refinements. The crystal data and other experimental details for compounds

2b, **4a**, **5**, and **6** are given in Table 7. Crystals of **2b**, **4a**, **5**, and **6** were selected on the basis of optical purity using a Zeiss Photomicroscope II, and a conoscopic study verified their optical homogeneity. For each data set, final unit cell parameters were obtained from the setting angle values of 25 accurately centered reflections. Periodic intensity measurements of three control reflections for each compound, monitored at 2 h intervals of collection time, revealed no sign of deterioration for compounds **2b**, **4a**, and **6**. Thus, the electronic hardware reliability and crystal stability were confirmed. For complex **5**, a decay of 6.1% dictated the use of the SDP program Decay,²⁸ which applied a linear decay correction to the data set. After removal of these check reflections and systematic absences, the data for each complex were corrected for Lorentz, polarization, and X-ray absorption effects. The latter corrections were based on an empirical method employing high-angle ψ scan data.²⁹ The data for **2b**, **4a**, **5**, and **6** were averaged ($R_{\text{int}} = 0.018$ (**2b**), 0.020 (**4a**), 0.023 (**5**), 0.035 (**6**)) and an additional examination of each data set using an $N(Z)$ analysis (cumulative probability distribution test) provided evidence that all were centrosymmetric and that none possessed higher symmetry.³⁰

Crystallographic analyses employing the heavy-atom Patterson technique of the reduced and averaged data and successive difference Fourier syntheses revealed the location of all non-

(28) Enraf-Nonius VAX Structure Determination Package, Delft, The Netherlands, 1985.

(29) North, A. C. T.; Phillips, D. C.; Rogers, D. *Acta Crystallogr.* **1968**, A24, 351.

hydrogen atoms. All hydrogen atoms except the bridging hydrogen atoms in **4a** and **6** were included at geometrically calculated positions (C-H = 0.96 Å and B-H = 1.10 Å) using a riding model with fixed isotropic thermal parameters ($U_{\text{iso}} = 80 \times 10^{-3}$ and 60×10^{-3} Å², respectively). The bridging hydrogen atoms in **4a** and **6** were located by difference Fourier mapping after anisotropically refining the non-hydrogen atoms while including the hydrogen atoms. All calculations were performed using the SHELXTL-PC package of programs.³¹ Atomic scattering factors with related anomalous dispersion correction factors were obtained from the usual source.³² Final atomic positional parameters for non-hydrogen atoms are given in Tables 8–11.

Acknowledgment. We thank the Robert A. Welch Foundation for support (Grants AA-1201 and -0668).

Supporting Information Available: Complete tables of bond lengths and angles, anisotropic thermal parameters, and atom positional and thermal parameters and ORTEP diagrams for **2b**, **4a**, **5**, and **6** (35 pages). Ordering information is given on any current masthead page.

OM950251U

(30) Howells, E. R.; Phillips, D. C.; Rogers, D. *Acta Crystallogr.* **1950**, 3, 210.

(31) Siemens, SHELXTL-PC Siemens X-ray Instruments, Madison, WI, 1989.

(32) *International Tables for X-ray Crystallography*; Kynoch Press: Birmingham, U.K., 1974; Vol. 4.

Signs and Magnitudes of Heteronuclear Coupling Constants in Octahedral Rhodium Complexes by High-Resolution 2D NMR

Martin G. Partridge, Barbara A. Messerle,* and Leslie D. Field*

Department of Organic Chemistry, University of Sydney, Sydney 2006, NSW, Australia

Received November 23, 1994[⊗]

The magnitude and sign of $^1\text{H}-^{31}\text{P}$ and $^1\text{H}-^{13}\text{C}$ coupling constants across the central metal atom ($^2J_{\text{X}-\text{Rh}-\text{H}}$) were measured in a series of octahedral rhodium hydrido phosphine complexes $[\text{Rh}(\text{PMe}_3)_2(\text{CO})(\text{Cl})(\text{X})\text{H}]$; X = Cl, phenyl (2 isomers)] using a ^1H detected, frequency-selective, two-dimensional NMR experiment. The relative and absolute signs of $^2J_{^{13}\text{C}-\text{Rh}-\text{H}}$, $^2J_{^{13}\text{C}-\text{Rh}-\text{P}}$, and $^2J_{\text{P}-\text{Rh}-\text{H}}$ were determined, and in the case of $^2J_{^{13}\text{C}-\text{Rh}-\text{H}}$ both the magnitude and sign of the coupling constant were found to depend on the relative disposition of the coupled nuclei about the central metal atom.

Introduction

The photoactive rhodium(I) complex *trans*-Rh(PMe₃)₂(CO)Cl (**1**) is one of the most efficient reagents for the catalytic activation and functionalization of hydrocarbons. *trans*-Rh(PMe₃)₂(CO)Cl (**1**) reacts with both linear and branched alkanes to give organorhodium complexes which eventually form organic products *e.g.* by carbonylation or dehydrogenation.¹ Recent studies of the mechanism of carbonylation of arenes have indicated that the reaction proceeds via six-coordinate rhodium hydrido species, and ^1H , ^{31}P , and ^{13}C NMR spectroscopy was used to determine the stereochemistry of the unstable intermediates.²

The measurement of coupling constants between NMR-active atoms in ligands and the metal center (where the metal is itself NMR-active) and also between the NMR-active atoms in different ligands has developed into an important tool for the characterization of organometallic compounds by NMR spectroscopy. In organic and organometallic compounds, both homonuclear and heteronuclear coupling constants are sensitive to the electronic structure of bonded atoms and molecular geometry in terms of dihedral angles.^{3–5} In organometallic compounds, the magnitude of homo- and heteronuclear coupling constants can provide information about the stereochemistry of metal complexes as well as the oxidation state and coordination geometry of the central metal atom.^{6,7} In six-coordinate iron(II) phosphine complexes the relative magnitude of $^{31}\text{P}-^{31}\text{P}$

coupling constants is characteristic of the relative position of the phosphorus nuclei around the iron center, with $^2J_{\text{P}-\text{M}-\text{P}(\text{trans})} > ^2J_{\text{P}-\text{M}-\text{P}(\text{cis})}$ and $^2J_{\text{P}-\text{M}-\text{P}(\text{trans})}$ of opposite sign to $^2J_{\text{P}-\text{M}-\text{P}(\text{cis})}$.⁷ Early studies⁶ suggested that similar trends were apparent in the heteronuclear $^{31}\text{P}-^1\text{H}$ coupling constants ($^2J_{\text{P}-\text{M}-\text{H}}$) in transition metal complexes containing both phosphine and hydride ligands, and this was confirmed recently for a series of octahedral Fe and Ru hydrido phosphine complexes.⁸

A number of NMR techniques are available to facilitate the measurement of coupling constants,^{9,10} and these include homonuclear 2D experiments such as ECOSY,^{10,11} selective excitation methods,¹² and heteronuclear 2D and 3D experiments.^{13,14} We recently reported⁸ the application of a proton-detected, frequency-selective 2D NMR experiment for measuring the detailed structure of phosphorus-coupled multiplets in the ^1H NMR spectra of metal hydrides. The method allowed the measurement of both the magnitude and the relative signs of the P–H, P–P, and C–H coupling constants in a series of iron and ruthenium hydrides.

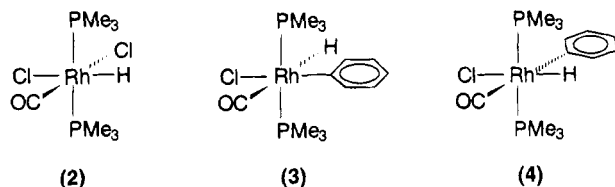
The relative signs of homonuclear and heteronuclear coupling constants have been established only for a limited number of organometallic complexes.¹⁵ The relative magnitudes of $^2J_{^{13}\text{C}-\text{M}-\text{H}}$ (*cis/trans*) couplings in octahedral Rh compounds have been measured in earlier work.¹⁶ In this paper we report the measurement of both the magnitudes and signs of $^2J_{^{13}\text{C}-\text{Rh}-\text{H}}$, $^2J_{^{13}\text{C}-\text{Rh}-\text{P}}$, and $^2J_{\text{P}-\text{Rh}-\text{H}}$ couplings for the complexes

- (6) (a) Moore, D. S.; Robinson, S. D. *Chem. Soc. Rev.* **1983**, *12*, 415.
 (b) Kaesz, H. D.; Saillant, R. B. *Chem. Rev.* **1972**, *72*, 231.
 (7) Field, L. D.; Baker, M. V. *Inorg. Chem.* **1987**, *26*, 2011.
 (8) Field, L. D.; Bampos, N.; Messerle, B. A. *Organometallics* **1993**, *12*, 2529.
 (9) (a) Bax, A.; Freeman, R. *J. Magn. Reson.* **1981**, *44*, 542. (b) Oschkinat, H.; Pastore, A.; Pfaendler, P.; Bodenhausen, G. *J. Magn. Reson.* **1986**, *69*, 559. (c) Mueller, L. *J. Magn. Reson.* **1987**, *71*, 191.
 (10) Griesinger, C.; Sorensen, O. W.; Ernst, R. R. *J. Am. Chem. Soc.* **1985**, *107*, 6394.
 (11) Griesinger, C.; Sorensen, O. W.; Ernst, R. R. *J. Magn. Reson.* **1987**, *75*, 474.
 (12) (a) Brueschweiler, R.; Madsen, J. C.; Griesinger, C.; Sorensen, O. W.; Ernst, R. R. *J. Magn. Reson.* **1987**, *73*, 380. (b) Emsley, L.; Bodenhausen, G. *J. Am. Chem. Soc.* **1991**, *113*, 3309. (c) Bodenhausen, G.; Freeman, R.; Morris, G. A. *J. Magn. Reson.* **1976**, *23*, 171.
 (13) Titman, J. J.; Neuhaus, D.; Keeler, J. *J. Magn. Reson.* **1989**, *85*, 111.
 (14) (a) Kessler, H.; Mronka, S.; Gemmecker, G. *Magn. Reson. Chem.* **1991**, *29*, 527. (b) Kessler, H.; Anders, U.; Gemmecker, G. *J. Magn. Reson.* **1988**, *78*, 382.

[⊗] Abstract published in *Advance ACS Abstracts*, May 15, 1995.

- (1) See for example: (a) Tanaka, M.; Sakakura, T. *Pure Appl. Chem.* **1990**, *62*, 1147. (b) Sakakura, T.; Sodeyama, T.; Tanaka, M. *Nouv. J. Chim.* **1989**, *13*, 737. (c) Sakakura, T.; Sodeyama, T.; Sasaki, K.; Wada, K.; Tanaka, M. *J. Am. Chem. Soc.* **1990**, *112*, 7221. (d) Nomura, K.; Saito, Y. *J. Chem. Soc., Chem. Commun.* **1988**, 161. (e) Tanaka, M.; Sakakura, T. In *Homogeneous Transition Metal Catalysed Reactions*; Moser, R.; Slocum, D. W., Eds.; American Chemical Society: Washington, DC, 1992; Vol. 230, p 181 and references therein. (f) Maguire, J. A.; Boese, W. T.; Goldman, A. S. *J. Am. Chem. Soc.* **1989**, *111*, 7088. (g) Maguire, J. A.; Boese, W. T.; Goldman, M. E.; Goldman, A. S. *Coord. Chem. Rev.* **1990**, *97*, 179. (h) Boese, W. T.; Goldman, A. S. *J. Am. Chem. Soc.* **1992**, *114*, 350.
 (2) Boyd, S. E.; Field, L. D.; Partridge, M. G. *J. Am. Chem. Soc.* **1994**, *116*, 9492.
 (3) Güntert, P.; Braun, W.; Billeter, M.; Wüthrich, K. *J. Am. Chem. Soc.* **1989**, *111*, 3997.
 (4) Karplus, M. *J. Am. Chem. Soc.* **1963**, *85*, 2870.
 (5) Bystrov, V. F. *Prog. NMR Spectrosc.* **1976**, *10*, 41.

Rh(PMe₃)₂(CO)(Cl)₂H (**2**) and Rh(PMe₃)₂(CO)(Cl)(C₆H₅)H (2 isomers **3** and **4**).



Results and Discussion

The activation of hydrocarbons has been achieved with a number of transition metal complexes.¹⁷ Where the product metal complexes are thermally unstable or short lived, it is necessary to obtain as much structural information as possible on the products *in situ* in solution before isolation or derivatization. Previously we have shown that irradiation of *trans*-Rh(PMe₃)₂(CO)Cl (**1**) in benzene/THF at 230 K generates 2 isomers of Rh(PMe₃)₂(CO)(Cl)(C₆H₅)H (**3** and **4**).² The ¹³CO-labeled complexes (**2**-¹³CO, **3**-¹³CO, and **4**-¹³CO) required for this study were generated from *trans*-Rh(PMe₃)₂(¹³CO)Cl (**1**-¹³CO). The assignment of the relative disposition of substituents about the metal center was achieved using NMR spectroscopy and described elsewhere.²

Magnitudes and Relative Signs of Coupling Constants. A selective two-dimensional heteronuclear correlation experiment (analogous to a homonuclear COSY-45 experiment^{9a}) was used to determine the relative signs of the couplings ²J¹³C-Rh-H, ²J¹³C-Rh-P, and ²J_{P-Rh-H}.⁸ The pulse sequence [(^π/2){X}-τ₀-(^π/2){X}, (^π/2){¹H-selective}-detect{¹H}], was applied with the selective proton excitation envelope centered on the resonance of the metal-bound hydride. Selective ¹H excitation was achieved using an E-BURP pulse,^{18,19} which maintains the pure in-phase character and detailed multiplet structure of the resonance. The magnitudes of all coupling constants were measured from the high-resolution 2D NMR spectra.

The fine structure observed in each cross peak of the two-dimensional spectrum is not symmetrical, but the pattern of resonances in the multiplet is skewed due to systematic peak absences. As in the COSY-45 experiment, the relative signs of coupling constants are

(15) See for example: (a) Pregosin, P. S.; Kunz, R. W. *NMR Basic Princ. Prog.* **1979**, *15*, 28–34, 86 and references therein. (b) Verkade, J. G. *Coord. Chem. Rev.* **1972/73**, *9*, 1. (c) Goodfellow, R. J.; Taylor, B. F. *J. Chem. Soc., Dalton Trans.* **1974**, 1676. (d) Pankowski, M.; Chodkiewicz, W.; Simonnin, M.-P. *Inorg. Chem.* **1985**, *24*, 533. (e) Hyde, E. M.; Kennedy, J. D.; Shaw, B. L.; McFarlane, W. *J. Chem. Soc., Dalton Trans.* **1977**, 1571.

(16) (a) Whitesides, G. M.; Maglio, G. *J. Am. Chem. Soc.* **1969**, *91*, 4980. (b) Brown, J. M.; Kent, A. G. *J. Chem. Soc., Perkin Trans. 2* **1987**, 1597.

(17) See for example: (a) Hoyano, J. K.; McMaster, A. D.; Graham, W. A. G. *J. Am. Chem. Soc.* **1983**, *105*, 7190. (b) Jones, W. D.; Feher, F. J. *Organometallics* **1983**, *2*, 562. (c) Wenzel, T. T.; Bergman, R. G. *J. Am. Chem. Soc.* **1986**, *108*, 4856. (d) Graham, W. A. G. *J. Organomet. Chem.* **1986**, *300*, 81. (e) Baker, M. V.; Field, L. D. *J. Am. Chem. Soc.* **1987**, *109*, 2825. (f) Field, L. D.; George, A. V.; Messerle, B. A. *J. Chem. Soc., Chem. Commun.* **1991**, *19*, 1339. (g) *Selective Hydrocarbon Activation; Principles and Progress*; Davies, J. A., Watson, P. L., Liebman, J. F., Greenberg, A., Eds; VCH Publishers, Inc.: New York, 1990; and references therein. (h) *Activation and Functionalisation of Alkanes*; Hill, C. L., Ed.; Wiley Interscience: New York, 1989; and references therein.

(18) Geen, H.; Wimperis, S.; Freeman, R. *J. Magn. Reson.* **1989**, *85*, 620.

(19) Geen, H.; Freeman, R. *J. Magn. Reson.* **1991**, *93*, 93.

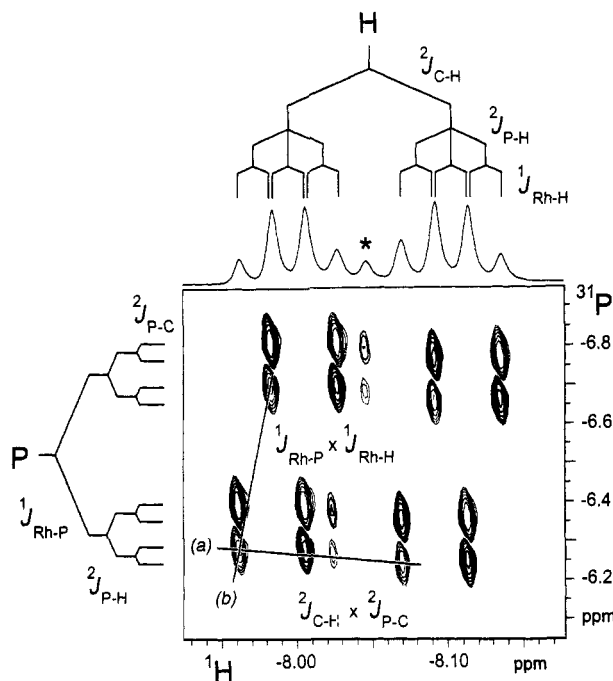


Figure 1. Two-dimensional, frequency-selective, proton-detected ¹H-³¹P correlation spectrum of **3**-¹³CO. The slopes of the two solid lines shown indicate the signs of the product (²J_{C-H}) × (²J_{P-C}) and the product (¹J_{Rh-H}) × (¹J_{Rh-P}). ¹H spectrum of **3**-¹³CO showing only the metal-bound hydride. The resonance from unlabeled **3** is indicated by an asterisk.

expressed in splittings arising from the passive rather than active couplings in each cross-peak.

An example of a typical multiplet observed from the ¹H spectrum of complex Rh(PMe₃)₂(¹³CO)(Cl)(C₆H₅)H (**3**-¹³CO) is given in Figure 1. In the normal (1D) NMR spectrum of **3**-¹³CO, the ¹H NMR spectrum shows a single complex multiplet in the high field (metal hydride) region at δ -8.05 ppm and a single multiplet in the ³¹P spectrum at δ -6.55 ppm. The spin system contains the NMR observable nuclei ¹H, ¹³C, ³¹P, and ¹⁰³Rh, and in the proton-detected ¹H-³¹P correlation experiment, the observed multiplet has only one active coupling (*J*_{P-H}) as well as passive heteronuclear couplings (*J*¹³C-H, *J*_{Rh-H} in F2 and *J*¹³C-³¹P, *J*_{Rh-³¹P} in F1).²⁰ In Figure 1, the active coupling defines four quadrants of antiphase transitions—each quadrant is displaced from another by a passive coupling in F1 (*J*_{P-Y}) and a passive coupling in F2 (*J*_{H-Y}). In this type of experiment, the number of quadrants observed depends on the number of passive couplings to ¹H and ³¹P and only transitions which are connected in F1 and F2, *i.e.* where the coupled ³¹P and ¹H nuclei have a common coupling partner Y, are visible. The slope of the line joining any two quadrants depends on the product of the passive couplings (*J*_{P-Y}) × (*J*_{H-Y}) by which they are separated. If the signs of *J*_{P-Y} and *J*_{H-Y} are different, the slope of the line will be opposite to that where *J*_{P-Y} and *J*_{H-Y} have the same sign. In Figure 1, the multiplets joined by the solid line (a) are separated by the passive coupling ²J_{C-H} in F2 and the passive coupling ²J_{P-C} in

(20) (a) Ernst, R. R.; Bodenhausen, G.; Wokaun, A. *Principles of Nuclear Magnetic Resonance in One and Two Dimensions*; Oxford University Press: Oxford, U.K., 1987; pp 414–22. (b) Bax, A. *Two Dimensional NMR in Liquids*; Delft University Press, D. Reidel Publishing Co.: Dordrecht, Holland, 1982; pp 78–84.

Table 1. Relative Magnitudes (Hz) and Signs of Heteronuclear Coupling Constants for the Hydride Resonances of Complexes 2–4^a

complex	no.	¹ J _{Rh-P} ^b	¹ J _{Rh-H} ^b	² J _{C-Rh-H}	² J _{P-Rh-H(cis)}	² J _{P-Rh-C(cis)}
	2	81.1	17.3	+3.8	+12.7	+12.0
	3	100.4	13.2	-65.0	+13.2	+9.0
	4	98.4	28.1	+4.7	+13.9	+9.6

^a NMR data for **2**²³ (THF-*d*₈, 230 K): ¹H δ -13.29 (Rh-H); ¹³C δ 187.3 (Rh-CO); ³¹P δ -3.34 (Rh-PMe₃). NMR data for **3**² (C₆H₆/THF-*d*₈, 230 K): ¹H δ -8.05 (Rh-H); ¹³C δ 191.6 (Rh-CO); ³¹P δ -6.55 (Rh-PMe₃). NMR data for **4**² (C₆H₆/THF-*d*₈, 230 K): ¹H δ -14.62 (Rh-H); ¹³C δ 190.9 (Rh-CO); ³¹P δ -8.53 (Rh-PMe₃).

^b Signs of coupling constants not determined.

F1; the multiplets joined by the solid line (*b*) are separated by the passive coupling ¹J_{Rh-H} in F2 and the passive coupling ¹J_{Rh-P} in F1. The lines *a* and *b* have opposite slopes, and this indicates that the product (²J_{C-H}) × (²J_{P-C}) has opposite sign to the product (¹J_{Rh-H}) × (¹J_{Rh-P}).

The absolute signs of the coupling constants were established by comparison of the selective two-dimensional spectra of the metal complexes with the equivalent two-dimensional spectrum of a known reference compound, trimethylphosphine, in which it has been established that ¹J_{C-H} > 0 and ¹J_{C-P} < 0.^{21,22}

The magnitudes and signs of the heteronuclear ²J_{C-Rh-H} couplings were measured for compounds **2–4**, and the values of the coupling constants are listed in Table 1.

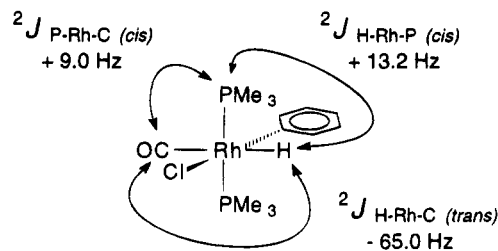
The relative magnitudes of heteronuclear ²J_{C-Rh-H} couplings have previously been reported and it was found that typically ²J_{13C-Rh-H(trans)} > ²J_{13C-Rh-H(cis)}.¹⁶ In complexes **2** and **4** it was found that ²J_{13C-Rh-H(cis)} is relatively small and has a positive sign, and ²J_{C-Rh-H(trans)} in **3** is relatively large and negative in sign. It should be possible to use the magnitude and signs of coupling constants to assign stereochemistry in closely related complexes without the need for full structural analysis. However, it should be noted that coupling constants are dependent on the specific aspects of the metal complex including the metal center in the complex, the metal oxidation state, the geometry of the complex, ligand types, etc., and extrapolation beyond closely related complexes is not possible.^{16a}

The relative magnitudes of ²J_{P-Rh-H} and ²J_{C-Rh-P} are unchanged for all the complexes studied, as would be expected since the relative stereochemistry of the metal-bound hydride and phosphine and metal-bound phosphine and carbonyl is the same for all the complexes. The signs of ²J_{P-Rh-H(cis)} and ²J_{C-Rh-P(cis)} are positive.

(21) Jameson, C. J. *J. Am. Chem. Soc.* **1969**, *91*, 6232.

(22) The ¹³C satellites of the methyl proton resonance of PMe₃ were observed, and the slope of the line connecting the quadrants of the passively coupled ¹³C satellites corresponds to a negative value of J_{13C-H} (F2) × J_{13C-P} (F1).

The absolute signs of the one bond couplings to rhodium could not be determined; however, ¹J_{C-Rh}, ¹J_{H-Rh}, and ¹J_{P-Rh} have the same sign.



Conclusions

A heteronuclear pulse sequence incorporating a band-selective pulse enabled high-resolution two-dimensional ¹H-³¹P and ¹H-¹³C NMR spectra of rhodium hydrides to be obtained. Heteronuclear ³¹P-¹H and ¹H-¹³C coupling constants were assigned and measured from the detailed structure of the complex cross-peak multiplets.

This is the first systematic study which has examined the relative signs and magnitudes of heteronuclear coupling constants in a series of related octahedral rhodium hydride complexes. The stereochemistry of the complexes was determined independently, and the absolute signs of some coupling constants were determined by reference to the C-H and C-P couplings in PMe₃. In complexes **2** and **4** it was found that ²J_{13C-Rh-H(cis)} is relatively small and has a positive sign, and ²J_{13C-Rh-H(trans)} in **3** is relatively large and negative in sign. In summary, in the octahedral rhodium hydride complexes studied the following is observed:

$${}^2J_{13\text{C-Rh-H(cis)}} > 0 \quad {}^2J_{13\text{C-Rh-H(trans)}} < 0$$

$$|{}^2J_{13\text{C-Rh-H(trans)}}| \gg |{}^2J_{13\text{C-Rh-H(cis)}}|$$

Experimental Section

Syntheses and manipulations of chemicals were carried out under nitrogen with standard Schlenk and high-vacuum techniques.

The samples for study were prepared in 5 mm NMR tubes with concentric Youngs PTFE valves connected. Low-temperature photolyses were carried out using a 125 W medium-pressure vapor lamp with the NMR tube being suspended in a double-walled Pyrex dewar containing ethanol cooled with a refrigeration coil.

Benzene and THF were dried by refluxing over sodium/benzophenone and distilled under nitrogen prior to use.

NMR Spectroscopy. Spectra were recorded on Bruker AMX400 and AMX600 spectrometers. Spectra of the rhodium complexes (**2–4**) were acquired at 230 K in THF-*d*₈. ³¹P NMR spectra were referenced to external, neat trimethyl phosphite, taken as 140.85 ppm at the temperature quoted; ¹H and ¹³C NMR spectra were referenced to residual solvent resonances.

The selective ¹H-X correlation spectra were acquired using a previously described pulse sequence:⁶ [(π/2){X} - τ₀ - (π/2){X}, (π/2){¹H-selective} - detect{¹H}], where τ₀ is the variable delay. Selective E-BURP pulses^{18,19} were applied using Bruker soft pulse hardware. Shaped pulses were defined by 256 points, centered on the resonance(s) of the metal-bound hydrides in the ¹H spectrum. Selective pulses were typically between 5 and 15 ms in duration giving excitation widths of approximately 200–1200 Hz. In 2D acquisitions, typically, 1024 data points were acquired over a sweep width of 1500 Hz in the ¹H spectrum, with 256 increments and 64 scans per increment. A relaxation delay of 2.5 s was left between acquisitions.

Spectra were zero-filled to 512 points in F_1 and 2048 points in F_2 . Sine-bell weightings were applied to the data in both dimensions (shifted by $\pi/2$ in F_2 and $\pi/4$ in F_1) prior to Fourier transformation.

Metal Complexes. $\text{Rh}(\text{PMe}_3)_2(\text{CO})\text{Cl}$ (**1**),²³ $\text{Rh}(\text{PMe}_3)_2(\text{CO})\text{Cl}$ (**1**- ^{13}C O),²⁴ $\text{Rh}(\text{PMe}_3)_2(\text{CO})(\text{Cl})_2\text{H}$ (**2**),²⁴ and $\text{Rh}(\text{PMe}_3)_2(\text{CO})(\text{Cl})(\text{C}_6\text{H}_5)\text{H}$ (2 isomers **3** and **4**)² were prepared by literature methods.

(23) Synthesis adapted from: Dunbar, K. R.; Haefner, S. C. *Inorg. Chem.* **1992**, *31*, 3676.

Acknowledgment. We gratefully acknowledge financial support from the Australian Research Council, the University of Sydney for the award of a H. B. and F. M. Gritton Research Fellowship (M.G.P.), and also Johnson-Matthey PLC for the generous loan of rhodium salts.

OM940894U

(24) Boyd, S. E.; Field, L. D.; Hambley T. W.; Partridge, M. G. *Organometallics* **1993**, *12*, 1720.

Alkynylcopper(I) Complexes with PPh₃ Ligands. Preparation, Structure, and Alkynyl Ligand Transfer to Palladium(II) Complexes

Kohtaro Osakada,* Tadashi Takizawa, and Takakazu Yamamoto*

Research Laboratory of Resources Utilization, Tokyo Institute of Technology, 4259 Nagatsuta, Midori-ku, Yokohama 226, Japan

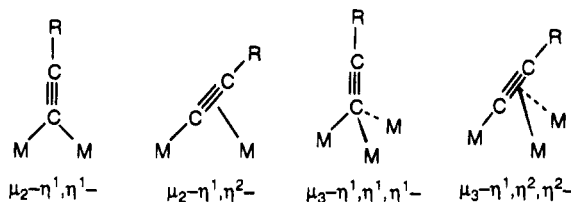
Received January 23, 1995*

Reactions of copper alkoxide complexes Cu(OCH(CF₃)₂)(PPh₃)₃, Cu(OCHPh₂)(PPh₃)₃, and [Cu(OPh)(PPh₃)₂]₂ with HC≡CCOOR (R = Me, Et, ^tBu) give alkynyl copper complexes formulated as Cu₂(C≡CCOOR)₂(PPh₃)₃ (**1**, R = Me; **2**, R = Et; **3**, R = ^tBu). The ¹H, ¹³C{¹H}, and ³¹P{¹H} NMR spectra agree with the structures containing two bridging alkynyl ligands that are coordinated to Cu(PPh₃) and to Cu(PPh₃)₂ units. The copper alkoxide complexes react with alkynes HC≡CSiMe₃, HC≡CPh, and HC≡CC₆H₄-*p*-Me to give alkynylcopper(I) complexes [Cu(C≡CR')(PPh₃)₄] (**4**, R' = SiMe₃; **5**, R' = Ph; **6**, R' = C₆H₄-*p*-Me). X-ray crystallography of **4**·Et₂O reveals a molecular structure containing a cubane-like core composed of four copper(I) centers bridged by four alkynyl ligands, each of which is coordinated to three Cu centers as a μ₃-η¹:η¹:η¹-ligand. Complex **5** undergoes ligand substitution by HC≡CCOOEt in the presence of PPh₃ to give **2**. Complexes **1**–**6** react with PdCl₂(PEt₃)₂ to cause alkynyl ligand transfer from Cu to Pd. Reactions of **1**–**3** with 0.5 equiv of PdCl₂(PEt₃)₂ in the presence of PPh₃ give *trans*-Pd(C≡CCOOR)₂(PEt₃)₂ accompanied by formation of CuCl(PPh₃)₃. Complex **4** undergoes alkynyl ligand transfer to give *trans*-PdCl(C≡CSiMe₃)(PEt₃)₂ exclusively, while similar reactions of **5** and **6** give mixtures of *trans*-Pd(C≡CAr)₂(PEt₃)₂ and *trans*-PdCl(C≡CAr)(PEt₃)₂ (Ar = Ph, C₆H₄-*p*-Me).

Introduction

Characterization of several alkynylcopper(I) complexes by X-ray crystallography has been recently reported to reveal multinuclear structures with bridging alkynyl ligands bonded to two or three Cu centers.^{1–5} No crystal structures of copper complexes with nonbridging alkynyl ligands have been reported, while nonbridging coordination of the alkynyl group is very common among the other transition metals.⁶ Complexes of group 6–10 transition metals with bridging alkynyl ligands have a μ₂-η¹:η²- or μ₃-η¹:η²:η²-coordination mode,^{7–9} while μ₂-η¹:η¹- or μ₃-η¹:η¹:η¹-coordination of the bridging alkynyl ligand is often observed in structural studies of alkynylcopper(I) complexes (Scheme 1). Alkynylcopper(I) complexes are of structural interest

Scheme 1. Coordination Mode of the Bridging Alkynyl Ligand



due to the above characteristics peculiar to alkynyl-copper bonding as well as to versatile multimetallic structures containing three to six Cu centers bridged by alkynyl ligands.

Chemical properties of alkynylcopper complexes are also intriguing since they are involved as the intermediates in copper complexes that promote C–C bond-forming reactions. Reports on copper complexes that promote homocoupling of alkynes^{10,11} are fewer than reports on the coupling reaction using alkyl, aryl, and vinyl copper reagents due to highly stable Cu–C bond of the copper(I) alkynyl compounds.^{12a,13} The higher

* Abstract published in *Advance ACS Abstracts*, June 15, 1995.

(1) Corfield, P. W. R.; Shearer, H. M. M. *Acta Crystallogr.* **1966**, *21*, 957.

(2) (a) ten Hoedt, R. W. M.; Noltes, J. G.; van Koten, G.; Spek, A. L. *J. Chem. Soc., Dalton Trans.* **1978**, 1800. (b) Knotter, D. M.; Spek, A. L.; Grove, D. M.; van Koten, G. *Organometallics* **1992**, *11*, 4083. (c) Knotter, D. M.; Grove, D. M.; Smeets, W. J. J.; Spek, A. L.; van Koten, G. *J. Am. Chem. Soc.* **1992**, *114*, 3400.

(3) Naldini, L.; Demartin, F.; Manassero, M.; Sansoni, M.; Rasso, G.; Zoroddu, M. A. *J. Organomet. Chem.* **1985**, *279*, C42.

(4) (a) Gamasa, M. P.; Gimeno, J.; Lastra, E.; Solans, X. *J. Organomet. Chem.* **1988**, *346*, 277. (b) Diez, J.; Gamasa, M. P.; Gimeno, J.; Lastra, E.; Aguirre, A.; García-Granda, S. *Organometallics* **1993**, *12*, 2213.

(5) Edwards, A. J.; Paver, M. A.; Raithby, P. R.; Rennie, M.-A.; Russell, C. A.; Wright, D. S. *Organometallics* **1994**, *13*, 4967.

(6) Nasta, R. *Coord. Chem. Rev.* **1982**, *47*, 89.

(7) Carty, A. *J. Pure Appl. Chem.* **1982**, *54*, 113.

(8) Sappa, E.; Tiripicchio, A.; Braunstein, P. *Chem. Rev.* **1983**, *83*, 203.

(9) (a) Akita, M.; Terada, M.; Oyama, S.; Moro-oka, Y. *Organometallics* **1990**, *9*, 816. (b) Akita, M.; Ishii, N.; Takabuchi, A.; Terada, M.; Tanaka, M.; Moro-oka, Y. *Organometallics* **1994**, *13*, 258 and references therein.

(10) Tsuda, T.; Hashimoto, T.; Saegusa, T. *J. Am. Chem. Soc.* **1972**, *94*, 658.

(11) Haglund, O.; Nilsson, M. *Synlett* **1991**, 723.

(12) (a) van Koten, G.; Noltes, J. G. In *Comprehensive Organometallic Chemistry*; Wilkinson, G.; Stone, F. G. A., Eds.; Pergamon: Tokyo, 1982; Vol. 2, pp 714–716. (b) Reference 12a, Vol. 2, pp 737–739 and references therein.

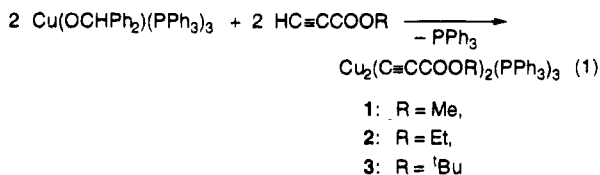
(13) The Cu–C bond of alkynyl copper complexes is believed to be much more stable than that of alkyl- and arylcopper complexes on the basis of comparison of decomposing temperature (ref 12). This tendency is similar to relative bond stability of late transition metal complexes (Bryndza, H. E.; Fong, L. K.; Paciello, R. A.; Tam, W.; Bercaw, J. E. *J. Am. Chem. Soc.* **1987**, *109*, 1444). However, precise determination of the relative bond stability of the Cu(I)–C bonds has not been examined.

stability of the alkynyl-copper(I) bond compared to the alkyl-copper(I) bond enables selective 1,4-addition of mixed organic cuprate, whose alkynyl ligand plays an important role as sacrificial ligand.¹⁴ Palladium complex-catalyzed cross-coupling reactions of 1-alkynes with vinyl and with aryl halides in the presence of CuI and tertiary amine provide 1,3-enynes and arylacetylenes, respectively. The reaction, which was reported at first by Sonogashira and Takahashi et al.,¹⁵ has been developed for the synthesis of various organic compounds¹⁶⁻¹⁹ as well as of π -conjugated polymers.²⁰ The reaction seems to involve initial formation of alkynylcopper(I) complex followed by alkynyl ligand transfer to the Pd(II) center giving the aryl (or vinyl) palladium alkynyl complex, Pd(Ar)(C \equiv CR)(PR₃)₂, which is responsible for reductive elimination of the product.

Recently we reported the preparation and structure of several copper alkoxide complexes with PPh₃ ligands, Cu(OCH(CF₃)₂)(PPh₃)₃ and Cu(OCHPh₂)(PPh₃)_n (n = 2, 3), which are highly soluble in common organic solvents.²¹ Since [Cu(O^tBu)]_n, which is also soluble in organic solvents, reacts with HC \equiv CPh to give [Cu(C \equiv CPh)]_n smoothly,¹⁰ the above alkoxide complexes would be suitable precursors of new alkynylcopper(I) complexes with PPh₃ ligands. In this paper we report reaction of the copper alkoxide complexes with terminal alkynes to provide various alkynylcopper(I) complexes, such as Cu₂(C \equiv CCOOR)₂(PPh₃)₃, [Cu(C \equiv CSiMe₃)(PPh₃)₄], and [Cu(C \equiv CAr)(PPh₃)₄]. The crystal structure of the tetranuclear (trimethylsilyl)ethynyl complex is also shown. The alkynyl copper complexes react easily with PdCl₂(PEt₃)₂ to give mono- and/or dialkynylpalladium(II) complexes through the alkynyl ligand transfer from the Cu(I) to the Pd(II) center.

Results and Discussion

Preparation and Structures of Alkynylcopper(I) Complexes. Reaction of Cu(OCHPh₂)(PPh₃)₃ with 1.2 equiv of HC \equiv CCOOMe gives Cu₂(μ -C \equiv CCOOMe)₂(PPh₃)₃ (**1**) in 63% yield. Complex **1** is also obtained from reaction of [Cu(OPh)(PPh₃)₂]₂ with the alkyne in 71%. Reactions of copper alkoxide complexes Cu(OCH(CF₃)₂)(PPh₃)₃, Cu(OCHPh₂)(PPh₃)₃, and [Cu(OPh)(PPh₃)₂]₂ with HC \equiv CCOOEt and with HC \equiv CCOO^tBu give the corresponding alkynylcopper complexes Cu₂(μ -C \equiv CCOOR)₂(PPh₃)₃ (**2**, R = Et; **3**, R = ^tBu), respectively (see eq 1). Very recently, (PCy₃)Cu(μ - η^1 : η^1 -C \equiv C^t-



Bu)₂Cu(PPh₃)₂, prepared from reaction of CpCu(PPh₃)

(14) (a) Carruthers, W. In *Comprehensive Organometallic Chemistry*; Wilkinson, G., Stone, F. G. A., Abel, E. W., Eds.; Pergamon: Tokyo, 1982; pp 722-724. (b) Lipshutz, B. H. In *Organometallics in Synthesis. A Manual*; Schlosser, M., Ed.; John Wiley: Chichester, 1994; pp 300-302 and references therein.

(15) (a) Sonogashira, K.; Tohda, Y.; Hagihara, N. *Tetrahedron Lett.* **1975**, 4467. (b) Takahashi, S.; Kuroyama, Y.; Sonogashira, K.; Hagihara, N. *Synthesis* **1980**, 627.

(16) Sabourin, E. T.; Onopchenko, A. *J. Org. Chem.* **1983**, *48*, 5135.

(17) Havens, S. J.; Hergenrother, P. M. *J. Org. Chem.* **1985**, *50*, 1763.

(18) Heck, R. F. *Palladium Reagents in Organic Synthesis*; Academic Press: London, 1985; p 299.

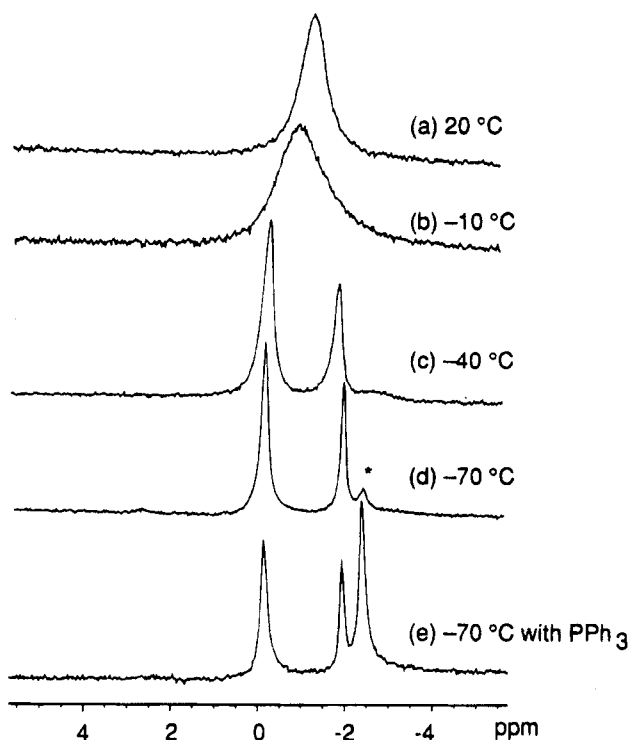


Figure 1. ³¹P{¹H} NMR spectra of **1** at (a) 20 °C, (b) -10 °C, (c) -40 °C, and (d) -70 °C. The peak with asterisk in d is assigned to Cu₂(C \equiv CCOOMe)₂(PPh₃)₄ contained in a small amount in the solution (see text). The spectrum of a mixture of **1** and PPh₃ at -70 °C is shown in e. Spectra were recorded at 160 MHz in CD₂Cl₂.

with LiC \equiv C^tBu and PCy₃, was characterized by X-ray crystallography.⁵

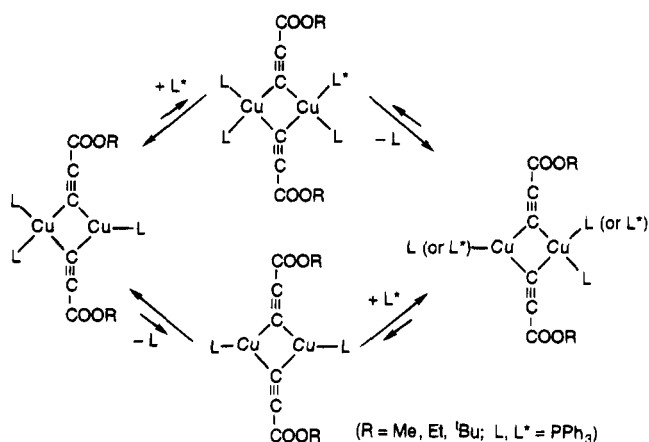
The NMR spectra as well as the elemental analyses of the complexes agree with the unsymmetrical structures, (PPh₃)Cu(μ -C \equiv CCOOR)₂Cu(PPh₃)₂. Figure 1 shows temperature dependent ³¹P{¹H} NMR spectra of **1**. The spectrum at -70 °C gives two peaks at -0.1 and -1.9 ppm in a 2:1 peak area ratio. These peaks are assigned to PPh₃ ligands bonded to the four-coordinated Cu center and to the three-coordinated Cu center, respectively. A small peak at -2.5 ppm can be attributed to the PPh₃ ligand of the symmetrical dinuclear complex, Cu₂(μ -C \equiv CCOOMe)₂(PPh₃)₄, which is in equilibrium with **1** in the solution since addition of PPh₃ to the solution caused an increase in the relative peak intensity (Figure 1e).²² Raising the temperature of the solution of **1** above -10 °C causes the above three peaks

(19) (a) Schreiber, S. L.; Kiessling, L. L. *J. Am. Chem. Soc.* **1988**, *110*, 631. (b) Mascarenas, J. L.; Sarandeses, L. A.; Castedo, L.; Mourino, A. *Tetrahedron* **1991**, *47*, 3485. (c) Curtin, M. L.; Okamura, W. H. *J. Am. Chem. Soc.* **1991**, *113*, 6958.

(20) (a) Sanechika, K.; Yamamoto, T.; Yamamoto, A. *Bull. Chem. Soc. Jpn.* **1984**, *57*, 752. (b) Yamamoto, T.; Takagi, M.; Kizu, K.; Maruyama, T.; Kubota, K.; Kanbara, H.; Kurihara, T.; Kaino, T. *J. Chem. Soc., Chem. Commun.* **1993**, 797. (c) Yamamoto, T.; Yamada, W.; Takagi, M.; Kizu, K.; Maruyama, T.; Ooba, N.; Tomaru, S.; Kurihara, T.; Kaino, T.; Kubota, K. *Macromolecules* **1994**, *27*, 6620.

(21) Osakada, K.; Takizawa, T.; Tanaka, M.; Yamamoto, T. *J. Organomet. Chem.* **1994**, *473*, 359.

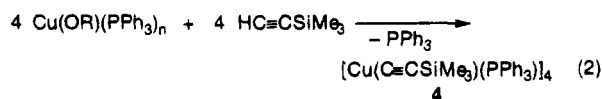
(22) It is not possible to obtain the NMR spectra of **1** free from peaks due to Cu₂(μ -C \equiv CCOOMe)₂(PPh₃)₄ despite purification of the complex by repeated recrystallization. The ¹H NMR spectra of **2** and **3** at -80 °C also show small peaks due to Cu₂(μ -C \equiv CCOOEt)₂(PPh₃)₄ (δ 4.2 (q, OCH₂, J = 9 Hz) and 1.4 (t, CH₃)) and Cu₂(μ -C \equiv CCOO^tBu)₂(PPh₃)₄ (δ 1.7 (s, C(CH₃)₃)), respectively. These peaks coalesce with the peaks due to **2** or **3** below room temperature. Appearance of the peaks due to symmetrical dicopper complexes may be attributed to partial disproportionation of Cu₂(μ -C \equiv CCOOR)₂(PPh₃)₃ into Cu₂(μ -C \equiv CCOOR)₂(PPh₃)₄ and Cu₂(μ -C \equiv CCOOR)₂(PPh₃)₂, although the presence of the latter compounds was not confirmed by NMR.

Scheme 2. Plausible Pathways for PPh₃ Exchange of 1–3


to coalesce to give a broadened peak near -1 ppm. Temperature dependent $^{31}\text{P}\{^1\text{H}\}$ NMR spectra of **2** and **3** are quite similar to those of **1**. The ^1H NMR spectra of **1–3** below -40 °C also indicate the presence of small amounts of $\text{Cu}_2(\mu_2\text{-C}\equiv\text{CCOOR})_2(\text{PPh}_3)_4$ (R = Me, Et, ^tBu) in the solutions. The ^1H NMR spectrum of **1** at -70 °C shows a slightly broadened peak at 3.4 ppm accompanied by a small peak at 3.9 ppm. Addition of PPh₃ to the solution causes growth of the latter peak. The above two peaks are assigned to Me hydrogens of **1** and $\text{Cu}_2(\mu_2\text{-C}\equiv\text{CCOOR})_2(\text{PPh}_3)_4$, respectively. The ^1H NMR spectra of **2** and **3** below -40 °C also show peaks due to ethyl and butyl hydrogens of $\text{Cu}_2(\mu_2\text{-C}\equiv\text{CCOOR})_2(\text{PPh}_3)_3$ and $\text{Cu}_2(\mu_2\text{-C}\equiv\text{CCOOR})_2(\text{PPh}_3)_4$. The ^1H NMR peaks due to $\text{Cu}_2(\mu_2\text{-C}\equiv\text{CCOOR})_2(\text{PPh}_3)_3$ and those due to $\text{Cu}_2(\mu_2\text{-C}\equiv\text{CCOOR})_2(\text{PPh}_3)_4$ coalesce above -20 °C.

Results of the above NMR measurements indicate that complexes **1–3** undergo PPh₃ ligand exchange between four-coordinated and three-coordinated Cu centers on the NMR time scale as well as ligand exchange with $\text{Cu}_2(\mu_2\text{-C}\equiv\text{CCOOR})_2(\text{PPh}_3)_4$. Scheme 2 shows plausible pathways for PPh₃ ligand exchange of **1–3**. Both the associative pathway involving $\text{Cu}_2(\mu_2\text{-C}\equiv\text{CCOOR})_2(\text{PPh}_3)_4$ as the intermediate and the dissociative pathway involving $\text{Cu}_2(\mu_2\text{-C}\equiv\text{CCOOR})_2(\text{PPh}_3)_2$ would explain the results of the NMR study. We are not able to decide which pathway is operative in the reaction, although the solutions of **1–3** contain small amounts of $\text{Cu}_2(\mu_2\text{-C}\equiv\text{CCOOR})_2(\text{PPh}_3)_4$.

$\text{Cu}(\text{OCH}(\text{CF}_3)_2)(\text{PPh}_3)_3$ reacts with 50 equiv of $\text{HC}\equiv\text{CSiMe}_3$ to give $[\text{Cu}(\mu_3\text{-C}\equiv\text{CSiMe}_3)(\text{PPh}_3)_4]$ (**4**) in 83% yield (eq 2).



Complex **4** is also obtained in moderate yields (35–57%) from a similar reaction with 1.5 equiv of $\text{HC}\equiv\text{CSiMe}_3$ as well as from reactions of $\text{CuMe}(\text{PPh}_3)_2(\text{Et}_2\text{O})_{0.5}$ and $\text{Cu}(\text{OCHPh}_2)(\text{PPh}_3)_3$ with $\text{HC}\equiv\text{CSiMe}_3$. Recrystallization of **4** from Et_2O at -30 °C gives single crystals of $4\cdot\text{Et}_2\text{O}$ in two crystal forms, both of which are characterized by X-ray crystallography. Figures 2 and 3 show molecular structures of two crystal forms of $4\cdot\text{Et}_2\text{O}$. Alkynylcopper cluster molecules of form I and form II have similar structures to each other and contain four copper centers bonded to four terminal PPh₃ ligands and to four μ_3 -bridging alkynyl ligands. Two different

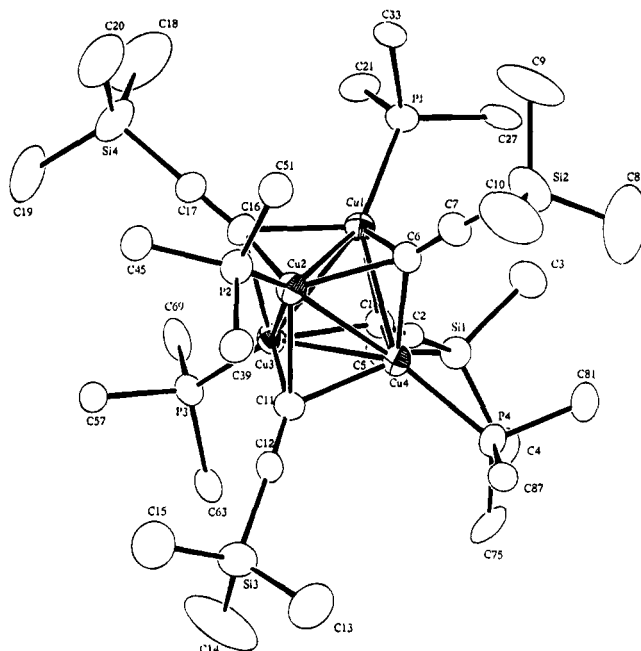


Figure 2. ORTEP drawing of $4\cdot\text{Et}_2\text{O}$ (from I) at 30% ellipsoidal level. Phenyl carbon atoms are omitted for simplicity except for the atoms bonded to P atoms.

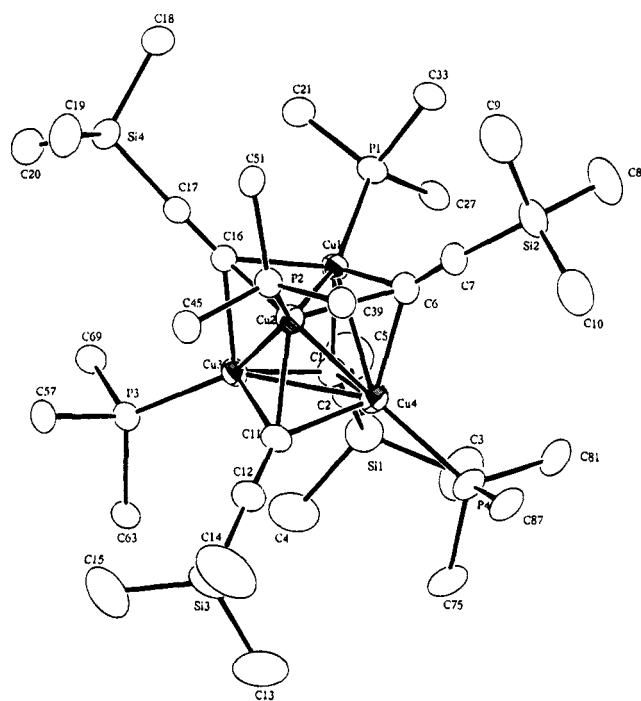
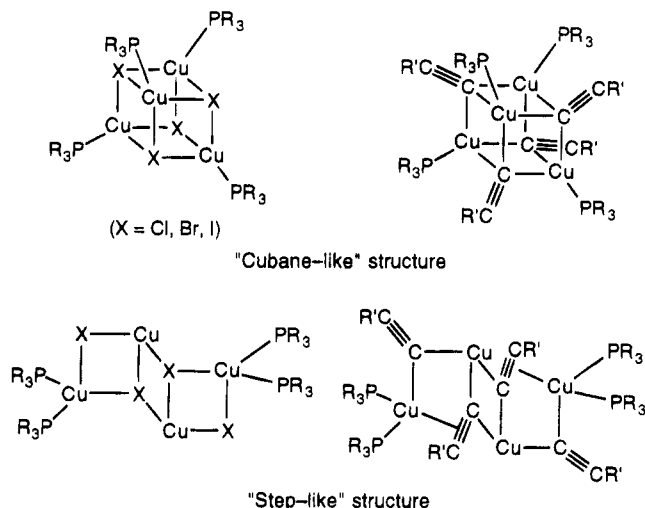


Figure 3. ORTEP drawing of $4\cdot\text{Et}_2\text{O}$ (from II) at 50% ellipsoidal level. Phenyl carbon atoms are omitted for simplicity except for the atoms bonded to P atoms.

structures have been already reported for tetranuclear alkynylcopper complexes with PPh₃ ligands formulated as $[\text{Cu}(\text{C}\equiv\text{CPh})(\text{PR}_3)_4]$, $[\text{Cu}(\mu_3\text{-C}\equiv\text{CPh})(\text{PPh}_3)_4]$ (**5**), prepared from reaction of $[\text{Cu}(\text{PPh}_3)_2(\text{BH}_4)]$ with phenylacetylene and KOH,³ as well as its PPh₂(py) analogue (py = 2-pyridyl),^{4a} has a cubane-like core composed of four Cu and four bridging phenylethynyl ligands. The trimethylphosphine-coordinated alkynylcopper tetramer, $[\text{Cu}_4(\mu_2\text{-}\eta^1\text{-}\eta^1\text{-C}\equiv\text{CPh})_2(\mu_3\text{-}\eta^1\text{-}\eta^1\text{-}\eta^2\text{-C}\equiv\text{CPh})_2(\text{PMe}_3)_4]$,¹ contains three four-membered rings, each of which is composed of two Cu and two bridging alkynyl ligands. The two different structures for tetranuclear alkynylcopper complexes with phosphine ligands are similar

Scheme 3. "Cubane-Like" and "Step-Like" Structures



to "cubane-like" and "step-like" isomers of $[\text{CuX}(\text{PR}_3)_4]$ (X = Cl, Br, and I; R = Et, Pr, and Ph).^{23,24}

Table 1 summarizes bond distances and angles of $4\text{-Et}_2\text{O}$. Cu–Cu distances are in the range 2.544(1)–2.642(1) Å, which is similar to those of **5** (2.523–2.676 Å) and $[\text{Cu}(\text{C}\equiv\text{CPh})(\text{PPh}_2\text{py})]_4$ (2.525(1)–2.686(1) Å)^{4a} but shorter than those of $[\text{CuCl}(\text{PPh}_3)]_4$ (3.118(1)–3.430(2) Å) and $[\text{CuBr}(\text{P}^t\text{Bu}_3)]_4$ (3.479(2)–3.491(2) Å).²⁵ Cu–C bond distances are in the range 2.13–2.17 Å, which is longer than usual transition metal–carbon bond. Similarity of distances among the three Cu–C bonds of the alkynyl ligands in structures of both crystal forms indicates $\eta^1:\eta^1:\eta^1$ -coordination of the ligand rather than $\eta^1:\eta^1:\eta^2$ - or $\eta^1:\eta^2:\eta^2$ -coordination. The Cu–C–Cu bond angles are in the range 70.7(1)–75.0(1)° and are as acute as the other copper complexes with bridging alkynyl ligands.^{4b} Similarly elongated Cu–C bonds as well as acute Cu–C–Cu angles in already characterized copper complexes with bridging aryl or alkynyl ligands were attributed to three-center two-electron or four-center three-electron bonding.^{12b,26,27}

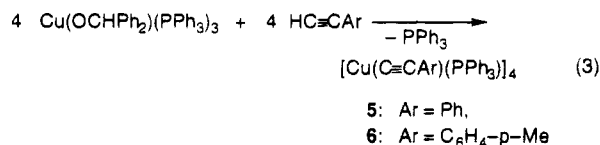
The structure of **4** is not rigid in solutions. The $^{31}\text{P}\{-^1\text{H}\}$ NMR spectrum of **4** at 25 °C shows a broad signal which turns into several peaks on cooling to –70 °C. The ^1H NMR spectra from –70 to 25 °C show three major and four minor SiMe_3 peaks around 0 ppm which shift peak positions and change peak area ratios as the temperature of the solution changes. Temperature dependent change of the NMR spectra is partly attributed to PPh_3 dissociation of **4** to give $[\text{Cu}_4(\text{C}\equiv\text{CSiMe}_3)_4(\text{PPh}_3)_{4-n}]$ ($n = 1, 2$, etc.) because addition of PPh_3 causes a change in the relative peak intensities.

Table 1. Selected Bond Distances (Å) and Angles (deg) of $4\text{-Et}_2\text{O}$ (Forms I and II)

Form I			
Cu1–Cu2	2.568(2)	Cu1–Cu3	2.586(3)
Cu1–Cu4	2.581(4)	Cu2–Cu3	2.567(3)
Cu2–Cu4	2.566(4)	Cu3–Cu4	2.584(4)
Cu1–C1	2.13(2)	Cu1–C6	2.15(2)
Cu1–C16	2.15(2)	Cu2–C6	2.16(2)
Cu2–C11	2.15(2)	Cu2–C16	2.15(2)
Cu3–C1	2.13(2)	Cu3–C11	2.15(2)
Cu3–C16	2.14(2)	Cu4–C1	2.13(2)
Cu4–C6	2.15(2)	Cu4–C11	2.16(2)
C1–C2	1.24(2)	C6–C7	1.20(3)
C11–C12	1.21(2)	C16–C17	1.21(4)
Cu1–C1–Cu3	74.7(7)	Cu1–C1–Cu4	74.4(5)
Cu3–C1–Cu4	74.6(5)	Cu1–C1–C2	135.1(1)
Cu3–C1–C2	136.1(1)	Cu4–C1–C2	135.2(1)
Cu1–C6–Cu2	73.1(7)	Cu1–C6–Cu4	73.7(5)
Cu2–C6–Cu4	73.1(5)	Cu1–C6–C7	133.1(1)
Cu2–C6–C7	140.1(1)	Cu4–C6–C7	135.2(1)
Cu2–C11–Cu3	73.3(7)	Cu2–C11–Cu4	73.0(5)
Cu3–C11–Cu4	73.5(5)	Cu2–C11–C12	141.1(1)
Cu3–C11–C12	134.1(1)	Cu4–C11–C12	132.2(1)
Cu1–C16–Cu2	73.4(8)	Cu1–C16–Cu3	74.0(8)
Cu2–C16–Cu3	73.5(8)	Cu1–C16–C17	134.1(1)
Cu2–C16–C17	141.1(1)	Cu3–C16–C17	132.1(1)
Form II			
Cu1–Cu2	2.642(1)	Cu1–Cu3	2.568(1)
Cu1–Cu4	2.544(2)	Cu2–Cu3	2.6269(8)
Cu2–Cu4	2.544(1)	Cu3–Cu4	2.628(2)
Cu1–C1	2.173(4)	Cu1–C6	2.119(4)
Cu1–C16	2.167(4)	Cu2–C6	2.220(4)
Cu2–C11	2.137(4)	Cu2–C16	2.184(4)
Cu3–C1	2.145(4)	Cu3–C11	2.235(4)
Cu3–C16	2.149(4)	Cu4–C1	2.180(4)
Cu4–C6	2.179(6)	Cu4–C11	2.143(4)
C1–C2	1.205(5)	C6–C7	1.211(5)
C11–C12	1.194(5)	C16–C17	1.197(5)
Cu1–C1–Cu3	73.0(1)	Cu1–C10–Cu4	71.5(1)
Cu3–C1–Cu4	74.8(1)	Cu1–C1–C2	139.2(3)
Cu3–C1–C2	135.9(3)	Cu4–C1–C2	134.4(3)
Cu1–C6–Cu2	75.0(1)	Cu1–C6–Cu4	72.6(1)
Cu2–C6–Cu4	70.7(1)	Cu1–C6–C7	142.2(3)
Cu2–C6–C7	125.5(3)	Cu4–C6–C7	140.6(3)
Cu2–C11–Cu3	73.8(1)	Cu2–C11–Cu4	72.9(1)
Cu3–C11–Cu4	73.7(1)	Cu2–C11–C12	140.2(3)
Cu3–C11–C12	126.1(3)	Cu4–C11–C12	141.2(3)
Cu1–C16–Cu2	74.8(1)	Cu1–C16–Cu3	73.0(1)
Cu2–C16–Cu3	74.6(1)	Cu1–C16–C17	136.1(3)
Cu2–C16–C17	132.4(3)	Cu3–C16–C17	139.1(3)

However, unambiguous assignment of the species in the solution is not feasible due to the complexity of the spectra.²⁸

Complexes **5** and $[\text{Cu}(\text{C}\equiv\text{CC}_6\text{H}_4\text{-}p\text{-Me})(\text{PPh}_3)_4]$ (**6**) are obtained from reactions of $\text{Cu}(\text{OCHPh}_2)(\text{PPh}_3)_2$ with $\text{HC}\equiv\text{CPh}$ and with $\text{HC}\equiv\text{CC}_6\text{H}_4\text{-}p\text{-Me}$, respectively (eq 3).



The reactions proceed smoothly on addition of 1.2 equiv of alkynes to the alkoxide complex, while reaction of $[\text{Cu}(\text{O}^t\text{Bu})]_n$ with $\text{HC}\equiv\text{CPh}$, giving $[\text{Cu}(\text{C}\equiv\text{CPh})]_n$, was reported to require 20 equiv of the alkyne to Cu.¹⁰ Elemental analyses of the complexes agree well with the proposed formula. The IR spectra of **5** and **6** show $\nu(\text{C}\equiv\text{C})$ vibrations at 2018 and 2014 cm^{-1} , respectively. The former peak position is quite similar to the corre-

(23) (a) Churchill, M. R.; Karla, K. L. *J. Am. Chem. Soc.* **1973**, *95*, 5772. (b) *Inorg. Chem.* **1974**, *13*, 1065. (c) **1974**, *13*, 1427. (d) **1974**, *13*, 1899.

(24) Goel, R. G.; Beauchamp, A. L. *Inorg. Chem.* **1983**, *22*, 395.

(25) Gill, J. T.; Mayerle, J. J.; Welcker, P. S.; Lewis, D. F.; Ucko, D. A.; Barton, D. J.; Stowens, D.; Lippard, S. J. *Inorg. Chem.* **1976**, *15*, 1155.

(26) van Koten, G. J. *Organomet. Chem.* **1990**, *400*, 283 and references therein.

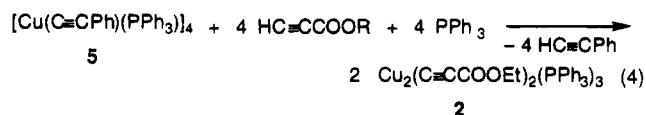
(27) Mason, R.; Mingos, D. M. P. *J. Organomet. Chem.* **1973**, *50*, 53.

(28) The NMR spectra and their temperature dependent change are not explained by assuming the presence of species formed only through PPh_3 dissociation from **4**. The complex seems to undergo some other reversible structural changes in the solution. Partial degradation of the complex into two $\text{Cu}_2(\mu_2\text{-C}\equiv\text{CSiMe}_2)_2(\text{PPh}_3)_2$ molecules and their redimerization may be also responsible for the spectroscopic change.

sponding peak of **5** (2020 cm⁻¹), which was prepared by an alternative reaction and has a cubane-like structure as determined by X-ray crystallography.³ Another structural isomer of [Cu(C≡CPh)(PPh₃)_n], which was prepared previously and not characterized well, showed two ν(C≡C) vibrations at 2060 and 1935 cm⁻¹.³

Many late transition metal alkoxide and amide complexes react smoothly with terminal alkyne to give the corresponding alkynyl complexes²⁹⁻³³ due to the high stability of the metal-alkynyl bond. Re(OMe)(CO)₃(PMe₃)₂ shows exceptionally low reactivity toward ligand substitution by an alkynyl group,³⁴ probably because the coordinatively saturated complex does not dissociate phosphine or CO ligands. Displacement of the alkoxide ligand of the copper complexes having coordinatively saturated structures²¹ by an alkynyl group proceeds smoothly, probably through PPh₃ dissociation due to the labile d¹⁰ configuration of the Cu center.

The alkynylcopper complexes with PPh₃ ligands obtained as above undergo substitution of the alkynyl ligand on addition of terminal alkynes. Complex **5** reacts with HC≡CCOOR in the presence or absence of PPh₃ to cause substitution of the alkynyl ligands (eq 4).

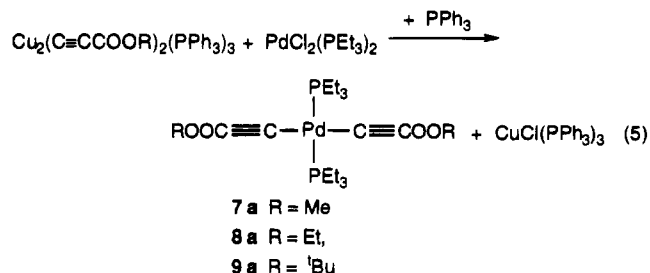


Reaction of **5** with equimolar amounts of HC≡CCOOEt and PPh₃ gives **2** (84%), which is characterized by IR and NMR spectra as well as elemental analyses. Similar reaction of **5** without addition of PPh₃ gives a mixture of copper complexes containing C≡CCOOMe ligands. The ³¹P{¹H} NMR spectrum of the product at -70 °C shows the peaks due to **1**, although several other peaks due to uncharacterized species are also observed. The ¹H NMR spectrum shows several peaks due to COOMe hydrogens in a peak area ratio of 3:15 between the Me and Ph hydrogens. All the results indicate that a Cu-C≡CCOOR bond is formed during the reaction due to its thermodynamically higher stability than a Cu-C≡CPh bond. Similarly a phenylethynyl ligand of Rh(C≡CPh)(L) (L = triphosphine) was readily replaced by a C≡CCOOR group on reaction with HC≡CCOOR.³⁵

Reactions of **3** with 2 equiv of HC≡CCOOMe and with 4 equiv of HC≡CCOOEt in Et₂O give **1** (63%) and **2** (73%), respectively. These results indicate that facile exchange of the alkynyl group between the alkynylcopper complex and alkyne occurs in solution. Preferential separation of **1** or **2** from the reaction mixtures is due to the lower solubility of complexes **1** and **2** compared to **3** rather than due to the difference in relative stability of the complexes. Estimation of relative stability among Cu-C≡CCOOR bonds is not feasible due to the pres-

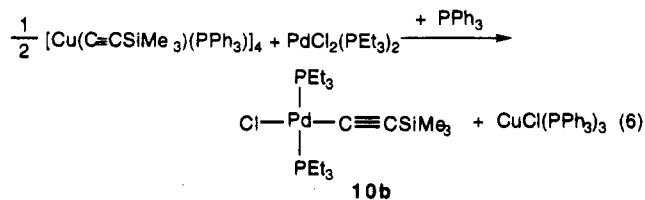
ence of several uncharacterized species observed in the NMR spectra of the reaction mixture.

Alkynyl Ligand Transfer from Copper to PdCl₂(PEt₃)₂. Reactions of **1-3** with 0.5 equiv of PdCl₂(PEt₃)₂ in the presence of PPh₃ give the corresponding dialkynylpalladium complexes, *trans*-Pd(C≡CCOOR)₂(PEt₃)₂ (**7a**, R = Me; **8a**, R = Et; **9a**, R = ^tBu), respectively, accompanied by formation of CuCl(PPh₃)₃ (eq 5).

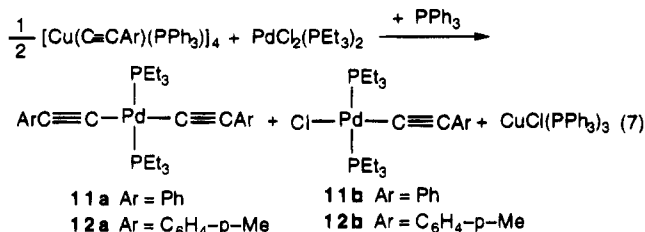


The ¹³C{¹H} NMR spectra of the complexes show the signals of the alkynyl carbons at 114.1-117.8 and 103.7-105.8 ppm as triplets due to ³¹P-¹³C coupling. The former signals, which show larger coupling constants (16-17 Hz) than the latter (3 Hz), are assigned to the carbon atoms bonded to the palladium center. The above results as well as the ³¹P{¹H} NMR spectrum showing a single peak indicate the *trans* structure of the complex. Formation of the monoalkynylpalladium complex, PdCl(C≡CCOOR)(PEt₃)₂, is not observed. CuCl(PPh₃)₃, separated from the reaction mixture as an Et₂O-insoluble solid, gives IR and ¹H NMR spectra which are identical with the authentic compound. Crystallographic parameters of single crystals of the product by X-ray measurement agree with the parameters already reported for CuCl(PPh₃)₃.²⁵ Reaction without addition of PPh₃ gives Cu₂Cl₂(PPh₃)₃ which is characterized on the basis of the IR spectrum as well as by comparison of crystallographic parameters of the single crystals.²⁵

Complex **4** reacts with 0.6 equiv of PdCl₂(PEt₃)₂ in the presence of PPh₃ to give CuCl(PPh₃)₃ and PdCl(C≡CSiMe₃)(PEt₃)₂ (**10b**, 82% based on PdCl₂(PEt₃)₂) (eq 6).



Complex **10b** gives satisfactory analytical and NMR results. Reaction of complex **5** with 0.63 equiv of PdCl₂(PEt₃)₂ in the presence of PPh₃ gives a mixture of *trans*-Pd(C≡CPh)₂(PEt₃)₂ (**11a**) (39%), *trans*-PdCl(C≡CPh)(PEt₃)₂ (**11b**) (56%), and CuCl(PPh₃)₃ (eq 7). Complexes



(29) Appleton, T. G.; Bennett, M. A. *Inorg. Chem.* **1978**, *17*, 738.

(30) Michelin, R. A.; Napoli, M.; Ros, R. *J. Organomet. Chem.* **1979**, *175*, 239.

(31) Fernández, M. J.; Esteruelas, M. A.; Covarrubias, M.; Oro, L. A.; Apreda, M.-C.; Foces-Foces, C.; Cano, F. H. *Organometallics* **1989**, *8*, 1158.

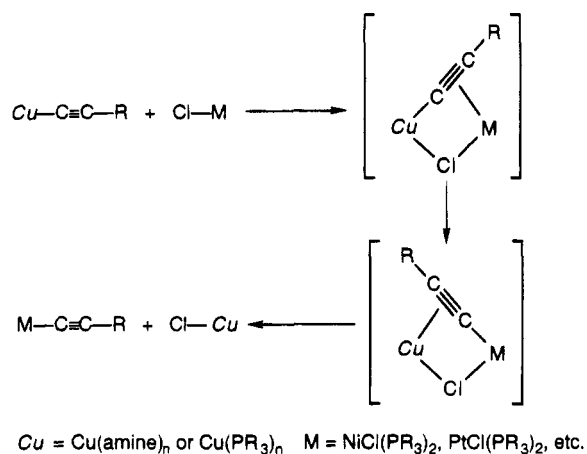
(32) Kim, Y.-J.; Osakada, K.; Yamamoto, A. *J. Organomet. Chem.* **1993**, *452*, 247.

(33) Rahim, M.; Bushweller, C. H.; Ahmed, K. J. *Organometallics* **1994**, *13*, 4952.

(34) Simpson, R. D.; Bergman, R. G. *Organometallics* **1992**, *11*, 3980.

(35) Bianchini, C.; Mealli, C.; Peruzzini, M.; Vizza, F.; Zanobini, F. *J. Organomet. Chem.* **1988**, *346*, C53.

Scheme 4. Plausible Pathway of Alkynyl Ligand Transfer from Cu to Ni, Pd, and Pt



11a and **11b** are isolated from each other by fractional crystallization of the reaction product after separation of $\text{CuCl}(\text{PPh}_3)_3$. Both complexes are characterized by the ^1H and $^{13}\text{C}\{^1\text{H}\}$ NMR spectra and are distinguished from each other on the basis of the peak area ratio of the ^1H NMR spectra as well as by elemental analyses. Similar reaction of **6** with $\text{PdCl}_2(\text{PET}_3)_2$ also gives a mixture of *trans*- $\text{Pd}(\text{C}\equiv\text{CC}_6\text{H}_4\text{-}p\text{-Me})_2(\text{PET}_3)_2$ (**12a**) and *trans*- $\text{PdCl}(\text{C}\equiv\text{CC}_6\text{H}_4\text{-}p\text{-Me})(\text{PET}_3)_2$ (**12b**) (76:24 molar ratio) accompanied by formation of $\text{CuCl}(\text{PPh}_3)_3$.

There have been no reports on reaction of alkynyl-copper phosphine complexes with dichloropalladium(II) complexes, although alkynyl ligand transfer from Cu to late transition metals was observed in reactions of phosphine-free copper alkynyl compounds with chloro complexes of late transition metals. The alkynylcopper compound, $[\text{Cu}(\text{C}\equiv\text{CPh})]_n$, reacts with $\text{PtCl}_2(\text{PET}_3)_2$ in the presence of TMEDA to give $\text{Pt}(\text{C}\equiv\text{CPh})_2(\text{PET}_3)_2$.³⁶ Reactions of $[\text{Cu}(\text{C}\equiv\text{CR})]_n$, prepared in situ from terminal alkynes CuI, and amines, with chloro complexes of Ni(II), Pd(II), and Pt(II) also give alkynyl complexes of these group 10 metals.³⁷ The reactions are believed to proceed through alkynyl ligand transfer from Cu(I) to Ni(II), Pd(II), and Pt(II) accompanied by transfer of the chloro ligand to the Cu center as shown in Scheme 4. Intermediate bimetallic or multimetallic complexes in which the alkynyl group is σ -bonded to the group 8 and 10 metals and π -bonded to the Cu center of the CuCl moiety are obtained from the reaction mixture of $[\text{Cu}(\text{C}\equiv\text{CPh})]_n$ and chloro complexes of Fe(II), Pt(II), and Ru(II).³⁸⁻⁴¹ Products of similar reactions of $[\text{Cu}(\text{C}\equiv\text{CPh})]_n$ with Ir(I) and Re(I) chloro complexes have multimetallic structures containing σ -bonding between

the alkynyl groups and Ir(I) or Re(I) centers, although the chloro ligand is eliminated from the products.^{42,43}

Change of the coordination mode of the $\mu_2\text{-}\eta^1\text{:}\eta^2$ -alkynyl ligand of bimetallic complex into a $\mu_2\text{-}\eta^2\text{:}\eta^1$ -structure is kinetically favored since rapid and reversible switching of the coordination between $\mu_2\text{-}\eta^1\text{:}\eta^2$ - and $\mu_2\text{-}\eta^2\text{:}\eta^1$ -bonding has been observed in an NMR study of Fe and Mo multimetallic complexes containing bridging alkynyl ligands.⁹ The irreversible alkynyl ligand transfer reactions from copper to other late transition metals shown above suggest lower thermodynamic stability of the Cu(I)-alkynyl σ -bond than of the σ -bond between the alkynyl group and group 6-10 transition metals.

Yields of dialkynylpalladium complexes in reactions 5-7 vary, depending on the alkynyl groups, in the order $\text{C}\equiv\text{CCOOR} > \text{C}\equiv\text{CPh}$ and $\text{C}\equiv\text{CC}_6\text{H}_4\text{-}p\text{-Me} > \text{C}\equiv\text{CSiMe}_3$. Electron-withdrawing groups, such as COOR, promote formation of the dialkynylpalladium complexes through stepwise displacement of two chloro ligands of $\text{PdCl}_2(\text{PET}_3)_2$. However, SiMe_3 -substituted alkynyl groups coordinated to Cu centers do not undergo transfer to *trans*- $\text{PdCl}(\text{C}\equiv\text{CSiMe}_3)(\text{PET}_3)_2$ under similar conditions. One of the possible reasons for enhancement of the alkynyl ligand transfer by the COOR group seems to be the significant stabilization of the Pd-C bond of the product caused by the electron-withdrawing group on the alkynyl group.⁴⁴

Conclusion

Labile alkoxide ligands bonded to copper(I) complexes with PPh_3 ligands undergo facile substitution by alkynyl groups on addition of terminal alkynes, giving the corresponding alkynylcopper complexes. The structure of the complexes varies depending on the kind of the alkynyl groups. Reactions of the alkoxide complexes with propiolic acid esters give unsymmetrical dinuclear complexes with two bridging alkynyl ligands, $(\text{PPh}_3)\text{-Cu}(\mu_2\text{-C}\equiv\text{CCOOR})_2\text{Cu}(\text{PPh}_3)_2$. Products of the reactions with $\text{HC}\equiv\text{CSiMe}_3$ and with $\text{HC}\equiv\text{CAr}$ show tetranuclear structures having cubane-like cores composed of four Cu and four alkynyl ligands, although the structures in the solutions are not rigid, which is mainly due to PPh_3 dissociation. Ligand exchange of the alkynylcopper complexes with alkynes occurs under mild conditions to give the thermodynamically more-favored alkynylcopper complexes. $\text{PdCl}_2(\text{PET}_3)_2$ activates the alkynyl-copper bond of the complexes to give alkynyl palladium complexes.

Experimental Section

General Procedures, Measurements, and Materials.

All manipulations of the complexes were carried out under nitrogen or argon using Schlenk techniques. $\text{Cu}(\text{OCH}(\text{CF}_3)_2)(\text{PPh}_3)_3$, $\text{Cu}(\text{OCHPh}_2)(\text{PPh}_3)_3$, and $[\text{Cu}(\text{OPh})(\text{PPh}_3)_2]_2$ were prepared according to the literature.^{21,45} IR spectra were measured on a JASCO 810 spectrophotometer. NMR spectra (^1H , ^{13}C , and ^{31}P) were recorded on JEOL FX-100, GX-270, EX-

(42) (a) Abu Salah, O. M.; Bruce, M. I. *J. Chem. Soc., Chem. Commun.* **1972**, 858. (b) Abu Salah, O. M.; Bruce, M. I.; Redhouse, A. D. *J. Chem. Soc., Chem. Commun.* **1974**, 855.

(43) Churchill, M. R.; Bezman, S. A. *Inorg. Chem.* **1974**, *13*, 1418.

(44) Masai, H.; Sonogashira, K.; Hagihara, N. *Bull. Chem. Soc. Jpn.* **1977**, *44*, 2226.

(45) (a) Kubota, M.; Yamamoto, A. *Bull. Chem. Soc. Jpn.* **1978**, *51*, 2909. (b) Kubota, M.; Yamamoto, T.; Yamamoto, A. *Bull. Chem. Soc. Jpn.* **1979**, *52*, 146.

(36) Sonogashira, K.; Fujikura, Y.; Yatake, T.; Toyoshima, N.; Takahashi, S.; Hagihara, N. *J. Organomet. Chem.* **1978**, *145*, 101.

(37) (a) Fujikura, Y.; Sonogashira, K.; Hagihara, N. *Chem. Lett.* **1975**, 1067. (b) Sonogashira, K.; Yatake, T.; Tohda, Y.; Takahashi, S.; Hagihara, N. *J. Chem. Soc., Chem. Commun.* **1977**, 291. (c) Ogawa, H.; Joh, T.; Takahashi, S.; Sonogashira, K. *J. Chem. Soc., Chem. Commun.* **1988**, 561.

(38) (a) Bruce, M. I.; Clark, R.; Howard, J.; Woodward, P. *J. Organomet. Chem.* **1972**, *42*, C107. (b) Abu Salah, O. M.; Bruce, M. I. *J. Chem. Soc., Dalton Trans.* **1974**, 2302. (c) Bruce, M. I.; Abu Salah, O. M.; Davis, R. E.; Reghavan, N. V. *J. Organomet. Chem.* **1974**, *64*, C48. (d) Abu Salah, O. M.; Bruce, M. I. *J. Chem. Soc., Dalton Trans.* **1975**, 2311.

(39) Clark, R.; Howard, J.; Woodward, P. *J. Chem. Soc., Dalton Trans.* **1974**, 2027.

(40) Yamazaki, S.; Deeming, A. J. *J. Chem. Soc., Dalton Trans.* **1993**, 3051.

(41) Tanaka, S.; Yoshida, T.; Adachi, T.; Yoshida, T.; Onitsuka, K.; Sonogashira, K. *Chem. Lett.* **1994**, 877.

400, and GX-500 spectrometers. Elemental analyses were carried out by Yanagimoto type MT-2 CHN autocorder.

Preparation of 1–3. To a toluene (5 mL) solution of Cu(OCHPh₂)(PPh₃)₃ (580 mg, 0.56 mmol) was added HC≡CCOOMe (56 mg, 0.67 mmol) at room temperature. Stirring the pale green solution caused the color to change to yellow, which was accompanied with gradual deposition of a white solid. After the reaction had proceeded for 7 h the insoluble material was dissolved by addition of toluene (9 mL) and a small amount of insoluble materials was removed by filtration. The filtrate was evaporated to dryness, and the remaining solid was washed repeatedly with hexane to give **1** as a white solid (190 mg, 63%). IR (KBr) $\nu(\text{C}=\text{C})$ 2042 cm⁻¹, $\nu(\text{C}=\text{O})$ 1683 cm⁻¹; ¹H NMR (CD₂Cl₂) δ 3.4 (s, 6H, CH₃), 7.1–7.5 (m, 45H, C₆H₅); ¹³C{¹H} NMR (CD₂Cl₂) δ 53.4 (s, CH₃), 113.1 and 119.4 (s, C≡C), 128–135 (C₆H₅), 154.2 (s, C=O). Anal. Found: C, 69.0; H, 5.1. Calcd for C₆₂H₅₁Cu₂O₄P₃: C, 68.9; H, 4.8.

Similar reactions with HC≡CCOOEt and HC≡CCOO^tBu gave **2** (67%) and **3** (60%), respectively. Spectroscopic data for **2**: IR (KBr), $\nu(\text{C}=\text{C})$ 2048 cm⁻¹, $\nu(\text{C}=\text{O})$ 1682 cm⁻¹; ¹H NMR (CD₂Cl₂) δ 1.1 (t, 6H, CH₃, *J* = 9 Hz), 3.8 (q, 4H, CH₂), 7.1–7.5 (m, 45H, C₆H₅); ¹³C{¹H} NMR (CD₂Cl₂) δ 14.5 (s, CH₃), 60.6 (s, CH₂), 113.8 and 119.2 (s, C≡C), 128–135 (C₆H₅), 153.9 (s, C=O). Anal. Found: C, 69.1; H, 5.1. Calcd for C₆₄H₅₅Cu₂O₄P₃: C, 69.4; H, 5.0. Spectroscopic data for **3**: IR (KBr) $\nu(\text{C}=\text{C})$ 2038 cm⁻¹, $\nu(\text{C}=\text{O})$ 1671 cm⁻¹; ¹H NMR (CD₂Cl₂) δ 1.3 (s, 18H, CH₃), 7.1–7.6 (m, 45H, C₆H₅); ¹³C{¹H} NMR (CD₂Cl₂) δ 28.3 (s, CH₃), 80.1 (s, C(CH₃)₃), 115.7 (br, C≡C), 128–134 (C₆H₅), 153.2 (s, C=O). Anal. Found: C, 70.8; H, 5.6. Calcd for C₆₈H₆₃Cu₂O₄P₃: C, 70.2; H, 5.5.

Preparation of 4–6. To an Et₂O (6 mL) solution of Cu(OCH(CF₃)₂)(PPh₃)₃ (200 mg, 0.20 mmol) was added HC≡CSiMe₃ (1.4 mL, 9.9 mmol) at room temperature. After the reaction mixture had been stirred for 4 h the colorless solution was filtered to remove a small amount of insoluble material. Addition of hexane (ca. 1 mL) to the filtrate followed by keeping the resulting mixture at -30 °C caused crystallization of [Cu(C≡CSiMe₃)(PPh₃)₄] (**4**) (70 mg, 83%).

Reaction of Cu(OCHPh₂)(PPh₃)₃ (300 mg, 0.29 mmol) with HC≡CSiMe₃ (43 mg, 0.43 mmol) for 25 h in toluene (3 mL) at room temperature resulted in formation of **4**, which was recrystallized from Et₂O to give **4**·H₂O (90 mg, 72%). IR (KBr) $\nu(\text{C}=\text{C})$ 1958 cm⁻¹; ¹H NMR (CD₂Cl₂) δ -0.9 to 0.2 (9H, Si(CH₃)₃), 7.2–7.7 (m, 15H, C₆H₅); ¹³C{¹H} NMR (CD₂Cl₂) δ -0.3 to 35.3 (Si(CH₃)₃), 90.3 and 93.3 (s, C≡C), 128–137 (C₆H₅). Anal. Found: C, 64.7; H, 6.1. Calcd for (C₂₃H₂₄CuPSi)₄·H₂O: C, 64.6; H, 5.8. Reaction of CuMe(PPh₃)₂(0.5Et₂O) (490 mg, 0.76 mmol) with HC≡CSiMe₃ (110 mg, 1.13 mmol) for 48 h in toluene at 0 °C also gave **4** (66 mg, 20%).

Reactions of Cu(OCHPh₂)(PPh₃)₃ with 1.2 equiv of HC≡CPh and with 1.2 equiv of HC≡CC₆H₄-*p*-Me gave **5** (87%) and **6** (83%), respectively. Spectroscopic data for **5**: IR (KBr) $\nu(\text{C}=\text{C})$ 2018 cm⁻¹; ¹H NMR (CD₂Cl₂) δ 6.0 (d, 2H, C₆H₅, *J* = 8 Hz), 6.7 (d, 2H, C₆H₅, *J* = 8 Hz), 6.8–7.7 (m, 16H, C₆H₅). Anal. Found: C, 73.6; H, 4.8. Calcd for (C₂₆H₂₀CuP)₄: C, 73.1; H, 4.7. Spectroscopic data for **6**: IR (KBr) $\nu(\text{C}=\text{C})$ 2014 cm⁻¹; ¹H NMR (CD₂Cl₂) δ 2.1 (s, 3H, CH₃), 5.9 (d, 2H, C₆H₄, *J* = 8 Hz), 6.4 (d, 2H, C₆H₄, *J* = 8 Hz), 6.9–7.8 (m, 15H, C₆H₅); ¹³C{¹H} NMR (C₆D₆) δ 2.12 (s, CH₃), 77.1 and 97.5 (s, C≡C), 124–136 (C₆H₅ and C₆H₄). Anal. Found: C, 73.7; H, 5.1. Calcd for (C₂₇H₂₂CuP)₄: C, 73.5; H, 5.0.

Crystal Structure Determination of 4·Et₂O. Single crystals of **4**·Et₂O were grown from Et₂O solutions of **4** at -30

Table 2. Crystal Data and Details of Structure Refinement of 4·Et₂O

	form I	form II
formula	C ₉₆ H ₁₀₆ Cu ₄ OP ₄ Si ₄	C ₉₆ H ₁₀₆ Cu ₄ OP ₄ Si ₄
mw	1766.32	1766.32
cryst size (mm ³)	0.4 × 0.4 × 0.6	0.5 × 0.3 × 0.4
cryst syst	triclinic	triclinic
space group	P $\bar{1}$	P $\bar{1}$
<i>a</i> (Å)	25.650(4)	15.59(1)
<i>b</i> (Å)	15.234(2)	20.47(1)
<i>c</i> (Å)	15.229(2)	14.844(5)
α (deg)	119.96(1)	90.89(4)
β (deg)	107.23(1)	94.60(5)
γ (deg)	72.74(1)	92.78(5)
<i>V</i> (Å ³)	4844	4717
<i>Z</i>	2	2
λ (Å)	0.710 69	0.710 69
<i>d</i> _{calcd} (g cm ⁻³)	1.211	1.244
μ (cm ⁻¹)	10.23	10.51
<i>F</i> (000)	1844	1844
<i>R</i>	0.060	0.036
<i>R</i> _w ^a	0.087	0.028
no. of variables	1044	1090
no. of measd reflns	12799	11980
no. of reflns used	5589	8913
	(<i>I</i> > 3 σ (<i>I</i>))	

$$^a w = [\sigma(F_o)]^{-2}.$$

°C.⁴⁶ Crystallographic data and results of structure refinement are summarized in Table 2. The unit cell parameters were obtained by least-squares refinement of 2 θ values of 25 reflections with 25° ≤ 2 θ ≤ 35°. Intensities were collected on Rigaku AFC-5R automated four-circle diffractometer by using Mo K α radiation (λ = 0.710 69 Å) and the ω -2 θ method. Calculations were carried out by using the program package TEXSAN on a DEC Micro VAXII computer.

Of the 13 217 collected reflections for form I of **4**·Et₂O 12 799 were unique (*R*_{int} = 0.039). No decay correction was applied. An empirical absorption correction based on azimuthal scans of several reflections was applied, which resulted in transmission factors ranging from 0.97 to 1.00. The data were corrected for Lorentz and polarization effects. The structure was solved by heavy-atom Patterson methods and expanded using Fourier techniques. The non-hydrogen atoms of the complex molecule were refined anisotropically, while the oxygen in the Et₂O molecule was refined isotropically. The hydrogen atoms were located at calculated positions and refined isotropically.

Of the 12 520 collected reflections for form II of **4**·Et₂O 11 980 were unique (*R*_{int} = 0.039). Over the data collection, the standards decreased by 1.3%. A linear correction factor was applied to the data to account for this phenomenon. An empirical absorption correction based on azimuthal scans of several reflections was applied, which resulted in transmission factors ranging from 0.89 to 1.00. The data were corrected for Lorentz and polarization effects. The structure was solved by direct methods and expanded using Fourier technique. The non-hydrogen atoms were refined anisotropically, while the hydrogen atoms were refined isotropically.

Reaction of 5 with HC≡CCOOEt in the Presence of PPh₃. To a toluene (9 mL) suspension of **5** (130 mg, 0.30 mmol of Cu) and PPh₃ (80 mg, 0.31 mmol) was added HC≡CCOOEt (59 mg, 0.60 mmol). When the reaction mixture was stirred at room temperature, **5** gradually dissolved to give a red solution. After the reaction had proceeded for 16 h a small amount of insoluble solid was removed by filtration. Evaporation of the solvent of the filtrate and ensuing addition of Et₂O (3 mL) gave **2** as a colorless solid (140 mg, 84%). Anal. Found: C, 69.4; H, 5.3. Calcd for C₆₄H₅₅Cu₂O₄P₃: C, 69.4; H, 5.0.

Reaction of 5 with HC≡CCOOMe. To a toluene (6 mL) suspension of **5** (290 mg, 0.68 mmol of Cu) was added HC≡CCOOMe (120 mg, 1.4 mmol) at room temperature. Stirring the reaction mixture for 8 h caused the color of the mixture to change from colorless to yellow brown. After the reaction mixture was diluted by addition of toluene (14 mL),

(46) Final D-map of the structure calculation of crystal form I of **4**·Et₂O shows a clear peak due to oxygen surrounded by several weaker peaks whose position are not reasonable as the carbon atoms of Et₂O. Although we initially assigned the crystal to the formula **4**·H₂O, we later improved the formula to **4**·Et₂O according to the comments by the reviewer who suggested the following points. The crystal (form I) has a larger volume of crystal cell than form II and has too large a vacancy to be filled by H₂O molecules around the O atom. We could not obtain further analytical or NMR results of the single crystal that was analyzed by X-ray crystallography to compare the two formulas for the crystal.

a small amount of insoluble product was removed by filtration. Evaporation of the solvent of the filtrate under vacuum followed by addition of Et₂O (5 mL) gave a yellow brown solid (270 mg). The spectroscopic results indicate that the product is a mixture of copper complexes having Cu-C≡C-COOE bonds. IR (KBr) $\nu(\text{C}\equiv\text{C})$ 2050, 2010, and 1904 cm⁻¹, $\nu(\text{C}=\text{O})$ 1671 cm⁻¹; ¹H NMR (CD₂Cl₂, -80 °C) δ 2.8–3.6 (br, 3H, CH₃), 7.7–7.0 (m, 15H, C₆H₅).

Reaction of 3 with HC≡CCOOEt and with HC≡CCOOEt. To an Et₂O (10 mL) solution of **3** (110 mg, 0.095 mmol) was added HC≡CCOOEt (18 mg, 0.21 mmol) at room temperature. Stirring the yellow solution for 20 h caused the color of the solution to change from pale yellow to colorless, which was accompanied by formation of a white solid precipitated. The solid was filtered, washed with Et₂O, and dried in vacuo (68 mg, 63%). The IR and the ¹H NMR spectra of the product were identical with **1**. Anal. Found: C, 68.5; H, 4.9. Calcd for C₆₂H₅₁Cu₂O₄P₃: C, 68.9; H, 4.8.

Similar reaction with 4 equiv of HC≡CCOOEt gave **2** in 73%. Anal. Found: C, 70.2; H, 5.0. Calcd for C₆₄H₅₅Cu₂O₄P₃: C, 69.4; H, 5.0.

Reactions of 1–3 with PdCl₂(PEt₃)₂. A mixture of **1** (160 mg, 0.30 mmol of Cu), PPh₃ (65 mg, 0.24 mmol) and PdCl₂(PEt₃)₂ (60 mg, 0.15 mmol) was dissolved in toluene (2 mL). Stirring the reaction mixture caused gradual precipitation of a white solid from the initially colorless solution. After the reaction had proceeded for 4 h, the deposited white solid (CuCl(PPh₃)₃, 190 mg, 88%) was removed by filtration. The filtrate and Et₂O washings of the solid were condensed to give the colorless residue. Recrystallization of the product from hexane at -30 °C gave *trans*-Pd(C≡CCOOEt)₂(PEt₃)₂ (**7a**) (64 mg, 80%). IR (KBr disk) $\nu(\text{C}\equiv\text{C})$ 2112 cm⁻¹, $\nu(\text{C}=\text{O})$ 1683 cm⁻¹; ¹H NMR (CD₂Cl₂) δ 1.2 (m, 18H, P(CH₂CH₃)₃), 1.9 (m, 12H, P(CH₂CH₃)₃), 3.6 (s, 6H, OCH₃); ¹³C{¹H} NMR (CD₂Cl₂) δ 8.6 (s, P(CH₂CH₃)₃), 17.2 (t, *J* = 15 Hz, P(CH₂CH₃)₃), 51.9 (s, OCH₃), 103.7 (t, *J* = 3 Hz, Pd-C≡C), 117.8 (t, *J* = 16 Hz, Pd-C), 154.5 (s, C=O); ³¹P{¹H} NMR (CD₂Cl₂) 19.4 ppm (s). Anal. Found: C, 47.5; H, 7.1. Calcd for C₂₀H₃₆O₄P₂Pd: C, 47.2; H, 7.1.

Similar reactions of **2** and **3** with PdCl₂(PEt₃)₂ gave *trans*-Pd(C≡CCOOEt)₂(PEt₃)₂ (**8a**) (84%) and *trans*-Pd(C≡CCOO^tBu)₂(PEt₃)₂ (**9a**) (100%), respectively. Spectroscopic data for **8a**: IR (KBr disk) $\nu(\text{C}\equiv\text{C})$ 2094 cm⁻¹, $\nu(\text{C}=\text{O})$ 1673 cm⁻¹; ¹H NMR (CD₂Cl₂) δ 1.2 (m, 18H, P(CH₂CH₃)₃), 1.2 (t, 6H, CH₃), 1.9 (m, 12H, P(CH₂CH₃)₃), 4.1 (q, 4H, OCH₂); ¹³C{¹H} NMR (CD₂Cl₂) δ 8.6 (s, P(CH₂CH₃)₃), 14.4 (s, CH₃), 17.2 (t, *J* = 15 Hz, P(CH₂CH₃)₃), 60.8 (s, OCH₂), 104.2 (t, *J* = 3 Hz, Pd-C≡C), 117.4 (t, *J* = 16 Hz, Pd-C), 154.5 (s, C=O); ³¹P{¹H} NMR (CD₂Cl₂) 19.8 ppm (s). Anal. Found: C, 49.5; H, 7.5. Calcd for C₂₂H₄₀O₄P₂Pd: C, 49.2; H, 7.5. Spectroscopic data for **9a**: IR (KBr disk) $\nu(\text{C}\equiv\text{C})$ 2090 cm⁻¹, $\nu(\text{C}=\text{O})$ 1669 cm⁻¹; ¹H NMR (CD₂Cl₂) δ 1.2 (m, 18H, P(CH₂CH₃)₃), 1.4 (s, 18H, CH₃), 1.9 (m, 12H, P(CH₂CH₃)₃); ¹³C{¹H} NMR (CD₂Cl₂) δ 8.6 (s, P(CH₂CH₃)₃), 14.4 (s, CH₃), 17.3 (t, *J* = 14 Hz, P(CH₂CH₃)₃), 28.3 (s, C(CH₃)₃), 80.5 (s, OC(CH₃)₃), 105.8 (t, *J* = 3 Hz, Pd-C≡C), 114.1 (t, *J* = 17 Hz, Pd-C), 153.5 (s, C=O); ³¹P{¹H} NMR (CD₂Cl₂) 19.7 ppm (s). Anal. Found: C, 53.2; H, 8.9. Calcd for C₂₆H₄₈O₂P₂Pd: C, 52.7; H, 8.2.

Reaction of 4 with PdCl₂(PEt₃)₂. A mixture of **4** (150 mg, 0.35 mmol of Cu), PPh₃ (180 mg, 0.68 mmol) and PdCl₂(PEt₃)₂ (85 mg, 0.21 mmol) was stirred in Et₂O (3 mL) under Ar for 6 h. The starting materials dissolved at once to give a pale yellow solution which gradually affords a white solid precipitate. After the mixture had been stirred for 6 h at room temperature the resulting white solid (CuCl(PPh₃)₃, 250 mg, 81%) was removed by filtration. The filtrate was evaporated to dryness to give a white residue, which was extracted with hexane several times. Cooling the hexane extract at -78 °C

gave *trans*-PdCl(C≡CSiMe₃)(PEt₃)₂ (**10b**) as colorless crystals (82 mg, 82%). IR (KBr) $\nu(\text{C}\equiv\text{C})$ 2048 cm⁻¹; ¹H NMR (CD₂Cl₂) δ 0.07 (s, 9H, Si(CH₃)₃), 1.2 (m, 18H, P(CH₂CH₃)₃), 1.9 (m, 12H, P(CH₂CH₃)₃); ¹³C{¹H} NMR (CD₂Cl₂) δ 0.8 (s, Si(CH₃)₃), 8.5 (s, P(CH₂CH₃)₃), 15.7 (t, *J* = 14 Hz, P(CH₂CH₃)₃), 112.1 (t, *J* = 4 Hz, Pd-C≡C), 116.0 (t, *J* = 16 Hz, Pd-C). ³¹P{¹H} NMR (CD₂Cl₂) 17.3 ppm (s). Anal. Found: C, 43.3; H, 8.3. Calcd for C₁₇H₃₉ClP₂PdSi: C, 43.0; H, 8.3.

Reactions of 5 and 6 with PdCl₂(PEt₃)₂. A mixture of **5** (530 mg, 1.2 mmol of Cu), PPh₃ (650 mg, 2.5 mmol), and PdCl₂(PEt₃)₂ (310 mg, 0.75 mmol) was stirred in toluene (12 mL) under Ar for 4 h. Evaporation of the solvent followed by addition of Et₂O caused precipitation of CuCl(PPh₃)₃, which was separated by filtration. Cooling the filtrate at -30 °C gave **11a** as a yellow crystalline solid (160 mg, 39%). Complex **11b** (200 mg, 56%) was obtained by addition of hexane to the filtrate after removal of **11a**. Spectroscopic data for **11a**: IR (KBr disk) $\nu(\text{C}\equiv\text{C})$ 2098 cm⁻¹; ¹H NMR (90 MHz, CD₂Cl₂) δ 1.2 (m, 18H, P(CH₂CH₃)₃), 2.0 (m, 12H, P(CH₂CH₃)₃), 7.0–7.4 (m, 10H, C₆H₅); ¹³C{¹H} NMR (125 MHz, CD₂Cl₂) δ 8.8 (s, P(CH₂CH₃)₃), 17.5 (t, *J* = 15 Hz, P(CH₂CH₃)₃), 110.9 (t, *J* = 3 Hz, Pd-C≡C), 111.9 (t, *J* = 17 Hz, Pd-C), 125–131 (C₆H₅). Anal. Found: C, 60.9; H, 7.7. Calcd for C₂₈H₄₀P₂Pd: C, 61.7; H, 7.4. Spectroscopic data for **11b**: IR (KBr disk) $\nu(\text{C}\equiv\text{C})$ 2114 cm⁻¹; ¹H NMR (90 MHz, CD₂Cl₂) δ 1.2 (m, 18H, P(CH₂CH₃)₃), 1.9 (m, 12H, P(CH₂CH₃)₃), 7.0–7.4 (m, 5H, C₆H₅); ¹³C{¹H} NMR (125 MHz, CD₂Cl₂) δ 8.5 (s, P(CH₂CH₃)₃), 15.8 (t, *J* = 14 Hz, P(CH₂CH₃)₃), 96.0 (t, *J* = 16 Hz, Pd-C), 106.7 (t, *J* = 6 Hz, Pd-C≡C), 125–131 (C₆H₅); ³¹P{¹H} NMR (CD₂Cl₂) ppm (s). Anal. Found: C, 51.0; H, 7.7. Calcd for C₂₀H₃₅ClP₂Pd: C, 50.1; H, 7.4. Slight disagreement of analytical values of **11a** and **11b** with calculated values is due to insufficient separation of the complexes from each other by fractional crystallization.

Reaction of **6** with PdCl₂(PEt₃)₂ was carried out analogously to give a mixture of *trans*-Pd(C≡CC₆H₄-*p*-Me)(PEt₃)₂ (**12a**) and *trans*-PdCl(C≡CC₆H₄-*p*-Me)(PEt₃)₂ (**12b**), which could not be separated from each other (yield 73%, **12a**:**12b** = 76:24). Spectroscopic data for **12a**: IR (KBr disk) $\nu(\text{C}\equiv\text{C})$ 2098 cm⁻¹; ¹H NMR (CD₂Cl₂) δ 1.2 (m, 18H, P(CH₂CH₃)₃), 2.0 (m, 12H, P(CH₂CH₃)₃), 2.3 (s, 6H, CH₃), 7.0 (d, 4H, *J* = 8 Hz), 7.4 (d, 4H, *J* = 8 Hz). ¹³C{¹H} NMR (CD₂Cl₂) δ 8.8 (s, P(CH₂CH₃)₃), 17.6 (t, *J* = 15 Hz, P(CH₂CH₃)₃), 21.3 (s, CH₃), 110.9 (t, *J* = 3 Hz, Pd-C≡C), 111.9 (t, *J* = 17 Hz, Pd-C), 126–135 (C₆H₄); ³¹P{¹H} NMR (CD₂Cl₂) 19.0 ppm (s). Spectroscopic data for **12b**: IR (KBr disk) $\nu(\text{C}\equiv\text{C})$ 2112 cm⁻¹; ¹H NMR (CD₂Cl₂) δ 1.2 (m, 18H, P(CH₂CH₃)₃), 1.9 (m, 12H, P(CH₂CH₃)₃), 2.3 (s, 6H, CH₃), 7.1 (d, 2H, *J* = 7 Hz), 7.3 (d, 2H). ¹³C{¹H} NMR ((125 MHz, CD₂Cl₂) δ 8.5 (s, P(CH₂CH₃)₃), 15.8 (t, *J* = 14 Hz, P(CH₂CH₃)₃), 21.3 (s, CH₃), 94.4 (t, *J* = 16 Hz, Pd-C), 106.6 (t, *J* = 6 Hz, Pd-C≡C), 125–136 (C₆H₄); ³¹P{¹H} NMR (CD₂Cl₂) 18.1 ppm (s).

Acknowledgment. This work was partially supported by a Grant-in-Aid for Scientific Research from the Ministry of Education, Science and Culture, Japan. Authors are grateful to Dr. Masako Tanaka of our laboratory for the crystallographic study and the reviewer who gave us helpful suggestions on the crystallographic results.

Supporting Information Available: Tables of positional parameters for all atoms, anisotropic displacement parameters of non-hydrogen atoms, and bond distances and angles of crystal forms I and II of 4·Et₂O (58 pages). Ordering information is given on any current masthead page.

OM950059S

Tetraaza Macrocycles as Ancillary Ligands in Early Metal Alkyl Chemistry. Synthesis and Characterization of Out-of-Plane (Me₄taen)ZrX₂ (X = Alkyl, Benzyl, NMe₂, Cl) and (Me₄taen)ZrX₂(NHMe₂) (X = Cl, CPh) Complexes

David G. Black, Dale C. Swenson, and Richard F. Jordan*

Department of Chemistry, University of Iowa, Iowa City, Iowa 52242

Robin D. Rogers

Department of Chemistry, Northern Illinois University, DeKalb, Illinois 60115

Received February 27, 1995*

The synthesis, properties, and structures of a series of out-of-plane (N₄-macrocycle)ZrX₂ complexes incorporating the tetraaza macrocycle Me₄taen²⁻ are described ((Me₄taen)H₂ = 5,7,12,14-tetramethyl-1,4,8,11-tetraazacyclotetradeca-4,6,11,13-tetraene). Alkane elimination reactions of (Me₄taen)H₂ (**1**) with ZrR₄ yield (Me₄taen)ZrR₂ (**2**, R = CH₂Ph; **3**, R = CH₂-SiMe₃). The amine elimination reaction of **1** with Zr(NMe₂)₄ yields (Me₄taen)Zr(NMe₂)₂ (**4**). Protonolysis of **4** with [HNHMe₂]Cl yields the seven-coordinate amine adduct (Me₄taen)-ZrCl₂(NHMe₂) (**5**), which loses amine under vacuum (120 °C, 10 h) to afford base-free (Me₄taen)ZrCl₂ (**6**). The reaction of **4** with phenylacetylene yields the seven-coordinate bisacetylide complex (Me₄taen)Zr(CPh)₂(NHMe₂) (**7**). The reaction of **6** with RLi reagents in toluene yields (Me₄taen)ZrR₂ (**8**, R = CH₂CMe₃; **9**, R = CH₃). Halide displacement does not provide facile access to **6**. Deprotonation of **1** yields [Li(THF)]₂[Me₄taen] (**10**), which readily loses THF to yield Li₂[Me₄taen] (**11**); however, the reaction of **11** with ZrCl₄(THF)₂ yields mixtures of **6** and (Me₄taen)₂Zr (**12**). Bismacrocycle complex **12** is formed in good yield via reaction of Zr(NMe₂)₄ with 2 equiv of **1**. Dialkyls **2** and **9** rearrange thermally by migration of an alkyl group from Zr to a macrocycle imine carbon. The solid state structures of **1**, **2**, **4**–**6**, and **10** have been determined. Compounds **1** and **10** exhibit rather planar Me₄taen conformations. Dichloride **6** adopts a trigonal prismatic structure in which the chlorides occupy adjacent edge sites, and the Me₄taen²⁻ conformation is similar to that in **1** and **10**. Dibenzyl complex **2** adopts a similar but more twisted trigonal prismatic structure. Bisamide complex **4** adopts a distorted octahedral structure in which the Me₄taen²⁻ ligand is significantly folded. These structural differences are rationalized in terms of the conformational preference of the Me₄taen²⁻ ligand, as deduced from the structures of **1** and **10**, and the π-donating ability of the X group. Seven-coordinate complex **5** adopts a side-capped trigonal prismatic structure with a tripodal arrangement of chloride and amine ligands. The structures and properties of these new compounds are compared to those of Cp₂MX₂ and other early metal analogues.

Introduction

Zirconium(IV) and hafnium(IV) complexes of 14- or 16-membered tetraaza macrocyclic ligands (N₄-macrocycle)MX₂ adopt “out-of-plane” cis structures because the large metal ions cannot fit in the macrocycle N₄-plane (A, Chart 1).^{1–11} Complexes of this type can coordinate one or two additional ligands cis to the X groups giving seven- or eight-coordinate adducts (B, C); coordination of ligands trans to the X groups is pre-

cluded by the out-of-plane structure. The potential availability of coordination sites cis to the X ligands

(5) For earlier work on cis (por)MX₂ compounds see: (a) Buchler, J. W.; Eikelmann, G.; Puppe, L.; Rohbock, K.; Schneehage, H. H.; Weck, D. *Liebigs Ann. Chem.* **1971**, *745*, 135. (b) Buchler, J. W.; Schneehage, H. H. *Z. Naturforsch. B* **1973**, *28*, 433. (c) Buchler, J. W.; Folz, M.; Habets, H.; van Kaam, J.; Rohbock, K. *Chem. Ber.* **1976**, *109*, 1477. (d) Buchler, J. W. In *The Porphyrins*; Dolphin, D., Ed.; Academic: New York, 1978; Vol. 1, p 390.

(6) For comparison, (por)TiX₂ compounds adopt trans structures in which the Ti^{IV} lies in the N₄ plane, while (phthalocyaninato)TiCl₂ adopts an out-of-plane cis structure. (a) Marchon, J.-C.; Latour, J.-M.; Grand, A.; Belakhovsky, M.; Loos, M.; Goulon, J. *Inorg. Chem.* **1990**, *29*, 57. (b) Lecomte, C.; Protas, J.; Marchon, J.-C.; Nakajima, M. *Acta Crystallogr., Sect. B: Struct. Crystallogr. Cryst. Chem.* **1978**, *34*, 2856. (c) Goedken, V. L.; Dessy, G.; Ercolani, C.; Fares, V.; Gastaldi, L. *Inorg. Chem.* **1985**, *24*, 991.

(7) Organotitanium porphyrin complexes have been characterized. (a) Woo, L. K.; Hays, J. A.; Jacobson, R. A.; Day, C. L. *Organometallics* **1991**, *10*, 2102. (b) Latour, J.-M.; Boreham, C. J.; Marchon, J.-C. *J. Organomet. Chem.* **1980**, *190*, C61. See also: (c) Berreau, L. M.; Young, V. G.; Woo, L. K. *Inorg. Chem.* **1995**, *34*, 527.

(8) (a) Shibata, K.; Aida, T.; Inoue, S. *Tetrahedron Lett.* **1992**, *33*, 1077. (b) Shibata, K.; Aida, T.; Inoue, S. *Chem. Lett.* **1992**, 1173.

(9) Me₄taa²⁻ is also referred to as taa²⁻ in the literature.

* Abstract published in *Advance ACS Abstracts*, June 15, 1995.

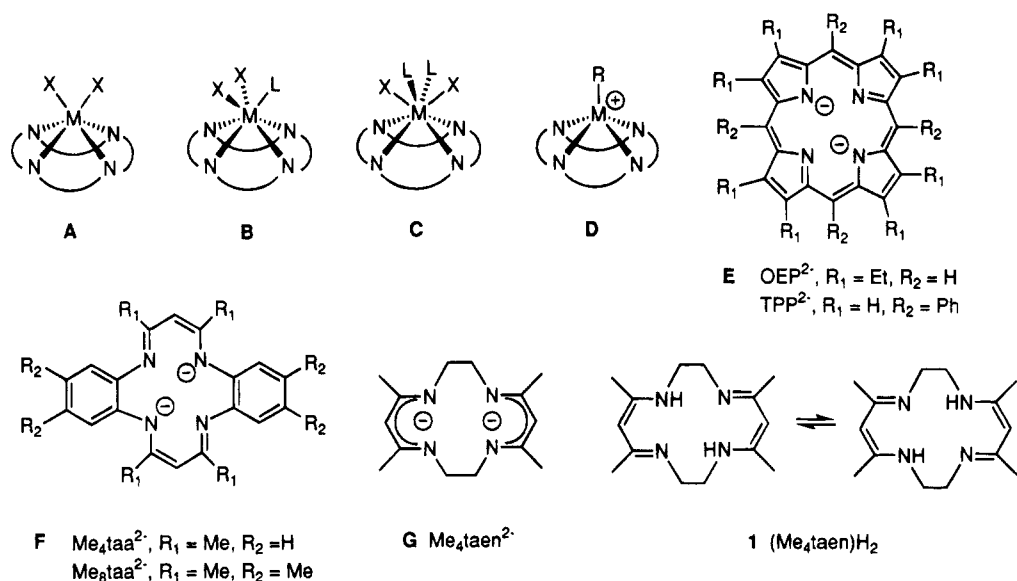
(1) Uhrhammer, R.; Black, D. G.; Gardner, T. G.; Olsen, J. D.; Jordan, R. F. *J. Am. Chem. Soc.* **1993**, *115*, 8493.

(2) OEP = octaethylporphyrin; TPP = tetraphenylporphyrin; taa = tetraazaannulene.

(3) (a) Brand, Holger; Arnold, J. *J. Am. Chem. Soc.* **1992**, *114*, 2266. (b) Brand, H.; Capriotti, J. A.; Arnold, J. *Organometallics* **1994**, *13*, 4469. (c) Brand, H.; Arnold, J. *Organometallics* **1993**, *12*, 3655. (d) Arnold, J. A.; Johnson, S. E.; Knobler, C. B.; Hawthorne, M. F. *J. Am. Chem. Soc.* **1992**, *114*, 3996.

(4) For related studies see: (a) Kim, H.; Whang, D.; Kim, K.; Do, Y. *Inorg. Chem.* **1993**, *32*, 360. (b) Ryu, S.; Whang, D.; Kim, J.; Yeo, W.; Kim, K. *J. Chem. Soc., Dalton Trans.* **1993**, 205.

Chart 1



makes organometallic derivatives of these systems of interest for synthetic and catalytic applications. Our own long-term goal in this area is to develop *cationic* (N₄-macrocyclic)M(R)⁺ alkyl complexes (**D**) which, given the *cis* structures of (N₄-macrocyclic)MX₂ species, should form *cis* (N₄-macrocyclic)M(R)(substrate)⁺ adducts, possibly leading to insertion and σ -bond metathesis chemistry.¹

To date, group 4 metal macrocycle chemistry has focused on porphyrin and tetraazaannulene (taa) ligands (**E** and **F**, Chart 1). Arnold has prepared an extensive series of out-of-plane *cis* (OEP)ZrR₂ dialkyls and investigated their reactivity.²⁻⁷ These complexes undergo rapid Zr–C protonolysis, yielding new (OEP)ZrX₂ (X⁻ = TfO⁻, R'CO₂⁻, R'O⁻, Cl⁻) and (OEP)Zr(R)⁺ derivatives, and also cleanly insert CO₂ and acetone, yielding carboxylate and alkoxide complexes. Hydrogenolysis of (OEP)Zr(CH₂SiMe₃)₂ yields hydride species which can be trapped by olefins yielding (OEP)Zr(CH₂SiMe₃)(CH₂CH₂R) and (OEP)Zr(CH₂CH₂R)₂ (R = H, Me). This system catalytically hydrogenates ethylene, presumably via an insertion/Zr–C hydrogenolysis process. Recently, Inoue reported that (TPP)ZrX₂ complexes (X⁻ = RCO₂⁻, Cl⁻)² catalyze the carboalumination of terminal alkynes.⁸

Goedken and Floriani have investigated (Me₄taa)MCl₂ (M = Ti, Zr, Hf) and several derivatives containing the 14-membered macrocycle Me₄taa²⁻.^{9,10} These complexes invariably exhibit out-of-plane *cis* structures in which the ligand adopts a relatively rigid saddle conformation due to steric interactions between the methyl and benzo groups.^{10f,g} However, the organometallic chemistry of this system is less well developed. Floriani showed that (Me₄taa)ZrCl₂ can be alkylated by PhCH₂MgCl to yield *cis* (Me₄taa)Zr(CH₂Ph)₂; however reaction with MeMgX

results in methylation at a Me₄taa imine carbon, yielding (Me₅taa)Zr(Me)(THF).¹¹ Recently, we prepared a series of (Me₈taa)MR₂ alkyls (M = Zr, Hf; R = Me, CH₂-Ph, CH₂SiMe₃) via salt metathesis or direct alkane elimination routes.¹ Protonolysis of these species with ammonium reagents yields (Me₈taa)M(R)⁺ cations which insert alkynes and polymerize ethylene. The potential utility of out-of-plane (Me_xtaa)MX_n compounds in organic synthesis is further demonstrated by Geoffroy's earlier discovery that (Me₄taa)Ti(=O) undergoes facile cycloaddition reactions with metal carbonyls, electrophilic ketones, epoxides, and other substances.¹²

In the present contribution we describe the synthesis and characterization of a series of neutral Zr(IV) complexes of the 12- π -electron, 14-membered macrocyclic ligand Me₄taen²⁻ (**G**), the dianion of (Me₄taen)H₂ (**1**).¹³ This ligand was chosen for study for several reasons. Macrocycle **1** is easily available in good yield by non-template ketoenamine/diamine condensation routes developed by Holm and Tokumitsu or by a Au^{III}-templated β -diketone/diamine condensation route developed by Everett.¹⁴⁻¹⁶ Analogues of **1** with different substituents on the diiminato or –CH₂CH₂– fragments, or an increased level of unsaturation, may be prepared by derivatization of **1** or by direct synthesis.¹⁷ The Me₄taen²⁻ ligand is more flexible than Me_xtaa²⁻ or porphyrin²⁻ ligands, which may allow for greater M–N

(12) (a) Housmekerides, C. E.; Pilato, R. S.; Geoffroy, G. L.; Rheingold, A. L. *J. Chem. Soc., Chem. Commun.* **1991**, 563. (b) Yang, C.; Ladd, J. A.; Goedken, V. L. *J. Coord. Chem.* **1988**, *19*, 235. (c) Yang, C.; Goedken, V. L. *Inorg. Chim. Acta* **1986**, *117*, L19.

(13) (Me₄taen)H₂ (**1**; 5,7,12,14-tetramethyl-1,4,8,11-tetraazacyclotetradeca-4,6,11,13-tetraene) is also referred to as H₂(MeHMe(en)₂) in the literature.

(14) Truex, T. J.; Holm, R. H. *J. Am. Chem. Soc.* **1972**, *94*, 4529.

(15) Tokumitsu, T.; Hayashi, T. *Bull. Chem. Soc. Jpn.* **1981**, *54*, 2348.

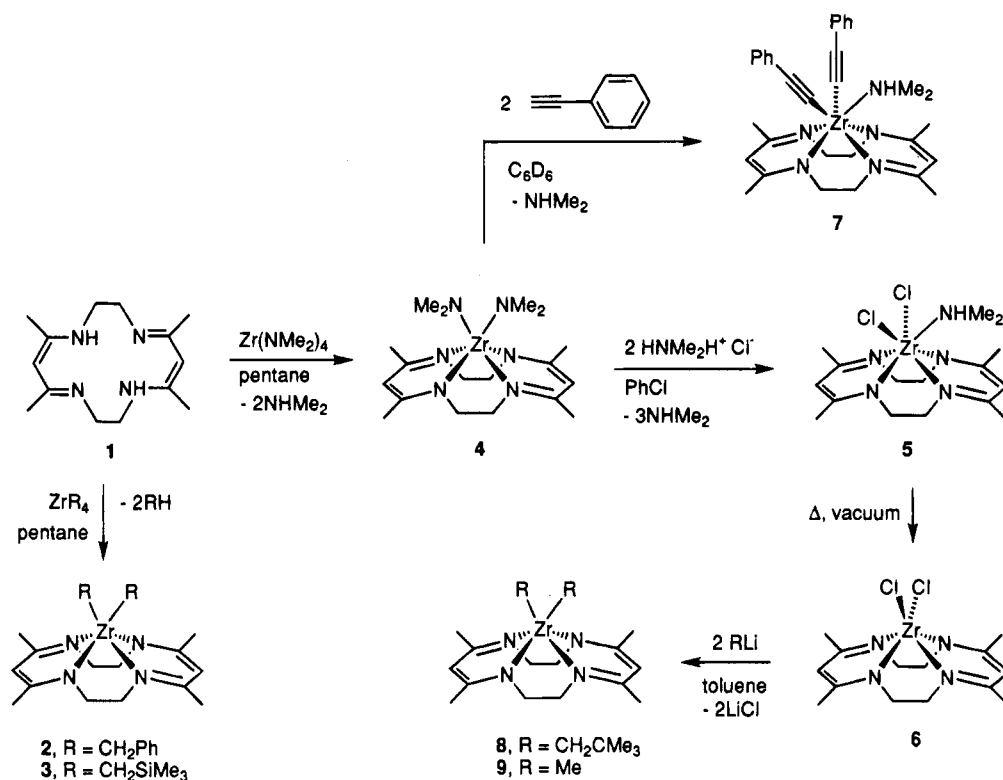
(16) (a) Kim, J.-H.; Everett, Jr., G. W. *Inorg. Chem.* **1979**, *18*, 3145. (b) Brawner, S. A.; Lin, I. J. B.; Kim, J.-H.; Everett, Jr., G. W. *Inorg. Chem.* **1978**, *17*, 1304.

(17) See the foregoing three refs and also the following: (a) Tang, S. C.; Koch, S.; Weinstein, G. N.; Lane, R. W.; Holm, R. H. *Inorg. Chem.* **1973**, *12*, 2589. (b) Fujiwara, M.; Nakajima, Y.; Matsushita, T.; Shono, T. *Polyhedron* **1985**, *4*, 1589. (c) Fujiwara, M.; Matsushita, T.; Shono, T. *Polyhedron* **1984**, *3*, 1357. (d) Sakata, K.; Hashimoto, M.; Tagami, N.; Murakami, Y. *Bull. Chem. Soc. Jpn.* **1980**, *53*, 2262. (e) Owston, P. G.; Peters, R.; Ramsamy, E.; Tasker, P. A.; Trotter, J. *J. Chem. Soc., Chem. Commun.* **1980**, 1218. (f) Bamfield, P. *J. Chem. Soc. A.* **1969**, 2021. (g) Jäger, E.-G. *Z. Chem.* **1968**, *8*, 30. (h) Jäger, E.-G. *Z. Chem.* **1968**, *8*, 30, 470.

(10) (a) Goedken, V. L.; Ladd, J. A. *J. Chem. Soc., Chem. Commun.* **1982**, 142. (b) Yang, C.; Goedken, V. L. *J. Chem. Soc., Chem. Commun.* **1986**, 1101. (c) Ciurli, S.; Floriani, C.; Chiesi-Villa, A.; Guastini, C. *J. Chem. Soc., Chem. Commun.* **1986**, 1401. (d) De Angelis, S.; Solari, E.; Gallo, E.; Floriani, C.; Chiesi-Villa, A.; Rizzoli, C. *Inorg. Chem.* **1992**, *31*, 2520. (e) Giannini, L.; Solari, E.; Floriani, C.; Chiesi-Villa, A.; Rizzoli, C. *Angew. Chem., Int. Ed. Engl.* **1994**, *33*, 2204. (f) Goedken, V. L.; Pluth, P. J.; Peng, S.; Bursten, B. *J. Am. Chem. Soc.* **1976**, *98*, 8014. (g) Weiss, M. C.; Bursten, B.; Peng, S.; Goedken, V. L. *J. Am. Chem. Soc.* **1976**, *98*, 8021. Review: (h) Cotton, F. A.; Czuchajowska, J. *Polyhedron* **1990**, *21*, 2553.

(11) Floriani, C.; Ciurli, S.; Chiesi-Villa, A.; Guastini, C. *Angew. Chem., Int. Ed. Engl.* **1987**, *26*, 70.

Scheme 1



π -bonding and concomitant greater stabilization of electron-deficient (N_4 -macrocycle) $M(R)^+$ species. The steric properties of Me_4taen^{2-} (i.e., macrocycle pocket size, degree of steric crowding above or below the N_4 -plane) are intermediate relative to those of Me_xtaa^{2-} and porphyrin $^{2-}$ ligands.

An extensive series of mid and late transition metal (Me_4taen) M^{n+} complexes ($n = 0$, $M = Fe^{II}$, Co^{II} , Ni^{II} , Cu^{II} , Zn^{II} ; $n = 1$, $M = Au^{III}$) and analogues containing differently substituted $taen^{2-}$ ligands has been prepared.¹⁸ The electronic, spectroscopic, and magnetic properties of these compounds are in accord with square planar structures. An X-ray diffraction study of $[(Me_4taen)Au]Cl \cdot H_2O$ established that the $(Me_4taen)Au^+$ cation adopts a nearly planar structure with square planar Au^{3+} coordination geometry.¹⁹ However, due to disorder problems, the conformation of the $-CH_2CH_2-$ fragments of the Me_4taen^{2-} ligand was not well determined.

The objectives of the present work were to develop efficient routes to $(Me_4taen)ZrR_2$ compounds and a general understanding of their structures and properties. The chemistry of cationic derivatives will be discussed in a subsequent paper.¹

Results and Discussion

Synthesis of $(Me_4taen)ZrR_2$ Complexes via Alkane Elimination. Alkane elimination reactions have been utilized to prepare a wide variety of group 4 metal complexes containing alkoxide, Schiff base, carborane, and other ligands.²⁰ Alkane elimination reactions of the

neutral macrocycle $(Me_4taen)H_2$ (1) and homoleptic ZrR_4 compounds provide the most efficient approach to $(Me_4taen)ZrR_2$ complexes. Compound 1 reacts readily with ZrR_4 ($R = CH_2Ph$, CH_2SiMe_3) in pentane at 23 °C affording $(Me_4taen)Zr(CH_2Ph)_2$ (2) and $(Me_4taen)Zr(CH_2SiMe_3)_2$ (3) in high yield (Scheme 1). Complexes 2 and 3 are isolated as orange solids after recrystallization and have been characterized by 1H and ^{13}C NMR and analysis. Complex 2 is sparingly soluble, 3 is quite soluble in benzene, and both are soluble and stable in THF and CH_2Cl_2 .

The 1H NMR spectra of 2 and 3 contain singlets for the Me_4taen methyl and methine hydrogens, and two multiplets for the $-CH_2CH_2-$ hydrogens. These data are consistent with *cis* C_{2v} -symmetric structures, in which the "upper" and "lower" $-CH_2CH_2-$ hydrogens are inequivalent. The $ZrCH_2 J_{CH}$ values for 2 (106 Hz) and 3 (105 Hz) are at the low end of the normal range observed for alkyl complexes of electropositive metals, and indicate that the hydrocarbyl ligands are not significantly distorted by non-classical η^2 -benzyl or α -agostic interactions.^{21,22}

(20) (a) Collier, M. R.; Lappert, M. F.; Pearce, R. *J. Chem. Soc., Dalton Trans.* **1973**, 445. (b) Lubben, T. V.; Wolczanski, P. T.; Van Duyne, G. G. *Organometallics* **1984**, *3*, 977. (c) Latesky, S. L.; McMullen, A. K.; Nicolai, G. P.; Rothwell, I. P. *Organometallics* **1985**, *4*, 902. (d) Chestnut, R. W.; Durfee, L. D.; Fanwick, P. E.; Rothwell, I. P. *Polyhedron* **1987**, *6*, 2019. (e) Crowther, D. J.; Baenziger, N. C.; Jordan, R. F. *J. Am. Chem. Soc.* **1991**, *113*, 1455. (f) Tjaden, E. B.; Swenson, D. C.; Jordan, R. F.; Petersen, J. L. *Organometallics* **1995**, *14*, 371.

(21) (a) Jordan, R. F.; LaPointe, R. E.; Bajgur, C. S.; Echols, S. F.; Willett, R. D. *J. Am. Chem. Soc.* **1987**, *109*, 4111. (b) Jordan, R. F.; LaPointe, R. E.; Baenziger, N. C.; Hinch, G. D. *Organometallics* **1990**, *9*, 1539. (c) Crowther, D. J.; Borkowsky, S. L.; Swenson, D.; Meyer, T. Y.; Jordan, R. F. *Organometallics* **1993**, *12*, 2897. (d) Latesky, S. L.; McMullen, A. K.; Nicolai, G. P.; Rothwell, I. P.; Huffman, J. C. *Organometallics* **1985**, *4*, 902. (e) Scholz, J.; Schlegel, M.; Thiele, K. H. *Chem. Ber.* **1987**, *120*, 1369.

(22) (a) Guo, Z.; Swenson, D. C.; Jordan, R. F. *Organometallics* **1994**, *13*, 1424. (b) Lee, L.; Berg, D.; Bushnell, G. W. *Organometallics* **1995**, *14*, 8 and references therein.

(18) See the foregoing four refs and also the following: (a) Fujiwara, M.; Wakita, H.; Matsushita, T.; Shono, T. *Bull. Chem. Soc. Jpn.* **1990**, *63*, 3443. (b) Sakata, K.; Taziri, H.; Yamaura, F.; Hashoto, M. *Synth. React. Inorg. Met.-Org. Chem.* **1990**, *20*, 757. (c) Green, M.; Tasker, P. A. *Inorg. Chim. Acta* **1971**, *5*, 65. (d) Nishida, Y.; Osha, H.; Kida, S. *Inorg. Chim. Acta* **1978**, *29*, L191.

(19) (a) Kim, J.-H.; Everett, Jr., G. W. *Inorg. Chem.* **1981**, *20*, 853. For a related structure see: (b) Park, C. H.; Lee, B.; Everett, G. W., Jr. *Inorg. Chem.* **1982**, *21*, 1681.

Synthesis of (Me₄taen)Zr(NMe₂)₂. The alkane elimination approach to (Me₄taen)ZrR₂ complexes is limited by the small pool of easily accessible homoleptic ZrR₄ compounds. It has been shown previously that group 4 metal amido complexes containing Cp, linked Cp₂, Cp-amido, carborane, and other ligands (L) may be prepared by amine elimination reactions of weakly acidic L-H species and M(NR₂)₄ complexes, and are useful precursors to other derivatives.²³ This approach also works well in the (Me₄taen)ZrX₂ system. The reaction of **1** with Zr(NMe₂)₄ proceeds readily in hydrocarbon solvents to afford (Me₄taen)Zr(NMe₂)₂ (**4**) in high yield (Scheme 1). Complex **4** is isolated as a yellow solid which is extremely soluble in aromatic solvents and moderately soluble in hot hexane, from which it may be recrystallized. The NMR data for **4** are similar to data for **2** and **3**, and confirm the expected cis structure. Complex **4** does not coordinate HNMe₂, which is a coproduct of its synthesis.

Synthesis of (Me₄taen)ZrCl₂(NHMe₂) and (Me₄taen)ZrCl₂. The reaction of **4** with 2 equiv of [HNHMe₂]-Cl (chlorobenzene, 0–23 °C) results in selective protonolysis of the Zr–NMe₂ bonds and quantitative formation of the seven-coordinate complex (Me₄taen)ZrCl₂(NHMe₂) (**5**, Scheme 1). Complex **5** is isolated as a yellow solid which is soluble in chlorinated solvents and slightly soluble in aromatic solvents. The ¹H and ¹³C NMR spectra of **5** (CDCl₂CDCl₂) contain amine resonances which are significantly shifted from those of free NHMe₂, indicating that the amine remains coordinated in solution. These spectra also indicate that **5** has effective C_{2v} symmetry on the NMR time scale, which may result from stereochemical nonrigidity (as expected for a seven-coordinate complex) or from rapid amine exchange. Complex **5** undergoes rapid (NMR time scale) exchange with free NHMe₂ at 23 °C.

Complex **5** retains the NHMe₂ ligand upon recrystallization from chlorobenzene/pentane and upon vacuum drying at 80 °C. However, thermolysis of solid **5** at 120 °C (10 h) under vacuum yields the base-free dichloride complex (Me₄taen)ZrCl₂ (**6**, Scheme 1) as an analytically pure yellow solid.²⁴ Complex **6** is moderately soluble in chlorinated solvents but only sparingly soluble in hydrocarbons.

Interestingly, **5** is formed directly by the reaction of **1** and Zr(NMe₂)₄ in CD₂Cl₂ (5 h, 0 °C; then 4 h, 23 °C). This reaction provides a convenient synthesis of **5**, although the yield (73%) is less than that described above. Control experiments show that Zr(NMe₂)₄ is stable in CH₂Cl₂ under these conditions but that **4** is converted to **5**, via an intermediate monoamido species (Me₄taen)Zr(NMe₂)Cl.²⁵ This reaction was not investigated in detail.

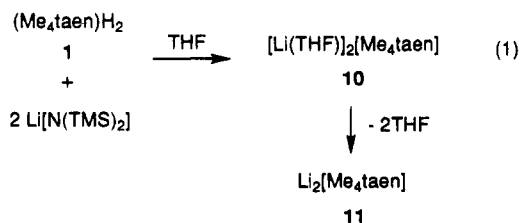
Generation of (Me₄taen)Zr(C≡CPh)₂(NHMe₂). The reaction of **4** with 2 equiv of PhC≡CH yields the

bisalkynyl complex (Me₄taen)Zr(C≡CPh)₂(NHMe₂) (**7**), which was characterized spectroscopically (Scheme 1). The ¹³C NMR spectrum of **7** contains resonances at δ 148.5 and 103.8, which are assigned to α and β alkynyl carbons, respectively, on the basis of comparisons to other acetylide complexes of electropositive metals.^{23b,26} The ¹H and ¹³C NMR data indicate that **7** has effective C_{2v} symmetry on the NMR time scale, as a result of amine exchange or stereochemical nonrigidity. Interestingly, the ¹H NMR resonances for the diastereotopic –CH₂CH₂– hydrogens in **7** are much more widely separated (Δδ = 1.1) than for other (Me₄taen)ZrX₂L_n species (**2–6**, **8**, and **9**, *vide infra*; Δδ < 0.5). This suggests that the predominant conformation of **7** in solution is that in which the alkynyl ligands point over the –CH₂CH₂– fragments of the Me₄taen ligand. This conformation is analogous to that observed in the solid state for **5** (*vide infra*), and places the “upper” –CH₂CH₂– hydrogens within the anisotropic shielding environment of the C≡C triple bonds.

Complex **7** is stable in benzene solution at 23 °C in the presence of excess NHMe₂. Exchange of free and coordinated NHMe₂ is rapid on the NMR time scale under these conditions. However, in the absence of added NHMe₂, **7** rapidly decomposes to insoluble product(s). Presumably NHMe₂ dissociation yields base-free (Me₄taen)Zr(CPh)₂, which is unstable.

Alkylation of (Me₄taen)ZrCl₂. Dichloride complex **6** is a useful precursor to (Me₄taen)ZrR₂ complexes (Scheme 1). The reaction of **6** with LiCH₂CMe₃ in toluene at 23 °C affords (Me₄taen)Zr(CH₂CMe₃)₂ (**8**) in high yield as an orange solid. Similarly, the reaction of **6** with solid LiMe (generated by removal of solvent from a Et₂O solution) in toluene yields (Me₄taen)ZrMe₂ (**9**) as a yellow solid. These alkylations are highly selective; there is no evidence for alkylation at the Me₄taen imine carbons as observed in alkylations of related systems, e.g., (Me₄taa)ZrCl₂, (salen)MCl₂, and (acen)-MCl₂ (M = Ti, Zr).^{11,20f,27} Bisneopentyl complex **8** is highly soluble in aromatic solvents, while dimethyl complex **9** is only sparingly so.

Attempted Synthesis of (Me₄taen)ZrCl₂ via Salt Elimination. The successful alkylations of **6** prompted us to explore more direct routes to this compound. However, simple salt elimination routes to **6** are problematic. The Me₄taen²⁻ reagent [Li(THF)]₂[Me₄taen] (**10**) is easily prepared as a red crystalline solid via double deprotonation of **1** with Li[N(SiMe₃)₂] in THF (eq 1). Solid **10** loses THF upon standing or under



vacuum, yielding the base-free reagent Li₂[Me₄taen] (**11**, eq 1) as a tan powder. However, the reaction of ZrCl₄(THF)₂ with 1 equiv of **11** in THF or dimethoxyethane under a variety of conditions yields mixtures of **6** and

(23) (a) Chandra, G.; Lappert, M. F. *J. Chem. Soc. A* **1968**, 1940. (b) Hughes, A. K.; Meetsma, A.; Teuben, J. H. *Organometallics* **1993**, *12*, 1936. (c) Herrmann, W. A.; Morawietz, M. J. A.; Priemermeier, T. *Angew. Chem., Int. Ed. Engl.* **1994**, *33*, 1946. (d) Diamond, G. M.; Rodewald, S.; Jordan, R. F. *Organometallics* **1995**, *14*, 5. (e) Bowen, D. E.; Jordan, R. F.; Rogers, R. D.; submitted. (f) Bradley, D. C.; Chisholm, M. H. *Acc. Chem. Res.* **1976**, *9*, 273.

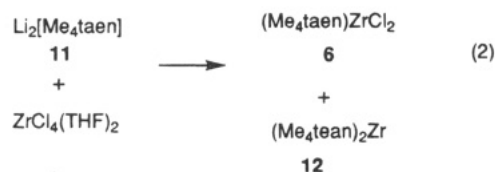
(24) In some experiments **6** was contaminated by small amounts (≤5%) of a C_{2v}-symmetric (Me₄taen)Zr hydrolysis product (¹H NMR: δ 5.12 (s, 2H), 4.00 (m, partially obscured), 3.60 (m, 4H), 1.97 (s, 12H)). This same species is formed by addition of H₂O to **6**; however, this issue was not studied further.

(25) ¹H NMR: δ 5.04 (s, 2H), 3.90, (m, 4H), 3.64 (m, 4H), 2.72 (s, 6H), 2.01 (s, 12H). ¹³C{¹H} NMR: δ 164.6 (C=N), 102.7 (CH), 50.5 (CH₂), 42.7 (NMe₂), 22.8 (CH₃).

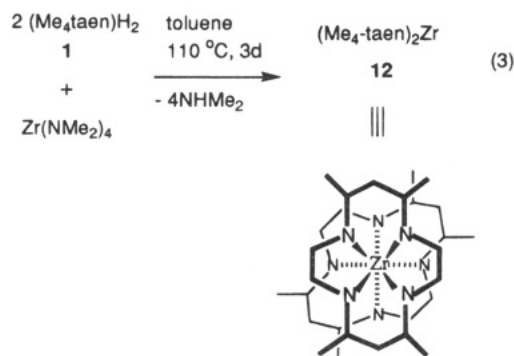
(26) (a) Erker, G.; Frömberg, W.; Benn, R.; Mynott, R.; Angermund, K.; Krüger, C. *Organometallics* **1989**, *8*, 911. (b) Sebald, A.; Fritz, P.; Wrackmeyer, B. *Spectrochim. Acta* **1985**, *41A*, 1405.

(27) Solari, E.; Floriani, C.; Chiesi-Villa, A.; Rizzoli, C. *J. Chem. Soc., Dalton Trans.* **1992**, 367.

the bis-ligand sandwich compound $(\text{Me}_4\text{taen})_2\text{Zr}$ (**12**, eq 2). Separation of these mixtures was not pursued because undesired compound **12** was generally the major component.

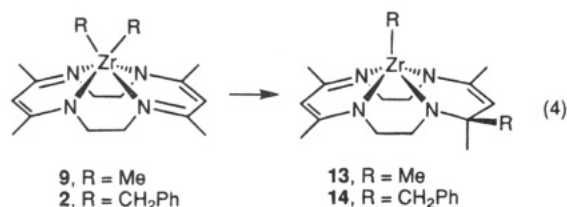


Synthesis of $(\text{Me}_4\text{taen})_2\text{Zr}$ (12**).** Compound **12** was prepared in pure form via the amine elimination reaction of $\text{Zr}(\text{NMe}_2)_4$ and 2 equiv of **1** (eq 3). The ^1H NMR



spectrum of **12** contains two Me resonances but only a single methine resonance, and the ^{13}C NMR spectrum contains two Me and imine carbon resonances but only a single methine resonance. These patterns establish that **12** adopts a square antiprismatic structure in which the $\text{Me}_4\text{taen}^{2-}$ ligands are rotated 45° with respect to each other. Complex **12** is an analogue of $\text{Zr}(\text{OEP})_2$, $\text{Zr}(\text{TPP})_2$, $\text{Ta}(\text{OEP})_2^+$, and related bisporphyrin complexes, and is structurally similar to $(\text{por})\text{Zr}(\text{acac})_2$ and $(\text{por})\text{Zr}(\text{OAc})_2$ species.²⁸

Thermal Rearrangement of $(\text{Me}_4\text{taen})\text{ZrR}_2$ Complexes. Dimethyl complex **9** undergoes facile rearrangement to a new species **13** (23°C , 24 h, toluene), which results from net migration of a methyl group from Zr to a Me_4taen imine carbon (eq 4). The NMR spectra



of **13** are complicated but consistent with the proposed highly unsymmetrical structure. The ^{13}C spectrum contains resonances at δ 163.8, 163.5, and 100.4 which are in the range observed for the imino and methine carbons of $(\text{Me}_4\text{taen})\text{ZrX}_2$ and $(\text{Me}_4\text{taen})\text{ZrX}_2\text{L}$ complexes, resonances at δ 147.5 and 91.7 which are assignable to the enamide sp^2 carbons, five resonances in the range δ 57.4–50.3 for the sp^3 carbons bonded to

(28) (a) Kim, K.; Lee, W. S.; Kim, H.; Cho, S.; Girolami, G. S.; Gorlin, P. A.; Suslick, K. S. *Inorg. Chem.* **1991**, *30*, 2652. (b) Buchler, J. W.; De Cian, A.; Fischer, J.; Hammerschmitt, P.; Weiss, R. *Chem. Ber.* **1991**, *124*, 1051. (c) Kim, H. J.; Whang, D.; Kim, J.; Kim, K. *Inorg. Chem.* **1992**, *31*, 3882. (d) Buchler, J. W.; De Cian, A.; Elschner, S.; Fischer, J.; Hammerschmitt, P.; Weiss, R. *Chem. Ber.* **1992**, *125*, 107. (e) Dawson, D. Y.; Brand, H.; Arnold, J. A. *J. Am. Chem. Soc.* **1994**, *116*, 9797.

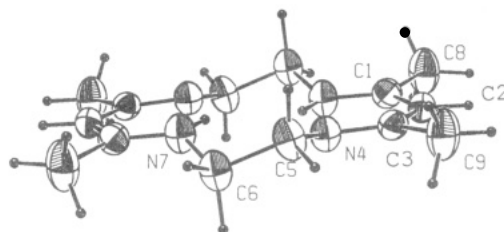


Figure 1. Molecular structure of $(\text{Me}_4\text{taen})\text{H}_2$ (**1**).

Table 1. Atomic Coordinates and Equivalent Isotropic Thermal Parameters (\AA^2) for $(\text{Me}_4\text{taen})\text{H}_2$ (**1**)

atom ^a	x/a	y/b	z/c	occ	B (\AA^2) ^b
N4	0.8969(1)	0.4055(2)	0.7865(2)	1.0	4.33(3)
N7	1.1658(1)	0.4218(2)	0.9743(2)	1.0	4.77(3)
C1	0.7125(1)	0.5759(2)	0.9170(2)	1.0	4.31(3)
C2	0.6812(1)	0.4951(2)	0.7622(2)	1.0	4.22(3)
C3	0.7711(1)	0.4177(2)	0.6966(2)	1.0	4.00(3)
C5	0.9951(3)	0.3553(3)	0.7043(3)	0.591	4.59(6)
C5'	0.9944(4)	0.3067(5)	0.7518(5)	0.409	5.23(8)
C6	1.1192(3)	0.3032(3)	0.8450(3)	0.591	4.30(5)
C6'	1.1245(4)	0.3752(6)	0.7912(5)	0.409	5.9(1)
C8	0.6046(2)	0.6652(3)	0.9570(3)	1.0	7.16(5)
C9	0.7185(2)	0.3493(3)	0.5189(2)	1.0	6.74(5)

^a C5' and C6' correspond to the disordered methylene carbons.

^b B values for anisotropically refined atoms are given in the form of the isotropic equivalent displacement parameter defined as $4/3[a^2B_{11} + b^2B_{22} + c^2B_{33} + ab(\cos \gamma)B_{12} + ac(\cos \beta)B_{13} + bc(\cos \alpha)B_{23}]$.

nitrogen, and six methyl resonances in the range 31.7–20.3. The ^1H NMR spectrum of **13** contains six methyl and two methine resonances, and a complicated pattern for the $-\text{CH}_2\text{CH}_2-$ hydrogens.²⁹

Dibenzyl complex **2** undergoes a similar but much slower rearrangement process to **14** (110°C , 3 days, eq 4). The NMR parameters of **14** are similar to those of **13** and are consistent with a highly unsymmetrical structure. The ^1H NMR spectrum of **14** contains an AB pattern with a small geminal J_{HH} value (8.9 Hz) for the diastereotopic $\text{Zr}-\text{CH}_2$ methylene hydrogens and a high field doublet for the ZrCH_2Ph ortho hydrogens (δ 6.51), which together indicate that the Zr benzyl group adopts a η^2 or η^{π} bonding mode.²¹

Structural Trends in $(\text{Me}_4\text{taen})\text{ZrX}_n$ Complexes. X-ray diffraction studies have been carried out on the parent macrocycle **1**, the $\text{Me}_4\text{taen}^{2-}$ salt **10**, and several representative $(\text{Me}_4\text{taen})\text{ZrX}_n$ complexes to investigate how deprotonation and metal complexation influence the structure and conformation of the macrocycle and to probe metal geometries.

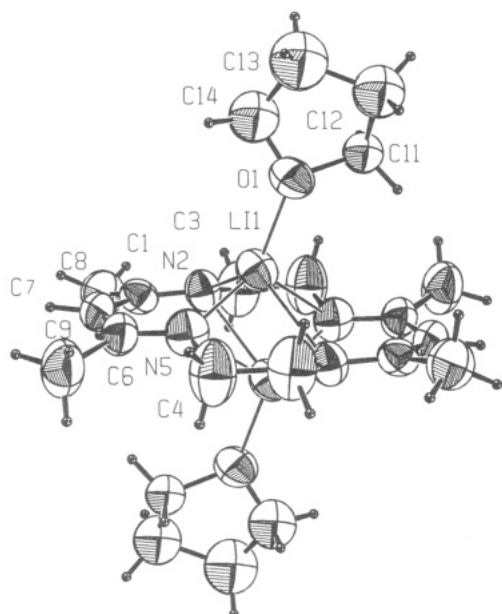
The structure of the free macrocycle $(\text{Me}_4\text{taen})\text{H}_2$ (**1**) resides around a center of inversion and is disordered between two orientations, one of which is shown in Figure 1; atomic coordinates and metrical parameters are listed in Tables 1 and 2. The orientations differ in the position of the imine hydrogen atoms (on N7 vs N4) and in the conformation of the $-\text{CH}_2\text{CH}_2-$ sectors, and correspond to two of the several possible tautomeric forms of **1** (Chart 1). The eight N4, C5, C6, and N7 atoms adopt a chair-like conformation (N4–C5–C6–N7 dihedral angle 54.1°), and the four nitrogens are coplanar. The two diiminato sectors are planar and are

(29) The rate of the rearrangement of **9** to **13** in toluene is unaffected by the addition of small amounts of THF (1 equiv) and **13** does not coordinate THF. Thus the methyl migration appears not to be ligand induced. The decomposition of bisalkynyl complex **7** may involve a similar rearrangement.

Table 2. Selected Bond Distances (Å) and Angles (deg) for (Me₄taen)H₂ (1)

N4-C3	1.315(2)	C1-C8	1.510(3)
N4-C5	1.464(7)	C2-C3	1.405(7)
N7-C1 ^a	1.322(2)	C3-C9	1.505(3)
N7-C6	1.471(4)	C5-C6	1.53(1)
C1-C2	1.396(2)		
C3-N4-C5	121.0(3)	N4-C3-C9	120.9(2)
C2-C1-C8	118.6(2)	N4-C5-C6	109.1(4)
C1-C2-C3	126.2(2)	N7-C6-C5	109.5(4)
N4-C3-C2	121.4(1)	C2-C3-C4	117.7(2)
C6-N7-C1 ^a	122.2(3)	C8-C1-N7 ^a	119.9(2)
C2-C1-N7 ^a	121.5(1)		

^a Symmetry code = 2 - x, 1 - y, 2 - z.

**Figure 2.** Molecular structure of [Li(THF)₂][Me₄taen] (10).

tipped by ca. 10° in opposite directions relative to the N₄ plane. An analysis of key dihedral angles indicates that the N-H bond and the nitrogen σ-lone pair in one diiminato unit point ca. 5° out of the N₄-plane, while those on the other diiminato unit point ca. 5° out of the N₄-plane in the opposite direction. The nitrogen-to-center distance (1.95 Å), which defines the size of the binding pocket, is intermediate relative to those of (Me₄taa)H₂ (1.90 Å) and porphyrin ligands (2.04 Å).^{10f}

The molecular structure of [Li(THF)₂][Me₄taen] (10, Figure 2, Tables 3 and 4) consists of a Me₄taen²⁻ dianion capped on both faces by Li(THF)⁺ cations. Compound 10 resides around a center of inversion. The conformation of the macrocycle is similar to that in 1. The large thermal parameters for C3 and C4 suggest that the CH₂-CH₂ units are disordered as in 1; however this disorder was not resolved. The bond distances and angles within the macrocycle are essentially unchanged from the corresponding parameters in 1. The geometry of the Li⁺ cations may be described as distorted square pyramidal; each Li⁺ cation coordinates one THF and interacts strongly with the nitrogens of one diiminato unit (average Li-N, 2.01 Å) and weakly with the nitrogens of the other (average Li-N, 2.42 Å). Similar though more symmetric square pyramidal structures have been observed in Li⁺ crown ether complexes.³⁰ The structure

Table 3. Atomic Coordinates and Equivalent Isotropic Thermal Parameters (Å²) for [Li(THF)₂][Me₄taen] (10)

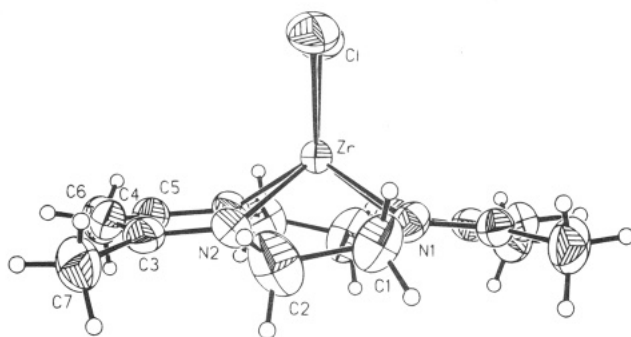
atom ^a	x/a	y/b	z/c	occ	B (Å ²) ^{b,c}
O1	0.1820(7)	0.6945(5)	0.9919(6)	1.0	8.9(2)
N2	-0.1466(8)	0.5715(6)	1.0895(6)	1.0	6.8(2)
N5	0.1318(8)	0.4599(6)	1.1441(6)	1.0	7.3(2)
C1	-0.1612(9)	0.5565(6)	1.2014(7)	1.0	6.2(2)
C3	-0.282(1)	0.6025(9)	1.0082(9)	1.0	10.3(3)
C4	0.251(1)	0.387(1)	1.1124(9)	1.0	11.3(4)
C6	0.087(1)	0.4565(7)	1.2515(7)	1.0	7.1(2)
C7	-0.046(1)	0.5087(7)	1.2800(7)	1.0	6.7(2)
C8	-0.310(1)	0.5829(8)	1.2544(9)	1.0	9.4(3)
C9	0.175(1)	0.3875(9)	1.3464(9)	1.0	11.2(4)
C11	0.162(3)	0.747(2)	0.871(2)	0.4	6.8(5)*
C12	0.323(2)	0.803(1)	0.879(1)	0.8	10.7(4)*
C13	0.338(2)	0.834(1)	1.015(11)	0.8	13.5(5)*
C14	0.213(3)	0.775(2)	1.066(2)	0.4	10.4(8)*
C15	0.248(3)	0.709(2)	0.878(2)	0.4	7.6(6)*
C18	0.304(3)	0.753(2)	1.073(2)	0.4	6.9(5)*
C19	0.324(6)	0.688(5)	0.962(4)	0.2	10(1)*
C20	0.392(4)	0.806(3)	0.951(3)	0.2	3.5(7)*
C21	0.288(4)	0.864(3)	0.955(3)	0.2	6(1)*
C22	0.133(7)	0.796(5)	0.974(5)	0.2	11(2)*
Li1	0.065(2)	0.572(1)	1.026(1)	1.0	7.0(4)

^a C11-C22 correspond to the disordered THF; see Experimental Section. ^b B values for anisotropically refined atoms are given in the form of the isotropic equivalent displacement parameter defined as $\frac{1}{3}[a^2B_{11} + b^2B_{22} + c^2B_{33} + ab(\cos \gamma)B_{12} + ac(\cos \beta)B_{13} + bc(\cos \alpha)B_{23}]$. ^c Starred values denote atoms refined isotropically.

Table 4. Selected Bond Distances (Å) and Angles (deg) for [Li(THF)₂][Me₄taen] (10)

O1-Li1	1.92(2)	N5-Li1	2.00(2)
N2-Li1	2.02(2)	N5-Li1 ^a	2.43(2)
N2-Li1 ^a	2.41(2)		
O1-Li1-N2	126(1)	N2-Li1-N5	88(1)
O1-Li1-N2 ^a	109(1)	N2-Li1-N2 ^a	121(1)
O1-Li1-N5	127(1)	N2-Li1-N5 ^a	73(1)
O1-Li1-N5 ^a	108(1)	N5-Li1-N5 ^a	121(1)

^a Symmetry code = -x, 1 - y, 2 - z.

**Figure 3.** Molecular structure of (Me₄taen)ZrCl₂ (6).

of 10 contrasts with that of the Li₂(THF)₄(OEP), which crystallizes as discrete Li(THF)₄⁺ and Li(OEP)⁻ ions.³¹

The dichloride complex (Me₄taen)ZrCl₂ (6, Figure 3, Tables 5 and 6) adopts a trigonal prismatic structure in which the chloride ligands occupy adjacent edge sites. The eight N1, C1, C2, and N2 atoms of the macrocycle adopt a twist-boat-like conformation which orients the four nitrogen σ lone pairs toward the same side of the macrocycle, as required for out-of-plane Zr coordination. The bond distances and angles within the macrocycle are very similar to those in 1 and 10; however, the ligand is somewhat flattened as assessed by the N1-C1-C2-N2 dihedral angle (19.9°). The structure is

(30) For reviews see (a) Setzer, W. N.; Schleyer, P. v. R. *Adv. Organomet. Chem.* **1985**, *24*, 353. (b) Gregory, K.; Schleyer, P. v. R.; Snaith, R. *Adv. Inorg. Chem.* **1992**, *37*, 47.

(31) (a) Arnold, J.; Dawson, D. Y.; Hoffman, C. G. *J. Am. Chem. Soc.* **1993**, *115*, 2707. (b) Arnold, J. *J. Chem. Soc., Chem. Commun.* **1990**, 976.

Table 5. Atomic Coordinates ($\times 10^4$) and Equivalent Isotropic Thermal Parameters ($\text{\AA}^2 \times 10^3$) for $(\text{Me}_4\text{taen})\text{ZrCl}_2$ (6**)**

atom	<i>x/a</i>	<i>y/b</i>	<i>z/c</i>	<i>U(eq)^a</i>
Zr	5000	7082(1)	2500	30(1)
C1	6465(1)	8441(1)	2012(1)	58(1)
N1	5450(3)	6409(2)	992(2)	38(1)
N2	6882(3)	6333(2)	2998(2)	37(1)
C1	6899(4)	6256(4)	960(3)	55(1)
C2	7607(5)	6035(4)	2072(4)	69(1)
C3	7476(4)	6246(3)	4024(3)	41(1)
C4	6778(4)	6349(3)	4938(3)	45(1)
C5	5386(4)	6345(3)	4935(3)	42(1)
C6	4868(5)	6224(4)	6036(3)	61(1)
C7	8949(4)	6008(4)	4252(4)	61(1)

^a *U*(eq) is defined as one-third of the trace of the orthogonalized U_{ij} tensor.

Table 6. Selected Bond Distances (\AA) and Angles (deg) for $(\text{Me}_4\text{taen})\text{ZrCl}_2$ (6**)**

Zr–N1	2.156(3)	Zr–Cl	2.503(1)
Zr–N2	2.171(3)		
N1–Zr–N1 ^a	128.7(2)	N1–Zr–N2 ^a	79.61(11)
N1–Zr–Cl	86.24(9)	N1–Zr–N2	76.45(12)
Cl–Zr–Cl	82.34(6)	N2–Zr–N2 ^a	122.8(2)
Cl–Zr–N1 ^a	135.85(9)	N2–Zr–Cl ^a	143.84(8)
N2–Zr–Cl	85.03(8)		

^a Symmetry code = 1 – *x*, *y*, 0.5 – *z*.

Table 7. Zr–Cl Distances and Cl–Zr–Cl Angles in Representative Zr(IV) Dichloride Complexes

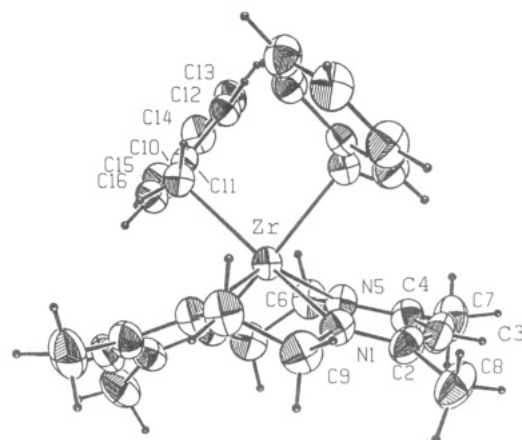
compd	Zr–Cl (\AA)	Cl–Zr–Cl (deg)	ref
Cp{N(SiMe ₃) ₂ }ZrCl ₂	2.380(1), 2.398(1)	97.53(5)	33c
Cp*(η^3 -allyl)ZrCl ₂	2.429(2)	96.12(9)	33e
(msal) ₂ ZrCl ₂ ^a	2.435(2), 2.440(3)	97.9(1)	33b
Cp ₂ ZrCl ₂	2.436(5), 2.446(5)	97.1(2)	33a
(OEP)ZrCl ₂	2.459(1), 2.473(1)	81.70(3)	3c
(acen)ZrCl ₂	2.465(1), 2.482(1)	87.2(1)	33b
(Me ₄ taa)ZrCl ₂	2.490(2), 2.493(2)	85.6(1)	10d
(COT)ZrCl ₂ (THF)	2.496(1)	87.2(1)	33d
(Me ₄ taen)ZrCl ₂ (6)	2.503(1)	82.34(6)	this work

^a msal = *N*-methylsalicylideneamine.

distorted from an ideal trigonal prism by a slight twist ($\Theta = 6^\circ$),³² which is also reflected in a slight relative twisting of the two diiminato units (N–N–N–N dihedral angle, 4.4°). The structure of **6** is similar to that of $(\text{Me}_4\text{taa})\text{ZrCl}_2$.^{10d} The Zr–N distances in **6** (2.164 \AA , average) and $(\text{Me}_4\text{taa})\text{ZrCl}_2$ (2.166 \AA , average) are nearly identical, while the Zr to N₄-plane distance in **6** (0.987 \AA) is slightly shorter than that in $(\text{Me}_4\text{taa})\text{ZrCl}_2$ (1.070 \AA) due to the larger pocket size of Me₄taen²⁻ vs Me₄taa²⁻. For comparison, in (OEP)ZrCl₂ the Zr–N distance is longer (average 2.221 \AA) and the Zr to N₄-plane distance is shorter (0.93 \AA), as a result of the larger pocket size (16- vs 14-membered macrocycle).^{3c} The Zr–Cl distances in **6** are at the extreme long end of the range observed for other cis L₂Zr^{IV}Cl₂ complexes (Table 7).³³ This suggests that net electron donor ability of Me₄taen²⁻ is comparable to or greater than that of other ancillary ligand sets such as OEP²⁻, Cp₂²⁻, Cp(amido)²⁻, and N₂O₂²⁻ Schiff bases.

(32) Huheey, J. E.; Keiter, E. A.; Keiter, R. L. *Inorganic Chemistry*, 4th ed.; Harper Collins: New York, NY, 1993; p 488–490.

(33) (a) Prout, K.; Cameron, T. S.; Forder, R. A.; Critchley, S. R.; Denton, B.; Rees, G. V. *Acta Crystallogr.* **1974**, *B30*, 2290. (b) Corazza, F.; Solari, E.; Floriani, C.; Chiesi-Villa, A.; Guastini, C. *J. Chem. Soc., Dalton Trans.* **1990**, 1335. (c) Coalter, J. N.; Pupi, R. M.; Petersen, J. L. unpublished results. (d) Brauer, D. J.; Krüger, C. *Inorg. Chem.* **1975**, *14*, 3053. (e) Vance, P. J.; Prins, T. J.; Hauger, B. E.; Silver, M. E.; Wemple, M. E.; Pederson, L. M.; Kort, D. A.; Kannisto, M. R.; Geerligs, S. J.; Kelly, R. S.; McCandless, J. J.; Huffman, J. C.; Peters, D. G. *Organometallics* **1991**, *10*, 917.

**Figure 4.** Molecular structure of $(\text{Me}_4\text{taen})\text{Zr}(\text{CH}_2\text{Ph})_2$ (**2**).**Table 8. Atomic Coordinates and Equivalent Isotropic Thermal Parameters for $(\text{Me}_4\text{taen})\text{Zr}(\text{CH}_2\text{Ph})_2$ (**2**)**

atom ^a	<i>x/z</i>	<i>y/b</i>	<i>z/c</i>	<i>B</i> (\AA^2) ^b
Zr	1.000	0.23679(2)	0.250	3.516(5)
N1	0.9050(1)	0.3269(1)	0.2992(1)	4.42(4)
N5	0.9546(1)	0.3005(2)	0.1076(1)	4.61(4)
C2	0.8418(1)	0.3569(2)	0.2420(2)	5.07(5)
C3	0.8294(1)	0.3475(2)	0.1393(2)	5.73(6)
C4	0.8824(1)	0.3265(2)	0.0747(2)	5.19(6)
C6	1.0152(2)	0.2953(2)	0.0435(2)	5.54(6)
C7	0.8558(2)	0.3361(3)	-0.0347(2)	7.38(8)
C8	0.7788(2)	0.4083(2)	0.2886(3)	7.33(8)
C9	0.9161(2)	0.3523(2)	0.4050(2)	5.73(6)
C10	1.0933(1)	0.1127(2)	0.2810(2)	4.19(5)
C11	1.1193(1)	0.0814(2)	0.1879(2)	3.79(4)
C12	1.0820(1)	0.0078(2)	0.1275(2)	4.48(5)
C13	1.1050(2)	-0.0185(2)	0.0383(2)	5.36(6)
C14	1.1656(2)	0.0292(2)	0.0056(2)	5.87(6)
C15	1.2037(1)	0.1010(2)	0.0631(2)	5.80(6)
C16	1.1816(1)	0.1272(2)	0.1526(2)	4.81(5)
C31	0.5386(3)	0.2159(6)	0.2724(5)	7.9(2)
C32	0.4733(4)	0.2557(4)	0.2341(6)	7.7(2)
C33	0.3988(3)	0.1976(5)	0.1854(5)	7.0(2)
C34	0.4063(3)	0.1056(5)	0.1873(5)	7.5(2)
C35	0.4783(4)	0.0629(4)	0.2313(6)	8.1(2)
C36	0.5408(4)	0.1174(5)	0.2732(5)	8.3(2)
C37	0.5940(6)	0.2812(7)	0.3054(7)	11.1(3)

^a C31–C37 correspond to the toluene solvent molecule. ^b *B* values for anisotropically refined atoms are given in the form of the isotropic equivalent displacement parameter defined as $\frac{1}{3}[a^2B_{11} + b^2B_{22} + c^2B_{33} + ab(\cos \gamma)B_{12} + ac(\cos \beta)B_{13} + bc(\cos \alpha)B_{23}]$.

Table 9. Selected Bond Distances (\AA) and Angles (deg) for $(\text{Me}_4\text{taen})\text{Zr}(\text{CH}_2\text{Ph})_2$ (2**)**

Zr–N1	2.244(2)	C11–C16	1.400(3)
Zr–N5	2.178(2)	C12–C13	1.387(4)
Zr–C10	2.338(3)	C13–C14	1.371(4)
C10–C11	1.478(3)	C14–C15	1.363(4)
C11–C12	1.395(4)	C15–C16	1.384(4)
N1–Zr–N5	82.13(8)	Zr–C10–C11	110.0(2)
N1–Zr–C10	149.82(8)	C10–Zr–C10 ^a	88.4(1)
N5–Zr–C10	127.09(8)	N1–Zr–N1 ^a	114.27(8)
N5–Zr–N5 ^a	133.46(8)		

^a Symmetry code = 2 – *x*, *y*, 0.5 – *z*.

The dibenzyl complex $(\text{Me}_4\text{taen})\text{Zr}(\text{CH}_2\text{Ph})_2$ (**2**, Figure 4, Tables 8 and 9), which crystallizes as a toluene solvate, adopts an out-of-plane cis structure with normal (undistorted) benzyl ligands (Zr–C–Ph angle, $110.0(2)^\circ$). The Zr coordination geometry is best described as a distorted trigonal prism (twist angle $\Theta = 17^\circ$) in which the benzyl ligands occupy adjacent edge sites. The larger twist angle (vs **6**) results in a more pronounced relative twisting of the two diiminato units (N–N–N–N

Table 10. Atomic Coordinates ($\times 10^4$) and Equivalent Isotropic Thermal Parameters ($\text{\AA}^2 \times 10^3$) for $(\text{Me}_4\text{taen})\text{Zr}(\text{NMe}_2)_2$ (4)

atom ^a	x/a	y/b	z/c	$U(\text{eq})^b$
Zr	6619(1)	6019(1)	8137(1)	25(1)
N(1)	5633(3)	4512(2)	6412(2)	30(1)
N(2)	8334(3)	6854(2)	7256(2)	31(1)
N(3)	6249(3)	7962(3)	8142(2)	33(1)
N(4)	4018(3)	5461(3)	7895(2)	34(1)
N(5)	7896(3)	7193(3)	9738(2)	35(1)
N(6)	6881(3)	4349(3)	8429(2)	31(1)
C(1)	6322(4)	4263(3)	5568(2)	34(1)
C(2)	7817(4)	5099(3)	5549(3)	35(1)
C(3)	8683(4)	6353(3)	6288(3)	33(1)
C(4)	9009(4)	8286(3)	7889(3)	39(1)
C(5)	7658(4)	8862(3)	7962(3)	43(1)
C(6)	5018(4)	8371(3)	8294(3)	37(1)
C(7)	3534(4)	7529(4)	8331(3)	41(1)
C(8)	3023(4)	6167(4)	8053(3)	38(1)
C(9)	3407(4)	4011(3)	7352(3)	39(1)
C(10)	3990(4)	3647(3)	6286(3)	37(1)
C(11)	5489(5)	3079(3)	4545(3)	45(1)
C(12)	10019(4)	7178(4)	5935(3)	46(1)
C(13)	5106(5)	9755(4)	8397(3)	60(1)
C(14)	1246(4)	5455(4)	7882(3)	51(1)
C(15)	7670(5)	8370(4)	10449(3)	50(1)
C(16)	9297(4)	7027(4)	10248(3)	46(1)
C(17)	6587(4)	4099(4)	9424(3)	45(1)
C(18)	7130(4)	3197(3)	7685(3)	43(1)
C(19)	9475(22)	9420(7)	4063(8)	120(4)
C(20)	8199(41)	9684(27)	4021(27)	171(13)
C(21)	7596(67)	10296(36)	5062(45)	130(16)
C(22)	9196(33)	10846(14)	6006(19)	99(5)
C(23)	10853(47)	9853(11)	4853(19)	144(11)
C(24)	11998(68)	9381(37)	4592(36)	115(12)

^a C19–C24 correspond to the disordered toluene molecule. C19 is present at full occupancy, and C20–C24 are present at half occupancy. ^b $U(\text{eq})$ is defined as one-third of the trace of the orthogonalized U_{ij} tensor.

Table 11. Selected Bond Distances (\AA) and Angles (deg) for $(\text{Me}_4\text{taen})\text{Zr}(\text{NMe}_2)_2$ (4)

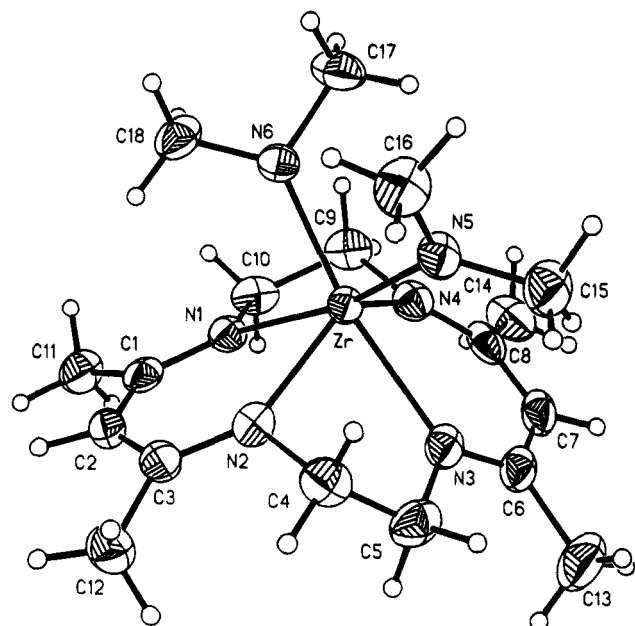
Zr–N6	2.108(3)	Zr–N5	2.117(3)
Zr–N4	2.193(3)	Zr–N2	2.197(3)
Zr–N1	2.285(3)	Zr–N3	2.306(3)
N6–Zr–N5	88.22(10)	N6–Zr–N4	98.87(10)
N5–Zr–N4	115.93(10)	N6–Zr–N2	114.90(10)
N5–Zr–N2	98.73(10)	N4–Zr–N2	132.16(10)
N6–Zr–N1	81.97(10)	N5–Zr–N1	167.42(9)
N4–Zr–N1	73.62(9)	N2–Zr–N1	78.52(9)
N6–Zr–N3	169.32(9)	N5–Zr–N3	83.67(10)
N4–Zr–N3	78.60(10)	N2–Zr–N3	73.36(10)
N1–Zr–N3	106.97(9)	C16–N5–Zr	124.1(2)
C15–N5–Zr	126.7(2)	C18–N6–Zr	128.5(2)
C17–N6–Zr	122.5(2)		

bonds (average 2.20 \AA). This unsymmetrical bonding reflects a balancing of the trans influence of the $-\text{NMe}_2$ ligands and the structural constraints of the macrocycle.

The structural differences between **4** (distorted octahedral) and **2** and **6** (distorted trigonal prismatic) may be traced to electronic factors.³⁶ Recent work has shown that trigonal prismatic structures are favored over octahedral structures for some d^0 ML_6 species (e.g., ZrMe_6^{2-} and WMe_6).³⁷ Mixing of empty d (e') orbitals

(35) Representative $\text{Zr}(\text{IV})$ amide complexes and average Zr–N distances. (a) $\text{Zr}(\text{NMe}_2)_4$, 2.07 \AA : Hagen, K.; Holwill, C. J.; Rice, D. A.; Runnacles, J. D. *Inorg. Chem.* **1988**, *27*, 2032. (b) $(\text{Me}_2\text{N})_2\text{Zr}(\mu\text{-N}^t\text{-Bu})_2\text{Zr}(\text{NMe}_2)_2$, 2.06 \AA : Nugent, W. A.; Harlow, R. L. *Inorg. Chem.* **1979**, *18*, 2030. (c) *rac*-(EBI) $\text{Zr}(\text{NMe}_2)_2$, 2.06 \AA : Diamond, G. M.; Petersen, J. L.; Jordan, R. F. unpublished results. (d) $\text{Cp}_2\text{Zr}(\text{NC}_4\text{H}_4)_2$, 2.17 \AA : Bynum, R. V.; Hunter, W. E.; Rogers, R. D.; Atwood, J. L. *Inorg. Chem.* **1980**, *19*, 2368.

(36) Inspection of space-filling computer models of **2**, **4**, and **6** indicates that these compounds are not highly crowded. In particular, in **4** there are no interligand H–H contacts < 2.5 \AA (closest contacts H16B–H17A, 2.67 \AA , and H9B–H17C, 2.54 \AA).

**Figure 5.** Molecular structure of $(\text{Me}_4\text{taen})\text{Zr}(\text{NMe}_2)_2$ (**4**).

dihedral angle, 14.8°), greater puckering of the $\text{NCH}_2\text{-CH}_2\text{N}$ units (N1-C9-C6'-N5' dihedral angle, 42.8°), and unequal Zr–N bond distances (2.244(2) and 2.178(2) \AA). The average Zr–N distance (2.21 \AA) and the Zr–(N_4 -plane) distance (1.038 \AA) in **2** are somewhat longer than in **6**, consistent with replacement of the chloride ligands by the stronger σ -donor benzyl ligands. The Zr–C distance (2.338(3) \AA) is slightly shorter than that in $(\text{Me}_4\text{taa})\text{Zr}(\text{CH}_2\text{Ph})_2$ (2.37(1) \AA),¹¹ and, consistent with the trend in Zr–Cl distances noted above, is at the long end of the range spanned by other Zr^{IV} η^1 -benzyl complexes (ca. 2.25–2.37 \AA).³⁴ However, detailed comparisons of M–benzyl bond distances are complicated by steric factors and the possibility of Zr– η^2 -benzyl interactions.

The molecular structure of $(\text{Me}_4\text{taen})\text{Zr}(\text{NMe}_2)_2$ (**4**, Figure 5, Tables 10 and 11), which crystallizes as a toluene hemisolvate, is quite different from those of **6** and **2**. Complex **4** adopts an out-of-plane cis structure, but the $\text{Me}_4\text{taen}^{2-}$ ligand is significantly folded such that the angle between the diimino planes is 53.0° . The zirconium coordination geometry is best described as distorted octahedral; two trans angles are nearly 180° (N6-Zr-N3 , $169.32(9)^\circ$; N5-Zr-N1 , $167.42(9)^\circ$) while the third is significantly contracted (N2-Zr-N4 , $132.2(1)^\circ$). There is clear evidence for π -donation from the $-\text{NMe}_2$ ligands in **4**. The amide nitrogens are flat (sum of angles around N, 359.5°), and the Zr– NMe_2 distances (2.11 \AA , average) are in the range observed for other unsaturated $\text{Zr}(\text{IV})$ amide complexes in which N–Zr π -donation is present (ca. 2.04–2.17 \AA).³⁵ The Zr– $\text{N}_{\text{macrocycle}}$ bonds trans to the $-\text{NMe}_2$ ligands are significantly longer (average, 2.30 \AA) than the cis Zr– $\text{N}_{\text{macrocycle}}$

(34) Representative examples of Zr^{IV} –(η^1 -benzyl) complexes and average Zr–C distances. (a) $(\text{OAr})_2\text{Zr}(\text{CH}_2\text{Ph})_2$, 2.258(8) \AA : Latesky, S. L.; McMullen, A. K.; Nicolai, G. P.; Rothwell, I. P. *Organometallics* **1985**, *4*, 902. (b) $\text{Cp}_2\text{ZrBr}(\text{CH}_2\text{Ph})$, 2.29(1) \AA : Randall, C. R.; Silver, M. E.; Ibers, J. A. *Inorg. Chim. Acta* **1987**, *128*, 39. (c) $(4,7\text{-F}_2\text{-indenyl})_2\text{Zr}(\text{CH}_2\text{Ph})_2$, 2.294(2) \AA : Piccolrovazzi, N.; Pino, P.; Consiglio, G.; Sironi, A.; Moret, M. *Organometallics* **1990**, *9*, 3098. (d) $\text{Cp}(\eta^6\text{-PhCH}_2\text{B}^{\text{C}^-})(\text{C}_6\text{F}_5)_3\text{Zr}^+(\text{CH}_2\text{Ph})_2$, 2.29(2) \AA : Pellicchia, C.; Immirzi, A.; Grassi, A.; Zambelli, A. *Organometallics* **1993**, *12*, 4473. (e) $(\text{EBTHI})\text{Zr}(\text{CH}_2\text{Ph})_2$, 2.314(4) \AA : Jordan, R. F.; LaPointe, R. E.; Baenziger, N.; Hinch, G. D. *Organometallics* **1990**, *9*, 1539. (f) $(\text{dmpe})(\eta^2\text{-CH}_2\text{Ph})\text{Zr}(\text{CH}_2\text{Ph})_2$, 2.346 \AA : Girolami, G. S.; Wilkinson, G.; Thornton-Pett, M.; Hursthouse, M. B. *J. Chem. Soc., Dalton Trans.* **1984**, 2789.

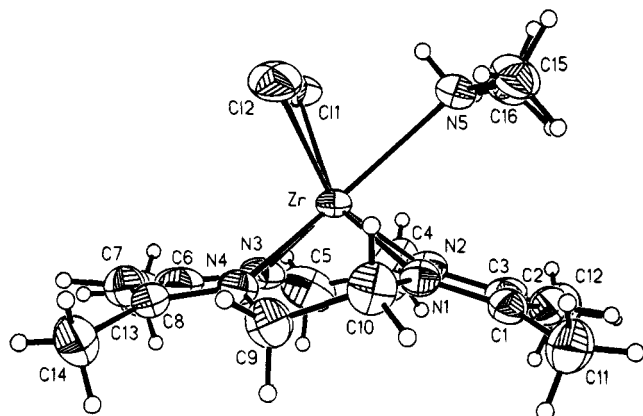


Figure 6. Molecular structure of $(\text{Me}_4\text{taen})\text{ZrCl}_2(\text{NHMe}_2)$ (**5**).

with filled M–L σ -bonding (e') orbitals is possible in the trigonal prismatic geometry and results in net stabilization versus an octahedral structure (second-order Jahn–Teller distortion).³⁸ However, factors which increase the energy gap between the empty d and filled M–L σ -bonding orbitals (ligand to metal π -donation or strong σ -donation) weaken the mixing and favor octahedral geometry.³⁹ The distorted trigonal prismatic structures of **6** and **2** are favored by the conformational preference of the $\text{Me}_4\text{taen}^{2-}$ ligand and the weak π -donor ability of the chloride and benzyl ligands.^{40,41} In **4**, destabilization of the metal d orbitals by strong π -donation from the amide ligands favors an octahedral structure, and the $\text{Me}_4\text{taen}^{2-}$ ligand distorts accordingly. Synthetic and theoretical studies to probe the electronic structures of these compounds in more detail are in progress.⁴²

The seven-coordinate amine adduct $(\text{Me}_4\text{taen})\text{ZrCl}_2(\text{NHMe}_2)$ (**5**, Figure 6, Tables 12 and 13) adopts an out-of-plane structure with a tripodal arrangement of chloride and amine ligands and a side-capped trigonal prismatic geometry around Zr. As a result of the higher coordination number, the Zr–N_{macrocycle} (average, 2.21 Å), Zr–(N₄-plane) (1.104 Å), and Zr–Cl (2.565(1) Å) distances are slightly longer in **5** than in base-free analogue **6**. Complex **5** is structurally related to $(\text{TPP})\text{ZrCl}_2(\text{THF})$, $\text{Hf}(\text{OEP})\text{Cl}_2(\text{H}_2\text{O})$, $[\text{NBu}_4][\text{Hf}(\text{OEP})(\text{P}_3\text{O}_9)]$,⁴ $\{(\text{TPP})\text{Zr}\}_2(\mu\text{-OH})_2(\mu\text{-O})$,⁴³ and $\text{U}(\text{TPP})\text{Cl}_2(\text{THF})$,⁴⁴ all of which are out-of-plane porphyrin complexes with three ligands on the top face. The structures of these (N₄-macrocycle) MX_3 species differ significantly from the

Table 12. Atomic Coordinates and Equivalent Isotropic Thermal Parameters (\AA^2) for $(\text{Me}_4\text{taen})\text{ZrCl}_2(\text{NHMe}_2)$ (**5**)

atom	x/a	y/b	z/c	B(eq) ^a
Zr	0.24646(4)	0.04235(4)	0.25596(3)	2.11
Cl1	0.2554(1)	-0.1120(1)	0.4220(1)	3.93
Cl2	0.4884(1)	-0.0536(2)	0.2297(1)	4.32
N1	0.3064(4)	0.2416(4)	0.1586(3)	2.46
N2	0.1137(4)	0.1983(4)	0.3155(3)	2.94
N3	0.0065(4)	-0.0891(4)	0.2436(3)	3.11
N4	0.1905(4)	-0.0461(4)	0.0866(3)	2.72
N5	0.4576(4)	0.2013(5)	0.3910(3)	3.02
C1	0.3089(5)	0.3890(5)	0.1797(3)	2.74
C2	0.2421(5)	0.4414(5)	0.2612(4)	3.23
C3	0.1423(5)	0.3515(5)	0.3199(3)	3.20
C4	-0.0088(8)	0.1170(7)	0.3698(5)	6.37
C5	-0.0867(6)	-0.0328(7)	0.3156(5)	4.96
C6	-0.0465(5)	-0.2280(6)	0.1952(4)	3.79
C7	0.0138(6)	-0.2792(5)	0.1108(4)	4.12
C8	0.1123(6)	-0.1867(5)	0.0512(4)	3.51
C9	0.2654(6)	0.0501(5)	0.0104(4)	3.74
C10	0.3686(6)	0.1972(5)	0.0650(4)	3.69
C11	0.3830(6)	0.5102(6)	0.1117(4)	4.17
C12	0.0640(7)	0.4363(7)	0.3918(5)	5.42
C13	-0.1852(7)	-0.3347(7)	0.2279(6)	5.90
C14	0.1188(7)	-0.2490(7)	-0.0594(4)	4.97
C15	0.5848(6)	0.3115(6)	0.3548(4)	4.26
C16	0.4174(6)	0.2667(6)	0.4886(4)	4.46

$${}^a B(\text{eq}) = (8\pi^2/3)[a^2U_{11}(a^*)^2 + b^2U_{22}(b^*)^2 + c^2U_{33}(c^*)^2 + ab(\cos \gamma)U_{12}a^*b^* + ac(\cos \beta)U_{13}a^*c^* + bc(\cos \alpha)U_{23}b^*c^*].$$

Table 13. Selected Bond Distances (\AA) and Angles (deg) for $(\text{Me}_4\text{taen})\text{ZrCl}_2(\text{NHMe}_2)$ (**5**)

Zr–Cl1	2.565(1)	Zr–Cl2	2.565(1)
Zr–N1	2.222(3)	Zr–N2	2.207(3)
Zr–N3	2.193(3)	Zr–N4	2.212(3)
Zr–N5	2.497(4)	N5–C15	1.475(6)
N5–C16	1.477(6)		
Cl1–Zr–Cl2	83.68(4)	Cl1–Zr–N1	157.16(9)
Cl2–Zr–N1	93.17(9)	Cl1–Zr–N2	95.4(1)
Cl2–Zr–N2	156.6(1)	N1–Zr–N2	78.6(1)
Cl1–Zr–N3	77.3(1)	Cl2–Zr–N3	128.7(1)
N1–Zr–N3	120.8(1)	N2–Zr–N3	73.2(1)
Cl1–Zr–N4	127.9(1)	Cl2–Zr–N4	77.96(9)
N1–Zr–N4	72.9(1)	N2–Zr–N4	119.2(1)
N3–Zr–N4	77.4(1)	Cl1–Zr–N5	74.4(1)
Cl2–Zr–N5	75.5(1)	N1–Zr–N5	82.9(1)
N2–Zr–N5	81.7(1)	N3–Zr–N5	139.8(1)
N4–Zr–N5	142.8(1)	Zr–N5–C15	119.4(3)
Zr–N5–C16	119.1(3)		

structures of Cp_2ML_3 species, in which the L ligands are invariably arranged in a meridional manner.⁴⁵

Conclusions

Alkane and amine elimination reactions of $(\text{Me}_4\text{taen})\text{-H}_2$ (**1**) and ZrR_4 or $\text{Zr}(\text{NMe}_2)_4$ provide convenient access to $(\text{Me}_4\text{taen})\text{ZrX}_2$ complexes (X = alkyl, benzyl, NMe_2). Additionally, $(\text{Me}_4\text{taen})\text{ZrCl}_2$ is formed by protonolysis of $(\text{Me}_4\text{taen})\text{Zr}(\text{NMe}_2)_2$ with $[\text{HNHMe}_2]\text{Cl}$ followed by vacuum thermolysis and can be alkylated to yield $(\text{Me}_4\text{taen})\text{ZrR}_2$ complexes.

$(\text{Me}_4\text{taen})\text{ZrX}_2$ complexes adopt out-of-plane, cis structures because the $\text{Me}_4\text{taen}^{2-}$ pocket size is too small to accommodate a Zr(IV) center in the N₄-plane. The flexibility of the $\text{Me}_4\text{taen}^{2-}$ ligand allows a variety of metal geometries in these complexes. The solid state structures of $(\text{Me}_4\text{taen})\text{ZrX}_2$ complexes range from nearly ideal trigonal prismatic for $(\text{Me}_4\text{taen})\text{ZrCl}_2$ (**6**) to distorted octahedral for $(\text{Me}_4\text{taen})\text{Zr}(\text{NMe}_2)_2$ (**4**).

(37) (a) Morse, P. M.; Girolami, G. S. *J. Am. Chem. Soc.* **1989**, *111*, 4114. (b) Haaland, A.; Hammel, A.; Rypdal, K.; Volden, H. V. *J. Am. Chem. Soc.* **1990**, *112*, 4547.

(38) (a) Kang, S. K.; Albright, T. A.; Eisenstein, O. *Inorg. Chem.* **1989**, *28*, 1611. (b) Demolliens, A.; Jean, Y.; Eisenstein, O. *Organometallics* **1986**, *5*, 1457. (c) Hoffmann, R.; Howell, J. M.; Rossi, A. R. *J. Am. Chem. Soc.* **1976**, *98*, 2484.

(39) Or, put in an alternative way, distortion of a trigonal prismatic structure toward an octahedral structure lowers the energies of the empty e' (d) orbitals, favoring π -donation.^{38a}

(40) (a) Zhu, L.; Kostic, N. M. *J. Organomet. Chem.* **1987**, *335*, 395. (b) Marsella, J. A.; Moloy, K. G.; Caulton, K. G. *J. Organomet. Chem.* **1980**, *201*, 389. (c) Chisholm, M. H.; Clark, D. L. *Comments Inorg. Chem.* **1987**, *6*, 23. (d) Poulton, J. T.; Folting, K.; Streib, W. E.; Caulton, K. G. *Inorg. Chem.* **1992**, *31*, 3190. (e) Johnson, T. J.; Folting, K.; Streib, W. E.; Martin, J. D.; Huffman, J. C.; Jackson, S. A.; Eisenstein, O.; Caulton, K. G. *Inorg. Chem.* **1995**, *34*, 488.

(41) The greater distortion from trigonal prismatic toward octahedral geometry of **2** versus **6** may be due to the greater σ -donor ability of the benzyl versus the chloride ligands.

(42) In particular, the π -donor ability of $\text{Me}_4\text{taen}^{2-}$ needs to be probed.

(43) Kim, H.-J.; Whang, D.; Do, Y.; Kim, K. *Chem. Lett.* **1993**, 807.

(44) Girolami, G. S.; Milam, S. N.; Suslick, K. S. *Inorg. Chem.* **1987**, *26*, 343.

(45) Cardin, D. J.; Lappert, M. F.; Raston, C. L. *Chemistry of Organo-Zirconium and Organo-Hafnium Compounds*; John Wiley: New York, 1986.

Comparison of the ligand conformations in **1**, [Li(THF)]₂-[Me₄taen] (**10**), and (Me₄taen)ZrX₂ complexes suggests that the trigonal prismatic extreme is favored by the Me₄taen²⁻ ligand, but that π -bonding from the X ligands can override this preference and distort the structure toward octahedral.

The long Zr-Cl bond distances observed in **6** suggest that the Me₄taen²⁻ is a stronger net electron donor than Cp₂²⁻ and other ancillary ligand sets commonly used in early metal chemistry. However, the formation of the seven-coordination amine adducts (Me₄taen)ZrX₂-(NHMe₂) (X = Cl, CPh) indicate that (Me₄taen)ZrX₂ species are effectively more Lewis acidic than Cp₂ZrX₂ species, which do not form such amine adducts. The relatively open structure of the (Me₄taen)ZrX₂ complexes favors coordination of an additional ligand.

Dialkyl species **2** and **9** rearrange via alkyl migration to a Me₄taen imine carbon. This reaction is favored by the electrophilic character of the Me₄taen imine carbons, and represents a potential obstacle to general application of the Me₄taen²⁻ ligand in early metal chemistry. Efforts to modify the ligand to disfavor this process are in progress.

Experimental Section

General Procedures. All manipulations were performed on a high-vacuum line or in a glovebox under a purified N₂ atmosphere. Solvents were distilled from Na/benzophenone ketyl, except for chlorinated solvents, which were distilled from activated molecular sieves (3 Å) or P₂O₅. (Me₄taen)H₂ (**1**),¹⁴ Zr(CH₂Ph)₄,⁴⁶ Zr(CH₂SiMe₃)₄,⁴⁷ ZrCl₂(THF)₂,⁴⁸ and Zr(NMe₂)₄^{23d,49} were prepared by literature procedures. NMR spectra were recorded on a Bruker AC-300 or an AMX 360 spectrometer in sealed or Teflon-valved tubes at ambient probe temperature unless otherwise indicated. ¹H and ¹³C chemical shifts are reported versus SiMe₄ and were determined by reference to the residual ¹H and ¹³C solvent peaks. Coupling constants *J* are in hertz. Elemental analyses were performed by E & R Microanalytical Laboratory, Inc.

(Me₄taen)Zr(CH₂Ph)₂ (2). A slurry of **1** (0.58 g, 2.3 mmol) and Zr(CH₂Ph)₄ (1.1 g, 2.3 mmol) in pentane (50 mL) was stirred for 3 h at 23 °C. The slurry was filtered to yield an orange solid, which was dried under high vacuum overnight (0.87 g, 87%). The product may be recrystallized from toluene/pentane. This compound strongly retains toluene from the recrystallization solvent and, even when toluene is not used for recrystallization, from the toluene byproduct of the synthesis. ¹H NMR (C₆D₆): δ 7.26–6.88 (m, Ph), 4.89 (s, 2 H, NC=CH-CN), 2.95 (m, 4H, NCH₂), 2.86 (m, 4H, NCH₂), 2.70 (s, 4H, ZrCH₂), 1.54 (s, 12H). ¹H NMR (THF-*d*₈): δ 6.99 (t, 4H), 6.89 (d, 4H), 6.55 (t, 2H), 5.04 (s, 2H), 3.42 (m, 4H, NCH₂), 3.19 (m, 4H, NCH₂), 2.11 (s, 4H, ZrCH₂), 1.94 (s, 12H). ¹³C-{¹H} NMR (THF-*d*₈): δ 165.4 (C=N), 150.4 (*i*-Ph), 128.0 (*o*- or *m*-Ph), 127.1 (*m*- or *o*-Ph), 119.0 (*p*-Ph), 102.0 (NC=CH-CN), 65 (ZrCH₂), 50.4 (NCH₂), 22.7. Anal. Calcd for C₂₈H₃₆N₄Zr: C, 64.69; H, 6.98; N, 10.78. Found: C, 63.20; H, 6.70; N, 11.66.⁵⁰

(Me₄taen)Zr(CH₂SiMe₃)₂ (3). A slurry of **1** (1.5 g, 6.2 mmol) and Zr(CH₂SiMe₃)₄ (2.9 g, 6.6 mmol) in pentane (50 mL) was stirred for 3 h at 23 °C. The solvent was removed under

vacuum, and the resulting brown solid was slurried in 25 mL of benzene and centrifuged. The supernate was decanted, and this process was repeated. The supernates were combined and evaporated under vacuum. The resulting brown solid was washed with cold pentane and dried under high vacuum for 20 min (2.4 g, 76%). The product may be recrystallized from toluene/pentane. ¹H NMR (C₆D₆): δ 4.94 (s, 2H, NC=CH-CN), 3.5 (m, 4H, NCH₂), 3.0 (m, 4H, NCH₂), 1.64 (s, 12H), 0.70 (s, 4H, ZrCH₂), 0.36 (s, 18H). ¹³C{gated-¹H} NMR (C₆D₆): δ 164.7 (m, C=N), 102.0 (dm, *J* = 157, NC=CH-CN), 50.4 (t, *J* = 105, ZrCH₂), 49.3 (t, *J* = 136, NCH₂), 22.6, 4.2. Anal. Calcd for C₂₂H₄₄N₄Si₂Zr: C, 51.61; H, 8.66; N, 10.94. Found: C, 51.44; H, 8.40; N, 11.05.

(Me₄taen)Zr(NMe₂)₂ (4). A slurry of **1** (1.12 g, 4.51 mmol) and Zr(NMe₂)₄ (1.19 g, 4.51 mmol) in pentane (25 mL) was stirred for 6 h at 23 °C. The volatiles were removed under vacuum, yielding analytically pure **4** (100%) as a yellow solid. This product was recrystallized from the hot hexane (57.3%). ¹H NMR (C₆D₆): δ 4.95 (s, 2H), 3.55 (m, 4H), 3.20 (s, 12H), 3.15 (m, 4H), 1.71 (s, 12H). ¹³C{gated-¹H} NMR (C₆D₆): δ 162.4 (s, N=C), 100.9 (d, *J* = 157, CH), 50.7 (t, *J* = 128, CH₂), 45.0 (qq, *J* = 130, 6, NCH₃), 22.1 (q, *J* = 126, CH₃). Anal. Calcd for C₁₈H₃₄N₆Zr: C, 50.78; H, 8.05; N, 19.73. Found: C, 50.56; H, 7.96; N, 19.92.

(Me₄taen)ZrCl₂(NHMe₂) (5). Method 1: A yellow slurry of (Me₄taen)Zr(NMe₂)₂ (**4**, 1.90 g, 4.46 mmol) and [Me₂NH₂]Cl (0.728 g, 8.92 mmol) in chlorobenzene (20 mL) was stirred at 0 °C for 4 h and at 23 °C for 3 h. The volatiles were removed under vacuum, yielding a yellow solid which was washed with cold chlorobenzene/pentane (2/1) and dried under vacuum, yielding analytically pure **5** (74.5%). Method 2: A yellow solution of **1** (1.00 g, 4.04 mmol) and Zr(NMe₂)₄ (1.06 g, 4.04 mmol) in CH₂Cl₂ (25 mL) was stirred for 5 h at 0 °C and for 4 h at 23 °C. The solution darkened during the last 2 h. The solvent was removed under vacuum, yielding an orange/brown solid which was recrystallized from chlorobenzene/pentane (10/2), washed with pentane (2 × 5 mL) and dried under vacuum (1.34 g, 73.2%). ¹H NMR (CDCl₂CDCl₂): δ 5.12 (s, 2H), 4.9 (br s, 1H), 4.23 (m, 4H), 3.76 (m, 4H), 2.40 (s, 6H), 1.98 (s, 12H). ¹³C{gated-¹H} NMR (CDCl₂CDCl₂): δ 162.3 (s, N=C), 102.4 (d, *J* = 158, CH), 49.0 (t, *J* = 138, CH₂), 36.1 (q, *J* = 139, NCH₃), 21.8 (qd, *J* = 127, 4, CH₃). IR (KBr ν_{NH} 3251 cm⁻¹). Anal. Calcd for C₁₆H₂₉Cl₂N₅Zr: C, 42.37; H, 6.44; N, 15.28; Cl, 15.63. Found: C, 42.22; H, 6.28, N, 15.44; Cl, 15.79.

(Me₄taen)ZrCl₂ (6). (Me₄taen)ZrCl₂(NHMe₂) was heated at 120 °C for 10 h under vacuum ¹H NMR (CDCl₂CDCl₂): δ 5.24 (s, 2H), 4.04 (m, 4H), 3.75 (m, 4H), 2.02 (s, 12H). ¹³C{gated-¹H} NMR (CDCl₂CDCl₂): δ 163.2 (s, N=C), 102.9 (d, *J* = 160, CH), 48.47 (t, *J* = 138, NCH₂), 21.3 (qd, *J* = 127, 3.9, CH₃). Anal. Calcd for C₁₄H₂₂Cl₂N₄Zr: C, 41.17; H, 5.40; N, 13.71; Cl, 17.36. Found: C, 41.15; H, 5.43, N, 13.58; Cl, 17.41.

(Me₄taen)Zr(CPh)₂(NHMe₂) (7). This compound was generated on an NMR scale only. An NMR tube was charged with (Me₄taen)Zr(NMe₂)₂ (0.053 g, 1.2 mmol) and phenylacetylene (27 μ L, 2.5 mmol) was added to the tube via microsyringe. Benzene-*d*₆ (0.3 mL) was added via vacuum transfer, and the tube was sealed and warmed to 23 °C. A brown solution formed. NMR spectra were recorded after 30 min and indicated complete conversion to **7**. ¹H NMR (C₆D₆): δ 7.58 (d, *J* = 7.7, 4H), 7.06 (t, *J* = 7.3, 4H), 6.95 (t, *J* = 7.5, 2H), 4.86 (s, 2H), 4.42 (m, 4H), 3.30 (m, 4H), 2.6 (broad singlet, 2H, free and coordinated HNMe₂), 2.35 (d, *J* = 6.2, 12H, free and coordinated HNMe₂), 2.35 (d, *J* = 6.2, 12H, free and coordinated HNMe₂), 1.70 (s, 12H). ¹³C{gated-¹H} NMR (C₆D₆): δ 162.2 (s, C=N), 148.5 (s, ZrC), 131.9 (dt, *J* = 158, 7, Ph), 128.3 (dt, *J* = 157, 7, Ph), 125.7 (dt, *J* = 159, 8, Ph), 103.8 (s, ZrCC), 103.0 (d, *J* = 152, CH), 51.4 (t, *J* = 135, CH₂), 39.8 (q, *J* = 133, HNMe₂), 22.4 (qd, *J* = 124, 4, Me₄taen). The Ph ipso carbon signal was observed at δ 128.5 in the {¹H} ¹³C spectrum. The volatiles were removed under vacuum, and the residue was redissolved in benzene-*d*₆, yielding a black solution. The ¹H NMR spectrum was identical to that listed above

(46) Zucchini, U.; Aldizzati, E.; Giannini, U. *J. Organomet. Chem.* **1971**, *26*, 357.

(47) Collier, M. R.; Lappert, M. F. *J. Chem. Soc., Dalton Trans.* **1973**, 445.

(48) Manzer, L. E. *Inorg. Synth.* **1982**, *21*, 135.

(49) (a) Bradley, D. C.; Thomas, I. M. *Proc. Chem. Soc.* **1959**, 225. (b) Bradley, D. C.; Thomas, I. M. *J. Chem. Soc.* **1960**, 3857. (c) Chisholm, M. H.; Hammond, C. E.; Huffman, J. C. *Polyhedron* **1988**, *7*, 2515.

(50) Poor C and N analyses were consistently obtained for spectroscopically pure samples of **2**.

Table 14. Summary of Crystallographic Data

compd	(Me ₄ taen)H ₂ (1)	[Li(THF)] ₂ [Me ₄ taen] (10)	(Me ₄ taen)ZrCl ₂ (6)	(Me ₄ taen)Zr(CH ₂ Ph) ₂ -PhMe (2)	(Me ₄ taen)Zr(NMe ₂) ₂ (0.5-PhMe) (4)	(Me ₄ taen)ZrCl ₂ (NHMe ₂) (5)
empirical formula	C ₁₄ H ₂₂ N ₄	C ₂₂ H ₃₈ Li ₂ N ₄ O ₂	C ₁₄ H ₂₂ Cl ₂ N ₄ Zr	C ₂₈ H ₃₈ N ₄ Zr-C ₇ H ₈	C ₁₈ H ₃₄ N ₆ Zr-0.5C ₇ H ₈	C ₁₆ H ₂₉ Cl ₂ N ₅ Zr
fw	248.37	404.46	408.48	612.87	471.80	453.57
cryst size (mm ³)	0.26 × 0.31 × 0.35	0.14 × 0.18 × 0.32	0.40 × 0.20 × 0.15	0.32 × 0.45 × 0.50	0.20 × 0.10 × 0.09	0.15 × 0.15 × 0.45
color/shape	colorless/ parallelepiped	yellow/parallelepiped	yellow/fragment	orange/fragment	yellow/fragment	colorless/parallelepiped
space group	<i>P</i> 2 ₁ / <i>c</i>	<i>P</i> 2 ₁ / <i>c</i>	<i>C</i> 2/ <i>c</i>	<i>C</i> 2/ <i>c</i>	<i>P</i> $\bar{1}$	<i>P</i> $\bar{1}$
<i>a</i> (Å)	10.587(3)	8.554(3)	10.008(2)	17.529(3)	8.946(3)	8.965(3)
<i>b</i> (Å)	9.005(2)	12.836(3)	13.862(5)	13.508(3)	11.277(4)	8.970(2)
<i>c</i> (Å)	8.069(2)	11.273(3)	12.174(4)	13.711(3)	13.288(5)	12.699(6)
α (deg)	90	90	90	90	108.415(5)	92.06(3)
β (deg)	107.54(2)	96.67(2)	97.03(2)	98.21(1)	95.453(6)	98.43(3)
γ (deg)	90	90	90	90	106.565(5)	102.80(3)
<i>V</i> (Å ³)	733.5(6)	1229(1)	1676.2(9)	3213(1)	1193.6(8)	982.6(1)
<i>Z</i>	2	2	4	4	2	2
<i>T</i> (K)	293	291	290	295	173	295
diffractometer	Enraf-Nonius CAD-4	Enraf-Nonius CAD-4	Enraf-Nonius CAD-4	Enraf-Nonius CAD-4	Siemens SMART/CCD area detector	Enraf-Nonius CAD-4
radiation, λ (Å)	Mo K α , 0.710 73	Mo K α , 0.710 73	Mo K α , 0.710 73	Mo K α , 0.710 73	Mo K α , 0.710 73	Mo K α , 0.710 73
2 θ range (deg)	4 < 2 θ < 60	4 < 2 θ < 40	5 < 2 θ < 50	4 < 2 θ < 60	3 < 2 θ < 46	2 < 2 θ < 50
data collected: <i>h</i> ; <i>k</i> ; <i>l</i>	±14; -11, 12; -11, 5	±8; -12, 10; ±10	+11; +16; ±14	-1, 6; -14, 17; ±22	±9; ±12; -14, 10	+10; ±10; ±15
no. of reflns	6104	4333	1558	8803	4686	3474
no. of unique reflns	2106	1141	1476	4650	3314	3216
<i>R</i> _{int}	0.008	0.028	0.0192	0.025	0.0296	
no. of obsd reflns	<i>I</i> > 2 σ (<i>I</i>), 1110	<i>I</i> > 2 σ (<i>I</i>), 671		<i>I</i> > 2 σ (<i>I</i>), 3014		<i>I</i> > 2.5 σ (<i>I</i>), 2862
μ (cm ⁻¹)	0.65	0.65	9.73	11.84	4.79	8.29
transmissn range (%)				97-100		92-100
structure soln	direct methods ^a	direct methods ^a	direct methods ^c	direct methods ^a	direct methods ^c	direct methods ^b
refinement	all non-H anisotropic; H refined, isotropic	non-H anisotropic; THF carbons isotropic; H isotropic, fixed	all non-H anisotropic; H isotropic, fixed	all non-H anisotropic; H isotropic, fixed	all non-H anisotropic; H isotropic, fixed	all non-H anisotropic; amine H isotropic; other H isotropic, fixed
GOF			1.063		1.025	0.97
<i>R</i>	0.047	0.093	0.0485 (R, all data)	0.036	0.0417 (R, all data)	0.039
<i>R</i> _w	0.066	0.102	0.0899 (wR, all data)	0.041	0.0858 (wR, all data)	0.050
max resid density (e/Å ³)	0.037	0.19	0.679	0.66	0.36	0.8

^a MOLEN; An (Interactive System for Crystal Structure Analysis; Fair, C. K. Enraf Nonius: Delft, The Netherlands, 1990). ^b SHELX-86 and SHELXS-93. ^c SHELXTL, PC Version 5; Siemens Analytical X-Ray Instruments, Inc.: Madison, WI.

except that (i) the amine resonances were shifted to δ 3.57 (NH) and 2.41 (NMe₂) and reduced to an intensity corresponding to 1 equiv vs Zr and (ii) ca. 5% decomposition was evident. Attempts to isolate this compound on a preparatory scale were unsuccessful due to thermal decomposition.

(Me₄taen)Zr(CH₂CMe₃)₂ (8). A slurry of (Me₄taen)ZrCl₂ (0.400 g, 0.979 mmol) and neopentyl lithium (0.153 g, 1.96 mmol) in toluene (12 mL) was stirred for 3 h at 23 °C and filtered twice through a frit. The orange filtrate was concentrated to 1 mL under vacuum and layered with pentane (5 mL). Filtration yielded an orange solid, which was washed with cold pentane and dried under vacuum (0.270 g). The filtrate was stored at -40 °C for 1 day and, an additional 82 mg was isolated in the same manner (total yield = 0.35 g, 75%), ¹H NMR (C₆D₆): δ 4.95 (s, 2H), 3.44 (m, 4H), 3.03 (m, 4H), 1.63 (s, 12H), 1.39 (s, 18H), 1.27 (s, 4H). ¹³C{gated-¹H} NMR (C₆D₆): δ 164.6 (s, N=C), 101.9 (d, J = 157, CH), 79.9 (t, J = 106, ZrCH₂), 49.1 (t, J = 135, NCH₂), 36.4 (s, CMe₃), 36.3 (q, J = 122, CMe₃), 22.7 (qd, J = 126, 4, CH₃). Anal. Calcd for C₂₄H₄₄N₄Zr: C, 60.01; H, 9.24; N, 11.67. Found: C, 59.80; H, 9.27; N, 11.43.

(Me₄taen)ZrMe₂ (9). A slurry of solid MeLi (2.45 mmol, prepared by removal of solvent from 1.75 mL of a 1.4 M MeLi/Et₂O solution under vacuum) and (Me₄taen)ZrCl₂ (0.500 g, 1.22 mmol) in toluene (12 mL) was stirred for 30 min at 23 °C. The reaction mixture was filtered through a glass fiber filter, yielding a homogeneous, brown solution. The precipitate was washed with toluene (8 mL). The combined filtrate and wash were concentrated to 7 mL under vacuum, layered with pentane, and cooled to -40 °C for 4 h to yield a bright yellow solid which was collected by filtration, washed with pentane (2 × 5 mL), and dried under vacuum (0.239 g, 53.3%). ¹H NMR (CD₂Cl₂): δ 5.00 (s, 2H), 3.98 (m, 4H), 3.67 (m, 4H), 2.00 (s, 12H), -0.17 (s, 6H). ¹³C{gated-¹H} NMR (CD₂Cl₂): δ 164.7 (s, N=C), 101.5 (d, J = 157, CH), 49.8 (J = 136 Hz, NCH₂), 37.7 (qd, J = 110, 4, ZrCH₂), 22.5 (J = 126, CH₃). Anal. Calcd for C₁₆H₂₈N₄Zr: C, 52.28; H 7.68; N, 15.23. Found: C, 51.95; H, 7.48; N, 15.46.

[Li(THF)]₂[Me₄taen] (10) and Li₂[Me₄taen] (11). A slurry of (Me₄taen)H₂ (1.17 g, 4.73 mmol) and Li(SiMe₃)₂ (1.58 g, 9.46 mmol) in THF (25 mL) was refluxed for 3 h. The resulting solution was cooled to ambient temperature and then -40 °C. Filtration yielded a red crystalline solid ([Li(THF)]₂[Me₄taen], **10**), which was washed with pentane (2 × 5 mL) and dried under vacuum overnight, yielding Li₂[Me₄taen] (**11**) as a tan powder (0.489 g). The red filtrate was concentrated to 10 mL, and an additional 0.289 g of **11** was isolated in the same manner (total 0.778 g, 63.2%). ¹H NMR (acetone-*d*₆): δ 4.29 (s, 2H), 3.65 (s, 8H), 1.82 (s, 12H). ¹³C{¹H} NMR (acetone-*d*₆): δ 160.4 (N=C), 95.3 (CH), 47.4 (CH₂), 19.6 (CH₃). Anal. Calcd for C₁₄H₂₂Li₂N₄: C, 64.62; H, 8.52; N, 21.52. Found: C, 64.40; H, 8.64; N, 21.51.

(Me₄taen)₂Zr (12). A slurry of **1** (0.208 g, 0.838 mmol) and Zr(NMe₂)₄ (0.110 g, 0.419 mmol) in toluene (5 mL) was heated to 110 °C for 3 days and cooled to -40 °C for 6 h. The slurry was filtered, yielding a tan solid which was washed with pentane (2 × 5 mL) and dried under vacuum for 30 min (0.143 g). The filtrate was concentrated to 2 mL, and pentane (3 mL) was added. The resulting slurry was cooled to -40 °C overnight and filtered, yielding an additional 0.061 g of product (total yield 0.204 g, 83.3%). ¹H NMR (CD₂Cl₂): δ 4.73 (s, 2H), 3.61 (m, 2H), 3.3 (m, 6H), 1.93 (s, 6H), 1.77 (s, 6H). ¹³C{¹H} NMR (CD₂Cl₂): δ 164.5 (N=C), 161.6 (N=C), 101.5 (CH), 52.2 (CH₂), 51.1, (CH₂), 24.4 (CH₃), 23.4 (CH₃). Anal. Calcd for C₂₈H₄₄N₈Zr: C, 57.60; H, 7.60; N, 19.18. Found: C, 57.27; H, 7.41; N, 19.32.

Rearrangement of (Me₄taen)₂ZrMe₂ to Compound 13. A solution (Me₄taen)ZrMe₂ in toluene-*d*₈ was maintained at 23 °C for 24 h. NMR analysis revealed complete conversion to **13**. Preparative scale: Methyl lithium (0.874 mL of a 1.40 M solution in ether, 1.22 mmol) was added to a frozen mixture of (Me₄taen)ZrCl₂ (0.250 g, 0.612 mmol) and toluene (15 mL) at -196 °C. The mixture was allowed to warm to 23 °C and

was stirred for 17 h. The resulting yellow slurry was filtered, concentrated to 5 mL under vacuum, layered with pentane (10 mL), and cooled to -40 °C for 1 day. The tan solid was isolated by filtration, washed with pentane (2 × 5 mL), and dried under vacuum (0.166 g, 73.8%). ¹H NMR (chlorobenzene-*d*₅): δ 4.82 (s, 1H), 4.21 (s, 1H), 3.93 (m, 2H), 3.53 (m, 4H), 3.23 (m, 2H), 1.93 (s, 3H), 1.83 (s, 3H), 1.78 (s, 3H), 1.41 (s, 3H), 1.18 (s, 3H). ¹³C{¹H} NMR (CD₂Cl₂): δ 163.8, 163.5, 147.5, 100.4, 91.7, 57.4, 54.2, 52.7, 50.8, 50.3, 31.7, 28.6, 22.7, 22.4, 21.8, 20.3. Anal. Calcd for C₁₆H₂₈N₄Zr: C, 52.28; H 7.68; N, 15.23. Found: C, 52.03; H, 7.48; N, 15.07.

Rearrangement of (Me₄taen)Zr(CH₂Ph)₂ to Compound

14. A slurry of (Me₄taen)Zr(CH₂Ph)₂ (50 mg) in benzene-*d*₆ (0.3 mL) in a sealed NMR tube was heated to 110 °C for 3 days yielding a black solution. ¹H NMR (benzene-*d*₆): δ 7.33 (m, 3H), 7.20 (m, 2H), 6.65 (t, 1H, J = 7.5), 6.51 (d, 2H, J = 7.2, ortho ZrCH₂Ph), 4.75 (s, 1H), 4.15 (s, 1H), 3.57 (m, 4H), 3.25 (m, 3H), 3.02 (d, J = 13.2), 2.98 (m, 1H), 2.73 (d, J = 13.1), 1.75 (d, J = 8.9, ZrCH₂) 1.68 (d, partially obscured, ZrCH₂), 1.67 (s, 3H), 1.61 (s, 3H), 1.58 (s, 3H), 1.37 (s, 3H). ¹³C{¹H} NMR (C₆D₆): 163.7, 163.0, 149.1, 144.8, 140.0, 138.9, 131.6, 129.0, 127.9, 126.3, 125.8, 119.8, 101.5, 86.8, 58.4, 57.9, 56.6, 52.5, 51.2, 51.0, 47.0, 23.3, 22.3, 22.0, 20.1. Two aryl resonances were not observed.

X-ray Structural Determinations. The structures of **1**, **2**, and **10** were determined at the University of Iowa by D. C. Swenson. The structures of **4**, **5**, and **6** were determined at Northern Illinois University by R. D. Rogers. Data collection, solution, and refinement procedures and parameters are summarized in Table 14. Additional comments specific to each structure follow.

The structure of **1** is disordered. The disorder is manifested in two ways. One is the existence of two orientations for the C5-C6 ethylene groups. The occupancies of the two orientations were refined and constrained to sum to 1.0. The second disorder is a superposition of two tautomeric forms for the diiminato groups which results in two partially occupied enamine hydrogen positions. The occupancies of the two partially occupied hydrogen atom positions were adjusted to give approximately equal thermal parameters. The resulting occupancies were nearly the same as those for the two orientations of the C5-C6 ethylene group (0.58 and 0.42 for H N7 and H N4 vs 0.59 and 0.41 for C5-C6 and C5'-C6') and were arbitrarily set to be the same. The enamine hydrogen atoms are involved in intramolecular hydrogen bonds (H7···N4, 2.05(2) Å; N7-H7···N4, 135(1)°; H4···N7, 2.12(2) Å; N4-H4···N7, 135(1)°). Conversion from one tautomer to the other involves moving the hydrogen atom ca. 1.4 Å and shifting of the single and double bonds.

The THF ligand in **10** is disordered between three orientations. The bonding scheme is as follows: orientation 1, O1, C11, C12, C13, C14 (occupancy 0.4); orientation 2, O1, C15, C13, C18 (occupancy 0.4); orientation 3, O1, C19, C20, C21, C22 (occupancy 0.2).

Crystals of **2** contain 1 equiv of toluene. Crystals of **4** contain 0.5 equiv of toluene which is located around a center of inversion and is disordered between two equally occupied orientations. C19 is present at full occupancy while C20-C24 are present at half occupancy.

Acknowledgment. This work was supported by DOE grant DE-FG02-88ER13935. The authors thank Dr. Roger Uhrhammer for helpful discussions and for preparing compound **3**, Dr. S. Rodewald and Dr. Gary Diamond for helpful discussions, and Professor Jeffrey Petersen for disclosure of results prior to publication.

Supporting Information Available: Summaries of crystallographic data, tables of bond distances, angles, anisotropic thermal parameters, hydrogen atom coordinates, and least-squares planes, and alternative views for **1**, **2**, **4-6**, and **10** (43 pages). Ordering information is given on any current masthead page.

Thiadisilacyclopropanes: Stereospecific Formation from Disilenes and Solid State Structures

John E. Mangette, Douglas R. Powell, and Robert West*

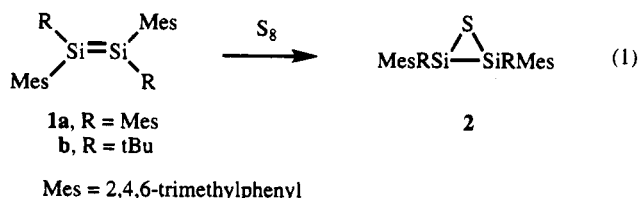
Department of Chemistry, University of Wisconsin, Madison, Wisconsin 53706

Received May 9, 1995*

The reactions of (*E*)-1,2-bis(2,4,6-triisopropylphenyl)-1,2-di-*tert*-butyldisilene, **E-1c**, (*Z*)-1,2-bis(2,4,6-triisopropylphenyl)-1,2-di-*tert*-butyldisilene, **Z-1c**, and an *E/Z* mixture of 1,2-dimesityl-1,2-di-*tert*-butyldisilenes, **1b**, with elemental sulfur and either ethylene or propylene sulfide and the reaction of (*E*)-1,2-dimesityl-1,2-di-*tert*-butyldisilene, **E-1b**, with ethylene sulfide were found to be stereospecific with retention of the original disilene stereochemistry, giving thiadisilacyclopropanes, **2**. X-ray crystal structures of *cis*- and *trans*-2,3-bis(2,4,6-triisopropylphenyl)-2,3-di-*tert*-butyl-1-thia-2,3-disilacyclopropanes, **2c**, and *trans*-2,3-dimesityl-2,3-di-*tert*-butyl-1-thia-2,3-disilacyclopropane, **trans-2b**, are reported and compared to the known structure of 2,2,3,3-tetramesityl-1-thia-2,3-disilacyclopropane, **2a**. Compound **cis-2c**, C₃₈H₆₄SSi₂, crystallized in the orthorhombic space group *Pna*2₁ with *Z* = 8 and lattice constants *a* = 18.846(2) Å, *b* = 9.555(2) Å, and *c* = 42.236(4) Å. Compound **trans-2c**, C₃₈H₆₄SSi₂, crystallized in the monoclinic space group *P*2₁ with *Z* = 2 and lattice constants *a* = 10.547(2) Å, *b* = 16.096(2) Å, *c* = 11.695(2) Å, and β = 107.330(11)°. Compound **trans-2b**, C₂₆H₄₀SSi₂, crystallized in the monoclinic space group *C*2/*c* with *Z* = 4 and lattice constants *a* = 12.6447(5) Å, *b* = 12.2663(5) Å, *c* = 16.9828(9) Å, and β = 102.549(4)°. The mechanistic consequences of stereospecific sulfur transfer are discussed.

Introduction

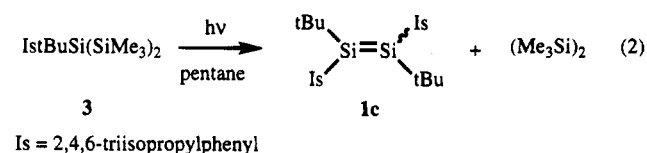
The three-membered ring thiadisilacyclopropanes have been synthesized by the reaction of isolable disilenes with elemental sulfur¹ and, more recently, with episulfides.² For example, tetramesitylthiadisilacyclopropane, **2a**, as well as the 2,3-dimesityl-2,3-di-*tert*-butyl compound, **2b**, have been made (eq 1).¹ The latter was



a single isomer produced from the reaction of S₈ with the pure *trans* disilene, but its stereochemistry was not determined. The reaction of **1a** with cyclohexene sulfide was shown by ¹H NMR to give exclusively **2a** and cyclohexene.²

From a mechanistic viewpoint it is of great interest to determine if sulfur transfer to disilenes is stereospecific, stereoselective, or neither. However, this cannot easily and unequivocally be done with **1b** since only its *E* isomer can be isolated pure.³ Fortunately, efforts in this group to develop new disilenes have produced 1,2-bis(2,4,6-triisopropylphenyl)-1,2-di-*tert*-butyldisilene, **1c**, a compound for which both geometrical isomers can be

isolated in pure form.⁴ Photolysis of the trisilane **3** (λ = 254 nm) generates **1c** as an *E/Z* mixture (eq 2). The



less soluble *E* isomer, the stereochemistry of which was determined by X-ray diffraction, precipitates cleanly from the reaction mixture. The *Z* isomer can be made on a small scale in >95% purity by complete photoisomerization (λ = 350 nm) of the *E* isomer. Its identity was supported by its characteristic downfield ²⁹Si chemical shift of +96.93 ppm and comparison of this value to that of **E-1c** at +87.39 ppm.

This report details stereospecific thiadisilacyclopropane syntheses by treatment of **E-1c** and **Z-1c** with sulfur and propylene sulfide. X-ray structures of both isomeric three-membered rings were obtained. The sulfurization of **E-1b** with ethylene sulfide and *E/Z* mixtures of **1b** with both sulfur and ethylene sulfide is also described. An X-ray structure of **trans-2b** was determined.

Results and Discussion

Reactions of 1 with S₈ and Episulfides. Separate solutions of *E*- and *Z*-**1c** in benzene were treated with sulfur at room temperature. The reactions were complete within 1 min, as evidenced by the loss of the characteristic bright yellow or orange disilene color. For NMR-scale reactions, only one new ²⁹Si resonance was

(4) Archibald, R. S.; Van den Winkel, Y.; Millevolte, A. J.; Desper, J. M.; West, R. *Organometallics* 1992, 11, 3276.

* Abstract published in *Advance ACS Abstracts*, June 15, 1995.
(1) West, R.; DeYoung, D. J.; Haller, K. J. *J. Am. Chem. Soc.* 1985, 107, 4942.

(2) Mangette, J. E.; Powell, D. R.; West, R. *J. Chem. Soc., Chem. Commun.* 1993, 1348.

(3) (a) Michalczyk, M. J.; West, R.; Michl, J. *J. Am. Chem. Soc.* 1984, 106, 821. (b) Michalczyk, M. J.; West, R.; Michl, J. *Organometallics* 1985, 4, 826. (c) Murakami, S.; Collins, S.; Masamune, S. *Tetrahedron Lett.* 1984, 25, 2131.

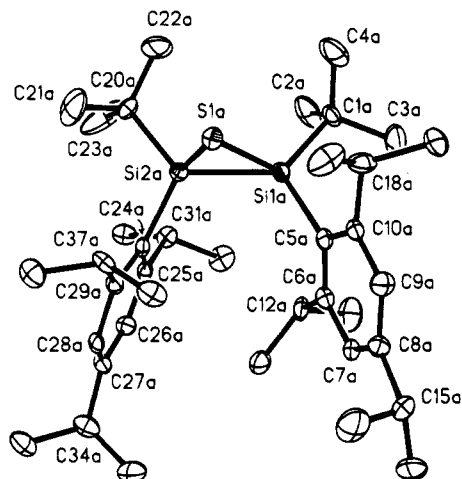


Figure 1. Thermal ellipsoid drawing of *cis-2c*, molecule A, at the 50% probability level. Hydrogens omitted for clarity.

observed for each isomer: -33.71 ppm from *E-1c*, assigned as *trans-2c*, and -28.91 ppm from *Z-1c*, assigned as *cis-2c*. The ^1H NMR spectra showed no contamination of either product with its diastereomer, implying stereospecific sulfur transfer.

Similar results were obtained with propylene sulfide, although reactions were much slower. Standard NMR-scale reactions (20 mg of disilene) were complete after 4 days at room temperature using ca. 1.5 equiv of episulfide. Several complex peaks at δ 5.0 and 5.7 in the ^1H NMR were assigned as propylene.⁵ Again the *E* disilene gave only a *trans* three-membered ring. The *Z* isomer gave nearly complete retention with a *cis/trans* ratio of 24:1.

Preparative- or semipreparative-scale reactions were also conducted. Products were purified by preparative thin layer chromatography or crystallization. Isolated yields of *cis-* and *trans-2c*, respectively, were 47 and 75% using elemental sulfur and 50 and 57% using propylene sulfide.

Disilene *E-1b* was treated with ethylene sulfide, giving ^1H and ^{29}Si (-35.96 ppm) NMR data consistent with *2b* as previously isolated.¹ *E/Z* mixtures [(3–3.5):1] of *1b*, generated by photolysis of the *E* isomer,³ were treated separately with sulfur and ethylene sulfide. Two ^{29}Si peaks were observed for each reaction; a large signal was seen at -35.96 ppm and a smaller one at -29.63 ppm. The minor product was not isolated but, based on the results from *1c*, was assumed to be the other diastereomer of *2b*. Integration of product peaks in the ^1H spectra gave ratios roughly equal to those of the disilene precursors.

Solid State Structures of *cis-* and *trans-2c* and *trans-2b*. Structural analyses of the three compounds listed above were undertaken to unequivocally establish the stereochemical course of sulfur transfer and for comparison to the known structure of *2a*.¹ Crystals of *cis-2c*, *trans-2c*, and *trans-2b* were isolated from preparative-scale reactions of *Z-1c*, *E-1c*, and *E-1b*, respectively, with sulfur. Thermal ellipsoid diagrams are given in Figures 1–3, and Tables 1–4 present X-ray acquisition data. Selected structural parameters are given in Table 5.

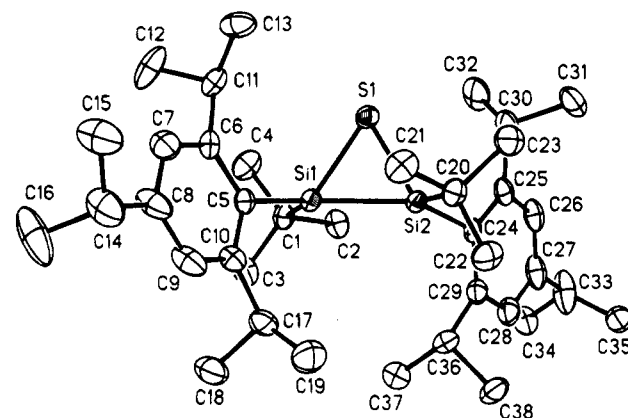


Figure 2. Thermal ellipsoid drawing of *trans-2c* at the 50% probability level. Hydrogens omitted for clarity.

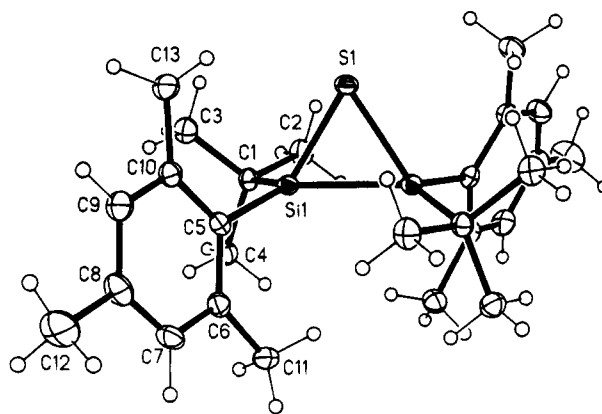
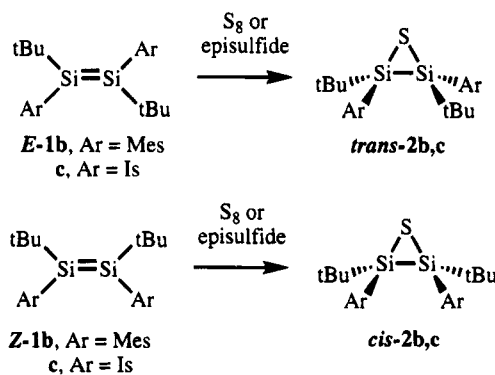


Figure 3. Thermal ellipsoid drawing for *trans-2b* at the 50% probability level.

Scheme 1



Clearly, from the X-ray data, sulfur transfer occurs with either exclusive (S_8) or predominant (episulfides) retention of the silicon-silicon double bond configuration (Scheme 1). As mentioned earlier, it is also evident that the unisolated product from sulfurization of *E/Z-1b* is *cis-2b*. Mechanistic ramifications are discussed in the next section.

As can be seen from Table 5, the structural parameters of *2b,c* are similar to those for *2a*. The exceptionally short silicon-silicon bond distances (versus the normal silicon-silicon single bond distance of 2.34–2.35 Å) and the near 360° summations of the $\text{C}_{\text{tBu}}\text{-Si-C}_{\text{Ar}}$, $\text{C}_{\text{tBu}}\text{-Si-Si}$, and $\text{C}_{\text{Ar}}\text{-Si-Si}$ angles about each silicon ($\Sigma\theta(\text{Si})$) are characteristic of reported structures of other disilacyclopropane derivatives. For instance 1,1,2,2-tetramesityl-3-oxa-1,2-disilacyclopropane⁶ and 1,1,2,2-tetrakis(2,6-dimethylphenyl)-1,2-disilacyclopropane⁷ have silicon-silicon bond distances of 2.227(2) and 2.272(2)

(5) The vinylic region of the spectrum agreed with an authentic sample of propylene generated by reaction of propylene sulfide with triphenylphosphine.

Table 1. Experimental Crystallographic Data for **2c** and *trans*-**2b**

	<i>cis</i> - 2c	<i>trans</i> - 2c	<i>trans</i> - 2b
empirical formula	C ₃₈ H ₆₄ SSi ₂	C ₃₈ H ₆₄ SSi ₂	C ₂₆ H ₄₀ SSi ₂
fw	609.13	609.13	440.82
cryst syst	orthorhombic	monoclinic	monoclinic
space group	<i>Pna</i> 2 ₁	<i>P</i> 2 ₁	<i>C</i> 2/c
<i>a</i> , Å	18.846(2)	10.547(2)	12.6447(5)
<i>b</i> , Å	9.555(2)	16.096(2)	12.2663(5)
<i>c</i> , Å	42.236(4)	11.695(2)	16.9828(9)
α, deg	90	90	90
β, deg	90	107.330(11)	102.549(4)
γ, deg	90	90	90
<i>V</i> , Å ³	7606(2)	1859.3(5)	2571.2(2)
<i>Z</i>	8	2	4
<i>d</i> (calcd), g/cm ³	1.064	1.067	1.139
cryst size, mm	0.40 × 0.30 × 0.10	0.30 × 0.20 × 0.20	0.30 × 0.15 × 0.05
abs coeff, mm ⁻¹	1.511	1.516	2.065
<i>F</i> (000)	2688	672	960
<i>T</i> , °C	-160(2)	-160(2)	-160(2)
2θ range, deg	4.0–114.0	4.0–114.0	4.0–114.0
scan type	ω	ω	ω
scan speed, deg/min	2.00–40.00	2.00–40.00	2.00–40.00
scan range (ω), deg	0.70	1.42	0.72
index ranges	0 ≤ <i>h</i> ≤ 20, 0 ≤ <i>k</i> ≤ 10, 0 ≤ <i>l</i> ≤ 45 + Friedel	0 ≤ <i>h</i> ≤ 11, 0 ≤ <i>k</i> ≤ 17, -12 ≤ <i>l</i> ≤ 12 + Friedel	0 ≤ <i>h</i> ≤ 13, 0 ≤ <i>k</i> ≤ 13, 0 ≤ <i>l</i> ≤ 18 + Friedel
no. of reflns colld	10 442	5607	3574
no. of ind reflns	10 274 (<i>R</i> _{int} = 3.37%)	5098 (<i>R</i> _{int} = 8.93%)	1744 (<i>R</i> _{int} = 4.87%)
final <i>R</i> indices (obs data), %	<i>R</i> = 5.39, <i>R</i> _w = 14.27	<i>R</i> = 6.53, <i>R</i> _w = 16.92	<i>R</i> = 3.90, <i>R</i> _w = 10.10
goodness of fit	1.036	1.074	1.085
largest and mean Δ/σ	0.004/0.000	-0.003/0.000	0.015/0.000
data-to-param ratio	13.9	13.7	12.8
largest diff peak/hol, e Å ⁻³	0.429/-0.421	0.705/-0.423	0.345/-0.470

Å, respectively, while, in the former compound, the sum of the angles about the silicons was reported to be 360°. Experimentalists and theoreticians have attributed these structural characteristics to a certain amount of π-bonding between the silicons.^{1,6,10} Thus the overall bonding is related to that in olefin-transition metal complexes where, according to the Dewar-Chatt-Duncanson model,¹² a σ bond is created by donation of π electron density from the olefin to the metal and an interaction of π symmetry allows back-donation of electron density from a d-orbital of the metal to the π*-orbital of the olefin. Note that for **2** and similar compounds a filled p-orbital on the heteroatom would have the proper symmetry for back-donation to the π*-orbital of the disilene-like unit.

Besides the basic similarities between the structures of **2**, several differences are also evident. The silicon-silicon bond distances, although all unusually short, show a steady increase following the order *trans*-**2b** < **2a** ≈ *trans*-**2c** < *cis*-**2c**. It is difficult to correlate this trend with the silicon-silicon double bond lengths of the parent disilenes since crystal packing forces and

crystallization conditions apparently affect the observed Si=Si distances. This fact is most evident with **1a** for which two significantly different double bond lengths, 2.143(2) and 2.160(1) Å, were reported.¹³

Perhaps a better correlation is with the degree of twisting of the bulky groups about the silicon-silicon single bond of **2**, as depicted in Figures 4 and 5 for the newly reported structures. The twist angle, φ, is defined as the average of the torsional angles between *cis* carbon atoms directly bonded to silicon, e.g. for *cis*-**2c**, φ = [θ(C(5)-Si(1)-Si(2)-C(24)) + θ(C(1)-Si(1)-Si(2)-C(20))]/2. As shown in Table 5, in general, as φ increases so does the silicon-silicon bond distance. The two extremes are represented by *trans*-**2b** with a φ of nearly 0° (Figure 5) and the shortest silicon-silicon bond length of the series and *cis*-**2c** with φ = 27.5° (Figure 4, bottom) and a relatively long silicon-silicon bond. Compounds **2a** and *trans*-**2c** (Figure 4, top) show comparatively modest twist angles with intermediate bond distances. Steric effects alone should influence the silicon-silicon bond lengths and could cause significant twisting. This is best illustrated for the most highly distorted structure, *cis*-**2c**, which has the bulkiest combination of substituents, foremost being the *cis tert*-butyl groups. However, a greater degree of twisting could, in and of itself, lead to longer Si-Si bonds considering the bonding model discussed above. The twisting distortion would decrease the π overlap between the silicons, thus reducing the bond order and increasing the bond length.

A second likely result of the combination of steric hindrance and large φ is the 0.02 Å difference in the silicon-sulfur bond lengths within a molecule for *cis*-**2c** (Table 5). In contrast, the structures of **2a** and *trans*-**2b** exhibit equal Si-S distances, while *trans*-**2c**

(6) Yokelson, H. B.; Millevolte, A. J.; Gillette, G. R.; West, R. *J. Am. Chem. Soc.* **1987**, *109*, 6865.

(7) Masamune, S.; Murakami, S.; Tobita, H. *J. Am. Chem. Soc.* **1983**, *105*, 7776.

(8) For comparison cyclotrisilanes have been shown by X-ray studies⁹ to have longer than normal silicon-silicon bond lengths (2.375–2.511 Å). In agreement with calculational work,^{10,11} and in contrast to the three-membered rings mentioned in the present discussion, several exhibit three equivalent silicon-silicon bond lengths.

(9) (a) Masamune, S.; Hanzawa, Y.; Murakami, S.; Bally, T.; Blount, J. F. *J. Am. Chem. Soc.* **1982**, *104*, 1150. (b) Schäfer, A.; Weidenbruch, M.; Peters, K.; von Schnering, H.-G. *Angew. Chem., Int. Ed. Engl.* **1984**, *23*, 302. (c) Dewan, J. C.; Murakami, S.; Snow, J. T.; Collins, S.; Masamune, S. *J. Chem. Soc., Chem. Commun.* **1985**, 892. (d) Weidenbruch, M.; Pohl, S.; Saak, W.; Thom, K. L. *J. Organomet. Chem.* **1987**, *329*, 151.

(10) (a) Grev, R. S.; Schaefer, H. F., III. *J. Am. Chem. Soc.* **1987**, *109*, 6577. (b) Cremer, D.; Gauss, J.; Cremer, E. *J. Mol. Struct.-Theochem.* **1988**, *169*, 531.

(11) Boatz, J. A.; Gordon, M. S. *J. Phys. Chem.* **1989**, *93*, 3025.

(12) (a) Dewar, M. J. S. *Bull. Soc. Chim. Fr.* **1951**, *18*, C71. (b) Chatt, J.; Duncanson, L. A. *J. Chem. Soc.* **1953**, 2939.

(13) (a) Fink, M. J.; Michalczyk, M. J.; Haller, K. J.; West, R.; Michl, J. *Organometallics* **1984**, *3*, 793. (b) Shepherd, B. D.; Campana, C. F.; West, R. *Heteroatom Chem.* **1990**, *1*, 1.

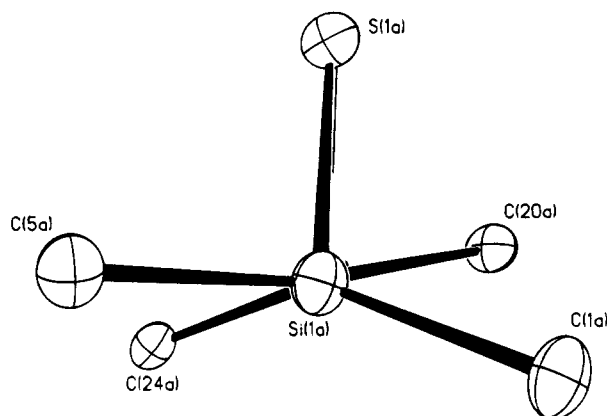
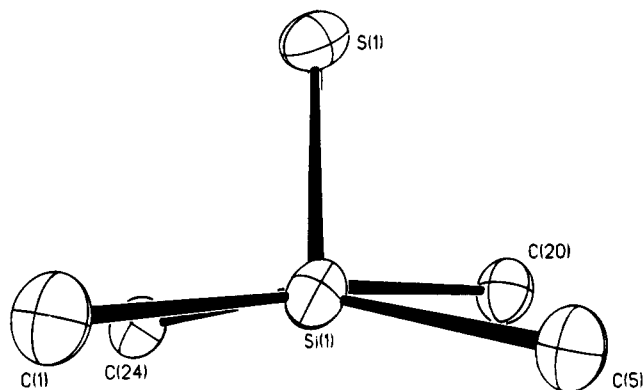


Figure 4. End-on views of the silicon-silicon bonds of *cis*-**2c** (bottom) and *trans*-**2c** (top).

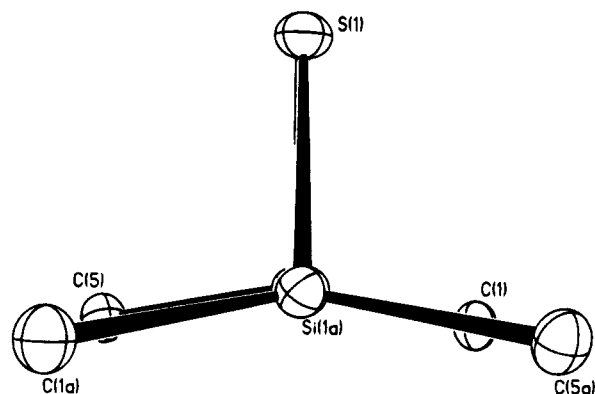


Figure 5. End-on view of the silicon-silicon bond of *trans*-**2b**.

has a comparatively small asymmetry with a bond length difference of less than 0.01 Å.

The twisting distortion in molecule A of *cis*-**2c**¹⁴ causes the C(20a) *tert*-butyl group and the C(5a) 2,4,6-triisopropylphenyl group to be closer to sulfur compared to the C(1a) *tert*-butyl group and the C(24a) 2,4,6-triisopropylphenyl group (Figure 4, bottom). The non-bonded distances in Table 6 demonstrate this. A significant difference in the steric requirements of the two closer groups could cause sulfur to be displaced

(14) Molecule B in the crystal structure of *cis*-**2c** exhibits structural features similar to those of molecule A. The general description also applies to it.

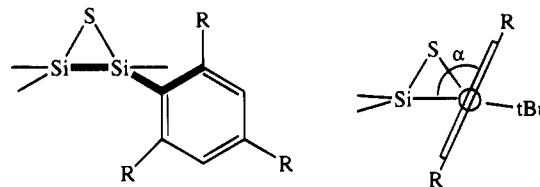


Figure 6. Visual description of the torsional angle, α .

along the silicon-silicon axis away from the larger group.¹⁵ The longer Si(2a)-S bond, under this premise, would correspond to the *tert*-butyl group of the pair of closer substituents exerting a greater steric influence. This should be expected considering the known steric dominance of the *tert*-butyl group. Furthermore, the dihedral angle, α , which the Si(1a) 2,4,6-triisopropylphenyl ring makes with the Si-Si-C plane (Figure 6) is $-115.5(4)^\circ$, a value which should correspond to a less than maximum steric influence.

In addition to the twisting distortion, the $86.0(4)^\circ$ α angle of the Si(2a) 2,4,6-triisopropylphenyl ring should result in a further steric encumbrance at Si(2a). Eclipsing interactions between sulfur and the *ortho* aromatic carbon which bears an isopropyl group would be expected.

Using this type of analysis the silicon-sulfur bond length difference in *trans*-**2c** should be small in comparison. Both *tert*-butyl groups are bent toward sulfur and have very similar conformations. The torsional angles between sulfur and the *tert*-butyl methyl groups are $-60.8(4)$, $58.6(4)$, and $-179.1(3)^\circ$ for C(1) and $-67.6(4)$, $50.3(4)$, and $174.6(4)^\circ$ for C(20). Also, there would likely be no difference in the steric influence of the 2,4,6-triisopropylphenyl groups since their α values differ by less than 2° .

A similar situation exists for **2a**. The two closer groups are both mesityl, and their effective bulk should be nearly equal since their α angles are comparable, 133 and 128° . The α angles of the two distant mesityl groups are somewhat different from each other, 85 and 73° , but due to the Si-Si twisting distortion they would be expected to have less influence on the orientation of sulfur than would the other rings. The equality of the silicon-sulfur bonds in *trans*-**2b** is a consequence of C_2 site symmetry.

Mechanistic Considerations. Certainly more experimentation must be done to establish mechanistic details with any confidence. But the present stereochemical results may suggest that a concerted mechanism is a dominant pathway for both sulfur transfer agents.

An attractive mechanism involving elemental sulfur is presented in A, Scheme 2. Steudel has proposed sulfuranes as possible intermediates in the well-known interconversion reactions of sulfur allotropes at elevated temperatures (Scheme 3),¹⁶ and to explain kinetic results of the redistribution reaction of R_2S_3 and R'_2S_3 to give $RR'S_3$.^{16a} Becker and Wojnowski have subsequently used this mechanism to rationalize the insertion of sulfur into a silicon-silicon bond of $(Me_2Si)_6$.¹⁷

(15) Complexes of transition metals to monosubstituted olefins exhibit a longer distance between the metal and the substituted carbon, attributed, at least in part, to sterics. Herberhold, M. *Metal π -Complexes*; Elsevier: New York, 1974; Vol. 2, Part 2, p 183.

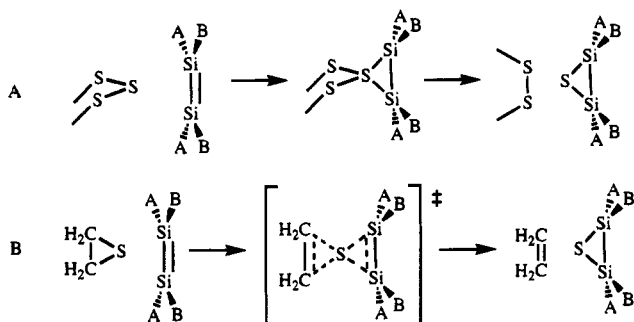
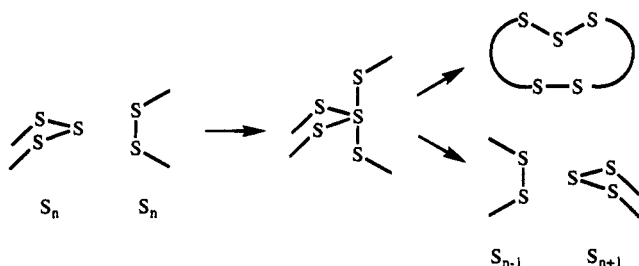
(16) (a) Steudel, R. *Top. Curr. Chem.* **1982**, *102*, 149. (b) Laitinen, R. S.; Pakkanen, T. A.; Steudel, R. *J. Am. Chem. Soc.* **1987**, *109*, 710.

(17) Becker, B.; Wojnowski, W. *J. Organomet. Chem.* **1988**, *346*, 287.

Table 2. Atomic Coordinates ($\times 10^4$) and Equivalent Isotropic Displacement Parameters ($\times 10^3$) for *cis*-2c

	x	y	z	$U(\text{eq}), \text{\AA}^2$		x	y	z	$U(\text{eq}), \text{\AA}^2$
S(1A)	6002(1)	7258(1)	7771(1)	21(1)	S(1B)	6446(1)	2774(1)	5397(1)	20(1)
Si(1A)	6617(1)	5744(1)	8025(1)	18(1)	Si(1B)	5964(1)	4398(1)	5687(1)	15(1)
Si(2A)	6482(1)	5660(1)	7480(1)	16(1)	Si(2B)	5848(1)	4335(1)	5141(1)	18(1)
C(1A)	7527(3)	6248(6)	8200(1)	23(1)	C(1B)	5496(3)	3351(5)	6017(1)	20(1)
C(2A)	8103(3)	5599(8)	7991(2)	45(2)	C(2B)	6105(4)	2575(7)	6178(2)	38(2)
C(3A)	7595(3)	5624(8)	8533(2)	43(2)	C(3B)	5106(4)	4187(7)	6265(2)	56(2)
C(4A)	7629(4)	7833(8)	8221(2)	45(2)	C(4B)	4994(4)	2257(8)	5882(2)	48(2)
C(5A)	5977(3)	4900(6)	8322(1)	20(1)	C(5B)	6494(2)	5901(6)	5858(1)	15(1)
C(6A)	5822(3)	3471(5)	8322(1)	19(1)	C(6B)	6124(3)	7152(7)	5931(1)	19(1)
C(7A)	5279(3)	2943(6)	8517(1)	21(1)	C(7B)	6497(3)	8349(6)	6021(1)	21(1)
C(8A)	4876(3)	3802(6)	8706(1)	25(1)	C(8B)	7235(3)	8386(6)	6031(1)	24(1)
C(9A)	5052(3)	5228(6)	8717(1)	25(1)	C(9B)	7594(3)	7142(7)	5964(2)	23(1)
C(10A)	5589(3)	5791(5)	8533(1)	20(1)	C(10B)	7246(3)	5920(6)	5886(1)	20(1)
C(11A)	6754(4)	1595(7)	8334(2)	43(2)	C(11B)	5036(3)	7746(6)	6255(2)	28(2)
C(12A)	6228(4)	2436(5)	8131(2)	24(2)	C(12B)	5308(3)	7247(6)	5929(2)	20(1)
C(13A)	5747(3)	1426(6)	7943(1)	34(1)	C(13B)	5015(3)	8209(7)	5674(2)	33(1)
C(14A)	4173(3)	1716(7)	8923(2)	40(2)	C(14B)	7981(4)	10282(8)	5814(2)	55(2)
C(15A)	4221(3)	3308(7)	8888(2)	29(2)	C(15B)	7622(3)	9723(6)	6108(1)	26(1)
C(16A)	3552(3)	3855(8)	8722(2)	46(2)	C(16B)	8160(3)	9566(6)	6375(1)	32(1)
C(17A)	5969(5)	7726(7)	8907(2)	43(2)	C(17B)	8203(3)	4347(6)	6109(2)	31(1)
C(18A)	5726(4)	7352(5)	8568(2)	28(2)	C(18B)	7696(3)	4608(6)	5834(1)	22(1)
C(19A)	5076(3)	8208(6)	8477(2)	42(2)	C(19B)	8096(3)	4691(7)	5517(1)	34(2)
C(20A)	6948(3)	6707(5)	7149(1)	20(1)	C(20B)	4957(3)	3852(6)	4954(1)	26(1)
C(21A)	6335(4)	7383(9)	6966(3)	63(3)	C(21B)	4361(3)	4532(8)	5152(2)	44(2)
C(22A)	7401(5)	7890(9)	7276(2)	63(3)	C(22B)	4907(3)	4453(7)	4616(2)	40(2)
C(23A)	7367(5)	5874(7)	6910(2)	73(3)	C(23B)	4826(4)	2280(7)	4944(2)	43(2)
C(24A)	5955(3)	4151(6)	7316(1)	16(1)	C(24B)	6498(3)	5175(6)	4851(1)	20(1)
C(25A)	6321(3)	2890(7)	7236(1)	17(1)	C(25B)	6635(3)	6624(6)	4847(1)	20(1)
C(26A)	5951(3)	1709(6)	7150(1)	21(1)	C(26B)	7175(3)	7161(6)	4654(2)	24(1)
C(27A)	5209(3)	1683(6)	7134(1)	21(1)	C(27B)	7585(3)	6309(6)	4461(1)	22(1)
C(28A)	4860(3)	2899(7)	7199(1)	22(1)	C(28B)	7424(3)	4900(6)	4458(1)	24(1)
C(29A)	5198(3)	4144(5)	7284(1)	18(1)	C(29B)	6898(3)	4310(5)	4644(1)	22(1)
C(30A)	7414(3)	2313(6)	6917(2)	26(2)	C(30B)	5694(4)	8463(7)	4832(2)	44(2)
C(31A)	7132(3)	2791(6)	7237(2)	21(1)	C(31B)	6213(3)	7652(6)	5042(2)	23(2)
C(32A)	7434(3)	1847(6)	7499(2)	31(1)	C(32B)	6682(3)	8664(7)	5227(2)	39(2)
C(33A)	4302(3)	465(6)	6794(1)	35(1)	C(33B)	8159(3)	8392(7)	4186(2)	38(2)
C(34A)	4825(3)	318(6)	7063(1)	28(1)	C(34B)	8206(3)	6863(7)	4268(2)	27(1)
C(35A)	4474(4)	-260(8)	7364(2)	50(2)	C(35B)	8903(3)	6571(8)	4448(2)	51(2)
C(36A)	4244(3)	5698(6)	7064(1)	30(1)	C(36B)	6563(4)	2352(7)	4274(2)	41(2)
C(37A)	4749(3)	5432(6)	7343(1)	21(1)	C(37B)	6785(4)	2744(6)	4611(2)	29(2)
C(38A)	4352(3)	5349(6)	7655(1)	29(1)	C(38B)	7444(4)	1926(7)	4711(2)	43(2)

^a Equivalent isotropic U defined as one-third of the trace of the orthogonalized U_{ij} tensor.

Scheme 2**Scheme 3**

A concerted sulfur transfer from episulfides, B, Scheme 2, might be analogous to the concerted alkene epoxidations with peroxy acids,¹⁸ oxaziridines,¹⁹ and dioxiranes²⁰ which are thought to involve similar butterfly

transition states. This comparison implies an electrophilic nature of the episulfide sulfur such as in the stereospecific concerted desulfurizations with phosphines,²¹ organolithium reagents,^{21,22} and catalytic thiophenoxide.²³ More probable, though, is an initial nucleophilic attack by sulfur on the disilene which, if concerted, would be more like the concerted episulfide desulfurizations on metal surfaces.²⁴

For episulfides a nonconcerted mechanism deserves some consideration, though, since the reaction of **Z-1c**

(18) For reviews see: (a) Rebek, J., Jr. *Heterocycles* **1981**, *15*, 517. (b) Dryuk, V. G. *Tetrahedron* **1976**, *32*, 2855. (c) Swern, D. *Chem. Rev.* **1949**, *45*, 1. For more recent work see: (d) Beak, P.; Woods, K. W. *J. Am. Chem. Soc.* **1991**, *113*, 6281. (e) Bach, R. D.; Owensby, A. L.; Gonzalez, C.; Schlegel, H. B.; McDouall, J. J. W. *J. Am. Chem. Soc.* **1991**, *113*, 2338.

(19) (a) Davis, F. A.; Billmers, J. M.; Gosciniak, D. J.; Towson, J. C.; Bach, R. D. *J. Org. Chem.* **1986**, *51*, 4240. (b) Bach, R. D.; Wolber, G. *J. Am. Chem. Soc.* **1984**, *106*, 1410. (c) Bach, R. D.; Coddens, B. A.; McDouall, J. J. W.; Schlegel, H. B.; Davis, F. A. *J. Org. Chem.* **1990**, *55*, 3325.

(20) (a) Baumstark, A. L.; McCloskey, C. J. *Tetrahedron Lett.* **1987**, *28*, 3311. (b) Baumstark, A. L.; Vasquez, P. C. *J. Org. Chem.* **1988**, *53*, 3437. (c) Murray, R. W.; Shiang, D. L. *J. Chem. Soc., Perkins Trans. 2* **1990**, 349. (d) Bach, R. D.; Andrés, J. L.; Owensby, A. L.; Schlegel, H. B.; McDouall, J. J. W. *J. Am. Chem. Soc.* **1992**, *114*, 7207.

(21) (a) Bordwell, F. G.; Andersen, H. M.; Pitt, B. M. *J. Am. Chem. Soc.* **1954**, *76*, 1082. (b) Neureiter, N. P.; Bordwell, F. G. *J. Am. Chem. Soc.* **1959**, *81*, 578. (c) Boskin, M. J.; Denney, D. B. *Chem. Ind.* **1959**, 330. (d) Boskin, M. J.; Denney, D. B. *J. Am. Chem. Soc.* **1960**, *82*, 4736.

(22) (a) Trost, B. M.; Ziman, S. D. *J. Org. Chem.* **1973**, *38*, 932. (b) Bonini, B. F.; Maccagnani, G.; Mazzanti, G.; Zani, P. *Gazz. Chim. Ital.* **1990**, *120*, 115.

(23) Huisgen, R. *Phosphorus Sulfur* **1989**, *43*, 63.

Table 3. Atomic Coordinates ($\times 10^4$) and Equivalent Isotropic Displacement Parameters ($\times 10^3$) for *trans*-2c

	x	y	z	U(eq), Å ²
S(1)	400(1)	7436(1)	4635(1)	25(1)
Si(1)	808(1)	6914(1)	3074(1)	21(1)
Si(2)	1675(1)	6347(1)	4944(1)	21(1)
C(1)	1756(5)	7724(3)	2434(5)	28(1)
C(2)	3049(5)	7968(3)	3380(5)	33(1)
C(3)	2055(6)	7399(4)	1316(5)	40(1)
C(4)	861(6)	8485(4)	2082(6)	40(2)
C(5)	-680(5)	6428(3)	1932(4)	23(1)
C(6)	-1981(5)	6738(3)	1711(4)	25(1)
C(7)	-3042(5)	6270(4)	1034(5)	37(1)
C(8)	-2867(6)	5491(4)	556(6)	42(2)
C(9)	-1581(6)	5219(4)	727(5)	40(2)
C(10)	-493(5)	5680(3)	1390(5)	30(1)
C(11)	-2294(5)	7580(3)	2153(5)	31(1)
C(12)	-2891(7)	8165(5)	1102(7)	60(2)
C(13)	-3185(6)	7506(4)	2961(6)	42(1)
C(14)	-4007(7)	4926(5)	-110(6)	52(2)
C(15)	-5210(6)	5044(5)	289(7)	56(2)
C(16)	-4271(8)	4995(7)	-1405(6)	80(3)
C(17)	881(6)	5332(3)	1492(5)	36(1)
C(18)	1120(6)	5288(5)	261(6)	48(2)
C(19)	1112(7)	4484(4)	2101(7)	54(2)
C(20)	871(5)	5460(3)	5572(5)	28(1)
C(21)	-573(5)	5326(4)	4800(6)	37(1)
C(22)	1656(6)	4660(3)	5693(5)	37(1)
C(23)	860(6)	5721(4)	6839(5)	37(1)
C(24)	3463(5)	6542(3)	5836(4)	23(1)
C(25)	3828(5)	7153(3)	6749(5)	29(1)
C(26)	5175(5)	7349(4)	7243(5)	35(1)
C(27)	6164(5)	6972(4)	6894(5)	39(1)
C(28)	5807(5)	6351(4)	6024(5)	37(1)
C(29)	4478(5)	6132(3)	5504(4)	26(1)
C(30)	2857(6)	7597(3)	7251(5)	35(1)
C(31)	3152(6)	7448(5)	8607(5)	48(2)
C(32)	2823(8)	8537(4)	6991(6)	51(2)
C(33)	7603(6)	7244(5)	7423(6)	57(2)
C(34)	8179(6)	7552(4)	6495(5)	39(1)
C(35)	8376(8)	6658(5)	8273(8)	38(3)
C(35')	8206(20)	7264(13)	8642(18)	37(7)
C(36)	4179(5)	5435(3)	4566(5)	32(1)
C(37)	4568(6)	5663(4)	3446(5)	40(1)
C(38)	4838(6)	4615(4)	5089(6)	42(2)

Table 4. Atomic Coordinates ($\times 10^4$) and Equivalent Isotropic Displacement Parameters ($\times 10^3$) for *trans*-2b^a

	x	y	z	U(eq), Å ²
S(1)	5000	2214(1)	7500	17(1)
Si(1)	5064(1)	3718(1)	6844(1)	14(1)
C(1)	3841(2)	3960(2)	5988(1)	16(1)
C(2)	2773(2)	3788(2)	6263(2)	22(1)
C(3)	3871(2)	3184(2)	5286(1)	22(1)
C(4)	3881(2)	5141(2)	5689(2)	22(1)
C(5)	6402(2)	3940(2)	6550(1)	15(1)
C(6)	6921(2)	4967(2)	6682(1)	19(1)
C(7)	7956(2)	5100(2)	6543(1)	23(1)
C(8)	8509(2)	4249(2)	6269(2)	25(1)
C(9)	7988(2)	3256(2)	6122(2)	23(1)
C(10)	6953(2)	3081(2)	6256(1)	18(1)
C(11)	6387(2)	5945(2)	6971(2)	22(1)
C(12)	9648(2)	4411(2)	6143(2)	40(1)
C(13)	6475(2)	1954(2)	6080(2)	22(1)

^a The compound sits on a 2-fold rotation axis in the crystal structure.

with propylene sulfide was not completely stereospecific. In fact, with neither sulfurization agent is it possible to dismiss stepwise mechanisms since it is not clear how

rapid silicon-silicon bond rotation would be in intermediates such as *S-S_n-S-SiRR'-Si*RR' and *CH₂-CH₂-S-SiRR'-Si*RR' (* = •, +, or -) relative to three-membered ring formation.

Conclusions

The present work has expanded upon the earlier thiadisilacyclopropane syntheses to show that sulfur transfer occurs with either exclusive (with sulfur) or predominant (with episulfides) retention of the disilene stereochemistry and that the newly reported structures possess features characteristic of other disilacyclopropane derivatives. Very few studies have been dedicated to disilene reaction mechanisms. However, this work can now serve as a starting point for further mechanistic study which will focus on the reactions of *cis*- and *trans*-1,2-disubstituted episulfides with disilenes.

Experimental Section

General Procedures. Reactions and manipulations of disilenes were conducted under a nitrogen atmosphere using standard Schlenk techniques. Solvents were dried over sodium benzophenone ketyl, distilled, and degassed prior to use. Disilenes **1b,c** were prepared as described in the literature.^{3b,4,13a} Commercial episulfides were distilled and degassed prior to use, while the sulfur was purified by sublimation. Chromatography was performed on 20 × 20 cm commercial preparative silica gel plates (Whatman, 60 Å, 1000 μm thickness). Reported melting points are uncorrected. ¹H NMR spectra were referenced to residual solvent resonances which were calibrated against tetramethylsilane. ²⁹Si NMR spectra were obtained using INEPT pulse sequences and were referenced to external tetramethylsilane.

NMR-Scale Sulfurization Reactions of 1c. A solution of 20 mg (0.035 mmol) of isomerically pure **1c** (*trans* as isolated from the original trisilane photolysis, *cis* from photolysis of pure *trans*) in ca. 0.75 mL of benzene-*d*₆ was mixed with either 2 mg-atoms of sulfur or 4 mg of propylene sulfide (0.05 mmol, 1.5 equiv) in an NMR tube. The sulfur reaction was complete within minutes, while the episulfide reaction required 4 days. ¹H NMR showed isomerically pure products for the reactions of **E-1c** with both reagents and of **Z-1c** with sulfur. The reaction of **Z-1c** with propylene sulfide gave a *cis*- and *trans*-2c ratio of 96:4. Characteristic spectra are given below.

NMR-Scale Sulfurization Reactions of *trans*-1b. To 12 mg (0.03 mmol) of pure *trans*-**1b** was added 1.0 mL of a 0.05 M solution of ethylene sulfide in benzene-*d*₆ (0.05 mmol of episulfide, 1.7 equiv). After 2 h, the following NMR spectra, which correspond to those reported for **2b**,¹ were observed: ¹H NMR (C₆D₆, 200 MHz) δ 6.78, 6.76 (2 s, Mes H), 2.82, 2.77 (2 s, *o*-Me), 2.08 (s, *p*-Me), 1.00 (s, *t*-Bu); ²⁹Si NMR (C₆D₆, 99.36 MHz) δ -35.94.

NMR-Scale Sulfurization Reactions of *E/Z* Mixtures of 1b. Two solutions of 15 mg of **E-1b** (0.037 mmol) in 0.75 mL of benzene-*d*₆ were photolyzed with light of λ = 350 nm until the *E* to *Z* ratios were (3-3.5):1. One solution with an *E* to *Z* ratio of 3.6:1 was treated with 10 mg of sulfur to give a mixture of two compounds assigned as *trans*- and *cis*-**2b**. ¹H NMR gave a *trans* to *cis* ratio of 4.1:1. The other solution, containing a 3:1 *E* to *Z* ratio was treated with 0.5 mL of a 0.13 M solution of ethylene sulfide (0.065 mmol of ethylene sulfide, 1.8 equiv) in benzene-*d*₆. After several hours the reaction was complete. ¹H NMR gave a *trans* to *cis* ratio of 3.5:1. NMR data for *cis*-**2b**: ¹H NMR (C₆D₆, 200 MHz) δ 6.56, 6.46 (2 s, Mes H), 2.69, 2.59 (2 s, *o*-Me), 1.87 (s, *p*-Me), 1.25 (s, *t*Bu groups); ²⁹Si NMR (C₆D₆, 53.67 MHz) δ -29.63.

Preparative Synthesis of *cis*-2c with Sulfur. Two NMR-scale reactions (40 mg of **Z-1c**, 0.07 mmol) were combined and concentrated in vacuo. The residue was chromatographed on silica gel in hexanes, giving a central major band

(24) (a) Thomas, T. M.; Grimm, F. A.; Carlson, T. A.; Agron, P. A. *J. Electron Spectrosc. Relat. Phenom.* **1982**, *25*, 159. (b) Friend, C. M.; Roberts, J. T. *J. Am. Chem. Soc.* **1987**, *109*, 7899. (c) Friend, C. M.; Roberts, J. T. *Acc. Chem. Res.* **1988**, *21*, 394. (d) Calhorda, M. J.; Hoffmann, R.; Friend, C. M. *J. Am. Chem. Soc.* **1990**, *112*, 50. (e) Wiegand, B. C.; Friend, C. M. *Chem. Rev.* **1992**, *92*, 491.

Table 5. Selected Structural Data for 2

	$r(\text{Si}-\text{Si})$ (Å)	$r(\text{S}-\text{Si})$ (Å)	$\theta(\text{Si}-\text{S}-\text{Si})$ (deg)	$\theta(\text{Si}-\text{Si}-\text{S})$ (deg)	$\Sigma\theta(\text{Si})^a$ (deg)	ϕ^b (deg)
2a^c	2.289(2)	2.161(2)	64.0(1)	58.0(1)	357.3(2)	12.7(3)
trans-2b	2.2697(12)	2.1655(8)	63.21(4)	58.39(2)	357.13(8)	0.42(8)
cis-2c^d	2.318(2)	2.159(2)	64.64(6)	58.03(7)	358.0(3)	27.5(3)
		2.176(2)		57.33(7)	359.2(3)	
	2.317(2)	2.158(2)	64.62(6)	58.11(7)	358.1(3)	27.6(3)
		2.178(2)		57.27(7)	359.2(3)	
trans-2c	2.294(2)	2.166(2)	63.84(6)	58.23(6)	358.4(3)	8.7(3)
		2.173(2)		57.93(6)	358.4(3)	

^a $\Sigma\theta(\text{Si}) = \theta(\text{C}_{\text{tBu}}-\text{Si}-\text{C}_{\text{Ar}}) + \theta(\text{C}_{\text{tBu}}-\text{Si}-\text{Si}) + \theta(\text{C}_{\text{Ar}}-\text{Si}-\text{Si})$. ^b The twist angle, ϕ , is defined as the average of the torsional angles between *cis* carbon atoms directly bonded to silicon. ^c Reference 1. ^d There are two molecules per asymmetric unit. Data for molecule A are given first.

Table 6. Selected Sulfur-Carbon Nonbonded Distances (Å) in Molecule A of *cis-2c*

S(1a)-C(1)	3.538(5)	S(1a)-C(20a)	3.222(5)
S(1a)-C(5a)	3.259(5)	S(1a)-C(24a)	3.560(5)

which provided 20 mg (47.0%) of *cis-2c*. Somewhat larger quantities of *cis-2c* (ca. 50 mg) were obtained by adding an excess of sulfur to the filtrate from the original synthesis/isolation of *E-1c*. After 3 h of stirring, the colorless solution was concentrated in vacuo, and the residue was dissolved in boiling diethyl ether. Elemental sulfur crystallized after 24 h at -25 °C. The mother liquor was removed, and crystals of *cis-2c* were isolated after 2 weeks at -25 °C. Analytical data: ¹H NMR (C_6D_6 , 300 MHz) δ 7.03, 6.98 (2 d, $J = 1.8$ Hz, 4 H, aromatic H), 4.04 (sept, $J = 6.6$ Hz, 2 H, *ortho* isopropyl methine H), 3.34 (sept, $J = 6.6$ Hz, 2 H, *ortho* isopropyl methine H), 2.67 (sept, $J = 7.0$ Hz, 2 H, *para* isopropyl methine H), 1.32, 1.32, 1.29, 1.29 (s, *t*Bu, 3 d, $J = 6.6$ Hz, six *ortho* isopropyl methyl groups, 36 H), 1.12 (d, $J = 7$ Hz, 12 H, four *para* isopropyl methyl groups), 0.96 (d, $J = 6.6$ Hz, 6 H, two *ortho* isopropyl methyl groups); ²⁹Si NMR (C_6D_6 , 99.36 MHz) δ -28.91 ; exact mass for $\text{C}_{38}\text{H}_{64}\text{SSi}_2$ calcd *m/e* 608.4267, found 608.4260; mp 158–161 °C.

Preparative Synthesis of *trans-2c* with Sulfur. An excess of elemental sulfur was added to a solution of *E-1c* (50 mg, 0.087 mmol) in 15 mL of hexanes, and the mixture was swirled for ca. 1 min. The resulting colorless suspension was concentrated in vacuo, and the residue chromatographed on silica gel in hexanes. The band with the second highest R_f provided 39.7 mg (75.2%) of *trans-2c*. Analytical data: ¹H NMR (C_6D_6 , 300 MHz) δ 7.17, 7.12 (2 d, $J = 1.5$ Hz, 4 H, aromatic H), 4.17 (sept, $J = 6.6$ Hz, 2 H, *ortho* isopropyl methine H), 3.76 (sept, $J = 6.6$ Hz, 2 H, *ortho* isopropyl methine H), 2.76 (sept, $J = 6.9$ Hz, 2 H, *para* isopropyl methine H), 1.60 (d, $J = 6.6$ Hz, 6 H, two *ortho* isopropyl methyl groups), 1.52 (d, $J = 6.6$ Hz, 6 H, two *ortho* isopropyl methyl groups), 1.39, 1.37 (2 d, $J = 6.6$ Hz, 12 H, four *ortho* isopropyl methyl groups), 1.19 (d, $J = 6.6$ Hz, 12 H, four *para* isopropyl methyl groups), 1.04 (s, 18 H, *t*Bu); ²⁹Si NMR (C_6D_6 , 99.36 MHz) δ -33.71 ; exact mass for $\text{C}_{38}\text{H}_{64}\text{SSi}_2$ calcd *m/e* 608.4267, found 608.4260; mp 231–233 °C.

Preparative Synthesis of *cis-2c* with Propylene Sulfide. Two NMR-scale reactions (40 mg of *Z-1c*, 0.07 mmol) were combined and concentrated in vacuo. The residue was chromatographed on silica gel in hexanes. The major band (second highest R_f) provided 21.3 mg (50.5%) of *cis-2c*.

Preparative Synthesis of *trans-2c* with Propylene Sulfide. A solution of 100 mg of propylene sulfide (1.35 mmol, 7.8 equiv) in 20 mL of benzene was added to 100 mg of *E-1c* (0.174 mmol). After stirring for 4 days at 25 °C, the colorless solution was concentrated in vacuo, and the residue was chromatographed on silica gel in hexanes. The fraction with the highest R_f gave 61 mg (57.8%) of *trans-2c*.

X-ray Structure Determinations. X-ray crystallographic analyses were performed on a Siemens P4 diffractometer equipped with a graphite crystal monochromator. Cu K α radiation ($\lambda = 1.54178$ Å) was used for all three structures. Suitable crystals of *trans-2c* were grown by slow evaporation from *n*-hexane at 25 °C, while those of *cis-2c* were grown from

diethyl ether at -25 °C, and of *trans-2b* by slow evaporation from benzene at 25 °C. The orientation matrices and unit cell parameters were determined by the least squares fitting of 36–38 centered reflections ($10^\circ \leq \theta \leq 27^\circ$). Intensities of three standard reflections were monitored every 100 reflections with a maximum variation of 0.04–0.075. All structures were solved using the SHELXS-86 program.²⁵ The non-hydrogen atoms were refined anisotropically using the SHELXL-93 program²⁶ by full-matrix least squares analysis on F^2 . The applied weighting scheme for all three structures was $w^{-1} = \sigma^2 F_o^2 + (xP)^2 + yP$, where $x = 0.1014$ and $y = 2.7839$ for *trans-2c*, $x = 0.0870$ and $y = 6.1493$ for *cis-2c*, and $x = 0.0479$ and $y = 3.2056$ for *trans-2b* and $P = (F_o^2 + 2F_c^2)/3$.²⁶ Extinction corrections were applied with the form $F_c^* = kF_c[1 + 0.001\chi F_c^2 \lambda^3 / \sin(2\theta)]^{-1/4}$ (ref 27) where $\chi = 0.0024(5)$ for *trans-2c*, $\chi = 0.00020(3)$ for *cis-2c*, and $\chi = 0.0008(1)$ for *trans-2b*. The positions of the hydrogen atoms were calculated by idealized geometry and refined using a riding model. Neutral atom scattering factors were taken from ref 28.

Space groups *Pnma* and *Pna2₁* were both possible for *cis-2c* based on the systematic absences. With $Z = 8$, there would be either one or two molecules, respectively, in the asymmetric units of these space groups. Attempts to solve the structure in *Pnma* were not successful, whereas solution was readily accomplished in *Pna2₁*. Refinement in *Pna2₁* produced correlations in a few of the atomic parameters in the two different molecules. An examination of the packing diagram revealed that no center of symmetry existed along the 2₁ axis which could relate the two independent molecules, as would be necessary if the space group were truly *Pnma*.

The results on *trans-2c* revealed that atom C(35) occurred in a major location with an occupancy of 0.72(2) and a minor location with an occupancy of 0.28(2). Both C(35) and C(35') were refined with isotropic thermal parameters.

Acknowledgment. This research was supported by a grant from the National Science Foundation. Funding for X-ray instruments and computers was provided by the National Science Foundation (Grant CHE-9105497) and the University of Wisconsin.

Supporting Information Available: Tables of all bond distances and angles, anisotropic displacement coefficients, and H-atom coordinates and isotropic displacement coefficients and packing diagrams (23 pages). This material is contained in many libraries on microfiche, immediately follows this article in the microfilm version of the journal, and can be ordered from the ACS; see any current masthead page for ordering information.

OM9503353

(25) Sheldrick, G. M. *Acta Crystallogr.* **1990**, *A46*, 467.

(26) Sheldrick, G. M. *J. Appl. Crystallogr.*, manuscript in preparation.

(27) Larsen, A. C. In *Crystallographic Computing*; Ahmed, F. K., Ed.; Mundsgaard: Copenhagen, 1970; pp 291–294.

(28) *International Tables for X-ray Crystallography*; Kynoch: Birmingham, U.K., 1992; Vol. C, Tables 6.1.1.4, 4.2.6.8, and 4.2.4.2 (Present distributors: Kluwer, Boston).

Notes

Five-Coordinate Organometallic Complexes of Gallium and Indium

Yuanlin Zhou and Darrin S. Richeson*

Department of Chemistry, University of Ottawa, Ottawa, Ontario, Canada K1N 6N5

Received March 30, 1995*

Summary: Using 2-benzylaminopyridine anion as a ligand, we have prepared a family of five- and six-coordinate organometallic complexes of Ga^{III} and In^{III}. The monomeric nature and unusual distorted square-based pyramidal coordination geometries of the metal centers for $M\{2-[N(CH_2C_6H_5)]NC_5H_4\}_2Me$ ($M = Ga$, **1**; $M = In$, **2**) were confirmed through single-crystal X-ray diffraction analyses. An intermediate in the formation of the gallium complex, $Ga\{2-[N(CH_2C_6H_5)]NC_5H_4\}Me_2(OEt_2)$, has been characterized spectroscopically. Further reaction of **2** with a third equivalent of amine yields a six-coordinate tris-ligand complex, $\{2-[N(CH_2C_6H_5)]NC_5H_4\}_3In$.

The organometallic complexes of aluminum, gallium, and indium are dominated by the appearance of four-coordinate metal centers.¹ Stimulated by efforts to clarify the steric and electronic effects on both the structure and the reactivity of group 13 organometallic species, there has been a recent resurgence of interest in the preparation of alkyl complexes of these elements having uncommon coordination geometries. For example, there are now several structurally characterized polynuclear and monomeric five- and six-coordinate organoaluminum complexes.²⁻⁵ However, as one moves down the group toward gallium and indium, the examples of such species decline.⁶⁻¹⁴ In fact, the dominant profile of aluminum is illustrated by the fact that the first structurally characterized five- and six-coordinate organometallic complexes of indium have been only very recently reported.⁷

Motivated by an interest in the effects of ligand geometry on the coordination environments of post-transition elements in general and of gallium and indium specifically, we began a systematic study of the use of bidentate, three-atom bridging ligands for organometallic gallium and indium compounds. This family of ligands has been important in preparing a wide variety of dinuclear transition-metal complexes, and a member of this class of ligands, the triazenide anion, has recently been used to stabilize unusual aluminum and indium alkyls.^{4,7} In addition, modification of the organic substituents on these ligands should allow tuning of their steric bulk and, as a result, the aggregation of the product compounds. This note reports the ready reaction of gallium and indium trialkyl complexes with 2-(benzylamino)pyridine to eliminate alkane and yield stable monomeric five-coordinate organometallic Ga^{III} and In^{III} compounds of the general formula $M\{2-[N(CH_2C_6H_5)]NC_5H_4\}_2Me$ ($M = Ga, In$). An intermediate in the formation of the gallium complex, $Ga\{2-[N(CH_2C_6H_5)]NC_5H_4\}Me_2(OEt_2)$ has been characterized spectroscopically. Further reaction of the indium species with a third equivalent of amine yields a six-coordinate tris-ligand complex, $\{2-[N(CH_2C_6H_5)]NC_5H_4\}_3In$.

Reaction of an ether solution of $Ga(CH_3)_3$ or $In(CH_3)_3$ (prepared *in situ* from a stoichiometric reaction of MCl_3 and $MeLi$) with 2 equiv of 2-(benzylamino)pyridine afforded, after crystallization, the new species **1** and **2** (Scheme 1) in 70% and 73% yield, respectively. The ¹H NMR spectra for the two compounds are similar and consistent with a 2:1 ratio of bidentate ligand to CH_3 as well as a single environment for the amido ligands. For example, the benzylic protons (4.34 ppm, $M = Ga$; 4.15 ppm, $M = In$) and carbon atoms (48.7 ppm, $M = Ga$; 48.8 ppm, $M = In$) exhibit single resonance signals. Elemental analysis confirmed the formulas of these species to be $[M\{2-[N(CH_2C_6H_5)]NC_5H_4\}_2(CH_3)]_n$. On the basis of the ready solubility of both **1** and **2** in organic solvents, the comparable ionic radius of In(III) with those of the transition metals, and the ability of indium to accommodate 5- or 6-fold coordination, we could not rule out the possibility that these complexes may be dinuclear species.¹⁵ A lantern-type arrangement with four bridging ligands was recently discovered in

* Abstract published in *Advance ACS Abstracts*, June 15, 1995.

(1) For a summary of Ga and In organometallic chemistry see: Tuck, D. G. In *Comprehensive Organometallic Chemistry*; Wilkinson, G., Stone, F. G. A., Abel, E. W., Eds.; Pergamon Press: Oxford, England, 1982; Vol. 1, Chapter 7.

(2) Robinson, G. H.; Sangokoya, S. A. *J. Am. Chem. Soc.* **1987**, *109*, 6852.

(3) Healy, M. D.; Barron, A. R. *J. Am. Chem. Soc.* **1989**, *111*, 398.

(4) Leman, J. T.; Barron, A. R. *Organometallics* **1989**, *8*, 1828.

(5) Self, M. F.; Pennington, W. T.; Laske, J. A.; Robinson, G. H. *Organometallics* **1991**, *10*, 36.

(6) Lee, B.; Pennington, W. T.; Robinson, G. H. *Organometallics* **1990**, *9*, 1709.

(7) Leman, J. T.; Roman, H. A.; Barron, A. R. *Organometallics* **1993**, *12*, 2986.

(8) Schumann, H.; Just, O.; Seuss, T. D.; Weiman, R. *J. Organomet. Chem.* **1994**, *472*, 15.

(9) Schumann, H.; Seuss, T. D.; Just, O.; Weiman, R.; Hemling, H.; Görlitz, F. H. *J. Organomet. Chem.* **1994**, *479*, 171.

(10) Reger, D. L.; Knox, S. J.; Rheingold, A. L.; Haggerty, B. S. *Organometallics* **1990**, *9*, 2581.

(11) Reger, D. L.; Mason, S. S.; Reger, L. B.; Rheingold, A. L.; Ostrander, R. L. *Inorg. Chem.* **1994**, *33*, 1803.

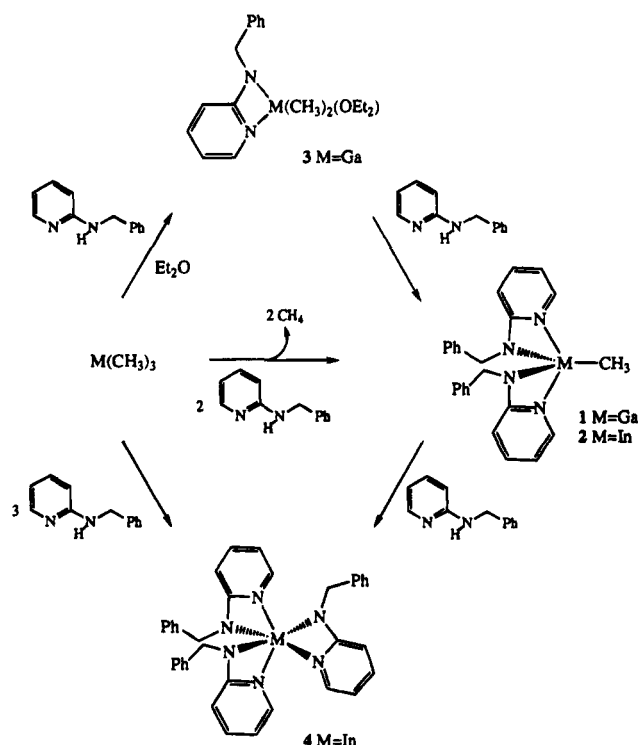
(12) Reger, D. L.; Mason, S. S.; Rheingold, A. L.; Ostrander, R. L. *Inorg. Chem.* **1994**, *33*, 1811.

(13) Rettig, S. J.; Storr, A.; Trotter, J. *Can. J. Chem.* **1976**, *54*, 1278.

(14) Rettig, S. J.; Storr, A.; Trotter, J. *Can. J. Chem.* **1975**, *53*, 58.

(15) (a) Gerstner, F.; Weidlein, J. *Z. Naturforsch.* **1978**, *33B*, 24.
(b) Hausen, H. D.; Gerstner, F.; Schwarz, W. *J. Organomet. Chem.* **1978**, *145*, 277.

Scheme 1



our laboratory for the indium formamidinate complex $\text{Cl}_2\text{In}_2(\text{CyNCHNCy})_4$ (Cy = cyclohexyl).¹⁶

The monomeric nature and the coordination geometries of the metal centers for both 1 and 2 were confirmed through single-crystal X-ray diffraction analyses. Complex 1 crystallized in the monoclinic space group $C2/c$ ($a = 20.884(5)$ Å, $b = 9.335(4)$ Å, $c = 25.769(9)$ Å, $\beta = 103.32(4)^\circ$) with one molecule of 1 and half of a solvent molecule (Et_2O) in the asymmetric unit. There are no anomalously short intermolecular contacts. The molecular geometry and atom-numbering scheme are shown in Figure 1. Complex 2 crystallized in the triclinic space group $P\bar{1}$ ($a = 10.475(4)$ Å, $b = 11.917(7)$ Å, $c = 9.683(5)$ Å, $\alpha = 97.16(5)^\circ$, $\beta = 101.08(4)^\circ$, $\gamma = 69.45(3)^\circ$, $Z = 2$). The molecular geometry and atom-numbering scheme are shown in Figure 2.

In both cases the structural analysis revealed a molecular core with the metal center in an unusual distorted square-based pyramidal environment consisting of the four nitrogen atoms of the two 2-(benzylamino)pyridine anions with an apical methyl group completing the coordination sphere.¹⁷ Within a given complex, the two nitrogen atoms of the pyridine rings as well as those of the amido groups are oriented in a trans configuration. Tables 1 and 2 present a summary of selected bond distances and angles for the two complexes. The principal structural parameter differences between 1 and 2, including M–C and M–N distances and angles, are in accord with the increased ionic radius of indium with respect to that of gallium.

In both 1 and 2, the metal center lies at the intersection of two planes; one contains the two pyridine

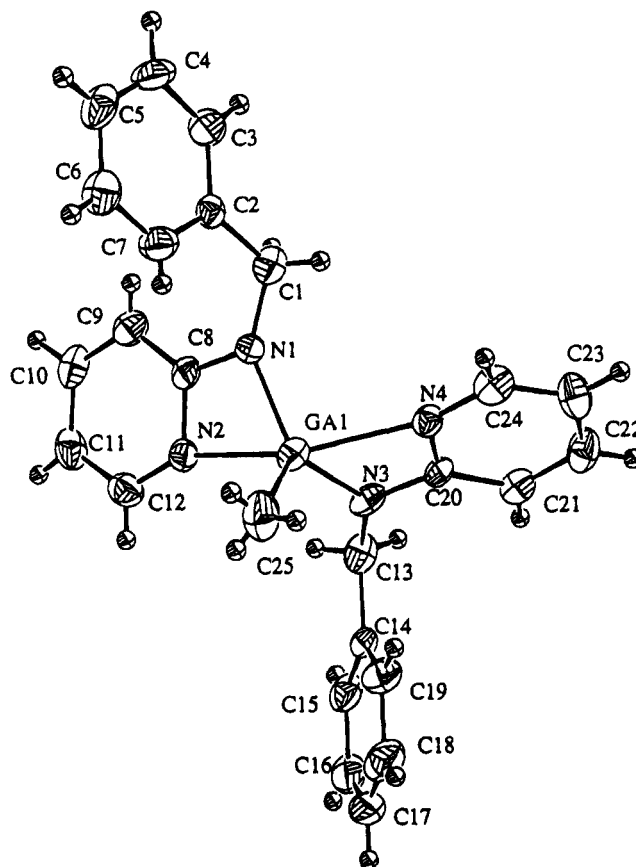


Figure 1. Molecular structure and atom-numbering scheme for $\text{MeGa}(\text{C}_6\text{H}_5\text{CH}_2\text{NC}_5\text{H}_4)_2$ (1). The solvent of crystallization has been omitted for clarity.

Table 1. Selected Atomic Bond Distances (in angstroms) for Compounds 1 and 2

compd 1		compd 2	
Ga1–N1	1.933(3)	In1–N1	2.146(2)
Ga1–N2	2.216(3)	In1–N2	2.349(3)
Ga1–N3	1.933(3)	In1–N3	2.169(2)
Ga1–N4	2.236(3)	In1–N4	2.341(3)
Ga1–C25	1.924(5)	In1–C25	2.158(3)
N1–C1	1.433(5)	N1–C1	1.443(4)
N1–C8	1.340(5)	N1–C8	1.343(4)
N2–C8	1.363(5)	N2–C8	1.365(4)
N2–C12	1.331(5)	N2–C12	1.338(4)
N3–C13	1.442(5)	N3–C13	1.434(4)
N3–C20	1.333(5)	N3–C20	1.340(4)
N4–C20	1.356(5)	N4–C20	1.365(4)
N4–C24	1.311(5)	N4–C24	1.335(4)
C1–C2	1.521(5)	C1–C2	1.499(5)
C8–C9	1.396(6)	C8–C9	1.416(4)

nitrogens, the metal, and the methyl carbon with the other consisting of the two amido nitrogens, the metal center, and the methyl carbon. The planarity of these groups is confirmed by the fact that the sum of the appropriate angles is 360° . Both compounds display M–N(amido) distances that are slightly shorter than the M–N(Py) bond lengths, a feature consistent with the literature.^{1,7,18,19} The Ga–CH₃ and In–CH₃ bond

(16) Zhou, Y.; Richeson, D. S. Unpublished results.

(17) References 6, 7, 13, and 14 present crystal structures of five-coordinate gallium and indium complexes in distorted-trigonal-bipyramidal coordination environments. The values for the angle along the pseudo-axial vectors in these reports fall in the range 149.7 – 157.2° . In all cases the methyl group is in the equatorial plane.

(18) For a summary of Ga coordination chemistry see: Taylor, M. J. In *Comprehensive Coordination Chemistry*; Wilkinson, G., Gillard, D., McCleverty, J. A., Eds.; Pergamon Press: Oxford, England, 1987; Vol. 3, Chapter 25.1.

(19) For a summary of In coordination chemistry see: Tuck, D. G. In *Comprehensive Coordination Chemistry*; Wilkinson, G., Gillard, D., McCleverty, J. A., Eds.; Pergamon Press: Oxford, England, 1987; Vol. 3, Chapter 25.2.

Table 2. Selected Atomic Bond Angles (in Degrees) for Compounds 1 and 2

compd 1		compd 2	
N1-Ga1-N2	63.7(1)	N1-In1-N2	59.46(9)
N1-Ga1-N3	113.2(1)	N1-In1-N3	115.5(1)
N1-Ga1-N4	99.2(1)	N1-In1-N4	101.6(9)
N1-Ga1-C25	124.7(2)	N1-In1-C25	123.8(1)
N2-Ga1-N3	97.2(1)	N2-In1-N3	98.2(9)
N2-Ga1-N4	148.1(1)	N2-In1-N4	143.0(9)
N2-Ga1-C25	106.2(2)	N2-In1-C25	110.9(1)
N3-Ga1-N4	63.5(1)	N3-In1-N4	59.3(9)
N3-Ga1-C25	122.0(2)	N3-In1-C25	120.6(1)
N4-Ga1-C25	105.7(2)	N4-In1-C25	105.9(1)
Ga1-N1-C1	138.8(3)	In1-N1-C1	139.3(2)
Ga1-N1-C8	100.2(2)	In1-N1-C8	99.4(2)
C1-N1-C8	121.0(3)	C1-N1-C8	120.9(3)
Ga1-N2-C8	87.0(2)	In1-N2-C8	89.7(2)
Ga1-N2-C12	154.6(3)	In1-N2-C12	149.4(2)
C8-N2-C12	118.4(3)	C8-N2-C12	120.2(3)
Ga1-N3-C13	135.8(3)	In1-N3-C13	141.0(2)
Ga1-N3-C20	99.9(2)	In1-N3-C20	98.6(2)
C13-N3-C20	124.0(3)	C13-N3-C20	120.3(3)
Ga1-N4-C20	85.9(2)	In1-N4-C20	90.3(2)
Ga1-N4-C24	155.0(3)	In1-N4-C24	148.5(2)
C20-N4-C24	118.8(3)	C20-N4-C24	120.2(3)
N1-C1-C2	117.1(3)	N1-C1-C2	112.7(3)
N1-C8-N2	109.1(3)	N1-C8-N2	111.3(3)
N3-C20-N4	110.4(3)	N3-C20-N4	111.6(3)

lengths correlate with the few reported values for five-coordinate complexes.^{7,13,14}

In an effort to isolate an intermediate in the formation of **1**, an ether solution of Ga(CH₃)₃ was mixed with 1 equiv of 2-(benzylamino)pyridine (Scheme 1). Various attempts were made to isolate the resulting material, but unfortunately, complex **3** proved to be too unstable and its identification relied on ¹H and ¹³C NMR and subsequent reactivity. The molecular formula for **3**, Me₂Ga{2-[N(CH₂C₆H₅)]NC₅H₄}(OEt₂), is confirmed by ¹H NMR and by the fact that reaction of **3** with a second equivalent of 2-[HN(CH₂C₆H₅)]NC₅H₄ resulted in isolation of complex **1**. We feel confident in assigning a coordinated Et₂O molecule as part of the five-coordinate structure of **3** on the basis of NMR integrations and the characteristic upfield shift of coordinated versus free diethyl ether (free ether, 3.27 ppm (q, CH₂), 1.13 ppm (t, CH₃); coordinated ether in **3**, 2.97 ppm (q, CH₂), 0.77 ppm (t, CH₃)). In addition, the presence of the gallium methyl carbon signal at -6.1 ppm is consistent with what we observed for complex **1**.

On the basis of the observation that the 2-(benzylamino)pyridine anion led to the ready formation of five-coordinate complexes, we were interested in the possibility of generating six-coordinate tris-ligand compounds. The interaction of In(CH₃)₃ with 3 equiv of 2-[HN(CH₂C₆H₅)]NC₅H₄ followed by crystallization from diethyl ether resulted in the isolation of the tris-ligand product In{2-[N(CH₂C₆H₅)]NC₅H₄}₃ (**4**) (Scheme 1). Microanalysis confirmed the stoichiometry of this product, and the spectroscopic parameters are consistent with the formulation of **4** as a six-coordinate complex. Alternatively, the same material can be prepared by the reaction of **2** with 2-(benzylamino)pyridine in a 1:1 mole ratio. Surprisingly, direct reaction of MCl₃ (M = Ga, In) with 1, 2, or 3 equiv of the lithium salt of the 2-(benzylamino)pyridine anion have, so far, led only to intractable mixtures.

The use of the 2-(benzylamino)pyridine anion as a ligand in the organometallic chemistry of gallium and indium leads to a family of five- and six-coordinate

organometallic complexes of these metals. X-ray crystallographic studies and spectroscopic parameters confirm that these complexes represent examples of rather unusual five- and six-coordinate geometries. Our continuing investigations are oriented at dissecting the steric and electronic features that influence the formation and reactivity of high-coordination-number organogallium and organoindium compounds.

Experimental Section

General Procedure. All reactions were carried out either in a nitrogen filled drybox or under nitrogen using standard Schlenk-line techniques. Diethyl ether, hexane, and benzene were distilled under nitrogen from potassium. Deuterated benzene was dried by vacuum transfer from potassium. 2-(Benzylamino)pyridine and MeLi (in diethyl ether) were purchased from Aldrich and used without further purification. InCl₃ and GaCl₃ (Aldrich) were sublimed prior to use.

Synthesis of MeGa(C₆H₅CH₂NC₅H₄)₂ (1**).** To a suspension of GaCl₃ (0.44 g, 2.50 mmol) in diethyl ether (30 mL) was added MeLi (5.4 mL, 1.4 M, 7.50 mmol) dropwise, and the mixture was then stirred for an additional 30 min. 2-(Benzylamino)pyridine (0.92 g, 5.00 mmol) was added, and the reaction mixture was stirred 24 h and then filtered. The solution was concentrated to ca. 8 mL and cooled to -30 °C. The resulting white crystalline solid was collected by filtration and dried under oil pump vacuum: yield 0.79 g, 70%, 1.75 mmol; mp (sealed) 84–86 °C. Spectroscopic data: IR (Nujol, cm⁻¹) 1605 (s), 1487 (s); ¹H NMR (C₆D₆, ppm) 7.30–7.05 (m, 14H, C₆H₅, and NC₅H₄), 5.91 (m, 4H, NC₅H₄), 4.34 (s, 4H, CH₂), 3.27 (q, 2H, CH₂, ether of crystallization), 1.13 (t, 3H, CH₃, ether of crystallization), 0.42 (s, 3H, GaMe); ¹³C NMR (C₆D₆, ppm) 165.9, 145.3, 141.6, 139.7, 128.7, 127.2, 126.7, 108.7, 104.2 (9 s, C₆H₅ and NC₅H₄), 65.9 (s, CH₂, ether of crystallization), 48.7 (s, CH₂), 15.6 (s, CH₃, ether of crystallization), -6.5 (s, GaCH₃). Elemental analysis was performed on a sample dried under vacuum. Anal. Calcd for C₂₅H₂₅GaN₄: C, 66.55; H, 5.58; N, 12.42. Found: C, 66.15; H, 5.72; N, 12.37.

Synthesis of MeIn(C₆H₅CH₂NC₅H₄)₂ (2**).** To a suspension of InCl₃ (0.71 g, 3.21 mmol) in diethyl ether (30 mL) was added MeLi (6.9 mL, 1.4 M, 9.63 mmol) dropwise, and the mixture was then stirred for an additional 20 min. 2-(Benzylamino)pyridine (1.18 g, 6.42 mmol) was added, and the reaction mixture was stirred overnight and then filtered. The solution was concentrated to ca. 8 mL and cooled to -30 °C. The resulting white crystalline solid was collected by filtration and dried under oil pump vacuum: yield 1.16 g, 73%, 2.34 mmol; mp (sealed) 119–121 °C. Spectroscopic data: IR (Nujol, cm⁻¹) 1604 (s), 1484 (s); ¹H NMR (C₆D₆, ppm) 7.18–6.85 (m, 14H, C₆H₅ and NC₅H₄), 5.85 (m, 4H, NC₅H₄), 4.15 (s, 4H, CH₂), 0.23 (s, 3H, InCH₃); ¹³C NMR (C₆D₆, ppm) 165.4, 146.4, 141.8, 138.9, 128.5, 127.6, 126.9, 108.9, 105.0 (9 s, C₆H₅ and NC₅H₄), 48.8 (s, CH₂), -8.2 (s, InCH₃). Anal. Calcd for C₂₅H₂₅InN₄: C, 60.50; H, 5.18; N, 11.29. Found: C, 60.55; H, 5.16; N, 11.33.

Synthesis of Me₂Ga(C₆H₅CH₂NC₅H₄) (3**).** To a suspension of GaCl₃ (0.68 g, 3.86 mmol) in diethyl ether (30 mL) was added MeLi (8.3 mL, 1.4 M, 11.58 mmol) dropwise, and the mixture was then stirred for an additional 30 min. 2-(Benzylamino)pyridine (0.71 g, 5.00 mmol) was added, and the reaction mixture was stirred 24 h and then filtered. The solution was removed under oil pump vacuum. The residue was dissolved in 10 mL of hexane/diethyl ether (9:1), and the solution was cooled to -30 °C. The resulting white crystalline solid was collected by filtration and dried under oil pump vacuum: yield 0.99 g, 73%, 2.82 mmol; mp (sealed) 78–80 °C. Spectroscopic data: IR (Nujol, cm⁻¹) 1606 (s), 1485 (s); ¹H NMR (C₆D₆, ppm) 7.55–6.05 (m, 9H, C₆H₅ and NC₅H₄), 4.69 (s, 2H, CH₂), 2.97 (q, 4H, CH₂, ether), 0.77 (t, 6H, CH₃, ether), -0.04 (s, 6H, GaMe); ¹³C NMR (C₆D₆, ppm) 167.5, 146.0, 142.8, 137.9,

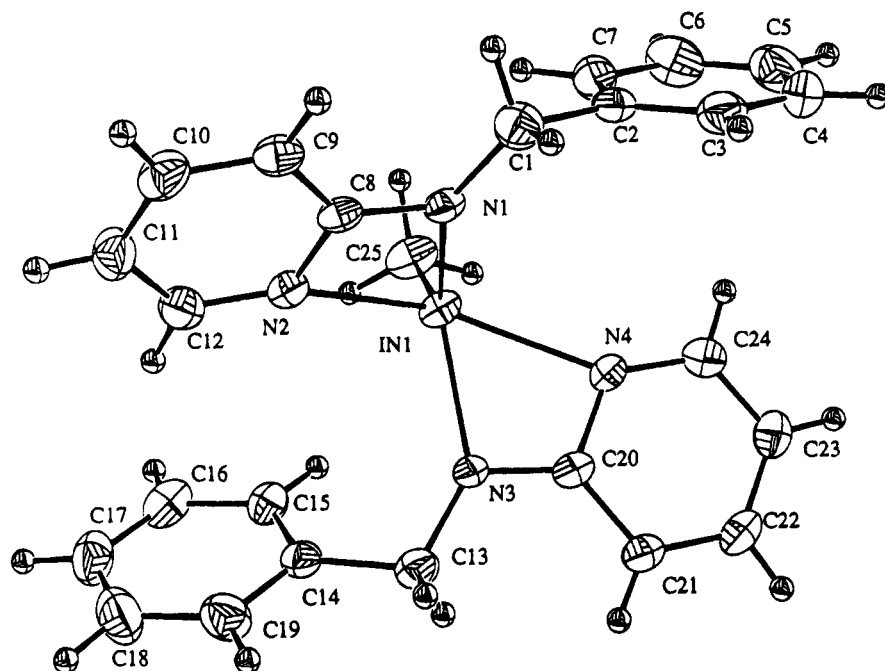


Figure 2. Molecular structure and atom-numbering scheme for $\text{MeIn}(\text{C}_6\text{H}_5\text{CH}_2\text{NC}_5\text{H}_4)_2$ (**2**).

128.3, 127.0, 126.2, 110.3, 108.3 (9 s, C_6H_5 and NC_5H_4), 65.9 (s, CH_2 , ether), 51.5 (s, CH_2), 14.5 (s, CH_3 , ether), -6.1 (s, GaCH_3).

Synthesis of $\text{In}(\text{C}_6\text{H}_5\text{CH}_2\text{NC}_5\text{H}_4)_3$ (4**).** To a suspension of InCl_3 (0.34 g, 1.54 mmol) in diethyl ether (25 mL) was added MeLi (3.3 mL, 1.4 M, 4.62 mmol) dropwise, and the mixture was then stirred for an additional 20 min. 2-(Benzylamino)pyridine (0.85 g, 4.62 mmol) was added, and the reaction mixture was stirred for 2 h and then filtered. The solution was concentrated to ca. 8 mL and cooled to -30 °C. The resulting crystalline solid was collected by filtration and dried under oil pump vacuum: yield 0.66 g, 65%, 1.00 mmol; mp (sealed) 98–100 °C. Spectroscopic data: IR (Nujol, cm^{-1}) 1602 (s), 1485 (s); ^1H NMR (C_6D_6 , ppm) 7.21–6.93 (m, 21H, C_6H_5 and NC_5H_4), 5.93 (m, 6H, NC_5H_4), 4.23 (s, 6H, CH_2). Anal. Calcd for $\text{C}_{36}\text{H}_{33}\text{InN}_6$: C, 65.07; H, 5.01; N, 12.65. Found: C, 65.17; H, 5.25; N, 12.32.

X-ray Crystallography. Intensity data were collected on a Rigaku diffractometer at -153 °C using the ω - 2θ scan technique to a maximum 2θ value of 47° (complex **1**) and 50° (complex **2**) for crystals mounted on glass fibers. Cell constants and orientation matrices were obtained from the least-squares refinement of 24 carefully centered high-angle reflections. Redundant reflections were removed from the data set. The intensities of 3 representative reflections were measured

after every 150 reflections to monitor the crystal and instrument stability. Data were corrected for Lorentz and polarization effects but not for absorption. The structures were solved by direct methods. The non-hydrogen atoms were refined anisotropically. Hydrogen atom positions were located in the difference Fourier maps and refined isotropically in the case of favorable observation/parameter ratios. The final cycle of full-matrix least-squares refinement was based on the number of observed reflections with $I > 2.5\sigma(I)$. Anomalous dispersion effects were included in F_o . All calculations were performed using the NRCVAX package. Details of the data collection and refinement and final atomic coordinates are reported in the supporting information.

Acknowledgment. This work was supported by the Natural Sciences and Engineering Research Council of Canada.

Supporting Information Available: Text giving a description of the structural solutions, tables of atomic positions, thermal parameters, crystallographic data, and bond distances and angles, and ORTEP drawings for compounds **1** and **2** (20 pages). Ordering information is given on any current masthead page.

OM950236P

First Example of an Aluminum–Phosphorus–Arsenic Mixed-Pnicogen Ring Compound: X-ray Crystal

Structure of $\text{Et}_2\text{AlP}(\text{SiMe}_3)_2\text{Al}(\text{Et})_2\text{As}(\text{SiMe}_3)_2$

Janeen A. Laske Cooke and Richard L. Wells*

Department of Chemistry, Paul M. Gross Chemical Laboratory, Duke University,
Durham, North Carolina 27708-0346

Peter S. White

Department of Chemistry, Venable Hall, University of North Carolina at Chapel Hill,
Chapel Hill, North Carolina 27514

Received April 6, 1995[®]

Summary: The aluminum mixed-pnicogen compound, $\text{Et}_2\text{AlP}(\text{SiMe}_3)_2\text{Al}(\text{Et})_2\text{As}(\text{SiMe}_3)_2$ (**1**), is the first structurally-characterized compound to contain a four-membered ring with two aluminum centers bridged by two different heavier group 15 atoms. Compound **1** was synthesized by the equilibration of $[\text{Et}_2\text{AlP}(\text{SiMe}_3)_2]_2$ (**2**) and $[\text{Et}_2\text{AlAs}(\text{SiMe}_3)_2]_2$ (**3**) in a 1:1 mole ratio under ultrasonic conditions. Low-temperature X-ray crystallographic analysis revealed that crystals of **1** are isomorphous with those of **2** and **3**. The electron ionization (20 eV) mass spectrum of **1** shows a fragmentation pattern, which is consistent with this compound, and no peaks above m/z 400, which is consistent with either **2** or **3**.

Introduction

Much of the research in our laboratory during the past decade has focused on the preparation of potential single-source precursors to group 13–15 binary semiconductor and electronic materials. Through various synthetic routes, we have been able to isolate several oligomeric, monomeric, and Lewis acid–base adduct compounds with novel compositions and structural characteristics.^{1–11} As an extension of this work, we have been investigating the preparation of compounds containing a group 13 metal and two different pnicogens, which might serve as single-source precursors to ternary group 13–15 materials. Our initial efforts to synthesize such metal–pnictogen compounds involved

attempted reactions of “mixed-bridge” binary group 13–15 compounds having M–E–M–Cl ($\text{M} = \text{In}$ or Ga , $\text{E} = \text{P}$, As) ring cores with the lithium salts of silylarsines and phosphines and resulted in unusual binary rearrangement products rather than preferred mixed-pnicogen compounds.¹²

As alternatives to the salt-elimination synthetic pathway, equilibration reactions of analogous group 13–15 dimeric compounds were explored and found to be successful methods of preparing ternary metal–pnictogen compounds. We have recently reported the isolation and structural characterization of $(\text{Me}_3\text{SiCH}_2)_2\text{InAs}(\text{SiMe}_3)_2\text{In}(\text{CH}_2\text{SiMe}_3)_2\text{P}(\text{SiMe}_3)_2$ (**4**)¹³ and $\text{I}_2\text{GaAs}(\text{SiMe}_3)_2\text{Ga}(\text{I})_2\text{P}(\text{SiMe}_3)_2$ (**5**),¹⁴ which are the first examples of four-membered ring compounds containing two group 13 metal centers bridged by both an arsenic and a phosphorus atom. Both **4** and **5** were prepared by the equilibration of equimolar amounts of two isostructural dimers of the formulae $[(\text{Me}_3\text{SiCH}_2)_2\text{InE}(\text{SiMe}_3)_2]_2$ ($\text{E} = \text{As}$ (**6**)¹⁵ and P (**7**)³) and $[\text{I}_2\text{GaE}(\text{SiMe}_3)_2]_2$ ($\text{E} = \text{As}$ (**8**)¹⁶ and P (**9**)¹⁴), respectively. These results led us to equilibrate two analogous organoaluminum dimeric compounds in a similar fashion in an effort to isolate an Al–P–As mixed-pnicogen product. To this end, the previously reported dimers, $[\text{Et}_2\text{AlP}(\text{SiMe}_3)_2]_2$ (**2**)⁸ and $[\text{Et}_2\text{AlAs}(\text{SiMe}_3)_2]_2$ (**3**)², were equilibrated in a 1:1 mole ratio under ultrasonic conditions, forming the ring compound **1**. Herein, we describe the synthesis and structural characterization of the aluminum mixed-group 15 compound, $\text{Et}_2\text{AlP}(\text{SiMe}_3)_2\text{Al}(\text{Et})_2\text{As}(\text{SiMe}_3)_2$ (**1**).

Experimental Section

General Considerations. All manipulations were performed by Schlenk techniques or in a Vacuum Atmospheres

(12) Wells, R. L.; McPhail, A. T.; Jones, L. J.; Self, M. F. *Organometallics* **1992**, *11*, 2694.

(13) Jones, L. J., III; McPhail, A. T.; Wells, R. L. *Organometallics* **1994**, *13*, 2504.

(14) Wells, R. L.; Aubuchon, S. R.; Lube, M. S.; White, P. S. *Main Group Chem.*, in press.

(15) Wells, R. L.; Jones, L. J.; McPhail, A. T.; Alvanipour, A. *Organometallics* **1991**, *10*, 2345.

(16) Johansen, J. D.; McPhail, A. T.; Wells, R. L. *Adv. Mater. Opt. Electron.* **1992**, *1*, 29.

* Author to whom correspondence should be addressed.

[®] Abstract published in *Advance ACS Abstracts*, June 15, 1995.

(1) Wells, R. L. *Coord. Chem. Rev.* **1992**, *112*, 273.

(2) Wells, R. L.; McPhail, A. T.; Speer, T. M. *Organometallics* **1992**, *11*, 960.

(3) Wells, R. L.; McPhail, A. T.; Self, M. F. *Organometallics* **1992**, *11*, 221.

(4) Wells, R. L.; McPhail, A. T.; Jones, L. J., III; Self, M. F.; Butcher, R. J. *Organometallics* **1992**, *11*, 2694.

(5) Wells, R. L.; Aubuchon, S. R.; Self, M. F.; Jasinski, J. P.; Woudenberg, R. C.; Butcher, R. J. *Organometallics* **1992**, *11*, 3370.

(6) Wells, R. L.; McPhail, A. T.; Jones, L. J., III; Self, M. F. *J. Organomet. Chem.* **1993**, *449*, 85.

(7) Wells, R. L.; Self, M. F.; McPhail, A. T.; Aubuchon, S. R.; Woudenberg, R. C.; Jasinski, J. P. *Organometallics* **1993**, *12*, 2832.

(8) Wells, R. L.; McPhail, A. T.; Self, M. F.; Laske, J. A. *Organometallics* **1993**, *12*, 3333.

(9) Wells, R. L.; Self, M. F.; Baldwin, R. A.; White, P. S. *J. Coord. Chem.* **1994**, *33*, 279.

(10) Wells, R. L.; Baldwin, R. A.; White, P. S. *Organometallics* **1995**, *14*, 2123.

(11) Wells, R. L.; McPhail, A. T.; Laske, J. A.; White, P. S. *Polyhedron* **1994**, *13*, 2737.

HE-493 Dri-Lab under argon. Pentane was dried over LiAlH_4 and distilled under dry nitrogen prior to use. Benzene- d_6 was distilled from sodium/benzophenone under dry nitrogen and toluene- d_8 was used as received from Aldrich Chemical Co., Milwaukee, WI. Sonication of reaction solutions was performed in an L&R Ultrasonics Quatrex 140H ultrasonic cleaning bath. Compounds **2**⁸ and **3**² were prepared by literature methods.

^1H , ^{27}Al , and $^{31}\text{P}\{^1\text{H}\}$ NMR spectra were acquired on a Varian Unity 500 (500.1, 130.3, and 202.4 MHz, respectively) spectrometer using 5-mm tubes. $^{13}\text{C}\{^1\text{H}\}$ NMR spectra were obtained on a Varian XL-300 (75.4 MHz) spectrometer also using 5-mm tubes. ^1H and $^{13}\text{C}\{^1\text{H}\}$ NMR spectra were referenced to TMS *via* the residual protons or carbons of benzene- d_6 and δ 7.15 or 128.0 ppm. ^{27}Al and $^{31}\text{P}\{^1\text{H}\}$ NMR spectra were externally referenced to $\text{Al}(\text{NO}_3)_3$ and H_3PO_4 , respectively, at δ 0.00 ppm. Melting points (uncorrected) were taken in flame-sealed capillaries on a Thomas-Hoover Unimelt apparatus. Elemental analyses were performed by E+R Microanalytical Laboratory, Inc., Corona, NY. Single-crystal data for **1** were collected at the University of North Carolina—Chapel Hill on a Rigaku AFC6/S diffractometer at -130°C , with graphite-monochromated Mo K α radiation.

Preparation of $\text{Et}_2\text{AlP}(\text{SiMe}_3)_2\text{Al}(\text{Et})_2\text{As}(\text{SiMe}_3)_2$ (1**).** A one-necked screw-top round-bottomed flask, equipped with a Teflon valve and stir-bar, was charged with 0.262 g (0.499 mmol) of **2** in 30 mL of pentane and 0.306 g (0.499 mmol) of **3** in 30 mL of pentane. The solution was sonicated at 45°C in an ultrasonic cleaning bath for 24 h, resulting in a clear, colorless solution. The volatiles were removed *in vacuo* leaving a white crystalline solid, which was dissolved in pentane and cooled to -20°C . After 3 days, colorless X-ray-quality single crystals of **1** were isolated (0.527 g, 92.6% yield), mp $261\text{--}264.5^\circ\text{C}$ (changes from crystalline to glassy, then melts to a colorless liquid). Anal. Calcd (Found) for $\text{C}_{20}\text{H}_{56}\text{Al}_2\text{AsPSi}_4$: C, 42.23 (41.91); H, 9.92 (10.29); Al, 9.49 (9.10); P, 5.44 (5.66). ^1H NMR (C_6D_6): δ 0.37 (d, 18 H, Me_3SiP , $J_{\text{P-H}} = 4.7$ Hz), 0.42 (s, 18 H, Me_3SiAs), 0.49 (q, 8 H, CH_2), 1.37 (m, 12 H, CH_3). $^{13}\text{C}\{^1\text{H}\}$ NMR: δ 4.38 (s, CH_2), 4.46 (s, Me_3SiAs), 4.67 (d, Me_3SiP , $J_{\text{P-C}} = 4.0$ Hz), 9.63 (m, CH_3). ^{27}Al NMR: δ 214.05 (br s). $^{31}\text{P}\{^1\text{H}\}$ NMR: δ -240.93 (s), -245.83 (s). The electron ionization (20 eV) mass spectrum shows a peak for $(\text{C}_{18}\text{H}_{51}\text{Al}_2\text{AsPSi}_4)^+$ at m/z 539.2, for $(\text{C}_{17}\text{H}_{47}\text{Al}_2\text{AsPSi}_3)^+$ m/z 495.2, for $(\text{C}_{14}\text{H}_{41}\text{Al}_2\text{AsPSi}_4)^+$ at m/z 481.2, for $(\text{C}_{14}\text{H}_{38}\text{Al}_2\text{AsSi}_2)^+$ at m/z 391.1, and for $(\text{C}_{14}\text{H}_{38}\text{Al}_2\text{PSi}_2)^+$ at m/z 347.2. These ions correspond to the fragmentation due to the elimination of an ethyl group, the elimination of a single trimethylsilyl group, the elimination of three ethyl groups, the elimination of $\text{P}(\text{SiMe}_3)_2$, and the elimination of $\text{As}(\text{SiMe}_3)_2$ from **1**, respectively.

Low-Temperature ^1H NMR Study of **1.** In a drybox, solid **1** (16.2 mg, 0.0248 mmol) was added to an NMR tube, which was sealed with a septum. A 0.7 mL amount of toluene- d_8 was added to the NMR tube *via* syringe. The tube was placed in the 500 MHz NMR probe, and ^1H NMR spectra were recorded from 25 to -42°C at 10°C increments, allowing 10 min for equilibration at each temperature. The compound readily dissolved at temperatures above -40°C , allowing for the acquisition of suitable spectra. At -42°C , colorless crystals of **1** began to grow out of solution, preventing further data acquisition at lower temperatures. ^1H NMR (-35°C): δ 0.37 (d, 18 H, Me_3SiP , $J_{\text{P-H}} = 4.5$ Hz), 0.42 (s, 18 H, Me_3SiAs), 0.52 (q, 8 H, CH_2), 1.41 (m, 12 H, CH_3).

X-ray Structural Analysis of **1.** Crystallographic data and measurements for **1** are summarized in Table 1. A single colorless crystal of **1** was affixed to the end of a glass fiber using a viscous oil under an inert nitrogen atmosphere and then transferred to a goniometer head and cooled to -130°C under a nitrogen flow. X-ray intensity data were recorded using the ω -scan mode (Mo K α radiation, $\lambda = 0.71073 \text{ \AA}$). Cell parameters and an orientation matrix corresponded to a

Table 1. Crystallographic Data and Measurements^a for $\text{Et}_2\text{AlP}(\text{SiMe}_3)_2\text{Al}(\text{Et})_2\text{As}(\text{SiMe}_3)_2$ (1**)**

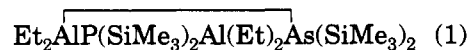
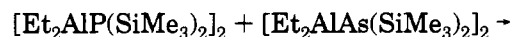
molecular formula	$\text{C}_{20}\text{H}_{56}\text{Al}_2\text{AsPSi}_4$
fw	568.87
cryst syst	monoclinic
space group	$C2/c$ (C_{2h}^6)
a , \AA	17.960(4)
b , \AA	9.328(1)
c , \AA	20.194(5)
β , deg	100.33(2)
V , \AA^3	3328(1)
Z	4
D_{calcd} , Mg m^{-3}	1.135
μ , mm^{-1}	1.266
temp, $^\circ\text{C}$	-130
cryst dimens, mm^3	$0.40 \times 0.40 \times 0.35$
$T_{\text{max}}:T_{\text{min}}$	0.706:0.613
scan type	$\omega-2\theta$
θ_{max} , deg	50
total no. of reflns recorded	3028
no. of nonequiv reflns	2909
R_{merge} , on I	0.058
no. of reflns retained, $I > 2.5\sigma(I)$	2178
no. of params refined	128
R , R_w^b	0.030, 0.037
goodness-of-fit ^c	1.19
max shift/ σ ratio; esd in final least-squares cycle	0.001
final $\Delta\rho$ ($\text{e}/\text{\AA}^3$) max, min	0.54, -0.23

^a Crystallographic calculations were performed on a DEC 3000/400 computer using the NRCVAX suite of structure determination programs.²¹ ^b $R = \sum||F_o| - |F_c||/\sum|F_o|$; $R_w = [\sum w(|F_o| - |F_c|)^2/\sum w|F_o|^2]^{1/2}$; $\sum w\Delta^2[w = 1/\sigma^2(|F_o|)]$, $\Delta = (|F_o| - |F_c|)$ was minimized. ^c Goodness-of-fit = $[\sum w\Delta^2/(N_{\text{observations}} - N_{\text{parameters}})]^{1/2}$.

monoclinic cell, space group $C2/c$ for **1**. The structure of **1** was solved by direct methods, and the refined unit-cell parameters were derived from the diffractometer setting angles for 51 reflections ($40^\circ < 2\theta < 50^\circ$). Intensity data were corrected for absorption using ψ -scans. Positional and thermal parameters were refined using least-squares adjustment techniques; the last least-squares cycle was calculated with 42 atoms, 128 parameters, and 2178 (with $I > 2.5\sigma(I)$) out of the 2909 reflections. In the final iterations, hydrogen atoms were incorporated at their calculated positions using a riding model, with parameter refinement converging at $R = 0.030$ ($R_w = 0.037$). An ORTEP¹⁷ diagram showing the solid-state structure and atom labeling scheme of **1** is shown in Figure 1. Neutral atom scattering factors and their anomalous dispersion corrections were taken from ref 18.

Results and Discussion

The equilibration reaction of $[\text{Et}_2\text{AlP}(\text{SiMe}_3)_2]_2$ (**2**)⁸ and $[\text{Et}_2\text{AlAs}(\text{SiMe}_3)_2]_2$ (**3**)² was carried out in a 1:1 mole ratio in pentane, under ultrasonic conditions at 45°C , and afforded a white crystalline solid, which was recrystallized from pentane and determined to be the aluminum mixed-pnictogen compound **1** (eq 1). A crys-



(17) Johnson, C. K. ORTEP-II: A Fortran Thermal Ellipsoid Plot Program for Crystal Structure Illustrations. Report ONRL-5138; National Technical Information Service, U.S. Department of Commerce: Springfield, Va, 1976.

(18) *International Tables for X-ray Crystallography*; Kynoch: Birmingham, England, 1974; Vol. IV (present distributor, D. Reidel, Dordrecht, The Netherlands).

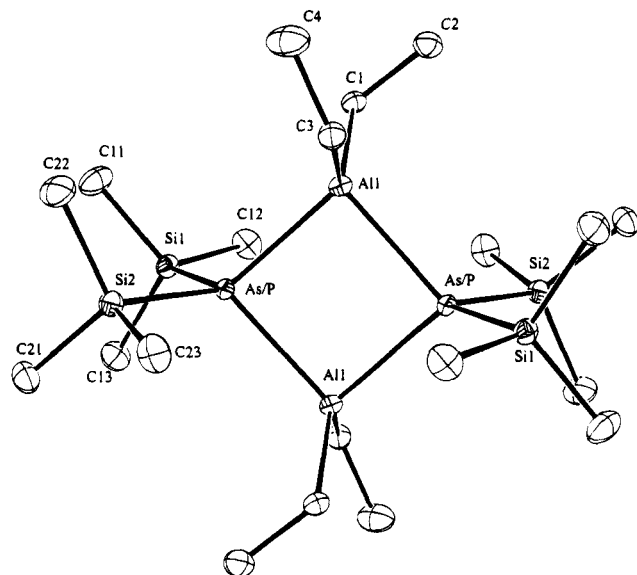


Figure 1. ORTEP diagram (30% probability ellipsoids) showing the solid state structure of $\text{Et}_2\text{AlP}(\text{SiMe}_3)_2\text{Al}(\text{Et})_2\text{As}(\text{SiMe}_3)_3$ (**1**). Hydrogen atoms have been omitted for clarity. Labeled and unlabeled atoms are related by a crystallographic 2-fold axis of symmetry.

tallographic study of **1** reveals that it is isomorphous with the isostructural compounds **2**⁸ and **3**.² Compound **1** lies on a crystallographic C_2 axis of symmetry and contains a planar, four-membered Al–E–Al–E ring (E = P/As). The unit cell parameters of **1** are all slightly smaller than those of **2** and **3** rather than being the averages of the starting dimers, which was the case with the indium mixed-pnicogen compound, **4**. Consistent with compound **4** and **5**, the pnicogen sites in **1** exhibit a 50:50 occupancy ratio for phosphorus and arsenic. The exact identification of the individual pnicogen sites in **1** as P or As is indeterminable by means of X-ray crystallographic analysis, leaving the possibility that crystals of **1** contain either discrete mixed-pnicogen molecules or cocrystallized starting materials, **2** and **3**.

To our knowledge, compound **1** is the first structurally-characterized aluminum mixed-pnicogen ring compound containing two Al centers bridged by two different heavier group 15 atoms. Previously, Schmidbaur and co-workers reported the structure of an aluminum mixed-pnicogen species, but it was an aluminum–nitrogen–phosphorus compound, $\{(\text{CH}_3)_2\text{Al}[\text{P}(\text{C}_6\text{H}_5)_2]\text{N}[\text{P}(\text{C}_6\text{H}_5)_2]\}_2$, containing a six-membered Al–N–P–Al–N–P ring in a twist-conformation.¹⁹ Cowley *et al.* have also reported the syntheses of two compounds containing ternary aluminum core rings; however they were mixed-metal dimers of the type $\text{Me}_2\text{ME}(\text{tBu})_2\text{M}'(\text{Me})_2\text{E}(\text{tBu})_2$ (M, M' = Al, Ga; E = P, As) and no structural information was provided.²⁰

Crystallographic data and data collection parameters for **1** are summarized in Table 1. An ORTEP¹⁷ diagram showing the solid-state conformation and atom-numbering scheme is presented in Figure 1. Table 2 lists the non-hydrogen atoms fractional coordinates and equivalent isotropic thermal parameters with estimated standard deviations in parentheses.

Table 2. Non-Hydrogen Atom Fractional Coordinates and Equivalent Isotropic Thermal Parameters for **1**, with Estimated Standard Deviations in Parentheses

atom	x	y	z	B_{eq} (\AA^2)
As/P	0.81190(2)	0.25627(4)	0.07800(2)	1.36(2)
Al(1)	0.68036(4)	0.16600(8)	0.03872(4)	1.62(3)
Si(1)	0.89269(4)	0.07306Z(8)	0.12009(3)	1.98(3)
Si(2)	0.82685(4)	0.43877(8)	0.15610(4)	2.03(3)
C(1)	0.6022(2)	0.2699(3)	0.0771(1)	2.0(1)
C(2)	0.6015(2)	0.2363(3)	0.1509(2)	2.9(1)
C(3)	0.6764(2)	-0.0455(3)	0.0466(1)	2.2(1)
C(4)	0.5979(2)	-0.1044(4)	0.0452(2)	4.2(2)
C(11)	0.9900(1)	0.1449(4)	0.1453(2)	3.6(2)
C(12)	0.8920(2)	-0.0652(3)	0.0538(2)	3.1(1)
C(13)	0.8617(2)	-0.0130(3)	0.1939(2)	3.3(1)
C(21)	0.8262(2)	0.3654(3)	0.2418(1)	2.9(1)
C(22)	0.9179(2)	0.5338(4)	0.1561(2)	3.6(2)
C(23)	0.7474(2)	0.5676(3)	0.1340(2)	3.2(1)

Table 3. Selected Bond Distances (\AA) and Angles (deg) for **1**, with Estimated Standard Deviations in Parentheses

Bond Lengths			
As/P–Al(1)	2.499(1)	Si(1)–C(12)	1.857(3)
As/P–Al(1a)	2.494(1)	Si(1)–C(13)	1.863(3)
As/P–Si(1)	2.304(1)	Si(2)–C(21)	1.863(3)
As/P–Si(2)	2.303(1)	Si(2)–C(22)	1.860(3)
Al(1)–C(1)	1.974(3)	Si(2)–C(23)	1.857(3)
Al(1)–C(3)	1.981(3)	C(1)–C(2)	1.525(4)
Si(1)–C(11)	1.856(3)	C(3)–C(4)	1.510(4)
Bond Angles			
Al(1)–As/P–Al(1a)	90.44(3)	As/P(1a)–Al(1)–C(1)	113.08(9)
Al(1)–As/P–Si(1)	111.35(3)	As/P(1a)–Al(1)–C(3)	111.96(9)
Al(1)–As/P–Si(2)	116.99(3)	C(1)–Al(1)–C(3)	114.8(1)
Al(1a)–As/P–Si(1)	115.23(3)	As/P–Si(1)–C(11)	109.5(1)
Al(1a)–As/P–Si(2)	114.38(3)	As/P–Si(1)–C(12)	109.1(1)
Si(1)–As/P–Si(2)	107.90(3)	As/P–Si(1)–C(13)	110.9(1)
As/P–Al(1)–As/P	89.56(3)	As/P–Si(2)–C(21)	110.2(1)
As/P–Si(2)–C(22)	110.3(1)	As/P–Si(2)–C(22)	110.3(1)
As/P–Al(1)–C(1)	114.06(8)	As/P–Si(2)–C(23)	108.9(1)
As/P–Al(1)–C(3)	110.81(9)		

lent isotropic thermal parameters with estimated standard deviations. Selected bond lengths and bond angles are provided in Table 3.

Compound **1** crystallizes in the monoclinic space group $C2/c$ (C_{2h}^6) and has a unit cell with four discrete molecules lying on crystallographic centers of symmetry. The pnicogen–aluminum bond lengths of 2.499(1) and 2.494(1) \AA in **1** are the averages of the Al–P bonds in **2** [2.460(1) and 2.454(1) \AA] and the Al–As bonds in **3** [2.539(1) and 2.531(1) \AA], respectively. Such similarities were previously observed when the In–As/P bond lengths of **4** were compared to those in the In–As and In–P bonds in **6** and **7**. The Al and the pnicogen centers in **1** reside in pseudotetrahedral environments. The Al–As/P–Al(a) angles in **1** are 90.44(3) $^\circ$ and are slightly larger than the As/P–Al–As/P(a) angles of 89.56(3) $^\circ$, an effect also observed in the indium mixed-pnicogen ring of **4**, and similar group 13–15 four-membered ring systems.^{3,7,13} The exocyclic angles at the pnicogen and aluminum centers in **1**, Si(1)–As/P–Si(2) (107.90(3) $^\circ$) and C(1)–Al–C(3) (114.8(1) $^\circ$), are nearly identical to the averages of the corresponding angles in **2** and **3** (107.8 $^\circ$ and 114.6 $^\circ$).

Electron ionization mass spectroscopy (20 eV) was used to investigate the gas-phase behavior of **1** as additional evidence of the proposed crystal structure.

(19) Schmidbaur, H.; Lauteschlager, S.; Milewski-Mahrla, B. *Chem. Ber.* **1983**, *116*, 1403.

(20) Arif, A. M.; Benac, B. L.; Cowley, A. H.; Jones, R. A.; Kidd, K. B.; Nunn, C. M. *New J. Chem.* **1988**, *12*, 553.

(21) Gabe, E. J.; Le Page, Y.; Charland, J. P.; Lee, R. L.; White, P. S. *J. Appl. Crystallogr.* **1989**, *22*, 384.

Although a peak for the molecular ion (M^+) was not observed, the mass spectrum of **1** shows an ion peak m/z 539.2, arising from the loss of an ethyl group, and at m/z 495.2 due to the loss of a (Me_3Si) group from the parent ion. A peak at m/z 481.2 can be attributed to the $(M - \text{Et}_3)^+$ ion. The noted presence of single gas-phase ions containing aluminum, arsenic, and phosphorus in the mass spectrum of **1** supports the results of the crystallographic analysis. No peaks corresponding to molecular ions of **2** (m/z for M^+ , 524.9) or **3** (m/z for M^+ , 613.0) were observed above m/z 400 in the mass spectrum. Melting point studies revealed a melting range of 261–264.5 °C for crystals of **1**, which is unique from those of the equilibrated dimers, **2** (280–282.5 °C) and **3** (201 °C). If compound **1** were composed of cocrystallized starting materials, one would expect a broad melting point range rather than the observed range of 3.5 °C.

Solution ^1H , ^{13}C , ^{27}Al , and ^{31}P NMR spectra are consistent with the solid-state structure of **1** described in Figure 1. The room temperature ^1H NMR spectrum of **1** is unique from those of the starting materials, **2** and **3**. The protons of the Me_3Si groups on the phosphorus and arsenic atoms give rise to a doublet at δ 0.37 ppm and a singlet at δ 0.42 ppm, respectively. Notably absent is the triplet which would be expected if the core ring of **1** contained two chemically-equivalent P atoms, as does dimer **2**. The ^{13}C NMR spectrum of **1** also exhibits a doublet at δ 4.67 ppm arising from the carbons in the phosphorus trimethylsilyl groups, indicating the presence of only one P center in the ring. A solution ^{27}Al NMR study of **1** showed a broad signal at δ 214.05 ppm, which is significantly shifted from the ^{27}Al signals for **2** and **3** (δ 164.3 and 187.87 ppm, respectively), but is still well within the expected ppm range for a four-coordinate tetrahedral Al center.

Two peaks are present in the ^{31}P NMR spectrum of **1**: a singlet at δ -240.93 ppm and a slightly smaller singlet at δ -245.83 ppm. The lone phosphorus nucleus in the Al–P–Al–As ring of **1** gives rise to the primary singlet at δ -240.93 ppm. The smaller peak at δ -245.83 ppm corresponds to a minor signal (δ -245.10 ppm) observed in a ^{31}P solution spectrum of **2**, which was obtained upon long-standing of an NMR sample of **2**. This upfield signal may be attributed to the presence of the $\text{Et}_2\text{AlP}(\text{SiMe}_3)_2$ moiety, which is generated by the dissociation of the core rings of both **1** and **2** in solution

to form monomeric species. The ^{31}P NMR spectral features of **1** correspond to those of the spectra for the mixed-pnicogen compounds, **4** and **5**, as do those of the ^1H and ^{13}C NMR spectra. Low-temperature ^1H NMR experiments were performed in order to investigate the possibility of dynamic behavior of compound **1** but proved inconclusive. No changes in peak shape or area were observed between 25 and -35 °C. However, additional cooling caused a broadening of all ^1H signals due to the recrystallization of the compound.

Conclusions

As demonstrated by the work reported herein, equilibration reactions between dimeric analogs, containing the same group 13 metal but different pnicogen atoms, can be used as synthetic routes to mixed-pnicogen compounds. Compound **1** is the first example of a ring containing two aluminum centers bridged by two different heavier group 15 elements, phosphorus and arsenic. Currently, our laboratory is studying the use of equilibration reactions to prepare other examples of mixed-pnicogen and mixed-metal group 13–15 compounds. The potential for these classes of compounds to act as single-source precursors to group 13–15 ternary electronic materials is also being investigated.

Acknowledgment. We are grateful for the financial support of this work provided by the Office of Naval Research AASERT Program. The National Science Foundation (Grant 9116161) and the North Carolina Biotechnology Center (Grant 9210-IDG-1008) are gratefully acknowledged for their financial support for the mass spectrometer. We also thank Dr. George R. Dubay and Dr. James Kenar of the P. M. Gross Chemical Laboratory at Duke University for performing the electron ionization mass spectroscopy of our compounds and Dr. Anthony A. Ribeiro of the Duke NMR Spectroscopy Center for assisting with the NMR studies of the title compound.

Supporting Information Available: Tables of non-hydrogen and hydrogen atom coordinates and isotropic thermal parameters, anisotropic temperature factors, and all interatomic bond distances and bond angles for **1** (4 pages). Ordering information is given on any current masthead page.

OM950248A

Novel Zirconium Borohydride Complexes: Syntheses and Molecular Structures of $[\text{Zr}(\eta\text{-C}_8\text{H}_6(\text{SiMe}_3)_2)(\eta^3\text{-BH}_4)(\eta^2\text{-BH}_4)]$ and $[(\eta\text{-C}_8\text{H}_6(\text{SiMe}_3)_2)\text{Zr}(\mu\text{-}\eta^6\text{:}\eta^4\text{-C}_8\text{H}_6(\text{SiMe}_3)_2)(\mu\text{-H})\text{Zr}(\eta^3\text{-BH}_4)]$

Stephen C. P. Joseph,[†] F. Geoffrey N. Cloke,^{*,†} Christine J. Cardin,[‡] and Peter B. Hitchcock[†]

School of Chemistry and Molecular Sciences, University of Sussex, Brighton BN1 9QJ, U.K., and Department of Chemistry, University of Reading, Reading RG6 2AD, U.K.

Received January 31, 1995[®]

Summary: The reaction between the dimer $[\{\text{Zr}(\text{COT}'')\text{Cl}_2\}_2]$ ($\text{COT}'' = 1,4\text{-bis}(\text{trimethylsilyl})\text{cyclooctatetraene}$) and $[\text{LiBH}_4]$ affords crystallographically characterized $[\text{Zr}(\eta\text{-C}_8\text{H}_6(\text{SiMe}_3)_2)(\eta^3\text{-BH}_4)(\eta^2\text{-BH}_4)]$. The latter reacts with Lewis bases to afford $[(\eta\text{-C}_8\text{H}_6(\text{SiMe}_3)_2)\text{Zr}(\mu\text{-}\eta^6\text{:}\eta^4\text{-C}_8\text{H}_6(\text{SiMe}_3)_2)(\mu\text{-H})\text{Zr}(\eta^3\text{-BH}_4)]$, whose X-ray structure reveals a novel bridging mode for one of the COT'' ligands.

Transition metal borohydride complexes are of interest because they may represent plausible models for CH_4 coordination in the transition state for C–H activation,¹ display extensive reactivity with organic substrates, and are useful starting materials for the preparation of transition metal hydrides and borides.² The tetrahydroborato ligand may also display a variety of coordination modes.³

We are currently investigating the reactivity of early transition metal complexes incorporating the ligand COT'' ($\text{COT}'' = 1,4\text{-bis}(\text{trimethylsilyl})\text{cyclooctatetraene}$), which can exhibit novel coordination modes for the eight-membered ring and can also give rise to unusual solid state structures and reactivity patterns.^{4–6} The bridging chloride dimer $[\{\text{Zr}(\text{COT}'')\text{Cl}_2\}_2]$ ^{5,7} is a particularly useful synthon for the preparation of complexes containing the $[\text{Zr}(\text{COT}'')]$ fragment, and herein we report the syntheses and characterization of novel Zr(COT'')-borohydride and -borohydride(hydride) complexes.

Results and Discussion

The reaction between $[\{\text{Zr}(\text{COT}'')\text{Cl}_2\}_2]$ and excess $[\text{LiBH}_4]$ affords $[\text{Zr}(\eta\text{-C}_8\text{H}_6(\text{SiMe}_3)_2)(\eta^3\text{-BH}_4)(\eta^2\text{-BH}_4)]$, **1**, as large orange moderately air sensitive crystals in 70% yield (see Scheme 1).

[†] University of Sussex.

[‡] University of Reading.

[®] Abstract published in *Advance ACS Abstracts*, June 15, 1995.

(1) Jensen, J. A.; Wilson, S. R.; Girolami, G. S. *J. Am. Chem. Soc.* **1988**, *110*, 4977. Jensen, J. A.; Girolami, G. S. *J. Chem. Soc., Chem. Commun.* **1986**, 1160.

(2) Dick, D. G.; Duchateau, R.; Edema, J. H.; Gambarotta, S. *Inorg. Chem.* **1993**, *32*, 1959 and references therein.

(3) Volatron, F.; Duran, M.; Lledos, A.; Jean, Y. *Inorg. Chem.* **1993**, *32*, 951. See also, ref 2.

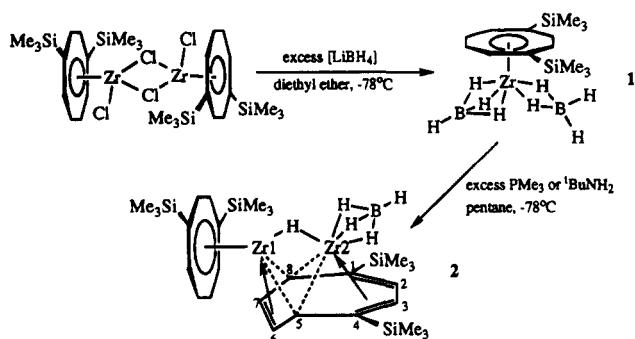
(4) Burton, N. C.; Cloke, F. G. N.; Hitchcock, P. B.; de Lemos, H. C.; Sameh, A. A. *J. Chem. Soc., Chem. Commun.* **1989**, 1462.

(5) Cloke, F. G. N.; Hitchcock, P. B.; Joseph, S. C. P. *J. Chem. Soc., Chem. Commun.* **1994**, 1207.

(6) Cloke, F. G. N.; Hitchcock, P. B.; Kaltsoyannis, N.; Joseph, S. C. P.; McCamley, A.; Mountford, P. *J. Chem. Soc., Dalton Trans.* **1994**, 2867.

(7) Berno, P.; Floriani, C.; Chiesi-Villa, A.; Rizzoli, C. *J. Chem. Soc., Dalton Trans.* **1991**, 3093.

Scheme 1. NMR Assignments for the Bridging Ring in **2**



The ^1H and ^{13}C NMR spectra of **1** show the typical resonances for a planar $\eta^8\text{-COT}''$ ring.⁸ The BH_4 ligands are observed as a broad hump (due to quadrupolar broadening from the ^{11}B nucleus and rapid exchange within the BH_4 ligands themselves) in the ^1H NMR spectrum, but appear as a sharp singlet ($\delta -19.66$ ppm) in the $^{11}\text{B}\{^1\text{H}\}$ NMR spectrum.

A single crystal structure determination of **1** (see Figure 1, Tables 1 and 2 for structural data and Table 3 for experimental data) shows asymmetric coordination modes for the two BH_4 ligands, a feature reflected in the Zr–B1 and Zr–B2 bond distances (2.368(3) and 2.605(3) Å, respectively). Location of the bridging hydrogens in the BH_4 ligands confirmed that both η^2 and η^3 bonding modes are present, but the latter feature could not be readily deduced from the infrared spectrum of **1**. It is also evident from the molecular structure of **1** that the $\eta^8\text{-COT}''$ ring is somewhat distorted. The eight ring carbon atoms (C1–C8) are all approximately equidistant from the metal center (*ca.* 2.441 Å), but the ring as a whole is distinctly dished such that the trimethylsilyl groups are directed downward toward Zr. The perpendicular displacements of Si1 and Si2 from the plane are 0.2376(7) and 0.3677(7) Å, respectively. Since there is no apparent steric constraint which would force the COT'' ring of **1** to adopt this geometry, it may be assumed that electronic factors are the major determinant, and it is likely that this distortion allows improved overlap of the p-orbitals of the ring carbon atoms with the valence orbitals on the metal; the nonplanarity of cyclopolyene ligands bound to transition metal fragments has been discussed by Hoffman *et al.* in these terms.⁹

(8) Burton, N. C.; Cloke, F. G. N.; Joseph, S. C. P.; Karamallakis, H.; Sameh, A. A. *J. Organomet. Chem.* **1993**, *462*, 39. See also refs 4–7 therein.

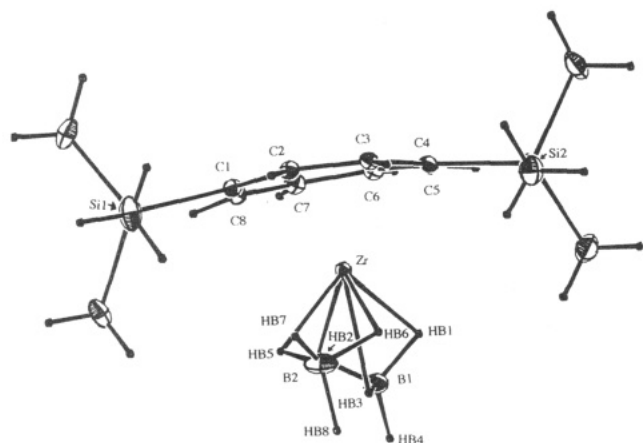


Figure 1. ORTEP¹⁷ drawing of the molecular structure of **1** with non-H atoms as 20% thermal ellipsoids and H atoms as arbitrary sized spheres.

Table 1. Fractional Atomic Coordinates and Equivalent Isotropic Thermal Parameters

	<i>x</i>	<i>y</i>	<i>z</i>	<i>U</i> _{eq} ^a or <i>U</i> _{iso} /Å ²
Zr	0.22343(1)	0.12877(2)	0.15255(2)	0.020(1)
Sn1	0.51699(5)	0.19276(6)	0.20961(5)	0.032(1)
Si2	0.13652(5)	-0.05730(5)	0.35498(5)	0.028(1)
C1	0.4057(2)	0.0982(2)	0.1951(2)	0.025(1)
C2	0.3906(2)	0.0736(2)	0.2964(2)	0.024(1)
C3	0.3142(2)	0.0244(2)	0.3270(2)	0.024(1)
C4	0.2178(2)	-0.0252(2)	0.2687(2)	0.024(1)
C5	0.1694(2)	-0.0604(2)	0.1533(2)	0.027(1)
C6	0.1891(2)	-0.0520(2)	0.0532(2)	0.028(1)
C7	0.2615(2)	0.0026(2)	0.0216(2)	0.028(1)
C8	0.3475(2)	0.0688(2)	0.0792(2)	0.026(1)
C9	0.5811(2)	0.2421(3)	0.3589(2)	0.054(1)
C10	0.4694(2)	0.3126(2)	0.1131(2)	0.049(1)
C11	0.6084(2)	0.1126(3)	0.1669(2)	0.055(1)
C12	0.1965(2)	-0.0007(3)	0.5022(2)	0.048(1)
C13	0.0062(2)	0.0012(3)	0.2812(2)	0.051(1)
C14	0.1300(2)	-0.2089(2)	0.3605(2)	0.052(1)
B1	0.0776(2)	0.2141(3)	0.0138(3)	0.039(1)
B2	0.2639(3)	0.3039(3)	0.2797(3)	0.047(1)
H(B1)	0.059(2)	0.131(2)	0.038(2)	0.060(9)
H(B2)	0.149(2)	0.206(2)	-0.007(2)	0.056(8)
H(B3)	0.116(2)	0.255(2)	0.094(2)	0.051(8)
H(B4)	0.011(2)	0.257(2)	-0.049(2)	0.045(8)
H(B5)	0.282(2)	0.285(2)	0.200(2)	0.043(7)
H(B6)	0.213(2)	0.230(2)	0.287(2)	0.055(8)
H(B7)	0.334(2)	0.304(3)	0.347(2)	0.068(9)
H(B8)	0.213(2)	0.378(2)	0.270(2)	0.054(9)

^a *U*_{eq} is defined as one-third of the trace of the orthogonalized *U*_{ij} tensor.

Table 2. Selected Interatomic Distances and Angles for [Zr(η⁸-C₈H₆(SiMe₃)₂)(η³-BH₄)(η²-BH₄)]

Interatomic Distances (Å)			
Zr-Cen ^a	1.605	Zr-B1	2.368(3)
av Zr-C for η ⁸ -COT' ring	2.441	Zr-B2	2.605(3)
Angles (deg)			
Zr-H(B3)-B1	91(2)	Zr-H(B1)-B1	84(1)
Zr-H(B2)-B1	88(2)	Zr-H(B5)-B2	104(2)
Zr-H(B6)-B2	99(2)		

^a Cen is the centroid of the C1-C8 ring.

Compound **1** reacts with excess PMe₃ or ^tBuNH₂ to afford [(η⁸-C₈H₆(SiMe₃)₂)Zr(μ-η⁶:η⁴-C₈H₆(SiMe₃)₂)(μ-H)-Zr(η³-BH₄)]**2** (see Scheme 1), together with 1 equiv of BH₃-L (by NMR, L = PMe₃ or ^tBuNH₂). **2** is cleanly isolated as a deep red powder following high-vacuum

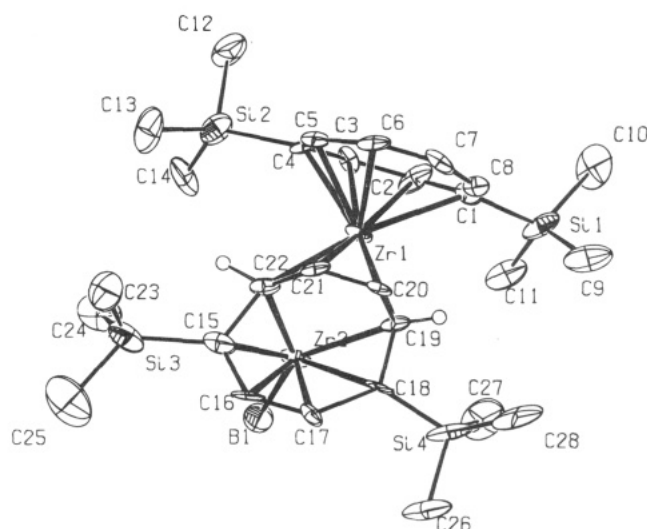


Figure 2. ORTEP¹⁷ drawing of the molecular structure of **2** with atoms as 20% thermal ellipsoids.

Table 3

	C ₁₄ H ₃₂ B ₂ Si ₂ Zr (1)	C ₂₈ H ₅₂ BSi ₄ Zr ₂ (2)
formula	C ₁₄ H ₃₂ B ₂ Si ₂ Zr (1)	C ₂₈ H ₅₂ BSi ₄ Zr ₂ (2)
fw	369.4	694.3
cryst syst	monoclinic	monoclinic
space group	<i>P</i> 2 ₁ / <i>c</i> (No. 14)	<i>P</i> 2 ₁ (<i>a</i> axis unique)
<i>a</i> /Å	14.093(3)	11.399(1)
<i>b</i> /Å	12.220(2)	12.822(1)
<i>c</i> /Å	12.661(2)	24.622(2)
<i>α</i> /deg	90	104.766(5)
<i>β</i> /deg	112.70(2)	90
<i>γ</i> /deg	90	90
cell vol/Å ³	2011.5	3479.7
<i>Z</i>	4	4
density (calcd)/g cm ⁻³	1.22	1.309
<i>F</i> (000)	776	1410
λ(Mo Kα)/Å	0.710 69	0.710 69
μ/cm ⁻¹	6.39	4.3
temp/K	173	293
cryst size/mm	0.35 × 0.25 × 0.2 (in oil)	0.2 × 0.2 × 0.2 (in capillary)
scan mode	θ-2θ	
2θ _{max} /deg	50	50
total no. of reflns	3878	17 887
measd		
no. of unique reflns	3715	5279
no. of significant reflns	3030	4976
soln	heavy-atom methods	heavy-atom and direct methods
refinement	full-matrix least squares	full-matrix least squares
quantity minimized	Σw(<i>F</i> _o - <i>F</i> _c) ²	Σw({ <i>F</i> _o } ² - { <i>F</i> _c } ²) ²
no. of variables	300	622
no. of obsd reflns	3030	4976
<i>R</i> , <i>R</i> '	0.024, 0.031	0.0947, 0.2548

sublimation of the reaction mixture residue. Recrystallization of the sublimate affords translucent red crystals of **2** in ca. 8% yield.

The single crystal X-ray structure determination of **2** is shown in Figure 2, Table 3 lists experimental data, and Tables 4 and 5 list structural data. Only one of the two molecules contained within the asymmetric unit is shown; the second molecule contains residual disorder (see Experimental Section). The molecular structure shows that **2** is dimeric, containing two zirconium metal centers (Zr1 and Zr2) bridged in the first instance by an unusually distorted COT' ring ligand. The second COT' ring ligand present in **2** is essentially planar and is bound in an η⁸ fashion to Zr1 (the average Zr1-η⁸-ring carbon distance is ca. 2.47 Å). The bridging COT' ring

Table 4. Atomic Coordinates ($\times 10^4$) and Equivalent Isotropic Displacement Parameters ($\text{\AA}^2 \times 10^3$) for **1**

	x	y	z	U_{eq}
Zr1	9148(2)	6631(1)	5030(1)	18(1)
Zr2	7564	8543	5039	24(1)
B1	7780(28)	10346(18)	5031(11)	41(7)
Si1	10931(7)	6141(6)	3577(3)	39(2)
Si3	6361(7)	8790(6)	6483(4)	52(2)
Si2	10995(7)	7467(6)	6463(3)	41(2)
Si4	6310(7)	7461(6)	3621(3)	46(2)
C1	10629(18)	5951(15)	4292(8)	22(4)
C2	11213(19)	6678(17)	4725(7)	25(4)
C3	11220(17)	6957(15)	5312(8)	23(4)
C4	10647(17)	6658(14)	5748(7)	16(3)
C5	9922(17)	5774(15)	5736(8)	20(3)
C6	9481(19)	4881(15)	5305(8)	26(4)
C7	9504(16)	4617(14)	4721(9)	24(4)
C8	9911(18)	5108(16)	4311(8)	23(4)
C9	9898(24)	5466(25)	3141(12)	59(7)
C10	12371(27)	5596(31)	3356(12)	70(8)
C11	11045(26)	7607(23)	3613(11)	52(6)
C12	12499(28)	6967(25)	6631(11)	60(7)
C13	9948(37)	7295(27)	7032(10)	70(8)
C14	11135(27)	8895(21)	6479(12)	62(8)
C15	6558(20)	8139(18)	5739(9)	34(4)
C16	5635(16)	8165(15)	5336(8)	22(4)
C17	5648(15)	7937(12)	4777(6)	13(3)
C18	6570(18)	7457(17)	4333(8)	29(4)
C19	7471(19)	6735(16)	4446(8)	24(3)
C20	7189(16)	5916(14)	4746(7)	17(3)
C21	7226(16)	6190(15)	5313(7)	18(3)
C22	7469(18)	7270(15)	5599(8)	23(3)
C23	6055(37)	7783(27)	6861(11)	74(9)
C24	7633(30)	9630(25)	6712(14)	66(7)
C25	5126(31)	9663(31)	6695(18)	98(11)
C26	5049(29)	8235(26)	3515(13)	65(7)
C27	7671(22)	8004(31)	3339(14)	76(8)
C28	5984(34)	6178(23)	3191(12)	71(8)
Zr3	8210(3)	3353(2)	9919(1)	54(1)
Zr4	9787	1455	9908	57(1)
B2	9628(52)	-370(26)	9928(20)	89(13)
Si5	6383(10)	3768(7)	11357(3)	62(2)
Si6	6257(11)	2517(9)	8486(3)	72(3)
Si7	11070(9)	1187(9)	8473(3)	66(3)
Si8	11184(9)	2508(8)	11337(3)	58(2)
C29	6847(29)	3926(26)	10643(13)	63(6)
C30	6150(32)	3179(25)	10244(13)	66(6)
C31	6250(30)	2937(27)	9602(11)	66(6)
C32	6772(33)	3367(29)	9189(13)	71(6)
C33	7544(37)	4284(26)	9241(14)	77(6)
C34	7920(30)	5046(27)	9666(14)	68(6)
C35	8008(36)	5343(28)	10231(14)	77(7)
C36	7552(34)	4844(25)	10644(14)	69(6)
C37	7743(36)	4404(30)	11911(12)	81(9)
C(38)	5069(36)	4360(31)	11513(12)	73(8)
C39	6515(47)	2436(30)	11451(18)	100(12)
C40	7512(46)	2864(32)	8079(17)	102(10)
C41	5080(40)	2842(38)	8382(17)	108(12)
C42	6360(50)	981(29)	8410(15)	109(13)
C43	10980(26)	2403(24)	10537(10)	65(6)
C44	11849(21)	1677(20)	10091(8)	45(6)
C45	11560(27)	1667(23)	9597(10)	66(7)
C46	10720(28)	1886(25)	9227(12)	60(6)
C47	9781(32)	2653(25)	9303(10)	60(5)
C48	10172(33)	3812(29)	9591(14)	74(6)
C49	10203(30)	4002(29)	10152(12)	65(6)
C50	9877(33)	3263(27)	10477(12)	68(6)
C51	12391(36)	1582(31)	11346(15)	85(9)
C52	9772(33)	2102(32)	11667(13)	80(9)
C53	11413(35)	4036(27)	11701(11)	78(9)
C54	9745(37)	543(31)	8119(11)	81(9)
C55	11142(49)	2468(34)	8084(17)	100(11)
C56	12324(11)	377(9)	8429(4)	76(8)

^a U_{eq} is defined as one-third of the trace of the orthogonalized U_{ij} tensor.

Table 5. Interatomic Distances and Angles for $[(\eta\text{-C}_8\text{H}_6(\text{SiMe}_3)_2)\text{Zr}(\mu\text{-}\eta^6\text{-}\eta^4\text{-C}_8\text{H}_6(\text{SiMe}_3)_2)(\mu\text{-H})\text{Zr}(\eta^3\text{-BH}_4)]$

Interatomic Distances (\AA)			
Zr1-Zr2	3.041(2)	Zr2-B1	2.33(2)
Zr1-C19	2.42(2)	Zr1-C22	2.39(2)
Zr2-C19	2.41(2)	Zr2-C22	2.39(2)
Angles (deg)			
C19-Zr1-C22	69.7(6)	C19-Zr2-C22	69.8(6)
C19-Zr1-C20	35.1(6)	C21-Zr1-C22	34.2(6)
B1-Zr2-Zr1	137.5(8)	C17-Zr2-C19	66.0(6)
C16-Zr2-C22	64.1(6)		

in **2** is bound through six carbon atoms (C15, C16, C17, C18, C19, and C22) to Zr2 and through four approximately coplanar carbon atoms to Zr1 (C19, C20, C21, and C22). The bond distances Zr1-C19, Zr1-C22, Zr2-C19, and Zr2-C22 are all essentially identical (*ca.* 2.40 \AA). Although bridging COT rings are known (*e.g.* in $[\text{M}_2(\text{C}_8\text{H}_8)_3]$, M = Cr, W),¹⁰ the geometry of the bridging ring in **2** is very unusual. The disorder in the crystal prevents a detailed description of the precise bonding that exists in the bridging COT' ligand; however the orientation of the two "bridgehead hydrogens" (H19 and H22) located from a difference Fourier map shows that carbon atoms C19 and C22 are sp^3 hybridized. C19 and C22 may thus be described as belonging to bridging alkyl groups. Although the hydrogen atoms associated with the BH_4 ligand could not be located, the Zr2-B1 distance of 2.33(2) \AA is indicative of an η^3 -coordination mode; compare, *e.g.*, the Zr-B1 bond distance of 2.368(3) \AA for the $\eta^3\text{-BH}_4$ group in **1**. Unfortunately, the hydride ligand could not be convincingly located from a difference Fourier map, but the gross molecular structure of **2** and NMR evidence (*vide infra*) suggest the hydride to be bridging. The Zr1-Zr2 distance of 3.041(2) \AA is remarkably short in comparison to other zirconium compounds which contain bridging hydride ligands.¹¹

Solution NMR data for **2** are consistent with the solid state structure described above. The ^1H and ^{13}C NMR spectra display the expected resonances for the $\eta^8\text{-COT}'$ ring⁸ and also reflect the unusual distortion of the second, bridging COT' ring. A singlet at δ 5.5 ppm in the proton spectrum is associated with the two equivalent protons in the 2 and 3 positions of the bridging ring (see Scheme 1). The remaining two sets of two protons (positions 6, 7 and 5, 8) for this ring are complex multiplets observed at *ca.* δ 5.0 and 2.2 ppm, respectively; the latter chemical shift is consistent with the hybridization of the carbon atoms bearing these protons noted in the discussion of the X-ray structure above. The broad singlet centered at *ca.* δ 6.22 ppm is attributed to the bridging hydride, observed as a triplet (due to coupling to protons in ring positions 5 and 8) under resolution enhancement. As in **1**, the protons associated with the BH_4 ligand in **2** are not well resolved in the room temperature ^1H NMR spectrum. The $^1\text{H}\{^{11}\text{B}\}$ NMR spectrum for **2** does, however, contain an additional resonance to the ^1H NMR spectrum centered at *ca.* δ -0.6 ppm, which can be assigned to the BH_4 ligand protons. The ring carbons of the bridging COT' ring in **2** occur as a set of four resonances in the ^{13}C -

(10) Elschenbroich, Ch.; Salzer, A. *Organometallics, A Concise Introduction*, 2nd ed.; VCH: New York, 1991; pp 367-369.

(11) Bochmann, M.; Lancaster, S. J.; Hursthouse, M. B.; Mazid, M. *Organometallics* **1993**, *12*, 4718 and references therein.

{¹H} NMR spectrum, and of particular note is the signal at *ca.* δ 66 ppm due to carbons 5 and 8 which have some bonding interaction with both Zr1 and Zr2 (see above); again, the chemical shift is indicative of substantial sp³ character, which is also reflected in the relatively low value for *J*_{CH} of 139 Hz (*J*_{CH} for the remaining carbons in this ring fall in the range 160–170 Hz).

The results presented herein illustrate the highly versatile ligating properties of the COT'' ring resulting from the steric and electronic effects of the SiMe₃ substituents, and further studies on the chemistry of mono-COT'' complexes of group 4 are in progress.

Experimental Section

All experiments were carried out under pure argon using Schlenk techniques, or in a MBraun glovebox under an atmosphere of dinitrogen (<2 ppm H₂O, <1 ppm O₂). Diethyl ether and *n*-pentane were predried over sodium wire, distilled from sodium/potassium alloy, and stored over potassium mirrors. Deuteriated solvents (²H₈toluene and ²H₆benzene) were refluxed over potassium and trap-to-trap distilled prior to use. [LiBH₄] and ⁴BuNH₂ were purchased from Aldrich and used without further purification. The compounds PMe₃¹² and [{Zr(COT'')Cl₂]₂] were prepared according to literature methods. NMR spectra were recorded on Bruker WM 360 or AC 250 instruments at probe temperature unless stated otherwise and were referenced internally to residual solvent resonances (¹H and ¹³C), external SiMe₄ (²⁹Si), or external [BF₃·Et₂O] (¹¹B). Low-resolution EI mass spectra were recorded on solid samples using a Kratos MS80RF spectrometer. Elemental analyses were carried out by the Canadian Microanalytical Service Ltd., Delta, BC, Canada.

Synthesis of [Zr(η-C₈H₆(SiMe₃)₂)(η³-BH₄)(η²-BH₄)]₂, 1. In a Schlenk flask was placed [{Zr(COT'')Cl₂]₂] (0.4 g, 0.48 mmol) and [LiBH₄] (0.056 g, 2.6 mmol). Diethyl ether (50 mL) was added at room temperature and the mixture stirred overnight. The solvent was removed *in vacuo* and the green-orange residue extracted with pentane and filtered through Celite on a glass frit. The pale orange filtrates were concentrated and cooled slowly to -30 °C to afford crystals of 1. Yield: 0.25 g, 70%. Mp: 119 °C. ¹H NMR (²H₆benzene, 293 K): δ 6.85 (2H, s, C₈H₆(SiMe₃)₂), 6.81 (2H, m, C₈H₆(SiMe₃)₂), 6.50 (2H, m, C₈H₆(SiMe₃)₂), 0.32 (18H, s, C₈H₆(SiMe₃)₂). ¹³C{¹H} NMR (²H₈toluene, 293 K): δ 109.2 (s, CSiMe₃ ring), 107.9 (s, CH ring), 105.4 (s, CH ring), 101.6 (s, CH ring), -0.15 (s, SiMe₃ ring). ²⁹Si{¹H} NMR (²H₈toluene, 293 K): δ 10.6 (s, SiMe₃). ¹¹B{¹H} NMR (²H₈toluene, 293 K): δ -19.7 (s, BH₄). ¹¹B NMR (²H₈toluene, 293 K): δ -19.7 (q, BH₄, ¹J(B,H) = 86 Hz). EI-MS (70 eV), *m/z* (%): 368 (7) [M⁺], 353 (100) [M⁺ - BH₄], 73 (65) [SiMe₃⁺]. Anal. Calcd for C₁₄H₃₂B₂Si₂Zr: C, 45.52; H, 8.73. Found: C, 45.38; H, 8.53.

Crystallographic data were collected on an Enraf-Nonius CAD4 diffractometer. A total of 3030 reflections with *I* > 3σ(*I*) were used; there was no correction for absorption and no crystal decay. Solution was by heavy atom methods (SHELXS-86¹³), and refinement, by full-matrix least squares with anisotropic thermal parameters for all non-hydrogen atoms using the molEN program package¹⁴ and scattering factors.¹⁵ The hydrogen atoms were all located and freely refined isotropically.

Synthesis of [(η-C₈H₆(SiMe₃)₂)Zr(μ-η⁶:η⁴-C₈H₆(SiMe₃)₂)-(μ-H)Zr(η³-BH₄)]₂, 2. To an orange pentane solution (30 mL)

of 1 (0.25 g, 0.67 mmol) cooled to -196 °C was added an excess of PMe₃ (*ca.* 1 mL) by vacuum transfer. The reaction mixture was then allowed to warm to room temperature and stirred overnight. Solvent and excess PMe₃ were removed *in vacuo* and the red-brown residue sublimed (180 °C/10⁻⁵ mmHg) to afford a red microcrystalline sublimate which was recrystallized from *n*-pentane at -30 °C to afford red air sensitive crystals of 2. The latter may also be obtained in an entirely analogous fashion using ⁴BuNH₂ in place of PMe₃. Yield: 0.038 g, 8%. Mp: 160 °C. ¹H NMR (²H₈toluene, 293 K): δ 6.52 (2H, s, C₈H₆(SiMe₃)₂), 6.22 (1H, s, Zr-H), 6.17 (2H, m, C₈H₆(SiMe₃)₂), 5.77 (2H, m, C₈H₆(SiMe₃)₂), 5.49 (2H, s, C₈H₆(SiMe₃)₂), 4.92 (2H, m, C₈H₆(SiMe₃)₂), 2.18 (2H, m, C₈H₆(SiMe₃)₂), 0.41 (18H, s, C₈H₆(SiMe₃)₂), 0.22 (18H, s, C₈H₆(SiMe₃)₂). ¹³C{¹H} NMR (²H₈toluene, 293 K): δ 122.3 (CH ring), 110.5 (s, CH ring), 106.2 (s, CSiMe₃ ring), 103.9 (s, CSiMe₃ ring), 101.1 (s, CH ring), 97.9 (s, CH ring) 97.0 (s, CH ring), 66.1 (s, CH ring), 0.5 (s, C₈H₆(SiMe₃)₂), 0.2 (s, C₈H₆(SiMe₃)₂). ¹H{¹¹B} NMR (²H₈toluene, 293 K): δ -0.59 (4H, s, BH₄). ¹¹B{¹H} NMR (²H₈toluene, 293 K): δ -15.7 (s, BH₄). ¹¹B NMR (²H₈toluene, 293 K): δ -15.7 (q, BH₄, ¹J(B,H) = 83 Hz). EI-MS (70 eV), *m/z* (%): 694 (12) [M⁺], 680 (20) [M⁺ - BH₄], 337 (25) [M⁺ - Zr(COT'')(BH₄H)], 73 (100) [SiMe₃⁺]. Anal. Calcd for C₂₈H₅₂BSi₄Zr₂: C, 48.37; H, 7.68. Found: C, 47.83; H, 7.53.

Crystallographic data were collected with a Mar Research image plate scanner and graphite-monochromated Mo Kα radiation. A total of 190 primary frames were measured, with an exposure time of 180 s per frame. Data were processed using the XDS package,¹⁶ to give 5279 unique reflections in space group *P*2₁, *R*(int) = 0.0231, *R*(σ) = 0.0256. The structure was solved and refined using the SHELXS and SHELXL packages,¹³ and the final *R* factor was 0.0947 for 4969 reflections measured for 3.13 < θ < 23.70° and +*h*, ±*k*, ±*l* for which |*F*| > 4σ(*F*), or 0.1021 for all 5279 data; there was no crystal decay, and no absorption correction was applied. Hydrogen atoms were placed geometrically with the exception of those on the "bridgehead" carbons of the bent COT'' ring, which were located from a difference map. The H atoms of the BH₄⁻ ligand could not be convincingly located. The asymmetric unit within the crystal contains two molecules in the space group used, but there is residual disorder associated with the second molecule in the crystal. The first molecule refines satisfactorily. The disorder in the second molecule manifested itself as a difficulty in refining the C atom positions C39–C42, which is evident from their high thermal parameters. The only way this could be modeled was by introducing bond length constraints for just this part of the second molecule. This problem persisted in spite of three different data collections on three different crystals. Further details of the crystal structure investigations are available on request from the Director of the Cambridge Crystallographic Data Centre, 12 Union Road, GB-Cambridge CB2 1EZ, U.K., on quoting the full journal citation.

Acknowledgment. We thank EPSERC and BP (Dr. J. P. McNally) for financial support (S.C.P.J.).

Supporting Information Available: Tables of crystal structure determination details, all bond distances and angles, atom parameters, displacement parameters, and least squares planes for 1 and 2 (29 pages). Ordering information is given on any current masthead page.

OM950081L

(12) Luetkens, M. L., Jr.; Sattelberger, A. P.; Murray, H. H.; Basil, J. D.; Fackler, J. P., Jr. *Inorg. Synth.* **1987**, *26*, 7.

(13) Courtesy of Professor G. M. Sheldrick, University of Göttingen.

(14) Enraf-Nonius molEN structure Determination System (1990).

(15) *International Tables for X-Ray Crystallography*; Kynoch Press: Birmingham, England, 1974; Vol. IV.

(16) Kabsch, W. *J. Appl. Crystallogr.* **1988**, *21*, 67.

(17) Johnson, C. K. ORTEP II; Report ORNL-5738; Oak Ridge National Laboratory: Oak Ridge, TN, 1976.

A New Chiral Tridentate Ferrocenyl Ligand. Synthesis and Characterization of Its Palladium(II) and Nickel(II) Complexes

Pierluigi Barbaro[†] and Antonio Togni^{*}

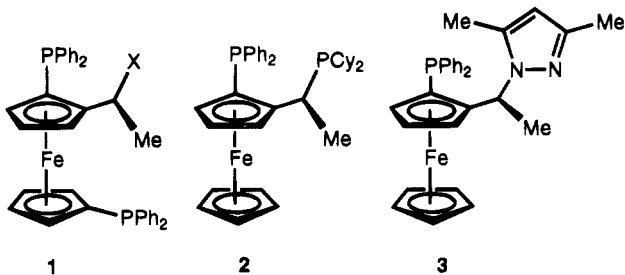
Laboratory of Inorganic Chemistry, Swiss Federal Institute of Technology, ETH-Zentrum, CH-8092 Zürich, Switzerland

Received March 21, 1995[©]

Summary: A novel chiral tridentate phosphine ligand based on ferrocene (**5**) can be readily obtained from cyclohexylphosphine and *N,N*-dimethyl-(*S*)-1-(*R*)-2-(diphenylphosphino)ferrocenylethylamine (**4**) in acetic acid. Ligand **5** adopts a meridional coordination geometry with *d*⁸-metal centers. The crystal structure of [Pd(**5**)Cl]PF₆ (**6**) has been determined.

Introduction

Chiral, enantiomerically pure ferrocenyl ligands have been very successful in asymmetric catalysis. Hayashi, Ito, and co-workers have demonstrated that bidentate ligands of type **1**, bearing the phosphino substituents



in the 1,1'-positions, can be adapted to the specific needs of a series of catalytic reactions by virtue of the variable side chain X.¹ We reported more recently a new generation of easily accessible and highly effective chelating ligands based on ferrocene, compounds **2** and **3** being representative examples.² The main feature of such new P,P and P,N ligands is their highly tunable character, with respect to both steric and electronic properties. The key reaction in their synthesis is the introduction of the ligating fragment attached to the stereogenic center. This is carried out in acetic acid using either a secondary phosphine or a pyrazole as the nucleophile. We extended this methodology to primary phosphines and now report the preparation and char-

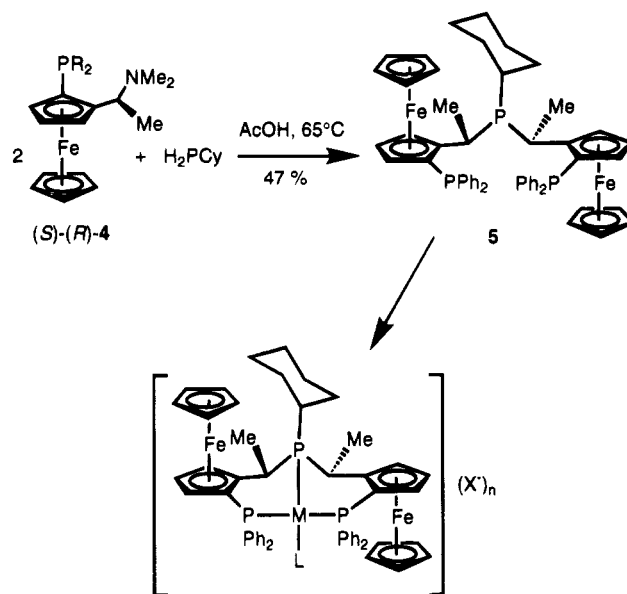
[†] Present address: ISSECC-CNR, via J. Nardi, 39, I-50132 Firenze, Italy.

[©] Abstract published in *Advance ACS Abstracts*, June 15, 1995.

(1) For reviews, see: (a) Hayashi, T. In *Ferrocenes. Homogeneous Catalysis, Organic Synthesis, Materials Science*; Togni, A., Hayashi, T., Eds.; VCH: Weinheim, 1995; pp 105–142. (b) Sawamura, M.; Ito, Y. *Chem. Rev.* **1992**, *92*, 857–871.

(2) (a) Togni, A.; Breutel, C.; Schnyder, A.; Spindler, F.; Landert, H.; Tijani, A. *J. Am. Chem. Soc.* **1994**, *116*, 4062–4066. (b) Breutel, C.; Pregosin, P. S.; Salzmann, R.; Togni, A. *J. Am. Chem. Soc.* **1994**, *116*, 4067–4068. (c) Togni, A.; Breutel, C.; Soares, M. C.; Zanetti, N.; Gerfin, T.; Gramlich, V.; Spindler, F.; Rihs, G. *Inorg. Chim. Acta* **1994**, *222*, 213–224. (d) Abbenhuis, H. C. L.; Burckhardt, U.; Gramlich, V.; Togni, A.; Albinati, A.; Müller, B. *Organometallics* **1994**, *13*, 4481–4493. (e) Abbenhuis, H. C. L.; Burckhardt, U.; Gramlich, V.; Köllner, C.; Pregosin, P. S.; Salzmann, R.; Togni, A. *Organometallics* **1995**, *14*, 759–766. (f) Schnyder, A.; Hintermann, L.; Togni, A. *Angew. Chem.* **1995**, *107*, 996–998; *Angew. Chem., Int. Ed. Engl.* **1995**, *34*, 931–933.

Scheme 1



6 (M = Pd; L = Cl⁻; (X')_n = PF₆⁻)

7a (M = Pd; L = MeCN; (X')_n = (PF₆⁻)₂)

7b (M = Pd; L = MeCN; (X')_n = (BF₄⁻)₂)

8 (M = Ni; L = MeCN; (X')_n = (ClO₄⁻)₂)

acterization of a novel tridentate phosphine that can potentially adopt both *meridional* or *facial* coordination geometries. This ligand is still a quite rare example of a chiral tridentate phosphine.³ We envisage applications in asymmetric Lewis-acid catalysis using late transition metal centers (see below).

Results and Discussion

Synthesis. The new chiral bis(ferrocenyl) chelating ligand "Pigiphos" (**5**)⁴ has been prepared as shown in Scheme 1. The reaction of the starting (*S*)-(*R*)-PPFA (**4**)⁵ with cyclohexylphosphine in acetic acid at 65 °C proceeds with retention of configuration on the side

(3) For a general review on polydentate phosphines, see: Cotton, F. A.; Hong, B. *Prog. Inorg. Chem.* **1992**, *40*, 179–289. For examples of chiral-tripodal phosphines, see, e.g.: (a) Burk, M. J.; Harlow, R. L. *Angew. Chem.* **1990**, *102*, 1511–1513. (b) Burk, M. J.; Feaster, J. E.; Harlow, R. L. *Tetrahedron: Asymmetry* **1991**, *2*, 569–592. (c) Ward, T. R.; Venanzi, L. M.; Albinati, A.; Lianza, F.; Gerfin, T.; Gramlich, V.; Ramos Tombo, G. M. *Helv. Chim. Acta* **1991**, *74*, 983–988.

(4) In order to avoid its long systematic name (Bis{(S)-1-(R)-2-(diphenylphosphino)ferrocenylethyl}cyclohexylphosphine), compound **5** is called "Pigiphos" in our laboratory, after the nickname of one of the authors (P.B.).

(5) Hayashi, T.; Mise, T.; Fukushima, M.; Kagotani, M.; Nagashima, N.; Hamada, Y.; Matsumoto, A.; Kawakami, S.; Konishi, M.; Yamamoto, K.; Kumada, M. *Bull. Chem. Soc. Jpn.* **1980**, *53*, 1138–1151.

chain stereocenters, leading to an (*S*)-(*R*) configuration on both the ferrocenyl units. The final product could be isolated in satisfactory yield after purification by column chromatography and recrystallization. Noteworthy, the use of phenylphosphine as the nucleophile under the same reaction conditions gave only a small amount of the elimination product 1-(diphenylphosphino)-2-vinylferrocene, along with unidentified species.

The two ferrocenyl moieties of "Pigiphos" are diastereotopic, as demonstrated by the ^{31}P and ^1H NMR spectra. The ^{31}P NMR spectrum of "Pigiphos" can be seen as the superposition of two AX spin systems ($A = \text{CyP}$, $X = \text{Ph}_2\text{P}$) in which the two Ph_2P phosphorus atoms have the same chemical shift but very different coupling constants to the central CyP nucleus ($^4J_{\text{PP}} = 28.1$ and $^4J_{\text{PP}} = 9.9$ Hz, respectively). The larger coupling is attributed to a 1,3-bis(phosphino) fragment assuming a conformation similar to that encountered for the ligand Josiphos (**2**, for which $^4J_{\text{PP}} = 30$ Hz).^{2a} The other subunit obviously adopts a different conformation, probably because of steric reasons.

The observed ^1H NMR parameters are rather routine and are in the range observed for the parent ligand Josiphos.^{2a} However, the ^1H NMR spectrum shows separated sets of resonances for each of the two ferrocenyl fragments, thus indicating the lack of any symmetry element relating them.

Orange crystals of the Pd complex **6** were afforded by treatment of $[\text{PdCl}_2(\text{NCCCH}_3)_2]$ with TlPF_6 in the presence of the ligand "Pigiphos". The compound is air-stable both in the solid state and in solution. The ^{31}P NMR spectrum of **6** consists of an ABX pattern, the two low-frequency resonances being attributed to the Ph_2P atoms showing a mutual $^2J_{\text{PP}}$ coupling constant of 411.5 Hz, consistent with their *trans* position. The observed moderate line broadening of the ^{31}P signals is indicative of a possible dynamic behavior of the molecule.

The dicationic derivative **7** is obtained either from complex **6** utilizing TlPF_6 as a chloride scavenger in CH_3CN solution (**7a**) or by treatment of the acetonitrile complex $[\text{Pd}(\text{NCCCH}_3)_4](\text{BF}_4)_2$ ⁶ with the ligand "Pigiphos" (**7b**). Compounds **7a,b** are stable under a nitrogen atmosphere in the solid state but decompose very slowly in solution. The IR spectrum shows bands at 2318 and 2289 cm^{-1} , assigned to $\nu(\text{C}\equiv\text{N})$ of a coordinated acetonitrile. The ^{31}P NMR spectrum of **7** consists of an ABX pattern similar to that observed for **6**, *trans* $^2J_{\text{PP}}$ coupling constant being 336.9 Hz, thus showing that the two complexes share the same primary structure. On the other hand, the CyP chemical shift falls ca. 14 ppm downfield compared to the corresponding resonance of **6**, indicating that this parameter is rather sensitive to the nature of the *trans* ligand.

The nickel complex **8** was prepared by treatment with the ligand "Pigiphos" of a $\text{Ni}^{2+}-\text{CH}_3\text{CN}$ adduct generated *in situ*. The compound is stable under a nitrogen atmosphere in the solid state but decomposes very slowly in solution, as was the case for derivatives **7**. The observed IR bands at 2319 and 2285 cm^{-1} $\nu(\text{C}\equiv\text{N})$ fall in the same range as those of **7**. The ^{31}P NMR spectrum of **8** shows the expected ABX pattern with a *trans* $^2J_{\text{PP}}$ coupling constant of 235.9 Hz. Comparison of the ^{31}P and ^1H NMR spectra of **8** with those of **7** suggests that

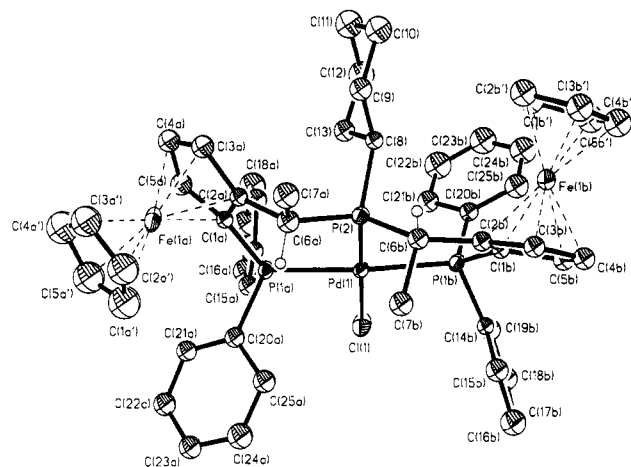


Figure 1. ORTEP view of the cation $[(\text{Pigiphos})\text{PdCl}]^+$ (**6**) and atom numbering scheme. Selected bond lengths (\AA) and angles (deg): $\text{Pd}(1)-\text{Cl}(1) = 2.339(5)$, $\text{Pd}(1)-\text{P}(1a) = 2.333(4)$, $\text{Pd}(1)-\text{P}(1b) = 2.331(4)$, $\text{Pd}(1)-\text{P}(2) = 2.255(4)$; $\text{Cl}(1)-\text{Pd}(1)-\text{P}(1a) = 84.8(1)$, $\text{Cl}(1)-\text{Pd}(1)-\text{P}(1b) = 89.0(1)$, $\text{Cl}(1)-\text{Pd}(1)-\text{P}(2) = 177.4(2)$, $\text{P}(1a)-\text{Pd}(1)-\text{P}(1b) = 168.2(2)$, $\text{P}(1a)-\text{Pd}(1)-\text{P}(2) = 95.4(1)$, $\text{P}(1b)-\text{Pd}(1)-\text{P}(2) = 91.4(1)$.

there are no drastic changes in the overall structure of the complexes on going from Pd to Ni.

Solid State Structure of 6. Compound **6** was characterized by X-ray crystal structural analysis and an ORTEP view of the cation $[\text{PdCl}(\text{Pigiphos})]^+$ is depicted in Figure 1. The coordination around the metal center approximates a square planar geometry in which the chlorine atom and the P(2) atom (CyP) assume a mutual *trans* position. A significant distortion from the idealized geometry is indicated by the displacement of the Cl-Pd vector from the plane containing the three phosphorus atoms, such that the chlorine atom is ca. 0.47 \AA above this plane. The nonideal square planar geometry is also reflected by the distance of the Pd atom from the same plane (0.18 \AA), and by the angles $\text{P}(2)-\text{Pd}-\text{P}(1a)$ and $\text{P}(2)-\text{Pd}-\text{P}(1b)$ of 95.4(1) and 91.4(1) $^\circ$, respectively.

Nevertheless, considering the best idealized coordination plane of Pd (maximum deviations of the donor atoms -0.12 to $+0.14$ \AA), it is instructive to analyze the position of different parts of the molecule with respect to this plane. Thus one observes that (a) one of the unsubstituted Cp rings (Cp_a) as well as the two methyl groups lie below this plane, while the other Cp ring (Cp_b) and the cyclohexyl group are above, and (b) the four phenyl rings are pairwise above and below the plane, overall assuming an approximately C_2 symmetric arrangement. Furthermore, important differences in the conformation of the two 1,3-bis(phosphino)ferrocenyl moieties are evident: (a) the phenyl rings bonded to P(1b) are closer to an axial/equatorial arrangement with respect to the coordination plane of Pd than those bonded to P(1a) [$\text{Cl}(1)-\text{Pd}(1)-\text{P}(1b)-\text{C}(20b) = 82.4(3)$, $\text{Cl}(1)-\text{Pd}(1)-\text{P}(1b)-\text{C}(14b) = -33.1(3)$, $\text{Cl}(1)-\text{Pd}(1)-\text{P}(1a)-\text{C}(20a) = 64.8(3)$, $\text{Cl}(1)-\text{Pd}(1)-\text{P}(1a)-\text{C}(14a) = -53.1(4)^\circ$], and (b) the side chains of the two moieties also adopt different conformations, as illustrated by the two torsion angles $\text{C}(1b)-\text{C}(2b)-\text{C}(6b)-\text{P}(2) = -28.3(2)$ and $\text{C}(1a)-\text{C}(2a)-\text{C}(6a)-\text{P}(2) = 60.8(3)^\circ$. The differing conformational features of the two side chains are also reflected by the relative positions of the two methyl

(6) Wayland, B. B.; Schramm, R. F. *Inorg. Chem.* **1969**, *8*, 971-976.

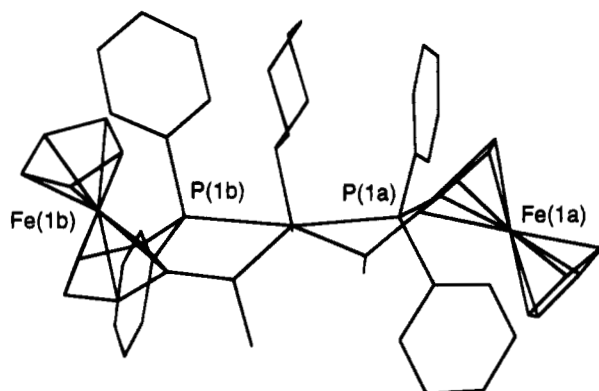


Figure 2. Schematic representation of the cation **6**, projected along the Cl(1)–Pd(1) axis.

groups (see the torsion angles C(1b)–C(2b)–C(6b)–C(7b) = 83.7(4) and C(1a)–C(2a)–C(6a)–C(7a) = 11.8(4)⁹). These structural characteristics are clearly visible in the schematic representation of Figure 2.⁷

Conclusions

The readily prepared ligand "Pigiphos" is suited for the formation of cationic d⁸-metal complexes in which the metal center is held in a rigid coordination environment. The system is thus suited for reactions involving the singular fourth coordination site. Preliminary experiments show that the dicationic Ni(II) complex **8** behaves as a Lewis acid and readily catalyzes the hetero Diels–Alder reaction of aldehydes with activated dienes.⁸ These investigations, as well as studies concerning the behavior of "Pigiphos" in an octahedral coordination geometry are under way and will be reported in due course.

Experimental Section

All manipulations were performed under an N₂ atmosphere using standard Schlenk techniques. ¹H and ³¹P NMR spectra were recorded at 250.13 and 101.3 MHz, respectively, on a Bruker 250-ACP spectrometer (unless otherwise stated), and IR spectra on a Perkin-Elmer Paragon 1000 FT-IR spectrometer using KBr pellets. Merck silica gel 60 (70–230 mesh) was used for column chromatography. Optical rotations were measured with a Perkin-Elmer 341 polarimeter using 10 cm cells. Elemental analyses were performed by the "Mikroelementar-analytisches Laboratorium der ETH".

Pigiphos⁴ (**5**). Cyclohexylphosphine (360 μL, 2.7 mmol) was added to a solution of (*S*)-(*R*)-PPFA (**4**, 2.22 g, 5.03 mmol) in acetic acid (50 mL) and the mixture stirred at 65 °C for 7 h. The solvent was then evaporated at 65 °C under reduced pressure and the residue chromatographed over silica using *n*-hexane:EtOAc = 3:1 as eluent (*R*_f = 0.68). Recrystallization from CH₂Cl₂/EtOH under a stream of nitrogen gave 855 mg of pure product (47% yield). [α]_D²⁰ = +398 (*c* = 1.0, CHCl₃). Anal. Calcd for C₅₄H₅₅Fe₂P₃: C, 71.38; H, 6.10. Found: C, 70.99; H, 6.30. ³¹P NMR (CDCl₃): δ 15.60 (dd, 1P, *J*_{PP} = 28.1, *J*_{PP} = 9.9), –26.04 (2d, 2P). ¹H NMR (CDCl₃): δ 0.55–1.60 (m, 11H), 1.53 (dd, 3H, *J* = 7.2), 1.64 (t, 3H, *J* = 7.4), 2.81 (dq_{quint}, 1H, *J* = 4.6, *J* = 7.4), 3.15 (qd, 1H, *J* = 7.4, *J* = 2.7),

3.82 (bs, 6H), 3.86 (s, 5H), 3.96 (bm, 2H), 4.07 (bm, 1H), 4.22 (t, 1H), 4.26 (bm, 1H), 7.12–7.70 (m, 20H).

[(Pigiphos)PdCl]PF₆ (**6**). "Pigiphos" (300 mg, 0.33 mmol) was slowly dissolved in acetone (40 mL), and solid [PdCl₂(CH₃CN)₂] (85 mg, 0.33 mmol) was then added. After the mixture was stirred for 10 min, solid TlPF₆ (115 mg, 0.33 mmol) was added. TlCl was then filtered off and the solution evaporated to ca. 10 mL under a stream of nitrogen. Addition of diethyl ether (30 mL) gave the product as an orange solid. Crystals were obtained by recrystallization from CH₂Cl₂/EtOH (252 mg, 64%). Anal. Calcd for C₅₄H₅₅ClF₆Fe₂P₄Pd: C, 54.26; H, 4.60. Found: C, 54.12; H, 4.56. ³¹P NMR (202.5 MHz, CD₂Cl₂): (ABX spin system) δ(*P*₂) 80.70 (*J*_{P₂P_{1a}} = 12.0, *J*_{P₂P_{1b}} = 29.0), δ(*P*_{1a}) 15.15 (*J*_{P_{1a}P_{1a}} = 411.5 Hz), δ(*P*_{1b}) 9.77. ¹H NMR (500.138 MHz, CD₂Cl₂): δ 0.66 (br q, 1H), 0.80 (qt, 1H), 1.03 (qt, 1H), 1.19 (q, 1H), 1.62 (m, 1H), 1.64 (dd, 3H), 1.67 (m, 1H), 1.85 (m, 2H), 2.05 (dd, 3H), 2.08 (m, 1H), 2.36 (br d, 1H), 3.02 (br q, 1H), 3.34 (m, 1H), 3.64 (dq, 1H), 3.73 (s, 5H), 3.95 (s, 5H), 4.28 (br s, 1H), 4.60 (m, 1H), 4.66 (t, 1H), 4.73 (q, 1H), 4.77 (m, 1H), 4.92 (m, 1H), 7.10–7.90 (several m, 20H).

[(Pigiphos)Pd(CH₃CN)]Y₂ (**Y** = PF₆ (**7a**), BF₄ (**7b**)). **7a**. Solid TlPF₆ (26 mg, 0.08 mmol) was added to a stirred solution of **6** (90 mg, 0.08 mmol) in CH₃CN (10 mL). After 1 h the mixture was filtered over Celite and the solvent removed under vacuum. Recrystallization from CH₃CN/diethyl ether gave **7a** as purple microcrystals in 62% yield. Anal. Calcd for C₅₆H₅₅NF₁₂Fe₂P₅Pd: C, 49.97; H, 4.34; N, 1.04. Found: C, 49.86; H, 4.36; N, 0.98.

7b. Solid Pigiphos (82 mg, 0.09 mmol) was added to a solution of [Pd(CH₃CN)₄](BF₄)₂ (40 mg, 0.09 mmol) in CH₃CN (10 mL). After the mixture was stirred until no ligand was detectable (1 h), the solvent was evaporated to ca. half under vacuum. Slow addition of diethyl ether (20 mL) gave **7b** as a purple solid in 85% yield. Anal. Calcd for C₅₆H₅₅NB₂F₈Fe₂P₃Pd: C, 54.69; H, 4.75; N, 1.14. Found: C, 54.55; H, 4.90; N, 1.20. ³¹P NMR (101.3 MHz, CD₂Cl₂): (ABX spin system) δ-(*CyP*) 94.57 (*J*_{PP} = 28.0, *J*_{PP} = 1.6), δ(*P*'') 7.43 (*J*_{PP} = 336.9), δ(*P*''') 16.34. ¹H NMR (500.138 MHz, CD₂Cl₂): δ 0.30 (qt, 1H), 0.45 (bm, 1H), 0.98 (qt, 1H), 1.08 (bm, 1H), 1.4–1.6 (m, 2H), 1.48 (s, 3H), 1.7–1.9 (m, 3H), 1.82 (dd, 3H, *J* = 6.9, *J* = 16.7), 2.13 (dd, 3H, *J* = 14.2), 2.44 (bd, 1H), 2.71 (bq, 1H), 3.33 (dq, 1H, *J* = 9.6, *J* = 7.6), 3.88 (s, 5H), 3.98 (bm, 1H, *J* = 9.5), 4.17 (s, 5H), 4.29 (bs, 1H), 4.70 (bs, 1H), 4.76 (t, 1H), 4.82 (q, 1H), 4.99 (bs, 1H), 5.08 (bs, 1H), 6.85 (m, 2H), 7.30–8.00 (m, 18H). IR: 2318, 2289 (ν(C≡N)) cm⁻¹.

[(Pigiphos)Ni(NCCH₃)](ClO₄)₂ (**8**). A solution of Ni(ClO₄)₂·6H₂O (30 mg, 0.08 mmol) in *n*-BuOH (20 mL) was gently concentrated by heating at boiling temperature to ca. 1 mL. The procedure was repeated twice; then 1 mL of CH₃CN was added. The resulting pale blue-green solution turned brown-red by treatment with Pigiphos (74 mg, 0.08 mmol) in CH₂Cl₂ (10 mL). Addition of diethyl ether (10 mL) followed by the slow flow of ether vapors through the solution under a stream of nitrogen gave deep purple crystals in a 70% yield. Anal. Calcd for C₅₆H₅₅NCl₂Fe₂O₈P₃Ni: C, 55.71; H, 4.84; N, 1.16. Found: C, 55.34; H, 4.92; N, 1.03. ³¹P NMR (CD₂Cl₂): (ABX spin system) δ(*CyP*) 83.42 (*J*_{PP} = 24.8, *J*_{PP} = 10.3), δ-(*P*'') 9.23 (*J*_{PP} = 235.9), δ(*P*''') 18.10. ¹H NMR (CD₂Cl₂): δ 0.50 (bm, 2H), 0.97 (q, 1H), 1.06 (bm, 1H), 1.4–1.6 (m, 3H), 1.51 (s, 3H), 1.7–1.8 (m, 2H), 1.91 (dd, 3H, *J* = 6.9, *J* = 16.7), 2.05 (dd, 3H, *J* = 14.2), 2.38 (bd, 1H), 2.77 (bq, 1H), 3.31 (quint, 1H, *J* = 9.6, *J* = 7.6), 3.71 (bm, 1H, *J* = 9.5), 3.88 (s, 5H), 4.17 (s, 5H), 4.21 (bs, 1H), 4.64 (bs, 1H), 4.75 (bs, 1H), 4.79 (bm, 1H), 4.96 (bs, 1H), 5.05 (bs, 1H), 6.88 (m, 2H), 7.40–8.10 (m, 18H). IR: 2319, 2285 cm⁻¹ (ν(C≡N)).

X-ray Crystallographic Study of 6. Red crystals of **6** suitable for X-ray crystallography were obtained by recrystallization from CH₂Cl₂/EtOH. Crystal data for C₅₄H₅₅ClF₆P₄Pd (*f*_w 1195.4): orthorhombic, space group P2₁2₁2₁, with cell dimensions at 293 K of *a* = 13.344(7) Å, *b* = 19.516(10) Å, *c* = 19.717(11) Å, and *V* = 5135(5) Å³ with *Z* = 4 and *D*_{calcd} = 1.546 Mg/m³, μ(Mo Kα) = 11.39 cm⁻¹ (graphite monochromated), λ

(7) Preliminary 500 MHz ¹H NOESY experiments on complex **6** indicate that the conformational features found in the solid state are essentially retained in solution.

(8) For an example of a chiral transition metal Lewis acid as catalyst for hetero Diels–Alder reactions, see, e.g.: (a) Togni, A. *Organometallics* **1990**, *9*, 3106–3113. (b) Togni, A.; Rist, G.; Rihs, G.; Schweiger, A. *J. Am. Chem. Soc.* **1993**, *115*, 1908–1915 and references quoted therein.

= 0.710 73 Å, $F(000) = 2432$. The data were collected on a Syntex P21 diffractometer using the ω scan mode (2θ range = 3.0–40.0°). Data were measured with variable scan speeds (1.0–4.0°/min in ω) to ensure constant statistical precision on the collected intensities. No absorption correction was applied. The structure was solved using direct methods. Of the 2718 independent reflections, 2117 with $F > 3.0\sigma(F)$ were used in the refinement. A total of 343 parameters were refined by full-matrix least squares using SHELXTL PLUS (data-to-parameter ratio 6.2:1, quantity minimized $\sum w(F_o - F_c)^2$). Due to the relatively low number of reflections, all carbon atoms were refined using isotropic displacement parameters. The contribution of the hydrogen atoms in their idealized positions (riding model with fixed isotropic $U = 0.080 \text{ \AA}^2$) was taken into account but not refined. The final residuals (on all data) were $R = 0.059$ and $R_w = 0.046$ (weighting scheme $w^{-1} = \sigma^2(F) + 0.0005F^2$; GOF = 1.01).

Acknowledgment. This research was supported by the Swiss National Science Foundation (Special Program "CHiral2", Grant No. 21-36700.92). We are grateful to U. Burckhardt and V. Gramlich for the X-ray structural analysis of compound **6**.

Supporting Information Available: Tables of crystal data and refinement details, atomic coordinates, bond distances and angles, anisotropic displacement coefficients for non-carbon atoms, and coordinates of hydrogen atoms for compound **6** (11 pages). Ordering information is given on any current masthead page. A table of calculated and observed structure factors (9 pages) may be obtained from the authors upon request.

OM950210Y

Oxidative Coupling of an Acyl Ligand with a Carbene Ligand on a Chromium Center To Produce α -Alkoxy Enones

G. M. Wieber, L. S. Hegedus,* and Celeste Gale

Department of Chemistry, Colorado State University, Fort Collins, Colorado 80523

Received February 16, 1995[®]

Summary: Treatment of chromium alkoxy carbene complexes having α -protons with 2 equivs of organolithium reagents led first to α -deprotonation followed by attack of the organolithium reagent at a metal-bound carbon monoxide to produce a species which, upon oxidation, led to coupling of the two organic fragments to produce α -alkoxy enones.

Introduction

Chromium alkoxy carbene complexes undergo facile deprotonation on the α -carbon ($pK_a \approx 12$)¹ by a wide range of bases, and facile nucleophilic attack at the carbene carbon,² in spite of the fact that both molecular orbital calculations³ and ESCA studies⁴ indicate that the greatest positive charge on these complexes is localized on the carbon of the carbonyl ligands. The rationale offered^{3,5} is that nucleophilic attack is frontier orbital controlled rather than charge controlled, and the LUMO of Fischer carbene complexes is spatially and energetically localized on the carbene carbon.⁶ When the carbene carbon bears a formally negatively charged group, such as "O⁻" as found in the anionic acylate complex precursors to carbene complexes, nucleophilic attack is directed to the CO ligand, with the ultimate production of bis(carbene) complexes.⁷ An alternate way to install a negatively charged group on the carbene carbon is to remove an α -proton. This, too, should suppress nucleophilic attack at the carbene carbon and redirect it to some other site in the complex (Figure 1). In an attempt to α -deprotonate pentacarbonyl(methylmethoxycarbene)chromium(0), 2 equivs of *n*-butyllithium was inadvertently used. Upon oxidative workup of the resulting complex, an α -alkoxy enone consisting of the carbene fragment, a butyl group from butyllithium, and a carbon monoxide was obtained (eq 1).

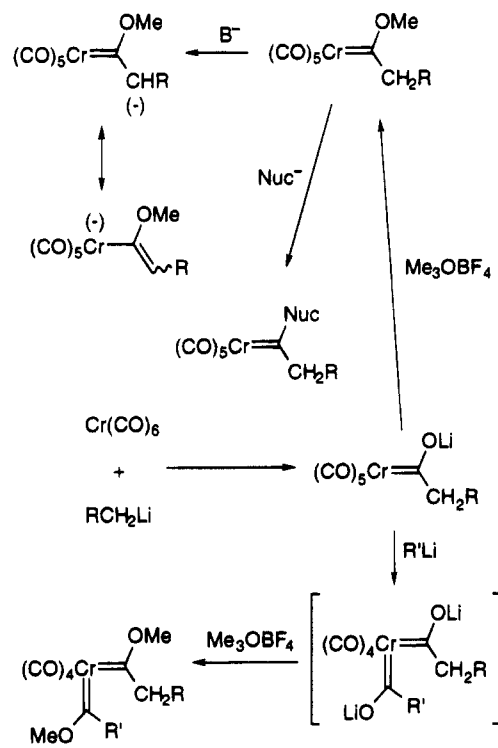
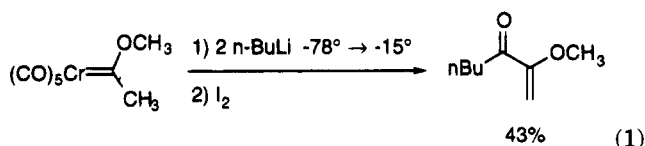


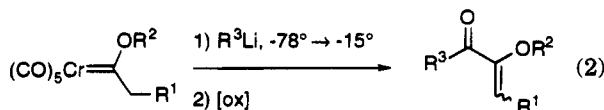
Figure 1.

Studies probing the course and generality of this reaction are described below.



Results and Discussion

To determine if this phenomenon was a special case or if it was general, a variety of alkoxy carbene complexes was treated with 2 equivs of an organolithium reagent and the resulting complexes were oxidized (eq 2). In general, iodine was used as oxidant, but in some



cases iodine-containing organic byproducts were obtained, necessitating the use of other oxidants. The results are summarized in Table 1. The process was quite general for carbene complexes having α -protons and for a number of organolithium reagents. (The modest yields are, at least in part, due to the relative

[®] Abstract published in *Advance ACS Abstracts*, June 1, 1995.

(1) (a) For an early measurement, see: Casey, C. P.; Anderson, R. L. *J. Am. Chem. Soc.* **1974**, *96*, 1230. (b) Gandler, J. R.; Bernasconi, C. F. *Organometallics* **1989**, *8*, 2282.

(2) For a review, see: Fischer, H. *Mechanistic Aspects of Carbene Complex Reactions*. In *Transition Metal Carbene Complexes*; Seyferth, D., Ed.; Verlag Chemie: Deerfield Beach, FL, 1983; pp 252-259.

(3) (a) Block, T. F.; Fenske, R. F.; Casey, C. P. *J. Am. Chem. Soc.* **1976**, *98*, 441. (b) Block, T. F.; Fenske, R. F. *J. Organomet. Chem.* **1977**, *139*, 235.

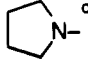
(4) Berry, W. B.; Schaaf, T. F.; Jolly, W. L.; Todd, L. J.; Cronin, D. L. *Inorg. Chem.* **1974**, *13*, 2038.

(5) Kostic, N. M.; Fenske, R. F. *Organometallics* **1982**, *1*, 974.

(6) For a review see: Hoffmann, D. *Electronic Structures of Transition Metal Carbene Complexes*. In *Transition Metal Carbene Complexes*; Seyferth, D., Ed.; Verlag Chemie: Deerfield Beach, FL, 1983; pp 114-149.

(7) (a) Fischer, E. O.; Kreissl, F. R.; Kreiter, C. G.; Meineke, E. W. *Chem. Ber.* **1972**, *105*, 2558. (b) Darst, K. P.; Lenhart, P. G.; Lukehart, C. M.; Warfield, L. T. *J. Organomet. Chem.* **1980**, *195*, 317. For synthesis of bis(carbene) complexes from bis(organolithium) compounds, see: (c) Hoa Tram Huy, N.; Pascard, C.; Tran Huu Dau, E.; Dotz, K. H. *Organometallics* **1988**, *7*, 590 and references therein.

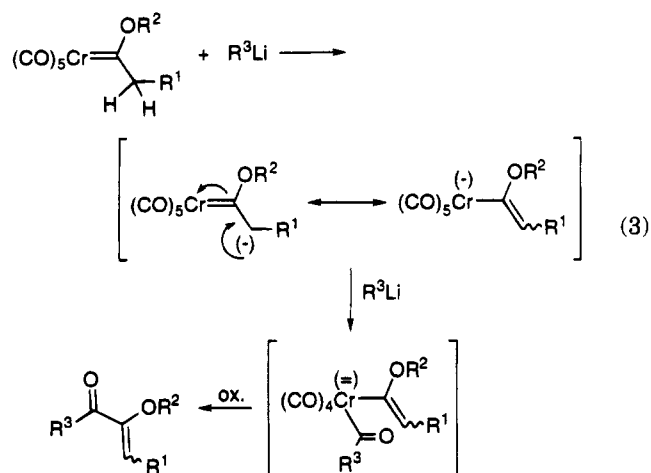
Table 1. Production of α -Alkoxy Enones as in Eq 2

R ¹	R ²	R ³	[ox]	Yield, % ^a
H	Bn	nBu	I ₂	50
H	Me	nBu	I ₂	43
H	Me	nC ₁₀ H ₂₁	BQ ^b	20
H	Bn	Ph	I ₂	14 ^c
H	tBuMe ₂ Si	nBu	I ₂	30
H	Bn		I ₂	7
	-(CH ₂) ₂	nBu	I ₂	43
	-(CH ₂) ₃	nBu	I ₂	51
CH ₃	Bn	nBu	Cr ^{VI} ^e	20
Ph	CH ₃	nBu	Cr ^{VI}	12

^a Yields are for isolated, purified material. ^b BQ = benzoquinone.
^c The major product (65%) was PhC(OBn)CH₂. ^d One equiv of *n*-BuLi was used for the initial deprotonation. ^e Cr^{VI} = Bu₄NCrO₃Cl.

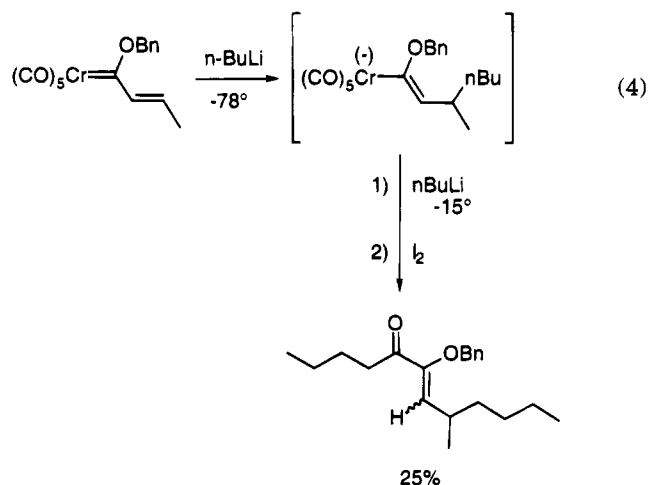
instability of the α -alkoxy enone products, which not only easily hydrolyze during isolation but, being captodative alkenes,⁸ readily undergo free radical reactions.⁹ In fact most compounds in Table 1 polymerized within a few hours, even when stored at -30 °C in the dark.) Thus butyllithium, *n*-decyllithium, and lithium pyrrolidide all led to the expected product. In contrast phenyllithium produced only a low yield of α -alkoxy enone, the major product (68%) being α -(benzyloxy)-styrene, resulting from the coupling of the carbene group and phenyllithium *without* incorporation of carbon monoxide. Methylithium failed to produce α -alkoxy enones. The sole product isolated was the ester corresponding to the oxidation product of the initial carbene complex.

The reaction is thought to proceed as shown in eq 3. Initial deprotonation of the α -position of the carbene



complex by the first equiv of organolithium reagent "protects" the carbene carbon from nucleophilic attack. The second equivalent of organolithium attacks at a metal-bound carbon monoxide, producing the dianionic (σ -acyl)(σ -vinyl)chromium complex, oxidation of which

leads to reductive elimination and coupling of the two organic fragments. When phenyllithium was used, the major product was that resulting from direct coupling of the carbene fragment and phenyllithium, without incorporation of carbon monoxide. In this case it is likely that the intermediate σ -benzoyl- σ -vinyl complex deinserted carbon monoxide prior to oxidation, giving a σ -phenyl- σ -vinyl intermediate. (From studies with anionic bis(acyl)rhenium complexes¹⁰ the deinsertion of a benzoyl group was thermodynamically more favored than that of an acetyl group.) Attempts to γ -deprotonate the (benzyloxy)propenylcarbene complex instead resulted in Michael addition of butyllithium to the carbene complex, followed by alkylation of a carbonyl group. Oxidation of this intermediate gave coupling product containing two *n*-butyl groups (eq 4). In this case, as



well as the last two entries in Table 2, only a single stereoisomer about the double bond was isolated, although in principle both are possible. Stereochemistry could not be assigned from spectroscopic data. It is likely that these compounds have (*Z*)-olefin geometry, since the (*Z*)-olefin isomer of the (σ -acyl)(σ -vinyl)-chromium complex intermediate (R¹ syn to the small OR² and anti to the bulky chromium fragment) would be the less sterically hindered.

This coupling reaction was restricted to α -carbanions of alkoxy carbene complexes. Treatment of chromium hexacarbonyl with 2 equivs of organolithium reagent (in an attempt to make the dianionic bis(acyl) species) followed by oxidation did not produce α -diketones. Similarly *N*-deprotonation of the phenyl(methylamino)-carbene complex followed by addition of excess butyl- or decyllithium and oxidation failed to yield any coupling product.

Experimental Section

General Methods. All reactions were performed under argon with argon-saturated solvents. Purification of crude reaction mixtures was achieved by column chromatography, using Alfa 70 μ m or 58 μ m silica gel or by radial-layer chromatography on a Model 7924 Chromatotron using Merck silica gel 60PF.

Triethylamine-treated silica gel was made by forming a slurry of silica in 4:1 hexane/Et₃N and removing excess solvent by filtration and drying under vacuum. Alkyl- and aryllithium

(8) Viehe, H. G.; Janousek, Z.; Merenyi, R. *Acc. Chem. Res.* **1985**, *18*, 148.

(9) Brodsky, L.; Agosta, W. C. *J. Org. Chem.* **1974**, *39*, 2928.

(10) Casey, C. P.; Scheck, D. M. *J. Am. Chem. Soc.* **1980**, *102*, 2723.

reagents were titrated with *sec*-butanol (Aldrich) in benzene using 1,10-phenanthroline (Fischer) as an indicator.

The carbene complexes studied were prepared by literature procedures.¹¹

General Procedure for the Synthesis of α -Alkoxy Enones. In each case, the appropriate carbene was dissolved in freshly distilled, argon-saturated solvent in a 10 mL Airlessware flask under an argon atmosphere. After the solution was cooled to the specified temperature, the alkyl lithium solution was added dropwise via syringe, generally down the cooled sides of the flask. After reaction at specified times and temperatures, the oxidant was generally added to the flask as a solid. The products were isolated by dilution of the crude reaction mixture with Et₂O (20 mL) washing with aqueous Na₂S₂O₃ to remove excess oxidant and drying over anhydrous MgSO₄. Remaining soluble chromium residues were precipitated by exposure of the solution to air and daylight for 2–8 h. Filtration through Celite and Et₃N-treated silica gel, concentration under vacuum, and purification by radial chromatography (1 mm silica gel plate, 1% triethylamine in hexane) gave pure material.

2-(Benzyloxy)-1-hepten-3-one. *n*-Butyllithium (2.0 M in hexanes, 0.93 mL, 1.9 mmol) was added to a –78 °C solution of [(benzyloxy)(methyl)carbene]pentacarbonylchromium(0) (242 mg, 0.74 mmol) in 7.0 mL of THF. The mixture was warmed to –16 °C for 30 min and then recooled to –78 °C before adding iodine (400 mg, 1.6 mmol). After being stirred at –78 °C for 5 min and warming to room temperature, the mixture was subjected to the standard isolation and purification procedure and gave 80.2 mg (50%) of the product.

¹H NMR (200 M Hz, CDCl₃): δ 0.90 (t, 3H, *J* = 7.3 Hz, CH₃), 1.31 (m, 2H, CH₃CH₂), 1.60 (m, 2H, CH₃CH₂CH₂), 2.71 (t, 2H, *J* = 7.3 Hz, CH₂CO), 4.49 (d, 1H, *J* = 2.5 Hz, =CH₂), 4.85 (s, 2H, CH₂Ph), 5.27 (d, 1H, *J* = 2.5 Hz, =CH₂), 7.38 (m, 5H, ArH) ppm. ¹³C NMR (75.5 M Hz, CDCl₃): δ 13.9 (CH₃), 22.3 (CH₃CH₂), 25.8 (CH₃CH₂CH₂), 37.8 (CH₂CO), 70.0 (CH₂Ph), 91.3 (=CH₂), 127.2, 128.0, 128.5, 136.2 (ArC), 157.6 (C=CH₂), 198.0 (CO) ppm. IR (film): ν 1732 (br, CO), 1609 cm⁻¹. Mass spectrum (EI): *m/z* 218, [M]⁺.

2-Methoxy-1-hepten-3-one. *n*-Butyllithium (1.95 M in hexanes, 1.20 mL, 2.34 mmol) was added to a –78 °C solution of [(methoxy)(methyl)carbene]pentacarbonylchromium(0) (234 mg, 0.94 mmol) in 9.0 mL of THF. The mixture was warmed to –15 °C for 30 min and then recooled to –78 °C. Iodine (499 mg, 1.97 mmol) was added, and the mixture was stirred for 5 min at –78 °C before warming to room temperature. Standard isolation and purification gave 56.6 mg (43%) of pure product.

¹H NMR (270 M Hz, CDCl₃): δ 0.92 (t, 3H, *J* = 7.3 Hz, CH₃CH₂), 1.34 (sextet 2H, *J* = 7.4, CH₃CH₂), 1.59 (pentet, 2H, *J* = 7.5 Hz, CH₃CH₂CH₂), 2.67 (t, 2H, *J* = 7.4 Hz, CH₂CO), 3.64 (s, 3H, CH₃O), 4.47 (d, 1H, *J* = 2.8 Hz, =CHH), 5.20 (d, 1H, *J* = 2.8 Hz, =CHH) ppm. ¹³C NMR (67.9 M Hz, CDCl₃): δ 13.7 (CH₃CH₂), 22.3 (CH₃CH₂), 25.8 (CH₃CH₂CH₂), 37.6 (CH₂CO), 55.2 (CH₃O), 90.4 (=CH₂), 158.6 (C=CH₂), 197.7 (CO) ppm. IR (film): ν 1709, 1613 cm⁻¹. Mass spectrum (EI): *m/z* 142, [M]⁺. FAB high-resolution mass spectrum: Calcd for C₈H₁₅O₂, *m/z* 143.1072; found, *m/z* 143.1083 \pm 0.0010.

2-Methoxy-1-tridecen-3-one. *n*-Decyllithium (1.6 M in Et₂O, 0.60 mL, 0.96 mmol) was added dropwise to a room temperature solution of [(methoxy)(methyl)carbene]pentacarbonylchromium(0) (230 mg, 0.92 mmol) in 10 mL of THF over 10 min and then cooled to –30 °C for 15 min before a second 0.60 mL portion of decyllithium was added over 10 min. After the mixture was stirred at –30 °C for 20 more min and cooled to –78 °C, benzoquinone (118 mg, 1.09 mL in 1 mL of THF) was added. The mixture was allowed to slowly warm to room temperature over 18 h and then filtered through a plug of silica gel with Et₂O. Concentration under vacuum and purification by radial chromatography (1 mm silica gel plate eluted with a

hexane to 9% Et₂O in hexane gradient) gave 50 mg of product contaminated with about 20% of an unidentified alkane compound (~20% yield).

¹H NMR (300 M Hz, CDCl₃): δ 0.88 (t, 3H, *J* = 6.6 Hz, CH₃CH₂), 1.25–1.50 (m, 14H (–CH₂–)₇), 1.60 (m, 2H, CH₂CH₂CO), 2.65 (t, 2H, *J* = 7.4 Hz, CH₂CO), 3.64 (s, 3H, CH₃O), 4.45 (d, 1H, *J* = 2.7 Hz, =CHH), 5.19 (d, 1H, *J* = 2.7 Hz, =CHH) ppm. ¹³C NMR (75.5 M Hz, CDCl₃): δ 14.1 (CH₃CH₂), 22.6, 23.8, 29.2, 29.3, 29.4, 29.5, 29.6, 31.9 ((–CH₂–)₈), 38.0 (CH₂CO), 55.2 (CH₃O), 90.4 (=CH₂), 158.6 (C=CH₂), 197.8 (CO) ppm.

2-(Benzyloxy)-3-phenyl-1-propen-3-one and 1-(Benzyloxy)-1-phenylethene. Phenyllithium (0.84 M in Et₂O, 1.85 mL, 1.6 mmol) was added to a –78 °C solution of [(benzyloxy)(methyl)carbene]pentacarbonylchromium(0) (203 mg, 0.62 mmol) in 6.0 mL of THF. The mixture was warmed to –17 °C for 30 min and then 0 °C for 30 min before recoiling to –78 °C. Iodine (332 mg, 1.3 mmol) was added and the mixture warmed to room temperature. Isolation by the standard procedure gave 21.6 mg (14%) of the α -alkoxy enone and 89.3 mg of α -(benzyloxy)styrene (~65% yield).

¹H NMR (300 M Hz, CDCl₃): δ 4.86 (d, 1H, *J* = 2.9 Hz, =CHH), 4.98 (s, 2H, CH₂Ph), 5.09 (d, 1H, *J* = 2.9 Hz, =CHH), 7.3–7.6 (m, 8H, ArH), 7.87 (dd, 2H, *J* = 1.3, 8.4 Hz, ArH) ppm. ¹³C NMR (75.5 M Hz, CDCl₃): δ 70.2 (CH₂Ph), 96.1 (=CH₂), 127.3, 128.0, 128.6, 129.0, 129.8, 132.7, 136.0, 136.6 (ArC), 157.9 (C=CH₂), 191.3 (CO) ppm. IR (film): ν 1734, 1670, 1607 cm⁻¹. Mass spectrum (EI): *m/z* 238, [M]⁺.

The α -(benzyloxy)styrene was found to be even more unstable than the α -alkoxy enones, so further purification was not pursued and only spectroscopic techniques were used for characterization of this material.

¹H NMR (270 M Hz, CDCl₃): δ 4.59 (d, 1H, *J* = 3.3 Hz, =CHH), 4.79 (d, 1H, *J* = 3.3 Hz, =CHH), 4.88 (s, 2H, CH₂Ph), 7.0–7.7 (m, 10H, ArH) ppm. ¹³C NMR (75.5 M Hz, CDCl₃): δ 73.8 (CH₂Ph), 94.8 (=CH₂), 127.1, 127.2, 128.1, 128.5, 128.5, 128.7, 130.2, 134.9, 137.4, 140.4, 141.2 (ArC, =C) ppm. IR (film): ν 1627, 1596 cm⁻¹.

2-(Benzyloxy)-3-pyrrolidino-1-propen-3-one. *n*-Butyllithium (1.93 M in hexanes, 0.34 mL, 0.66 mmol) was added to a –78 °C solution of [(benzyloxy)(methyl)carbene]pentacarbonylchromium(0) (208 mg, 0.64 mmol) in 5.0 mL of THF. In a second flask, *n*-butyllithium (0.50 mL, 0.97 mmol) was added to a –78 °C solution of pyrrolidine (80 μ L, 0.96 mmol) in 2.0 mL of THF and then warmed to 0 °C for 45 min. This lithium pyrrolidide solution was added via syringe to the flask containing the chromium complex, which was warmed to –17 °C for 30 min and recooled to –78 °C. Iodine (344 mg, 1.36 mmol) was added, and the mixture was warmed to room temperature. Isolation by the standard procedure gave 10.9 mg (7.4%) of pure product.

¹H NMR (300 M Hz, CDCl₃): δ 1.85 (m, 4H, CH₂CH₂N), 2.51 (t, 2H, *J* = 6.9 Hz, CH₂N), 3.54 (t, 2H, *J* = 6.7 Hz, CH₂N), 4.49 (d, 1H, *J* = 1.8 Hz, =CHH), 4.82 (s, 2H, CH₂Ph), 4.88 (d, 1H, *J* = 2.8 Hz, =CHH), 7.37 (m, 5H, ArH) ppm. ¹³C NMR (75.5 M Hz, CDCl₃): δ 23.9, 26.3 (CH₂CH₂N), 46.4, 48.2 (CH₂N), 70.1 (CH₂Ph), 89.4 (=CH₂), 127.8, 128.2, 128.6, 136.0 (ArC), 156.9 (C=CH₂), 164.1 (CO) ppm. IR (film): ν 1640, 1620 cm⁻¹. Mass spectrum (NH₃Cl): *m/z* 249, [M + 18]⁺.

2-(*tert*-Butyldimethylsilyloxy)-1-hepten-2-one. *n*-Butyllithium (1.93 M in hexanes, 0.83 mL, 1.6 mmol) was added to a –78 °C solution of [(*tert*-butyldimethylsilyloxy)methyl]carbene]pentacarbonylchromium(0) (227 mg, 0.65 mmol) in 6.5 mL of THF. The mixture was warmed to –15 °C for 30 min and recooled to –78 °C before iodine (347 mg, 1.37 mmol) was added. The mixture was warmed to room temperature. Isolation by the standard procedure gave 55.6 mg (30%) of desired product.

¹H NMR (270 M Hz, CDCl₃): δ 0.19 (s, 6H, (CH₃)₂Si), 0.91 (t, 3H, *J* = 7.3 Hz, CH₃CH₂), 0.97 (s, 9H, (CH₃)₃C), 1.34 (sextet, 2H, *J* = 7.4, CH₃CH₂), 1.59 (pentet, 2H, *J* = 7.5, CH₂CH₂CH₂), 2.64 (t, 2H, *J* = 7.4 Hz, CH₂CO), 4.73 (d, 1H, *J* = 1.4 Hz,

(11) Hafner, A.; Hegedus, L. S.; deWeck, G.; Hawkins, B. J. *J. Am. Chem. Soc.* **1988**, *110*, 8413 and references therein.

=CHH), 5.34 (d, 1H, $J = 1.5$ Hz, =CHH) ppm. ^{13}C NMR (75.5 M Hz, CDCl_3): δ -4.9 ((CH_3)₂Si), 13.9 (CH_3CH_2), 18.2 ((CH_3)₃C), 22.4 (CH_3CH_2), 25.6 ((CH_3)₃C), 26.1 ($\text{CH}_3\text{CH}_2\text{CH}_2$), 37.7 ($\text{CH}_2\text{-CO}$), 100.2 (=CH₂), 154.1 (C=CH₂), 199.3 (CO) ppm. IR (film) ν 1730, 1694, 1610 cm^{-1} . Mass spectrum (NH_3Cl) m/z 260 [$\text{M} + 18$]⁺.

6-Pentanoyl-2,3-dihydropyran. *n*-Butyllithium (1.96 M in hexanes, 0.52 mL, 1.0 mmol) was added to a -78 °C solution of (2-oxacyclohexylidene)pentacarbonylchromium(0) (125 mg, 0.45 mmol) in 7.0 mL of THF and then stirred at -78 °C for 25 min before removing the cooling bath for 20 min. After the mixture was recooled to -78 °C, iodine (137 mg, 0.54 mmol) was added and the mixture was allowed to warm slowly to room temperature over 18 h. Isolation by the standard procedure gave 38.6 mg (51%) of pure product.

^1H NMR (300 M Hz, CDCl_3): δ 0.91 (t, 3H, $J = 7.3$ Hz, CH_3), 1.34 (sextet, 2H, $J = 7.4$ Hz, CH_2CH_3), 1.58 (pentet, 2H, $J = 7.5$ Hz, $\text{CH}_3\text{CH}_2\text{CH}_2$), 1.85 (tt, 2H, $J = 6.2, 5.3$ Hz, $\text{CH}_2\text{CH}_2\text{O}$), 2.20 (dt, 2H, $J = 4.3, 6.3$ Hz, $\text{CH}_2\text{CH=}$), 2.59 (t, 2H, $J = 7.5$ Hz, CH_2CO), 4.08 (t, 2H, $J = 5.1$ Hz, CH_2O), 5.96 (t, 1H, $J = 4.2$ Hz, CH=C) ppm. ^{13}C NMR (75.5 M Hz, CDCl_3): δ 13.8 (CH_3), 20.6, 21.5, 22.3 (CH_3CH_2 , $\text{CH}_2\text{CH=}$, $\text{CH}_2\text{CH}_2\text{O}$), 26.2 ($\text{CH}_3\text{CH}_2\text{CH}_2$), 37.1 (CH_2CO), 66.1 (CH_2O), 109.3 (CH=), 151.2 (C=CH), 183.6 (C=O) ppm. IR (film): ν 1702 (CO), 1632 cm^{-1} . Mass spectrum (EI): m/z 168, [M]⁺. FAB high-resolution MS: Calcd for $\text{C}_{10}\text{H}_{17}\text{O}_2$, m/z 169.1228; found, m/z 169.1218 \pm 0.0006.

5-Pentanoyl-2,3-dihydrofuran. *n*-Butyllithium (1.93 M in hexanes, 1.06 mL, 2.1 mmol) was added to a -78 °C solution of (2-oxacyclopentylidene)pentacarbonylchromium(0) (214 mg, 0.82 mmol) in 8.0 mL of THF. After being warmed to -17 °C for 30 min, the mixture was recooled to -78 °C before iodide (439 mg, 1.73 mmol) was added. The mixture was stirred for 90 min at -78 °C and then warmed to room temperature. Isolation by the standard procedure gave 54.1 mg (43%) of pure product.

^1H NMR (300 M Hz, CDCl_3): δ 0.92 (t, 3H, $J = 7.3$ Hz, CH_3), 1.35 (sextet, 2H, $J = 7.4$ Hz, CH_2CH_3), 1.62 (pentet, 2H, $J = 7.5$ Hz, $\text{CH}_2\text{CH}_2\text{CH}_3$), 2.62 (t, 2H, $J = 7.5$ Hz, CH_2CO), 2.83 (dq, 2H, $J = 3.1, 9.8$ Hz, $\text{CH}_2\text{CH=}$), 4.47 (t, 2H, $J = 9.8$ Hz, CH_2O), 5.94 (t, 1H, $J = 3.1$ Hz, CH=C) ppm. ^{13}C NMR (75.5 M Hz, CDCl_3): δ 13.8 (CH_3), 22.3 (CH_3CH_2), 26.3 ($\text{CH}_3\text{CH}_2\text{CH}_2$), 30.6 ($\text{CH}_2\text{CH=}$), 38.6 (CH_2CO), 70.2 (CH_2O), 110.9 (CH=), 155.5 (C=CH), 193.3 (CO) ppm. IR (film): ν 1770, 1727 (CO), 1614 cm^{-1} . Mass spectrum (EI): m/z 154, [M]⁺. FAB high-resolution MS: Calcd for $\text{C}_9\text{H}_{15}\text{O}_2$, m/z 155.1072; found, m/z 155.1078 \pm 0.0007.

3-(Benzyloxy)-2-octen-4-one. *n*-Butyllithium (1.93 M in hexanes, 0.71 mL, 1.4 mmol) was added to a -78 °C solution of [(benzyloxy)(ethyl)carbene]pentacarbonylchromium(0) (187 mg, 0.55 mmol) in 6.0 mL of THF. The mixture was warmed to -15 °C for 40 min and recooled to -78 °C before tetrabutylammonium chlorochromate (273 mg, 0.72 mmol) was added. After being warmed to room temperature for 90 min, the mixture was worked up in the usual manner to give 33.6 mg of product (20% yield).

^1H NMR (300 M Hz, CDCl_3): δ 0.91 (t, 3H, $J = 7.3$ Hz, $\text{CH}_3\text{-CH}_2$), 1.33 (sextet, 2H, $J = 7.4$ Hz, CH_3CH_2), 1.59 (pentet, 2H, $J = 7.5$ Hz, $\text{CH}_3\text{CH}_2\text{CH}_2$), 1.74 (d, 3H, $J = 7.1$ Hz, CH_3CH), 2.58 (t, 2H, $J = 7.5$ Hz, CH_2CO), 4.83 (s, 2H, CH_2Ph) 6.30 (q, 1H, $J = 7.1$ Hz, CH_3CH), 7.35 (m, 5H, ArH) ppm. ^{13}C NMR (75.5 M Hz, CDCl_3): δ 11.6 (CH_3CH), 13.9 (CH_3CH_2), 22.4 (CH_3CH_2), 26.6 ($\text{CH}_3\text{CH}_2\text{CH}_2$), 37.7 (CH_2CO), 73.7 (CH_2Ph), 124.7 ($\text{CH}_3\text{CH=}$), 128.1, 128.4, 137.3 (ArC), 153.3 (C=CH), 198.1 (CO) ppm. IR (film): ν 1678, 1636 cm^{-1} . Mass spectrum (EI): m/z 232, [M]⁺.

2-Methoxy-1-phenyl-1-hepten-3-one. *n*-Butyllithium (2.13 mg in hexanes, 0.54 mL, 1.2 mmol) was added to a -78 °C solution of [(methoxy)(benzyl)carbene]pentacarbonylchromium(0) (150 mg, 0.46 mmol) in 6.0 mL of THF. The mixture was warmed to -15 °C for 30 min and then recooled to -78 °C before addition of tetrabutylammonium chlorochromate (221 mg, 0.58 mmol). The mixture was warmed to room temperature over 20 min and filtered through Celite before oxidation over 18 h. Isolation by the standard procedure gave 12.2 mg (12%) of pure product.

^1H NMR (270 M Hz, CDCl_3): δ 0.95 (t, 3H, $J = 7.5$ Hz, $\text{CH}_3\text{-CH}_2$), 1.39 (sextet, 2H, $J = 7.2$ Hz, CH_2CH_3), 1.67 (pentet, 2H, $J = 7.5$ Hz, $\text{CH}_2\text{CH}_2\text{CH}_3$), 2.73 (t, 2H, $J = 7.5$ Hz, CH_2CO), 3.72 (s, 3H, CH_3O), 6.86 (s, 1H, PhCH=), 7.30-7.42 (m, 3H, ArH), 7.74-7.77 (m, 2H, ArH) ppm. ^{13}C NMR (75.5 M Hz, CDCl_3): δ 13.9 (CH_3CH_2), 22.4 (CH_3CH_2), 26.6 ($\text{CH}_3\text{CH}_2\text{CH}_2$), 37.9 (CH_2CO), 59.1 (CH_3O), 123.1, 128.6, 129.1, 130.3, 133.4 (ArC, PhCH=), 153.2 (C=CHPh), 199.2 (CO) ppm. IR (film): ν 1677 (CO), 1614 cm^{-1} . Mass spectrum (EI): m/z 218, [M]⁺.

6-(Benzyloxy)-8-methyl-6-dodecen-5-one. *n*-Butyllithium (1.95 M in hexanes, 1.00 mL, 1.95 mmol) was added to a -78 °C solution of [(benzyloxy)(1-propenyl)carbene]pentacarbonylchromium(0) (274 mg, 0.78 mmol) in 7.8 mL of THF. After the mixture was warmed to -15 °C for 30 min and recooled to -78 °C, iodine (415 mg, 1.6 mmol) was added. The mixture was warmed to room temperature. Isolation by the standard procedure gave 59.0 mg (25%) of pure product.

^1H NMR (270 M Hz, CDCl_3): δ 0.80-1.00 (m, 9H, 3 \times CH_3), 1.1-1.4 (m, 8H, $\text{CH}_2\text{CH}_2\text{CH}_2\text{CO}$, $\text{CH}_3\text{CH}_2\text{CH}_2\text{CH}_2\text{CH}$), 1.60 (pentet, 2H, $J = 7.5$ Hz, $\text{CH}_2\text{CH}_2\text{CO}$), 2.59 (t, 2H, $J = 7.5$ Hz, CH_2CO), 2.70 (m, 1H, CHCH₂), 4.81 (s, 2H, CH_2Ph), 5.94 (d, 1H, $J = 10.0$ Hz, =CH), 7.35 (m, 5H, ArH) ppm. ^{13}C NMR (67.9 M Hz, CDCl_3): δ 13.9, 14.0 (2 \times CH_3CH_2), 20.2 ($\text{CH}_2\text{-CH}$), 22.4, 22.7 (2 \times CH_2CH_3), 26.7 (OCH_2CH_2), 29.7, 30.8, 36.6 ($\text{CH}_2\text{CH}_2\text{CH}$, CH_2CH , CHCH₃), 37.8 (CH_2O), 73.9 (CH_2Ph), 128.0, 128.2, 128.3, 135.7 (ArC), 137.4 (=CH), 151.3 (C=CH), 198.4 (C=O) ppm. IR (film): ν 3032 (ArC-H), 2958, 2929, 2871 (ArC-H), 1736, 1681, 1631 cm^{-1} . Mass spectrum (EI): m/z 302, [M]⁺.

Acknowledgment. Support for this research by National Science Foundation Grant CHE-9224489 is gratefully acknowledged. Mass spectra were obtained on instruments supported by the National Institutes of Health shared instrumentation Grant GM49631.

OM950130U

Synthesis and Molecular Structure of the Novel Imide-Bridged [3]Ferrocenophane

Toshiyuki Moriuchi, Isao Ikeda, and Toshikazu Hirao*

Department of Applied Chemistry, Faculty of Engineering, Osaka University,
Yamada-oka, Suita, Osaka 565, Japan

Received March 8, 1995[®]

Summary: The imide-bridged [3]ferrocenophane 2-pyridyl-1,1'-ferrocenedicarboximide was synthesized directly in one step. X-ray crystal structure determination indicated its characteristic structure; the two cyclopentadienyl rings are staggered and tilted 16.4° with respect to each other. In molecular packing, an intermolecular π -hydrogen bond interaction (edge-to-face interaction) was revealed between the cyclopentadienyl hydrogen and pyridyl ring.

Metallophenanes are structurally interesting aromatics, and redox of transition metals permits their potential utilization as materials and catalysts.¹ Synthesis of [n]metallophenanes has been addressed from these points of view.² The internal strain is a key factor in the design of [n]metallophenanes. A bridging unit containing heteroatoms is expected to expand the scope of metallophenane chemistry. We report herein a new synthesis and structural elucidation of the unique imide-bridged [3]ferrocenophane.

The imide-bridged [3]ferrocenophane was successfully synthesized in one step as follows. Treatment of 1,1'-ferrocenedicarboxylic acid chloride with 2 molar equiv of 2-aminopyridine in the presence of triethylamine and a catalytic amount of 4-(dimethylamino)pyridine afforded 2-pyridyl-1,1'-ferrocenedicarboximide (PFI) in 57% yield (Scheme 1). It is noteworthy that the imide ring is formed predominantly. The diamide, 2-BPFA, was obtained in only 4% yield. PFI appears to be the first example of the imide-bridged [3]ferrocenophanes to the best of our knowledge. This result is in sharp contrast to the finding that *N,N'*-bis(4-pyridyl)-1,1'-ferrocenedicarboxamide (4-BPFA) was produced exclusively in 74% yield in the case of 4-aminopyridine. No intramolecular imide formation was observed. This difference is referred to the site of the pyridyl nitrogens, suggesting the involvement of an acylpyridinium intermediate in the cyclization step to PFI.

The X-ray crystal structure determination of PFI indicated distortion of the ferrocenophane ring (Figure 1 and Table 1). The important bond distances and angles are listed in Table 2. It should be noted that the dihedral angle (16.4°) between the least-squares planes of the two cyclopentadienyl rings is unexpectedly large as compared with those of the known [3]ferro-

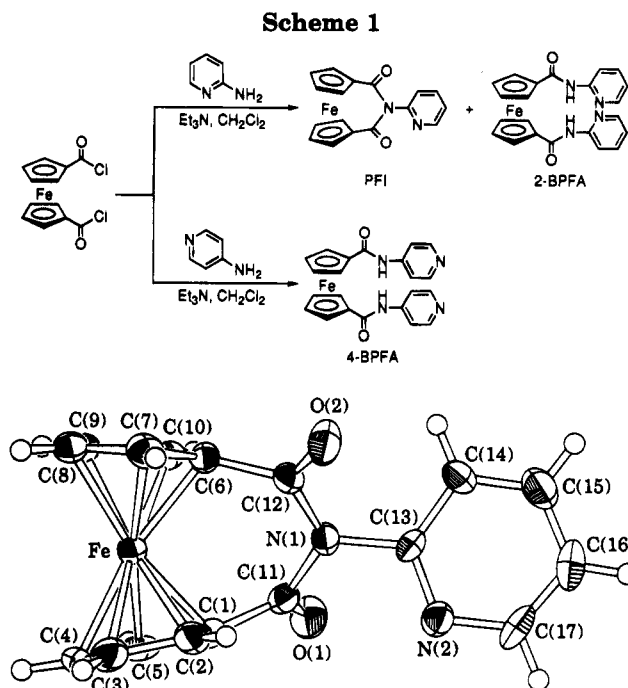


Figure 1. ORTEP view of the X-ray crystal structure of PFI (50% probability ellipsoids).

Table 1. Crystallographic Data for PFI

formula	C ₁₇ H ₁₂ N ₂ O ₂ Fe
mol wt	332.14
cryst syst	monoclinic
space group	P2 ₁ /c
a, Å	9.708(3)
b, Å	8.697(3)
c, Å	16.641(2)
β , deg	106.07(1)
V, Å ³	1350.2(5)
Z	4
D _{calcd} , g cm ⁻³	1.634
μ (Mo K α), cm ⁻¹	11.24
T, °C	23
λ (Mo K α), Å	0.710 69
R	0.063
R _w	0.073

cenophanes;²⁻⁵ the rings of [3]ferrocenophane-1,3-dione and cationic 2-*N,N*-dimethylammonium[3]ferrocenophane iodide are tilted 9.8 and 12.2°, respectively, with respect to each other.⁴

[®] Abstract published in *Advance ACS Abstracts*, June 15, 1995.
(1) (a) Sinn, H.; Kaminsky, W. *Adv. Organomet. Chem.* **1980**, *18*, 99. (b) Kaminsky, W.; Külper, K.; Brintzinger, H. H.; Wild, F. R. W. P. *Angew. Chem., Int. Ed. Engl.* **1985**, *24*, 507. (c) Röhl, W.; Brintzinger, H. H.; Rieger, B.; Zolk, R. *Ibid.* **1990**, *29*, 279. (d) Spaleck, W.; Antberg, M.; Rohrmann, J.; Winter, A.; Bachmann, B.; Kiprof, P.; Behm, J.; Herrmann, W. A. *Ibid.* **1992**, *31*, 1347 and references therein. (e) Erker, G.; Aulbach, M.; Wingbermühle, D.; Krüger, C.; Werner, S. *Chem. Ber.* **1993**, *126*, 755.

(2) Hisatome, M. *Rev. Heteroat. Chem.* **1992**, *6*, 142 and references therein.

(3) (a) Jones, N. D.; Marsh, R. E.; Richards, J. H. *Acta Crystallogr., Sect. B* **1965**, *19*, 330. (b) Lecomte, P. C.; Dusausay, Y.; Protas, J.; Moise, C.; Tirouflet, J. *Ibid.* **1973**, *29*, 488. (c) Lecomte, P. C.; Dusausay, Y.; Protas, J.; Moise, C. *Ibid.* **1973**, *29*, 1127. (d) Batail, P.; Grandjean, D.; Astruc, D.; Dabard, R. *J. Organomet. Chem.* **1975**, *102*, 79.

(4) (a) Gyepes, E.; Glowiak, T.; Toma, S.; Soldánová, J. *J. Organomet. Chem.* **1984**, *276*, 209. (b) Plenio, H.; Yang, J.; Diodone, R.; Heinze, J. *Inorg. Chem.* **1994**, *33*, 4098.

(5) Ogino, H.; Tobita, H.; Habazaki, H.; Shimoi, M. *J. Chem. Soc., Chem. Commun.* **1989**, 828.

Table 2. Selected Bond Distances (Å) and Bond Angles (deg) for PFI

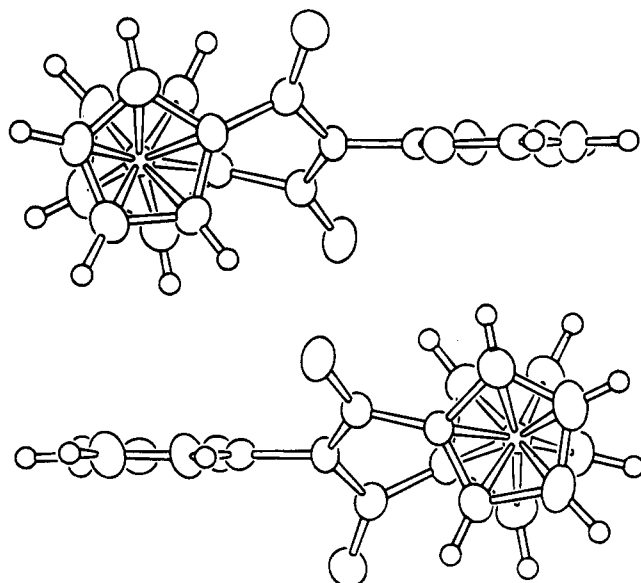
Bond Distances			
Fe-C(1)	1.971(6)	Fe-C(10)	2.014(7)
Fe-C(2)	2.011(7)	C(1)-C(11)	1.482(9)
Fe-C(3)	2.069(7)	C(6)-C(12)	1.493(9)
Fe-C(4)	2.085(6)	C(11)-O(1)	1.217(8)
Fe-C(5)	2.037(6)	C(12)-O(2)	1.214(8)
Fe-C(6)	1.974(6)	C(11)-N(1)	1.446(8)
Fe-C(7)	2.043(7)	C(12)-N(1)	1.408(8)
Fe-C(8)	2.079(6)	C(13)-N(1)	1.446(8)
Fe-C(9)	2.080(7)		
Bond Angles			
C(1)-C(11)-N(1)	117.0(5)	O(2)-C(12)-N(1)	120.9(6)
C(1)-C(11)-O(1)	123.5(6)	C(11)-N(1)-C(12)	124.8(5)
O(1)-C(11)-N(1)	119.5(6)	C(11)-N(1)-C(13)	115.8(5)
C(6)-C(12)-N(1)	118.0(5)	C(12)-N(1)-C(13)	119.4(5)
C(6)-C(12)-O(2)	121.1(6)		

The β -angle, defined as the angle between the plane of the cyclopentadienyl ring and C(ipso)-CO(bridging) bond, is 34.6° for C(1)-C(2)-C(3)-C(4)-C(5) and C(1)-C(11)O(1) and 45.7° for C(6)-C(7)-C(8)-C(9)-C(10) and C(6)-C(12)O(2). The β -angle effect was supported by the ^{13}C -NMR spectrum; the upfield chemical shift for the C(ipso) atom and the downfield shift for the C(α) and C(β) atoms of the cyclopentadienyl rings were observed in comparison with those of 2-BPFA.

Another interesting feature is that the staggered orientation of the two cyclopentadienyl rings is accompanied by the twisting of the bridge in the imide system. The degree of stagger, 35.5° , was defined here as the angle between the mean planes through the atoms Fe-C(1)-C(11) and Fe-C(6)-C(12). The two rings are approximately staggered, being in contrast with the eclipsed ones of the known [3]ferrocenophanes.²⁻⁵ This unique distorted structure including the above-mentioned larger tilt angle is considered to be attributed to the imide linkage.

It should be also noted that the calculated position of the hydrogen atom on the cyclopentadienyl C(α) atom is almost facing the π -electrons of the pyridyl ring of the neighboring molecule in the crystal packing of PFI (Figure 2). The distance between the hydrogen and the center of the pyridyl ring is 2.97 Å, suggesting a π -hydrogen bond⁶ in the crystal structure (edge-to-face interaction). The dihedral angle between the least-squares planes of the cyclopentadienyl and pyridyl rings is 90.4° , which is reasonable for the edge-to-face interaction.

The preferred orientation of the imide linkage would seem to be perpendicular to the cyclopentadienyl ring planes, leading to an eclipsed orientation of the rings. Because of steric interactions between the oxygen atoms, O(1) and O(2), and the pyridyl nitrogen atom and hydrogen atom at C(14) of the pyridyl ring, the orientation of the pyridyl ring would be within a limited range of parallel to the cyclopentadienyl ring. The packing interaction, however, requires rotation of the pyridyl

**Figure 2.** Molecular packing of PFI.

ring away from this orientation, which is considered to induce a twist in the imide bridge, resulting in the observed staggered conformation and the tilted rings at the bridgehead carbon atoms to set the observed dihedral angle.

An alternative explanation might involve the larger angle at the bridging nitrogen atom, which would lead to the two cyclopentadienyl rings being further apart in a favored eclipsed orientation. The most likely explanation might be based on a combination of these two effects.

The strained imide bridge is predicted to affect the electronic state. The electrochemical properties of the above-obtained ferrocene derivatives were studied by cyclic voltammetry. A reversible oxidation wave of the Fc^+/Fc couple was observed at $E_{1/2}$ values of 1018 (PFI), 947 (2-BPFA), and 904 (4-BPFA) mV vs SCE. PFI showed a large anodic shift of 71 mV in comparison with 2-BPFA. The difference is probably due to the distortion of the [3]ferrocenophane with the electron-withdrawing imide linkage.

The novel and readily obtained imide-bridged [3]ferrocenophane, PFI, is characteristic of the highly distorted structure and is thus in contrast with the known [3]ferrocenophanes.

Experimental Section

General Procedures. All chemicals and solvents were dried and purified by usual methods. Melting points were determined using a Yanagimoto micromelting point apparatus and are uncorrected. ^1H NMR spectra were recorded on a JEOL JNM-GSX400 spectrometer. ^{13}C NMR spectra were recorded on a Bruker AM-600 spectrometer. Infrared spectra were recorded on a Perkin-Elmer FT-IR 1600 infrared spectrometer. The fast atom bombardment mass spectra were run on a JEOL JMS-DX303HF spectrometer. Recycling preparative HPLC analysis was performed on a JAI LC-908. The X-ray crystallography was carried out on a Rigaku AFC5R diffractometer. The standard electrochemical instrumentation consisted of a Hokuto Denko potentiostat/galvanostat HA-301S and a Hokuto Denko function generator HB-104S with a three-electrode system consisting of a glassy carbon working electrode, a platinum auxiliary electrode, and a KCl-saturated calomel reference electrode. Cyclic voltammograms were recorded with Graphtec WX 1000.

(6) (a) Burley, S. K.; Petsko, G. A. *Science* **1985**, *229*, 23. (b) Nishio, M.; Hirota, M. *Tetrahedron* **1989**, *45*, 7201. (c) Jorgensen, W. L.; Severance, D. L. *J. Am. Chem. Soc.* **1990**, *112*, 4768. (d) Atwood, J. L.; Hamada, F.; Robinson, K. D.; Orr, G. W.; Vincent, R. L. *Nature* **1991**, *349*, 683. (e) Suzuki, S.; Green, P. G.; Bumgarner, R. E.; Dasgupta, S.; Goddard, W. A., III; Blake, G. A. *Science* **1992**, *257*, 942. (f) Cochran, J. E.; Parrott, T. J.; Whitlock, H. W. *J. Am. Chem. Soc.* **1992**, *114*, 2269. (g) Subramanian, S.; Wang, L.; Zaworotko, M. J. *Organometallics* **1993**, *12*, 310. (h) Sakaki, S.; Kato, K.; Miyazaki, T.; Musashi, Y.; Ohkubo, K.; Ihara, H.; Hirayama, C. *J. Chem. Soc., Faraday Trans.* **1993**, *89*, 659.

Synthesis of PFI and 2-BPFA. To a stirred mixture of 2-aminopyridine (0.377 g, 4.0 mmol), 4-(dimethylamino)pyridine (0.0122 g, 0.1 mmol), and triethylamine (2.8 mL, 20 mmol) in dichloromethane (10 mL) was added dropwise 1,1'-ferrocenedicarboxylic acid chloride (0.622 g, 2.0 mmol) in dichloromethane (30 mL) under nitrogen at 0 °C. The mixture was stirred at 0 °C for 7 h and at room temperature for 17 h. The resulting mixture was diluted with dichloromethane (20 mL), washed with saturated NaHCO₃ aqueous solution and brine, and dried over MgSO₄. An orange solid was obtained by evaporation of the dichloromethane solution in vacuo. PFI and 2-BPFA were isolated by recycling preparative HPLC and recrystallized from dichloromethane.

PFI. Orange prisms; yield, 57%; mp 215–219 °C (decomp); IR (KBr, cm⁻¹) 1702, 1655 (C=O), 1587 (C=C); ¹H NMR (400 MHz, CDCl₃) δ 8.62 (ddd, 1H, *J* = 4.9, 2.0, 0.7 Hz, Py), 7.86 (dt, 1H, *J* = 7.7, 2.0 Hz, Py), 7.38 (ddd, 1H, *J* = 7.7, 1.0, 0.7 Hz, Py), 7.33 (ddd, 1H, *J* = 7.7, 4.9, 1.0 Hz, Py), 4.82 (t, 4H, *J* = 2.0 Hz, Cp), 4.58 (t, 4H, *J* = 2.0 Hz, Cp); ¹³C NMR (150 MHz, CDCl₃) δ 171.4 (C=O), 153.2 (Py), 149.7 (Py), 138.4 (Py), 123.1 (Py), 122.9 (Py), 76.9 (ipso Cp), 75.3 (Cp), 72.8 (Cp); MS (FAB) *m/z* 333 (M⁺ + 1). Anal. Calcd for C₁₇H₁₂N₂O₂Fe: C, 61.48; H, 3.64; N, 8.43. Found: C, 61.27; H, 3.67; N, 8.38.

2-BPFA. Orange prisms; yield, 4%; mp 158–161 °C (decomp); IR (KBr, cm⁻¹) 3362 (NH), 1664 (C=O), 1576 (C=C); ¹H NMR (400 MHz, CDCl₃) δ 8.66 (bs, 2H, NH), 8.26 (ddd, 2H, *J* = 4.9, 2.1, 1.1 Hz, Py), 8.24 (dt, 2H, *J* = 8.3, 1.1 Hz, Py), 7.65 (ddd, 2H, *J* = 8.3, 7.3, 2.1 Hz, Py), 7.02 (ddd, 2H, *J* = 7.3, 4.9, 1.1 Hz, Py), 4.91 (t, 4H, *J* = 2.0 Hz, Cp), 4.53 (t, 4H, *J* = 2.0 Hz, Cp); ¹³C NMR (150 MHz, CDCl₃) δ 168.1 (C=O), 151.5 (Py), 147.6 (Py), 138.4 (Py), 119.5 (Py), 114.2 (Py), 77.7 (ipso Cp), 72.7 (Cp), 70.4 (Cp); MS (FAB) *m/z* 427 (M⁺ + 1). Anal. Calcd for C₂₂H₁₈N₄O₂Fe·0.25H₂O: C, 61.34; H, 4.33; N, 13.01. Found: C, 61.27; H, 4.42; N, 12.54.

Synthesis of 4-BPFA. To a stirred mixture of 4-aminopyridine (0.847 g, 9.0 mmol), 4-(dimethylamino)pyridine (0.0274 g, 0.23 mmol), and triethylamine (6.5 mL, 45 mmol) in dichloromethane (20 mL) was added dropwise 1,1'-ferrocenedicarboxylic acid chloride (1.40 g, 4.5 mmol) in dichloromethane (60 mL) under nitrogen at 0 °C. The mixture was stirred at 0 °C for 7 h and at room temperature for 17 h. The resulting mixture was diluted with dichloromethane (30 mL), washed with saturated NaHCO₃ aqueous solution and brine, and dried over MgSO₄. An orange solid was obtained by evaporation of the dichloromethane solution in vacuo. Recrystallization from chloroform gave a microcrystalline orange solid, 4-BPFA.

4-BPFA. Orange prisms; yield, 74%; mp 174–177 °C (decomp); IR (KBr, cm⁻¹) 3234 (NH), 1675 (C=O), 1581 (C=C); ¹H NMR (400 MHz, CDCl₃) δ 8.88 (bs, 2H, NH), 8.58 (dd, 4H,

J = 4.9, 1.6 Hz, Py), 7.73 (dd, 4H, *J* = 4.9, 1.6 Hz, Py), 4.69 (t, 4H, *J* = 1.8 Hz, Cp), 4.56 (t, 4H, *J* = 1.8 Hz, Cp); ¹³C NMR (150 MHz, CDCl₃) δ 170.0 (C=O), 150.9 (Py), 145.2 (Py), 113.7 (Py), 78.4 (ipso Cp), 71.9 (Cp), 71.5 (Cp); MS (FAB) *m/z* 427 (M⁺ + 1). Anal. Calcd for C₂₂H₁₈N₄O₂Fe·H₂O: C, 59.48; H, 4.54; N, 12.61. Found: C, 59.73; H, 4.41; N, 12.46.

Electrochemical Experiments. All electrochemical measurements were carried out at 25 °C under an atmospheric pressure of nitrogen, which was previously passed through a solution of the same composition as the electrolysis solution. Cyclic voltammograms were obtained in the dichloromethane solutions containing 0.1 M ⁿBu₄NClO₄ as a supporting electrolyte ([ferrocene derivatives] = 1 × 10⁻³ M). Potentials were determined with reference to a KCl-saturated calomel electrode at 100 mV s⁻¹ scan rate.

X-ray Crystal Structure Determination of PFI. An orange crystal of PFI with approximate dimensions of 0.50 × 0.30 × 0.30 mm was mounted on a glass fiber. The measurement was made on a Rigaku AFC5R diffractometer with graphite-monochromated Mo Kα radiation and a 12 kW rotating anode generator. Cell constants and an orientation matrix for data collection were obtained from a least-squares refinement using the setting angles of 25 carefully centered reflections in the range 27.15° < 2θ < 27.43° corresponded to a primitive monoclinic cell. The data were collected at a temperature of 23 ± 1 °C using the ω-2θ scan technique to a maximum 2θ value of 55.1°. A total of 3513 independent reflections was obtained, of which 3325 were unique (*R*_{int} = 0.061). The structure was solved by direct methods and expanded using Fourier techniques. The non-hydrogen atoms were refined anisotropically. The final cycle of full-matrix least-squares refinement was based on 2161 observed reflections (*I* > 3.00σ(*I*)) and 217 variable parameters: *R* = 0.063, *R*_w = 0.073. Crystallographic details are given in Table 1.

Acknowledgment. Thanks are due to the Analytical Center, Faculty of Engineering, Osaka University, for the use of the NMR and MS instruments. Partial financial support by Research Fellowships for Young Scientists of the Japan Society for the Promotion of Science and the Kurata Foundation are also acknowledged.

Supporting Information Available: Tables giving full details of the crystal data and data collection parameters, atomic coordinates, anisotropic displacement parameters, bond distances, bond angles, and torsion angles (23 pages). Ordering information is given on any current masthead page.

OM950180Z

New Method for the Determination of the Trialkylaluminum Content in Alumoxanes

Andrew R. Barron

Department of Chemistry, Harvard University, Cambridge, Massachusetts 02138

Received November 9, 1994[®]

Summary: Alkylalumoxanes (such as methylalumoxane, MAO) can contain "free" trialkylaluminum (AlR_3). The relative ratio of the latter in any sample may be determined by ^{31}P NMR spectroscopy upon addition of excess PPh_3 . The rapid exchange of free PPh_3 and $\text{Me}_3\text{-Al-PPh}_3$ results in the ^{31}P NMR signal being a weighted average from which an accurate determination of AlR_3 can be made, based on an external standard. This analysis method has been demonstrated for the determination of AlMe_3 , AlEt_3 , and Al^iBu_3 in methylalumoxane (MAO), ethylalumoxane (EAO), and isobutylalumoxane (IBAO) and bis(diisobutylaluminum oxide) (DBAO), respectively.

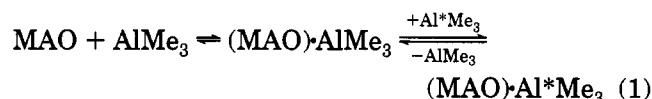
Introduction

Alumoxanes, $(\text{RAIO})_n$, formed by the controlled hydrolysis of trialkylaluminum compounds, are used commercially as active catalysts and cocatalysts for the oligomerization and polymerization of olefins and epoxides. Although alumoxanes traditionally were proposed to be rings or chains containing three-coordinate aluminum, we have demonstrated that the primary species are cage compounds in which the aluminum is four-coordinate.^{1–3} While we have isolated individual cage compounds for the *tert*-butylalumoxanes (e.g., $[(^t\text{Bu})\text{AlO}]_n$, $n = 6–9, 12$),^{1,2} commercial alumoxanes, in particular methylalumoxane (MAO), are known to contain significant quantities of the parent trialkyl as a residue from the hydrolysis reaction.⁴ Since the amount of AlMe_3 present has a significant effect on the catalytic activity of MAO,⁵ it is of importance to determine accurately the quantity of AlMe_3 in any single sample of alumoxane.

There are at present a number of methods for the determination of content of AlMe_3 in MAO: (a) volatilization of AlMe_3 , (b) ^1H NMR spectroscopy, and (c) titration of AlMe_3 with pyridine.⁶ None of these methods give an accurate measure of AlMe_3 content due to a number of insurmountable issues.

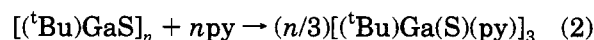
The AlMe_3 present in commercial samples of MAO is present in two forms: *free* (i.e., Al_2Me_6) and *complexed* (i.e., $(\text{MAO})\text{-AlMe}_3$). Removal of volatiles initially takes away the free AlMe_3 . That more free AlMe_3 is observed on standing of a sample from which the AlMe_3 has been

removed is due to the equilibrium between free and complexed trialkyl (eq 1).⁷ Thus, the determination of



volatile aluminum content is highly dependent on the experimental conditions. The equilibrium between free and complexed AlMe_3 (eq 1) also precludes accurate integration of the ^1H NMR spectra, notwithstanding the pathological overlap of the Al-CH_3 peaks for AlMe_3 and $(\text{MeAlO})_n$. Any methodology to determine AlMe_3 content must determine the total percentage of aluminum present as AlMe_3 .

With respect to the pyridine titration method, the basic assumption is that complexation only occurs with the AlMe_3 and not the alumoxane. However, we have reported that the isolobal gallium sulfide cages react *via* cage cleavage with pyridine (eq 2),⁸ and a similar

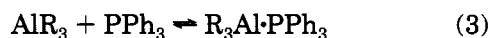


reaction is observed for alumoxanes.¹ The results of pyridine titration experiment are masked by side reactions. It is desirable, therefore, that any method for the determination of AlR_3 content should be specific for the trialkyl and preclude any reaction with the alumoxane.

Given the limitations of the analytical methods outlined above, we have developed a simple NMR method for the accurate determination of AlR_3 content in alumoxane solutions.

Results and Discussion

Rationalization of Method. Aluminum trialkyls react reversibly with triphenylphosphine to form a Lewis acid–base complex (eq 3).⁹ While the equilibrium



constant for this reaction is dependent on the steric hindrance of the alkyl substituent, the reaction is sufficiently shifted to the right so that complexation is complete. This is true even if the parent trialkyl is dimeric, e.g., Al_2Me_6 . In contrast to the cleavage of alkyl-bridged dimers, we have demonstrated that there is no reaction between PPh_3 and dimeric (or higher oligomeric) aluminum compounds where the bridging

(7) It should be noted that the AlR_3 content in alumoxanes is also dependent upon the age of the sample.

(8) Power, M. B.; Ziller, J. W.; Barron, A. R. *Organometallics* 1992, 11, 2783.

(9) Barron, A. R. *J. Chem. Soc., Dalton Trans.* 1988, 3047.

[®] Abstract published in *Advance ACS Abstracts*, June 1, 1995.

(1) Mason, M. R.; Smith, J. M.; Bott, S. G.; Barron, A. R. *J. Am. Chem. Soc.* 1993, 115, 4971.

(2) Harlan, C. J.; Mason, M. R.; Barron, A. R. *Organometallics* 1994, 13, 2957.

(3) Harlan, C. J.; Bott, S. G.; Barron, A. R. *J. Am. Chem. Soc.* 1995, 117, 6465.

(4) Pasynkiewicz, S. *Polyhedron* 1990, 9, 429.

(5) Increased amounts of AlMe_3 in MAO have been shown to decrease the catalytic activity of MAO in a number of systems, including the ring-opening polymerization of β -lactones; see: Wu, B.; Lenz, R. W.; Harlan, C. J.; Barron, A. R. *Can. J. Biochem.*, in press.

(6) See: Jordan, D. E. *Anal. Chem.* 1968, 40, 2150 and references therein.

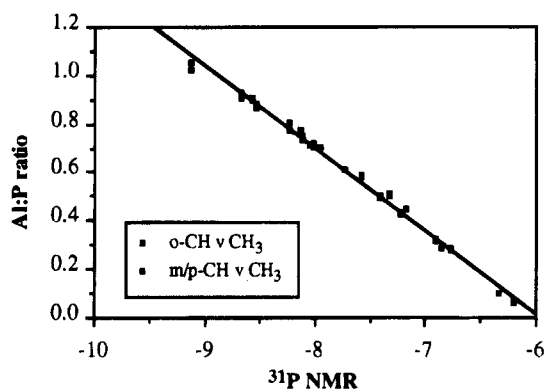


Figure 1. Plot of the ^{31}P NMR chemical shift of a mixture of AlMe_3 and PPh_3 in toluene- d_8 as a function of the Al:P ratio ($R = 0.993$).

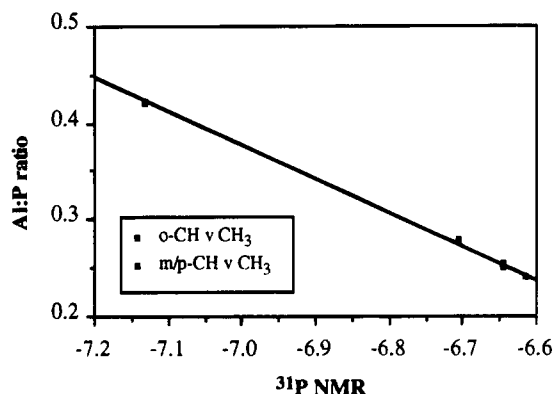


Figure 2. Plot of the ^{31}P NMR chemical shift of a mixture of AlEt_3 and PPh_3 in toluene- d_8 as a function of the Al:P ratio ($R = 0.998$).

ligand is an oxygen donor (e.g., oxide, alkoxide).¹⁰ Thus, addition of PPh_3 to a mixture of $\text{Al}(\text{}^i\text{Bu})_3$ and $[(\text{}^i\text{Bu})_2\text{Al}(\text{O}^i\text{Bu})]_2$ results in complexation of the former and not the latter.

Addition of an excess of PPh_3 to a solution of $\text{Me}_3\text{Al}\cdot\text{PPh}_3$ shifts the equilibrium shown in eq 3. Thus, in the presence of an excess of PPh_3 , essentially all the AlMe_3 will be complexed to the phosphine. An additional (concentration-independent) equilibrium between coordinated and free phosphine also is present (eq 4), such that the ^{31}P NMR spectrum of a sample



containing a mixture of AlMe_3 with an excess of PPh_3 will exhibit a single resonance whose shift is dependent on the $\text{AlMe}_3:\text{PPh}_3$ ratio. The relationship of the ^{31}P NMR spectral shift with respect to $\text{AlR}_3:\text{PPh}_3$ is shown in Figures 1 ($R = \text{Me}$), 2 ($R = \text{Et}$), and 3 ($R = \text{}^i\text{Bu}$). The shift dependence was determined from a series of standard solutions (see Experimental Section). In each case, the absolute ratio was determined as an average from the integration of the phosphine *o*-CH signal versus the Al-alkyl signal and, independently, from the signal for the phosphine's *p*- and *m*-CH groups versus the aluminum-alkyl signal.¹¹ This assures the minimization of errors due to both partial hydrolysis and/or accuracy in integration of the ^1H NMR resonances. In

(10) Healy, M. D.; Ziller, J. W.; Barron, A. R. *J. Am. Chem. Soc.* **1990**, *112*, 2949.

(11) The ^1H NMR signals for the triphenylphosphine *p*- and *m*-CH groups overlap and are observed as a broad unresolved multiplet.

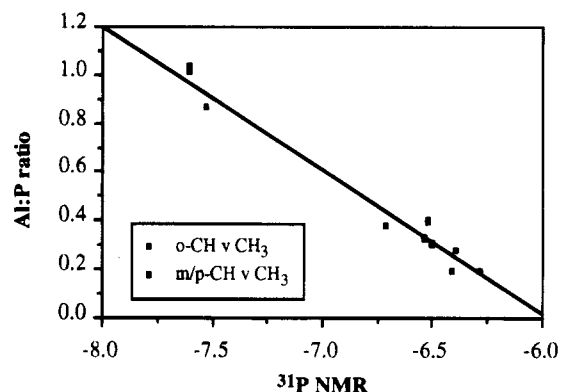


Figure 3. Plot of the ^{31}P NMR chemical shift of a mixture of $\text{Al}(\text{}^i\text{Bu})_3$ and PPh_3 in toluene- d_8 as a function of the Al:P ratio ($R = 0.969$).

each case, under conditions of excess PPh_3 , there is a linear relationship between the Al:P ratio and the ^{31}P NMR shift. The relationships between the AlR_3 to PPh_3 ratio (Al:P) and the ^{31}P NMR shift (δ) are given in eqs 5–7. The concentration independence of these relation-

$$R = \text{Me} \quad \text{Al:P} = -2.0323 - 0.34148(\delta) \quad (5)$$

$$R = \text{Et} \quad \text{Al:P} = -2.0675 - 0.34921(\delta) \quad (6)$$

$$R = \text{}^i\text{Bu} \quad \text{Al:P} = -3.5351 - 0.59143(\delta) \quad (7)$$

ships was tested by the preparation of multiple samples of varying concentrations. Furthermore, there were found to be negligible differences with different solvents: hexane, heptane, benzene, and toluene.¹²

It should be noted that, unlike the complexation of group 13 alkyls with phosphine oxides,¹³ the equilibrium shown in eq 3 is not frozen out at -80°C , precluding the direct integration of free and complexed species.

Analysis of Alumoxanes. The relationships shown in Figures 1–3 have been used to determine the AlR_3 content of several commercial and synthesized alumoxane samples for which either the density and Al weight percent or the aluminum concentration was known.¹⁴ A measured sample (5 mL) of alumoxane solution was added to an accurately weighed excess of PPh_3 , and the mixture was allowed to reach equilibrium.¹⁵ The ^{31}P NMR spectrum was obtained and the Al:P ratio determined. Since the total mass of PPh_3 is known and the proportion complexed to AlR_3 is calculated from eqs 5–7, then the mass (and/or molarity) of aluminum in the form of AlR_3 is readily calculated. The results for repeat runs of each sample are given in Table 1. From Table 2 it is clear that the internal precision of the technique is high: $\pm 2\%$ ($R = \text{Me}$).¹⁶

Two independent experiments are available to determine the validity of the phosphine approach. First, the

(12) Use of coordinating solvents, e.g., Et_2O and THF, should be avoided due to competing equilibria; see: Power, M. B.; Nash, J. R.; Healy, M. D.; Barron, A. R. *Organometallics* **1992**, *11*, 1830.

(13) Power, M. B.; Ziller, J. W.; Barron, A. R. *Organometallics* **1993**, *12*, 4908.

(14) The density and aluminum content, from which the total aluminum concentration can be calculated, are given for all commercial MAO samples. The aluminum concentration of "homemade" samples is readily calculated from the quantity of reactant employed.

(15) Separate NMR experiments indicate that equilibrium is reached within the mixing time of the solutions.

(16) Increased accuracy is obtained if an estimate of the Al:P ratio is made and the amount of PPh_3 added is proportioned to be ca. 1.5 greater.

Table 1. Analysis of AlR₃ in Samples of Alumoxanes

sample no.	alumoxane ^d	% Al as AlR ₃
1 ^a	MAO	43 ± 2
2 ^a	MAO	48 ± 1
3 ^a	MAO	36 ± 1
4 ^a	MAO	52 ± 2
5 ^b	MAO	25 ± 1
6 ^c	MAO (no AlMe ₃)	9.3 ± 0.1
7 ^b	EAO	31 ± 1
8 ^a	IBAO	5.4 ± 0.1
9 ^a	DBAO	8.0 ± 0.1

^a Commercial sample. ^b Synthesized by literature methods. ^c Volatiles removed from sample 2 under vacuum (10⁻³ Torr, 24 h). ^d Abbreviations: MAO = methylalumoxane, EAO = ethylalumoxane, IBAO = isobutylalumoxane, DBAO = bis(diisobutylaluminum oxide).

Table 2. Multiple Analysis of a Commercial MAO Sample^a

run no.	vol of MAO soln ^b (mL)	amt of PPh ₃ (g)	³¹ P NMR shift (ppm)	% Al as AlR ₃
1	5.0	5.480	-7.013	46.9
2	5.0	5.108	-7.110	47.8
3	5.0	5.532	-7.045	48.8

^a Sample 2 (see Table 1). ^b Conditions: toluene solution, 9.9 wt % Al, $\rho = 0.88 \text{ g cm}^{-3}$.

Al(ⁱBu)₃ content in a mixture with [(ⁱBu)₂Al(OⁱBu)]₂ was determined using the ³¹P NMR method described and direct integration of the ¹H NMR spectrum. On the basis of integration of the ¹H NMR spectrum, Al(ⁱBu)₃ was determined to be 45 ± 1% of the aluminum. A value of 45 ± 2% was obtained using the ³¹P NMR spectral method. Second, an accurately measured additional quantity of AlMe₃ was added to a sample of a previously analyzed MAO sample prior to phosphine addition. The experimentally determined level of AlMe₃ was 55% of the total aluminum content, which compares favorably with the calculated "ideal" value of 54%.

The values in Table 1 are lower than those obtained for the same samples by the pyridine titration, consistent with our observation that pyridines readily cleave Al-O-Al moieties.¹⁰ Furthermore, the values obtained for AlMe₃ content from the phosphine method are higher in comparison with those from the measurement of volatility, consistent with the observation of the incomplete removal of AlMe₃ from MAO solutions. The phosphine method may be used to determine the residual AlMe₃ in MAO from which the AlMe₃ has been "removed". A commercial sample of MAO was placed under vacuum (10⁻³ Torr) until no volatiles were collected in a liquid-N₂ trap. The sample was then analyzed by the phosphine method, and the AlMe₃ content was determined to be 9.3 ± 0.1% of the total aluminum content. The presence of AlMe₃ as opposed to another Lewis acidic species was confirmed by mass spectrometry.

It would appear, therefore, that the phosphine method for AlR₃ content determination is easier and more reproducible than previous methods. Furthermore, unlike previous methods, this is specific to AlR₃, is not affected by the presence of the alumoxane, and determines total (i.e., both "free" and "complexed") AlR₃ in an alumoxane solution.

Several additional points are worth making. First, it is clear that, unlike the *tert*-butylalumoxanes, samples of MAO contain varying quantities of AlMe₃. This

obviously makes comparison of the catalytic activity of alumoxanes from different sources and/or batches difficult and further highlights the importance of accurately determining the AlR₃ content in alumoxanes. Second, the relative AlR₃ content decreases with increased steric bulk of the aluminum alkyl (see Table 1), as exemplified by the absence of Al(^tBu)₃ in samples of TBAO (*tert*-butylalumoxane). Third, DBAO, which has been proposed to be a single species,¹⁷ i.e., [(ⁱBu)₂Al{OAl(ⁱBu)₂}]₂, clearly contains residual Al(ⁱBu)₃.

Finally, note should be taken of two assumptions that must be made with regard to EAO, IBAO, and DBAO. First, EAO commonly contains a quantity of *n*-butyl groups. If Al(ⁿBu)_x(Et)_{3-x} ($x = 1-3$) is formed, then substituent effects will cause a shift in the ³¹P NMR from that expected for Et₃Al·PPh₃. Second, the ethyl- and isobutylalumoxanes potentially contain Al-H groups. Since phosphines are known to cleave the Al(μ -H)₂Al unit,¹⁸ the alkyl hydrides would complex to PPh₃ and cause a shift in the expected NMR resonance. However, given that these impurities are a minor constituent, they should not significantly change the accuracy of the analysis for AlR₃.

Experimental Section

All manipulation were carried out under an inert atmosphere of predried nitrogen or argon. Reference NMR spectra were recorded in toluene-*d*₈ on a Bruker WM-500. Shifts are reported in ppm relative to external SiMe₄ (¹H, ¹³C) and external H₃PO₄ (H₂O) (³¹P). Trimethylaluminum (TMA), isobutylalumoxane (IBAO), bis(diisobutylaluminum oxide) (DBAO), triisobutylaluminum (TBA), and triethylaluminum (TEA) were obtained from Akzo Nobel. Samples of methylalumoxane (MAO) were obtained from Akzo Nobel and Albe-Marle. Ethylalumoxane (EAO) and Me₃Al(PPh₃) were prepared by following literature methods. PPh₃ (Aldrich) was recrystallized from EtOH prior to use.

Standard AlMe₃/PPh₃ samples were prepared in the drybox. Me₃Al(PPh₃) (ca. 50 mg) was placed in a 5 mm NMR tube. To this was added PPh₃ (1-300 mg) and toluene-*d*₈ (ca. 1 mL). Standards with low PPh₃ were prepared by the addition of AlMe₃ to Me₃Al·PPh₃.

Analysis of Alumoxane. In a typical experiment a measured sample of MAO solution (5.0 mL) with a known total aluminum content (sample 2, 9.9 wt %) is added to an excess of PPh₃ (5.108 g). The actual quantity of PPh₃ employed is not important; however, ca. 5.0 g measured to ±0.001 g is recommended. The resulting solution was stirred at room temperature for 2 h. An aliquot (ca. 1 mL) of the reaction mixture was then transferred to an NMR tube in which toluene-*d*₈ (ca. 0.2 mL) had already been added. The ³¹P NMR spectrum was obtained at 25 °C. From the NMR spectral shift and the appropriate equation ($R = \text{Me}$; eq 5) the Al:P ratio was determined (0.395). Given the mass of PPh₃ used, the mass of PPh₃ complexed to AlMe₃ (2.0176 g) and, hence, mass of Al existing as AlMe₃ (0.2079 g) were determined. The percentage of the total aluminum content existing as AlMe₃ is thus obtained (47.8%).

Acknowledgment. Financial support for this work was provided by the Office of Naval Research, and Akzo Nobel (Dobbs Ferry, NY) is acknowledged for a gift of chemicals.

OM940853Y

(17) Boleslawski, M.; Serwatowski, J. *J. Organomet. Chem.* **1983**, *254*, 159.

(18) Barron, A. R.; Motevalii, M.; Hursthouse, M. B.; Wilkinson, G. *J. Chem. Soc., Chem. Commun.* **1985**, 664.

Unusual Interaction of Ag⁺ with an Organopalladium Crown Ether. Synthesis and Structures of [PdCl(L)] and [Pd(H₂O)(L)(Ag)][CF₃SO₃]₂ (L = 5,8,11-Trioxa-2,14-dithia[15]-*m*-cyclophane)

James E. Kickham and Stephen J. Loeb*

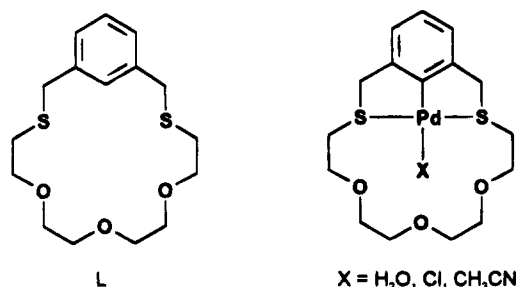
Department of Chemistry and Biochemistry, University of Windsor,
Windsor, Ontario, Canada N9B 3P4

Received December 13, 1994[®]

Summary: Reaction of 2 equiv of [Ag][CF₃SO₃] with the organopalladium crown ether [PdCl(L)] (L = 5,8,11-trioxa-2,14-dithia[15]-*m*-cyclophane) results in formation of AgCl and encapsulation of the second Ag⁺ ion to form the bimetallic complex [Pd(H₂O)(L)(Ag)][CF₃SO₃]₂. The X-ray structure of [Pd(H₂O)(L)(Ag)][CF₃SO₃]₂·CH₂Cl₂ shows that the electrophilic Ag⁺ ion is bound to the Pd-C(aryl) unit and that this interaction is complemented by peripheral coordination to the ether oxygens and a counterion.

Introduction

m-Thiacyclophanes can be palladated to produce organopalladium complexes that contain an open coordination site on palladium *trans* to the Pd-C bond.¹ If the thiacyclophane contains peripheral donor sites, such as the three oxygen atoms in the polyether chain of 5,8,11-trioxa-2,14-dithia[15]-*m*-cyclophane, L, there exists



the possibility of noncovalent (electrostatic, hydrogen-bonding) interactions accompanying coordination at the transition metal center.² Recent results from our laboratories, as well as others, have demonstrated that this phenomenon, known as simultaneous first- and second-sphere coordination,³ can be used for the molecular recognition of substrate molecules.²⁻⁷ Another interesting aspect of these systems is the possibility that this noncovalent, second-sphere coordination could be

used to stabilize otherwise weak bonding interactions in the first-sphere of coordination of a transition metal. This may, for example, have application to mechanistic studies in organometallic chemistry by allowing for the stabilization and thus detection of transient metal-substrate interactions.

Experimental Section

Silver triflate, pyrazine, and all deuterated solvents were purchased from Aldrich and used as received. [PdCl₂(PhCN)₂] and the thiacyclophane ligand 5,8,11-trioxa-2,14-dithia[15]-*m*-cyclophane, L, were prepared by literature methods.^{8,3c} All reactions were conducted under an atmosphere of N₂ using standard Schlenk techniques, and all solvents were degassed prior to use. ¹H and ¹³C{¹H} NMR spectra were recorded at 300.1 and 75.4 MHz, respectively, on a Bruker AC300 spectrometer locked to the deuterated solvent. Infrared spectra were recorded on a Nicolet 5DX FTIR spectrometer. Elemental analyses were performed by Canadian Microanalytical Services, Delta, British Columbia, Canada.

Preparation of [PdCl(L)]. [PdCl₂(PhCN)₂] (0.227 g, 0.592 mmol), [Ag][CF₃SO₃] (0.171 g, 0.667 mmol), and the thiacyclophane, L (0.194 g, 0.591 mmol), were dissolved in CH₃CN (50 mL). The yellow-colored solution was refluxed for 48 h, cooled, and filtered to remove a yellow precipitate, and then the solvent was removed in vacuo. The orange residue was dissolved in acetonitrile (10 mL), and diffusion of diethyl ether into this solution gave [PdCl(L)] as a yellow crystalline solid. Yield: 0.179 g (64%). ¹H NMR (CD₃CN): δ (ppm) 6.99 (m, 3H, aromatic), 4.41 (s, 4H, benzylic), 4.07 (s, br, 4H, OCH₂), 3.58 (s, 4H, OCH₂), 3.51 (s, 4H, OCH₂), 3.20 (s, br, 4H, SCH₂). ¹³C{¹H} NMR (CD₃CN): δ (ppm) 155.9, 151.7, 126.3, 123.5 (aromatic), 72.2, 71.2, 71.1 (OCH₂), 45.1 (benzylic), 38.1 (SCH₂). Anal. Calcd for C₁₆H₂₃ClO₃PdS₂: C, 40.94; H, 4.95. Found: C, 40.34; H, 4.88.

Preparation of [Pd(H₂O)(L)(Ag)][CF₃SO₃]₂. [Ag][CF₃SO₃] (0.089 g, 0.345 mmol), [PdCl(L)] (0.075 g, 0.160 mmol), and pyrazine (0.065 g, 0.081 mmol) in CH₂Cl₂ (8 mL) were stirred at room temperature overnight. The solution was filtered, and the volume of solvent was reduced to 2 mL. Diffusion of diethyl ether into this solution produced orange-colored crystals suitable for single-crystal X-ray diffraction.

(4) (a) van Staveren, C. J.; van Eerden, J.; van Veggel, F. C. J. M.; Harkema, S.; Reinhoudt, D. N. *J. Am. Chem. Soc.* **1988**, *110*, 4994. (b) van Doorn, A. R.; Rushton, D. J.; van Straaten-Nijenhuis, W. F.; Verboom, W.; Reinhoudt, D. N. *Recl. Trav. Chim. Pays-Bas* **1992**, *111*, 421.

(5) Reetz, M. T.; Niemeyer, C. M.; Hermes, M.; Goddard, M. *Angew. Chem., Int. Ed. Engl.* **1992**, *24*, 135.

(6) (a) Aoyama, Y.; Yamagishi, A.; Asagawa, M.; Toi, H.; Ogoshi, H. *J. Am. Chem. Soc.* **1988**, *110*, 4076. (b) Mizutani, T.; Ema, T.; Yoshida, T.; Kurado, Y.; Ogoshi, H. *Inorg. Chem.* **1993**, *32*, 2072.

(7) (a) Shionoya, M.; Kimura, E.; Shiro, S. *J. Am. Chem. Soc.* **1993**, *115*, 6730. (b) Shionoya, M.; Ikeda, T.; Kimura, E.; Shiro, S. *J. Am. Chem. Soc.* **1994**, *116*, 3848.

(8) Karash, M. S.; Seyler, R. C.; Mayo, F. F. *J. Am. Chem. Soc.* **1938**, *60*, 882.

[®] Abstract published in *Advance ACS Abstracts*, June 1, 1995.

(1) (a) Hanan, G. S.; Kickham, J. E.; Loeb, S. J. *J. Chem. Soc., Chem. Commun.* **1991**, 893. (b) Hanan, G. S.; Kickham, J. E.; Loeb, S. J. *Organometallics* **1992**, *11*, 3063. (c) Giesbrecht, G. R.; Hanan, G. S.; Kickham, J. E.; Loeb, S. J. *Inorg. Chem.* **1992**, *31*, 3286.

(2) (a) Colquhoun, H. M.; Stoddart, J. F.; Williams, D. J. *Angew. Chem., Int. Ed. Engl.* **1986**, *25*, 487. (b) Stoddart, J. F.; Zarzycki, R. *Cation Binding by Macrocycles*; Inoue, Y., Gokel, G. W., Eds.; Marcel Dekker: New York, 1990; p 631 and references therein.

(3) (a) Kickham, J. E.; Loeb, S. J.; Murphy, S. L. *J. Am. Chem. Soc.* **1993**, *115*, 7031. (b) Kickham, J. E.; Loeb, S. J. *J. Chem. Soc., Chem. Commun.* **1993**, 1848. (c) Kickham, J. E.; Loeb, S. J. *Inorg. Chem.* **1994**, *33*, 4351.

Table 1. Crystallographic Data for [PdCl(L)] and [Pd(H₂O)(L)(Ag)][CF₃SO₃]₂·CH₂Cl₂

compd	[PdCl(L)]	[{d(H ₂ O)(L)(Ag)}][CF ₃ SO ₃] ₂ ·CH ₂ Cl ₂
formula	C ₁₆ H ₂₃ ClO ₃ PdS ₂	C ₁₉ H ₂₇ AgCl ₂ F ₆ O ₁₀ PdS ₄
fw	469.40	942.82
a, Å	10.276(5)	12.746(5)
b, Å	10.343(5)	12.769(7)
c, Å	8.875(3)	10.224(8)
α, deg	94.04(4)	94.41(6)
β, deg	94.34(4)	104.87(4)
γ, deg	100.22(4)	90.61(4)
V, Å ³	922.3(1)	1603(2)
space group	P $\bar{1}$ (No. 2)	P $\bar{1}$ (No. 2)
Z	2	2
ρ, g/cm ⁻³	1.69	1.92
λ, Å	0.7107	0.7107
μ, cm ⁻¹	13.7	16.8
T, °C	23	23
R(F _o), % ^a	4.09	6.49
R _w (F _o), % ^a	5.10	7.92

^a $R = \sum |F_o| - |F_c| / \sum |F_o|$, $R_w = (\sum w(|F_o| - |F_c|)^2 / \sum w F_o^2)^{1/2}$, and $w = 1/\sigma^2(F)$.

Yield: 0.056 g (41%) as the CH₂Cl₂ solvate. Any attempt to obtain a solution NMR spectrum for this compound resulted in decomposition of the material. Anal. Calcd for C₁₆H₂₃AgF₆O₁₀PdS₄: C, 25.20; H, 2.94. Found: C, 25.02; H, 2.79.

Reaction of [Pd(CH₃CN)(L)]BF₄ with [Ag][CF₃SO₃]. [Ag][CF₃SO₃] (0.030 g, 0.116 mmol) and [Pd(CH₃CN)(L)]BF₄ (0.065 g, 0.116 mmol) were dissolved in CDCl₃ (2 mL), and the ¹H NMR spectrum was recorded immediately. ¹H NMR (CDCl₃): δ (ppm) 7.26 (t, 1H, aromatic), 7.06 (d, 2H, aromatic), 4.90 (br, s, 2H, benzylic), 4.48 (br, s, 2H, benzylic), 4.26 (br, s, 4H, OCH₂), 3.91 (s, 4H, OCH₂), 3.59 (s, 4H, OCH₂), 3.36 (s, br, 2H, SCH₂), 3.13 (s, br, 2H, SCH₂), 2.01 (s, br, 3H, CH₃CN).

General X-ray Crystallography. Diffraction experiments were performed on a four-circle Rigaku AFC6S diffractometer with graphite-monochromatized Mo Kα radiation. The unit cell constants and orientation matrices for data collection were obtained from 25 centered reflections (15° < 2θ < 35°). Machine parameters, crystal data, and data collection parameters are summarized in Tables 1 and S-1 (supporting information). The intensities of three standard reflections were recorded every 150 reflections and showed no statistically significant changes over the duration of the data collections. The intensity data were collected using the ω-2θ scan technique, in four shells (2θ < 30°, 40°, 45°, and 50°). Empirical absorption coefficients were calculated, and absorption corrections were applied to the data. The data were processed using the TEXSAN software package running on an SGI Challenge XL computer.⁹ Refinements were carried out by using full-matrix least-squares techniques on F by minimizing the function $w(|F_o| - |F_c|)^2$, where $w = 1/\sigma^2(F_o)$ and F_o and F_c are the observed and calculated structure factors. Atomic scattering factors¹⁰ and anomalous dispersion terms^{11,12} were taken from the usual sources. Fixed H atom contributions were included with C-H distances of 0.95 Å and thermal parameters 1.2 times the isotropic thermal parameter of the bonded C atoms. No H atoms were refined, but all values were updated as refinement continued.

Structures of [PdCl(L)] and [Pd(H₂O)(L)(Ag)][CF₃SO₃]₂. Yellow crystals of [PdCl(L)] and golden-yellow [Pd(H₂O)(L)(Ag)][CF₃SO₃]₂ were grown by diffusion of diethyl

Table 2. Selected Positional Parameters and B(eq) Values^a for [PdCl(L)]

atom	x	y	z	B(eq)
Pd	0.68850(6)	0.61461(6)	0.16299(6)	2.91(2)
Cl	0.8072(2)	0.5788(2)	-0.0550(2)	4.6(1)
S(1)	0.5221(2)	0.6910(2)	0.0317(2)	3.15(8)
S(2)	0.8307(2)	0.5312(2)	0.3238(2)	3.55(8)
O(1)	0.7133(5)	1.0649(5)	0.0669(6)	4.2(2)
O(2)	0.9786(5)	1.0604(5)	0.2541(6)	4.4(2)
O(3)	1.1322(6)	0.8353(6)	0.3175(8)	6.5(3)
C(1)	0.5991(7)	0.6574(6)	0.3462(7)	2.6(3)
C(2)	0.6526(7)	0.6380(6)	0.4912(7)	3.0(3)
C(3)	0.5895(8)	0.6636(7)	0.6178(7)	3.5(3)
C(4)	0.4737(8)	0.7113(8)	0.6033(8)	4.5(4)
C(5)	0.4188(8)	0.7353(8)	0.4632(8)	4.2(4)
C(6)	0.4818(7)	0.7080(7)	0.3337(7)	3.0(3)
C(7)	0.4173(7)	0.7225(7)	0.1788(8)	3.9(3)
C(8)	0.5974(7)	0.8544*7	-0.0094(8)	3.5(3)
C(9)	0.6830(7)	0.9396(7)	0.1175(8)	3.8(3)
C(10)	0.7966(9)	1.1622(7)	0.169(1)	4.7(4)
C(11)	0.939(1)	1.1618(8)	0.171(1)	5.0(4)
C(12)	1.1136(9)	1.0575(8)	0.253(1)	5.2(4)
C(13)	1.1610(8)	0.9706(9)	0.363(1)	5.7(4)
C(14)	0.9994(8)	0.7745(8)	0.314(1)	4.8(4)
C(15)	0.9955(8)	0.6289(8)	0.3174(8)	4.3(4)
C(16)	0.7819(8)	0.5869(8)	0.5068(8)	4.0(3)

$$^a B(\text{eq}) = (8\pi^2/3) \sum_{i=1}^3 \sum_{j=1}^3 U_{ij} a_i^* a_j^* \bar{a}_i \bar{a}_j.$$

ether into respective acetonitrile and CH₂Cl₂ solutions of the complexes. Statistical analysis of intensity distributions were consistent with the triclinic space group P $\bar{1}$ for both compounds. These assignments were confirmed by successful solution refinements. A total of 3462 reflections were collected and 2645 unique reflections with F_o² > 3σ(F_o²) were used in the refinement of [PdCl(L)], while a total of 4580 reflections were collected and 2515 unique reflections with F_o² > 3σ(F_o²) were used in the refinement of [Pd(H₂O)(L)(Ag)][CF₃SO₃]₂. The positions of the palladium, silver, and sulfur atoms were determined by direct methods from the initial E-maps with the highest figure of merit. The remaining non-hydrogen atoms were located from difference Fourier map calculations. In the final cycles of refinement for [PdCl(L)], all atoms were assigned anisotropic thermal parameters. This resulted in R = 0.0409 and R_w = 0.0510 at final convergence. In the final cycles of refinement for [Pd(H₂O)(L)(Ag)][CF₃SO₃]₂, the silver, palladium, chlorine, sulfur, fluorine, oxygen, and carbon atoms of the cation, the uncoordinated triflate ion, and the solvent molecule were all assigned anisotropic thermal parameters. The coordinated triflate was input as an anisotropic S atom, three independent isotropic O atoms, and a rigid CF₃ group with individual isotropic thermal parameters. This resulted in R = 0.0649 and R_w = 0.0792 at final convergence. The Δ/σ value for any parameter in the final cycles was less than 0.002, and final difference Fourier map calculations showed no peaks of chemical significance. Selected atomic positional parameters are summarized in Tables 2 and 4, and selected bond distances and angles are summarized in Tables 3 and 5. Full listings of atomic positional parameters (Tables S-2 and S-6), nonessential bonding parameters (Tables S-3 and S-7), thermal parameters (Tables S-4, S-8), and hydrogen atom parameters (Table S-5 and S-9) are deposited as supporting information.

Results and Discussion

The thiacyclopentane L is easily palladated by refluxing an acetonitrile solution of the ligand in the presence of 1 equiv each of [PdCl₂(PhCN)₂] and [Ag][CF₃SO₃]. The resulting complex [PdCl(L)] is a yellow, air-stable crystalline solid that is soluble in most polar organic solvents. ¹H and ¹³C NMR spectra show features that are diagnostic of a palladated structure for [PdCl(L)]; the absence of a downfield resonance in the aromatic

(9) TEXSAN-TEXRAY Structure Analysis Package; Molecular Structure Corp: The Woodlands, TX, 1985.

(10) Cromer, D. T.; Waber, J. T. *International Tables for X-ray Crystallography*; Kynoch Press: Birmingham, England, 1974; Vol. 4, Table 2.2A.

(11) Ibers, J. A.; Hamilton, H. A. *Acta Crystallogr.* 1974, 17, 781.

(12) Cromer, D. T. *International Tables for X-ray Crystallography*; Kynoch Press: Birmingham, England, 1974; Vol. 4, Table 2.3.1.

Table 3. Selected Bonding Parameters for [PdCl(L)]

Distances (Å)			
Pd-Cl	2.405(2)	Pd-S(1)	2.284(2)
Pd-S(2)	2.286(2)	Pd-C(1)	1.988(7)
S(1)-C(7)	1.802(8)	S(1)-C(8)	1.804(8)
S(2)-C(15)	1.818(8)	S(2)-C(16)	1.821(7)
O(1)-C(9)	1.392(8)	O(1)-C(10)	1.419(8)
O(2)-C(11)	1.420(9)	O(2)-C(12)	1.394(9)
O(3)-C(13)	1.402(9)	O(3)-C(14)	1.395(9)
C(2)-C(16)	1.516(9)	C(6)-C(7)	1.510(8)
C(8)-C(9)	1.501(9)	C(10)-C(11)	1.47(1)
C(12)-C(13)	1.48(1)	C(14)-C(15)	1.50(1)
Angles (deg)			
Cl-Pd-S(1)	94.96(7)	Cl-Pd-S(2)	93.91(8)
Cl-Pd-C(1)	175.7(2)	S(1)-Pd-S(2)	170.54(8)
S(1)-Pd-C(1)	85.4(2)	S(2)-Pd-C(1)	86.0(2)
C(7)-S(1)-C(8)	103.1(3)	C(15)-S(2)-C(16)	103.4(4)
C(11)-O(2)-C(12)	112.9(7)	C(9)-O(1)-C(10)	116.1(6)
C(13)-O(3)-C(14)	116.1(7)	S(1)-C(7)-C(6)	111.4(5)
S(1)-C(8)-C(9)	116.8(5)	O(1)-C(9)-C(8)	106.3(6)
O(1)-C(10)-C(11)	115.8(7)	O(2)-C(11)-C(10)	112.7(7)
O(2)-C(12)-C(13)	113.5(8)	O(3)-C(13)-C(12)	115.8(7)
O(3)-C(14)-C(15)	107.5(7)	S(2)-C(15)-C(14)	114.7(5)
S(2)-C(16)-C(2)	112.0(5)		

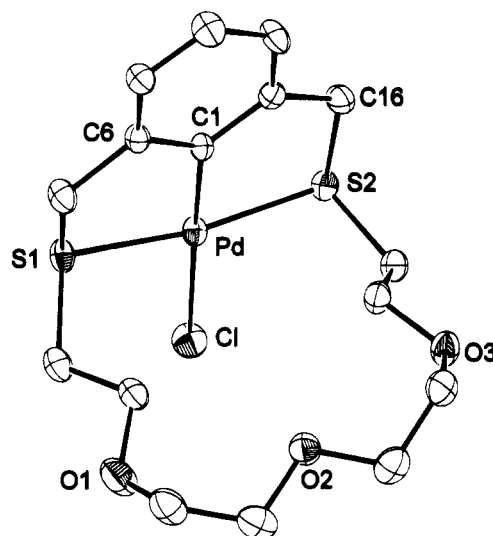
Table 4. Selected Positional Parameters and B(eq)^a for [Pd(H₂O)(L)(Ag)][CF₃SO₃]₂CH₂Cl₂

atom	x	y	z	B(eq)
Ag	0.2423(1)	0.9179(1)	0.2819(1)	3.77(7)
Pd	0.0950(1)	0.8293(1)	0.4189(1)	3.03(7)
S(1)	0.2083(4)	0.8712(4)	0.6308(4)	4.8(3)
S(2)	-0.0459(4)	0.8247(4)	0.2260(5)	4.4(2)
O(1)	0.401(1)	0.862(1)	0.478(1)	4.7(6)
O(2)	0.363(1)	0.803(1)	0.202(1)	5.4(7)
O(3)	0.139(1)	0.798(1)	0.060(1)	4.1(6)
O(4)	0.080(1)	0.665(1)	0.439(1)	5.0(6)
C(1)	0.108(1)	0.980(1)	0.393(2)	3.2(8)
C(2)	0.042(2)	1.022(2)	0.280(2)	4(1)
C(3)	0.040(2)	1.138(2)	0.282(3)	7(2)
C(4)	0.100(3)	1.204(2)	0.382(4)	9(2)
C(5)	0.164(2)	1.158(2)	0.487(3)	7(1)
C(6)	0.173(2)	1.049(2)	0.496(2)	4(1)
C(7)	0.245(2)	1.009(2)	0.613(2)	6(1)
C(8)	0.334(2)	0.803(2)	0.663(2)	5(1)
C(9)	0.379(2)	0.771(2)	0.543(2)	6(1)
C(10)	0.485(2)	0.847(2)	0.412(2)	6(1)
C(11)	0.456(2)	0.771(2)	0.291(3)	6(1)
C(12)	0.320(2)	0.734(1)	0.085(2)	5(1)
C(13)	0.224(2)	0.780(2)	-0.006(2)	5(1)
C(14)	0.087(2)	0.704(2)	0.088(2)	6(1)
C(15)	-0.029(2)	0.731(2)	0.094(2)	5(1)
C(16)	-0.029(2)	0.947(2)	0.165(2)	6(1)

$$^a B(\text{eq}) = (8\pi^2/3) \sum_{i=1}^3 \sum_{j=1}^3 U_{ij} a_i^* a_j^* \bar{a}_i \bar{a}_j.$$

region of the ¹H NMR spectrum normally assigned to a proton at the 2-position on the aromatic ring and the presence of a large downfield shift for one of the aromatic carbons in the ¹³C{¹H} NMR spectrum are indicative of Pd-C bond formation. These features are also consistent with those reported previously for other metalated thiacyclophanes.^{1,2}

A perspective ORTEP drawing of [PdCl(L)] is shown in Figure 1. The complex exhibits square planar geometry at Pd with three donor atoms provided by the rigid S₂C chelate and bond distances of Pd-S(1) 2.286(2), Pd-S(2) 2.284(2), and Pd-C(1) 1.988(7) Å. The two five-membered chelate rings display bite-angles of 85.4(2)° and 86.0(2)° for S(1)-Pd-C(1) and S(2)-Pd-C(1), respectively, while the S(1)-Pd-S(2) angle shows a minor distortion from ideal, square planar geometry with an angle of 170.54(8)°. The fourth site *trans* to the Pd-C bond is occupied by a chloride ion with Pd-

**Figure 1.** ORTEP drawing of [PdCl(L)] showing the atom numbering scheme. Thermal ellipsoids of 30% are shown.**Table 5. Selected Bonding Parameters for [Pd(H₂O)(L)(Ag)][CF₃SO₃]₂CH₂Cl₂**

Distances (Å)			
Ag-Pd	2.884(2)	Ag-O(1)	2.60(1)
Ag-O(2)	2.38(1)	Ag-O(3)	2.66(1)
Ag-O(8)	2.54(2)	Ag-C(1)	2.40(2)
Pd-S(1)	2.294(4)	Pd-S(2)	2.299(4)
Pd-O(4)	2.14(1)	Pd-C(1)	1.97(2)
S(1)-C(7)	1.85(2)	S(1)-C(8)	1.80(2)
S(2)-C(15)	1.79(2)	S(2)-C(16)	1.76(2)
O(1)-C(9)	1.44(3)	O(1)-C(10)	1.42(3)
O(2)-C(11)	1.39(2)	O(2)-C(12)	1.42(2)
O(3)-C(13)	1.43(3)	O(3)-C(14)	1.44(3)
C(2)-C(16)	1.54(3)	C(6)-C(7)	1.43(3)
C(8)-C(9)	1.51(3)	C(10)-C(11)	1.48(3)
C(12)-C(13)	1.49(3)	C(14)-C(15)	1.53(3)
Angles (deg)			
O(1)-Ag-O(2)	67.6(4)	O(1)-Ag-O(3)	126.6(4)
O(1)-Ag-C(1)	104.3(5)	O(1)-Ag-O(8)	131.3(6)
O(2)-Ag-O(3)	68.3(4)	O(2)-Ag-C(1)	160.5(6)
O(2)-Ag-O(8)	95.6(6)	O(3)-Ag-O(8)	81.4(5)
O(8)-Ag-C(1)	102.6(7)	S(1)-Pd-S(2)	163.9(2)
S(1)-Pd-O(4)	96.5(3)	S(1)-Pd-C(1)	85.3(5)
S(2)-Pd-O(4)	93.4(3)	S(2)-Pd-C(1)	85.0(5)
O(4)-Pd-C(1)	178.0(6)	C(7)-S(1)-C(8)	105(1)
C(15)-S(2)-C(16)	104(1)	C(9)-O(1)-C(10)	113(2)
C(11)-O(2)-C(12)	116(2)	C(13)-O(3)-C(14)	115(2)
S(1)-C(7)-C(6)	112(1)	S(1)-C(8)-C(9)	117(1)
O(1)-C(9)-C(8)	111(2)	O(1)-C(10)-C(11)	114(2)
O(2)-C(11)-C(10)	109(2)	O(2)-C(12)-C(13)	110(2)
O(3)-C(13)-C(12)	111(2)	O(3)-C(14)-C(15)	108(2)
S(2)-C(15)-C(14)	118(1)	S(2)-C(16)-C(2)	110(1)

Cl 2.405(2) Å and Cl-Pd-C(1) 175.7(2)°. The angles at sulfur are 103.1(3)° and 103.4(4)°, and this results in the polyether chain between the sulfur atoms being oriented away from and approximately perpendicular to the metal coordination plane.

We have previously shown that the treatment of [PdCl(L)] with 1 equiv of Ag⁺ ion in the presence of a donor solvent such as acetonitrile or an ancillary ligand (Y) such as an aromatic amine or phosphine results in the removal of chloride ion as AgCl and the formation of complexes of the type [Pd(Y)(L)]⁺.¹ In an attempt to form a neutral bridge between two molecules of [Pd(L)]⁺, 2 equiv of [PdCl(L)] and 1 equiv of pyrazine were inadvertently reacted with 4 equiv of [Ag][CF₃SO₃] rather than the 2 equiv required for the intended reaction. An unanticipated result was the almost

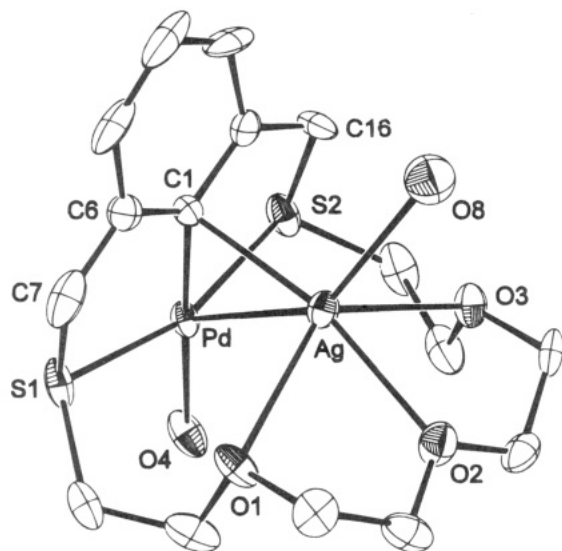


Figure 2. ORTEP drawing of the $[\text{Pd}(\text{H}_2\text{O})(\text{L})(\text{Ag})]^{2+}$ cation, plus O(8) from the coordinated triflate anion, showing the atom numbering scheme. Thermal ellipsoids of 30% are shown.

quantitative formation of the bimetallic Pd–Ag complex $[\text{Pd}(\text{H}_2\text{O})(\text{L})(\text{Ag})][\text{CF}_3\text{SO}_3]_2$. The pyrazine was recovered unchanged, and the same result was obtained in the absence of the aromatic amine. The source of water must presumably have been atmospheric moisture or incomplete drying of the solvent. Attempts to record solution NMR data on this compound were thwarted by the need for polar organic solvents such as acetonitrile which inevitably resulted in decomposition of the complex and formation of $[\text{Pd}(\text{CH}_3\text{CN})(\text{L})][\text{CF}_3\text{SO}_3]$. However, the ^1H NMR spectrum of a similar reaction between $[\text{Pd}(\text{CH}_3\text{CN})(\text{L})][\text{BF}_4]$ and 1 equiv of $[\text{Ag}][\text{CF}_3\text{SO}_3]$ in CDCl_3 showed significant downfield shifts for the aromatic protons consistent with the presence of an electrophile and thus a $\text{Ag}^+ \cdots \text{C}(\pi)$ interaction between the palladated aromatic system and the Ag^+ ion.

A perspective ORTEP drawing of the complex cation $[\text{Pd}(\text{H}_2\text{O})(\text{L})(\text{Ag})]^{2+}$ is shown in Figure 2. This complex has square planar geometry at Pd involving three donor atoms provided by the macrocycle and a water molecule

coordinated in the fourth site; Pd–S(1) 2.296(5), Pd–S(2) 2.298(5), Pd–O(4) 2.14(1), and Pd–C(1) 1.98(2) Å. The Ag^+ ion is bound in an unusual manner directly over the palladated carbon atom with a Ag–C bond distance of 2.40(2) Å and a $\text{Ag} \cdots \text{Pd}$ distance of 2.884(2) Å. The peripheral oxygen atoms of the polyether chain act to stabilize this interaction by encapsulating the Ag ion; Ag–O(1) 2.60(1), Ag–O(2) 2.38(1), Ag–O(3) 2.66(1) Å. A single oxygen atom from one of the CF_3SO_3^- groups, Ag–O(8) 2.54(2) Å, completes the coordination sphere. The geometry around the silver(I) ion is best described in terms of a distorted octahedron with C(1) *trans* to O(2), C(1)–Ag–O(2) 160.5(6)°, O(1) *trans* to O(3), O(1)–Ag–O(3) 126.6(4)°, and Pd *trans* to O(8), Pd–Ag–O(8) 137.6(5)°. The X-ray structure of $[\text{Pd}(\text{H}_2\text{O})(\text{L})(\text{Ag})][\text{CF}_3\text{SO}_3]_2 \cdot \text{CH}_2\text{Cl}_2$ demonstrates that the electrophilic Ag^+ ion is bound directly to the Pd–C(aryl) unit and that the interaction as a whole is supported by peripheral coordination to the ether oxygens and counterion.

A limited number of π -electron rich ligands or π -cryptands,¹³ are known to form weak complexes with Ag^+ . The complex $[\text{Pd}(\text{H}_2\text{O})(\text{L})(\text{Ag})][\text{CF}_3\text{SO}_3]_2 \cdot \text{CH}_2\text{Cl}_2$ described herein can be considered as another example of this class of compounds with the presumably weak Pd–C(π) $\cdots \text{Ag}^+$ interaction stabilized by peripheral coordination of Ag^+ to three ether oxygen atoms of the ligand.

Acknowledgment. We thank the NSERC of Canada for financial support of this research.

Supporting Information Available: Listings of crystallographic data collection parameters, positional parameters, thermal parameters, nonessential bonding parameters, and hydrogen atom parameters (9 pages). Ordering information is given on any current masthead page.

OM940952B

- (13) (a) Xu, W.; Puddephatt, R. J. *Organometallics* **1994**, *13*, 3054. (b) Gano, J. E.; Subramanian, G.; Birnbaum, R. J. *Org. Chem.* **1990**, *55*, 4760. (c) Pierre, J. L.; Baret, P.; Chautemps, P.; Armand, M. *J. Am. Chem. Soc.* **1981**, *103*, 2986. (d) Cohen-Addad, C.; Baret, P.; Chautemps, P.; Pierre, J. L. *Acta Crystallogr.* **1983**, *C39*, 1346. (e) Kang, H. C.; Hanson, A. W.; Eaton, B.; Boekelheide, V. *J. Am. Chem. Soc.* **1985**, *107*, 1979. (f) Terheijden, J.; van Koten, G.; Vinke, I. C.; Spek, A. L. *J. Am. Chem. Soc.* **1985**, *107*, 2891.

Insertion of ClPPh₂ into a Ta–H bond: Synthesis and Structure of the First Phosphido Derivative of Tantalocene

Georgii I. Nikonov,^{*,†} Ludmila G. Kuzmina,[‡] Philip Mountford,[§] and Dmitry A. Lemenovskii^{*,†}

Chemistry Department, Moscow University, Lenin Hills, 119899 Moscow, Russia, Institute of General and Inorganic Chemistry, RAS, Leninsky prosp. 31, 117907 Moscow, Russia, and Chemistry Department, University of Nottingham, University Park, Nottingham NG7 2RD, England

Received December 28, 1994[⊗]

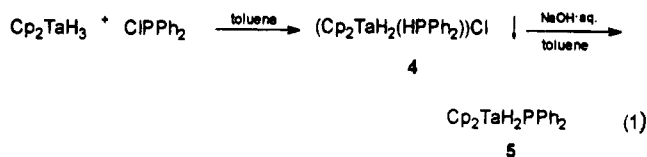
Summary: Ph₂PCl easily inserts into the Ta–H bond of Cp₂TaH₃ affording an ionic complex [Cp₂TaH₂(HPPH₂)]Cl (4). This species was deprotonated to give the first phosphido-substituted tantalocene complex Cp₂TaH₂PPh₂ (5), which was characterized by NMR spectroscopy and X-ray crystallography. Thermal decomposition of 5 as well as its reaction with HPPH₂ was studied.

Recently there has been an increased interest in phosphido-substituted metallocene chemistry.^{1–6} The usual approaches to these species are metathesis¹ and oxidative addition of HPR₂;² however, for the group 5 metallocenes these methods have yet shown little application due to the difficulties of isolation and low yields.^{3,4} For the basic d² metallocenes Cp₂MH(L) (M = Nb, Ta, L = two-electron donor; M = Mo, W, L = H) an alternative synthetic route was suggested,⁵ leading to [Cp₂ML(PHPH₂)]X and supposed to be a nucleophilic substitution of halogen in XPR₂ by a nucleophilic metallocene center.^{5a} Our recent investigation of the reaction of Cp₂NbH₃ with ClPR₂ (Scheme 1) has shown

that direct insertion of a halogenophosphine into the Nb–H bond of Cp₂NbH₃ is also possible, especially for complexes lacking metal-centered lone pairs.⁶ Deprotonation of the insertion product [Cp₂NbH₂(PHPH₂)]Cl (1) yields, however, only the phosphine hydride complex Cp₂NbH(HPPH₂) (3), whereas the possible intermediate isomeric dihydro phosphide Cp₂NbH₂PPh₂ (2) was not observed directly. The tantalum analogue of 2, i.e. Cp₂TaH₂PPh₂, was mentioned earlier in literature; however, neither the synthesis nor characterization was provided.⁴ Here we report the application of our insertion/deprotonation approach⁶ to the synthesis of Cp₂TaH₂PPh₂, together with its characterization and X-ray structure.

Results and Discussion

Similar to the case of niobocene, ClPPh₂ very smoothly inserts into the Ta–H bond of Cp₂TaH₃ yielding the ionic compound (Cp₂TaH₂(HPPH₂))Cl (4) (eq 1). The



compound 4 immediately precipitates as white voluminous flakes after mixing toluene solutions of Cp₂TaH₃ and ClPPh₂ at ambient temperature. Even at low temperatures (up to –20 °C) the rate of the reaction is very high.

The structure of 4 was established by comparison of its IR and NMR data with those of its niobocene analogue 1. In the ¹H NMR spectrum of 4, the P–H resonance appeared as a doublet of triplets at δ 7.09 ppm (¹J_{P–H} = 389 Hz, ³J_{H–H} = 4.3 Hz). This signal does not diminish rapidly in intensity with time (days), indicating that 4 is much more resistant to proton exchange with the solvent (CD₃OD), when compared to its niobium analogue 1 (hours).⁶ However, deprotonation of 4 in aqueous sodium hydroxide (0.25 M) results in a quite different product compared to that found in the case of 1. Thus the dihydride phosphido complex Cp₂TaH₂PPh₂ (5) was produced exclusively rather than the tantalocene analogue of 3. Complex 5 was isolated in high yield (90%) as pale yellow crystals after recrystallization from diethyl ether. Formation of pentavalent 5 versus trivalent 3 indicates an interesting isomerism existing for the complexes of HPPH₂. An analogous

[†] Moscow University.

[‡] RAS.

[§] University of Nottingham.

[⊗] Abstract published in *Advance ACS Abstracts*, May 1, 1995.

(1) (a) Ellerman, J.; Poersch, P. *Angew. Chem., Int. Ed. Engl.* **1967**, *6*, 335. (b) Issleib, K.; Hackert, H. *Z. Naturforsch.* **1966**, *21B*, 519. (c) Baker, R. T.; Whitney, J. F.; Wreford, S. S. *Organometallics* **1983**, *2*, 1049. (d) Wade, S. R.; Wallbridge, M. G. H.; Willey, G. R. *J. Chem. Soc., Dalton Trans.* **1983**, 2555. (e) Weber, L.; Meine, G.; Boese, R.; Augart, N. *Organometallics* **1987**, *6*, 2484. (f) Pagne, R.; Hachgene, J.; Fritz, G.; Fenske, D. *Z. Naturforsch.* **1986**, *41B*, 1535. (g) Chang, M. Y.; Gambarotta, S.; Bolhuis, F. V. *Organometallics* **1988**, *7*, 1864. (h) Benac, B. L.; Jones, R. A. *Polyhedron* **1989**, *8*, 177. (i) Baker, R. T.; Krusic, P. J.; Tulip, T. H.; Calabrese, J. C.; Wreford, S. S. *J. Am. Chem. Soc.* **1983**, *105*, 6763. (j) Roddick, D. M.; Santarsiero, B. D.; Bercaw, J. E. *J. Am. Chem. Soc.* **1985**, *107*, 4670. (k) Hey, E.; Bott, S. G.; Atwood, J. L. *Chem. Ber.* **1988**, *121*, 561. (l) Dick, D. G.; Stephan, D. W. *Can. J. Chem.* **1991**, *69*, 1146. (m) Dick, D. G.; Stephan, D. W. *Organometallics* **1991**, *10*, 2811. (n) Ho, J.; Drake, R. J.; Stephan, D. W. *J. Am. Chem. Soc.* **1993**, *115*, 3792. (o) Hou, Z.; Stephan, D. W. *J. Am. Chem. Soc.* **1992**, *114*, 10088.

(2) (a) Ho, J.; Stephan, D. W. *Organometallics* **1992**, *11*, 1014 (and references therein). (b) Ho, J.; Stephan, D. W. *Organometallics* **1991**, *10*, 3001. (c) Ho, J.; Hou, Z.; Drake, R. J.; Stephan, D. W. *Organometallics* **1993**, *12*, 3145. (d) Hou, Z.; Breen, T. L.; Stephan, D. W. *Organometallics* **1993**, *12*, 1358. (e) Vaughan, G. A.; Hillhouse, G. L.; Rheingold, A. L. *Organometallics* **1989**, *8*, 1760. (f) Nielsen-Marsh, S.; Growte, R. J.; Edwards, P. G. J. *Chem. Soc., Chem. Comm.* **1992**, 699.

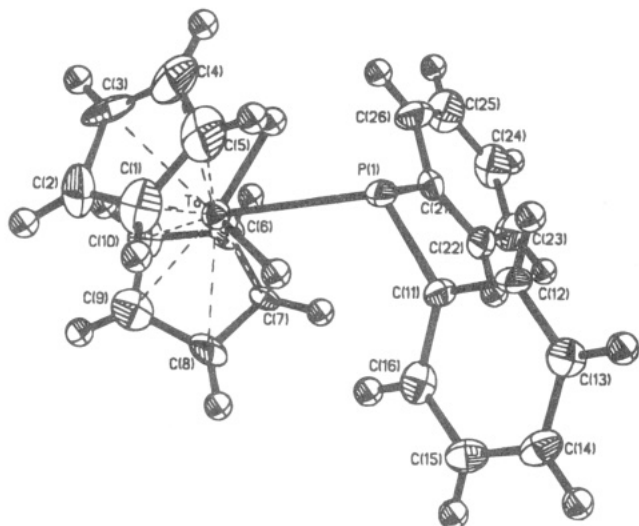
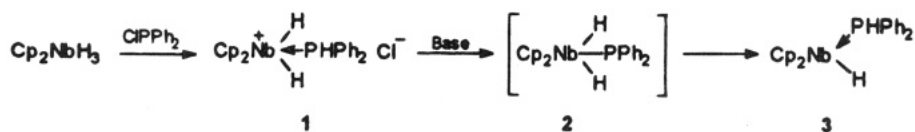
(3) Ol'dekop, Yu. A.; Knizhnikov, V. Z. *Zh. Obshch. Chem.* **1981**, *51*, 723.

(4) Leblanc, J.-C.; Moise, C. J. *Organomet. Chem.* **1989**, *364*, C3.

(5) Bonnet, G.; Lavastre, O.; Leblanc, J.-C.; Moise, C. *New J. Chem.* **1988**, *12*, 551. (b) Bonnet, G.; Kubicki, M. M.; Moise, C.; Lazzaroni, R.; Salvador, P.; Vitulli, G. *Organometallics* **1992**, *11*, 964. (c) Kubicki, M. M.; Kergoat, R.; Cariou, M.; Guerschais, J. E.; L'Haridon, P. *J. Organomet. Chem.* **1987**, *322*, 357. (d) Barre, C.; Kubicki, M. M.; Leblanc, J.-C.; Moise, C. *Inorg. Chem.* **1990**, *29*, 5244.

(6) Nikonov, G. I.; Lemenovskii, D. A.; Lorberth, J. *Organometallics* **1994**, *13*, 3127.

Scheme 1

Figure 1. Molecular structure of $\text{Cp}_2\text{TaH}_2\text{PPh}_2$.Table 1. Selected Bond Distances (Å) and Angles (deg) for $\text{Cp}_2\text{TaH}_2\text{PPh}_2$

Ta-P(1)	2.595(3)	Ta-H(1)	1.70
Ta-H(2)	1.70	Ta-X(1) ^a	2.058
Ta-X(2)	2.039	P(1)-C(21)	1.85(1)
P(1)-C(11)	1.85(1)		
P(1)-Ta-H(1)	54.0	P(1)-Ta-H(2)	53.5
H(1)-Ta-H(2)	102	C(11)-P(1)-C(21)	101.1(5)
Ta-P(1)-C(21)	108.8 (4)	Ta-P(1)-C(11)	113.9 (3)
Cp(1)-Cp(2) ^b	137.3		

^a X(1) and X(2) are the gravity centers of the cyclopentadienyl rings. ^b Cp(1)-Cp(2) denotes the angle between the normals to the cyclopentadienyl rings.

isomerism has recently been observed by Baker et al. for the pair $\text{Cp}^*\text{W}(\text{PMe}_3)(\text{PPh}_2)_2\text{H}$ and $\text{Cp}^*\text{Mo}(\text{PMe}_3)(\text{HPPH}_2)\text{PPh}_2$.⁷ In our opinion, the stabilization of hydrido phosphide complexes for the 3rd row transition metals is mainly due to the higher metal-hydrogen bond energy observed for the third transition row as compared with the second.⁸

An X-ray diffraction study of **5** confirmed the above formulation. Thus **5** was found to be a trisubstituted tantalocene with a centrally positioned PPh_2 substituent and two lateral hydride ligands. Structurally analogous silicon⁹ and tin¹⁰ compounds have been previously studied; a related disilicon hydride tantalocene has been reported by Berry et al.¹¹ The molecular structure of **5** is shown in Figure 1, and selected bond distances and angles are given in Table 1. It is a common bent tantalocene substituted by a pyramidal PPh_2 ligand. The Ta-P bond distance is 2.595(3) Å, which is in perfect agreement with the calculated distance of 2.60

Å obtained by combining the tantalum radius in d^0 tantalocene (1.50 Å)⁹ with the P radius of 1.10 Å.¹² This distance is somewhat longer than the Ta-P(phosphine) bond in $\text{Cp}_2\text{TaSiMe}_3(\text{PMe}_3)$ (2.516(4) Å)¹¹ and reflects the absence of any Ta-P multiple bond. In another structurally characterized phosphide derivative of tantalum, $\text{TaH}(\text{PPh}_2)_2(\text{dmp})_2$,¹³ having trigonal-planar phosphide ligands, the Ta-P(phosphide) bond distances are 2.430(6) and 2.404(6) Å, and the average bond order was assigned to be 1.5. Two hydrides were also located (but were not refined) at the distances of 1.700 Å, which are close to those found for Cp_2TaH_3 (average 1.774 (3) Å).¹⁴

The compound **5** was proposed earlier to be an intermediate in the reaction between Cp_2TaH_3 and HPPH_2 to give the diphosphene compound $\text{Cp}_2\text{TaH}(\eta^2\text{-PPhPPH})$ (**6**).⁴ According to these authors, **5** "is readily converted into **6** by heating with HPPH_2 ". In this context it would be of interest to compare the thermal decomposition of the tantalum complex **5** and niobium complex **3**. The latter was showed to lose easily dihydrogen giving an orthometalated complex **7**, probably, via an intermediate complex **2'**, isomeric to **2**.⁶



Wishing to obtain other possible intermediates on the way to **6**, we have studied the thermolysis of **5**. We have found that **5** does not decompose upon heating at 85 °C over 8 h (by ¹H and ¹³C NMR). However, when **5** was heated at 100 °C in the presence of an equivalent amount of HPPH_2 for 3.5 h, very small but detectable amounts of another phosphorus derivative of tantalocene were found. Its ¹H, ¹³C, and ³¹P NMR data were identical with those of $\text{Cp}_2\text{Ta}(\text{HPPH}_2)\text{PPh}_2$ (**8**), which was also synthesized by another method;¹⁵ the tantalum analogue of **7** was not found. Small amounts of Cp_2TaH_3 were also observed in the NMR spectra of the reaction mixture. This indirectly supports that elimination of dihydrogen from **5** proceeds via complex $\text{Cp}_2\text{TaH}_2\text{PPh}_2$ with a lateral position of the PPh_2 group, which is analogous to **2'** and isomeric to **5**. This compound can be formed by subsequent reductive elimination/oxidative addition steps of HPPH_2 from **5**, producing Cp_2TaH as an intermediate. Trapping of the latter by H_2 accounts for the formation of Cp_2TaH_3 .

Complex **6** was, however, formed after refluxing **5** in toluene for 2 days in the presence of HPPH_2 with a

(7) Baker, R. T.; Calabrese, J. C.; Harlow, R. L.; Williams, I. D. *Organometallics* **1993**, *12*, 830.

(8) Moore, D. S.; Robinson, S. D. *Chem. Soc. Rev.* **1983**, *12*, 415.

(9) Curtis, M. D.; Bell, L. G.; Buter, N. M. *Organometallics* **1985**, *4*, 701.

(10) Arkhireeva, T. M.; Bulychev, B. M.; Protsky, A. N.; Soloveichik, G. L.; Bel'sky, V. K. *J. Organomet. Chem.* **1986**, *317*, 33.

(11) Jiang, Q.; Carrol, P. J.; Berry, D. H. *Organometallics* **1991**, *10*, 3648.

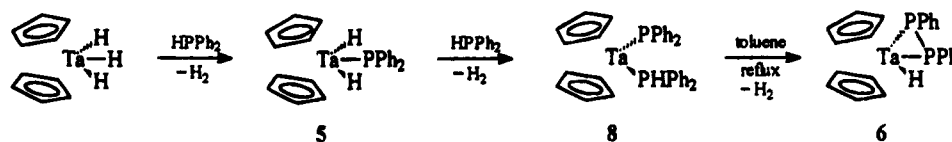
(12) Pauling, L. *The Nature of the Chemical Bond*, 3rd ed.; Cornell University Press: Ithaca, NY, 1960.

(13) Domaille, P. J.; Foxman, B. M.; McNeese, T. J.; Wreford, S. S. *J. Am. Chem. Soc.* **1980**, *102*, 4114.

(14) Wilson, R. D.; Koetzle, T. F.; Hart, D. W.; Kwick, A.; Tipton, D. L.; Bay, R. *J. Am. Chem. Soc.* **1977**, *99*, 1775.

(15) Preparation of this compound as well as further development of the chemistry described here will be reported in a following full paper.

Scheme 2



periodical removal of dihydrogen. The ^1H and ^{31}P NMR spectra of the reaction mixture revealed the presence of **8** and **6** in the ratio 3:7. Thus the reactions between Cp_2TaH_3 and HPPH_2 and between **5** and HPPH_2 can be presented by Scheme 2. The search for other intermediates of this interesting transformation of Cp_2TaH_3 to $\text{Cp}_2\text{TaH}(\eta^2\text{-PPhPPH})$ (**6**) continues.

Experimental Section

All manipulations were carried out *in vacuo* using conventional Schlenk techniques. Solvents were dried over sodium or sodium benzophenone ketyl and distilled into the reaction vessel by high-vacuum gas phase transfer. CIPPh_2 was purchased from Merck. NMR spectra were recorded on a Varian VXR-400 spectrometer (^1H , 400 MHz; ^{13}C , 100.4 MHz, ^{31}P , 162 MHz). IR spectra were obtained with an IKS-26 spectrometer. Elemental analysis was performed in the analytical laboratory of the Chemistry Department of Moscow University.

Preparation of $[\text{Cp}_2\text{TaH}_2(\text{HPPH}_2)]\text{Cl}$ (4**).** Excess of CIPPh_2 (1 mL, 5.57 mmol) was added dropwise to 100 mL of toluene solution of Cp_2TaH_3 (1.05 g, 3.35 mmol). A white voluminous precipitate was formed immediately. After filtration of the reaction solution, this powder was washed with an additional 10 mL of toluene and dried *in vacuo*. Yield: 1.30 g (2.61 mmol, 77.9%). IR (KBr): $\nu_{\text{P-H}} = 2290\text{ cm}^{-1}$, $\nu_{\text{Ta-H}} = 1780\text{ cm}^{-1}$. ^1H NMR (methanol- d_4): δ 7.70 (m, 4, Ph) and 7.58 (m, 6, Ph), 7.09 (dt, $^3J_{\text{H-H}} = 4.3\text{ Hz}$, $^1J_{\text{H-P}} = 389\text{ Hz}$, 1, P-H), 5.58 (d, $J_{\text{P-H}} = 0.9\text{ Hz}$, 10, Cp), -0.60 (dd, $^3J_{\text{H-H}} = 4.3\text{ Hz}$, $^1J_{\text{P-H}} = 71.9\text{ Hz}$, 2, Ta-H). ^{13}C NMR: 134.00, 132.88 (d, $^1J_{\text{C-P}} = 19\text{ Hz}$), 130.81, 120.68 (Ph), 94.13 (s, Cp). $^{31}\text{P}\{^1\text{H}\}$ NMR: 0.17 (s). Anal. Calcd for $\text{C}_{22}\text{TaH}_{23}\text{PCl}$: C, 49.41; H, 4.33. Found: C, 49.56; H, 3.97.

Preparation of $\text{Cp}_2\text{TaH}_2\text{PPh}_2$ (5**).** A 0.555 g (1.04 mmol) amount of **4** was suspended in 35 mL of toluene. A 15 mL volume of 0.25 M aqueous NaOH was added, and the mixture thus obtained was stirred for 1.5 h, until the precipitate was almost completely dissolved. The organic layer turned yellow. Then the toluene solution was decanted and all volatiles were removed *in vacuo* to give a light-orange oily substance. Recrystallization from Et_2O gives **5** as yellow crystals in 90.5% yield (0.939 mmol). IR (KBr): $\nu_{\text{Ta-H}} = 1815\text{ cm}^{-1}$. ^1H NMR (benzene- d_6): δ 7.73 (t, 2, Ph), 7.15 (m, 4, Ph) and 6.95 (m, 4, Ph), 4.66 (s, 10, Cp), -0.10 (d, $J_{\text{P-H}} = 56.9\text{ Hz}$, 2, Ta-H). ^{13}C NMR for **5**: 153.48 (d, $^1J_{\text{C-P}} = 25.3\text{ Hz}$), 134.4 (d, $^2J_{\text{C-P}} = 15.2\text{ Hz}$), 127.54 (d, $^3J_{\text{C-P}} = 5.3\text{ Hz}$), 124.50 (s, Phs), 91.67 (d, $J_{\text{C-P}} = 2.4\text{ Hz}$). $^{31}\text{P}\{^1\text{H}\}$ NMR: -48.91 (s). MS (EI): m/e 496 ($\text{Cp}_2\text{TaPPh}_2$), 798 ($(\text{Cp}_2\text{Ta})_2(\text{C}_{10}\text{H}_8)\text{PPh}_2$). Anal. Calcd for $\text{C}_{22}\text{TaH}_{22}\text{P}$: C, 53.02; H, 4.45. Found: C, 52.75; 4.30.

Thermolysis of $\text{Cp}_2\text{TaH}_2\text{PPh}_2$. A toluene solution of **5** was heated to $100\text{ }^\circ\text{C}$; a light red color appeared, but no reaction product was detected by ^1H NMR. One equivalent of HPPH_2 was added, and the reaction mixture was heated at $100\text{ }^\circ\text{C}$ for 3.5 h giving a red solution. NMR spectra indicated the presence of $\text{Cp}_2\text{Ta}(\text{HPPH}_2)\text{PPh}_2$. Spectral data for **8** are as follows. ^1H NMR (benzene- d_6): δ 7.60, 7.45, 7.32, 7.18 and 6.90 (m, 20, Phs), 7.34 (d, $^1J_{\text{P-H}} = 340.1\text{ Hz}$, 1, P-H), 4.30 (t, $J_{\text{P-H}} = 1.7\text{ Hz}$, 10, Cp). ^{13}C NMR: 89.35 (s, Cp). $^{31}\text{P}\{^1\text{H}\}$ NMR: -20.97 (d, $^2J_{\text{P-P}} = 0.09\text{ Hz}$, 1, PPh_2), 32.09 (d, $^2J_{\text{P-P}} = 15.3\text{ Hz}$, 1, HPPH_2).

X-ray Diffraction Study of **5.** Crystals suitable for X-ray diffraction were grown from an ether solution of **5**. Atomic coordinates are given in Table 2, and the crystal data and data collection parameters are summarized in Table 3. Unit cell

Table 2. Positional Parameters and U Values (\AA^2) and Their Estimated Standard Deviations for $\text{Cp}_2\text{TaH}_2\text{PPh}_2$

atom	x	y	z	$U(\text{iso})/U(\text{eq})$
Ta	0.0004(1)	0.2079(1)	0.7000(1)	0.0213(1)
P(1)	0.0927(3)	0.2945(2)	0.5634(2)	0.0228(7)
C(1)	-0.189(2)	0.3139(9)	0.762(1)	0.045(4)
C(2)	-0.0217(2)	0.2235(9)	0.7965(9)	0.044(4)
C(3)	-0.270(2)	0.1638(9)	0.725(1)	0.045(5)
C(4)	-0.0280(2)	0.219(1)	0.660(1)	0.053(5)
C(5)	-0.0227(2)	0.309(1)	0.675(1)	0.053(5)
C(6)	0.164(2)	0.0687(8)	0.6893(8)	0.035(4)
C(7)	0.264(1)	0.1501(9)	0.7036(6)	0.031(3)
C(8)	0.247(2)	0.1870(9)	0.7842(7)	0.033(4)
C(9)	0.122(2)	0.1334(9)	0.8211(9)	0.042(4)
C(10)	0.072(2)	0.0609(9)	0.7644(8)	0.040(4)
C(11)	0.237(1)	0.3942(7)	0.5837(6)	0.022(3)
C(12)	0.221(1)	0.4747(8)	0.5327(6)	0.024(3)
C(13)	0.323(1)	0.5536(8)	0.5439(7)	0.030(3)
C(14)	0.444(1)	0.5527(9)	0.6065(7)	0.032(3)
C(15)	0.462(1)	0.4730(8)	0.6573(8)	0.030(3)
C(16)	0.363(1)	0.3959(8)	0.6481(7)	0.032(3)
C(21)	0.221(1)	0.2119(8)	0.5020(6)	0.028(3)
C(22)	0.384(1)	0.2237(9)	0.4910(7)	0.029(3)
C(23)	0.475(2)	0.160(1)	0.4439(8)	0.037(4)
C(24)	0.398(2)	0.082(1)	0.4065(9)	0.046(4)
C(25)	0.237(2)	0.067(1)	0.4177(9)	0.051(5)
C(26)	0.145(2)	0.131(1)	0.4631(8)	0.038(4)
H(1)	0.073	0.321	0.695	
H(2)	-0.076	0.191	0.600	

Table 3. Crystal Data and Parameters of the Crystallographic Data Collection

empirical formula	$\text{C}_{22}\text{H}_{22}\text{PTa}$	monochromator	graphite
color	yellow	$d(\text{calc})$ (g/cm^3)	1.84
		abs coef (cm^{-1})	6.11
cryst system	monoclinic	$F(000)$	968.00
space group	$P2_1/c$ (No. 14)	temp (K)	173
unit cell		2θ range (deg)	2-54
params		scan mode	$\theta-2\theta$
a (\AA)	8.206 (4)	no. of rflns	3019
b (\AA)	13.970 (6)	colld	
c (\AA)	15.73 (1)	no. of obs rflns	2725
β (deg)	91.34 (6)	($F > 4.0 \sigma(F)$)	
V (\AA^3)	1803 (3)	weighting scheme	$w^{-1} = [\sigma^2(F) + 0.000256(F^2)]^{-1}$
Z	4	final R indices	$R = 0.0482$, $R_w = 0.0499$
radiation (\AA)	$\lambda(\text{Mo K}\alpha) = 0.71069$	(obs data)	$R_g = 0.0678$, $R_m = 0.0678$
diffractometer	Enraf-Nonius CAD-4	(all data)	0.0678
		goodness of fit	3.05

parameters were determined from least-squares refinement of a set of 25 centered reflections. Two reflections were measured every 2 h as an orientation and intensity check; significant decay of intensity was not observed. The data were corrected for Lorentz, polarization, and absorption (DIFABS¹⁶). The structure was solved by direct methods (SHELX-76¹⁷) and refined by full-matrix least-squares procedures (SHELX-86¹⁸) with anisotropic temperature factors for all the non-hydrogen atoms. Calculated idealized positions of all of the hydrogen atoms were included in further refinement. Two hydride hydrogens were found in the difference Fourier synthesis. In

(16) Walker, N.; Stuart, D. *Acta Crystallogr.*, Sect. A **1983**, 39, 158.

(17) Sheldrick, G. M. SHELX-76, Program for Crystal Structure Determination, University of Cambridge, 1976.

(18) Sheldrick, G. M. SHELX-86, Program for Crystal Structure Determination, Universität Göttingen, 1986.

further refinement, the non-hydride hydrogen atoms were refined using the "rider" scheme with fixed isotropic thermal parameters ($U = 0.08 \text{ \AA}^2$), and the positions of hydrides were fixed.

Acknowledgment. G.I.N. and D.A.L. thank The Russian Foundation for Fundamental Investigations for financial support of this work.

Supporting Information Available: Tables of thermal parameters for non-hydrogen atoms, hydrogen atom positional and thermal parameters, and bond distances and angles for **5** (4 pages). Ordering information is given on any current masthead page.

OM940991N

Ring Opening with Phosphorus–Carbon Bond Cleavage and Coupling in the Reaction of 1,2,3-Triphenylphosphirene (C_2Ph_3P) with $[Ru_3(CO)_{12}]$: X-ray Structure of $[Ru_3(CO)_8(\mu_3-C_4Ph_6P_2)]$

Alejandro J. Arce,^{*,†} Ysaura De Sanctis,[†] Rubén Machado,[†] Mario V. Capparelli,[†] Jorge Manzur,[‡] and Antony J. Deeming^{*,§}

Centro de Química, Instituto Venezolano de Investigaciones Científicas (IVIC), Apartado 21827, Caracas 1020-A, Venezuela, Departamento de Química, Universidad de Chile, Av. Tupper 2069, Casilla 2777, Santiago, Chile, and Department of Chemistry, University College London, 20 Gordon Street, London WC1H 0AJ, U.K.

Received January 23, 1995[®]

Summary: The title complex $[Ru_3(CO)_8(\mu_3, \eta^4-PhPCPh-CPhPPhCPhCPh)]$ is obtained along with $[Ru_4(CO)_{11}(\mu_4-PPh)(\mu_4-PhC_2Ph)]$ by reaction of $[Ru_3(CO)_{12}]$ with 1,2,3-triphenylphosphirene in refluxing tetrahydrofuran. The trinuclear cluster was characterized by NMR and IR spectroscopy, and its structure was determined by X-ray analysis. The dark red crystals are monoclinic, $P2_1/c$, $Z = 4$, $a = 15.439(3)$ Å, $b = 12.654(2)$ Å, $c = 23.313(3)$ Å, $\beta = 105.833(9)^\circ$. The structure was solved by direct methods and refined to $R = 0.022$, $R_w = 0.026$ for 3939 reflections with $[F > 4.0\sigma(F)]$. The molecule is a 48-electron cluster which contains two opened and coupled phosphirene rings acting as an 8-electron donor ligand to a $Ru_3(CO)_8$ unit.

Phosphirene rings are potentially very useful precursors to a range of organometallic ligands, acetylenes, phosphinidenes, and various linked systems. Reactions of phosphirene rings $PhPCPh=CPh$ with mononuclear transition metal complexes can lead to insertion of metal fragments like $[M(PR_3)_2]$ ($M = Pd, R = Et; M = Pt, R = Et, Ph, dppe$) into a P–C bond of the phosphirene ring.¹ Metal carbonyl complexes in which the phosphirene ring acts as a normal tertiary phosphine have been reported recently. Under forcing conditions, P–C bond cleavage occurs and CO or alkenes are inserted into a pentacarbonyl(phosphirene)metal skeleton ($M = Cr, Mo, W$).² We have recently examined a related heterocycle, 1-phenylphosphole, and found that simple substitution compounds $[M_3(CO)_{12-x}(PhPC_4H_4)_x]$ ($x = 1$ or $2, M = Os$) are formed initially with the heterocycle η^1 -coordinated through the P atom,³ which is the commonly found mode of coordination for phospholes. By thermal treatment of these simple substitution products, oxidative addition occurs with P–C bond cleavage to afford ring-opened clusters $[Os_3(CO)_9(PhPC_4H_4)]$ and $[Os_3(CO)_8(PhPC_4H_4)]$ in which the coordination of the P atom can be considered in terms of a μ -phosphido group as part of an eight-electron donating ligand, differently coordinated in the two clusters.

Here we report the results of the reaction of 1,2,3-triphenylphosphirene with $[Ru_3(CO)_{12}]$ in refluxing dry THF. A tetranuclear product was shown by spectroscopic and analytical data to be the pentagonal-bipyramidal *cis*- $[Ru_4(CO)_9(\mu-CO)_2(\mu_4-PPh)(\mu_4, \eta^2-PhC_2Ph)]$, **1**, already described by Carty as a product from the reaction of the phosphinidene complex $[Ru_4(CO)_{13}(\mu_3-PPh)]$ with diphenylacetylene.⁴ However the main product was the new cluster $[Ru_3(CO)_8(C_4Ph_6P_2)]$, complex **2**, which was formed by ring-opening and coupling of two phosphiridene rings. Complex **2** has been characterized by X-ray diffraction analysis, elemental analysis, and NMR and IR spectroscopy.

Results and Discussion

The reaction of $[Ru_3(CO)_{12}]$ with 1,2,3-triphenylphosphirene in refluxing THF yields complexes **1** (12%) and **2** (44%) that are shown in Scheme 1. Complex **1** was shown by analytical and spectroscopic methods to be the same compound that was formed previously by reaction of PhC_2Ph with the phosphinidene cluster $[Ru_4(CO)_{13}(\mu_3-Ph)]$ and structurally characterized.⁴ The phosphiridene is likely to coordinate initially through the P atom in the cluster $[Ru_3(CO)_{11}(C_2Ph_3P)]$, **A** (Scheme 1). Ring-opening would then give compound **B**, which structurally corresponds directly to the known compound $[Os_3(\mu-CO)(CO)_9(\mu_3-MePC_6H_4)]$, formed from $PMePh_2$ and $[Os_3(CO)_{12}]$,⁵ and an iron analogue, $[Fe_3(\mu-CO)(CO)_9(\mu_3-RPCR'=CR'')]$, in which $R = C_6H_4OMe-4$, $R' = H$, and $R'' = Ph$, is also known.⁶

Neither of the suggested intermediates **A** and **B** was detected experimentally. Reaction of **B** with $[Ru_3(CO)_{12}]$ to add a $Ru(CO)_2$ unit would give the known cluster **C**, which has been shown to decarbonylate under our reaction conditions to give the isolated product **1**. The main product is the 48-electron cluster **2**, which we believe to be formed by interception of the proposed intermediate **B** of 1,2,3-triphenylphosphirene. A moderate increase in the yield of **2** was obtained (**2**, 52%; **1**, 10%) by carrying out the reaction in a 2:1 ligand:cluster mole ratio. Spectroscopic and analytical results on **2**

[†] IVIC.

[‡] Universidad de Chile.

[§] University College London.

[®] Abstract published in *Advance ACS Abstracts*, May 1, 1995.

(1) Carmichael, D.; Hitchcock, P. B.; Nixon, J. F.; Mathey, F.; Pidcock, A. *J. Chem. Soc., Chem. Commun.* **1986**, 762.

(2) (a) Marinetti, A.; Fischer, J.; Mathey, F. *J. Am. Chem. Soc.* **1985**, *107*, 5001. (b) Svara, J.; Marinetti, A.; Mathey, F. *Organometallics* **1986**, *5*, 1161.

(3) (a) Arce, A. J.; De Sanctis, Y.; Manzur, J.; Deeming, A. J.; Powell, N. I. *J. Organomet. Chem.* **1991**, *408*, C18. (b) Deeming, A. J.; Powell, N. I.; Arce, A. J.; De Sanctis, Y.; Manzur, J. *J. Chem. Soc., Dalton Trans.* **1991**, 3381.

(4) (a) Corrigan, J. F.; Doherty, S.; Taylor, N. J.; Carty, A. J. *Organometallics* **1993**, *12*, 1365. (b) Lunniss, J.; MacLaughlin, S. A.; Taylor, N. J.; Carty, A. J.; Sappa, E. *Organometallics* **1985**, *4*, 2066.

(5) Deeming, A. J.; Kabir, S. E.; Powell, N. I.; Bates, P. A.; Hursthouse, M. B. *J. Chem. Soc., Dalton Trans.* **1987**, 1529.

(6) Knoll, K.; Orama, O.; Huttner, G. *Angew. Chem., Int. Ed. Engl.* **1984**, *23*, 976.

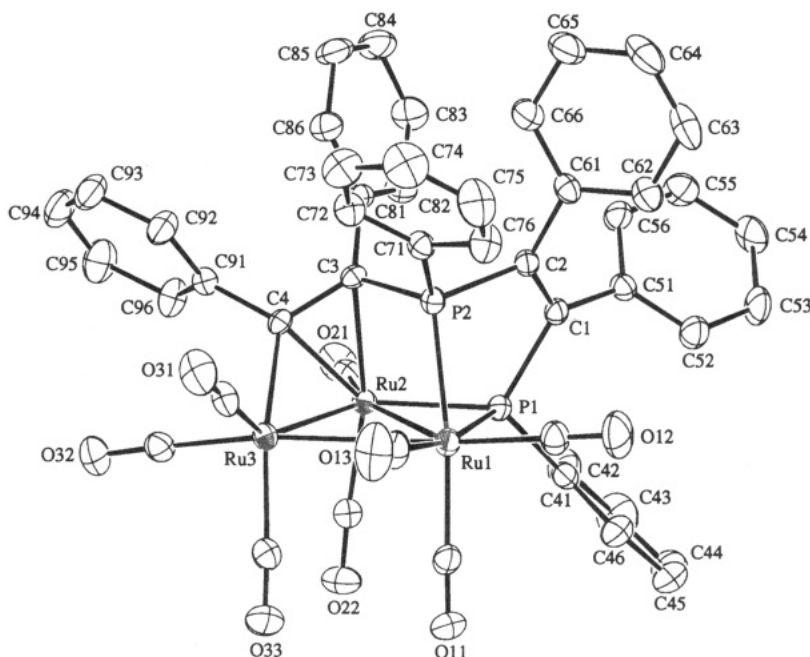
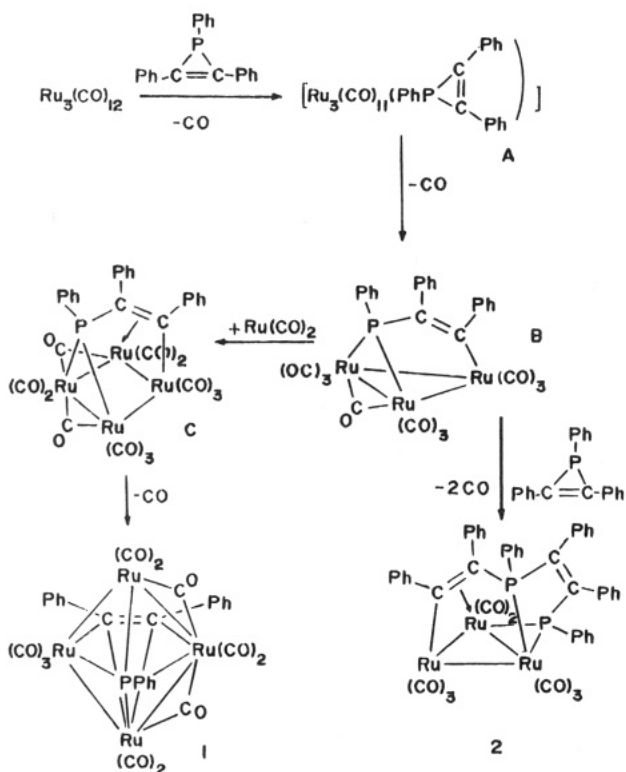


Figure 1. Molecular structure of compound **2** with displacement ellipsoids drawn at 30% probability. In the CO groups both atoms are identically numbered; only O atoms are labeled.

Scheme 1



confirm the stoichiometry $[\text{Ru}_3(\text{CO})_8(\text{C}_4\text{Ph}_6\text{P}_2)]$, while a single-crystal X-ray structure determination has established the mode of bonding of the organic ligand. Both phosphiridene ligands have opened by P–C bond cleavage, and these fragments have coupled head-to-tail through a P–C bond to give the ligand chain, PhPCPh-CPhPPhCPhCPh, bonded as an eight-electron donor. With three Ru–Ru bonds, the 48-electron cluster would be electron precise. The molecular structure of cluster **2** is shown in Figure 1.

There are three distinct types of linkage of the ligand to the metal atoms: a three-electron donating phosphido

Table 1. Crystal Data, Intensity Data Collection Parameters, and Final Refinement Results for Compound **2**

Crystal Data	
formula	$\text{C}_{48}\text{H}_{30}\text{O}_8\text{P}_2\text{Ru}_3$
fw	1099.02
color	dark red
morphology	prisms
specimen size (mm^3)	$0.44 \times 0.25 \times 0.17$
T (K)	295(1)
a (Å)	15.439(3)
b (Å)	12.654(2)
c (Å)	23.313(3)
β (deg)	105.833(9)
V (Å ³)	4382(1)
cryst syst	monoclinic
space group	$P2_1/c$ (No. 14)
Z	4
D_{calc} (g cm^{-3})	1.667
$F(000)$	2176
μ (Mo $K\alpha$) (mm^{-1})	1.148
2θ range for cell (deg)	24.5–31.9
no. of reflns for cell	25
Data Collection	
scan type	ω -2 θ
scan width (deg)	$1.42 + 0.35 \tan \theta$
ω scan speed (deg min^{-1})	8.0
2θ range (deg)	4.0–45.0
hkl range	0–14, 0–13, –24–24
no. of reflns measd	5165
no. of reflns unique	4899
R_{int}	0.046
Refinement (Last Cycle)	
absorption corr	empirical (ΔF)
transmissn factor	0.962–1.141
no. of params refined	550
no. of reflns obsd	3939 [$I > 2\sigma(I)$]
weighting scheme	$w = \sigma(F)^{-2}$
R	0.0217
R_w	0.0257
S (g.o.f.)	1.647
Δ/σ max	0.0005
$\Delta\rho_r$ min, max (e Å^{-3})	–0.27, 0.22

bridge [P(1) bridging Ru(1) and Ru(2)], a two-electron donating tertiary phosphine, P(2), and a three-electron donating μ_2, η^1, η^2 -vinyl bridge [atoms C(3) and C(4)

Table 2. Selected Geometric Parameters (Å, deg) for Compound 2

Bond Lengths			
Ru(1)–Ru(2)	2.8700(5)	Ru(3)–C(31)	1.888(5)
Ru(1)–Ru(3)	3.0482(6)	Ru(3)–C(32)	1.871(5)
Ru(1)–P(1)	2.397(1)	Ru(3)–C(33)	1.950(5)
Ru(1)–P(2)	2.337(1)	P(1)–C(1)	1.858(4)
Ru(1)–C(11)	1.947(5)	P(1)–C(41)	1.814(4)
Ru(1)–C(12)	1.925(5)	P(2)–C(2)	1.850(4)
Ru(1)–C(13)	1.942(5)	P(2)–C(3)	1.820(4)
Ru(2)–Ru(3)	2.6634(6)	P(2)–C(71)	1.813(4)
Ru(2)–P(1)	2.261(1)	C(1)–C(2)	1.348(5)
Ru(2)–C(3)	2.316(4)	C(1)–C(51)	1.474(5)
Ru(2)–C(4)	2.217(4)	C(2)–C(61)	1.493(6)
Ru(2)–C(21)	1.861(5)	C(3)–C(4)	1.429(5)
Ru(2)–C(22)	1.886(5)	C(3)–C(81)	1.516(5)
Ru(3)–C(4)	2.093(4)	C(4)–C(91)	1.496(5)
Bond Angles			
Ru(2)–Ru(1)–Ru(3)	53.39(1)	Ru(1)–Ru(3)–Ru(2)	59.88(1)
Ru(2)–Ru(1)–P(1)	49.87(3)	Ru(1)–Ru(3)–C(4)	88.1(1)
Ru(2)–Ru(1)–P(2)	70.35(3)	Ru(2)–Ru(3)–C(4)	54.0(1)
Ru(3)–Ru(1)–P(1)	103.25(3)	Ru(1)–P(1)–Ru(2)	76.01(3)
Ru(3)–Ru(1)–P(2)	82.02(3)	Ru(1)–P(1)–C(1)	105.1(1)
P(1)–Ru(1)–P(2)	74.90(4)	Ru(2)–P(1)–C(1)	119.1(1)
Ru(1)–Ru(2)–Ru(3)	66.73(1)	Ru(1)–P(2)–C(2)	106.1(1)
Ru(1)–Ru(2)–P(1)	54.12(3)	Ru(1)–P(2)–C(3)	109.4(1)
Ru(1)–Ru(2)–C(3)	81.32(9)	C(2)–P(2)–C(3)	105.2(2)
Ru(1)–Ru(2)–C(4)	90.4(1)	P(1)–C(1)–C(2)	114.6(3)
Ru(3)–Ru(2)–P(1)	120.84(3)	P(2)–C(2)–C(1)	114.1(3)
Ru(3)–Ru(2)–C(3)	78.13(9)	Ru(2)–C(3)–P(2)	93.5(2)
Ru(3)–Ru(2)–C(4)	49.8(1)	Ru(2)–C(3)–C(4)	67.9(2)
P(1)–Ru(2)–C(3)	93.3(1)	P(2)–C(3)–C(4)	118.6(3)
P(1)–Ru(2)–C(4)	126.0(1)	Ru(2)–C(4)–Ru(3)	76.3(1)
C(3)–Ru(2)–C(4)	36.7(1)	Ru(2)–C(4)–C(3)	75.4(2)
Ru(3)–C(4)–C(3)	125.8(3)		

bridging Ru(2) and Ru(3)]. The coordinated C(3)–C(4) bond is 1.429(5) Å, whereas the noncoordinated bond C(1)–C(2) is shorter, 1.348(5) Å (see Tables 1 and 2).

It is worth noting that the P(1)–C(1) bond lengths of 1.858(4) Å and P(2)–C(2) of 1.850(4) Å are elongated presumably due to the fact that the C(1)–C(2) double bond is not coordinated to the metal framework and also to the strain created by fitting the six-atom ligand chain around the three metal centers; this could also justify the notorious variation of metal–metal distances (Ru(1)–Ru(2), 2.8700(5) Å; Ru(1)–Ru(3), 3.0482(6) Å; and Ru(2)–Ru(3), 2.6634(6) Å) even though they must be considered as normal Ru–Ru single bonds as were found in a series of polyphosphido ruthenium clusters.⁷ The unsymmetrical nature of the electron distribution in the compound is also indicated by the very unsymmetrical phosphido bridge: Ru(1)–P(1), 2.307(1) Å, and Ru(2)–P(1), 2.261(1) Å (see Table 3).

Experimental Section

[Ru₃(CO)₁₂] was purchased from Strem Chemicals Inc. 1,2,3-Triphenylphosphirene was synthesized by the published method.⁸ All solvents were dried by conventional techniques and distilled under nitrogen prior to use. NMR spectra were obtained on a Bruker AM-300 instrument, and IR spectra (cyclohexane solutions) were recorded on a Nicolet 5DXC FTIR spectrometer.

Preparation of Complex 2. To a refluxing solution of 200 mg of [Ru₃(CO)₁₂] (0.31 mmol) in dried THF (50 mL) under nitrogen was added 84 mg (0.31 mmol) of 1,2,3-triphenylphosphirene. After 24 h, the IR spectrum showed that no [Ru₃(CO)₁₂] remained and the reaction was stopped. Removal of

Table 3. Fractional Coordinates and Equivalent Isotropic Displacement Parameters^a (Å²)

atom	x	y	z	B _{eq}
Ru(1)	0.18309(2)	-0.14244(3)	-0.18093(2)	2.68(2)
Ru(2)	0.32969(2)	-0.11395(3)	-0.07574(1)	2.27(1)
Ru(3)	0.20466(2)	0.03622(3)	-0.09042(2)	2.62(2)
P(1)	0.31664(7)	-0.24569(8)	-0.14310(5)	2.54(5)
P(2)	0.15656(7)	-0.24045(8)	-0.10247(5)	2.39(5)
O(11)	0.2707(3)	-0.0042(3)	-0.2583(1)	5.5(2)
O(12)	0.1104(3)	-0.3118(3)	-0.2745(2)	6.4(2)
O(13)	0.0004(3)	-0.0296(3)	-0.2101(2)	7.0(2)
O(21)	0.5085(2)	-0.1484(3)	0.0134(2)	4.8(2)
O(22)	0.4234(2)	0.0422(3)	-0.1373(1)	4.8(2)
O(31)	0.0152(2)	0.0813(3)	-0.0834(2)	5.7(2)
O(32)	0.2772(2)	0.2130(3)	-0.0042(2)	5.5(2)
O(33)	0.2154(3)	0.1883(3)	-0.1912(2)	6.6(2)
C(1)	0.2761(3)	-0.3774(3)	-0.1264(2)	2.6(2)
C(2)	0.1993(3)	-0.3751(3)	-0.1094(2)	2.6(2)
C(3)	0.2270(2)	-0.1901(3)	-0.0320(2)	2.2(2)
C(4)	0.2334(2)	-0.0783(3)	-0.0231(2)	2.2(2)
C(11)	0.2373(3)	-0.0536(4)	-0.2299(2)	3.6(2)
C(12)	0.1366(3)	-0.2488(4)	-0.2404(2)	3.7(2)
C(13)	0.0707(4)	-0.0644(4)	-0.1967(2)	4.1(2)
C(21)	0.4384(3)	-0.1374(3)	-0.0185(2)	3.0(2)
C(22)	0.3864(3)	-0.0140(4)	-0.1134(2)	3.2(2)
C(31)	0.0855(3)	0.0647(3)	-0.0885(2)	3.7(2)
C(32)	0.2501(3)	0.1446(4)	-0.0360(2)	3.5(2)
C(33)	0.2114(3)	0.1307(4)	-0.1551(2)	4.1(2)
C(41)	0.3980(3)	-0.2701(3)	-0.1849(2)	3.1(2)
C(42)	0.4858(4)	-0.2896(4)	-0.1535(2)	4.9(3)
C(43)	0.5501(4)	-0.3149(5)	-0.1838(3)	6.6(3)
C(44)	0.5246(5)	-0.3207(5)	-0.2445(4)	6.9(4)
C(45)	0.4383(5)	-0.2999(5)	-0.2764(3)	6.3(3)
C(46)	0.3751(3)	-0.2740(4)	-0.2463(2)	4.6(2)
C(51)	0.3286(3)	-0.4748(3)	-0.1258(2)	2.7(2)
C(52)	0.3493(3)	-0.5130(4)	-0.1763(2)	4.0(2)
C(53)	0.3957(4)	-0.6070(4)	-0.1745(2)	4.7(2)
C(54)	0.4209(3)	-0.6645(4)	-0.1235(2)	4.6(2)
C(55)	0.4026(3)	-0.6275(4)	-0.0725(2)	4.2(2)
C(56)	0.3567(3)	-0.5338(3)	-0.0740(2)	3.6(2)
C(61)	0.1482(3)	-0.4711(3)	-0.1006(2)	2.9(2)
C(62)	0.1249(3)	-0.5444(4)	-0.1464(2)	4.0(2)
C(63)	0.0732(3)	-0.6316(4)	-0.1412(3)	5.3(3)
C(64)	0.0440(4)	-0.6450(4)	-0.0915(3)	5.9(3)
C(65)	0.0673(4)	-0.5741(4)	-0.0461(3)	5.6(3)
C(66)	0.1195(3)	-0.4868(4)	-0.0503(2)	4.4(2)
C(71)	0.0402(3)	-0.2558(3)	-0.1016(2)	2.9(2)
C(72)	0.0054(3)	-0.2071(4)	-0.0600(2)	3.6(2)
C(73)	-0.0840(3)	-0.2194(4)	-0.0614(2)	5.1(3)
C(74)	-0.1395(3)	-0.2781(5)	-0.1049(3)	6.2(3)
C(75)	-0.1080(4)	-0.3244(5)	-0.1478(3)	6.0(3)
C(76)	-0.0183(3)	-0.3142(4)	-0.1471(2)	4.4(2)
C(81)	0.2526(3)	-0.2690(3)	0.0188(2)	2.5(2)
C(82)	0.3292(3)	-0.3293(3)	0.0291(2)	3.2(2)
C(83)	0.3506(3)	-0.4037(4)	0.0743(2)	4.2(2)
C(84)	0.2949(4)	-0.4183(4)	0.1107(2)	4.7(2)
C(85)	0.2187(4)	-0.3573(4)	0.1021(2)	4.6(2)
C(86)	0.1971(3)	-0.2829(4)	0.0562(2)	3.6(2)
C(91)	0.2565(3)	-0.0398(3)	0.0399(2)	2.5(2)
C(92)	0.1889(3)	-0.0307(4)	0.0684(2)	4.1(2)
C(93)	0.2047(4)	0.0094(4)	0.1251(2)	4.8(3)
C(94)	0.2888(4)	0.0407(4)	0.1552(2)	5.0(3)
C(95)	0.3570(3)	0.0339(4)	0.1286(2)	5.2(3)
C(96)	0.3403(3)	-0.0065(4)	0.0709(2)	4.1(2)

^a Equivalent isotropic displacement parameters are as follows: $B_{eq} = (1/3)\pi^2[(aa^*)^2U_{11} + (bb^*)^2U_{22} + (cc^*)^2U_{33} + 2aa^*bb^* \cos \gamma U_{12} + 2aa^*cc^* \cos \beta U_{13} + 2bb^*cc^* \cos \alpha U_{23}]$.

the solvent under reduced pressure and TLC of the orange-red residue (SiO₂, hexane/CH₂Cl₂ eluant, 1:1) gave a red-orange band characterized as [Ru₄(CO)₁₁(PPh)(PhC₂Ph)], **1**, (17 mg, 12%), as dark-red crystals, and a deep-orange band characterized as [Ru₃(CO)₈(C₄Ph₆P₂)], **2**, (62 mg, 44%) as dark-red crystals from hexane. **1**: IR (ν(CO), cm⁻¹) 2087 s, 2056 vs, 2045 vs, 2034 vs, 2021 s, 2008 m, 1987 m, 1975 w. ³¹P-¹H NMR (δ, ppm, C₇D₈) +350. Anal. Calcd (found) for C₃₁H₁₅O₁₁PRu₄: C, 37.27 (37.61); H, 1.52 (1.61). **2**: IR (ν(CO), cm⁻¹) 2073 vs, 2046 s, 2013 s, 1997 m, 1991 m, 1964 m, 1935

(7) Corrigan, J. F.; Sun, Y.; Carty, A. J. *New J. Chem.* **1994**, *18*, 77.

(8) Lochschmidt, S.; Mathey, F.; Schmidpeter, A. *Tetrahedron Lett.* **1986**, *27*, 2365.

m. $^{31}\text{P}\{^1\text{H}\}$ NMR (δ , ppm, CDCl_3) +249.3 (d, $J = 10.5$ Hz), +79.9 (d, $J = 10.5$ Hz). Anal. Calcd (found) for $\text{C}_{48}\text{H}_{30}\text{O}_8\text{P}_2\text{-Ru}_3$: C, 52.45 (52.87); H, 2.75 (2.88).

Crystallography. Crystal data, intensity data collection parameters and final refinement results are summarized in Table 1. Selected geometric parameters are given in Table 2.

All measurements were carried out on a Rigaku AFC-7S diffractometer, using graphite-monochromated Mo K α radiation ($\lambda = 0.71069$ Å). Unit-cell parameters were obtained from the least-squares fit of the setting angles of 25 automatically centered reflections. Intensities were recorded using fixed ω scan speed. Weak reflections [$I < 15\sigma(I)$] were rescanned up to four times, with accumulated counts. The check reflections, monitored every 150 measurements, showed an average decay of 8.9%. The data were scaled using the check reflections and corrected for Lorentz and polarization effects. In the latter stages of refinement an empirical absorption correction⁹ was applied.

The space group was uniquely determined by the systematic absences. The structure was solved by direct methods¹⁰ and refined on F by full-matrix least-squares. Non-hydrogen atoms were refined anisotropically, while H atoms were placed in calculated positions (C–H, 0.96 Å) and assigned fixed coordinates and fixed isotropic displacement parameters [$B_{\text{iso}} = 1.2B_{\text{eq}}(\text{C})$].

Data collection and cell refinement were carried out using the MSC/AFC Diffractometer Control program.¹¹ All other

calculations and drawings were made using the teXsan software package.¹² Neutral-atom scattering factors were taken from ref 13, anomalous scattering corrections from ref 14, and mass absorption coefficients from ref 15.

Acknowledgment. The authors acknowledge the Consejo Nacional de Investigaciones Científicas y Tecnológicas (CONICIT) of Venezuela (Project S1-2094) for providing funds for the purchase of the Rigaku AFC-7S diffractometer and auxiliary equipment (Project PI-092), the Comisión Nacional de Ciencia y Tecnología (CONICYT) of Chile, the University of London, and the Science and Engineering Research Council (SERC) of Great Britain for financial support of this work.

Supporting Information Available: Tables of positional and displacement parameters for the hydrogen atoms, anisotropic displacement parameters, bond lengths and angles, and least-squares mean planes (10 pages). Ordering information is given in any current masthead page.

OM9500533

(11) *MCS/AFC Diffractometer Control Software*; Molecular Structure Corporation: The Woodlands, TX, 1993.

(12) *teXsan. Single Crystal Structure Analysis Software*, Version 1.6; Molecular Structure Corporation: The Woodlands, TX, 1993.

(13) Cromer, D. T.; Waber, J. T. *International Tables for X-ray Crystallography*; Ibers, J. A., Hamilton, W. C., Eds.; Kynoch Press: Birmingham, U.K., 1974; Vol. IV, pp 71–147.

(14) Creagh, D. C.; Mc Auley, W. J. *International Tables for Crystallography*; Wilson, A. J. C., Ed.; Kluwer Academic Publishers: Boston, 1992; Vol. C, pp 219–222.

(15) Creagh, D. C.; Hubell, J. H. *International Tables for Crystallography*; Wilson, A. J. C., Ed.; Kluwer Academic Publishers: Boston, 1992; Vol. C, pp 200–206.

(9) Walker, N.; Stuart, D. *Acta Crystallogr.* **1983**, *A39*, 158.

(10) Beurskens, P. T.; Beurskens, G.; Bosman, W. P.; Garcia-Granda, S.; Smits, J. M. M.; Smykalla, C. *The DIRDIF Program System. Technical Report of the Crystallography Laboratory*; University of Nijmegen: Nijmegen, Holland, 1992.

Reaction of OsHCl(CO)(PiPr₃)₂ with Cyclohexylacetylene: Formation of a Hydrido–Vinylidene Complex via a 1,3-Hydrogen Shift

Miguel A. Esteruelas,* Luis A. Oro, and Cristina Valero

Departamento de Química Inorgánica, Instituto de Ciencia de Materiales de Aragón, Universidad de Zaragoza-CSIC, 50009 Zaragoza, Spain

Received November 28, 1994[Ⓞ]

Summary: The complex OsHCl(CO)(PiPr₃)₂ (**1**) reacts with cyclohexylacetylene to give OsHCl(=C=CHCy)(CO)(PiPr₃)₂ (**2**), which evolves in solution to OsCl{(E)-CH=CHCy}(CO)(PiPr₃)₂ (**3**). Complex **3** reacts with HCl to afford OsCl₂(=CHCH₂Cy)(CO)(PiPr₃)₂ (**4**). The reaction of OsDCI(CO)(PiPr₃)₂ (**1-d**) with cyclohexylacetylene leads to a mixture of OsDCI(=C=CHCy)(CO)(PiPr₃)₂ (**2-d_a**) and OsHCl(=C=CDCy)(CO)(PiPr₃)₂ (**2-d_b**) in a ca. 1:1 molar ratio, indicating that the formation of **2** involves a 1,3-hydrogen shift via an alkynyl intermediate. The dihydrogen or dihydride nature of this alkynyl intermediate is discussed.

Introduction

During studies designed to determine the mechanism of the reduction¹ and hydrosilylation² of terminal alkynes catalyzed by OsHCl(CO)(PiPr₃)₂, we have observed that the nature of the alkyne R group determines the type of the organometallic complexes obtained by reaction of the hydrido-osmium complex OsHCl(CO)(PiPr₃)₂ with terminal alkynes. Thus, it has been reported that this monohydrido compound reacts with acetylene, propyne, and phenylacetylene by insertion to give the five-coordinate vinyl–osmium compounds OsCl{(E)-CH=CHR}(CO)(PiPr₃)₂ (R = H, Me, Ph),³ while the reactions of the monohydride with HC≡CC(OH)R¹R² afford, in one step, vinylcarbene compounds of the type OsCl₂(=CHCH=CR¹R²)(CO)(PiPr₃)₂ in about 40% yield. When R¹ is hydrogen, small amounts of the complexes OsCl{CHCHC(O)R²}(CO)(PiPr₃)₂ can also be obtained.⁴ We have now observed that the reaction of OsHCl(CO)(PiPr₃)₂ with cyclohexylacetylene leads to the hydrido–vinylidene species OsHCl(=C=CHCy)(CO)(PiPr₃)₂.

Hydrido–vinylidene complexes are considered important intermediates in several homogeneous and heterogeneous catalytic reactions, including alkene oligomerization, polymerization, metathesis of olefins,⁵ and Fischer–Tropsch synthesis.⁶ To the best of our knowl-

edge, only three hydrido–vinylidene complexes have been previously isolated. Bercaw *et al.* have reported that the reaction of Cp*₂TaCl₂ and vinylmagnesium bromide gives the neutral hydrido–vinylidene species Cp*₂Ta(H)(=C=CH₂), which affords Cp*₂Ta(CH=CH₂)(CO) by reaction with CO.⁷ Bianchini *et al.* have observed that the 16-electron fragment [(PP₃)OsH]⁺ (PP₃ = P(CH₂CH₂P)₃) is capable of promoting the terminal alkyne to vinylidene tautomerism.⁸ We have shown that the OsH₃(η²-O₂CCH₃)(PiPr₃)₂ complex reacts with phenylacetylene to give OsH(η²-O₂CCH₃)(=C=CHPh)(PiPr₃)₂ and molecular hydrogen.⁹

In this note, we report on the reaction of OsHCl(CO)(PiPr₃)₂ (**1**) with cyclohexylacetylene to give OsHCl(=C=CHCy)(PiPr₃)₂ (**2**), its transformation into OsCl{(E)-CH=CHCy}(CO)(PiPr₃)₂ (**3**), and the reaction of **3** with HCl to afford OsCl₂(=CHCH₂Cy)(CO)(PiPr₃)₂ (**4**) (Scheme 1).

Results and Discussion

The reaction of the hydrido–osmium complex **1** with cyclohexylacetylene to give **2** was carried out in toluene at room temperature. Complex **2** was isolated after 30 min as a pale green solid in 70% yield by addition of pentane and was characterized by elemental analysis, IR, and ¹H, ³¹P{¹H}, and ¹³C{¹H} NMR spectroscopy.

The most noticeable absorptions of the IR spectrum in Nujol are three bands at 2030, 1935, and 1670 cm⁻¹, assigned to the ν(OsH), ν(CO), and ν(C=C) vibrations, respectively. The presence of a hydrido ligand in **2** was mainly inferred from ¹H and ³¹P{¹H} NMR spectra. In agreement with the mutually *trans* disposition of the hydrido and carbonyl ligands, the ¹H NMR spectrum in benzene-*d*₆ contains a triplet at -4.62 ppm¹⁰ with a P–H coupling constant of 28.8 Hz. The ³¹P{¹H} NMR spectrum shows a singlet at 44.8 ppm, which under off-resonance conditions splits into a doublet. The vinylidene group was characterized by a doublet of triplets at 3.19 ppm with P–H and H–H coupling constants of 4.1 and 10.6 Hz, respectively, and, in the ¹³C{¹H} NMR spectrum, by a triplet at 326.9 ppm due to the α-carbon atom with a P–C coupling constant of 2.0 Hz and a singlet at 121.9 ppm due to the β-carbon atom. Similar

* Abstract published in *Advance ACS Abstracts*, June 1, 1995.

(1) Andriollo, A.; Esteruelas, M. A.; Meyer, U.; Oro, L. A.; Sanchez-Delgado, R. A.; Sola, E.; Valero, C.; Werner, H. *J. Am. Chem. Soc.* **1989**, *111*, 7431.

(2) Esteruelas, M. A.; Oro, L. A.; Valero, C. *Organometallics* **1991**, *10*, 462.

(3) Werner, H.; Esteruelas, M. A.; Otto, H. *Organometallics* **1986**, *5*, 2295.

(4) Esteruelas, M. A.; Lahoz, F. J.; Oñate, E.; Oro, L. A.; Zeier, B. *Organometallics* **1994**, *13*, 1662.

(5) (a) Turner, H. W.; Schrock, R. R.; Fellman, J. D.; Holmes, S. J. *J. Am. Chem. Soc.* **1983**, *105*, 4942. (b) Green, J. C.; Green, M. L. H.; Morley, C. P. *Organometallics* **1985**, *4*, 1302.

(6) (a) McCanlish, L. E. *J. Catal.* **1983**, *83*, 362. (b) Erley, W.; McBreen, P. H.; Ibach, H. *J. Catal.* **1983**, *84*, 229. (c) Hoel, E. L.; Ansell, G. B.; Leta, S. *Organometallics* **1986**, *5*, 585. (d) Hoel, E. L. *Organometallics* **1986**, *5*, 587. (e) Zheng, C.; Apeloig, Y.; Hoffmann, R. *J. Am. Chem. Soc.* **1988**, *110*, 749.

(7) van Asselt, A.; Burger, B. J.; Gibson, V. C.; Bercaw, J. E. *J. Am. Chem. Soc.* **1986**, *108*, 5347.

(8) Barbaro, P.; Bianchini, C.; Peruzzini, M.; Polo, A.; Zanobini, F.; Frediani, P. *Inorg. Chim. Acta* **1994**, *5*, 220.

(9) Esteruelas, M. A.; Oro, L. A.; Ruiz, N. *Organometallics* **1994**, *13*, 1507.

(10) A similar δ value for Os–H has been found for related compounds containing a carbonyl ligand *trans* to a hydrido ligand. See: (a) Esteruelas, M. A.; Werner, H. *J. Organomet. Chem.* **1986**, *303*, 221. (b) Werner, H.; Esteruelas, M. A.; Meyer, U.; Wrackmeyer, B. *Chem. Ber.* **1987**, *120*, 11.

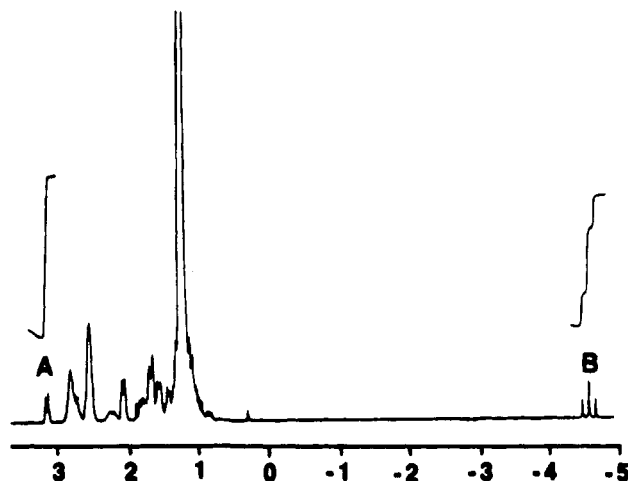
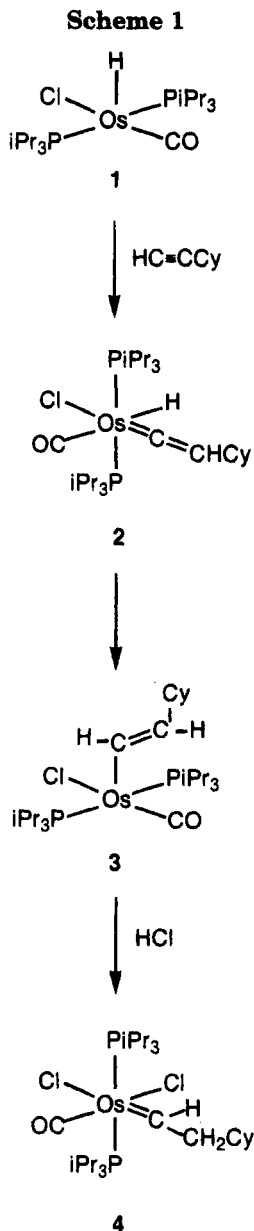


Figure 1. ^1H NMR spectrum of the reaction of $\text{OsDCl}(\text{CO})(\text{PiPr}_3)_2$ (**1-d**) with cyclohexylacetylene after 20 min in benzene- d_6 .

metal to the β -carbon atom of the alkyne group in the 1,3-hydrogen shift is prohibitive.¹⁴ In agreement with this, Werner *et al.* have proved that the mechanism for the formation of the complex $\text{Rh}(\eta^5\text{-C}_5\text{H}_5)(\text{C}=\text{CHPh})(\text{PiPr}_3)_2$ via a hydrido-alkynyl intermediate does not involve an intramolecular 1,3-hydrogen shift but a two-step elimination-addition reaction, in which the last step involves the protonation of the alkynyl ligand.¹⁵

In order to obtain information about the mechanism of formation of **2**, the reaction of $\text{OsDCl}(\text{CO})(\text{PiPr}_3)_2$ (**1-d**) with cyclohexylacetylene was studied by ^1H and ^2H NMR spectroscopy. Figure 1 shows the ^1H NMR spectrum of the solution formed by addition of the stoichiometric amount of cyclohexylacetylene to a benzene- d_6 solution of **1-d**, after 20 min. The most noticeable signals of this spectrum are the two resonances A (δ 3.19, dt, $J(\text{HH}) = 10.6$, $J(\text{HP}) = 4.1$ Hz) and B (δ -4.62, t, $J(\text{HP}) = 28.8$ Hz). Resonance A can be assigned to $\text{OsDCl}(\text{C}=\text{CHCy})(\text{PiPr}_3)_2$ (**2-d_a**), while resonance B can be assigned to $\text{OsHCl}(\text{C}=\text{CDCy})(\text{PiPr}_3)_2$ (**2-d_b**). The presence of the OsD and $\text{C}=\text{CDCy}$ fragments in complexes **2-d_a** and **2-d_b**, respectively, is strongly supported by the ^2H NMR spectrum, which contains two resonances, a broad singlet at 3.0 ppm for the $\text{C}=\text{CDCy}$ group of **2-d_b** and a triplet at -4.6 ppm with a P-D coupling constant of 4.0 Hz, assigned to Os-D of **2-d_a**. H,D-exchange between **1-d** and **2** was not observed in an additional experiment. This observation together with the formation of **2-d_a** and **2-d_b** in a ca. 1:1 molar ratio no doubt indicates that the alkyne \rightarrow vinylidene transformation involves a 1,3-hydrogen shift via an alkynyl intermediate. Furthermore, the second-order rate law for the reaction of **1** with cyclohexylacetylene suggests an intramolecular 1,3-hydrogen shift.

chemical shifts have been observed for related vinylidene compounds.¹¹

The reaction of **1** with cyclohexylacetylene to form **2** can be easily monitored by $^{31}\text{P}\{^1\text{H}\}$ NMR spectroscopy. Kinetic measurements for two different concentrations of **1** yield a second-order rate constant of $(6.0 \pm 0.2) \times 10^{-3} \text{ M}^{-1} \text{ s}^{-1}$ at -29°C .

The addition of terminal alkynes to coordinatively unsaturated metal-complex fragments is a general method of preparing vinylidene compounds.¹² It is generally agreed that, in the initial step, the alkyne molecule coordinates in a η^2 -fashion to the metallic center, undergoing transformation in the coordination sphere of the metal to give the corresponding vinylidene species. This transformation is generally viewed either as a 1,2-hydrogen shift or as a 1,3-hydrogen shift via hydrido-alkynyl intermediates.¹³ Theoretical studies suggest that the expenditure of energy to promote the concerted migration of the hydrido ligand from the

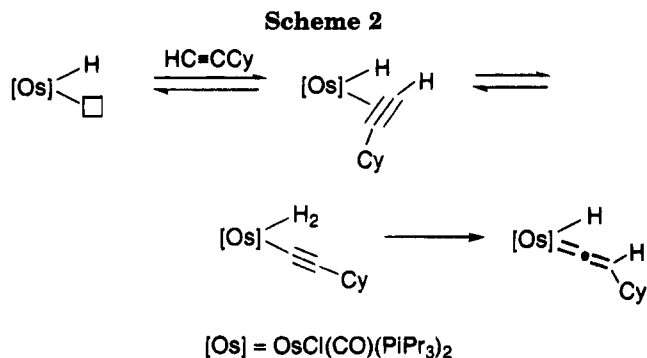
(11) See, for example: (a) Werner, H.; Rappert, T.; Wiedemann, R.; Wolf, J.; Mahr, N. *Organometallics* **1994**, *13*, 2721. (b) Ting, P. C.; Lin, Y. C.; Cheng, M. C.; Wang, Y. *Organometallics* **1994**, *13*, 2150.

(12) Bruce, M. I. *Chem. Rev.* **1991**, *91*, 197.

(13) (a) Garcia Alonso, F. J.; Höhn, A.; Wolf, J.; Otto, H.; Werner, H. *Angew. Chem., Int. Ed. Engl.* **1985**, *24*, 406. (b) Höhn, A.; Otto, H.; Dzialis, M.; Werner, H. *J. Chem. Soc., Chem. Commun.* **1987**, 852. (c) Bianchini, C.; Innocenti, P.; Meli, A.; Peruzzini, M.; Zanobini, F.; Zanello, P. *Organometallics* **1990**, *9*, 2514. (d) Bianchini, C.; Meli, A.; Peruzzini, M.; Zanobini, F.; Zanello, P. *Organometallics* **1990**, *9*, 241. (e) Bianchini, C.; Peruzzini, M.; Zanobini, F. *Organometallics* **1991**, *10*, 3415. (f) Bianchini, C.; Peruzzini, M.; Vacca, A.; Zanobini, F. *Organometallics* **1991**, *10*, 3697. (g) Lompfrey, J. R.; Selegue, J. P. *J. Am. Chem. Soc.* **1992**, *114*, 5518.

(14) Silvestre, J.; Hoffmann, R. *Helv. Chim. Acta* **1985**, *68*, 1461.

(15) Wolf, J.; Werner, H.; Serhadli, O.; Ziegler, M. L. *Angew. Chem., Int. Ed. Engl.* **1983**, *22*, 414.



The nature of this alkynyl intermediate merits further consideration. Its formation should occur by oxidative addition of the H–C_{sp} alkyne bond to give, at first glance, a dihydrido–osmium(IV) species, where both hydrido ligands should be nucleophilic centers. In addition, it should be noted that coordination of an acetylide, [RC≡C][−], to a metal center transfers the nucleophilicity from the α- to the β-carbon atom, and it has been proved that for these types of osmium systems the transfer is efficient.¹⁶ Thus, the direct attack of one of the two hydrido ligands at the β-carbon atom of the alkynyl group does not seem likely, given the nucleophilicity of these centers. Hence, it can be proposed that the H–C_{sp} activation leads to dihydrogen species. In this way, the formation of **2** could be rationalized as the electrophilic attack of an acidic proton of the dihydrogen ligand at the β-carbon atom of the alkynyl group (Scheme 2).

In favor of a dihydrogen intermediate, the following should be noted. (i) The addition of HX molecules to hydrido–osmium(II) complexes has been found to be an useful synthetic route for dihydrogen compounds. Thus, the alkynyl–hydrido–dihydrogen derivative OsH(C₂R)(η²-H₂)(CO)(PiPr₃)₂ (R = Ph, SiMe₃),¹⁷ the silyl–dihydrogen derivative Os(SiEt₃)Cl(η²-H₂)(CO)(PiPr₃)₂,² and the dichloro–dihydrogen complex OsCl₂(η²-H₂)(CO)(PiPr₃)₂¹⁸ have been prepared by reaction of OsH₂(CO)(PiPr₃)₂ with HC≡CR (R = Ph, SiMe₃) or OsHCl(CO)(PiPr₃)₂ with HSiEt₃ or HCl, respectively. (ii) The electrophilic character of the dihydrogen complexes has been previously demonstrated. A common feature of the dihydrogen complexes is that the coordinated dihydrogen ligand is readily deprotonated.¹⁹ (iii) The addition of electrophiles to metal alkynyl complexes is a general method of preparing vinylidene compounds.¹²

In benzene-*d*₆ or toluene as solvent, **2** evolves after 3 days into the vinyl derivative **3**. Complex **3** was isolated as a dark blue solid in 88% yield by addition of pentane. The IR spectrum of this solid in Nujol shows the ν(CO) and ν(C=C) absorptions at 1895 and 1590 cm^{−1}, respectively. The most noticeable resonances in the ¹H NMR spectrum are a doublet at 6.80 ppm with an H–H coupling constant of 12.6 Hz and a doublet of doublets

of triplets at 4.60 ppm with H–H coupling constants of 12.6 and 7.2 Hz and a P–H coupling constant of 2.1 Hz. These resonances are assigned to the protons attached to the α- and β-carbon atoms of the vinyl ligand, respectively. The α-carbon atom of the vinyl group appears in the ¹³C{¹H} NMR spectrum at 105.9 ppm with a P–C coupling constant of 7.0 Hz, while the β-carbon atom appears at 139.6 ppm as a triplet with a P–C coupling constant of 3.0 Hz. The ³¹P{¹H} NMR spectrum shows a singlet at 22.3 ppm.

These spectroscopic data agree well with those previously reported for the related compounds OsCl{(E)-CH=CHR}(CO)(PiPr₃)₂ (R = H, Me, Ph), where the square-pyramidal coordination of the osmium atom, and the *trans* position of the two substituents at the carbon–carbon double bond, have been determined by a single-crystal X-ray diffraction study on OsCl{(E)-CH=CHPh}(CO)(PiPr₃)₂.³

Previous studies of vinyl compounds have identified the localization of electron density at the β-carbon atom of the vinyl ligand. The chemical reactivity at this atom is thus oriented toward electrophiles.²⁰ In agreement with this, **3** reacts with a stoichiometric amount of a toluene–HCl solution to afford the dichloro–carbene compound **4**.

Complex **4** was isolated as a yellow solid in 70% yield. The presence of the carbene ligand in this complex can be inferred from the ¹H and the ¹³C{¹H} spectra. The ¹H NMR spectrum exhibits the Os=CH resonance at 19.20 ppm as a triplet with a H–H coupling constant of 5.7 Hz. In the ¹³C{¹H} NMR spectrum, the Os=C signal appears as a triplet at 273.05 ppm with a P–C coupling constant of 7.6 Hz. The ³¹P{¹H} NMR spectrum shows a singlet at 11.10 ppm, indicating that both triisopropylphosphine ligands are equivalent.

In conclusion, the reaction of the monohydrido–osmium(II) compound OsHCl(CO)(PiPr₃)₂ (**1**) with cyclohexylacetylene initially leads to the hydrido–vinylidene species OsHCl(=C=CHCy)(CO)(PiPr₃)₂ (**2**), which evolves in solution into OsCl{(E)-CH=CHCy}(CO)(PiPr₃)₂ (**3**). The reaction of this vinyl compound with HCl affords OsCl₂(=CHCH₂Cy)(CO)(PiPr₃)₂ (**4**). The process of formation of the vinylidene complex **2** is a real 1,3-hydrogen shift, which takes place via an alkynyl intermediate. The 1,3-hydrogen shift, most probably implies the presence of a dihydrogen molecule instead of two hydrido ligands in the alkynyl intermediate.

Experimental Section

General Considerations. All reactions were carried out with rigorous exclusion of air by using Schlenk-tube techniques. Solvents were dried by known procedures and distilled under argon prior to use. OsHCl(CO)(PiPr₃)₂^{10a} and OsDCl(CO)(PiPr₃)₂² were prepared by a published method.

Physical Measurements. Infrared spectra were recorded as Nujol mulls on polyethylene sheets using a Perkin-Elmer 883 or a Nicolet 550 spectrometer. NMR spectra were recorded on a Varian UNITY 300 or on a Bruker 300 AXR. Chemical shifts are expressed in ppm using C₆D₆ (7.15 ppm) as internal

(16) Esteruelas, M. A.; Lahoz, F. J.; López, A. M.; Oñate, E.; Oro, L. A.; Zeier, B. *Organometallics* **1994**, *13*, 1664.

(17) Espuelas, J.; Esteruelas, M. A.; Lahoz, F. J.; Oro, L. A.; Valero, C. *Organometallics* **1993**, *12*, 663.

(18) Esteruelas, M. A.; Oro, L. A.; Valero, C. Manuscript in preparation.

(19) (a) Jessop, P. G.; Morris, R. H. *Coord. Chem. Rev.* **1992**, *121*, 155 and references cited therein. (b) Cappellani, E. P.; Drouin, S. M.; Jia, G.; Maltby, P.; Morris, R. H.; Schweitzer, C. T. *J. Am. Chem. Soc.* **1994**, *116*, 3375. (c) Albéniz, M. J.; Buil, M. L.; Esteruelas, M. A.; López, A. M.; Oro, L. A.; Zeier, B. *Organometallics* **1994**, *13*, 3746.

(20) (a) Kremer, K. A. M.; Kuo, G. H.; O'Connor, E. J.; Helquist, P.; Kerber, R. C. *J. Am. Chem. Soc.* **1982**, *104*, 6119. (b) Bodner, G. S.; Smith, D. E.; Hatton, W. G.; Heah, P. C.; Georgiou, S.; Rheingold, A. L.; Geib, S. J.; Hutchinson, J. P.; Gladysz, J. A. *J. Am. Chem. Soc.* **1987**, *109*, 7688. (c) Feng, S. G.; White, P. S.; Templeton, J. L. *Organometallics* **1993**, *12*, 2131.

standard (^2H) or upfield from Me_4Si (^{13}C , ^1H) or 85% H_3PO_4 (^{31}P). Coupling constants J and N ($N = J(\text{HP}) + J(\text{HP}')$ for ^1H , and $N = J(\text{CP}) + J(\text{CP}')$ for ^{13}C) are given in hertz. C and H analyses were carried out with a Perkin-Elmer 2400 CHNS/O analyzer.

Reaction of $\text{OsHCl}(\text{CO})(\text{PiPr}_3)_2$ (1) with Cyclohexylacetylene: Preparation of $\text{OsHCl}(\text{C}=\text{CHCy})(\text{CO})(\text{PiPr}_3)_2$ (2). A solution of 1 (217 mg, 0.38 mmol) in 8 mL of toluene was treated with cyclohexylacetylene (63 μL , 0.49 mmol). After the mixture was stirred for 30 min at room temperature, it was evaporated to dryness. The green-violet residue was washed three times (3 mL) with cold pentane and dried in vacuo. The product is a pale green solid. Yield 181 mg (70%). Anal. Calcd for $\text{C}_{27}\text{H}_{55}\text{ClO}_2\text{Os}$: C, 47.43; H, 8.11. Found: C, 47.41; H, 7.85. IR (Nujol): $\nu(\text{OsH})$ 2030 (w), $\nu(\text{C}=\text{O})$ 1935 (s), $\nu(\text{Os}=\text{C}=\text{C})$ 1670 (m) cm^{-1} . ^1H NMR (300 MHz, C_6D_6): δ 3.19 (dt, $J(\text{HH}) = 10.6$, $J(\text{HP}) = 4.1$; $=\text{C}=\text{CHCy}$), 2.76 (m; PCH), 2.1–1.4 (H of Cy), 1.24 and 1.23 (both dvt, $N = 14.1$, $J(\text{HH}) = 6.9$; PCCH_3), -4.62 (t, $J(\text{HP}) = 28.8$; OsH). $^{13}\text{C}\{^1\text{H}\}$ NMR (75.43 MHz, C_6D_6): δ 326.9 (t, $J(\text{CP}) = 2.0$; OsC_α), 179.3 (t, $J(\text{CP}) = 8.6$; OsCO), 121.9 (br; $=\text{CC}_\beta$), 36.4, 32.4, 26.6, and 25.9 (each s; C of Cy), 24.9 (vt, $N = 28.0$; PCH), 19.1, 18.9 (both s; PCCH_3). $^{31}\text{P}\{^1\text{H}\}$ NMR (121.42 MHz, C_6D_6): δ 44.8 (s, d in off-resonance).

Reaction of $\text{OsDCl}(\text{CO})(\text{PiPr}_3)_2$ (1-d) with Cyclohexylacetylene: Formation of $\text{OsDCl}(\text{C}=\text{CHCy})(\text{CO})(\text{PiPr}_3)_2$ (2-d_a) and $\text{OsHCl}(\text{C}=\text{CDCy})(\text{CO})(\text{PiPr}_3)_2$ (2-d_b). To an NMR tube containing a benzene- d_6 solution of 1-d (0.035 mmol in 0.5 mL) was added cyclohexylacetylene (5 μL , 0.037 mmol). The reaction was followed by ^1H and ^2H NMR analysis. After 20 min, the two isotopomers were formed in the ratio 2-d_a:2-d_b = 1:0.84. Data for 2-d_a are as follows. ^1H NMR (300 MHz, C_6D_6): δ 3.19 (dt, $J(\text{HH}) = 10.6$, $J(\text{HP}) = 4.1$; $=\text{C}=\text{CHCy}$), 2.76 (m; PCH), 2.1–1.4 (H of Cy), 1.24 and 1.23 (both dvt, $N = 14.1$, $J(\text{HH}) = 6.9$; PCCH_3). ^2H NMR (46.07 MHz, C_6H_6): δ -4.6 (t, $J(\text{DP}) = 4.0$; OsD). Data for 2-d_b are as follows. ^1H NMR (300 MHz, C_6D_6): δ 2.76 (m; PCH), 2.1–1.4 (H of Cy), 1.24 and 1.23 (both dvt, $N = 14.1$, $J(\text{HH}) = 6.9$; PCCH_3), -4.62 (t, $J(\text{HP}) = 28.8$; OsH). ^2H NMR (46.07 MHz, C_6H_6): δ 3.0 (br; $=\text{C}=\text{CDCy}$). $^{31}\text{P}\{^1\text{H}\}$ NMR (121.42 MHz, C_6D_6) for 2-d_a and 2-d_b: δ 44.8 (br s).

Reaction of $\text{OsDCl}(\text{CO})(\text{PiPr}_3)_2$ (1-d) with $\text{OsHCl}(\text{C}=\text{CHCy})(\text{CO})(\text{PiPr}_3)_2$ (2). Complexes 1-d (15 mg, 0.026 mmol) and 2 (18 mg, 0.026 mmol) were dissolved in 0.5 mL of benzene- d_6 , and the resulting solution was transferred to an NMR tube. The ^1H NMR spectrum was recorded over the time. No reaction was observed after 1 h.

Preparation of $\text{OsCl}\{(\text{E})\text{-CH}=\text{CHCy}\}(\text{CO})(\text{PiPr}_3)_2$ (3). A solution of 2 (125 mg, 0.22 mmol) in 5 mL of toluene was stirred at room temperature under an argon atmosphere. After 3 days, the purification procedure was analogous to that described for 2. The product is a dark blue solid. Yield: 132

mg (88%). Anal. Calcd for $\text{C}_{27}\text{H}_{55}\text{ClO}_2\text{Os}$: C, 47.43; H, 8.11. Found: C, 47.38; H, 7.80. IR (Nujol): $\nu(\text{C}=\text{O})$ 1895 (vs), $\nu(\text{C}=\text{C})$ 1590 (s) cm^{-1} . ^1H NMR (300 MHz, C_6D_6): δ 6.8 (d, $J(\text{HH}) = 12.6$; $\text{OsCH}=\text{C}$), 4.6 (ddt, $J(\text{HH}) = 12.6$ and 7.2, $J(\text{HP}) = 2.1$; $=\text{CHCy}$), 2.90 (m; PCH), 2.4–1.4 (H of Cy), 1.22 (dvt, $N = 12.6$, $J(\text{HH}) = 6.0$; PCCH_3). ^{13}C NMR (75.43 MHz, C_6D_6): δ 182.9 (t, $J(\text{CP}) = 9.2$; OsCO), 139.6 (t, $J(\text{CP}) = 3.0$; CC_β), 105.9 (t, $J(\text{CP}) = 7.0$; OsC_α), 45.0, 34.8 and 26.8 (each s; C of Cy), 24.9 (vt, $N = 23.8$; PCH), 20.0 and 19.78 (both s; PCCH_3). $^{31}\text{P}\{^1\text{H}\}$ NMR (121.42 MHz, C_6D_6): δ 22.3 (s).

Reaction of 3 with HCl: Preparation of $\text{OsCl}_2(\text{C}=\text{CH}_2\text{Cy})(\text{CO})(\text{PiPr}_3)_2$ (4). A solution of 3 (70 mg, 0.10 mmol) in 4 mL of toluene was treated dropwise with toluene-HCl (0.123N; 0.8 mL, 0.31 mmol). After the mixture was stirred for 20 min at room temperature, the yellow-green solution was evaporated to dryness. The residue was washed twice for 10 min with 2 mL of pentane and dried in vacuo. The product is a yellow solid. Yield: 50 mg (70%). Anal. Calcd for $\text{C}_{27}\text{H}_{56}\text{Cl}_2\text{O}_2\text{Os}$: C, 44.96; H, 7.82. Found: C, 45.38; H, 7.83. IR (Nujol): $\nu(\text{C}=\text{O})$ 1930 (s) cm^{-1} . ^1H NMR (300 MHz, C_6D_6): δ 19.20 (t, $J(\text{HH}) = 5.7$; $\text{Os}=\text{CH}$), 2.75 (m; PCH), 2.15 (pseudo t, $J(\text{HH}) = 6.05$; $=\text{CCH}_2$), 2.0–1.1 (H of Cy), 1.35 (dvt, $N = 14.0$, $J(\text{HH}) = 7.1$; PCCH_3), 1.15 (dvt, $N = 13.7$, $J(\text{HH}) = 6.8$; PCCH_3). $^{13}\text{C}\{^1\text{H}\}$ NMR (75.43 MHz, C_6D_6): δ 273.05 (t, $J(\text{CP}) = 7.6$; OsC_α), 176 (t, $J(\text{CP}) = 8.5$; OsCO), 68.9 (s, $=\text{CC}_\beta$), 38.60, 33.50, 26.54, and 26.47 (each s; C of Cy), 25.3 (vt, $N = 25.1$; PCH), 20.1 and 19.4 (both s; PCCH_3). $^{31}\text{P}\{^1\text{H}\}$ NMR (121.42 MHz, CDCl_3): δ 11.1 (s).

Kinetics of formation of 2. The reaction of 1 with cyclohexylacetylene was monitored by $^{31}\text{P}\{^1\text{H}\}$ NMR at -29°C , assuming that the reaction occurs in a 1:1 molar ratio. Samples of 1 and cyclohexylacetylene in 0.5 mL of toluene- d_8 were stored under argon in NMR tubes at -120°C prior to measurements. Second-order rate constants were calculated by linear least-squares fitting of the kinetic data to the integrated second-order rate law

$$\ln(C_a/C_b) = (C_a^\circ - C_b^\circ)kt + \ln(C_a^\circ/C_b^\circ)$$

For two different samples of reactant 1 (0.052 M and 0.07 M) and cyclohexylacetylene (0.233 M), the calculated rate constants were $(6.1 \pm 0.3) \times 10^{-3}$ and $(5.9 \pm 0.1) \times 10^{-3}$ $\text{M}^{-1} \text{s}^{-1}$, respectively.

Acknowledgment. We thank the DGICYT (Project PB 92-0092, Programa de Promoción General del Conocimiento) and the EU (Project: Selective Processes and Catalysis Involving Small Molecules) for financial support. We thank Dr. E. Sola for assistance with the kinetic measurements.

OM940899R

^{103}Rh NMR Shielding Correlation with Rate Data for Aryl Migration in $\text{RhCp}^*\text{I}(\text{CO})(p\text{-XC}_6\text{H}_4)$: Mechanistic Implications[†]

Vanda Tedesco and Wolfgang von Philipsborn*

Organisch-chemisches Institut, Universität Zürich, Winterthurerstrasse 190,
CH-8057 Zürich, Switzerland

Received January 23, 1995[©]

Summary: The rhodium-103 NMR chemical shifts of the complexes $\text{RhCp}^*\text{I}(\text{CO})(p\text{-XC}_6\text{H}_4)\text{PPh}_3$ ($\text{Cp}^* = \text{C}_5\text{Me}_5$; $\text{X} = \text{H, Me, Cl, CHO, CN, NO}_2$) exhibit a linear correlation ($R^2 = 0.991$) with $\ln(k_{\text{rel}})$, where k_{rel} is the relative rate constant for the PPh_3 -assisted migration of a coordinated aryl group to a coordinated CO in the complexes $\text{RhCp}^*\text{I}(\text{CO})(p\text{-XC}_6\text{H}_4)$ reported by Bassetti et al. This is the first example of a correlation of the transition-metal chemical shifts of the product with reaction rates and leads to the postulate that such reactions are characterized by a product-like (late) transition state.

Rhodium-103 NMR spectroscopy has provided an elegant method for the study of reactivity and mechanism in stoichiometric² and catalytic³ reactions. Several papers have described successful attempts to correlate transition-metal NMR chemical shifts with various rate data,^{2,4} catalytic activity,⁵ steric parameters,⁶ electronic parameters,⁷ stability constants⁸ and phosphorus-31 NMR data.⁹ Although there are many examples of rhodium-103 NMR data in the literature¹⁰⁻¹² there is surprisingly little information concerning complexes containing the pentamethylcyclopentadienyl ligand, complexes which are widely studied for their potential catalytic activity and C-H bond activation properties.¹³⁻¹⁵

The syntheses of $\text{RhCp}^*\text{I}(\text{CO})(p\text{-XC}_6\text{H}_4)\text{PPh}_3$ (**3**; $\text{Cp}^* = \text{C}_5\text{Me}_5$; $\text{X} = \text{H, Me, Cl, CHO, CN, NO}_2$) have been described,^{16,17} and their synthetic route is shown in Figure 1.¹⁶⁻¹⁹ The kinetics of the migration step^{16,17} to

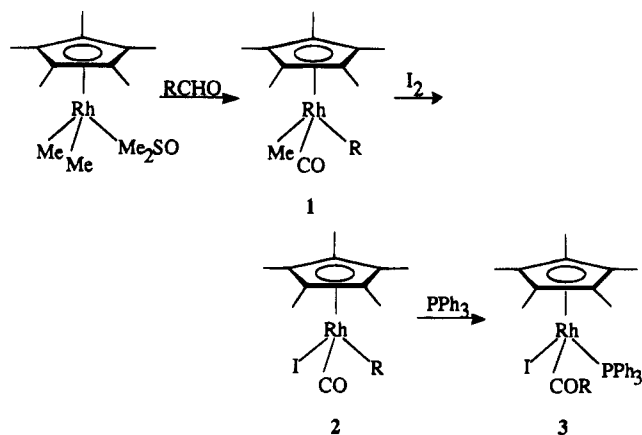


Figure 1. Reaction scheme (for R see Table 1).

give complexes **3** have been reported; it was found that the mechanism was associative and solvent independent,^{16,17} and it is also possible that ring slippage is not involved.^{20,21} The following discussion will present the results of a rhodium-103 NMR study of the complexes shown in Figure 1 in order to gain further insight into the mechanism of the migration reaction.

The ^{103}Rh resonances were measured by direct detection for complexes **2**, with the exception of the methyl derivative, for which 2D inverse detection via the methyl protons was applied. The same 2D (^1H , ^{103}Rh) experiment was used to detect the rhodium signals of complexes **1**, whereas a triple-resonance 2D (^{31}P , ^{103}Rh){ ^1H } inverse pulse sequence was utilized for complexes **3**. Figure 2 illustrates for $\text{RhCp}^*\text{MeCO}(p\text{-CNC}_6\text{H}_4)$ the successful use of $^2J(\text{Rh},\text{H})$ for inverse detection of the ^{103}Rh resonance. Because of the large sensitivity enhancement factors, $(\gamma_{\text{H}}/\gamma_{\text{Rh}})^{5/2} = 5689$ and $(\gamma_{\text{P}}/\gamma_{\text{Rh}})^{5/2} = 593$, respectively, for the inverse versus direct detection experiments, they constitute the method of choice for organometallic substrates.

Table 1 lists the rhodium-103 NMR chemical shifts for complexes **1-3**. The starting material $\text{RhCp}^*\text{Me}_2\text{SO}$ has a rhodium-103 chemical shift at -148 ppm. It was also found^{16,17} that in complexes **2** when $\text{X} = \text{CN}$ and NO_2 , substitution of CO for PPh_3 occurs in competi-

[†] Transition Metal NMR Spectroscopy. 25. Part 24: reference 1.
[©] Abstract published in *Advance ACS Abstracts*, June 1, 1995.
 (1) Torocheshnikov, V.; Rentsch, D.; von Philipsborn, W. *Magn. Reson. Chem.* **1994**, *32*, 348.
 (2) Koller, M.; von Philipsborn, W. *Organometallics* **1992**, *11*, 467.
 (3) Bender, B. R.; Koller, M.; Nanz, D.; von Philipsborn, W. *J. Am. Chem. Soc.* **1993**, *115*, 5889.
 (4) DeShong, P.; Sidler, D. R.; Rybczynski, P. J.; Ogilvie, A. A.; von Philipsborn, W. *J. Org. Chem.* **1989**, *54*, 5432.
 (5) Bönnemann, H.; Brijoux, W.; Brinkmann, R.; Meurers, W.; Mynott, R.; von Philipsborn, W.; Eglolf, T. *J. Organomet. Chem.* **1984**, *272*, 231.
 (6) Tavagnacco, C.; Balducci, G.; Costa, G.; Täschler, K.; von Philipsborn, W. *Helv. Chim. Acta* **1990**, *73*, 1469.
 (7) Graham, P. B.; Rausch, M. D.; Täschler, K.; von Philipsborn, W. *Organometallics* **1991**, *10*, 3049.
 (8) Åkermark, B.; Blomberg, M. R. A.; Glaser, J.; Öhrström, L.; Wahlberg, S.; Wärnmark, K.; Zetterberg, K. *J. Am. Chem. Soc.* **1994**, *116*, 3405.
 (9) Ernsting, J. M.; Elsevier, C. J.; de Lange, W. G. J.; Timmer, K. *Magn. Reson. Chem.* **1991**, *29*, S118.
 (10) Goodfellow, R. J. In *Multinuclear NMR*; Mason, J., Ed.; Plenum Press: New York, 1987.
 (11) Mann, B. E. In *NMR of Newly Accessible Nuclei*; Laszlo, P., Ed.; Academic Press: New York, 1983.
 (12) Mann, B. E. In *Transition Metal Nuclear Magnetic Resonance*; Pregosin, P. S., Ed.; Elsevier: Amsterdam, The Netherlands, 1991.
 (13) Maitlis, P. M. *Acc. Chem. Res.* **1978**, *11*, 301.
 (14) Jones, W. D.; Feher, F. J. *Acc. Chem. Res.* **1989**, *22*, 91.
 (15) Periana, R. A.; Bergman, R. G. *J. Am. Chem. Soc.* **1986**, *108*, 7332.

(16) Bassetti, M.; Sunley, G. J.; Maitlis, P. M. *J. Chem. Soc., Chem. Commun.* **1988**, 1012.
 (17) Bassetti, M.; Sunley, G. J.; Fanizzi, F. P.; Maitlis, P. M. *J. Chem. Soc., Dalton Trans.* **1990**, 1799.
 (18) de Miguel, A. V.; Gómez, M.; Isobe, K.; Taylor, B. F.; Mann, B. E.; Maitlis, P. M. *Organometallics* **1983**, *2*, 1724.
 (19) Gómez, M.; Kisenyi, J. M.; Sunley, G. J.; Maitlis, P. M. *J. Organomet. Chem.* **1985**, *296*, 197.
 (20) Bassetti, M.; Mannina, L.; Monti, D. *Organometallics* **1994**, *13*, 3293.
 (21) Monti, D.; Bassetti, M. *J. Am. Chem. Soc.* **1993**, *115*, 4658.

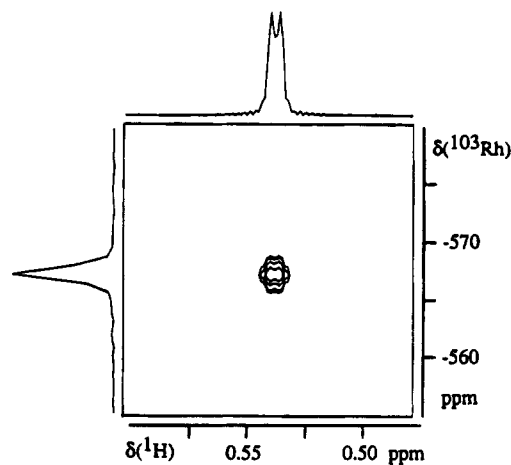


Figure 2. 2D(^1H , ^{103}Rh) NMR spectrum of RhCp^*MeCO -($p\text{-CNC}_6\text{H}_4$) ($^2J(\text{Rh},\text{H}) = 2.5$ Hz).

Table 1. Rhodium-103 NMR Chemical Shifts of the Complexes Shown in Figure 1 and Relative Rates for the Reaction 2 \rightarrow 3

R	$\delta(^{103}\text{Rh})$ (ppm)			relative rate ^a k_{rel}
	1	2	3	
Me	-829	-366	849	0.26
$p\text{-MeC}_6\text{H}_4$	-584	-106	813	2.8
Ph	-578	-102	804	1
$p\text{-ClC}_6\text{H}_4$	-582	-122	784	0.31
$p\text{-CHOC}_6\text{H}_4$	-566	-121	765	0.034
$p\text{-CNC}_6\text{H}_4$	-567	-127	748	0.008
$p\text{-NO}_2\text{C}_6\text{H}_4$	-565	-134	742	0.007

^a Reference 17.

tion with aryl migration to give $\text{RhCp}^*\text{I}(\text{PPh}_3)(p\text{-CNC}_6\text{H}_4)$ ($\delta(^{103}\text{Rh})$ 505 ppm) and $\text{RhCp}^*\text{I}(\text{PPh}_3)(p\text{-NO}_2\text{C}_6\text{H}_4)$ ($\delta(^{103}\text{Rh})$ 507 ppm), respectively, together with the expected complexes 3.

The rhodium nuclei in complexes 1 are, in general, deshielded when the substituent in the para position of the phenyl group is electron withdrawing ($\text{X} = \text{Cl}$, CHO , CN , NO_2) and shielded when the substituent is electron donating ($\text{X} = \text{Me}$). The shielding effects for complexes 2 are reverse to those observed for complexes 1; that is, electron-withdrawing substituents on the phenyl ring shield the rhodium nucleus. The difference between complexes 1 and 2 is that an electron-donating Me group has been substituted for an electron-withdrawing iodide ligand. The presence of the soft iodide ligand could cause some cooperative effect with the donor/acceptor properties of the X substituent in the aryl group that causes the shielding/deshielding effect on the rhodium nucleus to invert.

It was found^{16,17} that the rate of migration (Table 1) for complexes 2 was significantly slowed for those compounds containing electron-withdrawing substituents in the para position of the aryl group. The rates decrease with increasing shielding of the rhodium nucleus as for the CO/PPh_3 displacement reaction in ($\eta^5\text{-C}_5\text{H}_4\text{X}$) $\text{Rh}(\text{CO})_2$ complexes;² however, the range of chemical shifts is small ($\Delta\delta = 32$ ppm) and the correlation between the two parameters $\ln(k_{\text{rel}})$ and $\delta(\text{Rh})$ is insignificant ($R^2 = 0.813$).

In complexes 3, electron-withdrawing substituents also shield the rhodium nucleus, while electron-donating ones deshield it. A plot of $\ln(k_{\text{rel}})$ versus $\delta(^{103}\text{Rh})$ (Figure 3) for the aryl derivatives is linear with a high correlation coefficient; $R^2 = 0.991$. This is the first example of

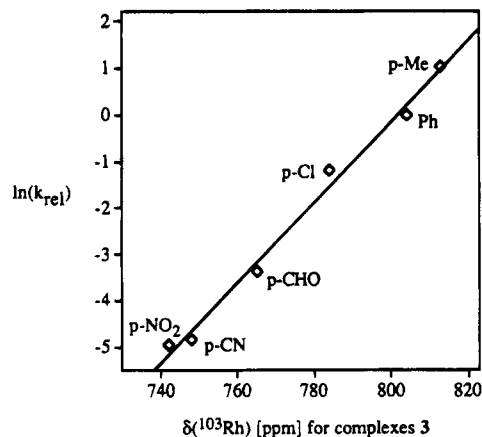


Figure 3. Plot of $\ln(k_{\text{rel}})$ versus $\delta(^{103}\text{Rh})$ for complexes 3.

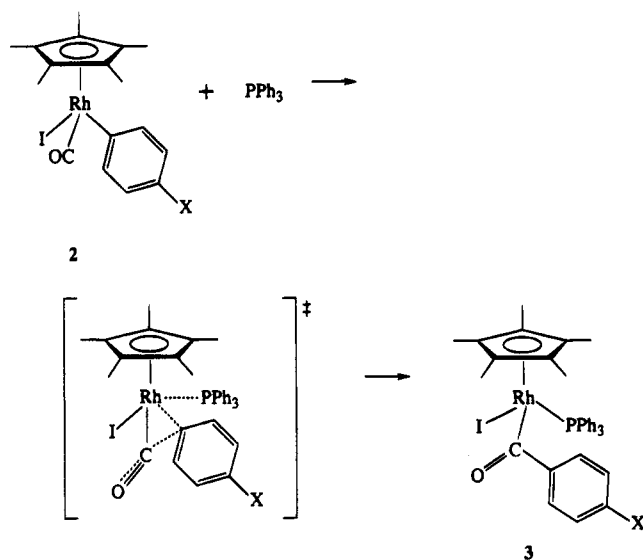


Figure 4. Proposed mechanism for the PPh_3 -assisted aryl migration reaction of 2 to give 3.

a correlation between transition-metal chemical shifts of the product with rate data. A plot of σ_p (Hammett electronic parameter²²) against $\delta(^{103}\text{Rh})$ is also linear with the correlation coefficient $R^2 = 0.991$.

A suggested mechanism for the PPh_3 -assisted aryl migration reaction 2 \rightarrow 3 is shown in Figure 4. It is most likely that aryl migration to CO occurs rather than CO insertion into the Rh-C(aryl) bond, as this would require the breaking of two Rh-C σ -bonds. There are many examples of CO insertion²³ into a metal-methyl bond, but these normally occur when CO is the incoming ligand. When both the CO and Me are coordinated to the metal center, then the migration mechanism is favored.^{23,24}

It was suggested¹⁷ that the mechanism of the aryl migration 2 \rightarrow 3 is associative and that the transition state $[\text{RhCp}^*(\text{aryl})(\text{CO})(\text{PPh}_3)\text{I}]^\ddagger$ is involved. It is also possible that a molecular complex of the type $[\text{RhCp}^*(\text{aryl})(\text{CO})\text{I}, \text{PPh}_3]$ is initially formed in a rapid pre-equilibrium before the rate-determining aryl migration similar to that proposed in the reaction of $\text{Fe}(\eta^5\text{-$

(22) Hansch, C.; Leo, A.; Taft, R. W. *Chem. Rev.* **1991**, *91*, 165.

(23) Collman, J. P.; Hegedus, L. S.; Norton, J. R.; Finke, R. G. *Principles and Applications of Organotransition Metal Chemistry*; University Science Books: Mill Valley, CA, 1987.

(24) Koga, N.; Morokuma, K. *J. Am. Chem. Soc.* **1986**, *108*, 6136.

indenyl)I(CO)Me (indenyl is C_9H_7) with PR_3 ,^{20,21} but there is no evidence for this.

A proposed transition state is shown in Figure 4. The linear relationship between $\ln(k_{rel})$ and the rhodium-103 NMR chemical shifts of the product rather than of the reactant leads to the postulate that the aryl migration proceeds via a late transition state, which is structurally more similar to the product, complex **3**, than the reactant, complex **2**. This implies that in the transition state the C(aryl)-C(O) and Rh-PPh₃ bonds are already formed to an appreciable extent with simultaneous breaking of the Rh-C(aryl) bond. Finally, complete breakage of the Rh-C(aryl) bond and formation of the Rh-P bond gives the final product, complex **3**.

Experimental Details

All compounds were prepared as previously described.^{16-19,25}

Direct detection of the rhodium-103 resonances was performed on a Bruker AMX600 NMR spectrometer operating at 18.9 MHz ($B_0 = 14.1$ T), without proton decoupling, using 20-30 mg of sample dissolved in 0.5 cm³ of CDCl₃ in 5 mm NMR tubes. Typically 1000-2000 scans were accumulated in 1-2 h using a spectral width of 5000 Hz, a pulse width of 20 μ s (corresponding to a flip angle of about 60°), an acquisition time of 1.4 s, and a relaxation delay of 2.5 s.

Inverse 2D NMR experiments, (¹H, ¹⁰³Rh) and (³¹P, ¹⁰³Rh)-{¹H}, were carried out on a Bruker AMX600 or AM400 NMR spectrometer operating at 18.9 MHz ($B_0 = 14.1$ T) or 12.6 MHz ($B_0 = 9.4$ T), respectively, using the pulse sequences reported by Bax et al.²⁶ and Benn et al.²⁷ For proton observation about

20 mg of sample dissolved in 0.5 cm³ of CDCl₃ in 5 mm NMR tubes was used, while for phosphorus observation 30-40 mg of sample under the same conditions was employed. An inverse broad-band probehead was employed for the 2D (¹H, ¹⁰³Rh) experiments. For the 2D (³¹P, ¹⁰³Rh)-{¹H} experiments on the AM400, a triple-resonance probehead (outer coil tunable to a low-frequency nucleus (¹⁵N to ¹⁸⁷O)) and an inner coil tunable to lock, proton, and phosphorus) was utilized together with a second PTS160 synthesizer and a BSV3 heterodecoupling unit for pulsing of the rhodium frequency. Coupling constants of the orders ²J(Rh,H) = 2.5 Hz and ¹J(Rh,P) = 160 Hz were used for the polarization transfer. Typically 128 increments, each of 4 (proton) or 8 (phosphorus) scans, were accumulated in 1-2 h: spectral width in the rhodium dimension 2000-5000 Hz, spectral width for proton or phosphorus 500-1000 Hz, 90° pulse length for rhodium 125 μ s (AMX600) or 40 μ s (AM400), 90° pulse length for proton 11 μ s, 90° pulse length for phosphorus 14 μ s, and relaxation delay 3.5 s. Before Fourier transformation, the data were zero-filled in the rhodium dimension and multiplied by sine window functions in both dimensions.

All samples were measured at 300 K. Rhodium chemical shifts are reported relative to a reference frequency of 3.16 MHz in a field where the protons of TMS resonate with exactly 100 MHz.¹⁰ All shifts to high frequency are positive. The estimated error in the chemical shifts is ± 1 ppm.

Acknowledgment. We thank the Swiss National Science Foundation for financial support.

OM950055N

(25) White, C.; Yates, A.; Maitlis, P. M.; Heinekey, D. M. *Inorg. Synth.* **1992**, *29*, 228.

(26) Bax, A.; Griffey, R. H.; Hawkins, B. L. *J. Magn. Reson.* **1983**, *55*, 301.

(27) Benn, R.; Brevard, C. *J. Am. Chem. Soc.* **1986**, *108*, 5622.

Synthesis, Structure, and Reactivity of the First Phosphaazaallene–Metal Complex

John B. Alexander and David S. Glueck*

6128 Burke Laboratory, Department of Chemistry, Dartmouth College,
Hanover, New Hampshire 03755

Glenn P. A. Yap and Arnold L. Rheingold

Department of Chemistry, University of Delaware, Newark, Delaware 19716

Received February 13, 1995[§]

Summary: The first phosphaazaallene metal complex, $Cp'_2Nb(Cl)[\eta^2-(N,C)-PhNCPMes^*][3]$; $Cp' = C_5H_4SiMe_3$, $Mes^* = 2,4,6-(t-Bu)_3C_6H_2$, was prepared from Cp'_2NbCl and the cumulene. Spectroscopic and crystallographic characterization of **3** and some transformations of the complexed phosphaazaallene are described.

Introduction

Phosphaazaallenes $RP=C=NR'$ are reactive molecules¹ which could conceivably bind to a transition metal either in a π (C,N or C,P) or in a σ (N or P) fashion. Cowley has shown that WL_4Cl_2 ($L = PMePh_2$) can cleave the P=C bond in $Mes^*P=C=NPh$ [**1**, $Mes^* = 2,4,6-(t-Bu)_3C_6H_2$] to generate the phosphinidene complex $trans-L_2WCl_2(CNPh)(PMes^*)$.² We recently described the related reaction of **1** with $Rh(PCy_3)_2Cl$ ($Cy = cyclo-C_6H_{11}$), which gives $trans-Rh(PCy_3)_2Cl(CNPh)$ and the phosphaindan [**2**, $4-(t-Bu)_2C_6H_2(6-CMe_2CH_2PH)$] (**2**),⁴ presumably via intramolecular decomposition of the free phosphinidene Mes^*P .⁵ However, the coordination chemistry of these cumulenes has been otherwise neglected. We report here the synthesis of the first phosphaazaallene–metal complex $Cp'_2Nb(Cl)[\eta^2-(N,C)-PhNCPMes^*]$ (**3**, $Cp' = C_5H_4SiMe_3$), its characterization by spectroscopic methods and by X-ray crystallography, and a brief survey of its reactivity (Scheme 1).

Results and Discussion

As reported for other heterocumulenes,⁶ **1** reacts with Cp'_2NbCl ⁷ to form complex **3** as red air-stable crystals, which are thermally stable in solution, remaining unchanged on heating to 80 °C in THF for 1 week.

From hard–soft considerations⁸ and the bulk of the Mes^* group, coordination of Nb to N or the N=C bond rather than to P or the P=C bond is predicted. The ³¹P NMR chemical shift of the phosphaazaallene changes from –106 to 14.3 ppm on coordination; the lack of broadening of the ³¹P signal by the ⁹³Nb quadrupole⁹ suggests the phosphorus is not coordinated. The coordination chemical shift of the central allene carbon from 200.8 to 171.5 ppm and the change in J_{PC} for this carbon from 67 to 155 Hz are consistent with $\pi(N,C)$ coordination. The IR spectrum shows a signal at 1505 cm^{-1} which may be assigned to an uncomplexed P=C group.

The $\pi(N,C)$ coordination of $Mes^*P=C=NPh$ in **3** was confirmed by X-ray crystallography (Figure 1). Crystal, data collection, and refinement parameters are given in Table 1. Atomic coordinates and equivalent isotropic displacement coefficients are given in Table 2, while selected bond lengths and angles are found in Tables 3–4. Complexation of **1**¹⁰ to Nb causes an increase in the C–N bond length (1.209(4) to 1.301(23) Å) and a decrease in the N–C–P bond angle (171.1(2) to 156.2(13)°). The isoelectronic ketenimine complex, $Cp'_2Nb(Cl)[\eta^2-(N,C)-PhNCCPh_2]$,¹¹ has a longer Nb–N bond than in **3** (2.140(4) Å vs 2.075(12) Å) and a smaller N–C–C bond angle than the N–C–P bond angle in **3** (140.0 (4)° vs 156.2 (14)°).

Photolysis of **3** in either benzene or THF with a Hg lamp forms $Cp'_2NbCl(CNPh)$ ¹² (**4**) and phosphaindan **2**. Monitoring the reaction in THF by ³¹P NMR showed that this transformation does not occur at the metal center. Instead, irradiation causes dissociation of **1** from **3**; the free phosphaazaallene is then converted to **2** as previously reported for the analogous phosphaketene $Mes^*P=C=O$ ¹³ and as confirmed by control experiments. The isocyanide formed is trapped by Cp'_2NbCl to give **4**.

Adding $HBf_4 \cdot OMe_2$ to **3** in petroleum ether gives white $\{Cp'_2Nb(Cl)[\eta^2-(N,C)-PhN=CPhMes^*]\}BF_4$ (**5**), the first example of a phospha–imino acyl complex. The P–H bond is observed in the ³¹P NMR spectrum (δ

[§] Abstract published in *Advance ACS Abstracts*, June 1, 1995.

(1) Appel, R.; Knoll, F. *Adv. Inorg. Chem.* **1989**, *33*, 259–361.

(2) Yoshifuji, M.; Toyota, K.; Shibayama, K.; Inamoto, N. *Tetrahedron Lett.* **1984**, *25*, 1809–1812.

(3) Cowley, A. H.; Pellerin, B.; Atwood, J. L.; Bott, S. G. *J. Am. Chem. Soc.* **1990**, *112*, 6734–6735.

(4) (a) Cowley, A. H.; Pakulski, M. *Tetrahedron Lett.* **1984**, *25*, 2125–2126. (b) Yoshifuji, M.; Sato, T.; Inamoto, N. *Chem. Lett.* **1988**, 1735–1738.

(5) David, M.-A.; Paisner, S. N.; Glueck, D. S. *Organometallics* **1995**, *14*, 17–19.

(6) (a) Antinolo, A.; Fajardo, M.; Jalon, F. A.; Lopez Mardomingo, C.; Otero, A.; Sanz-Bernabe, C. *J. Organomet. Chem.* **1989**, *369*, 187–196. (b) Halfon, S. E.; Fermin, M. C.; Bruno, J. W. *J. Am. Chem. Soc.* **1989**, *111*, 5490–5491. (c) Antinolo, A.; Fajardo, M.; Lopez Mardomingo, C.; Otero, A.; Mourad, Y.; Mugnier, Y.; Sanz-Aparicio, J.; Fonseca, I.; Florencio, F. *Organometallics* **1990**, *9*, 2919–2925. (d) Antinolo, A.; Garcia-Lledo, S.; Martinez de Ilarduya, J.; Otero, A. *J. Organomet. Chem.* **1987**, *335*, 85–90.

(7) See: (a) Reference 6d. (b) Fermin, M. C.; Hneihen, A. S.; Maas, J. J.; Bruno, J. W. *Organometallics* **1993**, *12*, 1845–1856.

(8) Pearson, R. G. *Inorg. Chem.* **1988**, *27*, 734.

(9) Antinolo, A.; Gomez-Sal, P.; Martinez de Ilarduya, J.; Otero, A.; Royo, P.; Martinez Carrera, S.; Garcia Blanco, S. *J. Chem. Soc., Dalton Trans.* **1987**, 975–980.

(10) Yoshifuji, M.; Niitsu, T.; Toyota, K.; Inamoto, N.; Hirotsu, K.; Odagaki, Y.; Higuchi, T.; Nagase, S. *Polyhedron* **1988**, *7*, 2213–2216.

(11) Antinolo, A.; Fajardo, M.; Lopez Mardomingo, C.; Otero, A.; Mourad, Y.; Mugnier, Y.; Sanz-Aparicio, J.; Fonseca, J.; Florencio, F. *Organometallics* **1990**, *9*, 2919–2925.

(12) Martinez de Ilarduya, J. M.; Otero, A.; Royo, P. *J. Organomet. Chem.* **1988**, *340*, 187–193.

(13) Cowley, A. H.; Gabbai, F.; Schluter, R.; Atwood, D. *J. Am. Chem. Soc.* **1992**, *114*, 3142–3144.

Scheme 1

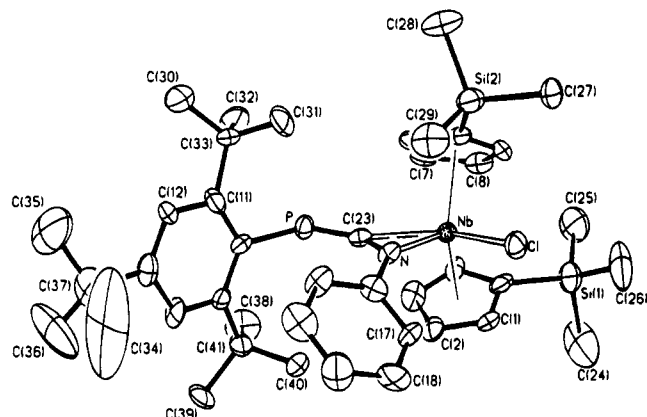
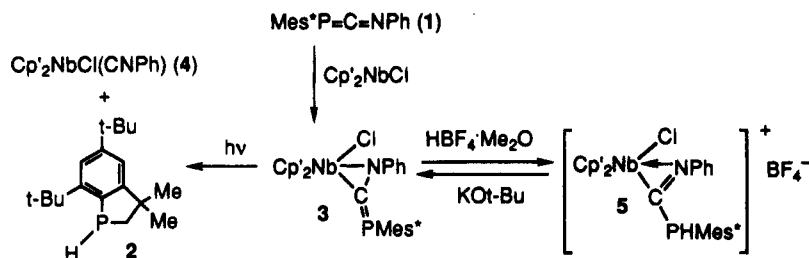


Figure 1. ORTEP diagram of complex **3**. The figure shows one of the two independent but chemically equivalent molecules found in the unit cell.

−37.4, d, $^1J_{PH} = 302$ Hz) and the 1H NMR spectrum (δ 7.32, $^1J_{PH} = 302$ Hz). Exchange with D_2O gives $\{[Cp'_2Nb(Cl)(PhN=CPDMes^*)]BF_4\}$ (**5D**), ($J_{PD} = 44.3$ Hz),¹⁴ confirming the unusual 1H NMR shift for the acidic P–H proton. Deprotonation of **5** with 1 equiv of potassium *tert*-butoxide affords **3** quantitatively by ^{31}P NMR.

Further studies of the reactivity of **3** and **5** with small molecules, and of related phosphacumulene complexes, are currently under way.

Experimental Section

General Experimental Details. All manipulations were carried out under a nitrogen atmosphere using either standard Schlenk apparatus or a glovebox. Solvents were distilled from sodium and benzophenone (toluene, THF, ether, petroleum ether) or from CaH_2 (methylene chloride) and stored under nitrogen in ampules until needed. IR spectra were recorded on a Perkin-Elmer 1600 Series FTIR infrared spectrometer. NMR spectra were obtained on a Varian 300 FT NMR spectrometer at the following frequencies (MHz): ^{31}P , 121.4; ^{13}C , 75.4; 1H , 299.9. Elemental analyses were done by Schwarzkopf Labs, Woodside, NY. The cumulene Mes*PCNPh² was prepared by the literature method.

Cp₂Nb(Cl)[(η^2 -N,C)PhNCPMes*] (3). Cp₂NbCl was prepared according to a literature method^{7b} and used without recrystallization; we found that an excess of this impure material must be used to get good yields. A brown solution of Cp₂NbCl (1.062 g, 2.63 mmol) and Mes*PCNPh (1.00 g, 2.63 mmol) in THF (10 mL) was stirred overnight at ambient temperature to give a red solution, whose ^{31}P NMR spectrum showed ~85% conversion of **1** to **3**. Addition of more Cp₂NbCl (180 mg, 0.48 mmol) induced complete conversion to **3** overnight. The solvent was removed under vacuum, and the red

(14) From the gyromagnetic ratios $\gamma_H/\gamma_D = 6.5144$, J_{PD} is expected to be 46.4 Hz: Sergeev, N. M. In *Isotope Effects in NMR Spectroscopy*; Diehl, P., Fluck, E., Günther, H., Kosfeld, R., Selig, J., Eds.; Springer Verlag: Berlin, 1990; p 42.

Table 1. Structure Determination Summary

Crystal Data	
empirical formula	C ₄₁ H ₆₀ ClNNbPSi ₂
color; habit	red block
cryst size	0.10 × 0.20 × 0.35 mm ³
cryst system	monoclinic
space group	<i>P2₁/c</i>
unit cell dimens	<i>a</i> = 15.361(8) Å, <i>b</i> = 18.898(8) Å, <i>c</i> = 31.849(9) Å, β = 98.03(6) ^o
<i>V</i>	9155(3) Å ³
<i>Z</i>	8
fw	782.4
<i>D</i> (calcd)	1.140 g/cm ³
abs coeff	0.437 mm ⁻¹
<i>F</i> (000)	3296
Data Collection	
diffractometer used	Siemens P4
radiation	Mo K α ($\lambda = 0.71073$ Å)
temp	296 K
monochromator	highly oriented graphite cryst
2 θ range	4.0–45.0 ^o
scan type	Wyckoff
scan speed	variable; 8.37–29.30 ^o /min in ω
scan range (ω)	1.00 ^o plus K α separation
bckgd measmt	stationary cryst and stationary counter at beginning and end of scan, each for 50.0% of tot. scan time
std reflns	3 measd every 197 reflns
index ranges	−15 ≤ <i>h</i> ≤ 15, 0 ≤ <i>k</i> ≤ 19, 0 ≤ <i>l</i> ≤ 32
reflncs collcd	10 747
independent reflncs	10514 (<i>R</i> _{int} = 2.41%)
obsd reflncs	6092 (<i>F</i> > 4.0 σ (<i>F</i>))
abs corr	N/A
Solution and Refinement	
system used	Siemens SHELXTL PLUS (PC Version)
solution	direct methods
refinement method	full-matrix least squares
quantity minimized	$\Sigma w(F_o - F_c)^2$
absolute structure	N/A
extinctn corr	N/A
H atoms	riding model, fixed isotropic <i>U</i>
weighting scheme	$w^{-1} = \sigma^2(F) + 0.0010F^2$
no. of params refined	763
final <i>R</i> indices (obsd data)	<i>R</i> = 9.61(<i>F</i>) + 0.0010 <i>F</i>
no. of params refined	763
final <i>R</i> indices (obsd data)	<i>R</i> = 9.61%, w <i>R</i> = 12.53%
<i>R</i> indices (all data)	<i>R</i> = 15.07%, w <i>R</i> = 14.22%
goodness-of-fit	2.22
largest and mean δ/σ	0.331, 0.011
data-to-param ratio	8.0:1
largest diff peak	1.08 e Å ⁻³
largest diff hole	−0.76 e Å ⁻³

solid was extracted with petroleum ether. Concentration of the resulting red solution gave a red powder, which was collected on a fine frit. The mother liquor was layered with nitromethane and cooled to induce further crystallization. In total, 908 mg (45%) of pure **3** was collected. Crystals suitable for X-ray crystallography were obtained by slow recrystallization from petroleum ether at −20 °C over 4 months.

1H NMR (C₆D₆) (δ): 7.51 (d, $J_{PH} = 0.9$ Hz, 2H, Mes*); 7.04 (d, $J = 6$ Hz, 2H, *o*-Ph); 6.97 (t, $J = 6$ Hz, 2H, *m*-Ph); 6.78 (t, $J = 6$ Hz, 1H, *p*-Ph); 6.28 (d, $J = 2.1$ Hz, 2H, Cp'); 6.07 (d, J

Table 2. Atomic Coordinates ($\times 10^4$) and Equivalent Isotropic Displacement Coefficients ($\text{\AA}^2 \times 10^3$)

	<i>x</i>	<i>y</i>	<i>z</i>	<i>U</i> (eq) ^a		<i>x</i>	<i>y</i>	<i>z</i>	<i>U</i> (eq) ^a
Nb	4361.9(9)	2371.7(8)	59.3(5)	35(1)	C(36)	4675(30)	-624(20)	2614(13)	212(26)
Nb'	9314(1)	2571.8(9)	-155(5)	43(1)	C(37)	5115(21)	47(17)	2553(9)	111(14)
Si(1)	3893(4)	2510(4)	-1193(2)	77(3)	C(38)	2495(12)	142(12)	925(7)	82(10)
Si(2)	5745(4)	3926(3)	619(2)	59(2)	C(39)	3512(16)	-824(10)	1204(6)	84(11)
Si(1')	10300(4)	1118(3)	-819(3)	85(3)	C(40)	4031(15)	50(10)	699(6)	72(10)
Si(2')	9549(5)	2272(4)	1083(2)	87(3)	C(41)	3468(15)	-25(10)	1068(6)	61(9)
P	3371(3)	1703(3)	944(2)	45(2)	C(1')	8599(10)	1701(7)	-673(4)	52(8)
P'	7859(3)	3330(3)	-1028(2)	53(2)	C(2')	8090	1752	-335	66(9)
N	5006(9)	1825(7)	576(4)	36(5)	C(3')	8607	1496	38	82(11)
N'	9671(9)	3189(7)	-638(4)	39(6)	C(4')	9435	1286	-69	57(9)
C1	5888(3)	2536(3)	-115(1)	53(2)	C(5')	9431	1413	-509	51(8)
C1'	10931(3)	2375(3)	16(2)	63(2)	C(6')	8362(8)	2903(8)	351(5)	62(9)
C(1)	4452(8)	1528(8)	-529(4)	51(8)	C(7')	8399	3496	81	51(8)
C(2)	4135	1142	-199	54(8)	C(8')	9268	3770	151	53(8)
C(3)	3309	1431	-138	68(10)	C(9')	9768	3346	465	53(8)
C(4)	3115	1995	-430	50(8)	C(10')	9208	2810	589	58(8)
C(5)	3821	2055	-672	56(8)	C(11')	8142(8)	4660(8)	-1433(3)	53(8)
C(6)	3964(9)	3292(6)	535(3)	43(7)	C(12')	8356	5085	-1762	65(9)
C(7)	3232	3209	213	55(8)	C(13')	8457	4783	-2152	60(9)
C(8)	3492	3426	-178	56(8)	C(14')	8344	4056	-2213	74(10)
C(9)	4385	3643	-98	51(8)	C(15')	8131	3631	-1884	62(9)
C(10)	4676	3560	343	43(7)	C(16')	8030	3933	-1494	60(9)
C(11)	4128(8)	1561(4)	1808(4)	50(8)	C(17')	10215(8)	3909(7)	-1192(4)	57(8)
C(12)	4543	1207	2165	50(8)	C(18')	10800	4414	-1308	89(11)
C(13)	4647	474	2156	57(8)	C(19')	11470	4674	-1006	90(12)
C(14)	4337	96	1789	59(8)	C(20')	11555	4431	-589	81(11)
C(15)	3923	450	1432	46(8)	C(21')	10969	3926	-473	46(7)
C(16)	3818	1183	1442	39(7)	C(22')	10300	3666	-774	48(8)
C(17)	6195(9)	1028(7)	457(3)	55(8)	C(23')	8836(12)	3161(8)	-736(5)	42(7)
C(18)	6832	527	606	68(9)	C(24')	9691(17)	529(14)	-1250(10)	143(16)
C(19)	6973	352	1036	86(11)	C(25')	10841(14)	1831(11)	-1083(7)	80(10)
C(20)	6479	677	1317	80(10)	C(26')	11167(15)	604(11)	-407(9)	110(13)
C(21)	5842	1178	1168	57(8)	C(27')	10497(28)	1701(29)	1080(10)	265(30)
C(22)	5700	1353	738	50(8)	C(28')	8541(26)	1729(19)	1211(9)	197(22)
C(23)	4207(12)	1864(9)	665(5)	39(7)	C(29')	9776(36)	2928(19)	1508(8)	262(31)
C(24)	3653(27)	1749(18)	-1588(8)	193(21)	C(30')	7860(17)	5917(11)	-1103(7)	88(11)
C(25)	3048(21)	3234(14)	-1287(8)	129(15)	C(31')	8721(13)	4961(11)	-674(5)	65(8)
C(26)	5004(21)	2876(17)	-1239(9)	155(18)	C(32')	7033(14)	4876(12)	-898(6)	79(10)
C(27)	6324(14)	4369(11)	198(7)	79(10)	C(33')	7969(14)	5100(10)	-1018(6)	57(8)
C(28)	5425(16)	4661(12)	985(7)	96(11)	C(34')	9685(19)	5489(16)	-2366(8)	131(15)
C(29)	6447(14)	3231(12)	942(7)	84(10)	C(35')	8682(25)	4897(20)	-2911(8)	188(21)
C(30)	4148(18)	2562(11)	2364(7)	98(11)	C(36')	8140(22)	5955(20)	-2547(10)	176(20)
C(31)	4611(22)	2806(12)	1664(7)	129(15)	C(37')	8750(15)	5275(16)	-2503(7)	88(12)
C(32)	3044(22)	2628(12)	1741(7)	123(14)	C(38')	7034(23)	2636(13)	-1901(8)	124(15)
C(33)	3974(18)	2375(10)	1886(6)	76(10)	C(39')	7875(19)	2756(15)	-2500(8)	124(14)
C(34)	5901(35)	-197(45)	2466(15)	452(60)	C(40')	8634(20)	2376(14)	-1803(8)	116(114)
C(35)	5117(27)	497(20)	2966(10)	198(23)	C(41')	7941(17)	2858(13)	-2019(8)	83(11)

^a Equivalent isotropic *U* defined as one-third of the trace of the orthogonalized U_{ij} tensor.

Table 3. Selected Bond Lengths (\AA)^a

Nb-N	2.075(12)	N-C(23)	1.301(23)
Nb-C(23)	2.198(17)	N-C(22)	1.429(18)
Nb-Cl	2.503(5)	P-C(23)	1.688(19)
Nb-Cp' centroid (Cnt)	2.13 (av)	P-C(16)	1.908(12)

^aThese data refer to one of the two independent but chemically equivalent molecules found in the unit cell. Complete lists of bond lengths and angles for both molecules are included in the supplementary material.

Table 4. Selected Bond Angles (deg)^a

N-Nb-Cl	83.1(4)	Nb-C(23)-N	67.2(9)
N-Nb-C(23)	35.3(6)	Nb-N-C(22)	147.8(10)
Cl-Nb-C(23)	117.9(5)	P-C(23)-N	156.2(13)
Cnt-Nb-Cnt	128 (av)	C(16)-P-C(23)	108.5(7)
Nb-N-C(23)	77.5(9)	C(22)-N-C(23)	129.5(13)

^aThese data refer to one of the two independent but chemically equivalent molecules found in the unit cell. Complete lists of bond lengths and angles for both molecules are included in the supplementary material.

= 2.1 Hz, 2H, Cp'); 5.92 (d, *J* = 2.1 Hz, 2H, Cp'); 5.60 (d, *J* = 2.1 Hz, 2H, Cp'); 1.80 (18H, *o*-*t*-Bu); 1.41 (9H, *p*-*t*-Bu); 0.20 (18H, SiMe₃). ¹³C{¹H} NMR (CD₂Cl₂) (δ): 171.5 (d, ¹J_{PC} = 155.3 Hz, P=C=N); 155.0 (d, ²J_{PC} = 3.8 Hz, *o*-Mes*); 148.9 (*p*-

Mes*); 144.3 (ipso Ph); 140.3 (d, *J*_{PC} = 87.7 Hz, ipso Mes*); 127.7 (*m*-Ph); 126.1 (d, *J*_{PC} = 1.6 Hz, Cp'); 124.0 (*o*-Ph); 123.0 (*p*-Ph); 121.9 (*m*-Mes*); 117.8 (Cp'C-SiMe₃); 112.5 (d, *J*_{PC} = 3.8 Hz, Cp'); 112.1 (Cp'); 108.8 (d, *J*_{PC} = 5.0 Hz, Cp'); 38.7 (d, *J*_{PC} = 1.6 Hz, *o*-CMe₃); 35.0 (*p*-CMe₃); 33.4 (d, *J*_{PC} = 4.4 Hz, *o*-CMe₃); 31.6 (*p*-CMe₃); 0.2 (d, *J*_{PC} = 1.1 Hz, SiMe₃). ³¹P{¹H} NMR (C₆D₆): δ 14.3. IR (KBr): 2951, 2361, 1652, 1592, 1558, 1540, 1505, 1456, 1387, 1358, 1248, 1170, 837 cm⁻¹. Anal. Calcd for C₄₁H₈₀ClNNbPSi₂: C, 62.94; H, 7.73; N, 1.77; Found: C, 62.89; H, 7.79; N, 1.83.

X-ray Crystal Structure Determination of 3. Crystal, data collection, and refinement parameters are given in Table 1. Suitable crystals were selected and mounted with epoxy cement to glass fibers. The unit-cell parameters were obtained by the least-squares refinement of the angular settings of 24 reflections ($2\theta \leq 25^\circ$).

The systematic absences in the diffraction data for **3** are uniquely consistent for space group *P2₁/c*. The structure was solved using direct methods, completed by subsequent difference Fourier syntheses and refined by full-matrix least-squares procedures. Two independent but chemically equiv compound molecules were located in the asymmetric unit. The centroid to niobium distances are 2.125(14), 2.131(15), 2.137(14), and 2.125(14) \AA . The centroid-niobium-centroid angles are 127.8(5) and 128.9(5)°. All non-hydrogen atoms were refined

with anisotropic displacement coefficients. Hydrogen atoms were ignored. Phenyl rings were refined as rigid planar hexagons and Cp rings as rigid pentagons to conserve data. Additional results of the structure determination are available as supporting information.

All software and sources of the scattering factors are contained in either the SHELXTL (5.1) or the SHELXTL PLUS (4.2) program libraries (G. Sheldrick, Siemens XRD, Madison, WI).

Photochemical Conversion of 3 to Cp₂NbCl(CNPh) (4) and 2,4-(*t*-Bu)₂-6-C₈H₂CMe₂PH (2). A red benzene-*d*₆ (1 mL) solution of **3** (10 mg, 13 μmol) with a tetramethylsilane internal standard was irradiated with a water-cooled 450 W Ace-Hanovia Mercury photochemical lamp for 5 h. The solution darkened to a deep brown. The ¹H NMR spectrum, after irradiation, showed formation of **2** and **4** in 79% yield. The isocyanide complex **4** was characterized by ¹H NMR and IR of the reaction mixture, while phosphaindan **2** was identified by ¹H and ³¹P NMR in comparison to an authentic sample.

In a separate experiment, a similar sample of **3** was irradiated for 1 h, after which the solution contained an ~2:3 mixture of **3** and **1** by ³¹P NMR. Additional irradiation (2 h) completed the conversion to **2** and **4**. In a third experiment, a sample of **1** (10 mg, 26 μmol) in benzene-*d*₆ (1 mL) was irradiated for 3 h and showed only **2** in the ³¹P NMR spectrum.

[Cp₂Nb(Cl){(η²-N,C)PhN=CPhMes*}]JBF₄ (5). Tetrafluoroboric acid dimethyl ether complex (14.9 μL, 0.128 mmol) was added to a solution of **3** (100 mg, 0.128 mmol) in petroleum ether (5 mL). The clear red solution became yellow after 1 h of stirring, with precipitation of the product. The white powder was collected on a fine frit and washed with petroleum ether (99 mg, 89%). An analytical sample, obtained from a 1:1 mixture of methylene chloride and petroleum ether (5 mL), cocrystallized with CH₂Cl₂, as confirmed quantitatively by ¹H NMR.

¹H NMR (CD₂Cl₂) (δ): 7.44 (d, ³J_{PH} = 2.4 Hz, 2H, Mes*); 7.32 (d, ¹J_{PH} = 302 Hz, 1 H, P-H); 7.19 (t, *J* = 8.0 Hz, 1 H, *p*-Ph); 7.04 (t, *J* = 8.0 Hz, 2H, *m*-Ph); 6.83 (2H, Cp'); 6.54 (d, *J* = 7.6 Hz, 2H, *o*-Ph); 6.36 (4H, Cp'); 6.03 (2H, Cp'); 1.47 (18H, *o*-*t*-Bu); 1.36 (9H, *p*-*t*-Bu); 0.17 (18H, SiMe₃). ¹³C{¹H} NMR

(CD₂Cl₂) (δ): 208.5 (d, ¹J_{PC} = 115.6 Hz, P-C≡N); 157.2 (d, ³J_{PC} = 11.0 Hz, ipso Ph); 154.6 (quat-Mes*); 137.4 (quat-Mes*); 130.8 (Cp'₂-SiMe₃); 128.95–128.9 (overlapping *p*-Ph and *m*-Ph); 126.2 (Cp'); 124.2 (*m*-Mes*); 123.9 (*o*-Ph); 121.4 (d, ¹J_{PC} = 35.0 Hz, ipso Mes*); 112.3 (Cp'); 110.2 (Cp'); 109.9 (Cp'); 38.3 (*o*-CMe₃); 35.7 (*p*-C Me₃); 33.8 (d, *J*_{PC} = 6.0 Hz, *o*-CMe₃); 31.4 (*p*-CMe₃); 0.3 (SiMe₃). ³¹P NMR (CD₂Cl₂): δ -37.4 ppm (d, *J*_{PH} = 302 Hz). IR (KBr): 3113, 2957, 2902, 1641, 1590, 1484, 1408, 1364, 1248, 1167, 1051, 904, 837, 755, 687, 636, 522 cm⁻¹. Anal. Calcd for C₄₁H₆₁BClF₄NNbPSi₂·0.95CH₂Cl₂: C, 52.98; H, 6.67; N, 1.47. Found: C, 52.63; H, 6.87, N, 1.53.

Reaction of 5 with D₂O. An excess of D₂O (~0.1 mL, 99.9% D) was added to a solution of **5** (10 mg, 11.5 μmol) in either nitromethane-*d*₃ or methylene-*d*₂ chloride in an NMR tube. After the tube was vigorously shaken for several minutes, the ³¹P and ¹H NMR spectra were recorded. The P-H signal disappeared in the ¹H spectrum, and the ³¹P spectrum showed a 1:1:1 triplet (δ -38.4, *J*_{PD} = 44.3 Hz).

Reaction of 5 with KO-*t*-Bu. A clear solution of **5** (14 mg, 16 μmol) in THF (1 mL) was added to solid KO-*t*-Bu (2 mg, 16 μmol). The solution became red, and ³¹P NMR showed that **3** was the only P-containing product.

Acknowledgment. We thank Dartmouth College and the Petroleum Research Fund, administered by the ACS, for partial support of this work. J.B.A. thanks Dartmouth College for a Presidential Scholarship and the NSF for a REU fellowship.

Supporting Information Available: Additional structural results for **3**, including complete tables of bond lengths and angles and anisotropic displacement coefficients (7 pages). This material is contained in many libraries on microfiche, immediately follows this article in the microfilm version of the journal, can be ordered from the ACS, and can be downloaded from the Internet; see any current masthead page for ordering information and Internet access instructions.

OM950116H